

INTERNATIONAL TABLES
FOR
CRYSTALLOGRAPHY

International Tables for Crystallography

Volume A: *Space-Group Symmetry*

Editor Theo Hahn

First Edition 1983, Fifth Edition 2002

Volume B: *Reciprocal Space*

Editor U. Shmueli

First Edition 1993, Second Edition 2001

Volume C: *Mathematical, Physical and Chemical Tables*

Editors A. J. C. Wilson and E. Prince

First Edition 1992, Second Edition 1999

Volume D: *Physical Properties of Crystals*

Editor A. Authier

First Edition 2003

Volume E: *Subperiodic Groups*

Editors V. Kopský and D. B. Litvin

First Edition 2002

Volume F: *Crystallography of Biological Macromolecules*

Editors Michael G. Rossmann and Eddy Arnold

First Edition 2001

Forthcoming volumes

Volume A1: *Symmetry Relations between Space Groups*

Editors H. Wondratschek and U. Müller

Volume G: *Definition and Exchange of Crystallographic Data*

Editors S. R. Hall and B. McMahon

INTERNATIONAL TABLES FOR CRYSTALLOGRAPHY

Volume D
PHYSICAL PROPERTIES OF CRYSTALS

Edited by
A. AUTHIER

Published for
THE INTERNATIONAL UNION OF CRYSTALLOGRAPHY
by
KLUWER ACADEMIC PUBLISHERS
DORDRECHT/BOSTON/LONDON
2003

A C.I.P. Catalogue record for this book
is available from the Library of Congress
ISBN 1-4020-0714-0 (acid-free paper)

Published by Kluwer Academic Publishers,
P.O. Box 17, 3300 AA Dordrecht, The Netherlands

Sold and distributed in North, Central and South America
by Kluwer Academic Publishers,
101 Philip Drive, Norwell, MA 02061, USA

In all other countries, sold and distributed
by Kluwer Academic Publishers,
P.O. Box 322, 3300 AH Dordrecht, The Netherlands

Technical Editors: N. J. Ashcroft and A. S. Berry
© International Union of Crystallography 2003

Short extracts may be
reproduced without formality, provided that the
source is acknowledged, but substantial portions
may not be reproduced by any process
without written permission from the
International Union of Crystallography

Printed in Denmark by P. J. Schmidt A/S

Contributing authors

- A. AUTHIER: Institut de Minéralogie et de la Physique des Milieux Condensés, Bâtiment 7, 140 rue de Lourmel, 75051 Paris, France. E-mail: AAuthier@wanadoo.fr. [1.1, 1.3]
- P. BOČEK: Institute of Information Theory and Automation, Academy of Sciences of the Czech Republic, Pod vodárenskou věží 4, 182 08 Prague 8, Czech Republic. E-mail: bocek@utia.cas.cz. [3.1.6, *GI★KoBo-1*]
- A. S. BOROVIK–ROMANOV†: P. L. Kapitza Institute for Physical Problems, Russian Academy of Sciences, Kosygin Street 2, 119334 Moscow, Russia. [1.5]
- B. BOULANGER: Laboratoire de Spectrométrie Physique, Université Joseph Fourier, 140 avenue de la Physique, BP 87, 38 402 Saint-Martin-d'Hères, France. E-mail: benoit.boulanger@ujf-grenoble.fr. [1.7]
- E. COURTENS: Laboratoire des Verres, Université Montpellier 2, Case 069, Place Eugène Bataillon, 34095 Montpellier CEDEX, France. E-mail: eric.courtens@ldv.univ-montp2.fr. [2.4]
- K. G. COX†: Department of Earth Sciences, University of Oxford, Parks Road, Oxford OX1 3PR, England. [1.6]
- G. ECKOLD: Institut für Physikalische Chemie, Universität Göttingen, Tammannstrasse 6, D-37077 Göttingen, Germany. E-mail: geckold@gwdg.de. [2.1]
- M. EPHRAÏM: Advisory Engineering Agency PROMIS, PO Box 854, 1180 AW Amstelveen, The Netherlands. E-mail: M.Ephraim@promisbv.com. [1.2.7, *Tenχar*]
- A. M. GLAZER: Department of Physics, University of Oxford, Parks Road, Oxford OX1 3PU, England. E-mail: glazer@physics.ox.ac.uk. [1.6]
- I. GREGORA: Institute of Physics, Academy of Sciences of the Czech Republic, Na Slovance 2, CZ-18221 Prague 8, Czech Republic. E-mail: gregora@fzu.cz. [2.3]
- H. GRIMMER: Labor für Neutronenstreuung, ETH Zurich, and Paul Scherrer Institute, CH-5234 Villigen PSI, Switzerland. E-mail: hans.grimmer@psi.ch. [1.5]
- TH. HAHN: Institut für Kristallographie, Rheinisch–Westfälische Technische Hochschule, D-52056 Aachen, Germany. E-mail: hahn@xtal.rwth-aachen.de. [3.2, 3.3]
- A. JANNER: Institute for Theoretical Physics, University of Nijmegen, 6525 ED Nijmegen, The Netherlands. E-mail: alo@sci.kun.nl. [1.2.7, *Tenχar*]
- V. JANOVEC: Department of Physics, Technical University of Liberec, Hálkova 6, 461 17 Liberec 1, Czech Republic. Email: janovec@fzu.cz. [3.1.3, 3.2, 3.4]
- T. JANSSEN: Institute for Theoretical Physics, University of Nijmegen, 6524 ED Nijmegen, The Netherlands. E-mail: ted@sci.kun.nl. [1.2, 1.10, *Tenχar*]
- H. KLAPPER: Mineralogisch-Petrologisches Institut, Universität Bonn, D-53113 Bonn, Germany. E-mail: klapper@uni-bonn.de. [3.2, 3.3]
- V. KOPSKÝ: Institute of Physics, Academy of Sciences of the Czech Republic, Na Slovance 2, 182 21 Prague 8, and Department of Physics, Technical University of Liberec, Hálkova 6, 461 17 Liberec 1, Czech Republic. E-mail: kopsky@fzu.cz. [3.1.3, 3.1.6, *GI★KoBo-1*]
- W. F. KUHS: GZG Abt. Kristallographie, Goldschmidtstrasse 1, 37077 Göttingen, Germany. E-mail: wkuhs1@gwdg.de. [1.9]
- H. KÜPPERS: Institut für Geowissenschaften, Universität Kiel, Olshausenstrasse 40, D-24098 Kiel, Germany. E-mail: kueppers@min.uni-kiel.de. [1.4]
- G. D. MAHAN: Department of Physics, 104 Davey Laboratory, Pennsylvania State University, University Park, Pennsylvania, USA. E-mail: gmahan@psu.edu. [1.8]
- J. PŘÍVRATSKÁ: Department of Mathematics and Didactics of Mathematics, Technical University of Liberec, Hálkova 6, 461 17 Liberec 1, Czech Republic. E-mail: jana.privratska@vslib.cz. [3.4]
- K. SCHWARZ: Institut für Materialchemie, Technische Universität Wien, Getreidemarkt 9/165-TC, A-1060 Vienna, Austria. Email: kschwarz@theochem.tuwien.ac.at. [2.2]
- J. F. SCOTT: Earth Sciences Department, University of Cambridge, Downing Street, Cambridge CB2 3EQ England. E-mail: JSCO99@esc.cam.ac.uk. [3.1.5]
- A. THIERS: AT Computing, Toernooiveld 104, 6525 EC Nijmegen, The Netherlands. Email: ad.thiers@ATConsultancy.nl. [1.2.7, *Tenχar*]
- J.-C. TOLÉDANO: Ecole Polytechnique, Route de Saclay, 91128 Palaiseau CEDEX France. E-mail: toledano@hp1sesi.polytechnique.fr. [3.1.1, 3.1.2, 3.1.4]
- R. VACHER: Laboratoire des Verres, Université Montpellier 2, Case 069, Place Eugène Bataillon, 34095 Montpellier CEDEX, France. E-mail: rene.vacher@ldv.univ-montp2.fr. [2.4]
- A. ZAREMBOWITCH: Laboratoire de Physique des Milieux Condensés, Université P. et M. Curie, 75252 Paris CEDEX 05, France. E-mail: Andre.Zarembowitch@pmc.jussieu.fr. [1.3]
- J. ZYSS: Laboratoire de Photonique Quantique et Moléculaire, Ecole Normale Supérieure de Cachan, 61 Avenue du Président Wilson, 94235 Cachan, France. E-mail: zyss.joseph@lpqm.ens-cachan.fr. [1.7]

† Deceased.

Contents

| | PAGE |
|--|------------|
| Preface (A. AUTHIER) | xi |
| PART 1. TENSORIAL ASPECTS OF PHYSICAL PROPERTIES | |
| 1.1. Introduction to the properties of tensors (A. AUTHIER) | 3 |
| 1.1.1. The matrix of physical properties | 3 |
| 1.1.2. Basic properties of vector spaces | 5 |
| 1.1.3. Mathematical notion of tensor | 7 |
| 1.1.4. Symmetry properties | 10 |
| 1.1.5. Thermodynamic functions and physical property tensors | 31 |
| 1.1.6. Glossary | 32 |
| 1.2. Representations of crystallographic groups (T. JANSSEN) | 34 |
| 1.2.1. Introduction | 34 |
| 1.2.2. Point groups | 35 |
| 1.2.3. Space groups | 46 |
| 1.2.4. Tensors | 51 |
| 1.2.5. Magnetic symmetry | 53 |
| 1.2.6. Tables | 56 |
| 1.2.7. Introduction to the accompanying software <i>Tenxar</i> (M. EPHRAÏM, T. JANSSEN, A. JANNER AND A. THIERS) | 62 |
| 1.2.8. Glossary | 70 |
| 1.3. Elastic properties (A. AUTHIER AND A. ZAREMBOWITCH) | 72 |
| 1.3.1. Strain tensor | 72 |
| 1.3.2. Stress tensor | 76 |
| 1.3.3. Linear elasticity | 80 |
| 1.3.4. Propagation of elastic waves in continuous media – dynamic elasticity | 86 |
| 1.3.5. Pressure dependence and temperature dependence of the elastic constants | 89 |
| 1.3.6. Nonlinear elasticity | 91 |
| 1.3.7. Nonlinear dynamic elasticity | 94 |
| 1.3.8. Glossary | 97 |
| 1.4. Thermal expansion (H. KÜPPERS) | 99 |
| 1.4.1. Definition, symmetry and representation surfaces | 99 |
| 1.4.2. Grüneisen relation | 100 |
| 1.4.3. Experimental methods | 101 |
| 1.4.4. Relation to crystal structure | 103 |
| 1.4.5. Glossary | 104 |
| 1.5. Magnetic properties (A. S. BOROVIK-ROMANOV AND H. GRIMMER) | 105 |
| 1.5.1. Introduction | 105 |
| 1.5.2. Magnetic symmetry | 109 |
| 1.5.3. Phase transitions into a magnetically ordered state | 116 |
| 1.5.4. Domain structure | 125 |
| 1.5.5. Weakly non-collinear magnetic structures | 127 |
| 1.5.6. Reorientation transitions | 131 |
| 1.5.7. Piezomagnetism | 132 |
| 1.5.8. Magnetoelectric effect | 137 |
| 1.5.9. Magnetostriction | 142 |
| 1.5.10. Transformation from Gaussian to SI units | 146 |
| 1.5.11. Glossary | 146 |

CONTENTS

| | |
|--|-----|
| 1.6. Classical linear crystal optics (A. M. GLAZER AND K. G. COX) | 150 |
| 1.6.1. Introduction | 150 |
| 1.6.2. Generalized optical, electro-optic and magneto-optic effects | 150 |
| 1.6.3. Linear optics | 152 |
| 1.6.4. Practical observation of crystals | 154 |
| 1.6.5. Optical rotation | 166 |
| 1.6.6. Linear electro-optic effect | 172 |
| 1.6.7. The linear photoelastic effect | 173 |
| 1.6.8. Glossary | 176 |
| 1.7. Nonlinear optical properties (B. BOULANGER AND J. ZYSS) | 178 |
| 1.7.1. Introduction | 178 |
| 1.7.2. Origin and symmetry of optical nonlinearities | 178 |
| 1.7.3. Propagation phenomena | 183 |
| 1.7.4. Determination of basic nonlinear parameters | 212 |
| 1.7.5. The main nonlinear crystals | 214 |
| 1.7.6. Glossary | 216 |
| 1.8. Transport properties (G. D. MAHAN) | 220 |
| 1.8.1. Introduction | 220 |
| 1.8.2. Macroscopic equations | 220 |
| 1.8.3. Electrical resistivity | 220 |
| 1.8.4. Thermal conductivity | 224 |
| 1.8.5. Seebeck coefficient | 226 |
| 1.8.6. Glossary | 227 |
| 1.9. Atomic displacement parameters (W. F. KUHS) | 228 |
| 1.9.1. Introduction | 228 |
| 1.9.2. The atomic displacement parameters (ADPs) | 228 |
| 1.9.3. Site-symmetry restrictions | 232 |
| 1.9.4. Graphical representation | 232 |
| 1.9.5. Glossary | 242 |
| 1.10. Tensors in quasiperiodic structures (T. JANSSEN) | 243 |
| 1.10.1. Quasiperiodic structures | 243 |
| 1.10.2. Symmetry | 245 |
| 1.10.3. Action of the symmetry group | 247 |
| 1.10.4. Tensors | 249 |
| 1.10.5. Tables | 255 |

PART 2. SYMMETRY ASPECTS OF EXCITATIONS

| | |
|---|-----|
| 2.1. Phonons (G. ECKOLD) | 266 |
| 2.1.1. Introduction | 266 |
| 2.1.2. Fundamentals of lattice dynamics in the harmonic approximation | 266 |
| 2.1.3. Symmetry of lattice vibrations | 274 |
| 2.1.4. Conclusion | 291 |
| 2.1.5. Glossary | 291 |
| 2.2. Electrons (K. SCHWARZ) | 294 |
| 2.2.1. Introduction | 294 |
| 2.2.2. The lattice | 294 |
| 2.2.3. Symmetry operators | 294 |
| 2.2.4. The Bloch theorem | 295 |
| 2.2.5. The free-electron (Sommerfeld) model | 297 |

CONTENTS

| | |
|--|------------|
| 2.2.6. Space-group symmetry | 297 |
| 2.2.7. The k vector and the Brillouin zone | 298 |
| 2.2.8. Bloch functions | 299 |
| 2.2.9. Quantum-mechanical treatment | 299 |
| 2.2.10. Density functional theory | 300 |
| 2.2.11. Band-theory methods | 301 |
| 2.2.12. The linearized augmented plane wave method | 303 |
| 2.2.13. The local coordinate system | 304 |
| 2.2.14. Characterization of Bloch states | 305 |
| 2.2.15. Electric field gradient tensor | 307 |
| 2.2.16. Examples | 310 |
| 2.2.17. Conclusion | 312 |
| 2.3. Raman scattering (I. GREGORA) | 314 |
| 2.3.1. Introduction | 314 |
| 2.3.2. Inelastic light scattering in crystals – basic notions | 314 |
| 2.3.3. First-order scattering by phonons | 315 |
| 2.3.4. Morphic effects in Raman scattering | 322 |
| 2.3.5. Spatial-dispersion effects | 325 |
| 2.3.6. Higher-order scattering | 326 |
| 2.3.7. Conclusions | 327 |
| 2.3.8. Glossary | 328 |
| 2.4. Brillouin scattering (R. VACHER AND E. COURTENS) | 329 |
| 2.4.1. Introduction | 329 |
| 2.4.2. Elastic waves | 329 |
| 2.4.3. Coupling of light with elastic waves | 330 |
| 2.4.4. Brillouin scattering in crystals | 330 |
| 2.4.5. Use of the tables | 331 |
| 2.4.6. Techniques of Brillouin spectroscopy | 331 |
| PART 3. SYMMETRY ASPECTS OF STRUCTURAL PHASE TRANSITIONS, TWINNING AND DOMAIN STRUCTURES | |
| 3.1. Structural phase transitions (J.-C. TOLÉDANO, V. JANOVEC, V. KOPSKÝ, J. F. SCOTT AND P. BOČEK) | 338 |
| 3.1.1. Introduction (J.-C. TOLÉDANO) | 338 |
| 3.1.2. Thermodynamics of structural transitions (J.-C. TOLÉDANO) | 340 |
| 3.1.3. Equitranslational phase transitions. Property tensors at ferroic phase transitions (V. JANOVEC AND V. KOPSKÝ) | 350 |
| 3.1.4. Example of a table for non-equitranslational phase transitions (J.-C. TOLÉDANO) | 361 |
| 3.1.5. Microscopic aspects of structural phase transitions and soft modes (J. F. SCOTT) | 361 |
| 3.1.6. Group informatics and tensor calculus (V. KOPSKÝ AND P. BOČEK) | 372 |
| 3.1.7. Glossary | 374 |
| 3.2. Twinning and domain structures (V. JANOVEC, TH. HAHN AND H. KLAPPER) | 377 |
| 3.2.1. Introduction and history | 377 |
| 3.2.2. A brief survey of bicrystallography | 378 |
| 3.2.3. Mathematical tools | 379 |
| 3.3. Twinning of crystals (TH. HAHN AND H. KLAPPER) | 393 |
| 3.3.1. Crystal aggregates and intergrowths | 393 |
| 3.3.2. Basic concepts and definitions of twinning | 394 |
| 3.3.3. Morphological classification, simple and multiple twinning | 398 |
| 3.3.4. Composite symmetry and the twin law | 399 |

CONTENTS

| | |
|--|-----|
| 3.3.5. Description of the twin law by black–white symmetry | 402 |
| 3.3.6. Examples of twinned crystals | 403 |
| 3.3.7. Genetic classification of twins | 412 |
| 3.3.8. Lattice aspects of twinning | 416 |
| 3.3.9. Twinning by merohedry and pseudo-merohedry | 422 |
| 3.3.10. Twin boundaries | 426 |
| 3.3.11. Glossary | 444 |
| 3.4. Domain structures (V. JANOVEC AND J. PŘÍVRATSKÁ) | 449 |
| 3.4.1. Introduction | 449 |
| 3.4.2. Domain states | 451 |
| 3.4.3. Domain pairs: domain twin laws, distinction of domain states and switching | 470 |
| 3.4.4. Domain twins and domain walls | 491 |
| 3.4.5. Glossary | 502 |
| List of terms and symbols used in this volume | 507 |
| Author index | 509 |
| Subject index | 514 |

Preface

BY ANDRÉ AUTHIER

The initial idea of having a volume of *International Tables for Crystallography* dedicated to the physical properties of crystals is due to Professor B. T. M. Willis. He submitted the proposal to the Executive Committee of the International Union of Crystallography during their meeting in Vienna in 1988. The principle was then adopted, with Professor Willis as Editor. After his resignation in 1990, I was asked by the Executive Committee to become the new Editor. Following a broad consultation with many colleagues, a nucleus of potential authors met in Paris in June 1991 to define the contents of the volume and to designate its contributors. This was followed by a meeting in 1995, hosted by Theo Hahn in Aachen, of the authors contributing to Part 3 and by another meeting in 1998, hosted by Vaclav Janovec and Vojtech Kopský in Prague, of the authors of the supplementary software.

The aim of Volume D is to provide an up-to-date account of the physical properties of crystals, with many useful tables, to a wide readership in the fields of mineralogy, crystallography, solid-state physics and materials science. An original feature of the volume is the bringing together of various topics that are usually to be found in quite different handbooks but that have in common their tensorial nature and the role of crystallographic symmetry. Part 3 thus confronts the properties of twinning, which traditionally pertains to crystallography and mineralogy, and the properties of ferroelectric or ferroelastic domains, which are usually studied in physics.

The volume comprises three parts and a CD-ROM of supplementary software.

The first part is devoted to the tensorial properties of physical quantities. After a presentation of the matrix of physical properties and an introduction to the mathematical notion of a tensor, the symmetry properties of tensors and the representations of crystallographic groups are discussed, with a special treatment for the case of quasiperiodic structures. The first part also includes several examples of physical property tensors developed in separate chapters: elastic properties, thermal expansion, magnetic properties, optical properties (both linear and nonlinear), transport properties and atomic displacement parameters.

The second part is concerned with the symmetry aspects of excitations in reciprocal space. It includes bases of solid-state physics and describes in the first two chapters the properties of phonons and electrons in crystals. The following two chapters deal with Raman and Brillouin scattering.

The third part concerns structural phase transitions and twinning. The first chapter includes an introduction to the

Landau theory, a description of the behaviour of physical property tensors at ferroic phase transitions and an approach to the microscopical aspect of structural transitions and soft modes, with practical examples. The second chapter explains the relationship between twinning and domain structures and introduces the group-theoretical tools needed for the analysis of domain structures and twins. In the third chapter, the basic concepts and definitions of twinning are presented, as well as the morphological, genetic and lattice classifications of twins and the properties of twin boundaries, with many examples. The fourth chapter is devoted to the symmetry and crystallographic analysis of domain structures. The relations that govern their formation are derived and tables with useful ready-to-use data on domain structures of ferroic phases are provided.

An innovation of Volume D is an accompanying CD-ROM containing two programs. The first, *TenChar (Calculations with Tensors and Characters)* supports Part 1 for the determination of irreducible group representations and tensor components. The second, *GI★KoBo-1*, supports Part 3 on structural phase transitions and enables the reader to find the changes in the tensor properties of physical quantities during ferroic phase transitions.

For various reasons, Volume D has taken quite a long time to produce, from the adoption of its principle in 1990 to its actual printing in 2003, and it is a particular pleasure for me to see the outcome of so many efforts. I would like to take this opportunity to thank all those who have contributed to the final result. Firstly, thanks are due to Terry Willis, whose idea the volume was and who made the initial push to have it accepted. I am very grateful to him for his encouragement and for having translated into English a set of notes that I had written for my students and which served as the nucleus of Chapter 1.1. I am greatly indebted to the Technical Editors who have worked tirelessly over the years: Sue Barnes in the early years and then Nicola Ashcroft, Amanda Berry and the staff of the Editorial Office in Chester, who did the hard work of editing all the chapters and translating them into Standard Generalized Markup Language (SGML); I thank them for their infinite patience and good humour. I am also very grateful to the Research and Development Officer, Brian McMahon, for his successful integration of the supplementary software and for his constant cooperation with its authors. Last but not least, I would like to thank all the authors who contributed to the volume and made it what it is.

1.1. Introduction to the properties of tensors

By A. AUTHIER

1.1.1. The matrix of physical properties

1.1.1.1. Notion of extensive and intensive quantities

Physical laws express in general the response of a medium to a certain influence. Most physical properties may therefore be defined by a relation coupling two or more measurable quantities. For instance, the specific heat characterizes the relation between a variation of temperature and a variation of entropy at a given temperature in a given medium, the dielectric susceptibility the relation between electric field and electric polarization, the elastic constants the relation between an applied stress and the resulting strain *etc.* These relations are between quantities of the same nature: thermal, electrical and mechanical, respectively. But there are also cross effects, for instance:

(a) *thermal expansion* and *piezocalorific effect*: mechanical reaction to a thermal impetus or the reverse;

(b) *pyroelectricity* and *electrocalorific effect*: electrical response to a thermal impetus or the reverse;

(c) *piezoelectricity* and *electrostriction*: electric response to a mechanical impetus;

(d) *piezomagnetism* and *magnetostriction*: magnetic response to a mechanical impetus;

(e) *photoelasticity*: birefringence produced by stress;

(f) *acousto-optic effect*: birefringence produced by an acoustic wave;

(g) *electro-optic effect*: birefringence produced by an electric field;

(h) *magneto-optic effect*: appearance of a rotatory polarization under the influence of a magnetic field.

The physical quantities that are involved in these relations can be divided into two categories:

(i) *extensive quantities*, which are proportional to the volume of matter or to the mass, that is to the number of molecules in the medium, for instance entropy, energy, quantity of electricity *etc.* One uses frequently specific extensive parameters, which are given per unit mass or per unit volume, such as the specific mass, the electric polarization (dipole moment per unit volume) *etc.*

(ii) *intensive parameters*, quantities whose product with an extensive quantity is homogeneous to an energy. For instance, volume is an extensive quantity; the energy stored by a gas undergoing a change of volume dV under pressure p is $p dV$. Pressure is therefore the intensive parameter associated with volume. Table 1.1.1.1 gives examples of extensive quantities and of the related intensive parameters.

1.1.1.2. Notion of tensor in physics

Each of the quantities mentioned in the preceding section is represented by a mathematical expression. Some are direction independent and are represented by *scalars*: specific mass, specific heat, volume, pressure, entropy, temperature, quantity of electricity, electric potential. Others are direction dependent and are represented by *vectors*: force, electric field, electric displacement, the gradient of a scalar quantity. Still others cannot be represented by scalars or vectors and are represented by more complicated mathematical expressions. Magnetic quantities are represented by *axial vectors* (or *pseudovectors*), which are a particular kind of tensor (see Section 1.1.4.5.3). A few examples will show the necessity of using tensors in physics and Section 1.1.3 will present elementary mathematical properties of tensors.

(i) *Thermal expansion*. In an isotropic medium, thermal expansion is represented by a single number, a scalar, but this is

not the case in an anisotropic medium: a sphere cut in an anisotropic medium becomes an ellipsoid when the temperature is varied and thermal expansion can no longer be represented by a single number. It is actually represented by a tensor of rank 2.

(ii) *Dielectric constant*. In an isotropic medium of a perfect dielectric we can write, in SI units,

$$\begin{aligned}\mathbf{P} &= \varepsilon_0 \chi_e \mathbf{E} \\ \mathbf{D} &= \varepsilon_0 \mathbf{E} + \mathbf{P} = \varepsilon_0 (1 + \chi_e) \mathbf{E} = \varepsilon \mathbf{E},\end{aligned}$$

where \mathbf{P} is the electric polarization (= dipole moment per unit volume), ε_0 the permittivity of vacuum, χ_e the dielectric susceptibility, \mathbf{D} the electric displacement and ε the dielectric constant, also called dielectric permittivity. These expressions indicate that the electric field, on the one hand, and polarization and displacement, on the other hand, are linearly related. In the general case of an anisotropic medium, this is no longer true and one must write expressions indicating that the components of the displacement are linearly related to the components of the field:

$$\begin{cases} D^1 = \varepsilon_1^1 E^1 + \varepsilon_1^2 E^2 + \varepsilon_1^3 E^3 \\ D^2 = \varepsilon_2^1 E^1 + \varepsilon_2^2 E^2 + \varepsilon_2^3 E^3 \\ D^3 = \varepsilon_3^1 E^1 + \varepsilon_3^2 E^2 + \varepsilon_3^3 E^3. \end{cases} \quad (1.1.1.1)$$

The dielectric constant is now characterized by a set of nine components ε_i^j ; they are the components of a tensor of rank 2. It will be seen in Section 1.1.4.5.2.1 that this tensor is symmetric ($\varepsilon_i^j = \varepsilon_j^i$) and that the number of independent components is equal to six.

(iii) *Stressed rod (Hooke's law)*. If one pulls a rod of length ℓ and cross section \mathcal{A} with a force F , its length is increased by a quantity $\Delta\ell$ given by $\Delta\ell/\ell = (1/E)F/\mathcal{A}$, where E is Young's modulus, or elastic stiffness (see Section 1.3.3.1). But, at the same time, the radius, r , decreases by Δr given by $\Delta r/r = -(\nu/E)F/\mathcal{A}$, where ν is Poisson's ratio (Section 1.3.3.4.3). It can be seen that a scalar is not sufficient to describe the elastic deformation of a material, even if it is isotropic. The number of independent components depends on the symmetry of the medium and it will be seen that they are the components of a tensor of rank 4. It was precisely to describe the properties of elasticity by a mathematical expression that the notion of a tensor was introduced in physics by W. Voigt in the 19th century (Voigt, 1910) and by L. Brillouin in the first half of the 20th century (Brillouin, 1949).

Table 1.1.1.1. Extensive quantities and associated intensive parameters

The last four lines of the table refer to properties that are time dependent.

| Extensive quantities | Intensive parameters |
|-------------------------|------------------------|
| Volume | Pressure |
| Strain | Stress |
| Displacement | Force |
| Entropy | Temperature |
| Quantity of electricity | Electric potential |
| Electric polarization | Electric field |
| Electric displacement | Electric field |
| Magnetization | Magnetic field |
| Magnetic induction | Magnetic field |
| Reaction rate | Chemical potential |
| Heat flow | Temperature gradient |
| Diffusion of matter | Concentration gradient |
| Electric current | Potential gradient |

1. TENSORIAL ASPECTS OF PHYSICAL PROPERTIES

(iv) *Expansion in Taylor series of a field of vectors.* Let us consider a field of vectors $\mathbf{u}(\mathbf{r})$ where \mathbf{r} is a position vector. The Taylor expansion of its components is given by

$$u^i(\mathbf{r} + d\mathbf{r}) = u^i(\mathbf{r}) + \left(\frac{\partial u^i}{\partial x^j}\right) dx^j + \frac{1}{2} \left(\frac{\partial^2 u^i}{\partial x^j \partial x^k}\right) dx^j dx^k + \dots \quad (1.1.1.2)$$

using the so-called Einstein convention, which implies that there is automatically a summation each time the same index appears twice, once as a superscript and once as a subscript. This index is called a *dummy* index. It will be shown in Section 1.1.3.8 that the nine partial differentials $\partial u^i / \partial x^j$ and the 27 partial differentials $\partial^2 u^i / (\partial x^j \partial x^k)$ are the components of tensors of rank 2 and 3, respectively.

Remark. Of the four examples given above, the first three (thermal expansion, dielectric constant, stressed rod) are related to *physical property tensors* (also called *material tensors*), which are characteristic of the medium and whose components have the same value everywhere in the medium if the latter is homogeneous, while the fourth one (expansion in Taylor series of a field of vectors) is related to a *field tensor* whose components vary at every point of the medium. This is the case, for instance, for the strain and for the stress tensors (see Sections 1.3.1 and 1.3.2).

1.1.1.3. The matrix of physical properties

Each extensive parameter is in principle a function of all the intensive parameters. For a variation di_q of a particular intensive parameter, there will be a variation de_p of every extensive parameter. One may therefore write

$$de_p = C_p^q di_q. \quad (1.1.1.3)$$

The summation is over all the intensive parameters that have varied.

One may use a matrix notation to write the equations relating the variations of each extensive parameter to the variations of all the intensive parameters:

$$(de) = (C)(di), \quad (1.1.1.4)$$

where the intensive and extensive parameters are arranged in column matrices, (di) and (de) , respectively. In a similar way, one could write the relations between intensive and extensive parameters as

$$\left. \begin{aligned} di_p &= R_p^q de_q \\ (di) &= (R)(de). \end{aligned} \right\} \quad (1.1.1.5)$$

Matrices (C) and (R) are inverse matrices. Their leading diagonal terms relate an extensive parameter and the associated intensive parameter (their product has the dimensions of energy), e.g. the elastic constants, the dielectric constant, the specific heat *etc.* The corresponding physical properties are called principal properties. If one only of the intensive parameters, i_q , varies, a variation di_q of this parameter is the *cause* of which the *effect* is a variation,

$$de_p = C_p^q di_q$$

(without summation), of each of the extensive parameters. The matrix coefficients C_p^q may therefore be considered as partial differentials:

$$C_p^q = \partial e_p / \partial i_q.$$

The parameters C_p^q that relate causes di_q and effects de_p represent physical properties and matrix (C) is called the *matrix of physical properties*. Let us consider the following intensive parameters: T stress, \mathbf{E} electric field, \mathbf{H} magnetic field, Θ

temperature and the associated extensive parameters: S strain, \mathbf{P} electric polarization, \mathbf{B} magnetic induction, σ entropy, respectively. Matrix equation (1.1.1.4) may then be written:

$$\begin{pmatrix} S \\ P \\ B \\ \delta\sigma \end{pmatrix} = \begin{pmatrix} C_S^T & C_S^E & C_S^H & C_S^\Theta \\ C_P^T & C_P^E & C_P^H & C_P^\Theta \\ C_B^T & C_B^E & C_B^H & C_B^\Theta \\ C_\sigma^T & C_\sigma^E & C_\sigma^H & C_\sigma^\Theta \end{pmatrix} \begin{pmatrix} T \\ E \\ H \\ \Theta \end{pmatrix}. \quad (1.1.1.6)$$

The various intensive and extensive parameters are represented by scalars, vectors or tensors of higher rank, and each has several components. The terms of matrix (C) are therefore actually submatrices containing all the coefficients C_p^q relating all the components of a given extensive parameter to the components of an intensive parameter. The leading diagonal terms, C_S^T , C_P^E , C_B^H , C_σ^Θ , correspond to the principal physical properties, which are elasticity, dielectric susceptibility, magnetic susceptibility and specific heat, respectively. The non-diagonal terms are also associated with physical properties, but they relate intensive and extensive parameters whose products do not have the dimension of energy. They may be coupled in pairs symmetrically with respect to the main diagonal:

C_S^E and C_P^T represent the piezoelectric effect and the converse piezoelectric effect, respectively;

C_S^H and C_B^T the piezomagnetic effect and the converse piezomagnetic effect;

C_S^Θ and C_σ^T thermal expansion and the piezocalorific effect;

C_P^T and C_σ^E the pyroelectric and the electrocalorific effects;

C_P^H and C_B^E the magnetoelectric effect and the converse magnetoelectric effect;

C_σ^H and C_B^Θ the pyromagnetic effect and the magnetocalorific effect.

It is important to note that equation (1.1.1.6) is of a thermodynamic nature and simply provides a general framework. It indicates the possibility for a given physical property to exist, but in no way states that a given material will exhibit it. Curie laws, which will be described in Section 1.1.4.2, show for instance that certain properties such as pyroelectricity or piezoelectricity may only appear in crystals that belong to certain point groups.

1.1.1.4. Symmetry of the matrix of physical properties

If parameter e_p varies by de_p , the specific energy varies by du , which is equal to

$$du = i_p de_p.$$

We have, therefore

$$i_p = \frac{\partial u}{\partial e_p}$$

and, using (1.1.1.5),

$$R_p^q = \frac{\partial i_p}{\partial e_q} = \frac{\partial^2 u}{\partial e_p \partial e_q}.$$

Since the energy is a state variable with a perfect differential, one can interchange the order of the differentiations:

$$R_p^q = \frac{\partial^2 u}{\partial e_q \partial e_p} = \frac{\partial i_q}{\partial e_p}.$$

Since p and q are dummy indices, they may be exchanged and the last term of this equation is equal to R_q^p . It follows that

$$R_p^q = R_q^p.$$

Matrices R_p^q and C_p^q are therefore symmetric. We may draw two important conclusions from this result:

1.1. INTRODUCTION TO THE PROPERTIES OF TENSORS

(i) The submatrices associated with the principal properties are symmetric with respect to interchange of the indices related to the causes and to the effects: these properties are represented by symmetric tensors. For instance, the dielectric constant and the elastic constants are represented by symmetric tensors of rank 2 and 4, respectively (see Section 1.1.3.4).

(ii) The submatrices associated with terms that are symmetric with respect to the main diagonal of matrices (C) and (R) and that represent cross effects are transpose to one another. For instance, matrix (C_S^E) representing the converse piezoelectric effect is the transpose of matrix (C_P^T) representing the piezoelectric effect. It will be shown in Section 1.1.3.4 that they are the components of tensors of rank 3.

1.1.1.5. Onsager relations

Let us now consider systems that are in steady state and not in thermodynamic equilibrium. The intensive and extensive parameters are time dependent and relation (1.1.1.3) can be written

$$J_m = L_{mn} X_n,$$

where the intensive parameters X_n are, for instance, a temperature gradient, a concentration gradient, a gradient of electric potential. The corresponding extensive parameters J_m are the heat flow, the diffusion of matter and the current density. The diagonal terms of matrix L_{mn} correspond to thermal conductivity (Fourier's law), diffusion coefficients (Fick's law) and electric conductivity (Ohm's law), respectively. Non-diagonal terms correspond to cross effects such as the thermoelectric effect, thermal diffusion *etc.* All the properties corresponding to these examples are represented by tensors of rank 2. The case of second-rank axial tensors where the symmetrical part of the tensors changes sign on time reversal was discussed by Zheludev (1986).

The *Onsager reciprocity relations* (Onsager, 1931a,b)

$$L_{mn} = L_{nm}$$

express the symmetry of matrix L_{mn} . They are justified by considerations of statistical thermodynamics and are not as obvious as those expressing the symmetry of matrix (C_p^q) . For instance, the symmetry of the tensor of rank 2 representing thermal conductivity is associated with the fact that a circulating flow is undetectable.

Transport properties are described in Chapter 1.8 of this volume.

1.1.2. Basic properties of vector spaces

[The reader may also refer to Section 1.1.4 of Volume B of *International Tables for Crystallography* (2000).]

1.1.2.1. Change of basis

Let us consider a vector space spanned by the set of n basis vectors $\mathbf{e}_1, \mathbf{e}_2, \mathbf{e}_3, \dots, \mathbf{e}_n$. The decomposition of a vector using this basis is written

$$\mathbf{x} = x^i \mathbf{e}_i \quad (1.1.2.1)$$

using the Einstein convention. The interpretation of the position of the indices is given below. For the present, we shall use the simple rules:

- (i) the index is a subscript when attached to basis vectors;
- (ii) the index is a superscript when attached to the components. The components are numerical coordinates and are therefore dimensionless numbers.

Let us now consider a second basis, \mathbf{e}'_j . The vector \mathbf{x} is independent of the choice of basis and it can be decomposed also in the second basis:

$$\mathbf{x} = x'^i \mathbf{e}'_i. \quad (1.1.2.2)$$

If A_i^j and B_j^i are the transformation matrices between the bases \mathbf{e}_i and \mathbf{e}'_j , the following relations hold between the two bases:

$$\left. \begin{aligned} \mathbf{e}_i &= A_i^j \mathbf{e}'_j; & \mathbf{e}'_j &= B_j^i \mathbf{e}_i \\ x^i &= B_j^i x'^j; & x'^j &= A_i^j x^i \end{aligned} \right\} \quad (1.1.2.3)$$

(summations over j and i , respectively). The matrices A_i^j and B_j^i are inverse matrices:

$$A_i^j B_j^k = \delta_i^k \quad (1.1.2.4)$$

(Kronecker symbol: $\delta_i^k = 0$ if $i \neq k$, $= 1$ if $i = k$).

Important Remark. The behaviour of the basis vectors and of the components of the vectors in a transformation are different. The roles of the matrices A_i^j and B_j^i are opposite in each case. The components are said to be *contravariant*. Everything that transforms like a basis vector is *covariant* and is characterized by an *inferior* index. Everything that transforms like a component is *contravariant* and is characterized by a *superior* index. The property describing the way a mathematical body transforms under a change of basis is called *variance*.

1.1.2.2. Metric tensor

We shall limit ourselves to a *Euclidean* space for which we have defined the scalar product. The analytical expression of the scalar product of two vectors $\mathbf{x} = x^i \mathbf{e}_i$ and $\mathbf{y} = y^j \mathbf{e}_j$ is

$$\mathbf{x} \cdot \mathbf{y} = x^i \mathbf{e}_i \cdot y^j \mathbf{e}_j.$$

Let us put

$$\mathbf{e}_i \cdot \mathbf{e}_j = g_{ij}. \quad (1.1.2.5)$$

The nine components g_{ij} are called the components of the *metric tensor*. Its tensor nature will be shown in Section 1.1.3.6.1. Owing to the commutativity of the scalar product, we have

$$g_{ij} = \mathbf{e}_i \cdot \mathbf{e}_j = \mathbf{e}_j \cdot \mathbf{e}_i = g_{ji}.$$

The table of the components g_{ij} is therefore symmetrical. One of the definition properties of the scalar product is that if $\mathbf{x} \cdot \mathbf{y} = 0$ for all \mathbf{x} , then $\mathbf{y} = \mathbf{0}$. This is translated as

$$x^i y^j g_{ij} = 0 \quad \forall x^i \implies y^j g_{ij} = 0.$$

In order that only the trivial solution ($y^j = 0$) exists, it is necessary that the determinant constructed from the g_{ij} 's is different from zero:

$$\Delta(g_{ij}) \neq 0.$$

This important property will be used in Section 1.1.2.4.1.

1.1.2.3. Orthonormal frames of coordinates – rotation matrix

An orthonormal coordinate frame is characterized by the fact that

$$g_{ij} = \delta_{ij} \quad (= 0 \text{ if } i \neq j \text{ and } = 1 \text{ if } i = j). \quad (1.1.2.6)$$

One deduces from this that the scalar product is written simply as

$$\mathbf{x} \cdot \mathbf{y} = x^i y^j g_{ij} = x^i y^i.$$

Let us consider a change of basis between two orthonormal systems of coordinates:

$$\mathbf{e}_i = A_i^j \mathbf{e}'_j.$$

Multiplying the two sides of this relation by \mathbf{e}'_p , it follows that

1. TENSORIAL ASPECTS OF PHYSICAL PROPERTIES

$$\mathbf{e}_i \cdot \mathbf{e}'_j = A_i^j \mathbf{e}'_k \cdot \mathbf{e}'_j = A_i^j g'_{kj} = A_i^j \delta_{kj} \quad (\text{written correctly}),$$

which can also be written, if one notes that variance is not apparent in an orthonormal frame of coordinates and that the position of indices is therefore not important, as

$$\mathbf{e}_i \cdot \mathbf{e}'_j = A_i^j \quad (\text{written incorrectly}).$$

The matrix coefficients, A_i^j , are the direction cosines of \mathbf{e}'_j with respect to the \mathbf{e}_i basis vectors. Similarly, we have

$$B_j^i = \mathbf{e}_i \cdot \mathbf{e}'_j$$

so that

$$A_i^j = B_j^i \quad \text{or} \quad A = B^T,$$

where T indicates transpose. It follows that

$$A = B^T \quad \text{and} \quad A = B^{-1}$$

so that

$$\left. \begin{aligned} A^T &= A^{-1} &\Rightarrow & A^T A = I \\ B^T &= B^{-1} &\Rightarrow & B^T B = I. \end{aligned} \right\} \quad (1.1.2.7)$$

The matrices A and B are unitary matrices or matrices of rotation and

$$\Delta(A)^2 = \Delta(B)^2 = 1 \Rightarrow \Delta(A) = \pm 1. \quad (1.1.2.8)$$

If $\Delta(A) = 1$ the senses of the axes are not changed – *proper* rotation.

If $\Delta(A) = -1$ the senses of the axes are changed – *improper* rotation. (The right hand is transformed into a left hand.)

One can write for the coefficients A_i^j

$$A_i^j B_j^k = \delta_i^k, \quad A_i^j A_j^k = \delta_i^k,$$

giving six relations between the nine coefficients A_i^j . There are thus *three* independent coefficients of the 3×3 matrix A .

1.1.2.4. Covariant coordinates – dual or reciprocal space

1.1.2.4.1. Covariant coordinates

Using the developments (1.1.2.1) and (1.1.2.5), the scalar products of a vector \mathbf{x} and of the basis vectors \mathbf{e}_i can be written

$$x_i = \mathbf{x} \cdot \mathbf{e}_i = x^j \mathbf{e}_j \cdot \mathbf{e}_i = x^j g_{ij}. \quad (1.1.2.9)$$

The n quantities x_i are called *covariant* components, and we shall see the reason for this a little later. The relations (1.1.2.9) can be considered as a system of equations of which the components x^j are the unknowns. One can solve it since $\Delta(g_{ij}) \neq 0$ (see the end of Section 1.1.2.2). It follows that

$$x^j = x_i g^{ij} \quad (1.1.2.10)$$

with

$$g^{ij} g_{jk} = \delta_k^i. \quad (1.1.2.11)$$

The table of the g^{ij} 's is the inverse of the table of the g_{ij} 's. Let us now take up the development of \mathbf{x} with respect to the basis \mathbf{e}_i :

$$\mathbf{x} = x^i \mathbf{e}_i.$$

Let us replace x^i by the expression (1.1.2.10):

$$\mathbf{x} = x_j g^{ji} \mathbf{e}_i, \quad (1.1.2.12)$$

and let us introduce the set of n vectors

$$\mathbf{e}^j = g^{ji} \mathbf{e}_i \quad (1.1.2.13)$$

which span the space E^n ($j = 1, \dots, n$). This set of n vectors forms a *basis* since (1.1.2.12) can be written with the aid of (1.1.2.13) as

$$\mathbf{x} = x_j \mathbf{e}^j. \quad (1.1.2.14)$$

The x_j 's are the components of \mathbf{x} in the basis \mathbf{e}^j . This basis is called the *dual basis*. By using (1.1.2.11) and (1.1.2.13), one can show in the same way that

$$\mathbf{e}_j = g_{ij} \mathbf{e}^i. \quad (1.1.2.15)$$

It can be shown that the basis vectors \mathbf{e}^j transform in a change of basis like the components x^j of the physical space. They are therefore *contravariant*. In a similar way, the components x_j of a vector \mathbf{x} with respect to the basis \mathbf{e}^j transform in a change of basis like the basis vectors in direct space, \mathbf{e}_j ; they are therefore *covariant*:

$$\left. \begin{aligned} \mathbf{e}^j &= B_k^j \mathbf{e}'^k; & \mathbf{e}'^k &= A_j^k \mathbf{e}^j \\ x_i &= A_i^j x'_j; & x'_j &= B_j^i x_i. \end{aligned} \right\} \quad (1.1.2.16)$$

1.1.2.4.2. Reciprocal space

Let us take the scalar products of a covariant vector \mathbf{e}_i and a contravariant vector \mathbf{e}^j :

$$\mathbf{e}_i \cdot \mathbf{e}^j = \mathbf{e}_i \cdot g^{jk} \mathbf{e}_k = \mathbf{e}_i \cdot \mathbf{e}_k g^{jk} = g_{ik} g^{jk} = \delta_i^j$$

[using expressions (1.1.2.5), (1.1.2.11) and (1.1.2.13)].

The relation we obtain, $\mathbf{e}_i \cdot \mathbf{e}^j = \delta_i^j$, is identical to the relations defining the reciprocal lattice in crystallography; *the reciprocal basis then is identical to the dual basis* \mathbf{e}^i .

1.1.2.4.3. Properties of the metric tensor

In a change of basis, following (1.1.2.3) and (1.1.2.5), the g_{ij} 's transform according to

$$\left. \begin{aligned} g_{ij} &= A_i^k A_j^m g'_{km} \\ g'_{ij} &= B_i^k B_j^m g_{km}. \end{aligned} \right\} \quad (1.1.2.17)$$

Let us now consider the scalar products, $\mathbf{e}^i \cdot \mathbf{e}^j$, of two contravariant basis vectors. Using (1.1.2.11) and (1.1.2.13), it can be shown that

$$\mathbf{e}^i \cdot \mathbf{e}^j = g^{ij}. \quad (1.1.2.18)$$

In a change of basis, following (1.1.2.16), the g^{ij} 's transform according to

$$\left. \begin{aligned} g^{ij} &= B_k^i B_m^j g'^{km} \\ g'^{ij} &= A_k^i A_m^j g^{km}. \end{aligned} \right\} \quad (1.1.2.19)$$

The volumes V' and V of the cells built on the basis vectors \mathbf{e}'_i and \mathbf{e}_i , respectively, are given by the triple scalar products of these two sets of basis vectors and are related by

$$\begin{aligned} V' &= (\mathbf{e}'_1, \mathbf{e}'_2, \mathbf{e}'_3) \\ &= \Delta(B_j^i) (\mathbf{e}_1, \mathbf{e}_2, \mathbf{e}_3) \\ &= \Delta(B_j^i) V, \end{aligned} \quad (1.1.2.20)$$

where $\Delta(B_j^i)$ is the determinant associated with the transformation matrix between the two bases. From (1.1.2.17) and (1.1.2.20), we can write

$$\Delta(g'_{ij}) = \Delta(B_i^k) \Delta(B_j^m) \Delta(g_{km}).$$

1.1. INTRODUCTION TO THE PROPERTIES OF TENSORS

If the basis \mathbf{e}_i is orthonormal, $\Delta(g_{km})$ and V are equal to one, $\Delta(B_j)$ is equal to the volume V' of the cell built on the basis vectors \mathbf{e}'_j and

$$\Delta(g'_{ij}) = V'^2.$$

This relation is actually general and one can remove the prime index:

$$\Delta(g_{ij}) = V^2. \quad (1.1.2.21)$$

In the same way, we have for the corresponding reciprocal basis

$$\Delta(g^{ij}) = V^{*2},$$

where V^* is the volume of the reciprocal cell. Since the tables of the g_{ij} 's and of the g^{ij} 's are inverse, so are their determinants, and therefore the volumes of the unit cells of the direct and reciprocal spaces are also inverse, which is a very well known result in crystallography.

1.1.3. Mathematical notion of tensor

1.1.3.1. Definition of a tensor

For the mathematical definition of tensors, the reader may consult, for instance, Lichnerowicz (1947), Schwartz (1975) or Sands (1995).

1.1.3.1.1. Linear forms

A linear form in the space E_n is written

$$T(\mathbf{x}) = t_i x^i,$$

where $T(\mathbf{x})$ is independent of the chosen basis and the t_i 's are the coordinates of T in the dual basis. Let us consider now a *bilinear* form in the product space $E_n \otimes F_p$ of two vector spaces with n and p dimensions, respectively:

$$T(\mathbf{x}, \mathbf{y}) = t_{ij} x^i y^j.$$

The np quantities t_{ij} 's are, by definition, the components of a tensor of rank 2 and the form $T(\mathbf{x}, \mathbf{y})$ is *invariant* if one changes the basis in the space $E_n \otimes F_p$. The tensor t_{ij} is said to be *twice covariant*. It is also possible to construct a bilinear form by replacing the spaces E_n and F_p by their respective conjugates E^n and F^p . Thus, one writes

$$T(\mathbf{x}, \mathbf{y}) = t_{ij} x^i y^j = t'^i_{ij} x^i y^j = t^i_{ij} x_i y_j = t^{ij} x_i y_j,$$

where t^{ij} is the doubly contravariant form of the tensor, whereas t'^i_{ij} and t^i_{ij} are mixed, once covariant and once contravariant.

We can generalize by defining in the same way tensors of rank 3 or higher by using trilinear or multilinear forms. A vector is a tensor of rank 1, and a scalar is a tensor of rank 0.

1.1.3.1.2. Tensor product

Let us consider two vector spaces, E_n with n dimensions and F_p with p dimensions, and let there be two linear forms, $T(\mathbf{x})$ in E_n and $S(\mathbf{y})$ in F_p . We shall associate with these forms a bilinear form called a *tensor product* which belongs to the product space with np dimensions, $E_n \otimes F_p$:

$$P(\mathbf{x}, \mathbf{y}) = T(\mathbf{x}) \otimes S(\mathbf{y}).$$

This correspondence possesses the following properties:

- (i) it is distributive from the right and from the left;
- (ii) it is associative for multiplication by a scalar;
- (iii) the tensor products of the vectors with a basis E_n and those with a basis F_p constitute a basis of the product space.

The analytical expression of the tensor product is then

$$\left. \begin{aligned} T(\mathbf{x}) &= t_i x^i \\ S(\mathbf{y}) &= s_j y^j \end{aligned} \right\} P(\mathbf{x}, \mathbf{y}) = p_{ij} x^i y^j = t_i x^i s_j y^j = t_i s_j x^i y^j.$$

One deduces from this that

$$p_{ij} = t_i s_j.$$

It is a tensor of rank 2. One can equally well envisage the tensor product of more than two spaces, for example, $E_n \otimes F_p \otimes G_q$ in npq dimensions. We shall limit ourselves in this study to the case of *affine* tensors, which are defined in a space constructed from the product of the space E_n with itself or with its conjugate E^n . Thus, a tensor product of rank 3 will have n^3 components. The tensor product can be generalized as the product of multilinear forms. One can write, for example,

$$\left. \begin{aligned} P(\mathbf{x}, \mathbf{y}, \mathbf{z}) &= T(\mathbf{x}, \mathbf{y}) \otimes S(\mathbf{z}) \\ p^j_{ik} x^i y_j z^k &= t^i_i x^i y_j s_k z^k \end{aligned} \right\} \quad (1.1.3.1)$$

1.1.3.2. Behaviour under a change of basis

A multilinear form is, by definition, invariant under a change of basis. Let us consider, for example, the trilinear form (1.1.3.1). If we change the system of coordinates, the components of vectors $\mathbf{x}, \mathbf{y}, \mathbf{z}$ become

$$x^i = B^i_{\alpha} x'^{\alpha}; \quad y_j = A^{\beta}_j y'_{\beta}; \quad z^k = B^k_{\gamma} z'^{\gamma}.$$

Let us put these expressions into the trilinear form (1.1.3.1):

$$P(\mathbf{x}, \mathbf{y}, \mathbf{z}) = p^j_{ik} B^i_{\alpha} x'^{\alpha} A^{\beta}_j y'_{\beta} B^k_{\gamma} z'^{\gamma}.$$

Now we can equally well make the components of the tensor appear in the new basis:

$$P(\mathbf{x}, \mathbf{y}, \mathbf{z}) = p'^{\beta}_{\alpha\gamma} x'^{\alpha} y'_{\beta} z'^{\gamma}.$$

As the decomposition is unique, one obtains

$$p'^{\beta}_{\alpha\gamma} = p^j_{ik} B^i_{\alpha} A^{\beta}_j B^k_{\gamma}. \quad (1.1.3.2)$$

One thus deduces the rule for transforming the components of a tensor q times covariant and r times contravariant: they transform like the product of q covariant components and r contravariant components.

This transformation rule can be taken inversely as the definition of the components of a tensor of rank $n = q + r$.

Example. The operator O representing a symmetry operation has the character of a tensor. In fact, under a change of basis, O transforms into O' :

$$O' = A O A^{-1}$$

so that

$$O'^i_j = A^i_k O^k_l (A^{-1})^l_j.$$

Now the matrices A and B are inverses of one another:

$$O^i_j = A^i_k O^k_l B^l_j.$$

The symmetry operator is a tensor of rank 2, once covariant and once contravariant.

1.1.3.3. Operations on tensors

1.1.3.3.1. Addition

It is necessary that the tensors are of the same nature (same rank and same variance).

1. TENSORIAL ASPECTS OF PHYSICAL PROPERTIES

1.1.3.3.2. Multiplication by a scalar

This is a particular case of the tensor product.

1.1.3.3.3. Contracted product, contraction

Here we are concerned with an operation that only exists in the case of tensors and that is very important because of its applications in physics. In practice, it is almost always the case that tensors enter into physics through the intermediary of a contracted product.

(i) *Contraction*. Let us consider a tensor of rank 2 that is once covariant and once contravariant. Let us write its transformation in a change of coordinate system:

$$t_i^j = A_p^j B_i^q t_q^p.$$

Now consider the quantity t_i^i derived by applying the Einstein convention ($t_i^i = t_1^1 + t_2^2 + t_3^3$). It follows that

$$t_i^i = A_p^i B_i^q t_q^p = \delta_p^q t_q^p \\ t_i^i = t_p^p.$$

This is an invariant quantity and so is a *scalar*. This operation can be carried out on any tensor of rank higher than or equal to two, provided that it is expressed in a form such that its components are (at least) once covariant and once contravariant.

The *contraction* consists therefore of equalizing a covariant index and a contravariant index, and then in summing over this index. Let us take, for example, the tensor t_i^{jk} . Its contracted form is t_i^{ik} , which, with a change of basis, becomes

$$t_i^{ik} = A_p^k t_q^{ip}.$$

The components t_i^{ik} are those of a vector, resulting from the contraction of the tensor t_i^{jk} . The rank of the tensor has changed from 3 to 1. In a general manner, the contraction reduces the rank of the tensor from n to $n - 2$.

Example. Let us take again the operator of symmetry O . The trace of the associated matrix is equal to

$$O_1^1 + O_2^2 + O_3^3 = O_i^i.$$

It is the resultant of the contraction of the tensor O . It is a tensor of rank 0, which is a scalar and is invariant under a change of basis.

(ii) *Contracted product*. Consider the product of two tensors of which one is contravariant at least once and the other covariant at least once:

$$p_i^{jk} = t_i^j z^k.$$

If we contract the indices i and k , it follows that

$$p_i^j = t_i^j z^i.$$

The contracted product is then a tensor of rank 1 and not 3. It is an operation that is very frequent in practice.

(iii) *Scalar product*. Next consider the tensor product of two vectors:

$$t_i^j = x_i y^j.$$

After contraction, we get the scalar product:

$$t_i^i = x_i y^i.$$

1.1.3.4. Tensor nature of physical quantities

Let us first consider the dielectric constant. In the introduction, we remarked that for an isotropic medium

$$\mathbf{D} = \varepsilon \mathbf{E}.$$

If the medium is anisotropic, we have, for one of the components,

$$D^1 = \varepsilon_1^1 E^1 + \varepsilon_2^1 E^2 + \varepsilon_3^1 E^3.$$

This relation and the equivalent ones for the other components can also be written

$$D^i = \varepsilon_j^i E^j \quad (1.1.3.3)$$

using the Einstein convention.

The scalar product of \mathbf{D} by an arbitrary vector \mathbf{x} is

$$D^i x_i = \varepsilon_j^i E^j x_i.$$

The right-hand member of this relation is a bilinear form that is invariant under a change of basis. The set of nine quantities ε_j^i constitutes therefore the set of components of a tensor of rank 2. Expression (1.1.3.3) is the contracted product of ε_j^i by E^j .

A similar demonstration may be used to show the tensor nature of the various physical properties described in Section 1.1.1, whatever the rank of the tensor. Let us for instance consider the piezoelectric effect (see Section 1.1.4.4.3). The components of the electric polarization, P^i , which appear in a medium submitted to a stress represented by the second-rank tensor T_{jk} are

$$P^i = d^{ijk} T_{jk},$$

where the tensor nature of T_{jk} will be shown in Section 1.3.2. If we take the contracted product of both sides of this equation by any vector of covariant components x_i , we obtain a linear form on the left-hand side, and a trilinear form on the right-hand side, which shows that the coefficients d^{ijk} are the components of a third-rank tensor. Let us now consider the piezo-optic (or photoelastic) effect (see Sections 1.1.4.10.5 and 1.6.7). The components of the variation $\Delta\eta^{ij}$ of the dielectric impermeability due to an applied stress are

$$\Delta\eta^{ij} = \pi^{ijkl} T_{jl}.$$

In a similar fashion, consider the contracted product of both sides of this relation by two vectors of covariant components x_i and y_j , respectively. We obtain a bilinear form on the left-hand side, and a quadrilinear form on the right-hand side, showing that the coefficients π^{ijkl} are the components of a fourth-rank tensor.

1.1.3.5. Representation surface of a tensor

1.1.3.5.1. Definition

Let us consider a tensor $t_{ijkl\dots}$ represented in an orthonormal frame where variance is not important. The value of component $t'_{1111\dots}$ in an arbitrary direction is given by

$$t'_{1111\dots} = t_{ijkl\dots} B_1^i B_1^j B_1^k B_1^l \dots,$$

where the B_1^i, B_1^j, \dots are the direction cosines of that direction with respect to the axes of the orthonormal frame.

The *representation surface* of the tensor is the polar plot of $t'_{1111\dots}$.

1.1.3.5.2. Representation surfaces of second-rank tensors

The representation surfaces of second-rank tensors are quadrics. The directions of their principal axes are obtained as follows. Let t_{ij} be a second-rank tensor and let $\mathbf{OM} = \mathbf{r}$ be a vector with coordinates x_i . The doubly contracted product, $t_{ij} x^i x^j$, is a scalar. The locus of points M such that

1.1. INTRODUCTION TO THE PROPERTIES OF TENSORS

$$t_{ij}x^ix^j = 1$$

is a quadric. Its principal axes are along the directions of the eigenvectors of the matrix with elements t_{ij} . They are solutions of the set of equations

$$t_{ij}x^i = \lambda x^j,$$

where the associated quantities λ are the eigenvalues.

Let us take as axes the principal axes. The equation of the quadric reduces to

$$t_{11}(x^1)^2 + t_{22}(x^2)^2 + t_{33}(x^3)^2 = 1.$$

If the eigenvalues are all of the same sign, the quadric is an ellipsoid; if two are positive and one is negative, the quadric is a hyperboloid with one sheet; if one is positive and two are negative, the quadric is a hyperboloid with two sheets (see Section 1.3.1).

Associated quadrics are very useful for the geometric representation of physical properties characterized by a tensor of rank 2, as shown by the following examples:

(i) *Index of refraction* of a medium. It is related to the dielectric constant by $n = \varepsilon^{1/2}$ and, like it, it is a tensor of rank 2. Its associated quadric is an ellipsoid, the optical indicatrix, which represents its variations with the direction in space (see Section 1.6.3.2).

(ii) *Thermal expansion*. If one cuts a sphere in a medium whose thermal expansion is anisotropic, and if one changes the temperature, the sphere becomes an ellipsoid. Thermal expansion is therefore represented by a tensor of rank 2 (see Chapter 1.4).

(iii) *Thermal conductivity*. Let us place a drop of wax on a plate of gypsum, and then apply a hot point at the centre. There appears a halo where the wax has melted: it is elliptical, indicating anisotropic conduction. Thermal conductivity is represented by a tensor of rank 2 and the elliptical halo of molten wax corresponds to the intersection of the associated ellipsoid with the plane of the plate of gypsum.

1.1.3.5.3. Representation surfaces of higher-rank tensors

Examples of representation surfaces of higher-rank tensors are given in Sections 1.3.3.4.4 and 1.9.4.2.

1.1.3.6. Change of variance of the components of a tensor

1.1.3.6.1. Tensor nature of the metric tensor

Equation (1.1.2.17) describing the behaviour of the quantities $g_{ij} = \mathbf{e}_i \cdot \mathbf{e}_j$ under a change of basis shows that they are the components of a tensor of rank 2, the *metric tensor*. In the same way, equation (1.1.2.19) shows that the g^{ij} 's transform under a change of basis like the product of two contravariant coordinates. The coefficients g^{ij} and g_{ij} are the components of a *unique tensor*, in one case doubly contravariant, in the other case doubly covariant. In a general way, the Euclidean tensors (constructed in a space where one has defined the scalar product) are geometrical entities that can have covariant, contravariant or mixed components.

1.1.3.6.2. How to change the variance of the components of a tensor

Let us take a tensor product

$$t^{ij} = x^iy^j.$$

We know that

$$x^i = g^{ik}x_k \quad \text{and} \quad y^j = g^{jl}y_l.$$

It follows that

$$t^{ij} = g^{ik}g^{jl}x_ky_l.$$

x_ky_l is a tensor product of two vectors expressed in the dual space:

$$x_ky_l = t_{kl}.$$

One can thus pass from the doubly covariant form to the doubly contravariant form of the tensor by means of the relation

$$t^{ij} = g^{ik}g^{jl}t_{kl}.$$

This result is general: to change the variance of a tensor (in practice, to raise or lower an index), it is necessary to make the contracted product of this tensor using g^{ij} or g_{ij} , according to the case. For instance,

$$t^l_k = g^{jl}t_{lk}; \quad t^{ij}_k = g_{kl}t^{ijl}.$$

Remark

$$g^i_j = g^{ik}g_{kj} = \delta^i_j.$$

This is a property of the metric tensor.

1.1.3.6.3. Examples of the use in physics of different representations of the same quantity

Let us consider, for example, the force, \mathbf{F} , which is a tensor quantity (tensor of rank 1). One can define it:

(i) by the fundamental law of dynamics:

$$\mathbf{F} = m\mathbf{\Gamma}, \quad \text{with } F^i = m \, d^2x^i/dt^2,$$

where m is the mass and $\mathbf{\Gamma}$ is the acceleration. The force appears here in a *contravariant* form.

(ii) as the derivative of the energy, W :

$$F_i = \partial W / \partial x^i = \partial_i W.$$

The force appears here in *covariant* form. In effect, we shall see in Section 1.1.3.8.1 that to form a derivative with respect to a variable contravariant augments the covariance by unity. The general expression of the law of dynamics is therefore written with the energy as follows:

$$m \, d^2x^i/dt^2 = g^{ij}\partial_j W.$$

1.1.3.7. Outer product

1.1.3.7.1. Definition

The tensor defined by

$$\mathbf{x} \bigwedge \mathbf{y} = \mathbf{x} \otimes \mathbf{y} - \mathbf{y} \otimes \mathbf{x}$$

is called the *outer product* of vectors \mathbf{x} and \mathbf{y} . (*Note:* The symbol is different from the symbol \wedge for the vector product.) The analytical expression of this tensor of rank 2 is

$$\left. \begin{array}{l} \mathbf{x} = x^i \mathbf{e}_i \\ \mathbf{y} = y^j \mathbf{e}_j \end{array} \right\} \implies \mathbf{x} \bigwedge \mathbf{y} = (x^i y^j - y^i x^j) \mathbf{e}_i \otimes \mathbf{e}_j.$$

The components $p^{ij} = x^i y^j - y^i x^j$ of this tensor satisfy the properties

$$p^{ij} = -p^{ji}; \quad p^{ii} = 0.$$

It is an *antisymmetric* tensor of rank 2.

1. TENSORIAL ASPECTS OF PHYSICAL PROPERTIES

1.1.3.7.2. Vector product

Consider the so-called permutation tensor of rank 3 (it is actually an axial tensor – see Section 1.1.4.5.3) defined by

$$\begin{cases} \varepsilon_{ijk} = +1 & \text{if the permutation } ijk \text{ is even} \\ \varepsilon_{ijk} = -1 & \text{if the permutation } ijk \text{ is odd} \\ \varepsilon_{ijk} = 0 & \text{if at least two of the three indices are equal} \end{cases}$$

and let us form the contracted product

$$z_k = \frac{1}{2} \varepsilon_{ijk} p^{ij} = \varepsilon_{ijk} x^i y^j. \quad (1.1.3.4)$$

It is easy to check that

$$\begin{cases} z_1 = x^2 y^3 - y^2 x^3 \\ z_2 = x^3 y^1 - y^3 x^1 \\ z_3 = x^1 y^2 - y^1 x^2 \end{cases}$$

One recognizes the coordinates of the vector product.

1.1.3.7.3. Properties of the vector product

Expression (1.1.3.4) of the vector product shows that it is of a covariant nature. This is indeed correct, and it is well known that the vector product of two vectors of the direct lattice is a vector of the reciprocal lattice [see Section 1.1.4 of Volume B of *International Tables for Crystallography* (2000)].

The vector product is a very particular vector which it is better not to call a vector: sometimes it is called a *pseudovector* or an *axial* vector in contrast to normal vectors or *polar* vectors. The components of the vector product are the independent components of the antisymmetric tensor p_{ij} . In the space of n dimensions, one would write

$$v_{i_3 i_4 \dots i_n} = \frac{1}{2} \varepsilon_{i_1 i_2 \dots i_n} p^{i_1 i_2}.$$

The number of independent components of p^{ij} is equal to $(n^2 - n)/2$ or 3 in the space of three dimensions and 6 in the space of four dimensions, and the independent components of p^{ij} are not the components of a vector in the space of four dimensions.

Let us also consider the behaviour of the vector product under the change of axes represented by the matrix

$$\begin{pmatrix} \bar{1} & 0 & 0 \\ 0 & \bar{1} & 0 \\ 0 & 0 & \bar{1} \end{pmatrix}.$$

This is a symmetry with respect to a point that transforms a right-handed set of axes into a left-handed set and reciprocally. In such a change, the components of a normal vector change sign. Those of the vector product, on the contrary, remain unchanged, indicating – as one well knows – that the orientation of the vector product has changed and that it is not, therefore, a vector in the normal sense, *i.e.* independent of the system of axes.

1.1.3.8. Tensor derivatives

1.1.3.8.1. Interpretation of the coefficients of the matrix – change of coordinates

We have under a change of axes:

$$x^i = A_j^i x^j.$$

This shows that the new components, x^i , can be considered linear functions of the old components, x^j , and one can write

$$A_j^i = \partial x^i / \partial x^j = \partial_j x^i.$$

It should be noted that the covariance has been increased.

1.1.3.8.2. Generalization

Consider a field of tensors t_i^j that are functions of space variables. In a change of coordinate system, one has

$$t_i^j = A_i^\alpha B_\beta^j t'_\alpha{}^\beta.$$

Differentiate with respect to x^k :

$$\begin{aligned} \frac{\partial t_i^j}{\partial x^k} &= \partial_k t_i^j = A_i^\alpha B_\beta^j \frac{\partial t'_\alpha{}^\beta}{\partial x'^\gamma} \frac{\partial x'^\gamma}{\partial x^k} \\ \partial_k t_i^j &= A_i^\alpha B_\beta^j A_k^\gamma \partial_\gamma t'_\alpha{}^\beta. \end{aligned}$$

It can be seen that the partial derivatives $\partial_k t_i^j$ behave under a change of axes like a tensor of rank 3 whose covariance has been increased by 1 with respect to that of the tensor t_i^j . It is therefore possible to introduce a tensor of rank 1, ∇ (nabla), of which the components are the operators given by the partial derivatives $\partial/\partial x^i$.

1.1.3.8.3. Differential operators

If one applies the operator nabla to a scalar φ , one obtains

$$\text{grad } \varphi = \nabla \varphi.$$

This is a covariant vector in reciprocal space.

Now let us form the tensor product of ∇ by a vector \mathbf{v} of variable components. We then have

$$\nabla \otimes \mathbf{v} = \frac{\partial v^j}{\partial x^i} \mathbf{e}_i \otimes \mathbf{e}^j.$$

The quantities $\partial_i v^j$ form a tensor of rank 2. If we contract it, we obtain the divergence of \mathbf{v} :

$$\text{div } \mathbf{v} = \partial_i v^i.$$

Taking the vector product, we get

$$\text{curl } \mathbf{v} = \nabla \wedge \mathbf{v}.$$

The curl is then an axial vector.

1.1.3.8.4. Development of a vector function in a Taylor series

Let $\mathbf{u}(\mathbf{r})$ be a vector function. Its development as a Taylor series is written

$$u^i(\mathbf{r} + d\mathbf{r}) = u^i(\mathbf{r}) + \frac{\partial u^i}{\partial x^j} dx^j + \frac{1}{2} \frac{\partial^2 u^i}{\partial x^j \partial x^k} dx^j dx^k + \dots \quad (1.1.3.5)$$

The coefficients of the expansion, $\partial u^i / \partial x^j$, $\partial^2 u^i / \partial x^j \partial x^k$, ... are tensors of rank 2, 3, ...

An example is given by the relation between displacement and electric field:

$$D^i = \varepsilon_j^i E^j + \chi_{jk}^i E^j E^k + \dots$$

(see Sections 1.6.2 and 1.7.2).

We see that the linear relation usually employed is in reality a development that is arrested at the first term. The second term corresponds to nonlinear optics. In general, it is very small but is not negligible in ferroelectric crystals in the neighbourhood of the ferroelectric–paraelectric transition. Nonlinear optics are studied in Chapter 1.7.

1.1.4. Symmetry properties

For the symmetry properties of the tensors used in physics, the reader may also consult Bhagavantam (1966), Billings (1969), Mason (1966), Nowick (1995), Nye (1985), Paufler (1986), Shuvalov (1988), Sirotn & Shaskol'skaya (1982), and Wooster (1973).

1.1. INTRODUCTION TO THE PROPERTIES OF TENSORS

1.1.4.1. Introduction – Neumann's principle

We saw in Section 1.1.1 that physical properties express in general the response of a medium to an impetus. It has been known for a long time that symmetry considerations play an important role in the study of physical phenomena. These considerations are often very fruitful and have led, for instance, to the discovery of piezoelectricity by the Curie brothers in 1880 (Curie & Curie, 1880, 1881). It is not unusual for physical properties to be related to asymmetries. This is the case in electrical polarization, optical activity *etc.* The first to codify this role was the German physicist and crystallographer F. E. Neumann, who expressed in 1833 the *symmetry principle*, now called *Neumann's principle*: *if a crystal is invariant with respect to certain symmetry elements, any of its physical properties must also be invariant with respect to the same symmetry elements* (Neumann, 1885).

This principle may be illustrated by considering the optical properties of a crystal. In an anisotropic medium, the index of refraction depends on direction. For a given wave normal, two waves may propagate, with different velocities; this is the double refraction effect. The indices of refraction of the two waves vary with direction and can be found by using the index ellipsoid known as the *optical indicatrix* (see Section 1.6.3.2). Consider the central section of the ellipsoid perpendicular to the direction of propagation of the wave. It is an ellipse. The indices of the two waves that may propagate along this direction are equal to the semi-axes of that ellipse. There are two directions for which the central section is circular, and therefore two wave directions for which there is no double refraction. These directions are called optic axes, and the medium is said to be *biaxial*. If the medium is invariant with respect to a threefold, a fourfold or a sixfold axis (as in a trigonal, tetragonal or hexagonal crystal, for instance), its ellipsoid must also be invariant with respect to the same axis, according to Neumann's principle. As an ellipsoid can only be ordinary or of revolution, the indicatrix of a trigonal, tetragonal or hexagonal crystal is necessarily an ellipsoid of revolution that has only one circular central section and one optic axis. These crystals are said to be *uniaxial*. In a cubic crystal that has four threefold axes, the indicatrix must have several axes of revolution, it is therefore a sphere, and cubic media behave as isotropic media for properties represented by a tensor of rank 2.

1.1.4.2. Curie laws

The example given above shows that the symmetry of the property may possess a higher symmetry than the medium. The property is represented in that case by the indicatrix. The symmetry of an ellipsoid is

$$\begin{aligned} \frac{A_2}{M} \frac{A'_2}{M'} \frac{A''_2}{M''} C &= mmm \text{ for any ellipsoid} \\ &\text{(orthorhombic symmetry)} \\ \frac{A_\infty}{M} \frac{\infty A_2}{\infty M} C &= \frac{\infty}{m} m \text{ for an ellipsoid of revolution} \\ &\text{(cylindrical symmetry)} \\ \infty \frac{A_\infty}{M} C &= \infty \frac{\infty}{m} \text{ for a sphere} \\ &\text{(spherical symmetry).} \end{aligned}$$

[Axes A_∞ are axes of revolution, or *axes of isotropy*, introduced by Curie (1884, 1894), cf. *International Tables for Crystallography* (2002), Vol. A, Table 10.1.4.2.]

The symmetry of the indicatrix is identical to that of the medium if the crystal belongs to the orthorhombic holohedry and is higher in all other cases.

This remark is the basis of the generalization of the symmetry principle by P. Curie (1859–1906). He stated that (Curie, 1894):

(i) *the symmetry characteristic of a phenomenon is the highest compatible with the existence of the phenomenon;*

(ii) *the phenomenon may exist in a medium that possesses that symmetry or that of a subgroup of that symmetry;*

and concludes that some symmetry elements may coexist with the phenomenon but that their presence is not necessary. On the contrary, what is necessary is the *absence* of certain symmetry elements: 'asymmetry creates the phenomenon' ('*C'est la dissymétrie qui crée le phénomène*'; Curie, 1894, p. 400). Noting that physical phenomena usually express relations between a cause and an effect (an influence and a response), P. Curie restated the two above propositions in the following way, now known as Curie laws, although they are not, properly speaking, laws:

- (i) *the asymmetry of the effects must pre-exist in the causes;*
- (ii) *the effects may be more symmetric than the causes.*

The application of the Curie laws enable one to determine the symmetry characteristic of a phenomenon. Let us consider the phenomenon first as an effect. If Φ is the symmetry of the phenomenon and C the symmetry of the cause that produces it,

$$C \leq \Phi.$$

Let us now consider the phenomenon as a cause producing a certain effect with symmetry E :

$$\Phi \leq E.$$

We can therefore conclude that

$$C \leq \Phi \leq E.$$

If we choose among the various possible causes the most symmetric one, and among the various possible effects the one with the lowest symmetry, we can then determine the symmetry that characterizes the phenomenon.

As an example, let us determine the symmetry associated with a mechanical force. A force can be considered as the result of a traction effort, the symmetry of which is $A_\infty \infty M$. If considered as a cause, its effect may be the motion of a sphere in a given direction (for example, a spherical ball falling under its own weight). Again, the symmetry is $A_\infty \infty M$. The symmetries associated with the force considered as a cause and as an effect being the same, we may conclude that $A_\infty \infty M$ is its characteristic symmetry.

1.1.4.3. Symmetries associated with an electric field and with magnetic induction (flux density)

1.1.4.3.1. Symmetry of an electric field

Considered as an effect, an electric field may have been produced by two circular coaxial electrodes, the first one carrying positive electric charges, the other one negative charges (Fig. 1.1.4.1). The cause possesses an axis of revolution and an infinity of mirrors parallel to it, $A_\infty \infty M$. Considered as a cause, the electric field induces for instance the motion of a spherical electric charge parallel to itself. The associated symmetry is the same in each case, and the symmetry of the electric field is identical to that of a force, $A_\infty \infty M$. The electric polarization or the electric displacement have the same symmetry.

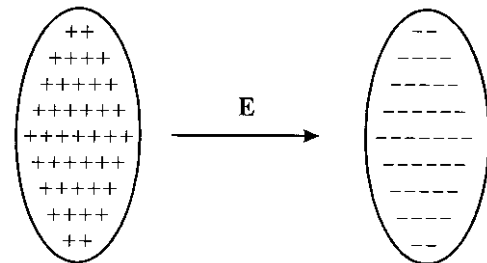


Fig. 1.1.4.1. Symmetry of an electric field.

1. TENSORIAL ASPECTS OF PHYSICAL PROPERTIES

1.1.4.3.2. Symmetry of magnetic induction

The determination of the symmetry of magnetic quantities is more delicate. Considered as an effect, magnetic induction may be obtained by passing an electric current in a loop (Fig. 1.1.4.2). The corresponding symmetry is that of a cylinder rotating around its axis, $(A_\infty/M)C$. Conversely, the variation of the flux of magnetic induction through a loop induces an electric current in the loop. If the magnetic induction is considered as a cause, its effect has the same symmetry. The symmetry associated with the magnetic induction is therefore $(A_\infty/M)C$.

This symmetry is completely different from that of the electric field. This difference can be understood by reference to Maxwell's equations, which relate electric and magnetic quantities:

$$\text{curl } \mathbf{E} = \nabla \wedge \mathbf{E} = -\frac{\partial \mathbf{B}}{\partial t}; \quad \text{curl } \mathbf{H} = \nabla \wedge \mathbf{H} = \frac{\partial \mathbf{D}}{\partial t}.$$

It was seen in Section 1.1.3.8.3 that the curl is an axial vector because it is a vector product. Maxwell's equations thus show that if the electric quantities (\mathbf{E} , \mathbf{D}) are polar vectors, the magnetic quantities (\mathbf{B} , \mathbf{H}) are axial vectors and *vice versa*; the equations of Maxwell are, in effect, perfectly symmetrical on this point. Indeed, one could have been tempted to determine the symmetry of the magnetic field by considering interactions between magnets, which would have led to the symmetry $A_\infty \propto M$ for the magnetic quantities. However, in the world where we live and where the origin of magnetism is in the spin of the electron, the magnetic field is an axial vector of symmetry $(A_\infty/M)C$ while the electric field is a polar vector of symmetry $A_\infty \propto M$.

1.1.4.4. Superposition of several causes in the same medium – pyroelectricity and piezoelectricity

1.1.4.4.1. Introduction

Let us now consider a phenomenon resulting from the superposition of several causes in the same medium. The symmetry of the global cause is the intersection of the groups of symmetry of the various causes: the asymmetries add up (Curie, 1894). This remark can be applied to the determination of the point groups where physical properties such as pyroelectricity or piezoelectricity are possible.

1.1.4.4.2. Pyroelectricity

Pyroelectricity is the property presented by certain materials that exhibit electric polarization when the temperature is changed uniformly. Actually, this property appears in crystals for which the centres of gravity of the positive and negative charges do not coincide in the unit cell. They present therefore a spontaneous polarization that varies with temperature because, owing to thermal expansion, the distances between these centres of gravity are temperature dependent. A very important case is that of the ferroelectric crystals where the direction of the polarization can be changed under the application of an external electric field.

From the viewpoint of symmetry, pyroelectricity can be considered as the superposition of two causes, namely the crystal

with its symmetry on one hand and the increase of temperature, which is isotropic, on the other. The intersection of the groups of symmetry of the two causes is in this case identical to the group of symmetry of the crystal. The symmetry associated with the effect is that of the electric polarization that is produced, $A_\infty \propto M$. Since the asymmetry of the cause must pre-exist in the causes, the latter may not possess more than one axis of symmetry nor mirrors other than those parallel to the single axis. The only crystal point groups compatible with this condition are

$$1, 2, 3, 4, 6, m, 2mm, 3m, 4mm, 6mm.$$

There are therefore only ten crystallographic groups that are compatible with the pyroelectric effect. For instance, tourmaline, in which the effect was first observed, belongs to $3m$.

1.1.4.4.3. Piezoelectricity

Piezoelectricity, discovered by the Curie brothers (Curie & Curie, 1880), is the property presented by certain materials that exhibit an electric polarization when submitted to an applied mechanical stress such as a uniaxial compression (see, for instance, Cady, 1964; Ikeda, 1990). Conversely, their shape changes when they are submitted to an external electric field; this is the converse piezoelectric effect. The physical interpretation of piezoelectricity is the following: under the action of the applied stress, the centres of gravity of negative and positive charges move to different positions in the unit cell, which produces an electric polarization.

From the viewpoint of symmetry, piezoelectricity can be considered as the superposition of two causes, the crystal with its own symmetry and the applied stress. The symmetry associated with a uniaxial compression is that of two equal and opposite forces, namely $A_\infty/M \propto A_2/\infty MC$. The effect is an electric polarization, of symmetry $A_\infty \propto M$, which must be higher than or equal to the intersection of the symmetries of the two causes:

$$\frac{A_\infty}{M} \frac{\infty A_2}{\infty M} C \cap S_{\text{crystal}} \leq A_\infty \propto M,$$

where S_{crystal} denotes the symmetry of the crystal.

It may be noted that the effect does not possess a centre of symmetry. The crystal point groups compatible with the property of piezoelectricity are therefore among the 21 noncentrosymmetric point groups. More elaborate symmetry considerations show further that group 432 is also not compatible with piezoelectricity. This will be proved in Section 1.1.4.10.4 using the symmetry properties of tensors. There are therefore 20 point groups compatible with piezoelectricity:

$$1, 2, m, 222, 2mm, \\ 3, 32, 3m, 4, \bar{4}, 422, 4mm, \bar{4}2m, 6, \bar{6}, 622, 6mm, \bar{6}2m \\ 23, \bar{4}3m.$$

The intersection of the symmetries of the crystal and of the applied stress depend of course on the orientation of this stress relative to the crystallographic axes. Let us take, for instance, a crystal of quartz, which belongs to group $32 = A_33A_2$. The above condition becomes

$$\frac{A_\infty}{M} \frac{\infty A_2}{\infty M} C \cap A_33A_2 \leq A_\infty \propto M.$$

If the applied compression is parallel to the threefold axis, the intersection is identical to the symmetry of the crystal, A_33A_2 , which possesses symmetry elements that do not exist in the effect, and piezoelectricity cannot appear. This is of course obvious because the threefold axis is not polar. For all other directions, piezoelectricity may appear.

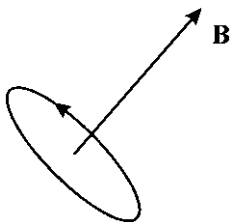


Fig. 1.1.4.2. Symmetry of magnetic induction.

1.1. INTRODUCTION TO THE PROPERTIES OF TENSORS

1.1.4.5. Intrinsic symmetry of tensors

1.1.4.5.1. Introduction

The symmetry of a tensor representing a physical property or a physical quantity may be due either to its own nature or to the symmetry of the medium. The former case is called intrinsic symmetry. It is a property that can be exhibited both by physical property tensors or by field tensors. The latter case is the consequence of Neumann's principle and will be discussed in Section 1.1.4.6. It applies to physical property tensors.

1.1.4.5.2. Symmetric tensors

1.1.4.5.2.1. Tensors of rank 2

A bilinear form is symmetric if

$$T(\mathbf{x}, \mathbf{y}) = T(\mathbf{y}, \mathbf{x}).$$

Its components satisfy the relations

$$t_{ij} = t_{ji}.$$

The associated matrix, T , is therefore equal to its transpose T^T :

$$T = \begin{pmatrix} t_{11} & t_{12} & t_{13} \\ t_{21} & t_{22} & t_{23} \\ t_{31} & t_{32} & t_{33} \end{pmatrix} = T^T = \begin{pmatrix} t_{11} & t_{21} & t_{31} \\ t_{12} & t_{22} & t_{32} \\ t_{13} & t_{23} & t_{33} \end{pmatrix}.$$

In a space with n dimensions, the number of independent components is equal to

$$(n^2 - n)/2 + n = (n^2 + n)/2.$$

Examples

(1) The metric tensor (Section 1.1.2.2) is symmetric because the scalar product is commutative.

(2) The tensors representing one of the physical properties associated with the leading diagonal of the matrix of physical properties (Section 1.1.1.4), such as the dielectric constant. Let us take up again the demonstration of this case and consider a capacitor being charged. The variation of the stored energy per unit volume for a variation $d\mathbf{D}$ of the displacement is

$$dW = \mathbf{E} \cdot d\mathbf{D},$$

where [equation (1.1.3.3)]

$$D^i = \varepsilon_j^i E^j.$$

Since both D^i and E^j are expressed through contravariant components, the expression for the energy should be written

$$dW = g_{ij} E^j dD^i.$$

If we replace D^i by its expression, we obtain

$$dW = g_{ij} \varepsilon_k^i E^j dE^k = \varepsilon_{jk} E^j dE^k,$$

where we have introduced the doubly covariant form of the dielectric constant tensor, ε_{jk} . Differentiating twice gives

$$\frac{\partial^2 W}{\partial E^k \partial E^j} = \varepsilon_{jk}.$$

If one can assume, as one usually does in physics, that the energy is a 'good' function and that the order of the derivatives is of little importance, then one can write

$$\frac{\partial^2 W}{\partial E^k \partial E^j} = \frac{\partial^2 W}{\partial E^j \partial E^k}.$$

As one can exchange the role of the dummy indices, one has

$$\partial^2 W / (\partial E^j \partial E^k) = \varepsilon_{kj}.$$

Hence one deduces that

$$\varepsilon_{jk} = \varepsilon_{kj}.$$

The dielectric constant tensor is therefore symmetric. One notes that the symmetry is conveyed on two indices of the same variance. One could show in a similar way that the tensor representing magnetic susceptibility is symmetric.

(3) There are other possible causes for the symmetry of a tensor of rank 2. The strain tensor (Section 1.3.1), which is a field tensor, is symmetric because one does not take into account the rotative part of the deformation; the stress tensor, also a field tensor (Section 1.3.1), is symmetric because one neglects body torques (couples per unit volume); the thermal conductivity tensor is symmetric because circulating flows do not produce any detectable effects *etc.*

1.1.4.5.2.2. Tensors of higher rank

A tensor of rank higher than 2 may be symmetric with respect to the indices of one or more couples of indices. For instance, by its very nature, the demonstration given in Section 1.1.1.4 shows that the tensors representing principal physical properties are of even rank. If n is the rank of the associated square matrix, the number of independent components is equal to $(n^2 + n)/2$. In the case of a tensor of rank 4, such as the tensor of elastic constants relating the strain and stress tensors (Section 1.3.3.2.1), the number of components of the tensor is $3^4 = 81$. The associated matrix is a 9×9 one, and the number of independent components is equal to 45.

1.1.4.5.3. Antisymmetric tensors – axial tensors

1.1.4.5.3.1. Tensors of rank 2

A bilinear form is said to be antisymmetric if

$$T(\mathbf{x}, \mathbf{y}) = -T(\mathbf{y}, \mathbf{x}).$$

Its components satisfy the relations

$$t_{ij} = -t_{ji}.$$

The associated matrix, T , is therefore also antisymmetric:

$$T = -T^T = \begin{pmatrix} 0 & t_{12} & t_{13} \\ -t_{12} & 0 & t_{23} \\ -t_{13} & -t_{23} & 0 \end{pmatrix}.$$

The number of independent components is equal to $(n^2 - n)/2$, where n is the number of dimensions of the space. It is equal to 3 in a three-dimensional space, and one can consider these components as those of a *pseudovector* or *axial* vector. It must never be forgotten that under a change of basis the components of an axial vector transform like those of a tensor of rank 2.

Every tensor can be decomposed into the sum of two tensors, one symmetric and the other one antisymmetric:

$$T = S + A,$$

with $S = (T + T^T)/2$ and $A = (T - T^T)/2$.

Example. As shown in Section 1.1.3.7.2, the components of the vector product of two vectors, \mathbf{x} and \mathbf{y} ,

$$z_k = \varepsilon_{ijk} x^i y^j,$$

are really the independent components of an antisymmetric tensor of rank 2. The magnetic quantities, \mathbf{B} , \mathbf{H} (Section 1.1.4.3.2), the tensor representing the pyromagnetic effect (Section 1.1.1.3) *etc.* are axial tensors.

1. TENSORIAL ASPECTS OF PHYSICAL PROPERTIES

1.1.4.5.3.2. Tensors of higher rank

If the rank of the tensor is higher than 2, the tensor may be antisymmetric with respect to the indices of one or several couples of indices.

(i) *Tensors of rank 3 antisymmetric with respect to every couple of indices.* A trilinear form $T(\mathbf{x}, \mathbf{y}, \mathbf{z}) = t_{ijk}x^i y^j z^k$ is said to be antisymmetric if it satisfies the relations

$$\left. \begin{aligned} T(\mathbf{x}, \mathbf{y}, \mathbf{z}) &= -T(\mathbf{y}, \mathbf{x}, \mathbf{z}) \\ &= -T(\mathbf{x}, \mathbf{z}, \mathbf{y}) \\ &= -T(\mathbf{z}, \mathbf{y}, \mathbf{x}). \end{aligned} \right\}$$

Tensor t_{ijk} has 27 components. It is found that all of them are equal to zero, except

$$t_{123} = t_{231} = t_{312} = -t_{213} = -t_{132} = -t_{321}.$$

The three-times contracted product with the permutations tensor (Section 1.1.3.7.2), $(1/6)\varepsilon_{ijk}t_{ijk}$, is a *pseudoscalar* or *axial scalar*. It is not a usual scalar: the sign of this product changes when one changes the hand of the reference axes, change of basis represented by the matrix

$$\begin{pmatrix} \bar{1} & 0 & 0 \\ 0 & \bar{1} & 0 \\ 0 & 0 & \bar{1} \end{pmatrix}.$$

Form $T(\mathbf{x}, \mathbf{y}, \mathbf{z})$ can also be written

$$T(\mathbf{x}, \mathbf{y}, \mathbf{z}) = P t_{123},$$

where

$$P = \varepsilon_{ijk}x^i y^j z^k = \begin{vmatrix} x^1 & x^2 & x^3 \\ y^1 & y^2 & y^3 \\ z^1 & z^2 & z^3 \end{vmatrix}$$

is the triple scalar product of the three vectors $\mathbf{x}, \mathbf{y}, \mathbf{z}$:

$$P = (\mathbf{x}, \mathbf{y}, \mathbf{z}) = (\mathbf{x} \wedge \mathbf{y}) \cdot \mathbf{z}.$$

It is also a pseudoscalar. The permutation tensor is not a real tensor of rank 3: if the hand of the axes is changed, the sign of P also changes; P is therefore not a trilinear form.

Another example of a pseudoscalar is given by the rotatory power of an optically active medium, which is expressed through the relation (see Section 1.6.5.4)

$$\theta = \rho d,$$

where θ is the rotation angle of the light wave, d the distance traversed in the material and ρ is a pseudoscalar: if one takes the mirror image of this medium, the sign of the rotation of the light wave also changes.

(ii) *Tensor of rank 3 antisymmetric with respect to one couple of indices.* Let us consider a trilinear form such that

$$T(\mathbf{x}, \mathbf{y}, \mathbf{z}) = -T(\mathbf{y}, \mathbf{x}, \mathbf{z}).$$

Its components satisfy the relation

$$t^{iil} = 0; \quad t^{ijl} = -t^{jil}.$$

The twice contracted product

$$t_k^l = \frac{1}{2}\varepsilon_{ijk}t^{ijl}$$

is an *axial* tensor of rank 2 whose components are the independent components of the antisymmetric tensor of rank 3, t^{ijl} .

Examples

(1) *Hall constant.* The Hall effect is observed in semiconductors. If one takes a semiconductor crystal and applies a

magnetic induction \mathbf{B} and at the same time imposes a current density \mathbf{j} at right angles to it, one observes an electric field \mathbf{E} at right angles to the other two fields (see Section 1.8.3.4). The expression for the field can be written

$$E_i = R_{H\,ikl}j_k B_l,$$

where $R_{H\,ikl}$ is the Hall constant, which is a tensor of rank 3. However, because the direction of the current density is imposed by the physical law (the set of vectors $\mathbf{B}, \mathbf{j}, \mathbf{E}$ constitutes a right-handed frame), one has

$$R_{H\,ikl} = -R_{H\,kil},$$

which shows that $R_{H\,ikl}$ is an antisymmetric (axial) tensor of rank 3. As can be seen from its physical properties, only the components such that $i \neq k \neq l$ are different from zero. These are

$$R_{H\,123} = -R_{H\,213}; \quad R_{H\,132} = -R_{H\,312}; \quad R_{H\,312}; \quad R_{H\,321}.$$

(2) *Optical rotation.* The gyration tensor used to describe the property of optical rotation presented by gyrotropic materials (see Section 1.6.5.4) is an axial tensor of rank 2, which is actually an antisymmetric tensor of rank 3.

(3) *Acoustic activity.* The acoustic gyrotropic tensor describes the rotation of the polarization plane of a transverse acoustic wave propagating along the acoustic axis (see for instance Kumaraswamy & Krishnamurthy, 1980). The elastic constants may be expanded as

$$c_{ijkl}(\omega, \mathbf{k}) = c_{ijkl}(\omega) + id_{ijklm}(\omega)k_m + \dots,$$

where d_{ijklm} is a fifth-rank tensor. Time-reversal invariance requires that $d_{ijklm} = -d_{jiklm}$, which shows that it is an antisymmetric (axial) tensor.

1.1.4.5.3.3. Properties of axial tensors

The two preceding sections have shown examples of axial tensors of ranks 0 (pseudoscalar), 1 (pseudovector) and 2. They have in common that all their components change sign when the sign of the basis is changed, and this can be taken as the definition of an axial tensor. Their components are the components of an antisymmetric tensor of higher rank. It is important to bear in mind that in order to obtain their behaviour in a change of basis, one should first determine the behaviour of the components of this antisymmetric tensor.

1.1.4.6. Symmetry of tensors imposed by the crystalline medium

Many papers have been devoted to the derivation of the invariant components of physical property tensors under the influence of the symmetry elements of the crystallographic point groups: see, for instance, Fumi (1951, 1952a,b,c, 1987), Fumi & Ripamonti (1980a,b), Nowick (1995), Nye (1957, 1985), Sands (1995), Sirotnin & Shaskol'skaya (1982), and Wooster (1973). There are three main methods for this derivation: the matrix method (described in Section 1.1.4.6.1), the direct inspection method (described in Section 1.1.4.6.3) and the group-theoretical method (described in Section 1.2.4 and used in the accompanying software, see Section 1.2.7.4).

1.1.4.6.1. Matrix method – application of Neumann's principle

An operation of symmetry turns back the crystalline edifice on itself; it allows the physical properties of the crystal and the tensors representing them to be invariant. An operation of symmetry is equivalent to a change of coordinate system. In a change of system, a tensor becomes

$$t_{\gamma\delta}^{\alpha\beta} = t_{kl}^{ij} A_i^\alpha A_j^\beta B_\gamma^k B_\delta^l.$$

If A represents a symmetry operation, it is a unitary matrix:

1.1. INTRODUCTION TO THE PROPERTIES OF TENSORS

$$A = B^T = B^{-1}.$$

Since the tensor is invariant under the action of the symmetry operator A , one has, according to Neumann's principle,

$$t'_{\gamma\delta}{}^{\alpha\beta} = t_{\gamma\delta}{}^{\alpha\beta}$$

and, therefore,

$$t_{\gamma\delta}{}^{\alpha\beta} = t_{kl}^{ij} A_i^\alpha A_j^\beta B_\gamma^k B_\delta^l. \quad (1.1.4.1)$$

There are therefore a certain number of linear relations between the components of the tensor and the number of independent components is reduced. If there are p components and q relations between the components, there are $p - q$ independent components. This number is *independent* of the system of axes. When applied to each of the 32 point groups, this reduction enables one to find the form of the tensor in each case. It depends on the rank of the tensor. In the present chapter, the reduction will be derived for tensors up to the fourth rank and for all crystallographic groups as well as for the isotropic groups. An orthonormal frame will be assumed in all cases, so that co- and contravariance will not be apparent and the positions of indices as subscripts or superscripts will not be meaningful. The Ox_3 axis will be chosen parallel to the threefold, fourfold or sixfold axis in the trigonal, tetragonal and hexagonal systems. The accompanying software to the present volume enables the reduction for tensors of any rank to be derived.

1.1.4.6.2. The operator A is in diagonal form

1.1.4.6.2.1. Introduction

If one takes as the system of axes the eigenvectors of the operator A , the matrix is written in the form

$$\begin{pmatrix} \exp i\theta & 0 & 0 \\ 0 & \exp -i\theta & 0 \\ 0 & 0 & \pm 1 \end{pmatrix},$$

where θ is the rotation angle, Ox_3 is taken parallel to the rotation axis and coefficient A_3 is equal to +1 or -1 depending on whether the rotation axis is direct or inverse (proper or improper operator).

The equations (1.1.4.1) can then be simplified and reduce to

$$t_{kl}^{ij} = t_{kl}^{ij} A_i^\alpha A_j^\beta B_\gamma^k B_\delta^l \quad (1.1.4.2)$$

(without any summation).

If the product $A_i^\alpha A_j^\beta B_\gamma^k B_\delta^l$ (without summation) is equal to unity, equation (1.1.4.2) is trivial and there is significance in the component t_{kl}^{ij} . On the contrary, if it is different from 1, the only solution for (1.1.4.2) is that $t_{kl}^{ij} = 0$. One then finds immediately that certain components of the tensor are zero and that others are unchanged.

1.1.4.6.2.2. Case of a centre of symmetry

All the diagonal components are in this case equal to -1. One thus has:

(i) *Tensors of even rank*, $t^{ij\dots} = (-1)^{2p} t^{ij\dots}$. The components are not affected by the presence of the centre of symmetry. The reduction of tensors of even rank is therefore the same in a centred group and in its noncentred subgroups, that is in any of the 11 *Laue classes*:

| | |
|--------------|--------------------------|
| $\bar{1}$ | 1 |
| $2/m$ | 2, m |
| mmm | 222, $2mm$ |
| $\bar{3}$ | 3 |
| $\bar{3}m$ | $\bar{3}2$, $3m$ |
| $4/m$ | $\bar{4}$, 4 |
| $4/m\bar{m}$ | $\bar{4}2m$, 422, $4mm$ |
| $6/m$ | $\bar{6}$, 6 |
| $6/m\bar{m}$ | $\bar{6}2m$, 622, $6mm$ |
| $m\bar{3}$ | $\bar{2}3$ |
| $m\bar{3}m$ | 432, $\bar{4}32$. |

If a tensor is invariant with respect to two elements of symmetry, it is invariant with respect to their product. It is then sufficient to make the reduction for the generating elements of the group and (since this concerns a tensor of even rank) for the 11 *Laue classes*.

(ii) *Tensors of odd rank*, $t^{ij\dots} = (-1)^{2p+1} t^{ij\dots}$. All the components are equal to zero. The physical properties represented by tensors of rank 3, such as piezoelectricity, piezomagnetism, nonlinear optics, for instance, will therefore not be present in a centrosymmetric crystal.

1.1.4.6.2.3. General case

By replacing the matrix coefficients A_i^α by their expression, (1.1.4.2) becomes, for a proper rotation,

$$t^{jk\dots} = t^{jk\dots} \exp(ir\theta) \exp(-is\theta) (1)^t = t^{jk\dots} \exp i(r-s)\theta,$$

where r is the number of indices equal to 1, s is the number of indices equal to 2, t is the number of indices equal to 3 and $r + s + t = p$ is the rank of the tensor. The component $t^{jk\dots}$ is not affected by the symmetry operation if

$$(r-s)\theta = 2K\pi,$$

where K is an integer, and is equal to zero if

$$(r-s)\theta \neq 2K\pi.$$

The angle of rotation θ can be put into the form $2\pi/q$, where q is the order of the axis. The condition for the component not to be zero is then

$$r-s = Kq.$$

The condition is fulfilled differently depending on the rank of the tensor, p , and the order of the axis, q . Indeed, we have $r-s \leq p$ and

- $p = 2, r-s \leq 2$: the result of the reduction will be the same for any $q \geq 3$;
- $p = 3, r-s \leq 3$: the result of the reduction will be the same for any $q \geq 4$;
- $p = 4, r-s \leq 4$: the result of the reduction will be the same for any $q \geq 5$.

It follows that:

- (i) for tensors of rank 2, the reduction will be the same for trigonal (threefold axis), tetragonal (fourfold axis) and hexagonal (sixfold axis) groups;
- (ii) for tensors of rank 3, the reduction will be the same for tetragonal and hexagonal groups;
- (iii) for tensors of rank 4, the reduction will be different for trigonal, tetragonal and hexagonal groups.

The inconvenience of the diagonalization method is that the vectors and eigenvalues are, in general, complex, so in practice one uses another method. For instance, we may note that equation (1.1.4.1) can be written in the case of $p = 2$ by associating with the tensor a 3×3 matrix T :

$$T = BTB^T,$$

1. TENSORIAL ASPECTS OF PHYSICAL PROPERTIES

where B is the symmetry operation. Through identification of homologous coefficients in matrices T and BTB^T , one obtains relations between components t_{ij} that enable the determination of the independent components.

1.1.4.6.3. The method of direct inspection

The method of ‘direct inspection’, due to Fumi (1952a,b, 1987), is very simple. It is based on the fundamental properties of tensors; the components transform under a change of basis like a product of vector components (Section 1.1.3.2).

Examples

(1) Let us consider a tensor of rank 3 invariant with respect to a twofold axis parallel to Ox_3 . The matrix representing this operator is

$$\begin{pmatrix} \bar{1} & 0 & 0 \\ 0 & \bar{1} & 0 \\ 0 & 0 & 1 \end{pmatrix}.$$

The component t_{ijk} behaves under a change of axes like the product of the components x_i, x_j, x_k . The components x_1, x_2, x_3 of a vector become, respectively, $-x_1, -x_2, x_3$. To simplify the notation, we shall denote the components of the tensor simply by ijk . If, amongst the indices i, j and k , there is an even number (including the number zero) of indices that are equal to 3, the product $x_i x_j x_k$ will become $-x_i x_j x_k$ under the rotation. As the component ‘ ijk ’ remains invariant and is also equal to its opposite, it must be zero. 14 components will thus be equal to zero:

111, 122, 133, 211, 222, 133, 112, 121, 212, 221, 323, 331, 332, 313.

(2) Let us now consider that the same tensor of rank 3 is invariant with respect to a fourfold axis parallel to Ox_3 . The matrix representing this operator and its action on a vector of coordinates x_1, x_2, x_3 is given by

$$\begin{pmatrix} x_2 \\ -x_1 \\ x_3 \end{pmatrix} = \begin{pmatrix} 0 & 1 & 0 \\ \bar{1} & 0 & 0 \\ 0 & 0 & 1 \end{pmatrix} \begin{pmatrix} x_1 \\ x_2 \\ x_3 \end{pmatrix}. \quad (1.1.4.3)$$

Coordinate x_1 becomes x_2 , x_2 becomes $-x_1$ and x_3 becomes x_3 . Component ijk transforms like product $x^i x^j x^k$ according to the rule given above. Since the twofold axis parallel to Ox_3 is a subgroup of the fourfold axis, we can start from the corresponding reduction. We find

$$\begin{array}{lll} 311 & \Longleftrightarrow & 322 : t_{311} = t_{322} \\ 123 & \Longleftrightarrow & -(213) : t_{123} = -t_{213} \\ 113 & \Longleftrightarrow & 223 : t_{113} = t_{223} \\ 333 & \Longleftrightarrow & 333 : t_{333} = t_{333} \\ 132 & \Longleftrightarrow & -(231) : t_{132} = -t_{231} \\ 131 & \Longleftrightarrow & 232 : t_{131} = t_{232} \\ 312 & \Longleftrightarrow & -(321) : t_{312} = -t_{321}. \end{array}$$

All the other components are equal to zero.

It is not possible to apply the method of direct inspection for point group 3. One must in this case use the matrix method described in Section 1.1.4.6.2; once this result is assumed, the method can be applied to all other point groups.

1.1.4.7. Reduction of the components of a tensor of rank 2

The reduction is given for each of the 11 Laue classes.

1.1.4.7.1. Triclinic system

Groups $\bar{1}, 1$: no reduction, the tensor has 9 independent components. The result is represented in the following symbolic way (Nye, 1957, 1985):

$$\begin{pmatrix} \bullet & \bullet & \bullet \\ \bullet & \bullet & \bullet \\ \bullet & \bullet & \bullet \end{pmatrix}$$

where the sign \bullet represents a nonzero component.

1.1.4.7.2. Monoclinic system

Groups $2m, 2, m$: it is sufficient to consider the twofold axis or the mirror. As the representative matrix is diagonal, the calculation is immediate. Taking the twofold axis to be parallel to Ox_3 , one has

$$t_3^1 = t_1^3 = t_3^2 = t_2^3 = 0.$$

The other components are not affected. The result is represented as

$$\begin{pmatrix} \bullet & \bullet & \\ \bullet & \bullet & \\ & & \bullet \end{pmatrix}$$

There are 5 independent components. If the twofold axis is taken along axis Ox_2 , which is the usual case in crystallography, the table of independent components becomes

$$\begin{pmatrix} \bullet & & \bullet \\ & \bullet & \\ \bullet & & \bullet \end{pmatrix}$$

1.1.4.7.3. Orthorhombic system

Groups $mmm, 2mm, 222$: the reduction is obtained by considering two perpendicular twofold axes, parallel to Ox_3 and to Ox_2 , respectively. One obtains

$$\begin{pmatrix} \bullet & & \\ & \bullet & \\ & & \bullet \end{pmatrix}$$

There are 3 independent components.

1.1.4.7.4. Trigonal, tetragonal, hexagonal and cylindrical systems

We remarked in Section 1.1.4.6.2.3 that, in the case of tensors of rank 2, the reduction is the same for threefold, fourfold or sixfold axes. It suffices therefore to perform the reduction for the tetragonal groups. That for the other systems follows automatically.

1.1.4.7.4.1. Groups $\bar{3}, 3; 4/m, \bar{4}, 4; 6/m, \bar{6}, 6; (A_\infty/M)C, A_\infty$

If we consider a fourfold axis parallel to Ox_3 represented by the matrix given in (1.1.4.3), by applying the direct inspection method one finds

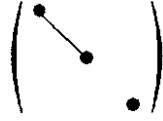
$$\begin{pmatrix} \bullet & \ominus & \\ \ominus & \bullet & \\ & & \bullet \end{pmatrix}$$

where the symbol \ominus means that the corresponding component is numerically equal to that to which it is linked, but of opposite sign. There are 3 independent components.

1.1. INTRODUCTION TO THE PROPERTIES OF TENSORS

1.1.4.7.4.2. Groups $\bar{3}m$, 32 , $3m$; $4/m\bar{m}$, 422 , $4mm$, $\bar{4}2m$; $6/m\bar{m}$, 622 , $6mm$, $62m$; $(A_\infty/M) \propto (A_2/M)C$, $A_\infty \propto A_2$

The result is obtained by combining the preceding result and that corresponding to a twofold axis normal to the fourfold axis. One finds



There are 2 independent components.

1.1.4.7.5. Cubic and spherical systems

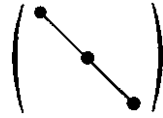
The cubic system is characterized by the presence of threefold axes along the $\langle 111 \rangle$ directions. The action of a threefold axis along $[111]$ on the components x_1, x_2, x_3 of a vector results in a permutation of these components, which become, respectively, x_2, x_3, x_1 and then x_3, x_1, x_2 . One deduces that the components of a tensor of rank 2 satisfy the relations

$$t_1^1 = t_2^2 = t_3^3.$$

The cubic groups all include as a subgroup the group 23 of which the generating elements are a twofold axis along Ox_3 and a threefold axis along $[111]$. If one combines the corresponding results, one deduces that

$$t_1^2 = t_2^3 = t_3^1 = t_1^3 = t_2^1 = t_3^2 = 0,$$

which can be summarized by

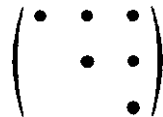


There is a single independent component and the medium behaves like a property represented by a tensor of rank 2, like an isotropic medium.

1.1.4.7.6. Symmetric tensors of rank 2

If the tensor is symmetric, the number of independent components is still reduced. One obtains the following, representing the nonzero components for the leading diagonal and for one half of the others.

1.1.4.7.6.1. Triclinic system



There are 6 independent components. It is possible to interpret the number of independent components of a tensor of rank 2 by considering the associated quadric, for instance the optical indicatrix. In the triclinic system, the quadric is any quadric. It is characterized by six parameters: the lengths of the three axes and the orientation of these axes relative to the crystallographic axes.

1.1.4.7.6.2. Monoclinic system (twofold axis parallel to Ox_2)



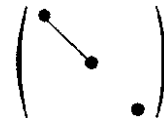
There are 4 independent components. The quadric is still any quadric, but one of its axes coincides with the twofold axis of the monoclinic lattice. Four parameters are required: the lengths of the axes and one angle.

1.1.4.7.6.3. Orthorhombic system



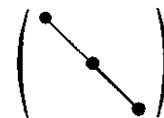
There are 3 independent components. The quadric is any quadric, the axes of which coincide with the crystallographic axes. Only three parameters are required.

1.1.4.7.6.4. Trigonal, tetragonal and hexagonal systems, isotropic groups



There are 2 independent components. The quadric is of revolution. It is characterized by two parameters: the lengths of its two axes.

1.1.4.7.6.5. Cubic system



There is 1 independent component. The associated quadric is a sphere.

1.1.4.8. Reduction of the components of a tensor of rank 3

1.1.4.8.1. Triclinic system

1.1.4.8.1.1. Group 1

All the components are independent. Their number is equal to 27. They are usually represented as a 3×9 matrix which can be subdivided into three 3×3 submatrices:

$$\begin{pmatrix} 111 & 122 & 133 & 123 & 131 & 112 & 132 & 113 & 121 \\ 211 & 222 & 233 & 223 & 231 & 212 & 232 & 213 & 221 \\ 311 & 322 & 333 & 323 & 331 & 312 & 332 & 313 & 321 \end{pmatrix}.$$

1.1.4.8.1.2. Group $\bar{1}$

All the components are equal to zero.

1. TENSORIAL ASPECTS OF PHYSICAL PROPERTIES

1.1.4.8.2. Monoclinic system

1.1.4.8.2.1. Group 2

Choosing the twofold axis parallel to Ox_3 and applying the direct inspection method, one finds

$$\left(\begin{array}{ccc|ccc} \bullet & & & \bullet & \bullet & \\ & \bullet & \bullet & & \bullet & \bullet \\ & & & \bullet & & \bullet \end{array} \right)$$

There are 13 independent components. If the twofold axis is parallel to Ox_2 , one finds

$$\left(\begin{array}{ccc|ccc} \bullet & & & \bullet & \bullet & \bullet \\ & \bullet & \bullet & & \bullet & \\ & & & \bullet & \bullet & \bullet \end{array} \right)$$

1.1.4.8.2.2. Group m

One obtains the matrix representing the operator m by multiplying by -1 the coefficients of the matrix representing a twofold axis. The result of the reduction will then be exactly complementary: the components of the tensor which include an odd number of 3's are now equal to zero. One writes the result as follows:

$$\left(\begin{array}{ccc|ccc} \bullet & \bullet & \bullet & \bullet & & \\ \bullet & \bullet & \bullet & & \bullet & \\ & & & \bullet & & \bullet \end{array} \right)$$

There are 14 independent components. If the mirror axis is normal to Ox_2 , one finds

$$\left(\begin{array}{ccc|ccc} \bullet & \bullet & \bullet & \bullet & & \\ & \bullet & \bullet & & \bullet & \\ \bullet & \bullet & \bullet & & \bullet & \end{array} \right)$$

1.1.4.8.2.3. Group $2/m$

All the components are equal to zero.

1.1.4.8.3. Orthorhombic system

1.1.4.8.3.1. Group 222

There are three orthonormal twofold axes. The reduction is obtained by combining the results associated with two twofold axes, parallel to Ox_3 and Ox_2 , respectively.

$$\left(\begin{array}{ccc|ccc} & & & \bullet & & \\ & & & & \bullet & \\ & & & & & \bullet \end{array} \right)$$

There are 6 independent components.

1.1.4.8.3.2. Group $mm2$

The reduction is obtained by combining the results associated with a twofold axis parallel to Ox_3 and with a mirror normal to Ox_2 :

$$\left(\begin{array}{ccc|ccc} & & & \bullet & & \\ & & & & \bullet & \\ & & & & & \bullet \end{array} \right)$$

There are 7 independent components.

1.1.4.8.3.3. Group mmm

All the components are equal to zero.

1.1.4.8.4. Trigonal system

1.1.4.8.4.1. Group 3

The threefold axis is parallel to Ox_3 . The matrix method should be used here. One finds

$$\left(\begin{array}{ccc|ccc} \bullet & \ominus & & \bullet & \bullet & \ominus \\ \ominus & \bullet & & \bullet & \bullet & \ominus \\ \bullet & \bullet & \bullet & \bullet & \bullet & \ominus \end{array} \right)$$

There are 9 independent components.

1.1.4.8.4.2. Group 32 with a twofold axis parallel to Ox_1

$$\left(\begin{array}{ccc|ccc} \bullet & \ominus & & \bullet & & \\ & & & \bullet & \ominus & \\ & & & & \ominus & \ominus \end{array} \right)$$

There are 4 independent components.

1.1.4.8.4.3. Group $3m$ with a mirror normal to Ox_1

$$\left(\begin{array}{ccc|ccc} \ominus & \bullet & & \bullet & & \\ \bullet & \bullet & \bullet & \bullet & \ominus & \\ & & & & \ominus & \ominus \end{array} \right)$$

There are 4 independent components.

1.1.4.8.4.4. Groups $\bar{3}$ and $\bar{3}m$

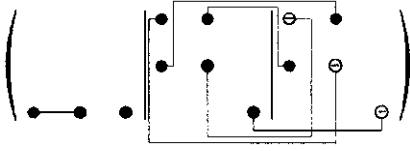
All the components are equal to zero.

1.1.4.8.5. Tetragonal system

1.1.4.8.5.1. Group 4

The method of direct inspection can be applied for a fourfold axis. One finds

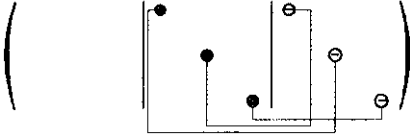
1.1. INTRODUCTION TO THE PROPERTIES OF TENSORS



There are 7 independent components.

1.1.4.8.5.2. Group 422

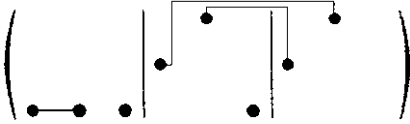
One combines the reductions for groups 4 and 222:



There are 3 independent components.

1.1.4.8.5.3. Group 4mm

One combines the reductions for groups 4 and 2m:



There are 4 independent components.

1.1.4.8.5.4. Group 4/m

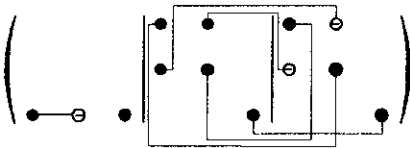
All the components are equal to zero.

1.1.4.8.5.5. Group $\bar{4}$

The matrix corresponding to axis $\bar{4}$ is

$$\begin{pmatrix} 0 & \bar{1} & 0 \\ 1 & 0 & 0 \\ 0 & 0 & \bar{1} \end{pmatrix}$$

and the form of the 3×9 matrix is

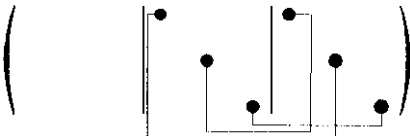


There are 6 independent components.

1.1.4.8.5.6. Group $\bar{4}2m$

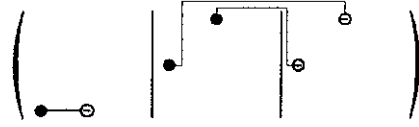
One combines either the reductions for groups $\bar{4}$ and 222, or the reductions for groups $\bar{4}$ and 2mm.

(i) Twofold axis parallel to Ox_1 :



There are 6 independent components.

(ii) Mirror perpendicular to Ox_1 (the twofold axis is at 45°)



The number of independent components is of course the same, 6.

1.1.4.8.5.7. Group 4/m

All the components are equal to zero.

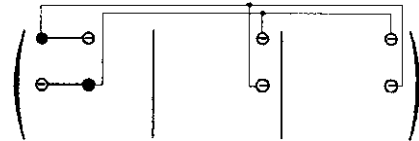
1.1.4.8.6. Hexagonal and cylindrical systems

1.1.4.8.6.1. Groups 6, A_∞ , 622, $A_\infty \infty A_2$, 6mm and $A_\infty \infty M$

It was shown in Section 1.1.4.6.2.3 that, in the case of tensors of rank 3, the reduction is the same for axes of order 4, 6 or higher. The reduction will then be the same as for the tetragonal system.

1.1.4.8.6.2. Group $\bar{6} = 3/m$

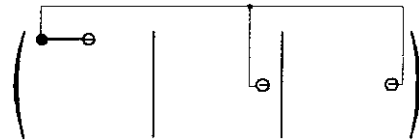
One combines the reductions for the groups corresponding to a threefold axis parallel to Ox_3 and to a mirror perpendicular to Ox_3 :



There are 2 independent components.

1.1.4.8.6.3. Group $\bar{6}2m$

One combines the reductions for groups 6 and 2mm:



There is 1 independent component.

1.1.4.8.6.4. Groups 6/m, $(A_\infty/M)C$, 6/mm and $(A_\infty/M) \infty (A_2/M)C$

All the components are equal to zero.

1.1.4.8.7. Cubic and spherical systems

1.1.4.8.7.1. Group 23

One combines the reductions corresponding to a twofold axis parallel to Ox_3 and to a threefold axis parallel to $[111]$:

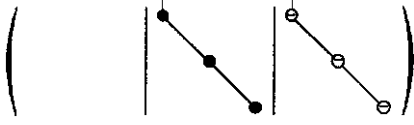


There are 2 independent components.

1. TENSORIAL ASPECTS OF PHYSICAL PROPERTIES

1.1.4.8.7.2. Groups 432 and $\infty A_\infty/M$

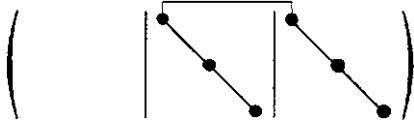
One combines the reductions corresponding to groups 422 and 23:



There is 1 independent component.

1.1.4.8.7.3. Group $\bar{4}3m$

One combines the reductions corresponding to groups $\bar{4}2m$ and 23:



There is 1 independent component.

1.1.4.8.7.4. Groups $m\bar{3}$, $m\bar{3}m$ and $\infty(A_\infty/M)C$

All the components are equal to zero.

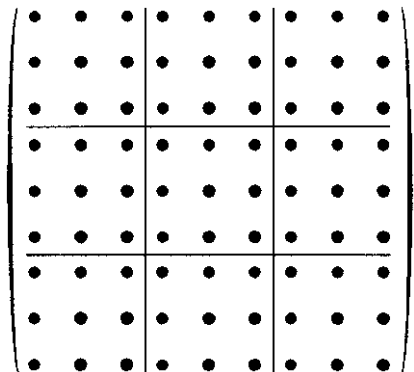
1.1.4.9. Reduction of the components of a tensor of rank 4

1.1.4.9.1. Triclinic system (groups $\bar{1}$, 1)

There is no reduction; all the components are independent. Their number is equal to 81. They are usually represented as a 9×9 matrix, where components t_{ijkl} are replaced by $ijkl$, for brevity:

| kl | 11 | 22 | 33 | 23 | 31 | 12 | 32 | 13 | 21 |
|------|------|------|------|------|------|------|------|------|------|
| ij | | | | | | | | | |
| 11 | 1111 | 1122 | 1133 | 1123 | 1131 | 1112 | 1132 | 1113 | 1121 |
| 22 | 2211 | 2222 | 2233 | 2223 | 2231 | 2212 | 2232 | 2213 | 2221 |
| 33 | 3311 | 3322 | 3333 | 3323 | 3331 | 3312 | 3332 | 3313 | 3321 |
| 23 | 2311 | 2322 | 2333 | 2323 | 2331 | 2312 | 2332 | 2313 | 2321 |
| 31 | 3111 | 3122 | 3133 | 3123 | 3131 | 3112 | 3132 | 3113 | 3121 |
| 12 | 1211 | 1222 | 1233 | 1223 | 1231 | 1212 | 1232 | 1213 | 1221 |
| 32 | 3211 | 3222 | 3233 | 3223 | 3231 | 3212 | 3232 | 3213 | 3221 |
| 13 | 1311 | 1322 | 1333 | 1323 | 1331 | 1312 | 1332 | 1313 | 1321 |
| 21 | 2111 | 2122 | 2133 | 2123 | 2131 | 2112 | 2132 | 2113 | 2121 |

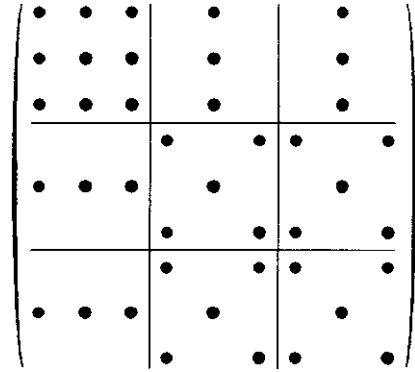
This matrix can be represented symbolically by



where the 9×9 matrix has been subdivided for clarity in to nine 3×3 submatrices.

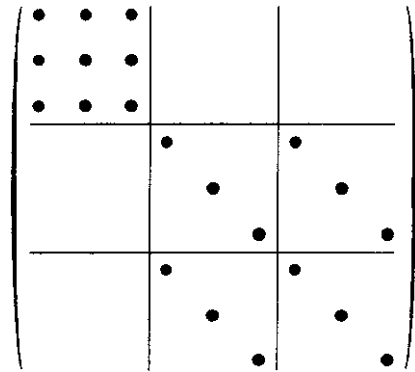
1.1.4.9.2. Monoclinic system (groups $2/m$, 2 , m)

The reduction is obtained by the method of direct inspection. For a twofold axis parallel to Ox_2 , one finds



There are 41 independent components.

1.1.4.9.3. Orthorhombic system (groups mmm , $2mm$, 222)



There are 21 independent components.

1.1.4.9.4. Trigonal system

1.1.4.9.4.1. Groups 3 and $\bar{3}$

The reduction is first applied in the system of axes tied to the eigenvectors of the operator representing a threefold axis. The system of axes is then changed to a system of orthonormal axes with Ox_3 parallel to the threefold axis:

| kl | 11 | 22 | 33 | 23 | 31 | 12 | 32 | 13 | 21 |
|------|-------|-------|-------|-------|-------|-------|-------|-------|-------|
| ij | | | | | | | | | |
| 11 | 1111 | 1122 | 1133 | 1123 | -2231 | 1112 | 1132 | -2213 | 1121 |
| 22 | 1122 | 1111 | 1133 | -1123 | 2231 | -1121 | -1132 | 2213 | -1112 |
| 33 | 3311 | 3311 | 3333 | | | 3312 | | | -3312 |
| 23 | 2311 | -2311 | | 2323 | 2331 | 1322 | 2332 | 2313 | 1322 |
| 31 | -3122 | 3122 | | 3123 | 3131 | 3211 | 3132 | 3113 | 3211 |
| 12 | 1211 | -2111 | 1233 | 2213 | 1132 | 1212 | 2231 | 1123 | 1221 |
| 32 | 3211 | -3211 | | 3113 | -3132 | 3122 | 3131 | -3123 | 3122 |
| 13 | -1322 | 1322 | | -2313 | 2332 | 2311 | -2331 | 2323 | 2311 |
| 21 | 2111 | -121 | -1233 | 2213 | 1132 | 1221 | 2231 | 1123 | 1212 |

with

$$\left. \begin{aligned} t_{1111} - t_{1122} &= t_{1212} + t_{1221} \\ t_{1112} + t_{1121} &= -(t_{1211} + t_{2111}). \end{aligned} \right\}$$

There are 27 independent components.

1.1. INTRODUCTION TO THE PROPERTIES OF TENSORS

1.1.4.9.4.2. Groups $\bar{3}m$, 32 , $3m$, with the twofold axis parallel to Ox_1

| kl | 11 | 22 | 33 | 23 | 31 | 12 | 32 | 13 | 21 |
|------|------|-------|------|-------|------|----|-------|------|----|
| ij | | | | | | | | | |
| 11 | 1111 | 1122 | 1133 | 1123 | | | 1132 | | |
| 22 | 1122 | 1111 | 1133 | -1123 | | | -1132 | | |
| 33 | 3311 | 3311 | 3333 | | | | | | |
| 23 | 2311 | -2311 | | 2323 | | | 2332 | | |
| 31 | | | | 3131 | 3211 | | 3113 | 3211 | |
| 12 | | | | 1132 | 1212 | | 1123 | 1221 | |
| 32 | 3211 | -3211 | | 3113 | | | 3131 | | |
| 13 | | | | 2332 | 2311 | | 2323 | 2311 | |
| 21 | | | | 1132 | 1221 | | 1123 | 1212 | |

with

$$t_{1111} - t_{1122} = t_{1212} + t_{1221}.$$

There are 14 independent components.

1.1.4.9.5. Tetragonal system

1.1.4.9.5.1. Groups $4/m$, 4 , $\bar{4}$

| kl | 11 | 22 | 33 | 23 | 31 | 12 | 32 | 13 | 21 |
|------|-------|-------|-------|-------|-------|------|-------|-------|-------|
| ij | | | | | | | | | |
| 11 | 1111 | 1122 | 1133 | | | 1112 | | | -2212 |
| 22 | 1122 | 1111 | 1133 | | | 2212 | | | -1112 |
| 33 | 3311 | 3311 | 3333 | | | 3312 | | | -3312 |
| 23 | | | | 2323 | 2331 | | 2332 | 2313 | |
| 31 | | | | 3123 | 3131 | | 3132 | 3113 | |
| 12 | 1211 | 1222 | 1233 | | | 1212 | | | 1221 |
| 32 | | | | 3113 | -3132 | | 3131 | -3123 | |
| 13 | | | | -2313 | 2332 | | -2331 | 2323 | |
| 21 | -1222 | -1211 | -1233 | | | | | | 1212 |

There are 21 independent components.

1.1.4.9.5.2. Groups $4/m\bar{m}2$, 422 , $4mm$, $\bar{4}2m$

| kl | 11 | 22 | 33 | 23 | 31 | 12 | 32 | 13 | 21 |
|------|------|------|------|------|------|------|------|------|------|
| ij | | | | | | | | | |
| 11 | 1111 | 1122 | 1133 | | | | | | |
| 22 | 1122 | 1111 | 1133 | | | | | | |
| 33 | 3311 | 3311 | 3333 | | | | | | |
| 23 | | | | 2323 | | | 2332 | | |
| 31 | | | | 3131 | | | 3113 | | |
| 12 | | | | | | 1212 | | | 1221 |
| 32 | | | | 3113 | | | 3131 | | |
| 13 | | | | | 2332 | | | 2323 | |
| 21 | | | | | | 1221 | | | 1212 |

There are 11 independent components.

1.1.4.9.6. Hexagonal and cylindrical systems

1.1.4.9.6.1. Groups $6/m$, $\bar{6}$, 6 ; $(A_\infty/M)C$, A_∞

| kl | 11 | 22 | 33 | 23 | 31 | 12 | 32 | 13 | 21 |
|------|------|-------|-------|-------|-------|-------|-------|-------|-------|
| ij | | | | | | | | | |
| 11 | 1111 | 1122 | 1133 | | | 1112 | | | 1121 |
| 22 | 1122 | 1111 | 1133 | | | -1121 | | | -1112 |
| 33 | 3311 | 3311 | 3333 | | | 3312 | | | -3312 |
| 23 | | | | 2323 | 2331 | | 2332 | 2313 | |
| 31 | | | | 3123 | 3131 | | 3132 | 3113 | |
| 12 | 1211 | -2111 | 1233 | | | 1212 | | | 1221 |
| 32 | | | | 3113 | -3132 | | 3131 | -3123 | |
| 13 | | | | -2313 | 2332 | | -2331 | 2323 | |
| 21 | 2111 | -1211 | -1233 | | | 1132 | 1221 | | 1123 |

with

$$\left. \begin{aligned} t_{1111} - t_{1122} &= t_{1212} + t_{1221} \\ t_{1112} + t_{1121} &= -(t_{1211} + t_{2111}). \end{aligned} \right\}$$

There are 19 independent components.

1.1.4.9.6.2. Groups $6/m\bar{m}2$, 622 , $6mm$, $\bar{6}2m$; $(A_\infty/M)\infty$; $(A_2/M)C$, $A_\infty \infty A_2$

| kl | 11 | 22 | 33 | 23 | 31 | 12 | 32 | 13 | 21 |
|------|------|------|------|------|------|------|------|------|------|
| ij | | | | | | | | | |
| 11 | 1111 | 1122 | 1133 | | | | | | |
| 22 | 1122 | 1111 | 1133 | | | | | | |
| 33 | 3311 | 3311 | 3333 | | | | | | |
| 23 | | | | 2323 | | | 2332 | | |
| 31 | | | | | 3131 | | | 3113 | |
| 12 | | | | | | 1212 | | | 1221 |
| 32 | | | | 3113 | | | 3131 | | |
| 13 | | | | | 2332 | | | 2323 | |
| 21 | | | | | | 1221 | | | 1212 |

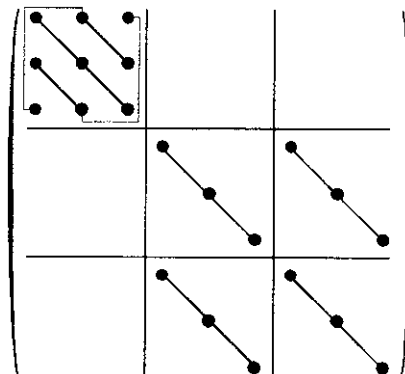
with

$$t_{1111} - t_{1122} = t_{1212} + t_{1221}.$$

There are 11 independent components.

1.1.4.9.7. Cubic system

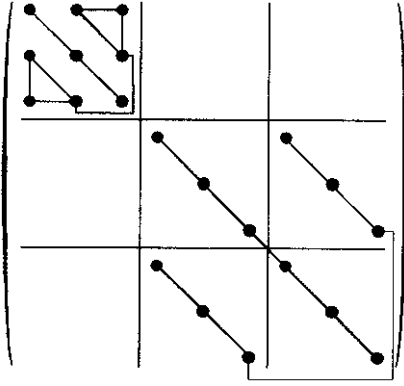
1.1.4.9.7.1. Groups 23 , $\bar{3}m$



There are 7 independent components.

1. TENSORIAL ASPECTS OF PHYSICAL PROPERTIES

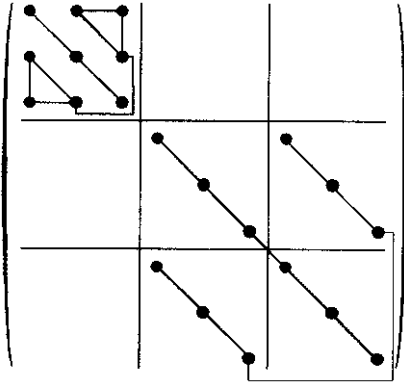
1.1.4.9.7.2. Groups $m\bar{3}m$, 432 , $\bar{4}3m$



There are 4 independent components. The tensor is symmetric.

1.1.4.9.8. Spherical system

1.1.4.9.8.1. Groups $\infty(A_\infty/M)C$ and ∞A_∞



with

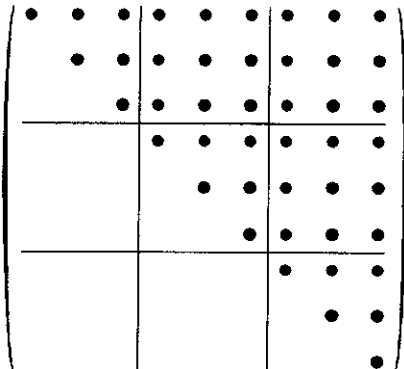
$$t_{1111} - t_{1122} = t_{1212} + t_{1221}.$$

There are 3 independent components. The tensor is symmetric.

1.1.4.9.9. Symmetric tensors of rank 4

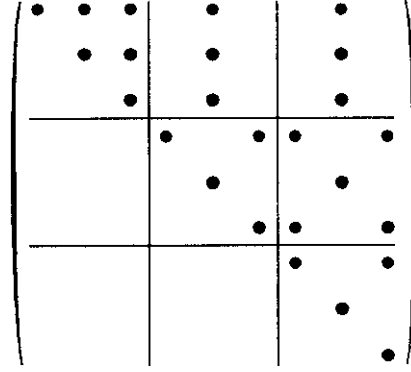
For symmetric tensors such as those representing principal properties, one finds the following, representing the nonzero components for the leading diagonal and for one half of the others.

1.1.4.9.9.1. Triclinic system



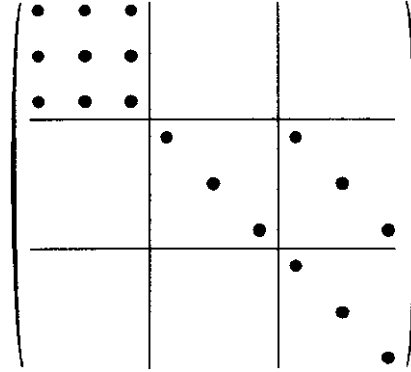
There are 45 independent coefficients.

1.1.4.9.9.2. Monoclinic system



There are 25 independent coefficients.

1.1.4.9.9.3. Orthorhombic system



There are 15 independent coefficients.

1.1.4.9.9.4. Trigonal system

(i) Groups 3 and $\bar{3}$

| kl | 11 | 22 | 33 | 23 | 31 | 12 | 32 | 13 | 21 |
|------|------|------|------|-------|-------|-------|-------|-------|-------|
| ij | | | | | | | | | |
| 11 | 1111 | 1122 | 1133 | 1123 | -2231 | 1112 | 1132 | -2213 | -1112 |
| 22 | | 1111 | 1133 | -1123 | 2231 | -1121 | -1132 | 2213 | -1112 |
| 33 | | | 3333 | | | 3312 | | | -3312 |
| 23 | | | | 2323 | 2331 | 2213 | 2332 | | 2213 |
| 31 | | | | | 3131 | 1132 | | 2332 | 1132 |
| 12 | | | | | | 1212 | 2231 | 1123 | 1221 |
| 32 | | | | | | | 3131 | -2331 | 2231 |
| 13 | | | | | | | | 2323 | 1123 |
| 21 | | | | | | | | | 1212 |

with

$$t_{1111} - t_{1122} = t_{1212} + t_{1221}.$$

There are 15 independent components.

1.1. INTRODUCTION TO THE PROPERTIES OF TENSORS

(ii) Groups $\bar{3}m$, 32 , $3m$

| kl | 11 | 22 | 33 | 23 | 31 | 12 | 32 | 13 | 21 |
|------|------|------|------|-------|------|------|-------|------|------|
| ij | | | | | | | | | |
| 11 | 1111 | 1122 | 1133 | 1123 | | | 1132 | | |
| 22 | | 1111 | 1133 | -1123 | | | -1132 | | |
| 33 | | | 3333 | | | | | | |
| 23 | | | | 2323 | | | 2332 | | |
| 31 | | | | | 3131 | 1132 | | 2332 | 1132 |
| 12 | | | | | | 1212 | | 1123 | 1221 |
| 32 | | | | | | | 3131 | | |
| 13 | | | | | | | | 2323 | 1123 |
| 21 | | | | | | | | | 1212 |

with

$$t_{1111} - t_{1122} = t_{1212} + t_{1221}.$$

There are 11 independent components.

1.1.4.9.5. *Tetragonal system*

(i) Groups $4/m$, 4 , $\bar{4}$

| kl | 11 | 22 | 33 | 23 | 31 | 12 | 32 | 13 | 21 |
|------|------|------|------|------|------|------|------|-------|-------|
| ij | | | | | | | | | |
| 11 | 1111 | 1122 | 1133 | | | 1112 | | | -2212 |
| 22 | | 1111 | 1133 | | | 2212 | | | -1112 |
| 33 | | | 3333 | | | 3312 | | | -3312 |
| 23 | | | | 2323 | 2331 | | 2332 | | |
| 31 | | | | | 3131 | | | 2332 | |
| 12 | | | | | | 1212 | | | 1221 |
| 32 | | | | | | | 3131 | -2331 | |
| 13 | | | | | | | | 2323 | |
| 21 | | | | | | | | | 1212 |

There are 13 independent components.

(ii) Groups $4/m\bar{m}2$, 422 , $4mm$, $\bar{4}2m$

| kl | 11 | 22 | 33 | 23 | 31 | 12 | 32 | 13 | 21 |
|------|------|------|------|------|------|------|------|------|------|
| ij | | | | | | | | | |
| 11 | 1111 | 1122 | 1133 | | | | | | |
| 22 | | 1111 | 1133 | | | | | | |
| 33 | | | 3333 | | | | | | |
| 23 | | | | 2323 | | | 2332 | | |
| 31 | | | | | 3131 | | | 3113 | |
| 12 | | | | | | 1212 | | | 1221 |
| 32 | | | | | | | 3131 | | |
| 13 | | | | | | | | 2323 | |
| 21 | | | | | | | | | 1212 |

There are 9 independent components.

1.1.4.9.6. *Hexagonal and cylindrical systems*

(i) Groups $6/m$, $\bar{6}$, 6 ; $(A_\infty/M)C$, A_∞

| kl | 11 | 22 | 33 | 23 | 31 | 12 | 32 | 13 | 21 |
|------|------|------|------|------|------|-------|------|-------|-------|
| ij | | | | | | | | | |
| 11 | 1111 | 1122 | 1133 | | | 1112 | | | 1121 |
| 22 | | 1111 | 1133 | | | -1121 | | | -1112 |
| 33 | | | 3333 | | | 3312 | | | -3312 |
| 23 | | | | 2323 | 2331 | | 2332 | | |
| 31 | | | | | 3131 | | 3132 | 2332 | |
| 12 | | | | | | 1212 | | | 1221 |
| 32 | | | | | | | 3131 | -2331 | |
| 13 | | | | | | | | 2323 | |
| 21 | | | | | | | | | 1212 |

with

$$t_{1111} - t_{1122} = t_{1212} + t_{1221}.$$

There are 12 independent components.

(ii) Groups $6/m\bar{m}2$, 622 , $6mm$, $\bar{6}2m$; $(A_\infty/M)\infty(A_2/M)C$, $A_\infty\infty A_2$

| kl | 11 | 22 | 33 | 23 | 31 | 12 | 32 | 13 | 21 |
|------|------|------|------|------|------|------|------|------|------|
| ij | | | | | | | | | |
| 11 | 1111 | 1122 | 1133 | | | | | | |
| 22 | | 1111 | 1133 | | | | | | |
| 33 | | | 3333 | | | | | | |
| 23 | | | | 2323 | | | 2332 | | |
| 31 | | | | | 3131 | | | 3113 | |
| 12 | | | | | | 1212 | | | 1221 |
| 32 | | | | | | | 3131 | | |
| 13 | | | | | | | | 2323 | |
| 21 | | | | | | | | | 1212 |

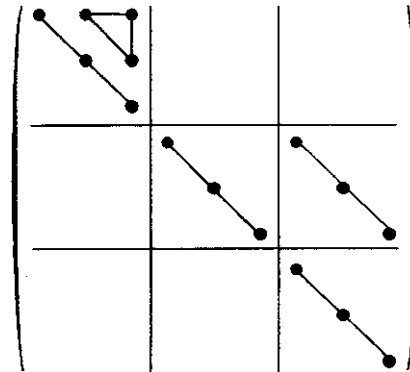
with

$$t_{1111} - t_{1122} = t_{1212} + t_{1221}.$$

There are 10 independent components.

1.1.4.9.7. *Cubic system*

(i) Groups 23 , $\bar{3}m$



with

$$t_{1111} - t_{1122} = t_{1212} + t_{1221}.$$

There are 5 independent components.

1. TENSORIAL ASPECTS OF PHYSICAL PROPERTIES

(ii) Groups $m\bar{3}m$, 432 , $\bar{4}3m$, and spherical system: the reduced tensors are already symmetric (see Sections 1.1.4.9.7 and 1.1.4.9.8).

1.1.4.10. Reduced form of polar and axial tensors – matrix representation

1.1.4.10.1. Introduction

Many tensors representing physical properties or physical quantities appear in relations involving symmetric tensors. Consider, for instance, the strain S_{ij} resulting from the application of an electric field \mathbf{E} (the piezoelectric effect):

$$S_{ij} = d_{ijk}E_k + Q_{ijkl}E_kE_l, \quad (1.1.4.4)$$

where the first-order terms d_{ijk} represent the components of the third-rank converse piezoelectric tensor and the second-order terms Q_{ijkl} represent the components of the fourth-rank electrostriction tensor. In a similar way, the direct piezoelectric effect corresponds to the appearance of an electric polarization \mathbf{P} when a stress T_{jk} is applied to a crystal:

$$P_i = d_{ijk}T_{jk}. \quad (1.1.4.5)$$

Owing to the symmetry properties of the strain and stress tensors (see Sections 1.3.1 and 1.3.2) and of the tensor product E_kE_l , there occurs a further reduction of the number of independent components of the tensors which are engaged in a contracted product with them, as is shown in Section 1.1.4.10.3 for third-rank tensors and in Section 1.1.4.10.5 for fourth-rank tensors.

1.1.4.10.2. Stress and strain tensors – Voigt matrices

The stress and strain tensors are symmetric because body torques and rotations are not taken into account, respectively (see Sections 1.3.1 and 1.3.2). Their components are usually represented using Voigt's one-index notation.

(i) Strain tensor

$$\left. \begin{aligned} S_1 &= S_{11}; & S_2 &= S_{22}; & S_3 &= S_{33}; \\ S_4 &= S_{23} + S_{32}; & S_5 &= S_{31} + S_{13}; & S_6 &= S_{12} + S_{21}; \\ S_4 &= 2S_{23} = 2S_{32}; & S_5 &= 2S_{31} = 2S_{13}; & S_6 &= 2S_{12} = 2S_{21}. \end{aligned} \right\} \quad (1.1.4.6)$$

The Voigt components S_α form a Voigt matrix:

$$\begin{pmatrix} S_1 & S_6 & S_5 \\ & S_2 & S_4 \\ & & S_3 \end{pmatrix}.$$

The terms of the leading diagonal represent the elongations (see Section 1.3.1). It is important to note that the non-diagonal terms, which represent the shears, are here equal to *twice* the corresponding components of the strain tensor. The components S_α of the Voigt strain matrix are therefore *not* the components of a tensor.

(ii) Stress tensor

$$\left. \begin{aligned} T_1 &= T_{11}; & T_2 &= T_{22}; & T_3 &= T_{33}; \\ T_4 &= T_{23} = T_{32}; & T_5 &= T_{31} = T_{13}; & T_6 &= T_{12} = T_{21}. \end{aligned} \right\}$$

The Voigt components T_α form a Voigt matrix:

$$\begin{pmatrix} T_1 & T_6 & T_5 \\ & T_2 & T_4 \\ & & T_3 \end{pmatrix}.$$

The terms of the leading diagonal correspond to principal normal constraints and the non-diagonal terms to shears (see Section 1.3.2).

1.1.4.10.3. Reduction of the number of independent components of third-rank polar tensors due to the symmetry of the strain and stress tensors

Equation (1.1.4.5) can be written

$$P_i = \sum_j d_{ijj}T_{jj} + \sum_{j \neq k} (d_{ijk} + d_{ikj})T_{jk}.$$

The sums $(d_{ijk} + d_{ikj})$ for $j \neq k$ have a definite physical meaning, but it is impossible to devise an experiment that permits d_{ijk} and d_{ikj} to be measured separately. It is therefore usual to set them equal:

$$d_{ijk} = d_{ikj}. \quad (1.1.4.7)$$

It was seen in Section 1.1.4.8.1 that the components of a third-rank tensor can be represented as a 9×3 matrix which can be subdivided into three 3×3 submatrices:

$$\left(\begin{array}{c|c|c} \mathbf{1} & \mathbf{2} & \mathbf{3} \end{array} \right).$$

Relation (1.1.4.7) shows that submatrices **1** and **2** are identical. One puts, introducing a two-index notation,

$$\left. \begin{aligned} d_{ijj} &= d_{i\alpha} \quad (\alpha = 1, 2, 3) \\ d_{ijk} + d_{ikj} \quad (j \neq k) &= d_{i\alpha} \quad (\alpha = 4, 5, 6). \end{aligned} \right\}$$

Relation (1.1.4.7) becomes

$$P_i = d_{i\alpha}T_\alpha.$$

The coefficients $d_{i\alpha}$ may be written as a 3×6 matrix:

$$\left(\begin{array}{ccc|ccc} 11 & 12 & 13 & 14 & 15 & 16 \\ 21 & 22 & 23 & 24 & 25 & 26 \\ 31 & 32 & 33 & 34 & 35 & 36 \end{array} \right).$$

This matrix is constituted by two 3×3 submatrices. The left-hand one is identical to the submatrix **1**, and the right-hand one is equal to the sum of the two submatrices **2** and **3**:

$$\left(\begin{array}{c|c} \mathbf{1} & \mathbf{2} + \mathbf{3} \end{array} \right).$$

The inverse piezoelectric effect expresses the strain in a crystal submitted to an applied electric field:

$$S_{ij} = d_{ijk}E_k,$$

where the matrix associated with the coefficients d_{ijk} is a 9×3 matrix which is the transpose of that of the coefficients used in equation (1.1.4.5), as shown in Section 1.1.1.4.

The components of the Voigt strain matrix S_α are then given by

$$\left. \begin{aligned} S_\alpha &= d_{i\alpha}E_k \quad (\alpha = 1, 2, 3) \\ S_\alpha &= S_{ij} + S_{ji} = (d_{ijk} + d_{jik})E_k \quad (\alpha = 4, 5, 6). \end{aligned} \right\}$$

This relation can be written simply as

$$S_\alpha = d_{\alpha k}E_k,$$

where the matrix of the coefficients $d_{\alpha k}$ is a 6×3 matrix which is the transpose of the $d_{i\alpha}$ matrix.

There is another set of piezoelectric constants (see Section 1.1.5) which relates the stress, T_{ij} , and the electric field, E_k , which are both intensive parameters:

$$T_{ij} = e_{ijk}E_k, \quad (1.1.4.8)$$

where a new piezoelectric tensor is introduced, e_{ijk} . Its components can be represented as a 3×9 matrix:

1.1. INTRODUCTION TO THE PROPERTIES OF TENSORS

$$\begin{pmatrix} 1 \\ - \\ 2 \\ - \\ 3 \end{pmatrix}.$$

Both sides of relation (1.1.4.8) remain unchanged if the indices i and j are interchanged, on account of the symmetry of the stress tensor. This shows that

$$e_{ijk} = e_{jik}.$$

Submatrices **2** and **3** are equal. One introduces here a two-index notation through the relation $e_{\alpha k} = e_{ijk}$, and the $e_{\alpha k}$ matrix can be written

$$\begin{pmatrix} 1 \\ 2+3 \end{pmatrix}.$$

The relation between the full and the reduced matrix is therefore different for the d_{ijk} and the e_{kij} tensors. This is due to the particular property of the strain Voigt matrix (1.1.4.6), and as a consequence the relations between nonzero components of the reduced matrices are different for certain point groups (3, 32, 3m, $\bar{6}$, $\bar{6}2m$).

1.1.4.10.4. *Independent components of the matrix associated with a third-rank polar tensor according to the following point groups*

1.1.4.10.4.1. *Triclinic system*

(i) Group 1: all the components are independent. There are 18 components.

(ii) Group $\bar{1}$: all the components are equal to zero.

1.1.4.10.4.2. *Monoclinic system*

(i) Group 2: twofold axis parallel to Ox_2 :

$$\begin{pmatrix} \cdot & \cdot & \cdot & | & \cdot & \cdot \\ \cdot & \cdot & \cdot & | & \cdot & \cdot \end{pmatrix}$$

There are 8 independent components.

(ii) Group m :

$$\begin{pmatrix} \cdot & \cdot & \cdot & | & \cdot & \cdot \\ \cdot & \cdot & \cdot & | & \cdot & \cdot \end{pmatrix}$$

There are 10 independent components.

(iii) Group $2/m$: all the components are equal to zero.

1.1.4.10.4.3. *Orthorhombic system*

(i) Group 222:

$$\begin{pmatrix} \cdot & \cdot & \cdot & | & \cdot & \cdot \\ \cdot & \cdot & \cdot & | & \cdot & \cdot \end{pmatrix}$$

There are 3 independent components.

(ii) Group $mm2$:

$$\begin{pmatrix} \cdot & \cdot & \cdot & | & \cdot & \cdot \\ \cdot & \cdot & \cdot & | & \cdot & \cdot \end{pmatrix}$$

There are 5 independent components.

(iii) Group mmm : all the components are equal to zero.

1.1.4.10.4.4. *Trigonal system*

(i) Group 3:

$$\begin{pmatrix} \cdot & \ominus & \cdot & | & \cdot & \cdot \\ \cdot & \cdot & \cdot & | & \cdot & \cdot \end{pmatrix}$$

where the symbol \ominus means that the corresponding component is equal to the opposite of that to which it is linked, \odot means that the component is equal to twice minus the value of the component to which it is linked for d_{ijk} and to minus the value of the component to which it is linked for e_{ijk} . There are 6 independent components.

(ii) Group 32, twofold axis parallel to Ox_1 :

$$\begin{pmatrix} \cdot & \ominus & \cdot & | & \cdot & \cdot \\ \cdot & \cdot & \cdot & | & \cdot & \cdot \end{pmatrix}$$

with the same conventions. There are 4 independent components.

(iii) Group $3m$, mirror perpendicular to Ox_1 :

$$\begin{pmatrix} \cdot & \cdot & \cdot & | & \cdot & \cdot \\ \cdot & \cdot & \cdot & | & \cdot & \cdot \end{pmatrix}$$

with the same conventions. There are 4 independent components.

(iv) Groups $\bar{3}$ and $\bar{3}m$: all the components are equal to zero.

1.1.4.10.4.5. *Tetragonal, hexagonal and cylindrical systems*

(i) Groups 4, 6 and A_∞ :

$$\begin{pmatrix} \cdot & \cdot & \cdot & | & \cdot & \cdot \\ \cdot & \cdot & \cdot & | & \cdot & \cdot \end{pmatrix}$$

There are 4 independent components.

(ii) Groups 422, 622 and $A_\infty \propto A_2$:

$$\begin{pmatrix} \cdot & \cdot & \cdot & | & \cdot & \cdot \\ \cdot & \cdot & \cdot & | & \cdot & \cdot \end{pmatrix}$$

There is 1 independent component.

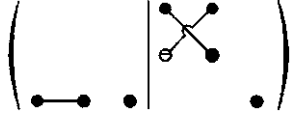
(iii) Groups $4mm$, $6mm$ and $A_\infty \propto M$:

$$\begin{pmatrix} \cdot & \cdot & \cdot & | & \cdot & \cdot \\ \cdot & \cdot & \cdot & | & \cdot & \cdot \end{pmatrix}$$

There are 3 independent components.

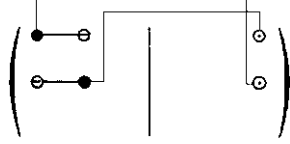
1. TENSORIAL ASPECTS OF PHYSICAL PROPERTIES

- (iv) Groups $4/m$, $6/m$ and $(A_\infty/M)C$: all the components are equal to zero.
(v) Group $\bar{4}$:



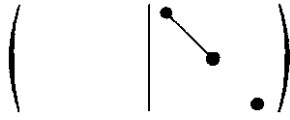
There are 4 independent components.

- (vi) Group $\bar{6} = 3/m$:



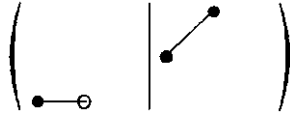
with the same conventions as for group 3. There are 2 independent components.

- (vii) Group $\bar{4}2m$ – twofold axis parallel to Ox_1 :



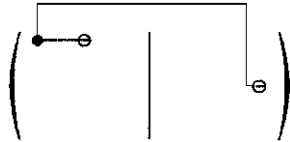
There are 2 independent components.

- (viii) Group $\bar{4}2m$ – mirror perpendicular to Ox_1 (twofold axis at 45°):



The number of independent components is of course the same.

- (ix) Group $\bar{6}2/m$:



with the same conventions as for group 3. There is 1 independent component.

- (x) Groups $4/mm$, $6/mm$ and $(A_\infty/M)\infty(A_2/M)C$: all the components are equal to zero.

1.1.4.10.4.6. Cubic and spherical systems

- (i) Groups 23 and $\bar{4}3m$:



There is 1 independent component.

- (ii) Groups $\bar{4}32$ and ∞A_∞ : it was seen in Section 1.1.4.8.6 that we have in this case

$$d_{123} = -d_{132}.$$

It follows that $d_{14} = 0$, all the components are equal to zero.

- (iii) Groups $m\bar{3}$, $m\bar{3}m$ and $\infty(A_\infty/M)C$: all the components are equal to zero.

1.1.4.10.5. Reduction of the number of independent components of fourth-rank polar tensors due to the symmetry of the strain and stress tensors

Let us consider five examples of fourth-rank tensors:

- (i) *Elastic compliances*, s_{ijkl} , relating the resulting strain tensor S_{ij} to an applied stress T_{ij} (see Section 1.3.3.2):

$$S_{ij} = s_{ijkl} T_{kl}, \quad (1.1.4.9)$$

where the compliances s_{ijkl} are the components of a tensor of rank 4.

- (ii) *Elastic stiffnesses*, c_{ijkl} (see Section 1.3.3.2):

$$T_{ij} = c_{ijkl} S_{kl}.$$

- (iii) *Piezo-optic coefficients*, π_{ijkl} , relating the variation $\Delta\eta_{ij}$ of the dielectric impermeability to an applied stress T_{kl} (*photoelastic effect* – see Section 1.6.7):

$$\Delta\eta_{ij} = \pi_{ijkl} T_{kl}.$$

- (iv) *Elasto-optic coefficients*, p_{ijkl} , relating the variation $\Delta\eta_{ij}$ of the dielectric impermeability to the strain S_{kl} :

$$\Delta\eta_{ij} = p_{ijkl} S_{kl}.$$

- (v) *Electrostriction coefficients*, Q_{ijkl} , which appear in equation (1.1.4.4):

$$S_{ij} = Q_{ijkl} E_k E_l, \quad (1.1.4.10)$$

where only the second-order terms are considered.

In each of the equations from (1.1.4.9) to (1.1.4.10), the contracted product of a fourth-rank tensor by a symmetric second-rank tensor is equal to a symmetric second-rank tensor. As in the case of the third-rank tensors, this results in a reduction of the number of independent components, but because of the properties of the strain Voigt matrix, and because two of the tensors are endowed with intrinsic symmetry (the elastic tensors), the reduction is different for each of the five tensors. The above relations can be written in matrix form:

$$\begin{pmatrix} 1 \\ 2 \\ 3 \end{pmatrix} = \begin{pmatrix} 1 & 2 & 3 \\ 4 & 5 & 6 \\ 7 & 8 & 9 \end{pmatrix} \times \begin{pmatrix} 1 \\ 2 \\ 3 \end{pmatrix}$$

where the second-rank tensors are represented by 1×9 column matrices, which can each be subdivided into three 1×3 submatrices and the 9×9 matrix associated with the fourth-rank tensors is subdivided into nine 3×3 submatrices, as shown in Section 1.1.4.9.1. The symmetry of the second-rank tensors means that submatrices **2** and **3** which are associated with them are equal.

Let us first consider the reduction of the tensor of elastic compliances. As in the case of the piezoelectric tensor, equation (1.1.4.9) can be written

$$S_{ij} = \sum_l s_{ijll} T_{ll} + \sum_{k \neq l} (s_{ijkl} + s_{ijlk}) T_{kl}. \quad (1.1.4.11)$$

The sums $(s_{ijkl} + s_{ijlk})$ for $k \neq l$ have a definite physical meaning, but it is impossible to devise an experiment permitting s_{ijkl} and s_{ijlk} to be measured separately. It is therefore usual to set them equal in order to avoid an unnecessary constant:

$$s_{ijkl} = s_{ijlk}.$$

1.1. INTRODUCTION TO THE PROPERTIES OF TENSORS

Furthermore, the left-hand term of (1.1.4.11) remains unchanged if we interchange the indices i and j . The terms on the right-hand side therefore also remain unchanged, whatever the value of T_{ll} or T_{kl} . It follows that

$$s_{ijll} = s_{jill}$$

$$s_{ijkl} = s_{ijlk} = s_{jikl} = s_{jilk}.$$

Similar relations hold for c_{ijkl} , Q_{ijkl} , p_{ijkl} and π_{ijkl} : the submatrices **2** and **3**, **4** and **7**, **5**, **6**, **8** and **9**, respectively, are equal.

Equation (1.4.1.11) can be rewritten, introducing the coefficients of the Voigt strain matrix:

$$S_\alpha = S_{ii} = \sum_l s_{iill} T_{ll} + \sum_{k \neq l} (s_{iikl} + s_{iilk}) T_{kl} \quad (\alpha = 1, 2, 3)$$

$$S_\alpha = S_{ij} + S_{ji} = \sum_l (s_{ijll} + s_{jill}) T_{ll} + \sum_{k \neq l} (s_{ijkl} + s_{ijlk} + s_{jikl} + s_{jilk}) T_{kl} \quad (\alpha = 4, 5, 6).$$

We shall now introduce a two-index notation for the elastic compliances, according to the following conventions:

$$\left. \begin{array}{ll} i = j; & k = l; & s_{\alpha\beta} = s_{iill} \\ i = j; & k \neq l; & s_{\alpha\beta} = s_{iikl} + s_{iilk} \\ i \neq j; & k = l; & s_{\alpha\beta} = s_{ijkk} + s_{jikk} \\ i \neq j; & k \neq l; & s_{\alpha\beta} = s_{ijkl} + s_{ijlk} + s_{jikl} + s_{jilk}. \end{array} \right\} \quad (1.1.4.12)$$

We have thus associated with the fourth-rank tensor a square 6×6 matrix with 36 coefficients:

| β | 1 | 2 | 3 | 4 | 5 | 6 |
|----------|----|----|----|----|----|----|
| α | | | | | | |
| 1 | 11 | 12 | 13 | 14 | 15 | 16 |
| 2 | 21 | 22 | 23 | 24 | 25 | 26 |
| 3 | 31 | 32 | 33 | 34 | 35 | 36 |
| 4 | 41 | 42 | 43 | 44 | 45 | 46 |
| 5 | 51 | 52 | 53 | 54 | 55 | 56 |
| 6 | 61 | 62 | 63 | 64 | 65 | 66 |

One can translate relation (1.1.4.12) using the 9×9 matrix representing s_{ijkl} by adding term by term the coefficients of submatrices **2** and **3**, **4** and **7** and **5**, **6**, **8** and **9**, respectively:

$$\left(\begin{array}{c} 1 \\ 2+3 \\ 2 \end{array} \right) = \left(\begin{array}{c|c} 1 & 2 \\ \hline 4+7 & 5+6+8+9 \end{array} \right) \times \left(\begin{array}{c} 1 \\ 2+3 \\ 2 \end{array} \right)$$

Using the two-index notation, equation (1.1.4.9) becomes

$$S_\alpha = s_{\alpha\beta} T_\beta. \quad (1.1.4.13)$$

A similar development can be applied to the other fourth-rank tensors π_{ijkl} , which will be replaced by 6×6 matrices with 36 coefficients, according to the following rules.

(i) *Elastic stiffnesses*, c_{ijkl} and *elasto-optic coefficients*, p_{ijkl} :

$$\left(\begin{array}{c} 1 \\ 2 \end{array} \right) = \left(\begin{array}{c|c} 1 & 2 \\ \hline 4 & 5 \end{array} \right) \times \left(\begin{array}{c} 1 \\ 2 \end{array} \right)$$

where

$$c_{\alpha\beta} = c_{ijkl}$$

$$p_{\alpha\beta} = p_{ijkl}.$$

(ii) *Piezo-optic coefficients*, π_{ijkl} :

$$\left(\begin{array}{c} 1 \\ 2 \end{array} \right) = \left(\begin{array}{c|c} 1 & 2+3 \\ \hline 4 & 5+6 \end{array} \right) \times \left(\begin{array}{c} 1 \\ 2 \end{array} \right)$$

where

$$\left. \begin{array}{ll} i = j; & k = l; & \pi_{\alpha\beta} = \pi_{iill} \\ i = j; & k \neq l; & \pi_{\alpha\beta} = \pi_{iikl} + \pi_{iilk} \\ i \neq j; & k = l; & \pi_{\alpha\beta} = \pi_{ijkk} = \pi_{jikk} \\ i \neq j; & k \neq l; & \pi_{\alpha\beta} = \pi_{ijkl} + \pi_{ijlk} = \pi_{jikl} + \pi_{jilk}. \end{array} \right\}$$

(iii) *Electrostriction coefficients*, Q_{ijkl} : same relation as for the elastic compliances.

1.1.4.10.6. *Independent components of the matrix associated with a fourth-rank tensor according to the following point groups*

1.1.4.10.6.1. *Triclinic system, groups $\bar{1}$, 1*

$$\left(\begin{array}{c} p_{\alpha\beta}, \pi_{\alpha\beta}, Q_{\alpha\beta} \\ c_{\alpha\beta}, s_{\alpha\beta} \end{array} \right) \left(\begin{array}{c} \bullet \bullet \bullet \bullet \bullet \bullet \\ \bullet \bullet \bullet \bullet \bullet \bullet \\ \bullet \bullet \bullet \bullet \bullet \bullet \\ \bullet \bullet \bullet \bullet \bullet \bullet \\ \bullet \bullet \bullet \bullet \bullet \bullet \\ \bullet \bullet \bullet \bullet \bullet \bullet \end{array} \right) \left(\begin{array}{c} \bullet \bullet \bullet \bullet \bullet \bullet \\ \bullet \bullet \bullet \bullet \bullet \bullet \\ \bullet \bullet \bullet \bullet \bullet \bullet \\ \bullet \bullet \bullet \bullet \bullet \bullet \\ \bullet \bullet \bullet \bullet \bullet \bullet \\ \bullet \bullet \bullet \bullet \bullet \bullet \end{array} \right)$$

36 independent components 21 independent components

1.1.4.10.6.2. *Monoclinic system*

Groups $2/m$, 2 , m , twofold axis parallel to Ox_2 :

$$\left(\begin{array}{c} p_{\alpha\beta}, \pi_{\alpha\beta}, Q_{\alpha\beta} \\ c_{\alpha\beta}, s_{\alpha\beta} \end{array} \right) \left(\begin{array}{c} \bullet \bullet \bullet \bullet \bullet \bullet \\ \bullet \bullet \bullet \bullet \bullet \bullet \\ \bullet \bullet \bullet \bullet \bullet \bullet \\ \bullet \bullet \bullet \bullet \bullet \bullet \\ \bullet \bullet \bullet \bullet \bullet \bullet \\ \bullet \bullet \bullet \bullet \bullet \bullet \end{array} \right) \left(\begin{array}{c} \bullet \bullet \bullet \bullet \bullet \bullet \\ \bullet \bullet \bullet \bullet \bullet \bullet \\ \bullet \bullet \bullet \bullet \bullet \bullet \\ \bullet \bullet \bullet \bullet \bullet \bullet \\ \bullet \bullet \bullet \bullet \bullet \bullet \\ \bullet \bullet \bullet \bullet \bullet \bullet \end{array} \right)$$

20 independent components 13 independent components

1.1.4.10.6.3. *Orthorhombic system*

Groups mmm , $2mm$, 222 :

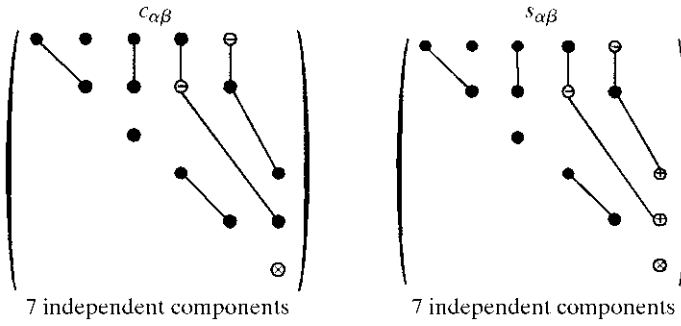
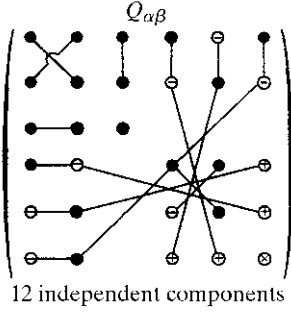
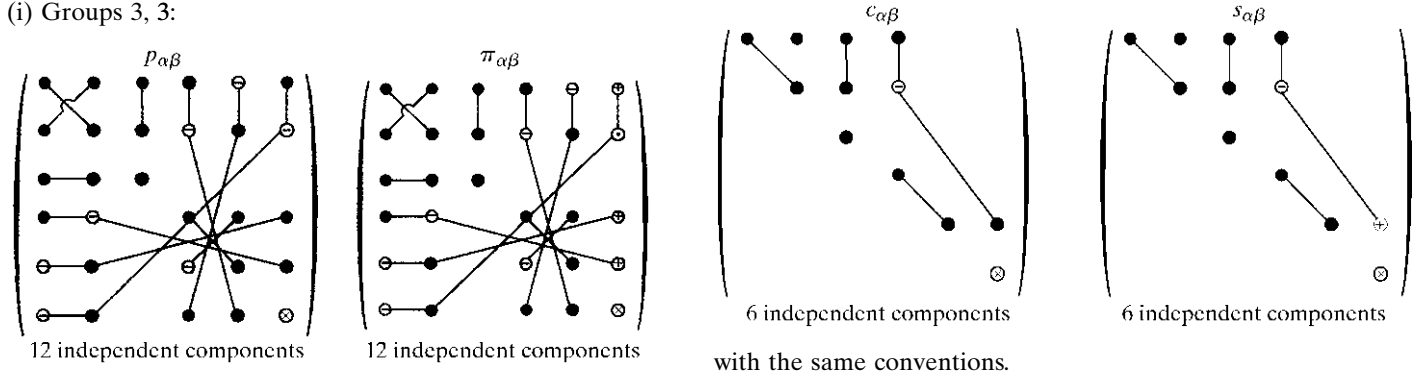
$$\left(\begin{array}{c} p_{\alpha\beta}, \pi_{\alpha\beta}, Q_{\alpha\beta} \\ c_{\alpha\beta}, s_{\alpha\beta} \end{array} \right) \left(\begin{array}{c} \bullet \bullet \bullet \bullet \bullet \bullet \\ \bullet \bullet \bullet \bullet \bullet \bullet \\ \bullet \bullet \bullet \bullet \bullet \bullet \\ \bullet \bullet \bullet \bullet \bullet \bullet \\ \bullet \bullet \bullet \bullet \bullet \bullet \\ \bullet \bullet \bullet \bullet \bullet \bullet \end{array} \right) \left(\begin{array}{c} \bullet \bullet \bullet \bullet \bullet \bullet \\ \bullet \bullet \bullet \bullet \bullet \bullet \\ \bullet \bullet \bullet \bullet \bullet \bullet \\ \bullet \bullet \bullet \bullet \bullet \bullet \\ \bullet \bullet \bullet \bullet \bullet \bullet \\ \bullet \bullet \bullet \bullet \bullet \bullet \end{array} \right)$$

12 independent components 9 independent components

1. TENSORIAL ASPECTS OF PHYSICAL PROPERTIES

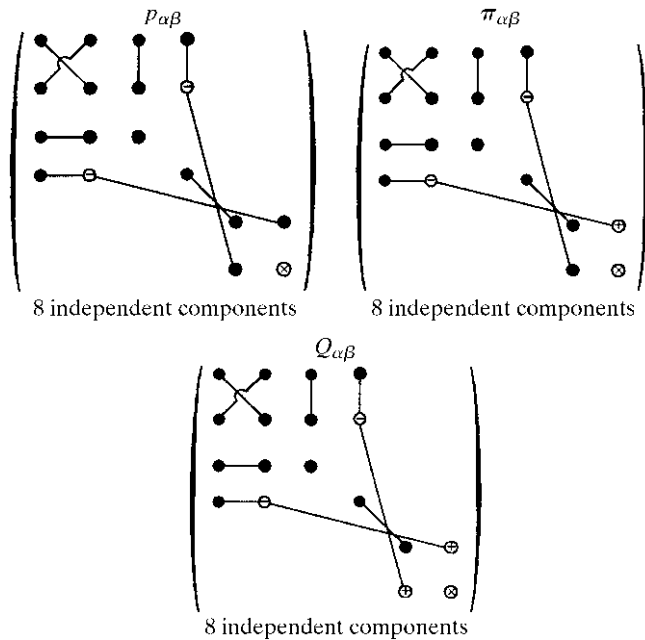
1.1.4.10.6.4. Trigonal system

(i) Groups 3, $\bar{3}$:



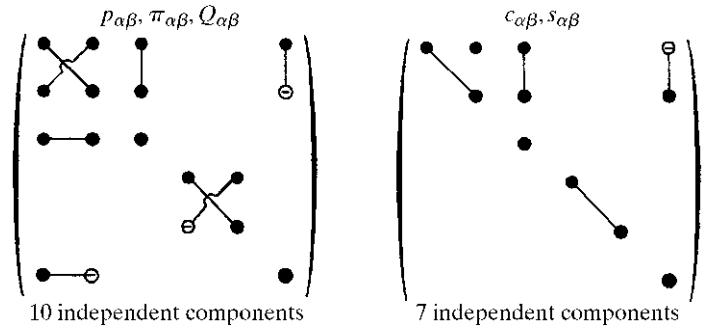
where \ominus is a component numerically equal but opposite in sign to the heavy dot component to which it is linked; \oplus is a component equal to twice the heavy dot component to which it is linked; \odot is a component equal to minus twice the heavy dot component to which it is linked; \otimes is equal to $1/2(p_{11} - p_{12})$, $(\pi_{11} - \pi_{12})$, $2(Q_{11} - Q_{12})$, $1/2(c_{11} - c_{12})$ and $2(s_{11} - s_{12})$, respectively.

(ii) Groups 32, $3m$, $\bar{3}m$:

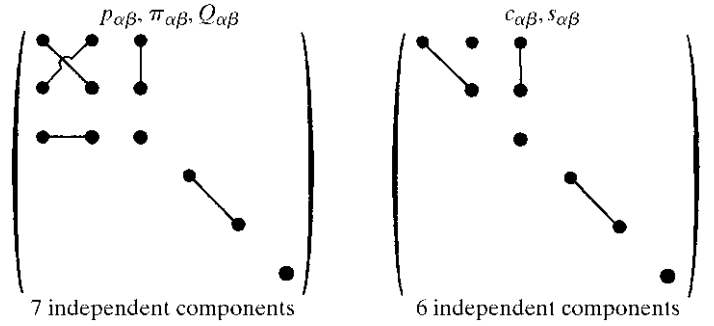


1.1.4.10.6.5. Tetragonal system

(i) Groups 4, $\bar{4}$ and $4/m$:

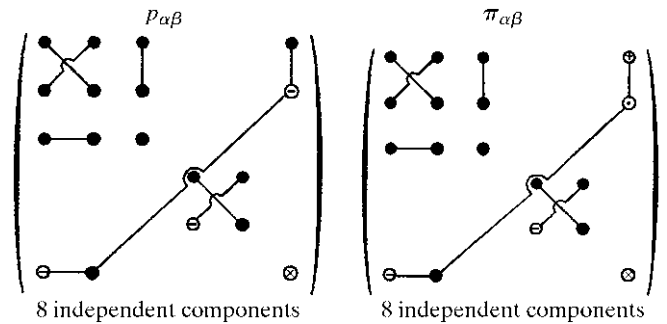


(ii) Groups 422, $4mm$, $\bar{4}2m$ and $4/m\bar{2}m$:



1.1.4.10.6.6. Hexagonal system

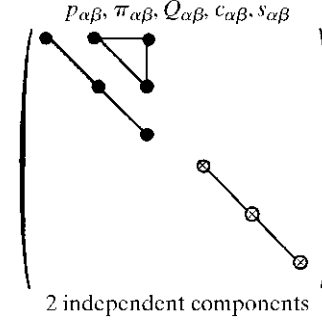
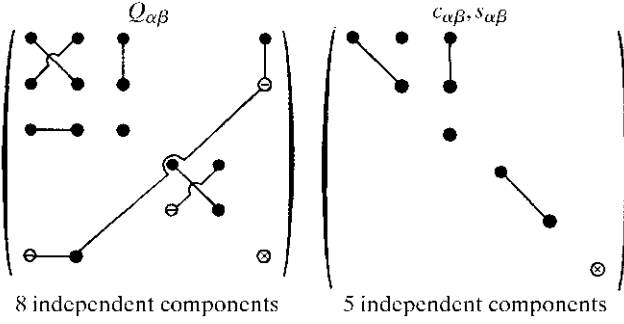
(i) Groups 6, $\bar{6}$ and $6/m$:



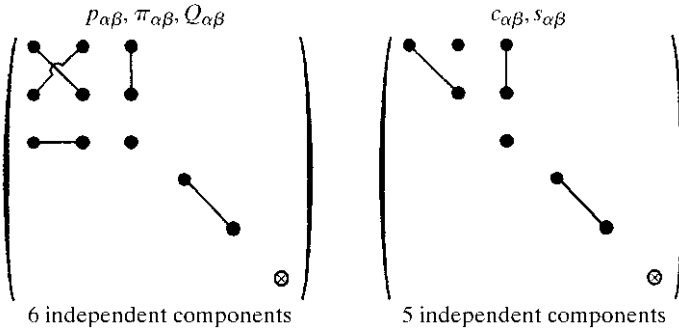
1.1. INTRODUCTION TO THE PROPERTIES OF TENSORS

1.1.4.10.6.8. Spherical system

For all tensors



(ii) Groups 622, 6mm, $\bar{6}2m$ and 6/mmm:



1.1.4.10.7. Reduction of the number of independent components of axial tensors of rank 2

It was shown in Section 1.1.4.5.3.2 that axial tensors of rank 2 are actually tensors of rank 3 antisymmetric with respect to two indices. The matrix of independent components of a tensor such that

$$g_{ijk} = -g_{jik}$$

is given by

$$\begin{pmatrix} & 122 & 133 \\ -121 & & 223 \\ -131 & -232 & \end{pmatrix} \begin{vmatrix} 123 & 131 \\ & 231 \\ -233 & \end{vmatrix} \begin{vmatrix} 132 & 121 \\ 232 & -123 \\ -133 & -231 \end{vmatrix}.$$

The second-rank axial tensor g_{kl} associated with this tensor is defined by

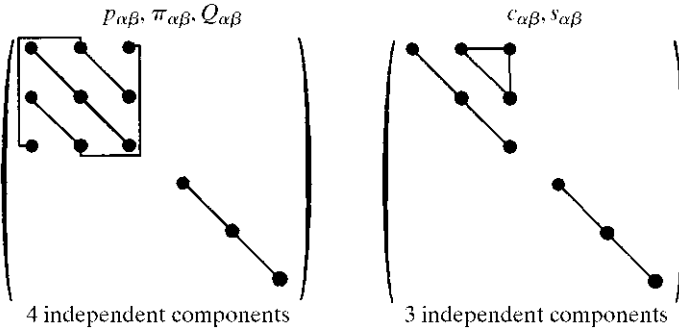
$$g_{kl} = \frac{1}{2} \epsilon_{ijk} g_{ijl}.$$

For instance, the piezomagnetic coefficients that give the magnetic moment M_i due to an applied stress T_α are the components of a second-rank axial tensor, $\Lambda_{i\alpha}$ (see Section 1.5.7.1):

$$M_i = \Lambda_{i\alpha} T_\alpha.$$

1.1.4.10.6.7. Cubic system

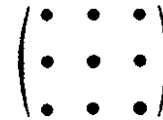
(i) Groups 23 and 3m:



1.1.4.10.7.1. Independent components according to the following point groups

(i) Triclinic system

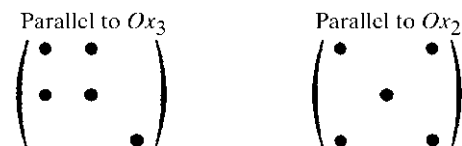
(a) Group 1:



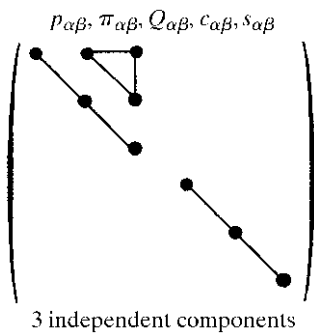
(b) Group $\bar{1}$: all components are equal to zero.

(ii) Monoclinic system

(a) Group 2:

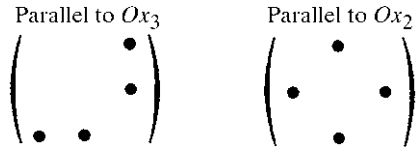


(ii) Groups 432, $\bar{4}3m$ and $m\bar{3}m$:



1. TENSORIAL ASPECTS OF PHYSICAL PROPERTIES

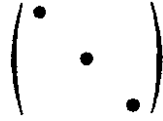
(b) Group m :



(c) Group $2/m$: all components are equal to zero.

(iii) *Orthorhombic system*

(a) Group 222:



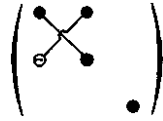
(b) Group $mm2$:



(c) Group mmm : all components are equal to zero.

(iv) *Trigonal, tetragonal, hexagonal and cylindrical systems*

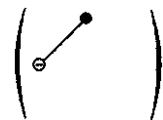
(a) Groups 3, 4, 6 and A_∞ :



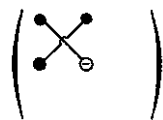
(b) Groups 32, 42, 62 and $A_\infty \infty A_2$:



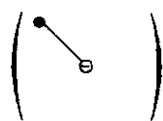
(c) Groups $3m$, $4m$, $6m$ and $A_\infty \infty M$:



(d) Group $\bar{4}$:



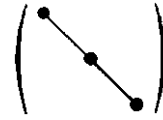
(e) Group $\bar{4}2m$:



(f) Groups $\bar{3}$, $4/m$, $\bar{6}2m$, $\bar{3}m$, $4/m\bar{m}$ and $6/m\bar{m}$: all components are equal to zero.

(v) *Cubic and spherical systems*

(a) Groups 23, 432 and ∞A_∞ :



The axial tensor is reduced to a pseudoscalar.

(b) Groups $m\bar{3}$, $\bar{4}3m$, $m\bar{3}m$ and $\infty(A_\infty/M)C$: all components are equal to zero.

1.1.4.10.7.2. *Independent components of symmetric axial tensors according to the following point groups*

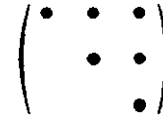
Some axial tensors are also symmetric. For instance, the optical rotatory power of a gyrotropic crystal in a given direction of direction cosines $\alpha_1, \alpha_2, \alpha_3$ is proportional to a quantity G defined by (see Section 1.6.5.4)

$$G = g_{ij}\alpha_i\alpha_j,$$

where the gyration tensor g_{ij} is an axial tensor. This expression shows that only the symmetric part of g_{ij} is relevant. This leads to a further reduction of the number of independent components:

(i) *Triclinic system*

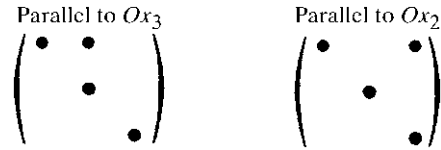
(a) Group 1:



(b) Group $\bar{1}$: all components are equal to zero.

(ii) *Monoclinic system*

(a) Group 2:



(b) Group m :



(c) Group $2/m$: all components are equal to zero.

(iii) *Orthorhombic system*

(a) Group 222:



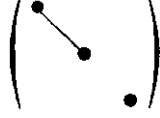
(b) Group $mm2$:



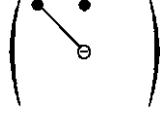
(c) Group mmm : all components are equal to zero.

1.1. INTRODUCTION TO THE PROPERTIES OF TENSORS

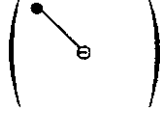
- (iv) *Trigonal, tetragonal and hexagonal systems*
 (a) Groups 3, 32, 4, 42, 6, 62:



- (b) Group $\bar{4}$:

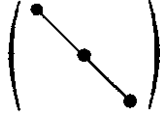


- (c) Group $\bar{4}2m$:



- (d) Groups $\bar{3}$, $3m$, $\bar{3}m$, $4/m$, $4mm$, $4/m\bar{m}$, $\bar{6}$, $\bar{6}2m$ and $6/m\bar{m}$: all components are equal to zero.

- (v) *Cubic and spherical systems*
 (a) Groups 23, 432 and $A_\infty \infty A_2$:



- (b) Groups $m\bar{3}$, $\bar{4}3m$, $m\bar{3}m$ and $\infty(A_\infty/M)C$: all components are equal to zero.

In practice, gyrotropic crystals are only found among the enantiomorphic groups: 1, 2, 222, 3, 32, 4, 422, 6, 622, 23, 432. Pasteur (1848a,b) was the first to establish the distinction between 'molecular dissymmetry' and 'crystalline dissymmetry'.

1.1.5. Thermodynamic functions and physical property tensors

[The reader may also consult Mason (1966), Nye (1985) or Sirotnin & Shaskol'skaya (1982).]

1.1.5.1. Isothermal study

The energy of a system is the sum of all the forms of energy: thermal, mechanical, electrical *etc.* Let us consider a system whose only variables are these three. For a small variation of the associated extensive parameters, the variation of the internal energy is

$$dU = E_n dD_n + T_{kl} dS_{kl} + \Theta d\sigma,$$

where Θ is the temperature and σ is the entropy; there is summation over all dummy indices; an orthonormal frame is assumed and variance is not apparent. The mechanical energy of deformation is given by $T_{kl} dS_{kl}$ (see Section 1.3.2.8). Let us consider the Gibbs free-energy function \mathcal{G} defined by

$$\mathcal{G} = U - E_n D_n - T_{kl} S_{kl} - \Theta \sigma.$$

Differentiation of \mathcal{G} gives

$$d\mathcal{G} = -D_n dE_n - S_{kl} dT_{kl} - \sigma d\Theta.$$

The extensive parameters are therefore partial derivatives of the free energy:

$$S_{kl} = -\frac{\partial \mathcal{G}}{\partial T_{kl}}; \quad D_n = -\frac{\partial \mathcal{G}}{\partial E_n}; \quad \sigma = -\frac{\partial \mathcal{G}}{\partial \Theta}.$$

Each of these quantities may be expanded by performing a further differentiation in terms of the intensive parameters, T_{kl} , E_n and Θ . We have, to the first order,

$$\begin{aligned} dS_{kl} &= \left[\frac{\partial S_{kl}}{\partial T_{ij}} \right]_{E, \Theta} dT_{ij} + \left[\frac{\partial S_{kl}}{\partial E_n} \right]_{T, \Theta} dE_n + \left[\frac{\partial S_{kl}}{\partial \Theta} \right]_{E, T} \delta\Theta \\ dD_n &= \left[\frac{\partial D_n}{\partial T_{kl}} \right]_{E, \Theta} dT_{kl} + \left[\frac{\partial D_n}{\partial E_m} \right]_{T, \Theta} dE_m + \left[\frac{\partial D_n}{\partial \Theta} \right]_{E, T} \delta\Theta \\ d\sigma &= \left[\frac{\partial \sigma}{\partial T_{ij}} \right]_{E, \Theta} dT_{ij} + \left[\frac{\partial \sigma}{\partial E_m} \right]_{T, \Theta} dE_m + \left[\frac{\partial \sigma}{\partial \Theta} \right]_{E, T} \delta\Theta. \end{aligned}$$

To a first approximation, the partial derivatives may be considered as constants, and the above relations may be integrated:

$$\left. \begin{aligned} S_{kl} &= (s_{klj})^{E, \Theta} T_{ij} + (d_{kln})^{T, \Theta} E_n + (\alpha_{kl})^{E, T} \delta\Theta \\ D_n &= (d_{nkl})^{E, \Theta} T_{kl} + (\varepsilon_{nm})^{T, \Theta} E_m + (p_n)^{E, T} \delta\Theta \\ \sigma &= (\alpha_{ij})^E T_{ij} + (p_m)^T E_m + (\rho C^{E, T} / \Theta) \delta\Theta. \end{aligned} \right\} \quad (1.1.5.1)$$

This set of equations is the equivalent of relation (1.1.1.6) of Section 1.1.1.3, which gives the coefficients of the matrix of physical properties. These coefficients are:

(i) For the principal properties: $(s_{klj})^{E, \Theta}$: elastic compliances at constant temperature and field; $(\varepsilon_{nm})^{T, \Theta}$: dielectric constant at constant temperatures and stress; $\rho C^{T, E}$: heat capacity per unit volume at constant stress and field (ρ is the specific mass and $C^{T, E}$ is the specific heat at constant stress and field).

(ii) For the other properties: $(d_{kln})^{T, \Theta}$ and $(d_{nkl})^{E, \Theta}$ are the components of the piezoelectric effect and of the converse effect. They are represented by 3×9 and 9×3 matrices, respectively. One may notice that

$$d_{kln} = \frac{\partial S_{kl}}{\partial E_n} = -\frac{\partial^2 \mathcal{G}}{\partial E_n \partial T_{kl}} = -\frac{\partial^2 \mathcal{G}}{\partial T_{kl} \partial E_n} = \frac{\partial D_n}{\partial T_{kl}} = d_{nkl},$$

which shows again that the components of two properties that are symmetric with respect to the leading diagonal of the matrix of physical properties are equal (Section 1.1.1.4) and that the corresponding matrices are transpose to one another.

In a similar way,

(a) the matrices $(\alpha_{kl})^{E, T}$ of the thermal expansion and $(\alpha_{ij})^E$ of the piezocalorific effect are transpose to one another;

(b) the components $(p_n)^T$ of the pyroelectric and of the electrocalorific effects are equal.

Remark. The piezoelectric effect, namely the existence of an electric polarization \mathbf{P} under an applied stress, is always measured at zero applied electric field and at constant temperature. The second equation of (1.1.5.1) becomes under these circumstances

$$P_n = D_n = (d_{nkl})^\Theta T_{kl}.$$

Remark. Equations (1.1.5.1) are, as has been said, first-order approximations because we have assumed the partial derivatives to be constants. Actually, this approximation is not correct, and in many cases it is necessary to take into account the higher-order terms as, for instance, in:

(a) nonlinear elasticity (see Sections 1.3.6 and 1.3.7);

(b) electrostriction;

(c) nonlinear optics (see Chapter 1.7);

(d) electro-optic and piezo-optic effects (see Sections 1.6.6 and 1.6.7).

1. TENSORIAL ASPECTS OF PHYSICAL PROPERTIES

1.1.5.2. Other forms of the piezoelectric constants

We use here another Gibbs function, the electric Gibbs function, \mathcal{G}_2 , defined by

$$\mathcal{G}_2 = \mathcal{U} - E_n D_n - \Theta \sigma.$$

Differentiation of \mathcal{G} gives

$$d\mathcal{G}_2 = -D_n dE_n + T_{ij} dS_{ij} - \sigma d\Theta.$$

It follows that

$$T_{ij} = \frac{\partial \mathcal{G}_2}{\partial S_{ij}}; \quad D_n = -\frac{\partial \mathcal{G}_2}{\partial E_n}; \quad \sigma = -\frac{\partial \mathcal{G}_2}{\partial \Theta}$$

and a set of relations analogous to (1.1.5.1):

$$\left. \begin{aligned} T_{ij} &= (c_{ijkl})^{E,\Theta} S_{kl} - (e_{ijn})^{S,\Theta} E_n - (\lambda_{ij})^{E,S} \delta\Theta \\ D_n &= (e_{nij})^{E,\Theta} S_{ij} + (\varepsilon_{nm})^{S,\Theta} E_m + (p_n)^S \delta\Theta \\ \delta\sigma &= (\lambda_{ij})^E S_{ij} + (p_n)^S E_n + \rho C^{E,S} \delta\Theta / \Theta, \end{aligned} \right\} \quad (1.1.5.2)$$

where the components $(c_{ijkl})^{E,\Theta}$ are the isothermal elastic stiffnesses at constant field and constant temperature,

$$e_{ijn} = -\frac{\partial T_{ij}}{\partial E_n} = -\frac{\partial^2 \mathcal{G}_2}{\partial E_n \partial S_{ij}} = -\frac{\partial^2 \mathcal{G}_2}{\partial S_{ij} \partial E_n} = \frac{\partial D_n}{\partial S_{ij}} = e_{nij}$$

are the piezoelectric stress coefficients at constant strain and constant temperature,

$$\lambda_{ij} = -\frac{\partial T_{ij}}{\partial \Theta} = -\frac{\partial^2 \mathcal{G}_2}{\partial \Theta \partial S_{ij}} = -\frac{\partial^2 \mathcal{G}_2}{\partial S_{ij} \partial \Theta} = \frac{\partial \delta\sigma}{\partial S_{ij}}$$

are the temperature-stress constants and

$$p_n = \frac{\partial D_n}{\partial \Theta} = -\frac{\partial^2 \mathcal{G}_2}{\partial \Theta \partial E_n} = -\frac{\partial^2 \mathcal{G}_2}{\partial E_n \partial \Theta} = \frac{\partial \delta\sigma}{\partial E_n}$$

are the components of the pyroelectric effect at constant strain.

The relations between these coefficients and the usual coefficients d_{kln} are easily obtained:

(i) At constant temperature and strain: if one puts $\delta\Theta = 0$ and $S_{kl} = 0$ in the first equation of (1.1.5.1) and (1.1.5.2), one obtains, respectively,

$$\begin{aligned} 0 &= s_{klij} T_{ij} + d_{kln} E_n \\ T_{ij} &= -e_{ijn} E_n, \end{aligned}$$

from which it follows that

$$d_{kln} = s_{klij} e_{ijn}$$

at constant temperature and strain.

(ii) At constant temperature and stress: if one puts $\delta\Theta = 0$ and $T_{ij} = 0$, one obtains in a similar way

$$\begin{aligned} S_{kl} &= d_{kln} E_n \\ 0 &= c_{ijkl} S_{kl} - e_{ijn} E_n, \end{aligned}$$

from which it follows that

$$e_{ijn} = c_{ijkl} d_{kln}$$

at constant temperature and stress.

1.1.5.3. Relation between the pyroelectric coefficients at constant stress and at constant strain

By combining relations (1.1.5.1) and (1.1.5.2), it is possible to obtain relations between the pyroelectric coefficients at constant stress, p_n^T , and the pyroelectric coefficients at constant strain, p_n^S , also called *real* pyroelectric coefficients, p_n^S . Let us put $T_{ij} = 0$ and

$E_n = 0$ in the first equation of (1.1.5.1). For a given variation of temperature, $\delta\Theta$, the observed strain is

$$S_{kl} = [\alpha_{kl}]^{E,T} \delta\Theta.$$

From the second equations of (1.1.5.1) and (1.1.5.2), it follows that

$$\begin{aligned} D_n &= p_n^T \delta\Theta \\ D_n &= e_{nkl} S_{kl} + p_n^S \delta\Theta. \end{aligned}$$

Substituting the expression S_{kl} and eliminating D_n , it follows that

$$p_n^T = e_{nkl} [\alpha_{kl}]^{E,T} + p_n^S. \quad (1.1.5.3)$$

This relation shows that part of the pyroelectric effect is actually due to the piezoelectric effect.

1.1.5.4. Adiabatic study

Piezoelectric resonators usually operate at a high frequency where there are no heat exchanges, and therefore in an adiabatic regime ($\Theta \delta\sigma = 0$). From the third equation of (1.1.5.1), we obtain a relation between the temperature variation, the applied stress and the electric field:

$$(\alpha_{ij})^E T_{ij} + (p_m)^T E_m + \frac{\rho C^{T,E}}{\Theta} \delta\Theta = 0.$$

If we substitute this relation in the two other relations of (1.1.5.1), we obtain two equivalent relations, but in the *adiabatic* regime:

$$\begin{aligned} S_{kl} &= (s_{klij})^{E,\sigma} T_{ij} + (d_{klm})^{T,\sigma} E_m \\ D_n &= (d_{nij})^{E,\sigma} T_{ij} + (\varepsilon_{nm})^{T,\sigma} E_m. \end{aligned}$$

By comparing these expressions with (1.1.5.1), we obtain the following relations between the adiabatic and the isothermal coefficients:

$$\begin{aligned} (s_{ijkl})^{E,\sigma} &= (s_{ijkl})^{E,\theta} - \frac{(\alpha_{ij})^E (\alpha_{kl})^E \Theta}{\rho C^{T,E}} \\ (d_{nij})^{E,\sigma} &= (d_{nij})^{E,\theta} - \frac{(p_n)^T (\alpha_{kl})^E \Theta}{\rho C^{T,E}} \\ (\varepsilon_{mn})^{T,\sigma} &= (\varepsilon_{mn})^{T,\theta} - \frac{(p_n)^T (p_m)^T \Theta}{\rho C^{T,E}}. \end{aligned}$$

1.1.6. Glossary

| | |
|---------------------|---|
| \mathbf{e}_i | basis vectors in direct space (covariant) |
| \mathbf{e}^i | basis vectors in reciprocal space (contravariant) |
| x^i | components of a vector in direct space (contravariant) |
| x_i | components of a vector in reciprocal space (covariant) |
| g_{ij} | components of the metric tensor |
| $i_1 \dots j_q$ | components of a tensor of rank n, p times covariant and q times contravariant ($n = p + q$) |
| $i_1 \dots i_p$ | |
| A^T | transpose of matrix A |
| \otimes | tensor product |
| \wedge | outer product |
| \wedge | vector product |
| ∂_i | partial derivative with respect to x_i |
| δ_i^j | Kronecker symbol |
| ε_{ijk} | permutation tensor |
| V | volume |

1.1. INTRODUCTION TO THE PROPERTIES OF TENSORS

| | |
|----------------------------|---|
| p | pressure |
| u_i | components of the displacement vector |
| S_{ij} | components of the strain tensor |
| S_{α} | components of the strain Voigt matrix |
| T_{ij} | components of the stress tensor |
| T_{α} | components of the stress Voigt matrix |
| s_{ijkl} | elastic compliances |
| $s_{\alpha\beta}$ | reduced elastic compliances |
| $(s_{ijkl})^{\sigma}$ | adiabatic elastic compliances |
| c_{ijkl} | elastic stiffnesses |
| $c_{\alpha\beta}$ | reduced elastic stiffnesses |
| ν | Poisson's ratio |
| E | Young's modulus |
| Θ | temperature |
| σ | entropy |
| α_{ij} | thermal expansion |
| λ_{ij} | temperature-stress constant |
| \mathcal{U} | internal energy |
| \mathcal{G} | Gibbs free energy |
| $C^{E,T}$ | specific heat at constant stress and applied electric field |
| E | electric field |
| D | electric displacement |
| H | magnetic field |
| B | magnetic induction |
| ϵ_0 | permittivity of vacuum |
| ϵ | dielectric constant |
| ϵ_{ij} | dielectric tensor |
| $(\epsilon_{ij})^{\sigma}$ | adiabatic dielectric tensor |
| χ_e | dielectric susceptibility |
| η_{ij} | dielectric impermeability |
| p_i | pyroelectric tensor |
| d_{ijk} | piezoelectric tensor |
| $d_{i\alpha}$ | reduced piezoelectric tensor |
| $d_{\alpha i}$ | reduced inverse piezoelectric tensor |
| $(d_{ijk})^{\sigma}$ | adiabatic piezoelectric tensor |
| e_{ijk} | piezoelectric tensor at constant strain |
| Q_{ijkl} | electrostriction tensor |
| $Q_{\alpha\beta}$ | reduced electrostriction tensor |
| π_{ijkl} | piezo-optic tensor |
| $\pi_{\alpha\beta}$ | reduced piezo-optic tensor |
| p_{ijkl} | elasto-optic tensor |
| $p_{\alpha\beta}$ | reduced elasto-optic tensor |
| $R_{H\ ij k}$ | Hall constant |

References

- Bhagavantam, S. (1966). *Crystal symmetry and physical properties*. London: Academic Press.
- Billings, A. (1969). *Tensor properties of materials*. London/New York: Wiley Interscience.
- Brillouin, L. (1949). *Les tenseurs en mécanique et en élasticité*. Paris: Masson & Cie.
- Cady, W. G. (1964). *Piezoelectricity*. New York: Dover.
- Curie, J. & Curie, P. (1880). Développement par pression de l'électricité polaire dans les cristaux hémiedres à faces inclinées. *C. R. Acad. Sci.* **91**, 294–295.
- Curie, J. & Curie, P. (1881). Contractions et dilatations produites par des tensions électriques dans les cristaux hémiedres à faces inclinées. *C. R. Acad. Sci.* **93**, 1137–1140.
- Curie, P. (1884). Sur les questions d'ordre: répétitions. *Bull. Soc. Fr. Minéral.* **7**, 89–110.
- Curie, P. (1894). Sur la symétrie dans les phénomènes physiques, symétrie d'un champ électrique et d'un champ magnétique. *J. Phys. (Paris)*, **3**, 393–415.
- Fumi, F. G. (1951). Third-order elastic coefficients of crystals. *Phys. Rev.* **83**, 1274–1275.
- Fumi, F. G. (1952a). Physical properties of crystals: the direct inspection method. *Acta Cryst.* **5**, 44–48.
- Fumi, F. G. (1952b). The direct-inspection method in systems with a principal axis of symmetry. *Acta Cryst.* **5**, 691–694.
- Fumi, F. G. (1952c). Third-order elastic coefficients in trigonal and hexagonal crystals. *Phys. Rev.* **86**, 561.
- Fumi, F. G. (1987). Tables for the third-order elastic tensors in crystals. *Acta Cryst.* **A43**, 587–588.
- Fumi, F. G. & Ripamonti, C. (1980a). Tensor properties and rotational symmetry of crystals. I. A new method for group $3(3_2)$ and its application to general tensors up to rank 8. *Acta Cryst.* **A36**, 535–551.
- Fumi, F. G. & Ripamonti, C. (1980b). Tensor properties and rotational symmetry of crystals. II. Groups with 1-, 2- and 4-fold principal symmetry and trigonal and hexagonal groups different from group 3. *Acta Cryst.* **A36**, 551–558.
- Ikeda, T. (1990). *Fundamentals of piezoelectricity*. Oxford University Press.
- International Tables for Crystallography* (2000). Vol. B. *Reciprocal space*, edited by U. Shmueli. Dordrecht: Kluwer Academic Publishers.
- International Tables for Crystallography* (2002). Vol. A. *Space-group symmetry*, edited by Th. Hahn. Dordrecht: Kluwer Academic Publishers.
- Kumaraswamy, K. & Krishnamurthy, N. (1980). The acoustic gyrotropic tensor in crystals. *Acta Cryst.* **A36**, 760–762.
- Lichnerowicz, A. (1947). *Algèbre et analyse linéaires*. Paris: Masson.
- Mason, W. P. (1966). *Crystal physics of interaction processes*. London: Academic Press.
- Neumann, F. (1885). *Vorlesungen über die Theorie der Elastizität der festen Körper und des Lichtäthers*, edited by O. E. Meyer. Leipzig: B. G. Teubner-Verlag.
- Nowick, A. S. (1995). *Crystal properties via group theory*. Cambridge University Press.
- Nye, J. F. (1957). *Physical properties of crystals*, 1st ed. Oxford: Clarendon Press.
- Nye, J. F. (1985). *Physical properties of crystals*, revised ed. Oxford University Press.
- Onsager, L. (1931a). Reciprocal relations in irreversible processes. I. *Phys. Rev.* **37**, 405–426.
- Onsager, L. (1931b). Reciprocal relations in irreversible processes. II. *Phys. Rev.* **38**, 2265–2279.
- Pasteur, L. (1848a). Recherches sur les relations qui peuvent exister entre la forme cristalline, la composition chimique et le sens de la polarisation rotatoire. *Ann. Chim. (Paris)*, **24**, 442–459.
- Pasteur, L. (1848b). Mémoire sur la relation entre la forme cristalline et la composition chimique, et sur la cause de la polarisation rotatoire. *C. R. Acad. Sci.* **26**, 535–538.
- Pauffer, P. (1986). *Physikalische Kristallographie*. Berlin: Akademie-Verlag.
- Sands, D. E. (1995). *Vectors and tensors in crystallography*. New York: Dover.
- Schwartz, L. (1975). *Les tenseurs*. Paris: Hermann.
- Shuvalov, L. A. (1988). *Modern crystallography IV (physical properties of crystals)*. Berlin: Springer-Verlag.
- Sirotnin, Y. I. & Shaskol'skaya, M. P. (1982). *Fundamentals of crystal physics*. Moscow: Mir.
- Voigt, W. (1910). *Lehrbuch der Kristallphysik*. Leipzig: Teubner. 2nd ed. (1929); photorep. (1966). New York: Johnson Reprint Corp. and Leipzig: Teubner.
- Wooster, W. A. (1973). *Tensors and group theory for the physical properties of crystals*. Oxford: Clarendon Press.
- Zheludev, I. S. (1986). Space and time inversion in physical crystallography. *Acta Cryst.* **A42**, 122–127.

1.2. Representations of crystallographic groups

BY T. JANSSEN

1.2.1. Introduction

Symmetry arguments play an important role in science. Often one can use them in a heuristic way, but the correct formulation is in terms of group theory. This remark is in fact superfluous for crystallographers, who are used to point groups and space groups as they occur in the description of structures. However, besides these structural problems there are many others where group theory may play a role. A central role in this context is played by representation theory, which treats the action of a group on physical quantities, and usually this is done in terms of linear transformations, although nonlinear representations may also occur.

To start with an example, consider a spin system, an arrangement of spins on sites with a certain symmetry, for example space-group symmetry. The elements of the space group map the sites onto other sites, but at the same time the spins are rotated or transformed otherwise in a well defined fashion. The spins can be seen as elements of a vector space (spin space) and the transformation in this space is an image of the space-group element. In a similar way, all symmetric tensors of rank 2 form a vector space, because one can add them and multiply them by a real factor. A linear change of coordinates changes the vectors, and the transformations in the space of tensors are the image of the coordinate transformations. Probably the most important use of such representations is in quantum mechanics, where transformations in coordinate space are mapped onto linear transformations in the quantum mechanical space of state vectors.

To see the relation between groups of transformations and the use of their representations in physics, consider a tensor which transforms under a certain point group. Let us take a symmetric rank 2 tensor T_{ij} in three dimensions. We take as example the point group 222. From Section 1.1.3.2 one knows how such a tensor transforms: it transforms into a tensor T'_{ij} according to

$$T'_{ij} = \sum_{k=1}^3 \sum_{m=1}^3 R_{ik} R_{jm} T_{km} \quad (1.2.1.1)$$

for all orthogonal transformations R in the group 222. This action of the point group 222 is obviously a linear one:

$$(c_1 T_{ij}^{(1)} + c_2 T_{ij}^{(2)})' = c_1 T_{ij}^{(1)'} + c_2 T_{ij}^{(2)'}$$

The transformations on the tensors really form an image of the group, because if one writes $D(R)T$ for T' , one has for two elements $R^{(1)}$ and $R^{(2)}$ the relation

$$(D(R^{(1)}R^{(2)}))T = D(R^{(1)})(D(R^{(2)})T)$$

or

$$D(R^{(1)}R^{(2)}) = D(R^{(1)})D(R^{(2)}). \quad (1.2.1.2)$$

This property is said to define a (linear) representation. Because of the representation property, it is sufficient to know how the tensor transforms under the generators of a group. In our example, one could be interested in symmetric tensors that are invariant under the group 222. Then it is sufficient to consider the rotations over 180° along the x and y axes. If the point group is a symmetry group of the system, a tensor describing the relation between two physical quantities should remain the same. For invariant tensors one has

$$\begin{pmatrix} a_{11} & a_{12} & a_{13} \\ a_{12} & a_{22} & a_{23} \\ a_{13} & a_{23} & a_{33} \end{pmatrix} = \begin{pmatrix} 1 & 0 & 0 \\ 0 & -1 & 0 \\ 0 & 0 & -1 \end{pmatrix} \begin{pmatrix} a_{11} & a_{12} & a_{13} \\ a_{12} & a_{22} & a_{23} \\ a_{13} & a_{23} & a_{33} \end{pmatrix} \begin{pmatrix} 1 & 0 & 0 \\ 0 & -1 & 0 \\ 0 & 0 & -1 \end{pmatrix},$$

$$\begin{pmatrix} a_{11} & a_{12} & a_{13} \\ a_{12} & a_{22} & a_{23} \\ a_{13} & a_{23} & a_{33} \end{pmatrix} = \begin{pmatrix} -1 & 0 & 0 \\ 0 & 1 & 0 \\ 0 & 0 & -1 \end{pmatrix} \begin{pmatrix} a_{11} & a_{12} & a_{13} \\ a_{12} & a_{22} & a_{23} \\ a_{13} & a_{23} & a_{33} \end{pmatrix} \begin{pmatrix} -1 & 0 & 0 \\ 0 & 1 & 0 \\ 0 & 0 & -1 \end{pmatrix}$$

and the solution of these equations is

$$\begin{pmatrix} a_{11} & a_{12} & a_{13} \\ a_{12} & a_{22} & a_{23} \\ a_{13} & a_{23} & a_{33} \end{pmatrix} = \begin{pmatrix} a_{11} & 0 & 0 \\ 0 & a_{22} & 0 \\ 0 & 0 & a_{33} \end{pmatrix}.$$

The matrices of rank 2 form a nine-dimensional vector space. The rotation over 180° around the x axis can also be written as

$$R \begin{pmatrix} a_{11} \\ a_{12} \\ a_{13} \\ a_{21} \\ a_{22} \\ a_{23} \\ a_{31} \\ a_{32} \\ a_{33} \end{pmatrix} = \begin{pmatrix} 1 & 0 & 0 & 0 & 0 & 0 & 0 & 0 & 0 \\ 0 & -1 & 0 & 0 & 0 & 0 & 0 & 0 & 0 \\ 0 & 0 & -1 & 0 & 0 & 0 & 0 & 0 & 0 \\ 0 & 0 & 0 & -1 & 0 & 0 & 0 & 0 & 0 \\ 0 & 0 & 0 & 0 & 1 & 0 & 0 & 0 & 0 \\ 0 & 0 & 0 & 0 & 0 & 1 & 0 & 0 & 0 \\ 0 & 0 & 0 & 0 & 0 & 0 & -1 & 0 & 0 \\ 0 & 0 & 0 & 0 & 0 & 0 & 0 & 1 & 0 \\ 0 & 0 & 0 & 0 & 0 & 0 & 0 & 0 & 1 \end{pmatrix} \begin{pmatrix} a_{11} \\ a_{12} \\ a_{13} \\ a_{21} \\ a_{22} \\ a_{23} \\ a_{31} \\ a_{32} \\ a_{33} \end{pmatrix}.$$

This nine-dimensional matrix together with the one corresponding to a rotation along the y axis generate a representation of the group 222 in the nine-dimensional space of three-dimensional rank 2 tensors. The invariant tensors form the subspace $(a_{11}, 0, 0, 0, a_{22}, 0, 0, 0, a_{33})$. In this simple case, group theory is barely needed. However, in more complex situations, the calculations may become quite cumbersome without group theory. Moreover, group theory may give a wealth of other information, such as selection rules and orthogonality relations, that can be obtained only with much effort without group theory, or in particular representation theory. Tables of tensor properties, and irreducible representations of point and space groups, have been in use for a long time. For point groups see, for example, Butler (1981) and Altmann & Herzog (1994); for space groups, see Miller & Love (1967), Kovalev (1987) and Stokes & Hatch (1988).

In the following, we shall discuss the representation theory of crystallographic groups. We shall adopt a slightly abstract language, which has the advantage of conciseness and generality, but we shall consider examples of the most important notions. Another point that could give rise to some problems is the fact that we shall consider in part the theory for crystallographic groups in arbitrary dimension. Of course, physics occurs in three-

1.2. REPRESENTATIONS OF CRYSTALLOGRAPHIC GROUPS

dimensional space, but often it is useful to see what is general and what is special for one, two or three dimensions. In Section 1.2.2, the point groups are discussed, together with their representations. In Section 1.2.3, the same is done for space groups. Tensors for point and space groups are then treated in terms of representation theory in Section 1.2.4. Besides transformations in space, transformations involving time reversal are important as well. They are discussed in Section 1.2.5. Information on crystallographic groups and their representations is presented in tabular form in Section 1.2.6. This section can be consulted independently.

1.2.2. Point groups

1.2.2.1. Finite point groups in one, two and three dimensions

The crystallographic point groups are treated in Volume A of *International Tables for Crystallography* (2002). Here we just give a brief summary of some important notions. To maintain generality, we consider the case of n -dimensional point groups.

Point groups in n dimensions are subgroups of the orthogonal group $O(n)$ in n dimensions. By definition they leave a point, the origin, invariant. They are of importance in physics because physical laws are invariant under such transformations. In this case $n = 1, 2$ or 3 . For crystallography, the crystallographic point groups are the most relevant ones. A *crystallographic point group* is a subgroup of $O(n)$ that leaves an n -dimensional lattice invariant. A *lattice* is a collection of points

$$\mathbf{r} = \mathbf{r}_o + \sum_{i=1}^n n_i \mathbf{e}_i, \quad n_i \in \mathbb{Z}, \quad (1.2.2.1)$$

where the n vectors \mathbf{e}_i form a basis of n -dimensional space. In other words, the points of the lattice can be obtained by the action of translations

$$\mathbf{t} = \sum_{i=1}^n n_i \mathbf{e}_i \quad (1.2.2.2)$$

on the lattice origin \mathbf{r}_o . These translations form a *lattice translation group* in n -dimensional space, i.e. a discrete subgroup of the group of all translations $T(n)$ in n dimensions, generated by n linearly independent translations.

Because a crystallographic point group leaves a lattice of points invariant, (a) it is a finite group of linear transformations and (b) on a basis of the lattice it is represented by integer matrices. On the other hand, as will be shown in Section 1.2.2.2, there is for every finite group of matrices an invariant scalar product, i.e. a positive definite metric tensor left invariant by the group. If one uses this metric tensor for the definition of the scalar product, the matrices represent orthogonal transformations. Moreover, when the matrices are integer, the group of matrices can be considered to be a crystallographic point group. In this sense, every finite group of integer matrices is a crystallographic point group. Consider as an example the group of matrices

$$\begin{pmatrix} 1 & 0 \\ 0 & 1 \end{pmatrix}, \quad \begin{pmatrix} 0 & -1 \\ 1 & -1 \end{pmatrix}, \quad \begin{pmatrix} -1 & 1 \\ -1 & 0 \end{pmatrix},$$

which leaves invariant the metric tensor

$$g = \begin{pmatrix} a & -a/2 \\ -a/2 & a \end{pmatrix}.$$

The lattice points $n_1 \mathbf{a}_1 + n_2 \mathbf{a}_2$ go over into lattice points and the transformation leaves the scalar product of two such vectors the same if the scalar product of the two vectors $n_1 \mathbf{a}_1 + n_2 \mathbf{a}_2$ and $n'_1 \mathbf{a}_1 + n'_2 \mathbf{a}_2$ is defined as

$$n_1 n'_1 a - n_1 n'_2 a/2 - n_2 n'_1 a/2 + n_2 n'_2 a.$$

After a basis transformation,

$$\mathbf{e}_1 = \mathbf{a}_1 / \sqrt{a}, \quad \mathbf{e}_2 = (\mathbf{a}_1 + 2\mathbf{a}_2) / \sqrt{3a},$$

the metric tensor is in standard form (see Section 1.1.2.2):

$$\mathbf{e}_i \cdot \mathbf{e}_j = \delta_{ij}.$$

This means that with respect to the basis $\mathbf{e}_1, \mathbf{e}_2$, the three transformations become orthogonal matrices.

To be able to give a list of all crystallographic point groups in n dimensions it is necessary to state which point groups should be considered as different. Two point groups belong to the same *geometric crystal class* if they are conjugated subgroups of $O(n)$. This means that $K \subset O(n)$ and $K' \subset O(n)$ belong to the same class if there is an element $R \in O(n)$ such that $K' = RKR^{-1}$, which implies that there are two orthonormal bases in the vector space related by an orthogonal transformation R such that the matrices of K for one basis are the same as those for K' on the second basis.

In *one-dimensional space*, there are only two different point groups, the first consisting of the identity, the second of the numbers ± 1 . These groups are isomorphic to C_1 and C_2 , respectively, where C_m is the cyclic group of integers modulo m (also denoted by \mathbb{Z}_m). Both are crystallographic because their 1×1 'matrices' are the integers ± 1 .

In *two-dimensional space*, the orthogonal group $O(2)$ is the union of the subgroup $SO(2)$, consisting of all orthogonal transformations with determinant $+1$, and the coset $O(2) \setminus SO(2)$, consisting of all orthogonal transformations with determinant -1 . The group $SO(2)$ is Abelian, and therefore all its subgroups are Abelian. The finite ones are the rotation groups denoted by n ($n \in \mathbb{Z}^+$). Every element of $O(2) \setminus SO(2)$ is of order two, and corresponds to a mirror line. Therefore, all the other finite point groups are nmm (n even) or nm (n odd). The rotation groups are isomorphic with the cyclic groups C_n and the others with the dihedral groups D_n . Only the groups $1, 2, 3, 4, 6, m, 2mm, 3m, 4mm$ and $6mm$ leave a lattice invariant and are crystallographic.

The isomorphism class of a group can be given by its *generators* and *defining relations*. For example, the elements of the group $4mm$ can be written as products (with generally more than two factors) of the two matrices

$$A = \begin{pmatrix} 0 & -1 \\ 1 & 0 \end{pmatrix}, \quad B = \begin{pmatrix} 1 & 0 \\ 0 & -1 \end{pmatrix},$$

which satisfy the relations $A^4 = B^2 = ABAB = E$, and every group whose elements are products of two generating elements with the same and not more independent relations is isomorphic. One calls the relations the defining relations. The set of generators and defining relations is not unique. In an extreme case, one can consider all elements of the group as generators, and the product rules $ab = c$ as the defining relations.

For the two-dimensional groups, the generators and defining relations are

C_n : one generator A , with $A^n = E$;

D_n : two generators A and B , with $A^n = B^2 = (AB)^2 = E$, where E is the unit element.

The determination of all finite point groups in *three-dimensional space* is more involved. A derivation can, for example, be found in Janssen (1973). The group $O(3)$ is again the union of $SO(3)$ and $O(3) \setminus SO(3)$, and in fact the direct product of $SO(3)$ and the group generated by the inversion $I = -E$. One may distinguish between three different classes of finite point groups:

(a) point groups that belong fully to the rotation group $SO(3)$;

(b) point groups that contain the inversion $-E$ and are, consequently, the direct product of a point group of the first class and the group generated by $-E$;

1. TENSORIAL ASPECTS OF PHYSICAL PROPERTIES

(c) point groups that have elements in common with $O(3)/SO(3)$ but do not contain $-E$; such groups are isomorphic to a group of the first class, as one can see if one multiplies all elements with determinant equal to -1 by $-E$.

The list of three-dimensional finite point groups is given in Table 1.2.6.1. All isomorphism classes of two-dimensional point groups occur in three dimensions as well. The isomorphism classes occurring here for the first time are:

$$\begin{aligned}
 C_n \times C_2: & A, B, \text{ with } A^n = B^2 = ABA^{-1}B^{-1} = E; \\
 D_n \times C_2: & A, B, C \text{ with } A^n = B^2 = (AB)^2 = C^2 = ACA^{-1}C^{-1} \\
 & = BCB^{-1}C^{-1} = E; \\
 T: & A, B, \text{ with } A^3 = B^2 = (AB)^3 = E; \\
 O: & A, B, \text{ with } A^4 = B^3 = (AB)^2 = E; \\
 T \times C_2: & A, B, C, \text{ with } A^3 = B^2 = (AB)^3 = C^2 = ACA^{-1}C^{-1} \\
 & = BCB^{-1}C^{-1} = E; \\
 O \times C_2: & A, B, C, \text{ with } A^4 = B^3 = (AB)^2 = C^2 = ACA^{-1}C^{-1} \\
 & = BCB^{-1}C^{-1} = E; \\
 I: & A, B, \text{ with } A^5 = B^3 = (AB)^2 = E; \\
 I \times C_2: & A, B, C, \text{ with } A^5 = B^3 = (AB)^2 = C^2 = ACA^{-1}C^{-1} \\
 & = BCB^{-1}C^{-1} = E.
 \end{aligned}$$

The crystallographic groups among them are given in Table 1.2.6.2.

1.2.2.2. Representations of finite groups

As stated in Section 1.2.1, elements of point groups act on physical properties (like tensorial properties) and on wave functions as linear operators. These linear operators therefore generally act in a different space than the three-dimensional configuration space. We denote this new space by V and consider a mapping D from the point group K to the group of nonsingular linear operators in V that satisfies

$$D(R)D(R') = D(RR') \quad \forall R, R' \in K. \quad (1.2.2.3)$$

In other words D is a *homomorphism* from K to the group of nonsingular linear transformations $GL(V)$ on the vector space V . Such a homomorphism is called a *representation* of K in V . Here we only consider finite-dimensional representations.

With respect to a basis \mathbf{e}_i ($i = 1, 2, \dots, n$) the linear transformations are given by matrices $\Gamma(R)$. The mapping Γ from K to the group of nonsingular $n \times n$ matrices $GL(n, R)$ (for a real vector space V) or $GL(n, C)$ (if V is complex) is called an *n -dimensional matrix representation* of K .

If one chooses another basis for V connected to the former one by a nonsingular matrix S , the same group of operators $D(K)$ is represented by another matrix group $\Gamma'(K)$, which is related to $\Gamma(K)$ by S according to $\Gamma'(R) = S^{-1}\Gamma(R)S$ ($\forall R \in K$). Two such matrix representations are called *equivalent*. On the other hand, two such equivalent matrix representations can be considered to describe two different groups of linear operators $[D(K)$ and $D'(K)]$ on the same basis. Then there is a nonsingular linear operator T such that $D(R)T = TD'(R)$ ($\forall R \in K$). In this case, the representations $D(K)$ and $D'(K)$ are also called equivalent.

It may happen that a representation $D(K)$ in V leaves a subspace W of V invariant. This means that for every vector $v \in W$ and every element $R \in K$ one has $D(R)v \in W$. Suppose that this subspace is of dimension $m < n$. Then one can choose m basis vectors for V inside the invariant subspace. With respect to this basis, the corresponding matrix representation has elements

$$\Gamma(R) = \begin{pmatrix} \Gamma_1(R) & \Gamma_3(R) \\ 0 & \Gamma_2(R) \end{pmatrix}, \quad (1.2.2.4)$$

where the matrices $\Gamma_1(R)$ form an m -dimensional matrix representation of K . In this situation, the representations $D(K)$ and $\Gamma(K)$ are called *reducible*. If there is no proper invariant subspace the representation is *irreducible*. If the representation is a direct sum of subspaces, each carrying an irreducible representation, the representation is called *fully reducible* or *decomposable*. In the latter case, a basis in V can be chosen such that the matrices $\Gamma(R)$ are direct sums of matrices $\Gamma_i(R)$ such that the $\Gamma_i(R)$ form an irreducible matrix representation. If $\Gamma_3(R)$ in (1.2.2.4) is zero and Γ_1 and Γ_2 form irreducible matrix representations, Γ is fully reducible. For finite groups, each reducible representation is fully reducible. That means that if $\Gamma(K)$ is reducible, there is a matrix S such that

$$\begin{aligned}
 \Gamma(R) &= S[\Gamma_1(R) \oplus \dots \oplus \Gamma_n(R)]S^{-1} \\
 &= S \begin{pmatrix} \Gamma_1(R) & 0 & \dots & 0 \\ 0 & \Gamma_2(R) & \dots & 0 \\ \vdots & \vdots & \ddots & \vdots \\ 0 & 0 & \dots & \Gamma_n(R) \end{pmatrix} S^{-1}.
 \end{aligned} \quad (1.2.2.5)$$

In this way one may proceed until all matrix representations $\Gamma_i(K)$ are *irreducible*, i.e. do not have invariant subspaces. Then each representation $\Gamma(K)$ can be written as a direct sum

$$\Gamma(R) = S[m_1\Gamma_1(R) \oplus \dots \oplus m_s\Gamma_s(R)]S^{-1}, \quad (1.2.2.6)$$

where the representations $\Gamma_1 \dots \Gamma_s$ are all nonequivalent and the *multiplicities* m_i are the numbers of times each irreducible representation occurs. The nonequivalent irreducible representations Γ_i for which the multiplicity is not zero are the *irreducible components* of $\Gamma(K)$.

We first discuss two special representations. The simplest representation in one-dimensional space is obtained by assigning the number 1 to all elements of K . Obviously this is a representation, called the *identity* or *trivial representation*. Another is the *regular representation*. To obtain this, one numbers the elements of K from 1 to the order N of the group ($|K| = N$). For a given $R \in K$ there is a one-to-one mapping from K to itself defined by $R_i \rightarrow R_j \equiv RR_i$. Consider the $N \times N$ matrix $\Gamma(R)$, which has in the i th column zeros except on line j , where the entry is unity. The matrix $\Gamma(R)$ then has as only entries 0 or 1 and satisfies

$$RR_i = \Gamma(R)_{ji}R_j, \quad (i = 1, 2, \dots, N). \quad (1.2.2.7)$$

These matrices $\Gamma(R)$ form a representation, the *regular representation* of K of dimension N , as one sees from

$$\begin{aligned}
 (R_i R_j)R_k &= R_i \sum_{l=1}^N \Gamma(R_j)_{lk} R_l = \sum_{l=1}^N \sum_{m=1}^N \Gamma(R_j)_{lk} \Gamma(R_i)_{ml} R_m \\
 &= \sum_{m=1}^N [\Gamma(R_i) \Gamma(R_j)]_{mk} R_m = \sum_{m=1}^N \Gamma(R_i R_j)_{mk} R_m.
 \end{aligned}$$

A representation in a real vector space that leaves a positive definite metric invariant can be considered on an orthonormal basis for that metric. Then the matrices satisfy

$$\Gamma(R)\Gamma(R)^T = E$$

(T denotes transposition of the matrix) and the representation is *orthogonal*. If V is a complex vector space with positive definite metric invariant under the representation, the latter gives on an orthonormal basis matrices satisfying

$$\Gamma(R)\Gamma(R)^\dagger = E$$

1.2. REPRESENTATIONS OF CRYSTALLOGRAPHIC GROUPS

(\dagger denotes Hermitian conjugation) and the representation is *unitary*. A real representation of a finite group is always equivalent with an orthogonal one, a complex representation of a finite group is always equivalent with a unitary one. As a proof of the latter statement, consider the standard Hermitian metric on V : $f(x, y) = \sum_i x_i^* y_i$. Then the positive definite form

$$F(x, y) = (1/N) \sum_{R \in K} f(D(R)x, D(R)y) \quad (1.2.2.8)$$

is invariant under the representation. To show this, take an arbitrary element R' . Then

$$\begin{aligned} F(D(R')x, D(R')y) &= (1/N) \sum_{R \in K} f(D(R'R)x, D(R'R)y) \\ &= F(x, y). \end{aligned} \quad (1.2.2.9)$$

With respect to an orthonormal basis for this metric $F(x, y)$, the matrices corresponding to $D(R)$ are unitary. The complex representation can be put into this unitary form by a basis transformation. For a real representation, the argument is fully analogous, and one obtains an orthogonal transformation.

From two representations, $D_1(K)$ in V_1 and $D_2(K)$ in V_2 , one can construct the sum and product representations. The *sum representation* acts in the direct sum space $V_1 \oplus V_2$, which has elements (\mathbf{a}, \mathbf{b}) with $\mathbf{a} \in V_1$ and $\mathbf{b} \in V_2$. The representation $D_1 \oplus D_2$ is defined by

$$[(D_1 \oplus D_2)(R)](\mathbf{a}, \mathbf{b}) = (D_1(R)\mathbf{a}, D_2(R)\mathbf{b}). \quad (1.2.2.10)$$

The matrices $\Gamma_1 \oplus \Gamma_2(R)$ are of dimension $n_1 + n_2$.

The *product representation* acts in the tensor space, which is the space spanned by the vectors $\mathbf{e}_i \otimes \mathbf{e}_j$ ($i = 1, 2, \dots, \dim V_1$; $j = 1, 2, \dots, \dim V_2$). The dimension of the tensor space is the product of the dimensions of both spaces. The action is given by

$$[(D_1 \otimes D_2)(R)]\mathbf{a} \otimes \mathbf{b} = D_1(R)\mathbf{a} \otimes D_2(R)\mathbf{b}. \quad (1.2.2.11)$$

For bases \mathbf{e}_i ($i = 1, 2, \dots, d_1$) for V_1 and \mathbf{e}'_j ($j = 1, 2, \dots, d_2$) for V_2 , a basis for the tensor product of spaces is given by

$$\mathbf{e}_i \otimes \mathbf{e}'_j, \quad i = 1, \dots, d_1; \quad j = 1, 2, \dots, d_2, \quad (1.2.2.12)$$

and with respect to this basis the representation of K is given by matrices

$$(\Gamma_1 \otimes \Gamma_2)(R)_{ik,jl} = \Gamma_1(R)_{ij} \Gamma_2(R)_{kl}. \quad (1.2.2.13)$$

As an example of these operations, consider

$$\begin{aligned} \begin{pmatrix} 1 & 0 \\ 0 & -1 \end{pmatrix} \oplus \begin{pmatrix} 0 & 1 \\ 1 & 0 \end{pmatrix} &= \begin{pmatrix} 1 & 0 & 0 & 0 \\ 0 & -1 & 0 & 0 \\ 0 & 0 & 0 & 1 \\ 0 & 0 & 1 & 0 \end{pmatrix}; \\ \begin{pmatrix} 1 & 0 \\ 0 & -1 \end{pmatrix} \otimes \begin{pmatrix} 0 & 1 \\ 1 & 0 \end{pmatrix} &= \begin{pmatrix} 0 & 1 & 0 & 0 \\ 1 & 0 & 0 & 0 \\ 0 & 0 & 0 & -1 \\ 0 & 0 & -1 & 0 \end{pmatrix}. \end{aligned}$$

If two representations $D_1(K)$ and $D_2(K)$ are equivalent, there is an operator S such that

$$SD_1(R) = D_2(R)S \quad \forall R \in K.$$

This relation may also hold between sets of operators that are not necessarily representations. Such an operator S is called an *intertwining operator*. With this concept we can formulate a theorem that strictly speaking does not deal with representations but with intertwining operators: *Schur's lemma*.

Proposition. Let M and N be two sets of nonsingular linear transformations in spaces V (dimension n) and W (dimension m), respectively. Suppose that both sets are irreducible (the only invariant subspaces are the full space and the origin). Let S be a linear transformation from V to W such that $SM = NS$. Then either S is the null operator or S is nonsingular and $SMS^{-1} = N$.

Proof: Consider the image of V under S : $\text{Im}_S V \subseteq W$. That means that $S\mathbf{r} \in \text{Im}_S V$ for all $\mathbf{r} \in V$. This implies that $NS\mathbf{r} = SM\mathbf{r} \in \text{Im}_S V$. Therefore, $\text{Im}_S V$ is an invariant subspace of W under N . Because N is irreducible, either $\text{Im}_S V = 0$ or $\text{Im}_S V = W$. In the first case, S is the null operator. In the second case, notice that the kernel of S , the subspace of V mapped on the null vector of W , is an invariant subspace of V under M : if $S\mathbf{r} = 0$ then $NS\mathbf{r} = 0$. Again, because of the irreducibility, either Ker_S is the whole of V , and then S is again the null operator, or $\text{Ker}_S = 0$. In the latter case, S is a one-to-one mapping and therefore nonsingular. Therefore, either S is the null operator or it is an isomorphism between the vector spaces V and W , which are then both of dimension n . With respect to bases in the two spaces, the operator S corresponds to a nonsingular matrix and $M = S^{-1}NS$.

This is a very fundamental theorem. Consequences of the theorem are:

(1) If N and M are nonequivalent irreducible representations and $SM = NS$, then $S = 0$.

(2) If a matrix S is singular and links two irreducible representations of the same dimension, then $S = 0$.

(3) A matrix S that commutes with all matrices of an irreducible complex representation is a multiple of the identity. Suppose that an $n \times n$ matrix S commutes with all matrices of a complex irreducible representation. S can be singular and is then the null matrix, or it is nonsingular. In the latter case it has an eigenvalue $\lambda \neq 0$ and $S - \lambda E$ commutes with all the matrices. However, $S - \lambda E$ is singular and therefore the null matrix: $S = \lambda E$. This reasoning is only valid in a complex space, because, generally, the eigenvalues λ are complex.

1.2.2.3. General tensors

Suppose a group K acts linearly on a d -dimensional space V : for any $v \in V$ one has

$$Rv \in V \quad \forall R \in K, v \in V.$$

For a basis \mathbf{a}_i in V this gives a matrix group $\Gamma(K)$ via

$$R\mathbf{a}_i = \sum_{j=1}^d \Gamma(R)_{ji} \mathbf{a}_j, \quad R \in K. \quad (1.2.2.14)$$

The matrix group $\Gamma(K)$ is a matrix representation of the group K .

Consider now a linear function f on V . Because

$$f\left(\sum_{i=1}^d \xi_i \mathbf{a}_i\right) = \sum_{i=1}^d \xi_i f(\mathbf{a}_i),$$

the function is completely determined by its value on the basis vectors \mathbf{a}_i . A second point is that these linear functions form a vector space because for two functions f_1 and f_2 the function $\alpha_1 f_1 + \alpha_2 f_2$ is a well defined linear function. The vector space is called the *dual space* and is denoted by V^* . A basis for this space is given by functions f_1, \dots, f_d such that

$$f_i(\mathbf{a}_j) = \delta_{ij},$$

because any linear function f can be written as a linear combination of these vectors with as coefficients the value of f on the basis vectors \mathbf{a}_i :

$$f = \sum_{i=1}^d f(\mathbf{a}_i) f_i \Leftrightarrow f\left(\sum_{k=1}^d \xi_k \mathbf{a}_k\right) = \sum_{k=1}^d \xi_k \sum_{i=1}^d f(\mathbf{a}_i) f_i(\mathbf{a}_k) = \sum_{k=1}^d \xi_k f(\mathbf{a}_k).$$

1. TENSORIAL ASPECTS OF PHYSICAL PROPERTIES

Therefore, the space V^* also has d dimensions. If V has in addition a nonsingular scalar product, there is for each linear function f a vector \mathbf{k} such that

$$f(\mathbf{r}) = \mathbf{k} \cdot \mathbf{r}, \quad (1.2.2.15)$$

and the vectors \mathbf{k}_i corresponding to the basis functions f_i above satisfy

$$\mathbf{k}_i \cdot \mathbf{a}_j = f_i(\mathbf{a}_j) = \delta_{ij}. \quad (1.2.2.16)$$

The vectors \mathbf{k}_i (with $i = 1, 2, \dots, d$) form the *reciprocal basis* (see also Section 1.1.2.4).

The transformation properties of the vectors in dual (or reciprocal) space can be derived from those of the vectors in V if one puts

$$(Rf)(R\mathbf{r}) = f(\mathbf{r}). \quad (1.2.2.17)$$

Then

$$Rf_i = \sum_{j=1}^d \Gamma^*(R)_{ji} f_j \leftrightarrow \sum_{i=1}^d \Gamma^*(R)_{ji} \sum_{l=1}^d \Gamma(R)_{lk} f_j(\mathbf{a}_l) = f_i(\mathbf{a}_k) = \delta_{ik},$$

from which follows the relation

$$\Gamma^*(R)_{ij} = \Gamma^{-1}(R)_{ji}. \quad (1.2.2.18)$$

The matrices $\Gamma^*(R)$ form also a representation of K , the *contragredient representation*. In general, the latter is not equivalent with the former. The elements of the space V^* are *dual vectors*.

One can generalize the procedure that gave the dual space, and this leads to a more abstract definition of a tensor. Consider a bilinear function on V .

$$f(r, s): f(\alpha r_1 + \beta r_2, \gamma s_1 + \delta s_2) = \alpha \gamma f(r_1, s_1) + \alpha \delta f(r_1, s_2) + \beta \gamma f(r_2, s_1) + \beta \delta f(r_2, s_2).$$

Again, such bilinear functions form a vector space of dimension d^2 . Any function $f(\mathbf{r}, \mathbf{s})$ is fixed by its value on the d^2 pairs of basis vectors, and these values are the coefficients of the function on a basis

$$f_{ij}(\mathbf{a}_k, \mathbf{a}_l) = \delta_{ik} \delta_{jl}. \quad (1.2.2.19)$$

One has

$$f(\mathbf{r}, \mathbf{s}) = \sum_{ij} f_{ij}(\mathbf{a}_i, \mathbf{a}_j) f_{ij}(\mathbf{r}, \mathbf{s}). \quad (1.2.2.20)$$

Analogously to the former case, one can determine the transformation properties of the elements of the *tensor space* $V^* \otimes V^*$:

$$Rf_{ij} = \sum_{k=1}^d \sum_{l=1}^d \Gamma^*(R)_{ki} \Gamma^*(R)_{lj} f_{kl}. \quad (1.2.2.21)$$

The space carries the product representation of the contragredient representation Γ^* with itself.

That this is really the same concept of tensor as usually used in physics can be seen from the example of the dielectric tensor ϵ_{ij} . For an electric field \mathbf{E} , the energy is given by $\sum_{ij} \epsilon_{ij} E_i E_j$ and this is a bilinear function $f_\epsilon(\mathbf{E}, \mathbf{E})$.

The most general situation occurs if one considers all multilinear functions of p vectors and q dual vectors. The function

$$f(\mathbf{r}_1, \dots, \mathbf{r}_p, \mathbf{k}_1, \dots, \mathbf{k}_q)$$

is linear in each of its arguments. Again, the function is determined by its value on the basis vectors \mathbf{a}_i of V and \mathbf{b}_j of V^* . The (p, q) -linear functions form a vector space with basis vectors $f_{i_1, \dots, i_p, j_1, \dots, j_q}$ given by

$$f_{i_1, \dots, i_p, j_1, \dots, j_q}(\mathbf{a}_{k_1}, \dots, \mathbf{b}_{l_q}) = \delta_{i_1 k_1} \dots \delta_{j_q l_q}.$$

The $d^{(p+q)}$ -dimensional space carries a representation of the group K :

$$Rf_{i_1, \dots, i_p, j_1, \dots, j_q} = \sum_{k_1=1}^d \dots \sum_{k_p=1}^d \sum_{l_1=1}^d \dots \sum_{l_q=1}^d \Gamma(R)_{k_1 i_1} \dots \Gamma(R)_{k_p i_p} \Gamma^*(R)_{l_1 j_1} \dots \Gamma^*(R)_{l_q j_q} f_{k_1, \dots, k_p, l_1, \dots, l_q}. \quad (1.2.2.22)$$

Therefore, the space of (p, q) tensors carries a representation which is the tensor product of the p th tensor power of $\Gamma(K)$ and the q th tensor power of the contragredient representation $\Gamma^*(K)$.

If the $(0, 2)$ tensor $f(\mathbf{r}, \mathbf{s})$ is symmetric in its arguments, the space of such tensors carries the symmetrized tensor product of the representation $\Gamma(K)$ with itself. Similarly the (anti)symmetric $(2, 0)$ tensors form a space that carries the symmetrized, respectively antisymmetrized, tensor product of $\Gamma^*(K)$ with itself. This can be generalized to (p, q) tensors with all kinds of symmetry. One can have a $(0, 4)$ tensor that is symmetric in all its four arguments. Such tensors form a space that not only carries a representation of K , but one of the symmetric group S_4 (the permutation group on four letters) as well. We shall come back to such symmetric tensors in Section 1.2.2.7.

1.2.2.4. Orthogonality relations

Important consequences from symmetry for physical systems are related to orthogonality relations. The vanishing of matrix elements is one example. Consider two irreducible representations $\Gamma_1(K)$ and $\Gamma_2(K)$ of dimensions d_1 and d_2 , respectively. Then take an arbitrary $d_1 \times d_2$ matrix M and construct with this a new matrix S :

$$S = \sum_{R \in K} \Gamma_1(R) M \Gamma_2^{-1}(R).$$

For this matrix one has

$$\begin{aligned} S \Gamma_2(R) &= \sum_{R' \in K} \Gamma_1(R') M \Gamma_2^{-1}(R') \Gamma_2(R) \\ &= \Gamma_1(R) \sum_{R' \in K} \Gamma_1^{-1}(R) \Gamma_1(R') M \Gamma_2^{-1}(R') \Gamma_2(R) \\ &= \Gamma_1(R) \sum_{R' \in K} \Gamma_1(R^{-1} R') M \Gamma_2^{-1}(R^{-1} R') = \Gamma_1(R) S. \end{aligned}$$

Because $\Gamma_1(K)$ and $\Gamma_2(K)$ are supposed to be irreducible, it follows from Schur's lemma that either Γ_1 and Γ_2 are not equivalent and S is the null matrix, or they are equivalent. If they are not equivalent one has

$$0 = S_{ij} = \sum_{R \in K} \sum_{kl} \Gamma_1(R)_{ik} M_{kl} \Gamma_2^{-1}(R^{-1})_{lj}. \quad (1.2.2.23)$$

Because we have taken an arbitrary matrix M , this implies that

$$\sum_{R \in K} \Gamma_1(R)_{ik} \Gamma_2^{-1}(R^{-1})_{lj} = 0 \quad (1.2.2.24)$$

whenever $\Gamma_1(K)$ and $\Gamma_2(K)$ are not equivalent.

When the two irreducible representations are equivalent we assume them to be identical. Then S commutes with all matrices $\Gamma_1(K)$ of an irreducible representation and is thus a multiple of the identity (in case one considers complex representations). Its trace is then $d\lambda$ if the dimension of the representation is denoted by d , but on the other hand it is

$$\text{Tr}(S) = \sum_{R \in K} \text{Tr}(\Gamma_1(R) M \Gamma_1^{-1}(R)) = N \text{Tr}(M).$$

Therefore,

$$S_{ij} = (N/d) \text{Tr}(M) \delta_{ij} = \sum_{R \in K} \sum_{kl} \Gamma_1(R)_{ik} M_{kl} \Gamma_1^{-1}(R^{-1})_{lj}. \quad (1.2.2.25)$$

Hence

1.2. REPRESENTATIONS OF CRYSTALLOGRAPHIC GROUPS

$$\sum_{R \in K} \Gamma_1(R)_{ik} \Gamma_1(R^{-1})_{lj} = (N/d) \delta_{ij} \delta_{kl}. \quad (1.2.2.26)$$

This leads to the following proposition.

Proposition. If $\Gamma_\alpha(K)$ and $\Gamma_\beta(K)$ are irreducible complex representations of the finite group K one has

$$\sum_{R \in K} \Gamma_\alpha(R)_{ik} \Gamma_\beta(R^{-1})_{lj} = (N/d) \delta_{ij} \delta_{kl} \delta'_{\alpha\beta}, \quad (1.2.2.27)$$

where $\delta'_{\alpha\beta}$ is zero if the representations are not equivalent, unity if they are identical and undefined if they are equivalent but not identical.

For unitary representations the orthogonality relations can be written as

$$\sum_{R \in K} \Gamma_\alpha(R)_{ik} \Gamma_\beta(R)_{jl}^* = (N/d) \delta_{ij} \delta_{kl} \delta'_{\alpha\beta}. \quad (1.2.2.28)$$

According to Section 1.2.2.2 for finite groups K , there is always an equivalent unitary representation.

1.2.2.5. Characters

Two equivalent representations of a group K are conjugate subgroups in the group of nonsingular linear transformations. Corresponding matrices therefore have the same invariants. It is a remarkable fact that one of these invariants suffices for characterizing the equivalence class of a representation, namely the trace. The *character* of an element $R \in K$ in a representation $D(K)$ is the trace $\chi(R) = \text{Tr}(D(R))$. It is a complex function on the group: for every $R \in K$ there is a complex number $\chi(R)$.

The character only depends on the conjugacy class: if two elements R and R' belong to the same class there is an element $T \in K$ such that $R' = TRT^{-1}$. Hence $\chi(R') = \text{Tr}(D(TRT^{-1})) = \text{Tr}(D(R)) = \chi(R)$. Notice that for the identity element one has $D(E) =$ the d -dimensional unit matrix and $\chi(E) = d$. For the same reason, the character for two equivalent representations is the same.

From the orthogonality relations for the matrix elements of two irreducible representations follow those for characters.

Proposition. For two irreducible complex representations of a finite group K , one has

$$\sum_{R \in K} \chi_\alpha(R) \chi_\beta^*(R) = N \delta_{\alpha\beta}. \quad (1.2.2.29)$$

Here one can use the Kronecker delta because characters of equivalent representations are equal, even if they are not identical.

The character of the sum of two representations is the sum of the characters. More generally, the character of the sum of irreducible representations D_α , each with multiplicity m_α , is

$$\chi(R) = \sum_\alpha m_\alpha \chi_\alpha(R).$$

This gives a *formula for the multiplicity* of an irreducible component:

$$\begin{aligned} m_\alpha &= \sum_\beta m_\beta \delta_{\alpha\beta} = (1/N) \sum_{R \in K} \sum_\beta m_\beta \chi_\beta(R) \chi_\alpha^*(R) \\ &= (1/N) \sum_{R \in K} \chi(R) \chi_\alpha^*(R). \end{aligned} \quad (1.2.2.30)$$

From the expression for the multiplicities follows:

Proposition. The representations $D_1(K)$ and $D_2(K)$ are equivalent if and only if their characters are the same: $\chi_1(R) = \chi_2(R)$. Two equivalent representations obviously have the same character. Nonequivalent irreducible representations have different

characters because of the orthogonality relations and the multiplicities and irreducible components are uniquely determined by the formula above.

Because the character is constant on a conjugacy class, (1.2.2.30) can also be written as

$$m_\alpha = (1/N) \sum_{i=1}^k n_i \chi(C_i) \chi_\alpha^*(C_i), \quad (1.2.2.31)$$

where C_i denotes the i th conjugacy class ($i = 1, 2, \dots, k$) and n_i the number of its elements.

Proposition. The representation $D(K)$ is irreducible if and only if

$$(1/N) \sum_{i=1}^k n_i |\chi(C_i)|^2 = 1.$$

Proof. For a representation that is equivalent to the sum of irreducible representations with multiplicities m_α one has

$$\begin{aligned} (1/N) \sum_{i=1}^k n_i |\chi(C_i)|^2 &= (1/N) \sum_{i=1}^k \sum_{\alpha\beta} n_i m_\alpha m_\beta \chi_\alpha(C_i) \chi_\beta^*(C_i) \\ &= \sum_{\alpha\beta} m_\alpha m_\beta \delta_{\alpha\beta} = \sum_\alpha m_\alpha^2. \end{aligned} \quad (1.2.2.32)$$

If the representation is irreducible, there is exactly one value of α for which $m_\alpha = 1$, whereas all other multiplicities vanish. If the representation is reducible, $\sum_\alpha m_\alpha^2 > 1$.

Proposition. (Burnside's theorem.) The sum of the squares of the dimensions of all nonequivalent irreducible representations is equal to the order of the group.

Proof. Consider the regular representation. The value of its character in an element R is given by the number of elements $R_i \in K$ for which $RR_i = R_i$. Therefore,

$$\chi(R) = \begin{cases} 0 & \text{for } R \neq E; \\ N & \text{for } R = E. \end{cases}$$

The multiplicity formula (1.2.2.30) then gives

$$m_\alpha = (1/N) \sum_{R \in K} \chi(R) \chi_\alpha^*(R) = (1/N) \chi(E) \chi_\alpha^*(E) = d_\alpha.$$

Each irreducible representation occurs in the regular representation with a multiplicity equal to its dimension. Therefore,

$$N = \chi(E) = \sum_\alpha m_\alpha \chi_\alpha(E) = \sum_\alpha d_\alpha^2.$$

Proposition. The number of nonequivalent irreducible representations of a finite group K is equal to the number of its conjugacy classes.

Proof. Take from each equivalence class of irreducible representations of K one unitary representative $\Gamma_\alpha(K)$. The matrix elements $\Gamma_\alpha(R)_{ij}$ are complex functions on the group. The number of these functions is the sum over α of d_α^2 and that is equal to the order of the group according to Burnside's theorem. The number of independent functions on K is, of course, also equal to the order N of the group. If one considers the usual scalar product of functions on the group,

$$f_1 \cdot f_2 \equiv \sum_{R \in K} f_1^*(R) f_2(R),$$

the scalar product of two of the N functions is

$$\sum_{R \in K} \Gamma_\alpha^*(R)_{ij} \Gamma_\beta(R)_{kl} = (N/d_\alpha) \delta_{\alpha\beta} \delta_{ik} \delta_{jl} \quad (1.2.2.33)$$

1. TENSORIAL ASPECTS OF PHYSICAL PROPERTIES

according to the orthogonality relations. This means that the N functions indeed form an orthogonal basis in the space of all functions on the group. In particular, consider a function $f(K)$ that is constant on conjugacy classes. This function can be expanded in the basis functions.

$$\begin{aligned} f(R) &= \sum_{\alpha ij} f_{\alpha ij} \Gamma_{\alpha}(R)_{ij} \\ &= \sum_{\alpha ij} f_{\alpha ij} (1/N) \sum_{T \in K} \Gamma_{\alpha}(TRT^{-1})_{ij} \\ &= (1/N) \sum_{\alpha ijk} f_{\alpha ij} \Gamma_{\alpha}(T)_{ik} \Gamma_{\alpha}(R)_{kl} \Gamma_{\alpha}(T^{-1})_{lj} \\ &= (1/N) \sum_{\alpha ijk} f_{\alpha ij} \Gamma_{\alpha}(R)_{kl} (N/d_{\alpha}) \delta_{ij} \delta_{kl} \\ &= \sum_{\alpha} \sum_{i=1}^{d_{\alpha}} (f_{\alpha ii} / d_{\alpha}) \chi_{\alpha}(R). \end{aligned}$$

This implies that every class function can be written as a linear combination of the character functions. Therefore, the number of such character functions must be equal to or larger than the number of conjugacy classes. On the other hand, the number of dimensions of the space of class functions is k , the number of conjugacy classes. For the scalar product in this space given by

$$f_1 \cdot f_2 \equiv \sum_{i=1}^k (n_i/N) f_1^*(C_i) f_2(C_i)$$

the character functions are orthogonal:

$$\sum_{i=1}^k (n_i/N) \chi_{\alpha}^*(C_i) \chi_{\beta}(C_i) = (1/N) \sum_{R \in K} \chi_{\alpha}^*(R) \chi_{\beta}(R) = \delta_{\alpha\beta}. \quad (1.2.2.34)$$

There are at most k mutually orthogonal functions, and consequently the number of nonequivalent irreducible characters $\chi_{\alpha}(K)$ is exactly equal to the number of conjugacy classes.

As additional result one has the following proposition.

Proposition. The functions $\Gamma_{\alpha}(R)_{ij}$ with $\alpha = 1, 2, \dots, k$ and $i, j = 1, 2, \dots, d_{\alpha}$ form an orthogonal basis in the space of complex functions on the group K . The characters χ_{α} form an orthogonal basis for the space of all class functions.

The characters of a group K can be combined into a square matrix, the *character table*, with entries $\chi_{\alpha}(C_i)$. Besides the orthogonality relations mentioned above, there are also relations connected with *class multiplication constants*. Consider the conjugacy classes C_i of the group K . Formally one can introduce the sum of all elements of a class:

$$M_i = \sum_{R \in C_i} R.$$

It can be proven that the multiplication of two such class sums is the sum of class sums, where such a class sum may occur more than once:

$$M_i M_j = \sum_k c_{ijk} M_k, \quad c_{ijk} \in \mathbb{Z}.$$

The coefficients c_{ijk} are called the *class multiplication constants*. The elements of the character table then have the following properties.

$$(1/N) \sum_{i=1}^k n_i \chi_{\alpha}(C_i) \chi_{\beta}^*(C_i) = \delta_{\alpha\beta}; \quad (1.2.2.35)$$

$$(1/N) \sum_{\alpha=1}^k \chi_{\alpha}(C_i) \chi_{\alpha}^*(C_j) = (1/n_i) \delta_{ij}; \quad (1.2.2.36)$$

$$n_i \chi_{\alpha}(C_i) n_j \chi_{\alpha}(C_j) = d_{\alpha} \sum_{l=1}^k c_{ijl} n_l \chi_{\alpha}(C_l). \quad (1.2.2.37)$$

As an example, consider the permutation group on three letters S_3 . It consists of six permutations. It is a group that is isomorphic with the point group 32. The character table is a 3×3 array, because there are three conjugacy classes (C_i , $i = 1, 2, 3$), and consequently three irreducible representations (Γ_i , $i = 1, 2, 3$) (see Table 1.2.2.1).

The two one-dimensional representations are equal to their character. A representative representation for the third character is generated by matrices

$$\Gamma_3(A) = \begin{pmatrix} 0 & -1 \\ 1 & -1 \end{pmatrix}, \quad \Gamma_3(B) = \begin{pmatrix} 1 & -1 \\ 0 & -1 \end{pmatrix}$$

and the group of matrices is equivalent to an orthogonal group with generators

$$\Gamma_3(A)' = \begin{pmatrix} -\frac{1}{2} & \frac{1}{2}\sqrt{3} \\ -\frac{1}{2}\sqrt{3} & -\frac{1}{2} \end{pmatrix}, \quad \Gamma_3(B)' = \begin{pmatrix} 1 & 0 \\ 0 & -1 \end{pmatrix}.$$

The character table is in agreement with the class multiplication table

$$\begin{array}{lll} C_1 C_1 = C_1 & C_2 C_1 = C_2 & C_3 C_1 = C_3 \\ C_1 C_2 = C_2 & C_2 C_2 = 2C_1 + C_2 & C_3 C_2 = 2C_3 \\ C_1 C_3 = C_3 & C_2 C_3 = 2C_3 & C_3 C_3 = 3C_1 + 3C_2. \end{array}$$

1.2.2.6. The representations for point groups in one, two and three dimensions

For the irreducible representations of the point groups, it is necessary to know something about the structure of these groups. Since the representations of isomorphic groups are the same, one can restrict oneself to representatives of the isomorphism classes. In the following, we give a brief description of the structure of the point groups in spaces up to three dimensions. The character tables are given in Section 1.2.6. For the infinite series of groups (C_n and D_n), the crystallographic members are given explicitly separately.

(i) C_n . Cyclic groups are Abelian. Therefore, each element is a conjugacy class on itself. Irreducible representations are one-dimensional. The representation is determined by its value on a generator. Since $A^n = E$, the character $\chi(A)$ of an irreducible representation is an n th root of unity. There are n one-dimensional representations. For the p th irreducible representation, one has $\chi^{(p)}(A) = \exp(2\pi i p/n)$.

(ii) D_n . From the defining relations, it follows that A^p and A^{-p} ($p = 1, 2, \dots, n$) form a conjugacy class and that $A^p B$ and $A^{p+2} B$ belong to the same class. Therefore, one has to distinguish the

Table 1.2.2.1. Character table for $S_3 \sim D_3$

| Elements Symbols | (1) E | (123) A | (132) A^2 | (23) B | (13) $A^2 B$ | (12) AB |
|---------------------|------------|--------------|----------------|-------------|-----------------|--------------|
| Class Order | C_1 1 | C_2 3 | | C_3 2 | | |
| Γ_1 | 1 | 1 | | 1 | | |
| Γ_2 | 1 | 1 | | -1 | | |
| Γ_3 | 2 | -1 | | 0 | | |

1.2. REPRESENTATIONS OF CRYSTALLOGRAPHIC GROUPS

cases of even n from those of odd n . For odd n , one has a class consisting of E (order 1), $(n-1)/2$ classes with elements $A^{\pm p}$, and one class with all elements $A^p B$ (order 2). For even n , there is a class consisting of E (order 1), one with $A^{n/2}$, and $(n-2)/2$ classes with $A^{\pm p}$. The other elements form two classes of order 2 elements, one with the elements $A^p B$ for p odd, the other with $A^p B$ for p even.

The number of one-dimensional irreducible representations is the order of the group (N) divided by the order of the *commutator group*, which is the group generated by all elements $aba^{-1}b^{-1}$ ($a, b \in K$). For n odd this number is 2, for n even it is 4. In addition there are two-dimensional irreducible representations: $(n-1)/2$ for odd n , $n/2 - 1$ for even n .

(iii) T, O, I . The conjugacy classes of the tetrahedral, the octahedral and the icosahedral groups T, O and I , respectively, are given in the tables in Section 1.2.6.

(iv) $K \times C_2$. Because the generator of C_2 commutes with all elements of the group, the number of conjugacy classes of the direct product $K \times C_2$ is twice that for K . If A is the generator of C_2 and C_i are the classes of K , then the classes of the direct product are C_i and $C_i A$. The element A , which commutes with all elements of the direct product, is in an irreducible representation represented by a multiple of the identity. Because A is of order 2, the factor is ± 1 . Therefore, the character table looks like

$$\chi(K \times C_2) = \begin{pmatrix} \chi(K) & \chi(K) \\ \chi(K) & -\chi(K) \end{pmatrix}.$$

The n irreducible representations where A is represented by $+E$ are called *gerade* representations, the other, where A is represented by $-E$, are called *ungerade*.

In general, if K and H are finite groups with irreducible representations $D_{1\alpha}(K)$ and $D_{2\beta}(H)$, the *outer tensor product* acts on the tensor product $V_1 \otimes V_2$ of representation spaces as

$$(D_{1\alpha}(R) \otimes D_{2\beta}(R')) \mathbf{a} \otimes \mathbf{b} = (D_{1\alpha}(R) \mathbf{a}) \otimes (D_{2\beta}(R') \mathbf{b}),$$

$$\mathbf{a} \in V_1, \mathbf{b} \in V_2. \quad (1.2.2.38)$$

With the irreducibility criterion, one checks that this is an irreducible representation of $K \times H$. Moreover, $D_{1\alpha} \otimes D_{2\beta}$ is equivalent with $D_{1\alpha'} \otimes D_{2\beta'}$ if and only if $\alpha = \alpha'$ and $\beta = \beta'$. This means that one obtains all nonequivalent irreducible representations of $K \times H$ from the outer tensor products of the irreducible representations of K and H . If the group H is C_2 , there are two irreducible representations of C_2 , both one-dimensional. That means that the tensor product simplifies to a normal product. If $H = C_2$ and $D_{2\beta}(H)$ is the trivial representation, one has from (1.2.2.38)

$$D_{\alpha g}(R) = D_{\alpha}(R), \quad D_{\alpha g}(RA) = D_{\alpha}(R), \quad R \in K$$

$$D_{\alpha u}(R) = D_{\alpha}(R), \quad D_{\alpha u}(RA) = -D_{\alpha}(R).$$

The letters g and u come from the German *gerade* (even) and *ungerade* (odd). They indicate the sign of the operator associated with the generator A of C_2 : $+1$ for g representations, -1 for u representations. The number of nonequivalent irreducible representations of $K \otimes C_2$ is twice that of K .

Schur's lemma and the orthogonality relations and theorems derived above are formulated for complex representations and are, generally, not valid for integer or real representations. Nevertheless, many physical properties can be described using representation theory, but being real quantities they sometimes require a slightly different treatment. Here we shall discuss the relation between the complex representations and *physical or real representations*. Consider a real matrix representation $\Gamma(K)$. If it is reducible over complex numbers, it can be fully reduced. When is an irreducible component itself real? A first condition is clearly that its character is real. This is, however, not sufficient. A real representation can by a complex basis transformation be put

into a complex form and such a transformation does not change the character. Therefore, a better question is: which complex irreducible representations can be brought into real form? Consider a complex irreducible representation with a real character. Then it is equivalent with its complex conjugate *via* a matrix S :

$$\Gamma(R) = S\Gamma^*(R)S^{-1}, \quad R \in K.$$

Here one has to distinguish two different cases. To make the distinction between the two cases one has the following:

Proposition. Suppose that $\Gamma(K)$ is a complex irreducible representation with real character, and S a matrix intertwining $\Gamma(K)$ and its complex conjugate. Then S satisfies either $SS^* = E$ or $SS^* = -E$. In the former case, there exists a basis transformation that brings $\Gamma(K)$ into real form, in the latter case there is no such basis transformation.

Proposition. If $\Gamma(K)$ is a complex irreducible representation with real character $\chi(K)$, the latter satisfies

$$(1/N) \sum_{R \in K} \chi(R^2) = \pm 1.$$

If the right-hand side is $+1$, the representation can be put into real form, if it is -1 it cannot. (Proofs are given in Section 1.2.5.5.)

Consequently, a complex irreducible representation $\Gamma(K)$ is equivalent with a real one if $\chi(R) = \chi^*(R)$ and $\sum_R \chi(R^2) = N$. If that is not the case, a real representation containing $\Gamma(K)$ as irreducible component is the matrix representation

$$\frac{1}{2} \begin{pmatrix} \Gamma(R) + \Gamma^*(R) & i(\Gamma(R) - \Gamma^*(R)) \\ -i(\Gamma(R) - \Gamma^*(R)) & \Gamma(R) + \Gamma^*(R) \end{pmatrix} \sim \begin{pmatrix} \Gamma(R) & 0 \\ 0 & \Gamma^*(R) \end{pmatrix}. \quad (1.2.2.39)$$

The basis transformation is given by

$$S = \begin{pmatrix} E & E \\ -iE & iE \end{pmatrix}.$$

The dimension of the physically irreducible representation is $2d$, if d is the dimension of the complex irreducible representation $\Gamma(K)$. In summary, there are three types of irreducible representation:

- (1) First kind: $\chi(K) = \chi^*(K)$, $\sum_{R \in K} \chi(R^2) = +N$, dimension of real representation d ;
- (2) Second kind: $\chi(K) = \chi^*(K)$, $\sum_{R \in K} \chi(R^2) = -N$, dimension of real representation $2d$;
- (3) Third kind: $\chi(R) \neq \chi(R)^*$, $\sum_{R \in K} \chi(R^2) = 0$, dimension of real representation $2d$.

Examples of the three cases:

- (1) The matrices

$$D(A) = \begin{pmatrix} 0 & i \\ i & 0 \end{pmatrix} \quad \text{and} \quad D(B) = \begin{pmatrix} 1 & 0 \\ 0 & -1 \end{pmatrix}$$

generate a group that forms a faithful representation of the dihedral group $D_4 = 422$, for which the character table is given in Table 1.2.6.5. If one uses the same numbering of conjugacy classes, its character is $\chi(C_i) = 2, 0, -2, 0, 0$. It is an irreducible representation ($2^2 + 2^2 = N = 8$) with real character. The sum of the characters of the squares of the elements is $2 + 2 \times (-2) + 2 + 2 \times 2 + 2 \times 2 = 8 = N$. Therefore, it is equivalent to a real matrix representation, e.g. with

$$D'(A) = \begin{pmatrix} 0 & -1 \\ 1 & 0 \end{pmatrix} \quad \text{and} \quad D'(B) = \begin{pmatrix} 0 & 1 \\ 1 & 0 \end{pmatrix}.$$

1. TENSORIAL ASPECTS OF PHYSICAL PROPERTIES

(2) The matrices

$$D(A) = \begin{pmatrix} 0 & i \\ i & 0 \end{pmatrix} \text{ and } D(B) = \begin{pmatrix} 0 & -1 \\ 1 & 0 \end{pmatrix}$$

generate a group that is a faithful representation of the quaternion group of order 8. This group has five classes: E , $\{A, A^3\}$, $\{B, B^3\}$, $\{BA, AB\}$ and A^2 . The character of the elements is $\chi(R) = 2, 0, 0, 0, -2$ for the five classes. Then

$$(1/8) \sum_R \chi(R^2) = -1,$$

which means that the representation is essentially complex. A real physically irreducible representation of the group is generated by

$$\begin{pmatrix} 0 & 0 & 0 & -1 \\ 0 & 0 & -1 & 0 \\ 0 & 1 & 0 & 0 \\ 1 & 0 & 0 & 0 \end{pmatrix} \text{ and } \begin{pmatrix} 0 & -1 & 0 & 0 \\ 1 & 0 & 0 & 0 \\ 0 & 0 & 0 & -1 \\ 0 & 0 & 1 & 0 \end{pmatrix},$$

and the generated group is a crystallographic group in four dimensions.

(3) The complex number $\exp(2\pi i/n)$ generates a representation of the cyclic group C_n . For $n > 2$ the representation is not equivalent with its complex conjugate. Therefore, it is not a physical representation. The physically irreducible representation that contains this complex irreducible component is generated by

$$\begin{pmatrix} \cos(2\pi/n) & -\sin(2\pi/n) \\ \sin(2\pi/n) & \cos(2\pi/n) \end{pmatrix} \simeq \begin{pmatrix} \exp(2\pi i/n) & 0 \\ 0 & \exp(-2\pi i/n) \end{pmatrix}.$$

All complex irreducible representations of the finite point groups in up to three dimensions with real character can be put into a real form. This is not true for higher dimensions, as we have seen in the example of the quaternion group.

1.2.2.7. Tensor representations

When V_1, \dots, V_n are linear vector spaces, one may construct tensor products of these spaces. There are many examples in physics where this notion plays a role. Take the example of a particle with spin. The wave function of the particle has two components, one in the usual three-dimensional space and one in spin space. The proper way to describe this situation is *via* the tensor product. In normal space, a basis is formed by spherical harmonics Y_{lm} , in spin space by the states $|ss_z\rangle$. Spin-orbit interaction then plays in the $(2l+1)(2s+1)$ -dimensional space with basis $|lm\rangle \otimes |ss_z\rangle$. Another example is a physical tensor, e.g. the dielectric tensor ε_{ij} of rank 2. It is a symmetric tensor that transforms under orthogonal transformations exactly like a symmetric bi-vector with components $v_i w_j + v_j w_i$, where v_i and w_i ($i = 1, 2, 3$) are the components of vectors \mathbf{v} and \mathbf{w} . A basis for the space of symmetric bi-vectors is given by the six vectors $(\mathbf{e}_i \otimes \mathbf{e}_j + \mathbf{e}_j \otimes \mathbf{e}_i)$ ($i \leq j$). The space of symmetric rank 2 tensors has the same transformation properties.

A basis for the tensor space $V_1 \otimes V_2 \otimes \dots \otimes V_n$ is given by $\mathbf{e}_{1i} \otimes \mathbf{e}_{2j} \otimes \dots \otimes \mathbf{e}_{nk}$, where $i = 1, 2, \dots, d_1; j = 1, 2, \dots, d_2; \dots; k = 1, 2, \dots, d_n$. Therefore the dimension of the tensor product is the product of the dimensions of the spaces V_i (see also Section 1.1.3.1.2). The tensor space consists of all linear combinations with real or complex coefficients of the basis vectors. In the summation one has the multilinear property

$$\left(\sum_{i=1}^{d_1} c_{1i} \mathbf{e}_{1i} \right) \otimes \left(\sum_{j=1}^{d_2} c_{2j} \mathbf{e}_{2j} \right) \otimes \dots = \sum_{ij\dots} c_{1i} c_{2j} \dots \mathbf{e}_{1i} \otimes \mathbf{e}_{2j} \otimes \dots \quad (1.2.2.40)$$

In many cases in practice, the spaces V_i are all identical and then the dimension of the tensor product $V^{\otimes n}$ is simply d^n .

The tensor product of n identical spaces carries in an obvious way a representation of the permutation group S_n of n elements. A permutation of n elements is always the product of pair exchanges. The action of the permutation (12), that interchanges spaces 1 and 2, is given by

$$P_{12} \mathbf{e}_i \otimes \mathbf{e}_j \otimes \mathbf{e}_k \otimes \dots = \mathbf{e}_j \otimes \mathbf{e}_i \otimes \mathbf{e}_k \otimes \dots \quad (1.2.2.41)$$

Two subspaces are then of particular interest, that of the tensors that are invariant under all elements of S_n and those that get a minus sign under pair exchanges. These spaces are the spaces of fully *symmetric* and *antisymmetric* tensors, respectively.

If the spaces V_1, \dots, V_n carry a representation of a finite group K , the tensor product space carries the product representation.

$$\begin{aligned} \mathbf{e}_{1j_1} \otimes \mathbf{e}_{2j_2} \otimes \dots \\ = \bigotimes_{i=1}^n \mathbf{e}_{ij_i} \rightarrow \sum_{k_1 k_2 \dots} \Gamma_1(R)_{k_1 j_1} \Gamma_2(R)_{k_2 j_2} \dots \mathbf{e}_{1k_1} \otimes \mathbf{e}_{2k_2} \otimes \dots \end{aligned} \quad (1.2.2.42)$$

The matrix $\Gamma(R)$ of the tensor representation is the tensor product of the matrices $\Gamma_i(R)$. In general, this representation is reducible, even if the representations Γ_i are irreducible. The special case of $n = 2$ has already been discussed in Section 1.2.2.3.

From the definition of the action of $R \in K$ on vectors in the tensor product space, it is easily seen that the character of R in the tensor product representation is the product of the characters of R in the representations Γ_i :

$$\chi(R) = \prod_{i=1}^n \chi_i(R). \quad (1.2.2.43)$$

The reduction in irreducible components then occurs with the multiplicity formula.

$$m_\alpha = (1/N) \sum_{R \in K} \chi_\alpha^*(R) \prod_{i=1}^n \chi_i(R). \quad (1.2.2.44)$$

If the tensor product representation is a real representation, the physically irreducible components can be found by first determining the complex irreducible components, and then combining with their complex conjugates the components that cannot be brought into real form.

The tensor product of the representation space V with itself has a basis $\mathbf{e}_i \otimes \mathbf{e}_j$ ($i, j = 1, 2, \dots, d$). The permutation (12) transforms this into $\mathbf{e}_j \otimes \mathbf{e}_i$. This action of the permutation becomes diagonal if one takes as basis $\mathbf{e}_i \otimes \mathbf{e}_j + \mathbf{e}_j \otimes \mathbf{e}_i$ ($1 \leq i \leq j \leq d$, spanning the space $V_s^{\otimes 2}$) and $\mathbf{e}_i \otimes \mathbf{e}_j - \mathbf{e}_j \otimes \mathbf{e}_i$ ($1 \leq i < j \leq d$, spanning the space $V_a^{\otimes 2}$). If one considers the action of K , one has with respect to the first basis $\chi(R) = \chi_\alpha(R)^2$ if V carries the representation with character $\chi_\alpha(K)$. With respect to the second basis, one sees that the character of the permutation $P = (12)$ is given by $\frac{1}{2}d(d+1) - \frac{1}{2}d(d-1) = d$. The action of the element $R \in K$ on the second basis is

$$R(\mathbf{e}_i \otimes \mathbf{e}_j \pm \mathbf{e}_j \otimes \mathbf{e}_i) = \sum_{kl} (\Gamma_\alpha \otimes \Gamma_\alpha)(R)_{kl,ij} (\mathbf{e}_i \otimes \mathbf{e}_j \pm \mathbf{e}_j \otimes \mathbf{e}_i).$$

This implies that both $V_s^{\otimes 2}$ and $V_a^{\otimes 2}$ are invariant under R . The character in the subspace is

$$\chi^+(R) = \sum_{k \leq l} (\Gamma_\alpha \otimes \Gamma_\alpha)(R)_{kl,kl} \quad (1.2.2.45)$$

for the symmetric subspace and

$$\chi^-(R) = \sum_{k < l} (\Gamma_\alpha \otimes \Gamma_\alpha)(R)_{kl,kl} \quad (1.2.2.46)$$

1.2. REPRESENTATIONS OF CRYSTALLOGRAPHIC GROUPS

for the antisymmetric one. Consequently one has

$$\chi^\pm(R) = \frac{1}{2}(\chi_\alpha(R)^2 \pm \chi_\alpha(R^2)); \quad d^\pm = \frac{1}{2}d_\alpha(d_\alpha \pm 1). \quad (1.2.2.47)$$

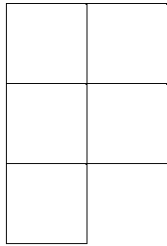
For $n > 2$, the tensor product space does not carry just a symmetric and an antisymmetric subspace, but also higher-dimensional representations of the permutation group S_n . The derivation of the character of the fully symmetric and fully antisymmetric subspaces remains rather similar. The formulae for the character of the representation of K carried by the fully symmetric (+) and fully antisymmetric (−) subspace, respectively, for $n = 1, 2, 3, 4, 5, 6$ are

$$\begin{aligned} n = 2 : \chi^\pm(R) &= \frac{1}{2!}(\chi(R)^2 \pm \chi(R^2)) \\ n = 3 : \chi^\pm(R) &= \frac{1}{3!}(\chi(R)^3 \pm 3\chi(R^2)\chi(R) + 2\chi(R^3)) \\ n = 4 : \chi^\pm(R) &= \frac{1}{4!}(\chi(R)^4 \pm 6\chi(R^2)\chi(R)^2 + 3\chi(R^2)^2 \\ &\quad + 8\chi(R^3)\chi(R) \pm 6\chi(R^4)) \\ n = 5 : \chi^\pm(R) &= \frac{1}{5!}(\chi(R)^5 \pm 10\chi(R^2)\chi(R)^3 + 15\chi(R^2)^2\chi(R) \\ &\quad + 20\chi(R^3)\chi(R)^2 \pm 20\chi(R^3)\chi(R^2) \\ &\quad \pm 30\chi(R^4)\chi(R) + 24\chi(R^5)) \\ n = 6 : \chi^\pm(R) &= \frac{1}{6!}(\chi(R)^6 \pm 15\chi(R^2)\chi(R)^4 + 45\chi(R^2)^2\chi(R)^2 \\ &\quad + 40\chi(R^3)^2 \pm 15\chi(R^2)^3 + 40\chi(R^3)\chi(R)^3 \\ &\quad \pm 120\chi(R^3)\chi(R^2)\chi(R) \pm 90\chi(R^4)\chi(R)^2 \\ &\quad + 90\chi(R^4)\chi(R^2) + 144\chi(R^5)\chi(R) \\ &\quad \pm 120\chi(R^6)) \end{aligned}$$

From this follows immediately the dimension of the two subspaces:

$$\begin{aligned} n = 2 : \frac{1}{2}(d^2 \pm d) \\ n = 3 : \frac{1}{6}(d^3 \pm 3d^2 + 2d) \\ n = 4 : \frac{1}{24}(d^4 \pm 6d^3 + 11d^2 \pm 6d) \\ n = 5 : \frac{1}{120}(d^5 \pm 10d^4 + 35d^3 \pm 50d^2 + 24d) \\ n = 6 : \frac{1}{720}(d^6 \pm 15d^5 + 85d^4 \pm 225d^3 + 274d^2 \pm 120d). \end{aligned}$$

These expressions are based on Young diagrams. The procedure will be exemplified for the case of $n = 5$. In the expression for χ^\pm occur the partitions of n in groups of integers:



$5 = 4 + 1 = 3 + 2 = 3 + 1 + 1 = 2 + 2 + 1 = 2 + 1 + 1 + 1 = 1 + 1 + 1 + 1 + 1$. Each partition corresponds with a Young diagram with as many rows as there are terms in the sum, and in each row the corresponding number of boxes. The total number of boxes is n . Each partition corresponds with a term $\chi(R^{i_1})\chi(R^{i_2})\dots$ such that $\sum_j i_j = n$. Here i_1 is the number of boxes in the first row etc. The prefactor then is the number of

possible permutations compatible with the partition. For example, the partition $2 + 2 + 1$ allows the permutations

$$\begin{aligned} (12)(34)(5) \quad (13)(24)(5) \quad (14)(23)(5) \quad (12)(35)(4) \quad (13)(25)(4) \\ (15)(23)(4) \quad (12)(45)(3) \quad (14)(25)(3) \quad (15)(24)(3) \quad (13)(45)(2) \\ (14)(35)(2) \quad (15)(34)(2) \quad (23)(45)(1) \quad (24)(35)(1) \quad (25)(34)(1) \end{aligned}$$

The sign of all these permutations is even: they are the product of an even number of pair interchanges. The prefactor for the term $\chi(R^2)\chi(R^2)\chi(R)$ is then $+15/5!$.

1.2.2.8. Projective representations

It is useful to consider a more general type of representation, one that gives only a homomorphism from a group to linear transformations up to a factor. In quantum mechanics, the relevance of such representations is a consequence of the freedom of the phase of the wave function, but they also occur in classical physics. In particular, we shall need this generalized concept for the determination of representations of crystallographic space groups.

A *projective representation* of a group K is a mapping from K to the group of nonsingular linear transformations of a vector space V such that

$$D(R)D(R') = \omega(R, R')D(RR') \quad \forall R, R' \in K,$$

where $\omega(R, R')$ is a nonzero real or complex number. The name stems from the fact that the mapping is a homomorphism if one identifies linear transformations that differ by a factor. Then one looks at the transformations of the lines through the origin, and these form a projective space. Other names are *multiplier* or *ray representations*. The mapping ω from $K \times K$ to the real or complex numbers is called the *factor system* of the projective representation. An ordinary representation is a projective representation with a trivial factor system that has only the value unity. A projective representation that can be identified with $D(H)$ is one with $D'(R) = u(R)D(R)$ for some real or complex function u on the group. It gives the same transformations of projective space. The projective representations $D(H)$ and $D'(H)$ are called *associated*. Their factor systems are related by

$$\omega'(R, R') = \frac{u(R)u(R')}{u(RR')} \omega(R, R'), \quad (1.2.2.48)$$

as one can check easily. Two factor systems that are related in this way are also called *associated*.

Not every mapping $\omega : K \times K \rightarrow$ complex numbers can be considered as a factor system. There is the following proposition:

Proposition. A mapping ω from $K \times K$ to the complex numbers can occur as factor system for a projective representation if and only if one has

$$\begin{aligned} \omega(R_1, R_2)\omega(R_1R_2, R_3) &= \omega(R_1, R_2R_3)\omega(R_2, R_3) \\ \forall R_1, R_2, R_3 \in K. \end{aligned} \quad (1.2.2.49)$$

If one has two mappings ω_1 and ω_2 satisfying this relation, the product $\omega(R, R') = \omega_1(R, R')\omega_2(R, R')$ also satisfies the relation. Therefore, factor systems form an Abelian multiplicative group. A subgroup is formed by all factor systems that are associated with the trivial one:

$$\omega(R, R') = \frac{u(R)u(R')}{u(RR')}$$

for some function u on the group. These form another Abelian group and the factor group consists of all essentially different factor systems. This factor group is called *Schur's multiplier group*.

1. TENSORIAL ASPECTS OF PHYSICAL PROPERTIES

A projective representation is called *reducible* if there is a proper invariant subspace. It is fully reducible if there is a basis on which the representation matrices form the direct sum of two representations. This is exactly as for ordinary representations. Equivalence of projective representations is slightly more subtle. Two projective representations are called *associated* if their factor systems are associated. They are *weakly equivalent* if there is a complex function $u(R)$ on the group and a nonsingular linear transformation S such that

$$D_2(R) = u(R)SD_1(R)S^{-1} \quad \forall R \in K. \quad (1.2.2.50)$$

This implies that their factor systems are associated. Two projective representations are *strongly equivalent* if their factor systems are identical and there exists a nonsingular linear transformation S such that $D_2(R)S = SD_1(R)$. Therefore, strong equivalence implies weak equivalence, which in turn implies association. The reason for this distinction will soon become clear.

For projective representations with identical factor systems there exist *orthogonality relations* for matrix elements and for characters. It is important to notice that for projective representations the character is generally not a class function, because one can multiply every operator with a separate constant.

Proposition. For given factor system ω there is a finite number r of strong equivalence classes of irreducible projective representations. The dimensions of the nonequivalent irreducible representations satisfy

$$\sum_{\alpha=1}^r d_{\alpha}^2 = N. \quad (1.2.2.51)$$

Proposition. For two irreducible projective matrix representations with the same factor system, the following holds:

$$\sum_{R \in K} \Gamma_{\alpha}(R)_{ij} \Gamma_{\beta}^{-1}(R)_{kl} = (N/d_{\alpha}) \delta'_{\alpha\beta} \delta_{il} \delta_{jk}. \quad (1.2.2.52)$$

Notice that, in general, for projective representations $\Gamma(R^{-1}) \neq \Gamma(R)^{-1}$! Every projective representation of a finite group is strongly equivalent with a unitary representation, for which one has

$$\sum_{R \in K} \Gamma_{\alpha}(R)_{ij} \Gamma_{\beta}^{*}(R)_{ik} = (N/d_{\alpha}) \delta'_{\alpha\beta} \delta_{il} \delta_{jk}, \quad (1.2.2.53)$$

and for the characters

$$\sum_{R \in K} \chi_{\alpha}(R) \chi_{\beta}^{*}(R) = N \delta_{\alpha\beta}. \quad (1.2.2.54)$$

For projective representations with the same factor system, one can construct the sum representation, which still has the same factor system: $(\Gamma_1 \oplus \Gamma_2)(R) = \Gamma_1(R) \oplus \Gamma_2(R)$. On the other hand, a reducible projective representation can be decomposed into irreducible components with the same factor system and multiplicities

$$m_{\alpha} = (1/N) \sum_{R \in K} \chi(R) \chi_{\alpha}^{*}(R), \quad (1.2.2.55)$$

as follows directly from the orthogonality conditions.

Projective representations of a group K may be constructed from the ordinary representations of a larger group R . Suppose that R has a subgroup A in the centre, which means that all its elements commute with all elements of R . Suppose furthermore that the factor group R/A is isomorphic with K . Therefore, the order of R is the product of the orders of A and K . Because K is the factor group, each element of R corresponds to a unique element of K and the elements of the subgroup A correspond to the unit element in K . Then consider an irreducible representa-

tion D of R . For two elements r_1 and r_2 of R there are elements k_1 and k_2 in K . Define linear operators $P(k_i) = D(r_i)$. Then $k_1 k_2$ corresponds to $r_1 r_2$ up to an element $a \in A$. This means

$$P(k_1)P(k_2) = D(a)P(k_1 k_2).$$

Because a commutes with all elements of R , the operator $D(a)$ commutes with all the operators of the irreducible representation $D(R)$. From Schur's lemma it follows that it is a multiple of the unit operator. Moreover, this multiple depends on k_1 and k_2 : $D(a) = \omega(k_1, k_2)E$. Therefore, an irreducible representation of R gives a projective representation of K . It has been shown by Schur that one obtains all projective representations of K , i.e. one representative from each strong equivalence class for each class of non-associated factor systems, in the way presented if one takes for the group A the multiplier group. The way to find all projective representations of K is then: determine the multiplier group, determine R , determine the ordinary irreducible representations of R . We shall not go into detail, but only present a way to characterize projective representations.

First we consider an example, the group $K = 2mm$, isomorphic to D_2 . It can be shown that the multiplier group is the group of two elements. Therefore, the representation group R has eight elements and one can show that it is isomorphic to D_4 or to the quaternion group (in general there is not a unique R). The character table of D_4 is given in Table 1.2.2.2.

The centre is generated by A^2 . If the elements of the factor group are e, a, b and ab , then E and A^2 correspond to e, A and A^3 to a, B and $A^2 B$ to b , and AB and $A^3 B$ to ab . Because A^2 is represented by the unit element for the four one-dimensional representations, each element of the factor group corresponds to a unique element of the representation. $P(a)$ can be chosen to be $D(A)$ or $D(A^3)$, but because $D(A^2) = E$ for the one-dimensional representations these are equal. Therefore, the one-dimensional representations of $K = D_2$ have a trivial factor system. For the two-dimensional representation one may choose

$$P(e) = \begin{pmatrix} 1 & 0 \\ 0 & 1 \end{pmatrix}, \quad P(a) = \begin{pmatrix} 0 & -1 \\ 1 & 0 \end{pmatrix}, \\ P(b) = \begin{pmatrix} 1 & 0 \\ 0 & -1 \end{pmatrix}, \quad P(ab) = \begin{pmatrix} 0 & 1 \\ 1 & 0 \end{pmatrix}.$$

It is easily checked that this forms a projective representation with a nontrivial factor system. One can characterize the projective representation starting from the defining relations $a^2 = b^2 = (ab)^2 = e$. One has $P(a)^2 = -E$, $P(b)^2 = E$, $(P(a)P(b))^2 = E$. It is easily seen that one cannot achieve a trivial factor system by multiplication of the P matrices by suitably chosen factors. Therefore, the factor system is not associated with the trivial one either. This is the general situation. The ordinary representations of R can be partitioned into groups, each group corresponding with one class of associated factor systems, and within each group one finds representatives of each strong equivalence class. For the example above, there is only one such class for the nontrivial factor system as one sees from $d^2 = 4 = N = |D_2|$.

The general procedure then is to characterize a factor system with expressions stemming from defining relations for the group K . Defining relations are expressions (words) in the generators that fix the isomorphism class of the group. They are of the form

Table 1.2.2.2. Character table of D_4

| | E | A, A^3 | A^2 | $B, A^2 B$ | $AB, A^3 B$ |
|------------|-----|----------|-------|------------|-------------|
| Γ_1 | 1 | 1 | 1 | 1 | 1 |
| Γ_2 | 1 | -1 | 1 | 1 | -1 |
| Γ_3 | 1 | 1 | 1 | -1 | -1 |
| Γ_4 | 1 | -1 | 1 | -1 | 1 |
| Γ_5 | 2 | 0 | -2 | 0 | 0 |

1.2. REPRESENTATIONS OF CRYSTALLOGRAPHIC GROUPS

$$W_i(A_1, A_2, \dots, A_p) = E, \quad i = 1, 2, \dots, s \quad (1.2.2.56)$$

if the A_i are the generators. For a projective representation the corresponding product

$$W_i(D(A_1), D(A_2), \dots, D(A_p)) = \lambda_i E$$

is a multiple of the identity operator. The defining relations are not unique for a group. Therefore, there is arbitrariness here. The complex numbers λ_i that correspond to the defining relations may be changed by multiplying the operators $D(R)$ by factors $u(R)$. This changes the factor system to an associated one. If in a table the factor systems are given by the numbers λ_i , one can identify the class of a given factor system by calculating the corresponding words and solving the problem of finding the table values by taking into account additional factors $u(R)$. For example, the factor system that gives the values of λ_i for D_2 above is associated with one that gives $\lambda_{1,2,3} = 1, 1, -1$, if one multiplies $P(a)$ by i .

1.2.2.9. Double groups and their representations

Three-dimensional rotation point groups are subgroups of $SO(3)$. In quantum mechanics, rotations act according to some representation of $SO(3)$. Because wave functions can be multiplied by an arbitrary phase factor, in principle projective representations play a role here. The projective representations of $SO(3)$ can be obtained from the ordinary representations of the representation group, which is $SU(2)$, the group of all 2×2 matrices

$$\begin{pmatrix} a & b \\ -b^* & a^* \end{pmatrix} \quad \text{with } |a|^2 + |b|^2 = 1.$$

For example, in spin space for a particle with spin $\frac{1}{2}$, a rotation over φ along the z axis acts according to

$$\begin{pmatrix} \exp(i\varphi/2) & 0 \\ 0 & \exp(-i\varphi/2) \end{pmatrix},$$

and in general the representation for a rotation over φ along an axis \hat{n} is

$$\cos(\varphi/2)E + i \sin(\varphi/2)(\boldsymbol{\sigma} \cdot \hat{n}),$$

where $\boldsymbol{\sigma}$ is a vector with the three Pauli spin matrices as components. Because the matrices for $\varphi = 2\pi$ become $-E$, the representation has a nontrivial factor system. As a representation of $SU(2)$, however, it is an ordinary representation.

To each rotation ($R \in SO(3)$) correspond two elements $\pm U(R) \in SU(2)$. To a point group $K \subset SO(3)$ corresponds a subset of $SU(2)$ which is in fact a subgroup, because $U(R)U(R') = \pm U(RR')$. This group is the *double group* K^d . It contains both E and $-E$, which are both mapped to the unit element of $SO(3)$ under the homomorphism $SU(2) \rightarrow SO(3)$. Because $\pm E$ commute with all elements of K^d , this group C_2 is an invariant subgroup and the factor group K^d/C_2 is isomorphic to K . Therefore, every representation of K is a representation of K^d , but in general there are other representations as well, the *extra representations*. Notice that the double group of K does not only depend on the isomorphism class of K , but also on the geometric class, because the realization as subgroup of $O(3)$ comes in.

As an example, we take the group $222 \subset SO(3)$. The two generators 2_x and 2_y correspond, respectively, to the matrices

$$\pm \begin{pmatrix} 0 & i \\ -i & 0 \end{pmatrix}, \quad \pm \begin{pmatrix} 0 & 1 \\ 1 & 0 \end{pmatrix}.$$

These matrices generate a group of order eight, which can also be presented by

$$A = \begin{pmatrix} i & 0 \\ 0 & -i \end{pmatrix}, \quad B = \begin{pmatrix} 0 & 1 \\ 1 & 0 \end{pmatrix}; \quad A^4 = B^2 = (AB)^2 = E.$$

This group is isomorphic with D_4 , a group with five irreducible representations: four one-dimensional and one two-dimensional. The former are the four ordinary representations of D_2 because both E and $-E$ are represented by the unit matrix. The two-dimensional representation has $\Gamma(-E) = -\Gamma(E)$ and is, therefore, not an ordinary representation for 222 . It is an extra representation for the double group 222^d , or a projective representation of 222 . Choosing one element from $SU(2)$ for each generator of 222 one obtains

$$\Gamma(2_x) = \begin{pmatrix} 0 & i \\ -i & 0 \end{pmatrix}, \quad \Gamma(2_y) = \begin{pmatrix} 0 & 1 \\ 1 & 0 \end{pmatrix},$$

$$\Gamma(2_x)^2 = \Gamma(2_y)^2 = E, \quad (\Gamma(2_x)\Gamma(2_y))^2 = -E.$$

The factor system fixed in this way is not associated to a trivial one (otherwise the irreducible representation could not be two-dimensional). The extra representation of the double group corresponds to a nontrivial projective representation of the point group itself.

To construct the character table of the double group, it is worthwhile to note that the elements of K^d mapped on one class of K form two classes, except when the class in K consists of 180° rotations and there exists for one element of this class another 180° rotation in K with its axis perpendicular to that of the former element. The example above illustrates this: there are four classes in $K = 222$ and five classes in K^d . The identity in K corresponds to $\pm E$ in K^d , and these form two classes. The other pairs $\pm A$, $\pm B$ and $\pm AB$ are mapped each on one class. This is, however, not the most general case. $\pm u(R)$ only belong to the same class if there is an element $S \in K$ such that $u(R)u(S) = -u(S)u(R)$. If one brings $u(R)$ into diagonal form, one sees that this is only possible if the diagonal elements are $\pm i$, i.e. when the rotation angle of R is π . In this case one has

$$u(S) \begin{pmatrix} i & 0 \\ 0 & -i \end{pmatrix} = - \begin{pmatrix} i & 0 \\ 0 & -i \end{pmatrix} u(S),$$

then

$$u(S) = \begin{pmatrix} 0 & \exp(i\varphi) \\ -\exp(-i\varphi) & 0 \end{pmatrix},$$

which is a twofold rotation with axis perpendicular to the z axis. Therefore, in general, if a class in K of 180° rotations does not exist or if there is not a perpendicular 180° rotation, the class in K corresponds to two classes in K^d .

As a second example, we consider the group $K = 32$ of order six. It is generated by a threefold rotation along the z axis and a twofold rotation perpendicular to the first one. Corresponding elements of $SU(2)$ are

$$A = \begin{pmatrix} \frac{1}{2} + \frac{1}{2}i\sqrt{3} & 0 \\ 0 & \frac{1}{2} - \frac{1}{2}i\sqrt{3} \end{pmatrix}, \quad B = \begin{pmatrix} 0 & 1 \\ -1 & 0 \end{pmatrix}.$$

The group K^d generated by these elements is of order 12 with six classes: E , $-E$, (A, A^5) , (A^2, A^4) , (B, A^2B, A^4B) and (AB, A^3B, A^5B) , which are mapped on the three classes of $K = 32$. Therefore, there are six irreducible representations for K^d : four one-dimensional ones and two two-dimensional ones. Two one-dimensional and one two-dimensional representations are the ordinary representations of K , the other ones are extra representations and have $\Gamma(-E) = -\Gamma(E)$. As projective representations of $K = 32$, they are associated with ordinary representations: for the one-dimensional ones this is obvious; for the two-dimensional one, generated by A and B , one can find an associated one $\Gamma(A) = -A$, $\Gamma(B) = iB$ such that

1. TENSORIAL ASPECTS OF PHYSICAL PROPERTIES

$$\Gamma(A)^3 = \Gamma(B)^2 = (\Gamma(A)\Gamma(B))^2 = E$$

and, consequently, this representation has a trivial factor system. This shows that, although 32^d has three extra representations, there are no nontrivial projective representations.

The characters for the double point groups are given in Table 1.2.6.7.

1.2.3. Space groups

1.2.3.1. Structure of space groups

The Euclidean group $E(n)$ in n dimensions is the group of all distance-preserving inhomogeneous linear transformations. In Euclidean space, an element is denoted by

$$g = \{R|\mathbf{a}\}$$

where $R \in O(n)$ and \mathbf{a} is an n -dimensional translation. On a point \mathbf{r} in n -dimensional space, g acts according to

$$\{R|\mathbf{a}\}\mathbf{r} = R\mathbf{r} + \mathbf{a}. \quad (1.2.3.1)$$

Therefore, $|\mathbf{g}\mathbf{r}_1 - \mathbf{g}\mathbf{r}_2| = |\mathbf{r}_1 - \mathbf{r}_2|$. The group multiplication law is given by

$$\{R|\mathbf{a}\}\{R'|\mathbf{a}'\} = \{RR'|\mathbf{a} + R\mathbf{a}'\}. \quad (1.2.3.2)$$

The elements $\{E|\mathbf{a}\}$ form an Abelian subgroup, the group of n -dimensional translations $T(n)$.

An n -dimensional space group is a subgroup of $E(n)$ such that its intersection with $T(n)$ is generated by n linearly independent basis translations. This means that this *lattice translation subgroup* A is isomorphic to the group of n -tuples of integers: each translation in A can be written as

$$\{E|\mathbf{a}\} = \prod_{i=1}^n \{E|\mathbf{e}_i\}^{n_i} = \{E|\sum_{i=1}^n n_i \mathbf{e}_i\}. \quad (1.2.3.3)$$

The lattice translation subgroup A is an invariant subgroup because

$$g\{E|\mathbf{a}\}g^{-1} = \{R|\mathbf{b}\}\{E|\mathbf{a}\}\{R|\mathbf{b}\}^{-1} = \{E|R\mathbf{a}\} \in A.$$

The factor group G/A , of the space group G and the lattice translation group A , is isomorphic to the group K formed by all elements R occurring in the elements $\{R|\mathbf{a}\} \in G$. This group is the *point group* of the space group G . It is a subgroup of $O(n)$.

The *unit cell* of the space group is a domain in n -dimensional space such that every point in space differs by a lattice translation from some point in the unit cell, and such that between any two points in the unit cell the difference is not a lattice translation. The unit cell is not unique. One choice is the n -dimensional parallelepiped spanned by the n basis vectors. The points in this unit cell have coordinates between 0 (inclusive) and 1. Another choice is not basis dependent: consider all points generated by the lattice translation group from an origin. This produces a lattice of points Λ . Consider now all points that are closer to the origin than to any other lattice point. This domain is a unit cell, if one takes care which part of the boundary belongs to it and which part not, and is called the *Wigner-Seitz cell*. In mathematics it is called the *Voronoi cell* or *Dirichlet domain* (or region).

Because the point group leaves the lattice of points invariant, it transforms the Wigner-Seitz cell into itself. This implies that points inside the unit cell may be related by a point-group element. Similarly, space-group elements may connect points inside the unit cell, up to lattice translations. A *fundamental region* or *asymmetric unit* is a part of the unit cell such that no points of the fundamental region are connected by a space-group element, and simultaneously that any point in space can be related to a point in the fundamental region by a space-group transformation.

Because $\{E|R\mathbf{a}\}$ belongs to the lattice translation group for every $R \in K$ and every lattice translation $\{E|\mathbf{a}\}$, the lattice Λ generated by the vectors \mathbf{e}_i ($i = 1, 2, \dots, n$) is invariant under the point group K . Therefore, the latter is a crystallographic point group. On a basis of the lattice Λ , the point group corresponds to a group $\Gamma(K)$ of integer matrices. One has the following situation. The space group G has an invariant subgroup A isomorphic to \mathbb{Z}^n , the factor group G/A is a crystallographic point group K which acts according to the integer representation $\Gamma(K)$ on A . In mathematical terms, G is an *extension* of K by A with homomorphism Γ from K to the group of automorphisms of A .

The vectors \mathbf{a} occurring in the elements $\{E|\mathbf{a}\} \in G$ are called *primitive translations*. They have integer coefficients with respect to the basis $\mathbf{e}_1, \dots, \mathbf{e}_n$. However, not all vectors \mathbf{a} in the space-group elements are necessarily primitive. One can decompose the space group G according to

$$G = A + g_2 A + g_3 A + \dots + g_N A. \quad (1.2.3.4)$$

To every element $R \in K$ there is a coset $g_i A$ with $g_i = \{R|\mathbf{a}(R)\}$ as representative. Such a representative is unique up to a lattice translation. Instead of $\mathbf{a}(R)$, one could as well have $\mathbf{a}(R) + \mathbf{n}$ as representative for any lattice translation \mathbf{n} . For a particular choice, the function $\mathbf{a}(R)$ from the point group to the group $T(n)$ is called the *system of nonprimitive translations* or *translation vector system*. It is a mapping from the point group K to $T(n)$, modulo A . Such a system of nonprimitive translations satisfies the relations

$$\mathbf{a}(R) + R\mathbf{a}(S) = \mathbf{a}(RS) \bmod A \quad \forall R, S \in K. \quad (1.2.3.5)$$

This follows immediately from the product of two representatives g_i .

If the lattice translation subgroup A acts on a point \mathbf{r} different from the origin, one obtains the set $\Lambda + \mathbf{r}$. One can describe the elements of G as well as combinations of an orthogonal transformation with \mathbf{r} as centre and a translation. This can be seen from

$$\{R|\mathbf{a}\} = \{E|\mathbf{a} - \mathbf{r} + R\mathbf{r}\}\{R|\mathbf{r} - R\mathbf{r}\}, \quad (1.2.3.6)$$

where now $\{R|\mathbf{r} - R\mathbf{r}\}$ leaves the point \mathbf{r} invariant. The new system of nonprimitive translations is given by

$$\mathbf{a}'(R) = \mathbf{a}(R) + (R - E)\mathbf{r}. \quad (1.2.3.7)$$

This is the effect of a *change of origin*. Therefore, for a space group, the systems of nonprimitive translations are only determined up to a primitive translation and up to a change of origin.

It is often convenient to describe a space group on another basis, the conventional lattice basis. This is the basis for a sublattice with the same, or higher, symmetry and with the same number of free parameters. Therefore, the sublattice is also invariant under K and with respect to the conventional basis, which is obtained from the original one *via* a basis transformation S , the point group has the form

$$\Gamma_{\text{conventional}}(R) = S\Gamma_{\text{primitive}}(R)S^{-1}, \quad (1.2.3.8)$$

where S is the *centring matrix*. It is a matrix with determinant equal to the inverse of the number of lattice points of the primitive lattice inside the unit cell of the conventional lattice. As an example, consider the primitive and centred rectangular lattices in two dimensions. Both have symmetry $2mm$, and two parameters a and b . The transformation from a basis of the conventional lattice $[(2a, 0) \text{ and } (0, 2b)]$ to a basis of the primitive lattice $[(a, -b) \text{ and } (a, b)]$ is given by S , and the relations between the generators of the point groups are

1.2. REPRESENTATIONS OF CRYSTALLOGRAPHIC GROUPS

$$\begin{pmatrix} -1 & 0 \\ 0 & 1 \end{pmatrix} = S \begin{pmatrix} 0 & -1 \\ -1 & 0 \end{pmatrix} S^{-1}, \quad S = \begin{pmatrix} \frac{1}{2} & \frac{1}{2} \\ -\frac{1}{2} & \frac{1}{2} \end{pmatrix}$$

$$\begin{pmatrix} 1 & 0 \\ 0 & -1 \end{pmatrix} = S \begin{pmatrix} 0 & 1 \\ 1 & 0 \end{pmatrix} S^{-1}.$$

1.2.3.2. Irreducible representations of lattice translation groups

The lattice translation group A is isomorphic to the group \mathbb{Z}^n of n -tuples of integers. This is an infinite group and, therefore, the usual techniques for finite groups cannot be applied. A way past this is the following. If \mathbf{a}_i are the basis vectors of the lattice Λ , the lattice translation group generated by the translations $\{E|N\mathbf{a}_i\}$ forms an Abelian subgroup A^N of A . The factor group A/A^N is a finite group isomorphic to the direct product of n cyclic groups of order N . Each representation of this group is a representation of A with the property that the elements of A^N are represented by the unit operator. This procedure is in fact that of periodic boundary conditions in solid-state physics. In the following, we shall consider only the representations of A that satisfy this condition.

The irreducible representations of the direct product of n cyclic groups of order N are all one-dimensional. According to Section 1.2.2.6 they can be characterized by n integers and read

$$\Gamma^{(p_j)} \left(\{E| \sum_{i=1}^n n_i \mathbf{e}_i\} \right) = \exp[2\pi i(n_1 p_1 + n_2 p_2 + \dots + n_n p_n)/N], \quad (1.2.3.9)$$

because a representation of the cyclic group C_N is determined by its value on the basis translations:

$$\Gamma^p(\{E|\mathbf{e}\}) = \exp(2\pi i p/N), \quad 0 \leq p < N.$$

There are exactly N^n nonequivalent irreducible representations.

If \mathbf{a}_i are basis vectors of the lattice Λ , its dual basis consists of vectors \mathbf{b}_j defined by

$$\mathbf{a}_i \cdot \mathbf{b}_j = 2\pi \delta_{ij}. \quad (1.2.3.10)$$

These vectors \mathbf{b}_j span the *reciprocal lattice* Λ^* . The scalar product of an arbitrary lattice vector \mathbf{a} and a reciprocal-lattice vector \mathbf{K} is then

$$\mathbf{K} \cdot \mathbf{a} = \left(\sum_{i=1}^n m_i \mathbf{b}_i \right) \cdot \left(\sum_{j=1}^n n_j \mathbf{a}_j \right) = 2\pi \sum_{i=1}^n n_i m_i. \quad (1.2.3.11)$$

The expression (1.2.3.9) then can be written more concisely if one introduces an n -dimensional vector \mathbf{k} :

$$\mathbf{k} = (1/N) \sum_{i=1}^n p_i \mathbf{b}_i. \quad (1.2.3.12)$$

Then (1.2.3.9) simplifies to

$$\Gamma^{(\mathbf{k})}(\{E|\mathbf{a}\}) = \exp(i\mathbf{k} \cdot \mathbf{a}). \quad (1.2.3.13)$$

Because $0 \leq p_i/N < 1$, the vector \mathbf{k} belongs to the unit cell of the reciprocal lattice. If one chooses that unit cell as the Voronoi cell for the reciprocal lattice, which in direct space would be the Wigner-Seitz cell, it is called the *Brillouin zone*. Therefore, representations of the lattice translation subgroup are characterized by a vector in the Brillouin zone. In fact, the vectors \mathbf{k} form a mesh inside the Brillouin zone, but this mesh becomes finer if N increases. In the limit of N going to ∞ , the wavevectors \mathbf{k} fill the Brillouin zone.

Just like the direct lattice, the reciprocal lattice is invariant under the point group K . The Brillouin zone, or at least its interior, is invariant under K as well. A *fundamental domain* in the Brillouin zone is a part of the zone such that no two points of

the fundamental region are related by a point-group transformation from K and that any point in the Brillouin zone can be obtained from a point in the fundamental region by a point-group transformation.

1.2.3.3. Irreducible representations of space groups

For representations of space groups, we use the same argumentation as for the lattice translation subgroup. Notice that the group A^N generated by the vectors $\{E|N\mathbf{e}_i\}$ is an invariant Abelian subgroup of the space group G as well.

$$\{R|\mathbf{a}\}\{E|N\mathbf{e}_i\}\{R^{-1}|-R^{-1}\mathbf{a}\} = \{E|N\mathbf{R}\mathbf{e}_i\} \in A^N.$$

The factor group G/A^N is a finite group of order N^n times the order of the point group K . Representations of this factor group are representations of G with the property that all elements of A^N are mapped on the unit operator. We shall consider here only such space-group representations.

Suppose that $\Gamma(G)$ is an irreducible representation of the space group G . Its restriction $\Gamma(A)$ to the lattice translation subgroup is then reducible, unless it is one-dimensional. Each irreducible representation of A is characterized by a vector \mathbf{k} in the Brillouin zone. Therefore,

$$\Gamma(\{E|\mathbf{a}\}) = \begin{pmatrix} \exp(i\mathbf{k}_1 \cdot \mathbf{a}) & 0 & 0 & \dots & 0 & 0 \\ 0 & \exp(i\mathbf{k}_2 \cdot \mathbf{a}) & 0 & \dots & 0 & 0 \\ 0 & 0 & \exp(i\mathbf{k}_3 \cdot \mathbf{a}) & \dots & 0 & 0 \\ 0 & 0 & 0 & \dots & \dots & 0 \\ 0 & 0 & 0 & \dots & 0 & \exp(i\mathbf{k}_n \cdot \mathbf{a}) \end{pmatrix}. \quad (1.2.3.14)$$

Some of the vectors \mathbf{k}_i may be identical. Therefore, the matrix representation can be written as

$$\Gamma(\{E|\mathbf{a}\}) = \begin{pmatrix} \exp(i\mathbf{k}_1 \cdot \mathbf{a})E & 0 & 0 & \dots & 0 & 0 \\ 0 & \exp(i\mathbf{k}_2 \cdot \mathbf{a})E & 0 & \dots & 0 & 0 \\ 0 & 0 & \exp(i\mathbf{k}_3 \cdot \mathbf{a})E & \dots & 0 & 0 \\ 0 & 0 & 0 & \dots & 0 & 0 \\ 0 & 0 & 0 & \dots & 0 & \exp(i\mathbf{k}_s \cdot \mathbf{a})E \end{pmatrix}. \quad (1.2.3.15)$$

It can be shown that the dimensions of the unit matrices E are all the same (and equal to d). Then

$$n = s \cdot d.$$

With respect to the basis on which the translation is of this form, every basis vector in the p th block is multiplied by a factor $\exp(i\mathbf{k}_p \cdot \mathbf{a})$.

Suppose that $\{R|\mathbf{u}\}$ is an element of the space group G . Consider a basis vector v of the representation space that gets a factor $\exp(i\mathbf{k} \cdot \mathbf{a})$ under the translation $\{E|\mathbf{a}\}$. Then one has

$$\begin{aligned} D(\{E|\mathbf{a}\})v &= \exp(i\mathbf{k} \cdot \mathbf{a})v \\ D(\{E|\mathbf{a}\})D(\{R|\mathbf{u}\})v &= D(\{R|\mathbf{u}\})D(\{E|R^{-1}\mathbf{a}\})v \\ &= \exp(iR\mathbf{k} \cdot \mathbf{a})D(\{R|\mathbf{u}\})v, \end{aligned}$$

and because $D(\{R|\mathbf{u}\})v$ also belongs to the representation space there are vectors that transform with the vector $R\mathbf{k}$ as well as vectors that transform with \mathbf{k} . This means that for every vector \mathbf{k} occurring in a block in (1.2.3.5), there is also a block for each vector $R\mathbf{k}$ as R runs over the point group K . The vectors $\{R\mathbf{k}|R \in K\}$ form the *star* of \mathbf{k} . Vectors $R\mathbf{k}$ that differ by a reciprocal-lattice vector ($\mathbf{k}' = \mathbf{k} + \mathbf{K}$ with $\mathbf{K} \in \Lambda^*$) correspond to the same representation and are therefore considered to be the same. Generally, a vector \mathbf{k} may be left invariant by a subgroup of the point group K . This point group $K_{\mathbf{k}}$ is the *point group* of \mathbf{k} .

1. TENSORIAL ASPECTS OF PHYSICAL PROPERTIES

$$K_{\mathbf{k}} \equiv \{R|\mathbf{R}\mathbf{k} \equiv \mathbf{k} \bmod \Lambda^*\}. \quad (1.2.3.16)$$

Then there are s point-group elements R_i such that

$$K = K_{\mathbf{k}} \cup R_2 K_{\mathbf{k}} \cup \dots \cup R_s K_{\mathbf{k}} \quad (1.2.3.17)$$

and each element R_i corresponds to a vector in the star:

$$\mathbf{k}_i = R_i \mathbf{k}_1; \quad \mathbf{k}_1 = \mathbf{k}, \quad i = 1, 2, \dots, s.$$

Therefore, the blocks in (1.2.3.15) for an irreducible representation of the space group G correspond to the s branches of the star of \mathbf{k} . They are all of the same dimension d . If the vectors \mathbf{k}_i in (1.2.3.15) belonged to two or more different stars, the representation would be reducible.

To the point group of \mathbf{k} corresponds a subgroup of the space group G that has $K_{\mathbf{k}}$ as point group. It is called *the group of \mathbf{k}* and is defined by

$$G_{\mathbf{k}} \equiv \{g = \{R|\mathbf{a}\} \in G | R \in K_{\mathbf{k}}\}. \quad (1.2.3.18)$$

Analogously to (1.2.3.17), one can write

$$G = G_{\mathbf{k}} \cup g_2 G_{\mathbf{k}} \cup \dots \cup g_s G_{\mathbf{k}} \quad (1.2.3.19)$$

for elements $g_i = \{R_i|\mathbf{a}_i\}$ of the space group G .

As one sees from (1.2.3.15), there is a subspace of vectors \mathbf{v} that get a factor $\exp(i\mathbf{k} \cdot \mathbf{a})$ for any lattice translation \mathbf{a} . If one considers the action of $D(g)$ with $g \in G_{\mathbf{k}}$, it follows immediately that a vector from this space is transformed into a vector of the same space: the subspace corresponding to a vector \mathbf{k} is invariant under $G_{\mathbf{k}}$. Therefore this space $V_{\mathbf{k}}$ carries a representation of $G_{\mathbf{k}}$. It can be seen as follows that one may construct the irreducible representation of the whole group G as soon as one knows the representation $D_{\mathbf{k}}$ of $G_{\mathbf{k}}$ in $V_{\mathbf{k}}$. To that end, consider a basis $\mathbf{e}_1, \dots, \mathbf{e}_d$ in $V_{\mathbf{k}}$. The vectors

$$\psi_{i\mu} = D(g_i)\mathbf{e}_{\mu} \quad (i = 1, 2, \dots, s; \mu = 1, 2, \dots, d), \quad (1.2.3.20)$$

form a basis of the whole representation space. Under a lattice-translation vector \mathbf{a} , the vector $\psi_{i\mu}$ gets a factor $\exp(i\mathbf{k}_i \cdot \mathbf{a})$. On this basis, one can determine the matrix representation $\Gamma(G)$. Take an element $\{R|\mathbf{u}\} \in G$. It belongs to a certain coset $g_m G_{\mathbf{k}}$ in the decomposition of G . In addition, the element $\{R|\mathbf{u}\}g_i$ belongs to a well defined $g_j G_{\mathbf{k}}$. This means that there is an element $\{S|\mathbf{v}\}$ in the group $G_{\mathbf{k}}$ such that

$$\{R|\mathbf{u}\}g_i = g_j \{S|\mathbf{v}\} \quad (i = 1, 2, \dots, s; \{S|\mathbf{v}\} \in G_{\mathbf{k}}).$$

Then one can write

$$\begin{aligned} D(\{R|\mathbf{u}\})\psi_{i\mu} &= D(\{R|\mathbf{u}\})D(g_i)\mathbf{e}_{\mu} \\ &= D(g_j)D(\{S|\mathbf{v}\})\mathbf{e}_{\mu} \\ &= D(g_j) \sum_{\nu=1}^d \Gamma_{\mathbf{k}}(\{S|\mathbf{v}\})_{\nu\mu} \mathbf{e}_{\nu} \\ &= \sum_{\nu=1}^d \Gamma_{\mathbf{k}}(\{S|\mathbf{v}\})_{\nu\mu} \psi_{j\nu} \\ &= \sum_{j=1}^s \sum_{\nu=1}^d \Gamma(\{R|\mathbf{u}\})_{j\nu, i\mu} \psi_{j\nu}. \end{aligned}$$

This means that the representation matrix $\Gamma(\{R|\mathbf{u}\})$ can be decomposed into $s \times s$ blocks of dimension d . In each row of blocks there is exactly one that is not a block of zeros, and the same is true for each column of blocks. Moreover, the only nonzero block in the i th column and in the j th row is

$$D_{\mathbf{k}}(\{S|\mathbf{v}\}) = D_{\mathbf{k}}(g_j^{-1}\{R|\mathbf{u}\}g_i), \quad (1.2.3.21)$$

where i and j are uniquely related by

$$\{R|\mathbf{u}\}g_i \in g_j G_{\mathbf{k}}. \quad (1.2.3.22)$$

It can be shown that $\Gamma(G)$ is irreducible if and only if $D_{\mathbf{k}}(G_{\mathbf{k}})$ is irreducible. From the construction, it is obvious that one may obtain all irreducible representations of G in this way. Moreover, one obtains all representations of G if one takes for the construction all stars and for each star all irreducible representations of $G_{\mathbf{k}}$.

So the final step is to determine all nonequivalent irreducible representations of $G_{\mathbf{k}}$. Notice that the lattice translation subgroup is a subgroup of $G_{\mathbf{k}}$. Therefore,

$$D_{\mathbf{k}}(\{E|\mathbf{a}\}) = \exp(i\mathbf{k} \cdot \mathbf{a})E.$$

If one makes a choice for the system of nonprimitive translations $\mathbf{u}(R)$, every element $g = \{S|\mathbf{v}\} \in G_{\mathbf{k}}$ can be written uniquely as

$$g = \{E|\mathbf{a}\}\{S|\mathbf{u}(S)\},$$

for a lattice translation \mathbf{a} . Therefore, one has

$$D_{\mathbf{k}}(\{S|\mathbf{v}\}) = \exp(i\mathbf{k} \cdot \mathbf{a})D_{\mathbf{k}}(\{S|\mathbf{u}(S)\}) \equiv \exp\{i\mathbf{k} \cdot [\mathbf{a} + \mathbf{u}(S)]\}\Gamma(S) \quad (1.2.3.23)$$

if one defines

$$\Gamma(S) = \exp[-i\mathbf{k} \cdot \mathbf{u}(S)]D_{\mathbf{k}}(\{S|\mathbf{u}(S)\}). \quad (1.2.3.24)$$

It is important to notice that this definition of Γ does not depend on the choice of the system of nonprimitive translations. If one takes $\mathbf{u}'(S) = \mathbf{u}(S) + \mathbf{b}$ ($\mathbf{b} \in A$), the result for $\Gamma(S)$ is the same. The product of two matrices $\Gamma(S)$ and $\Gamma(S')$ then becomes

$$\begin{aligned} \Gamma(S)\Gamma(S') &= \exp\{-i\mathbf{k} \cdot [\mathbf{u}(S) + \mathbf{u}(S')]\}D_{\mathbf{k}}(\{SS'|\mathbf{u}(S) + \mathbf{u}(S')\}) \\ &= \exp\{-i\mathbf{k} \cdot [\mathbf{u}(S') - \mathbf{u}(S)]\}\Gamma(S'). \end{aligned} \quad (1.2.3.25)$$

One sees that the matrices $\Gamma(R)$ form a projective representation of the point group of \mathbf{k} . The factor system is given by

$$\begin{aligned} \omega(S, S') &= \exp\{-i\mathbf{k} \cdot [\mathbf{u}(S') - \mathbf{u}(S)]\} \\ &= \exp[-i(\mathbf{k} - S^{-1}\mathbf{k}) \cdot \mathbf{u}(S')]. \end{aligned} \quad (1.2.3.26)$$

Such a factor system may, however, be equivalent to a trivial one.

If the space group $G_{\mathbf{k}}$ is symmorphic, one may choose the system of nonprimitive translations to be zero. Consequently, in this case the factor system $\omega(S, S')$ is unity and the matrices $\Gamma(S)$ form an ordinary representation of the space group $G_{\mathbf{k}}$. This is also the case if \mathbf{k} is not on the Brillouin-zone boundary. If \mathbf{k} is inside the Brillouin zone and $S \in K_{\mathbf{k}}$, one has $S\mathbf{k} = \mathbf{k} + \mathbf{K}$ only for $\mathbf{K} = 0$. So inside the Brillouin zone one has $S\mathbf{k} = \mathbf{k}$ for all $S \in K_{\mathbf{k}}$. This implies that

$$\exp\{-i\mathbf{k} \cdot [\mathbf{u}(S') - \mathbf{u}(S)]\} = \exp[-i(\mathbf{k} - S^{-1}\mathbf{k}) \cdot \mathbf{u}(S')] = 1.$$

A nontrivial factor system $\omega(S, S')$ can therefore only occur for a nonsymmorphic group $G_{\mathbf{k}}$ and for a \mathbf{k} on the Brillouin-zone boundary. But even then, it is possible that one may redefine the matrices $\Gamma(S)$ with an appropriate phase factor such that they form an ordinary representation. This is, for example, always the case if $K_{\mathbf{k}}$ is cyclic, because cyclic groups do not have genuine projective representations. These are always associated with an ordinary representation.

If the factor system $\omega(S, S')$ is not associated with a trivial one, one has to find the irreducible projective representations with the given factor system. As seen in the previous section, one may do this by using the defining relation for the point group $K_{\mathbf{k}}$. If these are words $W_i(A_1, \dots, A_r)$ in the generators A_1, \dots, A_r , the corresponding expressions in the representation

$$W_i(D_{\mathbf{k}}(A_1), \dots, D_{\mathbf{k}}(A_r)) = \lambda_i E$$

are multiples of the unit operator. The values of λ_i fix the class of the factor system completely. By multiplying the operators $D_{\mathbf{k}}(A_j)$ by proper phase factors, the values of λ_i can be trans-

1.2. REPRESENTATIONS OF CRYSTALLOGRAPHIC GROUPS

Table 1.2.3.1. Choices of \mathbf{k} in the fundamental domain of $Pnma$ and the elements of $K_{\mathbf{k}}$

| \mathbf{k} | Wyckoff position | $K_{\mathbf{k}}$ | Elements |
|-------------------------------------|------------------|------------------|---|
| 000 | a | mmm | $E \quad m_x \quad m_y \quad m_z \quad \bar{1} \quad 2_x \quad 2_y \quad 2_z$ |
| $\frac{1}{2}00$ | b | mmm | $E \quad m_x \quad m_y \quad m_z \quad \bar{1} \quad 2_x \quad 2_y \quad 2_z$ |
| $0\frac{1}{2}0$ | c | mmm | $E \quad m_x \quad m_y \quad m_z \quad \bar{1} \quad 2_x \quad 2_y \quad 2_z$ |
| $00\frac{1}{2}$ | c | mmm | $E \quad m_x \quad m_y \quad m_z \quad \bar{1} \quad 2_x \quad 2_y \quad 2_z$ |
| $0\frac{1}{2}\frac{1}{2}$ | g | mmm | $E \quad m_x \quad m_y \quad m_z \quad \bar{1} \quad 2_x \quad 2_y \quad 2_z$ |
| $\frac{1}{2}0\frac{1}{2}$ | d | mmm | $E \quad m_x \quad m_y \quad m_z \quad \bar{1} \quad 2_x \quad 2_y \quad 2_z$ |
| $\frac{1}{2}\frac{1}{2}0$ | f | mmm | $E \quad m_x \quad m_y \quad m_z \quad \bar{1} \quad 2_x \quad 2_y \quad 2_z$ |
| $\frac{1}{2}\frac{1}{2}\frac{1}{2}$ | h | mmm | $E \quad m_x \quad m_y \quad m_z \quad \bar{1} \quad 2_x \quad 2_y \quad 2_z$ |
| $\xi 00$ | i | $2mm$ | $E \quad m_y \quad m_z \quad 2_x$ |
| $\xi \frac{1}{2}0$ | k | $2mm$ | $E \quad m_y \quad m_z \quad 2_x$ |
| $\xi 0\frac{1}{2}$ | j | $2mm$ | $E \quad m_y \quad m_z \quad 2_x$ |
| $\xi \frac{1}{2}\frac{1}{2}$ | l | $2mm$ | $E \quad m_y \quad m_z \quad 2_x$ |
| $0\eta 0$ | m | $m2m$ | $E \quad m_x \quad m_z \quad 2_y$ |
| $\frac{1}{2}\eta 0$ | o | $m2m$ | $E \quad m_x \quad m_z \quad 2_y$ |
| $0\eta \frac{1}{2}$ | n | $m2m$ | $E \quad m_x \quad m_z \quad 2_y$ |
| $\frac{1}{2}\eta \frac{1}{2}$ | p | $m2m$ | $E \quad m_x \quad m_z \quad 2_y$ |
| 00ξ | q | $mm2$ | $E \quad m_x \quad m_y \quad 2_z$ |
| $\frac{1}{2}0\xi$ | s | $mm2$ | $E \quad m_x \quad m_y \quad 2_z$ |
| $0\frac{1}{2}\xi$ | r | $mm2$ | $E \quad m_x \quad m_y \quad 2_z$ |
| $\frac{1}{2}\frac{1}{2}\xi$ | t | $mm2$ | $E \quad m_x \quad m_y \quad 2_z$ |
| $0\eta\xi$ | u | $m11$ | $E \quad m_x$ |
| $\frac{1}{2}\eta\xi$ | v | $m11$ | $E \quad m_x$ |
| $\xi 0\xi$ | w | $1m1$ | $E \quad m_y$ |
| $\xi \frac{1}{2}\xi$ | x | $1m1$ | $E \quad m_y$ |
| $\xi \eta 0$ | y | $11m$ | $E \quad m_z$ |
| $\xi \eta \frac{1}{2}$ | z | $11m$ | $E \quad m_z$ |
| $\xi \eta \xi$ | α | 1 | E |

Table 1.2.3.2. Strata of irreducible representations of $Pmm2$ and $Pmmm$

| \mathbf{k} | Wyckoff position in $Pmm2$ | Wyckoff positions in $Pmmm$ | $K_{\mathbf{k}}$ |
|-----------------------------|----------------------------|-----------------------------|------------------|
| 00 ξ | a | a, c, q | $mm2$ |
| $0\frac{1}{2}\xi$ | b | e, g, r | $mm2$ |
| $\frac{1}{2}0\xi$ | c | b, d, s | $mm2$ |
| $\frac{1}{2}\frac{1}{2}\xi$ | d | f, h, t | $mm2$ |
| $\xi 0\xi$ | e | i, j, w | $1m1$ |
| $\xi \frac{1}{2}\xi$ | f | k, l, x | $1m1$ |
| $0\eta\xi$ | g | m, n, u | $m11$ |
| $\frac{1}{2}\eta\xi$ | h | o, p, v | $m11$ |
| $\xi \eta \xi$ | i | y, z, α | 1 |

representations are labelled μ . There are several conventions for the choice of this label, but an irreducible representation of G is always characterized by a pair (\mathbf{k}, μ) , where \mathbf{k} fixes the star and μ the irreducible point-group representation.

The projective representations of the group of \mathbf{k} , i.e. of $K_{\mathbf{k}}$, can be obtained from the ordinary representations of a larger group. If the factor system $\omega(R, R')$ is of order m , the order of this larger group $\hat{K}_{\mathbf{k}\omega}$ is m times the order of $K_{\mathbf{k}}$. Then the irreducible representations of the space group are labelled by the vector \mathbf{k} in the Brillouin zone and an irreducible ordinary representation of $\hat{K}_{\mathbf{k}\omega}$, where ω follows from (1.2.3.26).

Two stars such that one branch of the first one has the same $K_{\mathbf{k}}$ as one branch of the other determine representations that are quite similar. The only difference is the numerical value of the factors $\exp(i\mathbf{k} \cdot \mathbf{a})$, the form of the representation matrices being the same. Such irreducible representations of the space group are said to belong to the same *stratum*. Strata are denoted by a symbol for one vector \mathbf{k} in the Brillouin zone. For example, the origin, conventionally denoted by Γ , belongs to one stratum that corresponds to the ordinary representations of the point group K . For a simple cubic space group, the point $[\frac{1}{2}, 0, 0]$ is denoted by X . Its $K_{\mathbf{k}}$ is the tetragonal group $4/mmm$. All points $[\xi, 0, 0]$ with $\xi \neq 0$ and $-\frac{1}{2} < \xi < \frac{1}{2}$ form one stratum with point group $4mm$. This stratum is denoted by Δ etc. The strata can be compared with the Wyckoff positions in direct space. There a Wyckoff position is a manifold in the unit cell for which all points have the same site symmetry, modulo the lattice translations. Here it is a manifold of k vectors with the same symmetry group modulo the reciprocal lattice. The action of $G_{\mathbf{k}}$ does not involve the nonprimitive translations. Therefore, the strata correspond to Wyckoff positions of the corresponding symmorphic space group. The stratum symbols for the various three-dimensional Bravais classes are given in Table 1.2.6.11.

As an example, we consider here the orthorhombic space group $Pnma$. The orthorhombic Brillouin zone has a fundamental domain with volume that is one-eighth of that of the Brillouin zone. The various choices of \mathbf{k} in this fundamental domain, together with the corresponding point groups $K_{\mathbf{k}}$, are given in Table 1.2.3.1. The vectors \mathbf{k} correspond to Wyckoff positions of the group $Pmmm$.

In the tables, the vectors \mathbf{k} and their corresponding Wyckoff positions are given for the holohedral space groups. In general, the number of different strata is smaller for the other groups. One can still use the same symbols for these groups, or take the symbols for the Wyckoff positions for the groups that are not holohedral. Consider as an example the group $Pmm2$. Its holohedral space group is $Pmmm$. The strata of irreducible representations can be labelled by the symbols for Wyckoff positions of $Pmm2$ as well as those of $Pmmm$. This is shown in Table 1.2.3.2.

The defining relations for the point group mmm are

$$A^2 = B^2 = (AB)^2 = C^2 = E, \quad AC = CA, \quad BC = CB.$$

formed into those tabulated. Then the tables give all irreducible representations for this factor system.

In summary, the procedure for finding all irreducible representations of a space group G is as follows.

(1) Consider all stars of \mathbf{k} with respect to G . This means that one takes all vectors \mathbf{k} in a *fundamental region* of the Brillouin zone.

(2) For each star, one determines the group $K_{\mathbf{k}}$.

(3) For each $K_{\mathbf{k}}$, one determines the factor system $\omega(S, S')$.

(4) For this factor system, one looks for all nonequivalent irreducible (projective) representations.

(5) From the representations $D_{\mathbf{k}}(K_{\mathbf{k}})$, one determines the representations $\Gamma_{\mathbf{k}}(G_{\mathbf{k}})$ and $\Gamma(G)$ according to the procedure given above.

1.2.3.4. Characterization of space-group representations

The irreducible representations of space groups are characterized by a star of vectors in the Brillouin zone, and by the irreducible, possibly projective, representations of the point group of one point from that star.

The stars are sets of vectors in the Brillouin zone related mutually by transformations from the point group K of the space group G modulo reciprocal-lattice vectors. To obtain all stars, it is sufficient to take all vectors in the fundamental domain of the Brillouin zone, i.e. a part of the Brillouin zone such that no vectors in the domain are related by point-group elements (modulo Λ^*) and such that every point in the Brillouin zone is related to a vector in the fundamental domain by a point-group operation.

From each star one takes one point \mathbf{k} and determines the nonequivalent irreducible representations of the point group $K_{\mathbf{k}}$, the ordinary representations if the group $G_{\mathbf{k}}$ is symmorphic or \mathbf{k} is inside the Brillouin zone, or the projective representations with factor system ω [equation (1.2.3.26)] otherwise. These repre-

1. TENSORIAL ASPECTS OF PHYSICAL PROPERTIES

Table 1.2.3.3. Characteristic values of λ_i for the projective irreps of $K_{\mathbf{k}}$ for the point group mmm

| \mathbf{k} | A^2 λ_1 | B^2 λ_2 | $(AB)^2$ λ_3 | C^2 λ_4 | $AC = CA$ λ_5 | $BC = CB$ λ_6 | Representations | |
|-------------------------------------|----------------------|----------------------|-------------------------|----------------------|--------------------------|--------------------------|-----------------|-----------|
| | | | | | | | Number | Dimension |
| 000 | 1 | 1 | 1 | 1 | 1 | 1 | 8 | 1 |
| $\frac{1}{2}00$ | -1 | 1 | -1 | 1 | -1 | 1 | 2 | 2 |
| $0\frac{1}{2}0$ | 1 | -1 | 1 | 1 | 1 | 1 | 2 | 2 |
| $00\frac{1}{2}$ | 1 | 1 | 1 | -1 | -1 | 1 | 2 | 2 |
| $0\frac{1}{2}\frac{1}{2}$ | 1 | -1 | 1 | -1 | -1 | 1 | 2 | 2 |
| $\frac{1}{2}0\frac{1}{2}$ | -1 | 1 | -1 | -1 | 1 | 1 | 8 | 1 |
| $\frac{1}{2}\frac{1}{2}0$ | -1 | -1 | -1 | 1 | -1 | 1 | 2 | 2 |
| $\frac{1}{2}\frac{1}{2}\frac{1}{2}$ | -1 | -1 | -1 | -1 | 1 | 1 | 2 | 2 |
| $\xi 00$ | 1 | 1 | 1 | | | | 4 | 1 |
| $\xi \frac{1}{2}0$ | -1 | 1 | -1 | | | | 4 | 1 |
| $\xi 0\frac{1}{2}$ | 1 | -1 | -1 | | | | 4 | 1 |
| $\xi \frac{1}{2}\frac{1}{2}$ | -1 | -1 | 1 | | | | 4 | 1 |
| $0\eta 0$ | 1 | 1 | 1 | | | | 4 | 1 |
| $\frac{1}{2}\eta 0$ | -1 | 1 | 1 | | | | 1 | 2 |
| $0\eta \frac{1}{2}$ | 1 | -1 | 1 | | | | 1 | 2 |
| $\frac{1}{2}\eta \frac{1}{2}$ | -1 | -1 | 1 | | | | 4 | 1 |
| 00ζ | 1 | 1 | 1 | | | | 4 | 1 |
| $\frac{1}{2}0\zeta$ | -1 | 1 | -1 | | | | 1 | 2 |
| $0\frac{1}{2}\zeta$ | 1 | -1 | 1 | | | | 1 | 2 |
| $\frac{1}{2}\frac{1}{2}\zeta$ | -1 | -1 | -1 | | | | 1 | 2 |
| $0\eta\zeta$ | 1 | | | | | | 2 | 1 |
| $\frac{1}{2}\eta\zeta$ | -1 | | | | | | 2 | 1 |
| $\xi 0\zeta$ | 1 | | | | | | 2 | 1 |
| $\xi \frac{1}{2}\zeta$ | -1 | | | | | | 2 | 1 |
| $\xi \eta 0$ | 1 | | | | | | 2 | 1 |
| $\xi \eta \frac{1}{2}$ | -1 | | | | | | 2 | 1 |
| $\xi \eta \zeta$ | | | | | | | 1 | 1 |

For the subgroups, the defining relations follow from these. The corresponding expressions in the representation matrices $\Gamma(A_i)$ for the generators of the point groups give expressions

$$W_i^{\text{left}}(A_1, \dots, A_r) = \lambda_i W_i^{\text{right}}(A_1, \dots, A_r), \quad i = 1, \dots$$

In the example one has

$$\begin{aligned} \Gamma(A)^2 &= \lambda_1 E & \Gamma(B)^2 &= \lambda_2 E \\ (\Gamma(A)\Gamma(B))^2 &= \lambda_3 E & \Gamma(C)^2 &= \lambda_4 E \\ \Gamma(A)\Gamma(C) &= \lambda_5 \Gamma(C)\Gamma(A) & \Gamma(B)\Gamma(C) &= \lambda_6 \Gamma(C)\Gamma(B). \end{aligned}$$

The values for λ_i characterize the projective representation factor system and are given in Table 1.2.3.3. They are unity for ordinary representations.

By putting factors i in front of the representation matrices in the appropriate places, some of the values of λ_i can be changed from -1 to $+1$. In this way, one obtains either ordinary representations, which are necessarily one-dimensional for these Abelian groups, or projective representations, which are in this case two-dimensional. This is indicated as well in Table 1.2.3.3. The one-dimensional irreducible representations are ordinary representations of the group $K_{\mathbf{k}}$. The two-dimensional ones are projective representations, but correspond to ordinary representations of the larger groups isomorphic to $D_4 \times C_2$ and D_4 .

1.2.3.5. Double space groups and their representations

In Section 1.2.2.9, it was mentioned that the transformation properties of spin- $\frac{1}{2}$ particles under rotations are not given by the orthogonal group $O(3)$, but by the covering group $SU(2)$. Hence, the transformation of a spinor field under a Euclidean transformation g is given by

$$g\Psi(\mathbf{r}) = \pm U(R)\Psi(R^{-1}(\mathbf{r} - \mathbf{a})) \quad \forall g = \{R|\mathbf{a}\} \in E(3), \quad (1.2.3.27)$$

where the $SU(2)$ operator $U(R)$ is given by

$$U(R) = E \cos(\varphi/2) + (\boldsymbol{\sigma} \cdot \mathbf{n}) \sin(\varphi/2) \quad (1.2.3.28)$$

when the rotation R has angle φ and axis \mathbf{n} . When R does not belong to $SO(3)$ one has to take $U(-R)$.

For an ordinary space group, one can construct the double space group by

$$\{R|\mathbf{a}\} \rightarrow \{\pm U(R)|\mathbf{a}\} \quad (1.2.3.29)$$

with multiplication rule

$$\{U(R)|\mathbf{a}\}\{U(S)|\mathbf{b}\} = \{U(R)U(S)|\mathbf{a} + R\mathbf{b}\}. \quad (1.2.3.30)$$

An invariant subgroup of the double space group is the translation group A . The factor group is the double point group K^d of the point group K .

The representations of the double space groups can be constructed in the same way as those of ordinary space groups. They are characterized by a vector \mathbf{k} in the Brillouin zone and a label for an irreducible, generally projective, representation of the (double) point group $K_{\mathbf{k}}^d$ of \mathbf{k} , which is the double group of $K_{\mathbf{k}}$. Again, for nonsymmorphic space groups or wavevectors \mathbf{k} inside the Brillouin zone, the relevant irreducible representations of $K_{\mathbf{k}}^d$ are ordinary representations with a trivial factor system.

For an element g of the space group G , there are two elements of the double space group G^d . If one considers an irreducible representation $D(G^d)$ for the double space group and takes for each $g \in G$ one of the two corresponding elements in G^d , the resulting set of linear operators forms a projective representation of the space group. It is also characterized by a vector \mathbf{k} in the Brillouin zone and a projective representation of the point group (not its double) $K_{\mathbf{k}}$. This projective representation does not have the same factor system as discussed in Section 1.2.3.3, because the factor system now stems partly from the nonprimitive translations and partly from the fact that a double point group gives a projective representation of the ordinary point group $K_{\mathbf{k}}$.

The projective representations of a space group corresponding to ordinary representations of the double space group again are characterized by the star of a vector \mathbf{k} . The projective representation of the group $G_{\mathbf{k}}$ then is given by

$$P_{\mathbf{k}}(\{R|\mathbf{a}\}) = \exp(i\mathbf{k} \cdot \mathbf{a})\Gamma(R), \quad (1.2.3.31)$$

where the projective representation $\Gamma(K_{\mathbf{k}})$ has the factor system

$$\begin{aligned} \Gamma(R)\Gamma(S) &= \omega_s(R, S) \exp[-i(\mathbf{k} - R^{-1}\mathbf{k}) \cdot \mathbf{a}(S)]\Gamma(RS) \\ &= \omega(R, S)\Gamma(RS), \end{aligned} \quad (1.2.3.32)$$

where ω_s is the spin factor system for $K_{\mathbf{k}}$ and $\mathbf{a}(S)$ is the nonprimitive translation of the space-group element with orthogonal part S . The factor system ω can be characterized by the defining relations of $K_{\mathbf{k}}$. If these are the words

$$W_i(A_1, \dots, A_p) = E,$$

then the factor system ω is characterized by the factors λ_i in

$$W_i(\Gamma(A_1), \dots, \Gamma(A_p)) = \lambda_i E. \quad (1.2.3.33)$$

1.2. REPRESENTATIONS OF CRYSTALLOGRAPHIC GROUPS

The factors λ_i are the product of the values found from the spin factor system ω_s and those corresponding to the factor system for an ordinary representation [equation (1.2.3.26)].

1.2.4. Tensors

1.2.4.1. Transformation properties of tensors

A vector is an element of an N -dimensional vector space that transforms under an orthogonal transformation, an element of $O(n)$, as

$$x = \sum_{i=1}^n \xi_i \mathbf{a}_i \rightarrow x' = \sum_{i=1}^n \xi'_i \mathbf{a}_i = \sum_{ij} R_{ij} \xi_j \mathbf{a}_i, \quad \{R_{ij}\} \in O(n).$$

A tensor of rank r under $O(n)$ is an object with components $T_{i_1 \dots i_r}$ ($i_j = 1, 2, \dots, n$) that transforms as (see Section 1.1.3.2)

$$T_{i_1 \dots i_r} \rightarrow T'_{i_1 \dots i_r} = \sum_{j_1=1}^n \dots \sum_{j_r=1}^n R_{i_1 j_1} \dots R_{i_r j_r} T_{j_1 \dots j_r}.$$

A rank-zero tensor is a scalar, which is invariant under $O(n)$. A pseudovector (or axial vector) has components x_i and transforms according to

$$x_i \rightarrow x'_i = \text{Det}(R) \sum_j R_{ij} \xi_j$$

and analogously for pseudotensors (or axial tensors – see Section 1.1.4.5.3).

A vector field is a vector-valued function in n -dimensional space. Under an orthogonal transformation it transforms according to

$$F_i(\mathbf{r}') = \sum_{j=1}^n R_{ij} F_j(R^{-1} \mathbf{r}). \quad (1.2.4.1)$$

Under a Euclidean transformation, the function transforms according to

$$F_i(\mathbf{r}') = \sum_{j=1}^n R_{ij} F_j(R^{-1}(\mathbf{r} - \mathbf{a})), \quad \{R|\mathbf{a}\} \in E(n). \quad (1.2.4.2)$$

In a similar way, one has (pseudo)tensor functions under the orthogonal group or the Euclidean group. So it is important to specify under what group an object is a tensor, unless no confusion is possible.

The n -dimensional vectors form a vector space that carries a representation of the group $O(n)$. Moreover, it is an irreducible representation space. To stress this fact, one could speak of *irreducible tensors and vectors*. Vectors are here just rank-one tensors. The three-dimensional Euclidean vector space carries in this way an irreducible representation of $O(3)$. Such representations are characterized by an integer l and are $(2l+1)$ -dimensional. The usual three-dimensional space is therefore an irreducible $l=1$ space for $O(3)$.

Since point groups are subgroups of the orthogonal group and space groups are subgroups of the Euclidean group, tensors inherit their transformation properties from their supergroups. As we have seen in Sections 1.2.2.3 and 1.2.2.7, one can also define tensors in a quite abstract way. Irreducible tensors under a group are then elements of a vector space that carries an irreducible representation of that group. Generally, tensors are elements of a vector space that carries a tensor product representation and (anti)symmetric tensors belong to a space with an (anti)symmetrized tensor product representation.

Because the point groups one usually considers in physics are subgroups of $O(2)$ or $O(3)$, it is useful to consider the irreducible representations of these groups. They are not finite, but they are compact, and for compact groups most of the theorems for finite

groups are still valid if one replaces sums over group elements by integration over the group.

The group $O(3)$ is the direct product $SO(3) \times C_2$. Therefore, there are even and odd representations. They have the property

$$D^\pm(R) = \Delta(R), \quad D^\pm(-R) = \pm \Delta(R), \quad R \in SO(3).$$

The irreducible representations are labelled by non-negative integers ℓ and have character

$$\chi_\ell(R) = \frac{\sin(\ell + \frac{1}{2})\varphi}{\sin \frac{1}{2}\varphi} \quad (1.2.4.3)$$

if R is a rotation with rotation angle φ . From the character it follows that the dimension of the representation D_ℓ is equal to $(2\ell + 1)$.

The tensor product of two irreducible representations of $SO(3)$ is generally reducible:

$$D_\ell \otimes D_m = \bigoplus_{j=|\ell-m|}^{\ell+m} D_j \quad (1.2.4.4)$$

and the symmetrized and antisymmetrized tensor products are

$$(D_m \otimes D_m)_s = \bigoplus_{j=0}^m D_{2j}, \quad (1.2.4.5)$$

$$(D_m \otimes D_m)_a = \bigoplus_{j=1}^m D_{2j-1}. \quad (1.2.4.6)$$

If the components of the tensor $T_{i_1 \dots i_r}$ are taken with respect to an orthonormal basis, the tensor is called a *Cartesian tensor*. The orthogonal transformation R then is represented by an orthogonal matrix R_{ij} . Cartesian tensors of higher rank than one are generally no longer irreducible for the group $O(n)$. For example, the rank-two tensors in three dimensions have nine components T_{ij} . Under $SO(3)$, they transform according to the tensor product of two $\ell=1$ representations. Because

$$D_1 \otimes D_1 = D_0 \oplus D_1 \oplus D_2,$$

the space of rank 2 Cartesian tensors is the direct sum of three invariant subspaces. This corresponds to the fact that a general rank 2 tensor can be written as the sum of a diagonal tensor, an antisymmetric tensor and a symmetric tensor with trace zero. These three tensors are irreducible tensors, in this case also called *spherical tensors*, i.e. irreducible tensors for the orthogonal group.

An irreducible tensor with respect to the group $O(3)$ transforms, in general, according to some reducible representation of a point group $K \in O(3)$. If the group K is a symmetry of the physical system, the tensor should be invariant under K , i.e. it should transform according to the identity representation of K .

Consider, for example, a symmetric second-rank tensor under $O(3)$. This means that it belongs to the space that transforms according to the representation

$$D_0 \oplus D_2$$

[see (1.2.4.6)]. If the symmetry group of the system is the point group $K = 432$, the representation

$$D_0(K) \oplus D_2(K)$$

has character

| | | | | | |
|------------|---------------|---------------|-----------------------|-------------------|---------------------|
| $R:$ | ε | $\beta = C_3$ | $\alpha^2 = C_{4z}^2$ | $\alpha = C_{4z}$ | $\alpha\beta = C_2$ |
| $\chi(R):$ | 6 | 0 | 2 | 0 | 2 |

and is equivalent to the direct sum

1. TENSORIAL ASPECTS OF PHYSICAL PROPERTIES

$$\Gamma_1 \oplus \Gamma_3 \oplus \Gamma_5.$$

The multiplicity of Γ_1 is one. Therefore, the space of tensors invariant under K is one-dimensional. Consequently, there is only one parameter left to describe such a symmetric second-rank tensor invariant under the cubic group $K = 432$. Noninvariant symmetric second-rank tensors are sums of tensors which transform according to the Γ_3 and Γ_5 representations. Here we are especially interested in invariant tensors.

1.2.4.2. Invariants

The dimension of the space of tensors of a certain type which are invariant under a point group K is equal to the number of free parameters in such a tensor. This number can be found as the multiplicity of the identity representation in the tensor space. For the 32 three-dimensional point groups this number is given in Table 1.2.6.9 for general second-rank tensors, symmetric second-rank tensors and a number of higher-rank tensors.

Invariant tensors, *i.e.* tensors of a certain type left invariant by a given group, may be constructed in several ways. The first way is a direct calculation. Take as an example again a second-rank symmetric tensor invariant under the cubic group 432. This means that

$$Rf = f \quad \forall R \in K,$$

which is a concise notation for

$$(Rf)_{ij} = \sum_{kl} R_{ik} R_{jl} f_{kl} = f_{ij}.$$

The group has two generators. Because each element of K is the product of generators, a tensor is left invariant under a group if it is left invariant by the generators. Therefore, one has in this case for

$$f = \begin{pmatrix} a_1 & a_2 & a_3 \\ a_2 & a_4 & a_5 \\ a_3 & a_5 & a_6 \end{pmatrix}$$

the equation

$$\begin{pmatrix} 0 & -1 & 0 \\ 1 & 0 & 0 \\ 0 & 0 & 1 \end{pmatrix} f \begin{pmatrix} 0 & 1 & 0 \\ -1 & 0 & 0 \\ 0 & 0 & 1 \end{pmatrix} = \begin{pmatrix} 0 & 1 & 0 \\ 0 & 0 & 1 \\ 1 & 0 & 0 \end{pmatrix} f \begin{pmatrix} 0 & 0 & 1 \\ 1 & 0 & 0 \\ 0 & 1 & 0 \end{pmatrix} = f.$$

These equations form a system of 12 linear algebraic equations for the coefficients of f with the solution

$$a_1 = a_4 = a_6; \quad a_2 = a_3 = a_5 = 0.$$

Up to a factor there is only one such tensor:

$$f = \begin{pmatrix} a & 0 & 0 \\ 0 & a & 0 \\ 0 & 0 & a \end{pmatrix},$$

in agreement with the finding that the space of invariant second-rank symmetric tensors is one-dimensional. An overview of these relations for the 32 point groups can be found in Section 1.1.4 in this volume.

This method can always be used for groups with a finite number of generators. Another method for determining invariant tensors is using projection operators.

If a group, for example a point group, acts in some linear vector space, for example the space of tensors of a certain type, this space carries a representation. Then it is possible to construct a

basis such that the representation corresponds to a choice of matrix representation. In particular, if the representation is reducible, it is possible to construct a basis such that the matrix representation is in reduced form. This can be achieved with *projection operators*.

Suppose the element $R \in K$ acts in a space as an operator $D(R)$ such that the representation $D(K)$ is equivalent with a matrix representation $\Gamma(K)$ which has irreducible components $\Gamma_\alpha(K)$. Then choose a vector v in the representation space and construct the d_α vectors

$$v_i = (1/N) \sum_{R \in K} \Gamma_\alpha(R)_{ji}^* D(R) v \quad (1.2.4.7)$$

with j fixed. If v does not have a component in the invariant space of the irreducible representation D_α , these vectors are all zero, but for a sufficiently general vector the d_α vectors form a basis for the irreducible representation. This property follows from the orthogonality relations.

Using this relation one can write for an invariant symmetric second-rank tensor

$$f = (1/N) \sum_{R \in K} D(R) f' = (1/N) \sum_{R \in K} \Gamma(R) f' \Gamma(R)^T$$

for an arbitrary symmetric second-rank tensor f' . For the group $K = 432$ this would give a tensor with components $f_{ij} = a\delta_{ij}$. Of course, this is a rather impractical method if the order of the group is large. A simple example for a very small group is the construction of the symmetrical and antisymmetrical components of a function: $f_\pm(x) = [f(x) \pm f(-x)]/2$.

1.2.4.3. Clebsch–Gordan coefficients

The tensor product of two irreducible representations of a group K is, in general, reducible. If \mathbf{a}_i is a basis for the irreducible representation Γ_α ($i = 1, \dots, d_\alpha$) and \mathbf{b}_j one for Γ_β ($j = 1, \dots, d_\beta$), a basis for the tensor product space is given by

$$\mathbf{e}_{ij} = \mathbf{a}_i \otimes \mathbf{b}_j.$$

On this basis, the matrix representation is, in general, not in reduced form, even if the product representation is reducible. Suppose that

$$\Gamma_\alpha \otimes \Gamma_\beta \sim \sum_\gamma \oplus m_\gamma \Gamma_\gamma.$$

This means that there is a basis

$$\psi_{\gamma\ell k} \quad (\ell = 1, \dots, m_\gamma; k = 1, \dots, d_\gamma),$$

on which the representation is in reduced form. The multiplicity m_γ gives the number of times the irreducible component Γ_γ occurs in the tensor product. The basis transformation is given by

$$\psi_{\gamma\ell k} = \sum_{ij} \begin{pmatrix} \alpha & \beta & \gamma \\ i & j & k \end{pmatrix} \begin{matrix} \ell \\ \ell \end{matrix} \mathbf{a}_i \otimes \mathbf{b}_j. \quad (1.2.4.8)$$

The basis transformation is unitary if one starts with orthonormal bases and has coefficients

$$\begin{pmatrix} \alpha & \beta & \gamma \\ i & j & k \end{pmatrix} \begin{matrix} \ell \\ \ell \end{matrix} \quad (1.2.4.9)$$

called *Clebsch–Gordan coefficients*. For the group $O(3)$ they are the original Clebsch–Gordan coefficients; for bases $|\ell m\rangle$ and $|\ell' m'\rangle$ of the $(2\ell + 1)$ - and $(2\ell' + 1)$ -dimensional representations D_ℓ and $D_{\ell'}$, respectively, of $O(3)$ one has

1.2. REPRESENTATIONS OF CRYSTALLOGRAPHIC GROUPS

$$|JM\rangle = \sum_{mm'} \begin{pmatrix} \ell & \ell' & J \\ m & m' & M \end{pmatrix} |\ell m\rangle \otimes |\ell' m'\rangle, \quad (1.2.4.10)$$

$$(J = |\ell - \ell'|, \dots, \ell + \ell').$$

The multiplicity here is always zero or unity, which is the reason why one leaves out the number ℓ in the notation.

If the multiplicity m_γ is unity, the coefficients for given α, β, γ are unique up to a common factor for all i, j, k . This is no longer the case if the multiplicity is larger, because then one can make linear combinations of the basis vectors belonging to Γ_γ . Anyway, one has to follow certain conventions. In the case of $O(3)$, for example, there are the Condon–Shortley phase conventions. The degree of freedom of the Clebsch–Gordan coefficients for given matrix representations Γ_α can be seen as follows. Suppose that there are two basis transformations, S and S' , in the tensor product space which give the same reduced form:

$$S(D_\alpha \otimes D_\beta)S^{-1} = S'(D_\alpha \otimes D_\beta)S'^{-1} = D = \bigoplus m_\gamma D_\gamma. \quad (1.2.4.11)$$

Then the matrix $S'S^{-1}$ commutes with every matrix $D(R)$ ($R \in K$). If all multiplicities are zero or unity, it follows from Schur's lemma that $S'S^{-1}$ is the direct sum of unit matrices of dimension d_γ . If the multiplicities are larger, the matrix $S'S^{-1}$ is a direct sum of blocks which are of the form

$$\begin{pmatrix} \lambda_{11}E & \lambda_{12}E & \dots & \lambda_{1m_\gamma}E \\ \lambda_{21}E & \lambda_{22}E & \dots & \lambda_{2m_\gamma}E \\ \vdots & \vdots & \ddots & \vdots \\ \lambda_{m_\gamma 1}E & \dots & \dots & \lambda_{m_\gamma m_\gamma}E \end{pmatrix},$$

such that $\text{Det}(\lambda_{ij}) = 1$, and the E 's are d_γ -dimensional unit matrices. This means that for multiplicity-free ($m_\gamma \leq 1$) cases, the Clebsch–Gordan coefficients are unique up to a common factor for all coefficients involving one value of γ .

The Clebsch–Gordan coefficients satisfy the following rules:

$$\begin{pmatrix} \alpha & \beta & \gamma \\ i & j & k \end{pmatrix} \begin{pmatrix} \beta & \alpha & \gamma \\ j & i & k \end{pmatrix} = \begin{pmatrix} \alpha & \beta & \gamma \\ i & j & k \end{pmatrix} \begin{pmatrix} \beta & \alpha & \gamma \\ j & i & k \end{pmatrix}$$

$$\begin{pmatrix} \alpha & \beta & \gamma \\ i & j & k \end{pmatrix} = 0, \text{ if } D_\alpha \otimes D_\beta \text{ does not contain } D_\gamma$$

$$\sum_{k\ell} \begin{pmatrix} \alpha & \beta & \gamma \\ i & j & k \end{pmatrix}^* \begin{pmatrix} \alpha & \beta & \gamma \\ i' & j' & k \end{pmatrix} = \delta_{ii'} \delta_{jj'}$$

$$\sum_{ij} \begin{pmatrix} \alpha & \beta & \gamma \\ i & j & k \end{pmatrix}^* \begin{pmatrix} \alpha & \beta & \gamma \\ i & j & k' \end{pmatrix} = \delta_{kk'} \delta_{\ell\ell'}.$$

For the basis vectors of the invariant space belonging to the identity representation Γ_1 , one has $\gamma = d_\gamma = 1$. Consequently,

$$\psi_\ell = \sum_{ij} \begin{pmatrix} \alpha & \beta & 1 \\ i & j & 1 \end{pmatrix} \mathbf{a}_i \otimes \mathbf{b}_j.$$

1.2.5. Magnetic symmetry

1.2.5.1. Magnetic point groups

Until now, the symmetry transformations we have considered affect only spatial variables. In physics, however, time coordinates are also often essential, and time reversal is a very important transformation as well.

The time-reversal operation generates a group of order 2 with as elements the unit operator E and the time-reversal operator T . This transformation commutes with transformations of spatial

variables. One can consider the combined operation of T and a Euclidean transformation. In other words, we consider the direct product of the Euclidean group $E(d)$ and the time-reversal group of order 2. Elements of this direct product that belong to $E(d)$ are called *orthochronous*, whereas the elements of the coset which are combinations of a Euclidean transformation with T are called *antichronous*. We shall start by considering combinations of T and orthogonal transformations in the physical d -dimensional space. Such combinations generate a subgroup of the direct product of $O(d)$ and the time-reversal group.

There are three types of such groups. First, one can have a group that is already a subgroup of $O(d)$. This group does not have time-reversing elements. A second type of group contains the operator T and is, therefore, the direct product of a subgroup of $O(d)$ with the time-reversal group. The third type of group contains antichronous elements but not T itself. This means that the group contains a subgroup of index 2 that belongs to $O(d)$ and one coset of this subgroup, all elements of which can be obtained from those of the subgroup by multiplication with one fixed time-reversing element which is not T . If one then multiplies all elements of the coset by T , one obtains a group that belongs to $O(d)$ and is isomorphic to the original group. This is the same situation as for subgroups of $O(3)$, which is the direct product of $SO(3)$ with space inversion I . Here also all subgroups of $O(d) \times \mathbb{Z}_2$ are isomorphic to point groups or to the direct product of a point group and \mathbb{Z}_2 . Magnetic groups can be used to characterize spin arrangements. Because spin inverses sign under time reversal, a spin arrangement is never invariant under T . Therefore, the point groups of the second type are also called *nonmagnetic point groups*. Because time reversal does not play a role in groups of the first type, these are called *trivial magnetic point groups*, whereas the groups of the third type are called *nontrivial magnetic point groups*.

Magnetic point groups are discussed in Chapter 1.5. Orthochronous magnetic point groups (trivial magnetic groups) are denoted by their symbol as a normal point group. Magnetic point groups containing T are denoted by the symbol for the orthochronous subgroup, which is a trivial magnetic group, to which the symbol $1'$ is added. Magnetic point groups that are neither trivial nor contain T are isomorphic to a trivial magnetic point group. They are denoted by the symbol of the latter in which all symbols for antichronous elements are marked with a prime ($'$). For example, $\bar{1}$ is the trivial magnetic group generated by I , $\bar{1}1'$ is the group of four elements generated by I and T , and $\bar{1}'$ is the magnetic group of order 2 generated by the product IT .

Two magnetic point groups are called equivalent if they are conjugated in $O(d) \times \mathbb{Z}_2$ by an element in $O(d)$. This means that under the conjugation antichronous elements go to antichronous elements. The equivalence classes of magnetic point groups are the magnetic crystal classes. There are 32 classes of trivial crystallographic magnetic point groups, 32 classes of direct products with the time-reversal group and 58 classes of nontrivial magnetic crystallographic point groups. They are given in Table 1.2.6.12.

1.2.5.2. Magnetic space groups

Magnetic space groups are subgroups of the direct product of the Euclidean group $E(d)$ with the time-reversal group (this direct product is sometimes called the *Shubnikov group*) such that the orthochronous elements together with the products of the antichronous elements and T form a space group in d dimensions. As in the case of magnetic point groups, one can distinguish trivial magnetic groups, which are subgroups of $E(d)$, direct products of a trivial group with the time-reversal group (nonmagnetic) and nontrivial magnetic space groups with antichronous elements but without T . The groups of the third type can be transformed into groups of the first type by multiplication of all antichronous elements by T .

1. TENSORIAL ASPECTS OF PHYSICAL PROPERTIES

The translation subgroup U of a magnetic space group G is the intersection of G and $T(d) \times \{E, T\}$. The factor group G/U is (isomorphic to) a subgroup of $O(d) \times \{E, T\}$. For trivial magnetic space groups, the point group is a subgroup of $O(d)$. For direct products with $\{E, T\}$, the translation group is the direct product of an orthochronous lattice with $\{E, T\}$ and the point group is a subgroup of $O(d)$. Magnetic space groups with antichronous elements but without T have either a translation subgroup consisting of orthochronous elements or one with antichronous elements as well. In the first case, the point group is a subgroup of $O(d) \times \{E, T\}$ and contains antichronous elements; in the second case, one may always choose orthochronous elements for the coset representatives with respect to the translation group, and the point group is a subgroup of $O(d)$. Therefore, nontrivial magnetic space groups without T have either the same lattice or the same point group as the space group of orthochronous elements.

Two magnetic space groups are equivalent if they are affine conjugated *via* a transformation with positive determinant that maps antichronous elements on antichronous elements. Then there are 1656 equivalence classes: 230 classes of trivial groups with only orthochronous elements, 230 classes of direct products with $\{E, T\}$ and 1191 classes with nontrivial magnetic groups.

1.2.5.3. Transformation of tensors

Vectors and tensors transforming in the same way under Euclidean transformations may behave differently when time reversal is taken into account. As an example, both the electric field \mathbf{E} and magnetic field \mathbf{B} transform under a rotation as a position vector. Under time reversal, the former is invariant, but the latter changes sign. Therefore, the magnetic field is called a pseudovector field under time reversal. Under spatial inversion, the field \mathbf{E} changes sign, as does a position vector, but the field \mathbf{B} does not. Therefore, the magnetic field is also a pseudovector under central inversion. The electric polarization induced by an electric field is given by the electric susceptibility, a magnetic moment induced by a magnetic field is given by the magnetic susceptibility and in some crystals a magnetic moment is induced by an electric field *via* the magneto-electric susceptibility. Under the four elements of the group generated by $T = 1'$ and $I = \bar{1}$, the fields and susceptibility tensors transform according to

| | E | $\bar{1}$ | $1'$ | $\bar{1}'$ |
|--------------|-----|-----------|------|------------|
| \mathbf{E} | 1 | -1 | 1 | -1 |
| \mathbf{B} | 1 | 1 | -1 | -1 |
| χ_{ee} | 1 | 1 | 1 | 1 |
| χ_{mm} | 1 | 1 | 1 | 1 |
| χ_{me} | 1 | -1 | -1 | 1 |

Here $\bar{1}' = \bar{1}1'$.

In general, a vector transforms as the position vector \mathbf{r} under rotations and changes sign under $\bar{1}$, but not under $1'$. A pseudovector under $\bar{1}$ or (respectively and) $1'$ gets an additional minus sign. The generalization to tensors is straightforward.

$$gT_{i_1 \dots i_n} = \varepsilon_P \varepsilon_T \sum_{j_1 \dots j_n} \left(\prod_{k=1}^n R_{ikj_k} \right) T_{j_1 \dots j_n}, \quad (1.2.5.1)$$

where ε_P and ε_T are ± 1 , depending on the pseudotensor character with respect to space and time reversal, respectively.

Under a rotation $[R \in SO(d)]$, a vector transforms according to a representation characterized by the character $\chi(R)$ of the representation. In two dimensions $\chi = 2 \cos \varphi$ and in three dimensions $\chi = 1 + 2 \cos \varphi$, if φ is the rotation angle. Under IR the character gets an additional minus sign, under RT it is the same, and under RIT there is again an additional minus sign. For pseudovectors, either under I or T or both, there are the extra factors ε_P , ε_T and $\varepsilon_P \varepsilon_T$, respectively. As an example, the character

Table 1.2.5.1. Character of the representations corresponding to the electric and magnetic fields in point groups 222, 2'2'2 and 2'mm'

n_i is the number of invariants.

| Point group | \mathbf{E} | | | | n_i | \mathbf{B} | | | | n_i |
|-------------|--------------|----|----|----|-------|--------------|----|----|----|-------|
| 222 | 3 | -1 | -1 | -1 | 0 | 3 | -1 | -1 | -1 | 0 |
| 2'2'2 | 3 | -1 | -1 | -1 | 0 | 3 | 1 | 1 | -1 | 1 |
| 2'mm' | 3 | -1 | 1 | 1 | 1 | 3 | 1 | -1 | 1 | 1 |

of the representations corresponding to the electric and magnetic fields in two orthorhombic point groups (222, 2'2'2 and 2'mm') are given in Table 1.2.5.1.

The number of invariant components is the multiplicity of the trivial representation in the representation to which the tensor belongs. The nonzero invariant field components are B_z for 2'2'2, E_x and B_y for 2'mm'. These components can be constructed by means of projection-operator techniques, or more simply by solving the linear equations representing the invariance of the tensor under the generators of the point group. For example, the magnetic field vector \mathbf{B} transforms to $(-B_x, B_y, -B_z)$ under m_y and to $(B_x, B_y, -B_z)$ under m_z , and this gives the result that all components are zero except B_y .

1.2.5.4. Time-reversal operators

In quantum mechanics, symmetry transformations act on state vectors as unitary or anti-unitary operators. For the Schrödinger equation for one particle without spin,

$$\hbar i \frac{\partial}{\partial t} \Psi(\mathbf{r}, t) = H \Psi(\mathbf{r}, t), \quad (1.2.5.2)$$

the operator that reverses time is the complex conjugation operator θ with

$$\theta \Psi(\mathbf{r}, t) = \Psi^*(\mathbf{r}, t) \quad (1.2.5.3)$$

satisfying

$$\hbar i \frac{\partial}{\partial t} \Psi^*(\mathbf{r}, -t) = H \Psi^*(\mathbf{r}, -t),$$

which is the time-reversed equation.

This operator is *anti-linear* $[\theta(\alpha\Psi + \beta\Phi) = \alpha^*\theta\Psi + \beta^*\theta\Phi]$ and has the following commutation relations with the operators \mathbf{r} and \mathbf{p} for position and momentum:

$$\theta \mathbf{r} \theta^{-1} = \mathbf{r}, \quad \theta \mathbf{p} \theta^{-1} = -\mathbf{p}. \quad (1.2.5.4)$$

For a Euclidean transformation $g = \{R|\mathbf{a}\}$, the operation on the state vector is given by the unitary operator

$$T_g \Psi(\mathbf{r}) = \Psi(g^{-1}\mathbf{r}) = \Psi(R^{-1}(\mathbf{r} - \mathbf{a})). \quad (1.2.5.5)$$

The two operators θ and T_g commute. Therefore, if g is an orthochronous element of the symmetry group, the corresponding operator is T_g , and if gT is an antichronous element the operator is θT_g . The operator θT_g is also *anti-unitary*: it is anti-linear and conserves the absolute value of the Hermitian scalar product: $|\langle \theta T_g \Psi | \theta T_g \Phi \rangle| = |\langle \Psi | \Phi \rangle|$.

If the particle has a spin, the time-reversal operator has to have the commutation relation

$$\theta \mathbf{S} \theta^{-1} = -\mathbf{S} \quad (1.2.5.6)$$

with the spin operator \mathbf{S} . For a spin- $\frac{1}{2}$ particle, the spin operators are $S_i = \hbar \sigma_i / 2$ in terms of the Pauli matrices. Then the time-reversal operator is

$$T_T = \sigma_2 \theta. \quad (1.2.5.7)$$

1.2. REPRESENTATIONS OF CRYSTALLOGRAPHIC GROUPS

The operators corresponding to the elements of a magnetic symmetry group are generally (anti-)unitary operators on the state vectors. These operators form a representation of the magnetic symmetry group.

$$T_g T_{g'} = T_{gg'}. \quad (1.2.5.8)$$

In principle, they even form a projective representation, but as discussed before for particles without spin the factor system is trivial, and for particles with spin one can take as the symmetry group the double group of the symmetry group.

1.2.5.5. Co-representations

Suppose the magnetic point group G has an orthochronous subgroup H and an antichronous coset $H' = aH$ for some antichronous element a . The elements of H are represented by unitary operators, those of H' by anti-unitary operators. These operators correspond to matrices in the following way. Suppose Φ_j are the elements of a basis of the state vector space. Then

$$T_g \Phi_j = \sum_k M(g)_{kj} \Phi_k, \quad g \in G. \quad (1.2.5.9)$$

The matrices M do not form a matrix representation in the usual sense. They satisfy the relations

$$\begin{aligned} M(g_1 g_2) &= M(g_1) M(g_2) \quad g_1 \in H \\ &= M(g_1) M^*(g_2) \quad g_1 \in H', \end{aligned} \quad (1.2.5.10)$$

as one verifies easily. Matrices satisfying these relations are called *co-representations* of the group G .

A co-representation is irreducible if there is no proper invariant subspace. If a co-representation is reducible, there is a basis transformation S that brings the matrices into a block form. For co-representations, a basis transformation S with

$$S \Phi_i = \sum_{j=1}^m S_{ji} \Phi_j \quad (1.2.5.11)$$

transforms the matrices according to

$$M(h) \rightarrow S^{-1} M(h) S, \quad M(ah) \rightarrow S^{-1} M(ah) S^*, \quad (h \in H). \quad (1.2.5.12)$$

Here a is the coset representative of the antichronous elements. The co-representation restricted to the orthochronous subgroup H gives an ordinary representation of H which is not necessarily irreducible even if the co-representation is irreducible. Suppose that $\Phi_1 \dots \Phi_m$ form a basis for the irreducible co-representation of G and that the restriction to H is also irreducible. The elements $T_a \Phi_1, \dots, T_a \Phi_m$ form another basis for the space, and on this basis the representation matrices of H follow from

$$T_h T_a \Phi_i = T_a T_{a^{-1}ha} \Phi_i = \sum_{j=1}^m M(a^{-1}ha)_{ji}^* T_a \Phi_j. \quad (1.2.5.13)$$

Because both bases are bases for the same irreducible space, it means that the (ordinary) representations $M(H)$ and $M(a^{-1}Ha)^*$ are equivalent.

If the representation $M(H)$ is reducible, there is a basis $\varphi_1, \dots, \varphi_d$ for the irreducible representation $D(H)$. A basis for the whole space then is given by

$$\varphi_1, \dots, \varphi_d, T_a \varphi_1, \dots, T_a \varphi_d,$$

because the co-representation of G would be reducible if the last d vectors were dependent on the first d . On this basis, the matrices for the co-representation become

$$\begin{aligned} M(h) &= \begin{pmatrix} D(h) & 0 \\ 0 & D(a^{-1}ha)^* \end{pmatrix}, \\ M(ah) &= \begin{pmatrix} 0 & D(aha) \\ D(h)^* & 0 \end{pmatrix}, \quad h \in H, a \in H' \end{aligned} \quad (1.2.5.14)$$

because

$$\begin{aligned} T_a h \varphi_i &= T_a \sum_j D(h)_{ji} \varphi_j = \sum_j D(h)_{ji}^* T_a \varphi_j \\ T_a h T_a \varphi_i &= T_a h a \varphi_i = \sum_j D(aha)_{ji} \varphi_j. \end{aligned}$$

The two irreducible components for $M(H)$ can be either equivalent or non-equivalent. If they are not equivalent the co-representation is indeed irreducible, because a basis transformation S that leaves the matrices $M(h)$ the same is necessarily of the form $\lambda E \oplus \mu E$ because of Schur's lemma, and such a matrix cannot bring the matrices $D(ah)$ into a reduced form. In this case, the co-representation $M(G)$ is irreducible, in agreement with the starting assumption, and the dimension m is twice the dimension of the representation $D(H)$: $m = 2d$.

If the two irreducible components $D(H)$ and $D(a^{-1}Ha)^*$ are equivalent, there is a basis transformation U such that

$$D(a^{-1}ha)^* = U^{-1} D(h) U \quad \forall h \in H.$$

The basis transformation

$$T = \begin{pmatrix} 1 & 0 \\ 0 & U^{-1} \end{pmatrix}$$

then gives a new matrix co-representation for G :

$$\begin{aligned} M(h) &\rightarrow T^{-1} M(h) T = \begin{pmatrix} D(h) & 0 \\ 0 & D(h) \end{pmatrix}, \\ M(ah) &\rightarrow T^{-1} M(ah) T^* = \begin{pmatrix} 0 & D(aha) U^{*-1} \\ U D(h)^* & 0 \end{pmatrix}. \end{aligned}$$

The most general basis transformation S that leaves $M(h)$ in the same form is then

$$S = \begin{pmatrix} \lambda E & \mu E \\ \rho E & \sigma E \end{pmatrix}. \quad (1.2.5.15)$$

Under this basis transformation, the matrices $M(ah)$ become

$$S^{-1} M(ah) S^* = \frac{1}{(\lambda\sigma - \mu\rho)} \mathcal{M}$$

with

$$\begin{aligned} \mathcal{M}_{11} &= -\lambda^* \mu U D(h)^* + \rho^* \sigma D(aha) U^{*-1} \\ \mathcal{M}_{12} &= |\sigma|^2 D(aha) U^{*-1} - |\mu|^2 U D(h)^* \\ \mathcal{M}_{21} &= |\lambda|^2 U D(h)^* - |\rho|^2 D(aha) U^{*-1} \\ \mathcal{M}_{22} &= \lambda \mu^* U D(h)^* - \rho \sigma^* D(aha) U^{*-1}. \end{aligned}$$

This is block diagonal if

$$|\mu|^2 U U^* D(a^{-1}ha) U^{*-1} U^* = |\sigma|^2 D(aha)$$

and analogous expressions for $|\lambda|^2$ and $|\rho|^2$ also hold.

The transformation matrix U satisfies $U U^* = \pm D(a^2)$, as one can show as follows. From the definition

$$D(a^{-1}ha)^* = U^{-1} D(h) U$$

follow the two relations

1. TENSORIAL ASPECTS OF PHYSICAL PROPERTIES

$$D(a^{-2}ha^2) = U^{*-1}U^{-1}D(h)UU^*$$

$$D(a^{-2}ha^2) = D(a^2)^{-1}D(h)D(a^2).$$

(Notice that $a^2 \in H$.) Because $D(H)$ is irreducible, it follows that $UU^*D(a^{-2})$ is a multiple of the identity: $UU^* = \chi D(a^2)$. The factor χ is real because

$$D(a^2)^* = U^{-1}D(a^2)U = U^{-1}UU^*U/\chi$$

and

$$D(a^2)^* = U^*U/\chi^*.$$

Hence $\chi = \chi^* = \pm 1$.

The conditions for the transformed matrix $M(ah)$ to be block diagonal then read

$$\pm|\mu|^2 D(a^2)D(a^{-1}ha) = |\sigma|^2 D(aha), \quad (1.2.5.16)$$

with the corresponding expressions for λ and ρ . If χ is equal to -1 , these equations do not have a solution. However, when $\chi = +1$ there is a solution, which means that the co-representation is reducible, contrary to the assumption. Therefore, this situation can not occur.

One can summarize these considerations in the following theorem.

Theorem 1. If the restriction of an irreducible co-representation to the orthochronous subgroup is reducible, then either the (two) irreducible components are non-equivalent, or they are equivalent and connected by a basis transformation U for which $UU^* = -D(a^2)$. If the restriction $M(H)$ is irreducible, it is equivalent to $M(a^{-1}Ha)^*$.

In the former case, the dimension of the co-representation is twice that of the restriction, in the latter case they are equal. Therefore, one has the following corollary.

Corollary. A d -dimensional irreducible representation of the orthochronous subgroup H can occur as irreducible component of the restriction of an irreducible co-representation of G with dimension m with

$$m = 2d \text{ if } D(H) \text{ nonequivalent to } D(a^{-1}Ha)^*$$

$$m = 2d \text{ if } D(H) \text{ equivalent to } D(a^{-1}Ha)^* \text{ and } UU^* = -D(a^2)$$

$$m = d \text{ if } D(H) \text{ equivalent to } D(a^{-1}Ha)^* \text{ and } UU^* = +D(a^2).$$

The three cases from theorem (1) can be distinguished by the following theorem:

Theorem 2. The irreducible representation $D(H)$ with character $\chi(H)$ belongs to the respective cases of theorem (1) if

$$\sum_{h \in H} \chi(ahah) = \begin{cases} 0 & \text{for the first case} \\ -N & \text{for the second case} \\ N & \text{for the third case.} \end{cases} \quad (1.2.5.17)$$

The proof of theorem (2) goes as follows. We have

$$\begin{aligned} \sum_{h \in H} \chi(ahah) &= \sum_{h \in H} \sum_{i=1}^d D(ahah)_{ii} \\ &= \sum_{i,k,l} D(a^2)_{ik} \sum_{h \in H} D(a^{-1}ha)_{kl} D(h)_{li}, \end{aligned} \quad (1.2.5.18)$$

and this gives zero if $D(H)$ and $D(a^{-1}Ha)^*$ are non-equivalent, because of the orthogonality relations. If the two representations are equivalent, we take for convenience unitary representations. Then there is a unitary matrix U with

$$D(a^{-1}ha)^* = U^{-1}D(h)U.$$

Then we have

$$\begin{aligned} \sum_{h \in H} \chi(ahah) &= \sum_{ikl} D(a^2)_{ik} (U^{*-1})_{km} \sum_{h \in H} D(h)_{mn}^* U_{nl} D(h)_{li} \\ &= (N/d) \sum_{i,k,\ell} D(a^2)_{ik} (U^{*-1})_{k\ell} U_{i\ell}^* \\ &= (N/d) \sum_{i,k} D(a^2)_{ik} (U^*U)_{ik} \\ &= \pm(N/d) \sum_{i,k} D(a^2)_{ik} D(a^{-2})_{ki} = \pm N. \end{aligned}$$

This proves theorem (2).

In the special case of a group G in which the time reversal $1'$ occurs as element, one may choose $a = 1'$. In this case, a^2 is the identity and the expressions simplify. Theorem (1) now states that an irreducible d -dimensional representation $D(H)$ of an orthochronous group can occur as irreducible component in the restriction of an irreducible m -dimensional co-representation of $H \times \{E, 1'\}$, with

$$m = 2d \text{ if } D(H) \text{ nonequivalent to } D(H)^*$$

$$m = 2d \text{ if } D(H) = UD(H)^*U^{-1} \text{ and } UU^* = -E$$

$$m = d \text{ if } D(H) = UD(H)^*U^{-1} \text{ and } UU^* = +E,$$

which correspond to, respectively, [cf. theorem (2)]

$$\sum_{h \in H} \chi(h^2) = \begin{cases} 0 \\ -N \\ +N \end{cases} \quad (1.2.5.19)$$

For a spinless particle, the time-reversal operator is the complex conjugation θ . This generates a co-representation of the group \mathbb{Z}_2 . The symmetry group is the direct product of the point group H and \mathbb{Z}_2 . Compared to the degeneracy d of a state characterized by the irreducible representation $D(H)$, the degeneracy is double ($m = 2d$) for the first two cases and the same for the third case. When it is a particle with spin $\frac{1}{2}$, the time-reversal operator is $\sigma_2\theta$, which is of order 4. If one takes for the coset representative a the time reversal, one has $D(a^2) = -E$. Therefore, the degeneracy is now doubled in the first and third case, and the same for the second. This is Kramer's degeneracy.

1.2.6. Tables

In the following, a short description of the tables is given in order to facilitate consultation without reading the introductory theoretical Sections 1.2.2 to 1.2.5.

Table 1.2.6.1. Finite point groups in three dimensions. The point groups are grouped by isomorphism class. There are four infinite families and six other isomorphism classes. (Notation: C_n for the cyclic group of order n , D_n for the dihedral group of order $2n$, T , O and I the tetrahedral, octahedral and icosahedral groups, respectively). Point groups of the first class are subgroups of $SO(3)$, those of the second class contain $-E$, and those of the third class are not subgroups of $SO(3)$, but do not contain $-E$ either. The families C_n and D_n are also isomorphism classes of two-dimensional finite point groups.

Table 1.2.6.2. Among the infinite number of finite three-dimensional point groups, 32 are crystallographic.

Table 1.2.6.3. Character table for the cyclic groups C_n . The generator is denoted by α . The number of elements in the conjugacy classes (n_i) is one for each class. The order is the smallest nonnegative power p for which $A^p = E$. The n irreducible representations are denoted by Γ_i .

Table 1.2.6.4. Character tables for the dihedral groups D_n of order $2n$. n_i is the number of elements in the conjugacy class C_i . The irreducible representations are denoted by Γ_i .

1.2. REPRESENTATIONS OF CRYSTALLOGRAPHIC GROUPS

Table 1.2.6.1. Finite point groups in three dimensions

| Isomorphism class | First class with determinants > 0 | Second class with $-E$ | Third class without $-E$ | Order |
|-------------------|--|--|---|-------|
| C_n | n | | \bar{n} (n even, > 2) m ($n = 2$) | n |
| D_n | $n22$ (n even) $n2$ (n odd, > 1) | | mmm (n even) $\bar{n}2m$ (n even) nm (n odd) | $2n$ |
| $C_n \times C_2$ | | \bar{n} (n odd) n/m (n even) | | $2n$ |
| $D_n \times C_2$ | | n/mmm (n even, ≥ 4) mmm ($n = 2$) $\bar{n}m$ (n odd, > 0) | | $4n$ |
| T | 23 | | | 12 |
| O | 432 | | $\bar{4}3m$ | 24 |
| I | 532 | | | 60 |
| $T \times C_2$ | | $m\bar{3}$ | | 24 |
| $O \times C_2$ | | $m\bar{3}m$ | | 48 |
| $I \times C_2$ | | $\bar{5}3m$ | | 120 |

Table 1.2.6.5. The character tables for the 32 three-dimensional crystallographic point groups. The groups are grouped by isomorphism class (there are 18 isomorphism classes).

For each isomorphism class, the character table is given, including the symbol for the isomorphism class, the number n of elements per conjugacy class and the order of the elements in each such class. The conjugation classes are specified by representative elements expressed in terms of the generators α, β, \dots . The irreps are denoted by Γ_i , where i takes as many values as there are conjugation classes. In each isomorphism class for each point group, given by its international symbol and its Schoenflies symbol, identification is made between the generators of the abstract group (α, β) and the generating orthogonal transformations. Notation: C_{nx} is a rotation of $2\pi/n$ along the x axis, σ_x is a reflection from a plane perpendicular to the x axis, S_{nz} is a rotation over $2\pi/n$ along the z axis multiplied by $-E$ and σ_v is a reflection from a plane through the unique axis.

The notation for the irreducible representations can be given as Γ_i , but other systems have been used as well. Indicated below are the relations between Γ_i and a system that uses a characterization according to the dimension of the representation and (for

groups of the second kind) the sign of the representative of $-E$. This nomenclature is often used by spectroscopists.

| | |
|------------------------|-------------------|
| A, A_1, A_2, A', A'' | one-dimensional |
| B, B_1, B_2, B_3 | one-dimensional |
| E | two-dimensional |
| T, T_1, T_2 | three-dimensional |
| A_g, B_g etc. | gerade |
| A_u, B_u etc. | ungerade |

The other notation for which the relation with the present notation is indicated is that of Kopský, and is used on the accompanying CD-ROM.

The three functions x, y and z transform according to the vector representation of the point group, which is generally reducible. The reduction into irreducible components of this three-dimensional vector representation is indicated.

The six bilinear functions $x^2, xy, xz, y^2, yz, z^2$ transform according to the symmetrized product of the vector representation. The basis functions of the irreducible components are indicated. Because the basis functions are real, one should consider the physically irreducible representations.

Table 1.2.6.6. The point groups of the second class containing $-E$ are obtained from those of the first class by taking the direct product with the group generated by $\bar{1}$. From the point groups, one obtains nonmagnetic point groups by the direct product with the group generated by the time reversal $1'$. The relation between the characters of a point group and its direct products with

Table 1.2.6.2. Crystallographic point groups in three dimensions

| Isomorphism class | First class | Second class with $-E$ | Third class without $-E$ | Order |
|-------------------|-------------|------------------------|--------------------------|-------|
| C_1 | 1 | | | 1 |
| C_2 | 2 | $\bar{1}$ | m | 2 |
| C_3 | 3 | | | 3 |
| C_4 | 4 | | 4 | 4 |
| D_2 | 222 | $2/m$ | $2mm$ | 4 |
| C_6 | 6 | $\bar{3}$ | $\bar{6}$ | 6 |
| D_3 | 32 | | $3m$ | 6 |
| $C_4 \times C_2$ | | $4/m$ | | 8 |
| D_4 | 422 | | $4mm, \bar{4}2m$ | 8 |
| $D_2 \times C_2$ | | mmm | | 8 |
| D_6 | 622 | $\bar{3}m$ | $6mm, \bar{6}2m$ | 12 |
| T | 23 | | | 12 |
| $C_6 \times C_2$ | | $6/m$ | | 12 |
| $D_4 \times C_2$ | | $4/mmm$ | | 16 |
| O | 432 | | $\bar{4}3m$ | 24 |
| $D_6 \times C_2$ | | $6/mmm$ | | 24 |
| $T \times C_2$ | | $m\bar{3}$ | | 24 |
| $O \times C_2$ | | $m\bar{3}m$ | | 48 |

Table 1.2.6.3. Irreducible representations for cyclic groups C_n

$\omega = \exp(2\pi i/n)$, s.c.m. = smallest common multiple.

| n_i | ε | α | α^2 | α^3 | \dots | α^{n-1} |
|------------|---------------|---------------|------------------|------------------|----------|----------------|
| Order | 1 | n | s.c.m.($n, 2$) | s.c.m.($n, 3$) | \dots | n |
| Γ_1 | 1 | 1 | 1 | 1 | \dots | 1 |
| Γ_2 | 1 | ω | ω^2 | ω^3 | \dots | ω^{-1} |
| \vdots | 1 | \vdots | \vdots | \vdots | \ddots | \vdots |
| Γ_n | 1 | ω^{-1} | ω^{-2} | ω^{-3} | \dots | ω |

Table 1.2.6.4. Irreducible representations for dihedral groups D_n

(a) n odd. $m = 1, \dots, (n-1)/2$; $j = 1, \dots, (n-1)/2$, s.c.m. = smallest common multiple.

| n_i | ε | α^j | \dots | β |
|----------------|---------------|---------------------|---------|---------|
| Order | 1 | s.c.m.(n, j) | 2 | n |
| Γ_1 | 1 | 1 | \dots | 1 |
| Γ_2 | 1 | 1 | \dots | -1 |
| Γ_{2+m} | 2 | $2 \cos(2\pi mj/n)$ | \dots | 0 |

(b) n even. $m = 1, \dots, (n/2 - 1)$; $j = 1, \dots, (n/2 - 1)$, s.c.m. = smallest common multiple.

| n_i | ε | $\alpha^{n/2}$ | α^j | \dots | β | $\alpha\beta$ |
|----------------|---------------|----------------|---------------------|---------|---------|---------------|
| Order | 1 | 2 | s.c.m.(n, j) | \dots | $n/2$ | $n/2$ |
| Γ_1 | 1 | 1 | 1 | \dots | 1 | 1 |
| Γ_2 | 1 | 1 | 1 | \dots | -1 | -1 |
| Γ_3 | 1 | $(-1)^{n/2}$ | $(-1)^j$ | \dots | 1 | -1 |
| Γ_4 | 1 | $(-1)^{n/2}$ | $(-1)^j$ | \dots | -1 | 1 |
| Γ_{4+m} | 2 | $(-1)^{m/2}$ | $2 \cos(2\pi mj/n)$ | \dots | 0 | 0 |

1. TENSORIAL ASPECTS OF PHYSICAL PROPERTIES

Table 1.2.6.5. Irreducible representations and character tables for the 32 crystallographic point groups in three dimensions

(a) C_1

| | |
|------------|---------------|
| C_1 | ε |
| n | 1 |
| Order | 1 |
| Γ_1 | 1 |

$$1 \quad \Gamma_1 : A = \chi_1 \quad x, y, z \quad x^2, y^2, z^2, yz, xz, xy$$

(e) $C_6 [\omega = \exp(\pi i/3)]$.

| | | | | | | |
|------------|---------------|-------------|------------|------------|------------|-------------|
| C_6 | ε | α | α^2 | α^3 | α^4 | α^5 |
| n | 1 | 1 | 1 | 1 | 1 | 1 |
| Order | 1 | 6 | 3 | 2 | 3 | 6 |
| Γ_1 | 1 | 1 | 1 | 1 | 1 | 1 |
| Γ_2 | 1 | ω | ω^2 | -1 | $-\omega$ | $-\omega^2$ |
| Γ_3 | 1 | ω^2 | $-\omega$ | 1 | ω^2 | $-\omega$ |
| Γ_4 | 1 | -1 | 1 | -1 | 1 | -1 |
| Γ_5 | 1 | $-\omega$ | ω^2 | 1 | $-\omega$ | ω^2 |
| Γ_6 | 1 | $-\omega^2$ | $-\omega$ | -1 | ω^2 | ω |

(b) C_2

| | | |
|------------|---------------|----------|
| C_2 | ε | α |
| n | 1 | 1 |
| Order | 1 | 2 |
| Γ_1 | 1 | 1 |
| Γ_2 | 1 | -1 |

$$\begin{array}{ll} 2 & \alpha = C_{2z} \quad \Gamma_1 : A = \chi_1 \quad z \quad x^2, y^2, z^2, xy \\ & \Gamma_2 : B = \chi_3 \quad x, y \quad yz, xz \\ m & \alpha = \sigma_z \quad \Gamma_1 : A' = \chi_1 \quad x, y \quad x^2, y^2, z^2, xy \\ & \Gamma_2 : A'' = \chi_3 \quad z \quad yz, xz \\ \bar{1} & \alpha = I \quad \Gamma_1 : A_g = \chi_1^+ \quad x^2, y^2, z^2, yz, xz, xy \\ & \Gamma_2 : A_u = \chi_1^- \quad x, y, z \end{array}$$

(c) $C_3 [\omega = \exp(2\pi i/3)]$.

| | | | |
|------------|---------------|------------|------------|
| C_3 | ε | α | α^2 |
| n | 1 | 1 | 1 |
| Order | 1 | 3 | 3 |
| Γ_1 | 1 | 1 | 1 |
| Γ_2 | 1 | ω | ω^2 |
| Γ_3 | 1 | ω^2 | ω |

Matrices of the real two-dimensional representation:

| | | | |
|----------------------------|--|--|--|
| | ε | α | α^2 |
| $\Gamma_2 \oplus \Gamma_3$ | $\begin{pmatrix} 1 & 0 \\ 0 & 1 \end{pmatrix}$ | $\begin{pmatrix} 0 & -1 \\ 1 & -1 \end{pmatrix}$ | $\begin{pmatrix} -1 & 1 \\ -1 & 0 \end{pmatrix}$ |

$$\begin{array}{ll} 3 & \alpha = C_{3z} \quad \Gamma_1 : A = \chi_1 \quad z \quad x^2 + y^2, z^2 \\ & \Gamma_2 \oplus \Gamma_3 : E = \chi_{1c} + \chi_{1c}^* \quad x, y \quad x^2 - y^2, xz, yz, xy \end{array}$$

(d) C_4

| | | | | |
|------------|---------------|----------|------------|------------|
| C_4 | ε | α | α^2 | α^3 |
| n | 1 | 1 | 1 | 1 |
| Order | 1 | 4 | 2 | 4 |
| Γ_1 | 1 | 1 | 1 | 1 |
| Γ_2 | 1 | i | -1 | $-i$ |
| Γ_3 | 1 | -1 | 1 | -1 |
| Γ_4 | 1 | $-i$ | -1 | i |

Matrices of the real two-dimensional representation:

| | | | | |
|----------------------------|--|---|--|---|
| | ε | α | α^2 | α^3 |
| $\Gamma_2 \oplus \Gamma_4$ | $\begin{pmatrix} 1 & 0 \\ 0 & 1 \end{pmatrix}$ | $\begin{pmatrix} 0 & -1 \\ 1 & 0 \end{pmatrix}$ | $\begin{pmatrix} -1 & 0 \\ 0 & -1 \end{pmatrix}$ | $\begin{pmatrix} 0 & 1 \\ -1 & 0 \end{pmatrix}$ |

$$\begin{array}{ll} 4 & \alpha = C_{4z} \quad \Gamma_1 : A = \chi_1 \quad z \quad x^2 + y^2, z^2 \\ & \Gamma_3 : B = \chi_3 \quad x^2 - y^2, xy \\ & \Gamma_2 \oplus \Gamma_4 : E = \chi_{1c} + \chi_{1c}^* \quad x, y \quad yz, xz \\ \bar{4} & \alpha = S_4 \quad \Gamma_1 : A = \chi_1 \quad x^2 + y^2, z^2 \\ & \Gamma_3 : B = \chi_3 \quad x^2 - y^2, xy \\ & \Gamma_2 \oplus \Gamma_4 : E = \chi_{1c} + \chi_{1c}^* \quad x, y \quad yz, xz \end{array}$$

Matrices of the real representations:

| | | |
|---------------|--|--|
| | $\Gamma_2 \oplus \Gamma_6$ | $\Gamma_3 \oplus \Gamma_5$ |
| ε | $\begin{pmatrix} 1 & 0 \\ 0 & 1 \end{pmatrix}$ | $\begin{pmatrix} 1 & 0 \\ 0 & 1 \end{pmatrix}$ |
| α | $\begin{pmatrix} 1 & -1 \\ 1 & 0 \end{pmatrix}$ | $\begin{pmatrix} 0 & -1 \\ 1 & -1 \end{pmatrix}$ |
| α^2 | $\begin{pmatrix} 0 & -1 \\ 1 & -1 \end{pmatrix}$ | $\begin{pmatrix} -1 & 1 \\ -1 & 0 \end{pmatrix}$ |
| α^3 | $\begin{pmatrix} -1 & 0 \\ 0 & -1 \end{pmatrix}$ | $\begin{pmatrix} 1 & 0 \\ 0 & 1 \end{pmatrix}$ |
| α^4 | $\begin{pmatrix} -1 & 1 \\ -1 & 0 \end{pmatrix}$ | $\begin{pmatrix} 0 & -1 \\ 1 & -1 \end{pmatrix}$ |
| α^5 | $\begin{pmatrix} 0 & 1 \\ -1 & 1 \end{pmatrix}$ | $\begin{pmatrix} -1 & 1 \\ -1 & 0 \end{pmatrix}$ |

$$\begin{array}{ll} 6 & \alpha = C_{6z} \quad \Gamma_1 : A = \chi_1 \quad z \quad x^2 + y^2, z^2 \\ & \Gamma_4 : B = \chi_3 \quad xz, yz \\ & \Gamma_2 \oplus \Gamma_6 : E_1 = \chi_{1c} + \chi_{1c}^* \quad x, y \quad x^2 - y^2, xy \\ & \Gamma_3 \oplus \Gamma_5 : E_2 = \chi_{2c} + \chi_{2c}^* \end{array}$$

$$\begin{array}{ll} \bar{3} & \alpha = S_{3z} \quad \Gamma_1 : A_g = \chi_1^+ \quad x^2 + y^2, z^2 \\ & \Gamma_4 : A_u = \chi_1^- \quad z \\ & \Gamma_2 \oplus \Gamma_6 : E_u = \chi_{1c}^- + \chi_{1c}^{*-} \quad x, y \\ & \Gamma_3 \oplus \Gamma_5 : E_g = \chi_{1c}^+ + \chi_{1c}^{*+} \quad x^2 - y^2, xy, xz, yz \end{array}$$

$$\begin{array}{ll} \bar{6} & \alpha = S_{6z} \quad \Gamma_1 : A' = \chi_1 \quad x^2 + y^2, z^2 \\ & \Gamma_4 : A'' = \chi_3 \quad z \\ & \Gamma_2 \oplus \Gamma_6 : E' = \chi_{2c} + \chi_{2c}^* \quad xz, yz \\ & \Gamma_3 \oplus \Gamma_5 : E'' = \chi_{1c} + \chi_{1c}^* \quad x, y \quad x^2 - y^2, xy \end{array}$$

(f) D_2

| | | | | |
|------------|---------------|----------|---------|---------------|
| D_2 | ε | α | β | $\alpha\beta$ |
| n | 1 | 1 | 1 | 1 |
| Order | 1 | 2 | 2 | 2 |
| Γ_1 | 1 | 1 | 1 | 1 |
| Γ_2 | 1 | 1 | -1 | -1 |
| Γ_3 | 1 | -1 | 1 | -1 |
| Γ_4 | 1 | -1 | -1 | 1 |

$$\begin{array}{ll} 222 & \alpha = C_{2x} \quad \Gamma_1 : A_1 = \chi_1 \quad x^2, y^2, z^2 \\ & \beta = C_{2y} \quad \Gamma_2 : B_3 = \chi_3 \quad x \quad yz \\ & \alpha\beta = C_{2z} \quad \Gamma_3 : B_2 = \chi_4 \quad y \quad xz \\ & \quad \quad \quad \Gamma_4 : B_1 = \chi_2 \quad z \quad xz \end{array}$$

$$\begin{array}{ll} mm2 & \alpha = C_{2z} \quad \Gamma_1 : A_1 = \chi_1 \quad z \quad x^2, y^2, z^2 \\ & \beta = \sigma_x \quad \Gamma_2 : A_2 = \chi_2 \quad xy \\ & \alpha\beta = \sigma_y \quad \Gamma_3 : B_2 = \chi_3 \quad y \quad yz \\ & \quad \quad \quad \Gamma_4 : B_1 = \chi_4 \quad x \quad xz \end{array}$$

$$\begin{array}{ll} 2/m & \alpha = C_{2z} \quad \Gamma_1 : A_g = \chi_1^+ \quad x^2, y^2, z^2, xy \\ & \beta = \sigma_z \quad \Gamma_2 : A_u = \chi_1^- \quad z \quad z \\ & \alpha\beta = I \quad \Gamma_3 : B_u = \chi_3^- \quad x, y \\ & \quad \quad \quad \Gamma_4 : B_g = \chi_3^+ \end{array}$$

1.2. REPRESENTATIONS OF CRYSTALLOGRAPHIC GROUPS

Table 1.2.6.5 (cont.)

(g) D_3

| D_3 n Order | ε | α | β |
|-----------------------|---------------|----------|---------|
| | 1 | 2 | 3 |
| | 1 | 3 | 2 |
| Γ_1 | 1 | 1 | 1 |
| Γ_2 | 1 | 1 | -1 |
| Γ_3 | 2 | -1 | 0 |

Matrices of the two-dimensional representation:

| | ε | α | β |
|------------|--|--|---|
| Γ_3 | $\begin{pmatrix} 1 & 0 \\ 0 & 1 \end{pmatrix}$ | $\begin{pmatrix} 0 & -1 \\ 1 & -1 \end{pmatrix}$ | $\begin{pmatrix} -1 & 1 \\ 0 & 1 \end{pmatrix}$ |

| | | | |
|----------|--------------------|---------------------------|------------------------------------|
| 32 | $\alpha = C_{3z}$ | $\Gamma_1 : A_1 = \chi_1$ | $x^2 + y^2, z^2$ |
| D_3 | $\beta = C_{2x}$ | $\Gamma_2 : A_2 = \chi_2$ | z |
| | | $\Gamma_3 : E = \chi_1$ | $x, y \quad xz, yz, xy, x^2 - y^2$ |
| 3m | $\alpha = C_{3z}$ | $\Gamma_1 : A_1 = \chi_1$ | $x^2 + y^2, z^2$ |
| C_{3v} | $\beta = \sigma_v$ | $\Gamma_2 : A_2 = \chi_2$ | z |
| | | $\Gamma_3 : E = \chi_1$ | $x, y \quad xz, yz, xy, x^2 - y^2$ |

(h) D_4

| D_4 n Order | ε | α | α^2 | β | $\alpha\beta$ |
|-----------------------|---------------|----------|------------|---------|---------------|
| | 1 | 2 | 1 | 2 | 2 |
| | 1 | 4 | 2 | 2 | 2 |
| Γ_1 | 1 | 1 | 1 | 1 | 1 |
| Γ_2 | 1 | 1 | 1 | -1 | -1 |
| Γ_3 | 1 | -1 | 1 | 1 | -1 |
| Γ_4 | 1 | -1 | 1 | -1 | 1 |
| Γ_5 | 2 | 0 | -2 | 0 | 0 |

Matrices of the two-dimensional representation:

| | Γ_5 |
|---------------|--|
| ε | $\begin{pmatrix} 1 & 0 \\ 0 & 1 \end{pmatrix}$ |
| α | $\begin{pmatrix} 0 & -1 \\ 1 & 0 \end{pmatrix}$ |
| α^2 | $\begin{pmatrix} -1 & 0 \\ 0 & -1 \end{pmatrix}$ |
| β | $\begin{pmatrix} -1 & 0 \\ 0 & 1 \end{pmatrix}$ |
| $\alpha\beta$ | $\begin{pmatrix} 0 & -1 \\ -1 & 0 \end{pmatrix}$ |

| | | | |
|-------------|--------------------------|---------------------------|---------------------|
| 422 | $\alpha = C_{4z}$ | $\Gamma_1 : A_1 = \chi_1$ | $x^2 + y^2, z^2$ |
| D_4 | $\beta = C_{2x}$ | $\Gamma_2 : A_2 = \chi_2$ | z |
| | | $\Gamma_3 : B_1 = \chi_3$ | $x^2 - y^2$ |
| | | $\Gamma_4 : B_2 = \chi_4$ | xy |
| | | $\Gamma_5 : E = \chi_1$ | $x, y \quad xz, yz$ |
| 4mm | $\alpha = C_{4z}$ | $\Gamma_1 : A_1 = \chi_1$ | $x^2 + y^2, z^2$ |
| C_{4v} | $\beta = \sigma_v$ | $\Gamma_2 : A_2 = \chi_2$ | z |
| | | $\Gamma_3 : B_1 = \chi_3$ | $x^2 - y^2$ |
| | | $\Gamma_4 : B_2 = \chi_4$ | xy |
| | | $\Gamma_5 : E = \chi_1$ | $x, y \quad xz, yz$ |
| $\bar{4}2m$ | $\alpha = S_{4z}$ | $\Gamma_1 : A_1 = \chi_1$ | $x^2 + y^2, z^2$ |
| D_{2d} | $\beta = C_{2v}$ | $\Gamma_2 : A_2 = \chi_2$ | z |
| | $\alpha\beta = \sigma_d$ | $\Gamma_3 : B_1 = \chi_3$ | $x^2 - y^2$ |
| | | $\Gamma_4 : B_2 = \chi_4$ | xy |
| | | $\Gamma_5 : E = \chi_1$ | $x, y \quad xz, yz$ |

(i) D_6

| D_6 n Order | ε | α | α^2 | α^3 | β | $\alpha\beta$ |
|-----------------------|---------------|----------|------------|------------|---------|---------------|
| | 1 | 2 | 2 | 1 | 3 | 3 |
| | 1 | 6 | 3 | 2 | 2 | 2 |
| Γ_1 | 1 | 1 | 1 | 1 | 1 | 1 |
| Γ_2 | 1 | 1 | 1 | 1 | -1 | -1 |
| Γ_3 | 1 | -1 | 1 | -1 | 1 | -1 |
| Γ_4 | 1 | -1 | 1 | -1 | -1 | 1 |
| Γ_5 | 2 | 1 | -1 | -2 | 0 | 0 |
| Γ_6 | 2 | -1 | -1 | 2 | 0 | 0 |

Matrices of the two-dimensional representations:

| | Γ_5 | Γ_6 |
|---------------|--|--|
| ε | $\begin{pmatrix} 1 & 0 \\ 0 & 1 \end{pmatrix}$ | $\begin{pmatrix} 1 & 0 \\ 0 & 1 \end{pmatrix}$ |
| α | $\begin{pmatrix} 1 & -1 \\ 1 & 0 \end{pmatrix}$ | $\begin{pmatrix} 0 & -1 \\ 1 & -1 \end{pmatrix}$ |
| α^2 | $\begin{pmatrix} 0 & -1 \\ 1 & -1 \end{pmatrix}$ | $\begin{pmatrix} -1 & 1 \\ -1 & 0 \end{pmatrix}$ |
| α^3 | $\begin{pmatrix} -1 & 0 \\ 0 & -1 \end{pmatrix}$ | $\begin{pmatrix} 1 & 0 \\ 0 & 1 \end{pmatrix}$ |
| β | $\begin{pmatrix} -1 & 1 \\ 0 & 1 \end{pmatrix}$ | $\begin{pmatrix} -1 & 1 \\ 0 & 1 \end{pmatrix}$ |
| $\alpha\beta$ | $\begin{pmatrix} -1 & 0 \\ -1 & 1 \end{pmatrix}$ | $\begin{pmatrix} 0 & -1 \\ -1 & 0 \end{pmatrix}$ |

| | | | |
|-------------|--------------------------|--------------------------------|------------------------------------|
| 622 | $\alpha = C_{6z}$ | $\Gamma_1 : A_1 = \chi_1$ | $x^2 + y^2, z^2$ |
| D_6 | $\beta = C_{2x}$ | $\Gamma_2 : A_2 = \chi_2$ | z |
| | | $\Gamma_3 : B_1 = \chi_3$ | $x^2 - y^2$ |
| | | $\Gamma_4 : B_2 = \chi_4$ | xy |
| | | $\Gamma_5 : E_1 = \chi_1$ | $x, y \quad xz, yz$ |
| | | $\Gamma_6 : E_2 = \chi_2$ | |
| 6mm | $\alpha = C_{6z}$ | $\Gamma_1 : A_1 = \chi_1$ | $x^2 + y^2, z^2$ |
| C_{6v} | $\beta = \sigma_v$ | $\Gamma_2 : A_2 = \chi_2$ | z |
| | | $\Gamma_3 : B_1 = \chi_3$ | $x^2 - y^2$ |
| | | $\Gamma_4 : B_2 = \chi_4$ | xy |
| | | $\Gamma_5 : E_1 = \chi_1$ | $x, y \quad xz, yz$ |
| | | $\Gamma_6 : E_2 = \chi_2$ | |
| $\bar{6}2m$ | $\alpha = S_{6z}$ | $\Gamma_1 : A'_1 = \chi_1$ | $x^2 + y^2, z^2$ |
| D_{3h} | $\beta = C_{2v}$ | $\Gamma_2 : A'_2 = \chi_2$ | z |
| | $\alpha\beta = \sigma_d$ | $\Gamma_3 : A''_1 = \chi_3$ | $x^2 - y^2$ |
| | | $\Gamma_4 : A'_2 = \chi_4$ | xy |
| | | $\Gamma_5 : E' = \chi_2$ | xz, yz |
| | | $\Gamma_6 : E'' = \chi_1$ | x, y |
| $\bar{3}m$ | $\alpha = S_{3z}$ | $\Gamma_1 : A_{1g} = \chi_1^+$ | $x^2 + y^2, z^2$ |
| D_{3v} | $\beta = \sigma_d$ | $\Gamma_2 : A_{2g} = \chi_2^+$ | z |
| | | $\Gamma_3 : A_{1u} = \chi_1^-$ | $x^2 - y^2$ |
| | | $\Gamma_4 : A_{2u} = \chi_2^-$ | xy |
| | | $\Gamma_5 : E_u = \chi_1$ | xz, yz |
| | | $\Gamma_6 : E_g = \chi_1^+$ | $x, y \quad xz, yz, xy, x^2 - y^2$ |

(j) $T [\omega = \exp(2\pi i/3)]$.

| T n Order | ε | α | α^2 | β |
|---------------------|---------------|------------|------------|---------|
| | 1 | 4 | 4 | 3 |
| | 1 | 3 | 3 | 2 |
| Γ_1 | 1 | 1 | 1 | 1 |
| Γ_2 | 1 | ω | ω^2 | 1 |
| Γ_3 | 1 | ω^2 | ω | 1 |
| Γ_4 | 3 | 0 | 0 | -1 |

1. TENSORIAL ASPECTS OF PHYSICAL PROPERTIES

Table 1.2.6.5 (cont.)

Real representations of dimension $d > 1$:

| | $\Gamma_2 \oplus \Gamma_3$ | Γ_4 |
|---------------|--|---|
| ε | $\begin{pmatrix} 1 & 0 \\ 0 & 1 \end{pmatrix}$ | $\begin{pmatrix} 1 & 0 & 0 \\ 0 & 1 & 0 \\ 0 & 0 & 1 \end{pmatrix}$ |
| α | $\begin{pmatrix} 1 & -1 \\ 0 & -1 \end{pmatrix}$ | $\begin{pmatrix} 0 & 1 & 0 \\ 0 & 0 & 1 \\ 1 & 0 & 0 \end{pmatrix}$ |
| α^2 | $\begin{pmatrix} 1 & -1 \\ 0 & -1 \end{pmatrix}$ | $\begin{pmatrix} 0 & 0 & 1 \\ 1 & 0 & 0 \\ 0 & 1 & 0 \end{pmatrix}$ |
| β | $\begin{pmatrix} 1 & 0 \\ 0 & 1 \end{pmatrix}$ | $\begin{pmatrix} -1 & 0 & 0 \\ 0 & -1 & 0 \\ 0 & 0 & 1 \end{pmatrix}$ |

$$\begin{array}{llll}
 23 & \alpha = C_{3d} & \Gamma_1 : A = \chi_1 & x^2 + y^2 + z^2 \\
 T & \beta = C_{2z} & \Gamma_2 \oplus \Gamma_3 : E = \chi_{3c} + \chi_{3c}^* & x^2 - y^2, x^2 - z^2 \\
 & & \Gamma_4 : T = \chi_1 & xy, xz, yz
 \end{array}$$

(k) O

| O | ε | β | α^2 | α | $\alpha\beta$ |
|------------|---------------|---------|------------|----------|---------------|
| n | 1 | 8 | 3 | 6 | 6 |
| Order | 1 | 3 | 2 | 4 | 2 |
| Γ_1 | 1 | 1 | 1 | 1 | 1 |
| Γ_2 | 1 | 1 | 1 | -1 | -1 |
| Γ_3 | 2 | -1 | 2 | 0 | 0 |
| Γ_4 | 3 | 0 | -1 | 1 | -1 |
| Γ_5 | 3 | 0 | -1 | -1 | 1 |

Higher-dimensional representations:

| | Γ_3 | Γ_4 | Γ_5 |
|---------------|--|---|---|
| ε | $\begin{pmatrix} 1 & 0 \\ 0 & 1 \end{pmatrix}$ | $\begin{pmatrix} 1 & 0 & 0 \\ 0 & 1 & 0 \\ 0 & 0 & 1 \end{pmatrix}$ | $\begin{pmatrix} 1 & 0 & 0 \\ 0 & 1 & 0 \\ 0 & 0 & 1 \end{pmatrix}$ |
| β | $\begin{pmatrix} 0 & -1 \\ 1 & -1 \end{pmatrix}$ | $\begin{pmatrix} 0 & 0 & 1 \\ 1 & 0 & 0 \\ 0 & 1 & 0 \end{pmatrix}$ | $\begin{pmatrix} 0 & 0 & 1 \\ 1 & 0 & 0 \\ 0 & 1 & 0 \end{pmatrix}$ |
| α^2 | $\begin{pmatrix} 1 & 0 \\ 0 & 1 \end{pmatrix}$ | $\begin{pmatrix} -1 & 0 & 0 \\ 0 & -1 & 0 \\ 0 & 0 & 1 \end{pmatrix}$ | $\begin{pmatrix} -1 & 0 & 0 \\ 0 & -1 & 0 \\ 0 & 0 & 1 \end{pmatrix}$ |
| α | $\begin{pmatrix} 0 & 1 \\ 1 & 0 \end{pmatrix}$ | $\begin{pmatrix} 0 & -1 & 0 \\ 1 & 0 & 0 \\ 0 & 0 & 1 \end{pmatrix}$ | $\begin{pmatrix} 0 & 1 & 0 \\ -1 & 0 & 0 \\ 0 & 0 & -1 \end{pmatrix}$ |
| $\alpha\beta$ | $\begin{pmatrix} -1 & 0 \\ -1 & 1 \end{pmatrix}$ | $\begin{pmatrix} -1 & 0 & 0 \\ 0 & 0 & 1 \\ 0 & 1 & 0 \end{pmatrix}$ | $\begin{pmatrix} 1 & 0 & 0 \\ 0 & 0 & -1 \\ 0 & -1 & 0 \end{pmatrix}$ |

$$\begin{array}{llll}
 432 & \alpha = C_{4z} & \Gamma_1 : A_1 = \chi_1 & x^2 + y^2 + z^2 \\
 O & \beta = C_{3d} & \Gamma_2 : A_2 = \chi_2 & \\
 & \alpha\beta = C_2 & \Gamma_3 : E = \chi_3 & x^2 - y^2, y^2 - z^2 \\
 & & \Gamma_4 : T_1 = \chi_1 & xy, yz, xz \\
 & & \Gamma_5 : T_2 = \chi_2 & \\
 \bar{4}3m & \alpha = S_{4z} & \Gamma_1 : A_1 = \chi_1 & x^2 + y^2 + z^2 \\
 T_d & \beta = C_{3d} & \Gamma_2 : A_2 = \chi_2 & \\
 & \alpha\beta = \sigma_d & \Gamma_3 : E = \chi_3 & x^2 - y^2, y^2 - z^2 \\
 & & \Gamma_4 : T_1 = \chi_1 & \\
 & & \Gamma_5 : T_2 = \chi_2 & xy, yz, xz
 \end{array}$$

Other point groups which are of second class and contain $-E$. See Table 1.2.6.6(a).

| Group | Isomorphism class | Rotation subgroup |
|-------------|---------------------------|-------------------|
| $4/m$ | $C_4 \times \mathbb{Z}_2$ | 4 |
| $6/m$ | $C_6 \times \mathbb{Z}_2$ | 6 |
| mmm | $D_2 \times \mathbb{Z}_2$ | 222 |
| $4/mmm$ | $D_4 \times \mathbb{Z}_2$ | 422 |
| $6/mmm$ | $D_6 \times \mathbb{Z}_2$ | 622 |
| $m\bar{3}$ | $T \times \mathbb{Z}_2$ | 23 |
| $m\bar{3}m$ | $O \times \mathbb{Z}_2$ | 432 |

Table 1.2.6.6. Direct products with $\{E, \bar{1}\}$ and $\{E, 1'\}$

(a) With $\{E, \bar{1}\}$.

| $K \times \mathbb{Z}_2$ | $R \in K$ | \bar{R} |
|-------------------------|-----------|------------|
| Γ_g | $\chi(R)$ | $\chi(R)$ |
| Γ_u | $\chi(R)$ | $-\chi(R)$ |

| | | |
|-------------|---------------------------|---------|
| $4/m$ | $C_4 \times \mathbb{Z}_2$ | cf. 4 |
| $6/m$ | $C_6 \times \mathbb{Z}_2$ | cf. 6 |
| mmm | $D_2 \times \mathbb{Z}_2$ | cf. 222 |
| $4/mmm$ | $D_4 \times \mathbb{Z}_2$ | cf. 422 |
| $6/mmm$ | $D_6 \times \mathbb{Z}_2$ | cf. 622 |
| $m\bar{3}$ | $T \times \mathbb{Z}_2$ | cf. 23 |
| $m\bar{3}m$ | $O \times \mathbb{Z}_2$ | cf. 432 |

(b) With $\{E, 1'\}$.

| $K \times \mathbb{Z}_2$ | $R \in K$ | R' |
|-------------------------|-----------|------------|
| Γ_+ | $\chi(R)$ | $\chi(R)$ |
| Γ_- | $\chi(R)$ | $-\chi(R)$ |

| | | |
|---------------|---------------------------|-----------------|
| $1'$ | $C_1 \times \mathbb{Z}_2$ | cf. 1 |
| $21'$ | $C_2 \times \mathbb{Z}_2$ | cf. 2 |
| $m1'$ | $C_2 \times \mathbb{Z}_2$ | cf. m |
| $2221'$ | $D_2 \times \mathbb{Z}_2$ | cf. 222 |
| $2mm1'$ | $D_2 \times \mathbb{Z}_2$ | cf. $2mm$ |
| $41'$ | $C_4 \times \mathbb{Z}_2$ | cf. 4 |
| $\bar{4}1'$ | $C_4 \times \mathbb{Z}_2$ | cf. $\bar{4}$ |
| $4mm1'$ | $D_4 \times \mathbb{Z}_2$ | cf. $4mm$ |
| $4221'$ | $D_4 \times \mathbb{Z}_2$ | cf. 422 |
| $\bar{4}2m1'$ | $D_4 \times \mathbb{Z}_2$ | cf. $\bar{4}2m$ |
| $31'$ | $C_3 \times \mathbb{Z}_2$ | cf. 3 |
| $321'$ | $D_3 \times \mathbb{Z}_2$ | cf. 32 |
| $\bar{3}1'$ | $C_6 \times \mathbb{Z}_2$ | cf. $\bar{3}$ |
| $3m1'$ | $D_3 \times \mathbb{Z}_2$ | cf. $3m$ |
| $6mm1'$ | $D_6 \times \mathbb{Z}_2$ | cf. $6mm$ |
| $61'$ | $C_6 \times \mathbb{Z}_2$ | cf. 6 |
| $\bar{6}1'$ | $C_6 \times \mathbb{Z}_2$ | cf. $\bar{6}$ |
| $6221'$ | $D_6 \times \mathbb{Z}_2$ | cf. 622 |
| $\bar{6}2m1'$ | $D_6 \times \mathbb{Z}_2$ | cf. $\bar{6}2m$ |
| $231'$ | $T \times \mathbb{Z}_2$ | cf. 23 |
| $4321'$ | $O \times \mathbb{Z}_2$ | cf. 432 |
| $\bar{4}3m1'$ | $O \times \mathbb{Z}_2$ | cf. $\bar{4}3m$ |

(c) With $\{E, \bar{1}\}$ and $\{E, 1'\}$.

| $K \times \mathbb{Z}_2 \times \mathbb{Z}_2$ | $R \in K$ | \bar{R} | R' | \bar{R}' |
|---|-----------|------------|------------|------------|
| Γ_{g+} | $\chi(R)$ | $\chi(R)$ | $\chi(R)$ | $\chi(R)$ |
| Γ_{u+} | $\chi(R)$ | $-\chi(R)$ | $\chi(R)$ | $-\chi(R)$ |
| Γ_{g-} | $\chi(R)$ | $\chi(R)$ | $-\chi(R)$ | $-\chi(R)$ |
| Γ_{u-} | $\chi(R)$ | $-\chi(R)$ | $-\chi(R)$ | $\chi(R)$ |

| | | |
|-----------------|---|----------|
| $\bar{1}'$ | $C_1 \times \mathbb{Z}_2 \times \mathbb{Z}_2$ | cf. 1 |
| $21'/m$ | $C_2 \times \mathbb{Z}_2 \times \mathbb{Z}_2$ | cf. 2 |
| $4/m1'$ | $C_4 \times \mathbb{Z}_2 \times \mathbb{Z}_2$ | cf. 4 |
| $6/m1'$ | $C_6 \times \mathbb{Z}_2 \times \mathbb{Z}_2$ | cf. 6 |
| $mmm1'$ | $D_2 \times \mathbb{Z}_2 \times \mathbb{Z}_2$ | cf. 222 |
| $4/mmm1'$ | $D_4 \times \mathbb{Z}_2 \times \mathbb{Z}_2$ | cf. 422 |
| $\bar{3}m1'$ | $D_6 \times \mathbb{Z}_2 \times \mathbb{Z}_2$ | cf. $3m$ |
| $6/mmm1'$ | $D_6 \times \mathbb{Z}_2 \times \mathbb{Z}_2$ | cf. 622 |
| $m\bar{3}1'$ | $T \times \mathbb{Z}_2 \times \mathbb{Z}_2$ | cf. 23 |
| $m(\bar{3})m1'$ | $O \times \mathbb{Z}_2 \times \mathbb{Z}_2$ | cf. 432 |

1.2. REPRESENTATIONS OF CRYSTALLOGRAPHIC GROUPS

groups generated by $\bar{1}$, $1'$ and $\{\bar{1}, 1'\}$ are given in Tables 1.2.6.6(a), (b) and (c), respectively.

Table 1.2.6.7. The representations of a point group are also representations of their double groups. In addition, there are extra representations which give projective representations of the point groups. For several cases, these are associated with an ordinary representation. As extra representations, those irreducible representations of the double point groups that give rise to projective representations of the point groups with a factor system that is not associated with the trivial one are given. These do not correspond to ordinary representations of the single group.

Table 1.2.6.8. If one chooses for each element of a point group one of the two corresponding $SU(2)$ elements, the latter form a projective representation of the point group. If one selects for the rotation $R \in K \subset SO(3)$ the element

$$u(R) = E \cos(\varphi/2) + i(\boldsymbol{\sigma} \cdot \mathbf{n}) \sin(\varphi/2),$$

where φ is the rotation angle and \mathbf{n} the rotation axis, and for $R \in K \subset O(3) \setminus SO(3)$ the element

$$u(R) = E \cos(\psi/2) + i(\boldsymbol{\sigma} \cdot \mathbf{n}) \sin(\psi/2),$$

where ψ and \mathbf{n} are the rotation angle and axis of the rotation $-R$, the matrices $u(R)$ form a projective representation:

$$u(R)u(R') = \omega_s(R, R')u(RR').$$

The factor system ω_s is the spin factor system. It is determined *via* the generators and defining relations

$$W_i(A_1, \dots, A_p) = E$$

of the point group K . Then

$$W_i(u(A_1), \dots, u(A_p)) = \lambda_i E,$$

and the factors λ_i fix uniquely the class of the factor system ω_s . These factors are given in the table.

Because $\bar{1}$ is represented by the unit matrix in spin space, the double groups of two isomorphic point groups obtained from each other by replacing the elements $R \in O(3) \setminus SO(3)$ by $-R$ are the same.

The projective representations with factor system ω_s may sometimes be associated with one with a trivial factor system. If this is the case, there are actually no extra representations of the

Table 1.2.6.7. Extra representations of double groups

| | | | | | | | | | |
|--|-----|------|------------|-------------|-------------|-------------|-------------|-------------|-------------|
| 222^d Γ'_5 | E | $-E$ | $\pm A$ | $\pm B$ | $\pm AB$ | | | | |
| | 2 | -2 | 0 | 0 | 0 | | | | |
| 422^d Γ'_6 Γ'_7 | E | $-E$ | $\pm A^2$ | A | $-A$ | $\pm B$ | $\pm AB$ | | |
| | 2 | -2 | 0 | $\sqrt{2}$ | $-\sqrt{2}$ | 0 | 0 | | |
| | 2 | -2 | 0 | $-\sqrt{2}$ | $\sqrt{2}$ | 0 | 0 | | |
| 622^d Γ'_8 Γ'_9 Γ'_7 | E | $-E$ | A^2 | $-A^2$ | $\pm B$ | $\pm A^3$ | A^5 | $-A^5$ | $\pm A^3 B$ |
| | 2 | -2 | 1 | -1 | 0 | 0 | $\sqrt{3}$ | $-\sqrt{3}$ | 0 |
| | 2 | -2 | 1 | -1 | 0 | 0 | $-\sqrt{3}$ | $\sqrt{3}$ | 0 |
| | 2 | -2 | -2 | 2 | 0 | 0 | 0 | 0 | 0 |
| 23^d Γ'_5 Γ'_6 Γ'_7 | E | $-E$ | A | $-A$ | A^2 | $-A^2$ | $\pm B$ | | |
| | 2 | -2 | 1 | -1 | 1 | -1 | 0 | | |
| | 2 | -2 | ω | ω^4 | ω^2 | ω^5 | 0 | | |
| | 2 | -2 | ω^5 | ω^2 | ω^4 | ω | 0 | | |
| 432^d Γ'_6 Γ'_7 Γ'_8 | E | $-E$ | B | $-B$ | $\pm A^2$ | A | $-A$ | $\pm AB$ | |
| | 2 | -2 | 1 | -1 | 0 | $\sqrt{2}$ | $-\sqrt{2}$ | 0 | |
| | 2 | -2 | 1 | -1 | 0 | $-\sqrt{2}$ | $\sqrt{2}$ | 0 | |
| | 4 | -4 | -1 | 1 | 0 | 0 | 0 | 0 | |

Table 1.2.6.8. Projective spin representations of the 32 crystallographic point groups

| Point group | Relations giving λ_i | Double group | Extra representations |
|----------------------------------|---|--------------|-----------------------|
| $\bar{1}$ $\bar{1}$ | $A = E$ $A^2 = E$ | 1^d | No No |
| $2, m$ $2/m$ | $A^2 = -E$ $A^2 = B^2 = -E, (AB)^2 = E$ | 2^d | No |
| $222, 2mm$ mmm | $A^2 = B^2 = (AB)^2 = -E$ $A^2 = B^2 = (AB)^2 = -E$ $C^2 = E, AC = CA, BC = CB$ | 222^d | Yes |
| $4, \bar{4}$ $4/m$ | $A^4 = -E$ $A^4 = B^2 = -E, AB = BA$ | 4^d | No |
| $422, 4mm, \bar{4}2m$ $4/mmm$ | $A^4 = B^2 = (AB)^2 = -E$ As above, plus $C^2 = E, AC = CA, BC = CB$ | 422^d | Yes |
| $\bar{3}$ $\bar{3}$ | $A^3 = -E$ $A^6 = E$ | 3^d | No |
| $\bar{3}2, 3m$ $\bar{3}m$ | $A^3 = B^2 = (AB)^2 = -E$ $A^6 = E, B^2 = (AB)^2 = -E$ | 32^d | No |
| $6, \bar{6}$ $6/m$ | $A^6 = -E$ $A^6 = B^2 = -E, AB = BA$ | 6^d | No |
| $622, 6mm, \bar{6}2m$ $6/mmm$ | $A^6 = B^2 = (AB)^2 = -E$ As above, plus $C^2 = E, AC = CA, BC = CB$ | 622^d | Yes |
| 23 $m\bar{3}$ | $A^3 = B^2 = (AB)^3 = -E$ As above, plus $C^2 = E, AC = CA, BC = CB$ | 23^d | Yes |
| $432, \bar{4}3m$ $m\bar{3}m$ | $A^4 = B^3 = (AB)^2 = -E$ As above, plus $C^2 = E, AC = CA, BC = CB$ | 432^d | Yes |

1. TENSORIAL ASPECTS OF PHYSICAL PROPERTIES

double group. If there are extra representations, these are irreducible representations of the double group: see Table 1.2.6.7.

Table 1.2.6.9. For the 32 three-dimensional crystallographic point groups, the character of the vector representation Γ and the number of times the identity representation occurs in a number of tensor products of this vector representation are given. This is identical to the number of free parameters in a tensor of the corresponding type. For the direct products $K \times C_2$, the character is equal to that of K on the rotation subgroup, and its opposite $[\chi(-R) = -\chi(R)]$ for the coset $-K$.

Table 1.2.6.10. The irreducible projective representations of the 32 three-dimensional crystallographic point groups that have a factor system that is not associated to a trivial one. In three (and two) dimensions all factor systems are of order two.

Table 1.2.6.11. The special points in the Brillouin zones. Strata of irreducible representations of the space groups are characterized by the wavevector \mathbf{k} of such a point and a (possibly projective) irreducible representation of the point group $K_{\mathbf{k}}$. The latter is the intersection of the symmetry group of \mathbf{k} (the group of \mathbf{k} for the holohedral point group) and the point group of the space group. For each Bravais class the special points for the holohedry are given. These are given by their coordinates with respect to a basis of the reciprocal lattice of the conventional cell. These points correspond to Wyckoff positions in the corresponding dual lattice. The symbols for these Wyckoff positions and their site symmetry are given. A well known notation for the special points is that of Kovalev, as used in his book on representations of space groups. Correspondence with the notation in Kovalev (1987) is given.

Table 1.2.6.12. The three-dimensional crystallographic magnetic and nonmagnetic point groups of type I (trivial magnetic, no antichronous elements), type II (nonmagnetic, containing time reversal as an element) and type III (nontrivial magnetic, without time reversal itself, but with antichronous elements).

1.2.7. Introduction to the accompanying software *Tenχar*

BY M. EPHRAÏM, T. JANSSEN, A. JANNER AND
A. THIERS

1.2.7.1. Overview

The determination of tensors with specified properties often requires long calculations. In principle the algorithms are simple, but in complicated cases errors can be made. This is therefore a situation in which it is best to rely on computer calculations. For this reason, this volume is accompanied by software on a CD-ROM. Here we shall give a short introduction to the *Tenχar* package that deals with tensors with specific symmetry properties in the first module, and with characters of representations of point groups in the second module. The latter play a role when determining the number of independent elements of a tensor invariant under a given point group, but they are much more widely applicable.

The software package has a graphical interface with windows and buttons. When the program is started, a window opens up in which a choice may be made between the tensor part or the character part of the program.

Within each of the two sections of the program, the results of the calculations are given in numbered windows. It is possible to browse through the various pages. Each page may be sent to a separate window (by the command 'to window'), or to a file (by the command 'to file'). Opened windows may be closed again using a 'close' button.

Special features of the package are that it is dimension- and rank-independent, and that it performs the calculations in an exact way. The number of dimensions and the rank are only limited by the computer memory and by the time the program needs for higher dimensions and ranks. The calculations are exact in the sense of the computer algebra software. Here this is achieved by performing the calculations with integers and

Table 1.2.6.9. Number of free parameters of some tensors

| Group | Isomorphism class | Character of the vector representation | Multiplicity identity representation in | | | | |
|-------------|-------------------|--|---|------------------------|----------------------|---------------------------------------|--|
| | | | $\Gamma^{\otimes 2}$ | $\Gamma_s^{\otimes 2}$ | $\Gamma^{\otimes 3}$ | $\Gamma \otimes \Gamma_s^{\otimes 2}$ | $(\Gamma_s^{\otimes 2})_s^{\otimes 2}$ |
| 1 | C_1 | 3 | 9 | 6 | 27 | 18 | 21 |
| $\bar{1}$ | C_2 | 3, -3 | 9 | 6 | 0 | 0 | 21 |
| 2 | C_2 | 3, -1 | 5 | 4 | 13 | 8 | 13 |
| m | C_2 | 3, 1 | 5 | 4 | 14 | 10 | 13 |
| $2/m$ | $C_2 \times C_2$ | | 5 | 4 | 0 | 0 | 13 |
| 222 | D_2 | 3, -1, -1, -1 | 3 | 3 | 6 | 3 | 9 |
| $2mm$ | D_2 | 3, 1, 1, -1 | 3 | 3 | 7 | 5 | 9 |
| mmm | $D_2 \times C_2$ | | 3 | 3 | 0 | 0 | 9 |
| 3 | C_3 | 3, 0, 0 | 3 | 2 | 9 | 6 | 9 |
| $\bar{3}$ | $C_3 \times C_2$ | | 3 | 2 | 0 | 0 | 9 |
| 32 | D_3 | 3, 0, -1 | 2 | 2 | 4 | 2 | 6 |
| $3m$ | D_3 | 3, 0, 1 | 2 | 2 | 5 | 4 | 6 |
| $3m$ | $D_3 \times C_2$ | | 2 | 2 | 0 | 0 | 6 |
| 6 | C_6 | 3, 2, 0, -1, 0, 2 | 3 | 2 | 7 | 4 | 5 |
| $\bar{6}$ | C_6 | 3, 2, 0, 1, 0, -2 | 3 | 2 | 2 | 2 | 5 |
| $6/m$ | $C_6 \times C_2$ | | 3 | 2 | 0 | 0 | 5 |
| 622 | D_6 | 3, 2, 0, -1, -1, -1 | 2 | 2 | 3 | 1 | 5 |
| $6mm$ | D_6 | 3, 2, 0, -1, 1, 1 | 2 | 2 | 4 | 3 | 5 |
| $\bar{6}2m$ | D_6 | 3, -2, 0, 1, -1, 1 | 2 | 2 | 1 | 1 | 5 |
| $6/mmm$ | $D_6 \times C_2$ | | 2 | 2 | 0 | 0 | 5 |
| 4 | C_4 | 3, 1, -1, 1 | 3 | 2 | 7 | 4 | 7 |
| $\bar{4}$ | C_4 | 3, -1, -1, -1 | 3 | 2 | 6 | 4 | 7 |
| $4/m$ | $C_4 \times C_2$ | | 3 | 2 | 0 | 0 | 7 |
| 422 | D_4 | 3, 1, -1, -1, -1 | 2 | 2 | 3 | 1 | 6 |
| $4mm$ | D_4 | 3, 1, -1, 1, 1 | 2 | 2 | 4 | 3 | 6 |
| $42m$ | D_4 | 3, -1, -1, -1, 1 | 2 | 2 | 3 | 2 | 6 |
| $4/mmm$ | $D_4 \times C_2$ | | 2 | 2 | 0 | 0 | 6 |
| 23 | T | 3, 0, 0, -1 | 1 | 1 | 2 | 1 | 3 |
| $m\bar{3}$ | $T \times C_2$ | | 1 | 1 | 0 | 0 | 3 |
| 432 | O | 3, 0, -1, 1, -1 | 1 | 1 | 1 | 0 | 3 |
| $43m$ | O | 3, 0, -1, -1, 1 | 1 | 1 | 1 | 1 | 3 |
| $m\bar{3}m$ | $O \times C_2$ | | 1 | 1 | 0 | 0 | 3 |

1.2. REPRESENTATIONS OF CRYSTALLOGRAPHIC GROUPS

Table 1.2.6.10. Irreducible projective representations of the 32 crystallographic point groups

(a) D_2

| $A^2 = B^2 = E, (AB)^2 = -E$ | | | | |
|------------------------------|-----|-----|-----|------|
| Elements | E | A | B | AB |
| Γ'_5 | 2 | 0 | 0 | 0 |

(b) D_4

| $A^4 = -E, B^2 = (AB)^2 = E$ | | | | | | | | |
|------------------------------|-----|-------|--------------|--------------|-----|--------|------|--------|
| Elements | E | A^2 | A | A^3 | B | A^2B | AB | A^3B |
| Γ'_6 | 2 | 0 | $i\sqrt{2}$ | $i\sqrt{2}$ | 0 | 0 | 0 | 0 |
| Γ'_7 | 2 | 0 | $-i\sqrt{2}$ | $-i\sqrt{2}$ | 0 | 0 | 0 | 0 |

(c) D_6

| $A^6 = B^2 = E, (AB)^2 = -E$ | | | | | | | | | | | | |
|------------------------------|-----|-------|-------|-----|--------|--------|-------|--------------|--------------|------|--------|--------|
| Elements | E | A^2 | A^4 | B | A^2B | A^4B | A^3 | A | A^5 | AB | A^3B | A^5B |
| Γ'_7 | 2 | 2 | 2 | 0 | 0 | 0 | 0 | 0 | 0 | 0 | 0 | 0 |
| Γ'_8 | 2 | -1 | -1 | 0 | 0 | 0 | 0 | $i\sqrt{3}$ | $-i\sqrt{3}$ | 0 | 0 | 0 |
| Γ'_9 | 2 | -1 | -1 | 0 | 0 | 0 | 0 | $-i\sqrt{3}$ | $i\sqrt{3}$ | 0 | 0 | 0 |

(d) T [$\omega = \exp(2\pi i/3)$].

| $A^3 = E, B^2 = (AB)^3 = -E$ | | | | | | |
|------------------------------|------------|------------|------------|------------|------------|------------|
| Elements | E | A | BAB | BA | AB | A^2 |
| Γ'_5 | 2 | -1 | 1 | 1 | 1 | -1 |
| Γ'_6 | 2 | ω^5 | ω^2 | ω^2 | ω^2 | ω^5 |
| Γ'_7 | 2 | ω | ω^4 | ω^4 | ω^4 | ω |
| Elements | ABA | A^2B | BA^2 | B | ABA^2 | A^2BA |
| Γ'_5 | -1 | -1 | -1 | 0 | 0 | 0 |
| Γ'_6 | ω^5 | ω^5 | ω^5 | 0 | 0 | 0 |
| Γ'_7 | ω | ω | ω | 0 | 0 | 0 |

(e) O

| $A^4 = -E, B^3 = (AB)^2 = E$ | | | | | | |
|------------------------------|--------------|--------------|--------------|--------------|--------------|--------------|
| Elements | E | B | AB^2A | A^2B | BA^2 | B^2 |
| Γ'_6 | 2 | -1 | 1 | -1 | -1 | -1 |
| Γ'_7 | 2 | -1 | 1 | -1 | -1 | -1 |
| Γ'_8 | 4 | 1 | -1 | 1 | 1 | 1 |
| Elements | BA^2B | ABA^3 | A^2B^2 | A^2 | BA^2B^2 | B^2A^2B |
| Γ'_6 | 1 | 1 | 1 | 0 | 0 | 0 |
| Γ'_7 | 1 | 1 | 1 | 0 | 0 | 0 |
| Γ'_8 | -1 | -1 | -1 | 0 | 0 | 0 |
| Elements | A | A^3 | A^3B | BA^3 | B^2A | AB^2 |
| Γ'_6 | $i\sqrt{2}$ | $i\sqrt{2}$ | $-i\sqrt{2}$ | $-i\sqrt{2}$ | $-i\sqrt{2}$ | $-i\sqrt{2}$ |
| Γ'_7 | $-i\sqrt{2}$ | $-i\sqrt{2}$ | $i\sqrt{2}$ | $i\sqrt{2}$ | $i\sqrt{2}$ | $i\sqrt{2}$ |
| Γ'_8 | 0 | 0 | 0 | 0 | 0 | 0 |
| Elements | A^2B^2A | BA | AB | AB^2A^2 | AB^2A^2B | B^2AB^2 |
| Γ'_6 | 0 | 0 | 0 | 0 | 0 | 0 |
| Γ'_7 | 0 | 0 | 0 | 0 | 0 | 0 |
| Γ'_8 | 0 | 0 | 0 | 0 | 0 | 0 |

(f) $C_4 \times C_2$

| $A^4 = B^2 = E, AB = -BA$ | | | | | | | | |
|---------------------------|-----|-----|-------|-------|-----|------|--------|--------|
| Elements | E | A | A^2 | A^3 | B | AB | A^2B | A^3B |
| Γ'_9 | 2 | 0 | 2 | 0 | 0 | 0 | 0 | 0 |
| Γ'_{10} | 2 | 0 | -2 | 0 | 0 | 0 | 0 | 0 |

(g) $C_6 \times C_2$

| $A^6 = B^2 = E, AB = -BA$ | | | | | | | | | | | | |
|---------------------------|-----|-----|-------------|-------|-------------|-------|-----|------|--------|--------|--------|--------|
| Elements | E | A | A^2 | A^3 | A^4 | A^5 | B | AB | A^2B | A^3B | A^4B | A^5B |
| Γ'_{13} | 2 | 0 | 2 | 0 | 2 | 0 | 0 | 0 | 0 | 0 | 0 | 0 |
| Γ'_{14} | 2 | 0 | $2\omega^2$ | 0 | $2\omega^4$ | 0 | 0 | 0 | 0 | 0 | 0 | 0 |
| Γ'_{15} | 2 | 0 | $2\omega^4$ | 0 | $2\omega^4$ | 0 | 0 | 0 | 0 | 0 | 0 | 0 |

1. TENSORIAL ASPECTS OF PHYSICAL PROPERTIES

Table 1.2.6.10 (cont.)

| $(h) D_2 \times C_2$ | | | | | | | | |
|--|-----|-------|-----|-------|-----|-------|------|-------|
| $A^2 = -E, B^2 = C^2 = (AB)^2 = E, AC = CA, BC = CB$ | | | | | | | | |
| Elements | E | A | B | AB | C | AC | BC | ABC |
| Γ'_9 | 2 | 0 | 0 | 0 | 2 | 0 | 0 | 0 |
| Γ'_{10} | 2 | 0 | 0 | 0 | -2 | 0 | 0 | 0 |
| $A^2 = E, B^2 = C^2 = (AB)^2 = E, AC = -CA, BC = CB$ | | | | | | | | |
| Elements | E | A | B | AB | C | AC | BC | ABC |
| Γ'_{11} | 2 | 0 | 2 | 0 | 0 | 0 | 0 | 0 |
| Γ'_{12} | 2 | 0 | -2 | 0 | 0 | 0 | 0 | 0 |
| $A^2 = E, B^2 = C^2 = (AB)^2 = E, AC = CA, BC = -CB$ | | | | | | | | |
| Elements | E | A | B | AB | C | AC | BC | ABC |
| Γ'_{13} | 2 | $2i$ | 0 | 0 | 0 | 0 | 0 | 0 |
| Γ'_{14} | 2 | $-2i$ | 0 | 0 | 0 | 0 | 0 | 0 |
| $A^2 = -E, B^2 = C^2 = (AB)^2 = E, AC = -CA, BC = CB$ | | | | | | | | |
| Elements | E | A | B | AB | C | AC | BC | ABC |
| Γ'_{15} | 2 | 0 | 0 | 0 | 0 | 0 | 2 | 0 |
| Γ'_{16} | 2 | 0 | 0 | 0 | 0 | 0 | -2 | 0 |
| $A^2 = -E, B^2 = C^2 = (AB)^2 = E, AC = CA, BC = -CB$ | | | | | | | | |
| Elements | E | A | B | AB | C | AC | BC | ABC |
| Γ'_{17} | 2 | 0 | 0 | 0 | 0 | $2i$ | 0 | 0 |
| Γ'_{18} | 2 | 0 | 0 | 0 | 0 | $-2i$ | 0 | 0 |
| $A^2 = E, B^2 = C^2 = (AB)^2 = E, AC = -CA, BC = -CB$ | | | | | | | | |
| Elements | E | A | B | AB | C | AC | BC | ABC |
| Γ'_{19} | 2 | 0 | 0 | $2i$ | 0 | 0 | 0 | 0 |
| Γ'_{20} | 2 | 0 | 0 | $-2i$ | 0 | 0 | 0 | 0 |
| $A^2 = -E, B^2 = C^2 = (AB)^2 = E, AC = -CA, BC = -CB$ | | | | | | | | |
| Elements | E | A | B | AB | C | AC | BC | ABC |
| Γ'_{21} | 2 | 0 | 0 | 0 | 0 | 0 | 0 | $2i$ |
| Γ'_{22} | 2 | 0 | 0 | 0 | 0 | 0 | 0 | $-2i$ |

cyclotomics. Use of arbitrary real numbers would imply a finite precision.

Detailed instructions for the use of the program, together with a guided tour (*QuickStart*), can be found in the manual on the CD-ROM.

1.2.7.2. Tensors

The tensor module of *TenChar* determines the number of independent elements and the relations between the elements of tensors and pseudotensors invariant under a chosen point group and with specified permutation symmetry of the indices. Although the list of point groups provided in a database is limited to dimensions two and three, the program runs for arbitrary dimensions. Similarly, the choice of index permutation symmetry is limited to rank smaller than or equal to four. This is also not a restriction of the program, which works for arbitrary rank. For higher dimensions and higher ranks, the user needs to provide additional information. The limiting factors are in fact the speed, which becomes low for higher dimensions and/or higher rank, and the available memory, which must be sufficient to store the tensor elements.

When the program is started and the tensor part is chosen *via* a button, a selection box opens. The user can specify dimension and rank in open fields. A field without a coloured border has a formally correct content, but the user should check whether the pre-given numbers correspond to his wishes. In open fields with a coloured border, additional information must be given. Clicking on the button 'point group' results in the opening of a new selection window. A specific two- or three-dimensional point group may be chosen *via* geometric crystal classes. This point group may be viewed if wished. The chosen point group is given

by generating matrices and is the one under which the (pseudo)tensor is invariant.

The second symmetry is the index permutation symmetry. For tensors and pseudotensors up to rank four, all possible symmetries are tabulated after clicking 'permutation symmetry'. The indices are numbered from 0 to $r - 1$, where r is the rank. The symbol for a tensor symmetric in the indices 2 and 3 is (2 3), and it is [2 3] if the tensor gets a minus sign under permutation. Arbitrary combinations of symmetric and antisymmetric series can be made. For example, (0 1) 2 [3 4] is a rank-five tensor which is symmetric in the first two indices and antisymmetric in the last two indices. The symbol (0 1 2) characterizes a rank-three tensor that is fully symmetric in all indices. For (pseudo)tensors of rank five and higher, the user needs to specify the permutation symmetry using parentheses in this way. Symmetrization of other pairs is similar. For example, if the rank-three tensor T is symmetric in the first and last indices, the symbol for its permutation character is (0 2) 1. Then $T_{xyz} = T_{zyx}$.

Different settings of the point group may be specified. The standard setting of a point group as given in *International Tables for Crystallography* Volume A may be different from the one to be specified. In this case, the user may perform a basis transformation which transforms the standard setting to the desired setting. This is done *via* the button 'basis transformation'. The standard setting is chosen with 'no transformation'. The transformation from a hexagonal to an orthogonal (Cartesian) basis is performed by selecting 'hC transformation'.

Finally, the tensor or pseudotensor with the specified point group and permutation symmetry is calculated and displayed in a (numbered) window. The command for this is given by clicking on the button 'tensor' or 'pseudotensor', respectively. In the window appear the input data, such as the point group, the

1.2. REPRESENTATIONS OF CRYSTALLOGRAPHIC GROUPS

Table 1.2.6.11. *Special points in the Brillouin zones in three dimensions*

| (a) Triclinic | | | | | | | | |
|--|------------------|----------|--|------------------|----------|--|------------------|----------|
| k | $K_{\mathbf{k}}$ | Kovalev | k | $K_{\mathbf{k}}$ | Kovalev | k | $K_{\mathbf{k}}$ | Kovalev |
| $a\ 000$ | $\bar{1}$ | k_8 | $u\ 0\beta\gamma$ | m | k_1 | $-\frac{1}{2}\frac{1}{2}\frac{1}{2}$ | $\bar{1}$ | k_{11} |
| $b\ 00\frac{1}{2}$ | $\bar{1}$ | k_7 | $v\ \frac{1}{2}\beta\gamma$ | $m11$ | k_2 | $\frac{1}{2}-\frac{1}{2}\frac{1}{2}$ | $\bar{1}$ | k_{12} |
| $c\ 0\frac{1}{2}0$ | $\bar{1}$ | k_6 | $w\ \alpha0\gamma$ | $1m1$ | k_3 | $\frac{1}{2}\frac{1}{2}-\frac{1}{2}$ | $\bar{1}$ | k_{13} |
| $d\ \frac{1}{2}00$ | $\bar{1}$ | k_5 | $x\ \alpha\frac{1}{2}\gamma$ | $1m1$ | k_4 | $l\ 0\beta\gamma$ | $m11$ | k_1 |
| $e\ \frac{1}{2}\frac{1}{2}0$ | $\bar{1}$ | k_4 | $y\ \alpha\beta0$ | $11m$ | k_5 | $m\ \alpha0\gamma$ | $1m1$ | k_2 |
| $f\ \frac{1}{2}0\frac{1}{2}$ | $\bar{1}$ | k_3 | $z\ \alpha\beta\frac{1}{2}$ | $11m$ | k_6 | $n\ \alpha\beta0$ | $11m$ | k_3 |
| $g\ 0\frac{1}{2}\frac{1}{2}$ | $\bar{1}$ | k_2 | | | | | | |
| $h\ \frac{1}{2}\frac{1}{2}\frac{1}{2}$ | $\bar{1}$ | k_1 | | | | | | |
| (b) Monoclinic P | | | (e) Orthorhombic C | | | (h) Tetragonal P | | |
| k | $K_{\mathbf{k}}$ | Kovalev | k | $K_{\mathbf{k}}$ | Kovalev | k | $K_{\mathbf{k}}$ | Kovalev |
| $a\ 000$ | $2/m$ | k_7 | $a\ 000$ | mmm | k_{14} | $a\ 000$ | $4/mmm$ | k_{17} |
| $b\ 00\frac{1}{2}$ | $2/m$ | k_{11} | $b\ 010$ | mmm | k_{15} | $b\ 00\frac{1}{2}$ | $4/mmm$ | k_{19} |
| $c\ \frac{1}{2}00$ | $2/m$ | k_{12} | $c\ 01\frac{1}{2}$ | mmm | k_{17} | $c\ \frac{1}{2}\frac{1}{2}0$ | $4/mmm$ | k_{18} |
| $d\ 0\frac{1}{2}0$ | $2/m$ | k_{13} | $d\ 00\frac{1}{2}$ | mmm | k_{16} | $d\ \frac{1}{2}\frac{1}{2}\frac{1}{2}$ | $4/mmm$ | k_{20} |
| $e\ 0\frac{1}{2}\frac{1}{2}$ | $2/m$ | k_9 | $e\ \frac{1}{2}\frac{1}{2}0$ | $2/m$ | k_{12} | $e\ 0\frac{1}{2}\frac{1}{2}$ | mmm | k_{16} |
| $f\ \frac{1}{2}0\frac{1}{2}$ | $2/m$ | k_8 | $f\ \frac{1}{2}\frac{1}{2}\frac{1}{2}$ | $2/m$ | k_{13} | $f\ 0\frac{1}{2}0$ | mmm | k_{15} |
| $g\ \frac{1}{2}\frac{1}{2}0$ | $2/m$ | k_{14} | $g\ \alpha00$ | $2mm$ | k_8 | $g\ 00\gamma$ | $4mm$ | k_{13} |
| $h\ \frac{1}{2}\frac{1}{2}\frac{1}{2}$ | $2/m$ | k_{10} | $h\ \alpha0\frac{1}{2}$ | $2mm$ | k_9 | $h\ \frac{1}{2}\frac{1}{2}\gamma$ | $4mm$ | k_{14} |
| $i\ 00\gamma$ | 2 | k_3 | $i\ 0\beta0$ | $m2m$ | k_{10} | $i\ 0\frac{1}{2}\gamma$ | $mm2$ | k_{12} |
| $j\ 0\frac{1}{2}\gamma$ | 2 | k_5 | $j\ 0\beta\frac{1}{2}$ | $m2m$ | k_{11} | $j\ \alpha\alpha0$ | $2mm$ | k_{10} |
| $k\ \frac{1}{2}0\gamma$ | 2 | k_4 | $k\ 00\gamma$ | $mm2$ | k_6 | $k\ \alpha\alpha\frac{1}{2}$ | $2mm$ | k_{11} |
| $l\ \frac{1}{2}\frac{1}{2}\gamma$ | 2 | k_6 | $l\ 01\gamma$ | $mm2$ | k_7 | $l\ 0\beta0$ | $m2m$ | k_8 |
| $m\ \alpha\beta0$ | m | k_1 | $m\ \frac{1}{2}\frac{1}{2}\gamma$ | 112 | k_5 | $m\ 0\beta\frac{1}{2}$ | $m2m$ | k_9 |
| $n\ \alpha\beta\frac{1}{2}$ | m | k_2 | $n\ 0\beta\gamma$ | $m11$ | k_1 | $n\ \alpha\frac{1}{2}0$ | $2mm$ | k_6 |
| | | | $o\ \alpha0\gamma$ | $1m1$ | k_2 | $o\ \alpha\frac{1}{2}\frac{1}{2}$ | $2mm$ | k_7 |
| | | | $p\ \alpha\beta0$ | $11m$ | k_3 | $p\ \alpha\beta0$ | $11m$ | k_1 |
| | | | $q\ \alpha\beta\frac{1}{2}$ | $11m$ | k_4 | $q\ \alpha\beta\frac{1}{2}$ | $11m$ | k_2 |
| | | | | | | $r\ \alpha\alpha\gamma$ | m | k_5 |
| | | | | | | $s\ 0\beta\gamma$ | $m11$ | k_3 |
| | | | | | | $t\ \alpha\frac{1}{2}\gamma$ | $1m1$ | k_4 |
| (c) Monoclinic A | | | (f) Orthorhombic I | | | (i) Tetragonal I | | |
| k | $K_{\mathbf{k}}$ | Kovalev | k | $K_{\mathbf{k}}$ | Kovalev | k | $K_{\mathbf{k}}$ | Kovalev |
| $a\ 000$ | $2/m$ | k_6 | $a\ 000$ | mmm | k_{17} | $a\ 000$ | $4/mmm$ | k_{14} |
| $b\ 010$ | $2/m$ | k_8 | $b\ 001$ | mmm | k_{18} | $b\ 001$ | $4/mmm$ | k_{15} |
| $c\ \frac{1}{2}00$ | $2/m$ | k_9 | $c\ 0\frac{1}{2}\frac{1}{2}$ | $2/m11$ | k_{13} | $c\ \frac{1}{2}\frac{1}{2}0$ | mmm | k_{13} |
| $d\ \frac{1}{2}10$ | $2/m$ | k_9 | $1\ \frac{1}{2}\frac{1}{2}$ | $2/m11$ | k_{10} | $d\ \frac{1}{2}\frac{1}{2}\frac{1}{2}$ | $\bar{4}m2$ | k_{12} |
| $e\ 0\frac{1}{2}\frac{1}{2}$ | $\bar{1}$ | k_4 | $d\ \frac{1}{2}0\frac{1}{2}$ | $12/m1$ | k_{14} | $e\ 00\gamma$ | $4mm$ | k_{10} |
| $f\ \frac{1}{2}\frac{1}{2}\frac{1}{2}$ | $\bar{1}$ | k_5 | $\frac{1}{2}\frac{1}{2}\frac{1}{2}$ | $12/m1$ | k_{11} | $f\ \frac{1}{2}0\frac{1}{2}$ | $12/m1$ | k_{11} |
| $g\ 00\gamma$ | 2 | k_2 | $e\ \frac{1}{2}\frac{1}{2}0$ | $112/m$ | k_{15} | $g\ \frac{1}{2}\frac{1}{2}\gamma$ | $2mm$ | k_9 |
| $h\ \frac{1}{2}0\gamma$ | 2 | k_3 | $\frac{1}{2}\frac{1}{2}1$ | $112/m$ | k_{12} | $h\ \alpha\alpha0$ | $2mm$ | k_7 |
| $i\ \alpha\beta0$ | m | k_1 | $f\ \frac{1}{2}\frac{1}{2}\frac{1}{2}$ | 222 | k_{16} | $i\ \alpha00$ | $2mm$ | k_7 |
| | | | $g\ \alpha00$ | $2mm$ | k_7 | $j\ \alpha(1-\alpha)0$ | $2mm$ | k_8 |
| | | | $h\ 0\beta0$ | $m2m$ | k_8 | $k\ \frac{1}{2}\beta\frac{1}{2}$ | 121 | k_5 |
| | | | $i\ 00\gamma$ | $mm2$ | k_9 | $l\ \alpha\beta0$ | $11m$ | k_2 |
| | | | $j\ \frac{1}{2}\frac{1}{2}\gamma$ | 112 | k_6 | $m\ \alpha\alpha\gamma$ | m | k_3 |
| | | | $k\ \frac{1}{2}\beta\frac{1}{2}$ | 121 | k_5 | $\alpha(1-\alpha)\gamma$ | m | k_4 |
| | | | $l\ \alpha\frac{1}{2}\frac{1}{2}$ | 211 | k_4 | $n\ \alpha0\gamma$ | $1m1$ | k_1 |
| | | | $m\ 0\beta\gamma$ | $m11$ | k_1 | | | |
| | | | $n\ \alpha0\gamma$ | $1m1$ | k_2 | | | |
| | | | $o\ \alpha\beta0$ | $11m$ | k_3 | | | |
| | | | | | | | | |
| (d) Orthorhombic P | | | (g) Orthorhombic F | | | (j) Trigonal R (rhombohedral axes) | | |
| k | $K_{\mathbf{k}}$ | Kovalev | k | $K_{\mathbf{k}}$ | Kovalev | k | $K_{\mathbf{k}}$ | Kovalev |
| $a\ 000$ | mmm | k_{19} | $a\ 000$ | mmm | k_{14} | $a\ 000$ | $\bar{3}m$ | k_7 |
| $b\ \frac{1}{2}00$ | mmm | k_{20} | $b\ 100$ | mmm | k_{15} | $b\ \frac{1}{2}\frac{1}{2}\frac{1}{2}$ | $\bar{3}m$ | k_8 |
| $c\ 00\frac{1}{2}$ | mmm | k_{22} | $c\ 010$ | mmm | k_{16} | $c\ \alpha\alpha\alpha$ | $3m$ | k_6 |
| $d\ \frac{1}{2}0\frac{1}{2}$ | mmm | k_{24} | $d\ 001$ | mmm | k_{17} | $d\ 00\frac{1}{2}$ | $2/m$ | k_4 |
| $e\ 0\frac{1}{2}0$ | mmm | k_{21} | $e\ \alpha00$ | $2mm$ | k_4 | $e\ \frac{1}{2}\frac{1}{2}0$ | $2/m$ | k_5 |
| $f\ \frac{1}{2}\frac{1}{2}0$ | mmm | k_{25} | $f\ \alpha10$ | $2mm$ | k_5 | $f\ \alpha(-\alpha)0$ | 2 | k_2 |
| $g\ 0\frac{1}{2}\frac{1}{2}$ | mmm | k_{23} | $g\ 0\beta0$ | $m2m$ | k_6 | $g\ \alpha(-\alpha)\frac{1}{2}$ | 2 | k_2 |
| $h\ \frac{1}{2}\frac{1}{2}\frac{1}{2}$ | mmm | k_{26} | $h\ 1\beta0$ | $m2m$ | k_7 | $h\ \alpha\beta\beta$ | m | k_1 |
| $i\ \alpha00$ | $2mm$ | k_7 | $i\ 00\gamma$ | $mm2$ | k_8 | | | |
| $j\ \alpha0\frac{1}{2}$ | $2mm$ | k_{12} | $j\ 01\gamma$ | $mm2$ | k_9 | | | |
| $k\ \alpha\frac{1}{2}0$ | $2mm$ | k_{10} | $k\ \frac{1}{2}\frac{1}{2}\frac{1}{2}$ | $\bar{1}$ | k_{10} | | | |
| $l\ \alpha\frac{1}{2}\frac{1}{2}$ | $2mm$ | k_{11} | | | | | | |
| $m\ 0\beta0$ | $m2m$ | k_8 | | | | | | |
| $n\ 0\beta\frac{1}{2}$ | $m2m$ | k_{15} | | | | | | |
| $o\ \frac{1}{2}\beta0$ | $m2m$ | k_{13} | | | | | | |
| $p\ \frac{1}{2}\beta\frac{1}{2}$ | $m2m$ | k_{14} | | | | | | |
| $q\ 00\gamma$ | $mm2$ | k_9 | | | | | | |
| $r\ 0\frac{1}{2}\gamma$ | $mm2$ | k_{18} | | | | | | |
| $s\ \frac{1}{2}0\gamma$ | $mm2$ | k_{16} | | | | | | |
| $t\ \frac{1}{2}\frac{1}{2}\gamma$ | $mm2$ | k_{17} | | | | | | |

1. TENSORIAL ASPECTS OF PHYSICAL PROPERTIES

Table 1.2.6.11 (cont.)

(k) Hexagonal P

| \mathbf{k} | $K_{\mathbf{k}}$ | Kovalev |
|--|------------------|----------|
| $a\ 000$ | $6/mmm$ | k_{16} |
| $b\ 00\frac{1}{2}$ | $6/mmm$ | k_{17} |
| $c\ \frac{1}{3}\frac{1}{3}0$ | $\bar{6}m2$ | k_{13} |
| $d\ \frac{1}{3}\frac{1}{3}\frac{1}{2}$ | $\bar{6}m2$ | k_{15} |
| $e\ 00\gamma$ | $6mm$ | k_{11} |
| $f\ \frac{1}{2}00$ | mmm | k_{12} |
| $g\ \frac{1}{2}0\frac{1}{2}$ | mmm | k_{14} |
| $h\ \frac{1}{3}\frac{1}{3}\gamma$ | $3m$ | k_{10} |
| $i\ \frac{1}{2}0\gamma$ | $2mm$ | k_9 |
| $j\ \alpha 00$ | $2mm$ | k_5 |
| $k\ \alpha 0\frac{1}{2}$ | $2mm$ | k_7 |
| $l\ \alpha\alpha 0$ | $2mm$ | k_6 |
| $m\ \alpha\alpha\frac{1}{2}$ | $2mm$ | k_8 |
| $n\ \alpha 0\gamma$ | m | k_3 |
| $o\ \alpha\alpha\gamma$ | m | k_4 |
| $p\ \alpha\beta 0$ | m | k_1 |
| $q\ \alpha\beta\frac{1}{2}$ | m | k_2 |

(l) Cubic P

| \mathbf{k} | $K_{\mathbf{k}}$ | Kovalev |
|--|------------------|----------|
| $a\ 000$ | $m\bar{3}m$ | k_{12} |
| $b\ \frac{1}{2}\frac{1}{2}\frac{1}{2}$ | $m\bar{3}m$ | k_{13} |
| $c\ \frac{1}{2}\frac{1}{2}0$ | $4/mmm$ | k_{11} |
| $d\ 00\frac{1}{2}$ | $4/mmm$ | k_{10} |
| $e\ 00\gamma$ | $4mm$ | k_8 |
| $f\ \frac{1}{2}\frac{1}{2}\gamma$ | $4mm$ | k_7 |
| $g\ \alpha\alpha\alpha$ | $3m$ | k_9 |
| $h\ \frac{1}{2}0\gamma$ | $mm2$ | k_6 |
| $i\ \alpha\alpha 0$ | $2mm$ | k_4 |
| $j\ \alpha\alpha\frac{1}{2}$ | $2mm$ | k_5 |
| $k\ \alpha\beta 0$ | $11m$ | k_1 |
| $l\ \alpha\beta\frac{1}{2}$ | $11m$ | k_2 |
| $m\ \alpha\alpha\gamma$ | m | k_3 |

(m) Cubic F

| \mathbf{k} | $K_{\mathbf{k}}$ | Kovalev |
|--|------------------|----------|
| $a\ 000$ | $m\bar{3}m$ | k_{11} |
| $b\ 001$ | $4/mmm$ | k_{10} |
| $c\ \frac{1}{2}\frac{1}{2}\frac{1}{2}$ | $\bar{3}m$ | k_9 |
| $d\ 10\frac{1}{2}$ | $4m2$ | k_8 |
| $e\ \alpha 00$ | $4mm$ | k_6 |
| $f\ \alpha\alpha\alpha$ | $3m$ | k_5 |
| $g\ \alpha 01$ | $2mm$ | k_7 |
| $h\ \alpha\alpha 0$ | $2mm$ | k_4 |
| $i\ \alpha(1-\alpha)\frac{1}{2}$ | 2 | k_3 |
| $j\ \alpha\beta$ | $11m$ | k_1 |
| $k\ \alpha\alpha\gamma$ | m | k_2 |

(n) Cubic I

| \mathbf{k} | $K_{\mathbf{k}}$ | Kovalev |
|--|------------------|----------|
| $a\ 000$ | $m\bar{3}m$ | k_{11} |
| $b\ 001$ | $m\bar{3}m$ | k_{10} |
| $c\ \frac{1}{2}\frac{1}{2}\frac{1}{2}$ | $\bar{4}3m$ | k_{10} |
| $d\ \frac{1}{2}\frac{1}{2}0$ | mmm | k_9 |
| $e\ \alpha 00$ | $4mm$ | k_8 |
| $f\ \alpha\alpha\alpha$ | $3m$ | k_7 |
| $g\ \alpha\frac{1}{2}\frac{1}{2}$ | $2mm$ | k_6 |
| $h\ \alpha\alpha 0$ | $2mm$ | k_4 |
| $i\ \alpha(1-\alpha)0$ | $2mm$ | k_9 |
| $j\ \alpha\beta$ | $11m$ | k_1 |
| $k\ \alpha\alpha\gamma$ | m | k_2 |
| $\alpha(1-\alpha)\gamma$ | m | k_3 |

Table 1.2.6.12. Magnetic point groups

| Type I | Type II | Type III |
|---|---|--|
| 1 $\bar{1}$ | $1'$ $\bar{1}1'$ | $\bar{1}'$ |
| 2 m $2/m$ | $21'$ $m1'$ $21'/m$ | $2'$ m' $2'/m, 2/m', 2'/m',$ |
| 222 $2mm$ mmm | $2221'$ $2mm1'$ $mmm1'$ | $2'2'$ $2'mm', 2m'm'$ $m'mm, m'm'm, m'm'm'$ |
| 4 $\bar{4}$ $4/m$ 422 $4mm$ $42m$ $4/mmm$ | $41'$ $\bar{4}1'$ $41'/m$ $4221'$ $4mm1'$ $42m1'$ $4/mmm1'$ | $4'$ $\bar{4}'$ $4'/m, 4/m', 4'/m'$ $4'22', 42'2'$ $4'mm', 4m'm'$ $\bar{4}'2'm, \bar{4}'2m', \bar{4}'2'm'$ $4/m'mm, 4'/mm'm, 4'/m'm'm, 4/m'm'm'$ |
| 3 $\bar{3}$ 32 $3m$ $\bar{3}m$ | $31'$ $\bar{3}1'$ $321'$ $3m1'$ $\bar{3}m1'$ | $\bar{3}'$ $32'$ $3m'$ $\bar{3}'m, \bar{3}'m', \bar{3}'m'$ |
| 6 $\bar{6}$ $6/m$ 622 $6mm$ $62m$ $6/mmm$ | $61'$ $\bar{6}1'$ $61'/m$ $6221'$ $6mm1'$ $62m1'$ $6/mmm1'$ | $6'$ $\bar{6}'$ $6'/m, 6/m', 6'/m'$ $6'22', 62'2'$ $6'mm', 6m'm'$ $\bar{6}'2'm, \bar{6}'2m', \bar{6}'2'm'$ $6/m'mm, 6'/mm'm, 6'/m'm'm, 6/m'm'm'$ |
| 23 $m\bar{3}$ 432 $43m$ $m\bar{3}m$ | $231'$ $m\bar{3}1'$ $4321'$ $43m1'$ $m\bar{3}m1'$ | $m'\bar{3}$ $4'32'$ $4'3m'$ $m'\bar{3}m, m\bar{3}m', m'\bar{3}m'$ |

dimension, the rank, the permutation symmetry and the setting basis transformation, and the calculated data: the number of independent elements (f) and the relations of these elements. They are either zero or expressed in terms of the free parameters a_0, \dots, a_{f-1} . The tensor elements are given by sequences x, y, z, \dots . The four elements of a general rank-two tensor in two dimensions are xx, xy, yx, yy , corresponding to T_{11}, T_{12}, T_{21} and T_{22} , respectively.

1.2.7.3. Characters

Calculations with characters of representations of point groups can be done in the character module of the program. It is selected in the main window by clicking 'character'. A selection window opens in which a point group may be selected just as in the tensor module. The point groups are organized according to dimension and geometric crystal class. Selection of a point group leads to the display of the character table if one asks for it by selecting 'view character table'.

The character table consists of a square array of (complex) numbers. The number of rows is the number of nonequivalent irreducible representations and is equal to the number of columns, which is the number of conjugacy classes of the group. For crystallographic groups, the complex numbers that form the entries of the character table are cyclotomic numbers. These are linear combinations with fractions as coefficients of complex numbers of the form $\exp(2\pi i n/m)$. For example, the square root of -1 (i) can be written as $\exp(2\pi i/4)$. A real number like $\sqrt{2}$ can be written as

$$\sqrt{2} = \frac{1}{2}\sqrt{2}(1 + i + 1 - i) = \exp(2\pi i/8) + \exp(2\pi i/8).$$

Another example is

$$\sqrt{5} = 1 + 2\exp(2\pi i/5) + 2\exp(2\pi i/5).$$

1.2. REPRESENTATIONS OF CRYSTALLOGRAPHIC GROUPS

However, many entries for the three-dimensional point groups are simply integers.

The program provides the following information as rows above the characters of the irreducible representation:

(1) Representative elements of the conjugacy classes expressed in terms of the generators a, b, \dots

(2) The number of elements of each class.

(3) The order of the elements of the classes: the lowest positive power of an element that equals the identity.

Below the character table, the following information is displayed:

(1) In the m th row after the square character table, the class to which the $(m+1)$ th powers of the elements from this column belong is given. If a conjugacy class has elements of order p , then only the $p-1$ first entries are given, because in the column there exists p periodicity.

(2) The determinant of the three-dimensional matrix for the element of the point group (or the elements of the conjugacy class). This is the character of an irreducible representation.

(3) Finally, the character of the vector representation is given.

As an example, the generalized character table for the three-dimensional point group $4mm$ is given in Table 1.2.7.1.

The data connected with a character table can be seen by choosing 'view character table'. The characters of the irreducible representations, the determinant representation and the vector representation are shown in the main window after selection of 'accept character table'. From the character of these representations, characters of other representations may be calculated. The results are added as rows to the table, which is shown after each calculation.

Calculations using rows from the table may have one or more arguments. Operations with one argument will produce, for example, the decomposition into irreducible components, the character of the p th power, the symmetrized or antisymmetrized square, or the character of the corresponding physical (real) representation. Operations with two or more arguments yield products and sums of characters. The arguments of a unitary, binary or multiple operation are selected by clicking on the button in front of the corresponding characters. If the result is a new character (e.g. the product of two characters), it is added as a row to the list of characters. If the result is not a character (e.g. the decomposition into irreducible components), the result is given on the worksheet.

Suppose one wants to determine the number of elastic constants for a material with cubic 432 symmetry. After selecting the character table for the group 432, one clicks on the button in front of 'vector representation' in the character table. This yields the character of the three-dimensional vector representation of the group. The character of the symmetrized square is obtained by selecting 'symmetrized square'. This gives the character of a six-dimensional representation. Determining the number of times the trivial representation occurs by selecting 'decompose' gives the number of free parameters in the metric tensor, i.e. 1. Clicking on 'symmetrized square' for the character of the six-dimensional representation gives the character of a 21-dimen-

sional representation. Decomposition yields the multiplicity 3 for the trivial representation, which means that there are three independent tensor elements for a tensor of symmetry type $((01)(23))$, which in turn means that there are three elastic constants for the group 432 (see Table 1.2.6.9). For the explicit determination of the independent tensor elements, the tensor module of the program should be used.

Of course, many kinds of calculations unrelated to tensors can be carried out using the character module. Examples include the calculation of selection rules in spectroscopy or the splitting of energy levels under a symmetry-breaking perturbation.

1.2.7.4. Algorithms

1.2.7.4.1. Construction of a basis

As a basis for a tensor space without permutation symmetry, one may choose one consisting of non-commutative monomials. It has d^r elements, where d is the dimension and r is the rank. In two dimensions, these are x, y for $r=1$, xx, xy, yx, yy for $r=2$ and $xxx, xxy, xyx, xyy, yxx, yxy, yyy$ for $r=3$. Note that $xy \neq yx$.

If there is permutation symmetry among the indices i_1, \dots, i_p , only polynomials $x_{i_1}x_{i_2}\dots x_{i_p}$ occur in the basis for which $i_1 \leq i_2 \leq \dots \leq i_p$. Then $x_{i_1}x_{i_2} = x_{i_2}x_{i_1}$. If there is antisymmetry among these indices, one has the condition $i_1 < i_2 < \dots < i_p$ and $x_{i_1}x_{i_2} = -x_{i_2}x_{i_1}$. Therefore, in two dimensions, the basis for tensors of type $(1\ 3)2$ is $xxx, xxy, xyx, xyy, yxy, yyy$ and for those of type $[1\ 3]2$ it is xyx, xyy . These bases can be obtained from the general basis by elimination.

1.2.7.4.2. Action of the generators of the point group G on the basis

The transformation of the monomial $x_i x_j \dots$ under the matrix $g \in G$ is given by the polynomial

$$\left[\sum_{m=1}^d g_{im} x_m \right] \times \left[\sum_{n=1}^d g_{jn} x_n \right] \dots,$$

which is in principle non-commutative. This polynomial can be written as a sum of the monomials in the basis taking into account the eventual (anti)symmetry of xy and yx . In this way, basis element (a monomial) e_i is transformed to

$$ge_i = \sum_{j=1}^d M(g)_{ji} e_j.$$

To each generator of G corresponds such an action matrix M .

The action matrix changes if one considers pseudotensors. In the case of pseudotensors, the previous equation changes to

$$ge_i = \text{Det}(g) \sum_{j=1}^d M(g)_{ji} e_j.$$

The function $\text{Det}(g)$ is just a one-dimensional representation of the group G . The determinant is either $+1$ or -1 .

1.2.7.4.3. Diagonalization of the action matrix and determination of the invariant tensor

An invariant element of the tensor space under the group G is a vector v that is left invariant under each generator:

$$\begin{pmatrix} M_1 - E \\ M_2 - E \\ \vdots \\ M_s - E \end{pmatrix} v = \Omega v = 0.$$

If the number of generators is one, $\Omega = M - E$. This equation is solved by diagonalization:

Table 1.2.7.1. Data connected with the character table for point group $4mm$

| e | a | a^2 | b | ab |
|-----|-----|-------|-----|------|
| 1 | 2 | 1 | 2 | 2 |
| 1 | 4 | 2 | 2 | 2 |
| 1 | 1 | 1 | 1 | 1 |
| 1 | 1 | 1 | -1 | -1 |
| 1 | -1 | 1 | 1 | -1 |
| 1 | -1 | 1 | -1 | 1 |
| 2 | 0 | -2 | 0 | 0 |
| 1 | 3 | 1 | 1 | 1 |
| | 2 | | | |
| | 1 | | | |
| 1 | 1 | 1 | -1 | -1 |
| 3 | 1 | -1 | 1 | 1 |

1. TENSORIAL ASPECTS OF PHYSICAL PROPERTIES

$$P\Omega Q Q^{-1}v = DQ^{-1}v = 0,$$

where $D_{ij} = d_i \delta_{ij}$. The dimension of the solution space is the number of elements d_i that are equal to zero. The corresponding rows of Q form a basis for the solution space. (See example further on.)

1.2.7.4.4. Determination of the vector representation

For a point group G , its isomorphism class and its character table are known. For each conjugacy class, a representative element is given as word $A_1 A_2 \dots$ where the A_i 's correspond to generators. Replacing the letters by the generating matrices, one obtains as product a matrix for which the trace is the character of the vector representation in the conjugacy class. The characters of all conjugacy classes being known, the representation can be decomposed into irreducible components by means of

$$m_\alpha = (1/|G|) \sum_i n_i \chi_\alpha^*(i) \chi(i),$$

where α labels the irreducible representations (the row number in the character table), m_α the number of times the representation α occurs, $|G|$ the order of the group G , n_i the number of elements in the i th conjugacy class (given as the second row in the character table), $\chi_\alpha(i)$ the cyclotomic in the i th row and α th column of the character table, and $\chi(i)$ the calculated character in the i th conjugacy class.

1.2.7.4.5. Determination of tensor products and their decomposition

Given a character (for an irreducible representation from the character table, or for the vector representation, for example), the character of the standard rank n tensor is the n th power of the character and can be decomposed with the multiplicity formula for m_α given above.

Fully symmetrized or antisymmetrized tensor products have characters given by

$$\begin{aligned} n=2 : \chi^\pm(R) &= \frac{1}{2!} (\chi(R)^2 \pm \chi(R^2)) \\ n=3 : \chi^\pm(R) &= \frac{1}{3!} (\chi(R)^3 \pm 3\chi(R^2)\chi(R) + 2\chi(R^3)) \\ n=4 : \chi^\pm(R) &= \frac{1}{4!} (\chi(R)^4 \pm 6\chi(R^2)\chi(R)^2 + 3\chi(R^2)^2 \\ &\quad + 8\chi(R^3)\chi(R) \pm 6\chi(R^4)) \\ n=5 : \chi^\pm(R) &= \frac{1}{5!} (\chi(R)^5 \pm 10\chi(R^2)\chi(R)^3 + 15\chi(R^2)^2\chi(R) \\ &\quad + 20\chi(R^3)\chi(R)^2 \pm 20\chi(R^3)\chi(R^2) \\ &\quad \pm 30\chi(R^4)\chi(R) + 24\chi(R^5)) \\ n=6 : \chi^\pm(R) &= \frac{1}{6!} (\chi(R)^6 \pm 15\chi(R^2)\chi(R)^4 + 45\chi(R^2)^2\chi(R)^2 \\ &\quad + 40\chi(R^3)^2 \pm 15\chi(R^2)^3 + 40\chi(R^3)\chi(R)^3 \\ &\quad \pm 120\chi(R^3)\chi(R^2)\chi(R) \pm 90\chi(R^4)\chi(R)^2 \\ &\quad + 90\chi(R^4)\chi(R^2) + 144\chi(R^5)\chi(R) \\ &\quad \pm 120\chi(R^6)). \end{aligned}$$

From this follows immediately the dimension of the subspaces of symmetric and antisymmetric tensors:

$$\begin{aligned} n=2 : & \frac{1}{2}(d^2 \pm d) \\ n=3 : & \frac{1}{6}(d^3 \pm 3d^2 + 2d) \\ n=4 : & \frac{1}{24}(d^4 \pm 6d^3 + 11d^2 \pm 6d) \\ n=5 : & \frac{1}{120}(d^5 \pm 10d^4 + 35d^3 \pm 50d^2 + 24d) \\ n=6 : & \frac{1}{720}(d^6 \pm 15d^5 + 85d^4 \pm 225d^3 + 274d^2 \pm 120d). \end{aligned}$$

The general expression for arbitrary rank can be determined as follows. (See also Section 1.2.2.7)

(1) If n is the rank, the first step is to determine all possible decompositions

$$n = \sum_{i=1}^n f_i$$

with non-negative integers f_i satisfying $f_i \leq f_{i-1}$.

(2) For each such decomposition $m = 1, \dots, n_{\text{tot}}$ there is a term

$$P_m = \prod_{i=1}^p \binom{N_i}{f_i} (f_i - 1)!,$$

where $N_1 = n$, $N_i = N_{i-1} - f_{i-1}$ ($i > 1$) and p is the number of nonzero integers f_i .

(3) If there are equal values of f_i in the m th decomposition, P_m should be divided by $t!$ for each t -tuple of equal values ($f_{k+1} = \dots = f_{k+t}$).

(4) The sign of the term P_m is $+1$ for a symmetrized power and

$$\prod_{i=1}^p (-1)^{(f_i-1)}$$

for an antisymmetrized power.

(5) The expression for the character of the (anti)symmetrized power then is

$$\chi^\pm(R) = (1/M!) \sum_{m=1}^{n_{\text{tot}}} \text{sign}_m P_m \prod_{i=1}^p \chi(R^{f_i}).$$

1.2.7.4.6. Invariant tensors

Once one has the character of the properly symmetrized tensor, the number of invariants is just m_1 , the number of times the trivial representation occurs in the decomposition.

Example (1). Dimension 3, rank 3, symmetry type (123), group 3. Basis: $xxx, xxy, xxz, xyy, xyz, xzz, yyy, yyz, yzz, zzz$. Under

$$\begin{pmatrix} 0 & 1 & 0 \\ 0 & 0 & 1 \\ 1 & 0 & 0 \end{pmatrix}$$

the basis elements go to $yyy, yyz, yxx, yzz, yzx, yxx, zzz, zxx, zxx, xxx$, respectively, and these are equivalent to $yyy, yyz, xyy, yzz, xyz, xxy, zzz, xzz, xxz, xxx$, respectively. This gives the ten-dimensional matrix

1.2. REPRESENTATIONS OF CRYSTALLOGRAPHIC GROUPS

$$M = \begin{pmatrix} 0 & 0 & 0 & 0 & 0 & 0 & 0 & 0 & 0 & 1 \\ 0 & 0 & 0 & 0 & 0 & 1 & 0 & 0 & 0 & 0 \\ 0 & 0 & 0 & 0 & 0 & 0 & 0 & 0 & 1 & 0 \\ 0 & 0 & 1 & 0 & 0 & 0 & 0 & 0 & 0 & 0 \\ 0 & 0 & 0 & 0 & 1 & 0 & 0 & 0 & 0 & 0 \\ 0 & 0 & 0 & 0 & 0 & 0 & 0 & 1 & 0 & 0 \\ 1 & 0 & 0 & 0 & 0 & 0 & 0 & 0 & 0 & 0 \\ 0 & 1 & 0 & 0 & 0 & 0 & 0 & 0 & 0 & 0 \\ 0 & 0 & 0 & 1 & 0 & 0 & 0 & 0 & 0 & 0 \\ 0 & 0 & 0 & 0 & 0 & 0 & 1 & 0 & 0 & 0 \end{pmatrix}.$$

Then $P(M - E)Q = D$, with D diagonal. There are four diagonal elements of D which are zero, and the invariant tensors correspond to the corresponding four columns of the matrix Q . The invariant polynomials are

$$xxx + yyy + zzz, \quad xxy + xzz + yyz, \quad xxz + yzz + xyy, \quad xyz.$$

Example (2). Dimension 2, rank 2, symmetry type (12). Group generated by

$$\begin{pmatrix} 0 & -1 \\ 1 & -1 \end{pmatrix}.$$

Basis xx, xy, yy goes to $yy, -xy + yy, xx - 2xy + yy$. This gives

$$M = \begin{pmatrix} 0 & 0 & 1 \\ 0 & -1 & -2 \\ 1 & 1 & 1 \end{pmatrix}.$$

Because

$$\begin{pmatrix} 1 & 0 & 0 \\ 2 & 1 & 2 \\ 1 & 0 & 1 \end{pmatrix} (M - E) \begin{pmatrix} 1 & -1 & 1 \\ 0 & 1 & 0 \\ 0 & -1 & 1 \end{pmatrix} = \begin{pmatrix} -1 & 0 & 0 \\ 0 & 0 & 0 \\ 0 & 0 & 2 \end{pmatrix},$$

the invariant tensor corresponds to the second column of Q , which as a polynomial reads $-xx + xy - yy$. This can be written with the tensor T_{ij} as

$$-xx + xy - yy = -\sum_{i,j} T_{ij} x_i x_j, \quad T_{ij} = \begin{pmatrix} 1 & -\frac{1}{2} \\ -\frac{1}{2} & 1 \end{pmatrix}$$

This tensor T is invariant under the group.

Example (3). Dimension 3, rank 2, tensor type (12). Group generated by matrix $([[0 -1 0][1 0 0][0 0 1]])$. The basis xx, xy, xz, yy, yz, zz goes under the generator to $yy, -xy, -yz, xx, xz, zz$. The solution of $(M - E)v = 0$ is

$$\alpha_1(xx + yy) + \alpha_2 zz.$$

The matrix D has two zeros on the diagonal.

Example (4). Dimension 3, rank 3, type (123). Same group as in Example (3). Basis $xxx, xxy, xxz, xyy, xyz, xzz, yyy, yyz, yzz, zzz$. The solution

$$\alpha_1(xxz + yyz) + \alpha_2 zzz$$

corresponds to a tensor with relations $T_{113} = T_{223}$, $T_{111} = T_{112} = T_{122} = T_{123} = T_{133} = T_{222} = T_{233} = 0$.

Example (5). Dimension 3, rank 4, type $((12)(34))$. Not only $i_1 \leq i_2$ and $i_3 \leq i_4$, but also $(i_1 i_2)$, should come lexicographically before $(i_3 i_4)$. Basis $xxxx, xxxy, xxxz, xxyy, xxyz, xxzz, xyxy, xyxz, xyyy, xyyz, xyzx, xzxx, xzyy, xzyz, xzzz, yyyy, yyyz, yyyz, yzyz, yzzz, zzzz$. Under the same group as in example (3), there are seven invariants. Invariant polynomial:

$$\alpha_1(xxxx + yyyy) + \alpha_2(xxyy - xyyx) + \alpha_3(xxyy + \alpha_4 xyxy + \alpha_5 zzzz + \alpha_6(xxz + yyz) + \alpha_7(xzx + yzy).$$

Table 1.2.7.2. Calculation with characters

| Generator | Composite character | Characters | | | Decomposition | | |
|--|---|--|-----|------|----------------------|-----------------------------|---|
| $\begin{pmatrix} 0 & 1 & 0 \\ 0 & 0 & 1 \\ 1 & 0 & 0 \end{pmatrix}$ | R | E | A | AA | $4D_1 + 3D_2 + 3D_3$ | | |
| | $\chi(R)$ | 3 | 0 | 0 | | | |
| | $\chi(R)^3$ | 27 | 0 | 0 | | | |
| | $\chi(R^2)$ | 3 | 0 | 0 | | | |
| | $\chi(R^2)\chi(R)$ | 9 | 0 | 0 | | | |
| | $\chi(R^3)$ | 3 | 3 | 3 | | | |
| Example (1) | $\frac{1}{6}(\chi(R)^3 + 3\chi(R^2)\chi(R) + 2\chi(R^3))$ | 10 | 1 | 1 | | | |
| $\begin{pmatrix} 0 & -1 \\ 1 & -1 \end{pmatrix}$ | R | E | A | AA | $D_1 + D_2 + D_3$ | | |
| | $\chi(R)$ | 2 | -1 | -1 | | | |
| | $\chi(R)^2$ | 4 | 1 | 1 | | | |
| | $\chi(R^2)$ | 2 | -1 | -1 | | | |
| | $\frac{1}{2}(\chi(R)^2 + \chi(R^2))$ | 3 | 0 | 0 | | | |
| | | | | | | | |
| $\begin{pmatrix} 0 & -1 & 0 \\ 1 & 0 & 0 \\ 0 & 0 & 1 \end{pmatrix}$ | R | E | A | AA | AAA | $2D_1 + D_2 + 2D_3 + D_4$ | |
| | $\chi(R)$ | 3 | 1 | -1 | 1 | | |
| | $\chi(R)^2$ | 9 | 1 | 1 | 1 | | |
| | $\chi(R^2)$ | 3 | -1 | 3 | -1 | | |
| | $\frac{1}{2}(\chi(R)^2 + \chi(R^2))$ | 6 | 0 | 2 | 0 | | |
| | | | | | | | |
| As above | $\chi(R)$ | 3 | 1 | -1 | 1 | $2D_1 + 3D_2 + 2D_3 + 3D_4$ | |
| Example (4) | $\chi(R)^3$ | 27 | 1 | -1 | 1 | | |
| | $\chi(R^2)$ | 3 | -1 | 3 | -1 | | |
| | $\chi(R^2)\chi(R)$ | 9 | -1 | -3 | -1 | | |
| | $\chi(R^3)$ | 3 | 1 | -1 | 1 | | |
| | $\frac{1}{6}(\chi(R)^3 + 3\chi(R^2)\chi(R) + 2\chi(R^3))$ | 10 | 0 | -2 | 0 | | |
| As above | $\chi(R)$ | 3 | 1 | -1 | 1 | $7D_1 + 4D_2 + 6D_3 + 4D_4$ | |
| | Example (5) | $\frac{1}{2}(\chi(R)^2 + \chi(R^2)) = \chi_s(R)$ | 6 | 0 | 2 | | 0 |
| | | $\chi_s(R)^2$ | 36 | 0 | 4 | | 0 |
| | | $\chi_s(R^2)$ | 6 | 2 | 6 | | 2 |
| | | $((12)(34))$ | 21 | 1 | 5 | | 1 |
| | | | | | | | |
| As above, example (6) | $\frac{1}{2}(\chi(R)^2 - \chi(R^2))$ | 3 | 1 | -1 | 1 | $D_1 + D_2 + D_4$ | |
| As above, example (7) | $\frac{1}{6}(\chi(R)^3 - 3\chi(R^2)\chi(R) + 2\chi(R^3))$ | 1 | 1 | 1 | 1 | D_1 | |

1. TENSORIAL ASPECTS OF PHYSICAL PROPERTIES

This corresponds to the tensor relations

$$\begin{aligned}
 T_{xxxx} &= -T_{yyyy} & T_{xxxy} &= T_{xyyy} & T_{xxxz} &= 0 \\
 T_{xxyz} &= 0 & T_{xxzz} &= T_{yyzz} & T_{xyxz} &= 0 \\
 T_{xyyz} &= 0 & T_{xyzx} &= 0 & T_{xzxz} &= T_{yzyz} \\
 T_{xzyy} &= 0 & T_{xzyz} &= 0 & T_{xzzz} &= 0 \\
 T_{yyyz} &= 0 & T_{yzzz} &= 0 & &
 \end{aligned}$$

$$\rightarrow \begin{pmatrix} \alpha_1 & \alpha_3 & \alpha_6 & 0 & 0 & \alpha_2 \\ \alpha_3 & \alpha_1 & \alpha_6 & 0 & 0 & -\alpha_2 \\ \alpha_6 & \alpha_6 & \alpha_5 & 0 & 0 & 0 \\ 0 & 0 & 0 & \alpha_7 & 0 & 0 \\ 0 & 0 & 0 & 0 & \alpha_7 & 0 \\ \alpha_2 & -\alpha_2 & 0 & 0 & 0 & \alpha_4 \end{pmatrix}.$$

The latter form is that of an elastic tensor with the usual convention $1 = xx$, $2 = yy$, $3 = zz$, $4 = yz$, $5 = xz$, $6 = xy$.

Example (6). Dimension 3, rank 2, type [12]. The same group as in example (3). Basis $xy, xz, yz \rightarrow -yx, -yz, xz$, which are equivalent to $xy, -yz, xz$. The transformation in the tensor space is

$$M = \begin{pmatrix} 1 & 0 & 0 \\ 0 & 0 & 1 \\ 0 & -1 & 0 \end{pmatrix} \rightarrow \begin{pmatrix} 0 & 0 & 0 \\ 0 & -1 & 1 \\ 0 & -1 & -1 \end{pmatrix} v = 0:$$

$$v = \begin{pmatrix} 1 \\ 0 \\ 0 \end{pmatrix} \sim xy.$$

There is just one invariant antisymmetric polynomial $xy = -yx$ corresponding to the tensor

$$T = \begin{pmatrix} 0 & 1 \\ -1 & 0 \end{pmatrix}.$$

Example (7). Dimension 3, rank 3, type [123]. Basis xyz invariant under the group: $xyz \rightarrow -yxz \sim xyz$. The corresponding tensor is the fully antisymmetric rank 3 tensor: $T_{ijk} = 1$ if ijk is an even permutation of 123, $= -1$ if ijk is an odd permutation, and $= 0$ if two or three indices are equal (permutation tensor, see Section 1.1.3.7.2).

Example (8). Calculation with characters. See Table 1.2.7.2.

Example (9). The action matrix for a pseudotensor. Take the group $4/m$ with generators

$$\begin{pmatrix} 0 & -1 & 0 \\ 1 & 0 & 0 \\ 0 & 0 & 1 \end{pmatrix}, \quad \begin{pmatrix} 1 & 0 & 0 \\ 0 & 1 & 0 \\ 0 & 0 & -1 \end{pmatrix}.$$

Consider the rank 3 pseudotensor (123). The action matrix is determined from the action of the generators A and B on the basis:

| | A | B |
|-------|--------|--------|
| xxx | $-yyy$ | $-xxx$ |
| xyx | xyy | $-xxy$ |
| xxz | yyz | xxz |
| xyy | $-xxy$ | $-xyy$ |
| xyz | $-xyz$ | xyz |
| xzz | $-yzz$ | $-xzz$ |
| yyy | xxx | $-yyy$ |
| yyz | xxz | yyz |
| yzz | xzz | $-yzz$ |
| zzz | zzz | zzz |

Therefore, the action matrix becomes

$$\begin{pmatrix} 0 & 0 & 0 & 0 & 0 & 0 & 1 & 0 & 0 & 0 \\ 0 & 0 & 0 & -1 & 0 & 0 & 0 & 0 & 0 & 0 \\ 0 & 0 & 0 & 0 & 0 & 0 & 0 & 1 & 0 & 0 \\ 0 & 1 & 0 & 0 & 0 & 0 & 0 & 0 & 0 & 0 \\ 0 & 0 & 0 & 0 & -1 & 0 & 0 & 0 & 0 & 0 \\ 0 & 0 & 0 & 0 & 0 & 0 & 0 & 0 & 1 & 0 \\ -1 & 0 & 0 & 0 & 0 & 0 & 0 & 0 & 0 & 0 \\ 0 & 0 & 1 & 0 & 0 & 0 & 0 & 0 & 0 & 0 \\ 0 & 0 & 0 & 0 & 0 & -1 & 0 & 0 & 0 & 0 \\ 0 & 0 & 0 & 0 & 0 & 0 & 0 & 0 & 0 & 1 \\ -1 & 0 & 0 & 0 & 0 & 0 & 0 & 0 & 0 & 0 \\ 0 & -1 & 0 & 0 & 0 & 0 & 0 & 0 & 0 & 0 \\ 0 & 0 & 1 & 0 & 0 & 0 & 0 & 0 & 0 & 0 \\ 0 & 0 & 0 & -1 & 0 & 0 & 0 & 0 & 0 & 0 \\ 0 & 0 & 0 & 0 & 1 & 0 & 0 & 0 & 0 & 0 \\ 0 & 0 & 0 & 0 & 0 & -1 & 0 & 0 & 0 & 0 \\ 0 & 0 & 0 & 0 & 0 & 0 & -1 & 0 & 0 & 0 \\ 0 & 0 & 0 & 0 & 0 & 0 & 0 & 1 & 0 & 0 \\ 0 & 0 & 0 & 0 & 0 & 0 & 0 & 0 & -1 & 0 \\ 0 & 0 & 0 & 0 & 0 & 0 & 0 & 0 & 0 & 1 \end{pmatrix}.$$

After diagonalization, one finds two nonzero elements on the diagonal:

$$\begin{aligned}
 zzz &= a; & xxz &= yyz = b; \\
 xxx &= xxy = xyy = xyz = xzz = yyy = yzz = 0.
 \end{aligned}$$

1.2.8. Glossary

| | |
|---------------------|--|
| $T_{i_1 \dots i_n}$ | tensor of rank n |
| $O(n)$ | orthogonal group |
| \mathbb{Z} | ring of integers |
| \mathbf{e}_i | basis vectors |
| g | metric tensor |
| K | point group |
| R | orthogonal transformation |
| C_m | cyclic group of order m |
| $SO(n)$ | special orthogonal group |
| \mathbb{Z}^+ | positive integers |
| D_n | dihedral group of order n |
| E | unit transformation, matrix or element |
| I | inversion |
| $D(K)$ | representation of K |
| $\Gamma(K)$ | matrix representation of K |
| $ K $ | order of K |
| \oplus | sum of spaces or operators |
| \otimes | tensor product |
| \in | element of |
| \mathbf{a}_i | basis of space or lattice |

1.2. REPRESENTATIONS OF CRYSTALLOGRAPHIC GROUPS

| | | | |
|------------------------|--|---|-----------------------------|
| V^* | dual space | ω | factor system |
| S | basis transformation | $\text{Det}(R)$ | determinant of R |
| χ | character | $\left(\begin{array}{cc cc} \alpha & \beta & \gamma & \\ i & j & k & \ell \end{array} \right)$ | Clebsch–Gordan coefficients |
| $\chi(R)$ | value of χ at R | | |
| C_i | conjugacy class | θ | time-reversal operator |
| χ_α | irreducible character | | |
| m_α | multiplicity | | |
| N | order of K | | |
| d_α | dimension of irreducible representation α | | |
| n_i | order of class C_i | | |
| c_{ijk} | class multiplication constants | | |
| T | tetrahedral group | | |
| O | octahedral group | | |
| I | icosahedral group | | |
| $P(K)$ | projective representation | | |
| $W_i(A_1, \dots, A_p)$ | word in generators A_j | | |
| K^d | double group | | |
| $E(n)$ | Euclidean group | | |
| $g = \{R \mathbf{a}\}$ | element of $E(n)$ | | |
| $T(n)$ | translation group in n dimensions | | |
| Λ | lattice | | |
| Λ^* | reciprocal lattice | | |
| $\mathbf{a}(R)$ | translation vector system | | |
| \mathbf{k} | vector in dual space | | |
| $G_{\mathbf{k}}$ | group of \mathbf{k} | | |
| $K_{\mathbf{k}}$ | point group of $G_{\mathbf{k}}$ | | |

References

- Altmann, S. L. & Herzig, P. (1994). *Point-group theory tables*. Oxford: Clarendon Press.
- Butler, P. H. (1981). *Point group symmetry applications*. New York & London: Plenum Press.
- International Tables for Crystallography* (2002). Vol. A. *Space-group symmetry*, edited by Th. Hahn. Dordrecht: Kluwer Academic Publishers.
- Janssen, T. (1973). *Crystallographic groups*. Amsterdam: North-Holland.
- Kovalev, O. V. (1987). *Representations of the crystallographic space groups*. New York: Gordon and Breach.
- Miller, S. C. & Love, W. F. (1967). *Tables of irreducible representations of space groups and co-representations of magnetic space groups*. Boulder, Colorado: Pruett Press.
- Stokes, H. T. & Hatch, D. M. (1988). *Isotropy subgroups of the 230 crystallographic space groups*. Singapore: World Scientific.

1.3. Elastic properties

BY A. AUTHIER AND A. ZAREMBOWITCH

1.3.1. Strain tensor

1.3.1.1. Introduction, the notion of strain field

Let us consider a medium that undergoes a deformation. This means that the various points of the medium are displaced with respect to one another. Geometrical transformations of the medium that reduce to a translation of the medium as a whole will therefore not be considered. We may then suppose that there is an invariant point, O , whose position one can always return to by a suitable translation. A point P , with position vector $\mathbf{OP} = \mathbf{r}$, is displaced to the neighbouring point P' by the deformation defined by

$$\mathbf{PP}' = \mathbf{u}(\mathbf{r}).$$

The displacement vector $\mathbf{u}(\mathbf{r})$ constitutes a vector field. It is not a uniform field, unless the deformation reduces to a translation of the whole body, which is incompatible with the hypothesis that the medium undergoes a deformation. Let Q be a point that is near P before the deformation (Fig. 1.3.1.1). Then one can write

$$\mathbf{dr} = \mathbf{PQ}; \quad \mathbf{r} + \mathbf{dr} = \mathbf{OQ}.$$

After the deformation, Q is displaced to Q' defined by

$$\mathbf{QQ}' = \mathbf{u}(\mathbf{r} + \mathbf{dr}).$$

In a deformation, it is more interesting in general to analyse the local, or relative, deformation than the absolute displacement. The relative displacement is given by comparing the vectors $\mathbf{P'Q}' = \mathbf{dr}'$ and \mathbf{PQ} . Thus, one has

$$\mathbf{P'Q}' = \mathbf{P'P} + \mathbf{PQ} + \mathbf{QQ}'.$$

Let us set

$$\left. \begin{aligned} \mathbf{dr}' &= \mathbf{dr} + \mathbf{u}(\mathbf{r} + \mathbf{dr}) - \mathbf{u}(\mathbf{r}) \\ \mathbf{du} &= \mathbf{u}(\mathbf{r} + \mathbf{dr}) - \mathbf{u}(\mathbf{r}) = \mathbf{dr}' - \mathbf{dr}. \end{aligned} \right\} \quad (1.3.1.1)$$

Replacing $\mathbf{u}(\mathbf{r} + \mathbf{dr})$ by its expansion up to the first term gives

$$\left. \begin{aligned} \mathbf{du}_i &= \frac{\partial u_i}{\partial x_j} \mathbf{dx}_j \\ \mathbf{dx}'_i &= \mathbf{dx}_i + \frac{\partial u_i}{\partial x_j} \mathbf{dx}_j. \end{aligned} \right\} \quad (1.3.1.2)$$

If we assume the Einstein convention (see Section 1.1.2.1), there is summation over j in (1.3.1.2) and (1.3.1.3). We shall further assume orthonormal coordinates throughout Chapter 1.3; variance is therefore not apparent and the positions of the indices have no meaning; the Einstein convention then only assumes repetition of a dummy index. The elements \mathbf{dx}_i and \mathbf{dx}'_i are the components of \mathbf{dr} and \mathbf{dr}' , respectively. Let us put

$$M_{ij} = \partial u_i / \partial x_j; \quad B_{ij} = M_{ij} + \delta_{ij},$$

where δ_{ij} represents the Kronecker symbol; the δ_{ij} 's are the components of matrix unity, I . The expressions (1.3.1.2) can also be written using matrices M and B :

$$\left. \begin{aligned} \mathbf{du}_i &= M_{ij} \mathbf{dx}_j \\ \mathbf{dx}'_i &= B_{ij} \mathbf{dx}_j. \end{aligned} \right\} \quad (1.3.1.3)$$

The components of the tensor M_{ij} are nonzero, unless, as mentioned earlier, the deformation reduces to a simple translation. Two cases in particular are of interest and will be discussed in turn:

(i) The components M_{ij} are constants. In this case, the deformation is homogeneous.

(ii) The components M_{ij} are variables but are small compared with unity. This is the practical case to which we shall limit ourselves in considering an inhomogeneous deformation.

1.3.1.2. Homogeneous deformation

If the components M_{ij} are constants, equations (1.3.1.3) can be integrated directly. They become, to a translation,

$$\left. \begin{aligned} u_i &= M_{ij} x_j \\ x'_i &= B_{ij} x_j. \end{aligned} \right\} \quad (1.3.1.4)$$

1.3.1.2.1. Fundamental property of the homogeneous deformation

The fundamental property of the homogeneous deformation results from the fact that equations (1.3.1.4) are linear: a plane before the deformation remains a plane afterwards, a crystal lattice remains a lattice. Thermal expansion is a homogeneous deformation (see Chapter 1.4).

1.3.1.2.2. Spontaneous strain

Some crystals present a twin microstructure that is seen to change when the crystals are gently squeezed. At rest, the domains can have one of two different possible orientations and the influence of an applied stress is to switch them from one orientation to the other. If one measures the shape of the crystal lattice (the strain of the lattice) as a function of the applied stress, one obtains an elastic hysteresis loop analogous to the magnetic or electric hysteresis loops observed in ferromagnetic or ferroelectric crystals. For this reason, these materials are called *ferroelastic* (see Chapters 3.1 to 3.3 and Salje, 1990). The strain associated with one of the two possible shapes of the crystal when no stress is applied is called the macroscopic *spontaneous strain*.

1.3.1.2.3. Cubic dilatation

Let \mathbf{e}_i be the basis vectors before deformation. On account of the deformation, they are transformed into the three vectors

$$\mathbf{e}'_i = B_{ij} \mathbf{e}_j.$$

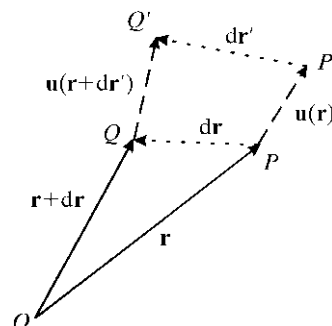


Fig. 1.3.1.1. Displacement vector, $\mathbf{u}(\mathbf{r})$.

1.3. ELASTIC PROPERTIES

The parallelepiped formed by these three vectors has a volume V' given by

$$V' = (\mathbf{e}'_1, \mathbf{e}'_2, \mathbf{e}'_3) = \Delta(B)(\mathbf{e}_1, \mathbf{e}_2, \mathbf{e}_3) = \Delta(B)V,$$

where $\Delta(B)$ is the determinant associated with matrix B , V is the volume before deformation and

$$(\mathbf{e}_1, \mathbf{e}_2, \mathbf{e}_3) = (\mathbf{e}_1 \wedge \mathbf{e}_2) \cdot \mathbf{e}_3$$

represents a triple scalar product.

The relative variation of the volume is

$$\frac{V' - V}{V} = \Delta(B) - 1. \quad (1.3.1.5)$$

It is what one calls the *cubic dilatation*. $\Delta(B)$ gives directly the volume of the parallelepiped that is formed from the three vectors obtained in the deformation when starting from vectors forming an orthonormal base.

1.3.1.2.4. *Expression of any homogeneous deformation as the product of a pure rotation and a pure deformation*

(i) *Pure rotation*: It is isometric. The moduli of the vectors remain unchanged and one direction remains invariant, the axis of rotation. The matrix B is unitary:

$$BB^T = 1.$$

(ii) *Pure deformation*: This is a deformation in which three orthogonal directions remain invariant. It can be shown that B is a symmetric matrix:

$$B = B^T.$$

The three invariant directions are those of the eigenvectors of the matrix; it is known in effect that the eigenvectors of a symmetric matrix are real.

(iii) *Arbitrary deformation*: the matrix B , representing an arbitrary deformation, can always be put into the form of the product of a unitary matrix B_1 , representing a pure rotation, and a symmetric matrix B_2 , representing a pure deformation. Let us put

$$B = B_1 B_2$$

and consider the transpose matrix of B :

$$B^T = B_2^T B_1^T = B_2 (B_1)^{-1}.$$

The product $B^T B$ is equal to

$$B^T B = (B_2)^2.$$

This shows that we can determine B_2 and therefore B_1 from B .

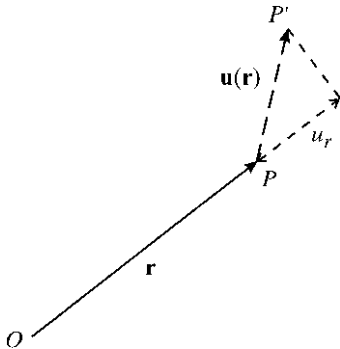


Fig. 1.3.1.2. Elongation, u_r/r .

1.3.1.2.5. Quadric of elongations

Let us project the displacement vector $\mathbf{u}(\mathbf{r})$ on the position vector \mathbf{OP} (Fig. 1.3.1.2), and let u_r be this projection. The *elongation* is the quantity defined by

$$\frac{u_r}{r} = \frac{\mathbf{u} \cdot \mathbf{r}}{r^2} = \frac{M_{ij}x_i x_j}{r^2},$$

where x_1, x_2, x_3 are the components of \mathbf{r} . The elongation is the relative variation of the length of the vector \mathbf{r} in the deformation. Let A and S be the antisymmetric and symmetric parts of M , respectively:

$$A = \frac{M - M^T}{2}; \quad S = \frac{M + M^T}{2}.$$

Only the symmetric part of M occurs in the expression of the elongation:

$$\frac{u_r}{r} = \frac{S_{ij}x_i x_j}{r^2}. \quad (1.3.1.6)$$

The geometrical study of the elongation as a function of the direction of \mathbf{r} is facilitated by introducing the quadric associated with M :

$$S_{ij}y_i y_j = \varepsilon, \quad (1.3.1.7)$$

where ε is a constant. This quadric is called the *quadric of elongations*, Q . S is a symmetric matrix with three real orthogonal eigenvectors and three real eigenvalues, $\lambda_1, \lambda_2, \lambda_3$. If it is referred to these axes, equation (1.3.1.7) is reduced to

$$\lambda_1(y_1)^2 + \lambda_2(y_2)^2 + \lambda_3(y_3)^2 = \varepsilon.$$

One can discuss the form of the quadric according to the sign of the eigenvalues λ_i :

(i) $\lambda_1, \lambda_2, \lambda_3$ have the same sign, and the sign of ε . The quadric is an ellipsoid (Fig. 1.3.1.3a). One chooses $\varepsilon = +1$ or $\varepsilon = -1$, depending on the sign of the eigenvalues.

(ii) $\lambda_1, \lambda_2, \lambda_3$ are of mixed signs: one of them is of opposite sign to the other two. One takes $\varepsilon = \pm 1$. The corresponding quadric is a hyperboloid whose asymptote is the cone

$$S_{ij}y_i y_j = 0.$$

According to the sign of ε , the hyperboloid will have one sheet outside the cone or two sheets inside the cone (Fig. 1.3.1.3b). If we wish to be able to consider any direction of the position vector \mathbf{r} in space, it is necessary to take into account the two quadrics.

In order to follow the variations of the elongation u_r/r with the orientation of the position vector, one associates with \mathbf{r} a vector \mathbf{y} , which is parallel to it and is defined by

$$\mathbf{y} = \mathbf{r}/k; \quad \mathbf{r} = k\mathbf{y},$$

where k is a constant. It can be seen that, in accordance with (1.3.1.6) and (1.3.1.7), the expression of the elongation in terms of \mathbf{y} is

$$u_r/r = \varepsilon/y^2.$$

Thus, the elongation is inversely proportional to the square of the radius vector of the quadric of elongations parallel to \mathbf{OP} . In practice, it is necessary to look for the intersection p of the parallel to \mathbf{OP} drawn from the centre O of the quadric of elongations (Fig. 1.3.1.3a):

(i) The eigenvalues all have the same sign; the quadric Q is an ellipsoid: the elongation has the same sign in all directions in space, positive for $\varepsilon = +1$ and negative for $\varepsilon = -1$.

(ii) The eigenvalues have different signs; two quadrics are to be taken into account: the hyperboloids corresponding, respectively, to $\varepsilon = \pm 1$. The sign of the elongation is different according to

1. TENSORIAL ASPECTS OF PHYSICAL PROPERTIES

whether the direction under consideration is outside or inside the asymptotic cone and intersects one or the other of the two hyperboloids.

Equally, one can connect the displacement vector $\mathbf{u}(\mathbf{r})$ directly with the quadric Q . Using the bilinear form

$$f(\mathbf{y}) = M_{ij}y_iy_j,$$

the gradient of $f(\mathbf{y})$, $\nabla(f)$, has as components

$$\partial f / \partial y^i = M_{ij}y_j = u_i.$$

One recognizes the components of the displacement vector \mathbf{u} , which is therefore parallel to the normal to the quadric Q at the extremity of the radius vector \mathbf{Op} parallel to \mathbf{r} .

The directions of the principal axes of Q correspond to the extremal values of y , i.e. to the stationary values (maximal or minimal) of the elongation. These values are the *principal elongations*.

If the deformation is a pure rotation

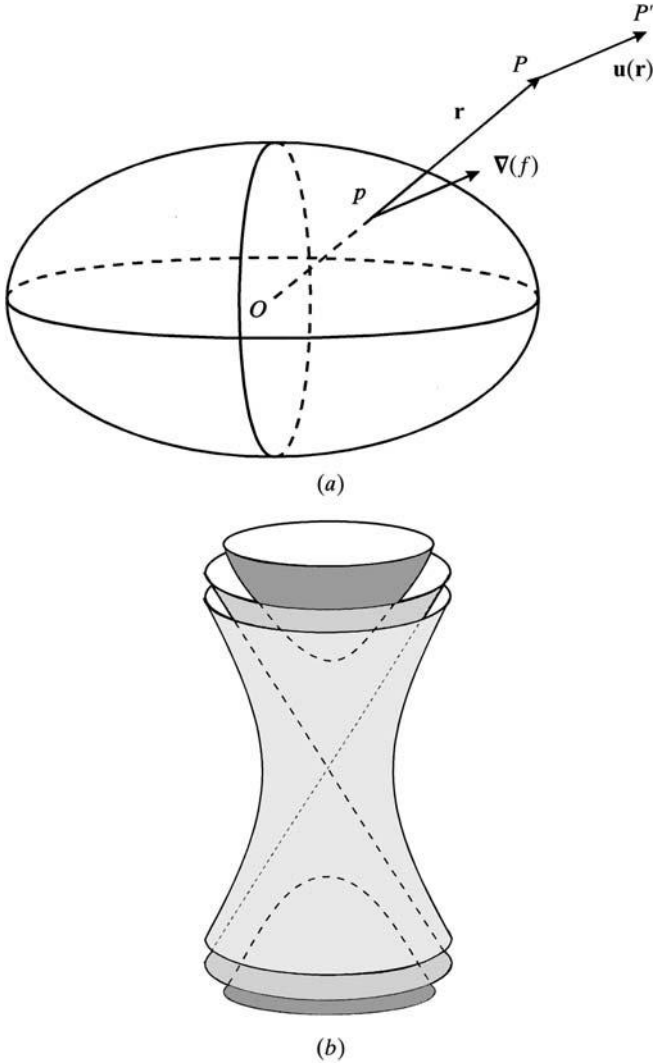


Fig. 1.3.1.3. Quadric of elongations. The displacement vector, $\mathbf{u}(\mathbf{r})$, at P in the deformed medium is parallel to the normal to the quadric at the intersection, p , of \mathbf{Op} with the quadric. (a) The eigenvalues all have the same sign, the quadric is an ellipsoid. (b) The eigenvalues have mixed signs, the quadric is a hyperboloid with either one sheet (shaded in light grey) or two sheets (shaded in dark grey), depending on the sign of the constant ε [see equation (1.3.1.7)]; the cone asymptote is represented in medium grey. For a practical application, see Fig. 1.4.1.1.

$$B = \begin{pmatrix} \cos \theta & \sin \theta & 0 \\ -\sin \theta & \cos \theta & 0 \\ 0 & 0 & 1 \end{pmatrix},$$

$$M = \begin{pmatrix} \cos \theta - 1 & \sin \theta & 0 \\ -\sin \theta & \cos \theta - 1 & 0 \\ 0 & 0 & 0 \end{pmatrix}.$$

Hence we have

$$M_{ij}y_iy_j = (\cos \theta - 1)(y_1 - y_2) = \varepsilon.$$

The quadric Q is a cylinder of revolution having the axis of rotation as axis.

1.3.1.3. Arbitrary but small deformations

1.3.1.3.1. Definition of the strain tensor

If the deformation is small but arbitrary, i.e. if the products of two or more components of M_{ij} can be neglected with respect to unity, one can describe the deformation locally as a homogeneous asymptotic deformation. As was shown in Section 1.3.1.2.4, it can be put in the form of the product of a pure deformation corresponding to the symmetric part of M_{ij} , S_{ij} , and a pure rotation corresponding to the asymmetric part, A_{ij} :

$$\left. \begin{aligned} S_{ij} &= S_{ji} = \frac{1}{2} \left(\frac{\partial u_i}{\partial x_j} + \frac{\partial u_j}{\partial x_i} \right) \\ A_{ij} &= -A_{ji} = \frac{1}{2} \left(\frac{\partial u_i}{\partial x_j} - \frac{\partial u_j}{\partial x_i} \right) \end{aligned} \right\} \quad (1.3.1.8)$$

Matrix B can be written

$$B = I + A + S,$$

where I is the matrix identity. As the coefficients $\partial u_i / \partial x_j$ of M_{ij} are small, one can neglect the product $A \times S$ and one has

$$B = (I + A)(I + S).$$

$(I + S)$ is a symmetric matrix that represents a pure deformation. $(I + A)$ is an antisymmetric unitary matrix and, since A is small,

$$(I + A)^{-1} = (I - A).$$

Thus, $(I + A)$ represents a rotation. The axis of rotation is parallel to the vector with coordinates

$$\left. \begin{aligned} \Omega_1 &= \frac{1}{2} \left(\frac{\partial u_3}{\partial x_2} - \frac{\partial u_2}{\partial x_3} \right) = A_{32} \\ \Omega_2 &= \frac{1}{2} \left(\frac{\partial u_1}{\partial x_3} - \frac{\partial u_3}{\partial x_1} \right) = A_{13} \\ \Omega_3 &= \frac{1}{2} \left(\frac{\partial u_2}{\partial x_1} - \frac{\partial u_1}{\partial x_2} \right) = A_{21}, \end{aligned} \right\}$$

which is an eigenvector of $(I + A)$. The magnitude of the rotation is equal to the modulus of this vector.

In general, one is only interested in the pure deformation, i.e. in the form of the deformed object. Thus, one only wishes to know the quantities $(I + S)$ and the symmetric part of M . It is this symmetric part that is called the deformation tensor or the strain tensor. It is very convenient for applications to use the simplified notation due to Voigt:

$$\begin{aligned} S_1 &= \frac{\partial u_1}{\partial x_1}; & S_2 &= \frac{\partial u_2}{\partial x_2}; & S_3 &= \frac{\partial u_3}{\partial x_3}; \\ S_4 &= \frac{\partial u_3}{\partial x_2} + \frac{\partial u_2}{\partial x_3}; & S_5 &= \frac{\partial u_3}{\partial x_1} + \frac{\partial u_1}{\partial x_3}; & S_6 &= \frac{\partial u_2}{\partial x_1} + \frac{\partial u_1}{\partial x_2}. \end{aligned}$$

1.3. ELASTIC PROPERTIES

One may note that

$$\begin{aligned} S_1 &= S_{11}; & S_2 &= S_{22}; & S_3 &= S_{33}; \\ S_4 &= S_{23} + S_{32}; & S_5 &= S_{31} + S_{13}; & S_6 &= S_{12} + S_{21}. \end{aligned}$$

The Voigt strain matrix S is of the form

$$\begin{pmatrix} S_1 & S_6 & S_5 \\ S_6 & S_2 & S_4 \\ S_5 & S_4 & S_3 \end{pmatrix}.$$

1.3.1.3.2. Geometrical interpretation of the coefficients of the strain tensor

Let us consider an orthonormal system of axes with centre P . We remove nothing from the generality of the following by limiting ourselves to a planar problem and assuming that point P' to which P goes in the deformation lies in the plane x_1Px_2 (Fig. 1.3.1.4). Let us consider two neighbouring points, Q and R , lying on axes Px_1 and Px_2 , respectively ($PQ = dx_1$, $PR = dx_2$). In the deformation, they go to points Q' and R' defined by

$$\begin{aligned} \mathbf{PQ}' : \begin{cases} dx'_1 = dx_1 + (\partial u_1/\partial x_1)dx_1 \\ dx'_2 = (\partial u_2/\partial x_1)dx_1 \\ dx'_3 = 0 \end{cases} \\ \mathbf{PR}' : \begin{cases} dx'_1 = (\partial u_1/\partial x_2)dx_2 \\ dx'_2 = dx_2 + (\partial u_2/\partial x_2)dx_2 \\ dx'_3 = 0. \end{cases} \end{aligned}$$

As the coefficients $\partial u_i/\partial x_j$ are small, the lengths of $P'Q'$ and $P'R'$ are hardly different from PQ and PR , respectively, and the elongations in the directions Px_1 and Px_2 are

$$\begin{aligned} \frac{P'Q' - PQ}{PQ} &= \frac{dx'_1 - dx_1}{dx_1} = \frac{\partial u_1}{\partial x_1} = S_1 \\ \frac{P'R' - PR}{PR} &= \frac{dx'_2 - dx_2}{dx_2} = \frac{\partial u_2}{\partial x_2} = S_2. \end{aligned}$$

The components S_1, S_2, S_3 of the principal diagonal of the Voigt matrix can then be interpreted as the elongations in the three directions Px_1, Px_2 and Px_3 . The angles α and β between \mathbf{PQ} and $\mathbf{P'Q'}$, and \mathbf{PR} and $\mathbf{P'R'}$, respectively, are given in the same way by

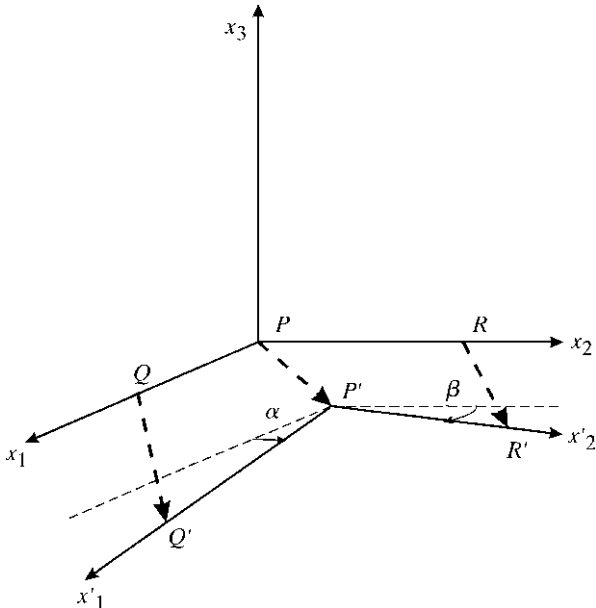


Fig. 1.3.1.4. Geometrical interpretation of the components of the strain tensor. Ox_1, Ox_2, Ox_3 : axes before deformation; Ox'_1, Ox'_2, Ox'_3 : axes after deformation.

$$\alpha = dx'_2/dx_1 = \partial u_2/\partial x_1; \quad \beta = dx'_1/dx_2 = \partial u_1/\partial x_2.$$

One sees that the coefficient S_6 of Voigt's matrix is therefore

$$S_6 = \frac{\partial u_2}{\partial x_1} + \frac{\partial u_1}{\partial x_2} = \alpha + \beta.$$

The angle $\alpha + \beta$ is equal to the difference between angles $\mathbf{PQ} \wedge \mathbf{PR}$ before deformation and $\mathbf{P'Q'} \wedge \mathbf{P'R'}$ after deformation. The nondiagonal terms of the Voigt matrix therefore represent the shears in the planes parallel to Px_1, Px_2 and Px_3 , respectively.

To summarize, if one considers a small cube before deformation, it becomes after deformation an arbitrary parallelepiped; the relative elongations of the three sides are given by the diagonal terms of the strain tensor and the variation of the angles by its nondiagonal terms.

The cubic dilatation (1.3.1.5) is

$$\Delta(B) - 1 = S_1 + S_2 + S_3$$

(taking into account the fact that the coefficients S_{ij} are small).

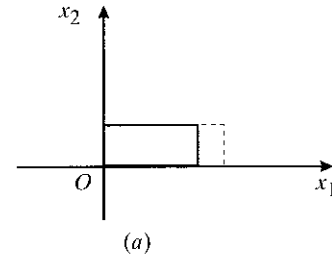
1.3.1.4. Particular components of the deformation

1.3.1.4.1. Simple elongation

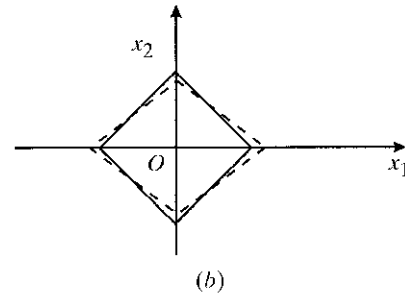
Matrix M has only one coefficient, e_1 , and reduces to (Fig. 1.3.1.5a)

$$\begin{pmatrix} e_1 & 0 & 0 \\ 0 & 0 & 0 \\ 0 & 0 & 0 \end{pmatrix}.$$

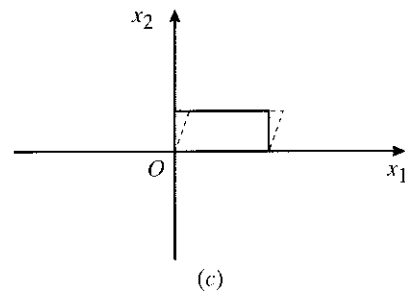
The quadric of elongations is reduced to two parallel planes, perpendicular to Ox_1 , with the equation $x_1 = \pm 1/\sqrt{|e|}$.



(a)



(b)



(c)

Fig. 1.3.1.5. Special deformations. The state after deformation is represented by a dashed line. (a) Simple elongation; (b) pure shear; (c) simple shear.

1. TENSORIAL ASPECTS OF PHYSICAL PROPERTIES

1.3.1.4.2. Pure shear

This is a pure deformation (without rotation) consisting of the superposition of two simple elongations along two perpendicular directions (Fig. 1.3.1.5b) and such that there is no change of volume (the cubic dilatation is zero):

$$\begin{pmatrix} e_1 & 0 & 0 \\ 0 & -e_1 & 0 \\ 0 & 0 & 0 \end{pmatrix}.$$

The quadric of elongations is a hyperbolic cylinder.

1.3.1.4.3. Simple shear

Matrix M_{ij} has one coefficient only, a shear (Fig. 1.3.1.5c):

$$\begin{pmatrix} 0 & s & 0 \\ 0 & 0 & 0 \\ 0 & 0 & 0 \end{pmatrix}.$$

The matrix is not symmetrical, as it contains a component of rotation. Thus we have

$$\left. \begin{aligned} x'_1 &= x_1 + sx_2 \\ x'_2 &= x_2 \\ x'_3 &= x_3. \end{aligned} \right\}$$

One can show that the deformation is a pure shear associated with a rotation around Ox_3 .

1.3.2. Stress tensor

1.3.2.1. General conditions of equilibrium of a solid

Let us consider a solid C , in movement or not, with a mass distribution defined by a specific mass ρ at each point. There are two types of force that are manifested in the interior of this solid.

(i) *Body forces* (or mass forces), which one can write in the form

$$\mathbf{F} dm = \mathbf{F} \rho d\tau,$$

where $d\tau$ is a volume element and dm a mass element. Gravity forces or inertial forces are examples of body forces. One can also envisage body torques (or volume couples), which can arise, for example, from magnetic or electric actions but which will be seen to be neglected in practice.

(ii) *Surface forces or stresses*. Let us imagine a cut in the solid along a surface element $d\sigma$ of normal \mathbf{n} (Fig. 1.3.2.1). The two lips of the cut that were in equilibrium are now subjected to equal and opposite forces, \mathbf{R} and $\mathbf{R}' = -\mathbf{R}$, which will tend to separate or draw together these two lips. One admits that, when the area element $d\sigma$ tends towards zero, the ratio $\mathbf{R}/d\sigma$ tends towards a finite limit, \mathbf{T}_n , which is called *stress*. It is a force per unit area of surface, homogeneous to a pressure. It will be considered as positive if it is oriented towards the same side of the surface-area element $d\sigma$ as the normal \mathbf{n} and negative in the other case. The choice of the orientation of \mathbf{n} is arbitrary. The pressure in a liquid is defined in a similar way but its magnitude is independent of the orientation of \mathbf{n} and its direction is always parallel to \mathbf{n} . On the other hand, in a solid the constraint \mathbf{T}_n applied to a surface element is not necessarily normal to the latter and the magnitude and the orientation with respect to the normal change when the orientation of \mathbf{n} changes. A stress is said to be *homogeneous* if the force per unit area acting on a surface element of given orientation and given shape is independent of the position of the element in the body. Other stresses are *inhomogeneous*. Pressure is represented by a scalar, and stress by a rank-two tensor, which will be defined in Section 1.3.2.2.

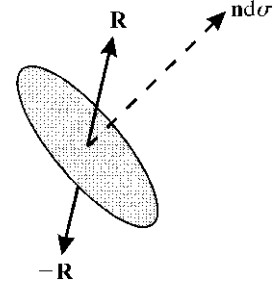


Fig. 1.3.2.1. Definition of stress: it is the limit of $\mathbf{R} d\sigma$ when the surface element $d\sigma$ tends towards zero. \mathbf{R} and \mathbf{R}' are the forces to which the two lips of the small surface element cut within the medium are subjected.

Now consider a volume V within the solid C and the surface S which surrounds it (Fig. 1.3.2.2). Among the influences that are exterior to V , we distinguish those that are external to the solid C and those that are internal. The first are translated by the body forces, eventually by volume couples. The second are translated by the local contact forces of the part external to V on the internal part; they are represented by a surface density of forces, i.e. by the stresses \mathbf{T}_n that depend only on the point Q of the surface S where they are applied and on the orientation of the normal \mathbf{n} of this surface at this point. If two surfaces S and S' are tangents at the same point Q , the same stress acts at the point of contact between them. The equilibrium of the volume V requires:

(i) For the resultant of the applied forces and the inertial forces:

$$\int_S \mathbf{T}_n d\sigma + \int_V \mathbf{F} \rho d\tau = \frac{d}{dt} \left\{ \int_V \mathbf{v} d\tau \right\}. \quad (1.3.2.1)$$

(ii) For the resultant moment:

$$\int_S \mathbf{OQ} \wedge \mathbf{T}_n d\sigma + \int_V \mathbf{OP} \wedge \mathbf{F} \rho d\tau = \frac{d}{dt} \left\{ \int_V \mathbf{OP} \wedge \mathbf{v} d\tau \right\}, \quad (1.3.2.2)$$

where Q is a point on the surface S , P a point in the volume V and \mathbf{v} the velocity of the volume element $d\tau$.

The equilibrium of the solid C requires that:

- (i) there are no stresses applied on its surface and
- (ii) the above conditions are satisfied for *any* volume V within the solid C .

1.3.2.2. Definition of the stress tensor

Using the condition on the resultant of forces, it is possible to show that the components of the stress \mathbf{T}_n can be determined from the knowledge of the orientation of the normal \mathbf{n} and of the components of a rank-two tensor. Let P be a point situated inside volume V , Px_1 , Px_2 and Px_3 three orthonormal axes, and consider a plane of arbitrary orientation that cuts the three axes at Q , R

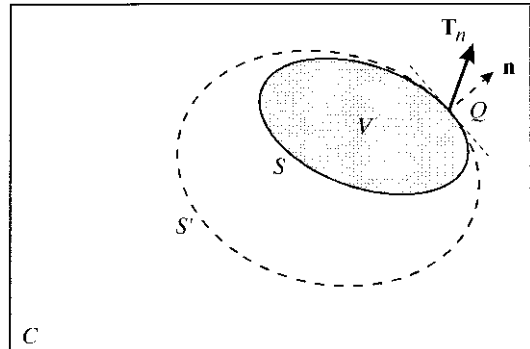


Fig. 1.3.2.2. Stress, \mathbf{T}_n , applied to the surface of an internal volume.

1.3. ELASTIC PROPERTIES

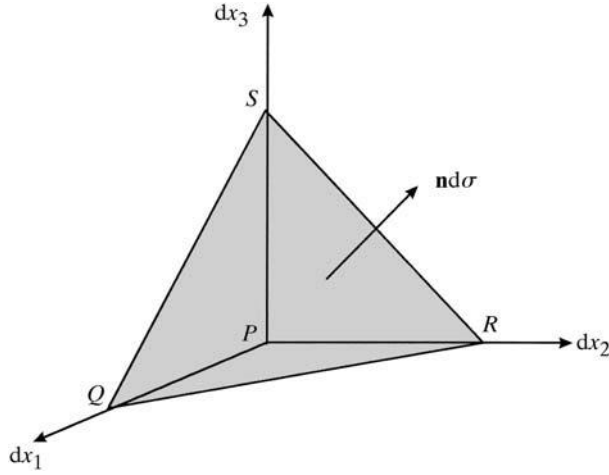


Fig. 1.3.2.3. Equilibrium of a small volume element.

and S , respectively (Fig. 1.3.2.3). The small volume element $PQRS$ is limited by four surfaces to which stresses are applied. The normals to the surfaces PRS , PSQ and PQR will be assumed to be directed towards the interior of the small volume. By contrast, for reasons that will become apparent later, the normal \mathbf{n} applied to the surface QRS will be oriented towards the exterior. The corresponding applied forces are thus given in Table 1.3.2.1. The volume $PQRS$ is subjected to five forces: the forces applied to each surface and the resultant of the volume forces and the inertial forces. The equilibrium of the small volume requires that the resultant of these forces be equal to zero and one can write

$$-\mathbf{T}_n d\sigma + \mathbf{T}_1 d\sigma_1 + \mathbf{T}_2 d\sigma_2 + \mathbf{T}_3 d\sigma_3 + \mathbf{F}\rho d\tau = 0$$

(including the inertial forces in the volume forces).

As long as the surface element $d\sigma$ is finite, however small, it is possible to divide both terms of the equation by it. If one introduces the direction cosines, α_i , the equation becomes

$$-\mathbf{T}_n + \mathbf{T}_1 d\alpha_1 + \mathbf{T}_2 d\alpha_2 + \mathbf{T}_3 d\alpha_3 + \mathbf{F}\rho d\tau/d\sigma = 0.$$

When $d\sigma$ tends to zero, the ratio $d\sigma/d\tau$ tends towards zero at the same time and may be neglected. The relation then becomes

$$\mathbf{T}_n = \mathbf{T}_i \alpha_i. \quad (1.3.2.3)$$

This relation is called the Cauchy relation, which allows the stress \mathbf{T}_n to be expressed as a function of the stresses \mathbf{T}_1 , \mathbf{T}_2 and \mathbf{T}_3 that are applied to the three faces perpendicular to the axes, Px_1 , Px_2 and Px_3 . Let us project this relation onto these three axes:

$$T_{nj} = T_{ij} \alpha_i. \quad (1.3.2.4)$$

The nine components T_{ij} are, by definition, the components of the stress tensor. In order to check that they are indeed the components of a tensor, it suffices to make the contracted product of each side of (1.3.2.4) by any vector x_i : the left-hand side is a scalar product and the right-hand side a bilinear form. The T_{ij} 's are therefore the components of a tensor. The index to the far left indicates the face to which the stress is applied (normal to the x_1 , x_2 or x_3 axis), while the second one indicates on which axis the stress is projected.

Table 1.3.2.1. Stresses applied to the faces surrounding a volume element

α_1 , α_2 and α_3 are the direction cosines of the normal \mathbf{n} to the small surface QRS .

| Face | Area | Applied stress | Applied force |
|-------|--------------------------------|-----------------|--------------------------|
| QRS | $d\sigma$ | $-\mathbf{T}_n$ | $-\mathbf{T}_n d\sigma$ |
| PRS | $d\sigma_1 = \alpha_1 d\sigma$ | \mathbf{T}_1 | $\mathbf{T}_1 d\sigma_1$ |
| PSQ | $d\sigma_2 = \alpha_2 d\sigma$ | \mathbf{T}_2 | $\mathbf{T}_2 d\sigma_2$ |
| PQR | $d\sigma_3 = \alpha_3 d\sigma$ | \mathbf{T}_3 | $\mathbf{T}_3 d\sigma_3$ |

1.3.2.3. Condition of continuity

Let us return to equation (1.3.2.1) expressing the equilibrium condition for the resultant of the forces. By replacing \mathbf{T}_n by the expression (1.3.2.4), we get, after projection on the three axes,

$$\int_S T_{ij} d\sigma_i + \int_V F_j \rho d\tau = 0,$$

where $d\sigma_i = \alpha_i d\sigma$ and the inertial forces are included in the volume forces. Applying Green's theorem to the first integral, we have

$$\int_S T_{ij} d\sigma_i = \int_V \int \left[\partial T_{ij} / \partial x_i \right] d\tau.$$

The equilibrium condition now becomes

$$\int_V \int \left[\partial T_{ij} / \partial x_i + F_j \rho \right] d\tau = 0.$$

In order that this relation applies to any volume V , the expression under the integral must be equal to zero,

$$\partial T_{ij} / \partial x_i + F_j \rho = 0, \quad (1.3.2.5)$$

or, if one includes explicitly the inertial forces,

$$\partial T_{ij} / \partial x_i + F_j \rho = -\rho \partial^2 x_j / \partial t^2. \quad (1.3.2.6)$$

This is the condition of continuity or of conservation. It expresses how constraints propagate throughout the solid. This is how the cohesion of the solid is ensured. The resolution of any elastic problem requires solving this equation in terms of the particular boundary conditions of that problem.

1.3.2.4. Symmetry of the stress tensor

Let us now consider the equilibrium condition (1.3.2.2) relative to the resultant moment. After projection on the three axes, and using the Cartesian expression (1.1.3.4) of the vectorial products, we obtain

$$\int_S \frac{1}{2} \varepsilon_{ijk} (x_i T_{lj} - x_j T_{li}) d\sigma_l + \int_V \int \left[\frac{1}{2} \varepsilon_{ijk} \rho (x_i F_j - x_j F_i) + \Gamma_k \right] d\tau = 0.$$

(including the inertial forces in the volume forces). ε_{ijk} is the permutation tensor. Applying Green's theorem to the first integral and putting the two terms together gives

$$\int_V \int \left\{ \frac{1}{2} \varepsilon_{ijk} \left[\frac{\partial}{\partial x_l} (x_i T_{lj} - x_j T_{li}) + \rho (x_i F_j - x_j F_i) \right] + \Gamma_k \right\} d\tau = 0.$$

In order that this relation applies to any volume V within the solid C , we must have

$$\frac{1}{2} \varepsilon_{ijk} \left[\frac{\partial}{\partial x_l} (x_i T_{lj} - x_j T_{li}) \right] + \Gamma_k = 0$$

or

$$\frac{1}{2} \varepsilon_{ijk} \left[x_i \left(\frac{\partial T_{lj}}{\partial x_l} + F_j \rho \right) - x_j \left(\frac{\partial T_{li}}{\partial x_l} + F_i \rho \right) + T_{ij} - T_{ji} \right] + \Gamma_k = 0.$$

Taking into account the continuity condition (1.3.2.5), this equation reduces to

$$\frac{1}{2} \varepsilon_{ijk} \rho [T_{ij} - T_{ji}] + \Gamma_k = 0.$$

A volume couple can occur for instance in the case of a magnetic or an electric field acting on a body that locally possesses magnetic or electric moments. In general, apart from very rare cases, one can ignore these volume couples. One can then deduce that the stress tensor is symmetrical:

1. TENSORIAL ASPECTS OF PHYSICAL PROPERTIES

$$T_{ij} - T_{ji} = 0.$$

This result can be recovered by applying the relation (1.3.2.2) to a small volume in the form of an elementary parallelepiped, thus illustrating the demonstration using Green's theorem but giving insight into the action of the constraints. Consider a rectangular parallelepiped, of sides $2\Delta x_1$, $2\Delta x_2$ and $2\Delta x_3$, with centre P at the origin of an orthonormal system whose axes Px_1 , Px_2 and Px_3 are normal to the sides of the parallelepiped (Fig. 1.3.2.4). In order that the resultant moment with respect to a point be zero, it is necessary that the resultant moments with respect to three axes concurrent in this point are zero. Let us write for instance that the resultant moment with respect to the axis Px_3 is zero. We note that the constraints applied to the faces perpendicular to Px_3 do not give rise to a moment and neither do the components T_{11} , T_{13} , T_{22} and T_{23} of the constraints applied to the faces normal to Px_1 and Px_2 (Fig. 1.3.2.4). The components T_{12} and T_{21} alone have a nonzero moment.

For face 1, the constraint is $T_{12} + (\partial T_{12}/\partial x_1)\Delta x_1$ if T_{12} is the magnitude of the constraint at P . The force applied at face 1 is

$$\left[T_{12} + \frac{\partial T_{12}}{\partial x_1} \Delta x_1 \right] 4\Delta x_2 \Delta x_3$$

and its moment is

$$\left[T_{12} + \frac{\partial T_{12}}{\partial x_1} \Delta x_1 \right] 4\Delta x_2 \Delta x_3 \Delta x_1.$$

Similarly, the moments of the force on the other faces are

$$\text{Face } 1' : - \left[T_{12} + \frac{\partial T_{12}}{\partial x_1} (-\Delta x_1) \right] 4\Delta x_2 \Delta x_3 (-\Delta x_1);$$

$$\text{Face } 2 : \left[T_{21} + \frac{\partial T_{21}}{\partial x_2} \Delta x_2 \right] 4\Delta x_1 \Delta x_3 \Delta x_2;$$

$$\text{Face } 2' : - \left[T_{21} + \frac{\partial T_{21}}{\partial x_2} (-\Delta x_2) \right] 4\Delta x_1 \Delta x_3 (-\Delta x_2).$$

Noting further that the moments applied to the faces 1 and 1' are of the same sense, and that those applied to faces 2 and 2' are of the opposite sense, we can state that the resultant moment is

$$[T_{12} - T_{21}] 8\Delta x_1 \Delta x_2 \Delta x_3 = [T_{12} - T_{21}] \Delta \tau,$$

where $8\Delta x_1 \Delta x_2 \Delta x_3 = \Delta \tau$ is the volume of the small parallelepiped. The resultant moment per unit volume, taking into account the couples in volume, is therefore

$$T_{12} - T_{21} + \Gamma_3.$$

It must equal zero and the relation given above is thus recovered.

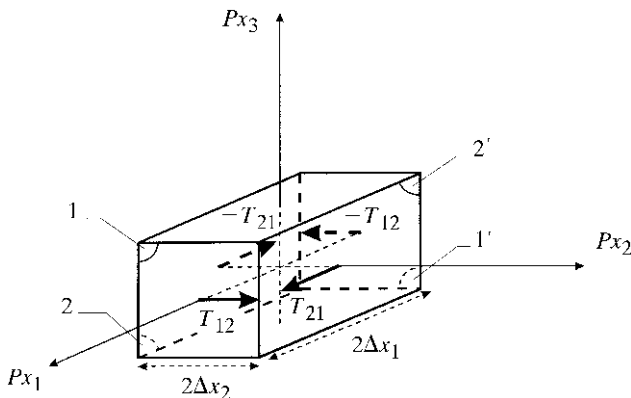


Fig. 1.3.2.4. Symmetry of the stress tensor: the moments of the couples applied to a parallelepiped compensate each other.

1.3.2.5. Voigt's notation – interpretation of the components of the stress tensor

1.3.2.5.1. Voigt's notation, reduced form of the stress tensor

We shall use frequently the notation due to Voigt (1910) in order to express the components of the stress tensor:

$$\begin{aligned} T_1 &= T_{11}; & T_2 &= T_{22}; & T_3 &= T_{33}; \\ T_4 &= T_{23} = T_{32}; & T_5 &= T_{31} = T_{13}; & T_6 &= T_{12} = T_{21}. \end{aligned}$$

It should be noted that the conventions are different for the Voigt matrices associated with the stress tensor and with the strain tensor (Section 1.3.1.3.1).

The Voigt matrix associated with the stress tensor is therefore of the form

$$\begin{pmatrix} T_1 & T_6 & T_5 \\ T_6 & T_2 & T_4 \\ T_5 & T_4 & T_3 \end{pmatrix}.$$

1.3.2.5.2. Interpretation of the components of the stress tensor – special forms of the stress tensor

(i) *Uniaxial stress*: let us consider a solid shaped like a parallelepiped whose faces are normal to three orthonormal axes (Fig. 1.3.2.5). The terms of the main diagonal of the stress tensor correspond to uniaxial stresses on these faces. If there is a single uniaxial stress, the tensor is of the form

$$\begin{pmatrix} 0 & 0 & 0 \\ 0 & 0 & 0 \\ 0 & 0 & T_3 \end{pmatrix}.$$

The solid is submitted to two equal and opposite forces, $T_{33}S_3$ and $-T_{33}S_3$, where S_3 is the area of the face of the parallelepiped that is normal to the Ox_3 axis (Fig. 1.3.2.5a). The convention used in general is that there is a uniaxial *compression* if $T_3 \leq 0$ and a uniaxial *traction* if $T_3 \geq 0$, but the opposite sign convention is sometimes used, for instance in applications such as piezoelectricity or photoelasticity.

(ii) *Pure shear stress*: the tensor reduces to two equal uniaxial constraints of opposite signs (Fig. 1.3.2.5b):

$$\begin{pmatrix} T_1 & 0 & 0 \\ 0 & -T_1 & 0 \\ 0 & 0 & 0 \end{pmatrix}.$$

(iii) *Hydrostatic pressure*: the tensor reduces to three equal uniaxial stresses of the same sign (it is spherical):

$$\begin{pmatrix} -p & 0 & 0 \\ 0 & -p & 0 \\ 0 & 0 & -p \end{pmatrix},$$

where p is a positive scalar.

(iv) *Simple shear stress*: the tensor reduces to two equal nondiagonal terms (Fig. 1.3.2.5c), for instance $T_{12} = T_{21} = T_6$. T_{12} represents the component parallel to Ox_2 of the stress applied to face 1 and T_{21} represents the component parallel to Ox_1 of the stress applied to face 2. These two stresses generate opposite couples that compensate each other. It is important to note that it is impossible to have one nondiagonal term only: its effect would be a couple of rotation of the solid and not a deformation.

1.3.2.6. Boundary conditions

If the surface of the solid C is free from all exterior action and is in equilibrium, the stress field T_{ij} inside C is zero at the surface. If C is subjected from the outside to a distribution of stresses T_n

1.3. ELASTIC PROPERTIES

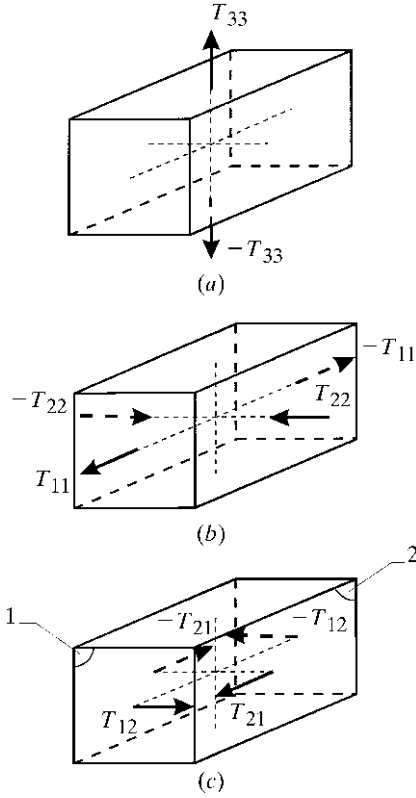


Fig. 1.3.2.5. Special forms of the stress tensor. (a) Uniaxial stress: the stress tensor has only one component, T_{33} ; (b) pure shear stress: $T_{22} = -T_{11}$; (c) simple shear stress: $T_{21} = T_{12}$.

(apart from the volume forces mentioned earlier), the stress field inside the solid is such that at each point of the surface

$$T_{nj} = T_{ij}\alpha_i,$$

where the α_j 's are the direction cosines of the normal to the surface at the point under consideration.

1.3.2.7. Local properties of the stress tensor

(i) *Normal stress and shearing stress*: let us consider a surface area element $d\sigma$ within the solid, the normal \mathbf{n} to this element and the stress \mathbf{T}_n that is applied to it (Fig. 1.3.2.6).

The *normal stress*, ν , is, by definition, the component of \mathbf{T}_n on \mathbf{n} ,

$$\nu = \mathbf{n}(\mathbf{T}_n \cdot \mathbf{n})$$

and the *shearing stress*, τ , is the projection of \mathbf{T}_n on the surface area element,

$$\tau = \mathbf{n} \wedge (\mathbf{T}_n \wedge \mathbf{n}) = \mathbf{T}_n - \nu \mathbf{n}.$$

(ii) *The stress quadric*: let us consider the bilinear form attached to the stress tensor:

$$f(\mathbf{y}) = T_{ij}y_i y_j.$$

The quadric represented by

$$f(\mathbf{y}) = \varepsilon$$

is called the stress quadric, where $\varepsilon = \pm 1$. It may be an ellipsoid or a hyperboloid. Referred to the principal axes, and using Voigt's notation, its equation is

$$y_i^2 T_i = \varepsilon.$$

To every direction \mathbf{n} of the medium, let us associate the radius vector \mathbf{y} of the quadric (Fig. 1.3.2.7) through the relation

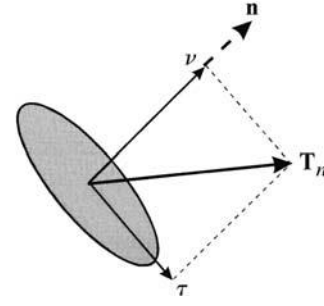


Fig. 1.3.2.6. Normal (ν) and shearing (τ) stress.

$$\mathbf{n} = k\mathbf{y}.$$

The stress applied to a small surface element $d\sigma$ normal to \mathbf{n} , \mathbf{T}_n , is

$$\mathbf{T}_n = k\nabla(f)$$

and the normal stress, ν , is

$$\nu = \alpha_i T_i = 1/y^2,$$

where the α_i 's are the direction cosines of \mathbf{n} .

(iii) *Principal normal stresses*: the stress tensor is symmetrical and has therefore real eigenvectors. If we represent the tensor with reference to a system of axes parallel to its eigenvectors, it is put in the form

$$\begin{pmatrix} T_1 & 0 & 0 \\ 0 & T_2 & 0 \\ 0 & 0 & T_3 \end{pmatrix}.$$

T_1 , T_2 and T_3 are the principal normal stresses. The mean normal stress, T , is defined by the relation

$$T = (T_1 + T_2 + T_3)/3$$

and is an invariant of the stress tensor.

1.3.2.8. Energy density in a deformed medium

Consider a medium that is subjected to a stress field T_{ij} . It has sustained a deformation indicated by the deformation tensor S . During this deformation, the forces of contact have performed work and the medium has accumulated a certain elastic energy W . The knowledge of the energy density thus acquired is useful for studying the properties of the elastic constants. Let the medium deform from the deformation S_{ij} to the deformation $S_{ij} + \delta S_{ij}$ under the influence of the stress field and let us evaluate the work of each component of the effort. Consider a small elementary rectangular parallelepiped of sides $2\Delta x_1$, $2\Delta x_2$, $2\Delta x_3$ (Fig. 1.3.2.8). We shall limit our calculation to the components T_{11} and T_{12} , which are applied to the faces 1 and 1', respectively.

In the deformation δS , the point P goes to the point P' , defined by

$$\mathbf{PP}' = \mathbf{u}(\mathbf{r}).$$

A neighbouring point Q goes to Q' such that (Fig. 1.3.1.1)

$$\mathbf{PQ} = \Delta \mathbf{r}; \quad \mathbf{P'Q'} = \delta \mathbf{r'}.$$

The coordinates of $\delta \mathbf{r'}$ are given by

$$\delta x'_i = \delta \Delta x_i + \delta S_{ij} \delta x_j.$$

Of sole importance is the relative displacement of Q with respect to P and the displacement that must be taken into account in calculating the forces applied at Q . The coordinates of the relative displacement are

1. TENSORIAL ASPECTS OF PHYSICAL PROPERTIES

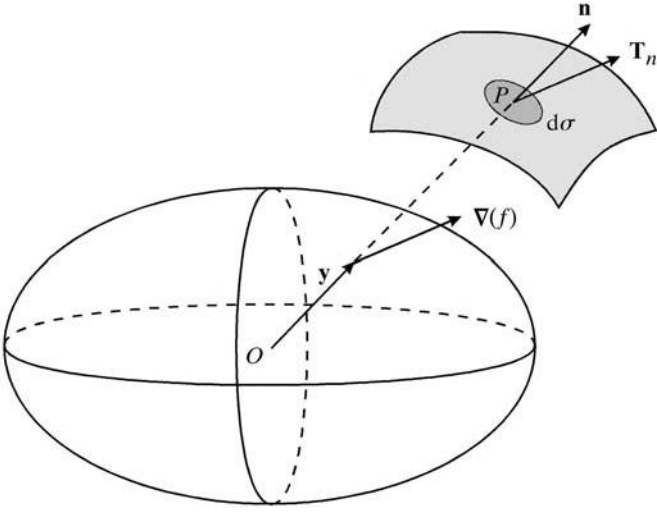


Fig. 1.3.2.7. The stress quadric: application to the determination of the stress applied to a surface element. The surface of the medium is shaded in light grey and a small surface element, $d\sigma$, is shaded in medium grey. The stress at P is proportional to $\nabla(f)$ at the intersection of \mathbf{OP} with the stress quadric.

$$\delta x'_i - \delta \Delta x_i = \delta S_{ij} \delta x_j.$$

We shall take as the position of Q the point of application of the forces at face 1, *i.e.* its centre with coordinates $\Delta x_1, 0, 0$ (Fig. 1.3.2.8). The area of face 1 is $4\Delta x_2 \Delta x_3$ and the forces arising from the stresses T_{11} and T_{12} are equal to $4\Delta x_2 \Delta x_3 T_{11}$ and $4\Delta x_2 \Delta x_3 T_{12}$, respectively. The relative displacement of Q parallel to the line of action of T_{11} is $\Delta x_1 \delta S_{11}$ and the corresponding displacement along the line of action of T_{12} is $\Delta x_1 \delta S_{21}$. The work of the corresponding forces is therefore

$$\begin{aligned} \text{for } T_{11} : & 4\Delta x_1 \Delta x_2 \Delta x_3 T_{11} \delta S_{11} \\ \text{for } T_{12} : & 4\Delta x_1 \Delta x_2 \Delta x_3 T_{12} \delta S_{21}. \end{aligned}$$

The work of the forces applied to the face 1' is the same (T_{11} , T_{12} and x_1 change sign simultaneously). The works corresponding to the faces 1 and 1' are thus $T_{11} \delta S_{11} \Delta \tau$ and $T_{12} \delta S_{21} \Delta \tau$ for the two stresses, respectively. One finds an analogous result for each of the other components of the stress tensor and the total work per unit volume is

$$\delta W = T_{ij} \delta S_{ji}. \quad (1.3.2.7)$$

1.3.3. Linear elasticity

1.3.3.1. Hooke's law

Let us consider a metallic bar of length l_o loaded in pure tension (Fig. 1.3.3.1). Under the action of the uniaxial stress $T = F/A$ (F applied force, A area of the section of the bar), the bar elongates and its length becomes $l = l_o + \Delta l$. Fig. 1.3.3.2 relates the variations of Δl and of the applied stress T . The curve representing the traction is very schematic and does not correspond to any real case. The following result, however, is common to all concrete situations:

(i) If $0 < T < T_o$, the deformation curve is reversible, *i.e.* if one releases the applied stress the bar resumes its original form. To a first approximation, the curve is linear, so that one can write *Hooke's law*:

$$\frac{\Delta l}{l} = \frac{1}{E} T, \quad (1.3.3.1)$$

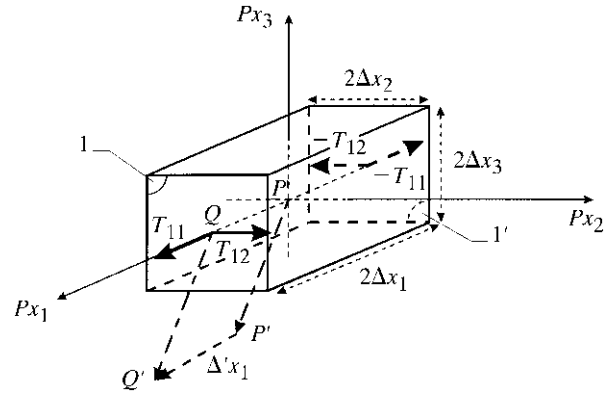


Fig. 1.3.2.8. Determination of the energy density in a deformed medium. $\mathbf{PP'}$ represents the displacement of the small parallelepiped during the deformation. The thick arrows represent the forces applied to the faces 1 and 1'.

where E is the elastic stiffness, also called Young's modulus. The physical mechanism at the origin of elasticity is the deformation of the chemical bonds between atoms, ions or molecules in the solid, which act as so many small springs. The reaction of these springs to an applied stress is actually anharmonic and Hooke's law is only an approximation: a Taylor expansion up to the first term. A rigorous treatment of elasticity requires nonlinear phenomena to be taken into account. This is done in Section 1.3.6. The stress below which the strain is recoverable when the stress is removed, T_o , is called the *elastic limit*.

(ii) If $T > T_o$, the deformation curve is no longer reversible. If one releases the applied stress, the bar assumes a permanent deformation. One says that it has undergone a *plastic* deformation. The region of the deformation is ultimately limited by rupture (symbolized by an asterisk on Fig. 1.3.3.2). The plastic deformation is due to the formation and to the movement of lattice defects such as dislocations. The material in its initial state, before the application of a stress, is not free in general from defects and it possesses a complicated history of deformations. The proportionality constant between stresses and deformations in the elastic region depends on the interatomic force constants and is an intrinsic property, very little affected by the presence of defects. By contrast, the limit, T_o , of the elastic region depends to a large extent on the defects in the material and on its history. It is

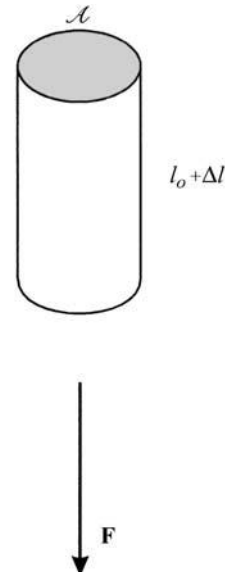


Fig. 1.3.3.1. Bar loaded in pure tension.

1.3. ELASTIC PROPERTIES

an extrinsic property. For example, the introduction of carbon into iron modifies considerably the extent of the elastic region.

The extents of the elastic and plastic regions vary appreciably from one material to another. Fragile materials, for instance, have a much reduced plastic region, with a clear break.

1.3.3.2. Elastic constants

1.3.3.2.1. Definition

Young's modulus is not sufficient to describe the deformation of the bar: its diameter is reduced, in effect, during the elongation. One other coefficient, at least, is therefore necessary. In a general way, let us consider the deformation of a continuous anisotropic medium under the action of a field of applied stresses. We will generalize Hooke's law by writing that at each point there is a linear relation between the components T_{ij} of the stress tensor and the components S_{ij} of the strain tensor:

$$\begin{aligned} S_{ij} &= s_{ijkl} T_{kl} \\ T_{ij} &= c_{ijkl} S_{kl} \end{aligned} \quad (1.3.3.2)$$

The quantities s_{ijkl} and c_{ijkl} are characteristic of the elastic properties of the medium if it is homogeneous and are independent of the point under consideration. Their tensorial nature can be shown using the demonstration illustrated in Section 1.1.3.4. Let us take the contracted product of the two sides of each of the two equations of (1.3.3.2) by the components x_i and y_j of any two vectors, \mathbf{x} and \mathbf{y} :

$$\begin{aligned} S_{ij} x_i y_j &= s_{ijkl} T_{kl} x_i y_j \\ T_{ij} x_i y_j &= c_{ijkl} S_{kl} x_i y_j \end{aligned}$$

The left-hand sides are bilinear forms since S_{ij} and T_{ij} are second-rank tensors and the right-hand sides are quadrilinear forms, which shows that s_{ijkl} and c_{ijkl} are the components of fourth-rank tensors, the tensor of elastic *compliances* (or moduli) and the tensor of elastic *stiffnesses* (or coefficients), respectively. The number of their components is equal to 81.

Equations (1.3.3.2) are Taylor expansions limited to the first term. The higher terms involve sixth-rank tensors, s_{ijklmn} and c_{ijklmn} , with $3^6 = 729$ coefficients, called third-order elastic compliances and stiffnesses and eighth-rank tensors with $3^8 = 6561$ coefficients, called fourth-order elastic compliances and stiffnesses. They will be defined in Section 1.3.6.4. Tables for third-order elastic constants are given in Fumi (1951, 1952, 1987). The accompanying software to this volume enables these tables to be derived for any point group.

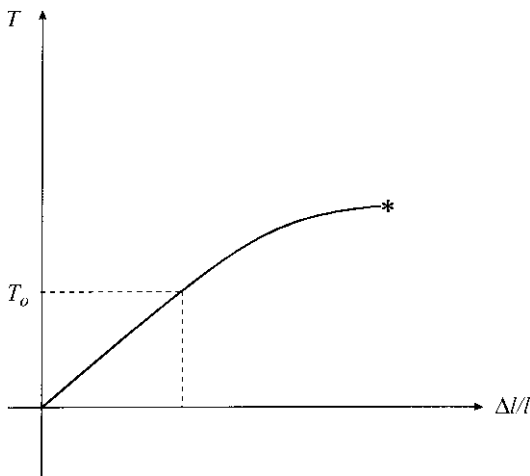


Fig. 1.3.3.2. Schematic stress-strain curve. T : stress; T_0 : elastic limit; $\Delta l/l$: elongation; the asterisk symbolizes the rupture.

1.3.3.2.2. Matrix notation – reduction of the number of independent components

It is convenient to write the relations (1.3.3.2) in matrix form by associating with the stress and strain tensors column matrices 1×9 and with the tensors of the elastic stiffnesses, c , and of the elastic compliances, s , square matrices 9×9 (Section 1.1.4.10.4); these two 9×9 matrices are inverse to one another. The number of independent components of the fourth-rank elastic tensors can be reduced by three types of consideration:

(i) *Intrinsic symmetry*: it was shown in Section 1.1.1.4 that tensors representing principal properties are symmetric. This is the case of the elastic tensors and can be shown directly using expression (1.3.2.7) of the energy stored per unit volume in the medium when we allow it to deform from the state S_{ij} to the state $S_{ij} + \delta S_{ij}$ under the action of the stress T_{ij} :

$$\delta W = T_{ij} \delta S_{ji}.$$

Applying relation (1.3.3.1), we get

$$\partial W / \partial S_{ij} = c_{ijkl} S_{kl}. \quad (1.3.3.3)$$

Hence, one has by further differentiation

$$\partial^2 W / (\partial S_{ij} \partial S_{kl}) = c_{ijkl}.$$

Nothing is changed by interchanging the role of the pairs of dummy indices ij and lk :

$$\partial^2 W / (\partial S_{kl} \partial S_{ij}) = c_{klij}.$$

Since the energy is a state function with a perfect differential, one can interchange the order of the differentiations: the members on the left-hand sides of these two equations are therefore equal; one then deduces

$$c_{ijkl} = c_{klij}. \quad (1.3.3.4)$$

The tensor of elastic stiffnesses (and also the tensor of elastic compliances) is thus symmetrical. As shown in Section 1.1.4.5.2.2, the number of their independent components is therefore reduced to 45.

(ii) *Symmetry of the strain and stress tensors*: the strain tensor S_{ij} is symmetric by definition (Section 1.3.1.3.1) because rotations are not taken into account and the stress tensor T_{ij} is symmetric (Section 1.3.2.4) because body torques are neglected. For this reason, summation (1.3.3.2), $S_{ij} = s_{ijkl} T_{kl}$, can be factorized [equation (1.1.4.11)]:

$$S_{ij} = \sum_l s_{ijll} T_{ll} + \sum_{k \neq l} (s_{ijkl} + s_{ijlk}) T_{kl}.$$

This shows that the number of independent components of tensor s_{ijkl} is reduced. This effect of the symmetry of the strain and stress tensors was discussed systematically in Section 1.1.4.10.4. It was shown that

$$\begin{aligned} s_{ijkl} &= s_{ijlk} = s_{jikl} = s_{jilk} \\ c_{ijkl} &= c_{ijlk} = c_{jikl} = c_{jilk} \end{aligned} \quad (1.3.3.5)$$

and that the number of independent elastic compliances or stiffnesses is reduced to 21. They are replaced by two-index coefficients constituting 6×6 matrices according to Voigt's notation:

1. TENSORIAL ASPECTS OF PHYSICAL PROPERTIES

$$\left. \begin{array}{l} i = j; \quad k = l \\ i = j; \quad k \neq l \\ i \neq j; \quad k = l \\ i \neq j; \quad k \neq l \end{array} \right\} \begin{array}{l} \text{compliances} \\ s_{\alpha\beta} = s_{iill} \\ s_{\alpha\beta} = s_{iill} + s_{iilk} \\ s_{\alpha\beta} = s_{ijll} + s_{jill} \\ s_{\alpha\beta} = s_{ijkl} + s_{jikl} + s_{ijlk} + s_{jilk} \end{array} \left. \begin{array}{l} \text{stiffnesses} \\ c_{\alpha\beta} = c_{ijkl} \end{array} \right\} \quad (1.3.3.6)$$

Using these notations and Voigt's notations for the strain and stress tensors, equations (1.3.3.2) become:

$$\begin{aligned} S_{\alpha\beta} &= s_{\alpha\beta} T_{\beta} \\ T_{\alpha\beta} &= c_{\alpha\beta} S_{\beta}. \end{aligned} \quad (1.3.3.7)$$

For instance, the first of these two relations is written, once developed, as

$$\begin{pmatrix} S_1 \\ S_2 \\ S_3 \\ S_4 \\ S_5 \\ S_6 \end{pmatrix} = \begin{pmatrix} s_{11} & s_{12} & s_{13} & s_{14} & s_{15} & s_{16} \\ s_{12} & s_{22} & s_{23} & s_{24} & s_{25} & s_{26} \\ s_{13} & s_{23} & s_{33} & s_{34} & s_{35} & s_{36} \\ s_{14} & s_{24} & s_{34} & s_{44} & s_{45} & s_{46} \\ s_{15} & s_{25} & s_{35} & s_{45} & s_{55} & s_{56} \\ s_{16} & s_{26} & s_{36} & s_{46} & s_{56} & s_{66} \end{pmatrix} \begin{pmatrix} T_1 \\ T_2 \\ T_3 \\ T_4 \\ T_5 \\ T_6 \end{pmatrix}. \quad (1.3.3.8)$$

Matrices $s_{\alpha\beta}$ and $c_{\alpha\beta}$ are the inverse of each another. It is important to note that they are matrices and not tensors. One cannot apply to them the usual rules of transformation under a change of base since they are only valid for the components of a tensor. In cases where the coordinate system is changed, it is necessary to use the components s_{ijkl} and c_{ijkl} or to establish the rules of transformation for $s_{\alpha\beta}$ and $c_{\alpha\beta}$.

(iii) *Symmetry of the crystal*: the reduction of the number of independent components of the matrices $s_{\alpha\beta}$ and $c_{\alpha\beta}$ was discussed in Section 1.1.4.10.6. As a summary, Table 1.3.3.1 gives the number of independent components for each Laue class.

(iv) *Cauchy relation*: the form that the strain energy of a discrete-particle structure takes when its potential energy depends only on the magnitude of the distance separating pairs of particles is called the central or point-to-point force law. It is shown that, when the cohesive forces have this special form, structures that are such that every atom is situated at a centre of symmetry have elastic constants that are totally symmetric in their four indices. Thus

$$c_{ijkl} = c_{ikjl} = c_{iljk}$$

in addition to the symmetries required by the previous considerations. This additional symmetry implies the following relations between the two-index components:

$$\begin{aligned} c_{23} &= c_{44}; & c_{14} &= c_{56} \\ c_{13} &= c_{55}; & c_{25} &= c_{46} \\ c_{12} &= c_{66}; & c_{36} &= c_{45}. \end{aligned}$$

Table 1.3.3.1. Number of independent components of the elastic compliances and stiffnesses for each Laue class

| Laue class | No. of independent components |
|---|-------------------------------|
| $\bar{1}, 1$ | 21 |
| $2/m, 2, m$ | 13 |
| $mmm, 222, 2mm$ | 9 |
| $\bar{3}, 3$ | 7 |
| $\bar{3}m, 32, 3m$ | 6 |
| $4/m, 4, 4$ | 7 |
| $4/mmm, 422, \bar{4}2m, 42m$ | 6 |
| $6/m, 6, 6$ | 5 |
| $6/mmm, 622, \bar{6}2m, 62m$ | 5 |
| $m\bar{3}, 23$ | 3 |
| $m\bar{3}m, 432, \bar{4}32$ | 3 |
| $\infty A_{\infty}/MC, \infty A_{\infty}$ | 2 |

These are known as the Cauchy relations. The further symmetry implied by the Cauchy relations reduces the maximum number of independent constants from 21 to 15. In crystal structures for which they might be valid, the extent to which these relations are fulfilled is often used to assess the validity of the assumption of a central-force law. It is important to apply such a test only to structures having the necessary symmetry properties for Cauchy relations to hold. For instance, f.c.c and b.c.c. metals have the required symmetry (an inversion centre at each atomic site), while diamond, silicon and germanium do not. Consequently, any apparent fulfilment of the Cauchy relation $c_{12} = c_{66}$ for a diamond-type structure offers no ground for conclusions about the nature of the force field.

1.3.3.2.3. Passage from elastic compliances $s_{\alpha\beta}$ to elastic stiffnesses $c_{\alpha\beta}$

We have noted already that the matrix $c_{\alpha\beta}$ is the inverse of the matrix $s_{\alpha\beta}$. These matrices can be written for cubic and isotropic materials as follows:

$$\begin{aligned} s_{\alpha\beta} &= \begin{pmatrix} s_{11} & s_{12} & s_{12} & 0 & 0 & 0 \\ s_{12} & s_{11} & s_{12} & 0 & 0 & 0 \\ s_{12} & s_{12} & s_{11} & 0 & 0 & 0 \\ 0 & 0 & 0 & s_{44} & 0 & 0 \\ 0 & 0 & 0 & 0 & s_{44} & 0 \\ 0 & 0 & 0 & 0 & 0 & s_{44} \end{pmatrix} \\ c_{\alpha\beta} &= \begin{pmatrix} c_{11} & c_{12} & c_{12} & 0 & 0 & 0 \\ c_{12} & c_{11} & c_{12} & 0 & 0 & 0 \\ c_{12} & c_{12} & c_{11} & 0 & 0 & 0 \\ 0 & 0 & 0 & c_{44} & 0 & 0 \\ 0 & 0 & 0 & 0 & c_{44} & 0 \\ 0 & 0 & 0 & 0 & 0 & c_{44} \end{pmatrix}, \end{aligned}$$

where we have, for isotropic materials,

$$\begin{aligned} s_{44} &= 2(s_{11} - s_{12}) \\ c_{44} &= \frac{1}{2}(c_{11} - c_{12}). \end{aligned} \quad (1.3.3.9)$$

We easily find that

$$\begin{aligned} s_{11} &= \frac{c_{11} + c_{12}}{(c_{11} - c_{12})(c_{11} + 2c_{12})}; & c_{11} &= \frac{s_{11} + s_{12}}{(s_{11} - s_{12})(s_{11} + 2s_{12})}; \\ s_{12} &= \frac{-c_{12}}{(c_{11} - c_{12})(c_{11} + 2c_{12})}; & c_{12} &= \frac{-s_{12}}{(s_{11} - s_{12})(s_{11} + 2s_{12})}; \\ s_{44} &= \frac{1}{c_{44}}; & c_{44} &= \frac{1}{s_{44}}. \end{aligned}$$

The coefficient c_{44} is sometimes called the *rigidity modulus*.

1.3.3.3. Elastic strain energy

Expression (1.3.2.7) of the strain energy stored per unit volume in a medium for a small deformation can be integrated when the medium is strained under a stress T_{ij} according to linear elasticity. Applying relation (1.3.3.2), one gets for the density of strain energy

$$W = \frac{1}{2} T_{ij} S_{ij} = \frac{1}{2} c_{ijkl} S_{ij} S_{kl}. \quad (1.3.3.10)$$

1.3.3.4. Particular elastic constants

1.3.3.4.1. Volume compressibility

Let us apply a hydrostatic pressure (Section 1.3.2.5.2). The medium undergoes a relative variation of volume $\Delta V/V = S_1 + S_2 + S_3$ (the cubic dilatation, Section 1.3.1.3.2). If one

1.3. ELASTIC PROPERTIES

replaces in (1.3.3.8) the stress distribution by a hydrostatic pressure, one obtains for the components of the strain tensor

$$\begin{aligned} S_1 &= -p(s_{11} + s_{12} + s_{13}) \\ S_2 &= -p(s_{12} + s_{22} + s_{23}) \\ S_3 &= -p(s_{13} + s_{23} + s_{33}). \end{aligned}$$

From this, we deduce the volume compressibility, χ , which is the inverse of the *bulk modulus*, κ :

$$\chi = \kappa^{-1} = -\frac{1}{p} \frac{\delta V}{V} = s_{11} + s_{22} + s_{33} + 2(s_{12} + s_{23} + s_{13}). \quad (1.3.3.11)$$

This expression reduces for a cubic or isotropic medium to

$$\chi = \kappa^{-1} = 3(s_{11} + 2s_{12}). \quad (1.3.3.12)$$

1.3.3.4.2. Linear compressibility

Under the action of a hydrostatic pressure, each vector assumes a different elongation. This elongation is given by equation (1.3.1.6):

$$\frac{u_r}{r} = \frac{S_{ij}x_i x_j}{r^2} = S_{ij}\alpha_i \alpha_j = s_{ijkl}T_{kl}\alpha_i \alpha_j,$$

where the α_i 's are the direction cosines of \mathbf{r} . The coefficient of linear compressibility is, by definition, $(-1/p)(u_r/r)$. Replacing T_{kl} by its value $-p\delta_{kl}$, we obtain for the coefficient of linear compressibility

$$-\frac{1}{p} \frac{u_r}{r} = s_{ijkl}\alpha_i \alpha_j.$$

In the case of a cubic or isotropic medium, this expression reduces to

$$-\frac{1}{p} \frac{u_r}{r} = s_{11} + 2s_{12}.$$

The coefficient of linear compressibility is then equal to one third of the coefficient of volume compressibility. We note that the quadric of elongations is a sphere.

1.3.3.4.3. Young's modulus, Poisson's ratio

If the applied stress reduces to a uniaxial stress, $T_{11} = T$, the strain tensor is of the form

$$S_{\alpha} = s_{1\alpha}T.$$

In particular,

$$S_1 = s_{11}T; \quad S_2 = s_{12}T.$$

We deduce from this that Young's modulus (equation 1.3.3.1) is

$$E = 1/s_{11}. \quad (1.3.3.13)$$

The elongation of a bar under the action of a uniaxial stress is characterized by S_1 and the diminution of the cross section is characterized by S_2 and S_3 . For a cubic material, the relative diminution of the diameter is

$$S_2 = S_3 = s_{12}T.$$

One deduces from this that s_{12} is necessarily of opposite sign to s_{11} and one calls the ratio $\nu = -s_{12}/s_{11}$ *Poisson's ratio*.

Putting this value into expression (1.3.3.12) for the coefficient of compressibility in cubic or isotropic materials gives

$$\kappa^{-1} = 3s_{11}(1 - 2\nu). \quad (1.3.3.14)$$

As the coefficient of compressibility, by definition, is always positive, we have

$$0 < \nu < 0.5.$$

In practice, Poisson's ratio is always close to 0.3. It is a dimensionless number. The quantity $s_{44}/2(s_{11} - s_{12})$ represents the departure from isotropy of the material and is the anisotropy factor. It is to be noted that cubic materials are not isotropic for elastic properties. Table 1.3.3.2 gives the values of s_{11} , s_{12} , s_{44} , ν and $s_{44}/2(s_{11} - s_{12})$ for a few cubic materials.

1.3.3.4.4. Variation of Young's modulus with orientation

It is interesting to calculate Young's modulus in any direction. For this it is sufficient to change the axes of the tensor s_{ijkl} . If A is the matrix associated with the change of axes, leading to the direction x_1 changing to the direction x'_1 , then Young's modulus in this new direction is

$$E' = 1/s'_{11}$$

with

$$s'_{11} = s'_{1111} = A_{1i}A_{1j}A_{1k}A_{1l}s_{ijkl}. \quad (1.3.3.15)$$

Table 1.3.3.2. Elastic compliances of some cubic materials in (GPa)⁻¹ (after Landolt-Börnstein, 1979)

| Material | s_{11} | s_{12} | s_{44} | ν | $s_{44}/2(s_{11} - s_{12})$ |
|---|----------|----------|----------|-------|-----------------------------|
| Ag | 22.9 | -9.8 | 22.1 | 0.428 | 0.338 |
| Al | 16.0 | -5.8 | 35.3 | 0.362 | 0.810 |
| C (diamond) | 1.12 | -0.14 | 1.83 | 0.125 | 0.726 |
| Cu | 15.0 | -6.3 | 13.3 | 0.42 | 0.312 |
| Fe | 7.67 | -2.83 | 8.57 | 0.369 | 0.408 |
| Ge | 9.73 | -2.64 | 14.9 | 0.271 | 0.602 |
| Mo | 2.71 | -0.74 | 9.00 | 0.273 | 1.304 |
| Ni | 7.67 | -2.93 | 8.23 | 0.382 | 0.388 |
| Pb | 93.7 | -43.04 | 68.0 | 0.459 | 0.249 |
| Si | 7.74 | -2.16 | 12.60 | 0.279 | 0.636 |
| W | 2.49 | -0.70 | 6.35 | 0.281 | 0.995 |
| LiF | 11.6 | -3.35 | 15.8 | 0.289 | 0.528 |
| MgO | 4.01 | -0.96 | 6.47 | 0.239 | 0.651 |
| NaCl | 23.9 | -3.20 | 78.7 | 0.133 | 1.452 |
| GaAs | 11.75 | -3.66 | 16.8 | 0.311 | 0.545 |
| ZnS | 19.7 | -7.6 | 22.6 | 0.386 | 0.414 |
| BaTiO ₃ | 8.33 | -2.68 | 9.24 | 0.322 | 0.420 |
| Adamantane | 240 | -79 | 295 | 0.329 | 0.462 |
| Almandine (Fe ₃ Al ₂ Si ₃ O ₁₂) | 4.036 | -1.093 | 10.77 | 0.271 | 1.050 |
| Spinel (MgAl ₂ O ₄) | 5.80 | -2.05 | 6.49 | 0.353 | 0.413 |

1. TENSORIAL ASPECTS OF PHYSICAL PROPERTIES

The matrix coefficients A_{li} are the direction cosines of Ox'_l with respect to the axes Ox_1 , Ox_2 and Ox_3 . In spherical coordinates, they are given by (Fig. 1.3.3.3)

$$A_{11} = \cos \theta \sin \varphi, \quad A_{12} = \sin \theta \sin \varphi, \quad A_{13} = \cos \varphi,$$

where θ is the angle between Ox'_1 and Ox_1 , and φ is the angle between Ox'_1 and Ox_3 . Using the reduction of s_{ijkl} for the various crystal classes (Section 1.1.4.9.9), we find, in terms of the reduced two-index components, the following.

(i) *Triclinic system* (groups 1, $\bar{1}$):

$$\begin{aligned} s'_{11} = & [s_{11} \cos^4 \theta + s_{22} \sin^4 \theta + (2s_{12} + s_{66}) \sin^2 2\theta/4 \\ & + (s_{16} \cos \theta + s_{26} \sin \theta) \sin 2\theta] \sin^4 \varphi \\ & + 2[(s_{25} + s_{46}) \sin \theta + (s_{14} + s_{56}) \cos \theta] \sin 2\theta/2 \\ & + s_{15} \cos^3 \theta + s_{24} \sin^3 \theta \} \cos \varphi \sin^3 \varphi \\ & + [(2s_{23} + s_{44}) \sin^2 \theta + (2s_{13} + s_{55}) \cos^2 \theta \\ & + (s_{36} + s_{45}) \sin 2\theta] \sin^2 2\varphi/4 \\ & + 2(s_{35} \cos \theta + s_{34} \sin \theta) \cos^3 \varphi \sin \varphi + s_{33} \cos^4 \varphi. \end{aligned}$$

(ii) *Monoclinic system* (groups 2, m , $2/m$):

$$\begin{aligned} s'_{11} = & [s_{11} \cos^4 \theta + s_{22} \sin^4 \theta + (2s_{12} + s_{66}) \sin^2 2\theta/4] \sin^4 \varphi \\ & + 2[(s_{25} + s_{46}) \sin^2 \theta + s_{15} \cos^2 \theta] \cos \varphi \sin^3 \varphi \cos \theta \\ & + [(2s_{23} + s_{44}) \sin^2 \theta + (2s_{13} + s_{55}) \cos^2 \theta] \sin^2 2\varphi/4 \\ & + 2s_{35} \cos^3 \varphi \sin \varphi \cos \theta + s_{33} \cos^4 \varphi. \end{aligned}$$

(iii) *Orthorhombic system* (groups 222, $2mm$, mmm):

$$\begin{aligned} s'_{11} = & [s_{11} \cos^4 \theta + s_{22} \sin^4 \theta + (2s_{12} + s_{66}) \sin^2 2\theta/4] \sin^4 \varphi \\ & + [(2s_{23} + s_{44}) \sin^2 \theta + (2s_{13} + s_{55}) \cos^2 \theta] \sin^2 2\varphi/4 \\ & + s_{33} \cos^4 \varphi. \end{aligned}$$

(iv) *Trigonal system* (groups 3, $\bar{3}$):

$$\begin{aligned} s'_{11} = & s_{11} \sin^4 \varphi + s_{33} \cos^4 \varphi + (2s_{13} + s_{44}) \sin^2 2\varphi/4 \\ & + (s_{14} \sin 3\theta - s_{25} \cos 3\theta) \sin 2\varphi \sin^2 \varphi. \end{aligned}$$

(v) *Trigonal system* (groups 32, $3m$, $\bar{3}m$):

$$\begin{aligned} s'_{11} = & s_{11} \sin^4 \varphi + s_{33} \cos^4 \varphi + (2s_{13} + s_{44}) \sin^2 2\varphi/4 \\ & + s_{14} \sin 3\theta \sin 2\varphi \sin^2 \varphi. \end{aligned}$$

(vi) *Tetragonal system* (groups 4, $\bar{4}$, $4/m$):

$$\begin{aligned} s'_{11} = & \{s_{11} + [s_{66} - 2(s_{11} - s_{12})] \sin^2 \theta/4\} \sin^4 \varphi + s_{33} \cos^4 \varphi \\ & + (2s_{13} + s_{44}) \sin^2 2\varphi/4 + s_{16} \sin 4\theta \sin^4 \varphi/2. \end{aligned}$$

(vii) *Tetragonal system* (groups 422, $\bar{4}2m$, $4mm$, $4/mmm$):

$$\begin{aligned} s'_{11} = & \{s_{11} + [s_{66} - 2(s_{11} - s_{12})] \sin^2 \theta/4\} \sin^4 \varphi + s_{33} \cos^4 \varphi \\ & + (2s_{13} + s_{44}) \sin^2 2\varphi/4. \end{aligned}$$

(viii) *Hexagonal system*:

$$s'_{11} = s_{11} \sin^4 \varphi + s_{33} \cos^4 \varphi + (2s_{13} + s_{44}) \sin^2 2\varphi/4.$$

(ix) *Cubic system*:

$$s'_{11} = s_{11} + [s_{44} - 2(s_{11} - s_{12})] \sin^2 \varphi [\cos^2 \varphi + \sin^2 2\theta \sin^2 \varphi/4].$$

This expression reduces to s_{11} if $s_{44} - 2(s_{11} - s_{12}) = 0$ and we retrieve the relation between elastic compliances in an isotropic material (Sections 1.1.4.10.4 and 1.3.3.2.3).

The representation surface of s_{11} , the inverse of Young's modulus, is illustrated in Figure 1.3.3.4 for crystals of different symmetries. As predicted by the Neumann principle, the representation surface is invariant with respect to the symmetry elements of the point group of the crystal but, as stated by the Curie laws, its symmetry can be larger. In the examples of Fig. 1.3.3.4, the symmetry of the surface is the same as that of the point group for sodium chloride (Fig. 1.3.3.4a), tungsten (Fig. 1.3.3.4b) and aluminium (Fig. 1.3.3.4c), which have $m\bar{3}m$ as point group, for tin (Fig. 1.3.3.4e, $4/mmm$) and for calcite (Fig. 1.3.3.4f, $\bar{3}m$). But in the case of zinc (Fig. 1.3.3.4d, $6/mmm$), the surface is of revolution and has a larger symmetry. It is interesting to compare the differences in shapes of the representation surfaces for the three cubic crystals, depending on the value of the anisotropy factor, which is larger than 1 for sodium chloride, smaller than 1 for aluminium and close to 1 for tungsten (see Table 1.3.3.2). In this latter case, the crystal is pseudo-isotropic and the surface is practically a sphere.

1.3.3.5. Isotropic materials

The isotropy relation between elastic compliances and elastic stiffnesses is given in Section 1.3.3.2.3. For reasons of symmetry, the directions of the eigenvectors of the stress and strain tensors are necessarily the same in an isotropic medium. If we take these directions as axes, the two tensors are automatically diagonalized and the second relation (1.3.3.7) becomes

$$T_1 = c_{11}S_1 + c_{12}(S_2 + S_3)$$

$$T_2 = c_{12}S_1 + c_{11}S_2 + c_{12}S_3$$

$$T_3 = c_{12}(S_1 + S_2) + c_{11}S_3.$$

These relations can equally well be written in the symmetrical form

$$T_1 = (c_{11} - c_{12})S_1 + c_{12}(S_1 + S_2 + S_3)$$

$$T_2 = (c_{11} - c_{12})S_2 + c_{12}(S_1 + S_2 + S_3)$$

$$T_3 = (c_{11} - c_{12})S_3 + c_{12}(S_1 + S_2 + S_3).$$

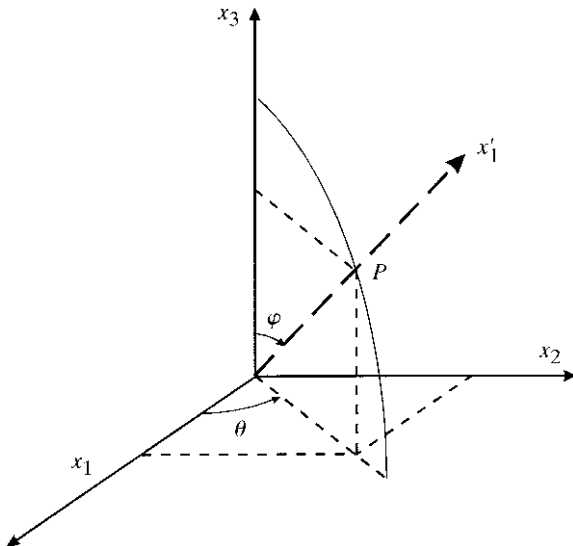


Fig. 1.3.3.3. Spherical coordinates.

1.3. ELASTIC PROPERTIES

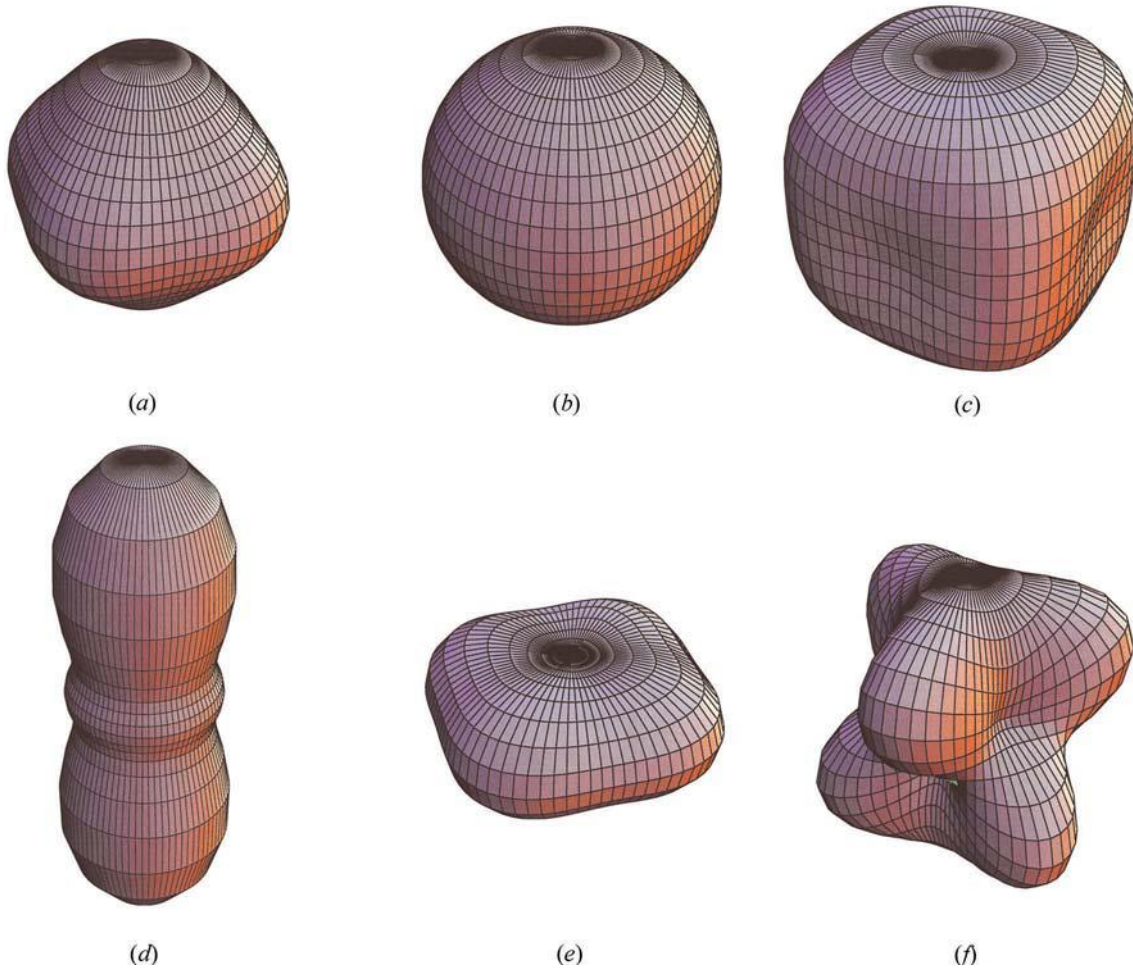


Fig. 1.3.3.4. Representation surface of the inverse of Young's modulus. (a) NaCl, cubic, anisotropy factor > 1 ; (b) W, cubic, anisotropy factor $= 1$; (c) Al, cubic, anisotropy factor < 1 ; (d) Zn, hexagonal; (e) Sn, tetragonal; (f) calcite, trigonal.

If one introduces the Lamé constants,

$$\begin{aligned}\mu &= (1/2)(c_{11} - c_{12}) = c_{44} \\ \lambda &= c_{12},\end{aligned}$$

the equations may be written in the form often used in mechanics:

$$\begin{aligned}T_1 &= 2\mu S_1 + \lambda(S_1 + S_2 + S_3) \\ T_2 &= 2\mu S_2 + \lambda(S_1 + S_2 + S_3) \\ T_3 &= 2\mu S_3 + \lambda(S_1 + S_2 + S_3).\end{aligned}\quad (1.3.3.16)$$

Two coefficients suffice to define the elastic properties of an isotropic material, s_{11} and s_{12} , c_{11} and c_{12} , μ and λ , μ and ν , etc. Table 1.3.3.3 gives the relations between the more common elastic coefficients.

1.3.3.6. Equilibrium conditions of elasticity for isotropic media

We saw in Section 1.3.2.3 that the condition of equilibrium is

$$\partial T_{ij} / \partial x_i + \rho F_j = 0.$$

If we use the relations of elasticity, equation (1.3.3.2), this condition can be rewritten as a condition on the components of the strain tensor:

$$c_{ijkl} \frac{\partial S_{kl}}{\partial x_j} + \rho F_i = 0.$$

Recalling that

$$S_{kl} = \frac{1}{2} \left[\frac{\partial u_k}{\partial x_l} + \frac{\partial u_l}{\partial x_k} \right],$$

the condition becomes a condition on the displacement vector, $\mathbf{u}(\mathbf{r})$:

$$c_{ijkl} \frac{\partial^2}{\partial x_i \partial x_j} + \rho F_i = 0.$$

In an isotropic orthonormal medium, this equation, projected on the axis $0x_1$, can be written with the aid of relations (1.3.3.5) and (1.3.3.9):

$$\begin{aligned}& c_{11} \frac{\partial^2 u_1}{(\partial x_1)^2} + c_{12} \left[\frac{\partial^2 u_2}{\partial x_1 \partial x_2} + \frac{\partial^2 u_3}{\partial x_1 \partial x_3} \right] \\ & + \frac{1}{2}(c_{11} - c_{12}) \left[\frac{\partial^2 u_1}{(\partial x_2)^2} + \frac{\partial^2 u_3}{\partial x_1 \partial x_3} + \frac{\partial^2 u_1}{(\partial x_3)^2} \right] + \rho F_1 \\ & = 0.\end{aligned}$$

This equation can finally be rearranged in one of the three following forms with the aid of Table 1.3.3.3.

$$\begin{aligned}& \frac{1}{2}(c_{11} - c_{12})\Delta \mathbf{u} + \frac{1}{2}(c_{11} + c_{12})\nabla(\nabla \cdot \mathbf{u}) + \rho \mathbf{F} = 0 \\ & \mu \Delta \mathbf{u} + (\mu + \lambda)\nabla(\nabla \cdot \mathbf{u}) + \rho \mathbf{F} = 0 \\ & \mu \left[\Delta \mathbf{u} + \frac{1}{1 - 2\nu} \nabla(\nabla \cdot \mathbf{u}) \right] + \rho \mathbf{F} = 0.\end{aligned}\quad (1.3.3.17)$$

1. TENSORIAL ASPECTS OF PHYSICAL PROPERTIES

1.3.4. Propagation of elastic waves in continuous media – dynamic elasticity

1.3.4.1. Introduction

The elastic properties of materials have been considered in the preceding section in the static state and the elastic constants have been defined in terms of the response of the material to particular static forces. It is effectively the way the elastic constants have been measured in the past, although the measurements could not be very precise. A way of proceeding frequently used now is to excite a mechanical wave in the crystal and measure its propagation velocity or the wavelength associated with a particular frequency. One method consists in sending a train of ultrasonic waves through the crystal; one uses a pulse generator and a piezoelectric transducer glued to the crystal. The elapsed time between the emission of the train of waves and its reception after reflection from the rear face of the sample is then measured. Another method involves producing a system of standing waves after reflection at the inner surface of the crystal and determining the set of resonance frequencies. The experimental techniques will be described in Section 1.3.4.6.

The purpose of the next sections is to establish relations between the wavelength – or the velocity of propagation – and the elastic constants.

1.3.4.2. Equation of propagation of a wave in a material

Consider the propagation of a wave in a continuous medium. The elongation of each point will be of the form

$$\mathbf{u} = \mathbf{u}_0 \exp(2\pi i \nu t) \exp(-2\pi i \mathbf{q} \cdot \mathbf{r}), \quad (1.3.4.1)$$

where ν is the frequency and \mathbf{q} is the wavevector. The velocity of propagation of the wave is

$$V = \nu/q. \quad (1.3.4.2)$$

We saw in Section 1.3.3.6 that the equilibrium condition is

$$c_{ijkl} \frac{\partial^2 u_k}{\partial x_i \partial x_j} + \rho F_i = 0.$$

Here the only volume forces that we must consider are the inertial forces:

$$c_{ijkl} \frac{\partial^2 u_k}{\partial x_i \partial x_j} = \rho \frac{\partial^2 x_i}{\partial t^2}. \quad (1.3.4.3)$$

The position vector of the point under consideration is of the form

$$\mathbf{r} = \mathbf{r}_0 + \mathbf{u},$$

where only \mathbf{u} depends on the time and \mathbf{r}_0 defines the mean position. Equation (1.3.4.3) is written therefore

$$c_{ijkl} \frac{\partial^2 u_k}{\partial x_i \partial x_j} = \rho \frac{\partial^2 u_i}{\partial t^2}. \quad (1.3.4.4)$$

Replacing \mathbf{u} by its value in (1.3.4.1), dividing by $-4\pi^2$ and using orthonormal coordinates, we get

$$c_{ijkl} u_k q_j q_l = \rho \nu^2 u_i. \quad (1.3.4.5)$$

It can be seen that, for a given wavevector, $\rho \nu^2$ appears as an eigenvalue of the matrix $c_{ijkl} u_k q_j q_l$ of which the vibration vector \mathbf{u} is an eigenvector. This matrix is called the dynamical matrix, or *Christoffel matrix*. In order that the system (1.3.4.5) has a solution other than a trivial one, it is necessary that the associated determinant be equal to zero. It is called the Christoffel determinant and it plays a fundamental role in the study of the propagation of elastic waves in crystals.

Let $\alpha_1, \alpha_2, \alpha_3$ be the direction cosines of the wavevector \mathbf{q} . The components of the wavevector are

$$q_i = q \alpha_i.$$

With this relation and (1.3.4.2), the system (1.3.4.5) becomes

$$c_{ijkl} u_k \alpha_j \alpha_l = \rho \nu^2 u_i. \quad (1.3.4.6)$$

Putting

$$\Gamma_{ik} = c_{ijkl} \alpha_j \alpha_l \quad (1.3.4.7)$$

in (1.3.4.6), the condition that the Christoffel determinant is zero can be written

$$\Delta(\Gamma_{ik} - \rho \nu^2 \delta_{ik}) = 0. \quad (1.3.4.8)$$

On account of the intrinsic symmetry of the tensor of elastic stiffnesses, the matrix Γ_{ik} is symmetrical.

If we introduce into expression (1.3.4.7) the elastic stiffnesses with two indices [equation (1.3.3.6)], we find, for instance, for Γ_{11} and Γ_{12}

$$\begin{aligned} \Gamma_{11} &= c_{11}(\alpha_1)^2 + c_{66}(\alpha_2)^2 + c_{55}(\alpha_3)^2 + 2c_{16}\alpha_1\alpha_2 \\ &\quad + 2c_{15}\alpha_1\alpha_3 + 2c_{56}\alpha_2\alpha_3 \\ \Gamma_{12} &= c_{16}(\alpha_1)^2 + c_{26}(\alpha_2)^2 + c_{45}(\alpha_3)^2 + (c_{12} + c_{66})\alpha_1\alpha_2 \\ &\quad + (c_{14} + c_{56})\alpha_1\alpha_3 + (c_{46} + c_{25})\alpha_2\alpha_3. \end{aligned}$$

The expression for the effective value, c_{ijkl}^e , of the ‘stiffened’ elastic stiffness in the case of piezoelectric crystals is given in Section 2.4.2.2.

1.3.4.3. Dynamic elastic stiffnesses

Equation (1.3.4.7) may be written

$$\Gamma_{ik} = \sum_{j \neq l} [c_{ijkl} + c_{ilkj}] \alpha_j \alpha_l.$$

This shows that in a dynamic process only the sums $[c_{ijkl} + c_{ilkj}]$ can be measured and not c_{ijkl} and c_{ilkj} separately. On the contrary, c_{ijij} can be measured directly. In the cubic system therefore, for instance, c_{1122} is determined from the measurement of $[c_{1122} + c_{1221}]$ on the one hand and from that of c_{1221} on the other hand.

1.3.4.4. Polarization of the elastic waves

The Christoffel determinant has three roots and the Christoffel matrix, being Hermitian with real coefficients, has three real eigenvalues and three orthogonal eigenvectors. The wavevector \mathbf{q} , therefore, encompasses three waves with vibration vectors $\mathbf{u}_1, \mathbf{u}_2, \mathbf{u}_3$ which are perpendicular to one another. In the general case, there is no particular angular relationship between the vibration vectors (or polarization vectors). However, if the latter are parallel to certain symmetry directions in the crystal, one of the vibration vectors is along this direction. The corresponding

Table 1.3.3.3. Relations between elastic coefficients in isotropic media

| Coefficient | In terms of μ and λ | In terms of μ and ν | In terms of c_{11} and c_{12} |
|------------------------|--|-------------------------------|-----------------------------------|
| c_{11} | $2\mu + \lambda$ | $2\mu(1 - \nu)(1 - 2\nu)$ | c_{11} |
| c_{12} | λ | $2\mu\nu(1 - 2\nu)$ | c_{12} |
| $c_{44} = 1/s_{44}$ | μ | μ | $(c_{11} - c_{12})/2$ |
| $E = 1/s_{11}$ | $\mu(2\mu + 3\lambda)/(\mu + \lambda)$ | $2\mu(1 + \nu)$ | See Section 1.3.3.2.3 |
| s_{12} | $-\lambda/[2\mu(2\mu + 3\lambda)]$ | $-\nu/[2\mu(1 + \nu)]$ | See Section 1.3.3.2.3 |
| κ | $3/(2\mu + 3\lambda)$ | $3(1 - 2\nu)/[2\mu(1 + \nu)]$ | $3/(c_{11} + 2c_{12})$ |
| $\nu = -s_{12}/s_{11}$ | $\lambda/[2\mu(2\mu + 3\lambda)]$ | ν | $c_{11}/(c_{11} + c_{12})$ |

1.3. ELASTIC PROPERTIES

wave is called longitudinal. The two other waves have their polarization direction perpendicular to the wavevector and are thus transverse. If one of the polarization vectors is almost parallel to the wavevector, which often happens, then one speaks of the vibration as being quasi-longitudinal.

1.3.4.5. Relation between velocity of propagation and elastic stiffnesses

We shall limit ourselves to cubic, hexagonal and tetragonal crystals and consider particular cases.

1.3.4.5.1. Cubic crystals

(i) *The wavevector is parallel to [100].* The Christoffel determinant reduces to

$$\begin{pmatrix} c_{11} - \rho v^2 & 0 & 0 \\ 0 & c_{44} - \rho v^2 & 0 \\ 0 & 0 & c_{44} - \rho v^2 \end{pmatrix} = 0.$$

The three solutions are given in Table 1.3.4.1. These results are valid for a wave propagating in any direction in an isotropic medium.

(ii) *The wavevector is parallel to [110].* The direction cosines of the wavevector are $1/\sqrt{2}$, $1/\sqrt{2}$, 0. The Christoffel determinant assumes the form

$$\begin{pmatrix} \frac{1}{2}(c_{11} + c_{44}) - \rho v^2 & \frac{1}{2}(c_{12} + c_{44}) & 0 \\ \frac{1}{2}(c_{12} + c_{44}) & \frac{1}{2}(c_{11} + c_{44}) - \rho v^2 & 0 \\ 0 & 0 & c_{44} - \rho v^2 \end{pmatrix} = 0.$$

The three solutions are given in Table 1.3.4.2.

(iii) *The wavevector is parallel to [111].* The Christoffel determinant assumes the form

$$\begin{pmatrix} c_{11} + 2c_{44} - \rho v^2 & c_{12} + c_{44} & c_{12} + c_{44} \\ c_{12} + c_{44} & c_{11} + 2c_{44} - \rho v^2 & c_{12} + c_{44} \\ c_{12} + c_{44} & c_{12} + c_{44} & c_{44} - \rho v^2 \end{pmatrix} = 0.$$

The solutions are given in Table 1.3.4.3.

1.3.4.5.2. Hexagonal crystals

In hexagonal crystals, there are five independent elastic stiffnesses, c_{11} , c_{33} , c_{12} , c_{13} , c_{44} and $c_{66} = (c_{11} - c_{12})/2$ (Section 1.1.4.10.4).

(i) *The wavevector is parallel to [001].* The Christoffel determinant reduces to

$$\begin{pmatrix} c_{44} - \rho v^2 & 0 & 0 \\ 0 & c_{44} - \rho v^2 & 0 \\ 0 & 0 & c_{33} - \rho v^2 \end{pmatrix} = 0.$$

The solutions are given in Table 1.3.4.4.

(ii) *The wavevector is parallel to [100].* The Christoffel determinant readily reduces to

$$\begin{pmatrix} c_{11} - \rho v^2 & 0 & 0 \\ 0 & c_{66} - \rho v^2 & 0 \\ 0 & 0 & c_{44} - \rho v^2 \end{pmatrix} = 0.$$

The three solutions are given in Table 1.3.4.5.

1.3.4.5.3. Tetragonal crystals (classes $4mm$, $\bar{4}2m$, $4/mmm$)

In tetragonal crystals, there are six independent elastic stiffnesses, c_{11} , c_{33} , c_{12} , c_{13} , c_{44} and c_{66} (Section 1.1.4.10.4).

(i) *The wavevector is parallel to [001].* The Christoffel determinant reduces to

$$\begin{pmatrix} c_{44} - \rho v^2 & 0 & 0 \\ 0 & c_{44} - \rho v^2 & 0 \\ 0 & 0 & c_{33} - \rho v^2 \end{pmatrix} = 0.$$

The three solutions are given in Table 1.3.4.6.

(ii) *The wavevector is parallel to [100].* The Christoffel determinant reduces to

$$\begin{pmatrix} c_{11} - \rho v^2 & 0 & 0 \\ 0 & c_{66} - \rho v^2 & 0 \\ 0 & 0 & c_{44} - \rho v^2 \end{pmatrix} = 0.$$

The three solutions are given in Table 1.3.4.7.

Table 1.3.4.1. Velocity of propagation when the wavevector is parallel to [100] (cubic crystals)

| Velocity of propagation | Polarization vector | Nature of the wave |
|--------------------------------------|----------------------------|--------------------|
| $v_{\parallel} = \sqrt{c_{11}/\rho}$ | [100] | Longitudinal |
| $v_{\perp} = \sqrt{c_{44}/\rho}$ | [010] | Transverse |
| $v_{\perp} = \sqrt{c_{44}/\rho}$ | Any vector normal to [100] | Transverse |

Table 1.3.4.2. Velocity of propagation when the wavevector is parallel to [110] (cubic crystals)

| Velocity of propagation | Polarization vector | Nature of the wave |
|---|-----------------------|--------------------|
| $v_{\parallel} = \sqrt{[c_{44} + \frac{1}{2}(c_{11} + c_{12})]/\rho}$ | [110] | Longitudinal |
| $v_{\perp} = \sqrt{\frac{1}{2}(c_{11} - c_{12})/\rho}$ | [$\bar{1}\bar{1}$ 0] | Transverse |
| $v_{\perp} = \sqrt{c_{44}/\rho}$ | [001] | Transverse |

Table 1.3.4.3. Velocity of propagation when the wavevector is parallel to [111] (cubic crystals)

| Velocity of propagation | Polarization vector | Nature of the wave |
|---|----------------------------|--------------------|
| $v_{\parallel} = \sqrt{(c_{11} + 2c_{12} + 4c_{44})/3\rho}$ | [111] | Longitudinal |
| $v_{\perp} = \sqrt{(c_{11} - c_{12} + c_{44})/3\rho}$ | Any vector normal to [111] | Transverse |

Table 1.3.4.4. Velocity of propagation when the wavevector is parallel to [001] (hexagonal crystals)

| Velocity of propagation | Polarization vector | Nature of the wave |
|--------------------------------------|----------------------------|--------------------|
| $v_{\parallel} = \sqrt{c_{33}/\rho}$ | [100] | Longitudinal |
| $v_{\perp} = \sqrt{c_{44}/\rho}$ | Any vector normal to [001] | Transverse |

Table 1.3.4.5. Velocity of propagation when the wavevector is parallel to [100] (hexagonal crystals)

| Velocity of propagation | Polarization vector | Nature of the wave |
|--------------------------------------|---------------------|--------------------|
| $v_{\parallel} = \sqrt{c_{11}/\rho}$ | [100] | Longitudinal |
| $v_{\perp} = \sqrt{c_{66}/\rho}$ | [010] | Transverse |
| $v_{\perp} = \sqrt{c_{44}/\rho}$ | [001] | Transverse |

Table 1.3.4.6. Velocity of propagation when the wavevector is parallel to [001] (tetragonal crystals)

| Velocity of propagation | Polarization vector | Nature of the wave |
|--------------------------------------|---------------------|--------------------|
| $v_{\parallel} = \sqrt{c_{33}/\rho}$ | [100] | Longitudinal |
| $v_{\perp} = \sqrt{c_{44}/\rho}$ | [010] | Transverse |
| $v_{\perp} = \sqrt{c_{44}/\rho}$ | [001] | Transverse |

Table 1.3.4.7. Velocity of propagation when the wavevector is parallel to [100] (tetragonal crystals)

| Velocity of propagation | Polarization vector | Nature of the wave |
|--------------------------------------|---------------------|--------------------|
| $v_{\parallel} = \sqrt{c_{11}/\rho}$ | [100] | Longitudinal |
| $v_{\perp} = \sqrt{c_{66}/\rho}$ | [010] | Transverse |
| $v_{\perp} = \sqrt{c_{44}/\rho}$ | [001] | Transverse |

1. TENSORIAL ASPECTS OF PHYSICAL PROPERTIES

1.3.4.6. Experimental determination of elastic constants

1.3.4.6.1. Introduction

As mentioned in Section 1.3.4.1, the elastic constants of a material can be obtained by the elastic response of the material to particular static forces; however, such measurements are not precise and the most often used approach nowadays consists of determining the velocity of ultrasonic waves propagating along different directions of the crystal and calculating the elastic constants from the Christoffel determinants (1.3.4.8). The experimental values are often accurate enough to justify the distinction between static and dynamic values of the elastic constants and between phase and group velocities, and the careful consideration of the frequency range of the experiments.

(i) *Static and dynamic elastic constants.* When one measures the elastic response of a material to external static forces, work is done and heat is produced. In general, the external forces are applied slowly (quasi-elastic processes) and the solid body remains in thermal equilibrium with its surroundings, which can be considered as a heat reservoir. In this case, the measured elastic constants are isothermal elastic constants as defined in Section 1.1.5.1. On the contrary, when ultrasonic waves propagate in a solid body, the compressed regions are slightly hotter than the expanded regions; the associated temperature gradients give rise to irreversible processes of thermal conduction. However, in the megahertz or higher-frequency ranges, the processes of heat exchange between different regions or between the solid and its surroundings are slow compared with the period of the ultrasonic wave and hence can be considered as isentropic. In this case, the measured velocities are isentropic and the elastic stiffnesses deduced from them are the adiabatic elastic stiffnesses as defined in Section 1.1.5.4. The differences between isothermal and adiabatic elastic stiffnesses can be calculated from equation (1.1.5.2):

$$\delta T_{ij} = (c_{ijkl})^\Theta \delta S_{kl} - \lambda_{ij} \delta \Theta$$

$$\delta \sigma = \lambda_{kl} \delta S_{kl} + \frac{\rho C^S}{\Theta} \delta \Theta.$$

By combining these two equations, it is possible to obtain relations between the isothermal elastic stiffnesses, $(c_{ijkl})^\Theta$, and the adiabatic elastic stiffnesses, $(c_{ijkl})^\sigma$:

$$(c_{ijkl})^\sigma = (c_{ijkl})^\Theta + \frac{\lambda_{ij} \lambda_{kl}}{\rho c^S},$$

where c^S is the specific heat at constant strain.

This relation shows that adiabatic elastic stiffnesses are larger than isothermal elastic stiffnesses, at least for the terms of the main diagonal of the elastic matrix. In general, the differences between isothermal and adiabatic elastic stiffnesses are less than 1%. An exception to this statement concerns the temperature region near the critical temperature T_c where a phase transition occurs.

(ii) *Frequency dependence of the elastic constants.* Dynamic measurements of the elastic constants can be performed at a wide range of ultrasonic frequencies. Currently used techniques for investigating a wide range of frequencies are electronic pulse-echo techniques in the megahertz frequency range and Brillouin scattering in the 10 GHz frequency range. To evaluate the possible differences between dynamic elastic constants determined in different frequency ranges, high-accuracy measurements of the *absolute value* of the elastic constants are required. From optical resonance techniques in the megahertz frequency range and Brillouin scattering in the gigahertz frequency range, it has been shown that the results are the same within 0.1 to 0.2% in the case of simple and stable crystals such as sodium chloride when the ultrasonic waves can be considered as a 'passive probe' (Michard *et al.*, 1971). Larger differences are observed when ultrasonic waves interact with the medium, when they favour or

impede structural changes of the material or when they are absorbed for a particular frequency.

(iii) *Phase velocity and group velocity.* When the velocity of ultrasonic waves is frequency dependent (dispersive medium), one has to distinguish phase velocity and group velocity. If a resonance technique is used, the resonance frequencies correspond to phase-matching conditions and the calculation of velocity from the resonance frequencies leads to 'phase velocity'. If a pulse-echo technique is used, the transit time of an elastic pulse is measured and the interpretation of the measurement is more complex. In this case, Brillouin (1932) has shown that the head and the tail of the pulse travel with the group velocity. Differences of a few per cent can be observed between phase and group velocities in dispersive media.

1.3.4.6.2. Resonance technique

The use of the resonance technique is a well established approach for determining the velocity of sound in a gas by observing nodes and antinodes of a system of standing waves produced in the so-called *Kund tube*. In the case of transparent solids, optical means allow us to visualize the standing waves and to measure the wavelength directly (Zarembowitch, 1965). An easier procedure can be used: let us consider a transparent crystal in the shape of a parallelepiped (Fig. 1.3.4.1). A piezoelectric transducer is glued to the crystal and excited at varying frequencies. If the bonding between the transducer and the crystal is loose enough, the crystal can be considered as free from stress and the sequence of its resonance frequencies is given by

$$v = nV/2l,$$

where n is an integer, V the phase velocity of the wave in the direction orthogonal to the parallel faces and l the distance between these faces.

The looseness of the bonding can be checked by the regularity of the arithmetic ratio, $V/2l$. On account of the elasto-optic coupling, a phase grating is associated with the elastic standing-wave system and a light beam can be diffracted by this grating. The intensity of the diffraction pattern is maximum when resonance occurs. A large number of resonance frequencies can be detected, usually more than 100, sometimes 1000 for non-attenuating materials. Consequently, in favourable cases the absolute value of the ultrasonic velocity can be determined with an uncertainty less than 10^{-3} .

1.3.4.6.3. Pulse-echo techniques

Pulse-echo techniques are valid for transparent and opaque materials. They are currently used for measuring ultrasonic velocities in solids and can be used in very simple as well as in sophisticated versions according to the required precision (McSkimmin, 1964). In the simplest version (Fig. 1.3.4.2), an electronic pulse generator excites the mechanical vibrations of a piezo-electric transducer glued to one of two plane-parallel faces of a specimen. An ultrasonic pulse whose duration is of the order of a microsecond is generated and transmitted through the specimen. After reflection at the opposite face, it returns and, when it arrives back at the transducer, it gives rise to an electronic signal, or echo. The whole sequence of such echos is displayed on the screen of an oscilloscope and it is possible to measure from them the time interval for transit. Usually, X-cut quartz crystals or ferroelectric ceramics are used to excite longitudinal waves and Y-cut quartz is used to excite transverse waves. In many cases, a circulator, or gate, is used to protect the receiver from saturation following the main 'bang'. This method is rough because the beginning and the end of a pulse are not well characterized. Several improvements have therefore been made, mainly based on interferometric techniques (pulse-superposition

1.3. ELASTIC PROPERTIES

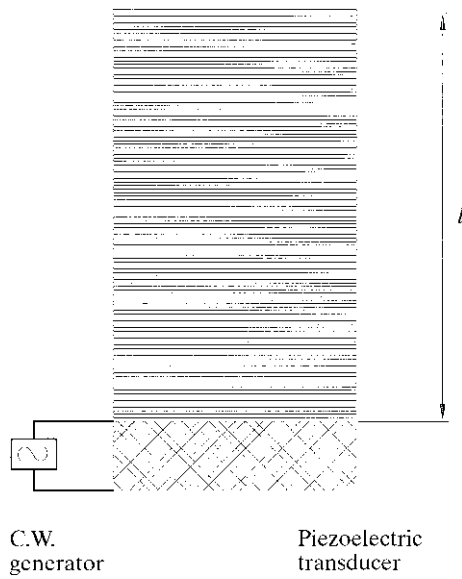


Fig. 1.3.4.1. Resonance technique: standing waves excited in a parallelepiped.

method, 'sing around' method *etc.*). Nevertheless, if the absolute value of the ultrasonic velocity is not determined with a high accuracy by using pulse-echo techniques, this approach has proved valuable when relative values of ultrasonic velocities are needed, *e.g.* temperature and pressure dependences of ultrasonic velocities.

(i) *Pulse-superposition method.* A piezoelectric transducer initiates ultrasonic pulses in the specimen. These pulses echo back and forth within the specimen. A continuous-wave oscillator is used to control the pulse repetition rate. When the repetition rate is adjusted so that the initiation of a pulse coincides with the return of the first echo from the preceding pulses, the change in the signal amplitude indicates superposition. The pulse rate is a measure of the travel time within the specimen.

(ii) *'Sing around method'.* The 'sing around' method for measuring the velocity of ultrasonic waves involves the use of two piezoelectric transducers, one at each end of the specimen. One transducer receives an impulse from the electronic generator and converts it into an ultrasonic pulse in the specimen. This pulse, after passing through the specimen, is detected by the receiving transducer. The received pulse triggers the electronic generator to initiate a succeeding pulse. The pulse repetition rate is a very sensitive probe for measuring changes of the ultrasonic velocity in the specimen. Relative variations of 10^{-7} can be measured, such as temperature or stress dependences of the velocity.

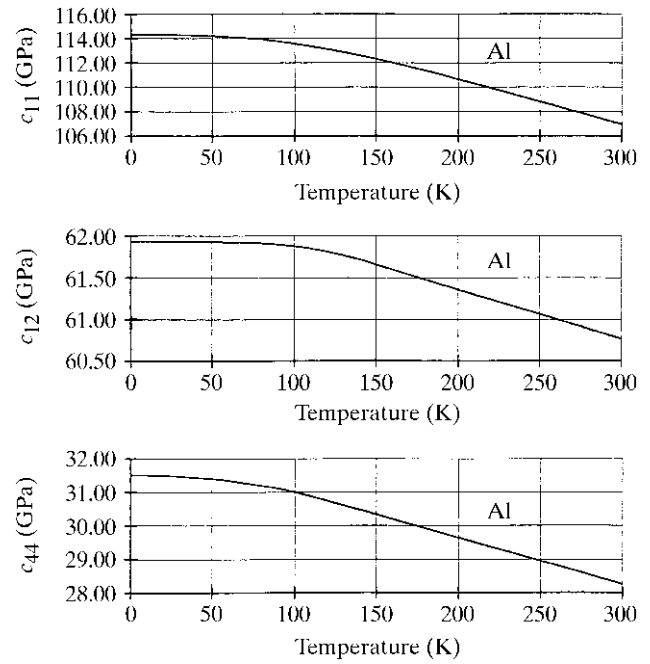


Fig. 1.3.5.1. Temperature dependence of the elastic stiffnesses of an aluminium single crystal (after Landolt-Börnstein, 1979).

1.3.5. Pressure dependence and temperature dependence of the elastic constants

1.3.5.1. Introduction

In a solid, the elastic constants are temperature and pressure dependent. As examples, the *temperature dependence* of the elastic stiffnesses of an aluminium single crystal within its stability domain (the melting point is 933 K) and the *pressure dependence* of the elastic stiffnesses of the ternary compound KZnF_3 within its stability domain (the crystal becomes unstable for a hydrostatic pressure of about 20 GPa) are shown in Figs. 1.3.5.1 and 1.3.5.2, respectively.

We can observe the following trends, which are general for stable crystals:

(i) From 0 K to about $\Theta_D/5$, where Θ_D is the Debye temperature, the elastic stiffnesses decrease according to a Θ^4 law. From $\Theta_D/5$ to the beginning of the instability domain, the dependence is linear with Θ . In addition, $(\partial c_{ii}/\partial \Theta)_p = 0$ at 0 K as predicted by the third principle of thermodynamics.

(ii) For stable crystals, the *pressure dependence* of the elastic stiffnesses is linear as long as the applied pressure is small compared to the elastic stiffnesses. As an example, a typical order

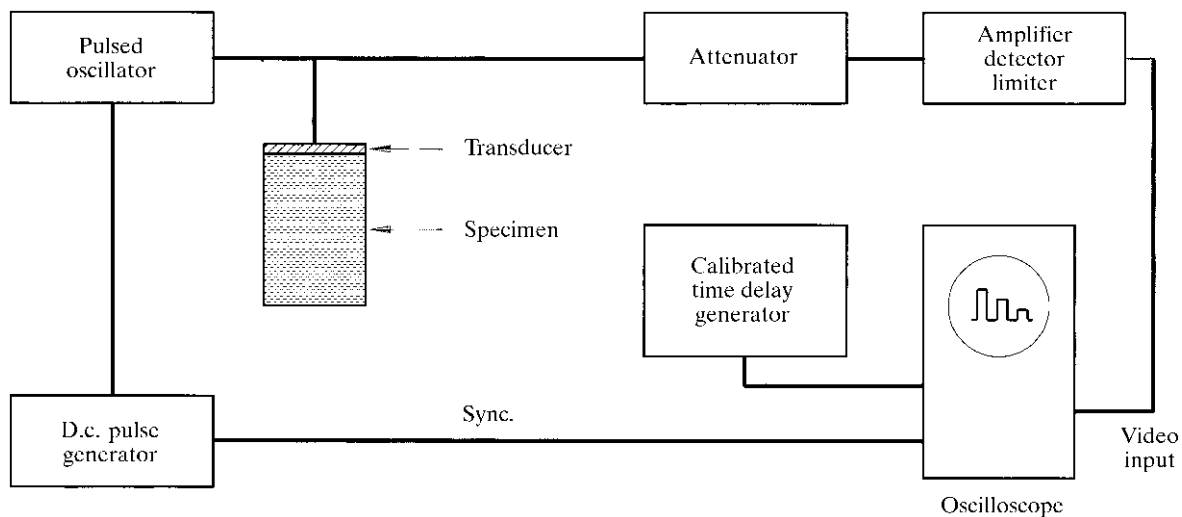


Fig. 1.3.4.2. Block diagram of the pulse-echo technique.

1. TENSORIAL ASPECTS OF PHYSICAL PROPERTIES

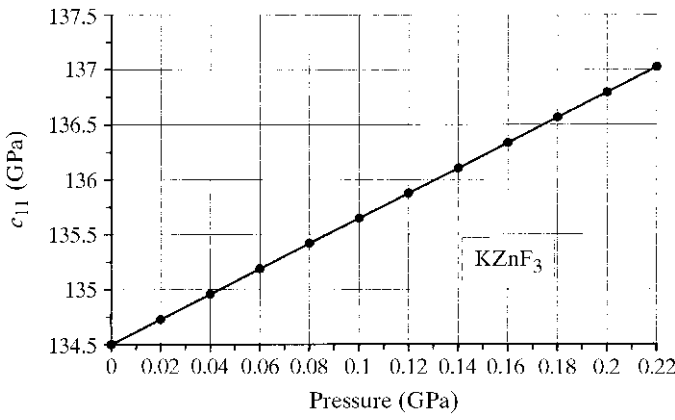


Fig. 1.3.5.2. Pressure dependence of the elastic stiffness c_{11} of a KZnF_3 crystal. Reproduced with permission from *Ultrasonics Symposium Proc. IEEE* (Fischer *et al.*, 1980). Copyright (1980) IEEE.

of magnitude for c_{11} in crystals is about 100 GPa and, within the experimental uncertainty, the pressure dependence of c_{11} does not depart from a linear behaviour up to at least 0.2 GPa.

These observations can be quantitatively justified on the basis of an equation of state of a solid:

$$f(T_{ij}, S_{ij}, X, \Theta) = 0,$$

where T_{ij} represents the stress tensor, S_{ij} the strain tensor, X the position of the elementary elements of the solid and Θ the temperature.

Different equations of state of solids have been proposed. They correspond to different degrees of approximation that can only be discussed and understood in a microscopic theory of lattice dynamics. The different steps in the development of lattice dynamics, the Einstein model, the Debye model and the Grüneisen model, will be presented in Section 2.1.2.7. Concerning the temperature and the pressure dependences of the elastic constants, we may notice that rather sophisticated models are needed to describe correctly the general trends mentioned above:

(a) In the *Einstein model*, where the N atoms of a crystal are considered as $3N$ independent harmonic oscillators, the temperature increase affects only the amplitude of the oscillations and not the average positions of the atoms; consequently, this model can explain neither the thermal expansion nor the *temperature dependence* of the elastic constants. In addition, this theory ignores the difference between isothermal and adiabatic elastic constants. Similarly, if the oscillators are harmonic, the stiffness of the ‘springs’ connecting atoms does not depend on the distances between atoms and the model cannot therefore explain the pressure dependence of the elastic constants, which requires anharmonic ‘springs’ or, more accurately, anharmonic potentials.

(b) In the *Debye model*, the $3N$ oscillators are not independent but they are still harmonic. The result is that here again the elastic constants are pressure and temperature independent.

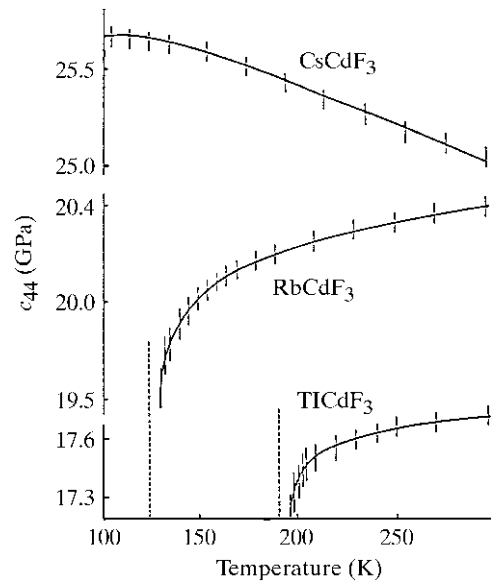


Fig. 1.3.5.3. Temperature dependence of the elastic constant c_{44} in RbCdF_3 , CsCdF_3 and TiCdF_3 crystals; the crystals of RbCdF_3 and TiCdF_3 undergo structural phase transitions (after Rousseau *et al.*, 1975).

(c) In the *Grüneisen model*, the frequencies of the oscillators are volume-dependent; this so-called ‘quasiharmonic approximation’ can justify the standard behaviour shown in Figs. 1.3.5.1 and 1.3.5.2.

1.3.5.2. Temperature dependence of the elastic constants

Table 1.3.5.1 gives typical values of $(\partial \ln c_{ij} / \partial \Theta)_p$ for some cubic crystals considered within their stability domain. In column 6, the ‘elastic Debye temperature’ of the crystal, $(\Theta_D)_{el}$, has been calculated according to the formula

$$(\Theta_D)_{el} = hv/k_B(3n/4\pi)^{1/3},$$

where h is the Planck constant, k_B is the Boltzmann constant, v is an average velocity (see for instance De Launay, 1956) and n is the number of atoms per unit volume.

It is interesting to compare $(\Theta_D)_{el}$, the ‘elastic Debye temperature’, with $(\Theta_D)_{cal}$, the ‘calorimetric Debye temperature’. The definition of $(\Theta_D)_{cal}$ will be given in Section 2.1.2.7. It results from the attempt at founding a universal description for the thermal properties of solids when the temperature is expressed as a reduced temperature, $\Theta/(\Theta_D)_{cal}$; $(\Theta_D)_{cal}$ is obtained from calorimetric measurements at low temperature. It is worth noting that accurate values of low-temperature elastic constants and low-temperature calorimetric measurements lead to an excellent agreement between $(\Theta_D)_{el}$ and $(\Theta_D)_{cal}$ [better than 2 or 3 K (De Launay, 1956)]. This agreement demonstrates the validity of the Debye model in the vicinity of 0 K. From Table 1.3.5.1, we can observe that for ionic crystals $(\partial \ln c_{11} / \partial \Theta)_p$ is, in general, greater than $(\partial \ln c_{44} / \partial \Theta)_p$. This remark is not valid for covalent and metallic crystals. Typical orders of magnitude are given in Table 1.3.5.2. These statements concern only general trends valid for stable crystals.

In the case of *temperature-induced phase transitions*, some elastic constants are softened in the vicinity and sometimes far from the critical temperature. As an example, Fig. 1.3.5.3 shows the temperature dependence of c_{44} in RbCdF_3 , CsCdF_3 and TiCdF_3 single crystals. RbCdF_3 and TiCdF_3 undergo structural phase transitions at 124 and 191 K, respectively, while CsCdF_3 remains stable in this temperature range.

Table 1.3.5.1. Temperature dependence of the elastic stiffnesses for some cubic crystals

| Material | Temperature range (K) | $(\partial \ln c_{11} / \partial \Theta)_p$ (10^{-4} K^{-1}) | $(\partial \ln c_{44} / \partial \Theta)_p$ (10^{-4} K^{-1}) | $(\partial \ln c_{12} / \partial \Theta)_p$ (10^{-4} K^{-1}) | Θ^{el} (K) |
|----------|-----------------------|---|---|---|----------------------|
| Al | 80–300 | −3.1 | −4.45 | −1.3 | 430 |
| Cu | 80–300 | −2.01 | −3.33 | −1.24 | 344 |
| Ag | 50–300 | −2.3 | −4.0 | −1.5 | 226 |
| Pb | 100–300 | −4.4 | −1.5 | −2.8 | 105 |
| Si | 80–300 | −0.81 | −10.6 | −1.10 | 648 |
| Ge | 150–1000 | −1.2 | −1.15 | −1.10 | 374 |
| ZnS | 100–300 | −1.2 | −0.65 | −0.8 | 347 |
| NaCl | 100–300 | −7.8 | −2.2 | −4.7 | 321 |
| KCl | 80–300 | −8.3 | −2.1 | −3.6 | 236 |
| KBr | 80–300 | −7.6 | −2.1 | 7 | 172 |

1.3. ELASTIC PROPERTIES

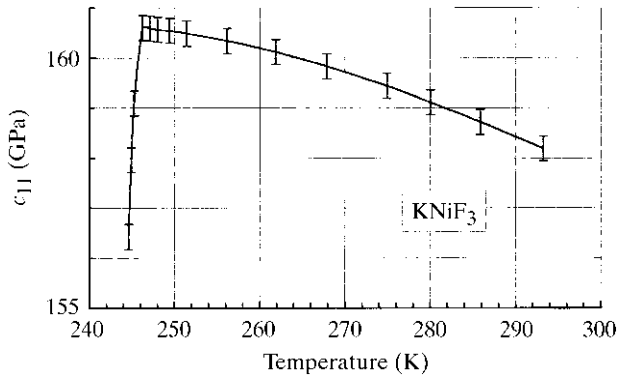


Fig. 1.3.5.4. Temperature dependence of the elastic constant c_{11} in KNiF_3 , which undergoes a para-antiferromagnetic phase transition. Reprinted with permission from *Appl. Phys. Lett.* (Nouet *et al.*, 1972). Copyright (1972) American Institute of Physics.

The softening of c_{44} when the temperature decreases starts more than 100 K before the critical temperature, Θ_c . In contrast, Fig. 1.3.5.4 shows the temperature dependence of c_{11} in KNiF_3 , a crystal that undergoes a para-antiferromagnetic phase transition at 246 K; the coupling between the elastic and the magnetic energy is weak, consequently c_{11} decreases abruptly only a few degrees before the critical temperature. We can generalize this observation and state that the softening of an elastic constant occurs over a large domain of temperature when this constant is the order parameter or is strongly coupled to the order parameter of the transformation; for instance, in the cooperative Jahn-Teller phase transition in DyVO_4 , $(c_{11} - c_{12})/2$ is the soft acoustic phonon mode leading to the phase transition and this parameter anticipates the phase transition 300 K before it occurs (Fig. 1.3.5.5).

1.3.5.3. Pressure dependence of the elastic constants

As mentioned above, anharmonic potentials are needed to explain the stress dependence of the elastic constants of a crystal. Thus, if the strain-energy density is developed in a polynomial in terms of the strain, only the first and the second elastic constants are used in linear elasticity (harmonic potentials), whereas higher-order elastic constants are also needed for nonlinear elasticity (anharmonic potentials).

Concerning the pressure dependence of the elastic constants (nonlinear elastic effect), considerable attention has been paid to their experimental determination since they are a unique source of significant information in many fields:

(i) In *geophysics*, a large part of the knowledge we have on the interior of the earth comes from the measurement of the transit time of elastic bursts propagating in the mantle and in the core (in the upper mantle, the average pressure is estimated to be about a few hundred GPa, a value which is comparable to that of the elastic stiffnesses of many materials).

(ii) In *solid-state physics*, the pressure dependence of the elastic constants gives significant indications concerning the stability of crystals. For example, Fig. 1.3.5.2 shows the pressure dependence of the elastic constants of KZnF_3 , a cubic crystal belonging to the perovskite family. As mentioned previously, this crystal is known to be stable over a wide range of temperature and the elastic stiffnesses c_{ij} depend linearly on pressure. It may be noted that, consequently, the third-order elastic constants

Table 1.3.5.2. Order of magnitude of the temperature dependence of the elastic stiffnesses for different types of crystals

| Type of crystal | $(\partial \ln c_{11} / \partial \Theta)_p$ (K^{-1}) | $(\partial \ln c_{44} / \partial \Theta)_p$ (K^{-1}) |
|-----------------|---|---|
| Ionic | -10^{-3} | -3×10^{-4} |
| Covalent | -10^{-4} | -8×10^{-5} |
| Metallic | -2×10^{-4} | -3×10^{-4} |

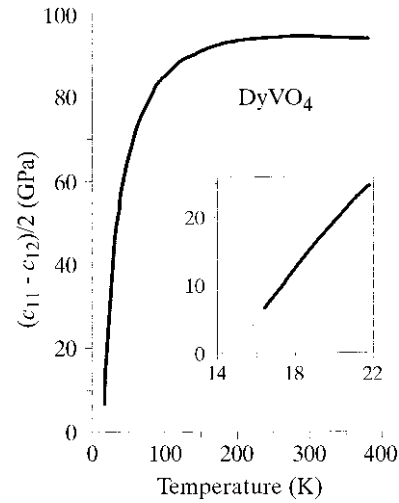


Fig. 1.3.5.5. Temperature dependence of $(c_{11} - c_{12})/2$ in DyVO_4 , which undergoes a cooperative Jahn-Teller phase transition (after Melcher & Scott, 1972).

(TOECs) are constant. On the contrary, we observe in Fig. 1.3.5.6 that the pressure dependence of the elastic constants of TlCdF_3 , a cubic crystal belonging to the same family but which is known to become unstable when the temperature is decreased to 191 K (Fischer, 1982), is nonlinear even at low pressures. In this case, the development of the strain-energy density in terms of strains cannot be stopped after the terms containing the third-order elastic constants; the contributions of the fourth- and fifth-order elastic constants are not negligible.

(iii) For practical use in the case of technical materials such as concrete or worked metals, the pressure dependence of the elastic moduli is also required for examining the effect of applied stresses or of an applied hydrostatic pressure, and for studying residual stresses resulting from loading (heating) and unloading (cooling) the materials.

1.3.6. Nonlinear elasticity

1.3.6.1. Introduction

In a solid body, the relation between the stress tensor T and the strain tensor S is usually described by Hooke's law, which postulates linear relations between the components of T and S (Section 1.3.3.1). Such relations can be summarized by (see equation 1.3.3.2)

$$T_{ij} = c_{ijkl} S_{kl},$$

where the c_{ijkl} 's are the elastic stiffnesses.

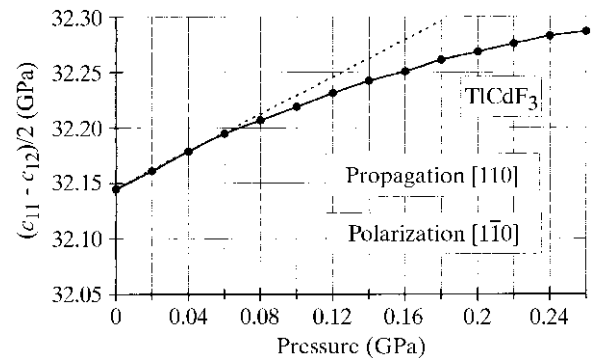


Fig. 1.3.5.6. Pressure dependence of the elastic constants $(c_{11} - c_{12})/2$ in TlCdF_3 . Reproduced with permission from *Ultrasonics Symposium Proc. IEEE* (Fischer *et al.*, 1980). Copyright (1980) IEEE.

1. TENSORIAL ASPECTS OF PHYSICAL PROPERTIES

For a solid under finite strain conditions, Hooke's law, valid for infinitesimal deformations, does not hold, and the fundamental definitions for stress and strain must be revisited.

1.3.6.2. Lagrangian and Eulerian description

Finite elastic strains may be treated from two different viewpoints using either the *Lagrangian (material)* or the *Eulerian (spatial)* descriptions.

Let us consider a fixed rectangular Cartesian coordinate system with axes x_i ($i = 1, 2, 3$). Any particular position vector \mathbf{r} of components (x_1, x_2, x_3) denotes a point in space. A point that always moves with the material is called a particle or *material point*. Let every particle be identified by its coordinates at some reference time t_0 . These reference coordinates, referred to the same Cartesian system, will be denoted by (a_1, a_2, a_3) and the corresponding position vector \mathbf{a} . A particular vector \mathbf{a} can serve as a name for the particle located at that position at the reference time t_0 .

The vectors \mathbf{r} and \mathbf{a} both specify a position in a fixed Cartesian frame of reference. At any time, we associate each \mathbf{r} with an \mathbf{a} by the rule that \mathbf{r} is the present position vector of the particle initially at \mathbf{a} . This connection between \mathbf{r} and \mathbf{a} is written symbolically as

$$\mathbf{r} = \mathbf{r}(t, \mathbf{a}) \quad \text{or} \quad x_i = x_i(t, a_1, a_2, a_3), \quad (1.3.6.1)$$

where

$$\mathbf{a} = \mathbf{r}(t_0, \mathbf{a}) \quad \text{or} \quad a_i = x_i(t_0, a_1, a_2, a_3). \quad (1.3.6.2)$$

The coordinates a_i that identify the particles are called *material coordinates*. A description that, like (1.3.6.1), uses (t, a_1, a_2, a_3) as independent variables is called a *material* or *Lagrangian* description.

The converse of (1.3.6.1) and (1.3.6.2) may be written

$$\mathbf{a} = \mathbf{a}(t, \mathbf{r}) \quad \text{or} \quad a_i = a_i(t, x_1, x_2, x_3), \quad (1.3.6.3)$$

where

$$\mathbf{r} = \mathbf{a}(t_0, \mathbf{r}) \quad \text{or} \quad x_i = a_i(t_0, x_1, x_2, x_3). \quad (1.3.6.4)$$

A spatial description or *Eulerian* description uses the independent variables (t, x_1, x_2, x_3) , the x_i being called *spatial coordinates*.

Now, for the sake of simplicity, we shall work with the Lagrangian formulation exclusively. For more details see, for instance, Thurston (1964) and Wallace (1970, 1972).

1.3.6.3. Strain and stress tensors

The displacement vector from the reference position of a particle to its new position has as components

$$u_i = x_i - a_i. \quad (1.3.6.5)$$

The term strain refers to a change in the relative positions of the material points in a body. Let a final configuration be described in terms of the reference configuration by setting t equal to a constant in (1.3.6.1). Then t no longer appears as a variable and (1.3.6.1) can be written

$$x_i = x_i(a_1, a_2, a_3),$$

where the a_i are the independent variables. It follows that

$$dx_j = \frac{\partial x_j}{\partial a_i} da_i = \left(\frac{\partial u_j}{\partial a_i} + \delta_{ij} \right) da_i. \quad (1.3.6.6)$$

Let now the particle initially at (a_1, a_2, a_3) move to (x_1, x_2, x_3) . The square of the initial distance to a neighbouring particle whose initial coordinates were $a_j + da_j$ is

$$ds^2 = da_j da_j.$$

The square of the final distance to the same neighbouring particle is

$$ds^2 = dx_j dx_j.$$

In a material description, the strain components S_{ik} are defined by the following equations:

$$dx_j dx_j - da_j da_j = 2S_{ik} da_i da_k. \quad (1.3.6.7)$$

Substituting (1.3.6.6) into (1.3.6.7), it follows that

$$\left(\frac{\partial u_j}{\partial a_i} + \delta_{ji} \right) \left(\frac{\partial u_j}{\partial a_k} + \delta_{jk} \right) da_i da_k - da_j da_j = 2S_{ik} da_i da_k.$$

Hence

$$S_{ik} = \frac{1}{2} \left(\frac{\partial u_k}{\partial a_i} + \frac{\partial u_i}{\partial a_k} + \frac{\partial u_j}{\partial a_i} \frac{\partial u_j}{\partial a_k} \right).$$

If the products and squares of the displacement derivatives are neglected, the strain components reduce to the usual form of 'infinitesimal elasticity' [see equation (1.3.1.8)]:

$$S_{ik} = \frac{1}{2} \left(\frac{\partial u_i}{\partial a_k} + \frac{\partial u_k}{\partial a_i} \right).$$

It is often useful to introduce the Jacobian matrix associated with the transformation (\mathbf{a}, \mathbf{x}) . The components of this matrix are

$$J = \begin{pmatrix} \alpha_{11} & \alpha_{12} & \alpha_{13} \\ \alpha_{21} & \alpha_{22} & \alpha_{23} \\ \alpha_{31} & \alpha_{32} & \alpha_{33} \end{pmatrix},$$

where

$$\alpha_{ik} = \frac{\partial x_i}{\partial a_k} = \frac{\partial u_j}{\partial a_k} + \delta_{jk}.$$

From the definition of matrix J , one has

$$d\mathbf{x} = J d\mathbf{a}$$

and

$$dx^2 - da^2 = (d\mathbf{x})^T d\mathbf{x} - (d\mathbf{a})^T d\mathbf{a} = (d\mathbf{a})^T (J^T J - \delta) d\mathbf{a},$$

where $(d\mathbf{a})^T$, $(d\mathbf{x})^T$ and J^T are the transpose matrices of $d\mathbf{a}$, $d\mathbf{x}$ and J , respectively, and δ is the Kronecker matrix.

The Lagrangian strain matrix S may then be written symbolically:

$$S = \frac{1}{2} (J^T J - \delta). \quad (1.3.6.8)$$

When finite strains are concerned, we have to distinguish three states of the medium: the natural state, the initial state and the final or present state: The *natural* state is a state free of stress. The *initial* state is deduced from the natural state by a homogeneous strain. The *final* state is deduced from the initial state by an arbitrary strain.

Concerning the stress tensor, as pointed out by Thurston (1964), the stress-deformation relation is complicated in nonlinear elasticity because 'the strain is often referred to a natural unstressed state, whereas the stress T_{ij} is defined per unit area of the deformed body'. For this reason, the differential of work done by the stress is not equal to the stress components times the differentials of the corresponding strain components. So, following Truesdell & Toupin (1960), we shall introduce a *thermodynamic tension tensor* t_{ij} defined as the first derivative of the energy with respect to strain. If the internal energy U per unit

1.3. ELASTIC PROPERTIES

mass is considered, the *thermodynamic tension* refers to an isentropic process. Then

$$t_{ij}^{\sigma} = \rho_0 \left(\frac{\partial U}{\partial S_{ij}} \right)_{\sigma},$$

where σ is the entropy and ρ_0 the volumic mass in the initial state.

If the Helmholtz free energy F is considered, the thermodynamic tension refers to an isothermal process. Then

$$t_{ij}^{\Theta} = \rho_0 \left(\frac{\partial U}{\partial S_{ij}} \right)_{\Theta},$$

where Θ is the temperature. It will be shown in Section 1.3.7.2 that

$$T_{ij} = (1/J) \alpha_{ik} \alpha_{jl} t_{kl}.$$

1.3.6.4. Second-order and higher-order elastic stiffnesses

Following Brugger (1964), the strain-energy density, or strain energy per unit volume Φ , is assumed to be a polynomial in the strain:

$$\Phi = \Phi_0 + c_{ij} S_{ij} + \frac{1}{2!} c_{ijkl} S_{ij} S_{kl} + \frac{1}{3!} c_{ijklmn} S_{ij} S_{kl} S_{mn}, \quad (1.3.6.9)$$

where $\Phi = \rho_0 U(X, S_{ij})$, $\Phi_0 = \rho_0 U(X, 0)$, X denotes the configuration of the initial state and the S_{ij} 's are the Lagrangian finite strain-tensor components.

If the initial energy and the deformation of the body are both zero, the first two terms in (1.3.6.9) are zero. Note that c_{ij} is a stress and not an intrinsic characteristic of the material. In this expression, the elastic stiffnesses c_{ijkl} and c_{ijklmn} are the second- and third-order stiffnesses, respectively. Since the strain tensor is symmetric, pairs of subscripts can be interchanged [see equation (1.3.3.4)]:

$$\begin{aligned} c_{ijkl} &= c_{jikl} = c_{ijlk} = c_{jilk}, \\ c_{ijklmn} &= c_{jiklmn} = c_{ijlkmn} = c_{jilkmn} = c_{ijklnm} \\ &= c_{jiklnm} = c_{ijlknm} = c_{jilknm}. \end{aligned}$$

More accurately, the isentropic and the isothermal elastic stiffnesses are defined as the n th partial derivatives of the internal energy and the Helmholtz free energy, respectively. For example, the third-order isentropic and isothermal stiffnesses are, respectively,

$$\begin{aligned} c_{ijklmn}^{\sigma} &= \rho_0 \frac{\partial^3 U}{\partial S_{ij} \partial S_{kl} \partial S_{mn}}, \\ c_{ijklmn}^{\Theta} &= \rho_0 \frac{\partial^3 F}{\partial S_{ij} \partial S_{kl} \partial S_{mn}}, \end{aligned}$$

where the internal energy, U , is a function of X , S_{ij} and σ , and the Helmholtz free energy, F , is a function of X , S_{ij} and Θ .

From these definitions, it follows that the Brugger stiffness coefficients depend on the initial state. *When no additional information is given, the initial state is the natural state.*

The third-order stiffnesses form a sixth-rank tensor containing $3^6 = 729$ components, of which 56 are independent for a triclinic crystal and 3 for isotropic materials (the independent components of a sixth-rank tensor can be obtained for any point group using the accompanying software to this volume). The three independent constants for isotropic materials are often taken as c_{123} , c_{144} and c_{456} and denoted respectively by ν_1 , ν_2 , ν_3 , the 'third-order Lamé constants'.

The 'third-order Murnaghan constants' (Murnaghan, 1951), denoted by l , m , n , are given in terms of the Brugger constants by the relations

$$l = \frac{1}{2} c_{112}; \quad m = c_{155}; \quad n = 4c_{456}.$$

Similarly, the fourth-order stiffnesses form an eighth-rank tensor containing $3^8 = 6561$ components, 126 of which are independent for a triclinic crystal and 11 for isotropic materials (the independent components of a sixth-rank tensor can be obtained for any point group using the accompanying software to this volume).

For a solid under finite strain conditions, the definition of the elastic compliance tensor has to be reconsidered. In linear elasticity, the second-order elastic compliances s_{ijkl} were defined through the relations (1.3.3.2):

$$S_{ij} = s_{ijkl} T_{kl} \quad \text{or} \quad s_{ijkl} = \frac{\partial S_{ij}}{\partial T_{kl}},$$

while, in nonlinear elasticity, one has

$$s_{ijkl} = \frac{\partial S_{ij}}{\partial t_{kl}},$$

where

$$t_{kl} = \rho_0 \frac{\partial U}{\partial S_{kl}}.$$

1.3.6.5. Expansion of elastic constants for small initial stress

In most experiments, the initial stress is small compared with the second-order elastic constants (for example, 1 GPa hydrostatic pressure compared with the usual value $c_{ijkl} = 100$ GPa). Consequently, the deformation between the initial (stressed) state and the natural (unstressed) state is small compared with 1. For this reason, it is convenient to expand the elastic constants in the initial state as a power series in the strain about the natural state. *To avoid confusion, we introduce new notations:* \bar{X} now represents the coordinates in the *natural* or unstressed state; X represents the coordinates in the *initial* or homogeneously strained state; $u_i = x_i - X_i$ are the components of displacement. All letters with superscript bar refer to the natural state; for example, \bar{S}_{ij} denotes the Lagrangian strain in the natural state; $\bar{U} = U(\bar{X}, \bar{S}_{ij})$.

Now, in order to relate the properties at X to those at \bar{X} , we need to specify the strain from \bar{X} to X . Let

$$a_{ij} = \frac{\partial X_i}{\partial \bar{X}_j} = \bar{\alpha}_{ij}.$$

Consequently,

$$\frac{\partial \bar{S}_{ij}}{\partial S_{mn}} = a_{mi} a_{nj}.$$

The second-order elastic constants at X can be expressed in terms of the second- and third-order elastic constants at \bar{X} :

$$c_{ijkl} = \rho_0 \frac{\partial^2 U}{\partial S_{ij} \partial S_{kl}} = \rho_0 \frac{\partial^2 \bar{U}}{\partial \bar{S}_{mn} \partial \bar{S}_{pq}} a_{im} a_{jn} a_{kp} a_{lq}$$

or

$$c_{ijkl} = \frac{\rho_0}{\bar{\rho}_0} \left(\bar{c}_{mnpq} + \bar{c}_{mnpqrs} S_{rs} + \frac{1}{2!} \bar{c}_{mnpqrstuv} S_{rs} S_{tu} + \dots \right) a_{im} a_{jn} a_{kp} a_{lq}.$$

This expression holds for both isentropic and isothermal elastic constants.

1. TENSORIAL ASPECTS OF PHYSICAL PROPERTIES

1.3.6.6. Elastic strain-energy density

The elastic strain-energy density has appeared in the literature in various forms. Most of the authors use the Murnaghan constants as long as isotropic solids are concerned. However, most of the literature uses Brugger's thermodynamic definition when anisotropic media are under consideration (Brugger, 1964).

The elastic strain-energy density for an isotropic medium, including third-order terms but omitting terms independent of strain, may be expressed in terms of three strain invariants, since an isotropic material is invariant with respect to rotation:

$$\Phi = \frac{\lambda + 2\mu}{2}(I_1)^2 - 2\mu I_2 + \frac{l + 2m}{3}(I_1)^3 - 2mI_1 I_2 + nI_3,$$

where λ and μ are the second-order Lamé constants, l, m, n are the third-order Murnaghan constants, and I_1, I_2, I_3 are the three invariants of the Lagrangian strain matrix. These invariants may be written in terms of the strain components as

$$\begin{aligned} I_1 &= S_{11} + S_{22} + S_{33} \\ I_2 &= \begin{vmatrix} S_{11} & S_{12} \\ S_{21} & S_{22} \end{vmatrix} + \begin{vmatrix} S_{22} & S_{23} \\ S_{32} & S_{33} \end{vmatrix} + \begin{vmatrix} S_{33} & S_{31} \\ S_{13} & S_{11} \end{vmatrix} \\ I_3 &= \begin{vmatrix} S_{11} & S_{12} & S_{13} \\ S_{21} & S_{22} & S_{23} \\ S_{31} & S_{32} & S_{33} \end{vmatrix}. \end{aligned}$$

The elastic strain-energy density for an *anisotropic* medium (for example a medium belonging to the most symmetrical groups of cubic crystals) is (Green, 1973)

$$\begin{aligned} \Phi &= \frac{1}{2}c_{11}[(S_{11})^2 + (S_{22})^2 + (S_{33})^2] + c_{12}[S_{11}S_{22} + S_{22}S_{33} + S_{33}S_{11}] \\ &+ c_{44}[(S_{12})^2 + (S_{21})^2 + (S_{23})^2 + (S_{32})^2 + (S_{31})^2 + (S_{13})^2] \\ &+ c_{111}[(S_{11})^3 + (S_{22})^3 + (S_{33})^3] \\ &+ c_{112}[(S_{11})^2(S_{22} + S_{33}) + (S_{22})^2(S_{33} + S_{11}) \\ &+ (S_{33})^2(S_{11} + S_{22})] \\ &+ \frac{1}{2}c_{144}\{S_{11}[(S_{23})^2 + (S_{32})^2] + S_{22}[(S_{31})^2 + (S_{13})^2] \\ &+ S_{33}[(S_{12})^2 + (S_{21})^2]\} \\ &+ \frac{1}{2}c_{166}\{[(S_{12})^2 + (S_{21})^2](S_{11} + S_{22}) \\ &+ [(S_{23})^2 + (S_{32})^2](S_{22} + S_{33}) \\ &+ [(S_{13})^2 + (S_{31})^2](S_{11} + S_{33})\} \\ &+ c_{123}S_{11}S_{22}S_{33} + c_{456}[S_{12}S_{23}S_{31} + S_{21}S_{32}S_{13}]. \end{aligned}$$

1.3.7. Nonlinear dynamic elasticity

1.3.7.1. Introduction

In recent years, the measurements of ultrasonic wave velocities as functions of stresses applied to the sample and the measurements of the amplitude of harmonics generated by the passage of an ultrasonic wave throughout the sample are in current use. These experiments and others, such as the interaction of two ultrasonic waves, are interpreted from the same theoretical basis, namely nonlinear dynamical elasticity.

A first step in the development of nonlinear dynamical elasticity is the derivation of the general equations of motion for elastic waves propagating in a solid under nonlinear elastic conditions. Then, these equations are restricted to elastic waves propagating either in an isotropic or in a cubic medium. The next step is the examination of two important cases:

(i) the generation of harmonics when *finite amplitude* ultrasonic waves travel throughout an *unstressed* medium;

(ii) the propagation of *small amplitude* ultrasonic waves when they travel throughout a *stressed* medium.

Finally, the concept of natural velocity is introduced and the experiments that can be used to determine the third- and higher-order elastic constants are described.

1.3.7.2. Equation of motion for elastic waves

For generality, these equations will be derived in the X configuration (initial state). It is convenient to obtain the equations of motion with the aid of Lagrange's equations. In the absence of body forces, these equations are

$$\frac{d}{dt} \frac{\partial L}{\partial \dot{x}_i} + \frac{\partial}{\partial X_i} \frac{\partial L}{\partial (\partial x_i / \partial X_j)} = 0 \quad (1.3.7.1)$$

or

$$\frac{d}{dt} \frac{\partial L}{\partial \dot{x}_i} + \frac{\partial}{\partial X_i} \frac{\partial L}{\partial \alpha_{ij}} = 0, \quad (1.3.7.2)$$

where L is the Lagrangian per unit initial volume and $\alpha_{ij} = \partial x_i / \partial X_j$ are the elements of the Jacobian matrix.

For adiabatic motion

$$L = \frac{1}{2} \rho_0 \dot{x}_i^2 - \rho_0 U, \quad (1.3.7.3)$$

where U is the internal energy per unit mass.

Combining (1.3.7.2) and (1.3.7.3), it follows that

$$\rho_0 \ddot{x}_i = \frac{\partial}{\partial X_j} \left(\rho_0 \frac{\partial U}{\partial S_{lm}} \frac{\partial S_{lm}}{\partial \alpha_{ij}} \right),$$

which can be written

$$\rho_0 \ddot{x}_i = \frac{\partial}{\partial X_j} \left(\alpha_{il} \alpha_{jm} \rho_0 \frac{\partial U}{\partial S_{lm}} \right)$$

since

$$\frac{\partial S_{lm}}{\partial \alpha_{ij}} = \frac{1}{2} (\alpha_{im} \delta_{jl} + \alpha_{il} \delta_{jm}).$$

Using now the equation of continuity or conservation of mass:

$$\frac{\rho_0}{\rho} = J = \det(\alpha_{ij}),$$

and the identity of Euler, Piola and Jacobi:

$$\frac{\partial}{\partial x_j} \left(\frac{1}{J} \frac{\partial x_j}{\partial X_i} \right) = 0,$$

we get an expression of Newton's law of motion:

$$\rho x_i'' = \frac{dT_{ij}}{dX_j} \text{ or } \rho u_i'' = \frac{dT_{ij}}{dX_j} \quad (1.3.7.4)$$

with

$$T_{ij} = \frac{\rho_0}{J} \alpha_{ik} \alpha_{jl} \frac{\partial U}{\partial S_{kl}} = \rho \alpha_{ik} \alpha_{jl} \frac{\partial U}{\partial S_{kl}}.$$

T_{ij} becomes

$$T_{ij} = \frac{1}{J} \alpha_{ik} \alpha_{jl} t_{kl}$$

since

$$t_{kl} = \rho_0 \frac{\partial U}{\partial S_{kl}}.$$

1.3. ELASTIC PROPERTIES

t_{kl} , the thermodynamic tensor conjugate to the variable S_{kl}/ρ_0 , is generally denoted as the ‘second Piola–Kirchoff stress tensor’.

Using Φ , the strain energy per unit volume, Newton’s law (1.3.7.4) takes the form

$$\rho x_i'' = \frac{\partial}{\partial X_j} \left(\alpha_{jk} \frac{\partial \Phi}{\partial S_{ik}} \right) \quad \text{or} \quad \rho u_i'' = \frac{\partial}{\partial X_j} \left(\alpha_{jk} \frac{\partial \Phi}{\partial S_{ik}} \right)$$

and

$$T_{ij} = \alpha_{jk} \frac{\partial \Phi}{\partial S_{ik}}. \quad (1.3.7.5)$$

1.3.7.3. Wave propagation in a nonlinear elastic medium

As an example, let us consider the case of a plane finite amplitude wave propagating along the x_1 axis. The displacement components in this case become

$$u_1 = u_1(X_1, t); \quad u_2 = u_2(X_1, t); \quad u_3 = u_3(X_1, t).$$

Thus, the Jacobian matrix α_{ij} reduces to

$$J = \begin{pmatrix} \alpha_{11} & 0 & 0 \\ \alpha_{21} & 0 & 0 \\ \alpha_{31} & 0 & 0 \end{pmatrix}.$$

The Lagrangian strain matrix is [equation (1.3.6.8)]

$$S = \frac{1}{2} (J^T J - \delta).$$

The only nonvanishing strain components are, therefore,

$$\begin{aligned} S_{11} &= \frac{1}{2} (\alpha_{11}^2 + \alpha_{21}^2 + \alpha_{31}^2) - 1 \\ &= \frac{\partial u_1}{\partial X_1} + \frac{1}{2} \left[\left(\frac{\partial u_1}{\partial X_1} \right)^2 + \left(\frac{\partial u_2}{\partial X_1} \right)^2 + \left(\frac{\partial u_3}{\partial X_1} \right)^2 \right] \\ S_{12} &= S_{21} = \frac{1}{2} \frac{\partial u_2}{\partial X_1} \\ S_{13} &= S_{31} = \frac{1}{2} \frac{\partial u_3}{\partial X_1} \end{aligned}$$

and the strain invariants reduce to

$$I_1 = S_{11}; \quad I_2 = -(S_{12}S_{21} + S_{13}S_{31}); \quad I_3 = 0.$$

1.3.7.3.1. Isotropic media

In this case, the strain-energy density becomes

$$\Phi = \frac{1}{2} (\lambda + 2\mu) (S_{11})^2 + 2\mu (S_{12}S_{21} + S_{13}S_{31}) + \frac{1}{3} (l + 2m) (S_{11})^3 + 2mS_{11}(S_{12}S_{21} + S_{13}S_{31}). \quad (1.3.7.6)$$

Differentiating (1.3.7.6) with respect to the strains, we get

$$\frac{\partial \Phi}{\partial S_{11}} = (\lambda + 2\mu) S_{11} + (l + 2m) (S_{11})^2 + 2m(S_{12}S_{21} + S_{13}S_{31})$$

$$\frac{\partial \Phi}{\partial S_{12}} = 2\mu S_{21} + 2mS_{11}S_{21}$$

$$\frac{\partial \Phi}{\partial S_{13}} = 2\mu S_{31} + 2mS_{11}S_{31}$$

$$\frac{\partial \Phi}{\partial S_{21}} = 2\mu S_{12} + 2mS_{11}S_{12}$$

$$\frac{\partial \Phi}{\partial S_{31}} = 2\mu S_{13} + 2mS_{11}S_{13}.$$

All the other $\partial \Phi / \partial S_{ij} = 0$.

From (1.3.7.5), we derive the stress components:

$$T_{11} = \alpha_{1k} \frac{\partial \Phi}{\partial S_{1k}}; \quad T_{12} = \alpha_{2k} \frac{\partial \Phi}{\partial S_{1k}}; \quad T_{13} = \alpha_{3k} \frac{\partial \Phi}{\partial S_{1k}};$$

$$T_{21} = \alpha_{1k} \frac{\partial \Phi}{\partial S_{2k}}; \quad T_{22} = \alpha_{2k} \frac{\partial \Phi}{\partial S_{2k}}; \quad T_{23} = \alpha_{3k} \frac{\partial \Phi}{\partial S_{2k}};$$

$$T_{31} = \alpha_{1k} \frac{\partial \Phi}{\partial S_{3k}}; \quad T_{32} = \alpha_{2k} \frac{\partial \Phi}{\partial S_{3k}}; \quad T_{33} = \alpha_{3k} \frac{\partial \Phi}{\partial S_{3k}}.$$

Note that this tensor is not symmetric.

For the particular problem discussed here, the three components of the equation of motion are

$$\rho u_1'' = dT_{11}/dX_1,$$

$$\rho u_2'' = dT_{21}/dX_1,$$

$$\rho u_3'' = dT_{31}/dX_1.$$

If we retain only terms up to the quadratic order in the displacement gradients, we obtain the following equations of motion:

$$\begin{aligned} \rho u_1'' &= (\lambda + 2\mu) \frac{\partial^2 u_1}{\partial X_1^2} + [3(\lambda + 2\mu) + 2(l + 2m)] \frac{\partial u_1}{\partial X_1} \frac{\partial^2 u_1}{\partial X_1^2} \\ &\quad + (\lambda + 2\mu + m) \left[\frac{\partial u_2}{\partial X_1} \frac{\partial^2 u_2}{\partial X_1^2} + \frac{\partial u_3}{\partial X_1} \frac{\partial^2 u_3}{\partial X_1^2} \right] \\ \rho u_2'' &= \mu \frac{\partial^2 u_2}{\partial X_1^2} + (\lambda + 2\mu + m) \left[\frac{\partial u_1}{\partial X_1} \frac{\partial^2 u_2}{\partial X_1^2} + \frac{\partial u_2}{\partial X_1} \frac{\partial^2 u_1}{\partial X_1^2} \right] \\ \rho u_3'' &= \mu \frac{\partial^2 u_3}{\partial X_1^2} + (\lambda + 2\mu + m) \left[\frac{\partial u_1}{\partial X_1} \frac{\partial^2 u_3}{\partial X_1^2} + \frac{\partial u_3}{\partial X_1} \frac{\partial^2 u_1}{\partial X_1^2} \right]. \end{aligned} \quad (1.3.7.7)$$

1.3.7.3.2. Cubic media (most symmetrical groups)

In this case, the strain-energy density becomes

$$\begin{aligned} \Phi &= \frac{1}{2} c_{11} (S_{11})^2 + c_{44} [(S_{12})^2 + (S_{21})^2 + (S_{31})^2 + (S_{13})^2] \\ &\quad + c_{111} (S_{11})^3 + \frac{1}{2} c_{166} S_{11} [(S_{12})^2 + (S_{21})^2 + (S_{31})^2 + (S_{13})^2]. \end{aligned} \quad (1.3.7.8)$$

Differentiating (1.3.7.8) with respect to the strain, one obtains

$$\begin{aligned} \frac{\partial \Phi}{\partial S_{11}} &= c_{11} S_{11} + 3c_{111} (S_{11})^2 + \frac{1}{2} c_{166} [(S_{12})^2 + (S_{21})^2 \\ &\quad + (S_{31})^2 + (S_{13})^2] \end{aligned}$$

$$\frac{\partial \Phi}{\partial S_{21}} = 2c_{44} S_{21} + c_{166} S_{11} S_{21}$$

$$\frac{\partial \Phi}{\partial S_{31}} = 2c_{44} S_{31} + c_{166} S_{11} S_{31}.$$

All other $\partial \Phi / \partial S_{ij} = 0$. From (1.3.7.5), we derive the stress components:

$$T_{11} = \alpha_{1k} \frac{\partial \Phi}{\partial S_{1k}}$$

$$T_{21} = \alpha_{1k} \frac{\partial \Phi}{\partial S_{2k}}$$

$$T_{31} = \alpha_{1k} \frac{\partial \Phi}{\partial S_{3k}}.$$

In this particular case, the three components of the equation of motion are

1. TENSORIAL ASPECTS OF PHYSICAL PROPERTIES

$$\begin{aligned}\rho u_1'' &= dT_{11}/dX_1 \\ \rho u_2'' &= dT_{21}/dX_1 \\ \rho u_3'' &= dT_{31}/dX_1.\end{aligned}$$

If we retain only terms up to the quadratic order in the displacement gradients, we obtain the following equations of motion:

$$\begin{aligned}\rho u_1'' &= c_{11} \frac{\partial^2 u_1}{\partial X_1^2} + [3c_{11} + c_{111}] \frac{\partial u_1}{\partial X_1} \frac{\partial^2 u_1}{\partial X_1^2} \\ &\quad + (c_{11} + c_{166}) \left[\frac{\partial u_2}{\partial X_1} \frac{\partial^2 u_2}{\partial X_1^2} + \frac{\partial u_3}{\partial X_1} \frac{\partial^2 u_3}{\partial X_1^2} \right] \\ \rho u_2'' &= c_{44} \frac{\partial^2 u_2}{\partial X_1^2} + (c_{11} + c_{166}) \left[\frac{\partial u_1}{\partial X_1} \frac{\partial^2 u_2}{\partial X_1^2} + \frac{\partial u_2}{\partial X_1} \frac{\partial^2 u_1}{\partial X_1^2} \right] \\ \rho u_3'' &= c_{44} \frac{\partial^2 u_3}{\partial X_1^2} + (c_{11} + c_{166}) \left[\frac{\partial u_1}{\partial X_1} \frac{\partial^2 u_3}{\partial X_1^2} + \frac{\partial u_3}{\partial X_1} \frac{\partial^2 u_1}{\partial X_1^2} \right],\end{aligned}\quad (1.3.7.9)$$

which are identical to (1.3.7.7) if we put

$$c_{11} = \lambda + 2\mu; \quad c_{44} = \mu; \quad c_{111} = 2(l + 2m); \quad c_{166} = m.$$

1.3.7.4. Harmonic generation

The coordinates in the medium free of stress are denoted either a or \bar{X} . The notation \bar{X} is used when we have to discriminate the natural configuration, \bar{X} , from the initial configuration X . Here, the process that we describe refers to the propagation of an elastic wave in a medium free of stress (natural state) and the coordinates will be denoted a_i .

Let us first examine the case of a pure longitudinal mode, *i.e.*

$$u_1 = u_1(a_1, t); \quad u_2 = u_3 = 0.$$

The equations of motion, (1.3.7.7) and (1.3.7.9), reduce to

$$\rho u_1'' = (\lambda + 2\mu) \frac{\partial^2 u_1}{\partial a_1^2} + [3(\lambda + 2\mu) + 2(l + 2m)] \frac{\partial u_1}{\partial a_1} \frac{\partial^2 u_1}{\partial a_1^2}$$

for an isotropic medium or

$$\rho u_1'' = c_{11} \frac{\partial^2 u_1}{\partial a_1^2} + [3c_{11} + c_{166}] \frac{\partial u_1}{\partial a_1} \frac{\partial^2 u_1}{\partial a_1^2}$$

for a cubic crystal (most symmetrical groups) when a pure longitudinal mode is propagated along [100].

For both cases, we have a one-dimensional problem; (1.3.7.7) and (1.3.7.9) can therefore be written

$$\rho u_1'' = K_2 \frac{\partial^2 u_1}{\partial a_1^2} + [3K_2 + K_3] \frac{\partial u_1}{\partial a_1} \frac{\partial^2 u_1}{\partial a_1^2}. \quad (1.3.7.10)$$

The same equation is also valid when a pure longitudinal mode is propagated along [110] and [111], with the following correspondence:

$$\begin{aligned}[100] \quad K_2 &= c_{11}, \quad K_3 = c_{111} \\ [110] \quad K_2 &= \frac{c_{11} + c_{12} + 2c_{44}}{2}, \quad K_3 = \frac{c_{111} + 3c_{112} + 12c_{166}}{4} \\ [111] \quad K_2 &= \frac{c_{11} + 2c_{12} + 4c_{44}}{3}, \\ K_3 &= \frac{c_{111} + 6c_{112} + 12c_{144} + 24c_{166} + 2c_{123} + 16c_{456}}{9}.\end{aligned}$$

Let us assume that $K_3 \ll K_2$; a perturbation solution to (1.3.7.10) is

$$u = u^0 + u^1,$$

where $u^1 \ll u^0$ with

$$u^0 = A \sin(ka - \omega t) \quad (1.3.7.11)$$

$$u^1 = Ba \sin 2(ka - \omega t) + Ca \cos 2(ka - \omega t). \quad (1.3.7.12)$$

If we substitute the trial solutions into (1.3.7.10), we find after one iteration the following approximate solution:

$$u = A \sin(ka - \omega t) - \frac{(kA)^2(3K_2 + K_3)}{8\rho c^2} a \cos 2(ka - \omega t),$$

which involves second-harmonic generation.

If additional iterations are performed, higher harmonic terms will be obtained. A well known property of the first-order nonlinear equation (1.3.7.10) is that its solutions exhibit discontinuous behaviour at some point in space and time. It can be seen that such a discontinuity would appear at a distance from the origin given by (Breazeale, 1984)

$$L = -2 \frac{(K_2)^2}{3K_2 + K_3} \rho \omega u_0',$$

where u_0' is the initial value for the particle velocity.

1.3.7.5. Small-amplitude waves in a strained medium

We now consider the propagation of small-amplitude elastic waves in a homogeneously strained medium. As defined previously, \bar{X} or a are the coordinates in the natural or unstressed state. X are the coordinates in the initial or homogeneously strained state. $u_i = x_i - X_i$ are the components of displacement from the initial state due to the wave.

Starting from (1.3.7.4), we get

$$T_{ij} = \frac{\rho_0}{J} \alpha_{ik} \alpha_{jl} \frac{\partial U}{\partial S_{kl}}.$$

Its partial derivative is

$$\frac{\partial T_{ij}}{\partial x_j} = \frac{1}{J} \frac{\partial}{\partial X_k} \left[\rho_0 \alpha_{il} \frac{\partial U}{\partial S_{kl}} \right].$$

If we expand the state function about the initial configuration, it follows that

$$\begin{aligned}\rho_0 U(X_k, S_{ij}) &= \rho_0 U(X_k) + c_{ij} S_{ij} + \frac{1}{2} c_{ijkl} S_{ij} S_{kl} \\ &\quad + \frac{1}{6} c_{ijklmn} S_{ij} S_{kl} S_{mn} + \dots\end{aligned}$$

The linearized stress derivatives become

$$\frac{\partial T_{ij}}{\partial x_j} = [c_{jl} \delta_{ik} + c_{ijkl}] \frac{\partial^2 x_k}{\partial X_j \partial X_l}.$$

If we let $D_{ijkl} = [c_{jl} \delta_{ik} + c_{ijkl}]$, the equation of motion in the initial state is

$$\rho_0 u_i'' = D_{jkli} \frac{\partial^2 u_k}{\partial X_j \partial X_l}. \quad (1.3.7.13)$$

The coefficients D_{ijkl} do not present the symmetry of the coefficients c_{ijkl} except in the natural state where D_{ijkl} and c_{ijkl} are equal.

The simplest solutions of the equation of motion are plane waves. We now assume plane sinusoidal waves of the form

$$u_i = A_i \exp[i(\omega t - \mathbf{k} \cdot \mathbf{X})], \quad (1.3.7.14)$$

where \mathbf{k} is the wavevector.

Substitution of (1.3.7.14) into (1.3.7.13) results in

$$\rho_0 \omega^2 A_j = D_{ijkl} k_j k_l A_k$$

1.3. ELASTIC PROPERTIES

Table 1.3.7.1. Relationships between ρW^2 , its pressure derivatives and the second- and third-order elastic constants

| Propagation | Polarization | $(\bar{\rho}_0 W^2)_0$ | $\partial(\bar{\rho}_0 W^2)_0/\partial p$ |
|-------------|--------------|--|--|
| [100] | [100] | \bar{c}_{11} | $-1 - (2\bar{c}_{11} + \Gamma_{1111})/3\bar{\kappa}$ |
| [100] | [010] | \bar{c}_{44} | $-1 - (2\bar{c}_{44} + \Gamma_{2323})/3\bar{\kappa}$ |
| [110] | [110] | $(\bar{c}_{11} + \bar{c}_{12} + 2\bar{c}_{44})/2$ | $-1 - (\bar{c}_{11} + \bar{c}_{12} + 2\bar{c}_{44} + 0.5[\Gamma_{1111} + \Gamma_{1122} + \Gamma_{2323}])/3\bar{\kappa}$ |
| [110] | [110] | $(\bar{c}_{11} - \bar{c}_{12} + \bar{c}_{44})/3$ | $-1 - (\bar{c}_{11} - \bar{c}_{12} + \bar{c}_{44} + 0.5[\Gamma_{1111} - \Gamma_{1122}])/3\bar{\kappa}$ |
| [110] | [001] | \bar{c}_{44} | $-1 - (2\bar{c}_{44} + \Gamma_{2323})/3\bar{\kappa}$ |
| [111] | [111] | $(\bar{c}_{11} + 2\bar{c}_{12} + 4\bar{c}_{44})/3$ | $-1 - (2\bar{c}_{11} + 4\bar{c}_{12} + 8\bar{c}_{44} + [\Gamma_{1111} + 2\Gamma_{1122} + 4\Gamma_{2323}])/9\bar{\kappa}$ |
| [111] | [110] | $(\bar{c}_{11} - \bar{c}_{12} + \bar{c}_{44})/3$ | $-1 - (2\bar{c}_{11} - 2\bar{c}_{12} + 2\bar{c}_{44} + [\Gamma_{1111} - \Gamma_{1122} + \Gamma_{2323}])/9\bar{\kappa}$ |

or

$$\rho_0 \omega^2 A_j = \Delta_{jk} A_k$$

with $\Delta_{jk} = D_{ijkl} k_j k_l$.

The quantities $\rho_0 \omega^2 A_j$ and A are, respectively, the *eigenvalues* and *eigenvectors of the matrix* Δ_{jk} . Since Δ_{jk} is a real symmetric matrix, the eigenvalues are real and the eigenvectors are orthogonal.

1.3.7.6. Experimental determination of third- and higher-order elastic constants

The main experimental procedures for determining the third- and higher-order elastic constants are based on the measurement of stress derivatives of ultrasonic velocities and on harmonic generation experiments. Hydrostatic pressure, which can be accurately measured, has been widely used; however, the measurement of ultrasonic velocities in a solid under hydrostatic pressure cannot lead to the whole set of third-order elastic constants, so uniaxial stress measurements or harmonic generation experiments are then necessary.

In order to interpret wave-propagation measurements in stressed crystals, Thurston (1964) and Brugger (1964) introduced the concept of natural velocity with the following comments:

‘According to equation of motion, the wave front is a material plane which has unit normal \mathbf{k} in the natural state; a wave front moves from the plane $\mathbf{k} \cdot \mathbf{a} = 0$ to the plane $\mathbf{k} \cdot \mathbf{a} = \mathbf{L}_0$ in the time L_0/W . Thus W , the *natural velocity*, is the wave speed referred to natural dimensions for propagation normal to a plane of natural normal \mathbf{k} .

In a typical ultrasonic experiment, plane waves are reflected between opposite parallel faces of a specimen, the wave fronts being parallel to these faces. One ordinarily measures a repetition frequency F , which is the inverse of the time required for a round trip between the opposite faces.’

Hence

$$W = 2L_0 F.$$

In most experiments, the third-order elastic constants and higher-order elastic constants are deduced from the stress derivatives of $\bar{\rho}_0 W^2$. For instance, Table 1.3.7.1 gives the expressions for $(\bar{\rho}_0 W^2)_0$ and $\partial(\bar{\rho}_0 W^2)_0/\partial p$ for a cubic crystal. These quantities refer to the natural state free of stress. In this table, p denotes the hydrostatic pressure and the Γ_{ijkl} ’s are the following linear combinations of third-order elastic constants:

$$\Gamma_{1111} = \bar{c}_{111} + 2\bar{c}_{111}$$

$$\Gamma_{1122} = 2\bar{c}_{112} + \bar{c}_{123}$$

$$\Gamma_{2323} = \bar{c}_{144} + 2\bar{c}_{166}.$$

1.3.8. Glossary

| | |
|---------------------|--|
| \mathbf{e}_i | covariant basis vector |
| A^T | transpose of matrix A |
| u_i | components of the displacement vector |
| S_{ij} | components of the strain tensor |
| S_α | components of the strain Voigt matrix |
| T_{ij} | components of the stress tensor |
| T_α | components of the stress Voigt matrix |
| p | pressure |
| ν | normal stress |
| τ | shear stress |
| s_{ijkl} | second-order elastic compliances |
| $s_{\alpha\beta}$ | reduced second-order elastic compliances |
| $(s_{ijkl})^\sigma$ | adiabatic second-order elastic compliances |
| s_{ijklmn} | third-order elastic compliances |
| c_{ijkl} | second-order elastic stiffnesses |
| $(c_{ijkl})^\sigma$ | adiabatic second-order elastic stiffnesses |
| $c_{\alpha\beta}$ | reduced second-order elastic stiffnesses |
| c_{ijklmn} | third-order elastic stiffnesses |
| ν | Poisson’s ratio |
| E | Young’s modulus |
| κ | bulk modulus (volume compressibility) |
| λ, μ | Lamé constants |
| Θ | temperature |
| c^S | specific heat at constant strain |
| ρ | volumic mass |
| Θ_D | Debye temperature |
| k_B | Boltzmann constant |
| U | internal energy |
| F | free energy |

References

- Breazeale, M. A. (1984). *Determination of third-order elastic constants from ultrasonic harmonic generation. Physical acoustics*, Vol. 17, edited by R. N. Thurston, pp. 2–75. New York: Academic Press.
- Brillouin, L. (1932). *Propagation des ondes électromagnétiques dans les milieux matériels. Congrès International d’Électricité*, Vol. 2, Section 1, pp. 739–788. Paris: Gauthier-Villars.
- Brugger, K. (1964). *Thermodynamic definition of higher-order elastic coefficients. Phys. Rev.* **133**, 1611–1612.
- De Launay, J. (1956). *The theory of specific heats and lattice vibrations. Solid state physics*, Vol. 2, edited by F. Seitz & D. Turnbull, pp. 219–303. New York: Academic Press.
- Fischer, M. (1982). *Third- and fourth-order elastic constants of fluoperovskites CsCdF₃, TlCdF₃, RbCdF₃, RbCaF₃. J. Phys. Chem. Solids*, **43**, 673–682.
- Fischer, M., Zarembowitch, A. & Breazeale, M. A. (1980). *Nonlinear elastic behavior and instabilities in crystals. Ultrasonics Symposium Proc. IEEE*, pp. 999–1002.
- Fumi, F. G. (1951). *Third-order elastic coefficients of crystals. Phys. Rev.* **83**, 1274–1275.
- Fumi, F. G. (1952). *Third-order elastic coefficients in trigonal and hexagonal crystals. Phys. Rev.* **86**, 561.
- Fumi, F. G. (1987). *Tables for the third-order elastic tensors in crystals. Acta Cryst.* **A43**, 587–588.

1. TENSORIAL ASPECTS OF PHYSICAL PROPERTIES

- Green, R. E. (1973). *Treatise on material science and technology*, Vol. 3. New York: Academic Press.
- Landoldt-Börnstein (1979). Group III. *Crystal and solid state physics*. Berlin: Springer-Verlag.
- McSkimmin, H. J. (1964). *Ultrasonic methods for measuring the mechanical properties of solids and fluids*. *Physical acoustics*, Vol. 1A, edited by W. P. Mason, pp. 271–334. New York: Academic Press.
- Melcher, R. L. & Scott, B. A. (1972). *Soft acoustic modes at the cooperative Jahn–Teller transition in DyVO₄*. *Phys. Rev. Lett.* **28**, 607–610.
- Michard, F., Zarembowitch, A., Vacher, R. & Boyer, L. (1971). *Premier son et son zéro dans les nitrates de strontium, barium et plomb. Phonons*, edited by M. A. Nusimovici, pp. 321–325. Paris: Flammarion.
- Murnaghan, F. D. (1951). *Finite deformation in an elastic solid*. New York: John Wiley and Sons.
- Nouet, J., Zarembowitch, A., Pisarev, R. V., Ferré, J. & Lecomte, M. (1972). *Determination of T_N for KNiF₃ through elastic, magneto-optical and heat capacity measurements*. *Appl. Phys. Lett.* **21**, 161–162.
- Rousseau, M., Gesland, J. Y., Julliard, J., Nouet, J., Zarembowitch, J. & Zarembowitch, A. (1975). *Crystallographic, elastic and Raman scattering investigations of structural phase transitions in RbCdF₃ and TlCdF₃*. *Phys. Rev.* **12**, 1579–1590.
- Salje, E. K. H. (1990). *Phase transitions in ferroelastic and co-elastic crystals*. Cambridge University Press.
- Thurston, R. N. (1964). *Wave propagation in fluids and normal solids*. *Physical acoustics*, Vol. 1A, edited by W. P. Mason, pp. 1–109. New York: Academic Press.
- Truesdell, C. & Toupin, R. (1960). *The classical field theories*. *Handbuch der Physik*, Vol. III/1, edited by S. Flügge. Berlin, Göttingen, Heidelberg: Springer-Verlag.
- Voigt, W. (1910). *Lehrbuch der Kristallphysik*. 2nd ed. (1929). Leipzig: Teubner. Photoreproduction (1966). New York: Johnson Reprint Corp.
- Wallace, D. C. (1970). *Thermoelastic theory of stressed crystals and higher-order elastic constants*. *Solid state physics*, Vol. 25. New York: Academic Press.
- Wallace, D. C. (1972). *Thermodynamics of crystals*. New York: John Wiley and Sons.
- Zarembowitch, A. (1965). *Etude théorique et détermination optique des constantes élastiques de monocristaux*. *Bull. Soc. Fr. Minéral. Cristallogr.* **28**, 17–49.

1.4. Thermal expansion

BY H. KÜPPERS

1.4.1. Definition, symmetry and representation surfaces

If the temperature T of a solid is raised by an amount ΔT , a deformation takes place that is described by the strain tensor u_{ij} :

$$u_{ij} = \alpha_{ij} \Delta T. \quad (1.4.1.1)$$

The quantities α_{ij} are the coefficients of thermal expansion. They have dimensions of T^{-1} and are usually given in units of 10^{-6} K^{-1} . Since u_{ij} is a symmetrical polar tensor of second rank and T is a scalar, α_{ij} is a symmetrical polar tensor of second rank ($\alpha_{ij} = \alpha_{ji}$). According to the properties of the strain tensor u_{ij} (cf. Section 1.3.1.3.2), the 'volume thermal expansion', β , is given by the (invariant) trace of the 'linear' coefficients α_{ij} :

$$\beta = \frac{1}{V} \frac{\Delta V}{\Delta T} = \alpha_{11} + \alpha_{22} + \alpha_{33} = \text{trace}(\alpha_{ij}). \quad (1.4.1.2)$$

The magnitudes of thermal expansion in different directions, α'_{11} , can be visualized in the following ways:

(1) The representation quadric (cf. Section 1.1.3.5.2)

$$\alpha_{ij} x_i x_j = C \quad (1.4.1.3)$$

can be transformed to principal axes X_1 , X_2 and X_3 with principal values α_1 , α_2 and α_3 :

$$\alpha_1 X_1^2 + \alpha_2 X_2^2 + \alpha_3 X_3^2 = C.$$

The length of any radius vector leading to the surface of the quadric ($C = 1$) represents the reciprocal of the square root of thermal expansion along that direction, $\alpha'_{11} = a_{1i} a_{1j} \alpha_{ij}$ (a_{kl} are the direction cosines of the particular direction).

If all α_i are positive, the quadric ($C = +1$) is represented by an ellipsoid, whose semiaxes have lengths $1/\sqrt{\alpha_i}$. In this case, the square of the reciprocal length of radius vector \mathbf{r} , r^{-2} , represents the amount of positive expansion in the particular direction, i.e. a *dilation* with increasing temperature. If all α_i are negative, C is set to -1 . Then, the quadric is again an ellipsoid, and r^{-2} represents a negative expansion, i.e. a *contraction* with increasing temperature.

If the α_i have different signs, the quadric is a hyperboloid. The asymptotic cone represents directions along which no thermal expansion occurs ($\alpha'_{11} = 0$).

If one of the α_i is negative, let us first choose $C = +1$. Then, the hyperboloid has one (belt-like) sheet (cf. Fig. 1.3.1.3) and the squares of reciprocal lengths of radius vectors leading to points on this sheet represent positive expansions (dilatations) along the particular directions. Along directions where the hyperboloid has no real values, negative expansions occur. To visualize these, C is set to -1 . The resulting hyperboloid has two (cap-like) sheets (cf. Fig. 1.3.1.3) and r^{-2} represents the amount of contraction along the particular direction.

If two of the α_i are negative, the situation is complementary to the previous case.

(2) A crystal sample having spherical shape (radius = 1 at temperature T) will change shape, after a temperature increase ΔT , to an ellipsoid with principal axes $(1 + \alpha_1 \Delta T)$, $(1 + \alpha_2 \Delta T)$ and $(1 + \alpha_3 \Delta T)$. This 'strain ellipsoid' is represented by the formula

$$\frac{X_1^2}{(1 + \alpha_1 \Delta T)^2} + \frac{X_2^2}{(1 + \alpha_2 \Delta T)^2} + \frac{X_3^2}{(1 + \alpha_3 \Delta T)^2} = 1.$$

Whereas the strain quadric (1.4.1.3) may be a real or imaginary ellipsoid or a hyperboloid, the strain ellipsoid is always a real ellipsoid.

(3) The magnitude of thermal expansion in a certain direction (the longitudinal effect), α'_{11} , if plotted as radius vector, yields an oval:

$$(\alpha_1 X_1^2 + \alpha_2 X_2^2 + \alpha_3 X_3^2)^2 = (X_1^2 + X_2^2 + X_3^2)^3.$$

If spherical coordinates (φ, ϑ) are used to specify the direction, the length of \mathbf{r} is

$$|\mathbf{r}| = \alpha'_{11} = (\alpha_1 \cos^2 \varphi + \alpha_2 \sin^2 \varphi) \sin^2 \vartheta + \alpha_3 \cos^2 \vartheta. \quad (1.4.1.4)$$

Sections through this representation surface are called polar diagrams.

The three possible graphical representations are shown in Fig. 1.4.1.1.

The maximum number of independent components of the tensor α_{ij} is six (in the triclinic system). With increasing symmetry, this number decreases as described in Chapter 1.1. Accordingly, the directions and lengths of the principal axes of the representation surfaces are restricted as described in Chapter 1.3 (e.g. in hexagonal, trigonal and tetragonal crystals, the representation surfaces are rotational sheets and the rotation axis is parallel to the n -fold axis). The essential results of these symmetry considerations, as deduced in Chapter 1.1 and relevant for thermal expansion, are compiled in Table 1.4.1.1.

The coefficients of thermal expansion depend on temperature. Therefore, the directions of the principal axes of the quadrics in triclinic and monoclinic crystals change with temperature (except the principal axis parallel to the twofold axis in monoclinic crystals).

The thermal expansion of a polycrystalline material can be approximately calculated if the α_{ij} tensor of the single crystal is known. Assuming that the grains are small and of comparable size, and that the orientations of the crystallites are randomly distributed, the following average of α'_{11} [(1.4.1.4)] can be calculated:

$$\bar{\alpha} = \frac{1}{4\pi} \int_0^{2\pi} \int_0^\pi \alpha'_{11} \sin \vartheta \, d\vartheta \, d\varphi = \frac{1}{3}(\alpha_1 + \alpha_2 + \alpha_3).$$

If the polycrystal consists of different phases, a similar procedure can be performed if the contribution of each phase is considered with an appropriate weight.

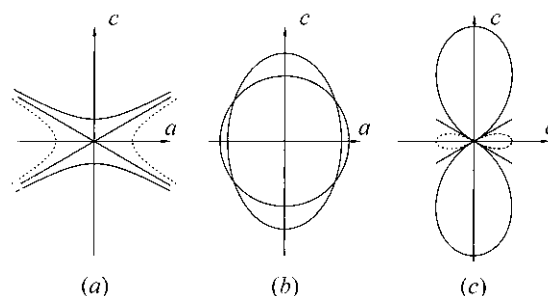


Fig. 1.4.1.1. Sections (ac plane) of representation surfaces for a trigonal (or tetragonal or hexagonal) crystal with $\alpha_{11} = \alpha_{22} = -1$ and $\alpha_{33} = +3 \times 10^{-5} \text{ K}^{-1}$ (similar to calcite). (a) Quadric, (b) strain ellipsoid (greatly exaggerated), (c) polar diagram. The c axis is the axis of revolution. Sectors with negative expansions are dashed.

1. TENSORIAL ASPECTS OF PHYSICAL PROPERTIES

It should be mentioned that the true situation is more complicated. The grain boundaries of anisotropic polycrystalline solids are subject to considerable stresses because the neighbouring grains have different amounts of expansion or contraction. These stresses may cause local plastic deformation and cracks may open up between or within the grains. These phenomena can lead to a hysteresis behaviour when the sample is heated up or cooled down. Of course, in polycrystals of a cubic crystal species, these problems do not occur.

If the polycrystalline sample exhibits a texture, the orientation distribution function (ODF) has to be considered in the averaging process. The resulting overall symmetry of a textured polycrystal is usually ∞m (see Section 1.1.4.7.4.2), showing the same tensor form as hexagonal crystals (Table 1.4.1.1), or mmm .

1.4.2. Grüneisen relation

Thermal expansion of a solid is a consequence of the anharmonicity of interatomic forces (see also Section 2.1.2.8). If the potentials were harmonic, the atoms would oscillate (even with large amplitudes) symmetrically about their equilibrium positions and their mean central position would remain unchanged. In order to describe thermal expansion, the anharmonicity is most conveniently accounted for by means of the so-called ‘quasi-harmonic approximation’, assuming the lattice vibration frequencies ω to be independent of temperature but dependent on volume $[(\partial\omega/\partial V) \neq 0]$. Anharmonicity is taken into account by letting the crystal expand, but it is assumed that the atoms vibrate about their new equilibrium positions harmonically, *i.e.* lattice dynamics are still treated in the harmonic approximation. The assumption $(\partial\omega/\partial V) = 0$, which is made for the harmonic oscillator, is a generalization of the postulate that the frequency of a harmonic oscillator does not depend on the amplitude of vibration.

This approach leads, as demonstrated below, to the Grüneisen relation, which combines thermal expansion with other material constants and, additionally, gives an approximate description of the temperature dependence of thermal expansion (*cf.* Krishnan *et al.*, 1979; Barron, 1998).

For isotropic media, the volume expansion $\beta [= 3\alpha = \alpha_{11} + \alpha_{22} + \alpha_{33}]$, *cf.* (1.4.1.2), can be expressed by the thermodynamic relation

$$\beta = \frac{1}{V} \left(\frac{\partial V}{\partial T} \right)_p = -\frac{1}{V} \left(\frac{\partial V}{\partial p} \right)_T \left(\frac{\partial p}{\partial T} \right)_V = \kappa \left(\frac{\partial p}{\partial T} \right)_V, \quad (1.4.2.1)$$

κ being the isothermal compressibility. To obtain the quantity $(\partial p/\partial T)_V$, the pressure p is deduced from the free energy F , whose differential is $dF = -S dT - p dV$, *i.e.* from

$$p = -(\partial F/\partial V)_T. \quad (1.4.2.2)$$

In a crystal consisting of N unit cells with p atoms in each unit cell, there are $3p$ normal modes with frequencies ω_s (denoted by an index s running from 1 to $3p$) and with N allowed wavevectors

Table 1.4.1.1. Shape of the quadric and symmetry restrictions

| System | Quadric | | No. of independent components | Nonzero components |
|---------------------------------|-------------------------------------|--|-------------------------------|--------------------|
| | Shape | Direction of principal axes | | |
| Triclinic | General ellipsoid or hyperboloid | No restrictions | 6 | |
| Monoclinic | | One axis parallel to twofold axis (b) | 4 | |
| Orthorhombic | | Parallel to crystallographic axes | 3 | |
| Trigonal, tetragonal, hexagonal | Revolution ellipsoid or hyperboloid | c axis is revolution axis | 2 | |
| Cubic, isotropic media | Sphere | Arbitrary, not defined | 1 | |

\mathbf{q}_t (denoted by an index t running from 1 to N). Each normal mode $\omega_s(\mathbf{q}_t)$ contributes to the free energy by the amount

$$f_{s,t} = \frac{\hbar}{2} \omega_s(\mathbf{q}_t) + kT \ln \left[1 - \exp \left(-\frac{\hbar \omega_s(\mathbf{q}_t)}{kT} \right) \right]. \quad (1.4.2.3)$$

The total free energy amounts, therefore, to

$$F = \sum_{s=1}^{3p} \sum_{t=1}^N f_{s,t} = \sum_{s=1}^{3p} \sum_{t=1}^N \left\{ \frac{\hbar}{2} \omega_s(\mathbf{q}_t) + kT \ln \left[1 - \exp \left(-\frac{\hbar \omega_s(\mathbf{q}_t)}{kT} \right) \right] \right\}. \quad (1.4.2.4)$$

From (1.4.2.2)

$$p = - \left(\frac{\partial F}{\partial V} \right)_T = - \sum_{s=1}^{3p} \sum_{t=1}^N \left\{ \frac{\hbar}{2} \frac{\partial \omega_s}{\partial V} + \frac{\exp(-\hbar \omega_s/kT) \hbar (\partial \omega_s/\partial V)}{1 - \exp(-\hbar \omega_s/kT)} \right\}. \quad (1.4.2.5)$$

The last term can be written as

$$\frac{\hbar (\partial \omega_s/\partial V)}{\exp(\hbar \omega_s/kT) - 1} = \hbar n(\omega_s(\mathbf{q}_t), T) \frac{\partial \omega_s}{\partial V}, \quad (1.4.2.6)$$

where $n(\omega_s, T)$ is the Bose–Einstein distribution

1.4. THERMAL EXPANSION

$$n(\omega_s, T) = \frac{1}{\exp(\hbar\omega_s/kT) - 1}. \quad (1.4.2.7)$$

Differentiation of (1.4.2.5) and (1.4.2.6) with respect to temperature at constant volume [see (1.4.2.1)] yields

$$\begin{aligned} \left(\frac{\partial p}{\partial T}\right)_V &= - \sum_s \sum_t \hbar \frac{\partial n(\omega_s, T)}{\partial T} \frac{\partial \omega_s(\mathbf{q}_t)}{\partial V} \\ &= - \sum_s \sum_t c_{s,t}^V \frac{1}{\omega_s(\mathbf{q}_t)} \frac{\partial \omega_s(\mathbf{q}_t)}{\partial V} \end{aligned} \quad (1.4.2.8)$$

with

$$c_{s,t}^V = \hbar\omega_s(\mathbf{q}_t) \frac{\partial n(\omega_s, T)}{\partial T} = k \frac{(\hbar\omega_s/kT)^2 \exp(\hbar\omega_s/kT)}{[\exp(\hbar\omega_s/kT) - 1]^2}. \quad (1.4.2.9)$$

This quantity, $c_{s,t}^V$ (the Einstein function), is the well known contribution of the normal mode $\omega_s(\mathbf{q}_t)$ to the specific heat (at constant volume):

$$c^V = \sum_s \sum_t c_{s,t}^V = \sum_s \sum_t \hbar\omega_s(\mathbf{q}_t) \frac{\partial n(\omega_s, T)}{\partial T}. \quad (1.4.2.10)$$

Equation (1.4.2.8) can be simplified by the introduction of an ‘individual Grüneisen parameter’ $\gamma_{s,t}$ for each normal mode $\omega_s(\mathbf{q}_t)$:

$$\gamma_{s,t} = - \frac{V}{\omega_s(\mathbf{q}_t)} \frac{\partial \omega_s(\mathbf{q}_t)}{\partial V} = - \frac{\partial[\ln \omega_s(\mathbf{q}_t)]}{\partial(\ln V)}. \quad (1.4.2.11)$$

Equation (1.4.2.8) then reads [with (1.4.2.1)]

$$\left(\frac{\partial p}{\partial T}\right)_V = \frac{1}{V} \sum_s \sum_t c_{s,t}^V \gamma_{s,t} = \frac{\beta}{\kappa}. \quad (1.4.2.12)$$

Based on these individual parameters $\gamma_{s,t}$, an average (or overall mode-independent) Grüneisen parameter $\bar{\gamma}$ can be defined as

$$\bar{\gamma} = \frac{\sum_s \sum_t \gamma_{s,t} c_{s,t}^V}{\sum_s \sum_t c_{s,t}^V} = \frac{\sum_s \sum_t \gamma_{s,t} c_{s,t}^V}{c^V}. \quad (1.4.2.13)$$

In this averaging process, the contribution of each normal mode to $\bar{\gamma}$ is weighted in the same way as it contributes to the specific heat c^V [see (1.4.2.10)]. Equations (1.4.2.12) and (1.4.2.13) lead to the Grüneisen relation

$$\beta = \bar{\gamma} \frac{\kappa c^V}{V}. \quad (1.4.2.14)$$

The above derivation was made for isotropic media. For anisotropic media, $\Delta V/V$ is replaced by the strain u_{kl} and κ^{-1} is replaced by the stiffness tensor c_{ijkl} [cf. Chapter 2.1 and equation (2.1.2.75)]. Then the Grüneisen parameter turns out to be a second-rank tensor γ_{ij} :

$$\gamma_{ij} = \frac{V}{c^V} c_{ijkl}^T \alpha_{kl}. \quad (1.4.2.15)$$

In the Debye approximation, the mode frequencies scale linearly with the cut-off frequency ω_D . Therefore, with $\hbar\omega_D = kT_D$, the average isotropic Grüneisen parameter is calculated to be

$$\gamma_D = - \frac{V}{\omega_D} \frac{\partial \omega_D}{\partial V} = - \frac{V}{T_D} \frac{\partial T_D}{\partial V} = - \frac{\partial(\ln T_D)}{\partial(\ln V)}.$$

Since, in the Debye theory, T_D is independent of temperature, γ_D turns out to be independent of temperature. As κ and V are only weakly temperature dependent, the thermal expansion β should then, according to (1.4.2.14), roughly behave like c^V , i.e. β should be proportional to T^3 at very low temperatures, and should be approximately constant for $T \gg T_D$ (the Dulong–Petit law). This

behaviour is found to be approximately satisfied for many compounds, even with different types of interatomic interaction, and γ takes values roughly between 1 and 2. Even in the case of crystals with highly anisotropic elastic and thermal behaviour, the three principal values of the tensor γ_{ij} [(1.4.2.15)] are comparably uniform, having values of about 2 (Küppers, 1974).

Effectively, γ shows a certain more or less pronounced dependence on temperature. The individual $\gamma_{s,t}$ are assumed to be temperature independent. However, being an average over the whole spectrum of excited modes [cf. (1.4.2.13)], $\bar{\gamma}$ will not necessarily have the same value at low temperatures (when only low frequencies are excited) as at high temperatures (when all modes are excited). Two limiting cases can be considered:

(1) At very high temperatures, all normal modes contribute by an equal amount and the overall $\bar{\gamma}$ becomes simply the mean value of all $\gamma_{s,t}$.

$$\gamma_\infty = \frac{1}{3pN} \sum_s \sum_t \gamma_{s,t}.$$

(2) At very low temperatures, only the lower frequencies contribute. If only the acoustic branches are considered, $\bar{\gamma}$ can be related to the velocities of elastic waves. In the long-wavelength limit, dispersion is neglected, i.e. $|\mathbf{q}|$ is proportional to ω :

$$|\mathbf{q}_t| = \frac{\omega_s(\mathbf{q}_t)}{v_s(\varphi, \vartheta)}, \quad (1.4.2.16)$$

where $v_s(\varphi, \vartheta)$ ($s = 1, 2, 3$) describes the velocities of the three elastic waves propagating in a direction (φ, ϑ) . The density of vibrational states for each acoustic branch in reciprocal space increases with $q^2 d\mathbf{q}$. From (1.4.2.16), it follows that the number of normal modes in an increment of solid angle in \mathbf{q} space, $d\Omega = \sin \vartheta d\vartheta d\varphi$, within a frequency interval ω to $\omega + d\omega$, is proportional to $(\omega^2 d\omega d\Omega)/v^3$. The summation over t can be converted into an integration over ω and Ω , leading to

$$\gamma_0 = \frac{\sum_{s=1}^3 \int \frac{\gamma_s(\vartheta, \varphi) d\Omega}{v_s^3(\vartheta, \varphi)}}{\sum_{s=1}^3 \int \frac{d\Omega}{v_s^3(\vartheta, \varphi)}}.$$

The $v_s(\varphi, \vartheta)$ can be calculated if the elastic constants are known. For isotropic solids, the term $\sum v_s^{-3}$ can be replaced (as done in Debye’s theory of heat capacity) by $(v_l^{-3} + 2v_{tr}^{-3})$, with v_l being the velocity of the longitudinal wave and v_{tr} the velocity of the transverse waves.

In metals, the conduction electrons and magnetic interactions yield contributions to the free energy and to the specific heat. Accordingly, expression (1.4.2.14) can be augmented by introduction of an ‘electronic Grüneisen parameter’, γ_e , and a ‘magnetic Grüneisen parameter’, γ_m , in addition to the ‘lattice Grüneisen parameter’, γ_l , considered so far:

$$\beta = \frac{\kappa}{V} (\gamma_l c_l^V + \gamma_e c_e^V + \gamma_m c_m^V).$$

1.4.3. Experimental methods

1.4.3.1. General remarks

Although the strain tensor u_{ij} and the thermal expansion tensor α_{ij} in general contain components with $i \neq j$ (shear strains), in practice only longitudinal effects, i.e. relative length changes $\Delta l/l$ with temperature changes ΔT , are measured along different directions and the results are later transformed to a common coordinate system. Diffraction methods directly yield this ratio $\Delta l/l$. Other measuring techniques require separate measurements of Δl and l . The error in the measurement of l can

1. TENSORIAL ASPECTS OF PHYSICAL PROPERTIES

usually be neglected. Thus, the accuracies of Δl and ΔT limit the accuracy of thermal expansion coefficients. The temperature interval ΔT is determined by two measurements of temperatures $T_2 > T_1$, with $T_2 - T_1 = \Delta T$. To increase the accuracy of the difference ΔT , this interval should be large. The measured thermal expansion $\Delta l/(l\Delta T)$ is usually assigned to a temperature at the midpoint of the temperature interval, $T_0 = (T_2 + T_1)/2$. This procedure is only justified if thermal expansion does not depend on temperature.

Since, in fact, thermal expansion depends on temperature, in principle, smaller intervals should be chosen, which, in turn, enlarge the error of ΔT . Here, a compromise has to be made. Sometimes, after completion of a first run and after reviewing the preliminary course of $\alpha(T)$, it is necessary to repeat some measurements using smaller temperature intervals in temperature ranges with large curvatures.

The more-or-less curved course of $\alpha_{ij}(T)$ is usually fitted by polynomials in powers of temperature. Here, those T terms should be selected that are physically meaningful in the particular temperature range. For the low-temperature behaviour of a metal, a polynomial of type $\alpha = AT + BT^3 + CT^5$ should be chosen. For minerals at higher temperatures, a polynomial $\alpha = \alpha_0 + AT + BT^{-1} + CT^{-2}$ is used (Saxena & Shen, 1992).

Temperature is usually measured by thermocouples and, in the cases of optical or electrical measurements (Sections 1.4.3.3 and 1.4.3.4) and at low temperatures also by platinum resistance thermometers. Above 1100 K, optical pyrometers can be used.

In order to measure the thermal expansion of a crystal, at least as many independent measurements are necessary as the tensor has independent components (fourth column in Table 1.4.1.1). It is advisable, however, to carry out more measurements than are necessary. In this case (of redundancy), a 'best' set of tensor components is to be determined by least-squares methods as described below.

Let us assume the most general case of a triclinic crystal, where $m > 6$ independent measurements of thermal expansions b_k ($k = 1, \dots, m$) were performed along m different directions with direction cosines $(\alpha_{ij})_k$ ($j = 1, 2, 3$) with respect to the chosen coordinate system. Each measurement b_k is related to the six unknown tensor components α_{ij} (to be determined) by

$$b_k = (\alpha'_{11})_k = (\alpha_{1i})_k (\alpha_{1j})_k \alpha_{ij}. \quad (1.4.3.1)$$

If the α_{ij} are replaced by α_γ ($\gamma = 1, \dots, 6$), using Voigt's one-index notation (Section 1.1.4.10.2), then $b_k = C_{k\gamma} \alpha_\gamma$ represents an overdetermined inhomogeneous system of m linear equations for the six unknowns α_γ . The coefficients $C_{k\gamma}$, forming an $m \times 6$ matrix, are products containing direction cosines according to (1.4.3.1). The solution is obtained after several matrix calculations which are indicated by the formula (Nye, 1985)

$$\alpha_\gamma = \left\{ \left[(C_{l\delta}^t \cdot C_{l\varepsilon})^{-1} \right]_{\gamma\eta} C_{k\eta}^t \right\} b_k \\ (\gamma, \delta, \varepsilon, \eta = 1, \dots, 6; \quad l, k = 1, \dots, m),$$

where a superscript 't' means transposed.

Instead of determining the tensor components of a triclinic or monoclinic crystal in a direct way, as outlined above, it is also possible to determine first the temperature change of the crystallographic unit cell and then, by formulae given e.g. by Schlenker *et al.* (1978), to deduce the tensor components α_{ij} . The direct approach is recommended, however, for reasons of the propagation of errors (Jessen & Küppers, 1991).

The experimental techniques of measuring relative length changes $\Delta l/l$ that are most widely used include diffraction, optical interferometry, pushrod dilatometry and electrical capacitance methods. If the specimens available are very small and/or irregular in shape, only diffraction methods can be used. The other methods require single-crystal parallelepipedal samples with at least 5 mm side lengths.

1.4.3.2. Diffraction

Thermal expansion expresses itself, on a microscopic scale, by a change of the interplanar spacings of lattice planes. These can be measured by use of diffraction methods from changes of Bragg angles θ . Differentiation of the Bragg equation $2d \sin \theta = \lambda$, giving $\Delta d/d = -\cot \theta \Delta \theta$, yields the thermal expansions α'_{11} in directions normal to lattice planes (hkl) (i.e. along $\mathbf{h} = h\mathbf{a}^* + k\mathbf{b}^* + l\mathbf{c}^*$) and, if \mathbf{h} has direction cosines $a_{ij}^{(hkl)}$ with respect to the chosen Cartesian coordinate system,

$$\alpha'_{11} = a_{1i}^{(hkl)} a_{1j}^{(hkl)} \alpha_{ij} = \frac{1}{d^{(hkl)}} \frac{\partial d^{(hkl)}}{\partial T} = -\cot \theta \frac{\partial \theta}{\partial T}.$$

The coefficient $\cot \theta$ permits a tremendous increase of sensitivity and accuracy if $\theta \rightarrow 90^\circ$. That means, if possible, high-angle ($\theta > 70^\circ$) reflections should be used for measurement because, for a given Δd , the changes of Bragg angles $|\Delta \theta|$ to be measured increase with $(\cot \theta)^{-1} = \tan \theta$.

The most important diffraction techniques (X-radiation is preferentially used) are: the rotating-crystal method, the Weissenberg method and diffractometers with counter recording. If small single crystals ($> \text{approximately } 50 \mu\text{m}$) are not available, powder methods (using a Debye-Scherrer film camera or powder diffractometer) must be used, although the advantage of the highly accurate back-reflections, in general, cannot be used.

Experimental aspects of measuring absolute d -values are discussed in detail in Volume C of *International Tables for Crystallography* (1999), Part 5. Since only relative displacements are to be measured in the present case, many complications connected with the determination of absolute values do not apply for thermal expansion measurements, such as zero-point correction, eccentricity of the mounted sample, refraction, absorption and diffraction profile.

1.4.3.3. Optical methods (interferometry)

The basic principle of measuring thermal expansion by interferometry consists of converting sample-length changes into variations of optical path differences of two coherent monochromatic light beams, which are reflected from two opposite end faces of the sample (or planes corresponding to them). An He-Ne laser usually serves as a light source. A beam expander produces a parallel beam and interference by two planes, which are slightly inclined to each other, produces fringes of equal thickness. Thermal expansion causes a movement of this fringe pattern, which is detected by photodiodes. The number of fringes passing a reference mark is counted and gives a measure of the relative movement of the two planes.

As examples for various realizations of interferometric devices (Hahn, 1998), two basic designs will be described.

(i) *Fizeau interferometer* (Fig. 1.4.3.1). The sample S is covered by a thin plate P_2 (with a polished upper surface and a coarsely ground and non-reflecting lower surface) and is placed in between a bottom plate P_3 and a wedge-shaped plate P_1 (wedge angle of about 1°). The upper surface of P_1 reflects the incident beam (i) to a reflected beam (r) so that it is removed from the interference process. The relevant interference takes place between ray (1) reflected by the lower surface of P_1 and ray (2) reflected by the upper surface of P_2 . A cylindrical tube T , which defines the distance between P_1 and P_3 as well as P_2 , is usually made of fused silica, a material of low and well known thermal expansion. The measured dilatation is caused, therefore, by the difference between thermal expansion of the sample and a portion of the fused silica tube of equal length. The whole apparatus is mounted in a thermostat.

(ii) *Michelson interferometer* (Fig. 1.4.3.2). The reference mirror M and the beam-splitter B are placed outside the thermostat. The upper face of the sample S is one interference plane and the upper surface of the bottom plate is the other. The

1.4. THERMAL EXPANSION

interference pattern IP is divided into two fields corresponding to the two ends of the sample. The difference of fringe movements within these two fields yields the absolute thermal expansion of the sample.

1.4.3.4. Electrical methods

1.4.3.4.1. Inductance changes (pushrod dilatometry)

With this method, the expansion of the crystal is transmitted out of the cooled or heated region to an external measuring device by a rod made of a reference material whose thermal expansion is low and well known (usually silica glass) (*cf.* Gaal, 1998). If this rod is inside a tube of the same material (silica glass), and the specimen is inside as well, then the difference in expansion between the crystal and an equal length of the reference material is measured. Above 1100 K, instead of silica glass, high-purity alumina or single-crystal sapphire or tungsten rods are used.

To measure the displacement of the rods, several techniques are used. The most important are:

(1) a ferrite core is moved in a coil to change the inductivity of the coil, which is detected by the change of resonance frequency of an electrical circuit having a fixed capacitance;

(2) linear-variable-differential transformers.

Temperature gradients in the rod and the tube can lead to severe complications. For every determination, the system should be calibrated by certified materials (White, 1998), such as α -Al₂O₃, Cu, Pt, fused silica, Si, W, Mg or Mo.

1.4.3.4.2. Capacitance methods

In a way similar to the interferometric methods, the change of the gap between the lower surface of P_1 and the upper surface of P_2 (Fig. 1.4.3.1) is used to determine the thermal expansion of the sample. This gap – with electrically conducting surfaces – is used as the capacitance in an electric circuit with a fixed inductance. The change of capacitance leads to a change of resonance frequency, which is measured.

1.4.4. Relation to crystal structure

The anharmonicities of the interatomic potentials gain importance with increasing vibration amplitudes of the atoms. Since, at a given temperature, weakly bonded atoms oscillate with larger amplitudes, they contribute to a larger degree to thermal expansion in comparison with stronger bonds. This correlation follows also from the Grüneisen relation (1.4.2.14) because α (or

β) is proportional to the compressibility, which, in turn, is a rough measure of the interatomic and intermolecular forces.

This simple consideration allows qualitative predictions of the thermal expansion behaviour of a crystal species if the structure is known:

(1) Covalent bonds are associated with very small thermal expansions (diamond, graphite perpendicular to the c axis), whereas van der Waals bonds give rise to large thermal expansions (N₂, graphite parallel to the c axis). In accordance with their relatively high elastic stiffness, hydrogen bonds, especially short hydrogen bonds, lead to comparably small thermal expansions.

(2) In layer-like structures, the maximum thermal expansion occurs normal to the layers (mica, graphite, pentaerythritol).

(3) Thermal expansion decreases when the density of weak bonds decreases: therefore, expansion is greater for crystals with small molecules (many van der Waals contacts per volume) than for their larger homologues (*e.g.* benzene–naphthalene–anthracene).

Buda *et al.* (1990) have calculated the thermal expansion of silicon by means of *ab initio* methods. It is to be expected that these methods, which are currently arduous, will be applicable to more complicated structures in the years to come and will gain increasing importance in this field (*cf.* Lazzeri & de Gironcoli, 1998).

It is observed rather frequently in anisotropic materials that an enhanced expansion occurs along one direction and a contraction (negative expansion) in directions perpendicular to that direction (*e.g.* in calcite). The volume expansion, *i.e.* the trace of α_{ij} , is usually positive in these cases, however. If the tensor of elastic constants is known, such negative expansions can mostly be explained by a lateral Poisson contraction caused by the large expansion (Küppers, 1974).

Only a few crystals show negative volume expansion and usually only over a narrow temperature range (*e.g.* Si and fused silica below about 120 K and quartz above 846 K) (White, 1993). Cubic ZrW₂O₈ was recently found to exhibit isotropic negative thermal expansion over the complete range of stability of this material (0.5–1050 K) (Mary *et al.*, 1996). This behaviour is explained by the librational motion of practically rigid polyhedra and a shortening of Zr–O–W bonds by transverse vibration of the oxygen atom. By tailoring the chemical content (of TiO₂ or

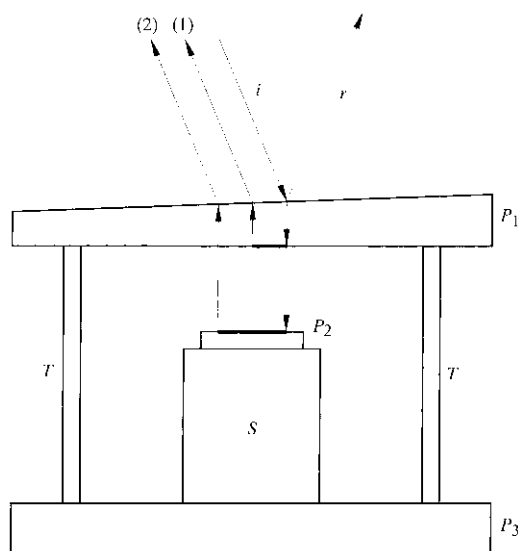


Fig. 1.4.3.1. Schematic diagram of a Fizeau interferometer.

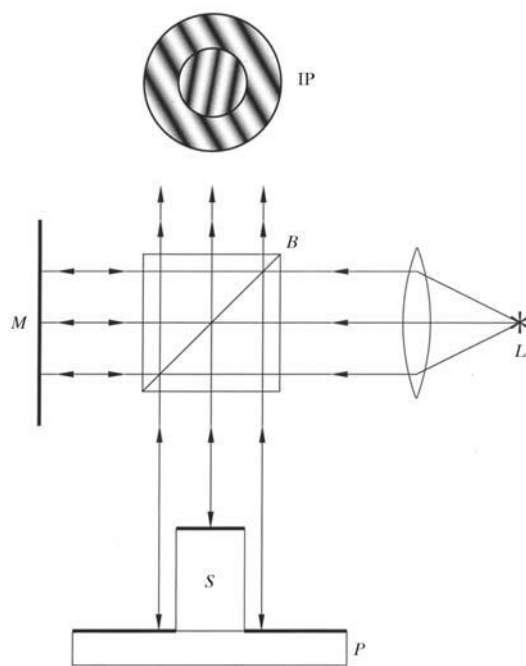


Fig. 1.4.3.2. Schematic diagram of a Michelson interferometer.

1. TENSORIAL ASPECTS OF PHYSICAL PROPERTIES

LiAlSiO₄) in a glassy matrix, an expansion coefficient can be achieved that is nearly zero over a desired temperature range.

A compilation of numerical values of the tensor components of more than 400 important crystals of different symmetry is given by Krishnan *et al.* (1979).

Phase transitions are accompanied and characterized by discontinuous changes of derivatives of the free energy. Since the thermal expansion β is a second-order derivative, discontinuities or changes of slope in the $\beta(T)$ curve are used to detect and to describe phase transitions (*cf.* Chapter 3.1).

1.4.5. Glossary

| | |
|---------------|----------------------------------|
| α_{ij} | thermal expansion |
| β | volume thermal expansion |
| γ | Grüneisen parameter |
| κ | isothermal compressibility |
| u_{ij} | strain tensor |
| c^V | specific heat at constant volume |
| F | free energy |
| p | pressure |
| S | entropy |
| T | temperature |
| V | volume |

References

- Barron, T. H. K. (1998). *Generalized theory of thermal expansion of solids*. In *Thermal expansion of solids*, edited by C. Y. Ho, ch. 1. Materials Park, Ohio: ASM International.
- Buda, F., Car, R. & Parrinello, M. (1990). *Thermal expansion of c-Si via ab initio molecular dynamics*. *Phys. Rev. B*, **41**, 1680–1683.
- Gaal, P. S. (1998). *Pushrod dilatometers*. In *Thermal expansion of solids*, edited by C. Y. Ho, ch. 5. Materials Park, Ohio: ASM International.
- Hahn, T. A. (1998). *Thermal expansion measurements using optical interferometry*. In *Thermal expansion of solids*, edited by C. Y. Ho, ch. 6. Materials Park, Ohio: ASM International.
- International Tables for Crystallography* (1999). Vol. C. *Mathematical, physical and chemical tables*, 2nd ed., edited by A. J. C. Wilson & E. Prince. Dordrecht: Kluwer Academic Publishers.
- Jessen, S. M. & Küppers, H. (1991). *The precision of thermal-expansion tensors of triclinic and monoclinic crystals*. *J. Appl. Cryst.* **24**, 239–242.
- Krishnan, R. S., Srinivasan, R. & Devanarayanan, S. (1979). *Thermal expansion of solids*. Oxford: Pergamon.
- Küppers, H. (1974). *Anisotropy of thermal expansion of ammonium and potassium oxalates*. *Z. Kristallogr.* **140**, 393–398.
- Lazzeri, M. & de Gironcoli, S. (1998). *Ab initio study of Be(001) surface thermal expansion*. *Phys. Rev. Lett.* **81**, 2096–2099.
- Mary, T. A., Evans, J. S. O., Vogt, T. & Sleight, A. W. (1996). *Negative thermal expansion from 0.3 to 1050 Kelvin in ZrW₂O₈*. *Science*, **272**, 90–92.
- Nye, J. F. (1985). *Physical properties of crystals*. Oxford: Clarendon Press.
- Saxena, S. K. & Shen, G. (1992). *Assessed data on heat capacity, thermal expansion, and compressibility of some oxides and silicates*. *J. Geophys. Res.* **97**, 19813–19825.
- Schlenker, J. L., Gibbs, G. V. & Boisen, M. B. (1978). *Strain-tensor components expressed in terms of lattice parameters*. *Acta Cryst.* **A34**, 52–54.
- White, G. K. (1993). *Solids: thermal expansion and contraction*. *Contemp. Phys.* **34**, 193–204.
- White, G. K. (1998). *Thermal expansion reference materials*. In *Thermal expansion of solids*, edited by C. Y. Ho, ch. 11. Materials Park, Ohio: ASM International.

1.5. Magnetic properties

BY A. S. BOROVIK-ROMANOV† AND H. GRIMMER

1.5.1. Introduction

In the present chapter, we shall give a short review of the structure and some properties of magnetic substances that depend mainly on the symmetry of these substances. Aspects related to the magnetic symmetry receive the most emphasis. The magnetic symmetry takes into account the fact that it is necessary to consider time inversion in addition to the usual spatial transformations in order to describe the invariance of the thermodynamic equilibrium states of a body.

The symmetry of magnetic materials depends not only on the mean charge density function $\rho(\mathbf{r})$, but also on the mean current density $\mathbf{j}(\mathbf{r})$ and the mean spin density $\mathbf{S}(\mathbf{r})$. The symmetry of the function $\rho(\mathbf{r})$ is called the crystallographic or crystallochemical symmetry of a body. If the current density $\mathbf{j}(\mathbf{r})$ in the crystal is not zero, an orbital magnetic moment is produced. It is obvious that there can be no macroscopic current in a substance which is in thermodynamic equilibrium and the integral $\int \mathbf{j} d\tau$ over the magnetic elementary cell is always equal to zero. The current \mathbf{j} , however, may produce a macroscopic nonzero magnetic moment $\mathbf{m}(\mathbf{r})$. We shall consider below the function $\mathbf{m}(\mathbf{r})$, which determines the space distribution of the total (spin and orbital) magnetic moment density. The symmetry of the distribution of the magnetic moment density $\mathbf{m}(\mathbf{r})$ may be considered as the symmetry of the arrangement and orientation of the mean atomic (or ionic) magnetic moments in the crystal (we shall not consider the magnetism of the conduction electrons in this chapter).

The first part of the chapter is devoted to a brief classification of magnetics. If $\mathbf{m}(\mathbf{r}) \equiv 0$ at every point, the substance is a disordered magnetic. There are two types of such magnetics: diamagnets and paramagnets. The most important features of these magnetics are briefly outlined in Section 1.5.1.1.

If $\mathbf{m}(\mathbf{r}) \neq 0$, the substance possesses a magnetic structure. There are two cases to be considered: (1) The integral of $\mathbf{m}(\mathbf{r})$ over the primitive cell is not zero ($\int \mathbf{m} d\tau \neq 0$); such a substance is called ferromagnetic. (2) $\int \mathbf{m} d\tau = 0$; such a substance is called antiferromagnetic. The integration is performed over the magnetic elementary cell, which may differ from the crystallographic one. This crude classification is extended in Section 1.5.1.2.

The classification of ferromagnets according to the type of the magnetic structure is given in Section 1.5.1.2.1. The concept of the magnetic sublattice is introduced and the ferromagnets are divided into two groups: one-sublattice ferromagnets and multi-sublattice ferro- and ferrimagnets. Collinear and non-collinear ferromagnets are described.

In Section 1.5.1.2.2, the antiferromagnets are classified by the types of their magnetic structures: collinear, weakly non-collinear and strongly non-collinear antiferromagnets.

Incommensurate structures are briefly mentioned in Section 1.5.1.2.3.

The study of ordered magnetics has led to an extension of the theory of crystallographic symmetry. This extension is based on the fact that $\mathbf{m}(\mathbf{r})$ changes sign under a specific transformation R , which is equivalent to time inversion. The invariance of the equation of motion is preserved under R . The symmetry that admits the operation R along with ordinary crystallographic transformations (translations, rotations and reflections) is called

the magnetic symmetry. Section 1.5.2 is devoted to magnetic symmetry. Different types of magnetic point (Section 1.5.2.1) and magnetic space (Section 1.5.2.3) groups are defined. The 22 magnetic Bravais lattices are displayed in Section 1.5.2.2. All magnetic groups (both point and space) are categorized into three types: (1) The groups that possess R as an additional element. The crystals which belong to such space groups satisfy $\mathbf{m}(\mathbf{r}) = -\mathbf{m}(\mathbf{r})$ at every point, hence $\mathbf{m}(\mathbf{r}) = 0$. Such crystals are found to be paramagnetic or diamagnetic. Crystals with a point group that possesses R as an additional element may also be antiferromagnetic. This is the case if R appears in the space group multiplied by some translations but not as a separate element. (2) The groups that do not possess R at all. (3) The groups that contain the element R only in combination with some other elements (translations, rotations, reflections). The latter two types of space groups describe ordered magnetics.

The transition from the paramagnetic state into the magnetically ordered state entails a transition from one magnetic group into another. These transitions are considered in Section 1.5.3. Section 1.5.3.1 gives an example of the analysis of such transitions in terms of magnetic symmetry and introduces the concept of ferromagnetic and antiferromagnetic vectors, which characterize the magnetic structures. The phenomenological theory of magnetic transitions is based on the Landau theory of second-order transitions. Section 1.5.3.3 is dedicated to this theory (see also Section 3.1.2). The Landau theory is based on the expansion of the thermodynamic potential into a series of the basic functions of irreducible representations of the space group of the crystal under consideration. It is essential to distinguish the exchange and relativistic terms in the expansion of the thermodynamic potential (see Section 1.5.3.2).

The domain structure of ferromagnets and antiferromagnets is considered in Section 1.5.4, where 180° and T-domains are described. The change from a multidomain structure to a single-domain structure under the action of an applied magnetic field explains the magnetization process in ferro- and ferrimagnets. The existence of 180° domains in antiferromagnets was shown in experiments on piezomagnetism and the linear magnetoelectric effect.

Non-collinear antiferromagnetic structures (weakly ferromagnetic, non-collinear and non-coplanar antiferromagnetic structures) are described in Section 1.5.5. The existence of these structures is directly connected with the magnetic symmetry. Such a structure arises if the irreducible representation responsible for the phase transition into the ordered state is two- or three-dimensional. Correspondingly, the magnetic group allows the coexistence of two or three different ferro- or antiferromagnetic vectors.

Besides the magnetic phase transition from the disordered into the ordered state, there exist transitions from one magnetic structure into another. Those of these that are obtained by a rotation of the ferromagnetic or antiferromagnetic vector relative to the crystallographic axis are called reorientation transitions and are analysed in Section 1.5.6.

Sections 1.5.7 and 1.5.8 are devoted to phenomena that can be (and were) predicted only on the basis of magnetic symmetry. These are piezomagnetism (Section 1.5.7) and the magnetoelectric effect (Section 1.5.8). The reciprocal of the piezomagnetic effect (Section 1.5.7.1) is linear magnetostriction (Section 1.5.7.2). The magnetoelectric effect has been investigated far more than piezomagnetism. In addition to the linear

† The sudden death of Andrey Stanislavovich Borovik-Romanov is deeply regretted. At the age of 77, he died on 31 July 1997 in Cairns, Australia, where he was taking part in the International Conference on Magnetism ICM'97.

1. TENSORIAL ASPECTS OF PHYSICAL PROPERTIES

magnetoelectric effect (Section 1.5.8.1), effects of higher order (Section 1.5.8.2) have also been observed. In connection with the magnetoelectric effect, ferromagnetic and antiferromagnetic ferroelectrics are also considered (Section 1.5.8.3).

In Section 1.5.9, the magnetostriction in ferromagnets is discussed. Only fundamental points of this problem are considered.

As noted above, only those problems of magnetism that are closely connected with magnetic symmetry are considered in this chapter. However, these problems are only outlined briefly here because of the restrictions on the extent of this volume. For the same reason, it is impossible to give an exhaustive list of references. The references given here include selected publications on magnetic symmetry and those describing the first experimental work devoted to the properties connected with magnetic symmetry.

1.5.1.1. Disordered magnetics

A crystal placed in a magnetic field \mathbf{H} is magnetized. The magnetized state is characterized by two vectors, the magnetization \mathbf{M} (the magnetic moment per unit volume) and the magnetic induction \mathbf{B} . The Gaussian system of units is used in this chapter (see Table 1.5.10.1 at the end of the chapter for a list of conversions from Gaussian to SI units). The magnetic induction is given by

$$\mathbf{B} = \mathbf{H} + 4\pi\mathbf{M}. \quad (1.5.1.1)$$

This equation shows that the dimensions of \mathbf{B} , \mathbf{H} and \mathbf{M} are the same in the Gaussian system. The unit for \mathbf{B} , the gauss (G), and for \mathbf{H} , the oersted (Oe), also coincide in magnitude, whereas the unit for \mathbf{M} , usually called emu cm⁻³, is 4π times larger. These units are related to the corresponding SI units as follows: 1 G = 10⁻⁴ tesla (T), 1 Oe = 10³/(4 π) A m⁻¹, 1 emu cm⁻³ = 10³ A m⁻¹.

In disordered magnetics, the vectors \mathbf{B} and \mathbf{M} are linear in the magnetic field. Using a Cartesian coordinate system, this can be expressed as

$$M_i = \chi_{ij}H_j \text{ and } B_i = \mu_{ij}H_j, \quad (1.5.1.2)$$

where χ_{ij} is the dimensionless magnetic susceptibility per unit volume and μ_{ij} is the magnetic permeability. The susceptibility is frequently referred to 1 g or to one mole of substance. The mass susceptibility is written as χ_g , the molar susceptibility as χ_{mol} .

All three vectors \mathbf{H} , \mathbf{M} and \mathbf{B} are axial vectors (see Section 1.1.4.5.3), the symmetry of which is ∞/m . Accordingly, the components of these vectors perpendicular to a mirror plane do not change sign on being reflected by this plane, whereas the components parallel to the plane do change sign. Consequently, these three vectors are invariant with respect to inversion. The quantities χ_{ij} and μ_{ij} are components of second-rank polar tensors. In principal axes, the tensors become diagonal and both the magnetic susceptibility and permeability of a crystal are characterized by the three values of the principal susceptibilities and principal permeabilities, respectively.

All disordered magnetics are divided into two types: diamagnets ($\chi < 0$) and paramagnets ($\chi > 0$).

Diamagnetism is a universal property of all materials. It is associated with the tendency of all the electrons to screen the applied external field according to the Lenz law. For materials in which the electron orbits are spherically symmetric, the relation for the diamagnetic susceptibility was calculated by Langevin. For monoatomic substances he obtained

$$\chi = -\frac{Ne^2}{6mc^2} \left(\sum_{i=1}^{i=Z} \overline{r_i^2} \right), \quad (1.5.1.3)$$

where N is the number of atoms per unit volume, Z is the number of electrons per atom, e and m are the charge and the mass of the electron, respectively, and $\overline{r_i^2}$ are the mean squares of the radii of the electron orbits. In polyatomic substances, the summation must be done over all types of atoms. In most chemical compounds, the orbits are not spherical and the calculation of the diamagnetic susceptibility becomes more complicated. In metals, the conduction electrons contribute significantly to the diamagnetic susceptibility. The diamagnetic susceptibility of most substances is very small ($\chi \sim 10^{-6}$) and isotropic. Rare exceptions are bismuth and some organic compounds, in which the diamagnetism is strongly anisotropic.

Most paramagnetic materials contain ions (or free atoms) with a partly filled inner electronic shell. Examples are the transition metals and the rare-earth and actinide elements. Atoms, molecules and point defects possessing an odd number of electrons are also paramagnetic. Ions with a partly filled inner electronic shell possess orbital \mathbf{L} and spin \mathbf{S} angular momenta, which determine the total angular momentum \mathbf{J} if the spin-orbit interaction is strong compared with the crystal field.

The magnetic susceptibility of paramagnets follows the Curie-Weiss law in low magnetic fields ($\mu_B B \ll k_B T$):

$$\chi = \frac{Np^2\mu_B^2}{3k_B(T - \Delta)}, \quad (1.5.1.4)$$

where N is the number of magnetic ions (or atoms) per cm³, μ_B is the Bohr magneton, p is the effective number of Bohr magnetons, k_B is the Boltzmann factor and Δ is the Weiss constant. The Weiss constant is related to the interaction between the magnetic moments (mostly exchange interaction) and to the effect of the splitting of electron levels of the paramagnetic ion in the crystalline electric field. Many paramagnets that obey the Curie-Weiss law transform into ordered magnetics at a temperature T_c , which is of the order of $|\Delta|$. The sign of Δ depends on the sign of the exchange constant J [see relation (1.5.1.7)]. For the substances that at low temperatures become ferromagnets, we have $\Delta > 0$, for antiferromagnets $\Delta < 0$, and for ferrimagnets the temperature dependence of χ is more complicated (see Fig. 1.5.1.1). For those paramagnets that do not go over into an ordered state, Δ is close to zero and equation (1.5.1.4) changes to the Curie law.

The value of the effective number of Bohr magnetons p depends strongly on the type of the magnetic ions and their environment. For most rare-earth compounds at room temperature, the number p has the same value as for free ions:

$$p = g[J(J+1)]^{1/2}, \quad (1.5.1.5)$$

where g is the Landé g -factor or the spectroscopic splitting factor ($1 \leq g \leq 2$). In this case, the paramagnetic susceptibility is practically isotropic. Some anisotropy can arise from the anisotropy of the Weiss constant Δ .

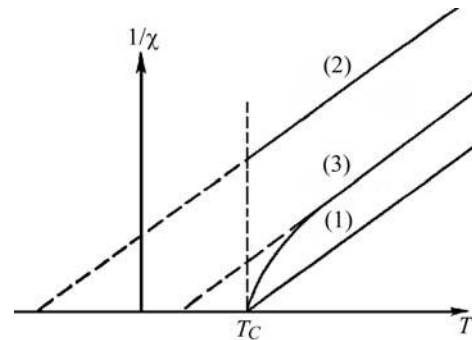


Fig. 1.5.1.1. Temperature dependence of $1/\chi$ at high temperatures for different types of magnetics: (1) ferromagnet; (2) antiferromagnet; (3) ferrimagnet.

1.5. MAGNETIC PROPERTIES

The behaviour of the transition-metal ions is very different. In contrast to the rare-earth ions, the electrons of the partly filled shell in transition metals interact strongly with the electric field of the crystal. As a result, their energy levels are split and the orbital moments can be ‘quenched’. This means that relation (1.5.1.5) transforms to

$$p_{ij} = (g_{\text{eff}})_{ij}[S(S+1)]^{1/2}. \quad (1.5.1.6)$$

Here the value of the effective spin S represents the degeneration of the lowest electronic energy level produced by the splitting in the crystalline field; $(g_{\text{eff}})_{ij}$ differs from the usual Landé g -factor. The values of its components lie between 0 and 10–20. The tensor $(g_{\text{eff}})_{ij}$ becomes diagonal in the principal axes. According to relation (1.5.1.6), the magnetic susceptibility also becomes a tensor. The anisotropy of $(g_{\text{eff}})_{ij}$ can be studied using electron paramagnetic resonance (EPR) techniques.

The Curie–Weiss law describes the behaviour of those paramagnets in which the magnetization results from the competition of two forces. One is connected with the reduction of the magnetic energy by orientation of the magnetic moments of ions in the applied magnetic field; the other arises from thermal fluctuations, which resist the tendency of the field to orient these moments. At low temperatures and in strong magnetic fields, the linear dependence of the magnetization *versus* magnetic field breaks down and the magnetization can be saturated in a sufficiently strong magnetic field. Most of the paramagnetic substances that obey the Curie–Weiss law ultimately transform to an ordered magnetic as the temperature is decreased.

The conduction electrons in metals possess paramagnetism in addition to diamagnetism. The paramagnetic susceptibility of the conduction electrons is small (of the same order of magnitude as the diamagnetic susceptibility) and does not depend on temperature. This is due to the fact that the conduction electrons are governed by the laws of Fermi–Dirac statistics.

1.5.1.2. Ordered magnetics

1.5.1.2.1. Ferromagnets (including ferrimagnets)

As stated above, all ordered magnetics that possess a spontaneous magnetization \mathbf{M}_s different from zero (a magnetization even in zero magnetic field) are called ferromagnets. The simplest type of ferromagnet is shown in Fig. 1.5.1.2(a). This type possesses only one kind of magnetic ion or atom. All their magnetic moments are aligned parallel to each other in the same direction. This magnetic structure is characterized by one vector \mathbf{M} . It turns out that there are very few ferromagnets of this type in which only atoms or ions are responsible for the ferromagnetic magnetization (CrBr_3 , EuO etc.). The overwhelming majority of ferromagnets of this simplest type are metals, in which the magnetization is the sum of the magnetic moments of the localized ions and of the conduction electrons, which are partly polarized.

More complicated is the type of ferromagnet which is called a ferrimagnet. This name is derived from the name of the oxides of the elements of the iron group. As an example, Fig. 1.5.1.2(b) schematically represents the magnetic structure of magnetite (Fe_3O_4). It contains two types of magnetic ions and the number of Fe^{3+} ions (μ_1 and μ_2) is twice the number of Fe^{2+} ions (μ_3). The values of the magnetic moments of these two types of ions differ. The magnetic moments of all Fe^{2+} ions are aligned in one direction. The Fe^{3+} ions are divided into two parts: the magnetic moments of one half of these ions are aligned parallel to the magnetic moments of Fe^{2+} and the magnetic moments of the other half are aligned antiparallel. The array of all magnetic moments of identical ions oriented in one direction is called a magnetic sublattice. The magnetization vector of a given sublattice will be denoted by \mathbf{M}_i . Hence the magnetic structure of Fe_3O_4

consists of three magnetic sublattices. The magnetizations of two of them are aligned in one direction, the magnetization of the third one is oriented in the opposite direction. The net ferromagnetic magnetization is $M_s = M_1 - M_2 + M_3 = M_3$.

The special feature of ferrimagnets, as well as of many antiferromagnets, is that they consist of sublattices aligned antiparallel to each other. Such a structure is governed by the nature of the main interaction responsible for the formation of the ordered magnetic structures, the exchange interaction. The energy of the exchange interaction does not depend on the direction of the interacting magnetic moments (or spins \mathbf{S}) rela-

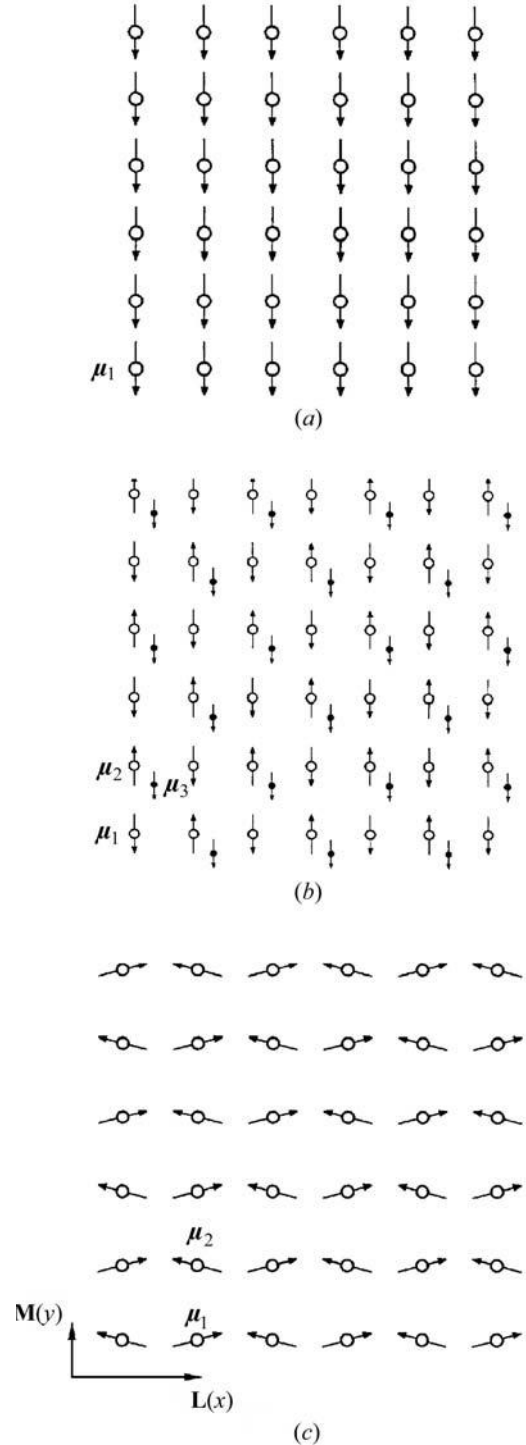


Fig. 1.5.1.2. Ordered arrangements of magnetic moments μ_i in: (a) an ordinary ferromagnet $\mathbf{M}_s = N\mu_i$; (b) a ferrimagnet $\mathbf{M}_s = (N/3)(\mu_1 + \mu_2 + \mu_3)$; (c) a weak ferromagnet $\mathbf{M} = \mathbf{M}_D = (N/2)(\mu_1 + \mu_2)$, $\mathbf{L} = (N/2)(\mu_1 - \mu_2)$, ($L_x \gg M_y$; $M_x = M_z = L_y = L_z = 0$). (N is the number of magnetic ions per cm^3 .)

1. TENSORIAL ASPECTS OF PHYSICAL PROPERTIES

tive to the crystallographic axes and is represented by the following relation:

$$U_{\text{ex}} = - \sum_{m,n} J_{mn} \mathbf{S}_m \mathbf{S}_n. \quad (1.5.1.7)$$

Here $\mathbf{S}_m, \mathbf{S}_n$ are the spins of magnetic atoms (ions) and J_{mn} is the exchange constant, which usually decreases fast when the distance between the atoms rises. Therefore, usually only the nearest neighbour interaction needs to be taken into account. Hence, according to (1.5.1.7), the exchange energy is a minimum for the state in which neighbouring spins are parallel (if $J > 0$) or antiparallel (if $J < 0$). If the nearest neighbour exchange interaction were the only interaction responsible for the magnetic ordering, only collinear magnetic structures would exist (except in triangle lattices). Together with the exchange interaction, there is also a magnetic dipole interaction between the magnetic moments of the atoms as well as an interaction of the atomic magnetic electrons with the crystalline electric field. These interactions are much smaller than the exchange interaction. They are often called relativistic interactions. The relativistic interactions and the exchange interaction between next-nearest atoms bring about the formation of non-collinear magnetic structures.

A simple non-collinear structure is the magnetic structure of a weak ferromagnet. It contains identical magnetic ions divided in equal amounts between an even number of sublattices. In the first approximation, the magnetizations of these sublattices are antiparallel, as in usual antiferromagnets. In fact, the magnetizations are not strictly antiparallel but are slightly canted, *i.e.* non-collinear, as shown in Fig. 1.5.1.2(c). There results a ferromagnetic moment M_D , which is small compared with the sublattice magnetization M_i . The magnetic properties of weak ferromagnets combine the properties of both ferromagnets and antiferromagnets. They will be discussed in detail in Section 1.5.5.1.

1.5.1.2.2. Antiferromagnets

As discussed above, the exchange interaction, which is of prime importance in the formation of magnetic order, can lead to a parallel alignment of the neighbouring magnetic moments as well as to an antiparallel one. In the latter case, the simplest magnetic structure is the collinear antiferromagnet, schematically shown in Fig. 1.5.1.3(a). Such an antiferromagnet consists of one or several pairs of magnetic sublattices of identical magnetic ions located in equivalent crystallographic positions. The magnetizations of the sublattices are oriented opposite to each other.

Fig. 1.5.1.3(b) shows a weakly non-collinear antiferromagnet, in which the vectors of magnetization of four equivalent sublattices form a cross with a small tilting angle 2α . Such a structure can be considered as an admixture of 'weak antiferromagnetism' \mathbf{L}_1 with easy axis Ox to an ordinary antiferromagnet \mathbf{L}_2 with easy axis Oy . This weak antiferromagnetism is of the same origin as weak ferromagnetism. Its nature will be discussed in detail in Section 1.5.5.2.

The minimum of the exchange interaction energy of three spins located at the corners of a triangle corresponds to a structure in which the angles between two adjacent spins are 120° . Correspondingly, many hexagonal crystals possess a triangular antiferromagnetic structure like the one shown in Fig. 1.5.1.3(c). The sum of the magnetizations of the three sublattices in this structure equals zero. In tetragonal crystals, there is a possibility of the existence of a 90° antiferromagnetic structure, which consists of four equivalent sublattices with magnetizations oriented along the positive and negative directions of the x and y axes.

Finally, it is worth noting that in addition to the electronic magnetically ordered substances, there exist nuclear ferro- and antiferromagnets (below 1 mK for some insulators and below 1 μ K for metals).

1.5.1.2.3. Helical and sinusoidal magnetics

There are many more complicated non-collinear magnetic structures. Fig. 1.5.1.4(a) shows an antiferromagnetic helical structure. It consists of planes perpendicular to the z axis in which all the magnetic moments are parallel to each other and are perpendicular to z . The polar angle of the direction of the moments changes from plane to plane by some constant δ . Thus the magnetization vectors describe a spiral along the axis of the crystal. Such structures were observed in hexagonal rare-earth metals. A specific feature is that they often are incommensurate structures. This means that $2\pi/\delta$ is not a rational number and that the period of the magnetic spiral is not a multiple of the period of the lattice.

Similar to the antiferromagnetic helix, ferromagnetic helical or spiral structures exist [see Fig. 1.5.1.4(b)] in which the magnetizations of the layers are tilted to the axis at an angle θ . As a result,

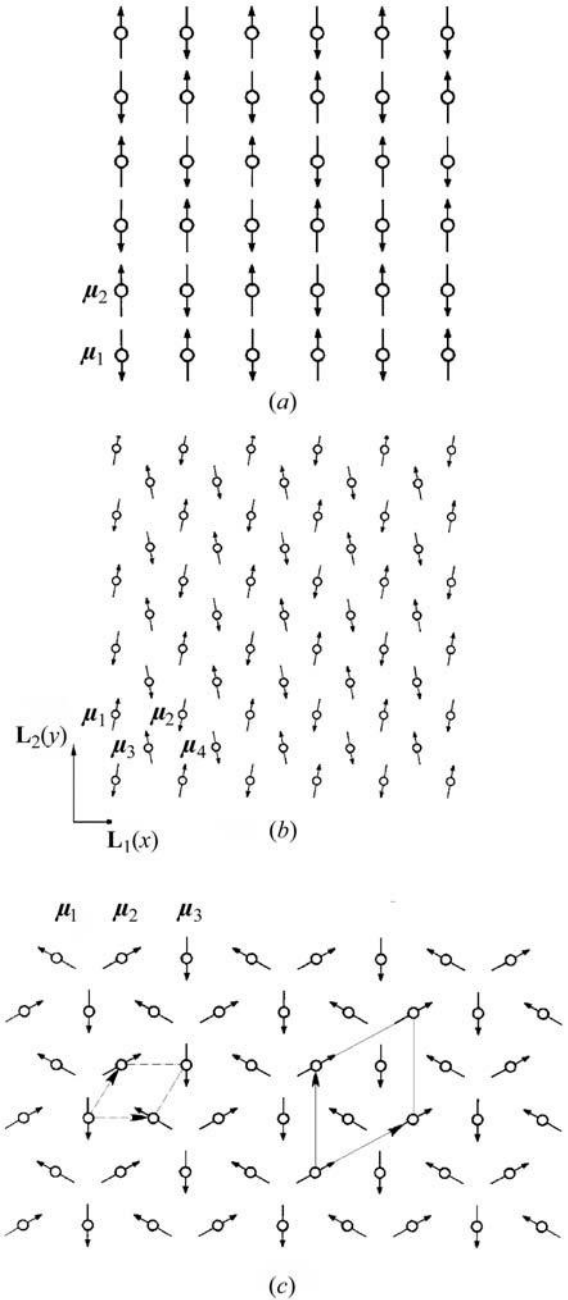


Fig. 1.5.1.3. Ordered arrangements of magnetic moments μ_i in: (a) an ordinary two-sublattice antiferromagnet $\mathbf{L} = (N/2)(\mu_1 - \mu_2)$; (b) a weakly non-collinear four-sublattice antiferromagnet $\mathbf{L}_1(x) = (N/4)(\mu_1 - \mu_2 - \mu_3 + \mu_4)$, $\mathbf{L}_2(y) = (N/4)(\mu_1 - \mu_2 + \mu_3 - \mu_4)$; (c) a strongly non-collinear three-sublattice antiferromagnet $\mathbf{L}_1 = (N/3)(\mu_2 - \mu_1)$, $\mathbf{L}_2 = (N/3)(\mu_1 + \mu_2 - \mu_3)$. The broken lines show the crystallographic primitive cell and the solid lines show the magnetic primitive cell.

1.5. MAGNETIC PROPERTIES

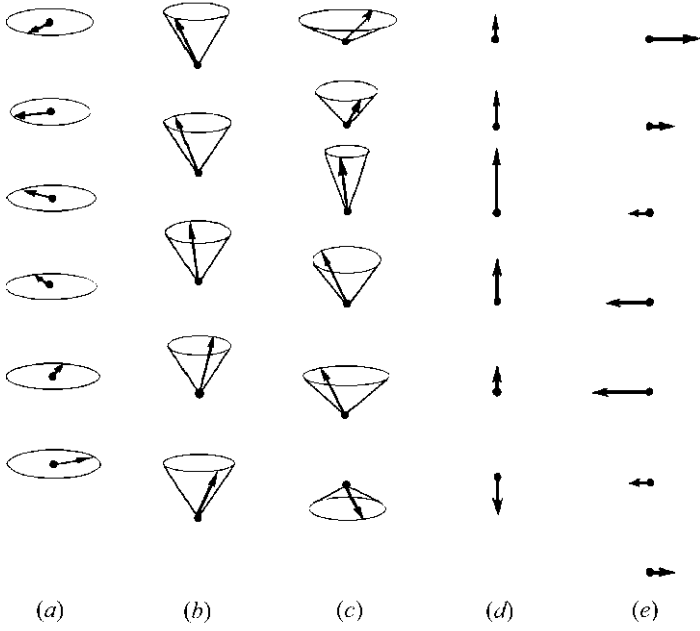


Fig. 1.5.1.4. Helical and sinusoidal magnetic structures. (a) An antiferromagnetic helix; (b) a cone spiral; (c) a cycloidal spiral; (d) a longitudinal spin-density wave; (e) a transverse spin-density wave.

the vectors of the magnetization of the layers are arranged on the surface of a cone. The ferromagnetic magnetization is aligned along the z axis. This structure is called a ferromagnetic helix. It usually belongs to the incommensurate magnetic structures.

More complicated antiferromagnetic structures also exist: sinusoidal structures, which also consist of layers in which all the magnetic moments are parallel to each other. Fig. 1.5.1.4(c) displays the cycloidal spiral and Figs. 1.5.1.4(d) and (e) display longitudinal and transverse spin density waves, respectively.

1.5.2. Magnetic symmetry

As discussed in Section 1.5.1, in studies of the symmetry of magnetics one should take into account not only the crystallographic elements of symmetry (rotations, reflections and translations) but also the time-inversion element, which causes the reversal of the magnetic moment density vector $\mathbf{m}(\mathbf{r})$. Following Landau & Lifshitz (1957), we shall denote this element by R . If combined with any crystallographic symmetry element G we get a product RG , which some authors call the space-time symmetry operator. We shall not use this terminology in the following.

To describe the symmetry properties of magnetics, one should use magnetic point and space groups instead of crystallographic ones. (See also Section 1.2.5.)

By investigating the ‘four-dimensional groups of three-dimensional space’, Heesch (1930) found not only the 122 groups that now are known as magnetic point groups but also the seven triclinic and 91 monoclinic magnetic space groups. He also recognized that these groups can be used to describe the symmetry of spin arrangements. The present interest in magnetic symmetry was much stimulated by Shubnikov (1951), who considered the symmetry groups of figures with black and white faces, which he called antisymmetry groups. The change of colour of the faces in antisymmetry (black–white symmetry, see also Section 3.3.5) corresponds to the element R . These antisymmetry classes were derived as magnetic symmetry point groups by Tavger & Zaitsev (1956). Beside antisymmetry, the concept of

Table 1.5.2.1. Comparison of different symbols for magnetic point groups

| Schoenflies | Hermann–Mauguin | Shubnikov | |
|-------------|-----------------|-----------|------|
| D_{4R} | 4221' | 4:21' | 4:21 |
| D_4 | 422 | 4:2 | 4:2 |
| $D_4(C_4)$ | 42'2' | 4:2' | 4:2 |
| $D_4(D_2)$ | 4'22' | 4':2 | 4:2 |

colour (or generalized) symmetry also was developed, in which the number of colours is not 2 but 3, 4 or 6 (see Belov *et al.*, 1964; Koptsik & Kuzhukeev, 1972). A different generalization to more than two colours was proposed by van der Waerden & Burckhardt (1961). The various approaches have been compared by Schwarzenberger (1984).

As the theories of antisymmetry and of magnetic symmetry evolved often independently, different authors denote the operation of time inversion (black–white exchange) by different symbols. Of the four frequently used symbols ($R = E' = \underline{1} = 1'$) we shall use in this article only two: R and $1'$.

1.5.2.1. Magnetic point groups

Magnetic point groups may contain rotations, reflections, the element R and their combinations. A set of such elements that satisfies the group properties is called a magnetic point group. It is obvious that there are 32 trivial magnetic point groups; these are the ordinary crystallographic point groups supplemented by the element R . Each of these point groups contains all the elements of the ordinary point group \mathcal{P} and also all the elements of this group \mathcal{P} multiplied by R . This type of magnetic point group \mathcal{M}_{P1} can be represented by

$$\mathcal{M}_{P1} = \mathcal{P} + R\mathcal{P}. \quad (1.5.2.1)$$

These groups are sometimes called ‘grey’ magnetic point groups. As pointed out above, all dia- and paramagnets belong to this type of point group. To this type belong also antiferromagnets with a magnetic space group that contains translations multiplied by R (space groups of type III^b).

The second type of magnetic point group, which is also trivial in some sense, contains all the 32 crystallographic point groups without the element R in any form. For this type $\mathcal{M}_{P2} = \mathcal{P}$. Thirteen of these point groups allow ferromagnetic spontaneous magnetization (ferromagnetism, ferrimagnetism, weak ferromagnetism). They are listed in Table 1.5.2.4. The remaining 19 point groups describe antiferromagnets. The groups \mathcal{M}_{P2} are often called ‘white’ magnetic point groups.

The third type of magnetic point group \mathcal{M}_{P3} , ‘black and white’ groups (which are the only nontrivial ones), contains those point groups in which R enters only in combination with rotations or reflections. There are 58 point groups of this type. Eighteen of them describe different types of ferromagnetism (see Table 1.5.2.4) and the others represent antiferromagnets.

Replacing R by the identity element E in the magnetic point groups of the third type does not change the number of elements in the point group. Thus each group of the third type \mathcal{M}_{P3} is isomorphic to a group \mathcal{P} of the second type.

The method of derivation of the nontrivial magnetic groups given below was proposed by Indenbom (1959). Let \mathcal{H} denote the set of those elements of the group \mathcal{P} which enter into the asso-

Table 1.5.2.2. Comparison of different symbols for the elements of magnetic point groups

| Magnetic point group | Elements | |
|----------------------|--|---|
| | Schoenflies | Hermann–Mauguin |
| $D_{4R} = 4221'$ | $E, C_2, 2C_4, 2U_2, 2U_2^a, R, RC_2, 2RC_4, 2RU_2, 2RU_2^a$ | $1, 2_x, 2_y, 2_z, 2_{xy}, 2_{-xy}, \pm 4_z, 1', 2'_x, 2'_y, 2'_z, 2'_{xy}, 2'_{-xy}, \pm 4'_z$ |
| $D_4 = 422$ | $E, C_2, 2C_4, 2U_2, 2U_2^a$ | $1, 2_x, 2_y, 2_z, 2_{xy}, 2_{-xy}, \pm 4_z$ |
| $D_4(C_4) = 42'2'$ | $E, C_2, 2C_4, 2RU_2, 2RU_2^a$ | $1, 2_z, \pm 4_z, 2'_x, 2'_y, 2'_{xy}, 2'_{-xy}$ |
| $D_4(D_2) = 4'22'$ | $E, C_2^x, C_2^y, C_2^z, 2RU_2^a, 2RC_4$ | $1, 2_x, 2_y, 2_z, 2'_{xy}, 2'_{-xy}, \pm 4'_z$ |

1. TENSORIAL ASPECTS OF PHYSICAL PROPERTIES

Table 1.5.2.3. The 90 magnetic point groups of types 2 and 3

| 1 | 2 | 3 | 4 | 5 | 6 |
|--------------|---|--|--|---|---|
| System | Symbol of magnetic point group \mathcal{M} | | | | Symmetry operators of group \mathcal{M} |
| | Schoenflies | Shubnikov | Hermann–Mauguin | | |
| | | | Short | Full | |
| Triclinic | C_1 C_i $C_i(C_1)$ | 1 $\bar{2}$ $\underline{\bar{2}}$ | 1 $\bar{1}$ $\bar{1}'$ | 1 $\bar{1}$ $\bar{1}'$ | 1 1, $\bar{1}$ 1, $\bar{1}'$ |
| Monoclinic | C_2 $C_2(C_1)$ C_s $C_s(C_1)$ C_{2h} $C_{2h}(C_i)$ $C_{2h}(C_2)$ $C_{2h}(C_s)$ | 2 $\underline{2}$ m \underline{m} $2 : m$ $\underline{2} : \underline{m}$ $2 : \underline{m}$ $\underline{2} : m$ | 2 2' m m' $2/m$ $2'/m'$ $2/m'$ $2'/m$ | 121 12'1 $1m1$ $1m'1$ $1\frac{2}{m}1$ $1\frac{2'}{m'}1$ $1\frac{2}{m'}1$ $1\frac{2'}{m}1$ | 1, 2_y 1, $2'_y$ 1, m_y 1, m'_y 1, $\bar{1}, 2_y, m_y$ 1, $\bar{1}, 2'_y, m'_y$ 1, $2_y, \bar{1}', m'_y$ 1, $m_y, \bar{1}', 2'_y$ |
| Orthorhombic | D_2 $D_2(C_2)$ C_{2v} $C_{2v}(C_2)$ $C_{2v}(C_s)$ D_{2h} $D_{2h}(C_{2h})$ $D_{2h}(D_2)$ $D_{2h}(C_{2v})$ | $2 : 2$ $2 : \underline{2}$ $2 \cdot m$ $2 \cdot \underline{m}$ $\underline{2} \cdot m$ $m \cdot 2 : m$ $\underline{m} \cdot 2 : m$ $\underline{m} \cdot 2 : \underline{m}$ $m \cdot 2 : \underline{m}$ | 222 $2'2'2$ $mm2$ $m'm'2$ $2'm'm$ mmm $mm'm'$ $m'm'm'$ $mm'm'$ | 222 $2'2'2$ $mm2$ $m'm'2$ $2'm'm$ $\underline{2} \cdot \underline{2} \cdot \underline{2}$ $\underline{2} \cdot \underline{2}' \cdot \underline{2}'$ $\underline{m}' \cdot \underline{m}' \cdot \underline{m}'$ $\underline{2}' \cdot \underline{2}' \cdot \underline{2}'$ | 1, $2_x, 2_y, 2_z$ 1, $2_z, 2'_x, 2'_y$ 1, $2_z, m_x, m_y$ 1, $2_z, m'_x, m'_y$ 1, $m_z, 2'_x, m'_y$ 1, $\bar{1}, 2_x, 2_y, 2_z, m_x, m_y, m_z$ 1, $\bar{1}, 2_x, m_x, 2'_y, 2'_z, m'_y, m'_z$ 1, $2_x, 2_y, 2_z, \bar{1}', m'_x, m'_y, m'_z$ 1, $2_z, m_x, m_y, \bar{1}', 2'_x, 2'_y, m'_z$ |
| Tetragonal | C_4 $C_4(C_2)$ S_4 $S_4(C_2)$ C_{4h} $C_{4h}(C_{2h})$ $C_{4h}(C_4)$ $C_{4h}(S_4)$ D_4 $D_4(D_2)$ $D_4(C_4)$ C_{4v} $C_{4v}(C_{2v})$ $C_{4v}(C_4)$ D_{2d} $D_{2d}(D_2)$ $D_{2d}(C_{2v})$ $D_{2d}(S_4)$ D_{4h} $D_{4h}(D_{2h})$ $D_{4h}(C_{4h})$ $D_{4h}(D_4)$ $D_{4h}(C_{4v})$ $D_{4h}(D_{2d})$ | 4 $\underline{4}$ $\bar{4}$ $\bar{\underline{4}}$ $4 : m$ $\underline{4} : m$ $4 : \underline{m}$ $\underline{4} : \underline{m}$ $4 : 2$ $\underline{4} : 2$ $4 : \underline{2}$ $4 \cdot m$ $\underline{4} \cdot m$ $4 \cdot \underline{m}$ $\bar{4} \cdot m$ $\bar{\underline{4}} \cdot m$ $\underline{4} \cdot \underline{m}$ $\bar{4} \cdot \underline{m}$ $m \cdot 4 : m$ $m \cdot \underline{4} : m$ $\underline{m} \cdot 4 : m$ $\underline{m} \cdot 4 : \underline{m}$ $m \cdot 4 : \underline{m}$ $m \cdot \underline{4} : \underline{m}$ | 4 4' $\bar{4}$ $\bar{4}'$ $4/m$ $4'/m$ $4/m'$ $4'/m'$ 422 $4'22'$ $42'2'$ $4mm$ $4'mm'$ $4m'm'$ $\bar{4}2m$ $\bar{4}'2m'$ $\bar{4}m2'$ $\bar{4}2'm'$ $4/mmm$ $4'/mmm'$ $4/mm'm'$ $4/m'm'm'$ $4/m'mm$ $4'/m'm'm$ | 4 4' $\bar{4}$ $\bar{4}'$ $\frac{4}{m}$ $\frac{4'}{m}$ $\frac{4}{m'}$ $\frac{4'}{m'}$ 422 $4'22'$ $42'2'$ $4mm$ $4'mm'$ $4m'm'$ $\bar{4}2m$ $\bar{4}'2m'$ $\bar{4}m2'$ $\bar{4}2'm'$ $\frac{4}{m} \cdot \frac{2}{m} \cdot \frac{2}{m}$ $\frac{4'}{m'} \cdot \frac{2'}{m'} \cdot \frac{2'}{m'}$ $\frac{4}{m} \cdot \frac{2'}{m'} \cdot \frac{2'}{m'}$ $\frac{4'}{m'} \cdot \frac{2}{m} \cdot \frac{2}{m}$ $\frac{4'}{m'} \cdot \frac{2'}{m'} \cdot \frac{2'}{m'}$ $\frac{4'}{m'} \cdot \frac{2}{m} \cdot \frac{2}{m}$ | 1, $2_z, \pm 4_z$ 1, $2_z, \pm 4'_z$ 1, $2_z, \pm \bar{4}_z$ 1, $2_z, \pm \bar{4}'_z$ 1, $\bar{1}, 2_z, m_z, \pm 4_z, \pm \bar{4}_z$ 1, $\bar{1}, 2_z, m_z, \pm 4'_z, \pm \bar{4}'_z$ 1, $2_z, \pm 4_z, \bar{1}', m'_z, \pm \bar{4}'_z$ 1, $2_z, \pm \bar{4}_z, \bar{1}', m'_z, \pm 4'_z$ 1, $2_x, 2_y, 2_z, 2_{xy}, 2_{-xy}, \pm 4_z$ 1, $2_x, 2_y, 2_z, 2'_{xy}, 2'_{-xy}, \pm 4'_z$ 1, $2_z, \pm 4_z, 2'_x, 2'_y, 2'_{xy}, 2'_{-xy}$ 1, $2_z, m_x, m_y, m_{xy}, m_{-xy}, \pm 4_z$ 1, $2_z, m_x, m_y, m'_{xy}, m'_{-xy}, \pm 4'_z$ 1, $2_z, \pm 4_z, m'_x, m'_y, m'_{xy}, m'_{-xy}$ 1, $2_x, 2_y, 2_z, m_{xy}, m_{-xy}, \pm \bar{4}_z$ 1, $2_x, 2_y, 2_z, m'_{xy}, m'_{-xy}, \pm \bar{4}'_z$ 1, $2_z, m_x, m_y, 2'_{xy}, 2'_{-xy}, \pm \bar{4}'_z$ 1, $2_z, \pm \bar{4}_z, 2'_x, 2'_y, m'_{xy}, m'_{-xy}$ 1, $\bar{1}, 2_x, 2_y, 2_z, 2_{xy}, 2_{-xy}, m_x, m_y, m_z, m_{xy}, m_{-xy}, \pm 4_z, \pm \bar{4}_z$ 1, $\bar{1}, 2_x, 2_y, 2_z, m_x, m_y, m_z, 2'_{xy}, 2'_{-xy}, m'_{xy}, m'_{-xy}, \pm 4'_z, \pm \bar{4}'_z$ 1, $\bar{1}, 2_z, m_z, \pm 4_z, \pm \bar{4}_z, 2'_x, 2'_y, 2'_{xy}, 2'_{-xy}, m'_x, m'_y, m'_{xy}, m'_{-xy}$ 1, $2_x, 2_y, 2_z, 2_{xy}, 2_{-xy}, \pm 4_z, \bar{1}', m'_x, m'_y, m'_z, m'_{xy}, m'_{-xy}, \pm \bar{4}'_z$ 1, $2_z, m_x, m_y, m_{xy}, m_{-xy}, \pm 4_z, \bar{1}', 2'_x, 2'_y, 2'_{xy}, 2'_{-xy}, m'_z, \pm \bar{4}'_z$ 1, $2_x, 2_y, 2_z, m_{xy}, m_{-xy}, \pm \bar{4}_z, \bar{1}', 2'_{xy}, 2'_{-xy}, m'_x, m'_y, m'_z, \pm 4'_z$ |

ciated magnetic group \mathcal{M}_{p_3} not multiplied by R . The set \mathcal{H} contains the identity element E , for each element H also its inverse H^{-1} , and for each pair H_1, H_2 also its products $H_1 H_2$ and $H_2 H_1$. Thus the set \mathcal{H} forms a group. It is a subgroup of the crystallographic group \mathcal{P} . Let P_i denote an element of $(\mathcal{P} - \mathcal{H})$. All these elements enter \mathcal{M}_{p_3} in the form of products RP_i because $RP_i = P_i R$ and $R^2 = 1$. Multiplying the elements of \mathcal{M}_{p_3} by a fixed element RP_1 corresponds to a permutation of the elements of \mathcal{M}_{p_3} . This permutation maps each element of the subgroup \mathcal{H} on an element of \mathcal{M}_{p_3} that does not belong to \mathcal{H} and *vice versa*. It follows that one half of the elements of \mathcal{M}_{p_3} are elements of $(\mathcal{P} - \mathcal{H})$ multiplied by R and the other half belong to \mathcal{H} . The relation for the magnetic point groups of the third type may therefore be written as

$$\mathcal{M}_{p_3} = \mathcal{H} + R(\mathcal{P} - \mathcal{H}) = \mathcal{H} + RP_1 \mathcal{H}. \quad (1.5.2.2)$$

\mathcal{H} is therefore a subgroup of index 2 of \mathcal{P} . The subgroups of index 2 of \mathcal{P} can easily be found using the tables of irreducible representations of the point groups. Every real non-unit one-dimensional representation of \mathcal{P} contains equal numbers of characters $+1$ and -1 . In the corresponding magnetic point group \mathcal{M}_{p_3} , the elements of \mathcal{P} with character -1 are multiplied by R and those with character $+1$ remain unchanged. The latter form the subgroup \mathcal{H} . This rule can be stated as a theorem: every real non-unit one-dimensional representation τ of a point group of symmetry \mathcal{P} produces an isomorphic mapping of this group upon a magnetic group \mathcal{M}_{p_3} (Indenbom, 1959). This concept will be developed in Section 1.5.3.

Using the Schoenflies symbols and the method described above, the point groups of magnetic symmetry (magnetic point groups) can be denoted by $\mathcal{P}(\mathcal{H})$, where \mathcal{P} is the symbol of the original crystallographic point group and \mathcal{H} is the symbol of that

1.5. MAGNETIC PROPERTIES

Table 1.5.2.3 (cont.)

| 1 | 2 | 3 | 4 | 5 | 6 |
|-----------|--|---|---|--|--|
| System | Symbol of magnetic point group \mathcal{M} | | | | Symmetry operators of group \mathcal{M} |
| | Schoenflies | Shubnikov | Hermann–Mauguin | | |
| | | | Short | Full | |
| Trigonal | C_3 S_6 $S_6(C_3)$ D_3 $D_3(C_3)$ C_{3v} $C_{3v}(C_3)$ D_{3d} $D_{3d}(S_6)$ $D_{3d}(D_3)$ $D_{3d}(C_{3v})$ | 3 $\bar{6}$ $\bar{6}$ 3 : 2 3 : $\underline{2}$ 3·m 3· \underline{m} $\bar{6}$ ·m $\bar{6}$ · \underline{m} $\bar{6}$ · \underline{m} $\bar{6}$ ·m | 3 $\bar{3}$ $\bar{3}'$ 32 32' 3m 3m' $\bar{3}m$ $\bar{3}m'$ $\bar{3}m'$ $\bar{3}m$ | 3 $\bar{3}$ $\bar{3}'$ 321 32'1 3m1 3m'1 $\bar{3}\frac{2}{m}1$ $\bar{3}\frac{2}{m'}1$ $\bar{3}\frac{2}{m'}1$ $\bar{3}\frac{2}{m}1$ | 1, $\pm 3_z$ 1, $\bar{1}$, $\pm 3_z$, $\pm \bar{3}_z$ 1, $\pm 3_z$, $\bar{1}'$, $\pm \bar{3}_z'$ 1, 3(2 $_{\perp}$), $\pm 3_z$ 1, $\pm 3_z$, 3(2' $_{\perp}$) 1, 3(m_{\perp}), $\pm 3_z$ 1, $\pm 3_z$, 3(m'_{\perp}) 1, $\bar{1}$, 3(2 $_{\perp}$), 3(m_{\perp}), $\pm 3_z$, $\pm \bar{3}_z$ 1, $\bar{1}$, $\pm 3_z$, $\pm \bar{3}_z$, 3(2' $_{\perp}$), 3(m'_{\perp}) 1, 3(2 $_{\perp}$), $\pm 3_z$, $\bar{1}'$, 3(m'_{\perp}), $\pm \bar{3}_z'$ 1, 3(m_{\perp}), $\pm 3_z$, $\bar{1}'$, 3(2' $_{\perp}$), $\pm \bar{3}_z'$ |
| Hexagonal | C_6 $C_6(C_3)$ C_{3h} $C_{3h}(C_3)$ C_{6h} $C_{6h}(S_6)$ $C_{6h}(C_6)$ $C_{6h}(C_{3h})$ D_6 $D_6(D_3)$ $D_6(C_6)$ C_{6v} $C_{6v}(C_{3v})$ $C_{6v}(C_6)$ D_{3h} $D_{3h}(D_3)$ $D_{3h}(C_{3v})$ $D_{3h}(C_{3h})$ D_{6h} $D_{6h}(D_{3d})$ $D_{6h}(C_{6h})$ $D_{6h}(D_6)$ $D_{6h}(C_{6v})$ $D_{6h}(D_{3h})$ | 6 $\bar{6}$ 3 : m 3 : \underline{m} 6 : m $\bar{6}$: \underline{m} 6 : \underline{m} $\bar{6}$: m 6 : 2 $\bar{6}$: 2 6 : $\underline{2}$ 6·m $\bar{6}$ ·m 6· \underline{m} m·3 : m $\bar{6}$ ·3 : \underline{m} m·3 : \underline{m} \underline{m} ·3 : m m·6 : m m· $\bar{6}$: \underline{m} \underline{m} ·6 : m \underline{m} ·6 : \underline{m} m·6 : \underline{m} m·6 : \underline{m} | 6 6' $\bar{6}$ $\bar{6}'$ 6/m 6'/m' 6/m' 6'/m 622 6'22' 62'2' 6mm 6'mm' 6m'm' $\bar{6}m2$ $\bar{6}'2m'$ $\bar{6}m2'$ $\bar{6}m'2'$ 6/mmm 6'/m'mm' 6/mmm' 6/m'mm 6'/mmm' | 6 6' $\bar{6}$ $\bar{6}'$ $\frac{6}{m}$ $\frac{6}{m'}$ $\frac{6}{m'}$ $\frac{6}{m}$ 622 6'22' 62'2' 6mm 6'mm' 6m'm' $\bar{6}m2$ $\bar{6}'2m'$ $\bar{6}m2'$ $\bar{6}m'2'$ $\frac{6}{m}\frac{2}{m}\frac{2}{m}$ $\frac{6'}{m'}\frac{2}{m'}\frac{2'}{m'}$ $\frac{6}{m}\frac{2'}{m'}\frac{2'}{m'}$ $\frac{6}{m'}\frac{2}{m'}\frac{2}{m'}$ $\frac{6}{m'}\frac{2}{m'}\frac{2'}{m}$ $\frac{6'}{m'}\frac{2'}{m'}\frac{2}{m}$ | 1, 2 $_z$, $\pm 3_z$, $\pm 6_z$ 1, $\pm 3_z$, 2' $_z$, $\pm 6'_z$ 1, m_z , $\pm 3_z$, $\pm \bar{6}_z$ 1, $\pm 3_z$, m'_z , $\pm \bar{6}_z'$ 1, $\bar{1}$, 2 $_z$, m_z , $\pm 3_z$, $\pm \bar{3}_z$, $\pm 6_z$, $\pm \bar{6}_z$ 1, $\bar{1}$, $\pm 3_z$, $\pm \bar{3}_z$, 2' $_z$, m'_z , $\pm 6'_z$, $\pm \bar{6}_z'$ 1, 2 $_z$, $\pm 3_z$, $\pm 6_z$, $\bar{1}'$, m'_z , $\pm \bar{3}_z'$, $\pm \bar{6}_z'$ 1, m_z , $\pm 3_z$, $\pm \bar{6}_z$, $\bar{1}'$, 2' $_z$, $\pm \bar{3}_z'$, $\pm 6'_z$ 1, 6(2 $_{\perp}$), 2 $_z$, $\pm 3_z$, $\pm 6_z$ 1, 3(2 $_{\perp}$), $\pm 3_z$, 3(2' $_{\perp}$), 2' $_z$, $\pm 6'_z$ 1, 2 $_z$, $\pm 3_z$, $\pm 6_z$, 6(2' $_{\perp}$) 1, 2 $_z$, 6(m_{\perp}), $\pm 3_z$, $\pm 6_z$ 1, 3(m_{\perp}), $\pm 3_z$, 2' $_z$, 3(m'_{\perp}), $\pm 6'_z$ 1, 2 $_z$, $\pm 3_z$, $\pm 6_z$, 6(m'_{\perp}) 1, 3(2 $_{\perp}$), 3(m_{\perp}), m_z , $\pm 3_z$, $\pm \bar{6}_z$ 1, 3(2 $_{\perp}$), $\pm 3_z$, 3(m'_{\perp}), m'_z , $\pm \bar{6}_z'$ 1, 3(m_{\perp}), $\pm 3_z$, 3(2' $_{\perp}$), m'_z , $\pm \bar{6}_z'$ 1, m_z , $\pm 3_z$, $\pm \bar{6}_z$, 3(2' $_{\perp}$), 3(m'_{\perp}) 1, $\bar{1}$, 6(2 $_{\perp}$), 2 $_z$, 6(m_{\perp}), m_z , $\pm 3_z$, $\pm \bar{3}_z$, $\pm 6_z$, $\pm \bar{6}_z$ 1, $\bar{1}$, 3(2 $_{\perp}$), 3(m_{\perp}), $\pm 3_z$, $\pm \bar{3}_z$, 3(2' $_{\perp}$), 2' $_z$, 3(m'_{\perp}), m'_z , $\pm 6'_z$, $\pm \bar{6}_z'$ 1, $\bar{1}$, 2 $_z$, m_z , $\pm 3_z$, $\pm \bar{3}_z$, $\pm 6_z$, $\pm \bar{6}_z$, 6(2' $_{\perp}$), 6(m'_{\perp}) 1, 6(2 $_{\perp}$), 2 $_z$, $\pm 3_z$, $\pm 6_z$, $\bar{1}'$, 6(m'_{\perp}), m'_z , $\pm \bar{3}_z'$, $\pm \bar{6}_z'$ 1, 2 $_z$, 6(m_{\perp}), $\pm 3_z$, $\pm 6_z$, $\bar{1}'$, 6(2' $_{\perp}$), m'_z , $\pm \bar{3}_z'$, $\pm \bar{6}_z'$ 1, 3(2 $_{\perp}$), 3(m_{\perp}), m_z , $\pm 3_z$, $\pm \bar{6}_z$, $\bar{1}'$, 3(2' $_{\perp}$), 2' $_z$, 3(m'_{\perp}), $\pm \bar{3}_z'$, $\pm 6'_z$ |
| Cubic | T T_h $T_h(T)$ O $O(T)$ T_d $T_d(T)$ O_h $O_h(T_h)$ $O_h(O)$ $O_h(T_d)$ | 3/2 $\bar{6}/2$ $\bar{6}/2$ 3/4 3/ $\underline{4}$ 3/4 3/ $\underline{4}$ $\bar{6}/4$ $\bar{6}/4$ $\bar{6}/4$ $\bar{6}/4$ | 23 $m\bar{3}$ $m'\bar{3}'$ 432 4'32' $\bar{4}3m$ $\bar{4}'3m'$ $m\bar{3}m$ $m\bar{3}m'$ $m'\bar{3}'m'$ $m'\bar{3}'m$ | 23 $\frac{2}{m}\bar{3}$ $\frac{2}{m'}\bar{3}'$ 432 4'32' $\bar{4}3m$ $\bar{4}'3m'$ $\frac{4}{m}\frac{3}{m}\frac{2}{m}$ $\frac{4}{m'}\frac{3}{m'}\frac{2'}{m'}$ $\frac{4}{m'}\frac{3}{m'}\frac{2}{m'}$ $\frac{4'}{m'}\frac{3}{m'}\frac{2'}{m}$ | 1, 3(2), 4(± 3) 1, $\bar{1}$, 3(2), 3(m), 4(± 3), 4($\pm \bar{3}$) 1, 3(2), 4(± 3), $\bar{1}'$, 3(m'), 4($\pm \bar{3}'$) 1, 9(2), 4(± 3), 3(± 4) 1, 3(2), 4(± 3), 6(2'), 3($\pm 4'$) 1, 3(2), 6(m), 4(± 3), 3(± 4) 1, 3(2), 4(± 3), 6(m'), 3($\pm 4'$) 1, $\bar{1}$, 9(2), 9(m), 4(± 3), 4($\pm \bar{3}$), 3(± 4), 3($\pm \bar{4}$) 1, $\bar{1}$, 3(2), 3(m), 4(± 3), 4($\pm \bar{3}$), 6(2'), 6(m'), 3($\pm 4'$), 3($\pm \bar{4}'$) 1, 9(2), 4(± 3), 3(± 4), $\bar{1}'$, 9(m'), 4($\pm \bar{3}'$), 3($\pm 4'$) 1, 3(2), 6(m), 4(± 3), 3(± 4), $\bar{1}'$, 6(2'), 3(m'), 4($\pm \bar{3}'$), 3($\pm 4'$) |

subgroup the elements of which are not multiplied by R . This notation is often used in the physics literature. In the crystallographic literature, the magnetic groups are defined by Hermann–Mauguin or Shubnikov symbols. In this type of designation, the symbols of elements multiplied by R are primed or underlined. The primed symbols are used in most of the recent publications. The Hermann–Mauguin and Shubnikov definitions differ slightly, as in the case of crystallographic groups. In Table 1.5.2.1, different symbols of magnetic point groups (trivial and nontrivial ones) are compared. This is done for the family that belongs to the crystallographic point group $D_4 = 422$. The symbols of the symmetry elements of these four magnetic point groups are compared in Table 1.5.2.2.

Table 1.5.2.3 gives a list of the 90 magnetic point groups belonging to types 2 and 3. The Schoenflies, Shubnikov and Hermann–Mauguin symbols of the point groups are given in the table. The entries in the Hermann–Mauguin symbol refer to symmetry directions, as explained in Section 2.2.4 of *International Tables for Crystallography*, Vol. A (2002). The elements of symmetry of each point group are displayed using the Hermann–Mauguin symbols. The symbol $N(2_{\perp})$ denotes N 180° rotations with axes perpendicular to the principal symmetry axis; $N(m_{\perp})$ denotes N mirror planes with normals perpendicular to the principal symmetry axis. Similar definitions hold for the primed symbols $N(2'_{\perp})$ and $N(m'_{\perp})$. The point groups are arranged in families. The part of the Schoenflies symbol before the bracket is

1. TENSORIAL ASPECTS OF PHYSICAL PROPERTIES

Table 1.5.2.4. List of the magnetic classes in which ferromagnetism is admitted

(a) Triclinic

| Symbol of symmetry class | | Allowed direction of \mathbf{M}_s |
|--------------------------|-----------------|-------------------------------------|
| Schoenflies | Hermann–Mauguin | |
| C_1 | 1 | Any |
| C_i | $\bar{1}$ | Any |

(b) Monoclinic

| Symbol of symmetry class | | Allowed direction of \mathbf{M}_s |
|--------------------------|-----------------|-------------------------------------|
| Schoenflies | Hermann–Mauguin | |
| C_2 | 2 | $\parallel 2$ |
| $C_2(C_1)$ | $2'$ | $\perp 2'$ |
| $C_s = C_{1h}$ | m | $\perp m$ |
| $C_s(C_1)$ | m' | $\parallel m'$ |
| C_{2h} | $2/m$ | $\parallel 2$ |
| $C_{2h}(C_i)$ | $2'/m'$ | $\parallel m'$ |

(c) Orthorhombic

| Symbol of symmetry class | | Allowed direction of \mathbf{M}_s |
|--------------------------|-----------------|-------------------------------------|
| Schoenflies | Hermann–Mauguin | |
| $D_2(C_2)$ | $22'2'$ | $\parallel 2$ |
| $C_{2v}(C_2)$ | $m'm'2$ | $\parallel 2$ |
| $C_{2v}(C_s)$ | $m'm'2'$ | $\perp m$ |
| $D_{2h}(C_{2h})$ | $mm'm'$ | $\perp m$ |

(d) Tetragonal

| Symbol of symmetry class | | Allowed direction of \mathbf{M}_s |
|--------------------------|-----------------|-------------------------------------|
| Schoenflies | Hermann–Mauguin | |
| C_4 | 4 | $\parallel 4$ |
| S_4 | $\bar{4}$ | $\parallel \bar{4}$ |
| C_{4h} | $4/m$ | $\parallel 4$ |
| $D_4(C_4)$ | $42'2'$ | $\parallel 4$ |
| $C_{4v}(C_4)$ | $4m'm'$ | $\parallel 4$ |
| $D_{2d}(S_4)$ | $\bar{4}2'm'$ | $\parallel \bar{4}$ |
| $D_{4h}(C_{4h})$ | $4/mmm'm'$ | $\parallel 4$ |

(e) Trigonal

| Symbol of symmetry class | | Allowed direction of \mathbf{M}_s |
|--------------------------|-----------------|-------------------------------------|
| Schoenflies | Hermann–Mauguin | |
| C_3 | 3 | $\parallel 3$ |
| S_6 | $\bar{3}$ | $\parallel \bar{3}$ |
| $D_3(C_3)$ | $32'$ | $\parallel 3$ |
| $C_{3v}(C_3)$ | $3m'$ | $\parallel 3$ |
| $D_{3d}(S_6)$ | $3m'$ | $\parallel 3$ |

(f) Hexagonal

| Symbol of symmetry class | | Allowed direction of \mathbf{M}_s |
|--------------------------|-----------------|-------------------------------------|
| Schoenflies | Hermann–Mauguin | |
| C_6 | 6 | $\parallel 6$ |
| C_{3h} | $\bar{6}$ | $\parallel \bar{6}$ |
| C_{6h} | $6/m$ | $\parallel 6$ |
| $D_6(C_6)$ | $62'2'$ | $\parallel 6$ |
| $C_{6v}(C_6)$ | $6m'm'$ | $\parallel 6$ |
| $D_{3h}(C_{3h})$ | $\bar{6}m'2'$ | $\parallel \bar{6}$ |
| $D_{6h}(C_{6h})$ | $6/mmm'm'$ | $\parallel 6$ |

the same for each member of a family. Each family begins with a trivial magnetic point group. It contains the same elements as the corresponding crystallographic point group; its Schoenflies symbol contains no brackets. For each nontrivial point group, the list of the elements of symmetry begins with the non-primed elements, which belong to a subgroup \mathcal{H} of the head of the family \mathcal{G} . The number of the primed elements is equal to the number of non-primed ones and the total number of the elements is the same for all point groups of one family.

The overall number of the magnetic point groups of all three types is 122. There are two general statements concerning the magnetic point groups. The element $RC_3 = 3'$ does not appear in any of the magnetic point groups of type 3. Only trivial magnetic point groups (of both first and second type) belong to the families containing the point groups $C_1 = 1$, $C_3 = 3$ and $T = 23$.

Only 31 magnetic point groups allow ferromagnetism. The different types of ferromagnetism (one-sublattice ferromagnet, ferrimagnet, weak ferromagnet, any magnetic order with nonzero magnetization) cannot be distinguished by their magnetic symmetry. Ferromagnetism is not admitted in any point group of type 1. For the magnetic point groups of the second type, ferromagnetism is not allowed if the point group contains more than one symmetry axis, more than one mirror plane or a mirror plane that is parallel to the axis. The same restrictions are valid for the point groups of type 3 (if the corresponding elements are not multiplied by R). If the point group contains $\bar{1}'$, ferromagnetic order is also forbidden. There are the following rules for the orientation of the axial vector of ferromagnetic magnetization \mathbf{M} : $\mathbf{M} \parallel N$, $\mathbf{M} \perp 2'$, $\mathbf{M} \perp m$, $\mathbf{M} \parallel m'$. Table 1.5.2.4 lists those magnetic point groups that admit ferromagnetic order (Tavger, 1958). The allowed direction of the magnetization vector is given for every point group. Ferromagnetic order is allowed in 13 point groups of the second type and 18 point groups of the third type.

All 31 point groups of magnetic symmetry allowing ferromagnetism are subgroups of the infinite noncrystallographic group

$$D_{\infty h}(C_{\infty h}) = \frac{\infty}{m} \frac{2'}{m'}.$$

The transition from a paramagnetic to a ferromagnetic state is always accompanied by a change of the magnetic symmetry.

1.5.2.2. Magnetic lattices

If the point group of symmetry describes the macroscopic properties of a crystal, its microscopic structure is determined by the space group, which contains the group of translations \mathcal{T} as a subgroup. The elements \mathbf{t} of \mathcal{T} are defined by the following relation:

$$\mathbf{t} = n_1 \mathbf{a}_1 + n_2 \mathbf{a}_2 + n_3 \mathbf{a}_3, \quad (1.5.2.3)$$

where $\mathbf{a}_1, \mathbf{a}_2, \mathbf{a}_3$ are basic primitive translation vectors and n_1, n_2, n_3 are arbitrary integers. The set of points \mathbf{r}' obtained by applying all the translations of the group \mathcal{T} to any point \mathbf{r} defines a lattice. All sites of the crystallographic lattice are equivalent.

The structure of the ordered magnetics is described by the magnetic lattices and corresponding magnetic translation groups \mathcal{M}_T . In the magnetic translation groups \mathcal{M}_T , some of the elements \mathbf{t} may be multiplied by R (we shall call them primed translations). The magnetic lattices then have two types of sites, which are not equivalent. One set is obtained by non-primed translations and the other set by the primed ones. The magnetic translation group \mathcal{M}_T is isometric to the crystallographic one \mathcal{G}_0 that is obtained by replacing R by E in \mathcal{M}_T .

There are trivial magnetic translation groups, in which none of the translation elements is multiplied by R . The magnetic lattices of these groups coincide with crystallographic lattices.

Nontrivial magnetic translation groups can be constructed in analogy to relation (1.5.2.2). Zamorzaev (1957) showed that every translation group \mathcal{T} has seven subgroups of index 2. If the basic primitive translations of the group \mathcal{T} are $\mathbf{a}_1, \mathbf{a}_2, \mathbf{a}_3$, then the basic primitive translations of the seven subgroups \mathcal{H} can be chosen as follows (see also Opechowski & Guccione, 1965)

1.5. MAGNETIC PROPERTIES

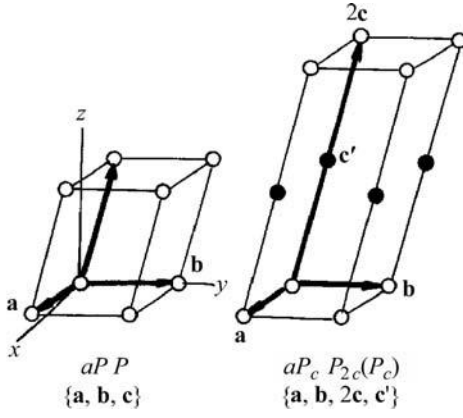


Fig. 1.5.2.1. Magnetic lattices of the triclinic system.

$$\mathcal{H}_1 : 2\mathbf{a}_1, \mathbf{a}_2, \mathbf{a}_3 \quad (1.5.2.4)$$

$$\mathcal{H}_2 : \mathbf{a}_1, 2\mathbf{a}_2, \mathbf{a}_3 \quad (1.5.2.5)$$

$$\mathcal{H}_3 : \mathbf{a}_1, \mathbf{a}_2, 2\mathbf{a}_3 \quad (1.5.2.6)$$

$$\mathcal{H}_4 : 2\mathbf{a}_1, \mathbf{a}_1 + \mathbf{a}_2, \mathbf{a}_3 \quad (1.5.2.7)$$

$$\mathcal{H}_5 : 2\mathbf{a}_2, \mathbf{a}_2 + \mathbf{a}_3, \mathbf{a}_1 \quad (1.5.2.8)$$

$$\mathcal{H}_6 : 2\mathbf{a}_3, \mathbf{a}_3 + \mathbf{a}_1, \mathbf{a}_2 \quad (1.5.2.9)$$

$$\mathcal{H}_7 : 2\mathbf{a}_1, \mathbf{a}_1 + \mathbf{a}_2, \mathbf{a}_1 + \mathbf{a}_3. \quad (1.5.2.10)$$

As an example, let us consider the case (1.5.2.5). In this case, the subgroup \mathcal{H} consists of the following translations:

$$\mathbf{t}(\mathcal{H}) = n_1\mathbf{a}_1 + 2n_2\mathbf{a}_2 + n_3\mathbf{a}_3. \quad (1.5.2.11)$$

Therefore the elements G_i of $(\mathcal{T} - \mathcal{H})$ [which corresponds to $(\mathcal{P} - \mathcal{H})$ in relation (1.5.2.2)] must have the following form:

$$\mathbf{t}(G_i) = n_1\mathbf{a}_1 + (2n_2 + 1)\mathbf{a}_2 + n_3\mathbf{a}_3. \quad (1.5.2.12)$$

The corresponding magnetic translation group consists of the elements (1.5.2.12) multiplied by R and the elements (1.5.2.11).

The crystallographic lattices are classified into Bravais types or Bravais lattices. The magnetic lattices are classified into Bravais types of magnetic lattices. It turns out that there are 22 nontrivial magnetic Bravais types. Together with the trivial ones, there are 36 magnetic Bravais lattices.

Two types of smallest translation-invariant cells are in common use for the description of magnetically ordered structures: the crystallographic cell obtained if the magnetic order is neglected and the magnetic cell, which takes the magnetic order into account. The list of the basic translations of all the magnetic Bravais lattices was given by Zamorzaev (1957). The diagrams of the magnetic unit cells were obtained by Belov *et al.* (1957).

In Figs. 1.5.2.1–1.5.2.7, the diagrams of the magnetic unit cells of all 36 Bravais types are sketched in such a way that it is clear to which family the given cell belongs. All the cells of one family are displayed in one row. Such a row begins with the cell of the trivial magnetic lattice. All nontrivial cells of a family change into the trivial one of this family if R is replaced by E (to draw these diagrams we used those published by Opechowski & Guccione, 1965). Open and full circles are used to show the primed and unprimed translations. A line connecting two circles of the same type is an unprimed translation; a line connecting two circles of different types is a primed translation. The arrows in the trivial magnetic cell represent the primitive (primed or unprimed) translations for all the magnetic lattices of the family. The arrows in the nontrivial cells are primitive translations of the magnetic unit cell. The magnetic unit cell of a nontrivial magnetic lattice is generated by unprimed translations only. Its volume is twice the volume of the smallest cell generated by all (primed and unprimed) translations. The reason for this is that one of the primitive translations of the magnetic cell is twice a primitive primed translation. The crystallographic cell of many simple collinear or weakly non-collinear structures coincides with the smallest cell generated by the primed and unprimed translations. However, there are also magnetic structures with more complicated transformations from the crystallographic to the magnetic unit cell. The second line after each part of Figs. 1.5.2.1–1.5.2.7 gives, between braces, an extended vector basis of the magnetic translation group (Shubnikov & Koptsik, 1972). The first line

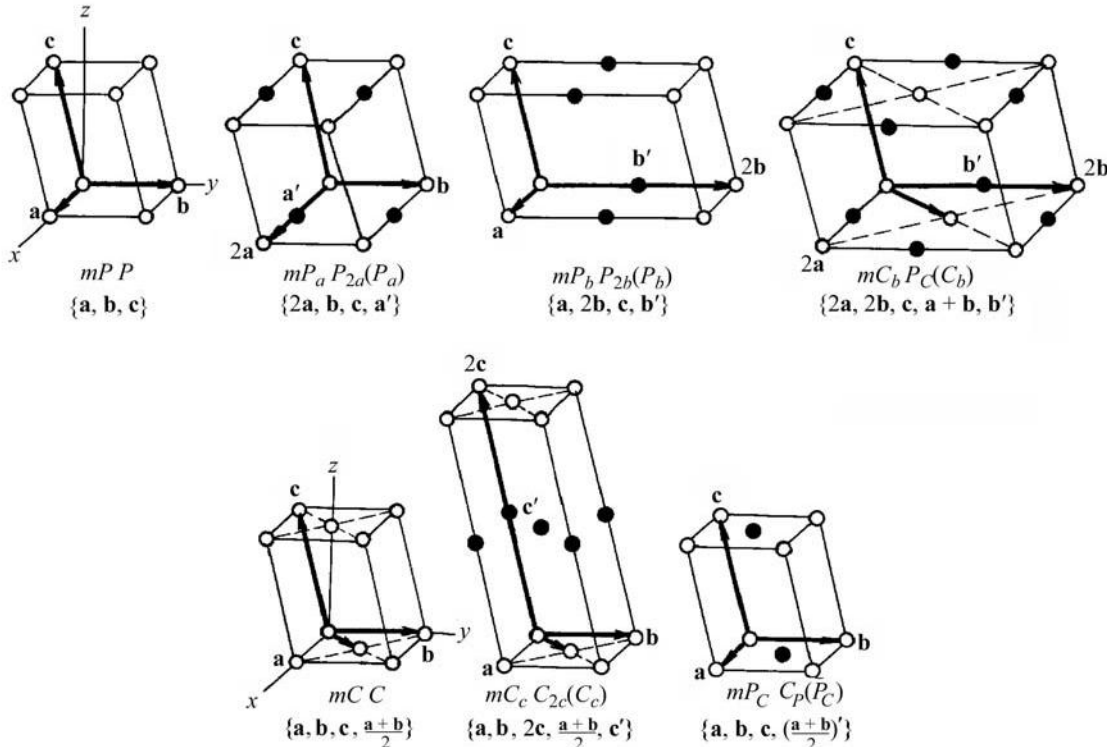


Fig. 1.5.2.2. Magnetic lattices of the monoclinic system (the y axis is the twofold axis).

1. TENSORIAL ASPECTS OF PHYSICAL PROPERTIES

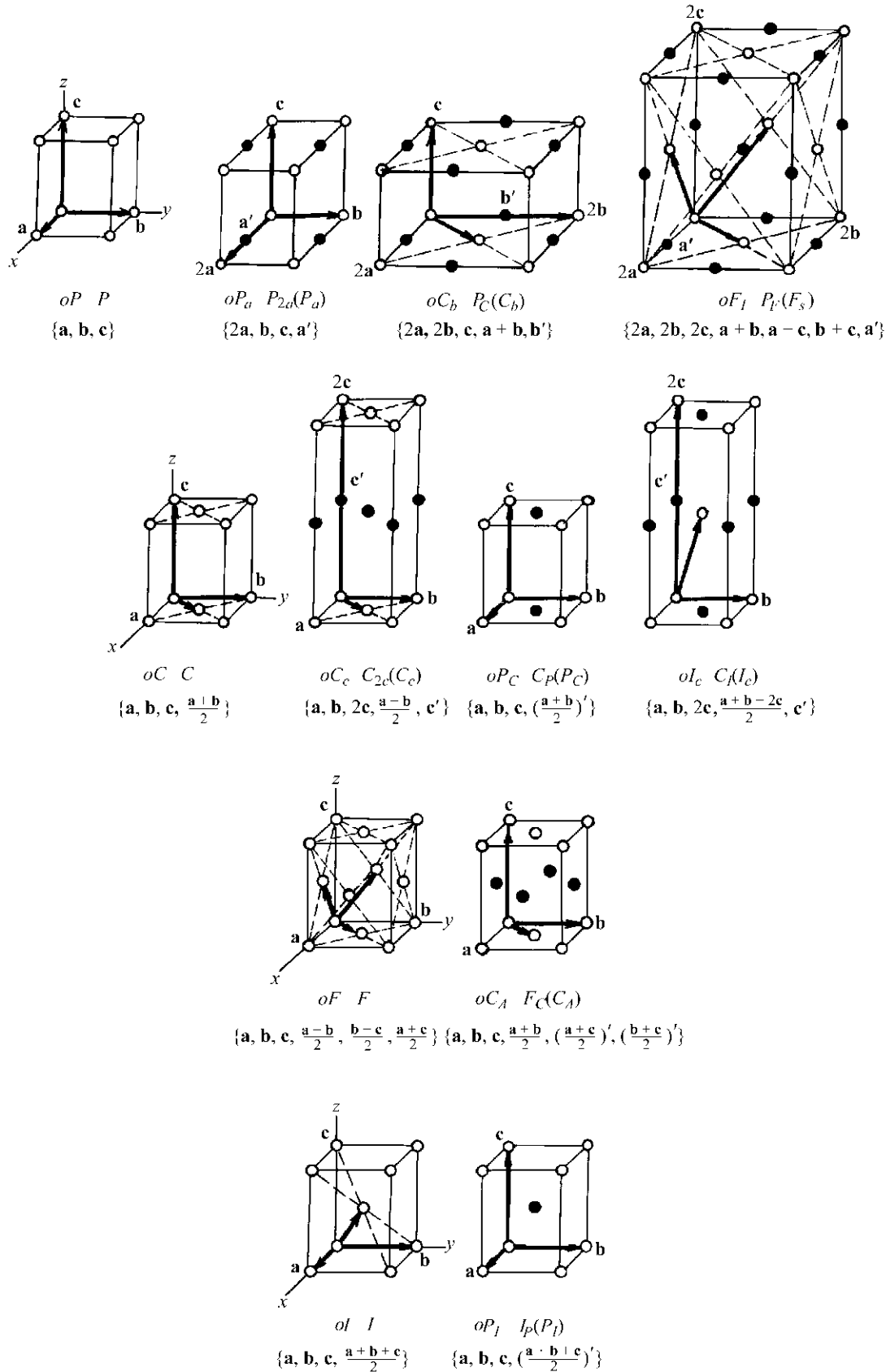


Fig. 1.5.2.3. Magnetic lattices of the orthorhombic system.

gives two symbols for each Bravais type: the symbol to the right was introduced by Opechowski & Guccione (1965). The symbol to the left starts with a lower-case letter giving the crystal system followed by a capital letter giving the centring type of the cell defined by the unprimed translations (P : primitive; C, A, B : C -, A -, B -centred; I : body-centred; F : all-face-centred). The

subscript, which appears for the nontrivial Bravais types, indicates the translations that are multiplied by time inversion R .

Ferromagnetism is allowed only in trivial magnetic Bravais lattices. All nontrivial magnetic lattices represent antiferromagnetic order. There are only two magnetic sublattices in the simplest antiferromagnetic structures; one sublattice consists

1.5. MAGNETIC PROPERTIES

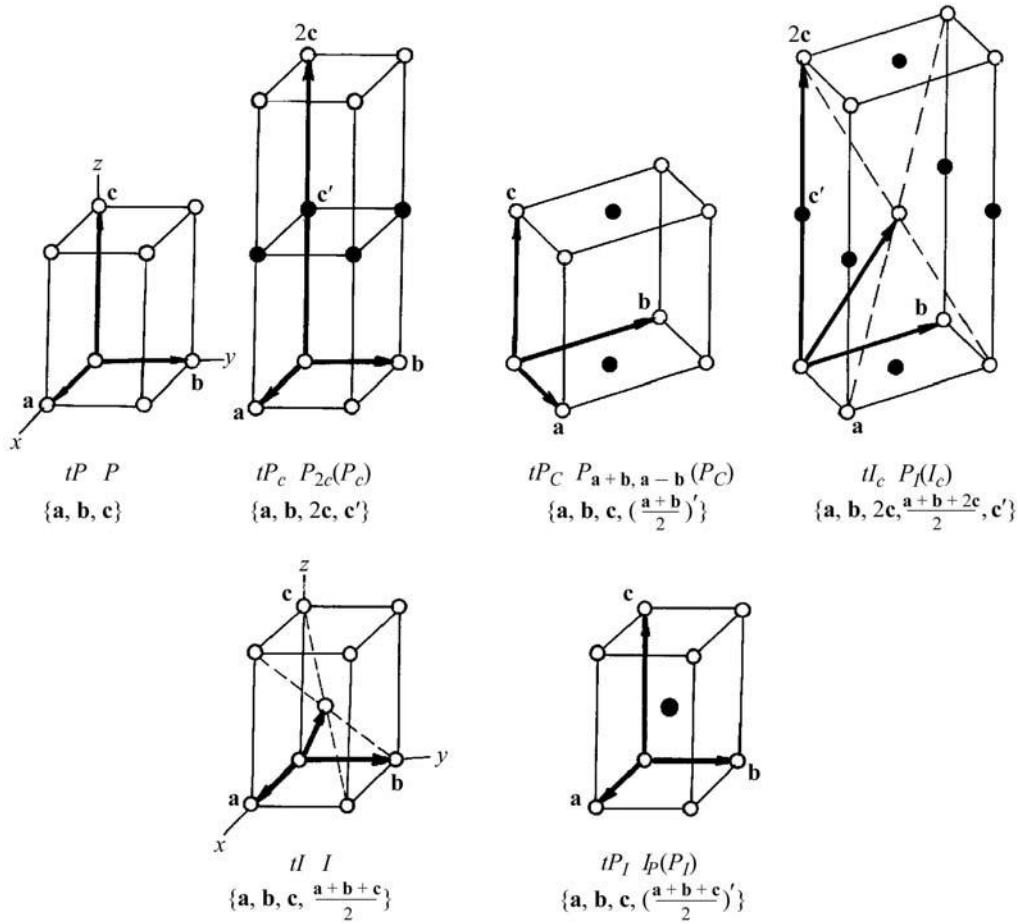


Fig. 1.5.2.4. Magnetic lattices of the tetragonal system.

of the magnetic ions located in the black sites and the other of the ions located in the white sites. All the magnetic moments of one sublattice are oriented in one direction and those of the other sublattice in the opposite direction. However, anti-ferromagnetism is allowed also in trivial lattices if the (trivial) magnetic cell contains more than one magnetic ion. The magnetic point group must be nontrivial in this case. The situation is more complicated in case of strongly non-collinear structures. In such structures (triangle, 90° etc.), the magnetic lattice can differ from the crystallographic one despite the fact that none of the translations is multiplied by R . The magnetic elementary cell will possess three or four magnetic ions although the crystallographic

cell possesses only one. An example of such a situation is shown in Fig. 1.5.1.3(c). More complicated structures in which the magnetic lattice is incommensurate with the crystallographic one also exist. We shall not discuss the problems of such systems in this chapter.

1.5.2.3. Magnetic space groups

There are 1651 magnetic space groups \mathcal{M}_G , which can be divided into three types. Type I, \mathcal{M}_{G1} , consists of the 230 crystallographic space groups to which R is added. Crystals belonging to these trivial magnetic space groups show no magnetic order; they are para- or diamagnetic.

Type II, \mathcal{M}_{G2} , consists of the same 230 crystallographic groups which do not include R in any form. In the ordered magnetics, which belong to the magnetic space groups of this type, the

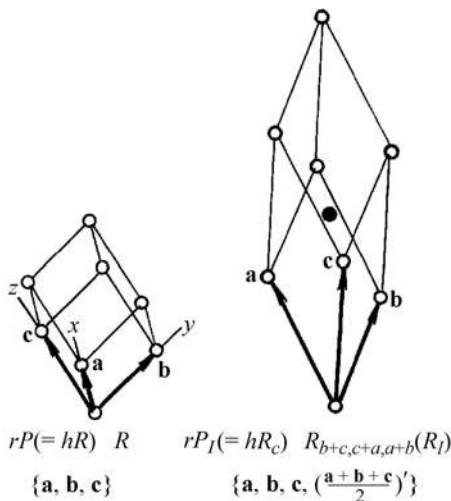


Fig. 1.5.2.5. Magnetic lattices of the rhombohedral system.

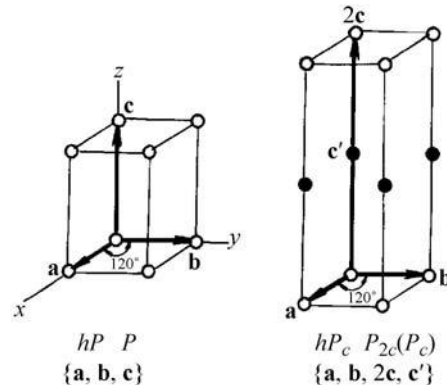


Fig. 1.5.2.6. Magnetic lattices of the hexagonal system.

1. TENSORIAL ASPECTS OF PHYSICAL PROPERTIES

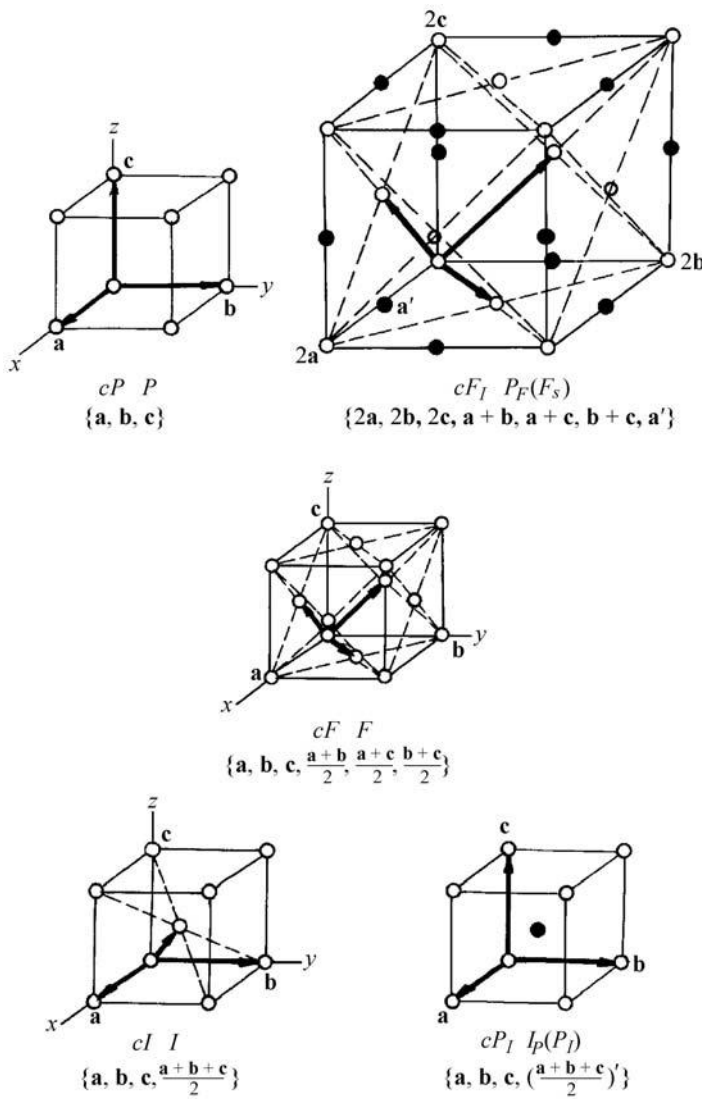


Fig. 1.5.2.7. Magnetic lattices of the cubic system.

magnetic unit cell coincides with the classical one. Forty-four groups of type II describe different ferromagnetic crystals; the remaining antiferromagnets.

The nontrivial magnetic space groups belong to type III, \mathcal{M}_{G_3} . This consists of 1191 groups, in which R enters only in combination with rotations, reflections or translations. These groups have the structure described by relation (1.5.2.2). The magnetic space groups of this type are divided into two subtypes.

Subtype III^a contains those magnetic space groups \mathcal{M}_{G_3} in which R is not combined with translations. In these groups, the magnetic translation group is trivial. To these space groups correspond magnetic point groups of type \mathcal{M}_{p_3} . There are 674 magnetic space groups of subtype III^a; 231 of them admit ferromagnetism, the remaining 443 describe antiferromagnets.

In the magnetic space groups of the subtype III^b, R is combined with translations and the corresponding point groups are of type \mathcal{M}_{p_1} . They have a nontrivial magnetic Bravais lattice. There are 517 magnetic space groups of this subtype; they describe antiferromagnets.

In summary, the 230 magnetic space groups that describe dia- and paramagnets are of type I, the 275 that admit spontaneous magnetization are of types II and III^a; the remaining 1146 magnetic space groups (types II, III^a and III^b) describe antiferromagnets.

1.5.2.4. Exchange symmetry

The classification of magnetic structures on the basis of the magnetic (point and space) groups is an exact classification.

However, it neglects the fundamental role of the exchange energy, which is responsible for the magnetic order (see Sections 1.5.1.2 and 1.5.3.2). To describe the symmetry of the magnetically ordered crystals only by the magnetic space groups means the loss of significant information concerning those properties of these materials that are connected with the higher symmetry of the exchange forces. Andreev & Marchenko (1976, 1980) have introduced the concept of exchange symmetry.

The exchange forces do not depend on the directions of the spins (magnetic moments) of the ions relative to the crystallographic axes and planes. They depend only on the relative directions of the spins. Thus the exchange group \mathcal{G}_{ex} contains an infinite number of rotations U of spin space, *i.e.* rotations of all the spins (magnetic moments) through the same angle about the same axis. The components of the magnetic moment density $\mathbf{m}(\mathbf{r})$ transform like scalars under all rotations of spin space. The exchange symmetry group \mathcal{G}_{ex} contains those combinations of the space transformation elements, the rotations U of spin space and the element R with respect to which the values $m(\mathbf{r})$ are invariant. Setting all the elements U and R equal to the identity transformation, we obtain one of the ordinary crystallographic space groups \mathcal{G} . This space group defines the symmetry of the charge density $\rho(\mathbf{r})$ and of all the magnetic scalars in the crystal. However, the vectors $\mathbf{m}(\mathbf{r})$ may not be invariant with respect to \mathcal{G} .

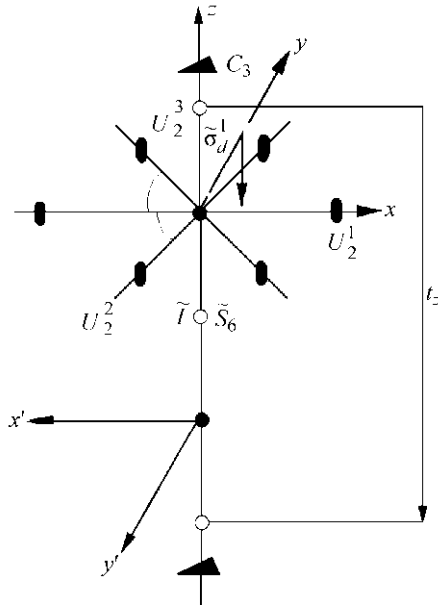
The concept of exchange symmetry makes it possible to classify all the magnetic structures (including the incommensurate ones) with the help of not more than three orthogonal magnetic vectors. We shall discuss this in more detail in Section 1.5.3.3.

More information about magnetic symmetry can be found in Birss (1964), Cracknell (1975), Joshua (1991), Koptsik (1966), Landau & Lifshitz (1957), Opechowski & Guccione (1965), and in Sirotn & Shaskol'skaya (1979).

1.5.3. Phase transitions into a magnetically ordered state

Most transitions from a paramagnetic into an ordered magnetic state are second-order phase transitions. A crystal with a given crystallographic symmetry can undergo transitions to different ordered states with different magnetic symmetry. In Section 1.5.3.3, we shall give a short review of the theory of magnetic second-order phase transitions. As was shown by Landau (1937), such a transition causes a change in the magnetic symmetry. The magnetic symmetry group of the ordered state is a subgroup of the magnetic group of the material in the paramagnetic state. But first we shall give a simple qualitative analysis of such transitions.

To find out what ordered magnetic structures may be obtained in a given material and to which magnetic group they belong, one has to start by considering the crystallographic space group \mathcal{G} of the crystal under consideration. It is obvious that a crystal in which the unit cell contains only one magnetic ion can change only into a ferromagnetic state if the magnetic unit cell of the ordered state coincides with the crystallographic one. If a transition into an antiferromagnetic state occurs, then the magnetic cell in the ordered state will be larger than the crystallographic one if the latter contains only one magnetic ion. Such antiferromagnets usually belong to the subtype III^b described in Section 1.5.2.3. In Section 1.5.3.1, we shall consider crystals that transform into an antiferromagnetic state without change of the unit cell. This is possible only if the unit cell possesses two or more magnetic ions. To find the possible magnetic structures in this case, one has to consider those elements of symmetry which interchange the positions of the ions inside the unit cell (especially glide planes and rotation axes). Some of these elements displace the magnetic ion without changing its magnetic moment, and others change the moment of the ion. It is also essential to know the positions of all these elements in the unit cell. All this information is contained in the space group \mathcal{G} . If the magnetic ordering occurs without change of the unit cell, the translation

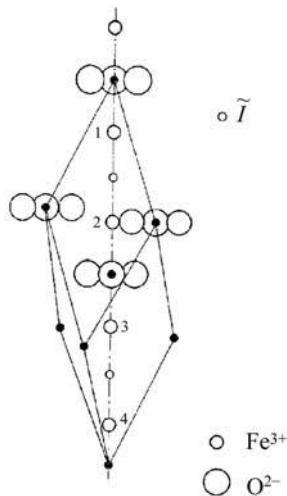
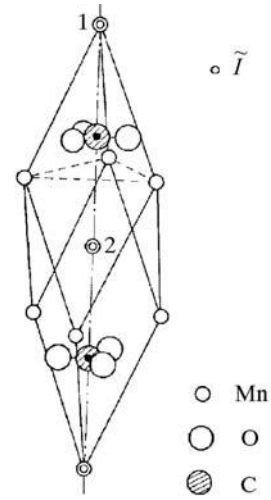

 Fig. 1.5.3.1. Arrangement of the symmetry elements of the group \tilde{D}_{3d}^6 .

group \mathcal{T} in the ordered state does not contain primed elements. Therefore, there is no need to consider the whole crystal space group \mathcal{G} . It will suffice to consider the cosets of \mathcal{T} in \mathcal{G} . Such a coset consists of all elements of \mathcal{G} that differ only by a translation. From each coset, a representative with minimum translative component is chosen. We denote a set of such representatives by $\tilde{\mathcal{G}}$; it can be made into a group by defining AB ($A, B \in \tilde{\mathcal{G}}$) as the representative of the coset that contains AB . Obviously, $\tilde{\mathcal{G}}$ is then isomorphic to the factor group \mathcal{G}/\mathcal{T} and therefore to the point group \mathcal{P} of \mathcal{G} .

Once more, we should like to stress that to construct the magnetic structures and the magnetic groups of a given crystal it is not enough to consider only the point group of the crystal, but it is necessary to perform the analysis with the help of its space group in the paramagnetic state or the corresponding group of coset representatives. An example of such an analysis will be given in the following section.

1.5.3.1. Magnetic structures in rhombohedral crystals

Following Dzyaloshinskii (1957a), we consider crystals belonging to the crystallographic space group $D_{3d}^6 = R\bar{3}c$. To this group belong α -Fe₂O₃ and the carbonates of Mn²⁺, Co²⁺ and Ni²⁺. Weak ferromagnetism was first observed in these materials.


 Fig. 1.5.3.2. Crystallographic structure of transition-metal oxides of the type α -Fe₂O₃.

 Fig. 1.5.3.3. Crystallographic structure of transition-metal carbonates of the type MnCO₃.

Cr₂O₃, in which the magnetoelectric effect was discovered, also belongs to this group. The magnetic ordering in these materials occurs without change of the unit cell.

The representatives of the cosets D_{3d}^6/\mathcal{T} form the group \tilde{D}_{3d}^6 . Its symmetry operations are shown in Fig. 1.5.3.1. Directed along the z axis is the threefold axis C_3 and the sixfold roto-inversion axis \tilde{S}_6 . Three twofold axes U_2 run through the points \bullet at right angles to the z axis. One of these axes is directed along the x axis. Arranged normal to each of the U_2 axes are three glide planes $\tilde{\sigma}_d$. The y axis is directed along one of these planes. The centre of inversion \tilde{I} is located at the point \circ , lying on the z axis halfway between two points \bullet . The sign \sim means that the corresponding operation is accompanied by a translation along the z axis through half the period of the crystal (\tilde{I} means that the inversion centre is shifted from the point \bullet to the point \circ). In Fig. 1.5.3.1, the elementary period of translation along the z axis is marked by t_z . Thus the crystallographic group \tilde{D}_{3d}^6 has the following elements:

$$E, 2C_3, 3U_2, \tilde{I}, 3\tilde{\sigma}_d, 2\tilde{S}_6 \quad \{1, \pm 3_z, 3(2_\perp), \tilde{1}, 3(c = \tilde{m}), \pm \tilde{3}_z\}. \quad (1.5.3.1)$$

In two types of crystals, considered below, the magnetic ions are arranged on the z axis. If we place the magnetic ion at point 1 located between points \circ and \bullet (see Fig. 1.5.3.2), then using symmetry operations (1.5.3.1) we obtain three additional positions for other magnetic ions (points 2, 3, 4). Thus, the elementary cell will contain four magnetic ions. This is the structure of oxides of trivalent ions of iron and chromium (Fe₂O₃, Cr₂O₃). The structure of these oxides is shown in Fig. 1.5.3.2. If the positions of the magnetic ions coincide with the positions of the inversion centre \circ , we obtain the structure of the carbonates of the transition metals (MnCO₃, CoCO₃, NiCO₃, FeCO₃), which is shown in Fig. 1.5.3.3.

Evidently, the formation of a magnetic structure in the crystal does not result in the appearance of new elements of symmetry. The magnetic groups of magnetically ordered crystals may lack some elements contained in the crystallographic group and some of the remaining elements may happen to be multiplied by R (primed). Let us find the groups of symmetry that correspond to all possible collinear magnetic structures in rhombohedral crystals with four magnetic ions in the elementary cell. We shall assume that the magnetic moments are located at the points of the ion positions 1–4; they will be marked μ_a . The symmetry transformations cannot change the length of the vectors of the magnetic moments but they can change the direction of these vectors and interchange the positions of the sites $1 \leftrightarrow 2, 3 \leftrightarrow 4$

1. TENSORIAL ASPECTS OF PHYSICAL PROPERTIES

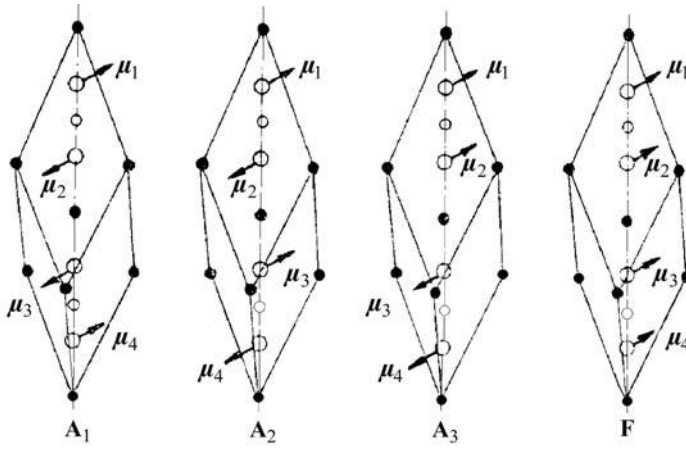


Fig. 1.5.3.4. Four types of magnetic structures of rhombohedral oxides of transition metals. The direction of μ_α is shown conventionally.

and $1 \leftrightarrow 3, 2 \leftrightarrow 4$. This interchange of the vectors $\mu_1, \mu_2, \mu_3, \mu_4$ means that these vectors form a basis of a reducible representation of the group \tilde{D}_{3d}^6 . The following linear combinations of μ_α form irreducible representations¹ of \tilde{D}_{3d}^6 :

$$\begin{aligned} \mathbf{l}_1 &= \mu_1 - \mu_2 - \mu_3 + \mu_4 \\ \mathbf{l}_2 &= \mu_1 - \mu_2 + \mu_3 - \mu_4 \\ \mathbf{l}_3 &= \mu_1 + \mu_2 - \mu_3 - \mu_4 \\ \mathbf{m} &= \mu_1 + \mu_2 + \mu_3 + \mu_4. \end{aligned} \quad (1.5.3.2)$$

Vectors \mathbf{l}_α characterize the antiferromagnetic states and are called antiferromagnetic vectors. The ferromagnetic vector \mathbf{m} gives the total magnetic moment of the elementary cell. These vectors describe the four possible collinear magnetic structures. Three are antiferromagnetic structures: A_1 ($\mathbf{l}_1 \neq 0, \mathbf{l}_2 = \mathbf{l}_3 = \mathbf{m} = 0$), A_2 ($\mathbf{l}_2 \neq 0, \mathbf{l}_3 = \mathbf{l}_1 = \mathbf{m} = 0$), A_3 ($\mathbf{l}_3 \neq 0, \mathbf{l}_1 = \mathbf{l}_2 = \mathbf{m} = 0$) and one is a ferromagnetic structure, F ($\mathbf{l}_1 = \mathbf{l}_2 = \mathbf{l}_3 = 0$). All these types are presented schematically in Fig. 1.5.3.4.

In the description of the structures of orthoferrites, other symbols were introduced to define the linear combinations of μ_α and to denote the antiferromagnetic structures under consideration (see Bertaut, 1963). The two types of symbols are compared in Table 1.5.3.1.

It should be borne in mind that in each of these types of magnetic ordering the respective vectors \mathbf{l}_α and \mathbf{m} may be directed along any direction. There are 12 types of such structures in which \mathbf{l}_α or \mathbf{m} are directed along one of the axes or planes of symmetry. To find out to which group of magnetic symmetry each of these structures belongs, one needs to investigate how each element of the crystallographic symmetry transforms the Cartesian components of the four vectors. This is shown in Table 1.5.3.2 for the group \tilde{D}_{3d}^6 . If the component keeps its direction, it is marked by the + sign; the - sign corresponds to reversal of the component direction. In some cases, the transformation results in a change of the direction of the components $l_{\alpha i}$ or m_i through an angle other than 0 or π . This is marked by 0. With the help of Table 1.5.3.2, we can easily describe all the elements of symmetry of the magnetic group that corresponds to each structure ($A_{\alpha i}$ or F_i) with the aid of the following rule. All the elements that yield the + sign are included in the magnetic group as they stand, while

Table 1.5.3.1. Two types of symbols for collinear antiferromagnetic and ferromagnetic structures

| Symbol | Alternative symbol |
|--------|--------------------|
| A_1 | A |
| A_2 | G |
| A_3 | C |
| F | F |

the elements yielding the - sign must be multiplied by R ; the elements which are marked by the sign 0 are not included in the magnetic group.² With the aid of this rule, Table 1.5.3.3 of the elements of the magnetic groups for the structures under consideration was compiled. In Table 1.5.3.4, the symbols of the magnetic point groups of all the 12 magnetic structures considered are listed. The crystals with two ions in the elementary cell have only two sublattices and their antiferromagnetic structures belong to the same groups as the structures $A_{3i} = C_i$.

One can see from Tables 1.5.3.3 and 1.5.3.4 that, in accordance with general theory, the magnetic point groups of the crystals under consideration are subgroups of the trivial magnetic point group $D_{3dR} = \tilde{3}m1'$ to which they belong in the paramagnetic state. In the example considered, the translation group does not change in going from the paramagnetic to the ordered state. Thus the same statement made for the point groups is also true for the space groups. Putting $R = E$ gives a subgroup of the crystallographic group of the crystal. For the magnetic structures with the ferromagnetic or antiferromagnetic vector directed along the z axis, it turns out that the magnetic group is isomorphic to the crystallographic group. This rule is obeyed by all (optically) uniaxial crystals if the transition occurs without change of the elementary cell. (Optically uniaxial are the non-cubic crystals with a point group possessing a threefold, fourfold or sixfold axis.)

Tables 1.5.3.3 and 1.5.3.4 show that different types of collinear structures may belong to the same point group (and also to the same space group). For the antiferromagnetic structure A_{3y} and the ferromagnetic F_x the group is $2/m$, and for the structures A_{3x} and F_y it is $2'/m'$. Thus the symmetry allows a phase to be simultaneously ferromagnetic and antiferromagnetic. That is not ferrimagnetic order because all the ions in the four sublattices are identical and their numbers are equal. The ferromagnetic vector \mathbf{m} and the antiferromagnetic one \mathbf{l}_3 are perpendicular and $|\mathbf{m}| \ll |\mathbf{l}_3|$. This phenomenon is called weak ferromagnetism and will be discussed in detail in Section 1.5.5.1. Like weak ferromagnetism, the symmetry also allows the coexistence of two orthogonal antiferromagnetic structures A_1 and A_2 . This gives rise to weakly non-collinear antiferromagnetic structures.

The strongly non-collinear structures are described by another set of basis vectors for the irreducible representations of the group \tilde{G} . If the magnetic ions μ_α in the crystal form triangular planes one gets instead of (1.5.3.2) the relations for the basis vectors:

$$\begin{aligned} \mathbf{l}_1 &= \sqrt{3}(\mu_1 - \mu_2) \\ \mathbf{l}_2 &= \mu_1 + \mu_2 - \mu_3 \\ \mathbf{m} &= \mu_1 + \mu_2 + \mu_3. \end{aligned} \quad (1.5.3.3)$$

1.5.3.2. Exchange and magnetic anisotropy energies

It is pertinent to compare the different kinds of interactions that are responsible for magnetic ordering. In general, all these interactions are much smaller than the electrostatic interactions between the atoms that determine the chemical bonds in the material. Therefore, if a crystal undergoes a transition into a magnetically ordered state, the deformations of the crystal that

¹ By omitting its translative part, each element of \tilde{D}_{3d}^6 is mapped on the corresponding element of the point group $D_{3d} = \tilde{3}m$. This mapping also establishes a one-to-one correspondence between the representations of \tilde{D}_{3d}^6 and those of $D_{3d} = \tilde{3}m$.

² In Section 1.5.3.3, we shall show that this rule corresponds in the Landau theory of phase transitions to the general law that the magnetically ordered state is described by $L_{\alpha i}$ or M_i , which form the basis of one of the irreducible representations of the paramagnetic space group of the crystal.

1.5. MAGNETIC PROPERTIES

Table 1.5.3.2. Sign variation of the components of antiferromagnetic and ferromagnetic vectors during transformations of the group \tilde{D}_{3d}^6 in rhombohedral crystals with four magnetic ions

| Vector components | Elements of symmetry | | | | | | | | | |
|-------------------|----------------------|----------|---------|---------|---------|-------------|----------------------|----------------------|----------------------|-----------------------|
| | E | $2C_3$ | U_2^1 | U_2^2 | U_2^3 | \tilde{I} | $\tilde{\sigma}_d^1$ | $\tilde{\sigma}_d^2$ | $\tilde{\sigma}_d^3$ | $2\tilde{\sigma}_d^3$ |
| | 1 | $\pm 3z$ | $2x$ | $2z$ | $2z$ | $\tilde{1}$ | c_x | $c_z^{(2)}$ | $c_z^{(3)}$ | $\pm \tilde{3}$ |
| l_{1x} | + | 0 | + | 0 | 0 | — | — | 0 | 0 | 0 |
| l_{1y} | + | 0 | — | 0 | 0 | — | + | 0 | 0 | 0 |
| l_{1z} | + | + | — | — | — | — | + | + | + | — |
| l_{2x} | + | 0 | — | 0 | 0 | — | + | 0 | 0 | 0 |
| l_{2y} | + | 0 | + | 0 | 0 | — | — | 0 | 0 | 0 |
| l_{2z} | + | + | + | + | + | — | — | — | — | — |
| l_{3x} | + | 0 | — | 0 | 0 | + | — | 0 | 0 | 0 |
| l_{3y} | + | 0 | + | 0 | 0 | + | + | 0 | 0 | 0 |
| l_{3z} | + | + | + | + | + | + | + | + | + | + |
| m_x | + | 0 | + | 0 | 0 | + | + | 0 | 0 | 0 |
| m_y | + | 0 | — | 0 | 0 | + | — | 0 | 0 | 0 |
| m_z | + | + | — | — | — | + | — | — | — | + |

give rise to the change of its crystallographic symmetry are comparatively small. It means that most of the non-magnetic properties do not change drastically. As an example, the anisotropic deformation of the crystal that accompanies the transition into the ordered state (see Section 1.5.9.1) is mostly not larger than 10^{-4} .

The formation of the ordered magnetic structures is due mainly to the exchange interaction between the spins \mathbf{S}_α (and corresponding magnetic moments $\boldsymbol{\mu}$ of the atoms or ions). The expression for the exchange energy can contain the following terms [see formula (1.5.1.7)]:

$$\mathbf{S}_\alpha \mathbf{S}_\beta, \mathbf{S}_\alpha [\mathbf{S}_\beta \mathbf{S}_\gamma]. \quad (1.5.3.4)$$

The exchange interaction decreases rapidly as the distance between the atoms rises. Thus, it is usually sufficient to consider the interaction only between nearest neighbours. The exchange interaction depends only on the relative alignment of the spin moments and does not depend on their alignment relative to the crystal lattice. Therefore, being responsible for the magnetic ordering in the crystal, it cannot define the direction of the spontaneous magnetization in ferromagnets or of the antiferromagnetic vector. This direction is determined by the spin-orbit and magnetic spin-spin interactions, which are often called relativistic interactions as they are small, of the order of v^2/c^2 , where v is the velocity of atomic electrons and c is the speed of light. The relativistic interactions are responsible for the magnetic anisotropy energy, which depends on the direction of the magnetic moments of the ions with regard to the crystal lattice. The value of the exchange energy can be represented by the effective exchange field H_e . For an ordered magnetic with a transition temperature of 100 K, $H_e \simeq 1000$ kOe. Thus the external magnetic field hardly changes the value of the magnetization \mathbf{M} or of the antiferromagnetic vector \mathbf{L} ; they are conserved quantities to a good approximation. The effective anisotropy field H_a in cubic crystals is very small: 1–10 Oe. In most non-cubic materials, H_a is not larger than 1–10 kOe. This means that by applying an external magnetic field we can change only the direction of \mathbf{M} , or sometimes of \mathbf{L} , but not their magnitudes.

The magnetic anisotropy energy U_a can be represented as an expansion in the powers of the components of the vectors \mathbf{M} or \mathbf{L} . The dependence of U_a on the direction of the magnetization is essential. Therefore, one usually considers the expansion of the spontaneous magnetization or antiferromagnetic vector in powers of the unit vector \mathbf{n} . The anisotropy energy is invariant under time reversal. Therefore, the general expression for this energy has the form

$$U_a = K_{ij} n_i n_j + K_{ijk\ell} n_i n_j n_k n_\ell + K_{ijk\ell mn} n_i n_j n_k n_\ell n_m n_n, \quad (1.5.3.5)$$

where K_{ij} , $K_{ijk\ell}$, $K_{ijk\ell mn}$ are tensors, the components of which have the dimension of an energy density. The forms of the tensors depend on the symmetry of the crystal. There are at most two independent components in K_{ij} . For a uniaxial crystal, the second-order term in the anisotropy energy expansion is determined by one anisotropy constant, K . Instead of using the components of the unit vector \mathbf{n} , its direction can be described by two angles: polar θ and azimuthal φ . Correspondingly, the anisotropy energy for a uniaxial crystal can be written as

$$U_a = K(n_x^2 + n_y^2) = K \sin^2 \theta. \quad (1.5.3.6)$$

This relation is equivalent to

$$U_a = K(1 - n_z^2) = K - K \cos^2 \theta. \quad (1.5.3.7)$$

The direction of the magnetization vector \mathbf{M} in a ferromagnet or of the antiferromagnetic vector \mathbf{L} in an antiferromagnet is called the direction or the axis of easy magnetization. The crystals in which this axis is aligned with a threefold, fourfold or sixfold axis of the magnetic point group are called easy-axis magnetics. The magnetic crystals with the main axis higher than twofold in the paramagnetic state in which, in the ordered state, \mathbf{L} (or \mathbf{M}) is perpendicular to this axis are often called easy-plane magnetics. The anisotropy in this plane is usually extremely small. In this case, the crystal possesses more than one axis of easy magnetization and the crystal is usually in a multidomain state (see Section 1.5.4).

If the anisotropy constant K is positive, then the vector \mathbf{n} is aligned along the z axis, and such a magnetic is an easy-axis one.

Table 1.5.3.3. Magnetic groups of symmetry in rhombohedral oxides of trivalent transition-metal ions

| Type of magnetic structure | Magnetic moments are directed along the axis | | |
|----------------------------|--|---|---|
| | x | y | z |
| $A_1 = A$ | $E; U_2; \tilde{I}R; \tilde{\sigma}_d R$ | $E; U_2 R; \tilde{I}R; \tilde{\sigma}_d$ | $E; 2C_3; 3U_2 R; \tilde{I}R; 3\tilde{\sigma}_d; 2\tilde{\sigma}_6 R$ |
| $A_2 = G$ | $E; U_2 R; \tilde{I}R; \tilde{\sigma}_d$ | $E; U_2; \tilde{I}R; \tilde{\sigma}_d R$ | $E; 2C_3; 3U_2; \tilde{I}R; 3\tilde{\sigma}_d R; 2\tilde{\sigma}_6 R$ |
| $A_3 = C$ | $E; U_2 R; \tilde{I}; \tilde{\sigma}_d R$ | $E; U_2; \tilde{I}; \tilde{\sigma}_d$ | $E; 2C_3; 3U_2; \tilde{I}; 3\tilde{\sigma}_d; 2\tilde{\sigma}_6$ |
| $F = F$ | $E; U_2; \tilde{I}; \tilde{\sigma}_d$ | $E; U_2 R; \tilde{I}; \tilde{\sigma}_d R$ | $E; 2C_3; 3U_2 R; \tilde{I}; 3\tilde{\sigma}_d R; 2\tilde{\sigma}_6$ |

Table 1.5.3.4. Magnetic point groups in rhombohedral oxides of transition metals

| Type of magnetic structure | Magnetic moments are directed along the axis | | |
|----------------------------|--|-----------------------|-------------------------------|
| | x | y | z |
| $A_1 = A$ | $C_{2h}(C_2) = 2/m'$ | $C_{2h}(C_s) = 2'/m$ | $D_{3d}(C_{3v}) = \tilde{3}m$ |
| $A_2 = G$ | $C_{2h}(C_i) = 2'/m$ | $C_{2h}(C_2) = 2/m'$ | $D_{3d}(D_3) = \tilde{3}'m'$ |
| $A_3 = C$ | $C_{2h}(C_i) = 2'/m'$ | $C_{2h} = 2/m$ | $D_{3d} = \tilde{3}m$ |
| $F = F$ | $C_{2h} = 2/m$ | $C_{2h}(C_i) = 2'/m'$ | $D_{3d}(S_6) = \tilde{3}m'$ |

1. TENSORIAL ASPECTS OF PHYSICAL PROPERTIES

For an easy-plane magnetic, K is negative. It is convenient to use equation (1.5.3.6) for easy-axis magnetics and equation (1.5.3.7) for easy-plane magnetics. In the latter case, the quantity K is included in the isotropic part of the thermodynamic potential Φ , and (1.5.3.7) becomes $U_a = -K \cos^2 \theta$. Instead we shall write $U_a = K \cos^2 \theta$ in the following, so that K becomes positive for easy-plane ferromagnetics as well.

Apart from the second-order term, terms of higher order must be taken into account. For tetragonal crystals, the symmetry allows the following invariant terms in the anisotropy energy:

$$\begin{aligned} U_a(4) &= K_1(n_x^2 + n_y^2) + K_2(n_x^2 + n_y^2)^2 + K_{xyy}n_x^2n_y^2 \\ &= K_1 \sin^2 \theta + K_2 \sin^4 \theta + K_{\perp} \sin^4 \theta \sin^2 2\varphi; \end{aligned} \quad (1.5.3.8)$$

the azimuthal angle φ is measured from the twofold axis x in the basal plane and the constant K_{\perp} determines the anisotropy in the basal plane.

Trigonal symmetry also allows second- and fourth-order invariants:

$$\begin{aligned} U_a(3) &= K_1(n_x^2 + n_y^2) + K_2(n_x^2 + n_y^2)^2 \\ &\quad + K'_{\perp} \frac{1}{2} n_z [(n_x + in_y)^3 + (n_x - in_y)^3] \\ &= K_1 \sin^2 \theta + K_2 \sin^4 \theta + K'_{\perp} \cos \theta \sin^3 \theta \cos 3\varphi, \end{aligned} \quad (1.5.3.9)$$

where φ is measured from the x axis, which is chosen parallel to one of the twofold axes. For easy-plane magnetics and $K'_{\perp} > 0$, the vector \mathbf{n} is directed along one of the twofold axes in the basal plane. If K'_{\perp} is negative, then \mathbf{n} lies in a vertical mirror plane directed at a small angle to the basal plane. For the complete solution of this problem, the sixth-order term must be taken into account. This term is similar to the one that characterizes the anisotropy of hexagonal crystals. The expression for the latter is of the following form:

$$\begin{aligned} U_a(6) &= K_1(n_x^2 + n_y^2) + K_2(n_x^2 + n_y^2)^2 \\ &\quad + K''_{\perp} \frac{1}{2} [(n_x + in_y)^6 + (n_x - in_y)^6] \\ &= K_1 \sin^2 \theta + K_2 \sin^4 \theta + K''_{\perp} \sin^6 \theta \cos 6\varphi, \end{aligned} \quad (1.5.3.10)$$

where x and φ have the same meaning as in (1.5.3.9).

The symmetry of cubic crystals does not allow any second-order terms in the expansion of the anisotropy energy. The expression for the anisotropy energy of cubic crystals contains the following invariants:

$$U_a(\text{cub}) = K_1(n_x^2n_y^2 + n_x^2n_z^2 + n_y^2n_z^2) + K_2n_x^2n_y^2n_z^2. \quad (1.5.3.11)$$

In considering the anisotropy energy, one has to take into account spontaneous magnetostriction and magnetoelastic energy (see Section 1.5.9). This is especially important in cubic crystals. Any collinear cubic magnetic (being brought into a single domain state) ceases to possess cubic crystallochemical symmetry as a result of spontaneous magnetostriction. If K_1 is positive, the easy axis is aligned along one of the edges of the cube and the crystal becomes tetragonal (like Fe). If K_1 is negative, the crystal becomes rhombohedral and can be an easy-axis magnetic with vector \mathbf{n} parallel to one of the spatial diagonals (like Ni) or an easy-plane magnetic with \mathbf{n} perpendicular to a spatial diagonal. We shall discuss this topic in more detail in Section 1.5.9.3.

The considerations presented above can be applied to all crystals belonging in the paramagnetic state to the tetragonal, trigonal or hexagonal system that become easy-plane magnetics in the ordered state. All of them, including the cubic crystals, may possess more than one allowed direction of easy magnetization.

In the example considered in the previous section, these directions can be aligned along the three twofold axes for the structures A_1^x, A_2^x, A_3^x, F^x and can be parallel to the three mirror planes for A_1^y, A_2^y, A_3^y, F^y .

It is worth noting that in some applications it is more convenient to use an expansion of the anisotropy energy in terms of surface spherical harmonics. This problem has been considered in detail by Birss (1964).

1.5.3.3. The thermodynamic theory of transitions into a magnetically ordered state

According to Landau (1937) (see also Landau & Lifshitz, 1951), a phase transition of the second kind can be described by an order parameter η , which varies smoothly in the neighbourhood of the transition temperature T_c . The order parameter $\eta = 0$ when $T \geq T_c$ and rises continuously as the temperature is decreased below T_c , but the symmetry of the crystal changes suddenly. The order parameter can be a scalar, a vector or a tensor.

Consider a crystal with known space group in the paramagnetic state. In this section, we show how the Landau theory allows us to determine the magnetic space groups that are possible after a second-kind phase transition into an ordered state. The application of the Landau theory to the magnetic transitions into different types of antiferromagnets was made by Dzyaloshinskii (1957a,c; 1964). In these cases, the order parameter is the magnetic moment density $\mathbf{m}(\mathbf{r})$. To determine the equilibrium form of this function, it is necessary to find the minimum of the thermodynamic potential Φ , which is a functional of $\mathbf{m}(\mathbf{r})$. Since the transition is continuous and $\mathbf{m}(\mathbf{r}) = 0$ for $T \geq T_c$, the value of $\mathbf{m}(\mathbf{r})$ must be very small in the neighbourhood below the transition point. In this region, the thermodynamic potential Φ will be expanded into a power series of $\mathbf{m}(\mathbf{r})$. To find the proper form of this expansion, it is convenient to represent $\mathbf{m}(\mathbf{r})$ as a linear combination of functions that form bases of the irreducible representations of the space group of the paramagnetic phase \mathcal{M}_G :

$$m^i(\mathbf{r}) = \sum_{n,\alpha} M_{n,\alpha}^i \varphi_{n,\alpha}(\mathbf{r}), \quad (1.5.3.12)$$

where $\varphi_{n,\alpha}(\mathbf{r})$ are functions that transform under the representation n (α is the number of the function in the representation) and $i = x, y, z$. In this expansion, the quantities $M_{n,\alpha}^i$ are independent of \mathbf{r} and transform with respect to i as the components of an axial vector. The functions $\varphi_{n,\alpha}(\mathbf{r})$ are transformed into combinations of one another by the elements of the group \mathcal{M}_G . Instead, these elements can be regarded as transforming the coefficients $M_{n,\alpha}^i$ and leaving the functions $\varphi_{n,\alpha}$ invariant. In this case, the quantities $M_{n,\alpha}^i$ transform according to the direct product of the representation n of \mathcal{M}_G and the representation formed by the components of the pseudovector. This representation is reducible in the general case. Irreducible representations p, q, \dots can be obtained by forming linear combinations of the $M_{n,\alpha}^i$. Let us denote these combinations by $c_{p,\alpha}, c_{q,\alpha}, \dots$. These variables can be considered as components of the order parameter, and the thermodynamic potential can be expanded into a power series of $c_{p,\alpha}$. The terms of this expansion must be invariant under the transformations of the magnetic space group of the crystal in the paramagnetic state \mathcal{M}_G . This group possesses R as a separate element. Therefore the expansion can contain only even terms. For each irreducible representation, there is only one invariant of second order – the sum of the squares. Consequently, retaining only the square terms, the expansion of the thermodynamic potential Φ has the form:

$$\Phi(T) = \Phi_0(T) + \sum_p A_p(T) \sum_{\alpha} c_{p,\alpha}^2. \quad (1.5.3.13)$$

1.5. MAGNETIC PROPERTIES

To minimize Φ , it is necessary to add the terms of the fourth power. All the coefficients $A_p(T)$ in the relation (1.5.3.13) depend on the temperature. At $T \geq T_c$ all $c_{p,\alpha} = 0$. This solution corresponds to the minimum of Φ if all $A_p(T)$ are positive. The transition into the ordered state occurs if one of the quantities $A_p(T)$ changes its sign. This means that the transition temperature T_c is the temperature at which one of the coefficients $A_p(T_c) = 0$. This coefficient has the form:

$$A_p(T) = \lambda(T - T_c). \quad (1.5.3.14)$$

Accordingly, the corresponding magnetic structure is defined by the order parameters $c_{p,\alpha}$ and belongs to the representation p .

The representation of the space group is realized by a set of functions of the following type:

$$\varphi_{\mathbf{k}_\beta}(\mathbf{r}) = u_{\mathbf{k}_\beta}(\mathbf{r}) \exp(i\mathbf{k}_\beta \mathbf{r}), \quad (1.5.3.15)$$

where the values of the vectors \mathbf{k} are confined to the Brillouin zone in the reciprocal lattice and the function $u_{\mathbf{k}_\beta}(\mathbf{r})$ is periodic in the real lattice. The irreducible representation defined by the vector \mathbf{k}_β contains the functions with all the vectors \mathbf{k}_β that belong to the same star. The star is the set of the vectors \mathbf{k}_β obtained by applying all the transformations g_i of the corresponding point group to any vector of the star (see also Section 1.2.3.3). If we denote it as \mathbf{k}_1 , then the set of the vectors of the star consists of all inequivalent vectors of the form $g_i \mathbf{k}_1$.

There are three types of transition we have to consider: (1) the magnetic lattice is commensurate with the crystallographic one and $\mathbf{k} \neq 0$; (2) the magnetic lattice is incommensurate with the crystallographic one; (3) $\mathbf{k} = 0$ and the magnetic lattice coincides with the crystallographic lattice. Below we shall discuss in detail only the first and the third type of transition.

(a) $\mathbf{k} \neq 0$.

It is found that the first type of transition occurs if the arms of the star \mathbf{k}_β are aligned along specific isolated crystallographic directions and its vectors are equal to 1/2, 1/3 or 1/4 of some translation in the reciprocal lattice (Lifshitz, 1942). Then the magnetic structure is described by one of the 22 nontrivial Bravais types of magnetic lattices shown in Figs. 1.5.2.1–1.5.2.7.

As an example, let us consider a magnetic transition in UO_2 . In the paramagnetic state, it is a crystal with a face-centred cubic structure (space group $\mathcal{O}_h^5 = Fm\bar{3}m$) (for details see Dzyaloshinskii & Man'ko, 1964; Izyumov & Naish, 1979; Izyumov, Naish & Petrov, 1979; Izyumov, Naish & Syromiatnikov, 1979; Barbara *et al.*, 1988). Primitive translations of the crystallographic lattice are (see Fig. 1.5.3.5):

$$\mathbf{a}_1 = (a/2)(0, 1, 1), \quad \mathbf{a}_2 = (a/2)(1, 0, 1), \quad \mathbf{a}_3 = (a/2)(1, 1, 0). \quad (1.5.3.16)$$

Primitive translations of the reciprocal lattice are:

$$\mathbf{b}_1 = (2\pi/a)(-1, 1, 1), \quad \mathbf{b}_2 = (2\pi/a)(1, -1, 1), \quad \mathbf{b}_3 = (2\pi/a)(1, 1, -1). \quad (1.5.3.17)$$

Let us assume that there is one magnetic ion in the primitive cell in the position $(0, 0, 0)$ and that the transition takes place over a three-armed star $\{\mathbf{K}_{10}\}$ (for the definition of the symbols of the stars see Kovalev, 1987):

$$\begin{aligned} \mathbf{k}_1 &= (\mathbf{b}_1 + \mathbf{b}_2)/2 = (2\pi/a)(0, 0, 1) \\ \mathbf{k}_2 &= (\mathbf{b}_1 + \mathbf{b}_3)/2 = (2\pi/a)(0, 1, 0) \\ \mathbf{k}_3 &= (\mathbf{b}_2 + \mathbf{b}_3)/2 = (2\pi/a)(1, 0, 0). \end{aligned} \quad (1.5.3.18)$$

If μ_1 is the magnetic moment at the site $(0, 0, 0)$, the value of $\mu_i(\mathbf{k}_j)$ at $\mathbf{t}_i = (a/2)(h_i, k_i, l_i)$ may be obtained for each \mathbf{k}_j with the help of the following relation:

$$\mu_i(\mathbf{k}_j) = \mu_1 \exp[i(\mathbf{k}_j \mathbf{t}_i)]. \quad (1.5.3.19)$$

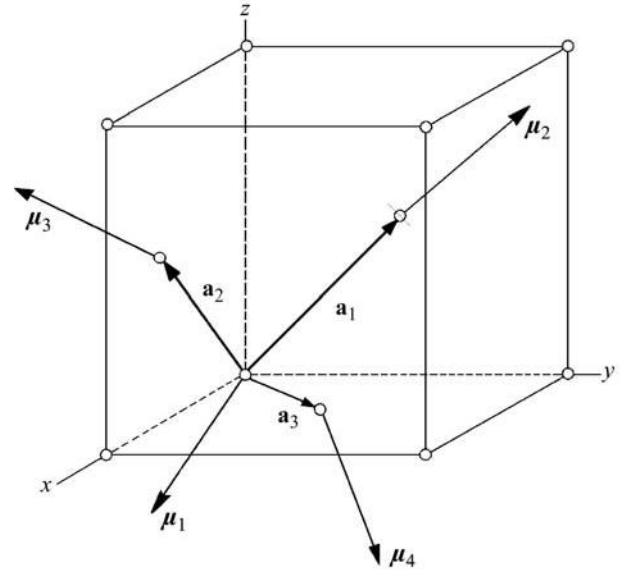


Fig. 1.5.3.5. The conventional unit cell of UO_2 . Only the positions of the magnetic U^{4+} ions are shown. The vectors $\mathbf{a}_1, \mathbf{a}_2, \mathbf{a}_3$ form a basis of a primitive cell of the crystallographic lattice; $\mu_1, \mu_2, \mu_3, \mu_4$ are the magnetic moments of the ions belonging to the four magnetic lattices.

From this relation, it follows that $\mu_i(\mathbf{k}_j) = \pm \mu_1$ for different combinations of \mathbf{t}_i and \mathbf{k}_j . The signs of the magnetic moments μ_i at the four sites at the corner and the face centres of the conventional unit cell are displayed in Table 1.5.3.5.

Table 1.5.3.5 shows that for each arm of the vector star \mathbf{k}_j , there exists a linear combination of the four vectors μ_i ($i = \text{lattice site}$) which is a basis of the representation of one of the arms. According to Table 1.5.3.5, these linear combinations have the following forms:

$$\begin{aligned} \mathbf{l}_1 &= \mu_1 - \mu_2 - \mu_3 + \mu_4 \\ \mathbf{l}_2 &= \mu_1 - \mu_2 + \mu_3 - \mu_4 \\ \mathbf{l}_3 &= \mu_1 + \mu_2 - \mu_3 - \mu_4. \end{aligned} \quad (1.5.3.20)$$

None of the vectors \mathbf{l}_α is a basis of an irreducible representation of the whole space group $\mathcal{O}_h^5 = Fm\bar{3}m$ in the case under consideration. The basis functions of the irreducible representation are formed by linear superposition of the basis functions of each arm. One of these representations, τ_3 , is a superposition of the following components of \mathbf{l}_α : l_{1z} , l_{2y} and l_{3x} . This corresponds to the following orientations of the magnetic moments located in different corners of the primitive unit cell:

$$\mu_1 \sim [\bar{1}, \bar{1}, \bar{1}], \quad \mu_2 \sim [\bar{1}, 1, 1], \quad \mu_3 \sim [1, \bar{1}, 1], \quad \mu_4 \sim [1, 1, \bar{1}]. \quad (1.5.3.21)$$

Thus the magnetic structure of UO_2 consists of four primitive cubic magnetic sublattices \mathbf{M}_i inserted into each other. According to (1.5.3.21), the magnetization vectors of these sublattices \mathbf{M}_i are aligned along the space diagonals of the cubic lattice. This magnetic structure for UO_2 was predicted theoretically by Dzyaloshinskii & Man'ko (1964) (using the representation approach in the way discussed above) and established by neutron scattering by Faber *et al.* (1975).

Table 1.5.3.5. The signs of $\mu_i(\mathbf{k}_j)$ for four sites \mathbf{t}_i of the conventional unit cell (the corners of a primitive cell)

| | \mathbf{t}_1 $a(0, 0, 0)$ | \mathbf{t}_2 $(a/2)(0, 1, 1)$ | \mathbf{t}_3 $(a/2)(1, 0, 1)$ | \mathbf{t}_4 $(a/2)(1, 1, 0)$ |
|----------------|--------------------------------|------------------------------------|------------------------------------|------------------------------------|
| \mathbf{k}_1 | + | − | − | + |
| \mathbf{k}_2 | + | − | + | − |
| \mathbf{k}_3 | + | + | − | − |

1. TENSORIAL ASPECTS OF PHYSICAL PROPERTIES

This example shows that the Landau theory can solve complicated problems of phase transitions where the magnetic lattice does not coincide with the crystallographic one and the magnetic structure is strongly non-collinear. Here only a qualitative analysis has been given; Section 1.5.3.3.1 and Section 1.5.3.3.2 will be devoted to quantitative solutions connected with phase transitions into an ordered state.

As was discussed in Section 1.5.2, Andreev & Marchenko (1976, 1980) introduced the concept of exchange magnetic symmetry. This concept is based on neglecting the relativistic interactions in comparison with the exchange interaction. In such an approach, the orientation of the magnetic moments relative to the crystallographic axis is arbitrary and the crystallographic transformations act on the magnetic moments not as on vectors but as on scalars. In the exchange approximation, three magnetic vectors can be introduced that describe any magnetic structure. These vectors are mutually orthogonal. All magnetic structures can be classified into four types. (1) Collinear ferromagnets or ferrimagnets are described by one ferromagnetic vector \mathbf{M} . (2) Collinear antiferromagnets are described by one antiferromagnetic vector \mathbf{L} . (3) Non-collinear ferromagnets are described by one ferromagnetic vector \mathbf{M} and one or two antiferromagnetic vectors \mathbf{L}_α . (4) Non-collinear antiferromagnets are described by two or three antiferromagnetic vectors \mathbf{L}_α . The Andreev and Marchenko approach describes the magnetic structure of UO_2 considered above by three antiferromagnetic vectors which are aligned along $[1, 0, 0]$, $[0, 1, 0]$ and $[0, 0, 1]$, respectively.

(b) *Incommensurate structures* (see also Section 1.10.1).

In the second type of transition, \mathbf{k}_β differs slightly from one of the rational values $(1/2, 1/3, 1/4)$. Then the magnetic structure is incommensurate with the crystallographic lattice. Such non-collinear structures are shown in Fig. 1.5.1.4 (antiferromagnetic and ferromagnetic helices). A detailed analysis of this problem is given by Andreev & Marchenko (1976, 1980).

(c) $\mathbf{k}_\beta = 0$.

To the third type belong transitions for which $\mathbf{k}_\beta = 0$. In this case, the magnetic primitive cell coincides with the crystallographic one and antiferromagnetic ordering is allowed only if there is more than one magnetic ion in the primitive cell. As stated above, only this type of ordering allows collinear ferromagnetism. Therefore, we shall discuss this type of transition later in more detail.

Let us consider the phase transition in a uniaxial crystal with four magnetic ions in the primitive cell, as was done by Dzyaloshinskii (1957a). Now the average density of the magnetic moment $m^i(\mathbf{r})$ in (1.5.3.12) is determined by the average values of the magnetic moments of each ion, $\mu_1, \mu_2, \mu_3, \mu_4$. In (1.5.3.12), there is no longer any need to distinguish the coefficients $M_{n\alpha}^i$ and the functions $\varphi_{n,\alpha}(\mathbf{r})$. Their product $M_{n,\alpha}^i \varphi_{n,\alpha}(\mathbf{r})$ is now replaced by the linear combinations of the components of $\mu_1, \mu_2, \mu_3, \mu_4$ transforming according to the corresponding irreducible representation of the point group \mathcal{P} of the crystal (the space group of which is \mathcal{G}). To illustrate this, we shall take for \mathcal{G} the group $D_{3d}^6 = R\bar{3}c$, which was discussed in Section 1.5.3.1. There we introduced the linear combinations (1.5.3.2) $\mathbf{l}_1, \mathbf{l}_2, \mathbf{l}_3, \mathbf{m}$ of the

vectors $\mu_1, \mu_2, \mu_3, \mu_4$. The components of these linear combinations are basis functions of the irreducible representations of the corresponding point group $D_{3d} = \bar{3}m$. The characters of the representations of this group are given in Table 1.5.3.6. It follows from this table that all z components of the vectors \mathbf{l}_α and \mathbf{m} are transformed according to different one-dimensional representations of D_{3d} (i.e. $\Gamma_1, \dots, \Gamma_4$). Following the rule introduced in Section 1.5.2.1 [see relation (1.5.2.2)], we established the magnetic point groups displayed in the last column of Table 1.5.3.6. The symbols for the magnetic structures are given in the corresponding column. The x, y components are transformed by two-dimensional representations: m_x, m_y and l_{3x}, l_{3y} are transformed according to the same representation Γ_5 ; a similar situation holds for the pairs l_{1x}, l_{1y} and l_{2x}, l_{2y} , which are transformed according to Γ_6 . It is obvious that if the magnetic structure possesses x, y components of the magnetic vectors, the magnetic point group (which must be a subgroup of D_{3d}) will contain only four elements of the group D_{3d} : $E, C_2, I, \sigma_{\perp}$. These elements form the point group $C_{2h} = 2/m$. The point group C_{2h} has four one-dimensional representations, which according to relation (1.5.2.2) generate the four magnetic point groups listed in the last column of Table 1.5.3.6. To each of these magnetic point groups corresponds a definite magnetic structure, which is a mixture of x and y components of \mathbf{l}_3 and \mathbf{m} or \mathbf{l}_1 and \mathbf{l}_2 . The symbols of these structures are also listed in the table (by definition, the twofold axis is aligned along the x axis).

According to the relation (1.5.3.13), the thermodynamic potential Φ contains a sum of quadratic terms of basis functions for each irreducible representation. Thus it contains the following invariants, which correspond to the one-dimensional representations:

$$A_1' l_{1z}^2 + A_2' l_{2z}^2 + A_3' l_{3z}^2 + B' m_z^2. \quad (1.5.3.22)$$

The invariants formed with the x, y components of the vectors $\mathbf{l}_1, \mathbf{l}_2, \mathbf{l}_3, \mathbf{m}$, which are basis functions of two-dimensional representations, have the following form:

$$A_1''(l_{1x}^2 + l_{1y}^2) + A_2''(l_{2x}^2 + l_{2y}^2) + A_3''(l_{3x}^2 + l_{3y}^2) + B''(m_x^2 + m_y^2). \quad (1.5.3.23)$$

The thermodynamic potential for any uniaxial crystal possesses such invariants of second order. For crystals belonging to the space group D_{3d}^6 it is possible to construct additional invariants, which are linear combinations of the mixed products of the x and y components of the pairs of vectors $\mathbf{l}_1, \mathbf{l}_2$ and \mathbf{l}_3, \mathbf{m} and are transformed according to the same two-dimensional representations. These invariants have the following form:

$$l_{1x}l_{2y} - l_{1y}l_{2x}, \quad l_{3x}m_y - l_{3y}m_x. \quad (1.5.3.24)$$

These terms are responsible for 'weakly non-collinear' structures; we discuss their properties in the Section 1.5.5 and shall not take them into account now.

Before writing the whole expression of the thermodynamic potential, let us combine expressions (1.5.3.22) and (1.5.3.23) to

Table 1.5.3.6. *Characters of the irreducible representations of the group $D_{3d} = \bar{3}m$ and corresponding magnetic structures*

| Representation | Magnetic vector components | Elements of symmetry | | | | | | Magnetic structure | Magnetic point group |
|----------------|----------------------------|----------------------|--------|--------|-----|--------|-------------|--------------------|------------------------------|
| | | E | $2C_3$ | $3C_2$ | I | $2S_6$ | $3\sigma_d$ | | |
| Γ_1 | l_{3z} | 1 | 1 | 1 | 1 | 1 | 1 | C_z | $D_{3d} = \bar{3}m$ |
| Γ_2 | m_z | 1 | 1 | -1 | 1 | 1 | -1 | F_z | $D_{3d}(S_6) = \bar{3}m'$ |
| Γ_3 | l_{1z} | 1 | 1 | -1 | -1 | -1 | 1 | A_z | $D_{3d}(C_{3v}) = \bar{3}'m$ |
| Γ_4 | l_{2z} | 1 | 1 | 1 | -1 | -1 | -1 | G_z | $D_{3d}(D_3) = \bar{3}'m'$ |
| Γ_5 | l_{3x}, m_y | 2 | -1 | 0 | 2 | -1 | 0 | C_x, F_y | $C_{2h}(C_i) = 2'/m'$ |
| | m_x, l_{3y} | | | | | | | C_y, F_x | $C_{2h} = 2/m$ |
| Γ_6 | l_{1x}, l_{2y} | 2 | -1 | 0 | -2 | 1 | 0 | A_x, G_y | $C_{2h}(C_2) = 2/m'$ |
| | l_{2x}, l_{1y} | | | | | | | A_y, G_x | $C_{2h}(C_i) = 2'/m$ |

1.5. MAGNETIC PROPERTIES

separate the exchange terms from the relativistic ones. This can be performed in two ways:

$$\begin{aligned} A_1' l_{1z}^2 + A_1''(l_{1x}^2 + l_{1y}^2) &= (A_1/2) \mathbf{l}_1^2 + (a_1/2) l_{1z}^2 \quad \text{or} \\ A_1' l_{1z}^2 + A_1''(l_{1x}^2 + l_{1y}^2) &= (A_1/2) \mathbf{l}_1^2 + (a_1/2)(l_{1x}^2 + l_{1y}^2). \end{aligned} \quad (1.5.3.25)$$

Similar rearrangements are performed for \mathbf{l}_2 , \mathbf{l}_3 and \mathbf{m} . Summing expressions (1.5.3.22) and (1.5.3.23) and taking into account expression (1.5.3.25), we obtain the final expression for the thermodynamic potential Φ limited to the terms of second order:

$$\begin{aligned} \Phi_1 &= \Phi_0 + (A_1/2) \mathbf{l}_1^2 + (A_2/2) \mathbf{l}_2^2 + (A_3/2) \mathbf{l}_3^2 + (B/2) \mathbf{m}^2 \\ &\quad + (a_1/2) l_{1z}^2 + (a_2/2) l_{2z}^2 + (a_3/2) l_{3z}^2 + (b/2) m_z^2. \end{aligned} \quad (1.5.3.26)$$

In this expression, the coefficients of the terms representing the exchange interaction are denoted by capital letters. It is mainly these terms that are responsible for the transition to the ordered state. The much smaller relativistic terms are responsible for the orientation of the vectors \mathbf{l}_α or \mathbf{m} . Their coefficients are denoted by small letters.

To minimize the potential (1.5.3.26), it is necessary to add terms of the fourth order, which are restricted to the exchange terms. The total expression for the thermodynamic potential Φ will then be

$$\Phi = \Phi_1 + \frac{1}{4} \sum_{\alpha} C_{\alpha} \mathbf{l}_{\alpha}^4 + \frac{1}{4} C' \mathbf{m}^4 + \frac{1}{2} \sum_{\alpha} D_{\alpha} (\mathbf{l}_{\alpha} \mathbf{m})^2 + \frac{1}{2} \sum_{\alpha} D'_{\alpha} \mathbf{l}_{\alpha}^2 \mathbf{m}^2. \quad (1.5.3.27)$$

As pointed out above, one of the coefficients A_{α} or B vanishes at the transition temperature T_0 . This coefficient may be expanded in a series of $(T - T_0)$ [see (1.5.3.14)]. At $T < T_0$, a ferro- or antiferromagnetic structure will be realized, the type of which is determined by minimization of the thermodynamic potential (1.5.3.27).

As an example, we shall consider in the next two sections the simplest cases, the uniaxial ferromagnet and the uniaxial antiferromagnet. When doing this, we shall not restrict ourselves to a certain crystallographic structure as in the case above. For the sake of simplicity, it will be assumed that the primitive cell contains only two magnetic ions and therefore there is only one antiferromagnetic vector \mathbf{l} . Further, we shall introduce new variables:

$$\mathbf{M} = (N/2) \mathbf{m}, \quad \mathbf{L} = (N/2) \mathbf{l}, \quad (1.5.3.28)$$

where N is the number of magnetic ions per cm^3 .

1.5.3.3.1. Uniaxial ferromagnet

The temperature of transition from the paramagnetic to the ferromagnetic state is called the Curie temperature. The thermodynamic treatment of the behaviour of uniaxial ferromagnets in the neighbourhood of the Curie temperature T_c is given below.

In the case of a ferromagnet ($\mathbf{L} = 0$), the thermodynamic potential (1.5.3.27) near T_c including the magnetic energy $-\mathbf{MH}$ is given by (see 1.5.3.25)

$$\tilde{\Phi} = \Phi_0 + (B/2) \mathbf{M}^2 + (b/2)(M_x^2 + M_y^2) + (C/4) \mathbf{M}^4 - \mathbf{MH}, \quad (1.5.3.29)$$

where $\tilde{\Phi}$ is used to designate the thermodynamic potential in variables p, T, \mathbf{H} [instead of $\Phi(p, T, \mathbf{M})$]; at the given field, $\tilde{\Phi}$ should be a minimum. The equilibrium value of the magnetization \mathbf{M} is found by minimizing the thermodynamic potential.

First consider the ferromagnet in the absence of the external field ($\mathbf{H} = 0$). The system of equations $\partial \tilde{\Phi} / \partial \mathbf{M} = 0$ has three solutions:

$$(I) \quad M_x = M_y = M_z = 0 \quad (1.5.3.30)$$

$$(II) \quad M_z = 0; \quad M_x^2 + M_y^2 = M_{\perp}^2 = -\frac{B+b}{C} \quad (1.5.3.31)$$

$$(III) \quad M_x = M_y = 0; \quad M_z^2 = -\frac{B}{C}. \quad (1.5.3.32)$$

In the whole range of temperatures $T > T_c$ when $B > 0$, the minimum of the potential is determined by solution (I) (*i.e.* absence of a spontaneous magnetization). The realization of the second or third state depends on the sign of the coefficient b . If $b > 0$, then the third state is realized, the magnetization \mathbf{M} being directed along the axis. In this case, the transition from the paramagnetic into the ferromagnetic state will take place at $T_c = T_0$ (when $B = 0$). If $b < 0$, the magnetization is directed perpendicular to the axis. In this case, the Curie temperature is $T_c = T_0 - b/\lambda$ (when $B + b = 0$). In the absence of a magnetic field, the difference between the two values of T_c has no physical meaning, since it only means another value of the coefficient B [see (1.5.3.25)]. In a magnetic field, both temperatures may be determined experimentally, *i.e.* when B becomes zero and when $B + b$ becomes zero.

If a magnetic field \mathbf{H} is applied parallel to the z axis and $b > 0$, the minimization of the thermodynamic potential Φ leads to

$$H/M = CM^2 + B. \quad (1.5.3.33)$$

This relation has been verified in many experiments and the corresponding graphical representations are known in the literature as Arrott-Belov-Kouvel plots (see Kouvel & Fisher, 1964). Putting $B = \lambda(T - T_c)$ according to (1.5.3.14), equations (1.5.3.32) and (1.5.3.33) may be used to derive expressions for the initial magnetic susceptibilities (for $H \rightarrow 0$):

$$\chi_0 = \frac{1}{2\lambda(T_c - T)^{\gamma}}, \quad T < T_c, \quad (1.5.3.34)$$

$$\chi_0 = \frac{1}{\lambda(T - T_c)^{\gamma}}, \quad T > T_c, \quad (1.5.3.35)$$

where $\gamma = 1$.

The Landau theory of phase transitions does not take account of fluctuations of the order parameter. It gives qualitative predictions of all the possible magnetic structures that are allowed for a given crystal if it undergoes a second-order transition. The theory also explains which of the coefficients in the expression for the thermodynamic potential is responsible for the corresponding magnetic structure. It describes also quantitative relations for the magnetic properties of the material if

$$1 \gg (T - T_c)/T_c \gg T_c B^2 / b\alpha^3, \quad (1.5.3.36)$$

where α is the coefficient in the term which describes the gradient energy. In this chapter, we shall not discuss the behaviour of the material in the fluctuation region. It should be pointed out that, in this region, γ in relations (1.5.3.34) and (1.5.3.35) depends on the dimensionality of the structure n and equals 1.24 for $n = 1$, 1.31 for $n = 2$ and 1.39 for $n = 3$. Similar considerations are relevant to the relations (1.5.3.31) and (1.5.3.32), which describe the temperature dependence of spontaneous magnetization.

The relations (1.5.3.31) and (1.5.3.32) describe the behaviour of the ferromagnet in the 'saturated' state when the applied magnetic field is strong enough to destroy the domain structure. The problem of the domains will be discussed later (see Section 1.5.4).

The transition from the paramagnetic to the ferromagnetic state is a second-order transition, provided that there is no magnetic field. In the presence of a magnetic field that is parallel to the easy axis of magnetization, the magnetic symmetry of the crystal is the same ($M_z \neq 0$) both above and below T_c . From the point of view of symmetry, no transition occurs in this case.

1. TENSORIAL ASPECTS OF PHYSICAL PROPERTIES

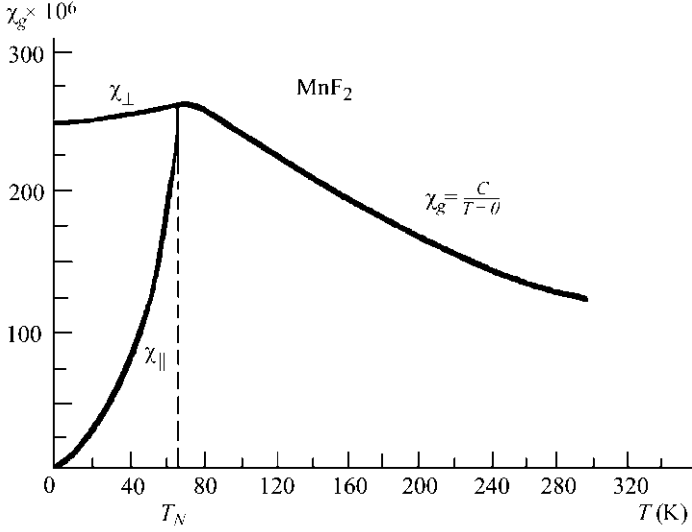


Fig. 1.5.3.6. Temperature dependence of the mass susceptibility χ_g for a uniaxial antiferromagnet along ($\chi_{||}$) and perpendicular (χ_{\perp}) to the axis of antiferromagnetism (see Foner, 1963).

1.5.3.3.2. Uniaxial antiferromagnet

Now let us proceed to the uniaxial antiferromagnet with two ions in the primitive cell. The thermodynamic potential $\tilde{\Phi}$ for such an antiferromagnet is given in accordance with (1.5.3.26) and (1.5.3.27) by (Landau, 1933)

$$\begin{aligned} \tilde{\Phi} = & \Phi_0 + (A/2)\mathbf{L}^2 + (B/2)\mathbf{M}^2 + (a/2)(L_x^2 + L_y^2) \\ & + (b/2)(M_x^2 + M_y^2) + (C/4)\mathbf{L}^4 + (D/2)(\mathbf{LM})^2 \\ & + (D'/2)\mathbf{L}^2\mathbf{M}^2 - \mathbf{MH}. \end{aligned} \quad (1.5.3.37)$$

If the magnetic field is absent ($\mathbf{H} = 0$), then $\mathbf{M} = 0$ because B , D and $D' > 0$. Then three possible magnetic states are obtained by minimizing the potential with respect to \mathbf{L} only:

$$(I) \quad L_x = L_y = L_z = 0 \quad (1.5.3.38)$$

$$(II) \quad L_z = 0; \quad L_x^2 + L_y^2 = L_{\perp}^2 = -\frac{A+a}{C} \quad (1.5.3.39)$$

$$(III) \quad L_x = L_y = 0; \quad L_z^2 = -\frac{A}{C}. \quad (1.5.3.40)$$

When $a < 0$, state (II) with $L_z = 0$ is thermodynamically stable. When $a > 0$, state (III) is stable and the antiferromagnetic vector is directed along the axis. This means that the term with the coefficient a is responsible for the anisotropy of the uniaxial antiferromagnet. We introduce the effective anisotropy field:

$$H_a = aL = 2aM_0, \quad (1.5.3.41)$$

where M_0 is the sublattice magnetization.

Formulas (1.5.3.39) and (1.5.3.14) in the form $A = \lambda(T - T_c)$ yield the expression for the temperature dependence of the sublattice magnetization:

$$L^2 = (\lambda/C)(T_N - T), \quad (1.5.3.42)$$

where T_N is the Néel temperature. The assertions relating to formulas (1.5.3.34) and (1.5.3.35) concerning the fluctuation region are also valid for the temperature dependence of the sublattice magnetization.

The minimization of the potential $\tilde{\Phi}$ with respect to \mathbf{M} for given $\mathbf{L} \neq 0$ when $\mathbf{H} \neq 0$ yields the following relation for the magnetization:

$$\mathbf{M} = \chi_{\perp}\mathbf{H} - (\chi_{\perp} - \chi_{||})(\mathbf{qH})\mathbf{q}, \quad (1.5.3.43)$$

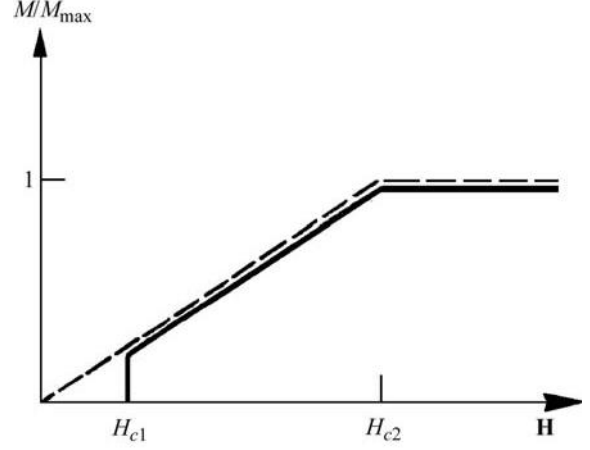


Fig. 1.5.3.7. Dependence of the relative magnetization M/M_{\max} on the magnetic field at $T = 0$. The dashed line corresponds to $\mathbf{H} \perp O_z$, the full line to $\mathbf{H} \parallel O_z$. H_{c1} is the field of spin-flop, H_{c2} is the field of spin-flip.

where $\mathbf{q} = \mathbf{L}/|\mathbf{L}|$. Thus the magnetization of an antiferromagnet is linear with the magnetic field, as for a paramagnet, if the magnetic field is not too strong. The main difference is in the anisotropy and temperature dependence of the susceptibility. The parallel susceptibility $\chi_{||}$ decreases when the temperature is lowered, and χ_{\perp} does not depend on temperature ($\chi_{\perp} = 1/B$) (see Fig. 1.5.3.6). The coefficient B belongs to the exchange term and defines the effective exchange field

$$H_e = \frac{1}{2}BL = BM_0. \quad (1.5.3.44)$$

As seen from Fig. 1.5.3.6, $\chi_{\perp} > \chi_{||}$. Therefore, when the magnetic field applied parallel to the axis of a uniaxial antiferromagnet reaches the critical value

$$H_{c1}^2 = aL^2/(\chi_{\perp} - \chi_{||}) \simeq aBL_0^2 = 2H_aH_e \quad (1.5.3.45)$$

(L_0 is the value of L at $T = 0$), a flopping of the sublattices from the direction along the axis to some direction in the plane perpendicular to the axis occurs. In this spin-flop transition (which is a first-order transition into a new magnetic structure), the magnetization jumps as shown in Fig. 1.5.3.7.

A second-order transition into a saturated paramagnetic state takes place in a much stronger magnetic field $H_{c2} = 2H_e$. This transition is called a spin-flip transition. Fig. 1.5.3.7 shows the magnetic field dependence of the magnetization of a uniaxial antiferromagnet. Fig. 1.5.3.8 shows the temperature dependence of both critical fields.

The quantitative behaviour of the critical magnetic fields in the neighbourhood of T_N for both directions of the magnetic field ($\mathbf{H} \parallel O_z$ and $\mathbf{H} \perp O_z$) can be determined from the theory of second-order phase transitions starting from the thermodynamic potential $\tilde{\Phi}$ and taking into account that L is small and $DL^2 \ll B$ close to T_N .

In the presence of the magnetic field $\mathbf{H} \perp O_z$, \mathbf{L} is parallel to O_z , $\mathbf{LM} = 0$, the coefficient A at L^2 is replaced by $A + 2D'H^2/B^2$ and the latter is zero at the new transition point. The critical field is given by the relation

$$H_{c2}^2 = (\lambda B^2/2D')(T_N - T), \quad \mathbf{H} \perp O_z. \quad (1.5.3.46)$$

If the field is applied parallel to the z axis, then \mathbf{L} remains parallel to O_z if $H < H_{c1}$ ($H_{c1} \simeq aB^2/D$ in the neighbourhood of T_N). Therefore,

$$H_{c2}^2 = \frac{\lambda B^2}{2(D + D')}(T_N - T), \quad \mathbf{H} \parallel O_z, \quad H < H_{c1}. \quad (1.5.3.47)$$

If $H > H_{c1}$, \mathbf{L} becomes perpendicular to the z axis and the anisotropy term has to be taken into account:

1.5. MAGNETIC PROPERTIES

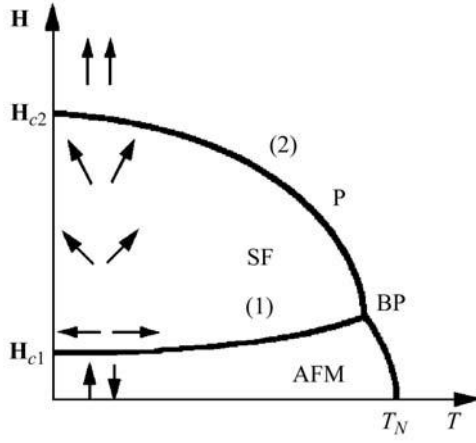


Fig. 1.5.3.8. Magnetic phase diagram for a uniaxial antiferromagnet in a magnetic field applied parallel to the axis. (1) The line of spin-flop transition (H_{c1}); (2) the line of spin-flip transition (H_{c2}); P, paramagnetic phase; AFM, easy-axis antiferromagnetic phase; SF, spin-flop phase; BP, bicritical point.

$$H_{c2}^2 = \frac{\lambda B^2}{2D'}(T_N - T - a/\lambda), \quad \mathbf{H} \parallel Oz, \quad H > H_{c1}. \quad (1.5.3.48)$$

Formulas (1.5.3.46)–(1.5.3.48) show that the transition temperature is reduced by applying the magnetic field. The displacement of the transition point is directly proportional to the square of the applied field. Fig. 1.5.3.9 shows the phase diagram of an antiferromagnet in the neighbourhood of T_N . Unlike ferromagnets, antiferromagnets maintain the second-order phase transition when a magnetic field is applied because the symmetry of the crystal in the antiferromagnetic state differs essentially from that in the paramagnetic state also if the crystal is placed into a magnetic field.

Formula (1.5.3.43) describes the magnetization process only in easy-axis antiferromagnets. For easy-plane antiferromagnets, the anisotropy in the plane is usually extremely small and the antiferromagnetic vector rotates freely in the basic plane. Therefore, for any direction of the magnetic field, the vector \mathbf{L} becomes

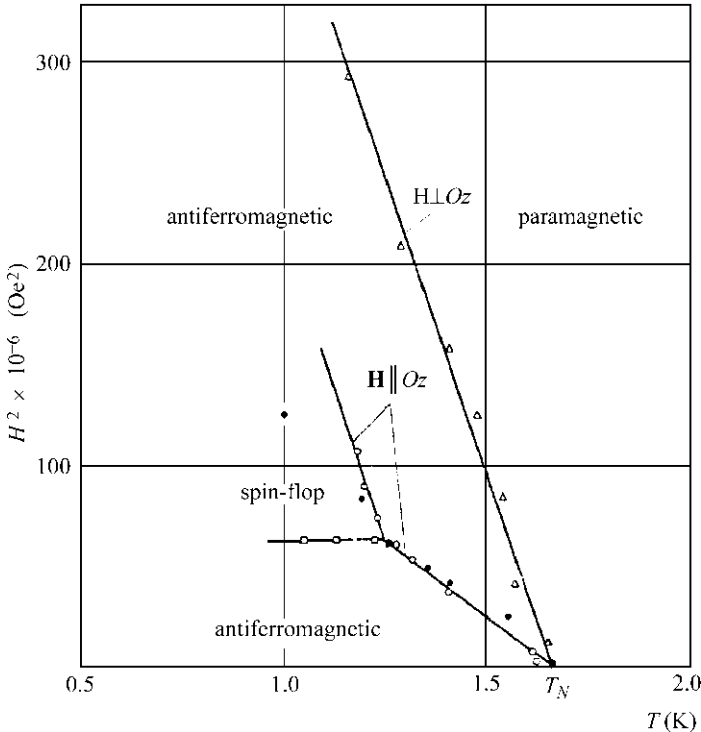


Fig. 1.5.3.9. Phase diagram for a uniaxial antiferromagnet in the proximity of T_N , calculated for $\text{MnCl}_2 \cdot 4\text{H}_2\text{O}$. Experimental data are taken from Gijsman *et al.* (1959).

aligned perpendicular to the applied magnetic field. Correspondingly the magnetization becomes

$$\mathbf{M} = \chi_z H_z \hat{\mathbf{z}} + \chi_\perp H_\perp \hat{\mathbf{x}}, \quad (1.5.3.49)$$

where $\hat{\mathbf{z}}$ and $\hat{\mathbf{x}}$ are unit vectors parallel and perpendicular to the axis.

1.5.4. Domain structure

1.5.4.1. 180° domains

Neither symmetry nor energy considerations can determine the alignment of the magnetization vector \mathbf{n} in a non-chiral easy-axis magnetic (of ferro- or antiferromagnetic type). The vector \mathbf{n} may be aligned parallel or antiparallel to the positive direction of the z axis. Therefore, specimens of any magnetic are usually split into separate regions called domains. In each domain of an easy-axis magnetic, the vector \mathbf{n} has one of its two possible directions. Such domains are called 180° domains. Adjacent domains are separated by a domain wall, in which the magnetic moments are no longer strictly parallel (or antiparallel). As a result of this, both the exchange and the anisotropy energy rise inside the volume of the domain wall.

In ferromagnets (and ferrimagnets), the loss in the exchange and anisotropy energy in a multidomain sample is compensated by the gain in the magnetostatic energy. The existence of the domain structure is responsible for the behaviour of a ferromagnet in an applied magnetic field. There are two kinds of magnetization processes that one has to distinguish: the displacement of the domain walls and the rotation of the spontaneous magnetization vector from the easy direction to the direction of the applied magnetic field. The magnetization process will first be considered without taking the demagnetizing field into account. If the magnetic field is applied parallel to the axis of an easy-axis ferromagnet, the displacement of the domain wall will completely determine the magnetization process. If the sample contains no impurities and crystal defects, such a displacement must take place in an infinitely small magnetic field [see curve (1) in Fig. 1.5.4.1 and Fig. 1.5.4.3a]. If the magnetic field is applied perpendicular to the easy axis, the size of the domains does not change but their magnetization vectors rotate. Let us denote the spontaneous magnetization by M_s . Then the sample magnetization M rises linearly with respect to the applied magnetic field:

$$M = HM_s^2/2K_1, \quad (1.5.4.1)$$

where K_1 is defined by relations (1.5.3.8)–(1.5.3.10). Some nonlinearity in H can arise from the fourth-order term with K_2 [see curve (2) in Fig. 1.5.4.1 and Fig. 1.5.4.3c]. When $H = 2K_1/M_s = H_s$, the magnetizations of all the domains are rotated by 90° and the magnetization of the sample becomes oriented along the magnetic field; its value is saturated and is equal to the spontaneous magnetization M_s . If $T \neq 0$ K, there is an additional rise in magnetization with the magnetic field. This rise, which is called true magnetization, is relatively very small at all temperatures except for the temperature region close to the transition temperature. If the magnetic field is applied at an arbitrary angle θ to the easy axis, the magnetization process occurs in two steps [see curves (2) in Fig. 1.5.4.2 and Fig. 1.5.4.3b]. First, as a result of the wall displacement, the magnetization jumps to the value M_1 in a small magnetic field. Next, the rotation process follows and at H_s the sample becomes saturated [see curves (2) in Fig. 1.5.4.2]. It is essential to take the shape of the sample into account in considering the problem of the magnetization processes in ferromagnets, as the demagnetizing field can be up to $4\pi M$. In real materials, the displacement process is partly (at low fields) reversible and partly (at higher fields) irreversible. Therefore, complicated hysteresis processes arise in magnetizing ferromagnets.

1. TENSORIAL ASPECTS OF PHYSICAL PROPERTIES

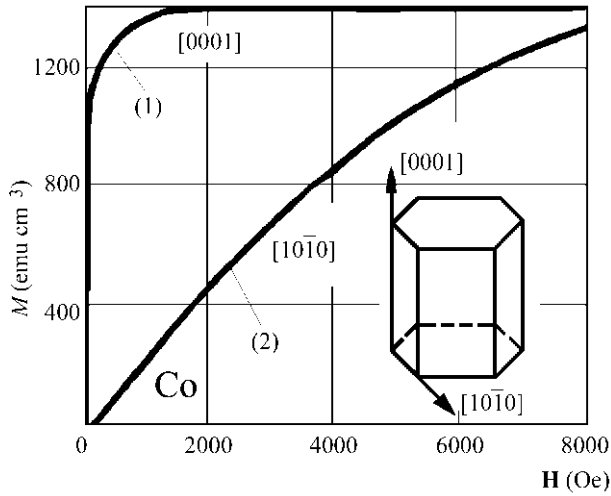


Fig. 1.5.4.1. Magnetization curves of hexagonal cobalt for two main crystallographic directions: (1) [0001] and (2) [10 $\bar{1}$ 0].

The problem of 180° domains in antiferromagnets is not as clear. These domains differ in the sign of the antiferromagnetic vector \mathbf{L} . This vector was defined as the difference of the vectors of sublattice magnetizations in a two-sublattice antiferromagnet, i.e. $\mathbf{M}_1 - \mathbf{M}_2$. Thus two such antiferromagnetic domains differ only by the numbering of the sites in the sublattices. Antiferromagnetic 180° domains are also called S-domains. The wall between two S-domains is schematically represented in Fig. 1.5.4.4.

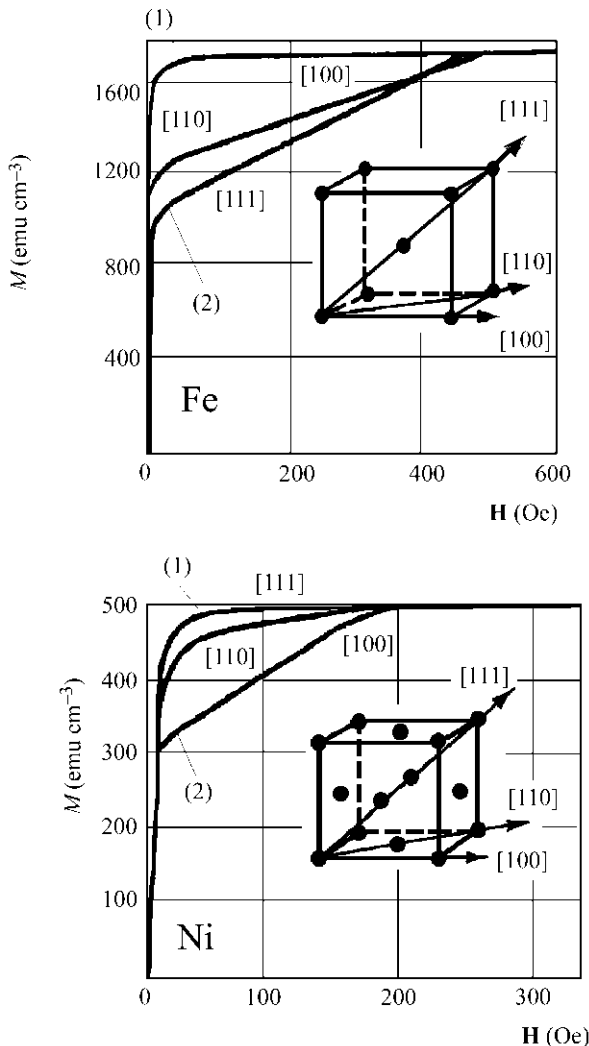


Fig. 1.5.4.2. Magnetization curves of two cubic crystals (iron and nickel) for three crystallographic directions.

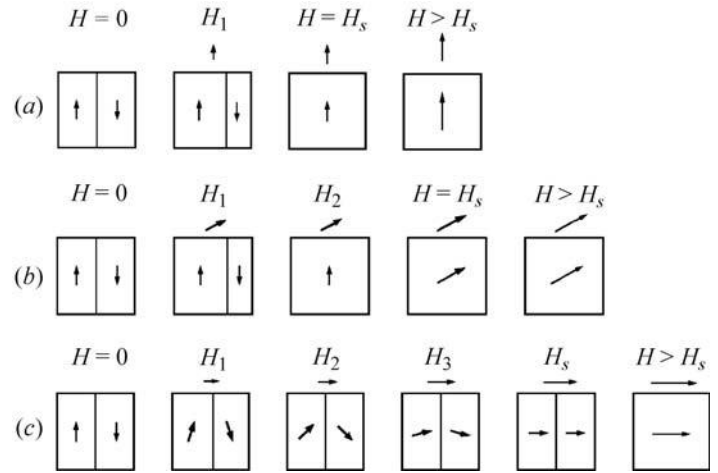


Fig. 1.5.4.3. Schematic display of the magnetization: (a) along the easy axis; (b) at an arbitrary angle to the easy axis; (c) perpendicular to the easy axis.

The origin of the antiferromagnetic S-domains cannot be explained from the point of view of energy balance as in a ferromagnet. These domains give rise to additional exchange and anisotropy energies which are not compensated by a decrease of any other kind of energy. Thus the S-domain structure is thermodynamically not stable. However, experiments show that S-domains exist in most easy-axis antiferromagnets.

The formation of S-domains can be explained by assuming that when the material is cooled down to the Néel temperature, antiferromagnetic ordering arises in different independent regions. The direction of the vector \mathbf{L} in these regions is accidental. When growing regions with different directions of \mathbf{L} meet, the regular alternation of the directions of magnetic moments of the ions is broken on the border between these regions. Domain walls are created on such borders. Such domain structures can be metastable.

The existence of S-domains in easy-axis antiferromagnets was first proved in experiments in which effects that depend on the sign of \mathbf{L} were investigated. These are piezomagnetism, linear magnetostriction and the linear magnetoelectric effect. The sign of these effects depends on the sign of \mathbf{L} . We shall discuss this problem in detail in Sections 1.5.7 and 1.5.8. Later, 180° domain walls were observed in neutron scattering experiments (Schlenker & Baruchel, 1978), and the domains themselves in magneto-optical experiments (see Kharchenko *et al.*, 1979; Kharchenko & Gnatchenko, 1981).

1.5.4.2. Twin domains

As pointed out in Section 1.5.3, in tetragonal non-easy-axis magnetics, in easy-plane hexagonal and trigonal and in cubic magnetics there is more than one easy magnetization direction (3, 4 or 6). As a result, domains arise in which vectors \mathbf{M}_s or \mathbf{L} are directed to each other at 120, 109.5, 90, 70.5 and 60°. Such domains are called twin or T-domains. The formation of magnetic

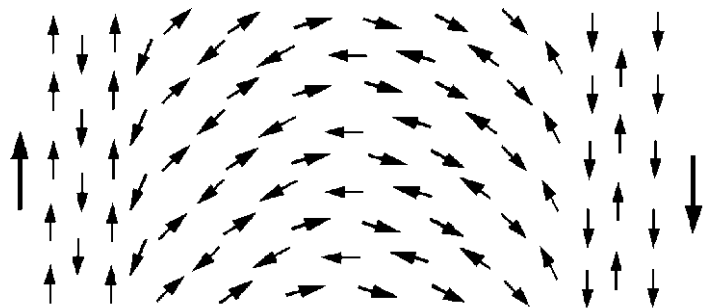


Fig. 1.5.4.4. A 180° domain wall in an antiferromagnet.

1.5. MAGNETIC PROPERTIES

T-domains is accompanied by the formation of crystallographic domains as a result of spontaneous magnetostriction. But mostly this is very small. Each of the T-domains may split into 180° domains.

The magnetization process in ferromagnets possessing T-domains is similar to the previously described magnetization of an easy-axis ferromagnet in a magnetic field directed at an oblique angle. First the displacement process allows those 180° domains that are directed unfavourably in each T-domain to disappear, and then the rotation process follows.

In easy-plane antiferromagnets, the T-domain structure is destroyed by a small magnetic field and the antiferromagnetic vector \mathbf{L} in the whole specimen becomes directed perpendicular to the applied magnetic field, as was explained in Section 1.5.3.

There are four kinds of T-domains in cubic antiferromagnets, in which the vectors \mathbf{L} are directed parallel or perpendicular to the four $\langle 111 \rangle$ axes. Such a T-domain structure can be destroyed only when the applied magnetic field is so strong that the antiferromagnetic order is destroyed at a spin-flip transition.

1.5.4.3. Ferroic domains

Aizu (1970) gave a classification of domain formation when a crystal undergoes a transition from an unordered to a magnetically ordered state that has a lower point-group symmetry (see also Section 3.1.1). The unordered state (called the prototype phase) has a grey point group. The number of elements in this group is equal to the product of the number of elements in the point group of the ordered state (called the ferroic state) times the number of domains. Aizu found that there are 773 possible combinations of the point-group symmetries of the prototype and the ferroic state, if crystallographically inequivalent orientations of the subgroup in the group of the prototype are distinguished. These 773 combinations are called ferroic species and are characterized by a symbol giving first the point group of the prototype, then the letter F, then the point group of the ferroic state and finally a letter between parentheses if different orientations are possible. As an example, the 2' axis of the ferroic state is parallel to the fourfold axis of the prototype in 4221'F2'(p) and perpendicular to it in 4221'F2'(s).

Let us discuss the ferroic states of rhombohedral transition-metal oxides given in Table 1.5.3.4. The paramagnetic prototype has point group $\bar{3}m1'$. The four monoclinic ferroic species have six domains ('orientation states') each, which form three pairs of 180° domains ('time-conjugate orientation states'). All four species are 'fully ferroelastic', i.e. the three pairs show different orientations of the spontaneous strain; two of the four species ($\bar{3}m1'F2'/m'$ and $\bar{3}m1'F2'/m$) are also 'fully ferromagnetic' because all six domains have different orientations of the spontaneous magnetization. Switching a domain into another with a different orientation of the spontaneous strain can be achieved by applying mechanical stress. If the domain was spontaneously magnetized, the orientation of the magnetization is changed simultaneously. Similarly, a domain can be switched into another with a different orientation of the spontaneous magnetization by means of a magnetic field. If the two spontaneous magnetizations have different directions (not just opposite sign), the direction of the spontaneous strain will change at the same time.

The Aizu classification is of interest for technological applications because it gives an overall view not only of domain formation but also of the possibilities for domain switching.

1.5.5. Weakly non-collinear magnetic structures

As was indicated above (see Tables 1.5.3.3 and 1.5.3.6), certain magnetic space groups allow the coexistence of two different types of magnetic ordering. Some magnetic structures can be described as a superposition of two antiferromagnetic structures with perpendicular antiferromagnetic vectors \mathbf{L}_α . Such structures

may be called weakly non-collinear antiferromagnets. There can also be a superposition of an antiferromagnetic structure \mathbf{L} with a ferromagnetic one \mathbf{M} (with $\mathbf{L} \perp \mathbf{M}$). This phenomenon is called weak ferromagnetism. We shall demonstrate in this section why one of the magnetic vectors has a much smaller value than the other in such mixed structures.

1.5.5.1. Weak ferromagnetism

The theory of weak ferromagnetism was developed by Dzyaloshinskii (1957a). He showed that the expansion of the thermodynamic potential Φ may contain terms of the following type: $L_i M_k$ ($i, k = x, y$). Such terms are invariant with respect to the transformations of many crystallographic space groups (see Section 1.5.3.3). If there is an antiferromagnetic ordering in the material ($L_i \neq 0$) and the thermodynamic potential of the material contains such a term, the minimum of the potential will be obtained only if $M_k \neq 0$ as well. The term $L_i M_k$ is a relativistic one. Therefore this effect must be small.

We shall consider as an example the origin of weak ferromagnetism in the two-sublattice antiferromagnets MnCO_3 , CoCO_3 and NiCO_3 , discussed in Section 1.5.3.1. The following analysis can be applied also to the four-sublattice antiferromagnet $\alpha\text{-Fe}_2\text{O}_3$ (assuming $\mathbf{L}_1 = \mathbf{L}_2 = 0$, $\mathbf{L}_3 = \mathbf{L}$). All these rhombohedral crystals belong to the crystallographic space group $D_{3d}^6 = R\bar{3}c$. The thermodynamic potential Φ for these crystals was derived in Section 1.5.3.3. For the case of a two-sublattice antiferromagnet, one has to add to the expression (1.5.3.26) the invariant (1.5.3.24):

$$\Phi = (A/2)\mathbf{L}^2 + (B/2)\mathbf{M}^2 + (a/2)L_z^2 + (b/2)M_z^2 + d(L_x M_y - L_y M_x) - \mathbf{M}\mathbf{H}. \quad (1.5.5.1)$$

The coefficients of the isotropic terms (A and B) are of exchange origin. They are much larger than the coefficients of the relativistic terms (a, b, d). Minimization of Φ for a fixed value of \mathbf{L}^2 and $\mathbf{H} = 0$ gives two solutions:

(1) $\mathbf{L} \parallel Oz$ ($L_x = L_y = 0$, $\mathbf{M} = 0$). FeCO_3 and the low-temperature modification of $\alpha\text{-Fe}_2\text{O}_3$ possess such purely antiferromagnetic structures.

(2) $\mathbf{L} \perp Oz$ [$M_x = (d/B)L_y$, $M_y = (d/B)L_x$, $M_z = 0$]. This structure exhibits a spontaneous ferromagnetic moment

$$M_D = (M_x^2 + M_y^2)^{1/2} = (d/B)L. \quad (1.5.5.2)$$

The magnetic moment M_D is smaller than the magnetization of the sublattices ($M_0 = L/2$) in the ratio $2d/B$. This phenomenon is therefore called weak ferromagnetism. The vectors \mathbf{M}_D and \mathbf{L} are mutually perpendicular. Their direction in the plane is determined by the sixth-order terms of the anisotropy energy (see Section 1.5.3.2). This anisotropy is extremely small in most materials. The vectors of magnetization of the sublattices \mathbf{M}_0 are deflected by a small angle $\varphi \simeq 2d/B$ away from the direction of the antiferromagnetic axis \mathbf{L} in such weak ferromagnets (see Fig. 1.5.5.1).

Weak ferromagnetism was first observed in the following trigonal crystals: the high-temperature modification of haematite, $\alpha\text{-Fe}_2\text{O}_3$ (Townsend Smith, 1916; Néel & Pauthenet, 1952), MnCO_3 (Borovik-Romanov & Orlova, 1956) and later also in CoCO_3 , NiCO_3 and FeBO_3 . In accordance with theory, weak ferromagnetism does not occur in trigonal crystals with a positive anisotropy coefficient a . Such crystals become easy-axis antiferromagnets. Of this type are FeCO_3 and the low-temperature modification of $\alpha\text{-Fe}_2\text{O}_3$. For four-sublattice antiferromagnets, the sequence of the directions of the magnetic moments of the sublattices is also essential. For example, the structures of the types \mathbf{A}_1 and \mathbf{A}_2 (see Fig. 1.5.3.4 and Table 1.5.3.3) do not exhibit weak ferromagnetism.

1. TENSORIAL ASPECTS OF PHYSICAL PROPERTIES

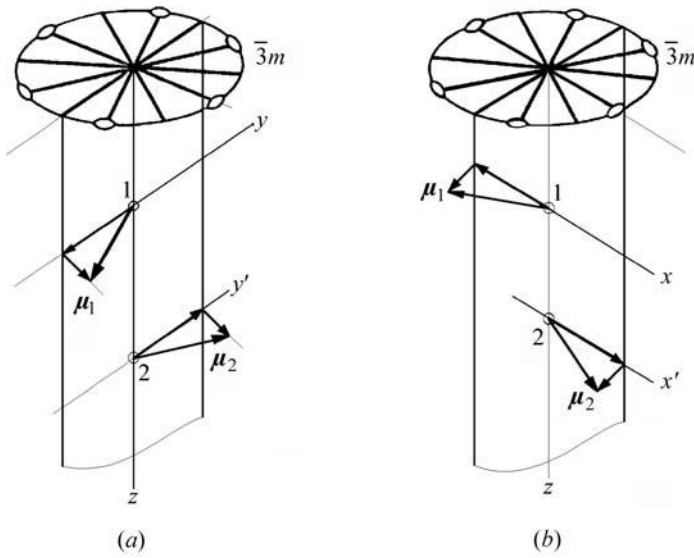


Fig. 1.5.5.1. Diagrams demonstrating two weakly ferromagnetic structures in rhombohedral crystals with two magnetic ions in the primitive cell (compare with Fig. 1.5.3.1). (a) Magnetic space group $P2/c$; (b) magnetic space group $P2'/c$.

The behaviour of weak ferromagnets in magnetic fields applied perpendicular (H_{\perp}) and parallel (H_{\parallel}) to the trigonal axis is described by the following relations:

$$M_{\perp} = M_D + \chi_{\perp} H_{\perp}, \quad M_{\parallel} = \chi_{\parallel} H_{\parallel}, \quad (1.5.5.3)$$

where

$$\chi_{\perp} = 1/B, \quad \chi_{\parallel} = 1/(B + b). \quad (1.5.5.4)$$

An external magnetic field can freely rotate the ferromagnetic moment in the basal plane of the easy-plane weak ferromagnets under consideration because their anisotropy in the basal plane is extremely small. During such a rotation, both vectors \mathbf{M} and \mathbf{L} move simultaneously as a rigid structure. On the other hand, it is impossible to deflect the vector \mathbf{M}_D out of the basal plane, as this is forbidden by symmetry. This is illustrated by the magnetization curves plotted in Fig. 1.5.5.2, which confirm the relations (1.5.5.3).

It is worth mentioning that when the weakly ferromagnetic structure is rotated in the basal plane, a change of the magnetic space groups occurs in the following order: $P2/c \leftrightarrow P\bar{1} \leftrightarrow P2'/c \leftrightarrow P\bar{1} \leftrightarrow P2/c \leftrightarrow \dots$. Each of these symmetry transformations corresponds to a second-order phase transition. Such transitions are allowed because $P\bar{1}$ is a subgroup of both groups $P2/c$ and $P2'/c$.

NiF_2 was one of the first weak ferromagnets to be discovered (Matarrese & Stout, 1954). In the paramagnetic state, it is a tetragonal crystal. Its crystallographic space group is $D_{4h}^{14} = P4_2/mnm$. In the ordered state its magnetic point group is $D_{2h}(C_{2h}) = mm'm'$ and the vectors \mathbf{L} and \mathbf{M} are directed along two twofold axes (one of which is primed) in the plane perpendicular to the former fourfold axis (see Fig. 1.5.5.3a). The invariant term responsible for the weak ferromagnetism in tetragonal fluorides has the form

$$d(L_x M_y + L_y M_x). \quad (1.5.5.5)$$

The anisotropy of the crystals of NiF_2 and the relation given above for the invariant lead to the same dependence on the magnetic field as for trigonal crystals. However, the anisotropy of the magnetic behaviour in the basal plane is much more complicated than for rhombohedral crystals (see Bazhan & Bazan, 1975). The anisotropy constant K_1 is positive for most other fluorides (MnF_2 , FeF_2 and CoF_2) and their magnetic structure is described by the magnetic point group

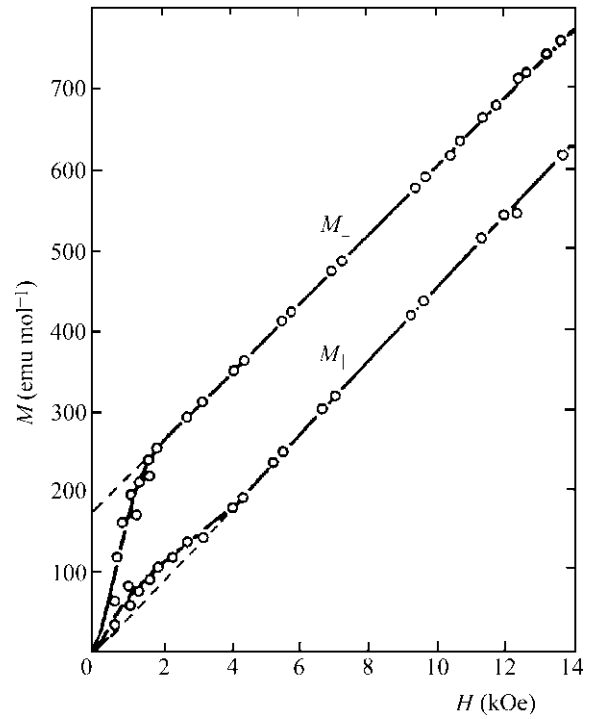


Fig. 1.5.5.2. Dependence of magnetization M_{\perp} and M_{\parallel} on the magnetic field H for the weak ferromagnet MnCO_3 at 4.2 K (Borovik-Romanov, 1959a).

$D_{4h}(D_{2h}) = 4'/mmm'$. They are easy-axis antiferromagnets without weak ferromagnetism.

The interaction described by the invariant $d(L_x M_y - L_y M_x)$ in equation (1.5.5.1) is called Dzyaloshinskii–Moriya interaction. It corresponds to the interaction between the spins of neighbouring ions, which can be represented in the form

$$d[\mathbf{S}_i \times \mathbf{S}_j], \quad (1.5.5.6)$$

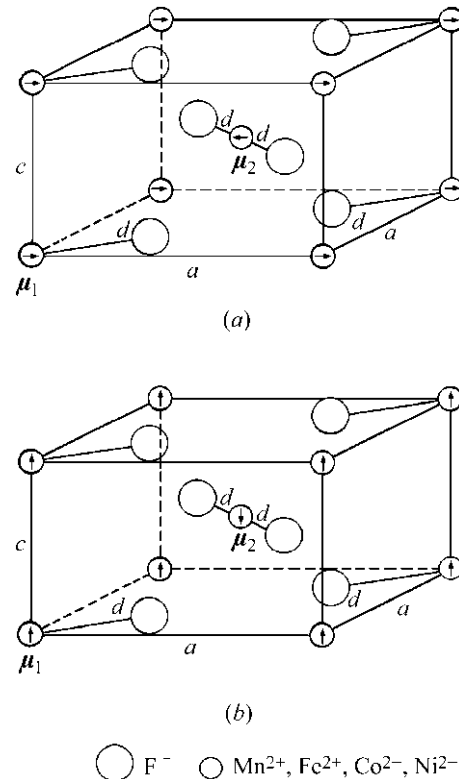


Fig. 1.5.5.3. Magnetic structures of fluorides of transition metals. (a) The weak ferromagnet NiF_2 ; (b) the easy-axis antiferromagnets MnF_2 , FeF_2 and CoF_2 .

1.5. MAGNETIC PROPERTIES

where the vector \mathbf{d} has the components $(0, 0, d_z)$. Terms of such type are allowed by symmetry for crystals that in the paramagnetic state belong to certain space groups of the trigonal, tetragonal and hexagonal systems. In some groups of the tetragonal system, weak ferromagnetism is governed by the term $d(L_x M_y + L_y M_x)$ (as for NiF_2) and in the orthorhombic system by $(d_1 L_i M_k + d_2 L_k M_i)$, $(i, k = x, y, z)$. In the monoclinic system, the latter sum contains four terms. The weak ferromagnetism in most groups of the hexagonal and cubic systems is governed by invariants of fourth and sixth order of L_i, M_k . Turov (1963) determined for all crystallographic space groups the form of the invariants of lowest order that allow a phase transition into a state with weak ferromagnetism. The corresponding list of the numbers of the space groups that allow the transition into an antiferromagnetic state with weak ferromagnetism is given in Table 1.5.5.1. The form of the invariant responsible for weak ferromagnetism is also displayed in the table. Turov (1963) showed that weak ferromagnetism is forbidden for the triclinic system, for 14 tetragonal groups, six trigonal groups and 12 cubic groups (those with point groups $T = 23$ or $T_h = m\bar{3}$).

The microscopic theory of the origin of weak ferromagnetism was given by Moriya (1960a,b, 1963). In this chapter, however, we have restricted our consideration to the phenomenological approach to this problem.

A large number of orthorhombic orthoferrites and orthochromites with the formula RMO_3 (where R is a trivalent rare-earth ion and M is Fe^{3+} or Cr^{3+}) have been investigated in many laboratories (cf. Wijn, 1994). Some of them exhibit weak ferromagnetism. The space group of these compounds is $\mathbf{D}_{2h}^{16} = Pnma$ in the paramagnetic state. The primitive cell is the same in the paramagnetic and magnetically ordered states. It contains four magnetic transition-metal ions (see Fig. 1.5.5.4). They determine to a large extent the properties of orthoferrites (outside the region of very low temperatures). For a four-sublattice antiferromagnet, there are four possible linear combinations of the sublattice vectors, which define three types of antiferromagnetic vectors \mathbf{L}_α and one ferromagnetic vector \mathbf{F} [see relations (1.5.3.2) and Table 1.5.3.1]. The exchange interaction in these compounds governs magnetic structures, which to a first approximation are described by the following antiferromagnetic vector (which is usually denoted by the symbol \mathbf{G}):

$$\mathbf{G} = \mathbf{L}_2 = (N/4)(\mu_1 - \mu_2 + \mu_3 - \mu_4). \quad (1.5.5.7)$$

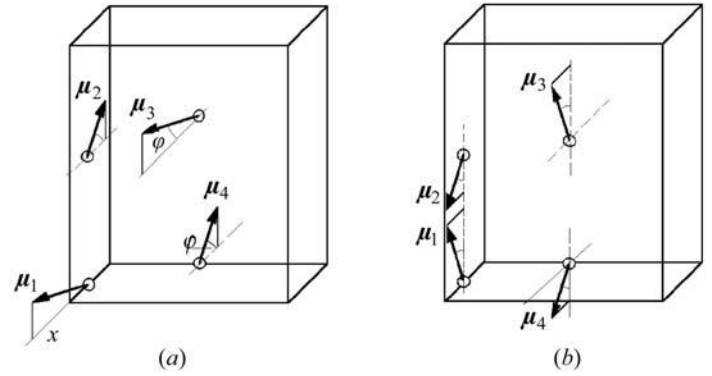
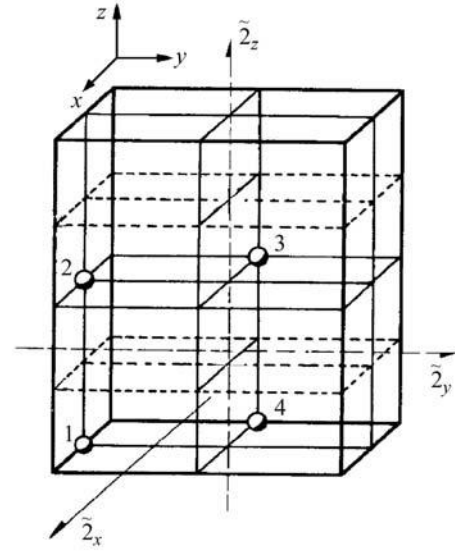


Fig. 1.5.5.4. Magnetic structures of orthoferrites and orthochromites RMO_3 . (Only the transition-metal ions are shown; the setting $Pnma$ is used.) (a) $\mathbf{G}_x \mathbf{F}_z$ weakly ferromagnetic state; (b) $\mathbf{G}_z \mathbf{F}_x$ weakly ferromagnetic state.

In the case of orthoferrites, the other two antiferromagnetic vectors \mathbf{L}_1 and \mathbf{L}_3 [see relations (1.5.3.2)] are named \mathbf{A} and \mathbf{C} , respectively.

The magnetic structure of the compounds under consideration is usually called the \mathbf{G}_i or $\mathbf{G}_i \mathbf{F}_k$ state. Depending on the signs and

Table 1.5.5.1. The numbers of the crystallographic space groups that allow a phase transition into a weakly ferromagnetic state and the invariants that are responsible for weak ferromagnetism (Turov, 1963)

| System | Nos. of the space groups | Invariants | Case No. |
|--------------|---------------------------|---|----------|
| Monoclinic | 3–15 | $M_x L_y, M_z L_y, M_y L_x, M_y L_z$ | 1 |
| Orthorhombic | 16–74 | $M_x L_y, M_y L_x$ | 2 |
| | | $M_y L_z, M_z L_y$ | 3 |
| | | $M_x L_z, M_z L_x$ | 4 |
| | | | |
| Tetragonal | 81–92, 101–142 | $M_x L_y + M_y L_x, M_x L_x - M_y L_y$ | 5 |
| | | $M_x L_y - M_y L_x$ | 6 |
| | | $M_x L_y + M_y L_x$ | 7 |
| | | $M_x L_x - M_y L_y$ | 8 |
| | | | |
| Trigonal | 147–159, 162–167 | $M_x L_y - M_y L_x$ | 9 |
| | | $M_x L_y - M_y L_x$ | 10 |
| | | | |
| Hexagonal | 168–173, 178, 179, 190 | $M_z (L_x \pm i L_y)^3, (M_x \pm i M_y)(L_x \pm i L_y)^2 L_z$ | 11 |
| | 174–177, 180–189, 191–194 | $M_x L_y - M_y L_x$ | 12 |
| | | $i M_z [(L_x + i L_y)^3 - (L_x - i L_y)^3],$ $i [(M_x + i M_y)(L_x + i L_y)^2 - (M_x - i M_y)(L_x - i L_y)^2] L_z$ | 13 |
| | | $M_z [(L_x + i L_y)^3 + (L_x - i L_y)^3],$ $[(M_x + i M_y)(L_x + i L_y)^2 + (M_x - i M_y)(L_x - i L_y)^2] L_z$ | 14 |
| | | | |
| Cubic | 207–230 | $M_x L_x (L_y^2 - L_z^2) + M_y L_y (L_z^2 - L_x^2) + M_z L_z (L_x^2 - L_y^2)$ | 15 |

1. TENSORIAL ASPECTS OF PHYSICAL PROPERTIES

the values of the anisotropy constants, there are three possible magnetic states:

$$(I) \quad \mathbf{G}_x \mathbf{F}_z \quad L_{2x} \neq 0; \quad M_{Dz} \neq 0, \quad (1.5.5.8)$$

$$(II) \quad \mathbf{G}_y \quad L_{2y} \neq 0; \quad \mathbf{M}_D = 0, \quad (1.5.5.9)$$

$$(III) \quad \mathbf{G}_z \mathbf{F}_x \quad L_{2z} \neq 0; \quad M_{Dx} \neq 0. \quad (1.5.5.10)$$

The magnetic structures (I) and (III) are weak ferromagnets. They are displayed schematically in Fig. 1.5.5.4. Both are described by the same magnetic point group $\mathbf{D}_{2h}(\mathbf{C}_{2h})$ yet in different orientations: $m'm'm'$ (i.e. $2'_x/m'_x \ 2'_y/m'_y \ 2_z/m_z$) for structure (I) and $mm'm'$ (i.e. $2_x/m_x \ 2'_y/m'_y \ 2'_z/m'_z$) for structure (III). The magnetic point group of structure (II) is $\mathbf{D}_{2h} = mmm$.

Weak ferromagnetism is observed in boracites with chemical formula $M_3B_7O_{13}X$ (where $M = \text{Co, Ni}$ and $X = \text{Br, Cl, I}$). These compounds are unique, being simultaneously antiferromagnets, weak ferromagnets and ferroelectrics. Section 1.5.8.3 is devoted to these ferromagnetoelectrics.

Concerning the magnetic groups that allow weak ferromagnetism, it should be noted that, as for any ferromagnetism, weak ferromagnetism is allowed only in those space groups that have a trivial magnetic Bravais lattice. There must be at least two magnetic ions in the primitive cell to get antiferromagnetic order. Among the 31 magnetic point groups that admit ferromagnetism (see Table 1.5.2.4), weak ferromagnetism is forbidden in the magnetic groups belonging to the tetragonal, trigonal and hexagonal systems. Twelve magnetic point groups that allow weak ferromagnetism remain. These groups are listed in Table 1.5.5.2.

A material that becomes a weak ferromagnet below the Néel temperature T_N differs from a collinear antiferromagnet in its behaviour above T_N . A magnetic field applied to such a material above T_N gives rise to an ordered antiferromagnetic state with vector \mathbf{L} directed perpendicular and magnetization \mathbf{M} parallel to the field. Thus, as in usual ferromagnets, the magnetic symmetry of a weak ferromagnet in a magnetic field is the same above and below T_N . As a result, the magnetic susceptibility has a maximum at $T = T_N$ [like the relations (1.5.3.34) and (1.5.3.35)]. This is true only if the magnetic field is aligned along the easy axis for weak ferromagnetism. Fig. 1.5.5.5 shows the anomalous anisotropy of the temperature dependence of the magnetic susceptibility in the neighbourhood of T_N for weak ferromagnets.

Similar anomalies in the neighbourhood of T_N are observed in materials with a symmetry allowing a transition into a weakly ferromagnetic state for which the sign of the anisotropy constant causes their transition into purely antiferromagnetic states.

1.5.5.2. Other weakly non-collinear magnetic structures

A thermodynamic potential $\tilde{\Phi}$ of the form (1.5.5.1) may give rise not only to the weak ferromagnetism considered above but also to the reverse phenomenon. If the coefficient B (instead of A) changes its sign and $b > 0$, the material will undergo a transition into a slightly canted ferromagnetic structure, in which $M_s \gg L_D$ and the expression for L_D is

$$L_D = (d/B)M_{s\perp}. \quad (1.5.5.11)$$

Experimental detection of such structures is a difficult problem and to date no-one has observed such a phenomenon.

The thermodynamic potential $\tilde{\Phi}$ of a four-sublattice antiferromagnet may contain the mixed invariant [see (1.5.3.24)]

$$d_1(L_{1x}L_{2y} - L_{1y}L_{2x}). \quad (1.5.5.12)$$

Such a term gives rise to a structure in which all four vectors of sublattice magnetization \mathbf{M}_α form a star, as shown in Fig. 1.5.5.6 (see also Fig. 1.5.1.3b). The angle 2α between the vectors μ_1 and μ_3 (or μ_2 and μ_4) is equal to d_1/A_2 if the main antiferromagnetic structure is defined by the vector \mathbf{l}_2 [see relation (1.5.3.2)]. Such a structure may occur in Cr_2O_3 . In most orthoferrites discussed above, such non-collinear structures are observed for all three cases: purely antiferromagnetic (\mathbf{G}_y) and weakly ferromagnetic ($\mathbf{G}_x \mathbf{F}_z$ and $\mathbf{G}_z \mathbf{F}_x$). The structure \mathbf{G}_y is not coplanar. Apart from the main antiferromagnetic vector \mathbf{G} aligned along the y axis, it possesses two other antiferromagnetic vectors: \mathbf{A} (aligned along the x axis) and \mathbf{C} (aligned along the z axis). The weakly ferromagnetic structure $\mathbf{G}_x \mathbf{F}_z$ has an admixture of the \mathbf{A}_y antiferromagnetic structure.

The helical (or spiral) structure described in Section 1.5.1.2.3 and depicted in Fig. 1.5.1.4 is also a weakly non-collinear antiferromagnetic structure. As mentioned above, this structure consists of atomic layers in which all the magnetic moments are

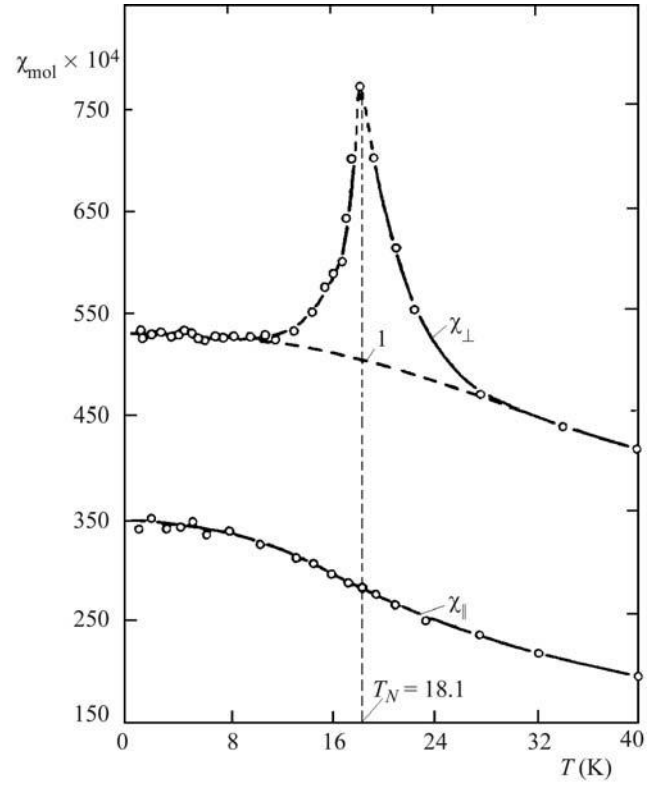


Fig. 1.5.5.5. Temperature dependence of the susceptibility for CoCO_3 (Borovik-Romanov & Ozhogin, 1960).

| Schoenflies | Hermann-Mauguin |
|------------------|-----------------|
| C_1 | 1 |
| C_i | $\bar{1}$ |
| C_2 | 2 |
| $C_2(C_1)$ | $2'$ |
| C_s | m |
| $C_s(C_1)$ | m' |
| C_{2h} | $2/m$ |
| $C_{2h}(C_i)$ | $2'/m'$ |
| $D_2(C_2)$ | $22'2'$ |
| $C_{2v}(C_2)$ | $m'm'2$ |
| $C_{2v}(C_s)$ | $m'm'2'$ |
| $D_{2h}(C_{2h})$ | mmm' |

Table 1.5.5.2. Magnetic point groups that allow weak ferromagnetism

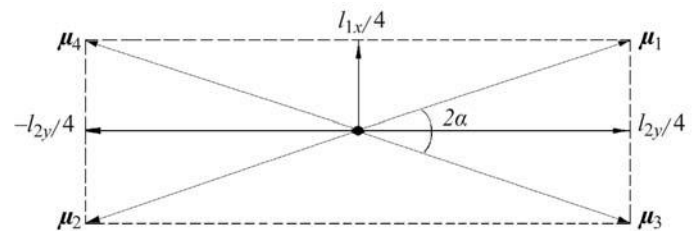


Fig. 1.5.5.6. A weakly non-collinear magnetic structure corresponding to (1.5.5.12).

1.5. MAGNETIC PROPERTIES

parallel to each other and parallel to the layer. The magnetizations of neighbouring layers are antiparallel to a first approximation; but, more specifically, there is a small deviation from a strictly antiparallel alignment. The layers are perpendicular to a vector \mathbf{k} , which is parallel to the axis of the helix. The two mutually perpendicular antiferromagnetic vectors \mathbf{L}_α are both perpendicular to \mathbf{k} . These vectors define the helical structure by the following relation for the density of the magnetization $\mathbf{M}(\mathbf{r})$ in the layer with the coordinate \mathbf{r} (Dzyaloshinskii, 1964; Andreev & Marchenko, 1980):

$$\mathbf{M}(\mathbf{r}) = \mathbf{L}_1 \sin \mathbf{k}\mathbf{r} - \mathbf{L}_2 \cos \mathbf{k}\mathbf{r}. \quad (1.5.5.13)$$

Most helical structures are incommensurate, which means that the representation defined by the vector \mathbf{k} does not satisfy the Lifshitz condition (see Section 1.5.3.3).

1.5.6. Reorientation transitions

In many materials, the anisotropy constants change sign at some temperature below the critical temperature. As a result, the direction of the vector \mathbf{L} (or \mathbf{M}_s) changes relative to the crystallographic axes. Correspondingly, the magnetic symmetry of the material also changes. Such phase transitions are called reorientation transitions.

Cobalt is a typical ferromagnet and experiences two such reorientation transitions. It is a hexagonal crystal, which at low temperatures behaves as an easy-axis ferromagnet; its magnetic point group is $D_{6h}(C_{6h}) = 6/m\bar{m}'m'$. If the anisotropy energy were described by the relations (1.5.3.6) and (1.5.3.7) with only one anisotropy constant K_1 , the change of the sign of this constant would give rise to a first-order transition from an easy-axis to an easy-plane antiferromagnet. This transition would occur at the temperature T_c at which $K_1(T) = 0$. In fact, the polar angle θ which determines the direction of the spontaneous magnetization increases progressively over a finite temperature interval. The behaviour of θ during the process of this reorientation may be obtained by minimizing the expression of the anisotropy energy (1.5.3.10), which contains two anisotropy coefficients K_1 and K_2 . If $K_2 > 0$, the minimum of U_a corresponds to three magnetic phases, which belong to the following magnetic point groups:

(1) $D_{6h}(C_{6h}) = 6/m\bar{m}'m'$; for this phase $\theta = 0, \pi$. It is realized at temperatures $T < T_1 = 520$ K, where $K_1 > 0$.

(2) $C_{2h}(C_i) = 2'/m'$; for this phase $\sin \theta = \pm(-K_1/2K_2)^{1/2}$. It is realized at temperatures $T_1 = 520 < T < T_2 = 580$ K, where $-2K_2 < K_1 < 0$.

(3) $D_{2h}(C_{2h}) = mm'm'$; for this phase $\theta = \pi/2$. It is realized at temperatures $T_2 = 580 < T < T_c = 690$ K, where $K_1 < -2K_2$.

The low-temperature phase is of the easy-axis type and the high-temperature phase is of the easy-plane type. The intermediate phase is called the angular phase. The two second-order phase transitions occur at temperatures which are the roots of the two equations

$$K_1(T_1) = 0; \quad K_1(T_2) + 2K_2(T_2) = 0. \quad (1.5.6.1)$$

The chain of these transitions (including the transition to the paramagnetic state at $T = T_c$) may be represented by the following chain of the corresponding magnetic point groups:

$$\begin{aligned} D_{6h}(C_{6h}) = 6/m\bar{m}'m' &\longleftrightarrow C_{2h}(C_i) = 2'/m' \\ &\longleftrightarrow D_{2h}(C_{2h}) = mm'm' \\ &\longleftrightarrow (D_{6h} + RD_{6h}) = 6/mmm1'. \end{aligned}$$

In Co and most of the other ferromagnets, the rotation of the spontaneous magnetization described above may be obtained by applying an external magnetic field in an appropriate direction. In many antiferromagnets, there occur similar reorientation

transitions, which cannot be achieved by means of a magnetic field.

The first reorientation transition in antiferromagnets was observed in haematite (α -Fe₂O₃), which at room temperature is a weak ferromagnet with magnetic structure A_{3x} or A_{3y} (see Tables 1.5.3.3 and 1.5.3.4 in Section 1.5.3.1). Morin (1950) found that the weak ferromagnetism in haematite disappears below $T_M \simeq 260$ K. At low temperature, haematite becomes an easy-axis antiferromagnet with the structure A_{3z} . Unlike in cobalt, the transition at T_M is a first-order transition in haematite. This is so because the anisotropy constant K_2 is negative in haematite. As a result, there are only two solutions for the angle θ that lead to a minimum of the anisotropy energy $U_a(3)$ [(1.5.3.9)], $\theta = 0$ if $K_1 > -K_2$ and $\theta = \pi/2$ if $K_1 < -K_2$. The transition temperature T_M is defined by

$$K_1(T_M) + K_2(T_M) = 0. \quad (1.5.6.2)$$

There is the following change in the magnetic space groups at this transition:

$$R\bar{3}c' \xrightarrow{T_M} \begin{cases} P2/c \\ P2'/c' \end{cases} \quad (1.5.6.3)$$

$$(1.5.6.4)$$

Which of the two groups is realized at high temperatures depends on the sign of the anisotropy constant K'_\perp in equation (1.5.3.9). Neither of the high-temperature magnetic space groups is a subgroup of the low-temperature group. Therefore the transition under consideration cannot be a second-order transition.

Reorientation transitions have been observed in many orthoferrites and orthochromites. Orthoferrites of Ho, Er, Tm, Nd, Sm and Dy possess the structure $G_x F_z$ [see (1.5.5.8)] at room temperature. The first five of them undergo reorientation transitions to the structure $G_z F_x$ at lower temperatures. This reorientation occurs gradually, as in Co. Both vectors \mathbf{L} and \mathbf{M}_D rotate simultaneously, as shown in Fig. 1.5.6.1. These vectors remain perpendicular to each other, but the value of \mathbf{M}_D varies from $(d_1/B)L$ for M_{Dz} to $(d_2/B)L$ for M_{Dx} . The coefficients d_1 and d_2 belong to the terms $L_x M_z$ and $L_z M_x$, respectively. The following magnetic point groups are observed when these transitions occur:

$$\frac{2'_x}{m'_x} \frac{2'_y}{m'_y} \frac{2'_z}{m'_z} \xrightarrow{T_1} \frac{2'_y}{m'_y} \xrightarrow{T_2} \frac{2'_x}{m'_x} \frac{2'_y}{m'_y} \frac{2'_z}{m'_z}. \quad (1.5.6.5)$$

Anomalies typical for second-order transitions were observed at the temperatures T_1 and T_2 . The interval $T_2 - T_1$ varies from 10 to 100 K.

At low temperatures, DyFeO₃ is an easy-axis antiferromagnet without weak ferromagnetism – G_y . It belongs to the trivial magnetic point group $D_{2h} = mmm$. At $T_M = 40$ K, DyFeO₃ transforms into a weak ferromagnet $G_x F_z$. This is a first-order reorientation transition of the type

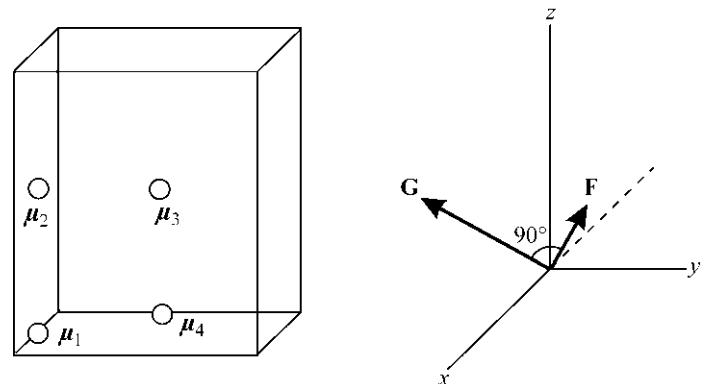


Fig. 1.5.6.1. Schematic representation of the rotation of the vectors \mathbf{G} and \mathbf{F} (in the xz plane) at a reorientation transition in orthoferrites.

1. TENSORIAL ASPECTS OF PHYSICAL PROPERTIES

$$\mathbf{D}_{2h} = mmm \xrightarrow{T_M} \mathbf{D}_{2h}(\mathbf{C}_{2h}) = m'm'm. \quad (1.5.6.6)$$

Reorientation transitions in antiferromagnets occur not only as a result of a sign change of the anisotropy constant. They can be governed by the applied magnetic field. In Section 1.5.3.3.2, we described the spin-flop first-order reorientation transition in an easy-axis antiferromagnet. This transition splits into two second-order transitions if the magnetic field is not strictly parallel to the axis of the crystal. There is a specific type of reorientation transition, which occurs in antiferromagnets that do not exhibit weak ferromagnetism, but would become weak ferromagnets if the antiferromagnetic vector was directed along another crystallographic direction. As an example, let us consider such a transition in CoF_2 . It is a tetragonal crystal with crystallographic space group $\mathbf{D}_{4h}^{14} = P4_2/mnm$. Below T_N , CoF_2 becomes an easy-axis antiferromagnet. The magnetic structure of this crystal is shown in Fig. 1.5.5.3. Its magnetic point group is $\mathbf{D}_{4h}(\mathbf{D}_{2h}) = 4'/mmm'$. Let us apply the magnetic field H parallel to the twofold axis x (see Fig. 1.5.6.2). In a typical antiferromagnet, the field stimulates a magnetization $\mathbf{M} = \chi_{\perp} \mathbf{H}$. The structure $\mathbf{D}_{4h}^{14} = P4_2/mnm$ allows weak ferromagnetism if \mathbf{L} is perpendicular to the z axis. As a result, if the vector \mathbf{L} is deflected from the z axis by an angle θ in the plane yz perpendicular to the x axis, the magnetization will rise according to the relation

$$\mathbf{M} = \chi_{\perp}(\mathbf{H} + H_D \sin \theta), \quad (1.5.6.7)$$

where $H_D = M_D/\chi_{\perp}$ [see (1.5.5.3) and (1.5.5.4)]. As a result, there is a gain in the magnetic energy, which compensates the loss in the anisotropy energy. The beginning of the deflection is a second-order transition. The balance of both energies determines the value of θ :

$$\sin \theta = (H_e/H_a H_D) H. \quad (1.5.6.8)$$

The second second-order transition occurs when θ becomes equal to $\pi/2$ at the critical field H_c :

$$H_c = H_D H_a / H_e. \quad (1.5.6.9)$$

After the reorientation transition, CoF_2 has the same magnetic point group as the weak ferromagnet NiF_2 , i.e. $\mathbf{D}_{2h}(\mathbf{C}_{2h}) = mm'm'$.

1.5.7. Piezomagnetism

As we have seen, the appearance of weak ferromagnetism in antiferromagnets is closely connected with their magnetic symmetry. If the magnetic point group of the antiferromagnetic crystal contains an axis of higher than twofold symmetry, the magnetic structure is purely antiferromagnetic. By applying an external force that disturbs the symmetry of the crystal and destroys the axis of high symmetry, one may create a structure possessing weak ferromagnetism. In the previous section, we considered such reduction of the symmetry with the aid of a magnetic field applied perpendicular to the main axis of the crystal. Another possibility for symmetry reduction is to apply an external pressure and to deform the crystal. Thus, in some antiferromagnetic crystals, a ferromagnetic moment may be produced on application of external stress. This phenomenon is called piezomagnetism.

To investigate the piezomagnetic effect from the phenomenological point of view, we have to add the terms of the magnetoelastic energy in the expansion of the thermodynamic potential. The magnetoelastic terms of the least degree in the expansion of the thermodynamic potential $\tilde{\Phi}$ for a given stable magnetic structure will be of the type $T_{ij} M_k L_l$ (T_{ij} are the components of the elastic stress tensor \mathbf{T}). These terms must be invariant relative to the crystallographic group of the material under examination.

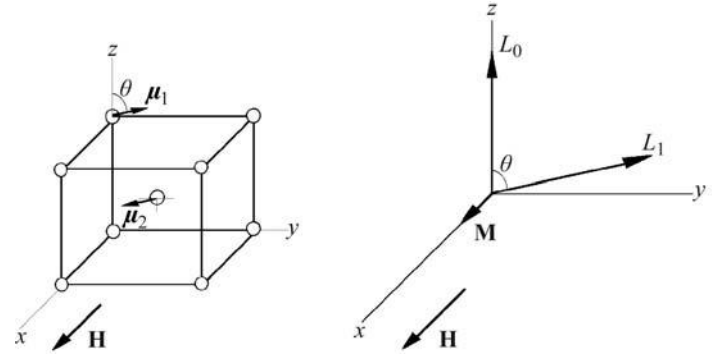


Fig. 1.5.6.2. Schematic representation of the rotation of the vector \mathbf{L} under the action of a magnetic field applied to CoF_2 perpendicular to the fourfold axis z (reorientation transition) (see Figs. 1.5.5.3a and b).

If we consider the potential Φ , which is a function of $T, \mathbf{T}, \mathbf{H}$, the terms of the magnetoelastic energy that are responsible for piezomagnetism are of the form $H_i T_{jk}$. Thus, for the piezomagnetic crystals the expansion of the thermodynamic potential should be expressed by

$$\Phi(T, \mathbf{T}, \mathbf{H}) = \Phi_0(T, \mathbf{H}) - \sum_{i,j,k} \Lambda_{ijk} H_i T_{jk}. \quad (1.5.7.1)$$

If at least one term of this expansion remains invariant under the magnetic symmetry of the given crystal, then the corresponding component Λ_{ijk} will not be zero and hence

$$M_i = -\partial\Phi/\partial H_i = -\partial\Phi_0/\partial H_i + \Lambda_{ijk} T_{jk}. \quad (1.5.7.2)$$

Thus, when a stress T_{jk} is applied, a magnetic moment is produced which is linear with the stress.

It follows from expression (1.5.7.1) that the converse of the piezomagnetic effect also exists, i.e. linear magnetostriction:

$$S_{jk} = -\partial\Phi/\partial T_{jk} = \Lambda_{ijk} H_i, \quad (1.5.7.3)$$

where S_{jk} are the components of the deformation tensor.

1.5.7.1. Piezomagnetic effect

The possibility of the existence of a piezomagnetic effect was first foreseen by Voigt (1928). However, he assumed that it is sufficient to consider only the crystallographic symmetry in order to predict this effect. In reality, the crystals that do not possess a magnetic structure are characterized by the transformation R being contained in the magnetic group as an independent element. The transformation R changes the sign of the magnetic vectors $\mathbf{H}, \mathbf{L}, \mathbf{M}$. Hence, for such crystals all values of Λ_{ijk} vanish and piezomagnetism is forbidden. The magnetic groups of magnetically ordered crystals (ferromagnets and antiferromagnets) contain R only in combination with other elements of symmetry, or do not contain this transformation at all. Hence the piezomagnetic effect may occur in such crystals. This statement was first made by Tavger & Zaitsev (1956). The most interesting manifestation of the piezomagnetic effect is observed in antiferromagnets, as there is no spontaneous magnetization in these materials.

From equation (1.5.7.1) it follows that Λ_{ijk} is an axial tensor of third rank. Hence, apart from the restriction that piezomagnetism is forbidden for all para- and diamagnetic materials, it must be absent from the 21 magnetic point groups that contain the element $C_i R = \bar{1}$ (see Table 1.5.7.1). The stress tensor T_{jk} is symmetrical ($T_{jk} = T_{kj}$); see Section 1.3.2.4. Thus the tensor Λ_{ijk} is symmetrical in its last two indices. This is the reason why piezomagnetism is prohibited for three more magnetic point groups: $\mathbf{O} = 432$, $\mathbf{T}_d = \bar{4}3m$ and $\mathbf{O}_h = m\bar{3}m$. The remaining 66 magnetic point groups were found by Tavger (1958), who also

1.5. MAGNETIC PROPERTIES

Table 1.5.7.1. *The forms of the matrix characterizing the piezomagnetic effect*

| Magnetic crystal class | | Matrix representation $\Lambda_{i\alpha}$ of the piezomagnetic tensor |
|---|---|---|
| Schoenflies | Hermann–Mauguin | |
| C_1 C_i | 1 $\bar{1}$ | $\begin{bmatrix} \Lambda_{11} & \Lambda_{12} & \Lambda_{13} & \Lambda_{14} & \Lambda_{15} & \Lambda_{16} \\ \Lambda_{21} & \Lambda_{22} & \Lambda_{23} & \Lambda_{24} & \Lambda_{25} & \Lambda_{26} \\ \Lambda_{31} & \Lambda_{32} & \Lambda_{33} & \Lambda_{34} & \Lambda_{35} & \Lambda_{36} \end{bmatrix}$ |
| C_2 C_s C_{2h} | 2 (= 121) m (= 1 m 1) $2/m$ (= 1 2/ m 1) (unique axis y) | $\begin{bmatrix} 0 & 0 & 0 & \Lambda_{14} & 0 & \Lambda_{16} \\ \Lambda_{21} & \Lambda_{22} & \Lambda_{23} & 0 & \Lambda_{25} & 0 \\ 0 & 0 & 0 & \Lambda_{34} & 0 & \Lambda_{36} \end{bmatrix}$ |
| $C_2(C_1)$ $C_3(C_1)$ $C_{2h}(C_i)$ | $2'$ (= 12'1) m' (= 1 m' 1) $2'/m'$ (= 1 2'/ m' 1) (unique axis y) | $\begin{bmatrix} \Lambda_{11} & \Lambda_{12} & \Lambda_{13} & 0 & \Lambda_{15} & 0 \\ 0 & 0 & 0 & \Lambda_{24} & 0 & \Lambda_{26} \\ \Lambda_{31} & \Lambda_{32} & \Lambda_{33} & 0 & \Lambda_{35} & 0 \end{bmatrix}$ |
| D_2 C_{2v} D_{2h} | 222 $mm2$ [$2mm$, $m2m$] mmm | $\begin{bmatrix} 0 & 0 & 0 & \Lambda_{14} & 0 & 0 \\ 0 & 0 & 0 & 0 & \Lambda_{25} & 0 \\ 0 & 0 & 0 & 0 & 0 & \Lambda_{36} \end{bmatrix}$ |
| $D_2(C_2)$ $C_{2v}(C_2)$ $C_{2v}(C_i)$ $D_{2h}(C_{2h})$ | $2'2'2$ $m'm'2$ $m'2'm$ [$2'm'm$] $m'm'm$ | $\begin{bmatrix} 0 & 0 & 0 & 0 & \Lambda_{15} & 0 \\ 0 & 0 & 0 & \Lambda_{24} & 0 & 0 \\ \Lambda_{31} & \Lambda_{32} & \Lambda_{33} & 0 & 0 & 0 \end{bmatrix}$ |
| C_4, C_6 S_4, C_3h C_{4h}, C_{6h} | 4, 6 $\bar{4}, \bar{6}$ $4/m, 6/m$ | $\begin{bmatrix} 0 & 0 & 0 & \Lambda_{14} & \Lambda_{15} & 0 \\ 0 & 0 & 0 & \Lambda_{15} & -\Lambda_{14} & 0 \\ \Lambda_{31} & \Lambda_{31} & \Lambda_{33} & 0 & 0 & 0 \end{bmatrix}$ |
| $C_4(C_2)$ $S_4(C_2)$ $C_{4h}(C_{2h})$ | $4'$ $\bar{4}'$ $4'/m$ | $\begin{bmatrix} 0 & 0 & 0 & \Lambda_{14} & \Lambda_{15} & 0 \\ 0 & 0 & 0 & -\Lambda_{15} & \Lambda_{14} & 0 \\ \Lambda_{31} & -\Lambda_{31} & 0 & 0 & 0 & \Lambda_{36} \end{bmatrix}$ |
| D_4, D_6 C_{4v}, C_{6v} D_{2d}, D_{3h} D_{4h}, D_{6h} | 422, 622 $4mm, 6mm$ $42m$ [$4m2$], $\bar{6}m2$ [$\bar{6}2m$] $4/mmm, 6/mmm$ | $\begin{bmatrix} 0 & 0 & 0 & \Lambda_{14} & 0 & 0 \\ 0 & 0 & 0 & 0 & -\Lambda_{14} & 0 \\ 0 & 0 & 0 & 0 & 0 & 0 \end{bmatrix}$ |
| $D_4(C_4), D_6(C_6)$ $C_{4v}(C_4), C_{6v}(C_6)$ $D_{2d}(S_4), D_{3h}(C_{3h})$ $D_{4h}(C_{4h}), D_{6h}(C_{6h})$ | $42'2', 62'2'$ $4m'm', 6m'm'$ $\bar{4}2'm'$ [$\bar{4}m'2'$], $\bar{6}m'2'$ [$\bar{6}2'm'$] $4/mm'm', 6/mmm'm'$ | $\begin{bmatrix} 0 & 0 & 0 & 0 & \Lambda_{15} & 0 \\ 0 & 0 & 0 & \Lambda_{15} & 0 & 0 \\ \Lambda_{31} & \Lambda_{31} & \Lambda_{33} & 0 & 0 & 0 \end{bmatrix}$ |
| $D_4(D_2)$ $C_{4v}(C_{2v})$ $D_{2d}(D_2), D_{2d}(C_{2v})$ $D_{4h}(D_{2h})$ | $4'22'$ $4'mm'$ $4'2m', \bar{4}'m2'$ $4'/mmm'$ | $\begin{bmatrix} 0 & 0 & 0 & \Lambda_{14} & 0 & 0 \\ 0 & 0 & 0 & 0 & \Lambda_{14} & 0 \\ 0 & 0 & 0 & 0 & 0 & \Lambda_{36} \end{bmatrix}$ |
| C_3 S_6 | 3 $\bar{3}$ | $\begin{bmatrix} \Lambda_{11} & -\Lambda_{11} & 0 & \Lambda_{14} & \Lambda_{15} & -2\Lambda_{22} \\ -\Lambda_{22} & \Lambda_{22} & 0 & \Lambda_{15} & -\Lambda_{14} & -2\Lambda_{11} \\ \Lambda_{31} & \Lambda_{31} & \Lambda_{33} & 0 & 0 & 0 \end{bmatrix}$ |
| D_3 C_{3v} D_{3d} | 32 (= 321) $3m$ (= 3 m 1) $\bar{3}m$ (= $\bar{3}m$ 1) | $\begin{bmatrix} \Lambda_{11} & -\Lambda_{11} & 0 & \Lambda_{14} & 0 & 0 \\ 0 & 0 & 0 & 0 & -\Lambda_{14} & -2\Lambda_{11} \\ 0 & 0 & 0 & 0 & 0 & 0 \end{bmatrix}$ |
| $D_3(C_3)$ $C_{3v}(C_3)$ $D_{3d}(S_6)$ | $32'$ (= 32'1) $3m'$ (= 3 m' 1) $\bar{3}m'$ (= $\bar{3}m'$ 1) | $\begin{bmatrix} 0 & 0 & 0 & 0 & \Lambda_{15} & -2\Lambda_{22} \\ -\Lambda_{22} & \Lambda_{22} & 0 & \Lambda_{15} & 0 & 0 \\ \Lambda_{31} & \Lambda_{31} & \Lambda_{33} & 0 & 0 & 0 \end{bmatrix}$ |
| $C_6(C_3)$ $C_{3h}(C_3)$ $C_{6h}(S_6)$ | $6'$ $\bar{6}'$ $6'/m'$ | $\begin{bmatrix} \Lambda_{11} & -\Lambda_{11} & 0 & 0 & 0 & -2\Lambda_{22} \\ -\Lambda_{22} & \Lambda_{22} & 0 & 0 & 0 & -2\Lambda_{11} \\ 0 & 0 & 0 & 0 & 0 & 0 \end{bmatrix}$ |
| $D_6(D_3)$ $C_{6v}(C_{3v})$ $D_{3h}(D_3), D_{3h}(C_{3v})$ $D_{6h}(D_{3d})$ | $6'22'$ $6'mm'$ $\bar{6}'2m', \bar{6}'m2'$ $6'/m'mm'$ | $\begin{bmatrix} \Lambda_{11} & -\Lambda_{11} & 0 & 0 & 0 & 0 \\ 0 & 0 & 0 & 0 & 0 & -2\Lambda_{11} \\ 0 & 0 & 0 & 0 & 0 & 0 \end{bmatrix}$ |
| T, T_h $O(T)$ $T_d(T)$ $O_h(T_h)$ | 23, $\bar{m}\bar{3}$ $4'32'$ $\bar{4}'3m'$ $m\bar{3}m'$ | $\begin{bmatrix} 0 & 0 & 0 & \Lambda_{14} & 0 & 0 \\ 0 & 0 & 0 & 0 & \Lambda_{14} & 0 \\ 0 & 0 & 0 & 0 & 0 & \Lambda_{14} \end{bmatrix}$ |

1. TENSORIAL ASPECTS OF PHYSICAL PROPERTIES

constructed the 16 corresponding forms of the piezomagnetic tensors appropriate to each point group. They are represented in Table 1.5.7.1. (See also Birss & Anderson, 1963; Birss, 1964.)

Since the stress tensor T_{jk} is symmetrical, it has only six independent components. Therefore the notation of its components can be replaced by a matrix notation (Voigt's notation, see Section 1.3.2.5) in the following manner:

| Tensor notation | Matrix notation |
|------------------|-----------------|
| T_{11} | T_1 |
| T_{22} | T_2 |
| T_{33} | T_3 |
| T_{23}, T_{32} | T_4 |
| T_{31}, T_{13} | T_5 |
| T_{12}, T_{21} | T_6 |

In matrix notation, equation (1.5.7.2) may be written in the form

$$M_i = \Lambda_{i\alpha} T_\alpha, \quad (1.5.7.4)$$

where $i = 1, 2, 3$ and $\alpha = 1, 2, 3, 4, 5, 6$. These notations are used in Table 1.5.7.1. Notice that $\Lambda_{ij} = \Lambda_{iji}$ for $j = 1, 2, 3$, $\Lambda_{i4} = 2\Lambda_{i23}$, $\Lambda_{i5} = 2\Lambda_{i31}$, and $\Lambda_{i6} = 2\Lambda_{i12}$.

The form of the matrix $\Lambda_{i\alpha}$ depends on the orientation of the axes of the Cartesian coordinate system (CCS) with respect to the symmetry axes of the point group of the crystal under consideration. These symmetry axes may be rotation axes, rotoinversion axes or mirror-plane normals, all possibly combined with time reversal. The usual orientations of the CCS with respect to the symmetry axes can be expressed by the order of the entries in the Hermann–Mauguin symbol. An entry consists (apart from possible primes and bars) of a number $N = 1, 2, 3, 4$ or 6 or the letter m or N/m ($= \frac{N}{m}$). The conventional rules will be followed: in the monoclinic and orthorhombic crystal systems the x, y and z axes of the CCS are parallel to the symmetry axes given in the first, second and third entries, respectively. In the monoclinic system, there is only one symmetry axis, which is usually chosen parallel to the y axis, and a short Hermann–Mauguin symbol with only one entry is usually used, e.g. $2/m$ instead of $12/m1$. In the trigonal and hexagonal systems, the z, x and y axes are parallel to the symmetry axes given in the first, second and third entries, respectively. In the tetragonal system, the z axis is parallel to the symmetry axis given in the first entry, and the x and y axes are parallel to the symmetry axes given in the second entry, which appear in two mutually perpendicular directions. In the cubic system, the symmetry axes given in the first entry appear in three mutually perpendicular directions; the x, y and z axes of the CCS are chosen parallel to these directions. Alternative orientations of the same point group that give rise to the same form of $\Lambda_{i\alpha}$ have been added between square brackets [] in Table 1.5.7.1. Notice that the Schoenflies notation does not allow us to distinguish different orientations of the CCS with respect to the symmetry axes.

The forms of $\Lambda_{i\alpha}$ for frequently encountered orientations of the CCS other than those given in Table 1.5.7.1 are

(1) $112, 11m, 112/m$ (unique axis z):

$$\begin{bmatrix} 0 & 0 & 0 & \Lambda_{14} & \Lambda_{15} & 0 \\ 0 & 0 & 0 & \Lambda_{24} & \Lambda_{25} & 0 \\ \Lambda_{31} & \Lambda_{32} & \Lambda_{33} & 0 & 0 & \Lambda_{36} \end{bmatrix};$$

(2) $112', 11m', 112'/m'$ (unique axis z):

$$\begin{bmatrix} \Lambda_{11} & \Lambda_{12} & \Lambda_{13} & 0 & 0 & \Lambda_{16} \\ \Lambda_{21} & \Lambda_{22} & \Lambda_{23} & 0 & 0 & \Lambda_{26} \\ 0 & 0 & 0 & \Lambda_{34} & \Lambda_{35} & 0 \end{bmatrix};$$

(3) $22'2', 2m'm', mm'2' [m2'm'], mm'm'$:

$$\begin{bmatrix} \Lambda_{11} & \Lambda_{12} & \Lambda_{13} & 0 & 0 & 0 \\ 0 & 0 & 0 & 0 & 0 & \Lambda_{26} \\ 0 & 0 & 0 & 0 & \Lambda_{35} & 0 \end{bmatrix};$$

(4) $2'22', m'2m', 2'mm' [m'm2'], m'mm'$:

$$\begin{bmatrix} 0 & 0 & 0 & 0 & 0 & \Lambda_{16} \\ \Lambda_{21} & \Lambda_{22} & \Lambda_{23} & 0 & 0 & 0 \\ 0 & 0 & 0 & \Lambda_{34} & 0 & 0 \end{bmatrix};$$

(5) $4'2'2, 4'm'm, \bar{4}'m'2, \bar{4}'2'm, 4'/mm'm$:

$$\begin{bmatrix} 0 & 0 & 0 & 0 & \Lambda_{15} & 0 \\ 0 & 0 & 0 & -\Lambda_{15} & 0 & 0 \\ \Lambda_{31} & -\Lambda_{31} & 0 & 0 & 0 & 0 \end{bmatrix};$$

(6) $6'2'2, 6'm'm, \bar{6}'m'2, \bar{6}'2'm, 6'/m'm'm$:

$$\begin{bmatrix} 0 & 0 & 0 & 0 & 0 & -2\Lambda_{22} \\ -\Lambda_{22} & \Lambda_{22} & 0 & 0 & 0 & 0 \\ 0 & 0 & 0 & 0 & 0 & 0 \end{bmatrix};$$

(7) $312, 31m, \bar{3}1m$:

$$\begin{bmatrix} 0 & 0 & 0 & \Lambda_{14} & 0 & -2\Lambda_{22} \\ -\Lambda_{22} & \Lambda_{22} & 0 & 0 & -\Lambda_{14} & 0 \\ 0 & 0 & 0 & 0 & 0 & 0 \end{bmatrix};$$

(8) $312', 31m', \bar{3}1m'$:

$$\begin{bmatrix} \Lambda_{11} & -\Lambda_{11} & 0 & 0 & \Lambda_{15} & 0 \\ 0 & 0 & 0 & \Lambda_{15} & 0 & -2\Lambda_{11} \\ \Lambda_{31} & \Lambda_{31} & \Lambda_{33} & 0 & 0 & 0 \end{bmatrix}.$$

Many connections between the different forms of $\Lambda_{i\alpha}$ given above and in Table 1.5.7.1 have been derived by Kopský (1979a,b) and Grimmer (1991). These connections between the forms that the matrix can assume for the various magnetic or crystallographic point groups hold for all matrices and tensors that describe properties of materials, not just for the special case of piezomagnetism.

Dzyaloshinskii (1957b) pointed out a number of antiferromagnets that may display the piezomagnetic effect. These include the fluorides of the transition metals, in which the piezomagnetic effect was first observed experimentally (see Fig. 1.5.7.1) (Borovik-Romanov, 1959b). Below we shall discuss the origin of the piezomagnetic effect in fluorides in more detail.

The fluorides of transition metals MnF_2 , CoF_2 and FeF_2 are tetragonal easy-axis antiferromagnets (see Fig. 1.5.5.3). It is easy to check that the expansion of the thermodynamic potential $\tilde{\Phi}$ up to terms that are linear in stress T_{ij} and invariant relative to the transformations of the crystallographic space group $D_{4h}^{14} = P4_2/mnm$ is represented by

1.5. MAGNETIC PROPERTIES

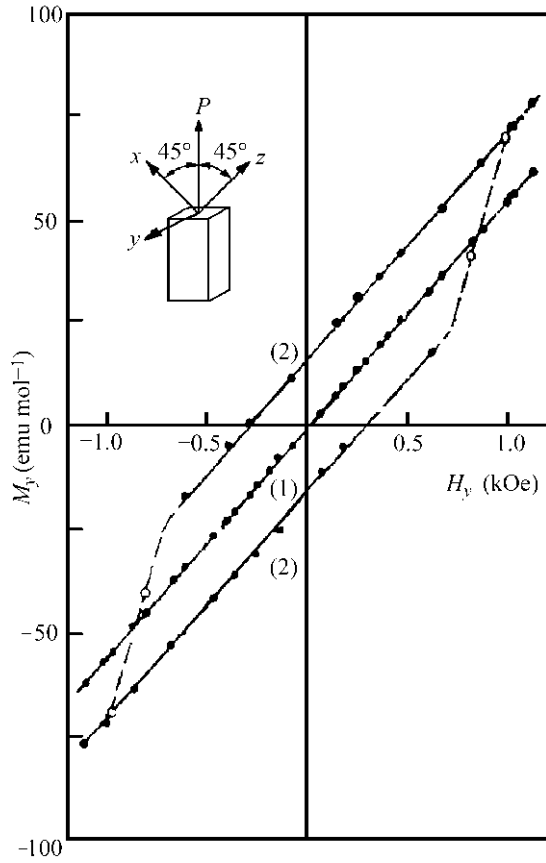


Fig. 1.5.7.1. The dependence of the magnetic moment of CoF₂ on the magnetic field. (1) Without stress; (2) under the stress $T_{xz} = 33.3$ MPa (Borovik-Romanov, 1960).

$$\begin{aligned} \tilde{\Phi} = & \tilde{\Phi}_0 + (A/2)\mathbf{L}^2 + (a/2)(L_x^2 + L_y^2) \\ & + (B/2)\mathbf{M}^2 + (b/2)(M_x^2 + M_y^2) \\ & + d(L_x M_y + L_y M_x) \\ & + 2\lambda_1(M_x T_{yz} + M_y T_{xz})L_z \\ & + 2\eta_1(L_y T_{yz} + L_x T_{xz})L_z \\ & + 2\lambda_2 M_z L_z T_{xy} + 2\eta_2 L_x L_y T_{xy} - \mathbf{M}\mathbf{H}. \end{aligned} \quad (1.5.7.5)$$

In this expression, the sums $(T_{ij} + T_{ji})$ that appear in the magnetoelastic terms have been replaced by $2T_{ij}$ as $T_{ij} \equiv T_{ji}$.

The analysis of expression (1.5.7.5) in the absence of stresses proves that fluorides may possess weak ferromagnetism provided that $a < 0$ ($L_z = 0$) (see Section 1.5.5.1). Here we shall discuss the easy-axis structure of the fluorides MnF₂, CoF₂, FeF₂ (see Fig. 1.5.5.3b). In the absence of magnetic fields and stresses only $L_z \neq 0$ for this structure. All other components of the vector \mathbf{L} and the magnetization vector \mathbf{M} are equal to zero. The magnetic point group is $\mathbf{D}_{4h}(\mathbf{D}_{2h}) = 4'/mmm'$.

To transform the potential $\tilde{\Phi}(L_i, M_j, T_{kl})$ [(1.5.7.5)] into the form $\Phi(T, \mathbf{T}, \mathbf{H})$ [(1.5.7.1)], one has to insert into the magnetoelastic terms the dependence of the components of \mathbf{L} and \mathbf{M} on the magnetic field. The corresponding relations, obtained by minimization of (1.5.7.5) without the magnetoelastic terms, are

$$\begin{aligned} M_x = \frac{a}{a(B+b)-d^2} H_x; \quad L_x = -\frac{d}{a(B+b)-d^2} H_y; \\ M_y = \frac{a}{a(B+b)-d^2} H_y; \quad L_y = -\frac{d}{a(B+b)-d^2} H_x; \quad (1.5.7.6) \\ M_z = \frac{1}{B} H_z; \quad L_z \simeq \text{constant}. \end{aligned}$$

To a first approximation, the component L_z does not depend on the magnetic field.

Inserting the relations (1.5.7.6) for M_i and L_i into the magnetoelastic terms of (1.5.7.5), one gets the following expression for the corresponding terms in $\Phi(T, H_i, T_{jk})$:

$$\begin{aligned} \Phi(T, H_i, T_{jk}) = & \Phi_0(T, H_i) + 2L_z \frac{a\lambda_1 - d\eta_1}{a(B+b) - d^2} T_{yz} H_x \\ & + 2L_z \frac{a\lambda_1 - d\eta_1}{a(B+b) - d^2} T_{xz} H_y + 2L_z \frac{\lambda_2}{B} T_{xy} H_z. \end{aligned} \quad (1.5.7.7)$$

In this case, the expression for the magnetoelastic energy contains only three components of the stress tensor: T_{yz} , T_{xz} and T_{xy} . Using (1.5.7.2), we get formulas for the three main components of the piezomagnetic effect:

$$M_x = 2L_z \frac{d\eta_1 - a\lambda_1}{a(B+b) - d^2} T_{yz} = 2\Lambda_{xyz} T_{yz} = \Lambda_{14} T_4, \quad (1.5.7.8)$$

$$M_y = 2L_z \frac{d\eta_1 - a\lambda_1}{a(B+b) - d^2} T_{xz} = 2\Lambda_{yxz} T_{xz} = \Lambda_{25} T_5, \quad (1.5.7.9)$$

$$M_z = -2L_z \frac{\lambda_2}{B} T_{xy} = 2\Lambda_{zxy} T_{xy} = \Lambda_{36} T_6. \quad (1.5.7.10)$$

In all three cases, the piezomagnetic moment is produced in the direction perpendicular to the shear plane. Comparing (1.5.7.8) and (1.5.7.9), we see that $\Lambda_{25} = \Lambda_{14}$. This is in agreement with the equivalence of the axes x and y in the tetragonal crystals. If the stress is applied in the plane xz (or yz), the vector \mathbf{L} turns in the shear plane and a component L_x (or L_y) is produced:

$$L_x = 2L_z \frac{\eta_1(B+b) - d\lambda_1}{a(B+b) - d^2} T_{xz}. \quad (1.5.7.11)$$

For T_{xy} stress, no rotation of the vector \mathbf{L} occurs.

Formulas (1.5.7.8)–(1.5.7.10) show that in accordance with Table 1.5.7.1 the form of the matrix $\Lambda_{i\alpha}$ for the magnetic point group $\mathbf{D}_{4h}(\mathbf{D}_{2h}) = 4'/mmm'$ is

$$\Lambda_{i\alpha} = \begin{bmatrix} 0 & 0 & 0 & \Lambda_{14} & 0 & 0 \\ 0 & 0 & 0 & 0 & \Lambda_{14} & 0 \\ 0 & 0 & 0 & 0 & 0 & \Lambda_{36} \end{bmatrix}. \quad (1.5.7.12)$$

The relations (1.5.7.8)–(1.5.7.10) show that the components of the piezomagnetic tensor Λ_{ijk} are proportional to the components of the antiferromagnetic vector \mathbf{L} . Thus the sign of the piezomagnetic moment depends on the sign of the vector \mathbf{L} and the value of the piezomagnetic effect depends on the domain structure of the sample (we are referring to S-domains). The piezomagnetic moment may become equal to zero in a poly-domain sample. On the other hand, piezomagnetism may be used to obtain single-domain antiferromagnetic samples by cooling them from the paramagnetic state in a magnetic field under suitably oriented external pressure.

There are relatively few publications devoted to experimental investigations of the piezomagnetic effect. As mentioned above, the first measurements of the values of the components of the tensor Λ_{ijk} were performed on crystals of MnF₂ and CoF₂ (Borovik-Romanov, 1960). In agreement with theoretical prediction, three components were observed: $\Lambda_{xyz} = \Lambda_{yxz}$ and Λ_{zxy} . The largest value obtained for these components was $\Lambda_{14} = 21 \times 10^{-10}$ Oe⁻¹. The piezomagnetic effect was also observed for two modifications of α -Fe₂O₃ (Andratskii & Borovik-Romanov, 1966). The magnetic point group of the low-temperature modification of this compound is $\mathbf{D}_{3d} = \bar{3}m$. In accordance with form (7) given above, the following nonzero components Λ_{ijk} were found for the low-temperature state:

$$\Lambda_{xyz} = -\Lambda_{yxz}, \quad (1.5.7.13)$$

$$\Lambda_{yyy} = -\Lambda_{yxx} = -\Lambda_{xxy}. \quad (1.5.7.14)$$

1. TENSORIAL ASPECTS OF PHYSICAL PROPERTIES

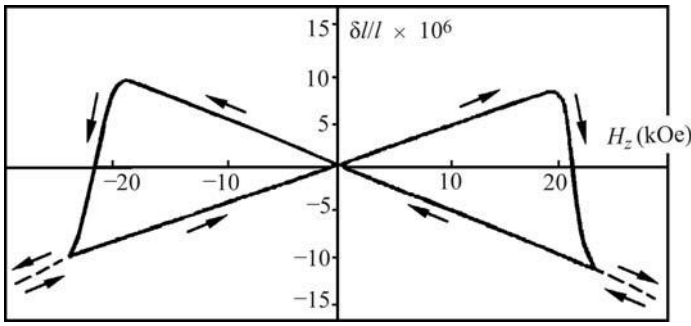


Fig. 1.5.7.2. Linear magnetostriction of CoF₂ (Prokhorov & Rudashevskii, 1975).

The values of these components are one order of magnitude smaller than for CoF₂.

The temperature dependence of the components is similar for the piezomagnetic tensor and the sublattice magnetization. This means that the magnetoelastic constants λ_1 and λ_2 (as well as the constants B and d) in the relations (1.5.7.7) and (1.5.7.8) depend only slightly on temperature.

1.5.7.2. Linear magnetostriction

From expression (1.5.7.3), it follows that a deformation of the sample may occur in a magnetic field. This deformation is linear with respect to the field. By its linear dependence, this effect differs essentially from ordinary magnetostriction, which is quadratic in the magnetic field. Most substances display such quadratic magnetostriction. The linear magnetostriction may be observed only in those ordered magnetics that belong to one of the 66 magnetic point groups that allow piezomagnetism and are listed in Table 1.5.7.1. The distinctive feature of linear magnetostriction is the dependence of its sign on the sign of the magnetic field and on the sign of the antiferromagnetic vector \mathbf{L} . The sign of \mathbf{L} characterizes the domain state of the specimen. Thus, observation of linear magnetostriction gives information about the domain state. In some materials, it has been observed that a sudden transition from one domain state to the opposite may occur in strong magnetic fields.

Linear magnetostriction (LM) was observed in CoF₂ by Borovik-Romanov & Yavelov (1963) in a magnetic field applied parallel to the fourfold axis. The relations for the LM in CoF₂ can be obtained by differentiating the expression of the thermodynamic potential Φ [(1.5.7.7)]. If the magnetic field is applied along the y axis, a deformation S_{xz} appears:

$$S_{xz} = -\partial\Phi/\partial T_{xz} = 2L_z \frac{d\eta_1 - a\lambda_1}{a(B+b) - d^2} H_y = 2\Lambda_{yz} H_y = \Lambda_{25} H_2. \quad (1.5.7.15)$$

A similar formula holds for S_{yz} if the magnetic field is applied parallel to the x axis (with Λ_{14} , which is equal to Λ_{25}).

If the magnetic field is applied parallel to the fourfold axis, the S_{xy} component of the deformation appears:

$$S_{xy} = -\partial\Phi/\partial T_{xy} = -2L_z(\lambda_2/B)H_z = -2L_z\lambda_2\chi_{\parallel}H_z = 2\Lambda_{zy}H_z = \Lambda_{36}H_3. \quad (1.5.7.16)$$

If the relations (1.5.7.15) and (1.5.7.16) are compared with (1.5.7.8)–(1.5.7.10), it is apparent that in accordance with theory the components of the tensors of the piezomagnetic effect (PM) and LM are identical.

Prokhorov & Rudashevskii (1969, 1975) extended the investigation of LM in CoF₂. They discovered that if the applied field becomes larger than 20 kOe, a jump in the magnetostriction occurs and it changes its sign (see Fig. 1.5.7.2). This jump is the result of a transition of the magnetic structure from one domain

state (\mathbf{L}_+) into the opposite state (\mathbf{L}_-). To explain such a transition, one has to take into account the term of third power in the expansion of the magnetic energy (Scott & Anderson, 1966),

$$U_m = A_i H_i + \frac{1}{2} \chi_{ij} H_i H_j + C_{ijk} H_i H_j H_k. \quad (1.5.7.17)$$

C_{ijk} is an axial time-antisymmetric tensor, the sign of which depends on the sign of the domain. This term defines the dependence of the magnetic energy on the sign of the antiferromagnetic domain.

To date, CoF₂ and MnF₂ are unique in that LM and PM occur without rotating the antiferromagnetic vector \mathbf{L} if the magnetic field is applied along the fourfold axis (or pressure along a $\langle 110 \rangle$ axis). In all other cases, these effects are accompanied by a rotation of \mathbf{L} and, as a result, the creation of new components L_i . To the latter belongs the LM in the low-temperature modification of α -Fe₂O₃, which was observed by Anderson *et al.* (1964) (see also Scott & Anderson, 1966; Levitin & Shchurov, 1973). This compound displays PM, therefore it is obvious that LM will also occur (see Table 1.5.7.1).

LM has been observed in some orthoferrites. One of the orthoferrites, DyFeO₃ at low temperatures, is a pure antiferromagnet, the vector \mathbf{L} of which is aligned along the y axis. Its magnetic point group ($\mathbf{D}_{2h} = mmm$) allows PM and LM. The latter was observed when a magnetic field was applied parallel to the z axis by Zvezdin *et al.* (1985). There it was shown that $\Lambda_{zxy} \neq 0$ if $0 < H < H_c$. At $H_c \simeq 4$ kOe, a first-order phase transition into a weakly ferromagnetic state with magnetic point group $\mathbf{D}_{2h}(\mathbf{C}_{2h}) = m'm'm$ ($\mathbf{L} \parallel Ox$, $\mathbf{M}_D \parallel Oz$) occurs.

Many orthoferrites and orthochromites that possess weak ferromagnetism belong to the same point group, which possesses an ordinary centre of symmetry. Thus PM and LM are allowed for these phases of orthoferrites. If the magnetic field is applied parallel to Ox , they undergo a reorientation transition at which both vectors, \mathbf{L} and \mathbf{M}_D , being orthogonal, rotate in the xz plane. These intermediate angular phases belong to the magnetic point group $\mathbf{C}_{2h}(\mathbf{C}_i) = 2'/m'$.

LM was observed by Kadomtseva and coworkers (Kadomtseva, Agafonov, Lukina *et al.*, 1981; Kadomtseva, Agafonov, Milov *et al.*, 1981) in two such compounds, YFeO₃ and YCrO₃. The Λ_{xxz} components of the LM tensor were measured, which are allowed for the $\mathbf{D}_{2h}(\mathbf{C}_{2h}) = m'm'm$ state.

The experimental data obtained to date for PM and LM are summarized in Table 1.5.7.2. The values of the components Λ_{iq} can be converted to SI units using $1 \text{ Oe}^{-1} = 4\pi \times 10^{-3} \text{ m A}^{-1} = 4\pi \times 10^{-3} \text{ T Pa}^{-1}$.

Table 1.5.7.2. Experimental data for the piezomagnetic effect (PM) and for linear magnetostriction (LM)

a : antiferromagnetic phase; w : weak ferromagnetic phase.

| Compound | $\Lambda_{iq} \times 10^{10} (\text{Oe}^{-1})$ | T (K) | PM or LM | Reference† |
|--|--|---------|----------|------------|
| MnF ₂ | $\Lambda_{14} \simeq 0.2$ | 20 | PM | (1) |
| CoF ₂ | $\Lambda_{14} = 21$ | 20 | PM | (1) |
| | $\Lambda_{36} = 8.2$ | 20 | PM | (1) |
| | $\Lambda_{36} = 9.8$ | 4 | LM | (3) |
| | $\Lambda_{36} = 6.0$ | 6 | LM | (8) |
| DyFeO ₃ | $\Lambda_{15} = 1.7$ | 6 | LM | (6) |
| YFeO ₃ | $\Lambda_{15} \simeq 1$ | 6 | LM | (7) |
| α -Fe ₂ O ₃ (a) | $\Lambda_{22} = 1.9$ | 78 | LM | (4) |
| | $\Lambda_{22} = 3.2$ | 77 | PM | (2) |
| | $\Lambda_{22} = 1.3$ | 100 | LM | (5) |
| | $\Lambda_{14} = 0.3$ | 78 | LM | (4) |
| | $\Lambda_{14} = 1.7$ | 77 | PM | (2) |
| | $\Lambda_{14} = 0.9$ | 100 | LM | (5) |
| α -Fe ₂ O ₃ (w) | $\Lambda_{23} = 2.5$ | 292 | PM | (2) |

† References: (1) Borovik-Romanov (1959b, 1960); (2) Andratskii & Borovik-Romanov (1966); (3) Prokhorov & Rudashevskii (1969, 1975); (4) Anderson *et al.* (1964); (5) Levitin & Shchurov (1973); (6) Kadomtseva, Agafonov, Milov *et al.* (1981); (7) Kadomtseva, Agafonov, Lukina *et al.* (1981); (8) Zvezdin *et al.* (1985).

1.5. MAGNETIC PROPERTIES

1.5.7.3. Linear magnetic birefringence

The magnetic contribution to the component of the dielectric permittivity $\delta\epsilon_{ij}$ can be represented as a series in the powers of the components of the magnetization and the antiferromagnetic vector. The magnetic birefringence (also called the Cotton–Mouton or Voigt effect) is described by the real symmetrical part of the tensor $\delta\epsilon_{ij}$. In paramagnetic crystals, the magnetization \mathbf{M} is proportional to the applied magnetic field \mathbf{H} , and the series has the form

$$\delta\epsilon_{ij} = Q_{ijkl}^{MM} M_k M_\ell = Q_{ijkl}^{MM} \chi_{kr}^M \chi_{ls}^M H_r H_s = \Gamma_{ijrs} H_r H_s. \quad (1.5.7.18)$$

The tensor Γ_{ijrs} is symmetric with respect to both the first and the second pair of indices. The symmetry of this tensor implies that the diagonal components of the permittivity tensor include magnetic corrections. The modification of the diagonal components gives rise to birefringence in cubic crystals and to a change Δn^{pm} of the birefringence in uniaxial and lower-symmetry crystals. It follows from (1.5.7.18) that this birefringence is bilinear in the applied field. Bilinear magnetic birefringence can be observed in uniaxial crystals if the magnetic field is applied along the x axis perpendicular to the principal z axis. In the simplest case, a difference in the refractive indices n_x and n_y arises:

$$\Delta n^{\text{pm}} = n_x - n_y = \frac{1}{2n_0} (\delta\epsilon_{xx} - \delta\epsilon_{yy}) = \frac{1}{2n_0} (\Gamma_{xxxx} - \Gamma_{yyxx}) H_x^2, \quad (1.5.7.19)$$

where n_0 is the refractive index for the ordinary beam.

Consider now a magnetically ordered crystal which can be characterized by an antiferromagnetic vector \mathbf{L}_0 and a magnetization vector \mathbf{M}_0 in the absence of a magnetic field. Applying a magnetic field with components H_r , we change the direction and size of \mathbf{L}_0 and \mathbf{M}_0 , getting additional components $L_k^H = \chi_{kr}^L H_r$ and $M_k^H = \chi_{kr}^M H_r$. This is illustrated by the relations (1.5.7.6). Instead of (1.5.7.18) we get

$$\begin{aligned} \delta\epsilon_{ij} &= Q_{ijkl}^{LL} L_k L_\ell + Q_{ijkl}^{ML} M_k L_\ell + Q_{ijkl}^{MM} M_k M_\ell \\ &= Q_{ijkl}^{LL} L_{0k} L_{0\ell} + Q_{ijkl}^{ML} M_{0k} L_{0\ell} + Q_{ijkl}^{MM} M_{0k} M_{0\ell} \\ &\quad + [2Q_{ijkl}^{LL} \chi_{kr}^L L_{0\ell} + Q_{ijkl}^{ML} (\chi_{kr}^M L_{0\ell} + M_{0k} \chi_{lr}^L) + 2Q_{ijkl}^{MM} \chi_{kr}^M M_{0\ell}] H_r. \end{aligned} \quad (1.5.7.20)$$

The terms in the middle line of (1.5.7.20) show that in an ordered state a change in the refractive indices occurs that is proportional to L_0^2 in antiferromagnets and to M_0^2 in ferromagnets. The terms in square brackets show that a linear magnetic birefringence may exist. In the special case of a tetragonal antiferromagnet belonging to the space group $D_{4h}^{14} = P4_2/mnm$ with \mathbf{L}_0 parallel to the principal axis z , the linear birefringence occurs in the xy plane if the magnetic field is applied along the z axis (see Fig. 1.5.5.3). In this case, $\mathbf{M}_0 = 0$, $\chi_{kz}^L = 0$ for all k , $\chi_{xz}^M = \chi_{yz}^M = 0$ and $\chi_{zz}^M = 1/B$ [see (1.5.7.6)]. Therefore the terms in square brackets in (1.5.7.20) differ from zero only for one component of $\delta\epsilon_{ij}$,

$$\delta\epsilon_{ij} = Q_{xyzx}^{ML} L_{0z} H_z / B = q_{zxy} H_z \text{sign}(L_{0z}). \quad (1.5.7.21)$$

As a result,

$$\Delta n^{\text{af}} = n_{x'} - n_{y'} = \frac{1}{2n_0} \delta\epsilon_{xy} = \frac{1}{2n_0} q_{zxy} H_z \text{sign}(L_{0z}), \quad (1.5.7.22)$$

where x', y' are the optic axes, which in these tetragonal crystals are rotated by $\pi/4$ relative to the crystallographic axes.

Comparing relation (1.5.7.22) with (1.5.7.3), one can see that like LM, there may be linear magnetic birefringence. The forms of the tensors that describe the two effects are the same.

Linear magnetic birefringence has been observed in the uniaxial antiferromagnetic low-temperature $\alpha\text{-Fe}_2\text{O}_3$ when the magnetic field was applied perpendicular to the threefold axis

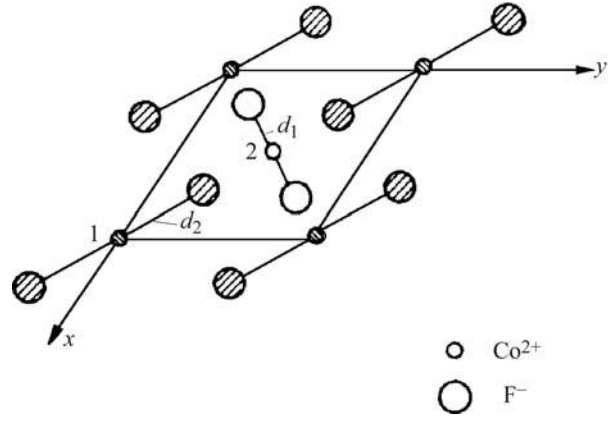


Fig. 1.5.7.3. Variation of symmetry of the crystal field in the presence of the piezomagnetic effect in CoF_2 . The unshaded atoms lie at height $c/2$ above the xy plane (see Fig. 1.5.5.3).

(Le Gall *et al.*, 1977; Merkulov *et al.*, 1981). The most impressive effect was observed in CoF_2 when the magnetic field was applied along the fourfold axis. The crystal ceased to be optically uniaxial and a difference $(n_{x'} - n_{y'}) \propto H_z$ was observed in accordance with (1.5.7.22). Such linear magnetic birefringence does not exist in the paramagnetic state. Linear birefringence has also been observed in CoCO_3 and DyFeO_3 . For details of these experiments, see Eremenko *et al.* (1989). These authors also used linear birefringence to make the antiferromagnetic domains visible. A further review of linear magnetic birefringence has been given by Ferré & Gehring (1984).

Piezomagnetism, linear magnetostriction and linear birefringence in fluorides can be clearly demonstrated qualitatively for one particular geometry. As shown in Fig. 1.5.7.3, the crystallographically equivalent points 1 and 2 are no longer equivalent after a shear deformation applied in the plane xy . During such a deformation, the distances from the magnetic ions to the nearest fluoride ions increase in points 1 and decrease in points 2. As a result, the values of the g -factors for the ions change. Evidently, the changes of the values of the g -factors for different sublattices are opposite in sign. Thus the sublattice magnetizations are no longer equal, and a magnetic moment arises along the direction of sublattice magnetization. On the other hand, if we increase the magnetization of one sublattice and decrease the magnetization of the other by applying a magnetic field parallel to the z axis, the interactions with the neighbouring fluoride ions also undergo changes with opposite signs. This gives rise to the magnetostriction. These considerations can be applied only to antiferromagnets with the fluoride structure. In these structures, single-ion anisotropy is responsible for the weak ferromagnetism, not the antisymmetric exchange interaction of the form $\mathbf{d}[\mathbf{S}_i \times \mathbf{S}_k]$.

1.5.8. Magnetoelectric effect

Curie (1894) stated that materials that develop an electric polarization in a magnetic field or a magnetization in an electric field may exist. This prediction was given a more precise form by Landau & Lifshitz (1957), who considered the invariants in the expansion of the thermodynamic potential up to linear terms in H_i . For materials belonging to certain magnetic point groups, the thermodynamic potential Φ can be written in the form

$$\Phi = \Phi_0 - \alpha_{ij} E_i H_j. \quad (1.5.8.1)$$

If (in the absence of a magnetic field) an electric field \mathbf{E} is applied to a crystal with potential (1.5.8.1), a magnetization will be produced:

$$M_j = -\frac{\partial \Phi}{\partial H_j} = \alpha_{ij} E_i. \quad (1.5.8.2)$$

1. TENSORIAL ASPECTS OF PHYSICAL PROPERTIES

Conversely, an electric polarization \mathbf{P} arises at zero electric field if a magnetic field is applied:

$$P_i = -\frac{\partial \Phi}{\partial E_i} = \alpha_{ij} H_j. \quad (1.5.8.3)$$

This phenomenon is called the magnetoelectric effect. A distinction is made between the linear magnetoelectric effect described above and two types of bilinear magnetoelectric effects. These bilinear effects arise if the thermodynamic potential contains terms of the form $E_i H_j H_k$ or $H_i E_j E_k$. They will be described in Section 1.5.8.2.

1.5.8.1. Linear magnetoelectric effect

It is obvious that the linear magnetoelectric effect is forbidden for all dia- and paramagnets as their magnetic groups possess R as a separate element. The effect is also forbidden if the magnetic

space group contains translations multiplied by R because in these cases the point group also possesses R as a separate element. Since \mathbf{H} is an axial vector that changes sign under R and \mathbf{E} is a polar vector that is invariant under time inversion, α_{ij} is an axial tensor of second rank, the components of which all change sign under time inversion (R). From relation (1.5.8.1), it follows that a magnetic group which allows the magnetoelectric effect cannot possess a centre of symmetry ($C_i = \bar{1}$). However, it can possess it multiplied by R ($C_i R = \bar{1}$) (see Table 1.5.8.1). There are 21 magnetic point groups that possess a centre of symmetry. The detailed analysis of the properties of the tensor α_{ij} shows that among the remaining 69 point groups there are 11 groups for which the linear magnetoelectric effect is also forbidden. These groups are $C_{3h} = \bar{6}$, $C_6(C_3) = 6'$, $C_{6h}(C_{3h}) = 6'/m$, $D_{3h} = \bar{6}m2$, $D_{3h}(C_{3h}) = \bar{6}m'2'$, $D_{6h}(D_{3h}) = 6'/mmm'$, $D_6(D_3) = 6'22'$, $C_{6v}(C_{3v}) = 6'm'm$, $T_d = \bar{4}3m$, $O(T) = 4'32'$ and $O_h(T_d) = m'\bar{3}'m$.

All remaining 58 magnetic point groups in which the linear magnetoelectric effect is possible are listed in Table 1.5.8.1. The 11 forms of tensors that describe this effect are also listed in this table.³ The orientation of the axes of the Cartesian coordinate system (CCS) with respect to the symmetry axes of the crystal is the same as in Table 1.5.7.1. Alternative orientations of the same point group that give rise to the same form of α_{ij} have been added between square brackets in Table 1.5.8.1. The tensor has the same form for 32 (= 321) and 312, $3m'1$ and $31m'$, $\bar{3}'m'1$ and $\bar{3}'1m'$; it also has the same form for $3m1$ and $31m$, $32'1$ and $312'$, $\bar{3}'m1$ and $\bar{3}'1m$.

The forms of α_{ij} for frequently encountered orientations of the CCS other than those given in Table 1.5.8.1 are (cf. Rivera, 1994)

(1) $112, 11m', 112/m'$ (unique axis z):

$$\begin{bmatrix} \alpha_{11} & \alpha_{12} & 0 \\ \alpha_{21} & \alpha_{22} & 0 \\ 0 & 0 & \alpha_{33} \end{bmatrix};$$

(2) $11m, 112', 112'/m$ (unique axis z):

$$\begin{bmatrix} 0 & 0 & \alpha_{13} \\ 0 & 0 & \alpha_{23} \\ \alpha_{31} & \alpha_{32} & 0 \end{bmatrix};$$

(3) $2mm, 22'2', m'm2' [m'2'm], m'mm$:

$$\begin{bmatrix} 0 & 0 & 0 \\ 0 & 0 & \alpha_{23} \\ 0 & \alpha_{32} & 0 \end{bmatrix};$$

(4) $m2m, 2'22', mm'2' [2'm'm], mm'm$:

$$\begin{bmatrix} 0 & 0 & \alpha_{13} \\ 0 & 0 & 0 \\ \alpha_{31} & 0 & 0 \end{bmatrix};$$

(5) $\bar{4}m2, \bar{4}2'm', 4'2'2, 4'mm', 4'/m'mm'$:

$$\begin{bmatrix} 0 & \alpha_{12} & 0 \\ \alpha_{12} & 0 & 0 \\ 0 & 0 & 0 \end{bmatrix}.$$

Table 1.5.8.1. The forms of the tensor characterizing the linear magnetoelectric effect

| Magnetic crystal class | | Matrix representation of the property tensor α_{ij} |
|--|--|---|
| Schoenflies | Hermann–Mauguin | |
| C_1 $C_i(C_1)$ | 1 $\bar{1}$ | $\begin{bmatrix} \alpha_{11} & \alpha_{12} & \alpha_{13} \\ \alpha_{21} & \alpha_{22} & \alpha_{23} \\ \alpha_{31} & \alpha_{32} & \alpha_{33} \end{bmatrix}$ |
| C_2 $C_s(C_1)$ $C_{2h}(C_2)$ | 2 (= 121) $m' (= 1m'1)$ $2/m' (= 12/m'1)$ (unique axis y) | $\begin{bmatrix} \alpha_{11} & 0 & \alpha_{13} \\ 0 & \alpha_{22} & 0 \\ \alpha_{31} & 0 & \alpha_{33} \end{bmatrix}$ |
| C_s $C_2(C_1)$ $C_{2h}(C_s)$ | $m (= 1m1)$ $2' (= 12'1)$ $2'/m (= 12'/m1)$ (unique axis y) | $\begin{bmatrix} 0 & \alpha_{12} & 0 \\ \alpha_{21} & 0 & \alpha_{23} \\ 0 & \alpha_{32} & 0 \end{bmatrix}$ |
| D_2 $C_{2v}(C_2)$ $D_{2h}(D_2)$ | 222 $m'm'2 [2m'm', m'2m']$ $m'm'm'$ | $\begin{bmatrix} \alpha_{11} & 0 & 0 \\ 0 & \alpha_{22} & 0 \\ 0 & 0 & \alpha_{33} \end{bmatrix}$ |
| C_{2v} $D_2(C_2)$ $C_{2v}(C_s)$ $D_{2h}(C_{2v})$ | $mm2$ $2'2'2$ $2'mm' [m2'm']$ mmm' | $\begin{bmatrix} 0 & \alpha_{12} & 0 \\ \alpha_{21} & 0 & 0 \\ 0 & 0 & 0 \end{bmatrix}$ |
| $C_4, S_4(C_2), C_{4h}(C_4)$ $C_3, S_6(C_3)$ $C_6, C_{3h}(C_3), C_{6h}(C_6)$ | 4, $\bar{4}$, $4/m'$ 3, $\bar{3}$ 6, $\bar{6}$, $6/m'$ | $\begin{bmatrix} \alpha_{11} & \alpha_{12} & 0 \\ -\alpha_{12} & \alpha_{11} & 0 \\ 0 & 0 & \alpha_{33} \end{bmatrix}$ |
| S_4 $C_4(C_2)$ $C_{4h}(S_4)$ | $\bar{4}$ $4'$ $4'/m'$ | $\begin{bmatrix} \alpha_{11} & \alpha_{12} & 0 \\ \alpha_{12} & -\alpha_{11} & 0 \\ 0 & 0 & 0 \end{bmatrix}$ |
| $D_4, C_{4v}(C_4)$ $D_{2d}(D_2), D_{4h}(D_4)$ $D_3, C_{3v}(C_3), D_{3d}(D_3)$ $D_6, C_{6v}(C_6)$ $D_{3h}(D_3), D_{6h}(D_6)$ | 422, $4m'm'$ $\bar{4}2m' [\bar{4}m'2]$, $4/m'm'm'$ 32, $3m'$, $\bar{3}'m'$ 622, $6m'm'$ $\bar{6}'m'2 [\bar{6}'2m']$, $6/m'm'm'$ | $\begin{bmatrix} \alpha_{11} & 0 & 0 \\ 0 & \alpha_{11} & 0 \\ 0 & 0 & \alpha_{33} \end{bmatrix}$ |
| $C_{4v}, D_4(C_4)$ $D_{2d}(C_{2v}), D_{4h}(C_{4v})$ $C_{3v}, D_3(C_3), D_{3d}(C_{3v})$ $C_{6v}, D_6(C_6)$ $D_{3h}(C_{3v}), D_{6h}(C_{6v})$ | $4mm, 42'2'$ $\bar{4}'2'm [\bar{4}'m2']$, $4/m'mm$ $3m, 32', \bar{3}'m$ $6mm, 62'2'$ $\bar{6}'m2' [\bar{6}'2'm]$, $6/m'mm$ | $\begin{bmatrix} 0 & \alpha_{12} & 0 \\ -\alpha_{12} & 0 & 0 \\ 0 & 0 & 0 \end{bmatrix}$ |
| $D_{2d}, D_{2d}(S_4)$ $D_4(D_2), C_{4v}(C_{2v})$ $D_{4h}(D_{2d})$ | $\bar{4}2m, \bar{4}m'2'$ $4'22', 4'm'm$ $4'/m'm'm$ | $\begin{bmatrix} \alpha_{11} & 0 & 0 \\ 0 & -\alpha_{11} & 0 \\ 0 & 0 & 0 \end{bmatrix}$ |
| $T, T_h(T)$ $O, T_d(T), O_h(O)$ | 23, $m'\bar{3}'$ 432, $\bar{4}3m', m'\bar{3}'m'$ | $\begin{bmatrix} \alpha_{11} & 0 & 0 \\ 0 & \alpha_{11} & 0 \\ 0 & 0 & \alpha_{11} \end{bmatrix}$ |

³ Table 1.5.8.1 shows that the tensor describing the magnetoelectric effect does not need to be symmetric for 31 of the 58 point groups. These 31 groups coincide with those that admit a spontaneous toroidal moment (Gorbatsevich & Kopaev, 1994); they were first determined by Ascher (1966) as the magnetic point groups admitting spontaneous currents.

1.5. MAGNETIC PROPERTIES

As mentioned above, the components of the linear magnetoelectric tensor change sign under time inversion. The sign of these components is defined by the sign of the antiferromagnetic vector \mathbf{L} , *i.e.* by the sign of the 180° domains (S-domains). This is like the behaviour of the piezomagnetic effect and therefore everything said above about the role of the domains can be applied to the magnetoelectric effect.

Dzyaloshinskii (1959) proposed the antiferromagnetic Cr_2O_3 as the first candidate for the observation of the magnetoelectric (ME) effect. He showed that the ME tensor for this compound has three nonzero components: $\alpha_{11} = \alpha_{22}$ and α_{33} . The ME effect in Cr_2O_3 was discovered experimentally by Astrov (1960) on an unoriented crystal. He verified that the effect is linear in the applied electric field. Folen *et al.* (1961) and later Astrov (1961) performed measurements on oriented crystals and revealed the anisotropy of the ME effect. In the first experiments, the ordinary magnetoelectric effect ME_E (the electrically induced magnetization) was investigated. This means the magnetic moment induced by the applied electric field was measured. Later Rado & Folen (1961) observed the converse effect ME_H (the electric polarization induced by the magnetic field). The temperature dependence of the components of the magnetoelectric tensor in Cr_2O_3 was studied in detail in both laboratories.

In the following years, many compounds that display the linear magnetoelectric effect were discovered. Both the electrically induced and the magnetically induced ME effect were observed. The values of the components of the magnetoelectric tensor range from 10^{-6} to 10^{-2} in compounds containing the ions of the iron group and from 10^{-4} to 10^{-2} in rare-earth compounds. Cox (1974) collected values of α_{max} of the known magnetoelectrics. Some are listed in Table 1.5.8.2 together with more recent results.

Table 1.5.8.2. A list of some magnetoelectrics

| Compound | T_N or T_C (K) | Magnetic point group | Maximum α_{obs} | References† |
|---|-----------------------|-------------------------|----------------------------------|------------------------|
| Fe_2TeO_6 | 219 | $4/m'm'm'$ | 3×10^{-5} | 7–9, 70 |
| DyAlO_3 | 3.5 | $m'm'm'$ | 2×10^{-3} | 11–13 |
| GdAlO_3 | 4.0 | $m'm'm'$ | 1×10^{-4} | 14 |
| TbAlO_3 | 4.0 | $m'm'm'$ | 1×10^{-3} | 12, 15–17 |
| TbCoO_3 | 3.3 | mmm' | 3×10^{-5} | 12, 16, 18 |
| Cr_2O_3 | 318 | $\bar{3}m'$ | 1×10^{-4} | 45–49, 70, 71, W162 |
| $\text{Nb}_2\text{Mn}_4\text{O}_9$ | 110 | $\bar{3}m'$ | 2×10^{-6} | 52, 53 |
| $\text{Nb}_2\text{Co}_4\text{O}_9$ | 27 | $\bar{3}m'$ | 2×10^{-5} | 52, 53 |
| $\text{Ta}_2\text{Mn}_4\text{O}_9$ | 104 | $\bar{3}m'$ | 1×10^{-5} | 53 |
| $\text{Ta}_2\text{Co}_4\text{O}_9$ | 21 | $\bar{3}m'$ | 1×10^{-4} | 53 |
| LiMnPO_4 | 35 | $m'm'm'$ | 2×10^{-5} | 55, 56, 58, 60 |
| LiFePO_4 | 50 | mmm' | 1×10^{-4} | 57, 58 |
| LiCoPO_4 | 22 | mmm' | 7×10^{-4} | 54, 55, R161 |
| LiNiPO_4 | 23 | mmm' | 4×10^{-5} | 54, 55, 61 |
| GdVO_4 | 2.4 | $4'/m'm'm$ | 3×10^{-4} | 70 |
| TbPO_4 | 2.2 | $4'/m'm'm$ | 1×10^{-2} | 66, 67 |
| DyPO_4 | 3.4 | $4'/m'm'm$ | 1×10^{-3} | 68, 69 |
| HoPO_4 | 1.4 | $4'/m'm'm$ | 2×10^{-4} | 72 |
| $\text{Mn}_3\text{B}_7\text{O}_{13}\text{I}$ | 26 | $m'm2'$ | 2×10^{-6} | C204 |
| $\text{Co}_3\text{B}_7\text{O}_{13}\text{Cl}$ | 12 | m' | 3×10^{-4} | S204 |
| $\text{Co}_3\text{B}_7\text{O}_{13}\text{Br}$ | 17 | $m'm2'$ | 2×10^{-3} | 88C1 |
| $\text{Co}_3\text{B}_7\text{O}_{13}\text{I}$ | 38 | $m'm2'$ | 1×10^{-3} | 90C3 |
| $\text{Ni}_3\text{B}_7\text{O}_{13}\text{I}$ | 61.5 | m' | 2×10^{-4} | 74, 75, 77–79, 90C2 |
| $\text{Ni}_3\text{B}_7\text{O}_{13}\text{Cl}$ | 9 | $m'm2'$ | 3×10^{-4} | 74R2, 91R1 |
| $\text{Cu}_3\text{B}_7\text{O}_{13}\text{Cl}$ | 8.4 | $m'm2'$ | 3×10^{-6} | 88R1 |
| FeGaO_3 | 305 | $m'm2'$ | 4×10^{-4} | 84–86 |
| TbOOH | 10.0 | $2/m'$ | 4×10^{-4} | 114 |
| DyOOH | 7.2 | $2/m'$ | 1×10^{-4} | 92, 114 |
| ErOOH | 4.1 | $2'/m$ | 5×10^{-4} | 93, 114 |
| Gd_2CuO_4 | 6.5 | mmm' | 1×10^{-4} | W161 |
| MnNb_2O_6 | 4.4 | mmm' | 3×10^{-6} | 101, 102 |
| MnGeO_3 | 16 | mmm' | 2×10^{-6} | 98–100 |
| CoGeO_3 | 31 | mmm' | 1×10^{-4} | 70 |
| CrTiNdO_5 | 13 | mmm' | 1×10^{-5} | 70, 89 |

† Numbers refer to references quoted by Cox (1974); codes 88C1, 90C3, 88R1, 90C2, 74R2, 91R1 refer to references quoted by Burzo (1993); and codes W162, R161, C204, S204 and W161 refer to articles in *Ferroelectrics*, **162**, 141, **161**, 147, **204**, 125, **204**, 57 and **161**, 133, respectively.

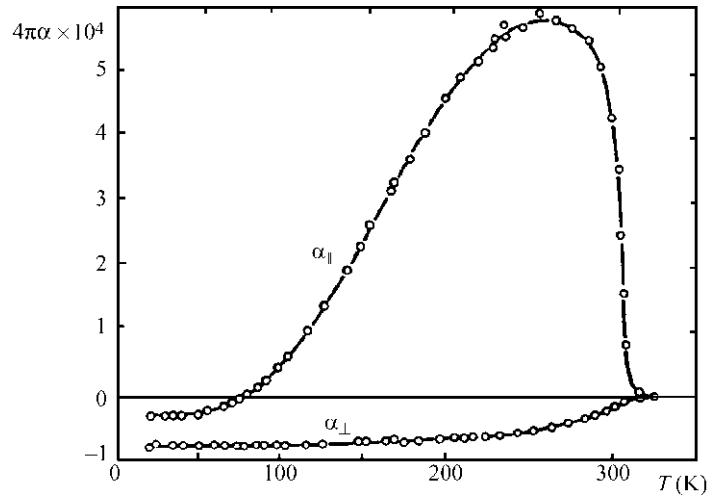


Fig. 1.5.8.1. Temperature dependence of the components α_{\parallel} and α_{\perp} in Cr_2O_3 (Astrov, 1961).

Additional information about the experimental data is presented in three conference proceedings (Freeman & Schmid, 1975; Schmid *et al.*, 1994; Bichurin, 1997).

The values of α_{ij} are given in rationalized Gaussian units, where α_{ij} is dimensionless. Some authors follow Dzyaloshinskii (1959) in writing (1.5.8.1) as $\Phi = \Phi_0 - (\alpha'_{ij}/4\pi)E_iH_j$, where α'_{ij} are the non-rationalized Gaussian values of the components of the magnetoelectric tensor. If SI units are used, then (1.5.8.1) becomes $\Phi = \Phi_0 - \alpha_{ij}^{\text{SI}}E_iH_j$. The connections between the values of a tensor component expressed in these three systems are

$$4\pi\alpha_{ij} = \alpha'_{ij} = 3 \times 10^8 \alpha_{ij}^{\text{SI}}. \quad (1.5.8.4)$$

The units of α_{ij}^{SI} are s m^{-1} . A detailed discussion of the relations between the descriptions of the magnetoelectric effect in different systems of units is given by Rivera (1994).

Most magnetoelectrics are oxides containing magnetic ions. The ions of the iron group are contained in corundum-type oxides [magnetic point group $\mathbf{D}_{3d}(\mathbf{D}_3) = \bar{3}m'$], triphylite-type oxides with different magnetic groups belonging to the orthorhombic crystallographic structure $\mathbf{D}_{2h} = mmm$ and other compounds. The rare-earth oxides are represented by the orthorhombic RMO_3 structure with R = rare earth, $M = \text{Fe}^{3+}$, Co^{3+} , Al^{3+} [magnetic point group $\mathbf{D}_{2h}(\mathbf{D}_2) = m'm'm'$], tetragonal zircon-type compounds RMO_4 (R = rare earth, $M = \text{P}$, V) [magnetic point group $\mathbf{D}_{4h}(\mathbf{D}_{2d}) = 4'/m'm'm$], monoclinic oxide hydroxides ROOH [magnetic point groups $\mathbf{C}_{2h}(\mathbf{C}_2) = 2/m'$, $\mathbf{C}_{2h}(\mathbf{C}_s) = 2'/m$] and other compounds. Of particular interest is TbPO_4 , which has the highest value of the magnetoelectric tensor components, 1.2×10^{-2} (Rado & Ferrari, 1973; Rado *et al.*, 1984). There are also some weak ferromagnets and ferrimagnets that exhibit the linear magnetoelectric effect. An example is the weakly ferromagnetic boracite $\text{Ni}_3\text{B}_7\text{O}_{13}\text{I}$. These orthorhombic compounds will be discussed in Section 1.5.8.3. Another orthorhombic magnetoelectric crystal is ferrimagnetic FeGaO_3 (Rado, 1964; see Table 1.5.8.2).

It has been shown in experiments on Cr_2O_3 that in the spin-flop phase α_{\parallel} becomes zero but a non-diagonal component α_{xz} arises (Popov *et al.*, 1992). Such behaviour is possible if under the spin-flop transition the magnetic point group of Cr_2O_3 transforms from $\mathbf{D}_{3d}(\mathbf{D}_3) = \bar{3}m'$ to $\mathbf{C}_{2h}(\mathbf{C}_s) = 112'/m$. For the latter magnetic point group, the ME tensor possesses only transverse components.

The temperature dependences determined for the ME moduli, α_{\parallel} and α_{\perp} , in Cr_2O_3 are quite different (see Fig. 1.5.8.1). The temperature dependence of α_{\perp} is similar to that of the order parameter (sublattice magnetization M_0), which can be explained easily, bearing in mind that the magnetoelectric moduli are

1. TENSORIAL ASPECTS OF PHYSICAL PROPERTIES

proportional to the magnitude of the antiferromagnetic vector ($\alpha \propto L_z = 2M_0$). However, to explain the rather complicated temperature dependence of α_{\parallel} it becomes necessary to assume that the moduli α are proportional to the magnetic susceptibility of the crystal so that (Rado, 1961; Rado & Folen, 1962)

$$\alpha_{\parallel} = a_{\parallel} \chi_{\parallel} L_z, \quad \alpha_{\perp} = a_{\perp} \chi_{\perp} L_z, \quad (1.5.8.5)$$

where a_{\parallel} and a_{\perp} are new constants of the magnetoelectric effect which do not depend on temperature. Formulas (1.5.8.5) provide a good explanation of the observed temperature dependence of α .

The linear relation between α and $L_z = 2M_0$ is also proved by the fact that when studying the ME effect, the domain structure of the sample is revealed. An annealing procedure to prepare a single-domain sample has been developed. To perform this annealing, the sample must be heated well above the Néel temperature and then cooled below T_N in the presence of electric and magnetic fields. The directions of these fields have to agree with the allowed components of the ME tensor. In some compounds, a single-domain state may be obtained by applying simultaneous pulses of both fields to a multidomain sample at temperatures below T_N (see O'Dell, 1970).

It was shown in the previous section that the piezomagnetic effect can be explained phenomenologically as weak ferromagnetism caused by the change of the symmetry produced by deformation of the lattice. The electric field may act indirectly inducing atomic displacement (similar to the displacement under stress) and as in piezomagnetism may cause the rise of a magnetic moment. Such ideas were proposed by Rado (1964) and expanded by White (1974).

The electric field may act directly to change the admixture of orbital states in the electron wavefunctions. As a result of such direct action, there may be a change of different terms in the microscopic spin Hamiltonian. Correspondingly, the following mechanisms are to be distinguished. Changes in the g -tensor can explain the ME effect in DyPO_4 (Rado, 1969). The electric-field-induced changes in single-ion anisotropy may represent the main mechanism of the ME effect in Cr_2O_3 (Rado, 1962). Two other mechanisms have to be taken into account: changes in symmetric and antisymmetric exchange. For details and references see the review article of de Alcantara Bonfim & Gehring (1980).

1.5.8.2. Nonlinear magnetoelectric effects

Along with linear terms in E and H , the thermodynamic potential Φ may also contain invariants of higher order in E_k, H_i :

$$\Phi = \Phi_0 - \alpha_{ik} E_i H_k - \frac{1}{2} \beta_{ijk} E_i H_j H_k - \frac{1}{2} \gamma_{ijk} H_i E_j E_k. \quad (1.5.8.6)$$

From this relation, one obtains the following formulas for the electric polarization P_i and the magnetization M_i :

$$P_i = \alpha_{ik} H_k + \frac{1}{2} \beta_{ijk} H_j H_k + \gamma_{jik} H_j E_k, \quad (1.5.8.7)$$

$$M_i = \alpha_{ki} E_k + \beta_{ijk} E_j H_k + \frac{1}{2} \gamma_{ijk} E_j E_k. \quad (1.5.8.8)$$

The third term in (1.5.8.7) describes the dependence of the dielectric susceptibility ($\chi_{ik}^e = P_i/E_k$) and, consequently, of the dielectric permittivity ε_{ik} , on the magnetic field. Similarly, the second term in (1.5.8.8) points out that the magnetic susceptibility χ^m may depend on the electric field ($\delta\chi_{ik}^m = \beta_{ijk} E_j$). The tensors β_{ijk} and γ_{ijk} are symmetric in their last two indices. Symmetry imposes on β_{ijk} the same restrictions as on the piezoelectric tensor and on γ_{ijk} the same restrictions as on the piezomagnetic tensor (see Table 1.5.7.1).

Ascher (1968) determined all the magnetic point groups that allow the terms EHH and HEE in the expansion of the thermodynamic potential Φ . These groups are given in Table 1.5.8.3, which has been adapted from a table given by Schmid (1973). It classifies the 122 magnetic point groups according to which types of magnetoelectric effects (EH, EHH or HEE) they admit and whether they admit spontaneous dielectric polarization (E) or spontaneous magnetization (H). It also classifies the 122 point groups according to whether they contain $\bar{1}, 1'$ or $\bar{1}'$, as in a table given by Mercier (1974). Ferromagnets, ferrimagnets and weak ferromagnets have a point group characterized by H (the 31 groups of types 4–7 in Table 1.5.8.3); dia- and paramagnets as well as antiferromagnets with a nontrivial magnetic Bravais lattice have a point group containing $1'$ (the 32 groups of types 1, 13, 17 and 19 in Table 1.5.8.3). The 59 remaining point groups describe antiferromagnets with a trivial Bravais lattice. The 31 point groups characterized by E , the 32 containing $\bar{1}$ and the 59 remaining ones correspond to a similar classification of crystals according to their electric properties (see Schmid, 1973).

Table 1.5.8.3 shows that for the 16 magnetic point groups of types 16–19, any kind of magnetoelectric effect is prohibited.

Table 1.5.8.3. Classification of the 122 magnetic point groups according to magnetoelectric types

| Type | Inversions in the group | Permitted terms in thermodynamic potential | | | | Magnetic point groups | Number of magnetic point groups | | | | |
|------|-------------------------------|---|----|----|-----|--|---|----|----|----|-----|
| 1 | 1' | E | | | EHH | 1', 21', m1', mm21', 41', 4mm1', 31', 3m1', 61', 6mm1' | 10 | 31 | | 49 | 122 |
| 2 | | E | | | EHH | HEE | 6', 6'mm' | | 2 | | |
| 3 | | E | | EH | EHH | HEE | mm2, 4mm, 4', 4'mm', 3m, 6mm | | 6 | | |
| 4 | 1̄ | E | H | EH | EHH | HEE | 1, 2, m, 2', m', m'm2', m'm'2, 4, 4m'm', 3, 3m', 6, 6m'm' | 13 | 31 | | |
| 5 | | | H | EH | EHH | HEE | 2'2'2, 42'2', 4, 42'm', 32', 62'2' | 6 | | | |
| 6 | | | H | | EHH | HEE | 6, 6'm'2' | 2 | | | |
| 7 | | | H | | | HEE | 1̄, 2/m, 2'/m', m'm'm, 4/m, 4/mmm'm', 3̄, 3̄m', 6/m, 6/mmm'm' | 10 | | | |
| 8 | | | | EH | EHH | HEE | 222, 4̄, 422, 4̄2m, 4'22', 4̄'2m', 4̄'2'm, 32, 6̄', 622, 6̄'m'2, 6m2', 23, 4̄'3m' | 14 | | | 73 |
| 9 | | | | | EHH | HEE | 6̄m2, 6'22' | 2 | | | |
| 10 | | | EH | | | 432 | 1 | 19 | | | |
| 11 | 1̄' | | EH | | | 1̄', 2/m', 2'/m, mmm'm', m'm'm', 4/m', 4'/m', 4/m'm'm', 4/m'mm, 4'/m'm'm, 3̄', 3̄m', 3̄m, 6/m', 6/m'm'm', 6/m'mm, m'3̄, m'3̄m' | 18 | | | | |
| 12 | 1' | | | | EHH | 43m | 1 | 11 | | | |
| 13 | | | | | EHH | 2221', 4̄1', 4221', 4̄2m1', 321', 6̄1', 6221', 6̄m21', 231', 4̄3m1' | 10 | | | | |
| 14 | | | | | HEE | 4'32' | 1 | | 11 | | |
| 15 | 1̄ | | | | HEE | mmm, 4'/m, 4'/mmm, 4'/mmm', 3̄m, 6'/m', 6'/mmm, 6'/m'm'm, m3̄, m3̄m' | 10 | | | | |
| 16 | 1̄' | | | | | 6'/m, 6'/mmm', m'3̄m | 3 | 16 | | | |
| 17 | 1' | | | | | 4321' | 1 | | | | |
| 18 | 1̄ | | | | | m3̄m | 1 | | | | |
| 19 | 1̄, 1', 1̄' | | | | | 11', 2/m1', mmm1', 4/m1', 4/mmm1', 3̄1', 3̄m1', 6/m1', 6/mmm1', m3̄1', m3̄m1' | 11 | | | | |

1.5. MAGNETIC PROPERTIES

These are the 11 grey point groups that contain all three inversions, the white group $O_h = m\bar{3}m$, the grey group $(O + RO) = 4321'$ and the three black-white groups $C_{6h}(C_{3h}) = 6'/m$, $D_{6h}(D_{3h}) = 6'/mmm'$ and $O_h(T_d) = m'\bar{3}'m$.

Among the 58 magnetic point groups that allow the linear magnetoelectric effect, there are 19 that do not allow the nonlinear effects EHH and HEE (types 10 and 11 in Table 1.5.8.3). The remaining 39 groups are compatible with all three effects, EH, EHH and HEE; 19 of these groups describe ferromagnets (including weak ferromagnets) and ferrimagnets (types 4 and 5 in Table 1.5.8.3).

The 21 point groups of types 7, 14 and 15 allow only the magnetoelectric effect HEE. These groups contain $C_i = \bar{1}$, except $4'32'$. The compounds belonging to these groups possess only one tensor of magnetoelectric susceptibility, the tensor γ_{ijk} of the nonlinear ME effect. The effect is described by

$$P_i = \gamma_{ijk} H_j E_k, \quad (1.5.8.9)$$

$$M_i = \frac{1}{2} \gamma_{ijk} E_j E_k. \quad (1.5.8.10)$$

The magnetic point group of ferrimagnetic rare-earth garnets RFe_5O_{12} ($R = \text{Gd, Y, Dy}$) is $D_{3d}(S_6) = \bar{3}m'$, which is of type 7. Therefore, the rare-earth garnets may show a nonlinear ME effect corresponding to relations (1.5.8.9) and (1.5.8.10). This was observed by O'Dell (1967) by means of a pulsed magnetic field. As mentioned above, this effect may be considered as the dependence of the dielectric permittivity on the magnetic field, which was the method used by Cardwell (1969) to investigate this ME effect experimentally. Later Lee *et al.* (1970) observed the ME effect defined by relation (1.5.8.10). Applying both static electric fields and alternating ones (at a frequency ω), they observed an alternating magnetization at both frequencies ω and 2ω . A nonlinear ME effect of the form HEE was also observed in the weakly ferromagnetic orthoferrites $TbFeO_3$ and $YbFeO_3$. Their magnetic point group is $D_{2h}(C_{2h}) = m'm'm$.

Moreover, paramagnets that do not possess an inversion centre $C_i = \bar{1}$ may show an ME effect if the point group is not $4321'$. They have one of the 20 grey point groups given as types 1 or 13 in Table 1.5.8.3. Bloembergen (1962) pointed out that all these paramagnets are piezoelectric crystals. He called the ME effect in these substances the *paramagnetoelectric* (PME) effect. It is defined by the nonzero components of the tensor β_{ijk} :

$$P_i = \frac{1}{2} \beta_{ijk} H_j H_k, \quad (1.5.8.11)$$

$$M_i = \beta_{ijk} E_j H_k. \quad (1.5.8.12)$$

The PME effect was discovered by Hou & Bloembergen (1965) in $NiSO_4 \cdot 6H_2O$, which belongs to the crystallographic point group $D_4 = 422$. The only nonvanishing components of the third-rank tensor are $\beta_{xyz} = \beta_{zyx} = -\beta_{yxz} = -\beta_{zyx} = \beta$ ($\beta_{14} = -\beta_{25} = 2\beta$ in matrix notation), so that $\mathbf{P} = \beta(H_y H_z, -H_x H_z, 0)$ and $\mathbf{M} = \beta(-E_y H_z, E_x H_z, E_x H_y - E_y H_x)$. Both effects were observed: the polarization \mathbf{P} by applying static (H_z) and alternating (H_x or H_y) magnetic fields and the magnetization \mathbf{M} by applying a static magnetic field H_z and an alternating electric field in the plane xy . As a function of temperature, the PME effect shows a peak at 3.0 K and changes sign at 1.38 K. The coefficient of the PME effect at 4.2 K is

$$\beta(4.2 \text{ K}) = 2.2 \times 10^{-9} \text{ cgs units.} \quad (1.5.8.13)$$

The theory developed by Hou and Bloembergen explains the PME effect by linear variation with the applied electric field of the crystal-field-splitting parameter D of the spin Hamiltonian.

Most white and black-white magnetic point groups that do not contain the inversion ($C_i = \bar{1}$), either by itself or multiplied by $R = 1'$, admit all three types of ME effect: the linear (EH) and two higher-order (EHH and HEE) effects. There are many magnetically ordered compounds in which the nonlinear ME

effect has been observed. Some of them are listed by Schmid (1973); more recent references are given in Schmid (1994a).

In principle, many ME effects of higher order may exist. As an example, let us consider the *piezomagnetoelectric* effect. This is a combination of piezomagnetism (or piezoelectricity) and the ME effect. The thermodynamic potential Φ must contain invariants of the form

$$\Phi = \Phi_0 - \pi_{ijk\ell} E_i H_j T_{k\ell}. \quad (1.5.8.14)$$

The problem of the piezomagnetoelectric effect was considered by Rado (1962), Lyubimov (1965) and recently in detail by Grimmer (1992). All 69 white and black-white magnetic point groups that possess neither $C_i = \bar{1}$ nor $R = 1'$ admit the piezomagnetoelectric effect. (These are the groups of types 2–6, 8–12, 14 and 16 in Table 1.5.8.3.) The tensor $\pi_{ijk\ell}$ that describes the piezomagnetoelectric effect is a tensor of rank 4, symmetric in the last two indices and invariant under space-time inversion. This effect has not been observed so far (Rivera & Schmid, 1994). Grimmer (1992) analyses in which antiferromagnets it could be observed.

1.5.8.3. Ferromagnetic and antiferromagnetic ferroelectrics

Neronova & Belov (1959) pointed out that there are ten magnetic point groups that admit the simultaneous existence of spontaneous dielectric polarization \mathbf{P} and magnetic polarization \mathbf{M} . Materials with such a complicated ordered structure are called ferromagnetoelectrics. Neronova and Belov considered only structures with parallel alignment of \mathbf{P} and \mathbf{M} (or \mathbf{L}). There are three more groups that allow the coexistence of ferroelectric and ferromagnetic order, in which \mathbf{P} and \mathbf{M} are perpendicular to each other. Shuvalov & Belov (1962) published a list of the 13 magnetic point groups that admit ferromagnetoelectric order. These are the groups of type 4 in Table 1.5.8.3; they are given with more details in Table 1.5.8.4.

Notice that \mathbf{P} and \mathbf{M} must be parallel in eight point groups, they may be parallel in 1 and m' , and they must be perpendicular in $2'$, m and $m'm'2'$ (see also Ascher, 1970). The magnetic point groups listed in Table 1.5.8.4 admit not only ferromagnetism (and ferrimagnetism) but the first seven also admit antiferromagnetism with weak ferromagnetism. Ferroelectric pure antiferromagnets of type III^a may also exist. They must belong to one of the following eight magnetic point groups (types 2 and 3 in Table 1.5.8.3): $C_4(C_2) = 4'$; $C_{4v}(C_{2v}) = 4'mm'$; $C_6(C_3) = 6'$; $C_{6v}(C_{3v}) = 6'mm'$; $C_{2v} = mm2$; $C_{4v} = 4mm$; $C_{3v} = 3m$; $C_{6v} = 6mm$.

The first experimental evidence to indicate that complex perovskites may become ferromagnetoelectric was observed by the Smolenskii group (see Smolenskii *et al.*, 1958). They investigated the temperature dependence of the magnetic susceptibility of the ferroelectric perovskites $Pb(Mn_{1/2}Nb_{1/2})O_3$ and $Pb(Fe_{1/2}Nb_{1/2})O_3$. The temperature dependence at $T > 77 \text{ K}$ followed the Curie–Weiss law with a very large antiferromagnetic

Table 1.5.8.4. List of the magnetic point groups of the ferromagnetoelectrics

| Symbol of symmetry group | | Allowed direction of | |
|--------------------------|-----------------|----------------------|----------------|
| Schoenflies | Hermann–Mauguin | \mathbf{P} | \mathbf{M} |
| C_1 | 1 | Any | Any |
| C_2 | 2 | $\parallel 2$ | $\parallel 2$ |
| $C_2(C_1)$ | $2'$ | $\parallel 2'$ | $\perp 2'$ |
| $C_s = C_{1h}$ | m | $\parallel m$ | $\perp m$ |
| $C_s(C_1)$ | m' | $\parallel m'$ | $\parallel m'$ |
| $C_{2v}(C_2)$ | $m'm'2$ | $\parallel 2$ | $\parallel 2$ |
| $C_{2v}(C_s)$ | $m'm'2'$ | $\parallel 2'$ | $\perp m$ |
| C_4 | 4 | $\parallel 4$ | $\parallel 4$ |
| $C_{4v}(C_4)$ | $4m'm'$ | $\parallel 4$ | $\parallel 4$ |
| C_3 | 3 | $\parallel 3$ | $\parallel 3$ |
| $C_{3v}(C_3)$ | $3m'$ | $\parallel 3$ | $\parallel 3$ |
| C_6 | 6 | $\parallel 6$ | $\parallel 6$ |
| $C_{6v}(C_6)$ | $6m'm'$ | $\parallel 6$ | $\parallel 6$ |

1. TENSORIAL ASPECTS OF PHYSICAL PROPERTIES

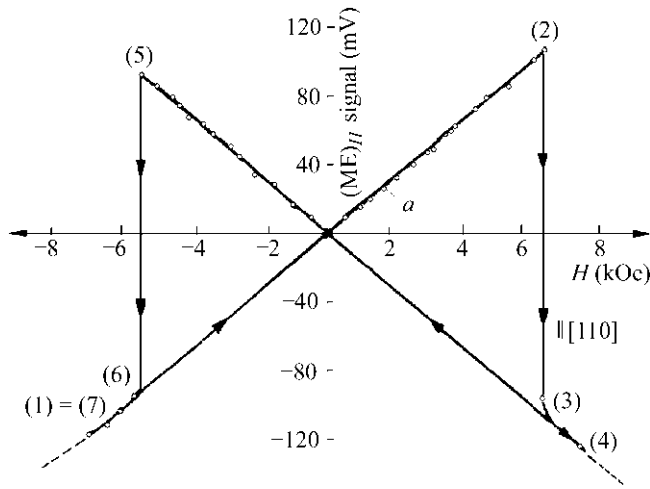


Fig. 1.5.8.2. The hysteresis loop in the linear magnetoelectric effect in ferromagnetoelectric $\text{Ni}_3\text{B}_7\text{O}_{13}\text{I}$ at 46 K (Ascher *et al.*, 1966).

Weiss constant. Later, Astrov *et al.* (1968) proved that these compounds undergo a transition into a weakly ferromagnetic state at temperatures $T_N = 11$ and 9 K, respectively.

BiFeO_3 is an antiferromagnet below $T_N = 643$ K. This was proved by neutron scattering (Kiselev *et al.*, 1962; Michel *et al.*, 1969) and magnetic measurements (Smolenskii *et al.*, 1962; see also Venevsev *et al.*, 1987). BiFeO_3 also possesses a spontaneous electric polarization. The magnetic point group above T_N is $3m1'$ and below it should have been $3m$ (Kiselev *et al.*, 1962), but in reality it possesses an antiferromagnetic spatially modulated spin structure (Sosnovska *et al.*, 1982). Another ferroelectric antiferromagnet, YMnO_3 , was found by Bertaut *et al.* (1964). It becomes ferroelectric at $T_c = 913$ K (with paramagnetic point group $6mm1'$) and antiferromagnetic at $T_N = 77$ K. Below this temperature, its magnetic point group is $6'mm'$. The antiferromagnetic ordering was also proved by investigating the Mössbauer effect (Chappert, 1965). The symmetries of both antiferromagnetic ferroelectrics described above do not allow weak ferromagnetism according to Table 1.5.5.2, and, experimentally, a spontaneous ferromagnetic moment has not been observed so far.

Since Schmid (1965) developed a technique for growing single crystals of boracites, these compounds have become the most interesting ferromagnetoelectrics. The boracites have the chemical formula $M_3\text{B}_7\text{O}_{13}X$ (where $M = \text{Cu}^{2+}, \text{Ni}^{2+}, \text{Co}^{2+}, \text{Fe}^{2+}, \text{Mn}^{2+}, \text{Cr}^{2+}$ and $X = \text{F}^-, \text{Cl}^-, \text{Br}^-, \text{I}^-, \text{OH}^-, \text{NO}_3^-$). Many of them are ferroelectrics and weak ferromagnets at low temperatures. This was first shown for $\text{Ni}_3\text{B}_7\text{O}_{13}\text{I}$ (see Ascher *et al.*, 1966). The symmetries of all the boracites are cubic at high temperatures and their magnetic point group is $43m1'$. As the temperature is lowered, most become ferroelectrics with the magnetic point group $mm21'$. At still lower temperatures, the spins of the magnetic ions in the boracites go into an antiferromagnetic state with weak ferromagnetism. For some the ferromagnetoelectric phase belongs to the group $m'm2'$ and for others to $m'm'2, m', m$ or 1. In accordance with Table 1.5.8.4, the spontaneous polarization \mathbf{P} is oriented perpendicular to the weak ferromagnetic moment \mathbf{M}_D for the groups $m'm2'$ and m . There results a complicated behaviour of boracites in external magnetic and electric fields. It depends strongly on the history of the samples. Changing the direction of the electric polarization by an electric field also changes the direction of the ferromagnetic vector (as well as the direction of the antiferromagnetic vector) and *vice versa*.

As an example, Fig. 1.5.8.2 shows the results of measurements on Ni-I boracite with spontaneous polarization along $[001]$ and spontaneous magnetization initially along $[110]$. A magnetic field was applied along $[110]$ and the polarization induced along $[001]$

was measured. If the applied field was increased beyond 6 kOe, the induced polarization changed sign because the spontaneous magnetization had been reversed. On reversing the applied magnetic field, the rest of the hysteresis loop describing the ME_{\parallel} response was obtained.

If the spontaneous polarization is reversed, *e.g.* by applying an electric field, the spontaneous magnetization will rotate simultaneously by 90° around the polarization axis. Applying magnetic fields as described above will no longer produce a measurable polarization. If, however, the crystal is rotated by 90° around the polarization axis before repeating the experiment, a hysteresis loop similar to Fig. 1.5.8.2 but turned upside down will be obtained (*cf.* Schmid, 1967).

The similarity of the jumps in the curves of linear magnetostriction (see Fig. 1.5.7.2) and magnetoelectric effect in Ni-I boracite is noteworthy. More details about the present state of investigation of the ferromagnetoelectrics are presented in the review article of Schmid (1994b).

The ferromagnetoelectrics appear as type 4 and the ferroelectric antiferromagnets of type III^a as types 2 and 3 in Table 1.5.8.3. The table shows that the linear magnetoelectric effect is admitted by all ferromagnetoelectrics and all ferroelectric antiferromagnets of type III^a , except those that belong to the two point groups $C_6(C_3) = 6'$ and $C_{6v}(C_{3v}) = 6'mm'$.

Concluding Section 1.5.8, it is worth noting that the magnetoelectric effect is still actively investigated. Recent results in this field can be found in papers presented at the 1993 and 1996 conferences devoted to this subject (see Schmid *et al.*, 1994; Bichurin, 1997, 2002).

1.5.9. Magnetostriction

The transition to an ordered magnetic state is accompanied by a spontaneous distortion of the lattice, which is denoted spontaneous magnetostriction. The lattice distortion may be specified by the deformation (strain) components S_{ij} . The undeformed state is defined as the crystal structure that would be realized if the crystal remained in the paramagnetic state at the given temperature. This means that it is necessary to separate the magnetostrictive deformation from the ordinary thermal expansion of the crystal. This can be done by measurements of the magnetostriction in external magnetic fields applied in different directions (see Section 1.5.9.2). The magnetostriction arises because the first derivatives of the exchange and relativistic energies responsible for the magnetic order do not vanish at $S_{ij} = 0$. Thus these energies depend linearly on the deformations around $S_{ij} = 0$. That part of the magnetic energy which depends on the deformations (and consequently on the stresses) is called the magnetoelastic energy, U_{me} . To find the equilibrium values of the spontaneous magnetostriction, one also has to take the elastic energy into account.

The magnetoelastic energy includes both an exchange and a relativistic part. In some ferromagnets that are cubic in the paramagnetic phase, the exchange interaction does not lower the cubic symmetry. Thus the exchange part of U_{me} satisfies the relations

$$\partial U_{me}/\partial S_{ii} = B'_0 \text{ and } \partial U_{me}/\partial S_{ij} = 0 \quad (i \neq j). \quad (1.5.9.1)$$

Such a form of the magnetoelastic energy gives rise to an isotropic spontaneous magnetostriction or volume change (volume striction) which does not depend on the direction of magnetization. In what follows, we shall analyse mainly the anisotropic magnetostriction.

The spontaneous magnetostriction deformations are so small (about 10^{-5}) for some ferro- and antiferromagnets that they cannot be observed by the usual X-ray techniques. However, in materials with ions possessing strong spin-orbit interactions (like Co^{2+}), it may be as large as 10^{-4} . The magnetostriction in rare-

1.5. MAGNETIC PROPERTIES

earth metals and their compounds with iron and cobalt are especially large (up to 10^{-3}).

Magnetostriction is observed experimentally as a change δl of the linear dimension along a direction specified by a unit vector $\beta = (\beta_1, \beta_2, \beta_3)$:

$$\lambda_\beta = \delta l/l = \sum_{ij} S_{ij} \beta_i \beta_j, \quad (1.5.9.2)$$

where S_{ij} are the deformation components, which are functions of the components of the unit vector \mathbf{n} aligned in the direction of the magnetization. Only the symmetric part of the deformation tensor S_{ij} has been taken into account, because the antisymmetric part represents a rotation of the crystal as a whole.

The magnetostriction that arises in an applied magnetic field will be discussed in Section 1.5.9.2; Section 1.5.9.1 is devoted to the spontaneous magnetostriction.

1.5.9.1. Spontaneous magnetostriction

In this section, we shall assume that the crystal under consideration undergoes a phase transition from the paramagnetic state into a magnetically ordered state. The latter is a single-domain state with the magnetization (or the antiferromagnetic vector) aligned along the vector \mathbf{n} . As was mentioned above, to solve the problem of the spontaneous magnetostriction we have to minimize the sum of magnetoelastic and elastic energy.

Like the anisotropy energy, the anisotropic part of the magnetoelastic energy can be represented as a series in the components of the unit vector \mathbf{n} :

$$U_{\text{me}} = Q_{k\ell mn} S_{k\ell} n_m n_n + Q_{k\ell mnop} S_{k\ell} n_m n_n n_o n_p + \dots = V_{k\ell}^0 S_{k\ell}. \quad (1.5.9.3)$$

As for every ordered magnetic, this relation contains only even powers of the magnetization unit vector. The components of the tensors \mathbf{Q} are called magnetostrictive or magnetoelastic coefficients. They are proportional to even powers of the magnetization M ($Q_{k\ell mn} \propto M^2$ and $Q_{k\ell mnop} \propto M^4$). The symmetry of the tensors $\mathbf{Q}_{k\ell mn}$ and $\mathbf{Q}_{k\ell mnop}$ is defined by the crystallographic point group of the initial paramagnetic phase of the crystal.

It is convenient to consider the magnetoelastic energy as part of a general expansion of the free energy of a magnetic into a series with respect to the deformation (as the magnetostrictive deformations are small):

$$V = V^0 + V_{k\ell}^0 S_{k\ell} + \frac{1}{2} V_{k\ell mn}^0 S_{k\ell} S_{mn} + \dots, \quad (1.5.9.4)$$

where all the expansion coefficients V^0 are functions of the components of the magnetization unit vector \mathbf{n} . The superscripts zero indicate that the expansion coefficients have been calculated relative to the undistorted lattice. Such a state in which, at a given temperature, there is no magnetic interaction to distort the crystal is not realizable practically. It will be shown below that the values of the coefficients $V_{k\ell}^0$ may be obtained experimentally by observing the magnetostriction in a magnetic field (see Section 1.5.9.2).

The first term in (1.5.9.4) is the anisotropy energy at zero deformation U_a^0 :

$$V^0 = U_a^0 = K_{ij}^0 n_i n_j + K_{ijk\ell}^0 n_i n_j n_k n_\ell + K_{ijk\ell mn}^0 n_i n_j n_k n_\ell n_m n_n. \quad (1.5.9.5)$$

This expression has to be compared with the expression for the anisotropy at zero stress introduced in Section 1.5.3.2 [see (1.5.3.5)]. It is obvious that symmetry imposes the same restrictions on the tensors \mathbf{K} in both expressions for the anisotropy. Later, we shall discuss these two relations for the anisotropy in more detail.

The second term in (1.5.9.4) is the magnetoelastic energy density, which is displayed in equation (1.5.9.3) and represents the energy of anisotropic deformation.

The third term in (1.5.9.4) is quadratic in $S_{k\ell}$ and can be considered as an additional contribution to the elastic energy arising from the distortion of the lattice by spontaneous magnetostriction. This term is small compared with the main part of the elastic energy, and the effect it produces is called a morphic effect and is usually neglected.

The equilibrium deformation components S_{ij}^* may be found by minimization of the sum of the magnetoelastic and elastic energies. The latter, U_{el} , is given by

$$U_{\text{el}} = \frac{1}{2} c_{ijk\ell} S_{ij} S_{k\ell}, \quad (1.5.9.6)$$

where $c_{ijk\ell}$ are the elastic stiffnesses. The minimization leads to

$$\partial(U_{\text{el}} + U_{\text{me}})/\partial S_{ij} = c_{ijk\ell} S_{k\ell}^* + V_{ij}^0 = 0. \quad (1.5.9.7)$$

We shall replace the elastic stiffnesses $c_{ijk\ell}$ in this equation by the elastic compliances $s_{ijk\ell}$, taking into account that Hooke's law may be written in two forms (see Section 1.3.3):

$$T_{ij} = c_{ijk\ell} S_{k\ell} \quad \text{or} \quad S_{ij} = s_{ijk\ell} T_{k\ell}. \quad (1.5.9.8)$$

Thus the relation for the equilibrium components of the strain S_{ij}^* becomes

$$S_{ij}^* = -s_{ijk\ell} V_{k\ell}^0. \quad (1.5.9.9)$$

Combining the relations (1.5.9.9) and (1.5.9.3), we get the following equation for the magnetostrictive strain components S_{ij} as a function of the magnitude M_s and direction $\mathbf{n} = \mathbf{M}_s/M_s$ of the magnetization \mathbf{M}_s :

$$\begin{aligned} S_{ij}^* &= -s_{ijk\ell} (Q_{k\ell mn} n_m n_n + Q_{k\ell mnop} n_m n_n n_o n_p + \dots) \\ &= M_s^2 N_{ijk\ell} n_k n_\ell + M_s^4 N_{ijk\ell mn} n_k n_\ell n_m n_n + \dots \end{aligned} \quad (1.5.9.10)$$

Let us denote the spontaneous magnetostriction by λ_β^0 (β defines the direction of the magnetostriction relative to the crystallographic axes). According to (1.5.9.2), we obtain

$$\lambda_\beta^0 = M_s^2 N_{ijk\ell} \beta_i \beta_j n_k n_\ell + M_s^4 N_{ijk\ell mn} \beta_i \beta_j n_k n_\ell n_m n_n. \quad (1.5.9.11)$$

Relation (1.5.9.11) shows that $N_{ijk\ell mn}$ can be chosen as symmetric in its first two indices and symmetric in its last four indices. It can therefore be represented by a 6×15 matrix $N_{\alpha A}$, where $\alpha = 1, \dots, 6$ and $A = 01, \dots, 15$. Table 1.5.9.1 lists the pairs ij that correspond to α and the quadruples $k\ell mn$ that correspond to A .

Similarly, $N_{ijk\ell}$ can be chosen as symmetric in its first two and in its last two indices. It can therefore be represented by a 6×6 matrix $N_{\alpha\beta}$, where $\alpha, \beta = 1, \dots, 6$. The correspondence between the numbers 1 to 6 and pairs ij or $k\ell$ is given in Table 1.5.9.1.

The tensors $N_{ijk\ell}$ and $N_{ijk\ell mn}$ must satisfy the symmetry of the paramagnetic state of the crystal under consideration. In the case of cubic crystals with fourfold axes (paramagnetic point groups $4321'$, $43m1'$ or $m3m1'$), the two matrices $N_{\alpha\beta}$ and $N_{\alpha A}$ possess instead of the 36 and 90 independent components only 3 and 6, i.e. N_{11}, N_{12}, N_{44} and $N_{101}, N_{102}, N_{104}, N_{105}, N_{407}, N_{410}$, respectively. The exact form of the two matrices will be given in the following.

(a) Cubic crystals.

If the point group of the paramagnetic crystal is $4321'$, $43m1'$ or $m3m1'$, it follows from the Neumann principle that the only nonvanishing components of $N_{\alpha\beta}$ are $N_{11} = N_{22} = N_{33}$, $N_{12} = N_{23} = N_{31} = N_{21} = N_{32} = N_{13}$ and $N_{44} = N_{55} = N_{66}$. Similarly, the only nonvanishing components of $N_{\alpha A}$ are $N_{101} = N_{202} = N_{303}$, $N_{102} = N_{203} = N_{301} = N_{103} = N_{201} = N_{302}$, $N_{104} = N_{205} = N_{306}$, $N_{105} = N_{206} = N_{304} = N_{106} = N_{204} = N_{305}$, $N_{407} = N_{508} = N_{609}$,

1. TENSORIAL ASPECTS OF PHYSICAL PROPERTIES

$N_{410} = N_{511} = N_{612} = N_{413} = N_{514} = N_{615}$. The spontaneous magnetostriction (1.5.9.11) can then be written as

$$\lambda_{\beta}^0 = h_0 + h_1 S(n_1^2 \beta_1^2) + 2h_2 S(n_1 n_2 \beta_1 \beta_2) + h_3 S(n_1^2 n_2^2) + h_4 S(n_1^4 \beta_1^2 + \frac{2}{3} n_1^2 n_2^2) + 2h_5 S(n_1 n_2 n_3^2 \beta_1 \beta_2). \quad (1.5.9.12)$$

Here an operator $S()$ has been introduced, which denotes the sum of the three quantities obtained by cyclic permutation of the suffixes in the expression within the brackets. For example, $S(n_1^2 n_2 n_3 \beta_2 \beta_3) = n_1^2 n_2 n_3 \beta_2 \beta_3 + n_2^2 n_3 n_1 \beta_3 \beta_1 + n_3^2 n_1 n_2 \beta_1 \beta_2$.

The coefficients h_i are related in the following way to the components of the matrices $N_{\alpha\beta}$ and $N_{\alpha A}$ and the spontaneous magnetization M_s :

$$\begin{aligned} h_0 &= N_{12} M_s^2 + N_{102} M_s^4, \\ h_1 &= (N_{11} - N_{12}) M_s^2 - 6(N_{104} - N_{105}) M_s^4, \\ h_2 &= 2N_{44} M_s^2 + 4N_{410} M_s^4, \\ h_3 &= [-\frac{2}{3}(N_{101} + 2N_{102}) + 2(N_{104} + 2N_{105})] M_s^4, \\ h_4 &= [N_{101} - N_{102} + 6(N_{104} - N_{105})] M_s^4, \\ h_5 &= 4(3N_{407} - N_{410}) M_s^4. \end{aligned} \quad (1.5.9.13)$$

(b) Hexagonal crystals.

The equation for the spontaneous magnetostriction of a crystal that, in its paramagnetic state, has a point group $6221'$, $6mm1'$, $\bar{6}m21'$ or $6/mmm1'$, is of the following form [if we restrict ourselves to the quadratic terms in (1.5.9.11)]:

$$\lambda_{\beta}^0 = h_0 + h_1 n_3^2 \beta_3^2 + h_2 (n_1^2 \beta_1^2 + n_2^2 \beta_2^2) + h_3 (n_1^2 \beta_2^2 + n_2^2 \beta_1^2) + 2h_4 n_1 n_2 \beta_1 \beta_2 + 2h_5 n_3 \beta_3 (n_1 \beta_1 + n_2 \beta_2) + h_6 \beta_3^2. \quad (1.5.9.14)$$

The coefficients h_i are related to the components $N_{\alpha\beta}$ and the spontaneous magnetization as follows:

$$\begin{aligned} h_0 &= N_{13} M_s^2 \\ h_1 &= (N_{33} - N_{31}) M_s^2 \\ h_2 &= (N_{11} - N_{13}) M_s^2 \\ h_3 &= (N_{12} - N_{13}) M_s^2 \\ h_4 &= (N_{11} - N_{12}) M_s^2 \\ h_5 &= 2N_{44} M_s^2 \\ h_6 &= (N_{31} - N_{13}) M_s^2 \end{aligned} \quad (1.5.9.15)$$

Table 1.5.9.1. Correspondence between matrix indices α , A and tensor indices of the tensors describing spontaneous magnetostriction

| α | ij | A | $k\ell mn$ |
|----------|--------|-----|--|
| 1 | 11 | 01 | 1111 |
| 2 | 22 | 02 | 2222 |
| 3 | 33 | 03 | 3333 |
| 4 | 23, 32 | 04 | 2233, 2323, 2332, 3223, 3232, 3322 |
| 5 | 31, 13 | 05 | 3311, 3131, 3113, 1331, 1313, 1133 |
| 6 | 12, 21 | 06 | 1122, 1212, 1221, 2112, 2121, 2211 |
| | | 07 | 1123, 1132, 1213, 1231, 1312, 1321, 2113, 2131, 2311, 3112, 3121, 3211 |
| | | 08 | 2231, 2213, 2321, 2312, 2123, 2132, 3221, 3212, 3122, 1223, 1232, 1322 |
| | | 09 | 3312, 3321, 3132, 3123, 3231, 3213, 1332, 1323, 1233, 2331, 2313, 2133 |
| | | 10 | 2223, 2232, 2322, 3222 |
| | | 11 | 3331, 3313, 3133, 1333 |
| | | 12 | 1112, 1121, 1211, 2111 |
| | | 13 | 3332, 3323, 3233, 2333 |
| | | 14 | 1113, 1131, 1311, 3111 |
| | | 15 | 2221, 2212, 2122, 1222 |

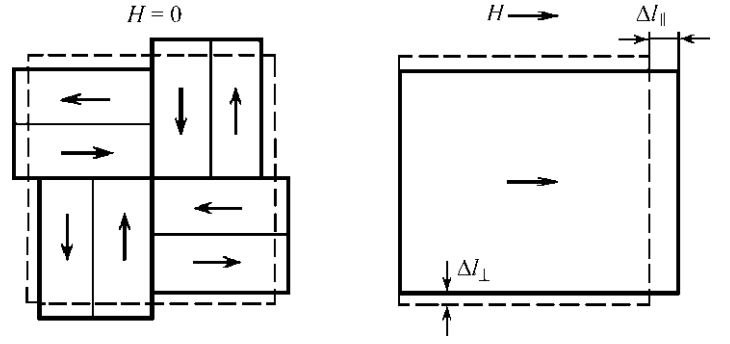


Fig. 1.5.9.1. Diagram explaining the occurrence of magnetostrictive strains in the demagnetized and saturated states of a cube-shaped crystal with a cubic prototype.

As mentioned above, the values of the magnetostrictive coefficients h_i and the spontaneous magnetostriction λ_{β}^0 may be obtained from measurements of magnetostriction in a magnetic field. The latter will be discussed in the next section.

Notice that there is some disagreement between our results (1.5.9.12)–(1.5.9.13) and the corresponding results of Mason (1951), and similarly between (1.5.9.14)–(1.5.9.15) and the results of Mason (1954).

1.5.9.2. Magnetostriction in an external magnetic field

There are three reasons for the magnetostriction arising in a magnetic field: (a) the transfer of the crystal into a single-domain state if the magnetic field is directed along one of the easy axes; (b) the deflection of the magnetization (or antiferromagnetic vector) by the magnetic field from the easy axis in a single-domain crystal; (c) the change of the magnetization in a sufficiently strong magnetic field.

Let us begin with case (a) and consider a crystal with cubic symmetry in the paramagnetic state (*i.e.* with a cubic prototype). We calculate the magnetostriction that occurs when the applied magnetic field transforms the crystal from the demagnetized multidomain state into the saturated single-domain state. This transformation is shown schematically in Fig. 1.5.9.1.

Each domain in the demagnetized state is distorted by spontaneous magnetostriction. The number of domains in the sample is usually much larger than shown in the figure. Thus a sample of a crystal with a cubic prototype which in the paramagnetic state has the form of a cube will retain this form in the ordered state. Its linear dimension will be changed as a result of magnetostriction. Averaging these strains over all the domains, one gets the spontaneous magnetostrictive change of the linear dimension of the sample, which is equal for any direction x , y or z :

$$(\delta l)_{\text{dem}}/l_0 = \lambda^{\text{dem}} = \overline{\lambda_{\beta}^0(n_k)}, \quad (1.5.9.16)$$

where n_k defines the directions parallel to all the easy axes of the crystal. For crystals with a cubic prototype, there are two principal ordered states: with the easy axis along the $\langle 111 \rangle$ directions as in nickel or along the $\langle 100 \rangle$ directions as in iron. Averaging the strains of all eight possible easy-axis directions of the domains in the $\langle 111 \rangle$ -type ferromagnet we obtain from (1.5.9.12) the following expression for the spontaneous magnetostriction of the demagnetized crystal:

$$\lambda^{\text{dem}} = h_0 + \frac{1}{3}(h_1 + h_3 + h_4). \quad (1.5.9.17)$$

In the case of the $\langle 100 \rangle$ -type ferromagnet, the averaging over the six groups of domains leads to

$$\lambda^{\text{dem}} = h_0 + \frac{1}{3}(h_1 + h_4). \quad (1.5.9.18)$$

1.5. MAGNETIC PROPERTIES

In the saturated state, the sample loses its cubic form. It becomes longer parallel to the magnetic field and thinner perpendicular to it. By definition, the demagnetized state is taken as a reference state for the magnetostriction in the magnetic field. Subtracting from the general relation for spontaneous magnetostriction (1.5.9.12) the expressions (1.5.9.17) and (1.5.9.18) for the demagnetized sample, Becker & Döring (1939) obtained the equations that describe the anisotropy of the magnetostriction caused by saturation magnetization of the $\langle 111 \rangle$ and $\langle 100 \rangle$ types of magnetic crystals:

$\langle 111 \rangle$ type:

$$\lambda_{\beta}^{\text{sat}} = h_1[S(n_1^2\beta_1^2) - \frac{1}{3}] + 2h_2S(n_1n_2\beta_1\beta_2) + h_3[S(n_1^2n_2^2) - \frac{1}{3}] + h_4[S(n_1^4\beta_1^2 + \frac{2}{3}n_1^2n_2^2) - \frac{1}{3}] + 2h_5S(n_1^2n_2n_3\beta_2\beta_3); \quad (1.5.9.19)$$

$\langle 100 \rangle$ type:

$$\lambda_{\beta}^{\text{sat}} = h_1[S(n_1^2\beta_1^2) - \frac{1}{3}] + 2h_2S(n_1n_2\beta_1\beta_2) + h_3S(n_1^2n_2^2) + h_4[S(n_1^4\beta_1^2 + \frac{2}{3}n_1^2n_2^2) - \frac{1}{3}] + 2h_5S(n_1^2n_2n_3\beta_2\beta_3). \quad (1.5.9.20)$$

Both types of magnetics with a cubic prototype are described by a two-constant equation if the terms of fourth power are neglected. This equation was obtained by Akulov (1928) in the form

$$\lambda_{\beta}^{\text{sat}} = \frac{3}{2}\lambda_{100}(n_1^2\beta_1^2 + n_2^2\beta_2^2 + n_3^2\beta_3^2 - \frac{1}{3}) + 3\lambda_{111}(n_1n_2\beta_1\beta_2 + n_2n_3\beta_2\beta_3 + n_3n_1\beta_3\beta_1), \quad (1.5.9.21)$$

where the constants λ_{100} and λ_{111} correspond to the magnetostrictive deformation of a 'cubic' ferromagnet along the direction of the magnetic field that is applied along the directions $\langle 100 \rangle$ and $\langle 111 \rangle$, respectively. Let us denote by Q_1 and Q_2 the following equal coefficients in the equation for the magnetoelastic energy (1.5.9.3):

$$Q_1 = Q_{xxxx} = Q_{yyyy} = Q_{zzzz}; \quad Q_2 = Q_{xyxy} = Q_{yzyz} = Q_{zxzx}. \quad (1.5.9.22)$$

According to (1.5.9.9), the coefficients λ_{100} and λ_{111} may be written as the following fractions of Q_i and the elastic stiffnesses $c_{\alpha\beta}$:

$$\lambda_{100} = \frac{Q_1}{c_{12} - c_{11}}, \quad \lambda_{111} = -\frac{1}{3} \frac{Q_2}{c_{44}}. \quad (1.5.9.23)$$

If the magnetic field transforms the crystal from the demagnetized to the saturated state and if the linear dimension of the sample along the magnetic field increases, then its dimension perpendicular to the field will decrease (see Fig. 1.5.9.1). It follows from relation (1.5.9.21) that the magnetostriction perpendicular to the magnetic field is

$$\lambda_{100}^{\perp} = -\frac{1}{2}\lambda_{100} \quad \text{and} \quad \lambda_{111}^{\perp} = -\frac{1}{2}\lambda_{111}. \quad (1.5.9.24)$$

Some data for magnetostriction of ferromagnets with prototype symmetry $m\bar{3}m1'$ are presented in Table 1.5.9.2.

In a uniaxial crystal, the magnetostriction in the magnetic field arises mainly as a result of the rotation of the magnetization vector from the direction of the easy axis to the direction of the applied field. The magnetostriction in the magnetic field of an easy-axis hexagonal ferromagnet can be obtained from the relation for the spontaneous magnetostriction (1.5.9.14). In the demagnetized state, such a ferromagnet possesses only two types of antiparallel domains, in which the magnetization is aligned

Table 1.5.9.2. *Magnetostriction data for ferromagnets with prototype symmetry $m\bar{3}m1'$*

| Compound | $\lambda_{100} \times 10^6$ | $\lambda_{111} \times 10^6$ | References† |
|--------------------------------|-----------------------------|-----------------------------|-------------|
| Fe | 20.7 | -21.2 | (1) |
| Ni | -45.9 | -24.3 | (1) |
| Fe ₃ O ₄ | -20 | 78 | (2) |
| YIG ($T = 300$ K) | -1.4 | -2.4 | (3) |
| DyIG ($T = 300$ K) | -12.5 | -5.9 | (3) |
| DyIG ($T = 4.2$ K) | -1400 | -550 | (4) |

† References: (1) Lee (1955); (2) Bickford *et al.* (1955); (3) Iida (1967); (4) Clark *et al.* (1966).

parallel or antiparallel to the hexagonal axis ($n_z = \pm 1$, $n_x = n_y = 0$).

Thus the magnetostriction of the demagnetized state is described by

$$\lambda_{\beta}^{\text{dem}} = h_0 + (h_1 + h_6)\beta_3^2. \quad (1.5.9.25)$$

The saturation magnetostriction can be calculated for different directions of the applied magnetic field using the equations (1.5.9.14), (1.5.9.15) and (1.5.9.25). If the magnetic field is applied along the x axis ($n_x = 1$, $n_y = n_z = 0$), the saturation magnetostrictions for three directions of the vector β : $\lambda_{\beta}^{\text{sat}} = \lambda_A, \lambda_B, \lambda_C$ are

$$\begin{aligned} \beta \parallel Ox \quad \lambda_A &= h_2, \\ \beta \parallel Oy \quad \lambda_B &= h_3, \\ \beta \parallel Oz \quad \lambda_C &= -h_1. \end{aligned} \quad (1.5.9.26)$$

If the magnetic field is applied at an angle of 45° to the hexagonal axis along the $[101]$ direction, the saturation magnetostriction along the magnetic field is described by

$$\lambda_D = \lambda_{101}^{\text{sat}} = \frac{1}{4}(h_2 - h_1 + 2h_5). \quad (1.5.9.27)$$

Using the constants $\lambda_A, \lambda_B, \lambda_C$ and λ_D introduced above, the general relation for the magnetostriction caused by magnetization to saturation can be presented in the form

$$\begin{aligned} \lambda_{\beta}^{\text{sat}} &= \lambda_A[(n_1\beta_1 + n_2\beta_2)^2 - (n_1\beta_1 + n_2\beta_2)n_3\beta_3] \\ &\quad + \lambda_B[(1 - n_3^2)(1 - \beta_3^2) - (n_1\beta_1 + n_2\beta_2)^2] \\ &\quad + \lambda_C[(1 - n_3^2)\beta_3^2 - (n_1\beta_1 + n_2\beta_2)n_3\beta_3] \\ &\quad + 4\lambda_D(n_1\beta_1 + n_2\beta_2)n_3\beta_3. \end{aligned} \quad (1.5.9.28)$$

A typical hexagonal ferromagnet is cobalt. The magnetostriction constants introduced above have the following values for Co at room temperature:

$$\begin{aligned} \lambda_A &= -45 \times 10^{-6} & \lambda_C &= +110 \times 10^{-6} \\ \lambda_B &= -95 \times 10^{-6} & \lambda_D &= -100 \times 10^{-6} \end{aligned}$$

A more sophisticated treatment of the symmetry of the magnetostriction constants is given in the monograph of Birss (1964) and in Zalesky (1981).

1.5.9.3. The difference between the magnetic anisotropies at zero strain and zero stress

The spontaneous magnetostriction makes a contribution to the magnetic anisotropy (especially in magnetics with a cubic prototype). Therefore, to find the full expression for the anisotropy energy one has to sum up the magnetic U_a^0 [see (1.5.9.5)], the magnetoelastic U_{me} [see (1.5.9.3)] and the elastic U_{el} [see (1.5.9.6)] energies. At zero strain ($S_{ij}^* = 0$), only $U_a^0 \neq 0$. At zero stress

$$\begin{aligned} U_a^0 + U_{\text{me}} + U_{\text{el}} &= U_a^0 + V_{ij}^0 S_{ij}^* + \frac{1}{2} c_{ijkl} S_{ij}^* S_{kl}^* \\ &= U_a^0 + \frac{1}{2} V_{ij}^0 S_{ij}^*. \end{aligned} \quad (1.5.9.29)$$

1. TENSORIAL ASPECTS OF PHYSICAL PROPERTIES

Table 1.5.10.1. *Conversion of Gaussian to SI units*

| Symbol | Quantity | Gaussian unit and its SI equivalent |
|---------------------|--|---|
| B | Magnetic induction | 1 gauss (G) = 10^{-4} tesla (T) |
| H | Magnetic field | 1 oersted (Oe) = $10^3/(4\pi)$ A m $^{-1}$ |
| M | Magnetization (= magnetic moment per unit volume) | 1 emu cm $^{-3}$ = 10^3 A m $^{-1}$ |
| α | Linear magnetoelectric tensor (rationalized units) | 1 (dimensionless units) = $4\pi \times 10^{-8}/3$ s m $^{-1}$ |
| Λ | Piezomagnetic tensor | 1 Oe $^{-1}$ = $4\pi \times 10^{-3}$ m A $^{-1}$ = $4\pi \times 10^{-3}$ T Pa $^{-1}$ |
| χ | Magnetic volume susceptibility | 1 (dimensionless units) = 4π (dimensionless units) |
| χ_g | Magnetic mass susceptibility | 1 cm 3 g $^{-1}$ = $4\pi \times 10^{-6}$ m 3 g $^{-1}$ |
| χ_{mol} | Magnetic molar susceptibility | 1 cm 3 mol $^{-1}$ = $4\pi \times 10^{-6}$ m 3 mol $^{-1}$ |

We used here the modified equation (1.5.9.7):

$$\frac{1}{2}c_{ijkl}S_{ij}^*S_{kl}^* = -\frac{1}{2}V_{ij}^0S_{ij}^*. \quad (1.5.9.30)$$

Substituting the values for the spontaneous magnetostriction, the final equation for the anisotropy energy measured at atmospheric pressure may be written as

$$\begin{aligned} U_a &= U_a^0 + \frac{1}{2}V_{ij}^0S_{ij}^* \\ &= (K_{ij}^0 + K_{ij}')n_i n_j + (K_{ijk\ell}^0 + K_{ijk\ell}')n_i n_j n_k n_\ell \\ &\quad + (K_{ijk\ell mn}^0 + K_{ijk\ell mn}')n_i n_j n_k n_\ell n_m n_n + \dots \end{aligned} \quad (1.5.9.31)$$

As an example, for the ferromagnets with a cubic prototype this equation may be written as

$$U_a = (K_1^0 + K_1')S(n_1^2 n_2^2) + (K_2^0 + K_2')n_1^2 n_2^2 n_3^2. \quad (1.5.9.32)$$

The coefficients K_1' and K_2' may be expressed in terms of the saturation magnetostriction constants h_0, \dots, h_5 [see (1.5.9.12)] and the elastic stiffnesses $c_{\alpha\beta}$:

$$\begin{aligned} K_1' &= c_{11}[h_0(2h_4 - 3h_3) + h_1(h_1 - h_3 + 3h_4) - h_4(h_3 - 2h_4)] \\ &\quad + c_{12}[2h_0(2h_4 - 3h_3) - (h_1 + h_4)(h_1 + 2h_3)] - \frac{1}{2}c_{44}h_2^2, \end{aligned} \quad (1.5.9.33)$$

$$\begin{aligned} K_2' &= -c_{11}[3h_4(h_1 + h_3) + (h_4 - h_3)(4h_4 - 3h_3)] \\ &\quad + c_{12}[3h_4(h_1 + h_3) + h_3(5h_4 - 6h_3)] \\ &\quad - \frac{1}{2}c_{44}(6h_2 + h_5)h_5. \end{aligned} \quad (1.5.9.34)$$

For cubic crystals, K_1^0 and K_1' are of the same magnitude. As an example, for Ni one has $K_1^0 = 80\,000$ erg cm $^{-3}$ = 8000 J m $^{-3}$ and $K_1' = -139\,000$ erg cm $^{-3}$ = $-13\,900$ J m $^{-3}$.

1.5.10. Transformation from Gaussian to SI units

Numerical values of magnetic quantities are given in Gaussian units in this chapter. For each quantity that appears in a table or figure, Table 1.5.10.1 gives the corresponding Gaussian unit and its value expressed in SI units. More details on the transformation between Gaussian and SI units are given *e.g.* in the Appendix of Jackson (1999).

1.5.11. Glossary

| | |
|---------------------|---|
| α_{ij} | (linear) magnetoelectric tensor |
| β_{ijk} | nonlinear magnetoelectric tensor <i>EHH</i> |
| γ_{ijk} | nonlinear magnetoelectric tensor <i>HEE</i> |
| Δ | Weiss constant |
| Δn | magnetic birefringence |
| ε_{ij} | dielectric permittivity |
| λ | constant describing magnetostriction |
| Λ_{ijk} | tensor describing the piezomagnetic effect |
| $\Lambda_{i\alpha}$ | matrix describing the piezomagnetic effect |
| μ_{ij} | magnetic permeability |

| | |
|--------------------------|---|
| μ | magnetic moment |
| μ_B | Bohr magneton |
| π_{ijkl} | piezomagnetoelectric tensor |
| $\rho(\mathbf{r})$ | charge density |
| Φ | thermodynamic potential |
| χ_{ij}^e | dielectric susceptibility |
| χ_{ij}, χ_{ij}^m | magnetic susceptibility |
| B | magnetic induction |
| c | speed of light |
| c_{ijkl} | elastic stiffness |
| $d\tau$ | volume element |
| e | charge of the electron |
| E | electric field |
| g | Landé g -factor |
| H | magnetic field |
| j(r) | current density |
| J | total angular momentum |
| k | position vector in reciprocal space |
| k_B | Boltzmann factor |
| l_i | sum of the magnetic moments in a unit cell, in which some of the moments are taken with opposite sign |
| L_i | antiferromagnetic vector |
| L | orbital angular momentum (Section 1.5.1.1), antiferromagnetic vector (remainder of this chapter) |
| m(r) | magnetic moment density |
| m | sum of the magnetic moments in a unit cell |
| M | magnetization (= magnetic moment per unit volume = ferromagnetic vector) |
| N | No. of atoms per unit volume |
| P | effective number of Bohr magnetons (Section 1.5.1), pressure (remainder of this chapter) |
| P | electric polarization |
| r | position vector in space |
| S(r) | spin density |
| S | spin angular momentum (of an atom or ion) |
| s_{ijkl} | elastic compliance |
| S_{ij} | strain tensor |
| T_{ij} | stress tensor |
| T | temperature |
| T_c | transition temperature, in particular Curie temperature |
| T_N | Néel temperature |
| U | energy |
| U_a | anisotropy energy |
| U_{el} | elastic energy |
| U_{me} | magnetoelastic energy |
| v | velocity |
| Z | atomic number (= number of electrons per atom) |

The authors express their gratitude to Dr Elena Zhdanova for her great support in the preparation of the figures, and to Professor Stephen Lovesey, Dr Jean-Pierre Rivera and Professor

Hans Schmid for suggesting numerous improvements to the manuscript.

References

- Aizu, K. (1970). Possible species of ferromagnetic, ferroelectric and ferroelastic crystals. *Phys. Rev. B*, **2**, 754–772.
- Akulov, N. (1928). Über die Magnetostraktion der Eisenkristalle. *Z. Phys.* **52**, 389–405.
- Alcantara Bonfim, O. F. de & Gehring, G. A. (1980). Magnetoelectric effect in antiferromagnetic crystals. *Adv. Phys.* **29**, 731–769.
- Anderson, J. C., Birss, R. R. & Scott, R. A. M. (1964). *Linear magnetostriction in hematite*. In *Proc. Int. Conf. Magnetism*, Nottingham, pp. 597–599. London: Institute of Physics and the Physical Society.
- Andratskii, V. P. & Borovik-Romanov, A. S. (1966). Piezomagnetic effect in α -Fe₂O₃. (In Russian.) *Zh. Eksp. Teor. Fiz.* **51**, 1030–1036. [English translation: *Sov. Phys. JETP*, **24** (1967), 687–691.]
- Andreev, A. F. & Marchenko, V. I. (1976). Macroscopic theory of spin waves. (In Russian.) *Zh. Eksp. Teor. Fiz.* **70**, 1522–1538. (English translation: *Sov. Phys. JETP*, **43**, 794–803.)
- Andreev, A. F. & Marchenko, V. I. (1980). Symmetry and the macroscopic dynamics of magnetic materials. (In Russian.) *Usp. Fiz. Nauk*, **130**, 39–63. (English translation: *Sov. Phys. Usp.* **23**, 21–34.)
- Ascher, E. (1966). Some properties of spontaneous currents. *Helv. Phys. Acta*, **39**, 40–48.
- Ascher, E. (1968). Higher-order magneto-electric effects. *Philos. Mag.* **17**, 149–157.
- Ascher, E. (1970). The interactions between magnetization and polarization: phenomenological symmetry considerations on boracites. *J. Phys. Soc. Jpn.* **28** Suppl., 7–14.
- Ascher, E., Rieder, H., Schmid, H. & Stössel, H. (1966). Some properties of ferromagnetoelectric nickel-iodine boracite, Ni₃B₇O₁₃I. *J. Appl. Phys.* **37**, 1404–1405.
- Astrov, D. N. (1960). The magnetoelectric effect in antiferromagnetics. (In Russian.) *Zh. Eksp. Teor. Fiz.* **38**, 984–985. (English translation: *Sov. Phys. JETP*, **11**, 708–709.)
- Astrov, D. N. (1961). Magnetoelectric effect in chromium oxide. (In Russian.) *Zh. Eksp. Teor. Fiz.* **40**, 1035–1041. (English translation: *Sov. Phys. JETP*, **13**, 729–733.)
- Astrov, D. N., Al'shin, B. I., Zorin, R. V. & Drobyshev, L. A. (1968). Spontaneous magnetoelectric effect. (In Russian.) *Zh. Eksp. Teor. Fiz.* **55**, 2122–2127. [English translation: *Sov. Phys. JETP*, **28** (1969), 1123–1125.]
- Barbara, B., Gignoux, D. & Vettier, C. (1988). *Lectures on modern magnetism*. Beijing: Science Press.
- Bazhan, A. N. & Bazan, Ch. (1975). Weak ferromagnetism in CoF₂ and NiF₂. (In Russian.) *Zh. Eksp. Teor. Fiz.* **69**, 1768–1781. (English translation: *Sov. Phys. JETP*, **42**, 898–904.)
- Becker, R. & Döring, W. (1939). *Ferromagnetismus*. Berlin: Springer.
- Belov, N. V., Belova, E. N. & Tarkhova, T. N. (1964). Polychromatic plane groups. In Shubnikov & Belov (1964). *Colored symmetry*, edited by W. T. Holser, pp. 228–237. Oxford: Pergamon.
- Belov, N. V., Neronova, N. N. & Smirnova, T. S. (1957). Shubnikov groups. (In Russian.) *Kristallografiya*, **2**, 315–325. (English translation: *Sov. Phys. Crystallogr.* **2**, 311–322.)
- Bertaut, E. F. (1963). Spin configurations of ionic structures: theory and practice. In *Magnetism*, Vol. III, edited by G. T. Rado & H. Suhl, pp. 149–209. New York: Academic Press.
- Bertaut, E. F., Mercier, M. & Pauthenet, R. (1964). Ordre magnétique et propriétés magnétiques de MnYO₃. *J. Phys.* **25**, 550–557.
- Bichurin, M. (1997). Editor. *Proceedings of the 3rd international conference on magnetoelectric interaction phenomena in crystals (MEIPIC-3)*. *Ferroelectrics*, **204**.
- Bichurin, M. (2002). Editor. *Proceedings of the 4th international conference on magnetoelectric interaction phenomena in crystals (MEIPIC-4)*. *Ferroelectrics*, **279–280**.
- Bickford, L. R. Jr, Pappis, J. & Stull, J. L. (1955). Magnetostriction and permeability of magnetite and cobalt-substituted magnetite. *Phys. Rev.* **99**, 1210–1214.
- Birss, R. R. (1964). *Symmetry and magnetism*. Amsterdam: North-Holland.
- Birss, R. R. & Anderson, J. C. (1963). Linear magnetostriction in antiferromagnetics. *Proc. Phys. Soc.* **81**, 1139–1140.
- Bloembergen, N. (1962). In *Proc. Int. Conf. High Magnetic Fields*, edited by B. Lax, p. 454. New York: John Wiley.
- Borovik-Romanov, A. S. (1959a). Investigation of weak ferromagnetism in the MnCO₃ single crystal. (In Russian.) *Zh. Eksp. Teor. Fiz.* **36**, 766–781. (English translation: *Sov. Phys. JETP*, **9**, 539–549.)
- Borovik-Romanov, A. S. (1959b). Piezomagnetism in the antiferromagnetic fluorides of cobalt and manganese. (In Russian.) *Zh. Eksp. Teor. Fiz.* **36**, 1954–1955. (English translation: *Sov. Phys. JETP*, **9**, 1390–1391.)
- Borovik-Romanov, A. S. (1960). Piezomagnetism in the antiferromagnetic fluorides of cobalt and manganese. (In Russian.) *Zh. Eksp. Teor. Fiz.* **38**, 1088–1098. (English translation: *Sov. Phys. JETP*, **11**, 786–793.)
- Borovik-Romanov, A. S. & Orlova, M. P. (1956). Magnetic properties of cobalt and manganese carbonates. (In Russian.) *Zh. Eksp. Teor. Fiz.* **31**, 579–582. [English translation: *Sov. Phys. JETP*, **4** (1957), 531–534.]
- Borovik-Romanov, A. S. & Ozhogin, V. I. (1960). Weak ferromagnetism in an antiferromagnetic CoCO₃ single crystal. (In Russian.) *Zh. Eksp. Teor. Fiz.* **39**, 27–36. (English translation: *Sov. Phys. JETP*, **12**, 18–24.)
- Borovik-Romanov, A. S. & Yavelov, B. E. (1963). Linear magnetostriction in antiferromagnetic CoF₂. In *Proc. 3rd Regional Conf. Prague*, 81–83.
- Burzo, E. (1993). Magnetic properties of non-metallic inorganic compounds based on transition elements. Boron containing oxides. Landolt-Börnstein **III** 27 h, Berlin: Springer.
- Cardwell, M. J. (1969). Measurements of the magnetic field dependent electric susceptibility of yttrium iron garnet. *Phil. Mag.* **20**, 1087–1089.
- Chappert, J. (1965). Etude par effet Mössbauer de la substitution partielle par le fer du manganèse dans les manganites de terres rares. *Phys. Lett.* **18**, 229–230.
- Clark, A. E., DeSavage, B. F., Tsuya, N. & Kawakami, S. (1966). Magnetostriction of dysprosium, holmium, and erbium iron garnets. *J. Appl. Phys.* **37**, 1324–1326.
- Cox, D. E. (1974). Spin ordering in magnetoelectrics. *Int. J. Magn.* **6**, 67–75. [Reprinted in Freeman & Schmid (1975), pp. 111–119.]
- Cracknell, A. P. (1975). *Magnetism in crystalline materials*. Oxford: Pergamon.
- Curie, P. (1894). Sur la symétrie dans les phénomènes physiques, symétrie d'un champ électrique et d'un champ magnétique. *J. Phys.*, 3rd series **III**, 393–415.
- Dzyaloshinskii, I. E. (1957a). Thermodynamic theory of 'weak' ferromagnetism in antiferromagnetic substances. (In Russian.) *Zh. Eksp. Teor. Fiz.* **32**, 1547–1562. (English translation: *Sov. Phys. JETP*, **5**, 1259–1272.)
- Dzyaloshinskii, I. E. (1957b). The problem of piezomagnetism. (In Russian.) *Zh. Eksp. Teor. Fiz.* **33**, 807–808. [English translation: *Sov. Phys. JETP*, **6** (1958), 621–622.]
- Dzyaloshinskii, I. E. (1957c). The magnetic structure of fluorides of the transition metals. (In Russian.) *Zh. Eksp. Teor. Fiz.* **33**, 1454–1456. [English translation: *Sov. Phys. JETP*, **6** (1958), 1120–1122.]
- Dzyaloshinskii, I. E. (1959). On the magneto-electrical effect in antiferromagnets. (In Russian.) *Zh. Eksp. Teor. Fiz.* **37**, 881–882. [English translation: *Sov. Phys. JETP*, **10** (1960), 628–629.]
- Dzyaloshinskii, I. E. (1964). Theory of helicoidal structures in antiferromagnets. (In Russian.) *Zh. Eksp. Teor. Fiz.* **46**, 1420–1437, **47**, 336–348 and 992–1002. [English translation: *Sov. Phys. JETP*, **19**, 960–971, **20** (1965), 223–231 and 665–671.]
- Dzyaloshinskii, I. E. & Man'ko, V. I. (1964). Nonlinear effects in antiferromagnets. 'Latent' antiferromagnetism. (In Russian.) *Zh. Eksp. Teor. Fiz.* **46**, 1352–1359. (English translation: *Sov. Phys. JETP*, **19**, 915–919.)
- Eremenko, V. V., Kharchenko, N. F., Litvinenko, Yu. G. & Naumenko, V. M. (1989). *Magneto-optics and spectroscopy of antiferromagnets*. (In Russian.) Kiev: Naukova Dumka. [English translation (1992): New York: Springer.]
- Faber, J., Lander, G. H. & Cooper, B. R. (1975). Neutron-diffraction study of UO₂: observation of an internal distortion. *Phys. Rev. Lett.* **35**, 1770–1773.
- Ferré, J. & Gehring, G. A. (1984). Linear optical birefringence of magnetic crystals. *Rep. Prog. Phys.* **47**, 513–611.
- Folen, V. J., Rado, G. T. & Stalder, E. W. (1961). Anisotropy of the magnetoelectric effect in Cr₂O₃. *Phys. Rev. Lett.* **6**, 607–608.
- Foner, S. (1963). Antiferromagnetic and ferrimagnetic resonance. In *Magnetism*, Vol. I, edited by G. T. Rado & H. Suhl, pp. 383–447. New York: Academic Press.

1. TENSORIAL ASPECTS OF PHYSICAL PROPERTIES

- Freeman, A. J. & Schmid, H. (1975). *Magnetoelectric interaction phenomena in crystals*. London: Gordon and Breach.
- Gijsman, H. M., Poulis, N. J. & Van den Handel, J. (1959). *Magnetic susceptibilities and phase transitions of two antiferromagnetic manganese salts*. *Physica*, **25**, 954–968.
- Gorbatsevich, A. A. & Kopaev, Yu. V. (1994). *Toroidal order in crystals*. *Ferroelectrics*, **161**, 321–334.
- Grimmer, H. (1991). *General connections for the form of the property tensors in the 122 Shubnikov point groups*. *Acta Cryst.* **A47**, 226–232.
- Grimmer, H. (1992). *The piezomagnetoelectric effect*. *Acta Cryst.* **A48**, 266–271.
- Heesch, H. (1930). *Über die vierdimensionalen Gruppen des dreidimensionalen Raumes*. *Z. Kristallogr.* **73**, 325–345.
- Hou, S. L. & Bloembergen, N. (1965). *Paramagnetoelectric effects in $\text{NiSO}_4 \cdot 6\text{H}_2\text{O}$* . *Phys. Rev. A*, **138**, 1218–1226.
- Iida, S. (1967). *Magnetostriction constants of rare earth iron garnets*. *J. Phys. Soc. Jpn.* **22**, 1201–1209.
- Indenbom, V. L. (1959). *Relation of the antisymmetry and color symmetry groups to one-dimensional representations of the ordinary symmetry groups. Isomorphism of the Shubnikov and space groups*. (In Russian.) *Kristallografiya*, **4**, 619–621. [English translation: *Sov. Phys. Cryst.* **4** (1960), 578–580.]
- International Tables for Crystallography* (2002). Vol. A. *Space-group symmetry*, edited by Th. Hahn. Dordrecht: Kluwer Academic Publishers.
- Izumov, Yu. A. & Naish, V. E. (1979). *Symmetry analysis in neutron diffraction studies of magnetic structures*. *J. Magn. Magn. Mater.* **12**, 239–248.
- Izumov, Yu. A., Naish, V. E. & Petrov, S. B. (1979). *Symmetry analysis in neutron diffraction studies of magnetic structures*. *J. Magn. Magn. Mater.* **13**, 267–274, 275–282.
- Izumov, Yu. A., Naish, V. E. & Syromiatnikov, V. N. (1979). *Symmetry analysis in neutron diffraction studies of magnetic structures*. *J. Magn. Magn. Mater.* **12**, 249–261.
- Jackson, J. D. (1999). *Classical electrodynamics*, 3rd ed. New York: Wiley.
- Joshua, S. J. (1991). *Symmetry principles and magnetic symmetry in solid state physics*. Graduate Student Series in Physics. Bristol: Hilger.
- Kadomtseva, A. M., Agafonov, A. P., Lukina, M. M., Milov, V. N., Moskvina, A. S. & Semenov, V. A. (1981). *Characteristic magnetoelastic properties of yttrium orthochromite*. (In Russian.) *Fiz. Tverd. Tela*, **23**, 3554–3557. (English translation: *Sov. Phys. Solid State*, **23**, 2065–2067.)
- Kadomtseva, A. M., Agafonov, A. P., Milov, V. N., Moskvina, A. S. & Semenov, V. A. (1981). *Direct observation of symmetry change induced in orthoferrite crystals by an external magnetic field*. (In Russian.) *Pis'ma Zh. Eksp. Teor. Fiz.* **33**, 400–403. (English translation: *JETP Lett.* **33**, 383–386.)
- Kharchenko, N. F., Eremenko, V. V. & Belyi, L. I. (1979). *Visual observation of 180-degree antiferromagnetic domains*. (In Russian.) *Pis'ma Zh. Eksp. Teor. Fiz.* **29**, 432–435. (English translation: *JETP Lett.* **29**, 392–395.)
- Kharchenko, N. F. & Gnatchenko, S. L. (1981). *Linear magneto-optic effect and visual observation of antiferromagnetic domains in an orthorhombic crystal of DyFeO_3* . (In Russian.) *Fiz. Nizk. Temp.* **7**, 475–493. (English translation: *Sov. J. Low Temp. Phys.* **7**, 234–243.)
- Kiselev, S. V., Ozerov, R. P. & Zhdanov, G. S. (1962). *Detection of magnetic order in ferroelectric BiFeO_3 by neutron diffraction*. (In Russian.) *Dokl. Akad. Nauk SSSR*, **145**, 1255–1258. [English translation: *Sov. Phys. Dokl.* **7** (1963), 742–744.]
- Kopský, V. (1979a). *Tensorial covariants for the 32 crystal point groups*. *Acta Cryst.* **A35**, 83–95.
- Kopský, V. (1979b). *A simplified calculation and tabulation of tensorial covariants for magnetic point groups belonging to the same Laue class*. *Acta Cryst.* **A35**, 95–101.
- Koptsik, V. A. (1966). *Shubnikov groups*. (In Russian.) Moscow: Izd. MGU.
- Koptsik, J. N. & Kuzhukeev, Zh.-N. M. (1972). *Derivation of the three-, four- and six-color Belov space groups from tables of irreducible representations*. (In Russian.) *Kristallografiya*, **17**, 705–711. [English translation: *Sov. Phys. Crystallogr.* **17** (1973), 622–627.]
- Kouvel, J. S. & Fisher, M. E. (1964). *Detailed magnetic behavior of nickel near its Curie point*. *Phys. Rev. A*, **136**, 1626–1632.
- Kovalev, O. V. (1987). *Representations of the crystallographic space groups*, 2nd ed. (In Russian.) Moscow: Nauka. [English translation (1993): New York: Gordon and Breach.]
- Landau, L. D. (1933). *Eine mögliche Erklärung der Feldabhängigkeit der Suszeptibilität bei niedrigen Temperaturen*. *Phys. Z. Sowjet.* **4**, 675–679.
- Landau, L. D. (1937). *Zur Theorie der Phasenumwandlungen. I*. *Phys. Z. Sowjet.* **11**, 26–47.
- Landau, L. D. & Lifshitz, E. M. (1951). *Statistical physics*. (In Russian.) Moscow: Gostekhizdat. [English translation (1958): London: Pergamon.]
- Landau, L. D. & Lifshitz, E. M. (1957). *Electrodynamics of continuous media*. (In Russian.) Moscow: Gostekhizdat. [English translation (1960): London: Pergamon.]
- Le Gall, H., Leycuras, C., Minella, D., Rudashevskii, E. G. & Merkulov, V. S. (1977). *Anomalous evolution of the magnetic and magneto-optical properties of hematite at temperature near and lower than the Morin phase transition*. *Physica B*, **86–88**, 1223–1225.
- Lee, E. W. (1955). *Magnetostriction and magnetomechanical effects*. *Rep. Prog. Phys.* **18**, 184–229.
- Lee, G., Mercier, M. & Bauer, P. (1970). *Mesures magnétoélectriques sur les grenats de Y, de Gd et de Dy aux basses températures*. In *Les éléments des terres rares*, Vol. II, pp. 389–399. Paris: Editions du CNRS.
- Levitin, R. Z. & Shchurov, V. A. (1973). *In Physics and chemistry of ferrites*, pp. 162–194. (In Russian.) Moscow: Izd. Mosk. Gos. Univ.
- Lifshitz, E. M. (1942). *On the theory of phase transitions of the second order*. *J. Phys. (Moscow)*, **6**, 61–74.
- Lyubimov, V. N. (1965). *The interaction of polarization and magnetization in crystals*. (In Russian.) *Kristallografiya*, **10**, 520–524. [English translation: *Sov. Phys. Crystallogr.* **10** (1966), 433–436.]
- Mason, W. P. (1951). *A phenomenological derivation of the first- and second-order magnetostriction and morphic effects for a nickel crystal*. *Phys. Rev.* **82**, 715–723; erratum (1952), **85**, 1065.
- Mason, W. P. (1954). *Derivation of magnetostriction and anisotropic energies for hexagonal, tetragonal, and orthorhombic crystals*. *Phys. Rev.* **96**, 302–310.
- Matarrese, L. M. & Stout, J. W. (1954). *Magnetic anisotropy of NiF_2* . *Phys. Rev.* **94**, 1792–1793.
- Mercier, R. (1974). *Magnetoelectric behaviour in garnets*. *Int. J. Magn.* **6**, 77–88. [Reprinted in Freeman & Schmid (1975), pp. 99–110.]
- Merkulov, V. S., Rudashevskii, E. G., Le Gall, H. & Leycuras, C. (1981). *Linear magnetic birefringence of hematite in the vicinity of the Morin temperature*. (In Russian.) *Zh. Eksp. Teor. Fiz.* **80**, 161–170. (English translation: *Sov. Phys. JETP*, **53**, 81–85.)
- Michel, Ch., Moreau, J.-M., Achenbach, G. D., Gerson, R. & James, W. J. (1969). *The atomic structure of BiFeO_3* . *Solid State Commun.* **7**, 701–704.
- Morin, F. J. (1950). *Magnetic susceptibility of $\alpha\text{-Fe}_2\text{O}_3$ and $\alpha\text{-Fe}_2\text{O}_3$ with added titanium*. *Phys. Rev.* **78**, 819–820.
- Moriya, T. (1960a). *Theory of magnetism of NiF_2* . *Phys. Rev.* **117**, 635–647.
- Moriya, T. (1960b). *Anisotropic superexchange interaction and weak ferromagnetism*. *Phys. Rev.* **120**, 91–98.
- Moriya, T. (1963). *Weak ferromagnetism*. In *Magnetism*, Vol. I, edited by G. T. Rado & H. Suhl, pp. 85–125. New York: Academic Press.
- Néel, L. & Pauthenet, R. (1952). *Étude thermomagnétique d'un monocristal de $\text{Fe}_2\text{O}_3 \cdot \alpha$* . *C. R. Acad. Sci.* **234**, 2172–2174.
- Neronova, N. N. & Belov, N. V. (1959). *Ferromagnetic and ferroelectric space groups*. (In Russian.) *Kristallografiya*, **4**, 807–812. (English translation: *Sov. Phys. Crystallogr.* **4**, 769–774.)
- O'Dell, T. H. (1967). *An induced magneto-electric effect in yttrium iron garnet*. *Philos. Mag.* **16**, 487–494.
- O'Dell, T. H. (1970). *The electrodynamics of magneto-electric media*. Amsterdam: North-Holland.
- Opechowski, W. & Guccione, R. (1965). *Magnetic symmetry*. In *Magnetism*, Vol. IIA, edited by G. T. Rado & H. Suhl, pp. 105–165. New York: Academic Press.
- Popov, Yu. F., Kazei, Z. A. & Kadomtseva, A. M. (1992). *Linear magnetoelectric effect in Cr_2O_3 in strong magnetic fields*. (In Russian.) *Pis'ma Zh. Eksp. Teor. Fiz.* **55**, 238–241. (English translation: *JETP Lett.* **55**, 234–238.)
- Prokhorov, A. S. & Rudashevskii, E. G. (1969). *Magnetostriction of antiferromagnetic cobalt fluoride*. (In Russian.) *Pis'ma Zh. Eksp. Teor. Fiz.* **10**, 175–179. (English translation: *JETP Lett.* **10**, 110–113.)
- Prokhorov, A. S. & Rudashevskii, E. G. (1975). *Magnetoelastic interactions and the single-domain antiferromagnetic state in cobalt fluoride*. (In Russian.) *Kratk. Soobshch. Fiz.* **11**, 3–6. (English translation: *Sov. Phys. Lebedev Inst. Rep.* **11**, 1–4.)

1.5. MAGNETIC PROPERTIES

- Rado, G. T. (1961). *Mechanism of the magnetoelectric effect in an antiferromagnet*. *Phys. Rev. Lett.* **6**, 609–610.
- Rado, G. T. (1962). *Statistical theory of magnetoelectric effects in antiferromagnets*. *Phys. Rev.* **128**, 2546–2556.
- Rado, G. T. (1964). *Observation and possible mechanisms of magnetoelectric effects in a ferromagnet*. *Phys. Rev. Lett.* **13**, 335–337.
- Rado, G. T. (1969). *Magnetoelectric evidence for the attainability of time-reversed antiferromagnetic configurations by metamagnetic transitions in DyPO₄*. *Phys. Rev. Lett.* **23**, 644–647, 946.
- Rado, G. T. & Ferrari, J. M. (1973). *Magnetoelectric effects in TbPO₄*. *AIP Conf. Proc.* **10**, 1417.
- Rado, G. T., Ferrari, J. M. & Maisch, W. G. (1984). *Magnetoelectric susceptibility and magnetic symmetry of magnetoelectrically annealed TbPO₄*. *Phys. Rev. B*, **29**, 4041–4048.
- Rado, G. T. & Folen, V. J. (1961). *Observation of the magnetically induced magnetoelectric effect and evidence for antiferromagnetic domains*. *Phys. Rev. Lett.* **7**, 310–311.
- Rado, G. T. & Folen, V. J. (1962). *Magnetoelectric effects in antiferromagnetics*. *J. Appl. Phys.* **33** Suppl., 1126–1132.
- Rivera, J.-P. (1994). *On definitions, units, measurements, tensor forms of the linear magnetoelectric effect and on a new dynamic method applied to Cr-Cl boracite*. *Ferroelectrics*, **161**, 165–180.
- Rivera, J.-P. & Schmid, H. (1994). *Search for the piezomagnetoelectric effect in LiCoPO₄*. *Ferroelectrics*, **161**, 91–97.
- Schlenker, M. & Baruchel, J. (1978). *Neutron techniques for the observation of ferro- and antiferromagnetic domains*. *J. Appl. Phys.* **49**, 1996–2001.
- Schmid, H. (1965). *Die Synthese von Boraziten mit Hilfe chemischer Transportreaktionen*. *J. Phys. Chem. Solids*, **26**, 973–988.
- Schmid, H. (1967). *Twining and sector growth in nickel boracites grown by transport reactions*. (In Russian.) *Rost Krist.* **7**, 32–65. (English translation: *Growth Cryst. USSR*, **7**, 25–52.)
- Schmid, H. (1973). *On a magnetoelectric classification of materials*. *Int. J. Magn.* **4**, 337–361. [Reprinted in Freeman & Schmid (1975) pp. 121–146.]
- Schmid, H. (1994a). *Introduction to the proceedings of the 2nd international conference on magnetoelectric interaction phenomena in crystals, MEIPIC-2*. *Ferroelectrics*, **161**, 1–28.
- Schmid, H. (1994b). *Multi-ferroic magnetoelectrics*. *Ferroelectrics*, **162**, 317–338.
- Schmid, H., Janner, A., Grimmer, H., Rivera, J.-P. & Ye, Z.-G. (1994). *Editors. Proceedings of the 2nd international conference on magnetoelectric interaction phenomena in crystals (MEIPIC-2)*. *Ferroelectrics*, **161**–**162**.
- Schwarzenberger, R. L. E. (1984). *Colour symmetry*. *Bull. London Math. Soc.* **16**, 209–240.
- Scott, R. A. M. & Anderson, J. C. (1966). *Indirect observation of antiferromagnetic domains by linear magnetostriction*. *J. Appl. Phys.* **37**, 234–237.
- Shubnikov, A. V. (1951). *Symmetry and antisymmetry of finite figures*. (In Russian.) Moscow: Acad. Sci. USSR. [English translation in Shubnikov & Belov (1964) pp. 3–172 and 249–252.]
- Shubnikov, A. V. & Belov, N. V. (1964). *Colored symmetry*, edited by W. T. Holser. Oxford: Pergamon.
- Shubnikov, A. V. & Koptsik, V. A. (1972). *Symmetry in science and art*. (In Russian.) Moscow: Nauka. [English translation (1974): New York: Plenum.]
- Shuvalov, L. A. & Belov, N. V. (1962). *The symmetry of crystals in which ferromagnetic and ferroelectric properties appear simultaneously*. (In Russian.) *Kristallografiya*, **7**, 192–194. (English translation: *Sov. Phys. Crystallogr.* **7**, 150–151.)
- Sirotnin, Y. I. & Shaskol'skaya, M. P. (1979). *Fundamentals of crystal physics*. (In Russian.) Moscow: Nauka. [English translation (1982): Moscow: Mir.]
- Smolenskii, G. A., Agranovskaya, A. I., Popov, S. N. & Isupov, V. A. (1958). *New ferroelectrics of complex composition*. (In Russian.) *Zh. Tekh. Fiz.* **28**, 2152–2153. (English translation: *Sov. Phys. Tech. Phys.* **3**, 1981–1982.)
- Smolenskii, G. A., Yudin, V. M., Sher, E. S. & Stolypin, Yu. E. (1962). *Antiferromagnetic properties of some perovskites*. (In Russian.) *Zh. Eksp. Teor. Fiz.* **43**, 877–880. [English translation: *Sov. Phys. JETP*, **16** (1963), 622–624.]
- Sosnovska, I., Peterlin-Neumaier, T. & Steichele, E. (1982). *Spiral magnetic ordering in bismuth ferrite*. *J. Phys. C*, **15**, 4835–4846.
- Tavger, B. A. (1958). *The symmetry of ferromagnetics and antiferromagnetics*. (In Russian.) *Kristallografiya*, **3**, 339–341. (English translation: *Sov. Phys. Crystallogr.* **3**, 341–343.)
- Tavger, B. A. & Zaitsev, V. M. (1956). *Magnetic symmetry of crystals*. (In Russian.) *Zh. Eksp. Teor. Fiz.* **30**, 564–568. (English translation: *Sov. Phys. JETP*, **3**, 430–436.)
- Townsend Smith, T. (1916). *The magnetic properties of hematite*. *Phys. Rev.* **8**, 721–737.
- Turov, E. A. (1963). *Physical properties of magnetically ordered crystals*. (In Russian.) Moscow: Akad. Nauk SSSR. [English translation (1965): New York: Academic Press.]
- Venevsev, Yu. N., Gagulin, V. V. & Zhitomirsky, I. D. (1987). *Material science aspects of seignette-magnetism problem*. *Ferroelectrics*, **73**, 221–248.
- Voigt, W. (1928). *Lehrbuch der Kristallphysik*. Leipzig: Teubner.
- Waerden, B. L. van der & Burckhardt, J. J. (1961). *Farbgruppen*. *Z. Kristallogr.* **115**, 231–234.
- White, R. L. (1974). *Microscopic origins of piezomagnetism and magnetoelectricity*. *Int. J. Magn.* **6**, 243–245. [Reprinted in Freeman & Schmid (1975), pp. 41–43.]
- Wijn, H. P. J. (1994). *Magnetic properties of non-metallic inorganic compounds based on transition elements. Perovskites. II. Oxides with corundum, ilmenite and amorphous structures*. Landolt-Börnstein **III**, 27, f3, Berlin: Springer.
- Zalessky, A. V. (1981). *Magnetic properties of crystals*. In *Modern crystallography*, Vol. IV, edited by L. A. Shuvalov. (In Russian.) Moscow: Nauka. [English translation (1988): Berlin: Springer.]
- Zamorzaev, A. M. (1957). *Generalization of Fedorov groups*. (In Russian.) *Kristallografiya*, **2**, 15–20. (English translation: *Sov. Phys. Crystallogr.* **2**, 10–15.)
- Zvezdin, A. K., Zorin, I. A., Kadomtseva, A. M., Krynetskii, I. B., Moskvina, A. S. & Mukhin, A. A. (1985). *Linear magnetostriction and antiferromagnetic domain structure in dysprosium orthoferrite*. (In Russian.) *Zh. Eksp. Teor. Fiz.* **88**, 1098–1102. (English translation: *Sov. Phys. JETP*, **61**, 645–647.)

1.6. Classical linear crystal optics

BY A. M. GLAZER AND K. G. COX†

1.6.1. Introduction

The field of classical crystal optics is an old one, and in the last century, in particular, it was the main subject of interest in the study of crystallography. Since the advent of X-ray diffraction, however, crystal optics tended to fall out of widespread use, except perhaps in mineralogy, where it has persisted as an important technique for the classification and identification of mineral specimens. In more recent times, however, with the growth in optical communications technologies, there has been a revival of interest in the optical properties of crystals, both linear and nonlinear. There are many good books dealing with classical crystal optics, which the reader is urged to consult (Hartshorne & Stuart, 1970; Wahlstrom, 1959; Bloss, 1961). In addition, large collections of optical data on crystals exist (Groth, 1906–1919; Winchell, 1931, 1939, 1951, 1954, 1965; Kerr, 1959). In this chapter, both linear and nonlinear optical effects will be introduced briefly in a generalized way. Then the classical derivation of the refractive index surface for a crystal will be derived. This leads on to a discussion on the practical means by which conventional crystal optics can be used in the study of crystalline materials, particularly in connection with mineralogical study, although the techniques described apply equally well to other types of crystals. Finally, some detailed explanations of certain linear optical tensors will be given.

1.6.2. Generalized optical, electro-optic and magneto-optic effects

When light of a particular cyclic frequency ω is incident on a crystal of the appropriate symmetry, in general an electrical polarization \mathbf{P} may be generated within the crystal. This can be expressed in terms of a power series with respect to the electric vector of the light wave (Nussbaum & Phillips, 1976; Butcher & Cotter, 1990; Kaminow, 1974):

$$\mathbf{P} = \sum \epsilon_o \chi^{(i)} E^i = \epsilon_o (\chi^{(1)} E + \chi^{(2)} E^2 + \chi^{(3)} E^3 + \dots), \quad (1.6.2.1)$$

where the $\chi^{(i)}$ are susceptibilities of order i . Those working in the field of electro-optics tend to use this notation as a matter of course. The susceptibility $\chi^{(1)}$ is a linear term, whereas the higher-order susceptibilities describe nonlinear behaviour.

However, it is convenient to generalize this concept to take into account other fields (*e.g.* electrical, magnetic and stress fields) that can be imposed on the crystal, not necessarily due to the incident light. The resulting polarization can be considered to arise from many different so-called electro-optic, magneto-optic and photoelastic (elasto-optic) effects, expressed as a series expansion of P_i in terms of susceptibilities $\chi_{ijkl\dots}$ and the applied fields \mathbf{E} , \mathbf{B} and T . This can be written in the following way:

$$\begin{aligned} P_i = & P_i^0 + \epsilon_o \chi_{ij} E_j^\omega + \epsilon_o \chi_{ij\ell} \nabla_\ell E_j^\omega + \epsilon_o \chi_{ijk} E_j^{\omega_1} E_k^{\omega_2} \\ & + \epsilon_o \chi_{ijk\ell} E_j^{\omega_1} E_k^{\omega_2} E_\ell^{\omega_3} + \epsilon_o \chi_{ijk} E_j^{\omega_1} B_k^{\omega_2} \\ & + \epsilon_o \chi_{ijk\ell} E_j^{\omega_1} B_k^{\omega_2} E_\ell^{\omega_3} + \epsilon_o \chi_{ijk\ell} E_j^{\omega_1} T_{kl}^{\omega_2} + \dots \end{aligned} \quad (1.6.2.2)$$

† The sudden death of Keith Cox is deeply regretted. He died in a sailing accident on 27 August 1998 in Scotland at the age of 65.

Here, the superscripts refer to the frequencies of the relevant field terms and the susceptibilities are expressed as tensor components. Each term in this expansion gives rise to a specific effect that may or may not be observed, depending on the crystal symmetry and the size of the susceptibility coefficients. Note a possible confusion: in the notation $\chi^{(i)}$, i is equal to one less than its rank. It is important to understand that these terms describe various properties, both linear and nonlinear. Those terms that describe the effect purely of optical frequencies propagating through the crystal give rise to *linear* and *nonlinear* optics. In the former case, the input and output frequencies are the same, whereas in the latter case, the output frequency results from sums or differences of the input frequencies. Furthermore, it is apparent that nonlinear optics depends on the intensity of the input field, and so is an effect that is induced by the strong optical field.

If the input electrical fields are static (the term ‘static’ is used here to mean zero or low frequency compared with that of light), the resulting effects are either linear or nonlinear electrical effects, in which case they are of no interest here. There is, however, an important class of effects in which both static and optical fields are involved: linear and nonlinear electro-optic effects. Here, the use of the terms linear and nonlinear is open to confusion, depending on whether it is the electrical part or the optical part to which reference is made (see for example below in the discussion of the linear electro-optic effect). Similar considerations apply to applied magnetic fields to give linear and nonlinear magneto-optic effects and to applied stresses, the *photoelastic* effects. Table 1.6.2.1 lists the most important effects according to the terms in this series. The susceptibilities are written in the form $\chi(\omega_1; \omega_2, \omega_3, \dots)$ to indicate the frequency ω_1 of the output electric field, followed after the semicolon by the input frequencies $\omega_1, \omega_2, \dots$

Table 1.6.2.1. Summary of linear and nonlinear optical properties

| Type of polarization term | Susceptibility | Effect |
|---|---|---|
| P_i^0 | $\chi(0; 0)$ | Spontaneous polarization |
| $\epsilon_o \chi_{ij} E_j^\omega$ | $\chi(\omega; \omega)$ | Dielectric polarization, refractive index, linear birefringence |
| $\epsilon_o \chi_{ij\ell} \nabla_\ell E_j^\omega$ | $\chi(\omega; \omega)$ | Optical rotation (gyration) |
| $\epsilon_o \chi_{ijk} E_j^{\omega_1} E_k^{\omega_2}$ | $\chi(0; 0, 0)$ | Quadratic electric effect |
| | $\chi(\omega; \omega, 0)$ | Linear electro-optic effect or Pockels effect |
| | $\chi(\omega_1 \pm \omega_2; \omega_1, \omega_2)$ | Sum/difference frequency generation, two-wave mixing |
| | $\chi(\omega; \omega/2, \omega/2)$ | Second harmonic generation (SHG) |
| | $\chi(0; \omega/2, \omega/2)$ | Optical rectification |
| | $\chi(\omega_3; \omega_1, \omega_2)$ | Parametric amplification |
| $\epsilon_o \chi_{ijk\ell} E_j^{\omega_1} E_k^{\omega_2} E_\ell^{\omega_3}$ | $\chi(\omega; 0, 0)$ | Quadratic electro-optic effect or Kerr effect |
| | $\chi(\omega; \omega/2, \omega/2, 0)$ | Electric-field induced second harmonic generation (EFISH) |
| | $\chi(-\omega_1; \omega_2, \omega_3, -\omega_4)$ | Four-wave mixing |
| $\epsilon_o \chi_{ijk} E_j^{\omega_1} B_k^{\omega_2}$ | $\chi(\omega; \omega, 0)$ | Faraday rotation |
| $\epsilon_o \chi_{ijk\ell} E_j^{\omega_1} B_k^{\omega_2} E_\ell^{\omega_3}$ | $\chi(\omega; \omega, 0, 0)$ | Quadratic magneto-optic effect or Cotton–Mouton effect |
| $\epsilon_o \chi_{ijk\ell} E_j^{\omega_1} T_{kl}^{\omega_2}$ | $\chi(\omega; \omega, 0)$ | Linear elasto-optic effect or photoelastic effect |
| | $\chi(\omega_1 \pm \omega_2; \omega_1, \omega_2)$ | Linear acousto-optic effect |

1.6. CLASSICAL LINEAR CRYSTAL OPTICS

1.6.2.1. Spontaneous polarization P_i^0

A spontaneous polarization of a crystal can be created in some polar crystals after a strong static electric field is first applied and then removed. Subsequent application of an electric field in the opposite direction can then reverse the sense of the spontaneous polarization. By analogy with the well known similar phenomenon of ferromagnetism, such crystals are known as ferroelectrics (Jona & Shirane, 1962; Lines & Glass, 1979). This effect is therefore not an optical effect, but is included here for the sake of completeness. For a crystal to be a ferroelectric, it cannot have a centre of symmetry.

1.6.2.2. Dielectric polarization $\varepsilon_o \chi_{ij} E_j^\omega$

Application of an electric field \mathbf{E} of frequency ω to a crystal results in a polarization response whose size depends on the dielectric susceptibility $\chi^{(1)}$. This is a second-rank tensor that is applicable to *all* materials, and is often quoted in terms of the dielectric constant $\varepsilon = \varepsilon_o(1 + \chi)$. For electric fields at optical frequencies, the dielectric constant is equal to the square of the refractive index for light propagating in a certain direction and in a particular polarization state. This effect can only be termed optical if the frequency of the electric field lies at optical frequencies. There is no difference between input and output frequencies, and so the susceptibility is written in the form $\chi_{ij}(\omega; \omega)$. Because there is no change in frequency, this is a linear optical effect.

1.6.2.3. Optical rotation (gyration) $\varepsilon_o \chi_{ij\ell} \nabla_\ell E_j^\omega$

This is the phenomenon often known as *optical activity* (Born & Wolf, 1993; Agranovich & Ginzburg, 1984) in which plane-polarized light of frequency ω passing through a medium has its polarization rotated through an angle depending on the path length through the medium. It is seen most easily along uniaxial directions in crystals with the appropriate symmetry. Centrosymmetric crystals cannot show optical rotation. Because no change in frequency occurs, it can be considered to be a linear optical effect.

1.6.2.4. Quadratic electric effect $\varepsilon_o \chi_{ijk} E_j^{\omega_1} E_k^{\omega_2}$

If $\omega_1 = \omega_2 = 0$, i.e. the susceptibility is $\chi_{ijk}(0; 0, 0)$, the resulting polarization is given by

$$P_i^0 = \varepsilon_o \chi_{ijk} E_j^0 E_k^0.$$

This is therefore a polarization induced in the crystal by a strong static electric field. It is a nonlinear electrical effect, and so it is not an optical property.

1.6.2.5. Linear electro-optic effect $\varepsilon_o \chi_{ijk} E_j^{\omega_1} E_k^{\omega_2}$

If $\omega_1 = \omega$ and $\omega_2 = 0$, i.e. $\chi_{ijk}(\omega; \omega, 0)$, this contribution becomes

$$P_i^\omega = \varepsilon_o \chi_{ijk} E_j^\omega E_k^0$$

and corresponds to the situation where light of frequency ω passes into the crystal at the same time as a static electric field is applied. The effect, sometimes known as the *Pockels effect*, is to change the polarization state of the incident light, effectively by altering the refractive indices of the crystal. This physical property is governed by the third-rank electro-optic susceptibility $\chi^{(2)}$, components χ_{ijk} , which follow the same symmetry constraints as the piezoelectric tensor. Crystals therefore must lack a centre of symmetry for this effect to be observable. Although this can be classified as a nonlinear effect, because more than one incident field is involved, it is customary to call it a linear electro-optic effect, as only a single electrical field is used, and moreover there is no change in the frequency of the incident light.

1.6.2.6. Sum/difference frequency generation (two-wave mixing) $\varepsilon_o \chi_{ijk} E_j^{\omega_1} E_k^{\omega_2}$

It can happen that when two different light fields of frequencies ω_1 and ω_2 , such as can be obtained from two lasers, propagate through a crystal, the resulting output frequency can be the sum or difference of the two incident frequencies, through the susceptibility $\chi_{ijk}(\omega_1 \pm \omega_2; \omega_1, \omega_2)$. A particular case is of interest: suppose $\omega_1 = \omega_2 = \omega/2$ i.e. $\chi_{ijk}(\omega; \omega/2, \omega/2)$, to get

$$P_i^\omega = \varepsilon_o \chi_{ijk} E_j^{\omega/2} E_k^{\omega/2}.$$

Here, the light, on passing through the crystal, interacts with itself to produce a doubling of the frequency. This important effect is known as *second harmonic generation* or SHG and is used for generating different laser frequencies starting from a fundamental frequency. The observation of SHG is also often a good indicator of the lack of a centre of inversion in a crystal. As two optical fields are involved, the incident field inducing the second one, this is a true nonlinear optical effect.

Another effect can be envisaged in which the susceptibility is $\chi_{ijk}(0; \omega/2, -\omega/2)$, i.e. there is a cancellation of the two incident frequencies to produce a polarization in the crystal. This is called *optical rectification*.

Parametric amplification is an effect caused when an incident beam at frequency ω_1 is incident on a nonlinear optical crystal at the same time as an intense pump beam frequency ω_2 , where $\omega_2 > \omega_1$. The ω_1 wave is then amplified accompanied by an 'idler' wave of frequency $\omega_3 = \omega_2 - \omega_1$.

1.6.2.7. Quadratic electro-optic effect $\varepsilon_o \chi_{ijk\ell} E_j^{\omega_1} E_k^{\omega_2} E_\ell^{\omega_3}$

This effect, known also as the *Kerr effect*, results from setting $\omega_1 = \omega$, $\omega_2 = \omega_3 = 0$, i.e. the susceptibility is $\chi_{ijk\ell}(\omega; \omega, 0, 0)$, thus:

$$P_i^\omega = \varepsilon_o \chi_{ijk\ell} E_j^\omega E_k^0 E_\ell^0.$$

Like the linear electro-optic effect described above, a static electric field applied to the medium causes a change in the refractive indices, which then affects the polarization of the transmitted light. The difference here is that the Kerr effect is displayed by all transparent media, including liquids. In an otherwise optically isotropic system, application of a strong static field makes the system optically anisotropic: this change from isotropic to anisotropic can be used to produce a fast optical shutter. Because the light frequency is unchanged, this can be termed a linear optical effect, but on the other hand, because it depends on the square of the static electric field, it is a nonlinear electrical effect.

1.6.2.8. Electric-field induced second harmonic generation $\varepsilon_o \chi_{ijk\ell} E_j^{\omega_1} E_k^{\omega_2} E_\ell^{\omega_3}$

If $\omega_1 = \omega_2 = \omega/2$ and $\omega_3 = 0$, i.e. the susceptibility is $\chi_{ijk\ell}(\omega; \omega/2, \omega/2, 0)$, the resulting polarization is

$$P_i^\omega = \varepsilon_o \chi_{ijk\ell} E_j^{\omega/2} E_k^{\omega/2} E_\ell^0.$$

A second-harmonic response is obtained, but this time induced by a static electric field. This is called *electric-field-induced SHG* or EFISH. It is a nonlinear optical effect that is created by a linear electric effect.

1.6.2.9. Four-wave mixing $\varepsilon_o \chi_{ijk\ell} E_j^{\omega_1} E_k^{\omega_2} E_\ell^{\omega_3}$

One use of a third-order nonlinear optical susceptibility is in the important area of four-wave mixing. In this case, the complex amplitude of the induced polarization at the frequency $\omega_1 = \omega_2 + \omega_3 - \omega_4$ is given by

$$P_i^{\omega_1} = \varepsilon_o \chi_{ijk\ell} (-\omega_1; \omega_2, \omega_3, -\omega_4) E_j^{\omega_2} E_k^{\omega_3} E_\ell^{*\omega_4}.$$

1. TENSORIAL ASPECTS OF PHYSICAL PROPERTIES

Thus if a nonlinear crystal is pumped by two counter-propagating beams of frequency $\omega_1 = \omega_2 = \omega$, and another beam $\omega_4 = \omega$ is input at some angle, a fourth beam $\omega_3 = \omega$ results whose complex amplitude will be the complex conjugate of the ω_4 beam. Thus four-wave mixing is an important arrangement for producing *phase conjugation*.

1.6.2.10. Faraday rotation $\varepsilon_o \chi_{ijk} E_j^{\omega_1} B_k^{\omega_2}$

Application of a static magnetic field to certain crystals through which light of frequency ω passes causes a change in polarization state *via*

$$P_i^\omega = \varepsilon_o \chi_{ijk} E_j^\omega B_k^0.$$

The effect is to rotate the plane of polarization of the incident light, the size of the effect depending not only on the length of the medium traversed, but also on the size of the applied magnetic field. An interesting difference from ordinary optical rotation is that on reflecting the light beam back through the medium, the plane of polarization is *further* rotated rather than cancelled: this property has been used in making optical isolators.

1.6.2.11. Quadratic magneto-optic effect $\varepsilon_o \chi_{ijkl} E_j^{\omega_1} B_k^{\omega_2} B_\ell^{\omega_3}$

By analogy with the quadratic electro-optic effect, application of a strong static magnetic field can modulate the polarization state of the incident light *via*

$$P_i^\omega = \varepsilon_o \chi_{ijkl} E_j^\omega B_k^0 B_\ell^0.$$

This effect is also known as the *Cotton-Mouton effect*.

1.6.2.12. Linear photoelastic effect $\varepsilon_o \chi_{ijkl} E_j^{\omega_1} T_{kl}^{\omega_2}$

Also known as the *piezo-optic* effect (or *elasto-optic* effect), this is usually observed through $\chi_{ijkl}(\omega; \omega, 0)$, *i.e.* the applied stress is static. Thus the application of a force to an elasto-optic material results in a change in birefringence. This effect can be seen not only in crystals, but also in isotropic materials such as glass or transparent plastics. By observation of a stressed material between crossed polars, the resulting strains can be seen as coloured fringes, a useful way of examining engineering structures.

1.6.2.13. Linear acousto-optic effect $\varepsilon_o \chi_{ijkl} E_j^{\omega_1} T_{kl}^{\omega_2}$

In the acousto-optic effect, the applied stress is at an acoustic frequency ω_2 , *i.e.* the relevant susceptibility is $\chi_{ijkl}(\omega_1 \pm \omega_2; \omega_1, \omega_2)$. Thus a sound wave passing through an acousto-optic crystal modulates the refractive index *via*

$$P_i^{\omega_1 \pm \omega_2} = \varepsilon_o \chi_{ijkl} E_j^{\omega_1} T_{kl}^{\omega_2}.$$

A beam of light of frequency ω_1 passing through the crystal can then be diffracted by the refractive index modulation, and so such a crystal is a useful device for converting sound waves into an optical signal for long-distance transmission along optical fibres. As $\omega_1 \gg \omega_2$, the frequency of the input light is only very slightly altered by the sound wave, and for most purposes can be neglected.

1.6.3. Linear optics

1.6.3.1. The fundamental equation of crystal optics

It is necessary, in order to understand fully the propagation of light through a general anisotropic crystal, to address the question of the way in which an electromagnetic wave is affected by its passage through a regular array of atoms or molecules. A full analysis of this problem at a microscopical level is complicated and was treated, for example, by Ewald (1916), who showed through consideration of a 'half-crystal' how to link the electro-

magnetic field outside the crystal to that inside (a good description of Ewald's work on this can be read in the book *P. P. Ewald and his Dynamical Theory of X-ray Diffraction*, published by the International Union of Crystallography, Oxford Science Publications, 1992). For the purposes needed here, it is sufficient to apply Maxwell's equations to a bulk anisotropic continuum crystal, thus taking a macroscopic approach. The treatment here follows that given by Nussbaum & Phillips (1976).

Consider the relationship between the dielectric displacement \mathbf{D} and an electric field \mathbf{E} which in tensor terms is given by

$$D_i = \varepsilon_o \varepsilon_{ij} E_j, \quad (1.6.3.1)$$

where ε_o is the vacuum dielectric permittivity and ε_{ij} is a second-rank tensor, the relative dielectric tensor. Correspondingly, there is an induced polarization \mathbf{P} related to \mathbf{E} *via*

$$P_k = \varepsilon_o \chi_{kl} E_\ell, \quad (1.6.3.2)$$

where χ_{kl} is another second-rank tensor, called the dielectric susceptibility tensor. Note that the restriction to a linear relationship between \mathbf{D} and \mathbf{E} (or \mathbf{P} and \mathbf{E}) confines the theory to the region of *linear optics*. Addition of higher-order terms (see above) gives *nonlinear optics*. (Nonlinear optics is discussed in Chapter 1.7.)

$$\text{curl } \mathbf{H} = \partial \mathbf{D} / \partial t \quad (1.6.3.3)$$

$$\text{curl } \mathbf{E} = -\partial \mathbf{B} / \partial t, \quad (1.6.3.4)$$

where \mathbf{B} and \mathbf{H} are the magnetic induction and magnetic field intensity, respectively. It is customary at this point to assume that the crystal is non-magnetic, so that $\mathbf{B} = \mu_o \mathbf{H}$, where μ_o is the vacuum magnetic permeability. If plane-wave solutions of the form

$$\mathbf{E} = \mathbf{E}_o \exp[i(\mathbf{k} \cdot \mathbf{r} - \omega t)] \quad (1.6.3.5)$$

$$\mathbf{H} = \mathbf{H}_o \exp[i(\mathbf{k} \cdot \mathbf{r} - \omega t)] \quad (1.6.3.6)$$

$$\mathbf{D} = \mathbf{D}_o \exp[i(\mathbf{k} \cdot \mathbf{r} - \omega t)] \quad (1.6.3.7)$$

are substituted into equations (1.6.3.3) and (1.6.3.4), the following results are obtained:

$$\mathbf{k} \times \mathbf{H} = \omega \mathbf{D} \quad (1.6.3.8)$$

$$\mathbf{k} \times \mathbf{E} = -\omega \mathbf{B}. \quad (1.6.3.9)$$

These equations taken together imply that \mathbf{D} , \mathbf{H} and \mathbf{k} are vectors that are mutually orthogonal to one another: note that in general \mathbf{E} and \mathbf{D} need not be parallel. Similarly \mathbf{B} (and hence \mathbf{H}), \mathbf{E} and \mathbf{k} are mutually orthogonal. Now, on substituting (1.6.3.9) into (1.6.3.8),

$$\frac{1}{\mu_o \omega^2} \mathbf{k} \times (\mathbf{k} \times \mathbf{E}) = -\mathbf{D}. \quad (1.6.3.10)$$

Defining the propagation vector (or wave normal) \mathbf{s} by

$$\mathbf{s} = \frac{c}{\omega} \mathbf{k} = n \hat{\mathbf{s}}, \quad (1.6.3.11)$$

where $\hat{\mathbf{s}}$ is the unit vector in the direction of \mathbf{s} and n is the *refractive index* for light propagating in this direction, equation (1.6.3.10) then becomes

$$\frac{1}{\mu_o c^2} \mathbf{s} \times (\mathbf{s} \times \mathbf{E}) = -\mathbf{D}. \quad (1.6.3.12)$$

Via the vector identity $\mathbf{A} \times (\mathbf{B} \times \mathbf{C}) = (\mathbf{A} \cdot \mathbf{C})\mathbf{B} - (\mathbf{A} \cdot \mathbf{B})\mathbf{C}$, this result can be transformed to

$$-(\mathbf{s} \cdot \mathbf{s})\mathbf{E} + (\mathbf{s} \cdot \mathbf{E})\mathbf{s} = -\mu_o c^2 \mathbf{D}. \quad (1.6.3.13)$$

1.6. CLASSICAL LINEAR CRYSTAL OPTICS

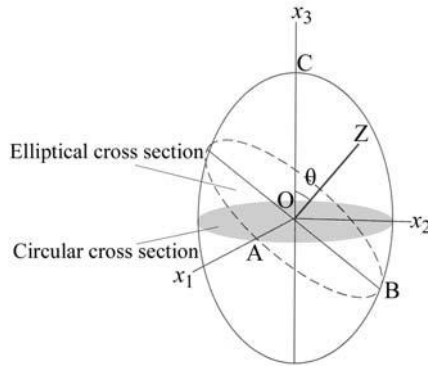


Fig. 1.6.3.1. The optical indicatrix.

$\mathbf{s} \cdot \mathbf{s}$ is equal to n^2 and $\mathbf{s} \cdot \mathbf{E}$ can be expressed simply in tensor form as $\sum_j s_j E_j$. Now, with equation (1.6.3.1), the fundamental equation of linear crystal optics is found:

$$\sum_j (\varepsilon_{ij} + s_i s_j) E_j = n^2 I E_i, \quad (1.6.3.14)$$

where I is the unit matrix.

1.6.3.2. The optical indicatrix

Equation (1.6.3.14) is the relevant starting point for the derivation of the way in which light propagates in an anisotropic medium. To solve it in a particular case, treat it as an eigenvector-eigenvalue problem: the E_i are the eigenvectors and n^2 the eigenvalues. For example, take the case of a uniaxial crystal. The dielectric tensor is then given by

$$\begin{pmatrix} \varepsilon_{11} & 0 & 0 \\ 0 & \varepsilon_{11} & 0 \\ 0 & 0 & \varepsilon_{33} \end{pmatrix}. \quad (1.6.3.15)$$

Assume that light propagates along a direction in the x_2x_3 plane, at an angle θ to the x_3 axis. Then, using (1.6.3.11), it is seen that

$$\begin{aligned} s_1 &= 0 \\ s_2 &= n \sin \theta \\ s_3 &= n \cos \theta \end{aligned} \quad (1.6.3.16)$$

and

$$s_i s_j = \begin{pmatrix} 0 & 0 & 0 \\ 0 & n^2 \sin^2 \theta & n^2 \sin \theta \cos \theta \\ 0 & n^2 \sin \theta \cos \theta & n^2 \cos^2 \theta \end{pmatrix}. \quad (1.6.3.17)$$

Substituting into equation (1.6.3.14) yields

$$\begin{aligned} & \begin{pmatrix} \varepsilon_{11} & 0 & 0 \\ 0 & \varepsilon_{11} + n^2 \sin^2 \theta & n^2 \sin \theta \cos \theta \\ 0 & n^2 \sin \theta \cos \theta & \varepsilon_{33} + n^2 \cos^2 \theta \end{pmatrix} \begin{pmatrix} E_1 \\ E_2 \\ E_3 \end{pmatrix} \\ &= \begin{pmatrix} n^2 & 0 & 0 \\ 0 & n^2 & 0 \\ 0 & 0 & n^2 \end{pmatrix} \begin{pmatrix} E_1 \\ E_2 \\ E_3 \end{pmatrix}. \end{aligned} \quad (1.6.3.18)$$

Solving this for the eigenvalues n gives

$$n_1^2 = \varepsilon_{11} \quad (1.6.3.19)$$

as one solution and

$$\frac{1}{n_2^2} = \frac{\cos^2 \theta}{\varepsilon_{11}} + \frac{\sin^2 \theta}{\varepsilon_{33}} \quad (1.6.3.20)$$

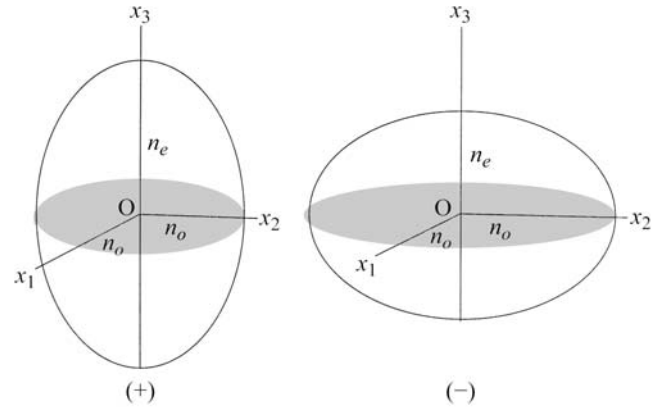


Fig. 1.6.3.2. Positive and negative uniaxial indicatrix.

as the other. This latter solution can be rewritten as

$$\frac{1}{n_2^2} = \frac{\cos^2 \theta}{n_o^2} + \frac{\sin^2 \theta}{n_e^2}, \quad (1.6.3.21)$$

showing how the observed refractive index n_2 varies between the limits set by n_o and n_e , called the *ordinary* and *extraordinary* refractive index, respectively (sometimes these are denoted by ω and ε , respectively). Equation (1.6.3.21) can be thought of as the equation of a uniaxial ellipsoid (circular cross section) with the lengths of the semi-axes given by n_o and n_e . This is illustrated in Fig. 1.6.3.1, where \mathbf{OZ} is the direction of propagation of the light ray at an angle θ to x_3 . Perpendicular to \mathbf{OZ} , an elliptical cross section is cut from the uniaxial ellipsoid with semi-axes OA equal to n_o and OB given by (1.6.3.21); the directions \mathbf{OA} and \mathbf{OB} also correspond to the eigenvectors of equation (1.6.3.4).

Direction \mathbf{OA} is therefore the direction of the electric polarization transverse to the propagation direction, so that the refractive index measured for light polarized along \mathbf{OA} is given by the value n_o . For light polarized along \mathbf{OB} , the refractive index would be given by equation (1.6.3.7). When \mathbf{OZ} is aligned along x_3 , a circular cross section of radius n_o is obtained, indicating that for light travelling along \mathbf{OZ} and with any polarization the crystal would appear to be optically isotropic. The ellipsoid described here is commonly known as the *optical indicatrix*, in this case a *uniaxial indicatrix*.

Two cases are recognized (Fig. 1.6.3.2). When $n_o < n_e$, the indicatrix is a prolate ellipsoid and is defined to be positive; when $n_o > n_e$, it is oblate and defined to be negative. Note that when $n_o = n_e$ the indicatrix is a sphere, indicating that the refractive index is the same for light travelling in any direction, i.e. the crystal is optically isotropic. The quantity $\Delta n = n_e - n_o$ is called the *linear birefringence* (often simply called *birefringence*). In general, then, for light travelling in any direction through a uniaxial crystal, there will be two rays, the ordinary and the extraordinary, polarized perpendicular to each other and travelling with different velocities. This splitting of a ray of light into two rays in the crystal is also known as *double refraction*.

The origin of the birefringence in terms of the underlying crystal structure has been the subject of many investigations. It is obvious that birefringence is a form of optical anisotropy (the indicatrix is not spherical) and so it must be linked to anisotropy in the crystal structure. Perhaps the most famous early study of this link, which is still worth reading, is that of Bragg (1924), who showed that it was possible to calculate rough values for the refractive indices, and hence birefringence, of calcite and aragonite. His theory relied upon the summation of polarizability contributions from the Ca^{2+} and O^{2-} ions.

Returning now to the theory of the indicatrix, more general solution of the fundamental equation (1.6.3.14) leads to a triaxial

1. TENSORIAL ASPECTS OF PHYSICAL PROPERTIES

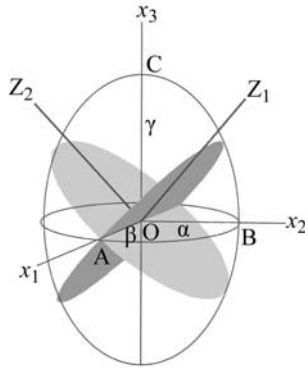


Fig. 1.6.3.3. Biaxial indicatrix, showing the two optic axes and corresponding circular cross sections.

ellipsoid, *i.e.* one in which all three semi-axes are different from one another (Fig. 1.6.3.3).

It is conventional to label the three axes according to the size of the refractive index by $n_\gamma > n_\beta > n_\alpha$ (or simply $\gamma > \beta > \alpha$). In such an ellipsoid, there are always two special directions lying in the γ - α plane, known as the *optic axial plane*, and perpendicular to which there are circular cross sections (shown shaded) of radius β . Thus these two directions are optic axes down which the crystal appears to be optically isotropic, with a measured refractive index β for light of any polarization. For this reason, crystals with this type of indicatrix are known as *biaxial*. When the angle between the optic axes, denoted conventionally as $2V$, is acute about the γ axis, the crystal is *positive biaxial*, and when it is acute about α the crystal is *negative biaxial*. Note that as $2V$ becomes smaller, the biaxial indicatrix becomes closer to a uniaxial indicatrix (positive or negative). In all general directions the crystal is optically anisotropic. Thus, for light along x_3 , the measured refractive indices will be α and β for light polarized along x_1 and x_2 , respectively; for light along x_2 , α and γ are measured for light polarized along x_1 and x_3 , respectively; and along x_1 , β and γ are measured for light polarized along x_2 and x_3 , respectively. There are therefore three different linear birefringences to measure: $\gamma - \beta$, $\beta - \alpha$ and $\gamma - \alpha$.

The different indicatrices are oriented in the crystal according to symmetry considerations (Table 1.6.3.1), and so their observation can form valuable and reliable indicators of the crystal system.

1.6.3.3. The dielectric impermeability tensor

It has been seen how the refractive indices can be described in a crystal in terms of an ellipsoid, known as the indicatrix. Thus for orthogonal axes chosen to coincide with the ellipsoid axes, one can write

$$\frac{x_1^2}{n_1^2} + \frac{x_2^2}{n_2^2} + \frac{x_3^2}{n_3^2} = 1, \quad (1.6.3.22)$$

where $n_1 = (\epsilon_{11})^{1/2}$, $n_2 = (\epsilon_{22})^{1/2}$ and $n_3 = (\epsilon_{33})^{1/2}$. One can write this equation alternatively as

$$\eta_{11}x_1^2 + \eta_{22}x_2^2 + \eta_{33}x_3^2 = 1, \quad (1.6.3.23)$$

where the $\eta_{ii} = 1/\epsilon_{ii}$ are the *relative dielectric impermeabilities*. For the indicatrix in any general orientation with respect to the coordinate axes

$$\eta_{11}x_1^2 + \eta_{22}x_2^2 + \eta_{33}x_3^2 + 2\eta_{12}x_1x_2 + 2\eta_{23}x_2x_3 + 2\eta_{31}x_3x_1 = 1. \quad (1.6.3.24)$$

Thus the dielectric impermeability tensor is described by a second-rank tensor, related inversely to the dielectric tensor.

1.6.4. Practical observation of crystals

1.6.4.1. The polarizing microscope

There are countless applications of polarizing microscopy. One of the largest fields of use is in mineralogy and petrology, where the requirement is to identify naturally occurring minerals, the optical properties of which have already been determined elsewhere. Medical applications of a similar sort exist, for instance in the identification of the minerals present in bladder or kidney stones. The chemist or materials scientist who has synthesised a crystalline material may also wish to identify it from known properties, or it may be a new substance that needs to be described. For other purposes it might, for example, be necessary to determine the orientation (relative to crystallographic axes) of mineral specimens, *e.g.* in the cutting of synthetic corundum for the manufacture of watch jewels. This section explains the point of view of an observer who wishes to record and measure optical properties, for whatever reason. Although much of what follows is discussed in terms of mineral crystals, it is equally valid for crystals in general, whether organic or inorganic.

The polarizing microscope incorporates five major features not found in ordinary microscopes. These are:

(i) A *polarizer*, normally a sheet of Polaroid, which is part of the microscope substage assembly. This produces plane-polarized light before the light reaches the specimen. In some microscopes, the polarizer can be rotated, though applications of this technique are rare. In the commonly used petrological microscope, the vibration direction of the polarizer is set in what is called the E-W direction, that is, as the user of the microscope sees the field of view, the vibration direction is from side to side.

(ii) An extra, high-power *condenser* situated in the substage immediately below the specimen. The condenser is switched in and out of the optical path as required.

(iii) A *rotating stage*, circular in plan and graduated in degrees. For a number of purposes, specimens can be rotated through known angles.

(iv) An *analyser*, a second polarizing device, situated in the microscope tube above the specimen. Its vibration direction is set at right angles to that of the polarizer, *i.e.* usually N-S. Like the condenser, this can be inserted into the optical path as needed.

(v) A *Bertrand lens*, also in the microscope tube and insertable as required, which has the function of transferring images from the back (upper) focal plane of the objective to the front (lower) focal plane of the eyepiece. The Bertrand lens and the extra substage condenser are used together to convert the microscope from the *orthoscopic* to the *conoscopic* configuration (see later).

In addition, polarizing microscopes have slotted tubes that allow the insertion of a variety of extra devices generally known as accessory plates. Most common amongst these are the sensitive-tint plate (or λ plate) and the quartz wedge.

Objective lenses of various magnifying powers are mounted in a rotating turret. Apart from magnification (typically $\times 5$ for low power, and $\times 40$ or more for high power), the *numerical aperture* (n.a.) of a lens is an important feature. This is defined as the diameter divided by the focal length. This is a measure of the angle of the cone of light that can enter the objective. In the

Table 1.6.3.1. Symmetry constraints on the optical indicatrix

| Crystal system | Indicatrix | Orientation constraints |
|-------------------------------------|--------------------|--|
| Cubic | Isotropic (sphere) | None |
| Tetragonal Trigonal Hexagonal | Uniaxial | Circular cross section perpendicular to c |
| Orthorhombic | Biaxial | All indicatrix axes aligned along a , b and c |
| Monoclinic | Biaxial | One indicatrix axis aligned along b (second setting) |
| Triclinic | Biaxial | None |

1.6. CLASSICAL LINEAR CRYSTAL OPTICS

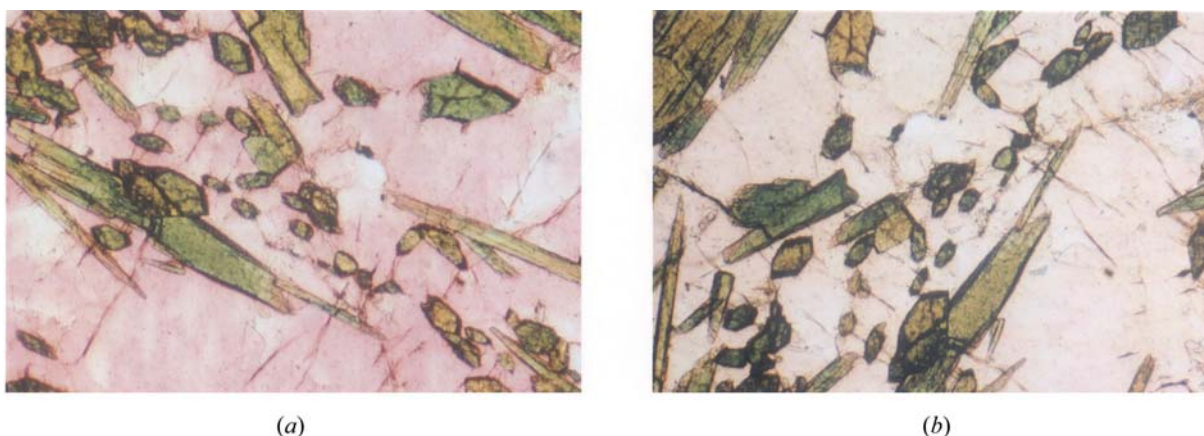


Fig. 1.6.4.1. A thin section of a rock containing the minerals aegirine (elongated crystals) and eudyalite (the matrix) viewed in plane-polarized light in two positions at right angles to each other [(a) and (b)]. Aegirine shows pleochroism from grass-green to yellow-green (compare specific crystals in the two photographs). Eudyalite shows pleochroism from pink to almost colourless.

conoscopic use of the microscope (see Section 1.6.4.11), this angle is required to be as large as possible so that the properties of rays travelling through the crystal in a variety of directions can be observed. Numerical apertures of more than *ca* 0.9 can not be achieved with 'dry' objectives, but higher values are obtained by inserting a drop of immersion oil between the specimen and the lens.

Eyepieces in polarizing microscopes are set in a short tube, at the lower end of which is mounted a set of cross wires, which lie in the front focal plane of the lens. When the microscope is properly focused, a real image of the specimen, created by the objective, is made to coincide with the cross wires. The cross wires are conventionally oriented vertically (N–S) and horizontally (E–W) in the field of view, and coincide with the vibration directions of the polarizer and analyser.

1.6.4.2. Specimen preparation

Specimens for examination with the polarizing microscope are usually of two different sorts: collections of small crystals or grains (and individual crystals), and thin sections cut from larger solid samples. In the first category, the material is often crushed to a fine sand, scattered on a microscope slide, a drop of immersion oil is applied, and a cover slip is placed on top. For special applications, an individual crystal may, for example, be mounted on the end of a glass fibre, and similarly examined under immersion oil. The thin-section technique is more widely used in petrology. Here a rock sample is cut into a section of standard thickness (0.03 mm) and mounted on a glass slide, using a resinous mounting material, formerly Canada Balsam but now synthetic. Small single crystals can also be used by mounting them on a spindle stage, or similar device, which allows one to orient the crystal in the microscope.

1.6.4.3. The indicatrix as an aid to practical microscopy

It is convenient for the microscopist to imagine the indicatrix sitting inside the crystal under observation. The indicatrix ellipsoid is fixed with respect to the crystallographic axes, according to different crystal systems (Table 1.6.3.1). The radial dimensions of the ellipsoid, in whatever direction, are a measure of the refractive index of a ray vibrating in that direction. Hence, because ray directions are approximately parallel to the microscope axis, a planar section across the indicatrix at right angles to the axis approximately contains the vibration directions of the ray. Such a section is in general an ellipse, the magnitudes of the major and minor axes of which represent the relative refractive indices, and the directions of which represent the vibration directions of the two transmitted rays. In all cases, the ray with the greater refractive index is known as the *slow ray* and the other as the *fast ray*. In uniaxial crystals the ordinary ray may be

slow or fast, depending on the optic sign. This mental image of the indicatrix acts as the microscopist's guide in the practical operations that follow.

1.6.4.4. Vibration directions

For the microscopist, the overriding feature of the behaviour of light transmitted through crystals is double refraction. Many of the observations that can be made with the polarizing microscope depend on the ability to distinguish the *individual* properties of the two rays. In general, they have different refractive indices, and in coloured crystals they may show different absorptions (*i.e.* the rays show different colours after transmission, the phenomenon known as *pleochroism* – see Fig. 1.6.4.1).

When the microscope is used for observations in *plane-polarized* light, the polarizer is inserted into the optical path but the analyser is not. The light before entering the crystal is polarized E–W. On entry, in the general case where the vibration directions of the crystal happen to lie in a random orientation relative to the vibration direction of the polarizer, the light is transmitted as two rays resolved into the two vibration directions of the specimen. These reach the observer's eye unchanged, and the effects observed are an average of what each ray would individually demonstrate.

Two cases can be used to illustrate this fundamental concept. The mineral calcite (CaCO_3) is always given as an example of extreme double refraction. In sections cut parallel to the *c* crystallographic axis, the two rays have refractive indices of 1.486 and 1.658, and this is the maximum difference they can show. Crystals in other orientations always show a smaller difference. The numerical difference between the two refractive indices, when we have identified the maximum difference, is what is quoted as the *birefringence* of the mineral, and for calcite it is unusually large (0.172) by the standards of other commonly occurring minerals (*cf.* quartz = 0.009). Birefringence is an important quantitative optical property, because in thin sections it is easily measurable. It is also useful to refer to the birefringence of individual grains, but this should not be confused with the use of the same term, based on maximum birefringence, as a diagnostic optical property of the material concerned.

Consider a calcite crystal lying with its *c* axis in the plane of the microscope slide. The vibration directions are parallel and at right angles to the crystallographic axis. On rotation of the stage, the *c* axis may be brought into parallelism with the vibration direction of the polarizer, in which case all the light is transmitted using only one of the vibration directions, which in this case has a refractive index of 1.486. On turning the stage through a right angle, all the effects seen are completely due to the other ray, with a refractive index of 1.658. The mounting medium in standard thin-section preparations has a refractive index of *ca* 1.54.

1. TENSORIAL ASPECTS OF PHYSICAL PROPERTIES

Hence, in the first position there is quite a large contrast between the refractive index of the crystal grain and the mounting medium, and in the other it is considerably smaller. Calcite is usually a highly transparent and virtually colourless substance, and whether the observer can even see the crystals depends on the refractive index difference between it and the mounting medium. In the first case, it is highly visible and in the second case it is harder to see. It is of course the roughness of the surface of the thin section, or the angularities of the form of the crushed crystal, which create small refractions, if there is a refractive-index contrast between it and the mounting medium, and thus make the crystal visible. The general property is known as *relief*. High relief means highly visible in this sense. Calcite shows such extreme changes in relief on rotation of the stage that the phenomenon is known as *twinkling*. Relief is not a measurable property, but to the experienced microscopist it is a subtle and useful guide to identification.

As a second example consider the mineral biotite, which shows extremely strong pleochroism. Biotite is for practical purposes a hexagonal mineral having a platy form dominated by a strong cleavage on (001.1). In thin sections, biotite crystals cut across the cleavage, *i.e.* parallel to the direction [00.1], are typically very dark brown in plane-polarized light when the cleavage lies parallel to the polarizer direction. When turned through 90° , the same crystals are only a very pale brown, pale yellow, or almost colourless. The colour contrast, a consequence of the different absorbing properties of the two rays, is striking. Examples of pleochroism are shown in Fig. 1.6.4.1.

From these examples it should be clear that the different rays show different things. However, the microscopist needs to be certain that the observations made refer exactly to one ray or the other. When the analyser is inserted into the optical path, most crystals (excluding those of the cubic system, and crystallites lying in special orientations) will show *polarization colours*, a consequence of the interference between the two rays once they are recombined vibrating in the analyser plane. Details will be discussed below, but for the present purpose it is the *extinction position* that is of importance. On rotation, a crystal viewed with both analyser and polarizer in position (a configuration known as *crossed Nicols*, after the Nicol prism, the forerunner of Polaroid) will transmit no light in two positions at right angles to each other. This happens when the vibration direction of a transmitted ray coincides with that of the polarizer. In this case, all the light transmitted through the crystal vibrates in a single direction, at right angles to the vibration direction of the analyser, and it is consequently unable to reach the observer. Thus, for all observations of the effects of a particular ray, crossing the polars (inserting the analyser), turning the stage to an extinction position, and then uncrossing the polars (removing the analyser) leaves the specimen showing the pure effects of whichever ray vibrates in the same direction as the polarizer. Much that follows depends on this simple operation.

1.6.4.5. Measuring refractive indices

Refractive indices measured carefully can be extremely useful aids in crystal identification, as well as being of importance as physical properties of interest. Apart from distinguishing crystalline species that may look similar under the microscope but have widely different refractive indices, the precise composition of crystalline materials belonging to important solid-solution series (*e.g.* the plagioclase feldspars or the olivines, in geological applications) can also be determined.

The direct measurement of refractive indices is often made by the examination of crystal grains mounted in an immersion oil, using the so-called *Becke line* test. This is observed in plane-polarized light with the substage diaphragm closed down to produce a narrow beam of essentially parallel rays. A medium-

power lens is usually suitable. When the oil has a refractive index different from that of the crystal, the Becke line appears as a bright rim of light around the edge of the crystal. However, as the microscope tube is racked up and down slightly (*i.e.* the position of focus is changed), the Becke line moves in or out relative to the crystal edge. As the position of focus is *lowered* the line moves towards the medium with the *lower* refractive index, *e.g.* if the oil has a higher refractive index than the crystal, lowering the focus (racking down) causes the Becke line to contract into the crystal. It is of course important to set the specimen in an extinction position before making the observation. If the oil has a refractive index between those of the two rays passing through the crystal, then the behaviour of the Becke line will reverse if the crystal is rotated to the other extinction position. In cases where there is a very large contrast between the crystal and the surrounding medium, a line as such may not be observed, but rather the specimen may appear to glow with concentrated light. The equivalent of Becke line movement is then the expansion or contraction of the light pool with changing focus.

The general objective of the observations is eventually to achieve an exact match between the immersion medium and the crystal. This is done by choosing different oils, or mixtures of oils, in sequence, the refractive indices of which are measured by a suitable refractometer. Ideally monochromatic or near-monochromatic light (*e.g.* the Na doublet with $\lambda = ca\ 590\text{ nm}$) is used, in which case the Becke line simply disappears when the crystal and the oil match. In white light however, because of dispersion by the oil, a match is shown by the presence of *two* faint Becke lines, one red and one greenish blue, which migrate in opposite directions as the focus is changed.

The general strategy of refractive-index determination is perfectly straightforward for cubic crystals, but requires the separate determination of values of n_e and n_o in uniaxial crystals, and n_α , n_β and n_γ in biaxial crystals. The most general case is that of the biaxial crystal. If a large number of crystal grains in the mount are examined, a number of cases may be distinguished.

(i) All grains have both refractive indices higher than the oil. The oil has a refractive index below n_α .

(ii) All grains have both refractive indices below that of the oil. The oil has a refractive index above n_γ .

(iii) Some grains have both refractive indices above that of the oil, while others have one above and one below. The oil has a refractive index between n_α and n_β .

(iv) Conversely, some grains have both refractive indices below the oil, while others have one above and one below. The oil has a refractive index between n_β and n_γ .

Uniaxial crystals present a simpler series of cases, in which the crystal may show both refractive indices higher than the oil (*i.e.* the refractive index of the oil is less than that of the fast ray), both lower than the oil, or one higher and one lower.

Systematic application of the above techniques leads to the determination of all the refractive indices required, and constitutes one of the most powerful methods of crystal identification or description. However, it is useful to make an additional check using the fact that, in anisotropic crystals, any specimen that fails to show polarization colours between crossed polars (*i.e.* remains dark in all stage positions) must lie with an optic axis parallel to the microscope axis. Such a crystal directly shows n_o (uniaxial crystals) or n_β (biaxial crystals). Furthermore, crystal grains showing maximum birefringence (see below) can be checked to see if they give a centred flash figure (see later), and if they do, their two vibration directions will show n_e and n_o , or n_α and n_γ , that is, the optic axis or axes lie in the plane of the microscope slide.

In larger crystalline specimens, several other techniques are available for measuring the refractive index. Perhaps the simplest and also the most convenient is to cut the crystal into a prism, and use minimum-deviation measurements on a spectrometer table. In addition, large plates can be inserted directly into a commer-

1.6. CLASSICAL LINEAR CRYSTAL OPTICS

cial refractometer, in order to measure the refractive index directly.

1.6.4.6. Determination of linear birefringence

The numerical determination of linear birefringence gives less information than a full set of refractive-index measurements, but is nevertheless highly useful in crystal identification, particularly in mineralogical and petrological applications where the thin section is the norm. It is also a most sensitive indicator of changes in the crystal structure at a phase transformation or as a function of temperature, pressure *etc.* Refractive-index determination is tedious, but birefringence determination is quick and easy.

Double refraction generates polarization colours when crystals are viewed between crossed polars, except where the crystal is by chance in an extinction position, or cut normal to an optic axis. The colours result from the interference of the two transmitted rays when they are combined into one vibration direction in the analyser. Polarization colours are best observed with the substage diaphragm moderately closed down, so that the transmitted light corresponds to a roughly parallel bundle of rays (if the diaphragm is wide open, and the supplementary condenser is inserted, the resultant rays are far from parallel, and the polarization colours will immediately be seen to degrade in the direction of whitening).

Considering a section showing two refractive indices, n_1 and n_2 , the time difference required for a ray to traverse the section is

$$t = \frac{nz}{c}, \quad (1.6.4.1)$$

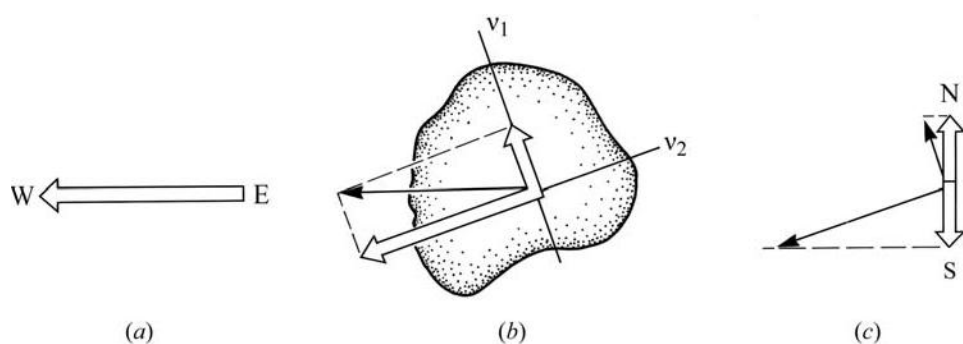


Fig. 1.6.4.2. Successive sections across the optical path of the microscope. (a) Above the polarizer, beneath the crystal. Polarized light vibrates E-W. (b) Within the crystal. Transmitted light is resolved into the two vibration directions of the crystal (v_1 and v_2). (c) Above the analyser. The two transmitted rays are resolved into the N-S direction. Amplitudes are shown, but phase difference is not.

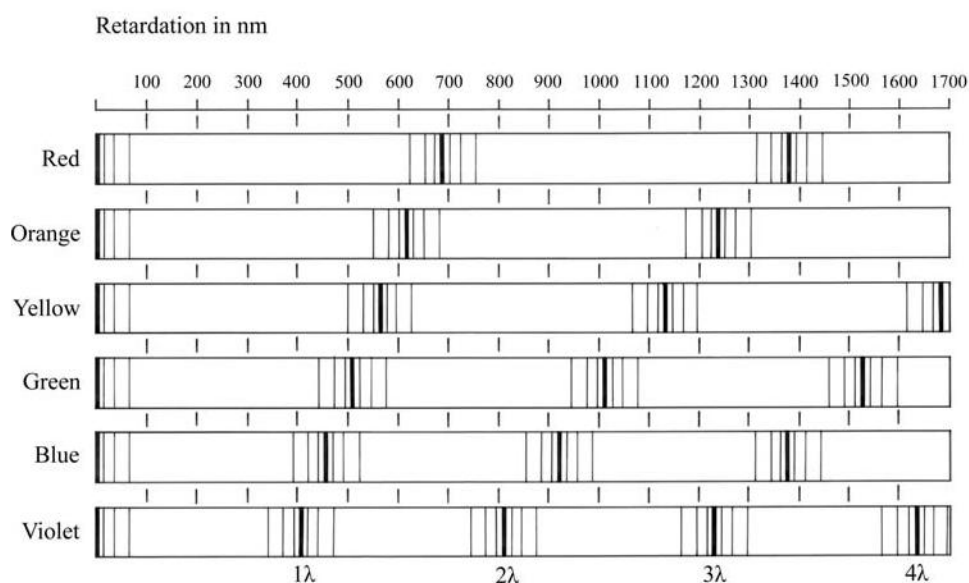


Fig. 1.6.4.3. Plot of retardation, R , versus wavelength, showing how polarization colours are formed.

where z is the thickness of the section. The time difference between the two rays is then

$$t_1 - t_2 = \frac{(n_1 - n_2)z}{c}, \quad (1.6.4.2)$$

which is referred to as the *retardation*. Multiplication by c gives the *relative retardation* or *optical path difference*, R , where

$$R = c(t_1 - t_2) = (n_1 - n_2)z. \quad (1.6.4.3)$$

R is usually expressed in nm (formerly $\mu\mu$).

The possibilities of interference clearly depend on R , but also on wavelength. For complete destructive interference, because of the way the transmitted rays are resolved into the vibration direction of the analyser (see Fig. 1.6.4.2), R must either be zero (as in cubic crystals, and sections normal to optic axes in anisotropic crystals) or a whole number of wavelengths. Thus as R changes, either with thickness, orientation of the crystals or with variation in birefringence in different substances, a variety of colours are produced, essentially formed from white light with various wavelengths *subtracted*. There is a good discussion of this point in Wahlstrom (1959).

Fig. 1.6.4.3 shows the effect of increasing R on a variety of visible-light wavelengths. When R is zero, no light is transmitted since all wavelengths show total destructive interference. As R increases a little, all wavelengths continue to show interference, and the polarization colours are essentially greys, which decrease in darkness until the middle of the first order where the grey is very pale, almost white. Most wavelengths at this stage are

showing relatively strong transmission. With increasing R , the region is reached where the shortest wavelengths of the visible light spectrum (violet) are beginning to approach a phase difference of 1λ . The transmitted light then takes on first a yellow tinge and then bright orange, as violet light (at $R \approx 400$ nm) and then blue are completely removed. Next, the removal of green light ($R \approx 500$ nm) results in the transmitted light being red and at $R \approx 560$ nm the top of the *first-order* colours is reached with the removal of yellow light. The resultant polarization colour is a distinctive magenta colour known as sensitive tint. The accessory plate known as the 'sensitive-tint' or ' 1λ ' plate is made to have $R = 560$ nm. Its use will be explained below, but meanwhile note that the polarization colour is so-called because with only very slight changes in R it becomes obviously red (falling R) or blue (rising R).

Between $R = 560$ nm and $R = 1120$ nm, the second-order colours are produced, and are similar in appearance to the colours of the rainbow (blue, green, yellow, orange and red in sequence), as orange, red, violet, blue, and green are successively cut out. The *third-order* colours ($R = 1120$ – 1680 nm) are essentially a repeat of the second-order, but there is a subtle change of quality about them, as they take on slightly garish hues compared with rainbow colours (the red at the top of the order has for example a distinct air of 'shocking pink' or even lipstick about it). This effect is a consequence of the increasing chances that two wavelengths

1. TENSORIAL ASPECTS OF PHYSICAL PROPERTIES

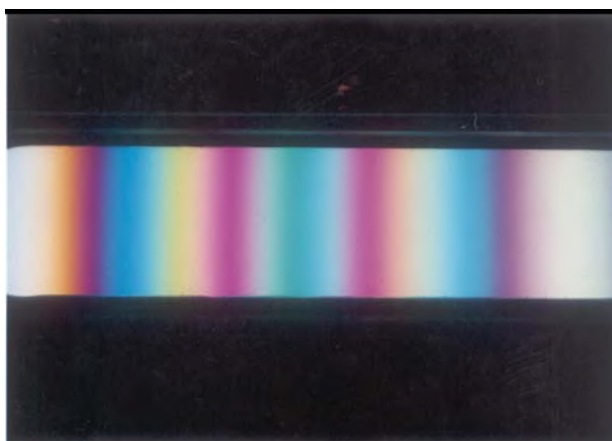


Fig. 1.6.4.4. A quartz wedge between crossed Nicols. The thin end is on the left. The colours shown vary between about the middle of the first order up to high fifth order.

will be cut out simultaneously (see Fig. 1.6.4.3), *e.g.* while first-order red results from the removal of green, second-order red results from the removal of both violet and yellow.

With increasing R , the distinction of colours within each order becomes weaker as the number of wavelengths simultaneously removed increases. Colours are diluted towards grey or white, so that from the fifth order upwards the range is little more than an alternation of pale pinkish and pale greenish tints. Eventually, at higher orders the polarization colours become a more-or-less uniform dull white. Fig. 1.6.4.4 shows the colours produced by a quartz crystal cut into a wedge shape.

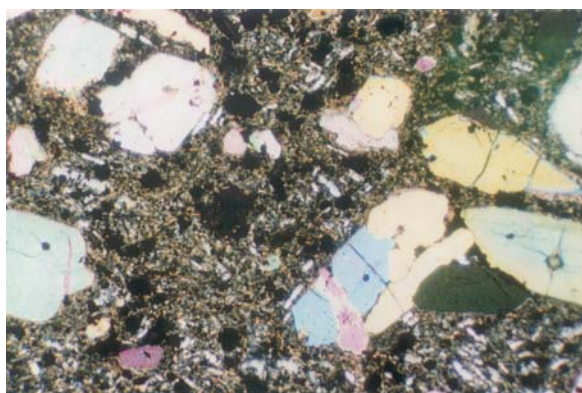
1.6.4.7. Identification of polarization colours

Birefringence can be determined quantitatively if the polarization colour can be correctly identified, and the section is of known thickness (see Fig. 1.6.4.6). It is of course necessary to distinguish between the birefringence of an individual grain, which will depend on orientation (see Fig. 1.6.4.5a), and the maximum birefringence (highest polarization colour) shown by the crystals concerned. It is the latter that is diagnostic, and in general it will be necessary to examine as many grains as possible to determine it.

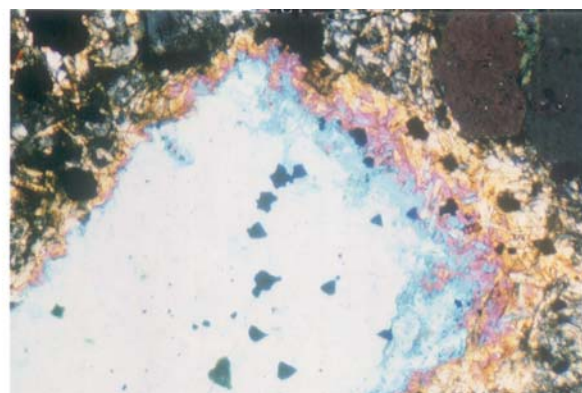
The grey colours of the lower part of the first-order colours are unique and immediately identifiable, but all other colours are at least superficially ambiguous. Even first-order white may be confused with a high-order white. There are essentially two methods of determining the order of an ambiguous colour, the first of which, fringe counting, is discussed here. Other methods depending on the use of the quartz wedge and sensitive-tint plate will be considered later.

1.6.4.8. Fringe counting

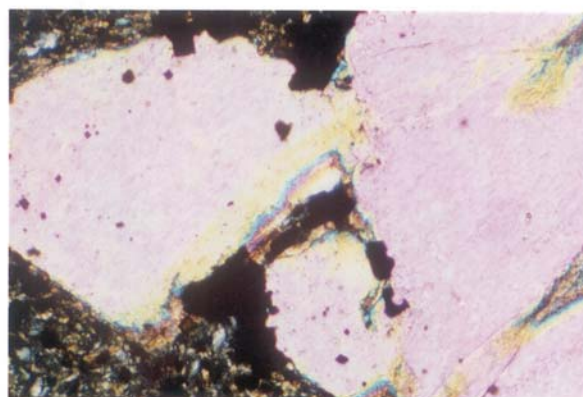
In a well made thin section, most crystals show a uniform polarization colour because of uniform orientation and thickness. Crystal edges, however, frequently taper off to near-zero thickness. In this case, the edge acts as a natural wedge of variable R and displays a series of fringes corresponding to the orders within the complete spectrum of interference colours, from first-order grey up to the main colour shown by the body of the crystal (Figs. 1.6.4.5b and c). Using a moderately high power objective, it is often easy to identify the individual bands and thus count up to the order concerned. The colour band red-sensitive tint-blue



(a)



(b)



(c)

Fig. 1.6.4.5. (a) Photomicrograph between crossed polars of a thin section of rock containing large olivine crystals set in a fine-grained matrix. The olivine crystals show a variety of polarization colours (first-order to high second-order) depending on their orientation. (b) Thin section between crossed polars of a rock containing a large pyroxene crystal, intergrown with other phases marginally. The edges of the crystal are wedge-like, and therefore thinner than the main body. The first-order white to orange colours make a prominent fringe on the right, grading inwards to sensitive tint and then to blue. The main body of the crystal is thus determined as second-order blue. (c) A similar section to that in (a) (centre of photograph) but here the second-order blue fringe is narrow and is succeeded by a second-order yellow fringe. Hence the main body of the crystal must be showing second-order pink.

1.6. CLASSICAL LINEAR CRYSTAL OPTICS

marking the first/second-order change is particularly easy to spot because of its generally dark colour. The method is also usable when the crystal grain has a sloping contact with a different crystal, and is especially easy when the latter has significantly lower birefringence. In this case, there are effectively two superimposed wedges (leading to some interesting addition or subtraction effects on R), but counting the fringes in ascending order will lead correctly to the identification of the polarization colour of the high-birefringence grain.

1.6.4.9. Fast and slow vibration directions

Before discussing other methods of identifying polarization colours, it is necessary to explain the use of the sensitive-tint plate and the quartz wedge. Both devices consist of a crystal mounted in an elongated holder that can be inserted into a slot in the microscope tube set at 45° to the vibration directions of the polarizer and analyser. The vibration directions of the plates themselves are normally oriented so that the slow ray vibrates NE–SW and the fast ray NW–SE.

The sensitive-tint (or 1λ) plate is made from a cleavage sheet of the white mica, muscovite, and has a thickness such that $R = 560$ nm. To determine fast and slow directions in an unknown specimen, the crystal grain is set to an extinction position and then rotated 45° in either direction. Thus its own vibration directions lie in diagonal positions, and when the tint plate is inserted, the vibration directions of plate and grain are parallel to each other. There are two possible cases depending whether the fast and slow directions coincide or not, *i.e.* slow vibration direction of plate parallel to the slow direction of the crystal (and fast parallel to fast) or slow direction of plate parallel to the fast direction of the crystal.

In the first case, the relative retardation is increased by 560 nm and the observed polarization colour jumps up the scale by one complete order as the plate is inserted. Thus, for example, first-order white ($R = 230$ nm) changes to second-order yellow/green ($R = 790$ nm), second-order blue changes to third-order blue *etc.*

When this effect is seen, it shows that the slow direction of the crystal lies NE–SW.

In the converse case, the observed polarization colour also changes, and, if the original colour is at least as high as second-order, will move down the scale by one complete order, *e.g.* second-order orange ($R = 950$ nm) changes to first-order yellow/orange ($R = 390$ nm). If the original colour is, however, within the first order (*i.e.* $R < 560$ nm), the new colour is still a consequence of subtracting 560 nm from R , but it is the absolute value of the new R (not the sign) which is relevant. For example, if the original colour is a first-order grey ($R = 100$ nm), the new colour corresponds to $R = 460$ nm, *i.e.* first-order orange. As a rapid mental aid, it is useful to think of the original colour falling to the bottom of the scale ($R = 0$) and then ‘bouncing’ back up until a change of one order has been reached, *e.g.* a first-order white, in the middle of the first order, hardly changes (half an order down followed by half an order up); first-order red changes to first-order grey (a fall of 90% of an order, followed by a rise of 10%).

If there is any doubt about the identification of the new colour, the crystal should be rotated through 90° and the second new colour examined. A comparison of the two options available, before and after rotation, rarely leaves any doubt about which is the higher colour (*i.e.* the slow-parallel-to-slow case). In all cases, whether or not the original colour is in the first order, one of the two new colours is higher than the other.

The sensitive-tint plate is so-called because it allows investigation of crystals showing very low birefringence (*e.g.* dark greys with $R \approx 50$ nm or less). In the parallel position, the new colour will lie just on the blue side of sensitive tint, and in the crossed position, just on the red side. These two colours are very easy to distinguish even though they represent only a small change in R .

From the above, it should be clear what an important aid the sensitive-tint plate can be in the actual identification of an unknown polarization colour, whether it be the body colour of the crystal or something observed in a set of grain-margin fringes. There are always two other colours that can be generated using the plate, and their relationship to the original colour is known in terms of R change, so that there are altogether three colours providing information.

The quartz wedge (Fig. 1.6.4.6) is an elongated wedge-shaped plate of progressively increasing thickness, usually cut parallel to the c axis so that the slow vibration direction is parallel to the length of the wedge. In this form it is inserted into a NE–SW slot so that the slow direction has this orientation. Some microscopes are, however, fitted with a NW–SE slot, and are provided with wedges (and sensitive-tint plates) that are ‘length fast’ rather than ‘length slow’. The optical effects are of course the same in both cases, but it is always a good idea to examine an accessory plate for its vibration directions (marked by the manufacturer) to be on the safe side.

The wedge varies in thickness from almost zero to about 0.2 mm, and typically shows a range of polarization colours from dark first-order grey up to the fourth order or so, as it is progressively inserted into the slot. The wedge can thus be used to change the polarization colour of an observed crystal by any desired amount of R within the available range (roughly 0–2500 nm). By using the two vibration directions of the crystal, these changes can be made additive or subtractive at will. In its simplest possible

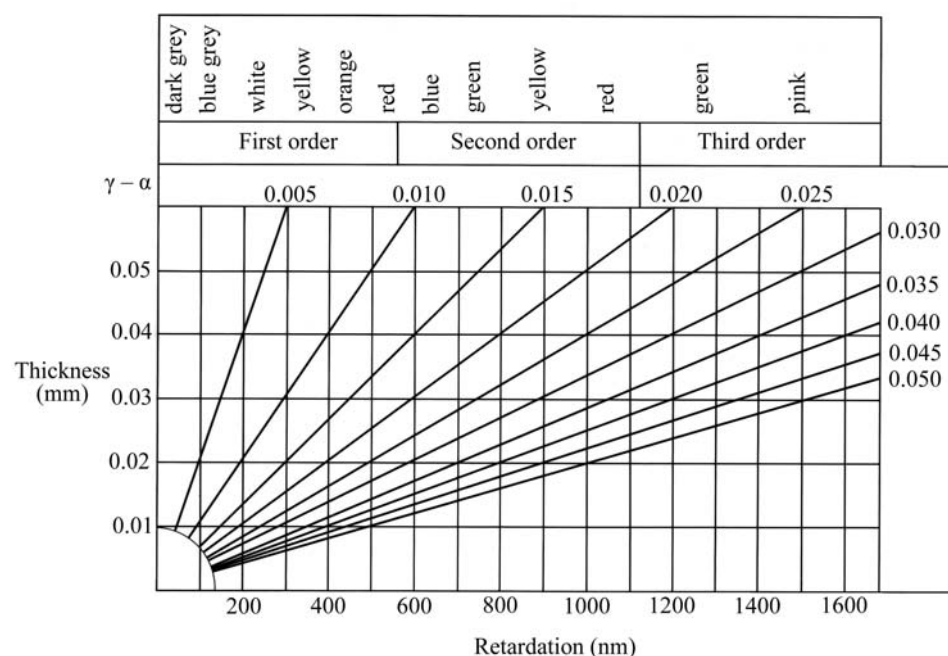


Fig. 1.6.4.6. Polarization colours *versus* thickness. The lines radiating from the origin are of equal birefringence (numerical values are given at the top and the right-hand side of the figure). The diagram may be used to determine thickness if birefringence is known, or birefringence if thickness is known. For example, the diagonal line for birefringence = 0.009 (*e.g.* quartz) intersects the standard thin-section thickness (0.03 mm) on first-order white. This is the polarization colour shown by quartz in a standard thin section.

1. TENSORIAL ASPECTS OF PHYSICAL PROPERTIES

application, the crystal is set so that slow is against fast and the wedge is inserted until the crystal shows as close to zero birefringence as possible, *i.e.* the relative retardations of the wedge and the crystal are equal and opposite (this is called *compensation*). Next, the specimen is removed, the colour shown by the wedge noted, and the wedge is slowly pulled out, counting the orders as they go past. This is an accurate and simple alternative method of determining polarization colours.

The accessory plates are useful in identifying the order of polarization colours, but their most frequent application is in determining which of the vibration directions shown by a crystal is fast and which is slow. For example, in a specimen of a biaxial crystal lying with the optic axial plane in the plane of the slide, the slow ray represents γ and the fast ray α . To determine which is which, the vibration directions are set in the 45° position and the tint plate is inserted. If the polarization colour goes up by an order, then the slow direction of the plate is parallel to the slow direction of the crystal. Conversely, if the colour goes down by an order, or goes up by less than a complete order (when the original $R < 560$ nm), fast in the crystal is parallel to slow in the plate.

1.6.4.10. Other methods of measuring birefringence

While the use of compensating plates is convenient, more precise techniques have been developed for the measurement of linear birefringence, both in an absolute and in a relative sense. The main methods of making absolute measurements use commercially available compensators mounted on a microscope. The main types are used with a polarizing microscope with crossed polars:

(i) *Babinet compensator*: This is mounted instead of the eyepiece of the microscope, and uses two quartz wedges sliding in opposite directions to each other. The wedges are so designed that when they fully overlap, but without a birefringent specimen in the microscope, a black compensation band is seen in the centre of the field of view. Then when the specimen is placed on the microscope stage in one of the two possible 45° positions, the compensation band is shifted. When in the correct 45° position, as found by trial, the lower wedge is then screwed out to recentre the compensation band, and the distance moved is read from an internal scale. This distance is calibrated in terms of relative retardation.

(ii) *Berek and Ehringhaus compensators*: These use a rotating birefringent crystal to change their effective retardation in order to compensate against the retardation of the specimen. The Berek compensator uses a calcite plate 0.01 mm thick, whereas the Ehringhaus compensator has compound compensating plates of either quartz or calcite, made of two sections of equal thickness cut parallel to the optic axes and cemented above one another at right angles. The compensator is inserted in the slot used for accessory plates with the specimen in one of the two 45° positions. Then by tilting the compensator plate, the apparent retardations are varied until the combined retardation matches that of the specimen, thus giving rise to the compensation band appearing in the centre of the field of view. The angle of tilt can then be converted to relative rotation by the use of suitable tables provided by the manufacturer.

In order to measure birefringence in a relative sense, the following techniques have been devised. All are capable of phenomenal precision in measuring *changes* in birefringence, in some instances to one part in 10^7 .

(i) *Sénarmont compensator*: A $\lambda/4$ plate is inserted above the specimen, with one of its principal vibration directions, say the slow direction, parallel to the vibration direction of the polarizer. The analyser is rotatable with a divided circle so that the angle of rotation can be measured. It can be shown that the phase shift of the light δ is given in terms of the angle θ through which the analyser is turned to achieve extinction by

$$\delta = \frac{2\pi}{\lambda} \Delta n z = 2\theta.$$

Thus if the birefringence, or more correctly the relative retardation, of the specimen is changed, say by altering the temperature, one can follow the change simply by monitoring the angle θ . This can be done either manually, or electronically using a phase meter attached to a photomultiplier to measure the intensity as a function of the angle of the analyser, which is rotated at some frequency by a motor.

(ii) *Intensity between crossed polars*: In this case the specimen is placed in the 45° position between crossed polars and the intensity of the light through the system is measured by a photomultiplier and presented typically on a recorder. On changing the retardation of the specimen, say by heating, this intensity changes according to

$$I = I_o \sin^2 \delta/2.$$

Thus on heating a set of \sin^2 fringes is drawn out, and by counting the fringes exact measurements of δ can be made. This technique is of great sensitivity, but suffers from the fact that the specimen must be maintained throughout in the 45° position.

(iii) *Rotating analyser*: In this system (Wood & Glazer, 1980), a $\lambda/4$ plate is inserted below the substage but above the polarizer in order to produce circularly polarized light. On passing through a birefringent crystal specimen, this is generally converted to elliptical polarization. This then passes through a Polaroid analyser set to rotate about the axis of the light at a predetermined frequency ω . The resulting intensity is then given by

$$I = (I_o/2)[1 + \sin(2\omega t - 2\varphi) \sin \delta],$$

where φ is the angle between the analyser at any time and an allowed vibration direction of the specimen. Thus by measuring the light intensity with a photomultiplier and then by using, say, phase-sensitive detection to examine the signal at 2ω , a plot of $\sin \delta$ can be made as the specimen's retardation is changed. The fact that circularly polarized light is incident on the specimen means that it is not necessary to align the specimen to any particular angle. Recently, a new type of optical microscope (Glazer *et al.*, 1996) has been developed using this principle, in which false colour images representing I_o , φ and $|\sin \delta|$ can be formed (Fig. 1.6.4.7).

1.6.4.11. Interference figures

Interference figures provide one of the most powerful tools for obtaining information about a crystal. The simplest applications allow the division of crystals into uniaxial and biaxial classes, hence constraining the crystal system. Within these classes, crystals are easily divided into the subclasses of positive and negative. More advanced techniques enable the orientation of the indicatrix relative to crystallographic features to be fully established.

Interference figures are obtained when the microscope is used in its *conoscopic* configuration. This means that light is made to pass through the specimen in as wide a range of directions as possible. A powerful substage condenser is inserted to produce a wide cone of incident light and the substage diaphragm is set wide open. A diffusing screen makes a good substitute for the condenser, as it also produces light with a variety of ray directions. However, some brightness is inevitably lost. In either case, a high-power objective with a large numerical aperture is used to collect the light above the specimen, and the polarizer and analyser are crossed.

The distinction between conoscopic and orthoscopic (parallel-light) applications of the microscope is important. For observations of birefringence, the orthoscopic arrangement is required so that optical path lengths through the crystal are constant. The

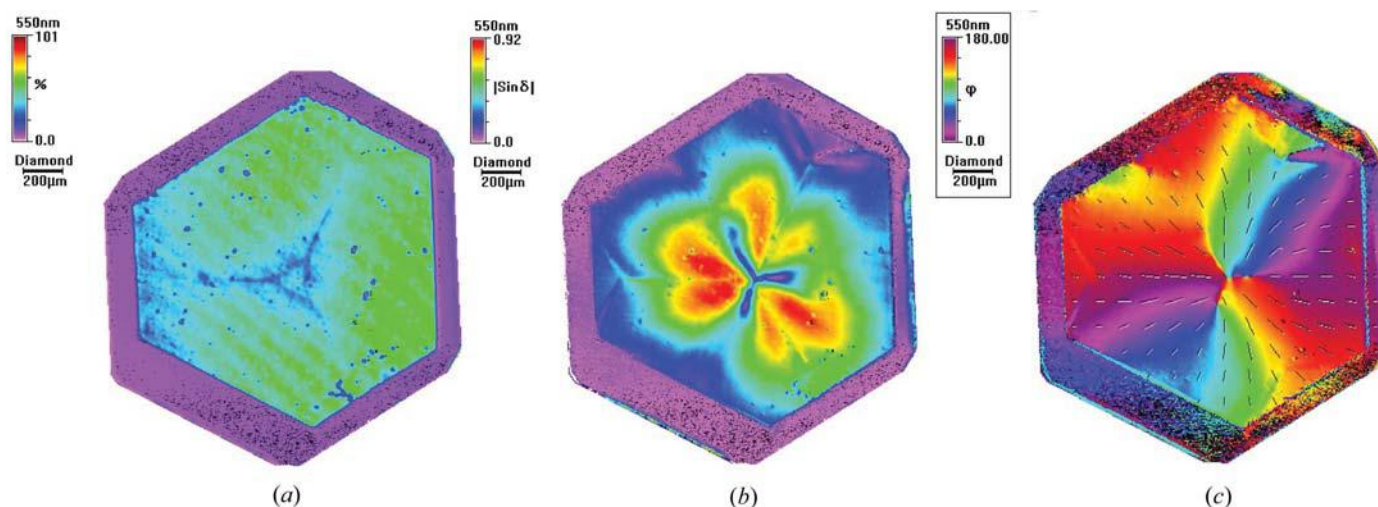


Fig. 1.6.4.7. Three birefringence images of industrial diamond viewed along $[111]$ taken with the rotating analyser system. (a) I_0 ; (b) $|\sin \delta|$; (c) orientation φ of slow axis with respect to horizontal.

images observed in plane-polarized light rely on scattering from point sources within the specimen, and do not depend strictly on whether the configuration is conoscopic or orthoscopic. Nevertheless, relief and the Becke line are much more clearly observable in orthoscopic use.

The principle of conoscopic use is quite different. Here, the image is formed in the *back focal plane* of the objective. Any group of parallel rays passing through the specimen is brought to a focus in this plane, at a specific point depending on the direction of transmission. Hence every point in the image corresponds to a different transmission direction (see Fig. 1.6.4.8). Moreover, the visible effects are entirely caused by interference, and there is no image of the details of the specimen itself. That image is of course also present, towards the top of the tube at or near the cross wires, but the two are not simultaneously visible. The conoscopic image may be viewed simply by removing the eyepiece and looking down the tube, where it appears as a small but bright circle. More commonly however, the Bertrand lens is inserted in the tube, which has the effect of transferring the conoscopic image from the back focal plane of the objective to the front focal plane of the eyepiece, where it coincides with the cross wires and may be examined as usual.

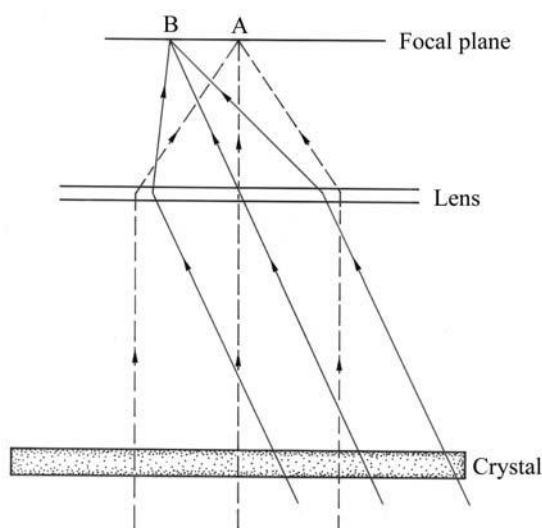


Fig. 1.6.4.8. Formation of the interference figure. The microscope axis lies vertically in the plane of the paper. A bundle of rays travelling through the crystal parallel to the microscope axis (dashed lines) is brought to a focus at A in the back focal plane of the objective. This is the centre of the interference figure. A bundle of oblique rays (solid lines) is brought to a focus at B, towards the edge of the figure.

It is useful to think of the conoscopic image as analogous to the gnomonic projection as used in crystallography. The geometrical principles are the same, as each direction through the crystal is projected directly through the centre of the lens into the back focal plane.

1.6.4.12. Uniaxial figures

To understand the formation of an interference figure, consider a simple example, a specimen of calcite cut at right angles to the c crystallographic axis. Calcite is uniaxial negative, with the optic axis parallel to c . The rays that have passed most obliquely through the specimen are focused around the edge of the figure, while the centre is occupied by rays that have travelled parallel to the optic axis (see Fig. 1.6.4.8). The birefringence within the image clearly must increase from nil in the centre to some higher value at the edges, because the rays here have had longer path lengths through the crystal. Furthermore, the image must have radial symmetry, so that the first most obvious feature of the figure is a series of coloured rings, corresponding in outward sequence to the successive orders. The number of rings visible will of course depend on the thickness of the sample, and when birefringence is low enough no rings will be obvious because all colours lie well within the first order (Figs. 1.6.4.9a and b). Fig. 1.6.4.10(a) illustrates, by reference to the indicatrix, the way in which the vibration directions of the o and e rays are disposed. Fig. 1.6.4.10(b) shows the disposition of vibration directions in the figure. Note that o rays always vibrate tangentially and e rays radially. The o -ray vibration directions lie in the plane of the figure, but e -ray vibration directions become progressively more inclined to the plane of the figure towards the edge.

The shaded cross on the figure illustrates the position of dark 'brushes' known as *isogyres* (Fig. 1.6.4.10b). These develop wherever vibration directions lie N-S or E-W, hence corresponding to the vibration directions of the analyser and polarizer. As the stage is rotated, as long as the optic axis is truly parallel to the microscope axis, the figure will not change. This is an example of a centred uniaxial optic axis figure, and such a figure identifies the crystal as belonging to the tetragonal, trigonal or hexagonal systems (see Fig. 1.6.4.11a).

From the point of crystal identification, one can also determine whether the figure coincides with the uniaxial positive ($n_e > n_o$) or uniaxial negative ($n_e < n_o$) cases. Inserting the sensitive-tint plate will move the coloured ring up or down the birefringence scale by a complete order. Fig. 1.6.4.11(c) shows the centred optic axis figure for calcite, which is optically negative. The insertion of a tint plate with its slow vibration direction lying NE-SW lowers the colours in the NE and SW quadrants of the figure, and raises

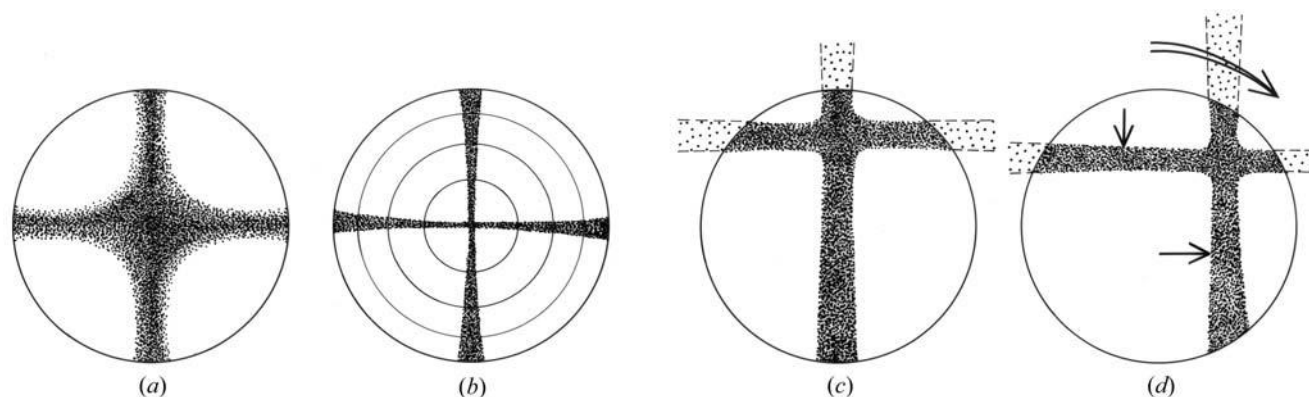


Fig. 1.6.4.9. (a) Centred uniaxial optic axis figure of a crystal with low birefringence. The isogyres are diffuse and the polarization colours in the quadrants are likely to be first-order grey. (b) As above, but for a crystal with high birefringence. The isogyres are narrower, and circular rings of polarization colours are seen, progressing outwards from first order to higher orders. (c) Off-centre uniaxial optic axis figure in the straight position (extinction position of crystal). (d) The same rotated to 45° . The curved arrow shows the rotation of the figure as the stage is turned clockwise. Arrows inside the field of view show directions of motions of isogyres. If the optic axis lies outside the field of view, such figures are difficult to interpret and may easily be confused with an off-centre biaxial optic axis figure when $2V$ is small to moderate.

those in the other quadrants (Fig. 1.6.4.11b). The simplest general rule is to look at the dark first-order grey in the original figure, lying immediately adjacent to the optic axis, *i.e.* the centre of the cross formed by the isogyres (Figs. 1.6.4.11b and c). If the crystal is optically negative, this colour changes to first-order yellow in the NE quadrant, if positive to blue. When the crystal has low birefringence, these colours may occupy the whole quadrant.

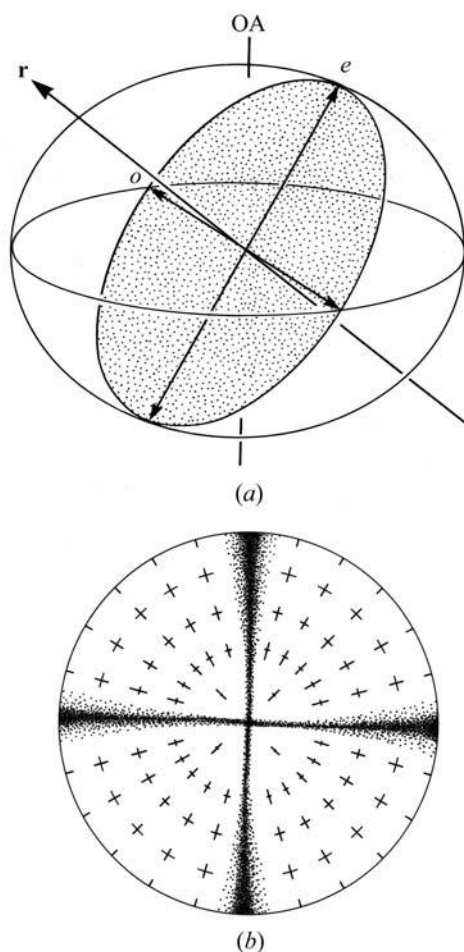


Fig. 1.6.4.10. (a) Vibration directions of an oblique ray passing through calcite, viewed relative to the indicatrix. OA is the optic axis, normal to the circular cross section of indicatrix, \mathbf{r} is the ray direction, e and o are, respectively, the vibration directions of the extraordinary and ordinary rays in the plane of the elliptical cross section of the indicatrix normal to \mathbf{r} . (b) Vibration directions as seen in the figure. The tangential set represents the o rays, the radial set represents e rays. The isogyres are also shown.

An *off-centre* uniaxial optic axis figure is obtained when the optic axis is inclined to the microscope axis by an amount which is small enough for it still to be visible within the figure (roughly within 25° of the microscope axis, using a normal high-power objective). Such figures show an isogyre cross with attendant rings, but the centre of the cross does not lie in the centre of the figure, and as the stage is rotated the centre of the cross moves round the figure in a circle (Figs. 1.6.4.9c and d). The isogyres remain NS and EW throughout. If the figure is so off-centre that the centre of the cross is not visible, the behaviour of the figure becomes difficult to interpret, and may easily be confused with some sorts of off-centre biaxial figures (see below). In the extreme case, when the optic axis lies in the plane of the slide, a quite different figure, known as a *flash figure*, is obtained. This is similar to many of the figures obtained from biaxial crystals, and will be considered further below.

1.6.4.13. Biaxial figures

(i) *Acute bisectrix figures*: Biaxial figures may be introduced by considering a crystal with a small $2V$ angle, oriented so that the acute bisectrix is parallel to the microscope axis. The conoscopic figure will have much in common with the uniaxial case already discussed (and indeed will become identical as $2V$ tends to zero), and some form of bilateral rather than radial symmetry is to be expected.

Vibration directions within the figure can be deduced by consideration of the *Biot-Fresnel* construction. Given that the form of the indicatrix is known, this is used to determine vibration directions in any orientation required. A general case presented in the form of a stereographic projection is given in Fig. 1.6.4.12(a). It is first necessary to know the positions of the optic axes and the position of a ray direction. Two planes are constructed, each containing one optic axis and the ray direction. Two *additional* planes are constructed, each containing the microscope axis and *bisecting* the angles between the first two planes. The plane in which the vibration directions lie is plotted normal to the ray direction, and the two vibration directions in this plane are fixed by the intersections of this plane with the two additional planes. This is also a very powerful construction to use in conjunction with orthoscopic methods. If crystallographic features, *e.g.* traces of cleavage planes, crystallographic axes, twin planes *etc.* (twinning is discussed in Chapter 3.3) are added to the stereogram, it becomes possible to determine the predicted angles between vibration directions and crystallographic features. One of the most fundamental aims of polarizing microscopy is the determination of the complete orientation of the indicatrix relative to crystallographic directions. Familiarity with the Biot-Fresnel construction is a substantial aid.

1.6. CLASSICAL LINEAR CRYSTAL OPTICS

Returning to the interference figure, a modified version of the Biot-Fresnel construction is illustrated in Fig. 1.6.4.12(b). Since the interference figure is analogous to a gnomonic rather than a stereographic projection, the various constructional planes required are straight lines. The vibration directions for the complete figure are given in Fig. 1.6.4.12(c).

Considering first the isogyres (brushes), if the optic axial plane lies N-S, as in Fig. 1.6.4.13(a), clearly the isogyres form a cross, as in the uniaxial case. There is a small difference, however. Because the vibration directions curve round more rapidly near the optic axial plane, the N-S isogyre is sharper than the E-W, which is relatively broadened and less dark.

If the slide is rotated so that the optic axial plane lies NE-SW, inspection of the vibration directions in Fig. 1.6.4.13(b) shows that the isogyres must part in the direction shown. Rotation of the stage through a full 180° will thus show two positions at which the brushes cross – once when the optic axial plane lies N-S, the other when it lies E-W – and two positions of maximum separation of the isogyres – when the optic axial plane lies NE-SW and NW-SE (see Fig. 1.6.4.14a). The position of the broader, more diffuse, brush will alternate. The amount by which the two

isogyres are separated in the 45° position depends on the size of $2V$. Since the field of view is usually about 60° , when $2V$ is 60° the isogyres will retreat right to the edge of the field of view in the 45° position, and then come back as rotation continues. When $2V > 60^\circ$, the brushes will entirely leave the field of view for part of the rotation (Fig. 1.6.4.14c). Approximate estimates of $2V$ can be made on this basis.

As in the uniaxial case, coloured fringes are also part of the figure, and are most obvious when birefringence is high (Fig. 1.6.4.14a and Fig. 1.6.4.15a). The outermost fringes have an elliptical form, but towards the centre of the figure they are distorted into a dumbbell-like or figure-of-eight form. This arises

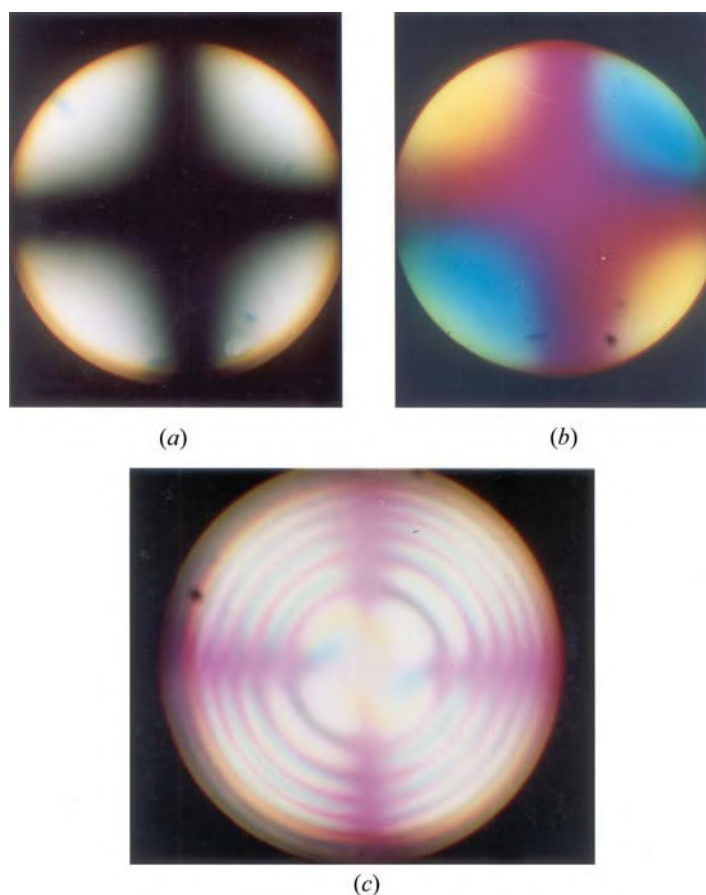


Fig. 1.6.4.11. (a) Centred optic axis figure of quartz (uniaxial). The birefringence is low, resulting in a diffuse cross and quadrant colours in the lower half of the first order. (b) The same figure with the sensitive-tint plate inserted (slow vibration direction NE-SW). The isogyres take on the sensitive-tint colour. Compensation takes place in the NE and SW quadrants (slow directions of crystal and plate parallel to each other) resulting in second-order blue, that is, one whole order above the original. In the other quadrants, the colours also apparently rise, but are restricted to yellow (high first-order). Thus the crystal is optically positive, that is, e rays (radial) are slow and o rays (tangential) are fast. (c) Centred optic axis figure of calcite with sensitive-tint plate (slow direction lying NE-SW) inserted. The birefringence is very high so there are many coloured rings. In the top right quadrant, the colour immediately adjacent to the cross is first-order yellow, whereas in the top left it is second-order blue. Calcite is hence optically negative. It can be observed that all the coloured rings in the top right and bottom left quadrants are an order lower than their counterparts in the top left and bottom right.

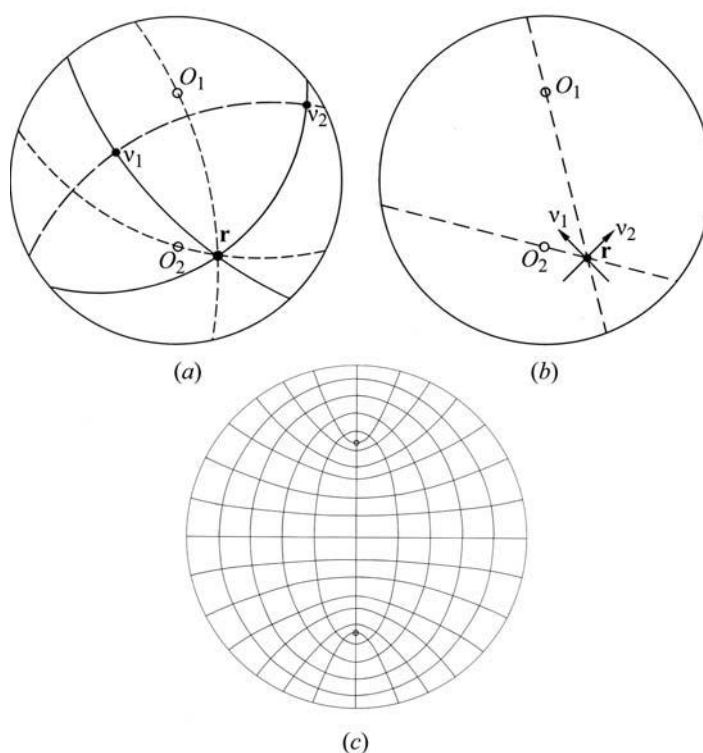


Fig. 1.6.4.12. (a) The Biot-Fresnel construction illustrated on the stereographic projection. (b) Method of determining vibration directions in a biaxial acute bisectrix figure using the Biot-Fresnel construction and a gnomonic projection. (c) Complete vibration directions of a figure similar to the above. As noted in the text, the directions shown are components resolved into the plane of the figure, and the true vibration directions are in general somewhat inclined.

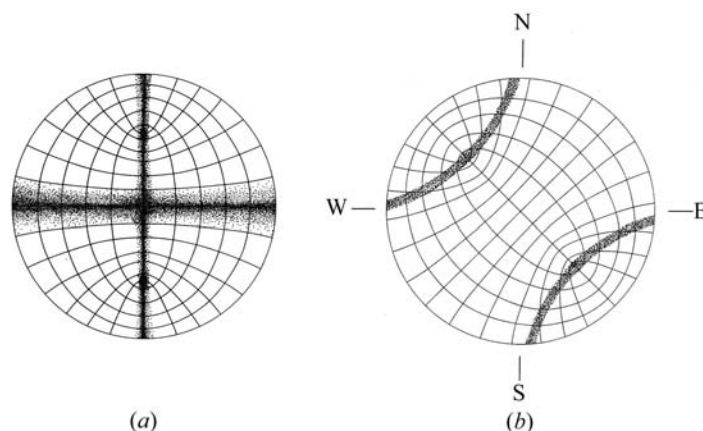


Fig. 1.6.4.13. (a) Illustration of the formation of crossed isogyres when the optic axial plane of a biaxial figure lies N-S. The shaded lines illustrate the zones in which vibration directions are N-S and E-W, leading to the formation of the isogyres. Along the E-W line, the zone across which vibration directions depart little from N-S and E-W is broad, hence this isogyre is wider than the N-S isogyre. (b) Illustration of the formation of separated curved isogyres when the same crystal is in the 45° position (optic axial plane NE-SW).

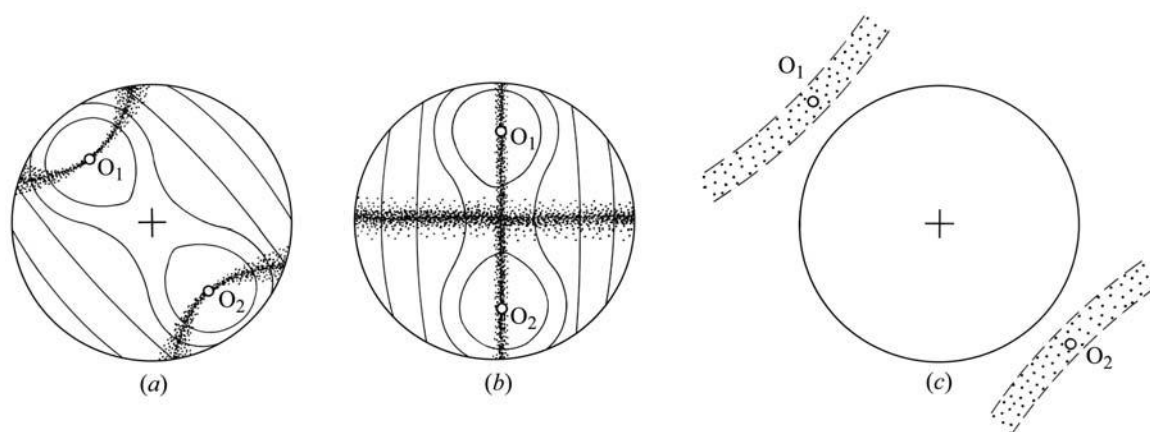


Fig. 1.6.4.14. (a) Drawing of biaxial optic axis figures set in the 45° position with the optic axial plane set NW-SE. $2V$, represented by the angle O_1-O_2 , is about 40° (cf. total field of view of ca 60°). The distribution of coloured fringes is represented, with near-circular areas of first-order colours around the optic axes, progressing outwards to higher orders (see also Fig. 1.6.4.15a). (b) The same figure in the straight position (optic axial plane N-S). Note that the isogyre along the optic axial plane is sharper than the E-W isogyre. (c) Representation of a biaxial figure in the 45° position when $2V > 60^\circ$. The isogyres leave the field completely.

because the areas of minimum birefringence must lie adjacent to the optic axes, and birefringence, although generally increasing outwards, must also increase towards a point midway between the optic axes. This effect is slight when birefringence is low, but is prominent when birefringence is high, in which case each optic axis is surrounded by its own set of almost-circular fringes, set within the general elliptical array.

Optic sign can be determined from the acute bisectrix biaxial figure in a way analogous to the uniaxial case. The stage is rotated to the 45° position, *i.e.* with maximum separation of the isogyres, and the analogues of the uniaxial quadrants are identified. The difference here is that in one of the 45° positions the NE and SW quadrants join through the space between the optic axes, and in the other the NW and SE quadrants are connected. The sensitive-tint plate is employed just as in the uniaxial case, and the same rules apply to change of colour (Fig. 1.6.4.15a and b). For example, suppose that the stage is turned so that the NE and SW quadrants are separated from each other. Optically positive crystals show second-order blue close to the isogyre within the quadrant (on the concave side of the isogyre), while first-order yellow appears on the convex side, which is part of the combined NW and SE quadrants. Optically negative crystals show the reverse.

Slightly off-centre acute bisectrix figures are easy to interpret if $2V$ is low, but as the degree of off-centring increases, and as $2V$ increases, it is obvious that interpretational difficulties will rapidly increase, and recourse must be made to the optic axis figure.

(ii) *Optic axis figures*: Although the acute bisectrix figure forms the most convenient introduction to the subject, it is in practice quite difficult to find a suitable section without trial and error. In monoclinic and triclinic crystals, for example, the acute bisectrix section is not in general identifiable by reference to crystallographic features (cleavage, faces *etc.*), nor by any special optical properties observable under orthoscopic conditions. As in the uniaxial case, however, the optic axis section is identifiable by its low-to-nil birefringence. The optic axis figure is the workhorse of the microscopist.

The essential feature of this figure is that, as the stage is rotated, one of the optic axes is positioned permanently in the centre of the field of view, while the other rotates around it. One of the isogyres is always visible. When $2V$ is small, on rotation of the stage the figure simply looks like a wobbly version of the acute bisectrix figure. Both isogyres are visible, and determination of optic sign, using the sensitive-tint plate, is as described above.

As $2V$ increases, however, the second isogyre leaves the field during part of the rotation, and the point where the isogyres cross, when the optic axial plane lies N-S or E-W, moves towards the edge of the field of view. Eventually, with further increase of $2V$, the second isogyre does not enter the field of view at all, and the figure consists of a single brush rotating about the optic axis. The brush changes from straight, when it lies N-S or E-W, to curved, when the crystal is in the 45° position, and the degree of curvature decreases with rising $2V$. When $2V = 90^\circ$, the brush remains straight in all positions. With experience, the maximum curvature of the isogyre can be used for rough estimation of $2V$.

Optic sign is readily determined from any sort of optic axis figure by setting the crystal in the 45° position and using the curvature of the isogyre to identify the various 'quadrants' as described above. This of course is not possible when

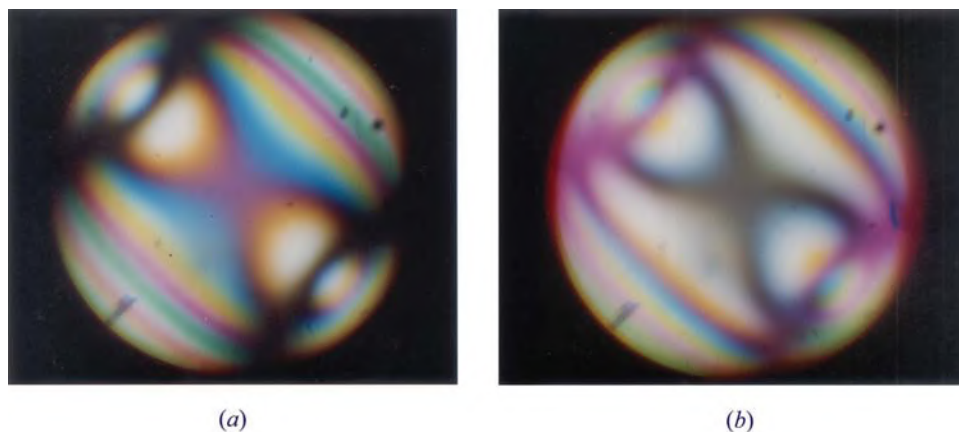


Fig. 1.6.4.15. (a) Acute bisectrix figure of a biaxial crystal with $2V \approx 40^\circ$. The optic axial plane is oriented NW-SE. First-order colours are confined to the two circular 'eyes' or melatopes around the optic axes, with sensitive tint itself making a figure-of-eight shape ('dumbbell'). At the edge of the figure in the NE and SW directions the coloured fringes reach third-order pink. (b) The same figure with the sensitive-tint plate inserted (slow direction NE-SW). The isogyres have taken on the sensitive-tint colour. Between the optic axes (*e.g.* the centre of the figure), the original sensitive-tint dumbbell has become black, and to the NW and SE of the centre all the fringes have dropped by one order. Conversely, in the extreme NW and SE directions all fringes have gained an order. The little patches of yellow lying just inside the optic axes, and the accompanying blue patches just outside, indicate by analogy with the uniaxial figure that the crystal is optically negative.

1.6. CLASSICAL LINEAR CRYSTAL OPTICS

$2V = 90^\circ$, and such crystals are described as optically neutral.

A further piece of useful information is derivable from optic axis (and acute bisectrix) figures, *i.e.* the direction of the optic axial plane, that is, the line joining the two optic axes. Even if the second isogyre is never visible, the position of the second optic axis, outside the field of view, is easily judged. By reverting to orthoscopic observation without moving the specimen, it is easy to see how the optic axial plane relates to crystallographic features such as faces, cleavages or twin planes.

(iii) *Other biaxial figures*: Several special figures are occasionally useful, and their behaviour is readily explained by comparison with the acute bisectrix figure. The obtuse bisectrix figure behaves like the acute bisectrix figure, but as if $2V$ were very large. The isogyres form a diffuse cross in the centre of the field, and then, on rotation, rapidly depart from the field, either *via* the NE and SW quadrants or *via* the NW and SE. As rotation approaches 90° , they re-enter the field of view from the other direction. When $2V$ approaches 90° , there is of course very little difference between the acute and obtuse bisectrix figures, and to determine which is which it is necessary to measure the speed at which isogyres leave the field of view during rotation (for a given rotation the obtuse bisectrix isogyres move further).

The optic normal figure (often known as a *flash figure* because of the extreme speed of isogyre movement) is formed when the optic axial plane lies in the plane of the slide. Its behaviour on rotation of the stage is an extremely rapidly moving version of the obtuse bisectrix figure. The isogyres are very broad and diffuse, and when the cross is formed there is little more than a momentary darkening of the whole field of view. The brushes vanish completely from the field with only a very small rotation from this position. Often it requires careful inspection even to be certain that the cross splits into two brushes that vanish diagonally from the field.

The optic normal figure is useful in orientation studies and, as mentioned above, grain mounts of orthorhombic crystals may naturally give rise to suitably oriented crystals. In thin sections, the figure is useful to confirm that grains apparently showing maximum birefringence do in fact lie with their optic axial planes normal to the microscope axis. When only a small number of grains are available, this check is important.

In the most general sense, this exercise illustrates that all figures are variations on a single theme, in which the vibration direction diagram of Fig. 1.6.4.12(c) can be thought of as being viewed from different distances (delimiting the size of the area viewed) and different directions (*i.e.* where the centre of the field of view is, relative to the centre of the diagram). For, example, the figure shown represents a centred uniaxial optic axis figure if viewed from infinite distance in a direction corresponding to the centre of the diagram. On the other hand, if viewed from close up in the same direction (so that the field of view is thought of as a rather small circle in the middle of the diagram), the figure becomes analogous to the acute bisectrix figure of a crystal with a large $2V$, the obtuse bisectrix figure, or even the uniaxial flash figure (but see below), with increasing distance of the viewpoint. Off-centre figures can be equally well explained by placing the viewpoint non-centrally.

Only the uniaxial flash figure and the biaxial optic normal figure seem, at first sight, to defy exact interpretation, because the optic axes, lying in the plane of the figure, seem to require to be plotted at infinity in the plane of the paper. This then requires that the map of the vibration directions consists of two linear sets at a right angle to each other. No explanation of the rapid separation of the diffuse isogyres accompanying a small rotation from the extinction position is forthcoming. Rather, a simple extinction of the whole field is predicted at every 90° .

In fact, the vibration directions seen in such figures still retain the 'barrel-shaped' configuration seen in Fig. 1.6.4.12(c), though degrees of curvature can be very small. This arises because the

true vibration directions of, for example, the *e* rays in the uniaxial case, do not lie in the plane of the figure (except at the centre). A curved surface is required for the true description of the vibration directions. We have up to this point regarded the diagram as flat, but in fact the vibration directions, as we view them, become distorted into the barrel shape.

1.6.4.14. Orientation studies

The full skills of the microscopist are required in the production of an accurate description of the optical orientation of a sample, that is the relationship of the indicatrix to the crystallographic axes.

It is best to start by determining the crystal system. Completely isotropic crystals are cubic, uniaxial crystals are tetragonal, trigonal or hexagonal, while biaxial crystals are orthorhombic, monoclinic or triclinic. Crystallographic features such as edges, faces, crystal outlines, shapes, cleavages and twin planes give the additional information required to subdivide the uniaxial and biaxial classes.

In uniaxial cases, a grain giving a centred optic axis figure is required. If the crystals look square, or have cleavages and/or twin planes intersecting at right angles, then the system is most likely to be tetragonal. Features disposed as equilateral triangles indicate triclinic, and hexagonal arrangements may indicate triclinic or hexagonal. The cases are often impossible to distinguish.

Orthorhombic crystals are usually fairly easy to identify because, although biaxial, they still show parallelism between many optical and crystallographic properties. For example, vibration directions commonly lie parallel to the traces of cleavage planes or crystal outlines (so-called *straight extinction*). Alternatively, vibration directions may bisect the angles between such features (*symmetrical extinction*). Furthermore, crystals with obviously special orientations can be identified, *e.g.* a section showing two sharply defined cleavages (*i.e.* lying at right angles to the plane of the slide) perhaps at right angles to each other, or producing a diamond pattern, is obviously cut normal to an important crystallographic direction, perhaps containing two of the crystallographic axes. The interference figure of such a section should be examined carefully as it is likely to be a centred version of the acute bisectrix, obtuse bisectrix or flash figure.

Monoclinic crystals are extremely common, and, while biaxial, do not generally show the parallelism of optical and crystallographic features typical of the orthorhombic system. There is no general recipe for success in determining the optical orientation of such crystals, other than systematic observation of crystals in different orientations. The most important observations are the relationships between extinction positions and crystallographic features, and the nature of the interference figures. All monoclinic crystals have one plane that, if at right angles to the slide, shows symmetrical or straight extinction. This plane is observed when the twofold symmetry axis lies in the plane of the slide. In crystals that show two cleavages, their intersection is also likely to mark a crystallographic axis. From consideration of such features it is often possible to identify a crucial special section, that lying perpendicular to the twofold axis. This is an important section, because two crystallographic axes now lie in the plane of the slide and their directions may be indicated by cleavage traces, crystal edges *etc.* Determination of the angles between vibration directions and supposed crystallographic axis directions then gives the important angle (*e.g.* n_p , **c**) which expresses the tilt of the indicatrix within the plane normal to the twofold axis.

If everything fails, and no relationship can be found between crystallographic and optical directions, the crystal is probably triclinic, and it is not possible to say very much about its orientation using the flat-stage microscope. Recourse must then be had

1. TENSORIAL ASPECTS OF PHYSICAL PROPERTIES

to the *universal stage*, a device that allows rotation of the slide in three dimensions. This is rarely done these days.

Orientation studies are completed by assigning specific axes of the indicatrix to specific crystallographic axes. The identification of the principal axes of the indicatrix is easy. For example, in uniaxial cases, sections showing maximum birefringence contain the unique crystallographic axis, which is parallel to the n_e direction. Knowledge of the optic sign shows which of the two vibration directions coincides with n_e , on the basis of being fast or slow. In biaxial cases, the maximum birefringence section has n_α and n_γ lying in the plane of the slide, and of these n_γ corresponds of course to the slow ray. In biaxial crystals, the identification of the optic axial plane direction in a figure enables immediate identification of the n_β direction, which is normal to it.

1.6.4.15. Absorption colours

Many crystalline substances are coloured in transmitted light under the microscope, as a result of the absorption of certain visible-light wave bands. Though there may be much variability between one sample of a substance and another, colour is nevertheless often a great aid in identification.

Absorption, like other optical phenomena, is capable of showing marked anisotropy, the phenomenon known as pleochroism. Pleochroism is usually obvious in both grain mounts and thin sections, because grains change colour when rotated in plane-polarized light. The effect can be subtle (*e.g.* the mineral hypersthene is almost colourless in thin sections but often shows pleochroism from a very faint pink to a very faint green), or very marked (*e.g.* dark brown to colourless or pale yellow in the mineral biotite). The full description of pleochroism involves the assigning of different colours to specific axes of the indicatrix. Uniaxial crystals are *dichroic*, that is, two colours describe the effects. Sections showing centred optic axis figures do not exhibit pleochroism, showing only the pure absorption colours of light vibrating normal to the optic axis (n_o). In biotite for example (which is for practical purposes uniaxial), this colour is usually dark brown. Maximum birefringence sections, or those showing centred flash figures in grain mounts, show maximum pleochroism, one vibration direction exhibiting the n_o absorption already noted, and the other the pure effects of absorption on n_e (in the case of biotite, colourless to pale yellow). Random sections show less pleochroism, and colours that are combinations of the pure end members.

Biaxial crystals can be notably trichroic, and colours are readily assigned by looking at maximum birefringence (flash figure) sections to obtain n_α (fast ray) and n_γ (slow ray) absorptions, and optic axis sections to obtain that for n_β .

The other notable thing about absorption colours is that they can occasionally severely mask polarization colours. Once this is appreciated, the use of the sensitive-tint plate is often sufficient to identify the latter.

1.6.4.16. Dispersion

Dispersion, that is to say variation of refractive index depending on wavelength, is a common phenomenon in crystals, and occasionally an important aid in identification. In extreme cases, it results in the production of highly anomalous polarization colours, often browns, blue greys or brownish purples, or bright colours which just look slightly unusual compared with normal second- or third-order colours. Anomalous colours are highly diagnostic of certain substances (*e.g.* the minerals chlorite, zoisite and epidote).

Dispersion also results in a lack of definition of extinction positions, because in biaxial crystals there may effectively be differently oriented indicatrices for different wavelengths. In extreme cases, it may be impossible to locate the extinction position with any accuracy. As an example of a milder case, the very common mineral plagioclase (triclinic) shows subtle, though

highly characteristic, features between crossed polars in sections cut approximately normal to the b crystallographic axis. The normal polarization colours seen in between the extinction positions are pure first-order greys and whites, but as a grain is rotated slowly through an extinction position the colours darken and take on a bluish (cold) tinge before going black, and then lighten again with a yellowish (warm) tinge. This is the result of a slight mismatch of the orientations of the indicatrices for long and short wavelengths.

Such dispersion is also often obvious (at least, when looked for) in the interference figures of biaxial crystals. Isogyres become edged with 'cold' (*i.e.* bluish) and 'warm' (tending to red or orange) fringes on opposite sides, indicating that optic axes for different wavelengths have slightly different positions.

Dispersion is a difficult phenomenon to investigate fully with the polarizing microscope. In cubic crystals, it can only be studied systematically by the determination of refractive indices using a number of monochromatic light sources of different wavelengths. Uniaxial crystals can show anomalous polarization colours, but they do not show fringes in interference figures, nor vagueness in extinction position, because the indicatrices for different wavelengths all have the same orientation. Like cubic crystals, however, the dispersion can be investigated by monochromatic light studies of refractive index. Biaxial crystals present the most complex cases. Not only can the shape of the indicatrix vary with wavelength (*i.e.* the relative values of the principal refractive indices), but so can orientation relative to the crystallographic axes. There are even substances known (admittedly with small $2V$) in which the optic axial plane for red light is at right angles to the optic axial plane for violet light. The phenomenon is known as 'crossed axial plane dispersion', a real challenge for the microscopist.

1.6.5. Optical rotation

1.6.5.1. Introduction

Optical rotation or gyration, as it is sometimes known, was first recorded by Arago in 1811. Since then, a great deal of work has been done to try to explain this phenomenon, and at the present time it is one of the few physical properties of a crystal that can be successfully understood in terms of the underlying crystal structure (Glazer & Stadnicka, 1986). Lowry (1935) has given a good historical account of the subject.

Optical rotation is the phenomenon observed in some crystals (and in some solutions of, usually, organic compounds) of the rotation of plane-polarized light on passing through the crystal. If the rotation, as seen by the observer, is to the left or counter-clockwise it is known as *laevorotation*; if to the right or clockwise it is known as *dextrorotation*. A crystal that shows this effect is sometimes called *optically active* or *gyrotropic*. It is therefore clear that, from a symmetry point of view, optical rotation can only occur in a crystal in which one direction is not equivalent to its opposite, *i.e.* there are no inversion symmetry operations that can change chirality.

One of the earliest theories to explain the origin of optical rotation was given by Fresnel. This was based on the idea that a plane-polarized wave can be equally described by two opposing circularly polarized waves propagating along the same direction. In Fig. 1.6.5.1(a), the polarization vector **OA** is simply given by the vector sum of **OB** and **OC**, polarization vectors at some instant of time belonging to a right-circular and a left-circular wave, respectively. Here it is assumed that the light propagates in a direction towards the viewer. If the light now passes through a gyrotropic material, one of the circularly polarized waves will be slowed down with respect to the other (this corresponds to having a small difference in refractive indices for the two waves). Thus on emerging from the crystal, there will be a phase difference between the circular waves, so that on recombining, the resulting

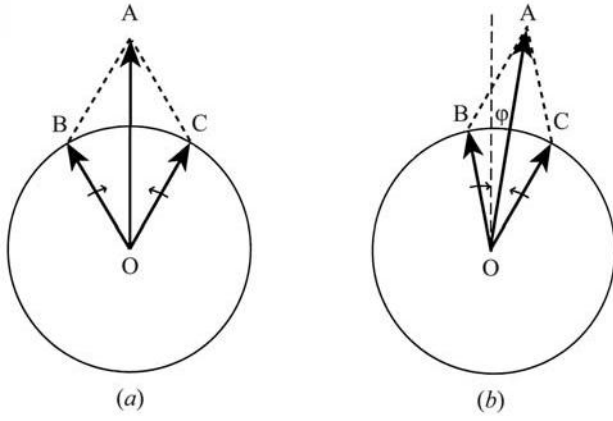


Fig. 1.6.5.1. Fresnel's explanation of optical rotation.

plane of linear polarization **OA** will have rotated through an angle ϕ . This is shown in Fig. 1.6.5.1(b), where the right-circular (clockwise) component travels faster than the left-circular (anticlockwise) component. Because of this, in a given time, the electric vector for the right-circular wave, observed in a fixed plane perpendicular to the line of sight, will have rotated through a larger angle clockwise than the electric vector for the left-circular wave will have rotated anticlockwise. The result is a net rotation to the right, *i.e.* dextrorotation, of the vector **OA**. The left and right-circular refractive indices, n_L and n_R , are inversely related to the velocities of the waves, and so Fig. 1.6.5.1(b) corresponds to the case where $n_L > n_R$. Thus this theory shows that a positive value of $n_L - n_R$ defines dextrorotation and that optical rotation is in fact a form of *circular birefringence*.

Fig. 1.6.5.2 illustrates in a more generalized way the nature of the birefringences possible in a crystal. Formally, the refractive index of a medium can be written in terms of real and imaginary components:

$$n = n' + in'', \quad (1.6.5.1)$$

the imaginary component referring to the absorption of the light (the real and imaginary terms are related as usual by the Kramers–Kronig relationship). Similarly, the linear and circular birefringences can also be written in real and imaginary terms:

$$\begin{aligned} \Delta n_{\text{linear}} &= (n_1 - n_2)' + i(n_1 - n_2)'' \\ \Delta n_{\text{circular}} &= (n_L - n_R)' + i(n_L - n_R)''. \end{aligned} \quad (1.6.5.2)$$

The real linear birefringence (a) shows a resonance, changing sign, at a particular wavelength. Its variation with wavelength is known as *birefringent dispersion*. The imaginary component (b) peaks at this wavelength and corresponds to the difference in absorption between linear polarization states. This is called *linear dichroism* (LD) and is determined by quantum-mechanical selection rules resulting from matrix elements of the type $\langle \Psi_1 | \hat{p} | \Psi_0 \rangle$, where \hat{p} is the electric dipole operator. The circular components follow similar behaviour. The real circular birefringence (c) corresponds to the optical rotation and its change with wavelength is known as *optical rotatory dispersion* (ORD). The imaginary circular birefringence (d) corresponds to the difference in absorption of opposite circularly polarized states. This is called *circular dichroism* (CD) and is determined by the matrix elements of the type $\langle \Psi_1 | \hat{\alpha} | \Psi_0 \rangle$, where $\hat{\alpha}$ is the polarizability operator. Since $\hat{\alpha}$ is an even function, whereas \hat{p} is an odd function, the selection rules for LD and CD are different, and each type of spectrum gives different information.

The link between optical rotation and crystal structure has been the subject of a great deal of work from the 18th century to date. Experimental methods for determining absolute chirality (Glazer & Stadnicka, 1989) of crystals only became routine in the late 1940s with the use of the X-ray anomalous dispersion effect,

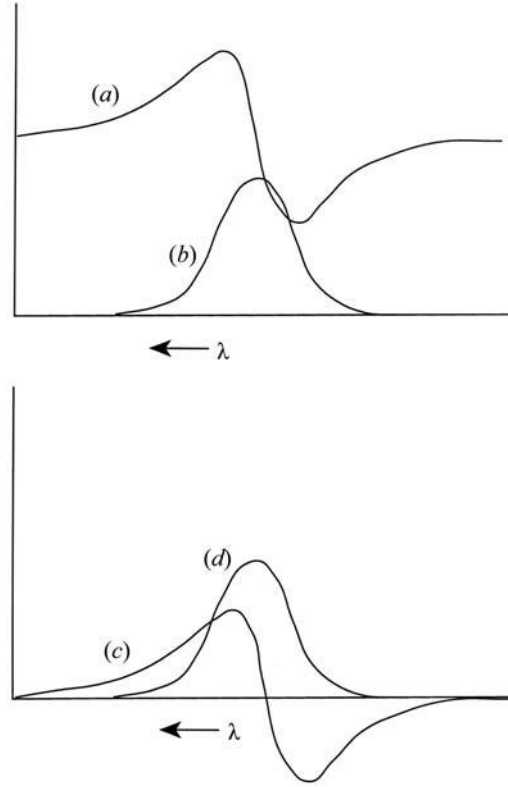


Fig. 1.6.5.2. Real and imaginary birefringence as a function of wavelength: (a) real linear; (b) imaginary linear; (c) real circular; (d) imaginary circular.

which made it possible to determine the absolute sense of the chiral nature of a crystal and then to link this to the sense of optical rotation. However, despite the preponderance of a great many complex theories, until recently, experimental evidence to support these theories has been fragmentary. It was shown by Glazer & Stadnicka (1986) that, at least for inorganic crystals, the problem lay in mistakes in the experiments or publications describing the experiments, rather than in the underlying theories. Once these errors are taken into account, it is possible to find a direct link between the chiral nature of the structure and the optical rotation, which appears to work in almost all cases. It has even been possible to produce a computer program *OPTACT* (Devarajan & Glazer, 1986; Glazer, 2002), using a polarizability theory based on earlier work by Born (1933), that is capable of calculating both the sign and magnitude of the effect with reasonable precision in many cases. *OPTACT* also calculates the refractive indices with good reliability.

1.6.5.2. The dielectric tensor and spatial dispersion

The relevant polarization term to consider here is

$$P_i^\omega = \omega_0 \chi_{ij\ell} \nabla_\ell E_j^\omega. \quad (1.6.5.3)$$

The important part of this expression is the use of the field gradient, which implies a variation of the electric field across the unit cell of the crystal rather than the assumption that **E** is everywhere constant. This variation in **E** is known as *spatial dispersion* (Agranovich & Ginzburg, 1984).

Assume propagation of a plane wave given by **E** = **E**₀ exp(**i****k** · **r**) through an optically active crystal. Substituting into the expression for the polarization gives

$$P_i^\omega = i\omega_0 \chi_{ij\ell} E_j^\omega k_\ell. \quad (1.6.5.4)$$

This term can now be treated as a perturbation to the dielectric tensor $\varepsilon_{ij}(\omega)$ to form the *effective* dielectric tensor $\varepsilon_{ij}(\omega, \mathbf{k})$:

$$\varepsilon_{ij}(\omega, \mathbf{k}) = \varepsilon_{ij}(\omega) + i\gamma_{ij\ell} k_\ell, \quad (1.6.5.5)$$

1. TENSORIAL ASPECTS OF PHYSICAL PROPERTIES

where $\gamma_{ij\ell}$ has been written for the susceptibility $\chi_{ij\ell}$ in order to distinguish it from the use of χ elsewhere. Note that this can be expressed more generally as a power-series expansion in the vector \mathbf{k} (Agranovich & Ginzburg, 1984) to allow for a generalization to include all possible spatial dispersion effects:

$$\varepsilon_{ij}(\omega, \mathbf{k}) = \varepsilon_{ij}(\omega) + i\gamma_{ij\ell}(\omega)k_\ell + \alpha_{ij\ell m}(\omega)k_\ell k_m, \quad (1.6.5.6)$$

where the susceptibilities are in general themselves dependent on frequency.

1.6.5.3. Symmetry of effective dielectric tensor

To determine the symmetry constraints on the effective dielectric tensor, it should be recognized that the application of a real electric field \mathbf{E} must lead to a real dielectric displacement \mathbf{D} . This therefore implies that one can write

$$\varepsilon_{ij}(\omega, \mathbf{k}) = \varepsilon_{ij}^*(-\omega^*, -\mathbf{k}^*)$$

or

$$\varepsilon_{ij}(\omega^*, \mathbf{k}^*) = \varepsilon_{ij}^*(-\omega, -\mathbf{k}). \quad (1.6.5.7)$$

Furthermore, in the absence of any absorptive processes, ε_{ij} must be Hermitian, that is

$$\varepsilon_{ij}(\omega, \mathbf{k}) = \varepsilon_{ji}(\omega, -\mathbf{k}). \quad (1.6.5.8)$$

This is fulfilled by the following symmetry constraints for the leading terms in the effective dielectric tensor:

$$\varepsilon_{ij}(\omega) = \varepsilon_{ji}(\omega); \quad \gamma_{ij\ell}(\omega) = -\gamma_{ji\ell}(\omega); \quad \alpha_{ij\ell m}(\omega) = \alpha_{ji\ell m}(\omega). \quad (1.6.5.9)$$

In a gyrotropic crystal, there must be at least one direction that is not equivalent to its opposite, and so such a crystal cannot have a centre of symmetry. (Only a noncentrosymmetric crystal can be gyrotropic. However, it is true to say that all non-gyrotropic crystals must be centrosymmetric.) Therefore, for a non-gyrotropic crystal,

$$\varepsilon_{ij}(\omega, \mathbf{k}) = \varepsilon_{ji}(\omega, -\mathbf{k}). \quad (1.6.5.10)$$

It follows therefore in such a case that

$$\gamma_{ij\ell}(\omega) = 0. \quad (1.6.5.11)$$

It is obvious then that the susceptibility $\gamma_{ij\ell}(\omega)$ has the required symmetry for gyration and that it forms an antisymmetric tensor of rank 3 (see Section 1.1.4.5.3 for the properties of antisymmetric tensors).

1.6.5.4. Gyration tensor

It is convenient to rewrite the effective dielectric expression in the following way (just keeping the first two terms):

$$\varepsilon_{ij}(\omega, \mathbf{k}) = \varepsilon_{ij}(\omega) + i\hat{\varepsilon}_{ijm}g_{m\ell}k_\ell, \quad (1.6.5.12)$$

where $\hat{\varepsilon}_{ijm}$ is a unit antisymmetric pseudotensor of rank 3 or permutation tensor ($\hat{\varepsilon}_{123} = 1$, $\hat{\varepsilon}_{213} = -1$, $\hat{\varepsilon}_{112} = 0$ etc.; $\hat{\varepsilon}_{ijm}$ is not affected by mirror reflection) and $g_{m\ell}$ represents a pseudotensor (i.e. axial tensor) of rank 2. One can then write further

$$\varepsilon_{ij}(\omega, \mathbf{k}) = \varepsilon_{ij}(\omega) + i\hat{\varepsilon}_{ijm}G_m, \quad (1.6.5.13)$$

where $G_m = g_{m\ell}k_\ell$ is a component of a pseudovector (i.e. axial vector), known as the gyration vector. The formula for the dielectric displacement can then be expressed in the form

$$D_i = \varepsilon_o \varepsilon_{ij}(\omega, \mathbf{k}) E_j = \varepsilon_o [\varepsilon_{ij}(\omega) E_j - i(\mathbf{G} \times \mathbf{E})_i]. \quad (1.6.5.14)$$

The operation $\mathbf{G} \times \mathbf{E}$ can also be represented by the product of an antisymmetric tensor $[G]$ with the vector \mathbf{E} :

$$\begin{pmatrix} 0 & G_{12} & G_{13} \\ -G_{12} & 0 & G_{23} \\ -G_{13} & -G_{23} & 0 \end{pmatrix} \begin{pmatrix} E_1 \\ E_2 \\ E_3 \end{pmatrix} = \begin{pmatrix} G_{12}E_2 + G_{13}E_3 \\ G_{23}E_3 - G_{12}E_1 \\ -G_{13}E_1 - G_{23}E_2 \end{pmatrix} \\ = \begin{pmatrix} -G_3E_2 + G_2E_3 \\ -G_1E_3 + G_3E_1 \\ -G_2E_1 + G_1E_2 \end{pmatrix}, \quad (1.6.5.15)$$

where $-G_1 = G_{23} = -G_{32}$, $-G_2 = -G_{13} = G_{31}$ and $-G_3 = G_{12} = -G_{21}$. If $\hat{\mathbf{s}}$ is the unit vector in the propagation direction, then

$$\mathbf{G} = G\hat{\mathbf{s}} \quad (1.6.5.16)$$

and G represents the magnitude of the gyration vector. Thus,

$$\hat{\mathbf{s}} \cdot \mathbf{G} = \hat{\mathbf{s}} \cdot G\hat{\mathbf{s}} = G\hat{\mathbf{s}} \cdot \hat{\mathbf{s}} = G. \quad (1.6.5.17)$$

Consequently, if one knows the direction of propagation inside the crystal, the coefficient G can be calculated via

$$G = \hat{s}_1 G_1 + \hat{s}_2 G_2 + \hat{s}_3 G_3 \quad (1.6.5.18)$$

and then the optical *rotatory power* is defined as

$$\rho = \frac{\pi G}{\lambda n}, \quad (1.6.5.19)$$

where ρ is the angle of rotation in degrees per millimetre. According to the way in which the sign of G has been defined here, a positive value of ρ means dextrorotation and a negative value means laevorotation.

There is a possibility of confusion here in terminology with respect to the term ‘gyration tensor’. It is seen that there exists an antisymmetric tensor $[G]$: this is sometimes referred to as the gyration tensor. However, returning to equation (1.6.5.12), it is the pseudotensor given by $g_{m\ell}$ that is more often described as the gyration tensor. The difference between them is really one of emphasis. The $[G]$ tensor refers to the polarization directions of the wave, whereas the g tensor is referred to the direction of wave propagation. Thus, for example, G_{23} refers to a wave whose polarization lies in the x_2x_3 plane, and so propagates in the x_1 direction, according to the axial gyration vector component $-G_1$. The gyration is equally described by the tensor component g_{11} . Being an axial tensor, g_{11} corresponds to a wave travelling along x_1 , along which direction one observes a rotation in the x_2x_3 plane.

Although g is in general an antisymmetric tensor, since it is only the scalar products $g_{m\ell}\hat{s}_m\hat{s}_\ell$ that are important in determining the rotation of the plane of polarization, the components of \mathbf{D} , and hence the refractive index behaviour, are independent of the antisymmetric part of $g_{m\ell}$. It is thus possible to construct a table of tensor invariances for the symmetric part of the gyration tensor with regard to the possible symmetry classes of a crystal (Table 1.6.5.1). For a discussion of the importance of the antisymmetric terms, see Agranovich & Ginzburg (1984).

1.6.5.5. Optical rotation along the optic axis of a uniaxial crystal

Consider a uniaxial crystal such as quartz, crystallizing in point group 32. In this case, the only dielectric tensor terms (for the effect of symmetry, see Section 1.1.4.10) are $\varepsilon_{11} = \varepsilon_{22} \neq \varepsilon_{33}$, with the off-diagonal terms equal to zero. The equations for the dielectric displacements along the three coordinate axes x_1 , x_2 and x_3 are then given, according to equations (1.6.5.14) and (1.6.5.15), by

1.6. CLASSICAL LINEAR CRYSTAL OPTICS

Table 1.6.5.1. Symmetry constraints (see Section 1.1.4.10) on the gyration tensor g_{ij}

All g_{ij} components are zero for the centrosymmetric point groups plus $4mm$, $\bar{4}3m$, $3m$, $6mm$, $\bar{6}$ and $\bar{6}m2$.

| Triclinic | Monoclinic | | Orthorhombic |
|--|--|---|--|
| Point group 1 | Point group 2 ($2 \parallel x_2$) | Point group m ($m \perp x_2$) | Point group 222 |
| $\begin{pmatrix} g_{11} & g_{12} & g_{13} \\ g_{12} & g_{22} & g_{23} \\ g_{13} & g_{23} & g_{33} \end{pmatrix}$ | $\begin{pmatrix} g_{11} & 0 & g_{13} \\ 0 & g_{22} & 0 \\ g_{13} & 0 & g_{33} \end{pmatrix}$ | $\begin{pmatrix} 0 & g_{12} & 0 \\ g_{12} & 0 & g_{23} \\ 0 & g_{23} & 0 \end{pmatrix}$ | $\begin{pmatrix} g_{11} & 0 & 0 \\ 0 & g_{22} & 0 \\ 0 & 0 & g_{33} \end{pmatrix}$ |
| | Point group 2 ($2 \parallel x_3$) | Point group m ($m \perp x_3$) | Point group $mm2$ |
| | $\begin{pmatrix} g_{11} & g_{12} & 0 \\ g_{12} & g_{22} & 0 \\ 0 & 0 & g_{33} \end{pmatrix}$ | $\begin{pmatrix} 0 & & g_{13} \\ & 0 & g_{23} \\ g_{13} & g_{23} & 0 \end{pmatrix}$ | $\begin{pmatrix} 0 & g_{12} & 0 \\ g_{12} & 0 & 0 \\ 0 & 0 & 0 \end{pmatrix}$ |

| Tetragonal | Trigonal and hexagonal | | Cubic and isotropic |
|--|--|--|--|
| Point groups 4, 422 | Point group $\bar{4}$ | Point groups 3, 32, 6, 622 | Point groups 432, 23 |
| $\begin{pmatrix} g_{11} & 0 & 0 \\ 0 & g_{11} & 0 \\ 0 & 0 & g_{33} \end{pmatrix}$ | $\begin{pmatrix} g_{11} & g_{12} & 0 \\ g_{12} & -g_{11} & 0 \\ 0 & 0 & 0 \end{pmatrix}$ | $\begin{pmatrix} g_{11} & 0 & 0 \\ 0 & g_{11} & 0 \\ 0 & 0 & g_{33} \end{pmatrix}$ | $\begin{pmatrix} g_{11} & 0 & 0 \\ 0 & g_{11} & 0 \\ 0 & 0 & g_{11} \end{pmatrix}$ |
| Point group $\bar{4}2m$ | | | Isotropic, no centre of symmetry |
| $\begin{pmatrix} g_{11} & 0 & 0 \\ 0 & -g_{11} & 0 \\ 0 & 0 & 0 \end{pmatrix}$ | | | $\begin{pmatrix} g_{11} & 0 & 0 \\ 0 & g_{11} & 0 \\ 0 & 0 & g_{11} \end{pmatrix}$ |

$$\begin{aligned} D_1 &= \varepsilon_o \varepsilon_{11} E_1 - i \varepsilon_o [G_{12} E_2 + G_{13} E_3] \\ D_2 &= \varepsilon_o \varepsilon_{22} E_2 - i \varepsilon_o [G_{23} E_3 - G_{21} E_1] \\ D_3 &= \varepsilon_o \varepsilon_{33} E_3 - i \varepsilon_o [G_{31} E_1 - G_{32} E_2]. \end{aligned} \quad (1.6.5.20)$$

$$n_1 - n_2 = \frac{G_{12}}{\bar{n}} = -\frac{G_3}{\bar{n}}. \quad (1.6.5.26)$$

If the light is taken to propagate along x_3 , the optic axis, the fundamental optics equation (1.6.3.14) is expressed as

$$\begin{pmatrix} \varepsilon_{11} & -iG_{12} & -iG_{13} \\ iG_{12} & \varepsilon_{11} & -iG_{23} \\ iG_{13} & iG_{23} & \varepsilon_{33} + n^2 \end{pmatrix} \begin{pmatrix} E_1 \\ E_2 \\ E_3 \end{pmatrix} = \begin{pmatrix} n^2 & 0 & 0 \\ 0 & n^2 & 0 \\ 0 & 0 & n^2 \end{pmatrix} \begin{pmatrix} E_1 \\ E_2 \\ E_3 \end{pmatrix}. \quad (1.6.5.21)$$

As usual, the longitudinal solution given by

$$iG_{13}E_1 + iG_{23}E_2 + \varepsilon_{33}E_3 = 0 \quad (1.6.5.22)$$

can be ignored, as one normally deals with a transverse electric field in the normal case of propagating light. For a non-trivial solution, then,

$$\begin{vmatrix} \varepsilon_{11} - n^2 & -iG_{12} \\ iG_{12} & \varepsilon_{11} - n^2 \end{vmatrix} = 0, \quad (1.6.5.23)$$

which gives

$$n^2 = \varepsilon_{11} \pm G_{12}. \quad (1.6.5.24)$$

This results in two eigenvalue solutions, n_1 and n_2 , from which one has

$$(n_1 - n_2)(n_1 + n_2) = 2G_{12} = -2G_3 \quad (1.6.5.25)$$

and thus

The optical rotatory power (1.6.5.19) is then given by

$$\rho = \frac{\pi G_3}{\lambda \bar{n}} = \frac{\pi(n_2 - n_1)}{\lambda}. \quad (1.6.5.27)$$

Note that in order to be consistent with the definition of rotatory power used here, $n_2 > n_1$ for a dextrorotatory solution. This implies that n_2 should be identified with n_L and n_1 with n_R . To check this, find the eigenvectors corresponding to the two solutions (1.6.5.24).

For $n_1^2 = \varepsilon_{11} - G_3$, the following matrix is found from (1.6.5.21):

$$\begin{pmatrix} G_3 & iG_3 \\ -iG_3 & G_3 \end{pmatrix} = 0, \quad (1.6.5.28)$$

giving the Jones matrix

$$(1/2^{1/2}) \begin{pmatrix} 1 \\ -i \end{pmatrix} = 0. \quad (1.6.5.29)$$

This corresponds to a right-circularly polarized wave. It should be noted that there is confusion in the optics textbooks over the Jones matrices for circular polarizations. Jones (1948) writes a right-circular wave as

$$\begin{pmatrix} 1 \\ i \end{pmatrix},$$

but this is for a definition of right-circularly polarized light as that for which an instantaneous picture of the space distribution of its electric vector describes a right spiral. The modern usage is to define the sense of circular polarization through the time variation of the electric vector in a given plane as seen by an observer

1. TENSORIAL ASPECTS OF PHYSICAL PROPERTIES

looking towards the source of the light. This reverses the definition given by Jones.

For $n_2^2 = \varepsilon_{11} + G_3$, the following matrix is found:

$$\begin{pmatrix} -G_3 & iG_3 \\ -iG_3 & -G_3 \end{pmatrix} = 0, \quad (1.6.5.30)$$

giving

$$(1/2^{1/2}) \begin{pmatrix} 1 \\ i \end{pmatrix} = 0. \quad (1.6.5.31)$$

This corresponds to a left-circularly polarized wave. Therefore it is proved that the optical rotation arises from a competition between two circularly polarized waves and that in equation (1.6.5.26) $n_1 = n_R$ and $n_2 = n_L$, the refractive indices for right- and left-circularly polarized light, respectively. Note that Fresnel's original idea of counter-rotating circular polarizations fits nicely with the eigenvectors rigorously determined in (1.6.5.29) and (1.6.5.31). Thus

$$\rho = \frac{\pi(n_L - n_R)}{\lambda}. \quad (1.6.5.32)$$

Finally, for light propagating along x_3 in quartz, one can write the direction of the wave normal as

$$\hat{s}_1 = 0; \quad \hat{s}_2 = 0; \quad \hat{s}_3 = 1 \quad (1.6.5.33)$$

and then the gyration vector is given by

$$G = g_{\beta\gamma}\hat{s}_\beta\hat{s}_\gamma = g_{13} + g_{23} + g_{33} = g_{33} \quad (1.6.5.34)$$

as $g_{12} = g_{23} = 0$ in point group 32. Thus from (1.6.5.26) it is seen that

$$g_{33} = G_3 = -G_{12}, \quad (1.6.5.35)$$

thus linking one of the components of the gyration tensor $g_{m\ell}$ with a component of the gyration vector \mathbf{G} and a tensor component of $[G]$.

1.6.5.6. Optical rotation perpendicular to the optic axis of a uniaxial crystal

The magnitude of circular birefringence is typically about 10^{-4} times smaller than that of linear birefringence. For this reason, optical rotation has usually been observed only in directions where the linear birefringence is absent, such as in optic axial directions. However, it has been clear for some time that optical rotation also exists in other directions and that with specialized techniques it is even possible to measure it. The techniques (Moxon & Renshaw, 1990; Moxon *et al.*, 1991) are complex and require very precise measuring capabilities, and therefore are generally not commonly available.

Probably the best known case where optical rotation has been measured in a linearly birefringent section is that of quartz. It has been seen that it is easy to measure the rotation along the optic axial direction, since this is the direction along which the crystal looks isotropic. Szivessy & Münster (1934) measured the rotation in a direction perpendicular to the optic axis and found that its magnitude was smaller and opposite in sign to that along the optic axis of the same crystal.

To see the relationship between the linear and circular birefringences, consider light travelling along x_1 in quartz. The fundamental equation (1.6.3.14) then becomes

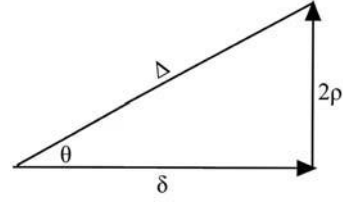


Fig. 1.6.5.3. The principle of superposition.

$$\begin{pmatrix} \varepsilon_{11} - n^2 & -iG_{12} & -iG_{13} \\ iG_{12} & \varepsilon_{11} & -iG_{23} \\ iG_{13} & iG_{23} & \varepsilon_{33} \end{pmatrix} \begin{pmatrix} E_1 \\ E_2 \\ E_3 \end{pmatrix} = \begin{pmatrix} n^2 & 0 & 0 \\ 0 & n^2 & 0 \\ 0 & 0 & n^2 \end{pmatrix} \begin{pmatrix} E_1 \\ E_2 \\ E_3 \end{pmatrix}. \quad (1.6.5.36)$$

Solving for the non-trivial transverse solutions

$$\begin{vmatrix} \varepsilon_{11} - n^2 & -iG_{23} \\ iG_{23} & \varepsilon_{33} - n^2 \end{vmatrix} = 0 \quad (1.6.5.37)$$

and then

$$n^4 - n^2(\varepsilon_{11} + \varepsilon_{33}) + \varepsilon_{11}\varepsilon_{33} - G_{23}^2 = 0. \quad (1.6.5.38)$$

Finding the roots of this equation considered as a quadratic in n^2 , the following birefringence is obtained:

$$n_1 - n_2 = [(n_o - n_e)^2 + (G_{23}^2/\bar{n}^2)]^{1/2}. \quad (1.6.5.39)$$

The eigenvectors for the two solutions n_1 and n_2 can easily be shown to correspond to elliptical polarizations. Notice that in equation (1.6.5.39), two refractive-index solutions are obtained whose difference depends on two terms, one with respect to the linear birefringence $n_o - n_e$ and the other to the circular birefringence represented by the gyration component $G_{23} = -G_1$. The refractive-index difference $n_1 - n_2$ gives rise to a phase shift between the two elliptically polarized components of the light, given by

$$\Delta = (2\pi/\lambda)(n_1 - n_2), \quad (1.6.5.40)$$

from which

$$\begin{aligned} \Delta^2 &= (4\pi^2/\lambda^2)[(n_o - n_e)^2 + (G_{23}^2/\bar{n}^2)] \\ &= \delta^2 + (2\rho)^2, \end{aligned} \quad (1.6.5.41)$$

where

$$\delta = \frac{2\pi}{\lambda}(n_o - n_e) \quad \text{and} \quad \rho = \frac{-\pi G_{23}}{\lambda\bar{n}} = \frac{-\pi G_1}{\lambda\bar{n}}. \quad (1.6.5.42)$$

δ is the phase difference when there is no optical rotation and 2ρ is the phase difference corresponding to a normal optical rotation ρ when there is no linear birefringence. (1.6.5.41) shows that the linear and circular terms simply add, and this is known as the *principle of superposition*.

This reveals that an elliptical polarization is created by the simple vector addition of a linearly polarized wave to a circularly polarized wave, as indicated in Fig. 1.6.5.3. From this, the ellipticity κ of the polarization is given by

$$\kappa = \tan(\frac{1}{2}\theta), \quad (1.6.5.43)$$

where

$$\tan \theta = \frac{2\rho}{\delta}. \quad (1.6.5.44)$$

1.6. CLASSICAL LINEAR CRYSTAL OPTICS

Table 1.6.6.1. *Symmetry constraints (see Section 1.1.4.10) on the linear electro-optic tensor r_{ij} (contracted notation)*

| Triclinic | Monoclinic | | Orthorhombic |
|--|--|--|---|
| Point group 1 | Point group 2 ($2 \parallel x_2$) | Point group m ($m \perp x_2$) | Point group 222 |
| $\begin{pmatrix} r_{11} & r_{12} & r_{13} \\ r_{21} & r_{22} & r_{23} \\ r_{31} & r_{32} & r_{33} \\ r_{41} & r_{42} & r_{43} \\ r_{51} & r_{52} & r_{53} \\ r_{61} & r_{62} & r_{63} \end{pmatrix}$ | $\begin{pmatrix} 0 & r_{12} & 0 \\ 0 & r_{22} & 0 \\ 0 & r_{32} & 0 \\ r_{41} & 0 & r_{43} \\ 0 & r_{52} & 0 \\ r_{61} & 0 & r_{63} \end{pmatrix}$ | $\begin{pmatrix} r_{11} & 0 & r_{13} \\ r_{21} & 0 & r_{23} \\ r_{31} & 0 & r_{33} \\ 0 & r_{42} & 0 \\ r_{51} & 0 & r_{53} \\ 0 & r_{62} & 0 \end{pmatrix}$ | $\begin{pmatrix} 0 & 0 & 0 \\ 0 & 0 & 0 \\ 0 & 0 & 0 \\ r_{41} & 0 & 0 \\ 0 & r_{52} & 0 \\ 0 & 0 & r_{63} \end{pmatrix}$ |
| | Point group 2 ($2 \parallel x_3$) | Point group m ($m \perp x_3$) | Point group $mm2$ |
| | $\begin{pmatrix} 0 & 0 & r_{13} \\ 0 & 0 & r_{23} \\ 0 & 0 & r_{33} \\ r_{41} & r_{42} & 0 \\ r_{51} & r_{52} & 0 \\ 0 & 0 & r_{63} \end{pmatrix}$ | $\begin{pmatrix} r_{11} & r_{12} & 0 \\ r_{21} & r_{22} & 0 \\ r_{31} & r_{32} & 0 \\ 0 & 0 & r_{43} \\ 0 & 0 & r_{53} \\ r_{61} & r_{62} & 0 \end{pmatrix}$ | $\begin{pmatrix} 0 & 0 & r_{13} \\ 0 & 0 & r_{23} \\ 0 & 0 & r_{33} \\ 0 & r_{42} & 0 \\ r_{51} & 0 & 0 \\ 0 & 0 & 0 \end{pmatrix}$ |

| Tetragonal | | Trigonal | |
|--|---|--|--|
| Point group 4 | Point group $\bar{4}$ | Point group 3 | Point group 32 |
| $\begin{pmatrix} 0 & 0 & r_{13} \\ 0 & 0 & r_{13} \\ 0 & 0 & r_{33} \\ r_{41} & r_{51} & 0 \\ r_{51} & -r_{41} & 0 \\ 0 & 0 & 0 \end{pmatrix}$ | $\begin{pmatrix} 0 & 0 & r_{13} \\ 0 & 0 & -r_{13} \\ 0 & 0 & 0 \\ r_{41} & -r_{51} & 0 \\ r_{51} & r_{41} & 0 \\ 0 & 0 & r_{63} \end{pmatrix}$ | $\begin{pmatrix} r_{11} & -r_{22} & r_{13} \\ -r_{11} & r_{22} & r_{13} \\ 0 & 0 & r_{33} \\ r_{41} & r_{51} & 0 \\ r_{51} & -r_{41} & 0 \\ -r_{22} & -r_{11} & 0 \end{pmatrix}$ | $\begin{pmatrix} r_{11} & 0 & 0 \\ -r_{11} & 0 & 0 \\ 0 & 0 & 0 \\ r_{41} & 0 & 0 \\ 0 & -r_{41} & 0 \\ 0 & -r_{11} & 0 \end{pmatrix}$ |
| Point group $\bar{4}2m$ | Point group 422 | Point group $3m1$ ($m \perp x_1$) | Point group $31m$ ($m \perp x_2$) |
| $\begin{pmatrix} 0 & 0 & 0 \\ 0 & 0 & 0 \\ 0 & 0 & 0 \\ r_{41} & 0 & 0 \\ 0 & r_{41} & 0 \\ 0 & 0 & r_{63} \end{pmatrix}$ | $\begin{pmatrix} 0 & 0 & 0 \\ 0 & 0 & 0 \\ 0 & 0 & 0 \\ r_{41} & 0 & 0 \\ 0 & -r_{41} & 0 \\ 0 & 0 & 0 \end{pmatrix}$ | $\begin{pmatrix} 0 & -r_{22} & r_{13} \\ 0 & r_{22} & r_{13} \\ 0 & 0 & r_{33} \\ 0 & r_{51} & 0 \\ r_{51} & 0 & 0 \\ -r_{22} & 0 & 0 \end{pmatrix}$ | $\begin{pmatrix} r_{11} & 0 & r_{13} \\ -r_{11} & 0 & r_{13} \\ 0 & 0 & r_{33} \\ 0 & r_{51} & 0 \\ r_{51} & 0 & 0 \\ 0 & -r_{11} & 0 \end{pmatrix}$ |
| Point group $4mm$ | | | |
| $\begin{pmatrix} 0 & 0 & r_{13} \\ 0 & 0 & r_{13} \\ 0 & 0 & r_{33} \\ 0 & r_{51} & 0 \\ r_{51} & 0 & 0 \\ 0 & 0 & 0 \end{pmatrix}$ | | | |

| Hexagonal | | | Cubic |
|--|---|---|---|
| Point group 6 | Point group $6mm$ | Point group 622 | Point groups $\bar{4}3m, 23$ |
| $\begin{pmatrix} 0 & 0 & r_{13} \\ 0 & 0 & r_{13} \\ 0 & 0 & r_{33} \\ r_{41} & r_{51} & 0 \\ r_{51} & -r_{41} & 0 \\ 0 & 0 & 0 \end{pmatrix}$ | $\begin{pmatrix} 0 & 0 & r_{13} \\ 0 & 0 & r_{13} \\ 0 & 0 & r_{33} \\ 0 & r_{51} & 0 \\ r_{51} & 0 & 0 \\ 0 & 0 & 0 \end{pmatrix}$ | $\begin{pmatrix} 0 & 0 & 0 \\ 0 & 0 & 0 \\ 0 & 0 & 0 \\ r_{41} & 0 & 0 \\ 0 & -r_{41} & 0 \\ 0 & 0 & 0 \end{pmatrix}$ | $\begin{pmatrix} 0 & 0 & 0 \\ 0 & 0 & 0 \\ 0 & 0 & 0 \\ r_{41} & 0 & 0 \\ 0 & r_{41} & 0 \\ 0 & 0 & r_{41} \end{pmatrix}$ |
| Point group $\bar{6}$ | Point group $\bar{6}m2$ ($m \perp x_1$) | Point group $\bar{6}2m$ ($m \perp x_2$) | Point group 432 |
| $\begin{pmatrix} r_{11} & -r_{22} & 0 \\ -r_{11} & r_{22} & 0 \\ 0 & 0 & 0 \\ 0 & 0 & 0 \\ 0 & 0 & 0 \\ -r_{22} & -r_{11} & 0 \end{pmatrix}$ | $\begin{pmatrix} 0 & -r_{22} & 0 \\ 0 & r_{22} & 0 \\ 0 & 0 & 0 \\ 0 & 0 & 0 \\ 0 & 0 & 0 \\ -r_{22} & 0 & 0 \end{pmatrix}$ | $\begin{pmatrix} r_{11} & 0 & 0 \\ -r_{11} & 0 & 0 \\ 0 & 0 & 0 \\ 0 & 0 & 0 \\ 0 & 0 & 0 \\ 0 & -r_{11} & 0 \end{pmatrix}$ | $\begin{pmatrix} 0 & 0 & 0 \\ 0 & 0 & 0 \\ 0 & 0 & 0 \\ 0 & 0 & 0 \\ 0 & 0 & 0 \\ 0 & 0 & 0 \end{pmatrix}$ |

1. TENSORIAL ASPECTS OF PHYSICAL PROPERTIES

Thus

$$\tan \theta = \frac{G_1}{\bar{n}(n_o - n_e)} = \frac{g_{11}}{\bar{n}(n_o - n_e)}. \quad (1.6.5.45)$$

Generally speaking, the ellipticity is extremely small and difficult to measure (Moxon & Renshaw, 1990). In right-handed quartz (right-handed with respect to optical rotation observed along the c axis), $n_o = 1.544$, $n_e = 1.553$, $g_{11} = g_{22} = -5.82 \times 10^{-5}$ and $g_{33} = 12.96 \times 10^{-5}$ measured at $\lambda = 5100 \text{ \AA}$. Since the c axis is also the optic axis, $\delta = 0$ for the (0001) plane, and thus $\kappa = 1$ for this section [equations (1.6.5.44) and (1.6.5.43)]. This value of $\kappa = 1$ means that the two waves are circular (see Section 1.6.5.5), *i.e.* there is no linear birefringence, only a pure rotation. In this direction, the gyration g_{33} means a rotation of $\rho = 29.5^\circ \text{ mm}^{-1}$ [using equation (1.6.5.27)]. In a direction normal to the optic axis, from equation (1.6.5.40) one finds $\rho = -13.3^\circ \text{ mm}^{-1}$. However, in this direction, the crystal appears linearly birefringent with $\delta = 110.88 \text{ mm}^{-1}$ [equation (1.6.5.42)]. Thus the ellipticity $\kappa = -0.00209$, as calculated from equations (1.6.5.44) and (1.6.5.43). In other words, the two waves are very slightly elliptical, and the sense of rotation of the two ellipses is reversed. Because of the change in sign of the gyration coefficients, it is found that at an angle of $56^\circ 10'$ down from the optic axis $\kappa = 0$, meaning that waves travelling along this direction show no optical rotation, only linear birefringence.

1.6.6. Linear electro-optic effect

The linear electro-optic effect, given by $P_i^\omega = \varepsilon_o \chi_{ijk} E_j^\omega E_k^0$ is conventionally expressed in terms of the change in dielectric impermeability caused by imposition of a static electric field on the crystal. Thus one may write the linear electro-optic effect as

$$\Delta \eta_{ij} = r_{ijk} E_k^0, \quad (1.6.6.1)$$

where the coefficients r_{ijk} form the so-called *linear electro-optic tensor*. These have identical symmetry with the piezoelectric tensor and so obey the same rules (see Table 1.6.6.1). Like the piezoelectric tensor, there is a maximum of 18 independent coefficients (triclinic case) (see Section 1.1.4.10.3). However, unlike in piezoelectricity, in using the Voigt contracted notation there are two major differences:

(1) In writing the electro-optic tensor components as r_{ij} , the first suffix refers to the column number and the second suffix is the row number.

(2) There are no factors of 1/2 or 2.

Typical values of linear electro-optic coefficients are around 10^{-12} mV^{-1} .

1.6.6.1. Primary and secondary effects

In considering the electro-optic effect, it is necessary to bear in mind that, in addition to the primary effect of changing the refractive index, the applied electric field may also cause a strain in the crystal *via* the converse piezoelectric effect, and this can then change the refractive index, as a secondary effect, through the elasto-optic effect. Both these effects, which are of comparable magnitude in practice, will occur if the crystal is free. However, if the crystal is mechanically clamped, it is not possible to induce any strain, and in this case therefore only the primary electro-optic effect is seen. In practice, the free and clamped behaviour can be investigated by measuring the linear birefringence when applying electric fields of varying frequencies. When the electric field is static or of low frequency, the effect is measured at constant stress, so that both primary and secondary effects are measured together. For electric fields at frequencies above the natural mechanical resonance of the crystal, the strains are very small, and in this case only the primary effect is measured.

1.6.6.2. Example of LiNbO_3

In order to understand how tensors can be used in calculating the optical changes induced by an applied electric field, it is instructive to take a particular example and work out the change in refractive index for a given electric field. LiNbO_3 is the most widely used electro-optic material in industry and so this forms a useful example for calculation purposes. This material crystallizes in point group $3m$, for which the electro-optic tensor has the form (for the effect of symmetry, see Section 1.1.4.10) (with x_1 perpendicular to m)

$$\begin{pmatrix} 0 & -r_{22} & r_{13} \\ 0 & r_{22} & r_{13} \\ 0 & 0 & r_{33} \\ 0 & r_{51} & 0 \\ r_{51} & 0 & 0 \\ -r_{22} & 0 & 0 \end{pmatrix}, \quad (1.6.6.2)$$

with $r_{13} = 9.6$, $r_{22} = 6.8$, $r_{33} = 30.9$ and $r_{51} = 32.5 \times 10^{-12} \text{ mV}^{-1}$, under the normal measuring conditions where the crystal is unclamped.

Calculation using dielectric impermeability tensor. Suppose, for example, a static electric field E_3^0 is imposed along the x_3 axis. One can then write

$$\begin{pmatrix} \Delta \eta_1 \\ \Delta \eta_2 \\ \Delta \eta_3 \\ \Delta \eta_4 \\ \Delta \eta_5 \\ \Delta \eta_6 \end{pmatrix} = \begin{pmatrix} 0 & -r_{22} & r_{13} \\ 0 & r_{22} & r_{13} \\ 0 & 0 & r_{33} \\ 0 & r_{51} & 0 \\ r_{51} & 0 & 0 \\ -r_{22} & 0 & 0 \end{pmatrix} \begin{pmatrix} 0 \\ 0 \\ E_3^0 \end{pmatrix} = \begin{pmatrix} r_{13} E_3^0 \\ r_{13} E_3^0 \\ r_{33} E_3^0 \\ 0 \\ 0 \\ 0 \end{pmatrix}. \quad (1.6.6.3)$$

Thus

$$\begin{aligned} \Delta \eta_1 &= r_{13} E_3^0 = \Delta \eta_2 \\ \Delta \eta_3 &= r_{33} E_3^0 \\ \Delta \eta_4 &= \Delta \eta_5 = \Delta \eta_6 = 0. \end{aligned} \quad (1.6.6.4)$$

Since the original indicatrix of LiNbO_3 before application of the field is uniaxial,

$$\begin{aligned} \eta_1 &= \frac{1}{n_o^2} = \eta_2 \\ \eta_3 &= \frac{1}{n_e^2}, \end{aligned} \quad (1.6.6.5)$$

and so differentiating, the following are obtained:

$$\begin{aligned} \Delta \eta_1 &= \Delta \eta_2 = -\frac{2}{n_o^3} \Delta n_o \\ \Delta \eta_3 &= -\frac{2}{n_e^3} \Delta n_e. \end{aligned} \quad (1.6.6.6)$$

Thus, the induced changes in refractive index are given by

$$\begin{aligned} \Delta n_1 &= \Delta n_2 = -\frac{n_o^3}{2} r_{13} E_3^0 \\ \Delta n_3 &= -\frac{n_e^3}{2} r_{33} E_3^0. \end{aligned} \quad (1.6.6.7)$$

It can be seen from this that the effect is simply to change the refractive indices by deforming the indicatrix, but maintain the uniaxial symmetry of the crystal. Note that if light is now propagated along, say, x_1 , the observed linear birefringence is given by

$$(n_e - n_o) - \frac{1}{2}(n_e^3 r_{33} - n_o^3 r_{13}) E_3^0. \quad (1.6.6.8)$$

1.6. CLASSICAL LINEAR CRYSTAL OPTICS

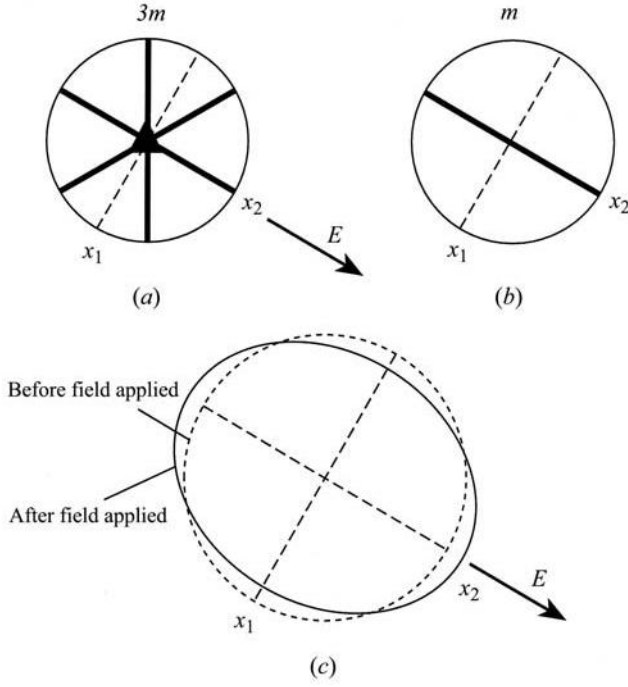


Fig. 1.6.6.1. (a) Symmetry elements of point group $3m$. (b) Symmetry elements after field applied along x_2 . (c) Effect on circular section of uniaxial indicatrix.

If, on the other hand, the electric field E_2^0 is applied along x_2 , i.e. within the mirror plane, one finds

$$\begin{aligned}\Delta\eta_1 &= -r_{22}E_2^0 \\ \Delta\eta_2 &= +r_{22}E_2^0 \\ \Delta\eta_4 &= +r_{51}E_2^0 \\ \Delta\eta_3 &= \Delta\eta_5 = \Delta\eta_6 = 0.\end{aligned}\quad (1.6.6.9)$$

Diagonalization of the matrix

$$\begin{pmatrix} \Delta\eta_1 & 0 & 0 \\ 0 & \Delta\eta_2 & \Delta\eta_4 \\ 0 & \Delta\eta_4 & \Delta\eta_3 \end{pmatrix} \quad (1.6.6.10)$$

containing these terms gives three eigenvalue solutions for the changes in dielectric impermeabilities:

$$\begin{aligned}(1) \quad & -r_{22}E_2^0 \\ (2) \quad & \frac{r_{22} + (r_{22}^2 + 4r_{51}^2)^{1/2}}{2}E_2^0 \\ (3) \quad & \frac{r_{22} - (r_{22}^2 + 4r_{51}^2)^{1/2}}{2}E_2^0.\end{aligned}\quad (1.6.6.11)$$

On calculating the eigenfunctions, it is found that solution (1) lies along x_1 , thus representing a change in the value of the indicatrix axis in this direction. Solutions (2) and (3) give the other two axes of the indicatrix: these are different in length, but mutually perpendicular, and lie in the x_2x_3 plane. Thus a biaxial indicatrix is formed with one refractive index fixed along x_1 and the other two in the plane perpendicular. The effect of having the electric field imposed within the mirror plane is thus to remove the threefold axis in point group $3m$ and to form the point subgroup m (Fig. 1.6.6.1).

Relationship between linear electro-optic coefficients r_{ijk} and the susceptibility tensor $\chi_{ijk}^{(2)}$. It is instructive to repeat the above calculation using the normal susceptibility tensor and equation (1.6.3.14). Consider, again, a static electric field along x_3 and light propagating along x_1 . As before, the only coefficients that need to

be considered with the static field along x_3 are $\chi_{113} = \chi_{223}$ and χ_{333} . Equation (1.6.3.14) can then be written as

$$\begin{pmatrix} \varepsilon_1 + \varepsilon_o\chi_{13}E_3^0 + n^2 & 0 & 0 \\ 0 & \varepsilon_1 + \varepsilon_o\chi_{13}E_3^0 & 0 \\ 0 & 0 & \varepsilon_3 + \varepsilon_o\chi_{33}E_3^0 \end{pmatrix} \begin{pmatrix} E_1 \\ E_2 \\ E_3 \end{pmatrix} = \begin{pmatrix} n^2 & 0 & 0 \\ 0 & n^2 & 0 \\ 0 & 0 & n^2 \end{pmatrix} \begin{pmatrix} E_1 \\ E_2 \\ E_3 \end{pmatrix}, \quad (1.6.6.12)$$

where for simplicity the Voigt notation has been used. The first line of the matrix equation gives

$$(\varepsilon_1 + \varepsilon_o\chi_{13}E_3^0 + n^2)E_1 = n^2E_1. \quad (1.6.6.13)$$

Since only a transverse electric field is relevant for an optical wave (plasma waves are not considered here), it can be assumed that the longitudinal field $E_1 = 0$. The remaining two equations can be solved by forming the determinantal equation

$$\begin{vmatrix} \varepsilon_1 + \varepsilon_o\chi_{13}E_3^0 - n^2 & 0 \\ 0 & \varepsilon_3 + \varepsilon_o\chi_{33}E_3^0 - n^2 \end{vmatrix} = 0, \quad (1.6.6.14)$$

which leads to the results

$$n_1^2 = \varepsilon_1 + \varepsilon_o\chi_{13}E_3^0 \quad \text{and} \quad n_2^2 = \varepsilon_3 + \varepsilon_o\chi_{33}E_3^0. \quad (1.6.6.15)$$

Thus

$$n_1^2 = n_o^2 + \varepsilon_o\chi_{13}E_3^0 \quad \text{and} \quad n_2^2 = n_e^2 + \varepsilon_o\chi_{33}E_3^0, \quad (1.6.6.16)$$

and so

$$(n_1 - n_o)(n_1 + n_o) = \varepsilon_o\chi_{13}E_3^0 \quad \text{and} \quad (n_2 - n_e)(n_2 + n_e) = \varepsilon_o\chi_{33}E_3^0, \quad (1.6.6.17)$$

and since $n_1 \simeq n_o$ and $n_2 \simeq n_e$,

$$n_1 - n_o = \frac{\varepsilon_o\chi_{13}E_3^0}{2n_o} \quad \text{and} \quad n_2 - n_e = \frac{\varepsilon_o\chi_{33}E_3^0}{2n_e}. \quad (1.6.6.18)$$

Subtracting these two results, the induced birefringence is found:

$$(n_e - n_o) - \frac{1}{2}\left(\frac{\varepsilon_o\chi_{33}}{n_e} - \frac{\varepsilon_o\chi_{13}}{n_o}\right)E_3^0. \quad (1.6.6.19)$$

Comparing with the equation (1.6.6.8) calculated for the linear electro-optic coefficients,

$$(n_e - n_o) - \frac{1}{2}(n_e^3r_{33} - n_o^3r_{13})E_3^0, \quad (1.6.6.20)$$

one finds the following relationships between the linear electro-optic coefficients and the susceptibilities $\chi^{(2)}$:

$$r_{13} = \frac{\varepsilon_o\chi_{13}}{n_o^4} \quad \text{and} \quad r_{33} = \frac{\varepsilon_o\chi_{33}}{n_e^4}. \quad (1.6.6.21)$$

1.6.7. The linear photoelastic effect

1.6.7.1. Introduction

The linear photoelastic (or piezo-optic) effect (Narasimhamurthy, 1981) is given by $P_i^o = \varepsilon_o\chi_{ijkl}E_j^o S_{kl}^o$, and, like the electro-optic effect, it can be discussed in terms of the change in dielectric impermeability caused by a static (or low-frequency) field, in this case a stress, applied to the crystal. This can be written in the form

$$\Delta\eta_{ij} = \pi_{ijkl}T_{kl}^o. \quad (1.6.7.1)$$

1. TENSORIAL ASPECTS OF PHYSICAL PROPERTIES

The coefficients π_{ijkl} form a fourth-rank tensor known as the *linear piezo-optic* tensor. Typically, the piezo-optic coefficients are of the order of $10^{-12} \text{ m}^2 \text{ N}^{-1}$. It is, however, more usual to express the effect as an *elasto-optic effect* by making use of the relationship between stress and strain (see Section 1.3.3.2), thus

$$T_{k\ell} = c_{k\ell mn} S_{mn}, \quad (1.6.7.2)$$

where the $c_{k\ell mn}$ are the elastic stiffness coefficients. Therefore equation (1.6.7.2) can be rewritten in the form

$$\Delta\eta_{ij} = \pi_{ijkl} c_{k\ell mn} S_{mn} = p_{ijmn} S_{mn} \quad (1.6.7.3)$$

or, in contracted notation,

$$\Delta\eta_i = p_{ij} S_j, \quad (1.6.7.4)$$

where, for convenience, the superscript 0 has been dropped, the elastic strain being considered as essentially static or of low frequency compared with the natural mechanical resonances of the crystal. The p_{ijmn} are coefficients that form the *linear elasto-optic* (or *strain-optic*) tensor (Table 1.6.7.1). Note that these coefficients are dimensionless, and typically of order 10^{-1} , showing that the change to the optical indicatrix is roughly one-tenth of the strain.

The elasto-optic effect can arise in several ways. The most obvious way is through application of an external stress, applied to the surfaces of the crystal. However, strains, and hence changes to the refractive indices, can arise in a crystal through other ways that are less obvious. Thus, it is a common finding that crystals can be twinned, and thus the boundary between twin domains, which corresponds to a mismatch between the crystal structures either side of the domain boundary, will exhibit a strain. Such a crystal, when viewed between crossed polars under a microscope will produce birefringence colours that will highlight the contrast between the domains. This is known as *strain birefringence*. Similarly, when a crystal undergoes a phase transition involving a change in crystal system, a so-called *ferroelastic transition*, there will be a change in strain owing to the difference in unit-cell shapes. Hence there will be a corresponding change in the optical indicatrix. Often the phase transition is one going from a high-temperature optically isotropic section to a low-temperature optically anisotropic section. In this case, the high-temperature section has no internal strain, but the low-temperature phase acquires a strain, which is often called the *spontaneous strain* (by analogy with the term spontaneous polarization in ferroelectrics).

1.6.7.2. Spontaneous strain in BaTiO_3

As an example of the calculation of the relationship between spontaneous strain and linear birefringence, consider the high-temperature phase transition of the well known perovskite BaTiO_3 . This substance undergoes a transition at around 403 K on cooling from its high-temperature $Pm\bar{3}m$ phase to the room-temperature $P4mm$ phase. The $P4mm$ phase is both ferroelectric and ferroelastic. In this tetragonal phase, there is a small distortion of the unit cell along $[001]$ and a contraction along $\langle 100 \rangle$ compared with the unit cell of the high-temperature cubic phase, and so the room-temperature phase can be expected to have a uniaxial optical indicatrix.

The elasto-optic tensor for the $m\bar{3}m$ phase is (Table 1.6.7.1)

$$\begin{pmatrix} p_{11} & p_{12} & p_{12} & 0 & 0 & 0 \\ p_{12} & p_{11} & p_{12} & 0 & 0 & 0 \\ p_{12} & p_{12} & p_{11} & 0 & 0 & 0 \\ 0 & 0 & 0 & p_{44} & 0 & 0 \\ 0 & 0 & 0 & 0 & p_{44} & 0 \\ 0 & 0 & 0 & 0 & 0 & p_{44} \end{pmatrix}. \quad (1.6.7.5)$$

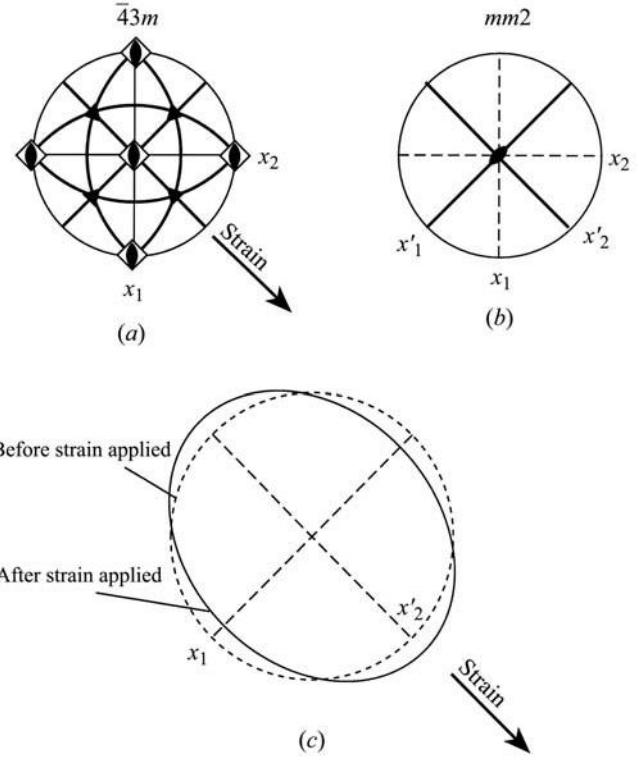


Fig. 1.6.7.1. (a) Symmetry elements of point group $\bar{4}3m$. (b) Symmetry elements after strain applied along $[110]$. (c) Effect on spherical indicatrix.

Consider the low-temperature tetragonal phase to arise as a small distortion of this cubic phase, with a spontaneous strain S_3^s given by the lattice parameters of the tetragonal phase:

$$S_3^s = [(c - a)/a]. \quad (1.6.7.6)$$

Therefore, the equations (1.6.7.4) for the dielectric impermeability in terms of the spontaneous strain component are given in matrix form as

$$\begin{pmatrix} \Delta\eta_1 \\ \Delta\eta_2 \\ \Delta\eta_3 \\ \Delta\eta_4 \\ \Delta\eta_5 \\ \Delta\eta_6 \end{pmatrix} = \begin{pmatrix} p_{11} & p_{12} & p_{12} & 0 & 0 & 0 \\ p_{12} & p_{11} & p_{12} & 0 & 0 & 0 \\ p_{12} & p_{12} & p_{11} & 0 & 0 & 0 \\ 0 & 0 & 0 & p_{44} & 0 & 0 \\ 0 & 0 & 0 & 0 & p_{44} & 0 \\ 0 & 0 & 0 & 0 & 0 & p_{44} \end{pmatrix} \begin{pmatrix} 0 \\ 0 \\ S_3^s \\ 0 \\ 0 \\ 0 \end{pmatrix} = \begin{pmatrix} p_{12} S_3^s \\ p_{12} S_3^s \\ p_{11} S_3^s \\ 0 \\ 0 \\ 0 \end{pmatrix} \quad (1.6.7.7)$$

so that

$$\begin{aligned} \Delta\eta_1 &= \Delta\eta_2 = p_{12} S_3^s \\ \Delta\eta_3 &= p_{11} S_3^s \\ \Delta\eta_4 &= \Delta\eta_5 = \Delta\eta_6 = 0. \end{aligned} \quad (1.6.7.8)$$

By analogy with equations (1.6.6.5) and (1.6.6.6), the induced changes in refractive index are then

1.6. CLASSICAL LINEAR CRYSTAL OPTICS

Table 1.6.7.1. Symmetry constraints on the linear elasto-optic (strain-optic) tensor p_{ij} (contracted notation) (see Section 1.1.4.10.6)

| Triclinic | Orthorhombic | Tetragonal | Trigonal |
|--|--|--|---|
| Point group 1 | Point groups 222, $mm2$, mmm | Point groups 4, $\bar{4}$, $4/m$ | Point groups 3, $\bar{3}$ |
| $\begin{pmatrix} p_{11} & p_{12} & p_{13} & p_{14} & p_{15} & p_{16} \\ p_{21} & p_{22} & p_{23} & p_{24} & p_{25} & p_{26} \\ p_{31} & p_{32} & p_{33} & p_{34} & p_{35} & p_{36} \\ p_{41} & p_{42} & p_{43} & p_{44} & p_{45} & p_{46} \\ p_{51} & p_{52} & p_{53} & p_{54} & p_{55} & p_{56} \\ p_{61} & p_{62} & p_{63} & p_{64} & p_{65} & p_{66} \end{pmatrix}$ | $\begin{pmatrix} p_{11} & p_{12} & p_{13} & 0 & 0 & 0 \\ p_{21} & p_{22} & p_{23} & 0 & 0 & 0 \\ p_{31} & p_{32} & p_{33} & 0 & 0 & 0 \\ 0 & 0 & 0 & p_{44} & 0 & 0 \\ 0 & 0 & 0 & & p_{55} & 0 \\ 0 & 0 & 0 & 0 & 0 & p_{66} \end{pmatrix}$ | $\begin{pmatrix} p_{11} & p_{12} & p_{13} & 0 & 0 & p_{16} \\ p_{12} & p_{22} & p_{13} & 0 & 0 & -p_{16} \\ p_{31} & p_{31} & p_{33} & 0 & 0 & 0 \\ 0 & 0 & 0 & p_{44} & p_{45} & 0 \\ 0 & 0 & 0 & -p_{45} & p_{55} & 0 \\ p_{61} & -p_{61} & 0 & & 0 & p_{66} \end{pmatrix}$ | $\begin{pmatrix} p_{11} & p_{12} & p_{13} & p_{14} & p_{15} & p_{16} \\ p_{12} & p_{11} & p_{13} & -p_{14} & -p_{15} & -p_{16} \\ p_{31} & p_{31} & p_{33} & 0 & 0 & 0 \\ p_{41} & -p_{41} & 0 & p_{44} & p_{45} & -p_{51} \\ p_{51} & -p_{51} & 0 & -p_{44} & p_{44} & p_{41} \\ -p_{16} & p_{16} & 0 & -p_{15} & p_{14} & \frac{1}{2}(p_{11} - p_{12}) \end{pmatrix}$ |
| Monoclinic | | Point groups $4mm$, $\bar{4}2m$, 422 , $4/mmm$ | Point groups $3m$, $\bar{3}m$, 32 |
| Point groups 2, m , $2/m$ ($2 \parallel x_2$) | Point groups 2, m , $2/m$ ($2 \parallel x_3$) | | |
| $\begin{pmatrix} p_{11} & p_{12} & p_{13} & 0 & p_{15} & 0 \\ p_{21} & p_{22} & p_{23} & 0 & p_{25} & 0 \\ p_{31} & p_{32} & p_{33} & 0 & p_{35} & 0 \\ 0 & 0 & 0 & p_{44} & 0 & p_{46} \\ p_{51} & p_{52} & p_{53} & 0 & p_{55} & 0 \\ 0 & 0 & 0 & p_{64} & 0 & p_{66} \end{pmatrix}$ | $\begin{pmatrix} p_{11} & p_{12} & p_{13} & 0 & 0 & p_{16} \\ p_{21} & p_{22} & p_{23} & 0 & 0 & p_{26} \\ p_{31} & p_{32} & p_{33} & 0 & 0 & p_{36} \\ 0 & 0 & 0 & p_{44} & p_{45} & 0 \\ 0 & 0 & 0 & p_{54} & p_{55} & 0 \\ p_{61} & p_{62} & p_{63} & 0 & 0 & p_{66} \end{pmatrix}$ | $\begin{pmatrix} p_{11} & p_{12} & p_{13} & p_{14} & 0 & 0 \\ p_{12} & p_{11} & p_{13} & -p_{14} & 0 & 0 \\ p_{13} & p_{13} & p_{33} & 0 & 0 & 0 \\ p_{41} & -p_{41} & 0 & p_{44} & 0 & 0 \\ 0 & 0 & 0 & 0 & p_{44} & p_{41} \\ 0 & 0 & 0 & 0 & p_{14} & \frac{1}{2}(p_{11} - p_{12}) \end{pmatrix}$ | |

| Hexagonal | Cubic | Isotropic |
|---|--|--|
| Point groups 6, $\bar{6}$, $6/m$ | Point groups $m\bar{3}$, 23 | |
| $\begin{pmatrix} p_{11} & p_{12} & p_{13} & 0 & 0 & p_{16} \\ p_{12} & p_{11} & p_{13} & 0 & 0 & -p_{16} \\ p_{31} & p_{31} & p_{33} & 0 & 0 & 0 \\ 0 & 0 & 0 & p_{44} & p_{45} & 0 \\ 0 & 0 & 0 & -p_{45} & p_{44} & 0 \\ -p_{16} & p_{16} & 0 & 0 & 0 & \frac{1}{2}(p_{11} - p_{12}) \end{pmatrix}$ | $\begin{pmatrix} p_{11} & p_{12} & p_{21} & 0 & 0 & 0 \\ p_{12} & p_{11} & p_{12} & 0 & 0 & 0 \\ p_{21} & p_{12} & p_{11} & 0 & 0 & 0 \\ 0 & 0 & 0 & p_{44} & 0 & 0 \\ 0 & 0 & 0 & 0 & p_{44} & 0 \\ 0 & 0 & 0 & 0 & 0 & p_{44} \end{pmatrix}$ | $\begin{pmatrix} p_{11} & p_{12} & p_{12} & 0 & 0 & 0 \\ p_{12} & p_{11} & p_{13} & 0 & 0 & 0 \\ p_{12} & p_{12} & p_{11} & 0 & 0 & 0 \\ 0 & 0 & 0 & \frac{1}{2}(p_{11} - p_{12}) & 0 & 0 \\ 0 & 0 & 0 & 0 & \frac{1}{2}(p_{11} - p_{12}) & 0 \\ 0 & 0 & 0 & 0 & 0 & \frac{1}{2}(p_{11} - p_{12}) \end{pmatrix}$ |
| Point groups $6mm$, $\bar{6}m2$, 622 , $6/mmm$ | Point groups $\bar{4}3m$, 432 , $m\bar{3}m$ | |
| $\begin{pmatrix} p_{11} & p_{12} & p_{13} & 0 & 0 & 0 \\ p_{12} & p_{11} & p_{13} & 0 & 0 & 0 \\ p_{13} & p_{13} & p_{33} & 0 & 0 & 0 \\ 0 & 0 & 0 & p_{44} & 0 & 0 \\ 0 & 0 & 0 & 0 & p_{44} & 0 \\ 0 & 0 & 0 & 0 & 0 & \frac{1}{2}(p_{11} - p_{12}) \end{pmatrix}$ | $\begin{pmatrix} p_{11} & p_{12} & p_{12} & 0 & 0 & 0 \\ p_{12} & p_{11} & p_{13} & 0 & 0 & 0 \\ p_{12} & p_{12} & p_{11} & 0 & 0 & 0 \\ 0 & 0 & 0 & p_{44} & 0 & 0 \\ 0 & 0 & 0 & 0 & p_{44} & 0 \\ 0 & 0 & 0 & 0 & 0 & p_{44} \end{pmatrix}$ | |

$$\begin{aligned} \Delta n_1 &= \Delta n_2 = -\frac{n_{\text{cub}}^3}{2} p_{12} S_3^s \\ \Delta n_3 &= -\frac{n_{\text{cub}}^3}{2} p_{11} S_3^s, \end{aligned} \quad (1.6.7.9)$$

where n_{cub} is the refractive index of the cubic phase. Thus the birefringence in the tetragonal phase as seen by light travelling along x_1 is given by

$$\Delta n_3 - \Delta n_2 = -\frac{n_{\text{cub}}^3}{2} (p_{11} - p_{12}) S_3^s. \quad (1.6.7.10)$$

Thus a direct connection is made between the birefringence of the tetragonal phase of BaTiO_3 and its lattice parameters *via* the spontaneous strain. As in the case of the linear electro-optic effect, the calculation can be repeated using equation (1.6.3.14) with the susceptibilities χ_{11} and χ_{12} to yield the relationship

$$p_{11} = \frac{c_{1111} \epsilon_o \chi_{11}}{n_o^4}; \quad p_{12} = \frac{c_{1122} \epsilon_o \chi_{12}}{n_o^4}. \quad (1.6.7.11)$$

1.6.7.3. The acousto-optic effect

The acousto-optic effect (Sapriel, 1976) is really a variant of the elasto-optic effect, in that the strain field is created by the passage of a sound wave through the crystal. If this wave has frequency ω_1 , the resulting polarization in the presence of a light

wave of frequency ω_2 is given by $P_i^\omega = \chi_{ijkl} E_j^{\omega_2} S_{kl}^{\omega_1}$, where $\omega = \omega_1 \pm \omega_2$. However, since the sound-wave frequency is very small compared with that of the light, to all intents and purposes the change in frequency of the light field can be ignored. The effect then of the sound wave is to produce within an acousto-optic crystal a spatially modulated change in refractive index: a beam of light can then be diffracted by this spatial modulation, the resulting optical diffraction pattern thus changing with the changing sound signal. Acousto-optic materials therefore can be used as transducers for converting sound signals into optical signals for transmission down optical fibres in communications systems. Consider, for instance, a sound wave propagating along the $[110]$ direction in gallium arsenide (GaAs), which crystallizes in point group $\bar{4}3m$. Suppose that this sound wave is longitudinally polarized. With respect to the cube axes, this corresponds to an oscillatory shear strain $S_{12} \sin(\omega t - k\xi)$, where ξ is a distance along the $[110]$ direction (Fig. 1.6.7.1). Then one can write

$$\Delta \eta_{ij} = p_{ij12} S_{12} \sin(\omega t - k\xi) \quad (1.6.7.12)$$

or in contracted notation

$$\Delta \eta_i = p_{i6} S_6 \sin(\omega t - k\xi). \quad (1.6.7.13)$$

From Table 1.6.7.1, it seen that the change in dielectric impermeability tensor is

1. TENSORIAL ASPECTS OF PHYSICAL PROPERTIES

$$\Delta\eta_6 = p_{66}S_6 \sin(\omega t - k\xi) = p_{44}S_6 \sin(\omega t - k\xi) \quad (1.6.7.14)$$

since all other components are zero. This means that the original spherical indicatrix of the cubic crystal has been distorted to form a biaxial indicatrix whose axes oscillate in length according to

$$\begin{aligned} n_1 &= n_{\text{cub}} + \frac{n_{\text{cub}}^3}{2} p_{44} S_6 \sin(\omega t - k\xi) \\ n_2 &= n_{\text{cub}} - \frac{n_{\text{cub}}^3}{2} p_{44} S_6 \sin(\omega t - k\xi) \\ n_3 &= n_{\text{cub}}, \end{aligned} \quad (1.6.7.15)$$

thus forming an optical grating of spatial periodicity given by the $k\xi$ term. In gallium arsenide, at a wavelength of light equal to $1.15 \mu\text{m}$, $p_{11} = -0.165$, $p_{12} = -0.140$ and $p_{44} = -0.072$. It is convenient to define a figure of merit for acousto-optic materials (Yariv & Yeh, 1983) given by

$$M = \frac{n^6 p^2}{d v^3}, \quad (1.6.7.16)$$

where v is the velocity of the sound wave and d is the density of the solid. For gallium arsenide, $d = 5340 \text{ kg m}^{-3}$, and for a sound wave propagating as above $v = 5.15 \text{ m s}^{-1}$. At the wavelength $\lambda = 1.15 \mu\text{m}$, $n = 3.37$, and so it is found that $M = 104$. In practice, figures of merits can range from less than 0.001 up to as high as 4400 in the case of Te, and so the value for gallium arsenide makes it potentially useful as an acousto-optic material for infrared signals.

1.6.8. Glossary

| | |
|-------------------------------|--|
| α, β, γ | refractive indices of biaxial indicatrix, $\alpha < \beta < \gamma$ |
| $\hat{\alpha}$ | polarizability operator |
| B_i | i th component of magnetic induction |
| c | velocity of light |
| c_{klmn} | $klmn$ th component of elastic stiffness tensor |
| $\chi_{ijk\dots}$ | $ijk\dots$ th component of generalized susceptibility |
| d | density |
| D_i | i th component of dielectric displacement |
| Δ | phase difference of light |
| \hat{e}_{ijm} | unit antisymmetric pseudotensor of rank 3 |
| E_i | i th component of electric field |
| g_{ij}, G_{ij} | ij th component of gyration tensor |
| \mathbf{G} | gyration vector |
| $\gamma_{ij\ell}$ | third-rank optical gyration susceptibility |
| \mathbf{H} | magnetic field intensity |
| η_{ij} | ij th component of dielectric impermeability tensor |
| ϵ_o | permittivity of free space |
| ϵ_{ij} | ij th component of dielectric tensor |
| κ | ellipticity of wave |
| \mathbf{k} | wavevector of light propagating in crystal ($ k = 2\pi/\lambda$) |
| λ | wavelength of light |
| μ_o | vacuum magnetic permeability |
| n | refractive index of light |
| $n_\alpha, n_\beta, n_\gamma$ | refractive indices for biaxial indicatrix, $n_\alpha < n_\beta < n_\gamma$ |
| n_o | ordinary refractive index |
| n_e | extraordinary refractive index |
| Ψ_i | wavefunction of state i |
| P_i | i th component of electric polarization |
| p_{ijkl} | $ijkl$ th component of elasto-optic (strain-optic) tensor |
| \hat{p} | electric dipole operator |

| | |
|--------------|--|
| ρ | optical rotatory power |
| π_{ijkl} | $ijkl$ th component of linear piezo-optic tensor |
| r_{ijk} | ijk th component of linear electro-optic tensor |
| \hat{s} | unit vector in the direction of \mathbf{s} , the wave normal |
| S_{ij} | ij th component of strain tensor |
| T_{ij} | ij th component of stress tensor |
| v | velocity of sound |
| V | half the angle between optic axes |
| ω | cyclic frequency |
| x_i | direction of i th Cartesian axis, $i = 1, 2, 3$ |

References

- Agranovich, V. M. & Ginzburg, V. C. (1984). *Crystal optics with spatial dispersion, and excitons*. Berlin: Springer.
- Bloss, F. D. (1961). *An introduction to the methods of optical crystallography*. New York: Holt, Rinehart and Winston.
- Born, M. (1933). *Dynamische Gittertheorie der Kristalle*. In *Handbuch der Physik*, **24**, 623–794.
- Born, M. & Wolf, E. (1993). *Principles of optics*. Sixth corrected edition. Oxford: Pergamon Press. Reissued (1999) by Cambridge University Press.
- Bragg, W. L. (1924). *The refractive indices of calcite and aragonite*. *Proc. R. Soc. London Ser. A*, **105**, 370.
- Butcher, P. N. & Cotter, D. (1990). *The elements of nonlinear optics*. Cambridge University Press.
- Devarajan, V. & Glazer, A. M. (1986). *Theory and computation of optical rotatory power in inorganic crystals*. *Acta Cryst.* **A42**, 560–569.
- Ewald, P. P. (1916). *Zur Begründung der Kristalloptik*. *Ann. Phys. (Leipzig)*, **49**, 1–38, 117–143.
- Glazer, A. M. (2002). WINOPTACT: a computer program to calculate optical rotatory power and refractive indices from crystal structure data. *J. Appl. Cryst.* **35**, 652.
- Glazer, A. M., Lewis, J. G. & Kaminsky, W. (1996). *An automatic optical imaging system for birefringent media*. *Proc. R. Soc. London Ser. A*, **452**, 2751–2765.
- Glazer, A. M. & Stadnicka, K. (1986). *On the origin of optical activity in crystal structures*. *J. Appl. Cryst.* **19**, 108–122.
- Glazer, A. M. & Stadnicka, K. (1989). *On the use of the term 'absolute' in crystallography*. *Acta Cryst.* **A45**, 234–238.
- Groth, P. (1906–1919). *Chemische Kristallographie*. Vols. I–V. Leipzig: Engelmann.
- Hartshorne, N. H. & Stuart, A. (1970). *Crystals and the polarising microscope*. London: Arnold.
- Jona, F. & Shirane, G. (1962). *Ferroelectric crystals*. Oxford: Pergamon.
- Jones, R. C. (1948). *A new calculus for the treatment of optical systems. VII. Properties of N-matrices*. *J. Opt. Soc. Am.* **38**, 671–685.
- Kaminow, I. P. (1974). *An introduction to electro-optic devices*. New York: Academic Press.
- Kerr, P. F. (1959). *Optical mineralogy*. New York: McGraw-Hill.
- Lines, M. E. & Glass, A. M. (1979). *Principles and applications of ferroelectrics and related materials*. Oxford: Clarendon.
- Lowry, T. M. (1935). *Optical rotatory power*. London: Longmans.
- Moxon, J. R. L. & Renshaw, A. R. (1990). *The simultaneous measurement of optical activity and circular dichroism in birefringent linearly dichroic crystal sections: I. Introduction and description of the method*. *J. Phys. Condens. Matter*, **2**, 6807–6836.
- Moxon, J. R. L., Renshaw, A. R. & Tebbutt, I. J. (1991). *The simultaneous measurement of optical activity and circular dichroism in birefringent linearly dichroic crystal sections: II. Description of the apparatus and results for quartz, nickel sulphate hexahydrate and benzil*. *J. Phys. D Appl. Phys.* **24**, 1187–1192.
- Narasimhamurthy, T. S. (1981). *Photoelastic and electro-optic properties of crystals*. New York: Plenum.
- Nussbaum, A. & Phillips, R. A. (1976). *Contemporary optics for scientists and engineers*. New Jersey: Prentice Hall.
- Sapriel, J. (1976). *Acousto-optics*. Chichester: Wiley.
- Szivessy, G. & Münster, C. (1934). *Über die Prüfung der Gitteroptik bei aktiven Kristallen*. *Ann. Phys. (Leipzig)*, **20**, 703–736.

1.6. CLASSICAL LINEAR CRYSTAL OPTICS

- Wahlstrom, E. E. (1959). *Optical crystallography*. New York: Wiley.
- Winchell, A. N. (1931). *Microscopic characters of artificial inorganic solid substances or artificial minerals*. New York: Wiley. [New edition (1964). New York: Academic Press.]
- Winchell, A. N. (1939). *Elements of optical mineralogy, Part III*. New York: Wiley.
- Winchell, A. N. (1951). *Elements of optical mineralogy, Part II*. New York: Wiley.
- Winchell, A. N. (1954). *The optical properties of organic compounds*. New York: Academic Press.
- Winchell, A. N. (1965). *Optical properties of minerals. A determinative table*. New York: Academic Press.
- Wood, I. G. & Glazer, A. M. (1980). Ferroelastic phase transition in BiVO_4 . I. Birefringence measurements using the rotating-analyser method. *J. Appl. Cryst.* **13**, 217–223.
- Yariv, A. & Yeh, P. (1983). *Optical waves in crystals*. New York: Wiley.

1.7. Nonlinear optical properties

By B. BOULANGER AND J. ZYSS

1.7.1. Introduction

The first nonlinear optical phenomenon was observed by Franken *et al.* (1961): ultraviolet radiation at 0.3471 μm was detected at the exit of a quartz crystal illuminated with a ruby laser beam at 0.6942 μm . This was the first demonstration of second harmonic generation at optical wavelengths. A coherent light of a few W cm^{-2} is necessary for the observation of nonlinear optical interactions, which thus requires the use of laser beams.

The basis of nonlinear optics, including quantum-mechanical perturbation theory and Maxwell equations, is given in the paper published by Armstrong *et al.* (1962).

It would take too long here to give a complete historical account of nonlinear optics, because it involves an impressive range of different aspects, from theory to applications, from physics to chemistry, from microscopic to macroscopic aspects, from quantum mechanics of materials to classical and quantum electrodynamics, from gases to solids, from mineral to organic compounds, from bulk to surface, from waveguides to fibres and so on.

Among the main nonlinear optical effects are harmonic generation, parametric wave mixing, stimulated Raman scattering, self-focusing, multiphoton absorption, optical bistability, phase conjugation and optical solitons.

This chapter deals mainly with harmonic generation and parametric interactions in anisotropic crystals, which stand out as one of the most important fields in nonlinear optics and certainly one of its oldest and most rigorously treated topics. Indeed, there is a great deal of interest in the development of solid-state laser sources, be they tunable or not, in the ultraviolet, visible and infrared ranges. Spectroscopy, telecommunications, telemetry and optical storage are some of the numerous applications.

The electric field of light interacts with the electric field of matter by inducing a dipole due to the displacement of the electron density away from its equilibrium position. The induced dipole moment is termed polarization and is a vector: it is related to the applied electric field *via* the dielectric susceptibility tensor. For fields with small to moderate amplitude, the polarization remains linearly proportional to the field magnitude and defines the linear optical properties. For increasing field amplitudes, the polarization is a nonlinear function of the applied electric field and gives rise to nonlinear optical effects. The polarization is properly modelled by a Taylor power series of the applied electric field if its strength does not exceed the atomic electric field (10^8 – 10^9 V cm^{-1}) and if the frequency of the electric field is far away from the resonance frequencies of matter. Our purpose lies within this framework because it encompasses the most frequently encountered cases, in which laser intensities remain in the kW to MW per cm^2 range, that is to say with electric fields from 10^3 to 10^4 V cm^{-1} . The electric field products appearing in the Taylor series express the interactions of different optical waves. Indeed, a wave at the circular frequency ω can be radiated by the second-order polarization induced by two waves at ω_a and ω_b such as $\omega = \omega_a \pm \omega_b$: these interactions correspond to sum-frequency generation ($\omega = \omega_a + \omega_b$), with the particular cases of second harmonic generation ($2\omega_a = \omega_a + \omega_a$) and indirect third harmonic generation ($3\omega_a = \omega_a + 2\omega_a$); the other three-wave process is difference-frequency generation, including optical parametric amplification and optical parametric oscillation. In the same way, the third-order polarization governs four-wave mixing: direct third harmonic generation ($3\omega_a = \omega_a + \omega_a + \omega_a$)

and more generally sum- and difference-frequency generations ($\omega = \omega_a \pm \omega_b \pm \omega_c$).

Here, we do not consider optical interactions at the microscopic level, and we ignore the way in which the atomic or molecular dielectric susceptibility determines the macroscopic optical properties. Microscopic solid-state considerations and the relations between microscopic and macroscopic optical properties, particularly successful in the realm of organic crystals, play a considerable role in materials engineering and optimization. This important topic, known as molecular and crystalline engineering, lies beyond the scope of this chapter. Therefore, all the phenomena studied here are connected to the macroscopic first-, second- and third-order dielectric susceptibility tensors $\chi^{(1)}$, $\chi^{(2)}$ and $\chi^{(3)}$, respectively; we give these tensors for all the crystal point groups.

We shall mainly emphasize propagation aspects, on the basis of Maxwell equations which are expressed for each Fourier component of the optical field in the nonlinear crystal. The reader will then follow how the linear optical properties come to play a pivotal role in the nonlinear optical interactions. Indeed, an efficient quadratic or cubic interaction requires not only a high magnitude of $\chi^{(2)}$ or $\chi^{(3)}$, respectively, but also specific conditions governed by $\chi^{(1)}$: existence of phase matching between the induced nonlinear polarization and the radiated wave; suitable symmetry of the field tensor, which is defined by the tensor product of the electric field vectors of the interacting waves; and small or nil double refraction angles. Quadratic and cubic processes cannot be considered as fully independent in the context of cascading. Significant phase shifts driven by a sequence of sum- and difference-frequency generation processes attached to a $\chi^{(2)} \cdot \chi^{(2)}$ contracted tensor expression have been reported (Bosshard, 2000). These results point out the relevance of polar structures to cubic phenomena in both inorganic and organic structures, thus somewhat blurring the borders between quadratic and cubic NLO.

We analyse in detail second harmonic generation, which is the prototypical interaction of frequency conversion. We also present indirect and direct third harmonic generations, sum-frequency generation and difference-frequency generation, with the specific cases of optical parametric amplification and optical parametric oscillation.

An overview of the methods of measurement of the nonlinear optical properties is provided, and the chapter concludes with a comparison of the main mineral and organic crystals showing nonlinear optical properties.

1.7.2. Origin and symmetry of optical nonlinearities

1.7.2.1. Induced polarization and susceptibility

The macroscopic electronic polarization of a unit volume of the material system is classically expanded in a Taylor power series of the applied electric field \mathbf{E} , according to Bloembergen (1965):

$$\mathbf{P} = \mathbf{P}_0 + \varepsilon_0(\chi^{(1)} \cdot \mathbf{E} + \chi^{(2)} \cdot \mathbf{E}^2 + \dots + \chi^{(n)} \cdot \mathbf{E}^n + \dots), \quad (1.7.2.1)$$

where $\chi^{(n)}$ is a tensor of rank $n + 1$, \mathbf{E}^n is a shorthand abbreviation for the n th order tensor product $\mathbf{E} \otimes \mathbf{E} \otimes \dots \otimes \mathbf{E} = \otimes^n \mathbf{E}$ and the dot stands for the contraction of the last n indices of the

1.7. NONLINEAR OPTICAL PROPERTIES

tensor $\chi^{(n)}$ with the full \mathbf{E}^n tensor. More details on tensor algebra can be found in Chapter 1.1 and in Schwartz (1981).

A more compact expression for (1.7.2.1) is

$$\mathbf{P} = \mathbf{P}_0 + \mathbf{P}_1(t) + \mathbf{P}_2(t) + \dots + \mathbf{P}_n(t) + \dots, \quad (1.7.2.2)$$

where \mathbf{P}_0 represents the static polarization and \mathbf{P}_n represents the n th order polarization. The properties of the linear and nonlinear responses will be assumed in the following to comply with time invariance and locality. In other words, time displacement of the applied fields will lead to a corresponding time displacement of the induced polarizations and the polarization effects are assumed to occur at the site of the polarizing field with no remote interactions. In the following, we shall refer to the classical formalism and related notations developed in Butcher (1965) and Butcher & Cotter (1990).

Tensorial expressions will be formulated within the Cartesian formalism and subsequent multiple lower index notation. The alternative irreducible tensor representation, as initially implemented in the domain of nonlinear optics by Jerphagnon *et al.* (1978) and more recently revived by Brasselet & Zyss (1998) in the realm of molecular-engineering studies, is particularly advantageous for connecting the nonlinear hyperpolarizabilities of microscopic (*e.g.* molecular) building blocks of molecular materials to the macroscopic (*e.g.* crystalline) susceptibility level. Such considerations fall beyond the scope of the present chapter, which concentrates mainly on the crystalline level, regardless of the microscopic origin of phenomena.

1.7.2.1.1. Linear and nonlinear responses

1.7.2.1.1.1. Linear response

Let us first consider the first-order linear response in (1.7.2.1) and (1.7.2.2): the most general possible linear relation between $\mathbf{P}(t)$ and $\mathbf{E}(t)$ is

$$\mathbf{P}^{(1)}(t) = \varepsilon_o \int_{-\infty}^{+\infty} d\tau T^{(1)}(t, \tau) \cdot \mathbf{E}(\tau), \quad (1.7.2.3)$$

where $T^{(1)}$ is a rank-two tensor, or in Cartesian index notation

$$P_{\mu}^{(1)}(t) = \varepsilon_o \int_{-\infty}^{+\infty} d\tau T_{\mu\alpha}^{(1)}(t, \tau) E_{\alpha}(\tau). \quad (1.7.2.4)$$

Applying the time-invariance assumption to (1.7.2.4) leads to

$$\begin{aligned} \mathbf{P}^{(1)}(t + t_0) &= \varepsilon_o \int_{-\infty}^{+\infty} d\tau T^{(1)}(t + t_0, \tau) \cdot \mathbf{E}(\tau) \\ &= \varepsilon_o \int_{-\infty}^{+\infty} d\tau T^{(1)}(t, \tau + t_0) \cdot \mathbf{E}(\tau) \\ &= \varepsilon_o \int_{-\infty}^{+\infty} d\tau' T^{(1)}(t, \tau' - t_0) \cdot \mathbf{E}(\tau'), \end{aligned} \quad (1.7.2.5)$$

hence $T^{(1)}(t + t_0, \tau) = T^{(1)}(t, \tau - t_0)$ or, setting $t = 0$ and $t_0 = t$,

$$T^{(1)}(t, \tau) = T^{(1)}(0, \tau - t) = R^{(1)}(t - \tau), \quad (1.7.2.6)$$

where $R^{(1)}$ is a rank-two tensor referred to as the linear polarization response function, which depends only on the time difference $t - \tau$. Substitution in (1.7.2.5) leads to

$$\begin{aligned} \mathbf{P}^{(1)}(t) &= \varepsilon_o \int_{-\infty}^{+\infty} d\tau R^{(1)}(t - \tau) \mathbf{E}(\tau) \\ &= \varepsilon_o \int_{-\infty}^{+\infty} d\tau R^{(1)}(\tau) \mathbf{E}(t - \tau). \end{aligned} \quad (1.7.2.7)$$

$R^{(1)}$ can be viewed as the tensorial analogue of the linear impulse function in electric circuit theory. The causality principle imposes that $R^{(1)}(\tau)$ should vanish for $\tau < 0$ so that $\mathbf{P}^{(1)}(t)$ at time t will

depend only on polarizing field values before t . $R^{(1)}$, $\mathbf{P}^{(1)}$ and \mathbf{E} are real functions of time.

1.7.2.1.1.2. Quadratic response

The most general expression for $\mathbf{P}^{(2)}(t)$ which is quadratic in $\mathbf{E}(t)$ is

$$\mathbf{P}^{(2)}(t) = \varepsilon_o \int_{-\infty}^{+\infty} \int_{-\infty}^{+\infty} d\tau_1 d\tau_2 T^{(2)}(t, \tau_1, \tau_2) \cdot \mathbf{E}(\tau_1) \otimes \mathbf{E}(\tau_2) \quad (1.7.2.8)$$

or in Cartesian notation

$$P_{\mu}^{(2)}(t) = \varepsilon_o \int_{-\infty}^{+\infty} \int_{-\infty}^{+\infty} d\tau_1 d\tau_2 T_{\mu\alpha\beta}^{(2)}(t, \tau_1, \tau_2) E_{\alpha}(\tau_1) E_{\beta}(\tau_2). \quad (1.7.2.9)$$

It can easily be proved by decomposition of $T^{(2)}$ into symmetric and antisymmetric parts and permutation of dummy variables (α, τ_1) and (β, τ_2) , that $T^{(2)}$ can be reduced to its symmetric part, satisfying

$$T_{\mu\alpha\beta}^{(2)}(t, \tau_1, \tau_2) = T_{\mu\alpha\beta}^{(2)}(t, \tau_2, \tau_1). \quad (1.7.2.10)$$

From time invariance

$$T^{(2)}(t, \tau_1, \tau_2) = R^{(2)}(t - \tau_1, t - \tau_2), \quad (1.7.2.11)$$

$$\begin{aligned} \mathbf{P}^{(2)}(t) &= \varepsilon_o \int_{-\infty}^{+\infty} \int_{-\infty}^{+\infty} d\tau_1 d\tau_2 R^{(2)}(t - \tau_1, t - \tau_2) \cdot \mathbf{E}(\tau_1) \otimes \mathbf{E}(\tau_2), \\ \mathbf{P}^{(2)}(t) &= \varepsilon_o \int_{-\infty}^{+\infty} \int_{-\infty}^{+\infty} d\tau_1 d\tau_2 R^{(2)}(\tau_1, \tau_2) \cdot \mathbf{E}(t - \tau_1) \otimes \mathbf{E}(t - \tau_2). \end{aligned} \quad (1.7.2.12)$$

Causality demands that $R^{(2)}(\tau_1, \tau_2)$ cancels for either τ_1 or τ_2 negative while $R^{(2)}$ is real. Intrinsic permutation symmetry implies that $R_{\mu\alpha\beta}^{(2)}(\tau_1, \tau_2)$ is invariant by interchange of (α, τ_1) and (β, τ_2) pairs.

1.7.2.1.1.3. Higher-order response

The n th order polarization can be expressed in terms of the $(n + 1)$ -rank tensor $T^{(n)}(t, \tau_1, \tau_2, \dots, \tau_n)$ as

$$\begin{aligned} \mathbf{P}^{(n)}(t) &= \varepsilon_o \int_{-\infty}^{+\infty} d\tau_1 \int_{-\infty}^{+\infty} d\tau_2 \dots \int_{-\infty}^{+\infty} d\tau_n T^{(n)}(t, \tau_1, \tau_2, \dots, \tau_n) \\ &\quad \cdot \mathbf{E}(\tau_1) \otimes \mathbf{E}(\tau_2) \otimes \dots \otimes \mathbf{E}(\tau_n). \end{aligned} \quad (1.7.2.13)$$

For similar reasons to those previously stated, it is sufficient to consider the symmetric part of $T^{(n)}$ with respect to the $n!$ permutations of the n pairs $(\alpha_1, \tau_1), (\alpha_2, \tau_2) \dots (\alpha_n, \tau_n)$. The $T^{(n)}$ tensor will then exhibit intrinsic permutation symmetry at the n th order. Time-invariance considerations will then allow the introduction of the $(n + 1)$ th-rank real tensor $R^{(n)}$, which generalizes the previously introduced R operators:

$$\begin{aligned} \mathbf{P}_{\mu}^{(n)}(t) &= \varepsilon_o \int_{-\infty}^{+\infty} d\tau_1 \int_{-\infty}^{+\infty} d\tau_2 \dots \int_{-\infty}^{+\infty} d\tau_n R_{\mu\alpha_1\alpha_2\dots\alpha_n}^{(n)}(\tau_1, \tau_2, \dots, \tau_n) \\ &\quad \times E_{\alpha_1}(t - \tau_1) E_{\alpha_2}(t - \tau_2) \dots E_{\alpha_n}(t - \tau_n). \end{aligned} \quad (1.7.2.14)$$

$R^{(n)}$ cancels when one of the τ_i 's is negative and is invariant under any of the $n!$ permutations of the (α_i, τ_i) pairs.

1.7.2.1.2. Linear and nonlinear susceptibilities

Whereas the polarization response has been expressed so far in the time domain, in which causality and time invariance are most naturally expressed, Fourier transformation into the frequency domain permits further simplification of the equations given above and the introduction of the susceptibility tensors according to the following derivation.

1. TENSORIAL ASPECTS OF PHYSICAL PROPERTIES

The direct and inverse Fourier transforms of the field are defined as

$$\mathbf{E}(t) = \int_{-\infty}^{+\infty} d\omega \mathbf{E}(\omega) \exp(-i\omega t) \quad (1.7.2.15)$$

$$\mathbf{E}(\omega) = (1/2\pi) \int_{-\infty}^{+\infty} dt \mathbf{E}(t) \exp(i\omega t), \quad (1.7.2.16)$$

where $\mathbf{E}(\omega)^* = \mathbf{E}(-\omega)$ as $\mathbf{E}(t)$ is real.

1.7.2.1.2.1. Linear susceptibility

By substitution of (1.7.2.15) in (1.7.2.7),

$$\begin{aligned} \mathbf{P}^{(1)}(t) &= \varepsilon_o \int_{-\infty}^{+\infty} d\omega \int_{-\infty}^{+\infty} d\tau R^{(1)}(\tau) \cdot \mathbf{E}(\omega) \exp[-i\omega(t - \tau)] \\ \mathbf{P}^{(1)}(t) &= \varepsilon_o \int_{-\infty}^{+\infty} d\omega \chi^{(1)}(-\omega_\sigma; \omega) \mathbf{E}(\omega) \exp(-i\omega_\sigma t), \end{aligned} \quad (1.7.2.17)$$

where

$$\chi^{(1)}(-\omega_\sigma; \omega) = \int_{-\infty}^{+\infty} d\tau R^{(1)}(\tau) \exp(i\omega\tau).$$

In these equations, $\omega_\sigma = \omega$ to satisfy the energy conservation condition that will be generalized in the following. In order to ensure convergence of $\chi^{(1)}$, ω has to be taken in the upper half plane of the complex plane. The reality of $R^{(1)}$ implies that $\chi^{(1)}(-\omega_\sigma; \omega)^* = \chi^{(1)}(\omega_\sigma^*; -\omega^*)$.

1.7.2.1.2.2. Second-order susceptibility

Substitution of (1.7.2.15) in (1.7.2.12) yields

$$\begin{aligned} \mathbf{P}^{(2)}(t) &= \varepsilon_o \int_{-\infty}^{+\infty} d\omega_1 \int_{-\infty}^{+\infty} d\omega_2 \int_{-\infty}^{+\infty} d\tau_1 \int_{-\infty}^{+\infty} d\tau_2 R^{(2)}(\tau_1, \tau_2) \\ &\quad \cdot \mathbf{E}(\omega_1) \otimes \mathbf{E}(\omega_2) \exp\{-i[\omega_1(t - \tau_1) + \omega_2(t - \tau_2)]\} \end{aligned} \quad (1.7.2.18)$$

or

$$\begin{aligned} \mathbf{P}^{(2)}(t) &= \varepsilon_o \int_{-\infty}^{+\infty} d\omega_1 \int_{-\infty}^{+\infty} d\omega_2 \chi^{(2)}(-\omega_\sigma; \omega_1, \omega_2) \cdot \mathbf{E}(\omega_1) \otimes \mathbf{E}(\omega_2) \\ &\quad \times \exp(-i\omega_\sigma t) \end{aligned} \quad (1.7.2.19)$$

with

$$\begin{aligned} \chi^{(2)}(-\omega_\sigma; \omega_1, \omega_2) &= \int_{-\infty}^{+\infty} d\tau_1 \int_{-\infty}^{+\infty} d\tau_2 R^{(2)}(\tau_1, \tau_2) \\ &\quad \times \exp[i(\omega_1\tau_1 + \omega_2\tau_2)] \end{aligned}$$

and $\omega_\sigma = \omega_1 + \omega_2$. Frequencies ω_1 and ω_2 must be in the upper half of the complex plane to ensure convergence. Reality of $R^{(2)}$ implies $\chi^{(2)}(-\omega_\sigma; \omega_1, \omega_2)^* = \chi^{(2)}(\omega_\sigma^*; -\omega_1^*, -\omega_2^*)$. $\chi_{\mu\alpha\beta}^{(2)}(-\omega_\sigma; \omega_1, \omega_2)$ is invariant under the interchange of the (α, ω_1) and (β, ω_2) pairs.

1.7.2.1.2.3. nth-order susceptibility

Substitution of (1.7.2.15) in (1.7.2.14) provides

$$\begin{aligned} \mathbf{P}^{(n)}(t) &= \varepsilon_o \int_{-\infty}^{+\infty} d\omega_1 \int_{-\infty}^{+\infty} d\omega_2 \dots \int_{-\infty}^{+\infty} d\omega_n \chi^{(n)}(-\omega_\sigma; \omega_1, \omega_2, \dots, \omega_n) \\ &\quad \cdot \mathbf{E}(\omega_1) \otimes \mathbf{E}(\omega_2) \otimes \dots \otimes \mathbf{E}(\omega_n) \exp(-i\omega_\sigma t) \end{aligned} \quad (1.7.2.20)$$

where

$$\begin{aligned} \chi^{(n)}(-\omega_\sigma; \omega_1, \omega_2, \dots, \omega_n) &= \int_{-\infty}^{+\infty} d\tau_1 \int_{-\infty}^{+\infty} d\tau_2 \dots \int_{-\infty}^{+\infty} d\tau_n R^{(n)}(\tau_1, \tau_2, \dots, \tau_n) \exp\left(i \sum_{j=1}^n \omega_j \tau_j\right) \end{aligned} \quad (1.7.2.21)$$

and $\omega_\sigma = \omega_1 + \omega_2 + \dots + \omega_n$.

All frequencies must lie in the upper half complex plane and reality of $\chi^{(n)}$ imposes

$$\chi^{(n)}(-\omega_\sigma; \omega_1, \omega_2, \dots, \omega_n)^* = \chi^{(n)}(\omega_\sigma^*; -\omega_1^*, -\omega_2^*, \dots, -\omega_n^*). \quad (1.7.2.22)$$

Intrinsic permutation symmetry implies that $\chi_{\mu\alpha_1\alpha_2\dots\alpha_n}^{(n)}(-\omega_\sigma; \omega_1, \omega_2, \dots, \omega_n)$ is invariant with respect to the $n!$ permutations of the (α_i, ω_i) pairs.

1.7.2.1.3. Superposition of monochromatic waves

Optical fields are often superpositions of monochromatic waves which, due to spectral discretization, will introduce considerable simplifications in previous expressions such as (1.7.2.20) relating the induced polarization to a continuous spectral distribution of polarizing field amplitudes.

The Fourier transform of the induced polarization is given by

$$\mathbf{P}^{(n)}(\omega) = (1/2\pi) \int_{-\infty}^{+\infty} dt \mathbf{P}^{(n)}(t) \exp(i\omega t). \quad (1.7.2.23)$$

Replacing $\mathbf{P}^{(n)}(t)$ by its expression as from (1.7.2.20) and applying the well known identity

$$(1/2\pi) \int_{-\infty}^{+\infty} dt \exp[i(\omega - \omega_\sigma)t] = \delta(\omega - \omega_\sigma) \quad (1.7.2.24)$$

leads to

$$\begin{aligned} \mathbf{P}^{(n)}(\omega) &= \varepsilon_o \int_{-\infty}^{+\infty} d\omega_1 \int_{-\infty}^{+\infty} d\omega_2 \dots \int_{-\infty}^{+\infty} d\omega_n \chi^{(n)}(-\omega_\sigma; \omega_1, \omega_2, \dots, \omega_n) \\ &\quad \times \mathbf{E}(\omega_1) \mathbf{E}(\omega_2) \dots \mathbf{E}(\omega_n) \delta(\omega - \omega_\sigma). \end{aligned} \quad (1.7.2.25)$$

In practical cases where the applied field is a superposition of monochromatic waves

$$\mathbf{E}(t) = (1/2) \sum_{\omega'} [E_{\omega'} \exp(-i\omega' t) + E_{-\omega'} \exp(i\omega' t)] \quad (1.7.2.26)$$

with $E_{-\omega'} = E_{\omega'}^*$. By Fourier transformation of (1.7.2.26)

$$\mathbf{E}(\omega) = (1/2) \sum_{\omega'} [E_{\omega'} \delta(\omega - \omega') + E_{-\omega'} \delta(\omega + \omega')]. \quad (1.7.2.27)$$

The optical intensity for a wave at frequency ω' is related to the squared field amplitude by

$$I_{\omega'} = \varepsilon_o c n(\omega') \langle \mathbf{E}^2(t) \rangle_t = \frac{1}{2} \varepsilon_o c n(\omega') |E_{\omega'}|^2. \quad (1.7.2.28)$$

The averaging as represented above by brackets is performed over a time cycle and $n(\omega')$ is the index of refraction at frequency ω' .

1.7.2.1.4. Conventions for nonlinear susceptibilities

1.7.2.1.4.1. Classical convention

Insertion of (1.7.2.26) in (1.7.2.25) together with permutation symmetry provides

$$\begin{aligned} P_{\mu}^{(n)}(\omega_\sigma) &= \varepsilon_o \sum_{\alpha_1\alpha_2\dots\alpha_n} \sum_{\omega} K(-\omega_\sigma; \omega_1, \omega_2, \dots, \omega_n) \\ &\quad \times \chi_{\mu\alpha_1\alpha_2\dots\alpha_n}^{(n)}(-\omega_\sigma; \omega_1, \omega_2, \dots, \omega_n) \\ &\quad \times E_{\alpha_1}(\omega_1) E_{\alpha_2}(\omega_2) \dots E_{\alpha_n}(\omega_n), \end{aligned} \quad (1.7.2.29)$$

1.7. NONLINEAR OPTICAL PROPERTIES

Table 1.7.2.1. *The most common nonlinear effects and the corresponding susceptibility tensors in the frequency domain*

| Process | Order n | $-\omega_\sigma; \omega_1, \omega_2, \dots, \omega_n$ | K |
|---|-----------|---|-----------|
| Linear absorption | 1 | $-\omega; \omega$ | 1 |
| Optical rectification | 2 | $0; -\omega, \omega$ | 1/2 |
| Linear electro-optic effect | 2 | $-\omega; \omega, 0$ | 2 |
| Second harmonic generation | 2 | $-2\omega; \omega, \omega$ | 1/2 |
| Three-wave mixing | 2 | $-\omega_3; \omega_1, \omega_2$ | 1 |
| D.c. Kerr effect | 3 | $-\omega; \omega, 0, 0$ | 3 |
| D.c. induced second harmonic generation | 3 | $-2\omega; \omega, \omega, 0$ | 3/2 |
| Third harmonic generation | 3 | $-3\omega; \omega, \omega, \omega$ | 1/4 |
| Four-wave mixing | 3 | $-\omega_4; \omega_1, \omega_2, \omega_3$ | 3/2 |
| Coherent anti-Stokes Raman scattering | 3 | $-\omega_{as}; \omega_p, -\omega_p, -\omega_s$ | 3/4 |
| Intensity-dependent refractive index | 3 | $-\omega; \omega, -\omega, \omega$ | 3/4 |
| n th harmonic generation | n | $-n\omega; \omega, \omega, \dots, \omega$ | 2^{1-n} |

where the summation over ω stands for all distinguishable permutation of $\omega_1, \omega_2, \dots, \omega_n$, K being a numerical factor given by

$$K(-\omega_\sigma; \omega_1, \omega_2, \dots, \omega_n) = 2^{s+m-n} p, \quad (1.7.2.30)$$

where p is the number of distinct permutations of $\omega_1, \omega_2, \dots, \omega_n$, n is the order of the nonlinear process, m is the number of d.c. fields (e.g. corresponding to $\omega_i = 0$) within the n frequencies and $s = 0$ when $\omega_\sigma = 0$, otherwise $s = 1$. For example, in the absence of a d.c. field and when the ω_i 's are different, $K = 2^{s-n} n!$.

The K factor allows the avoidance of discontinuous jumps in magnitude of the $\chi_{\mu\alpha_1\alpha_2\dots\alpha_n}^{(n)}$ elements when some frequencies are equal or tend to zero, which is not the case for the other conventions (Shen, 1984).

The induced nonlinear polarization is often expressed in terms of a tensor $d^{(n)}$ by replacing $\chi^{(n)}$ in (1.7.2.29) by

$$\chi^{(n)} = 2^{-s-m+n} d^{(n)}. \quad (1.7.2.31)$$

Table 1.7.2.1 summarizes the most common classical nonlinear phenomena, following the notations defined above. Then, according to Table 1.7.2.1, the n th harmonic generation induced nonlinear polarization is written

$$P_\mu^{(2)}(n\omega) = \varepsilon_o \sum_{\alpha_1\alpha_2\dots\alpha_n} 2^{n-1} \chi_{\mu\alpha_1\alpha_2\dots\alpha_n}^{(n)}(-n\omega; \omega, \omega, \dots, \omega) \times E_{\alpha_1}(\omega) E_{\alpha_2}(\omega) \dots E_{\alpha_n}(\omega). \quad (1.7.2.32)$$

The E_{α_i} are the components of the total electric field $\mathbf{E}(\omega)$.

1.7.2.1.4.2. Convention used in this chapter

The K convention described above is often used, but may lead to errors in cases where two of the interacting waves have the same frequency but different polarization states. Indeed, as demonstrated in Chapter 1.6 and recalled in Section 1.7.3, a direction of propagation in an anisotropic crystal allows in the general case two different directions of polarization of the electric field vector, written \mathbf{E}^+ and \mathbf{E}^- . Then any nonlinear coupling in this medium occurs necessarily between these eigen modes at the frequencies concerned.

Because of the possible non-degeneracy with respect to the direction of polarization of the electric fields at the same frequency, it is suitable to consider a harmonic generation process, second harmonic generation (SHG) or third harmonic generation (THG) for example, like any other non-degenerated interaction. We do so for the rest of this chapter. Then all terms derived from the permutation of the fields with the same frequency are taken into account in the expression of the induced nonlinear polarization and the K factor in equation (1.7.2.29) disappears: hence, in the general case, the induced nonlinear polarization is written

$$P_\mu^{(n)}(\omega_\sigma) = \varepsilon_o \sum_{\alpha_1, \dots, \alpha_n} \chi_{\mu\alpha_1\dots\alpha_n}^{(n)}(-\omega_\sigma; \omega_1, \dots, \omega_n) \times E_{\alpha_1}^\pm(\omega_1) \dots E_{\alpha_n}^\pm(\omega_n), \quad (1.7.2.33)$$

where $+$ and $-$ refer to the eigen polarization modes.

According to (1.7.2.33), the n th harmonic generation induced polarization is expressed as

$$P_\mu^{(n)}(n\omega) = \varepsilon_o \sum_{\alpha_1, \dots, \alpha_n} \chi_{\mu\alpha_1\dots\alpha_n}^{(n)}(-n\omega; \omega, \dots, \omega) \times E_{\alpha_1}^\pm(\omega_1) \dots E_{\alpha_n}^\pm(\omega_n). \quad (1.7.2.34)$$

For example, in the particular case of SHG where the two waves at ω have different directions of polarization $\mathbf{E}^+(\omega)$ and $\mathbf{E}^-(\omega)$ and where the only nonzero $\chi_{yij}^{(2)}$ coefficients are χ_{yxz} and χ_{yzx} , (1.7.2.34) gives

$$P_y^{(2)}(2\omega) = \varepsilon_o [\chi_{yxz}(-2\omega; \omega, \omega) E_x^+(\omega) E_z^-(\omega) + \chi_{yzx}(-2\omega; \omega, \omega) E_z^+(\omega) E_x^-(\omega)]. \quad (1.7.2.35)$$

The two field component products are equal only if the two eigen modes are the same, i.e. $+$ or $-$.

According to (1.7.2.33) and (1.7.2.34), we note that $\chi_{\mu\alpha_1\dots\alpha_n}^{(n)}(-\omega_\sigma; \omega_1, \dots, \omega_n)$ changes smoothly to $\chi_{\mu\alpha_1\dots\alpha_n}^{(n)}(-n\omega; \omega, \dots, \omega)$ when all the $\omega_1, \dots, \omega_n$ approach continuously the same value ω .

1.7.2.2. Symmetry properties

1.7.2.2.1. Intrinsic permutation symmetry

1.7.2.2.1.1. ABDP and Kleinman symmetries

Intrinsic permutation symmetry, as already discussed, imposes the condition that the n th order susceptibility $\chi_{\mu\alpha_1\alpha_2\dots\alpha_n}^{(n)}(-\omega_\sigma; \omega_1, \omega_2, \dots, \omega_n)$ be invariant under the $n!$ permutations of the (α_i, ω_i) pairs as a result of time invariance and causality. Furthermore, the overall permutation symmetry, i.e. the invariance over the $(n+1)!$ permutations of the (α_i, ω_i) and $(\mu, -\omega_\sigma)$ pairs, may be valid when all the optical frequencies occurring in the susceptibility and combinations of these appearing in the denominators of quantum expressions are far removed from the transitions, making the medium transparent at these frequencies. This property is termed *ABDP symmetry*, from the initials of the authors of the pioneering article by Armstrong *et al.* (1962).

Let us consider as an application the quantum expression of the quadratic susceptibility (with damping factors neglected), the derivation of which being beyond the scope of this chapter, but which can be found in nonlinear optics treatises dealing with microscopic interactions, such as in Boyd (1992):

$$\chi_{\mu\alpha\beta}^{(2)}(-\omega_\sigma; \omega_1, \omega_2) = \frac{Ne^3}{\varepsilon_o^2 \hbar^2} S_T \sum_{abc} \rho_o(a) \frac{r_{ab}^\mu r_{bc}^\alpha r_{ca}^\beta}{(\Omega_{ba} - \omega_1 - \omega_2)(\Omega_{ca} - \omega_1)}, \quad (1.7.2.36)$$

where N is the number of microscopic units (e.g. molecules in the case of organic crystals) per unit volume, a, b and c are the eigen states of the system, Ω_{ba} and Ω_{ca} are transition energies, r_{ab}^μ is the μ component of the transition dipole connecting states a and b , and $\rho_o(a)$ is the population of level a as given by the corresponding diagonal term of the density operator. S_T is the summation operator over the six permutations of the $(\mu, -\omega_\sigma)$, (α, ω_1) , (β, ω_2) . Provided all frequencies at the denominator are much smaller than the transition frequencies Ω_{ba} and Ω_{ca} , the optical frequencies $-\omega_\sigma, \omega_1, \omega_2$ can be permuted without significant variation of the susceptibility. It follows correspondingly that the susceptibility is invariant with respect to the

1. TENSORIAL ASPECTS OF PHYSICAL PROPERTIES

permutation of Cartesian indices appearing only in the numerator of (1.7.2.36), regardless of frequency. This property, which can be generalized to higher-order susceptibilities, is known as *Kleinman symmetry*. Its validity can help reduce the number of non-vanishing terms in the susceptibility, as will be shown later.

1.7.2.2.1.2. Manley–Rowe relations

An important consequence of overall permutation symmetry is the *Manley–Rowe* power relations, which account for energy exchange between electromagnetic waves in a purely reactive (e.g. non-dissipative) medium. Calling W_i the power input at frequency ω_i into a unit volume of a dielectric polarizable medium,

$$W_i = \left\langle \mathbf{E}(t) \cdot \frac{d\mathbf{P}}{dt}(t) \right\rangle, \quad (1.7.2.37)$$

where the averaging is performed over a cycle and

$$\begin{aligned} \mathbf{E}(t) &= \text{Re}[E_{\omega_i} \exp(-j\omega_i t)] \\ \mathbf{P}(t) &= \text{Re}[P_{\omega_i} \exp(-j\omega_i t)]. \end{aligned} \quad (1.7.2.38)$$

The following expressions can be derived straightforwardly:

$$W_i = \frac{1}{2} \omega_i \text{Re}(iE_{\omega_i} \cdot P_{\omega_i}) = \frac{1}{2} \omega_i \text{Im}(E_{\omega_i}^* \cdot P_{\omega_i}). \quad (1.7.2.39)$$

Introducing the quadratic induced polarization $P^{(2)}$, Manley–Rowe relations for sum-frequency generation state

$$\frac{W_1}{\omega_1} = \frac{W_2}{\omega_2} = -\frac{W_3}{\omega_3}. \quad (1.7.2.40)$$

Since $\omega_1 + \omega_2 = \omega_3$, (1.7.2.40) leads to an energy conservation condition, namely $W_3 + W_1 + W_2 = 0$, which expresses that the power generated at ω_3 is equal to the sum of the powers lost at ω_1 and ω_2 .

A quantum mechanical interpretation of these expressions in terms of photon fusion or splitting can be given, remembering that $W_i/\hbar\omega_i$ is precisely the number of photons generated or annihilated per unit volume in unit time in the course of the nonlinear interactions.

1.7.2.2.1.3. Contracted notation for susceptibility tensors

The tensors $\chi_{\mu\alpha\beta}^{(2)}(-2\omega; \omega, \omega)$ or $d_{\mu\alpha\beta}^{(2)}(-2\omega; \omega, \omega)$ are invariant with respect to (α, β) permutation as a consequence of the intrinsic permutation symmetry. Independently, it is not possible to distinguish the coefficients $\chi_{ijk}^{(2)}(-2\omega; \omega, \omega)$ and $\chi_{ikj}^{(2)}(-2\omega; \omega, \omega)$ by SHG experiments, even if the two fundamental waves have different directions of polarization.

Therefore, these third-rank tensors can be represented in contracted form as 3×6 matrices $\chi_{\mu m}(-2\omega; \omega, \omega)$ and $d_{\mu m}(-2\omega; \omega, \omega)$, where the suffix m runs over the six possible (α, β) Cartesian index pairs according to the classical convention of contraction:

$$\begin{aligned} \text{for } \mu: x \rightarrow 1 \quad y \rightarrow 2 \quad z \rightarrow 3 \\ \text{for } m: xx \rightarrow 1 \quad yy \rightarrow 2 \quad zz \rightarrow 3 \quad yz = zy \rightarrow 4 \\ \quad \quad \quad xz = zx \rightarrow 5 \quad xy = yx \rightarrow 6. \end{aligned}$$

The 27 elements of $\chi_{\mu\alpha\beta}^{(2)}(-2\omega; \omega, \omega)$ are then reduced to 18 in the $\chi_{\mu m}$ contracted tensor notation (see Section 1.1.4.10).

For example, (1.7.2.35) can be written

$$\begin{aligned} P_y^{(2)}(2\omega) &= \varepsilon_o \chi_{25}(-2\omega; \omega, \omega) [e_x^+(\omega) \mathbf{E}^+(\omega) e_z^-(\omega) \mathbf{E}^-(\omega) \\ &\quad + e_z^+(\omega) \mathbf{E}^+(\omega) e_x^-(\omega) \mathbf{E}^-(\omega)]. \end{aligned} \quad (1.7.2.41)$$

The same considerations can be applied to THG. Then the 81 elements of $\chi_{\mu\alpha\beta\gamma}^{(3)}(-3\omega; \omega, \omega, \omega)$ can be reduced to 30 in the $\chi_{\mu m}$

contracted tensor notation with the following contraction convention:

$$\begin{aligned} \text{for } \mu: x \rightarrow 1 \quad y \rightarrow 2 \quad z \rightarrow 3 \\ \text{for } m: xxx \rightarrow 1 \quad yyy \rightarrow 2 \quad zzz \rightarrow 3 \quad yzz \rightarrow 4 \quad yyz \rightarrow 5 \\ \quad \quad \quad xzz \rightarrow 6 \quad xxz \rightarrow 7 \quad xyy \rightarrow 8 \quad xxy \rightarrow 9 \quad xyz \rightarrow 0. \end{aligned}$$

If Kleinman symmetry holds, the contracted tensor can be further extended beyond SHG and THG to any other processes where all the frequencies are different.

1.7.2.2.2. Implications of spatial symmetry on the susceptibility tensors

Centrosymmetry is the most detrimental crystalline symmetry constraint that will fully cancel all odd-rank tensors such as the $d^{(2)}$ [or $\chi^{(2)}$] susceptibilities. Intermediate situations, corresponding to noncentrosymmetric crystalline point groups, will reduce the number of nonzero coefficients without fully depleting the tensors.

Tables 1.7.2.2 to 1.7.2.5 detail, for each crystal point group, the remaining nonzero $\chi^{(2)}$ and $\chi^{(3)}$ coefficients and the eventual connections between them. $\chi^{(2)}$ and $\chi^{(3)}$ are expressed in the principal axes x, y and z of the second-rank $\chi^{(1)}$ tensor. (x, y, z) is usually called the optical frame; it is linked to the crystal-

Table 1.7.2.2. Nonzero $\chi^{(2)}$ coefficients and equalities between them in the general case

| Symmetry class | $\chi^{(2)}$ nonzero elements |
|--|--|
| Triclinic C_1 (1) | All 27 elements are independent and nonzero |
| Monoclinic C_2 (2) (twofold axis parallel to z) C_s (m) (mirror perpendicular to z) | $xyz, xzy, xxz, xzx, yyz, yzy, yxz, yzx, zxx, zyy, zzz, zxy, zyx$ $xxx, xyy, xzz, xxy, xyx, yxx, yyy, yzz, yxy, yyx, yyz, zzy, zxz, zzx$ |
| Orthorhombic C_{2v} ($mm2$) (twofold axis parallel to z) D_2 (222) | $xzx, xxz, yyz, yzy, zxx, zyy, zzz$ $xyz, xzy, yzx, yxz, zxy, zyx$ |
| Tetragonal C_4 (4) S_4 ($\bar{4}$) D_4 (422) C_{4v} ($4mm$) D_{2d} ($42m$) | $xyz = -yxz, xzy = -yzx, xzx = yzy, xxz = yyz, zxx = zyy, zzz, zxy = -zyx$ $xyz = yxz, xzy = yzx, xzx = -yzy, xxz = -yyz, zxx = -zyy, zxy = zyx$ $xyz = -yxz, xzy = -yzx, zxy = -zyx$ $xzx = yzy, xxz = yyz, zxx = zyy, zzz$ $xyz = yxz, xzy = yzx, zxy = zyx$ |
| Hexagonal C_6 (6) C_{3h} ($\bar{6}$) D_6 (622) C_{6v} ($6mm$) D_{3h} ($62m$) (mirror perpendicular to x) | $xyz = -yxz, xzy = -yzx, xzx = yzy, xxz = yyz, zxx = zyy, zzz, zxy = -zyx$ $xxx = -xyy = -yyx = -yxy, yyy = -yxx = -xxy = -xyx, zxx = zyy, zzz, zxy = -zyx$ $xyz = -yxz, xzy = -yzx, zxy = -zyx$ $xzx = yzy, xxz = yyz, zxx = zyy, zzz$ $yyy = -yxx = -xxy = -xyx$ |
| Trigonal C_3 (3) D_3 (32) C_{3v} ($3m$) (mirror perpendicular to x) | $xxx = -xyy = -yyx = -yxy, xyz = -yxz, xzy = -yzx, xzx = yzy, xxz = yyz, yyy = -yxx = -xxy = -xyx, zxx = zyy, zzz, zxy = -zyx$ $xxx = -xyy = -yyx = -yxy, xyz = -yxz, xzy = -yzx, zxy = -zyx$ $yyy = -yxx = -xxy = -xyx, xzx = yzy, xxz = yyz, zxx = zyy, zzz$ |
| Cubic T (23), T_d ($\bar{4}3m$) O (432) | $xyz = xzy = yzx = yxz = zxy = zyx$ $xyz = -xzy = yzx = -yxz = zxy = -zyx$ |

1.7. NONLINEAR OPTICAL PROPERTIES

lographical frame by the standard conventions given in Chapter 1.6.

1.7.3. Propagation phenomena

1.7.3.1. Crystalline linear optical properties

We summarize here the main linear optical properties that govern the nonlinear propagation phenomena. The reader may refer to Chapter 1.6 for the basic equations.

1.7.3.1.1. Index surface and electric field vectors

The relations between the different field vectors relative to a propagating electromagnetic wave are obtained from the constitutive relations of the medium and from Maxwell equations.

In the case of a non-magnetic and non-conducting medium, Maxwell equations lead to the following wave propagation equation for the Fourier component at the circular frequency ω defined by (1.7.2.15) and (1.7.2.16) (Butcher & Cotter, 1990):

$$\nabla \mathbf{x} \nabla \mathbf{x} \mathbf{E}(\omega) = (\omega^2/c^2) \mathbf{E}(\omega) + \omega^2 \mu_0 \mathbf{P}(\omega), \quad (1.7.3.1)$$

where $\omega = 2\pi c/\lambda$, λ is the wavelength and c is the velocity of light in a vacuum; μ_0 is the free-space permeability, $\mathbf{E}(\omega)$ is the electric field vector and $\mathbf{P}(\omega)$ is the polarization vector.

Table 1.7.2.3. Nonzero $\chi^{(2)}$ coefficients and equalities between them under the Kleinman symmetry assumption

| Symmetry class | Independent nonzero $\chi^{(2)}$ elements under Kleinman symmetry |
|---|---|
| Triclinic C_1 (1) | $xxx, xxy = yxy = yyx, xzz = zxz = zzx,$ $xyz = xzy = yxz = yzx = zxy = zyx,$ $xxz = xzx = zxx, xxy = xyx = yxx, yyy,$ $yyz = yzy = zzy, yyz = yzy = zyy, zzz$ |
| Monoclinic C_2 (2) (twofold axis parallel to z) C_s (m) (mirror perpendicular to z) | $xyz = xzy = yxz = yzx = zxy = zyx,$ $xxz = xzx = zxx, yyz = yzy = zyy, zzz$ $xxx, xxy = yxy = yyx, xzz = zxx = zzx,$ $xyx = yxx = yxx, yyy, yzz = zyz = zzy$ |
| Orthorhombic C_{2v} ($mm2$) (twofold axis parallel to z) D_2 (222) | $xzx = xxz = zxx, yyz = yzy = zyy, zzz$ $xyz = xzy = yxz = yzx = zxy = zyx$ |
| Tetragonal C_4 (4) S_4 (4) | $xzx = xxz = zxx = yzy = yyz = zyy, zzz$ $xyz = xzy = yxz = yzx = zxy = zyx, xzx = xxz$ $= zxx = -yzy = -yyz = -zyy$ |
| D_4 (422) C_{4v} ($4mm$) D_{2d} ($42m$) | All elements are nil $xzx = xxz = zxx = yyz = yzy = zyy, zzz$ $xyz = xzy = yxz = yzx = zxy = zyx$ |
| Hexagonal C_6 (6) C_{3h} (6) | $xzx = xxz = zxx = yyz = yzy = zyy, zzz$ $xxx = -xyy = -yxy = -yyx, yyy = -yxx = -xyx = -xxy$ |
| D_6 (622) C_{6v} ($6mm$) D_{3h} ($62m$) (mirror perpendicular to x) | All elements are nil $xzx = xxz = zxx = yyz = yzy = zyy, zzz$ $yyy = -yxx = -xxy = -xyx$ |
| Trigonal C_3 (3) | $xxx = -xyy = -yyx = -yxy, xzx = xxz = zxx$ $= yyz = yzy = zyy, yyy = -yxx = -xxy = -xyx, zzz$ |
| D_3 (32) C_{3v} ($3m$) (mirror perpendicular to x) | $xxx = -xyy = -yyx = -yxy$ $yyy = -yxx = -xxy = -xyx, xzx = xxz = zxx$ $= yyz = yzy = zyy, zzz$ |
| Cubic T (23), T_d ($\bar{4}3m$) O (432) | $xyz = xzy = yxz = yzx = zxy = zyx$ All elements are nil |

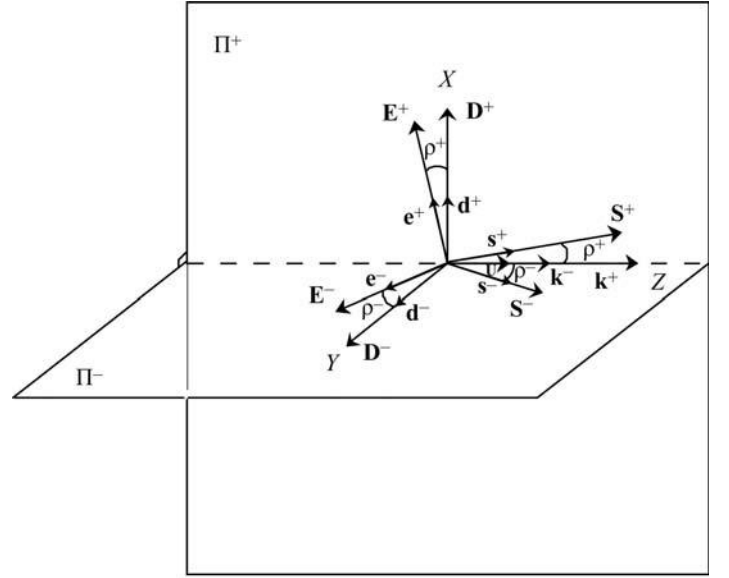


Fig. 1.7.3.1. Field vectors of a plane wave propagating in an anisotropic medium. (X, Y, Z) is the wave frame. Z is along the direction of propagation, X and Y are contained in Π^+ and Π^- respectively, by an arbitrary convention.

In the linear regime, $\mathbf{P}(\omega) = \varepsilon_0 \chi^{(1)}(\omega) \mathbf{E}(\omega)$, where ε_0 is the free-space permittivity and $\chi^{(1)}(\omega)$ is the first-order electric susceptibility tensor. Then (1.7.3.1) becomes

$$\nabla \mathbf{x} \nabla \mathbf{x} \mathbf{E}(\omega) = (\omega^2/c^2) \varepsilon(\omega) \mathbf{E}(\omega). \quad (1.7.3.2)$$

$\varepsilon(\omega) = 1 + \chi^{(1)}(\omega)$ is the dielectric tensor. In the general case, $\chi^{(1)}(\omega)$ is a complex quantity i.e. $\chi^{(1)} = \chi^{(1)'} + i\chi^{(1)''}$. For the following, we consider a medium for which the losses are small ($\chi^{(1)'} \gg \chi^{(1)''}$); it is one of the necessary characteristics of an efficient nonlinear medium. In this case, the dielectric tensor is real: $\varepsilon = 1 + \chi^{(1)'}$.

The plane wave is a solution of equation (1.7.3.2):

$$\mathbf{E}(\omega, X, Y, Z) = \mathbf{e}(\omega) \mathbf{E}(\omega, X, Y, Z) \exp[\pm ik(\omega)Z]. \quad (1.7.3.3)$$

(X, Y, Z) is the orthonormal frame linked to the wave, where Z is along the direction of propagation.

We consider a linearly polarized wave so that the unit vector \mathbf{e} of the electric field is real ($\mathbf{e} = \mathbf{e}^*$), contained in the XZ or YZ planes.

$\mathbf{E}(\omega, X, Y, Z) = A(\omega, X, Y, Z) \exp[i\Phi(\omega, Z)]$ is the scalar complex amplitude of the electric field where $\Phi(\omega, Z)$ is the phase, and $\mathbf{E}^*(-\omega, X, Y, Z) = \mathbf{E}(\omega, X, Y, Z)$. In the linear regime, the amplitude of the electric field varies with Z only if there is absorption.

k is the modulus of the wavevector, real in a lossless medium: $+kZ$ corresponds to forward propagation along Z , and $-kZ$ to backward propagation. We consider that the plane wave propagates in an anisotropic medium, so there are two possible wavevectors, \mathbf{k}^+ and \mathbf{k}^- , for a given direction of propagation of unit vector \mathbf{u} :

$$\mathbf{k}^\pm(\omega, \theta, \varphi) = (\omega/c) n^\pm(\omega, \theta, \varphi) \mathbf{u}(\theta, \varphi). \quad (1.7.3.4)$$

(θ, φ) are the spherical coordinates of the direction of the unit wavevector \mathbf{u} in the optical frame; (x, y, z) is the optical frame defined in Section 1.7.2.

The spherical coordinates are related to the Cartesian coordinates (u_x, u_y, u_z) by

$$u_x = \cos \varphi \sin \theta \quad u_y = \sin \varphi \sin \theta \quad u_z = \cos \theta. \quad (1.7.3.5)$$

1.7. NONLINEAR OPTICAL PROPERTIES

frame. We obtain, for each wave, three equations which relate the three components (e_x, e_y, e_z) to the unit wavevector components (u_x, u_y, u_z) (Shuvalov, 1981):

$$(n^\pm)^2(e_p^\pm - u_p[u_x e_x^\pm + u_y e_y^\pm + u_z e_z^\pm]) = (n_p)^2 e_p^\pm \quad (p = x, y \text{ and } z) \quad (1.7.3.9)$$

with $(e_x^\pm)^2 + (e_y^\pm)^2 + (e_z^\pm)^2 = 1$.

The vibration planes Π^\pm relative to the eigen polarization modes \mathbf{e}^\pm are called the neutral vibration planes associated with \mathbf{u} : an incident linearly polarized wave with a vibration plane parallel to Π^+ or Π^- is refracted inside the crystal without depolarization, that is to say in a linearly polarized wave, \mathbf{e}^+ or \mathbf{e}^- , respectively. For any other incident polarization the wave is refracted in the two waves \mathbf{e}^+ and \mathbf{e}^- , which propagate with the difference of phase $(\omega/c)(n^+ - n^-)Z$.

The existence of equalities between the principal refractive indices determines the three optical classes: isotropic for the cubic system; uniaxial for the tetragonal, hexagonal and trigonal systems; and generally biaxial for the orthorhombic, monoclinic and triclinic systems [Nye (1957) and Sections 1.1.4.1 and 1.6.3.2].

1.7.3.1.2. Isotropic class

The isotropic class corresponds to the equality of the three principal indices: the index surface is a one-sheeted sphere, so $n^+ = n^-$, $\rho^+ = \rho^- = 0$ for all directions of propagation, and any electric field vector direction is allowed as in an amorphous material.

1.7.3.1.3. *Uniaxial class*

The uniaxial class is characterized by the equality of two principal indices, called ordinary indices ($n_x = n_y = n_o$); the

other index is called the extraordinary index ($n_z = n_e$). Then, according to (1.7.3.6), the index surface has one umbilicus along the z axis, $n^+(\theta = 0) = n^-(\theta = 0)$, called the optic axis, which is along the fold rotation axis of greatest order of the crystal. The two other principal axes are related to the symmetry elements of the orientation class according to the standard conventions (Nye, 1957). The ordinary sheet is spherical *i.e.* $n_o(\theta, \varphi) = n_o$, so an ordinary wave has no walk-off for any direction of propagation in a uniaxial crystal; the extraordinary sheet is ellipsoidal *i.e.* $n_e(\theta, \varphi) = [(\cos^2 \theta)/(n_o^2) + (\sin^2 \theta)/(n_e^2)]^{-1/2}$. The sign of the uniaxial class is defined by the sign of the birefringence $n_e - n_o$. Thus, according to these definitions, (n_e, n_o) corresponds to (n^+, n^-) for the positive class ($n_e > n_o$) and to (n^-, n^+) for the negative class ($n_e < n_o$), as shown in Fig. 1.7.3.2.

The ordinary electric field vector is orthogonal to the optic axis ($e_z^o = 0$), and also to the extraordinary electric field vector, leading to

$$\mathbf{e}^o(\omega_i, \theta, \varphi) \cdot \mathbf{e}^e(\omega_i, \theta, \varphi) = 0. \quad (1.7.3.10)$$

This relation is satisfied when ω_i and ω_j are equal or different and for any direction of propagation (θ, φ) .

According to these results, the coplanarity of the field vectors imposes the condition that the double-refraction angle of the extraordinary wave is in a plane containing the optic axis. Thus, the components of the ordinary and extraordinary unit electric field vectors \mathbf{e}^o and \mathbf{e}^e at the circular frequency ω are

$$e_x^o = -\sin \varphi \quad e_v^o = +\cos \varphi \quad e_z^o = 0 \quad (1.7.3.11)$$

$$e_x^e = -\cos[\theta \pm \rho^\mp(\theta, \omega)] \cdot \cos \varphi$$

$$e_v^e = -\cos[\theta \pm \rho^\mp(\theta, \omega)] \cdot \sin \varphi$$

$$e^e_\tau = \sin[\theta \pm \rho^\mp(\theta, \omega)] \quad (1.7.3.12)$$

Table 1.7.2.5. *Nonzero $\chi^{(3)}$ coefficients and equalities between them under the Kleinman symmetry assumption*

| Symmetry class | Independent nonzero elements of $\chi^{(3)}$ under Kleinman symmetry |
|---|---|
| Triclinic C_1 (1), C_i ($\bar{1}$) | $xxxx, xyyy = yxyy = yyxy = yyyx, xzzz = xzxz = zxxz = zzzx, xyzz = xzyz = xzzy = yxzz = yzxx = yzzx = zxyz = zxzy$ $= zyxx = zyzx = zxyy = zzyx, xyyz = xzyy = xzyx = yxyz = yxzy = yyxz = yyzx = yzxy = yzyx = zxyy = zyxy = zyyx,$ $xxzz = xzxz = xzzx = zxxz = zxzx = zxxz, xxxz = xxzx = xzxx = zxxx, xxyy = xyxy = xyyx = yxxy = yxyx = yyyx,$ $xxxy = xxyx = xyxx = yxxx, xxyz = xxzy = xyxz = xyzx = xzxy = xzyx = yxxz = yxzx = yzxx = zxxxy = zxyx = zyxx,$ $yyyy, yzzz = zyzz = zzyz = zzzz, yyzz = yzyz = yzzy = zyyz = zyzy = zzyy, yyyz = yyzy = yzzy = zyyy, zzzz$ |
| Monoclinic C_s (m), C_2 (2), C_{2h} ($\frac{2}{m}$) (twofold axis parallel to z) | $xxxx, xyyy = yxyy = yyxy = yyyx, xyzz = xzyz = xzzy = yxzz = yzxx = yzzx = zxyz = zxzy = zyxx = zzyx = zzzx = zzyx,$ $xxzz = xzxz = xzzx = zxxz = zxzx = zxxz, xxyy = xyxy = xyyx = yxxy = yxyx = yyxx, xxxy = xxyx = xyxx = yxxx,$ $yyyy, yyzz = yzyz = yzzy = zyyz = zyzy = zzyy, zzzz$ |
| Orthorhombic C_{2v} ($mm2$), D_2 (222), D_{2h} (mmm) (twofold axis parallel to z) | $xxxx, xxzz = xzxz = xzzx = zxxz = zxzx = zxxz, xxyy = xyxy = xyyx = yxxy = yxyx = yyxx, yyyy, yyzz = yzyz = yzzy =$ $zyyz = zyzy = zzyy, zzzz$ |
| Tetragonal S_4 ($\bar{4}$), C_4 (4), C_{4h} ($\frac{4}{m}$) | $xxxx = yyyy, xyyy = yxyy = yyxy = yyyx = -xxxy = -xxyx = -xyxx = -yxxx, xxzz = xzxz = xzzx = yyzz = yzyz = yzzz$ $= zyyz = zyzy = zzyy = zxxz = zxzx = zxxz, xxyy = xyxy = xyyx = yxxy = yxyx = yyxx, zzzz$ |
| C_{4v} ($4mm$), D_{2d} ($\bar{4}2m$), D_4 (422), D_{4h} ($\frac{4}{m}mm$) | $xxxx = yyyy, xxzz = xzxz = xzzx = yyzz = yzyz = yzzy = zyyz = zyzy = zzyy = zxxz = zxzx = zxxz, xxyy = xyxy = xyyx$ $= yxxy = yxyx = yyxx, zzzz$ |
| Hexagonal C_{3h} ($\bar{6}$), C_6 (6), C_{6h} ($\frac{6}{m}$), C_{6v} ($6mm$), D_{3h} ($\bar{6}2m$), D_6 (622), D_{6h} ($\frac{6}{m}mm$) | $xxxx = yyyy = xxyy + xyxy + yxyx, xxzz = xzxz = xzzx = yyzz = yzyz = yzzy = zyyz = zyzy = zzyy = zxxz = zxzx =$ $zxxz, xxyy = xyxy = xyyx = yxxy = yxyx = yyxx, zzzz$ |
| Trigonal C_3 (3), C_{3i} ($\bar{3}$) | $xxxx = yyyy = xxyy + xyxy + yxyx, xyyz = xyzy = xzyy = -xxxz = -xxzx = -xzxx = yxyz = yxzy = yyxz = yyzx = yzxy$ $= yzyx = -zxxx = zxyy = zyxy = zyxx, xxzz = xzxz = xzzx = yyzz = yzyz = yzzy = zyyz = zyzy = zzyy = zxxz = zxzx =$ $zxxz, xxyy = xyxy = xyyx = yxxy = yxyx = yyxx, xxyz = xzyx = xxyx = yxxx, xxyz = xzyx = xzxz = xzyx = -yyyz = -yyzy =$ $-yzyy = yxxz = yxzx = yzxx = -zyyy = zxxxy = zxyx = zyxx, zzzz$ |
| C_{3v} ($3m$), D_3 (32), D_{3d} ($\bar{3}m$) (mirror perpendicular to x) (twofold axis parallel to x) | $xxxx = yyyy = xxyy + xyxy + yxyx, xxzz = xzxz = xzzx = yyzz = yzyz = yzzy = zyyz = zyzy = zzyy = zxxz = zxzx =$ $zxxz, xxyy = xyxy = xyyx = yxxy = yxyx = yyxx, xxyz = xxzy = yxzx = xyzx = xzxy = xzyx = -yyyz = -yyzy = -yzyy$ $= yxxz = yxzx = yzxx = -zyyy = zxxxy = zxyx = zyxx, zzzz$ |
| Cubic T (23), T_h ($m\bar{3}$), T_d ($\bar{4}3m$), O (432), O_h ($m\bar{3}m$) | $xxxx = yyyy = zzzz, xxzz = xzxz = xzzx = xxyy = xyxy = xyyx = yyzz = yzyz = yzzy = yyxx = yxyx = yxxy = zzyy =$ $zyzy = zyyz = zxxz = xzxz = zxxz$ |

1. TENSORIAL ASPECTS OF PHYSICAL PROPERTIES

with $-\rho^+(\theta, \omega)$ for the positive class and $+\rho^-(\theta, \omega)$ for the negative class. $\rho^\pm(\theta, \omega)$ is given by

$$\begin{aligned}\rho^\pm(\theta, \omega) &= \arccos(\mathbf{d}^\pm \cdot \mathbf{e}^\pm) = \arccos(\mathbf{u}^\pm \cdot \mathbf{s}^\pm) \\ &= \arccos \left\{ \left[\frac{\cos^2 \theta}{n_o^2(\omega)} + \frac{\sin^2 \theta}{n_e^2(\omega)} \right] \left[\frac{\cos^2 \theta}{n_o^4(\omega)} + \frac{\sin^2 \theta}{n_e^4(\omega)} \right]^{-1/2} \right\}.\end{aligned}\quad (1.7.3.13)$$

Note that the extraordinary walk-off angle is nil for a propagation along the optic axis ($\theta = 0$) and everywhere in the xy plane ($\theta = \pi/2$).

1.7.3.1.4. Biaxial class

In a biaxial crystal, the three principal refractive indices are all different. The graphical representations of the index surfaces are given in Fig. 1.7.3.3 for the positive biaxial class ($n_x < n_y < n_z$) and for the negative one ($n_x > n_y > n_z$), both with the usual

conventional orientation of the optical frame. If this is not the case, the appropriate permutation of the principal refractive indices is required.

In the orthorhombic system, the three principal axes are fixed by the symmetry; one is fixed in the monoclinic system; and none are fixed in the triclinic system. The index surface of the biaxial class has two umbilici contained in the xz plane, making an angle V with the z axis:

$$\sin^2 V(\omega) = \frac{n_y^{-2}(\omega) - n_x^{-2}(\omega)}{n_z^{-2}(\omega) - n_x^{-2}(\omega)}. \quad (1.7.3.14)$$

The propagation along the optic axes leads to the internal conical refraction effect (Schell & Bloembergen, 1978; Fève *et al.*, 1994).

1.7.3.1.4.1. Propagation in the principal planes

It is possible to define ordinary and extraordinary waves, but only in the principal planes of the biaxial crystal: the ordinary electric field vector is perpendicular to the z axis and to the extraordinary one. The walk-off properties of the waves are not the same in the xy plane as in the xz and yz planes.

(1) In the xy plane, the extraordinary wave has no walk-off, in contrast to the ordinary wave. The components of the electric field vectors can be established easily with the same considerations as for the uniaxial class:

$$\begin{aligned}e_x^o &= -\sin[\varphi \pm \rho^\mp(\varphi, \omega)] \\ e_y^o &= \cos[\varphi \pm \rho^\mp(\varphi, \omega)] \\ e_z^o &= 0,\end{aligned}\quad (1.7.3.15)$$

with $+\rho^-(\varphi, \omega)$ for the positive class and $-\rho^+(\varphi, \omega)$ for the negative class. $\rho^\pm(\varphi, \omega)$ is the walk-off angle given by (1.7.3.13), where θ is replaced by φ , n_o by n_y and n_e by n_x :

$$e_x^e = 0 \quad e_y^e = 0 \quad e_z^e = 1. \quad (1.7.3.16)$$

(2) The yz plane of a biaxial crystal has exactly the same characteristics as any plane containing the optic axis of a uniaxial crystal. The electric field vector components are given by (1.7.3.11) and (1.7.3.12) with $\varphi = \pi/2$. The ordinary walk-off is nil and the extraordinary one is given by (1.7.3.13) with $n_o = n_y$ and $n_e = n_z$.

(3) In the xz plane, the optic axes create a discontinuity of the shape of the internal and external sheets of the index surface leading to a discontinuity of the optic sign and of the electric field vector. The birefringence, $n_e - n_o$, is nil along the optic axis, and its sign changes on either side. Then the yz plane, xy plane and xz plane from the x axis to the optic axis have the same optic sign, the opposite of the optic sign from the optic axis to the z axis. Thus a positive biaxial crystal is negative from the optic axis to the z axis. The situation is inverted for a negative biaxial crystal. It implies the following configuration of polarization:

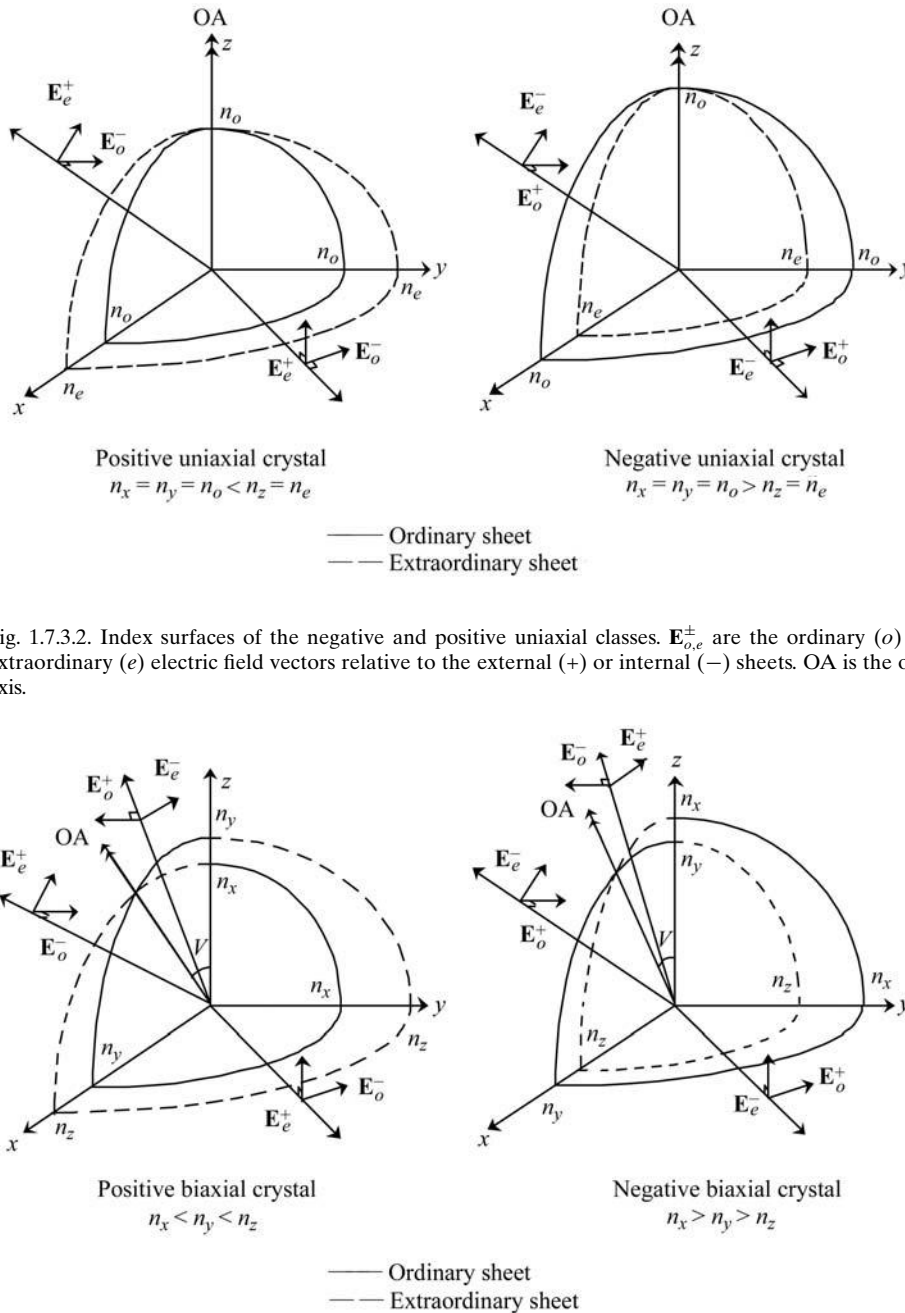


Fig. 1.7.3.2. Index surfaces of the negative and positive uniaxial classes. $\mathbf{E}_{o,e}^\pm$ are the ordinary (o) and extraordinary (e) electric field vectors relative to the external (+) or internal (−) sheets. OA is the optic axis.

Fig. 1.7.3.3. Index surfaces of the negative and positive biaxial classes. $\mathbf{E}_{o,e}^\pm$ are the ordinary (o) and extraordinary (e) electric field vectors relative to the external (+) or internal (−) sheets for a propagation in the principal planes. OA is the optic axis.

1.7. NONLINEAR OPTICAL PROPERTIES

(i) From the x axis to the optic axis, \mathbf{e}^o and \mathbf{e}^e are given by (1.7.3.11) and (1.7.3.12) with $\varphi = 0$. The walk-off is relative to the extraordinary wave and is calculated from (1.7.3.13) with $n_o = n_x$ and $n_e = n_z$.

(ii) From the optic axis to the z axis, the vibration plane of the ordinary and extraordinary waves corresponds respectively to a rotation of $\pi/2$ of the vibration plane of the extraordinary and ordinary waves for a propagation in the areas of the principal planes of opposite sign; the extraordinary electric field vector is given by (1.7.3.12) with $\varphi = 0$, $-\rho^-(\varphi, \omega)$ for the positive class and $+\rho^+(\varphi, \omega)$ for the negative class, and the ordinary electric field vector is out of phase by π in relation to (1.7.3.11), that is

$$e_x^o = 0 \quad e_y^o = -1 \quad e_z^o = 0. \quad (1.7.3.17)$$

The extraordinary walk-off angle is given by (1.7.3.13) with $n_o = n_x$ and $n_e = n_z$.

The $\pi/2$ rotation on either side of the optic axes is well observed during internal conical refraction (Fève *et al.*, 1994).

Note that for a biaxial crystal, the walk-off angles are all nil only for a propagation along the principal axes.

1.7.3.1.4.2. Propagation out of the principal planes

It is impossible to define ordinary and extraordinary waves out of the principal planes of a biaxial crystal: according to (1.7.3.6) and (1.7.3.9), \mathbf{e}^+ and \mathbf{e}^- have a nonzero projection on the z axis. According to these relations, it appears that \mathbf{e}^+ and \mathbf{e}^- are not perpendicular, so relation (1.7.3.10) is never verified. The walk-off angles ρ^+ and ρ^- are nonzero, different, and can be calculated from the electric field vectors:

$$\rho^\pm(\theta, \varphi, \omega) = \varepsilon \arccos[\mathbf{e}^\pm(\theta, \varphi, \omega) \cdot \mathbf{u}(\theta, \varphi, \omega)] - \varepsilon\pi/2. \quad (1.7.3.18)$$

$\varepsilon = +1$ or -1 for a positive or a negative optic sign, respectively.

1.7.3.2. Equations of propagation of three-wave and four-wave interactions

1.7.3.2.1. Coupled electric fields amplitudes equations

The nonlinear crystals considered here are homogeneous, lossless, non-conducting, without optical activity, non-magnetic and are optically anisotropic. The nonlinear regime allows interactions between γ waves with different circular frequencies $\omega_i, i = 1, \dots, \gamma$. The Fourier component of the polarization vector at ω_i is $\mathbf{P}(\omega_i) = \varepsilon_0 \chi^{(1)}(\omega_i) \mathbf{E}(\omega_i) + \mathbf{P}^{NL}(\omega_i)$, where $\mathbf{P}^{NL}(\omega_i)$ is the nonlinear polarization corresponding to the orders of the power series greater than 1 defined in Section 1.7.2.

Thus the propagation equation of each interacting wave ω_i is (Bloembergen, 1965)

$$\nabla_x \nabla_x \mathbf{E}(\omega_i) = (\omega_i^2/c^2) \varepsilon(\omega_i) \mathbf{E}(\omega_i) + \omega_i^2 \mu_0 \mathbf{P}^{NL}(\omega_i). \quad (1.7.3.19)$$

The γ propagation equations are coupled by $\mathbf{P}^{NL}(\omega_i)$:

(1) for a three-wave interaction, $\gamma = 3$,

$$\begin{aligned} \mathbf{P}^{NL}(\omega_1) &= \mathbf{P}^{(2)}(\omega_1) = \varepsilon_0 \chi^{(2)}(\omega_1 = \omega_3 - \omega_2) \cdot \mathbf{E}(\omega_3) \otimes \mathbf{E}^*(\omega_2), \\ \mathbf{P}^{NL}(\omega_2) &= \mathbf{P}^{(2)}(\omega_2) = \varepsilon_0 \chi^{(2)}(\omega_2 = \omega_3 - \omega_1) \cdot \mathbf{E}(\omega_3) \otimes \mathbf{E}^*(\omega_1), \\ \mathbf{P}^{NL}(\omega_3) &= \mathbf{P}^{(2)}(\omega_3) = \varepsilon_0 \chi^{(2)}(\omega_3 = \omega_1 + \omega_2) \cdot \mathbf{E}(\omega_1) \otimes \mathbf{E}^*(\omega_2); \end{aligned}$$

(2) for a four-wave interaction

$$\begin{aligned} \mathbf{P}^{NL}(\omega_1) &= \mathbf{P}^{(3)}(\omega_1) = \varepsilon_0 \chi^{(3)}(\omega_1 = \omega_4 - \omega_2 - \omega_3) \\ &\quad \cdot \mathbf{E}(\omega_4) \otimes \mathbf{E}^*(\omega_2) \otimes \mathbf{E}^*(\omega_3), \\ \mathbf{P}^{NL}(\omega_2) &= \mathbf{P}^{(3)}(\omega_2) = \varepsilon_0 \chi^{(3)}(\omega_2 = \omega_4 - \omega_1 - \omega_3) \\ &\quad \cdot \mathbf{E}(\omega_4) \otimes \mathbf{E}^*(\omega_1) \otimes \mathbf{E}^*(\omega_3), \end{aligned}$$

$$\begin{aligned} \mathbf{P}^{NL}(\omega_3) &= \mathbf{P}^{(3)}(\omega_3) = \varepsilon_0 \chi^{(3)}(\omega_3 = \omega_4 - \omega_1 - \omega_2) \\ &\quad \cdot \mathbf{E}(\omega_4) \otimes \mathbf{E}^*(\omega_1) \otimes \mathbf{E}^*(\omega_2) \\ \mathbf{P}^{NL}(\omega_4) &= \mathbf{P}^{(3)}(\omega_4) = \varepsilon_0 \chi^{(3)}(\omega_4 = \omega_1 + \omega_2 + \omega_3) \\ &\quad \cdot \mathbf{E}(\omega_1) \otimes \mathbf{E}(\omega_2) \otimes \mathbf{E}(\omega_3). \end{aligned}$$

The complex conjugates $\mathbf{E}^*(\omega_i)$ come from the relation $\mathbf{E}^*(\omega_i) = \mathbf{E}(-\omega_i)$.

We consider the plane wave, (1.7.3.3), as a solution of (1.7.3.19), and we assume that all the interacting waves propagate in the same direction Z . Each linearly polarized plane wave corresponds to an eigen mode \mathbf{E}^+ or \mathbf{E}^- defined above. For the usual case of beams with a finite transversal profile and when Z is along a direction where the double-refraction angles can be nonzero, *i.e.* out of the principal axes of the index surface, it is necessary to specify a frame for each interacting wave in order to calculate the corresponding powers as a function of Z : the coordinates linked to the wave at ω_i are written (X_i, Y_i, Z) , which can be relative to the mode $(+)$ or $(-)$. The systems are then linked by the double-refraction angles ρ : according to Fig. 1.7.3.1, we have $X_j^+ = X_i^+ + Z \tan[\rho^+(\omega_j) - \rho^+(\omega_i)]$, $Y_j^+ = Y_i^+$ for two waves $(+)$ with $\rho^+(\omega_j) > \rho^+(\omega_i)$, and $X_j^- = X_i^-$, $Y_j^- = Y_i^- + Z \tan[\rho^-(\omega_j) - \rho^-(\omega_i)]$ for two waves $(-)$ with $\rho^-(\omega_j) > \rho^-(\omega_i)$.

The presence of $\mathbf{P}^{NL}(\omega_i)$ in equations (1.7.3.19) leads to a variation of the γ amplitudes $E(\omega_i)$ with Z . In order to establish the equations of evolution of the wave amplitudes, we assume that their variations are small over one wavelength λ_i , which is usually true. Thus we can state

$$\begin{aligned} \frac{1}{k(\omega_i)} \left| \frac{\partial E(\omega_i, X_i, Y_i, Z)}{\partial Z} \right| &\ll |E(\omega_i, X_i, Y_i, Z)| \text{ or} \\ \left| \frac{\partial^2 E(\omega_i, X_i, Y_i, Z)}{\partial Z^2} \right| &\ll k(\omega_i) \left| \frac{\partial E(\omega_i, X_i, Y_i, Z)}{\partial Z} \right|. \end{aligned} \quad (1.7.3.20)$$

This is called the slowly varying envelope approximation.

Stating (1.7.3.20), the wave equation (1.7.3.19) for a forward propagation of a plane wave leads to

$$\begin{aligned} \frac{\partial E(\omega_i, X_i, Y_i, Z)}{\partial Z} &= j\mu_0 \frac{\omega_i^2}{2k(\omega_i) \cos^2 \rho(\omega_i)} \mathbf{e}(\omega_i) \cdot \mathbf{P}^{NL}(\omega_i, X_i, Y_i, Z) \\ &\quad \times \exp[-jk(\omega_i)Z]. \end{aligned} \quad (1.7.3.21)$$

We choose the optical frame (x, y, z) for the calculation of all the scalar products $\mathbf{e}(\omega_i) \cdot \mathbf{P}^{NL}(\omega_i)$, the electric susceptibility tensors being known in this frame.

For a three-wave interaction, (1.7.3.21) leads to

$$\begin{aligned} \frac{\partial E_1(X_1, Y_1, Z)}{\partial Z} &= j\kappa_1 [\mathbf{e}_1 \cdot \varepsilon_0 \chi^{(2)}(\omega_1 = \omega_3 - \omega_2) \cdot \mathbf{e}_3 \otimes \mathbf{e}_2] \\ &\quad \times E_3(X_3, Y_3, Z) E_2^*(X_2, Y_2, Z) \exp(j\Delta k Z) \\ \frac{\partial E_2(X_2, Y_2, Z)}{\partial Z} &= j\kappa_2 [\mathbf{e}_2 \cdot \varepsilon_0 \chi^{(2)}(\omega_2 = \omega_3 - \omega_1) \cdot \mathbf{e}_3 \otimes \mathbf{e}_1] \\ &\quad \times E_3(X_3, Y_3, Z) E_1^*(X_1, Y_1, Z) \exp(j\Delta k Z) \\ \frac{\partial E_3(X_3, Y_3, Z)}{\partial Z} &= j\kappa_3 [\mathbf{e}_3 \cdot \varepsilon_0 \chi^{(2)}(\omega_3 = \omega_1 + \omega_2) \cdot \mathbf{e}_1 \otimes \mathbf{e}_2] \\ &\quad \times E_1(X_1, Y_1, Z) E_2(X_2, Y_2, Z) \exp(-j\Delta k Z), \end{aligned} \quad (1.7.3.22)$$

with $\mathbf{e}_i = \mathbf{e}(\omega_i)$, $E_i(X_i, Y_i, Z_i) = E(\omega_i, X_i, Y_i, Z)$, $\kappa_i = (\mu_0 \omega_i^2) / [2k(\omega_i) \cos^2 \rho(\omega_i)]$ and $\Delta k = k(\omega_3) - [k(\omega_1) + k(\omega_2)]$, called the phase mismatch. We take by convention $\omega_1 < \omega_2 (< \omega_3)$.

1. TENSORIAL ASPECTS OF PHYSICAL PROPERTIES

If ABDP relations, defined in Section 1.7.2.2.1, are verified, then the three tensorial contractions in equations (1.7.3.22) are equal to the same quantity, which we write $\varepsilon_0 \chi_{\text{eff}}^{(2)}$, where $\chi_{\text{eff}}^{(2)}$ is called the effective coefficient:

$$\begin{aligned}\chi_{\text{eff}}^{(2)} &= \mathbf{e}_1 \cdot \chi^{(2)}(\omega_1 = \omega_3 - \omega_2) \cdot \mathbf{e}_3 \otimes \mathbf{e}_2 \\ &= \mathbf{e}_2 \cdot \chi^{(2)}(\omega_2 = \omega_3 - \omega_1) \cdot \mathbf{e}_3 \otimes \mathbf{e}_1 \\ &= \mathbf{e}_3 \cdot \chi^{(2)}(\omega_3 = \omega_1 + \omega_2) \cdot \mathbf{e}_1 \otimes \mathbf{e}_2.\end{aligned}\quad (1.7.3.23)$$

The same considerations lead to the same kind of equations for a four-wave interaction:

$$\begin{aligned}\frac{\partial E_1(X_1, Y_1, Z)}{\partial Z} &= j\kappa_1 \varepsilon_0 \chi_{\text{eff}}^{(3)} E_4(X_4, Y_4, Z) E_2^*(X_2, Y_2, Z) \\ &\quad \times E_3^*(X_3, Y_3, Z) \exp(j\Delta k Z) \\ \frac{\partial E_2(X_2, Y_2, Z)}{\partial Z} &= j\kappa_2 \varepsilon_0 \chi_{\text{eff}}^{(3)} E_4(X_4, Y_4, Z) E_1^*(X_1, Y_1, Z) \\ &\quad \times E_3^*(X_3, Y_3, Z) \exp(j\Delta k Z) \\ \frac{\partial E_3(X_3, Y_3, Z)}{\partial Z} &= j\kappa_3 \varepsilon_0 \chi_{\text{eff}}^{(3)} E_4(X_4, Y_4, Z) E_1^*(X_1, Y_1, Z) \\ &\quad \times E_2^*(X_2, Y_2, Z) \exp(j\Delta k Z) \\ \frac{\partial E_4(X_4, Y_4, Z)}{\partial Z} &= j\kappa_4 \varepsilon_0 \chi_{\text{eff}}^{(3)} E_1(X_1, Y_1, Z) E_2(X_2, Y_2, Z) \\ &\quad \times E_3(X_3, Y_3, Z) \exp(-j\Delta k Z).\end{aligned}\quad (1.7.3.24)$$

The conventions of notation are the same as previously and the phase mismatch is $\Delta k = k(\omega_4) - [k(\omega_1) + k(\omega_2) + k(\omega_3)]$. The effective coefficient is

$$\begin{aligned}\chi_{\text{eff}}^{(3)} &= \mathbf{e}_1 \cdot \chi^{(3)}(\omega_1 = \omega_4 - \omega_2 - \omega_3) \cdot \mathbf{e}_4 \otimes \mathbf{e}_2 \otimes \mathbf{e}_3 \\ &= \mathbf{e}_2 \cdot \chi^{(3)}(\omega_2 = \omega_4 - \omega_1 - \omega_3) \cdot \mathbf{e}_4 \otimes \mathbf{e}_1 \otimes \mathbf{e}_3 \\ &= \mathbf{e}_3 \cdot \chi^{(3)}(\omega_3 = \omega_4 - \omega_1 - \omega_2) \cdot \mathbf{e}_4 \otimes \mathbf{e}_1 \otimes \mathbf{e}_2 \\ &= \mathbf{e}_4 \cdot \chi^{(3)}(\omega_4 = \omega_1 + \omega_2 + \omega_3) \cdot \mathbf{e}_1 \otimes \mathbf{e}_2 \otimes \mathbf{e}_3.\end{aligned}\quad (1.7.3.25)$$

Expressions (1.7.3.23) for $\chi_{\text{eff}}^{(2)}$ and (1.7.3.25) for $\chi_{\text{eff}}^{(3)}$ can be condensed by introducing adequate third- and fourth-rank tensors to be contracted, respectively, with $\chi^{(2)}$ and $\chi^{(3)}$. For example, $\chi_{\text{eff}}^{(2)} = \chi^{(2)} \cdot e_3 \otimes e_1 \otimes e_2$ or $\chi_{\text{eff}}^{(3)} = \chi^{(3)} \cdot e_4 \otimes e_1 \otimes e_2 \otimes e_3$, and similar expressions. By substituting (1.7.3.8) in (1.7.3.22), we obtain the derivatives of Manley–Rowe relations (1.7.2.40) $\partial N(\omega_3, Z)/\partial Z = -\partial N(\omega_k, Z)/\partial Z$ ($k = 1, 2$) for a three-wave mixing, where $N(\omega_i, Z)$ is the Z photon flow. Identically with (1.7.3.24), we have $\partial N(\omega_4, Z)/\partial Z = -\partial N(\omega_k, Z)/\partial Z$ ($k = 1, 2, 3$) for a four-wave mixing.

In the general case, the nonlinear polarization wave and the generated wave travel at different phase velocities, $(\omega_1 + \omega_2)/[k(\omega_1) + k(\omega_2)]$ and $\omega_3/[k(\omega_3)]$, respectively, because of the frequency dispersion of the refractive indices in the crystal. Then the work per unit time $W(\omega_i)$, given in (1.7.2.39), which is done on the generated wave $\mathbf{E}(\omega_i, Z)$ by the nonlinear polar-

ization $\mathbf{P}^{\text{NL}}(\omega_i, Z)$, alternates in sign for each phase shift of π during the Z -propagation, which leads to a reversal of the energy flow (Bloembergen, 1965). The length leading to the phase shift of π is called the coherence length, $L_c = \pi/\Delta k$, where Δk is the phase mismatch given by (1.7.3.22) or (1.7.3.24).

1.7.3.2.2. Phase matching

The transfer of energy between the waves is maximum for $\Delta k = 0$, which defines phase matching: the energy flow does not alternate in sign and the generated field grows continuously. Note that a condition relative to the phases $\Phi(\omega_i, Z)$ also exists: the work of $\mathbf{P}^{\text{NL}}(\omega_i, Z)$ on $\mathbf{E}(\omega_i, Z)$ is maximum if these two waves are $\pi/2$ out of phase, that is to say if $\Delta k Z + \Delta \Phi(Z) = \pi/2$, where $\Delta \Phi(Z) = \Phi(\omega_3, Z) - [\Phi(\omega_1, Z) + \Phi(\omega_2, Z)]$; thus in the case of phase matching, the phase relation is $\Phi(\omega_3, Z) = \Phi(\omega_1, Z) + \Phi(\omega_2, Z) + \pi/2$ (Armstrong *et al.*, 1962). The complete initial phase matching is necessarily achieved when at least one wave among all the interacting waves is not incident but is generated inside the nonlinear crystal: in this case, its initial phase is locked on the good one. Phase matching is usually realized by the matching of the refractive indices using birefringence of anisotropic media as it is studied here. From the point of view of the quantum theory of light, the phase matching of the waves corresponds to the total photon-momentum conservation *i.e.*

$$\sum_{i=1}^{\gamma-1} \hbar k(\omega_i) = \hbar k(\omega_\gamma) \quad (1.7.3.26)$$

with $\gamma = 3$ for a three-photon interaction and $\gamma = 4$ for a four-photon interaction.

According to (1.7.3.4), the phase-matching condition (1.7.3.26) is expressed as a function of the refractive indices in the direction of propagation considered (θ, φ) ; for an interaction where the γ wavevectors are collinear, it is written

$$\sum_{i=1}^{\gamma-1} \omega_i n(\omega_i, \theta, \varphi) = \omega_\gamma n(\omega_\gamma, \theta, \varphi) \quad (1.7.3.27)$$

with

$$\sum_{i=1}^{\gamma-1} \omega_i = \omega_\gamma. \quad (1.7.3.28)$$

(1.7.3.28) is the relation of the energy conservation.

The efficiency of a nonlinear crystal directly depends on the existence of phase-matching directions. We shall see by considering in detail the effective coefficient that phase matching is a necessary but insufficient condition for the best expression of the nonlinear optical properties.

In an hypothetical non-dispersive medium $[\partial n(\omega)/\partial \omega = 0]$, (1.7.3.27) is always verified for each of the eigen refractive indices n^+ or n^- ; then any direction of propagation is a phase-matching direction. In a dispersive medium, phase matching can be achieved only if the direction of propagation has a birefringence which compensates the dispersion. Except for a propagation along the optic axis, there are two possible values, n^+ and n^- given by (1.7.3.6), for each of the three or four refractive indices involved in the phase-matching relations, that is to say 2^3 or 2^4 possible combinations of refractive indices for a three-wave or a four-wave process, respectively.

For a three-wave process, only three combinations among the 2^3 are compatible with the dispersion in frequency (1.7.3.7) and with the momentum and energy conservations (1.7.3.27) and (1.7.3.28). Thus the phase matching of a

Table 1.7.3.1. Correspondence between the phase-matching relations, the configurations of polarization and the types according to the sum- and difference-frequency generation processes SFG ($\omega_3 = \omega_1 + \omega_2$), DFG ($\omega_1 = \omega_3 - \omega_2$) and DFG ($\omega_2 = \omega_3 - \omega_1$)

| Phase-matching relations | Configurations of polarization | | | Types of interaction | | |
|--|--------------------------------|----------------|----------------|----------------------|--------------------|--------------------|
| | ω_3 | ω_1 | ω_2 | SFG (ω_3) | DFG (ω_1) | DFG (ω_2) |
| $\omega_3 n_3^- = \omega_1 n_1^+ = \omega_2 n_2^+$ | \mathbf{e}^- | \mathbf{e}^+ | \mathbf{e}^+ | I | II | III |
| $\omega_3 n_3^- = \omega_1 n_1^- = \omega_2 n_2^+$ | \mathbf{e}^- | \mathbf{e}^- | \mathbf{e}^+ | II | III | I |
| $\omega_3 n_3^- = \omega_1 n_1^+ = \omega_2 n_2^-$ | \mathbf{e}^- | \mathbf{e}^+ | \mathbf{e}^- | III | I | II |

\mathbf{e}^\pm are the unit electric field vectors relative to the refractive indices n^\pm in the phase-matching direction (Boulanger & Marnier, 1991).

1.7. NONLINEAR OPTICAL PROPERTIES

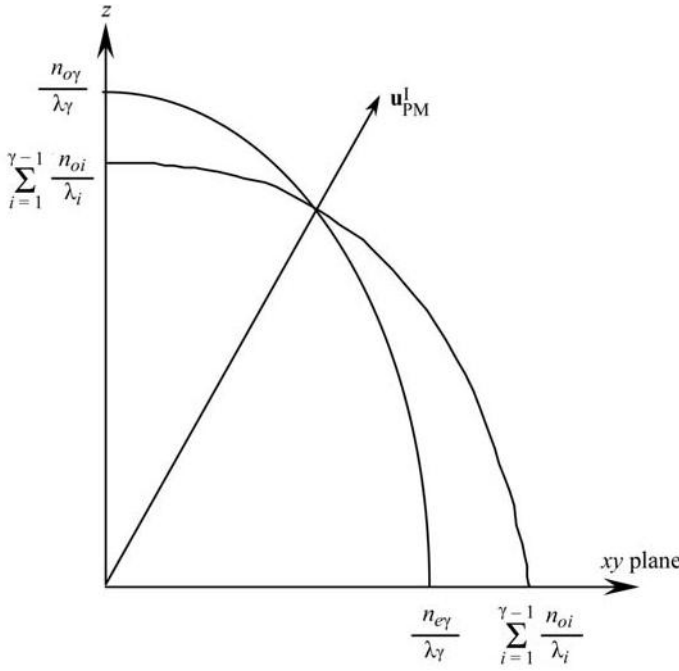


Fig. 1.7.3.4. Index surface sections in a plane containing the optic axis z of a negative uniaxial crystal allowing collinear type-I phase matching for SFG ($\omega_3 = \omega_1 + \omega_2$), $\gamma = 3$, or for SFG ($\omega_4 = \omega_1 + \omega_2 + \omega_3$), $\gamma = 4$. $\mathbf{u}_{\text{PM}}^{\text{I}}$ is the corresponding phase-matching direction.

three-wave interaction is allowed for three configurations of polarization given in Table 1.7.3.1.

The designation of the type of phase matching, I, II or III, is defined according to the polarization states at the frequencies which are added or subtracted. Type I characterizes interactions for which these two waves are identically polarized; the two corresponding polarizations are different for types II and III. Note that each phase-matching relation corresponds to one sum-frequency generation SFG ($\omega_3 = \omega_1 + \omega_2$) and two difference-frequency generation processes, DFG ($\omega_1 = \omega_3 - \omega_2$) and DFG ($\omega_2 = \omega_3 - \omega_1$). Types II and III are equivalent for SHG because $\omega_1 = \omega_2$.

For a four-wave process, only seven combinations of refractive indices allow phase matching in the case of normal dispersion; they are given in Table 1.7.3.2 with the corresponding configurations of polarization and types of SFG and DFG.

The convention of designation of the types is the same as for three-wave interactions for the situations where one polarization state is different from the three others, leading to the types I, II, III and IV. The criterion corresponding to type I cannot be applied to the three other phase-matching relations where two waves have the same polarization state, different from the two others. In this case, it is convenient to refer to each phase-matching relation by the same roman numeral, but with a different index: V^i , VI^i and VII^i , with the index $i = 1, 2, 3, 4$ corresponding to the index of the frequency generated by the SFG or DFG. For THG ($\omega_1 = \omega_2 = \omega_3$), types II, III and IV are equivalent, and so are types V^4 , VI^4 and VII^4 .

The index surface allows the geometrical determination of the phase-matching directions, which depend on the relative ellipticity of the internal (–) and external (+) sheets divided by the corresponding wavelengths: according to Tables 1.7.3.1 and 1.7.3.2 the directions are given by the intersection of the internal sheet of the lowest wavelength $[n^-(\lambda_\gamma, \theta, \varphi)]/(\lambda_\gamma)$ with a linear combination of the internal and external sheets at the other frequencies $\sum_{i=1}^{\gamma-1} [n^\pm(\lambda_i, \theta, \varphi)]/(\lambda_i)$. The existence and loci of these intersections depend on specific inequalities between the principal refractive indices at the different wavelengths. Note that independently of phase-matching considerations, normal dispersion and energy conservation impose $\sum_{i=1}^{\gamma-1} [n_a(\lambda_i)]/(\lambda_i) < [n_a(\lambda_\gamma)]/(\lambda_\gamma)$ with $a = x, y, z$.

1.7.3.2.2.1. Cubic crystals

There is no possibility of collinear phase matching in a dispersive cubic crystal because of the absence of birefringence. In a hypothetical non-dispersive anaxial crystal, the 2^3 three-wave and 2^4 four-wave phase-matching configurations would be allowed in any direction of propagation.

1.7.3.2.2.2. Uniaxial crystals

The configurations of polarization in terms of ordinary and extraordinary waves depend on the optic sign of the phase-matching direction with the convention given in Section 1.7.3.1: Tables 1.7.3.1 and 1.7.3.2 must be read by substituting (+, –) by (e , o) for a positive crystal and by (o , e) for a negative one.

Because of the symmetry of the index surface, all the phase-matching directions for a given type describe a cone with the optic axis as a revolution axis. Note that the previous comment on the anaxial class is valid for a propagation along the optic axis ($n_o = n_e$).

Fig. 1.7.3.4 shows the example of negative uniaxial crystals ($n_o > n_e$) like $\beta\text{-BaB}_2\text{O}_4$ (BBO) and KH_2PO_4 (KDP).

From Fig. 1.7.3.4, it clearly appears that the intersection of the sheets is possible only if $(n_{e\gamma})/(\lambda_\gamma) < \sum_{i=1}^{\gamma-1} (n_{oi})/(\lambda_i)$ [$< (n_{o\gamma})/(\lambda_\gamma)$] with $\gamma = 3$ for a three-wave process and $\gamma = 4$ for a four-wave one. The same considerations can be made for the positive sign and for all the other types of phase matching. There are different situations of inequalities allowing zero, one or several types: Table 1.7.3.3 gives the five possible situations for the three-wave interactions and Table 1.7.3.4 the 19 situations for the four-wave processes.

1.7.3.2.2.3. Biaxial crystals

The situation of biaxial crystals is more complicated, because the two sheets that must intersect are both elliptical in several cases. For a given interaction, all the phase-matching directions generate a complicated cone which joins two directions in the principal planes; the possible loci a , b , c , d are shown on the stereographic projection given in Fig. 1.7.3.5.

The basic inequalities of normal dispersion (1.7.3.7) forbid collinear phase matching for all the directions of propagation located between two optic axes at the two frequencies concerned.

Table 1.7.3.2. Correspondence between the phase-matching relations, the configurations of polarization and the types according to SFG ($\omega_4 = \omega_1 + \omega_2 + \omega_3$), DFG ($\omega_1 = \omega_4 - \omega_2 - \omega_3$), DFG ($\omega_2 = \omega_4 - \omega_1 - \omega_3$) and DFG ($\omega_3 = \omega_4 - \omega_1 - \omega_2$) (Boulanger et al., 1993)

| Phase-matching relations | Configurations of polarization | | | | Types of interaction | | | |
|---|--------------------------------|------------|------------|------------|----------------------|--------------------|--------------------|--------------------|
| | ω_4 | ω_1 | ω_2 | ω_3 | SFG (ω_4) | DFG (ω_1) | DFG (ω_2) | DFG (ω_3) |
| $\omega_4 n_4^+ = \omega_1 n_1^+ + \omega_2 n_2^+ + \omega_3 n_3^+$ | e^- | e^+ | e^+ | e^+ | I | II | III | IV |
| $\omega_4 n_4^- = \omega_1 n_1^- + \omega_2 n_2^- + \omega_3 n_3^-$ | e^- | e^- | e^- | e^- | II | III | IV | I |
| $\omega_4 n_4^+ = \omega_1 n_1^- + \omega_2 n_2^+ + \omega_3 n_3^-$ | e^- | e^- | e^+ | e^- | III | IV | I | II |
| $\omega_4 n_4^- = \omega_1 n_1^+ + \omega_2 n_2^- + \omega_3 n_3^+$ | e^- | e^+ | e^- | e^- | IV | I | II | IV |
| $\omega_4 n_4^- = \omega_1 n_1^- + \omega_2 n_2^+ + \omega_3 n_3^+$ | e^- | e^- | e^+ | e^+ | V^4 | V^1 | V^2 | V^3 |
| $\omega_4 n_4^+ = \omega_1 n_1^+ + \omega_2 n_2^- + \omega_3 n_3^-$ | e^- | e^+ | e^- | e^+ | VI^4 | VI^1 | VI^2 | VI^3 |
| $\omega_4 n_4^+ = \omega_1 n_1^- + \omega_2 n_2^+ + \omega_3 n_3^-$ | e^- | e^+ | e^+ | e^- | VII^4 | VII^1 | VII^2 | VII^3 |

1. TENSORIAL ASPECTS OF PHYSICAL PROPERTIES

Table 1.7.3.3. *Classes of refractive-index inequalities for collinear phase matching of three-wave interactions in positive and negative uniaxial crystals*

Types I, II and III refer to SFG; the types of the corresponding DFG are given in Table 1.7.3.1 (Fève *et al.*, 1993).

| Positive sign ($n_e > n_o$) | Negative sign ($n_o > n_e$) | Types of SFG |
|---|---|--------------|
| $\frac{n_{o3}}{\lambda_3} < \frac{n_{o1}}{\lambda_1} + \frac{n_{e2}}{\lambda_2}, \frac{n_{e1}}{\lambda_1} + \frac{n_{o2}}{\lambda_2}$ | $\frac{n_{o1}}{\lambda_1} + \frac{n_{e2}}{\lambda_2}, \frac{n_{e1}}{\lambda_1} + \frac{n_{o2}}{\lambda_2} < \frac{n_{e3}}{\lambda_3}$ | I, II, III |
| $\frac{n_{e1}}{\lambda_1} + \frac{n_{o2}}{\lambda_2} < \frac{n_{o3}}{\lambda_3} < \frac{n_{o1}}{\lambda_1} + \frac{n_{e2}}{\lambda_2}$ | $\frac{n_{o1}}{\lambda_1} + \frac{n_{e2}}{\lambda_2} < \frac{n_{e3}}{\lambda_3} < \frac{n_{e1}}{\lambda_1} + \frac{n_{o2}}{\lambda_2}$ | I, II |
| $\frac{n_{o1}}{\lambda_1} + \frac{n_{e2}}{\lambda_2} < \frac{n_{o3}}{\lambda_3} < \frac{n_{e1}}{\lambda_1} + \frac{n_{o2}}{\lambda_2}$ | $\frac{n_{e1}}{\lambda_1} + \frac{n_{o2}}{\lambda_2} < \frac{n_{e3}}{\lambda_3} < \frac{n_{o1}}{\lambda_1} + \frac{n_{e2}}{\lambda_2}$ | I, III |
| $\frac{n_{o1}}{\lambda_1} + \frac{n_{e2}}{\lambda_2}, \frac{n_{e1}}{\lambda_1} + \frac{n_{o2}}{\lambda_2} < \frac{n_{o3}}{\lambda_3} < \frac{n_{e1}}{\lambda_1} + \frac{n_{e2}}{\lambda_2}$ | $\frac{n_{o1}}{\lambda_1} + \frac{n_{e2}}{\lambda_2}, \frac{n_{e1}}{\lambda_1} + \frac{n_{o2}}{\lambda_2} < \frac{n_{e3}}{\lambda_3} < \frac{n_{o1}}{\lambda_1} + \frac{n_{o2}}{\lambda_2}$ | I |
| $\frac{n_{e1}}{\lambda_1} + \frac{n_{e2}}{\lambda_2} < \frac{n_{o3}}{\lambda_3}$ | $\frac{n_{o1}}{\lambda_1} + \frac{n_{o2}}{\lambda_2} < \frac{n_{e3}}{\lambda_3}$ | None |

Table 1.7.3.4. *Classes of refractive-index inequalities for collinear phase matching of four-wave interactions in positive ($n_a = n_e, n_b = n_o$) and negative ($n_a = n_o, n_b = n_e$) uniaxial crystals with $(n_{b4}/\lambda_4) < (n_{a1}/\lambda_1) + (n_{a2}/\lambda_2) + (n_{a3}/\lambda_3)$*

If this inequality is not verified, no phase matching is allowed. The types of phase matching refer to SFG; the types of the corresponding DFG are given in Table 1.7.3.2 (Fève, 1994).

| Positive sign ($n_e > n_o$) | Negative sign ($n_o > n_e$) | Types of SFG |
|--|--|--|
| $\frac{n_{a1}}{\lambda_1} + \frac{n_{a2}}{\lambda_2} + \frac{n_{b3}}{\lambda_3}, \frac{n_{a1}}{\lambda_1} + \frac{n_{b2}}{\lambda_2} + \frac{n_{a3}}{\lambda_3}, \frac{n_{b1}}{\lambda_1} + \frac{n_{a2}}{\lambda_2} + \frac{n_{a3}}{\lambda_3} < \frac{n_{b4}}{\lambda_4}$ | | I |
| $\frac{n_{a1}}{\lambda_1} + \frac{n_{a2}}{\lambda_2} + \frac{n_{b3}}{\lambda_3}, \frac{n_{a1}}{\lambda_1} + \frac{n_{b2}}{\lambda_2} + \frac{n_{a3}}{\lambda_3} < \frac{n_{b4}}{\lambda_4} < \frac{n_{b1}}{\lambda_1} + \frac{n_{a2}}{\lambda_2} + \frac{n_{a3}}{\lambda_3}$ | | I, V ⁴ |
| $\frac{n_{a1}}{\lambda_1} + \frac{n_{a2}}{\lambda_2} + \frac{n_{b3}}{\lambda_3}, \frac{n_{b1}}{\lambda_1} + \frac{n_{a2}}{\lambda_2} + \frac{n_{a3}}{\lambda_3} < \frac{n_{b4}}{\lambda_4} < \frac{n_{a1}}{\lambda_1} + \frac{n_{b2}}{\lambda_2} + \frac{n_{a3}}{\lambda_3}$ | | I, VI ⁴ |
| $\frac{n_{a1}}{\lambda_1} + \frac{n_{b2}}{\lambda_2} + \frac{n_{a3}}{\lambda_3}, \frac{n_{b1}}{\lambda_1} + \frac{n_{a2}}{\lambda_2} + \frac{n_{a3}}{\lambda_3} < \frac{n_{b4}}{\lambda_4} < \frac{n_{a1}}{\lambda_1} + \frac{n_{a2}}{\lambda_2} + \frac{n_{b3}}{\lambda_3}$ | | I, VII ⁴ |
| $\frac{n_{a1}}{\lambda_1} + \frac{n_{a2}}{\lambda_2} + \frac{n_{b3}}{\lambda_3} < \frac{n_{b4}}{\lambda_4} < \frac{n_{a1}}{\lambda_1} + \frac{n_{b2}}{\lambda_2} + \frac{n_{a3}}{\lambda_3}, \frac{n_{b1}}{\lambda_1} + \frac{n_{a2}}{\lambda_2} + \frac{n_{a3}}{\lambda_3}$ | $\frac{n_{b1}}{\lambda_1} + \frac{n_{b2}}{\lambda_2} + \frac{n_{a3}}{\lambda_3} < \frac{n_{b4}}{\lambda_4}$ $\frac{n_{b4}}{\lambda_4} < \frac{n_{b1}}{\lambda_1} + \frac{n_{b2}}{\lambda_2} + \frac{n_{a3}}{\lambda_3}$ | I, V ⁴ , VI ⁴ I, II, V ⁴ , VI ⁴ |
| $\frac{n_{a1}}{\lambda_1} + \frac{n_{b2}}{\lambda_2} + \frac{n_{a3}}{\lambda_3} < \frac{n_{b4}}{\lambda_4} < \frac{n_{a1}}{\lambda_1} + \frac{n_{a2}}{\lambda_2} + \frac{n_{b3}}{\lambda_3}, \frac{n_{b1}}{\lambda_1} + \frac{n_{a2}}{\lambda_2} + \frac{n_{a3}}{\lambda_3}$ | $\frac{n_{b1}}{\lambda_1} + \frac{n_{a2}}{\lambda_2} + \frac{n_{b3}}{\lambda_3} < \frac{n_{b4}}{\lambda_4}$ $\frac{n_{b4}}{\lambda_4} < \frac{n_{b1}}{\lambda_1} + \frac{n_{a2}}{\lambda_2} + \frac{n_{b3}}{\lambda_3}$ | I, V ⁴ , VII ⁴ I, III, V ⁴ , VII ⁴ |
| $\frac{n_{b1}}{\lambda_1} + \frac{n_{a2}}{\lambda_2} + \frac{n_{a3}}{\lambda_3} < \frac{n_{b4}}{\lambda_4} < \frac{n_{a1}}{\lambda_1} + \frac{n_{b2}}{\lambda_2} + \frac{n_{a3}}{\lambda_3}, \frac{n_{a1}}{\lambda_1} + \frac{n_{a2}}{\lambda_2} + \frac{n_{b3}}{\lambda_3}$ | $\frac{n_{a1}}{\lambda_1} + \frac{n_{b2}}{\lambda_2} + \frac{n_{b3}}{\lambda_3} < \frac{n_{b4}}{\lambda_4}$ $\frac{n_{b4}}{\lambda_4} < \frac{n_{a1}}{\lambda_1} + \frac{n_{b2}}{\lambda_2} + \frac{n_{b3}}{\lambda_3}$ | I, VI ⁴ , VII ⁴ I, IV, VI ⁴ , VII ⁴ |
| $\frac{n_{b4}}{\lambda_4} < \frac{n_{a1}}{\lambda_1} + \frac{n_{a2}}{\lambda_2} + \frac{n_{b3}}{\lambda_3}, \frac{n_{a1}}{\lambda_1} + \frac{n_{b2}}{\lambda_2} + \frac{n_{a3}}{\lambda_3}, \frac{n_{b1}}{\lambda_1} + \frac{n_{a2}}{\lambda_2} + \frac{n_{a3}}{\lambda_3}$ | $\frac{n_{b1}}{\lambda_1} + \frac{n_{b2}}{\lambda_2} + \frac{n_{a3}}{\lambda_3}, \frac{n_{b1}}{\lambda_1} + \frac{n_{a2}}{\lambda_2} + \frac{n_{b3}}{\lambda_3}, \frac{n_{a1}}{\lambda_1} + \frac{n_{b2}}{\lambda_2} + \frac{n_{b3}}{\lambda_3} < \frac{n_{b4}}{\lambda_4}$ $\frac{n_{a1}}{\lambda_1} + \frac{n_{b2}}{\lambda_2} + \frac{n_{b3}}{\lambda_3}, \frac{n_{b1}}{\lambda_1} + \frac{n_{a2}}{\lambda_2} + \frac{n_{b3}}{\lambda_3} < \frac{n_{b4}}{\lambda_4} < \frac{n_{b1}}{\lambda_1} + \frac{n_{b2}}{\lambda_2} + \frac{n_{a3}}{\lambda_3}$ $\frac{n_{a1}}{\lambda_1} + \frac{n_{b2}}{\lambda_2} + \frac{n_{b3}}{\lambda_3}, \frac{n_{b1}}{\lambda_1} + \frac{n_{b2}}{\lambda_2} + \frac{n_{a3}}{\lambda_3} < \frac{n_{b4}}{\lambda_4} < \frac{n_{a1}}{\lambda_1} + \frac{n_{a2}}{\lambda_2} + \frac{n_{b3}}{\lambda_3}$ $\frac{n_{b1}}{\lambda_1} + \frac{n_{a2}}{\lambda_2} + \frac{n_{b3}}{\lambda_3}, \frac{n_{b1}}{\lambda_1} + \frac{n_{b2}}{\lambda_2} + \frac{n_{a3}}{\lambda_3} < \frac{n_{b4}}{\lambda_4} < \frac{n_{a1}}{\lambda_1} + \frac{n_{b2}}{\lambda_2} + \frac{n_{b3}}{\lambda_3}$ $\frac{n_{a1}}{\lambda_1} + \frac{n_{b2}}{\lambda_2} + \frac{n_{b3}}{\lambda_3} < \frac{n_{b4}}{\lambda_4} < \frac{n_{b1}}{\lambda_1} + \frac{n_{a2}}{\lambda_2} + \frac{n_{b3}}{\lambda_3}, \frac{n_{b1}}{\lambda_1} + \frac{n_{b2}}{\lambda_2} + \frac{n_{a3}}{\lambda_3}$ $\frac{n_{b1}}{\lambda_1} + \frac{n_{a2}}{\lambda_2} + \frac{n_{b3}}{\lambda_3} < \frac{n_{b4}}{\lambda_4} < \frac{n_{a1}}{\lambda_1} + \frac{n_{b2}}{\lambda_2} + \frac{n_{b3}}{\lambda_3}, \frac{n_{b1}}{\lambda_1} + \frac{n_{b2}}{\lambda_2} + \frac{n_{a3}}{\lambda_3}$ $\frac{n_{b1}}{\lambda_1} + \frac{n_{b2}}{\lambda_2} + \frac{n_{a3}}{\lambda_3} < \frac{n_{b4}}{\lambda_4} < \frac{n_{a1}}{\lambda_1} + \frac{n_{b2}}{\lambda_2} + \frac{n_{b3}}{\lambda_3}, \frac{n_{b1}}{\lambda_1} + \frac{n_{a2}}{\lambda_2} + \frac{n_{b3}}{\lambda_3}$ $\frac{n_{b4}}{\lambda_4} < \frac{n_{a1}}{\lambda_1} + \frac{n_{b2}}{\lambda_2} + \frac{n_{b3}}{\lambda_3}, \frac{n_{b1}}{\lambda_1} + \frac{n_{a2}}{\lambda_2} + \frac{n_{b3}}{\lambda_3}, \frac{n_{b1}}{\lambda_1} + \frac{n_{b2}}{\lambda_2} + \frac{n_{a3}}{\lambda_3}$ | I, V ⁴ , VI ⁴ , VII ⁴ I, II, V ⁴ , VI ⁴ , VII ⁴ I, III, V ⁴ , VI ⁴ , VII ⁴ I, IV, V ⁴ , VI ⁴ , VII ⁴ I, II, III, V ⁴ , VI ⁴ , VII ⁴ I, II, IV, V ⁴ , VI ⁴ , VII ⁴ I, III, IV, V ⁴ , VI ⁴ , VII ⁴ All |

1.7. NONLINEAR OPTICAL PROPERTIES

Table 1.7.3.5. *Refractive-index conditions that determine collinear phase-matching loci in the principal planes of positive and negative biaxial crystals for three-wave SFG*

a, b, c, d refer to the areas given in Fig. 1.7.3.5. The types corresponding to the different DFGs are given in Table 1.7.3.1 (Fève *et al.*, 1993).

| Types of SFG | Phase-matching loci in the principal planes | Inequalities determining three-wave collinear phase matching in biaxial crystals | |
|--------------------------------------|---|--|--|
| | | Positive biaxial crystal | Negative biaxial crystal |
| | | $n_x(\omega_i) < n_y(\omega_i) < n_z(\omega_i)$ | $n_x(\omega_i) > n_y(\omega_i) > n_z(\omega_i)$ |
| Type I | a | $\frac{n_{x3}}{\lambda_3} < \frac{n_{y1}}{\lambda_1} + \frac{n_{y2}}{\lambda_2} < \frac{n_{z3}}{\lambda_3}$ | $\frac{n_{x1}}{\lambda_1} + \frac{n_{x2}}{\lambda_2} > \frac{n_{y3}}{\lambda_3} > \frac{n_{z1}}{\lambda_1} + \frac{n_{z2}}{\lambda_2}$ |
| | b | $\frac{n_{x1}}{\lambda_1} + \frac{n_{x2}}{\lambda_2} < \frac{n_{y3}}{\lambda_3} < \frac{n_{z1}}{\lambda_1} + \frac{n_{z2}}{\lambda_2}$ | $\frac{n_{x3}}{\lambda_3} > \frac{n_{y1}}{\lambda_1} + \frac{n_{y2}}{\lambda_2} > \frac{n_{z3}}{\lambda_3}$ |
| | c | $\frac{n_{x3}}{\lambda_3} < \frac{n_{z1}}{\lambda_1} + \frac{n_{z2}}{\lambda_2} < \frac{n_{y3}}{\lambda_3}$ | $\frac{n_{x1}}{\lambda_1} + \frac{n_{x2}}{\lambda_2} > \frac{n_{z3}}{\lambda_3} > \frac{n_{y1}}{\lambda_1} + \frac{n_{y2}}{\lambda_2}$ |
| | d | $\frac{n_{y1}}{\lambda_1} + \frac{n_{y2}}{\lambda_2} < \frac{n_{x3}}{\lambda_3} < \frac{n_{z1}}{\lambda_1} + \frac{n_{z2}}{\lambda_2}$ | $\frac{n_{y3}}{\lambda_3} > \frac{n_{x1}}{\lambda_1} + \frac{n_{x2}}{\lambda_2} > \frac{n_{z3}}{\lambda_3}$ |
| Type II | a | $\frac{n_{x3}}{\lambda_3} < \frac{n_{x1}}{\lambda_1} + \frac{n_{y2}}{\lambda_2}; \frac{n_{z1}}{\lambda_1} + \frac{n_{y2}}{\lambda_2} < \frac{n_{z3}}{\lambda_3}$ | $\frac{n_{y1}}{\lambda_1} + \frac{n_{x2}}{\lambda_2} > \frac{n_{y3}}{\lambda_3} > \frac{n_{y1}}{\lambda_1} + \frac{n_{z2}}{\lambda_2}$ |
| | b | $\frac{n_{y1}}{\lambda_1} + \frac{n_{x2}}{\lambda_2} > \frac{n_{y3}}{\lambda_3} > \frac{n_{y1}}{\lambda_1} + \frac{n_{z2}}{\lambda_2}$ | $\frac{n_{x3}}{\lambda_3} > \frac{n_{x1}}{\lambda_1} + \frac{n_{y2}}{\lambda_2}; \frac{n_{z1}}{\lambda_1} + \frac{n_{y2}}{\lambda_2} > \frac{n_{z3}}{\lambda_3}$ |
| | c | $\frac{n_{x3}}{\lambda_3} < \frac{n_{x1}}{\lambda_1} + \frac{n_{z2}}{\lambda_2}; \frac{n_{y1}}{\lambda_1} + \frac{n_{z2}}{\lambda_2} < \frac{n_{y3}}{\lambda_3}$ | $\frac{n_{z1}}{\lambda_1} + \frac{n_{x2}}{\lambda_2} > \frac{n_{z3}}{\lambda_3} > \frac{n_{z1}}{\lambda_1} + \frac{n_{y2}}{\lambda_2}$ |
| | c^* | $\frac{n_{x1}}{\lambda_1} + \frac{n_{z2}}{\lambda_2} < \frac{n_{x3}}{\lambda_3}; \frac{n_{y3}}{\lambda_3} < \frac{n_{y1}}{\lambda_1} + \frac{n_{z2}}{\lambda_2}$ | $\frac{n_{z1}}{\lambda_1} + \frac{n_{x2}}{\lambda_2} > \frac{n_{z3}}{\lambda_3} > \frac{n_{z1}}{\lambda_1} + \frac{n_{y2}}{\lambda_2}$ |
| | d | $\frac{n_{x1}}{\lambda_1} + \frac{n_{y2}}{\lambda_2} < \frac{n_{x3}}{\lambda_3} < \frac{n_{x1}}{\lambda_1} + \frac{n_{z2}}{\lambda_2}$ | $\frac{n_{y3}}{\lambda_3} > \frac{n_{y1}}{\lambda_1} + \frac{n_{x2}}{\lambda_2}; \frac{n_{z1}}{\lambda_1} + \frac{n_{x2}}{\lambda_2} > \frac{n_{z3}}{\lambda_3}$ |
| | d^* | $\frac{n_{x1}}{\lambda_1} + \frac{n_{y2}}{\lambda_2} < \frac{n_{x3}}{\lambda_3} < \frac{n_{x1}}{\lambda_1} + \frac{n_{z2}}{\lambda_2}$ | $\frac{n_{y1}}{\lambda_1} + \frac{n_{x2}}{\lambda_2} > \frac{n_{y3}}{\lambda_3}; \frac{n_{z3}}{\lambda_3} > \frac{n_{z1}}{\lambda_1} + \frac{n_{x2}}{\lambda_2}$ |
| Type III | a | $\frac{n_{x3}}{\lambda_3} < \frac{n_{y1}}{\lambda_1} + \frac{n_{x2}}{\lambda_2}; \frac{n_{y1}}{\lambda_1} + \frac{n_{z2}}{\lambda_2} < \frac{n_{z3}}{\lambda_3}$ | $\frac{n_{x1}}{\lambda_1} + \frac{n_{y2}}{\lambda_2} > \frac{n_{y3}}{\lambda_3} > \frac{n_{z1}}{\lambda_1} + \frac{n_{y2}}{\lambda_2}$ |
| | b | $\frac{n_{x1}}{\lambda_1} + \frac{n_{y2}}{\lambda_2} < \frac{n_{y3}}{\lambda_3} < \frac{n_{z1}}{\lambda_1} + \frac{n_{y2}}{\lambda_2}$ | $\frac{n_{x3}}{\lambda_3} > \frac{n_{y1}}{\lambda_1} + \frac{n_{x2}}{\lambda_2}; \frac{n_{y1}}{\lambda_1} + \frac{n_{z2}}{\lambda_2} > \frac{n_{z3}}{\lambda_3}$ |
| | c | $\frac{n_{x3}}{\lambda_3} < \frac{n_{z1}}{\lambda_1} + \frac{n_{x2}}{\lambda_2}; \frac{n_{z1}}{\lambda_1} + \frac{n_{y2}}{\lambda_2} < \frac{n_{y3}}{\lambda_3}$ | $\frac{n_{x1}}{\lambda_1} + \frac{n_{z2}}{\lambda_2} > \frac{n_{z3}}{\lambda_3} > \frac{n_{y1}}{\lambda_1} + \frac{n_{z2}}{\lambda_2}$ |
| | c^* | $\frac{n_{z1}}{\lambda_1} + \frac{n_{x2}}{\lambda_2} < \frac{n_{x3}}{\lambda_3}; \frac{n_{y3}}{\lambda_3} < \frac{n_{z1}}{\lambda_1} + \frac{n_{y2}}{\lambda_2}$ | $\frac{n_{x1}}{\lambda_1} + \frac{n_{z2}}{\lambda_2} > \frac{n_{z3}}{\lambda_3} > \frac{n_{y1}}{\lambda_1} + \frac{n_{z2}}{\lambda_2}$ |
| | d | $\frac{n_{y1}}{\lambda_1} + \frac{n_{x2}}{\lambda_2} < \frac{n_{x3}}{\lambda_3} < \frac{n_{z1}}{\lambda_1} + \frac{n_{x2}}{\lambda_2}$ | $\frac{n_{y3}}{\lambda_3} > \frac{n_{x1}}{\lambda_1} + \frac{n_{y2}}{\lambda_2}; \frac{n_{x1}}{\lambda_1} + \frac{n_{z2}}{\lambda_2} > \frac{n_{z3}}{\lambda_3}$ |
| | d^* | $\frac{n_{y1}}{\lambda_1} + \frac{n_{x2}}{\lambda_2} < \frac{n_{x3}}{\lambda_3} < \frac{n_{z1}}{\lambda_1} + \frac{n_{x2}}{\lambda_2}$ | $\frac{n_{x1}}{\lambda_1} + \frac{n_{y2}}{\lambda_2} > \frac{n_{y3}}{\lambda_3}; \frac{n_{z3}}{\lambda_3} > \frac{n_{x1}}{\lambda_1} + \frac{n_{z2}}{\lambda_2}$ |
| Conditions c, d are applied if | | $\frac{n_{y1}}{\lambda_1} - \frac{n_{x1}}{\lambda_1}, \frac{n_{y2}}{\lambda_2} - \frac{n_{x2}}{\lambda_2} < \frac{n_{y3}}{\lambda_3} - \frac{n_{x3}}{\lambda_3}$ | $\frac{n_{y1}}{\lambda_1} - \frac{n_{z1}}{\lambda_1}, \frac{n_{y2}}{\lambda_2} - \frac{n_{z2}}{\lambda_2} < \frac{n_{y3}}{\lambda_3} - \frac{n_{z3}}{\lambda_3}$ |
| Conditions c^*, d^* are applied if | | $\frac{n_{y3}}{\lambda_3} - \frac{n_{x3}}{\lambda_3} < \frac{n_{y1}}{\lambda_1} - \frac{n_{x1}}{\lambda_1}, \frac{n_{y2}}{\lambda_2} - \frac{n_{x2}}{\lambda_2}$ | $\frac{n_{y3}}{\lambda_3} - \frac{n_{z3}}{\lambda_3} < \frac{n_{y1}}{\lambda_1} - \frac{n_{z1}}{\lambda_1}, \frac{n_{y2}}{\lambda_2} - \frac{n_{z2}}{\lambda_2}$ |

Tables 1.7.3.5 and 1.7.3.6 give, respectively, the inequalities that determine collinear phase matching in the principal planes for the three types of three-wave SFG and for the seven types of four-wave SFG.

The inequalities in Table 1.7.3.5 show that a phase-matching cone which would join the directions a and d is not possible for any type of interaction, because the corresponding inequalities have an opposite sense. It is the same for a hypothetical cone joining b and c .

The existence of type-II or type-III SFG phase matching imposes the existence of type I, because the inequalities relative to type I are always satisfied whenever type II or type III exists.

However, type I can exist even if type II or type III is not allowed. A type-I phase-matched SFG in area c forbids phase-matching directions in area b for type-II and type-III SFG. The exclusion is the same between d and a . The consideration of all the possible combinations of the inequalities of Table 1.7.3.5 leads to 84 possible classes of phase-matching cones for both positive and negative biaxial crystals (Fève *et al.*, 1993; Fève, 1994). There are 14 classes for second harmonic generation (SHG) which correspond to the degenerated case ($\omega_1 = \omega_2$) (Hobden, 1967).

The coexistence of the different types of four-wave phase matching is limited as for the three-wave case: a cone joining a and d or b and c is impossible for type-I SFG. Type I in area d

1. TENSORIAL ASPECTS OF PHYSICAL PROPERTIES

Table 1.7.3.6. *Refractive-index conditions that determine collinear phase-matching loci in the principal planes of positive and negative biaxial crystals for four-wave SFG*

The types corresponding to the different DFGs are given in Table 1.7.3.2 (Boulanger *et al.*, 1993).

(a) SFG type I.

| Phase-matching loci in the principal planes | Inequalities determining four-wave collinear phase matching in biaxial crystals | |
|---|--|--|
| | Positive sign | Negative sign |
| <i>a</i> | $\frac{n_{x4}}{\lambda_4} < \frac{n_{y1}}{\lambda_1} + \frac{n_{y2}}{\lambda_2} + \frac{n_{y3}}{\lambda_3} < \frac{n_{z4}}{\lambda_4}$ | $\frac{n_{z1}}{\lambda_1} + \frac{n_{z2}}{\lambda_2} + \frac{n_{z3}}{\lambda_3} < \frac{n_{y4}}{\lambda_4} < \frac{n_{x1}}{\lambda_1} + \frac{n_{x2}}{\lambda_2} + \frac{n_{x3}}{\lambda_3}$ |
| <i>b</i> | $\frac{n_{x1}}{\lambda_1} + \frac{n_{x2}}{\lambda_2} + \frac{n_{x3}}{\lambda_3} < \frac{n_{y4}}{\lambda_4} < \frac{n_{z1}}{\lambda_1} + \frac{n_{z2}}{\lambda_2} + \frac{n_{z3}}{\lambda_3}$ | $\frac{n_{z4}}{\lambda_4} < \frac{n_{y1}}{\lambda_1} + \frac{n_{y2}}{\lambda_2} + \frac{n_{y3}}{\lambda_3} < \frac{n_{x4}}{\lambda_4}$ |
| <i>c</i> | $\frac{n_{x4}}{\lambda_4} < \frac{n_{z1}}{\lambda_1} + \frac{n_{z2}}{\lambda_2} + \frac{n_{z3}}{\lambda_3} < \frac{n_{y4}}{\lambda_4}$ | $\frac{n_{y1}}{\lambda_1} + \frac{n_{y2}}{\lambda_2} + \frac{n_{y3}}{\lambda_3} < \frac{n_{z4}}{\lambda_4} < \frac{n_{x1}}{\lambda_1} + \frac{n_{x2}}{\lambda_2} + \frac{n_{x3}}{\lambda_3}$ |
| <i>d</i> | $\frac{n_{y1}}{\lambda_1} + \frac{n_{y2}}{\lambda_2} + \frac{n_{y3}}{\lambda_3} < \frac{n_{x4}}{\lambda_4} < \frac{n_{z1}}{\lambda_1} + \frac{n_{z2}}{\lambda_2} + \frac{n_{z3}}{\lambda_3}$ | $\frac{n_{z4}}{\lambda_4} < \frac{n_{x1}}{\lambda_1} + \frac{n_{x2}}{\lambda_2} + \frac{n_{x3}}{\lambda_3} < \frac{n_{y4}}{\lambda_4}$ |

(b) SFG type II ($i = 1, j = 2, k = 3$), SFG type III ($i = 3, j = 1, k = 2$), SFG type IV ($i = 2, j = 3, k = 1$).

| Phase-matching loci in the principal planes | Inequalities determining four-wave collinear phase matching in biaxial crystals | |
|--|--|--|
| | Positive sign | Negative sign |
| <i>a</i> | $\frac{n_{x4}}{\lambda_4} < \frac{n_{xi}}{\lambda_i} + \frac{n_{xj}}{\lambda_j} + \frac{n_{yk}}{\lambda_k}; \frac{n_{zi}}{\lambda_i} + \frac{n_{zj}}{\lambda_j} + \frac{n_{yk}}{\lambda_k} < \frac{n_{z4}}{\lambda_4}$ | $\frac{n_{yi}}{\lambda_i} + \frac{n_{yj}}{\lambda_j} + \frac{n_{zk}}{\lambda_k} < \frac{n_{y4}}{\lambda_4} < \frac{n_{xi}}{\lambda_i} + \frac{n_{yj}}{\lambda_j} + \frac{n_{xk}}{\lambda_k}$ |
| <i>b</i> | $\frac{n_{yi}}{\lambda_i} + \frac{n_{yj}}{\lambda_j} + \frac{n_{xk}}{\lambda_k} < \frac{n_{y4}}{\lambda_4} < \frac{n_{zi}}{\lambda_i} + \frac{n_{zj}}{\lambda_j} + \frac{n_{zk}}{\lambda_k}$ | $\frac{n_{z4}}{\lambda_4} < \frac{n_{zi}}{\lambda_i} + \frac{n_{zj}}{\lambda_j} + \frac{n_{yk}}{\lambda_k}; \frac{n_{xi}}{\lambda_i} + \frac{n_{xj}}{\lambda_j} + \frac{n_{yk}}{\lambda_k} < \frac{n_{x4}}{\lambda_4}$ |
| <i>c</i> | $\frac{n_{x4}}{\lambda_4} < \frac{n_{xi}}{\lambda_i} + \frac{n_{xj}}{\lambda_j} + \frac{n_{zk}}{\lambda_k}; \frac{n_{yi}}{\lambda_i} + \frac{n_{yj}}{\lambda_j} + \frac{n_{zk}}{\lambda_k} < \frac{n_{y4}}{\lambda_4}$ | $\frac{n_{zi}}{\lambda_i} + \frac{n_{zj}}{\lambda_j} + \frac{n_{yk}}{\lambda_k} < \frac{n_{z4}}{\lambda_4} < \frac{n_{xi}}{\lambda_i} + \frac{n_{zj}}{\lambda_j} + \frac{n_{xk}}{\lambda_k}$ |
| <i>c*</i> | $\frac{n_{xi}}{\lambda_i} + \frac{n_{xj}}{\lambda_j} + \frac{n_{zk}}{\lambda_k} < \frac{n_{x4}}{\lambda_4}; \frac{n_{y4}}{\lambda_4} < \frac{n_{yi}}{\lambda_i} + \frac{n_{yj}}{\lambda_j} + \frac{n_{zk}}{\lambda_k}$ | $\frac{n_{zi}}{\lambda_i} + \frac{n_{zj}}{\lambda_j} + \frac{n_{yk}}{\lambda_k} < \frac{n_{z4}}{\lambda_4} < \frac{n_{xi}}{\lambda_i} + \frac{n_{zj}}{\lambda_j} + \frac{n_{xk}}{\lambda_k}$ |
| <i>d</i> | $\frac{n_{xi}}{\lambda_i} + \frac{n_{xj}}{\lambda_j} + \frac{n_{yk}}{\lambda_k} < \frac{n_{x4}}{\lambda_4} < \frac{n_{zi}}{\lambda_i} + \frac{n_{zj}}{\lambda_j} + \frac{n_{zk}}{\lambda_k}$ | $\frac{n_{z4}}{\lambda_4} < \frac{n_{zi}}{\lambda_i} + \frac{n_{zj}}{\lambda_j} + \frac{n_{xk}}{\lambda_k}; \frac{n_{yi}}{\lambda_i} + \frac{n_{yj}}{\lambda_j} + \frac{n_{xk}}{\lambda_k} < \frac{n_{y4}}{\lambda_4}$ |
| <i>d*</i> | $\frac{n_{xi}}{\lambda_i} + \frac{n_{xj}}{\lambda_j} + \frac{n_{yk}}{\lambda_k} < \frac{n_{x4}}{\lambda_4} < \frac{n_{xi}}{\lambda_i} + \frac{n_{xj}}{\lambda_j} + \frac{n_{zk}}{\lambda_k}$ | $\frac{n_{zi}}{\lambda_i} + \frac{n_{zj}}{\lambda_j} + \frac{n_{xk}}{\lambda_k} < \frac{n_{z4}}{\lambda_4}; \frac{n_{y4}}{\lambda_4} < \frac{n_{yi}}{\lambda_i} + \frac{n_{yj}}{\lambda_j} + \frac{n_{xk}}{\lambda_k}$ |
| SFG type II (i, j) = (1, 2); SFG type III (i, j) = (1, 3); SFG type IV (i, j) = (2, 3) | | |
| Conditions <i>c, d</i> are applied if | $\frac{n_{yi}}{\lambda_i} + \frac{n_{yj}}{\lambda_j} - \frac{n_{xi}}{\lambda_i} - \frac{n_{xj}}{\lambda_j} < \frac{n_{y4}}{\lambda_4} - \frac{n_{x4}}{\lambda_4}$ | $\frac{n_{yi}}{\lambda_i} + \frac{n_{yj}}{\lambda_j} - \frac{n_{zi}}{\lambda_i} - \frac{n_{zj}}{\lambda_j} < \frac{n_{y4}}{\lambda_4} - \frac{n_{z4}}{\lambda_4}$ |
| Conditions <i>c*, d*</i> are applied if | $\frac{n_{y4}}{\lambda_4} - \frac{n_{x4}}{\lambda_4} < \frac{n_{yi}}{\lambda_i} + \frac{n_{yj}}{\lambda_j} - \frac{n_{xi}}{\lambda_i} - \frac{n_{xj}}{\lambda_j}$ | $\frac{n_{y4}}{\lambda_4} - \frac{n_{z4}}{\lambda_4} < \frac{n_{yi}}{\lambda_i} + \frac{n_{yj}}{\lambda_j} - \frac{n_{zi}}{\lambda_i} - \frac{n_{zj}}{\lambda_j}$ |

forbids the six other types in *a*. The same restriction exists between *c* and *b*. Types II, III, IV, V⁴, VI⁴ and VII⁴ cannot exist without type I; other restrictions concern the relations between types II, III, IV and types V⁴, VI⁴, VII⁴ (Fève, 1994). The counting of the classes of four-wave phase-matching cones obtained from all the possible combinations of the inequalities of Table 1.7.3.6 is complex and it has not yet been done.

For reasons explained later, it can be interesting to consider a non-collinear interaction. In this case, the projection of the vectorial phase-matching relation (1.7.3.26) on the wavevector $\mathbf{k}(\omega_\gamma, \theta_\gamma, \varphi_\gamma)$ of highest frequency ω_γ leads to

$$\sum_{i=1}^{\gamma-1} \omega_i n(\omega_i, \theta_i, \varphi_i) \cos \alpha_{i\gamma} = \omega_\gamma n(\omega_\gamma, \theta_\gamma, \varphi_\gamma), \quad (1.7.3.29)$$

where $\alpha_{i\gamma}$ is the angle between $\mathbf{k}(\omega_i, \theta_i, \varphi_i)$ and $\mathbf{k}(\omega_\gamma, \theta_\gamma, \varphi_\gamma)$, with $\gamma = 3$ for a three-wave interaction and $\gamma = 4$ for a four-wave

interaction. The phase-matching angles $(\theta_\gamma, \varphi_\gamma)$ can be expressed as a function of the different (θ_i, φ_i) by the projection of (1.7.3.26) on the three principal axes of the optical frame.

The configurations of polarization allowing non-collinear phase matching are the same as for collinear phase matching. Furthermore, non-collinear phase matching exists only if collinear phase matching is allowed; the converse is not true (Fève, 1994). Note that collinear or non-collinear phase-matching conditions are rarely satisfied over the entire transparency range of the crystal.

1.7.3.2.3. Quasi phase matching

When index matching is not allowed, it is possible to increase the energy of the generated wave continuously during the propagation by introducing a periodic change in the sign of the nonlinear electric susceptibility, which leads to a periodic reset of

1.7. NONLINEAR OPTICAL PROPERTIES

Table 1.7.3.6 (cont.)

(c) SFG type VI⁴ ($i = 1, j = 2, k = 3$), SFG type VI⁴ ($i = 2, j = 3, k = 1$), SFG type VII⁴ ($i = 3, j = 1, k = 2$).

| Phase-matching loci in the principal planes | Inequalities determining four-wave collinear phase matching in biaxial crystals | |
|---|--|--|
| | Positive sign | Negative sign |
| a | $\frac{n_{x4}}{\lambda_4} < \frac{n_{xi}}{\lambda_i} + \frac{n_{yj}}{\lambda_j} + \frac{n_{yk}}{\lambda_k}; \frac{n_{zi}}{\lambda_i} + \frac{n_{yj}}{\lambda_j} + \frac{n_{yk}}{\lambda_k} < \frac{n_{z4}}{\lambda_4}$ | $\frac{n_{yi}}{\lambda_i} + \frac{n_{zj}}{\lambda_j} + \frac{n_{zk}}{\lambda_k} < \frac{n_{y4}}{\lambda_4} < \frac{n_{yi}}{\lambda_i} + \frac{n_{xj}}{\lambda_j} + \frac{n_{xk}}{\lambda_k}$ |
| b | $\frac{n_{yi}}{\lambda_i} + \frac{n_{xj}}{\lambda_j} + \frac{n_{xk}}{\lambda_k} < \frac{n_{y4}}{\lambda_4} < \frac{n_{yi}}{\lambda_i} + \frac{n_{zj}}{\lambda_j} + \frac{n_{zk}}{\lambda_k}$ | $\frac{n_{z4}}{\lambda_4} < \frac{n_{zi}}{\lambda_i} + \frac{n_{yj}}{\lambda_j} + \frac{n_{yk}}{\lambda_k}; \frac{n_{xi}}{\lambda_i} + \frac{n_{yj}}{\lambda_j} + \frac{n_{yk}}{\lambda_k} < \frac{n_{x4}}{\lambda_4}$ |
| c' | $\frac{n_{x4}}{\lambda_4} < \frac{n_{xi}}{\lambda_i} + \frac{n_{zj}}{\lambda_j} + \frac{n_{zk}}{\lambda_k}; \frac{n_{yi}}{\lambda_i} + \frac{n_{zj}}{\lambda_j} + \frac{n_{zk}}{\lambda_k} < \frac{n_{y4}}{\lambda_4}$ | $\frac{n_{zi}}{\lambda_i} + \frac{n_{yj}}{\lambda_j} + \frac{n_{yk}}{\lambda_k} < \frac{n_{z4}}{\lambda_4} < \frac{n_{zi}}{\lambda_i} + \frac{n_{xj}}{\lambda_j} + \frac{n_{xk}}{\lambda_k}$ |
| c^{**} | $\frac{n_{xi}}{\lambda_i} + \frac{n_{zj}}{\lambda_j} + \frac{n_{zk}}{\lambda_k} < \frac{n_{x4}}{\lambda_4}; \frac{n_{y4}}{\lambda_4} < \frac{n_{yi}}{\lambda_i} + \frac{n_{zj}}{\lambda_j} + \frac{n_{zk}}{\lambda_k}$ | $\frac{n_{zi}}{\lambda_i} + \frac{n_{yj}}{\lambda_j} + \frac{n_{yk}}{\lambda_k} < \frac{n_{z4}}{\lambda_4} < \frac{n_{zi}}{\lambda_i} + \frac{n_{xj}}{\lambda_j} + \frac{n_{xk}}{\lambda_k}$ |
| d' | $\frac{n_{xi}}{\lambda_i} + \frac{n_{yj}}{\lambda_j} + \frac{n_{yk}}{\lambda_k} < \frac{n_{x4}}{\lambda_4} < \frac{n_{xi}}{\lambda_i} + \frac{n_{zj}}{\lambda_j} + \frac{n_{zk}}{\lambda_k}$ | $\frac{n_{z4}}{\lambda_4} < \frac{n_{zi}}{\lambda_i} + \frac{n_{xj}}{\lambda_j} + \frac{n_{xk}}{\lambda_k}; \frac{n_{yi}}{\lambda_i} + \frac{n_{xj}}{\lambda_j} + \frac{n_{xk}}{\lambda_k} < \frac{n_{y4}}{\lambda_4}$ |
| d^{**} | $\frac{n_{xi}}{\lambda_i} + \frac{n_{yj}}{\lambda_j} + \frac{n_{yk}}{\lambda_k} < \frac{n_{x4}}{\lambda_4} < \frac{n_{xi}}{\lambda_i} + \frac{n_{zj}}{\lambda_j} + \frac{n_{zk}}{\lambda_k}$ | $\frac{n_{zi}}{\lambda_i} + \frac{n_{xj}}{\lambda_j} + \frac{n_{xk}}{\lambda_k} < \frac{n_{z4}}{\lambda_4}; \frac{n_{y4}}{\lambda_4} < \frac{n_{yi}}{\lambda_i} + \frac{n_{xj}}{\lambda_j} + \frac{n_{xk}}{\lambda_k}$ |
| SFG type VI ⁴ ($i = 1$); SFG type VI ⁴ ($i = 2$); SFG type VII ⁴ ($i = 3$) | | |
| Conditions c', d' are applied if | $\frac{n_{yi}}{\lambda_i} - \frac{n_{xi}}{\lambda_i} < \frac{n_{y4}}{\lambda_4} - \frac{n_{x4}}{\lambda_4}$ | $\frac{n_{yi}}{\lambda_i} - \frac{n_{zi}}{\lambda_i} < \frac{n_{y4}}{\lambda_4} - \frac{n_{z4}}{\lambda_4}$ |
| Conditions c^{**}, d^{**} are applied if | $\frac{n_{y4}}{\lambda_4} - \frac{n_{x4}}{\lambda_4} < \frac{n_{yi}}{\lambda_i} - \frac{n_{xi}}{\lambda_i}$ | $\frac{n_{y4}}{\lambda_4} - \frac{n_{z4}}{\lambda_4} < \frac{n_{yi}}{\lambda_i} - \frac{n_{zi}}{\lambda_i}$ |

π between the waves (Armstrong *et al.*, 1962). This method is called quasi phase matching (QPM). The transfer of energy between the nonlinear polarization and the generated electric field never alternates if the reset is made at each coherence length. In this case and for a three-wave SFG, the nonlinear polarization sequence is the following:

(i) from 0 to L_c , $\mathbf{P}^{NL}(\omega_3) = \varepsilon_0 \chi^{(2)}(\omega_3) \mathbf{e}_1 \mathbf{e}_2 E_1 E_2 \exp\{i[k(\omega_1) + k(\omega_2)]Z\}$;

(ii) from L_c to $2L_c$, $\mathbf{P}^{NL}(\omega_3) = -\varepsilon_0 \chi^{(2)}(\omega_3) \mathbf{e}_1 \mathbf{e}_2 E_1 E_2 \exp\{i[k(\omega_1) + k(\omega_2)]Z\}$, which is equivalent to $\mathbf{P}^{NL}(\omega_3) = \varepsilon_0 \chi^{(2)}(\omega_3) \mathbf{e}_1 \mathbf{e}_2 E_1 E_2 \exp\{i[k(\omega_1) + k(\omega_2)]Z - \pi\}$.

QPM devices are a recent development and are increasingly being considered for applications (Fejer *et al.*, 1992). The nonlinear medium can be formed by the bonding of thin wafers alternately rotated by π ; this has been done for GaAs (Gordon *et al.*, 1993). For ferroelectric crystals, it is possible to form periodic reversing of the spontaneous polarization in the same sample by proton- or ion-exchange techniques, or by applying an electric field, which leads to periodically poled (pp) materials like ppLiNbO₃ or ppKTP (Myers *et al.*, 1995; Karlsson & Laurell, 1997; Rosenman *et al.*, 1998).

Quasi phase matching offers three main advantages when compared with phase matching: it may be used for any configuration of polarization of the interacting waves, which allows us to use the largest coefficient of the $\chi^{(2)}$ tensor, as explained in the following section; QPM can be achieved over the entire transparency range of the crystal, since the periodicity can be adjusted; and, finally, double refraction and its harmful effect on the nonlinear efficiency can be avoided because QPM can be realized in the principal plane of a uniaxial crystal or in the principal axes of biaxial crystals. Nevertheless, there are limitations due to the difficulty in fabricating the corresponding materials: diffusion-bonded GaAs has strong reflection losses and periodic patterns of ppKTP or ppLN can only be written over a thickness that does not exceed 3 mm, which limits the input energy.

1.7.3.2.4. Effective coefficient and field tensor

1.7.3.2.4.1. Definitions and symmetry properties

The refractive indices and their dispersion in frequency determine the existence and loci of the phase-matching directions, and so impose the direction of the unit electric field vectors of the interacting waves according to (1.7.3.9). The effective coefficient, given by (1.7.3.23) and (1.7.3.25), depends in part on the linear optical properties *via* the field tensor, which is the tensor product of the interacting unit electric field vectors (Boulanger, 1989; Boulanger & Marnier, 1991; Boulanger *et al.*, 1993; Zyss, 1993). Indeed, the effective coefficient is the contraction between the field tensor and the electric susceptibility tensor of corresponding order:

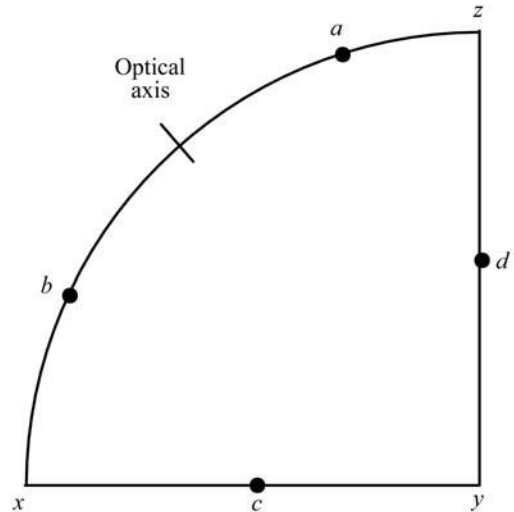


Fig. 1.7.3.5. Stereographic projection on the optical frame of the possible loci of phase-matching directions in the principal planes of a biaxial crystal.

1. TENSORIAL ASPECTS OF PHYSICAL PROPERTIES

(i) For three-wave mixing,

$$\begin{aligned}\chi_{\text{eff}}^{(2)}(\omega_a, \omega_b, \omega_c, \theta, \varphi) &= \sum_{ijk} \chi_{ijk}(\omega_a) F_{ijk}(\omega_a, \omega_b, \omega_c, \theta, \varphi) \\ &= \chi^{(2)}(\omega_a) \cdot F^{(2)}(\omega_a, \omega_b, \omega_c, \theta, \varphi),\end{aligned}\quad (1.7.3.30)$$

with

$$F^{(2)}(\omega_a, \omega_b, \omega_c, \theta, \varphi) = \mathbf{e}(\omega_a, \theta, \varphi) \otimes \mathbf{e}(\omega_b, \theta, \varphi) \otimes \mathbf{e}(\omega_c, \theta, \varphi), \quad (1.7.3.31)$$

where $\omega_a, \omega_b, \omega_c$ correspond to $\omega_3, \omega_1, \omega_2$ for SFG ($\omega_3 = \omega_1 + \omega_2$); to $\omega_1, \omega_3, \omega_2$ for DFG ($\omega_1 = \omega_3 - \omega_2$); and to $\omega_2, \omega_3, \omega_1$ for DFG ($\omega_2 = \omega_3 - \omega_1$).

(ii) For four-wave mixing,

$$\begin{aligned}\chi_{\text{eff}}^{(3)}(\omega_a, \omega_b, \omega_c, \omega_d, \theta, \varphi) &= \sum_{ijkl} \chi_{ijkl}(\omega_a) F_{ijkl}(\omega_a, \omega_b, \omega_c, \omega_d, \theta, \varphi) \\ &= \chi^{(3)}(\omega_a) \cdot F^{(3)}(\omega_a, \omega_b, \omega_c, \omega_d, \theta, \varphi),\end{aligned}\quad (1.7.3.32)$$

with

$$\begin{aligned}F^{(3)}(\omega_a, \omega_b, \omega_c, \omega_d, \theta, \varphi) &= \mathbf{e}(\omega_a, \theta, \varphi) \otimes \mathbf{e}(\omega_b, \theta, \varphi) \otimes \mathbf{e}(\omega_c, \theta, \varphi) \otimes \mathbf{e}(\omega_d, \theta, \varphi),\end{aligned}\quad (1.7.3.33)$$

where $\omega_a, \omega_b, \omega_c, \omega_d$ correspond to $\omega_4, \omega_1, \omega_2, \omega_3$ for SFG ($\omega_4 = \omega_1 + \omega_2 + \omega_3$); to $\omega_1, \omega_4, \omega_2, \omega_3$ for DFG ($\omega_1 = \omega_4 - \omega_2 - \omega_3$); to $\omega_2, \omega_4, \omega_1, \omega_3$ for DFG ($\omega_2 = \omega_4 - \omega_1 - \omega_3$); and to $\omega_3, \omega_4, \omega_1, \omega_2$ for DFG ($\omega_3 = \omega_4 - \omega_1 - \omega_2$).

Each $\mathbf{e}(\omega_i, \theta, \varphi)$ corresponds to a given eigen electric field vector.

The components of the field tensor are trigonometric functions of the direction of propagation.

Particular relations exist between field-tensor components of SFG and DFG which are valid for any direction of propagation. Indeed, from (1.7.3.31) and (1.7.3.33), it is obvious that the field-tensor components remain unchanged by concomitant permutations of the electric field vectors at the different frequencies and the corresponding Cartesian indices (Boulanger & Marnier, 1991; Boulanger *et al.*, 1993):

$$\begin{aligned}F_{ijk}^{\mathbf{e}_3 \mathbf{e}_1 \mathbf{e}_2}(\omega_3 = \omega_1 + \omega_2) &= F_{jik}^{\mathbf{e}_1 \mathbf{e}_3 \mathbf{e}_2}(\omega_1 = \omega_3 - \omega_2) \\ &= F_{kij}^{\mathbf{e}_2 \mathbf{e}_3 \mathbf{e}_1}(\omega_2 = \omega_3 - \omega_1)\end{aligned}\quad (1.7.3.34)$$

and

$$\begin{aligned}F_{ijkl}^{\mathbf{e}_4 \mathbf{e}_1 \mathbf{e}_2 \mathbf{e}_3}(\omega_4 = \omega_1 + \omega_2 + \omega_3) &= F_{jikl}^{\mathbf{e}_1 \mathbf{e}_4 \mathbf{e}_2 \mathbf{e}_3}(\omega_1 = \omega_4 - \omega_2 - \omega_3) \\ &= F_{kijl}^{\mathbf{e}_2 \mathbf{e}_4 \mathbf{e}_1 \mathbf{e}_3}(\omega_2 = \omega_4 - \omega_1 - \omega_3) \\ &= F_{lijk}^{\mathbf{e}_3 \mathbf{e}_4 \mathbf{e}_1 \mathbf{e}_2}(\omega_3 = \omega_4 - \omega_1 - \omega_2),\end{aligned}\quad (1.7.3.35)$$

where \mathbf{e}_i is the unit electric field vector at ω_i .

For a given interaction, the symmetry of the field tensor is governed by the vectorial properties of the electric fields, detailed in Section 1.7.3.1. This symmetry is then characteristic of both the optical class and the direction of propagation. These properties lead to four kinds of relations between the field-tensor components described later (Boulanger & Marnier, 1991; Boulanger *et al.*, 1993). Because of their interest for phase matching, we consider only the uniaxial and biaxial classes.

(a) The number of zero components varies with the direction of propagation according to the existence of nil electric field vector components. The only case where all the components are

nonzero concerns any direction of propagation out of the principal planes in biaxial crystals.

(b) The orthogonality relation (1.7.3.10) between any ordinary and extraordinary waves propagating in the same direction leads to specific relations independent of the direction of propagation. For example, the field tensor of an (*eo*) configuration of polarization (one extraordinary wave relative to the first Cartesian index and three ordinary waves relative to the three other indices) verifies $F_{xxij} + F_{yyij} (+ F_{zzij} = 0) = F_{xixj} + F_{yiyj} (+ F_{zizj} = 0) = F_{xijx} + F_{yijy} (+ F_{zizj} = 0) = 0$, with i and j equal to x or y ; the combination of these three relations leads to $F_{xxxx} = -F_{yyxx} = -F_{yxyx} = -F_{yxxy} = -F_{xyyy} = -F_{xyxy} = -F_{xyyx}$ and $F_{xyyy} = F_{yxyx} = F_{yyxx} = -F_{xyxx} = F_{xxyy} = -F_{xxxy}$. In a biaxial crystal, this kind of relation does not exist out of the principal planes.

(c) The fact that the direction of the ordinary electric field vectors in uniaxial crystals does not depend on the frequency, (1.7.3.11), leads to symmetry in the Cartesian indices relative to the ordinary waves. These relations can be redundant in comparison with certain orthogonality relations and are valid for any direction of propagation in uniaxial crystals. It is also the case for biaxial crystals, but only in the principal planes xz and yz . In the xy plane of biaxial crystals, the ordinary wave, (1.7.3.15), has a walk-off angle which depends on the frequency, and the extraordinary wave, (1.7.3.16), has no walk-off angle: then the field tensor is symmetric in the Cartesian indices relative to the extraordinary waves. The walk-off angles of ordinary and extraordinary waves are nil along the principal axes of the index surface of biaxial and uniaxial crystals and so everywhere in the xy plane of uniaxial crystals. Thus, any field tensor associated with these directions of propagation is symmetric in the Cartesian indices relative to both the ordinary and extraordinary waves.

(d) Equalities between frequencies can create new symmetries: the field tensors of the uniaxial class for any direction of propagation and of the biaxial class in only the principal planes xz and yz become symmetric in the Cartesian indices relative to the extraordinary waves at the same frequency; in the xy plane of a biaxial crystal, this symmetry concerns the indices relative to the ordinary waves. Equalities between frequencies are the only situations for which the field tensors are partly symmetric out of the principal planes of a biaxial crystal: the symmetry concerns the indices relative to the waves (+) with identical frequencies; it is the same for the waves (-): for example, $F_{ijk}^{++}(2\omega = \omega + \omega) = F_{ikj}^{++}(2\omega = \omega + \omega)$, $F_{ijkl}^{++}(\omega_4 = \omega + \omega + \omega_3) = F_{ikjl}^{++}(\omega_4 = \omega + \omega + \omega_3)$, $F_{ijkl}^{--}(\omega_4 = \omega + \omega + \omega_3) = F_{ikjl}^{--}(\omega_4 = \omega + \omega + \omega_3)$ and so on.

1.7.3.2.4.2. Uniaxial class

The field-tensor components are calculated from (1.7.3.11) and (1.7.3.12). The phase-matching case is the only one considered here: according to Tables 1.7.3.1 and 1.7.3.2, the allowed configurations of polarization of three-wave and four-wave interactions, respectively, are the *2o.e* (two ordinary and one extraordinary waves), the *2e.o* and the *3o.e*, *3e.o*, *2o.2e*.

Tables 1.7.3.7 and 1.7.3.8 give, respectively, the matrix representations of the three-wave interactions (*eo*), (*oee*) and of the four-wave (*oeoe*), (*eo*), (*ooee*) interactions for any direction of propagation in the general case where all the frequencies are different. In this situation, the number of independent components of the field tensors are: 7 for *2o.e*, 12 for *2e.o*, 9 for *3o.e*, 28 for *3e.o* and 16 for *2o.2e*. Note that the increase of the number of ordinary waves leads to an enhancement of symmetry of the field tensors.

If there are equalities between frequencies, the field tensors *oe*, *oeoe* and *oeoe* become totally symmetric in the Cartesian indices relative to the extraordinary waves and the tensors *eo* and *eo* remain unchanged.

Table 1.7.3.9 gives the field-tensor components specifically nil in the principal planes of uniaxial and biaxial crystals. The nil

1.7. NONLINEAR OPTICAL PROPERTIES

components for the other configurations of polarization are obtained by permutation of the Cartesian indices and the corresponding polarizations.

From Tables 1.7.3.7 and 1.7.3.8, it is possible to deduce all the other $2e.o$ interactions (eeo), (oeo), the $2o.e$ interactions (ooe), (oeo), the $3o.e$ interactions ($oooe$), ($oeoo$), ($ooeo$), the $3e.o$ interactions ($eeoe$), ($eeoe$), ($eeeo$) and the $2o.2e$ interactions ($oeoe$), ($eeoe$), ($eeeo$), ($oeeo$), ($eeoe$). The corresponding interactions and types are given in Tables 1.7.3.1 and 1.7.3.2. According to (1.7.3.31) and (1.7.3.33), the magnitudes of two permuted components are equal if the permutation of polarizations are associated with the corresponding frequencies. For example, according to Table 1.7.3.2, two permuted field-tensor components have the same magnitude for permutation between the following $3o.e$ interactions:

(i) ($eeoo$) SFG (ω_4) type I < 0 and the three ($oeoo$) interactions, DFG (ω_1) type II < 0, DFG (ω_2) type III < 0, DFG (ω_3) type IV < 0;

(ii) the three ($oooe$) interactions, SFG (ω_4) type II > 0, DFG (ω_1) type III > 0, DFG (ω_2) type IV > 0 and ($eeoo$) DFG (ω_3) type I > 0;

(iii) the two ($ooeo$) interactions SFG (ω_4) type III > 0, DFG (ω_1) type IV > 0, ($eeoo$) DFG (ω_2) type I > 0, and ($oooe$) DFG (ω_3) type II > 0;

(iv) ($oeoo$) SFG (ω_4) type IV > 0, ($eeoo$) DFG (ω_1) type I > 0, and the two interactions ($ooeo$) DFG (ω_2) type II > 0, DFG (ω_3) type III > 0.

The contraction of the field tensor and the uniaxial dielectric susceptibility tensor of corresponding order, given in Tables 1.7.2.2 to 1.7.2.5, is nil for the following uniaxial crystal classes

Table 1.7.3.7. Matrix representations of the (oeo) and (eeo) field tensors of the uniaxial class and of the biaxial class in the principal planes xz and yz , with $\omega_1 \neq \omega_2$ (Boulanger & Marnier, 1991)

$\bullet \quad F_{ijk} = 0$
 $\bullet \text{---} \bullet \quad F_{ijk} = F_{lmn}$
 $\bullet \text{---} \circ \quad F_{ijk} = -F_{lmn}$

| Interactions | Three-rank $F_{ijk}(\theta, \varphi)$ field tensors |
|---|---|
| Type eeo SFG (ω_3) type I < 0 DFG (ω_1) type I > 0 DFG (ω_2) type I > 0 | $F = \begin{pmatrix} x & y & z \\ y & x & z \\ z & x & y \end{pmatrix}$ |
| Type oeo SFG (ω_3) type I > 0 DFG (ω_1) type I < 0 DFG (ω_2) type I < 0 | $F = \begin{pmatrix} x & y & z \\ y & x & z \\ z & x & y \end{pmatrix}$ |

Table 1.7.3.8. Matrix representations of the ($oeoe$), ($eeoo$) and ($ooee$) field tensors of the uniaxial class and of the biaxial class in the principal planes xz and yz , with $\omega_1 \neq \omega_2 \neq \omega_3$ (Boulanger et al., 1993)

$\bullet \quad F_{ijkl} = 0$
 $\bullet \text{---} \bullet \quad F_{ijkl} = F_{mnop}$
 $\bullet \text{---} \circ \quad F_{ijkl} = -F_{mnop}$

| Interactions | Four-rank $F_{ijkl}(\theta, \varphi)$ field tensors |
|---|--|
| Type $oeoe$ SFG (ω_4) type I > 0 DFG (ω_1) type I < 0 DFG (ω_2) type I < 0 DFG (ω_3) type I < 0 | $F(3) = \begin{pmatrix} x & y & z \\ y & x & z \\ z & x & y \end{pmatrix}$ |
| Type $eeoo$ SFG (ω_4) type I < 0 DFG (ω_1) type I > 0 DFG (ω_2) type I > 0 DFG (ω_3) type I > 0 | $F(3) = \begin{pmatrix} x & y & z \\ y & x & z \\ z & x & y \end{pmatrix}$ |
| Type $ooee$ SFG (ω_4) type $V^4 > 0$ DFG (ω_1) type $V^1 > 0$ DFG (ω_2) type $V^2 > 0$ DFG (ω_3) type $V^3 > 0$ | $F(3) = \begin{pmatrix} x & y & z \\ y & x & z \\ z & x & y \end{pmatrix}$ |

1. TENSORIAL ASPECTS OF PHYSICAL PROPERTIES

Table 1.7.3.9. Field-tensor components specifically nil in the principal planes of uniaxial and biaxial crystals for three-wave and four-wave interactions

(i, j, k) = x, y or z.

| Configurations of polarization | Nil field-tensor components | | |
|--------------------------------|--|--|--|
| | (xy) plane | (xz) plane | (yz) plane |
| ooo | $F_{xjk} = 0; F_{yjk} = 0$ | $F_{ixk} = F_{ijx} = 0$ $F_{yjk} = 0$ | $F_{iyk} = F_{ijy} = 0$ $F_{xjk} = 0$ |
| oeo | $F_{ixk} = F_{ijx} = 0$ $F_{iyk} = F_{ijy} = 0$ | $F_{iyk} = F_{ijy} = 0$ $F_{xik} = 0$ | $F_{ixk} = F_{ijx} = 0$ $F_{yjk} = 0$ |
| oooo | $F_{xjkl} = 0; F_{yjkl} = 0$ | $F_{ixkl} = F_{ijxl} = F_{ijkx} = 0$ $F_{yjkl} = 0$ | $F_{iykl} = F_{ijyl} = F_{ijkx} = 0$ $F_{xjkl} = 0$ |
| oeoe | $F_{ixkl} = F_{ijxl} = F_{ijkx} = 0$ $F_{iykl} = F_{ijyl} = F_{ijkx} = 0$ | $F_{ixkl} = F_{ijxl} = F_{ijkx} = 0$ $F_{yjkl} = 0$ | $F_{ixkl} = F_{ijxl} = F_{ijkx} = 0$ $F_{yjkl} = 0$ |
| ooee | $F_{ixl} = F_{ijkx} = 0$ $F_{ijyl} = F_{ijkx} = 0$ | $F_{xjkl} = F_{ixkl} = 0$ $F_{ijyl} = F_{ijkx} = 0$ | $F_{yjl} = F_{ijkx} = 0$ $F_{ixl} = F_{ijkx} = 0$ |

and configurations of polarization: D_4 and D_6 for $2o.e$, C_{4v} and C_{6v} for $2e.o$, D_6 , D_{6h} , D_{3h} and C_{6v} for $3o.e$ and $3e.o$. Thus, even if phase-matching directions exist, the effective coefficient in these situations is nil, which forbids the interactions considered (Boulanger & Marnier, 1991; Boulanger *et al.*, 1993). The number of forbidden crystal classes is greater under the Kleinman approximation. The forbidden crystal classes have been determined for the particular case of third harmonic generation assuming Kleinman conjecture and without consideration of the field tensor (Midwinter & Warner, 1965).

1.7.3.2.4.3. Biaxial class

The symmetry of the biaxial field tensors is the same as for the uniaxial class, though only for a propagation in the principal planes xz and yz ; the associated matrix representations are given in Tables 1.7.3.7 and 1.7.3.8, and the nil components are listed in Table 1.7.3.9. Because of the change of optic sign from either side of the optic axis, the field tensors of the interactions for which the phase-matching cone joins areas b and a or a and c , given in Fig. 1.7.3.5, change from one area to another: for example, the field tensor ($oeoe$) becomes an ($oooo$) and so the solicited components of the electric susceptibility tensor are not the same.

The nonzero field-tensor components for a propagation in the xy plane of a biaxial crystal are: F_{zxx} , F_{zyy} , $F_{zxy} \neq F_{zyx}$ for (ooo); F_{xzz} , F_{yzz} for (oeo); F_{zxxx} , F_{zyyy} , $F_{zxyy} \neq F_{zyxy} \neq F_{zyyx}$, $F_{zxyx} \neq F_{zyxx} \neq F_{zyyx}$ for ($oooo$); F_{xzzz} , F_{yzzz} for ($oeoe$); $F_{xyzz} \neq F_{yxzz}$, F_{xxzz} , F_{yyzz} for ($ooee$). The nonzero components for the other configurations of polarization are obtained by the associated permutations of the Cartesian indices and the corresponding polarizations.

The field tensors are not symmetric for a propagation out of the principal planes in the general case where all the frequencies are different: in this case there are 27 independent components for the three-wave interactions and 81 for the four-wave interactions, and so all the electric susceptibility tensor components are solicited.

As phase matching imposes the directions of the electric fields of the interacting waves, it also determines the field tensor and hence the effective coefficient. Thus there is no possibility of choice of the $\chi^{(2)}$ coefficients, since a given type of phase matching is considered. In general, the largest coefficients of polar crystals, *i.e.* χ_{zzz} , are implicated at a very low level when phase matching is achieved, because the corresponding field tensor, *i.e.* F_{zzz} , is often weak (Boulanger *et al.*, 1997). In contrast, QPM authorizes the coupling between three waves polarized along the z axis, which leads to an effective coefficient which is purely χ_{zzz} , *i.e.* $\chi_{\text{eff}} = (2/\pi)\chi_{zzz}$, where the numerical factor comes from the periodic character of the rectangular function of modulation (Fejer *et al.*, 1992).

1.7.3.3. Integration of the propagation equations

1.7.3.3.1. Spatial and temporal profiles

The resolution of the coupled equations (1.7.3.22) or (1.7.3.24) over the crystal length L leads to the electric field amplitude $E_i(X, Y, L)$ of each interacting wave. The general solutions are Jacobian elliptic functions (Armstrong *et al.*, 1962; Fève, Boulanger & Douady, 2002). The integration of the systems is simplified for cases where one or several beams are held constant, which is called the undepleted pump approximation. We consider mainly this kind of situation here. The power of each interacting wave is calculated by integrating the intensity over the cross section of each beam according to (1.7.3.8). For our main purpose, we consider the simple case of plane-wave beams with two kinds of transverse profile:

$$\begin{aligned} \mathbf{E}(X, Y, Z) &= \mathbf{e}E_o(Z) \quad \text{for } (X, Y) \in [-w_o, +w_o] \\ \mathbf{E}(X, Y, Z) &= 0 \quad \text{elsewhere} \end{aligned} \quad (1.7.3.36)$$

for a flat distribution over a radius w_o ;

$$\mathbf{E}(X, Y, Z) = \mathbf{e}E_o(Z) \exp[-(X^2 + Y^2)/w_o^2] \quad (1.7.3.37)$$

for a Gaussian distribution, where w_o is the radius at $(1/e)$ of the electric field and so at $(1/e^2)$ of the intensity.

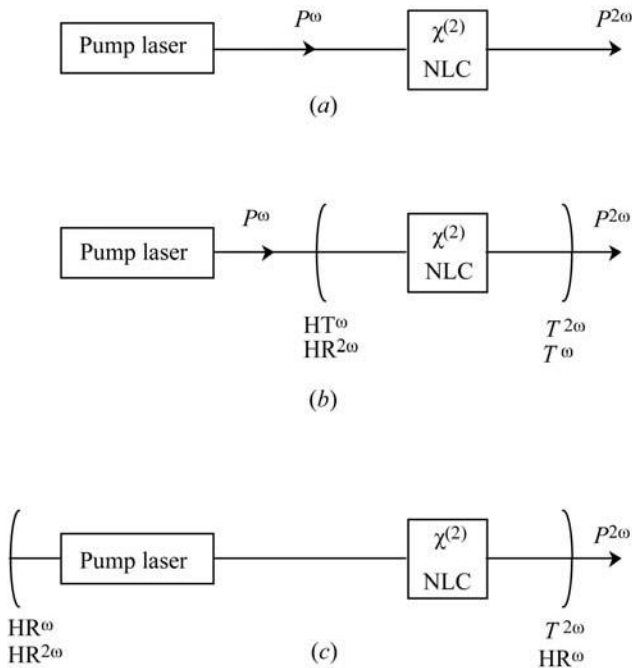


Fig. 1.7.3.6. Schematic configurations for second harmonic generation: (a) non-resonant SHG; (b) external resonant SHG: the resonant wave may either be the fundamental or the harmonic one; (c) internal resonant SHG. $P^{\omega, 2\omega}$ are the fundamental and harmonic powers; HT^{ω} and $HR^{\omega, 2\omega}$ are the high-transmission and high-reflection mirrors at ω or 2ω and $T^{\omega, 2\omega}$ are the transmission coefficients of the output mirror at ω or 2ω . NLC is the nonlinear crystal with a nonzero $\chi^{(2)}$.

1.7. NONLINEAR OPTICAL PROPERTIES

The associated powers are calculated according to (1.7.3.8), which leads to

$$P(L) = m(n/2)(\varepsilon_o/\mu_o)^{1/2}|E_o|^2\pi w_o^2 \quad (1.7.3.38)$$

where $m = 1$ for a flat distribution and $m = 1/2$ for a Gaussian profile.

The nonlinear interaction is characterized by the conversion efficiency, which is defined as the ratio of the generated power to the power of one or several incident beams, according to the different kinds of interactions.

For pulsed beams, it is necessary to consider the temporal shape, usually Gaussian:

$$P(t) = P_c \exp(-2t^2/\tau^2) \quad (1.7.3.39)$$

where P_c is the peak power and τ the half ($1/e^2$) width.

For a repetition rate f (s^{-1}), the average power \bar{P} is then given by

$$\bar{P} = P_c \tau f (\pi/2)^{1/2} = \tilde{E} f \quad (1.7.3.40)$$

where \tilde{E} is the energy per Gaussian pulse.

When the pulse shape is not well defined, it is suitable to consider the energies per pulse of the incident and generated waves for the definition of the conversion efficiency.

The interactions studied here are sum-frequency generation (SFG), including second harmonic generation (SHG: $\omega + \omega = 2\omega$), cascading third harmonic generation (THG: $\omega + 2\omega = 3\omega$) and direct third harmonic generation (THG: $\omega + \omega + \omega = 3\omega$). The difference-frequency generation (DFG) is also considered, including optical parametric amplification (OPA) and oscillation (OPO).

We choose to analyse in detail the different parameters relative to conversion efficiency (figure of merit, acceptance bandwidths, walk-off effect *etc.*) for SHG, which is the prototypical second-order nonlinear interaction. This discussion will be valid for the other nonlinear processes of frequency generation which will be considered later.

1.7.3.3.2. Second harmonic generation (SHG)

According to Table 1.7.3.1, there are two types of phase matching for SHG: type I and type II (equivalent to type III).

The fundamental waves at ω define the pump. Two situations are classically distinguished: the undepleted pump approximation, when the power conversion efficiency is sufficiently low to consider the fundamental power to be undepleted, and the depleted case for higher efficiency. There are different ways to realize SHG, as shown in Fig. 1.7.3.6: the simplest one is non-resonant SHG, outside the laser cavity; other ways are external or internal resonant cavity SHG, which allow an enhancement of the single-pass efficiency conversion.

1.7.3.3.2.1. Non-resonant SHG with undepleted pump in the parallel-beam limit with a Gaussian transverse profile

We first consider the case where the crystal length is short enough to be located in the near-field region of the laser beam where the parallel-beam limit is a good approximation. We make another simplification by considering a propagation along a principal axis of the index surface: then the walk-off angle of each interacting wave is nil so that the three waves have the same coordinate system (X, Y, Z) .

The integration of equations (1.7.3.22) over the crystal length Z in the undepleted pump approximation, *i.e.* $\partial E_1^\omega(X, Y, Z)/\partial Z = \partial E_2^\omega(X, Y, Z)/\partial Z = 0$, with $E_3^{2\omega}(X, Y, 0) = 0$, leads to

$$|E_3^{2\omega}(X, Y, L)|^2 = \{K_3^{2\omega}[\varepsilon_o \chi_{\text{eff}}^{(2)}]\}^2 |E_1^\omega(X, Y, 0)E_2^\omega(X, Y, 0)|^2 \times L^2 \sin^2 c^2[(\Delta k \cdot L)/2]. \quad (1.7.3.41)$$

(1.7.3.41) implies a Gaussian transversal profile for $|E_3^{2\omega}(X, Y, L)|$ if $|E_1^\omega(X, Y, 0)|$ and $|E_2^\omega(X, Y, 0)|$ are Gaussian. The three beam radii are related by $(1/w_{o3}^2) = (1/w_{o1}^2) + (1/w_{o2}^2)$, so if we assume that the two fundamental beams have the same radius w_o^ω , which is not an approximation for type I, then $w_o^{2\omega} = [w_o^\omega/(2^{1/2})]$. Two incident beams with a flat distribution of radius w_o^ω lead to the generation of a flat harmonic beam with the same radius $w_o^{2\omega} = w_o^\omega$.

The integration of (1.7.3.41) according to (1.7.3.36)–(1.7.3.38) for a Gaussian profile gives in the SI system

$$P^{2\omega}(L) = BP_1^\omega(0)P_2^\omega(0)\frac{L^2}{w_o^2}\sin^2 c^2\left(\frac{\Delta k \cdot L}{2}\right) \\ B = \frac{32\pi}{\varepsilon_o c} \frac{2N-1}{N} \frac{d_{\text{eff}}^2}{\lambda_\omega^2} \frac{T_3^{2\omega}T_1^\omega T_2^\omega}{n_3^{2\omega}n_1^\omega n_2^\omega}, \quad (W^{-1}) \quad (1.7.3.42)$$

where $c = 3 \times 10^8 \text{ m s}^{-1}$, $\varepsilon_o = 8.854 \times 10^{-12} \text{ A s V}^{-1} \text{ m}^{-1}$ and so $(32\pi/\varepsilon_o c) = 37.85 \times 10^3 \text{ V A}^{-1}$. L (m) is the crystal length in the direction of propagation. $\Delta k = k_3^{2\omega} - k_1^\omega - k_2^\omega$ is the phase mismatch. $n_3^{2\omega}$, n_1^ω and n_2^ω are the refractive indices at the harmonic and fundamental wavelengths $\lambda_{2\omega}$ and λ_ω (μm): for the phase-matching case, $\Delta k = 0$, $n_3^{2\omega} = n^-(2\omega)$, $n_1^\omega = n_2^\omega = n^+(\omega)$ for type I (the two incident fundamental beams have the same polarization contained in Π^+ , with the harmonic polarization contained in Π^-) and $n_1^\omega = n^+(\omega) \neq n_2^\omega = n^-(\omega)$ for type II (the two solicited eigen modes at the fundamental wavelength are in Π^+ and Π^- , with the harmonic polarization contained in Π^-). $T_3^{2\omega}$, T_1^ω and T_2^ω are the transmission coefficients given by $T_i = 4n_i/(n_i + 1)^2$. d_{eff} (pm V^{-1}) $= (1/2)\chi_{\text{eff}}^{(2)} = (1/2)[F^{(2)} \cdot \chi^{(2)}]$ is the effective coefficient given by (1.7.3.30) and (1.7.3.31). $P_1^\omega(0)$ and $P_2^\omega(0)$ are the two incident fundamental powers, which are not necessarily equal for type II; for type I we have obviously $P_1^\omega(0) = P_2^\omega(0) = (P_{\text{tot}}^\omega/2)$. N is the number of independently oscillating modes at the fundamental wavelength: every longitudinal mode at the harmonic pulsation can be generated by many combinations of two fundamental modes; the $(2N-1)/N$ factor takes into account the fluctuations between these longitudinal modes (Bloembergen, 1963).

The powers in (1.7.3.42) are instantaneous powers $P(t)$.

The second harmonic (SH) conversion efficiency, η_{SHG} , is usually defined as the ratio of peak powers $P^{2\omega}(L)/P_{\text{c,tot}}^\omega(0)$, or as the ratio of the pulse total energy $\tilde{E}^{2\omega}(L)/\tilde{E}_{\text{tot}}^\omega(0)$. For Gaussian temporal profiles, the SH ($1/e^2$) pulse duration $\tau_{2\omega}$ is equal to $\tau_\omega/(2^{1/2})$, because $P_{2\omega}$ is proportional to P_ω^2 , and so, according to (1.7.3.40), the pulse average energy conversion efficiency is $1/(2^{1/2})$ smaller than the peak power conversion efficiency given by (1.7.3.42). Note that the pulse total energy conversion efficiency is equivalent to the average power conversion efficiency $\tilde{P}^{2\omega}(L)/\tilde{P}_{\text{tot}}^\omega(0)$, with $\tilde{P} = \tilde{E} \cdot f$ where f is the repetition rate.

Formula (1.7.3.42) shows the importance of the contribution of the linear optical properties to the nonlinear process. Indeed, the field tensor $F^{(2)}$, the transmission coefficients T_i and the phase mismatch Δk only depend on the refractive indices in the direction of propagation considered.

(i) Figure of merit.

The contribution of $F^{(2)}$ was discussed previously, where it was shown that the field tensor is nil in particular directions of propagation or everywhere for particular crystal classes and configurations of polarization (even if the nonlinearity $\chi^{(2)}$ is high).

The field tensor $F^{(2)}$ of SHG can be written with the contracted notation of $d^{(2)}$; according to Table 1.7.3.1 and to the contraction

1. TENSORIAL ASPECTS OF PHYSICAL PROPERTIES

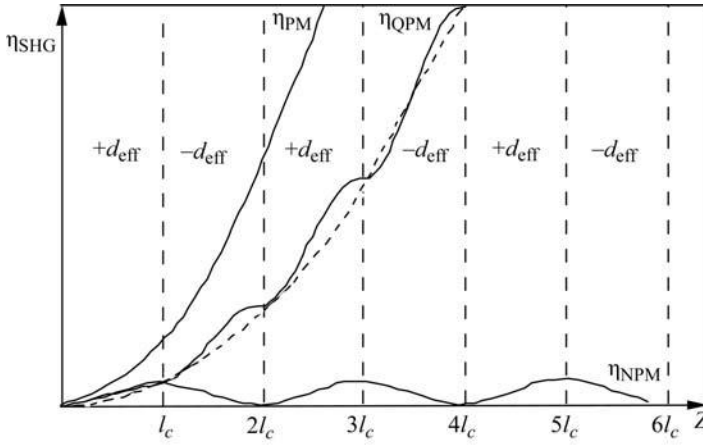


Fig. 1.7.3.7. Spatial growth evolution of second harmonic conversion efficiency, η_{SHG} , for non phase matching (NPM), $\Delta k \neq 0$, and phase matching (PM), $\Delta k = 0$, in a 'continuous' crystal, and for quasi phase matching (QPM) in a periodic structure. The dashed curve corresponds to $(4/\pi^2)\eta_{\text{PM}}(Z)$ where η_{PM} is the conversion efficiency of the phase-matched SHG. $l_c = \pi/\Delta k$ is the coherence length.

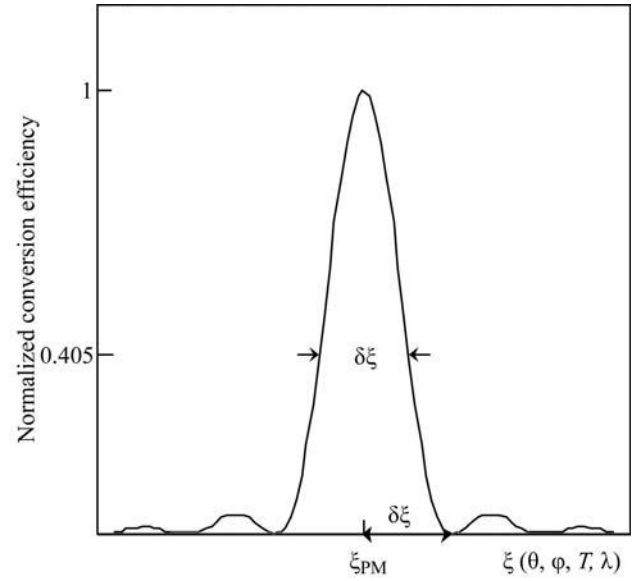


Fig. 1.7.3.8. Conversion efficiency evolution as a function of ξ for a given crystal length. ξ denotes the angle (θ or φ), the temperature (T) or the wavelength (λ). ξ_{PM} represents the parameter allowing phase matching.

conventions given in Section 1.7.2.2, the contracted field-tensor components for the phase-matched SHG are

$$\begin{aligned} F_{i1} &= \mathbf{e}_i^-(2\omega)[\mathbf{e}_x^+(\omega)]^2 \\ F_{i2} &= \mathbf{e}_i^-(2\omega)[\mathbf{e}_y^+(\omega)]^2 \\ F_{i3} &= \mathbf{e}_i^-(2\omega)[\mathbf{e}_z^+(\omega)]^2 \\ F_{i4} &= 2\mathbf{e}_i^-(2\omega)\mathbf{e}_x^+(\omega)\mathbf{e}_z^+(\omega) \\ F_{i5} &= 2\mathbf{e}_i^-(2\omega)\mathbf{e}_x^+(\omega)\mathbf{e}_y^+(\omega) \\ F_{i6} &= 2\mathbf{e}_i^-(2\omega)\mathbf{e}_x^+(\omega)\mathbf{e}_y^+(\omega) \end{aligned}$$

for type I and

$$\begin{aligned} F_{i1} &= \mathbf{e}_i^-(2\omega)\mathbf{e}_x^+(\omega)\mathbf{e}_x^-(\omega) \\ F_{i2} &= \mathbf{e}_i^-(2\omega)\mathbf{e}_y^+(\omega)\mathbf{e}_y^-(\omega) \\ F_{i3} &= \mathbf{e}_i^-(2\omega)\mathbf{e}_z^+(\omega)\mathbf{e}_z^-(\omega) \\ F_{i4} &= \mathbf{e}_i^-(2\omega)[\mathbf{e}_y^+(\omega)\mathbf{e}_z^-(\omega) + \mathbf{e}_y^-(\omega)\mathbf{e}_z^+(\omega)] \\ F_{i5} &= \mathbf{e}_i^-(2\omega)[\mathbf{e}_x^+(\omega)\mathbf{e}_z^-(\omega) + \mathbf{e}_x^-(\omega)\mathbf{e}_z^+(\omega)] \\ F_{i6} &= \mathbf{e}_i^-(2\omega)[\mathbf{e}_x^+(\omega)\mathbf{e}_y^-(\omega) + \mathbf{e}_x^-(\omega)\mathbf{e}_y^+(\omega)] \end{aligned}$$

for type II, with $i = (1, 2, 3)$ for F_{ij} , corresponding to $i = (x, y, z)$ for $\mathbf{e}_i^-(2\omega)$.

The ratio $d_{\text{eff}}^2/n_3^2\omega_1^2\omega_2^2$ in formula (1.7.3.42) is called the figure of merit of the direction considered. The effective coefficient is given in Section 1.7.5 for the main nonlinear crystals and for chosen SHG wavelengths.

(ii) *Effect of the phase mismatch.*

The interference function $\sin^2(\Delta kL/2)$ is a maximum and equal to unity only for $\Delta k = 0$, which defines the phase-matching condition. Fig. 1.7.3.7 shows the effect of the phase mismatch on the growth of second harmonic conversion efficiency, η_{SHG} , with interaction distance Z .

The conversion efficiency has a Z^2 dependence in the case of phase matching. The harmonic power oscillates around Z^2 for quasi phase matching, but is reduced by a factor of $4/\pi^2$ compared with that of phase-matched interaction (Fejer *et al.*, 1992).

An SHG phase-matching direction ($\theta_{\text{PM}}, \varphi_{\text{PM}}$) for given fundamental wavelength (λ_{PM}) and type of interaction, I or II, is defined at a given temperature (T_{PM}). It is important to consider the effect of deviation of Δk from 0 due to variations of angles ($\theta_{\text{PM}} \pm d\theta, \varphi_{\text{PM}} \pm d\varphi$), of temperature ($T_{\text{PM}} \pm dT$) and of wave-

length ($\lambda_{\text{PM}} \pm d\lambda$) on the conversion efficiency. The quantities that characterize these effects are the acceptance bandwidths $\delta\xi$ ($\xi = \theta, \varphi, T, \lambda$), usually defined as the deviation from the phase-matching value ξ_{PM} leading to a phase-mismatch variation Δk from 0 to $2\pi/L$, where L is the crystal length. Then $\delta\xi$ is also the full width of the peak efficiency curve plotted as a function of ξ at 0.405 of the maximum, as shown in Fig. 1.7.3.8.

Thus $L\delta\xi$ is a characteristic of the phase-matching direction. Small angular, thermal and spectral dispersion of the refractive indices lead to high acceptance bandwidths. The higher $L\delta\xi$, the lower is the decrease of the conversion efficiency corresponding to a given angular shift, to the heating of the crystal due to absorption or external heating, or to the spectral bandwidth of the fundamental beam.

The knowledge of the angular, thermal and spectral dispersion of the refractive indices allows an estimation of $\delta\xi$ by expanding Δk in a Taylor series about ξ_{PM} :

$$\frac{2\pi}{L} = \Delta k = \left. \frac{\partial(\Delta k)}{\partial\xi} \right|_{\xi_{\text{PM}}} \delta\xi + \frac{1}{2} \left. \frac{\partial^2(\Delta k)}{\partial\xi^2} \right|_{\xi_{\text{PM}}} (\delta\xi)^2 + \dots \quad (1.7.3.43)$$

When the second- and higher-order differential terms in (1.7.3.43) are negligible, the phase matching is called critical (CPM), because $L\delta\xi \simeq |2\pi/[\partial(\Delta k)/\partial\xi]_{\xi_{\text{PM}}}|$ is small. For the particular cases where $\partial(\Delta k)/\partial\xi|_{\xi_{\text{PM}}} = 0$, $L\delta\xi = \{|4\pi L/[\partial^2(\Delta k)/\partial\xi^2]_{\xi_{\text{PM}}}| \}^{1/2}$ is larger than the CPM acceptance and the phase matching is called non-critical (NCPM) for the parameter ξ considered.

We first consider the case of angular acceptances. In uniaxial crystals, the refractive indices do not vary in φ , leading to an infinite φ angular acceptance bandwidth. $\delta\theta$ is then the only one to consider. For directions of propagation out of the principal plane ($\theta_{\text{PM}} \neq \pi/2$), the phase matching is critical. According to the expressions of n_o and $n_e(\theta)$ given in Section 1.7.3.1, we have

(1) for type I in positive crystals, $n_e(\theta, \omega) = n_o(2\omega)$ and

$$L\delta\theta \simeq 2\pi/\{-(\omega/c)n_o^3(2\omega)[n_e^{-2}(\omega) - n_o^{-2}(\omega)] \sin 2\theta_{\text{PM}}\}; \quad (1.7.3.44)$$

(2) for type II in positive crystals, $2n_o(2\omega) = n_e(\theta, \omega) + n_o(\omega)$ and

1.7. NONLINEAR OPTICAL PROPERTIES

$$L\delta\theta \simeq 2\pi/\{-(\omega/2c)[2n_o(2\omega) - n_o(\omega)]^3 \\ \times [n_e^{-2}(\omega) - n_o^{-2}(\omega)] \sin 2\theta_{\text{PM}}\}; \quad (1.7.3.45)$$

(3) for type I in negative crystals, $n_e(\theta, 2\omega) = n_o(\omega)$ and

$$L\delta\theta \simeq 2\pi/\{-(\omega/c)n_o^3(\omega)[n_o^{-2}(2\omega) - n_e^{-2}(2\omega)] \sin 2\theta_{\text{PM}}\}; \quad (1.7.3.46)$$

(4) for type II in negative crystals, $2n_e(\theta, 2\omega) = n_e(\theta, \omega) + n_o(\omega)$ and

$$L\delta\theta \simeq |2\pi/\{-(\omega/c)n_e^3(\theta, 2\omega)[n_e^{-2}(2\omega) - n_o^{-2}(2\omega)] \sin 2\theta_{\text{PM}} \\ + (\omega/2c)n_e^3(\theta, \omega)[n_e^{-2}(\omega) - n_o^{-2}(\omega)] \sin 2\theta_{\text{PM}}\}|. \quad (1.7.3.47)$$

CPM acceptance bandwidths are small, typically about one mrad cm, as shown in Section 1.7.5 for the classical nonlinear crystals.

When $\theta_{\text{PM}} = \pi/2$, $\partial\Delta k/\partial\theta = 0$ and the phase matching is non-critical:

(1) for type I in positive crystals, $n_e(\omega) = n_o(2\omega)$ and

$$L\delta\theta \simeq (2\pi L/\{-(\omega/c)n_o^3(2\omega)[n_e^{-2}(\omega) - n_o^{-2}(\omega)]\})^{1/2}; \quad (1.7.3.48)$$

(2) for type II in positive crystals, $2n_o(2\omega) = n_e(\omega) + n_o(\omega)$ and

$$L\delta\theta \simeq (2\pi L/\{-(\omega/2c)n_e^3(\omega)[n_e^{-2}(\omega) - n_o^{-2}(\omega)]\})^{1/2}; \quad (1.7.3.49)$$

(3) for type I in negative crystals, $n_o(\omega) = n_e(2\omega)$ and

$$L\delta\theta \simeq (2\pi L/\{(\omega/c)n_o^3(\omega)[n_e^{-2}(2\omega) - n_o^{-2}(2\omega)]\})^{1/2}; \quad (1.7.3.50)$$

(4) for type II in negative crystals, $2n_e(2\omega) = n_e(\omega) + n_o(\omega)$ and

$$L\delta\theta \simeq (|2\pi L/\{-(\omega/c)n_e^3(2\omega)[n_e^{-2}(2\omega) - n_o^{-2}(2\omega)] \\ + (\omega/2c)n_e^3(\omega)[n_e^{-2}(\omega) - n_o^{-2}(\omega)]\}|)^{1/2}. \quad (1.7.3.51)$$

Values of NCPM acceptance bandwidths are given in Section 1.7.5 for the usual crystals. From the previous expressions for CPM and NCPM angular acceptances, it appears that the angular bandwidth is all the smaller since the birefringence is high.

The situation is obviously more complex in the case of biaxial crystals. The φ acceptance bandwidth is not infinite, leading to a smaller anisotropy of the angular acceptance in comparison with uniaxial crystals. The expressions of the θ and φ acceptance bandwidths have the same form as for the uniaxial class only in the principal planes. The phase matching is critical (CPM) for all directions of propagation out of the principal axes x , y and z : in this case, the mismatch Δk is a linear function of small angular deviations from the phase-matching direction as for uniaxial crystals. There exist six possibilities of NCPM for SHG, types I and II along the three principal axes, corresponding to twelve different index conditions (Hobden, 1967):

(1) for positive biaxial crystals

$$\begin{array}{ll} \text{Type I (x)} & n_{2\omega}^y = n_{\omega}^z \\ \text{Type I (y)} & n_{2\omega}^x = n_{\omega}^z \\ \text{Type I (z)} & n_{2\omega}^y = n_{\omega}^x \\ \text{Type II (x)} & n_{2\omega}^y = \frac{1}{2}(n_{\omega}^y + n_{\omega}^z) \\ \text{Type II (y)} & n_{2\omega}^x = \frac{1}{2}(n_{\omega}^x + n_{\omega}^z) \\ \text{Type II (z)} & n_{2\omega}^x = \frac{1}{2}(n_{\omega}^x + n_{\omega}^y); \end{array} \quad (1.7.3.52)$$

(2) for negative biaxial crystals

$$\begin{array}{ll} \text{Type I (x)} & n_{2\omega}^z = n_{\omega}^y \\ \text{Type I (y)} & n_{2\omega}^z = n_{\omega}^x \\ \text{Type I (z)} & n_{2\omega}^y = n_{\omega}^x \\ \text{Type II (x)} & n_{2\omega}^z = \frac{1}{2}(n_{\omega}^y + n_{\omega}^z) \\ \text{Type II (y)} & n_{2\omega}^z = \frac{1}{2}(n_{\omega}^x + n_{\omega}^z) \\ \text{Type II (z)} & n_{2\omega}^y = \frac{1}{2}(n_{\omega}^x + n_{\omega}^y). \end{array}$$

The NCPM angular acceptances along the three principal axes of biaxial crystals can be deduced from the expressions relative to the uniaxial class by the following substitutions:

Along the x axis:

$$L\delta\varphi \text{ (type I } > 0) = (1.7.3.50) \text{ with } n_o(\omega) \rightarrow n_z(\omega),$$

$$n_e(2\omega) \rightarrow n_y(2\omega) \text{ and } n_o(2\omega) \rightarrow n_x(2\omega)$$

$$L\delta\theta \text{ (type I } > 0) = (1.7.3.48) \text{ with } n_o(2\omega) \rightarrow n_y(2\omega),$$

$$n_e(\omega) \rightarrow n_z(\omega) \text{ and } n_o(\omega) \rightarrow n_x(\omega)$$

$$L\delta\varphi \text{ (type II } > 0) = (1.7.3.51) \text{ with } n_e \rightarrow n_y \text{ and } n_o \rightarrow n_x$$

$$L\delta\theta \text{ (type II } > 0) = (1.7.3.49) \text{ with } n_e(\omega) \rightarrow n_z(\omega)$$

$$\text{and } n_o(\omega) \rightarrow n_x(\omega)$$

$$L\delta\varphi \text{ (type I } < 0) = (1.7.3.48) \text{ with } n_o(2\omega) \rightarrow n_z(2\omega),$$

$$n_e(\omega) \rightarrow n_x(\omega) \text{ and } n_o(\omega) \rightarrow n_y(\omega)$$

$$L\delta\theta \text{ (type I } < 0) = (1.7.3.50) \text{ with } n_o(\omega) \rightarrow n_y(\omega),$$

$$n_e(2\omega) \rightarrow n_z(2\omega) \text{ and } n_o(2\omega) \rightarrow n_x(2\omega)$$

$$L\delta\varphi \text{ (type II } < 0) = (1.7.3.49) \text{ with } n_e(\omega) \rightarrow n_x(\omega)$$

$$\text{and } n_o(\omega) \rightarrow n_y(\omega)$$

$$L\delta\theta \text{ (type II } < 0) = (1.7.3.51) \text{ with } n_e \rightarrow n_z \text{ and } n_o \rightarrow n_x.$$

Along the y axis:

$$L\delta\varphi \text{ is the same as along the } x \text{ axis for all interactions}$$

$$L\delta\theta \text{ (type I } > 0) = (1.7.3.48) \text{ with } n_o(2\omega) \rightarrow n_x(2\omega),$$

$$n_e(\omega) \rightarrow n_z(\omega) \text{ and } n_o(\omega) \rightarrow n_y(\omega)$$

$$L\delta\theta \text{ (type II } > 0) = (1.7.3.49) \text{ with } n_e(\omega) \rightarrow n_z(\omega)$$

$$\text{and } n_o(\omega) \rightarrow n_y(\omega)$$

$$L\delta\theta \text{ (type I } < 0) = (1.7.3.50) \text{ with } n_o(\omega) \rightarrow n_x(\omega),$$

$$n_e(2\omega) \rightarrow n_z(2\omega) \text{ and } n_o(2\omega) \rightarrow n_y(2\omega)$$

$$L\delta\theta \text{ (type II } < 0) = (1.7.3.51) \text{ with } n_e \rightarrow n_z \text{ and } n_o \rightarrow n_y.$$

Along the z axis:

$$L\delta\theta_{xz} \text{ (type I } > 0) = (1.7.3.48) \text{ with } n_o(2\omega) \rightarrow n_y(2\omega),$$

$$n_e(\omega) \rightarrow n_x(\omega) \text{ and } n_o(\omega) \rightarrow n_z(\omega)$$

$$L\delta\theta_{yz} \text{ (type I } > 0) = (1.7.3.48) \text{ with } n_o(2\omega) \rightarrow n_x(2\omega),$$

$$n_e(\omega) \rightarrow n_y(\omega) \text{ and } n_o(\omega) \rightarrow n_z(\omega)$$

$$L\delta\theta_{xz} \text{ (type II } > 0) = (1.7.3.49) \text{ with } n_e(\omega) \rightarrow n_x(\omega)$$

$$\text{and } n_o(\omega) \rightarrow n_z(\omega)$$

$$L\delta\theta_{yz} \text{ (type II } > 0) = (1.7.3.49) \text{ with } n_e(\omega) \rightarrow n_y(\omega)$$

$$\text{and } n_o(\omega) \rightarrow n_z(\omega)$$

$$L\delta\theta_{xz} \text{ (type I } < 0) = (1.7.3.50) \text{ with } n_o(\omega) \rightarrow n_y(\omega),$$

$$n_e(2\omega) \rightarrow n_z(2\omega) \text{ and } n_o(2\omega) \rightarrow n_x(2\omega)$$

$$L\delta\theta_{yz} \text{ (type I } < 0) = (1.7.3.50) \text{ with } n_o(\omega) \rightarrow n_x(\omega),$$

$$n_e(2\omega) \rightarrow n_z(2\omega) \text{ and } n_o(2\omega) \rightarrow n_y(2\omega)$$

1. TENSORIAL ASPECTS OF PHYSICAL PROPERTIES

$$L\delta\theta_{xz} \text{ (type II } < 0) = (1.7.3.51) \text{ with } n_e \rightarrow n_x \text{ and } n_o \rightarrow n_z$$

$$L\delta\theta_{yz} \text{ (type II } < 0) = (1.7.3.51) \text{ with } n_e \rightarrow n_y \text{ and } n_o \rightarrow n_z.$$

The above formulae are relative to the internal angular acceptance bandwidths. The external acceptance angles are enlarged by a factor of approximately $n(\omega)$ for type I or $[n_1(\omega) + n_2(\omega)]/2$ for type II, due to refraction at the input plane face of the crystal. The angular acceptance is an important issue connected with the accuracy of cutting of the crystal.

Temperature tuning is a possible alternative for achieving NCPM in a few materials. The corresponding temperatures for different interactions are given in Section 1.7.5.

Another alternative is to use a special non-collinear configuration known as one-beam non-critical non-collinear phase matching (OBNC): it is non-critical with respect to the phase-matching angle of one of the input beams (referred to as the non-critical beam). It has been demonstrated that the angular acceptance bandwidth for the non-critical beam is exceptionally large, for example about 50 times that for the critical beam for type-I SHG at 1.338 μm in 3-methyl-4-nitropyridine-*N*-oxide (POM) (Dou *et al.*, 1992).

The typical values of thermal acceptance bandwidth, given in Section 1.7.5, are of the order of 0.5 to 50 K cm. The thermal acceptance is an important issue for the stability of the harmonic power when the absorption at the wavelengths concerned is high or when temperature tuning is used for the achievement of angular NCPM. Typical spectral acceptance bandwidths for SHG are given in Section 1.7.5. The values are of the order of 1 nm cm, which is much larger than the linewidth of a single-frequency laser, except for some diode or for sub-picosecond lasers with a large spectral bandwidth.

Note that a degeneracy of the first-order temperature or spectral derivatives ($\partial\Delta k/\partial T|_{T_{PM}} = 0$ or $\partial\Delta k/\partial\lambda|_{\lambda_{PM}} = 0$) can occur and lead to thermal or spectral NCPM.

Consideration of the phase-matching function $\lambda_{PM} = f(\xi_{PM})$, where $\chi_{PM} = T_{PM}, \theta_{PM}, \varphi_{PM}$ or all other dispersion parameters of the refractive indices, is useful for a direct comparison of the situation of non-criticality of the phase matching relative to λ_{PM} and to the other parameters ξ_{PM} : a nil derivative of λ_{PM} with respect to ξ_{PM} , *i.e.* $d\lambda_{PM}/d\xi_{PM} = 0$ at the point $(\lambda_{PM}^0, \xi_{PM}^0)$, means that the phase matching is non-critical with respect to ξ_{PM} and so strongly critical with respect to λ_{PM} , *i.e.* $d\xi_{PM}/d\lambda_{PM} = \infty$ at this point. Then, for example, an angular NCPM direction is a spectral CPM direction and the reverse is also so.

(iii) Effect of spatial walk-off.

The interest of the NCPM directions is increased by the fact that the walk-off angle of any wave is nil: the beam overlap is complete inside the nonlinear crystal. Under CPM, the interacting waves propagate with different walk-off angles: the conversion efficiency is then attenuated because the different Poynting vectors are not collinear and the beams do not overlap. Type I and type II are not equivalent in terms of walk-off angles. For type I, the two fundamental waves have the same polarization \mathbf{E}^+ and the same walk-off angle ρ^+ , which is different from the harmonic one; thus the coordinate systems that are involved in equations (1.7.3.22) are $(X_1, Y_1, Z) = (X_2, Y_2, Z) = (X_\omega^+, Y_\omega^+, Z)$ and $(X_3, Y_3, Z) = (X_{2\omega}^-, Y_{2\omega}^-, Z)$. For type II, the two fundamental waves have necessarily different walk-off angles ρ^+ and ρ^- , which forbids the nonlinear interaction beyond the plane where the two fundamental beams are completely separated. In this case we have three different coordinate systems: $(X_1, Y_1, Z) = (X_\omega^+, Y_\omega^+, Z)$, $(X_2, Y_2, Z) = (X_\omega^-, Y_\omega^-, Z)$ and $(X_3, Y_3, Z) = (X_{2\omega}^-, Y_{2\omega}^-, Z)$.

The three coordinate systems are linked by the refraction angles ρ of the three waves as explained in Section 1.7.3.2.1. We consider Gaussian transverse profiles: the electric field amplitude is then given by (1.7.3.37). In these conditions, the integration of (1.7.3.22) over (X, Y, Z) by assuming $\tan \rho = \rho$, the non-deple-

tion of the pump and, in the case of phase matching, $\Delta k = 0$ leads to the efficiency $\eta_{SHG}(L)$ given by formula (1.7.3.42) with $\sin^2(\Delta k L/2) = 1$ and multiplied by the factor $[G(L, w_o, \rho)]/[\cos^2 \rho(2\omega)]$ where $\rho(2\omega)$ is the harmonic walk-off angle and $G(L, w_o, \rho)$ is the walk-off attenuation function.

For type I, the walk-off attenuation is given by (Boyd *et al.*, 1965)

$$G_I(t) = (\pi^{1/2}/t) \text{erf}(t) - (1/t^2)[1 - \exp(-t^2)]$$

with

$$t = (\rho L/w_o) \quad (1.7.3.53)$$

and

$$\text{erf}(x) = (2/\pi^{1/2}) \int_0^x \exp(-t^2) dt.$$

For uniaxial crystals, $\rho = \rho^e(2\omega)$ for a *2oe* interaction and $\rho = \rho^e(\omega)$ for a *2eo* interaction. For the biaxial class, $\rho = \rho^e(2\omega)$ for a *2oe* interaction and $\rho = \rho^e(\omega)$ for a *2eo* interaction in the *xz* and *yz* planes, $\rho = \rho^o(\omega)$ for a *2oe* interaction and $\rho = \rho^o(2\omega)$ for a *2eo* interaction in the *xy* plane. For any direction of propagation not contained in the principal planes of a biaxial crystal, the fundamental and harmonic waves have nonzero walk-off angles, respectively $\rho^+(\omega)$ and $\rho^-(2\omega)$. In this case, (1.7.3.53) can be used with $\rho = |\rho^+(\omega) - \rho^-(2\omega)|$.

(a) For small t ($t \ll 1$), $G_I(t) \simeq 1$ and $P^{2\omega}(L) \equiv L^2$,

(b) For large t ($t \gg 1$), $G_I(t) \simeq (\pi^{1/2}/t)$ and so $P^{2\omega}(L) \equiv L/\rho$ according to (1.7.3.42) with $\Delta k = 0$.

For type II, we have (Mehendale & Gupta, 1988)

$$G_{II}(t) = (2/\pi^{1/2}) \int_{-\infty}^{+\infty} F^2(a, t) da$$

with

$$F(a, t) = (1/t) \exp(-a^2) \int_0^t \exp[-(a + \tau)^2] d\tau \quad (1.7.3.54)$$

and

$$a = \frac{r}{w_o} \quad \tau = \frac{\rho u}{w_o} \quad t = \frac{\rho L}{w_o}.$$

r and u are the Cartesian coordinates in the walk-off plane where u is collinear with the three wavevectors, *i.e.* the phase-matching direction.

$\rho = \rho^e(\omega)$ for (*oeo*) in uniaxial crystals and in the *xz* and *yz* planes of biaxial crystals. $\rho = \rho^o(\omega)$ in the *xy* plane of biaxial crystals for an (*eo*e) interaction.

For the interactions where $\rho^-(2\omega)$ and $\rho^-(\omega)$ are nonzero, we assume that they are close and contained in the same plane, which is generally the case. Then we classically take ρ to be the maximum value between $|\rho^-(2\omega) - \rho^+(\omega)|$ and $|\rho^-(\omega) - \rho^+(\omega)|$. This approximation concerns the (*eo*e) configuration of polarization in uniaxial crystals and for biaxial crystals in the *xz* and *yz* planes, in the *xy* plane for (*oeo*) and out of the principal planes for all the configurations of polarization.

The exact calculation of G , which takes into account the three walk-off angles, $\rho^-(\omega)$, $\rho^+(\omega)$ and $\rho^-(2\omega)$, was performed in the case where these three angles were coplanar (Asaumi, 1992). The exact calculation in the case of KTiOPO_4 (KTP) for type-II SHG at 1.064 μm gives the same result for $L/z_R < 1$ as for one angle defined as previously (Fève *et al.*, 1995), which includes the parallel-beam limit $L/z_R < 0.3\text{--}0.4$: $z_R = [k(\omega)w_o^2]/2$ is the Rayleigh length of the fundamental beam inside the crystal.

(a) For $t \ll 1$, $G_{II}(t) \simeq 1$, leading to the L^2 dependence of $P^{2\omega}(L)$.

1.7. NONLINEAR OPTICAL PROPERTIES

(b) For $t \gg 1$, $G_{II}(t) \simeq (t_a^2/t^2)$ with $t_a = [(2)^{1/2} \arctan(2^{1/2})]^{1/2}$, corresponding to a saturation of $P^{2\omega}(L)$ because of the walk-off between the two fundamental beams as shown in Fig. 1.7.3.9.

The saturation length, L_{sat} , is defined as $2.3t_a w_o / \rho$, which corresponds to the length beyond which the SHG conversion

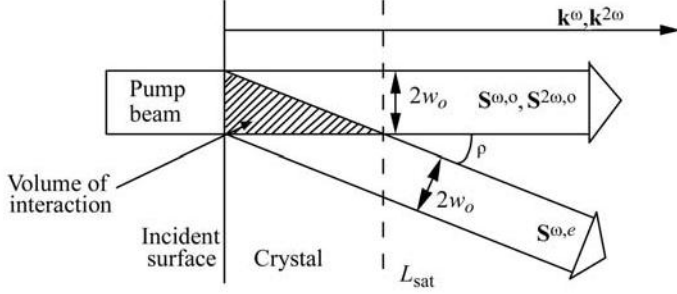


Fig. 1.7.3.9. Beam separation in the particular case of type-II (*oeo*) SHG out of the *xy* plane of a positive uniaxial crystal or in the *xz* and *yz* planes of a positive biaxial crystal. $\mathbf{S}^{\omega,o}$, $\mathbf{S}^{\omega,e}$ and $\mathbf{S}^{2\omega,o}$ are the fundamental and harmonic Poynting vectors; \mathbf{k}^{ω} and $\mathbf{k}^{2\omega}$ are the associated wavevectors collinear to the CPM direction. w_o is the fundamental beam radius and ρ is the walk-off angle. L_{sat} is the saturation length.

efficiency varies less than 1% from its saturation value $BP^{\omega}(0)t_a^2/\rho^2$.

The complete splitting of the two fundamental beams does not occur for type I, making it more suitable than type II for strong focusing. The fundamental beam splitting for type II also leads to a saturation of the acceptance bandwidths $\delta\xi$ ($\xi = \theta, \varphi, T, \lambda$), which is not the case for type I (Fève *et al.*, 1995). The walk-off angles also modify the transversal distribution of the generated harmonic beam (Boyd *et al.*, 1965; Mehendale & Gupta, 1988): the profile is larger than that of the fundamental beam for type I, contrary to type II.

The walk-off can be compensated by the use of two crystals placed one behind the other, with the same length and cut in the same CPM direction (Akhmanov *et al.*, 1975): the arrangement of the second crystal is obtained from that of the first one by a π rotation around the direction of propagation or around the direction orthogonal to the direction of propagation and contained in the walk-off plane as shown in Fig. 1.7.3.10 for the particular case of type II (*oeo*) in a positive uniaxial crystal out of the *xy* plane.

The twin-crystal device is potentially valid for both types I and II. The relative sign of the effective coefficients of the twin

crystals depends on the configuration of polarization, on the relative arrangement of the two crystals and on the crystal class. The interference between the waves generated in the two crystals is destructive and so cancels the SHG conversion efficiency if the two effective coefficients have opposite signs: it is always the case for certain crystal classes and configurations of polarization (Moore & Koch, 1996).

Such a tandem crystal was used, for example, with KTiOPO_4 (KTP) for type-II SHG at $\lambda_o = 1.3 \mu\text{m}$ ($\rho = 2.47^\circ$) and $\lambda_o = 2.532 \mu\text{m}$ ($\rho = 2.51^\circ$): the conversion efficiency was about 3.3 times the efficiency in a single crystal of length $2L$, where L is the length of each crystal of the twin device (Zondy *et al.*, 1994). The two crystals have to be antireflection coated or contacted in order to avoid Fresnel reflection losses.

Non-collinear phase matching is another method allowing a reduction of the walk-off, but only in the case of type II (Dou *et al.*, 1992). Fig. 1.7.3.11 illustrates the particular case of (*oeo*) type-II SHG for a propagation out of the *xy* plane of a uniaxial crystal, or in the *xz* or *yz* plane of a biaxial crystal.

In the configuration of special non-collinear phase matching, the angle between the fundamental beams inside the crystal is chosen to be equal to the walk-off angle ρ . Then the associated Poynting vectors $\mathbf{S}^{\omega,o}$ and $\mathbf{S}^{\omega,e}$ are along the same direction, while that of the generated wave deviates from them only by approximately $\rho/2$. The calculation performed in the case of special non-collinear phase matching indicates that it is possible to increase type-II SHG conversion efficiency by 17% for near-field undepleted Gaussian beams (Dou *et al.*, 1992). Another advantage of such geometry is to turn type II into a pseudo type I with respect to the walk-off,

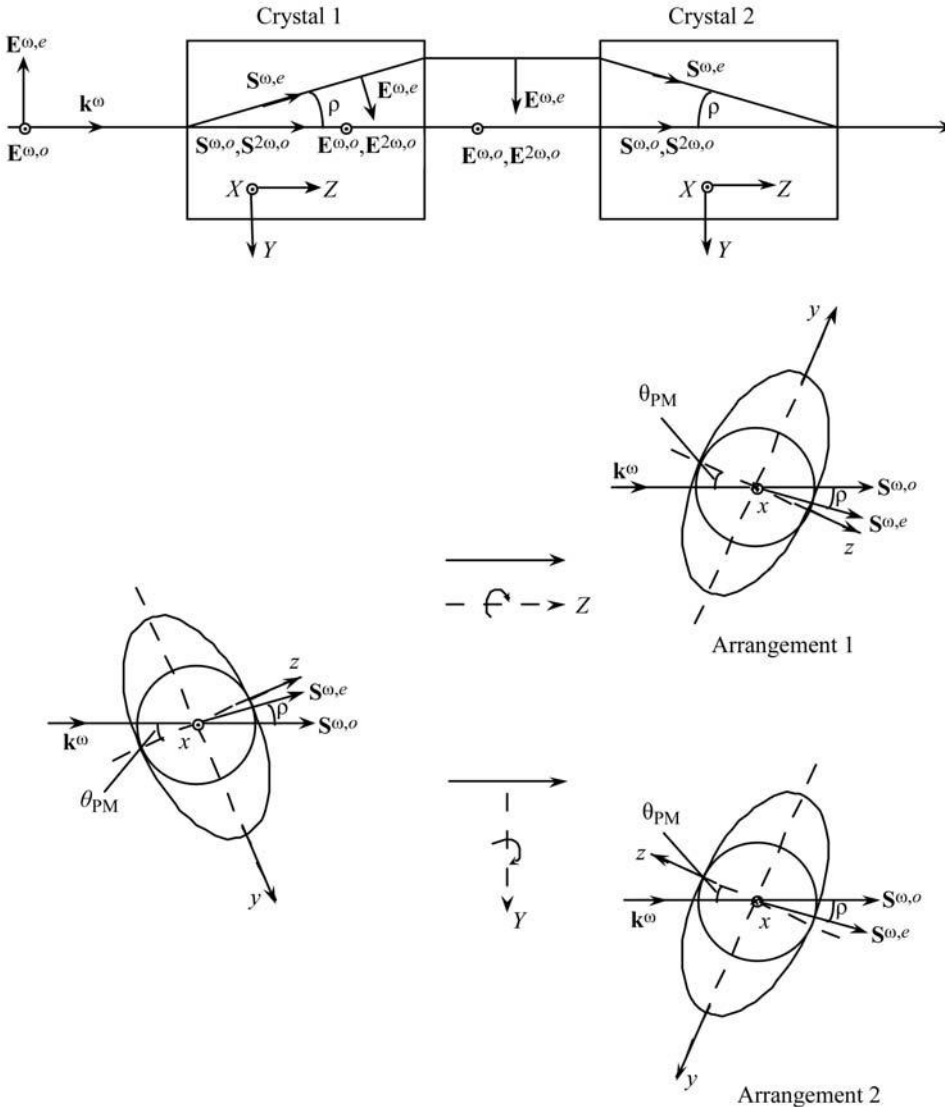


Fig. 1.7.3.10. Twin-crystal device allowing walk-off compensation for a direction of propagation θ_{PM} in the *yz* plane of a positive uniaxial crystal. (*X, Y, Z*) is the wave frame and (*x, y, z*) is the optical frame. The index surface is given in the *yz* plane. \mathbf{k}^{ω} is the incident fundamental wavevector. The refracted wavevectors $\mathbf{k}^{\omega,o}$, $\mathbf{k}^{\omega,e}$ and $\mathbf{k}^{2\omega,o}$ are collinear and along \mathbf{k}^{ω} . $\mathbf{S}^{\omega,o}$, $\mathbf{S}^{\omega,e}$ and $\mathbf{S}^{2\omega,o}$ are the Poynting vectors of the fundamental and harmonic waves. $\mathbf{E}^{\omega,o}$, $\mathbf{E}^{\omega,e}$ and $\mathbf{E}^{2\omega,o}$ are the electric field vectors. ρ is the walk-off angle.

1. TENSORIAL ASPECTS OF PHYSICAL PROPERTIES

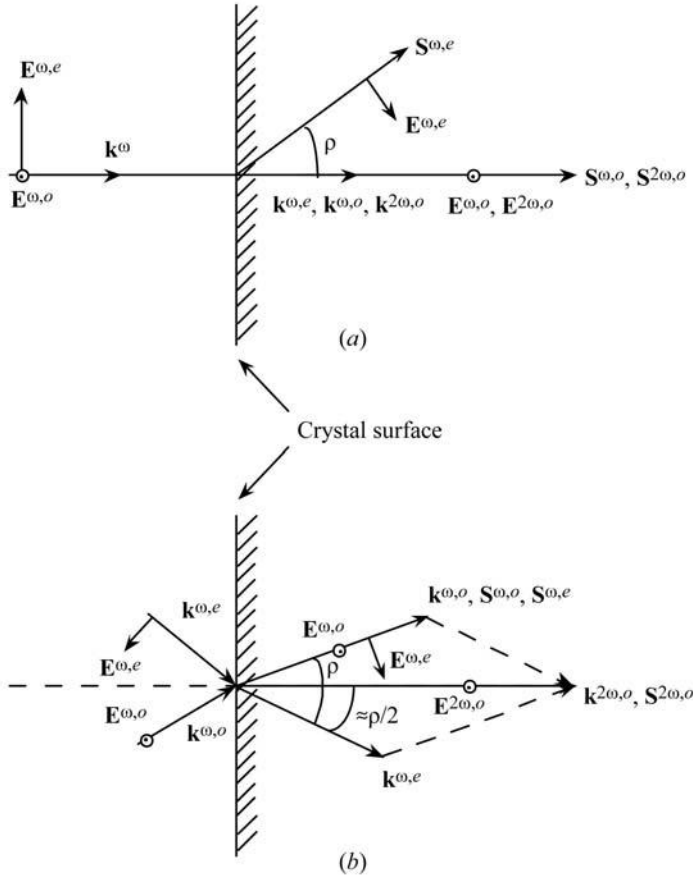


Fig. 1.7.3.11. Comparison between (a) collinear and (b) special non-collinear phase matching for (o eo) type-II SHG. $\mathbf{k}^{\omega,o}$, $\mathbf{k}^{\omega,e}$ and $\mathbf{k}^{2\omega,o}$ are the wavevectors, $\mathbf{S}^{\omega,o}$, $\mathbf{S}^{\omega,e}$ and $\mathbf{S}^{2\omega,o}$ are the Poynting vectors of the fundamental and harmonic waves, and $\mathbf{E}^{\omega,o}$, $\mathbf{E}^{\omega,e}$ and $\mathbf{E}^{2\omega,o}$ are the electric field vectors; ρ is the walk-off angle in the collinear case and the angle between $\mathbf{k}^{\omega,o}$ and $\mathbf{k}^{\omega,e}$ inside the crystal for the non-collinear interaction.

because the saturation phenomenon of type-II CPM is avoided.

(iv) Effect of temporal walk-off.

Even if the SHG is phase matched, the fundamental and harmonic group velocities, $v_g(\omega) = \partial\omega/\partial k$, are generally mismatched. This has no effect with continuous wave (c.w.) lasers. For pulsed beams, the temporal separation of the different beams during the propagation can lead to a decrease of the temporal overlap of the pulses. Indeed, this walk-off in the time domain affects the conversion efficiency when the pulse separations are close to the pulse durations. Then after a certain distance, L_τ , the pulses are completely separated, which entails a saturation of the conversion efficiency, for both types I and II (Tomov *et al.*, 1982). Three group velocities must be considered for type II. Type I is simpler, because the two fundamental waves have the same velocity, so $L_\tau = \tau/[v_g^{-1}(\omega) - v_g^{-1}(2\omega)]$, which defines the optimum crystal length, where τ is the pulse duration. For type-I SHG of 532 nm in KH_2PO_4 (KDP), $v_g(266 \text{ nm}) = 1.84 \times 10^8 \text{ m s}^{-1}$ and $v_g(532 \text{ nm}) = 1.94 \times 10^8 \text{ m s}^{-1}$, so $L_\tau = 3.5 \text{ mm}$ for 1 ps. For the usual nonlinear crystals, the temporal walk-off must be taken into account for pico- and femtosecond pulses.

1.7.3.3.2.2. Non-resonant SHG with undepleted pump and transverse and longitudinal Gaussian beams

We now consider the general situation where the crystal length can be larger than the Rayleigh length.

The Gaussian electric field amplitudes of the two eigen electric field vectors inside the nonlinear crystal are given by

$$E^\pm(X, Y, Z) = E_o^\pm \frac{w_o}{w(Z)} \exp \left[-\frac{(X + \rho^+ Z)^2 + (Y + \rho^- Z)^2}{w^2(Z)} \right] \times \exp \left(i \left\{ k^\pm Z - \arctan(Z/z_R) + \frac{k^\pm [(X + \rho^+ Z)^2 + (Y + \rho^- Z)^2]}{2Z[1 + (z_R^2/Z^2)]} \right\} \right) \quad (1.7.3.55)$$

with $\rho^- = 0$ for E^+ and $\rho^+ = 0$ for E^- .

(X, Y, Z) is the wave frame defined in Fig. 1.7.3.1. E_o^\pm is the scalar complex amplitude at $(X, Y, Z) = (0, 0, 0)$ in the vibration planes Π^\pm .

We consider the refracted waves E^+ and E^- to have the same longitudinal profile inside the crystal. Then the $(1/e^2)$ beam radius is given by $w(Z)^2 = w_o^2[1 + (Z^2/z_R^2)]$, where w_o is the minimum beam radius located at $Z = 0$ and $z_R = kw_o^2/2$, with $k = (k^+ + k^-)/2$; z_R is the Rayleigh length, the length over which the beam radius remains essentially collimated; k^\pm are the wavevectors at the wavelength λ in the direction of propagation Z . The far-field half divergence angle is $\Delta\alpha = 2/kw_o$.

The coordinate systems of (1.7.3.22) are identical to those of the parallel-beam limit defined in (iii).

In these conditions and by assuming the undepleted pump approximation, the integration of (1.7.3.22) over (X, Y, Z) leads to the following expression of the power conversion efficiency (Zondy, 1991):

$$\eta_{\text{SHG}}(L) = \frac{P^{2\omega}(L)}{P^\omega(0)} = CLP^\omega(0) \frac{h(L, w_o, \rho, f, \Delta k)}{\cos^2 \rho_{2\omega}}$$

with

$$C = 5.95 \times 10^{-2} \frac{2N-1}{N} \frac{d_{\text{eff}}^2}{\lambda_\omega^3} \frac{n_1^\omega + n_2^\omega}{2} \frac{T_3^\omega T_1^\omega T_2^\omega}{n_3^{2\omega} n_1^\omega n_2^\omega} \quad (\text{W}^{-1} \text{ m}^{-1}) \quad (1.7.3.56)$$

in the same units as equation (1.7.3.42).

For type I, $n_1^\omega = n_2^\omega$, $T_1^\omega = T_2^\omega$, and for type II $n_1^\omega \neq n_2^\omega$, $T_1^\omega \neq T_2^\omega$.

The attenuation coefficient is written

$$h(L, w_o, \rho, f, \Delta k) = [2z_R(\pi)^{1/2}/L] \int_{-\infty}^{+\infty} |H(a)|^2 \exp(-4a^2) da$$

with

$$H(a) = \frac{1}{(2\pi)^{1/2}} \int_{-fL/z_R}^{L(1-f)/z_R} \frac{d\tau}{1+i\tau} \exp \left[-\gamma^2 \left(\tau + \frac{fL}{z_R} \right)^2 - i\sigma\tau \right] \quad \text{for type I: } \gamma = 0 \text{ and } \sigma = \Delta k z_R + 4 \frac{\rho z_R}{w_o} a$$

$$\text{for type II: } \gamma = \frac{\rho z_R}{w_o(2)^{1/2}} \text{ and } \sigma = \Delta k z_R + 2 \frac{\rho z_R}{w_o} a, \quad (1.7.3.57)$$

where f gives the position of the beam waist inside the crystal: $f = 0$ at the entrance and $f = 1$ at the exit surface. The definition and approximations relative to ρ are the same as those discussed for the parallel-beam limit. Δk is the mismatch parameter, which takes into account first a possible shift of the pump beam direction from the collinear phase-matching direction and secondly the distribution of mismatch, including collinear and non-collinear interactions, due to the divergence of the beam, even if the beam axis is phase-matched.

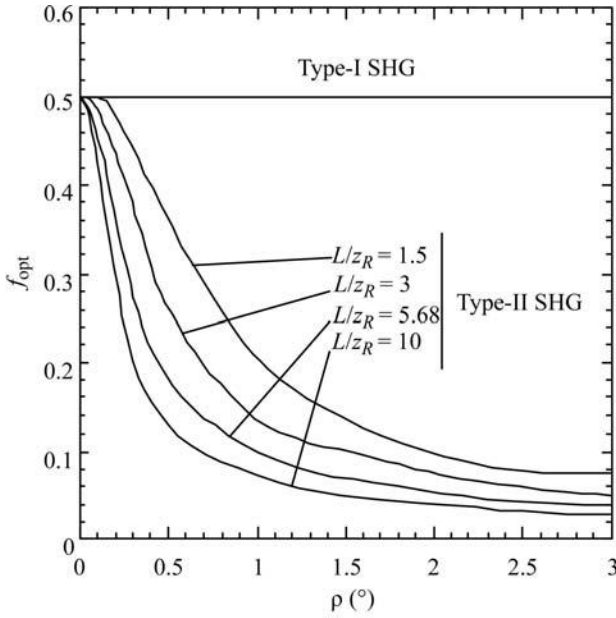


Fig. 1.7.3.12. Position f_{opt} of the beam waist for different values of walk-off angles and L/z_R , leading to an optimum SHG conversion efficiency. The value $f_{\text{opt}} = 0.5$ corresponds to the middle of the crystal and $f_{\text{opt}} = 0$ corresponds to the entrance surface (Fève & Zondy, 1996).

The computation of $h(L, w_o, \rho, f, \Delta k)$ allows an optimization of the SHG conversion efficiency which takes into account L/z_R , the waist location f inside the crystal and the phase mismatch Δk .

Fig. 1.7.3.12 shows the calculated waist location which allows an optimal SHG conversion efficiency for types I and II with optimum phase matching. From Fig. 1.7.3.12, it appears that the optimum waist location for type I, which leads to an optimum conversion efficiency, is exactly at the centre of the crystal, $f_{\text{opt}} = 0.5$. For type II, the focusing (L/z_R) is stronger and the walk-off angle is larger, and the optimum waist location is nearer the entrance of the crystal. These facts can be physically understood: for type I, there is no walk-off for the fundamental beam, so the whole crystal length is efficient and the symmetrical configuration is obviously the best one; for type II, the two fundamental rays can be completely separated in the waist area, which has the strongest intensity, when the waist location is far from the entrance face; for a waist location nearer the entrance, the waist area can be selected and the enlargement of the beams from this area allows a spatial overlap up to the exit face, which leads to a higher conversion efficiency.

The divergence of the pump beam imposes non-collinear interactions such that it could be necessary to shift the direction of propagation of the beam from the collinear phase-matching direction in order to optimize the conversion efficiency. This leads to the definition of an optimum phase-mismatch parameter $\Delta k_{\text{opt}} (\neq 0)$ for a given L/z_R and a fixed position of the beam waist f inside the crystal.

The function $h(L, w_o, \rho, f_{\text{opt}}, \Delta k_{\text{opt}})$, written $h_m(B, L)$, is plotted in Fig. 1.7.3.13 as a function of L/z_R for different values of the walk-off parameter, defined as $B = (1/2)\rho\{(k_o^\omega + k_e^\omega)/2\}^{1/2}$, at the optimal waist location and phase mismatch.

Consider first the case of angular NCPM ($B = 0$) where type-I and -II conversion efficiencies obviously have the same L/z_R evolutions. An optimum focusing at $L/z_R = 5.68$ exists which defines the optimum focusing $z_{R_{\text{opt}}}$ for a given crystal length or the optimal length L_{opt} for a given focusing. The conversion efficiency decreases for $L/z_R > 5.68$ because the increase of the 'average' beam radius over the crystal length due to the strong focusing becomes more significant than the increased peak power in the waist area.

In the case of angular CPM ($B \neq 0$), the L/z_R variation of type-I conversion efficiency is different from that of type II. For

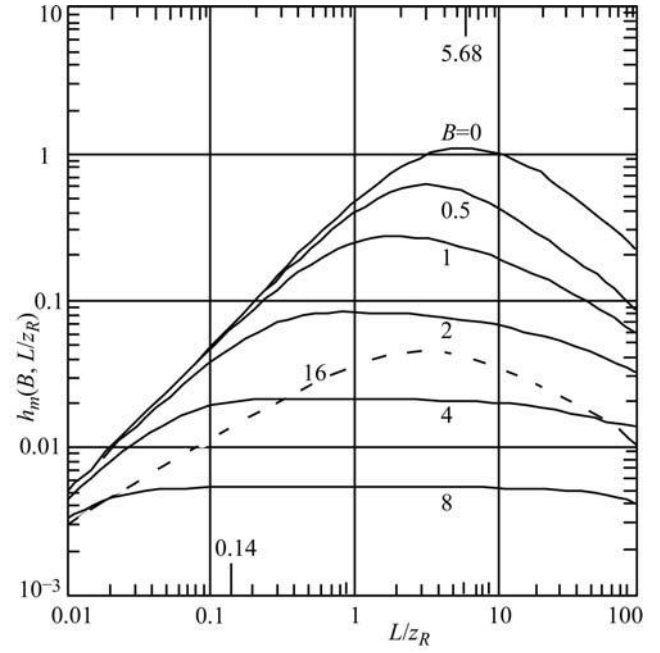


Fig. 1.7.3.13. Optimum walk-off function $h_m(B, L)$ as a function of L/z_R for various values of $B = (1/2)\rho\{(k_o^\omega + k_e^\omega)/2\}^{1/2}$. The curve at $B = 0$ is the same for both type-I and type-II phase matching. The full lines at $B \neq 0$ are for type II and the dashed line at $B = 16$ is for type I. (From Zondy, 1990).

type I, as B increases, the efficiency curves keep the same shape, with their maxima abscissa shifting from $L/z_R = 5.68$ ($B = 0$) to 2.98 ($B = 16$) as the corresponding amplitudes decrease. For type II, an optimum focusing becomes less and less apparent, while $(L/z_R)_{\text{opt}}$ shifts to much smaller values than for type I for the same variation of B ; the decrease of the maximum amplitude is stronger in the case of type II. The calculation of the conversion efficiency as a function of the crystal length L at a fixed z_R shows a saturation for type II, in contrast to type I. The saturation occurs at $B \simeq 3$ with a corresponding focusing parameter $L/z_R \simeq 0.4$, which is the limit of validity of the parallel-beam approximation. These results show that weak focusing is suitable for type II, whereas type I allows higher focusing.

The curves of Fig. 1.7.3.14 give a clear illustration of the walk-off effect in several usual situations of crystal length, walk-off angle and Gaussian laser beam. The SHG conversion efficiency is calculated from formula (1.7.3.56) and from the function (1.7.3.57) at f_{opt} and Δk_{opt} .

1.7.3.3.2.3. Non-resonant SHG with depleted pump in the parallel-beam limit

The analytical integration of the three coupled equations (1.7.3.22) with depletion of the pump and phase mismatch has only been done in the parallel-beam limit and by neglecting the walk-off effect (Armstrong *et al.*, 1962; Eckardt & Reintjes, 1984; Eimerl, 1987; Milton, 1992). In this case, the three coordinate systems of equations (1.7.3.22) are identical, (X, Y, Z) , and the general solution may be written in terms of the Jacobian elliptic function $\text{sn}(m, \alpha)$.

For the simple case of type I, i.e. $E_1^\omega(X, Y, Z) = E_2^\omega(X, Y, Z) = E^\omega(X, Y, Z) = E_{\text{tot}}^\omega(X, Y, Z)/(2^{1/2})$, the exit second harmonic intensity generated over a length L is given by (Eckardt & Reintjes, 1984)

$$I^{2\omega}(X, Y, L) = I_{\text{tot}}^\omega(X, Y, 0) T^{2\omega} v_b^2 \text{sn}^2 \left[\frac{\Gamma(X, Y) L}{v_b}, v_b^4 \right]. \quad (1.7.3.58)$$

1. TENSORIAL ASPECTS OF PHYSICAL PROPERTIES

$I_{\text{tot}}^\omega(X, Y, 0) = 2I^\omega(X, Y, 0)$ is the total initial fundamental intensity, $T^{2\omega}$ and T^ω are the transmission coefficients,

$$\frac{1}{v_b} = \frac{\Delta s}{4} + \left[1 + \left(\frac{\Delta s}{4} \right)^2 \right]^{1/2}$$

with

$$\Delta s = (k^{2\omega} - k^\omega)/\Gamma$$

and

$$\Gamma(X, Y) = \frac{\omega d_{\text{eff}}}{cn^{2\omega}} (T^\omega)^{1/2} |E_{\text{tot}}^\omega(X, Y, 0)|. \quad (1.7.3.59)$$

For the case of phase matching ($k^\omega = k^{2\omega}$, $T^\omega = T^{2\omega}$), we have $\Delta s = 0$ and $v_b = 1$, and the Jacobian elliptic function $\text{sn}(m, 1)$ is equal to $\tanh(m)$. Then formula (1.7.3.58) becomes

$$I^{2\omega}(X, Y, L) = I_{\text{tot}}^\omega(X, Y, 0) (T^\omega)^2 \tanh^2[\Gamma(X, Y)L], \quad (1.7.3.60)$$

where $\Gamma(X, Y)$ is given by (1.7.3.59).

The exit fundamental intensity $I^\omega(X, Y, L)$ can be established easily from the harmonic intensity (1.7.3.60) according to the Manley–Rowe relations (1.7.2.40), i.e.

$$I^\omega(X, Y, L) = I_{\text{tot}}^\omega(X, Y, 0) (T^\omega)^2 \text{sech}^2[\Gamma(X, Y)L]. \quad (1.7.3.61)$$

For small ΓL , the functions $\tanh^2(\Gamma L) \simeq \Gamma^2 L^2$ and $\text{sn}^2[(\Gamma L/v_b), v_b^4] \simeq \sin^2(\Gamma L/v_b)$ with $v_b \simeq 2/\Delta s$.

The first consequence of formulae (1.7.3.58)–(1.7.3.59) is that the various acceptance bandwidths decrease with increasing ΓL . This fact is important in relation to all the acceptances but in particular for the thermal and angular ones. Indeed, high efficiencies are often reached with high power, which can lead to an important heating due to absorption. Furthermore, the divergence of the beams, even small, creates a significant dephasing: in this case, and even for a propagation along a phase-matching direction, formula (1.7.3.60) is not valid and may be replaced by (1.7.3.58) where $k(2\omega) - k(\omega)$ is considered as the ‘average’ mismatch of a parallel beam.

In fact, there always exists a residual mismatch due to the divergence of real beams, even if not focused, which forbids asymptotically reaching a 100% conversion efficiency: $I^{2\omega}(L)$ increases as a function of ΓL until a maximum value has been reached and then decreases; $I^{2\omega}(L)$ will continue to rise and fall as ΓL is increased because of the periodic nature of the Jacobian elliptic sine function. Thus the maximum of the conversion efficiency is reached for a particular value $(\Gamma L)_{\text{opt}}$. The determination of $(\Gamma L)_{\text{opt}}$ by numerical computation allows us to define the optimum incident fundamental intensity I_{opt}^ω for a given phase-matching direction, characterized by K , and a given crystal length L .

The crystal length must be optimized in order to work with an incident intensity I_{opt}^ω smaller than the damage threshold intensity I_{dam}^ω of the nonlinear crystal, given in Section 1.7.5 for the main materials.

Formula (1.7.3.57) is established for type I. For type II, the second harmonic intensity is also an sn^2 function where the

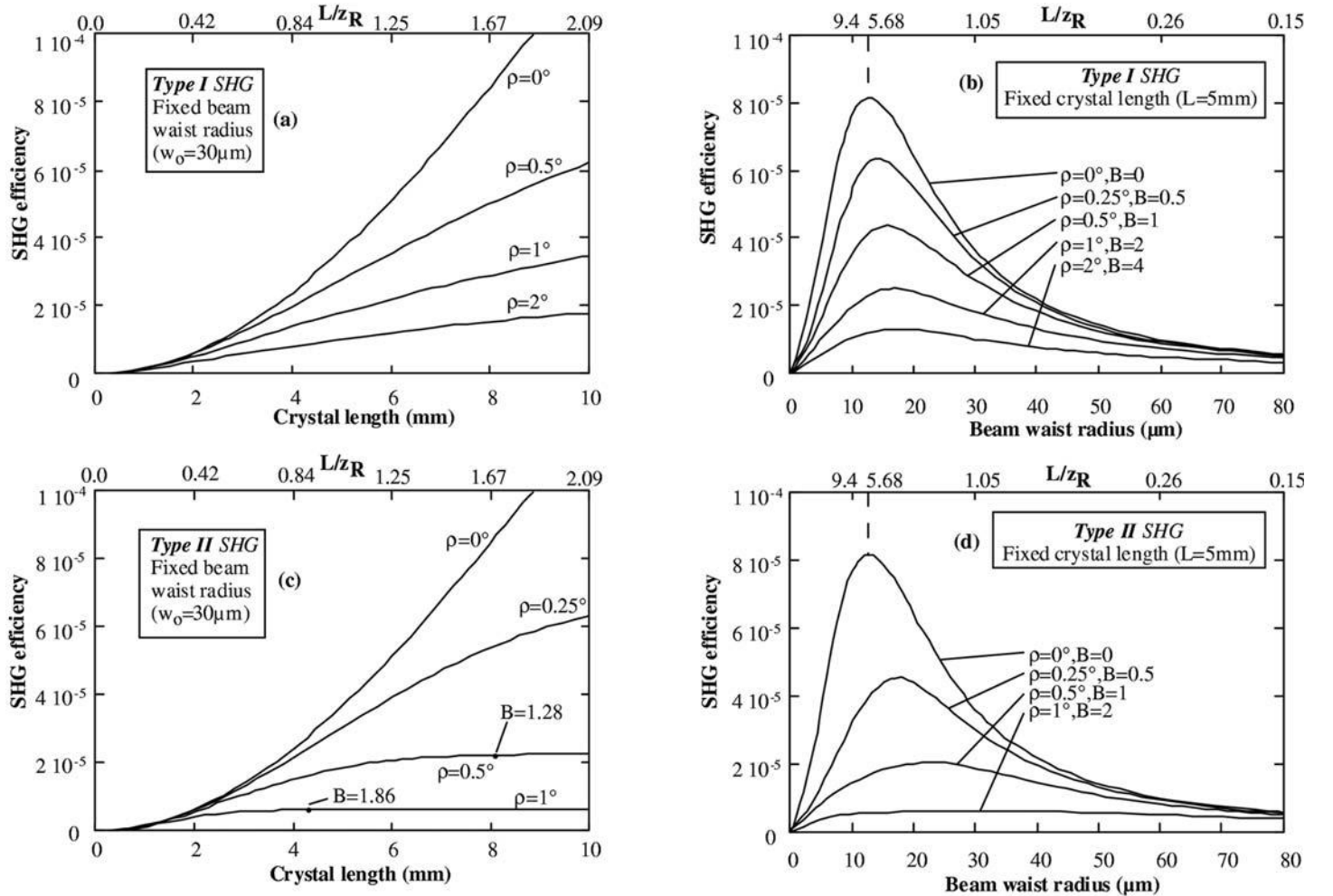


Fig. 1.7.3.14. Type-I and -II conversion efficiencies calculated as a function of L/z_R for different typical walk-off angles ρ : (a) and (c) correspond to a fixed focusing condition ($w_0 = 30 \mu\text{m}$); the curves (b) and (d) are plotted for a constant crystal length ($L = 5 \text{ mm}$); all the calculations are performed with the same effective coefficient ($d_{\text{eff}} = 1 \text{ pm V}^{-1}$), refractive indices ($n_3^{\omega} n_1^{\omega} n_2^{\omega} = 5.83$) and fundamental power [$P_\omega(0) = 1 \text{ W}$]. B is the walk-off parameter defined in the text (Fève & Zondy, 1996).

1.7. NONLINEAR OPTICAL PROPERTIES

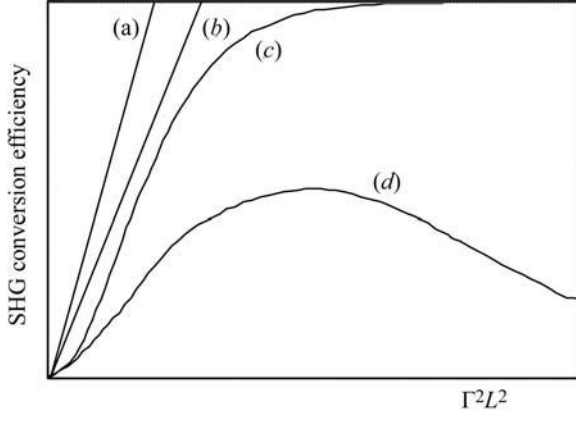


Fig. 1.7.3.15. Schematic SHG conversion efficiency for different situations of pump depletion and dephasing: (a) no depletion, no dephasing, $\eta = \Gamma^2 L^2$; (b) no depletion with constant dephasing δ , $\eta = \Gamma^2 L^2 \sin^2 \delta$; (c) depletion without dephasing, $\eta = \tanh^2(\Gamma L)$; (d) depletion and dephasing, $\eta = \eta_m \text{sn}^2(\Gamma L/v_b, v_b^2)$.

intensities of the two fundamental beams $I_1^\omega(X, Y, 0)$ and $I_2^\omega(X, Y, 0)$, which are not necessarily equal, are taken into account (Eimerl, 1987): the \tanh^2 function is valid only if perfect phase matching is achieved and if $I_1^\omega(X, Y, 0) = I_2^\omega(X, Y, 0)$, these conditions being never satisfied in real cases.

The situations described above are summarized in Fig. 1.7.3.15.

We give the example of type-II SHG experiments performed with a 10 Hz injection-seeded single-longitudinal-mode ($N = 1$) 1064 nm Nd:YAG (Spectra-Physics DCR-2A-10) laser equipped with super Gaussian mirrors; the pulse is 10 ns in duration and is near a Gaussian single-transverse mode, the beam radius is 4 mm, non-focused and polarized at $\pi/4$ to the principal axes of a 10 mm long KTP crystal ($L\delta\theta = 15$ mrad cm, $L\delta\varphi = 100$ mrad cm). The fundamental energy increases from 78 mJ (62 MW cm⁻²) to 590 mJ (470 MW cm⁻²), which corresponds to the damage of the exit surface of the crystal; for each experiment, the crystal was rotated in order to obtain the maximum conversion efficiency. The peak power SHG conversion efficiency is estimated from the measured energy conversion efficiency multiplied by the ratio between the fundamental and harmonic pulse duration ($\tau_\omega/\tau_{2\omega} = 2^{1/2}$). It increases from 50% at 63 MW cm⁻² to a maximum value of 85% at 200 MW cm⁻² and decreases for higher intensities, reaching 50% at 470 MW cm⁻² (Boulanger, Fejer *et al.*, 1994).

The integration of the intensity profiles (1.7.3.58) and (1.7.3.60) is obvious in the case of incident fundamental beams with a flat energy distribution (1.7.3.36). In this case, the fundamental and harmonic beams inside the crystal have the same profile and radius as the incident beam. Thus the powers are obtained from formulae (1.7.3.58) and (1.7.3.60) by expressing the intensity and electric field modulus as a function of the power, which is given by (1.7.3.38) with $m = 1$.

For a Gaussian incident fundamental beam, (1.7.3.37), the fundamental and harmonic beams are not Gaussian (Eckardt & Reintjes, 1984; Pliszka & Banerjee, 1993).

All the previous intensities are the peak values in the case of pulsed beams. The relation between average and peak powers, and then SHG efficiencies, is much more complicated than the ratio $\tau^{2\omega}/\tau^\omega$ of the undepleted case.

1.7.3.3.2.4. Resonant SHG

When the single-pass conversion efficiency SHG is too low, with c.w. lasers for example, it is possible to put the nonlinear crystal in a Fabry-Perot cavity external to the pump laser or directly inside the pump laser cavity, as shown in Figs. 1.7.3.6(b) and (c). The second solution, described later, is generally used because the available internal pump intensity is much larger.

We first recall some basic and simplified results of laser cavity theory without a nonlinear medium. We consider a laser in which one mirror is 100% reflecting and the second has a transmission T at the laser pulsation ω . The power within the cavity, $P_{\text{in}}(\omega)$, is evaluated at the steady state by setting the round-trip saturated gain of the laser equal to the sum of all the losses. The output laser cavity, $P_{\text{out}}(\omega)$, is given by (Siegman, 1986)

$$P_{\text{out}}(\omega) = TP_{\text{in}}(\omega)$$

with

$$P_{\text{in}}(\omega) = \frac{2g_o L' - (\gamma + T)}{2S(T + \gamma)}. \quad (1.7.3.62)$$

L' is the laser medium length, $g_o = \sigma N_o$ is the small-signal gain coefficient per unit length of laser medium, σ is the stimulated-emission cross section, N_o is the population inversion without oscillation, S is a saturation parameter characteristic of the nonlinearity of the laser transition, and $\gamma = \gamma_L = 2\alpha_L L' + \beta$ is the loss coefficient where α_L is the laser material absorption coefficient per unit length and β is another loss coefficient including absorption in the mirrors and scattering in both the laser medium and mirrors. For given g_o , S , α_L , β and L' , the output power reaches a maximum value for an optimal transmission coefficient T_{opt} defined by $[\partial P_{\text{out}}(\omega)/\partial T]_{T_{\text{opt}}} = 0$, which gives

$$T_{\text{opt}} = (2g_o L' \gamma)^{1/2} - \gamma. \quad (1.7.3.63)$$

The maximum output power is then given by

$$P_{\text{out}}^{\text{max}}(\omega) = (1/2S)[(2g_o L')^{1/2} - \gamma^{1/2}]^2. \quad (1.7.3.64)$$

In an intracavity SHG device, the two cavity mirrors are 100% reflecting at ω but one mirror is perfectly transmitting at 2ω . The presence of the nonlinear medium inside the cavity then leads to losses at ω equal to the round-trip-generated second harmonic (SH) power: half of the SH produced flows in the forward direction and half in the backward direction. Hence the highly transmitting mirror at 2ω is equivalent to a nonlinear transmission coefficient at ω which is equal to twice the single-pass SHG conversion efficiency η_{SHG} .

The fundamental power inside the cavity $P_{\text{in}}(\omega)$ is given at the steady state by setting, for a round trip, the saturated gain equal to the sum of the linear and nonlinear losses. $P_{\text{in}}(\omega)$ is then given by (1.7.3.62), where T and γ are (Geusic *et al.*, 1968; Smith, 1970)

$$T = 2\eta_{\text{SHG}} = [P_{\text{out}}(2\omega)/P_{\text{in}}(\omega)] \quad (1.7.3.65)$$

and

$$\gamma = \gamma_L + \gamma_{NL}. \quad (1.7.3.66)$$

η_{SHG} is the single-pass conversion efficiency. γ_L and γ_{NL} are the loss coefficients at ω of the laser medium and of the nonlinear crystal, respectively. L is the nonlinear medium length. The two faces of the nonlinear crystal are assumed to be antireflection-coated at ω .

In the undepleted pump approximation, the backward and forward power generated outside the nonlinear crystal at 2ω is

$$P_{\text{out}}(2\omega) = 2KP_{\text{in}}^2(\omega) \quad (1.7.3.67)$$

with

$$K = B(L^2/w_o^2) \sin^2(\Delta k L/2),$$

where

$$B = \frac{32\pi 2N - 1}{\epsilon_o c} \frac{d_{\text{eff}}^2}{N} \frac{T_3^{2\omega} T_1^\omega T_2^\omega}{\lambda_\omega^2 n_3^{2\omega} n_1^\omega n_2^\omega} \quad (\text{W}^{-1}).$$

1. TENSORIAL ASPECTS OF PHYSICAL PROPERTIES

The intracavity SHG conversion efficiency is usually defined as the ratio of the SH output power to the maximum output power that would be obtained from the laser without the nonlinear crystal by optimal linear output coupling.

Maximizing (1.7.3.67) with respect to K according to (1.7.3.62), (1.7.3.65) and (1.7.3.66) gives (Perkins & Fahlen, 1987)

$$K_{\text{opt}} = (\gamma_L + \gamma_{NL})S \quad (1.7.3.68)$$

and

$$P_{\text{out}}^{\text{max}}(2\omega) = (1/2S)[(2g_o L')^{1/2} - (\gamma_L + \gamma_{NL})^{1/2}]^2. \quad (1.7.3.69)$$

(1.7.3.69) shows that for the case where $\gamma_{NL} \ll \gamma_L$ ($\gamma \simeq \gamma_L$), the maximum SH power is identically equal to the maximum fundamental power, (1.7.3.64), available from the same laser for the same value of loss, which, according to the previous definition of the intracavity efficiency, corresponds to an SHG conversion efficiency of 100%. $P_{\text{out}}^{\text{max}}(2\omega)$ strongly decreases as the losses ($\gamma_L + \gamma_{NL}$) increase. Thus an efficient intracavity device requires the reduction of all losses at ω and 2ω to an absolute minimum.

(1.7.3.68) indicates that K_{opt} is independent of the operating power level of the laser, in contrast to the optimum transmitting mirror where T_{opt} , given by (1.7.3.63), depends on the laser gain. K_{opt} depends only on the total losses and saturation parameter. For given losses, the knowledge of K_{opt} allows us to define the optimal parameters of the nonlinear crystal, in particular the figure of merit, $d_{\text{eff}}^2/n_3^2 n_1^{\omega} n_2^{\omega}$ and the ratio $(L/w_o)^2$, in which the walk-off effect and the damage threshold must also be taken into account.

Some examples: a power of 1.1 W at 0.532 μm was generated in a TEM₀₀ c.w. SHG intracavity device using a 3.4 mm Ba₂Nb₅O₁₅ crystal within a 1.064 μm Nd:YAG laser cavity (Geusic *et al.*, 1968). A power of 9.0 W has been generated at 0.532 μm using a more complicated geometry based on an Nd:YAG intracavity-lens folded-arm cavity configuration using KTP (Perkins & Fahlen, 1987). High-average-power SHG has also been demonstrated with output powers greater than 100 W at 0.532 μm in a KTP crystal inside the cavity of a diode side-pumped Nd:YAG laser (LeGarrec *et al.*, 1996).

For type-II phase matching, a rotated quarter waveplate is useful in order to reinstate the initial polarization of the fundamental waves after a round trip through the nonlinear crystal, the retardation plate and the mirror (Perkins & Driscoll, 1987).

If the nonlinear crystal surface on the laser medium side has a 100% reflecting coating at 2ω and if the other surface is 100% transmitting at 2ω , it is possible to extract the full SH power in one direction (Smith, 1970). Furthermore, such geometry allows us to avoid losses of the backward SH beam in the laser medium and in other optical components behind.

External-cavity SHG also leads to good results. The resonated wave may be the fundamental or the harmonic one. The corresponding theoretical background is detailed in Ashkin *et al.* (1966). For example, a bow-tie configuration allowed the generation of 6.5 W of TEM₀₀ c.w. 0.532 μm radiation in a 6 mm LiB₃O₅ (LBO) crystal; the Nd:YAG laser was an 18 W c.w. laser with an injection-locked single frequency (Yang *et al.*, 1991).

1.7.3.3.3. Third harmonic generation (THG)

Fig. 1.7.3.16 shows the three possible ways of achieving THG: a cascading interaction involving two $\chi^{(2)}$ processes, *i.e.* $\omega + \omega = 2\omega$ and $\omega + 2\omega = 3\omega$, in two crystals or in the same crystal, and direct THG, which involves $\chi^{(3)}$, *i.e.* $\omega + \omega + \omega = 3\omega$.

1.7.3.3.3.1. SHG ($\omega + \omega = 2\omega$) and SFG ($\omega + 2\omega = 3\omega$) in different crystals

We consider the case of the situation in which the SHG is phase-matched with or without pump depletion and in which the sum-frequency generation (SFG) process ($\omega + 2\omega = 3\omega$), phase-

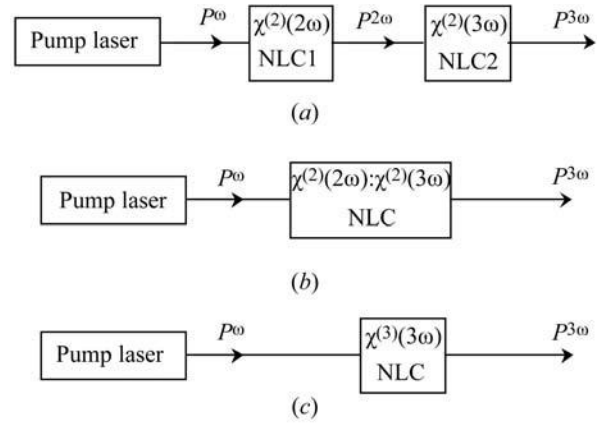


Fig. 1.7.3.16. Configurations for third harmonic generation: (a) cascading process SHG ($\omega + \omega = 2\omega$): SFG ($\omega + 2\omega = 3\omega$) in two crystals NLC1 and NLC2 and (b) in a single nonlinear crystal NLC; (c) direct process THG ($\omega + \omega + \omega = 3\omega$) in a single nonlinear crystal NLC.

matched or not, is without pump depletion at ω and 2ω . All the waves are assumed to have a flat distribution given by (1.7.3.36) and the walk-off angles are nil, in order to simplify the calculations.

This configuration is the most frequently occurring case because it is unusual to get simultaneous phase matching of the two processes in a single crystal. The integration of equations (1.7.3.22) over Z for the SFG in the undepleted pump approximation with $E_1^{\omega}(Z_{\text{SFG}} = 0) = E_1^{\omega}(L_{\text{SHG}})$, $E_2^{2\omega}(Z_{\text{SFG}} = 0) = E_2^{2\omega}(L_{\text{SHG}})$ and $E_3^{3\omega}(Z_{\text{SFG}} = 0) = 0$, followed by the integration over the cross section leads to

$$P^{3\omega}(L_{\text{SFG}}) = B_{\text{SFG}}[aP^{\omega}(L_{\text{SHG}})]P^{2\omega}(L_{\text{SHG}})\frac{L_{\text{SFG}}^2}{w_o^2}\sin^2 c^2 \frac{\Delta k_{\text{SFG}} L_{\text{SFG}}}{2} \quad (\text{W})$$

with

$$B_{\text{SFG}} = \frac{72\pi 2N - 1}{\epsilon_o c} \frac{d_{\text{eff}}^2}{N} \frac{T_3^{\omega} T_1^{\omega} T_2^{2\omega}}{\lambda_{\omega}^2 n_3^{\omega} n_1^{\omega} n_2^{2\omega}} \quad (\text{W}^{-1})$$

$$a = 1 \text{ for type-I SHG, } a = \frac{1}{2} \text{ for type-II SHG.}$$

(1.7.3.70)

$P^{\omega}(L_{\text{SHG}})$ and $P^{2\omega}(L_{\text{SHG}})$ are the fundamental and harmonic powers, respectively, at the exit of the first crystal. L_{SHG} and L_{SFG} are the lengths of the first and the second crystal, respectively. $\Delta k_{\text{SFG}} = k^{3\omega} - (k^{\omega} + k^{2\omega})$ is the SFG phase mismatch. λ_{ω} is the fundamental wavelength. The units and other parameters are as defined in (1.7.3.42).

For type-II SHG, the fundamental waves are polarized in two orthogonal vibration planes, so only half of the fundamental power can be used for type-I, -II or -III SFG ($a = 1/2$), in contrast to type-I SHG ($a = 1$). In the latter case, and for type-I SFG, it is necessary to set the fundamental and second harmonic polarizations parallel.

The cascading conversion efficiency is calculated according to (1.7.3.61) and (1.7.3.70); the case of type-I SHG gives, for example,

$$\begin{aligned} \eta_{\text{THG}}(L_{\text{SHG}}, L_{\text{SFG}}) &= \frac{P^{3\omega}(L_{\text{SFG}})}{P_{\text{tot}}^{\omega}(0)} \\ &= B_{\text{SFG}}(T^{\omega})^4 P_{\text{tot}}^{\omega}(0) \tanh^2(\Gamma L_{\text{SHG}}) \\ &\quad \times \text{sech}^2(\Gamma L_{\text{SHG}}) \frac{L_{\text{SFG}}^2}{w_o^2} \sin^2 c^2 \left(\frac{\Delta k_{\text{SFG}} L_{\text{SFG}}}{2} \right), \end{aligned} \quad (1.7.3.71)$$

where Γ is as in (1.7.3.59).

1.7. NONLINEAR OPTICAL PROPERTIES

(n^ω, T^ω) are relative to the phase-matched SHG crystal and $(n_1^\omega, n_2^\omega, n_3^\omega, T_1^\omega, T_2^\omega, T_3^\omega)$ correspond to the SFG crystal.

In the undepleted pump approximation for SHG, (1.7.3.71) becomes (Qiu & Penzkofer, 1988)

$$\eta_{\text{THG}}(L_{\text{SHG}}, L_{\text{SFG}}) = BT^\omega \left[\frac{P^\omega(0)}{w_o^2} \right]^2 L_{\text{SHG}}^2 L_{\text{SFG}}^2 \sin^2 \left(\frac{\Delta k_{\text{SFG}} L_{\text{SFG}}}{2} \right) \quad (1.7.3.72)$$

with

$$B = B_{\text{SHG}} \cdot B_{\text{SFG}} = \frac{576\pi^2}{\varepsilon_o^2 c^2} \left(\frac{2N-1}{N} \right)^2 \frac{d_{\text{effSHG}}^2 d_{\text{effSFG}}^2}{\lambda_\omega^4} \left(\frac{T_{\text{SHG}}^3}{n_{\text{SHG}}^3} \right) \left(\frac{T_{\text{SFG}}^3}{n_{\text{SFG}}^3} \right)$$

in W^{-2} , where

$$\frac{T_{\text{SHG}}^3}{n_{\text{SHG}}^3} = \frac{(T^\omega)^3}{(n^\omega)^3} \quad \text{and} \quad \frac{T_{\text{SFG}}^3}{n_{\text{SFG}}^3} = \frac{T_3^{3\omega} T_1^\omega T_2^{2\omega}}{n_3^{3\omega} n_1^\omega n_2^{2\omega}}.$$

The units are the same as in (1.7.3.42).

A more general case of SFG, where one of the two pump beams is depleted, is given in Section 1.7.3.3.4.

1.7.3.3.3.2. *SHG* ($\omega + \omega = 2\omega$) and *SFG* ($\omega + 2\omega = 3\omega$) in the same crystal

When the SFG conversion efficiency is sufficiently low in comparison with that of the SHG, it is possible to integrate the equations relative to SHG and those relative to SFG separately (Boulanger, Fejer *et al.*, 1994). In order to compare this situation with the example taken for the previous case, we consider a type-I configuration of polarization for SHG. By assuming a perfect phase matching for SHG, the amplitude of the third harmonic field inside the crystal is (Boulanger, 1994)

$$E^{3\omega}(X, Y, Z) = jK^{3\omega}(\varepsilon_o \chi_{\text{effSFG}}) \times \int_0^L E_{\text{tot}}^\omega(X, Y, Z) E^{2\omega}(X, Y, Z) \exp(j\Delta k_{\text{SFG}} Z) dZ \quad (1.7.3.73)$$

with

$$E^{2\omega}(X, Y, Z) = (T^\omega)^{1/2} |E_{\text{tot}}^\omega(0)| \tanh(\Gamma Z) \quad \text{and} \quad E_{\text{tot}}^\omega(X, Y, Z) = (T^\omega)^{1/2} |E_{\text{tot}}^\omega(0)| \text{sech}(\Gamma Z). \quad (1.7.3.74)$$

Γ is as in (1.7.3.59).

(1.7.3.73) can be analytically integrated for undepleted pump SHG; $\text{sech}(m) \rightarrow 1$, $\tanh(m) \rightarrow m$, and so we have

$$\eta_{\text{THG}}(L) = P^{3\omega}(L)/P_{\text{tot}}^\omega(0) \quad (1.7.3.75)$$

with

$$P^{3\omega}(L) = \frac{576\pi^2}{\varepsilon_o^2 c^2} \left(\frac{2N-1}{N} \right)^2 T^{3\omega} \frac{d_{\text{effSHG}}^2 d_{\text{effSFG}}^2}{n^{3\omega} (n^\omega)^3 (n^{2\omega})^2} \frac{[T^\omega P_{\text{tot}}^\omega(0)]^3}{w_o^4 \lambda_\omega^4} J(L),$$

where the integral $J(L)$ is

$$J(L) = \left| \int_0^L Z \exp(i\Delta k_{\text{SFG}} Z) dZ \right|^2. \quad (1.7.3.76)$$

For a nonzero SFG phase mismatch, $\Delta k_{\text{SFG}} \neq 0$,

$$J(L) \simeq L^2 / (\Delta k_{\text{SFG}})^2. \quad (1.7.3.77)$$

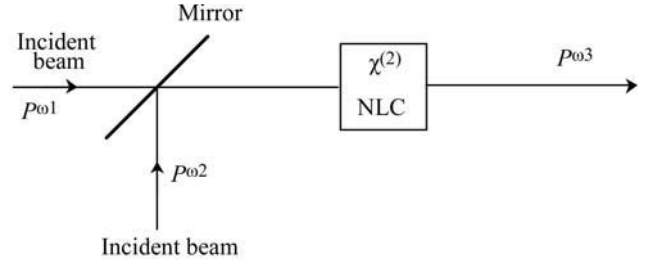


Fig. 1.7.3.17. Frequency up-conversion process $\omega_1 + \omega_2 = \omega_3$. The beam at ω_1 is mixed with the beam at ω_2 in the nonlinear crystal NLC in order to generate a beam at ω_3 . $P^{\omega_1, \omega_2, \omega_3}$ are the different powers.

For phase-matched SFG, $\Delta k_{\text{SFG}} = 0$,

$$J(L) = L^4/4. \quad (1.7.3.78)$$

Therefore (1.7.3.75) according to (1.7.3.78) is equal to (1.7.3.72) with $L_{\text{SHG}} = L_{\text{SFG}} = L/2$, $\Delta k_{\text{SFG}} = 0$ and 100% transmission coefficients at ω and 2ω between the two crystals.

1.7.3.3.3.3. *Direct THG* ($\omega + \omega + \omega = 3\omega$)

As for the cascading process, we consider a flat plane wave which propagates in a direction without walk-off. The integration of equations (1.7.3.24) over the crystal length L , with $E_4^{3\omega}(X, Y, 0) = 0$ and in the undepleted pump approximation, leads to

$$E_4^{3\omega}(X, Y, L) = jK_4^{3\omega} [\varepsilon_o \chi_{\text{eff}}^{(3)}] E_1^\omega(X, Y, 0) E_2^\omega(X, Y, 0) E_3^\omega(X, Y, 0) \times L \sin c[(\Delta k \cdot L)/2] \exp(-j\Delta k L/2). \quad (1.7.3.79)$$

According to (1.7.3.36) and (1.7.3.38), the integration of (1.7.3.79) over the cross section, which is the same for the four beams, leads to

$$\eta_{\text{THG}}(L) = \frac{P^{3\omega}(L)}{P^\omega(0)} = B_{\text{THG}} [P^\omega(0)]^2 \frac{L^2}{w_o^4} \sin^2[(\Delta k \cdot L)/2]$$

with

$$B_{\text{THG}} = \frac{576 d_{\text{eff}}^2 T_4^{3\omega} (T_1^\omega)^2 T_2^\omega}{\varepsilon_o^2 c^2 \lambda_\omega^2 n_4^{3\omega} (n_1^\omega)^2 n_2^\omega} \quad (\text{m}^2 \text{W}^{-2}), \quad (1.7.3.80)$$

where $d_{\text{eff}} = (1/4)\chi_{\text{eff}}^{(3)}$ is in $\text{m}^2 \text{V}^{-2}$ and λ_ω is in m. The statistical factor is assumed to be equal to 1, which corresponds to a longitudinal single-mode laser.

The different types of phase matching and the associated relations and configurations of polarization are given in Table 1.7.3.2 by considering the SFG case with $\omega_1 = \omega_2 = \omega_3 = \omega_4/3$.

1.7.3.3.4. *Sum-frequency generation (SFG)*

SHG ($\omega + \omega = 2\omega$) and SFG ($\omega + 2\omega = 3\omega$) are particular cases of three-wave SFG. We consider here the general situation where the two incident beams at ω_1 and ω_2 , with $\omega_1 < \omega_2$, interact with the generated beam at ω_3 , with $\omega_3 = \omega_1 + \omega_2$, as shown in Fig. 1.7.3.17. The phase-matching configurations are given in Table 1.7.3.1.

From the general point of view, SFG is a frequency up-conversion parametric process which is used for the conversion of laser beams at low circular frequency: for example, conversion of infrared to visible radiation.

The resolution of system (1.7.3.22) leads to Jacobian elliptic functions if the waves at ω_1 and ω_2 are both depleted. The calculation is simplified in two particular situations which are often encountered: on the one hand undepletion for the waves at ω_1 and ω_2 , and on the other hand depletion of only one wave at

1. TENSORIAL ASPECTS OF PHYSICAL PROPERTIES

ω_1 or ω_2 . For the following, we consider plane waves which propagate in a direction without walk-off so we consider a single wave frame; the energy distribution is assumed to be flat, so the three beams have the same radius w_o .

1.7.3.3.4.1. SFG ($\omega_1 + \omega_2 = \omega_3$) with undepletion at ω_1 and ω_2

The resolution of system (1.7.3.22) with $E_1(X, Y, 0) \neq 0$, $E_2(X, Y, 0) \neq 0$, $\partial E_1(X, Y, Z)/\partial Z = \partial E_2(X, Y, Z)/\partial Z = 0$ and $E_3(X, Y, 0) = 0$, followed by integration over (X, Y) , leads to

$$P^{\omega_1}(L) = (T^{\omega_1})^2 P^{\omega_1}(0) \quad (1.7.3.81)$$

$$P^{\omega_2}(L) = (T^{\omega_2})^2 P^{\omega_2}(0) \quad (1.7.3.82)$$

$$P^{\omega_3}(L) = B P^{\omega_1}(0) P^{\omega_2}(0) \frac{L^2}{w_o^2} \sin^2 \frac{\Delta k \cdot L}{2} \quad (1.7.3.83)$$

with

$$B_{\text{SFG}} = \frac{72\pi}{\varepsilon_o c} \frac{2N-1}{N} \frac{d_{\text{eff}}^2}{\lambda_{\omega}^2} \frac{T^{\omega_3} T^{\omega_1} T^{\omega_2}}{n^{\omega_3} n^{\omega_1} n^{\omega_2}} \quad (W^{-1})$$

in the same units as equation (1.7.3.70).

1.7.3.3.4.2. SFG ($\omega_s + \omega_p = \omega_i$) with undepletion at ω_p

$(\omega_s, \omega_p, \omega_i) = (\omega_1, \omega_2, \omega_3)$ or $(\omega_2, \omega_1, \omega_3)$.

The undepleted wave at ω_p , the pump, is mixed in the nonlinear crystal with the depleted wave at ω_s , the signal, in order to generate the idler wave at $\omega_i = \omega_s + \omega_p$. The integrations of the coupled amplitude equations over (X, Y, Z) with $E_s(X, Y, 0) \neq 0$, $E_p(X, Y, 0) \neq 0$, $\partial E_p(X, Y, Z)/\partial Z = 0$ and $E_i(X, Y, 0) = 0$ give

$$P_p(L) = T_p^2 P_p(0) \quad (1.7.3.84)$$

$$P_i(L) = \frac{\omega_i}{\omega_s} P_s(0) \Gamma^2 L^2 \frac{\sin^2 \{ \Gamma^2 L^2 + [(\Delta k \cdot L)/2]^2 \}^{1/2}}{\Gamma^2 L^2 + [(\Delta k \cdot L)/2]^2} \quad (1.7.3.85)$$

$$P_s(L) = P_s(0) \left[1 - \frac{\omega_s}{\omega_i} \frac{P_i(L)}{P_s(0)} \right], \quad (1.7.3.86)$$

with $\Delta k = k_i - (k_s + k_p)$ and $\Gamma^2 = [B_s P_p(0)]/w_o^2$, where

$$B_s = \frac{8\pi}{\varepsilon_o c} \frac{2N-1}{N} \frac{d_{\text{eff}}^2}{\lambda_s \lambda_i} \frac{T_s T_p T_i}{n_s n_p n_i}.$$

Thus, even if the up-conversion process is phase-matched ($\Delta k = 0$), the power transfers are periodic: the photon transfer efficiency is then 100% for $\Gamma L = (2m+1)(\pi/2)$, where m is an integer, which allows a maximum power gain ω_i/ω_s for the idler. A nonlinear crystal with length $L = (\pi/2\Gamma)$ is sufficient for an optimized device.

For a small conversion efficiency, *i.e.* ΓL weak, (1.7.3.85) and (1.7.3.86) become

$$P_i(L) \simeq P_s(0) \frac{\omega_i}{\omega_s} \Gamma^2 L^2 \sin^2 \frac{\Delta k \cdot L}{2} \quad (1.7.3.87)$$

and

$$P_s(L) \simeq P_s(0). \quad (1.7.3.88)$$

The expression for $P_i(L)$ with $\Delta k = 0$ is then equivalent to (1.7.3.83) with $\omega_p = \omega_1$ or ω_2 , $\omega_i = \omega_3$ and $\omega_s = \omega_2$ or ω_1 .

For example, the frequency up-conversion interaction can be of great interest for the detection of a signal, ω_s , comprising IR radiation with a strong divergence and a wide spectral bandwidth. In this case, the achievement of a good conversion efficiency, $P_i(L)/P_s(0)$, requires both wide spectral and angular acceptance bandwidths with respect to the signal. The double non-criticality in frequency and angle (DNPM) can then be used with one-beam

non-critical non-collinear phase matching (OBNC) associated with vectorial group phase matching (VGPM) (Dolinchuk *et al.*, 1994); this corresponds to the equality of the absolute magnitudes and directions of the signal and idler group velocity vectors *i.e.* $d\omega_i/d\mathbf{k}_i = d\omega_s/d\mathbf{k}_s$.

1.7.3.3.5. Difference-frequency generation (DFG)

DFG is defined by $\omega_3 - \omega_1 = \omega_2$ with $E_2(X, Y, 0) = 0$ or $\omega_3 - \omega_2 = \omega_1$ with $E_1(X, Y, 0) = 0$. The DFG phase-matching configurations are given in Table 1.7.3.1. As for SFG, the solutions of system (1.7.3.22) are Jacobian elliptic functions when the incident waves are both depleted. We consider here the simplified situations of undepletion of the two incident waves and depletion of only one incident wave. In the latter, the solutions differ according to whether the circular frequency of the undepleted wave is the highest one, *i.e.* ω_3 , or not. We consider the case of plane waves that propagate in a direction without walk-off and we assume a flat energy distribution for the three beams.

1.7.3.3.5.1. DFG ($\omega_p - \omega_s = \omega_i$) with undepletion at ω_p and ω_s

$(\omega_s, \omega_i, \omega_p) = (\omega_1, \omega_2, \omega_3)$ or $(\omega_2, \omega_1, \omega_3)$.

The resolution of system (1.7.3.22) with $E_s(X, Y, 0) \neq 0$, $E_p(X, Y, 0) \neq 0$, $\partial E_p(X, Y, Z)/\partial Z = \partial E_s(X, Y, Z)/\partial Z = 0$ and $E_i(X, Y, 0) = 0$, followed by integration over (X, Y) , leads to the same solutions as for SFG with undepletion at ω_1 and ω_2 , *i.e.* formulae (1.7.3.81), (1.7.3.82) and (1.7.3.83), by replacing ω_1 by ω_s , ω_2 by ω_p and ω_3 by ω_i . A schematic device is given in Fig. 1.7.3.17 by replacing $(\omega_1, \omega_2, \omega_3)$ by $(\omega_1, \omega_3, \omega_2)$ or $(\omega_2, \omega_3, \omega_1)$.

1.7.3.3.5.2. DFG ($\omega_s - \omega_p = \omega_i$) with undepletion at ω_p

$(\omega_s, \omega_i, \omega_p) = (\omega_3, \omega_1, \omega_2)$ or $(\omega_3, \omega_2, \omega_1)$.

The resolution of system (1.7.3.22) with $E_s(X, Y, 0) \neq 0$, $E_p(X, Y, 0) \neq 0$, $\partial E_p(X, Y, Z)/\partial Z = 0$ and $E_i(X, Y, 0) = 0$, followed by the integration over (X, Y) , leads to the same solutions as for SFG with undepletion at ω_1 or ω_2 : formulae (1.7.3.84), (1.7.3.85) and (1.7.3.86).

1.7.3.3.5.3. DFG ($\omega_p - \omega_s = \omega_i$) with undepletion at ω_p – optical parametric amplification (OPA), optical parametric oscillation (OPO)

$(\omega_s, \omega_i, \omega_p) = (\omega_1, \omega_2, \omega_3)$ or $(\omega_2, \omega_1, \omega_3)$.

The initial conditions are the same as in Section 1.7.3.3.5.2, except that the undepleted wave has the highest circular frequency. In this case, the integrations of the coupled amplitude equations over (X, Y, Z) lead to

$$P_p(L) = T_p^2 P_p(0), \quad (1.7.3.89)$$

$$P_i(L) = P_s(0) \frac{\omega_i}{\omega_s} \Gamma^2 L^2 \frac{\sinh^2 \{ \Gamma^2 L^2 - [(\Delta k \cdot L)/2]^2 \}^{1/2}}{\Gamma^2 L^2 - [(\Delta k \cdot L)/2]^2} \quad (1.7.3.90)$$

and

$$\begin{aligned} P_s(L) &= P_s(0) \left[1 + \frac{\omega_s}{\omega_i} \frac{P_i(L)}{P_s(0)} \right] \\ &= P_s(0) \left(1 + \Gamma^2 L^2 \frac{\sinh^2 \{ \Gamma^2 L^2 - [(\Delta k \cdot L)/2]^2 \}^{1/2}}{\Gamma^2 L^2 - [(\Delta k \cdot L)/2]^2} \right) \end{aligned} \quad (1.7.3.91)$$

with $\Delta k = k_p - (k_i + k_s)$ and $\Gamma^2 = [B_i P_p(0)]/w_o^2$, where w_o is the beam radius of the three beams and

$$B_i = \frac{8\pi}{\varepsilon_o c} \frac{2N-1}{N} \frac{d_{\text{eff}}^2}{\lambda_s \lambda_i} \frac{T_s T_p T_i}{n_s n_p n_i}.$$

1.7. NONLINEAR OPTICAL PROPERTIES

The units are the same as in equation (1.7.3.42).

Equations (1.7.3.90) and (1.7.3.91) show that both idler and signal powers grow exponentially. So, firstly, the generation of the idler is not detrimental to the signal power, in contrast to DFG ($\omega_s - \omega_p = \omega_i$) and SFG ($\omega_s + \omega_p = \omega_i$), and, secondly, the signal power is amplified. Thus DFG ($\omega_p - \omega_s = \omega_i$) combines two interesting functions: generation at ω_i and amplification at ω_s . The last function is called optical parametric amplification (OPA).

The gain of OPA can be defined as (Harris, 1969)

$$G(L) = \left| \frac{P_s(L)}{P_s(0)} - 1 \right|. \quad (1.7.3.92)$$

For example, Baumgartner & Byer (1979) obtained a gain of about 10 for the amplification of a beam at $0.355 \mu\text{m}$ by a pump at $1.064 \mu\text{m}$ in a 5 cm long KH_2PO_4 crystal, with a pump intensity of 28 MW cm^{-2} .

According to (1.7.3.91), for $\Delta k^2 L^2 / 4 \gg \Gamma^2 L^2$, $\sinh(im) \rightarrow -\sin^2(m)$ and so the gain is given by

$$G_{\text{small gain}} \simeq \Gamma^2 L^2 \sin^2 \left(\frac{\Delta k \cdot L}{2} \right). \quad (1.7.3.93)$$

Formula (1.7.3.93) shows that frequencies can be generated around ω_s . The full gain linewidth of the signal, $\Delta\omega_s$, is defined as the linewidth leading to a maximum phase mismatch $\Delta k = 2\pi/L$. If we assume that the pump wave linewidth is negligible, i.e. $\Delta\omega_p = 0$, it follows, by expanding Δk in a Taylor series around ω_i and ω_s , and by only considering the first order, that

$$|\Delta\omega_s^{\text{small gain}}| = |\Delta\omega_i^{\text{small gain}}| \simeq (2\pi/Lb) \quad (1.7.3.94)$$

with $b = [1/v_g(\omega_i)] - [1/v_g(\omega_s)]$, where $v_g(\omega) = \partial\omega/\partial k$ is the group velocity.

This linewidth can be termed intrinsic because it exists even if the pump beam is parallel and has a narrow spectral spread.

For type I, the spectral linewidth of the signal and idler waves is largest at the degeneracy: $b = 0$ because the idler and signal waves have the same polarization and so the same group velocity at degeneracy, i.e. $\omega_i = \omega_s = \omega_p/2$. In this case, it is necessary to consider the dispersion of the group velocity $\partial^2\omega/\partial^2 k$ for the calculation of $\Delta\omega_s$ and $\Delta\omega_i$. Note that an increase in the crystal length allows a reduction in the linewidth.

For type II, b is never nil, even at degeneracy.

A parametric amplifier placed inside a resonant cavity constitutes an optical parametric oscillator (OPO) (Harris, 1969; Byer, 1973; Brosnan & Byer, 1979; Yang *et al.*, 1993). In this case, it is not necessary to have an incident signal wave because both signal and idler photons can be generated by spontaneous parametric emission, also called parametric noise or parametric scattering (Louisell *et al.*, 1961): when a laser beam at ω_p propagates in a $\chi^{(2)}$ medium, it is possible for pump photons to spontaneously break down into pairs of lower-energy photons of circular frequencies ω_s and ω_i with the total photon energy conserved for each pair, i.e. $\omega_s + \omega_i = \omega_p$. The pairs of generated waves for which the phase-matching condition is satisfied are the only ones to be efficiently coupled by the nonlinear medium. The OPO can be singly resonant (SROPO) at ω_s or ω_i (Yang *et al.*, 1993; Chung & Siegman, 1993), doubly resonant (DROPO) at both ω_s and ω_i (Yang *et al.*, 1993; Breitenbach *et al.*, 1995) or triply resonant (TROPO) (Debuisschert *et al.*, 1993; Scheidt *et al.*, 1995). Two main techniques for the pump injection exist: the pump can propagate through the cavity mirrors, which allows the smallest cavity length; for continuous waves or pulsed waves with a pulsed duration greater than 1 ns, it is possible to increase the cavity length in order to put two 45° mirrors in the cavity for the pump, as shown in Fig. 1.7.3.18. This second technique allows us to use simpler mirror coatings because they are not illuminated by the strong pump beam.

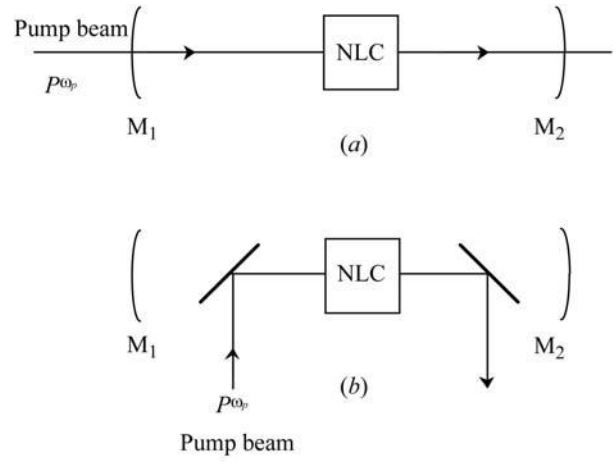


Fig. 1.7.3.18. Schematic OPO configurations. P^{ω_p} is the pump power. (a) can be a SROPO, DROPO or TROPO and (b) can be a SROPO or DROPO, according to the reflectivity of the cavity mirrors (M_1, M_2).

The only requirement for making an oscillator is that the parametric gain exceeds the losses of the resonator. The minimum intensity above which the OPO has to be pumped for an oscillation is termed the threshold oscillation intensity I_{th} . The oscillation threshold decreases when the number of resonant frequencies increases: $I_{\text{th}}^{\omega_p}(\text{SROPO}) > I_{\text{th}}^{\omega_p}(\text{DROPO}) > I_{\text{th}}^{\omega_p}(\text{TROPO})$; on the other hand the instability increases because the condition of simultaneous resonance is critical.

The oscillation threshold of a SROPO or DROPO can be decreased by reflecting the pump from the output coupling mirror M_2 in configuration (a) of Fig. 1.7.3.18 (Marshall & Kaz, 1993). It is necessary to pump an OPO by a beam with a smooth optical profile because hot spots could damage all the optical components in the OPO, including mirrors and nonlinear crystals. A very high beam quality is required with regard to other parameters such as the spectral bandwidth, the pointing stability, the divergence and the pulse duration.

The intensity threshold is calculated by assuming that the pump beam is undepleted. For a phase-matched SROPO, resonant at ω_s or ω_i , and for nanosecond pulsed beams with intensities that are assumed to be constant over one single pass, $I_{\text{th}}^{\omega_p}$ is given by

$$I_{\text{th}}^{\omega_p} = \frac{1.8}{KL^2(1+\gamma)^2} \left\{ \frac{25L}{c\tau} + 2\alpha L + Ln \left[\frac{1}{(1-T)^{1/2}} \right] + Ln(2) \right\}^2. \quad (1.7.3.95)$$

$K = (\omega_s \omega_i \chi_{\text{eff}}^2) / [2n(\omega_s)n(\omega_i)n(\omega_p)\epsilon_0 c^3]$; L is the crystal length; γ is the ratio of the backward to the forward pump intensity; τ is the $1/e^2$ half width duration of the pump beam pulse; and 2α and T are the linear absorption and transmission coefficients at the circular frequency of the resonant wave ω_s or ω_i . In the nanosecond regime, typical values of $I_{\text{th}}^{\omega_p}$ are in the range 10 – 100 MW cm^{-2} .

(1.7.3.95) shows that a small threshold is achieved for long crystal lengths, high effective coefficient and for weak linear losses at the resonant frequency. The pump intensity threshold must be less than the optical damage threshold of the nonlinear crystal, including surface and bulk, and of the dielectric coating of any optical component of the OPO. For example, a SROPO using an 8 mm long KNbO_3 crystal ($d_{\text{eff}} \simeq 10 \text{ pm V}^{-1}$) as a nonlinear crystal was performed with a pump threshold intensity of 65 MW cm^{-2} (Unschel *et al.*, 1995): the 3 mm-diameter pump beam was a 10 Hz injection-seeded single-longitudinal-mode Nd:YAG laser at $1.064 \mu\text{m}$ with a 9 ns pulse of 100 mJ; the SROPO was pumped as in Fig. 1.7.3.18(a) with a cavity length of 12 mm, a mirror M_1 reflecting 100% at the signal, from 1.4 to

1. TENSORIAL ASPECTS OF PHYSICAL PROPERTIES

2 μm , and a coupling mirror M_2 reflecting 90% at the signal and transmitting 100% at the idler, from 2 to 4 μm .

For increasing pump powers above the oscillation threshold, the idler and signal powers grow with a possible depletion of the pump.

The total signal or idler conversion efficiency from the pump depends on the device design and pump source. The greatest values are obtained with pulsed beams. As an example, 70% peak power conversion efficiency and 65% energy conversion of the pump to both signal ($\lambda_s = 1.61 \mu\text{m}$) and idler ($\lambda_i = 3.14 \mu\text{m}$) outputs were obtained in a SROPO using a 20 mm long KTP crystal ($d_{\text{eff}} = 2.7 \text{ pm V}^{-1}$) pumped by an Nd:YAG laser ($\lambda_p = 1.064 \mu\text{m}$) for eye-safe source applications (Marshall & Kaz, 1993): the configuration is the same as in Fig. 1.7.3.18(a) where M_1 has high reflection at 1.61 μm and high transmission at 1.064 μm , and M_2 has high reflection at 1.064 μm and a 10% transmission coefficient at 1.61 μm ; the Q-switched pump laser produces a 15 ns pulse duration (full width at half maximum), giving a focal intensity around 8 MW cm^{-2} per mJ of pulse energy; the energy conversion efficiency from the pump relative to the signal alone was estimated to be 44%.

OPOs can operate in the continuous-wave (cw) or pulsed regimes. Because the threshold intensity is generally high for the usual nonlinear materials, the cw regime requires the use of DROPO or TROPO configurations. However, cw-SROPO can run when the OPO is placed within the pump-laser cavity (Ebrahimzadeh *et al.*, 1999). The SROPO in the classical external pumping configuration, which leads to the most practical devices, runs very well with a pulsed pump beam, *i.e.* Q-switched laser running in the nanosecond regime and mode-locked laser emitting picosecond or femtosecond pulses. For nanosecond operation, the optical parametric oscillation is ensured by the same pulse, because several cavity round trips of the pump are allowed during the pulse duration. It is not possible in the ultrafast regimes (picosecond or femtosecond). In these cases, it is necessary to use synchronous pumping: the round-trip transit time in the OPO cavity is taken to be equal to the repetition period of the pump pulse train, so that the resonating wave pulse is amplified by successive pump pulses [see for example Ruffing *et al.* (1998) and Reid *et al.* (1998)].

OPOs are used for the generation of a fixed wavelength, idler or signal, but have potential for continuous wavelength tuning over a broad range, from the near UV to the mid-IR. The tuning is based on the dispersion of the refractive indices with the wavelength, the direction of propagation, the temperature or any other variable of dispersion. More particularly, the crystal must be phase-matched for DFG over the widest spectral range for a reasonable variation of the dispersion parameter to be used. Several methods are used: variation of the pump wavelength at a fixed direction, fixed temperature *etc.*; rotation of the crystal at a fixed pump wavelength, fixed temperature *etc.*; or variation of the crystal temperature at a fixed pump wavelength, fixed direction *etc.*

We consider here two of the most frequently encountered methods at present: for birefringence phase matching, angle tuning and pump-wavelength tuning; and the case of quasi phase matching.

(i) OPO with angle tuning.

The function of a tunable OPO is to generate the signal and idler waves over a broad range, $\Delta\omega_s$ and $\Delta\omega_i$, respectively, from a fixed pump wave at ω_p . The spectral shifts $\Delta\omega_s = \omega_s^+ - \omega_s^-$ and $\Delta\omega_i = \omega_i^+ - \omega_i^-$ are obtained by rotating the nonlinear crystal by an angle $\Delta\alpha = \alpha^+ - \alpha^-$ in order to achieve phase matching over the spectral range considered: $\omega_p n(\omega_p, \alpha) = \omega_s n(\omega_s, \alpha) + \omega_i n(\omega_i, \alpha)$ with $\omega_p = \omega_i + \omega_s$ from $(\omega_s^+, \omega_i^-, \alpha^\pm)$ to $(\omega_s^-, \omega_i^+, \alpha^\mp)$, where $(-)$ and $(+)$, respectively, denote the minimum and maximum values of the data considered. Note that $\Delta\omega_s = -\Delta\omega_i$ and so $(\Delta\lambda_i/\lambda_i^+ \lambda_i^-) = -(\Delta\lambda_s/\lambda_s^+ \lambda_s^-)$ if the spectral bandwidth of the pump, $\delta\omega_p$, is zero.

In the case of parallelepipedal nonlinear crystals, the tuning rate $\Delta\omega_{i,s}/\Delta\alpha$ has to be high because $\Delta\alpha$ cannot exceed about 30° of arc, *i.e.* 15° on either side of the direction normal to the plane surface of the nonlinear crystal: in fact, the refraction can lead to an attenuation of the efficiency of the parametric interaction for larger angles. For this reason, a broad-band OPO necessarily requires angular critical phase matching (CPM) directions over a broad spectral range. However, the angular criticality is detrimental to the spectral stability of the signal and idler waves with regard to the pointing fluctuations of the pump beam: a pointing instability of the order of 100 μrad is considered to be acceptable for OPOs based on KTP or BBO crystals. Fig. 1.7.3.19 shows the phase-matching tuning curves $\lambda_i(\alpha)$ and $\lambda_s(\alpha)$ for (a) BBO pumped at $\lambda_p = 355 \text{ nm}$ and (b) KTP pumped at $\lambda_p = 1064 \text{ nm}$, where $\alpha = \theta$ or φ is an internal angle: the calculations were carried out using the refractive indices given in Kato (1986) for BBO and in Kato (1991) for KTP.

The divergence of the pump beam may increase the spectral bandwidths $\delta\omega_s$ and $\delta\omega_i$: the higher the derivatives $\partial\lambda_{i,s}/\partial\alpha$ are, the higher the spectral bandwidths for a given pump divergence are. Furthermore, $\partial\lambda_{i,s}/\partial\alpha$ vary as a function of the phase-matching angle α . The derivative is a maximum at the degeneracy $\lambda_i = \lambda_s = 2\lambda_p$, when the idler and signal waves are identically polarized: this is the case for BBO as shown in Fig. 1.7.3.19(a). We give another example of a type-I BBO OPO pumped at 308 nm by a narrow-band injection-seeded ultraviolet XeCl excimer laser (Ebrahimzadeh *et al.*, 1990): the spectral bandwidth, expressed in cm^{-1} ($\partial\lambda_{i,s}/\lambda_{i,s}^2 = \partial\omega_{i,s}/2\pi c$), varies from $\sim 78 \text{ cm}^{-1}$ to $\sim 500 \text{ cm}^{-1}$ for a crystal length of 1.2 cm, corresponding to a signal bandwidth $\delta\lambda_s \simeq 1.8 \text{ nm}$ at 480 nm and $\delta\lambda_s \simeq 18 \text{ nm}$ at 600 nm, respectively. The degeneracy is not a particular situation with respect to the derivative of the phase-matching curve when the idler and signal waves are orthogonally polarized as shown in Fig. 1.7.3.19(b) with the example of KTP.

The way currently used for substantial reduction of the spectral bandwidth is to introduce bandwidth-limiting elements in the OPO cavity, such as a grazing grating associated with a tuning mirror reflecting either the signal or the idler according to the chosen resonant wavelength. The rotations of the nonlinear crystal and of the restricting element have to be synchronized in order to be active over all the wavelength range generated. Narrow bandwidths of about 0.1 cm^{-1} can be obtained in this way, but the gain of such a device is low. High energy and narrow spectral bandwidth can be obtained at the same time by the association of two OPOs: an OPO pumped at ω_p and without a restricting element inside the cavity is seeded by the idler or signal beam emitted by a narrow spectral bandwidth OPO also pumped at ω_p .

The disadvantages of parallelepipedal crystals can be circumvented by using a nonlinear crystal cut as a cylindrical plate, with the cylinder axis orthogonal to the OPO cavity axis and to the plane of the useful phase-matching directions (Boulanger *et al.*, 1999; Pacaud *et al.*, 2000; Fève, Pacaud *et al.*, 2002). Such a geometry allows us to consider any phase-matching range by rotation of the cylinder around its revolution axis. It is then possible to use interactions with a weak angular tuning rate to reduce the spectral bandwidth and increase the stability of the generated beams. Moreover, the propagation of the beams is at normal incidence for any direction, so collinear phase matching can be maintained, leading to better spatial and spectral transverse profiles. Because of the cylindrical geometry of the nonlinear crystal, it is necessary to focus the pump beam and to collect the signal and idler beams with cylindrical lenses. The cavity mirrors, plane or cylindrical, are then placed between the nonlinear crystal and the lenses. The diameter of the crystal being about a few tenths of a millimetre, the associated focal distance is short, *i.e.* a few millimetres, which leads to a strong spatial filtering effect, preventing the oscillation of beams with a quality factor M^2 bigger than about 1.5.

1.7. NONLINEAR OPTICAL PROPERTIES

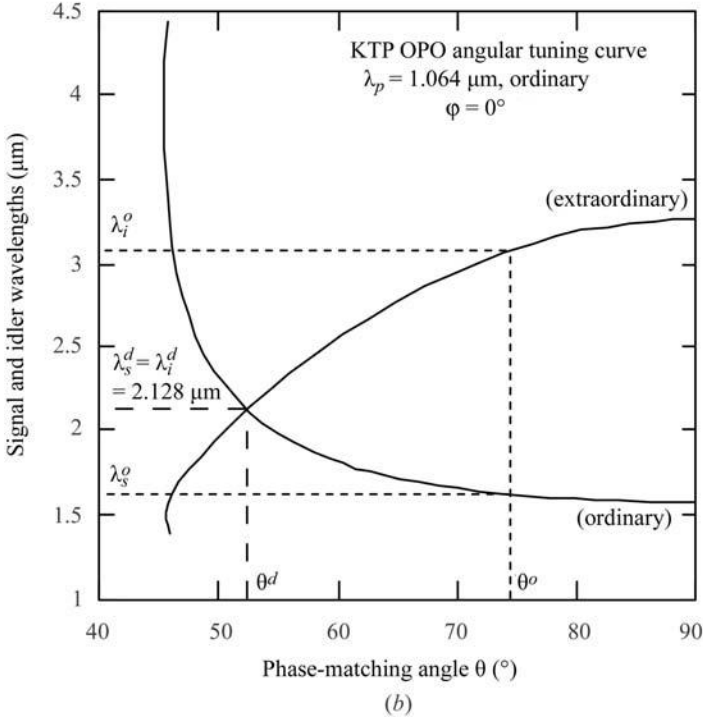
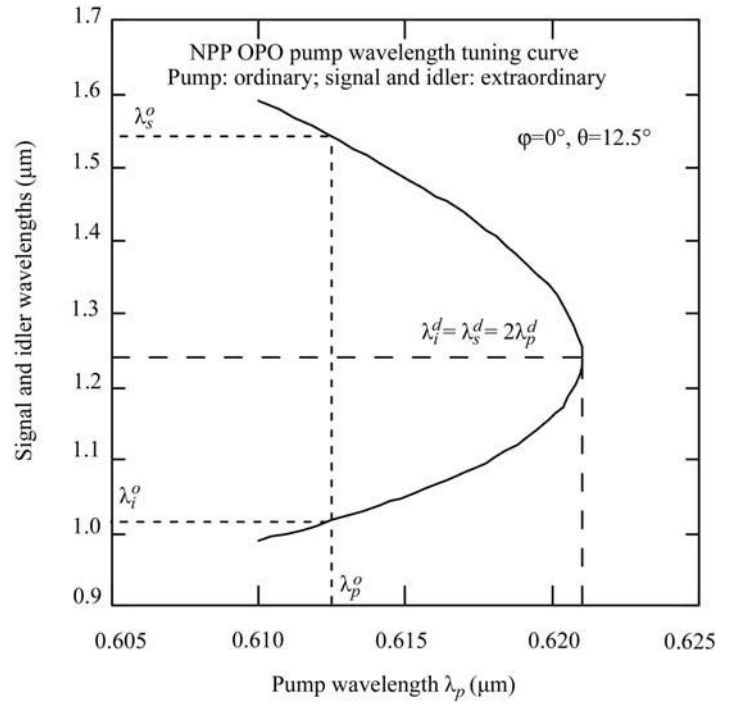
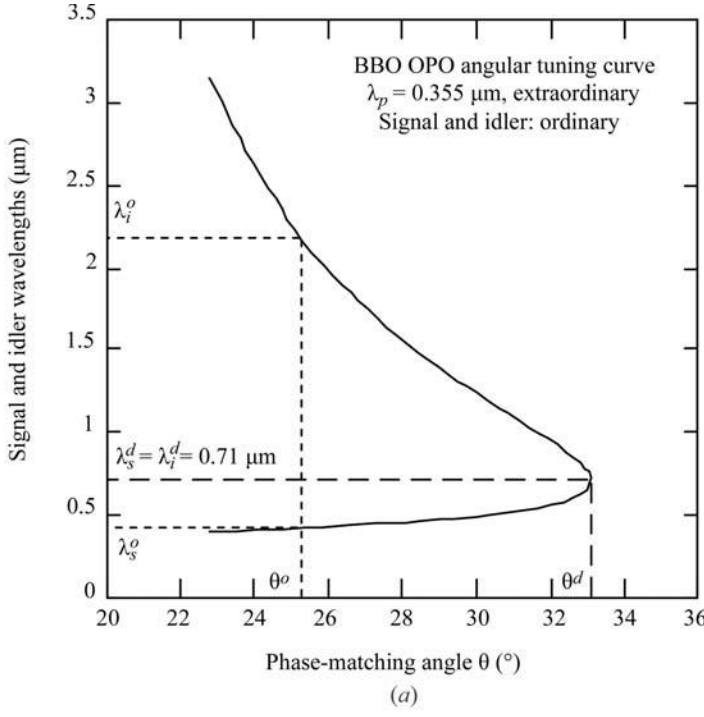


Fig. 1.7.3.19. Calculated angular tuning curves. θ and φ are the spherical coordinates of the phase-matching directions. θ^d is the phase-matching angle of the degeneracy process ($\lambda_i^d = \lambda_s^d = 2\lambda_p$). λ_i^o and λ_s^o are the idler and signal wavelengths, respectively, generated at θ^o . Ordinary and extraordinary refer to the polarization.

(ii) OPO with a tuning pump.

The nonlinear crystal is fixed and the pump frequency can vary over $\Delta\omega_p$, leading to a variation of the signal and idler frequencies such that $\Delta\omega_i + \Delta\omega_s = \Delta\omega_p$.

In Fig. 1.7.3.20, the example of *N*-(4-nitrophenyl)-L-propinol (NPP) pumped between 610 and 621 nm is shown (Ledoux *et al.*, 1990; Khodja *et al.*, 1995a). The phase-matching curve $\lambda_{i,s}(\lambda_p)$ is calculated from the Sellmeier equations of Ledoux *et al.* (1990) for the case of identical polarizations for the signal and idler waves. The tuning rate is a maximum at the degeneracy, as for angular tuning with identical polarizations.

Fig. 1.7.3.20. Calculated pump wavelength tuning curve. λ_p^d is the pump wavelength leading to degeneracy for the direction considered ($\theta = 12.5^\circ$, $\varphi = 0^\circ$). Ordinary and extraordinary refer to the polarization.

For any configuration of polarization, the most favourable direction of propagation of an OPO with a tuning pump is a principal axis of the index surface, because the phase matching is angular non-critical and so wavelength critical. In this optimal situation, the OPO has a low sensitivity to the divergence and pointing stability of the pump beam; furthermore, the walk-off angle is nil, which provides a higher conversion efficiency.

(iii) Quasi-phase-matched OPO with a tunable periodicity.

In a QPM device, the interacting frequencies are fixed by the frequency dispersion of the birefringence of the nonlinear material and by the periodicity of the grating. A first possibility is to fabricate a series of gratings with different periodicities in the same nonlinear crystal; the translation of this crystal with respect to the fixed pump beam allows us to address the different gratings and thus to generate different couples (ω_s , ω_i). Because the tuning is obtained in discrete steps, it is necessary to combine temperature or angle tuning with the translation of the sample in order to interpolate smoothly between the steps. For example, a device based on a periodically poled LiNbO₃ (ppLN) crystal with a thickness of 0.5 mm and a length along the periodicity vector of 1 cm has been developed (Myers *et al.*, 1996). A total of 25 gratings with periods between 26 and 32 μm were realized in 0.25 μm increments. The OPO was pumped at 1.064 μm and generated a signal between 1.35 and 1.98 μm , with the corresponding idler between 4.83 and 2.30 μm .

Fan-shaped gratings have been demonstrated as an alternative approach for continuous tuning (Powers *et al.*, 1998). However, such a structure has the disadvantage of introducing large spectral heterogeneity to the generated beams, because the grating period is not constant over the pump beam diameter.

Finally, the most satisfactory alternative for continuous tuning is the use of a cylindrical crystal with one single grating (Fève *et al.*, 2001). The variations of the signal and idler wavelengths are then obtained by rotation of the cylinder around its revolution axis, which is orthogonal to the OPO cavity axis and to the plane containing the frame vector Λ . For a direction of propagation making an angle α with Λ , the effective period of the grating as seen by the collinear interacting wavevectors is $\Lambda_\alpha = (\Lambda / \cos \alpha)$, leading to a continuous spectral tuning. For example, a rotation over an α range of 26° of a ppKTP cylinder pumped at 1064 nm

1. TENSORIAL ASPECTS OF PHYSICAL PROPERTIES

leads to a signal tuning range of 520 nm, between 1515 and 2040 nm, while the corresponding idler is tuned over 1340 nm, between 2220 and 3560 nm.

For an overview of OPO and OPA, the reader may refer to the following special issues of the *Journal of the Optical Society of America B*: (1993), **10**(9), 1656–1794; (1993), **10**(11), 2148–2239 and (1995), **12**(11), 2084–2310; and to the *Handbook of Optics* devoted to OPO (Ebrahimzadeh & Dunn, 2000).

1.7.4. Determination of basic nonlinear parameters

We review here the different methods that are used for the study of nonlinear crystals.

1.7.4.1. Phase-matching directions and associated acceptance bandwidths

The very early stage of crystal growth of a new material usually provides a powder with particle sizes less than 100 μm . It is then impossible to measure the phase-matching loci. Nevertheless, careful SHG experiments performed on high-quality crystalline material may indicate whether the SHG is phase-matched or not by considering the dependence of the SHG intensity on the following parameters: the angle between the detector and the direction of the incident fundamental beam, the powder layer thickness, the average particle size and the laser beam diameter (Kurtz & Perry, 1968). However, powder measurements are essentially used for the detection in a simple and quick way of noncentrosymmetry of crystals, this criterion being necessary to have a nonzero $\chi^{(2)}$ tensor (Kurtz & Dougherty, 1978). They also allow, for example, the measurement of the temperature of a possible centrosymmetric/noncentrosymmetric transition (Marnier *et al.*, 1989).

For crystal sizes greater than few hundred μm , it is possible to perform direct measurements of phase-matching directions. The methods developed at present are based on the use of a single crystal ground into an ellipsoidal (Velsko, 1989) or spherical shape (Marnier & Boulanger, 1989; Boulanger, 1989; Boulanger *et al.*, 1998); a sphere is difficult to obtain for sample diameters less than 2 mm, but it is the best geometry for large numbers and accurate measurements because of normal refraction for every chosen direction of propagation. The sample is oriented using X-rays, placed at the centre of an Euler circle and illuminated with fixed and appropriately focused laser beams. The experiments are usually performed with SHG of different fundamental wavelengths. The sample is rotated in order to propagate the fundamental beam in different directions: a phase-matching direction is then detected when the SHG conversion efficiency is a maximum. It is then possible to describe the whole phase-matching cone with an accuracy of 1° . A spherical crystal also allows easy measurement of the walk-off angle of each of the waves (Boulanger *et al.*, 1998). It is also possible to perform a precise observation and study of the internal conical refraction in biaxial crystals, which leads to the determination of the optic axis angle $V(\omega)$, given by relation (1.7.3.14), for different frequencies (Fève *et al.*, 1994).

Phase-matching relations are often poorly calculated when using refractive indices determined by the prism method or by measurement of the critical angle of total reflection. Indeed, all the refractive indices concerned have to be measured with an accuracy of 10^{-4} in order to calculate the phase-matching angles with a precision of about 1° . Such accuracies can be reached in the visible spectrum, but it is more difficult for infrared wavelengths. Furthermore, it is difficult to cut a prism of few mm size with plane faces.

If the refractive indices are known with the required accuracy at several wavelengths well distributed across the transparency region, it is possible to fit the data with a Sellmeier equation of the following type, for example:

$$n_i^2(\lambda) = A_i + \frac{B_i \lambda^2}{\lambda^2 - C_i} + D_i \lambda^2. \quad (1.7.4.1)$$

n_i is the principal refractive index, where $i = o$ (ordinary) and e (extraordinary) for uniaxial crystals and $i = x, y$ and z for biaxial crystals.

It is then easy to calculate the phase-matching angles (θ_{PM} , φ_{PM}) from (1.7.4.1) using equations (1.7.3.27) or (1.7.3.29) where the angular variation of the refractive indices is given by equation (1.7.3.6).

The measurement of the variation of intensity of the generated beam as a function of the angle of incidence can be performed on a sphere or slab, leading, respectively, to internal and external angular acceptances. The thermal acceptance is usually measured on a slab which is heated or cooled during the frequency conversion process. The spectral acceptance is not often measured, but essentially calculated from Sellmeier equations (1.7.4.1) and the expansion of Δk in the Taylor series (1.7.3.43) with $\xi = \lambda$.

1.7.4.2. Nonlinear coefficients

The knowledge of the absolute magnitude and of the relative sign of the independent elements of the tensors $\chi^{(2)}$ and $\chi^{(3)}$ is of prime importance not only for the qualification of a new crystal, but also for the fundamental engineering of nonlinear optical materials in connection with microscopic aspects.

However, disparities in the published values of the nonlinear coefficients of the same crystal exist, even if it is a well known material that has been used for a long time in efficient devices (Eckardt & Byer, 1991; Boulanger, Fève *et al.*, 1994). The disagreement between the different absolute magnitudes is sometimes a result of variation in the quality of the crystals, but mainly arises from differences in the measurement techniques. Furthermore, a considerable amount of confusion exists as a consequence of the difference between the conventions taken for the relation between the induced nonlinear polarization and the nonlinear susceptibility, as explained in Section 1.7.2.1.4.

Accurate measurements require mm-size crystals with high optical quality of both surface and bulk.

1.7.4.2.1. Non-phase-matched interaction method

The main techniques used are based on non-phase-matched SHG and THG performed in several samples cut in different directions. The classical method, termed the Maker-fringes technique (Jerphagnon & Kurtz, 1970; Herman & Hayden, 1995), consists of the measurement of the harmonic power as a function of the angle between the fundamental laser beam and the rotated slab sample, as shown in Fig. 1.7.4.1(a).

The conversion efficiency is weak because the interaction is non-phase-matched. In normal incidence, the waves are collinear and so formulae (1.7.3.42) for SHG and (1.7.3.80) for THG are valid. These can be written in a more convenient form where the coherence length appears:

$$\begin{aligned} P^{n\omega}(L) &= A^{n\omega} [P^\omega(0)]^n (d_{\text{eff}}^{n\omega} \cdot l_c^{n\omega})^2 \sin^2(\pi L / 2l_c^{n\omega}) \\ l_c^{2\omega} &= (\pi c / \omega) (2n_3^{2\omega} - n_1^\omega - n_2^\omega)^{-1} \\ l_c^{3\omega} &= (\pi c / \omega) (3n_4^{3\omega} - n_1^\omega - n_2^\omega - n_3^\omega)^{-1}. \end{aligned} \quad (1.7.4.2)$$

The coefficient $A^{n\omega}$ depends on the refractive indices in the direction of propagation and on the fundamental beam geometry: $A^{2\omega}$ and $A^{3\omega}$ can be easily expressed by identifying (1.7.4.2) with (1.7.3.42) and (1.7.3.80), respectively.

When the crystal is rotated, the harmonic and fundamental waves are refracted with different angles, which leads to a variation of the coherence length and consequently to an oscillation of the harmonic power as a function of the angle of incidence, α , of the fundamental beam. Note that the oscillation

1.7. NONLINEAR OPTICAL PROPERTIES

Table 1.7.5.1. *Mineral nonlinear crystals*

The letters (*a*, *b*, *c*) refer to the crystallographic frame. These data are mainly extracted from Bordui & Fejer (1993).

(*a*) SHG (1.064–0.532 μm).

| | KD ₂ PO ₄ (KD*P) | NH ₄ H ₂ PO ₄ (ADP) | CsD ₂ AsO ₄ (CD*A) | β -BaB ₂ O ₄ (BBO) | LiB ₃ O ₅ (LBO) |
|--|--|---|---|---|---|
| Crystal class | $\bar{4}2m$ | $\bar{4}2m$ | $\bar{4}2m$ | $3m$ | $mm2$ |
| Transparency (μm) | 0.18–1.8 | 0.184–1.5 | 0.27–1.66 | 0.198–2.6 | 0.16–2.3 |
| Non-critical λ_{pump} at room temperature (μm) | | | | | |
| Type I | 0.519 | 0.524 | 1.045 | 0.409 | 0.554 (<i>c</i>) 1.212 (<i>a</i>) 1.19 (<i>b</i>) |
| Type II | — | — | — | — | |
| T_{pm} (K) | | | 385 | | 421 |
| Type of phase matching | II | II | I | I | I (<i>a</i>) |
| θ ($^{\circ}$) | 54 | 62 | 90 | 23 | 90 |
| φ ($^{\circ}$) | — | — | — | — | 0 |
| Effective coefficient d_{eff} (pm V ⁻¹) | 0.35 | 0.39 | 0.30 | 1.9 | 0.85 |
| Angular bandwidth (mrad cm) | 2.3 | 2.2 | 51 | 0.53 | 72 |
| Walk-off angles | | | | | |
| ρ^{ω} ($^{\circ}$) | 1.3 | 1.2 | 0 | 0 | 0 |
| $\rho^{2\omega}$ ($^{\circ}$) | 1.4 | 1.5 | 0 | 3.2 | 0 |
| Thermal bandwidth (K cm) | 12 | 2.1 | 3.3 | 51 | 3.9 |
| Spectral bandwidth (nm cm) | 5.6 | 26 | 2.5 | 2 | 3.6 |
| Surface optical damage threshold (GW cm ⁻²) | 5 (1 ns) >8 (0.6 ns at 0.53 μm) | 6 (15 ns) >8 (0.6 ns at 0.53 μm) | 0.25 (12 ns) | 13.5 (1 ns) 23 (14 ns) 32 (8 ns at 0.53 μm) | 25 (0.1 ns) 1.4 (12 ns at 0.78 μm) |

SHG (1.064–0.532 μm) (*cont.*).

| | KTiOPO ₄ (KTP) | KNbO ₃ | 5% MgO:LiNbO ₃ | LiIO ₃ |
|--|---|--|---------------------------|---|
| Crystal class | $mm2$ | $mm2$ | $3m$ | $6mm$ |
| Transparency (μm) | 0.35–4.5 | 0.4–5.5 | 0.35–5 | 0.31–5 to c , 0.34–4 \perp to c |
| Non-critical λ_{pump} at room temperature (μm) | | | | |
| Type I | — | 0.860 (<i>a</i>) 0.982 (<i>b</i>) | | 0.756 |
| Type II | 0.990 (<i>b</i>) 1.081 (<i>a</i>) | — | | — |
| T_{pm} (K) | | 456 | 380 | |
| Type of phase matching | II (<i>a</i> , <i>b</i>) | I (<i>b</i>) | I | I |
| θ ($^{\circ}$) | 90 | 90 | 90 | 30 |
| φ ($^{\circ}$) | 23 | 90 | — | — |
| Effective coefficient d_{eff} (pm V ⁻¹) | 2.4 | —13 | 4.7 | 1.8 |
| Angular bandwidth (mrad cm) | 9 | 13 | 33 | 0.34 |
| Walk-off angles | | | | |
| ρ^{ω} ($^{\circ}$) | 0.20 | 0 | 0 | 0 |
| $\rho^{2\omega}$ ($^{\circ}$) | 0.27 | 0 | 0 | 4.3 |
| Thermal bandwidth (K cm) | 17 | 0.3 | 0.75 | 23 |
| Spectral bandwidth (nm cm) | 0.46 | 0.12 | 0.31 | 0.82 |
| Surface optical damage threshold (GW cm ⁻²) | 9–20 (1 ns) >2 (10 ns at 0.5 μm) | 7 (1 ns) >1 (10 ns) | | 2 (1 ns) 1 (0.1 ns at 0.53 μm) |

(*b*) SHG (532–266 nm).

| | KD ₂ PO ₄ (KD*P) | NH ₄ H ₂ PO ₄ (ADP) | β -BaB ₂ O ₄ (BBO) |
|--|--|--|---|
| Crystal class | $\bar{4}2m$ | $\bar{4}2m$ | $\bar{4}2m$ |
| Transparency (μm) | 0.18–1.8 | 0.184–1.5 | 0.198–2.6 |
| Non-critical λ_{pump} at room temperature (μm) | 0.519 | 0.524 | 0.409 |
| T_{pm} (K) | 308 | 324 | |
| Type of phase matching | I | I | I |
| θ ($^{\circ}$) | 90 | 90 | 47 |
| φ ($^{\circ}$) | — | — | — |
| Effective coefficient d_{eff} (pm V ⁻¹) | 0.44 | 0.57 | 2.0 |
| Angular bandwidth (mrad cm) | 16 | 16 | 0.16 |
| Walk-off angles | | | |
| ρ^{ω} ($^{\circ}$) | 0 | 0 | 0 |
| $\rho^{2\omega}$ ($^{\circ}$) | 0 | 0 | 4.8 |
| Thermal bandwidth (K cm) | 3.0 | 0.54 | 4.0 |
| Spectral bandwidth (nm cm) | 0.13 | 0.13 | 0.073 |
| Surface optical damage threshold (GW cm ⁻²) | 5 (1 ns) >8 (0.6 ns at 0.53 μm) | 6 (15 ns) >8 (0.6 ns at 0.53 μm) | 13.5 (1 ns) 23 (14 ns) 32 (8 ns at 0.53 μm) |

1. TENSORIAL ASPECTS OF PHYSICAL PROPERTIES

Table 1.7.5.1 (cont.)

(c) SHG (4000–2000 nm).

| | AgGaS ₂ | AgGaSe ₂ | ZnGeP ₂ | Tl ₃ AsSe ₃ (TAS) |
|--|--------------------|---|---|---|
| Crystal class | $\bar{4}2m$ | $\bar{4}2m$ | $\bar{4}2m$ | $3m$ |
| Transparency (μm) | 0.5–13 | 0.78–18 | 0.74–12 | 1.3–17 |
| Non-critical λ_{pump} at room temperature (μm) | 1.8 and 11.2 | 3.1 12.8 | 3.2 10.3 | — |
| Type of phase matching | I | I | I | I |
| θ ($^\circ$) | 31 | 52 | 56 | 33 |
| φ ($^\circ$) | — | — | — | — |
| Effective coefficient d_{eff} (pm V ⁻¹) | 10.4 | 28 | 70 | 68 |
| Angular bandwidth (mrad cm) | 3.7 | 6.0 | 5.0 | 4.2 |
| Walk-off angles | | | | |
| ρ^ω ($^\circ$) | 0 | 0 | 0.65 | 0 |
| $\rho^{2\omega}$ ($^\circ$) | 1.2 | 0.64 | 0 | 3.1 |
| Thermal bandwidth (K cm) | 50 | 50 | 40 | 5.7 (SHG at 10.6 μm) |
| Spectral bandwidth (nm cm) | 11 | 22 | 20 | — |
| Surface optical damage threshold (GW cm ⁻²) | 0.5 (10 ns bulk) | 0.01–0.04 (50 ns, 2 μm) 0.02–0.03 (10 ns at 10.6 μm) | 0.05 (25 ns at 2 μm) 1 (2 ns at 10.6 μm) | 0.016 (250 ns at 10.6 μm) |

exists even if the refractive indices do not vary with the direction of propagation, which would be the case for an interaction involving only ordinary waves during the rotation. The most general expression of the generated harmonic power, *i.e.* $P^{n\omega}(\alpha) = j(\alpha) \sin^2 \Psi(\alpha)$, must take into account the angular dependence of all the refractive indices, in particular for the calculation of the coherence length and transmission coefficients (Herman & Hayden, 1995). The effective coefficient is then deduced from the angular spacing of the Maker fringes and from the conversion efficiency at the maxima of oscillation.

A continuous variation of the phase mismatch can also be performed by translating a wedged sample as shown in Fig. 1.7.4.1(b) (Perry, 1991). The harmonic power oscillates as a function of the displacement x . In this case, the interacting waves stay collinear and the oscillation is only caused by the variation of the crystal length. Relation (1.7.4.2) is then valid, by considering a variable crystal length $L(x) = x \tan \beta$; $A^{n\omega}$ and $l_c^{n\omega}$ are constant. The space between two maxima of the wedge fringes is $\Delta x_c = 2l_c / \tan \beta$, which allows the determination of l_c . Then the measurement of the harmonic power, $P_{\text{max}}^{n\omega}$, generated at a maximum leads to the absolute value of the effective coefficient:

$$|d_{\text{eff}}^{n\omega}| = \left\{ \frac{P_{\text{max}}^{n\omega}}{A^{n\omega} [P^\omega(0)]^2 l_c^2} \right\}^{1/2} \quad (1.7.4.3)$$

$$l_c = (\Delta x_c \tan \beta / 2).$$

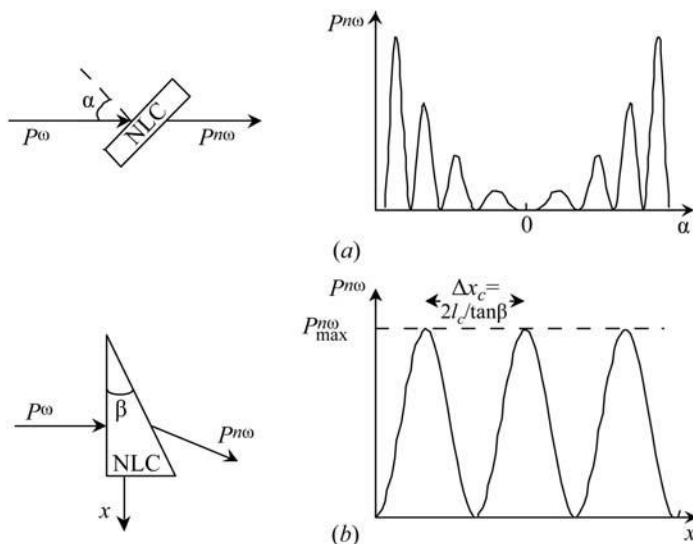


Fig. 1.7.4.1. (a) The Maker-fringes technique; (b) the wedge-fringes technique.

It is necessary to take into account a multiple reflection factor in the expression of $A^{n\omega}$.

The Maker-fringes and wedge-fringes techniques are essentially used for relative measurements referenced to a standard, usually KH₂PO₄ (KDP) or quartz (α -SiO₂).

1.7.4.2.2. Phase-matched interaction method

The use of phase-matched interactions is suitable for absolute and accurate measurements (Eckardt & Byer, 1991; Boulanger, Fève *et al.*, 1994). The sample studied is usually a slab cut in a phase-matching direction. The effective coefficient is determined from the measurement of the conversion efficiency using the theoretical expressions given by (1.7.3.30) and (1.7.3.42) for SHG, and by (1.7.3.80) for THG, according to the validity of the corresponding approximations. Because of phase matching, the generated harmonic power is not weak and it is measurable with very good accuracy, even with a c.w. conversion efficiency.

Recent experiments have been performed in a KTP crystal cut as a sphere (Boulanger *et al.*, 1997, 1998): the absolute magnitudes of the quadratic effective coefficients are measured with an accuracy of 10%, which is comparable with typical experiments on a slab.

For both non-phase-matched and phase-matched techniques, it is important to know the refractive indices and to characterize the spatial, temporal and spectral properties of the pump beam carefully. The considerations developed in Section 1.7.3 about effective coefficients and field tensors allow judicious choices of configurations of polarization and directions of propagation for the determination of the absolute value and relative sign of the independent coefficients of tensors $\chi^{(2)}$ and $\chi^{(3)}$, given in Tables 1.7.2.2 to 1.7.2.5 for the different crystal point groups.

1.7.5. The main nonlinear crystals

Tables 1.7.5.1 and 1.7.5.2 give some characteristics of the main nonlinear crystals. No single nonlinear crystal is the best for all applications, so the different materials must be seen as complementary to each other.

A complete review of mineral crystals is given in Bordui & Fejer (1993). General references for organic crystals may be found, for example, in Chemla & Zyss (1987), Zyss (1994), and Dmitriev *et al.* (1991). Perry (1991) deals with both organic and inorganic materials.

A new generation of materials has been developed since 1995 for the design of new compact all-solid-state laser sources. These optical materials are multifunction crystals, such as LiNbO₃:Nd³⁺, Ba₂NaNb₅O₁₅:Nd³⁺, CaGd₄(BO₃)₃O:Nd³⁺ or YAl₃(BO₃)₄:Yb³⁺, for example, in which the laser effect and the nonlinear frequency

1.7. NONLINEAR OPTICAL PROPERTIES

Table 1.7.5.2. *Organic and organo-mineral crystals*

Abbreviations for crystals: 5-NU: 5-nitouracil; MAP: methyl-(2,4-dinitrophenyl)-aminopropanoate; MNA: 2-methyl-4-nitroaniline; POM: 3-methyl-4-nitropyridine-*N*-oxide; NPP: *N*-(4-nitrophenyl)-*L*-prolinol; 2A5NPDP: 2-amino-5-nitropyridine dihydrogen phosphate. OPA, OPO and SROPO are abbreviations for optical parametric amplification, oscillation and single resonant optical parametric oscillator, respectively. 1 e.s.u. = 4.19×10^{-4} m V⁻¹.

| Crystal | Space group | Transparency | Refractive index phase matching (PM) | Damage threshold |
|---------|----------------|------------------------|---|--|
| Urea | $P\bar{4}2_1m$ | 220 nm to 2 μ m | 90° type-II PM at 597 nm PM to 238 nm | 1.4 GW cm ⁻² at 354.7 nm |
| 5-NU | $P2_12_12_1$ | 410 nm to 2 μ m | $n_b > n_c > n_a$ Types I and II for SHG and SFG ($\omega + 2\omega \rightarrow 3\omega$) | |
| MAP | $P2_1$ | 500 nm to 2 μ m | $n_x < n_y < n_z$ Non-critical PM: at 1.083 μ m (along z); at 1.06 μ m (between room temperature and liquid N ₂) | >3 GW cm ⁻² at 1.06 μ m, 10 ns, 10 Hz >150 MW cm ⁻² at 532 nm, 7 ns, 10 Hz |
| MNA | Cc | 500 nm to 2 μ m | $n_x = 2.093$ and $n_y = 2.494$ at 1.06 μ m | |
| POM | $P2_12_12_1$ | 500 nm to 2 μ m | $n_b > n_a > n_c$ Type-I PM tunable from 2 μ m to 0.8 μ m | ~1 TW cm ⁻² at 610 nm (10 Hz, 100 fs) 2 GW cm ⁻² at 1.06 μ m (20 ps) 150 MW cm ⁻² at 0.532 μ m (20 ps) 50 MW cm ⁻² at 0.532 μ m (10 ns) |
| NPP | $P2_1$ | 500 nm to 2 μ m | $n_y > n_x > n_z$ $n_x - n_z = 0.78$ at 532 nm Non-critical PM at 1.15 μ m $d\theta_{PM}/dT = -0.303$ mrad K ⁻¹ | 10 GW cm ⁻² at 620 nm (100 fs, 10 Hz) |
| 2A5NPDP | $Pna2_1$ | 0.420 to 1.7 μ m | $n_x < n_y < n_z$ $n_z - n_x = 0.158$ at 546 nm $n_z - n_y = 0.152$ at 546 nm Type-II non-critical PM at 1.06 μ m at 210 K Type-I ($d_{eff} = 2.25$ pm V ⁻¹) PM at 1.34 μ m Type-II ($d_{eff} = 4.5$ pm V ⁻¹) PM at 1.34 μ m $d\theta_{PM}/dT = -0.137$ mrad K ⁻¹ for type II at 1.34 μ m $d\lambda/dT = 0.176$ nm K ⁻¹ for PM (295 < T < 343 K) | |
| DAST | Cc | 700 nm to 2 μ m | $n_1(720 \text{ nm}) = 2.519$ $n_2(720 \text{ nm}) = 1.720$ $n_3(720 \text{ nm}) = 1.635$ | |
| 2A5NPCl | $P2_1$ | 410 nm to 1.65 μ m | See Horiuchi <i>et al.</i> (2002) | |

| Crystal | Nonlinear coefficients SHG (d_{ij}) and EO (r_{ij}) | OPO/OPA | References† |
|---------|---|---|------------------------------|
| Urea | $d_{14} = 1.4$ pm V ⁻¹ $r_{41} = 56 \times 10^{-9}$ e.s.u. $r_{63} = 25 \times 10^{-9}$ e.s.u. | SRO $\lambda_p = 354.7$ nm $t_p = 7$ ns Yield: 20.5% Threshold: 45 mW Output: 6 mW at 1.22 μ m Tunability: 0.499 to 1.23 μ m | (a), (b), (c), (d) |
| 5-NU | $d_{14} = d_{25} = d_{36} = 8.7$ pm V ⁻¹ at 1.06 μ m | | (e) |
| MAP | $d_{21} = 40 \pm 5 \times 10^{-9}$ e.s.u. $d_{22} = 44 \pm 5 \times 10^{-9}$ e.s.u. $d_{23} = 8.8 \pm 2 \times 10^{-9}$ e.s.u. $d_{25} = -1.3 \pm 2 \times 10^{-9}$ e.s.u. | | (f) |
| MNA | $d_{11} = 250$ pm V ⁻¹ at 1.06 μ m $d_{11} = 190$ pm V ⁻¹ at 1.2 μ m $d_{11} = 165$ pm V ⁻¹ at 1.3 μ m $d_{11} = 145$ pm V ⁻¹ at 1.47 μ m $d_{11} = 125$ pm V ⁻¹ at 1.54 μ m (d_{11}^2/n^3) _{MNA} = 2000(d_{11}^2/n^3) _{LiNbO₃} $r_{11} = 67 \pm 25$ pm V ⁻¹ at 632.8 nm $\frac{1}{2}(n_1^3 r_{11} - n_3^3 r_{31}) = 270 \pm 50$ pm V ⁻¹ | | (g), (h), (i) |
| POM | $d_{14} = d_{25} = d_{36} = 23 \pm 3$ pm V ⁻¹ at 1.06 μ m $r_{41} = 3.6 \pm 0.6$ pm V ⁻¹ at 632.8 nm $r_{52} = 5.1 \pm 0.4$ pm V ⁻¹ at 632.8 nm $r_{63} = 2.6 \pm 0.3$ pm V ⁻¹ at 632.8 nm | OPA: $G = 10^3$ $\lambda_p = 532$ nm, 10 Hz, 25 ps $I_p = 130$ MW cm ⁻² Infrared input: 5 kW cm ⁻² at degeneracy | (j), (k), (l), (m), (n) |
| NPP | $d_{21} = 56.5 \pm 5$ pm V ⁻¹ at 1.34 μ m $d_{22} = 18.7 \pm 2$ pm V ⁻¹ at 1.34 μ m $d_{22} = 128$ pm V ⁻¹ at 1.06 μ m $r_{12} = 25.5$ pm V ⁻¹ at 632.8 nm $r_{22} = 24$ pm V ⁻¹ at 632.8 nm $n^3 r_{eff} = 60$ pm V ⁻¹ at 1.34 μ m | OPA: $G \simeq 10^4$ at degeneracy (1.24 μ m); pump: 620 nm, 100 fs, 10 Hz OPO, λ_{pump} tuning: 593 < λ_p < 670 nm, 1000 < $\lambda_{i,s}$ < 1500 nm OPO, birefringence tuning: $\lambda_p = 670$ nm, 900 < $\lambda_{i,s}$ < 1700 nm DRO threshold at 670 nm: 0.45 MW cm ⁻² , pump: 2.3 MW cm ⁻² (60 ns, 10 Hz). Yield: 4.5%, IR _{output} 90 μ J | (m), (o), (p), (q), (r), (s) |
| 2A5NPDP | At 1.34 μ m: $d_{33} = 12 \pm 1$ pm V ⁻¹ , $d_{15} = 6 \pm 1$ pm V ⁻¹ At 1.06 μ m: $d_{24} = 1 \pm 0.4$ pm V ⁻¹ , $d_{15} = 7 \pm 1$ pm V ⁻¹ | OPA: $\Gamma = 29 \pm 3$ cm ⁻¹ ($I_p = 30$ GW cm ⁻²); $d_{eff} = 2.6 \pm 0.5$ pm V ⁻¹ ; $\lambda_s = 1.005$ μ m, $\lambda_p = 612$ nm OPA: $\Gamma = 19 \pm 3$ cm ⁻¹ , $G = 10^6$, $\lambda_s = 1$ μ m, $\lambda_i = 1.5$ μ m, $\lambda_p = 612$ nm OPO: λ_{pump} tuning: 565 < λ_p < 590 nm; $\lambda_s \simeq 1.003$ μ m; 1286 < λ_i < 1500 nm SRO: threshold: 6 MW cm ⁻² ; $I_p = 37.2$ MW cm ⁻² (7 ns, 10 Hz); yield 3%, IR _{output} 150 μ J | (r), (s), (t), (u) |

1. TENSORIAL ASPECTS OF PHYSICAL PROPERTIES

Table 1.7.5.2 (cont.)

| Crystal | Nonlinear coefficients SHG (d_{ij}) and EO (r_{ij}) | OPO/OPA | References† |
|---------|--|--|-------------|
| DAST | d_{11} (1318 nm) = 1010 pm V ⁻¹ d_{11} (1542 nm) = 290 pm V ⁻¹ d_{26} (1542 nm) = 39 pm V ⁻¹ r_{11} (720 nm) = 92 pm V ⁻¹ r_{11} (1313 nm) = 53 pm V ⁻¹ r_{11} (1535 nm) = 47 pm V ⁻¹ | Terahertz generation (difference frequency mixing) | (v), (w) |
| 2A5NPCl | $d_{11} = 9 \pm 4$ pm V ⁻¹ $d_{12} = 8 \pm 3$ pm V ⁻¹ $d_{13} = 11 \pm 4$ pm V ⁻¹ $d_{\text{eff}} = 5.1$ pm V ⁻¹ or 9.7 pm V ⁻¹ | | (x) |

† References: (a) Halbout *et al.*, 1979; (b) Morrell *et al.*, 1979; (c) Donaldson & Tang, 1984; (d) Rosker *et al.*, 1985; (e) Puccetti *et al.*, 1993; (f) Oudar & Hierle, 1977; (g) Levine *et al.*, 1979; (h) Lipscomb *et al.*, 1981; (i) Morita *et al.*, 1988; (j) Zyss *et al.*, 1981; (k) Sigelle & Hierle, 1981; (l) Zyss *et al.*, 1985; (m) Ledoux *et al.*, 1987; (n) Josse *et al.*, 1988; (o) Ledoux *et al.*, 1990; (p) Josse *et al.*, 1992; (q) Khodja *et al.*, 1995(b); (r) Khodja, 1995; (s) Zyss *et al.*, 1984; (t) Kotler *et al.*, 1992; (u) Fève *et al.*, 1999; (v) Bosshard, 2000; (w) Kawase *et al.*, 2000; (x) Horiuchi *et al.*, 2002.

conversion occur simultaneously inside the same crystal. An overview of these attractive materials is given in Brenier (2000).

1.7.6. Glossary

| | |
|--------------------------|--|
| μ_0 | vacuum magnetic permeability |
| ϵ_0 | permittivity of free space |
| c | velocity of light in a vacuum |
| \mathbf{P} | electronic polarization |
| \mathbf{P}_n | n th order electronic polarization |
| \mathbf{P}^{NL} | nonlinear polarization |
| $\chi^{(n)}$ | n th order dielectric susceptibility tensor |
| ϵ | dielectric tensor |
| n | refractive index |
| n_x, n_y, n_z | principal refractive indices |
| (x, y, z) | principal axes of the index surface (optical frame) |
| n_o, n_e | refractive indices of the ordinary and extraordinary eigen modes |
| T | transmission coefficient |
| V | half of the angle between optic axes |
| ω | laser circular frequency |
| λ | laser wavelength |
| φ | laser phase |
| v_g | laser group velocity |
| \mathbf{k} | wavevector |
| \mathbf{u} | unit wavevector |
| (θ, φ) | spherical coordinates of the wavevector in the optical frame |
| Π | neutral vibration plane |
| \mathbf{E} | electric field vector |
| (\mathbf{e}, E) | unit vector and amplitude of the electric field |
| \mathbf{D} | dielectric displacement vector |
| \mathbf{d} | unit dielectric displacement vector |
| \mathbf{H} | magnetic field vector |
| \mathbf{S} | Poynting vector |
| \mathbf{s} | unit Poynting vector |
| W | work done per unit time |
| (X, Y, Z) | orthonormal wave frame where Z is along the wavevector |
| ρ | double refraction angle (walk-off angle) |
| ∇ | nabla operator |
| \otimes | tensorial product |
| \cdot | tensorial contraction |
| \times | vectorial product |
| Q^* | complex conjugate of Q |
| w_0 | laser beam waist radius |
| Z_R | Rayleigh length of the laser beam |
| τ | laser pulse half duration |
| f | repetition rate of the pulsed laser |
| $P, P(t)$ | laser instantaneous power |

| | |
|-------------------------------------|---|
| I | instantaneous laser intensity |
| \tilde{E} | total energy per laser pulse |
| \tilde{P} | average laser power |
| P_c | laser peak power |
| L | crystal length |
| $\chi_{\text{eff}}, d_{\text{eff}}$ | effective coefficient |
| $\mathbf{F}^{(n)}$ | n th order field tensor |
| Δk | phase mismatch |
| η_{SHG} | conversion efficiency of second harmonic generation |
| G, h | spatial walk-off attenuation functions |

We thank Dr J. P. Fève for his valuable assistance and critical reading of the manuscript.

References

- Akhmanov, S. A., Kovrygin, A. I. & Sukhorukov, A. P. (1975). *Treatise in quantum electronics*, edited by H. Rabin & C. L. Tang. New York: Academic Press.
- Armstrong, J. A., Bloembergen, N., Ducuing, J. & Pershan, P. (1962). *Interactions between light waves in a nonlinear dielectric*. *Phys. Rev.* **127**, 1918–1939.
- Asaumi, K. (1992). *Second harmonic power of KTiOPO₄ with double refraction*. *Appl. Phys. B*, **54**, 265–270.
- Ashkin, A., Boyd, G. D. & Dziedzic, J. M. (1966). *Resonant optical second harmonic generation and mixing*. *IEEE J. Quantum Electron.* **QE2**, 109–124.
- Baumgartner, R. A. & Byer, R. L. (1979). *Optical parametric amplification*. *IEEE J. Quantum Electron.* **QE15**, 432–444.
- Bloembergen, N. (1963). *Some theoretical problems in quantum electronics*. *Symposium on optical masers*, edited by J. Fox, pp. 13–22. New York: Intersciences Publishers.
- Bloembergen, N. (1965). *Nonlinear optics*. New York: Benjamin.
- Bordui, P. F. & Fejer, M. M. (1993). *Inorganic crystals for nonlinear optical frequency conversion*. *Annu. Rev. Mater. Sci.* **23**, 321–379.
- Bosshard, C. (2000). *Third order nonlinear optics in polar materials*. In *Nonlinear optical effects and materials*, edited by P. Günter, pp. 7–161. Berlin: Springer Verlag.
- Boulanger, B. (1989). *Synthèse en flux et étude des propriétés optiques cristallines linéaires et non linéaires par la méthode de la sphère de KTiOPO₄ et des nouveaux composés isotypes et solutions solides de formule générale (K,Rb,Cs)TiO(P,As)O₄*. PhD Dissertation, Université de Nancy I, France.
- Boulanger, B. (1994). CNRS–NSF Report, Stanford University.
- Boulanger, B., Fejer, M. M., Blachman, R. & Bordui, P. F. (1994). *Study of KTiOPO₄ gray-tracking at 1064, 532 and 355 nm*. *Appl. Phys. Lett.* **65**(19), 2401–2403.
- Boulanger, B., Fève, J. P. & Marnier, G. (1993). *Field factor formalism for the study of the tensorial symmetry of the four-wave non linear optical parametric interactions in uniaxial and biaxial crystal classes*. *Phys. Rev. E*, **48**(6), 4730–4751.

1.7. NONLINEAR OPTICAL PROPERTIES

- Boulanger, B., Fève, J. P., Marnier, G., Bonnin, C., Villeval, P. & Zondy, J. (1997). *Absolute measurement of quadratic nonlinearities from phase-matched second-harmonic-generation in a single crystal cut as a sphere*. *J. Opt. Soc. Am. B*, **14**, 1380–1386.
- Boulanger, B., Fève, J. P., Marnier, G. & Ménaert, B. (1998). *Methodology for nonlinear optical studies: application to the isomorph family KTiOPO_4 , KTiOAsO_4 , RbTiOAsO_4 and CsTiOAsO_4* . *Pure Appl. Opt.* **7**, 239–256.
- Boulanger, B., Fève, J. P., Marnier, G., Ménaert, B., Cabirol, X., Villeval, P. & Bonnin, C. (1994). *Relative sign and absolute magnitude of $d^{(2)}$ nonlinear coefficients of KTP from second-harmonic-generation measurements*. *J. Opt. Soc. Am. B*, **11**(5), 750–757.
- Boulanger, B., Fève, J. P., Ménaert, B. & Marnier, G. (1999). PCT/FR98/02563 Patent No. WO99/28785.
- Boulanger, B. & Marnier, G. (1991). *Field factor calculation for the study of the relationships between all the three-wave non linear optical interactions in uniaxial and biaxial crystals*. *J. Phys. Condens. Matter*, **3**, 8327–8350.
- Boyd, R. W. (1992). *Nonlinear optics*. San Diego: Academic Press.
- Boyd, G. D., Ashkin, A., Dziedzic, J. M. & Kleinman, D. A. (1965). *Second-harmonic generation of light with double refraction*. *Phys. Rev.* **137**, 1305–1320.
- Brasselet, S. & Zyss, J. (1998). *Multipolar molecules and multipolar fields: probing and controlling the tensorial nature of nonlinear molecular media*. *J. Opt. Soc. Am. B*, **15**, 257–288.
- Breitenbach, G., Schiller, S. & Mlynek, J. (1995). *81% conversion efficiency in frequency-stable continuous wave parametric oscillator*. *J. Opt. Soc. Am. B*, **12**(11), 2095–2101.
- Brenier, A. (2000). *The self-doubling and summing lasers: overview and modelling*. *J. Lumin.* **91**, 121–132.
- Brosnan, S. J. & Byer, R. L. (1979). *Optical parametric oscillator threshold and linewidth studies*. *IEEE J. Quantum Electron.* **QE15**(6), 415–431.
- Butcher, P. N. (1965). *Nonlinear optical phenomena*. Bulletin 200, Engineering Experiment Station, Ohio State University, USA.
- Butcher, P. N. & Cotter, D. (1990). *The elements of nonlinear optics*. Cambridge series in modern optics. Cambridge University Press.
- Byer, R. L. (1973). *Treatise in quantum electronics*, edited by H. Rabin & C. L. Tang. New York: Academic Press.
- Chemla, D. S. & Zyss, J. (1987). *Nonlinear optical properties of organic molecules and crystals*. Quantum electronic principles and applications series. New York: Academic Press.
- Chung, J. & Siegman, E. (1993). *Singly resonant continuous-wave mode-locked KTiOPO_4 optical parametric oscillator pumped by a Nd:YAG laser*. *J. Opt. Soc. Am. B*, **10**(9), 2201–2210.
- Debuisschert, T., Sizmann, A., Giacobino, E. & Fabre, C. (1993). *Type-II continuous-wave optical parametric oscillator: oscillation and frequency tuning characteristics*. *J. Opt. Soc. Am. B*, **10**(9), 1668–1690.
- Dmitriev, V. G., Gurzadian, G. G. & Nikogosyan, D. N. (1991). *Handbook of nonlinear optical crystals*. Heidelberg: Springer-Verlag.
- Dolinchuk, S. G., Kornienko, N. E. & Zadorozhnyi, V. I. (1994). *Noncritical vectorial phase matchings in nonlinear optics of crystals and infrared up-conversion*. *Infrared Phys. Technol.* **35**(7), 881–895.
- Donaldson, W. R. & Tang, C. L. (1984). *Urea optical parametric oscillator*. *Appl. Phys. Lett.* **44**, 25–27.
- Dou, S. X., Josse, D., Hierle, R. & Zyss, J. (1992). *Comparison between collinear and noncollinear phase matching for second-harmonic and sum-frequency generation in 3-methyl-4-nitropyridine-1-oxide*. *J. Opt. Soc. Am. B*, **9**(5), 687–697.
- Ebrahimzadeh, M. & Dunn, M. H. (2000). *Optical parametric oscillators*. In *Handbook of optics*, Vol. IV, pp. 2201–2272. New York: McGraw-Hill.
- Ebrahimzadeh, M., Henderson, A. J. & Dunn, M. H. (1990). *An excimer-pumped $\beta\text{-BaB}_2\text{O}_4$ optical parametric oscillator tunable from 354 nm to 2.370 μm* . *IEEE J. Quantum Electron.* **QE26**(7), 1241–1252.
- Ebrahimzadeh, M., Turnbull, G. A., Edwards, T. J., Stothard, D. J. M., Lindsay, I. D. & Dunn, M. H. (1999). *Intracavity continuous-wave singly resonant optical parametric oscillators*. *J. Opt. Soc. Am. B*, **16**, 1499–1511.
- Eckardt, R. C. & Byer, R. L. (1991). *Measurement of nonlinear optical coefficients by phase-matched harmonic generation*. *SPIE. Inorganic crystals for optics, electro-optics and frequency conversion*, **1561**, 119–127.
- Eckardt, R. C. & Reintjes, J. (1984). *Phase matching limitations of high efficiency second harmonic generation*. *IEEE J. Quantum Electron.* **20**(10), 1178–1187.
- Eimerl, D. (1987). *High average power harmonic generation*. *IEEE J. Quantum Electron.* **23**, 575–592.
- Fejer, M. M., Magel, G. A., Jundt, D. H. & Byer, R. L. (1992). *Quasi-phase-matched second harmonic generation: tuning and tolerances*. *IEEE J. Quantum Electron.* **28**(11), 2631–2653.
- Fève, J. P. (1994). *Existence et symétrie des interactions à 3 et 4 photons dans les cristaux anisotropes. Méthodes de mesure des paramètres affectant les couplages à 3 ondes: étude de KTP et isotopes*. PhD Dissertation, Université de Nancy I, France.
- Fève, J. P., Boulanger, B. & Douady, J. (2002). *Specific properties of cubic optical parametric interactions compared with quadratic interactions*. *Phys. Rev. A*, **66**, 063817-1-11.
- Fève, J. P., Boulanger, B. & Marnier, G. (1993). *Calculation and classification of the direction loci for collinear types I, II and III phase-matching of three-wave non linear optical parametric interactions in uniaxial and biaxial acentric crystals*. *Optics Comm.* **99**, 284–302.
- Fève, J. P., Boulanger, B. & Marnier, G. (1994). *Experimental study of internal and external conical refractions in KTP*. *Optics Comm.* **105**, 243–252.
- Fève, J. P., Boulanger, B. & Marnier, G. (1995). *Experimental study of walk-off attenuation for type II second harmonic generation in KTP*. *IEEE J. Quantum Electron.* **31**(8), 1569–1571.
- Fève, J. P., Boulanger, B., Rousseau, I., Marnier, G., Zaccaro, J. & Ibanez, A. (1999). *Second-harmonic generation properties of 2-amino-5-nitropyridinium dihydrogenarsenate and dihydrogenphosphate organic-inorganic crystals*. *IEEE J. Quantum Electron.* **35**, 66–71.
- Fève, J. P., Pacaud, O., Boulanger, B., Ménaert, B., Hellström, J., Pasiskevicius, V. & Laurell, F. (2001). *Widely and continuously tuneable optical parametric oscillator using a cylindrical periodically poled KTiOPO_4 crystal*. *Opt. Lett.* **26**, 1882–1884.
- Fève, J. P., Pacaud, O., Boulanger, B., Ménaert, B. & Renard, M. (2002). *Tunable phase-matched optical parametric oscillators based on a cylindrical crystal*. *J. Opt. Soc. Am. B*, **19**, 222–233.
- Fève, J. P. & Zondy, J. J. (1996). Private communication.
- Franken, P., Hill, A. E., Peters, C. W. & Weinreich, G. (1961). *Generation of optical harmonics*. *Phys. Rev. Lett.* **7**, 118.
- Geusic, J. E., Levinstein, H. J., Singh, S., Smith, R. G. & Van Uitert, L. G. (1968). *Continuous 0.532- μm solid state source using $\text{Ba}_2\text{NaNbO}_{15}$* . *Appl. Phys. Lett.* **12**(9), 306–308.
- Gordon, L. A., Woods, G. L., Eckardt, R. C., Route, R. K., Feigelson, R. S., Fejer, M. M. & Byer, R. L. (1993). *Diffusion-bonded stacked GaAs for quasi-phase-matched second-harmonic generation of carbon dioxide laser*. *Electron. Lett.* **29**, 1942–1944.
- Hadni, A. (1967). *Essentials of modern physics applied to the study of the infrared*. Oxford: Pergamon Press.
- Halbout, J. M., Blit, S., Donaldson, W. & Tang, C. L. (1979). *Efficient phase-matched second harmonic generation and sum frequency mixing in urea*. *IEEE J. Quantum Electron.* **QE15**, 1176–1180.
- Harris, S. E. (1969). *Tunable optical parametric oscillators*. *Proc. IEEE*, **57**(12), 2096–2113.
- Herman, W. N. & Hayden, L. M. (1995). *Maker fringes revisited: second-harmonic generation from birefringent or absorbing materials*. *J. Opt. Soc. Am. B*, **12**, 416–427.
- Hobden, M. V. (1967). *Phase-matched second harmonic generation in biaxial crystals*. *J. Appl. Phys.* **38**, 4365–4372.
- Horiuchi, N., Lefaucheux, F., Ibanez, A., Josse, D. & Zyss, J. (2002). *Quadratic nonlinear optical coefficients of organic-inorganic crystal 2-amino-5-nitropyridinium chloride*. *J. Opt. Soc. Am. B*, **19**, 1830–1838.
- Jerphagnon, J., Chemla, D. S. & Bonneville, R. (1978). *The description of physical properties of condensed matter using irreducible tensors*. *Adv. Phys.* **27**, 609–650.
- Jerphagnon, J. & Kurtz, S. K. (1970). *Optical nonlinear susceptibilities: accurate relative values for quartz, ammonium dihydrogen phosphate, and potassium dihydrogen phosphate*. *Phys. Rev. B*, **1**(4), 1739–1744.
- Josse, D., Dou, S. X., Andreazza, P., Zyss, J. & Perigaud, A. (1992). *Near infrared optical parametric oscillation in a N-(4-nitrophenyl)-L-prolinol*. *Appl. Phys. Lett.* **61**, 121–123.
- Josse, D., Hierle, R., Ledoux, I. & Zyss, J. (1988). *Highly efficient second-harmonic generation of picosecond pulses at 1.32 μm in 3-methyl-4-nitropyridine-1-oxide*. *Appl. Phys. Lett.* **53**, 2251–2253.
- Karlsson, H. & Laurell, F. (1997). *Electric field poling of flux grown KTiOPO_4* . *Appl. Phys. Lett.* **71**, 3474–3476.

1. TENSORIAL ASPECTS OF PHYSICAL PROPERTIES

- Kato, K. (1986). *Second-harmonic generation to 2048 Å in β -BaB₂O₄*. *IEEE J. Quantum Electron.* **QE22**, 1013–1014.
- Kato, K. (1991). *Parametric oscillation at 3.3 μ m in KTP pumped at 1.064 μ m*. *IEEE J. Quantum Electron.* **QE27**, 1137–1140.
- Kawase, K., Hatanaka, T., Takahashi, H., Nakamura, K., Taniuchi, T. & Ito, H. (2000). *Tunable terahertz-wave generation from DAST crystal by dual signal-wave parametric oscillation of periodically poled lithium niobate*. *Opt. Lett.* **25**, 1714–1716.
- Khodja, S. (1995). *Interactions paramétriques optiques dans les cristaux organiques et organo-minéraux*. PhD Dissertation, Ecole Polytechnique, Palaiseau, France.
- Khodja, S., Josse, D. & Zyss, J. (1995a). *First demonstration of an efficient near-infrared optical parametric oscillator with an organomineral crystal*. *Proc. CThC2, CLEO'95* (Baltimore), pp. 267–268.
- Khodja, S., Josse, D. & Zyss, J. (1995b). *Thermo-optic tuning sensitivity of phase matched second-harmonic generation in 2-amino-5-nitropyridinium-dihydrogen crystals*. *Appl. Phys. Lett.* **67**, 3081–3083.
- Kotler, Z., Hierle, R., Josse, D., Zyss, J. & Masse, R. (1992). *Quadratic nonlinear-optical properties of a new transparent and highly efficient organic-inorganic crystal: 2-amino-5-nitropyridinium-dihydrogen phosphate (2A5NPDP)*. *J. Opt. Soc. Am. B*, **9**, 534–547.
- Kurtz, S. K. & Dougherty, J. P. (1978). *Systematic materials analysis*. Vol. IV, edited by J. H. Richardson. New York: Academic Press.
- Kurtz, S. K. & Perry, T. T. (1968). *A powder technique for the evaluation of nonlinear optical materials*. *J. Appl. Phys.* **39**(8), 3978–3813.
- Ledoux, I., Badan, J., Zyss, J., Migus, A., Hulin, D., Etchepare, J., Grillon, G. & Antonetti, A. (1987). *Generation of high-peak-power tunable infrared femtosecond pulses in an organic crystal: application to time resolution of weak infrared signals*. *J. Opt. Soc. Am. B*, **4**, 987–997.
- Ledoux, I., Lepers, C., Perigaud, A., Badan, J. & Zyss, J. (1990). *Linear and nonlinear optical properties of N-4-nitrophenyl-L-prolinol single crystals*. *Optics Comm.* **80**, 149–154.
- LeGarrec, B., Razé, G., Thro, P. Y. & Gillert, M. (1996). *High-average-power diode-array-pumped frequency-doubled YAG laser*. *Opt. Lett.* **21**, 1990–1992.
- Levine, B. F., Bethea, C. G., Thurmond, C. D., Lynch, R. T. & Bernstein, J. L. (1979). *An organic crystal with an exceptionally large optical second harmonic coefficient: 2-methyl-4-nitroaniline*. *J. Appl. Phys.* **50**, 2523–2527.
- Lipscomb, G. F., Garito, A. F. & Narang, R. S. (1981). *An exceptionally large linear electrooptic effect in the organic solid MNA*. *J. Chem. Phys.* **75**, 1509–1516.
- Louisell, W. H., Yariv, A. & Siegman, A. E. (1961). *Quantum fluctuations and noise in parametric processes*. *I. Phys. Rev.* **124**, 1646.
- Marnier, G. & Boulanger, B. (1989). *The sphere method: a new technique in linear and non linear crystalline optical studies*. *Optics Comm.* **72**(3–4), 139–143.
- Marnier, G., Boulanger, B. & Ménaert, B. (1989). *Melting and ferroelectric transition temperature of new compounds: CsTiOAsO₄ and Cs_xM_{1-x}TiOAs_{1-y}O₄ with M = K or Rb*. *J. Phys. Condens. Matter*, **1**, 5509–5513.
- Marshall, L. R. & Kaz, A. (1993). *Eye-safe output from noncritically phase-matched parametric oscillators*. *J. Opt. Soc. Am. B*, **10**(9), 1730–1736.
- Mehendale, S. C. & Gupta, P. K. (1988). *Effect of double refraction on type II phase matched second harmonic generation*. *Optics Comm.* **68**, 301–304.
- Midwinter, J. E. & Warner, J. (1965). *The effects of phase matching method and of crystal symmetry on the polar dependence of third-order non-linear optical polarization*. *J. Appl. Phys.* **16**, 1667–1674.
- Milton, J. T. (1992). *General expressions for the efficiency of phase-matched and nonphase-matched second-order nonlinear interactions between plane waves*. *IEEE J. Quantum Electron.* **28**(3), 739–749.
- Moore, G. T. & Koch, K. (1996). *Phasing of tandem crystals for nonlinear optical frequency conversion*. *Optics Comm.* **124**, 292–294.
- Morita, R., Kondo, T., Kaned, Y., Sugihashi, A., Ogasawara, N., Umegaki, S. & Ito, R. (1988). *Dispersion of second-order nonlinear optical coefficient d₁₁ of 2-methyl-4-nitroaniline (MNA)*. *Jpn. J. Appl. Phys.* **27**, L1131–L1133.
- Morrell, J. A., Albrecht, A. C., Levin, K. H. & Tang, C. L. (1979). *The electro-optic coefficients of urea*. *J. Chem. Phys.* **71**, 5063–5068.
- Myers, L. E., Eckardt, R. C., Fejer, M. M., Byer, R. L. & Bosenberg, W. R. (1996). *Multigrating quasi-phase-matched optical parametric oscillator in periodically poled LiNbO₃*. *Opt. Lett.* **21**(8), 591–593.
- Myers, L. E., Eckardt, R. C., Fejer, M. M., Byer, R. L., Bosenberg, W. R. & Pierce, J. W. (1995). *Quasi-phase-matched optical parametric oscillators in bulk periodically poled LiNbO₃*. *J. Opt. Soc. Am. B*, **12**, 2102–2116.
- Nye, J. F. (1957). *Physical properties of crystals*. Oxford: Clarendon Press.
- Oudar, J. L. & Hierle, R. (1977). *An efficient organic crystal for nonlinear optics: methyl-(2,4-dinitrophenyl)-aminopropanoate*. *J. Appl. Phys.* **48**, 2699–2704.
- Pacaud, O., Fève, J. P., Boulanger, B. & Ménaert, B. (2000). *Cylindrical KTiOPO₄ crystal for enhanced angular tunability of phase-matched optical parametric oscillators*. *Opt. Lett.* **25**, 737–739.
- Perkins, P. E. & Driscoll, T. A. (1987). *Efficient intracavity doubling in flash-lamp-pumped Nd:YLF*. *J. Opt. Soc. Am. B*, **4**(8), 1281–1285.
- Perkins, P. E. & Fahlen, T. S. (1987). *20-W average-power KTP intracavity-doubled Nd:YAG laser*. *J. Opt. Soc. Am. B*, **4**(7), 1066–1071.
- Perry, J. W. (1991). *Nonlinear optical properties of molecules and materials*. In *Materials for nonlinear optics, chemical perspectives*, edited by S. R. Marder, J. E. Sohn & G. D. Stucky, pp. 67–88. ACS Symp. Ser. No. 455. Washington: American Chemical Society.
- Pliszka, P. & Banerjee, P. P. (1993). *Nonlinear transverse effects in second-harmonic generation*. *J. Opt. Soc. Am. B*, **10**(10), 1810–1819.
- Powers, P. E., Kulp, T. J. & Bisson, S. E. (1998). *Continuous tuning of a continuous-wave periodically poled lithium niobate optical parametric oscillator by use of a fan-out grating design*. *Opt. Lett.* **23**, 159–161.
- Puccetti, G., Périgaud, A., Badan, J., Ledoux, I. & Zyss, J. (1993). *5-nitroauracil: a transparent and efficient nonlinear organic crystal*. *J. Opt. Soc. Am. B*, **10**, 733–744.
- Qiu, P. & Penzkofer, A. (1988). *Picosecond third-harmonic light generation in β -BaB₂O₄*. *Appl. Phys. B*, **45**, 225–236.
- Reid, D. T., Kennedy, G. T., Miller, A., Sibbett, W. & Ebrahimzadeh, M. (1998). *Widely tunable near- to mid-infrared femtosecond and picosecond optical parametric oscillators using periodically poled LiNbO₃ and RbTiOAsO₄*. *IEEE J. Sel. Top. Quantum Electron.* **4**, 238–248.
- Rosenman, G., Skliar, A., Eger, D., Oron, M. & Katz, M. (1998). *Low temperature periodic electrical poling of flux-grown KTiOPO₄ and isomorphic crystals*. *Appl. Phys. Lett.* **73**, 3650–3652.
- Rosker, M. J., Cheng, K. & Tang, C. L. (1985). *Practical urea optical parametric oscillator for tunable generation throughout the visible and near-infrared*. *IEEE J. Quantum Electron.* **QE21**, 1600–1606.
- Ruffing, B., Nebel, A. & Wallenstein, R. (1998). *All-solid-state CW mode-locked picosecond KTiOAsO₄ (KTA) optical parametric oscillator*. *Appl. Phys. B*, **67**, 537–544.
- Scheidt, M., Beier, B., Knappe, R., Bolle, K. J. & Wallenstein, R. (1995). *Diode-laser-pumped continuous wave KTP optical parametric oscillator*. *J. Opt. Soc. Am. B*, **12**(11), 2087–2094.
- Schell, A. J. & Bloembergen, N. (1978). *Laser studies of internal conical refraction. I. Quantitative comparison of experimental and theoretical conical intensity distribution in aragonite*. *J. Opt. Soc. Am.* **68**, 1093–1106.
- Schwartz, L. (1981). *Les tenseurs*. Paris: Hermann.
- Shen, Y. R. (1984). *The principles of nonlinear optics*. New York: Wiley.
- Shuvalov, L. A. (1981). *Modern crystallography IV – Physical properties of crystals*. Springer Series in solid-state sciences No. 37. Heidelberg: Springer Verlag.
- Siegman, A. E. (1986). *Lasers*. Mill Valley, California: University Science Books.
- Sigelle, M. & Hierle, R. (1981). *Determination of the electrooptic coefficients of 3-methyl-4-nitropyridine-1-oxide by an interferometric phase modulation technique*. *J. Appl. Phys.* **52**, 4199–4204.
- Smith, R. G. (1970). *Theory of intracavity optical second-harmonic generation*. *IEEE J. Quantum Electron.* **6**(4), 215–223.
- Tomov, I. V., Fedosejevs, R. & Offenberger, A. (1982). *Up-conversion of subpicosecond light pulses*. *IEEE J. Quantum Electron.* **12**, 2048–2056.
- Unschel, R., Fix, A., Wallenstein, R., Rytz, D. & Zysset, B. (1995). *Generation of tunable narrow-band midinfrared radiation in a type I potassium niobate optical parametric oscillator*. *J. Opt. Soc. Am. B*, **12**, 726–730.
- Velsko, S. P. (1989). *Direct measurements of phase matching properties in small single crystals of new nonlinear materials*. *Soc. Photo-Opt. Instrum. Eng. Conf. Laser Nonlinear Opt. Eng.* **28**, 76–84.
- Yang, S. T., Eckardt, R. C. & Byer, R. L. (1993). *Power and spectral characteristics of continuous-wave parametric oscillators: the doubly to singly resonant transition*. *J. Opt. Soc. Am. B*, **10**(9), 1684–1695.

1.7. NONLINEAR OPTICAL PROPERTIES

- Yang, S. T., Pohalski, C. C., Gustafson, E. K., Byer, R. L., Feigelson, R. S., Raymakers, R. J. & Route, R. K. (1991). 6.5-W, 532-nm radiation by CW resonant external-cavity second-harmonic generation of an 18-W Nd:YAG laser in LiB_3O_5 . *Optics Lett.* **16**(19), 1493–1495.
- Yao, J. Q. & Fahlen, T. S. (1984). Calculations of optimum phase match parameters for the biaxial crystal KTiOPO_4 . *J. Appl. Phys.* **55**, 65–68.
- Yariv, A. & Yeh, P. (2002). *Optical waves in crystals*. New York: Wiley.
- Zondy, J. J. (1990). Private communication.
- Zondy, J. J. (1991). Comparative theory of walkoff-limited type II versus type-I second harmonic generation with Gaussian beams. *Optics Comm.* **81**(6), 427–440.
- Zondy, J. J., Abed, M. & Khodja, S. (1994). Twin-crystal walk-off-compensated type-II second-harmonic generation: single-pass and cavity-enhanced experiments in KTiOPO_4 . *J. Opt. Soc. Am. B*, **11**(12), 2368–2379.
- Zyss, J. (1993). Molecular engineering implications of rotational invariance in quadratic nonlinear optics: from dipolar to octupolar molecules and materials. *J. Chem. Phys.* **98**(9), 6583–6599.
- Zyss, J. (1994). Editor. *Molecular nonlinear optics: materials, physics and devices*. Quantum electronic principles and applications series. New York: Academic Press.
- Zyss, J., Chemla, D. S. & Nicoud, J. F. (1981). Demonstration of efficient nonlinear optical crystals with vanishing molecular dipole moment: second-harmonic generation in 3-methyl-4-nitropyridine-1-oxide. *J. Chem. Phys.* **74**, 4800–4811.
- Zyss, J., Ledoux, I., Hierle, R., Raj, R. & Oudar, J. L. (1985). Optical parametric interactions in 3-methyl-4-nitropyridine-1-oxide (POM) single crystal. *IEEE J. Quantum Electron.* **21**, 1286–1295.
- Zyss, J., Nicoud, J. F. & Coquillay, A. (1984). Chirality and hydrogen bonding in molecular crystals for phase-matched second-harmonic generation: N-(4-nitrophenyl)-(L)-prolinol (NPP). *J. Chem. Phys.* **81**, 4160–4167.

1.8. Transport properties

BY G. D. MAHAN

1.8.1. Introduction

The flow of either electricity or heat is regarded as ‘transport’. These flows are an extremely important characteristic of crystals. Some materials conduct heat or electricity well, while others conduct them poorly. Such properties are important for the use of materials in manufactured products, as some applications require good conductors, while others require poor conductors.

In this chapter, we review the transport properties of crystals. The primary concern is the flow of either electricity or of heat. The topic is restricted to steady-state flows and we do not treat a.c. currents. We also limit our discussion to *linear response*, which is defined precisely below. In general, it means that the flows of electricity and heat are small.

1.8.2. Macroscopic equations

The basic equations of transport are given below (Ziman, 1962; Goldsmid, 1986; Mahan, 1990). (The symbols used in this chapter are defined in Section 1.8.6.)

$$\mathbf{J} = \sigma(\mathbf{E} - \mathbf{S} \nabla T) \quad (1.8.2.1)$$

$$\mathbf{J}_Q = \mathbf{J}TS - \mathbf{K} \nabla T, \quad (1.8.2.2)$$

where \mathbf{J} and \mathbf{J}_Q are the current density and the heat current, respectively. The three main transport coefficients are the electrical conductivity σ , the thermal conductivity K and the Seebeck coefficient S . The electrical resistivity ρ is the inverse of the conductivity, $\rho = 1/\sigma$. In general, the currents, electric field and ∇T are vectors while σ , S and K are second-rank tensors. The number of independent tensor components is determined by the symmetry of the crystal (see Chapter 1.1). We assume cubic symmetry, so all of the quantities can be treated as scalars. Onsager relations require that the Seebeck coefficient S is the same in the two equations. A description of the transport properties of most crystals is simply given as a graph, or table, of how each of the three parameters (σ , S , K) varies with temperature. The range of variation among crystals is enormous.

The above equations assume that there is no magnetic field and have to be changed if a magnetic field is present. This special case is discussed below.

1.8.3. Electrical resistivity

1.8.3.1. Properties of the electrical resistivity

The electrical conductivity is usually written as (Ziman, 1962; Goldsmid, 1986; Mahan, 1990)

$$\sigma = \frac{n_0 e^2 \tau}{m^*}, \quad (1.8.3.1)$$

where n_0 is the density of conduction electrons in units of m^{-3} , e is the charge on the electron, τ is the lifetime of the electron and m^* is the effective mass. Here we are assuming parabolic bands, so the energy of the electron is $\varepsilon(k) = \hbar^2 k^2 / 2m^*$.

If one measures σ as a function of temperature, then one has determined $\tau(T)$, assuming that one knows n_0 and m^* from other measurements, e.g. Allen *et al.* (1986). The electron density n_0 can sometimes be determined from the Hall effect, as discussed in Section 1.8.3.4. The effective mass m^* can be determined by a

cyclotron resonance experiment or a similar experiment that measures the properties of the Fermi surface. Also, the ratio n_0/m^* can be found by measuring the frequency dependence of the dielectric function in the infrared (Sievers, 1980): $\epsilon(\omega) = \epsilon_\infty - 4\pi n_0 e^2 / (m^* \omega^2)$. Here the factors $n_0 e^2 / m^*$ occur in the same combination as found in the d.c. conductivity. The factors n_0 and m^* can also be determined by numerical calculations of the band structure of the solid. In any case, we assume that these parameters are known. The only difficult parameter to find is the lifetime.

The lifetime of the electrons is usually determined by solving a Boltzmann equation for the distribution function of the electrons. The method of solution is described in many references (Ziman, 1962; Goldsmid, 1986; Mahan, 1990) and will not be repeated here. The Boltzmann equation is itself an approximate equation, since one must do some averaging over the particles in deriving it. This approximate equation can then be solved by a variety of methods: analytical with approximations, variationally or numerically with great accuracy. The latter is done quite easily with today's computers. Here we shall summarize the main contributions to the lifetime.

The electrical resistivity is the inverse of the conductivity,

$$\rho = \frac{m^*}{n_0 e^2 \tau}. \quad (1.8.3.2)$$

The scattering rate of the electron can often be calculated using Fermi's golden rule, which is an equation of the form

$$\frac{1}{\tau_i} = \frac{2\pi}{\hbar} \sum_f |M_{if}|^2 [1 - \cos \theta] \delta(E_i - E_f). \quad (1.8.3.3)$$

Here the lifetime of an initial state i is given by summing over all of the final states f that can be reached by a matrix element M_{if} . The factor of $[1 - \cos \theta]$ is included to measure the amount of scattering, where θ is the angle through which the electron scatters. Anything that scatters or interacts with an electron contributes to the lifetime. This includes the thermal vibrations of the ions, which is an intrinsic effect. There are also extrinsic effects such as scattering from impurities, grain boundaries, dislocations and the boundaries of the crystal. The latter is important in thin films or wires.

Matthiessen's rule (Matthiessen & Vogt, 1864) states that the resistivities from each type of scattering process can simply be added. The total resistivity can be written as

$$\rho = \frac{m^*}{n_0 e^2} \sum_j \frac{1}{\tau_j}, \quad (1.8.3.4)$$

where τ_j is the lifetime from one of the scattering mechanisms. There are several important disclaimers regarding this rule. It is far from rigorous. It is often untrue. Yet it works very well 95% of the time. We shall adopt the rule here for our discussion of the resistivity.

The major contributions to the resistivity of solids are:

(1) *Impurities*. Every crystal has impurities, as it is not possible to make a crystal without some defects. The reasons for this are well understood and here we just assume this fact. The formula for the lifetime contains two factors (Mahan, 1990): (a) the concentration of impurities n_i and (b) the phase shifts $\delta_l(k)$ for scattering an electron of wavevector k and angular momentum l ,

1.8. TRANSPORT PROPERTIES

$$\frac{1}{\tau_i(k)} = \frac{4\pi n_i \hbar}{m^* k} \sum_l l \sin^2[\delta_l(k) - \delta_{l-1}(k)]. \quad (1.8.3.5)$$

Although this expression appears complicated, one can view it as consisting of three parts:

$$\frac{1}{\tau_i} = n_i v_k \sigma_c(k), \quad (1.8.3.6)$$

$$v_k = \frac{\hbar k}{m^*}, \quad (1.8.3.7)$$

$$\sigma_c = \frac{4\pi}{k^2} \sum_l l \sin^2[\delta_l(k) - \delta_{l-1}(k)]. \quad (1.8.3.8)$$

The three factors are the concentration n_i of impurities, the electron velocity v_k and the cross section σ_c . For each impurity, the cross section is a function of k . The lifetime is the density of impurities multiplied by a simple function of electron energy and is independent of temperature. A careful analysis shows that there is a temperature dependence to the scattering by impurities. However, this dependence is rather slight, and is dwarfed by the large temperature dependence of the electron scattering by phonons (Bass *et al.*, 1990). It is a common approximation to treat τ_i as a constant independent of temperature. It is easy to determine this constant experimentally: the resistivity in the limit of zero temperature contains just the contribution from impurities and defects.

It is possible to add a known amount of impurities intentionally. Then a measurement of the impurity resistance provides a measurement of the cross section σ_c , since the Fermi velocity v_F is usually known.

(2) *Phonons in metals.* Crystals are composed of atoms, which vibrate. As the temperature increases, they vibrate with larger amplitude. These vibrations provide a noise spectrum for the electrons and cause the electrons to scatter. The scattering of electrons by phonons is an intrinsic process. For most solids, this process is the dominant contribution to the electrical resistivity at temperatures above 100 K.

Ziman (1962) first derived the following expression for the resistivity due to the scattering of electrons by phonons in a metal:

$$\rho(T) = C' \sum_{\lambda} \int q \, d^3 q |M_{\lambda}(\mathbf{q})|^2 (\hat{\xi}_{\lambda} \cdot \mathbf{q})^2 \left[-\frac{\partial n_B(\omega)}{\partial \omega} \right]_{\omega=\omega_{\lambda}(\mathbf{q})} \quad (1.8.3.9)$$

$$C' = \frac{3\hbar v_0}{Me^2 16v_F^2 k_F^4}. \quad (1.8.3.10)$$

The constant C' collects numerous constants including the Fermi wavevector k_F , the Fermi velocity v_F , the ion mass M and the unit-cell volume v_0 . The phonons have wavevector \mathbf{q} and different phonon bands (e.g. TA, LA, TO) are denoted by λ . The phonon frequencies are $\omega_{\lambda}(\mathbf{q})$ and the matrix element for scattering the electron by wavevector \mathbf{q} is $M_{\lambda}(\mathbf{q})$.

Equation (1.8.3.9) is easy to evaluate using a computer code that generates all of the phonons at different points in the Brillouin zone. It is the formula used most often to calculate the temperature dependence of the resistivity of metals. However, the reader is warned that this formula is not exact, as it represents an approximate solution of the Boltzmann equation. In the only case in which the accuracy of equation (1.8.3.9) has been tested against numerically accurate solutions of the Boltzmann equation, Wu & Mahan (1984) found that (1.8.3.9) had an error of a few per cent. However, the formula is useful because it gives an answer that only errs by a few per cent and is relatively easy to calculate.

Equation (1.8.3.9) has one feature that is simple and important. At high temperature, the resistivity becomes proportional to

temperature. The Bose–Einstein occupation number $n_B(\omega) \simeq k_B T / \hbar \omega$ and then the derivative with respect to ω is simple. This gives the expression

$$\rho(T) = \frac{m^*}{n_0 e^2} \frac{1}{\tau(T)} \quad (1.8.3.11)$$

$$\frac{1}{\tau} = \frac{2\pi}{\hbar} \lambda_i k_B T \quad (1.8.3.12)$$

$$\lambda_i = \frac{m}{M} \frac{v_0}{16\pi^2 k_F^3} \int q \, d^3 q \frac{|M_{\lambda}(\mathbf{q})|^2 (\hat{\xi}_{\lambda} \cdot \mathbf{q})^2}{[\hbar \omega_{\lambda}(\mathbf{q})]^2}. \quad (1.8.3.13)$$

At high temperature, which in practice is above half of the Debye temperature, the inverse lifetime of the electron is proportional to the temperature. The coefficient is the dimensionless constant λ_i , which is called the ‘transport form of lambda’ (see Grimvall, 1981). This parameter gives the strength of the interaction between the electrons and the phonons. It ranges from very small values ($\lambda_i \sim 0.1$) for the noble metals to values above 4 for heavy metals such as lead and mercury (see Grimvall, 1981).

Now we give some examples of the resistivity of common metals and show that the above formulas give a good account of the resistivity. Fig. 1.8.3.1 shows the intrinsic resistivity as a function of temperature for a simple metal (sodium). The data are taken from Bass *et al.* (1990). The impurity resistivity has been subtracted away. The resistivity is lowest at low temperature, increases at higher temperature and becomes linear at very high temperatures. In actual crystals, the low-temperature value is determined by scattering from impurities and is different for each piece of metal. If one subtracts the constant value and plots $\rho(T) - \rho(0)$, then the curve is the same for each crystal of sodium. This is just the phonon contribution to the resistivity.

At very high temperatures, the resistivity is found to deviate from being linear with temperature. This deviation is due to the thermal expansion of the crystal at high temperature. This can be suppressed by taking measurements at constant volume, as is the case for the results shown in Fig. 1.8.3.1. If the crystal is put under pressure to maintain constant volume, then the high-temperature resistivity is highly linear with temperature.

Also interesting is the behaviour of the resistivity at very low temperatures, say less than 1 K. For the alkali metals, the temperature dependence was found by Bass *et al.* (1990) to be

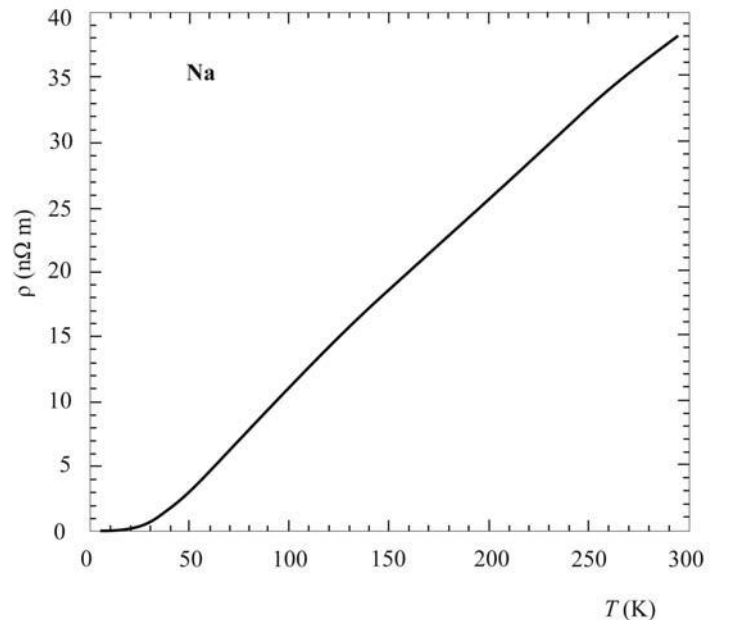


Fig. 1.8.3.1. The temperature dependence of the intrinsic electrical resistivity of sodium at constant density. The data are taken from Bass *et al.* (1990).

1. TENSORIAL ASPECTS OF PHYSICAL PROPERTIES

$$\rho(T) = \rho_i(1 + BT^2) + AT^2. \quad (1.8.3.14)$$

The term ρ_i is the constant due to the impurity scattering. There is also a term proportional to BT^2 , which is proportional to the impurity resistance. This factor is due to the Koshino–Taylor effect (Koshino, 1960; Taylor, 1964), which has been treated rigorously by Mahan & Wang (1989). It is the inelastic scattering of electrons by impurities. The impurity is part of the lattice and phonons can be excited when the impurity scatters the electrons. The term AT^2 is due to electron–electron interactions. The Coulomb interaction between electrons is highly screened and makes only a small contribution to A . The largest contribution to A is caused by phonons. MacDonald *et al.* (1981) showed that electrons can interact by exchanging phonons. There are also terms due to boundary scattering, which is important in thin films: see Bruls *et al.* (1985).

Note that (1.8.3.14) has no term from phonons of $O(T^5)$. Such a term is lacking in simple metals, contrary to the assertion in most textbooks. Its absence is due to *phonon drag*. For a review and explanation of this behaviour, see Wiser (1984). The T^5 term is found in the noble metals, where phonon drag is less important owing to the complexities of the Fermi surface.

1.8.3.2. Metal alloys

Alloys are solids composed of a mixture of two or more elements that do not form a stoichiometric compound. An example is $\text{Cu}_x\text{Ni}_{1-x}$, in which x can have any value. For small values of x , or of $(1-x)$, the atoms of one element just serve as impurities in the other element. This results in the type of behaviour described above. However, in the range $0.2 < x < 0.8$, a different type of resistivity is found. This was first summarized by Mooij (1973), who found a remarkable range of behaviours. He measured the resistivity of hundreds of alloys and also surveyed the published literature for additional results. He represented the resistivity at $T = 300$ K by two values: the resistivity itself, $\rho(T = 300)$, and its logarithmic derivative, $\alpha = d \ln(\rho)/dT$. He produced the graph shown in Fig. 1.8.3.2, where these two values are plotted against each other. Each point is one sample as represented by these two numbers. He found that all of the results fit within a band of numbers, in which larger values of $\rho(T = 300)$ are accompanied by negative values of α . Alloys with very high values of resistivity generally have a resistivity $\rho(T)$ that decreases with increasing temperature. The region where $\alpha = 0$ corresponds to a resistivity of $\rho^* = 150 \mu\Omega \text{ cm}$, which appears to be a fixed point. As the temperature is increased, the resistivities of alloys with $\rho > \rho^*$ decrease to this value, while the resistivities of alloys with $\rho < \rho^*$ increase to this value.

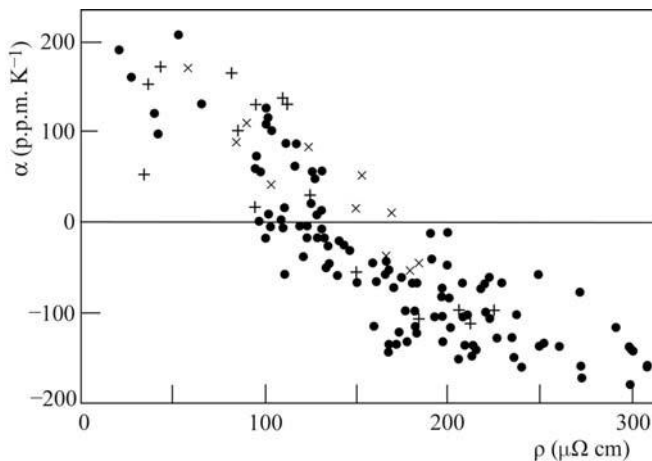


Fig. 1.8.3.2. The temperature coefficient of resistance *versus* resistivity for alloys according to Mooij (1973). Data are shown for bulk alloys (+), thin films (•) and amorphous alloys (x).

Mooij's observations are obviously important, but the reason for this behaviour is not certain. Several different explanations have been proposed and all are plausible: see Jonson & Girvin (1979), Allen & Chakraborty (1981) or Tsuei (1986).

Recently, another group of alloys have been found that are called *bad metals*. The ruthenates (see Allen *et al.*, 1996; Klein *et al.*, 1996) have a resistivity $\rho > \rho^*$ that increases at high temperatures. Their values are outliers on Mooij's plot.

1.8.3.3. Semiconductors

The resistivity of semiconductors varies from sample to sample, even of the same material. The conductivity can be written as $\sigma = n_0 e \mu$, where e is the charge on the electron, $\mu = e\tau/m^*$ is the mobility and n_0 is the density of conducting particles (electrons or holes). It is the density of particles n_0 that varies from sample to sample. It depends upon the impurity content of the semiconductor as well as upon temperature. Since no two samples have exactly the same number of impurities, they do not have the same values of n_0 . In semiconductors and insulators, the conducting particles are extrinsic – they come from defects, impurities or thermal excitation – in contrast to metals, where the density of the conducting electrons is usually an intrinsic property.

In semiconductors, instead of talking about the conductivity, the more fundamental transport quantity (Rode, 1975) is the mobility μ . It is the same for each sample at high temperature if the density of impurities and defects is low. There is an intrinsic mobility, which can be calculated assuming there are no impurities and can be measured in samples with a very low density of impurities. We shall discuss the intrinsic mobility first.

Fig. 1.8.3.3 shows the intrinsic mobility of electrons in silicon, from Rode (1972), as a function of temperature. The mobility generally decreases with increasing temperature. This behaviour is found in all common semiconductors. The mobility also decreases with an increasing concentration of impurities: see Jacoboni *et al.* (1977).

The intrinsic mobility of semiconductors is due to the scattering of electrons and holes by phonons. The phonons come in various branches called TA, LA, TO and LO, where T is transverse, L is longitudinal, A is acoustic and O is optical. At long wavelengths, the acoustic modes are just the sound waves, which

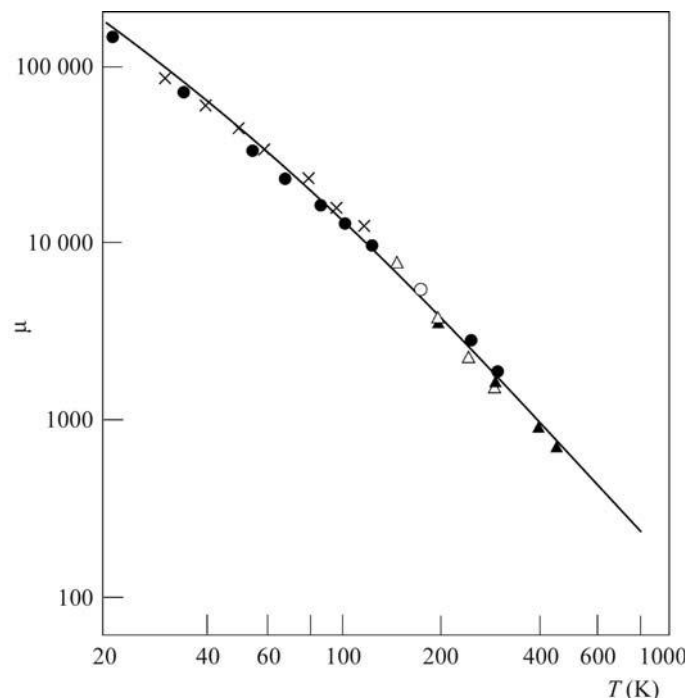


Fig. 1.8.3.3. The intrinsic mobility of electrons in silicon. Solid line: theory; points: experimental. After Rode (1972).

1.8. TRANSPORT PROPERTIES

can be modelled by a Debye model, $\omega_j(\mathbf{q}) = c_j q$, where c_j is the speed of sound for the mode j . At long wavelengths, the optical modes have a constant frequency which is represented by an Einstein model, $\omega_j(\mathbf{q}) = \omega_{j0}$.

The intrinsic mobility is that for a low density of electrons or holes. The existing conducting particles are then confined to the lowest wavevector states near the minimum of the conduction band (electrons) or near the maximum of the valence band (holes). The phonons scatter the particles locally, so that the wavevector changes by small amounts, which can only be done by phonons of long wavelength. The above approximations, of using a Debye model for A modes and an Einstein model for O modes, is accurate. This is because one only needs to consider phonons of long wavelength: the approximations are inaccurate for phonons of short wavelength, but they are irrelevant.

The exception to this general behaviour is where the conduction band has several equivalent minima and the phonons scatter an electron from one minimum to another. This is called intervalley scattering. If the minima of the two electron pockets are separated by a wavevector \mathbf{q}_m , then one needs phonons of energy $\omega_j(\mathbf{q}_m)$. Again, these are a fixed set of constants, so one can assume an Einstein model with these phonons as the frequency. For the calculation of the intrinsic mobility of a semiconductor, one does not need to know all of the phonon modes in the solid, as one does for a metal. Instead, one needs to know only the phonons at selected points in the Brillouin zone.

The inverse lifetimes for each scattering process are simply added:

$$\frac{1}{\tau(k)} = \frac{1}{\tau_A(k)} + \frac{1}{\tau_O(k)} + \frac{1}{\tau_I(k)}. \quad (1.8.3.15)$$

The three terms are acoustic, optical and intervalley. First, we discuss the scattering by optical phonons. The inverse lifetime is proportional to the density of optical phonons N_0 :

$$\frac{1}{\tau_0} = \frac{N_0}{\tau'}, \quad (1.8.3.16)$$

$$N_0 = \frac{1}{\exp(\hbar\omega_0/k_B T) - 1}. \quad (1.8.3.17)$$

The lifetime $\tau_0 \propto N_0^{-1} = \exp(\hbar\omega_0/k_B T) - 1$. This shows that the mobility increases exponentially at lower temperatures according to the factor $\exp(\hbar\omega_0/k_B T) - 1$. This feature is common to nearly all semiconductors.

The factor N_0 occurs because the electrons must absorb an optical phonon in order to scatter. The density of optical phonons in the crystal is proportional to the factor N_0 . Since usually $k_B T < \hbar\omega_0$ at room temperature, the thermally excited electrons have less energy than an optical phonon. In this case, the electrons cannot emit a phonon, since they are unable to lose that much energy: the process has no final state.

Notice that we have not yet discussed the mechanism by which the electron couples to the optical phonons. In general, there are two: the polar interaction and the deformation potential interaction. Polar interactions are found in crystals with different atoms and where there is some ionic bonding. When the charged ions vibrate, it results in oscillating dipoles that create long-range electric fields. Polar interactions are important in III-V and II-VI semiconductors such as GaAs or CdS. Polar interactions are not present in elemental semiconductors such as silicon and germanium, since each ion is neutral. However, the deformation potential interaction is present in these and could scatter strongly.

Next we discuss the intervalley scattering, where an electron moves between equivalent conduction-band minima. Here the phonons have a discrete energy $\hbar\omega_j(\mathbf{q}_m)$. At low temperatures, the electron can only absorb this phonon and the process is proportional to $N(\omega_j(\mathbf{q}_m))$. This behaves, in many ways, like the scattering by optical phonons. However, since $\omega_j(\mathbf{q}_m) < \omega_0$, the

temperature at which phonon emission can occur is lower. At low temperatures, the intervalley scattering also contributes exponentially to the inverse lifetime. These contributions are usually lower than the optical phonon scattering. However, in silicon, Rode (1972) showed that the intervalley scattering dominates over the optical phonon scattering.

The scattering by acoustic phonons only is important at low temperature. For most semiconductors, the interaction between electrons and acoustic phonons is due to the deformation potential interaction. The standard calculation gives the inverse lifetime as proportional to $T^{3/2}$, which becomes smaller at low temperature. However, since the other phonon contributions become smaller with an exponential dependence upon temperature, at small enough temperatures the acoustic phonon term makes the largest contribution to the inverse lifetime. Therefore, at low temperatures, the scattering by acoustic phonons limits the mobility of the electron. Of course, this presumes that there is no contribution from the scattering by impurities. Since this contribution is a constant at low temperature, it is always the dominant contribution at low temperatures. Only in samples with a small concentration of impurities can one actually observe the limitation by acoustic phonons. For most samples, with a moderate density of impurities, the optical-phonon part forms the limit at intermediate temperatures, the impurity scattering forms the limit at low temperatures and one never observes the limit from acoustic phonons.

The discussion above covers the behaviour in the majority of cases. There are special types of crystal that show special behaviour. One of these is crystals that are strongly piezoelectric. The size of the electron-phonon interaction due to piezoelectricity is governed by the electromechanical coupling constant. In crystals where this number is relatively large, the scattering of electrons by acoustic phonons gives $\tau \propto T^{1/2}$ at low temperature, as shown by Mahan (1990). So far, the only class of crystals where this is found is the II-VI semiconductors with the wurtzite structure: ZnO and CdS. These are the most piezoelectric crystals found so far. They both show a dependence of the mobility upon $T^{1/2}$ at low temperature.

Finally, we should mention that semiconductors have an intrinsic conductivity that provides an absolute minimum to the conductivity of any sample. The value of this conductivity depends upon temperature. An electron is thermally excited above the energy gap, creating an electron and a hole. The density of electrons or holes is usually determined by the density of the various impurities or native defects, such as vacancies or interstitials. However, in a perfect crystal without defects, there will still be electrons and holes. The density of electrons (n) and holes (p) obeys the relationship

$$np = 4N_c N_v \left(\frac{2\pi\hbar^2}{m_c k_B T} \right)^{3/2} \left(\frac{2\pi\hbar^2}{m_v k_B T} \right)^{3/2} \exp(-E_G/k_B T), \quad (1.8.3.18)$$

where E_G is the energy gap between the electron and hole bands, and N_j and m_j are the number of equivalent bands and their effective masses. This formula comes from chemical equilibrium: the recombination of electrons and holes is controlled by phase space and the energy gap. The absolute minimum number of electrons and holes is where $n = p$, so that each is equal to the square root of the right-hand side of (1.8.3.18). If this minimum value is called $n_m = p_m$, then the minimum conductivity is $\sigma_m = n_m(\mu_c + \mu_v)$, where μ_c and μ_v are the mobilities of the electrons and the holes, respectively. The conductivity is never lower than this value.

1.8.3.4. The Hall effect

Measurement of the Hall effect is simple and often useful. One takes a crystal and applies a magnetic field B_z along the z axis.

1. TENSORIAL ASPECTS OF PHYSICAL PROPERTIES

Then one imposes a current density j_x along the x axis. One finds that the Lorentz force induces a voltage, or the equivalent electric field E_y , in the y direction. The electric field is proportional to both the current and magnetic field. The ratio $E_y/(j_x B_z)$ is the *Hall constant* R_H . The inverse of R_H is just the charge e and the speed of light c multiplied by the density of electrons n_0 :

$$\frac{E_y}{j_x B_z} = R_H = \frac{1}{n_0 e c}. \quad (1.8.3.19)$$

This provides a simple and accurate method of measuring the density of electrons. It works well when there is only one kind of current carrier and works well in semiconductors with a low density of carriers. A typical experiment for a semiconductor is to measure the conductivity σ and the Hall constant R_H ; the mobility is then $\mu = c R_H \sigma$. If the conducting particles are holes in a semiconductor, the Hall constant has the opposite sign, which indicates positive charge carriers.

Measurement of the Hall effect does not work well if the semiconductor contains a mixture of different carriers, such as electrons and holes, or even electrons from different kinds of conduction bands. In these cases, the constant R_H is not easily interpreted. Similarly, measuring the Hall effect is rarely useful in metals. It only works well in the alkali metals, which have all of the electrons in the first Brillouin zone on a spherical Fermi surface. In most metals, the Fermi surface extends over several Brillouin zones and has numerous pockets or regions of different curvatures. Regions of positive curvature act as electrons and give a negative Hall constant; regions of negative curvature act as holes and give a positive contribution to the Hall constant. Again, it is difficult to interpret the Hall constant when both contributions are present. In general, the Hall effect is most useful in semiconductors.

1.8.3.5. Insulators

Insulators are crystals that do not conduct electricity by the flow of electrons or holes. We shall not mention this case. The band gaps E_G are sufficiently large that the intrinsic mobility is very small.

1.8.3.6. Ionic conductors

There are many ionic solids that have an appreciable electrical conductivity from the diffusive motion of ions. Any material in which the conductivity from the motion of ions is very much larger than that from the motion of electrons is useful as a battery material. For this reason, such materials have been investigated extensively, see *e.g.* Mahan & Roth (1976) or Salamon (1979).

1.8.4. Thermal conductivity

1.8.4.1. Introduction

The thermal conductivity determines the ability of the crystal to conduct heat. Device applications of crystals usually need an extreme value of the thermal conductivity: some applications need a low thermal conductivity, while others need a high thermal conductivity. At room temperature, the largest value of thermal conductivity is for diamond, which has $K = 1.8 \text{ kW m}^{-1} \text{ K}^{-1}$; see *e.g.* Spitzer (1970), Slack (1979) or Berman (1976). The lowest values are for amorphous materials, which have $K = 0.1 \text{ W m}^{-1} \text{ K}^{-1}$.

Heat flow can be carried by two kinds of excitations: phonons and electrons. The phonons carry most of the heat in insulators and semiconductors. Electrons carry appreciable amounts of heat only if there is a high density of conduction electrons, as in a metal. In metals, the electrons usually carry most of the heat. Of course, the heat conduction by phonons and electrons depends upon temperature. At high temperatures, the standard assumption is that the heat flows from phonons and electrons are inde-

pendent and can be calculated separately. However, there is an electron-phonon interaction, which causes a correlation between the two kinds of heat flow. This is called *phonon drag* and is an important phenomenon at low temperatures – typically less than 50 K. We are concerned mostly with higher temperatures, so will not discuss phonon drag here.

First consider the heat flow carried by phonons. As a rule of thumb, crystals with high values of thermal conductivity are those that are: (1) tetrahedrally bonded, (2) contain elements of low atomic number, and (3) lack impurities and defects (Spitzer, 1970; Berman, 1976; Slack, 1979).

The inverse of the thermal conductivity is called the thermal resistivity. There is an equivalent of Matthiessen's rule for thermal conductivity: it is a reasonable approximation to take the various contributions to the thermal resistivity and simply to add them. This is not a rigorous theorem; it is just a process that gives a reasonable answer most of the time. Here we shall discuss four contributions to the thermal resistivity: boundary scattering, impurity scattering, isotope scattering and anharmonic interactions:

$$R_K = R_B + R_i + R_l + R_A. \quad (1.8.4.1)$$

These various terms are discussed in order.

1.8.4.2. Boundary scattering

At low temperatures, the phonons that are thermally excited are those which have an energy near to or less than the thermal energy $\hbar\Omega(q) \leq k_B T$. This usually means acoustic modes of long wavelength. They tend to have a long mean free path, which can extend to the size of the crystal. In this case, the limiting process on the phonon scattering is simply bouncing off the walls of the crystal. The formula for this process is best derived from the classical formula for the thermal conductivity (see Ziman, 1962),

$$K = (1/3)C\bar{v}\Lambda, \quad (1.8.4.2)$$

where C is the heat capacity, \bar{v} is the average velocity and Λ is the mean free path. To apply this to the present problem, take Λ to be equal to the average dimension of the crystal and \bar{v} to be the speed of sound averaged over the various directions. At low temperatures, the heat capacity $C \propto T^3$, as given by the Debye theory. Since Λ and \bar{v} are constants, then $K \propto T^3$, which agrees well with the dependence found experimentally. Of course, the thermal resistance R_B is just the inverse of $R_B \propto T^{-3}$.

1.8.4.3. Impurity scattering

Impurities can be either point defects or extended defects such as dislocations. Here we confine our remarks to point defects. When acoustic phonons of long wavelength scatter from point defects, the process is very much like the Rayleigh scattering of light. The basic cross section varies as the fourth power of the frequency. Equivalently, at long wavelength, it varies as the fourth power of the wave number q of the phonons (see Ziman, 1962):

$$\frac{1}{\tau_i(q)} = n_i q^4 C_i, \quad (1.8.4.3)$$

where n_i is the concentration of impurities and C_i is a constant characteristic of the impurity. Of course, this lifetime for the phonon of wave number q must be averaged over all of the wavevectors in the crystal as a function of temperature. This averaging is actually mathematically delicate. At temperatures T less than the Debye temperature Θ , the average value of q is $q \sim k_B T/(\hbar v)$ and $R_i \sim T^4$. At high temperatures ($T > \Theta$), the average of $1/\tau(q)$ is a constant, since all values of q in the Brillouin zone are equally accessible. In this limit, $R_i \sim \text{constant}$.

1.8. TRANSPORT PROPERTIES

1.8.4.4. Isotope scattering

The perfect crystal is defined as having each atom in its expected position, with no vacancies, interstitials or other defects. Such a crystal would still have a type of disorder that scatters phonons. Most elements have several natural isotopes for their nuclei. Natural crystals usually reflect this mixture of isotopes. Special crystals can be made that are composed of a single isotope, and these lack the resistive term from isotope scattering. However, most crystals have isotope scattering. The scattering is from the mass difference of the nuclei. The interaction term comes from the kinetic energy of the ion vibrational motion. If there are two isotopes with masses M_1 and M_2 , with concentrations c and $(1 - c)$, respectively, then the average of the mass in the kinetic energy term as discussed by Klemens (1955) is

$$\left\langle \frac{1}{M} \right\rangle = \frac{c}{M_1} + \frac{1-c}{M_2}. \quad (1.8.4.4)$$

The kinetic energy term of the ions is then

$$\sum_i \frac{P_i^2}{2M_i} = \sum_i \frac{1}{2} P_i^2 \left[\left\langle \frac{1}{M} \right\rangle + \left(\frac{1}{M_i} - \left\langle \frac{1}{M} \right\rangle \right) \right]. \quad (1.8.4.5)$$

The second term is the perturbation. When we evaluate the golden rule for scattering, we square the matrix element and then average the square:

$$\left\langle \left(\frac{1}{M_i} - \left\langle \frac{1}{M} \right\rangle \right)^2 \right\rangle = c \left(\frac{1}{M_1} - \left\langle \frac{1}{M} \right\rangle \right)^2 + (1-c) \left(\frac{1}{M_2} - \left\langle \frac{1}{M} \right\rangle \right)^2 \quad (1.8.4.6)$$

$$= c(1-c) \left(\frac{1}{M_1} - \frac{1}{M_2} \right)^2 \quad (1.8.4.7)$$

$$= c(1-c) \left(\frac{\Delta M}{M_1 M_2} \right)^2. \quad (1.8.4.8)$$

The isotope scattering depends upon the concentration in the form $c(1 - c)$ and upon the square of the mass difference $\Delta M = M_2 - M_1$. The isotope fluctuations act as point defects. The total expression for the scattering cross section also includes a factor of q^4 in addition to the factors given above. Thus their temperature dependence is identical to that of the point defects: $R_I \sim T^4$ at low temperature and $R_I \sim \text{constant}$ at high temperature.

This behaviour is found experimentally. The isotope scattering is usually a small contribution to the thermal resistivity. It is only important in temperature regions where the other resistivities are small. This occurs, of course, at the maximum value of the thermal conductivity, since that is where all of the resistivities are small. Changing the isotopic mix of a crystal changes the thermal conductivity in the temperature regions where it is large. One example is diamond, which is usually 99% ^{12}C and 1% ^{13}C . Anthony *et al.* (1990) showed that eliminating the ^{13}C increases the thermal conductivity by a factor of nearly two (1.8 to $3.2 \text{ kW m}^{-1} \text{ K}^{-1}$) at room temperature. Another example is germanium, where isotope scattering makes a sizeable contribution to the thermal resistance (see Berman, 1976).

1.8.4.5. Alloy scattering

Alloys are mixtures of two or more different crystal ‘ingredients’. We assume that the atoms are randomly located on the different atom sites. Some alloys are ordered, but that makes them crystals. An example of a disordered alloy is $\text{Ga}_x\text{Al}_{1-x}\text{As}$. Since GaAs and AlAs have the same crystal structure and nearly the same lattice constant, the mixed crystal permits any value of x . The Ga and Al atoms randomly occupy the cation site in the

zinc blende lattice. Experimentally, it is found that the thermal resistance as a function of x is (see Ziman, 1962; Berman, 1976)

$$R(x) = xR_{\text{GaAs}} + (1-x)R_{\text{AlAs}} + x(1-x)R_A. \quad (1.8.4.9)$$

The first two terms just average the thermal resistance of the two lattices. The third term is the scattering of the phonons from the alloy fluctuations. It is derived in the same way as the equivalent factor of $c(1 - c)$ in the discussion of isotope scattering in Section 1.8.4.4. In alloys, the fluctuations are due to two factors: the mass difference at the atoms sites (as in isotope scattering) and the difference in the bonding between Ga and Al. The constant R_A depends on these factors. It is not small: Yao (1987) showed that the term $x(1 - x)R_A$ is four or five times larger than the others at $x = 1/2$. Although we have cited a particular example of alloy scattering, this dependence is quite universal. Alloy fluctuations typically dominate the thermal resistivity of alloys.

1.8.4.6. Anharmonic interactions

In crystals that are relatively pure, *i.e.* those that lack large numbers of impurities, the important limitation on thermal conductivity at high temperature is from anharmonic interactions (Ziman, 1962). The vibrational potential between neighbouring atoms is not perfectly harmonic. Besides the quadratic dependence on vibrational distance, there is usually a term that depends upon the third and perhaps fourth powers of the relative displacements of the ions. These latter terms are the anharmonic part of the vibrational potential energy. They cause the crystal to expand with temperature and also contribute to the thermal resistance.

For most crystals, the cubic term is important. Its contribution is best explained using the language of phonons. The cubic term means that three phonons are involved. This usually means that one phonon decays into two others, or two phonons combine into one. Both processes contribute to the lifetime of the phonons. On rare occasions, the phase space of the phonons does not permit these events. For example, silicon has a very high frequency optical phonon branch (62 meV at the zone centre) while the acoustic phonons have rather low frequencies. The optical phonons are unable to decay into two of lower frequency, since the two do not have enough energy. This explains, in part, why silicon has a high thermal conductivity. However, this case is unusual. In most crystals, the phonons have similar energy and one can decay into two of lower energy.

The three-phonon events have a simple dependence upon temperature. When one phonon goes to two, or *vice versa*, the rate depends upon the density of phonons $n_B(\omega_q)$ as given by the Bose–Einstein occupation number. At high temperature, *i.e.* about half of the Debye temperature, this function can be expanded to

$$n_B(\omega_q) = \frac{1}{\exp(\hbar\omega_q/k_B T) - 1} \simeq \frac{k_B T}{\hbar\omega_q} \quad (1.8.4.10)$$

and the thermal resistance is proportional to temperature. Thus a plot of the inverse thermal conductivity *versus* temperature usually shows a linear behaviour at high temperature. This linear term is from the anharmonic interactions. There are two main reasons for deviations from linear behaviour: the thermal expansion of the crystal and the contribution of the anharmonic quartic terms, which tend to go as $O(T^2)$.

1.8.4.7. Thermal conductivity of metals

Heat conduction in metals can occur by either phonons or electrons. The conduction by phonons has been discussed above. In metals, there is another contribution to the thermal resistance: the absorption of the phonons by the electrons. Metals have low-energy excitations, which consist of exciting an electron just below the chemical potential to an occupied state just above the

1. TENSORIAL ASPECTS OF PHYSICAL PROPERTIES

chemical potential. The separation in energy between these two electron states can be arbitrarily small and can be small enough to be equal to the energy of a phonon. By this process, the energy of the phonon can be absorbed by the electron gas, which contributes to the thermal resistance of the phonons.

However, in metals, the electrons tend to carry more heat than the phonons. The latter play a secondary role. Thus, we divide the thermal conductivity into electronic and phonon parts, $K = K_e + K_p$. This choice of separation is rather interesting. Note that we do not combine their inverses, as we do for the components of each separate contribution.

The thermal resistance due to the electrons is related to the electrical resistance. Both depend upon the lifetime of the electrons. Because of this, there is a simple relationship between the electronic part of the thermal conductivity and the electrical conductivity σ . This relationship is called the *Wiedemann–Franz law* (Wiedemann & Franz, 1853).

$$K_e = \mathcal{L}_0 \sigma T \quad (1.8.4.11)$$

$$\mathcal{L}_0 = \frac{\pi^2}{3} \left(\frac{k_B}{e} \right)^2. \quad (1.8.4.12)$$

The parameter \mathcal{L}_0 is called the *Lorenz number*. The value given above is for a metal with a well defined Fermi surface, so the electrons obey Fermi–Dirac statistics. In the other limit of classical statistics, its value is $2(k_B/e)^2$. We caution that this simple relation between the electrical and thermal conductivities is not exact. The reason for this is that the two lifetimes are not identical: the electrical conductivity uses the lifetime for changing the momentum of the electron, while the thermal conductivity uses the lifetime for changing the energy current. However, the two lifetimes are similar. In practice, the Wiedemann–Franz law is found to work quite well. It seems to be valid regardless of the mechanisms that scatter the electrons: whether the scattering is by phonons, impurities or spin excitations. It can be used to estimate the thermal conductivity from electrons in metals, or in semiconductors with large densities of conduction electrons or holes.

1.8.5. Seebeck coefficient

The Seebeck coefficient S is the third transport coefficient that enters into the fundamental equations (1.8.2.1) and (1.8.2.2). Here we discuss some of its basic properties. First, we write down three integrals for the transport coefficients according to Goldsmid (1986):

$$\sigma = e^2 \int_{-\infty}^{+\infty} d\varepsilon \left(-\frac{\partial n_F}{\partial \varepsilon} \right) \Sigma(\varepsilon) \quad (1.8.5.1)$$

$$T\sigma S = e \int_{-\infty}^{+\infty} d\varepsilon \left(-\frac{\partial n_F}{\partial \varepsilon} \right) \Sigma(\varepsilon)(\varepsilon - \mu) \quad (1.8.5.2)$$

$$TK_e = \int_{-\infty}^{+\infty} d\varepsilon \left(-\frac{\partial n_F}{\partial \varepsilon} \right) \Sigma(\varepsilon)(\varepsilon - \mu)^2, \quad (1.8.5.3)$$

where μ is the chemical potential, e is the electron charge,

$$\left(-\frac{\partial n_F}{\partial \varepsilon} \right) = \frac{1}{k_B T} \frac{\exp[(\varepsilon - \mu)/k_B T]}{\{\exp[(\varepsilon - \mu)/k_B T] + 1\}^2}, \quad (1.8.5.4)$$

$\Sigma(\varepsilon)$, which we will call the transport distribution function, is given by

$$\Sigma(\varepsilon) = \sum_{\mathbf{k}} v_x(\mathbf{k})^2 \tau(\mathbf{k}) \delta(\varepsilon - \varepsilon(\mathbf{k})), \quad (1.8.5.5)$$

where the summation is over the first Brillouin zone, $v_x(\mathbf{k})$ is the group velocity of the carriers with wavevector \mathbf{k} in the direction of the applied field, $\tau(\mathbf{k})$ is the lifetime of the carriers and $\varepsilon(\mathbf{k})$ is

the dispersion relation for the carriers. In cases in which many bands contribute to the transport process, the summation has to be extended to all the bands. In some particular cases, such as for parabolic bands, the transport distribution defined in (1.8.5.5) takes a much simpler form:

$$\Sigma(\varepsilon) = N(\varepsilon) v_x(\varepsilon)^2 \tau(\varepsilon), \quad (1.8.5.6)$$

where $N(\varepsilon)$ is the density of states.

The Seebeck coefficient is defined in (1.8.5.2). Since the left-hand side of this equation contains σTS , S is defined as the ratio of the two integrals in (1.8.5.1) and (1.8.5.2). The magnitude of the function $\Sigma(\varepsilon)$ is immaterial for S , since the magnitude cancels in the ratio. All that matters is the dependence of $\Sigma(\varepsilon)$ upon the energy ε . The function $\partial n_F / \partial \varepsilon$ is a symmetric function of ε . Furthermore, it becomes very small when ε is more than a few thermal energies ($k_B T$) away from the chemical potential. The Seebeck coefficient depends upon how $\Sigma(\varepsilon)$ varies within this small energy range. The usual case is that it is a smooth function of ε that can be expanded in a Taylor series:

$$\Sigma(\varepsilon) \simeq \Sigma(\mu) + (\varepsilon - \mu) \frac{\partial \Sigma(\mu)}{\partial \mu} + O((\varepsilon - \mu)^2) \quad (1.8.5.7)$$

$$\sigma = e^2 \Sigma(\mu) \quad (1.8.5.8)$$

$$S = \frac{\pi^2 k_B^2 T}{3e} \frac{\partial}{\partial \mu} \ln[\Sigma(\mu)]. \quad (1.8.5.9)$$

The Seebeck coefficient has a linear dependence upon temperature. The coefficient of this term depends upon the energy variations in $\Sigma(\varepsilon)$ at the chemical potential. In most metals, a linear dependence upon temperature is observed (e.g. Rowe, 1995), particularly at high temperature. This linearity is found when one simple criterion is satisfied: that the function $\Sigma(\varepsilon)$ has a smooth dependence upon energy near the chemical potential.

Any deviation from linear behaviour in the Seebeck coefficient implies that the function $\Sigma(\varepsilon)$ has a more complicated behaviour near the chemical potential. Here we review several possible shapes. One is a simple Lorentzian peak:

$$\Sigma = 1 + C \frac{\gamma^2}{(\varepsilon - \mu - \varepsilon_0)^2 + \gamma^2}. \quad (1.8.5.10)$$

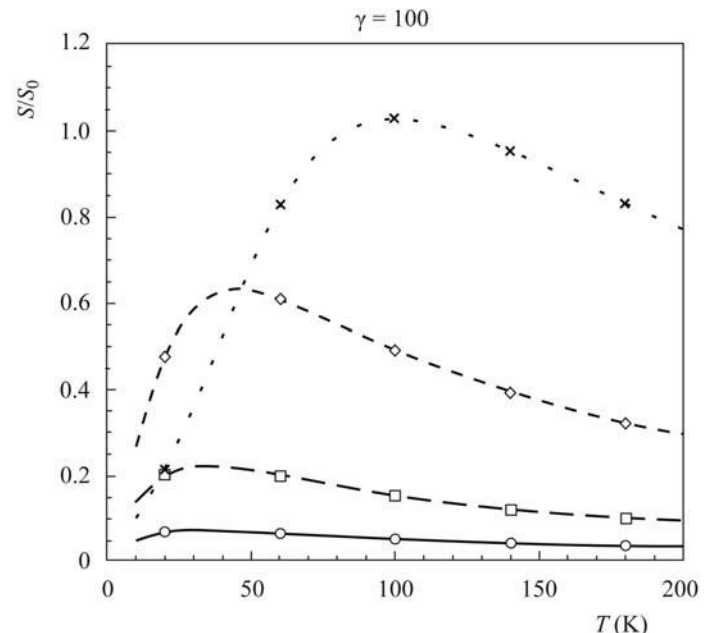


Fig. 1.8.5.1. The Seebeck coefficient S in units of $S_0 = k_B/e$ for $\Sigma(\varepsilon)$ containing a Lorentzian peak. The values of S increase as the resonance energy E_0 increases away from the chemical potential.

1.8. TRANSPORT PROPERTIES

The peak of the Lorentzian is at ε_0 and the width is γ . Fig. 1.8.5.1 shows the Seebeck coefficient calculated with this functional form. We arbitrarily took $\gamma = k_B T_\gamma$ and $T_\gamma = 100$ K. The four curves are for $\varepsilon_0/k_B = 10, 30, 100$ and 300 K, and the larger ε_0 has the larger Seebeck coefficient. All of the curves have a broad peak as a function of temperature. If $\varepsilon_0 = 0$, then $S = 0$, since the integrand is an odd function of $(\varepsilon - \mu)$. The vertical scale is S/S_0 where $S_0 = k_B/e = 86.17 \mu\text{V K}^{-1}$. We see from Fig. 1.8.5.1 that it is difficult to get values of S/S_0 very much larger than unity.

Another example is that of mixed-valence materials with f electrons. The f shells make electron states of narrow energy, which are approximated as Lorentzians. In this case, $\Sigma(\varepsilon)$ equals the inverse of the right-hand side of (1.8.5.10). The argument for this is that $1/\tau(\varepsilon)$ is proportional to the right-hand side of (1.8.5.10). Since $\Sigma \propto \tau$, it contains the inverse of (1.8.5.10). Interestingly enough, plots of the Seebeck coefficient by Jaccard & Sierro (1982) for this case also contain broad peaks in energy, where S/S_0 has a maximum of about unity. In this case, a proper calculation includes the fact that both C and γ are functions of temperature. For a review, see Mahan (1997).

We give these examples of the Seebeck coefficient because they are the cases that occur most often. In many metals, the Seebeck coefficient is either linear with temperature or has broad peaks. The broad peaks are due to structure in Σ near the chemical potential. This structure is usually due either to variations in the density of states or in the electron lifetime.

In insulators, the Seebeck coefficient can become relatively large. The exact value depends upon the energy gap, the temperature and the density of impurities. This example is treated in many references, e.g. Goldsmid (1986) and Rowe (1995).

1.8.6. Glossary

| | |
|----------------|--|
| T | temperature (K) |
| \mathbf{J} | current density (A m^{-2}) |
| \mathbf{J}_Q | heat current (W m^{-2}) |
| σ | electrical conductivity (S m^{-1}) |
| ρ | electrical resistivity |
| K | thermal conductivity ($\text{W m}^{-1} \text{K}^{-1}$) |
| \mathbf{E} | electric field (V m^{-1}) |
| S | Seebeck coefficient (V K^{-1}) |
| k_B | Boltzmann constant |
| R_H | Hall constant |
| m^* | effective mass of the electron |
| τ | lifetime of the electron |

Research support from the University of Tennessee and from Oak Ridge National Laboratory, managed by Lockheed Martin Energy Research Corporation for the US Department of Energy under contract No. DE-AC05-96OR22464, is gratefully acknowledged.

References

- Allen, P. B., Beaulac, T. P., Khan, F. S., Butler, W. H., Pinski, F. J. & Swihart, J. C. (1986). *D.c. transport in metals*. *Phys. Rev. B*, **34**, 4331–4333.
- Allen, P. B., Berger, H., Chauvet, O., Forro, L., Jarlborg, T., Junod, A., Revaz, B. & Santi, G. (1996). *Transport properties, thermodynamic properties, and electronic structure of SrRuO_3* . *Phys. Rev. B*, **53**, 4393–4398.
- Allen, P. B. & Chakraborty, B. (1981). *Infrared and d.c. conductivity in metals with strong scattering: nonclassical behavior from a generalized Boltzmann equation containing band-mixing effects*. *Phys. Rev. B*, **23**, 4815–4827.

- Anthony, T. R., Banholzer, W. F., Fleischer, J. F., Wei, L., Kuo, P. K., Thomas, R. L. & Pryor, R. W. (1990). *Thermal diffusivity of isotropically enriched ^{12}C diamond*. *Phys. Rev. B*, **42**, 1104–1111.
- Bass, J., Pratt, W. P. & Schroeder, P. A. (1990). *The temperature dependent electrical resistivities of the alkali metals*. *Rev. Mod. Phys.* **62**, 645–744.
- Berman, R. (1976). *Thermal conduction in solids*. Oxford University Press.
- Bruls, G. J. C. L., Bass, J., van Gelder, A. P., van Kempen, H. & Wyder, P. (1985). *Linear magnetoresistance due to sample thickness variations: applications to aluminum*. *Phys. Rev. B*, **32**, 1927–1939.
- Goldsmid, H. J. (1986). *Electronic refrigeration*. London: Pion Limited.
- Grimvall, G. (1981). *The electron–phonon interaction in metals*. Amsterdam: North-Holland.
- Jaccard, D. & Sierro, J. (1982). *Thermoelectric power of some intermediate valence compounds*. In *Valence instabilities*, edited by P. Wachter & H. Boppart, pp. 409–413. Amsterdam: North-Holland.
- Jacoboni, C., Canali, C., Ottaviani, G. & Quaranta, A. A. (1977). *A review of some charge transport properties of silicon*. *Solid State Electron.* **20**, 77–89.
- Jonson, M. & Girvin, S. M. (1979). *Electron–phonon dynamics and transport anomalies in random metal alloys*. *Phys. Rev. Lett.* **43**, 1447–1451.
- Klein, L., Dodge, J. S., Ahn, C. H., Snyder, G. J., Geballe, T. H., Beasley, M. R. & Kapitulnik, A. (1996). *Anomalous spin scattering effects in the badly metallic itinerant ferromagnet SrRuO_3* . *Phys. Rev. Lett.* **77**, 2774–2777.
- Klemens, P. G. (1955). *The scattering of low-frequency lattice waves by static imperfections*. *Proc. Phys. Soc. London Sect. A*, **68**, 1113–1128.
- Koshino, S. (1960). *Scattering of electrons by the thermal motion of impurity ions*. *Prog. Theor. Phys.* **24**, 484–494.
- MacDonald, A. H., Taylor, R. & Geldart, D. J. W. (1981). *Umklapp electron–electron scattering and the low-temperature electrical resistivity of the alkali metals*. *Phys. Rev. B*, **23**, 2718–2730.
- Mahan, G. D. (1990). *Many-particle physics*, 2nd ed. New York: Plenum.
- Mahan, G. D. (1997). *Good thermoelectrics*. In *Solid state physics*, Vol. 51, edited by H. Ehrenreich & F. Spaepen, pp. 81–157. New York: Academic Press.
- Mahan, G. D. & Roth, W. L. (1976). Editors. *Superionic conductors*. New York: Plenum.
- Mahan, G. D. & Wang, Z. (1989). *Koshino–Taylor coefficient in electrical conductivity*. *Phys. Rev. B*, **39**, 4926–4929.
- Matthiessen, A. & Vogt, C. (1864). *Ann. Phys. (Leipzig)*, **129**, 19.
- Mooij, J. H. (1973). *Electrical conduction in concentrated disordered transition metal alloys*. *Phys. Status Solidi A*, **17**, 521–530.
- Rode, D. L. (1972). *Electron mobility in Ge, Si, and GaP*. *Phys. Status Solidi B*, **53**, 245–254.
- Rode, D. L. (1975). *Low field electron transport*. In *Semiconductors and semimetals*, Vol. 10, edited by R. K. Willardson & A. C. Beer, pp. 1–89. New York: Academic Press.
- Rowe, D. M. (1995). Editor. *CRC handbook of thermoelectrics*. New York: CRC Press.
- Salamon, M. B. (1979). Editor. *Physics of superionic conductors*. New York: Springer-Verlag.
- Sievers, A. J. (1980). *Infrared and optical properties of Na, K, and Rb metals*. *Phys. Rev. B*, **22**, 1600–1611.
- Slack, G. A. (1979). *The thermal conductivity of nonmetallic crystals*. In *Solid state physics*, Vol. 34, edited by H. Ehrenreich, F. Seitz & D. Turnbull, pp. 1–71. New York: Academic Press.
- Spitzer, D. P. (1970). *Lattice thermal conductivity of semiconductors: a chemical bond approach*. *J. Phys. Chem. Solids*, **31**, 19–40.
- Taylor, P. L. (1964). *Changes in electrical resistance caused by incoherent electron–photon scattering*. *Phys. Rev. A*, **135**, 1333–1335.
- Tsuei, C. C. (1986). *Nonuniversality of the Mooij correlation – the temperature coefficient of electrical resistivity of disordered metals*. *Phys. Rev. Lett.* **57**, 1943–1946.
- Wiedemann, G. & Franz, R. (1853). *Ann. Phys. (Leipzig)*, **89**, 497.
- Wiser, N. (1984). *The electrical resistivity of simple metals*. *Contemp. Phys.* **25**, 211–249.
- Wu, J. W. & Mahan, G. D. (1984). *Transport equation at finite frequency: infrared absorption in metals*. *Phys. Rev. B*, **29**, 1769–1782.
- Yao, T. (1987). *Thermal properties of AlAs/GaAs superlattices*. *Appl. Phys. Lett.* **51**, 1798–1782.
- Ziman, J. M. (1962). *Electrons and phonons*. Oxford University Press.

1.9. Atomic displacement parameters

BY W. F. KUHS

1.9.1. Introduction

Atomic thermal motion and positional disorder is at the origin of a systematic intensity reduction of Bragg reflections as a function of scattering vector \mathbf{Q} . The intensity reduction is given as the well known *Debye–Waller factor* (DWF); the DWF may be of purely thermal origin (*thermal DWF* or *temperature factor*) or it may contain contributions of static atomic disorder (*static DWF*). As atoms of chemically or isotopically different elements behave differently, the individual atomic contributions to the global DWF (describing the weakening of Bragg intensities) vary. Formally, one may split the global DWF into the individual atomic contributions. Crystallographic experiments usually measure the global weakening of Bragg intensities and the individual contributions have to be assessed by adjusting individual atomic parameters in a least-squares refinement.

The theory of lattice dynamics (see *e.g.* Willis & Pryor, 1975) shows that the atomic thermal DWF T_α is given by an exponential of the form

$$T_\alpha(\mathbf{Q}) = \langle \exp(i\mathbf{Q}\mathbf{u}_\alpha) \rangle, \quad (1.9.1.1)$$

where \mathbf{u}_α are the individual atomic displacement vectors and the brackets symbolize the thermodynamic (time–space) average over all contributions \mathbf{u}_α . In the harmonic (Gaussian) approximation, (1.9.1.1) reduces to

$$T_\alpha(\mathbf{Q}) = \exp[(-1/2)\langle (\mathbf{Q}\mathbf{u}_\alpha)^2 \rangle]. \quad (1.9.1.2)$$

The thermodynamically averaged atomic mean-square displacements (of thermal origin) are given as $U^{ij} = \langle u^i u^j \rangle$, *i.e.* they are the thermodynamic average of the product of the displacements along the i and j coordinate directions. Thus (1.9.1.2) may be expressed with $\mathbf{Q} = 4\pi\mathbf{h}|\mathbf{a}|$ in a form more familiar to the crystallographer as

$$T_\alpha(\mathbf{h}) = \exp(-2\pi^2 h_i |a^i| h_j |a^j| U_\alpha^{ij}), \quad (1.9.1.3)$$

where h_i are the covariant Miller indices, \mathbf{a}^i are the reciprocal-cell basis vectors and $1 \leq i, j \leq 3$. Here and in the following, tensor notation is employed; implicit summation over repeated indices is assumed unless stated otherwise. For computational convenience one often writes

$$T_\alpha(\mathbf{h}) = \exp(-h_i h_j \beta_\alpha^{ij}) \quad (1.9.1.4)$$

with $\beta_\alpha^{ij} = 2\pi^2 |\mathbf{a}^i| |\mathbf{a}^j| U_\alpha^{ij}$ (no summation). Both \mathbf{h} and β are dimensionless tensorial quantities; \mathbf{h} transforms as a covariant tensor of rank 1, β as a contravariant tensor of rank 2 (for details of the mathematical notion of a tensor, see Chapter 1.1).

Similar formulations are found for the static atomic DWF S_α , where the average of the atomic static displacements $\Delta\mathbf{u}_\alpha$ may also be approximated [though with weaker theoretical justification, see Kuhs (1992)] by a Gaussian distribution:

$$S_\alpha(\mathbf{Q}) = \exp[(-1/2)\langle (\mathbf{Q}\Delta\mathbf{u}_\alpha)^2 \rangle]. \quad (1.9.1.5)$$

As in equation (1.9.1.3), the static atomic DWF may be formulated with the mean-square disorder displacements $\Delta U^{ij} = \langle \Delta u^i \Delta u^j \rangle$ as

$$S_\alpha(\mathbf{h}) = \exp(-2\pi^2 h_i |a^i| h_j |a^j| \Delta U_\alpha^{ij}). \quad (1.9.1.6)$$

It is usually difficult to separate thermal and static contributions, and it is often wise to use the sum of both and call them simply (mean-square) atomic displacements. A separation may however be achieved by a temperature-dependent study of atomic displacements. A harmonic diagonal tensor component of purely thermal origin extrapolates linearly to zero at 0 K; zero-point motion causes a deviation from this linear behaviour at low temperatures, but an extrapolation from higher temperatures (where the contribution from zero-point motion becomes negligibly small) still yields a zero intercept. Any positive intercept in such extrapolations is then due to a (temperature-independent) static contribution to the total atomic displacements. Care has to be taken in such extrapolations, as pronounced anharmonicity (frequently encountered at temperatures higher than the Debye temperature) will change the slope, thus invalidating the linear extrapolation (see *e.g.* Willis & Pryor, 1975). Owing to the difficulty in separating thermal and static displacements in a standard crystallographic structure analysis, a subcommittee of the IUCr Commission on Crystallographic Nomenclature has recommended the use of the term *atomic displacement parameters* (ADPs) for U^{ij} and β^{ij} (Trueblood *et al.*, 1996).

1.9.2. The atomic displacement parameters (ADPs)

One notes that in the Gaussian approximation, the mean-square atomic displacements (composed of thermal and static contributions) are fully described by six coefficients β^{ij} , which transform on a change of the direct-lattice base (according to $\mathbf{a}_k = A_{ki}\mathbf{a}_i$) as

$$\beta^{kl} = A_{ki} A_{lj} \beta^{ij}. \quad (1.9.2.1)$$

This is the transformation law of a tensor (see Section 1.1.3.2); the mean-square atomic displacements are thus tensorial properties of an atom α . As the tensor is contravariant and in general is described in a (non-Cartesian) crystallographic basis system, its indices are written as superscripts. It is convenient for comparison purposes to quote the dimensionless coefficients β^{ij} as their dimensioned representations U^{ij} .

In the harmonic approximation, the atomic displacements are fully described by the fully symmetric second-order tensor given in (1.9.2.1). Anharmonicity and disorder, however, cause deviations from a Gaussian distribution of the atomic displacements around the atomic position. In fact, anharmonicity in the thermal motion also provokes a shift of the atomic position as a function of temperature. A generalized description of atomic displacements therefore also involves first-, third-, fourth- and even higher-order displacement terms. These terms are defined by a moment-generating function $M(\mathbf{Q})$ which expresses $\langle \exp(i\mathbf{Q}\mathbf{u}_\alpha) \rangle$ in terms of an infinite number of moments; for a Gaussian distribution of displacement vectors, all moments of order > 2 are identically equal to zero. Thus

$$M(\mathbf{Q}) = \langle \exp(i\mathbf{Q}\mathbf{u}_\alpha) \rangle = \sum_{N=0}^{\infty} (i^N / N!) \langle (\mathbf{Q}\mathbf{u}_\alpha)^N \rangle. \quad (1.9.2.2)$$

The moments $\langle (\mathbf{Q}\mathbf{u}_\alpha)^N \rangle$ of order N may be expressed in terms of cumulants $\langle (\mathbf{Q}\mathbf{u}_\alpha)^N \rangle_{\text{cum}}$ by the identity

$$\sum_{N=0}^{\infty} (1/N!) \langle (\mathbf{Q}\mathbf{u}_\alpha)^N \rangle \equiv \exp \sum_{N=1}^{\infty} (1/N!) \langle (\mathbf{Q}\mathbf{u}_\alpha)^N \rangle_{\text{cum}}. \quad (1.9.2.3)$$

1.9. ATOMIC DISPLACEMENT PARAMETERS

Separating the powers of \mathbf{Q} and \mathbf{u} in (1.9.2.2) and (1.9.2.3), one may obtain expressions involving moments μ and cumulants k explicitly as

$$M(\mathbf{Q}) = \sum_{N=0}^{\infty} (i^N/N!) Q_i Q_j Q_k \dots Q_n \mu^{ijk\dots n} \quad (1.9.2.4)$$

and the cumulant-generating function $K(\mathbf{Q})$ as

$$K(\mathbf{Q}) = \exp[M(\mathbf{Q})] = \sum_{N=1}^{\infty} (i^N/N!) Q_i Q_j Q_k \dots Q_n k^{ijk\dots n}. \quad (1.9.2.5)$$

The indices i, j, k, \dots, n run in three-dimensional space from 1 to 3 and refer to the crystallographic basis system. Moments may be expressed in terms of cumulants (and *vice versa*); the transformation laws are given in *IT B* (2001), equation (1.2.12.9) and more completely in Kuhs (1988, 1992). The moment- and cumulant-generating functions are two ways of expressing the Fourier transform of the atomic probability density function (p.d.f.). If all terms up to infinity are taken into account, $M(\mathbf{Q})$ and $K(\mathbf{Q})$ are [by virtue of the identity $\exp(i\mathbf{Q}) = \sum (i\mathbf{Q})^N/N!$] identical. For a finite series, however, the cumulants of order N carry implicit information on contributions of order N^2, N^3 etc. in contrast to the moments. Equations (1.9.2.4) and (1.9.2.5) are useful, as they can be entered directly in a structure-factor equation (see Chapter 1.2 in *IT B*); however, the moments (and thus the cumulants) may also be calculated directly from the atomic p.d.f. as

$$\mu^{ijk\dots n} = \int u^i u^j u^k \dots u^n \text{p.d.f.}(\mathbf{u}) \, d\mathbf{u}. \quad (1.9.2.6)$$

The real-space expression of the p.d.f. obtained from a Fourier transform of (1.9.2.5) is called an *Edgeworth series* expansion. If one assumes that the underlying atomic p.d.f. is close to a Gaussian distribution, one may separate out the Gaussian contributions to the moment-generating function as suggested by Kuznetsov *et al.* (1960) and formulate a generating function for quasimoments as

$$\tilde{M}(\mathbf{Q}) = \exp[(1/2)\langle(\mathbf{Q}\mathbf{u})^2\rangle] \sum_{N=3}^{\infty} (i^N/N!) Q_i Q_j Q_k \dots Q_n \tilde{\mu}^{ijk\dots n}. \quad (1.9.2.7)$$

These quasimoments are especially useful in crystallographic structure-factor equations, as they just modify the harmonic case. The real-space expression of the p.d.f. obtained from a Fourier transformation of (1.9.2.7) is called a *Gram–Charlier series* expansion. Discussions of its merits as compared to the Edgeworth series are given in Zucker & Schulz (1982a,b), Kuhs (1983, 1988, 1992) and Scheringer (1985).

1.9.2.1. Tensorial properties of (quasi)moments and cumulants

By separating the powers of \mathbf{Q} and \mathbf{u} , one obtains in equations (1.9.2.4), (1.9.2.5) and (1.9.2.7) the higher-order displacement tensors in the form of moments, cumulants or quasimoments, which we shall denote in a general way as $b^{ijk\dots}$; note that b^{ij} is identical to β^{ij} . They transform on a change of the direct-lattice base according to

$$b^{pqr\dots} = A_{pi} A_{qj} A_{rk} \dots b^{ijk\dots}. \quad (1.9.2.8)$$

The higher-order displacement tensors are fully symmetric with respect to the interchange of any of their indices; in the nomenclature of Jahn (1949), their tensor symmetry thus is $[b^N]$. The number of independent tensor coefficients depends on the site symmetry of the atom and is tabulated in Sirotnin (1960) as well as in Tables 1.9.3.1–1.9.3.6. For triclinic site symmetry, the numbers of independent tensor coefficients are 1, 3, 6, 10, 15, 21 and 28 for the zeroth to sixth order. Symmetry may further

reduce the number of independent coefficients, as discussed in Section 1.9.3.

In many least-squares programs for structure refinement, the atomic displacement parameters are used in a dimensionless form [as given in (1.9.1.4) for the harmonic case]. These dimensionless quantities may be transformed according to

$$U^{ijk\dots n} = [N!/(2\pi)^N] b^{ijk\dots n} |\mathbf{a}^i| |\mathbf{a}^j| |\mathbf{a}^k| \dots |\mathbf{a}^n| \quad (1.9.2.9)$$

(no summation) into quantities of units \AA^N (or pm^N); \mathbf{a}^i etc. are reciprocal-lattice vectors. Nowadays, the published structural results usually quote U^{ij} for the second-order terms; it would be good practice to publish only dimensioned atomic displacements for the higher-order terms as well.

1.9.2.2. Contraction, expansion and invariants of atomic displacement tensors

Anisotropic or higher-order atomic displacement tensors may contain a wealth of information. However, this information content is not always worth publishing in full, either because the physical meaning is not of importance or the significance is only marginal. Quantities of higher significance or better clarity are obtained by an operation known as tensor contraction. Likewise, lower-order terms may be expanded to higher order to impose certain (chemically implied) symmetries on the displacement tensors or to provide initial parameters for least-squares refinements. A contraction is obtained by multiplying the contravariant tensor components (referring to the real-space basis vectors) with the covariant components of the real-space metric tensor g_{ij} ; for further details on tensor contraction, see Section 1.1.3.3.3. In the general case of atomic displacement tensors of (even) rank N , one obtains

$${}^N I_0 = g_{ij} g_{kl} \dots g_{mn} b^{ijkl\dots mn}. \quad (1.9.2.10)$$

${}^N I_0$ is called the trace of a tensor of rank N and is a scalar invariant; it is given in units of length^N and provides an easily interpretable quantity: In the case of ${}^4 I_0$, a positive sign indicates that the corresponding (real-space) p.d.f. is peaked, a negative sign indicates flatness of the p.d.f. The larger ${}^N I_0$, the stronger the deviation from a Gaussian p.d.f. provoked by the atomic displacements of order N . The frequently quoted isotropic equivalent U value U_{eq} is also obtained by this contraction process. Noting that U^{ij} may be expressed in terms of b^{ij} ($= \beta^{ij}$) according to (1.9.2.9) and that the trace of the matrix \mathbf{U} is given as $\text{Tr}(\mathbf{U}) = (2\pi^2)^{-1.2} I_0$, one obtains

$$U_{\text{eq}} = (1/3)(2\pi^2)^{-1} g_{ij} b^{ij}. \quad (1.9.2.11)$$

Note that in all non-orthogonal bases, $\text{Tr}(\mathbf{U}) \neq U^{11} + U^{22} + U^{33}$. In older literature, the isotropic equivalent displacement parameter is often quoted as B_{eq} , which is related to U_{eq} through the identity $B_{\text{eq}} = 8\pi^2 U_{\text{eq}}$. The use of B_{eq} is now discouraged (Trueblood *et al.*, 1996). Higher atomic displacement tensors of odd rank N may be reduced to simple vectors \mathbf{v} by the following contraction:

$${}^N v^i = g_{jk} g_{lm} \dots g_{np} b^{ijklm\dots np}. \quad (1.9.2.12)$$

where v^1 is the 23 trace etc. ${}^N v^i$ is sometimes called a vector invariant, as it can be uniquely assigned to the tensor in question (Pach & Frey, 1964) and its units are length^{N-1} . The vector \mathbf{v} is oriented along the line of maximum projected asymmetry for a given atom and vanishes for atoms with positional parameters fixed by symmetry; Johnson (1970) has named a vector closely related to ${}^3 \mathbf{v}$ the vector of skew divergence. The calculation of \mathbf{v} is useful as it gives the direction of the largest antisymmetric displacements contained in odd-rank higher-order thermal-motion tensors.

1. TENSORIAL ASPECTS OF PHYSICAL PROPERTIES

Table 1.9.3.1. Site-symmetry table giving key to Tables 1.9.3.2 to 1.9.3.6 for restrictions on the symmetry of various thermal-motion tensors

Hex denotes hexagonal axes.

| Point symmetry at special position | | | | Position x, y, z | Cross-reference for tensor tables | | | | | |
|------------------------------------|-----|------------------------|---------------------|-----------------------|-----------------------------------|-----|-----|-----|-----|-----|
| Symmetry axes | | Point-group generators | | | 1B | 1C | 1D | 1E | 1F | |
| $m\bar{3}m$ | | 4[0, 0, 1] | 3[1, 1, 1] | $\bar{1}$ | 0, 0, 0 | B1 | C0 | D1 | E0 | F1 |
| $\bar{4}3m$ | | 4[0, 0, 1] | 3[1, 1, 1] | | 0, 0, 0 | B1 | C1 | D1 | E1 | F1 |
| 432 | | 4[0, 0, 1] | 3[1, 1, 1] | | 0, 0, 0 | B1 | C0 | D1 | E0 | F1 |
| $m\bar{3}$ | | 3[1, 1, 1] | 2[0, 0, 1] | $\bar{1}$ | 0, 0, 0 | B1 | C0 | D1 | E0 | F2 |
| 23 | | 3[1, 1, 1] | 2[0, 0, 1] | | 0, 0, 0 | B1 | C1 | D1 | E1 | F2 |
| $6/mmm$ | Hex | 6[0, 0, 1] | 2[1, 0, 0] | $\bar{1}$ | 0, 0, 0 | B9 | C0 | D2 | E0 | F3 |
| $\bar{6}m2$ | Hex | 6[0, 0, 1] | 2[1, 0, 0] | | 0, 0, 0 | B9 | C9 | D2 | E5 | F3 |
| $\bar{6}m2$ | Hex | 6[0, 0, 1] | 2[1, 2, 0] | | 0, 0, 0 | B9 | C10 | D2 | E6 | F3 |
| $6mm$ | Hex | 6[0, 0, 1] | 2[1, 0, 0] | | 0, 0, z | B9 | C19 | D2 | E17 | F3 |
| 622 | Hex | 6[0, 0, 1] | 2[1, 0, 0] | | 0, 0, 0 | B9 | C0 | D2 | E0 | F4 |
| $6/m$ | Hex | 6[0, 0, 1] | $\bar{1}$ | | 0, 0, 0 | B9 | C0 | D2 | E0 | F4 |
| $\bar{6}$ | Hex | 6[0, 0, 1] | | | 0, 0, 0 | B9 | C20 | D2 | E24 | F4 |
| 6 | Hex | 6[0, 0, 1] | | | 0, 0, z | B9 | C19 | D2 | E17 | F4 |
| $4/mmm$ | | 4[0, 0, 1] | 2[1, 0, 0] | $\bar{1}$ | 0, 0, 0 | B2 | C0 | D3 | E0 | F5 |
| $4/mmm$ | | 4[0, 1, 0] | 2[0, 0, 1] | $\bar{1}$ | 0, 0, 0 | B3 | C0 | D4 | E0 | F6 |
| $4/mmm$ | | 4[1, 0, 0] | 2[0, 1, 0] | $\bar{1}$ | 0, 0, 0 | B4 | C0 | D5 | E0 | F7 |
| $\bar{4}2m$ | | 4[0, 0, 1] | 2[1, 0, 0] | | 0, 0, 0 | B2 | C1 | D3 | E7 | F5 |
| $\bar{4}2m$ | | 4[0, 0, 1] | 2[1, 1, 0] | | 0, 0, 0 | B2 | C2 | D3 | E8 | F5 |
| $\bar{4}2m$ | | 4[0, 1, 0] | 2[0, 0, 1] | | 0, 0, 0 | B3 | C1 | D4 | E9 | F6 |
| $\bar{4}2m$ | | 4[0, 1, 0] | 2[1, 0, 1] | | 0, 0, 0 | B3 | C3 | D4 | E10 | F6 |
| $\bar{4}2m$ | | 4[1, 0, 0] | 2[0, 1, 0] | | 0, 0, 0 | B4 | C1 | D5 | E11 | F7 |
| $\bar{4}2m$ | | 4[1, 0, 0] | 2[0, 1, 1] | | 0, 0, 0 | B4 | C4 | D5 | E12 | F7 |
| $4mm$ | | 4[0, 0, 1] | 2[1, 0, 0] | | 0, 0, z | B2 | C13 | D3 | E25 | F5 |
| $4mm$ | | 4[0, 1, 0] | 2[0, 0, 1] | | 0, y , 0 | B3 | C14 | D4 | E26 | F6 |
| $4mm$ | | 4[1, 0, 0] | 2[0, 1, 0] | | x , 0, 0 | B4 | C15 | D5 | E27 | F7 |
| 422 | | 4[0, 0, 1] | 2[1, 0, 0] | | 0, 0, 0 | B2 | C0 | D3 | E2 | F5 |
| 422 | | 4[0, 1, 0] | 2[0, 0, 1] | | 0, 0, 0 | B3 | C0 | D4 | E3 | F6 |
| 422 | | 4[1, 0, 0] | 2[0, 1, 0] | | 0, 0, 0 | B4 | C0 | D5 | E4 | F7 |
| $4/m$ | | 4[0, 0, 1] | $\bar{1}$ | | 0, 0, 0 | B2 | C0 | D12 | E0 | F14 |
| $4/m$ | | 4[0, 1, 0] | $\bar{1}$ | | 0, 0, 0 | B3 | C0 | D13 | E0 | F15 |
| $4/m$ | | 4[1, 0, 0] | $\bar{1}$ | | 0, 0, 0 | B4 | C0 | D14 | E0 | F16 |
| $\bar{4}$ | | 4[0, 0, 1] | | | 0, 0, 0 | B2 | C16 | D12 | E28 | F14 |
| $\bar{4}$ | | 4[0, 1, 0] | | | 0, 0, 0 | B3 | C17 | D13 | E29 | F15 |
| $\bar{4}$ | | 4[1, 0, 0] | | | 0, 0, 0 | B4 | C18 | D14 | E30 | F16 |
| 4 | | 4[0, 0, 1] | | | 0, 0, z | B2 | C13 | D12 | E31 | F14 |
| 4 | | 4[0, 1, 0] | | | 0, y , 0 | B3 | C14 | D13 | E32 | F15 |
| 4 | | 4[1, 0, 0] | | | x , 0, 0 | B4 | C15 | D14 | E33 | F16 |
| $\bar{3}m$ | | 3[1, 1, 1] | 2[1, $\bar{1}$, 0] | $\bar{1}$ | 0, 0, 0 | B5 | C0 | D6 | E0 | F8 |
| $\bar{3}m$ | | 3[1, 1, 1] | 2[1, $\bar{1}$, 0] | $\bar{1}$ | 0, 0, 0 | B6 | C0 | D7 | E0 | F9 |
| $\bar{3}m$ | | 3[1, $\bar{1}$, 1] | 2[1, 1, 0] | $\bar{1}$ | 0, 0, 0 | B7 | C0 | D8 | E0 | F10 |
| $\bar{3}m$ | | 3[1, 1, 1] | 2[1, 1, 0] | $\bar{1}$ | 0, 0, 0 | B8 | C0 | D9 | E0 | F11 |
| $\bar{3}m$ | Hex | 3[0, 0, 1] | 2[1, 0, 0] | $\bar{1}$ | 0, 0, 0 | B9 | C0 | D10 | E0 | F12 |
| $\bar{3}m$ | Hex | 3[0, 0, 1] | 2[1, 2, 0] | $\bar{1}$ | 0, 0, 0 | B9 | C0 | D11 | E0 | F13 |
| $3m$ | | 3[1, 1, 1] | 2[1, $\bar{1}$, 0] | | x, x, x | B5 | C33 | D6 | E34 | F8 |
| $3m$ | | 3[1, 1, $\bar{1}$] | 2[1, $\bar{1}$, 0] | | x, x, \bar{x} | B6 | C34 | D7 | E35 | F9 |
| $3m$ | | 3[1, $\bar{1}$, 1] | 2[1, 1, 0] | | x, \bar{x}, x | B7 | C35 | D8 | E36 | F10 |
| $3m$ | | 3[1, 1, 1] | 2[1, 1, 0] | | \bar{x}, x, x | B8 | C36 | D9 | D37 | F11 |
| $3m$ | Hex | 3[0, 0, 1] | 2[1, 0, 0] | | 0, 0, z | B9 | C37 | D10 | E38 | F12 |
| $3m$ | Hex | 3[0, 0, 1] | 2[1, 2, 0] | | 0, 0, z | B9 | C38 | D11 | E39 | F13 |
| 32 | | 3[1, 1, 1] | 2[1, $\bar{1}$, 0] | | 0, 0, 0 | B5 | C5 | D6 | E13 | F8 |
| 32 | | 3[1, 1, $\bar{1}$] | 2[1, $\bar{1}$, 0] | | 0, 0, 0 | B6 | C6 | D7 | E14 | F9 |
| 32 | | 3[1, $\bar{1}$, 1] | 2[1, 1, 0] | | 0, 0, 0 | B7 | C7 | D8 | E15 | F10 |
| 32 | | 3[1, 1, 1] | 2[1, 1, 0] | | 0, 0, 0 | B8 | C8 | D9 | E16 | F11 |
| 32 | Hex | 3[0, 0, 1] | 2[1, 0, 0] | | 0, 0, 0 | B9 | C9 | D10 | E5 | F12 |
| 32 | Hex | 3[0, 0, 1] | 2[1, 2, 0] | | 0, 0, 0 | B9 | C10 | D11 | E6 | F13 |
| $\bar{3}$ | | 3[1, 1, 1] | | | 0, 0, 0 | B5 | C0 | D15 | E0 | F17 |
| $\bar{3}$ | | 3[1, 1, $\bar{1}$] | | | 0, 0, 0 | B6 | C0 | D16 | E0 | F18 |
| $\bar{3}$ | | 3[1, $\bar{1}$, 1] | | | 0, 0, 0 | B7 | C0 | D17 | E0 | F19 |
| $\bar{3}$ | | 3[1, 1, 1] | | | 0, 0, 0 | B8 | C0 | D18 | E0 | F20 |
| $\bar{3}$ | Hex | 3[0, 0, 1] | | | 0, 0, 0 | B9 | C0 | D19 | E0 | F21 |
| 3 | | 3[1, 1, 1] | | | x, x, x | B5 | C54 | D15 | E58 | F17 |
| 3 | | 3[1, 1, $\bar{1}$] | | | x, x, \bar{x} | B6 | C55 | D16 | E59 | F18 |
| 3 | | 3[1, 1, 1] | | | x, \bar{x}, x | B7 | C56 | D17 | E60 | F19 |
| 3 | Hex | 3[1, 1, 1] | | | \bar{x}, x, x | B8 | C57 | D18 | E61 | F20 |
| 3 | | 3[0, 0, 1] | | | 0, 0, z | B9 | C58 | D19 | E62 | F21 |
| mmm | | 2[0, 0, 1] | 2[1, 0, 0] | $\bar{1}$ | 0, 0, 0 | B10 | C0 | D20 | E0 | F22 |
| mmm | | 2[0, 0, 1] | 2[1, 1, 0] | $\bar{1}$ | 0, 0, 0 | B11 | C0 | D21 | E0 | F23 |
| mmm | | 2[0, 1, 0] | 2[1, 0, 1] | $\bar{1}$ | 0, 0, 0 | B12 | C0 | D22 | E0 | F24 |
| mmm | | 2[1, 0, 0] | 2[0, 1, 1] | $\bar{1}$ | 0, 0, 0 | B13 | C0 | D23 | E0 | F25 |
| mmm | Hex | 2[0, 0, 1] | 2[1, 0, 0] | $\bar{1}$ | 0, 0, 0 | B14 | C0 | D24 | E0 | F26 |
| mmm | Hex | 2[0, 0, 1] | 2[1, 1, 0] | $\bar{1}$ | 0, 0, 0 | B11 | C0 | D21 | E0 | F23 |
| mmm | Hex | 2[0, 0, 1] | 2[0, 1, 0] | $\bar{1}$ | 0, 0, 0 | B15 | C0 | D25 | E0 | F27 |
| mm | | 2[0, 0, 1] | 2[1, 0, 0] | | 0, 0, z | B10 | C21 | D20 | E40 | F22 |
| mm | | 2[0, 0, 1] | 2[1, 1, 0] | | 0, 0, z | B11 | C22 | D21 | E41 | F23 |
| mm | | 2[0, 1, 0] | 2[0, 0, 1] | | 0, y , 0 | B10 | C23 | D20 | E42 | F22 |
| mm | | 2[0, 1, 0] | 2[1, 0, 1] | | 0, y , 0 | B12 | C24 | D22 | E43 | F24 |
| mm | | 2[1, 0, 0] | 2[0, 0, 1] | | x , 0, 0 | B10 | C25 | D20 | E44 | F22 |

1.9. ATOMIC DISPLACEMENT PARAMETERS

Table 1.9.3.1 (cont.)

| Point symmetry at special position | | | Position x, y, z | Cross-reference for tensor tables | | | | | |
|------------------------------------|------------------------|--------------------------|-----------------------|-----------------------------------|-----|-----|-----|-----|-----|
| Symmetry axes | Point-group generators | | | 1B | 1C | 1D | 1E | 1F | |
| mm | | $2[1, 0, 0]$ | $\bar{2}[0, 1, 1]$ | $x, 0, 0$ | B13 | C26 | D23 | E45 | F25 |
| mm | | $2[1, 1, 0]$ | $\bar{2}[0, 0, 1]$ | $x, x, 0$ | B11 | C27 | D21 | E46 | F23 |
| mm | | $2[1, \bar{1}, 0]$ | $\bar{2}[0, 0, 1]$ | $x, \bar{x}, 0$ | B11 | C28 | D21 | E47 | F23 |
| mm | | $2[1, 0, 1]$ | $\bar{2}[0, 1, 0]$ | $x, 0, x$ | B12 | C29 | D22 | E48 | F24 |
| mm | | $2[1, 0, \bar{1}]$ | $\bar{2}[0, 1, 0]$ | $x, 0, \bar{x}$ | B12 | C30 | D22 | E49 | F24 |
| mm | | $2[0, 1, 1]$ | $\bar{2}[1, 0, 0]$ | $0, y, y$ | B13 | C31 | D23 | E50 | F25 |
| mm | | $2[0, 1, \bar{1}]$ | $\bar{2}[1, 0, 0]$ | $0, y, \bar{y}$ | B13 | C32 | D23 | E51 | F25 |
| mm | Hex | $2[0, 0, 1]$ | $\bar{2}[1, 0, 0]$ | $0, 0, z$ | B14 | C40 | D24 | E52 | F26 |
| mm | Hex | $2[0, 0, 1]$ | $\bar{2}[1, 1, 0]$ | $0, 0, z$ | B11 | C22 | D21 | E41 | F23 |
| mm | Hex | $2[0, 0, 1]$ | $\bar{2}[1, 1, 0]$ | $0, 0, z$ | B15 | C39 | D25 | E53 | F27 |
| mm | Hex | $2[1, 0, 0]$ | $\bar{2}[0, 0, 1]$ | $x, 0, 0$ | B14 | C41 | D24 | E54 | F26 |
| mm | Hex | $2[2, 1, 0]$ | $\bar{2}[0, 0, 1]$ | $2x, x, 0$ | B15 | C42 | D25 | E55 | F27 |
| mm | Hex | $2[1, 1, 0]$ | $\bar{2}[0, 0, 1]$ | $x, x, 0$ | B11 | C27 | D21 | E46 | F23 |
| mm | Hex | $2[1, 2, 0]$ | $\bar{2}[0, 0, 1]$ | $x, 2x, 0$ | B14 | C43 | D24 | E56 | F26 |
| mm | Hex | $2[0, 1, 0]$ | $\bar{2}[0, 0, 1]$ | $0, y, 0$ | B15 | C44 | D25 | E57 | F27 |
| mm | Hex | $2[1, 1, 0]$ | $\bar{2}[0, 0, 1]$ | $x, \bar{x}, 0$ | B11 | C28 | D21 | E47 | F23 |
| 222 | | $2[0, 0, 1]$ | $\bar{2}[1, 0, 0]$ | $0, 0, 0$ | B10 | C1 | D20 | E18 | F22 |
| 222 | | $2[0, 0, 1]$ | $\bar{2}[1, 1, 0]$ | $0, 0, 0$ | B11 | C2 | D21 | E19 | F23 |
| 222 | | $2[0, 1, 0]$ | $\bar{2}[1, 0, 1]$ | $0, 0, 0$ | B12 | C3 | D22 | E20 | F24 |
| 222 | | $2[1, 0, 0]$ | $\bar{2}[0, 1, 1]$ | $0, 0, 0$ | B13 | C4 | D23 | E21 | F25 |
| 222 | Hex | $2[0, 0, 1]$ | $\bar{2}[1, 0, 0]$ | $0, 0, 0$ | B14 | C11 | D24 | E22 | F26 |
| 222 | Hex | $2[0, 0, 1]$ | $\bar{2}[1, 1, 0]$ | $0, 0, 0$ | B11 | C2 | D21 | E19 | F23 |
| 222 | Hex | $2[0, 0, 1]$ | $\bar{2}[0, 1, 0]$ | $0, 0, 0$ | B15 | C12 | D25 | E23 | F27 |
| 2/m | | $2[0, 0, 1]$ | $\bar{1}$ | $0, 0, 0$ | B16 | C0 | D26 | E0 | F28 |
| 2/m | | $2[0, 1, 0]$ | $\bar{1}$ | $0, 0, 0$ | B17 | C0 | D27 | E0 | F29 |
| 2/m | | $2[1, 0, 0]$ | $\bar{1}$ | $0, 0, 0$ | B18 | C0 | D28 | E0 | F30 |
| 2/m | | $2[1, 1, 0]$ | $\bar{1}$ | $0, 0, 0$ | B19 | C0 | D29 | E0 | F31 |
| 2/m | | $2[1, 1, 0]$ | $\bar{1}$ | $0, 0, 0$ | B20 | C0 | D30 | E0 | F32 |
| 2/m | | $2[1, 0, \bar{1}]$ | $\bar{1}$ | $0, 0, 0$ | B21 | C0 | D31 | E0 | F33 |
| 2/m | | $2[1, 0, \bar{1}]$ | $\bar{1}$ | $0, 0, 0$ | B22 | C0 | D32 | E0 | F34 |
| 2/m | | $2[0, 1, \bar{1}]$ | $\bar{1}$ | $0, 0, 0$ | B23 | C0 | D33 | E0 | F35 |
| 2/m | | $2[0, 1, \bar{1}]$ | $\bar{1}$ | $0, 0, 0$ | B24 | C0 | D34 | E0 | F36 |
| 2/m | Hex | $2[0, 0, 1]$ | $\bar{1}$ | $0, 0, 0$ | B16 | C0 | D26 | E0 | F28 |
| 2/m | Hex | $2[1, 0, 0]$ | $\bar{1}$ | $0, 0, 0$ | B25 | C0 | D35 | E0 | F37 |
| 2/m | Hex | $2[2, 1, 0]$ | $\bar{1}$ | $0, 0, 0$ | B26 | C0 | D36 | E0 | F38 |
| 2/m | Hex | $2[1, 1, 0]$ | $\bar{1}$ | $0, 0, 0$ | B19 | C0 | D29 | E0 | F31 |
| 2/m | Hex | $2[1, 2, 0]$ | $\bar{1}$ | $0, 0, 0$ | B27 | C0 | D37 | E0 | F39 |
| 2/m | Hex | $2[0, 1, 0]$ | $\bar{1}$ | $0, 0, 0$ | B28 | C0 | D38 | E0 | F40 |
| 2/m | Hex | $2[1, \bar{1}, 0]$ | $\bar{1}$ | $0, 0, 0$ | B20 | C0 | D30 | E0 | F32 |
| m | | $\bar{2}[0, 1, 0]$ | $2[1, 0, 1]$ | $x, 0, z$ | B17 | C64 | D27 | E77 | F29 |
| m | | $\bar{2}[1, 0, 0]$ | $2[0, 1, 1]$ | $0, y, z$ | B18 | C65 | D28 | E78 | F30 |
| m | | $\bar{2}[1, 1, 0]$ | $2[0, 1, 1]$ | x, \bar{x}, z | B19 | C66 | D29 | E79 | F31 |
| m | | $\bar{2}[1, \bar{1}, 0]$ | $2[0, 1, 1]$ | x, x, z | B20 | C67 | D30 | E80 | F32 |
| m | | $\bar{2}[1, 0, 1]$ | $2[0, 1, 1]$ | x, y, \bar{x} | B21 | C68 | D31 | E81 | F33 |
| m | | $\bar{2}[1, 0, \bar{1}]$ | $2[0, 1, 1]$ | x, y, x | B22 | C69 | D32 | E82 | F34 |
| m | | $\bar{2}[0, 1, 1]$ | $2[0, 1, 1]$ | x, y, \bar{y} | B23 | C70 | D33 | E83 | F35 |
| m | | $\bar{2}[0, 1, \bar{1}]$ | $2[0, 1, 1]$ | x, y, y | B24 | C71 | D34 | E84 | F36 |
| m | Hex | $\bar{2}[0, 0, 1]$ | $2[1, 0, 0]$ | $x, y, 0$ | B16 | C63 | D26 | E76 | F28 |
| m | Hex | $\bar{2}[1, 0, 0]$ | $2[0, 1, 0]$ | $x, 2x, z$ | B25 | C72 | D35 | E85 | F37 |
| m | Hex | $\bar{2}[2, 1, 0]$ | $2[0, 1, 0]$ | $0, y, z$ | B26 | C73 | D36 | E86 | F38 |
| m | Hex | $\bar{2}[1, 1, 0]$ | $2[0, 1, 0]$ | x, \bar{x}, z | B19 | C66 | D29 | E79 | F31 |
| m | Hex | $\bar{2}[1, 2, 0]$ | $2[0, 1, 0]$ | $x, 0, z$ | B27 | C74 | D37 | E87 | F39 |
| m | Hex | $\bar{2}[0, 1, 0]$ | $2[0, 1, 0]$ | $2x, x, z$ | B28 | C75 | D38 | E88 | F40 |
| m | Hex | $\bar{2}[1, 1, 0]$ | $2[0, 1, 0]$ | x, x, z | B20 | C67 | D30 | E80 | F32 |
| 2 | | $2[0, 0, 1]$ | $\bar{1}$ | $0, 0, z$ | B16 | C45 | D26 | E63 | F28 |
| 2 | | $2[0, 1, 0]$ | $\bar{1}$ | $0, y, 0$ | B17 | C46 | D27 | E64 | F29 |
| 2 | | $2[1, 0, 0]$ | $\bar{1}$ | $x, 0, 0$ | B18 | C47 | D28 | E65 | F30 |
| 2 | | $2[1, 1, 0]$ | $\bar{1}$ | $x, x, 0$ | B19 | C48 | D29 | E66 | F31 |
| 2 | | $2[1, \bar{1}, 0]$ | $\bar{1}$ | $x, \bar{x}, 0$ | B20 | C49 | D30 | E67 | F32 |
| 2 | | $2[1, 0, 1]$ | $\bar{1}$ | $x, 0, x$ | B21 | C50 | D31 | E68 | F33 |
| 2 | | $2[1, 0, \bar{1}]$ | $\bar{1}$ | $x, 0, \bar{x}$ | B22 | C51 | D32 | E69 | F34 |
| 2 | | $2[0, 1, 1]$ | $\bar{1}$ | $0, y, y$ | B23 | C52 | D33 | E70 | F35 |
| 2 | | $2[0, 1, \bar{1}]$ | $\bar{1}$ | $0, y, \bar{y}$ | B24 | C53 | D34 | E71 | F36 |
| 2 | Hex | $2[0, 0, 1]$ | $\bar{1}$ | $0, 0, z$ | B16 | C45 | D26 | E63 | F28 |
| 2 | Hex | $2[1, 0, 0]$ | $\bar{1}$ | $x, 0, 0$ | B25 | C59 | D35 | E72 | F37 |
| 2 | Hex | $2[2, 1, 0]$ | $\bar{1}$ | $2x, x, 0$ | B26 | C60 | D36 | E73 | F38 |
| 2 | Hex | $2[1, 1, 0]$ | $\bar{1}$ | $x, x, 0$ | B19 | C48 | D29 | E66 | F31 |
| 2 | Hex | $2[1, 2, 0]$ | $\bar{1}$ | $x, 2x, 0$ | B27 | C61 | D37 | E74 | F39 |
| 2 | Hex | $2[0, 1, 0]$ | $\bar{1}$ | $0, y, 0$ | B28 | C62 | D38 | E75 | F40 |
| 2 | Hex | $2[1, \bar{1}, 0]$ | $\bar{1}$ | $x, \bar{x}, 0$ | B20 | C49 | D30 | E67 | F32 |
| $\bar{1}$ | | $\bar{1}$ | 1 | $0, 0, 0$ | B29 | C0 | D39 | E0 | F41 |
| $\bar{1}$ | Hex | $\bar{1}$ | 1 | $0, 0, 0$ | B29 | C0 | D39 | E0 | F41 |
| 1 | | 1 | 1 | x, y, z | B29 | C76 | D39 | E89 | F41 |
| 1 | Hex | 1 | 1 | x, y, z | B29 | C76 | D39 | E89 | F41 |

1. TENSORIAL ASPECTS OF PHYSICAL PROPERTIES

Atomic displacement tensors may also be partially contracted or expanded; rules for these operations are found in Kuhs (1992).

1.9.3. Site-symmetry restrictions

Atoms (or molecules) situated on special positions of a space group exhibit (time-space averaged) probability distributions with a symmetry corresponding to the site symmetry. The p.d.f.'s describing these distributions contain the atomic displacement tensors. The displacement tensors enter into the structure-factor equation, which is the Fourier transform of the scattering density of the unit cell, *via* the atomic Debye–Waller factor, which is the Fourier transform of the atomic p.d.f. (see Chapter 1.2 of *IT B*). As discussed above, the tensor is fully symmetric with respect to the interchange of indices (*inner symmetry*). The site-symmetry restrictions (*outer symmetry*) of atomic displacement tensors of rank 2 are given in Chapter 8.3 of *IT C* (1999), where the tabulation of the constraints on the tensor coefficients are quoted for every Wyckoff position in each space group. Here the constraints for atomic displacement tensors of ranks 2, 3, 4, 5 and 6 for any crystallographic site symmetry are tabulated; some restrictions for tensors of rank 7 and 8 can be found in Kuhs (1984). To use these tables, first the site symmetry has to be identified. The site symmetries are given in *IT A* (2002) for the first equipoint of every Wyckoff position in each space group. The tabulated constraints may be introduced in least-squares refinements (some programs have the constraints of second-order displacement tensor components already imbedded). It should also be remembered that, due to arbitrary phase shifts in the structure-factor equation in a least-squares refinement of a noncentrosymmetric structure, for all odd-order tensors *one* coefficient corresponding to a nonzero entry for the corresponding acentric space group has to be kept fixed (in very much the same way as for positional parameters); *e.g.* the term b^{123} has to be kept fixed for *one* atom for all refinements in all space groups belonging to the point groups $43m$ or 23 , while all other terms b^{ijk} are allowed to vary freely for all atoms (Hazell & Willis, 1978). Even if this is strictly true only for the Edgeworth-series expansion, it also holds in practice for the Gram–Charlier case (Kuhs, 1992).

1.9.3.1. Calculation procedures

Levy (1956) and Peterse & Palm (1966) have given algorithms for determining the constraints on anisotropic displacement tensor coefficients, which are also applicable to higher-order tensors. The basic idea is that a tensor transformation according to the symmetry operation of the site symmetry under consideration (represented by the point-group generators) should leave the tensor unchanged. For symmetries higher than the identity 1, this only holds true if some of the tensor coefficients are either zero or interrelated. The constraints may be obtained explicitly from solving the homogeneous system of equations of tensor transformations (with one equation for each coefficient).

1.9.3.2. Key to tables

After identification of the site symmetry of the atomic site under consideration, the entry point (cross-reference) for the tabulation of the displacement tensors of a given rank (Tables 1.9.3.2–1.9.3.6) needs to be looked up in Table 1.9.3.1. The line entry corresponding to the cross-reference number in Tables 1.9.3.2–1.9.3.6 holds the information on the constraints imposed by the outer symmetry on the tensor coefficients. The order of assignment of independency of the coefficients is as for increasing indices of the coefficients (first 1, then 2, then 3, where 1, 2 and 3 refer to the three crystallographic axes), except for the unmixed coefficients, which have highest priority in every case; this order of priority is the same as the order in the tables reading from left to right. For better readability, each coefficient is assigned a letter (or 0 if the component is equal to zero by symmetry). Constraints

Table 1.9.3.2. Symmetry restrictions on coefficients in second-order tensors

| Cross-reference | No. of independent variables | Symbols and coefficient indices | | | | | |
|-----------------|------------------------------|---------------------------------|------------|------------|------------|------------|------------|
| | | A | B | C | D | E | F |
| | | (1) (1) | (2) (2) | (3) (3) | (1) (2) | (1) (3) | (2) (3) |
| B1 | 1 | A | A | A | 0 | 0 | 0 |
| B2 | 2 | A | A | C | 0 | 0 | 0 |
| B3 | 2 | A | B | A | 0 | 0 | 0 |
| B4 | 2 | A | B | B | 0 | 0 | 0 |
| B5 | 2 | A | A | A | D | D | D |
| B6 | 2 | A | A | A | D | −D | −D |
| B7 | 2 | A | A | A | D | −D | D |
| B8 | 2 | A | A | A | D | D | −D |
| B9 | 2 | A | A | C | A/2 | 0 | 0 |
| B10 | 3 | A | B | C | 0 | 0 | 0 |
| B11 | 3 | A | A | C | D | 0 | 0 |
| B12 | 3 | A | B | A | 0 | E | 0 |
| B13 | 3 | A | B | B | 0 | 0 | F |
| B14 | 3 | A | B | C | B/2 | 0 | 0 |
| B15 | 3 | A | B | C | A/2 | 0 | 0 |
| B16 | 4 | A | B | C | D | 0 | 0 |
| B17 | 4 | A | B | C | 0 | E | 0 |
| B18 | 4 | A | B | C | 0 | 0 | F |
| B19 | 4 | A | A | C | D | E | −E |
| B20 | 4 | A | A | C | D | E | E |
| B21 | 4 | A | B | A | D | E | −D |
| B22 | 4 | A | B | A | D | E | D |
| B23 | 4 | A | B | B | D | −D | F |
| B24 | 4 | A | B | B | D | D | F |
| B25 | 4 | A | B | C | B/2 | E | 2E |
| B26 | 4 | A | B | C | A/2 | 0 | F |
| B27 | 4 | A | B | C | B/2 | E | 0 |
| B28 | 4 | A | B | C | A/2 | E | E/2 |
| B29 | 6 | A | B | C | D | E | F |

thus read as algebraic relations between letter variables. Some more complicated constraint relations are quoted as footnotes to the tables.

1.9.4. Graphical representation

Atomic displacement tensors (ADTs) described by their tensor coefficients may be represented graphically to clarify their physical meaning. Different graphical representations exist and will be discussed separately for second- and higher-order tensors in the following.

1.9.4.1. Representation surfaces of second-order ADTs

Numerous examples of graphical representations of thermal-motion tensors (or, more generally speaking, atomic displacement tensors) have appeared in the literature since the early days of the computer program *ORTEP* written by C. K. Johnson (1965), yet the equal-probability surface usually displayed is only one of the possible representations of a second-order atomic displacement tensor. Representation surfaces are usually calculated in a Cartesian coordinate system. Accordingly, one has to transform the second-order ADT \mathbf{b} into \mathbf{U}_C described in a Cartesian frame:

$$\mathbf{U}_C = (2\pi^2)^{-1} \mathbf{F}^T \mathbf{b} \mathbf{F}. \quad (1.9.4.1)$$

The transformation matrix depends on the choice of Cartesian axes \mathbf{e}_i with respect to the reciprocal-cell axes \mathbf{a}^i (or equally well with respect to the direct axes \mathbf{a}_i). Choosing \mathbf{e}_1 along \mathbf{a}^1 , \mathbf{e}_2 in the $\mathbf{a}^1\mathbf{a}^2$ plane and \mathbf{e}_3 completing the right-handed set, one obtains for the transformation matrix \mathbf{F} (see also Willis & Pryor, 1975)

$$\mathbf{F} = \begin{pmatrix} 1/a^1 & a^2 \cos \gamma^* & a^3 \cos \beta^* \\ 0 & a^2 \sin \gamma^* & -a^3 \sin \beta^* \cos \alpha \\ 0 & 0 & 1/a_3 \end{pmatrix}. \quad (1.9.4.2)$$

Clearly, there is an infinite number of possible choices for relating a Cartesian frame to a crystallographic coordinate

1.9. ATOMIC DISPLACEMENT PARAMETERS

Table 1.9.3.3. Symmetry restrictions on coefficients in third-rank symmetric polar tensors

| Cross-reference | No. of independent variables | Symbols and coefficient indices | | | | | | | | | |
|-----------------|------------------------------|---------------------------------|-----|-----|------------|------------|-----|-----|-----|-----|-----|
| | | A | B | C | D | E | F | G | H | I | J |
| | | (1) | (2) | (3) | (1) | (1) | (1) | (1) | (2) | (2) | (1) |
| | | (1) | (2) | (3) | (1) | (2) | (1) | (3) | (2) | (3) | (2) |
| | | (1) | (2) | (3) | (2) | (2) | (3) | (3) | (3) | (3) | (3) |
| C0 | 0 | 0 | 0 | 0 | 0 | 0 | 0 | 0 | 0 | 0 | 0 |
| C1 | 1 | 0 | 0 | 0 | 0 | 0 | 0 | 0 | 0 | 0 | J |
| C2 | 1 | 0 | 0 | 0 | 0 | 0 | F | 0 | -F | 0 | 0 |
| C3 | 1 | 0 | 0 | 0 | D | 0 | 0 | 0 | 0 | -D | 0 |
| C4 | 1 | 0 | 0 | 0 | 0 | E | 0 | -E | 0 | 0 | 0 |
| C5 | 1 | 0 | 0 | 0 | D | -D | -D | D | D | -D | 0 |
| C6 | 1 | 0 | 0 | 0 | D | -D | D | D | -D | -D | 0 |
| C7 | 1 | 0 | 0 | 0 | D | D | D | -D | -D | -D | 0 |
| C8 | 1 | 0 | 0 | 0 | D | D | -D | -D | D | -D | 0 |
| C9 | 1 | 0 | 0 | 0 | D | D | 0 | 0 | 0 | 0 | 0 |
| C10 | 1 | A | -A | 0 | A/2 | -A/2 | 0 | 0 | 0 | 0 | 0 |
| C11 | 1 | 0 | 0 | 0 | 0 | 0 | F | 0 | 0 | 0 | F |
| C12 | 1 | 0 | 0 | 0 | 0 | 0 | 0 | 0 | H | 0 | H |
| C13 | 2 | 0 | 0 | C | 0 | 0 | F | 0 | F | 0 | 0 |
| C14 | 2 | 0 | B | 0 | D | 0 | 0 | 0 | 0 | D | 0 |
| C15 | 2 | A | 0 | 0 | 0 | E | 0 | E | 0 | 0 | 0 |
| C16 | 2 | 0 | 0 | 0 | 0 | 0 | F | 0 | -F | 0 | J |
| C17 | 2 | 0 | 0 | 0 | D | 0 | 0 | 0 | 0 | -D | J |
| C18 | 2 | 0 | 0 | 0 | 0 | E | 0 | -E | 0 | 0 | J |
| C19 | 2 | 0 | 0 | C | 0 | 0 | F | 0 | F | 0 | F/2 |
| C20 | 2 | A | -A | 0 | D | D - A | 0 | 0 | 0 | 0 | 0 |
| C21 | 3 | 0 | 0 | C | 0 | 0 | F | 0 | H | 0 | 0 |
| C22 | 3 | 0 | 0 | C | 0 | 0 | F | 0 | F | 0 | J |
| C23 | 3 | 0 | B | 0 | D | 0 | 0 | 0 | 0 | I | 0 |
| C24 | 3 | 0 | B | 0 | D | 0 | 0 | 0 | 0 | D | J |
| C25 | 3 | A | 0 | 0 | 0 | E | 0 | G | 0 | 0 | 0 |
| C26 | 3 | A | 0 | 0 | 0 | E | 0 | E | 0 | 0 | J |
| C27 | 3 | A | A | 0 | D | D | 0 | G | 0 | G | 0 |
| C28 | 3 | A | -A | 0 | D | -D | 0 | G | 0 | -G | 0 |
| C29 | 3 | A | 0 | A | 0 | E | F | F | E | 0 | 0 |
| C30 | 3 | A | 0 | -A | 0 | E | F | -F | -E | 0 | 0 |
| C31 | 3 | 0 | B | B | D | 0 | D | 0 | H | H | 0 |
| C32 | 3 | 0 | B | -B | D | 0 | -D | 0 | H | -H | 0 |
| C33 | 3 | A | A | A | D | D | D | D | D | D | J |
| C34 | 3 | A | A | -A | D | D | -D | D | -D | D | J |
| C35 | 3 | A | -A | A | D | -D | -D | -D | -D | D | J |
| C36 | 3 | A | -A | -A | D | -D | D | -D | D | D | J |
| C37 | 3 | A | -A | C | A/2 | -A/2 | F | 0 | F | 0 | F/2 |
| C38 | 3 | 0 | 0 | C | D | D | F | 0 | F | 0 | F/2 |
| C39 | 3 | 0 | 0 | C | 0 | 0 | F | 0 | H | 0 | F/2 |
| C40 | 3 | 0 | 0 | C | 0 | 0 | F | 0 | H | 0 | H/2 |
| C41 | 3 | A | 0 | 0 | D | D | 0 | G | 0 | 0 | 0 |
| C42 | 3 | A | B | 0 | A/2 | A/6 + 2B/3 | 0 | G | 0 | G/2 | 0 |
| C43 | 3 | A | B | 0 | B/6 + 2A/3 | B/2 | 0 | G | 0 | 2G | 0 |
| C44 | 3 | 0 | B | 0 | D | D | 0 | 0 | 0 | I | 0 |
| C45 | 4 | 0 | 0 | C | 0 | 0 | F | 0 | H | 0 | J |
| C46 | 4 | 0 | B | 0 | D | 0 | 0 | 0 | 0 | I | J |
| C47 | 4 | A | 0 | 0 | 0 | E | 0 | G | 0 | 0 | J |
| C48 | 4 | A | A | 0 | D | D | F | G | -F | G | 0 |
| C49 | 4 | A | -A | 0 | D | -D | F | G | -F | -G | 0 |
| C50 | 4 | A | 0 | A | D | E | F | F | E | -D | 0 |
| C51 | 4 | A | 0 | -A | D | E | F | -F | -E | -D | 0 |
| C52 | 4 | 0 | B | B | D | E | D | -E | H | H | 0 |
| C53 | 4 | 0 | B | -B | D | E | -D | -E | H | -H | 0 |
| C54 | 4 | A | A | A | D | E | E | D | D | E | J |
| C55 | 4 | A | A | -A | D | E | -E | D | -D | E | J |
| C56 | 4 | A | -A | A | D | E | E | -D | -D | -E | J |
| C57 | 4 | A | -A | -A | D | E | -E | -D | D | -E | J |
| C58 | 4 | A | -A | C | D | D - A | F | 0 | F | 0 | F/2 |
| C59 | 4 | A | 0 | 0 | D | D | F | G | 0 | 0 | F |
| C60 | 4 | A | B | 0 | A/2 | A/6 + 2B/3 | 0 | G | H | G/2 | H |
| C61 | 4 | A | B | 0 | B/6 + 2A/3 | B/2 | F | G | 0 | 2G | F |
| C62 | 4 | 0 | B | 0 | D | D | 0 | 0 | H | I | H |
| C63 | 6 | A | B | 0 | D | E | 0 | G | 0 | I | 0 |
| C64 | 6 | A | 0 | C | 0 | E | F | G | H | 0 | 0 |
| C65 | 6 | 0 | B | C | D | 0 | F | 0 | H | I | 0 |
| C66 | 6 | A | -A | C | D | -D | F | G | F | -G | J |
| C67 | 6 | A | A | C | D | D | F | G | F | G | J |
| C68 | 6 | A | B | -A | D | E | F | -F | -E | D | J |
| C69 | 6 | A | B | A | D | E | F | F | E | D | J |
| C70 | 6 | A | B | -B | D | E | -D | E | H | -H | J |
| C71 | 6 | A | B | B | D | E | D | E | H | H | J |
| C72 | 6 | A | B | C | B/6 + 2A/3 | B/2 | F | G | H | 2G | H/2 |
| C73 | 6 | 0 | B | C | D | D | F | 0 | H | I | F/2 |
| C74 | 6 | A | 0 | C | D | D | F | G | H | 0 | H/2 |
| C75 | 6 | A | B | C | A/2 | A/6 + 2B/3 | F | G | H | G/2 | F/2 |
| C76 | 10 | A | B | C | D | E | F | G | H | I | J |

1. TENSORIAL ASPECTS OF PHYSICAL PROPERTIES

Table 1.9.3.4. *Symmetry restrictions on coefficients in fourth-rank symmetric polar tensors*

(a) A–H.

| Cross-reference | No. of independent variables | Symbols and coefficient indices | | | | | | | |
|-----------------|------------------------------|---------------------------------|-----|-----|-----|-----|------------|-----|-----|
| | | A | B | C | D | E | F | G | H |
| | | (1) | (2) | (3) | (1) | (1) | (1) | (1) | (1) |
| | | (1) | (2) | (3) | (1) | (1) | (1) | (1) | (1) |
| | | (1) | (2) | (3) | (1) | (1) | (2) | (2) | (3) |
| | | (1) | (2) | (3) | (2) | (3) | (2) | (3) | (3) |
| D1 | 2 | A | A | A | 0 | 0 | F | 0 | F |
| D2 | 3 | A | A | C | A/2 | 0 | A/2 | 0 | H |
| D3 | 4 | A | A | C | 0 | 0 | F | 0 | H |
| D4 | 4 | A | B | A | 0 | 0 | F | 0 | H |
| D5 | 4 | A | B | B | 0 | 0 | F | 0 | F |
| D6 | 4 | A | A | A | D | D | F | G | F |
| D7 | 4 | A | A | A | D | −D | F | G | F |
| D8 | 4 | A | A | A | D | −D | F | G | F |
| D9 | 4 | A | A | A | D | D | F | G | F |
| D10 | 4 | A | A | C | A/2 | E | A/2 | E/2 | H |
| D11 | 4 | A | A | C | A/2 | 0 | A/2 | G | H |
| D12 | 5 | A | A | C | D | 0 | F | 0 | H |
| D13 | 5 | A | B | A | 0 | E | F | 0 | H |
| D14 | 5 | A | B | B | 0 | 0 | F | 0 | F |
| D15 | 5 | A | A | A | D | E | F | G | F |
| D16 | 5 | A | A | A | D | E | F | G | F |
| D17 | 5 | A | A | A | D | E | F | G | F |
| D18 | 5 | A | A | A | D | E | F | G | F |
| D19 | 5 | A | A | C | A/2 | E | A/2 | G | H |
| D20 | 6 | A | B | C | 0 | 0 | F | 0 | H |
| D21 | 6 | A | A | C | D | 0 | F | 0 | H |
| D22 | 6 | A | B | A | 0 | E | F | 0 | H |
| D23 | 6 | A | B | B | 0 | 0 | F | G | F |
| D24 | 6 | A | B | C | D | 0 | B/6 + 2D/3 | 0 | H |
| D25 | 6 | A | B | C | A/2 | 0 | F | 0 | H |
| D26 | 9 | A | B | C | D | 0 | F | 0 | H |
| D27 | 9 | A | B | C | 0 | E | F | 0 | H |
| D28 | 9 | A | B | C | 0 | 0 | F | G | H |
| D29 | 9 | A | A | C | D | E | F | G | H |
| D30 | 9 | A | A | C | D | E | F | G | H |
| D31 | 9 | A | B | A | D | E | F | G | H |
| D32 | 9 | A | B | A | D | E | F | G | H |
| D33 | 9 | A | B | B | D | −D | F | G | F |
| D34 | 9 | A | B | B | D | D | F | G | F |
| D35 | 9 | A | B | C | D | E | B/6 + 2D/3 | G | H |
| D36 | 9 | A | B | C | A/2 | 0 | F | G | H |
| D37 | 9 | A | B | C | D | E | B/6 + 2D/3 | G | H |
| D38 | 9 | A | B | C | A/2 | E | F | E/2 | H |
| D39 | 15 | A | B | C | D | E | F | G | H |

(b) I–P.

| Cross-reference | No. of independent variables | Symbols and coefficient indices | | | | | | |
|-----------------|------------------------------|---------------------------------|-------|-----|-----|-----|-----|-----|
| | | I | J | K | L | M | N | P |
| | | (1) | (1) | (1) | (1) | (2) | (2) | (2) |
| | | (2) | (2) | (2) | (3) | (2) | (2) | (3) |
| | | (2) | (2) | (3) | (3) | (2) | (3) | (3) |
| | | (2) | (3) | (3) | (3) | (3) | (3) | |
| D1 | 2 | 0 | 0 | 0 | 0 | 0 | F | 0 |
| D2 | 3 | A/2 | 0 | H/2 | 0 | 0 | H | 0 |
| D3 | 4 | 0 | 0 | 0 | 0 | 0 | H | 0 |
| D4 | 4 | 0 | 0 | 0 | 0 | 0 | F | 0 |
| D5 | 4 | 0 | 0 | 0 | 0 | 0 | N | 0 |
| D6 | 4 | D | G | G | D | D | F | D |
| D7 | 4 | D | G | −G | −D | −D | F | −D |
| D8 | 4 | D | −G | G | −D | D | F | D |
| D9 | 4 | D | −G | −G | D | −D | F | −D |
| D10 | 4 | A/2 | −E/2 | H/2 | 0 | −E | H | 0 |
| D11 | 4 | A/2 | G | H/2 | 0 | 0 | H | 0 |
| D12 | 5 | −D | 0 | 0 | 0 | 0 | H | 0 |
| D13 | 5 | 0 | 0 | 0 | −E | 0 | F | 0 |
| D14 | 5 | 0 | 0 | 0 | 0 | M | N | −M |
| D15 | 5 | E | G | G | D | D | F | E |
| D16 | 5 | −E | G | −G | −D | −D | F | −E |
| D17 | 5 | −E | −G | G | −D | D | F | E |
| D18 | 5 | E | −G | −G | D | −D | F | −E |
| D19 | 5 | A/2 | G − E | H/2 | 0 | −E | H | 0 |
| D20 | 6 | 0 | 0 | 0 | 0 | 0 | N | 0 |
| D21 | 6 | D | 0 | K | 0 | 0 | H | 0 |
| D22 | 6 | 0 | J | 0 | E | 0 | F | 0 |
| D23 | 6 | 0 | 0 | 0 | 0 | M | N | M |
| D24 | 6 | B/2 | 0 | K | 0 | 0 | 2K | 0 |

1.9. ATOMIC DISPLACEMENT PARAMETERS

Table 1.9.3.4 (cont.)

| Cross-reference | No. of independent variables | Symbols and coefficient indices | | | | | | |
|-----------------|------------------------------|---------------------------------|-------------|------|------|---------------|-----|------|
| | | I | J | K | L | M | N | P |
| | | (1) | (1) | (1) | (1) | (2) | (2) | (2) |
| | | (2) | (2) | (2) | (3) | (2) | (2) | (3) |
| | | (2) | (2) | (3) | (3) | (2) | (3) | (3) |
| D25 | 6 | $-A/4 + 3F/2$ | 0 | H/2 | 0 | 0 | N | 0 |
| D26 | 9 | I | 0 | K | 0 | 0 | N | 0 |
| D27 | 9 | 0 | J | 0 | L | 0 | N | 0 |
| D28 | 9 | 0 | 0 | 0 | 0 | M | N | P |
| D29 | 9 | D | $-G$ | K | L | $-E$ | H | $-L$ |
| D30 | 9 | D | G | K | L | E | H | L |
| D31 | 9 | I | J | $-G$ | E | $-I$ | F | $-D$ |
| D32 | 9 | I | J | G | E | I | F | D |
| D33 | 9 | I | J | $-J$ | $-I$ | M | N | M |
| D34 | 9 | I | J | J | I | M | N | M |
| D35 | 9 | B/2 | $-E/8 + 3G$ | K | L | $-E/4 + 6G$ | 2K | 2L |
| D36 | 9 | $-A/4 + 3F/2$ | G | H/2 | 0 | M | N | P |
| D37 | 9 | B/2 | G | K | L | 0 | 2K | 0 |
| D38 | 9 | $-A/4 + 3F/2$ | J | H/2 | L | $-E/4 + 3J/2$ | N | L/2 |
| D39 | 15 | I | J | K | L | M | N | P |

Table 1.9.3.5. Symmetry restrictions on coefficients in fifth-rank symmetric polar tensors

(a) A-K.

| Cross-reference | No. of independent coefficients | Symbols and coefficient indices | | | | | | | | | | |
|-----------------|---------------------------------|---------------------------------|------|------|-----|------|------|-----|------|---------|-----|------|
| | | A | B | C | D | E | F | G | H | I | J | K |
| | | 1 | 2 | 3 | 1 | 1 | 1 | 1 | 1 | 1 | 1 | 1 |
| | | 1 | 2 | 3 | 1 | 1 | 1 | 1 | 1 | 1 | 1 | 1 |
| | | 1 | 2 | 3 | 1 | 1 | 1 | 1 | 1 | 2 | 2 | 2 |
| E0 | 0 | 0 | 0 | 0 | 0 | 0 | 0 | 0 | 0 | 0 | 0 | 0 |
| E1 | 1 | 0 | 0 | 0 | 0 | 0 | 0 | G | 0 | 0 | 0 | 0 |
| E2 | 1 | 0 | 0 | 0 | 0 | 0 | 0 | G | 0 | 0 | 0 | 0 |
| E3 | 1 | 0 | 0 | 0 | 0 | 0 | 0 | G | 0 | 0 | 0 | 0 |
| E4 | 1 | 0 | 0 | 0 | 0 | 0 | 0 | 0 | 0 | 0 | 0 | 0 |
| E5 | 2 | 0 | 0 | 0 | D | 0 | D | 0 | 0 | D | 0 | K |
| E6 | 2 | A | $-A$ | 0 | A/2 | 0 | A/10 | 0 | H | $-A/10$ | 0 | H/2 |
| E7 | 2 | 0 | 0 | 0 | 0 | 0 | 0 | G | 0 | 0 | 0 | 0 |
| E8 | 2 | 0 | 0 | 0 | 0 | E | 0 | 0 | 0 | 0 | 0 | 0 |
| E9 | 2 | 0 | 0 | 0 | 0 | 0 | 0 | G | 0 | 0 | 0 | 0 |
| E10 | 2 | 0 | 0 | 0 | D | 0 | 0 | 0 | 0 | I | 0 | 0 |
| E11 | 2 | 0 | 0 | 0 | 0 | 0 | 0 | G | 0 | 0 | 0 | 0 |
| E12 | 2 | 0 | 0 | 0 | 0 | 0 | F | 0 | $-F$ | 0 | 0 | 0 |
| E13 | 2 | 0 | 0 | 0 | D | $-D$ | F | 0 | $-F$ | $-F$ | 0 | 0 |
| E14 | 2 | 0 | 0 | 0 | D | D | F | 0 | $-F$ | $-F$ | 0 | 0 |
| E15 | 2 | 0 | 0 | 0 | D | D | F | 0 | $-F$ | F | 0 | 0 |
| E16 | 2 | 0 | 0 | 0 | D | $-D$ | F | 0 | $-F$ | F | 0 | 0 |
| E17 | 3 | 0 | 0 | C | 0 | E | 0 | E/2 | 0 | 0 | E/2 | 0 |
| E18 | 3 | 0 | 0 | 0 | 0 | 0 | 0 | G | 0 | 0 | 0 | 0 |
| E19 | 3 | 0 | 0 | 0 | 0 | E | 0 | G | 0 | 0 | 0 | 0 |
| E20 | 3 | 0 | 0 | 0 | D | 0 | 0 | G | 0 | I | 0 | 0 |
| E21 | 3 | 0 | 0 | 0 | 0 | 0 | F | 0 | $-F$ | 0 | 0 | 0 |
| E22 | 3 | 0 | 0 | 0 | 0 | 0 | 0 | G | 0 | 0 | 2G | 0 |
| E23 | 3 | 0 | 0 | 0 | 0 | 0 | 0 | G | 0 | 0 | G | 0 |
| E24 | 4 | A | $-A$ | 0 | D | 0 | (1)† | 0 | H | (3)† | 0 | K |
| E25 | 4 | 0 | 0 | C | 0 | E | 0 | 0 | 0 | 0 | J | 0 |
| E26 | 4 | 0 | B | 0 | D | 0 | 0 | 0 | 0 | I | 0 | K |
| E27 | 4 | A | 0 | 0 | 0 | 0 | F | 0 | F | 0 | 0 | 0 |
| E28 | 4 | 0 | 0 | 0 | 0 | E | 0 | G | 0 | 0 | 0 | 0 |
| E29 | 4 | 0 | 0 | 0 | D | 0 | 0 | G | 0 | I | 0 | 0 |
| E30 | 4 | 0 | 0 | 0 | 0 | 0 | F | G | $-F$ | 0 | 0 | 0 |
| E31 | 5 | 0 | 0 | C | 0 | E | 0 | G | 0 | 0 | J | 0 |
| E32 | 5 | 0 | B | 0 | D | 0 | 0 | G | 0 | I | 0 | K |
| E33 | 5 | A | 0 | 0 | 0 | 0 | F | 0 | F | 0 | 0 | 0 |
| E34 | 5 | A | A | A | D | D | F | G | F | F | J | J |
| E35 | 5 | A | A | $-A$ | D | $-D$ | F | G | F | F | J | $-J$ |
| E36 | 5 | A | $-A$ | A | D | $-D$ | F | G | F | $-F$ | J | $-J$ |
| E37 | 5 | A | $-A$ | $-A$ | D | D | F | G | F | $-F$ | J | J |
| E38 | 5 | A | $-A$ | C | A/2 | E | A/10 | E/2 | H | $-A/10$ | E/2 | H/2 |
| E39 | 5 | 0 | 0 | C | D | E | D | E/2 | 0 | D | E/2 | K |
| E40 | 6 | 0 | 0 | C | 0 | E | 0 | 0 | 0 | 0 | J | 0 |
| E41 | 6 | 0 | 0 | C | 0 | E | 0 | G | 0 | 0 | J | 0 |
| E42 | 6 | 0 | B | 0 | D | 0 | 0 | 0 | 0 | I | 0 | K |
| E43 | 6 | 0 | B | 0 | D | 0 | 0 | G | 0 | I | 0 | K |
| E44 | 6 | A | 0 | 0 | 0 | 0 | F | 0 | H | 0 | 0 | 0 |
| E45 | 6 | A | 0 | 0 | 0 | 0 | F | G | H | 0 | 0 | 0 |
| E46 | 6 | A | $-A$ | 0 | D | 0 | F | 0 | H | F | 0 | K |

1. TENSORIAL ASPECTS OF PHYSICAL PROPERTIES

Table 1.9.3.5 (cont.)

| Cross-reference | No. of independent coefficients | Symbols and coefficient indices | | | | | | | | | | |
|-----------------|---------------------------------|---------------------------------|----|----|-----|----|------------------|-----|----|------------------|-----|-----|
| | | A | B | C | D | E | F | G | H | I | J | K |
| | | 1 | 2 | 3 | 1 | 1 | 1 | 1 | 1 | 1 | 1 | 1 |
| | | 1 | 2 | 3 | 1 | 1 | 1 | 1 | 1 | 1 | 1 | 1 |
| | | 1 | 2 | 3 | 1 | 1 | 1 | 1 | 1 | 2 | 2 | 2 |
| | | 1 | 2 | 3 | 1 | 1 | 2 | 2 | 3 | 2 | 2 | 3 |
| | | 1 | 2 | 3 | 2 | 3 | 2 | 3 | 3 | 2 | 3 | 3 |
| E47 | 6 | A | -A | 0 | D | 0 | F | 0 | H | -F | 0 | K |
| E48 | 6 | A | 0 | A | 0 | E | F | 0 | H | 0 | J | 0 |
| E49 | 6 | A | 0 | -A | 0 | E | F | 0 | H | 0 | G | 0 |
| E50 | 6 | 0 | B | B | D | D | 0 | 0 | 0 | I | J | J |
| E51 | 6 | 0 | B | -B | D | -D | 0 | 0 | 0 | I | J | -J |
| E52 | 6 | 0 | 0 | C | 0 | E | 0 | G | 0 | 0 | J | 0 |
| E53 | 6 | 0 | 0 | C | 0 | E | 0 | E/2 | 0 | 0 | J | 0 |
| E54 | 6 | A | 0 | 0 | D | 0 | F | 0 | H | (4) [†] | 0 | K |
| E55 | 6 | A | B | 0 | A/2 | 0 | F | 0 | H | (5) [†] | 0 | H/2 |
| E56 | 6 | A | B | 0 | D | 0 | (2) [†] | 0 | H | (6) [†] | 0 | K |
| E57 | 6 | 0 | B | 0 | D | 0 | D | 0 | 0 | I | 0 | K |
| E58 | 7 | A | A | A | D | E | F | G | H | H | J | J |
| E59 | 7 | A | A | -A | D | E | F | G | H | H | J | -J |
| E60 | 7 | A | -A | A | D | E | F | G | H | -H | J | -J |
| E61 | 7 | A | -A | -A | D | E | F | G | H | -H | J | J |
| E62 | 7 | A | -A | C | D | E | (1) [†] | E/2 | H | (3) [†] | E/2 | K |
| E63 | 9 | 0 | 0 | C | 0 | E | 0 | G | 0 | 0 | J | 0 |
| E64 | 9 | 0 | B | 0 | D | 0 | 0 | G | 0 | I | 0 | K |
| E65 | 9 | A | 0 | 0 | 0 | 0 | F | G | H | 0 | 0 | 0 |
| E66 | 9 | A | A | 0 | D | E | F | G | H | F | 0 | K |
| E67 | 9 | A | -A | 0 | D | E | F | G | H | -F | 0 | K |
| E68 | 9 | A | 0 | A | D | E | F | G | H | I | J | 0 |
| E69 | 9 | A | 0 | -A | D | E | F | G | H | I | J | 0 |
| E70 | 9 | 0 | B | B | D | D | F | 0 | -F | I | J | J |
| E71 | 9 | 0 | B | -B | D | -D | F | 0 | -F | I | J | -J |
| E72 | 9 | A | 0 | 0 | D | E | F | G | H | (4) [†] | 2G | K |
| E73 | 9 | A | B | 0 | A/2 | 0 | F | G | H | (5) [†] | G | H/2 |
| E74 | 9 | A | B | 0 | D | E | (2) [†] | G | H | (6) [†] | 2G | K |
| E75 | 9 | 0 | B | 0 | D | 0 | D | G | 0 | I | G | K |
| E76 | 12 | A | B | 0 | D | 0 | F | 0 | H | I | 0 | K |
| E77 | 12 | A | 0 | C | 0 | E | F | 0 | H | 0 | J | 0 |
| E78 | 12 | 0 | B | C | D | E | 0 | 0 | 0 | I | J | K |
| E79 | 12 | A | -A | C | D | E | F | G | H | -F | J | K |
| E80 | 12 | A | A | C | D | E | F | G | H | F | J | K |
| E81 | 12 | A | B | -A | D | E | F | G | H | I | J | K |
| E82 | 12 | A | B | A | D | E | F | G | H | I | J | K |
| E83 | 12 | A | B | -B | D | -D | F | G | F | I | J | -J |
| E84 | 12 | A | B | B | D | D | F | G | F | I | J | J |
| E85 | 12 | A | B | C | D | E | (2) [†] | G | H | (6) [†] | J | K |
| E86 | 12 | 0 | B | C | D | E | D | E/2 | 0 | I | J | K |
| E87 | 12 | A | 0 | C | D | E | F | G | H | (4) [†] | J | K |
| E88 | 12 | A | B | C | A/2 | E | F | E/2 | H | (5) [†] | J | H/2 |
| E89 | 21 | A | B | C | D | E | F | G | H | I | J | K |

(b) L-V.

| Cross-reference | No. of independent coefficients | Symbols and coefficient indices | | | | | | | | | |
|-----------------|---------------------------------|---------------------------------|------|-----|------|-----|----|----|----|----|----|
| | | L | M | N | P | Q | R | S | T | U | V |
| | | 1 | 1 | 1 | 1 | 1 | 1 | 2 | 2 | 2 | 2 |
| | | 1 | 2 | 2 | 2 | 2 | 3 | 2 | 2 | 2 | 3 |
| | | 3 | 2 | 2 | 2 | 3 | 3 | 2 | 2 | 3 | 3 |
| | | 3 | 2 | 2 | 3 | 3 | 3 | 2 | 3 | 3 | 3 |
| | | 3 | 2 | 3 | 3 | 3 | 3 | 3 | 3 | 3 | 3 |
| E0 | 0 | 0 | 0 | 0 | 0 | 0 | 0 | 0 | 0 | 0 | 0 |
| E1 | 1 | 0 | 0 | G | 0 | G | 0 | 0 | 0 | 0 | 0 |
| E2 | 1 | 0 | 0 | -G | 0 | 0 | 0 | 0 | 0 | 0 | 0 |
| E3 | 1 | 0 | 0 | 0 | 0 | -G | 0 | 0 | 0 | 0 | 0 |
| E4 | 1 | 0 | 0 | N | 0 | -N | 0 | 0 | 0 | 0 | 0 |
| E5 | 2 | 0 | D | 0 | K | 0 | 0 | 0 | 0 | 0 | 0 |
| E6 | 2 | 0 | -A/2 | 0 | -H/2 | 0 | 0 | 0 | 0 | -H | 0 |
| E7 | 2 | 0 | 0 | G | 0 | Q | 0 | 0 | 0 | 0 | 0 |
| E8 | 2 | L | 0 | 0 | 0 | 0 | 0 | -E | 0 | -L | 0 |
| E9 | 2 | 0 | 0 | N | 0 | G | 0 | 0 | 0 | 0 | 0 |
| E10 | 2 | 0 | 0 | 0 | 0 | 0 | 0 | 0 | -I | 0 | -D |
| E11 | 2 | 0 | 0 | N | 0 | N | 0 | 0 | 0 | 0 | 0 |
| E12 | 2 | 0 | M | 0 | 0 | 0 | -M | 0 | 0 | 0 | 0 |
| E13 | 2 | F | -D | 0 | 0 | 0 | D | D | F | -F | -D |
| E14 | 2 | -F | -D | 0 | 0 | 0 | D | -D | F | F | -D |
| E15 | 2 | F | D | 0 | 0 | 0 | -D | -D | -F | -F | -D |
| E16 | 2 | -F | D | 0 | 0 | 0 | -D | D | -F | F | -D |
| E17 | 3 | L | 0 | E/2 | 0 | L/2 | 0 | E | 0 | L | 0 |
| E18 | 3 | 0 | 0 | N | 0 | Q | 0 | 0 | 0 | 0 | 0 |
| E19 | 3 | L | 0 | -G | 0 | 0 | 0 | -E | 0 | -L | 0 |

1.9. ATOMIC DISPLACEMENT PARAMETERS

Table 1.9.3.5 (cont.)

| Cross-reference | No. of independent coefficients | Symbols and coefficient indices | | | | | | | | | |
|-----------------|---------------------------------|---------------------------------|------|-------|-------|-----|----|-------|-------|----|-----|
| | | L | M | N | P | Q | R | S | T | U | V |
| | | 1 | 1 | 1 | 1 | 1 | 1 | 2 | 2 | 2 | 2 |
| | | 1 | 2 | 2 | 2 | 2 | 3 | 2 | 2 | 2 | 3 |
| | | 3 | 2 | 2 | 2 | 3 | 3 | 2 | 2 | 3 | 3 |
| | | 3 | 2 | 2 | 3 | 3 | 3 | 2 | 3 | 3 | 3 |
| | | 3 | 2 | 3 | 3 | 3 | 3 | 3 | 3 | 3 | 3 |
| | | 3 | 2 | 3 | 3 | 3 | 3 | 3 | 3 | 3 | 3 |
| | | 3 | 2 | 3 | 3 | 3 | 3 | 3 | 3 | 3 | 3 |
| | | 3 | 2 | 3 | 3 | 3 | 3 | 3 | 3 | 3 | 3 |
| E20 | 3 | 0 | 0 | 0 | 0 | -G | 0 | 0 | -I | 0 | -D |
| E21 | 3 | 0 | M | N | 0 | -N | -M | 0 | 0 | 0 | 0 |
| E22 | 3 | L | 0 | 2G | 0 | L | 0 | S | 0 | 0 | 0 |
| E23 | 3 | 0 | 0 | N | 0 | Q | 0 | (14)† | 0 | Q | 0 |
| E24 | 4 | 0 | (7)† | 0 | (13)† | 0 | 0 | 0 | -H | 0 | 0 |
| E25 | 4 | L | 0 | 0 | 0 | 0 | 0 | E | 0 | L | 0 |
| E26 | 4 | 0 | 0 | 0 | 0 | 0 | 0 | 0 | I | 0 | D |
| E27 | 4 | 0 | M | 0 | P | 0 | M | 0 | 0 | 0 | 0 |
| E28 | 4 | L | 0 | G | 0 | Q | 0 | -E | 0 | -L | 0 |
| E29 | 4 | 0 | 0 | N | 0 | G | 0 | 0 | -I | 0 | -D |
| E30 | 4 | 0 | M | N | 0 | N | -M | 0 | 0 | 0 | 0 |
| E31 | 5 | L | 0 | -G | 0 | 0 | 0 | E | 0 | L | 0 |
| E32 | 5 | 0 | 0 | 0 | 0 | -G | 0 | 0 | I | 0 | D |
| E33 | 5 | 0 | M | N | P | -N | M | 0 | 0 | 0 | 0 |
| E34 | 5 | F | D | G | J | G | D | D | F | F | D |
| E35 | 5 | -F | D | G | -J | G | D | -D | F | -F | D |
| E36 | 5 | F | -D | G | J | G | -D | -D | -F | F | D |
| E37 | 5 | -F | -D | G | -J | G | -D | D | -F | -F | D |
| E38 | 5 | L | -A/2 | E/2 | -H/2 | L/2 | 0 | E | -H | L | 0 |
| E39 | 5 | L | D | E/2 | K | L/2 | 0 | E | 0 | L | 0 |
| E40 | 6 | L | 0 | 0 | 0 | 0 | 0 | S | 0 | U | 0 |
| E41 | 6 | L | 0 | G | 0 | Q | 0 | E | 0 | L | 0 |
| E42 | 6 | 0 | 0 | 0 | 0 | 0 | 0 | 0 | T | 0 | V |
| E43 | 6 | 0 | 0 | N | 0 | G | 0 | 0 | I | 0 | D |
| E44 | 6 | 0 | M | 0 | P | 0 | R | 0 | 0 | 0 | 0 |
| E45 | 6 | 0 | M | N | P | N | M | 0 | 0 | 0 | 0 |
| E46 | 6 | 0 | D | 0 | K | 0 | R | 0 | H | 0 | R |
| E47 | 6 | 0 | -D | 0 | -K | 0 | R | 0 | -H | 0 | -R |
| E48 | 6 | H | M | 0 | J | 0 | E | M | 0 | F | 0 |
| E49 | 6 | -H | M | 0 | -J | 0 | -E | -M | 0 | -F | 0 |
| E50 | 6 | I | 0 | 0 | 0 | 0 | 0 | S | T | T | S |
| E51 | 6 | -I | 0 | 0 | 0 | 0 | 0 | S | T | -T | -S |
| E52 | 6 | L | 0 | (10)† | 0 | Q | 0 | (15)† | 0 | 2Q | 0 |
| E53 | 6 | L | 0 | (11)† | 0 | L/2 | 0 | S | 0 | U | 0 |
| E54 | 6 | 0 | (4)† | 0 | K | 0 | R | 0 | 0 | 0 | 0 |
| E55 | 6 | 0 | (8)† | 0 | P | 0 | R | 0 | (16)† | 0 | R/2 |
| E56 | 6 | 0 | B/2 | 0 | (12)† | 0 | R | 0 | (17)† | 0 | 2R |
| E57 | 6 | 0 | (9)† | 0 | K | 0 | 0 | 0 | T | 0 | V |
| E58 | 7 | F | E | G | J | G | D | D | F | H | E |
| E59 | 7 | -F | -E | G | -J | G | D | -D | F | -H | -E |
| E60 | 7 | F | E | G | J | G | -D | -D | -F | H | -E |
| E61 | 7 | -F | -E | G | -J | G | -D | D | -F | -H | E |
| E62 | 7 | L | (7)† | E/2 | (13)† | L/2 | 0 | E | -H | L | 0 |
| E63 | 9 | L | 0 | N | 0 | Q | 0 | S | 0 | U | 0 |
| E64 | 9 | 0 | 0 | N | 0 | Q | 0 | 0 | T | 0 | V |
| E65 | 9 | 0 | M | N | P | Q | R | 0 | 0 | 0 | 0 |
| E66 | 9 | L | D | -G | K | 0 | R | -E | H | -L | R |
| E67 | 9 | L | -D | -G | -K | 0 | R | -E | -H | -L | -R |
| E68 | 9 | H | M | 0 | J | -G | E | M | -I | F | -D |
| E69 | 9 | -H | M | 0 | -J | -G | -E | -M | -I | -F | -D |
| E70 | 9 | I | M | N | 0 | -N | -M | S | T | T | S |
| E71 | 9 | -I | M | N | 0 | -N | -M | S | T | -T | -S |
| E72 | 9 | L | (4)† | 2G | K | L | R | 0 | 0 | 0 | 0 |
| E73 | 9 | 0 | (8)† | N | P | Q | R | (14)† | (16)† | Q | R/2 |
| E74 | 9 | L | B/2 | 2G | (12)† | L | R | 0 | (17)† | 0 | 2R |
| E75 | 9 | 0 | (9)† | N | K | Q | 0 | (14)† | T | Q | V |
| E76 | 12 | 0 | M | 0 | P | 0 | R | 0 | T | 0 | V |
| E77 | 12 | L | M | 0 | P | 0 | R | S | 0 | U | 0 |
| E78 | 12 | L | 0 | 0 | 0 | 0 | 0 | S | T | U | V |
| E79 | 12 | L | -D | G | -K | Q | R | E | -H | L | -R |
| E80 | 12 | L | D | G | J | Q | R | E | H | L | R |
| E81 | 12 | -H | M | N | -J | G | -E | -M | I | -F | D |
| E82 | 12 | H | M | N | J | G | E | M | I | F | D |
| E83 | 12 | -I | M | N | P | N | M | S | T | -T | -S |
| E84 | 12 | I | M | N | P | N | M | S | T | T | S |
| E85 | 12 | L | B/2 | (10)† | (12)† | N | M | (15)† | (17)† | 2N | 2M |
| E86 | 12 | L | 2I | (11)† | K | L/2 | 0 | S | T | U | V |
| E87 | 12 | L | (4)† | (10)† | K | N | M | (15)† | 0 | 2N | 0 |
| E88 | 12 | L | (8)† | (11)† | P | L/2 | R | S | (16)† | U | U/2 |
| E89 | 21 | L | M | N | P | Q | R | S | T | U | V |

† (1) $-2A/5 + D$; (2) $-3A/5 + B/10 + 3D/2$; (3) $-3A/5 + D$; (4) $-D + 2F$; (5) $-A/4 + 3F/2$; (6) $-2A/5 + B/5 + D$; (7) $-A + D$; (8) $-A/5 + 2B/5 + F$; (9) $-D + 2I$; (10) $-2G + 3J$; (11) $-E/4 + 3J/2$; (12) $-2H + 3K$; (13) $-H + K$; (14) $-G + 2N$; (15) $-4G + 6J$; (16) $-H/4 + 3P/2$; (17) $-4H + 6K$.

1. TENSORIAL ASPECTS OF PHYSICAL PROPERTIES

Table 1.9.3.6. *Symmetry restrictions on coefficients in sixth-rank symmetric polar tensors*

(a) A–N.

| Cross-reference | No. of independent parameters | Symbols and coefficient indices | | | | | | | | | | | | | |
|-----------------|-------------------------------|---------------------------------|---|---|-----|----|---|-----|---|------------------|------------------|-----|----|------------------|-------------------|
| | | A | B | C | D | E | F | G | H | I | J | K | L | M | N |
| | | 1 | 2 | 3 | 1 | 1 | 1 | 1 | 1 | 1 | 1 | 1 | 1 | 1 | 1 |
| | | 1 | 2 | 3 | 1 | 1 | 1 | 1 | 1 | 1 | 1 | 1 | 1 | 1 | 1 |
| | | 1 | 2 | 3 | 1 | 1 | 1 | 1 | 1 | 1 | 1 | 1 | 1 | 2 | 2 |
| | | 1 | 2 | 3 | 1 | 1 | 1 | 1 | 1 | 2 | 2 | 2 | 3 | 2 | 2 |
| | | 1 | 2 | 3 | 1 | 1 | 2 | 2 | 3 | 2 | 2 | 3 | 3 | 2 | 2 |
| | | 1 | 2 | 3 | 2 | 3 | 2 | 3 | 3 | 2 | 3 | 3 | 3 | 2 | 3 |
| F1 | 3 | A | A | A | 0 | 0 | F | 0 | F | 0 | 0 | 0 | 0 | F | 0 |
| F2 | 4 | A | A | A | 0 | 0 | F | 0 | H | 0 | 0 | 0 | 0 | H | 0 |
| F3 | 5 | A | A | C | A/2 | 0 | F | 0 | H | (1) [†] | 0 | H/2 | 0 | F | 0 |
| F4 | 6 | A | A | C | D | 0 | F | 0 | H | (2) [†] | 0 | H/2 | 0 | (5) [†] | 0 |
| F5 | 6 | A | A | C | 0 | 0 | F | 0 | H | 0 | 0 | 0 | 0 | F | 0 |
| F6 | 6 | A | B | A | 0 | 0 | F | 0 | H | 0 | 0 | 0 | 0 | M | 0 |
| F7 | 6 | A | B | B | 0 | 0 | F | 0 | F | 0 | 0 | 0 | 0 | M | 0 |
| F8 | 7 | A | A | A | D | D | F | G | F | I | J | J | I | F | J |
| F9 | 7 | A | A | A | D | −D | F | G | F | I | J | −J | −I | F | J |
| F10 | 7 | A | A | A | D | −D | F | G | F | I | J | −J | −I | F | −J |
| F11 | 7 | A | A | A | D | D | F | G | F | I | J | J | I | F | −J |
| F12 | 7 | A | A | C | A/2 | E | F | E/2 | H | (1) [†] | E/10 | H/2 | I | F | −E/10 |
| F13 | 7 | A | A | C | A/2 | 0 | F | G | H | (1) [†] | G | H/2 | 0 | F | G |
| F14 | 8 | A | A | C | D | 0 | F | 0 | H | 0 | 0 | K | 0 | F | 0 |
| F15 | 8 | A | B | A | 0 | E | F | 0 | H | 0 | J | 0 | 0 | M | 0 |
| F16 | 8 | A | B | B | 0 | 0 | F | 0 | H | 0 | 0 | 0 | 0 | M | N |
| F17 | 10 | A | A | A | D | E | F | G | H | I | J | K | I | H | K |
| F18 | 10 | A | A | A | D | E | F | G | H | I | J | K | −I | H | −K |
| F19 | 10 | A | A | A | D | E | F | G | H | I | J | K | −I | H | K |
| F20 | 10 | A | A | A | D | E | F | G | H | I | J | K | I | H | −K |
| F21 | 10 | A | A | C | D | E | F | G | H | (2) [†] | (4) [†] | H/2 | L | (5) [†] | (7) [†] |
| F22 | 10 | A | B | C | 0 | 0 | F | 0 | H | 0 | 0 | 0 | 0 | M | 0 |
| F23 | 10 | A | A | C | D | 0 | F | 0 | H | I | 0 | K | 0 | F | 0 |
| F24 | 10 | A | B | A | 0 | E | F | 0 | H | 0 | J | 0 | L | M | 0 |
| F25 | 10 | A | B | B | 0 | 0 | F | G | F | 0 | 0 | 0 | 0 | M | N |
| F26 | 10 | A | B | C | D | 0 | F | 0 | H | (3) [†] | 0 | K | 0 | (6) [†] | 0 |
| F27 | 10 | A | B | C | A/2 | 0 | F | 0 | H | (1) [†] | 0 | H/2 | 0 | M | 0 |
| F28 | 16 | A | B | C | D | 0 | F | 0 | H | I | 0 | K | 0 | M | 0 |
| F29 | 16 | A | B | C | 0 | E | F | 0 | H | 0 | J | 0 | L | M | 0 |
| F30 | 16 | A | B | C | 0 | 0 | F | G | H | 0 | 0 | 0 | 0 | M | N |
| F31 | 16 | A | A | C | D | E | F | G | H | I | J | K | L | F | −J |
| F32 | 16 | A | A | C | D | E | F | G | H | I | J | K | L | F | J |
| F33 | 16 | A | B | A | D | E | F | G | H | I | J | K | L | M | N |
| F34 | 16 | A | B | A | D | E | F | G | H | I | J | K | L | M | N |
| F35 | 16 | A | B | B | D | −D | F | G | F | I | J | −J | −I | M | N |
| F36 | 16 | A | B | B | D | D | F | G | F | I | J | J | I | M | N |
| F37 | 16 | A | B | C | D | E | F | G | H | (3) [†] | J | K | L | (6) [†] | (8) [†] |
| F38 | 16 | A | B | C | A/2 | 0 | F | G | H | (1) [†] | G | H/2 | 0 | M | N |
| F39 | 16 | A | B | C | D | E | F | G | H | (3) [†] | J | K | L | (6) [†] | (9) [†] |
| F40 | 16 | A | B | C | A/2 | E | F | E/2 | H | (1) [†] | J | H/2 | L | M | (10) [†] |
| F41 | 28 | A | B | C | D | E | F | G | H | I | J | K | L | M | N |

(b) P–c.

| Cross-reference | No. of independent parameters | Symbols and coefficient indices | | | | | | | | | | | | | |
|-----------------|-------------------------------|---------------------------------|-----|---|-------------------|------|-----|------|-----|----|----|---|----|---|----|
| | | P | Q | R | S | T | U | V | W | X | Y | Z | a | b | c |
| | | 1 | 1 | 1 | 1 | 1 | 1 | 1 | 1 | 1 | 2 | 2 | 2 | 2 | 2 |
| | | 1 | 1 | 1 | 2 | 2 | 2 | 2 | 2 | 3 | 2 | 2 | 2 | 2 | 3 |
| | | 2 | 2 | 3 | 2 | 2 | 2 | 2 | 3 | 3 | 2 | 2 | 2 | 3 | 3 |
| | | 2 | 3 | 3 | 2 | 2 | 2 | 3 | 3 | 3 | 2 | 2 | 3 | 3 | 3 |
| | | 3 | 3 | 3 | 2 | 2 | 3 | 3 | 3 | 3 | 2 | 3 | 3 | 3 | 3 |
| | | 3 | 3 | 3 | 2 | 3 | 3 | 3 | 3 | 3 | 3 | 3 | 3 | 3 | 3 |
| F1 | 3 | P | 0 | F | 0 | 0 | 0 | 0 | 0 | 0 | 0 | F | 0 | F | 0 |
| F2 | 4 | P | 0 | F | 0 | 0 | 0 | 0 | 0 | 0 | 0 | F | 0 | H | 0 |
| F3 | 5 | H/2 | 0 | R | A/2 | 0 | H/2 | 0 | R/2 | 0 | 0 | H | 0 | R | 0 |
| F4 | 6 | H/2 | 0 | R | (11) [†] | 0 | H/2 | 0 | R/2 | 0 | 0 | H | 0 | R | 0 |
| F5 | 6 | P | 0 | R | 0 | 0 | 0 | 0 | 0 | 0 | 0 | H | 0 | R | 0 |
| F6 | 6 | P | 0 | H | 0 | 0 | 0 | 0 | 0 | 0 | 0 | M | 0 | F | 0 |
| F7 | 6 | P | 0 | M | 0 | 0 | 0 | 0 | 0 | 0 | 0 | Z | 0 | Z | 0 |
| F8 | 7 | P | J | F | D | G | J | J | G | D | D | F | I | F | D |
| F9 | 7 | P | J | F | D | G | −J | J | −G | −D | −D | F | −I | F | −D |
| F10 | 7 | P | −J | F | D | −G | −J | −J | G | −D | D | F | I | F | D |
| F11 | 7 | P | −J | F | D | −G | J | −J | −G | D | −D | F | −I | F | −D |
| F12 | 7 | H/2 | I/2 | R | A/2 | −E/2 | H/2 | −I/2 | R/2 | 0 | −E | H | −I | R | 0 |
| F13 | 7 | H/2 | Q | R | A/2 | G | H/2 | Q | R/2 | 0 | 0 | H | 0 | R | 0 |
| F14 | 8 | P | 0 | R | −D | 0 | −K | 0 | 0 | 0 | 0 | H | 0 | R | 0 |
| F15 | 8 | P | 0 | H | 0 | 0 | 0 | −J | 0 | −E | 0 | M | 0 | F | 0 |
| F16 | 8 | P | −N | M | 0 | 0 | 0 | 0 | 0 | 0 | Y | Z | 0 | Z | −Y |
| F17 | 10 | P | J | F | E | G | J | K | G | D | D | F | I | H | E |
| F18 | 10 | P | J | F | −E | G | −J | −K | −G | −D | −D | F | −I | H | E |

1.9. ATOMIC DISPLACEMENT PARAMETERS

Table 1.9.3.6 (*cont.*)

| Cross-reference | No. of independent parameters | Symbols and coefficient indices | | | | | | | | | | | | | | |
|-----------------|-------------------------------|---------------------------------|-----|---|-------|-------|-------|-------|-----|----|-------|-------|-------|----|-----|--|
| | | P | Q | R | S | T | U | V | W | X | Y | Z | a | b | c | |
| | | 1 | 1 | 1 | 1 | 1 | 1 | 1 | 1 | 1 | 2 | 2 | 2 | 2 | 2 | |
| | | 1 | 1 | 1 | 2 | 2 | 2 | 2 | 2 | 3 | 2 | 2 | 2 | 2 | 3 | |
| | | 2 | 2 | 3 | 2 | 2 | 2 | 2 | 3 | 3 | 2 | 2 | 2 | 3 | 3 | |
| | | 2 | 3 | 3 | 2 | 2 | 2 | 3 | 3 | 3 | 2 | 2 | 3 | 3 | 3 | |
| | | 3 | 3 | 3 | 2 | 2 | 3 | 3 | 3 | 3 | 2 | 3 | 3 | 3 | 3 | |
| | | 3 | 3 | 3 | 2 | 3 | 3 | 3 | 3 | 3 | 3 | 3 | 3 | 3 | 3 | |
| F19 | 10 | P | −J | F | −E | −G | −J | −K | G | −D | D | F | I | H | −E | |
| F20 | 10 | P | −J | F | E | −G | J | K | −G | D | −D | F | −I | H | −E | |
| F21 | 10 | H/2 | Q | R | (11)† | (13)† | H/2 | (18)† | R/2 | 0 | −E | H | −L | R | 0 | |
| F22 | 10 | P | 0 | R | 0 | 0 | 0 | 0 | 0 | 0 | 0 | Z | 0 | b | 0 | |
| F23 | 10 | P | 0 | R | D | 0 | K | 0 | W | 0 | 0 | H | 0 | R | 0 | |
| F24 | 10 | P | 0 | H | 0 | T | 0 | J | 0 | E | 0 | M | 0 | F | 0 | |
| F25 | 10 | P | N | M | 0 | 0 | 0 | 0 | 0 | 0 | Y | Z | a | Z | Y | |
| F26 | 10 | P | 0 | R | B/2 | 0 | (16)† | 0 | W | 0 | 0 | (22)† | 0 | 2W | 0 | |
| F27 | 10 | P | 0 | R | (12)† | 0 | (17)† | 0 | R/2 | 0 | 0 | Z | 0 | b | 0 | |
| F28 | 16 | P | 0 | R | S | 0 | U | 0 | W | 0 | 0 | Z | 0 | b | 0 | |
| F29 | 16 | P | 0 | R | 0 | T | 0 | V | 0 | X | 0 | Z | 0 | b | 0 | |
| F30 | 16 | P | Q | R | 0 | 0 | 0 | 0 | 0 | 0 | Y | Z | a | b | c | |
| F31 | 16 | P | Q | R | D | −G | K | −Q | W | X | −E | H | −L | R | −X | |
| F32 | 16 | P | Q | R | D | G | K | Q | W | X | E | H | L | R | X | |
| F33 | 16 | P | −K | H | S | T | −N | J | −G | E | −S | M | −I | F | −D | |
| F34 | 16 | P | K | H | S | T | N | J | G | E | S | M | I | F | D | |
| F35 | 16 | P | N | M | S | T | U | −U | −T | −S | Y | Z | a | Z | Y | |
| F36 | 16 | P | N | M | S | T | U | U | T | S | Y | Z | a | Z | Y | |
| F37 | 16 | P | Q | R | B/2 | (14)† | (16)† | (19)† | W | X | (20)† | (22)† | (23)† | 2W | 2X | |
| F38 | 16 | P | Q | R | (12)† | (15)† | (17)† | Q | R/2 | 0 | Y | Z | a | b | c | |
| F39 | 16 | P | Q | R | B/2 | (9)† | (16)† | Q | W | X | 0 | (22)† | 0 | 2W | 0 | |
| F40 | 16 | P | L/2 | R | (12)† | T | (17)† | V | R/2 | X | (21)† | Z | (24)† | b | X/2 | |
| F41 | 28 | P | Q | R | S | T | U | V | W | X | Y | Z | a | b | c | |

† (1) $-A/4 + F/2$; (2) $A/2 - 3D/2 + 3F/2$; (3) $B/20 - 3D/5 + 3F/2$; (4) $-2E/5 + G$; (5) $A - 2D + F$; (6) $B/5 - 2D/5 + F$; (7) $-3E/5 + G$; (8) $2E - 5G + 4J$; (9) $-G + 2J$; (10) $-E/4 + 3J/2$; (11) $A - D$; (12) $A/2 - 5F/2 + 5M/2$; (13) $-E + G$; (14) $6E - 15G + 10J$; (15) $-G + 2N$; (16) $-2K + 3P$; (17) $-H/4 + 3P/2$; (18) $-L + Q$; (19) $-2L + 3Q$; (20) $12E - 30G + 20J$; (21) $E/2 - 5J/2 + 5T/2$; (22) $-4K + 6P$; (23) $-4L + 6Q$; (24) $-L/4 + 3V/2$.

system with correspondingly different transformation matrices \mathbf{F} (see *e.g.* Chapter 1.1 of *IT B*). The most useful representation surface of the second-order atomic displacement tensor \mathbf{U}_C is the representation quadric defined by the tensor invariant

$$^2I_0 = \mathbf{u}^T \mathbf{U}_C^{-1} \mathbf{u} \quad (1.9.4.3)$$

where \mathbf{u} is a displacement vector; \mathbf{U}^{-1} is often called the *variance-covariance matrix* and has (in a general axes frame) covariant components. Under the conditions of *positive definiteness*,

$$\left. \begin{array}{l} \text{Det}(\mathbf{U}_C) \\ \mathbf{U}_C^{ij} \\ \mathbf{U}_C^{ij} - \mathbf{U}_C^{ij} \text{ (no summation)} \end{array} \right\} \text{all positive}, \quad (1.9.4.4)$$

the surface of the representation quadric is an ellipsoid whose semi-major axes (for $^2I_0 = 0$) are of lengths equal to the root-mean-square displacements (r.m.s.d.'s) along the axes directions. The *thermal vibration ellipsoids* calculated in *ORTEP* are related to this surface; considering the discussion in Section 1.9.1, they should more appropriately be called *atomic displacement ellipsoids* or simply *ORTEP ellipsoids*. One notes that the Fourier transform of the atomic DWF, the atomic probability density function $P(\mathbf{u})$, is given in the case of a second-order tensor as a trivariate Gaussian distribution,

$$P(\mathbf{u}) = \frac{[\text{Det}(\mathbf{U}_C^{-1})]^{1/2}}{(2\pi)^{3/2}} \exp\left\{-\frac{1}{2}\mathbf{u}^T \mathbf{U}_C^{-1} \mathbf{u}\right\}. \quad (1.9.4.5)$$

On comparing (1.9.4.3) and (1.9.4.5), it is evident that (1.9.4.3) defines a surface of constant probability of finding a (displaced) atom. The integral of (1.9.4.5) over the volume inside the ellipsoid is a constant. For $^2I_0 = C^2$ with the integration limit $C = 1.5382$ (2.5003), the integral is equal to one half (nine tenths), and the ellipsoid is then called a 50 (90) per cent probability ellipsoid.

Other representation surfaces can be defined and are useful for special considerations. The quantities of interest are either the r.m.s.d.'s or the mean-square displacements (m.s.d.'s) defined in direct space. Here a distinction has to be made between the averaged squared displacement along a certain direction and the average for all squared displacements of an atom projected onto a given direction. Representation surfaces may also be calculated in reciprocal space, related to surfaces in direct space by Fourier transformation. For further details, see Nelmes (1969) and Hummel *et al.* (1990).

1.9.4.2. Higher-order representations

Representation surfaces of higher-order tensors may be calculated from their invariants. While for second-order tensors surfaces can be found that fully describe the directional aspects of the tensor involved, higher-order tensors need several different surfaces for a full description (see *e.g.* Wondratschek, 1958; Sirotnin, 1961). This makes the graphical representation of the displacements somewhat cumbersome and it is therefore rarely used. Instead, the probability density functions [given in equations (6.1.1.46), (6.1.1.48) or (6.1.1.49) of *IT C*] are calculated from the tensor coefficients and displayed in sections or as three-dimensional surfaces. If the higher-order terms are small, it is more appropriate to display only the difference between the total p.d.f. and the related Gaussian p.d.f., which may be calculated from the second-order displacement tensor using equation (1.9.4.5). Here, the second-order terms that were refined together with the higher-order terms are usually used (not the best-fitting second-order terms of a fit in the harmonic approximation):

$$P_{\text{deformation}}(\mathbf{u}) = P_{\text{general}}(\mathbf{u}) - P_{\text{Gaussian}}(\mathbf{u}). \quad (1.9.4.6)$$

The resulting *anharmonic deformation densities* (or *disorder deformation densities* in the case of static disorder) $P_{\text{deformation}}(\mathbf{u})$ may be displayed in a similar way to the total p.d.f.'s $P_{\text{general}}(\mathbf{u})$. The graphical representations appropriate for displaying those densities are similar to those used for electronic deformation

1. TENSORIAL ASPECTS OF PHYSICAL PROPERTIES

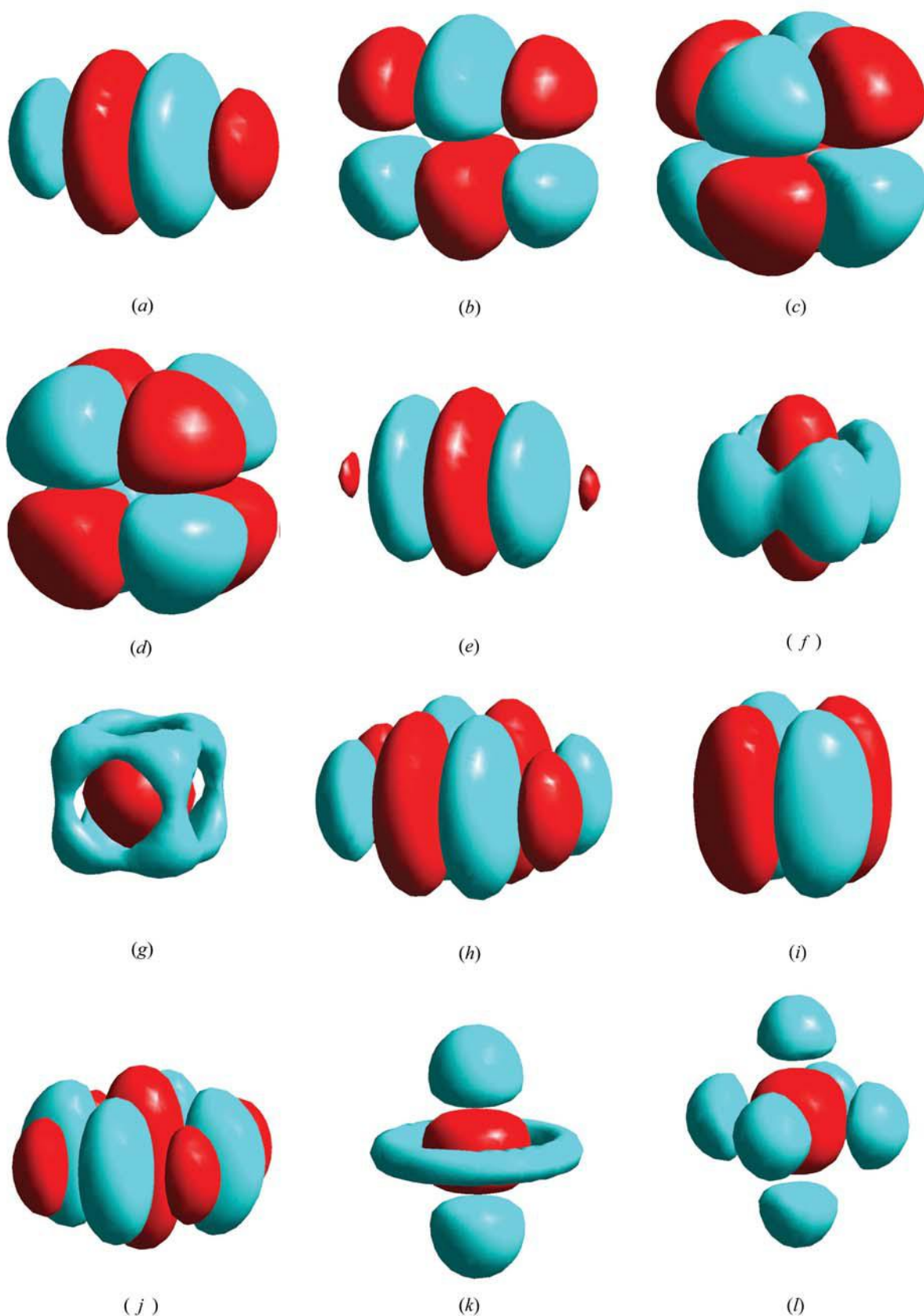


Fig. 1.9.4.1. A selection of graphical representations of density modulations due to higher-order terms in the Gram-Charlier series expansion of a Gaussian atomic probability density function. All figures are drawn on a common scale and have a common orientation. All terms within any given order of expansion are numerically identical and refer to the same underlying isotropic second-order term; the higher-order terms of different order of expansion differ by one order of magnitude, but refer again to the same underlying isotropic second-order term. The orthonormal crystallographic axes are oriented as follows: x oblique out of the plane of the paper towards the observer, y in the plane of the paper and to the right, and z in the plane of the paper and upwards. All surfaces are scaled to 1% of the absolute value of the maximum modulation within each density distribution. Positive modulations (*i.e.* an increase of density) are shown in red, negative modulations are shown in blue. The source of illumination is located approximately on the $[111]$ axis. The following graphs are shown (with typical point groups for specific cases given in parentheses). Third-order terms: (a) b^{222} ; (b) b^{223} ; (c) $b^{113} = -b^{223}$ (point group $\bar{4}$); (d) b^{123} (point group $43m$). Fourth-order terms: (e) b^{2222} ; (f) $b^{1111} = b^{2222}$; (g) $b^{1111} = b^{2222} = b^{3333}$ (point group $m\bar{3}m$); (h) b^{1222} ; (i) $b^{1112} = b^{1222}$; (j) b^{1122} ; (k) $b^{1133} = b^{2233}$; (l) $b^{1122} = b^{1133} = b^{2233}$ (point group $m\bar{3}m$).

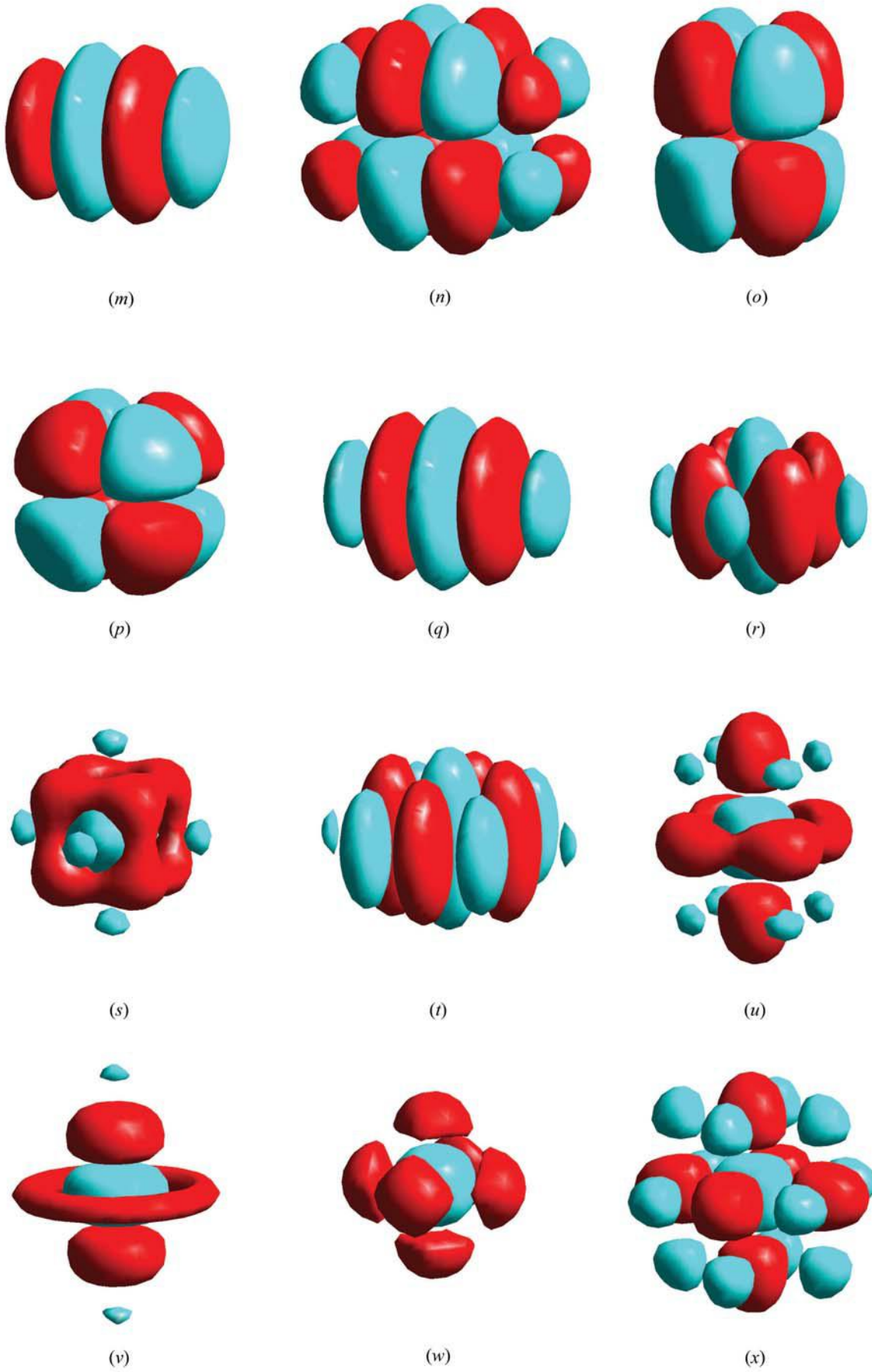


Fig. 1.9.4.1 (cont.). Fifth-order terms: (m) b^{22222} ; (n) b^{12223} ; (o) $b^{11123} = b^{12223}$; (p) $b^{11123} = b^{12223} = b^{12333}$ (point group $\bar{4}3m$). Sixth-order terms: (q) b^{222222} ; (r) $b^{111111} = b^{222222}$; (s) $b^{111111} = b^{222222} = b^{333333}$ (point group $m\bar{3}m$); (t) b^{112222} ; (u) $b^{111133} = b^{222233}$; (v) $b^{113333} = b^{223333}$; (w) $b^{111122} = b^{112222} = b^{111133} = b^{113333} = b^{222233} = b^{223333}$ (point group $m\bar{3}m$); (x) b^{112233} (point group $m\bar{3}m$).

1. TENSORIAL ASPECTS OF PHYSICAL PROPERTIES

densities (see *e.g.* Smith *et al.*, 1977). A number of examples of displacement deformation densities of high symmetry are shown in Fig. 1.9.4.1 as three-dimensional contour maps.

1.9.5. Glossary

| | |
|--------------------------|------------------------------------|
| $b^{ijk}...$ | atomic displacement tensor |
| $\beta^{ij}, U^{ijk}...$ | atomic displacement parameter |
| g_{ij} | metric tensor |
| S_{α} | atomic static Debye–Waller factor |
| T_{α} | atomic thermal Debye–Waller factor |
| \mathbf{Q} | scattering vector |
| u^i | atomic displacement |

References

- Hazell, R. G. & Willis, B. T. M. (1978). *Correlations between third cumulants in the refinement of noncentrosymmetric structures*. *Acta Cryst.* **A34**, 809–811.
- Hummel, W., Raselli, A. & Bürgi, H.-B. (1990). *Analysis of atomic displacement parameters and molecular motion in crystals*. *Acta Cryst.* **B46**, 683–692.
- International Tables for Crystallography* (1999). Vol. C. *Mathematical, physical and chemical tables*, edited by A. J. C. Wilson & E. Prince. Dordrecht: Kluwer Academic Publishers.
- International Tables for Crystallography* (2001). Vol. B. *Reciprocal space*, edited by U. Shmueli. Dordrecht: Kluwer Academic Publishers.
- International Tables for Crystallography* (2002). Vol. A. *Space-group symmetry*, edited by Th. Hahn. Dordrecht: Kluwer Academic Publishers.
- Jahn, H. A. (1949). *Note on the Bhagavantam–Suryanarayana method of enumerating the physical constants of crystals*. *Acta Cryst.* **2**, 30–33.
- Johnson, C. K. (1965). *ORTEP – a FORTRAN thermal ellipsoid plot program*. Report ORNL-3794. Oak Ridge National Laboratory, Tennessee, USA.
- Johnson, C. K. (1970). *Generalized treatments for thermal motion*. In *Thermal neutron diffraction*, edited by B. T. M. Willis, pp. 132–160. Oxford University Press.
- Kuhs, W. F. (1983). *Statistical description of multimodal atomic probability densities*. *Acta Cryst.* **A39**, 148–158.
- Kuhs, W. F. (1984). *Site-symmetry restrictions on thermal-motion-tensor coefficients up to rank 8*. *Acta Cryst.* **A40**, 133–137.
- Kuhs, W. F. (1988). *The anharmonic temperature factor in crystallographic structure analysis*. *Aust. J. Phys.* **41**, 369–382.
- Kuhs, W. F. (1992). *Generalized atomic displacements in crystallographic structure analysis*. *Acta Cryst.* **A48**, 80–98.
- Kuznetsov, P. I., Stratonovich, R. L. & Tikhonov, V. I. (1960). *Quasi-moment functions in the theory of random processes*. *Theory Probab. Its Appl. (USSR)*, **5**, 80–97.
- Levy, H. A. (1956). *Symmetry relations among coefficients of the anisotropic temperature factor*. *Acta Cryst.* **9**, 679.
- Nelmes, R. J. (1969). *Representational surfaces for thermal motion*. *Acta Cryst.* **A25**, 523–526.
- Pach, K. & Frey, T. (1964). *Vector and tensor analysis*. Budapest: Terra.
- Peterse, W. J. A. M. & Palm, J. H. (1966). *The anisotropic temperature factor of atoms in special positions*. *Acta Cryst.* **20**, 147–150.
- Scheringer, C. (1985). *A deficiency of the cumulant expansion of the anharmonic temperature factor*. *Acta Cryst.* **A41**, 79–81.
- Sirotnin, Yu. I. (1960). *Group tensor spaces*. *Sov. Phys. Crystallogr.* **5**, 157–165.
- Sirotnin, Yu. I. (1961). *Plotting tensors of a given symmetry*. *Sov. Phys. Crystallogr.* **6**, 263–271.
- Smith, V. H. Jr, Price, P. F. & Absar, I. (1977). *Representations of electron density and its topographical features*. *Isr. J. Chem.* **16**, 187–197.
- Trueblood, K. N., Bürgi, H.-B., Burzlaff, H., Dunitz, J. D., Gramaccioni, C. M., Schulz, H. H., Shmueli, U. & Abrahams, S. C. (1996). *Atomic displacement parameter nomenclature. Report of a subcommittee on atomic displacement parameter nomenclature*. *Acta Cryst.* **A52**, 770–781.
- Willis, B. T. M. & Pryor, A. W. (1975). *Thermal vibrations in crystallography*. Cambridge University Press.
- Wondratschek, H. (1958). *Über die Möglichkeit der Beschreibung kristallphysikalischer Eigenschaften durch Flächen*. *Z. Kristallogr.* **110**, 127–135.
- Zucker, U. H. & Schulz, H. (1982a). *Statistical approaches for the treatment of anharmonic thermal motion in crystals. I. A comparison of the most frequently used formalisms of anharmonic thermal vibrations*. *Acta Cryst.* **A38**, 563–568.
- Zucker, U. H. & Schulz, H. (1982b). *Statistical approaches for the treatment of anharmonic thermal motion in crystals. II. Anharmonic thermal vibrations and effective atomic potentials in the fast ionic conductor lithium nitride Li₃N*. *Acta Cryst.* **A38**, 568–576.

1.10. Tensors in quasiperiodic structures

By T. JANSSEN

1.10.1. Quasiperiodic structures

1.10.1.1. Introduction

Many materials are known which show a well ordered state without lattice translation symmetry, often in a restricted temperature or composition range. This can be seen in the diffraction pattern from the appearance of sharp spots that cannot be labelled in the usual way with three integer indices. The widths of the peaks are comparable with those of perfect lattice periodic crystals, and this is a sign that the coherence length is comparable as well.

A typical example is K_2SeO_4 , which has a normal lattice periodic structure above 128 K with space group $Pcmn$, but below this temperature shows satellites at positions $\gamma\mathbf{c}^*$, where γ is an irrational number, which in addition depends on temperature. These satellites cannot be labelled with integer indices with respect to the reciprocal basis \mathbf{a}^* , \mathbf{b}^* , \mathbf{c}^* of the structure above the transition temperature. Therefore, the corresponding structure cannot be lattice periodic.

The diffraction pattern of K_2SeO_4 arises because the original lattice periodic *basic structure* is deformed below 128 K. The atoms are displaced from their positions in the basic structure such that the displacement itself is again periodic, but with a period that is *incommensurate* with respect to the lattice of the basic structure.

Such a *modulated structure* is just a special case of a more general type of structure. These structures are characterized by the fact that the diffraction pattern has sharp Bragg peaks at positions \mathbf{H} that are linear combinations of a finite number of basic vectors:

$$\mathbf{H} = \sum_{i=1}^n h_i \mathbf{a}_i^* \quad (\text{integer } h_i). \quad (1.10.1.1)$$

Structures that have this property are called *quasiperiodic*. The minimal number n of basis vectors such that all h_i are integers is called the *rank* of the structure. If the rank is three and the vectors \mathbf{a}_i do not all fall on a line or in a plane, the structure is just lattice periodic. Lattice periodic structures form special cases of quasiperiodic structures. The collection of vectors \mathbf{H} forms the *Fourier module* of the structure. For rank three, this is just the *reciprocal lattice* of the lattice periodic structure.

The definition given above results in some important practical difficulties. In the first place, it is not possible to show experimentally that a wavevector has irrational components instead of rational ones, because an irrational number can be approximated by a rational number arbitrarily well. Very often the wavevector of the satellite changes with temperature. It has been reported that in some compounds the variation shows plateaux, but even when the change seems to be continuous and smooth one can not be sure about the irrationality. On the other hand, if the wavevector jumps from one rational position to another, the structure would always be lattice periodic, but the unit cell of this structure would vary wildly with temperature. This means that, if one wishes to describe the incommensurate phases in a unified fashion, it is more convenient to treat the wavevector as generically irrational. This experimental situation is by no means dramatic. It is similar to the way in which one can never be sure that the angles between the basis vectors of an orthorhombic

lattice are really 90° , although this is a concept that no-one has problems understanding.

A second problem stems from the fact that the wavevectors of the Fourier module are dense. For example, in the case of K_2SeO_4 the linear combinations of \mathbf{c}^* and $\gamma\mathbf{c}^*$ cover the c axis uniformly. To pick out a basis here could be problematic, but the intensity of the spots is usually such that choosing a basis is not a problem. In fact, one only observes peaks with an intensity above a certain threshold, and these form a discrete set. At most, the occurrence of scale symmetry may make the choice less obvious.

1.10.1.2. Types of quasiperiodic crystals

One may distinguish various families of quasiperiodic systems. [Sometimes these are also called incommensurate systems (Janssen & Janner, 1987).] It is not a strict classification, because one may have intermediate cases belonging to more than one family as well. Here we shall consider a number of pure cases.

An *incommensurately modulated structure* or *incommensurate crystal (IC)* phase is a periodically modified structure that without the modification would be lattice periodic. Hence there is a *basic structure* with space-group symmetry. The periodicity of the modification should be incommensurate with respect to the basic structure. The position of the j th atom in the unit cell with origin at the lattice point \mathbf{n} is $\mathbf{n} + \mathbf{r}_j$ ($j = 1, 2, \dots, s$).

For a *displacive modulation*, the positions of the atoms are shifted from a lattice periodic basic structure. A simple example is a structure that can be derived from the positions of the basic structure with a simple displacement wave. The positions of the atoms in the IC phase are then

$$\mathbf{n} + \mathbf{r}_j + \mathbf{f}_j(\mathbf{Q} \cdot \mathbf{n}) \quad [\mathbf{f}_j(x) = \mathbf{f}_j(x + 1)]. \quad (1.10.1.2)$$

Here the *modulation wavevector* \mathbf{Q} has irrational components with respect to the reciprocal lattice of the basic structure. One has

$$\mathbf{Q} = \alpha\mathbf{a}^* + \beta\mathbf{b}^* + \gamma\mathbf{c}^*, \quad (1.10.1.3)$$

where at least one of α , β or γ is irrational. A simple example is the function $\mathbf{f}_j(x) = \mathbf{A}_j \cos(2\pi x + \varphi_j)$, where \mathbf{A}_j is the *polarization vector* and φ_j is the phase of the modulation. The diffraction pattern of the structure (1.10.1.2) shows spots at positions

$$\mathbf{H} = h_1\mathbf{a}^* + h_2\mathbf{b}^* + h_3\mathbf{c}^* + h_4\mathbf{Q}. \quad (1.10.1.4)$$

Therefore, the rank is four and $\mathbf{a}_4^* = \mathbf{Q}$. In a more general situation, the components of the atom positions in the IC phase are given by

$$\mathbf{n}^\alpha + \mathbf{r}_j^\alpha + \sum_m \mathbf{A}_j^\alpha(\mathbf{Q}_m) \cos(2\pi \mathbf{Q}_m \cdot \mathbf{n} + \varphi_{jma}), \quad \alpha = x, y, z. \quad (1.10.1.5)$$

Here the vectors \mathbf{Q}_m belong to the Fourier module of the structure. Then there are vectors \mathbf{Q}_j such that any spot in the diffraction pattern can be written as

$$\mathbf{H} = \sum_{i=1}^3 h_i \mathbf{a}_i^* + \sum_{j=1}^d h_{3+j} \mathbf{Q}_j \quad (1.10.1.6)$$

and the rank is $3 + d$. The peaks corresponding to the basic structure [the combinations of the three reciprocal-lattice vectors

1. TENSORIAL ASPECTS OF PHYSICAL PROPERTIES

\mathbf{a}_i^* ($i = 1, 2, 3$) are called the *main reflections*, the other peaks are *satellites*. For the latter, at least one of the h_4, \dots, h_n is different from zero.

A second type of modulation is the *occupation* or *composition* modulation. Here the structure can again be described on the basis of a basic structure with space-group symmetry. The basic structure positions are occupied with a certain probability by different atom species, or by molecules in different orientations. In CuAu(II), the two lattice positions in a b.c.c. structure are occupied by either Cu and Au or by Au and Cu with a certain probability. This probability function is periodic in one direction with a period that is not a multiple of the lattice constant. In NaNO₂, the NO₂ molecules are situated at the centre of the orthorhombic unit cell. There are two possible orientations for the V-shaped molecule, and the probability for one of the orientations is a periodic function with periodicity along the a axis. In this case, the modulation wavevector $\alpha\mathbf{a}^*$ has a component α that strongly depends on temperature in a very narrow temperature range.

If the probability of finding species A in position $\mathbf{n} + \mathbf{r}_j$ or of finding one orientation of a molecule in that point is given by $P_j(\mathbf{Q} \cdot \mathbf{n})$, the probability for species B or the other orientation is of course $1 - P_j(\mathbf{Q} \cdot \mathbf{n})$. In the diffraction pattern, the spots belong to the Fourier module with basic vectors $\mathbf{a}^*, \mathbf{b}^*, \mathbf{c}^*$ and \mathbf{Q} . The analogous expression for a more general situation with more modulation wavevectors, or with more species or orientations, is a straightforward generalization.

The first examples of IC phases were found in *magnetic systems* (see Section 1.5.1.2.3). For example, holmium has a spiral spin arrangement with a periodicity of the spiral that does not fit with the underlying lattice. For the α component ($\alpha = x, y, z$) of the magnetic moment at position $\mathbf{n} + \mathbf{r}_j$ one has in an incommensurate magnetic system a superposition of waves

$$S_\alpha(\mathbf{n}) = \sum_m M_{maj} \cos(2\pi\mathbf{Q}_m \cdot \mathbf{n} + \varphi_{m\alpha}). \quad (1.10.1.7)$$

The most general expression is

$$S_\alpha(\mathbf{n}) = \sum_{\mathbf{H} \in M^*} M_{\alpha j}(\mathbf{H}) \exp(i\mathbf{H} \cdot \mathbf{n}), \quad (1.10.1.8)$$

where M^* is the Fourier module (1.10.1.1).

A following class of quasiperiodic materials is formed by *incommensurate composite structures*. To this belong misfit structures, intercalates and incommensurate adsorbed layers. An example is Hg_{3-x}AsF₆. This consists of a subsystem of AsF₆ octahedra forming a (modulated) tetragonal system and two other subsystems consisting of Hg chains, one system of chains in the x direction and one in the y direction. Because the average spacing between the Hg atoms is irrational with respect to the lattice constant of the host AsF₆ system in the same direction, the total structure does not have lattice periodicity in the a or b direction.

In general, there are two or more subsystems, labelled by v , and the atomic positions are given by

$$\mathbf{n}_v + \mathbf{r}_{vj} + \text{modulation}, \quad (1.10.1.9)$$

where \mathbf{n}_v belongs to the v th lattice, and where the modulation is a quasiperiodic displacement from the basic structure. The diffraction pattern has wavevectors

$$\mathbf{H} = \sum_v \sum_{i_v=1}^3 h_{i_v} \mathbf{a}_{vi_v}^* = \sum_{i=1}^n h_i \mathbf{a}_i^*. \quad (1.10.1.10)$$

Each of the reciprocal-lattice vectors \mathbf{a}_{vj}^* belongs to the Fourier module M^* and can be expressed as a linear combination with integer coefficients of the n basis vectors \mathbf{a}_i^* .

Very often, composite structures consist of a host system in the channels of which another material diffuses with a different, and

incommensurate, lattice constant. Examples are layer systems in which foreign atoms intercalate. Another type of structure that belongs to this class is formed by adsorbed monolayers, for example a noble gas on a substrate of graphite. If the natural lattice constant of the adsorbed material is incommensurate with the lattice constant of the substrate, the layer as a whole will be quasiperiodic.

In general, the subsystems can not exist as such. They form idealized lattice periodic structures. Because of the interaction between the subsystems the latter will, generally, become modulated, and even incommensurately modulated because of the mutual incommensurability of the subsystems. The displacive modulation will, generally, contain wavevectors that belong to the Fourier module (1.10.1.10). However, in principle, additional satellites may occur due to other mechanisms, and this increases the rank of the Fourier module.

The last class to be discussed here is that of *quasicrystals*. In 1984 it was found (Shechtman *et al.*, 1984) that in the diffraction pattern of a rapidly cooled AlMn alloy the spots were relatively sharp and the point-group symmetry was that of an icosahedron, a group with 120 elements and one that can not occur as point group of a three-dimensional space group. Later, ternary alloys were found with the same symmetry of the diffraction pattern, but with spots as sharp as those in ordinary crystals. These structures were called quasicrystals. Others have been found with eight-, ten- or 12-fold rotation symmetry of the diffraction pattern. Such symmetries are also *noncrystallographic symmetries* in three dimensions. Sometimes this noncrystallographic symmetry is considered as characteristic of quasicrystals.

Mathematical models for quasicrystals are quasiperiodic *two- and three-dimensional tilings*, plane or space coverings, without voids or overlaps, by copies of a finite number of 'tiles'. Examples are the Penrose tiling or the standard octagonal tiling in two dimensions, and a three-dimensional version of Penrose tiling, a quasiperiodic space filling by means of two types of rhombohedra. For Penrose tiling, all spots of the diffraction pattern are linear combinations of the five basis vectors

$$\mathbf{a}_m^* = \{a \cos[2\pi(m-1)/5], a \sin[2\pi(m-1)/5]\} \quad (m = 1, \dots, 5). \quad (1.10.1.11)$$

Because the sum of these five vectors is zero, the rank of the spanned Fourier module is four. The Fourier module of the standard octagonal tiling is spanned by

$$\mathbf{a}_m^* = \{a \cos[(m-1)\pi/4], a \sin[(m-1)\pi/4]\} \quad (m = 1, \dots, 4). \quad (1.10.1.12)$$

The rank of the Fourier module is four. The rank of the Fourier module of the three-dimensional Penrose tiling, consisting of two types of rhombohedra with a ratio of volumes of $(\sqrt{5} + 1)/2$, is six and basis vectors point to the faces of a regular dodecahedron.

An atomic model can be obtained by decorating the tiles with atoms, each type of tile in a specific way. Some quasicrystals can really be considered as decorated tilings.

1.10.1.3. Embedding in superspace

A simple example of a quasiperiodic function is obtained in the following way. Consider a function of n variables which is periodic with period one in each variable.

$$f(x_1, \dots, x_n) = f(x_1 + 1, x_2, \dots, x_n), \dots \quad (1.10.1.13)$$

Now take n mutually irrational numbers α_i and define the function $g(x)$ with one variable as

$$g(x) = f(\alpha_1 x, \alpha_2 x, \dots, \alpha_n x). \quad (1.10.1.14)$$

Because of the irrationality, the function $g(x)$ is not periodic. If we consider the Fourier transform of $f(x_1, \dots, x_n)$ we get

1.10. TENSORS IN QUASIPERIODIC STRUCTURES

$$f(x_1, \dots, x_n) = \sum_{m_1} \dots \sum_{m_n} A_{m_1, \dots, m_n} \exp[2\pi i(m_1 x_1 + \dots + m_n x_n)] \quad (1.10.1.15)$$

and consequently

$$g(x) = \sum_{m_1, \dots, m_n} A_{m_1, \dots, m_n} \exp\left[2\pi i \left(\sum_{i=1}^n m_i \alpha_i\right) x\right], \quad (1.10.1.16)$$

which proves that the function is quasiperiodic of rank n with n basis vectors $2\pi\alpha_i$ in one dimension.

The quasiperiodic function $g(x)$ is therefore the restriction to the line $(\alpha_1 x, \dots, \alpha_n x)$ in n -dimensional space. This is a general situation. Each quasiperiodic function can be obtained as the restriction of a periodic function in n dimensions to a subspace that can be identified with the physical space. We denote the n -dimensional space in which one finds the lattice periodic structure (the *superspace*) by V_s , the *physical space* by V_E and the additional space, called *internal space*, by V_I , such that V_s is the direct sum of V_E and V_I . In the field of quasicrystals, one often uses the name *parallel space* for V_E and *perpendicular space* for V_I .

On the other hand, one can embed the quasiperiodic function in superspace, which means that one constructs a lattice periodic function in n dimensions such that its restriction to physical space is the quasiperiodic function. Take as an example the displacively modulated structure of equation (1.10.1.2). Compare this three-dimensional structure with the array of lines

$$(\mathbf{n} + \mathbf{r}_j + \mathbf{f}_j(\mathbf{Q} \cdot \mathbf{n} + t), t) \quad (\text{real } t) \quad (1.10.1.17)$$

in four-dimensional space. The restriction to the three-dimensional hyperplane $t = 0$ gives exactly the structure (1.10.1.2). Moreover, the four-dimensional array of lines is lattice periodic. Because \mathbf{f}_j is periodic, the array is left invariant if one replaces t by $t + 1$, and for every lattice vector \mathbf{m} of the basic structure the array is left invariant if one replaces simultaneously t by $t - \mathbf{Q} \cdot \mathbf{m}$. This means that the array is left invariant by all four-dimensional lattice vectors of the lattice Σ with basis

$$\mathbf{a}_{si} = (\mathbf{a}_i, -\mathbf{Q} \cdot \mathbf{a}_i) \quad (i = 1, 2, 3), \quad \mathbf{a}_4 = (0, 1). \quad (1.10.1.18)$$

Indeed the quasiperiodic IC phase is the restriction to V_E ($t = 0$) of the lattice periodic function in four dimensions.

The reciprocal basis for (1.10.1.18) consists of the basis vectors

$$\mathbf{a}_{si}^* = (\mathbf{a}_i^*, 0) \quad (i = 1, 2, 3), \quad \mathbf{a}_4^* = (\mathbf{Q}, 1). \quad (1.10.1.19)$$

These span the reciprocal lattice Σ^* . The projection of this basis on V_E consists of the four vectors \mathbf{a}_i^* ($i = 1, 2, 3$) and \mathbf{Q} , and these form the basis for the Fourier module of the quasiperiodic structure.

This is a well known situation. From the theory of Fourier transformation one knows that the projection of the Fourier transform of a function in n dimensions on a d -dimensional subspace is the Fourier transform of the restriction of that n -dimensional function to the same d -dimensional subspace. This gives a way to embed the quasiperiodic structure in a space with as many dimensions as the rank of the Fourier module. One considers the basis of the Fourier module as the projection of n linearly independent vectors in n -dimensional space. This means that for every vector of the Fourier module one has exactly one reciprocal-lattice vector in V_s . Suppose the quasiperiodic structure is given by some function, for example the density $\rho(\mathbf{r})$. Then

$$\rho(\mathbf{r}) = \sum_{\mathbf{H} \in M^*} \hat{\rho}(\mathbf{H}) \exp(i\mathbf{H} \cdot \mathbf{r}). \quad (1.10.1.20)$$

One may define a function in n -dimensional space by

$$\rho_s(\mathbf{r}_s) = \sum_{\mathbf{H}_s \in \Sigma^*} \hat{\rho}(\mathbf{H}) \exp(i\mathbf{H}_s \cdot \mathbf{r}_s), \quad (1.10.1.21)$$

where \mathbf{H}_s is the unique reciprocal-lattice vector that is projected on the Fourier module vector \mathbf{H} . It is immediately clear that the restriction of ρ_s to physical space is exactly ρ . Moreover, the function ρ_s is lattice periodic with lattice Σ , for which Σ^* is the reciprocal lattice.

This construction can be performed in the following equivalent way. Consider a point \mathbf{r} in physical space, where one has the quasiperiodic function $\rho(\mathbf{r})$. The Fourier module of this function is the projection on physical space of the n -dimensional reciprocal lattice Σ^* with basis vectors \mathbf{a}_{si}^* ($i = 1, 2, \dots, n$). The reciprocal lattice Σ^* corresponds to the direct lattice Σ . A point \mathbf{r} in V_E can also be considered as an element $(\mathbf{r}, 0)$ in n -dimensional space. By the translations of Σ , this point is equivalent with a point \mathbf{r}_s with lattice coordinates

$$\xi_i = \text{Frac}(\mathbf{a}_{si}^* \cdot (\mathbf{r}, 0)) = \text{Frac}(\mathbf{a}_i^* \cdot \mathbf{r}) \quad (1.10.1.22)$$

in the unit cell of Σ , where $\text{Frac}(x)$ is x minus the largest integer smaller than x . If one puts $\rho_s(\mathbf{r}_s) = \rho(\mathbf{r})$, the function ρ determines the function ρ_s in the unit cell, and consequently in the whole n -dimensional space V_s . This means that all the information about the structure in V_E is mapped onto the information inside the n -dimensional unit cell. *The information in three dimensions is exactly the same as that in superspace.* Only the presentation is different.

In the case in which the crystal consists of point atoms, the corresponding points in d -dimensional physical space V_E are the intersection of $(n - d)$ -dimensional hypersurfaces with V_E . For displacively modulated IC phases in three dimensions with one modulation wavevector, one has $n = 4$, $d = 3$ and the hypersurfaces are just lines in superspace, as we have seen. For more independent modulation vectors the dimension of the hypersurfaces is larger than one. In this case, as often in the case of composite structures, the $(n - d)$ -dimensional surfaces do not have borders. This in contrast to quasicrystals, where they are bounded. All these hypersurfaces for which the intersection with physical space gives the atomic positions are called *atomic surfaces*.

1.10.2. Symmetry

1.10.2.1. Symmetry transformations

Because the embedded periodic structure in n dimensions has lattice periodicity, it has n -dimensional space-group symmetry as well. It is not *a priori* clear that such a symmetry group in the unphysical n -dimensional space is relevant for the physical structure, but we shall show here that the superspace description is indeed useful for the description of quasiperiodic systems. First we shall discuss some of the structures of these higher-dimensional space transformations.

Suppose the diffraction pattern has rotational symmetry. Consider for example an orthogonal transformation R that leaves the diffraction pattern invariant. In particular, any basis vector of the module is transformed into an element of the module, *i.e.* an integral linear combination of the basis vectors.

$$R\mathbf{a}_i^* = \sum_{j=1}^n M_{ji} \mathbf{a}_j^*, \quad i = 1, 2, \dots, n. \quad (1.10.2.1)$$

Because the matrix M depends on R and acts in reciprocal space, we denote it by $\Gamma^*(R) = M$. The matrix $\Gamma^*(R)$ has integer entries. Because the intensity of the diffraction pattern is not constant on circles around the origin (that would imply that one can not distinguish separate peaks), the orthogonal transformation R is of finite order. Then a theorem from group theory states that $\Gamma^*(R)$ is similar to an n -dimensional orthogonal transformation R_s . The latter certainly has an invariant subspace: the physical space. Therefore, one can find a basis transformation S such that the matrix $\Gamma^*(R)$ is conjugated to the direct sum of an orthogonal

1. TENSORIAL ASPECTS OF PHYSICAL PROPERTIES

transformation R in V_E and an additional orthogonal transformation in V_I :

$$S\Gamma^*(R)S^{-1} = \begin{pmatrix} R & 0 \\ 0 & R_I \end{pmatrix}, \quad R \in O(d), \quad R_I \in O(n-d). \quad (1.10.2.2)$$

We denote this orthogonal transformation in V_s as R_s or as a couple (R, R_I) . Clearly, the transformation R_s leaves the embedded reciprocal lattice Σ^* invariant. Moreover, this transformation leaves the direct lattice Σ invariant as well. As always, the action of R_s on the basis of Σ for which \mathbf{a}_{si}^* form the reciprocal basis is then given by

$$R_s \mathbf{a}_{si} = \sum_{j=1}^n \Gamma(R)_{ji} \mathbf{a}_{sj} \quad \text{with} \quad \Gamma(R)_{ij} = \Gamma^*(R^{-1})_{ji}. \quad (1.10.2.3)$$

This is the usual relation between the action on a basis and the action on the reciprocal basis.

By construction, the orthogonal transformation $R_s = (R, R_I)$ leaves the lattice Σ invariant, and can therefore belong to the point group of a periodic structure with this lattice. In general, such a point-group element does not leave the periodic structure itself invariant, just as a point group in three dimensions does not leave a crystal with a nonsymmorphic space group invariant. One then has to combine the orthogonal transformation with a translation that in general does not belong to the lattice. Here a translation has components in physical as well as in internal space. A translation can be denoted by $(\mathbf{a}_E, \mathbf{a}_I)$. Then a general solid motion can be written as

$$g = \{(R, R_I) | (\mathbf{a}_E, \mathbf{a}_I)\}. \quad (1.10.2.4)$$

The action of such a transformation on a point r_s in superspace is given by

$$gr_s = g(\mathbf{r}_E, \mathbf{r}_I) = (R\mathbf{r}_E + \mathbf{a}_E, R_I\mathbf{r}_I + \mathbf{a}_I). \quad (1.10.2.5)$$

If such a transformation leaves the periodic array of atomic surfaces in superspace invariant, it is a symmetry transformation. In particular, the elements $(\mathbf{a}_E, \mathbf{a}_I)$ of the translation group Σ are such symmetry transformations.

1.10.2.2. Point groups

The orthogonal transformations that leave the diffraction pattern invariant form a point group K , a finite subgroup of $O(d)$, where d is the dimension of the physical space. All elements act on the basis of the Fourier module as in (1.10.2.1) and the matrices $\Gamma^*(K)$ form a representation of the group K , an integral representation because the matrices have all integer entries, and reducible because the physical space is an invariant subspace for $\Gamma^*(K)$. Because K is finite, this representation is equivalent with a representation in terms of orthogonal matrices. Moreover, by construction $\Gamma^*(K)$ leaves the n -dimensional reciprocal lattice Σ^* invariant. It is an n -dimensional crystallographic point group. The components R of R_s form a d -dimensional point group K_E , which is not necessarily crystallographic, and the components R_I form an $(n-d)$ -dimensional point group K_I .

Consider as an example an IC phase with orthorhombic basic structure and one independent modulation wavevector $\gamma\mathbf{c}^*$ along the c axis. Suppose that the Fourier module, which is of rank four, is invariant under the point group mmm . Then one has for the three generators

$$\begin{aligned} m_x \mathbf{a}_1^* &= -\mathbf{a}_1^*, & m_x \mathbf{a}_2^* &= \mathbf{a}_2^*, & m_x \mathbf{a}_3^* &= \mathbf{a}_3^*, & m_x \mathbf{a}_4^* &= \mathbf{a}_4^* \\ m_y \mathbf{a}_1^* &= \mathbf{a}_1^*, & m_y \mathbf{a}_2^* &= -\mathbf{a}_2^*, & m_y \mathbf{a}_3^* &= \mathbf{a}_3^*, & m_y \mathbf{a}_4^* &= \mathbf{a}_4^* \\ m_z \mathbf{a}_1^* &= \mathbf{a}_1^*, & m_z \mathbf{a}_2^* &= \mathbf{a}_2^*, & m_z \mathbf{a}_3^* &= -\mathbf{a}_3^*, & m_z \mathbf{a}_4^* &= -\mathbf{a}_4^*. \end{aligned}$$

Therefore, the corresponding matrices $\Gamma^*(R)$ are

$$\begin{pmatrix} -1 & 0 & 0 & 0 \\ 0 & 1 & 0 & 0 \\ 0 & 0 & 1 & 0 \\ 0 & 0 & 0 & 1 \end{pmatrix}, \quad \begin{pmatrix} 1 & 0 & 0 & 0 \\ 0 & -1 & 0 & 0 \\ 0 & 0 & 1 & 0 \\ 0 & 0 & 0 & 1 \end{pmatrix}, \quad (1.10.2.6)$$

$$\begin{pmatrix} 1 & 0 & 0 & 0 \\ 0 & 1 & 0 & 0 \\ 0 & 0 & -1 & 0 \\ 0 & 0 & 0 & -1 \end{pmatrix},$$

which implies that the three generators of the four-dimensional point group are $(m_x, 1)$, $(m_y, 1)$ and $(m_z, 1)$.

The diffraction pattern of the standard octagonal tiling has rank four, basis vectors of the Fourier module are

$$(1, 0), \quad (\sqrt{1/2}, \sqrt{1/2}), \quad (0, 1), \quad (-\sqrt{1/2}, \sqrt{1/2})$$

and the pattern is invariant under a rotation of $\pi/4$ and a mirror symmetry. The action of these elements on the given basis of the Fourier module is

$$\Gamma^*(R_1) = \begin{pmatrix} 0 & 0 & 0 & -1 \\ 1 & 0 & 0 & 0 \\ 0 & 1 & 0 & 0 \\ 0 & 0 & 1 & 0 \end{pmatrix}, \quad \Gamma^*(R_2) = \begin{pmatrix} 0 & 0 & 0 & 1 \\ 0 & 0 & 1 & 0 \\ 0 & 1 & 0 & 0 \\ 1 & 0 & 0 & 0 \end{pmatrix}.$$

By a basis transformation, one may bring these transformations into the form

$$\begin{pmatrix} \cos(\pi/4) & -\sin(\pi/4) & 0 & 0 \\ \sin(\pi/4) & \cos(\pi/4) & 0 & 0 \\ 0 & 0 & \cos(3\pi/4) & -\sin(3\pi/4) \\ 0 & 0 & \sin(3\pi/4) & \cos(3\pi/4) \end{pmatrix},$$

$$\begin{pmatrix} -1 & 0 & 0 & 0 \\ 0 & 1 & 0 & 0 \\ 0 & 0 & -1 & 0 \\ 0 & 0 & 0 & 1 \end{pmatrix}.$$

Therefore, the $\pi/4$ rotation in physical space is combined with a $3\pi/4$ rotation in internal space in order to get a transformation that leaves a lattice invariant.

A three-dimensional example is the case of a quasicrystal with icosahedral symmetry. For the diffraction pattern all spots may be labelled with six indices with respect to a basis with basis vectors

$$\begin{aligned} \mathbf{a}_1^* &= (0, 0, 1) \\ \mathbf{a}_2^* &= (a, 0, b) \\ \mathbf{a}_3^* &= (a \cos(2\pi/5), a \sin(2\pi/5), b) \\ \mathbf{a}_4^* &= (a \cos(4\pi/5), a \sin(4\pi/5), b) \\ \mathbf{a}_5^* &= (a \cos(4\pi/5), -a \sin(4\pi/5), b) \\ \mathbf{a}_6^* &= (a \cos(2\pi/5), -a \sin(2\pi/5), b), \end{aligned}$$

with $a = 2/\sqrt{5}$ and $b = 1/\sqrt{5}$. The rotation subgroup that leaves the Fourier module invariant is generated by

$$\Gamma^*(A) = \begin{pmatrix} 1 & 0 & 0 & 0 & 0 & 0 \\ 0 & 0 & 1 & 0 & 0 & 0 \\ 0 & 0 & 0 & 1 & 0 & 0 \\ 0 & 0 & 0 & 0 & 1 & 0 \\ 0 & 0 & 0 & 0 & 0 & 1 \\ 0 & 1 & 0 & 0 & 0 & 0 \end{pmatrix},$$

$$\Gamma^*(B) = \begin{pmatrix} 0 & 0 & 0 & 0 & 0 & 1 \\ 1 & 0 & 0 & 0 & 0 & 0 \\ 0 & 0 & 0 & 0 & 1 & 0 \\ 0 & 0 & -1 & 0 & 0 & 0 \\ 0 & 0 & 0 & -1 & 0 & 0 \\ 0 & 1 & 0 & 0 & 0 & 0 \end{pmatrix}.$$
(1.10.2.7)

Moreover, there is the central inversion $-E$. The six-dimensional representation of the symmetry group, which is the icosahedral group $\bar{5}3m$, is reducible into the sum of two nonequivalent three-dimensional irreducible representations. A basis for this representation in the six-dimensional space is then given by

$$\begin{pmatrix} \mathbf{a}_1^* & c\mathbf{a}_1^* & \mathbf{a}_2^* & -c\mathbf{a}_2^* & \mathbf{a}_3^* & -c\mathbf{a}_3^* \\ \mathbf{a}_4^* & -c\mathbf{a}_4^* & \mathbf{a}_5^* & -c\mathbf{a}_5^* & \mathbf{a}_6^* & -c\mathbf{a}_6^* \end{pmatrix},$$
(1.10.2.8)

which projects on the given basis in V_E .

The point-group elements considered here are pairs of orthogonal transformations in physical and internal space. Orthogonal transformations that do not leave these two spaces invariant have not been considered. The reason for this is that the information about the reciprocal lattice comes from its projection on the Fourier module in physical space. By changing the length scale in internal space one does not change the projection but one would break a symmetry that mixes the two spaces. Nevertheless, quasicrystals are often described starting from an n -dimensional periodic structure with a lattice of higher symmetry. For example, the icosahedral 3D Penrose tiling can be obtained from a structure with a hypercubic six-dimensional lattice. Its reciprocal lattice is that spanned by the vectors (1.10.2.8) where one puts $c = 1$. The symmetry of the periodic structure, however, is lower than that of the lattice and has a point group in reducible form. Therefore, we shall consider here only reducible point groups, subgroups of the orthogonal group $O(n)$ which have a d -dimensional invariant subspace, identified with the physical space.

The fact that the spaces V_E and V_I are usually taken as mutually perpendicular does not have any physical relevance. One could as well consider oblique projections of a reciprocal lattice Σ^* on V_E . What is important is that the intersection of the periodic structure with the physical space should be the same in all descriptions. The metric in internal space V_I follows naturally from the fact that there is a finite group K_I .

1.10.2.3. Superspace groups

The quasiperiodic function $\rho(\mathbf{r})$ in d dimensions can be embedded as lattice periodic function $\rho_s(\mathbf{r}_s)$ in n dimensions. The symmetry group of the latter is the group of all elements g (1.10.2.4) for which

$$\rho_s(\mathbf{r}_s) = \rho_s(g\mathbf{r}_s) = \rho_s(R_E\mathbf{r} + \mathbf{a}_E, R_I\mathbf{r}_I + \mathbf{a}_I). \quad (1.10.2.9)$$

This group is an n -dimensional space group G . It has an invariant subgroup of translations, which is formed by the lattice translations Σ , and the quotient G/Σ is isomorphic to the n -dimensional point group K . However, not every n -dimensional space group can occur here because we made the restriction to reducible point

groups. For example, the n -dimensional hypercubic groups do not occur in this way as symmetry groups of quasiperiodic systems.

The product of two superspace group elements is

$$\{R_{s1}|\mathbf{a}_{s1}\}\{R_{s2}|\mathbf{a}_{s2}\} = \{R_{s1}R_{s2}|\mathbf{a}_{s1} + R_{s1}\mathbf{a}_{s2}\}. \quad (1.10.2.10)$$

On a lattice basis for Σ , the orthogonal transformations R_{s1} and R_{s2} are integer $n \times n$ matrices and the translations \mathbf{a}_{s1} and \mathbf{a}_{s2} are column vectors. The orthogonal transformations R_s leave the origin invariant. The translations depend on the choice of this origin. For a symmorphic space group there is a choice of origin such that the translations \mathbf{a} are lattice translations.

The point-group elements are reducible, which means that in the physical space one has the usual situation. If $d = 3$ then the only intrinsic nonprimitive translations are those in screw axes or glide planes. An n -dimensional orthogonal transformation can always be written as the sum of a number r of two-dimensional rotations with rotation angle different from π , a p -dimensional total inversion and a q -dimensional identity transformation. The integers r, p, q may be zero and $2r + p + q = n$. The possible intrinsic nonprimitive translations belong to the q -dimensional space in which the identity acts. For the three examples in the previous section, the internal component of the nonprimitive translation for m_x and m_y in the first example can be different from zero, but that for m_z in the same example is zero. For the octagonal case, only the second generator can have an intrinsic nonprimitive translation in the fourth direction, and for the icosahedral case the two generators have one two-dimensional invariant plane and one pointwise invariant line in V_I .

In the diffraction pattern of an IC phase one can distinguish between main reflections and satellites. A symmetry operation cannot transform a main reflection into a satellite. This implies that for these structures the reciprocal lattice of the basic structure is left invariant by the point group, and consequently the latter must be a three-dimensional crystallographic point group. Therefore, the point groups for IC phases are the same as those for lattice periodic systems. They act in superspace as a representation of a three-dimensional crystallographic point group. This is not true for an arbitrary quasiperiodic structure. The restriction in the general case comes from the requirement that the three-dimensional point group must have a faithful integer matrix representation in superspace. There is a mathematical statement to the effect that the lowest dimension in which a p -fold rotation can be represented as an integer matrix is given by the Euler function, the number of integers smaller than p that do not divide p . For example, for a prime number p this number is $p - 1$. This implies that if one restricts the rank of the Fourier module (*i.e.* the dimension of the superspace) to six, only values 1, 2, 3, 4, 5, 6, 7, 8, 9, 10, 12, 14 and 18 are possible for p . The values 7, 9, 14 and 18 only occur for two-dimensional quasiperiodic structures of rank six. Therefore, the allowable three-dimensional point groups for systems up to rank six are limited to the groups given in Table 1.10.2.1. The possible superspace groups for IC modulated phases of rank four are given in Chapter 9.8 of Volume C of *International Tables* (1999). Superspace groups for quasicrystals of rank $n \leq 6$ are given in Janssen (1988).

The notation of higher-dimensional symmetry groups is discussed in two IUCr reports (Janssen *et al.*, 1999, 2002).

1.10.3. Action of the symmetry group

1.10.3.1. Action of superspace groups

The action of the symmetry group on the periodic density function ρ_s in n dimensions is given by (1.10.2.9). The real physical structure, however, lives in physical space. One can derive from the action of the superspace group on the periodic structure its action on the quasiperiodic d -dimensional one. One knows that the density function in V_E is just the restriction of that in V_s . The same holds for the transformed function.

1. TENSORIAL ASPECTS OF PHYSICAL PROPERTIES

$$g\rho_s(\mathbf{r}_s) = \rho_s(g^{-1}\mathbf{r}_s) \rightarrow g\rho(\mathbf{r}) = \rho_s[R^{-1}(\mathbf{r} - \mathbf{a}_E), -R_I^{-1}\mathbf{a}_I]. \quad (1.10.3.1)$$

This transformation property differs from that under an n -dimensional Euclidean transformation by the ‘phase shift’ $-R_I^{-1}\mathbf{a}_I$. Take for example the IC phase with a sinusoidal modulation. If the positions of the atoms are given by

$$\mathbf{n} + \mathbf{r}_j + \mathbf{A}_j \cos(2\pi\mathbf{Q} \cdot \mathbf{n} + \varphi_j),$$

then the transformed positions are

$$R(\mathbf{n} + \mathbf{r}_j) + R\mathbf{A}_j \cos(2\pi\mathbf{Q} \cdot \mathbf{n} + \varphi_j - R_I^{-1}\mathbf{a}_I) + \mathbf{a}_E. \quad (1.10.3.2)$$

If the transformation g is a symmetry operation, this means that the original and the transformed positions are the same.

$$R(\mathbf{n} + \mathbf{r}_j) + \mathbf{a}_E = \mathbf{n}' + \mathbf{r}_j$$

and

$$R\mathbf{A}_j \cos(2\pi\mathbf{Q} \cdot \mathbf{n} + \varphi_j - R_I^{-1}\mathbf{a}_I) = \mathbf{A}_j \cos(2\pi\mathbf{Q} \cdot \mathbf{n}' + \varphi_j).$$

This puts, in general, restrictions on the modulation.

Another view of the same transformation property is given by Fourier transforming (1.10.2.9). The result for the Fourier transform is

$$g\hat{\rho}_s(\mathbf{k}_s) = \hat{\rho}_s(R_s^{-1}\mathbf{k}_s) \exp(-i\mathbf{k}_s \cdot \mathbf{a}_s) \quad (1.10.3.3)$$

and because there is a one-to-one correspondence between the vectors \mathbf{k}_s in the reciprocal lattice and the vectors \mathbf{k} in the Fourier module one can rewrite this as

$$g\hat{\rho}(\mathbf{k}) = \hat{\rho}(R^{-1}\mathbf{k}) \exp(-i\mathbf{k} \cdot \mathbf{a}_E - \mathbf{k}_I \cdot \mathbf{a}_I). \quad (1.10.3.4)$$

For a symmetry element one has $g\hat{\rho}(\mathbf{k}) = \hat{\rho}(\mathbf{k})$. Therefore, the superspace group element g is a symmetry transformation of the quasiperiodic function ρ if

$$\hat{\rho}(\mathbf{k}) = \hat{\rho}(R^{-1}\mathbf{k}) \exp(-i\mathbf{k} \cdot \mathbf{a}_E - \mathbf{k}_I \cdot \mathbf{a}_I). \quad (1.10.3.5)$$

This relation is at the basis of the *systematic extinctions*. If one has an orthogonal transformation R such that this in combination with a translation $(\mathbf{a}_E, \mathbf{a}_I)$ is a symmetry element and such that $R\mathbf{k} = \mathbf{k}$, then

$$\hat{\rho}(\mathbf{k}) = 0 \text{ if } \mathbf{k} \cdot \mathbf{a}_E + \mathbf{k}_I \cdot \mathbf{a}_I \neq 2\pi \times \text{integer}. \quad (1.10.3.6)$$

Because the structure factor is the Fourier transform of a density function which consists of δ functions on the positions of the atoms, for a quasiperiodic crystal it is the Fourier transform of a quasiperiodic function $\rho(\mathbf{r})$. Therefore, symmetry-determined absence of Fourier components leads to zero intensity of the corresponding diffraction peaks. Therefore, although there is no lattice periodicity for aperiodic crystals, systematic extinctions follow in the same way from the symmetry as in lattice periodic systems if one considers the n -dimensional space group as the symmetry group.

1.10.3.2. Compensating gauge transformations

The transformation property of the Fourier transform of the density given in the previous section can be formulated in another way. Consider a function $\rho(\mathbf{r})$ which is invariant under a d -dimensional Euclidean transformation $\{R|\mathbf{a}\}$ in physical space. Then its Fourier transform satisfies

$$\hat{\rho}(\mathbf{k}) = \hat{\rho}(R^{-1}\mathbf{k}) \exp(-i\mathbf{k} \cdot \mathbf{a}). \quad (1.10.3.7)$$

Conversely, if the Fourier transform satisfies this relation, the Euclidean transformation is a symmetry operation for $\rho(\mathbf{r})$. The

Table 1.10.2.1. Allowable three-dimensional point groups for systems up to rank six

| Isomorphism class | Order | Three-dimensional point groups |
|---------------------|-------|--|
| C_1 | 1 | 1 |
| C_2 | 2 | 2, $\bar{1}$, m |
| C_3 | 3 | 3 |
| C_4 | 4 | 4, $\bar{4}$ |
| C_5 | 5 | 5 |
| C_6 | 6 | 6, $\bar{6}$, $\bar{3}$ |
| C_8 | 8 | 8, $\bar{8}$ |
| C_{10} | 10 | 10, $\bar{10}$, $\bar{5}$ |
| C_{12} | 12 | 12, $\bar{12}$ |
| D_2 | 4 | 222, $2/m$, $2mm$ |
| D_3 | 6 | 32, $3m$ |
| D_4 | 8 | 422, $4mm$, $\bar{4}2m$ |
| D_5 | 10 | 52, $5m$ |
| D_6 | 12 | 622, $\bar{3}m$, $6mm$, $\bar{6}2m$ |
| D_8 | 16 | 822, $8mm$, $\bar{8}2m$ |
| D_{10} | 20 | 1022, $10mm$, $\bar{10}2m$, $\bar{5}m$ |
| D_{12} | 24 | 1222, $12mm$, $\bar{12}2m$ |
| $C_4 \times C_2$ | 8 | $4/m$ |
| $C_6 \times C_2$ | 12 | $6/m$ |
| $C_8 \times C_2$ | 16 | $8/m$ |
| $C_{10} \times C_2$ | 20 | $10/m$ |
| $C_{12} \times C_2$ | 24 | $12/m$ |
| $D_2 \times C_2$ | 8 | mmm |
| $D_4 \times C_2$ | 16 | $4/mmm$ |
| $D_6 \times C_2$ | 24 | $6/mmm$ |
| $D_8 \times C_2$ | 32 | $8/mmm$ |
| $D_{10} \times C_2$ | 40 | $10/mmm$ |
| $D_{12} \times C_2$ | 48 | $12/mmm$ |
| T | 12 | 23 |
| O | 24 | 432, $\bar{4}3m$ |
| I | 60 | 532 |
| $T \times C_2$ | 24 | $m\bar{3}$ |
| $O \times C_2$ | 48 | $m\bar{3}m$ |
| $I \times C_2$ | 120 | $\bar{5}3m$ |

two equations (1.10.3.5) and (1.10.3.7) are closely related. One can also write (1.10.3.5) as

$$\hat{\rho}(\mathbf{k}) = \hat{\rho}(R^{-1}\mathbf{k}) \exp(-i\mathbf{k} \cdot \mathbf{a}) \exp[i\Phi(R, \mathbf{k})], \quad (1.10.3.8)$$

where $\Phi(R, \mathbf{k})$ can be considered as a gauge transformation that compensates for the phase shift: it is a *compensating gauge transformation*. It is a function that is linear in \mathbf{k} ,

$$\Phi(R, \mathbf{k} + \mathbf{k}') = \Phi(R, \mathbf{k}) + \Phi(R, \mathbf{k}') \pmod{2\pi}, \quad (1.10.3.9)$$

and satisfies a relation closely related to the one satisfied by nonprimitive translations.

$$\Phi(R, \mathbf{k}) + \Phi(S, R\mathbf{k}) = \Phi(RS, \mathbf{k}) \pmod{2\pi}. \quad (1.10.3.10)$$

[Recall that a system of nonprimitive translations $\mathbf{u}(R)$ satisfies $\mathbf{u}(R) + R\mathbf{u}(S) = \mathbf{u}(RS)$ modulo lattice translations.] Therefore, the Euclidean transformation $\{R|\mathbf{a}\}$ combined with the compensating gauge transformation with gauge function $\Phi(R, \mathbf{k})$ is a symmetry transformation for $\rho(\mathbf{r})$ if equation (1.10.3.8) is satisfied. This is a three-dimensional formulation of the superspace group symmetry relation (1.10.3.5).

1.10.3.3. Irreducible representations of three-dimensional space groups

A third way to describe the symmetry of a quasiperiodic function is by means of irreducible representations of a space group. For the theory of these representations we refer to Chapter 1.2 on representations of crystallographic groups.

Consider first a modulated IC phase. Suppose the positions of the atoms are given by

$$\mathbf{n} + \mathbf{r}_j + \mathbf{u}_{nj}, \quad (1.10.3.11)$$

where \mathbf{n} belongs to the lattice, \mathbf{r}_j is a position inside the unit cell and \mathbf{u}_{nj} is a displacement. If the structure is quasiperiodic with

1.10. TENSORS IN QUASIPERIODIC STRUCTURES

Fourier module M^* , the vectors $\mathbf{u}_{\mathbf{n}j}$ can be written as a superposition of normal modes.

$$\mathbf{u}_{\mathbf{n}j} = \sum_{\mathbf{k} \in M^*, \nu} Q_{\mathbf{k}\nu} \boldsymbol{\epsilon}(\mathbf{k}\nu|j) e^{i\mathbf{k} \cdot \mathbf{n}} + c.c., \quad (1.10.3.12)$$

where the coefficient $Q_{\mathbf{k}\nu}$ is a normal coordinate, ν denotes the band index and $\boldsymbol{\epsilon}(\mathbf{k}\nu|j)$ denotes the polarization of the normal mode. The normal coordinates transform under a space group according to one of its irreducible representations. The relevant space group here is that of the basic structure. For the simple case of a one-dimensional irreducible representation, for each \mathbf{k} the effect is simply multiplication by a factor of absolute value unity. For example, for the modulated phase with basic space group $Pcmn$ and wavevector $\mathbf{k} = \gamma\mathbf{c}^*$ there are four non-equivalent one-dimensional representations. It depends on the band index which representation occurs in the decomposition. The space-group element $\{R|\mathbf{a}\}$, for which $R\mathbf{q} = \mathbf{q}$ (modulo reciprocal lattice) acts on $Q_{\mathbf{k}\nu}$ according to

$$Q_{\mathbf{k}\nu} \rightarrow Q_{\mathbf{k}\nu} \exp(i\mathbf{k} \cdot \mathbf{a}) \chi_\nu(R),$$

where $\chi_\nu(R)$ is the character of R in an irreducible representation associated with the branch ν . Because the character of a one-dimensional representation is of absolute value unity, one may write it as $\exp[i\varphi_\nu(R, \mathbf{k})]$. Consequently, if the decomposition of the displacement contains only the vectors $\pm\mathbf{k}$, the factor $\exp[i\varphi_\nu(R, \mathbf{k})]$ describes a shift in the modulation function.

Consider again as an example a basic structure with space group $Pcmn$ and a modulation wavevector $\gamma\mathbf{c}^*$. The point group $K_{\mathbf{k}}$ that leaves the modulation wavevector invariant is generated by m_y and m_x . This point group $mm2$ has four elements and four irreducible representations, all one-dimensional. One of them has for the character $\chi(m_x) = +1$, $\chi(m_y) = -1$. If the displacements of the atoms are described by a normal mode belonging to this irreducible representation, then the compensating phase shifts for c_x and m_y are, respectively, 0 and π . In the notation for superspace groups, this is the group $Pcmn(00\gamma)1s1$. The same structure can be described by the irreducible representation characterized as Δ_3 , because the modulation wavevector is the point Δ in the Brillouin zone and the irreducible representation Γ_3 has the character mentioned above.

In this way there is a correspondence between superspace groups for $(3+1)$ -dimensional modulated structures and two-dimensional irreducible representations of three-dimensional space groups.

1.10.4. Tensors

1.10.4.1. Tensors in higher-dimensional spaces

A vector in an n -dimensional space V transforms under an element of a point group as $\mathbf{r} \rightarrow R\mathbf{r}$. With respect to a basis \mathbf{a}_i , the coordinates and basis vectors transform according to

$$\begin{aligned} \mathbf{a}'_i &= \sum_{j=1}^n R_{ji} \mathbf{a}_j \\ \mathbf{r} &= \sum_{i=1}^n x_i \mathbf{a}_i \rightarrow \mathbf{r}' = \sum_{i=1}^n x'_i \mathbf{a}'_i, \quad x'_i = \sum_{j=1}^n R_{ij} x_j \end{aligned}$$

and the reciprocal basis vectors and coordinates in reciprocal space according to

$$\begin{aligned} \mathbf{a}^*_i &= \sum_{j=1}^n R_{ij} \mathbf{a}^*_{j'} \\ \mathbf{k} &= \sum_{i=1}^n \kappa_i \mathbf{a}^*_i \rightarrow \mathbf{k}' = \sum_{i=1}^n \kappa'_i \mathbf{a}^*_{i'}, \quad \kappa'_i = \sum_{j=1}^n R_{ji}^{-1} \kappa_j. \end{aligned}$$

With respect to an orthonormal basis in V the transformations are represented by orthogonal matrices. For orthogonal matrices

$R^{-1} = R^T$, the vectors in reciprocal space transform in exactly the same way as in direct space:

$$\begin{aligned} \mathbf{r} &= \sum_{i=1}^n x_i \mathbf{e}_i \rightarrow \mathbf{r}' = \sum_{i=1}^n x'_i \mathbf{e}_i \quad x'_i = \sum_{j=1}^n R_{ij} x_j \\ \mathbf{k} &= \sum_{i=1}^n \kappa_i \mathbf{e}_i^* \rightarrow \mathbf{k}' = \sum_{i=1}^n \kappa'_i \mathbf{e}_i^* \quad \kappa'_i = \sum_{j=1}^n R_{ij} \kappa_j. \end{aligned}$$

As discussed in Section 1.2.4, a tensor is a multilinear function of vectors and reciprocal vectors. Consider for example a tensor of rank two, the metric tensor g . It is a function of two vectors \mathbf{r}_1 and \mathbf{r}_2 which results in the scalar product of the two.

$$g(\mathbf{r}_1, \mathbf{r}_2) = \mathbf{r}_1 \cdot \mathbf{r}_2.$$

It clearly is a symmetric function because $g(\mathbf{r}_1, \mathbf{r}_2) = g(\mathbf{r}_2, \mathbf{r}_1)$. It is a function that is linear in each of its arguments and therefore

$$g(\mathbf{r}_1, \mathbf{r}_2) = g\left(\sum_{i=1}^n x_i \mathbf{e}_i, \sum_{j=1}^n y_j \mathbf{e}_j\right) = \sum_{ij} x_i y_j \delta_{ij} = \sum_i x_i y_i$$

if x_i and y_j are Cartesian coordinates of \mathbf{r}_1 and \mathbf{r}_2 , respectively. For another basis, for example a lattice basis, one has coordinates ξ_i and η_j , and the same function becomes

$$g(\mathbf{r}_1, \mathbf{r}_2) = g\left(\sum_{i=1}^n \xi_i \mathbf{a}_i, \sum_{j=1}^n \eta_j \mathbf{a}_j\right) = \sum_{ij} \xi_i \eta_j g_{ij} \quad (1.10.4.1)$$

with $g_{ij} = g(\mathbf{a}_i, \mathbf{a}_j)$. The relation between the Cartesian tensor components and the lattice tensor components follows from the basis transformation from orthonormal to a lattice basis. If

$$\mathbf{a}_j = \sum_k S_{kj} \mathbf{e}_k, \quad (1.10.4.2)$$

then the lattice tensor components are

$$g_{ij} = \sum_k S_{ki} S_{kj}.$$

For example, in the two-dimensional plane a lattice spanned by $a(1, 0)$ and $a(-\frac{1}{2}, \frac{\sqrt{3}}{2})$ has a basis obtained from an orthonormal basis by the basis transformation

$$S = a \begin{pmatrix} 1 & -\frac{1}{2} \\ 0 & \frac{\sqrt{3}}{2} \end{pmatrix}$$

and consequently the tensor components in lattice coordinates are

$$g_{ij} = \begin{pmatrix} a^2 & -\frac{1}{2}a^2 \\ -\frac{1}{2}a^2 & a^2 \end{pmatrix}.$$

The transformation of the tensor g under an orthogonal transformation follows from its definition. The transformation of the Cartesian tensor under the orthogonal transformation R is

$$g'_{ij} = \sum_{kl} R_{ki} R_{lj} g_{kl} = \sum_{kl} R_{ki} R_{lj} \delta_{kl} = \delta_{ij}$$

because of the fact that the matrix R_{ij} is orthogonal. The transformation of the tensor components with respect to the lattice basis, on which R is given by $\Gamma(R)$, is

$$g'_{ij} = \sum_{kl} \Gamma(R)_{ki} \Gamma(R)_{lj} g_{kl}, \quad (1.10.4.3)$$

or in matrix form $g' = \Gamma(R)^T g \Gamma(R)$.

The metric tensor is invariant under a point group K if

$$g_{ij} = \sum_{kl} \Gamma(R)_{ki} \Gamma(R)_{lj} g_{kl} \quad \forall R \in K. \quad (1.10.4.4)$$

1. TENSORIAL ASPECTS OF PHYSICAL PROPERTIES

On the one hand this formula can be used to determine the symmetry of a lattice with metric tensor g and on the other hand one may use it to determine the general form of a metric tensor invariant under a given point group. This comes down to the determination of the free parameters in g for given group of matrices $\Gamma(K)$. These are the coordinates in the space of invariant tensors.

1.10.4.2. Tensors in superspace

The tensors occurring for quasiperiodic structures are defined in a higher-dimensional space, but this space contains as privileged subspace the physical space. Since physical properties are measured in this physical space, the coordinates are not all on the same footing. This implies that sometimes one has to make a distinction between the various tensor elements as well.

The distinction between physical and internal (or perpendicular) coordinates can be made explicit by using a *split basis*. This is a basis for the superspace such that the first d basis vectors span the physical subspace and the other $n - d$ basis vectors span the internal space. A lattice basis is, generally, not a split basis.

Let us consider again the metric tensor which is used to characterize higher-dimensional lattices as well, and in particular those corresponding to quasiperiodic structures. The elements $g_{ij} = g(\mathbf{a}_i, \mathbf{a}_j)$ transform according to

$$g'_{ij} = g(\mathbf{a}'_i, \mathbf{a}'_j) = \sum_{kl} R_{ki} R_{lj} g_{kl}.$$

The symmetry of an n -dimensional lattice with metric tensor g is the group of nonsingular $n \times n$ integer matrices S satisfying

$$g = S^T g S, \quad (1.10.4.5)$$

where T means the transpose. For a lattice corresponding to a quasiperiodic structure, this group is reducible into a d - and an $(n - d)$ -dimensional component, where d is the dimension of physical space. This means that the d -dimensional component, which forms a finite group, is equivalent with a d -dimensional group of orthogonal transformations. In general, however, this does not leave a lattice in physical space invariant. However, it leaves the Fourier module of the quasiperiodic structure invariant. The basis vectors, for which the metric tensor determines the mutual relation, belong to the higher-dimensional superspace. Therefore, in this case the external and internal components of the basis vectors do not need to be treated differently. For the metric tensor g on a split basis one has

$$g_{ij} = 0 \quad \text{if } i \leq d, j > d \text{ or } i > d, j \leq d.$$

A quasiperiodic structure has an n -dimensional lattice embedding such that the intersection of Σ with the physical space V_E does not contain a d -dimensional lattice. Because of the incommensurability, however, there are lattice points of Σ arbitrarily close to V_E . This means that by an arbitrarily small shear deformation one may get a lattice in the physical space. The deformed quasiperiodic structure then becomes periodic. In general, the symmetry of the lattice then changes. This is certainly the case if the point group of the quasiperiodic structure is noncrystallographic, because then there cannot be a lattice in physical space left invariant by such a point group. For a given lattice Σ with symmetry group K one may ask which subgroups allow a deformation of the lattice that gives periodicity in V_E .

Physical tensors give often relations between vectorial or tensorial properties. Then they are multilinear functions of p vectors (and possibly q reciprocal vectors). An example is the dielectric tensor ε that gives the relation between E and D fields. This relation and the corresponding expression for the free energy F are

$$D_i = \sum_j \varepsilon_{ij} E_j \quad \text{or} \quad F = \sum_{ij} E_i \varepsilon_{ij} E_j = \varepsilon(\mathbf{E}, \mathbf{E}). \quad (1.10.4.6)$$

Therefore, the ε tensor is a bilinear function of vectors. The difference from the metric tensor is that here the vectors E and D are physical quantities which have d components and lie in physical space. The transformation properties therefore only depend on the physical-space components R_E of the superspace point group, and not on the full transformations R .

An intermediate case occurs for the strain. The strain tensor S gives the relation between a displacement and its origin: the point \mathbf{r} is displaced to $\mathbf{r} + \Delta\mathbf{r}$ with $\Delta\mathbf{r}$ linear in \mathbf{r} :

$$\Delta\mathbf{r}_i = \sum_j S_{ij} \mathbf{r}_j.$$

In ordinary elasticity, both \mathbf{r} and $\Delta\mathbf{r}$ belong to the physical space, and the relevant tensor is the symmetric part of S :

$$\frac{1}{2}(\partial_i \Delta\mathbf{r}_j + \partial_j \Delta\mathbf{r}_i).$$

For a quasiperiodic structure, $\Delta\mathbf{r}$ may be either a vector in physical space or in superspace and may depend both on physical and internal coordinates. That means that the matrix σ is either $d \times d$, or $n \times d$ or $n \times n$. Displacements in physical space are said to affect the *phonon degrees of freedom*, those in internal space the *phason degrees of freedom*. The phonon and phason displacements are functions of the physical-space coordinates. The transformation of the strain tensor under an element of a superspace group is

$$S'_{ij} = \sum_{k=1}^d \sum_{l=1}^d R_{Eki} R_{Elj} S_{kl} \quad \text{for phonon degrees,}$$

$$S'_{ij} = \sum_{k=d+1}^n \sum_{l=1}^d R_{Iki} R_{Elj} S_{kl} \quad \text{for phason degrees,}$$

$$S'_{ij} = \sum_{k=1}^n \sum_{l=1}^n R_{ski} R_{slj} S_{kl} \quad \text{for the general case.}$$

The first two of these expressions apply only to a split basis, but the third can be written on a lattice basis.

$$\sum_{k,l=1}^n \Gamma(R)_{ki} \Gamma(R)_{lj} S_{kl}. \quad (1.10.4.7)$$

The tensor of elastic stiffnesses c gives the relation between stress T and strain S . The stress tensor is a physical tensor of rank two and dimension three. For the phonon strain one has

$$S_{ij} = \sum_{kl} c_{ijkl} T_{kl}, \quad (i, j = 1, \dots, 3). \quad (1.10.4.8)$$

The phonon part of the elasticity tensor is symmetric under interchange of ij and kl , i and j , and k and l . It can be written in the usual notation $c_{\mu\nu}$ with $\mu, \nu = 1, 2, \dots, 6$ with $1 = (11)$, $2 = (22)$, $3 = (33)$, $4 = (23)$, $5 = (13)$, $6 = (12)$. Its transformation property under a three-dimensional orthogonal transformation is

$$c'_{ijkl} = \sum_{i'j'k'l'} R_{i'i} R_{j'j} R_{k'k} R_{l'l} c_{i'j'k'l'}.$$

For the phason part a similar elasticity tensor is defined. This and the third elastic contribution, the coupling between phonons and phasons, will be discussed in Section 1.10.4.5.

1.10.4.3. Inhomogeneous tensors

A vector field in d -dimensional space assigns a vector to each point of the space. This vector-valued function may, for a quasi-

1.10. TENSORS IN QUASIPERIODIC STRUCTURES

periodic system, have values in physical space or in superspace. In both cases one has the transformation property

$$g\mathbf{f}_i(\mathbf{r}) = \sum_j R_{ji}\mathbf{f}_j(g^{-1}\mathbf{r}). \quad (1.10.4.9)$$

For a vector field in physical space, i and j run over the values 1, 2, 3. This vector field may, however, be quasiperiodic. This means that it may be embedded in superspace. Then

$$g\mathbf{f}_i(\mathbf{r}_s) = \sum_{j=1}^3 R_{Eji}\mathbf{f}_j[R_E^{-1}(\mathbf{r} - \mathbf{a}), R_I^{-1}(\mathbf{r}_I - \mathbf{a}_I)]. \quad (1.10.4.10)$$

Here $i = 1, 2, 3$. If the vector field has values in superspace, as one can have for a displacement, one has

$$g\mathbf{f}_i(\mathbf{r}_s) = \sum_{j=1}^n R_{sji}\mathbf{f}_j[R_E^{-1}(\mathbf{r} - \mathbf{a}), R_I^{-1}(\mathbf{r}_I - \mathbf{a}_I)]. \quad (1.10.4.11)$$

Here $i = 1, \dots, n$. For Cartesian coordinates with respect to a split basis, R_s acts separately on physical and internal space and one has

$$g\mathbf{f}_i(\mathbf{r}_s) = \sum_{j=d+1}^n R_{iji}\mathbf{f}_j[R_E^{-1}(\mathbf{r} - \mathbf{a}), R_I^{-1}(\mathbf{r}_I - \mathbf{a}_I)] \quad (1.10.4.12)$$

for $i = d + 1, \dots, n$.

Just as for homogeneous tensors, inhomogeneous tensors may be divided into physical tensors with components in physical space only and others that have components with respect to an n -dimensional lattice. A physical tensor of rank two transforms under a space-group element $g = \{R_s|\mathbf{a}_s\}$ as

$$(gT)_{ij}(\mathbf{r}_s) = \sum_{k=1}^d \sum_{l=1}^d R_{Eki}R_{Elj}T_{kl}[R_E^{-1}(\mathbf{r}_E - \mathbf{a}_E), R_I^{-1}(\mathbf{r}_I - \mathbf{a}_I)]. \quad (1.10.4.13)$$

This implies the following transformation property for the Fourier components:

$$(g\hat{T})_{ij}(\mathbf{k}) = \sum_{k=1}^d \sum_{l=1}^d R_{Eki}R_{Elj}T_{kl}(R_E^{-1}\mathbf{k}) \exp(iR_E\mathbf{k} \cdot \mathbf{a}_E + iR_I\mathbf{k}_I \cdot \mathbf{a}_I). \quad (1.10.4.14)$$

This gives relations between various Fourier components and restrictions for wavevectors \mathbf{k} for which $R_E\mathbf{k} = \mathbf{k}$:

$$\hat{T}_{ij}(\mathbf{k}) = \sum_{k=1}^d \sum_{l=1}^d R_{Eki}R_{Elj}T_{kl}(\mathbf{k}) \exp(iR_E\mathbf{k} \cdot \mathbf{a}_E + iR_I\mathbf{k}_I \cdot \mathbf{a}_I). \quad (1.10.4.15)$$

For tensors with superspace components, the summation over the indices runs from 1 to n . An invariant tensor then satisfies

$$\hat{T}_{ij}(\mathbf{k}) = \sum_{k=1}^n \sum_{l=1}^n R_{ski}R_{slj}T_{kl}(\mathbf{k}) \exp(iR_E\mathbf{k} \cdot \mathbf{a}_E + iR_I\mathbf{k}_I \cdot \mathbf{a}_I). \quad (1.10.4.16)$$

The generalization to higher-rank tensors is straightforward.

1.10.4.4. Irreducible representations

For the characterization of vectors and tensors one needs the irreducible and vector representations of the point groups. If the point group is crystallographic in three dimensions, these can be found in Chapter 1.2. All point groups for IC phases or composite structures belong to this category. Exceptions are the point groups for quasicrystals. For the finite point groups for structures

up to rank six these are given in Table 1.10.5.1. This table presents:

(1) The character tables for the point groups

$$\begin{aligned} &5, \bar{5}, 5m, 52, \bar{5}m \\ &10, \bar{10}, 10/m, 10mm, 1022, \bar{10}2m, 10/mmm \\ &8, \bar{8}, 8/m, 8mm, 822, \bar{8}2m, 8/mmm \\ &12, \bar{12}, 12/m, 12mm, 1222, \bar{12}2m, 12/mmm \\ &532, \bar{5}3m. \end{aligned}$$

(2) Matrices for the generators in the irreducible representations of the groups

$$\bar{5}m, 10/mmm, 8/mmm, 12/mmm, \bar{5}3m.$$

(3) The vector representations and some tensor representations for the groups in the systems

$$\bar{5}m, 10/mmm, 8/mmm, 12/mmm, \bar{5}3m.$$

The character tables can be used to determine the number of independent tensor elements. This is the dimension of subspace of tensors transforming with the identity representation. Tensors transform according to (properly symmetrized or anti-symmetrized) tensor products of vector representations. The number of times the identity representation occurs in the decomposition of the tensor product into irreducible components is equal to the number of independent tensor elements and can be calculated with the multiplicity formula. A number of examples are given in the following section.

1.10.4.5. Determining the number of independent tensor elements

1.10.4.5.1. Piezoelectric tensor

(See Sections 1.1.4.4.3 and 1.1.4.10.1.) The strain in a crystal is determined by its displacement field. For a quasiperiodic crystal, this displacement can have components in the physical space V_E as well as in the internal space V_I . The first implies a local displacement of the material, the latter corresponds to a local deformation because of the shift in the internal coordinate, which is, for example, the phase of a modulation wave or a phason jump for a quasicrystal. The displacement in the point \mathbf{r} is $u = [u_E(\mathbf{r}), u_I(\mathbf{r})]$. Denote u_E by \mathbf{v} and u_I by \mathbf{w} . The strain tensor then is given by $\partial_i v_j$ and by $\partial_i w_k$. Here i and j run from 1 to the physical dimension d , and k from 1 to the internal dimension $n - d$. The antisymmetric part of $\partial_i v_j$ corresponds to a global rotation, which does not lead to an energy change. Therefore, the relevant tensors are

$$\begin{aligned} e_{ij} &= (\partial_i v_j + \partial_j v_i)/2, \quad f_{ik} = \partial_i w_k, \\ (i, j &= 1, \dots, d; k = 1, \dots, n - d). \end{aligned} \quad (1.10.4.17)$$

Both the phonon part e and the phason part f may be coupled to an external electric field E . A linear coupling is given by the piezoelectric tensor p_{ijk} . The free energy is given by

$$F = \int d\mathbf{r} \left(\sum_{ijk} p_{ijk}^e e_{ij} E_k + \sum_{ijk} p_{ijk}^f f_{ij} E_k \right).$$

The tensor e transforms with the symmetrized square of the vector representation in physical space, the tensor f according to the product of the vector representations in physical and internal space. Then p^e and p^f transform according to the product of these two representations with the vector representation in physical space, because E is a physical vector.

As an example, consider the decagonal phase with point group $10mm(10^3mm)$. The physical space is three-dimensional and

1. TENSORIAL ASPECTS OF PHYSICAL PROPERTIES

Table 1.10.4.1. Characters of the point group $10mm(10^3mm)$ for representations relevant for elasticity

$$\tau = (\sqrt{5} - 1)/2.$$

| Representation | Classes | | | | | Reduction |
|---------------------------------------|---------|------------|------------|-----|------|--|
| | E | A | A^2 | B | AB | |
| | 1 | 12 | 12 | 20 | 15 | |
| Γ_E | 3 | $1 + \tau$ | $-\tau$ | 0 | -1 | Γ_2 |
| Γ_I | 3 | $-\tau$ | $1 + \tau$ | 0 | -1 | Γ_3 |
| Γ_E^2 | 9 | $2 + \tau$ | $1 - \tau$ | 0 | 1 | |
| $\Gamma_e(g^2)$ | 3 | $-\tau$ | $1 + \tau$ | 0 | 3 | |
| $\Gamma_e = (\Gamma_E)_s^2$ | 6 | 1 | 1 | 0 | 2 | $\Gamma_1 + \Gamma_5$ |
| Γ_e^2 | 36 | 1 | 1 | 0 | 4 | |
| $\Gamma_e(g^2)$ | 6 | 1 | 1 | 0 | 6 | |
| $(\Gamma_e)_s^2$ | 21 | 1 | 1 | 0 | 5 | $2\Gamma_1 + \Gamma_4 + 3\Gamma_5$ |
| $\Gamma_f = \Gamma_E \times \Gamma_I$ | 9 | -1 | -1 | 0 | 1 | $\Gamma_4 + \Gamma_5$ |
| $(\Gamma_f)_s^2$ | 45 | 0 | 0 | 0 | 5 | $2\Gamma_1 + \Gamma_2 + \Gamma_3 + 3\Gamma_4 + 5\Gamma_5$ |
| $\Gamma_e \times \Gamma_f$ | 54 | -1 | -1 | 0 | 2 | $\Gamma_1 + 2\Gamma_2 + 2\Gamma_3 + 4\Gamma_4 + 5\Gamma_5$ |

carries a $(2 + 1)$ -reducible representation $(\Gamma_i \oplus \Gamma_5)$, the internal space an irreducible two-dimensional representation (Γ_8) . The symmetrized square of the first is six-dimensional, and the product of first and second is also six-dimensional. The products of these two with the three-dimensional vector representation in physical space are both 18-dimensional. The first contains the identity representation three times, the other does not contain the identity representation. This implies that the piezoelectric tensor has three independent tensor elements, all belonging to p^e . The tensor p^f is zero.

1.10.4.5.2. Elasticity tensor

(See Section 1.3.3.2.) As an example of a fourth-rank tensor, we consider the elasticity tensor. The lowest-order elastic energy is a bilinear expression in e and f :

$$F = \int d\mathbf{r} \left(\frac{1}{2} \sum_{ijkl} c_{ijkl}^E e_{ij} e_{kl} + \frac{1}{2} \sum_{ijkl} c_{ijkl}^I f_{ij} f_{kl} + \sum_{ijkl} c_{ijkl}^{EI} e_{ij} f_{kl} \right). \quad (1.10.4.18)$$

The elastic free energy is a scalar function. The integrand must be invariant under the operations of the symmetry group. When $\Gamma_E(K)$ is the vector representation of K in the physical space (*i.e.* the vectors in V_E transform according to this representation) and $\Gamma_I(K)$ the vector representation in V_I , the tensor e_{ij} transforms according to the symmetrized square of Γ_E and the tensor f_{ij} transforms according to the product $\Gamma_E \otimes \Gamma_I$. Let us call these representations Γ_e and Γ_f , respectively. This implies that the term that is bilinear in e transforms according to the symmetrized square of Γ_e , that the term bilinear in f transforms according to the symmetrized square of Γ_f , and that the mixed term transforms according to $\Gamma_e \otimes \Gamma_f$. The number of elastic constants follows from their transformation properties. If $d = 3$ and $n = 3 + p$, the number of constants c^E is 21, the number of constants c^I is $3p(3p + 1)/2$ and the number of c^{EI} is 18p. Therefore, without symmetry conditions, there are altogether $3(2 + p)(7 + 3p)/2$ elastic constants. For arbitrary dimension d of the physical space and dimension n of the superspace this number is

$$\begin{aligned} & d(d + 1)(d^2 + d + 2)/8 + pd(pd + 1)/2 + d^2(d + 1)p/2 \\ & = d(2p + d + 1)(2 + d + d^2 + 2pd)/8. \end{aligned}$$

The number of independent elastic constants is the number of independent coefficients in F , and this is given by the number of invariants, *i.e.* the number of times the identity representation occurs as irreducible component of, respectively, the symmetrized square of Γ_e , the symmetrized square of Γ_f , and of $\Gamma_e \otimes \Gamma_f$. The

first number is the number of elastic constants in classical theory. The other elastic constants involve the phason degrees of freedom, which exist for quasiperiodic structures. The theory of the generalized elasticity theory for quasiperiodic crystals has been given by Bak (1985), Lubensky *et al.* (1985), Socolar *et al.* (1986) and Ding *et al.* (1993).

As an example, we consider an icosahedral quasicrystal. The symmetry group 532 has five classes, which are given in Table 1.10.5.1. The vector representation is Γ_2 . It has character $\chi(R) = 3, 1 + \tau, -\tau, 0, -1$. The character of its symmetrized square is 6, 1, 1, 0, 2. Then the character of the representation with which the elasticity tensor transforms is 21, 1, 1, 0, 5. This representation contains

the trivial representation twice. Therefore, there are two free parameters (c_{1111} and c_{1122}) in the elasticity tensor for the phonon degrees of freedom.

For the phason degrees of freedom, the displacements transform with the representation Γ_3 . In this case, the phason elasticity tensor transforms with the symmetrized square of the product of Γ_2 and Γ_3 . Its character is 45, 0, 0, 0, 5. This representation contains the identity representation twice. This implies that this tensor also has two free parameters.

Finally, the coupling term transforms with the product of the symmetrized square of Γ_2 , Γ_2 and Γ_3 . This representation has character 54, -1, -1, 0, 2 and consequently contains the identity representation once. In total, the number of independent elastic constants is five for icosahedral tensors. The fact that we have only used the rotation subgroup 532, instead of the full group $\bar{5}3m$, does not change this number. The additional central inversion makes the irreducible representations either even or odd. The elasticity tensors should be even, and there are exactly as many even irreducible representations as odd ones. This is shown in Table 1.10.4.1 (*cf.* Table 1.10.5.1 for the character table of the group 532).

1.10.4.5.3. Electric field gradient tensor

As an example, we consider a symmetric rank-two tensor, *e.g.* an electric field gradient tensor, in a system with superspace group symmetry $Pcmn(00\gamma)1s\bar{1}$. The Fourier transform of the tensor T_{ij} is nonzero only for multiples of the vector $\gamma\mathbf{c}^*$. The symmetry element consisting of a mirror operation M_y and a shift $\frac{1}{2}\mathbf{a}_4$ in V_I then has

$$R_E \mathbf{k} = \mathbf{k}, \quad \mathbf{k} \cdot \mathbf{a}_E = 0, \quad R_I = +1, \quad \mathbf{k}_I \cdot \mathbf{a}_I = \pi.$$

Then equation (1.10.4.15) leads to the relation

$$\begin{aligned} \hat{T}(m\gamma\mathbf{c}^*) &= \begin{pmatrix} a_{11} & a_{12} & a_{13} \\ a_{21} & a_{22} & a_{23} \\ a_{31} & a_{32} & a_{33} \end{pmatrix} \\ &= (-1)^m \begin{pmatrix} 1 & 0 & 0 \\ 0 & -1 & 0 \\ 0 & 0 & 1 \end{pmatrix} \begin{pmatrix} a_{11} & a_{12} & a_{13} \\ a_{21} & a_{22} & a_{23} \\ a_{31} & a_{32} & a_{33} \end{pmatrix} \begin{pmatrix} 1 & 0 & 0 \\ 0 & -1 & 0 \\ 0 & 0 & 1 \end{pmatrix} \end{aligned}$$

with solution

1.10. TENSORS IN QUASIPERIODIC STRUCTURES

$$\hat{T} = \begin{pmatrix} a_{11} & 0 & a_{13} \\ 0 & a_{22} & 0 \\ a_{13} & 0 & a_{33} \end{pmatrix} \quad (m \text{ even}),$$

$$\hat{T} = \begin{pmatrix} 0 & a_{12} & 0 \\ a_{12} & 0 & a_{23} \\ 0 & a_{23} & 0 \end{pmatrix} \quad (m \text{ odd}).$$

This symmetry of the tensor can, for example, be checked by NMR (van Beest *et al.*, 1983).

1.10.4.6. Determining the independent tensor elements

In the previous sections some physical tensors have been studied, for which in a number of cases the number of the independent tensor elements has been determined. In this section the problem of determining the invariant tensor elements themselves will be addressed.

Consider an orthogonal transformation R acting on the vector space V . Its action on basis vectors is given by

$$\mathbf{e}'_i = \sum_j R_{ji} \mathbf{e}_j. \quad (1.10.4.19)$$

If the basis is orthonormal, the matrix R_{ij} is orthogonal ($RR^T = E$). For a point group in superspace the action of R in V_E differs, in general, from that on V_I .

$$\mathbf{e}'_{Ei} = \sum_j R_{Eji} \mathbf{e}_{Ej}; \quad \mathbf{e}'_{Ii} = \sum_j R_{Iji} \mathbf{e}_{Ij}. \quad (1.10.4.20)$$

The action of R on the tensor product space $V_1 \otimes V_2$, with V_i either V_E or V_I , is given by

$$\mathbf{e}'_{1i} \otimes \mathbf{e}'_{2j} = \sum_k \sum_l R_{ki}^1 R_{lj}^2 \mathbf{e}_{1k} \otimes \mathbf{e}_{2l}. \quad (1.10.4.21)$$

If both R_i are orthogonal matrices, the tensor product is also orthogonal. For the symmetrized tensor square $(V \otimes V)_{\text{sym}}$ the basis formed by $\mathbf{e}_i \otimes \mathbf{e}_i$ ($i = 1, \dots$) and $(\mathbf{e}_i \otimes \mathbf{e}_j + \mathbf{e}_j \otimes \mathbf{e}_i)/\sqrt{2}$ ($i < j$) is orthogonal.

A vector $\sum_{ij} c_{ij} \mathbf{e}_i \otimes \mathbf{e}_j$ in the tensor product space is invariant if

$$RcR^T = c. \quad (1.10.4.22)$$

A tensor as a (possibly symmetric or antisymmetric) bilinear function with coefficients $f_{ij} = f(\mathbf{e}_i, \mathbf{e}_j)$ is invariant if the matrix f_{ij} satisfies

$$R^T f R = f. \quad (1.10.4.23)$$

For orthogonal bases the equations (1.10.4.22) and (1.10.4.23) are equivalent.

Which spaces have to be chosen for V_i depends on the physical tensor property. The algorithm for determining invariant tensors starts from the transformation of the basis vectors \mathbf{e}_i , from which the basis transformation in tensor space follows after due orthogonalization in the case of (anti)symmetric tensors. This

procedure can be continued to obtain higher-rank tensors. For orthogonal bases the invariant subspace is spanned by vectors corresponding to the independent tensor elements. We give a number of examples below.

1.10.4.6.1. Metric tensor for an octagonal three-dimensional quasicrystal

From the Fourier module for an octagonal quasicrystal in 3D the generators of the point group can be expressed as 5D integer matrices. They are

$$A = 8(8^3) = \begin{pmatrix} 0 & 0 & 0 & -1 & 0 \\ 1 & 0 & 0 & 0 & 0 \\ 0 & 1 & 0 & 0 & 0 \\ 0 & 0 & 1 & 0 & 0 \\ 0 & 0 & 0 & 0 & 1 \end{pmatrix}$$

$$B = m_z(1) = \begin{pmatrix} 1 & 0 & 0 & 0 & 0 \\ 0 & 1 & 0 & 0 & 0 \\ 0 & 0 & 1 & 0 & 0 \\ 0 & 0 & 0 & 1 & 0 \\ 0 & 0 & 0 & 0 & -1 \end{pmatrix}$$

and

$$C = m(m) = \begin{pmatrix} -1 & 0 & 0 & 0 & 0 \\ 0 & 0 & 0 & 1 & 0 \\ 0 & 0 & 1 & 0 & 0 \\ 0 & 1 & 0 & 0 & 0 \\ 0 & 0 & 0 & 0 & 1 \end{pmatrix},$$

and span an integer representation of the point group $8/mmm(8^3 1mm)$. Solution of the three simultaneous equations $S^T g S = g$ is equivalent with the determination of the subspace of the 15D symmetric tensor space that is invariant under the point group. The space has as basis the elements e_{ij} with $i \leq j$. The solution is given by

$$g = \begin{pmatrix} g_{11} & g_{12} & 0 & -g_{12} & 0 \\ g_{12} & g_{11} & g_{12} & 0 & 0 \\ 0 & g_{12} & g_{11} & g_{12} & 0 \\ -g_{12} & 0 & g_{12} & g_{11} & 0 \\ 0 & 0 & 0 & 0 & g_{55} \end{pmatrix}.$$

If $\mathbf{e}_i \otimes \mathbf{e}_j$ is denoted by ij , the solution follows because 55 is left invariant by A , B and C , whereas the orbits of 11 and 12 are $11 \rightarrow 22 \rightarrow 33 \rightarrow 44 \rightarrow 11$ and $12 \rightarrow 23 \rightarrow 34 \rightarrow -14 \rightarrow 12$, respectively.

1.10.4.6.2. EFG tensor for $Pcmn$

The electric field gradient tensor transforms as the product of a reciprocal vector and a vector. In Cartesian coordinates the transformation properties are the same. The point group for the basic structure of many IC phases of the family of A_2BX_4 compounds is mmm , and the point group for the modulated phase is the 4D group $mmm(1\bar{1}\bar{1})$, with generators

Table 1.10.4.2. Sign change of $\partial_i E_j$ under the generators A , B , C

| | A | B | C |
|----|-----|-----|-----|
| 11 | + | + | + |
| 12 | − | − | + |
| 13 | − | + | − |
| 21 | − | − | + |
| 22 | + | + | + |
| 23 | + | − | − |
| 31 | − | + | − |
| 32 | + | − | − |
| 33 | + | + | + |
| 41 | − | + | − |
| 42 | + | − | − |
| 43 | + | + | + |

1. TENSORIAL ASPECTS OF PHYSICAL PROPERTIES

$$A = \begin{pmatrix} -1 & 0 & 0 & 0 \\ 0 & 1 & 0 & 0 \\ 0 & 0 & 1 & 0 \\ 0 & 0 & 0 & 1 \end{pmatrix}, \quad B = \begin{pmatrix} 1 & 0 & 0 & 0 \\ 0 & -1 & 0 & 0 \\ 0 & 0 & 1 & 0 \\ 0 & 0 & 0 & 1 \end{pmatrix},$$

$$C = \begin{pmatrix} 1 & 0 & 0 & 0 \\ 0 & 1 & 0 & 0 \\ 0 & 0 & -1 & 0 \\ 0 & 0 & 0 & -1 \end{pmatrix}.$$

The tensor elements $\partial_i E_j$ being indicated by ij , the transformation under the generators gives a factor ± 1 as shown in Table 1.10.4.2.

From this, it follows that the four independent tensor elements are $\partial_1 E_1$, $\partial_2 E_2$, $\partial_3 E_3$ and the phason part $\partial_4 E_3$.

1.10.4.6.3. Elasticity tensor for a two-dimensional octagonal quasicrystal

The point group of the standard octagonal tiling is generated by the 2D orthogonal matrices

$$A = \begin{pmatrix} \sqrt{1/2} & -\sqrt{1/2} \\ \sqrt{1/2} & \sqrt{1/2} \end{pmatrix}, \quad B = \begin{pmatrix} -1 & 0 \\ 0 & 1 \end{pmatrix}.$$

In the tensor space one has the following transformations of the basis vectors; they are denoted by ij for $\mathbf{e}_i \otimes \mathbf{e}_j$:

$$\begin{aligned} 11 &\rightarrow \frac{1}{2}(11 + 12 + 21 + 22) \\ 12 &\rightarrow \frac{1}{2}(-11 + 12 - 21 + 22) \\ 21 &\rightarrow \frac{1}{2}(-11 - 12 + 21 + 22) \\ 22 &\rightarrow \frac{1}{2}(11 - 12 - 21 + 22). \end{aligned}$$

In the space spanned by $a = 11$, $b = \sqrt{1/2}(12 + 21)$ and $c = 22$, the eightfold rotation is represented by the matrix

$$S_E = \begin{pmatrix} \frac{1}{2} & -\sqrt{1/2} & \frac{1}{2} \\ \sqrt{1/2} & 0 & -\sqrt{1/2} \\ \frac{1}{2} & \sqrt{1/2} & \frac{1}{2} \end{pmatrix}.$$

In the six-dimensional space with basis aa , $\sqrt{1/2}(ab + ba)$, $\sqrt{1/2}(ac + ca)$, bb , $\sqrt{1/2}(bc + cb)$ and cc , the rotation gives the transformation

$$\begin{pmatrix} \frac{1}{4} & \frac{1}{2} & \sqrt{2}/4 & \frac{1}{2} & \frac{1}{2} & \frac{1}{4} \\ -\frac{1}{2} & -\frac{1}{2} & 0 & 0 & \frac{1}{2} & \frac{1}{2} \\ \sqrt{2}/4 & 0 & \frac{1}{2} & -\sqrt{1/2} & 0 & \sqrt{2}/4 \\ \frac{1}{2} & 0 & -\sqrt{1/2} & 0 & 0 & \frac{1}{2} \\ -\frac{1}{2} & \frac{1}{2} & 0 & 0 & -\frac{1}{2} & \frac{1}{2} \\ \frac{1}{4} & -\frac{1}{2} & \sqrt{2}/4 & \frac{1}{2} & -\frac{1}{2} & \frac{1}{4} \end{pmatrix}.$$

The vector \mathbf{v} such that $\mathbf{S} \cdot \mathbf{v} = \mathbf{v}$ then is then of the form

$$\mathbf{v} = (v_1, 0, (v_1 - v_4)\sqrt{2}, v_4, 0, v_1)^T.$$

This vector is also invariant under the mirror B . This means that there are two independent phonon elastic constants c_{1111}^E and c_{1212}^E , whereas the other tensor elements satisfy the relations

$$\begin{aligned} c_{1112}^E &= c_{1222}^E = 0, \quad c_{2222}^E = c_{1111}^E, \\ c_{1122}^E &= (c_{1111}^E + c_{1212}^E)\sqrt{1/2}. \end{aligned}$$

The internal component of the eightfold rotation is A^3 , that of the mirror B is B itself. The phason strain tensor transforms with the tensor product of external and internal components. This implies that the basis vectors, denoted by ij ($i = 1, 2; j = 3, 4$), transform under the eightfold rotation according to

$$\begin{aligned} 13 &\rightarrow (-13 + 14 - 23 + 24)/2 \\ 14 &\rightarrow (-13 - 14 - 23 - 24)/2 \\ 23 &\rightarrow (13 - 14 - 23 + 24)/2 \\ 24 &\rightarrow (13 + 14 - 23 - 24)/2. \end{aligned}$$

The symmetrized tensor square of this matrix gives the transformation in the space of phason-phason elasticity tensors, the direct product of the transformations in the 3D phonon strain space and the 4D phason strain space gives the transformation in the space of phonon-phason elasticity tensors. The first matrix is given by

$$\frac{1}{16} \begin{pmatrix} 1 & \sqrt{2} & -\sqrt{2} & -\sqrt{2} & 1 & -\sqrt{2} & -\sqrt{2} & 1 & \sqrt{2} & 1 \\ -\sqrt{2} & 0 & 2 & 0 & \sqrt{2} & 0 & -2 & -\sqrt{2} & 0 & \sqrt{2} \\ \sqrt{2} & 2 & 0 & 0 & \sqrt{2} & 0 & 0 & -\sqrt{2} & -2 & -\sqrt{2} \\ -\sqrt{2} & 0 & 0 & 2 & \sqrt{2} & -2 & 0 & \sqrt{2} & 0 & -\sqrt{2} \\ 1 & -\sqrt{2} & -\sqrt{2} & \sqrt{2} & 1 & \sqrt{2} & -\sqrt{2} & 1 & -\sqrt{2} & 1 \\ -\sqrt{2} & 0 & 0 & -2 & \sqrt{2} & 2 & 0 & \sqrt{2} & 0 & -\sqrt{2} \\ \sqrt{2} & -2 & 0 & 0 & \sqrt{2} & 0 & 0 & -\sqrt{2} & 2 & -\sqrt{2} \\ 1 & \sqrt{2} & \sqrt{2} & \sqrt{2} & 1 & \sqrt{2} & \sqrt{2} & 1 & \sqrt{2} & 1 \\ -\sqrt{2} & 0 & -2 & 0 & \sqrt{2} & 0 & 2 & -\sqrt{2} & 0 & \sqrt{2} \\ 1 & -\sqrt{2} & \sqrt{2} & -\sqrt{2} & 1 & -\sqrt{2} & \sqrt{2} & 1 & -\sqrt{2} & 1 \end{pmatrix}.$$

Vectors invariant under this operation and the transformation corresponding to the mirror B correspond to invariant elasticity tensors. For the transformation B , all tensor elements with an odd number of indices 1 or 3 are zero. In the space of phason-phason tensors the general invariant vector is

$$(x_1, 0, 0, -x_6 + (x_5 - x_1)\sqrt{2}, x_5, x_6, 0, x_5, 0, x_1).$$

There are three independent elastic constants, $x_1 = c_{1313}$, $x_5 = c_{1414}$ and $x_6 = c_{1423}$. For the phonon-phason elastic constants the corresponding invariant vector is

$$(x, 0, 0, x, 0, x/\sqrt{2}, -x/\sqrt{2}, 0, -x, 0, 0, -x).$$

The independent elastic constant is $x = c_{1113} = c_{1124} = c_{1214}\sqrt{2} = -c_{1223}\sqrt{2} = -c_{2213} = -c_{2224}$.

1.10.4.6.4. Piezoelectric tensor for a three-dimensional octagonal quasicrystal

A quasicrystal with octagonal point group $8/mmm(8^3 1mm)$ will not show a piezoelectric effect because the point group contains the central inversion. We consider here the point group $8mm(8^3 mm)$ which is a subgroup without central inversion. It is generated by the matrices

$$A = \begin{pmatrix} \alpha & -\alpha & 0 & 0 & 0 \\ \alpha & \alpha & 0 & 0 & 0 \\ 0 & 0 & 1 & 0 & 0 \\ 0 & 0 & 0 & -\alpha & -\alpha \\ 0 & 0 & 0 & \alpha & -\alpha \end{pmatrix},$$

$$B = \begin{pmatrix} -1 & 0 & 0 & 0 & 0 \\ 0 & 1 & 0 & 0 & 0 \\ 0 & 0 & 1 & 0 & 0 \\ 0 & 0 & 0 & -1 & 0 \\ 0 & 0 & 0 & 0 & 1 \end{pmatrix}.$$

Here $\alpha = \sqrt{2}/2$. There are two components for the strain, a phonon component e and a phason component f . The phonon strain tensors form a 6D space, the phason strain tensors also a 6D space. The phonon strain space transforms with the symmetrized square of the physical parts of the operations, the phason strain space with the product of physical and internal parts. For the eightfold rotation the corresponding matrices are

1.10. TENSORS IN QUASIPERIODIC STRUCTURES

$$S_e = \begin{pmatrix} \frac{1}{2} & -\alpha & 0 & \frac{1}{2} & 0 & 0 \\ \alpha & 0 & 0 & -\alpha & 0 & 0 \\ 0 & 0 & \alpha & 0 & -\alpha & 0 \\ \frac{1}{2} & \alpha & 0 & \frac{1}{2} & 0 & 0 \\ 0 & 0 & \alpha & 0 & \alpha & 0 \\ 0 & 0 & 0 & 0 & 0 & 1 \end{pmatrix},$$

$$S_f = \begin{pmatrix} -\frac{1}{2} & -\frac{1}{2} & \frac{1}{2} & \frac{1}{2} & 0 & 0 \\ \frac{1}{2} & -\frac{1}{2} & -\frac{1}{2} & \frac{1}{2} & 0 & 0 \\ -\frac{1}{2} & -\frac{1}{2} & -\frac{1}{2} & -\frac{1}{2} & 0 & 0 \\ \frac{1}{2} & -\frac{1}{2} & \frac{1}{2} & -\frac{1}{2} & 0 & 0 \\ 0 & 0 & 0 & 0 & -\alpha & -\alpha \\ 0 & 0 & 0 & 0 & \alpha & -\alpha \end{pmatrix}.$$

The action on the space of piezoelectric tensors is given, for the phonon and the phason part, by taking the product of these matrices with the physical part A_E . The invariant vectors under these matrices give the invariant tensors. If the second generator is taken into account, which requires that the number of indices 1 or 4 is even, this results in the independent tensor elements

$$x_3 = c_{113}, \quad x_{16} = c_{322}, \quad x_{18} = c_{333}$$

with relation $c_{223} = c_{113}$, whereas all other elements are zero for the coupling between the electric field and phonon strain. There is no nontrivial invariant vector in the second case. Therefore, all tensor elements for the coupling between the electric field and phason strain are zero.

1.10.4.6.5. Elasticity tensor for an icosahedral quasicrystal

The point group of an icosahedral quasicrystal is $532(5^232)$ with generators having components

$$A_E = \begin{pmatrix} 1 & \tau & -1-\tau \\ \tau & 1+\tau & 1 \\ 1+\tau & -1 & \tau \end{pmatrix}/2,$$

$$B_E = \begin{pmatrix} -\tau & 1+\tau & -1 \\ 1+\tau & 1 & \tau \\ 1 & -\tau & -1-\tau \end{pmatrix}/2$$

in physical space and components

$$A_I = \begin{pmatrix} -1 & \tau & -1-\tau \\ -\tau & \tau^{-1} & 1 \\ 1+\tau & 1 & -\tau \end{pmatrix}/2, \quad B_I = \begin{pmatrix} 0 & 0 & -1 \\ -1 & 0 & 0 \\ 0 & 1 & 0 \end{pmatrix}$$

in internal space (see Table 1.10.5.2). The phonon and phason strain tensors form a 6D, respectively 9D, vector space, in which the point group acts with matrices

$$S_e = \frac{1}{4} \begin{pmatrix} 1 & \tau\sqrt{2} & -\varphi\sqrt{2} & 1-\tau & -\sqrt{2} & 2+\tau \\ \tau\sqrt{2} & 2 & 0 & \sqrt{2} & -2 & -\varphi\sqrt{2} \\ \varphi\sqrt{2} & 0 & -2 & -\tau\sqrt{2} & 2 & -\sqrt{2} \\ 1-\tau & \sqrt{2} & \tau\sqrt{2} & 2+\tau & \varphi\sqrt{2} & 1 \\ \sqrt{2} & 2 & 2 & -\varphi\sqrt{2} & 0 & \tau\sqrt{2} \\ 2+\tau & -\varphi\sqrt{2} & \sqrt{2} & 1 & -\tau\sqrt{2} & 1-\tau \end{pmatrix},$$

$$S_f = \frac{1}{4} \begin{pmatrix} -\tau & \varphi & -1 & \tau-1 & 1 & -\tau & 1 & -2-\tau & \varphi \\ \varphi & 1 & \tau & 1 & \tau & 1-\tau & -2-\tau & -\varphi & -1 \\ 1 & -\tau & -\varphi & \tau & \tau-1 & -1 & -\varphi & 1 & 2+\tau \\ \tau-1 & 1 & -\tau & -1 & 2+\tau & -\varphi & -\tau & \varphi & -1 \\ 1 & \tau & 1-\tau & 2+\tau & \varphi & 1 & \varphi & 1 & \tau \\ \tau & \tau-1 & -1 & \varphi & -1 & -2-\tau & 1 & -\tau & -\varphi \\ -1 & 2+\tau & -\varphi & \tau & -\varphi & 1 & \tau-1 & 1 & -\tau \\ 2+\tau & \varphi & 1 & -\varphi & -1 & -\tau & 1 & \tau & 1-\tau \\ \varphi & -1 & -2-\tau & -1 & \tau & \varphi & \tau & \tau-1 & -1 \end{pmatrix}$$

and

$$T_e = \frac{1}{4} \begin{pmatrix} 1 & -\tau\sqrt{2} & \varphi\sqrt{2} & 1-\tau & -\sqrt{2} & 2+\tau \\ \tau\sqrt{2} & -2 & 0 & \sqrt{2} & -2 & -\varphi\sqrt{2} \\ -\varphi\sqrt{2} & 0 & -2 & \tau\sqrt{2} & -2 & \sqrt{2} \\ 1-\tau & -\sqrt{2} & -\tau\sqrt{2} & 2+\tau & \varphi\sqrt{2} & 1 \\ -\sqrt{2} & 2 & 2 & \varphi\sqrt{2} & 0 & -\tau\sqrt{2} \\ 2+\tau & \varphi\sqrt{2} & -\sqrt{2} & 1 & -\tau\sqrt{2} & 1-\tau \end{pmatrix},$$

$$T_f = \frac{1}{2} \begin{pmatrix} 0 & 0 & 1 & 0 & 0 & -\tau & 0 & 0 & \varphi \\ 1 & 0 & 0 & -\tau & 0 & 0 & \varphi & 0 & 0 \\ 0 & -1 & 0 & 0 & \tau & 0 & 0 & -\varphi & 0 \\ 0 & 0 & \tau & 0 & 0 & -\varphi & 0 & 0 & -1 \\ \tau & 0 & 0 & -\varphi & 0 & 0 & -1 & 0 & 0 \\ 0 & -\tau & 0 & 0 & \varphi & 0 & 0 & 1 & 0 \\ 0 & 0 & -\varphi & 0 & 0 & -1 & 0 & 0 & \tau \\ -\varphi & 0 & 0 & -1 & 0 & 0 & \tau & 0 & 0 \\ 0 & \varphi & 0 & 0 & 1 & 0 & 0 & -\tau & 0 \end{pmatrix}.$$

This implies that the phonon elasticity tensors form a 21D space, the phason elasticity tensors a 45D space and the phonon-phason coupling a 54D space. The invariant vectors under these orthogonal transformations correspond to invariant elastic tensors. Their coordinates are the elastic constants. For the given presentation of the point group, these are given in Table 1.10.4.3. The tensor elements are expressed in parameters x and y where there are two independent tensor elements. The tensor elements that are not given are zero or equal to that given by the permutation symmetry. If bases for the phonon and phason strain are introduced by

$$[1] = 11, [2] = 12, [3] = 13, [4] = 22, [5] = 23, [6] = 33$$

for the phonon part and

$$[1] = 14, [2] = 15, [3] = 16, [4] = 24, [5] = 25, [6] = 26,$$

$$[7] = 34, [8] = 35, [9] = 36$$

for the phason part, the elastic tensors may be given in matrix form as

$$c^{ee} = \begin{pmatrix} x+y & 0 & 0 & x & 0 & x \\ 0 & y & 0 & 0 & 0 & 0 \\ 0 & 0 & y & 0 & 0 & 0 \\ x & 0 & 0 & x+y & 0 & x \\ 0 & 0 & 0 & 0 & y & 0 \\ x & 0 & 0 & x & 0 & x+y \end{pmatrix},$$

$$c^{ef} = \begin{pmatrix} z & \tau^2 u & -\tau u & -\tau u & \tau u & -\tau u & -u & 0 & \tau u \\ \tau^2 u & z - 2\tau u & u & \tau u & u & 0 & 0 & \tau^2 u & \tau u \\ -\tau u & u & z & -\tau u & 0 & -\tau^2 u & \tau u & \tau u & \tau u \\ -\tau u & \tau u & -\tau u & z & \tau u & u & -\tau^2 u & \tau u & 0 \\ \tau u & u & 0 & \tau u & z & -\tau^2 u & \tau u & -\tau u & -\tau u \\ -\tau u & 0 & -\tau^2 u & u & -\tau^2 u & z - 2\tau u & 0 & -\tau u & u \\ -u & 0 & \tau u & -\tau^2 u & \tau u & 0 & z - 2\tau u & -u & -\tau^2 u \\ 0 & \tau^2 u & \tau u & \tau u & -\tau u & -\tau u & -u & z & -\tau u \\ \tau u & \tau u & \tau u & 0 & -\tau u & u & -\tau^2 u & -\tau u & z \end{pmatrix},$$

$$c^{ff} = \begin{pmatrix} -v & -\tau v & -\tau^2 v & -\tau^3 v & \tau v & -\tau^2 v & v & -\tau v & -\tau^{-1} v \\ -\tau^3 v & \tau v & -\tau^2 v & \tau^2 v & v & \tau v & 0 & 0 & 0 \\ v & -\tau v & -\tau^{-1} v & 0 & 0 & 0 & -\tau v & -\tau^2 v & -\tau^3 v \\ \tau^{-1} v & v & \tau v & -\tau^2 v & v & -\tau v & -\tau^2 v & -\tau^3 v & \tau v \\ 0 & 0 & 0 & -\tau^2 v & \tau^3 v & \tau v & \tau v & -\tau^{-1} v & v \\ -\tau v & -\tau^2 v & -\tau^3 v & \tau v & -\tau^{-1} v & v & -\tau v & \tau^2 v & v \end{pmatrix}.$$

The parameters x, y, z, u, v are the five independent elastic constants.

1.10.5. Tables

In this section are presented the irreducible representations of point groups of quasiperiodic structures up to rank six that do not occur as three-dimensional crystallographic point groups.

1. TENSORIAL ASPECTS OF PHYSICAL PROPERTIES

Table 1.10.4.3. Elastic constants for icosahedral quasicrystals

| Type | Free parameters | Relations |
|---------------|-----------------|---|
| Phonon-phonon | 2 | $c_{1111} = c_{2222} = c_{3333} = x$ $c_{1122} = c_{1133} = c_{2233} = y$ $c_{1212} = c_{1313} = c_{2323} = x - y$ |
| Phason-phason | 2 | $c_{1414} = c_{1616} = c_{2424} = c_{2525} = c_{3535} = c_{3636} = x$ $c_{1416} = c_{1424} = -c_{1425} = c_{1426} = -c_{1436} = y$ $c_{1524} = c_{1536} = -c_{1624} = c_{1634} = c_{1635} = -y$ $c_{1636} = c_{2425} = c_{2435} = c_{2534} = -c_{2535} = -y$ $c_{2536} = c_{2635} = c_{3536} = y, c_{1515} = c_{2626} = c_{3434} = x + 2y$ $c_{1415} = c_{1535} = -c_{1626} = -c_{2434} = -c_{2526} = -c_{3436} = y\tau$ $c_{1434} = -c_{11516} = -c_{1525} = -c_{2426} = -c_{2636} = c_{3435} = y/\tau$ |
| Phonon-phason | 1 | $-c_{1114} = c_{1134} = c_{1225} = c_{2225} = c_{2336} = c_{3326} = c_{3336}$ $= -c_{1115}/\tau = c_{1125}/\tau = -c_{1135}\tau = c_{1215}\tau = c_{1226}\tau$ $= -c_{1334}\tau = -c_{2226}\tau = c_{2236}\tau = c_{2326}\tau = c_{2334}\tau$ $= -c_{3334}\tau = -c_{1116}\tau^2 = -c_{1126}\tau^2 = -c_{1216}\tau^2$ $= -c_{1335}\tau^2 = -c_{2224}\tau^2 = -c_{2234}\tau^2 = c_{3335}\tau^2$ $= -c_{1136}\tau = c_{1224}\tau = -c_{1316}\tau = -c_{2335}\tau$ $= -c_{1124}/\tau^3 = -c_{1336}/\tau^3 = c_{2235}/\tau^3 = c_{2325}/\tau^3$ |

Table 1.10.5.1. Character tables of some point groups for quasicrystals

(a) C_5 [$\omega = \exp(2\pi i/5)$].

| C_5 n Order | ε | α | α^2 | α^3 | α^4 |
|-----------------------|---------------|------------|------------|------------|------------|
| | 1 | 1 | 1 | 1 | 1 |
| | 1 | 5 | 5 | 5 | 5 |
| Γ_1 | 1 | 1 | 1 | 1 | 1 |
| Γ_2 | 1 | ω | ω^2 | ω^3 | ω^4 |
| Γ_3 | 1 | ω^2 | ω^4 | ω | ω^3 |
| Γ_4 | 1 | ω^3 | ω | ω^4 | ω^2 |
| Γ_5 | 1 | ω^4 | ω^3 | ω^2 | ω |

| | Generators | Vector representation | Perpendicular representation |
|---|-------------------|--|------------------------------|
| 5 | $\alpha = C_{5z}$ | $\Gamma_1 \oplus \Gamma_2 \oplus \Gamma_5$ | $\Gamma_3 \oplus \Gamma_4$ |

(b) D_5 [$\tau = (\sqrt{5} - 1)/2$].

| D_5 n Order | ε | α | α^2 | β |
|-----------------------|---------------|-------------|-------------|---------|
| | 1 | 2 | 2 | 5 |
| | 1 | 5 | 5 | 2 |
| Γ_1 | 1 | 1 | 1 | 1 |
| Γ_2 | 1 | 1 | 1 | -1 |
| Γ_3 | 2 | τ | $-1 - \tau$ | 0 |
| Γ_4 | 2 | $-1 - \tau$ | τ | 0 |

| | Generators | Vector representation | Perpendicular representation |
|------------|--|----------------------------------|------------------------------|
| 52 | $\alpha = C_{5z}$ | $\Gamma_2 \oplus \Gamma_3$ | Γ_4 |
| $5m$ | $\beta = C_{2x}$ $\alpha = C_{5z}$ $\beta = m_x$ | $\Gamma_1 \oplus \Gamma_3$ | Γ_4 |
| $\bar{5}m$ | $\sim 52 \times \mathbb{Z}_2$ | $\Gamma_{1u} \oplus \Gamma_{3u}$ | Γ_{4u} |

(c) C_8 [$\omega = \exp(\pi i/4) = (1 + i)/\sqrt{2}$].

| C_8 n Order | ε | α | α^2 | α^3 | α^4 | α^5 | α^6 | α^7 |
|-----------------------|---------------|------------|------------|------------|------------|------------|------------|------------|
| | 1 | 1 | 1 | 1 | 1 | 1 | 1 | 1 |
| | 1 | 8 | 4 | 8 | 2 | 8 | 6 | 8 |
| Γ_1 | 1 | 1 | 1 | 1 | 1 | 1 | 1 | 1 |
| Γ_2 | 1 | ω | i | ω^3 | -1 | ω^5 | -i | ω^7 |
| Γ_3 | 1 | i | -1 | -i | 1 | i | -1 | -i |
| Γ_4 | 1 | ω^3 | -i | ω | -1 | ω^7 | i | ω^5 |
| Γ_5 | 1 | -1 | 1 | -1 | 1 | -1 | 1 | -1 |
| Γ_6 | 1 | ω^5 | i | ω^7 | -1 | ω | -i | ω^3 |
| Γ_7 | 1 | -i | -1 | i | 1 | -i | -1 | i |
| Γ_8 | 1 | ω^7 | -i | ω^5 | -1 | ω^3 | i | ω |

| | Generators | Vector representation | Perpendicular representation |
|-----------|------------------------------|---|----------------------------------|
| 8 | $\alpha = C_{8z}$ | $\Gamma_1 \oplus \Gamma_2 \oplus \Gamma_8$ | $\Gamma_4 \oplus \Gamma_6$ |
| $\bar{8}$ | $\alpha = S_{8z}$ | $\Gamma_4 \oplus \Gamma_5 \oplus \Gamma_6$ | $\Gamma_2 \oplus \Gamma_8$ |
| $8/m$ | $\sim 8 \times \mathbb{Z}_2$ | $\Gamma_{1u} \oplus \Gamma_{2u} \oplus \Gamma_{8u}$ | $\Gamma_{4u} \oplus \Gamma_{6u}$ |

(d) D_8

| D_8 n Order | ε | α | α^2 | α^3 | α^4 | β | $\alpha\beta$ |
|-----------------------|---------------|-------------|------------|-------------|------------|---------|---------------|
| | 1 | 2 | 2 | 2 | 1 | 4 | 4 |
| | 1 | 8 | 4 | 8 | 2 | 2 | 2 |
| Γ_1 | 1 | 1 | 1 | 1 | 1 | 1 | 1 |
| Γ_2 | 1 | 1 | 1 | 1 | 1 | -1 | -1 |
| Γ_3 | 1 | -1 | 1 | -1 | 1 | 1 | -1 |
| Γ_4 | 1 | -1 | 1 | -1 | 1 | -1 | 1 |
| Γ_5 | 2 | $\sqrt{2}$ | 0 | $-\sqrt{2}$ | -2 | 0 | 0 |
| Γ_6 | 2 | 0 | -2 | 0 | 2 | 0 | 0 |
| Γ_7 | 2 | $-\sqrt{2}$ | 0 | $\sqrt{2}$ | -2 | 0 | 0 |

| | Generators | Vector representation | Perpendicular representation |
|-------------|--|----------------------------------|------------------------------|
| 822 | $\alpha = C_{8z}$ | $\Gamma_2 \oplus \Gamma_5$ | Γ_7 |
| $8mm$ | $\beta = C_{2x}$ $\alpha = C_{8z}$ $\beta = m_x$ | $\Gamma_1 \oplus \Gamma_5$ | Γ_7 |
| $\bar{8}2m$ | $\alpha = S_{8z}$ $\beta = 2_{2x}$ | $\Gamma_3 \oplus \Gamma_7$ | Γ_5 |
| $8/mmm$ | $\sim 822 \times \mathbb{Z}_2$ | $\Gamma_{2u} \oplus \Gamma_{5u}$ | Γ_{7u} |

(e) C_{10} [$\omega = \exp(2\pi i/5)$].

| C_{10} n Order | ε | α^2 | α^4 | α^6 | α^8 |
|--------------------------|---------------|------------|------------|------------|------------|
| | 1 | 1 | 1 | 1 | 1 |
| | 1 | 5 | 5 | 5 | 5 |
| Γ_1 | 1 | 1 | 1 | 1 | 1 |
| Γ_2 | 1 | ω | ω^2 | ω^3 | ω^4 |
| Γ_3 | 1 | ω^2 | ω^4 | ω | ω^3 |
| Γ_4 | 1 | ω^3 | ω | ω^4 | ω^2 |
| Γ_5 | 1 | ω^4 | ω^3 | ω^2 | ω |
| Γ_6 | 1 | 1 | 1 | 1 | 1 |
| Γ_7 | 1 | ω | ω^2 | ω^3 | ω^4 |
| Γ_8 | 1 | ω^2 | ω^4 | ω | ω^3 |
| Γ_9 | 1 | ω^3 | ω | ω^4 | ω^2 |
| Γ_{10} | 1 | ω^4 | ω^3 | ω^2 | ω |

| C_{10} n Order | α^5 | α^7 | α^9 | α | α^3 |
|--------------------------|------------|-------------|-------------|-------------|-------------|
| | 1 | 1 | 1 | 1 | 1 |
| | 2 | 10 | 10 | 10 | 10 |
| Γ_1 | 1 | 1 | 1 | 1 | 1 |
| Γ_2 | 1 | ω | ω^2 | ω^3 | ω^4 |
| Γ_3 | 1 | ω^2 | ω^4 | ω | ω^3 |
| Γ_4 | 1 | ω^3 | ω | ω^4 | ω^2 |
| Γ_5 | 1 | ω^4 | ω^3 | ω^2 | ω |
| Γ_6 | -1 | -1 | -1 | -1 | -1 |
| Γ_7 | -1 | $-\omega$ | $-\omega^2$ | $-\omega^3$ | $-\omega^4$ |
| Γ_8 | -1 | $-\omega^2$ | $-\omega^4$ | $-\omega$ | $-\omega^3$ |
| Γ_9 | -1 | $-\omega^3$ | $-\omega$ | $-\omega^4$ | $-\omega^2$ |
| Γ_{10} | -1 | $-\omega^4$ | $-\omega^3$ | $-\omega^2$ | $-\omega$ |

1.10. TENSORS IN QUASIPERIODIC STRUCTURES

Table 1.10.5.1 (*cont.*)

| | Generators | Vector representation | Perpendicular representation |
|-----------------|-------------------------------|--|----------------------------------|
| $\frac{10}{5}$ | $\alpha = C_{10z}$ | $\Gamma_1 \oplus \Gamma_7 \oplus \Gamma_{10}$ | $\Gamma_8 \oplus \Gamma_9$ |
| $\frac{5}{10}$ | $\alpha = S_{5z}$ | $\Gamma_6 \oplus \Gamma_8 \oplus \Gamma_9$ | $\Gamma_7 \oplus \Gamma_{10}$ |
| $\frac{10}{10}$ | $\alpha = S_{10z}$ | $\Gamma_2 \oplus \Gamma_4 \oplus \Gamma_6$ | $\Gamma_3 \oplus \Gamma_5$ |
| $10/m$ | $\sim 10 \times \mathbb{Z}_2$ | $\Gamma_{1u} \oplus \Gamma_{7u} \oplus \Gamma_{10u}$ | $\Gamma_{8u} \oplus \Gamma_{9u}$ |

| C_{12} n Order | α^6 | α^7 | α^8 | α^9 | α^{10} | α^{11} |
|--------------------------|------------|-------------|-------------|------------|---------------|---------------|
| 1 | 1 | 1 | 1 | 1 | 1 | 1 |
| 2 | 12 | 12 | 3 | 4 | 6 | 12 |
| Γ_0 | 1 | $-\omega^2$ | ω^4 | 1 | $-\omega^2$ | ω^4 |
| Γ_{10} | -1 | i | 1 | $-i$ | -1 | i |
| Γ_{11} | 1 | $-\omega^4$ | $-\omega^2$ | -1 | ω^4 | ω^2 |
| Γ_{12} | -1 | ω^5 | ω^4 | i | ω^2 | ω |

(f) D_{10} [$\tau = (\sqrt{5} - 1)/2$].

| D_{10} n Order | ε | α | α^2 | α^3 |
|--------------------------|---------------|-------------|-------------|-------------|
| 1 | 1 | 2 | 2 | 2 |
| 10 | 1 | 10 | 5 | 10 |
| Γ_1 | 1 | 1 | 1 | 1 |
| Γ_2 | 1 | 1 | 1 | 1 |
| Γ_3 | 1 | -1 | 1 | -1 |
| Γ_4 | 1 | -1 | 1 | -1 |
| Γ_5 | 2 | $1 + \tau$ | τ | $-\tau$ |
| Γ_6 | 2 | τ | $-1 - \tau$ | $-1 - \tau$ |
| Γ_7 | 2 | $-\tau$ | $-1 - \tau$ | $1 + \tau$ |
| Γ_8 | 2 | $-1 - \tau$ | τ | τ |

| D_{10} n Order | α^4 | α^5 | β | $\alpha\beta$ |
|--------------------------|-------------|------------|---------|---------------|
| 2 | 2 | 1 | 5 | 5 |
| 5 | 5 | 2 | 2 | 2 |
| Γ_1 | 1 | 1 | 1 | 1 |
| Γ_2 | 1 | 1 | -1 | -1 |
| Γ_3 | 1 | -1 | 1 | -1 |
| Γ_4 | 1 | -1 | -1 | 1 |
| Γ_5 | $-1 - \tau$ | -2 | 0 | 0 |
| Γ_6 | τ | 2 | 0 | 0 |
| Γ_7 | τ | -2 | 0 | 0 |
| Γ_8 | $-1 - \tau$ | 2 | 0 | 0 |

| | Generators | Vector representation | Perpendicular representation |
|-------------------|--------------------|----------------------------------|------------------------------|
| 1022 | $\alpha = C_{8z}$ | $\Gamma_2 \oplus \Gamma_5$ | Γ_7 |
| $10mm$ | $\beta = C_{2x}$ | $\Gamma_1 \oplus \Gamma_5$ | Γ_7 |
| $\overline{10}2m$ | $\alpha = C_{8z}$ | $\Gamma_3 \oplus \Gamma_7$ | Γ_5 |
| $\tilde{5}m$ | $\beta = m_x$ | $\Gamma_3 \oplus \Gamma_7$ | Γ_5 |
| $10/mmm$ | $\alpha = S_{10z}$ | $\Gamma_{2u} \oplus \Gamma_{5u}$ | Γ_{7u} |

| | Generator | Vector representation | Perpendicular representation |
|-----------------|-------------------------------|--|----------------------------------|
| $\frac{12}{12}$ | C_{12z} | $\Gamma_1 \oplus \Gamma_2 \oplus \Gamma_{12}$ | $\Gamma_6 \oplus \Gamma_8$ |
| $\frac{12}{12}$ | S_{12z} | $\Gamma_6 \oplus \Gamma_7 \oplus \Gamma_8$ | $\Gamma_2 \oplus \Gamma_{12}$ |
| $12/m$ | $\sim 12 \times \mathbb{Z}_2$ | $\Gamma_{1u} \oplus \Gamma_{2u} \oplus \Gamma_{12u}$ | $\Gamma_{6u} \oplus \Gamma_{8u}$ |

(h) D_{12}

| D_{12} n Order | ε | α | α^2 | α^3 |
|--------------------------|---------------|-------------|------------|------------|
| 1 | 1 | 2 | 2 | 2 |
| 12 | 1 | 12 | 6 | 4 |
| Γ_1 | 1 | 1 | 1 | 1 |
| Γ_2 | 1 | 1 | 1 | 1 |
| Γ_3 | 1 | -1 | 1 | -1 |
| Γ_4 | 1 | -1 | 1 | -1 |
| Γ_5 | 2 | $\sqrt{3}$ | 1 | 0 |
| Γ_6 | 2 | 1 | -1 | -2 |
| Γ_7 | 2 | 0 | -2 | 0 |
| Γ_8 | 2 | -1 | -1 | 2 |
| Γ_9 | 2 | $-\sqrt{3}$ | 1 | 0 |

| D_{12} n Order | α^4 | α^5 | α^6 | β | $\alpha\beta$ |
|--------------------------|------------|-------------|------------|---------|---------------|
| 2 | 2 | 2 | 1 | 6 | 6 |
| 3 | 3 | 12 | 2 | 2 | 2 |
| Γ_1 | 1 | 1 | 1 | 1 | 1 |
| Γ_2 | 1 | 1 | 1 | -1 | -1 |
| Γ_3 | 1 | -1 | 1 | 1 | -1 |
| Γ_4 | 1 | -1 | 1 | -1 | 1 |
| Γ_5 | -1 | $-\sqrt{3}$ | -2 | 0 | 0 |
| Γ_6 | -1 | 1 | 2 | 0 | 0 |
| Γ_7 | 2 | 0 | -2 | 0 | 0 |
| Γ_8 | -1 | -1 | 2 | 0 | 0 |
| Γ_9 | -1 | $\sqrt{3}$ | -2 | 0 | 0 |

(g) C_{12} [$\omega = \exp(\pi i/6)$].

| C_{12} n Order | ε | α | α^2 | α^3 | α^4 | α^5 |
|--------------------------|---------------|-------------|-------------|------------|-------------|-------------|
| 1 | 1 | 1 | 1 | 1 | 1 | 1 |
| 12 | 1 | 12 | 6 | 4 | 3 | 12 |
| Γ_1 | 1 | 1 | 1 | 1 | 1 | 1 |
| Γ_2 | 1 | ω | ω^2 | i | ω^4 | ω^5 |
| Γ_3 | 1 | ω^2 | ω^4 | -1 | $-\omega^2$ | $-\omega^4$ |
| Γ_4 | 1 | i | -1 | -i | 1 | i |
| Γ_5 | 1 | ω^4 | $-\omega^2$ | 1 | ω^4 | $-\omega^2$ |
| Γ_6 | 1 | ω^5 | $-\omega^4$ | i | $-\omega^2$ | ω |
| Γ_7 | 1 | -1 | 1 | -1 | 1 | -1 |
| Γ_8 | 1 | $-\omega$ | ω^2 | -i | ω^4 | $-\omega^5$ |
| Γ_9 | 1 | $-\omega^2$ | ω^4 | 1 | $-\omega^2$ | ω^4 |
| Γ_{10} | 1 | -i | -1 | i | 1 | -i |
| Γ_{11} | 1 | $-\omega^4$ | $-\omega^2$ | -1 | ω^4 | ω^2 |
| Γ_{12} | 1 | $-\omega^5$ | $-\omega^4$ | -i | $-\omega^2$ | $-\omega$ |

| C_{12} n Order | α^6 | α^7 | α^8 | α^9 | α^{10} | α^{11} |
|--------------------------|------------|-------------|-------------|------------|---------------|---------------|
| 1 | 1 | 1 | 1 | 1 | 1 | 1 |
| 2 | 12 | 12 | 3 | 4 | 6 | 12 |
| Γ_1 | 1 | 1 | 1 | 1 | 1 | 1 |
| Γ_2 | -1 | $-\omega$ | $-\omega^2$ | -i | $-\omega^4$ | $-\omega^5$ |
| Γ_3 | 1 | ω^2 | ω^4 | -1 | $-\omega^2$ | $-\omega^4$ |
| Γ_4 | -1 | -i | 1 | i | -1 | -i |
| Γ_5 | 1 | ω^4 | $-\omega^2$ | 1 | ω^4 | $-\omega^2$ |
| Γ_6 | -1 | $-\omega^5$ | ω^4 | -i | ω^2 | $-\omega$ |
| Γ_7 | 1 | -1 | 1 | -1 | 1 | -1 |
| Γ_8 | -1 | ω | $-\omega^2$ | i | $-\omega^4$ | ω^5 |

| | Generators | Vector representation | Perpendicular representation |
|-------------------|--------------------|----------------------------------|------------------------------|
| 1222 | $\alpha = C_{12z}$ | $\Gamma_2 \oplus \Gamma_5$ | Γ_9 |
| $12mm$ | $\beta = C_{2x}$ | $\Gamma_1 \oplus \Gamma_5$ | Γ_9 |
| $\overline{12}2m$ | $\alpha = C_{12z}$ | $\Gamma_4 \oplus \Gamma_9$ | Γ_5 |
| $12/mmm$ | $\beta = m_x$ | $\Gamma_{2u} \oplus \Gamma_{5u}$ | Γ_{9u} |

(i) I [$\tau = (\sqrt{5} - 1)/2$].

| I n Order | ε | α | α^2 | β | $\alpha\beta$ |
|---------------------|---------------|------------|------------|---------|---------------|
| 1 | 1 | 12 | 12 | 20 | 15 |
| 5 | 1 | 5 | 5 | 3 | 2 |
| Γ_1 | 1 | 1 | 1 | 1 | 1 |
| Γ_2 | 3 | $1 + \tau$ | $-\tau$ | 0 | -1 |
| Γ_3 | 3 | $-\tau$ | $1 + \tau$ | 0 | -1 |
| Γ_4 | 4 | -1 | -1 | 1 | 0 |
| Γ_5 | 5 | 0 | 0 | -1 | 1 |

| | Generators | Vector representation | Perpendicular representation |
|---------------|------------------|-----------------------|------------------------------|
| 532 | $\alpha = C_5$ | Γ_2 | Γ_3 |
| $\tilde{5}3m$ | $\beta = C_{3d}$ | Γ_{2u} | Γ_{3u} |

1. TENSORIAL ASPECTS OF PHYSICAL PROPERTIES

Table 1.10.5.2. Matrices of the irreducible representations of dimension $d \geq 2$ corresponding to the irreps of Table 1.10.5.1

(a) D_5

| Representation | $D(\alpha^p)$ | $D(\beta)$ |
|----------------|---|--|
| Γ_3 | $\begin{pmatrix} \cos(2\pi p/5) & -\sin(2\pi p/5) \\ \sin(2\pi p/5) & \cos(2\pi p/5) \end{pmatrix}$ | $\begin{pmatrix} 0 & 1 \\ 1 & 0 \end{pmatrix}$ |
| Γ_4 | $\begin{pmatrix} \cos(4\pi p/5) & -\sin(4\pi p/5) \\ \sin(4\pi p/5) & \cos(4\pi p/5) \end{pmatrix}$ | $\begin{pmatrix} 0 & 1 \\ 1 & 0 \end{pmatrix}$ |

(b) D_8

| Representation | $D(\alpha^p)$ | $D(\beta)$ |
|----------------|---|--|
| Γ_5 | $\begin{pmatrix} \cos(\pi p/4) & -\sin(\pi p/4) \\ \sin(\pi p/4) & \cos(\pi p/4) \end{pmatrix}$ | $\begin{pmatrix} 0 & 1 \\ 1 & 0 \end{pmatrix}$ |
| Γ_6 | $\begin{pmatrix} \cos(\pi p/2) & -\sin(\pi p/2) \\ \sin(\pi p/2) & \cos(\pi p/2) \end{pmatrix}$ | $\begin{pmatrix} 0 & 1 \\ 1 & 0 \end{pmatrix}$ |
| Γ_7 | $\begin{pmatrix} \cos(3\pi p/4) & -\sin(3\pi p/4) \\ \sin(3\pi p/4) & \cos(3\pi p/4) \end{pmatrix}$ | $\begin{pmatrix} 0 & 1 \\ 1 & 0 \end{pmatrix}$ |

(c) D_{10}

| Representation | $D(\alpha^p)$ | $D(\beta)$ |
|----------------|---|--|
| Γ_5 | $\begin{pmatrix} \cos(\pi p/5) & -\sin(\pi p/5) \\ \sin(\pi p/5) & \cos(\pi p/5) \end{pmatrix}$ | $\begin{pmatrix} 0 & 1 \\ 1 & 0 \end{pmatrix}$ |
| Γ_6 | $\begin{pmatrix} \cos(2\pi p/5) & -\sin(2\pi p/5) \\ \sin(2\pi p/5) & \cos(2\pi p/5) \end{pmatrix}$ | $\begin{pmatrix} 0 & 1 \\ 1 & 0 \end{pmatrix}$ |
| Γ_7 | $\begin{pmatrix} \cos(3\pi p/5) & -\sin(3\pi p/5) \\ \sin(3\pi p/5) & \cos(3\pi p/5) \end{pmatrix}$ | $\begin{pmatrix} 0 & 1 \\ 1 & 0 \end{pmatrix}$ |
| Γ_8 | $\begin{pmatrix} \cos(4\pi p/5) & -\sin(4\pi p/5) \\ \sin(4\pi p/5) & \cos(4\pi p/5) \end{pmatrix}$ | $\begin{pmatrix} 0 & 1 \\ 1 & 0 \end{pmatrix}$ |

(d) D_{12}

| Representation | $D(\alpha^p)$ | $D(\beta)$ |
|----------------|---|--|
| Γ_5 | $\begin{pmatrix} \cos(\pi p/6) & -\sin(\pi p/6) \\ \sin(\pi p/6) & \cos(\pi p/6) \end{pmatrix}$ | $\begin{pmatrix} 0 & 1 \\ 1 & 0 \end{pmatrix}$ |
| Γ_6 | $\begin{pmatrix} \cos(\pi p/3) & -\sin(\pi p/3) \\ \sin(\pi p/3) & \cos(\pi p/3) \end{pmatrix}$ | $\begin{pmatrix} 0 & 1 \\ 1 & 0 \end{pmatrix}$ |
| Γ_7 | $\begin{pmatrix} \cos(\pi p/2) & -\sin(\pi p/2) \\ \sin(\pi p/2) & \cos(\pi p/2) \end{pmatrix}$ | $\begin{pmatrix} 0 & 1 \\ 1 & 0 \end{pmatrix}$ |
| Γ_8 | $\begin{pmatrix} \cos(2\pi p/3) & -\sin(2\pi p/3) \\ \sin(2\pi p/3) & \cos(2\pi p/3) \end{pmatrix}$ | $\begin{pmatrix} 0 & 1 \\ 1 & 0 \end{pmatrix}$ |
| Γ_9 | $\begin{pmatrix} \cos(5\pi p/6) & -\sin(5\pi p/6) \\ \sin(5\pi p/6) & \cos(5\pi p/6) \end{pmatrix}$ | $\begin{pmatrix} 0 & 1 \\ 1 & 0 \end{pmatrix}$ |

Table 1.10.5.1 gives the characters of the point groups C_n with $n = 5, 8, 10, 12$, D_n with $n = 5, 8, 10, 12$, and the icosahedral group I . The direct products with \mathbb{Z}_2 then follow easily. Although these direct products of a group K with \mathbb{Z}_2 do not belong to the isomorphism class of K , their irreducible representations are nevertheless given in the table for K because these irreducible representations have the same labels as those for K apart from an additional subindex u . The representations of the subgroup K of $K \times \mathbb{Z}_2$ are the same as for K itself, those for the cosets get an additional minus sign. In the tables, the characters for the groups $K \times \mathbb{Z}_2$ are separated from those for K by a horizontal rule. In addition to the characters are given the realizations of crystal-

lographic point groups, and the irreducible components of the vector representations in direct space V_E and internal space V_I for these realizations. The vector representation in V_I is called the perpendicular representation.

In Table 1.10.5.2 the representation matrices for the irreducible representations in more than one dimension are given (one-dimensional representations are just the characters). For the cyclic groups there are only one-dimensional representations, for the dihedral groups there are one- and two-dimensional irreducible representations. There are four irreducible representations of I of dimension larger than one. The four- and five-dimensional ones are given as integer representations. They form

1.10. TENSORS IN QUASIPERIODIC STRUCTURES

Table 1.10.5.2 (*cont.*)

(e) *I*. First column: numbering of the elements. $f = (1 + \sqrt{5})/2$, $t = (\sqrt{5} - 1)/2$. Horizontal rules separate conjugation classes.

| No. | Order | Γ_2 | Γ_4 | Γ_5 |
|-----|-------|---|--|--|
| 1 | 1 | $\begin{pmatrix} 1 & 0 & 0 \\ 0 & 1 & 0 \\ 0 & 0 & 1 \end{pmatrix}$ | $\begin{pmatrix} 1 & 0 & 0 & 0 \\ 0 & 1 & 0 & 0 \\ 0 & 0 & 1 & 0 \\ 0 & 0 & 0 & 1 \end{pmatrix}$ | $\begin{pmatrix} 1 & 0 & 0 & 0 & 0 \\ 0 & 1 & 0 & 0 & 0 \\ 0 & 0 & 1 & 0 & 0 \\ 0 & 0 & 0 & 1 & 0 \\ 0 & 0 & 0 & 0 & 1 \end{pmatrix}$ |
| 2 | 5 | $\begin{pmatrix} 1/2 & t/2 & -f/2 \\ t/2 & f/2 & 1/2 \\ f/2 & -1/2 & t/2 \end{pmatrix}$ | $\begin{pmatrix} 0 & 0 & 0 & -1 \\ 1 & 0 & 0 & -1 \\ 0 & 1 & 0 & -1 \\ 0 & 0 & 1 & -1 \end{pmatrix}$ | $\begin{pmatrix} 1 & 0 & 0 & 0 & -1 \\ 0 & 0 & 0 & 0 & -1 \\ 0 & 1 & 0 & 0 & -1 \\ 0 & 0 & 1 & 0 & -1 \\ 0 & 0 & 0 & 1 & -1 \end{pmatrix}$ |
| 3 | 5 | $\begin{pmatrix} 1/2 & -t/2 & f/2 \\ -t/2 & f/2 & 1/2 \\ f/2 & -1/2 & t/2 \end{pmatrix}$ | $\begin{pmatrix} 0 & 0 & 1 & -1 \\ 1 & 0 & 0 & -1 \\ 0 & 0 & 0 & -1 \\ 0 & 1 & 0 & -1 \end{pmatrix}$ | $\begin{pmatrix} 0 & -1 & 1 & 0 & 0 \\ 0 & -1 & 0 & 0 & 1 \\ 0 & -1 & 0 & 0 & 0 \\ 0 & -1 & 0 & 1 & 0 \\ 1 & -1 & 0 & 0 & 0 \end{pmatrix}$ |
| 4 | 5 | $\begin{pmatrix} 1/2 & t/2 & f/2 \\ t/2 & f/2 & -1/2 \\ -f/2 & 1/2 & t/2 \end{pmatrix}$ | $\begin{pmatrix} -1 & 1 & 0 & 0 \\ -1 & 0 & 1 & 0 \\ -1 & 0 & 0 & 1 \\ -1 & 0 & 0 & 0 \end{pmatrix}$ | $\begin{pmatrix} 1 & -1 & 0 & 0 & 0 \\ 0 & -1 & 1 & 0 & 0 \\ 0 & -1 & 0 & 1 & 0 \\ 0 & -1 & 0 & 0 & 1 \\ 0 & -1 & 0 & 0 & 0 \end{pmatrix}$ |
| 5 | 5 | $\begin{pmatrix} t/2 & -f/2 & 1/2 \\ f/2 & 1/2 & t/2 \\ -1/2 & t/2 & f/2 \end{pmatrix}$ | $\begin{pmatrix} 0 & -1 & 0 & 0 \\ 0 & -1 & 0 & 1 \\ 1 & -1 & 0 & 0 \\ 0 & -1 & 1 & 0 \end{pmatrix}$ | $\begin{pmatrix} 0 & 1 & 0 & -1 & 0 \\ 0 & 0 & 0 & -1 & 1 \\ 0 & 0 & 1 & -1 & 0 \\ 1 & 0 & 0 & -1 & 0 \\ 0 & 0 & 0 & -1 & 0 \end{pmatrix}$ |
| 6 | 5 | $\begin{pmatrix} f/2 & -1/2 & -t/2 \\ 1/2 & t/2 & f/2 \\ -t/2 & -f/2 & 1/2 \end{pmatrix}$ | $\begin{pmatrix} 0 & 1 & -1 & 0 \\ 0 & 0 & -1 & 0 \\ 0 & 0 & -1 & 1 \\ 1 & 0 & -1 & 0 \end{pmatrix}$ | $\begin{pmatrix} 0 & 1 & 0 & 0 & 0 \\ 0 & 0 & 0 & 1 & 0 \\ 0 & 0 & 0 & 0 & 1 \\ 0 & 0 & 1 & 0 & 0 \\ 1 & 0 & 0 & 0 & 0 \end{pmatrix}$ |
| 7 | 5 | $\begin{pmatrix} f/2 & 1/2 & t/2 \\ -1/2 & t/2 & f/2 \\ t/2 & -f/2 & 1/2 \end{pmatrix}$ | $\begin{pmatrix} 0 & -1 & 0 & 1 \\ 0 & -1 & 1 & 0 \\ 1 & -1 & 0 & 0 \\ 0 & -1 & 0 & 0 \end{pmatrix}$ | $\begin{pmatrix} -1 & 0 & 1 & 0 & 0 \\ -1 & 1 & 0 & 0 & 0 \\ -1 & 0 & 0 & 0 & 1 \\ -1 & 0 & 0 & 0 & 0 \\ -1 & 0 & 0 & 1 & 0 \end{pmatrix}$ |
| 8 | 5 | $\begin{pmatrix} t/2 & f/2 & -1/2 \\ -f/2 & 1/2 & t/2 \\ 1/2 & t/2 & f/2 \end{pmatrix}$ | $\begin{pmatrix} -1 & 0 & 1 & 0 \\ -1 & 0 & 0 & 0 \\ -1 & 0 & 0 & 1 \\ -1 & 1 & 0 & 0 \end{pmatrix}$ | $\begin{pmatrix} 0 & 0 & 0 & 1 & -1 \\ 1 & 0 & 0 & 0 & -1 \\ 0 & 0 & 1 & 0 & -1 \\ 0 & 0 & 0 & 0 & -1 \\ 0 & 1 & 0 & 0 & -1 \end{pmatrix}$ |
| 9 | 5 | $\begin{pmatrix} t/2 & f/2 & 1/2 \\ -f/2 & 1/2 & -t/2 \\ -1/2 & -t/2 & f/2 \end{pmatrix}$ | $\begin{pmatrix} 0 & 0 & -1 & 0 \\ 0 & 0 & -1 & 1 \\ 0 & 1 & -1 & 0 \\ 1 & 0 & -1 & 0 \end{pmatrix}$ | $\begin{pmatrix} -1 & 0 & 0 & 1 & 0 \\ -1 & 0 & 1 & 0 & 0 \\ -1 & 0 & 0 & 0 & 0 \\ -1 & 1 & 0 & 0 & 0 \\ -1 & 0 & 0 & 0 & 1 \end{pmatrix}$ |
| 10 | 5 | $\begin{pmatrix} f/2 & 1/2 & -t/2 \\ -1/2 & t/2 & -f/2 \\ -t/2 & f/2 & 1/2 \end{pmatrix}$ | $\begin{pmatrix} 0 & -1 & 0 & 1 \\ 1 & -1 & 0 & 0 \\ 0 & -1 & 0 & 0 \\ 0 & -1 & 1 & 0 \end{pmatrix}$ | $\begin{pmatrix} 0 & 0 & 0 & 0 & 1 \\ 1 & 0 & 0 & 0 & 0 \\ 0 & 0 & 0 & 1 & 0 \\ 0 & 1 & 0 & 0 & 0 \\ 0 & 0 & 1 & 0 & 0 \end{pmatrix}$ |
| 11 | 5 | $\begin{pmatrix} 1/2 & -t/2 & -f/2 \\ -t/2 & f/2 & -1/2 \\ f/2 & 1/2 & t/2 \end{pmatrix}$ | $\begin{pmatrix} 0 & 1 & -1 & 0 \\ 0 & 0 & -1 & 1 \\ 1 & 0 & -1 & 0 \\ 0 & 0 & -1 & 0 \end{pmatrix}$ | $\begin{pmatrix} 0 & 0 & -1 & 0 & 1 \\ 0 & 0 & -1 & 0 & 0 \\ 1 & 0 & -1 & 0 & 0 \\ 0 & 0 & -1 & 1 & 0 \\ 0 & 1 & -1 & 0 & 0 \end{pmatrix}$ |
| 12 | 5 | $\begin{pmatrix} f/2 & -1/2 & t/2 \\ 1/2 & t/2 & -f/2 \\ t/2 & f/2 & 1/2 \end{pmatrix}$ | $\begin{pmatrix} 0 & 0 & 1 & -1 \\ 0 & 0 & 0 & -1 \\ 0 & 1 & 0 & -1 \\ 1 & 0 & 0 & -1 \end{pmatrix}$ | $\begin{pmatrix} 0 & 0 & 0 & -1 & 0 \\ 0 & 1 & 0 & -1 & 0 \\ 1 & 0 & 0 & -1 & 0 \\ 0 & 0 & 0 & -1 & 1 \\ 0 & 0 & 1 & -1 & 0 \end{pmatrix}$ |

1. TENSORIAL ASPECTS OF PHYSICAL PROPERTIES

Table 1.10.5.2 (*cont.*)

| No. | Order | Γ_2 | Γ_4 | Γ_5 |
|-----|-------|---|--|--|
| 13 | 5 | $\begin{pmatrix} t/2 & -f/2 & -1/2 \\ f/2 & 1/2 & -t/2 \\ 1/2 & -t/2 & f/2 \end{pmatrix}$ | $\begin{pmatrix} -1 & 0 & 0 & 1 \\ -1 & 0 & 1 & 0 \\ -1 & 0 & 0 & 0 \\ -1 & 1 & 0 & 0 \end{pmatrix}$ | $\begin{pmatrix} 0 & 0 & -1 & 0 & 0 \\ 0 & 0 & -1 & 1 & 0 \\ 0 & 1 & -1 & 0 & 0 \\ 1 & 0 & -1 & 0 & 0 \\ 0 & 0 & -1 & 0 & 1 \end{pmatrix}$ |
| 14 | 5 | $\begin{pmatrix} -t/2 & f/2 & -1/2 \\ f/2 & 1/2 & t/2 \\ 1/2 & -t/2 & -f/2 \end{pmatrix}$ | $\begin{pmatrix} 0 & 0 & -1 & 1 \\ 0 & 0 & -1 & 0 \\ 1 & 0 & -1 & 0 \\ 0 & 1 & -1 & 0 \end{pmatrix}$ | $\begin{pmatrix} 1 & 0 & 0 & -1 & 0 \\ 0 & 0 & 0 & -1 & 1 \\ 0 & 0 & 0 & -1 & 0 \\ 0 & 1 & 0 & -1 & 0 \\ 0 & 0 & 1 & -1 & 0 \end{pmatrix}$ |
| 15 | 5 | $\begin{pmatrix} -t/2 & f/2 & 1/2 \\ f/2 & 1/2 & -t/2 \\ -1/2 & t/2 & -f/2 \end{pmatrix}$ | $\begin{pmatrix} 0 & -1 & 1 & 0 \\ 0 & -1 & 0 & 1 \\ 0 & -1 & 0 & 0 \\ 1 & -1 & 0 & 0 \end{pmatrix}$ | $\begin{pmatrix} 1 & 0 & -1 & 0 & 0 \\ 0 & 0 & -1 & 1 & 0 \\ 0 & 0 & -1 & 0 & 1 \\ 0 & 0 & -1 & 0 & 0 \\ 0 & 1 & -1 & 0 & 0 \end{pmatrix}$ |
| 16 | 5 | $\begin{pmatrix} -f/2 & 1/2 & -t/2 \\ -1/2 & -t/2 & f/2 \\ t/2 & f/2 & 1/2 \end{pmatrix}$ | $\begin{pmatrix} 0 & 0 & -1 & 1 \\ 1 & 0 & -1 & 0 \\ 0 & 1 & -1 & 0 \\ 0 & 0 & -1 & 0 \end{pmatrix}$ | $\begin{pmatrix} 0 & -1 & 0 & 0 & 0 \\ 0 & -1 & 0 & 1 & 0 \\ 0 & -1 & 1 & 0 & 0 \\ 0 & -1 & 0 & 0 & 1 \\ 1 & -1 & 0 & 0 & 0 \end{pmatrix}$ |
| 17 | 5 | $\begin{pmatrix} -t/2 & -f/2 & 1/2 \\ -f/2 & 1/2 & t/2 \\ -1/2 & -t/2 & -f/2 \end{pmatrix}$ | $\begin{pmatrix} 0 & -1 & 0 & 0 \\ 0 & -1 & 1 & 0 \\ 0 & -1 & 0 & 1 \\ 1 & -1 & 0 & 0 \end{pmatrix}$ | $\begin{pmatrix} 0 & 0 & 0 & 0 & -1 \\ 1 & 0 & 0 & 0 & -1 \\ 0 & 1 & 0 & 0 & -1 \\ 0 & 0 & 0 & 1 & -1 \\ 0 & 0 & 1 & 0 & -1 \end{pmatrix}$ |
| 18 | 5 | $\begin{pmatrix} -t/2 & -f/2 & -1/2 \\ -f/2 & 1/2 & -t/2 \\ 1/2 & t/2 & -f/2 \end{pmatrix}$ | $\begin{pmatrix} -1 & 0 & 0 & 1 \\ -1 & 0 & 0 & 0 \\ -1 & 1 & 0 & 0 \\ -1 & 0 & 1 & 0 \end{pmatrix}$ | $\begin{pmatrix} -1 & 1 & 0 & 0 & 0 \\ -1 & 0 & 1 & 0 & 0 \\ -1 & 0 & 0 & 0 & 1 \\ -1 & 0 & 0 & 1 & 0 \\ -1 & 0 & 0 & 0 & 0 \end{pmatrix}$ |
| 19 | 5 | $\begin{pmatrix} -f/2 & -1/2 & t/2 \\ 1/2 & -t/2 & f/2 \\ -t/2 & f/2 & 1/2 \end{pmatrix}$ | $\begin{pmatrix} 0 & 1 & 0 & -1 \\ 0 & 0 & 1 & -1 \\ 0 & 0 & 0 & -1 \\ 1 & 0 & 0 & -1 \end{pmatrix}$ | $\begin{pmatrix} -1 & 0 & 0 & 0 & 1 \\ -1 & 0 & 0 & 0 & 0 \\ -1 & 0 & 1 & 0 & 0 \\ -1 & 1 & 0 & 0 & 0 \\ -1 & 0 & 0 & 1 & 0 \end{pmatrix}$ |
| 20 | 5 | $\begin{pmatrix} -f/2 & 1/2 & t/2 \\ -1/2 & -t/2 & -f/2 \\ -t/2 & -f/2 & 1/2 \end{pmatrix}$ | $\begin{pmatrix} 0 & -1 & 1 & 0 \\ 1 & -1 & 0 & 0 \\ 0 & -1 & 0 & 1 \\ 0 & -1 & 0 & 0 \end{pmatrix}$ | $\begin{pmatrix} 0 & 1 & 0 & -1 & 0 \\ 0 & 0 & 0 & -1 & 0 \\ 1 & 0 & 0 & -1 & 0 \\ 0 & 0 & 1 & -1 & 0 \\ 0 & 0 & 0 & -1 & 1 \end{pmatrix}$ |
| 21 | 5 | $\begin{pmatrix} 1/2 & -t/2 & f/2 \\ t/2 & -f/2 & -1/2 \\ f/2 & 1/2 & -t/2 \end{pmatrix}$ | $\begin{pmatrix} -1 & 1 & 0 & 0 \\ -1 & 0 & 0 & 1 \\ -1 & 0 & 0 & 0 \\ -1 & 0 & 1 & 0 \end{pmatrix}$ | $\begin{pmatrix} 0 & 0 & 0 & 1 & -1 \\ 0 & 1 & 0 & 0 & -1 \\ 0 & 0 & 0 & 0 & -1 \\ 0 & 0 & 1 & 0 & -1 \\ 1 & 0 & 0 & 0 & -1 \end{pmatrix}$ |
| 22 | 5 | $\begin{pmatrix} 1/2 & -t/2 & -f/2 \\ t/2 & -f/2 & 1/2 \\ -f/2 & -1/2 & -t/2 \end{pmatrix}$ | $\begin{pmatrix} 0 & 0 & 0 & -1 \\ 0 & 0 & 1 & -1 \\ 1 & 0 & 0 & -1 \\ 0 & 1 & 0 & -1 \end{pmatrix}$ | $\begin{pmatrix} 0 & 0 & 0 & 1 & 0 \\ 0 & 0 & 1 & 0 & 0 \\ 1 & 0 & 0 & 0 & 0 \\ 0 & 0 & 0 & 0 & 1 \\ 0 & 1 & 0 & 0 & 0 \end{pmatrix}$ |
| 23 | 5 | $\begin{pmatrix} 1/2 & t/2 & f/2 \\ -t/2 & -f/2 & 1/2 \\ f/2 & -1/2 & -t/2 \end{pmatrix}$ | $\begin{pmatrix} 0 & 0 & -1 & 0 \\ 1 & 0 & -1 & 0 \\ 0 & 0 & -1 & 1 \\ 0 & 1 & -1 & 0 \end{pmatrix}$ | $\begin{pmatrix} 0 & 0 & -1 & 0 & 1 \\ 0 & 1 & -1 & 0 & 0 \\ 0 & 0 & -1 & 1 & 0 \\ 1 & 0 & -1 & 0 & 0 \\ 0 & 0 & -1 & 0 & 0 \end{pmatrix}$ |
| 24 | 5 | $\begin{pmatrix} 1/2 & t/2 & -f/2 \\ -t/2 & -f/2 & -1/2 \\ -f/2 & 1/2 & -t/2 \end{pmatrix}$ | $\begin{pmatrix} -1 & 0 & 1 & 0 \\ -1 & 0 & 0 & 1 \\ -1 & 1 & 0 & 0 \\ -1 & 0 & 0 & 0 \end{pmatrix}$ | $\begin{pmatrix} 0 & 0 & 1 & 0 & 0 \\ 0 & 0 & 0 & 0 & 1 \\ 0 & 1 & 0 & 0 & 0 \\ 1 & 0 & 0 & 0 & 0 \\ 0 & 0 & 0 & 1 & 0 \end{pmatrix}$ |

1.10. TENSORS IN QUASIPERIODIC STRUCTURES

Table 1.10.5.2 (cont.)

| No. | Order | Γ_2 | Γ_4 | Γ_5 |
|-----|-------|---|--|--|
| 25 | 5 | $\begin{pmatrix} -f/2 & -1/2 & -t/2 \\ 1/2 & -t/2 & -f/2 \\ t/2 & -f/2 & 1/2 \end{pmatrix}$ | $\begin{pmatrix} 0 & 1 & 0 & -1 \\ 0 & 0 & 0 & -1 \\ 1 & 0 & 0 & -1 \\ 0 & 0 & 1 & -1 \end{pmatrix}$ | $\begin{pmatrix} 0 & -1 & 1 & 0 & 0 \\ 1 & -1 & 0 & 0 & 0 \\ 0 & -1 & 0 & 1 & 0 \\ 0 & -1 & 0 & 0 & 0 \\ 0 & -1 & 0 & 0 & 1 \end{pmatrix}$ |
| 26 | 3 | $\begin{pmatrix} -1/2 & t/2 & -f/2 \\ -t/2 & f/2 & 1/2 \\ f/2 & 1/2 & -t/2 \end{pmatrix}$ | $\begin{pmatrix} 1 & -1 & 0 & 0 \\ 0 & -1 & 1 & 0 \\ 0 & -1 & 0 & 0 \\ 0 & -1 & 0 & 1 \end{pmatrix}$ | $\begin{pmatrix} 0 & -1 & 0 & 1 & 0 \\ 0 & -1 & 0 & 0 & 1 \\ 1 & -1 & 0 & 0 & 0 \\ 0 & -1 & 1 & 0 & 0 \\ 0 & -1 & 0 & 0 & 0 \end{pmatrix}$ |
| 27 | 3 | $\begin{pmatrix} -1/2 & -t/2 & f/2 \\ t/2 & f/2 & 1/2 \\ -f/2 & 1/2 & -t/2 \end{pmatrix}$ | $\begin{pmatrix} 1 & 0 & -1 & 0 \\ 0 & 0 & -1 & 0 \\ 0 & 1 & -1 & 0 \\ 0 & 0 & -1 & 1 \end{pmatrix}$ | $\begin{pmatrix} 0 & 0 & 1 & 0 & -1 \\ 0 & 0 & 0 & 0 & -1 \\ 0 & 0 & 0 & 1 & -1 \\ 1 & 0 & 0 & 0 & -1 \\ 0 & 1 & 0 & 0 & -1 \end{pmatrix}$ |
| 28 | 3 | $\begin{pmatrix} -1/2 & t/2 & f/2 \\ -t/2 & f/2 & -1/2 \\ -f/2 & -1/2 & -t/2 \end{pmatrix}$ | $\begin{pmatrix} 0 & 0 & 0 & 1 \\ 0 & 1 & 0 & 0 \\ 1 & 0 & 0 & 0 \\ 0 & 0 & 1 & 0 \end{pmatrix}$ | $\begin{pmatrix} 0 & 0 & -1 & 1 & 0 \\ 0 & 0 & -1 & 0 & 0 \\ 0 & 1 & -1 & 0 & 0 \\ 0 & 0 & -1 & 0 & 1 \\ 1 & 0 & -1 & 0 & 0 \end{pmatrix}$ |
| 29 | 3 | $\begin{pmatrix} 0 & 0 & 1 \\ 1 & 0 & 0 \\ 0 & 1 & 0 \end{pmatrix}$ | $\begin{pmatrix} 0 & 0 & 0 & 1 \\ 1 & 0 & 0 & 0 \\ 0 & 0 & 1 & 0 \\ 0 & 1 & 0 & 0 \end{pmatrix}$ | $\begin{pmatrix} 0 & 1 & 0 & 0 & -1 \\ 0 & 0 & 1 & 0 & -1 \\ 1 & 0 & 0 & 0 & -1 \\ 0 & 0 & 0 & 0 & -1 \\ 0 & 0 & 0 & 1 & -1 \end{pmatrix}$ |
| 30 | 3 | $\begin{pmatrix} -1/2 & -t/2 & -f/2 \\ t/2 & f/2 & -1/2 \\ f/2 & -1/2 & -t/2 \end{pmatrix}$ | $\begin{pmatrix} 0 & 0 & 1 & 0 \\ 0 & 1 & 0 & 0 \\ 0 & 0 & 0 & 1 \\ 1 & 0 & 0 & 0 \end{pmatrix}$ | $\begin{pmatrix} 0 & -1 & 0 & 0 & 1 \\ 0 & -1 & 1 & 0 & 0 \\ 0 & -1 & 0 & 0 & 0 \\ 1 & -1 & 0 & 0 & 0 \\ 0 & -1 & 0 & 1 & 0 \end{pmatrix}$ |
| 31 | 3 | $\begin{pmatrix} 0 & 0 & -1 \\ 1 & 0 & 0 \\ 0 & -1 & 0 \end{pmatrix}$ | $\begin{pmatrix} 1 & -1 & 0 & 0 \\ 0 & -1 & 0 & 1 \\ 0 & -1 & 1 & 0 \\ 0 & -1 & 0 & 0 \end{pmatrix}$ | $\begin{pmatrix} 0 & 0 & 0 & 0 & -1 \\ 0 & 0 & 1 & 0 & -1 \\ 0 & 0 & 0 & 1 & -1 \\ 0 & 1 & 0 & 0 & -1 \\ 1 & 0 & 0 & 0 & -1 \end{pmatrix}$ |
| 32 | 3 | $\begin{pmatrix} f/2 & 1/2 & -t/2 \\ 1/2 & -t/2 & f/2 \\ t/2 & -f/2 & -1/2 \end{pmatrix}$ | $\begin{pmatrix} -1 & 0 & 1 & 0 \\ -1 & 1 & 0 & 0 \\ -1 & 0 & 0 & 0 \\ -1 & 0 & 0 & 1 \end{pmatrix}$ | $\begin{pmatrix} -1 & 1 & 0 & 0 & 0 \\ -1 & 0 & 0 & 0 & 0 \\ -1 & 0 & 0 & 1 & 0 \\ -1 & 0 & 0 & 0 & 1 \\ -1 & 0 & 1 & 0 & 0 \end{pmatrix}$ |
| 33 | 3 | $\begin{pmatrix} 0 & 1 & 0 \\ 0 & 0 & 1 \\ 1 & 0 & 0 \end{pmatrix}$ | $\begin{pmatrix} 0 & 1 & 0 & 0 \\ 0 & 0 & 0 & 1 \\ 0 & 0 & 1 & 0 \\ 1 & 0 & 0 & 0 \end{pmatrix}$ | $\begin{pmatrix} 0 & 0 & 1 & -1 & 0 \\ 1 & 0 & 0 & -1 & 0 \\ 0 & 1 & 0 & -1 & 0 \\ 0 & 0 & 0 & -1 & 1 \\ 0 & 0 & 0 & -1 & 0 \end{pmatrix}$ |
| 34 | 3 | $\begin{pmatrix} 0 & 0 & -1 \\ -1 & 0 & 0 \\ 0 & 1 & 0 \end{pmatrix}$ | $\begin{pmatrix} 0 & 0 & 0 & -1 \\ 0 & 1 & 0 & -1 \\ 0 & 0 & 1 & -1 \\ 1 & 0 & 0 & -1 \end{pmatrix}$ | $\begin{pmatrix} 0 & 1 & -1 & 0 & 0 \\ 0 & 0 & -1 & 0 & 1 \\ 0 & 0 & -1 & 1 & 0 \\ 0 & 0 & -1 & 0 & 0 \\ 1 & 0 & -1 & 0 & 0 \end{pmatrix}$ |
| 35 | 3 | $\begin{pmatrix} 0 & -1 & 0 \\ 0 & 0 & 1 \\ -1 & 0 & 0 \end{pmatrix}$ | $\begin{pmatrix} -1 & 0 & 0 & 1 \\ -1 & 1 & 0 & 0 \\ -1 & 0 & 1 & 0 \\ -1 & 0 & 0 & 0 \end{pmatrix}$ | $\begin{pmatrix} 0 & 0 & 0 & -1 & 1 \\ 1 & 0 & 0 & -1 & 0 \\ 0 & 0 & 0 & -1 & 0 \\ 0 & 0 & 1 & -1 & 0 \\ 0 & 1 & 0 & -1 & 0 \end{pmatrix}$ |
| 36 | 3 | $\begin{pmatrix} f/2 & -1/2 & t/2 \\ -1/2 & -t/2 & f/2 \\ -t/2 & -f/2 & -1/2 \end{pmatrix}$ | $\begin{pmatrix} 1 & 0 & 0 & 0 \\ 0 & 0 & 0 & 1 \\ 0 & 1 & 0 & 0 \\ 0 & 0 & 1 & 0 \end{pmatrix}$ | $\begin{pmatrix} 0 & -1 & 0 & 0 & 1 \\ 0 & -1 & 0 & 1 & 0 \\ 1 & -1 & 0 & 0 & 0 \\ 0 & -1 & 0 & 0 & 0 \\ 0 & -1 & 1 & 0 & 0 \end{pmatrix}$ |

1. TENSORIAL ASPECTS OF PHYSICAL PROPERTIES

Table 1.10.5.2 (*cont.*)

| No. | Order | Γ_2 | Γ_4 | Γ_5 |
|-----|-------|---|--|--|
| 37 | 3 | $\begin{pmatrix} 0 & 0 & 1 \\ -1 & 0 & 0 \\ 0 & -1 & 0 \end{pmatrix}$ | $\begin{pmatrix} -1 & 1 & 0 & 0 \\ -1 & 0 & 0 & 0 \\ -1 & 0 & 1 & 0 \\ -1 & 0 & 0 & 1 \end{pmatrix}$ | $\begin{pmatrix} 0 & 0 & -1 & 0 & 0 \\ 0 & 0 & -1 & 0 & 1 \\ 1 & 0 & -1 & 0 & 0 \\ 0 & 1 & -1 & 0 & 0 \\ 0 & 0 & -1 & 1 & 0 \end{pmatrix}$ |
| 38 | 3 | $\begin{pmatrix} 0 & 1 & 0 \\ 0 & 0 & -1 \\ -1 & 0 & 0 \end{pmatrix}$ | $\begin{pmatrix} 1 & 0 & 0 & -1 \\ 0 & 0 & 0 & -1 \\ 0 & 0 & 1 & -1 \\ 0 & 1 & 0 & -1 \end{pmatrix}$ | $\begin{pmatrix} -1 & 0 & 0 & 0 & 1 \\ -1 & 0 & 0 & 1 & 0 \\ -1 & 1 & 0 & 0 & 0 \\ -1 & 0 & 1 & 0 & 0 \\ -1 & 0 & 0 & 0 & 0 \end{pmatrix}$ |
| 39 | 3 | $\begin{pmatrix} f/2 & 1/2 & t/2 \\ 1/2 & -t/2 & -f/2 \\ -t/2 & f/2 & -1/2 \end{pmatrix}$ | $\begin{pmatrix} 0 & 0 & -1 & 0 \\ 0 & 1 & -1 & 0 \\ 1 & 0 & -1 & 0 \\ 0 & 0 & -1 & 1 \end{pmatrix}$ | $\begin{pmatrix} 0 & -1 & 0 & 0 & 0 \\ 1 & -1 & 0 & 0 & 0 \\ 0 & -1 & 0 & 0 & 1 \\ 0 & -1 & 1 & 0 & 0 \\ 0 & -1 & 0 & 1 & 0 \end{pmatrix}$ |
| 40 | 3 | $\begin{pmatrix} -t/2 & -f/2 & 1/2 \\ f/2 & -1/2 & -t/2 \\ 1/2 & t/2 & f/2 \end{pmatrix}$ | $\begin{pmatrix} 1 & 0 & -1 & 0 \\ 0 & 1 & -1 & 0 \\ 0 & 0 & -1 & 1 \\ 0 & 0 & -1 & 0 \end{pmatrix}$ | $\begin{pmatrix} -1 & 0 & 0 & 1 & 0 \\ -1 & 0 & 0 & 0 & 1 \\ -1 & 1 & 0 & 0 & 0 \\ -1 & 0 & 0 & 0 & 0 \\ -1 & 0 & 1 & 0 & 0 \end{pmatrix}$ |
| 41 | 3 | $\begin{pmatrix} -t/2 & -f/2 & -1/2 \\ f/2 & -1/2 & t/2 \\ -1/2 & -t/2 & f/2 \end{pmatrix}$ | $\begin{pmatrix} 0 & 0 & 1 & 0 \\ 1 & 0 & 0 & 0 \\ 0 & 1 & 0 & 0 \\ 0 & 0 & 0 & 1 \end{pmatrix}$ | $\begin{pmatrix} 0 & 0 & -1 & 1 & 0 \\ 1 & 0 & -1 & 0 & 0 \\ 0 & 0 & -1 & 0 & 1 \\ 0 & 1 & -1 & 0 & 0 \\ 0 & 0 & -1 & 0 & 0 \end{pmatrix}$ |
| 42 | 3 | $\begin{pmatrix} -t/2 & f/2 & 1/2 \\ -f/2 & -1/2 & t/2 \\ 1/2 & -t/2 & f/2 \end{pmatrix}$ | $\begin{pmatrix} 1 & 0 & 0 & -1 \\ 0 & 1 & 0 & -1 \\ 0 & 0 & 0 & -1 \\ 0 & 0 & 1 & -1 \end{pmatrix}$ | $\begin{pmatrix} 0 & 0 & 0 & -1 & 0 \\ 0 & 0 & 1 & -1 & 0 \\ 0 & 0 & 0 & -1 & 1 \\ 1 & 0 & 0 & -1 & 0 \\ 0 & 1 & 0 & -1 & 0 \end{pmatrix}$ |
| 43 | 3 | $\begin{pmatrix} -t/2 & f/2 & -1/2 \\ -f/2 & -1/2 & -t/2 \\ -1/2 & t/2 & f/2 \end{pmatrix}$ | $\begin{pmatrix} 0 & 1 & 0 & 0 \\ 0 & 0 & 1 & 0 \\ 1 & 0 & 0 & 0 \\ 0 & 0 & 0 & 1 \end{pmatrix}$ | $\begin{pmatrix} 0 & 1 & 0 & 0 & -1 \\ 0 & 0 & 0 & 1 & -1 \\ 0 & 0 & 0 & 0 & -1 \\ 1 & 0 & 0 & 0 & -1 \\ 0 & 0 & 1 & 0 & -1 \end{pmatrix}$ |
| 44 | 3 | $\begin{pmatrix} f/2 & -1/2 & -t/2 \\ -1/2 & -t/2 & -f/2 \\ t/2 & f/2 & -1/2 \end{pmatrix}$ | $\begin{pmatrix} 1 & 0 & 0 & 0 \\ 0 & 0 & 1 & 0 \\ 0 & 0 & 0 & 1 \\ 0 & 1 & 0 & 0 \end{pmatrix}$ | $\begin{pmatrix} 0 & 0 & 1 & -1 & 0 \\ 0 & 0 & 0 & -1 & 0 \\ 0 & 0 & 0 & -1 & 1 \\ 0 & 1 & 0 & -1 & 0 \\ 1 & 0 & 0 & -1 & 0 \end{pmatrix}$ |
| 45 | 3 | $\begin{pmatrix} 0 & -1 & 0 \\ 0 & 0 & -1 \\ 1 & 0 & 0 \end{pmatrix}$ | $\begin{pmatrix} 0 & -1 & 0 & 0 \\ 1 & -1 & 0 & 0 \\ 0 & -1 & 1 & 0 \\ 0 & -1 & 0 & 1 \end{pmatrix}$ | $\begin{pmatrix} -1 & 0 & 1 & 0 & 0 \\ -1 & 0 & 0 & 1 & 0 \\ -1 & 0 & 0 & 0 & 0 \\ -1 & 0 & 0 & 0 & 1 \\ -1 & 1 & 0 & 0 & 0 \end{pmatrix}$ |
| 46 | 2 | $\begin{pmatrix} -1 & 0 & 0 \\ 0 & 1 & 0 \\ 0 & 0 & -1 \end{pmatrix}$ | $\begin{pmatrix} 0 & 1 & 0 & -1 \\ 1 & 0 & 0 & -1 \\ 0 & 0 & 1 & -1 \\ 0 & 0 & 0 & -1 \end{pmatrix}$ | $\begin{pmatrix} 0 & 0 & 0 & 1 & 0 \\ 0 & 1 & 0 & 0 & 0 \\ 0 & 0 & 0 & 0 & 1 \\ 1 & 0 & 0 & 0 & 0 \\ 0 & 0 & 1 & 0 & 0 \end{pmatrix}$ |
| 47 | 2 | $\begin{pmatrix} -f/2 & 1/2 & t/2 \\ 1/2 & t/2 & f/2 \\ t/2 & f/2 & -1/2 \end{pmatrix}$ | $\begin{pmatrix} -1 & 0 & 0 & 0 \\ -1 & 1 & 0 & 0 \\ -1 & 0 & 0 & 1 \\ -1 & 0 & 1 & 0 \end{pmatrix}$ | $\begin{pmatrix} 0 & 0 & 1 & 0 & 0 \\ 0 & 0 & 0 & 1 & 0 \\ 1 & 0 & 0 & 0 & 0 \\ 0 & 1 & 0 & 0 & 0 \\ 0 & 0 & 0 & 0 & 1 \end{pmatrix}$ |
| 48 | 2 | $\begin{pmatrix} -f/2 & -1/2 & -t/2 \\ -1/2 & t/2 & f/2 \\ -t/2 & f/2 & -1/2 \end{pmatrix}$ | $\begin{pmatrix} 0 & 0 & 1 & 0 \\ 0 & 0 & 0 & 1 \\ 1 & 0 & 0 & 0 \\ 0 & 1 & 0 & 0 \end{pmatrix}$ | $\begin{pmatrix} -1 & 0 & 0 & 0 & 0 \\ -1 & 1 & 0 & 0 & 0 \\ -1 & 0 & 0 & 1 & 0 \\ -1 & 0 & 1 & 0 & 0 \\ -1 & 0 & 0 & 0 & 1 \end{pmatrix}$ |

1.10. TENSORS IN QUASIPERIODIC STRUCTURES

Table 1.10.5.2 (cont.)

| No. | Order | Γ_2 | Γ_4 | Γ_5 |
|-----|-------|---|--|--|
| 49 | 2 | $\begin{pmatrix} -f/2 & -1/2 & t/2 \\ -1/2 & t/2 & -f/2 \\ t/2 & -f/2 & -1/2 \end{pmatrix}$ | $\begin{pmatrix} 1 & 0 & -1 & 0 \\ 0 & 0 & -1 & 1 \\ 0 & 0 & -1 & 0 \\ 0 & 1 & -1 & 0 \end{pmatrix}$ | $\begin{pmatrix} 0 & 1 & 0 & 0 & 0 \\ 1 & 0 & 0 & 0 & 0 \\ 0 & 0 & 1 & 0 & 0 \\ 0 & 0 & 0 & 0 & 1 \\ 0 & 0 & 0 & 1 & 0 \end{pmatrix}$ |
| 50 | 2 | $\begin{pmatrix} -f/2 & 1/2 & -t/2 \\ 1/2 & t/2 & -f/2 \\ -t/2 & -f/2 & -1/2 \end{pmatrix}$ | $\begin{pmatrix} -1 & 0 & 0 & 0 \\ -1 & 0 & 1 & 0 \\ -1 & 1 & 0 & 0 \\ -1 & 0 & 0 & 1 \end{pmatrix}$ | $\begin{pmatrix} 0 & 0 & 0 & -1 & 1 \\ 0 & 1 & 0 & -1 & 0 \\ 0 & 0 & 1 & -1 & 0 \\ 0 & 0 & 0 & -1 & 0 \\ 1 & 0 & 0 & -1 & 0 \end{pmatrix}$ |
| 51 | 2 | $\begin{pmatrix} t/2 & f/2 & -1/2 \\ f/2 & -1/2 & -t/2 \\ -1/2 & -t/2 & -f/2 \end{pmatrix}$ | $\begin{pmatrix} 0 & 1 & 0 & 0 \\ 1 & 0 & 0 & 0 \\ 0 & 0 & 0 & 1 \\ 0 & 0 & 1 & 0 \end{pmatrix}$ | $\begin{pmatrix} -1 & 0 & 0 & 0 & 0 \\ -1 & 0 & 0 & 0 & 1 \\ -1 & 0 & 1 & 0 & 0 \\ -1 & 0 & 0 & 1 & 0 \\ -1 & 1 & 0 & 0 & 0 \end{pmatrix}$ |
| 52 | 2 | $\begin{pmatrix} t/2 & f/2 & 1/2 \\ f/2 & -1/2 & t/2 \\ 1/2 & t/2 & -f/2 \end{pmatrix}$ | $\begin{pmatrix} 1 & 0 & 0 & -1 \\ 0 & 0 & 1 & -1 \\ 0 & 1 & 0 & -1 \\ 0 & 0 & 0 & -1 \end{pmatrix}$ | $\begin{pmatrix} 0 & 1 & -1 & 0 & 0 \\ 1 & 0 & -1 & 0 & 0 \\ 0 & 0 & -1 & 0 & 0 \\ 0 & 0 & -1 & 1 & 0 \\ 0 & 0 & -1 & 0 & 1 \end{pmatrix}$ |
| 53 | 2 | $\begin{pmatrix} -1/2 & t/2 & f/2 \\ t/2 & -f/2 & 1/2 \\ f/2 & 1/2 & t/2 \end{pmatrix}$ | $\begin{pmatrix} 0 & -1 & 1 & 0 \\ 0 & -1 & 0 & 0 \\ 1 & -1 & 0 & 0 \\ 0 & -1 & 0 & 1 \end{pmatrix}$ | $\begin{pmatrix} 0 & 0 & 0 & 0 & 1 \\ 0 & 0 & 1 & 0 & 0 \\ 0 & 1 & 0 & 0 & 0 \\ 0 & 0 & 0 & 1 & 0 \\ 1 & 0 & 0 & 0 & 0 \end{pmatrix}$ |
| 54 | 2 | $\begin{pmatrix} -1/2 & t/2 & -f/2 \\ t/2 & -f/2 & -1/2 \\ -f/2 & -1/2 & t/2 \end{pmatrix}$ | $\begin{pmatrix} 0 & 0 & -1 & 1 \\ 0 & 1 & -1 & 0 \\ 0 & 0 & -1 & 0 \\ 1 & 0 & -1 & 0 \end{pmatrix}$ | $\begin{pmatrix} 0 & 0 & 1 & 0 & -1 \\ 0 & 1 & 0 & 0 & -1 \\ 1 & 0 & 0 & 0 & -1 \\ 0 & 0 & 0 & 1 & -1 \\ 0 & 0 & 0 & 0 & -1 \end{pmatrix}$ |
| 55 | 2 | $\begin{pmatrix} 1 & 0 & 0 \\ 0 & -1 & 0 \\ 0 & 0 & -1 \end{pmatrix}$ | $\begin{pmatrix} 0 & -1 & 0 & 1 \\ 0 & -1 & 0 & 0 \\ 0 & -1 & 1 & 0 \\ 1 & -1 & 0 & 0 \end{pmatrix}$ | $\begin{pmatrix} 0 & -1 & 0 & 1 & 0 \\ 0 & -1 & 0 & 0 & 0 \\ 0 & -1 & 1 & 0 & 0 \\ 1 & -1 & 0 & 0 & 0 \\ 0 & -1 & 0 & 0 & 1 \end{pmatrix}$ |
| 56 | 2 | $\begin{pmatrix} -1 & 0 & 0 \\ 0 & -1 & 0 \\ 0 & 0 & 1 \end{pmatrix}$ | $\begin{pmatrix} -1 & 0 & 0 & 0 \\ -1 & 0 & 0 & 1 \\ -1 & 0 & 1 & 0 \\ -1 & 1 & 0 & 0 \end{pmatrix}$ | $\begin{pmatrix} 1 & -1 & 0 & 0 & 0 \\ 0 & -1 & 0 & 0 & 0 \\ 0 & -1 & 0 & 0 & 1 \\ 0 & -1 & 0 & 1 & 0 \\ 0 & -1 & 1 & 0 & 0 \end{pmatrix}$ |
| 57 | 2 | $\begin{pmatrix} -1/2 & -t/2 & -f/2 \\ -t/2 & -f/2 & 1/2 \\ -f/2 & 1/2 & t/2 \end{pmatrix}$ | $\begin{pmatrix} 1 & -1 & 0 & 0 \\ 0 & -1 & 0 & 0 \\ 0 & -1 & 0 & 1 \\ 0 & -1 & 1 & 0 \end{pmatrix}$ | $\begin{pmatrix} 1 & 0 & -1 & 0 & 0 \\ 0 & 1 & -1 & 0 & 0 \\ 0 & 0 & -1 & 0 & 0 \\ 0 & 0 & -1 & 0 & 1 \\ 0 & 0 & -1 & 1 & 0 \end{pmatrix}$ |
| 58 | 2 | $\begin{pmatrix} t/2 & -f/2 & -1/2 \\ -f/2 & -1/2 & t/2 \\ -1/2 & t/2 & -f/2 \end{pmatrix}$ | $\begin{pmatrix} 0 & 1 & -1 & 0 \\ 1 & 0 & -1 & 0 \\ 0 & 0 & -1 & 0 \\ 0 & 0 & -1 & 1 \end{pmatrix}$ | $\begin{pmatrix} 1 & 0 & 0 & -1 & 0 \\ 0 & 0 & 1 & -1 & 0 \\ 0 & 1 & 0 & -1 & 0 \\ 0 & 0 & 0 & -1 & 0 \\ 0 & 0 & 0 & -1 & 1 \end{pmatrix}$ |
| 59 | 2 | $\begin{pmatrix} t/2 & -f/2 & 1/2 \\ -f/2 & -1/2 & -t/2 \\ 1/2 & -t/2 & -f/2 \end{pmatrix}$ | $\begin{pmatrix} 0 & 0 & 1 & -1 \\ 0 & 1 & 0 & -1 \\ 1 & 0 & 0 & -1 \\ 0 & 0 & 0 & -1 \end{pmatrix}$ | $\begin{pmatrix} 1 & 0 & 0 & 0 & -1 \\ 0 & 0 & 0 & 1 & -1 \\ 0 & 0 & 1 & 0 & -1 \\ 0 & 1 & 0 & 0 & -1 \\ 0 & 0 & 0 & 0 & -1 \end{pmatrix}$ |
| 60 | 2 | $\begin{pmatrix} -1/2 & -t/2 & f/2 \\ -t/2 & -f/2 & -1/2 \\ f/2 & -1/2 & t/2 \end{pmatrix}$ | $\begin{pmatrix} 0 & 0 & 0 & 1 \\ 0 & 0 & 1 & 0 \\ 0 & 1 & 0 & 0 \\ 1 & 0 & 0 & 0 \end{pmatrix}$ | $\begin{pmatrix} 1 & 0 & 0 & 0 & 0 \\ 0 & 0 & 0 & 0 & 1 \\ 0 & 0 & 0 & 1 & 0 \\ 0 & 0 & 1 & 0 & 0 \\ 0 & 1 & 0 & 0 & 0 \end{pmatrix}$ |

1. TENSORIAL ASPECTS OF PHYSICAL PROPERTIES

Table 1.10.5.3. *The representation matrices for Γ_3*

The representation matrices for Γ_3 are the same as for Γ_2 . Correspondences are given as pairs i, j : $\Gamma_3(R_i) = \Gamma_2(R_j)$.

| i | j | i | j | i | j | i | j | i | j | i | j |
|-----|-----|-----|-----|-----|-----|-----|-----|-----|-----|-----|-----|
| 1 | 1 | 11 | 21 | 21 | 5 | 31 | 42 | 41 | 29 | 51 | 48 |
| 2 | 14 | 12 | 16 | 22 | 6 | 32 | 45 | 42 | 39 | 52 | 54 |
| 3 | 23 | 13 | 17 | 23 | 8 | 33 | 36 | 43 | 33 | 53 | 46 |
| 4 | 15 | 14 | 4 | 24 | 10 | 34 | 27 | 44 | 30 | 54 | 50 |
| 5 | 25 | 15 | 2 | 25 | 11 | 35 | 26 | 45 | 38 | 55 | 52 |
| 6 | 24 | 16 | 13 | 26 | 34 | 36 | 28 | 46 | 49 | 56 | 57 |
| 7 | 19 | 17 | 12 | 27 | 35 | 37 | 31 | 47 | 53 | 57 | 59 |
| 8 | 20 | 18 | 7 | 28 | 43 | 38 | 40 | 48 | 51 | 58 | 56 |
| 9 | 18 | 19 | 9 | 29 | 44 | 39 | 37 | 49 | 47 | 59 | 58 |
| 10 | 22 | 20 | 3 | 30 | 41 | 40 | 32 | 50 | 55 | 60 | 60 |

crystallographic groups in 4D and 5D. The two three-dimensional representations have the same matrices. The elements, however, are connected by an outer automorphism. That means that the i th element R_i is represented by $\Gamma_2(R_i)$ in the representation Γ_2 , and by $\Gamma_3(R_i) = \Gamma_2(\varphi R_i)$ in Γ_3 . The element φR_i is another element R_j . The corresponding j for each i is given in Table 1.10.5.3.

References

Bak, P. (1985). *Symmetry, stability, and elastic properties of icosahedral incommensurate crystals*. *Phys. Rev. B*, **32**, 5764–5772.

- Beest, B. W. van, Janner, A. & Blinc, R. (1983). ^{87}Rb electric field gradient tensors and the symmetry of the incommensurate phase in Rb_2ZnBr_4 and Rb_2ZnCl_4 . *J. Phys. C*, **16**, 5409–5416.
- Ding, D.-H., Yang, W.-G., Hu, C.-Z. & Wang, R.-H. (1993). *Generalized elasticity theory of quasicrystals*. *Phys. Rev. B*, **48**, 7003–7010.
- International Tables for Crystallography* (1999). Vol. C. *Mathematical, physical and chemical tables*, edited by A. J. C. Wilson & E. Prince. Dordrecht: Kluwer Academic Publishers.
- Janssen, T. (1988). *Aperiodic crystals: a contradictio in terminis?* *Phys. Rep.* **168**, 57–113.
- Janssen, T., Birman, J. L., Dénoyer, F., Koptsik, V. A., Verger-Gaugry, J. L., Weigel, D., Yamamoto, A., Abrahams, S. C. & Kopsky, V. (2002). *Report of a subcommittee on the nomenclature of n-dimensional crystallography. II. Symbols for arithmetic crystal classes, Bravais classes and space groups*. *Acta Cryst. A* **58**, 605–621.
- Janssen, T., Birman, J. L., Koptsik, V. A., Senechal, M., Weigel, D., Yamamoto, A., Abrahams, S. C. & Hahn, Th. (1999). *Report of a subcommittee on the nomenclature of n-dimensional crystallography. I. Symbols for point-group transformations, families, systems and geometric crystal classes*. *Acta Cryst. A* **55**, 761–782.
- Janssen, T. & Janner, A. (1987). *Incommensurability in crystals*. *Adv. Phys.* **36**, 519–624.
- Lubensky, T. C., Ramaswamy, S. & Toner, J. (1985). *Hydrodynamics of icosahedral quasicrystals*. *Phys. Rev. B*, **32**, 7444–7452.
- Shechtman, D., Blech, I., Gratias, D. & Cahn, J. W. (1984). *Metallic phase with long-range orientational order and no translational symmetry*. *Phys. Rev. Lett.* **53**, 1951–1953.
- Socolar, J. E. S., Lubensky, T. C. & Steinhardt, P. J. (1986). *Phonons, phasons and dislocations in quasicrystals*. *Phys. Rev. B*, **34**, 3345–3360.

2.1. Phonons

BY G. ECKOLD

2.1.1. Introduction

Interatomic interactions in crystalline solids not only determine the equilibrium atomic structure but also the possible excitations of the lattice: the motions of atoms, molecules or ions. The investigation of dynamical processes provides us with detailed information about the interatomic forces. Obviously, there are a huge variety of possible collective motions within a solid, which represents a multiparticle system with 10^{23} degrees of freedom. As long as the solid may be described by an equilibrium structure and atomic displacements from the average positions are small compared with interatomic distances, the dynamical behaviour of the lattice is essentially determined by well defined lattice vibrations or phonons. These elementary excitations of a solid are described by eigenvectors and eigenfrequencies reflecting the strength of interatomic interactions. Owing to the symmetry (space group) of the equilibrium structure there are constraints for the individual eigenvectors. In special high-symmetry cases, phonon eigenvectors can even be predicted merely on the basis of group-theoretical considerations.

This chapter is devoted to the implications of lattice symmetry on the form, *i.e.* on the eigenvectors, of lattice vibrations. We restrict ourselves to the consideration of perfect crystals and harmonic vibrations. In addition, some aspects of anharmonicity are discussed in terms of a quasi-harmonic model, yielding the connection between microscopic dynamics and macroscopic thermodynamic quantities such as thermal expansion. However, intrinsic anharmonic effects associated with the interaction of phonons, phonon damping or localized vibrations due to defects, for example, are beyond the scope of this article. In Section 2.1.2 we present the fundamentals of lattice dynamics with special emphasis on the role of the dynamical matrix. Section 2.1.3 deals with the symmetry properties of this matrix along with its eigenvectors and eigenfrequencies. Symmetry-induced degeneracies will be considered in some detail as well as compatibility relations for phonon wavevectors corresponding to points of higher symmetry within the reciprocal space. Finally, the optical selection rules for long wavelength vibrations are presented. Some examples are included in order to illustrate the theoretical results.

For a further discussion of other phenomena associated with lattice vibrations the reader is referred to the monographs of Leibfried (1955), Maradudin *et al.* (1971), Reissland (1973), Srivastava (1990) or Dove (1993).

2.1.2. Fundamentals of lattice dynamics in the harmonic approximation

2.1.2.1. Hamiltonian and equations of motion

In order to reduce the complexity of lattice dynamical considerations, we describe the crystal's periodicity by the smallest unit needed to generate the whole (infinite) lattice by translation, *i.e.* the *primitive cell*. Each individual primitive cell may be characterized by a running index l and a vector \mathbf{r}_l pointing to its origin. Let there be N atoms per cell, the equilibrium positions of which are given by

$$\mathbf{r}_{kl}^o = \mathbf{r}_l + \mathbf{r}_\kappa^o \quad \kappa = 1, \dots, N \quad l = 1, 2, \dots, \quad (2.1.2.1)$$

\mathbf{r}_κ^o being the vector of the κ th atom with respect to the origin of the primitive cell (see Fig. 2.1.2.1).

The set of vectors \mathbf{r}_{kl}^o describes the structure of the perfect lattice. At a particular time t , however, the κ th atom within the l th primitive cell, denoted by (κl) , may be found at a position $\mathbf{r}_{kl}(t)$ which differs slightly from the equilibrium position, the time-dependent displacement being

$$\mathbf{u}_{kl}(t) = \mathbf{r}_{kl}(t) - \mathbf{r}_{kl}^o = \mathbf{r}_{kl}(t) - \mathbf{r}_l - \mathbf{r}_\kappa^o. \quad (2.1.2.2)$$

The potential energy V of the whole crystal depends on the position vectors of all atoms,

$$V = V(\mathbf{r}_1, \mathbf{r}_2, \dots, \mathbf{r}_{kl}, \dots), \quad (2.1.2.3)$$

and is minimal if all atoms occupy their equilibrium positions. For small displacements, it can be expanded in a Taylor series with respect to $\mathbf{u}_{kl}(t)$:

$$V = V^o + \frac{1}{2} \sum_{\kappa l} \sum_{\kappa' l'} \sum_{\alpha=1}^3 \sum_{\beta=1}^3 u_{\kappa l}^\alpha(t) V_{\alpha\beta}(\kappa l, \kappa' l') u_{\kappa' l'}^\beta(t) + \dots, \quad (2.1.2.4)$$

where $u_{\kappa l}^\alpha(t)$ denotes the Cartesian coordinate of $\mathbf{u}_{kl}(t)$ in direction α . In the *harmonic approximation*, third and higher-order terms are neglected. In order to simplify the formulae, we now drop the time argument, keeping in mind that we are always dealing with dynamical displacements. The expansion coefficients in equation (2.1.2.4) are the partial derivatives of the potential energy with respect to the atomic displacements taken at the equilibrium positions:

$$V_{\alpha\beta}(\kappa l, \kappa' l') = \left. \frac{\partial^2 V}{\partial u_{\kappa l}^\alpha \partial u_{\kappa' l'}^\beta} \right|_o. \quad (2.1.2.5)$$

Using the matrix notation

$$\mathbf{V}(\kappa l, \kappa' l') = \begin{pmatrix} V_{11}(\kappa l, \kappa' l') & V_{12}(\kappa l, \kappa' l') & V_{13}(\kappa l, \kappa' l') \\ V_{21}(\kappa l, \kappa' l') & V_{22}(\kappa l, \kappa' l') & V_{23}(\kappa l, \kappa' l') \\ V_{31}(\kappa l, \kappa' l') & V_{32}(\kappa l, \kappa' l') & V_{33}(\kappa l, \kappa' l') \end{pmatrix} \quad (2.1.2.6)$$

and dropping the constant V^o , equation (2.1.2.4) reads

$$V = \frac{1}{2} \sum_{\kappa l} \sum_{\kappa' l'} \mathbf{u}_{\kappa l} \mathbf{V}(\kappa l, \kappa' l') \mathbf{u}_{\kappa' l'} + \dots \quad (2.1.2.7)$$

The product $-\mathbf{V}(\kappa l, \kappa' l') \mathbf{u}_{\kappa' l'}$ is just the force $\mathbf{f}(\kappa l)$ acting upon atom (κl) if the atom $(\kappa' l')$ is displaced by $\mathbf{u}_{\kappa' l'}$ (Fig. 2.1.2.2). Hence, the matrix $\mathbf{V}(\kappa l, \kappa' l')$ may be regarded as a *force constant matrix* and its elements $V_{\alpha\beta}(\kappa l, \kappa' l')$ as *force constants*. These parameters may be calculated with the help of specific interaction models such as pair potentials, tensor-force models or more complicated many-body interactions.

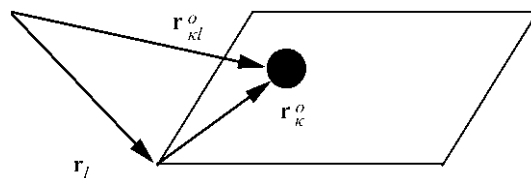


Fig. 2.1.2.1. Definition of position vectors.

2.1. PHONONS

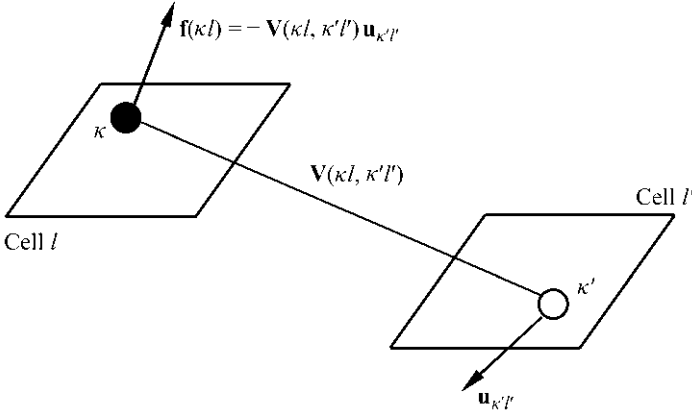


Fig. 2.1.2.2. Definition of the force acting on atom (κl) when atom $(\kappa' l')$ is displaced by $\mathbf{u}_{\kappa' l'}$.

The Hamiltonian of the perfect harmonic crystal can now be written in the form

$$H = \sum_{\kappa l} \frac{\mathbf{p}_{\kappa l}^2}{2m_{\kappa}} + \frac{1}{2} \sum_{\kappa l} \sum_{\kappa' l'} \mathbf{u}_{\kappa l} \mathbf{V}(\kappa l, \kappa' l') \mathbf{u}_{\kappa' l'} \quad (2.1.2.8)$$

if $\mathbf{p}_{\kappa l}$ and m_{κ} are the momentum and the mass of atom (κl) , respectively. Consequently, the equation of motion for a particular atom (κl) is given by

$$m_{\kappa} \frac{d^2 \mathbf{u}_{\kappa l}}{dt^2} = - \sum_{\kappa' l'} \mathbf{V}(\kappa l, \kappa' l') \mathbf{u}_{\kappa' l'}. \quad (2.1.2.9)$$

Solutions of this set of coupled differential equations are of the form

$$\mathbf{u}_{\kappa l}^{\pm} = \frac{1}{\sqrt{Nm_{\kappa}}} \mathbf{e}_{\kappa} \exp[i(\mathbf{q}\mathbf{r}_l \pm \omega t)], \quad (2.1.2.10)$$

which are plane waves with wavevector \mathbf{q} and polarization vector \mathbf{e}_{κ} . If a finite crystal is considered or if periodic boundary conditions are applied, the wavevector is restricted to a sequence of discrete and equidistant values which are, however, very close to each other. Thus, for practical work \mathbf{q} can be treated as a continuous variable. The polarization vectors \mathbf{e}_{κ} are, in general, different for every atom κ . Moreover, they depend on \mathbf{q} and for each wavevector there are $3N$ different modes of vibration characterized not only by different \mathbf{e}_{κ} 's but also by different vibrational frequencies ω . Hence, equation (2.1.2.10) can be written more specifically as

$$\mathbf{u}_{\kappa l}^{\pm}(\mathbf{q}, j) = \frac{1}{\sqrt{Nm_{\kappa}}} \mathbf{e}_{\kappa}(\mathbf{q}, j) \exp[i(\mathbf{q}\mathbf{r}_l \pm \omega_{\mathbf{q}, j} t)], \quad (2.1.2.10a)$$

where the running index $j = 1, \dots, 3N$ labels the different fundamental vibrations or *phonons*. The upper index \pm distinguishes two waves with identical frequencies which are travelling in opposite directions.

2.1.2.2. Stability conditions

Not all of the elements of the force-constant matrix are independent. From its definition, equation (2.1.2.5), it is clear that the force-constant matrix is symmetric:

$$V_{\beta\alpha}(\kappa' l', \kappa l) = V_{\alpha\beta}(\kappa l, \kappa' l'). \quad (2.1.2.11)$$

Moreover, there are general stability conditions arising from the fact that a crystal as a whole is in mechanical equilibrium: If a macroscopic crystal is rigidly translated by a vector \mathbf{u}_o , no interatomic interactions are affected and, hence, the force acting on any particular atom must vanish:

$$\sum_{\kappa' l'} V_{\alpha\beta}(\kappa l, \kappa' l') u_o^{\beta} = 0 \quad \text{for arbitrary } \mathbf{u}_o \quad (2.1.2.12)$$

and, consequently,

$$\sum_{\kappa' l'} V_{\alpha\beta}(\kappa l, \kappa' l') = 0. \quad (2.1.2.12a)$$

This relation is known as the condition of *translational invariance*.

In a similar way, it is argued that no interatomic interactions are affected when the crystal is rigidly rotated by infinitesimal amounts about arbitrary axes. This condition of *rotational invariance* leads to the following restrictions for the force constants:

$$\sum_{\kappa' l'} [V_{\alpha\beta}(\kappa l, \kappa' l') r_{\kappa' l'}^{\alpha\gamma} - V_{\alpha\gamma}(\kappa l, \kappa' l') r_{\kappa' l'}^{\alpha\beta}] = 0 \quad (2.1.2.13)$$

for all $\kappa = 1, \dots, N$ and $\alpha, \beta, \gamma = 1, 2, 3$.

In mechanical equilibrium, there must not be any strains within the crystal. The conditions of an *unstrained crystal* are also known as *Huang conditions* and may be formulated as

$$\begin{aligned} \sum_{\kappa l} \sum_{\kappa' l'} \{ & V_{\alpha\beta}(\kappa l, \kappa' l') [r_{\kappa l}^{\alpha\gamma} - r_{\kappa' l'}^{\alpha\gamma}] [r_{\kappa l}^{\alpha\delta} - r_{\kappa' l'}^{\alpha\delta}] \\ & - V_{\gamma\delta}(\kappa l, \kappa' l') [r_{\kappa l}^{\alpha\alpha} - r_{\kappa' l'}^{\alpha\alpha}] [r_{\kappa l}^{\alpha\beta} - r_{\kappa' l'}^{\alpha\beta}] \} = 0 \end{aligned} \quad (2.1.2.14)$$

for all $\alpha, \beta, \gamma, \delta = 1, 2, 3$.

All these stability conditions are independent of the particular crystal structure. There are other restrictions that are due to the symmetry of the atomic arrangement. They will be considered in detail in Section 2.1.3.

2.1.2.3. The dynamical matrix

If the *ansatz* (2.1.2.10a) is inserted into the equation of motion (2.1.2.9), the following eigenvalue equation is obtained:

$$\begin{aligned} \omega_{\mathbf{q}, j}^2 \mathbf{e}_{\kappa}(\mathbf{q}, j) &= \sum_{\kappa' l'} \sqrt{\frac{1}{m_{\kappa} m_{\kappa'}}} \mathbf{V}(\kappa l, \kappa' l') \exp[i\mathbf{q}(\mathbf{r}_{l'} - \mathbf{r}_l)] \mathbf{e}_{\kappa'}(\mathbf{q}, j) \\ &= \sum_{\kappa} \sqrt{\frac{1}{m_{\kappa} m_{\kappa'}}} \left[\sum_{l'} \mathbf{V}(\kappa l, \kappa' l') \exp[i\mathbf{q}(\mathbf{r}_{l'} - \mathbf{r}_l)] \right] \mathbf{e}_{\kappa'}(\mathbf{q}, j). \end{aligned} \quad (2.1.2.15)$$

The summation over all primitive cells on the right-hand side of equation (2.1.2.15) yields the Fourier-transformed force-constant matrix

$$\mathbf{F}_{\kappa\kappa'}(\mathbf{q}) = \sum_{l'} \mathbf{V}(\kappa l, \kappa' l') \exp[i\mathbf{q}(\mathbf{r}_{l'} - \mathbf{r}_l)], \quad (2.1.2.16)$$

which is independent of l for infinite crystals. $\mathbf{F}_{\kappa\kappa'}(\mathbf{q})$ contains all interactions of type κ atoms with type κ' atoms. Using this notation, equation (2.1.2.15) reduces to

$$\omega_{\mathbf{q}, j}^2 \mathbf{e}_{\kappa}(\mathbf{q}, j) = \sum_{\kappa'} \sqrt{\frac{1}{m_{\kappa} m_{\kappa'}}} \mathbf{F}_{\kappa\kappa'}(\mathbf{q}) \mathbf{e}_{\kappa'}(\mathbf{q}, j). \quad (2.1.2.17)$$

If for a given vibration characterized by (\mathbf{q}, j) we combine the three-dimensional polarization vectors $\mathbf{e}_{\kappa}(\mathbf{q}, j)$ of all atoms within a primitive cell to a $3N$ -dimensional polarization vector $\mathbf{e}(\mathbf{q}, j)$,

2. SYMMETRY ASPECTS OF EXCITATIONS

$$\mathbf{e}(\mathbf{q}, j) = \begin{pmatrix} \mathbf{e}_1(\mathbf{q}, j) \\ \vdots \\ \mathbf{e}_N(\mathbf{q}, j) \end{pmatrix} = \begin{pmatrix} e_1^x(\mathbf{q}, j) \\ e_1^y(\mathbf{q}, j) \\ e_1^z(\mathbf{q}, j) \\ \vdots \\ e_N^x(\mathbf{q}, j) \\ e_N^y(\mathbf{q}, j) \\ e_N^z(\mathbf{q}, j) \end{pmatrix} \quad (2.1.2.18)$$

and simultaneously the 3×3 matrices $\mathbf{F}_{\kappa\kappa'}(\mathbf{q})$ to a $3N \times 3N$ matrix $\mathbf{F}(\mathbf{q})$

$$\mathbf{F}(\mathbf{q}) = \begin{pmatrix} F_{11}^{xx} & F_{11}^{xy} & F_{11}^{xz} & & & F_{1N}^{xx} & F_{1N}^{xy} & F_{1N}^{xz} \\ F_{11}^{yx} & F_{11}^{yy} & F_{11}^{yz} & & & F_{1N}^{yx} & F_{1N}^{yy} & F_{1N}^{yz} \\ F_{11}^{zx} & F_{11}^{zy} & F_{11}^{zz} & & & F_{1N}^{zx} & F_{1N}^{zy} & F_{1N}^{zz} \\ & & & F_{\kappa\kappa'}^{xx} & F_{\kappa\kappa'}^{xy} & F_{\kappa\kappa'}^{xz} & & \\ & & & F_{\kappa\kappa'}^{yx} & F_{\kappa\kappa'}^{yy} & F_{\kappa\kappa'}^{yz} & & \\ & & & F_{\kappa\kappa'}^{zx} & F_{\kappa\kappa'}^{zy} & F_{\kappa\kappa'}^{zz} & & \\ & \vdots & & & & & \vdots & \\ & & & F_{NN}^{xx} & F_{NN}^{xy} & F_{NN}^{xz} & & \\ & & & F_{NN}^{yx} & F_{NN}^{yy} & F_{NN}^{yz} & & \\ & & & F_{NN}^{zx} & F_{NN}^{zy} & F_{NN}^{zz} & & \end{pmatrix}, \quad (2.1.2.19)$$

equation (2.1.2.17) can be written in matrix notation and takes the simple form

$$\omega_{\mathbf{q},j}^2 \mathbf{e}(\mathbf{q}, j) = [\mathbf{M}\mathbf{F}(\mathbf{q})\mathbf{M}] \mathbf{e}(\mathbf{q}, j) = \mathbf{D}(\mathbf{q}) \mathbf{e}(\mathbf{q}, j), \quad (2.1.2.20)$$

where the diagonal matrix

$$\mathbf{M} = \begin{pmatrix} \frac{1}{\sqrt{m_1}} & 0 & 0 & & & \\ 0 & \frac{1}{\sqrt{m_1}} & 0 & & & \\ 0 & 0 & \frac{1}{\sqrt{m_1}} & & & \\ \vdots & & & \ddots & & \\ & & & & \frac{1}{\sqrt{m_N}} & 0 & 0 \\ & & & & 0 & \frac{1}{\sqrt{m_N}} & 0 \\ & & & & 0 & 0 & \frac{1}{\sqrt{m_N}} \end{pmatrix} \quad (2.1.2.21)$$

contains the masses of all atoms. The $3N \times 3N$ matrix

$$\mathbf{D}(\mathbf{q}) = \mathbf{M}\mathbf{F}(\mathbf{q})\mathbf{M} \quad (2.1.2.22)$$

is called the *dynamical matrix*. It contains all the information about the dynamical behaviour of the crystal and can be calculated on the basis of specific models for interatomic interactions. In analogy to the 3×3 matrices $\mathbf{F}_{\kappa\kappa'}(\mathbf{q})$, we introduce the submatrices of the dynamical matrix:

$$\mathbf{D}_{\kappa\kappa'}(\mathbf{q}) = \frac{1}{\sqrt{m_\kappa m_{\kappa'}}} \mathbf{F}_{\kappa\kappa'}(\mathbf{q}). \quad (2.1.2.22a)$$

Owing to the symmetry of the force-constant matrix,

$$V_{\alpha\beta}(\kappa l, \kappa' l') = V_{\beta\alpha}(\kappa' l', \kappa l), \quad (2.1.2.23)$$

the dynamical matrix is Hermitian:¹

$$\mathbf{D}^T(\mathbf{q}) = \mathbf{D}^*(\mathbf{q}) = \mathbf{D}(-\mathbf{q}) \quad (2.1.2.24)$$

or more specifically

$$D_{\kappa\kappa'}^{\alpha\beta}(\mathbf{q}) = D_{\kappa'\kappa}^{\beta\alpha*}(\mathbf{q}) = D_{\kappa\kappa'}^{\beta\alpha}(-\mathbf{q}). \quad (2.1.2.24a)$$

Obviously, the squares of the vibrational frequency $\omega_{\mathbf{q},j}$ and the polarization vectors $\mathbf{e}(\mathbf{q}, j)$ are eigenvalues and corresponding eigenvectors of the dynamical matrix. As a direct consequence of

¹ The superscripts T and $*$ are used to denote the transposed and the complex conjugate matrix, respectively.

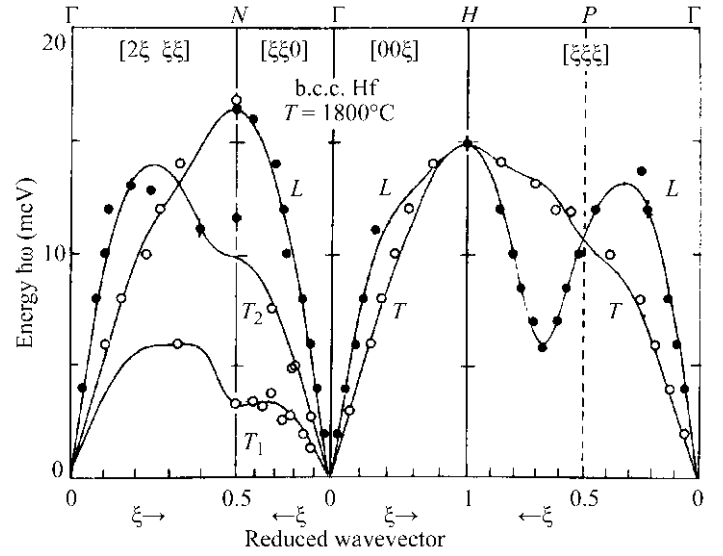


Fig. 2.1.2.3. Phonon dispersion of b.c.c. hafnium for wavevectors along the main symmetry directions of the cubic structure. The symbols represent experimental data obtained by inelastic neutron scattering and the full lines are the results of the model. From Trampenau *et al.* (1991). Copyright (1991) by the American Physical Society.

equation (2.1.2.20), the eigenvalues $\omega_{\mathbf{q},j}^2$ are real quantities and the following relations hold:

$$\omega_{\mathbf{q},j}^2 = \omega_{-\mathbf{q},j}^2, \quad (2.1.2.25)$$

$$\mathbf{e}^*(\mathbf{q}, j) = \mathbf{e}(-\mathbf{q}, j). \quad (2.1.2.26)$$

Moreover, the eigenvectors are mutually orthogonal and can be chosen to be normalized.

2.1.2.4. Eigenvalues and phonon dispersion, acoustic modes

The wavevector dependence of the vibrational frequencies is called *phonon dispersion*. For each wavevector \mathbf{q} there are $3N$ fundamental frequencies yielding $3N$ phonon *branches* when $\omega_{\mathbf{q},j}$ is plotted *versus* \mathbf{q} . In most cases, the phonon dispersion is displayed for wavevectors along high-symmetry directions. These dispersion curves are, however, only special projections of the dispersion hypersurface in the four-dimensional \mathbf{q} - ω space. As a simple example, the phonon dispersion of b.c.c. hafnium is displayed in Fig. 2.1.2.3. The wavevectors are restricted to the first Brillouin zone (see Section 2.1.3.1) and the phonon dispersion for different directions of the wavevector are combined in one single diagram making use of the fact that different high-symmetry directions meet at the Brillouin-zone boundary. Note that in Fig. 2.1.2.3, the moduli of the wavevectors are scaled by the Brillouin-zone boundary values and represented by the reduced coordinates ξ . Owing to the simple b.c.c. structure of hafnium with one atom per primitive cell, there are only three phonon branches. Moreover, for all wavevectors along the directions $[00\xi]$ and $[\xi\xi\xi]$, two exhibit the same frequencies – they are said to be *degenerate*. Hence in the corresponding parts of Fig. 2.1.2.3 only two branches can be distinguished.

Whereas in this simple example the different branches can be separated quite easily, this is no longer true for more complicated crystal structures. For illustration, the phonon dispersion of the high- T_c superconductor Nd_2CuO_4 is shown in Fig. 2.1.2.4 for the main symmetry directions of the tetragonal structure (space group $I4/mmm$, seven atoms per primitive cell). Note that in many publications on lattice dynamics the frequency $\nu = \omega/2\pi$ is used rather than the angular frequency ω .

The 21 phonon branches of Nd_2CuO_4 with their more complicated dispersion reflect the details of the interatomic interactions between all atoms of the structure. The phonon frequencies ν cover a range from 0 to 18 THz. In crystals with

2.1. PHONONS

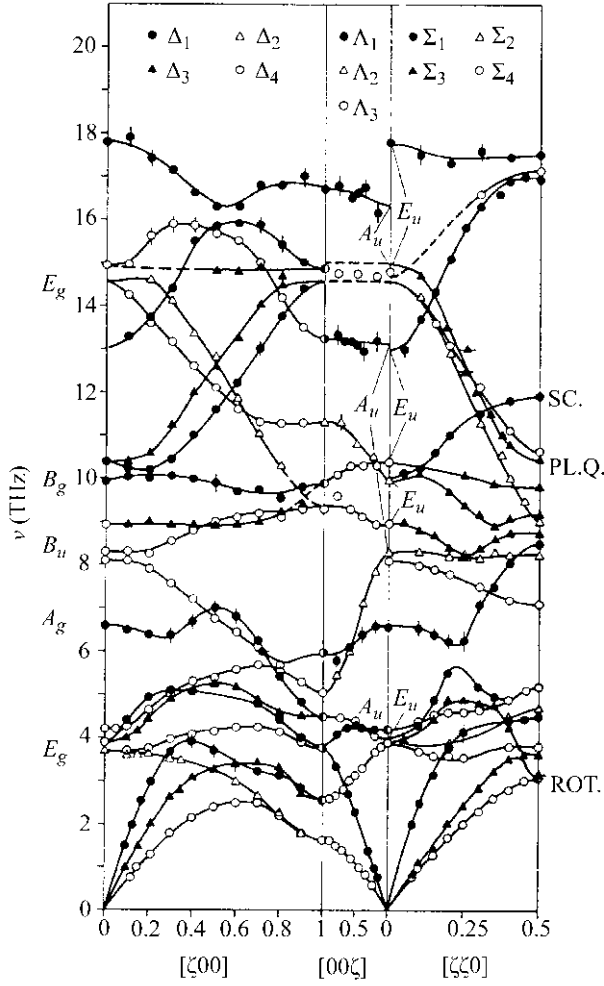


Fig. 2.1.2.4. Phonon dispersion of Nd_2CuO_4 along the main symmetry directions of the tetragonal structure. The symbols represent experimental data obtained by inelastic neutron scattering and the full lines are drawn to guide the eye. Reprinted from Pintschovius *et al.* (1991), copyright (1991), with permission from Elsevier.

strongly bonded molecular groups, like SiO_4 tetrahedra in quartz or SO_4 tetrahedra in sulfates, for example, the highest frequencies are found near 35 THz and correspond to bond-stretching vibrations. Soft materials like organic molecular crystals, on the other hand, exhibit a large number of phonon branches within a rather small frequency range which cannot easily be separated. Deuterated naphthalene (C_{10}D_8) is a well investigated example. The low-frequency part of its phonon dispersion is shown in Fig. 2.1.2.5.

Whereas neutron inelastic scattering is the most powerful method for the determination of phonons at arbitrary wavevectors, long wavelength ($\mathbf{q} \rightarrow \mathbf{0}$) phonons may also be detected by optical spectroscopy. The determination of phonon frequencies alone is, however, not sufficient for a concise determination of dispersion branches. Rather, individual phonons have to be assigned uniquely to one of the $3N$ branches, and this may prove a rather hard task if N is large. Here, symmetry considerations of eigenvectors are of special importance since phonons belonging to the same branch must exhibit the same symmetry properties. Moreover, inspection of Figs. 2.1.2.3 to 2.1.2.5 shows that some of the branches cross each other and others do not. It is a general statement that crossing is only allowed for branches with different symmetries – a property which yields a classification scheme for the different phonon branches. The symmetry of fundamental vibrations of a lattice will be discussed in some detail in Section 2.1.3.

In the limit of long wavelengths, there are always three particular modes with identical polarization vectors for all atoms,

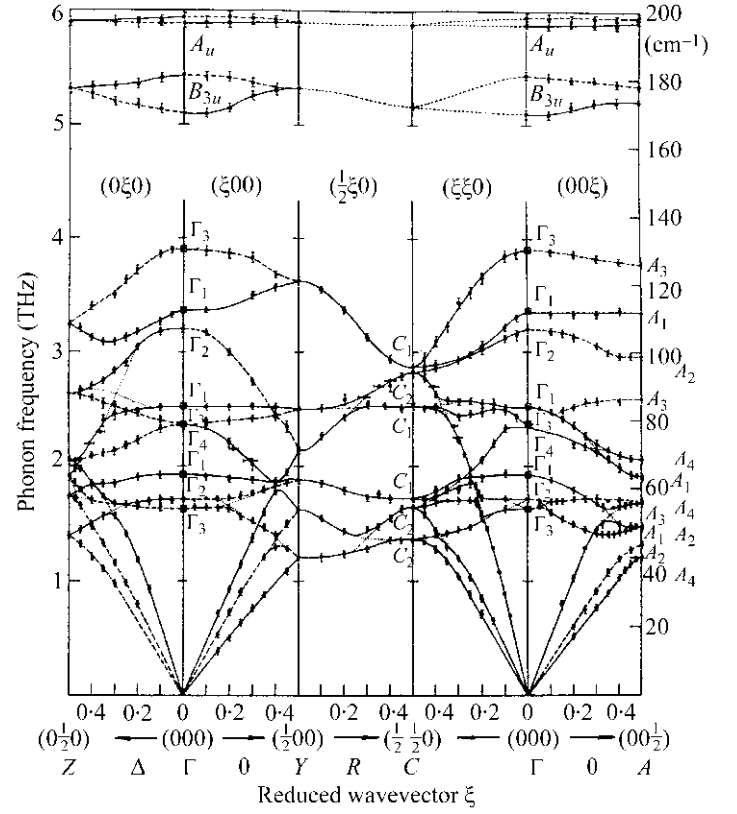


Fig. 2.1.2.5. Low-frequency part of the phonon dispersion of deuterated naphthalene at 6 K. The symbols represent experimental data obtained by inelastic neutron scattering and the full lines are drawn to guide the eye. Reproduced with permission from Natkaniec *et al.* (1980). Copyright (1980) IOP Publishing Limited.

which will be considered in the following. At exactly $\mathbf{q} = \mathbf{0}$ (the Γ point) or infinite wavelength, the eigenvalue equation (2.1.2.15) reduces to

$$\omega_{0,j}^2 \mathbf{e}_\kappa(\mathbf{0}, j) = \sum_{\kappa'l'} \frac{1}{\sqrt{m_\kappa m_{\kappa'}}} \mathbf{V}(\kappa l, \kappa' l') \mathbf{e}_{\kappa'}(\mathbf{0}, j). \quad (2.1.2.27)$$

One immediately recognizes that there are special solutions with

$$\frac{1}{\sqrt{m_\kappa}} \mathbf{e}_\kappa(\mathbf{0}, j) = \mathbf{u}_o \text{ for all } \kappa, \quad (2.1.2.28)$$

i.e. the (mass-weighted) eigenvectors of all atoms are identical. There are three orthogonal eigenvectors of this kind and the displacement pattern of such phonons corresponds to rigid translations of the whole lattice along the three orthogonal coordinates in direct space. These motions do not affect any interatomic interaction. Hence, there is no change in potential energy and the condition of translational invariance (*cf.* Section 2.1.2.2) guarantees that the frequencies of these modes are zero:

$$\omega_{0,j}^2 = \sum_{\kappa'l'} \mathbf{V}(\kappa l, \kappa' l') = 0 \text{ for } j = 1, 2, 3. \quad (2.1.2.29)$$

The phonon branches that lead to zero frequency at the Γ point ($\mathbf{q} = \mathbf{0}$) are called *acoustic*, whereas all other branches are called *optic*. The dispersion of acoustic branches in the vicinity of the Γ point can be investigated by expanding the phase factor in equation (2.1.2.15) in powers of \mathbf{q} . Using (2.1.2.28) one obtains

$$\begin{aligned} m_\kappa \omega_{\mathbf{q} \rightarrow \mathbf{0}, j}^2 \mathbf{u}_o &= \sum_{\kappa'l'} \mathbf{V}(\kappa l, \kappa' l') \{1 + i\mathbf{q}(\mathbf{r}_{l'} - \mathbf{r}_l) - \frac{1}{2}[\mathbf{q}(\mathbf{r}_{l'} - \mathbf{r}_l)]^2 + \dots\} \mathbf{u}_o. \end{aligned} \quad (2.1.2.30)$$

2. SYMMETRY ASPECTS OF EXCITATIONS

Neglecting higher-order terms, summing up both sides of equation (2.1.2.30) over κ and multiplying by \mathbf{u}_o yields

$$\begin{aligned} M \omega_{\mathbf{q} \rightarrow 0, j}^2 \mathbf{u}_o^2 &= \sum_{\kappa} \sum_{\kappa' l'} \sum_{\alpha \beta} u_o^\alpha \mathbf{V}_{\alpha \beta}(\kappa l, \kappa' l') u_o^\beta \\ &+ i \sum_{\gamma} q_{\gamma} \sum_{\kappa} \sum_{\kappa' l'} \sum_{\alpha \beta} u_o^\alpha V_{\alpha \beta}(\kappa l, \kappa' l') (r_l^{\alpha \gamma} - r_l^{\alpha \gamma}) u_o^\beta \\ &- \frac{1}{2} \sum_{\delta} \sum_{\gamma} q_{\gamma} q_{\delta} \sum_{\kappa} \sum_{\kappa' l'} \sum_{\alpha \beta} u_o^\alpha V_{\alpha \beta}(\kappa l, \kappa' l') \\ &\times (r_l^{\alpha \gamma} - r_l^{\alpha \gamma}) (r_l^{\alpha \delta} - r_l^{\alpha \delta}) u_o^\beta, \end{aligned} \quad (2.1.2.31)$$

M being the total mass of all atoms within the primitive cell ($M = \sum_{\kappa=1}^N m_{\kappa}$). The first term on the right-hand side is zero according to equation (2.1.2.29). The second term vanishes due to the symmetry property of the force-constant matrices, equation (2.1.2.23). Hence (2.1.2.31) is simplified to

$$\begin{aligned} M \left(\frac{\omega_{\mathbf{q} \rightarrow 0, j}}{|\mathbf{q}|} \right)^2 &= -\frac{1}{2} \sum_{\delta} \sum_{\gamma} \frac{q_{\gamma} q_{\delta}}{\mathbf{q}^2} \sum_{\kappa} \sum_{\kappa' l'} \sum_{\alpha \beta} V_{\alpha \beta}(\kappa l, \kappa' l') \\ &\times (r_l^{\alpha \gamma} - r_l^{\alpha \gamma}) (r_l^{\alpha \delta} - r_l^{\alpha \delta}) \frac{u_o^\alpha u_o^\beta}{\mathbf{u}_o^2}. \end{aligned} \quad (2.1.2.32)$$

The right-hand side no longer depends on the moduli of the wavevector and displacement but only on their orientation with respect to the crystal lattice. Consequently, acoustic dispersion curves always leave the Γ point as a straight line with a constant slope ($\omega/|\mathbf{q}|$).

The displacement pattern of these long-wavelength modes corresponds to a continuous deformation of a rigid body. Hence, acoustic phonons near the Γ point can be regarded as sound waves and the slope of the dispersion curve is given by the corresponding sound velocity,

$$v_s = \omega/|\mathbf{q}|. \quad (2.1.2.33)$$

Sound velocities, on the other hand, can be calculated from macroscopic elastic constants using the theory of macroscopic elasticity (cf. Chapter 1.3). Thus we are able to correlate macroscopic and microscopic dynamic properties of crystals. Using the generalized Hooke's law, the equation of motion for the dynamic deformation of a macroscopic body may be written as

$$\rho \frac{\partial^2 u_i(t)}{\partial t^2} = \sum_{k=1}^3 \sum_{l=1}^3 \sum_{m=1}^3 c_{ijklm} \frac{\partial^2 u_l}{\partial r^k \partial r^m}, \quad (2.1.2.34)$$

ρ being the macroscopic density, u_i the i th Cartesian component of the deformation and (c_{ijklm}) the symmetric tensor of elastic stiffnesses, which is discussed in detail in Chapter 1.3. The solution of this differential equation using plane waves,

$$\mathbf{u} = \mathbf{u}_o \exp[i(\mathbf{q}\mathbf{r} - \omega t)], \quad (2.1.2.35)$$

leads to the following relation:

$$\rho \left(\frac{\omega}{|\mathbf{q}|} \right)^2 u_o^i = \sum_{k=1}^3 \sum_{l=1}^3 \sum_{m=1}^3 c_{ijklm} \frac{q_k q_m}{\mathbf{q}^2} u_o^l. \quad (2.1.2.36)$$

If we define the components of the *propagation tensor* by

$$\Gamma_{jl} = \sum_{k=1}^3 \sum_{m=1}^3 c_{ijklm} \frac{q_k q_m}{\mathbf{q}^2}, \quad (2.1.2.37)$$

equation (2.1.2.36) may be written as the eigenvector equation

$$\rho v_s^2 \mathbf{u}_o = \mathbf{\Gamma} \mathbf{u}_o. \quad (2.1.2.38)$$

For a given propagation direction as defined by the Cartesian components of \mathbf{q} , the eigenvectors of the corresponding propagation tensor yield the polarization of three mutually orthogonal deformation waves. Its eigenvalues are related to the respective sound velocities $v_s = \omega/|\mathbf{q}|$. If the tensor of elastic stiffnesses is known, the elements of $\mathbf{\Gamma}$ and, hence, the velocity of elastic (sound) waves can be calculated for arbitrary propagation directions (see Section 1.3.4). These data, in turn, allow the prediction of the slopes of acoustic phonon dispersion curves near $\mathbf{q} = 0$.

2.1.2.5. Eigenvectors and normal coordinates

The plane-wave solutions (2.1.2.10) of the equations of motion form a complete set of orthogonal functions if \mathbf{q} is restricted to the first Brillouin zone. Hence, the actual displacement of an atom (κl) can be represented by a linear combination of the $\mathbf{u}_{\kappa l}^{\pm}(\mathbf{q}, j)$:

$$\mathbf{u}_{\kappa l} = \sum_{\mathbf{q}} \sum_j [A_{\mathbf{q}, j} \mathbf{u}_{\kappa l}^{+}(\mathbf{q}, j) + A'_{\mathbf{q}, j} \mathbf{u}_{\kappa l}^{-}(\mathbf{q}, j)]. \quad (2.1.2.39)$$

Since this displacement is an observable quantity, it must correspond to a real vector, not a complex one. Hence, the coefficients $A_{\mathbf{q}, j}$ obey the relation

$$A'_{\mathbf{q}, j} = A_{\mathbf{q}, j}^* \quad (2.1.2.40)$$

and equation (2.1.2.39) reduces to

$$\mathbf{u}_{\kappa l} = \frac{1}{\sqrt{Nm_{\kappa}}} \sum_{\mathbf{q}} \sum_j Q_{\mathbf{q}, j} \mathbf{e}_{\kappa}(\mathbf{q}, j) \exp(i\mathbf{q}\mathbf{r}_l), \quad (2.1.2.41)$$

where

$$Q_{\mathbf{q}, j} = A_{\mathbf{q}, j} \exp(-i\omega_{\mathbf{q}, j} t) + A_{-\mathbf{q}, j}^* \exp(i\omega_{\mathbf{q}, j} t) = Q_{-\mathbf{q}, j}^*. \quad (2.1.2.42)$$

If the displacement vectors $\mathbf{u}_{\kappa l}$ are combined to form a $3N$ -dimensional vector \mathbf{u}_l in analogy to the formation of the eigenvector $\mathbf{e}(\mathbf{q}, j)$ from the individual polarization vectors $\mathbf{e}_{\kappa}(\mathbf{q}, j)$ [equation (2.1.2.18)] we obtain

$$\mathbf{u}_l = \frac{1}{\sqrt{N}} \sum_{\mathbf{q}} \sum_j Q_{\mathbf{q}, j} \mathbf{M} \mathbf{e}(\mathbf{q}, j) \exp(i\mathbf{q}\mathbf{r}_l). \quad (2.1.2.43)$$

Thus, the atomic displacement is a linear combination of the eigenvectors $\mathbf{e}(\mathbf{q}, j)$ of the dynamical matrix. The coefficients $Q_{\mathbf{q}, j}$ are called *normal coordinates*. They reflect the relative weight and amplitude of a particular vibrational mode (\mathbf{q}, j) which is temperature-dependent and may be determined by statistical methods.

In terms of these normal coordinates, the Hamiltonian of the lattice (2.1.2.8) is reduced to a sum of independent harmonic oscillators. These are called *phonons* and may be regarded as quantum quasiparticles.

$$H = \frac{N_Z}{2N} \sum_{\mathbf{q}} \sum_j \left[\left| \frac{dQ_{\mathbf{q}, j}}{dt} \right|^2 + \omega_{\mathbf{q}, j}^2 |Q_{\mathbf{q}, j}|^2 \right]. \quad (2.1.2.44)$$

(N_Z is the number of primitive cells within the crystal.)

2.1.2.6. Amplitudes of lattice vibrations

Lattice vibrations that are characterized by both the frequencies $\omega_{\mathbf{q}, j}$ and the normal coordinates $Q_{\mathbf{q}, j}$ are elementary excitations of the harmonic lattice. As long as anharmonic effects are neglected, there are no interactions between the individual phonons. The respective amplitudes depend on the excitation level and can be determined by quantum statistical methods. The energy levels of a lattice vibration (\mathbf{q}, j) are those of a single harmonic oscillator:

2.1. PHONONS

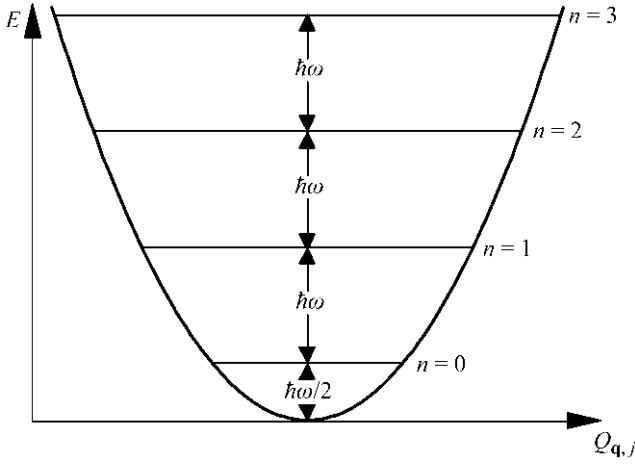


Fig. 2.1.2.6. Energy levels of a quantum-mechanical harmonic oscillator.

$$E_n = (n + \frac{1}{2})\hbar\omega_{q,j}, \quad (2.1.2.45)$$

as illustrated in Fig. 2.1.2.6. The levels are equidistant and the respective occupation probabilities are given by Boltzmann statistics:

$$p_n = \frac{\exp[-(n + 1/2)(\hbar\omega_{q,j}/kT)]}{\sum_{m=0}^{\infty} \exp[-(m + 1/2)(\hbar\omega_{q,j}/kT)]}. \quad (2.1.2.46)$$

In the quasiparticle description, this quantity is just the probability that at a temperature T there are n excited phonons of frequency $\omega_{q,j}$. Moreover, in thermal equilibrium the average number of phonons is given by the Bose factor:

$$n_{q,j} = \frac{1}{\exp(\hbar\omega_{q,j}/kT) - 1} \quad (2.1.2.47)$$

and the corresponding contribution of these phonons to the lattice energy is

$$E_{q,j} = (n_{q,j} + \frac{1}{2})\hbar\omega_{q,j}. \quad (2.1.2.48)$$

The mean-square amplitude of the normal oscillator coordinate is obtained as

$$\langle |Q_{q,j}|^2 \rangle = \frac{\hbar}{\omega_{q,j}} (n_{q,j} + \frac{1}{2}). \quad (2.1.2.49)$$

At high temperatures ($kT \gg \hbar\omega_{q,j}$), the phonon number, the corresponding energy and the amplitude approach the classical values of

$$n_{q,j} \xrightarrow{T \rightarrow \infty} \frac{kT}{\hbar\omega_{q,j}}, \quad (2.1.2.50)$$

$$E_{q,j} \xrightarrow{T \rightarrow \infty} 3NN_Z kT \text{ and} \quad (2.1.2.51)$$

$$\langle |Q_{q,j}|^2 \rangle \xrightarrow{T \rightarrow \infty} \frac{kT}{\omega_{q,j}^2},$$

respectively. Note that occupation number, energy and amplitude merely depend on the frequency of the particular lattice vibration. The form of the corresponding eigenvector $\mathbf{e}(\mathbf{q}, j)$ is irrelevant.

2.1.2.7. Density of states and the lattice heat capacity

The total energy stored in the harmonic phonon system is given by the sum over all phonon states (\mathbf{q}, j) :

$$E_{ph} = \sum_{\mathbf{q}} \sum_j \hbar\omega_{q,j} (n_{q,j} + \frac{1}{2}). \quad (2.1.2.52)$$

Related thermodynamic quantities like the internal energy or the heat capacity are determined by the frequency distribution of the lattice vibrations rather than by details of the phonon dispersion. Hence, it is useful to introduce the *phonon density of states* $G(\omega)$ in such a way that $G(\omega) d\omega$ is the number of phonons with frequencies between ω and $\omega + d\omega$. Using this quantity, the sum in (2.1.2.52) may be replaced by an integral expression:

$$E_{ph} - E_o = \int_0^{\infty} \frac{\hbar\omega}{\exp(\hbar\omega/kT) - 1} G(\omega) d\omega. \quad (2.1.2.53)$$

Here, E_o is the energy at $T = 0$. The derivative with respect to temperature provides the lattice heat capacity at constant volume:

$$c_V = k \int_0^{\infty} \left(\frac{\hbar\omega}{kT} \right)^2 \frac{\exp(\hbar\omega/kT)}{[\exp(\hbar\omega/kT) - 1]^2} G(\omega) d\omega. \quad (2.1.2.54)$$

As an example, Fig. 2.1.2.7 displays the phonon dispersion of GaAs as determined by inelastic neutron scattering along with the phonon density of states. Obviously, even in this relatively simple substance $G(\omega)$ (DOS) exhibits a rather complicated multi-peak structure. Integral properties like the heat capacity are, however, not very sensitive to details of $G(\omega)$. There are two well known approximations for $G(\omega)$ that are able to reproduce some prominent features of c_V :

(1) The Einstein model.

In the Einstein model, it is assumed that all phonons exhibit the same frequency ω_E (Einstein oscillator) and $G(\omega)$ is represented by a delta function:

$$G^{\text{Einstein}}(\omega) = 3NN_Z \delta(\omega - \omega_E). \quad (2.1.2.55)$$

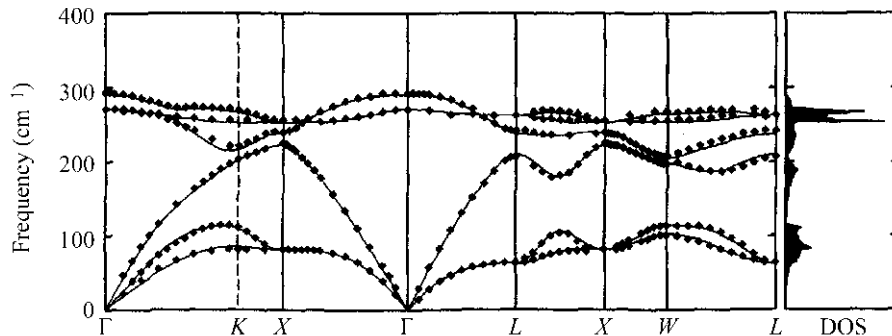


Fig. 2.1.2.7. Phonon dispersion and density of states for GaAs. The experimental data are from Strauch & Dorner (1990); the full lines and the density of states (DOS) are results of *ab initio* model calculations by Giannozzi *et al.* (1991). From Giannozzi *et al.* (1991). Copyright (1991) by the American Physical Society.

2. SYMMETRY ASPECTS OF EXCITATIONS

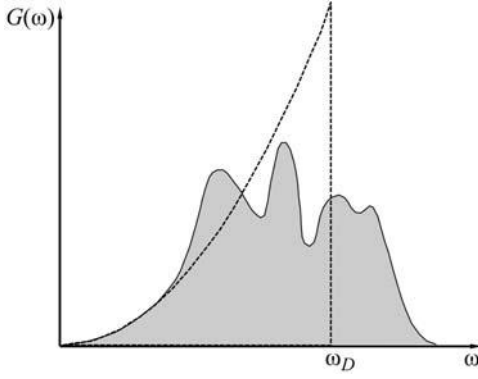


Fig. 2.1.2.8. Schematic representation of the true phonon density of states (solid line) along with the Debye approximation (dotted line). Note that the areas under the two curves are identical.

Consequently, the heat capacity turns out to be

$$c_V^{\text{Einstein}} = 3NN_Z k \left(\frac{\Theta_E}{T} \right)^2 \frac{\exp(\Theta_E/T)}{[\exp(\Theta_E/T) - 1]^2}, \quad (2.1.2.56)$$

where we use the abbreviation

$$\Theta_E = \hbar\omega_E/k, \quad (2.1.2.57)$$

which is the *Einstein temperature*.

At low temperatures, this model predicts an exponential temperature dependence of the heat capacity [$c_V \propto \exp(\Theta_E/T)$], which does not correspond to the experimental findings in most substances. Here, the *Debye model* provides a significant improvement.

(2) *The Debye model.*

In contrast to the Einstein model, which takes only one optic mode into account, the Debye model is restricted to acoustic modes that exhibit a linear dispersion close to the Γ point (see Section 2.1.2.4). Neglecting any deviation from linear behaviour, we get the simple result that the density of states is proportional to the square of the phonon frequency. The total number of phonon states is, however, given by $3NN_Z$, which is the number of all dynamical degrees of freedom of the whole system. Consequently, the frequency spectrum is assumed to be limited to frequencies below a particular value ω_D according to

$$3NN_Z = \int_0^{\omega_D} G^{\text{Debye}}(\omega) d\omega. \quad (2.1.2.58)$$

This limiting frequency is called the *Debye frequency* and is related to an appropriate average of (longitudinal and transverse) sound velocities and exhibits large values for hard materials. Fig. 2.1.2.8 compares schematically the true phonon density of states with the Debye approximation. The density of phonon states may thus be represented by

$$G^{\text{Debye}}(\omega) = 9NN_Z(\omega^2/\omega_D^3) \quad (2.1.2.59)$$

and, correspondingly, the heat capacity is

$$c_V^{\text{Debye}} = 9NN_Z k \left(\frac{T}{\Theta_D} \right)^3 \int_0^{\Theta_D/T} \frac{x^4 \exp(x)}{[\exp(x) - 1]^2} dx, \quad (2.1.2.60)$$

yielding a temperature dependence as shown in Fig. 2.1.2.9.

Θ_D is the *Debye temperature*, which is defined as

$$\Theta_D = \hbar\omega_D/k. \quad (2.1.2.61)$$

At low temperatures, the heat capacity is proportional to T^3 , in excellent agreement with most experiments:

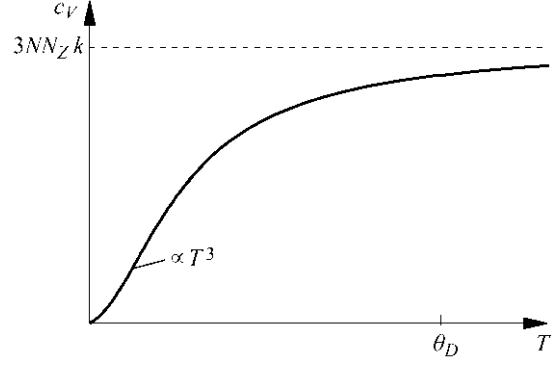


Fig. 2.1.2.9. Temperature dependence of the heat capacity at constant volume according to the Debye model.

$$c_V^{\text{Debye}} \xrightarrow{T \rightarrow 0} \frac{12}{5} \pi^4 NN_Z k (T/\Theta_D)^3. \quad (2.1.2.62)$$

It is not surprising that the Debye model provides a reasonable description of the low-temperature heat capacity, since in this temperature regime well below the Debye temperature, optical phonons are hardly excited and the heat capacity is dominated by the low-frequency acoustic modes which are modelled exactly. At higher temperatures it is, however, necessary to take into account the thermal excitation of (in general less dispersive) optic modes. This can be achieved either by introducing a temperature dependence of the Debye temperature or by mixing a Debye term like (2.1.2.60) and Einstein terms like (2.1.2.56).

As an example, we consider the case of GaAs, the density of states of which is shown in Fig. 2.1.2.7. Obviously there are two very pronounced peaks at high frequencies, which are due to nearly dispersionless optical phonon branches. These modes may therefore be regarded as Einstein oscillators. The remaining acoustic branches lead to the more continuous part of the spectrum at lower frequencies, which may be approximated by a Debye law.

2.1.2.8. Thermal expansion, compressibility and Grüneisen parameters

So far, we have always assumed that the crystal volume is constant. As long as we are dealing with harmonic solids, the thermal excitation of phonons does not result in a mean displacement of any atom. Consequently, thermal expansion cannot be understood in the harmonic approximation. It is due to the fact that there are anharmonic contributions to the lattice energy, *i.e.* third- and higher-order terms in the expansion with respect to atomic displacements [equation (2.1.2.4)]. Moreover, in an anharmonic lattice phonons are no longer independent elementary excitations. Rather, different lattice vibrations interact with each other leading to temperature-dependent frequency shifts, damping *etc.* Quantitatively, anharmonic effects may be analysed by means of perturbation theory, which is, however, beyond the scope of the present article. Details may be found, for example, in the monograph *The Physics of Phonons* (Reissland, 1973).

Some aspects of anharmonicity can, however, be discussed on the basis of the *quasi-harmonic model*. This approach makes use of the fact that the atomic interactions vary with the interatomic spacing and, hence, with the volume or, more generally, with any type of lattice deformation. The phonon frequencies will therefore depend on the deformation as well. Using the deformed lattice as a new reference frame for lattice dynamical calculations, the corresponding frequencies may be obtained again on the basis of a harmonic model with modified effective force constants. The comparison of phonons of both the original and the (arbitrarily) deformed lattice finally yields the partial derivatives of the frequencies $\omega_{\mathbf{q},j}$ with respect to the components ε_{kl} of the strain tensor.

2.1. PHONONS

If the deformation is exclusively due to a change of temperature, the phonon frequency shifts can thus be related to the coefficients of thermal expansion. In this approximation, any intrinsic temperature dependence of phonon frequencies due to phonon interactions is neglected. Note that just those effects are, however, of particular importance if displacive phase transitions that are associated with soft phonon modes are considered.

In the quasi-harmonic approximation, we use the thermodynamic relation between the Helmholtz free energy A and the partition function Z :

$$A = -kT \ln Z. \quad (2.1.2.63)$$

Z is given in terms of the energy levels of the independent harmonic oscillators:

$$Z = \exp(-\Phi/kT) \prod_{\mathbf{q},j} \frac{\exp(-\hbar\omega_{\mathbf{q},j}/2kT)}{1 - \exp(-\hbar\omega_{\mathbf{q},j}/kT)}, \quad (2.1.2.64)$$

where Φ is the potential energy of the crystal if all atoms occupy their equilibrium positions. Hence, the following expression for A results:

$$A = \Phi + \frac{1}{2} \sum_{\mathbf{q},j} \hbar\omega_{\mathbf{q},j} + kT \sum_{\mathbf{q},j} \ln[1 - \exp(-\hbar\omega_{\mathbf{q},j}/kT)]. \quad (2.1.2.65)$$

Elementary thermodynamics yields the pressure p as the partial derivative of A with respect to the volume at constant temperature:

$$p = -(\partial A / \partial V)_T. \quad (2.1.2.66)$$

This relation may be generalized if not only volume changes are taken into account but also arbitrary deformations as described by the strain tensor $\boldsymbol{\varepsilon} = (\varepsilon_{kl})$:

$$\sigma_{kl} = -(1/V)(\partial A / \partial \varepsilon_{kl})_T \quad (2.1.2.67)$$

with the stress tensor $\boldsymbol{\sigma} = (\sigma_{kl})$. Note that the hydrostatic pressure p and the relative volume change are given by the traces of $\boldsymbol{\sigma}$ and $\boldsymbol{\varepsilon}$, respectively:

$$p = -\frac{1}{3} \sum_{k=1}^3 \sigma_{kk}, \quad (\Delta V/V) = \sum_{k=1}^3 \varepsilon_{kk}. \quad (2.1.2.68)$$

Taking the temperature derivative of (2.1.2.66), we obtain

$$\left(\frac{\partial \sigma_{kl}}{\partial T} \right)_\varepsilon = -\frac{1}{V} \left(\frac{\partial}{\partial T} \left(\frac{\partial A}{\partial \varepsilon_{kl}} \right)_T \right)_\varepsilon. \quad (2.1.2.69)$$

Using Euler's relations, the left-hand side may be written as

$$\begin{aligned} \left(\frac{\partial \sigma_{kl}}{\partial T} \right)_\varepsilon &= - \sum_{mn} \left(\frac{\partial \sigma_{kl}}{\partial \varepsilon_{mn}} \right)_{T, \varepsilon_{m'n'}} \left(\frac{\partial \varepsilon_{mn}}{\partial T} \right)_\sigma \\ &= - \sum_{mn} c_{klmn} \alpha_{mn}, \end{aligned} \quad (2.1.2.70)$$

where the tensor of the elastic stiffnesses

$$c_{klmn} = \left(\frac{\partial \sigma_{kl}}{\partial \varepsilon_{mn}} \right)_{T, \varepsilon_{m'n'}} \quad (2.1.2.71)$$

and the tensor of thermal expansion

$$\alpha_{kl} = \left(\frac{\partial \varepsilon_{kl}}{\partial T} \right)_\sigma \quad (2.1.2.72)$$

have been introduced.

The free energy depends on the lattice deformations *via* the phonon frequencies. Hence, using (2.1.2.65), the right-hand side of (2.1.2.69) is evaluated as

$$\begin{aligned} \left(\frac{\partial}{\partial T} \left(\frac{\partial A}{\partial \varepsilon_{kl}} \right)_T \right)_\varepsilon &= \left(\frac{\partial}{\partial T} \left(\hbar \sum_{\mathbf{q},j} \frac{1}{\exp(\hbar\omega_{\mathbf{q},j}/kT) - 1} \left(\frac{\partial \omega_{\mathbf{q},j}}{\partial \varepsilon_{kl}} \right)_T \right) \right)_\varepsilon \\ &= \hbar \sum_{\mathbf{q},j} \frac{\partial n_{\mathbf{q},j}}{\partial T} \left(\frac{\partial \omega_{\mathbf{q},j}}{\partial \varepsilon_{kl}} \right)_T \end{aligned} \quad (2.1.2.73)$$

under the assumption that the phonon frequencies do not depend explicitly on the temperature. [$n_{\mathbf{q},j}$ is the Bose factor, (2.1.2.47)].

Let us denote the contribution of a single phonon (\mathbf{q}, j) to the heat capacity at constant volume by

$$\tilde{c}_{\mathbf{q},j} = \hbar\omega_{\mathbf{q},j} \frac{\partial n_{\mathbf{q},j}}{\partial T}. \quad (2.1.2.74)$$

Then the combination of (2.1.2.69), (2.1.2.70) and (2.1.2.71) yields the result

$$V \sum_{mn} c_{klmn} \alpha_{mn} = \sum_{\mathbf{q},j} \tilde{c}_{\mathbf{q},j} \frac{\partial \ln \omega_{\mathbf{q},j}}{\partial \varepsilon_{kl}} = \sum_{\mathbf{q},j} \tilde{c}_{\mathbf{q},j} \gamma_{\mathbf{q},kl} \quad (2.1.2.75)$$

with the *generalized-mode Grüneisen parameters*

$$\gamma_{\mathbf{q},kl} = \frac{\partial \ln \omega_{\mathbf{q},j}}{\partial \varepsilon_{kl}}. \quad (2.1.2.76)$$

The set of equations (2.1.2.75) (for $k, l = 1, 2, 3$) provide relations between the variation of phonon frequencies with the lattice deformations on the one hand and the tensors of elastic stiffnesses and thermal expansion on the other hand.

For cubic crystals, the tensor of the thermal expansion is diagonal,

$$\alpha_{kl} = \frac{1}{3} \beta \delta_{kl}, \quad (2.1.2.77)$$

where β represents the coefficient of volume expansion. If Voigt's notation is used for the elastic stiffnesses (*cf.* Section 1.3.3.2.2), equation (2.1.2.75) reduces to

$$\frac{1}{3} V \beta (c_{11} + 2c_{12}) = \sum_{\mathbf{q},j} \tilde{c}_{\mathbf{q},j} \gamma_{\mathbf{q},11} = \sum_{\mathbf{q},j} \tilde{c}_{\mathbf{q},j} \gamma_{\mathbf{q},22} = \sum_{\mathbf{q},j} \tilde{c}_{\mathbf{q},j} \gamma_{\mathbf{q},33}. \quad (2.1.2.78)$$

If there is an isotropic deformation, the shift of phonon frequencies may be described by an *averaged-mode Grüneisen parameter*:

$$\gamma_{\mathbf{q},j} = \frac{1}{3} \sum_{m=1}^3 \gamma_{\mathbf{q},mm} \quad (2.1.2.79)$$

and (2.1.2.78) may be rewritten as

$$\frac{1}{3} V \beta (c_{11} + 2c_{12}) = \sum_{\mathbf{q},j} \tilde{c}_{\mathbf{q},j} \gamma_{\mathbf{q},j}. \quad (2.1.2.80)$$

Introducing the *mean Grüneisen parameter* γ by the summation over all phonon states,

$$\gamma = \frac{\sum_{\mathbf{q},j} \gamma_{\mathbf{q},j} \tilde{c}_{\mathbf{q},j}}{c_V}, \quad (2.1.2.81)$$

we arrive at

$$\frac{1}{3} V \beta (c_{11} + 2c_{12}) = \gamma c_V. \quad (2.1.2.82)$$

Remembering that in cubic crystals the expression

$$\kappa = \frac{3}{c_{11} + 2c_{12}} \quad (2.1.2.83)$$

represents the isothermal compressibility, we find the commonly used scalar form of equation (2.1.2.75):

2. SYMMETRY ASPECTS OF EXCITATIONS

$$\beta = \kappa \frac{c_V \gamma}{V}, \quad (2.1.2.84)$$

which relates the thermodynamic quantities thermal expansion, compressibility and heat capacity with the mean Grüneisen parameter. For most substances, γ exhibits values between 1 and 4 which are hardly temperature dependent. Hence, equation (2.1.2.84) may be regarded as an equation of state for solid systems.

Experimentally, it is almost impossible to determine the heat capacity at constant volume c_V since the thermal expansion cannot be easily compensated. The more convenient quantity is c_p , the heat capacity at constant pressure. There is a simple thermodynamic relation between the two quantities,

$$c_p = c_V + \frac{TV\beta^2}{\kappa}, \quad (2.1.2.85)$$

and hence the following equation is obtained:

$$c_p = \left(\frac{1}{\gamma} + \beta T \right) \frac{\beta V}{\kappa}. \quad (2.1.2.86)$$

2.1.3. Symmetry of lattice vibrations

Having presented the basic formulation of lattice dynamics in Section 2.1.2, we will now consider the constraints that arise due to the symmetry of the particular atomic arrangement within a crystal. We shall see in the following how group-theoretical methods can be used in order:

- (a) to reduce the number of independent elements of the dynamical matrix;
 - (b) to provide a unique labelling of individual phonon branches according to the symmetries of the respective eigenvectors; and
 - (c) to deal with degeneracies of particular phonon modes.
- The theoretical aspects will be illustrated by means of simple examples which may serve as a guide for the application of the formalism to other systems of interest.

2.1.3.1. Symmetry constraints for the dynamical matrix

The elements of the $3N \times 3N$ dynamical matrix as introduced in Section 2.1.2.3 are given by

$$D_{\kappa\kappa'}^{\alpha\beta}(\mathbf{q}) = \frac{1}{\sqrt{m_\kappa m_{\kappa'}}} \sum_{l'} V_{\alpha\beta}(\kappa l, \kappa' l') \exp[i\mathbf{q}(\mathbf{r}_{l'} - \mathbf{r}_l)]. \quad (2.1.3.1)$$

Using the matrix notation for the 3×3 submatrices introduced in (2.1.2.22a), this equation reads

$$\mathbf{D}_{\kappa\kappa'}(\mathbf{q}) = \frac{1}{\sqrt{m_\kappa m_{\kappa'}}} \sum_{l'} \mathbf{V}(\kappa l, \kappa' l') \exp[i\mathbf{q}(\mathbf{r}_{l'} - \mathbf{r}_l)]. \quad (2.1.3.1a)$$

Since the vector $\mathbf{r}_{l'} - \mathbf{r}_l$ corresponds to a vector of the direct lattice, the right-hand side of equation (2.1.3.1) is invariant with respect to changes of the wavevector \mathbf{q} by an arbitrary reciprocal lattice vector \mathbf{g} . Hence, the elements of the dynamical matrix represent periodic functions within the reciprocal space:

$$\mathbf{D}(\mathbf{q} + \mathbf{g}) = \mathbf{D}(\mathbf{q}). \quad (2.1.3.2)$$

² If for a given wavevector \mathbf{q} the dynamical matrix exhibits degenerate eigenvalues, the most one can strictly infer from equation (2.1.3.2) is that the eigenvector $\mathbf{e}(\mathbf{q} + \mathbf{g}, j)$ may be represented by some linear combination of those eigenvectors $\mathbf{e}(\mathbf{q}, j')$ that correspond to the same eigenvalue. One always can choose, however, an appropriate labelling of the degenerate phonon modes and appropriate phase factors for the eigenvectors in order to guarantee that the simple relation (2.1.3.3) holds.

The same periodicity can also be assumed for the eigenvalues, or eigenfrequencies, and for the eigenvectors:²

$$\begin{aligned} \omega_{\mathbf{q}+\mathbf{g},j} &= \omega_{\mathbf{q},j}, \\ \mathbf{e}(\mathbf{q} + \mathbf{g}, j) &= \mathbf{e}(\mathbf{q}, j). \end{aligned} \quad (2.1.3.3)$$

Consequently, we can restrict our discussion to wavevectors within the first Brillouin zone.

Owing to the symmetry of the atomic structure, not all of the force constants $V_{\alpha\beta}(\kappa l, \kappa' l')$ reflecting the interaction between atoms (κl) and $(\kappa' l')$ are independent. Rather, there are constraints to the elements of the dynamical matrix according to the space group of the crystal. In the following, these constraints will be considered in some detail. Suppose the space group contains a symmetry operation $\{\mathbf{S}|\mathbf{v}(\mathbf{S}) + \mathbf{x}(m)\}$.³ When applied to the crystal, this symmetry operation sends atom (κl) into another atom $(K L)$ and simultaneously atom $(\kappa' l')$ into $(K' L')$. At the same time, the wavevector of a phonon is rotated from \mathbf{q} into $\mathbf{S}\mathbf{q}$. Hence, the elements of the dynamical matrix that describes the dynamics of the crystal after application of the symmetry operation may be written as

$$\begin{aligned} D_{KK'}^{\alpha\beta}(\mathbf{S}\mathbf{q}) &= \frac{1}{\sqrt{m_K m_{K'}}} \sum_{L'} V_{\alpha\beta}(KL, K' L') \exp[i(\mathbf{S}\mathbf{q})(\mathbf{r}_{L'} - \mathbf{r}_L)] \end{aligned} \quad (2.1.3.4)$$

or in submatrix notation

$$\mathbf{D}_{KK'}(\mathbf{S}\mathbf{q}) = \frac{1}{\sqrt{m_K m_{K'}}} \sum_{L'} \mathbf{V}(KL, K' L') \exp[i(\mathbf{S}\mathbf{q})(\mathbf{r}_{L'} - \mathbf{r}_L)]. \quad (2.1.3.4a)$$

This submatrix can be related to the corresponding matrix $\mathbf{D}_{\kappa\kappa'}(\mathbf{q})$ that describes the same dynamical behaviour, but in the unrotated crystal. To this end, we first consider the transformation of the force-constant matrices under the symmetry operation. Obviously, the interaction between atoms (κl) and $(\kappa' l')$ has to be of the same type as the interaction between (KL) and $(K' L')$.

Since the potential energy is invariant with respect to symmetry operations, the force constants are related via

$$\begin{aligned} \sum_{\alpha\beta} \sum_{\kappa l} \sum_{\kappa' l'} V_{\alpha\beta}(\kappa l, \kappa' l') u_{\kappa l}^\alpha u_{\kappa' l'}^\beta &= \sum_{\alpha\beta} \sum_{KL} \sum_{K' L'} V_{\alpha\beta}(KL, K' L') u_{KL}^\alpha u_{K' L'}^\beta \end{aligned} \quad (2.1.3.5)$$

or in matrix notation

$$\sum_{\kappa l} \sum_{\kappa' l'} \mathbf{u}_{\kappa l} \mathbf{V}(\kappa l, \kappa' l') \mathbf{u}_{\kappa' l'} = \sum_{KL} \sum_{K' L'} \mathbf{u}_{KL} \mathbf{V}(KL, K' L') \mathbf{u}_{K' L'}. \quad (2.1.3.5a)$$

Owing to the symmetry operation, the displacements of atoms (κl) and $(\kappa' l')$ are rotated and transferred to atoms (KL) and $(K' L')$, respectively (see Fig. 2.1.3.1). Thus, (2.1.3.5) can be rewritten as

$$\begin{aligned} \sum_{\alpha\beta} \sum_{\kappa l} \sum_{\kappa' l'} V_{\alpha\beta}(\kappa l, \kappa' l') u_\alpha(\kappa l) u_\beta(\kappa' l') &= \sum_{\alpha\beta} \sum_{\kappa l} \sum_{\kappa' l'} V_{\alpha\beta}(KL, K' L') \sum_\mu S_{\alpha\mu} u_\mu(\kappa l) \sum_\nu S_{\beta\nu} u_\nu(\kappa' l'). \end{aligned} \quad (2.1.3.6)$$

³ We use the Seitz notation for symmetry operations: \mathbf{S} denotes a rigid rotation of the lattice, $\mathbf{v}(\mathbf{S})$ is the corresponding vector of a fractional translation in the case of screw axes, glide planes etc. and $\mathbf{x}(m)$ is a lattice vector.

2.1. PHONONS

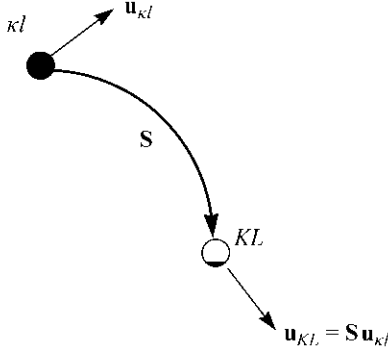


Fig. 2.1.3.1. Transformation of atomic displacements by a symmetry operation.

Moreover, this relation is valid for arbitrary displacements and, hence, the matrices of force constants transform according to

$$V_{\mu\nu}(\kappa l, \kappa' l') = \sum_{\alpha\beta} V_{\alpha\beta}(KL, K' L') S_{\alpha\mu} S_{\beta\nu} \quad (2.1.3.7)$$

or

$$\mathbf{V}(\kappa l, \kappa' l') = \mathbf{S}^T \mathbf{V}(KL, K' L') \mathbf{S}. \quad (2.1.3.7a)$$

Using the fact that the matrix of rotation \mathbf{S} is unitary ($\mathbf{S}^{-1} = \mathbf{S}^T$), the inverse relation is obtained:

$$\mathbf{V}(KL, K' L') = \mathbf{S} \mathbf{V}(\kappa l, \kappa' l') \mathbf{S}^T. \quad (2.1.3.7b)$$

Hence, the force-constant submatrices transform like tensors do. One has to bear in mind, however, that the matrices in equation (2.1.3.7b) correspond to different pairs of atoms as illustrated by Fig. 2.1.3.2. Using this result in equation (2.1.3.4a) and remembering the fact that atoms related by a symmetry operation have the same mass, we obtain

$$\begin{aligned} D_{KK'}^{\alpha\beta}(\mathbf{S}\mathbf{q}) &= \frac{1}{\sqrt{m_\kappa m_{\kappa'}}} \sum_{\mu\nu} S_{\alpha\mu} S_{\beta\nu} \sum_{l'} V_{\mu\nu}(\kappa l, \kappa' l') \exp[i(\mathbf{S}\mathbf{q})(\mathbf{r}_{L'} - \mathbf{r}_L)] \\ &= \frac{1}{\sqrt{m_\kappa m_{\kappa'}}} \sum_{\mu\nu} S_{\alpha\mu} S_{\beta\nu} \sum_{l'} V_{\mu\nu}(\kappa l, \kappa' l') \exp[i\mathbf{q} \mathbf{S}^{-1}(\mathbf{r}_{L'} - \mathbf{r}_L)]. \end{aligned} \quad (2.1.3.8)$$

The phase factor on the right-hand side contains the indices L and L' of those primitive cells into which the atoms (κl) and ($\kappa' l'$) are sent by the symmetry operation $\{\mathbf{S}|\mathbf{v}(\mathbf{S}) + \mathbf{x}(m)\}$. In general, the phase is not conserved during the transformation and, hence, the sum over l' cannot simply be replaced by the matrix elements $D_{\kappa\kappa'}^{\mu\nu}(\mathbf{q})$. Rather, we have to consider the phase factor in more detail in order to find the transformation law for the dynamical matrix.

The position vectors of particles (κl) and (KL) are related via

$$\begin{aligned} \mathbf{r}_{KL}^o &= \mathbf{r}_K^o + \mathbf{r}_L = \{\mathbf{S}|\mathbf{v}(\mathbf{S}) + \mathbf{x}(m)\} \mathbf{r}_{\kappa l}^o \\ &= \mathbf{S} \mathbf{r}_{\kappa l}^o + \mathbf{v}(\mathbf{S}) + \mathbf{x}(m) \\ &= \mathbf{S}(\mathbf{r}_\kappa^o + \mathbf{r}_l) + \mathbf{v}(\mathbf{S}) + \mathbf{x}(m) \end{aligned} \quad (2.1.3.9)$$

and

$$\begin{aligned} \mathbf{r}_\kappa^o + \mathbf{r}_l &= \mathbf{S}^{-1}(\mathbf{r}_K^o + \mathbf{r}_L) - \mathbf{v}(\mathbf{S}) - \mathbf{x}(m) \\ &= \{\mathbf{S}|\mathbf{v}(\mathbf{S}) + \mathbf{x}(m)\}^{-1} \mathbf{r}_K^o + \mathbf{S}^{-1} \mathbf{r}_L. \end{aligned} \quad (2.1.3.9a)$$

Consequently, the vector appearing in the phase factor of equation (2.1.3.8) can be expressed as

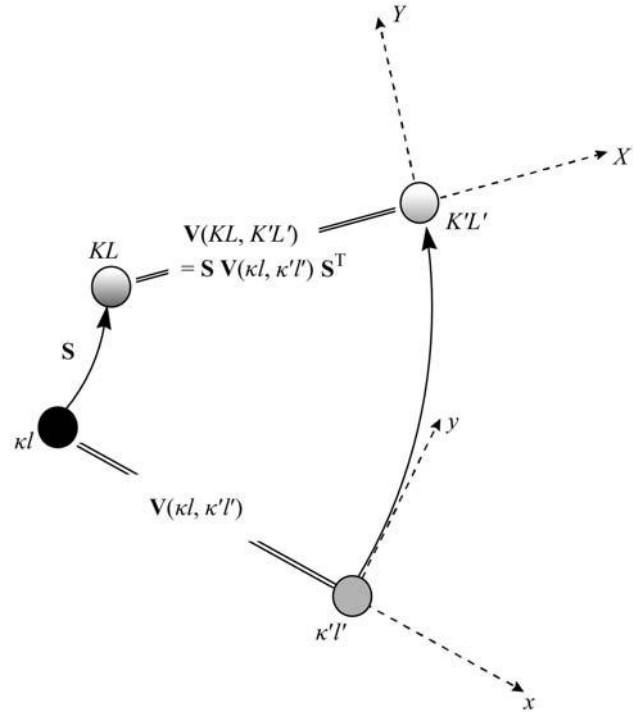


Fig. 2.1.3.2. Relation between interaction of symmetry-related atoms.

$$\mathbf{S}^{-1} \mathbf{r}_L = \mathbf{r}_\kappa^o + \mathbf{r}_l - \{\mathbf{S}|\mathbf{v}(\mathbf{S}) + \mathbf{x}(m)\}^{-1} \mathbf{r}_K^o. \quad (2.1.3.10)$$

When inserted into equation (2.1.3.8), the required transformation law for the dynamical matrix is obtained:

$$\begin{aligned} D_{KK'}^{\alpha\beta}(\mathbf{S}\mathbf{q}) &= \frac{1}{\sqrt{m_\kappa m_{\kappa'}}} \sum_{\mu\nu} S_{\alpha\mu} S_{\beta\nu} \sum_{l'} V_{\mu\nu}(\kappa l, \kappa' l') \\ &\quad \times \exp[i\mathbf{q}(\mathbf{r}_{l'} - \mathbf{r}_l)] \\ &\quad \times \exp[i\mathbf{q}(\{\mathbf{S}|\mathbf{v}(\mathbf{S}) + \mathbf{x}(m)\}^{-1} \mathbf{r}_K^o - \mathbf{r}_\kappa^o)] \\ &\quad \times \exp[-i\mathbf{q}(\{\mathbf{S}|\mathbf{v}(\mathbf{S}) + \mathbf{x}(m)\}^{-1} \mathbf{r}_{K'}^o - \mathbf{r}_{\kappa'}^o)] \end{aligned} \quad (2.1.3.11)$$

or

$$\begin{aligned} D_{KK'}^{\alpha\beta}(\mathbf{S}\mathbf{q}) &= \sum_{\mu\nu} S_{\alpha\mu} S_{\beta\nu} D_{\kappa\kappa'}^{\mu\nu}(\mathbf{q}) \\ &\quad \times \exp[i\mathbf{q}(\{\mathbf{S}|\mathbf{v}(\mathbf{S}) + \mathbf{x}(m)\}^{-1} \mathbf{r}_K^o - \mathbf{r}_\kappa^o)] \\ &\quad \times \exp[-i\mathbf{q}(\{\mathbf{S}|\mathbf{v}(\mathbf{S}) + \mathbf{x}(m)\}^{-1} \mathbf{r}_{K'}^o - \mathbf{r}_{\kappa'}^o)], \end{aligned} \quad (2.1.3.11a)$$

or in submatrix notation

$$\begin{aligned} \mathbf{D}_{KK'}(\mathbf{S}\mathbf{q}) &= \mathbf{S}^T \mathbf{D}_{\kappa\kappa'}(\mathbf{q}) \mathbf{S} \\ &\quad \times \exp[i\mathbf{q}(\{\mathbf{S}|\mathbf{v}(\mathbf{S}) + \mathbf{x}(m)\}^{-1} \mathbf{r}_K^o - \mathbf{r}_\kappa^o)] \\ &\quad \times \exp[-i\mathbf{q}(\{\mathbf{S}|\mathbf{v}(\mathbf{S}) + \mathbf{x}(m)\}^{-1} \mathbf{r}_{K'}^o - \mathbf{r}_{\kappa'}^o)]. \end{aligned} \quad (2.1.3.11b)$$

Again, these are relations between pairs of submatrices of the dynamical matrix. In contrast to the matrices of force constants, however, phase factors have to be considered here. This is because the symmetry operation $\{\mathbf{S}|\mathbf{v}(\mathbf{S}) + \mathbf{x}(m)\}$ may send different atoms κ and κ' located within the same primitive cell (0) into atoms (KL) and ($K' L'$) within different primitive cells L and L' as illustrated in Fig. 2.1.3.3. Therefore, the product of phase factors in equation (2.1.3.11) is in general different from unity.

Irrespective of the particular primitive cells in which the atoms are located, however, the labels κ and K of those atoms that are related by a symmetry operation are uniquely determined. Given

2. SYMMETRY ASPECTS OF EXCITATIONS

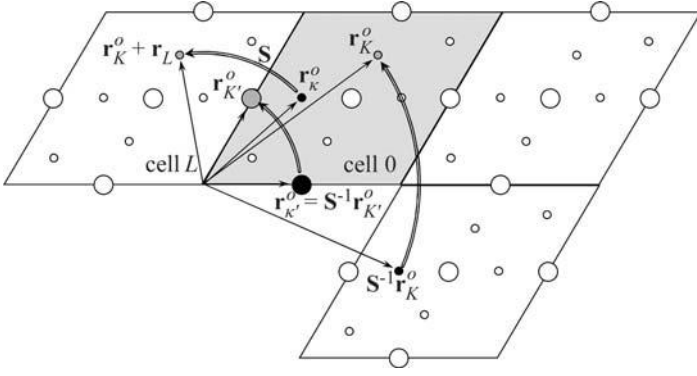


Fig. 2.1.3.3. Symmetry-related atoms in different primitive cells.

the label κ and a particular symmetry operation $\{S|\mathbf{v}(S) + \mathbf{x}(m)\}$, the label K may be represented by the function

$$K = F_o(\kappa, S), \quad (2.1.3.12)$$

which represents the atom transformation table.⁴ With the definition of unitary transformation matrices

$$\begin{aligned} \Gamma_{K\kappa}^{\alpha\mu}(\mathbf{q}, \{S|\mathbf{v}(S) + \mathbf{x}(m)\}) \\ = S_{\alpha\mu} \delta(\kappa, F_o^{-1}(K, S)) \exp[i\mathbf{q} \cdot (\{S|\mathbf{v}(S) + \mathbf{x}(m)\}^{-1} \mathbf{r}_K^o - \mathbf{r}_\kappa^o)], \end{aligned} \quad (2.1.3.13)$$

we are now able to formulate the transformation law for the dynamical matrix briefly as

$$\begin{aligned} \mathbf{D}(S\mathbf{q}) \\ = \Gamma(\mathbf{q}, \{S|\mathbf{v}(S) + \mathbf{x}(m)\}) \mathbf{D}(\mathbf{q}) \Gamma^+(\mathbf{q}, \{S|\mathbf{v}(S) + \mathbf{x}(m)\}). \end{aligned} \quad (2.1.3.14)$$

Obviously, with the help of equation (2.1.3.13), we can allocate a unitary matrix to each symmetry operation. These Γ matrices, however, do not form a representation of the crystal space group in the mathematical sense since the mapping

$$\{S|\mathbf{v}(S) + \mathbf{x}(m)\} \rightarrow \Gamma(\mathbf{q}, \{S|\mathbf{v}(S) + \mathbf{x}(m)\})$$

is not a linear one. Rather, we obtain the following transformation matrix for the product of two symmetry operations:

$$\begin{aligned} \Gamma(\mathbf{q}, \{S_1|\mathbf{v}(S_1) + \mathbf{x}(m_1)\} \circ \{S_2|\mathbf{v}(S_2) + \mathbf{x}(m_2)\}) \\ = \Gamma(S_2\mathbf{q}, \{S_1|\mathbf{v}(S_1) + \mathbf{x}(m_1)\}) \Gamma(\mathbf{q}, \{S_2|\mathbf{v}(S_2) + \mathbf{x}(m_2)\}). \end{aligned} \quad (2.1.3.15)$$

The nonlinearity of the mapping is due to the fact that the first matrix on the right-hand side of this equation depends on the wavevector $S_2\mathbf{q}$ rather than on \mathbf{q} . If we restrict our considerations to the symmetry operations of the *space group* $G(\mathbf{q})$ of the wavevector \mathbf{q} that leave the wavevector invariant modulo some reciprocal-lattice vector $\mathbf{g}(\mathbf{q}, S)$,

$$S\mathbf{q} = \mathbf{q} - \mathbf{g}(\mathbf{q}, S), \quad (2.1.3.16)$$

then equation (2.1.3.13) provides an ordinary (3N-dimensional) representation of this symmetry group.⁵ In the following, we denote the elements of the subgroup $G(\mathbf{q})$ by $\{\mathbf{R}|\mathbf{v}(\mathbf{R}) + \mathbf{x}(m)\}$.

⁴ Since the rotation S uniquely defines the fractional translation $\mathbf{v}(S)$ and since a lattice translation $\mathbf{x}(m)$ never changes the label of an atom within the primitive cell, the function F_o depends only on S .

⁵ According to (2.1.3.10), the vector $\{S|\mathbf{v}(S) + \mathbf{x}(m)\}^{-1} \mathbf{r}_K^o - \mathbf{r}_\kappa^o$ is always a lattice vector. Hence, the transformation matrix remains invariant when the wavevector is shifted by a reciprocal-lattice vector. If wavevectors within the first Brillouin zone are considered, $\mathbf{g}(\mathbf{q}, S)$ is always zero. For wavevectors on the Brillouin-zone boundary, however, there may be symmetry operations like the inversion that transform \mathbf{q} into another equivalent but not identical vector $\mathbf{q}' = \mathbf{q} + \mathbf{g}$.

The corresponding unitary and Hermitian transformation matrices can be reduced to

$$\begin{aligned} \Gamma_{K\kappa}^{\alpha\mu}(\mathbf{q}, \{\mathbf{R}|\mathbf{v}(\mathbf{R}) + \mathbf{x}(m)\}) \\ = R_{\alpha\mu} \delta(\kappa, F_o^{-1}(K; \mathbf{R})) \\ \times \exp[i\mathbf{q} \cdot (\mathbf{R}^{-1} \mathbf{r}_K^o - \mathbf{R}^{-1} \mathbf{v}(\mathbf{R}) - \mathbf{R}^{-1} \mathbf{x}(m) - \mathbf{r}_\kappa^o)] \\ = R_{\alpha\mu} \delta(\kappa, F_o^{-1}(K; \mathbf{R})) \\ \times \exp[i\mathbf{R} \mathbf{q} \cdot (\mathbf{r}_K^o - \{\mathbf{R}|\mathbf{v}(\mathbf{R}) + \mathbf{x}(m)\} \mathbf{r}_\kappa^o)] \\ = R_{\alpha\mu} \delta(\kappa, F_o^{-1}(K; \mathbf{R})) \\ \times \exp[i\mathbf{q} \cdot (\mathbf{r}_K^o - \{\mathbf{R}|\mathbf{v}(\mathbf{R}) + \mathbf{x}(m)\} \mathbf{r}_\kappa^o)]. \end{aligned} \quad (2.1.3.17)$$

According to equation (2.1.3.14), they commute with the dynamical matrix:

$$\Gamma(\mathbf{q}, \{\mathbf{R}|\mathbf{v}(\mathbf{R}) + \mathbf{x}(m)\}) \mathbf{D}(\mathbf{q}) \Gamma^{-1}(\mathbf{q}, \{\mathbf{R}|\mathbf{v}(\mathbf{R}) + \mathbf{x}(m)\}) = \mathbf{D}(\mathbf{q}). \quad (2.1.3.18)$$

This relation contains the symmetry constraints for the dynamical matrix. The independent elements of $\mathbf{D}(\mathbf{q})$ may be obtained by application of equation (2.1.3.18) for every operation of the space group of the wavevector.

Another approach to the symmetry reduction of the dynamical matrix is based on group-theoretical considerations making use of the well known irreducible representations of symmetry groups. It is especially useful for the prediction of the form of eigenvectors and the investigation of degeneracies. Following the treatment of Maradudin & Vosko (1968), we consider the purely rotational elements of the space group $G(\mathbf{q})$ that form the *point group of the wavevector* $G_o(\mathbf{q}) = \{\mathbf{R}\}$. According to equation (2.1.3.17), we associate a matrix operator

$$\mathbf{T}(\mathbf{q}, \mathbf{R}) = \exp[i\mathbf{q} \cdot (\mathbf{v}(\mathbf{R}) + \mathbf{x}(m))] \Gamma(\mathbf{q}, \{\mathbf{R}|\mathbf{v}(\mathbf{R}) + \mathbf{x}(m)\}) \quad (2.1.3.19)$$

to each of the elements of $G_o(\mathbf{q})$. These matrix operators are uniquely determined by the rotations \mathbf{R} and do not depend on the translational parts of the space-group operation $\{\mathbf{R}|\mathbf{v}(\mathbf{R}) + \mathbf{x}(m)\}$, as proven by inspection of the individual matrix elements:

$$\mathbf{T}_{K\kappa}^{\alpha\mu}(\mathbf{q}, \mathbf{R}) = R_{\alpha\mu} \delta(\kappa, F_o^{-1}(K, \mathbf{R})) \exp[i\mathbf{q} \cdot (\mathbf{r}_K^o - \mathbf{R} \mathbf{r}_\kappa^o)]. \quad (2.1.3.19a)$$

These \mathbf{T} matrices again commute with the dynamical matrix,

$$\mathbf{T}(\mathbf{q}, \mathbf{R}) \mathbf{D}(\mathbf{q}) \mathbf{T}^{-1}(\mathbf{q}, \mathbf{R}) = \mathbf{D}(\mathbf{q}), \quad (2.1.3.20)$$

but in contrast to the Γ matrices they do not provide an ordinary representation of the group $G_o(\mathbf{q})$. For the multiplication of two symmetry elements \mathbf{R}_i and \mathbf{R}_j the following relation holds:

$$\begin{aligned} \mathbf{T}(\mathbf{q}, \mathbf{R}_i) \mathbf{T}(\mathbf{q}, \mathbf{R}_j) \\ = \exp[i(\mathbf{q} - \mathbf{R}_i^{-1} \mathbf{q}) \cdot (\mathbf{v}(\mathbf{R}_j) + \mathbf{x}(m_j))] \mathbf{T}(\mathbf{q}, \mathbf{R}_i \circ \mathbf{R}_j). \end{aligned} \quad (2.1.3.21)$$

According to equation (2.1.3.16), $\mathbf{q} - \mathbf{R}_i^{-1} \mathbf{q}$ is a reciprocal-lattice vector $\mathbf{g}(\mathbf{q}, \mathbf{R}_i^{-1})$ and hence

$$\begin{aligned} \mathbf{T}(\mathbf{q}, \mathbf{R}_i) \mathbf{T}(\mathbf{q}, \mathbf{R}_j) &= \exp[i\mathbf{g}(\mathbf{q}, \mathbf{R}_i^{-1}) \cdot \mathbf{v}(\mathbf{R}_j)] \mathbf{T}(\mathbf{q}, \mathbf{R}_i \circ \mathbf{R}_j) \\ &= \varphi(\mathbf{q}, \mathbf{R}_i, \mathbf{R}_j) \mathbf{T}(\mathbf{q}, \mathbf{R}_i \circ \mathbf{R}_j). \end{aligned} \quad (2.1.3.21a)$$

Thus, the \mathbf{T} matrices provide not a normal but a *multiplier representation* of the group $G_o(\mathbf{q})$. The phase factor on the right-hand side of equation (2.1.3.21a) is the complex multiplier characteristic for the (ordered) product of symmetry operations.

2.1. PHONONS

For wavevectors within the first Brillouin zone, the reciprocal-lattice vectors $\mathbf{g}(\mathbf{q}, \mathbf{R}_i^{-1})$ are identically zero (see last footnote) and the \mathbf{T} representation is an ordinary one. The same is true if none of the symmetry elements of $G_o(\mathbf{q})$ contains a fractional translation, *i.e.* for symmorphic space groups. Therefore, multipliers have to be taken into account only if nonsymmorphic space groups and wavevectors on the Brillouin-zone boundary are considered.

There are some other restrictions for the dynamical matrix arising from the fact that inverting the wavevector is equivalent to taking the complex conjugate dynamical matrix [*c.f.* equation (2.1.2.24)]:

$$\mathbf{D}^*(\mathbf{q}) = \mathbf{D}(-\mathbf{q}). \quad (2.1.3.22)$$

Hence it is useful to extend our discussion to those symmetry operations that invert the phonon wavevector. Let us assume that the space group of the crystal contains an element $\{\mathbf{S}_-|\mathbf{v}(\mathbf{S}_-)\}$ with

$$\mathbf{S}_- \mathbf{q} = -\mathbf{q}. \quad (2.1.3.23)$$

Using equation (2.1.3.14) we obtain

$$\mathbf{D}(-\mathbf{q}) = \mathbf{D}^*(\mathbf{q}) = \Gamma(\mathbf{q}, \{\mathbf{S}_-|\mathbf{v}(\mathbf{S}_-)\}) \mathbf{D}(\mathbf{q}) \Gamma^+(\mathbf{q}, \{\mathbf{S}_-|\mathbf{v}(\mathbf{S}_-)\}). \quad (2.1.3.24)$$

In order to provide a consistent description, we introduce an anti-unitary operator \mathbf{K}_o which transforms an arbitrary vector Ψ into its complex conjugate counterpart Ψ^*

$$\mathbf{K}_o \Psi = \Psi^*. \quad (2.1.3.25)$$

Obviously, \mathbf{K}_o does not commute with the dynamical matrix but exhibits the following transformation behaviour:

$$\mathbf{K}_o \mathbf{D}(\mathbf{q}) \mathbf{K}_o = \mathbf{D}^*(\mathbf{q}). \quad (2.1.3.26)$$

On the other hand, we infer from equation (2.1.3.24) that

$$\begin{aligned} & \mathbf{K}_o \Gamma(\mathbf{q}, \{\mathbf{S}_-|\mathbf{v}(\mathbf{S}_-)\}) \mathbf{D}(\mathbf{q}) \Gamma^+(\mathbf{q}, \{\mathbf{S}_-|\mathbf{v}(\mathbf{S}_-)\}) \mathbf{K}_o \\ &= \mathbf{K}_o \mathbf{D}(-\mathbf{q}) \mathbf{K}_o \\ &= \mathbf{D}^*(-\mathbf{q}) \\ &= \mathbf{D}(\mathbf{q}), \end{aligned} \quad (2.1.3.27)$$

which provide the additional constraints for the dynamical matrix. In component form, this last relation can be written explicitly as

$$\begin{aligned} & [\exp(-i\mathbf{q}\mathbf{r}_K) D_{KK'}^{\mu\nu}(\mathbf{q}) \exp(i\mathbf{q}\mathbf{r}_{K'})]^* \\ &= \sum_{\alpha\beta} (S_-)_{\mu\alpha} [\exp(-i\mathbf{q}\mathbf{r}_K) D_{KK'}^{\alpha\beta}(\mathbf{q}) \exp(i\mathbf{q}\mathbf{r}_{K'})] (S_-)_{\nu\beta} \end{aligned} \quad (2.1.3.28)$$

if particles (κl) and ($\kappa' l'$) are sent into (KL) and ($K'L'$) by the symmetry operation $\{\mathbf{S}_-|\mathbf{v}(\mathbf{S}_-)\}$, respectively.

If \mathbf{S}_- represents the inversion $((S_-)_{\alpha\beta} = -\delta_{\alpha\beta})$, in particular, then (2.1.3.28) reduces to

$$[\exp(-i\mathbf{q}\mathbf{r}_K) D_{KK'}^{\mu\nu}(\mathbf{q}) \exp(i\mathbf{q}\mathbf{r}_{K'})]^* = [\exp(-i\mathbf{q}\mathbf{r}_K) D_{KK'}^{\mu\nu}(\mathbf{q}) \exp(i\mathbf{q}\mathbf{r}_{K'})]. \quad (2.1.3.29)$$

Moreover, if every atom is itself a centre of inversion (*e.g.* the NaCl structure) ($K = \kappa$ and $K' = \kappa'$), the matrix $\mathbf{C}(\mathbf{q})$ defined by

$$C_{\kappa\kappa'}^{\alpha\beta}(\mathbf{q}) = \exp(-i\mathbf{q}\mathbf{r}_\kappa) D_{\kappa\kappa'}^{\alpha\beta}(\mathbf{q}) \exp(i\mathbf{q}\mathbf{r}_{\kappa'}) \quad (2.1.3.30)$$

is a real and symmetric matrix with real eigenvectors for arbitrary wavevectors \mathbf{q} .

In terms of group theory we proceed as follows: We add to the space group of the wavevector $G(\mathbf{q})$ the elements of the coset $\{\mathbf{S}_-|\mathbf{v}(\mathbf{S}_-)\} \circ G(\mathbf{q})$.⁶ This will result in a new space group which we call $G(\mathbf{q}, -\mathbf{q})$. If instead of the matrix operator $\Gamma(\mathbf{q}, \{\mathbf{S}_-|\mathbf{v}(\mathbf{S}_-) + \mathbf{x}(m)\})$ the anti-unitary operator $\mathbf{K}_o \Gamma(\mathbf{q}, \{\mathbf{S}_-|\mathbf{v}(\mathbf{S}_-) + \mathbf{x}(m)\})$ is assigned to those symmetry operations that invert the wavevector, then a representation of the whole group $G(\mathbf{q}, -\mathbf{q})$ is provided. Moreover, all these matrix operators commute with the dynamical matrix.

As before, let us restrict ourselves to the rotational parts of the symmetry operations. The point group of the wavevector $G_o(\mathbf{q})$ is enlarged by the coset $\mathbf{S}_- \circ G_o(\mathbf{q})$ yielding the group $G_o(\mathbf{q}, -\mathbf{q})$. In analogy to equation (2.1.3.19), the elements of the left coset will be represented by the matrix operator

$$\begin{aligned} \mathbf{T}(\mathbf{q}, \mathbf{S}_- \circ \mathbf{R}) &= \mathbf{K}_o \exp[-i\mathbf{q}(\mathbf{v}(\mathbf{S}_- \circ \mathbf{R}) + \mathbf{x}(m))] \\ &\quad \times \Gamma(\mathbf{q}, \{\mathbf{S}_- \circ \mathbf{R}|\mathbf{v}(\mathbf{S}_- \circ \mathbf{R}) + \mathbf{x}(m)\}) \\ &= \exp[i\mathbf{q}(\mathbf{v}(\mathbf{S}_- \circ \mathbf{R}) + \mathbf{x}(m))] \\ &\quad \times \mathbf{K}_o \Gamma(\mathbf{q}, \{\mathbf{S}_- \circ \mathbf{R}|\mathbf{v}(\mathbf{S}_- \circ \mathbf{R}) + \mathbf{x}(m)\}). \end{aligned} \quad (2.1.3.31)$$

The \mathbf{T} matrix operators provide a *multiplier corepresentation*. The multipliers are not uniquely defined as in equation (2.1.3.21a). Rather, the definition depends on the type and the order of the symmetry operations involved. In order to distinguish between the different kinds of symmetry operations, we introduce the following notation:

$\mathbf{R} \in G_o(\mathbf{q}, -\mathbf{q})$ is an arbitrary element of the point group.

$\mathbf{R} \in G_o(\mathbf{q})$ is an element of the point group of the wavevector $G_o(\mathbf{q})$ which is a subgroup of $G_o(\mathbf{q}, -\mathbf{q})$. This element is represented by an unitary matrix operator.

$\mathbf{A} \in \mathbf{S}_- \circ G_o(\mathbf{q})$ is an element of the coset $\mathbf{S}_- \circ G_o(\mathbf{q})$, represented by an anti-unitary operator.

The multiplication rule

$$\mathbf{T}(\mathbf{q}, \bar{\mathbf{R}}_i) \mathbf{T}(\mathbf{q}, \bar{\mathbf{R}}_j) = \varphi(\mathbf{q}, \bar{\mathbf{R}}_i, \bar{\mathbf{R}}_j) \mathbf{T}(\mathbf{q}, \bar{\mathbf{R}}_i \circ \bar{\mathbf{R}}_j) \quad (2.1.3.32)$$

is determined by the multipliers

$$\begin{aligned} \varphi(\mathbf{q}, \mathbf{R}_i, \bar{\mathbf{R}}_j) &= \exp[i(\mathbf{q} - \mathbf{R}_i^{-1} \mathbf{q}) \mathbf{v}(\bar{\mathbf{R}}_j)] \\ \varphi(\mathbf{q}, \mathbf{A}_i, \bar{\mathbf{R}}_j) &= \exp[-i(\mathbf{q} + \mathbf{A}_i^{-1} \mathbf{q}) \mathbf{v}(\bar{\mathbf{R}}_j)]. \end{aligned} \quad (2.1.3.33)$$

Again, this representation reduces to an ordinary representation either for symmorphic space groups [all $\mathbf{v}(\bar{\mathbf{R}}_i) = \mathbf{0}$] or for wavevectors within the interior of the Brillouin zone.

All matrix operators of the \mathbf{T} representation commute with the dynamical matrix. Hence, they may be used for the determination of independent elements of the dynamical matrix as well as for the determination of the form of eigenvectors compatible with the atomic structure.

2.1.3.1.1. Example

As an example, we consider a crystal of tetragonal symmetry, space group $P4mm$, with lattice parameters a and c . The primitive cell spanned by the three mutually orthogonal vectors \mathbf{a} , \mathbf{b} and \mathbf{c} contains ten atoms at the positions listed in Table 2.1.3.1 and shown in Fig. 2.1.3.4. Consequently, the dynamical matrix has 30×30 elements.

The space group $P4mm$ contains eight symmetry operations, namely

- (1) the identity, denoted E ;
- (2) a 90° rotation around the z axis, denoted D_{90}^z ;
- (3) a 180° rotation around the z axis, denoted D_{180}^z ;
- (4) a 270° rotation around the z axis, denoted D_{270}^z ;

⁶ The choice of the left coset is arbitrary. We could also consider the right coset $G(\mathbf{q}) \circ \{\mathbf{S}_-|\mathbf{v}(\mathbf{S}_-)\}$. The same enlarged group and the same representations are obtained.

2. SYMMETRY ASPECTS OF EXCITATIONS

Table 2.1.3.1. Example structure in space group $P4mm$

| Atom No. | x | y | z |
|----------|-----|-----|-----|
| 1 | 0 | 0 | 0 |
| 2 | 0.5 | 0.5 | 0.6 |
| 3 | 0.2 | 0.1 | 0 |
| 4 | 0.8 | 0.9 | 0 |
| 5 | 0.9 | 0.8 | 0 |
| 6 | 0.1 | 0.8 | 0 |
| 7 | 0.2 | 0.9 | 0 |
| 8 | 0.8 | 0.1 | 0 |
| 9 | 0.9 | 0.2 | 0 |
| 10 | 0.1 | 0.2 | 0 |

- (5) a mirror plane normal to the x axis, denoted m_x ;
(6) a mirror plane normal to the y axis, denoted m_y ;
(7) a mirror plane normal to the $[\bar{1}10]$ axis, denoted $m_{[\bar{1}10]}$; and
(8) a mirror plane normal to the $[110]$ axis, denoted $m_{[110]}$.

Obviously, atoms No. 3 to 10 are chemically identical and have the same mass.

For the reduction of the dynamical matrix, we need the function $F_o(\kappa, \mathbf{S})$, yielding the label of that atom into which κ is sent by the symmetry operation \mathbf{S} . This function can be represented by the atom transformations shown in Table 2.1.3.2. This table displays the labels of atoms κ and K related by a particular symmetry operation and also the relative position $\mathbf{r}_l - \mathbf{r}_L$ of the primitive cells l and L where both atoms are located. This information is needed for the calculation of phase factors in the expression for the matrix operators \mathbf{T} . Via the twofold axis, atom 6, for example, is transformed into atom 9 located within the cell which is shifted by the vector $-\mathbf{a} - \mathbf{b}$.

Let us first consider the case of phonons with infinite wavelengths and, hence, the symmetry reduction of the dynamical matrix at zero wavevector (the Γ point). Here, the point group of the wavevector is equivalent to the point group $4mm$ of the lattice. According to equation (2.1.3.19a), we can immediately write down the transformation matrix for any of these symmetry operations. Using the notation

$$\begin{aligned} \mathbf{E} &= \begin{pmatrix} 1 & 0 & 0 \\ 0 & 1 & 0 \\ 0 & 0 & 1 \end{pmatrix} & \mathbf{D}_{90}^z &= \begin{pmatrix} 0 & -1 & 0 \\ 1 & 0 & 0 \\ 0 & 0 & 1 \end{pmatrix} \\ \mathbf{D}_{180}^z &= \begin{pmatrix} -1 & 0 & 0 \\ 0 & -1 & 0 \\ 0 & 0 & 1 \end{pmatrix} & \mathbf{D}_{270}^z &= \begin{pmatrix} 0 & 1 & 0 \\ -1 & 0 & 0 \\ 0 & 0 & 1 \end{pmatrix} \\ \mathbf{m}_x &= \begin{pmatrix} -1 & 0 & 0 \\ 0 & 1 & 0 \\ 0 & 0 & 1 \end{pmatrix} & \mathbf{m}_y &= \begin{pmatrix} 1 & 0 & 0 \\ 0 & -1 & 0 \\ 0 & 0 & 1 \end{pmatrix} \\ \mathbf{m}_{[\bar{1}10]} &= \begin{pmatrix} 0 & 1 & 0 \\ 1 & 0 & 0 \\ 0 & 0 & 1 \end{pmatrix} & \mathbf{m}_{[110]} &= \begin{pmatrix} 0 & -1 & 0 \\ -1 & 0 & 0 \\ 0 & 0 & 1 \end{pmatrix} \end{aligned}$$

for the three-dimensional vector representation of the symmetry elements, we obtain the \mathbf{T} matrix operators

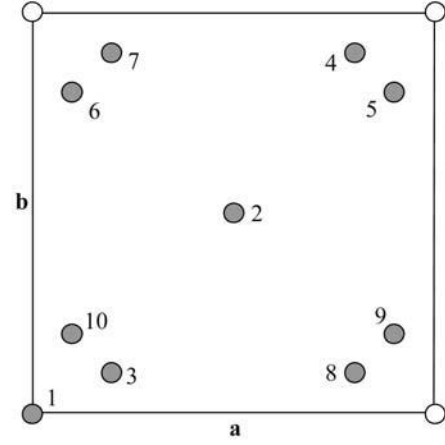


Fig. 2.1.3.4. Projection along the tetragonal z axis of the example structure given in Table 2.1.3.1.

$$\mathbf{T}(\mathbf{0}, \mathbf{E}) = \begin{pmatrix} \mathbf{E} & 0 & 0 & 0 & 0 & 0 & 0 & 0 & 0 & 0 \\ 0 & \mathbf{E} & 0 & 0 & 0 & 0 & 0 & 0 & 0 & 0 \\ 0 & 0 & \mathbf{E} & 0 & 0 & 0 & 0 & 0 & 0 & 0 \\ 0 & 0 & 0 & \mathbf{E} & 0 & 0 & 0 & 0 & 0 & 0 \\ 0 & 0 & 0 & 0 & \mathbf{E} & 0 & 0 & 0 & 0 & 0 \\ 0 & 0 & 0 & 0 & 0 & \mathbf{E} & 0 & 0 & 0 & 0 \\ 0 & 0 & 0 & 0 & 0 & 0 & \mathbf{E} & 0 & 0 & 0 \\ 0 & 0 & 0 & 0 & 0 & 0 & 0 & \mathbf{E} & 0 & 0 \\ 0 & 0 & 0 & 0 & 0 & 0 & 0 & 0 & \mathbf{E} & 0 \\ 0 & 0 & 0 & 0 & 0 & 0 & 0 & 0 & 0 & \mathbf{E} \end{pmatrix},$$

$$\mathbf{T}(\mathbf{0}, \mathbf{D}_{90}^z) = \begin{pmatrix} \mathbf{D}_{90}^z & 0 & 0 & 0 & 0 & 0 & 0 & 0 & 0 & 0 \\ 0 & \mathbf{D}_{90}^z & 0 & 0 & 0 & 0 & 0 & 0 & 0 & 0 \\ 0 & 0 & 0 & 0 & 0 & \mathbf{D}_{90}^z & 0 & 0 & 0 & 0 \\ 0 & 0 & 0 & 0 & 0 & 0 & 0 & 0 & \mathbf{D}_{90}^z & 0 \\ 0 & 0 & 0 & 0 & 0 & 0 & 0 & \mathbf{D}_{90}^z & 0 & 0 \\ 0 & 0 & 0 & \mathbf{D}_{90}^z & 0 & 0 & 0 & 0 & 0 & 0 \\ 0 & 0 & 0 & 0 & \mathbf{D}_{90}^z & 0 & 0 & 0 & 0 & 0 \\ 0 & 0 & 0 & 0 & 0 & 0 & 0 & 0 & 0 & \mathbf{D}_{90}^z \\ 0 & 0 & \mathbf{D}_{90}^z & 0 & 0 & 0 & 0 & 0 & 0 & 0 \\ 0 & 0 & 0 & 0 & 0 & 0 & \mathbf{D}_{90}^z & 0 & 0 & 0 \end{pmatrix},$$

$$\mathbf{T}(\mathbf{0}, \mathbf{D}_{180}^z) = \begin{pmatrix} \mathbf{D}_{180}^z & 0 & 0 & 0 & 0 & 0 & 0 & 0 & 0 & 0 \\ 0 & \mathbf{D}_{180}^z & 0 & 0 & 0 & 0 & 0 & 0 & 0 & 0 \\ 0 & 0 & 0 & \mathbf{D}_{180}^z & 0 & 0 & 0 & 0 & 0 & 0 \\ 0 & 0 & \mathbf{D}_{180}^z & 0 & 0 & 0 & 0 & 0 & 0 & 0 \\ 0 & 0 & 0 & 0 & 0 & 0 & 0 & 0 & 0 & \mathbf{D}_{180}^z \\ 0 & 0 & 0 & 0 & 0 & 0 & 0 & 0 & \mathbf{D}_{180}^z & 0 \\ 0 & 0 & 0 & 0 & 0 & 0 & 0 & \mathbf{D}_{180}^z & 0 & 0 \\ 0 & 0 & 0 & 0 & 0 & 0 & \mathbf{D}_{180}^z & 0 & 0 & 0 \\ 0 & 0 & 0 & 0 & 0 & \mathbf{D}_{180}^z & 0 & 0 & 0 & 0 \\ 0 & 0 & 0 & 0 & \mathbf{D}_{180}^z & 0 & 0 & 0 & 0 & 0 \end{pmatrix},$$

Table 2.1.3.2. Atom transformation table

| $P4mm$ | Symmetry operation | | | | | | | |
|----------|--------------------|-------------------|--------------------------------|-------------------|-------------------|-------------------|-------------------|--------------------------------|
| Atom No. | E | D_{90}^z | D_{180}^z | D_{270}^z | m_x | m_y | $m_{[\bar{1}10]}$ | $m_{[110]}$ |
| 1 | 1 | 1 | 1 | 1 | 1 | 1 | 1 | 1 |
| 2 | 2 | 2 - \mathbf{a} | 2 - $\mathbf{a} - \mathbf{b}$ | 2 - \mathbf{b} | 2 - \mathbf{a} | 2 - \mathbf{b} | 2 | 2 - $\mathbf{a} - \mathbf{b}$ |
| 3 | 3 | 9 - \mathbf{a} | 4 - $\mathbf{a} - \mathbf{b}$ | 6 - \mathbf{b} | 8 - \mathbf{a} | 7 - \mathbf{b} | 10 | 5 - $\mathbf{a} - \mathbf{b}$ |
| 4 | 4 | 6 - \mathbf{a} | 3 - $\mathbf{a} - \mathbf{b}$ | 9 - \mathbf{b} | 7 - \mathbf{a} | 8 - \mathbf{b} | 5 | 10 - $\mathbf{a} - \mathbf{b}$ |
| 5 | 5 | 7 - \mathbf{a} | 10 - $\mathbf{a} - \mathbf{b}$ | 8 - \mathbf{b} | 6 - \mathbf{a} | 9 - \mathbf{b} | 4 | 3 - $\mathbf{a} - \mathbf{b}$ |
| 6 | 6 | 3 - \mathbf{a} | 9 - $\mathbf{a} - \mathbf{b}$ | 4 - \mathbf{b} | 5 - \mathbf{a} | 10 - \mathbf{b} | 8 | 7 - $\mathbf{a} - \mathbf{b}$ |
| 7 | 7 | 10 - \mathbf{a} | 8 - $\mathbf{a} - \mathbf{b}$ | 5 - \mathbf{b} | 4 - \mathbf{a} | 3 - \mathbf{b} | 9 | 6 - $\mathbf{a} - \mathbf{b}$ |
| 8 | 8 | 5 - \mathbf{a} | 7 - $\mathbf{a} - \mathbf{b}$ | 10 - \mathbf{b} | 3 - \mathbf{a} | 4 - \mathbf{b} | 6 | 9 - $\mathbf{a} - \mathbf{b}$ |
| 9 | 9 | 4 - \mathbf{a} | 6 - $\mathbf{a} - \mathbf{b}$ | 3 - \mathbf{b} | 10 - \mathbf{a} | 5 - \mathbf{b} | 7 | 8 - $\mathbf{a} - \mathbf{b}$ |
| 10 | 10 | 8 - \mathbf{a} | 5 - $\mathbf{a} - \mathbf{b}$ | 7 - \mathbf{b} | 9 - \mathbf{a} | 6 - \mathbf{b} | 3 | 4 - $\mathbf{a} - \mathbf{b}$ |

2.1. PHONONS

$$\mathbf{T}(\mathbf{0}, \mathbf{D}_{270}^z) = \begin{pmatrix} \mathbf{D}_{270}^z & 0 & 0 & 0 & 0 & 0 & 0 & 0 & 0 & 0 \\ 0 & \mathbf{D}_{270}^z & 0 & 0 & 0 & 0 & 0 & 0 & 0 & 0 \\ 0 & 0 & 0 & 0 & 0 & 0 & 0 & 0 & \mathbf{D}_{270}^z & 0 \\ 0 & 0 & 0 & 0 & 0 & \mathbf{D}_{270}^z & 0 & 0 & 0 & 0 \\ 0 & 0 & 0 & 0 & 0 & 0 & \mathbf{D}_{270}^z & 0 & 0 & 0 \\ 0 & 0 & \mathbf{D}_{270}^z & 0 & 0 & 0 & 0 & 0 & 0 & 0 \\ 0 & 0 & 0 & 0 & 0 & 0 & 0 & 0 & 0 & \mathbf{D}_{270}^z \\ 0 & 0 & 0 & 0 & \mathbf{D}_{270}^z & 0 & 0 & 0 & 0 & 0 \\ 0 & 0 & 0 & \mathbf{D}_{270}^z & 0 & 0 & 0 & 0 & 0 & 0 \\ 0 & 0 & 0 & 0 & 0 & 0 & \mathbf{D}_{270}^z & 0 & 0 & 0 \end{pmatrix},$$

$$\mathbf{T}(\mathbf{0}, \mathbf{m}_x) = \begin{pmatrix} \mathbf{m}_x & 0 & 0 & 0 & 0 & 0 & 0 & 0 & 0 & 0 \\ 0 & \mathbf{m}_x & 0 & 0 & 0 & 0 & 0 & 0 & 0 & 0 \\ 0 & 0 & 0 & 0 & 0 & 0 & 0 & \mathbf{m}_x & 0 & 0 \\ 0 & 0 & 0 & 0 & 0 & 0 & \mathbf{m}_x & 0 & 0 & 0 \\ 0 & 0 & 0 & 0 & 0 & \mathbf{m}_x & 0 & 0 & 0 & 0 \\ 0 & 0 & 0 & 0 & \mathbf{m}_x & 0 & 0 & 0 & 0 & 0 \\ 0 & 0 & 0 & \mathbf{m}_x & 0 & 0 & 0 & 0 & 0 & 0 \\ 0 & 0 & \mathbf{m}_x & 0 & 0 & 0 & 0 & 0 & 0 & 0 \\ 0 & 0 & 0 & 0 & 0 & 0 & 0 & 0 & \mathbf{m}_x & 0 \\ 0 & 0 & 0 & 0 & 0 & 0 & 0 & \mathbf{m}_x & 0 & 0 \end{pmatrix},$$

$$\mathbf{T}(\mathbf{0}, \mathbf{m}_y) = \begin{pmatrix} \mathbf{m}_y & 0 & 0 & 0 & 0 & 0 & 0 & 0 & 0 & 0 \\ 0 & \mathbf{m}_y & 0 & 0 & 0 & 0 & 0 & 0 & 0 & 0 \\ 0 & 0 & 0 & 0 & 0 & 0 & \mathbf{m}_y & 0 & 0 & 0 \\ 0 & 0 & 0 & 0 & 0 & 0 & 0 & \mathbf{m}_y & 0 & 0 \\ 0 & 0 & 0 & 0 & 0 & 0 & 0 & 0 & \mathbf{m}_y & 0 \\ 0 & 0 & 0 & 0 & 0 & 0 & 0 & 0 & 0 & \mathbf{m}_y \\ 0 & 0 & \mathbf{m}_y & 0 & 0 & 0 & 0 & 0 & 0 & 0 \\ 0 & 0 & 0 & \mathbf{m}_y & 0 & 0 & 0 & 0 & 0 & 0 \\ 0 & 0 & 0 & 0 & \mathbf{m}_y & 0 & 0 & 0 & 0 & 0 \\ 0 & 0 & 0 & 0 & 0 & \mathbf{m}_y & 0 & 0 & 0 & 0 \end{pmatrix},$$

$$\mathbf{T}(\mathbf{0}, \mathbf{m}_{[\bar{1}10]}) = \begin{pmatrix} \mathbf{m}_{[\bar{1}10]} & 0 & 0 & 0 & 0 & 0 & 0 & 0 & 0 & 0 \\ 0 & \mathbf{m}_{[\bar{1}10]} & 0 & 0 & 0 & 0 & 0 & 0 & 0 & 0 \\ 0 & 0 & 0 & 0 & 0 & 0 & 0 & 0 & \mathbf{m}_{[\bar{1}10]} & 0 \\ 0 & 0 & 0 & 0 & \mathbf{m}_{[\bar{1}10]} & 0 & 0 & 0 & 0 & 0 \\ 0 & 0 & 0 & \mathbf{m}_{[\bar{1}10]} & 0 & 0 & 0 & 0 & 0 & 0 \\ 0 & 0 & 0 & 0 & 0 & 0 & \mathbf{m}_{[\bar{1}10]} & 0 & \mathbf{m}_y & 0 \\ 0 & 0 & 0 & 0 & 0 & 0 & 0 & \mathbf{m}_{[\bar{1}10]} & 0 & 0 \\ 0 & 0 & 0 & 0 & 0 & \mathbf{m}_{[\bar{1}10]} & 0 & 0 & 0 & 0 \\ 0 & 0 & 0 & 0 & 0 & 0 & \mathbf{m}_{[\bar{1}10]} & 0 & 0 & 0 \\ 0 & 0 & \mathbf{m}_{[\bar{1}10]} & 0 & 0 & 0 & 0 & 0 & 0 & 0 \end{pmatrix}$$

and

$$\mathbf{T}(\mathbf{0}, \mathbf{m}_{[110]}) = \begin{pmatrix} \mathbf{m}_{[110]} & 0 & 0 & 0 & 0 & 0 & 0 & 0 & 0 & 0 \\ 0 & \mathbf{m}_{[110]} & 0 & 0 & 0 & 0 & 0 & 0 & 0 & 0 \\ 0 & 0 & 0 & 0 & \mathbf{m}_{[110]} & 0 & 0 & 0 & 0 & 0 \\ 0 & 0 & 0 & 0 & 0 & 0 & 0 & 0 & \mathbf{m}_{[110]} & 0 \\ 0 & 0 & \mathbf{m}_{[110]} & 0 & 0 & 0 & 0 & 0 & 0 & 0 \\ 0 & 0 & 0 & 0 & 0 & \mathbf{m}_{[110]} & 0 & 0 & 0 & 0 \\ 0 & 0 & 0 & 0 & 0 & 0 & 0 & \mathbf{m}_{[110]} & 0 & 0 \\ 0 & 0 & 0 & 0 & 0 & 0 & 0 & 0 & \mathbf{m}_{[110]} & 0 \\ 0 & 0 & 0 & 0 & 0 & 0 & \mathbf{m}_{[110]} & 0 & 0 & 0 \\ 0 & 0 & 0 & \mathbf{m}_{[110]} & 0 & 0 & 0 & 0 & 0 & 0 \end{pmatrix}.$$

Since each of these matrices commutes with the dynamical matrix ($\mathbf{T}^{-1} \mathbf{D} \mathbf{T} = \mathbf{D}$, with $\mathbf{T}^{-1} = \mathbf{T}^T$), the following relations are obtained for the $\mathbf{D}_{\mathbf{K}\mathbf{K}'}(\mathbf{0})$ submatrices:

$$\mathbf{D}_{11}(\mathbf{0}) = \begin{pmatrix} D_{11}^{11} & 0 & 0 \\ 0 & D_{11}^{11} & 0 \\ 0 & 0 & D_{11}^{33} \end{pmatrix},$$

$$\mathbf{D}_{22}(\mathbf{0}) = \begin{pmatrix} D_{22}^{11} & 0 & 0 \\ 0 & D_{22}^{11} & 0 \\ 0 & 0 & D_{22}^{33} \end{pmatrix},$$

$$\mathbf{D}_{13}(\mathbf{0}) = \mathbf{D}_{270}^z \mathbf{D}_{16}(\mathbf{0}) \mathbf{D}_{90}^z = \begin{pmatrix} D_{16}^{22} & -D_{16}^{12} & -D_{16}^{23} \\ -D_{16}^{12} & D_{16}^{11} & D_{16}^{13} \\ -D_{16}^{23} & D_{16}^{13} & D_{16}^{33} \end{pmatrix},$$

$$= \mathbf{D}_{180}^z \mathbf{D}_{14}(\mathbf{0}) \mathbf{D}_{180}^z = \begin{pmatrix} D_{14}^{11} & D_{14}^{12} & -D_{14}^{13} \\ D_{14}^{12} & D_{14}^{22} & -D_{14}^{23} \\ -D_{14}^{13} & -D_{14}^{23} & D_{14}^{33} \end{pmatrix},$$

$$= \mathbf{D}_{90}^z \mathbf{D}_{19}(\mathbf{0}) \mathbf{D}_{270}^z = \begin{pmatrix} D_{19}^{22} & -D_{19}^{12} & D_{19}^{23} \\ -D_{19}^{12} & D_{19}^{11} & -D_{19}^{13} \\ D_{19}^{23} & -D_{19}^{13} & D_{19}^{33} \end{pmatrix},$$

$$= \mathbf{m}_x \mathbf{D}_{18}(\mathbf{0}) \mathbf{m}_x = \begin{pmatrix} D_{18}^{11} & -D_{18}^{12} & -D_{18}^{13} \\ -D_{18}^{12} & D_{18}^{22} & D_{18}^{23} \\ -D_{18}^{13} & D_{18}^{23} & D_{18}^{33} \end{pmatrix},$$

$$= \mathbf{m}_y \mathbf{D}_{17}(\mathbf{0}) \mathbf{m}_y = \begin{pmatrix} D_{17}^{11} & -D_{17}^{12} & D_{17}^{13} \\ -D_{17}^{12} & D_{17}^{22} & -D_{17}^{23} \\ D_{17}^{13} & -D_{17}^{23} & D_{17}^{33} \end{pmatrix},$$

$$= \mathbf{m}_{[\bar{1}10]} \mathbf{D}_{1,10}(\mathbf{0}) \mathbf{m}_{[\bar{1}10]} = \begin{pmatrix} D_{1,10}^{22} & D_{1,10}^{12} & D_{1,10}^{23} \\ D_{1,10}^{12} & D_{1,10}^{11} & D_{1,10}^{13} \\ D_{1,10}^{23} & D_{1,10}^{13} & D_{1,10}^{33} \end{pmatrix},$$

$$= \mathbf{m}_{[110]} \mathbf{D}_{15}(\mathbf{0}) \mathbf{m}_{[110]} = \begin{pmatrix} D_{15}^{22} & D_{15}^{12} & -D_{15}^{23} \\ D_{15}^{12} & D_{15}^{11} & -D_{15}^{13} \\ -D_{15}^{23} & -D_{15}^{13} & D_{15}^{33} \end{pmatrix},$$

and so on for the other submatrices.

For nonzero wavevectors \mathbf{q} along \mathbf{a}^* ($\mathbf{q} = h\mathbf{a}^*$), the point group $G_o(\mathbf{q})$ contains the identity and the mirror plane m_y only. The respective \mathbf{T} matrix operators are the same as for the Γ point:

$$\mathbf{T}(\mathbf{q}, \mathbf{m}_y) = \mathbf{T}(\mathbf{0}, \mathbf{m}_y).$$

There are, however, symmetry elements that invert the wavevector, namely D_{180}^z and m_x . Hence the enlarged group $G_o(\mathbf{q}, -\mathbf{q})$ consists of the elements E , m_y , m_x and D_{180}^z . Inspection of the atom transformation table yields the remaining matrix operators:

$$\mathbf{T}(h\mathbf{a}^*, \mathbf{D}_{180}^z) = \exp(-2\pi i h) \begin{pmatrix} \mathbf{D}_{180}^z \exp(2\pi i h) & 0 & 0 & 0 & 0 & 0 & 0 & 0 & 0 & 0 \\ 0 & \mathbf{D}_{180}^z & 0 & 0 & 0 & 0 & 0 & 0 & 0 & 0 \\ 0 & 0 & 0 & \mathbf{D}_{180}^z & 0 & 0 & 0 & 0 & 0 & 0 \\ 0 & 0 & 0 & 0 & 0 & 0 & 0 & 0 & 0 & 0 \\ 0 & 0 & 0 & 0 & 0 & 0 & 0 & 0 & \mathbf{D}_{180}^z & 0 \\ 0 & 0 & 0 & 0 & 0 & 0 & 0 & 0 & 0 & \mathbf{D}_{180}^z \\ 0 & 0 & 0 & 0 & 0 & 0 & 0 & \mathbf{D}_{180}^z & 0 & 0 \\ 0 & 0 & 0 & 0 & 0 & 0 & \mathbf{D}_{180}^z & 0 & 0 & 0 \\ 0 & 0 & 0 & 0 & 0 & \mathbf{D}_{180}^z & 0 & 0 & 0 & 0 \\ 0 & 0 & 0 & 0 & \mathbf{D}_{180}^z & 0 & 0 & 0 & 0 & 0 \end{pmatrix} \mathbf{K}_o$$

and

2. SYMMETRY ASPECTS OF EXCITATIONS

$$\mathbf{T}(h\mathbf{a}^*, \mathbf{m}_x) = \exp(-2\pi i h) \begin{pmatrix} \mathbf{m}_x \exp(2\pi i h) & 0 & 0 & 0 & 0 & 0 & 0 & 0 & 0 & 0 \\ 0 & \mathbf{m}_x & 0 & 0 & 0 & 0 & 0 & 0 & 0 & 0 \\ 0 & 0 & 0 & 0 & 0 & 0 & 0 & \mathbf{m}_x & 0 & 0 \\ 0 & 0 & 0 & 0 & 0 & 0 & \mathbf{m}_x & 0 & 0 & 0 \\ 0 & 0 & 0 & 0 & 0 & \mathbf{m}_x & 0 & 0 & 0 & 0 \\ 0 & 0 & 0 & 0 & \mathbf{m}_x & 0 & 0 & 0 & 0 & 0 \\ 0 & 0 & 0 & \mathbf{m}_x & 0 & 0 & 0 & 0 & 0 & 0 \\ 0 & 0 & \mathbf{m}_x & 0 & 0 & 0 & 0 & 0 & 0 & 0 \\ 0 & 0 & 0 & 0 & 0 & 0 & 0 & 0 & 0 & \mathbf{m}_x \\ 0 & 0 & 0 & 0 & 0 & 0 & 0 & 0 & \mathbf{m}_x & 0 \end{pmatrix} \mathbf{K}_o.$$

Being anti-unitary, the corresponding inverse operators are⁷

$$\begin{aligned}\mathbf{T}^{-1}(h\mathbf{a}^*, \mathbf{D}_{180}^z) &= \mathbf{K}_o \mathbf{T}^+(h\mathbf{a}^*, \mathbf{D}_{180}^z), \\ \mathbf{T}^{-1}(h\mathbf{a}^*, \mathbf{m}_x) &= \mathbf{K}_o \mathbf{T}^+(h\mathbf{a}^*, \mathbf{m}_x).\end{aligned}$$

$$\text{for } \mathbf{R} = \mathbf{D}_{180}^c : \quad \left(\begin{array}{cccccccccccc} \mathbf{D}_{11} & \mathbf{D}_{12} & \mathbf{D}_{13} & \mathbf{D}_{14} & \mathbf{D}_{15} & \mathbf{D}_{16} & \mathbf{D}_{17} & \mathbf{D}_{18} & \mathbf{D}_{19} & \mathbf{D}_{1,10} \\ & \mathbf{D}_{22} & \mathbf{D}_{23} & \mathbf{D}_{24} & \mathbf{D}_{25} & \mathbf{D}_{26} & \mathbf{D}_{27} & \mathbf{D}_{28} & \mathbf{D}_{29} & \mathbf{D}_{2,10} \\ & & \mathbf{D}_{33} & \mathbf{D}_{34} & \mathbf{D}_{35} & \mathbf{D}_{36} & \mathbf{D}_{37} & \mathbf{D}_{38} & \mathbf{D}_{39} & \mathbf{D}_{3,10} \\ & & & \mathbf{D}_{44} & \mathbf{D}_{45} & \mathbf{D}_{46} & \mathbf{D}_{47} & \mathbf{D}_{48} & \mathbf{D}_{49} & \mathbf{D}_{4,10} \\ & & & & \mathbf{D}_{55} & \mathbf{D}_{56} & \mathbf{D}_{57} & \mathbf{D}_{58} & \mathbf{D}_{59} & \mathbf{D}_{5,10} \\ & & & & & \mathbf{D}_{66} & \mathbf{D}_{67} & \mathbf{D}_{68} & \mathbf{D}_{69} & \mathbf{D}_{6,10} \\ & & & & & & \mathbf{D}_{77} & \mathbf{D}_{78} & \mathbf{D}_{79} & \mathbf{D}_{7,10} \\ & & & & & & & \mathbf{D}_{88} & \mathbf{D}_{89} & \mathbf{D}_{8,10} \\ & & & & & & & & \mathbf{D}_{99} & \mathbf{D}_{9,10} \\ & & & & & & & & & \mathbf{D}_{10,10} \end{array} \right)$$

$$= \left(\begin{array}{cccccccccccc} \tilde{\mathbf{D}}_{11}^* & \tilde{\mathbf{D}}_{12}^* & \tilde{\mathbf{D}}_{14}^* & \tilde{\mathbf{D}}_{13}^* & \tilde{\mathbf{D}}_{1,10}^* & \tilde{\mathbf{D}}_{19}^* & \tilde{\mathbf{D}}_{18}^* & \tilde{\mathbf{D}}_{17}^* & \tilde{\mathbf{D}}_{16}^* & \tilde{\mathbf{D}}_{15}^* \\ & \tilde{\mathbf{D}}_{22}^* & \tilde{\mathbf{D}}_{24}^* & \tilde{\mathbf{D}}_{23}^* & \tilde{\mathbf{D}}_{2,10}^* & \tilde{\mathbf{D}}_{29}^* & \tilde{\mathbf{D}}_{28}^* & \tilde{\mathbf{D}}_{27}^* & \tilde{\mathbf{D}}_{26}^* & \tilde{\mathbf{D}}_{25}^* \\ & & \tilde{\mathbf{D}}_{44}^* & \tilde{\mathbf{D}}_{43}^* & \tilde{\mathbf{D}}_{4,10}^* & \tilde{\mathbf{D}}_{49}^* & \tilde{\mathbf{D}}_{48}^* & \tilde{\mathbf{D}}_{47}^* & \tilde{\mathbf{D}}_{46}^* & \tilde{\mathbf{D}}_{45}^* \\ & & & \tilde{\mathbf{D}}_{33}^* & \tilde{\mathbf{D}}_{3,10}^* & \tilde{\mathbf{D}}_{39}^* & \tilde{\mathbf{D}}_{38}^* & \tilde{\mathbf{D}}_{37}^* & \tilde{\mathbf{D}}_{36}^* & \tilde{\mathbf{D}}_{35}^* \\ & & & & \tilde{\mathbf{D}}_{10,10}^* & \tilde{\mathbf{D}}_{10,9}^* & \tilde{\mathbf{D}}_{10,8}^* & \tilde{\mathbf{D}}_{10,7}^* & \tilde{\mathbf{D}}_{10,6}^* & \tilde{\mathbf{D}}_{10,5}^* \\ & & & & & \tilde{\mathbf{D}}_{99}^* & \tilde{\mathbf{D}}_{98}^* & \tilde{\mathbf{D}}_{97}^* & \tilde{\mathbf{D}}_{96}^* & \tilde{\mathbf{D}}_{95}^* \\ & & & & & & \tilde{\mathbf{D}}_{88}^* & \tilde{\mathbf{D}}_{87}^* & \tilde{\mathbf{D}}_{86}^* & \tilde{\mathbf{D}}_{85}^* \\ & & & & & & & \tilde{\mathbf{D}}_{77}^* & \tilde{\mathbf{D}}_{76}^* & \tilde{\mathbf{D}}_{75}^* \\ & & & & & & & & \tilde{\mathbf{D}}_{66}^* & \tilde{\mathbf{D}}_{65}^* \\ & & & & & & & & & \tilde{\mathbf{D}}_{55}^* \end{array} \right)$$

$$\text{with } \tilde{\mathbf{D}}_{kl} = \mathbf{D}_{180}^c \mathbf{D}_{kl} \mathbf{D}_{180}^c = \begin{pmatrix} D_{kl}^{11} & D_{kl}^{12} & -D_{kl}^{13} \\ D_{kl}^{21} & D_{kl}^{22} & -D_{kl}^{23} \\ -D_{kl}^{31} & -D_{kl}^{32} & D_{kl}^{33} \end{pmatrix}$$

and

The invariance of the dynamical matrix with respect to the similarity transformation ($\mathbf{T}^{-1} \mathbf{D} \mathbf{T} = \mathbf{D}$) using any of these operators leads to the following relations for wavevectors along \mathbf{a}^* .⁸

$$\text{For } \mathbf{R} = \mathbf{m}_y : \quad \begin{pmatrix} \mathbf{D}_{11} & \mathbf{D}_{12} & \mathbf{D}_{13} & \mathbf{D}_{14} & \mathbf{D}_{15} & \mathbf{D}_{16} & \mathbf{D}_{17} & \mathbf{D}_{18} & \mathbf{D}_{19} & \mathbf{D}_{1,10} \\ & \mathbf{D}_{22} & \mathbf{D}_{23} & \mathbf{D}_{24} & \mathbf{D}_{25} & \mathbf{D}_{26} & \mathbf{D}_{27} & \mathbf{D}_{28} & \mathbf{D}_{29} & \mathbf{D}_{2,10} \\ & & \mathbf{D}_{33} & \mathbf{D}_{34} & \mathbf{D}_{35} & \mathbf{D}_{36} & \mathbf{D}_{37} & \mathbf{D}_{38} & \mathbf{D}_{39} & \mathbf{D}_{3,10} \\ & & & \mathbf{D}_{44} & \mathbf{D}_{45} & \mathbf{D}_{46} & \mathbf{D}_{47} & \mathbf{D}_{48} & \mathbf{D}_{49} & \mathbf{D}_{4,10} \\ & & & & \mathbf{D}_{55} & \mathbf{D}_{56} & \mathbf{D}_{57} & \mathbf{D}_{58} & \mathbf{D}_{59} & \mathbf{D}_{5,10} \\ & & & & & \mathbf{D}_{66} & \mathbf{D}_{67} & \mathbf{D}_{68} & \mathbf{D}_{69} & \mathbf{D}_{6,10} \\ & & & & & & \mathbf{D}_{77} & \mathbf{D}_{78} & \mathbf{D}_{79} & \mathbf{D}_{7,10} \\ & & & & & & & \mathbf{D}_{88} & \mathbf{D}_{89} & \mathbf{D}_{8,10} \\ & & & & & & & & \mathbf{D}_{99} & \mathbf{D}_{9,10} \\ & & & & & & & & & \mathbf{D}_{10,10} \end{pmatrix}$$

$$= \begin{pmatrix} \tilde{\mathbf{D}}_{11} & \tilde{\mathbf{D}}_{12} & \tilde{\mathbf{D}}_{17} & \tilde{\mathbf{D}}_{18} & \tilde{\mathbf{D}}_{19} & \tilde{\mathbf{D}}_{1,10} & \tilde{\mathbf{D}}_{13} & \tilde{\mathbf{D}}_{14} & \tilde{\mathbf{D}}_{15} & \tilde{\mathbf{D}}_{16} \\ & \tilde{\mathbf{D}}_{22} & \tilde{\mathbf{D}}_{27} & \tilde{\mathbf{D}}_{28} & \tilde{\mathbf{D}}_{29} & \tilde{\mathbf{D}}_{2,10} & \tilde{\mathbf{D}}_{23} & \tilde{\mathbf{D}}_{24} & \tilde{\mathbf{D}}_{25} & \tilde{\mathbf{D}}_{26} \\ & & \tilde{\mathbf{D}}_{77} & \tilde{\mathbf{D}}_{78} & \tilde{\mathbf{D}}_{79} & \tilde{\mathbf{D}}_{7,10} & \tilde{\mathbf{D}}_{73} & \tilde{\mathbf{D}}_{74} & \tilde{\mathbf{D}}_{75} & \tilde{\mathbf{D}}_{76} \\ & & & \tilde{\mathbf{D}}_{88} & \tilde{\mathbf{D}}_{89} & \tilde{\mathbf{D}}_{8,10} & \tilde{\mathbf{D}}_{83} & \tilde{\mathbf{D}}_{84} & \tilde{\mathbf{D}}_{85} & \tilde{\mathbf{D}}_{86} \\ & & & & \tilde{\mathbf{D}}_{99} & \tilde{\mathbf{D}}_{9,10} & \tilde{\mathbf{D}}_{93} & \tilde{\mathbf{D}}_{94} & \tilde{\mathbf{D}}_{95} & \tilde{\mathbf{D}}_{96} \\ & & & & & \tilde{\mathbf{D}}_{10,10} & \tilde{\mathbf{D}}_{10,3} & \tilde{\mathbf{D}}_{10,4} & \tilde{\mathbf{D}}_{10,5} & \tilde{\mathbf{D}}_{10,6} \\ & & & & & & \tilde{\mathbf{D}}_{33} & \tilde{\mathbf{D}}_{34} & \tilde{\mathbf{D}}_{35} & \tilde{\mathbf{D}}_{36} \\ & & & & & & & \tilde{\mathbf{D}}_{44} & \tilde{\mathbf{D}}_{45} & \tilde{\mathbf{D}}_{46} \\ & & & & & & & & \tilde{\mathbf{D}}_{55} & \tilde{\mathbf{D}}_{56} \\ & & & & & & & & & \tilde{\mathbf{D}}_{66} \end{pmatrix},$$

with $\tilde{\mathbf{D}}_{kl} = \mathbf{m}_y \mathbf{D}_{kl} \mathbf{m}_y = \begin{pmatrix} D_{kl}^{11} & -D_{kl}^{12} & D_{kl}^{13} \\ -D_{kl}^{21} & D_{kl}^{22} & -D_{kl}^{23} \\ D_{kl}^{31} & -D_{kl}^{32} & D_{kl}^{33} \end{pmatrix}$

$$\begin{aligned} & \text{for } \mathbf{R} = \mathbf{m}_x : \\ & \left(\begin{array}{cccccccccccc} \mathbf{D}_{11} & \mathbf{D}_{12} & \mathbf{D}_{13} & \mathbf{D}_{14} & \mathbf{D}_{15} & \mathbf{D}_{16} & \mathbf{D}_{17} & \mathbf{D}_{18} & \mathbf{D}_{19} & \mathbf{D}_{1,10} \\ & \mathbf{D}_{22} & \mathbf{D}_{23} & \mathbf{D}_{24} & \mathbf{D}_{25} & \mathbf{D}_{26} & \mathbf{D}_{27} & \mathbf{D}_{28} & \mathbf{D}_{29} & \mathbf{D}_{2,10} \\ & & \mathbf{D}_{33} & \mathbf{D}_{34} & \mathbf{D}_{35} & \mathbf{D}_{36} & \mathbf{D}_{37} & \mathbf{D}_{38} & \mathbf{D}_{39} & \mathbf{D}_{3,10} \\ & & & \mathbf{D}_{44} & \mathbf{D}_{45} & \mathbf{D}_{46} & \mathbf{D}_{47} & \mathbf{D}_{48} & \mathbf{D}_{49} & \mathbf{D}_{4,10} \\ & & & & \mathbf{D}_{55} & \mathbf{D}_{56} & \mathbf{D}_{57} & \mathbf{D}_{58} & \mathbf{D}_{59} & \mathbf{D}_{5,10} \\ & & & & & \mathbf{D}_{66} & \mathbf{D}_{67} & \mathbf{D}_{68} & \mathbf{D}_{69} & \mathbf{D}_{6,10} \\ & & & & & & \mathbf{D}_{77} & \mathbf{D}_{78} & \mathbf{D}_{79} & \mathbf{D}_{7,10} \\ & & & & & & & \mathbf{D}_{88} & \mathbf{D}_{89} & \mathbf{D}_{8,10} \\ & & & & & & & & \mathbf{D}_{99} & \mathbf{D}_{9,10} \\ & & & & & & & & & \mathbf{D}_{10,10} \end{array} \right) \\ & = \left(\begin{array}{cccccccccccc} \tilde{\mathbf{D}}_{11}^* & \tilde{\mathbf{D}}_{12}^* & \tilde{\mathbf{D}}_{18}^* & \tilde{\mathbf{D}}_{17}^* & \tilde{\mathbf{D}}_{16}^* & \tilde{\mathbf{D}}_{15}^* & \tilde{\mathbf{D}}_{14}^* & \tilde{\mathbf{D}}_{13}^* & \tilde{\mathbf{D}}_{1,10}^* & \tilde{\mathbf{D}}_{19}^* \\ & \tilde{\mathbf{D}}_{22}^* & \tilde{\mathbf{D}}_{28}^* & \tilde{\mathbf{D}}_{27}^* & \tilde{\mathbf{D}}_{26}^* & \tilde{\mathbf{D}}_{25}^* & \tilde{\mathbf{D}}_{24}^* & \tilde{\mathbf{D}}_{23}^* & \tilde{\mathbf{D}}_{2,10}^* & \tilde{\mathbf{D}}_{29}^* \\ & & \tilde{\mathbf{D}}_{88}^* & \tilde{\mathbf{D}}_{87}^* & \tilde{\mathbf{D}}_{86}^* & \tilde{\mathbf{D}}_{85}^* & \tilde{\mathbf{D}}_{84}^* & \tilde{\mathbf{D}}_{83}^* & \tilde{\mathbf{D}}_{8,10}^* & \tilde{\mathbf{D}}_{89}^* \\ & & & \tilde{\mathbf{D}}_{77}^* & \tilde{\mathbf{D}}_{76}^* & \tilde{\mathbf{D}}_{75}^* & \tilde{\mathbf{D}}_{74}^* & \tilde{\mathbf{D}}_{73}^* & \tilde{\mathbf{D}}_{7,10}^* & \tilde{\mathbf{D}}_{79}^* \\ & & & & \tilde{\mathbf{D}}_{66}^* & \tilde{\mathbf{D}}_{65}^* & \tilde{\mathbf{D}}_{64}^* & \tilde{\mathbf{D}}_{63}^* & \tilde{\mathbf{D}}_{6,10}^* & \tilde{\mathbf{D}}_{69}^* \\ & & & & & \tilde{\mathbf{D}}_{55}^* & \tilde{\mathbf{D}}_{54}^* & \tilde{\mathbf{D}}_{53}^* & \tilde{\mathbf{D}}_{5,10}^* & \tilde{\mathbf{D}}_{59}^* \\ & & & & & & \tilde{\mathbf{D}}_{44}^* & \tilde{\mathbf{D}}_{43}^* & \tilde{\mathbf{D}}_{4,10}^* & \tilde{\mathbf{D}}_{49}^* \\ & & & & & & & \tilde{\mathbf{D}}_{33}^* & \tilde{\mathbf{D}}_{3,10}^* & \tilde{\mathbf{D}}_{39}^* \\ & & & & & & & & \tilde{\mathbf{D}}_{10,10}^* & \tilde{\mathbf{D}}_{10,9}^* \\ & & & & & & & & & \tilde{\mathbf{D}}_{99}^* \end{array} \right) \end{aligned}$$

For the submatrix \mathbf{D}_{11} (and similarly also for \mathbf{D}_{12} and \mathbf{D}_{22}) we can combine the three relations and obtain

$$\begin{aligned} \mathbf{D}_{11} &= \mathbf{m}_x \mathbf{D}_{11}^* \mathbf{m}_x = \begin{pmatrix} D_{11}^{1*} & -D_{11}^{12*} & -D_{11}^{13*} \\ -D_{11}^{12} & D_{11}^{22*} & D_{11}^{23*} \\ -D_{11}^{13} & D_{11}^{23} & D_{11}^{33*} \end{pmatrix} \\ &= \mathbf{m}_y \mathbf{D}_{11} \mathbf{m}_y = \begin{pmatrix} D_{11}^{11} & -D_{11}^{12} & D_{11}^{13} \\ -D_{11}^{12*} & D_{11}^{22} & -D_{11}^{23} \\ D_{11}^{13*} & -D_{11}^{23*} & D_{11}^{33} \end{pmatrix} \\ &= \mathbf{D}_{180}^z \mathbf{D}_{11}^* \mathbf{D}_{180}^z = \begin{pmatrix} D_{11}^{1*} & D_{11}^{12*} & -D_{11}^{13*} \\ D_{11}^{12} & D_{11}^{22*} & -D_{11}^{23*} \\ -D_{11}^{13} & -D_{11}^{23} & D_{11}^{33*} \end{pmatrix}. \end{aligned}$$

⁷ \mathbf{T}^+ denotes the Hermitian conjugate matrix.

⁸ Note that the lower half of the Hermitian matrix in each case is omitted for clarity.

2.1. PHONONS

Hence

$$\begin{aligned} D_{11}^{11} &= D_{11}^{11*} = \alpha \quad \text{real} \\ D_{11}^{12} &= -D_{11}^{12} = 0 \\ D_{11}^{13} &= -D_{11}^{13*} = i\beta \quad \text{imaginary} \\ D_{11}^{22} &= D_{11}^{22*} = \gamma \quad \text{real} \\ D_{11}^{23} &= -D_{11}^{23} = 0 \\ D_{11}^{33} &= D_{11}^{33*} = \delta \quad \text{real} \end{aligned} \Rightarrow \mathbf{D}_{11} = \begin{pmatrix} \alpha & 0 & i\beta \\ 0 & \gamma & 0 \\ -i\beta & 0 & \delta \end{pmatrix}.$$

Obviously, the symmetry considerations lead to a remarkable reduction of the independent elements of the dynamical matrix.

2.1.3.2. Symmetry of dispersion planes

According to equation (2.1.3.3), the phonon dispersion is periodic within the reciprocal space:

$$\omega(\mathbf{q}+\mathbf{g})_j = \omega_{\mathbf{q},j}. \quad (2.1.3.34)$$

Moreover, for each symmetry operation of the space group of the crystal, the eigenvalue equation may be written in the form

$$\mathbf{D}(\mathbf{S}\mathbf{q}) \mathbf{e}(\mathbf{S}\mathbf{q}, j) = \omega_{(\mathbf{S}\mathbf{q}),j}^2 \mathbf{e}(\mathbf{S}\mathbf{q}, j) \quad (2.1.3.35)$$

and due to the transformation property of the dynamical matrix, equation (2.1.3.14),

$$\begin{aligned} \mathbf{D}(\mathbf{q}) \Gamma^+(\mathbf{q}, \{\mathbf{S}|\mathbf{v}(\mathbf{S}) + \mathbf{x}(m)\}) \mathbf{e}(\mathbf{S}\mathbf{q}, j) \\ = \omega_{(\mathbf{S}\mathbf{q}),j}^2 \Gamma^+(\mathbf{q}, \{\mathbf{S}|\mathbf{v}(\mathbf{S}) + \mathbf{x}(m)\}) \mathbf{e}(\mathbf{S}\mathbf{q}, j). \end{aligned} \quad (2.1.3.36)$$

Hence $\omega_{(\mathbf{S}\mathbf{q}),j}^2$ is an eigenvalue of the dynamical matrix $\mathbf{D}(\mathbf{q})$ at the wavevector \mathbf{q} as is $\omega_{\mathbf{q},j}^2$ itself. If the eigenvalues are not degenerate, i.e. if there is not more than one linear independent eigenvector for each eigenvalue, then

$$\omega_{(\mathbf{S}\mathbf{q}),j}^2 = \omega_{\mathbf{q},j}^2. \quad (2.1.3.37)$$

If, on the other hand, there are degenerate phonon modes ($\omega_{\mathbf{q},j} = \omega_{\mathbf{q},j'}, j \neq j'$), the most we can strictly infer from equation (2.1.3.36) is

$$\omega_{(\mathbf{S}\mathbf{q}),j}^2 = \omega_{\mathbf{q},j'}^2. \quad (2.1.3.37a)$$

Without any loss of generality, however, it is possible to label the modes at $\mathbf{S}\mathbf{q}$ in terms of those modes at wavevector \mathbf{q} in such a way that equation (2.1.3.37) remains valid. Hence, we conclude that the phonon dispersion $\omega(\mathbf{q})^9$ in the three-dimensional reciprocal space exhibits the full symmetry of the point group of the crystal, as illustrated in Fig. 2.1.3.5.

Moreover, $\omega_{\mathbf{q},j}$ is an even function of \mathbf{q} (Fig. 2.1.3.6). This is always true even if the space group does not contain the inversion, since the dynamical matrix is Hermitian. From the eigenvector equation (2.1.2.20) we have

$$\mathbf{D}(-\mathbf{q}) \mathbf{e}(-\mathbf{q}, j) = \mathbf{D}^*(\mathbf{q}) \mathbf{e}(-\mathbf{q}, j) = \omega_{-\mathbf{q},j}^2 \mathbf{e}(-\mathbf{q}, j). \quad (2.1.3.38)$$

Taking the complex conjugate and remembering that the eigenvalues of a Hermitian matrix are real quantities,

$$\mathbf{D}(\mathbf{q}) \mathbf{e}^*(-\mathbf{q}, j) = \omega_{-\mathbf{q},j}^2 \mathbf{e}^*(-\mathbf{q}, j). \quad (2.1.3.38a)$$

Obviously, $\omega_{-\mathbf{q},j}^2$ is an eigenvalue of $\mathbf{D}(\mathbf{q})$ just as $\omega_{\mathbf{q},j}^2$ is. Hence, with the same arguments as above we conclude that

$$\omega_{-\mathbf{q},j} = \omega_{\mathbf{q},j}. \quad (2.1.3.39)$$

⁹ Note that we always choose the positive root $\omega(\mathbf{q}) = +\sqrt{\omega^2(\mathbf{q})}$ for the phonon frequency.

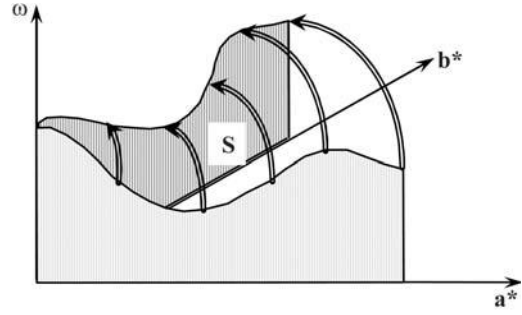


Fig. 2.1.3.5. Symmetry of the dispersion surface.

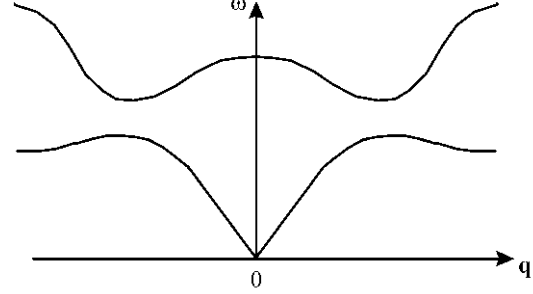


Fig. 2.1.3.6. The dispersion relation is an even function of \mathbf{q} .

2.1.3.3. Symmetry properties of eigenvectors

In the previous section we used the symmetry properties of the dynamical matrix to derive equation (2.1.3.36). Since the phonon dispersion $\omega(\mathbf{q}, j)$ is invariant with respect to all symmetry operations $\{\mathbf{S}|\mathbf{v}(\mathbf{S}) + \mathbf{x}(m)\}$ of the space group [equation (2.1.3.37)], we conclude that not only is $\mathbf{e}(\mathbf{q}, j)$ an eigenvector of the dynamical matrix $\mathbf{D}(\mathbf{q})$ but so is the vector $\Gamma^+(\mathbf{q}, \{\mathbf{S}|\mathbf{v}(\mathbf{S}) + \mathbf{x}(m)\}) \mathbf{e}(\mathbf{S}\mathbf{q}, j)$. If the corresponding eigenvalue $\omega_{\mathbf{q},j}^2$ is not degenerate, the (normalized) eigenvectors are uniquely determined except for a phase factor of unit modulus. Hence, the following relation holds:

$$\begin{aligned} \mathbf{e}(\mathbf{S}\mathbf{q}, j) &= \exp(i\varphi) \Gamma(\mathbf{q}, \{\mathbf{S}|\mathbf{v}(\mathbf{S}) + \mathbf{x}(m)\}) \mathbf{e}(\mathbf{q}, j) \\ &= \exp(i\varphi) \Gamma(\mathbf{S}\mathbf{q}, \{\mathbf{E}|\mathbf{x}(m)\}) \Gamma(\mathbf{q}, \{\mathbf{S}|\mathbf{v}(\mathbf{S})\}) \mathbf{e}(\mathbf{q}, j) \\ &= \exp(i\varphi) \exp[-i(\mathbf{S}\mathbf{q})\mathbf{x}(m)] \Gamma(\mathbf{q}, \{\mathbf{S}|\mathbf{v}(\mathbf{S})\}) \mathbf{e}(\mathbf{q}, j). \end{aligned} \quad (2.1.3.40)$$

The statement giving the atomic displacements as solutions of the equations of motion (cf. Section 2.1.2) was based on Bloch waves, the polarization vector being invariant with respect to lattice translations. It is therefore convenient to choose the arbitrary phase factor in the transformation law for eigenvectors in such a way as to leave the right-hand side of equation (2.1.3.40) independent of $\mathbf{x}(m)$. Setting the phase angle φ equal to $(\mathbf{S}\mathbf{q})\mathbf{x}(m)$, we obtain the simple form of the transformation law

$$\mathbf{e}(\mathbf{S}\mathbf{q}, j) = \Gamma(\mathbf{q}, \{\mathbf{S}|\mathbf{v}(\mathbf{S})\}) \mathbf{e}(\mathbf{q}, j). \quad (2.1.3.41)$$

This choice is, however, not always possible. If there is a symmetry operation \mathbf{S}_- that inverts the wavevector, then in addition to equation (2.1.3.40) there is another relation between $\mathbf{e}(-\mathbf{q}, j)$ and $\mathbf{e}(\mathbf{q}, j)$ due to the Hermitian nature of the dynamical matrix. Hence in this case the transformation law may differ from equation (2.1.3.41), as discussed in Section 2.1.3.5.2.

If the dynamical matrix exhibits degenerate eigenvalues for the wavevector \mathbf{q} , the most that can be said is that the symmetry operation $\{\mathbf{S}|\mathbf{v}(\mathbf{S}) + \mathbf{x}(m)\}$ sends an eigenvector $\mathbf{e}(\mathbf{q}, j)$ into some linear combination of all those eigenvectors that correspond to the same eigenvalue. Without any loss of generality we may,

2. SYMMETRY ASPECTS OF EXCITATIONS

however, demand that equation (2.1.3.41) remains valid even in this case, since if we would have determined eigenvectors $\mathbf{e}(\mathbf{q}, j)$ at \mathbf{q} then among the variety of possible and equivalent orthonormal sets of eigenvectors at $\mathbf{S}\mathbf{q}$ we simply choose that particular one which is given by (2.1.3.41). There is, however, one exception, which applies to wavevectors on the Brillouin-zone boundary and symmetry operations with $\mathbf{S}\mathbf{q} = \mathbf{q} + \mathbf{g}$ (where \mathbf{g} is a reciprocal-lattice vector): owing to the periodicity $\mathbf{e}(\mathbf{q} + \mathbf{g}, j) = \mathbf{e}(\mathbf{q}, j)$, equation (2.1.3.3), the eigenvectors $\mathbf{e}(\mathbf{S}\mathbf{q}, j)$ and $\mathbf{e}(\mathbf{q}, j)$ have to be identical in this case.

If we consider those symmetry operations that leave the wavevector invariant (except for an additional reciprocal-lattice vector), we are able to obtain special conditions for the eigenvectors themselves. In Section 2.1.3.1 we found that the dynamical matrix commutes with the \mathbf{T} matrix operators defined by equation (2.1.3.19a). Hence, if \mathbf{R} is an arbitrary element of the point group $G_o(\mathbf{q})$, the vector $\mathbf{T}(\mathbf{q}, \mathbf{R})\mathbf{e}(\mathbf{q}, j)$ is an eigenvector with respect to the eigenvalue $\omega_{\mathbf{q},j}^2$ as well as $\mathbf{e}(\mathbf{q}, j)$:

$$\mathbf{D}(\mathbf{q}) \{\mathbf{T}(\mathbf{q}, \mathbf{R})\mathbf{e}(\mathbf{q}, j)\} = \omega_{\mathbf{q},j}^2 \{\mathbf{T}(\mathbf{q}, \mathbf{R})\mathbf{e}(\mathbf{q}, j)\}. \quad (2.1.3.42)$$

Since eigenvalues may be degenerate, we now replace the index j that labels the $3N$ different phonon branches by the double index $\sigma\lambda$: σ labels all different eigenvalues whereas λ distinguishes those phonons that are degenerate by symmetry,¹⁰ i.e. that have the same frequency but different eigenvectors,

$$j \rightarrow \sigma, \lambda.$$

λ runs from 1 to f_σ if f_σ is the degeneracy of the eigenfrequency $\omega_{\mathbf{q},\sigma}$. With this notation, equation (2.1.3.42) can be rewritten as

$$\mathbf{D}(\mathbf{q}) \{\mathbf{T}(\mathbf{q}, \mathbf{R})\mathbf{e}(\mathbf{q}, \sigma\lambda)\} = \omega_{\mathbf{q},\sigma}^2 \{\mathbf{T}(\mathbf{q}, \mathbf{R})\mathbf{e}(\mathbf{q}, \sigma\lambda)\}. \quad (2.1.3.42a)$$

Consequently, the vector $\mathbf{T}(\mathbf{q}, \mathbf{R})\mathbf{e}(\mathbf{q}, \sigma\lambda)$ has to be some linear combination of all eigenvectors $\mathbf{e}(\mathbf{q}, \sigma\lambda')$, $\lambda' = 1, \dots, f_\sigma$, corresponding to the same eigenvalue $\omega_{\mathbf{q},\sigma}^2$,

$$\mathbf{T}(\mathbf{q}, \mathbf{R})\mathbf{e}(\mathbf{q}, \sigma\lambda) = \sum_{\lambda'=1}^{f_\sigma} \tau_{\lambda\lambda'}^{(\sigma)}(\mathbf{q}, \mathbf{R})\mathbf{e}(\mathbf{q}, \sigma\lambda'). \quad (2.1.3.43)$$

Obviously, the eigenvectors $\mathbf{e}(\mathbf{q}, \sigma\lambda)$ ($\lambda = 1, \dots, f_\sigma$) span a vector space that is invariant with respect to all symmetry operations of the point group of the wavevector. Moreover, this vector space does not contain any proper invariant subspaces and is therefore *irreducible*. Under the symmetry operations of the group $G_o(\mathbf{q})$, the f_σ eigenvectors transform into each other. The corresponding coefficients $\tau_{\lambda\lambda'}^{(\sigma)}(\mathbf{q}, \mathbf{R})$ can be regarded as the elements of a complex ($f_\sigma \times f_\sigma$) matrix $\boldsymbol{\tau}^{(\sigma)}(\mathbf{q}, \mathbf{R})$ that induces a unitary irreducible multiplier representation (IMR) of the point group of the wavevector. The complex multiplier is exactly the same as for the $3N$ -dimensional reducible representation provided by the \mathbf{T} matrix operators [cf. equation (2.1.3.21)].

For a given point group $G_o(\mathbf{q})$ there is only a limited number of irreducible representations. These can be calculated by group-theoretical methods and are tabulated, for example, in the monographs of Kovalev (1965) or Bradley & Cracknell (1972). The multipliers are specific for the individual space groups $G(\mathbf{q})$ and depend merely on the fractional translations $\mathbf{v}(\mathbf{R})$ associated with a symmetry element \mathbf{R} . It should be noted that for wavevectors within the Brillouin zone and for symmorphic space groups all multipliers are unity and we are left with ordinary irreducible representations. Hence, merely on the basis of group-theoretical considerations, restrictions for the phonon eigenvectors can be obtained.

A particular phonon can now be characterized by the symmetry of the corresponding eigenvector, i.e. the irreducible

multiplier representation (IMR) that describes its transformation behaviour. All degenerate phonons obviously belong to the same IMR. Moreover, phonons with different frequencies may belong to the same IMR. On the other hand, there may also be IMRs to which no phonon belongs at all. For a given crystalline structure it is possible, however, to predict the number of phonons with eigenvectors transforming according to a particular irreducible multiplier representation:

Let us arrange all eigenvectors $\mathbf{e}(\mathbf{q}, \sigma\lambda)$ of the dynamical matrix as columns of a unitary matrix $\mathbf{e}(\mathbf{q})$ in such a way that eigenvectors of the same irreducible representation occupy neighbouring columns:

$$\mathbf{e}(\mathbf{q}) = (\mathbf{e}(\mathbf{q}, 11) \dots \mathbf{e}(\mathbf{q}, 1f_1) \mathbf{e}(\mathbf{q}, 21) \dots \mathbf{e}(\mathbf{q}, 2f_2) \dots). \quad (2.1.3.44)$$

This matrix can now be used for a similarity transformation of the \mathbf{T} matrix operators:

$$\mathbf{e}(\mathbf{q})^{-1} \mathbf{T}(\mathbf{q}, \mathbf{R}) \mathbf{e}(\mathbf{q}) = \Delta(\mathbf{q}, \mathbf{R}). \quad (2.1.3.45)$$

Since an eigenvector can never change its symmetry by the multiplication with the \mathbf{T} matrix operator and since all eigenvectors are pairwise orthonormal, the resulting matrix $\Delta(\mathbf{q}, \mathbf{R})$ has block-diagonal form. Moreover, each block on the diagonal consists of the matrix of a particular irreducible multiplier representation:

$$\Delta(\mathbf{q}, \mathbf{R}) = \begin{pmatrix} \boldsymbol{\tau}^{(1)}(\mathbf{q}, \mathbf{R}) & 0 & s & 0 & 0 \\ 0 & \boldsymbol{\tau}^{(2)}(\mathbf{q}, \mathbf{R}) & s & 0 & 0 \\ \vdots & \vdots & \ddots & \vdots & \vdots \\ 0 & 0 & 0 & \ddots & 0 \\ 0 & 0 & 0 & 0 & \ddots \end{pmatrix}. \quad (2.1.3.46)$$

The matrix of eigenvectors thus reduces the operators \mathbf{T} to block-diagonal form.

There may be several phonons with different frequencies that belong to the same symmetry (irreducible representation). All purely longitudinally polarized lattice vibrations, irrespective of whether these are acoustic or optic modes, belong to the totally symmetric representation. This is because each vector parallel to \mathbf{q} – and in purely longitudinal modes the polarization vectors of each individual atom are parallel to the wavevector – is left invariant by any of the symmetry elements of $G_o(\mathbf{q})$. A particular irreducible representation may thus appear more than once in the decomposition of the \mathbf{T} matrix and, consequently, two or more of the blocks within the matrix $\Delta(\mathbf{q}, \mathbf{R})$ may be identical. Therefore, it is convenient to split the index σ that labels the modes of different frequency into two indices s and a ,

$$\sigma \rightarrow s, a.$$

s characterizes the inequivalent irreducible multiplier representations and a is the running index over all modes of the same symmetry but of different frequency. If c_s denotes the multiplicity of the representation s , then a takes the values $1, \dots, c_s$. Using this notation, the transformation law for the eigenvectors can be rewritten as

$$\begin{aligned} \mathbf{T}(\mathbf{q}, \mathbf{R})\mathbf{e}(\mathbf{q}, sa\lambda) &= \sum_{\lambda'=1}^{f_s} \tau_{\lambda\lambda'}^{(s)}(\mathbf{q}, \mathbf{R})\mathbf{e}(\mathbf{q}, sa\lambda') \\ \text{for } \lambda &= 1, \dots, f_s \text{ and } a = 1, \dots, c_s. \end{aligned} \quad (2.1.3.47)$$

As a well known result from group theory, the multiplicity c_s of a particular irreducible multiplier representation s in the decomposition of the reducible $3N$ -dimensional \mathbf{T} -matrix representation can be calculated from the respective characters

¹⁰ Accidental degeneracies that are due to the specific strength of interatomic forces are not considered here.

2.1. PHONONS

$$\begin{aligned}\chi(\mathbf{q}, \mathbf{R}) &= \sum_{\kappa\alpha} T_{\kappa\kappa}^{\alpha\alpha}(\mathbf{q}, \mathbf{R}) \\ &= \sum_{\kappa\alpha} R_{\alpha\alpha} \delta(\kappa, F_o(\kappa, \mathbf{R})) \exp[i\mathbf{q}(\mathbf{r}_\kappa - \mathbf{R}\mathbf{r}_\kappa)]\end{aligned}\quad (2.1.3.48)$$

and

$$\chi^{(s)}(\mathbf{q}, \mathbf{R}) = \sum_{\lambda=1}^{f_s} \tau_{\lambda\lambda}^{(s)}(\mathbf{q}, \mathbf{R}) \quad (2.1.3.49)$$

according to

$$c_s = (1/|G|) \sum_{\mathbf{R}} \chi(\mathbf{q}, \mathbf{R}) \chi^{(s)*}(\mathbf{q}, \mathbf{R}). \quad (2.1.3.50)$$

The summation index runs over all symmetry elements of the point group $G_o(\mathbf{q})$, the order of which is denoted by $|G|$. Hence we are able to predict the number of non-degenerate phonon modes for any of the different irreducible multiplier representations on the basis of group-theoretical considerations. Obviously, there are exactly $c_s \times f_s$ modes with eigenvectors that transform according to the irreducible multiplier representation s . Among these, groups of always f_s phonons have the same frequency. *The degeneracy corresponds to the dimensionality of the irreducible representation.* The crystallographic space groups give rise to one-, two- or three-dimensional irreducible representations. A maximum of three fundamental lattice vibrations can therefore be degenerate by symmetry, a situation that is observed for some prominent wavevectors within cubic crystals.

Symmetry considerations not only provide a means for a concise labelling of phonons; group theory can also be used to predict the form of eigenvectors that are compatible with the lattice structure. This aspect leads to the concept of symmetry coordinates, which is presented in Section 2.1.3.4.

2.1.3.3.1. Example

Let us return to the example presented in Section 2.1.3.1.1. At the Γ point, the point group of the wavevector is identical to the point group of the crystal, namely $4mm$. It contains all eight symmetry operations and there are five different irreducible representations, denoted $\tau^{(1+)}$, $\tau^{(1-)}$, $\tau^{(3+)}$, $\tau^{(3-)}$ and $\tau^{(2)}$. The corresponding character table including the reducible representation provided by the \mathbf{T} -matrix operators (*cf.* Section 2.1.3.1.1) has the form shown in Table 2.1.3.3. The representations $\tau^{(1+)}$, $\tau^{(1-)}$, $\tau^{(3+)}$ and $\tau^{(3-)}$ are one-dimensional, and $\tau^{(2)}$ is two-dimensional. The upper index, + or -, refers to the symmetry with respect to the mirror plane m_x . According to (2.1.3.50), we may calculate the multiplicities of these irreducible representations in the decomposition of the 30-dimensional \mathbf{T} representation. As the result we obtain

$$c_{\tau^{(1+)}} = 5, \quad c_{\tau^{(1-)}} = 3, \quad c_{\tau^{(3+)}} = 3, \quad c_{\tau^{(3-)}} = 3, \quad c_{\tau^{(2)}} = 8.$$

Hence for the sample structure presented in Section 2.1.3.1.1 we expect to have five phonon modes of symmetry $\tau^{(1+)}$, three modes

for each of the symmetries $\tau^{(1-)}$, $\tau^{(3+)}$ and $\tau^{(3-)}$, and 16 modes of symmetry $\tau^{(2)}$, the latter being divided into pairs of doubly degenerate phonons.

2.1.3.4. Symmetry coordinates

So far, we have used the $3N$ Cartesian coordinates of all atoms within a primitive cell in order to describe the dynamics of the crystal lattice. Within this coordinate system, the elements of the dynamical matrix can be calculated on the basis of specific models for interatomic interactions. The corresponding eigenvectors or normal coordinates are some linear combinations of the Cartesian components. With respect to these normal coordinates, which are specific to each particular crystal, the dynamical matrix has diagonal form and contains the squares of the eigenfrequencies reflecting the interatomic forces.

As shown in Sections 2.1.3.1 and 2.1.3.3, there are constraints for the dynamical matrix due to the symmetry of the crystal lattice and, hence, eigenvectors must obey certain transformation laws. Not all arbitrary linear combinations of the Cartesian coordinates can form an eigenvector. Rather, there are *symmetry-adapted coordinates* or simply *symmetry coordinates* compatible with a given structure that can be used to predict the general form of eigenvectors without the need for any particular model of interatomic interactions. These symmetry coordinates can be determined on the basis of the irreducible multiplier representations introduced in the previous section.

From the \mathbf{T} -matrix operators and the representation matrices $\tau^{(s)}(\mathbf{q}, \mathbf{R})$ of a particular irreducible multiplier representation we may define another matrix operator $\mathbf{P}^{(s)}(\mathbf{q})$ with the elements

$$\mathbf{P}_{\lambda\lambda'}^{(s)}(\mathbf{q}) = (f_s/|G|) \sum_{\mathbf{R}} \tau_{\lambda\lambda'}^{(s)*}(\mathbf{q}, \mathbf{R}) \mathbf{T}(\mathbf{q}, \mathbf{R}). \quad (2.1.3.51)$$

When applied to an arbitrary $3N$ -dimensional vector Ψ built from the Cartesian coordinates of the individual atoms, this operator yields the particular component of Ψ that transforms according to the irreducible representation s . Hence it acts as a *projection operator*. Defining a set of f_s vectors by

$$\mathbf{E}(\mathbf{q}, s\lambda) = \mathbf{P}_{\lambda\lambda'}^{(s)}(\mathbf{q}) \Psi, \quad \lambda = 1, \dots, f_s, \quad (2.1.3.52)$$

we obtain

$$\mathbf{T}(\mathbf{q}, \mathbf{R}') \mathbf{E}(\mathbf{q}, s\lambda) = (f_s/|G|) \sum_{\mathbf{R}} \tau_{\lambda\lambda'}^{(s)*}(\mathbf{q}, \mathbf{R}) \mathbf{T}(\mathbf{q}, \mathbf{R}') \mathbf{T}(\mathbf{q}, \mathbf{R}) \Psi. \quad (2.1.3.53)$$

Using the multiplication rule (2.1.3.21a), it can be shown that the right-hand side of this equation reduces to

$$(f_s/|G|) \sum_{\mathbf{R}} \sum_{\lambda''=1}^{f_s} \tau_{\lambda''\lambda}^{(s)}(\mathbf{q}, \mathbf{R}') \tau_{\lambda''\lambda'}^{(s)*}(\mathbf{q}, \mathbf{R}' \circ \mathbf{R}) \mathbf{T}(\mathbf{q}, \mathbf{R}' \circ \mathbf{R}) \Psi,$$

which can also be written in the form

Table 2.1.3.3. Character table of the point group $4mm$

| $4mm$ | Symmetry operation | | | | | | | |
|----------------------|--|---|--|---|--|--|---|---|
| | E | D_{90}^z | D_{180}^z | D_{270}^z | m_x | m_y | $m_{[110]}$ | $m_{[1\bar{1}0]}$ |
| χ_T | 30 | 2 | -2 | 2 | 2 | 2 | 2 | 2 |
| $\chi_{\tau^{(1+)}}$ | 1 | 1 | 1 | 1 | 1 | 1 | 1 | 1 |
| $\chi_{\tau^{(1-)}}$ | 1 | 1 | 1 | 1 | -1 | -1 | -1 | -1 |
| $\chi_{\tau^{(3+)}}$ | 1 | -1 | 1 | -1 | 1 | 1 | -1 | -1 |
| $\chi_{\tau^{(3-)}}$ | 1 | -1 | 1 | -1 | -1 | -1 | 1 | 1 |
| $\tau^{(2)}$ | $\begin{pmatrix} 1 & 0 \\ 0 & 1 \end{pmatrix}$ | $\begin{pmatrix} i & 0 \\ 0 & -i \end{pmatrix}$ | $\begin{pmatrix} -1 & 0 \\ 0 & -1 \end{pmatrix}$ | $\begin{pmatrix} -i & 0 \\ 0 & i \end{pmatrix}$ | $\begin{pmatrix} 0 & 1 \\ 1 & 0 \end{pmatrix}$ | $\begin{pmatrix} 0 & -1 \\ -1 & 0 \end{pmatrix}$ | $\begin{pmatrix} 0 & -i \\ i & 0 \end{pmatrix}$ | $\begin{pmatrix} 1 & i \\ -i & 0 \end{pmatrix}$ |
| $\chi_{\tau^{(2)}}$ | 2 | 0 | -2 | 0 | 0 | 0 | 0 | 0 |

2. SYMMETRY ASPECTS OF EXCITATIONS

$$\sum_{\lambda''=1}^{f_s} \tau_{\lambda''\lambda}^{(s)}(\mathbf{q}, \mathbf{R}') (f_s/|G|) \sum_{\mathbf{R}} \tau_{\lambda''\lambda'}^{(s)*}(\mathbf{q}, \mathbf{R}) \mathbf{T}(\mathbf{q}, \mathbf{R}) \Psi,$$

since if \mathbf{R} runs over all symmetry operations of the group $G_o(\mathbf{q})$ the same is true for the product $\mathbf{R}' \circ \mathbf{R}$. Comparing this expression with the definitions (2.1.3.51) and (2.1.3.52) we obtain

$$\mathbf{T}(\mathbf{q}, \mathbf{R}') \mathbf{E}(\mathbf{q}, s\lambda) = \sum_{\lambda''=1}^{f_s} \tau_{\lambda''\lambda}^{(s)}(\mathbf{q}, \mathbf{R}') \mathbf{E}(\mathbf{q}, s\lambda''). \quad (2.1.3.54)$$

Hence the set of vectors $\mathbf{E}(\mathbf{q}, s\lambda)$ span an irreducible vector space and transform into each other in just the same way as the eigenvectors $\mathbf{e}(\mathbf{q}, sa\lambda)$ of the dynamical matrix do.

If the corresponding irreducible representation s appears only once in the decomposition of the $3N$ -dimensional \mathbf{T} representation, then the vector space provided by the $\mathbf{E}(\mathbf{q}, s\lambda)$, $\lambda = 1, \dots, f_s$, is uniquely determined. Consequently, these basis vectors themselves may be regarded as eigenvectors of the dynamical matrix. In this case, symmetry considerations alone determine the polarization of lattice vibrations irrespective of the particular interatomic interactions.

If, on the other hand, the multiplicity c_s of the representation s is larger than 1, the most that can be inferred is that each of the vectors $\mathbf{E}(\mathbf{q}, s\lambda)$ is some linear combination of the c_s eigenvectors $\mathbf{e}(\mathbf{q}, sa\lambda)$, $a = 1, \dots, c_s$. By an appropriate choice of the different generating vectors Ψ_a in (2.1.3.52), it is, however, always possible to find a set of c_s pairwise orthogonal vectors $\mathbf{E}(\mathbf{q}, sa\lambda)$ that span the same vector space as the eigenvectors $\mathbf{e}(\mathbf{q}, sa\lambda)$. If we repeat this procedure for every irreducible representation s contributing to the \mathbf{T} representation, we obtain $3N$ linearly independent vectors, the *symmetry coordinates*, that generate a new coordinate system within the $3N$ -dimensional space of atomic displacements. With respect to this coordinate system the dynamical matrix is reduced to a symmetry-adapted block-diagonal form.

In order to show this, let us denote the matrix elements of the transformed dynamical matrix by $\bar{D}_{sa\lambda}^{s'a'\lambda'}(\mathbf{q})$ ($\lambda = 1, \dots, f_s$, $a = 1, \dots, c_s$) and the components of the symmetry coordinates by $E_{\kappa}^{\alpha}(\mathbf{q}, sa\lambda)$ ($\kappa = 1, \dots, N$, $\alpha = 1, 2, 3$). Then the following equation holds, since the dynamical matrix $\mathbf{D}(\mathbf{q})$ commutes with the \mathbf{T} -matrix operators and since the symmetry coordinates transform according to (2.1.3.54):

$$\begin{aligned} \bar{D}_{sa\lambda}^{s'a'\lambda'}(\mathbf{q}) &= \sum_{\kappa\alpha} \sum_{\kappa'\beta} E_{\kappa}^{\alpha*}(\mathbf{q}, sa\lambda) D_{\kappa\kappa'}^{\alpha\beta}(\mathbf{q}) E_{\kappa'}^{\beta}(\mathbf{q}, s'a'\lambda') \\ &= \sum_{\kappa\alpha} \sum_{\kappa'\beta} E_{\kappa}^{\alpha*}(\mathbf{q}, sa\lambda) \\ &\quad \times \sum_{\kappa_1\alpha_1} \sum_{\kappa_2\alpha_2} \{ (T^{-1}(\mathbf{q}, \mathbf{R}))_{\kappa\kappa_1}^{\alpha\alpha_1} D_{\kappa_1\kappa_2}^{\alpha_1\alpha_2}(\mathbf{q}) (T(\mathbf{q}, \mathbf{R}))_{\kappa_2\kappa'}^{\alpha_2\beta} \} \\ &\quad \times E_{\kappa'}^{\beta}(\mathbf{q}, s'a'\lambda') \\ &= \sum_{\kappa_1\alpha_1} \sum_{\kappa_2\alpha_2} \sum_{\mu=1}^{f_s} \sum_{\mu'=1}^{f_s} \tau_{\mu\lambda}^{(s)*}(\mathbf{q}, \mathbf{R}) E_{\kappa_1}^{\alpha_1*}(\mathbf{q}, sa\mu) \\ &\quad \times D_{\kappa_1\kappa_2}^{\alpha_1\alpha_2}(\mathbf{q}) \tau_{\mu'\lambda'}^{(s')}(\mathbf{q}, \mathbf{R}) E_{\kappa_2}^{\alpha_2}(\mathbf{q}, s'a'\lambda') \\ &= \sum_{\mu=1}^{f_s} \sum_{\mu'=1}^{f_s} \tau_{\mu\lambda}^{(s)*}(\mathbf{q}, \mathbf{R}) \tau_{\mu'\lambda'}^{(s')}(\mathbf{q}, \mathbf{R}) \bar{D}_{sa\mu}^{s'a'\mu'}(\mathbf{q}). \end{aligned} \quad (2.1.3.55)$$

Owing to the orthogonality of the irreducible representation, we obtain after summation over all symmetry elements \mathbf{R} and division by the order of the group

$$\begin{aligned} \bar{D}_{sa\lambda}^{s'a'\lambda'}(\mathbf{q}) &= (1/|G|) \sum_{\mathbf{R}} \sum_{\mu=1}^{f_s} \sum_{\mu'=1}^{f_s} \tau_{\mu\lambda}^{(s)*}(\mathbf{q}, \mathbf{R}) \tau_{\mu'\lambda'}^{(s')}(\mathbf{q}, \mathbf{R}) \bar{D}_{sa\mu}^{s'a'\mu'}(\mathbf{q}) \\ &= (1/f_s) \sum_{\mu=1}^{f_s} \sum_{\mu'=1}^{f_s} \delta_{\mu\mu'} \delta_{\lambda\lambda'} \delta_{ss'} \bar{D}_{sa\mu}^{s'a'\mu'}(\mathbf{q}) \\ &= (1/f_s) \delta_{\lambda\lambda'} \delta_{ss'} \sum_{\mu=1}^{f_s} \bar{D}_{sa\mu}^{s'a'\mu}(\mathbf{q}). \end{aligned} \quad (2.1.3.56)$$

This equation proves the block-diagonal form of the transformed dynamical matrix $\bar{\mathbf{D}}$. Hence, with respect to the symmetry coordinates, the dynamical matrix can be represented by submatrices $\bar{\mathbf{D}}^{(s)}(\mathbf{q})$ of dimension $c_s \times c_s$ that are determined by the individual irreducible representations (s):

$$\bar{\mathbf{D}}(\mathbf{q}) = \begin{pmatrix} \bar{\mathbf{D}}^{(1)}(\mathbf{q}) & \mathbf{0} & s & \mathbf{0} \\ \mathbf{0} & \bar{\mathbf{D}}^{(2)}(\mathbf{q}) & s & \mathbf{0} \\ \vdots & \vdots & \ddots & \vdots \\ \mathbf{0} & \mathbf{0} & s & \ddots \end{pmatrix}. \quad (2.1.3.57)$$

The elements of the submatrices are given by

$$\bar{D}_{aa'}^{(s)}(\mathbf{q}) = \sum_{\kappa\alpha} \sum_{\kappa'\beta} E_{\kappa}^{\alpha*}(\mathbf{q}, sa\lambda) D_{\kappa\kappa'}^{\alpha\beta}(\mathbf{q}) E_{\kappa'}^{\beta}(\mathbf{q}, sa'\lambda), \quad (2.1.3.58)$$

and must be independent of λ . Obviously, a submatrix $\bar{\mathbf{D}}^{(s)}(\mathbf{q})$ may appear once, twice or three times on the diagonal, according to the dimensionality f_s of the respective irreducible representation.

The eigenvectors and eigenvalues of the block-diagonalized dynamical matrix can be collected from the eigenvectors and eigenvalues of the individual submatrices. Hence, the eigenvectors of $\bar{\mathbf{D}}^{(s)}(\mathbf{q})$ correspond to the c_s non-degenerate phonons of symmetry s .

2.1.3.4.1. Example

Let us try to find the symmetry coordinates corresponding to our sample structure introduced in Section 2.1.3.1.1 for $\mathbf{q} = \mathbf{0}$. Using the irreducible representations displayed in Section 2.1.3.3.1, we write down the projection operator for representation $\tau^{(1\pm)}$ according to equation (2.1.3.51):

$$\mathbf{P}_{11}^{(1\pm)}(\mathbf{0}) = \frac{1}{8} \begin{pmatrix} \Sigma_1^{\pm} & 0 & 0 & 0 & 0 & 0 & 0 & 0 & 0 & 0 \\ 0 & \Sigma_1^{\pm} & 0 & 0 & 0 & 0 & 0 & 0 & 0 & 0 \\ 0 & 0 & \mathbf{E} & \mathbf{D}_{180}^z & \pm \mathbf{m}_{[110]} & \mathbf{D}_{90}^z & \pm \mathbf{m}_y & \pm \mathbf{m}_x & \mathbf{D}_{270}^z & \pm \mathbf{m}_{[110]} \\ 0 & 0 & \mathbf{D}_{180}^z & \mathbf{E} & \pm \mathbf{m}_{[110]} & \mathbf{D}_{270}^z & \pm \mathbf{m}_x & \pm \mathbf{m}_y & \mathbf{D}_{90}^z & \pm \mathbf{m}_{[110]} \\ 0 & 0 & \pm \mathbf{m}_{[110]} & \pm \mathbf{m}_{[110]} & \mathbf{E} & \pm \mathbf{m}_x & \mathbf{D}_{270}^z & \mathbf{D}_{90}^z & \pm \mathbf{m}_y & \mathbf{D}_{180}^z \\ 0 & 0 & \mathbf{D}_{270}^z & \mathbf{D}_{90}^z & \pm \mathbf{m}_x & \mathbf{E} & \pm \mathbf{m}_{[110]} & \pm \mathbf{m}_{[110]} & \mathbf{D}_{180}^z & \pm \mathbf{m}_y \\ 0 & 0 & \pm \mathbf{m}_y & \pm \mathbf{m}_x & \mathbf{D}_{90}^z & \pm \mathbf{m}_{[110]} & \mathbf{E} & \mathbf{D}_{180}^z & \pm \mathbf{m}_{[110]} & \mathbf{D}_{270}^z \\ 0 & 0 & \pm \mathbf{m}_x & \pm \mathbf{m}_y & \mathbf{D}_{270}^z & \pm \mathbf{m}_{[110]} & \mathbf{D}_{180}^z & \mathbf{E} & \pm \mathbf{m}_{[110]} & \mathbf{D}_{90}^z \\ 0 & 0 & \mathbf{D}_{90}^z & \mathbf{D}_{270}^z & \pm \mathbf{m}_y & \mathbf{D}_{180}^z & \pm \mathbf{m}_{[110]} & \pm \mathbf{m}_{[110]} & \mathbf{E} & \pm \mathbf{m}_x \\ 0 & 0 & \pm \mathbf{m}_{[110]} & \pm \mathbf{m}_{[110]} & \mathbf{D}_{180}^z & \pm \mathbf{m}_y & \mathbf{D}_{90}^z & \mathbf{D}_{270}^z & \pm \mathbf{m}_x & \mathbf{E} \end{pmatrix}$$

with the abbreviations

$$\begin{aligned} \Sigma_1^+ &= \mathbf{E} + \mathbf{D}_{90}^z + \mathbf{D}_{180}^z + \mathbf{D}_{270}^z + \mathbf{m}_x + \mathbf{m}_y + \mathbf{m}_{[110]} + \mathbf{m}_{[110]} \\ &= \begin{pmatrix} 0 & 0 & 0 \\ 0 & 0 & 0 \\ 0 & 0 & 8 \end{pmatrix}, \\ \Sigma_1^- &= \mathbf{E} + \mathbf{D}_{90}^z + \mathbf{D}_{180}^z + \mathbf{D}_{270}^z - \mathbf{m}_x - \mathbf{m}_y - \mathbf{m}_{[110]} - \mathbf{m}_{[110]} \\ &= \begin{pmatrix} 0 & 0 & 0 \\ 0 & 0 & 0 \\ 0 & 0 & 0 \end{pmatrix} = \mathbf{0}. \end{aligned}$$

2.1. PHONONS

From the results in Section 2.1.3.4, we expect to have five symmetry coordinates corresponding to representation $\tau^{(1+)}$ and three for $\tau^{(1-)}$ according to the respective multiplicities. Let $\mathbf{x}_1, \mathbf{y}_1, \mathbf{z}_1, \mathbf{x}_2, \mathbf{y}_2, \mathbf{z}_2, \dots, \mathbf{x}_{10}, \mathbf{y}_{10}, \mathbf{z}_{10}$ denote the basis of the 30-dimensional space generated by the displacements of the ten atoms in the x, y and z directions, respectively. If we apply the projection operator $\mathbf{P}_{11}^{(1+)}(\mathbf{0})$ to the basis vector \mathbf{z}_1 , we obtain the first symmetry coordinate according to equation (2.1.3.52):

$$\mathbf{E}(\mathbf{0}, 1^{+11}) = \mathbf{P}_{11}^{(1+)}(\mathbf{0}) \begin{pmatrix} 0 \\ 0 \\ 1 \\ 0 \\ 0 \\ 0 \\ \vdots \\ 0 \\ 0 \\ 0 \\ 0 \end{pmatrix} = \mathbf{P}_{11}^{(1+)}(\mathbf{0}) \mathbf{z}_1 = \mathbf{z}_1.$$

In a similar way we may use the basis vectors $\mathbf{z}_2, \mathbf{x}_3, \mathbf{z}_3$ and \mathbf{x}_5 in order to generate the other symmetry coordinates:

$$\begin{aligned} \mathbf{E}(\mathbf{0}, 1^{+21}) &= \mathbf{P}_{11}^{(1+)}(\mathbf{0}) \mathbf{z}_2 = \mathbf{z}_2 \\ \mathbf{E}(\mathbf{0}, 1^{+31}) &= \mathbf{P}_{11}^{(1+)}(\mathbf{0}) \mathbf{x}_3 \\ &= \frac{1}{8}[\mathbf{x}_3 - \mathbf{x}_4 - \mathbf{y}_5 - \mathbf{y}_6 + \mathbf{x}_7 - \mathbf{x}_8 + \mathbf{y}_9 + \mathbf{y}_{10}] \\ \mathbf{E}(\mathbf{0}, 1^{+41}) &= \mathbf{P}_{11}^{(1+)}(\mathbf{0}) \mathbf{z}_3 \\ &= \frac{1}{8}[\mathbf{z}_3 + \mathbf{z}_4 + \mathbf{z}_5 + \mathbf{z}_6 + \mathbf{z}_7 + \mathbf{z}_8 + \mathbf{z}_9 + \mathbf{z}_{10}] \\ \mathbf{E}(\mathbf{0}, 1^{+51}) &= \mathbf{P}_{11}^{(1+)}(\mathbf{0}) \mathbf{x}_5 \\ &= \frac{1}{8}[-\mathbf{y}_3 + \mathbf{y}_4 + \mathbf{x}_5 - \mathbf{x}_6 + \mathbf{y}_7 - \mathbf{y}_8 + \mathbf{x}_9 - \mathbf{x}_{10}]. \end{aligned}$$

(It can easily be shown that all the other basis vectors would lead to linearly dependent symmetry coordinates.)

Any eigenvector of the dynamical matrix corresponding to the irreducible representation $\tau^{(1+)}$ is necessarily some linear combination of these five symmetry coordinates. Hence it may be concluded that for all lattice vibrations of this symmetry, the displacements of atoms 1 and 2 can only be along the tetragonal axis. Moreover, the displacements of atoms 3 to 10 have to be identical along \mathbf{z} , and pairs of atoms vibrate in opposite directions within the xy plane.

For the representation $\tau^{(1-)}$ we obtain the following symmetry coordinates when $\mathbf{P}_{11}^{(1-)}(\mathbf{0})$ is applied to $\mathbf{x}_3, \mathbf{z}_3$ and \mathbf{x}_5 :

$$\begin{aligned} \mathbf{E}(\mathbf{0}, 1^{-11}) &= \mathbf{P}_{11}^{(1-)}(\mathbf{0}) \mathbf{x}_3 \\ &= \frac{1}{8}[\mathbf{x}_3 - \mathbf{x}_4 + \mathbf{y}_5 - \mathbf{y}_6 - \mathbf{x}_7 + \mathbf{x}_8 + \mathbf{y}_9 - \mathbf{y}_{10}] \\ \mathbf{E}(\mathbf{0}, 1^{-21}) &= \mathbf{P}_{11}^{(1-)}(\mathbf{0}) \mathbf{z}_3 \\ &= \frac{1}{8}[\mathbf{z}_3 + \mathbf{z}_4 - \mathbf{z}_5 + \mathbf{z}_6 - \mathbf{z}_7 - \mathbf{z}_8 + \mathbf{z}_9 - \mathbf{z}_{10}] \\ \mathbf{E}(\mathbf{0}, 1^{-31}) &= \mathbf{P}_{11}^{(1-)}(\mathbf{0}) \mathbf{x}_5 \\ &= \frac{1}{8}[\mathbf{y}_3 - \mathbf{y}_4 + \mathbf{x}_5 + \mathbf{x}_6 + \mathbf{y}_7 - \mathbf{y}_8 - \mathbf{x}_9 - \mathbf{x}_{10}]. \end{aligned}$$

Obviously, none of the corresponding phonons exhibits any displacement of atoms 1 and 2. There is an antiphase motion of pairs of atoms not only within the tetragonal plane but also along the tetragonal z axis.

For the representations $\tau^{(3\pm)}$ we obtain the following projection operators:

$$\mathbf{P}_{11}^{(3\pm)}(\mathbf{0}) = \frac{1}{8} \begin{pmatrix} \Sigma_3^\pm & 0 & 0 & 0 & 0 & 0 & 0 & 0 & 0 & 0 \\ 0 & \Sigma_3^\pm & 0 & 0 & 0 & 0 & 0 & 0 & 0 & 0 \\ 0 & 0 & \mathbf{E} & \mathbf{D}_{180}^z & \mp \mathbf{m}_{[110]} & -\mathbf{D}_{90}^z & \pm \mathbf{m}_y & \pm \mathbf{m}_x & -\mathbf{D}_{270}^z & \mp \mathbf{m}_{[110]} \\ 0 & 0 & \mathbf{D}_{180}^z & \mathbf{E} & \mp \mathbf{m}_{[110]} & -\mathbf{D}_{270}^z & \pm \mathbf{m}_x & \pm \mathbf{m}_y & -\mathbf{D}_{90}^z & \mp \mathbf{m}_{[110]} \\ 0 & 0 & \mp \mathbf{m}_{[110]} & \mp \mathbf{m}_{[110]} & \mathbf{E} & \pm \mathbf{m}_x & -\mathbf{D}_{270}^z & -\mathbf{D}_{90}^z & \pm \mathbf{m}_y & \mathbf{D}_{180}^z \\ 0 & 0 & -\mathbf{D}_{270}^z & -\mathbf{D}_{90}^z & \pm \mathbf{m}_x & \mathbf{E} & \mp \mathbf{m}_{[110]} & \mp \mathbf{m}_{[110]} & \mathbf{D}_{180}^z & \pm \mathbf{m}_y \\ 0 & 0 & \pm \mathbf{m}_y & \pm \mathbf{m}_x & -\mathbf{D}_{90}^z & \mp \mathbf{m}_{[110]} & \mathbf{E} & \mathbf{D}_{180}^z & \mp \mathbf{m}_{[110]} & -\mathbf{D}_{270}^z \\ 0 & 0 & \pm \mathbf{m}_x & \pm \mathbf{m}_y & -\mathbf{D}_{270}^z & \mp \mathbf{m}_{[110]} & \mathbf{D}_{180}^z & \mathbf{E} & \mp \mathbf{m}_{[110]} & -\mathbf{D}_{90}^z \\ 0 & 0 & -\mathbf{D}_{90}^z & -\mathbf{D}_{270}^z & \pm \mathbf{m}_y & \mathbf{D}_{180}^z & \mp \mathbf{m}_{[110]} & \mp \mathbf{m}_{[110]} & \mathbf{E} & \pm \mathbf{m}_x \\ 0 & 0 & \mp \mathbf{m}_{[110]} & \mp \mathbf{m}_{[110]} & \mathbf{D}_{180}^z & \pm \mathbf{m}_y & -\mathbf{D}_{90}^z & -\mathbf{D}_{270}^z & \pm \mathbf{m}_x & \mathbf{E} \end{pmatrix}$$

with

$$\Sigma_3^\pm = \mathbf{E} - \mathbf{D}_{90}^z + \mathbf{D}_{180}^z - \mathbf{D}_{270}^z \pm \mathbf{m}_x \pm \mathbf{m}_y \mp \mathbf{m}_{[110]} \mp \mathbf{m}_{[110]} = \mathbf{0}.$$

Both representations appear three times in the decomposition of the \mathbf{T} representation. Hence, we expect three phonons of each symmetry and also three linearly independent symmetry coordinates. These are generated if the projection operators are applied to the basis vectors $\mathbf{x}_3, \mathbf{z}_3$ and \mathbf{x}_5 :

$$\begin{aligned} \mathbf{E}(\mathbf{0}, 3^{+11}) &= \mathbf{P}_{11}^{(3+)}(\mathbf{0}) \mathbf{x}_3 \\ &= \frac{1}{8}[\mathbf{x}_3 - \mathbf{x}_4 \pm \mathbf{y}_5 + \mathbf{y}_6 \pm \mathbf{x}_7 \mp \mathbf{x}_8 - \mathbf{y}_9 \mp \mathbf{y}_{10}] \\ \mathbf{E}(\mathbf{0}, 3^{+21}) &= \mathbf{P}_{11}^{(3+)}(\mathbf{0}) \mathbf{z}_3 \\ &= \frac{1}{8}[\mathbf{z}_3 + \mathbf{z}_4 \mp \mathbf{z}_5 - \mathbf{z}_6 \pm \mathbf{z}_7 \pm \mathbf{z}_8 - \mathbf{z}_9 \mp \mathbf{z}_{10}] \\ \mathbf{E}(\mathbf{0}, 3^{+11}) &= \mathbf{P}_{11}^{(3+)}(\mathbf{0}) \mathbf{x}_5 \\ &= \frac{1}{8}[\pm \mathbf{y}_3 \mp \mathbf{y}_4 + \mathbf{x}_5 \mp \mathbf{x}_6 - \mathbf{y}_7 + \mathbf{y}_8 \pm \mathbf{x}_9 - \mathbf{x}_{10}]. \end{aligned}$$

Just as for representation $\tau^{(1-)}$, the symmetry coordinates corresponding to representations $\tau^{(3\pm)}$ do not contain any component of atoms 1 and 2. Consequently, all lattice modes of these symmetries leave the atoms on the fourfold axis at their equilibrium positions at rest.

Representation $\tau^{(2)}$ is two-dimensional and appears eight times in the decomposition of the \mathbf{T} representation. Hence, there are 16 doubly degenerate phonons of this symmetry. According to (2.1.3.51), four projection operators $\mathbf{P}_{11}^{(2)}(\mathbf{0})$, $\mathbf{P}_{21}^{(2)}(\mathbf{0})$, $\mathbf{P}_{12}^{(2)}(\mathbf{0})$ and $\mathbf{P}_{22}^{(2)}(\mathbf{0})$ can in principle be constructed, the latter two being, however, equivalent to the former ones:

$$\mathbf{P}_{11}^{(2)}(\mathbf{0}) = \frac{1}{4} \begin{pmatrix} \Sigma_2^\pm & 0 & 0 & 0 & 0 & 0 & 0 & 0 & 0 & 0 \\ 0 & \Sigma_2^\pm & 0 & 0 & 0 & 0 & 0 & 0 & 0 & 0 \\ 0 & 0 & \mathbf{E} & -\mathbf{D}_{180}^z & 0 & \pm i\mathbf{D}_{90}^z & 0 & 0 & \mp i\mathbf{D}_{270}^z & 0 \\ 0 & 0 & -\mathbf{D}_{180}^z & \mathbf{E} & 0 & \mp i\mathbf{D}_{270}^z & 0 & 0 & \pm i\mathbf{D}_{90}^z & 0 \\ 0 & 0 & 0 & 0 & \mathbf{E} & 0 & \mp i\mathbf{D}_{270}^z & \pm i\mathbf{D}_{90}^z & 0 & -\mathbf{D}_{180}^z \\ 0 & 0 & \mp i\mathbf{D}_{270}^z & \pm i\mathbf{D}_{90}^z & 0 & \mathbf{E} & 0 & 0 & -\mathbf{D}_{180}^z & 0 \\ 0 & 0 & 0 & 0 & \pm i\mathbf{D}_{90}^z & 0 & \mathbf{E} & -\mathbf{D}_{180}^z & 0 & \mp i\mathbf{D}_{270}^z \\ 0 & 0 & 0 & 0 & \mp i\mathbf{D}_{270}^z & 0 & -\mathbf{D}_{180}^z & \mathbf{E} & 0 & \pm i\mathbf{D}_{90}^z \\ 0 & 0 & \pm i\mathbf{D}_{90}^z & \mp i\mathbf{D}_{270}^z & 0 & -\mathbf{D}_{180}^z & 0 & 0 & \mathbf{E} & 0 \\ 0 & 0 & 0 & 0 & -\mathbf{D}_{180}^z & 0 & \pm i\mathbf{D}_{90}^z & \mp i\mathbf{D}_{270}^z & 0 & \mathbf{E} \end{pmatrix}$$

and

$$\mathbf{P}_{21}^{(2)}(\mathbf{0}) = \frac{1}{4} \begin{pmatrix} \Delta_2^\pm & 0 & 0 & 0 & 0 & 0 & 0 & 0 & 0 & 0 \\ 0 & \Delta_2^\pm & 0 & 0 & 0 & 0 & 0 & 0 & 0 & 0 \\ 0 & 0 & 0 & 0 & \pm i\mathbf{m}_{[110]} & 0 & -\mathbf{m}_y & \mathbf{m}_x & 0 & \mp i\mathbf{m}_{[110]} \\ 0 & 0 & 0 & 0 & \mp i\mathbf{m}_{[110]} & 0 & \mathbf{m}_x & -\mathbf{m}_y & 0 & \pm i\mathbf{m}_{[110]} \\ 0 & 0 & \pm i\mathbf{m}_{[110]} & \mp i\mathbf{m}_{[110]} & 0 & \mathbf{m}_x & 0 & 0 & -\mathbf{m}_y & 0 \\ 0 & 0 & 0 & 0 & \mathbf{m}_x & 0 & \pm i\mathbf{m}_{[110]} & \mp i\mathbf{m}_{[110]} & 0 & -\mathbf{m}_y \\ 0 & 0 & -\mathbf{m}_y & \mathbf{m}_x & 0 & \pm i\mathbf{m}_{[110]} & 0 & 0 & \mp i\mathbf{m}_{[110]} & 0 \\ 0 & 0 & \mathbf{m}_x & -\mathbf{m}_y & 0 & \mp i\mathbf{m}_{[110]} & 0 & 0 & \pm i\mathbf{m}_{[110]} & 0 \\ 0 & 0 & 0 & 0 & -\mathbf{m}_y & 0 & \mp i\mathbf{m}_{[110]} & \pm i\mathbf{m}_{[110]} & 0 & \mathbf{m}_x \\ 0 & 0 & \mp i\mathbf{m}_{[110]} & \pm i\mathbf{m}_{[110]} & 0 & -\mathbf{m}_y & 0 & 0 & \mathbf{m}_x & 0 \end{pmatrix}$$

2. SYMMETRY ASPECTS OF EXCITATIONS

with

$$\Sigma_2^\pm = \mathbf{E} \pm i\mathbf{D}_{90}^z - \mathbf{D}_{180}^z \mp i\mathbf{D}_{270}^z = \begin{pmatrix} 2 & \mp 2i & 0 \\ \pm 2i & 2 & 0 \\ 0 & 0 & 0 \end{pmatrix},$$

$$\Delta_2^\pm = \mathbf{m}_x - \mathbf{m}_y \pm i\mathbf{m}_{[110]} \mp i\mathbf{m}_{[\bar{1}10]} = \begin{pmatrix} -2 & \mp 2i & 0 \\ \mp 2i & 2 & 0 \\ 0 & 0 & 0 \end{pmatrix}.$$

The projection operator $\mathbf{P}_{11}^{(2)}(\mathbf{0})$ applied to the basis vectors $\mathbf{x}_1, \mathbf{x}_2, \mathbf{x}_3, \mathbf{x}_5, \mathbf{x}_6, \mathbf{x}_7, \mathbf{z}_3$ and \mathbf{z}_5 yields eight symmetry coordinates for eight phonon modes with different eigenfrequencies. Owing to the degeneracy, each of these phonons has a counterpart with the same frequency but with a different linearly independent eigenvector. These new eigenvectors are built from another set of symmetry coordinates, which is generated if the other operator $\mathbf{P}_{21}^{(2)}(\mathbf{0})$ is applied to the same vectors $\mathbf{x}_1, \mathbf{x}_2, \mathbf{x}_3, \mathbf{x}_5, \mathbf{x}_6, \mathbf{x}_7, \mathbf{z}_3$ and \mathbf{z}_5 . The two sets of symmetry coordinates are

$$\begin{aligned} \mathbf{E}(\mathbf{0}, 211) &= \mathbf{P}_{11}^{(2)}(\mathbf{0}) \mathbf{x}_1 = \frac{1}{2}[\mathbf{x}_1 + i\mathbf{y}_1] \\ \mathbf{E}(\mathbf{0}, 221) &= \mathbf{P}_{11}^{(2)}(\mathbf{0}) \mathbf{x}_2 = \frac{1}{2}[\mathbf{x}_2 + i\mathbf{y}_2] \\ \mathbf{E}(\mathbf{0}, 231) &= \mathbf{P}_{11}^{(2)}(\mathbf{0}) \mathbf{x}_3 = \frac{1}{4}[\mathbf{x}_3 + \mathbf{x}_4 + i\mathbf{y}_6 + i\mathbf{y}_9] \\ \mathbf{E}(\mathbf{0}, 241) &= \mathbf{P}_{11}^{(2)}(\mathbf{0}) \mathbf{x}_5 = \frac{1}{4}[\mathbf{x}_5 + \mathbf{x}_{10} + i\mathbf{y}_7 + i\mathbf{y}_8] \\ \mathbf{E}(\mathbf{0}, 251) &= \mathbf{P}_{11}^{(2)}(\mathbf{0}) \mathbf{x}_6 = \frac{1}{4}[\mathbf{x}_6 + \mathbf{x}_9 + i\mathbf{y}_3 + i\mathbf{y}_4] \\ \mathbf{E}(\mathbf{0}, 261) &= \mathbf{P}_{11}^{(2)}(\mathbf{0}) \mathbf{x}_7 = \frac{1}{4}[\mathbf{x}_7 + \mathbf{x}_8 + i\mathbf{y}_5 + i\mathbf{y}_{10}] \\ \mathbf{E}(\mathbf{0}, 271) &= \mathbf{P}_{11}^{(2)}(\mathbf{0}) \mathbf{z}_3 = \frac{1}{4}[\mathbf{z}_3 - \mathbf{z}_4 - i\mathbf{z}_6 + i\mathbf{z}_9] \\ \mathbf{E}(\mathbf{0}, 281) &= \mathbf{P}_{11}^{(2)}(\mathbf{0}) \mathbf{z}_5 = \frac{1}{4}[\mathbf{z}_5 - \mathbf{z}_{10} + i\mathbf{z}_7 - i\mathbf{z}_8] \\ \\ \mathbf{E}(\mathbf{0}, 212) &= \mathbf{P}_{21}^{(2)}(\mathbf{0}) \mathbf{x}_1 = \frac{1}{2}[-\mathbf{x}_1 + i\mathbf{y}_1] \\ \mathbf{E}(\mathbf{0}, 222) &= \mathbf{P}_{21}^{(2)}(\mathbf{0}) \mathbf{x}_2 = \frac{1}{2}[-\mathbf{x}_2 + i\mathbf{y}_2] \\ \mathbf{E}(\mathbf{0}, 232) &= \mathbf{P}_{21}^{(2)}(\mathbf{0}) \mathbf{x}_3 = \frac{1}{4}[-\mathbf{x}_7 - \mathbf{x}_8 + i\mathbf{y}_5 + i\mathbf{y}_{10}] \\ \mathbf{E}(\mathbf{0}, 242) &= \mathbf{P}_{21}^{(2)}(\mathbf{0}) \mathbf{x}_5 = \frac{1}{4}[-\mathbf{x}_6 - \mathbf{x}_9 + i\mathbf{y}_3 + i\mathbf{y}_4] \\ \mathbf{E}(\mathbf{0}, 252) &= \mathbf{P}_{21}^{(2)}(\mathbf{0}) \mathbf{x}_6 = \frac{1}{4}[-\mathbf{x}_5 - \mathbf{x}_{10} + i\mathbf{y}_7 + i\mathbf{y}_8] \\ \mathbf{E}(\mathbf{0}, 262) &= \mathbf{P}_{21}^{(2)}(\mathbf{0}) \mathbf{x}_7 = \frac{1}{4}[-\mathbf{x}_3 - \mathbf{x}_4 + i\mathbf{y}_6 + i\mathbf{y}_9] \\ \mathbf{E}(\mathbf{0}, 272) &= \mathbf{P}_{21}^{(2)}(\mathbf{0}) \mathbf{z}_3 = \frac{1}{4}[-\mathbf{z}_7 + \mathbf{z}_8 - i\mathbf{z}_5 + i\mathbf{z}_{10}] \\ \mathbf{E}(\mathbf{0}, 282) &= \mathbf{P}_{21}^{(2)}(\mathbf{0}) \mathbf{z}_5 = \frac{1}{4}[\mathbf{z}_6 - \mathbf{z}_9 - i\mathbf{z}_3 + i\mathbf{z}_4]. \end{aligned}$$

Looking carefully at these sets of symmetry coordinates, one recognises that both vector spaces are spanned by mutually complex conjugate symmetry coordinates.

Collecting all symmetry coordinates as column vectors within a 30×30 matrix we finally obtain the matrix shown in Fig. 2.1.3.7. For simplicity, only nonzero elements are displayed. This matrix can be used for the block-diagonalization of any dynamical matrix that describes the dynamical behaviour of our model crystal.

2.1.3.5. Degeneracy of lattice vibrations

Whenever two phonon modes of the same wavevector exhibit identical frequencies but linearly independent eigenvectors, these modes are called *degenerate*. As discussed in the preceding sections, the symmetry of the crystal lattice may cause degeneracies if there are higher-dimensional irreducible representations of the point group of the phonon wavevector. Two-dimensional representations yield twofold degenerate lattice vibrations, whereas threefold degeneracy may be found for special wavevectors in cubic crystals exhibiting three-dimensional irreducible representations. In addition, there are two other reasons for the possible existence of degenerate lattice vibra-

tions: *accidental degeneracy* and degeneracy due to *time-reversal invariance* of the lattice vibrations. Both phenomena will be described in the following.

2.1.3.5.1. Accidental degeneracy

The symmetry analysis of lattice vibrations provides a powerful tool not only for the characterization of eigenvectors but also for the presentation of experimental results. In neutron scattering experiments, for example, a series of single phonons may be detected but symmetry determines which of these phonons belong to the same branch, *i.e.* how the single phonons have to be connected by a dispersion curve. The decision as to which of Figs. 2.1.3.8(a) or (b), which represent the same experimental results as full circles, is the correct one can be made by symmetry arguments only. In Fig. 2.1.3.8(a) the two phonon branches intersect. Thus, there are two degenerate phonons at the single wavevector \mathbf{q}^* . From the symmetry point of view, this particular wavevector has no special properties, *i.e.* the point group $G_o(\mathbf{q}^*)$ is just the same as for neighbouring wavevectors. Hence, the degeneracy cannot be due to symmetry and the respective eigenvectors \mathbf{e}_1 and \mathbf{e}_2 are not related by any transformation matrix. As a consequence, the two phonons cannot belong to the same irreducible representation, because otherwise every linear combination $\alpha\mathbf{e}_1 + \beta\mathbf{e}_2$ would equally well represent a valid eigenvector to the same eigenvalue with the same symmetry. It is, however, highly improbable that the special nature of the interatomic interactions gives rise to this uncertainty of eigenvectors at some wavevector within the Brillouin zone. Rather, it is expected that any infinitesimal change of force constants will favour one particular linear combination which, consequently, must correspond to a phonon of lower frequency. At the same time, there will be another well defined orthogonal eigenvector with slightly higher frequency – just as is represented in Fig. 2.1.3.8(b). Hence, two phonon branches of the same symmetry do not intersect and yield a frequency gap. This phenomenon is sometimes called *anticrossing* behaviour. It is associated with an eigenvector exchange between the two branches.

Accidental degeneracy according to Fig. 2.1.3.8(a), on the other hand, can only be observed if the two phonon branches belong to different irreducible representations. In this case, the eigenvectors are uniquely determined even at \mathbf{q}^* since a mixing is forbidden by symmetry.

2.1.3.5.2. Time-reversal degeneracy

In Section 2.1.3.3, we considered in some detail the symmetry of phonon eigenvectors with respect to the symmetry operations contained in the point group $G_o(\mathbf{q})$ of the wavevector. We know, however, that those symmetry operations that invert the wavevector give rise to additional constraints for the dynamical matrix. A lattice vibration with wavevector $-\mathbf{q}$ can also be regarded as a wave travelling in the opposite direction $+\mathbf{q}$ on a reversed timescale. Since the classical equations of motion are invariant with respect to time reversal, both phonon eigenvectors, $\mathbf{e}(\mathbf{q})$ and $\mathbf{e}(-\mathbf{q})$, are related and additional degeneracies may appear if there are symmetry operations that transform \mathbf{q} into $-\mathbf{q}$.

Let \mathbf{A} be the rotational part of such a symmetry operation. We have shown in Section 2.1.3.1 that anti-unitary matrix operators $\mathbf{T}(\mathbf{q}, \mathbf{A})$ can be defined that commute with the dynamical matrix. Not only the eigenvectors $\mathbf{e}(\mathbf{q}, s\lambda)$, $\lambda = 1, \dots, f_s$, but also

$$\bar{\mathbf{e}}(\mathbf{q}, s\lambda) = \mathbf{T}(\mathbf{q}, \mathbf{A}) \mathbf{e}(\mathbf{q}, s\lambda) \quad (2.1.3.59)$$

are therefore eigenvectors corresponding to the same eigenfrequency. If the latter are linear combinations of the former ones, no new information about degeneracies can be expected. If, on the other hand, $\mathbf{T}(\mathbf{q}, \mathbf{A}) \mathbf{e}(\mathbf{q}, s\lambda)$ is orthogonal to all vectors $\mathbf{e}(\mathbf{q}, s'\lambda')$, it belongs to another vector space corresponding to different indices s' and λ' . In this case, the eigenfrequencies $\omega_{\mathbf{q},sa}$

2.1. PHONONS

| $\tau^{(1+)}$ | $\tau^{(1-)}$ | $\tau^{(3+)}$ | $\tau^{(3-)}$ | $\tau^{(2)}$ | |
|---------------|---------------|---------------|---------------|--------------|----|
| 1 | | | | 1 | 1 |
| | | | | i | -i |
| 1 | | | | 1 | 1 |
| | | | | i | -i |
| 1 | 1 | 1 | 1 | 1 | -1 |
| | -1 | | | i | i |
| 1 | | 1 | 1 | 1 | -i |
| | 1 | | | i | -1 |
| 1 | 1 | -1 | -1 | 1 | i |
| | -1 | | | -1 | -1 |
| 1 | | 1 | 1 | 1 | -i |
| | 1 | | | i | 1 |
| 1 | 1 | -1 | -1 | 1 | -1 |
| | -1 | | | i | i |
| 1 | | 1 | 1 | 1 | -1 |
| | 1 | | | i | 1 |
| 1 | 1 | -1 | -1 | 1 | -1 |
| | -1 | | | i | i |
| 1 | | 1 | 1 | 1 | -1 |
| | 1 | | | i | 1 |
| 1 | 1 | -1 | -1 | 1 | -1 |
| | -1 | | | i | i |
| 1 | | 1 | 1 | 1 | -1 |
| | 1 | | | i | 1 |

Fig. 2.1.3.7. Matrix of symmetry coordinates at $\mathbf{q} = \mathbf{0}$ for the example structure given in Fig. 2.1.3.4 and Table 2.1.3.1.

and $\omega_{\mathbf{q},s'a'}$ have to be identical and additional degeneracies appear that may even relate different irreducible representations s and s' .

In order to distinguish between the two possibilities, we have to consider the transformation behaviour of the vector $\bar{\mathbf{e}}(\mathbf{q}, s\lambda)$. According to the multiplication rule for the \mathbf{T} -matrix operators, (2.1.3.32), we obtain

$$\begin{aligned} \mathbf{T}(\mathbf{q}, \mathbf{R}) \bar{\mathbf{e}}(\mathbf{q}, s\lambda) &= \mathbf{T}(\mathbf{q}, \mathbf{R}) \mathbf{T}(\mathbf{q}, \mathbf{A}) \mathbf{e}(\mathbf{q}, s\lambda) \\ &= \varphi^*(\mathbf{q}, \mathbf{A}, \mathbf{A}^{-1} \circ \mathbf{R} \circ \mathbf{A}) \varphi(\mathbf{q}, \mathbf{R}, \mathbf{A}) \\ &\quad \times \mathbf{T}(\mathbf{q}, \mathbf{A}) \mathbf{T}(\mathbf{q}, \mathbf{A}^{-1} \circ \mathbf{R} \circ \mathbf{A}) \mathbf{e}(\mathbf{q}, s\lambda). \end{aligned} \quad (2.1.3.60)$$

The operation $\mathbf{A}^{-1} \circ \mathbf{R} \circ \mathbf{A}$ leaves the wavevector invariant and is therefore an element of the point group $G_o(\mathbf{q})$. Hence the right-hand side can be expressed in terms of the irreducible representation $\tau^{(s)}(\mathbf{q}, \mathbf{R})$:

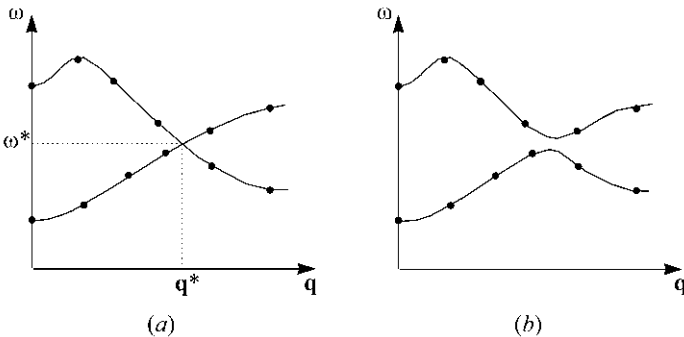


Fig. 2.1.3.8. (a) Accidental degeneracy of phonons with different symmetry. (b) Anticrossing of phonons with the same symmetry (no degeneracy).

$$\mathbf{T}(\mathbf{q}, \mathbf{R}) \bar{\mathbf{e}}(\mathbf{q}, s\lambda) = \varphi^*(\mathbf{q}, \mathbf{A}, \mathbf{A}^{-1} \circ \mathbf{R} \circ \mathbf{A}) \varphi(\mathbf{q}, \mathbf{R}, \mathbf{A}) \mathbf{T}(\mathbf{q}, \mathbf{A})$$

$$\begin{aligned} &\times \sum_{\lambda'=1}^{f_s} \tau_{\lambda'\lambda}^{(s)}(\mathbf{q}, \mathbf{A}^{-1} \circ \mathbf{R} \circ \mathbf{A}) \mathbf{e}(\mathbf{q}, s\lambda') \\ &= \varphi^*(\mathbf{q}, \mathbf{A}, \mathbf{A}^{-1} \circ \mathbf{R}) \varphi^*(\mathbf{q}, \mathbf{A}^{-1} \circ \mathbf{R}, \mathbf{A}) \\ &\quad \times \sum_{\lambda'=1}^{f_s} \tau_{\lambda'\lambda}^{(s)*}(\mathbf{q}, \mathbf{A}^{-1} \circ \mathbf{R} \circ \mathbf{A}) \bar{\mathbf{e}}(\mathbf{q}, s\lambda'). \end{aligned} \quad (2.1.3.61)$$

Obviously, the new eigenvectors $\bar{\mathbf{e}}(\mathbf{q}, s\lambda)$ transform according to the conjugated representation $\bar{\tau}^{(s)}(\mathbf{q}, \mathbf{R})$ defined by

$$\begin{aligned} \bar{\tau}^{(s)}(\mathbf{q}, \mathbf{R}) &= \varphi^*(\mathbf{q}, \mathbf{A}, \mathbf{A}^{-1} \circ \mathbf{R}) \varphi^*(\mathbf{q}, \mathbf{A}^{-1} \circ \mathbf{R}, \mathbf{A}) \\ &\quad \times \tau^{(s)*}(\mathbf{q}, \mathbf{A}^{-1} \circ \mathbf{R} \circ \mathbf{A}), \end{aligned} \quad (2.1.3.62)$$

\mathbf{A} being an arbitrary representative of those symmetry operations that invert the wavevector \mathbf{q} .

If the irreducible representations $\bar{\tau}^{(s)}(\mathbf{q}, \mathbf{R})$ and $\tau^{(s)}(\mathbf{q}, \mathbf{R})$ are not equivalent, the eigenvectors $\bar{\mathbf{e}}(\mathbf{q}, s\lambda)$ and $\mathbf{e}(\mathbf{q}, s\lambda')$ are linearly independent and, hence, the vibrations of the two representations are degenerate. In this case, $\tau^{(s)}(\mathbf{q}, \mathbf{R})$ is called a representation of the third kind. Within the decomposition of the \mathbf{T} representation, $\tau^{(s)}(\mathbf{q}, \mathbf{R})$ and $\bar{\tau}^{(s)}(\mathbf{q}, \mathbf{R})$ always appear in pairs.

If, on the other hand, the two representations are equivalent, there is a matrix β with

$$\bar{\tau}^{(s)}(\mathbf{q}, \mathbf{R}) = \beta^{-1} \tau^{(s)}(\mathbf{q}, \mathbf{R}) \beta \quad (2.1.3.63)$$

corresponding to a transformation of the coordinate system. It can be shown that the product $\beta \beta^*$ has the following form:

$$\beta \beta^* = \pm \varphi(\mathbf{q}, \mathbf{A}, \mathbf{A}) \tau^{(s)}(\mathbf{q}, \mathbf{A}^2). \quad (2.1.3.64)$$

In many cases, \mathbf{A} is of order 2, i.e. $\mathbf{A}^2 = \mathbf{E}$ (for $\mathbf{A} = \mathbf{i}$ or $\mathbf{A} = \mathbf{m}$, for example), and the right-hand side of (2.1.3.64) reduces to $\pm \mathbf{E}$.

Those representations for which the + sign in (2.1.3.64) holds have come to be called *representations of the first kind* [$\beta \beta^* = +\varphi(\mathbf{q}, \mathbf{A}, \mathbf{A}) \tau^{(s)}(\mathbf{q}, \mathbf{A}^2)$] and those that correspond to the - sign

2. SYMMETRY ASPECTS OF EXCITATIONS

representations of the second kind [$\beta\beta^* = -\varphi(\mathbf{q}, \mathbf{A}, \mathbf{A})\tau^{(s)}(\mathbf{q}, \mathbf{A}^2)$]. Without going into the details of the two cases, we merely wish to present the results that are most relevant for our discussion. For a more detailed presentation see *e.g.* Maradudin & Vosko (1968).

For representations of the first kind, the eigenvectors $\bar{\mathbf{e}}(\mathbf{q}, sa\lambda)$ and $\mathbf{e}(\mathbf{q}, sa\lambda')$ are related by a linear transformation. Hence there are no additional degeneracies due to the time-reversal invariance of the equation of motion. Let us consider the special case of a point group $G_o(\mathbf{q})$ whose elements commute with the symmetry operation \mathbf{A} . Crystals with a centre of inversion always meet this condition. For wavevectors within the Brillouin zone or for symmorphic space groups all multipliers are unity and $\tau^{(s)}(\mathbf{q}, \mathbf{R}) = \tau^{(s)*}(\mathbf{q}, \mathbf{R})$. In this case, representations are of the first kind if they are real representations.

For representations of the second kind, $\bar{\mathbf{e}}(\mathbf{q}, sa\lambda)$ and $\mathbf{e}(\mathbf{q}, sa\lambda')$ are linearly independent. The corresponding lattice vibrations are degenerate due to time-reversal invariance. Consequently, the multiplicity of the representation $\tau^{(s)}(\mathbf{q}, \mathbf{R})$ in the decomposition of the \mathbf{T} representation is an even number and pairs of eigenfrequencies are identical:

$$\omega_{\mathbf{q},sa} = \omega_{\mathbf{q},sa'} \text{ with } a \neq a'. \quad (2.1.3.65)$$

The theory of characters provides us with a rather simple criterion for the distinction between representations of the first, second or third kind. Without any proof, we simply present the result that is particularly important for practical work:

$$(1/|G|) \sum_{\mathbf{R}} \varphi(\mathbf{q}, \mathbf{A} \circ \mathbf{R}, \mathbf{A} \circ \mathbf{R}) \chi_{\tau^{(s)}}(\mathbf{q}, (\mathbf{A} \circ \mathbf{R})^2) = \begin{cases} +1 & \text{for representations of the first kind} \\ -1 & \text{for representations of the second kind} \\ 0 & \text{for representations of the third kind} \end{cases} \quad (2.1.3.66)$$

Finally, let us consider the special case of a real dynamical matrix. This can be found for crystals in which each atom is a centre of inversion or for special wavevectors on the Brillouin-zone boundary or at the Γ point, for example. In this case, the dynamical matrix commutes with the operator \mathbf{K}_o that transforms arbitrary vectors into their complex-conjugate counterparts. Hence, the vectors $\mathbf{K}_o \mathbf{e}(\mathbf{q}, sa\lambda) = \mathbf{e}^*(\mathbf{q}, sa\lambda)$ are eigenvectors to the eigenvalue $\omega_{\mathbf{q},sa}^2$ as well as $\mathbf{e}(\mathbf{q}, sa\lambda)$ itself. Since $\mathbf{e}(\mathbf{q}, sa\lambda)$ transforms under the elements of the point group $G_o(\mathbf{q})$ according to the irreducible representation $\tau^{(s)}(\mathbf{q})$, $\mathbf{e}^*(\mathbf{q}, sa\lambda)$ belongs to the complex-conjugate representation. If the two representations are not real ones and therefore not identical, the corresponding lattice vibrations have to be degenerate. Every linear combination of the eigenvectors $\mathbf{e}(\mathbf{q}, sa\lambda)$ and $\mathbf{e}^*(\mathbf{q}, sa\lambda)$ is an eigenvector as well. Thus, we are free to choose real eigenvectors, namely: $(1/\sqrt{2})[\mathbf{e}(\mathbf{q}, sa\lambda) + \mathbf{e}^*(\mathbf{q}, sa\lambda)]$ and $(1/\sqrt{2}i)[\mathbf{e}(\mathbf{q}, sa\lambda) - \mathbf{e}^*(\mathbf{q}, sa\lambda)]$.

2.1.3.5.3. Example

Let us consider the space group $P\bar{6}$. For wavevectors along the hexagonal axis, the point group $G_o(\mathbf{q})$ consists of the three symmetry operations E , D_{120}^z and D_{240}^z . Being a cyclic group, its irreducible representations are one-dimensional (see Table 2.1.3.4). The mirror plane m_z inverts the wavevector and the two threefold rotations are self-conjugated with respect to m_z :

$$\begin{aligned} \mathbf{m}_z D_{120}^z \mathbf{m}_z &= D_{120}^z \\ \mathbf{m}_z D_{240}^z \mathbf{m}_z &= D_{240}^z. \end{aligned}$$

If we remember that for symmorphic space groups all multipliers are unity, we obtain the following conjugate representations according to (2.1.3.62):

$$\begin{aligned} \bar{\tau}^{(1)} &= \tau^{(1)*} = \tau^{(1)} \\ \bar{\tau}^{(2)} &= \tau^{(2)*} = \tau^{(3)} \\ \bar{\tau}^{(3)} &= \tau^{(3)*} = \tau^{(2)}. \end{aligned}$$

Obviously, $\bar{\tau}^{(2)}$ and $\tau^{(2)}$ are inequivalent and, hence, pairs of phonons corresponding to representations $\tau^{(2)}$ and $\tau^{(3)}$, respectively, are degenerate. The two transverse acoustic phonon branches in particular not only leave the Γ point with the same slope as determined by the elastic stiffness $c_{44} = c_{2323}$ (*cf.* Section 2.1.2.4 and Chapter 1.3) but are strictly identical throughout the whole Brillouin zone.

Another example may illustrate the degeneracy of phonons at special wavevectors where the elements of the dynamical matrix are real quantities. Let us consider the nonsymmorphic space group $P6_3$. For the Γ point ($\mathbf{q} = \mathbf{0}$), the one-dimensional representations of this cyclic group are collected in Table 2.1.3.5. Obviously, $\tau^{(2)}(\mathbf{0})$ and $\tau^{(6)}(\mathbf{0})$ form a pair of complex-conjugated representations as well as $\tau^{(3)}(\mathbf{0})$ and $\tau^{(5)}(\mathbf{0})$. Therefore, always two lattice vibrations of these symmetries exhibit the same frequencies. The eigenvectors for representation $\tau^{(6)}(\mathbf{0})$ or $\tau^{(5)}(\mathbf{0})$ can be combined with the eigenvectors of corresponding modes of representations $\tau^{(2)}(\mathbf{0})$ or $\tau^{(3)}(\mathbf{0})$, respectively, to yield real quantities.

For wavevectors within the Brillouin zone along the hexagonal axis, the irreducible representations are the same as for the Γ point. However, the elements of the dynamical matrix are complex and symmetry does not yield any degeneracies. Hence phonons can be distinguished according to the six different representations.

At the Brillouin-zone boundary along the hexagonal axis ($\mathbf{q} = \mathbf{c}^*/2$, the A point), one has to take into account multipliers of the form $\exp[i\mathbf{q} \cdot \mathbf{v}(\mathbf{R})]$ since the space group is nonsymmorphic. For symmetry operations without fractional translation (E , D_{120}^z , D_{240}^z) this factor is unity, whereas it equals the complex unit i for the other elements of the point group (D_{60}^z , D_{180}^z , D_{300}^z). Hence the six irreducible multiplier representations are as shown in Table 2.1.3.6. Now we have three pairs of complex-conjugate representations, namely: $\tau^{(1)}(\mathbf{c}^*/2)$ and $\tau^{(4)}(\mathbf{c}^*/2)$; $\tau^{(2)}(\mathbf{c}^*/2)$ and $\tau^{(3)}(\mathbf{c}^*/2)$; and $\tau^{(5)}(\mathbf{c}^*/2)$ and $\tau^{(6)}(\mathbf{c}^*/2)$. Again, pairs of phonons of corresponding representations are degenerate. As a consequence, the phonon dispersion curves need not approach the Brillouin-zone boundary with a horizontal slope but meet another branch with the opposite slope.

In conclusion, group-theoretical considerations for wavevectors along the hexagonal axis yield at the centre (Γ point) as well as at the boundary (A point) of the first Brillouin zone pairs of degenerate phonon modes. Both modes belong to complex-conjugate representations. This result can be used in order to display the dispersion curves very clearly in an *extended zone scheme* plotting the phonon branches of different symmetries alternately from Γ to A and from A back to Γ as illustrated in Fig. 2.1.3.9. Here, the phonon dispersion for the room-temperature phase of KLiSO_4 is shown as an example. Note that irreducible representations are frequently denoted by the letters A, B, E, T instead of our notation $\tau^{(i)}$. T and E are reserved for representations that (at the Γ point) are triply and doubly degenerate, respectively. An index \pm or g/u is often used to distinguish representations that are symmetric (*gerade*) and antisymmetric (*ungerade*) with respect to a prominent symmetry operation, *e.g.* a centre of inversion or, in the case of $P6_3$, the twofold axis. The total symmetric representation is always denoted by A. Hence in

Table 2.1.3.4. Irreducible representations of the point group 3

| 3 | E | D_{120}^z | D_{240}^z |
|--------------|-----|------------------|------------------|
| $\tau^{(1)}$ | 1 | 1 | 1 |
| $\tau^{(2)}$ | 1 | $\exp(i2\pi/3)$ | $\exp(-i2\pi/3)$ |
| $\tau^{(3)}$ | 1 | $\exp(-i2\pi/3)$ | $\exp(i2\pi/3)$ |

2.1. PHONONS

Table 2.1.3.5. Irreducible representations of the space group $P6_3$ for $\mathbf{q} = \mathbf{0}$ (the Γ point)

| $P6_3$ | E | D_{60}^z | D_{120}^z | D_{180}^z | D_{240}^z | D_{300}^z |
|--------------------------|-----|----------------------------------|----------------------------------|-------------|----------------------------------|----------------------------------|
| $\tau^{(1)}(\mathbf{0})$ | 1 | 1 | 1 | 1 | 1 | 1 |
| $\tau^{(2)}(\mathbf{0})$ | 1 | $\exp(i\pi/3)$ | $\exp(i2\pi/3)$ | -1 | $\exp(i4\pi/3) = \exp(-i2\pi/3)$ | $\exp(i5\pi/3) = \exp(-i\pi/3)$ |
| $\tau^{(3)}(\mathbf{0})$ | 1 | $\exp(i2\pi/3)$ | $\exp(i4\pi/3) = \exp(-i2\pi/3)$ | 1 | $\exp(i2\pi/3)$ | $\exp(i4\pi/3) = \exp(-i2\pi/3)$ |
| $\tau^{(4)}(\mathbf{0})$ | 1 | -1 | 1 | -1 | 1 | -1 |
| $\tau^{(5)}(\mathbf{0})$ | 1 | $\exp(i4\pi/3) = \exp(-i2\pi/3)$ | $\exp(i2\pi/3)$ | 1 | $\exp(i4\pi/3) = \exp(-i2\pi/3)$ | $\exp(i2\pi/3)$ |
| $\tau^{(6)}(\mathbf{0})$ | 1 | $\exp(i5\pi/3) = \exp(-i\pi/3)$ | $\exp(i4\pi/3) = \exp(-i2\pi/3)$ | -1 | $\exp(i2\pi/3)$ | $\exp(i\pi/3)$ |

Table 2.1.3.6. Irreducible representations of the space group $P6_3$ for $\mathbf{q} = \mathbf{c}^*/2$ (the A point)

| $P6_3$ | E | D_{60}^z | D_{120}^z | D_{180}^z | D_{240}^z | D_{300}^z |
|------------------------------|-----|------------------------------------|----------------------------------|-------------|----------------------------------|------------------------------------|
| $\tau^{(1)}(\mathbf{c}^*/2)$ | 1 | i | 1 | i | 1 | i |
| $\tau^{(2)}(\mathbf{c}^*/2)$ | 1 | $i \exp(i\pi/3) = \exp(-i\pi/6)$ | $\exp(i2\pi/3)$ | - i | $\exp(i4\pi/3) = \exp(-i2\pi/3)$ | $i \exp(-i\pi/3) = \exp(i\pi/6)$ |
| $\tau^{(3)}(\mathbf{c}^*/2)$ | 1 | $i \exp(i2\pi/3) = \exp(i\pi/6)$ | $\exp(i4\pi/3) = \exp(-i2\pi/3)$ | i | $\exp(i2\pi/3)$ | $i \exp(-i2\pi/3) = \exp(-i\pi/6)$ |
| $\tau^{(4)}(\mathbf{c}^*/2)$ | 1 | - i | 1 | - i | 1 | - i |
| $\tau^{(5)}(\mathbf{c}^*/2)$ | 1 | $i \exp(-i2\pi/3) = \exp(-i\pi/6)$ | $\exp(i2\pi/3)$ | i | $\exp(i4\pi/3) = \exp(-i2\pi/3)$ | $i \exp(i2\pi/3) = \exp(i\pi/6)$ |
| $\tau^{(6)}(\mathbf{c}^*/2)$ | 1 | $i \exp(-i\pi/3) = \exp(i\pi/6)$ | $\exp(i4\pi/3) = \exp(-i2\pi/3)$ | - i | $\exp(i2\pi/3)$ | $i \exp(i\pi/3) = \exp(-i\pi/6)$ |

the preceding example all the representations $\tau^{(2)}$, $\tau^{(3)}$, $\tau^{(5)}$ and $\tau^{(6)}$ are E-type representations since they are doubly degenerate at the zone centre due to time-reversal degeneracy. Moreover, $\tau^{(3)}$ and $\tau^{(5)}$ are symmetric with respect to D_{180}^z . Therefore, the irreducible representations of Fig. 2.1.3.9 can be identified as $A = \tau^{(1)}$, $B = \tau^{(2)}$, $E_1 = \tau^{(2)}$, $E_1^+ = \tau^{(6)}$, $E_1^- = \tau^{(5)}$ and $E_2 = \tau^{(3)}$.

It can be seen that all phonon branches cross the zone boundary continuously while changing their symmetry. This behaviour is a direct consequence of the time-reversal degeneracy.

2.1.3.6. Compatibility relations

In our last example, we recognized that the group of the wavevector consists of the same elements, irrespective of whether the Γ point, the zone-boundary A point or any other wavevector along the hexagonal axis is concerned. This behaviour, however, is the exception rather than the rule. In general, wavevectors on the Brillouin-zone boundary exhibit different point groups to wavevectors within the Brillouin zone and the Γ point yields the full point group of the crystal. Obviously, the symmetry of the lattice vibrations changes discontinuously when approaching prominent wavevectors. Phonon branches, on the other hand, represent continuous functions $\omega(\mathbf{q})$ within the reciprocal space. Hence the question arises as to how the different irreducible (multiplier) representations associated with one particular phonon branch at different wavevectors are interrelated, *i.e.* which of the individual representations are *compatible*.

The solution of this problem is quite simple as long as all of the irreducible multiplier representations are one-dimensional. For arbitrary wavevectors within the Brillouin zone, the point group $G_o(\mathbf{q})$ is always a subgroup of $G_o(0)$ as well as of $G_o(\mathbf{q}_{\text{BZ}})$, where

\mathbf{q}_{BZ} represents a wavevector at the Brillouin-zone boundary in the direction of \mathbf{q} . When leaving a prominent wavevector ($\mathbf{q} = \mathbf{0}$ or $\mathbf{q} = \mathbf{q}_{\text{BZ}}$), the transformation properties of lattice vibrations with respect to all those symmetry operations that are conserved do not change. Hence, the compatibility relations for one-dimensional irreducible multiplier representations can be formulated as

$$\tau(\mathbf{q}, \mathbf{R}) = \tau(\mathbf{0}, \mathbf{R}) = \tau(\mathbf{q}_{\text{BZ}}, \mathbf{R}) \quad \forall \mathbf{R} \in G_o(\mathbf{q}). \quad (2.1.3.67)$$

The simple relation (2.1.3.67) does not hold, however, if higher-dimensional representations have to be considered at prominent wavevectors. With respect only to the symmetry elements of the subgroup $G_o(\mathbf{q})$, those representations are not necessarily irreducible. Rather, they may be decomposed into several (up to three) irreducible components $\tau^{(s)}(\mathbf{q})$. The multiplicities are given by the characters using the following equation:

$$c_s = \sum_{\mathbf{R} \in G_o(\mathbf{q})} \chi_{\tau(\mathbf{0}, \mathbf{R})} \chi_{\tau^{(s)}(\mathbf{q}, \mathbf{R})} \quad (2.1.3.68)$$

or

$$c'_s = \sum_{\mathbf{R} \in G_o(\mathbf{q})} \chi_{\tau(\mathbf{q}_{\text{BZ}}, \mathbf{R})} \chi_{\tau^{(s)}(\mathbf{q}, \mathbf{R})}.$$

Hence, phonons corresponding to irreducible representations $\tau^{(s)}(\mathbf{q})$ with nonzero multiplicities c_s (c'_s) will mix at the Γ point (zone boundary) to yield degenerate modes corresponding to the higher-dimensional representation.

In conclusion, group theory provides an important tool not only for the labelling of lattice vibrations according to irreducible multiplier representations but also for the assignment of branches at points of degeneracy within the reciprocal space.

2.1.3.6.1. Example

To illustrate compatibility relations, let us once more consider the example of space group $P4mm$ as introduced in Sections 2.1.3.1.1, 2.1.3.3.1 and 2.1.3.4.1. For wavevectors along \mathbf{a}^* we have $G_o(\mathbf{q}) = \{E, m_y\}$ and there are two irreducible representations, a symmetric one (with respect to m_y) $\tau^+(\mathbf{q})$ with $\tau^+(\mathbf{q}, m_y) = 1$ and an antisymmetric one with $\tau^-(\mathbf{q}, m_y) = -1$. Remember the representations for the Γ point, shown in Table 2.1.3.7. We immediately recognize that the Γ -point representations $\tau^{(1^+)}(\mathbf{0})$ and $\tau^{(3^+)}(\mathbf{0})$ are related to the symmetric representation τ^+ for nonzero wavevectors along \mathbf{a}^* . $\tau^{(1^-)}(\mathbf{0})$ and $\tau^{(3^-)}(\mathbf{0})$, on the

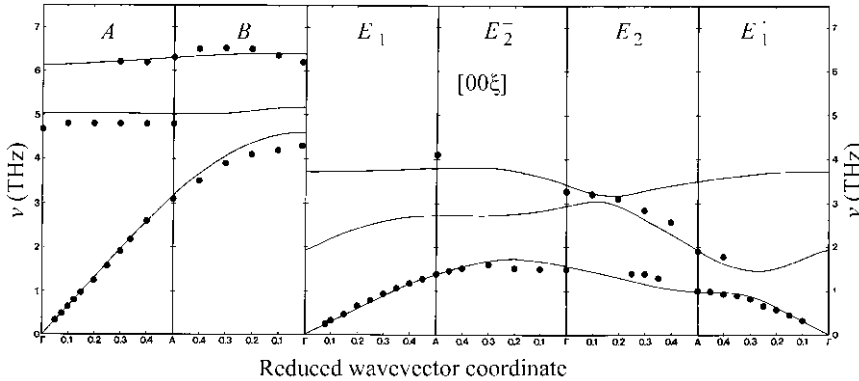


Fig. 2.1.3.9. Low-frequency part of the phonon dispersion of KLiSO_4 at room temperature (space group $P6_3$). The phonons are arranged in an extended zone scheme according to the different irreducible representations [after Eckold & Hahn (1987)]. The symbols represent experimental data and the lines represent the results of model calculations.

2. SYMMETRY ASPECTS OF EXCITATIONS

Table 2.1.3.7. Irreducible representations of the space group $P4mm$ for $\mathbf{q} = \mathbf{0}$ (the Γ point)

| $P4mm$ | Symmetry operation | | | | | | | |
|---------------------------------|--|---|--|---|--|--|---|---|
| | E | D_{90}^z | D_{180}^z | D_{270}^z | m_x | m_y | $m_{[110]}$ | $m_{[1\bar{1}0]}$ |
| $\tau^{(1+)}(\mathbf{0})$ | 1 | 1 | 1 | 1 | 1 | 1 | 1 | 1 |
| $\tau^{(1-)}(\mathbf{0})$ | 1 | 1 | 1 | 1 | -1 | -1 | -1 | -1 |
| $\tau^{(3+)}(\mathbf{0})$ | 1 | -1 | 1 | -1 | 1 | 1 | -1 | -1 |
| $\tau^{(3-)}(\mathbf{0})$ | 1 | -1 | 1 | -1 | -1 | -1 | 1 | 1 |
| $\tau^{(2)}(\mathbf{0})$ | $\begin{pmatrix} 1 & 0 \\ 0 & 1 \end{pmatrix}$ | $\begin{pmatrix} i & 0 \\ 0 & -i \end{pmatrix}$ | $\begin{pmatrix} -1 & 0 \\ 0 & -1 \end{pmatrix}$ | $\begin{pmatrix} -i & 0 \\ 0 & i \end{pmatrix}$ | $\begin{pmatrix} 0 & 1 \\ 1 & 0 \end{pmatrix}$ | $\begin{pmatrix} 0 & -1 \\ -1 & 0 \end{pmatrix}$ | $\begin{pmatrix} 0 & -i \\ i & 0 \end{pmatrix}$ | $\begin{pmatrix} 0 & i \\ -i & 0 \end{pmatrix}$ |
| $\chi_{\tau^{(2)}(\mathbf{0})}$ | 2 | 0 | -2 | 0 | 0 | 0 | 0 | 0 |

other hand, are related to the antisymmetric representation τ^- .

The two-dimensional representation $\tau^{(2)}(\mathbf{0})$ exhibits the character $\chi_{\tau^{(2)}(\mathbf{0}, \mathbf{m}_y)} = 0$. When leaving the Γ point along \mathbf{a}^* , it therefore splits into the symmetric representation with $\chi_{\tau^+(\mathbf{q}, \mathbf{m}_y)} = 1$ and the antisymmetric one with $\chi_{\tau^-(\mathbf{q}, \mathbf{m}_y)} = -1$. Consequently, there are always pairs of a symmetric and an antisymmetric lattice vibration which degenerate at the Brillouin-zone centre and the phonon dispersion along \mathbf{a}^* exhibits the principal behaviour as shown in Fig. 2.1.3.10. Here, six modes are displayed which illustrate the six possibilities for relating symmetric and antisymmetric vibrations to the Γ -point representations.

2.1.3.7. Optical selection rules

Inelastic neutron scattering is the unique experimental method for the determination of phonons at arbitrary wavevectors. Additional information can be obtained by optical methods, infrared absorption and Raman spectroscopy. For the detection of lattice vibrations, electromagnetic radiation of appropriate frequencies in the THz regime is needed. The corresponding wavelengths are of the order of 10^{-2} cm and are therefore very large compared with typical lattice parameters. Consequently, optical spectroscopy is sensitive to long-wavelength phonons only, *i.e.* to Γ -point modes. Moreover, the visibility of lattice vibrations in infrared or Raman experiments is governed by selection rules which, in turn, are determined by the symmetry of the corresponding eigenvectors. We may distinguish infrared-active modes, Raman-active modes and ‘silent’ modes that are neither infrared- nor Raman-active. Some simple group-theoretical arguments lead to the criteria for infrared or Raman activity.

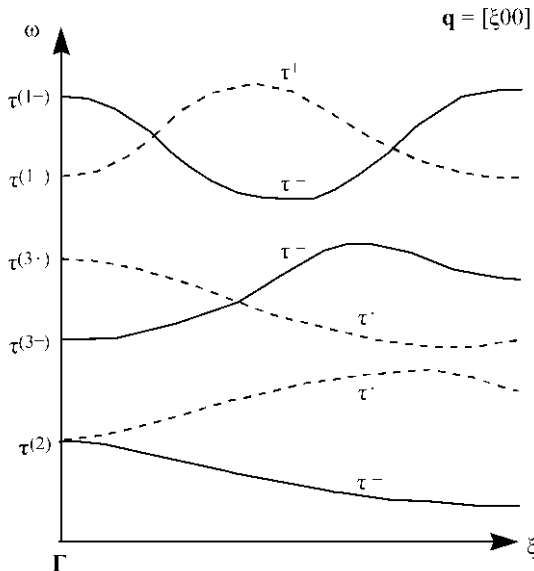


Fig. 2.1.3.10. Illustration of the compatibility relations for phonons in a tetragonal crystal with space group $P4mm$ for wavevectors along $[\xi 00]$.

Infrared spectroscopy is based on the absorption of electromagnetic radiation by phonons, as shown in Fig. 2.1.3.11. Photons can only be absorbed by those lattice vibrations that are associated with a periodic variation of an electric dipole moment. Since the dipole moment is a vector, it transforms under the symmetry operations of the crystal according to the vector representation τ_v , which is provided by the ordinary 3×3 matrices describing the effect of any rotation, mirror plane *etc.* upon an arbitrary vector of our three-dimensional space. It should be noted that the vector representation is in general reducible and can be regarded as the direct product of some irreducible representations. Lattice vibrations can carry an electric dipole moment only if their symmetry is compatible with the symmetry of a vector, *i.e.* if the corresponding irreducible representation is contained within the vector representation. The multiplicity of a particular irreducible Γ -point representation τ within the decomposition of the vector representation τ_v can be calculated from the respective characters χ_τ and χ_{τ_v} . Hence we may formulate the criterion for infrared activity as follows: Phonons corresponding to an irreducible representation τ are infrared active if

$$c_\tau = (1/|G|) \sum_{\mathbf{R}} \chi_\tau(\mathbf{R}) \chi_{\tau_v}(\mathbf{R}) \neq 0. \quad (2.1.3.69)$$

(First order) *Raman spectroscopy*, on the other hand, is based on the scattering of electromagnetic waves by phonons (see Fig. 2.1.3.12). Scattered intensity can only be obtained if the incident wave polarizes the crystal in such a way that it acts as a source for the outgoing wave. This is achieved if the tensor of the polarizability exhibits nonzero elements that relate electric field

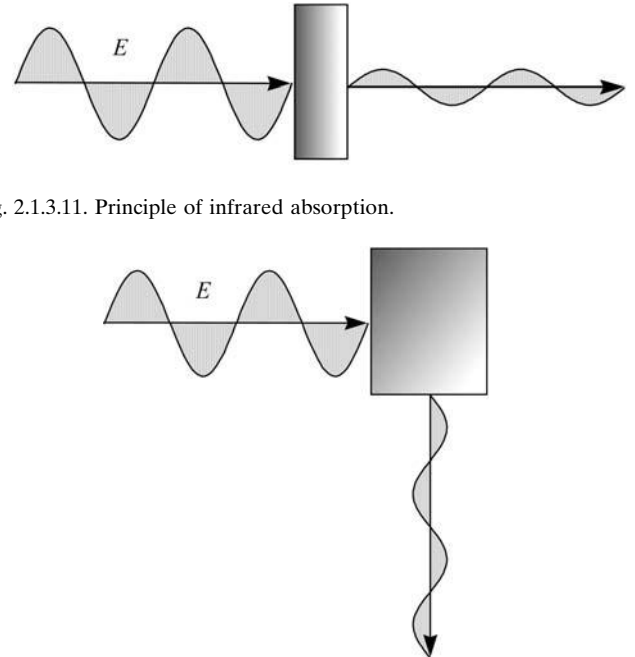


Fig. 2.1.3.11. Principle of infrared absorption.

Fig. 2.1.3.12. Principle of Raman spectroscopy.

2.1. PHONONS

Table 2.1.3.8. Character table of the space group $P4mm$ for $\mathbf{q} = \mathbf{0}$ (the Γ point)

| $P4mm$ | Symmetry operation | | | | | | | |
|----------------------|---|--|---|--|--|--|---|---|
| | E | D_{90}^z | D_{180}^z | D_{270}^z | m_x | m_y | $m_{[\bar{1}10]}$ | $m_{[110]}$ |
| $\chi_{\tau^{(1+)}}$ | 1 | 1 | 1 | 1 | 1 | 1 | 1 | 1 |
| $\chi_{\tau^{(1-)}}$ | 1 | 1 | 1 | 1 | -1 | -1 | -1 | -1 |
| $\chi_{\tau^{(3+)}}$ | 1 | -1 | 1 | -1 | 1 | 1 | -1 | -1 |
| $\chi_{\tau^{(3-)}}$ | 1 | -1 | 1 | -1 | -1 | -1 | 1 | 1 |
| $\chi_{\tau^{(2)}}$ | 2 | 0 | -2 | 0 | 0 | 0 | 0 | 0 |
| τ_v | $\begin{pmatrix} 1 & 0 & 0 \\ 0 & 1 & 0 \\ 0 & 0 & 1 \end{pmatrix}$ | $\begin{pmatrix} 0 & -1 & 0 \\ 1 & 0 & 0 \\ 0 & 0 & 1 \end{pmatrix}$ | $\begin{pmatrix} -1 & 0 & 0 \\ 0 & -1 & 0 \\ 0 & 0 & 1 \end{pmatrix}$ | $\begin{pmatrix} 0 & 1 & 0 \\ -1 & 0 & 0 \\ 0 & 0 & 1 \end{pmatrix}$ | $\begin{pmatrix} -1 & 0 & 0 \\ 0 & 1 & 0 \\ 0 & 0 & 1 \end{pmatrix}$ | $\begin{pmatrix} 1 & 0 & 0 \\ 0 & -1 & 0 \\ 0 & 0 & 1 \end{pmatrix}$ | $\begin{pmatrix} 0 & 1 & 0 \\ 1 & 0 & 0 \\ 0 & 0 & 1 \end{pmatrix}$ | $\begin{pmatrix} 0 & -1 & 0 \\ -1 & 0 & 0 \\ 0 & 0 & 1 \end{pmatrix}$ |
| χ_{τ_v} | 3 | 1 | -1 | 1 | 1 | 1 | 1 | 1 |
| χ_{τ_T} | 6 | 0 | 2 | 0 | 2 | 2 | 2 | 2 |

components in the directions of the incident and scattered waves. Hence, only those lattice vibrations that are associated with a periodic variation of the polarizability tensor can yield (first-order) Raman intensity. Their symmetry has to be compatible with the symmetry of a tensor, *i.e.* the corresponding irreducible representation has to be contained within the (reducible) tensor representation τ_T . As for infrared activity, we may therefore formulate the criterion for Raman-active phonons with the help of the characters χ_τ and χ_{τ_v} : Phonons corresponding to an irreducible representation τ are Raman active if

$$c_\tau = (1/|G|) \sum_{\mathbf{R}} \chi_\tau(\mathbf{R}) \chi_{\tau_T}(\mathbf{R}) \neq 0. \quad (2.1.3.70)$$

Without going into details, we note that the tensor representation τ_T is the symmetric square of the vector representation τ_v and its character may be calculated from the character of τ_v ,

$$\chi_{\tau_T}(\mathbf{R}) = \frac{1}{2}[\chi_v^2(\mathbf{R}) + \chi_v(\mathbf{R}^2)]. \quad (2.1.3.71)$$

It should be noted that group-theoretical considerations yield *necessary conditions* for the visibility of phonons. They cannot predict, however, intensities of active modes since these depend on crystal-specific properties like dipole moments or elements of the polarizability tensor.

2.1.3.7.1. Example

As an example, let us once more consider the space group $P4mm$. For $\mathbf{q} = \mathbf{0}$, the character table shown in Table 2.1.3.8 summarizes all essential information about irreducible, vector and tensor representations. Obviously, the vector representation consists of the irreducible representations $\tau^{(1+)}$ and $\tau^{(2)}$, the latter being two-dimensional. Γ -point phonons corresponding to these two representations are infrared active. All other lattice vibrations cannot be detected by absorption experiments.

Using the multiplicities as calculated from (2.1.3.70), we obtain the decomposition of the tensor representation:

$$\tau_T = 2\tau^{(1+)} + \tau^{(3+)} + \tau^{(3-)} + \tau^{(2)}.$$

Hence phonons corresponding to the representations $\tau^{(1+)}$, $\tau^{(3+)}$, $\tau^{(3-)}$ and $\tau^{(2)}$ are Raman active.

All lattice vibrations that belong to the representation $\tau^{(1-)}$ are neither infrared nor Raman active. They cannot be detected in (first-order) optical experiments and are therefore called silent modes.

2.1.4. Conclusion

Phonon investigations provide one of the most powerful tools for the determination of interatomic interactions within crystals since the phonon dispersion reflects all aspects of microscopic forces acting between the individual atoms. The symmetry of the atomic arrangement leads to certain restrictions for the actual

type of lattice vibrations. In this chapter, we have presented the fundamental ideas about phonon dispersion with special emphasis on the symmetry properties of the vibrations of a lattice.

Experimental phonon data are frequently interpreted in terms of either phenomenological interatomic potentials or *ab initio* band-structure calculations. In most cases, rather specific models are used for the theoretical calculation of the phonon dispersion for particular substances. This aspect is, however, beyond the scope of the present article. The interested reader is therefore referred to the original literature and a compilation by Bilz & Kress (1979), where phonon dispersion curves for more than a hundred insulating crystals are collected.

In the present chapter we have restricted ourselves to the general aspects of the symmetry reduction of both the dynamical matrix and its eigenvectors. It has been shown that group-theoretical methods play an important role in the labelling of phonons, in the consideration of degeneracies and, in particular, in the correct interpretation of experimental results.

It should be added that there is a computer program written by Warren & Worlton (1974) that enables the calculation of symmetry coordinates for arbitrary structures, for example. As part of a general lattice-dynamical program package for phenomenological model calculations written by Eckold *et al.* (1987; see also Eckold, 1992), it provides the symmetry reduction of the dynamical matrix and the assignment of individual phonon modes to the respective irreducible multiplier representations.

2.1.5. Glossary

| | |
|--|--|
| $\mathbf{a}^*, \mathbf{b}^*, \mathbf{c}^*$ | reciprocal-lattice vectors |
| A | Helmholtz free energy |
| \mathbf{A} | element of the coset $\mathbf{S}_- \circ G_o(\mathbf{q})$ |
| $\mathbf{C}(\mathbf{q}) = (C_{\kappa\kappa'}^{\alpha\beta}(\mathbf{q}))$ | modified dynamical matrix |
| c_{ij} | elastic stiffness in Voigt notation |
| (c_{ijklm}) | tensor of elastic stiffnesses |
| c_p | lattice heat capacity at constant pressure |
| $\tilde{c}_{\mathbf{q},j}$ | contribution of phonon state (\mathbf{q}, j) to the heat capacity at constant volume |
| c_s | multiplicity of irreducible representation s |
| c_V | lattice heat capacity at constant volume |
| c_V^{Debye} | lattice heat capacity at constant volume according to the Debye model |
| c_V^{Einstein} | lattice heat capacity at constant volume according to the Einstein model |
| $\mathbf{D}(\mathbf{q}) = (D_{\kappa\kappa'}^{\alpha\beta}(\mathbf{q}))$ | dynamical matrix |
| $\overline{\mathbf{D}}^{(s)}(\mathbf{q})$ | submatrix of the block-diagonalized dynamical matrix corresponding to irreducible multiplier representation σ |

2. SYMMETRY ASPECTS OF EXCITATIONS

| | | | |
|---|--|--|--|
| $\mathbf{D}_{\kappa\kappa'}(\mathbf{q})$ | 3×3 submatrix of the dynamical matrix | \mathbf{S}_- | space-group element that inverts the wavevector |
| \mathbf{D}_α^i | matrix of rotation about axis i by the angle α | t | time |
| $\mathbf{e}_\kappa(\mathbf{q}, j)$ | polarization vector of atom κ corresponding to the phonon (\mathbf{q}, j) | T | temperature |
| $\mathbf{e}(\mathbf{q}, j)$ | eigenvector of the dynamical matrix corresponding to the phonon (\mathbf{q}, j) | $\mathbf{T}(\mathbf{q}, \mathbf{R})$ $= (T_{\kappa\kappa'}^{\alpha\mu}(\mathbf{q}, \mathbf{R}))$ | matrix operator associated with a symmetry operation \mathbf{r} of the point group of the wavevector \mathbf{q} |
| E | identity | \mathbf{u}^o | polarization vector for elastic waves |
| $\mathbf{E}(\mathbf{q}, s\alpha\lambda)$ $= (E_\kappa^\alpha(\mathbf{q}, s\alpha\lambda))$ | matrix of symmetry coordinates | $\mathbf{u}_{\kappa l}(t)$ | displacement vector of atom (κl) |
| E_o | zero-point energy | V | potential energy |
| E_{ph} | lattice energy | V | volume |
| $E_{\mathbf{q}, j}$ | contribution of the phonon (\mathbf{q}, j) to the energy of the lattice | $\mathbf{V}(\kappa l, \kappa' l')$ $= (V_{\alpha\beta}(\kappa l, \kappa' l'))$ | matrix of force constants acting between atoms (κl) and $(\kappa' l')$ |
| $f_o(\kappa, S)$ | atom transformation table | v_s | sound velocity |
| f_σ | degeneracy of the eigenfrequency $\omega_{\mathbf{q}, \sigma}$ | $\mathbf{v}(\mathbf{S})$ | fractional translation associated with symmetry operation \mathbf{S} |
| $\mathbf{F}(\mathbf{q}) = (\mathbf{F}_{\kappa, \kappa'}(\mathbf{q}))$ | Fourier-transformed force-constant matrix | $\mathbf{x}(m)$ | lattice translation |
| \mathbf{g} | reciprocal-lattice vector | Z | partition function |
| $G(\mathbf{q})$ | space group of the wavevector \mathbf{q} | $\alpha = (\alpha_{\kappa l})$ | tensor of thermal expansion |
| $G_o(\mathbf{q})$ | point group of the wavevector \mathbf{q} | β | coefficient of volume expansion |
| $G_o(\mathbf{q}, -\mathbf{q})$ | augmented point group of the wavevector \mathbf{q} | γ | mean Grüneisen parameter |
| $ G $ | order of group G | $\gamma_{\mathbf{q}, j}$ | averaged-mode Grüneisen parameter |
| $G(\omega)$ | density of phonon states | $\gamma_{\mathbf{q}, \kappa l}$ | generalized-mode Grüneisen parameters |
| $G^{\text{Debye}}(\omega)$ | density of phonon states according to the Debye model | $\Gamma = (\Gamma_{jl})$ | propagation tensor |
| $G^{\text{Einstein}}(\omega)$ | density of phonon states according to the Einstein model | $\Gamma = (\Gamma_{\kappa\kappa'}^{\alpha\mu}(\mathbf{q}, \{\mathbf{S} \mathbf{v}(\mathbf{S}) + \mathbf{x}(m)\}))$ | transformation matrix |
| H | Hamiltonian | δ_{kl} | Kronecker delta |
| \hbar | Planck constant (1.0546×10^{-34} J s) | $\delta(\omega)$ | Dirac delta function |
| I | inversion | $\Delta(\mathbf{q}, \mathbf{R})$ | block-diagonal matrix of irreducible representations |
| k | Boltzmann constant (1.381×10^{-23} J K $^{-1}$) | $\boldsymbol{\varepsilon} = (\varepsilon_{\kappa l})$ | strain tensor |
| \mathbf{K}_o | anti-unitary operator | χ | character of a representation |
| \mathbf{M} | mass tensor | $\varphi(\mathbf{q}, \mathbf{r}_i, \mathbf{r}_j)$ | multiplier associated with two symmetry operations \mathbf{r}_i and \mathbf{r}_j of the point group of the wavevector \mathbf{q} |
| m_i | mirror plane perpendicular to axis i | Φ | potential energy |
| m_κ | mass of atom κ | κ | isothermal compressibility |
| $n_{\mathbf{q}, j}$ | Bose factor corresponding to the phonon state (\mathbf{q}, j) | Θ_D | Debye temperature |
| N | number of atoms within the primitive cell | Θ_E | Einstein temperature |
| N_Z | number of primitive cells | ρ | density |
| p | pressure | $\boldsymbol{\sigma} = (\sigma_{\kappa l})$ | stress tensor |
| $\mathbf{p}_{\kappa l}$ | momentum of atom (κl) | $\boldsymbol{\tau}^{(s)}(\mathbf{q}, \mathbf{R})$ $= (\tau_{\lambda\lambda'}^{(s)}(\mathbf{q}, \mathbf{R}))$ | irreducible representation |
| p_n | occupation probability of quantum state n | $\overline{\boldsymbol{\tau}^{(s)}}(\mathbf{q}, \mathbf{R})$ | conjugated representation |
| $\mathbf{P}^{(s)}(\mathbf{q}) = (P_{\lambda\lambda'}^{(s)}(\mathbf{q}))$ | projection operator | $\boldsymbol{\tau}_v$ | vector representation |
| \mathbf{q} | phonon wavevector | $\boldsymbol{\tau}_T$ | tensor representation |
| \mathbf{q}_{BZ} | wavevector on the Brillouin-zone boundary | ω_D | Debye frequency |
| $Q_{\mathbf{q}, j}$ | normal coordinate corresponding to the phonon (\mathbf{q}, j) | ω_E | Einstein frequency |
| \mathbf{r}_l | vector to the origin of the l th primitive cell | $\omega_{\mathbf{q}, j}$ | frequency of phonon (\mathbf{q}, j) |
| $\mathbf{r}_{\kappa l}(t)$ | time-dependent position vector of atom (κl) | $\boldsymbol{\Psi}$ | arbitrary vector |
| \mathbf{r}_κ^o | equilibrium position of atom κ with respect to the origin of the primitive cell | $*$ | denotes the complex-conjugate quantity |
| $\mathbf{r}_{\kappa l}^o$ | equilibrium position of atom κ within the l th primitive cell | $+$ | denotes the Hermitian conjugate matrix |
| \mathbf{R} | element of the point group of the wavevector $G_o(\mathbf{q})$ | T | denotes the transposed matrix |
| $\bar{\mathbf{R}}$ | element of $G_o(\mathbf{q}, -\mathbf{q})$ | | |
| $\{\mathbf{S} \mathbf{v}(\mathbf{S}) + \mathbf{x}(m)\}$ | symmetry operation (Seitz notation) | | |
| $\mathbf{S} = (S_{\alpha\beta})$ | matrix of rotation | | |

References

- Bilz, H. & Kress, W. (1979). *Phonon dispersion relations in insulators*. Springer Series in Solid State Sciences, Vol. 10. Berlin: Springer. (ISBN 3-540-09399-0.)
- Bradley, C. J. & Cracknell, A. P. (1972). *The mathematical theory of symmetry in solids*. Oxford: Clarendon Press.
- Dove, M. T. (1993). *Introduction to lattice dynamics*. Cambridge University Press. (ISBN 0-521-39293-4.)

2.1. PHONONS

- Eckold, G. (1992). *UNISOFT – a program package for lattice-dynamical calculations: user manual*. JÜL-2639, Jülich. (ISSN 0366-0885.)
- Eckold, G. & Hahn, Th. (1987). *Gitterdynamik von KLiSO_4* . In *Neutronenspektrometer UNIDAS – Ergebnisbericht 1981–1986*. JÜL-Spez-410, pp. 57–61. (ISSN 0343-7639.)
- Eckold, G., Stein-Arsic, M. & Weber, H. J. (1987). *UNISOFT – a program package for lattice-dynamical calculations*. *J. Appl. Cryst.* **20**, 134–139.
- Giannozzi, P., de Gironcoli, S., Pavone, P. & Baroni, S. (1991). *Ab initio calculation of phonon dispersions in semiconductors*. *Phys. Rev. B*, **43**, 7231–7242.
- Kovalev, O. V. (1965). *Irreducible representations of the space groups*. New York: Gordon & Breach.
- Leibfried, G. (1955). *Gittertheorie der mechanischen und thermischen Eigenschaften der Kristalle*. In *Handbuch der Physik VII/1*, edited by S. Flügge, pp. 105–324. Berlin: Springer.
- Maradudin, A. A., Montroll, E. W., Weiss, G. H. & Ipatova, I. P. (1971). *Theory of lattice dynamics in the harmonic approximation*. In *Solid state physics*, Suppl. 3, edited by H. Ehrenreich, F. Seitz & D. Turnbull. New York: Academic Press.
- Maradudin, A. A. & Vosko, S. H. (1968). *Symmetry properties of the normal vibrations of a crystal*. *Rev. Mod. Phys.* **40**, 1–37.
- Natkaniec, I., Bokhenkov, E. L., Dorner, B., Kalus, J., Mackenzie, G. A., Pawley, G. S., Schmelzer, U. & Sheka, E. F. (1980). *Phonon dispersion in d_8 -naphthalene crystal at 6 K*. *J. Phys. C*, **13**, 4265–4283.
- Pintschovius, L., Pyka, N., Reichardt, W., Rumiantsev, A. Yu., Mitrofanov, N. L., Ivanov, A. S., Collin, G. & Bourges, P. (1991). *Lattice dynamical studies of HTSC materials*. *Physica C*, **185–189**, 156–161.
- Reissland, J. A. (1973). *The physics of phonons*. London: Wiley. (ISBN 0-471-71585-9.)
- Srivastava, G. P. (1990). *The physics of phonons*. Bristol: Adam Hilger. (ISBN 0-85274-153-7.)
- Strauch, D. & Dorner, B. (1990). *Phonon dispersion in GaAs*. *J. Phys. Condens. Matter*, **2**, 1457–1474.
- Trampenau, J., Heiming, A., Petry, W., Alba, M., Herzig, C., Miekeley, W. & Schober, H. R. (1991). *Phonon dispersion of the bcc phase of group-IV metals. III. Bcc hafnium*. *Phys. Rev. B*, **43**, 10963–10969.
- Warren, J. L. & Worlton, T. G. (1974). *Improved version of group-theoretical analysis of lattice dynamics*. *Comput. Phys. Commun.* **8**, 71–84.

2.2. Electrons

BY K. SCHWARZ

2.2.1. Introduction

The electronic structure of a solid, characterized by its energy band structure, is the fundamental quantity that determines the ground state of the solid and a series of excitations involving electronic states. In this chapter, we first summarize several basic concepts in order to establish the notation used here and to repeat essential theorems from group theory and solid-state physics that provide definitions which we need in this context. Next the quantum-mechanical treatment, especially density functional theory, is described and the commonly used methods of band theory are outlined. One scheme is presented explicitly so that concepts in connection with energy bands can be explained. The electric field gradient is discussed to illustrate a tensorial quantity and a few examples illustrate the topics of this chapter.

2.2.2. The lattice

2.2.2.1. The direct lattice and the Wigner–Seitz cell

The three unit-cell vectors \mathbf{a}_1 , \mathbf{a}_2 and \mathbf{a}_3 define the parallelepiped of the unit cell. We define

(i) a translation vector *of* the lattice (upper case) as a primitive vector (integral linear combination) of all translations

$$\mathbf{T}_n = n_1\mathbf{a}_1 + n_2\mathbf{a}_2 + n_3\mathbf{a}_3 \text{ with } n_i \text{ integer,} \quad (2.2.2.1)$$

(ii) but a vector *in* the lattice (lower case) as

$$\mathbf{r} = x_1\mathbf{a}_1 + x_2\mathbf{a}_2 + x_3\mathbf{a}_3 \text{ with } x_i \text{ real.} \quad (2.2.2.2)$$

From the seven possible crystal systems one arrives at the 14 possible space lattices, based on both primitive and non-primitive (body-centred, face-centred and base-centred) cells, called the *Bravais lattices* [see Chapter 9.1 of *International Tables for Crystallography*, Volume A (2002)]. Instead of describing these cells as parallelepipeds, we can find several types of polyhedra with which we can fill space by translation. A very important type of space filling is obtained by the *Dirichlet construction*. Each lattice point is connected to its nearest neighbours and the corresponding bisecting (perpendicular) planes will delimit a region of space which is called the *Dirichlet region*, the *Wigner–Seitz cell* or the *Voronoi cell*. This cell is uniquely defined and has additional symmetry properties.

When we add a basis to the lattice (*i.e.* the atomic positions in the unit cell) we arrive at the well known 230 space groups [see Part 3 of *International Tables for Crystallography*, Volume A (2002)].

2.2.2.2. The reciprocal lattice and the Brillouin zone

Owing to the translational symmetry of a crystal, it is convenient to define a reciprocal lattice, which plays a dominating role in describing electrons in a solid. The three unit vectors of the reciprocal lattice \mathbf{b}_i are given according to the standard definition by

$$\mathbf{a}_i\mathbf{b}_j = 2\pi\delta_{ij}, \quad (2.2.2.3)$$

where the factor 2π is commonly used in solid-state physics in order to simplify many expressions. Strictly speaking (in terms of mathematics) this factor should not be included [see Section 1.1.2.4 of the present volume and Chapter 1.1 of *International*

Tables for Crystallography, Volume B (2000)], since the (complete) reciprocity is lost, *i.e.* the reciprocal lattice of the reciprocal lattice is no longer the direct lattice.

$$\mathbf{b}_1 = 2\pi \frac{\mathbf{a}_2 \times \mathbf{a}_3}{\mathbf{a}_1 \cdot \mathbf{a}_2 \times \mathbf{a}_3} \text{ and cyclic permutations.} \quad (2.2.2.4)$$

In analogy to the direct lattice we define

(i) a vector *of* the reciprocal lattice (upper case) as

$$\mathbf{K}_m = m_1\mathbf{b}_1 + m_2\mathbf{b}_2 + m_3\mathbf{b}_3 \text{ with } m_i \text{ integer;} \quad (2.2.2.5)$$

(ii) a vector *in* the lattice (lower case) as

$$\mathbf{k} = k_1\mathbf{b}_1 + k_2\mathbf{b}_2 + k_3\mathbf{b}_3 \text{ with } k_i \text{ real.} \quad (2.2.2.6)$$

From (2.2.2.5) and (2.2.2.1) it follows immediately that

$$\mathbf{T}_n\mathbf{K}_m = 2\pi N \text{ with } N \text{ an integer.} \quad (2.2.2.7)$$

A construction identical to the Wigner–Seitz cell delimits in reciprocal space a cell conventionally known as the *first Brillouin zone* (BZ), which is very important in the band theory of solids. There are 14 first Brillouin zones according to the 14 Bravais lattices.

2.2.3. Symmetry operators

The concepts of symmetry operations in connection with a quantum-mechanical treatment of the electronic states are essential for an understanding of the electronic structure. In this context the reader is referred, for example, to the book by Altmann (1994).

For the definition of symmetry operators we use in the whole of this chapter the *active picture*, which has become the standard in solid-state physics. This means that the whole configuration space is rotated, reflected or translated, while the coordinate axes are kept fixed.

A translation is given by

$$\mathbf{r}' = \mathbf{r} + \mathbf{T} \quad (2.2.3.1)$$

$$t\mathbf{r} = \mathbf{r} + \mathbf{T}, \quad (2.2.3.2)$$

where t on the left-hand side corresponds to a symmetry (configuration-space) operator.

2.2.3.1. Transformation of functions

Often we are interested in a function (*e.g.* a wavefunction) $f(\mathbf{r})$ and wish to know how it transforms under the configuration operator g which acts on \mathbf{r} . For this purpose it is useful to introduce a function-space operator \tilde{g} which defines how to modify the function in the transformed configuration space so that it agrees with the original function $f(\mathbf{r})$ at the original coordinate \mathbf{r} :

$$\tilde{g}f(g\mathbf{r}) = f(\mathbf{r}). \quad (2.2.3.3)$$

This must be valid for all points \mathbf{r} and thus also for $g^{-1}\mathbf{r}$, leading to the alternative formulation

$$\tilde{g}f(\mathbf{r}) = f(g^{-1}\mathbf{r}). \quad (2.2.3.4)$$

2.2. ELECTRONS

The symmetry operations form a group \tilde{G} of configuration-space operations \tilde{g}_i with the related group \tilde{G} of the function-shape operators \tilde{g}_i . Since the multiplication rules

$$g_i g_j = g_k \rightarrow \tilde{g}_i \tilde{g}_j = \tilde{g}_k \quad (2.2.3.5)$$

are preserved, these two groups are isomorphic.

2.2.3.2. Transformation of operators

In a quantum-mechanical treatment of the electronic states in a solid we have the following different entities: points in configuration space, functions defined at these points and (quantum-mechanical) operators acting on these functions. A symmetry operation transforms the points, the functions and the operators in a clearly defined way.

Consider an eigenvalue equation of operator \mathbb{A} (e.g. the Hamiltonian):

$$\mathbb{A}\varphi = a\varphi, \quad (2.2.3.6)$$

where $\varphi(\mathbf{r})$ is a function of \mathbf{r} . When g acts on \mathbf{r} , the function-space operator \tilde{g} acts [according to (2.2.3.4)] on φ yielding ψ :

$$\psi = \tilde{g}\varphi \rightarrow \varphi = \tilde{g}^{-1}\psi. \quad (2.2.3.7)$$

By putting φ from (2.2.3.7) into (2.2.3.6), we obtain

$$\mathbb{A}\tilde{g}^{-1}\psi = a\tilde{g}^{-1}\psi. \quad (2.2.3.8)$$

Multiplication from the left by \tilde{g} yields

$$\tilde{g}\mathbb{A}\tilde{g}^{-1}\psi = a\tilde{g}\tilde{g}^{-1}\psi = a\psi. \quad (2.2.3.9)$$

This defines the transformed operator $\tilde{g}\mathbb{A}\tilde{g}^{-1}$ which acts on the transformed function ψ that is given by the original function φ but at position $g^{-1}\mathbf{r}$.

2.2.3.3. The Seitz operators

The most general space-group operation is of the form $w p$ with the point-group operation p (a rotation, reflection or inversion) followed by a translation w :

$$w p = \{p|\mathbf{w}\}. \quad (2.2.3.10)$$

With the definition

$$\{p|\mathbf{w}\}\mathbf{r} = w p \mathbf{r} = w(p\mathbf{r}) = p\mathbf{r} + \mathbf{w} \quad (2.2.3.11)$$

it is easy to prove the multiplication rule

$$\{p|\mathbf{w}\}\{p'|\mathbf{w}'\} = \{pp'|\mathbf{w} + \mathbf{w}'\} \quad (2.2.3.12)$$

and define the inverse of a Seitz operator as

$$\{p|\mathbf{w}\}^{-1} = \{p^{-1}|\mathbf{w}'\}, \quad (2.2.3.13)$$

which satisfies

$$\{p|\mathbf{w}\}\{p|\mathbf{w}\}^{-1} = \{E|\mathbf{0}\}, \quad (2.2.3.14)$$

where $\{E|\mathbf{0}\}$ does not change anything and thus is the identity of the space group G .

2.2.3.4. The important groups and their first classification

Using the Seitz operators, we can classify the most important groups as we need them at the beginning of this chapter:

(i) the *space group*, which consists of all elements $G = \{\{p|\mathbf{w}\}\}$;
(ii) the *point group* (without any translations) $P = \{\{p|\mathbf{0}\}\}$; and

(iii) the *lattice translation subgroup* $T = \{\{E|\mathbf{T}\}\}$, which is an invariant subgroup of G , i.e. $T \triangleleft G$. Furthermore T is an Abelian group, i.e. the operation of two translations commute ($t_1 t_2 = t_2 t_1$) (see also Section 1.2.3.1 of the present volume). A useful

consequence of the commutation property is that T can be written as a direct product of the corresponding one-dimensional translations,

$$T = T_x \otimes T_y \otimes T_z. \quad (2.2.3.15)$$

(iv) A *symmorphic* space group contains no fractional translation vectors and thus P is a subgroup of G , i.e. $P \triangleleft G$.

(v) In a *non-symmorphic* space group, however, some p are associated with fractional translation vectors \mathbf{v} . These \mathbf{v} do not belong to the translation lattice but when they are repeated a specific integer number of times they give a vector of the lattice. In this case, $\{p|\mathbf{0}\}$ can not belong to G for all p .

(vi) The *Schrödinger group* is the group S of all operations \tilde{g} that leave the Hamiltonian invariant, i.e. $\tilde{g}\mathbb{H}\tilde{g}^{-1} = \mathbb{H}$ for all $\tilde{g} \in S$. This is equivalent to the statement that \tilde{g} and \mathbb{H} commute: $\tilde{g}\mathbb{H} = \mathbb{H}\tilde{g}$. From this commutator relation we find the degenerate states in the Schrödinger equation, namely that $\tilde{g}\varphi$ and φ are degenerate with the eigenvalue E whenever $\tilde{g} \in S$, as follows from the three equations

$$\mathbb{H}\varphi = E\varphi \quad (2.2.3.16)$$

$$\tilde{g}\mathbb{H}\varphi = E\tilde{g}\varphi \quad (2.2.3.17)$$

$$\mathbb{H}\tilde{g}\varphi = E\tilde{g}\varphi. \quad (2.2.3.18)$$

2.2.4. The Bloch theorem

The electronic structure of an infinite solid looks so complicated that it would seem impossible to calculate it. Two important steps make the problem feasible. One is the *single-particle approach*, in which each electron moves in an average potential $V(\mathbf{r})$ according to a Schrödinger equation,

$$\mathbb{H}\psi(\mathbf{r}) = \left\{ -\frac{\hbar^2}{2m} \nabla^2 + V(\mathbf{r}) \right\} \psi(\mathbf{r}) = E\psi(\mathbf{r}), \quad (2.2.4.1)$$

and has its kinetic energy represented by the first operator. The second important concept is the *translational symmetry*, which leads to Bloch functions. The single-particle aspect will be discussed later (for details see Sections 2.2.9 and 2.2.10).

2.2.4.1. A simple quantum-mechanical derivation

In order to derive the Bloch theorem, we can simplify the problem by considering a one-dimensional case with a lattice constant a . [The generalization to the three-dimensional case can be done easily according to (2.2.3.15).] The one-dimensional Schrödinger equation is

$$\left\{ -\frac{\hbar^2}{2m} \frac{d^2}{dx^2} + V(x) \right\} \psi(x) = E\psi(x), \quad (2.2.4.2)$$

where $V(x)$ is invariant under translations, i.e. $V(x+a) = V(x)$. We define a translation operator t according to (2.2.3.1) for the translation by one lattice constant as

$$tx = x + a \quad (2.2.4.3)$$

and apply its functional counterpart \tilde{t} to the potential, which gives [according to (2.2.3.4)]

$$\tilde{t}V(x) = V(t^{-1}x) = V(x-a) = V(x). \quad (2.2.4.4)$$

The first part in \mathbb{H} corresponds to the kinetic energy operator, which is also invariant under translations. Therefore, since $\tilde{t} \in T$ (the lattice translation subgroup) and $\tilde{t} \in S$ (the Schrödinger group), \tilde{t} commutes with \mathbb{H} , i.e. the commutator vanishes, $[\tilde{t}, \mathbb{H}] = 0$ or $\tilde{t}\mathbb{H} = \mathbb{H}\tilde{t}$. This situation was described above [see (2.2.3.16)–(2.2.3.18)] and leads to the fundamental theorem of quantum mechanics which states that when two operators

2. SYMMETRY ASPECTS OF EXCITATIONS

commute the eigenvectors of the first must also be eigenvectors of the second. Consequently we have

$$\mathbb{H}\psi(x) = E\psi(x) \quad (2.2.4.5)$$

$$\tilde{t}\psi(x) = \mu\psi(x), \quad (2.2.4.6)$$

where μ is the eigenvalue corresponding to the translation by the lattice constant a . The second equation can be written explicitly as

$$\tilde{t}\psi(x) = \psi(t^{-1}x) = \psi(x - a) = \mu\psi(x) \quad (2.2.4.7)$$

and tells us how the wavefunction changes from one unit cell to the neighbouring unit cell. Notice that the electron density must be translationally invariant and thus it follows

$$\text{from } \psi^*(x - a)\psi(x - a) = \psi^*(x)\psi(x) \text{ that } \mu^*\mu = 1, \quad (2.2.4.8)$$

which is a necessary (but not sufficient) condition for defining μ .

2.2.4.2. Periodic boundary conditions

We can expect the bulk properties of a crystal to be insensitive to the surface and also to the boundary conditions imposed, which we therefore may choose to be of the most convenient form. Symmetry operations are covering transformations and thus we have an *infinite* number of translations in T , which is most inconvenient. A way of avoiding this is provided by periodic boundary conditions (*Born-von Karman*). In the present one-dimensional case this means that the wavefunction $\psi(x)$ becomes periodic in a domain $L = Na$ (with integer N number of lattice constants a), *i.e.*

$$\psi(x + Na) = \psi(x + L) = \psi(x). \quad (2.2.4.9)$$

According to our operator notation (2.2.4.6), we have the following situation when the translation t is applied n times:

$$\tilde{t}^n\psi(x) = \psi(x - na) = \mu^n\psi(x). \quad (2.2.4.10)$$

It follows immediately from the periodic boundary condition (2.2.4.9) that

$$\mu^N = 1 \quad (2.2.4.11)$$

with the obvious solution

$$\mu = \exp[2\pi i(n/N)] \quad \text{with } n = 0 \pm 1, \pm 2, \dots \quad (2.2.4.12)$$

Here it is convenient to introduce a notation

$$k = \frac{2\pi n}{a N} \quad (2.2.4.13)$$

so that we can write $\mu = \exp(ika)$. Note that k is quantized due to the periodic boundary conditions according to (2.2.4.13). Summarizing, we have the Bloch condition (for the one-dimensional case):

$$\psi(x + a) = \exp(ika)\psi(x), \quad (2.2.4.14)$$

i.e. when we change x by one lattice constant a the wavefunction at x is multiplied by a phase factor $\exp(ika)$. At the moment (2.2.4.13) suggests the use of k as label for the wavefunction $\psi_k(x)$.

Generalization to three dimensions leads to the exponential $\exp(i\mathbf{k}\mathbf{T})$ with

$$\sum_{i=1}^3 k_i n_i = \mathbf{k} \cdot \mathbf{T} \quad \text{using (2.2.2.6) and (2.2.2.1)} \quad (2.2.4.15)$$

and thus to the Bloch condition

$$\psi_{\mathbf{k}}(\mathbf{r} + \mathbf{T}) = \exp(i\mathbf{k}\mathbf{T})\psi_{\mathbf{k}}(\mathbf{r}), \quad (2.2.4.16)$$

or written in terms of the translational operator $\{E|\mathbf{T}\}$ [see (2.2.3.15)]

$$\{E|\mathbf{T}\}\psi_{\mathbf{k}}(\mathbf{r}) = \psi_{\mathbf{k}}(\mathbf{r} - \mathbf{T}) = \exp(-i\mathbf{k}\mathbf{T})\psi_{\mathbf{k}}(\mathbf{r}). \quad (2.2.4.17)$$

The eigenfunctions that satisfy (2.2.4.17) are called Bloch functions and have the form

$$\psi_{\mathbf{k}}(\mathbf{r}) = \exp(i\mathbf{k}\mathbf{r})u_{\mathbf{k}}(\mathbf{r}), \quad (2.2.4.18)$$

where $u_{\mathbf{k}}(\mathbf{r})$ is a periodic function in the lattice,

$$u_{\mathbf{k}}(\mathbf{r}) = u_{\mathbf{k}}(\mathbf{r} + \mathbf{T}) \quad \text{for all } \mathbf{T}, \quad (2.2.4.19)$$

and \mathbf{k} is a vector in the reciprocal lattice [see (2.2.2.6)] that plays the role of the quantum number in solids. The \mathbf{k} vector can be chosen in the first BZ, because any \mathbf{k}' that differs from \mathbf{k} by just a lattice vector \mathbf{K} of the reciprocal lattice has the same Bloch factor and the corresponding wavefunction $\psi_{\mathbf{k}+\mathbf{K}}(\mathbf{r})$ satisfies the Bloch condition again, since

$$\exp[i(\mathbf{k} + \mathbf{K})\mathbf{T}] = \exp(i\mathbf{k}\mathbf{T})\exp(i\mathbf{K}\mathbf{T}) = \exp(i\mathbf{k}\mathbf{T}), \quad (2.2.4.20)$$

where the factor $\exp(i\mathbf{K}\mathbf{T})$ is unity according to (2.2.2.7). Since these two functions, $\psi_{\mathbf{k}+\mathbf{K}}(\mathbf{r})$ and $\psi_{\mathbf{k}}(\mathbf{r})$, belong to the same Bloch factor $\exp(i\mathbf{k}\mathbf{T})$ they are equivalent. A physical interpretation of the Bloch states will be given in Section 2.2.8.

2.2.4.3. A simple group-theoretical approach

Let us repeat a few fundamental definitions of group theory: For any symmetry operation $g_i \in G$, the product $gg_i g^{-1}$ can always be formed for any $g \in G$ and defines the conjugate element of g_i by g . Given any operation g_i , its class $C(g_i)$ is defined as the set of all its conjugates under all operations $g \in G$. What we need here is an important property of classes, namely that no two classes have any element in common so that any group can be considered as a sum of classes.

Assuming periodic boundary conditions with N_1, N_2, N_3 number of primitive cells along the axes $\mathbf{a}_1, \mathbf{a}_2, \mathbf{a}_3$, respectively, a lump of crystal with $N = N_1 N_2 N_3$ unit cells is studied. The translation subgroup T contains the general translation operators \mathbf{T} , which [using (2.2.3.15)] can be written as

$$\{E|\mathbf{T}\} = \{E|n_1\mathbf{a}_1\}\{E|n_2\mathbf{a}_2\}\{E|n_3\mathbf{a}_3\}, \quad (2.2.4.21)$$

where each factor belongs to one of the three axes. Since T is commutative (Abelian), each operation of T is its own class and thus the number of classes equals its order, namely N . From the general theorem that the squares of the dimensions of all irreducible representations of a group must equal the order of the group, it follows immediately that all N irreducible representations of T must be one-dimensional (see also Section 1.2.3.2 of the present volume). Taking the subgroup along the \mathbf{a}_1 axis, we must have N_1 different irreducible representations, which we label (for later convenience) by k_1 and denote as

$${}_{k_1}\hat{T}\{E|n_1\mathbf{a}_1\}. \quad (2.2.4.22)$$

These representations are one-dimensional matrices, *i.e.* numbers, and must be exponentials, often chosen of the form $\exp(-2\pi i k_1 n_1)$. The constant k_1 must be related to the corresponding label of the irreducible representation. In the three-dimensional case, we have the corresponding representation

$${}_{k_1 k_2 k_3}\hat{T}\{E|\mathbf{T}\} = \exp[-2\pi i(k_1 n_1 + k_2 n_2 + k_3 n_3)] = \exp(-i\mathbf{k} \cdot \mathbf{T}), \quad (2.2.4.23)$$

where we have used the definitions (2.2.2.6) and (2.2.2.1). Within the present derivation, the vector \mathbf{k} corresponds to the label of the irreducible representation of the lattice translation subgroup.

2.2. ELECTRONS

2.2.5. The free-electron (Sommerfeld) model

The free-electron model corresponds to the special case of taking a constant potential in the Schrödinger equation (2.2.4.1). The physical picture relies on the assumption that the (metallic) valence electrons can move freely in the field of the positively charged nuclei and the tightly bound core electrons. Each valence electron moves in a potential which is nearly constant due to the screening of the remaining valence electrons. This situation can be idealized by assuming the potential to be constant [$V(\mathbf{r}) = 0$]. This simple picture represents a crude model for simple metals but has its importance mainly because the corresponding equation can be solved analytically. By rewriting equation (2.2.4.1), we have

$$\nabla^2 \psi_{\mathbf{k}}(\mathbf{r}) = -\frac{2mE}{\hbar^2} \psi_{\mathbf{k}}(\mathbf{r}) = -|\mathbf{k}|^2 \psi_{\mathbf{k}}(\mathbf{r}), \quad (2.2.5.1)$$

where in the last step the constants are abbreviated (for later convenience) by $|\mathbf{k}|^2$. The solutions of this equation are plane waves (PWs)

$$\psi_{\mathbf{k}}(\mathbf{r}) = C \exp(i\mathbf{k} \cdot \mathbf{r}), \quad (2.2.5.2)$$

where C is a normalization constant which is defined from the integral over one unit cell with volume Ω . The PWs satisfy the Bloch condition and can be written (using the bra-ket notation) as

$$|\mathbf{k}\rangle = \psi_{\mathbf{k}}(\mathbf{r}) = \Omega^{1/2} \exp(i\mathbf{k} \cdot \mathbf{r}). \quad (2.2.5.3)$$

From (2.2.5.1) we see that the corresponding energy (labelled by \mathbf{k}) is given by

$$E_{\mathbf{k}} = \frac{\hbar^2}{2m} |\mathbf{k}|^2. \quad (2.2.5.4)$$

In this context it is useful to consider the momentum of the electron, which classically is the vector $\mathbf{p} = m\mathbf{v}$, where m and \mathbf{v} are the mass and velocity, respectively. In quantum mechanics we must replace \mathbf{p} by the corresponding operator $\hat{\mathbf{p}}$.

$$\hat{\mathbf{p}}|\mathbf{k}\rangle = \frac{\hbar}{i} \frac{\partial}{\partial \mathbf{r}} |\mathbf{k}\rangle = \frac{\hbar}{i} i\mathbf{k} |\mathbf{k}\rangle = \hbar \mathbf{k} |\mathbf{k}\rangle. \quad (2.2.5.5)$$

Thus a PW is an eigenfunction of the momentum operator with eigenvalue $\hbar \mathbf{k}$. Therefore the \mathbf{k} vector is also called the *momentum* vector. Note that this is strictly true for a vanishing potential but is otherwise only approximately true (referred to as *pseudomomentum*).

Another feature of a PW is that its phase is constant in a plane perpendicular to the vector \mathbf{k} (see Fig. 2.2.5.1). For this purpose, consider a periodic function in space and time,

$$\varphi_{\mathbf{k}}(\mathbf{r}, t) = \exp[i(\mathbf{k} \cdot \mathbf{r} - \omega t)], \quad (2.2.5.6)$$

which has a constant phase factor $\exp(i\omega t)$ within such a plane. We can characterize the spatial part of \mathbf{r} within this plane. Taking the nearest parallel plane (with vector \mathbf{r}') for which the same phase factors occur again but at a distance λ away (with the unit vector \mathbf{e} normal to the plane),

$$\mathbf{r}' = \mathbf{r} + \lambda \mathbf{e} = \mathbf{r} + \lambda \frac{\mathbf{k}}{|\mathbf{k}|}, \quad (2.2.5.7)$$

then $\mathbf{k} \cdot \mathbf{r}'$ must differ from $\mathbf{k} \cdot \mathbf{r}$ by 2π . This is easily obtained from (2.2.5.7) by multiplication with \mathbf{k} leading to

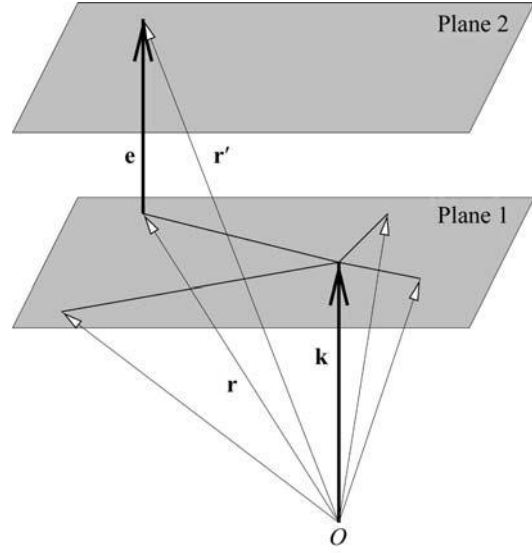


Fig. 2.2.5.1. Plane waves. The wavevector \mathbf{k} and the unit vector \mathbf{e} are normal to the two planes and the vectors \mathbf{r} in plane 1 and \mathbf{r}' in plane 2.

$$\mathbf{k} \cdot \mathbf{r}' = \mathbf{k} \cdot \mathbf{r} + \lambda \frac{|\mathbf{k}|^2}{|\mathbf{k}|} = \mathbf{k} \cdot \mathbf{r} + \lambda |\mathbf{k}| \quad (2.2.5.8)$$

$$\mathbf{k} \cdot \mathbf{r}' - \mathbf{k} \cdot \mathbf{r} = \lambda |\mathbf{k}| = 2\pi \quad (2.2.5.9)$$

$$\lambda = \frac{2\pi}{|\mathbf{k}|} \text{ or } |\mathbf{k}| = \frac{2\pi}{\lambda}. \quad (2.2.5.10)$$

Consequently λ is the wavelength and thus the \mathbf{k} vector is called the *wavevector* or *propagation vector*.

2.2.6. Space-group symmetry

2.2.6.1. Representations and bases of the space group

The effect of a space-group operation $\{p|\mathbf{w}\}$ on a Bloch function, labelled by \mathbf{k} , is to transform it into a Bloch function that corresponds to a vector $p\mathbf{k}$,

$$\{p|\mathbf{w}\} \psi_{\mathbf{k}} = \psi_{p\mathbf{k}}, \quad (2.2.6.1)$$

which can be proven by using the multiplication rule of Seitz operators (2.2.3.12) and the definition of a Bloch state (2.2.4.17).

A special case is the inversion operator, which leads to

$$\{i|\mathbf{E}\} \psi_{\mathbf{k}} = \psi_{-\mathbf{k}}. \quad (2.2.6.2)$$

The Bloch functions $\psi_{\mathbf{k}}$ and $\psi_{p\mathbf{k}}$, where p is any operation of the point group P , belong to the same basis for a representation of the space group G .

$$\langle \psi_{\mathbf{k}} | = \langle \psi_{p\mathbf{k}} | \text{ for all } p \in P \text{ for all } p\mathbf{k} \in \text{BZ}. \quad (2.2.6.3)$$

The same $p\mathbf{k}$ cannot appear in two different bases, thus the two bases $\psi_{\mathbf{k}}$ and $\psi_{\mathbf{k}'}$ are either identical or have no \mathbf{k} in common.

Irreducible representations of T are labelled by the N distinct \mathbf{k} vectors in the BZ, which separate in disjoint bases of G (with no \mathbf{k} vector in common). If a \mathbf{k} vector falls on the BZ edge, application of the point-group operation p can lead to an equivalent \mathbf{k}' vector that differs from the original by \mathbf{K} (a vector of the reciprocal lattice). The set of all mutually inequivalent \mathbf{k} vectors of $p\mathbf{k}$ ($p \in P$) define the *star of the \mathbf{k} vector* ($S_{\mathbf{k}}$) (see also Section 1.2.3.3 of the present volume).

The set of all operations that leave a \mathbf{k} vector invariant (or transform it into an equivalent $\mathbf{k} + \mathbf{K}$) forms the *group* $G_{\mathbf{k}}$ of the \mathbf{k} vector. Application of q , an element of $G_{\mathbf{k}}$, to a Bloch function (Section 2.2.8) gives

$$q \psi_{\mathbf{k}}^j(\mathbf{r}) = \psi_{\mathbf{k}}^j(\mathbf{r}) \text{ for } q \in G_{\mathbf{k}}, \quad (2.2.6.4)$$

2. SYMMETRY ASPECTS OF EXCITATIONS

where the band index j (described below) may change to j' . The Bloch factor stays constant under the operation of q and thus the periodic cell function $u_{\mathbf{k}}^j(\mathbf{r})$ must show this symmetry, namely

$$qu_{\mathbf{k}}^j(\mathbf{r}) = u_{\mathbf{k}}^{j'}(\mathbf{r}) \text{ for } q \in G_{\mathbf{k}}. \quad (2.2.6.5)$$

For example, a p_x -like orbital may be transformed into a p_y -like orbital if the two are degenerate, as in a tetragonal lattice.

A star of \mathbf{k} determines an irreducible basis, provided that the functions of the star are symmetrized with respect to the irreducible representation of the group of \mathbf{k} vectors, which are called *small representations*. The basis functions for the irreducible representations are given according to Seitz (1937) by

$$\langle s\psi_{\mathbf{k}}^j |, \text{ where } s \in S_{\mathbf{k}},$$

written as a row vector $\langle |$ with $j = 1, \dots, n$, where n is the dimension of the irreducible representation of $S_{\mathbf{k}}$ with the order $|S_{\mathbf{k}}|$. Such a basis consists of $n|S_{\mathbf{k}}|$ functions and forms an $n|S_{\mathbf{k}}|$ -dimensional irreducible representation of the space group. The degeneracies of these representations come from the star of \mathbf{k} (not crucial for band calculations except for determining the weight of the \mathbf{k} vector) and the degeneracy from $G_{\mathbf{k}}$. The latter is essential for characterizing the energy bands and using the compatibility relations (Bouckaert *et al.*, 1930; Bradley & Cracknell, 1972).

2.2.6.2. Energy bands

Each irreducible representation of the space group, labelled by \mathbf{k} , denotes an energy $E^j(\mathbf{k})$, where \mathbf{k} varies quasi-continuously over the BZ and the superscript j numbers the band states. The quantization of \mathbf{k} according to (2.2.4.13) and (2.2.4.15) can be done in arbitrary fine steps by choosing corresponding periodic boundary conditions (see Section 2.2.4.2). Since \mathbf{k} and $\mathbf{k} + \mathbf{K}$ belong to the same Bloch state, the energy is periodic in reciprocal space:

$$E^j(\mathbf{k}) = E^j(\mathbf{k} + \mathbf{K}). \quad (2.2.6.6)$$

Therefore it is sufficient to consider \mathbf{k} vectors within the first BZ. For a given \mathbf{k} , two bands will not have the same energy unless there is a multidimensional small representation in the group of \mathbf{k} or the bands belong to different irreducible representations and thus can have an accidental degeneracy. Consequently, this can not occur for a general \mathbf{k} vector (without symmetry).

2.2.7. The \mathbf{k} vector and the Brillouin zone

2.2.7.1. Various aspects of the \mathbf{k} vector

The \mathbf{k} vector plays a fundamental role in the electronic structure of a solid. In the above, several interpretations have been given for the \mathbf{k} vector that

- (a) is given in reciprocal space,
- (b) can be restricted to the first Brillouin zone,
- (c) is the quantum number for the electronic states in a solid,
- (d) is quantized due to the periodic boundary conditions,
- (e) labels the irreducible representation of the lattice translation subgroup T (see Section 2.2.4.3)
- (f) is related to the momentum [according to (2.2.5.5)] in the free-electron case and
- (g) is the propagation vector (wavevector) associated with the plane-wave part of the wavefunction (see Fig. 2.2.5.1).

2.2.7.2. The Brillouin zone (BZ)

Starting with one of the 14 Bravais lattices, one can define the reciprocal lattice [according to (2.2.2.4)] by the Wigner–Seitz construction as discussed in Section 2.2.2.2. The advantage of using the BZ instead of the parallelepiped spanned by the three unit vectors is its symmetry. Let us take a simple example first,

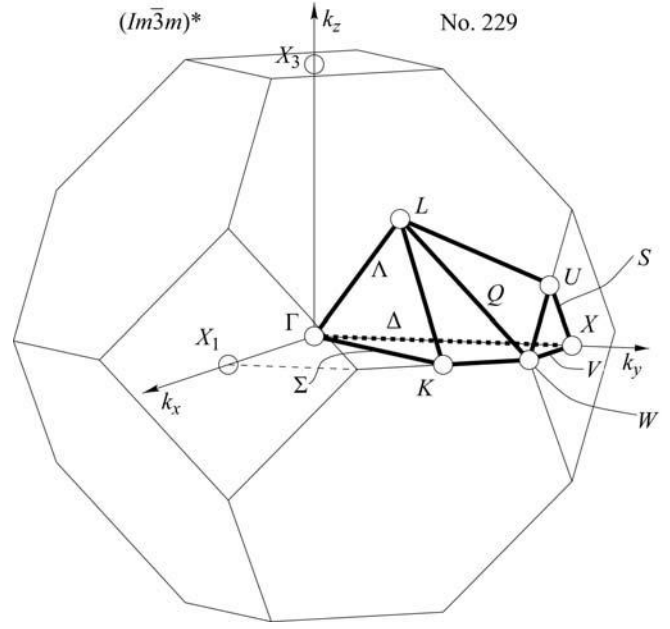


Fig. 2.2.7.1. The Brillouin zone (BZ) and the irreducible wedge of the BZ for the f.c.c. direct lattice. After the corresponding figure from the Bilbao Crystallographic Server (<http://www.cryst.ehu.es/cryst/>). The IBZ for any space group can be obtained by using the option KVEC and specifying the space group (in this case No. 225).

namely an element (say copper) that crystallizes in the face-centred-cubic (f.c.c.) structure. With (2.2.2.4) we easily find that the reciprocal lattice is body-centred-cubic (bcc) and the corresponding BZ is shown in Fig. 2.2.7.1. In this case, f.c.c. Cu has O_h symmetry with 48 symmetry operations $p \in P$ (point group). The energy eigenvalues within a star of \mathbf{k} (i.e. $\mathbf{k} \in S_{\mathbf{k}}$) are the same, and therefore it is sufficient to calculate one member in the star. Consequently, it is enough to consider the irreducible wedge of the BZ (called the IBZ). In the present example, this corresponds to 1/48th of the BZ shown in Fig. 2.2.7.1. To count the number of states in the BZ, one counts each \mathbf{k} point in the IBZ with a proper weight $w_{\mathbf{k}}$ to represent the star of this \mathbf{k} vector.

2.2.7.3. The symmetry of the Brillouin zone

The BZ is purely constructed from the reciprocal lattice and thus only follows from the translational symmetry (of the 14 Bravais lattices). However, the energy bands $E^j(\mathbf{k})$, with \mathbf{k} lying within the first BZ, possess a symmetry associated with one of the 230 space groups. Therefore one *can not* simply use the *geometrical symmetry* of the BZ to find its irreducible wedge, although this is tempting. Since the effort of computing energy eigenvalues increases with the number of \mathbf{k} points, one wishes to restrict such calculations to the basic domain, but the latter can only be found by considering the space group of the corresponding crystal (including the basis with all atomic positions).

One possible procedure for finding the IBZ is the following. First a uniform grid in reciprocal space is generated by dividing the three unit-cell vectors \mathbf{b}_i by an integer number of times. This is easy to do in the parallelepiped, spanned by the three unit-cell vectors, and yields a (more-or-less) uniform grid of \mathbf{k} points. Now one must go through the complete grid of \mathbf{k} points and extract a list of non-equivalent \mathbf{k} points by applying to each \mathbf{k} point in the grid the point-group operations. If a \mathbf{k} point is found that is already in the list, its weight is increased by 1, otherwise it is added to the list. This procedure can easily be programmed and is often used when \mathbf{k} integrations are needed. The disadvantage of this scheme is that the generated \mathbf{k} points in the IBZ are not necessarily in a connected region of the BZ, since one member of the star of \mathbf{k} is chosen arbitrarily, namely the first that is found by going through the complete list.

2.2. ELECTRONS

2.2.8. Bloch functions

We can provide a physical interpretation for a Bloch function by the following considerations. By combining the group-theoretical concepts based on the translational symmetry with the free-electron model, we can rewrite a Bloch function [see (2.2.4.18)] in the form

$$\psi_{\mathbf{k}}^j(\mathbf{r}) = |\mathbf{k}\rangle u_{\mathbf{k}}^j(\mathbf{r}), \quad (2.2.8.1)$$

where $|\mathbf{k}\rangle$ denotes the plane wave (ignoring normalization) in Dirac's ket notation (2.2.5.3). The additional superscript j denotes the band index associated with $E^j(\mathbf{k})$ (see Section 2.2.6.2). The two factors can be interpreted most easily for the two limiting cases, namely:

(i) For a constant potential, for which the first factor corresponds to a plane wave with momentum $\hbar\mathbf{k}$ [see (2.2.5.5)] but the second factor becomes a constant. Note that for a realistic (non-vanishing) potential, the \mathbf{k} vector of a Bloch function is no longer the momentum and thus is often denoted as pseudomomentum.

(ii) If the atoms in a crystal are infinitely separated (*i.e.* for infinite lattice constants) the BZ collapses to a point, making the first factor a constant. In this case, the second factor must correspond to atomic orbitals and the label j denotes the atomic states $1s, 2s, 2p$ etc. In the intermediate case, \mathbf{k} is quantized [see (2.2.4.13)] and can take N values (or $2N$ states including spin) for N cells contained in the volume of the periodic boundary condition [see (2.2.4.21)]. Therefore, as the interatomic distance is reduced from infinity to the equilibrium separations, an atomic level j is broadened into a band $E^j(\mathbf{k})$ with the quasi-continuous \mathbf{k} vectors and thus shows dispersion.

According to another theorem, the mean velocity of an electron in a Bloch state with wavevector \mathbf{k} and energy $E^j(\mathbf{k})$ is given by

$$\mathbf{v}^j(\mathbf{k}) = \frac{1}{\hbar} \frac{\partial}{\partial \mathbf{k}} E^j(\mathbf{k}). \quad (2.2.8.2)$$

If the energy is independent of \mathbf{k} , its derivative with respect to \mathbf{k} vanishes and thus the corresponding velocity. This situation corresponds to the genuinely isolated atomic levels (with band width zero) and electrons that are tied to individual atoms. If, however, there is any nonzero overlap in the atomic wavefunctions, then $E^j(\mathbf{k})$ will not be constant throughout the zone.

In the general case, different notations are used to characterize band states. Sometimes it is more appropriate to label an energy band by the atomic level from which it originates, especially for narrow bands. In other cases (with a large band width) the free-electron behaviour may be dominant and thus the corresponding free-electron notation is more appropriate.

2.2.9. Quantum-mechanical treatment

A description of the electronic structure of solids requires a quantum-mechanical (QM) treatment which can be parameterized (in semi-empirical schemes) but is often obtained from *ab initio* calculations. The latter are more demanding in terms of computational effort but they have the advantage that no experimental knowledge is needed in order to adjust parameters. The following brief summary is restricted to the commonly used types of *ab initio* methods and their main characteristics.

2.2.9.1. Exchange and correlation treatment

Hartree-Fock-based (HF-based) methods (for a general description see, for example, Pisani, 1996) are based on a wavefunction description (with one Slater determinant in the HF method). The single-particle HF equations (written for an atom in Rydberg atomic units) can be written in the following form, which is convenient for further discussions:

$$\begin{aligned} & \left[-\nabla^2 + V_{Ne}(\mathbf{r}) + \sum_{j=1}^N \int |\psi_j^{\text{HF}}(\mathbf{r}')|^2 \frac{2}{|\mathbf{r} - \mathbf{r}'|} d\mathbf{r}' \right. \\ & \left. - \sum_{j=1}^N \int \psi_j^{\text{HF}}(\mathbf{r}')^* \frac{1}{|\mathbf{r} - \mathbf{r}'|} P_{rr'} \psi_j^{\text{HF}}(\mathbf{r}') d\mathbf{r}' \right] \psi_i^{\text{HF}}(\mathbf{r}) \\ & = \epsilon_i^{\text{HF}} \psi_i^{\text{HF}}(\mathbf{r}), \end{aligned} \quad (2.2.9.1)$$

with terms for the kinetic energy, the nuclear electronic potential, the classical electrostatic Coulomb potential and the exchange, a function potential which involves the permutation operator $P_{rr'}$, which interchanges the arguments of the subsequent product of two functions. This exchange term can not be rewritten as a potential times the function $\psi_i^{\text{HF}}(\mathbf{r})$ but is truly non-local (*i.e.* depends on \mathbf{r} and \mathbf{r}'). The interaction of orbital j with itself (contained in the third term) is unphysical, but this self-interaction is exactly cancelled in the fourth term. This is no longer true in the approximate DFT method discussed below. The HF method treats exchange exactly but contains – by definition – no correlation effects. The latter can be added in an approximate form in post-HF procedures such as that proposed by Colle & Salvetti (1990).

Density functional theory (DFT) is an alternative approach in which both effects, exchange and correlation, are treated in a combined scheme but both approximately. Several forms of DFT functionals are available now that have reached high accuracy, so many structural problems can be solved adequately. Further details will be given in Section 2.2.10.

2.2.9.2. The choice of basis sets and wavefunctions

Most calculations of the electronic structure in solids (Pisani, 1996; Singh, 1994; Altmann, 1994) use a linear combination of basis functions in one form or another but differ in the basis sets. Some use a linear combination of atomic orbitals (LCAO) where the AOs are given as Gaussian- or Slater-type orbitals (GTOs or STOs); others use plane-wave (PW) basis sets with or without augmentations; and still others make use of muffin-tin orbitals (MTOs) as in LMTO (linear combination of MTOs; Skriver, 1984) or ASW (augmented spherical wave; Williams *et al.*, 1979). In the former cases, the basis functions are given in analytic form, but in the latter the radial wavefunctions are obtained numerically by integrating the radial Schrödinger equation (Singh, 1994) (see Section 2.2.11).

Closely related to the choice of basis sets is the explicit form of the wavefunctions, which can be well represented by them, whether they are nodeless pseudo-wavefunctions or all-electron wavefunctions including the complete radial nodal structure and a proper description close to the nucleus.

2.2.9.3. The form of the potential

In the muffin-tin or the atomic sphere approximation (MTA or ASA), each atom in the crystal is surrounded by an atomic sphere in which the potential is assumed to be spherically symmetric [see (2.2.12.5) and the discussion thereof]. While these schemes work reasonably well in highly coordinated, closely packed systems (such as face-centred-cubic metals), they become very approximate in all non-isotropic cases (*e.g.* layered compounds, semiconductors, open structures or molecular crystals). Schemes that make no shape approximation in the form of the potential are termed full-potential schemes (Singh, 1994; Blaha *et al.*, 1990; Schwarz & Blaha, 1996).

With a proper choice of pseudo-potential one can focus on the valence electrons, which are relevant for chemical bonding, and replace the inner part of their wavefunctions by a nodeless pseudo-function that can be expanded in PWs with good convergence.

2. SYMMETRY ASPECTS OF EXCITATIONS

2.2.9.4. Relativistic effects

If a solid contains only light elements, non-relativistic calculations are well justified, but as soon as heavier elements are present in the system of interest relativistic effects can no longer be neglected. In the medium range of atomic numbers (up to about 54), so-called scalar relativistic schemes are often used (Koelling & Harmon, 1977), which describe the main contraction or expansion of various orbitals (due to the Darwin s -shift or the mass-velocity term) but omit spin-orbit splitting. Unfortunately, the spin-orbit term couples spin-up and spin-down wavefunctions. If one has n basis functions without spin-orbit coupling, then including spin-orbit coupling in the Hamiltonian would lead to a $2n \times 2n$ matrix equation, which requires about eight times as much computer time to solve it (due to the n^3 scaling). Since the spin-orbit effect is generally small (at least for the valence states), one can simplify the procedure by diagonalizing the Hamiltonian including spin-orbit coupling in the space of the low-lying bands as obtained in a scalar relativistic step. This version is called second variational method (see e.g. Singh, 1994). For very heavy elements it may be necessary to solve Dirac's equation, which has all these terms (Darwin s -shift, mass-velocity and spin-orbit) included. Additional aspects are illustrated in Section 2.2.14 in connection with the uranium atom.

2.2.10. Density functional theory

The most widely used scheme for calculating the electronic structure of solids is based on density functional theory (DFT). It is described in many excellent books, for example that by Dreizler & Gross (1990), which contains many useful definitions, explanations and references. Hohenberg & Kohn (1964) have shown that for determining the ground-state properties of a system all one needs to know is the electron density $\rho(\mathbf{r})$. This is a tremendous simplification considering the complicated wavefunction of a crystal with (in principle infinitely) many electrons. This means that the total energy of a system (a solid in the present case) is a functional of the density $E[\rho(r)]$, which is independent of the external potential provided by all nuclei. At first it was just proved that such a functional exists, but in order to make this fundamental theorem of practical use Kohn & Sham (1965) introduced orbitals and suggested the following procedure.

In the universal approach of DFT to the quantum-mechanical many-body problem, the interacting system is mapped in a unique manner onto an effective non-interacting system of quasi-electrons with the same total density. Therefore the electron density plays the key role in this formalism. The non-interacting particles of this auxiliary system move in an effective local one-particle potential, which consists of a mean-field (Hartree) part and an exchange-correlation part that, in principle, incorporates all correlation effects exactly. However, the functional form of this potential is not known and thus one needs to make approximations.

Magnetic systems (with collinear spin alignments) require a generalization, namely a different treatment for spin-up and spin-down electrons. In this generalized form the key quantities are the spin densities $\rho_\sigma(r)$, in terms of which the total energy E_{tot} is

$$E_{\text{tot}}(\rho_\uparrow, \rho_\downarrow) = T_s(\rho_\uparrow, \rho_\downarrow) + E_{ee}(\rho_\uparrow, \rho_\downarrow) + E_{Ne}(\rho_\uparrow, \rho_\downarrow) + E_{xc}(\rho_\uparrow, \rho_\downarrow) + E_{NN}, \quad (2.2.10.1)$$

with the electronic contributions, labelled conventionally as, respectively, the kinetic energy (of the non-interacting particles), the electron-electron repulsion, the nuclear-electron attraction and the exchange-correlation energies. The last term E_{NN} is the repulsive Coulomb energy of the fixed nuclei. This expression is still exact but has the advantage that all terms but one can be calculated very accurately and are the dominating (large) quantities.

The exception is the exchange-correlation energy E_{xc} , which is defined by (2.2.10.1) but must be approximated. The first important methods for this were the local density approximation (LDA) or its spin-polarized generalization, the local spin density approximation (LSDA). The latter comprises two assumptions:

(i) That E_{xc} can be written in terms of a local exchange-correlation energy density ε_{xc} times the total (spin-up plus spin-down) electron density as

$$E_{xc} = \int \varepsilon_{xc}(\rho_\uparrow, \rho_\downarrow) * [\rho_\uparrow + \rho_\downarrow] dr. \quad (2.2.10.2)$$

(ii) The particular form chosen for ε_{xc} . For a homogeneous electron gas ε_{xc} is known from quantum Monte Carlo simulations, e.g. by Ceperley & Alder (1984). The LDA can be described in the following way. At each point \mathbf{r} in space we know the electron density $\rho(\mathbf{r})$. If we locally replace the system by a homogeneous electron gas of the same density, then we know its exchange-correlation energy. By integrating over all space we can calculate E_{xc} .

The most effective way known to minimize E_{tot} by means of the variational principle is to introduce (spin) orbitals χ_{jk}^σ constrained to construct the spin densities [see (2.2.10.7) below]. According to Kohn and Sham (KS), the variation of E_{tot} gives the following effective one-particle Schrödinger equations, the so-called Kohn-Sham equations (Kohn & Sham, 1965) (written for an atom in Rydberg atomic units with the obvious generalization to solids):

$$[-\nabla^2 + V_{Ne} + V_{ee} + V_{xc}^\sigma] \chi_{jk}^\sigma(r) = \epsilon_{jk}^\sigma(r) \chi_{jk}^\sigma(r), \quad (2.2.10.3)$$

with the external potential (the attractive interaction of the electrons by the nucleus) given by

$$V_{Ne}(r) = \frac{2Z}{r}, \quad (2.2.10.4)$$

the Coulomb potential (the electrostatic interaction between the electrons) given by

$$V_{ee}(\mathbf{r}) = V_C(\mathbf{r}) = \int \frac{\rho(\mathbf{r}')}{|\mathbf{r} - \mathbf{r}'|} d\mathbf{r}' \quad (2.2.10.5)$$

and the exchange-correlation potential (due to quantum mechanics) given by the functional derivative

$$V_{xc}(\mathbf{r}) = \frac{\delta E_{xc}[\rho(r)]}{\delta \rho}. \quad (2.2.10.6)$$

In the KS scheme, the (spin) electron densities are obtained by summing over all occupied states, i.e. by filling the KS orbitals (with increasing energy) according to the *Aufbau* principle.

$$\rho_\sigma(r) = \sum_{j,k} \rho_{jk}^\sigma |\chi_{jk}^\sigma(r)|^2. \quad (2.2.10.7)$$

Here ρ_{jk}^σ are occupation numbers such that $0 \leq \rho_{jk}^\sigma \leq 1/w_k$, where w_k is the symmetry-required weight of point \mathbf{k} . These KS equations (2.2.10.3) must be solved self-consistently in an iterative process, since finding the KS orbitals requires the knowledge of the potentials, which themselves depend on the (spin) density and thus on the orbitals again. Note the similarity to (and difference from) the Hartree-Fock equation (2.2.9.1). This version of the DFT leads to a (spin) density that is close to the exact density provided that the DFT functional is sufficiently accurate.

In early applications, the local density approximation (LDA) was frequently used and several forms of functionals exist in the literature, for example by Hedin & Lundqvist (1971), von Barth & Hedin (1972), Gunnarsson & Lundqvist (1976), Vosko *et al.* (1980) or accurate fits of the Monte Carlo simulations of Ceperley & Alder (1984). The LDA has some shortcomings, mostly due to the tendency of overbinding, which causes, for example, too-small lattice constants. Recent progress has been

2.2. ELECTRONS

made going beyond the LSDA by adding gradient terms or higher derivatives ($\nabla\rho$ and $\nabla^2\rho$) of the electron density to the exchange–correlation energy or its corresponding potential. In this context several physical constraints can be formulated, which an exact theory should obey. Most approximations, however, satisfy only part of them. For example, the exchange density (needed in the construction of these two quantities) should integrate to -1 according to the Fermi exclusion principle (Fermi hole). Such considerations led to the generalized gradient approximation (GGA), which exists in various parameterizations, *e.g.* in the one by Perdew *et al.* (1996). This is an active field of research and thus new functionals are being developed and their accuracy tested in various applications.

The Coulomb potential $V_c(\mathbf{r})$ in (2.2.10.5) is that of all N electrons. That is, any electron is also moving in its own field, which is physically unrealistic but may be mathematically convenient. Within the HF method (and related schemes) this self-interaction is cancelled exactly by an equivalent term in the exchange interaction [see (2.2.9.1)]. For the currently used approximate density functionals, the self-interaction cancellation is not complete and thus an error remains that may be significant, at least for states (*e.g.* 4f or 5f) for which the respective orbital is not delocalized. Note that delocalized states have a negligibly small self-interaction. This problem has led to the proposal of self-interaction corrections (SICs), which remove most of this error and have impacts on both the single-particle eigenvalues and the total energy (Parr *et al.*, 1978).

The Hohenberg–Kohn theorems state that the total energy (of the ground state) is a functional of the density, but the introduction of the KS orbitals (describing quasi-electrons) are only a tool in arriving at this density and consequently the total energy. Rigorously, the Kohn–Sham orbitals are *not electronic orbitals* and the KS eigenvalues ε_i (which correspond to E_k in a solids) are *not* directly related to electronic *excitation energies*. From a formal (mathematical) point of view, the ε_i are just Lagrange multipliers without a physical meaning.

Nevertheless, it is often a good approximation (and common practice) to partly ignore these formal inconsistencies and use the orbitals and their energies in discussing electronic properties. The gross features of the eigenvalue sequence depend only to a smaller extent on the details of the potential, whether it is orbital-based as in the HF method or density-based as in DFT. In this sense, the eigenvalues are mainly determined by orthogonality conditions and by the strong nuclear potential, common to DFT and the HF method.

In processes in which one removes (ionization) or adds (electron affinity) an electron, one compares the N electron system with one with $N - 1$ or $N + 1$ electrons. Here another conceptual difference occurs between the HF method and DFT. In the HF method one may use Koopmans’ theorem, which states that the $\varepsilon_i^{\text{HF}}$ agree with the ionization energies from state i assuming that the corresponding orbitals do not change in the ionization process. In DFT, the ε_i can be interpreted according to Janak’s theorem (Janak, 1978) as the partial derivative with respect to the occupation number n_i ,

$$\varepsilon_i = \frac{\partial E}{\partial n_i}. \quad (2.2.10.8)$$

Thus in the HF method ε_i is the total energy difference for $\Delta n = 1$, in contrast to DFT where a differential change in the occupation number defines ε_i , the proper quantity for describing metallic systems. It has been proven that for the exact density functional the eigenvalue of the highest occupied orbital is the first ionization potential (Perdew & Levy, 1983). Roughly, one can state that the further an orbital energy is away from the highest occupied state, the poorer becomes the approximation to use ε_i as excitation energy. For core energies the deviation can be significant, but one may use Slater’s transition state (Slater,

1974), in which half an electron is removed from the corresponding orbital, and then use the $\varepsilon_i^{\text{TS}}$ to represent the ionization from that orbital.

Another excitation from the valence to the conduction band is given by the energy gap, separating the occupied from the unoccupied single-particle levels. It is well known that the gap is not given well by taking $\Delta\varepsilon_i$ as excitation energy. Current DFT methods significantly underestimate the gap (half the experimental value), whereas the HF method usually overestimates gaps (by a factor of about two). A trivial solution, applying the ‘scissor operator’, is to shift the DFT bands to agree with the experimental gap. An improved but much more elaborate approach for obtaining electronic excitation energies within DFT is the GW method in which quasi-particle energies are calculated (Hybertsen & Louie, 1984; Godby *et al.*, 1986; Perdew, 1986). This scheme is based on calculating the dielectric matrix, which contains information on the response of the system to an external perturbation, such as the excitation of an electron.

In some cases, one can rely on the total energy of the states involved. The original Hohenberg–Kohn theorems (Hohenberg & Kohn, 1964) apply only to the ground state. The theorems may, however, be generalized to the energetically lowest state of any symmetry representation for which any property is a functional of the corresponding density. This allows (in cases where applicable) the calculation of excitation energies by taking total energy differences.

Many aspects of DFT from formalism to applications are discussed and many references are given in the book by Springborg (1997).

2.2.11. Band-theory methods

There are several methods for calculating the electronic structure of solids. They have advantages and disadvantages, different accuracies and computational requirements (speed or memory), and are based on different approximations. Some of these aspects have been discussed in Section 2.2.9. This is a rapidly changing field and thus only the basic concepts of a few approaches in current use are outlined below.

2.2.11.1. LCAO (linear combination of atomic orbitals)

For the description of crystalline wavefunctions (Bloch functions), one often starts with a simple concept of placing atomic orbitals (AOs) at each site in a crystal denoted by $|m\rangle$, from which one forms Bloch sums in order to have proper translational symmetry:

$$\chi_{\mathbf{k}}(\mathbf{r}) = \sum_m \exp(i\mathbf{k}\mathbf{T}_m) |m\rangle. \quad (2.2.11.1)$$

Then Bloch functions can be constructed by taking a linear combination of such Bloch sums, where the linear-combination coefficients are determined by the variational principle in which a secular equation must be solved. The LCAO can be used in combination with both the Hartree–Fock method and DFT.

2.2.11.2. TB (tight binding)

A simple version of the LCAO is found by parameterizing the matrix elements $\langle m' | \mathbb{H} | m \rangle$ and $\langle m' | m \rangle$ in a way similar to the Hückel molecular orbital (HMO) method, where the only non-vanishing matrix elements are the on-site integrals and the nearest-neighbour interactions (hopping integrals). For a particular class of solids the parameters can be adjusted to fit experimental values. With these parameters, the electronic structures of rather complicated solids can be described and yield quite satisfactory results, but only for the class of materials for which such a parametrization is available. Chemical bonding and symmetry aspects can be well described with such schemes, as Hoffmann has illustrated in many applications (Hoffmann, 1988).

2. SYMMETRY ASPECTS OF EXCITATIONS

In more complicated situations, however, such a simple scheme fails.

2.2.11.3. *The pseudo-potential schemes*

In many respects, core electrons are unimportant for determining the stability, structure and low-energy response properties of crystals. It is a well established practice to modify the one-electron part of the Hamiltonian by replacing the bare nuclear attraction with a pseudo-potential (PP) operator, which allows us to restrict our calculation to the valence electrons. The PP operator must reproduce screened nuclear attractions, but must also account for the Pauli exclusion principle, which requires that valence orbitals are orthogonal to core ones. The PPs are not uniquely defined and thus one seeks to satisfy the following characteristics as well as possible:

- (1) PP eigenvalues should coincide with the true (all-electron) ones;
- (2) PP orbitals should resemble as closely as possible the all-electron orbitals in an external region as well as being smooth and nodeless in the core region;
- (3) PP orbitals should be properly normalized;
- (4) the functional form of the PP should allow the simplification of their use in computations;
- (5) the PP should be transferable (independent of the system); and
- (6) relativistic effects should be taken into account (especially for heavy elements); this concerns mainly the indirect relativistic effects (*e.g.* core contraction, Darwin *s*-shift), but not the spin-orbit coupling.

There are many versions of the PP method (norm-conserving, ultrasoft *etc.*) and the actual accuracy of a calculation is governed by which is used. For standard applications, PP techniques can be quite successful in solid-state calculations. However, there are cases that require higher accuracy, *e.g.* when core electrons are involved, as in high-pressure studies or electric field gradient calculations (see Section 2.2.15), where the polarization of the charge density close to the nucleus is crucial for describing the physical effects properly.

2.2.11.4. *APW (augmented plane wave) and LAPW methods*

The partition of space (*i.e.* the unit cell) between (non-overlapping) atomic spheres and an interstitial region (see Fig. 2.2.12.1) is used in several schemes, one of which is the augmented plane wave (APW) method, originally proposed by Slater (Slater, 1937) and described by Loucks (1967), and its linearized version (the LAPW method), which is chosen as the one representative method that is described in detail in Section 2.2.12.

The basis set is constructed using the muffin-tin approximation (MTA) for the potential [see the discussion below in connection with (2.2.12.5)]. In the interstitial region the wavefunction is well described by plane waves, but inside the spheres atomic-like functions are used which are matched continuously (at the sphere boundary) to each plane wave.

2.2.11.5. *KKR (Korringa–Kohn–Rostocker) method*

In the KKR scheme (Korringa, 1947; Kohn & Rostocker, 1954), the solution of the KS equations (2.2.10.3) uses a Green-function technique and solves a Lippman–Schwinger integral equation. The basic concepts come from a multiple scattering approach which is conceptually different but mathematically equivalent to the APW method. The building blocks are spherical waves which are products of spherical harmonics and spherical Hankel, Bessel and Neumann functions. Like plane waves, they solve the KS equations for a constant potential. Augmenting the spherical waves with numerical solutions inside the atomic spheres as in the APW method yields the KKR basis set.

Compared with methods based on plane waves, spherical waves require fewer basis functions and thus smaller secular equations.

The radial functions in the APW and KKR methods are energy-dependent and so are the corresponding basis functions. This leads to a nonlinear eigenvalue problem that is computationally demanding. Andersen (1975) modelled the weak energy dependence by a Taylor expansion where only the first term is kept and thereby arrived at the so-called linear methods LMTO and LAPW.

2.2.11.6. *LMTO (linear combination of muffin-tin orbitals) method*

The LMTO method (Andersen, 1975; Skriver, 1984) is the linearized counterpart to the KKR method, in the same way as the LAPW method is the linearized counterpart to the APW method. This widely used method originally adopted the atomic sphere approximation (ASA) with overlapping atomic spheres in which the potential was assumed to be spherically symmetric. Although the ASA simplified the computation so that systems with many atoms could be studied, the accuracy was not high enough for application to certain questions in solid-state physics.

Following the ideas of Andersen, the augmented spherical wave (ASW) method was developed by Williams *et al.* (1979). The ASW method is quite similar to the LMTO scheme.

It should be noted that the MTA and the ASA are not really a restriction on the method. In particular, when employing the MTA only for the construction of the basis functions but including a generally shaped potential in the construction of the matrix elements, one arrives at a scheme of very high accuracy which allows, for instance, the evaluation of elastic properties. Methods using the unrestricted potential together with basis functions developed from the muffin-tin potential are called *full-potential* methods. Now for almost every method based on the MTA (or ASA) there exists a counterpart employing the full potential.

2.2.11.7. *CP (Car–Parrinello) method*

Conventional quantum-mechanical calculations are done using the Born–Oppenheimer approximation, in which one assumes (in most cases to a very good approximation) that the electrons are decoupled from the nuclear motion. Therefore the electronic structure is calculated for fixed atomic (nuclear) positions. Car & Parrinello (1985) suggested a new method in which they combined the motion of the nuclei (at finite temperature) with the electronic degrees of freedom. They started with a fictitious Lagrangian in which the wavefunctions follow a dynamics equation of motion. Therefore, the CP method combines the motion of the nuclei (following Newton's equation) with the electrons (described within DFT) into one formalism by solving equations of motion for both subsystems. This simplifies the computational effort and allows *ab initio* molecular dynamics calculations to be performed in which the forces acting on the atoms are calculated from the wavefunctions within DFT. The CP method has attracted much interest and is widely used, with a plane-wave basis, extended with pseudo-potentials and recently enhanced into an all-electron method using the projector augmented wave (PAW) method (Blöchl, 1994). Such CP schemes can also be used to find equilibrium structures and to explore the electronic structure.

2.2.11.8. *Order N schemes*

The various techniques outlined so far have one thing in common, namely the scaling. In a system containing N atoms the computational effort scales as N^3 , since one must determine a number of orbitals that is proportional to N which requires diagonalization of $(kN) \times (kN)$ matrices, where the prefactor k depends on the basis set and the method used. In recent years

2.2. ELECTRONS

much work has been done to devise algorithms that vary linearly with N , at least for very large N (Ordejon *et al.*, 1995). First results are already available and look promising. When such schemes become generally available, it will be possible to study very large systems with relatively little computational effort. This interesting development could drastically change the accessibility of electronic structure results for large systems.

2.2.12. The linearized augmented plane wave method

The electronic structure of solids can be calculated with a variety of methods as described above (Section 2.2.11). One representative example is the (full-potential) linearized augmented plane wave (LAPW) method. The LAPW method is one among the most accurate schemes for solving the effective one-particle (the so-called Kohn–Sham) equations (2.2.10.3) and is based on DFT (Section 2.2.10) for the treatment of exchange and correlation.

The LAPW formalism is described in many references, starting with the pioneering work by Andersen (1975) and by Koelling & Arberman (1975), which led to the development and the description of the computer code *WIEN* (Blaha *et al.*, 1990; Schwarz & Blaha, 1996). An excellent book by Singh (1994) is highly recommended to the interested reader. Here only the basic ideas are summarized, while details are left to the articles and references therein.

In the LAPW method, the unit cell is partitioned into (non-overlapping) atomic spheres centred around the atomic sites (type I) and an interstitial region (II) as shown schematically in Fig. 2.2.12.1. For the construction of basis functions (and only for this purpose), the muffin-tin approximation (MTA) is used. In the MTA, the potential is assumed to be spherically symmetric within the atomic spheres but constant outside; in the former atomic-like functions and in the latter plane waves are used in order to adapt the basis set optimally to the problem. Specifically, the following basis sets are used in the two types of regions:

(1) Inside the atomic sphere t of radius R_t (region I), a linear combination of radial functions times spherical harmonics $Y_{\ell m}(\hat{r})$ is used (we omit the index t when it is clear from the context):

$$\phi_{\mathbf{k}_n} = \sum_{\ell m} [A_{\ell m} u_{\ell}(r, E_{\ell}) + B_{\ell m} \dot{u}_{\ell}(r, E_{\ell})] Y_{\ell m}(\hat{r}), \quad (2.2.12.1)$$

where \hat{r} represents the angles ϑ and φ of the polar coordinates. The radial functions $u_{\ell}(r, E)$ depend on the energy E . Within a certain energy range this energy dependence can be accounted for by using a linear combination of the solution $u_{\ell}(r, E_{\ell})$ and its energy derivative $\dot{u}_{\ell}(r, E_{\ell})$, both taken at the same energy E_{ℓ} (which is normally chosen at the centre of the band with the corresponding ℓ -like character). This is the linearization in the LAPW method. These two functions are obtained on a radial mesh inside the atomic sphere by numerical integration of the radial Schrödinger equation using the spherical part of the potential inside sphere t and choosing the solution that is regular at the origin $r = 0$. The coefficients $A_{\ell m}$ and $B_{\ell m}$ are chosen by matching conditions (see below).

(2) In the interstitial region (II), a plane-wave expansion (see the Sommerfeld model, Section 2.2.5) is used:

$$\phi_{\mathbf{k}_n} = (1/\sqrt{\Omega}) \exp(i\mathbf{k}_n \cdot \mathbf{r}), \quad (2.2.12.2)$$

where $\mathbf{k}_n = \mathbf{k} + \mathbf{K}_n$, \mathbf{K}_n are vectors of the reciprocal lattice, \mathbf{k} is the wavevector in the first Brillouin zone and Ω is the unit-cell volume [see (2.2.5.3)]. This corresponds to writing the periodic function $u_{\mathbf{k}}(\mathbf{r})$ (2.2.4.19) as a Fourier series and combining it with the Bloch function (2.2.4.18). Each plane wave (corresponding to \mathbf{k}_n) is augmented by an atomic-like function in every atomic sphere, where the coefficients $A_{\ell m}$ and $B_{\ell m}$ in (2.2.12.1) are chosen to match (in value and slope) the atomic solution with the

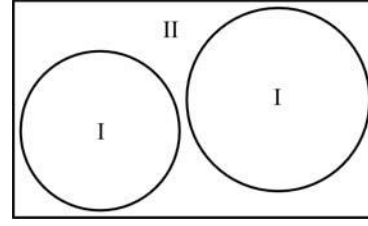


Fig. 2.2.12.1. Schematic partitioning of the unit cell into atomic spheres (I) and an interstitial region (II).

corresponding plane-wave basis function of the interstitial region.

The solutions to the Kohn–Sham equations are expanded in this combined basis set of LAPWs,

$$\psi_{\mathbf{k}} = \sum_n c_n \phi_{\mathbf{k}_n}, \quad (2.2.12.3)$$

where the coefficients c_n are determined by the Rayleigh–Ritz variational principle. The convergence of this basis set is controlled by the number of PWs, *i.e.* by the magnitude of the largest \mathbf{K} vector in equation (2.2.12.3).

In order to improve upon the linearization (*i.e.* to increase the flexibility of the basis) and to make possible a consistent treatment of semi-core and valence states in one energy window (to ensure orthogonality), additional (k_n -independent) basis functions can be added. They are called ‘local orbitals’ (Singh, 1994) and consist of a linear combination of two radial functions at two different energies (*e.g.* at the 3s and 4s energy) and one energy derivative (at one of these energies):

$$\phi_{\ell m}^{\text{LO}} = [A_{\ell m} u_{\ell}(r, E_{1,\ell}) + B_{\ell m} \dot{u}_{\ell}(r, E_{1,\ell}) + C_{\ell m} u_{\ell}(r, E_{2,\ell})] Y_{\ell m}(\hat{r}). \quad (2.2.12.4)$$

The coefficients $A_{\ell m}$, $B_{\ell m}$ and $C_{\ell m}$ are determined by the requirements that ϕ^{LO} should be normalized and has zero value and slope at the sphere boundary.

In its general form, the LAPW method expands the potential in the following form:

$$V(r) = \begin{cases} \sum_{LM} V_{LM}(r) K_{LM}(\hat{r}) & \text{inside sphere} \\ \sum_K V_K \exp(i\mathbf{K} \cdot \mathbf{r}) & \text{outside sphere} \end{cases} \quad (2.2.12.5)$$

where K_{LM} are the crystal harmonics compatible with the point-group symmetry of the corresponding atom represented in a local coordinate system (see Section 2.2.13). An analogous expression holds for the charge density. Thus no shape approximations are made, a procedure frequently called the ‘full-potential LAPW’ (FLAPW) method.

The muffin-tin approximation (MTA) used in early band calculations corresponds to retaining only the $L = 0$ and $M = 0$ component in the first expression of (2.2.12.5) and only the $K = 0$ component in the second. This (much older) procedure corresponds to taking the spherical average inside the spheres and the volume average in the interstitial region. The MTA was frequently used in the 1970s and works reasonable well in highly coordinated (metallic) systems such as face-centred-cubic (f.c.c.) metals. For covalently bonded solids, open or layered structures, however, the MTA is a poor approximation and leads to serious discrepancies with experiment. In all these cases a full-potential treatment is essential.

The choice of sphere radii is not very critical in full-potential calculations, in contrast to the MTA, where this choice may affect the results significantly. Furthermore, different radii would be found when one uses one of the two plausible criteria, namely based on the potential (maximum between two adjacent atoms) or the charge density (minimum between two adjacent atoms).

2. SYMMETRY ASPECTS OF EXCITATIONS

Table 2.2.13.1. Picking rules for the local coordinate axes and the corresponding LM combinations (ℓmp) of non-cubic groups taken from Kurki-Suonio (1977)

| Symmetry | Coordinate axes | ℓ, m, p of $y_{\ell mp}$ | Crystal system |
|--|---|--|----------------|
| 1 $\bar{1}$ | Any Any | All (ℓ, m, \pm) $(2\ell, m, \pm)$ | Triclinic |
| 2 m $2/m$ | $2 \parallel z$ $m \perp z$ $2 \parallel z, m \perp z$ | $(\ell, 2m, \pm)$ $(\ell, \ell - 2m, \pm)$ $(2\ell, 2m, \pm)$ | Monoclinic |
| 222 $mm2$ mmm | $2 \parallel z, 2 \parallel y (2 \parallel x)$ $2 \parallel z, m \perp y (2 \perp x)$ $2 \perp z, m \perp y, 2 \perp x$ | $(2\ell, 2m, +), (2\ell + 1, 2m, -)$ $(\ell, 2m, +)$ $(2\ell, 2m, +)$ | Orthorhombic |
| 4 $\bar{4}$ $4/m$ 422 4mm $\bar{4}2m$ 4mmm | $4 \parallel z$ $-4 \parallel z$ $4 \parallel z, m \perp z$ $4 \parallel z, 2 \parallel y (2 \parallel x)$ $4 \parallel z, m \perp y (2 \perp x)$ $-4 \parallel z, 2 \parallel x (m = xy \rightarrow yx)$ $4 \parallel z, m \perp z, m \perp x$ | $(\ell, 4m, \pm)$ $(2\ell, 4m, \pm), (2\ell + 1, 4m + 2, \pm)$ $(2\ell, 4m, \pm)$ $(2\ell, 4m, +), (2\ell + 1, 4m, -)$ $(\ell, 4m, +)$ $(2\ell, 4m, +), (2\ell + 1, 4m + 2, -)$ $(2\ell, 4m, +)$ | Tetragonal |
| 3 $\bar{3}$ 32 3m $\bar{3}m$ | $3 \parallel z$ $-3 \parallel z$ $3 \parallel z, 2 \parallel y$ $3 \parallel z, m \perp y$ $-3 \parallel z, m \perp y$ | $(\ell, 3m, \pm)$ $(2\ell, 3m, \pm)$ $(2\ell, 3m, +), (2\ell + 1, 3m, -)$ $(\ell, 3m, +)$ $(2\ell, 3m, +)$ | Rhombohedral |
| 6 $\bar{6}$ $6/m$ 622 6mm $\bar{6}2m$ 6mmm | $6 \parallel z$ $-6 \parallel z$ $6 \parallel z, m \perp z$ $6 \parallel z, 2 \parallel y (2 \parallel x)$ $6 \parallel z, m \perp y (m \perp x)$ $-6 \parallel z, m \perp y (2 \parallel x)$ $6 \parallel z, m \perp z, m \perp y (m \perp x)$ | $(\ell, 6m, \pm)$ $(2\ell, 6m, +), (2\ell + 1, 6m + 3, \pm)$ $(2\ell, 6m, \pm)$ $(2\ell, 6m, +), (2\ell + 1, 6m, -)$ $(\ell, 6m, +)$ $(2\ell, 6m, +), (2\ell + 1, 6m + 3, +)$ $(2\ell, 6m, +)$ | Hexagonal |

Therefore in the MTA one must make a compromise, whereas in full-potential calculations this problem practically disappears.

2.2.13. The local coordinate system

The partition of a crystal into atoms (or molecules) is ambiguous and thus the atomic contribution cannot be defined uniquely. However, whatever the definition, it must follow the relevant site symmetry for each atom. There are at least two reasons why one would want to use a *local coordinate system* at each atomic site: the concept of crystal harmonics and the interpretation of bonding features.

2.2.13.1. Crystal harmonics

All spatial observables of the bound atom (*e.g.* the potential or the charge density) must have the crystal symmetry, *i.e.* the point-group symmetry around an atom. Therefore they must be representable as an expansion in terms of site-symmetrized spherical harmonics. Any point-symmetry operation transforms a spherical harmonic into another of the same ℓ . We start with the usual complex spherical harmonics,

$$Y_{\ell m}(\vartheta, \varphi) = N_{\ell m} P_{\ell}^m(\cos \vartheta) \exp(im\varphi), \quad (2.2.13.1)$$

which satisfy Laplacian's differential equation. The $P_{\ell}^m(\cos \vartheta)$ are the associated Legendre polynomials and the normalization $N_{\ell m}$ is according to the convention of Condon & Shortley (1953). For the φ -dependent part one can use the real and imaginary part and thus use $\cos(m\varphi)$ and $\sin(m\varphi)$ instead of the $\exp(im\varphi)$ functions,

Table 2.2.13.2. LM combinations of cubic groups as linear combinations of $y_{\ell mp}$'s (given in parentheses)

The linear-combination coefficients can be found in Kurki-Suonio (1977).

| Symmetry | LM combinations |
|-------------|---|
| 23 | (0 0), (3 2-), (4 0, 4 4+), (6 0, 6 4+), (6 2+, 6 6+) |
| $m\bar{3}$ | (0 0), (4 0, 4 4+), (6 0, 6 4+) (6 2+, 6 6+) |
| 432 | (0 0), (4 0, 4 4+), (6 0, 6 4+) |
| $\bar{4}3m$ | (0 0), (3 2-), (4 0, 4 4+), (6 0, 6 4+), |
| $m\bar{3}m$ | (0 0), (4 0, 4 4+), (6 0, 6 4+) |

but we must introduce a parity p to distinguish the functions with the same $|m|$. For convenience we take real spherical harmonics, since physical observables are real. The even and odd polynomials are given by the combination of the complex spherical harmonics with the parity p either + or - by

$$y_{\ell mp} = \begin{cases} y_{\ell m+} = (1/\sqrt{2})(Y_{\ell m} + Y_{\ell \bar{m}}) & + \text{parity} \\ y_{\ell m-} = -(i/\sqrt{2})(Y_{\ell m} - Y_{\ell \bar{m}}) & - \text{parity} \end{cases}, m = 2n$$

$$y_{\ell mp} = \begin{cases} y_{\ell m+} = -(1/\sqrt{2})(Y_{\ell m} - Y_{\ell \bar{m}}) & + \text{parity} \\ y_{\ell m-} = (i/\sqrt{2})(Y_{\ell m} + Y_{\ell \bar{m}}) & - \text{parity} \end{cases}, m = 2n + 1. \quad (2.2.13.2)$$

The expansion of - for example - the charge density $\rho(\mathbf{r})$ around an atomic site can be written using the LAPW method [see the analogous equation (2.2.12.5) for the potential] in the form

$$\rho(\mathbf{r}) = \sum_{LM} \rho_{LM}(r) K_{LM}(\hat{\mathbf{r}}) \text{ inside an atomic sphere,} \quad (2.2.13.3)$$

where we use capital letters LM for the indices (i) to distinguish this expansion from that of the wavefunctions in which complex spherical harmonics are used [see (2.2.12.1)] and (ii) to include the parity p in the index M (which represents the combined index mp). With these conventions, K_{LM} can be written as a linear combination of real spherical harmonics $y_{\ell mp}$ which are symmetry-adapted to the site symmetry,

$$K_{LM}(\hat{\mathbf{r}}) = \begin{cases} y_{\ell mp} & \text{non-cubic} \\ \sum_j c_{Lj} y_{\ell jp} & \text{cubic} \end{cases} \quad (2.2.13.4)$$

i.e. they are either $y_{\ell mp}$ [(2.2.13.2)] in the non-cubic cases (Table 2.2.13.1) or are well defined combinations of $y_{\ell mp}$'s in the five cubic cases (Table 2.2.13.2), where the coefficients c_{Lj} depend on the normalization of the spherical harmonics and can be found in Kurki-Suonio (1977).

According to Kurki-Suonio, the number of (non-vanishing) LM terms [*e.g.* in (2.2.13.3)] is minimized by choosing for each atom a local Cartesian coordinate system adapted to its site

2.2. ELECTRONS

symmetry. In this case, other LM terms would vanish, so using only these terms corresponds to the application of a projection operator, *i.e.* equivalent to averaging the quantity of interest [*e.g.* $\rho(\mathbf{r})$] over the star of \mathbf{k} . Note that in another coordinate system (for the L values listed) additional M terms could appear. The group-theoretical derivation led to rules as to how the local coordinate system must be chosen. For example, the z axis is taken along the highest symmetry axis, or the x and y axes are chosen in or perpendicular to mirror planes. Since these coordinate systems are specific for each atom and may differ from the (global) crystal axes, we call them ‘local’ coordinate systems, which can be related by a transformation matrix to the global coordinate system of the crystal.

The symmetry constraints according to (2.2.13.4) are summarized by Kurki-Suonio, who has defined picking rules to choose the local coordinate system for any of the 27 non-cubic site symmetries (Table 2.2.13.1) and has listed the LM combinations, which are defined by (a linear combination of) functions $y_{\ell mp}$ [see (2.2.13.2)]. If the \pm parity appears, both the $+$ and the $-$ combination must be taken. An application of a local coordinate system to rutile TiO_2 is described in Section 2.2.16.2.

In the case of the five cubic site symmetries, which all have a threefold axis in (111), a well defined linear combination of $y_{\ell mp}$ functions (given in Table 2.2.13.2) leads to the cubic harmonics.

2.2.13.2. Interpretation for bonding

Chemical bonding is often described by considering orbitals (*e.g.* a p_z or a d_{z^2} atomic orbital) which are defined in polar coordinates, where the z axis is special, in contrast to Cartesian coordinates, where x , y and z are equivalent. Consider for example an atom coordinated by ligands (*e.g.* forming an octahedron). Then the application of group theory, ligand-field theory *etc.* requires a certain coordinate system provided one wishes to keep the standard notation of the corresponding spherical harmonics. If this octahedron is rotated or tilted with respect to the global (unit-cell) coordinate system, a local coordinate system is needed to allow an easy orbital interpretation of the interactions between the central atom and its ligands. This applies also to spectroscopy or electric field gradients.

The two types of reasons mentioned above may or may not lead to the same choice of a local coordinate system, as is illustrated for the example of rutile in Section 2.2.16.2.

2.2.14. Characterization of Bloch states

The electronic structure of a solid is specified by energy bands $E^j(\mathbf{k})$ and the corresponding wavefunctions, the Bloch functions $\psi_{\mathbf{k}}^j(\mathbf{r})$. In order to characterize energy bands there are various schemes with quite different emphasis. The most important concepts are described below and are illustrated using selected examples in the following sections.

2.2.14.1. Characterization by group theory

The energy bands are primarily characterized by the wave-vector \mathbf{k} in the first BZ that is associated with the translational symmetry according to (2.2.4.23). The star of \mathbf{k} determines an irreducible basis provided that the functions of the star are symmetrized with respect to the small representations, as discussed in Section 2.2.6. Along symmetry lines in the BZ (*e.g.* from Γ along Δ towards X in the BZ shown in Fig. 2.2.7.1), the corresponding group of the \mathbf{k} vector may show a group–subgroup relation, as for example for Γ and Δ . The corresponding irreducible representations can then be found by deduction (or by induction in the case of a group–supergroup relation). These concepts define the compatibility relations (Bouckaert *et al.*, 1930; Bradley & Cracknell, 1972), which tell us how to connect energy bands. For example, the twofold degenerate representation Γ_{12} (the e_g symmetry in a cubic system) splits into the Δ_1 and

Δ_2 manifold in the Δ direction, both of which are one-dimensional. The compatibility relations tell us how to connect bands. In addition, one can also find an orbital representation and thus knows from the group-theoretical analysis which orbitals belong to a certain energy band. This is very useful for interpretations.

2.2.14.2. Energy regions

In chemistry and physics it is quite common to separate the electronic states of an atom into those from core and valence electrons, but sometimes this distinction is not well defined, as will be discussed in connection with the so-called semi-core states. For the sake of argument, let us discuss the situation in a solid using the concepts of the LAPW method, keeping in mind that very similar considerations hold for all other band-structure schemes.

A core state is characterized by a low-lying energy (*i.e.* with a large negative energy value with respect to the Fermi energy) and a corresponding wavefunction that is completely confined inside the sphere of the respective atom. Therefore there is effectively no overlap with the wavefunctions from neighbouring atoms and, consequently, the associated band width is practically zero.

The valence electrons occupy the highest states and have wavefunctions that strongly overlap with their counterparts at adjacent sites, leading to chemical bonding, large dispersion (*i.e.* a strong variation of the band energy with \mathbf{k}) and a significant band width.

The semi-core states are in between these two categories. For example, the $3s$ and $3p$ states of the $3d$ transition metals belong here. They are about 2–6 Ry (1 Ry = 13.6 eV) below the valence bands and have most of the wavefunctions inside their atomic spheres, but a small fraction (a few per cent) of the corresponding charge lies outside this sphere. This causes weak interactions with neighbouring atoms and a finite width of the corresponding energy bands.

Above the valence states are the unoccupied states, which often (*e.g.* in DFT or the HF method) require special attention.

2.2.14.3. Decomposition according to wavefunctions

For interpreting chemical bonding or the physical origin of a given Bloch state at $E^j(\mathbf{k})$, a decomposition according to its wavefunction is extremely useful but always model-dependent. The charge density $\psi_{\mathbf{k}}^j(\mathbf{r})^* \psi_{\mathbf{k}}^j(\mathbf{r})$ corresponding to the Bloch state at $E^j(\mathbf{k})$ can be normalized to one per unit cell and is (in principle) an observable, while its decomposition depends on the model used. The following considerations are useful in this context:

(1) *Site-centred orbitals.* In many band-structure methods, the Bloch functions are expressed as a linear combination of atomic orbitals (LCAO). These orbitals are centred at the various nuclei that constitute the solid. The linear-combination coefficients determine how much of a given orbital contributes to the wavefunction (Mulliken population analysis).

(2) *Spatially confined functions.* In many schemes (LMTO, LAPW, KKR; see Section 2.2.11), atomic spheres are used in which the wavefunctions are described in terms of atomic-like orbitals. See, for example, the representation (2.2.12.1) in the LAPW method (Section 2.2.12), where inside the atomic sphere the wavefunction is written as an ℓ -like radial function times spherical harmonics (termed partial waves). The latter require a local coordinate system (Section 2.2.13) which need not to be the same as the global coordinate system of the unit cell. The reasons for choosing a special local coordinate system are twofold: one is a simplification due to the use of the point-group symmetry, and the other is the interpretation, as will be illustrated below for TiO_2 in the rutile structure (see Section 2.2.16.2).

(3) *Orbital decomposition.* In all cases in which ℓ -like orbitals are used (they do not require a local coordinate system) to construct the crystalline wavefunction, an ℓ -like decomposition

2. SYMMETRY ASPECTS OF EXCITATIONS

can be done. This is true for both atom-centred orbitals and spatially confined partial waves. A corresponding decomposition can be done on the basis of partial electronic charges, as discussed below. A further decomposition into the m components can only be done in a local coordinate system with respect to which the spherical harmonics are defined.

(4) *Bonding character.* As in a diatomic molecule with an orbital on atom A and another on atom B, we can form bonding and antibonding states by adding or subtracting the corresponding orbitals. The bonding interaction causes a lowering in energy with respect to the atomic state and corresponds to a constructive interference of the orbitals. For the antibonding state, the interaction raises the energy and leads to a change in sign of the wavefunction, causing a nodal plane that is perpendicular to the line connecting the nuclei. If the symmetry does not allow an interaction between two orbitals, a nonbonding state occurs. Analogous concepts can also be applied to solids.

(5) *Partial charges.* The charge corresponding to a Bloch function of state $E(\mathbf{k})$ – averaged over the star of \mathbf{k} – can be normalized to 1 in the unit cell. A corresponding decomposition of the charge can be done into partial electronic charges. This is illustrated first within the LAPW scheme. Using the resolution of the identity this 1 (unit charge) of each state $E_{\mathbf{k}}^j$ can be spatially decomposed into the contribution $q^{\text{out}}(E_{\mathbf{k}}^j)$ from the region outside all atomic spheres (interstitial region II) and a sum over all atomic spheres (with superscript i) which contain the charges $q^i(E_{\mathbf{k}}^j)$ (confined within atomic sphere i). The latter can be further decomposed into the partial ℓ -like charges $q_{\ell}^i(E_{\mathbf{k}}^j)$, leading to $1 = q^{\text{out}}(E_{\mathbf{k}}^j) + \sum_i \sum_{\ell} q_{\ell}^i(E_{\mathbf{k}}^j)$. In a site-centred basis a similar decomposition can be done, but without the term $q^{\text{out}}(E_{\mathbf{k}}^j)$. The interpretation, however, is different, as will be discussed for Cu (see Section 2.2.16). If the site symmetry (point group) permits, another partitioning according to m can be made, e.g. into the t_{2g} and e_g manifold of the fivefold degenerate d orbitals in an octahedral ligand field. The latter scheme requires a local coordinate system in which the spherical harmonics are defined (see Section 2.2.13). In general, the proper m combinations are given by the irreducible representations corresponding to the site symmetry.

2.2.14.4. Localized versus itinerant electrons

Simple metals with valence electrons originating from s - and p -type orbitals form wide bands which are approximately free-electron like (with a large band width W). Such a case corresponds to itinerant electrons that are delocalized and thus cause metallic conductivity.

The other extreme case is a system with $4f$ (and some $5f$) electrons, such as the lanthanides. Although the orbital energies

of these electrons are in the energy range of the valence electrons, they act more like core electrons and thus are tightly bound to the corresponding atomic site. Such electrons are termed localized, since they do not hop to neighbouring sites (controlled by a hopping parameter t) and thus do not contribute to metallic conductivity. Adding another of these electrons to a given site would increase the Coulomb repulsion U . A large U (i.e. $U > t$) prevents them from hopping.

There are – as usual – borderline cases (e.g. the late $3d$ transition-metal oxides) in which a delicate balance between t and U , the energy gain by delocalizing electrons and the Coulomb repulsion, determines whether a system is metallic or insulating. This problem of metal/insulator transitions is an active field of research of solid-state physics which shall not be discussed here.

In one example, however, the dual role of f electrons is illustrated for the uranium atom using relativistic wavefunctions (with a large and a small component) characterized by the quantum numbers n , ℓ and j . Fig. 2.2.14.1 shows the outermost lobe (the large component) of the electrons beyond the [Xe] core without the $4f$ and $5d$ core-like states. One can see the $6s_{1/2}$, $6p_{1/2}$ and $6p_{3/2}$ (semi-core) electrons, and the $6d_{3/2}$ and $7s_{1/2}$ (valence) electrons.

On the one hand, the radial wavefunction of the $5f_{5/2}$ orbital has its peak closer to the nucleus than the main lobes of the semi-core states $6s_{1/2}$, $6p_{1/2}$ and $6p_{3/2}$, and thus demonstrates the *core nature* of these $5f$ electrons. On the other hand, the $5f_{5/2}$ orbital decays (with distance) much less than the semi-core states and electrons in this orbital can thus also play the role of *valence electrons*, like electrons in the $6d_{3/2}$ and $7s_{1/2}$ orbitals. This dual role of the f electrons has been discussed, for example, by Schwarz & Herzig (1979).

2.2.14.5. Spin polarization

In a non-fully-relativistic treatment, spin remains a good quantum number. Associated with the spin is a spin magnetic moment. If atoms have net magnetic moments they can couple in various orders in a solid. The simplest cases are the collinear spin alignments as found in ferromagnetic (FM) or antiferromagnetic (AF) systems with parallel (FM) and antiparallel (AF) moments on neighbouring sites. Ferrimagnets have opposite spin alignments but differ in the magnitude of their moments on neighbouring sites, leading to a finite net magnetization. These cases are characterized by the electronic structure of spin-up and spin-down electrons. More complicated spin structures (e.g. canted spins, spin spirals, spin glasses) often require a special treatment beyond simple spin-polarized calculations. In favourable cases, however, as in spin spirals, it is possible to formulate a generalized Bloch theorem and treat such systems by band theory (Sandratskii, 1990).

In a fully relativistic formalism, an additional orbital moment may occur. Note that the orientation of the total magnetic moment (spin and orbital moment) with respect to the crystal axis is only defined in a relativistic treatment including spin-orbit interactions. In a spin-polarized calculation without spin-orbit coupling this is not the case and only the relative orientation (majority-spin and minority-spin) is known. The magnetic structures may lead to a lowering of symmetry, a topic beyond this book.

2.2.14.6. The density of states (DOS)

The density of states (DOS) is the number of one-electron states (in the HF method or DFT) per unit energy interval and per unit cell volume. It is better to start with the integral quantity $I(\varepsilon)$, the number of states below a certain energy ε ,

$$I(\varepsilon) = \frac{2}{V_{\text{BZ}}} \sum_j \int_{\text{BZ}} \vartheta(\varepsilon - \varepsilon_{\mathbf{k}}^j) d\mathbf{k}, \quad (2.2.14.1)$$

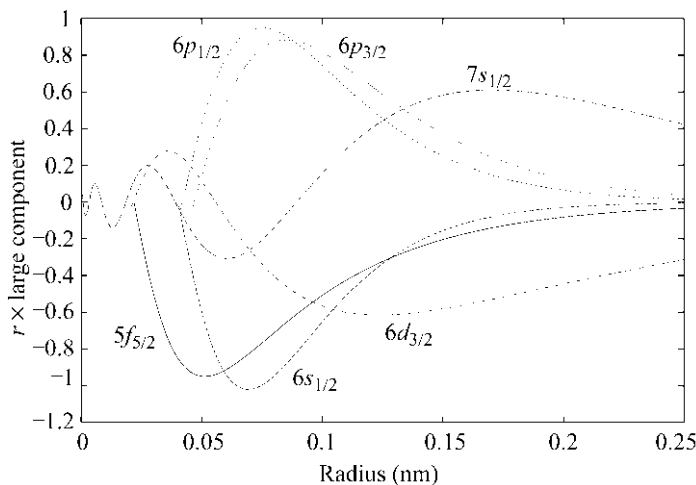


Fig. 2.2.14.1. Relativistic radial wavefunctions (large component) of the uranium atom. Shown are the outer lobes of valence and semi-core states excluding the [Xe] core, and the $4f$ and $5d$ core states.

2.2. ELECTRONS

where V_{BZ} is the volume of the BZ, the factor 2 accounts for the occupation with spin-up and spin-down electrons (in a non-spin-polarized case), and $\vartheta(\varepsilon - \varepsilon_{\mathbf{k}})$ is the step function, the value of which is 1 if $\varepsilon_{\mathbf{k}}$ is less than ε and 0 otherwise. The sum over \mathbf{k} points has been replaced by an integral over the BZ, since the \mathbf{k} points are uniformly distributed. Both expressions, sum and integral, are used in different derivations or applications. The Fermi energy is defined by imposing that $I(E_F) = N$, the number of (valence) electrons per unit cell.

The total DOS is defined as the energy derivative of $I(\varepsilon)$ as

$$n(\varepsilon) = \frac{dI(\varepsilon)}{d\varepsilon}, \quad (2.2.14.2)$$

with the normalization

$$N = \int_{-\infty}^{E_F} n(\varepsilon) d\varepsilon, \quad (2.2.14.3)$$

where the integral is taken from $-\infty$ if all core states are included or from the bottom of the valence bands, often taken to be at zero. This defines the Fermi energy (note that the energy range must be consistent with N). In a bulk material, the origin of the energy scale is arbitrary and thus only relative energies are important. In a realistic case with a surface (*i.e.* a vacuum) one can take the potential at infinity as the energy zero, but this situation is not discussed here.

The total DOS $n(\varepsilon)$ can be decomposed into a partial (or projected) DOS by using information from the wavefunctions as described above in Section 2.2.14.3. If the charge corresponding to the wavefunction of an energy state is partitioned into contributions from the atoms, a site-projected DOS can be defined as $n^t(\varepsilon)$, where the superscript t labels the atom t . These quantities can be further decomposed into ℓ -like contributions within each atom to give $n_\ell^t(\varepsilon)$. As discussed above for the partial charges, a further partitioning of the ℓ -like terms according to the site symmetry (point group) can be done (in certain cases) by taking the proper m combinations, *e.g.* the t_{2g} and e_g manifold of the fivefold degenerate d orbitals in an octahedral ligand field. The latter scheme requires a local coordinate system in which the spherical harmonics are defined (see Section 2.2.13). In this context all considerations as discussed above for the partial charges apply again. Note in particular the difference between site-centred and spatially decomposed wavefunctions, which affects the partition of the DOS into its wavefunction-dependent contributions. For example, in atomic sphere representations as in LAPW we have the decomposition

$$n(\varepsilon) = n^{\text{out}}(\varepsilon) + \sum_t \sum_\ell n_\ell^t(\varepsilon). \quad (2.2.14.4)$$

In the case of spin-polarized calculations, one can also define a spin-projected DOS for spin-up and spin-down electrons.

2.2.15. Electric field gradient tensor

2.2.15.1. Introduction

The study of hyperfine interactions is a powerful way to characterize different atomic sites in a given sample. There are many experimental techniques, such as Mössbauer spectroscopy, nuclear magnetic and nuclear quadrupole resonance (NMR and NQR), perturbed angular correlations (PAC) measurements *etc.*, which access hyperfine parameters in fundamentally different ways. Hyperfine parameters describe the interaction of a nucleus with the electric and magnetic fields created by the chemical environment of the corresponding atom. Hence the resulting level splitting of the nucleus is determined by the product of a nuclear and an extra-nuclear quantity. In the case of quadrupole interactions, the nuclear quantity is the nuclear quadrupole moment (Q) that interacts with the electric field gradient (EFG)

produced by the charges outside the nucleus. For a review see, for example, Kaufmann & Vianden (1979).

The EFG tensor is defined by the second derivative of the electrostatic potential V with respect to the Cartesian coordinates x_i , $i = 1, 2, 3$, taken at the nuclear site n ,

$$\Phi_{ij} = \left. \frac{\partial^2 V}{\partial x_i \partial x_j} \right|_n - \frac{1}{3} \delta_{ij} \nabla^2 \Big|_n, \quad (2.2.15.1)$$

where the second term is included to make it a traceless tensor. This is more appropriate, since there is no interaction of a nuclear quadrupole and a potential caused by s electrons. From a theoretical point of view it is more convenient to use the spherical tensor notation because electrostatic potentials (the negative of the potential energy of the electron) and the charge densities are usually given as expansions in terms of spherical harmonics. In this way one automatically deals with traceless tensors (for further details see Herzig, 1985).

The analysis of experimental results faces two obstacles: (i) The nuclear quadrupole moments (Pyykkö, 1992) are often known only with a large uncertainty, as this is still an active research field of nuclear physics. (ii) EFGs depend very sensitively on the anisotropy of the charge density close to the nucleus, and thus pose a severe challenge to electronic structure methods, since an accuracy of the density in the per cent range is required.

In the absence of a better tool, a simple point-charge model was used in combination with so-called Sternheimer (anti-) shielding factors in order to interpret the experimental results. However, these early model calculations depended on empirical parameters, were not very reliable and often showed large deviations from experimental values.

In their pioneering work, Blaha *et al.* (1985) showed that the LAPW method was able to calculate EFGs in solids accurately without empirical parameters. Since then, this method has been applied to a large variety of systems (Schwarz & Blaha, 1992) from insulators (Blaha *et al.*, 1985), metals (Blaha *et al.*, 1988) and superconductors (Schwarz *et al.*, 1990) to minerals (Winkler *et al.*, 1996).

Several other electronic structure methods have been applied to the calculation of EFGs in solids, for example the LMTO method for periodic (Methfessel & Frota-Pessoa, 1990) or non-periodic (Petrilli & Frota-Pessoa, 1990) systems, the KKR method (Akai *et al.*, 1990), the DVM (discrete variational method; Ellis *et al.*, 1983), the PAW method (Petrilli *et al.*, 1998) and others (Meyer *et al.*, 1995). These methods achieve different degrees of accuracy and are more or less suitable for different classes of systems.

As pointed out above, measured EFGs have an intrinsic uncertainty related to the accuracy with which the nuclear quadrupole moment is known. On the other hand, the quadrupole moment can be obtained by comparing experimental hyperfine splittings with very accurate electronic structure calculations. This has recently been done by Dufek *et al.* (1995a) to determine the quadrupole moment of ^{57}Fe . Hence the calculation of accurate EFGs is to date an active and challenging research field.

2.2.15.2. EFG conversion formulas

The nuclear quadrupole interaction (NQI) represents the interaction of Q (the nuclear quadrupole moment) with the electric field gradient (EFG) created by the charges surrounding the nucleus, as described above. Here we briefly summarize the main ideas (following Petrilli *et al.*, 1998) and provide conversions between experimental NQI splittings and electric field gradients.

Let us consider a nucleus in a state with nuclear spin quantum number $I > 1/2$ with the corresponding nuclear quadrupole moment $Q_{ij} = (1/e) \int d^3r \rho_n(r) r_i r_j$, where $\rho_n(r)$ is the nuclear

2. SYMMETRY ASPECTS OF EXCITATIONS

charge density around point \mathbf{r} and e is the proton's charge. The interaction of this Q with an electric field gradient tensor V_{ij} ,

$$H = e \sum_{i,j} Q_{i,j} V_{i,j}, \quad (2.2.15.2)$$

splits the energy levels E_Q for different magnetic spin quantum numbers $m_I = I, I-1, \dots, -I$ of the nucleus according to

$$E_Q = \frac{eQV_{zz}[3m_I^2 - I(I+1)](1 + \eta^2/3)^{1/2}}{4I(2I-1)} \quad (2.2.15.3)$$

in first order of V_{ij} , where Q represents the largest component of the nuclear quadrupole moment tensor in the state characterized by $m_I = I$. (Note that the quantum-mechanical expectation value of the charge distribution in an angular momentum eigenstate is cylindrical, which renders the expectation value of the remaining two components with half the value and opposite sign.) The conventional choice is $|V_{zz}| > |V_{yy}| \geq |V_{xx}|$. Hence, V_{zz} is the principal component (largest eigenvalue) of the electric field gradient tensor and the asymmetry parameter η is defined by the remaining two eigenvalues V_{xx}, V_{yy} through

$$\eta = \frac{|(V_{xx} - V_{yy})|}{|V_{zz}|}. \quad (2.2.15.4)$$

(2.2.15.3) shows that the electric quadrupole interaction splits the $(2I+1)$ -fold degenerate energy levels of a nuclear state with spin quantum number I ($I > 1/2$) into I doubly degenerate substates (and one singly degenerate state for integer I). Experiments determine the energy difference Δ between the levels, which is called the quadrupole splitting. The remaining degeneracy can be lifted further using magnetic fields.

Next we illustrate these definitions for ^{57}Fe , which is the most common probe nucleus in Mössbauer spectroscopy measurements and thus deserves special attention. For this probe, the nuclear transition occurs between the $I = 3/2$ excited state and $I = 1/2$ ground state, with a 14.4 KeV γ radiation emission. The quadrupole splitting between the $m_I = \pm(1/2)$ and the $m_I = \pm(3/2)$ state can be obtained by exploiting the Doppler shift of the γ radiation of the vibrating sample.

$$\Delta = \frac{V_{zz}eQ(1 + \eta^2/3)^{1/2}}{2}. \quad (2.2.15.5)$$

For systems in which the ^{57}Fe nucleus has a crystalline environment with axial symmetry (a threefold or fourfold rotation axis), the asymmetry parameter η is zero and Δ is given directly by

$$\Delta = \frac{V_{zz}eQ}{2}. \quad (2.2.15.6)$$

As η can never be greater than unity, the difference between the values of Δ given by equation (2.2.15.5) and equation (2.2.15.6) cannot be more than about 15%. In the remainder of this section we simplify the expressions, as is often done, by assuming that $\eta = 0$. As Mössbauer experiments exploit the Doppler shift of the γ radiation, the splitting is expressed in terms of the velocity between sample and detector. The quadrupole splitting can be obtained from the velocity, which we denote here by Δ_v , by

$$\Delta = \frac{E_\gamma}{c} \Delta_v, \quad (2.2.15.7)$$

where $c = 2.9979245580 \times 10^8 \text{ m s}^{-1}$ is the speed of light and $E_\gamma = 14.41 \times 10^3 \text{ eV}$ is the energy of the emitted γ radiation of the ^{57}Fe nucleus.

Finally, we still need to know the nuclear quadrupole moment Q of the Fe nucleus itself. Despite its utmost importance, its value has been heavily debated. Recently, however, Dufek *et al.* (1995b) have determined the value $Q = 0.16 \text{ b}$ for ^{57}Fe ($1 \text{ b} = 10^{-28} \text{ m}^2$) by comparing for fifteen different compounds

theoretical V_{zz} values, which were obtained using the linearized augmented plane wave (LAPW) method, with the measured quadrupole splitting at the Fe site.

Now we relate the electric field gradient V_{zz} to the Doppler velocity *via*

$$\Delta_v = \frac{eQc}{2E_\gamma} V_{zz}. \quad (2.2.15.8)$$

In the special case of the ^{57}Fe nucleus, we obtain

$$\begin{aligned} V_{zz} [10^{21} \text{ V m}^{-2}] &= 10^4 \frac{2E_\gamma [\text{eV}]}{c [\text{m s}^{-1}] Q [\text{b}]} \Delta_v [\text{mm s}^{-1}] \\ &\approx 6 \Delta_v [\text{mm s}^{-1}]. \end{aligned} \quad (2.2.15.9)$$

EFGs can also be obtained by techniques like NMR or NQR, where a convenient measure of the strength of the quadrupole interaction is expressed as a frequency ν_q , related to V_{zz} by

$$\nu_q = \frac{3eQV_{zz}}{2hI(2I-1)}. \quad (2.2.15.10)$$

The value V_{zz} can then be calculated from the frequency in MHz by

$$V_{zz} [10^{21} \text{ V m}^{-2}] = 0.02771 \frac{I(2I-1)}{Q [\text{b}]} \nu_q [\text{MHz}], \quad (2.2.15.11)$$

where $(h/e) = 4.1356692 \times 10^{-15} \text{ V Hz}^{-1}$. The principal component V_{zz} is also often denoted as $eq = V_{zz}$.

In the literature, two conflicting definitions of ν_q are in use. One is given by (2.2.15.10), and the other, defined as

$$\nu_q [\text{Hz}] = \frac{e^2 q Q}{2h}, \quad (2.2.15.12)$$

differs from the first by a factor of 2 and assumes the value $I = 3/2$. Finally, the definition of $q = V_{zz}/e$ has been introduced here. In order to avoid confusion, we will refer here only to the definition given by (2.2.15.10). Furthermore, we also adopt the same sign convention for V_{zz} as Schwarz *et al.* (1990) because it has been found to be consistent with the majority of experimental results.

2.2.15.3. Theoretical approach

Since the EFG is a ground-state property that is uniquely determined by the charge density distribution (of electrons and nuclei), it can be calculated within DFT without further approximations. Here we describe the basic formalism to calculate EFGs with the LAPW method (see Section 2.2.12). In the LAPW method, the unit cell is divided into non-overlapping atomic spheres and an interstitial region. Inside each sphere the charge density (and analogously the potential) is written as radial functions $\rho_{LM}(r)$ times crystal harmonics (2.2.13.4) and in the interstitial region as Fourier series:

$$\rho(r) = \begin{cases} \sum_{LM} \rho_{LM}(r) K_{LM}(\hat{r}) & \text{inside sphere} \\ \sum_K \rho_K \exp(iKr) & \text{outside sphere} \end{cases} \quad (2.2.15.13)$$

The charge density coefficients $\rho_{LM}(r)$ can be obtained from the wavefunctions (KS orbitals) by (in shorthand notation)

$$\rho_{LM}(r) = \sum_{E_k^j < E_F} \sum_{\ell m} \sum_{\ell' m'} R_{\ell m}(r) R_{\ell' m'}(r) G_{L\ell\ell'}^{Mmm'}, \quad (2.2.15.14)$$

where $G_{L\ell\ell'}^{Mmm'}$ are Gaunt numbers (integrals over three spherical harmonics) and $R_{\ell m}(r)$ denote the LAPW radial functions [see (2.2.12.1)] of the occupied states E_k^j below the Fermi energy E_F . The dependence on the energy bands in $R_{\ell m}(r)$ has been omitted in order to simplify the notation.

2.2. ELECTRONS

For a given charge density, the Coulomb potential is obtained numerically by solving Poisson's equation in form of a boundary-value problem using a method proposed by Weinert (1981). This yields the Coulomb potential coefficients $v_{LM}(r)$ in analogy to (2.2.15.13) [see also (2.2.12.5)]. The most important contribution to the EFG comes from a region close to the nucleus of interest, where only the $L = 2$ terms are needed (Herzig, 1985). In the limit $r \rightarrow 0$ (the position of the nucleus), the asymptotic form of the potential $r^L v_{LM} K_{LM}$ can be used and this procedure yields (Schwarz *et al.*, 1990) for $L = 2$:

$$V_{2M} = -C_{2M} \int_0^R \frac{\rho_{2M}(r)}{r^3} r^2 dr + C_{2M} \int_0^R \frac{\rho_{2M}(r)}{r} \left(\frac{r}{R}\right)^5 dr + 5 \frac{C_{2M}}{R^2} \sum_K V(K) j_2(KR) K_{2M}(K), \quad (2.2.15.15)$$

with $C_{2M} = 2\sqrt{4\pi/5}$, $C_{22} = \sqrt{3/4}C_{20}$ and the spherical Bessel function j_2 . The first term in (2.2.15.15) (called the *valence* EFG) corresponds to the integral over the respective atomic sphere (with radius R). The second and third terms in (2.2.15.15) (called the *lattice* EFG) arise from the boundary-value problem and from the charge distribution outside the sphere considered. Note that our definition of the lattice EFG differs from that based on the point-charge model (Kaufmann & Vianden, 1979). With these definitions the tensor components are given as

$$\begin{aligned} V_{xx} &= C \left[V_{22+} - \left(1/\sqrt{3}\right) V_{20} \right] \\ V_{yy} &= C \left[-V_{22+} - \left(1/\sqrt{3}\right) V_{20} \right] \\ V_{zz} &= C \left(2/\sqrt{3} \right) V_{20} \\ V_{xy} &= C V_{22-} \\ V_{xz} &= C V_{21+} \\ V_{yz} &= C V_{21-} \end{aligned} \quad (2.2.15.16)$$

where $C = \sqrt{15/4\pi}$ and the index M combines m and the parity p (e.g. $2+$). Note that the prefactors depend on the normalization used for the spherical harmonics.

The non-spherical components of the potential v_{LM} come from the non-spherical charge density ρ_{LM} . For the EFG only the $L = 2$ terms (in the potential) are needed. If the site symmetry does not contain such a non-vanishing term (as for example in a cubic system with $L = 4$ in the lowest LM combination), the corresponding EFG vanishes by definition. According to the Gaunt numbers in (2.2.15.14) only a few non-vanishing terms remain (ignoring f orbitals), such as the p - p , d - d or s - d combinations (for f orbitals, p - f and f - f would appear), where this shorthand notation denotes the products of the two radial functions $R_{\ell m}(r) R_{\ell' m'}(r)$. The s - d term is often small and thus is not relevant to the interpretation. This decomposition of the density can be used to partition the EFG (illustrated for the V_{zz} component),

$$V_{zz} \approx V_{zz}^p + V_{zz}^d + \text{small contributions}, \quad (2.2.15.17)$$

where the superscripts p and d are a shorthand notation for the product of two p - or d -like functions.

Table 2.2.15.1. Partial O 2p charges (in electrons) and electric field gradient tensor O EFG (in 10^{21} V m^{-2}) for $\text{YBa}_2\text{Cu}_3\text{O}_7$

Numbers in bold represent the main deviation from spherical symmetry in the 2p charges and the related principal component of the EFG tensor.

| Atom | p_x | p_y | p_z | V_{aa} | V_{bb} | V_{cc} |
|------|-------------|-------------|-------------|-------------|-------------|-------------|
| O1 | 1.18 | 0.91 | 1.25 | -6.1 | 18.3 | -12.2 |
| O2 | 1.01 | 1.21 | 1.18 | 11.8 | -7.0 | -4.8 |
| O3 | 1.21 | 1.00 | 1.18 | -7.0 | 11.9 | -4.9 |
| O4 | 1.18 | 1.19 | 0.99 | -4.7 | -7.0 | 11.7 |

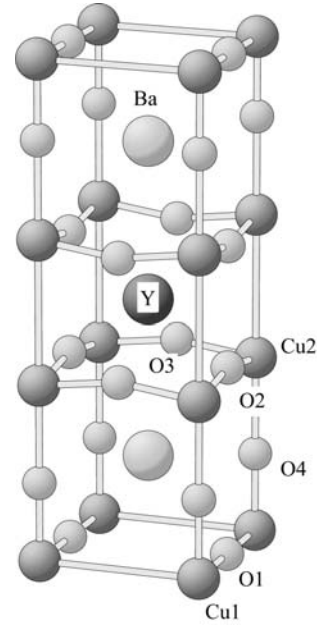


Fig. 2.2.15.1. Unit cell of the high-temperature superconductor $\text{YBa}_2\text{Cu}_3\text{O}_7$ with four non-equivalent oxygen sites.

From our experience we find that the first term in (2.2.15.15) is usually by far the most important and often a radial range up to the first node in the corresponding radial function is all that contributes. In this case the contribution from the other two terms is rather small (a few per cent). For first-row elements, however, which have no node in their $2p$ functions, this is no longer true and thus the first term amounts only to about 50–70%.

In some cases interpretation is simplified by defining a so-called asymmetry count, illustrated below for the oxygen sites in $\text{YBa}_2\text{Cu}_3\text{O}_7$ (Schwarz *et al.*, 1990), the unit cell of which is shown in Fig. 2.2.15.1.

In this case essentially only the O 2p orbitals contribute to the O EFG. Inside the oxygen spheres (all taken with a radius of 0.82 \AA) we can determine the partial charges q_i corresponding to the p_x , p_y and p_z orbitals, denoted in short as p_x , p_y and p_z charges.

With these definitions we can define the p -like asymmetry count as

$$\Delta n_p = \frac{1}{2}(p_x + p_y) - p_z \quad (2.2.15.18)$$

and obtain the proportionality

$$V_{zz} \propto \langle 1/r^3 \rangle_p \Delta n_p, \quad (2.2.15.19)$$

where $\langle 1/r^3 \rangle_p$ is the expectation value taken with the p orbitals. A similar equation can be defined for the d orbitals. The factor $1/r^3$ enhances the EFG contribution from the density anisotropies close to the nucleus. Since the radial wavefunctions have an asymptotic behaviour near the origin as r^ℓ , the p orbitals are more sensitive than the d orbitals. Therefore even a very small p anisotropy can cause an EFG contribution, provided that the asymmetry count is enhanced by a large expectation value.

Often the anisotropy in the p_x , p_y and p_z occupation numbers can be traced back to the electronic structure. Such a physical interpretation is illustrated below for the four non-equivalent oxygen sites in $\text{YBa}_2\text{Cu}_3\text{O}_7$ (Table 2.2.15.1). Let us focus first on O1, the oxygen atom that forms the linear chain with the Cu1 atoms along the b axis. In this case, the p_y orbital of O1 points towards Cu1 and forms a covalent bond, leading to bonding and antibonding states, whereas the other two p orbitals have no bonding partner and thus are essentially nonbonding. Part of the corresponding antibonding states lies above the Fermi energy

2. SYMMETRY ASPECTS OF EXCITATIONS

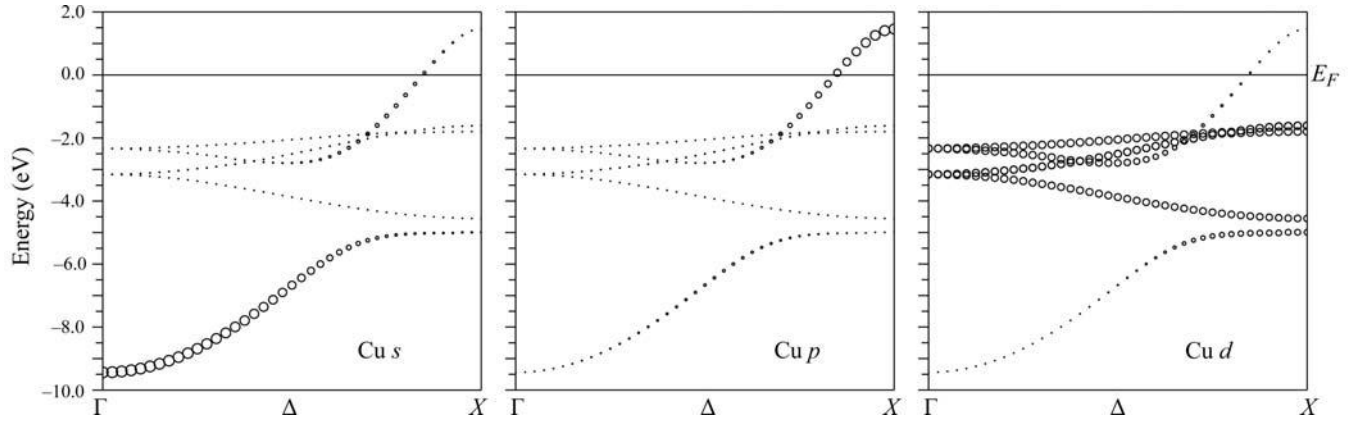


Fig. 2.2.16.1. Character of energy bands of f.c.c. copper in the Δ direction. The radius of each circle is proportional to the respective partial charge of the given state.

and thus is not occupied, leading to a smaller p_z charge of 0.91 e, in contrast to the fully occupied nonbonding states with occupation numbers around 1.2 e. (Note that only a fraction of the charge stemming from the oxygen 2p orbitals is found inside the relatively small oxygen sphere.) This anisotropy causes a finite asymmetry count [(2.2.15.18)] that leads – according to (2.2.15.19) – to a corresponding EFG.

In this simple case, the anisotropy in the charge distribution, given here by the different p occupation numbers, is directly proportional to the EFG, which is given with respect to the crystal axes and is thus labelled V_{aa} , V_{bb} and V_{cc} (Table 2.2.15.1). The principal component of the EFG is in the direction where the p occupation number is smallest, *i.e.* where the density has its highest anisotropy. The other oxygen atoms behave very similarly: O2, O3 and O4 have a near neighbour in the a , b and c direction, respectively, but not in the other two directions. Consequently, the occupation number is lower in the direction in which the bond is formed, whereas it is normal (around 1.2 e) in the other two directions. The principal axis falls in the direction of the low occupation. The higher the anisotropy, the larger the EFG (compare O1 with the other three oxygen sites). Excellent agreement with experiment is found (Schwarz *et al.*, 1990). In a more complicated situation, where p and d contributions to the EFG occur [see (2.2.15.17)], which often have opposite sign, the interpretation can be more difficult [see *e.g.* the copper sites in $\text{YBa}_2\text{Cu}_3\text{O}_7$; Schwarz *et al.* (1990)].

The importance of semi-core states has been illustrated for rutile, where the proper treatment of 3p and 4p states is essential to finding good agreement with experiment (Blaha *et al.*, 1992). The orthogonality between ℓ -like bands belonging to different principal quantum numbers (3p and 4p) is important and can be treated, for example, by means of local orbitals [see (2.2.12.4)].

In many simple cases, the off-diagonal elements of the EFG tensor vanish due to symmetry, but if they don't, diagonalization of the EFG tensor is required, which defines the orientation of the principal axis of the tensor. Note that in this case the orientation is given with respect to the local coordinate axes (see Section 2.2.13) in which the LM components are defined.

2.2.16. Examples

The general concepts described above are used in many band-structure applications and thus can be found in the corresponding literature. Here only a few examples are given in order to illustrate certain aspects.

2.2.16.1. F.c.c. copper

For the simple case of an element, namely copper in the f.c.c. structure, the band structure is shown in Fig. 2.2.16.1 along the Δ

symmetry direction from Γ to X . The character of the bands can be illustrated by showing for each band state the crucial information that is contained in the wavefunctions. In the LAPW method (Section 2.2.12), the wavefunction is expanded in atomic like functions inside the atomic spheres (partial waves), and thus a spatial decomposition of the associated charge and its portion of ℓ -like charge (s -, p -, d -like) inside the Cu sphere, $q_\ell^{\text{Cu}}(E_{\mathbf{k}}^i)$, provides such a quantity. Fig. 2.2.16.1 shows for each state $E_{\mathbf{k}}^i$ a circle the radius of which is proportional to the ℓ -like charge of that state. The band originating from the Cu 4s and 4p orbitals shows an approximately free-electron behaviour and thus a k^2 energy dependence, but it hybridizes with one of the d bands in the middle of the Δ direction and thus the ℓ -like character changes along the Δ direction.

This can easily be understood from a group-theoretical point of view. Since the d states in an octahedral environment split into the e_g and t_{2g} manifold, the d bands can be further partitioned into the two subsets as illustrated in Fig. 2.2.16.2. The s band ranges from about -9.5 eV below E_F to about 2 eV above. In the Δ direction, the s band has Δ_1 symmetry, the same as one of the d bands from the e_g manifold, which consists of Δ_1 and Δ_2 . As a consequence of the ‘non-crossing rule’, the two states, both with Δ_1 symmetry, must split due to the quantum-mechanical interaction between states with the same symmetry. This leads to the avoided crossing seen in the middle of the Δ direction (Fig. 2.2.16.1). Therefore the lowest band starts out as an ‘ s band’ but ends near X as a ‘ d band’. This also shows that bands belonging to different irreducible representations (small representations) may cross. The fact that Γ_{12} splits into the subgroups Δ_1 and Δ_2 is an example of the compatibility relations. In addition, group-theoretical arguments can be used (Altmann, 1994) to show that in certain symmetry directions the bands must enter the face of the BZ with zero slope.

Note that in a site-centred description of the wavefunctions a similar ℓ -like decomposition of the charge can be defined as $1 = \sum_i \sum_\ell q_\ell^i$ (without the q^{out} term), but here the partial charges have a different meaning than in the spatial decomposition. In one case (*e.g.* LAPW), q_ℓ^i refers to the partial charge of ℓ -like character inside sphere i , while in the other case (LCAO), it means ℓ -like charge coming from orbitals centred at site i . For the main components (for example Cu d) these two procedures will give roughly similar results, but the small components have quite a different interpretation. For this purpose consider an orbital that is centred on the neighbouring site j , but whose tail enters the atomic sphere i . In the spatial representation this tail coming from the j site must be represented by the (s , p , d etc.) partial waves inside sphere i and consequently will be associated with site i , leading to a small partial charge component. This situation is sometimes called the off-site component, in contrast to the on-site component, which

2.2. ELECTRONS

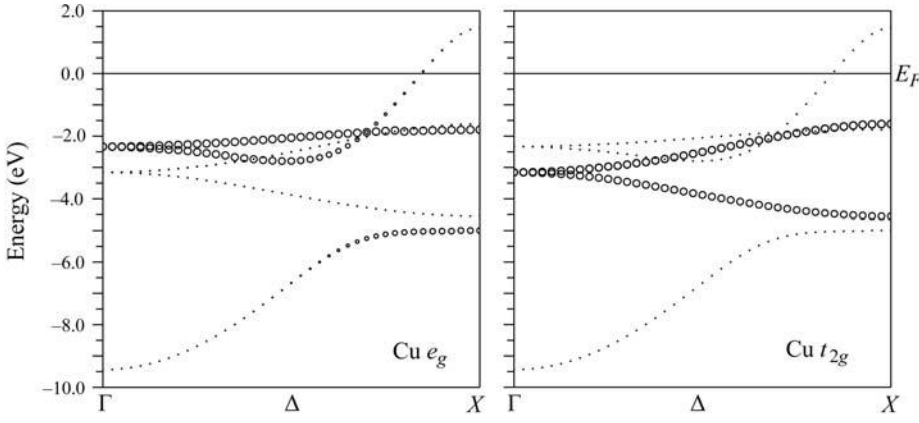


Fig. 2.2.16.2. Decomposition of the Cu d bands into the e_g and t_{2g} manifold. The radius of each circle is proportional to the corresponding partial charge.

will appear at its own site or in its own sphere, depending on the representation, site-centred or spatially confined.

2.2.16.2. The rutile TiO_2

The well known rutile structure (e.g. TiO_2) is tetragonal (see Fig. 2.2.16.3) with the basis consisting of the metal atoms at the $2a$ Wyckoff positions, $(0, 0, 0)$ and $(\frac{1}{2}, \frac{1}{2}, \frac{1}{2})$, and anions at the $4f$ position, located at $(\pm u, \pm u, 0)$ and $(\frac{1}{2} \pm u, \frac{1}{2} \mp u, \frac{1}{2})$ with a typical value of about 0.3 for the internal coordinate u . Rutile belongs to the non-symmorphic space group $P4_2/mmm$ (D_{4h}^{14}) in which the metal positions are transformed into each other by a rotation by 90° around the crystal c axis followed by a non-primitive translation of $(\frac{1}{2}, \frac{1}{2}, \frac{1}{2})$. The two metal positions at the centre and at the corner of the unit cell are equivalent when the surrounding octahedra are properly rotated. The metal atoms are octahedrally coordinated by anions which, however, do not form an ideal octahedron. The distortion depends on the structure parameters a , c/a and u , and results in two different metal–anion distances, namely the apical distance d_a and the equatorial distance d_e , the height (z axis) and the basal spacing of the octahedron. For a certain value u^* the two distances d_a and d_e become equal:

$$u = u^* = \frac{1}{4}[1 + \frac{1}{2}(c/a)^2]. \quad (2.2.16.1)$$

For this special value u^* and an ideal c/a ratio, the basal plane of the octahedron is quadratic and the two distances are equal. An ideal octahedral coordination is thus obtained with

$$d_a = d_e, \quad c = \sqrt{2}(1 - 2u)a \quad (2.2.16.2)$$

$$u_{\text{ideal}} = \frac{1}{2}(2 - \sqrt{2}) = 0.293 \quad (2.2.16.3)$$

$$(c/a)_{\text{ideal}} = 2 - \sqrt{2} = 0.586. \quad (2.2.16.4)$$

Although the actual coordination of the metal atoms deviates from the ideal octahedron (as in all other systems that crystallize in the rutile structure), we still use this concept for symmetry arguments and call it *octahedral coordination*.

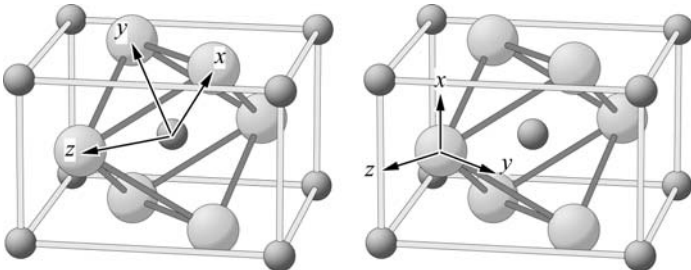


Fig. 2.2.16.3. The local coordinate system in rutile for titanium (small spheres) and oxygen (large spheres).

The concept of a local coordinate system is illustrated for rutile (TiO_2) from two different aspects, namely the crystal harmonics expansion (see Section 2.2.13) and the interpretation of chemical bonding (for further details see Sorantin & Schwarz, 1992).

(i) The expansion in crystal harmonics.

We know that titanium occupies the Wyckoff position $2a$ with point group mmm . From Table 2.2.13.1 we see that for point group mmm (listed under the orthorhombic structure) we must choose the x axis parallel to $[\bar{1}10]$, the y axis parallel to $[110]$ and the z axis parallel to $[001]$. We can transform the global coordinate system (i.e. that of the unit cell) into the local coordinate system around Ti. The following first LM combinations

appear in the series (2.2.12.5): $(LM) = (0, 0), (2, 0), (2, 2), (4, 0), (4, 2), (4, 4), \dots$, etc.

(ii) *The interpretation of bonding.* The second reason for choosing a local coordinate system is that it allows the use of symmetry-adapted orbitals for interpreting bonding, interactions or crystal-field effects. For this purpose, one likes to have the axes pointing to the six oxygen ligands, i.e. the x and y axes towards the oxygen atoms in the octahedral basal plane, and the z axis towards the apical oxygen (Fig. 2.2.16.3). The Cartesian x and y axes, however, are not exactly (but approximately) directed toward the oxygen ligands due to the rectangular distortion of the octahedral basal plane.

For oxygen in TiO_2 with point group $mm2$, the two types of local systems are identical and are shown in Fig. 2.2.16.3 for the position $(\frac{1}{2} - u, \frac{1}{2} + u, \frac{1}{2})$. The z axis coincides with that of the Ti atom, while it points to the neighbouring oxygen of the basal plane in the octahedron around Ti at the origin. Only in this local coordinate system are the orbitals arranged in the usual way for an octahedron, where the d orbitals split (into the three orbitals of t_{2g} and the two of e_g symmetry) and thus allow an easy interpretation of the interactions, e.g. one of the two e_g orbitals, namely the Ti d_{z^2} can form a σ bond with the O p_z orbital.

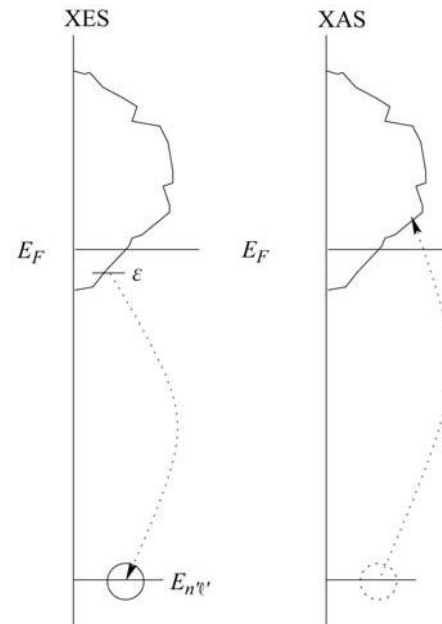


Fig. 2.2.16.4. Schematic transitions in X-ray emission and absorption spectra.

2. SYMMETRY ASPECTS OF EXCITATIONS

Table 2.2.16.1. $W_{\ell\ell'}$ factors for X-ray emission spectra showing the $\Delta\ell = \pm 1$ selection rule

| ℓ' | ℓ | | | | |
|---------|--------|-----|-----|-----|------|
| | 0 | 1 | 2 | 3 | 4 |
| 0 | 1 | 1/3 | 2/5 | | |
| 1 | | 2/3 | | 3/7 | |
| 2 | | | 3/5 | | 4/11 |
| 3 | | | | | |

2.2.16.3. Core electron spectra

In excitations involving core electrons, simplifications are possible that allow an easier interpretation. As one example, (soft) X-ray emission (XES) or absorption (XAS) spectra are briefly discussed. In the one-electron picture, the XES process can be described as sketched in Fig. 2.2.16.4. First a core electron of atom A in state $n'\ell'$ is knocked out (by electrons or photons), and then a transition occurs between the occupied valence states at energy ε and the core hole (the transitions between inner core levels are ignored).

According to Fermi's golden rule, the intensity of such a transition can be described by

$$I_{An'\ell'}(\nu) = \nu^3 \sum_{\ell} W_{\ell\ell'} n_{\ell}^A(\varepsilon) M_A(\ell, n'\ell', \varepsilon)^2 \delta(\varepsilon - E_{n'\ell'}^A - h\nu), \quad (2.2.16.5)$$

where $W_{\ell\ell'}$ comes from the integral over the angular components (Table 2.2.16.1) and contains the $\Delta\ell = \pm 1$ selection rule, $n_{\ell}^A(\varepsilon)$ is the local (within atomic sphere A) partial (ℓ -like) DOS, $M_A(\ell, n'\ell', \varepsilon)^2$ is the radial transition probability [see (2.2.16.6) below], and the last term takes the energy conservation into account.

The $M_A(\ell, n'\ell', \varepsilon)^2$ are defined as the dipole transition (with the dipole operator r) probability between the valence state at ε and the core state characterized by quantum numbers $n'\ell'$,

$$M_A(\ell, n'\ell', \varepsilon)^2 = \frac{[\int_0^{R_A} u_{\ell}^A(r, \varepsilon) r^3 R_{n'\ell'}^{A \text{ core}}(r) dr]^2}{\int_0^{R_A} [u_{\ell}^A(r, \varepsilon)]^2 r^2 dr}. \quad (2.2.16.6)$$

In this derivation one makes use of the fact that core states are completely confined inside the atomic sphere. Therefore the integral, which should be taken over the entire space, can be restricted to one atomic sphere (namely A), since the core wavefunction $R_{n'\ell'}^{A \text{ core}}(r)$ and thus the integrand vanishes outside this sphere. This is also the reason why XES (or XAS) are related to $n_{\ell}^A(\varepsilon)$, the local DOS weighted with the ℓ -like charge within the atomic sphere A .

The interpretation of XES intensities is as follows. Besides the ν^3 factor from Fermi's golden rule, the intensity is governed by the $\Delta\ell = \pm 1$ selection rule and the energy conservation. In addition, it depends on the number of available states at ε which reside inside sphere A and have an ℓ -like contribution, times the probability for the transition to take place from the valence and to the core hole under energy conservation. For an application, see for example the comparison between theory and experiment for the compounds NbC and NbN (Schwarz, 1977).

Note again that the present description is based on an atomic sphere representation with partial waves inside the spheres, in contrast to an LCAO-like treatment with site-centred basis functions. In the latter, an equivalent formalism can be defined which differs in details, especially for the small components (off-site contributions). If the tails of an orbital enter a neighbouring sphere and are crucial for the interpretation of XES, there is a semantic difference between the two schemes as discussed above in connection with f.c.c. Cu in Section 2.2.16.1. In the present framework, all contributions come exclusively from the sphere where the core hole resides, whereas in an LCAO representation 'cross transitions' from the valence states on one atom to the core

hole of a neighbouring atom may be important. The latter contributions must be (and are) included in the partial waves within the sphere in schemes such as LAPW. There is no physical difference between the two descriptions.

In XES, spectra are interpreted on the basis of results from ground-state calculations, although there could be relaxations due to the presence of a core hole. As early as 1979, von Barth and Grossmann formulated a 'final state rule' for XES in metallic systems (von Barth & Grossmann, 1979). In this case, the initial state is one with a missing core electron (core hole), whereas the final state is close to the ground state, since the hole in the valence bands (after a valence electron has filled the core hole) has a very short lifetime and is very quickly filled by other valence electrons. They applied time-dependent perturbation theory and could show by model calculations that the main XES spectrum can be explained by ground-state results, whereas the satellite spectrum (starting with two core holes and ending with one) requires a treatment of the core-hole relaxation. This example illustrates the importance of the relevant physical process in experiments related to the energy-band structure: it may not always be the just the ground states that are involved and sometimes excited states must be considered.

2.2.17. Conclusion

There are many more applications of band theory to solids and thus an enormous amount of literature has not been covered here. In this chapter, an attempt has been made to collect relevant concepts, definitions and examples from group theory, solid-state physics and crystallography in order to understand symmetry aspects in combination with a quantum-mechanical treatment of the electronic structure of solids.

The author wishes to thank the following persons who contributed to this chapter: P. Blaha, the main author of *WIEN*; J. Luitz, for help with the figures; and P. Herzig, with whom the author discussed the group-theoretical aspects.

References

- Akai, H., Akai, M., Blügel, S., Drittler, B., Ebert, H., Terakura, K., Zeller, R. & Dederichs, P. H. (1990). *Theory of hyperfine interactions in metals*. *Prog. Theor. Phys. Suppl.* **101**, 11–77.
- Altmann, S. L. (1994). *Band theory of solids: An introduction from the view of symmetry*. Oxford: Clarendon Press.
- Andersen, O. K. (1975). *Linear methods in band theory*. *Phys. Rev. B*, **12**, 3060–3083.
- Barth, U. von & Grossmann, G. (1979). *The effect of the core hole on X-ray emission spectra in simple metals*. *Solid State Commun.* **32**, 645–649.
- Barth, U. von & Hedin, L. (1972). *A local exchange-correlation potential for the spin-polarized case: I*. *J. Phys. C*, **5**, 1629–1642.
- Blaha, P., Schwarz, K. & Dederichs, P. H. (1988). *First-principles calculation of the electric field gradient in hcp metals*. *Phys. Rev. B*, **37**, 2792–2796.
- Blaha, P., Schwarz, K. & Herzig, P. (1985). *First-principles calculation of the electric field gradient of Li_3N* . *Phys. Rev. Lett.* **54**, 1192–1195.
- Blaha, P., Schwarz, K., Sorantin, P. I. & Trickey, S. B. (1990). *Full-potential linearized augmented plane wave programs for crystalline systems*. *Comput. Phys. Commun.* **59**, 399–415.
- Blaha, P., Singh, D. J., Sorantin, P. I. & Schwarz, K. (1992). *Electric field gradient calculations for systems with large extended core state contributions*. *Phys. Rev. B*, **46**, 5849–5852.
- Blöchl, P. E. (1994). *Projector augmented-wave method*. *Phys. Rev. B*, **50**, 17953–17979.
- Bouckaert, L. P., Smoluchowski, R. & Wigner, E. (1930). *Theory of Brillouin zones and symmetry properties of wavefunctions in crystals*. *Phys. Rev.* **50**, 58–67.
- Bradley, C. J. & Cracknell, A. P. (1972). *The mathematical theory of symmetry in solids*. Oxford: Clarendon Press.

- Car, R. & Parrinello, M. (1985). *Unified approach for molecular dynamics and density-functional theory*. *Phys. Rev. Lett.* **55**, 2471–2474.
- Ceperley, D. M. & Alder, B. J. (1984). *Ground state of the electron gas by a stochastic method*. *Phys. Rev. Lett.* **45**, 566–572.
- Colle, R. & Salvetti, O. (1990). *Generalisation of the Colle–Salvetti correlation energy method to a many determinant wavefunction*. *J. Chem. Phys.* **93**, 534–544.
- Condon, E. U. & Shortley, G. H. (1953). *The mathematical theory of symmetry in crystals*. Cambridge University Press.
- Dreizler, R. M. & Gross, E. K. U. (1990). *Density functional theory*. Berlin, Heidelberg, New York: Springer-Verlag.
- Dufek, P., Blaha, P. & Schwarz, K. (1995a). *Theoretical investigation of the pressure induced metallization and the collapse of the antiferromagnetic states in NiI₂*. *Phys. Rev. B*, **51**, 4122–4127.
- Dufek, P., Blaha, P. & Schwarz, K. (1995b). *Determination of the nuclear quadrupole moment of ⁵⁷Fe*. *Phys. Rev. Lett.* **75**, 3545–3548.
- Ellis, D. E., Guenzburger, D. & Jansen, H. B. (1983). *Electric field gradient and electronic structure of linear-bonded halide compounds*. *Phys. Rev. B*, **28**, 3697–3705.
- Godby, R. W., Schlüter, M. & Sham, L. J. (1986). *Accurate exchange-correlation potential for silicon and its discontinuity of addition of an electron*. *Phys. Rev. Lett.* **56**, 2415–2418.
- Gunnarsson, O. & Lundqvist, B. I. (1976). *Exchange and correlation in atoms, molecules, and solids by the spin-density-functional formation*. *Phys. Rev. B*, **13**, 4274–4298.
- Hedin, L. & Lundqvist, B. I. (1971). *Explicit local exchange-correlation potentials*. *J. Phys. C*, **4**, 2064–2083.
- Herzig, P. (1985). *Electrostatic potentials, field gradients from a general crystalline charge density*. *Theoret. Chim. Acta*, **67**, 323–333.
- Hoffmann, R. (1988). *Solids and surfaces: A chemist's view of bonding in extended structures*. New York: VCH Publishers, Inc.
- Hohenberg, P. & Kohn, W. (1964). *Inhomogeneous electron gas*. *Phys. Rev.* **136**, B864–B871.
- Hybertsen, M. S. & Louie, G. (1984). *Non-local density functional theory for the electronic and structural properties of semiconductors*. *Solid State Commun.* **51**, 451–454.
- International Tables for Crystallography* (2000). Vol. B. Reciprocal space, edited by U. Shmueli, 2nd ed. Dordrecht: Kluwer Academic Publishers.
- International Tables for Crystallography* (2002). Vol. A. Space-group symmetry, edited by Th. Hahn, 5th ed. Dordrecht: Kluwer Academic Publishers.
- Janak, J. F. (1978). *Proof that $\partial E/\partial n_i = \epsilon_i$ in density-functional theory*. *Phys. Rev. B*, **18**, 7165–7168.
- Kaufmann, E. N. & Vianden, R. J. (1979). *The electric field gradient in noncubic metals*. *Rev. Mod. Phys.* **51**, 161–214.
- Koelling, D. D. & Arbmán, G. O. (1975). *Use of energy derivative of the radial solution in an augmented plane wave method: application to copper*. *J. Phys. F Metal Phys.* **5**, 2041–2054.
- Koelling, D. D. & Harmon, B. N. (1977). *A technique for relativistic spin-polarized calculations*. *J. Phys. C Solid State Phys.* **10**, 3107–3114.
- Kohn, W. & Rostocker, N. (1954). *Solution of the Schrödinger equation in periodic lattice with an application to metallic lithium*. *Phys. Rev.* **94**, A1111–A1120.
- Kohn, W. & Sham, L. J. (1965). *Self-consistent equations including exchange*. *Phys. Rev.* **140**, A1133–A1138.
- Korringa, J. (1947). *On the calculation of the energy of a Bloch wave in a metal*. *Physica*, **13**, 392–400.
- Kurki-Suonio, K. (1977). *Symmetry and its implications*. *Isr. J. Chem.* **16**, 115–123.
- Loucks, T. L. (1967). *Augmented plane wave method*. New York, Amsterdam: W. A. Benjamin, Inc.
- Methfessel, M. & Frota-Pessoa, S. (1990). *Real-space method for calculation of the electric-field gradient: Comparison with K-space results*. *J. Phys. Condens. Matter*, **2**, 149–158.
- Meyer, B., Hummler, K., Elsässer, C. & Fähnle, M. (1995). *Reconstruction of the true wavefunction from the pseudo-wavefunctions in a crystal and calculation of electric field gradients*. *J. Phys. Condens. Matter*, **7**, 9201–9218.
- Ordejon, P., Drabold, D. A., Martin, R. A. & Grumbach, M. P. (1995). *Linear system-size scaling methods for electronic-structure calculations*. *Phys. Rev. B*, **51**, 1456–1476.
- Parr, R., Donnelly, R. A., Levy, M. & Palke, W. A. (1978). *Electronegativity: the density functional viewpoint*. *J. Chem. Phys.* **68**, 3801–3807.
- Perdew, J. P. (1986). *Density functional theory and the band gap problem*. *Int. J. Quantum Chem.* **19**, 497–523.
- Perdew, J. P., Burke, K. & Ernzerhof, M. (1996). *Generalized gradient approximation made simple*. *Phys. Rev. Lett.* **77**, 3865–3868.
- Perdew, J. P. & Levy, M. (1983). *Physical content of the exact Kohn–Sham orbital energies: band gaps and derivative discontinuities*. *Phys. Rev. Lett.* **51**, 1884–1887.
- Petrilli, H. M., Blöchl, P. E., Blaha, P. & Schwarz, K. (1998). *Electric-field-gradient calculations using the projector augmented wave method*. *Phys. Rev. B*, **57**, 14690–14697.
- Petrilli, H. M. & Frota-Pessoa, S. (1990). *Real-space method for calculation of the electric field gradient in systems without symmetry*. *J. Phys. Condens. Matter*, **2**, 135–147.
- Pisani, C. (1996). *Quantum-mechanical ab-initio calculation of properties of crystalline materials. Lecture notes in chemistry*, **67**, 1–327. Berlin, Heidelberg, New York: Springer-Verlag.
- Pyykkö, P. (1992). *The nuclear quadrupole moments of the 20 first elements: High-precision calculations on atoms and small molecules*. *Z. Naturforsch. A*, **47**, 189–196.
- Sandraskii, L. M. (1990). *Symmetry properties of electronic states of crystals with spiral magnetic order*. *Solid State Commun.* **75**, 527–529.
- Schwarz, K. (1977). *The electronic structure of NbC and NbN*. *J. Phys. C Solid State Phys.* **10**, 195–210.
- Schwarz, K., Ambrosch-Draxl, C. & Blaha, P. (1990). *Charge distribution and electric field gradients in YBa₂Cu₃O_{7-x}*. *Phys. Rev. B*, **42**, 2051–2061.
- Schwarz, K. & Blaha, P. (1992). *Ab initio calculations of the electric field gradients in solids in relation to the charge distribution*. *Z. Naturforsch. A*, **47**, 197–202.
- Schwarz, K. & Blaha, P. (1996). *Description of an LAPW DF program (WIEN95)*. In *Lecture notes in chemistry*, Vol. 67, *Quantum-mechanical ab initio calculation of properties of crystalline materials*, edited by C. Pisani. Berlin, Heidelberg, New York: Springer-Verlag.
- Schwarz, K. & Herzig, P. (1979). *The sensitivity of partially filled f bands to configuration and relativistic effects*. *J. Phys. C Solid State Phys.* **12**, 2277–2288.
- Seitz, F. (1937). *On the reduction of space groups*. *Ann. Math.* **37**, 17–28.
- Singh, D. J. (1994). *Plane waves, pseudopotentials and the LAPW method*. Boston, Dordrecht, London: Kluwer Academic Publishers.
- Skriver, H. L. (1984). *The LMTO method. Springer series in solid-state sciences*, Vol. 41. Berlin, Heidelberg, New York, Tokyo: Springer.
- Slater, J. C. (1937). *Wavefunctions in a periodic crystal*. *Phys. Rev.* **51**, 846–851.
- Slater, J. C. (1974). *The self-consistent field for molecules and solids*. New York: McGraw-Hill.
- Sorantin, P. & Schwarz, K. (1992). *Chemical bonding in rutile-type compounds*. *Inorg. Chem.* **31**, 567–576.
- Springborg, M. (1997). *Density-functional methods in chemistry and material science*. Chichester, New York, Weinheim, Brisbane, Singapore, Toronto: John Wiley and Sons Ltd.
- Vosko, S. H., Wilk, L. & Nusair, M. (1980). *Accurate spin-dependent electron liquid correlation energies for local spin density calculations*. *Can. J. Phys.* **58**, 1200–1211.
- Weinert, M. (1981). *Solution of Poisson's equation: beyond Ewald-type methods*. *J. Math. Phys.* **22**, 2433–2439.
- Williams, A. R., Kübler, J. & Gelatt, C. D. Jr (1979). *Cohesive properties of metallic compounds: Augmented-spherical-wave calculations*. *Phys. Rev. B*, **19**, 6094–6118.
- Winkler, B., Blaha, P. & Schwarz, K. (1996). *Ab initio calculation of electric field gradient tensors of fosterite*. *Am. Mineral.* **81**, 545–549.

2.3. Raman scattering

BY I. GREGORA

2.3.1. Introduction

The term Raman scattering, traditionally used for light scattering by molecular vibrations or optical lattice vibrations in crystals, is often applied in a general sense to a vast variety of phenomena of inelastic scattering of photons by various excitations in molecules, solids or liquids. In crystals these excitations may be collective (phonons, plasmons, polaritons, magnons) or single-particle (electrons, electron–hole pairs, vibrational and electronic excitation of impurities). Raman scattering provides an important tool for the study of the properties of these excitations. In the present chapter, we shall briefly review the general features of Raman scattering in perfect crystals on a phenomenological basis, paying special attention to the consequences of the crystal symmetry. Our focus will be mainly on Raman scattering by vibrational excitations of the crystal lattice – *phonons*. Nevertheless, most of the conclusions have general validity and may be (with possible minor modifications) transferred also to inelastic scattering by other excitations.

2.3.2. Inelastic light scattering in crystals – basic notions

Although quantum concepts must be used in any complete theory of inelastic scattering, basic insight into the problem may be obtained from a semiclassical treatment. In classical terms, the origin of inelastically scattered light in solids should be seen in the modulation of the dielectric susceptibility of a solid by elementary excitations. The exciting light polarizes the solid and the polarization induced *via* the modulated part of the susceptibility is re-radiated at differently shifted frequencies. Thus inelastic scattering of light by the temporal and spatial fluctuations of the dielectric susceptibility that are induced by elementary excitations provides information about the symmetry and wavevector-dependent frequencies of the excitations themselves as well as about their interaction with electromagnetic waves.

2.3.2.1. Kinematics

Let us consider the incident electromagnetic radiation, the scattered electromagnetic radiation and the elementary excitation to be described by plane waves. The incident radiation is characterized by frequency ω_I , wavevector \mathbf{k}_I and polarization vector \mathbf{e}_I . Likewise, the scattered radiation is characterized by ω_S , \mathbf{k}_S and \mathbf{e}_S :

$$\mathbf{E}_{I,S}(\mathbf{r}, t) = E_{I,S} \mathbf{e}_{I,S} \exp(i\mathbf{k}_{I,S} \cdot \mathbf{r} - \omega t). \quad (2.3.2.1)$$

The scattering process involves the annihilation of the incident photon, the emission or annihilation of one or more quanta of elementary excitations and the emission of a scattered photon. The scattering is characterised by a *scattering frequency* ω (also termed the *Raman shift*) corresponding to the energy transfer $\hbar\omega$ from the radiation field to the crystal, and by a *scattering wavevector* \mathbf{q} corresponding to the respective momentum transfer $\hbar\mathbf{q}$. Since the energy and momentum must be conserved in the scattering process, we have the conditions

$$\begin{aligned} \omega_I - \omega_S &= \omega, \\ \mathbf{k}_I - \mathbf{k}_S &= \mathbf{q}. \end{aligned} \quad (2.3.2.2)$$

Strictly speaking, the momentum conservation condition is valid only for sufficiently large, perfectly periodic crystals. It is further assumed that there is no significant absorption of the incident and

scattered light beams, so that the wavevectors may be considered real quantities.

Since the photon wavevectors (\mathbf{k}_I , \mathbf{k}_S) and frequencies (ω_I , ω_S) are related by the dispersion relation $\omega = ck/n$, where c is the speed of light in free space and n is the refractive index of the medium at the respective frequency, the energy and wavevector conservation conditions imply for the magnitude of the scattering wavevector q

$$c^2 q^2 = n_I^2 \omega_I^2 + n_S^2 (\omega_I - \omega)^2 - 2n_I n_S \omega_I (\omega_I - \omega) \cos \varphi, \quad (2.3.2.3)$$

where φ is the *scattering angle* (the angle between \mathbf{k}_I and \mathbf{k}_S). This relation defines in the (ω, q) plane the region of wavevectors and frequencies accessible to the scattering. This relation is particularly important for scattering by excitations whose frequencies depend markedly on the scattering wavevector (e.g. acoustic phonons, polaritons *etc.*).

2.3.2.2. Cross section

In the absence of any excitations, the incident field \mathbf{E}_I at frequency ω_I induces in the crystal the polarization \mathbf{P} , related to the field by the *linear* dielectric susceptibility tensor χ (ϵ_0 is the permittivity of free space):

$$\mathbf{P} = \epsilon_0 \chi(\omega_I) \mathbf{E}_I. \quad (2.3.2.4)$$

The linear susceptibility $\chi(\omega_I)$ is understood to be independent of position, depending on the crystal characteristics and on the frequency of the radiation field only. In the realm of nonlinear optics, additional terms of higher order in the fields may be considered; they are expressed through the respective *nonlinear* susceptibilities.

The effect of the excitations is to modulate the wavefunctions and the energy levels of the medium, and can be represented macroscopically as an additional contribution to the linear susceptibility. Treating this modulation as a perturbation, the resulting contribution to the susceptibility tensor, the so-called *transition susceptibility* $\delta\chi$ can be expressed as a Taylor expansion in terms of *normal coordinates* Q_j of the excitations:

$$\chi \rightarrow \chi + \delta\chi, \quad \text{where } \delta\chi = \sum_j \chi^{(j)} Q_j + \sum_{j,j'} \chi^{(j,j')} Q_j Q_{j'} + \dots \quad (2.3.2.5)$$

The tensorial coefficients $\chi^{(j)}$, $\chi^{(j,j')}$, ... in this expansion are, in a sense, *higher-order susceptibilities* and are often referred to as *Raman tensors* (of the first, second and higher orders). They are obviously related to *susceptibility derivatives* with respect to the normal coordinates of the excitations. The time-dependent polarization induced by $\delta\chi$ *via* time dependence of the normal coordinates can be regarded as the source of the inelastically scattered radiation.

The central quantity in the description of Raman scattering is the *spectral differential cross section*, defined as the relative rate of energy loss from the incident beam (frequency ω_I , polarization \mathbf{e}_I) as a result of its scattering (frequency ω_S , polarization \mathbf{e}_S) in volume V into a unit solid angle and unit frequency interval. The corresponding formula may be concisely written as (see e.g. Hayes & Loudon, 1978)

$$\frac{d^2\sigma}{d\Omega d\omega_S} = \frac{\omega_S^3 \omega_I V^2 n_S}{(4\pi)^2 c^4 n_I} \left| \mathbf{e}_I \delta\chi \mathbf{e}_S \right|_{\omega}^2. \quad (2.3.2.6)$$

2.3. RAMAN SCATTERING

The symbol $\langle \dots \rangle_\omega$ stands for the power spectrum (correlation function) of the transition susceptibility fluctuations. The spectral differential cross section is the quantity that can be directly measured in a Raman scattering experiment by analysing the frequency spectrum of the light scattered into a certain direction. By integrating over frequencies ω_s for a particular Raman band and, in addition, over the solid angle, one obtains, respectively, the *differential cross section* ($d\sigma/d\Omega$) and the *total cross section* (σ_{tot}):

$$\frac{d\sigma}{d\Omega} = \int \left(\frac{d^2\sigma}{d\Omega d\omega_s} \right) d\omega_s, \quad \sigma_{\text{tot}} = \int \left(\frac{d\sigma}{d\Omega} \right) d\Omega.$$

These quantities are useful in comparing the integrated scattered intensity by different excitations.

2.3.2.3. Experimental aspects

In a scattering experiment on crystals, the choice of the scattering geometry implies setting the propagation directions \mathbf{k}_i and \mathbf{k}_s and the polarization of the incident and scattered light with respect to the crystallographic axes and defining thus the direction of the scattering wavevector \mathbf{q} as well as the particular component (or a combination of components) of the transition susceptibility tensor $\delta\chi$. In practice, the incident radiation is almost exclusively produced by a suitable laser source, which yields a monochromatic, polarized narrow beam, with a well defined wavevector \mathbf{k}_i . The light scattered in the direction of \mathbf{k}_s is collected over a certain finite solid angle $\Delta\Omega$. Its polarization is analysed with a suitable polarization analyser, and the scattered intensity as a function of frequency ω_s (or Raman shift ω) is analysed using a spectrometer.

To characterize the Raman scattering geometry in a particular experimental arrangement, standard notation for the scattering geometry is often used, giving the orientation of the wavevectors and polarization vectors with respect to a reference Cartesian coordinate system, namely: $\mathbf{k}_i(\mathbf{e}_i, \mathbf{e}_s)\mathbf{k}_s$. Thus, for example, the symbol $x(z)y$ means that right-angle scattering geometry is used, where the incident beam polarized in the $z = [001]$ direction propagates along the $x = [100]$ axis, while the scattered beam is collected in the z direction and the polarization analyser is set parallel with the $y = [010]$ direction. The measured intensity, being proportional to $|\chi_{zy}|^2$, gives information on this particular component of the transition susceptibility tensor. By virtue of the momentum conservation, the scattering wavevector \mathbf{q} in this case is oriented along the $[101]$ direction.

In a typical Raman experiment with visible light ($\omega \ll \omega_i \approx \omega_s$), the magnitudes of the wavevectors $k_i \approx k_s = k$ are of the order of 10^5 cm^{-1} , much lower than those of the reciprocal-lattice vectors K ($\approx 10^8 \text{ cm}^{-1}$). Consequently, the range of the magnitudes of the scattering wavevectors q accessible by varying the scattering geometry from $\varphi = 0^\circ$ (forward scattering) to $\varphi = 180^\circ$ (back scattering) is $0 \leq q \leq 2k$, i.e. by about three orders of magnitude lower than the usual dimensions of the Brillouin zone. The use of back-scattering geometry is imperative in the case of opaque samples, which show stronger absorption for the exciting (or scattered) light.

It should be noted that the general formula for the spectral differential cross section (2.3.2.5) applies to the situation *inside* the crystal. Since in real experiments the observer is always *outside* the crystal, several corrections have to be taken into account. These are in particular due to refraction, reflection and transmission of the incident and scattered light at the interfaces, as well as absorption of light in the crystal. Attention must be paid in the case of anisotropic or gyrotropic crystals, where birefringence or rotation of the polarization direction of both incident and scattered light may occur on their paths through the crystal, between the interfaces and the scattering volume.

We conclude this section by remarking that, owing to the obvious difficulties in taking all the properties of the experimental setup and the corrections into consideration, measurements of absolute Raman intensities tend to be extremely rare. There exist, however, several crystals for which absolute determination of the cross section for particular excitations has been made with reasonable reliability and which may serve as secondary standards.

2.3.3. First-order scattering by phonons

In what follows, we shall be more specific and by underlying excitations we shall explicitly understand lattice vibrations – *phonons* – although the treatment is also applicable to other types of collective excitations in a crystal.

Let us recall (see Chapter 2.1) that atomic displacements in the crystal lattice can be expressed as linear combinations of the *normal modes of vibrations* – eigenvectors of the dynamical matrix.

$$\mathbf{u}_{\kappa\mathbf{l}} = \sum_{\mathbf{q}} \sum_j \mathbf{u}_{\kappa\mathbf{l}}(\mathbf{q}, j) = \frac{1}{\sqrt{Nm_\kappa}} \sum_{\mathbf{q}} \sum_j Q_j(\mathbf{q}) \mathbf{e}_\kappa(\mathbf{q}, j) \exp(i\mathbf{q}\mathbf{r}_\mathbf{l}), \quad (2.3.3.1)$$

where \mathbf{l} denotes the *primitive* unit cell, κ ($\kappa = 1, \dots, s$) is the index of the atom (mass m_κ) in the unit cell and N is the number of unit cells in the crystal. The *eigenvectors* $\mathbf{e}_\kappa(\mathbf{q}, j)$, also called *polarization vectors*, are normalized vectors describing the displacement pattern of atoms in the reference unit cell in a j th normal mode of vibration ($j = 1, 2, 3, \dots, 3s$) with a wavevector \mathbf{q} . The normal modes can be classified according to irreducible representations of the crystal space group and labelled correspondingly. In the case of degeneracy, the branch index j stands, in fact, for two indices: one for the irreducible representation, and the other distinguishing the degenerate partners of the same frequency. The coefficients $Q_j(\mathbf{q})$ are called *normal coordinates* and represent the time-dependent amplitudes of the normal modes, vibrating with frequencies $\omega_j(\mathbf{q})$. The reality of the displacements and the hermiticity of the dynamical matrix impose the following conditions:

$$\mathbf{e}_\kappa(\mathbf{q}, j) = \mathbf{e}_\kappa^*(-\mathbf{q}, j), \quad \omega_j(\mathbf{q}) = \omega_j(-\mathbf{q}), \quad Q_j(\mathbf{q}) = Q_j^*(-\mathbf{q}). \quad (2.3.3.2)$$

In the limit of $\mathbf{q} \rightarrow 0$, three of the vibrational branches correspond to homogeneous displacements of the crystal with vanishing frequency along three independent directions. These branches are termed *acoustic*. The remaining $3s - 3$ branches (provided that $s > 1$) are called *optic*; they correspond to relative displacement of sublattices with nonzero frequency.

For completeness, we note that in a phenomenological treatment the amplitude of the polarization set up by atomic displacements of the normal modes with wavevector \mathbf{q} can be expressed as

$$P_\alpha(\mathbf{q}) = \sum_j Z_{j\alpha}(\mathbf{q}) Q_j(\mathbf{q}), \quad (2.3.3.3)$$

introducing the $(3s \times 3)$ *effective charge* matrix of the j th normal mode of vibration (per unit cell of volume V_c),

$$Z_{j\alpha}(\mathbf{q}) = \left(\frac{\partial P_\alpha(\mathbf{q})}{\partial Q_j(\mathbf{q})} \right) = \frac{1}{V_c} \sum_{\kappa} z_{\alpha\kappa}^{(\kappa)} \frac{e_{\kappa\beta}(\mathbf{q}, j)}{\sqrt{Nm_\kappa}}. \quad (2.3.3.4)$$

The quantity $z_{\alpha\beta}^{(\kappa)}$ represents the *microscopic* effective charge of the κ th atom in the unit cell. Owing to dynamic contributions of ionic deformability, it is not a scalar but rather a (3×3) tensor in general. Hence, in general, the direction of the contribution of a mode to the electrical polarization (2.3.3.3) need not correspond

2. SYMMETRY ASPECTS OF EXCITATIONS

to its mechanical polarization, as given by the mode eigenvectors $\mathbf{e}_\kappa(\mathbf{q}, j)$.

In some cases, the optic modes carrying a nonzero effective charge \mathbf{Z}_j (so-called *polar optic* modes) may be classified as *transverse* (TO) or *longitudinal* (LO). Whenever applicable, this classification should be understood in the correct sense, *i.e.* according to the orientation of the associated *electric* polarization $\mathbf{P}_j(\mathbf{q}) = \mathbf{Z}_j(\mathbf{q})Q_j(\mathbf{q})$ relative to the wavevector \mathbf{q} .

2.3.3.1. First-order scattering cross section and Raman spectral line shapes

In the *first-order* scattering by a single excitation of the normal mode (\mathbf{q}, j) of frequency ω_j and wavevector \mathbf{q}_j , the energy and wavevector conservation conditions give

$$\begin{aligned}\omega &= \pm\omega_j \\ \mathbf{q} &= \pm\mathbf{q}_j,\end{aligned}$$

with the $+$ sign corresponding to a *Stokes* process (one excitation quantum is created) and the $-$ sign to an *anti-Stokes* process (one quantum is annihilated).

Let us explicitly consider the Stokes component, described by the term linear in the normal coordinate Q_j of the excitation. Inserting the plane-wave expressions for the quantities into the first term of the expansion (2.3.2.5) for $\delta\chi$ and comparing the terms with common time dependence, we get for the Stokes polarization due to the normal mode (\mathbf{q}, j)

$$\mathbf{P}(\mathbf{k}_S) = \varepsilon_0 \chi^{(j)}(\mathbf{q}, \omega_I, -\omega) Q_j^*(\mathbf{q}, \omega) \mathbf{E}_I(\mathbf{k}_I),$$

which corresponds to a plane wave at a frequency of $\omega_S = \omega_I - \omega$.

Since, in the harmonic approximation, the normal modes (\mathbf{q}, j) are *dynamically independent*, *i.e.* uncorrelated, the cross section for the Stokes component of the first-order scattering by phonons can be written as a sum over contributions from individual excitations. A summation convention over repeated Cartesian indices is understood throughout this chapter:

$$\begin{aligned}\frac{d^2\sigma}{d\Omega d\omega_S} &= \frac{\omega_S^3 \omega_I V^2 n_S}{(4\pi)^2 c^4 n_I} \sum_j \left| e_{I\alpha} \chi_{\alpha\beta}^{(j)}(\mathbf{q}, \omega_I, -\omega) e_{S\beta} \right|^2 \langle Q_j(\mathbf{q}) Q_j^*(\mathbf{q}) \rangle_\omega. \\ (2.3.3.5)\end{aligned}$$

Let us first briefly review the last term in this expression, which – together with the universal frequency-dependent first factor – essentially determines the shape of the scattered light spectrum, *i.e.* the frequency and temperature dependence of the spectral differential cross section. It depends exclusively on the fluctuation properties of the excitations participating in the scattering process.

The power spectrum of the fluctuations can be calculated using the linear response theory. The normal coordinates, *i.e.* excitation amplitudes of the normal modes, satisfy the decoupled equations of motion (with phenomenological damping constant $\gamma_{j,\mathbf{q}}$ added to take into account the finite lifetime of excitations in real crystals within the quasi-harmonic approximation):

$$\ddot{Q}_j(\mathbf{q}) + \gamma_{j,\mathbf{q}} \dot{Q}_j(\mathbf{q}) + \omega_j^2 Q_j(\mathbf{q}) = 0.$$

If a fictitious generalized force $F(t)$ with Fourier components $F(\omega)$ is applied to the system, the average of the Fourier components of the excitation amplitude and the force are proportional,

$$\bar{Q}_j(\mathbf{q}, \omega) = T_j(\mathbf{q}, \omega) F(\omega),$$

where the proportionality coefficient $T_j(\mathbf{q}, \omega)$ is called a *linear response function*.

The fluctuation–dissipation theorem (or, more exactly, its quantum version) relates the power spectrum $\langle \dots \rangle_\omega$ of a fluctuating quantity to the imaginary part of the corresponding response function. The results for the Stokes and anti-Stokes components of the scattering are, respectively:

$$\begin{aligned}\langle Q_j(\mathbf{q}) Q_j^*(\mathbf{q}) \rangle_\omega &= (\hbar/\pi) [n(\omega) + 1] \text{Im} T_j(\mathbf{q}, \omega) \text{ and} \\ \langle Q_j^*(\mathbf{q}) Q_j(\mathbf{q}) \rangle_\omega &= (\hbar/\pi) n(\omega) \text{Im} T_j(\mathbf{q}, \omega),\end{aligned} \quad (2.3.3.6)$$

where $n(\omega)$ is the Bose–Einstein statistical factor

$$n(\omega) = [\exp(\hbar\omega/k_B T) - 1]^{-1}, \quad (2.3.3.7)$$

which gives the occupation number of phonon states.

The linear response function of the normal coordinates is readily obtained from the equation of motion (N being the number of primitive cells in the crystal):

$$\begin{aligned}T_j(\mathbf{q}, \omega) &= \frac{1}{N} \frac{1}{\omega_j^2(\mathbf{q}) - \omega^2 - i\omega\gamma_{j,\mathbf{q}}}, \text{ hence} \\ \text{Im} T_j(\mathbf{q}, \omega) &= \frac{1}{N} \frac{\omega \gamma_{j,\mathbf{q}}}{[\omega_j^2(\mathbf{q}) - \omega^2]^2 + \omega^2 \gamma_{j,\mathbf{q}}^2}.\end{aligned}$$

If the damping parameter $\gamma_{j,\mathbf{q}}$ of the excitations is much smaller than the frequency $\omega_j(\mathbf{q})$, as is usually the case for phonons in perfect crystals, this function is closely approximated by a Lorentzian centred at $\omega_j(\mathbf{q})$, with a full width $\gamma_{j,\mathbf{q}}$ at half maximum. Hence, introducing a suitably normalized *lineshape function* $L_j(\omega)$,

$$\int_{-\infty}^{\infty} L_j(\omega) d\omega = 1,$$

we can write for the power spectra (2.3.3.5) of the j th normal mode in the spectral differential cross section

$$\begin{aligned}\langle Q_j(\mathbf{q}) Q_j^*(\mathbf{q}) \rangle_\omega &= \frac{\hbar}{2N\omega_j(\mathbf{q})} \{n[\omega_j(\mathbf{q})] + 1\} L_j(\omega) \text{ and} \\ \langle Q_j^*(\mathbf{q}) Q_j(\mathbf{q}) \rangle_\omega &= \frac{\hbar}{2N\omega_j(\mathbf{q})} n[\omega_j(\mathbf{q})] L_j(\omega)\end{aligned} \quad (2.3.3.8)$$

for the Stokes and anti-Stokes case, respectively.

Note that at low temperatures the differential cross section of the anti-Stokes component in the spectrum becomes vanishingly small, because the mean number of thermally excited phonons vanishes at $T = 0$.

Information about the interaction of photons with individual excitations is contained in the central term in the expression for the cross section (2.3.3.5), *i.e.* in the nonlinear susceptibility $\chi_{\alpha\beta}^{(j)}(\mathbf{q}, \omega_I, -\omega)$.

2.3.3.2. Symmetry properties of the scattering cross section

The quantity that controls the symmetry properties of the scattering cross section due to excitation $Q_j(\mathbf{q})$ is the squared modulus of the corresponding second-order susceptibility (second-rank tensor), contracted with the two polarization vectors of the incident and scattered light:

$$|\mathbf{e}_S \chi^{(j)}(\mathbf{q}, \omega_I, -\omega) \mathbf{e}_I|^2 \equiv |e_{S\alpha} \chi_{\alpha\beta}^{(j)}(\mathbf{q}, \omega_I, -\omega) e_{I\beta}|^2. \quad (2.3.3.9)$$

The nonlinear susceptibility tensor $\chi^{(j)}(\mathbf{q}, \omega_I, -\omega)$ is usually referred to as the first-order *Raman tensor* (defined in the literature to within a factor). Before discussing the consequences of the crystal symmetry on the form of the Raman tensor, let us mention two important approximations on which conventional analysis of its symmetry properties is based.

2.3. RAMAN SCATTERING

In a general case, the second-order susceptibilities are not necessarily symmetric. However, they fulfil a general symmetry property which follows from the symmetry of the scattering with respect to time inversion. Since the anti-Stokes process can be regarded as a time-inverted Stokes process (exchanging the role of the incident and scattered photons), it can be shown that in non-magnetic materials the susceptibilities obey the relation

$$\chi_{\beta\alpha}^{(j)}(-\mathbf{q}, \omega_s, \omega) = \chi_{\alpha\beta}^{(j)}(\mathbf{q}, \omega_I, -\omega). \quad (2.3.3.10)$$

In the *quasi-static* limit, *i.e.* if the scattering frequency is negligibly small compared with the incident photon frequency ($0 \approx \omega \ll \omega_I \approx \omega_s$), it follows that the susceptibilities of non-magnetic materials become *symmetric* in the Cartesian indices α, β . This symmetry is very well fulfilled in a great majority of cases. Appreciable antisymmetric contributions are known to occur, *e.g.* under *resonant conditions*, where the quasi-static approximation breaks down as the energy of the incident (or scattered) photon approaches those of electronic transitions.

Thus, in the first approximation, we set ω equal to zero and remove the time dependence in the phonon amplitudes, treating the normal coordinates as *static*. Then the nonlinear susceptibilities correspond to susceptibility derivatives,

$$\chi_{\alpha\beta}^{(j)}(\mathbf{q}, \omega_I, -\omega) \rightarrow R_{\alpha\beta}^j(\mathbf{q}) \equiv \chi_{\alpha\beta}^{(j)}(\mathbf{q}, \omega_I) = \frac{\partial \chi_{\alpha\beta}(\omega_I)}{\partial Q_j^*(\mathbf{q})}, \quad (2.3.3.11)$$

where we suppressed the explicit dependence on ω_I and introduced a simplified notation for the Raman tensor $\mathbf{R}^j(\mathbf{q})$, still keeping the dependence on the scattering wavevector.

In deriving the symmetry properties of the Raman tensor $\mathbf{R}^j(\mathbf{q})$ that follow from the crystal lattice symmetry, the main point is thus to determine its transformation properties under the symmetry operation of the crystal *space group*.

Since the magnitude of the scattering vector $q \equiv |\mathbf{q}|$ is very small compared with the Brillouin-zone dimensions, another conventional approximation is to neglect the \mathbf{q} dependence of the susceptibilities. Setting $\mathbf{q} \rightarrow 0$ enables us to analyse the symmetry of the Raman tensor in terms of the *factor group* G_0 , which is isomorphous to the point group of the crystal lattice. This approach is, again, appropriate for the vast majority of cases. An important exception is, for instance, the scattering by acoustic modes (*Brillouin scattering*) or scattering by longitudinal plasma waves in semiconductors (*plasmons*): in these cases the Raman tensor vanishes for $\mathbf{q} = 0$, since this limit corresponds to a homogeneous displacement of the system. Possible \mathbf{q} -dependent effects can be treated by expanding the Raman tensor in powers of \mathbf{q} and using compatibility relations between the symmetries at $\mathbf{q} = 0$ and at the full symmetries applicable in the $\mathbf{q} \neq 0$ case.

Let us mention that another notation is sometimes used in the literature for the Raman tensor. Since the square modulus of a second-rank tensor contracted with two vectors can be written as a fourth-rank tensor contracted with four vectors, one can introduce a fourth-rank tensor $\mathbf{I}^{(j)}$,

$$I_{\alpha\beta\mu\nu}^{(j)} = \frac{\partial \chi_{\alpha\beta}^*}{\partial Q_j} \frac{\partial \chi_{\mu\nu}}{\partial Q_j^*},$$

so that the scattering cross section of the j th mode is

$$\frac{d\sigma^{(j)}}{d\Omega d\omega_s} \approx e_{I\alpha} e_{I\mu} e_{S\beta} e_{S\nu} I_{\alpha\beta\mu\nu}^{(j)}.$$

If there are no antisymmetric components in the susceptibility derivatives, it can be shown that the fourth-rank tensor $\mathbf{I} = (I_{\alpha\beta\mu\nu})$ has at most 21 independent components, as for the elastic constants tensor.

2.3.3.3. Raman tensor and selection rules at $\mathbf{q} \approx 0$

The scattering cross section, being a scalar quantity, must be invariant with respect to all symmetry elements of the space group of the crystal. This invariance has two important consequences: it determines which normal modes (j) can contribute to the scattering (*Raman activity* of the modes) and it also gives the restrictions on the number of independent components of the Raman tensor (*polarization selection rules*).

At $\mathbf{q} \approx 0$, the transformation properties of the incident and scattered light are described by the three-dimensional *polar vector representation* Γ_{PV} of the appropriate point group of the crystal, since the quantities that characterize the light ($\mathbf{E}_I, \mathbf{E}_S, \mathbf{P} \dots$) are all *polar vectors*, *i.e.* first-rank polar tensors (T_α). The transformation properties of a normal mode j must correspond to an irreducible matrix representation $\Gamma(j)$ of the crystal point group. We recall that in cases of two- or three-dimensional representations (degeneracy), the index j represents two indices.

In order that a particular normal mode j in a given crystal be Raman active, *i.e.* *symmetry-allowed* to contribute to the (first-order) scattering cross section, the necessary condition is that the corresponding irreducible representation $\Gamma(j)$ must be contained in the decomposition of the direct Kronecker product representation $\Gamma_{\text{PV}} \otimes \Gamma_{\text{PV}}$ at least once:

$$\Gamma_{\text{PV}} \otimes \Gamma_{\text{PV}} \supset \Gamma(j). \quad (2.3.3.12)$$

In this case, the Kronecker product $\Gamma_{\text{PV}} \otimes \Gamma_{\text{PV}} \otimes \Gamma(j)$ contains the identity representation at least once, so the cross section remains invariant under the transformation of the crystal point group. In the phenomenological formulation, the susceptibility derivatives correspond to third derivatives of a particular potential energy Φ (interaction Hamiltonian),

$$R_{\alpha\beta}^j = \left(\frac{\partial \chi_{\alpha\beta}}{\partial Q_j^*} \right) \sim \left(\frac{\partial^3 \Phi}{\partial E_{I\alpha} \partial E_{S\beta}^* \partial Q_j^*} \right), \quad (2.3.3.13)$$

such that the product $\Gamma_{\text{PV}} \otimes \Gamma_{\text{PV}} \otimes \Gamma(j)$ is the reducible representation of the Raman tensor. If condition (2.3.3.12) holds, then the Raman tensor \mathbf{R}^j does not vanish identically and may have at least one independent nonzero component. As the representation $\Gamma_{\text{PV}} \otimes \Gamma_{\text{PV}}$ is that of a second-rank polar tensor, equivalent formulation of the Raman activity of a normal mode j is that the corresponding normal coordinate Q_j must transform like one or more components of a polar tensor. The transition susceptibility $\delta\chi^{(j)}$ transforms accordingly. The task of determining whether a given normal mode j is Raman active or not thus consists of simply decomposing the representation $\Gamma_{\text{PV}} \otimes \Gamma_{\text{PV}}$ and identifying the irreducible components $\Gamma(j)$.

The second consequence of the invariance condition is the imposition of restrictions on the Cartesian components of the Raman tensor for modes allowed to participate in the scattering. By virtue of the properties of the irreducible representations $\Gamma(j)$, some components of the corresponding Raman tensor are required to vanish whereas others may have related values. This fact results in anisotropies in the observed cross section depending on the polarization directions of the incident and scattered light, and is usually referred to as *polarization selection rules*. As the scattering cross section of the excitation (j) is proportional to the scalar quantity

$$|\mathbf{e}_S \mathbf{R}^j \mathbf{e}_I|^2 \equiv |e_{S\alpha} R_{\alpha\beta}^j e_{I\beta}|^2,$$

one can generally ‘isolate’ a given component of the Raman tensor by suitably arranging the scattering geometry in the experiment, *i.e.* by choosing the orientation of the wavevectors \mathbf{k}_I and \mathbf{k}_S and the polarization vectors \mathbf{e}_I and \mathbf{e}_S with respect to crystallographic axes.

2. SYMMETRY ASPECTS OF EXCITATIONS

For each normal mode (j) allowed in the scattering, the number of independent components of its Raman tensor is given by the multiplicity coefficients $c^{(j)}$ of the irreducible representation $\Gamma(j)$ in the decomposition

$$\Gamma_{\text{PV}} \otimes \Gamma_{\text{PV}} = c^{(1)}\Gamma(1) \oplus c^{(2)}\Gamma(2) \oplus \dots, \quad (2.3.3.14)$$

where the multiplicity coefficient $c^{(j)}$ corresponds to the number of times the given irreducible representation $\Gamma(j)$ enters the decomposition. If the representation $\Gamma(j)$ is two- or three-dimensional, then for each occurrence of $\Gamma(j)$ in (2.3.3.14) there are two or three degenerate partners (of the same frequency) whose Raman tensors are symmetry-related.

The matrix form of the Raman tensor corresponding to a given irreducible representation – i.e. *symmetry species* – $\Gamma(j)$ can be readily constructed by finding the appropriate bilinear basis functions that transform according to the corresponding irreducible representation $\Gamma(j)$. The required number of such independent bases is given by the multiplicity coefficient $c^{(j)}$. Alternatively, one may construct invariant polynomials (transforming as scalars) of order *four*, i.e. of the same order as the product $E_{I\alpha}E_{S\beta}Q_j$.

Making allowance for possible *antisymmetric* scattering, we have not explicitly supposed that the Raman tensor is symmetric. We recall that the derivative (2.3.3.13) is not necessarily symmetric in the α and β indices as long as the fields $E_{I\alpha}$ and $E_{S\beta}$ correspond to different frequencies (inelastic scattering). However, each second-rank polar tensor $T_{\alpha\beta}$ (nine components), transforming according to $\Gamma_{\text{PV}} \otimes \Gamma_{\text{PV}}$, can be decomposed into a symmetric part $T'_{\alpha\beta} = T'_{\beta\alpha}$ (six components), transforming like a symmetric polar tensor $[\Gamma_{\text{PV}} \otimes \Gamma_{\text{PV}}]_S$, and an antisymmetric part $T''_{\alpha\beta} = -T''_{\beta\alpha}$ (three components), transforming like an axial vector (for the definition of axial tensors, see Section 1.1.4.5.3) according to $\Gamma_{\text{AV}} = [\Gamma_{\text{PV}} \otimes \Gamma_{\text{PV}}]_A$.

The symmetry-restricted forms of the (3×3) Raman tensors corresponding to all Raman-active symmetry species are summarized in Table 2.3.3.1 (see e.g. Hayes & Loudon, 1978) for each of the 32 crystal symmetry classes. Spectroscopic notation is used for the irreducible representations of the point groups. The symbols (x , y or z) for some Raman-active symmetry species in the noncentrosymmetric classes indicate that the respective components of polar vectors also transform according to these irreducible representations. Hence the normal coordinates of the phonons of these *polar* symmetry species (polar phonons) transform in the same way and, consequently, the corresponding component of the effective charge tensor $Z_{j\alpha}(\mathbf{q} = 0)$, see (2.3.3.4), is not required by symmetry to vanish. Polar phonons thus may carry a nonzero dipole moment and contribute to the polarization in the crystal, which manifests itself in *infrared activity* and also in the Raman scattering cross section (see Section 2.3.3.5).

For convenience, the Raman tensors are explicitly split into a symmetric and possible antisymmetric part (upper and lower row of each part of the table, respectively, in each case). The conventional *symmetric* Raman tensors are *appropriate for most cases of practical interest*. Besides the resonant conditions mentioned above, there are other exceptions. For instance, there are optical phonons that transform like *axial vectors*, such as in the case of A_2 (or A_{2g} , A'_2) modes in some uniaxial crystal classes, where the Raman tensor is *purely antisymmetric*. Antisymmetric scattering by these modes may become allowed at finite wave-vector \mathbf{q} . Antisymmetric Raman tensors are also needed for analysing the symmetry of scattering in magnetic materials (scattering by spin waves – *magnons*), or non-magnetic materials under a magnetic field, where the susceptibility itself is essentially nonsymmetric.

We note that the matrix form of the Raman tensors depends on the setting of the Cartesian axes with respect to the crystallographic axes. To avoid ambiguities and apparent disagreement with other sources, we give the results for alternative orientations

Table 2.3.3.1. *Symmetry of Raman tensors in the 32 crystal classes*

The symbols a, b, c, d, e, f, g, h and i in the matrices stand for arbitrary parameters denoting possible independent nonzero components (in general complex) of the Raman tensors. Upper row: conventional symmetric Raman tensors; lower row: antisymmetric part. Alternative orientations of the point group are distinguished by subscripts at 2 or m in the class symbol indicating the direction of the twofold axis or of the normal to the mirror plane.

Triclinic

| | |
|---------------|--|
| | $\begin{pmatrix} a & d & f \\ d & b & h \\ f & h & c \end{pmatrix}$ |
| $\frac{1}{1}$ | $\begin{matrix} A(x, y, z) \\ A_g \end{matrix}$ |
| | $\begin{pmatrix} . & e & g \\ -e & . & i \\ -g & -i & . \end{pmatrix}$ |

Monoclinic, unique axis z

| | | |
|---------------------------|--|---|
| | $\begin{pmatrix} a & d & . \\ d & b & . \\ . & . & c \end{pmatrix}$ | $\begin{pmatrix} . & . & f \\ . & . & h \\ f & h & . \end{pmatrix}$ |
| 2_z m_z $2_z/m$ | $\begin{matrix} A(z) \\ A'(x, y) \\ A_g \end{matrix}$ | $\begin{matrix} B(x, y) \\ A''(z) \\ B_g \end{matrix}$ |
| | $\begin{pmatrix} . & e & . \\ -e & . & . \\ . & . & . \end{pmatrix}$ | $\begin{pmatrix} . & . & g \\ . & . & i \\ -g & -i & . \end{pmatrix}$ |

Monoclinic, unique axis y

| | | |
|---------------------------|--|---|
| | $\begin{pmatrix} a & . & d \\ . & b & . \\ d & . & c \end{pmatrix}$ | $\begin{pmatrix} . & f & . \\ f & . & h \\ . & h & . \end{pmatrix}$ |
| 2_y m_y $2_y/m$ | $\begin{matrix} A(y) \\ A'(x, z) \\ A_g \end{matrix}$ | $\begin{matrix} B(x, z) \\ A''(y) \\ B_g \end{matrix}$ |
| | $\begin{pmatrix} . & . & e \\ . & . & . \\ -e & . & . \end{pmatrix}$ | $\begin{pmatrix} . & g & . \\ -g & . & i \\ . & -i & . \end{pmatrix}$ |

Orthorhombic

| | | | | |
|-------------------------|---|--|--|--|
| | $\begin{pmatrix} a & . & . \\ . & b & . \\ . & . & c \end{pmatrix}$ | $\begin{pmatrix} . & d & . \\ d & . & . \\ . & . & . \end{pmatrix}$ | $\begin{pmatrix} . & . & f \\ . & . & . \\ f & . & . \end{pmatrix}$ | $\begin{pmatrix} . & . & . \\ . & . & h \\ . & h & . \end{pmatrix}$ |
| 222 $mm2$ mmm | $\begin{matrix} A \\ A_1(z) \\ A_g \end{matrix}$ | $\begin{matrix} B_1(z) \\ A_2 \\ B_{1g} \end{matrix}$ | $\begin{matrix} B_2(y) \\ B_1(x) \\ B_{2g} \end{matrix}$ | $\begin{matrix} B_3(x) \\ B_2(y) \\ B_{3g} \end{matrix}$ |
| | | $\begin{pmatrix} . & e & . \\ -e & . & . \\ . & . & . \end{pmatrix}$ | $\begin{pmatrix} . & . & g \\ . & . & . \\ -g & . & . \end{pmatrix}$ | $\begin{pmatrix} . & . & . \\ . & . & i \\ . & -i & . \end{pmatrix}$ |

of the point groups in several cases where different settings of the twofold axes or mirror planes with respect to the Cartesian axes are commonly used. This concerns all monoclinic classes (unique

2.3. RAMAN SCATTERING

Table 2.3.3.1 (*cont.*)

Tetragonal

| | | | | |
|------------------------|--|--|---|---|
| | $\begin{pmatrix} a & . & . \\ . & a & . \\ . & . & b \end{pmatrix}$ | $\begin{pmatrix} d & e & . \\ e & -d & . \\ . & . & . \end{pmatrix}$ | $\begin{pmatrix} . & . & f \\ . & . & h \\ f & h & . \end{pmatrix}$ | $\begin{pmatrix} . & . & -h \\ . & . & f \\ -h & f & . \end{pmatrix}$ |
| $\frac{4}{4}$ $4/m$ | A(z) A A _g | B B(z) B _g | E(x, y) E(x, -y) E _g | |
| | $\begin{pmatrix} . & c & . \\ -c & . & . \\ . & . & . \end{pmatrix}$ | | $\begin{pmatrix} . & . & g \\ . & . & i \\ -g & -i & . \end{pmatrix}$ | $\begin{pmatrix} . & . & -i \\ . & . & g \\ i & -g & . \end{pmatrix}$ |

| | | | | | | |
|---|---|---|---|---|--|--|
| | $\begin{pmatrix} a & . & . \\ . & a & . \\ . & . & b \end{pmatrix}$ | | $\begin{pmatrix} d & . & . \\ . & -d & . \\ . & . & . \end{pmatrix}$ | $\begin{pmatrix} . & e & . \\ e & . & . \\ . & . & . \end{pmatrix}$ | $\begin{pmatrix} . & . & f \\ . & . & . \\ f & . & . \end{pmatrix}$ | $\begin{pmatrix} . & . & . \\ . & . & f \\ . & f & . \end{pmatrix}$ |
| 422 4mm $\bar{4}2_x m_{xy}$ 4m _x 2 _{xy} 4/mmm | A ₁ A ₁ (z) A ₁ A ₁ A _{1g} | A ₂ (z) A ₂ A ₂ A ₂ A _{2g} | B ₁ B ₁ B ₁ B ₁ B _{1g} | B ₂ B ₂ B ₂ (z) B ₂ (z) B _{2g} | E(-y, x) E(x, y) E(y, x) E(-x, y) E _g | |
| | | $\begin{pmatrix} . & c & . \\ -c & . & . \\ . & . & . \end{pmatrix}$ | | | $\begin{pmatrix} . & . & g \\ . & . & . \\ -g & . & . \end{pmatrix}$ | $\begin{pmatrix} . & . & . \\ . & . & g \\ . & -g & . \end{pmatrix}$ |

Trigonal

| | | | |
|---------------|--|---|--|
| | $\begin{pmatrix} a & . & . \\ . & a & . \\ . & . & b \end{pmatrix}$ | $\begin{pmatrix} c & f & e \\ f & -c & d \\ e & d & . \end{pmatrix}$ | $\begin{pmatrix} f & -c & -d \\ -c & -f & e \\ -d & e & . \end{pmatrix}$ |
| $\frac{3}{3}$ | A(z) A _g | E(x, y) E _g | |
| | $\begin{pmatrix} . & h & . \\ -h & . & . \\ . & . & . \end{pmatrix}$ | $\begin{pmatrix} . & . & i \\ . & . & g \\ -i & -g & . \end{pmatrix}$ | $\begin{pmatrix} . & . & -g \\ . & . & i \\ g & -i & . \end{pmatrix}$ |

| | | | | |
|--|---|--|--|---|
| | $\begin{pmatrix} a & . & . \\ . & a & . \\ . & . & b \end{pmatrix}$ | | $\begin{pmatrix} f & . & . \\ . & -f & d \\ . & d & . \end{pmatrix}$ | $\begin{pmatrix} . & -f & -d \\ -f & . & . \\ -d & . & . \end{pmatrix}$ |
| 32 _x 3m _x $\bar{3}m_x$ | A ₁ A ₁ (z) A _{1g} | A ₂ (z) A ₂ A _{2g} | E(x, y) E(y, -x) E _g | |
| | | $\begin{pmatrix} . & h & . \\ -h & . & . \\ . & . & . \end{pmatrix}$ | $\begin{pmatrix} . & . & . \\ . & . & g \\ . & -g & . \end{pmatrix}$ | $\begin{pmatrix} . & . & -g \\ . & . & . \\ g & . & . \end{pmatrix}$ |

| | | | | |
|--|---|--|--|--|
| | $\begin{pmatrix} a & . & . \\ . & a & . \\ . & . & b \end{pmatrix}$ | | $\begin{pmatrix} . & f & . \\ f & . & d \\ . & d & . \end{pmatrix}$ | $\begin{pmatrix} f & . & -d \\ . & -f & . \\ -d & . & . \end{pmatrix}$ |
| 32 _y 3m _y $\bar{3}m_y$ | A ₁ A ₁ (z) A _{1g} | A ₂ (z) A ₂ A _{2g} | E(x, y) E(y, -x) E _g | |
| | | $\begin{pmatrix} . & h & . \\ -h & . & . \\ . & . & . \end{pmatrix}$ | $\begin{pmatrix} . & . & . \\ . & . & g \\ . & -g & . \end{pmatrix}$ | $\begin{pmatrix} . & . & -g \\ . & . & . \\ g & . & . \end{pmatrix}$ |

direction parallel to **y** or **z**), tetragonal class $\bar{4}2m$, trigonal classes 32, 3m and $\bar{3}m$, as well as hexagonal class $\bar{6}2m$.

$\bar{1}$, 2/m, mmm, 4/m, 4/mmm, $\bar{3}$, $\bar{3}m$, 6/m, 6/mmm, m3, m3m,

2.3.3.4. Centrosymmetric crystals

In those point groups that contain the inversion operation, *i.e.* in the eleven centrosymmetric (*nonpolar*) crystal classes

the irreducible representations are divided into two groups, odd and even, according to the parity. Since second-rank polar tensors must transform according to the *even* parity representations only, whereas polar vectors transform according to *odd* parity representations, the selection rules for electric dipole absorption

2. SYMMETRY ASPECTS OF EXCITATIONS

Table 2.3.3.1 (cont.)

Hexagonal

| | | | | | |
|---|--|---|---|--|--|
| | $\begin{pmatrix} a & . & . \\ . & a & . \\ . & . & b \end{pmatrix}$ | $\begin{pmatrix} . & . & e \\ . & . & d \\ e & d & . \end{pmatrix}$ | $\begin{pmatrix} . & . & -d \\ . & . & e \\ -d & e & . \end{pmatrix}$ | $\begin{pmatrix} c & f & . \\ f & -c & . \\ . & . & . \end{pmatrix}$ | $\begin{pmatrix} f & -c & . \\ -c & -f & . \\ . & . & . \end{pmatrix}$ |
| $\begin{matrix} 6 \\ \bar{6} \\ 6/m \end{matrix}$ | $\begin{matrix} A(z) \\ A' \\ A_g \end{matrix}$ | $\begin{matrix} E_1(x, y) \\ E'' \\ E_{1g} \end{matrix}$ | | $\begin{matrix} E_2 \\ E'(x, y) \\ E_{2g} \end{matrix}$ | |
| | $\begin{pmatrix} . & h & . \\ -h & . & . \\ . & . & . \end{pmatrix}$ | $\begin{pmatrix} . & . & i \\ . & . & g \\ -i & -g & . \end{pmatrix}$ | $\begin{pmatrix} . & . & -g \\ . & . & i \\ g & -i & . \end{pmatrix}$ | | |

| | | | | | | |
|---|---|---|---|---|---|--|
| | $\begin{pmatrix} a & . & . \\ . & a & . \\ . & . & b \end{pmatrix}$ | | $\begin{pmatrix} . & . & . \\ . & . & d \\ . & d & . \end{pmatrix}$ | $\begin{pmatrix} . & . & -d \\ . & . & . \\ -d & . & . \end{pmatrix}$ | $\begin{pmatrix} . & f & . \\ f & . & . \\ . & . & . \end{pmatrix}$ | $\begin{pmatrix} f & . & . \\ . & -f & . \\ . & . & . \end{pmatrix}$ |
| $\begin{matrix} 622 \\ 6mm \\ \bar{6}m_2 \\ \bar{6}2_x m_y \\ 6/mmm \end{matrix}$ | $\begin{matrix} A_1 \\ A_1(z) \\ A_1' \\ A_1' \\ A_{1g} \end{matrix}$ | $\begin{matrix} A_2(z) \\ A_2 \\ A_2' \\ A_2' \\ A_{2g} \end{matrix}$ | $\begin{matrix} E_1(x, y) \\ E_1(y, -x) \\ E'' \\ E'' \\ E_{1g} \end{matrix}$ | | $\begin{matrix} E_2 \\ E_2 \\ E'(x, y) \\ E'(y, -x) \\ E_{2g} \end{matrix}$ | |
| | | $\begin{pmatrix} . & h & . \\ -h & . & . \\ . & . & . \end{pmatrix}$ | $\begin{pmatrix} . & . & . \\ . & . & g \\ . & -g & . \end{pmatrix}$ | $\begin{pmatrix} . & . & -g \\ . & . & . \\ g & . & . \end{pmatrix}$ | | |

Cubic

| | | | | | | |
|--|---|---|--|--|--|--|
| | $\begin{pmatrix} a & . & . \\ . & a & . \\ . & . & a \end{pmatrix}$ | $\begin{pmatrix} b & . & . \\ . & b & . \\ . & . & -2b \end{pmatrix}$ | $\begin{pmatrix} -\sqrt{3}b & . & . \\ . & \sqrt{3}b & . \\ . & . & . \end{pmatrix}$ | $\begin{pmatrix} . & . & . \\ . & . & c \\ . & c & . \end{pmatrix}$ | $\begin{pmatrix} . & . & c \\ . & . & . \\ c & . & . \end{pmatrix}$ | $\begin{pmatrix} . & c & . \\ c & . & . \\ . & . & . \end{pmatrix}$ |
| $\begin{matrix} 23 \\ m\bar{3} \end{matrix}$ | $\begin{matrix} A \\ A_g \end{matrix}$ | $\begin{matrix} E \\ E_g \end{matrix}$ | | $\begin{matrix} F(x, y, z) \\ F_g \end{matrix}$ | | |
| | | | | $\begin{pmatrix} . & . & . \\ . & . & d \\ . & -d & . \end{pmatrix}$ | $\begin{pmatrix} . & . & d \\ . & . & . \\ -d & . & . \end{pmatrix}$ | $\begin{pmatrix} . & d & . \\ -d & . & . \\ . & . & . \end{pmatrix}$ |

| | | | | | | | |
|---|---|---|--|--|--|---|---|
| | $\begin{pmatrix} a & . & . \\ . & a & . \\ . & . & a \end{pmatrix}$ | $\begin{pmatrix} b & . & . \\ . & b & . \\ . & . & -2b \end{pmatrix}$ | $\begin{pmatrix} -\sqrt{3}b & . & . \\ . & \sqrt{3}b & . \\ . & . & . \end{pmatrix}$ | | $\begin{pmatrix} . & . & . \\ . & . & c \\ . & c & . \end{pmatrix}$ | $\begin{pmatrix} . & . & c \\ . & . & . \\ c & . & . \end{pmatrix}$ | $\begin{pmatrix} . & c & . \\ c & . & . \\ . & . & . \end{pmatrix}$ |
| $\begin{matrix} 432 \\ \bar{4}3m \\ m\bar{3}m \end{matrix}$ | $\begin{matrix} A_1 \\ A_1 \\ A_{1g} \end{matrix}$ | $\begin{matrix} E \\ E \\ E_g \end{matrix}$ | $\begin{matrix} F_1(x, y, z) \\ F_1 \\ F_{1g} \end{matrix}$ | | $\begin{matrix} F_2 \\ F_2(x, y, z) \\ F_{2g} \end{matrix}$ | | |
| | | | $\begin{pmatrix} . & . & . \\ . & . & d \\ . & -d & . \end{pmatrix}$ | $\begin{pmatrix} . & . & d \\ . & . & . \\ -d & . & . \end{pmatrix}$ | $\begin{pmatrix} . & d & . \\ -d & . & . \\ . & . & . \end{pmatrix}$ | | |

(infrared activity) and for Raman scattering are incompatible. This is often expressed as the *mutual exclusion rule* or *complementarity principle*: The excitations in a crystal belonging to a centrosymmetric class cannot be simultaneously active in infrared absorption and in Raman scattering. Let us note, however, that even-parity excitations are not necessarily all Raman active, and that odd-parity excitations are not necessarily infrared active.

In the remaining noncentrosymmetric crystal classes, the excitations have no defined parity with respect to inversion and can be, in principle, both Raman and infrared active.

Example: Consider a Raman scattering experiment on a crystal of tetragonal symmetry, class $4/mmm$. Raman-active phonons, allowed in conventional symmetric scattering, are of the symmetry species A_{1g} , B_{1g} , B_{2g} and E_g . (the A_{2g} species admits purely antisymmetric scattering only). Straightforward application of Table 2.3.3.1 makes it possible to determine the polar-

ization selection rules, *i.e.* to determine which symmetry species will contribute to the scattering cross section in various experimental configurations. Choosing the Cartesian axes $x \equiv [100]$, $y \equiv [010]$, $z \equiv [001]$ consistent with the standard setting of the $4/mmm$ point group, *i.e.* the fourfold rotation axis $4 \parallel \mathbf{z}$, let us further introduce the notation $x' \equiv [110]$, $y' \equiv [\bar{1}10]$. Then the contributions to the cross section for different symmetry species can be distinguished by their dependence on the polarization vectors \mathbf{e}_I and \mathbf{e}_S of the incident and scattered light:

$$A_{1g} : |(e_{Ix}e_{Sx} + e_{Iy}e_{Sy})a + e_{Iz}e_{Sz}b|^2$$

$$B_{1g} : |(e_{Ix}e_{Sx} - e_{Iy}e_{Sy})d|^2$$

$$B_{2g} : |(e_{Ix}e_{Sy} + e_{Iy}e_{Sx})e|^2$$

$$E_g : [(e_{Ix}e_{Sz} + e_{Iz}e_{Sx})^2 + (e_{Iy}e_{Sz} + e_{Iz}e_{Sy})^2]|f|^2.$$

2.3. RAMAN SCATTERING

Table 2.3.3.2. Raman selection rules in crystals of the 4/*mmm* class

| Scattering configuration | | Cross section for symmetry species | | | |
|------------------------------|------------------------|------------------------------------|-----------------|-----------------|----------------|
| Back scattering | Right-angle scattering | A _{1g} | B _{1g} | B _{2g} | E _g |
| $\bar{z}(xx)z, \bar{z}(yy)z$ | $y(xx)z, x(yy)z$ | $\sim a ^2$ | $\sim d ^2$ | — | — |
| $\bar{x}(zz)x, \bar{y}(zz)y$ | $x(zz)y$ | $\sim b ^2$ | — | — | — |
| $\bar{z}(xy)z$ | $y(xy)x, z(xy)x$ | — | — | $\sim e ^2$ | — |
| $\bar{y}(xz)y, \bar{x}(yz)x$ | $y(xz)x, x(yz)y$ | — | — | — | $\sim f ^2$ |
| $\bar{z}(x'x')z$ | $y'(x'x')z$ | $\sim a ^2$ | — | $\sim e ^2$ | — |
| $\bar{z}(x'y')z$ | $y'(x'y')z$ | — | $\sim d ^2$ | — | — |

Examples of some special scattering geometries that permit the separation of the contributions of different symmetry species are shown in Table 2.3.3.2 (five distinct configurations are sufficient to determine the five independent parameters a, b, d, e, f of the symmetric Raman tensors).

If, for some reason, antisymmetric scattering is allowed, possible contribution of the A_{2g} modes should be considered as well. The contribution to cross section from these modes is proportional to $|(e_{Ix}e_{Sy} - e_{Iy}e_{Sx})c|^2$, hence it can be distinguished from the contribution of the B_{2g} symmetry species by a suitable choice of the scattering geometry.

2.3.3.5. Noncentrosymmetric crystals

Special care is required in treating the scattering by those optical phonons in the 21 noncentrosymmetric (*polar*) crystal classes (1, 2, *m*, 222, *mm*2, 4, $\bar{4}$, 422, 4*mm*, $\bar{4}2m$, 3, 32, 3*m*, 6, $\bar{6}$, 622, 6*mm*, 6*m*2, 23, 432, 43*m*) that are simultaneously infrared-active. Since these polar modes carry a nonzero macroscopic effective charge (2.3.3.4), they contribute to the total polarization in the crystal, hence also to the macroscopic electric field, which in turn leads to a coupling between these modes. The polarization being a *polar vector*, the modes that contribute have the same symmetry character, *i.e.* they must also transform like the components of polar vectors.

An important consequence of the macroscopic field associated with polar modes in the crystal is the partial lifting of the degeneracies of the long-wavelength ($\mathbf{q} \approx 0$) mode frequencies (so-called TO–LO splitting). Since the macroscopic field in the crystal is longitudinal, it must be proportional to the longitudinal component of the polarization. Hence, the equations of motion for all polar modes carrying a nonzero longitudinal polarization (*i.e.* $\mathbf{P}_j \cdot \mathbf{q} \neq 0$) become coupled by the field and, consequently, their frequencies depend on the direction of \mathbf{q} . This phenomenon is called *directional dispersion* and is connected with the fact that in the electrostatic approximation the dynamical matrix with long-range Coulomb forces shows non-analytic behaviour for $\mathbf{q} \rightarrow 0$. In lattice dynamics, the limit can be treated correctly by taking into account the retardation effects in the range where cq becomes comparable to $\omega_j(\mathbf{q})$, *i.e.* in the crossing region of free photon and optical phonon dispersion curves. As a result, one finds that for small \mathbf{q} the true eigenmodes of the system – *polaritons* – have a mixed phonon–photon character and their frequencies show strong dispersion in the very close vicinity of $\mathbf{q} = 0$. Experimentally, this *polariton* region is partially accessible only in near-forward Raman scattering [see (2.3.2.3)]. For larger scattering wavevectors in the usual right-angle or back-scattering geometries, the electrostatic approximation, $cq \gg \omega$, is well applicable and the excitations behave like phonons. Owing to the coupling *via* the longitudinal macroscopic electric field, however, the directional dispersion of these phonon branches remains.

Detailed analysis is complicated in the general case of a low-symmetry crystal with more polar modes (see *e.g.* Claus *et al.*, 1975). In crystals with at least orthorhombic symmetry, the principal axes of the susceptibility tensor are fixed by symmetry

and for the wavevectors oriented along these principal axes the polar optic modes have purely transverse (TO) or longitudinal (LO) character with respect to the associated polarization. The character of a mode is usually mixed for a general direction of the wavevector.

Strictly speaking, conventional symmetry analysis in terms of irreducible representations of the factor group (point group) of the crystal, though giving a true description of polaritons at $\mathbf{q} = 0$, cannot account for the lifting of degeneracies and for the directional dispersion of polar modes. A correct picture of the symmetries and degeneracies is, however, obtained by taking into account the finiteness of the wavevector \mathbf{q} and classifying the vibrations according to the irreducible (*multiplier*) corepresentations of the *point group of the wavevector* $G_0(\mathbf{q})$, which is a subgroup of the factor group. Compatibility relations of the representations at $\mathbf{q} \rightarrow 0$ can then be used to establish a correspondence between the two approaches.

The oscillating macroscopic field associated with long-wavelength LO polar modes acts as another source of modulation of the susceptibility. In addition to the standard atomic displacement contribution connected with the mechanical displacements of atoms, one also has to consider that the transition susceptibility also contains the electro-optic term arising from the distortion of electron shells of atoms in the accompanying macroscopic field \mathbf{E} . Separating both contributions, we may write

$$\begin{aligned} \delta\chi_{\alpha\beta}^{(j)}(\mathbf{q} \approx 0, \omega_l) &= \frac{d\chi_{\alpha\beta}}{dQ_j} Q_j \\ &= \frac{\partial\chi_{\alpha\beta}}{\partial Q_j} Q_j + \frac{\partial\chi_{\alpha\beta}}{\partial E_\gamma} E_\gamma^j \\ &= \left(\frac{\partial\chi_{\alpha\beta}}{\partial Q_j} + \frac{\partial\chi_{\alpha\beta}}{\partial E_\gamma} \frac{dE_\gamma}{dQ_j} \right) Q_j, \end{aligned} \quad (2.3.3.15)$$

or, in terms of the Raman tensor,

$$\delta\chi = \sum_j \mathbf{R}^j Q_j = \sum_j (\mathbf{a}^j Q_j + \mathbf{b} E^j) = \sum_j [\mathbf{a}^j + \mathbf{b}(d\mathbf{E}/dQ_j)] Q_j,$$

where we introduce the notation \mathbf{a}^j and $\mathbf{b}(d\mathbf{E}/dQ_j)$ for the *atomic displacement* and *electro-optic* contributions to the Raman tensor \mathbf{R}^j . As usual, Q_j stands for the normal coordinate of the j th mode and \mathbf{E} for the total macroscopic electric field resulting from the longitudinal polarization of all optic modes. The modes that contribute to \mathbf{E} are only LO polar modes; they transform as Cartesian components of polar vectors (x, y, z). Hence the electro-optic term contributes to the Raman cross section only if $\mathbf{E}^j = (d\mathbf{E}/dQ_j) \neq 0$, *i.e.* if the mode has at least partially longitudinal character. Hence, not only the frequencies but also the scattering cross sections of the TO and LO components of polar modes belonging to the same symmetry species are, in general, different.

Nevertheless, in view of the fact that the macroscopic electric field associated with LO polar phonons transforms in the same way as its polarization vector, the symmetry properties of both the atomic displacement and the electro-optic contributions to the Raman tensors of polar modes are identical. They correspond to *third-rank polar* tensors, which have nonzero components only in *piezoelectric crystals*. The symmetry-restricted form of these tensors can also be derived from Table 2.3.3.1 by combining the matrices corresponding to the x, y and z components. Note that these may belong to different irreducible representations in lower-symmetry classes (*e.g.* z cannot mix with x, y), and that in some uniaxial classes the z component is missing completely. Finally, in the noncentrosymmetric class 32 of the cubic system, the Raman tensors of the triply degenerate polar modes (F_1) are purely antisymmetric; therefore all components of the piezoelectric tensor also vanish.

2. SYMMETRY ASPECTS OF EXCITATIONS

Table 2.3.3.3. Raman selection rules in crystals of the 4mm class

| Scattering configuration | | Cross section for symmetry species | |
|--------------------------|------------------------------|------------------------------------|---|
| | | A ₁ | E |
| q z | $z(xx)z, z(yy)z$ | $\sim a_{LO} ^2$ | — |
| q ⊥ z | $x(zx)x, x(zz)y$ | $\sim b_{TO} ^2$ | — |
| | $\bar{y}(xz)y, \bar{x}(yz)x$ | — | $\sim f_{TO} ^2$ |
| | $x'(zx')y', x'(y'z)y'$ | — | $\frac{1}{2} f_{TO} ^2 + \frac{1}{2} f_{LO} ^2$ |

Example: To illustrate the salient features of polar-mode scattering let us consider a crystal of the 4mm class, where of the Raman-active symmetry species the modes A₁(z) and E(x, y) are polar. According to Table 2.3.3.1, their (**q** = 0) Raman tensors are identical to those of the A_{1g} and E_g modes in the preceding example of a 4/mmm-class crystal. Owing to the macroscopic electric field, however, here one has to expect directional dispersion of the frequencies of the long wavelength (**q** ≈ 0) A₁ and E optic phonon modes according to their longitudinal or transverse character. Consequently, in determining the polarization selection rules, account has to be taken of the direction of the phonon wavevector (*i.e.* the scattering wavevector) **q** with respect to the crystallographic axes. Since for a general direction of **q** the modes are coupled by the field, a suitable experimental arrangement permitting the efficient separation of their respective contributions should have the scattering wavevector **q** oriented along principal directions. At **q** || **z**, the A₁ phonons are longitudinal (LO_{||}) and both E modes (2TO_⊥) are transverse, remaining degenerate, whereas at **q** || **x** or **q** || **y**, the A₁ phonons become transverse (TO_⊥) and the E phonons split into a pair of (TO_⊥, LO_⊥) modes of different frequencies. The subscripts || or ⊥ explicitly indicate the orientation of the electric dipole moment carried by the mode with respect to the fourfold axis (4 || **c** ≡ **z**).

Schematically, the situation (*i.e.* frequency shifts and splittings) at **q** ≈ 0 can be represented by

$$\begin{array}{ccccc}
 & \mathbf{q} \parallel \mathbf{z} & \mathbf{q} \parallel \mathbf{x} & & \\
 A_1(LO_{||}) & - & - & A_1(TO_{||}) & \\
 & & - & E_x(LO_{\perp}) & \\
 E(2TO_{\perp}) & - & - & E_y(TO_{\perp}) &
 \end{array}$$

For a general direction of **q**, the modes are of a mixed character and their frequencies show directional (angular) dispersion. The overall picture depends on the number of A₁ and E phonons present in the given crystal, as well as on their effective charges and on the ordering of their eigenfrequencies. In fact, only the E(TO_⊥) modes remain unaffected by the directional dispersion.

Table 2.3.3.3 gives the corresponding contributions of these modes to the cross section for several representative scattering geometries, where subscripts TO and LO indicate that the components of the total Raman tensor may take on different values for TO and LO modes due to electro-optic contributions in the latter case.

2.3.3.6. **q**-dependent terms

So far, we have not explicitly considered the dependence of the Raman tensor on the magnitude of the scattering wavevector, assuming **q** → 0 (the effects of directional dispersion in the case of scattering by polar modes were briefly mentioned in the preceding section). In some cases, however, the Raman tensors vanish in this limit, or **q**-dependent corrections to the scattering may appear. Formally, we may expand the susceptibility in a Taylor series in **q**. The coefficients in this expansion are higher-order susceptibility derivatives taken at **q** = 0. The symmetry-restricted form of these tensorial coefficients may be determined in the same way as that of the zero-order term, *i.e.* by decomposing the reducible representation of the third-, fourth- and

higher-order polar Cartesian tensors into irreducible components $\Gamma(j)$. General properties of the **q**-dependent terms can be advantageously discussed in connection with the so-called *morphic* effects (see Sections 2.3.4 and 2.3.5).

2.3.4. Morphic effects in Raman scattering

By *morphic* effects we understand the effects that arise from a reduction of the symmetry of a system caused by the application of *external forces*. The relevant consequences of morphic effects for Raman scattering are changes in the selection rules. Applications of external forces may, for instance, render it possible to observe scattering by excitations that are otherwise inactive. Again, group-theoretical arguments may be applied to obtain the symmetry-restricted component form of the Raman tensors under applied forces.

It should be noted that under external forces in this sense various ‘built-in’ fields can be included, *e.g.* electric fields or elastic strains typically occurring near the crystal surfaces. Effects of ‘intrinsic’ macroscopic electric fields associated with long-wavelength LO polar phonons can be treated on the same footing. Spatial-dispersion effects connected with the finiteness of the wavevectors, **q** or **k**, may also be included among morphic effects, since they may be regarded as being due to the gradients of the fields (displacement or electric) propagating in the crystal.

2.3.4.1. General remarks

Various types of applied forces – in a general sense – can be classified according to symmetry, *i.e.* according to their transformation properties. Thus a force is characterized as a *polar* force if it transforms under the symmetry operation of the crystal like a polar tensor of appropriate rank (rank 1: electric field **E**; rank 2: electric field gradient $\nabla \mathbf{E}$, stress **T** or strain **S**). It is an *axial* force if it transforms like an axial tensor (rank 1: magnetic field **H**). Here we shall deal briefly with the most important cases within the macroscopic approach of the susceptibility derivatives. We shall treat explicitly the first-order scattering only and neglect, for the moment, **q**-dependent terms.

In a perturbation approach, the first-order transition susceptibility $\delta\chi$ in the presence of an applied force **F** can be expressed in terms of Raman tensors **R**^{*i*}(**F**) expanded in powers of **F**:

$$\delta\chi(\mathbf{F}) = \sum_j \mathbf{R}^j(\mathbf{F})Q_j,$$

$$\text{where } \mathbf{R}^j(\mathbf{F}) = \mathbf{R}^{j0} + \mathbf{R}^{jF}\mathbf{F} + \frac{1}{2}\mathbf{R}^{jFF}\mathbf{F}\mathbf{F} + \dots$$

$$(2.3.4.1)$$

Here, $\mathbf{R}^{j0} = \chi^{(j)}(0) = (\partial\chi_{\alpha\beta}/\partial Q_j)$ is the zero-field *intrinsic* Raman tensor, whereas the tensors

$$\mathbf{R}^{jF}\mathbf{F} = \left(\frac{\partial^2 \chi_{\alpha\beta}}{\partial Q_j \partial F_\mu} \right) F_\mu,$$

$$\mathbf{R}^{jFF}\mathbf{F}\mathbf{F} = \left(\frac{\partial^3 \chi_{\alpha\beta}}{\partial Q_j \partial F_\mu \partial F_\nu} \right) F_\mu F_\nu \text{ etc.} \quad (2.3.4.2)$$

are the *force-induced* Raman tensors of the respective order in the field, associated with the *j*th normal mode. The scattering cross section for the *j*th mode becomes proportional to $|\mathbf{e}_s(\mathbf{R}^{j0} + \mathbf{R}^{jF}\mathbf{F} + \frac{1}{2}\mathbf{R}^{jFF}\mathbf{F}\mathbf{F} + \dots)\mathbf{e}_l|^2$, which, in general, may modify the polarization selection rules. If, for example, the mode is *intrinsically* Raman inactive, *i.e.* $\mathbf{R}^{j0} = 0$ whereas $\mathbf{R}^{jF} \neq 0$, we deal with purely force-induced Raman scattering; its intensity is proportional to F^2 in the first order. Higher-order terms must be investigated if, for symmetry reasons, the first-order terms vanish.

For force-induced Raman activity, in accordance with general rules, invariance again requires that a particular symmetry species $\Gamma(j)$ can contribute to the first-order transition susceptibility by terms of order *n* in the force only if the identity

2.3. RAMAN SCATTERING

representation is contained in the reducible representation of the n th-order Raman tensor.

An equivalent formulation is that the n th-order tensor-like coefficients in the corresponding force-induced Raman tensor, *i.e.*

$$R_{\alpha\beta\mu\dots\nu}^{iF\dots F} = \left(\frac{\partial^{1+n} \chi_{\alpha\beta}}{\partial Q_j \partial F_\mu \dots \partial F_\nu} \right) \text{ in the term } \mathbf{R}^{iF\dots F} \mathbf{F} \dots \mathbf{F},$$

vanish identically for symmetry reasons unless $[\Gamma_{\text{PV}} \otimes \Gamma_{\text{PV}}] \otimes [\Gamma(\mathbf{F})]_S^n \supset \Gamma(j)$. Here $[\Gamma(\mathbf{F})]_S^n = [\Gamma(\mathbf{F}) \otimes \Gamma(\mathbf{F}) \otimes \dots \otimes \Gamma(\mathbf{F})]_S$ is the *symmetrized n th power* of the representation $\Gamma(\mathbf{F})$ according to which the generalized force \mathbf{F} transforms under the operation of the point group. The requirement for the symmetrized part is dictated by the interchangeability of the higher-order derivatives with respect to the components of the force. We recall that the first factor representing the susceptibility, $[\Gamma_{\text{PV}} \otimes \Gamma_{\text{PV}}]$, need not be symmetric in general. However, for most purposes (non-resonant conditions, non-magnetic crystals in the absence of a magnetic field) it can be replaced by its symmetrized part $[\Gamma_{\text{PV}} \otimes \Gamma_{\text{PV}}]_S$.

Standard group-theoretical methods can be used to determine the force-induced Raman activity in a given order of the field and to derive the matrix form of the corresponding Raman tensors. Before treating several important cases of morphic effects in more detail in the following sections, let us make a few comments.

Beside the force-induced effects on the scattering tensors, there are also the direct morphic effects of the forces on the excitations themselves (possible frequency shifts, lifting of mode degeneracies *etc.*), which can be investigated by an analogous perturbation treatment, *i.e.* by expanding the dynamical matrix in powers of \mathbf{F} and determining the corresponding force-induced corrections in the respective orders.

The lifting of degeneracies is a typical sign of the fact that the symmetry of the problem is reduced. The extended system *crystal + applied force* corresponds to a new symmetry group resulting from those symmetry operations that leave the extended system invariant. Consequently, the new normal modes (in the long-wavelength limit) can be formally classified according to the new point group appropriate for the extended system, which qualitatively accounts for the new reduced symmetries and degeneracies.

The force-induced Raman tensors referring to the original crystal symmetry should thus be equivalent to the Raman tensors of the corresponding modes in the new point group *via* the compatibility relations. The new point-group symmetry of the extended system is often used to investigate Raman-induced activity. It should be noted, however, that this approach generally fails to predict to what order in the force the induced changes in the Raman tensors appear. Such information is usually of prime importance for the scattering experiment, where appropriate

setup and detection techniques can be applied to search for a force-induced effect of a particular order. Thus the perturbation method is usually preferable (Anastassakis, 1980).

In the following sections, we shall briefly treat the most important cases in the conventional limit $\mathbf{q} \rightarrow 0$ (neglecting for the moment the spatial dispersion).

2.3.4.2. Electric-field-induced scattering

Expanding the linear dielectric susceptibility into a Taylor series in the field, we write

$$\chi_{\alpha\beta}(\mathbf{E}) = \chi_{\alpha\beta}(0) + \frac{\partial \chi_{\alpha\beta}}{\partial E_\gamma} E_\gamma + \frac{\partial^2 \chi_{\alpha\beta}}{\partial E_\gamma \partial E_\delta} E_\gamma E_\delta + \dots \quad (2.3.4.3)$$

The coefficients of the field-dependent terms in this expansion are, respectively, third-, fourth- and higher-rank polar tensors; they describe linear, quadratic and higher-order *electro-optic effects*. The corresponding expansion of the Raman tensor of the j th optic mode is written as $\mathbf{R}'(\mathbf{E}) = \mathbf{R}^0 + \mathbf{R}^I \mathbf{E} + \frac{1}{2} \mathbf{R}^{IE} \mathbf{E} \mathbf{E} + \dots$

Since the representation $\Gamma(\mathbf{E}) = \Gamma_{\text{PV}}$, the coefficients of the linear term in the expansion for χ , *i.e.* the third-rank tensor $b_{\alpha\beta\gamma} = (\partial \chi_{\alpha\beta} / \partial E_\gamma)$, transform according to the reducible representation given by the direct product:

$$[\Gamma_{\text{PV}} \otimes \Gamma_{\text{PV}}]_S \otimes \Gamma_{\text{PV}}.$$

First-order field-induced Raman activity (conventional symmetric scattering) is thus obtained by reducing this representation into irreducible components $\Gamma(j)$. Higher-order contributions are treated analogously.

It is clear that in centrosymmetric crystals the reduction of a third-rank polar tensor cannot contain even-parity representations; consequently, electric-field-induced scattering by even-parity modes is forbidden in the first order (and in all odd orders) in the field. The lowest non-vanishing contributions to the field-induced Raman tensors of even-parity modes in these crystals are thus quadratic in \mathbf{E} ; their form is obtained by reducing the representation of a fourth-rank symmetric polar tensor $[\Gamma_{\text{PV}} \otimes \Gamma_{\text{PV}}]_S \otimes [\Gamma_{\text{PV}} \otimes \Gamma_{\text{PV}}]_S$ into irreducible components $\Gamma(j)$. On the other hand, since the electric field removes the centre of inversion, scattering by odd-parity modes becomes allowed in first order in the field but remains forbidden in all even orders. In noncentrosymmetric crystals, parity considerations do not apply.

For completeness, we note that, besides the direct electro-optic contribution to the Raman tensor due to field-induced distortion of the electronic states of the atoms in the unit cell, there are two additional mechanisms contributing to the total first-order change of the dielectric susceptibility in an external electric field \mathbf{E} . They come, respectively, from field-induced relative displacements of atoms due to field-induced excitation of polar optical phonons $Q_p(\mathbf{E}) \sim \mathbf{E}$ and from field-induced elastic deformation $\mathbf{S}(\mathbf{E}) = \mathbf{d}\mathbf{E}$ (*piezoelectric effect*, \mathbf{d} being the piezoelectric tensor).

Table 2.3.4.1. Symmetrized (*s*) and antisymmetrized (*a*) sets of trilinear basis functions corresponding to symmetry species of the $4mm$ class

| Species | Basis functions | Symmetry |
|---------|---|------------------------------|
| A_1 | $(x_1 x_2 + y_1 y_2) z_3; z_1 z_2 z_3; (x_1 z_2 + z_1 x_2) x_3 + (y_1 z_2 + z_1 y_2) y_3$ $(x_1 z_2 - z_1 x_2) x_3 + (y_1 z_2 - z_1 y_2) y_3$ | (<i>s</i>) (<i>a</i>) |
| A_2 | $(x_1 z_2 + z_1 x_2) y_3 - (y_1 z_2 + z_1 y_2) x_3$ $(x_1 y_2 - y_1 x_2) z_3; (x_1 z_2 - z_1 x_2) y_3 - (y_1 z_2 - z_1 y_2) x_3$ | (<i>s</i>) (<i>a</i>) |
| B_1 | $(x_1 x_2 - y_1 y_2) z_3; (x_1 z_2 + z_1 x_2) x_3 - (y_1 z_2 + z_1 y_2) y_3$ $(x_1 z_2 - z_1 x_2) x_3 - (y_1 z_2 - z_1 y_2) y_3$ | (<i>s</i>) (<i>a</i>) |
| B_2 | $(x_1 y_2 + y_1 x_2) z_3; (x_1 z_2 + z_1 x_2) y_3 + (y_1 z_2 + z_1 y_2) x_3$ $(x_1 z_2 - z_1 x_2) y_3 + (y_1 z_2 - z_1 y_2) x_3$ | (<i>s</i>) (<i>a</i>) |
| E | $[(x_1 x_2 + y_1 y_2) x_3, (x_1 x_2 + y_1 y_2) y_3]; [z_1 z_2 x_3, z_1 z_2 y_3];$ $[(x_1 z_2 + z_1 x_2) z_3, (y_1 z_2 + z_1 y_2) z_3]; [(x_1 x_2 - y_1 y_2) x_3,$ $-(x_1 x_2 - y_1 y_2) y_3]; [(x_1 y_2 + y_1 x_2) y_3, (x_1 y_2 + y_1 x_2) x_3]$ $[(x_1 z_2 - z_1 x_2) z_3, (y_1 z_2 - z_1 y_2) z_3]; [(x_1 y_2 - y_1 x_2) y_3,$ $-(x_1 y_2 - y_1 x_2) x_3]$ | (<i>s</i>) (<i>a</i>) |

2. SYMMETRY ASPECTS OF EXCITATIONS

In order to separate these contributions, we write formally $\chi(\mathbf{E}) = \chi(\mathbf{E}, Q_p(\mathbf{E}), \mathbf{S}(\mathbf{E}))$ and get, to first order in the field,

$$\begin{aligned} \delta\chi(\mathbf{E}) &= (\partial\chi/\partial\mathbf{E})\mathbf{E} + \sum_p (\partial\chi/\partial Q_p)Q_p(\mathbf{E}) + (\partial\chi/\partial\mathbf{S})\mathbf{S}(\mathbf{E}) \\ &= \sum_j \mathbf{R}^j \mathbf{E} Q_j, \text{ where we define} \\ \mathbf{R}^j &= (\partial\mathbf{R}^j/\partial\mathbf{E}) + \sum_p (\partial\mathbf{R}^j/\partial Q_p)(dQ_p/d\mathbf{E}) + (\partial\mathbf{R}^j/\partial\mathbf{S})\mathbf{d}. \end{aligned} \quad (2.3.4.4)$$

The first term in these equations involves the susceptibility derivative $\mathbf{b} = (\partial\chi/\partial\mathbf{E})$ at constant Q_p and \mathbf{S} . The second term involves the second-order susceptibility derivatives with respect to the normal coordinates: $\chi^{(j,p)} = (\partial^2\chi/\partial Q_j\partial Q_p) = (\partial R_{\alpha\beta}^j/\partial Q_p)$. Since $Q_p(\mathbf{E}) \sim Z_{pv}E_v$, where the quantity $\mathbf{Z}_p = (Z_{pv})$ is the effective charge tensor (2.3.3.4) of the normal mode p , its nonzero contributions are possible only if there are infrared-active optical phonons (for which, in principle, $\mathbf{Z}_p \neq 0$) in the crystal. The third term is proportional to the field-induced elastic strain $\mathbf{S}(\mathbf{E}) = \mathbf{dE}$ via the elasto-optic tensor $\mathbf{p} = (\partial\chi/\partial\mathbf{S})$ and can occur only in piezoelectric crystals.

Example: As an illustration, we derive the matrix form of linear electric-field-induced Raman tensors (including possible antisymmetric part) in a tetragonal crystal of the $4mm$ class. The corresponding representation $[\Gamma_{PV} \otimes \Gamma_{PV}] \otimes \Gamma_{PV}$ in this class reduces as follows:

$$\begin{aligned} [\Gamma_{PV} \otimes \Gamma_{PV}]_S \otimes \Gamma_{PV} &= 3A_1 \oplus A_2 \oplus 2B_1 \oplus 2B_2 \oplus 5E, \\ [\Gamma_{PV} \otimes \Gamma_{PV}]_A \otimes \Gamma_{PV} &= A_1 \oplus 2A_2 \oplus B_1 \oplus B_2 \oplus 2E. \end{aligned}$$

Suitable sets of symmetrized (s) and antisymmetrized (a) basis functions (third-order polynomials) for the representations of the $4mm$ point group can be easily derived by inspection or using projection operators. The results are given in Table 2.3.4.1. Using these basis functions, one can readily construct the Cartesian form of the linear contributions to the electric-field-induced Raman tensors $\mathbf{R}^i(\mathbf{E}) = \mathbf{R}^{iE}\mathbf{E}$ for all symmetry species of the $4mm$ -class crystals. The tensors are split into symmetric (conventional allowed scattering) and antisymmetric part.

| Symmetric | Antisymmetric |
|--|--|
| $A_1 : \begin{pmatrix} a_1 E_z & . & a_2 E_x \\ . & a_1 E_z & a_2 E_y \\ a_2 E_x & a_2 E_y & b_1 E_z \end{pmatrix}$ | $+ \begin{pmatrix} . & . & a_3 E_x \\ . & . & a_3 E_y \\ -a_3 E_x & -a_3 E_y & . \end{pmatrix}$ |
| $A_2 : \begin{pmatrix} . & . & c_2 E_y \\ . & . & -c_2 E_x \\ c_2 E_y & -c_2 E_x & . \end{pmatrix}$ | $+ \begin{pmatrix} . & c_1 E_z & c_3 E_y \\ -c_1 E_z & . & -c_3 E_x \\ -c_3 E_y & c_3 E_x & . \end{pmatrix}$ |
| $B_1 : \begin{pmatrix} d_1 E_z & . & d_2 E_x \\ . & -d_1 E_z & -d_2 E_y \\ d_2 E_x & -d_2 E_y & . \end{pmatrix}$ | $+ \begin{pmatrix} . & . & d_3 E_x \\ . & . & -d_3 E_y \\ -d_3 E_x & d_3 E_y & . \end{pmatrix}$ |
| $B_2 : \begin{pmatrix} . & e_1 E_z & e_2 E_y \\ e_1 E_z & . & e_2 E_x \\ e_2 E_y & e_2 E_x & . \end{pmatrix}$ | $+ \begin{pmatrix} . & . & e_3 E_y \\ . & . & e_3 E_x \\ -e_3 E_y & -e_3 E_x & . \end{pmatrix}$ |
| $E : \begin{pmatrix} (f_1 + f_2)E_x & f_4 E_y & f_5 E_z \\ f_4 E_y & (f_1 - f_2)E_x & . \\ f_5 E_z & . & f_3 E_x \\ (f_1 - f_2)E_y & f_4 E_x & . \\ f_4 E_x & (f_1 + f_2)E_y & f_3 E_z \\ . & f_5 E_z & f_3 E_y \end{pmatrix}$ | $+ \begin{pmatrix} . & g_4 E_y & g_5 E_z \\ -g_4 E_y & . & . \\ -g_5 E_z & . & . \\ . & -g_4 E_x & . \\ g_4 E_x & . & g_5 E_z \\ . & -g_5 E_z & . \end{pmatrix}$ |

2.3.4.3. Raman scattering in a magnetic field

In a magnetic field, the dielectric susceptibility tensor of a crystal is known to obey the general relation (Onsager reciprocity theorem for generalized kinetic coefficients)

$$\chi_{\alpha\beta}(\mathbf{H}) = \chi_{\beta\alpha}(-\mathbf{H}). \quad (2.3.4.5)$$

Further, in the absence of absorption, the susceptibility must be Hermitian, *i.e.*

$$\chi_{\alpha\beta}(\mathbf{H}) = \chi_{\beta\alpha}^*(\mathbf{H}). \quad (2.3.4.6)$$

Hence, $\chi(\mathbf{H})$ is neither symmetric nor real. Expanding $\chi(\mathbf{H})$ in the powers of the field,

$$\chi_{\alpha\beta}(\mathbf{H}) = \chi_{\alpha\beta}(0) + \frac{\partial\chi_{\alpha\beta}}{\partial H_\mu} H_\mu + \frac{\partial^2\chi_{\alpha\beta}}{\partial H_\mu \partial H_\nu} H_\mu H_\nu + \dots, \quad (2.3.4.7)$$

it follows that all terms of the magnetic-field-induced Raman tensor that are of odd powers in \mathbf{H} are purely imaginary and antisymmetric in α and β , whereas all terms of even powers in \mathbf{H} are real and symmetric.

Let us discuss in more detail the symmetry properties of the first-order term, which can be written as

$$\Delta\chi_{\alpha\beta}(\mathbf{H}) = if_{\alpha\beta\mu} H_\mu, \quad (2.3.4.8)$$

where the tensor \mathbf{f} , referred to as the *magneto-optic tensor*, is real and purely antisymmetric in the first two indices:

$$f_{\alpha\beta\nu} \equiv -i(\partial\chi_{\alpha\beta}/\partial H_\nu) = -f_{\beta\alpha\nu}.$$

The representation $\Gamma(\mathbf{f})$ of the magneto-optic tensor \mathbf{f} may thus be symbolically written as

$$\begin{aligned} \Gamma(\mathbf{f}) &= [\Gamma_{PV} \otimes \Gamma_{PV}]_A \otimes \Gamma_{AV} = \Gamma_{AV} \otimes \Gamma_{AV} = \Gamma_{PV} \otimes \Gamma_{PV} \\ &= \Gamma(T_\alpha T_\beta), \end{aligned} \quad (2.3.4.9)$$

since the antisymmetric part of the product of two polar vectors transforms like an axial vector, and the product of two axial vectors transforms exactly like the product of two polar vectors. Hence, the representation $\Gamma(\mathbf{f})$ is equivalent to the representation of a general nonsymmetric second-rank tensor and reduces in exactly the same way (2.3.3.14).

$$\Gamma(\mathbf{f}) = \Gamma_{PV} \otimes \Gamma_{PV} = c^{(1)}\Gamma(1) \oplus c^{(2)}\Gamma(2) \oplus \dots$$

We arrive thus at the important conclusion that, to first order in the field, only the modes that normally show intrinsic Raman activity (either symmetric and antisymmetric) can take part in magnetic-field-induced scattering. Moreover, the magnetic-field-induced Raman tensors for these symmetry species must have the same number of components as the general nonsymmetric Raman tensors at zero field.

In order to determine the symmetry-restricted matrix form of the corresponding field-induced Raman tensors (linear in \mathbf{H}) in Cartesian coordinates, one can use the general method and construct the tensors from the respective (antisymmetric) basis functions. In this case, however, a simpler method can be adopted, which makes use of the transformation properties of the magneto-optic tensor as follows.

From the definition of the tensor \mathbf{f} , it is clear that its Cartesian components $f_{\alpha\beta\nu}$ must have the same symmetry properties as the product $[E_\alpha E_\beta]_A H_\nu$. The antisymmetric factor $[E_\alpha E_\beta]_A$ transforms, however, as $\varepsilon_{\alpha\beta\mu} H_\mu$, where $\varepsilon_{\alpha\beta\mu}$ is the fully antisymmetric third-rank pseudotensor (*Levi-Civita tensor*). Consequently, $f_{\alpha\beta\nu}$ must transform in the same way as $\varepsilon_{\alpha\beta\mu} H_\mu H_\nu$, which in turn transforms identically to $\varepsilon_{\alpha\beta\mu} E_\mu E_\nu$. Therefore, comparison of the matrices corresponding to the irreducible components $\Gamma(j)$ provides a simple mapping between the components of the Cartesian forms of the linear field-induced Raman tensors $\mathbf{R}^j(\mathbf{H}) = \mathbf{R}^{jh}\mathbf{H}$ and the intrinsic Raman tensors \mathbf{R}^j . Explicitly, this mapping is given by

$$R_{\alpha\beta\nu}^{jh} \equiv \frac{\partial^2\chi_{\alpha\beta}}{\partial Q_j \partial H_\nu} = if_{\alpha\beta\nu}^{(j)} \leftarrow i\varepsilon_{\alpha\beta\mu} R_{\mu\nu}^{j0}. \quad (2.3.4.10)$$

2.3. RAMAN SCATTERING

For any given symmetry species, this relation can be used to deduce the matrix form of the first-order field-induced Raman tensors from the tensors given in Table 2.3.3.1.

Example: We consider again the $4mm$ class crystal. The representation $\Gamma(\mathbf{f})$ of the magneto-optic tensor \mathbf{f} in the $4mm$ class reduces as follows:

$$\Gamma(\mathbf{f}) = \Gamma_{\text{PV}} \otimes \Gamma_{\text{PV}} = 2A_1 \oplus A_2 \oplus B_1 \oplus B_2 \oplus 2E.$$

Straightforward application of the mapping mentioned above then gives the following symmetry-restricted matrix forms of contributions to the magnetic-field-induced Raman tensors $\mathbf{R}^{iH}\mathbf{H}$ for all symmetry species of the $4mm$ -class crystals. The number of independent parameters for each species is the same as in the intrinsic nonsymmetric zero-field Raman tensors:

$$\begin{aligned} A_1 : & \begin{pmatrix} . & ib'H_z & -ia'H_y \\ -ib'H_z & . & ia'H_x \\ ia'H_y & -ia'H_x & . \end{pmatrix} \\ A_2 : & \begin{pmatrix} . & . & ic'H_x \\ . & . & ic'H_y \\ -ic'H_x & -ic'H_y & . \end{pmatrix} \\ B_1 : & \begin{pmatrix} . & . & id'H_y \\ . & . & id'H_x \\ -id'H_y & -id'H_x & . \end{pmatrix} \\ B_2 : & \begin{pmatrix} . & . & -ie'H_x \\ . & . & ie'H_y \\ ie'H_x & -ie'H_y & . \end{pmatrix} \\ E : & \begin{pmatrix} . & ig'H_x & . \\ -ig'H_x & . & if'H_z \\ . & -if'H_z & . \end{pmatrix} \\ & \begin{pmatrix} . & ig'H_y & -if'H_z \\ -ig'H_y & . & . \\ if'H_z & . & . \end{pmatrix}. \end{aligned}$$

Let us note that the conclusions mentioned above apply, strictly speaking, to non-magnetic crystals. In magnetic materials in the presence of spontaneous ordering (*ferro-* or *antiferromagnetic* crystals) the analysis has to be based on magnetic point groups.

2.3.4.4. Stress- (strain-) induced Raman scattering

Stress-induced Raman scattering is an example of the case when the external ‘force’ is a higher-rank tensor. In the case of stress, we deal with a symmetric second-rank tensor. Since symmetric stress (\mathbf{T}) and strain (\mathbf{S}) tensors have the same symmetry and are uniquely related *via* the fourth-rank *elastic stiffness tensor* (\mathbf{c}),

$$T_{\alpha\beta} = c_{\alpha\beta\mu\nu} S_{\mu\nu},$$

it is immaterial for symmetry purposes whether stress- or strain-induced effects are considered. The linear strain-induced contribution to the susceptibility can be written as

$$\Delta\chi_{\alpha\beta}(\mathbf{S}) = \left(\frac{\partial\chi_{\alpha\beta}}{\partial S_{\mu\nu}} \right) S_{\mu\nu}$$

so that the respective strain coefficients (conventional symmetric scattering) transform evidently as

$$[\Gamma_{\text{PV}} \otimes \Gamma_{\text{PV}}]_S \otimes [\Gamma_{\text{PV}} \otimes \Gamma_{\text{PV}}]_S,$$

i.e. they have the same symmetry as the *piezo-optic* or *elasto-optic* tensor. Reducing this representation into irreducible components $\Gamma(j)$, we obtain the symmetry-restricted form of the linear strain-induced Raman tensors. Evidently, their matrix form is the same as for quadratic electric-field-induced Raman tensors. In centrosymmetric crystals, strain-induced Raman scattering (in any order in the strain) is thus allowed for even-parity modes only.

2.3.5. Spatial-dispersion effects

For $\mathbf{q} = 0$, the normal modes correspond to a homogeneous phonon displacement pattern (all cells vibrate in phase). Phenomenologically, the \mathbf{q} -dependence of Raman tensors can be understood as a kind of morphic effect due to the gradients of the displacement field. Developing the contribution of the long-wavelength j th normal mode to the susceptibility in Cartesian components of the displacement of atoms in the primitive cell and their gradients, we obtain

$$\delta\chi_{\alpha\beta}^{(j)}(\mathbf{q}) = \sum_{\kappa} \left(\frac{\partial\chi_{\alpha\beta}}{\partial u_{\kappa,\gamma}^{(j)}} \right)_0 u_{\kappa,\gamma}^{(j)}(\mathbf{q}) + i \sum_{\kappa} \left(\frac{\partial\chi_{\alpha\beta}}{\partial (\nabla u_{\kappa,\gamma}^{(j)})_{\delta}} \right)_0 q_{\delta} u_{\kappa,\gamma}^{(j)}(\mathbf{q}), \quad (2.3.5.1)$$

where the derivatives are taken at $\mathbf{q} = 0$, and we use the obvious relation $\nabla u_{\kappa,\gamma}^{(j)} = i\mathbf{q}u_{\kappa,\gamma}^{(j)}$.

Transforming to normal coordinates, using (2.3.3.1), we identify the $\mathbf{q} = 0$ intrinsic Raman tensor \mathbf{R}^{j0} of the j th normal mode, explicitly expressed *via* Cartesian displacements of atoms,

$$R_{\alpha\beta}^{j0} \equiv \chi_{\alpha\beta}^{(j)}(0) \equiv \left(\frac{\partial\chi_{\alpha\beta}}{\partial Q_j} \right) = \sum_{\kappa} \left(\frac{\partial\chi_{\alpha\beta}}{\partial u_{\kappa,\mu}^{(j)}} \right) \frac{e_{\kappa,\mu}(0, j)}{\sqrt{Nm_{\kappa}}}, \quad (2.3.5.2)$$

and introduce the first-order \mathbf{q} -induced atomic displacement Raman tensor coefficients \mathbf{R}^{jq} :

$$\begin{aligned} R_{\alpha\beta\gamma}^{jq} & \equiv -i \left(\frac{\partial\chi_{\alpha\beta}}{\partial q_{\gamma}} \right) = -i \left(\frac{\partial^2\chi_{\alpha\beta}}{\partial Q_j \partial q_{\gamma}} \right) \\ & = \sum_{\kappa} \left(\frac{\partial\chi_{\alpha\beta}}{\partial (\nabla u_{\kappa,\mu}^{(j)})_{\gamma}} \right) \frac{e_{\kappa,\mu}(0, j)}{\sqrt{Nm_{\kappa}}}. \end{aligned} \quad (2.3.5.3)$$

Hence, to the lowest order in \mathbf{q} , the transition susceptibility is expressed as

$$\delta\chi_{\alpha\beta}^{(j)}(\mathbf{q}) \cong \left(R_{\alpha\beta}^{j0} + iR_{\alpha\beta\gamma}^{jq} q_{\gamma} \right) Q_j(0). \quad (2.3.5.4)$$

In a more general case, spatial dispersion should be considered together with the electro-optic contributions due to the internal macroscopic field \mathbf{E} and its gradients. Assuming the linear susceptibility to be modulated by the atomic displacements Q_j and the macroscopic electric field \mathbf{E} as well as by their gradients ∇Q_j and $\nabla \mathbf{E}$, we can expand the transition susceptibility of the j th phonon mode $Q_j(\mathbf{q})$ to terms linear in \mathbf{q} and formally separate the atomic displacement and electro-optic parts of the Raman tensor [see (2.3.3.15)]:

$$\begin{aligned} \delta\chi^{(j)}(\mathbf{q}) & = (\partial\chi/\partial Q_j) Q_j(\mathbf{q}) + i(\partial\chi/\partial \nabla Q_j) \mathbf{q} Q_j(\mathbf{q}) \\ & \quad + (\partial\chi/\partial \mathbf{E}) \mathbf{E}^j(\mathbf{q}) + i(\partial\chi/\partial \nabla \mathbf{E}) \mathbf{q} \mathbf{E}^j(\mathbf{q}), \end{aligned}$$

or concisely

$$\delta\chi^{(j)}(\mathbf{q}) = \mathbf{a}^j(\mathbf{q}) Q_j(\mathbf{q}) + \mathbf{b}(\mathbf{q}) \mathbf{E}^j(\mathbf{q}),$$

with

$$\mathbf{a}^j(\mathbf{q}) = (\mathbf{a}^{j0} + i\mathbf{a}^{jq}\mathbf{q}), \quad \mathbf{b}(\mathbf{q}) = (\mathbf{b}^0 + i\mathbf{b}^q\mathbf{q}). \quad (2.3.5.5)$$

2. SYMMETRY ASPECTS OF EXCITATIONS

Hence, setting $\mathbf{E}^j(\mathbf{q}) = (d\mathbf{E}/dQ_j)Q_j(\mathbf{q})$, we write for the total Raman tensor

$$\mathbf{R}^j(\mathbf{q}) = \mathbf{a}^j(\mathbf{q}) + \mathbf{b}(\mathbf{q})(d\mathbf{E}/dQ_j). \quad (2.3.5.6)$$

The definitions of the tensors \mathbf{a}^j and \mathbf{a}^{jq} correspond to (2.3.5.2) and (2.3.5.3). Analogously, the tensors \mathbf{b}^0 and \mathbf{b}^q are defined by

$$b_{\alpha\beta\gamma}^0 = \left(\frac{\partial \chi_{\alpha\beta}}{\partial E_\gamma} \right), \quad b_{\alpha\beta\gamma\delta}^q = -i \left(\frac{\partial^2 \chi_{\alpha\beta}}{\partial q_\gamma \partial E_\delta} \right) = \left(\frac{\partial \chi_{\alpha\beta}}{\partial (\nabla E_\delta)_\gamma} \right). \quad (2.3.5.7)$$

The \mathbf{q} -independent part \mathbf{a}^{j0} of the atomic displacement Raman tensor corresponds to the standard $\mathbf{q} = 0$ Raman tensors \mathbf{R}^{j0} , whose symmetry properties and matrix form were discussed in Section 2.3.3.3.

Like \mathbf{a}^{j0} , the form of the \mathbf{q} -dependent contribution \mathbf{a}^{jq} also depends on the symmetry properties of the corresponding normal coordinate $Q_j(\mathbf{q} \approx 0)$. Since \mathbf{q} (or ∇Q_j) and \mathbf{E} are polar vectors, the symmetry properties of the \mathbf{a}^{jq} are identical to those of the coefficients \mathbf{R}^{jE} of the electric-field-induced Raman tensor discussed in Section 2.3.4.2: they transform according to the $\mathbf{q} = 0$ representation $[\Gamma_{\text{PV}} \otimes \Gamma_{\text{PV}}]_S \otimes \Gamma_{\text{PV}} \otimes \Gamma(j)$. Hence, the symmetry-restricted matrix form of the \mathbf{q} -dependent contribution to the atomic displacement Raman tensor \mathbf{a}^{jq} is exactly the same as that of the corresponding electric-field-induced Raman tensor \mathbf{R}^{jE} . In general, these linear terms must vanish for even-parity modes in centrosymmetric crystals (where the lowest-order non-vanishing contributions to the Raman tensor are quadratic). The third-rank tensor \mathbf{b}^0 corresponds to the first-order susceptibility derivative \mathbf{b} and the fourth-rank tensor \mathbf{b}^q to its first-order \mathbf{q} -dependent part.

As mentioned above, the \mathbf{q} -independent third-rank polar tensor \mathbf{b}^0 is nonzero only in noncentrosymmetric (piezoelectric) crystals, where it contributes to Raman tensors for polar longitudinal optical (LO) phonons. The corresponding electro-optic terms in \mathbf{R}^j , connected with the accompanying longitudinal electric field \mathbf{E} , are given by $\mathbf{b}^0(d\mathbf{E}/dQ_j)$. Symmetry arguments imply that the \mathbf{q} -independent part of such terms must have the same form as the atomic displacement Raman tensor for polar LO phonons, since the corresponding normal coordinates transform as components of polar vectors.

The \mathbf{q} -dependent part of the electro-optic contribution, the polar fourth-rank tensor $\mathbf{b}^q = (b_{\alpha\beta\gamma\delta}^q)$, transforms as $[\Gamma_{\text{PV}} \otimes \Gamma_{\text{PV}}]_S^2 \otimes \Gamma_{\text{PV}} \otimes \Gamma_{\text{PV}}$ and its symmetry properties are similar to those of the quadratic electro-optic tensor (however, as \mathbf{q} and \mathbf{E} are not interchangeable, there is no symmetry in the last two indices γ, δ). Thus, for finite \mathbf{q} , the term $\mathbf{b}^q\mathbf{q}$ has nonzero components in all crystal classes. The corresponding contribution to the Raman tensor, however, is possible only in noncentrosymmetric crystals. Again, because of the $(d\mathbf{E}/dQ_j)$ factor, the symmetry-restricted matrix form of this contribution for polar LO phonons will be equivalent to that of the $\mathbf{a}^j\mathbf{q}$ term. As far as symmetry is concerned, the distinction between atomic displacement and electro-optic contributions is therefore immaterial.

The occurrence of \mathbf{q} -dependent terms leads to polarization selection rules that are generally different from those of intrinsically ($\mathbf{q} = 0$) Raman-active modes. For this reason, this phenomenon is sometimes referred to as *forbidden* scattering. It is often observed under resonance conditions.

We recall that the terms linear in \mathbf{q} , *i.e.* proportional to displacement gradients and elastic strains, are fundamental for the description of inelastic light scattering by those excitations for which the transition susceptibility identically vanishes in the limit $\mathbf{q} \rightarrow 0$ regardless of lattice point symmetry. This is the case for scattering by acoustic phonons (*Brillouin scattering*) and also for scattering by plasma waves (plasmons in semiconductors).

We have explicitly considered only the \mathbf{q} -dependent effects, due to gradients of phonon fields. In general, spatial dispersion

may be also due to the gradients of the electric (or magnetic) field of the incident or scattered photons. The corresponding effects are often referred to as \mathbf{k} -dependent effects. In view of the wavevector conservation condition (2.3.2.2), the three wavevectors \mathbf{q} , \mathbf{k}_i and \mathbf{k}_s are always related, which simplifies the symmetry analysis. Without going into details, we note that, microscopically, the \mathbf{k} -dependent effects come from photon–electron interactions beyond the usual dipole approximation, *i.e.* from multipolar effects. The symmetry-allowed matrix form of the \mathbf{k} -induced contributions, depending on the nature of the leading microscopic mechanism, can be obtained by standard group-theoretical techniques.

Example: As an example we give the symmetry-restricted form for the linear \mathbf{q} -dependent contribution to the Raman tensors for *Raman-inactive* triply degenerate F_{1u} modes in the $m3m$ (O_h) class:

$$\mathbf{R}^j = 0; \quad \mathbf{R}^{jq} = \begin{pmatrix} cq_x & bq_y & bq_z \\ bq_y & aq_x & . \\ bq_z & . & aq_x \end{pmatrix}, \begin{pmatrix} aq_y & bq_x & . \\ bq_x & cq_y & bq_z \\ . & bq_z & aq_y \end{pmatrix}, \begin{pmatrix} aq_z & . & bq_x \\ . & aq_z & bq_y \\ bq_x & bq_y & cq_z \end{pmatrix}.$$

The same form of the \mathbf{q} -dependent contribution holds for Raman-active optic F_2 modes in the $\bar{4}3m$ (T_d) class. The conventional ($\mathbf{q} = 0$) intrinsic Raman tensor of F_2 is nonzero, but has off-diagonal components only. Since these modes are also infrared-active, there is a concomitant splitting of LO and TO frequencies as well as a possible electro-optic contribution to the Raman tensor due to the accompanying longitudinal macroscopic field. If one chooses $\mathbf{q} \parallel \mathbf{z}$, for instance, the first two matrices correspond to two degenerate TO modes and the third one to the LO mode. Combining the \mathbf{q} -independent and \mathbf{q} -dependent contributions, we get for each triplet of (2TO + LO) F_2 modes

$$\mathbf{R}^{j0} + \mathbf{R}^{jq} = \begin{pmatrix} . & . & bq_z \\ . & . & c_{\text{TO}} \\ bq_z & c_{\text{TO}} & . \end{pmatrix} \quad j_1 = F_2(\text{TO}_x),$$

$$\begin{pmatrix} . & . & c_{\text{TO}} \\ . & . & bq_z \\ c_{\text{TO}} & bq_z & . \end{pmatrix} \quad j_2 = F_2(\text{TO}_y),$$

$$\begin{pmatrix} aq_z & c_{\text{LO}} & . \\ c_{\text{LO}} & aq_z & . \\ . & . & dq_z \end{pmatrix} \quad j_3 = F_2(\text{LO}_z).$$

The difference in the parameters c_{TO} and c_{LO} is due to the electro-optic contribution to the Raman tensor for the LO mode. In the back-scattering geometry for scattering from the (001) face of the crystal, only the LO_z modes can take part. Intrinsic allowed components $|c_{\text{LO}}|^2$ are observable in the crossed (xy) polarization geometry, whereas the \mathbf{q} -dependent terms $|aq_z|^2$ appear as ‘forbidden’ scattering in parallel (xx) or (yy) geometries.

2.3.6. Higher-order scattering

In higher-order processes, the scattering involves participation of two or more quanta (j and j') of the elementary excitations. Let us discuss briefly the second-order scattering by phonons, where the energy and wavevector conservation conditions read

2.3. RAMAN SCATTERING

$$\begin{aligned}\omega_I - \omega_S &= \omega = \pm\omega_j \pm \omega_{j'}, \\ \mathbf{k}_I - \mathbf{k}_S &= \mathbf{q} = \pm\mathbf{q}_j \pm \mathbf{q}_{j'}.\end{aligned}\quad (2.3.6.1)$$

The combinations of signs in these equations correspond to four possibilities, in which either both phonons, j and j' , are created (Stokes process: ++), both annihilated (anti-Stokes process: --), or one is created and the other annihilated (difference process: +-, -+). If in the Stokes or anti-Stokes case both excitations are of the same type, $j = j'$, one speaks of *overtones*. The corresponding terms in the transition susceptibility are the coefficients of a bilinear combination of normal coordinates in the expansion of $\delta\chi$.

In the quasi-static limit, the transition susceptibilities for the second-order scattering correspond, again, to the susceptibility derivatives. Thus, the spectral differential cross section for the second-order scattering (Stokes component) can be formally written as

$$\begin{aligned}\frac{d^2\sigma}{d\omega d\Omega} &\approx \sum_{\substack{j,j' \\ \mathbf{q}_j + \mathbf{q}_{j'} = \mathbf{q} \approx 0}} \left| e_{S\alpha} \frac{\partial^2 \chi_{\alpha\beta}}{\partial Q_j^*(\mathbf{q}_j) \partial Q_{j'}^*(\mathbf{q}_{j'})} e_{I\beta} \right|^2 \\ &\times \delta[\omega_j(\mathbf{q}_j) + \omega_{j'}(\mathbf{q}_{j'}) - \omega],\end{aligned}$$

with $\omega = \omega_I - \omega_S > 0$. In this formula, we have suppressed the universal factors [see (2.3.3.5)] and the explicit expression for the response function (thermal factors). Instead, the *delta* function (response function in the limit of zero damping) expresses the energy-conservation condition.

The wavevector selection rules in the long-wavelength limit, with $\mathbf{q} = 0$, imply that $\mathbf{q}_j = -\mathbf{q}_{j'}$ (the same holds for anti-Stokes components, while $\mathbf{q}_j = \mathbf{q}_{j'}$ for difference scattering), so the wavevectors themselves need not be small and, in principle, scattering by phonons with all wavevectors from the Brillouin zone can be observed.

Without invoking any symmetry arguments for the Raman activity, such as the restrictions imposed by crystal symmetry on the susceptibility derivatives, it is clear that the intensity of second-order scattering at a frequency ω is controlled by the number of those combinations of phonons whose frequencies obey $\omega = \omega_j(\mathbf{q}) + \omega_{j'}(-\mathbf{q})$. The quantity determining this number is the combined density of states of phonon pairs, *i.e.*

$$\rho_2(\omega) = \sum_{j,j'} \sum_{\mathbf{q}} \delta[\omega_j(\mathbf{q}) + \omega_{j'}(-\mathbf{q}) - \omega]. \quad (2.3.6.2)$$

This function can be calculated provided the *dispersion curves* $\omega_j(\mathbf{q})$ of the excitations are known. The density of states is a continuous function and shows features known as the van Hove singularities corresponding to the *critical points*, where one or more components of the gradient $\nabla_{\mathbf{q}}[\omega_j(\mathbf{q}) + \omega_{j'}(-\mathbf{q})]$ vanish. Most of the critical points occur for wavevectors on the boundary, where the vanishing gradients of the individual dispersion curves are often dictated by the crystal symmetry, but they also occur in those regions of the reciprocal space where both dispersion curves have opposite or equal slopes at the same wavevector \mathbf{q} . To a first approximation, the second-order spectrum is thus essentially continuous, reflecting the two-phonon density of states, with peaks and sharp features at frequencies close to the positions of the van Hove singularities. This is to be contrasted with the first-order scattering, where (in perfect crystals) only single peaks corresponding to long-wavelength ($\mathbf{q} \approx 0$) phonons occur.

Group-theoretical arguments may again be invoked in deriving the selection rules that determine the Raman activity of a particular combination of excitations (Birman, 1974). The susceptibility derivative again transforms as a tensor. For a given pair of excitations (j, \mathbf{q}) and ($j', -\mathbf{q}$) responsible for the modu-

Table 2.3.6.1. Thermal factors for second-order Raman scattering

$n(\omega)$ is given by (2.3.3.7).

| Factor | Process | Raman shift |
|---|-------------|--------------------------------------|
| $[n(\omega_j) + 1][n(\omega_{j'}) + 1]$ | Stokes | $(\omega = \omega_j + \omega_{j'})$ |
| $[n(\omega_j) + 1]n(\omega_{j'})$ | Difference | $(\omega = \omega_j - \omega_{j'})$ |
| $n(\omega_j)n(\omega_{j'})$ | Anti-Stokes | $(\omega = -\omega_j - \omega_{j'})$ |

lation, the combined excitation symmetry is obtained by taking the direct product of the irreducible representations of the space group corresponding to the participating excitations,

$$\Gamma(j, j') = D_{j,\mathbf{q}} \otimes D_{j',-\mathbf{q}}. \quad (2.3.6.3)$$

The representation $\Gamma(j, j')$, unlike $D_{j,\mathbf{q}}$, corresponds to a zero-wavevector representation of the crystal space group and is therefore equivalent to a (reducible) representation of the crystal point group. It can be decomposed into irreducible components. Raman scattering of the pair is allowed if a Raman-active $\mathbf{q} = 0$ representation is contained in this decomposition of $\Gamma(j, j')$ or, alternatively, if the product $[\Gamma_{\text{PV}} \otimes \Gamma_{\text{PV}}]_S \otimes \Gamma(j, j')$ contains the totally symmetric representation $\Gamma(1)$.

The selection rules for the second-order scattering are, in general, far less restrictive than in the first-order case. For example, it can be shown that for a general wavevector \mathbf{q} in the Brillouin zone there are no selection rules on the participation of phonons in the second-order scattering, since the representations $\Gamma(j, j')$ contain all Raman-active symmetries. In specific crystal structures, however, restrictions occur for the wavevectors corresponding to special symmetry positions (points, lines or planes) in the Brillouin zone. This implies that the selection rules may suppress some of the van Hove singularities in the second-order spectra.

Morphic effects in second-order scattering, due to an applied external force \mathbf{F} (see Section 2.3.4.1), may be investigated using the same criteria as in first-order scattering, *i.e.* decomposing the $\mathbf{q} = 0$ representation $\Gamma(\mathbf{F}) \otimes [\Gamma_{\text{PV}} \otimes \Gamma_{\text{PV}}]_S \otimes \Gamma(j, j')$ and searching for the matrix form of the corresponding second-order Raman tensors.

Generalization to third- and higher-order processes is obvious.

Concluding this section, we note that in a Raman-scattering experiment, higher-order features in the spectra can in principle be distinguished from first-order features by different behaviour of the differential scattering cross section with temperature. For example, the respective thermal factors entering the expression for the second-order scattering cross section are given in Table 2.3.6.1.

2.3.7. Conclusions

In this overview of Raman scattering in crystals, we have almost exclusively based our considerations on a phenomenological, semi-classical viewpoint without going into details of the underlying microscopic theory. This is surely an appropriate approach to a discussion of the fundamental consequences of crystal symmetry on the selection rules governing the varied phenomena of inelastic light scattering and on the symmetry-restricted form of the corresponding tensorial quantities encountered in this vast and fruitful field. We have attempted to treat the most important symmetry aspects of the inelastic scattering of light by collective excitations in perfect crystals, concentrating on scattering by optical phonons – in the traditional sense of Raman scattering studies. Within a limited scope, we tried to give some insight into the nature of the phenomena relevant in connection with this topic. Our coverage is certainly not exhaustive (nor original); we have also deliberately omitted all scattering phenomena connected with purely electronic excitations, although the corresponding symmetry aspects can be analysed on the same footing. The essence of the truth is rather simple: As long as the

2. SYMMETRY ASPECTS OF EXCITATIONS

excitations are characterized by *irreducible representations* of the symmetry group of the system, the well proven tools of the theory of representations are at hand to work out the consequences (if common sense does not readily provide the answer).

For an experimental physicist, symmetry analysis is invaluable in designing the experimental arrangement expected to give evidence of some particular phenomenon. The type of answer one may expect from such analysis is characteristic of the group-theoretical predictions. One can learn whether a particular effect is *allowed* or *forbidden*, and – if it is allowed – one can learn *how many* independent coefficients may be needed to describe it. Symmetry analysis alone cannot predict *how large* the effect is, or *why* it occurs, though it may well indicate the way to make it more easily observable. In order to understand or justify its actual magnitude, one has to analyse in greater detail the underlying microphysical mechanisms; however, the analysis must be consistent with restrictions dictated by the symmetry of the problem and, here again, symmetry arguments with powerful group-theoretical tools provide reliable guidance.

For the sake of brevity, citations have been largely suppressed in the present overview. Instead, the relevant sources are included in the list of references.

For detailed information about all the varied aspects of light scattering in solids and recent advances in this vast and fruitful field, the reader is referred to specialized monographs, e.g. Turrell (1972), Hayes & Loudon (1978), and to a comprehensive series edited by Cardona & Güntherodt (1975–).

2.3.8. Glossary

$\alpha, \beta, \gamma, \delta, \dots, \mu, \nu$: Greek indices are used for Cartesian components of vectors and tensors (summation over repeated indices is understood).

| | |
|------------------------------------|---|
| \mathbf{a}_j | atomic displacement Raman tensor of the j th phonon mode, defined as $\partial\chi/\partial Q_j$ |
| \mathbf{b} | susceptibility derivative $\partial\chi/\partial\mathbf{E}$ (closely related to the electro-optic tensor \mathbf{r}) |
| c | velocity of light |
| \mathbf{c} | elastic stiffness tensor |
| \mathbf{d} | piezoelectric tensor |
| χ | susceptibility tensor |
| $\mathbf{e}_{l,s}$ | polarization vector of incident and scattered light |
| $\mathbf{e}_\kappa(\mathbf{q}, j)$ | phonon eigenvector of the j th phonon mode of wavevector \mathbf{q} |
| \mathbf{E} | electric field intensity |
| \mathbf{f} | magneto-optic tensor |

| | |
|--------------------------|---|
| $\gamma_{j,\mathbf{q}}$ | damping constant of mode (j, \mathbf{q}) |
| \mathbf{H} | magnetic field intensity |
| ϵ_0 | permittivity of free space |
| $\boldsymbol{\epsilon}$ | permittivity tensor |
| $\mathbf{k}_{l,s}$ | wavevector of incident and scattered light |
| $n_{l,s}$ | refractive index for incident and scattered light |
| \mathbf{P} | polarization |
| \mathbf{q} | phonon wavevector |
| $Q_j(\mathbf{q})$ | normal coordinate (amplitude of the j th phonon mode of wavevector \mathbf{q}) |
| \mathbf{R}^j | Raman tensor of j th phonon mode |
| \mathbf{S} | strain tensor |
| \mathbf{T} | stress tensor |
| σ | scattering cross section |
| ω | angular frequency |
| $\mathbf{Z}(\mathbf{q})$ | effective charge matrix |

References

- Agranovich, V. M. & Ginzburg, V. L. (1984). *Crystal optics with spatial dispersion, and excitons*. Berlin, Heidelberg, New York, Tokyo: Springer.
- Anastassakis, E. M. (1980). In *Dynamical properties of solids*, edited by G. K. Horton & A. A. Maradudin, Vol. 4, pp. 159–375. Amsterdam, New York, Oxford: North-Holland.
- Birman, J. L. (1974). *Theory of crystal space groups and infrared and Raman lattice processes of insulating crystals*. *Handbuch der Physik*, Vol. 25/2b. Berlin, Heidelberg, New York: Springer.
- Burstein, E. & Pinczuk, A. (1971). *The physics of opto-electronic materials*, edited by W. A. Albers, pp. 33–79. New York: Plenum Press.
- Callen, H. (1968). *Crystal symmetry and macroscopic laws*. *Am. J. Phys.* **36**, 735–748.
- Cardona, M. & Güntherodt, G. (1975–). Editors. *Light scattering in solids*, Vols. I–IV. Berlin, Heidelberg, New York, Tokyo: Springer.
- Claus, R., Merten, L. & Brandmüller, J. (1975). *Light scattering by phonon-polaritons*. Berlin, Heidelberg, New York: Springer.
- Hayes, W. & Loudon, R. (1978). *Scattering of light by crystals*. New York: John Wiley & Sons.
- Lax, M. J. (1974). *Symmetry principles in solid state and molecular physics*. New York: John Wiley & Sons.
- Nye, J. F. (1964). *Physical properties of crystals*. Oxford: Clarendon Press.
- Poulet, H. & Mathieu, J. P. (1976). *Vibration spectra and symmetry of crystals*. Paris: Gordon & Breach.
- Rousseau, D. L., Bauman, R. P. & Porto, S. P. S. (1981). *Normal mode determination in crystals*. *J. Raman Spectrosc.* **10**, 253–290.
- Turrell, G. (1972). *Infrared and Raman spectra of crystals*. London, New York: Academic Press.

2.4. Brillouin scattering

BY R. VACHER AND E. COURTENS

2.4.1. Introduction

Brillouin scattering originates from the interaction of an incident radiation with thermal acoustic vibrations in matter. The phenomenon was predicted by Brillouin in 1922 (Brillouin, 1922) and first observed in light scattering by Gross (Gross, 1930a,b). However, owing to specific spectrometric difficulties, precise experimental studies of Brillouin lines in crystals were not performed until the 1960s (Cecchi, 1964; Benedek & Fritsch, 1966; Gornall & Stoicheff, 1970) and Brillouin scattering became commonly used for the investigation of elastic properties of condensed matter with the advent of laser sources and multipass Fabry–Perot interferometers (Hariharan & Sen, 1961; Sandercock, 1971). More recently, Brillouin scattering of neutrons (Egelstaff *et al.*, 1989) and X-rays (Sette *et al.*, 1998) has been observed.

Brillouin scattering of light probes long-wavelength acoustic phonons. Thus, the detailed atomic structure is irrelevant and the vibrations of the scattering medium are determined by macroscopic parameters, in particular the density ρ and the elastic coefficients c_{ijkl} . For this reason, Brillouin scattering is observed in gases, in liquids and in crystals as well as in disordered solids.

Vacher & Boyer (1972) and Cummins & Schoen (1972) have performed a detailed investigation of the selection rules for Brillouin scattering in materials of various symmetries. In this chapter, calculations of the sound velocities and scattered intensities for the most commonly investigated vibrational modes in bulk condensed matter are presented. Brillouin scattering from surfaces will not be discussed. The current state of the art for Brillouin spectroscopy is also briefly summarized.

2.4.2. Elastic waves

2.4.2.1. Non-piezoelectric media

The fundamental equation of dynamics (see Section 1.3.4.2), applied to the displacement \mathbf{u} of an elementary volume at \mathbf{r} in a homogeneous material is

$$\rho \ddot{\mathbf{u}}_i = \frac{\partial T_{ij}}{\partial x_j}. \quad (2.4.2.1)$$

Summation over repeated indices will always be implied, and \mathbf{T} is the stress tensor. In non-piezoelectric media, the constitutive equation for small strains \mathbf{S} is simply

$$T_{ij} = c_{ijkl} S_{kl}. \quad (2.4.2.2)$$

The strain being the symmetrized spatial derivative of \mathbf{u} , and \mathbf{c} being symmetric upon interchange of k and ℓ , the introduction of (2.4.2.2) in (2.4.2.1) gives (see also Section 1.3.4.2)

$$\rho \ddot{\mathbf{u}}_i = c_{ijkl} \frac{\partial^2 \mathbf{u}_k}{\partial x_j \partial x_\ell}. \quad (2.4.2.3)$$

One considers harmonic plane-wave solutions of wavevector \mathbf{Q} and frequency ω ,

$$\mathbf{u}(\mathbf{r}, t) = \mathbf{u}_0 \exp i(\mathbf{Q} \cdot \mathbf{r} - \omega t). \quad (2.4.2.4)$$

For \mathbf{u}_0 small compared with the wavelength $2\pi/Q$, the total derivative $\ddot{\mathbf{u}}$ can be replaced by the partial $\partial^2 \mathbf{u} / \partial t^2$ in (2.4.2.3). Introducing (2.4.2.4) into (2.4.2.3), one obtains

$$c_{ijkl} \hat{\mathbf{Q}}_j \hat{\mathbf{Q}}_\ell \mathbf{u}_{0k} = C \delta_{ik} \mathbf{u}_{0k}, \quad (2.4.2.5)$$

where $\hat{\mathbf{Q}} = \mathbf{Q}/|\mathbf{Q}|$ is the unit vector in the propagation direction, δ_{ik} is the unit tensor and $C \equiv \rho V^2$, where $V = \omega/|\mathbf{Q}|$ is the phase velocity of the wave. This shows that \mathbf{u}_0 is an eigenvector of the tensor $c_{ijkl} \hat{\mathbf{Q}}_j \hat{\mathbf{Q}}_\ell$. For a given propagation direction \mathbf{Q} , the three eigenvalues $C^{(s)}$ are obtained by solving

$$\left| c_{ijkl} \hat{\mathbf{Q}}_j \hat{\mathbf{Q}}_\ell - C \delta_{ik} \right| = 0. \quad (2.4.2.6)$$

To each $C^{(s)}$ there is an eigenvector $\mathbf{u}^{(s)}$ given by (2.4.2.5) and an associated phase velocity

$$V^{(s)} = \sqrt{C^{(s)}/\rho}. \quad (2.4.2.7)$$

The tensor $c_{ijkl} \hat{\mathbf{Q}}_j \hat{\mathbf{Q}}_\ell$ is symmetric upon interchange of the indices (i, k) because $c_{ijkl} = c_{klij}$. Its eigenvalues are real positive, and the three directions of vibration $\hat{\mathbf{u}}^{(s)}$ are mutually perpendicular. The notation $\hat{\mathbf{u}}^{(s)}$ indicates a unit vector. The tensor $c_{ijkl} \hat{\mathbf{Q}}_j \hat{\mathbf{Q}}_\ell$ is also invariant upon a change of sign of the propagation direction. This implies that the solution of (2.4.2.5) is the same for all symmetry classes belonging to the same Laue class.

For a general direction $\hat{\mathbf{Q}}$, and for a symmetry lower than isotropic, $\hat{\mathbf{u}}^{(s)}$ is neither parallel nor perpendicular to $\hat{\mathbf{Q}}$, so that the modes are neither purely longitudinal nor purely transverse. In this case (2.4.2.6) is also difficult to solve. The situation is much simpler when $\hat{\mathbf{Q}}$ is parallel to a symmetry axis of the Laue class. Then, one of the vibrations is purely longitudinal (LA), while the other two are purely transverse (TA). A pure mode also exists when $\hat{\mathbf{Q}}$ belongs to a symmetry plane of the Laue class, in which case there is a transverse vibration with $\hat{\mathbf{u}}$ perpendicular to the symmetry plane. For all these *pure mode directions*, (2.4.2.6) can be factorized to obtain simple analytical solutions. In this chapter, only pure mode directions are considered.

2.4.2.2. Piezoelectric media

In piezoelectric crystals, a stress component is also produced by the internal electric field \mathbf{E} , so that the constitutive equation (2.4.2.2) has an additional term (see Section 1.1.5.2),

$$T_{ij} = c_{ijkl} S_{kl} - e_{mij} E_m, \quad (2.4.2.8)$$

where \mathbf{e} is the piezoelectric tensor at constant strain.

The electrical displacement vector \mathbf{D} , related to \mathbf{E} by the dielectric tensor $\boldsymbol{\epsilon}$, also contains a contribution from the strain,

$$\mathbf{D}_m = \epsilon_{mn} E_n + e_{mkl} S_{kl}, \quad (2.4.2.9)$$

where $\boldsymbol{\epsilon}$ is at the frequency of the elastic wave.

In the absence of free charges, $\text{div } \mathbf{D} = 0$, and (2.4.2.9) provides a relation between \mathbf{E} and \mathbf{S} ,

$$\epsilon_{mn} Q_n E_m + e_{mkl} Q_m S_{kl} = 0. \quad (2.4.2.10)$$

For long waves, it can be shown that \mathbf{E} and \mathbf{Q} are parallel. (2.4.2.10) can then be solved for \mathbf{E} , and this value is replaced in (2.4.2.8) to give

$$T_{ij} = \left[c_{ijkl} + \frac{e_{mij} e_{nkl} \hat{\mathbf{Q}}_m \hat{\mathbf{Q}}_n}{\epsilon_{gh} \hat{\mathbf{Q}}_g \hat{\mathbf{Q}}_h} \right] S_{kl} \equiv c_{ijkl}^{(e)} S_{kl}. \quad (2.4.2.11)$$

2. SYMMETRY ASPECTS OF EXCITATIONS

Comparing (2.4.2.11) and (2.4.2.2), one sees that the effective elastic tensor $\mathbf{c}^{(e)}$ now depends on the propagation direction \mathbf{Q} . Otherwise, all considerations of the previous section, starting from (2.4.2.6), remain, with \mathbf{c} simply replaced by $\mathbf{c}^{(e)}$.

2.4.3. Coupling of light with elastic waves

2.4.3.1. Direct coupling to displacements

The change in the relative optical dielectric tensor κ produced by an elastic wave is usually expressed in terms of the strain, using the Pockels piezo-optic tensor \mathbf{p} , as

$$(\Delta\kappa^{-1})_{ij} = p_{ijk\ell} S_{k\ell}. \quad (2.4.3.1)$$

The elastic wave should, however, be characterized by both strain \mathbf{S} and rotation \mathbf{A} (Nelson & Lax, 1971; see also Section 1.3.1.3):

$$A_{[k\ell]} = \frac{1}{2} \left(\frac{\partial u_k}{\partial x_\ell} - \frac{\partial u_\ell}{\partial x_k} \right). \quad (2.4.3.2)$$

The square brackets on the left-hand side are there to emphasize that the component is antisymmetric upon interchange of the indices, $A_{[k\ell]} = -A_{[\ell k]}$. For birefringent crystals, the rotations induce a change of the local κ in the laboratory frame. In this case, (2.4.3.1) must be replaced by

$$(\Delta\kappa^{-1})_{ij} = p'_{ijk\ell} \frac{\partial u_k}{\partial x_\ell}, \quad (2.4.3.3)$$

where \mathbf{p}' is the new piezo-optic tensor given by

$$p'_{ijk\ell} = p_{ijk\ell} + p_{ij[k\ell]}. \quad (2.4.3.4)$$

One finds for the rotational part

$$p_{ij[k\ell]} = \frac{1}{2} [(\kappa^{-1})_{ik} \delta_{\ell j} + (\kappa^{-1})_{\ell j} \delta_{ik} - (\kappa^{-1})_{ik} \delta_{\ell j} - (\kappa^{-1})_{\ell j} \delta_{ik}]. \quad (2.4.3.5)$$

If the principal axes of the dielectric tensor coincide with the crystallographic axes, this gives

$$p_{ij[k\ell]} = \frac{1}{2} (\delta_{i\ell} \delta_{kj} - \delta_{ik} \delta_{\ell j}) (1/n_i^2 - 1/n_j^2). \quad (2.4.3.6)$$

This is the expression used in this chapter, as monoclinic and triclinic groups are not listed in the tables below.

For the calculation of the Brillouin scattering, it is more convenient to use

$$(\Delta\kappa)_{mn} = -\kappa_{mi} \kappa_{nj} p'_{ijk\ell} \frac{\partial u_k}{\partial x_\ell}, \quad (2.4.3.7)$$

which is valid for small $\Delta\kappa$.

2.4.3.2. Coupling via the electro-optic effect

Piezoelectric media also exhibit an electro-optic effect linear in the applied electric field or in the field-induced crystal polarization. This effect is described in terms of the third-rank electro-optic tensor \mathbf{r} defined by

$$(\Delta\kappa^{-1})_{ij} = r_{ijm} E_m. \quad (2.4.3.8)$$

Using the same approach as in (2.4.2.10), for long waves E_m can be expressed in terms of $S_{k\ell}$, and (2.4.3.8) leads to an effective Pockels tensor \mathbf{p}^e accounting for both the piezo-optic and the electro-optic effects:

$$p_{ijk\ell}^e = p_{ijk\ell} - \frac{r_{ijm} e_{nkl} \hat{Q}_m \hat{Q}_n}{\epsilon_{gh} \hat{Q}_g \hat{Q}_h}. \quad (2.4.3.9)$$

The total change in the inverse dielectric tensor is then

$$(\Delta\kappa^{-1})_{ij} = (p_{ijk\ell}^e + p_{ij[k\ell]}) \frac{\partial u_k}{\partial x_\ell} = p'_{ijk\ell} \frac{\partial u_k}{\partial x_\ell}. \quad (2.4.3.10)$$

The same equation (2.4.3.7) applies.

2.4.4. Brillouin scattering in crystals

2.4.4.1. Kinematics

Brillouin scattering occurs when an incident photon at frequency ν_i interacts with the crystal to either produce or absorb an acoustic phonon at $\delta\nu$, while a scattered photon at ν_s is simultaneously emitted. Conservation of energy gives

$$\delta\nu = \nu_s - \nu_i, \quad (2.4.4.1)$$

where positive $\delta\nu$ corresponds to the anti-Stokes process. Conservation of momentum can be written

$$\mathbf{Q} = \mathbf{k}_s - \mathbf{k}_i, \quad (2.4.4.2)$$

where \mathbf{Q} is the wavevector of the emitted phonon, and $\mathbf{k}_s, \mathbf{k}_i$ are those of the scattered and incident photons, respectively. One can define unit vectors \mathbf{q} in the direction of the wavevectors \mathbf{k} by

$$\mathbf{k}_i = 2\pi \mathbf{q} n / \lambda_0, \quad (2.4.4.3a)$$

$$\mathbf{k}_s = 2\pi \mathbf{q}' n' / \lambda_0, \quad (2.4.4.3b)$$

where n and n' are the appropriate refractive indices, and λ_0 is the vacuum wavelength of the radiation. Equation (2.4.4.3b) assumes that $\delta\nu \ll \nu_i$ so that λ_0 is not appreciably changed in the scattering. The incident and scattered waves have unit polarization vectors \mathbf{e} and \mathbf{e}' , respectively, and corresponding indices n and n' . The polarization vectors are the principal directions of vibration derived from the sections of the ellipsoid of indices by planes perpendicular to \mathbf{q} and \mathbf{q}' , respectively. We assume that the electric vector of the light field \mathbf{E}_{opt} is parallel to the displacement \mathbf{D}_{opt} . This is exactly true for many cases listed in the tables below. In the other cases (such as skew directions in the orthorhombic group) this assumes that the birefringence is sufficiently small for the effect of the angle between \mathbf{E}_{opt} and \mathbf{D}_{opt} to be negligible. A full treatment, including this effect, has been given by Nelson *et al.* (1972).

After substituting (2.4.4.3) in (2.4.4.2), the unit vector in the direction of the phonon wavevector is given by

$$\hat{\mathbf{Q}} = \frac{n' \mathbf{q}' - n \mathbf{q}}{|n' \mathbf{q}' - n \mathbf{q}|}. \quad (2.4.4.4)$$

The Brillouin shift $\delta\nu$ is related to the phonon velocity V by

$$\delta\nu = VQ/2\pi. \quad (2.4.4.5)$$

Since $\nu\lambda_0 = c$, from (2.4.4.5) and (2.4.4.3), (2.4.4.4) one finds

$$\delta\nu \cong (V/\lambda_0) [n^2 + (n')^2 - 2nn' \cos \theta]^{1/2}, \quad (2.4.4.6)$$

where θ is the angle between \mathbf{q} and \mathbf{q}' .

2.4.4.2. Scattering cross section

The power dP_{in} , scattered from the illuminated volume V in a solid angle $d\Omega_{\text{in}}$, where P_{in} and Ω_{in} are measured inside the sample, is given by

$$\frac{dP_{\text{in}}}{d\Omega_{\text{in}}} = V \frac{k_B T \pi^2 n'}{2n\lambda_0^4 C} M I_{\text{in}}, \quad (2.4.4.7)$$

where I_{in} is the incident light intensity inside the material, $C = \rho V^2$ is the appropriate elastic constant for the observed phonon, and the factor $k_B T$ results from taking the fluctuation-

2.4. BRILLOUIN SCATTERING

dissipation theorem in the classical limit for $h\delta\nu \ll k_B T$ (Hayes & Loudon, 1978). The coupling coefficient M is given by

$$M = |e_m e'_n \kappa_{mi} \kappa_{nj} p'_{ijk\ell} \hat{\mathbf{u}}_k \hat{\mathbf{Q}}_\ell|^2. \quad (2.4.4.8)$$

In practice, the incident intensity is defined outside the scattering volume, I_{out} , and for normal incidence one can write

$$I_{\text{in}} = \frac{4n}{(n+1)^2} I_{\text{out}}. \quad (2.4.4.9a)$$

Similarly, the scattered power is observed outside as P_{out} , and

$$P_{\text{out}} = \frac{4n'}{(n'+1)^2} P_{\text{in}}, \quad (2.4.4.9b)$$

again for normal incidence. Finally, the approximative relation between the scattering solid angle Ω_{out} , outside the sample, and the solid angle Ω_{in} , in the sample, is

$$\Omega_{\text{out}} = (n')^2 \Omega_{\text{in}}. \quad (2.4.4.9c)$$

Substituting (2.4.4.9a,b,c) in (2.4.4.7), one obtains (Vacher & Boyer, 1972)

$$\frac{dP_{\text{out}}}{d\Omega_{\text{out}}} = \frac{8\pi^2 k_B T}{\lambda_0^4} \frac{n^4}{(n+1)^2} \frac{(n')^4}{(n'+1)^2} \beta V I_{\text{out}}, \quad (2.4.4.10)$$

where the coupling coefficient β is

$$\beta = \frac{1}{n^4 (n')^4} \frac{|e_m e'_n \kappa_{mi} \kappa_{nj} p'_{ijk\ell} \hat{\mathbf{u}}_k \hat{\mathbf{Q}}_\ell|^2}{C}. \quad (2.4.4.11)$$

In the cases of interest here, the tensor κ is diagonal, $\kappa_{ij} = n_i^2 \delta_{ij}$ without summation on i , and (2.4.4.11) can be written in the simpler form

$$\beta = \frac{1}{n^4 (n')^4} \frac{|e_i n_i^2 p'_{ijk\ell} \hat{\mathbf{u}}_k \hat{\mathbf{Q}}_\ell e'_j n_j'^2|^2}{C}. \quad (2.4.4.12)$$

2.4.5. Use of the tables

The tables in this chapter give information on modes and scattering geometries that are in most common use in the study of hypersound in single crystals. Just as in the case of X-rays, Brillouin scattering is not sensitive to the presence or absence of a centre of symmetry (Friedel, 1913). Hence, the results are the same for all crystalline classes belonging to the same centric group, also called Laue class. The correspondence between the point groups and the Laue classes analysed here is shown in Table 2.4.5.1. The monoclinic and triclinic cases, being too cumbersome, will not be treated here.

For tensor components $c_{ijk\ell}$ and $p_{ijk\ell}$, the tables make use of the usual contracted notation for index pairs running from 1 to 6. However, as the tensor $p'_{ijk\ell}$ is not symmetric upon interchange of (k, ℓ) , it is necessary to distinguish the order (k, ℓ) and (ℓ, k) . This is accomplished with the following correspondence:

$$\begin{aligned} 1, 1 &\rightarrow 1 & 2, 2 &\rightarrow 2 & 3, 3 &\rightarrow 3 \\ 1, 2 &\rightarrow 6 & 2, 3 &\rightarrow 4 & 3, 1 &\rightarrow 5 \\ 2, 1 &\rightarrow \bar{6} & 3, 2 &\rightarrow \bar{4} & 1, 3 &\rightarrow \bar{5}. \end{aligned}$$

Geometries for longitudinal modes (LA) are listed in Tables 2.4.5.2 to 2.4.5.8. The first column gives the direction of the scattering vector $\hat{\mathbf{Q}}$ that is parallel to the displacement $\hat{\mathbf{u}}$. The second column gives the elastic coefficient according to (2.4.2.6). In piezoelectric materials, effective elastic coefficients defined in (2.4.2.11) must be used in this column. The third column gives the direction of the light polarizations $\hat{\mathbf{e}}$ and $\hat{\mathbf{e}}'$, and the last column

gives the corresponding coupling coefficient β [equation (2.5.5.11)]. In general, the strongest scattering intensity is obtained for polarized scattering ($\hat{\mathbf{e}} = \hat{\mathbf{e}}'$), which is the only situation listed in the tables. In this case, the coupling to light (β) is independent of the scattering angle θ , and thus the tables apply to any θ value.

Tables 2.4.5.9 to 2.4.5.15 list the geometries usually used for the observation of TA modes in backscattering ($\theta = 180^\circ$). In this case, $\hat{\mathbf{u}}$ is always perpendicular to $\hat{\mathbf{Q}}$ (pure transverse modes), and $\hat{\mathbf{e}}'$ is not necessarily parallel to $\hat{\mathbf{e}}$. Cases where pure TA modes with $\hat{\mathbf{u}}$ in the plane perpendicular to $\hat{\mathbf{Q}}$ are degenerate are indicated by the symbol D in the column for $\hat{\mathbf{u}}$. For the Pockels tensor components, the notation is $p_{\alpha\beta}$ if the rotational term vanishes by symmetry, and it is $p'_{\alpha\beta}$ otherwise.

Tables 2.4.5.16 to 2.4.5.22 list the common geometries used for the observation of TA modes in 90° scattering. In these tables, the polarization vector $\hat{\mathbf{e}}$ is always perpendicular to the scattering plane and $\hat{\mathbf{e}}'$ is always parallel to the incident wavevector of light \mathbf{q} . Owing to birefringence, the scattering vector $\hat{\mathbf{Q}}$ does not exactly bisect \mathbf{q} and \mathbf{q}' [equation (2.4.4.4)]. The tables are written for strict 90° scattering, $\mathbf{q} \cdot \mathbf{q}' = 0$, and in the case of birefringence the values of $\mathbf{q}^{(m)}$ to be used are listed separately in Table 2.4.5.23. The latter assumes that the birefringences are not large, so that the values of $\mathbf{q}^{(m)}$ are given only to first order in the birefringence.

2.4.6. Techniques of Brillouin spectroscopy

Brillouin spectroscopy with visible laser light requires observing frequency shifts falling typically in the range ~ 1 to ~ 100 GHz, or ~ 0.03 to ~ 3 cm^{-1} . To achieve this with good resolution one mostly employs interferometry. For experiments at very small angles (near forward scattering), photocorrelation spectroscopy can also be used. If the observed frequency shifts are ≥ 1 cm^{-1} , rough measurements of spectra can sometimes be obtained with modern grating instruments. Recently, it has also become possible to perform Brillouin scattering using other excitations, in particular neutrons or X-rays. In these cases, the coupling does not occur *via* the Pockels effect, and the frequency shifts that are observed are much larger. The following discussion is restricted to optical interferometry.

The most common interferometer that has been used for this purpose is the single-pass planar Fabry–Perot (Born & Wolf, 1993). Upon illumination with monochromatic light, the frequency response of this instrument is given by the Airy function, which consists of a regular comb of maxima obtained as the optical path separating the mirrors is increased. Successive maxima are separated by $\lambda/2$. The ratio of the maxima separation to the width of a single peak is called the finesse F , which increases as the mirror reflectivity increases. The finesse is also limited by the planarity of the mirrors. A practical limit is $F \sim 100$. The resolving power of such an instrument is $R = 2\ell/\lambda$, where ℓ is the optical thickness. Values of R around 10^6 to 10^7 can be achieved. It is impractical to increase ℓ above ~ 5 cm because the luminosity of the instrument is proportional to $1/\ell$. If higher

Table 2.4.5.1. Definition of Laue classes

| Crystal system | Laue class | Point groups |
|----------------|----------------|--|
| Cubic | C_1 C_2 | 432, $\bar{4}3m$, $m\bar{3}m$ 23, $\bar{3}m$ |
| Hexagonal | H_1 H_2 | 622, $6mm$, $\bar{6}2m$, $6/mmm$ 6, $\bar{6}$, $6/m$ |
| Tetragonal | T_1 T_2 | 422, $4mm$, $\bar{4}2m$, $4/mmm$ 4, $\bar{4}$, $4/m$ |
| Trigonal | R_1 R_2 | 32, $3m$, $\bar{3}m$ 3, $\bar{3}$ |
| Orthorhombic | O | mmm , $2mm$, 222 |

2. SYMMETRY ASPECTS OF EXCITATIONS

Table 2.4.5.2. Cubic Laue classes C_1 and C_2 : longitudinal modes

This table, written for the class C_2 , is also valid for the class C_1 with the additional relation $p_{12} = p_{13}$. It can also be used for the spherical system where $c_{44} = \frac{1}{2}(c_{11} - c_{12})$, $p_{44} = \frac{1}{2}(p_{11} - p_{12})$.

| $\hat{\mathbf{Q}} = \hat{\mathbf{u}}$ | C | $\mathbf{e} = \mathbf{e}'$ | β |
|---------------------------------------|---|----------------------------|---|
| (1, 0, 0) | c_{11} | (0, 1, 0) | p_{13}^2/c_{11} |
| (1, 0, 0) | c_{11} | (0, 0, 1) | p_{12}^2/c_{11} |
| (1, 1, 0)/ $\sqrt{2}$ | $\frac{1}{2}(c_{11} + c_{12}) + c_{44}$ | (0, 0, 1) | $(p_{12} + p_{13})^2/4C$ |
| (1, 1, 0)/ $\sqrt{2}$ | $\frac{1}{2}(c_{11} + c_{12}) + c_{44}$ | (1, -1, 0)/ $\sqrt{2}$ | $(2p_{11} + p_{12} + p_{13} - 4p_{44})^2/16C$ |
| (1, 1, 1)/ $\sqrt{3}$ | $\frac{1}{3}(c_{11} + 2c_{12} + 4c_{44})$ | (1, 1, -2)/ $\sqrt{6}$ | $(p_{11} + p_{12} + p_{13} - 2p_{44})^2/9C$ |
| (1, 1, 1)/ $\sqrt{3}$ | $\frac{1}{3}(c_{11} + 2c_{12} + 4c_{44})$ | (1, -1, 0)/ $\sqrt{2}$ | $(p_{11} + p_{12} + p_{13} - 2p_{44})^2/9C$ |

Table 2.4.5.3. Tetragonal T_1 and hexagonal H_1 Laue classes: longitudinal modes

This table, written for the class T_1 , is also valid for the class H_1 with the additional relations $c_{66} = \frac{1}{2}(c_{11} - c_{12})$; $p_{66} = \frac{1}{2}(p_{11} - p_{12})$.

| $\hat{\mathbf{Q}} = \hat{\mathbf{u}}$ | C | $\mathbf{e} = \mathbf{e}'$ | β |
|---------------------------------------|---|----------------------------|------------------------------------|
| (1, 0, 0) | c_{11} | (0, 1, 0) | p_{12}^2/c_{11} |
| (1, 0, 0) | c_{11} | (0, 0, 1) | p_{31}^2/c_{11} |
| (0, 0, 1) | c_{33} | (1, 0, 0) | p_{13}^2/c_{33} |
| (0, 0, 1) | c_{33} | (0, 1, 0) | p_{12}^2/c_{33} |
| (1, 1, 0)/ $\sqrt{2}$ | $\frac{1}{2}(c_{11} + c_{12}) + c_{66}$ | (0, 0, 1) | p_{31}^2/C |
| (1, 1, 0)/ $\sqrt{2}$ | $\frac{1}{2}(c_{11} + c_{12}) + c_{66}$ | (1, -1, 0)/ $\sqrt{2}$ | $(p_{11} + p_{12} - 2p_{66})^2/4C$ |

Table 2.4.5.4. Hexagonal Laue class H_2 : longitudinal modes

| $\hat{\mathbf{Q}} = \hat{\mathbf{u}}$ | C | $\mathbf{e} = \mathbf{e}'$ | β |
|---------------------------------------|----------|----------------------------|-------------------|
| (1, 0, 0) | c_{11} | (0, 1, 0) | p_{12}^2/c_{11} |
| (1, 0, 0) | c_{11} | (0, 0, 1) | p_{31}^2/c_{11} |
| (0, 0, 1) | c_{33} | (1, 0, 0) | p_{13}^2/c_{33} |
| (0, 0, 1) | c_{33} | (0, 1, 0) | p_{12}^2/c_{33} |
| (1, 1, 0)/ $\sqrt{2}$ | c_{11} | (0, 0, 1) | p_{31}^2/c_{11} |
| (1, 1, 0)/ $\sqrt{2}$ | c_{11} | (1, -1, 0)/ $\sqrt{2}$ | p_{12}^2/c_{11} |

Table 2.4.5.5. Tetragonal Laue class T_2 : longitudinal modes

| $\hat{\mathbf{Q}} = \hat{\mathbf{u}}$ | C | $\mathbf{e} = \mathbf{e}'$ | β |
|---------------------------------------|----------|----------------------------|-------------------|
| (0, 0, 1) | c_{33} | (1, 0, 0) | p_{13}^2/c_{33} |
| (0, 0, 1) | c_{33} | (0, 1, 0) | p_{12}^2/c_{33} |

Table 2.4.5.6. Orthorhombic Laue class O : longitudinal modes

| $\hat{\mathbf{Q}} = \hat{\mathbf{u}}$ | C | $\mathbf{e} = \mathbf{e}'$ | β |
|---------------------------------------|----------|----------------------------|-------------------|
| (1, 0, 0) | c_{11} | (0, 1, 0) | p_{21}^2/c_{11} |
| (1, 0, 0) | c_{11} | (0, 0, 1) | p_{31}^2/c_{11} |
| (0, 1, 0) | c_{22} | (0, 0, 1) | p_{32}^2/c_{22} |
| (0, 1, 0) | c_{22} | (1, 0, 0) | p_{12}^2/c_{22} |
| (0, 0, 1) | c_{33} | (1, 0, 0) | p_{13}^2/c_{33} |
| (0, 0, 1) | c_{33} | (0, 1, 0) | p_{23}^2/c_{33} |

Table 2.4.5.7. Trigonal Laue class R_1 : longitudinal modes

| $\hat{\mathbf{Q}} = \hat{\mathbf{u}}$ | C | \mathbf{e} | \mathbf{e}' | β |
|---------------------------------------|----------|--------------|---------------|-------------------|
| (1, 0, 0) | c_{11} | (0, 1, 0) | (0, 1, 0) | p_{12}^2/c_{11} |
| (1, 0, 0) | c_{11} | (0, 0, 1) | (0, 0, 1) | p_{31}^2/c_{11} |
| (1, 0, 0) | c_{11} | (0, 1, 0) | (0, 0, 1) | p_{41}^2/c_{11} |
| (0, 0, 1) | c_{33} | (1, 0, 0) | (1, 0, 0) | p_{13}^2/c_{33} |
| (0, 0, 1) | c_{33} | (0, 1, 0) | (0, 1, 0) | p_{12}^2/c_{33} |

Table 2.4.5.8. Trigonal Laue class R_2 : longitudinal modes

| $\hat{\mathbf{Q}} = \hat{\mathbf{u}}$ | C | \mathbf{e} | \mathbf{e}' | β |
|---------------------------------------|----------|--------------|---------------|-------------------|
| (0, 0, 1) | c_{33} | (1, 0, 0) | (1, 0, 0) | p_{13}^2/c_{33} |
| (0, 0, 1) | c_{33} | (0, 1, 0) | (0, 1, 0) | p_{12}^2/c_{33} |

resolutions are required, one uses a spherical interferometer as described below.

A major limitation of the Fabry–Perot interferometer is its poor contrast, namely the ratio between the maximum and the minimum of the Airy function, which is typically ~ 1000 . This limits the use of this instrument to samples of very high optical quality, as otherwise the generally weak Brillouin signals are masked by the elastically scattered light. To avert this effect, several passes are made through the same instrument, thus elevating the Airy function to the corresponding power (Hariharan & Sen, 1961; Sandercock, 1971). Multiple-pass instruments with three, four or five passes are common. Another limitation of the standard Fabry–Perot interferometer is that the interference pattern is repeated at each order. Hence, if the spectrum has a broad spectral spread, the overlap of adjacent orders can greatly complicate the interpretation of measurements. In this case, tandem instruments can be of considerable help. They consist of two Fabry–Perot interferometers with combs of different periods placed in series (Chantrel, 1959; Mach *et al.*, 1963). These are operated around a position where the peak transmission of the first interferometer coincides with that of the second one. The two Fabry–Perot interferometers are scanned simultaneously. With this setup, the successive orders are reduced to small ghosts and overlap is not a problem. A convenient commercial instrument has been designed by Sandercock (1982).

To achieve higher resolutions, one uses the spherical Fabry–Perot interferometer (Connes, 1958; Hercher, 1968). This consists

of two spherical mirrors placed in a near-confocal configuration. Their spacing ℓ is scanned over a distance of the order of λ . The peculiarity of this instrument is that its luminosity increases with its resolution. One obvious drawback is that a change of resolving power, *i.e.* of ℓ , requires other mirrors. Of course, the single spherical Fabry–Perot interferometer suffers the same limitations regarding contrast and order overlap that were discussed above for the planar case. Multipassing the spherical Fabry–Perot interferometer is possible but not very convenient. It is preferable to use tandem instruments that combine a multipass planar instrument of low resolution followed by a spherical instrument of high resolution (Pine, 1972; Vacher, 1972). To analyse the linewidth of narrow phonon lines, the planar standard is adjusted dynamically to transmit the Brillouin line and the spherical interferometer is scanned across the line. With such a device, resolving powers of $\sim 10^8$ have been achieved. For the dynamical adjustment of this instrument one can use a reference signal near the frequency of the phonon line, which is derived by electro-optic modulation of the exciting laser (Sussner & Vacher, 1979). In this case, not only the width of the phonon, but also its absolute frequency shift, can be determined with an accuracy of ~ 1 MHz. It is obvious that to achieve this kind of resolution, the laser source itself must be appropriately stabilized.

In closing, it should be stressed that the practice of interferometry is still an art that requires suitable skills and training in spite of the availability of commercial instruments. The experimenter must take care of a large number of aspects relating to the

2.4. BRILLOUIN SCATTERING

Table 2.4.5.9. Cubic Laue classes C_1 and C_2 : transverse modes, backscattering

This table, written for the class C_2 , is also valid for the class C_1 with the additional relation $p_{12} = p_{13}$.
It can also be used for the spherical system where $c_{44} = \frac{1}{2}(c_{11} - c_{12})$, $p_{44} = \frac{1}{2}(p_{11} - p_{12})$.

| $\hat{\mathbf{Q}}$ | $\hat{\mathbf{u}}$ | C | \mathbf{e} | \mathbf{e}' | β |
|----------------------|-----------------------|---|-----------------------|-----------------------|--|
| $(1, 1, 0)/\sqrt{2}$ | $(1, -1, 0)/\sqrt{2}$ | $\frac{1}{2}(c_{11} - c_{12})$ | $(0, 0, 1)$ | $(0, 0, 1)$ | $(p_{12} - p_{13})^2/2(c_{11} - c_{12})$ |
| $(1, 1, 1)/\sqrt{3}$ | D | $\frac{1}{3}(c_{11} - c_{12} + c_{44})$ | $(1, 1, -2)/\sqrt{6}$ | $(1, -1, 0)/\sqrt{2}$ | $[3(p_{12} - p_{13})^2 + (p_{12} + p_{13} + 4p_{44} - 2p_{11})^2]/72C$ |

Table 2.4.5.10. Tetragonal T_1 and hexagonal H_1 Laue classes: transverse modes, backscattering

This table, written for the class T_1 , is also valid for the class H_1 with the additional relations $c_{66} = \frac{1}{2}(c_{11} - c_{12})$; $p_{66} = \frac{1}{2}(p_{11} - p_{12})$.

| $\hat{\mathbf{Q}}$ | $\hat{\mathbf{u}}$ | C | \mathbf{e} | \mathbf{e}' | β |
|----------------------|--------------------|--------------------------------|--------------|-----------------------|---|
| $(0, 1, 1)/\sqrt{2}$ | $(1, 0, 0)$ | $\frac{1}{2}(c_{44} + c_{66})$ | $(1, 0, 0)$ | $(0, 1, -1)/\sqrt{2}$ | $[(n_1^2 + n_3^2)^2/16n_1^4n_3^4C](n_1^2p_{66} - n_3^2p'_{44})^2$ |

Table 2.4.5.11. Hexagonal Laue class H_2 : transverse modes, backscattering

$$c_{66} = \frac{1}{2}(c_{11} - c_{12}); p_{66} = \frac{1}{2}(p_{11} - p_{12}).$$

| $\hat{\mathbf{Q}}$ | $\hat{\mathbf{u}}$ | C | \mathbf{e} | \mathbf{e}' | β |
|----------------------|--------------------|--------------------------------|--------------|-----------------------|---|
| $(1, 0, 0)$ | $(0, 1, 0)$ | c_{66} | $(0, 1, 0)$ | $(0, 1, 0)$ | p_{16}^2/c_{66} |
| $(1, 0, 0)$ | $(0, 0, 1)$ | c_{44} | $(0, 1, 0)$ | $(0, 0, 1)$ | p_{45}^2/c_{44} |
| $(0, 1, 1)/\sqrt{2}$ | $(1, 0, 0)$ | $\frac{1}{2}(c_{44} + c_{66})$ | $(1, 0, 0)$ | $(1, 0, 0)$ | $p_{16}^2/(c_{44} + c_{66})$ |
| $(0, 1, 1)/\sqrt{2}$ | $(1, 0, 0)$ | $\frac{1}{2}(c_{44} + c_{66})$ | $(1, 0, 0)$ | $(0, 1, -1)/\sqrt{2}$ | $[(n_1^2 + n_3^2)^2/16n_1^4n_3^4C](n_1^2p_{66} - n_3^2p'_{44})^2$ |

Table 2.4.5.12. Tetragonal Laue class T_2 : transverse modes, backscattering

| $\hat{\mathbf{Q}}$ | $\hat{\mathbf{u}}$ | C | \mathbf{e} | \mathbf{e}' | β |
|----------------------|--------------------|----------|--------------|-----------------------|-------------------|
| $(1, 0, 0)$ | $(0, 0, 1)$ | c_{44} | $(0, 1, 0)$ | $(0, 0, 1)$ | p_{45}^2/c_{44} |
| $(1, 1, 0)/\sqrt{2}$ | $(0, 0, 1)$ | c_{44} | $(0, 0, 1)$ | $(1, -1, 0)/\sqrt{2}$ | p_{45}^2/c_{44} |

Table 2.4.5.13. Orthorhombic Laue class O : transverse modes, backscattering

| $\hat{\mathbf{Q}}$ | $\hat{\mathbf{u}}$ | C | \mathbf{e} | \mathbf{e}' | β |
|----------------------|--------------------|--------------------------------|--------------|-----------------------|--|
| $(1, 1, 0)/\sqrt{2}$ | $(0, 0, 1)$ | $\frac{1}{2}(c_{44} + c_{55})$ | $(0, 0, 1)$ | $(1, -1, 0)/\sqrt{2}$ | $[(n_1^2 + n_2^2)^2/16n_1^4n_2^4C](n_1^2p'_{55} - n_2^2p'_{44})^2$ |
| $(0, 1, 1)/\sqrt{2}$ | $(1, 0, 0)$ | $\frac{1}{2}(c_{55} + c_{66})$ | $(1, 0, 0)$ | $(0, 1, -1)/\sqrt{2}$ | $[(n_2^2 + n_3^2)^2/16n_2^4n_3^4C](n_2^2p'_{66} - n_3^2p'_{55})^2$ |
| $(1, 0, 1)/\sqrt{2}$ | $(0, 1, 0)$ | $\frac{1}{2}(c_{44} + c_{66})$ | $(0, 1, 0)$ | $(-1, 0, 1)/\sqrt{2}$ | $[(n_1^2 + n_3^2)^2/16n_1^4n_3^4C](n_3^2p'_{44} - n_1^2p'_{66})^2$ |

Table 2.4.5.14. Trigonal Laue class R_1 : transverse modes, backscattering

$$c_{66} = \frac{1}{2}(c_{11} - c_{12}); p_{66} = \frac{1}{2}(p_{11} - p_{12}).$$

| $\hat{\mathbf{Q}}$ | $\hat{\mathbf{u}}$ | C | \mathbf{e} | \mathbf{e}' | β |
|-----------------------|--------------------|---|--------------|-----------------------|---|
| $(0, 1, 0)$ | $(1, 0, 0)$ | c_{66} | $(0, 0, 1)$ | $(1, 0, 0)$ | p_{41}^2/c_{66} |
| $(0, 0, 1)$ | D | c_{44} | $(1, 0, 0)$ | $(1, 0, 0)$ | p_{14}^2/c_{44} |
| $(0, 0, 1)$ | D | c_{44} | $(0, 1, 0)$ | $(1, 0, 0)$ | p_{14}^2/c_{44} |
| $(0, 1, 1)/\sqrt{2}$ | $(1, 0, 0)$ | $\frac{1}{2}(c_{44} + c_{66}) + c_{14}$ | $(1, 0, 0)$ | $(0, 1, -1)/\sqrt{2}$ | $[(n_1^2 + n_3^2)^2/16n_1^4n_3^4C][n_1^2(p_{66} + p_{14}) - n_3^2(p'_{44} + p_{41})]^2$ |
| $(0, 1, -1)/\sqrt{2}$ | $(1, 0, 0)$ | $\frac{1}{2}(c_{44} + c_{66}) - c_{14}$ | $(1, 0, 0)$ | $(0, 1, 1)/\sqrt{2}$ | $[(n_1^2 + n_3^2)^2/16n_1^4n_3^4C][n_1^2(p_{66} - p_{14}) + n_3^2(p_{41} - p'_{44})]^2$ |

Table 2.4.5.15. Trigonal Laue class R_2 : transverse modes, backscattering

| $\hat{\mathbf{Q}}$ | $\hat{\mathbf{u}}$ | C | \mathbf{e} | \mathbf{e}' | β |
|--------------------|--------------------|----------|--------------|---------------|--------------------------------|
| $(0, 0, 1)$ | D | c_{44} | $(1, 0, 0)$ | $(1, 0, 0)$ | $(p_{14}^2 + p_{15}^2)/c_{44}$ |
| $(0, 0, 1)$ | D | c_{44} | $(0, 1, 0)$ | $(1, 0, 0)$ | $(p_{14}^2 + p_{15}^2)/c_{44}$ |

2. SYMMETRY ASPECTS OF EXCITATIONS

Table 2.4.5.16. Cubic Laue classes C_1 and C_2 : transverse modes, right-angle scattering

This table, written for the class C_2 , is also valid for the class C_1 with the additional relation $p_{12} = p_{13}$.
It can also be used for the spherical system where $c_{44} = \frac{1}{2}(c_{11} - c_{12})$, $p_{44} = \frac{1}{2}(p_{11} - p_{12})$.

| $\hat{\mathbf{Q}}$ | $\hat{\mathbf{u}}$ | C | Scattering plane | \mathbf{e} | \mathbf{e}' | β |
|-----------------------|-----------------------|--------------------------------|------------------|-----------------------|-----------------------|-------------------------------------|
| (1, 0, 0) | D | c_{44} | (001) | (0, 0, 1) | $(1, -1, 0)/\sqrt{2}$ | $p_{44}^2/2c_{44}$ |
| (1, 0, 0) | D | c_{44} | (010) | (0, 1, 0) | $(1, 0, 1)/\sqrt{2}$ | $p_{44}^2/2c_{44}$ |
| (1, 1, 0)/ $\sqrt{2}$ | (0, 0, 1) | c_{44} | (001) | (0, 0, 1) | (1, 0, 0) | $p_{44}^2/2c_{44}$ |
| (1, 1, 0)/ $\sqrt{2}$ | $(-1, 1, 0)/\sqrt{2}$ | $\frac{1}{2}(c_{11} - c_{12})$ | (001) | (0, 0, 1) | (0, 0, 1) | $(p_{12} - p_{13})^2/4C$ |
| (1, 1, 0)/ $\sqrt{2}$ | $(-1, 1, 0)/\sqrt{2}$ | $\frac{1}{2}(c_{11} - c_{12})$ | (1-10) | $(1, -1, 0)/\sqrt{2}$ | $(1, 1, -\sqrt{2})/2$ | $(2p_{11} - p_{12} - p_{13})^2/32C$ |

Table 2.4.5.17. Tetragonal T_1 and hexagonal H_1 Laue classes: transverse modes, right-angle scattering

This table, written for the class T_1 , is also valid for the class H_1 with the additional relations $c_{66} = \frac{1}{2}(c_{11} - c_{12})$; $p_{66} = \frac{1}{2}(p_{11} - p_{12})$.

| $\hat{\mathbf{Q}}$ | $\hat{\mathbf{u}}$ | C | Scattering plane | \mathbf{e} | \mathbf{e}' | β |
|-----------------------|-----------------------|--------------------------------|------------------|-----------------------|--|---|
| (1, 0, 0) | (0, 0, 1) | c_{44} | (001) | (0, 0, 1) | $(q_1^{(1)}, q_2^{(1)}, 0)$ | $(q_1^{(1)} p_{44}')^2/c_{44}$ |
| (1, 0, 0) | (0, 1, 0) | c_{66} | (010) | (0, 1, 0) | $(q_1^{(2)}, 0, q_3^{(2)})$ | $\{[(n_3 q_1^{(2)})^2 + (n_1 q_3^{(2)})^2]/n_3^4 c_{66}\}(q_1^{(2)} p_{66}')^2$ |
| (0, 0, 1) | D | c_{44} | (010) | (0, 1, 0) | $(q_1^{(5)}, 0, q_3^{(5)})$ | $\{[(n_3 q_1^{(5)})^2 + (n_1 q_3^{(5)})^2]/n_1^4 c_{44}\}(q_3^{(5)} p_{44}')^2$ |
| (1, 1, 0)/ $\sqrt{2}$ | (0, 0, 1) | c_{44} | (001) | (0, 0, 1) | $(q_1^{(7)}, q_2^{(7)}, 0)$ | $[(q_1^{(7)} + q_2^{(7)}) p_{44}']^2/2c_{44}$ |
| (1, 1, 0)/ $\sqrt{2}$ | $(1, -1, 0)/\sqrt{2}$ | $\frac{1}{2}(c_{11} - c_{12})$ | (1-10) | $(1, -1, 0)/\sqrt{2}$ | $(q_1^{(10)}, q_1^{(10)}, q_3^{(10)})$ | $\{[2(n_3 q_1^{(10)})^2 + (n_1 q_3^{(10)})^2]/n_3^4 (c_{11} - c_{12})\}[q_1^{(10)}(p_{11} - p_{12})]^2$ |
| (0, 1, 1)/ $\sqrt{2}$ | (1, 0, 0) | $\frac{1}{2}(c_{44} + c_{66})$ | (100) | (1, 0, 0) | (0, 1, 0) | $p_{66}^2/(c_{44} + c_{66})$ |

Table 2.4.5.18. Hexagonal H_2 Laue class: transverse modes, right-angle scattering

$$c_{66} = \frac{1}{2}(c_{11} - c_{12}); p_{66} = \frac{1}{2}(p_{11} - p_{12}).$$

| $\hat{\mathbf{Q}}$ | $\hat{\mathbf{u}}$ | C | Scattering plane | \mathbf{e} | \mathbf{e}' | β |
|-----------------------|--------------------|--------------------------------|------------------|----------------------|-----------------------------|---|
| (1, 0, 0) | (0, 0, 1) | c_{44} | (001) | (0, 0, 1) | $(q_1^{(1)}, q_2^{(1)}, 0)$ | $(q_1^{(1)} p_{44}' + q_2^{(1)} p_{45}')^2/c_{44}$ |
| (1, 0, 0) | (0, 1, 0) | c_{66} | (001) | $(1, 1, 0)/\sqrt{2}$ | $(1, -1, 0)/\sqrt{2}$ | p_{16}^2/c_{66} |
| (1, 0, 0) | (0, 1, 0) | c_{66} | (010) | (0, 1, 0) | $(q_1^{(2)}, 0, q_3^{(2)})$ | $\{[(n_3 q_1^{(2)})^2 + (n_1 q_3^{(2)})^2]/n_3^4 c_{66}\}(q_1^{(2)} p_{66}')^2$ |
| (0, 0, 1) | D | c_{44} | (010) | (0, 1, 0) | $(q_1^{(5)}, 0, q_3^{(5)})$ | $\{[(n_3 q_1^{(5)})^2 + (n_1 q_3^{(5)})^2]/n_1^4 c_{44}\}(q_3^{(5)} p_{44}')^2$ |
| (0, 1, 1)/ $\sqrt{2}$ | (1, 0, 0) | $\frac{1}{2}(c_{44} + c_{66})$ | (100) | (1, 0, 0) | (1, 0, 0) | $p_{16}^2/(c_{44} + c_{66})$ |
| (0, 1, 1)/ $\sqrt{2}$ | (1, 0, 0) | $\frac{1}{2}(c_{44} + c_{66})$ | (100) | (1, 0, 0) | (0, 1, 0) | $p_{66}^2/(c_{44} + c_{66})$ |

Table 2.4.5.19. Tetragonal T_2 Laue class: transverse modes, right-angle scattering

| $\hat{\mathbf{Q}}$ | $\hat{\mathbf{u}}$ | C | Scattering plane | \mathbf{e} | \mathbf{e}' | β |
|-----------------------|--------------------|----------|------------------|--------------|-----------------------------|---|
| (1, 0, 0) | (0, 0, 1) | c_{44} | (001) | (0, 0, 1) | $(q_1^{(1)}, q_2^{(1)}, 0)$ | $(q_1^{(1)} p_{44}' + q_2^{(1)} p_{45}')^2/c_{44}$ |
| (1, 0, 0) | (0, 0, 1) | c_{44} | (010) | (0, 1, 0) | $(q_1^{(2)}, 0, q_3^{(2)})$ | $\{[(n_3 q_1^{(2)})^2 + (n_1 q_3^{(2)})^2]/n_1^4 c_{44}\}(q_3^{(2)} p_{45}')^2$ |
| (0, 0, 1) | D | c_{44} | (010) | (0, 1, 0) | $(q_1^{(5)}, 0, q_3^{(5)})$ | $\{[(n_3 q_1^{(5)})^2 + (n_1 q_3^{(5)})^2]/n_1^4 c_{44}\}(q_3^{(5)} p_{44}')^2$ |
| (1, 1, 0)/ $\sqrt{2}$ | (0, 0, 1) | c_{44} | (001) | (0, 0, 1) | $(q_1^{(7)}, q_2^{(7)}, 0)$ | $[(q_1^{(7)} + q_2^{(7)}) p_{44}' + (q_2^{(7)} - q_1^{(7)}) p_{45}']^2/2c_{44}$ |

Table 2.4.5.20. Orthorhombic Laue class O : transverse modes, right-angle scattering

| $\hat{\mathbf{Q}}$ | $\hat{\mathbf{u}}$ | C | Scattering plane | \mathbf{e} | \mathbf{e}' | β |
|-----------------------|--------------------|--------------------------------|------------------|--------------|-----------------------------|--|
| (1, 0, 0) | (0, 0, 1) | c_{55} | (001) | (0, 0, 1) | $(q_1^{(1)}, q_2^{(1)}, 0)$ | $\{[(n_2 q_1^{(1)})^2 + (n_1 q_2^{(1)})^2]/n_2^4 c_{55}\}(q_1^{(1)} p_{55}')^2$ |
| (1, 0, 0) | (0, 1, 0) | c_{66} | (010) | (0, 1, 0) | $(q_1^{(2)}, 0, q_3^{(2)})$ | $\{[(n_3 q_1^{(2)})^2 + (n_1 q_3^{(2)})^2]/n_3^4 c_{66}\}(q_1^{(2)} p_{66}')^2$ |
| (0, 1, 0) | (1, 0, 0) | c_{66} | (100) | (1, 0, 0) | $(0, q_2^{(3)}, q_3^{(3)})$ | $\{[(n_3 q_2^{(3)})^2 + (n_2 q_3^{(3)})^2]/n_3^4 c_{66}\}(q_2^{(3)} p_{66}')^2$ |
| (0, 1, 0) | (0, 0, 1) | c_{44} | (001) | (0, 0, 1) | $(q_1^{(4)}, q_2^{(4)}, 0)$ | $\{[(n_2 q_1^{(4)})^2 + (n_1 q_2^{(4)})^2]/n_1^4 c_{44}\}(q_2^{(4)} p_{44}')^2$ |
| (0, 0, 1) | (0, 1, 0) | c_{44} | (010) | (0, 1, 0) | $(q_1^{(5)}, 0, q_3^{(5)})$ | $\{[(n_3 q_1^{(5)})^2 + (n_1 q_3^{(5)})^2]/n_1^4 c_{44}\}(q_3^{(5)} p_{44}')^2$ |
| (0, 0, 1) | (1, 0, 0) | c_{55} | (100) | (1, 0, 0) | $(0, q_2^{(6)}, q_3^{(6)})$ | $\{[(n_3 q_2^{(6)})^2 + (n_2 q_3^{(6)})^2]/n_2^4 c_{55}\}(q_3^{(6)} p_{55}')^2$ |
| (1, 1, 0)/ $\sqrt{2}$ | (0, 0, 1) | $\frac{1}{2}(c_{44} + c_{55})$ | (001) | (0, 0, 1) | $(q_1^{(7)}, q_2^{(7)}, 0)$ | $\{[(n_2 q_1^{(7)})^2 + (n_1 q_2^{(7)})^2]/n_1^4 n_2^4 (c_{44} + c_{55})\} \times (n_2^2 q_1^{(7)} p_{55}' + n_2^2 q_2^{(7)} p_{44}')^2$ |
| (0, 1, 1)/ $\sqrt{2}$ | (1, 0, 0) | $\frac{1}{2}(c_{55} + c_{66})$ | (100) | (1, 0, 0) | $(0, q_2^{(8)}, q_3^{(8)})$ | $\{[(n_3 q_2^{(8)})^2 + (n_2 q_3^{(8)})^2]/n_2^4 n_3^4 (c_{55} + c_{66})\} \times (n_2^2 q_2^{(8)} p_{66}' + n_2^2 q_3^{(8)} p_{55}')^2$ |
| (1, 0, 1)/ $\sqrt{2}$ | (0, 1, 0) | $\frac{1}{2}(c_{44} + c_{66})$ | (010) | (0, 1, 0) | $(q_1^{(9)}, 0, q_3^{(9)})$ | $\{[(n_1 q_3^{(9)})^2 + (n_3 q_1^{(9)})^2]/n_1^4 n_3^4 (c_{44} + c_{66})\} \times (n_3^2 q_3^{(9)} p_{44}' + n_1^2 q_1^{(9)} p_{66}')^2$ |

2.4. BRILLOUIN SCATTERING

Table 2.4.5.21. Trigonal Laue class R_1 : transverse modes, right-angle scattering

$$c_{66} = \frac{1}{2}(c_{11} - c_{12}); p_{66} = \frac{1}{2}(p_{11} - p_{12}).$$

| $\hat{\mathbf{Q}}$ | $\hat{\mathbf{u}}$ | C | Scattering plane | \mathbf{e} | \mathbf{e}' | β |
|-----------------------|--------------------|---|------------------|--------------|-----------------------------|---|
| (0, 1, 0) | (1, 0, 0) | c_{66} | (100) | (1, 0, 0) | $(0, q_2^{(3)}, q_3^{(3)})$ | $\{[(n_3 q_2^{(3)})^2 + (n_1 q_3^{(3)})^2] / n_1^4 n_3^4 c_{66}\} (n_1^2 q_2^{(3)} p_{66} + n_3^2 q_3^{(3)} p_{41})^2$ |
| (0, 1, 0) | (1, 0, 0) | c_{66} | (001) | (0, 0, 1) | $(q_1^{(4)}, q_2^{(4)}, 0)$ | $(q_1^{(4)} p_{41})^2 / c_{66}$ |
| (0, 0, 1) | D | c_{44} | (010) | (0, 1, 0) | (0, 1, 0) | p_{14}^2 / c_{44} |
| (0, 0, 1) | D | c_{44} | (010) | (0, 1, 0) | $(q_1^{(5)}, 0, q_3^{(5)})$ | $\{[(n_3 q_1^{(5)})^2 + (n_1 q_3^{(5)})^2] / n_1^4 n_3^4 c_{44}\} [n_1^4 (q_1^{(5)} p_{14})^2 + n_3^4 (q_3^{(5)} p'_{44})^2]$ |
| $(0, 1, 1)/\sqrt{2}$ | (1, 0, 0) | $\frac{1}{2}(c_{44} + c_{66}) + c_{14}$ | (100) | (1, 0, 0) | (0, 1, 0) | $(p_{66} + p_{14})^2 / 2C$ |
| $(0, -1, 1)/\sqrt{2}$ | (1, 0, 0) | $\frac{1}{2}(c_{44} + c_{66}) - c_{14}$ | (100) | (1, 0, 0) | (0, 1, 0) | $(p_{66} - p_{14})^2 / 2C$ |

Table 2.4.5.22. Trigonal Laue class R_2 : transverse modes, right-angle scattering

$$c_{66} = \frac{1}{2}(c_{11} - c_{12}); p_{66} = \frac{1}{2}(p_{11} - p_{12}).$$

| $\hat{\mathbf{Q}}$ | $\hat{\mathbf{u}}$ | C | Scattering plane | \mathbf{e} | \mathbf{e}' | β |
|--------------------|--------------------|----------|------------------|--------------|-----------------------------|---|
| (0, 0, 1) | D | c_{44} | (010) | (0, 1, 0) | (0, 1, 0) | p_{14}^2 / c_{44} |
| (0, 0, 1) | D | c_{44} | (010) | (0, 1, 0) | $(q_1^{(5)}, 0, q_3^{(5)})$ | $\{[(n_3 q_1^{(5)})^2 + (n_1 q_3^{(5)})^2] / n_1^4 n_3^4 c_{44}\} [n_1^4 (q_1^{(5)} p_{14})^2 + n_3^4 (q_3^{(5)} p'_{44})^2]$ |

Table 2.4.5.23. Particular directions of incident light used in Tables 2.4.5.17 to 2.4.5.22

$$\varepsilon_1 = (n_2 + n_3 - 2n_1)/4n_1, \varepsilon_2 = (n_1 + n_3 - 2n_2)/4n_2, \varepsilon_3 = (n_1 + n_2 - 2n_3)/4n_3.$$

| Notation | q_1 | q_2 | q_3 |
|---------------------|--|--|--|
| $\mathbf{q}^{(1)}$ | $-2^{(-1/2)}(1 - \varepsilon_3)$ | $2^{(-1/2)}(1 + \varepsilon_3)$ | 0 |
| $\mathbf{q}^{(2)}$ | $-2^{(-1/2)}(1 - \varepsilon_2)$ | 0 | $2^{(-1/2)}(1 + \varepsilon_2)$ |
| $\mathbf{q}^{(3)}$ | 0 | $-2^{(-1/2)}(1 - \varepsilon_1)$ | $2^{(-1/2)}(1 + \varepsilon_1)$ |
| $\mathbf{q}^{(4)}$ | $2^{(-1/2)}(1 + \varepsilon_3)$ | $-2^{(-1/2)}(1 - \varepsilon_3)$ | 0 |
| $\mathbf{q}^{(5)}$ | $2^{(-1/2)}(1 + \varepsilon_2)$ | 0 | $-2^{(-1/2)}(1 + \varepsilon_2)$ |
| $\mathbf{q}^{(6)}$ | 0 | $2^{(-1/2)}(1 + \varepsilon_1)$ | $-2^{(-1/2)}(1 - \varepsilon_1)$ |
| $\mathbf{q}^{(7)}$ | $-2^{(-1/2)}(n_1 + n_3)(n_1^2 + n_3^2)^{(-1/2)}$ | $2^{(-1/2)}(n_1 - n_3)(n_1^2 + n_3^2)^{(-1/2)}$ | 0 |
| $\mathbf{q}^{(8)}$ | 0 | $-2^{(-1/2)}(n_1 + n_2)(n_1^2 + n_2^2)^{(-1/2)}$ | $2^{(-1/2)}(n_2 - n_1)(n_1^2 + n_2^2)^{(-1/2)}$ |
| $\mathbf{q}^{(9)}$ | $2^{(-1/2)}(n_3 - n_2)(n_2^2 + n_3^2)^{(-1/2)}$ | 0 | $-2^{(-1/2)}(n_2 + n_3)(n_2^2 + n_3^2)^{(-1/2)}$ |
| $\mathbf{q}^{(10)}$ | $-\frac{1}{2}(1 - \varepsilon_2)$ | $-\frac{1}{2}(1 - \varepsilon_2)$ | $2^{(-1/2)}(1 + \varepsilon_2)$ |

optical setup, the collection and acceptance angles of the instruments, spurious reflections and spurious interferences, etc. A full list is too long to be given here. However, when properly executed, interferometry is a fine tool, the performance of which is unequalled in its frequency range.

References

- Benedek, G. & Fritsch, K. (1966). *Brillouin scattering in cubic crystals*. *Phys. Rev.* **149**, 647–662.
- Born, M. & Wolf, E. (1993). *Principles of optics*. Sixth corrected edition. Oxford: Pergamon Press. Reissued (1999) by Cambridge University Press.
- Brillouin, L. (1922). *Diffusion de la lumière et des rayons X par un corps transparent homogène. Influence de l'agitation thermique*. *Ann. Phys. Paris*, **17**, 88–122.
- Cecchi, L. (1964). *Etude interférométrique de la diffusion Rayleigh dans les cristaux – diffusion Brillouin*. Doctoral Thesis, University of Montpellier.
- Chantrel, H. (1959). *Spectromètres interférentiels à un et deux étalons de Fabry–Perot*. *J. Rech. CNRS*, **46**, 17–33.
- Connes, P. (1958). *L'étalon de Fabry–Perot sphérique*. *J. Phys. Radium*, **19**, 262–269.
- Cummins, H. Z. & Schoen, P. E. (1972). *Linear scattering from thermal fluctuations*. In *Laser handbook*, Vol. 2, edited by F. T. Arecchi & E. O. Schulz-Dubois, pp. 1029–1075. Amsterdam: North-Holland.
- Egelstaff, P. A., Kearley, G., Suck, J.-B. & Youden, J. P. A. (1989). *Neutron Brillouin scattering in dense nitrogen gas*. *Europhys. Lett.* **10**, 37–42.
- Friedel, G. (1913). *Sur les symétries cristallines que peut révéler la diffraction des rayons Röntgen*. *C. R. Acad. Sci. Paris*, **157**, 1533–1536.
- Gornall, W. S. & Stoicheff, B. P. (1970). *The Brillouin spectrum and elastic constants of xenon single crystals*. *Solid State Commun.* **8**, 1529–1533.
- Gross, E. (1930a). *Change of wave-length of light due to elastic heat waves at scattering in liquids*. *Nature (London)*, **126**, 201–202.

- Gross, E. (1930b). *The splitting of spectral lines at scattering of light by liquids*. *Nature (London)*, **126**, 400.
- Hariharan, P. & Sen, J. (1961). *Double-passed Fabry–Perot interferometer*. *J. Opt. Soc. Am.* **51**, 398–399.
- Hayes, W. & Loudon, R. (1978). *Scattering of light by crystals*. New York: Wiley.
- Hercher, M. (1968). *The spherical mirror Fabry–Perot interferometer*. *Appl. Opt.* **7**, 951–966.
- Mach, J. E., McNutt, D. P., Roessler, F. L. & Chabbal, R. (1963). *The PEPSIOS purely interferometric high-resolution scanning spectrometer. I. The pilot model*. *Appl. Opt.* **2**, 873–885.
- Nelson, D. F. & Lax, M. (1971). *Theory of photoelastic interaction*. *Phys. Rev. B*, **3**, 2778–2794.
- Nelson, D. F., Lazay, P. D. & Lax, M. (1972). *Brillouin scattering in anisotropic media: calcite*. *Phys. Rev. B*, **6**, 3109–3120.
- Pine, A. S. (1972). *Thermal Brillouin scattering in cadmium sulfide: velocity and attenuation of sound; acoustoelectric effects*. *Phys. Rev. B*, **5**, 2997–3003.
- Sandercock, J. R. (1971). *The design and use of a stabilised multipassed interferometer of high contrast ratio*. In *Light scattering in solids*, edited by M. Balkanski, pp. 9–12. Paris: Flammarion.
- Sandercock, J. R. (1982). *Trends in Brillouin scattering: studies of opaque materials, supported films, and central modes*. In *Light scattering in solids III. Topics in applied physics*, Vol. 51, edited by M. Cardona & G. Güntherodt, pp. 173–206. Berlin: Springer.
- Sette, F., Krisch, M. H., Masciovecchio, C., Ruocco, G. & Monaco, G. (1998). *Dynamics of glasses and glass-forming liquids studied by inelastic X-ray scattering*. *Science*, **280**, 1550–1555.
- Sussner, H. & Vacher, R. (1979). *High-precision measurements of Brillouin scattering frequencies*. *Appl. Opt.* **18**, 3815–3818.
- Vacher, R. (1972). *Contribution à l'étude de la dynamique du réseau cristallin par analyse du spectre de diffusion Brillouin*. Doctoral Thesis, University of Montpellier II.
- Vacher, R. & Boyer, L. (1972). *Brillouin scattering: a tool for the measurement of elastic and photoelastic constants*. *Phys. Rev. B*, **6**, 639–673.

3.1. Structural phase transitions

BY J.-C. TOLÉDANO, V. JANOVEC, V. KOPSKÝ, J. F. SCOTT AND P. BOČEK

This chapter contains six contributions describing aspects of phase transitions in crystals that are of interest to crystallographers. The first contribution (Section 3.1.1) is a brief introduction aimed at defining the field of *structural transitions*. This restricted field constitutes, at present, the background of the clearest set of experimental and theoretical considerations. In this section, the terminology is specified. The second section (Section 3.1.2) describes the ideas and methods of the *theory of structural phase transitions*. This theory relates the symmetry characteristics of the transitions to their physical characteristics. The application of the symmetry principles that derive from this theory is illustrated by the results contained in Tables 3.1.3.1 and 3.1.4.1. The first of these two tables concerns the simple but experimentally widespread situation in which a structural transition is not accompanied by a change in the number of atoms per *primitive* crystal cell. The second table concerns the general case, in which the number of atoms changes, and which corresponds to the onset of superlattice reflections at the phase transition. This table provides, for a set of hypothetical transformations, the various symmetry-based predictions of the theory. Section 3.1.5 is devoted to the important topic of *soft modes*, which is related to the microscopic mechanism of a structural transition. Finally, Section 3.1.6 is an introduction to the software package *Group Informatics* contained in the accompanying CD-ROM.

3.1.1. Introduction

BY J.-C. TOLÉDANO

Phase transformations (the term *transitions* can be considered as a synonym) are experimentally recognized to exist in a large variety of systems submitted to a change in temperature or pressure: fluids, solids or mesophases, crystalline or disordered solids, metals or insulators.

This recognition is sometimes based on very obvious effects. This is, for instance, the case for the boiling or the freezing of a liquid, because the different *phases*, vapour, liquid, solid, differ greatly in their physical properties (*e.g.* the difference of density between the two fluids, or the difference of mechanical hardness between the liquid and the solid). In these cases, a phase transformation appears as an abrupt and major change of the physical properties.

In other systems, solids in particular, the existence of a phase transformation is generally revealed by more subtle effects only. The nature of these effects differs from one system to another: minor discontinuities in the lattice parameters of a crystalline phase; occurrence over a narrow temperature range of anomalies in certain specific physical properties; onset of a definite pattern of crystal twins *etc.*

Systems undergoing phase transitions constitute an important field of interest for crystallographers. This is due to the fact that, at the microscopic level, a phase transformation is generally accompanied by a change of the global or local atomic configuration. The structural data, *i.e.* the specification of the differences in atomic configurations between the two phases, or the study of the local ordering precursor to a transition, are thus essential, or at least important, clues to the understanding of the mechanism of the transition considered.

Conversely, the investigation of phase transitions has stimulated new developments in the techniques and concepts used by

crystallographers. For instance, it has been necessary to improve the precision of goniometric measurements and the control of temperature in order to detect accurately anomalies affecting the lattice parameters across a phase transition or to study the asymmetry of diffraction spots caused by the domain structure in a ‘low-symmetry’ phase. On the other hand, new methods of structural determination, relying on concepts of *n*-dimensional crystallography, had to be developed in order to study transitions to incommensurate phases.

Standard crystallographic considerations, based on the determination of the characteristics of a lattice and of a basis, appear to be most useful in the study of phase transformations between crystalline phases, due to the fact that, at a microscopic level, each phase is entirely described by its periodic crystal structure. There are a wide variety of such transformations and the task of classifying them has been attempted from several standpoints.

The most important distinction is that made between *reconstructive* and *non-reconstructive* transitions. This distinction stems from a comparison of the crystal structures of the two phases. In a *reconstructive transition*, the distances between certain atoms change by amounts similar to the dimension of the unit cell, and certain chemical bonds between neighbouring atoms are then necessarily broken (see Tolédano & Dmitriev, 1996, and references therein). The graphite–diamond transformation and many transformations in metals and alloys are examples of reconstructive transitions. If, instead, a transition preserves approximately the configuration of the chemical bonds between constituents, the transition is *non-reconstructive*.

Other classifications, which partly overlap with the preceding one, involve distinctions between *diffusionless* and *diffusion-assisted* transitions (*i.e.* those that require random hopping of atoms to achieve the change of atomic configuration) or between *displacive* and *order–disorder* transitions. Likewise, a number of transformations in metals or alloys are assigned to the class of *martensitic* transformations that is defined by a set of specific experimental observations (twinning behaviour, mechanical properties *etc.*). Finally, the distinction between *ferroic* and *non-ferroic* transitions has been progressively adopted in the recent years.

Owing to an insufficient understanding of the observations, the relationships between these various classifications is not fully clear at present. It is not even clear whether the same definitions and concepts can be applied to the description of all phase transformations between solid phases. For instance, one observes in certain solids (*e.g.* mixed lead magnesium niobates with an average perovskite structure) very broad anomalies of the physical properties (*i.e.* extending over a wide range of temperatures). These systems, which have stimulated many studies in recent years, are known to be chemically and structurally heterogeneous *simultaneously at several length scales*. The relevance to these systems of standard concepts defined for phase transitions in homogeneous systems, in which the anomalies of the physical properties are sharp, is uncertain.

It is therefore reasonable to restrict a review of basic concepts and theories to the simple reference case of *structural phase transitions*. We consider this terminology, in its *restricted* meaning, as pertaining to the situation of only a fraction of the phase transitions that take place in solids and imply a modification of the crystal structure. These are part of *non-reconstructive* transitions between homogeneous crystalline phases. It is customary to specify that a structural transition only *slightly*

3.1. STRUCTURAL PHASE TRANSITIONS

alters the chemical bond lengths (by less than *e.g.* 0.1 Å) and their relative orientations (by less than *e.g.* a few degrees).

Experimentally, such transitions are characterized by small values of the heat of transformation (less than a few calories per gram), weak discontinuities in the relevant physical quantities (*e.g.* lattice parameters) and *the occurrence of a symmetry relationship between the two phases surrounding the transition*.

In the simplest case, this relationship consists of the fact that the space group of one of the phases is a *subgroup* of the space group of the other phase, and that there is specific correspondence between the symmetry elements of the two phases. For example, for the phase transition occurring at 322 K in triglycine sulfate (Lines & Glass, 1977), the same binary axis can be found in the two phases. Likewise, the vector defining one of the primitive translations in one phase can be a multiple of the vector defining a primitive translation in the other phase.

In a more general way, the crystal structures of the two phases considered are both slight distortions of a *reference* structure, termed the *prototype* (or *parent*) structure. In this case, the space groups of the two phases are both subgroups of the space group of the prototype structure, with, as in the simple case above, a specific correspondence between the symmetry elements of the two phases and of the prototype structure. A well documented example of this situation is provided by two of the three transitions occurring in barium titanate (Lines & Glass, 1977).

A subclassification of *structural* transitions into *ferroic classes* is of interest (Aizu, 1969; Tolédano & Tolédano, 1987, and references therein). Indeed the distinction of ferroic classes allows one to establish a relationship between the point symmetries of the two phases surrounding a phase transition, the observed twinning, and the nature of the physical properties mainly affected by the phase transition.

The group-subgroup relationship that exists, in the standard situation, between the *space groups* of the two phases adjacent to a structural transition implies that the *point group* of one phase is either a *subgroup* of the point group of the other phase or is *identical* to it.

If the two point groups are *identical*, the corresponding transition is classified as *non-ferroic*.

In the general case, the point group of one phase (the *ferroic phase*) is a strict subgroup of the point group of the other phase (the *prototype phase*). The transition is then classified as *ferroic*. Originally, a somewhat more abstract definition was given (Aizu, 1969): a crystal was said to be ferroic if it can exist in two or more *orientation states* having equal stabilities in the absence of external forces, and when the various orientation states have crystal structures that only differ in their global spatial orientations. The latter definition, which focuses on the situation of the *ferroic phase*, derives from the former one: the *lowering of point symmetry* that accompanies the transition between the prototype phase and the ferroic phase results in the existence of various *variants* or twin orientations having the same structures within a

global reorientation (see also Sections 3.2.1, 3.2.3, 3.3.7, 3.3.10 and 3.4.1).

The various orientation states can coexist in a given sample and then determine a *twinning pattern*. Geometrical and physical considerations pertaining to twinned structures are developed in Chapters 3.2 and 3.3 of this volume. In particular, it can be shown that the structure of one orientation state can be brought to coincide with the structure of another orientation state by means of a set of geometrical transformations *R* which all belong to the space group of the *prototype phase*.

If we adopt a common frame of reference for all the orientation states of the ferroic phase, the tensors representing certain macroscopic quantities (see Chapter 1.1) will have different values in the different states (*e.g.* distinct nonzero components). If a certain macroscopic tensor has components differing in two states, *a* and *b*, these components are thus modified by the action of the geometrical transformations *R* which transforms (reorients) one structure into the other. Hence they are *not invariant* by geometrical operations belonging to the group of symmetry of the *prototype phase*: their value is necessarily zero in this phase.

Ferroic transitions therefore possess three characteristics:

(i) They are associated with a lowering of crystallographic point symmetry.

(ii) Components of certain macroscopic tensors acquire nonzero values below T_c .

(iii) The same tensors allow one to distinguish, at a macroscopic level, the various orientation states arising in the ferroic phase.

The subclassification of ferroics into *ferroic classes* has a crystallographic and a physical content. The crystallographic aspect is based on the type of point-symmetry lowering occurring at the transition, while the physical aspect focuses on the *rank of the tensor* (necessarily traceless) characterizing the different orientation states of the crystal in the ferroic phase and on the nature of the physical quantity (electrical, mechanical, ...) related to the relevant tensor (see Chapter 1.1). Table 3.1.1.1 specifies this twofold classification.

Note that a given transition related to a class defined by a tensor of rank *n* can belong to several classes defined by tensors of higher rank: *e.g.* a ferroelectric transition can also be ferroelastic and will also display characteristics of a higher-order ferroic.

The point-symmetry changes defining each class have been enumerated in various works (see for instance Aizu, 1973, and references therein).

The interest of the above classification is that it provides a guiding framework for the experimental investigations. Hence, the recognition that a transition is ferroelectric (respectively, ferroelastic) directs the investigation of the transition towards the examination of the dielectric (respectively, mechanical) properties of the system in the expectation that these will be the quantities mainly affected by the transition. This expectation is

Table 3.1.1.1. *Ferroic classification of structural parameters*

| | Class | | |
|---|--|--|--|
| | Ferroelectric | Ferroelastic | Higher-order ferroic |
| Symmetry change | (1) Non-polar to polar crystal point group (reference situation) or (2) polar to polar group with additional polar axes | Change of crystal system (syngony) (except from hexagonal to rhombohedral) | Change of point group not complying with the two preceding classes |
| Examples | (1) $2/m \Rightarrow 2$ (2) $mm2 \Rightarrow m$ | $mmm \Rightarrow 2/m$ (orthorhombic \Rightarrow monoclinic) | $622 \Rightarrow 32$ $4/mmm \Rightarrow 4/m$ |
| Rank of relevant tensor | 1 (vector) | 2 | ≥ 3 |
| Physical nature of the tensorial quantity | Dielectric polarization | Strain | Component of the piezoelectric or elastic tensor |
| Main physical properties affected by the transition | Dielectric, optical | Mechanical, elastic | Piezoelectric |
| Prototype example (temperature of transition) | Triglycine sulfate (322 K) | Lanthanum pentaphosphate, $\text{LaP}_5\text{O}_{14}$ (420 K) | Quartz, SiO_2 (846 K); niobium dioxide, NbO_2 (1080 K) |

3. PHASE TRANSITIONS, TWINNING AND DOMAIN STRUCTURES

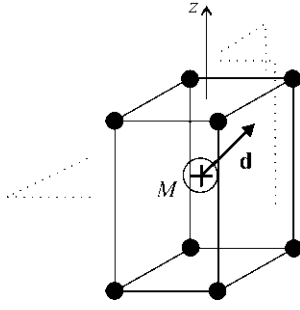


Fig. 3.1.2.1. Model of a structural transition. The filled circles at the vertices of the cell are singly charged negative ions and the empty circle at the centre is a singly charged positive ion. \mathbf{d} is an arbitrary displacement of the central ion.

based on the fact that the dielectric polarization (respectively, the thermal strain tensor) acquires spontaneous components across the transition.

Conversely, if neither of these two classes of ferroics is involved in the transition considered, one knows that one must focus the study on components of higher-rank macroscopic tensors in order to reveal the characteristic anomalies associated with the transition. Also, the knowledge of the ferroic class of a transition specifies the nature of the macroscopic tensorial quantity that must be measured in order to reveal the domain structure. For instance, ferroelastic domains correspond to different values of symmetric second-rank tensors. Aside from the spontaneous strain tensor, we can consider the dielectric permittivity tensor at optical frequencies. The latter tensor determines the optical indicatrix, which will be differently oriented in space for the distinct domains. Consequently, with suitably polarized light one should always be able to ‘visualize’ ferroelastic domains. Conversely, such visualization will never be possible by the same method for a non-ferroelastic system.

3.1.2. Thermodynamics of structural transitions

BY J.-C. TOLÉDANO

3.1.2.1. Introduction

In the study of structural phase transitions, the crystallographer is often confronted by an ambiguous situation. Small changes in atomic positions determine structures having different space groups, and the data are generally compatible with several possible symmetry assignments. In order to make a choice, the crystallographer must be able to rely on some theoretical substrate, which will allow him to discard certain of the possible assignments.

The relevant theoretical framework in this field is the thermodynamical and symmetry considerations that form the *Landau theory of phase transitions*. In this chapter, we describe the ideas and results of this theory.

In the next section, we give an introduction to the main ideas of the theory by using an example consisting of a simple speculative type of structural phase transition. In Section 3.1.2.3, we discuss various situations of experimental interest relative to the thermodynamical aspect of the theory: first and second order of the transition, metastable states and thermal hysteresis. In Section 3.1.2.4, we provide a brief description, in two steps, of the general arguments constituting the foundation of the theory. In Section 3.1.2.5, we discuss the case of a structural transition actually occurring in nature and having a greater complexity than the speculative case considered in Section 3.1.2.2. In this section we also analyse the relationship between the *ferroic* character of a transition (see Section 3.1.1) and its order-parameter symmetry.

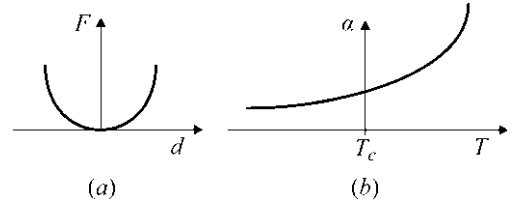


Fig. 3.1.2.2. (a) Variation of the free energy as function of the amplitude of the displacement of the central ion in Fig. 3.1.2.1. (b) Typical temperature dependence in the vicinity of T_c of the coefficient of a second-degree term in the Landau expansion (3.1.2.1) whenever this coefficient is strictly positive at T_c : one can see that this positivity is also valid slightly above and below T_c .

3.1.2.2. Basic ideas of Landau’s theory of phase transitions

The Landau theory of phase transitions is a phenomenological theory. It does not aim to establish that a phase transition exists in a given system. The existence of a transition is an experimental fact considered as a starting point of the theory. The explanatory power of the theory is to establish the overall consistency of the microscopic characteristics of the transition (space symmetry and structural changes, anomalies in the phonon spectrum *etc.*) and the results of the measurement of various relevant macroscopic quantities of thermal, dielectric, optical or mechanical nature.

The continuous (‘second-order’) character of the transition plays an essential role in working out the general foundations of the theory. However, though its strict field of validity is that of continuous transitions, the theory also satisfactorily applies to a large fraction of discontinuous transitions.

The Landau theory defines two basic concepts: the *order parameter* (OP) and the *transition free energy* (LFE). It is worth pointing out that these concepts keep their usefulness in the modern statistical theory of critical phenomena, even though these phenomena do not generally comply with the results of Landau’s theory. From the symmetry properties of the *order parameter* and of the *Landau free energy*, it is possible to infer, on the one hand, a certain number of observable symmetry characteristics of the system: degeneracy of the ‘low-symmetry’ phase (*i.e.* number of energetically equivalent domain orientations in this phase), enumeration of the possible symmetries of the ‘low-symmetry’ phase for a given symmetry of the ‘high-symmetry’ phase. On the other hand, macroscopic physical quantities can be classified as functions of their symmetries with respect to the order parameter. This classification leads to that of the various types of anomalous behaviours that can be induced by the occurrence of a phase transition.

In order to give an intuitive approach to the basic arguments of the Landau theory, and to its use, we first analyse an artificially simplified example of a crystalline phase transition.

3.1.2.2.1. Description of a prototype example

Fig. 3.1.2.1 represents a unit cell of a speculative crystalline structure with a simple tetragonal Bravais lattice, in which a phase transition is assumed to take place. Negative ions (filled circles) occupy the vertices of the tetragonal cell (lattice constants $a = b \neq c$). A positive ion M^+ is at the centre of the cell.

This configuration is assumed to be the equilibrium state of the system above the temperature T_c of the transition (see Fig. 3.1.2.2). Below T_c , equilibrium is assumed to correspond to a structure that only differs from the high-temperature structure by the fact that M^+ lies out of the centre of the cell in an unspecified direction. Hence the latter equilibrium is characterized by the magnitude and direction of the displacement $\mathbf{d}_0 = (d_x, d_y, d_z)$ of the central ion. At high temperature, the equilibrium corresponds to $\mathbf{d}_0 = 0$.

3.1. STRUCTURAL PHASE TRANSITIONS

3.1.2.2.2. Basic assumptions and strategy

Our aim is to determine the above displacement as a function of temperature. Landau's strategy is to determine \mathbf{d}_0 by a *variational method*. One considers an arbitrary displacement \mathbf{d} of the M^+ ion. For given temperature T and pressure p (or volume V), and specified values of the components of \mathbf{d} , there is, in principle, a definite value $F(T, p, d_x, d_y, d_z)$ for the free energy F of the system. This function is a *variational free energy* since it is calculated for an arbitrary displacement. The equilibrium displacement $\mathbf{d}_0(T, p)$ is defined as the displacement that minimizes the variational free energy F . The equilibrium free energy of the system is $F_{eq}(T, p) = F(T, p, \mathbf{d}_0)$. Note that, strictly speaking, in the case of a given pressure, one would have to consider a variational Gibbs function $(F + pV)$ in order to determine the equilibrium of the system. We will respect the current use in the framework of Landau's theory of denoting this function F and call it a *free energy*, though this function might actually be a Gibbs potential.

The former strategy is not very useful as long as one does not know the form of the variational free energy as a function of the components of the displacement. The second step of Landau's theory is to show that, given general assumptions, one is able to determine simply the form of $F(T, p, \mathbf{d})$ in the required range of values of the functions' arguments.

The basic assumption is that of *continuity of the phase transition*. It is in fact a dual assumption. On the one hand, one assumes that the equilibrium displacement $\mathbf{d}_0(T, p)$ has components varying continuously across the transition at T_c . On the other hand, one assumes that F is a continuous and derivable function of (T, p, \mathbf{d}) , which can be expanded in the form of a *Taylor expansion* as function of these arguments.

Invoking the continuity leads to the observation that, on either side of T_c , $|\mathbf{d}_0|$ is small, and that, accordingly, one can restrict the determination of the functional form of $F(T, p, \mathbf{d})$ to small values of (d_x, d_y, d_z) and of $|T - T_c|$. F will then be equal to the sum of the first relevant terms of a Taylor series in the preceding variables.

3.1.2.2.3. Symmetry constraints and form of the free energy

The central property of the variational free energy which allows one to specify its form is a symmetry property. F is a function of (d_x, d_y, d_z) which is *invariant by the symmetry transformations of the high-temperature equilibrium structure*. In other terms, an arbitrary displacement \mathbf{d} and the displacement \mathbf{d}' obtained by applying to \mathbf{d} one of the latter symmetry transformations correspond to the same value of the free energy.

Indeed, both displacements determine an identical set of mutual distances between the positive and negative ions of the system and the free energy only depends on this 'internal' configuration of the ions.

Note that, in the case considered here (Fig. 3.1.2.1), the set of symmetry transformations comprises, aside from the lattice translations, fourfold rotations around the z axis, mirror symmetries into planes and the products of these transformations. The set of rotations and reflections forms a *group* G of order 16, which is the crystallographic point group $4/mmm$ (or D_{4h}).

Also note that this symmetry property of the free energy also holds for each degree of the Taylor expansion of F since the geometrical transformations of G act linearly on the components of \mathbf{d} . Hence, terms of different degrees belonging to the expansion of F will not 'mix', and must be separately invariant.

Let us implement these remarks in the case in Fig. 3.1.2.1. It is easy to check that by successive application to the components of \mathbf{d} of the mirror symmetries perpendicular to the three axes, no linear combination of these components is invariant by G : each of the three former symmetry transformations reverses one

component of \mathbf{d} and preserves the two others. *Linear terms are therefore absent from the expansion.*

As for second-degree terms, the same symmetry transformations preclude the existence of combinations of bilinear products of the type $d_x d_y$. Actually, one finds that the fourfold symmetry imposes that the most general form of the second-degree contribution to the variational free energy is a linear combination of d_z^2 and of $(d_x^2 + d_y^2)$. Hence the Taylor expansion of F , restricted to its lowest-degree terms, is

$$F = F_0(T, p) + \frac{\alpha_1(T, p)}{2} d_z^2 + \frac{\alpha_2(T, p)}{2} (d_x^2 + d_y^2). \quad (3.1.2.1)$$

3.1.2.2.4. Reduction of the number of relevant degrees of freedom: order parameter

Let us now derive the *key result of the theory*, namely, that either the component d_z or the pair of components (d_x, d_y) will take nonzero values below T_c (but not both). The meaning of this result will be clarified by symmetry considerations.

The derivation of this result relies on the fact that one, and one only, of the two coefficients α_i in equation (3.1.2.1) must vanish and change sign at T_c , and that the other coefficient must remain positive in the neighbourhood of T_c .

(a) Before establishing the latter property in (b) hereunder, let us show that its validity implies the stated key result of the theory. Indeed, if one α_i coefficient is strictly positive (e.g. $\alpha_1 > 0$), then the minimum of F with respect to the components of \mathbf{d} (e.g. d_z) multiplying this coefficient in (3.1.2.1) occurs for zero equilibrium values of these components (e.g. $d_z^0 = 0$) in the vicinity of T_c , above and below this temperature. Hence, depending on the coefficient α_i which remains positive, either d_z or the pair (d_x, d_y) can be omitted, in the first place, from the free-energy expansion. *The remaining set of components is called the order parameter of the transition.* At this stage, this fundamental quantity is defined as the set of degrees of freedom, the coefficient of which in the second-degree contribution to F vanishes and changes sign at T_c . The number of independent components of the order parameter (one in the case of d_z , two in the case of the pair d_x, d_y) is called the dimension of the order parameter.

Note that the preceding result means that the displacement of the M^+ ion below T_c cannot occur in an arbitrary direction of space. It is either directed along the z axis, or in the (x, y) plane.

(b) Let us now establish the property of the α_i postulated above.

At T_c , the equilibrium values of the components of \mathbf{d} are zero. Therefore, at this temperature, the variational free energy (3.1.2.1) is minimum for $d_x, d_y, d_z = 0$. Considering the form (3.1.2.1) of F , this property implies that we have (Fig. 3.1.2.2) $\alpha_i(T_c) \geq 0$ ($i = 1, 2$).

Note that these inequalities cannot be strict for both coefficients α_i , because their positiveness would hold on either side of T_c in the vicinity of this temperature. Consequently, the minimum of F would correspond to $\mathbf{d} = 0$ on either side of the transition while the situation assumed is only compatible with this result above T_c . Using the converse argument that the equilibrium values of the components of \mathbf{d} are not *all* equal to zero below T_c leads easily to the conclusion that one, at least, of the two coefficients α_i must vanish at T_c and become negative below this temperature.

Let us now show that the two coefficients α_i cannot vanish simultaneously at T_c . This result relies on the 'reasonable' assumption that the two coefficients α_i are *different* functions of temperature and pressure (or volume), no constraint in this respect being imposed by the symmetry of the system.

Fig. 3.1.2.3 shows, in the (T, p) plane, the two lines corresponding to the vanishing of the two functions α_i . The simultaneous vanishing of the two coefficients occurs at an isolated point

3. PHASE TRANSITIONS, TWINNING AND DOMAIN STRUCTURES

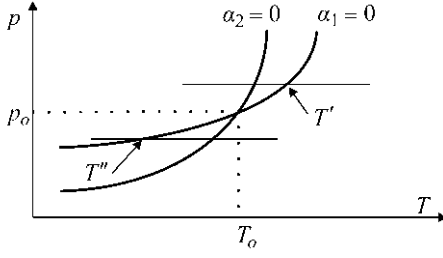


Fig. 3.1.2.3. Plots representative of the equations $\alpha_1(p, T) = 0$ and $\alpha_2(p, T) = 0$. The simultaneous vanishing of these coefficients occurs for a single couple of temperature and pressure (p_0, T_0) .

(T_0, p_0) . Let us consider, for instance, the situation depicted in Fig. 3.1.2.3. For $p > p_0$, on lowering the temperature, α_1 vanishes at T' and α_2 remains positive in the neighbourhood of T' . Hence, the equilibrium value of the set (d_x, d_y) remains equal to zero on either side of T' . A transition at this temperature will only concern a possible change in d_z^0 .

Likewise for p below p_0 , a transition at T'' will only concern a possible change of the set of components (d_x^0, d_y^0) , the third component d_z remaining equal to zero on either sides of T'' . Hence an infinitesimal change of the pressure (for instance a small fluctuation of the atmospheric pressure) from above p_0 to below p_0 will *modify qualitatively the nature of the phase transformation* with the direction of the displacement changing abruptly from z to the (x, y) plane. As will be seen below, the crystalline symmetries of the phases stable below T' and T'' are different. This is a singular situation, of *instability*, of the type of phase transition, not encountered in real systems. Rather, the standard situation corresponds to pressures away from p_0 , for which a slight change of the pressure does not modify significantly the direction of the displacement. In this case, one coefficient α_i only vanishes and changes sign at the transition temperature, as stated above.

3.1.2.2.5. Stable state below T_c and physical anomalies induced by the transition

We have seen that either d_z or the couple (d_x, d_y) of components of the displacement constitute the order parameter of the transition and that the free energy needs only to be expanded as a function of the components of the order parameter. Below the transition, the corresponding coefficient α_i is negative and, accordingly, the free energy, limited to its second-degree terms, has a maximum for $\mathbf{d} = 0$ and no minimum. Such a truncated expansion is not sufficient to determine the equilibrium state of the system. The stable state of the system must be determined by positive terms of higher degrees. Let us examine first the simplest case, for which the order parameter coincides with the d_z component.

The same symmetry argument used to establish the form (3.1.2.1) of the Landau free energy allows one straightforwardly to assert the absence of a third-degree term in the expansion of F as a function of the order parameter d_z , and to check the effective occurrence of a fourth-degree term. If we assume that this simplest form of expansion is sufficient to determine the equilibrium state of the system, the coefficient of the fourth-degree term must be positive in the neighbourhood of T_c . Up to the latter degree, the form of the relevant contributions to the free energy is therefore

$$F = F_0(T, p) + \frac{\alpha(T - T_c)}{2} d_z^2 + \frac{\beta}{4} d_z^4. \quad (3.1.2.2)$$

In this expression, α_1 , which is an odd function of $(T - T_c)$ since it vanishes and changes sign at T_c , has been expanded linearly. Likewise, the lowest-degree expansion of the function $\beta(T - T_c)$ is a *positive constant* in the vicinity of T_c . The function F_0 , which is the zeroth-degree term in the expansion, represents

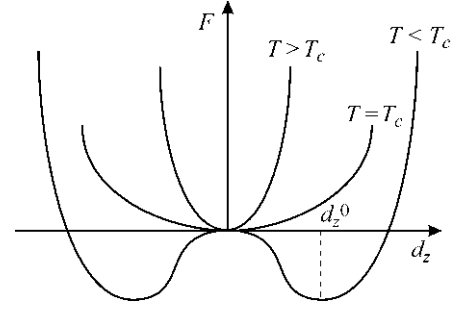


Fig. 3.1.2.4. Plots of the Landau free energy as a function of the order parameter, for values of the temperature above or below T_c or coincident with T_c . The shape of the plot changes qualitatively from a one-minimum plot to a two-minimum plot.

the normal ‘background’ part of the free energy. It behaves smoothly since it does not depend on the order parameter. A plot of $[F(d_z) - F_0]$ for three characteristic temperatures is shown in Fig. 3.1.2.4.

The minima of F , determined by the set of conditions

$$\frac{\partial F}{\partial d_z} = 0; \quad \frac{\partial^2 F}{\partial^2 d_z} > 0, \quad (3.1.2.3)$$

occur above T_c for $d_z = 0$, as expected. For $T < T_c$ they occur for

$$d_z^0 = \pm \sqrt{\alpha \frac{(T_c - T)}{\beta}}. \quad (3.1.2.4)$$

This behaviour has a general validity: the order parameter of a transition is expected, in the framework of Landau’s theory, to possess a square-root dependence as a function of the deviation of the temperature from T_c .

Note that one finds two minima corresponding to the same value of the free energy and opposite values of d_z^0 . The corresponding upward and downward displacements of the M^+ ion (Fig. 3.1.2.1) are distinct states of the system possessing the same stability.

Other physical consequences of the form (3.1.2.2) of the free energy can be drawn: absence of latent heat associated with the crossing of the transition, anomalous behaviour of the specific heat, anomalous behaviour of the *dielectric susceptibility* related to the order parameter.

The *latent heat* is $L = T\Delta S$, where ΔS is the difference in entropy between the two phases at T_c . We can derive S in each phase from the equilibrium free energy $F(T, p, d_z^0(T, p))$ using the expression

$$S = -\frac{dF}{dT} \Big|_{d_z^0} = -\left[\frac{\partial F}{\partial T} \Big|_{d_z^0} + \frac{\partial F}{\partial d_z} \frac{d(d_z^0)}{dT} \Big|_{d_z^0} \right]. \quad (3.1.2.5)$$

However, since F is a minimum for $d_z = d_z^0$, the second contribution vanishes. Hence

$$S = -\frac{\alpha}{2} (d_z^0)^2 - \frac{\partial F_0}{\partial T}. \quad (3.1.2.6)$$

Since both d_z^0 and $(\partial F_0 / \partial T)$ are continuous at T_c , there is no entropy jump $\Delta S = 0$, and *no latent heat at the transition*.

Several values of the specific heat can be considered for a system, depending on the quantity that is maintained constant. In the above example, the displacement \mathbf{d} of a positive ion determines the occurrence of an electric dipole (or of a macroscopic polarization \mathbf{P}). The quantity ϵ , which is thermodynamically conjugated to d_z , is therefore proportional to an electric field (the conjugation between quantities η and ζ is expressed by the fact that infinitesimal work on the system has the form $\zeta d\eta - c f$).

3.1. STRUCTURAL PHASE TRANSITIONS

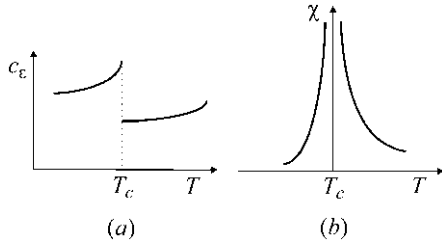


Fig. 3.1.2.5. (a) Qualitative temperature dependence of the specific heat at a continuous transition. (b) Temperature dependence of the susceptibility at a continuous transition.

Sections 1.1.1.4 and 1.1.5). Let us show that the specific heat at *constant electric field* has a specific type of anomaly.

This specific heat is expressed by

$$c_\varepsilon = T \left. \frac{\partial S}{\partial T} \right|_\varepsilon. \quad (3.1.2.7)$$

Using (3.1.2.6), we find

$$T > T_c: \quad c_\varepsilon^0 = -\frac{\partial^2 F_0(T, p)}{\partial T^2}, \quad (3.1.2.8)$$

$$T < T_c: \quad c_\varepsilon = -\frac{\partial^2 F_0(T, p)}{\partial T^2} - \frac{\alpha}{2} \frac{d(d_z^0)^2}{dT} T = c_\varepsilon^0 + \frac{\alpha^2}{2\beta}. \quad (3.1.2.8a)$$

Hence above and below T_c the specific heat is a different, smoothly varying function of temperature, determined by the background free energy $F_0(T, p)$ and by the smooth variation of the β coefficient. Fig. 3.1.2.5(a) reproduces the anomaly of the specific heat, which, on cooling through T_c , has the form of an upward step.

Finally, let us consider the anomaly of the susceptibility χ , which, in the case considered, is proportional to the dielectric susceptibility of the material. It is defined as

$$\chi = \lim_{\varepsilon \rightarrow 0} \left. \frac{\partial d_z}{\partial \varepsilon} \right| d_z^0. \quad (3.1.2.9)$$

In order to calculate χ , it is necessary to examine the behaviour of the system in the presence of a small field, ε , conjugated to the order parameter. In this case, the appropriate thermodynamical potential whose minimum determines the equilibrium of the system is not F but $G = F - d_z \varepsilon$. Minimizing G with respect to d_z leads to

$$d_z \{ \alpha(T - T_c) + \beta d_z^2 \} = \varepsilon. \quad (3.1.2.10)$$

For small values of ε , the solution of this equation must tend towards the equilibrium values $d_z = 0$. Deriving these solutions with respect to ε , we obtain

$$\chi(T > T_c) = \frac{1}{\alpha(T - T_c)}; \quad \chi(T < T_c) = \frac{1}{2\alpha(T - T_c)}. \quad (3.1.2.11)$$

The susceptibility goes to infinity when $T \rightarrow T_c$ from either side of the transition (Fig. 3.1.2.5b). The set of anomalies in c_ε and χ described in this paragraph represents the basic effects of temperature on quantities that are affected by a phase transition. They constitute the ‘canonical signature’ of a phase transition of the *continuous* type.

Certain complications arise in the cases where the transition is not strictly continuous, where the order parameter is coupled to other degrees of freedom, and where the order parameter is not

one-dimensional. We consider one of these complications in Section 3.1.2.3.

3.1.2.2.6. Symmetry considerations

3.1.2.2.6.1. Order-parameter symmetry

Up to now, we have defined the order parameter as a set of degrees of freedom determining a second-degree contribution to the free energy, the coefficient of which has a specific temperature dependence proportional to $(T - T_c)$. Actually, the order parameter can also be defined on the basis of its specific symmetry characteristics.

Let us consider the manner by which the components (d_x, d_y, d_z) transform when we apply to the crystal each of the 16 symmetry operations of the group $G = 4/mmm$. Table 3.1.2.1 specifies the results of these transformations.

In the first place, we note that d_z is transformed either into itself or into $(-d_z)$. If we consider this coordinate as the basis vector of a one-dimensional vector space, we can conclude that this *vector space* (i.e. the space formed by the set of vectors that are linear combinations of the basis) is *invariant* by all the transformations of the group G . Such a space, containing obviously no space of smaller dimension, is, according to the definitions given in Chapter 1.2, a *one-dimensional irreducible invariant space with respect to the group G*.

Each of the components (d_x, d_y) is not transformed into a proportional component by *all* the elements of G . Certain of these elements transform d_x into $\pm d_y$, and conversely. Hence d_x and d_y are not, separately, bases for one-dimensional irreducible invariant spaces. However, their set generates a two-dimensional vector space that has the property to be invariant and irreducible by all the transformations of G .

Note that the set of the three components (d_x, d_y, d_z) carries a three-dimensional vector space which, obviously, has the property to be invariant by all the transformations of G . However, this vector space *contains* the two invariant spaces carried respectively by d_z and by (d_x, d_y) . Hence it is not irreducible.

In conclusion, from a symmetry standpoint, the order parameter of a phase transition is a set of degrees of freedom that carries an irreducible vector space (an irreducible representation) with respect to the action of the group G , the latter group being the symmetry group of the high-symmetry phase.

3.1.2.2.6.2. Degeneracy of the low-symmetry phase

We had noted above that the structure is invariant by G in the stable state of the system above T_c . When $\mathbf{d} \neq 0$, the structure becomes invariant by a smaller set of transformations. Let us enumerate these transformations for each possible stable state of the system below T_c .

When the order parameter coincides with d_z , we determined, below T_c , two stable states, $d_z^0 = \pm[\alpha(T_c - T)/\beta]^{1/2}$. The crystalline structures determined by these displacements of the M^+ ion parallel to the z axis are both invariant by the same set of eight symmetry transformations. These comprise the cyclic group of order 4 generated by the fourfold rotation around z , and by the reflections in planes containing this axis. This set is the group

Table 3.1.2.1. Transformation of the components of \mathbf{d} under the symmetry operations of group $G = 4/mmm$

| G | E | C_4 | C_2 | C_4^3 | σ_x | σ_y | σ_{xy} | $\sigma_{xy'}$ |
|-------|--------|---------|------------|---------|------------|------------|---------------|----------------|
| d_z | d_z | d_z | d_z | d_z | d_z | d_z | d_z | d_z |
| d_x | d_x | d_y | $-d_x$ | $-d_y$ | $-d_x$ | d_x | $-d_y$ | d_y |
| d_y | d_y | $-d_x$ | $-d_y$ | d_x | d_y | $-d_y$ | $-d_x$ | d_x |
| G | I | S_4^3 | σ_z | S_4 | U_x | U_y | U_{xy} | $U_{xy'}$ |
| d_z | $-d_z$ | $-d_z$ | $-d_z$ | $-d_z$ | $-d_z$ | $-d_z$ | $-d_z$ | $-d_z$ |
| d_x | $-d_x$ | $-d_y$ | d_x | d_y | d_x | $-d_x$ | $-d_y$ | d_y |
| d_y | $-d_y$ | d_x | d_y | $-d_x$ | $-d_y$ | d_y | d_x | $-d_x$ |

3. PHASE TRANSITIONS, TWINNING AND DOMAIN STRUCTURES

$C_{4v} = 4mm$, a subgroup F of G . The transition is thus accompanied by a lowering of the symmetry of the system.

Also note that the two states $\pm d_z^z$ are transformed into each other by certain of the symmetry operations such as the mirror symmetry σ_z 'lost' below T_c . These two states correspond to the same value of the free energy [the minimum value determined in equation (3.1.2.3)]: they are equally stable. This can also be checked by applying to the system the mirror symmetry σ_z . This transformation keeps unchanged the value of F since the free energy is invariant by all the transformations belonging to G (to which σ_z belongs). The state d_z^z is, however, not preserved, and is transformed into $(-d_z^z)$.

We have not determined explicitly the stable states of the system in the case of a two-dimensional order parameter (d_x, d_y). A simple discussion along the line developed for the one-dimensional order parameter d_z^z would show that the relevant form of the free energy is

$$F = F_0 + \frac{\alpha(T - T_c)}{2}(d_x^2 + d_y^2) + \beta_1(d_x^4 + d_y^4) + \beta_2 d_x^2 d_y^2 \quad (3.1.2.12)$$

and that the possible stable states below T_c are:

- (i) $d_x^0 = \pm[\alpha(T_c - T)/\beta_1]^{1/2}$, $d_y = 0$;
- (ii) $d_y^0 = \pm[\alpha(T_c - T)/\beta_2]^{1/2}$, $d_x = 0$;
- (iii) and (iv) $d_x^0 = \pm d_y^0 = \pm[\alpha(T_c - T)/(\beta_1 + \beta_2)]^{1/2}$.

Like the case of d_z^z , there is a lowering of the crystal symmetry below T_c . In the four cases, one finds that the respective symmetry groups of the structure are (i) $F = C_{2v} = mm2_x$; (ii) $F' = C_{2v} = mm2_y$; (iii) $F = C_{2v} = mm2_{xy}$; (iv) $F' = C_{2v} = mm2_{xy}$.

States (i) and (ii) correspond to each other through one of the 'lost' transformations of G (the rotations by $\pi/2$). They therefore possess the same free energy and stability. The second set of states (iii) and (iv) also constitute, for the same reason, a pair of states with the same value of the equilibrium free energy.

Note that the symmetry groups associated with equally stable states are conjugate relative to G , that is they satisfy the relationship $F' = gFg^{-1}$, with g belonging to G .

3.1.2.3. Free-energy models for discontinuous transitions

Expression (3.1.2.2) for the free energy, discussed in the preceding section, only contains terms of even degrees as a function of the order parameter. We have stressed that this property derives from symmetry considerations. Let us provisionally ignore the symmetry constraints and assume that the phase transition in a given system is described by a free energy containing a term of degree three as a function of the order parameter.

$$F = F_0 + \frac{\alpha(T - T_0)}{2}\eta^2 + \frac{\delta}{3}\eta^3 + \frac{\beta}{4}\eta^4. \quad (3.1.2.13)$$

The stable state of this system at each temperature is determined by the minimum of F . The extrema of this function are provided by

$$\frac{\partial F}{\partial \eta} = \eta[\alpha(T - T_0) + \delta\eta + \beta\eta^2] = 0, \quad (3.1.2.14)$$

the solutions of which are

$$\eta = 0 \quad \text{and} \quad \eta = \frac{1}{2\beta}[-\delta \pm \sqrt{\delta^2 + 4\alpha\beta(T_0 - T)}]. \quad (3.1.2.15)$$

A straightforward analysis based on (3.1.2.13) and (3.1.2.15) shows that, depending on the range of temperatures, the free energy has one of the forms schematically represented in Fig. 3.1.2.6(a). This form changes at three characteristic temperatures.

(i) Above $T_1 = (T_0 + \delta^2/4\alpha\beta)$, the free energy has one extremum (a minimum) for $\eta = 0$. The stable state of the system corresponds to a zero value of the order parameter.

(ii) For $T_0 < T < T_1$, the free energy has two minima, one for $\eta = 0$ and the other one for $\eta = (1/2\beta)\{-\delta \pm [\delta^2 + 4\alpha\beta(T_1 - T)]^{1/2}\}$. These minima define one stable state (the deepest minimum) and one metastable state. Note that the zero value of the order parameter constitutes the stable state in the range $T_c < T < T_1$ with $T_c = T_0 + \delta^2/9\beta\alpha$. Hence, the observed phase transition corresponding to a change from a zero value to a nonzero value of the order parameter occurs at T_c . Below this temperature, and down to T_0 , the system has a stable state at $\eta \neq 0$ and a metastable state at $\eta = 0$.

(iii) Finally, below T_0 , the free energy has two minima both corresponding to $\eta \neq 0$, the value $\eta = 0$ being a relative maximum.

The remarkable physical consequences of this sequence of shapes are the following.

In the first place, it appears that the equilibrium value of the order parameter changes discontinuously at T_c . The free energy (3.1.2.13) therefore provides us with a model of discontinuous phase transitions. Referring to equation (3.1.2.6), we can see that a discontinuity of the order parameter is necessarily associated with a nonzero latent heat (or entropy) for the transition. More precisely, the downward jump experienced, on heating, by the equilibrium value of the order parameter corresponds to an endothermal transition. Such a transition is also termed (following Ehrenfest's classification) a *first-order transition*, since the entropy, which is a *first derivative* of the free energy, is discontinuous.

On the other hand, the occurrence of metastable states, in certain temperature ranges, generates *thermal hysteresis*. Indeed, on cooling from above T_1 , the system is likely to remain in the state $\eta = 0$ down to the temperature T_0 , even though between T_1 and T_0 this state is not the stable state of the system. Conversely, on heating, the system will remain in a state $\eta \neq 0$ up to T_1 , even though this state does not constitute the stable state of the system between T_c and T_1 . Hence, the variations of the order parameter will schematically vary as in Fig. 3.1.2.6(b), the temperature dependence below the discontinuity being determined by equation (3.1.2.15). Likewise, the susceptibility will vary as in Fig. 3.1.2.6(c).

The form (3.1.2.13) of the free energy is not the only model form for discontinuous transitions. Another canonical form is

$$F = F_0 + \frac{\alpha(T - T_0)}{2}\eta^2 - \frac{\beta}{4}\eta^4 + \frac{\gamma}{6}\eta^6, \quad (3.1.2.16)$$

where η , β and γ are positive coefficients. The negative coefficient of the fourth-degree term has the effect of introducing more than one minimum in a certain temperature range. Fig. 3.1.2.7 shows the different shapes of the plot of $F(\eta)$ over different temperature ranges. The situation is similar to the one already discussed in the presence of a third-degree contribution to the free energy. It corresponds to a discontinuous transition associated with a latent heat as well as to the existence of a range of thermal hysteresis.

Two relevant questions arise from consideration of the above models of first-order transitions.

In the first place, one can object to the use of a polynomial expansion of the free energy in cases involving a discontinuity of the order parameter while the assumption of continuity of the phase transition has been used as an essential substrate of the argument developed. However, the approach will clearly keep its validity if a transition, though discontinuous, involves 'small' discontinuities. The criterion for estimating if a discontinuity is small relies on the comparison between the atomic displacements involved by the transition and the distances between atoms in the structure. If the displacements are a small fraction of the distances between atoms, then the method used can be consid-

3.1. STRUCTURAL PHASE TRANSITIONS

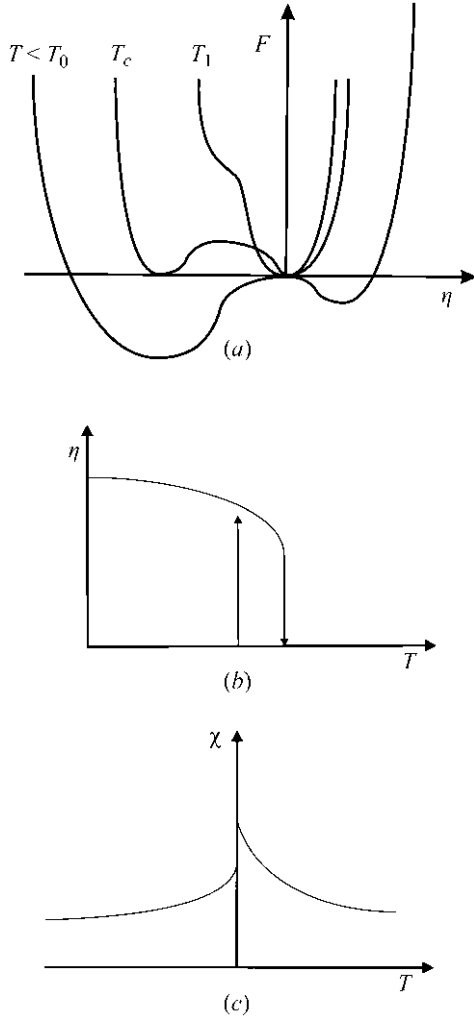


Fig. 3.1.2.6. (a) Plots of the free energy as a function of the order parameter for various temperature values in the framework of the model of a discontinuous transition associated with equation (3.1.2.13). (b) Temperature dependence of the equilibrium value of the order parameter, as determined by the model of a discontinuous transition. (c) Temperature dependence of the susceptibility in this model.

ered as valid. Indeed, the total free energy of the system depends on the distance between atoms, because this distance controls the strength of the interaction energy within the system. Hence, the transition only changes in a minor way the value of the system's free energy.

On the other hand, one has to check that there are systems of physical interest for which the crystallographic symmetry allows free-energy forms of the type (3.1.2.13), (3.1.2.16). Indeed, the crystallographic symmetry relative to the example in Section 3.1.2.2 was such that the presence of a third-degree term in the Landau free energy was excluded.

Such verification is not necessary for the free energy of type (3.1.2.16). This free energy is only characterized by a *specific sign* of the coefficient of the fourth-degree term, a circumstance that is not defined by symmetry considerations.

By contrast, an actual crystallographic model of a transition described by (3.1.2.13), which involves a term of degree three, is required to support the relevance of the corresponding model. Such a model is provided, for instance, by a crystal the high-temperature phase of which has a rhombohedral symmetry (e.g. $R3m$), and which undergoes a transition corresponding to an atomic displacement \mathbf{d} perpendicular to the ternary axis (Fig. 3.1.2.8).

If we refer the components to a rectangular frame of coordinates, the matrices representing the mode of transformation of the components (d_x, d_y) under application of the generating

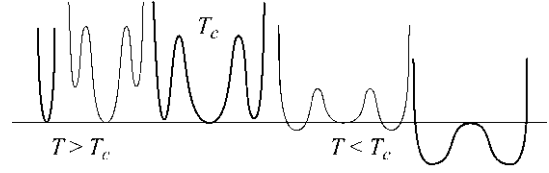


Fig. 3.1.2.7. Plots of the free energy as a function of the order parameter for various temperatures in the framework of the model of a discontinuous transition associated with equation (3.1.2.16). The temperature decreases from right to left, the transition being reached for the temperature corresponding to the third plot.

elements of the group $R3m$ have a form reproduced in existing tables. It is easy to check that the form of the Landau free energy resulting from a search of invariant polynomials of successive degrees is

$$F = F_0 + \frac{\alpha(T - T_0)}{2}(d_x^2 + d_y^2) + \frac{\delta}{3}(d_x^2 - 3d_y^2) + \frac{\beta}{4}(d_x^2 + d_y^2)^2. \quad (3.1.2.17)$$

We note that the form of the free energy of this system, determined by its symmetry, involves a third-degree term. Let us show that the thermodynamic properties corresponding to this form are qualitatively identical to the ones derived from the canonical free energy (3.1.2.13). In this view, let us put $d_x = \eta \cos \theta$ and $d_y = \eta \sin \theta$. The free energy takes the form

$$F = F_0 + \frac{\alpha(T - T_0)}{2}\eta^2 + \frac{\delta}{3}\eta^3 \cos \theta (\cos^2 \theta - 3 \sin^2 \theta) + \frac{\beta}{4}\eta^4. \quad (3.1.2.18)$$

For such a free energy, it is remarkable that for $\eta \neq 0$ the directions θ of the extrema, which are determined by $\partial F / \partial \theta = 0$, are independent of the value of η . These directions form two sets which we denote A ($\theta = 0, 2\pi/3, 4\pi/3$) and B ($\pi/3, \pi, -\pi/3$). If we replace in equation (3.1.2.18) η by one of these values, we obtain

$$F = F_0 + \frac{\alpha(T - T_0)}{2}\eta^2 \pm \frac{\delta}{3}\eta^3 + \frac{\beta}{4}\eta^4, \quad (3.1.2.19)$$

the sign in front of the δ coefficient being $+$ for the A set of θ angles and $-$ for the B set. We are therefore brought back to a form close to the canonical one [equation (3.1.2.13)]. Note that for $\delta > 0$, the stable second minimum of the free energy [equation (3.1.2.15)] corresponded to $\eta < 0$, i.e. to $\delta\eta < 0$. Hence in (3.1.2.19), η being a positive modulus, the second stable minimum will correspond to a negative coefficient for η^3 . Depending on the sign of δ , the direction θ of this minimum will either be the set A or the set B of θ values.

3.1.2.4. Generalization of the approach

Let us summarize the results obtained in the study of the specific models described in the preceding sections. We have shown that an order parameter (e.g. d_z or d_x, d_y) is a set of scalar degrees of freedom that allows the description of the symmetry and physical changes accompanying the phase transition in a system. The equilibrium values of the n components of the order parameter are zero for $T \geq T_c$ and *not all zero* for $T < T_c$. The n components define a vector space that is an irreducible invariant

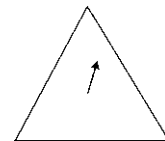


Fig. 3.1.2.8. Schematic representation of the displacement associated with the order parameter in a crystal having trigonal (rhombohedral) symmetry.

3. PHASE TRANSITIONS, TWINNING AND DOMAIN STRUCTURES

space by the group G , which is the crystallographic symmetry group of the high-temperature phase. A variational free energy F associated with the transition, and termed the Landau free energy, can be expanded as a function of the components of the order parameter. The second-degree term of this expansion has a coefficient that vanishes and changes sign at the transition temperature. The form of F is determined by the symmetry properties of the order parameter, *i.e.* by the mode of transformation of the components of the order parameter into each other when the operations of G are applied to them. The specific form of F determines the symmetries of the potentially stable phases below T_c , the degeneracy of these phases, the temperature dependencies of relevant physical quantities and, in certain cases, the thermodynamic order of the phase transition.

In this section, let us briefly outline the arguments used in order to formulate the theory in a general framework.

These arguments rely in part on the properties of the irreducible representations of a group. The reader can refer to Chapter 1.2 for a comprehensive presentation of irreducible representations. We will consider here representations of a group G carried by a set of degrees of freedom $(\eta_1, \eta_2, \eta_3, \dots)$, and use essentially the following properties.

(a) If the set is irreducible and non-totally symmetric (trivial), there is no linear combination $f_1(\eta_i) = \alpha_1\eta_1 + \alpha_2\eta_2 + \dots$ of the η_i that is invariant by all the elements of G .

(b) If the set is irreducible, there is a single homogeneous polynomial of degree two that is invariant by the group G . Its form is $f_2 = \sum \eta_i^2$.

(c) If $g(\mathbf{r})$ is an arbitrary function of the space coordinates $[\mathbf{r} = (x, y, z)]$, one can always write

$$g(\mathbf{r}) = \sum_{\gamma} \sum_j \varphi_{\gamma,j}(\mathbf{r}), \quad (3.1.2.20)$$

where each set of functions $\varphi_{\gamma,j}$ ($j = 1, 2, \dots, p$) defines a space generated by the p functions which is invariant and irreducible by the group G and corresponds to the irreducible representation labelled τ_{γ} of G .

3.1.2.4.1. Description of the phase transition

In order to generalize the considerations developed in the preceding sections, we have to define, independently from any specific structure, the basic ingredients of the theory: definition of a variational set of degrees of freedom; construction of a free energy; determination of the stable states on either side of a transition temperature.

In a first step, we describe an arbitrary atomic configuration of a system by the set of densities $\rho_i(\mathbf{r})$ of the particles of type (i) . This set constitutes variational degrees of freedom, which can be used to construct the variational free energy of the system $F[T, \rho_i(\mathbf{r})]$. The equilibrium of the system is defined by the set of functions $\rho_i^{\text{eq}}(T, \mathbf{r})$ that minimize the free energy.

The symmetry of the system at a given temperature is defined as the set of geometrical transformations that leave invariant all the ρ_i^{eq} . This set forms a group.

We are then in a position to define a *continuous transition* at T_c by two conditions:

(i) The $\rho_i^{\text{eq}}(T, \mathbf{r})$ are functions whose forms change continuously across T_c .

(ii) The symmetry group of the system just above T_c is different to the symmetry just below T_c . Hence the phase transition, though associated with a *continuous* change of the spatial configuration of the atoms, is associated with a *sudden* change of the symmetry.

3.1.2.4.2. Order parameter

As compared with the set (d_x, d_y, d_z) used in the example of Section 3.1.2.2, the variational functions $\rho_i(\mathbf{r})$ have the drawback

of not being *small and scalar* quantities, thus making an expansion of the free energy more complicated.

Without loss of generality, let us restrict ourselves to a single type of (i) particles. In order to remove the difficulty mentioned above we put

$$\rho(\mathbf{r}) = \rho_0(\mathbf{r}) + \sum \sum \eta_{\gamma,j} \varphi_{\gamma,j}(\mathbf{r}), \quad (3.1.2.21)$$

where $\rho_0 = \rho^{\text{eq}}(T_c, \mathbf{r})$ is the equilibrium density at T_c . Let us denote by G the symmetry group of this equilibrium density. The sum in the second part of (3.1.2.21) is a small increment since the transition is continuous. This increment has been expanded, as in (3.1.2.20), as a function of irreducible functions with respect to the group G . Moreover, each function has been expressed as the product of a normalized function $\varphi_{\gamma,j}$ and of small scalar parameters $\eta_{\gamma,j}$. It is easy to convince oneself that it is possible to consider that under the action of G either the $\varphi_{\gamma,j}$ transform into each other, the $\eta_{\gamma,j}$ being fixed coefficients, or the $\eta_{\gamma,j}$ transform into each other, the functions $\varphi_{\gamma,j}$ being fixed. *We shall adopt the second convention.* The variational free energy can then be written in the form

$$F = F[T, \eta_{\gamma,j}, \varphi_{\gamma,j}(\mathbf{r})]. \quad (3.1.2.22)$$

At each temperature, the characteristics of the system are specified by the following conditions:

(i) The equilibrium corresponds to the values $\eta_{\gamma,j}$ that make the free energy a minimum. These values define through (3.1.2.21) the equilibrium density of particles in the system.

(ii) The symmetry of the system is defined as the group of invariance of the determined equilibrium density.

Note that, in $(\rho - \rho_0)$, the contribution of the degrees of freedom $\eta_{\gamma,j}$ spanning a *totally symmetric representation* can be ignored in the first place. One can show that such a contribution would have the same symmetry on either side of the transition. Therefore it is not crucially associated with the symmetry change defining the phase transition.

Following the ideas introduced in Section 3.1.2.2, the free-energy form is obtained as a Taylor expansion as a function of the small parameters $\eta_{\gamma,j}$. Besides, each polynomial term of a given degree of this expansion is invariant by G . Indeed, F , being a scalar, is unchanged by any rotation or reflection. Among the transformations, those belonging to G have the additional property of leaving invariant the density ρ_0 which is, besides T and the $\eta_{\gamma,j}$, an argument of the function F .

It is easy to check that the group-theoretical rules recalled at the beginning of this section determine the absence of an invariant linear term in the expansion. Moreover, these rules specify the form of the second-degree contribution. We have

$$F = F_0(T) + \sum \alpha_{\gamma} (\sum \eta_{\gamma,j}^2). \quad (3.1.2.23)$$

On the other hand, the equilibrium density is

$$\rho^{\text{eq}} - \rho_0 = \sum \sum \eta_{\gamma,j}^0 \varphi_{\gamma,j}(\mathbf{r}). \quad (3.1.2.24)$$

Let us first consider the system at T_c . The equilibrium values of all the $\eta_{\gamma,j}$ are zero. Hence, on the basis of (3.1.2.23), we conclude that all the α_{γ} satisfy the condition $\alpha_{\gamma} > 0$ (since the second-degree expansion must be minimum at the origin). Note that this condition *cannot be strict for all γ* . Otherwise, these coefficients would also be positive in the vicinity of T_c , on either side of this temperature. As a consequence, the equilibrium values $\eta_{\gamma,j}^0$ would all be zero and the symmetry would be unchanged. *Hence, one at least of the α_{γ} has to vanish and to change sign at T_c .* An argument already invoked in Section 3.1.2.2 allows one to assert that one α_{γ} coefficient only has this property. The $\eta_{\gamma,j}$ corresponding to the other indices γ keep zero equilibrium values in the vicinity of T_c and can be ignored in the first place. We can therefore drop in (3.1.2.23) all degrees of freedom except the ones associated with

3.1. STRUCTURAL PHASE TRANSITIONS

the α_γ coefficient that vanishes at T_c . The set $\eta_{\gamma,j}$ ($j = 1, 2, \dots, m$) constitutes the m -dimensional order parameter of the transition considered. As this set comprises all the degrees of freedom contributing to a single second-degree term in the free energy, it necessarily constitutes a basis for an irreducible vector space with respect to G , according to the group-theoretical rules recalled above.

3.1.2.4.3. Stable states and symmetry in the vicinity of T_c

Above T_c , due to the positivity of α (we can drop the γ index), the equilibrium values of the η_j are zero and the symmetry is G , identical to the symmetry at T_c . Below T_c , α is negative and the minimum of F occurs away from the origin in the $\{\eta_j\}$ space. The symmetry of the system is defined by all the transformations leaving invariant the density:

$$\rho^{\text{eq}} = \rho_0 + \sum \eta_j^0 \varphi_j(\mathbf{r}). \quad (3.1.2.25)$$

Since the η_j^0 contribution to the second member is small, these transformations have to be selected among those belonging to the invariance group of ρ_0 . The space $\{\eta_j\}$ defines a *non-trivial representation* of the latter group since the linear combination of the order-parameter components present in ρ^{eq} cannot be invariant by all the transformations of G . The symmetry group of the system below T_c is therefore a subgroup F of G .

As pointed out in Section 3.1.2.2, in order to determine the minimum of F below T_c , it is necessary to expand the free energy to degrees higher than two. The relevant expression of the free energy is then

$$F = F_0(T, \rho_0) + \frac{1}{2}\alpha(T - T_c)(\sum \eta_j^2) + f_3(\eta_j) + f_4(\eta_j) + \dots, \quad (3.1.2.26)$$

where we have developed the coefficient α , which is an odd function of $(T - T_c)$ to the lowest degree in $(T - T_c)$. It can be shown that the existence of a third-degree term $f_3(\eta_j)$ depends exclusively on the nature of the representation τ_γ associated with the order parameter. If the symmetry of the order parameter is such that a third-degree term is not symmetry forbidden, the transition will be of the type analysed in Section 3.1.2.3: it will be discontinuous.

For any symmetry of the order parameter, fourth-degree terms $f_4(\eta_j)$ will always be present in the free-energy expansion (there will be at least one such term that is the square of the second-degree term). No further general statement can be made. Depending on the form and coefficients of this term, a continuous or discontinuous transition will be possible towards one or several distinct low-symmetry phases. The form of the $f_4(\eta_j)$ term can be determined by searching the most general fourth-degree polynomial that is invariant by the set of transformations belonging to G .

In summary, in the light of the preceding considerations, the study of a phase transition according to the Landau scheme can be developed along the following lines:

(a) Search, as a starting information on the system, the symmetry group G of the more symmetric phase surrounding the transition and the nature of the irreducible representation τ_γ associated with the order parameter. Both can be obtained from a crystallographic investigation as illustrated by the example in the next section.

(b) Check the possibility of a third-degree invariant on symmetry grounds.

(c) Construct the free energy by determining the form of the invariant polynomials of the required degrees.

(d) Determine, as a function of the coefficients of the free-energy expansion, the absolute minimum of F .

(e) For each minimum, determine the invariance group of the density ρ^{eq} , i.e. the 'low-symmetry' group of the system.

(f) Derive the temperature dependence of the quantities related to the order parameter component η_j .

(g) Consider (as discussed in the next section) the coupling of the order parameter to other relevant 'secondary' degrees of freedom, and derive the temperature dependence of these quantities.

3.1.2.5. Application to the structural transformation in a real system

Let us examine the particular ingredients needed to apply Landau's theory to an example of *structural* transitions, i.e. a transition between crystalline phases.

3.1.2.5.1. Nature of the groups and of their irreducible representations

The phases considered being crystalline, their invariance groups, G or F , coincide with *crystallographic space groups*. Let us only recall here that each of these groups of infinite order is constituted by elements of the form $\{R|\mathbf{t}\}$ where R is a point-symmetry operation and \mathbf{t} a translation. The symmetry operations R generate the point group of the crystal. On the other hand, among the translations \mathbf{t} there is a subset forming an infinite group of 'primitive' translations \mathbf{T} generating the three-dimensional Bravais lattice of the crystal.

For a space group G , there is an infinite set of unequivalent irreducible representations. An introduction to their properties can be found in Chapter 1.2 as well as in a number of textbooks. They cannot be tabulated in a synthetic manner as the better-known representations of finite groups. They have to be constructed starting from simpler representations. Namely, each representation is labelled by a double index.

(i) The first index is a \mathbf{k} vector in reciprocal space, belonging to the first Brillouin zone of this space. The former vector defines a subgroup $G(\mathbf{k})$ of G . This group is the set of elements $\{R|\mathbf{t}\}$ of G whose component R leaves \mathbf{k} unmoved, or transforms it into an 'equivalent' vector (i.e. differing from \mathbf{k} by a reciprocal-lattice vector). The group $G(\mathbf{k})$ has irreducible representations labelled $\tau_m(\mathbf{k})$ of dimension n_m which are defined in available tables.

(ii) A representation of G can be denoted $\Gamma_{\mathbf{k},m}$. It can be constructed according to systematic rules on the basis of the knowledge of $\tau_m(\mathbf{k})$. Its dimension is $n_m r$ where r is the number of vectors in the 'star' of \mathbf{k} . This star is the set of vectors, unequivalent to \mathbf{k} , having the same modulus as \mathbf{k} and obtained from \mathbf{k} by application of all the point-symmetry elements R of G .

3.1.2.5.2. The example of gadolinium molybdate, $Gd_2(MoO_4)_3$

Gadolinium molybdate (GMO) is a substance showing one complication with respect to the example in Section 3.1.2.2. Like the prototype example already studied, it possesses below its phase transition an electric dipole (and a spontaneous polarization) resulting from the displacement of ions. However, one does not observe the expected divergence of the associated susceptibility (Fig. 3.1.2.5).

3.1.2.5.2.1. Experimental identification of the order-parameter symmetry

The high-temperature space group G is known for GMO from X-ray diffraction experiments. It is the tetragonal space group $P4_2/m$. The corresponding point group $42m$ has eight elements, represented in Fig. 3.1.2.9.

The \mathbf{k} vector labelling the irreducible representation associated with the order parameter can be directly deduced from a comparison of the diffraction spectra above and below T_c . We have seen that the difference of the two stable structures surrounding the transition is specified by the equilibrium density:

$$\rho(T, \mathbf{r}) - \rho(T_c, \mathbf{r}) = \sum \eta_{\mathbf{k},m} \varphi_{\mathbf{k},m}(\mathbf{r}). \quad (3.1.2.27)$$

3. PHASE TRANSITIONS, TWINNING AND DOMAIN STRUCTURES

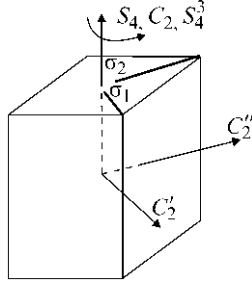


Fig. 3.1.2.9. Rotations/reflections belonging to the point group of gadolinium molybdate.

One can show, using the properties of the irreducible representations of the space groups, that the Fourier transform of the difference of densities given above is proportional to $\delta(\mathbf{K} - \mathbf{k})$, i.e. this Fourier transform is nonzero only for a \mathbf{K} vector equal to the \mathbf{k} vector indexing the order parameter. The implication of this property is that below T_c , the X-ray spectrum of the system will contain additional reflections whose locations in reciprocal space are defined by the vector of the order parameter. Experimentally, the vectors joining the Bragg spots existing in both phases to the *closest superlattice spots only appearing below T_c* are the vectors \mathbf{k} defining partly the irreducible representation $\Gamma_{\mathbf{k},m}$ that specifies the symmetry properties of the order parameter.

In GMO, X-ray diffraction measurements show that superlattice spots appear below T_c at one of the four equivalent \mathbf{k} vectors

$$\pm \frac{\mathbf{a}_1^* \pm \mathbf{a}_2^*}{2}. \quad (3.1.2.28)$$

The operations of the point group $\bar{4}2m$ transform these vectors into each other. The star of \mathbf{k} is therefore reduced to a single vector. On the other hand, consultation of available tables provides us with the possible representations $\tau_{\mathbf{k},m}$ necessary to construct the representation $\Gamma_{\mathbf{k},m}$ of the order parameter (the entries of the tables being the \mathbf{k} vector determined and the space group G). There are three unequivalent $\tau_{\mathbf{k},m}$, which are reproduced in Table 3.1.2.2.

The ambiguity in the symmetry of the order parameter has now to be lifted. In this approach, the method is to work out for each τ_m the symmetries G of the phases that are possibly stable below T_c . One then compares the results with the observed space group below T_c , which, for GMO, is the orthorhombic space group $Pba2$.

The group F of interest is the invariance group of the density difference [equation (3.1.2.27)]. Note that this difference can be considered as a 'vector' with components η_i in the irreducible space of the order parameter. In each irreducible space, the action of the elements of G on a vector is represented by the set

of matrices reproduced in Table 3.1.2.2. Let us first examine τ_1 in this table. Clearly, the matrices relative to $\{S_4|0\}$, $\{S_4^3|0\}$, $\{C_2'|t\}$ and $\{C_2''|t\}$ rotate by $\pi/2$ any vector of the two-dimensional space carrying the representation. These elements will not leave any direction unmoved and consequently they will not belong to F . The other elements either preserve any vector (and they then obviously belong to F) or they reverse any direction. However, in the latter case, the product of any two of these elements belongs to F .

Summarizing these remarks, we obtain a single possible group F consisting of the elements $\{E|0\}$, $\{C_2|a_1\}$, $\{\sigma_1|t\}$, $\{\sigma_2|t + a_1\}$ and by the infinite translation group generated by the vectors $(a_1 \pm a_2)$ and a_3 . The symbol for this space group is $Pmm2$.

A similar inspection yields for the representation τ_2 the group $Pba2$ and for τ_3 three possible groups ($P4$, $Pbm2$ and $P2$). Comparison with the experimental observation, recalled above, allows one to identify unambiguously the appropriate representation as τ_2 . In conclusion, the irreducible representation associated with the order parameter of the transition in GMO can be denoted $\Gamma_{\mathbf{k},m}$. Its \mathbf{k} vector is $\mathbf{k} = \pm(\mathbf{a}_1^* \pm \mathbf{a}_2^*)/2$, and its 'small representation' is $\tau_2(\mathbf{k})$. The number of components of the order parameter is two, equal to the dimension of $\Gamma_{\mathbf{k},m}$, which itself is equal to the product of the number of vectors in the star of \mathbf{k} (one) and of the dimension of τ_2 (two).

3.1.2.5.2.2. Construction of the free energy and stable states

Denote by (η_1, η_2) the two components of the order parameter. The Landau free energy can be constructed by selecting the homogeneous polynomials of different degrees that are invariant by the *distinct* matrices of τ_2 . There are four such matrices. It is easy to check that the most general form of fourth-degree polynomial invariant by the action of these four matrices is

$$F = F_0 + \frac{\alpha(T - T_c)}{2}(\eta_1^2 + \eta_2^2) + \frac{\beta_1}{4}(\eta_1^4 + \eta_2^4) + \frac{\beta_2}{2}\eta_1^2\eta_2^2 + \frac{\beta_3}{2}\eta_1\eta_2(\eta_1^2 - \eta_2^2). \quad (3.1.2.29)$$

A discussion of the minima of this free energy can be made according to the same method as in Section 3.1.2.3, by putting $\eta_1 = \rho \cos \theta$, $\eta_2 = \rho \sin \theta$. One then finds that, in accordance with the symmetry considerations developed in Section 3.1.2.5.2.1, there is a single possible symmetry below T_c . The equilibrium state of the system corresponds to an angle θ whose value depends on the values of the coefficients in the expansion. The modulus ρ has the standard temperature dependence $\rho \propto (T_c - T)^{1/2}$.

As in the model/example described in Section 3.1.2.2, below T_c there are several stable states having the same free energy. Indeed, one can easily check in expression (3.1.2.29) that if (η_1^0, η_2^0) is an absolute minimum of the free energy (3.1.2.29), the states $(-\eta_2^0, \eta_1^0)$, $(-\eta_1^0, \eta_2^0)$, $(-\eta_1^0, -\eta_2^0)$ are symmetry-related

Table 3.1.2.2. Matrices defining the irreducible representations of $Pba2$ for $\mathbf{k} = \mathbf{a}_1^* + \mathbf{a}_2^*$

| | G | | | | | | | | | | |
|----------|------------|-------------|--------------|---------------|------------------|------------------|--------------|---------------|----------------|----------------|----------------|
| | $\{E 0\}$ | $\{S_4 0\}$ | $\{C_2 0\}$ | $\{S_4^3 0\}$ | $\{\sigma_1 t\}$ | $\{\sigma_2 t\}$ | $\{C_2' t\}$ | $\{C_2'' t\}$ | \mathbf{a}_1 | \mathbf{a}_2 | \mathbf{a}_3 |
| τ_1 | 1 0 0 1 | 0 1 -1 0 | -1 0 0 -1 | 0 -1 1 0 | 1 0 0 1 | -1 0 0 -1 | 0 1 -1 0 | 0 -1 1 0 | -1 0 0 -1 | -1 0 0 -1 | 1 0 0 1 |
| τ_2 | 1 0 0 1 | 0 1 -1 0 | -1 0 0 -1 | 0 -1 1 0 | -1 0 0 -1 | 1 0 0 1 | 0 -1 1 0 | 0 1 -1 0 | -1 0 0 -1 | -1 0 0 -1 | 1 0 0 1 |
| τ_3 | 1 0 0 1 | 1 0 0 -1 | 1 0 0 1 | 1 0 0 -1 | 0 1 1 0 | 0 1 1 0 | 0 -1 1 0 | 0 -1 1 0 | -1 0 0 -1 | -1 0 0 -1 | 1 0 0 1 |

3.1. STRUCTURAL PHASE TRANSITIONS

minima corresponding to the same value of the equilibrium free energy.

The intensities of the diffraction ‘superlattice’ spots, being proportional to the square of the atomic displacement ρ , vary linearly as a function of temperature. On the other hand, the diverging susceptibility associated with the order parameter is related to a rapid increase of the diffuse scattering of X-rays or neutrons at the location of the superlattice spots in reciprocal space. Hence, consistent with the macroscopic measurements, it is not related to a divergence of the dielectric susceptibility.

3.1.2.5.2.3. Macroscopic behaviour of GMO

In GMO, macroscopic quantities are degrees of freedom that are distinct from the order parameter. Indeed, their symmetry properties are different, since any lattice translation will leave them invariant, while this is not the case for the order parameter (see Section 3.1.2.5.2.1). Nevertheless, certain of the macroscopic quantities behave singularly at the transition. These degrees of freedom can be decomposed, as shown in Section 3.1.2.4, as the sum of irreducible degrees of freedom. Having a symmetry different from that of the order parameter, they were neglected in the first step of the description of the phase transition. In a more detailed description, they have to be taken into account.

Let us, for instance, consider the P_z component of the dielectric polarization of GMO, as well as the ε component of the strain tensor which represents a shear in the xy plane of the crystal. The matrices in Table 3.1.2.3 recall the mode of transformation of the order-parameter components as well as those of these two quantities under the action of the G group.

We can complete the expression of the free energy of the system by adding to F in (3.1.2.29) the contributions of the preceding degrees of freedom up to the second degree (which, as will be seen, is comparable to the fourth degree used for the order parameter). The resulting expression is provided by (3.1.2.30) below, in which we have neglected a bilinear term in P_z and ε as this term does not change the qualitative result we want to establish.

$$F_1 = F + \frac{b}{2}P_z^2 + \frac{c}{2}\varepsilon^2 + \delta_1 P_z(\eta_1^2 - \eta_2^2) + \delta_2 \varepsilon(\eta_1^2 - \eta_2^2), \quad (3.1.2.30)$$

where F is provided by equation (3.1.2.29). At equilibrium, the derivatives of F_1 with respect to P_z and ε vanish. These conditions yield

$$P_z = -\frac{\delta_1}{b}(\eta_1^2 - \eta_2^2); \quad \varepsilon = -\frac{\delta_2}{c}(\eta_1^2 - \eta_2^2). \quad (3.1.2.31)$$

As stressed in Section 3.1.2.5.2.2, the equilibrium direction in the order-parameter space corresponds to the trivial $\theta = 0$ angle. Hence $(\eta_1^2 - \eta_2^2) \neq 0$ below T_c , resulting in the fact that nonzero values of P_z and ε will onset below the transition temperature. Besides, the form (3.1.2.31) indicates that the two macroscopic quantities considered, which are proportional to the square of the order parameter, are expected to vary linearly as a function of temperature below T_c . Note that terms such as P_z^2 are of the same order of magnitude as fourth-degree terms of the order parameter.

We can also determine the behaviour of the dielectric susceptibility χ , by calculating the variations of the equilibrium

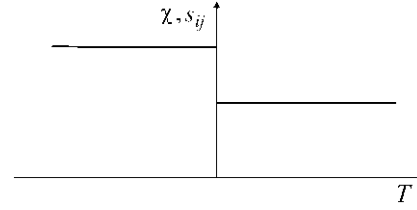


Fig. 3.1.2.10. Temperature dependence of the macroscopic susceptibility (or elastic compliance, s_{ij}) in gadolinium molybdate. Compare with the ‘normal’ behaviour in Fig. 3.1.2.5(b).

value of P_z as a function of an applied electric field \mathbf{E} parallel to the polarization. We proceed as in Section 3.1.2.2, and minimize the potential $G_1 = (F_1 - P_z E)$ with respect to the order parameter and to the polarization. In order to obtain the qualitative behaviour of χ , we simplify the free energy by considering a single component of the order parameter. We also neglect the shear strain component ε . The set of simplified equations

$$\chi = \frac{\partial P_z}{\partial E} | E = 0; \quad bP_z + \delta\eta^2 = E \quad (3.1.2.32)$$

$$\frac{\partial F_1}{\partial E} = \eta \left\{ \alpha(T - T_c) + \left(\beta - \frac{2\delta_1^2}{b} \right) \eta^2 + \frac{2\delta_1}{b} E \right\}$$

yields the following expression of the susceptibility:

$$\chi = \frac{1}{b} \quad \text{for } T > T_c \quad \text{and} \quad \chi = \frac{1}{b} + \frac{2\delta_1^2}{b(\beta - 2\delta_1^2/b)} \quad \text{for } T < T_c. \quad (3.1.2.33)$$

We find an upward step of the dielectric susceptibility on cooling. Likewise, consideration of the ‘elastic’ susceptibility relative to the shear strain component ε would determine an upward step of the elastic compliance (Fig. 3.1.2.10). The more usually measured elastic constant, which is the inverse of the compliance, undergoes a downward step on cooling.

We have seen in the preceding paragraph that the low-symmetry phase of gadolinium molybdate possesses four equally stable states differing by the values of the order-parameter components. Equation (3.1.2.31) shows that two of the states are associated with the same sign of the polarization P_z or of the shear strain ε , while the two other states possess opposite values of P_z and ε . According to the definitions given in Section 3.1.1, gadolinium molybdate belongs to the category of ferroelectrics as well as to that of ferroelastics.

The example of GMO clearly shows that the ferroic classification is less informative than the one based on the order-parameter symmetry. The latter determines the full symmetry change (orientational and translational), while the former only specifies the orientational symmetry change. On the other hand, the ferroic classification is not informative about the physical behaviour as a function of temperature. Thus, the model ferroelectric in Section 3.1.2.2 has a diverging dielectric susceptibility at T_c , while a GMO-type ferroelectric keeps a finite susceptibility. The ferroic classification has nevertheless the advantage of specifying the nature of the macroscopic quantities that are expected to behave anomalously at the transition, and are therefore worth measuring.

Table 3.1.2.3. Action of the generators of $P6_3/m2$ on the order parameter and on the polarization and strain components

| | E | S_4 | σ_1 | \mathbf{a}_1 | \mathbf{a}_2 | \mathbf{a}_3 |
|---------------|-----|-------|------------|----------------|----------------|----------------|
| η_1 | 1 0 | 0 1 | -1 0 | -1 0 | -1 0 | 1 0 |
| η_2 | 0 1 | -1 0 | 0 -1 | 0 -1 | 0 -1 | 0 1 |
| P_z | 1 | -1 | 1 | 1 | 1 | 1 |
| ε | 1 | -1 | 1 | 1 | 1 | 1 |

3. PHASE TRANSITIONS, TWINNING AND DOMAIN STRUCTURES

3.1.3. Equitranslational phase transitions. Property tensors at ferroic phase transitions

BY V. JANOVEC AND V. KOPSKÝ

In the Landau theory, presented in the preceding Section 3.1.2, symmetry considerations and thermodynamics are closely interwoven. These two aspects can be, at least to some extent, disentangled and some basic symmetry conditions formulated and utilized without explicitly invoking thermodynamics. Statements which follow directly from symmetry are exact but usually do not yield numerical results. These can be obtained by a subsequent thermodynamic or statistical treatment.

The central point of this section is Table 3.1.3.1, which contains results of symmetry analysis for a large class of equitranslational phase transitions and presents data on changes of property tensors at most ferroic phase transitions. Notions and statements relevant to these two applications are explained in Sections 3.1.3.1 and 3.1.3.2, respectively. Table 3.1.3.1 with a detailed explanation is displayed in Section 3.1.3.3. Examples illustrating possible uses of the table are given in Section 3.1.3.4.

3.1.3.1. Equitranslational phase transitions and their order parameters

A basic role is played in symmetry considerations by the relation between the space group \mathcal{G} of the high symmetry *parent* or *prototype* phase, the space group \mathcal{F} of the low-symmetry *ferroic* phase and the order parameter η : The low-symmetry group \mathcal{F} consists of all operations of the high-symmetry group \mathcal{G} that leave the order parameter η invariant. By the term *order parameter* we mean the primary order parameter, *i.e.* that set of degrees of freedom whose coefficient of the quadratic invariant changes sign at the phase-transition temperature (see Sections 3.1.2.2.4 and 3.1.2.4.2).

What matters in these considerations is not the physical nature of η but the transformation properties of η , which are expressed by the representation Γ_η of \mathcal{G} . The order parameter η with d_η components can be treated as a vector in a d_η -dimensional carrier space V_η of the representation Γ_η , and the low-symmetry group \mathcal{F} comprises all operations of \mathcal{G} that do not change this vector. If Γ_η is a real one-dimensional representation, then the low-symmetry group \mathcal{F} consists of those operations $g \in \mathcal{G}$ for which the matrices $D^{(\eta)}(g)$ [or characters $\chi_\eta(g)$] of the representation Γ_η equal one, $D^{(\eta)}(g) = \chi_\eta(g) = 1$. This condition is satisfied by one half of all operations of \mathcal{G} (index of \mathcal{F} in \mathcal{G} is two) and thus the real one-dimensional representation Γ_η determines the ferroic group \mathcal{F} unambiguously.

A real multidimensional representation Γ_η can induce several low-symmetry groups. A *general vector* of the carrier space V_η of Γ_η is invariant under all operations of a group $\text{Ker } \Gamma_\eta$, called the *kernel of representation* Γ_η , which is a normal subgroup of \mathcal{G} comprising all operations $g \in \mathcal{G}$ for which the matrix $D^{(\eta)}(g)$ is the unit matrix. Besides that, *special vectors* of V_η – specified by relations restricting values of order-parameter components (*e.g.* some components of η equal zero, some components are equal *etc.*) – may be invariant under larger groups than the kernel $\text{Ker } \Gamma_\eta$. These groups are called *epikernels* of Γ_η (Ascher & Kobayashi, 1977). The kernel and epikernels of Γ_η represent potential symmetries of the ferroic phases associated with the representation Γ_η . Thermodynamic considerations can decide which of these phases is stable at a given temperature and external fields.

Another fundamental result of the Landau theory is that components of the order parameter of all continuous (second-order) and some discontinuous (first-order) phase transitions transform according to an irreducible representation of the space group \mathcal{G} of the high-symmetry phase (see Sections 3.1.2.4.2 and 3.1.2.3). Since the components of the order parameter are real numbers, this condition requires irreducibility over the field of

real numbers (so-called *physical irreducibility* or *R-irreducibility*). This means that the matrices $D^{(\eta)}(g)$ of *R-irreducible* representations (abbreviated *R-ireps*) can contain only real numbers. (Physically irreducible matrix representations are denoted by $D^{(\omega)}$ instead of the symbol Γ_α used in general considerations.)

As explained in Section 1.2.3 and illustrated by the example of gadolinium molybdate in Section 3.1.2.5, an irreducible representation $\Gamma_{\mathbf{k},m}$ of a space group is specified by a vector \mathbf{k} of the first Brillouin zone, and by an irreducible representation $\tau_m(\mathbf{k})$ of the little group of \mathbf{k} , denoted $G(\mathbf{k})$. It turns out that the vector \mathbf{k} determines the change of the translational symmetry at the phase transition (see *e.g.* Tolédano & Tolédano, 1987; Izyumov & Syromiatnikov, 1990; Tolédano & Dmitriev, 1996). Thus, unless one restricts the choice of the vector \mathbf{k} , one would have an infinite number of phase transitions with different changes of the translational symmetry.

In this section, we restrict ourselves to representations with zero \mathbf{k} vector (this situation is conveniently denoted as the Γ point). Then there is no change of translational symmetry at the transition. In this case, the group \mathcal{F} is called an *equitranslational* or *translationengleiche* (*t*) *subgroup* of \mathcal{G} , and this change of symmetry will be called an *equitranslational symmetry descent* $\mathcal{G} \Downarrow^t \mathcal{F}$. An *equitranslational phase transition* is a transition with an equitranslational symmetry descent $\mathcal{G} \Downarrow^t \mathcal{F}$.

Any ferroic space-group-symmetry descent $\mathcal{G} \Downarrow \mathcal{F}$ uniquely defines the corresponding symmetry descent $G \Downarrow F$, where G and F are the point groups of the space groups \mathcal{G} and \mathcal{F} , respectively. Conversely, the equitranslational subgroup \mathcal{F} of a given space group \mathcal{G} is uniquely determined by the point-group symmetry descent $G \Downarrow F$, where G and F are point groups of space groups \mathcal{G} and \mathcal{F} , respectively. In other words, a point-group symmetry descent $G \Downarrow F$ defines the set of all equitranslational space-group symmetry descents $\mathcal{G} \Downarrow^t \mathcal{F}$, where \mathcal{G} runs through all space groups with the point group G . All equitranslational space-group symmetry descents $\mathcal{G} \Downarrow^t \mathcal{F}$ are available in the software *GI*KoBo-1*, where more details about the equitranslational subgroups can also be found.

Irreducible and reducible representations of the parent point group G are related in a similar way to irreducible representations with vector $\mathbf{k} = \mathbf{0}$ for all space groups \mathcal{G} with the point group G by a simple process called *engendering* (Jansen & Boon, 1967). The translation subgroup \mathbf{T}_G of \mathcal{G} is a normal subgroup and the point group G is isomorphic to a factor group \mathcal{G}/\mathbf{T}_G . This means that to every element $g \in G$ there correspond all elements $\{g|\mathbf{t} + \mathbf{u}_G(g)\}$ of the space group \mathcal{G} with the same linear constituent g , the same non-primitive translation $\mathbf{u}_G(g)$ and any vector \mathbf{t} of the translation group \mathbf{T}_G (see Section 1.2.3.1). If a representation of the point group G is given by matrices $D(g)$, then the corresponding engendered representation of a space group \mathcal{G} with vector $\mathbf{k} = \mathbf{0}$ assigns the same matrix $D(g)$ to all elements $\{g|\mathbf{t} + \mathbf{u}_G(g)\}$ of \mathcal{G} .

From this it further follows that a representation Γ_η of a point group G describes transformation properties of the primary order parameter for all equitranslational phase transitions with point-symmetry descent $G \Downarrow F$. This result is utilized in the presentation of Table 3.1.3.1.

3.1.3.2. Property tensors at ferroic phase transitions. Tensor parameters

The primary order parameter expresses the ‘difference’ between the low-symmetry and high-symmetry structures and can be, in a microscopic description, identified with spontaneous displacements of atoms (frozen in soft mode) or with an increase of order of molecular arrangement. To find a microscopic interpretation of order parameters, it is necessary to perform mode analysis (see *e.g.* Rousseau *et al.*, 1981; Aroyo & Perez-Mato, 1998), which takes into account the microscopic structure of the parent phase.

3.1. STRUCTURAL PHASE TRANSITIONS

Physical properties of crystals in a continuum description are described by *physical property tensors* (see Section 1.1.1.2), for short *property tensors* [equivalent expressions are *matter tensors* (Nowick, 1995; Wadhawan, 2000) or *material tensors* (Shuvalov, 1988)]. Property tensors are usually expressed in a Cartesian (rectangular) coordinate system [in Russian textbooks called a *crystallophysical system of coordinates* (Sirotnin & Shaskolskaya, 1982; Shuvalov, 1988)] which is related to the *crystallographic coordinate system* (IT A, 2002) by convention (see *IEEE Standard on Piezoelectricity*, 1987; Sirotnin & Shaskolskaya, 1982; Shuvalov, 1988). In what follows, *Cartesian coordinates* will mean coordinates in the crystallophysical system and tensor components will mean components in this coordinate system.

As explained in Section 1.1.4, the number of independent components of property tensors depends on the point-group symmetry of the crystal: the higher this symmetry is, the smaller this number is. Lowering of point-group symmetry at ferroic phase transitions is, therefore, always accompanied by an increased number of independent components of some property tensors. This effect manifests itself by the appearance of *morphic* (Strukov & Levanyuk, 1998) or *spontaneous tensor components*, which are zero in the parent phase and nonzero in the ferroic phase, and/or by symmetry-breaking increments of nonzero components in the ferroic phase that break relations between these tensor components which hold in the parent phase. Thus, for example, the strain tensor has two independent components $u_{11} = u_{22}, u_{33}$ in a tetragonal phase and four independent components $u_{11} \neq u_{22}, u_{33}, u_{12}$ in a monoclinic phase. In a tetragonal-to-monoclinic phase transition there is one morphic component u_{12} and one relation $u_{11} = u_{22}$ is broken by the *symmetry-breaking increment* $\delta u_{11} = -\delta u_{22}$.

Changes of property tensors at a ferroic phase transition can be described in an alternative manner in which no symmetry-breaking increments but only morphic terms appear. As we have seen, the transformation properties of the primary order parameter η are described by a d_η -dimensional R -irreducible matrix representation $D^{(\eta)}$ of the group G . One can form d_η linear combinations of Cartesian tensor components that transform according to the same representation $D^{(\eta)}$. These linear combinations will be called *components of a principal tensor parameter* of the ferroic phase transition with a symmetry descent $G \Downarrow F$. Equivalent designations are *covariant tensor components* (Kopský, 1979a) or *symmetry coordinates* (Nowick, 1995) of representation Γ_η of group G . Unlike the primary order parameter of a ferroic phase transition, a principal tensor parameter is not uniquely defined since one can always form further principal tensor parameters from Cartesian components of higher-rank tensors. However, only the principal tensor parameters formed from components of one, or even several, property tensors up to rank four are physically significant.

A principal tensor parameter introduced in this way has the same basic properties as the primary order parameter: it is zero in the parent phase and nonzero in the ferroic phase, and transforms according to the same R -irrep $D^{(\eta)}$. However, these two quantities have different physical nature: the primary order parameter of an equitranslational phase transition is a homogeneous microscopic distortion of the parent phase, whereas the principal tensor parameter describes the macroscopic manifestation of this microscopic distortion. Equitranslational phase transitions thus possess the unique property that their primary order parameter can be represented by principal tensor parameters which can be identified and measured by macroscopic techniques.

If the primary order parameter transforms as a vector, the corresponding principal tensor parameter is a dielectric polarization (*spontaneous polarization*) and the equitranslational phase transition is called a *proper ferroelectric phase transition*. Similarly, if the primary order parameter transforms as components of a symmetric second-rank tensor, the corresponding

principal tensor parameter is a *spontaneous strain* (or *spontaneous deformation*) and the equitranslational phase transition is called a *proper ferroelastic phase transition*.

A conspicuous feature of equitranslational phase transitions is a steep anomaly (theoretically an infinite singularity for continuous transitions) of the generalized susceptibility associated with the primary order parameter, especially the dielectric susceptibility near a proper ferroelectric transition (see Section 3.1.2.2.5) and the elastic compliance near a proper ferroelastic transition (see e.g. Tolédano & Tolédano, 1987; Tolédano & Dmitriev, 1996; Strukov & Levanyuk, 1998).

Any symmetry property of a ferroic phase transition has its pendant in domain structure. Thus it appears that any two ferroic single domain states differ in the values of the principal tensor parameters, i.e. principal tensor parameters ensure tensor distinction of any two ferroic domain states. If, in particular, the principal order parameter is polarization, then any two ferroic domain states differ in the direction of spontaneous polarization. Such a ferroic phase is called a *full ferroelectric phase* (Aizu, 1970). In this case, the number of ferroic domain states equals the number of ferroelectric domain states. Similarly, if any two ferroic domain states exhibit different spontaneous strain, then the ferroic phase is a *full ferroelastic phase*. An equivalent condition is an equal number of ferroic and ferroelastic domain states (see Sections 3.4.2.1 and 3.4.2.2).

The principal tensor parameters do not cover all changes of property tensors at the phase transition. Let $D^{(\lambda)}$ be a d_λ -dimensional matrix R -irrep of G with an epikernel (or kernel) L which is an intermediate group between F and G , in other words, L is a supergroup of F and a subgroup of G ,

$$F \subset L \subset G. \quad (3.1.3.1)$$

This means that a vector λ of the d_λ -dimensional carrier space V_λ of $D^{(\lambda)}$ is invariant under operations of L . The vector λ specifies a *secondary order parameter* of the transition, i.e. λ is a morphic quantity, the appearance of which lowers the symmetry from G to L (for more details on secondary order parameters see Tolédano & Tolédano, 1987; Tolédano & Dmitriev, 1996). Intermediate groups (3.1.3.1) can be conveniently traced in lattices of subgroups displayed in Figs. 3.1.3.1 and 3.1.3.2.

One can form linear combinations of Cartesian tensor components that transform according to $D^{(\lambda)}$. These combinations are components of a *secondary tensor parameter* which represents a macroscopic appearance of the secondary order parameter λ .

If a secondary tensor parameter is a spontaneous polarization and no primary order parameter with this property exists, the phase transition is called an *improper ferroelectric phase transition* (Dvořák, 1974; Levanyuk & Sannikov, 1974). Similarly, an *improper ferroelastic phase transition* is specified by existence of a secondary tensor parameter that transforms as components of the symmetric second-rank tensor (spontaneous strain) and by absence of a primary order parameter with this property. Unlike proper ferroelectric and proper ferroelastic phase transitions, which are confined to equitranslational phase transitions, the improper ferroelectric and improper ferroelastic phase transitions appear most often in non-equitranslational phase transitions. Classic examples are an improper ferroelectric phase transition in gadolinium molybdate (see Section 3.1.2.5.2) and an improper ferroelastic phase transition in strontium titanate (see Section 3.1.5.2.3). Examples of equitranslational improper ferroelectric and ferroelastic symmetry descents can be found in Table 3.1.3.2.

Secondary tensor parameters and corresponding susceptibilities exhibit less pronounced changes near the transition than those associated with the primary order parameter (see e.g. Tolédano & Tolédano, 1987; Tolédano & Dmitriev, 1996; Strukov & Levanyuk, 1998).

3. PHASE TRANSITIONS, TWINNING AND DOMAIN STRUCTURES

Table 3.1.3.1. *Point-group symmetry descents associated with irreducible representations*

Property tensors that appear in this table: ε enantiomorphism, chirality; P_i dielectric polarization; u_μ strain; g_μ optical activity; $d_{i\mu}$ piezoelectric tensor; $A_{i\mu}$ electrogyration tensor; $\pi_{\mu\nu}$ piezo-optic tensor ($i = 1, 2, 3$; $\mu, \nu = 1, 2, \dots, 6$). Applications of this table to symmetry analysis of equitranslational phase transitions and to changes of property tensors at ferroic transitions are explained in Section 3.1.3.3.

(a) Triclinic parent groups

| R -irep Γ_η | Standard variables | Ferroic symmetry | | Principal tensor parameters | Domain states | | | |
|--|-----------------------|------------------|-------|-----------------------------|--------------------------------------|-------|-------|---|
| | | F_1 | n_F | | n_f | n_a | n_e | |
| Parent symmetry G : $\mathbf{1} \ C_1$ | | | | | | | | |
| No ferroic symmetry descent | | | | | | | | |
| Parent symmetry G : $\bar{\mathbf{1}} \ C_i$ | | | | | | | | |
| A_u | x_1^- | 1 | C_1 | 1 | All components of odd parity tensors | 2 | 1 | 2 |

(b) Monoclinic parent groups

| R -irep Γ_η | Standard variables | Ferroic symmetry | | Principal tensor parameters | Domain states | | |
|---|-----------------------|------------------|-------|------------------------------|---------------|-------|-------|
| | | F_1 | n_F | | n_f | n_a | n_e |
| Parent symmetry G: $2_z \ C_{2z}$ | | | | | | | |
| B | x_3 | $1 \ C_1$ | 1 | $P_1, P_2; u_4, u_5$ | 2 | 2 | 2 |
| Parent symmetry G: $m_z \ C_{sz}$ | | | | | | | |
| A'' | x_3 | $1 \ C_1$ | 1 | $\varepsilon; P_3; u_4, u_5$ | 2 | 2 | 2 |
| Parent symmetry G: $2_z/m_z \ C_{2hz}$ | | | | | | | |
| B_g | x_3^+ | $\bar{1} \ C_i$ | 1 | u_4, u_5 | 2 | 2 | 0 |
| A_u | x_1^- | $2_z \ C_{2z}$ | 1 | $\varepsilon; P_3$ | 2 | 1 | 2 |
| B_u | x_3^- | $m_z \ C_{sz}$ | 1 | P_1, P_2 | 2 | 1 | 2 |

(c) Orthorhombic parent groups

| R -irep Γ_η | Standard variables | Ferroic symmetry | | Principal tensor parameters | Domain states | | | |
|--|-----------------------|-------------------------------|-----------|-----------------------------|--|-------|-------|---|
| | | F_1 | n_F | | n_f | n_a | n_e | |
| Parent symmetry G: $\mathbf{2}_x\mathbf{2}_y\mathbf{2}_z \ D_2$ | | | | | | | | |
| B_{1g} | x_2 | 2_z | C_{2z} | 1 | $P_3; u_6$ | 2 | 2 | 2 |
| B_{3g} | x_3 | 2_x | C_{2x} | 1 | $P_1; u_4$ | 2 | 2 | 2 |
| B_{2g} | x_4 | 2_y | C_{2y} | 1 | $P_2; u_5$ | 2 | 2 | 2 |
| Parent symmetry G: $m_xm_y\mathbf{2}_z \ C_{2vz}$ | | | | | | | | |
| A_2 | x_2 | 2_z | C_{2z} | 1 | u_6 | 2 | 2 | 1 |
| B_2 | x_3 | m_x | C_{xx} | 1 | $P_2; u_4$ | 2 | 2 | 2 |
| B_1 | x_4 | m_y | C_{yy} | 1 | $P_1; u_5$ | 2 | 2 | 2 |
| Parent symmetry G: $m_xm_ym_z \ D_{2h}$ | | | | | | | | |
| B_{1g} | x_2^+ | $2_z/m_z$ | C_{2hz} | 1 | u_6 | 2 | 2 | 0 |
| B_{3g} | x_3^+ | $2_x/m_x$ | C_{2hx} | 1 | u_4 | 2 | 2 | 0 |
| B_{2g} | x_4^+ | $2_y/m_y$ | C_{2hy} | 1 | u_5 | 2 | 2 | 0 |
| A_{1u} | x_1^- | $2_x\mathbf{2}_y\mathbf{2}_z$ | D_2 | 1 | $\varepsilon; g_1, g_2, g_3; d_{14}, d_{25}, d_{36}$ | 2 | 1 | 0 |
| B_{1u} | x_2^- | $m_xm_y\mathbf{2}_z$ | C_{2vz} | 1 | P_3 | 2 | 1 | 2 |
| B_{3u} | x_3^- | $2_xm_y\mathbf{2}_z$ | C_{2vx} | 1 | P_1 | 2 | 1 | 2 |
| B_{2u} | x_4^- | $m_x\mathbf{2}_ym_z$ | C_{2vy} | 1 | P_2 | 2 | 1 | 2 |

(d) Tetragonal parent groups

| R -irep Γ_η | Standard variables | Ferroic symmetry | | Principal tensor parameters | Domain states | | | |
|--|-----------------------|------------------|-----------|-----------------------------|--|-------|-------|---|
| | | F_1 | n_F | | n_f | n_a | n_e | |
| Parent symmetry G: $4_z \ C_{4z}$ | | | | | | | | |
| B | x_3 | 2_z | C_{2z} | 1 | $\delta u_1 = -\delta u_2, u_6$ | 2 | 2 | 1 |
| $^1E \oplus ^2E$ (Li) | (x_1, y_1) | 1 | C_1 | 1 | $(P_1, P_2); (u_4, -u_5)$ | 4 | 4 | 4 |
| Parent symmetry G: $\bar{4}_z \ S_{4z}$ | | | | | | | | |
| B | x_3 | 2_z | C_{2z} | 1 | $\varepsilon; P_3; \delta u_1 = -\delta u_2, u_6$ | 2 | 2 | 2 |
| $^1E \oplus ^2E$ | (x_1, y_1) | 1 | C_1 | 1 | $(P_1, -P_2); (u_4, -u_5)$ | 4 | 4 | 4 |
| Parent symmetry G: $4_z/m_z \ C_{4hz}$ | | | | | | | | |
| B_g | x_3^+ | $2_z/m_z$ | C_{2hz} | 1 | $\delta u_1 = -\delta u_2, u_6$ | 2 | 2 | 0 |
| A_u | x_1^- | 4_z | C_{4z} | 1 | $\varepsilon; P_3$ | 2 | 1 | 2 |
| B_u | x_3^- | $\bar{4}_z$ | S_{4z} | 1 | $g_1 = -g_2, g_6; d_{31} = -d_{32}, d_{36}, d_{14} = d_{25}, d_{15} = -d_{24}$ | 2 | 1 | 0 |
| $^1E_g \oplus ^2E_g$ | (x_1^+, y_1^+) | $\bar{1}$ | C_i | 1 | $(u_4, -u_5)$ | 4 | 4 | 0 |
| $^1E_u \oplus ^2E_u$ | (x_1^-, y_1^-) | m_z | C_{sz} | 1 | (P_1, P_2) | 4 | 2 | 4 |

3.1. STRUCTURAL PHASE TRANSITIONS

Table 3.1.3.1 (cont.)

| R-irep Γ_η | Standard variables | Ferroic symmetry | | Principal tensor parameters | Domain states | | | |
|--|-----------------------|------------------------|-----------------|-----------------------------|---|-------|-------|---|
| | | F_1 | n_F | | n_f | n_a | n_e | |
| Parent symmetry G : $4_2 2_x 2_{xy} D_{4z}$ | | | | | | | | |
| A_2 | x_2 | 4_z | C_{4z} | 1 | P_3 | 2 | 1 | 2 |
| B_1 | x_3 | $2_x 2_y 2_z$ | \hat{D}_2 | 1 | $\delta u_1 = -\delta u_2$ | 2 | 2 | 0 |
| B_2 | x_4 | $2_{xy} 2_{xy} 2_z$ | \hat{D}_{2z} | 1 | u_6 | 2 | 2 | 0 |
| E | $(x_1, 0)$ | 2_x | C_{2x} | 2 | $P_1; u_4$ | 4 | 4 | 4 |
| | (x_1, x_1) | 2_{xy} | C_{2xy} | 2 | $P_1 = P_2; u_4 = -u_5$ | 4 | 4 | 4 |
| (Li) | (x_1, y_1) | 1 | C_1 | 1 | $(P_1, P_2); (u_4, -u_5)$ | 8 | 8 | 8 |
| Parent symmetry G : $4_2 m_x m_{xy} C_{4vz}$ | | | | | | | | |
| A_2 | x_2 | 4_z | C_{4z} | 1 | $\varepsilon; g_1 = g_2, g_3; d_{14} = -d_{25}$ | 2 | 1 | 1 |
| B_1 | x_3 | $m_x m_y 2_z$ | C_{2vz} | 1 | $\delta u_1 = -\delta u_2$ | 2 | 2 | 1 |
| B_2 | x_4 | $m_{xy} m_{xy} 2_z$ | \hat{C}_{2vz} | 1 | u_6 | 2 | 2 | 1 |
| E | $(x_1, 0)$ | m_x | C_{xx} | 2 | $P_2; u_4$ | 4 | 4 | 4 |
| | (x_1, x_1) | m_{xy} | C_{xxy} | 2 | $P_2 = -P_1; u_4 = -u_5$ | 4 | 4 | 4 |
| | (x_1, y_1) | 1 | C_1 | 1 | $(P_2, -P_1); (u_4, -u_5)$ | 8 | 8 | 8 |
| Parent symmetry G : $\bar{4}_2 2_x m_{xy} D_{2dz}$ | | | | | | | | |
| A_2 | x_2 | $\bar{4}_z$ | S_{4z} | 1 | $g_6; d_{31} = -d_{32}, d_{15} = -d_{24}$ | 2 | 1 | 0 |
| B_1 | x_3 | $2_x 2_y 2_z$ | \hat{D}_2 | 1 | $\varepsilon; \delta u_1 = -\delta u_2$ | 2 | 2 | 0 |
| B_2 | x_4 | $m_{xy} m_{xy} 2_z$ | \hat{C}_{2vz} | 1 | $P_3; u_6$ | 2 | 2 | 2 |
| E | $(x_1, 0)$ | 2_x | C_{2x} | 2 | $P_1; u_4$ | 4 | 4 | 4 |
| | (x_1, x_1) | m_{xy} | C_{xxy} | 2 | $P_1 = -P_2; u_4 = -u_5$ | 4 | 4 | 4 |
| | (x_1, y_1) | 1 | C_1 | 1 | $(P_1, -P_2); (u_4, -u_5)$ | 8 | 8 | 8 |
| Parent symmetry G : $\bar{4}_2 m_x 2_{xy} \hat{D}_{2dz}$ | | | | | | | | |
| A_2 | x_2 | $\bar{4}_z$ | S_{4z} | 1 | $g_1 = -g_2; d_{36}, d_{14} = d_{25}$ | 2 | 1 | 0 |
| B_2 | x_3 | $m_x m_y 2_z$ | C_{2vz} | 1 | $P_3; \delta u_1 = -\delta u_2$ | 2 | 2 | 2 |
| B_1 | x_4 | $2_{xy} 2_{xy} 2_z$ | \hat{D}_{2z} | 1 | $\varepsilon; u_6$ | 2 | 2 | 0 |
| E | $(x_1, 0)$ | m_x | C_{xx} | 2 | $P_2; u_4$ | 4 | 4 | 4 |
| | (x_1, x_1) | 2_{xy} | C_{2xy} | 2 | $P_2 = P_1; u_4 = -u_5$ | 4 | 4 | 4 |
| | (x_1, y_1) | 1 | C_1 | 1 | $(P_2, P_1); (u_4, -u_5)$ | 8 | 8 | 8 |
| Parent symmetry G : $4_z/m_x m_x m_{xy} D_{4hz}$ | | | | | | | | |
| A_{2g} | x_2^+ | $4_z/m_x$ | C_{4hz} | 1 | $A_{31} = A_{32}, A_{33}, A_{15} = A_{24}$ | 2 | 1 | 0 |
| B_{1g} | x_3^+ | $m_x m_y m_z$ | \hat{D}_{2h} | 1 | $\delta u_1 = -\delta u_2$ | 2 | 2 | 0 |
| B_{2g} | x_4^+ | $m_{xy} m_{xy} m_z$ | \hat{D}_{2hz} | 1 | u_6 | 2 | 2 | 0 |
| A_{1u} | x_1^- | $4_z 2_x 2_{xy}$ | D_{4z} | 1 | $\varepsilon; g_1 = g_2, g_3; d_{14} = -d_{25}$ | 2 | 1 | 0 |
| A_{2u} | x_2^- | $4_z m_x m_{xy}$ | C_{4vz} | 1 | P_3 | 2 | 1 | 2 |
| B_{1u} | x_3^- | $\bar{4}_z 2_x m_{xy}$ | D_{2dz} | 1 | $g_1 = -g_2; d_{14} = d_{25}, d_{36}$ | 2 | 1 | 0 |
| B_{2u} | x_4^- | $\bar{4}_z m_x 2_{xy}$ | \hat{D}_{2dz} | 1 | $g_6; d_{31} = -d_{32}, d_{15} = -d_{24}$ | 2 | 1 | 0 |
| E_g | $(x_1^+, 0)$ | $2_x/m_x$ | C_{2hx} | 2 | u_4 | 4 | 4 | 0 |
| | (x_1^+, x_1^+) | $2_{xy}/m_{xy}$ | C_{2hxy} | 2 | $u_4 = -u_5$ | 4 | 4 | 0 |
| | (x_1^+, y_1^+) | 1 | C_i | 1 | $(u_4, -u_5)$ | 8 | 8 | 0 |
| E_u | $(x_1^-, 0)$ | $2_x m_y m_z$ | C_{2vx} | 2 | P_1 | 4 | 2 | 4 |
| | (x_1^-, x_1^-) | $m_{xy} 2_{xy} m_z$ | C_{2vxy} | 2 | $P_1 = P_2$ | 4 | 2 | 4 |
| | (x_1^-, y_1^-) | m_z | C_{sz} | 1 | (P_1, P_2) | 8 | 8 | 8 |

(e) Trigonal parent groups

| R -irep Γ_η | Standard variables | Ferroic symmetry | | Principal tensor parameters | Domain states | | |
|--|----------------------------|----------------------------------|--------|--|---------------|--------|--------|
| | | F_1 | n_F | | n_f | n_a | n_e |
| Parent symmetry G: $3_z \quad C_3$ | | | | | | | |
| E (La, Li) | (x_1, y_1) | 1 C_1 | 1 | (P_1, P_2) $(u_1 - u_2, -2u_6), (u_4, -u_5)$ $\delta u_1 = -\delta u_2$ | 3 | 3 | 3 |
| Parent symmetry G: $\bar{3}_z \quad C_{3i}$ | | | | | | | |
| A_u | x_1^- | $3_z \quad C_3$ | 1 | $\varepsilon; P_3$ | 2 | 1 | 2 |
| E_g (La) | (x_1^+, y_1^+) | $\bar{1} \quad C_i$ | 1 | $(u_1 - u_2, -2u_6), (u_4, -u_5)$ $\delta u_1 = -\delta u_2$ | 3 | 3 | 0 |
| E_u | (x_1^-, y_1^-) | 1 C_1 | 1 | (P_1, P_2) | 6 | 3 | 6 |
| Parent symmetry G: $3_z 2_x \quad D_{3x}$ | | | | | | | |
| A_2 | x_2 | $3_z \quad C_3$ | 1 | P_3 | 2 | 1 | 2 |
| E (La, Li) | $(x_1, 0)$ (x_1, y_1) | $2_x \quad C_{2x}$ 1 C_1 | 3 1 | $P_1; \delta u_1 = -\delta u_2, u_4$ $(P_1, P_2); (u_1 - u_2, -2u_6), (u_4, -u_5)$ | 3 6 | 3 6 | 3 6 |
| Parent symmetry G: $3_z m_x \quad C_{3vx}$ | | | | | | | |
| A_2 | x_2 | $3_z \quad C_3$ | 1 | $\varepsilon; g_1 = g_2, g_3; d_{11} = -d_{12} = -d_{26}, d_{14} = -d_{25}$ | 2 | 1 | 1 |
| E (La) | $(x_1, 0)$ (x_1, y_1) | $m_x \quad C_{xx}$ 1 C_1 | 3 1 | $P_2; \delta u_1 = -\delta u_2, u_4$ $(P_2, -P_1); (u_1 - u_2, -2u_6), (u_4, -u_5)$ | 3 6 | 3 6 | 3 6 |

3. PHASE TRANSITIONS, TWINNING AND DOMAIN STRUCTURES

Table 3.1.3.1 (cont.)

| R -irep Γ_η | Standard variables | Ferroic symmetry | | Principal tensor parameters | Domain states | | | |
|---|-----------------------|------------------|-----------|-----------------------------|---|-------|-------|----|
| | | F_1 | n_F | | n_f | n_a | n_e | |
| Parent symmetry G: $\bar{3}_z m_x D_{3dx}$ | | | | | | | | |
| A_{2g} | x_2^+ | $\bar{3}_z$ | C_{3i} | 1 | $A_{22} = -A_{21} = -A_{16}, A_{31} = A_{32}, A_{33}, A_{15} = A_{24}$ | 2 | 1 | 0 |
| A_{1u} | x_1^- | $3_z 2_x$ | D_{3x} | 1 | $\varepsilon; g_1 = g_2, g_3; d_{11} = -d_{12} = -d_{26}, d_{14} = -d_{25}$ | 2 | 1 | 0 |
| A_{2u} | x_2^- | $3_z m_x$ | C_{3vx} | 1 | P_3 | 2 | 1 | 2 |
| E_g | $(x_1^+, 0)$ | $2_x/m_x$ | C_{2hx} | 3 | $\delta u_1 = -\delta u_2, u_4$ | 3 | 3 | 0 |
| (La) | (x_1^+, y_1^+) | $\bar{1}$ | C_i | 1 | $(u_1 - u_2, -2u_6), (u_4, -u_5)$ | 6 | 6 | 0 |
| E_u | $(0, y_1^-)$ | m_x | C_{xx} | 3 | P_2 | 6 | 3 | 6 |
| | $(x_1^-, 0)$ | 2_x | C_{2x} | 3 | P_1 | 6 | 3 | 6 |
| | (x_1^-, y_1^-) | $\bar{1}$ | C_1 | 1 | (P_1, P_2) | 12 | 6 | 12 |
| Parent symmetry G: $3_z 2_y D_{3y}$ | | | | | | | | |
| A_2 | x_2 | 3_z | C_3 | 1 | P_3 | 2 | 1 | 2 |
| E | $(0, y_1)$ | 2_y | C_{2y} | 3 | $P_2; \delta u_1 = -\delta u_2, u_5$ | 3 | 3 | 3 |
| (La, Li) | (x_1, y_1) | $\bar{1}$ | C_1 | 1 | $(P_1, P_2); (2u_6, u_1 - u_2), (u_4, -u_5)$ | 6 | 6 | 6 |
| Parent symmetry G: $3_z m_y C_{3vy}$ | | | | | | | | |
| A_2 | x_2 | 3_z | C_3 | 1 | $\varepsilon; g_1 = g_2, g_3; d_{22} = -d_{21} = -d_{16}, d_{14} = -d_{25}$ | 2 | 1 | 1 |
| E | $(0, y_1)$ | m_y | C_{sy} | 3 | $P_1; \delta u_1 = -\delta u_2, u_5$ | 3 | 3 | 3 |
| (La) | (x_1, y_1) | $\bar{1}$ | C_1 | 1 | $(P_2, -P_1); (2u_6, u_1 - u_2), (u_4, -u_5)$ | 6 | 6 | 6 |
| Parent symmetry G: $\bar{3}_z m_y D_{3dy}$ | | | | | | | | |
| A_{2g} | x_2^+ | $\bar{3}_z$ | C_{3i} | 1 | $A_{11} = -A_{12} = -A_{26}, A_{31} = A_{32}, A_{33}, A_{15} = A_{24}$ | 2 | 1 | 0 |
| A_{1u} | x_1^- | $3_z 2_y$ | D_{3y} | 1 | $\varepsilon; g_1 = g_2, g_3; d_{22} = -d_{21} = -d_{16}, d_{14} = -d_{25}$ | 2 | 1 | 0 |
| A_{2u} | x_2^- | $3_z m_y$ | C_{3vy} | 1 | P_3 | 2 | 1 | 2 |
| E_g | $(0, y_1^+)$ | $2_y/m_y$ | C_{2hy} | 3 | $\delta u_1 = -\delta u_2, u_5$ | 3 | 3 | 0 |
| (La) | (x_1^+, y_1^+) | $\bar{1}$ | C_i | 1 | $(2u_6, u_1 - u_2), (u_4, -u_5)$ | 6 | 6 | 0 |
| E_u | $(0, y_1^-)$ | 2_y | C_{2y} | 3 | P_2 | 6 | 3 | 6 |
| | $(x_1^-, 0)$ | m_y | C_{sy} | 3 | P_1 | 6 | 3 | 6 |
| | (x_1^-, y_1^-) | $\bar{1}$ | C_1 | 1 | (P_1, P_2) | 12 | 6 | 12 |

(f) Hexagonal parent groups

Covariants with standardized labels and conversion equations:

$$\begin{aligned}
 g_1^- &= g_1 + g_2; & g_{2x}^- &= g_1 - g_2, & g_{2y}^- &= 2g_6 \\
 g_1 &= \frac{1}{2}(g_1^- + g_{2x}^-), & g_2 &= \frac{1}{2}(g_1^- - g_{2x}^-); & \delta g_1 &= -\delta g_2 = \frac{1}{2}g_{2x}^- \\
 d_1^- &= d_{14} - d_{25}; & d_{2x,2}^- &= d_{14} + d_{25}, & d_{2y,2}^- &= d_{24} - d_{15} \\
 d_{2,1}^- &= d_{31} + d_{32}; & d_{2x,1}^- &= 2d_{36}, & d_{2y,1}^- &= d_{32} - d_{31} \\
 d_{14} &= \frac{1}{2}(d_1^- + d_{2x,2}^-), & d_{25} &= \frac{1}{2}(-d_1^- + d_{2x,2}^-); & \delta d_{14} &= \delta d_{25} = \frac{1}{2}d_{2x}^- \\
 d_{36} &= \frac{1}{2}d_{2x,1}^-, & d_{31} &= \frac{1}{2}(d_{2,1}^- - d_{2y,1}^-); & d_{32} &= \frac{1}{2}(d_{2,1}^- + d_{2y,1}^-).
 \end{aligned}$$

| R -irep Γ_η | Standard variables | Ferroic symmetry | | Principal tensor parameters | Domain states | | | |
|--|-----------------------|------------------|-----------|-----------------------------|--|-------|-------|---|
| | | F_1 | n_F | | n_f | n_a | n_e | |
| Parent symmetry G: $6_z \quad C_6$ | | | | | | | | |
| B | x_3 | 3_z | C_3 | 1 | $d_{11} = -d_{12} = -d_{26}, d_{22} = -d_{21} = -d_{16}$ | 2 | 1 | 1 |
| E_2 (La, Li) | (x_2, y_2) | 2_z | C_{2z} | 1 | $(u_1 - u_2, 2u_6) \delta u_1 = -\delta u_2$ | 3 | 3 | 1 |
| E_1 (Li) | (x_1, y_1) | 1 | C_1 | 1 | (P_1, P_2) $(u_4, -u_5)$ | 6 | 6 | 6 |
| Parent symmetry G: $\bar{6}_z \quad C_{3h}$ | | | | | | | | |
| A'' | x_3 | 3_z | C_3 | 1 | $\varepsilon; P_3$ | 2 | 1 | 2 |
| E' (La) | (x_2, y_2) | m_z | C_{sz} | 1 | (P_2, P_1) $(u_1 - u_2, 2u_6) \delta u_1 = -\delta u_2$ | 3 | 3 | 3 |
| E'' | (x_1, y_1) | 1 | C_1 | 1 | $(u_4, -u_5)$ | 6 | 6 | 6 |
| Parent symmetry G: $6_z/m_z \quad C_{6h}$ | | | | | | | | |
| B_g | X_3^+ | $\bar{3}_z$ | C_{3i} | 1 | $A_{11} = -A_{12} = -A_{26}, A_{22} = -A_{21} = -A_{16}$ | 2 | 1 | 0 |
| A_u | X_1^- | 6_z | C_6 | 1 | $\varepsilon; P_3$ | 2 | 1 | 2 |
| B_u | X_3^- | $\bar{6}_z$ | C_{3h} | 1 | $d_{11} = -d_{12} = -d_{26}, d_{22} = -d_{21} = -d_{16}$ | 2 | 1 | 0 |
| E_{2g} (La) | (x_2^+, y_2^+) | $2_z/m_z$ | C_{2hz} | 1 | $(u_1 - u_2, 2u_6) \delta u_1 = -\delta u_2$ | 3 | 3 | 0 |
| E_{1g} | (x_1^+, y_1^+) | $\bar{1}$ | C_i | 1 | $(u_4, -u_5)$ | 6 | 6 | 0 |
| E_{2u} | (x_2^-, y_2^-) | 2_z | C_{2z} | 1 | $(g_1 - g_2, 2g_6) \ g_1 = -g_2, g_6$ $(2d_{36}, d_{32} - d_{31}) \ d_{32} = -d_{31}, d_{36}$ $(d_{14} + d_{25}, d_{24} - d_{15}) \ d_{14} = d_{25}, d_{24} = -d_{15}$ | 6 | 3 | 2 |
| E_{1u} | (x_1^-, y_1^-) | m_z | C_{sz} | 1 | (P_1, P_2) | 6 | 3 | 6 |

3.1. STRUCTURAL PHASE TRANSITIONS

Table 3.1.3.1 (cont.)

| R -irep Γ_η | Standard variables | Ferroic symmetry | | | Principal tensor parameters | Domain states | | |
|--|--|-------------------------------------|------------------------------------|-------------|---|---------------|--------------|--------------|
| | | F_1 | | n_F | | n_f | n_o | n_e |
| Parent symmetry G: $6_{\bar{z}}2_x2_y \quad D_6$ | | | | | | | | |
| A_2 | x_2 | 6_z | C_6 | 1 | P_3 | 2 | 1 | 2 |
| B_1 | x_3 | 3_z2_x | D_{3x} | 1 | $d_{11} = -d_{12} = -d_{26}$ | 2 | 1 | 0 |
| B_2 | x_4 | 3_z2_y | D_{3y} | 1 | $d_{22} = -d_{21} = -d_{16}$ | 2 | 1 | 0 |
| E_2 (La, Li) | $(x_2, 0)$ (x_2, y_2) | $2_x2_y2_z$ 2_z | D_2 C_{2z} | 3 1 | $\delta u_1 = -\delta u_2$ $(u_1 - u_2, 2u_6)$ | 3 6 | 3 6 | 0 2 |
| E_1 (Li) | $(x_1, 0)$ $(0, y_1)$ (x_1, y_1) | 2_x 2_y 1 | C_{2x} C_{2y} C_1 | 3 3 1 | $P_1; u_4$ $P_2; u_5$ $(P_1, P_2); (u_4, -u_5)$ | 6 6 12 | 6 6 12 | 6 6 12 |
| Parent symmetry G: $6_zm_xm_y \quad C_{6v}$ | | | | | | | | |
| A_2 | x_2 | 6_z | C_6 | 1 | $\varepsilon; g_1 = g_2, g_3; d_{14} = -d_{25}$ | 2 | 1 | 1 |
| B_2 | x_3 | 3_zm_x | C_{3vx} | 1 | $d_{22} = -d_{21} = -d_{16}$ | 2 | 1 | 1 |
| B_1 | x_4 | 3_zm_y | C_{3vy} | 1 | $d_{11} = -d_{12} = -d_{26}$ | 2 | 1 | 1 |
| E_2 (La) | $(x_2, 0)$ (x_2, y_2) | $m_xm_y2_z$ 2_z | C_{2vz} C_{2z} | 3 1 | $\delta u_1 = -\delta u_2$ $(u_1 - u_2, 2u_6)$ | 3 6 | 3 6 | 1 1 |
| E_1 | $(x_1, 0)$ $(0, y_1)$ (x_1, y_1) | m_x m_y 1 | C_{xx} C_{yy} C_1 | 3 3 1 | $P_2; u_4$ $P_1; u_5$ $(P_2, -P_1); (u_4, -u_5)$ | 6 6 12 | 6 6 12 | 6 6 12 |
| Parent symmetry G: $\bar{6}_z2_xm_y \quad D_{3h}$ | | | | | | | | |
| A_2' | x_2 | $\bar{6}_z$ | C_{3h} | 1 | $d_{22} = -d_{21} = -d_{16}$ | 2 | 1 | 0 |
| A_1'' | x_3 | 3_z2_x | D_{3x} | 1 | $\varepsilon; g_1 = g_2, g_3; d_{14} = -d_{25}$ | 2 | 1 | 0 |
| A_2'' | x_4 | 3_zm_y | C_{3vy} | 1 | P_3 | 2 | 1 | 2 |
| E' (La) | $(x_2, 0)$ (x_2, y_2) | $2_xm_y2_z$ m_z | C_{2vx} C_{sz} | 3 1 | $P_1; \delta u_1 = -\delta u_2$ $(P_1, -P_2); (u_1 - u_2, 2u_6)$ | 3 6 | 3 6 | 3 6 |
| E'' | $(x_1, 0)$ $(0, y_1)$ (x_1, y_1) | 2_x m_y 1 | C_{2x} C_{yy} C_1 | 3 3 1 | u_4 u_5 $(u_4, -u_5)$ | 6 6 12 | 6 6 12 | 3 6 12 |
| Parent symmetry G: $\bar{6}_zm_x2_y \quad \hat{D}_{3h}$ | | | | | | | | |
| A_2' | x_2 | $\bar{6}_z$ | C_{3h} | 1 | $d_{11} = -d_{12} = -d_{26}$ | 2 | 1 | 0 |
| A_2'' | x_3 | 3_zm_x | C_{3vx} | 1 | P_3 | 2 | 1 | 2 |
| A_1' | x_4 | 3_z2_y | D_{3y} | 1 | $\varepsilon; g_1 = g_2, g_3; d_{14} = -d_{25}$ | 2 | 1 | 0 |
| E' (La) | $(x_2, 0)$ (x_2, y_2) | $m_x2_y2_z$ m_z | C_{2vy} C_{sz} | 3 1 | $P_2; \delta u_1 = -\delta u_2$ $(P_2, P_1); (u_1 - u_2, 2u_6)$ | 3 6 | 3 6 | 3 6 |
| E'' | $(x_1, 0)$ $(0, y_1)$ (x_1, y_1) | m_x 2_y 1 | C_{xx} C_{2y} C_1 | 3 3 1 | u_4 u_5 $(u_4, -u_5)$ | 6 6 12 | 6 6 12 | 6 3 12 |
| Parent symmetry G: $6_z/m_xm_xm_y \quad D_{6h}$ | | | | | | | | |
| A_{2g} | x_2^+ | $6_z/m_z$ | C_{6h} | 1 | $A_{31} = A_{32}, A_{33}, A_{15} = A_{24}$ | 2 | 1 | 0 |
| B_{1g} | x_3^+ | 3_zm_x | D_{3dx} | 1 | $A_{11} = -A_{12} = -A_{26}$ | 2 | 1 | 0 |
| B_{2g} | x_4^+ | 3_zm_y | D_{3dy} | 1 | $A_{22} = -A_{21} = -A_{16}$ | 2 | 1 | 0 |
| A_{1u} | x_1^- | $6_z2_x2_y$ | D_6 | 1 | $\varepsilon; g_1 = g_2, g_3; d_{14} = -d_{25}$ | 2 | 1 | 0 |
| A_{2u} | x_2^- | $6_zm_xm_y$ | C_{6v} | 1 | P_3 | 2 | 1 | 2 |
| B_{1u} | x_3^- | $\bar{6}_z2_xm_y$ | D_{3h} | 1 | $d_{11} = -d_{12} = -d_{26}$ | 2 | 1 | 0 |
| B_{2u} | x_4^- | $\bar{6}_zm_x2_y$ | \hat{D}_{3h} | 1 | $d_{22} = -d_{21} = -d_{16}$ | 2 | 1 | 0 |
| E_{2g} (La) | $(x_2^+, 0)$ (x_2^+, y_2^+) | $m_xm_y2_z$ $2_z/m_z$ | D_{2h} C_{2hz} | 3 1 | $\delta u_1 = -\delta u_2$ $(u_1 - u_2, 2u_6)$ | 3 6 | 3 6 | 0 0 |
| E_{1g} | $(x_1^+, 0)$ $(0, y_1^+)$ (x_1^+, y_1^+) | $2_x/m_x$ $2_y/m_y$ 1 | C_{2hx} C_{2hy} C_i | 3 3 1 | u_4 u_5 $(u_4, -u_5)$ | 6 6 12 | 6 6 12 | 0 0 0 |
| E_{1u} | $(x_1^-, 0)$ $(0, y_1^-)$ (x_1^-, y_1^-) | $2_xm_y2_z$ $m_x2_y2_z$ m_z | C_{2vx} C_{2vy} C_{sz} | 3 3 1 | P_1 P_2 (P_1, P_2) | 6 6 12 | 3 3 6 | 6 6 12 |
| E_{2u} | $(x_2^-, 0)$ $(0, y_2^-)$ (x_2^-, y_2^-) | $2_x2_y2_z$ $m_xm_y2_z$ 2_z | D_2 C_{2vz} C_{2z} | 3 3 1 | $\delta g_1 = -\delta g_2; d_{36}, \delta d_{14} = \delta d_{25}$ $g_6; d_{32} = -d_{31}, d_{24} = -d_{15}$ $(g_1 - g_2, 2g_6); (2d_{36}, d_{32} - d_{31}), (d_{14} + d_{25}, d_{24} - d_{15})$ | 6 6 12 | 3 3 6 | 0 2 2 |

In tensor distinction of domains, the secondary tensor parameters play a secondary role in a sense that some but not all ferroic domain states exhibit different values of the secondary tensor parameters. This property forms a basis for the concept of partial ferroic phases (Aizu, 1970): A ferroic phase is a *partial ferroelectric (ferroelastic)* one if some but not all domain states differ in spontaneous polarization (spontaneous strain). A non-ferroelectric phase denotes a ferroic phase which is either non-polar or which possesses a unique polar direction available

already in the parent phase. A non-ferroelastic phase exhibits no spontaneous strain.

3.1.3.3. Tables of equitranslational phase transitions associated with irreducible representations

The first systematic symmetry analysis of Landau-type phase transitions was performed by Indenbom (1960), who found all equitranslational phase transitions that can be accomplished

3. PHASE TRANSITIONS, TWINNING AND DOMAIN STRUCTURES

Table 3.1.3.1 (*cont.*)

(g) Cubic parent groups

Covariants with standardized labels and conversion equations:

$$\begin{aligned}
 u_{3x} &= u_{3x}^+ = u_3 - a(u_1 + u_2); & u_{3y} &= u_{3y}^+ = b(u_1 - u_2) \\
 \delta u_1 &= -\frac{1}{3}u_{3x}^+ + \frac{1}{\sqrt{3}}u_{3y}^+; & \delta u_2 &= -\frac{1}{3}u_{3x}^+ - \frac{1}{\sqrt{3}}u_{3y}^+; & \delta u_3 &= \frac{2}{3}u_{3x}^+ \\
 g_1^- &= g_1 + g_2 + g_3; & g_{3x}^- &= g_3 - a(g_1 + g_2); & g_{3y}^- &= b(g_1 - g_2) \\
 g_1 &= \frac{1}{3}g_1^- - \frac{1}{3}g_{3x}^- + \frac{1}{\sqrt{3}}g_{3y}^-; & g_2 &= \frac{1}{3}g_1^- - \frac{1}{3}g_{3x}^- - \frac{1}{\sqrt{3}}g_{3y}^-; & g_3 &= \frac{1}{3}g_1^- + \frac{2}{3}g_{3x}^- \\
 d_1^- &= d_{14} + d_{25} + d_{36}; & d_{3x}^- &= b(d_{14} - d_{25}); & d_{3y}^- &= a(d_{14} + d_{25}) - d_{36} \\
 d_{14} &= \frac{1}{3}d_1^- + \frac{1}{\sqrt{3}}d_{3x}^- + \frac{1}{3}d_{3y}^-; & d_{25} &= \frac{1}{3}d_1^- - \frac{1}{\sqrt{3}}d_{3x}^- + \frac{1}{3}d_{3y}^-; & d_{36} &= \frac{1}{3}d_1^- - \frac{2}{3}d_{3y}^- \\
 d_{1x} &= d_{13} - d_{12}; & d_{1y} &= d_{21} - d_{23}; & d_{1z} &= d_{32} - d_{31} \\
 d_{2x} &= d_{13} + d_{12}; & d_{2y} &= d_{21} + d_{23}; & d_{2z} &= d_{32} + d_{31} \\
 d_{13} &= \frac{1}{2}(d_{1x} + d_{2x}); & d_{21} &= \frac{1}{2}(d_{1y} + d_{2y}); & d_{32} &= \frac{1}{2}(d_{1z} + d_{2z}) \\
 d_{12} &= \frac{1}{2}(d_{2x} - d_{1x}); & d_{23} &= \frac{1}{2}(d_{2y} - d_{1y}); & d_{31} &= \frac{1}{2}(d_{2z} - d_{1z})
 \end{aligned}$$

$$a = \frac{1}{2}, b = \frac{\sqrt{3}}{2}, \pi_{\mu\nu}^a = (\pi_{\mu\nu} - \pi_{\nu\mu}), \mu = 1, 2, \dots, 6, \nu = 1, 2, \dots, 6.$$

| R-irep Γ_η | Standard variables | Ferroic symmetry | | n_F | Principal tensor parameters | Domain states | | |
|--------------------------------------|-------------------------|---------------------|----------------|-------|--|---------------|-------|-------|
| | | F_1 | | | | n_f | n_a | n_e |
| Parent symmetry G : 23 T | | | | | | | | |
| E (La) | (x_3, y_3) | $2_x 2_y 2_z$ | D_2 | 1 | $[u_3 - a(u_1 + u_2), b(u_1 - u_2)]$ $\delta u_1 + \delta u_2 + \delta u_3 = 0$ | 3 | 3 | 0 |
| T (La, Li) | $(0, 0, z_1)$ | 2_z | C_{2z} | 3 | $P_3; u_6$ | 6 | 6 | 6 |
| | (x_1, x_1, x_1) | 3_p | C_{3p} | 4 | $P_1 = P_2 = P_3; u_4 = u_5 = u_6$ | 4 | 4 | 4 |
| | (x_1, y_1, z_1) | 1 | C_1 | 1 | $(P_1, P_2, P_3); (u_4, u_5, u_6)$ | 12 | 12 | 12 |
| Parent symmetry G : $\bar{m}3 T_h$ | | | | | | | | |
| A_u | x_1^- | 23 | T | 1 | $\varepsilon; g_1 = g_2 = g_3; d_{14} = d_{25} = d_{36}$ | 2 | 1 | 0 |
| E_g (La) | (x_3^+, y_3^+) | $m_x m_y m_z$ | D_{2h} | 1 | $[u_3 - a(u_1 + u_2), b(u_1 - u_2)]$ $\delta u_1 + \delta u_2 + \delta u_3 = 0$ | 3 | 3 | 0 |
| E_u | (x_3^-, y_3^-) | $2_x 2_y 2_z$ | D_2 | 1 | $[g_3 - a(g_1 + g_2), b(g_1 - g_2)]$ $\delta g_1 + \delta g_2 + \delta g_3 = 0$ $[b(d_{14} - d_{25}), a(d_{14} + d_{25}) - d_{36}]$ $\delta d_{14} + \delta d_{25} + \delta d_{36} = 0$ | 6 | 3 | 0 |
| T_g (La) | $(0, 0, z_1^+)$ | $2_z/m_z$ | C_{2hz} | 3 | u_6 | 6 | 6 | 0 |
| | (x_1^+, x_1^+, x_1^+) | $\bar{3}_p$ | C_{3ip} | 4 | $u_4 = u_5 = u_6$ | 4 | 4 | 0 |
| | (x_1^+, y_1^+, z_1^+) | 1 | C_i | 1 | (u_4, u_5, u_6) | 12 | 12 | 0 |
| T_u | $(0, 0, z_1^-)$ | $m_x m_y 2_z$ | C_{2vz} | 3 | P_3 | 6 | 3 | 6 |
| | (x_1^-, x_1^-, x_1^-) | 3_p | C_{3p} | 4 | $P_1 = P_2 = P_3$ | 8 | 4 | 8 |
| | (x_1^-, y_1^-, z_1^-) | 1 | C_1 | 1 | (P_1, P_2, P_3) | 24 | 12 | 24 |
| Parent symmetry G : 432 O | | | | | | | | |
| A_2 | x_2 | 23 | T | 1 | $d_{14} = d_{25} = d_{36}$ | 2 | 1 | 0 |
| E (La) | $(x_3, 0)$ | $4_z 2_x 2_{xy}$ | D_{4z} | 3 | $\delta u_1 = \delta u_2 = -\frac{1}{2}\delta u_3$ | 3 | 3 | 0 |
| | (x_3, y_3) | $2_x 2_y 2_z$ | D_2 | 1 | $[u_3 - a(u_1 + u_2), b(u_1 - u_2)]$ $\delta u_1 + \delta u_2 + \delta u_3 = 0$ | 6 | 6 | 0 |
| T_1 (Li) | $(0, 0, z_1)$ | 4_z | C_{4z} | 3 | P_3 | 6 | 3 | 6 |
| | $(x_1, x_1, 0)$ | 2_{xy} | C_{2xy} | 6 | $P_1 = P_2$ | 12 | 12 | 12 |
| | (x_1, x_1, x_1) | 3_p | C_{3p} | 4 | $P_1 = P_2 = P_3$ | 8 | 4 | 8 |
| | (x_1, y_1, z_1) | 1 | C_1 | 1 | (P_1, P_2, P_3) | 24 | 24 | 24 |
| T_2 (La, Li) | $(0, 0, z_2)$ | $2_{xy} 2_{xy} 2_z$ | \hat{D}_{2z} | 3 | u_6 | 6 | 6 | 0 |
| | $(x_2, -x_2, z_2)$ | 2_{xy} | C_{2xy} | 6 | $u_4 = -u_5, u_6$ | 12 | 12 | 12 |
| | (x_2, x_2, x_2) | $3_p 2_{x\bar{y}}$ | D_{3p} | 4 | $u_4 = u_5 = u_6$ | 4 | 4 | 0 |
| | (x_2, y_2, z_2) | 1 | C_1 | 1 | (u_4, u_5, u_6) | 24 | 24 | 24 |

continuously. A table of all crystallographic point groups G along with all their physically irreducible representations, corresponding ferroic point groups F and related data has been compiled by Janovec *et al.* (1975). These data are presented in an improved form in Table 3.1.3.1 together with corresponding principal tensor parameters and numbers of ferroic, ferroelectric and ferroelastic domain states. This table facilitates solving of the following typical problems:

(1) *Inverse Landau problem* (Ascher & Kobayashi, 1977) of equitranslational phase transitions: For a given equitranslational symmetry descent $\mathcal{G} \Downarrow^t \mathcal{F}$ (determined for example from diffraction experiments), find the representation Γ_η of \mathcal{G} that specifies the transformation properties of the primary order parameter. Solution: In Table 3.1.3.1, one finds a physically irre-

ducible representation Γ_η of the point group G of \mathcal{G} with epikernel F (point group of \mathcal{F}). For some symmetry descents from cubic point groups $G = 432, 43m$ and $m\bar{3}m$, the inverse Landau problem has two solutions, which are given in Table 3.1.3.2.

If for a given symmetry descent $\mathcal{G} \Downarrow^t \mathcal{F}$ no appropriate R -irep exists in Table 3.1.3.1, then the primary order parameter η transforms according to a reducible representation of G . These transitions are always discontinuous and can be accomplished with several reducible representations. Some symmetry descents can be associated with an irreducible representation and with several reducible representations. All these transitions are treated in the software *GI★KoBo-1* and in Kopský (2001). All point-group symmetry descents are listed in Table 3.4.2.7 and can be traced in lattices of subgroups (see Figs. 3.1.3.1 and 3.1.3.2).

3.1. STRUCTURAL PHASE TRANSITIONS

Table 3.1.3.1 (*cont.*)

| R -irep Γ_η | Standard variables | Ferroic symmetry | | Principal tensor parameters | Domain states | | | |
|---|--|--|--|-----------------------------|---|---------------|--------------|--------------|
| | | F_1 | n_F | | n_f | n_a | n_e | |
| Parent symmetry G : $\bar{4}3m$ T_d | | | | | | | | |
| A_2 | x_2 | 23 | T | 1 | $\varepsilon; g_1 = g_2 = g_3$ $A_{14} = A_{25} = A_{36}; \pi_{23}^a = \pi_{31}^a = \pi_{12}^a$ | 2 | 1 | 0 |
| E (La) | $(x_3, 0)$ (x_3, y_3) | $\bar{4}_z 2_x m_{xy}$ $2_x 2_y 2_z$ | D_{2dz} D_2 | 3 1 | $\delta u_1 = \delta u_2 = -\frac{1}{2} \delta u_3$ $[u_3 - a(u_1 + u_2), b(u_1 - u_2)]$ $\delta u_1 + \delta u_2 + \delta u_3 = 0$ | 3 6 | 3 6 | 0 0 |
| T_1 | $(0, 0, z_1)$ $(x_1, x_1, 0)$ | $\bar{4}_z$ m_{xy} | S_{4z} C_{sxy} | 3 6 | $g_6; d_{32} = -d_{31}, d_{24} = -d_{15}$ $g_4 = g_5$ $d_{13} = -d_{23}, d_{12} = -d_{21}$ $d_{35} = -d_{34}, d_{26} = -d_{16}$ | 6 12 | 3 12 | 0 12 |
| | (x_1, x_1, x_1) | 3_p | C_{3p} | 4 | $g_4 = g_5 = g_6$ $d_{13} = d_{21} = d_{32}, d_{12} = d_{23} = d_{31}$ $d_{35} = d_{16} = d_{24}, d_{26} = d_{34} = d_{15}$ | 8 | 4 | 4 |
| | (x_1, y_1, z_1) | 1 | C_1 | 1 | (g_4, g_5, g_6) $(d_{13} - d_{12}, d_{21} - d_{23}, d_{32} - d_{31})$ $(d_{35} - d_{26}, d_{16} - d_{34}, d_{24} - d_{15})$ | 24 | 24 | 24 |
| | | | | | | | | |
| T_2 | $(0, 0, z_2)$ $(x_2, -x_2, z_2)$ (x_2, x_2, x_2) | $m_{x\bar{y}} m_{xy} 2_z$ m_{xy} $3_p m_{x\bar{y}}$ | \hat{C}_{2vz} C_{sxy} C_{3vp} | 3 6 4 | $P_3; u_6$ $P_1 = -P_2, P_3; u_4 = -u_5, u_6$ $P_1 = P_2 = P_3; u_4 = u_5 = u_6$ | 6 12 4 | 6 12 4 | 6 12 4 |
| (La) | (x_2, y_2, z_2) | 1 | C_1 | 1 | $(P_1, P_2, P_3); (u_4, u_5, u_6)$ | 24 | 24 | 24 |
| Parent symmetry G : $m\bar{3}m$ O_h | | | | | | | | |
| A_{2g} | x_2^+ | $m\bar{3}$ | T_h | 1 | $A_{14} = A_{25} = A_{36}; \pi_{23}^a = \pi_{31}^a = \pi_{12}^a$ | 2 | 1 | 0 |
| A_{1u} | x_1^- | 432 | O | 1 | $\varepsilon; g_1 = g_2 = g_3;$ | 2 | 1 | 0 |
| A_{2u} | x_2^- | $\bar{4}3m$ | T_d | 1 | $d_{14} = d_{25} = d_{36}$ | 2 | 1 | 0 |
| E_g (La) | $(x_3^+, 0)$ (x_3^+, y_3^+) | $4_z/m_z m_x m_{xy}$ $m_x m_y m_z$ | D_{4hz} D_{2h} | 3 1 | δu_3 $[\delta u_3 - a(\delta u_1 + \delta u_2), b(\delta u_1 - \delta u_2)]$ | 3 6 | 3 6 | 0 0 |
| E_u | $(x_3^-, 0)$ $(0, y_3^-)$ (x_3^-, y_3^-) | $4_z 2_x 2_{xy}$ $\bar{4}_z 2_x m_{xy}$ $2_x 2_y 2_z$ | D_{4z} D_{2dz} D_2 | 3 3 1 | $g_1 = g_2, g_3; d_{14} = -d_{25}$ $g_1 = -g_2; d_{14} = d_{25} = d_{36}$ $[g_3 - a(g_1 + g_2), b(g_1 - g_2)]$ $[b(d_{14} - d_{25}), a(d_{14} + d_{25}) - d_{36}]$ | 12 6 12 | 3 3 6 | 0 0 0 |
| | | | | | | | | |
| | | | | | | | | |
| T_{1g} | $(0, 0, z_1^+)$ $(x_1^+, x_1^+, 0)$ | $4_z/m_z$ $2_{xy}/m_{xy}$ | C_{4hz} C_{2hxy} | 3 6 | $A_{33}, A_{32} = A_{31}, A_{24} = A_{15}, A_{14} = -A_{25}$ $A_{11} = A_{22},$ $A_{13} = A_{23}, A_{12} = A_{21}$ $A_{35} = A_{34}, A_{26} = A_{16}$ | 6 12 | 3 12 | 0 0 |
| | (x_1^+, x_1^+, x_1^+) | $\bar{3}_p$ | C_{3ip} | 4 | $A_{11} = A_{22} = A_{33}$ $A_{13} = A_{21} = A_{32}, A_{12} = A_{32} = A_{31}$ $A_{35} = A_{16} = A_{24}, A_{26} = A_{34} = A_{15}$ | 8 | 4 | 0 |
| | (x_1^+, y_1^+, z_1^+) | $\bar{1}$ | C_i | 1 | (A_{11}, A_{22}, A_{33}) $(A_{13} + A_{12}, A_{21} + A_{23}, A_{32} + A_{31})$ $(A_{35} + A_{26}, A_{16} + A_{34}, A_{24} + A_{15})$ | 24 | 24 | 0 |
| T_{2g} | $(0, 0, z_2^+)$ $(x_2^+, -x_2^+, z_2^+)$ (x_2^+, x_2^+, x_2^+) | $m_{x\bar{y}} m_{xy} m_z$ $2_{xy}/m_{xy}$ $\bar{3}_p m_{x\bar{y}}$ | \hat{D}_{2hz} C_{2hxy} D_{3dp} | 3 6 4 | u_6 $u_4 = -u_5, u_6$ $u_4 = u_5 = u_6$ | 6 24 4 | 6 12 4 | 0 12 0 |
| (La) | (x_2^+, y_2^+, z_2^+) | $\bar{1}$ | C_i | 1 | (u_4, u_5, u_6) | 24 | 24 | 0 |
| T_{1u} | $(0, 0, z_1^-)$ | $4_z m_x m_{xy}$ | C_{4vz} | 3 | P_3 | 6 | 3 | 6 |
| | $(x_1^-, y_1^-, 0)$ | m_z | C_{sz} | 3 | P_1, P_2 | 24 | 12 | 24 |
| | $(x_1^-, x_1^-, 0)$ | $m_{x\bar{y}} 2_{xy} m_z$ | \hat{C}_{2vxy} | 6 | $P_1 = P_2$ | 12 | 6 | 12 |
| | $(x_1^-, -x_1^-, z_1^-)$ | m_{xy} | C_{sxy} | 6 | $P_1 = -P_2, P_3$ | 24 | 12 | 24 |
| | (x_1^-, x_1^-, x_1^-) | $3_p m_{x\bar{y}}$ | C_{3vp} | 4 | $P_1 = P_2 = P_3$ | 8 | 4 | 8 |
| | (x_1^-, y_1^-, z_1^-) | 1 | C_1 | 1 | (P_1, P_2, P_3) | 48 | 24 | 48 |
| | | | | | | | | |
| T_{2u} | $(0, 0, z_2^-)$ $(x_2^-, y_2^-, 0)$ | $\bar{4}_z m_x 2_{xy}$ m_z | \hat{D}_{2dz} C_{sz} | 3 3 | $g_6; d_{32} = -d_{31}, d_{24} = -d_{15}$ $g_4, g_5; d_{13}, d_{12}, d_{21}, d_{23}$ $d_{35}, d_{26}, d_{16}, d_{34}$ | 6 24 | 3 12 | 0 24 |
| | $(x_2^-, -x_2^-, 0)$ | $m_{x\bar{y}} 2_{xy} m_z$ | \hat{C}_{2vxy} | 6 | $g_4 = -g_5; d_{13} = d_{23}, d_{21} = d_{21}$ $d_{35} = d_{34}, d_{16} = d_{26}$ | 12 | 6 | 12 |
| | $(x_2^-, -x_2^-, z_2^-)$ | 2_{xy} | C_{2xy} | 6 | $g_4 = -g_5, g_6; d_{13} = d_{23}, d_{21} = d_{21}$ $d_{35} = d_{34}, d_{16} = d_{26}$ $d_{32} = -d_{31}, d_{24} = -d_{15}$ | 24 | 12 | 12 |
| | (x_2^-, x_2^-, x_2^-) | $3_p 2_{x\bar{y}}$ | D_{3p} | 4 | $g_4 = g_5 = g_6;$ $d_{13} = -d_{12} = d_{21} = -d_{23} = d_{32} - d_{31}$ $d_{35} = -d_{26} = d_{16} = -d_{34} = d_{24} = -d_{15}$ | 8 | 4 | 0 |
| | (x_2^-, y_2^-, z_2^-) | 1 | C_1 | 1 | (g_4, g_5, g_6) $(d_{13} - d_{12}, d_{21} - d_{23}, d_{32} - d_{31})$ $(d_{35} - d_{26}, d_{16} - d_{34}, d_{24} - d_{15})$ | 48 | 24 | 48 |
| | | | | | | | | |
| | | | | | | | | |

3. PHASE TRANSITIONS, TWINNING AND DOMAIN STRUCTURES

The solution of the inverse Landau problem – *i.e.* the identification of the representation Γ_η relevant to symmetry descent $G \Downarrow F$ – enables one to determine the corresponding normal mode (so-called soft mode) of the transition (see *e.g.* Rousseau *et al.*, 1981). We note that this step requires additional knowledge of the crystal structure, whereas other conclusions of the analysis hold for *any* crystal structure with a given symmetry descent $G \Downarrow F$. Normal-mode determination reveals the dynamic microscopic nature of the instability of the crystal lattice which leads to the phase transition (for more details and examples, see Section 3.1.5).

The representation Γ_η further determines the principal tensor parameters associated with the primary order parameter η . If one of them is a vector (polarization) the soft mode is infrared-active in the parent phase; if it is a symmetric second-rank tensor (spontaneous strain), the soft mode is Raman active in this phase. Furthermore, the *R*-irrep Γ_η determines the polynomial in components of η in the Landau free energy (basic invariant polynomials, called *integrity bases*, are available in the software *GI★KoBo-1* and in Kopský, 2001) and allows one to decide whether the necessary conditions of continuity of the transition (so-called Landau and Lifshitz conditions) are fulfilled.

(2) *Direct Landau problem of equitranslational phase transitions*: For a given space group \mathcal{G} of the parent phase and the *R*-irrep Γ_η (specifying the transformation properties of the primary order parameter η), find the corresponding equitranslational space group \mathcal{F} of the ferroic phase. To solve this task, one first finds in Table 3.1.3.1 the point group F that corresponds to point group G of space group \mathcal{G} and to the given *R*-irrep Γ_η . The point-group symmetry descent $G \Downarrow F$ thus obtained specifies uniquely the equitranslational subgroup \mathcal{F} of \mathcal{G} that can be found in the lattices of equitranslational subgroups of space groups available in the software *GI★KoBo-1* (see Section 3.1.6).

(3) *Secondary tensor parameters of an equitranslational phase transition $\mathcal{G} \Downarrow \mathcal{F}$* . These parameters are specified by the representation Γ_λ of G associated with a symmetry descent $\Gamma \Downarrow L$, where L is an intermediate group [see equation (3.1.3.1)]. In other words, the secondary tensor parameters of the transition $G \Downarrow F$ are identical with principal tensor parameters of the transition $G \Downarrow L$. To each intermediate group L there corresponds a set of secondary tensor parameters. All intermediate subgroups of a symmetry descent $G \Downarrow F$ can be deduced from lattices of subgroups in Figs. 3.1.3.1 and 3.1.3.2.

The representation Γ_λ specifies transformation properties of the secondary tensor parameter λ and thus determines *e.g.* its

infrared and Raman activity in the parent phase and enables one to make a mode analysis. Representation Γ_λ together with Γ_η determine the coupling between secondary and primary tensor parameters. The explicit form of these faint interactions (Aizu, 1973; Kopský, 1979d) can be found in the software *GI★KoBo-1* and in Kopský (2001).

(4) *Changes of property tensors at a ferroic phase transition*. These changes are described by tensor parameters that depend only on the point-group-symmetry descent $G \Downarrow F$. This means that *the same principal tensor parameters and secondary tensor parameters appear in all equitranslational and in all non-equitranslational transitions with the same $G \Downarrow F$* . The only difference is that in non-equitranslational ferroic phase transitions a principal tensor parameter corresponds to a secondary ferroic order parameter. It still plays a leading role in tensor distinction of domains, since it exhibits different values in any two ferroic domain states (see Section 3.4.2.3). Changes of property tensors at ferroic phase transitions are treated in detail in the software *GI★KoBo-1* and in Kopský (2001).

We note that Table 3.1.3.1 covers only those point-group symmetry descents $G \Downarrow F$ that are ‘driven’ by *R*-ireps of G . All possible point-group symmetry descents $G \Downarrow F$ are listed in Table 3.4.2.7. Principal and secondary tensor parameters of symmetry descents associated with reducible representations are combinations of tensor parameters appearing in Table 3.1.3.1 (for a detailed explanation, see the manual of the software *GI★KoBo-1* and Kopský, 2000). Necessary data for treating these cases are available in the software *GI★KoBo-1* and Kopský (2001).

3.1.3.3.1. Explanation of Table 3.1.3.1

Parent symmetry G : the short international (Hermann–Mauguin) and the Schoenflies symbol of the point group G of the parent phase are given. Subscripts specify the orientation of symmetry elements (generators) in the Cartesian crystallophysical coordinate system of the group G (see Figs. 3.4.2.3 and 3.4.2.4, and Tables 3.4.2.5 and 3.4.2.6).

R-irrep Γ_η : physically irreducible representation Γ_η of the group G in the spectroscopic notation. This representation defines transformation properties of the primary order parameter η and of the principal tensor parameters. Each complex irreducible representation is combined with its complex conjugate and thus a real physically irreducible representation *R*-irrep is formed. Matrices $D^{(\alpha)}$ of *R*-ireps are given explicitly in the the software *GI★KoBo-1*.

Table 3.1.3.2. Symmetry descents $G \Downarrow F_1$ associated with two irreducible representations

| G | Γ_η | F_1 | Proper or improper | | Domain states | | | Full or partial | |
|-------------|---------------|-------------------|--------------------|--------------|---------------|-------|-------|-----------------|--------------|
| | | | Ferroelectric | Ferroelastic | n_f | n_e | n_a | Ferroelectric | Ferroelastic |
| 432 | T_1 | 2_{xy} | proper | improper | 12 | 12 | 12 | full | full |
| | T_2 | | improper | proper | | | | | |
| | T_1 | 1 | improper | improper | 24 | 24 | 24 | full | full |
| | T_2 | | proper | proper | | | | | |
| $\bar{4}3m$ | T_1 | m_{xy} | improper | improper | 12 | 12 | 12 | full | full |
| | T_2 | | proper | proper | | | | | |
| | T_1 | 1 | improper | improper | 24 | 24 | 24 | full | full |
| | T_2 | | proper | proper | | | | | |
| $m\bar{3}m$ | T_{1g} | $2_{xy}/m_{xy}$ | non | improper | 12 | 0 | 12 | non | full |
| | T_{2g} | | non | proper | | | | | |
| | T_{1g} | $\bar{1}$ | non | improper | 24 | 0 | 24 | non | full |
| | T_{2g} | | non | proper | | | | | |
| | T_{1u} | $m_{xy}2_{xy}m_z$ | proper | improper | 12 | 12 | 6 | full | partial |
| | T_{2u} | | improper | improper | | | | | |
| | T_{1u} | m_z | proper | improper | 24 | 24 | 12 | full | partial |
| | T_{2u} | | improper | improper | | | | | |
| | T_{1u} | 1 | proper | improper | 48 | 48 | 24 | full | partial |
| | T_{2u} | | improper | improper | | | | | |

3.1. STRUCTURAL PHASE TRANSITIONS

(La) below the symbol of the irreducible representation Γ_η indicates that the *Landau condition* is violated, hence the transition cannot be continuous (second order). The Landau condition requires the absence of the third-degree invariant polynomial of the order-parameter components (the symmetrized triple product $[\Gamma_\eta]^3$ must not contain the identity representation of G). For more details see Lyubarskii (1960), Kociński (1983, 1990), Tolédano & Tolédano (1987), Izyumov & Syromiatnikov (1990) and Tolédano & Dmitriev (1996).

(Li) below the symbol of the irreducible representation Γ_η means that the *Lifshitz condition* is violated, hence the transition to a homogeneous ferroic phase is not continuous. The Lifshitz condition demands the absence of invariant terms that couple bilinearly the order-parameter components with their spatial derivatives that are not exact differentials (the antisymmetric

square $\{\Gamma_\eta\}^2$ has no representation in common with the vector representation of G). For more details see Lyubarskii (1960), Kociński (1983, 1990), Tolédano & Tolédano (1987), Izyumov & Syromiatnikov (1990) and Tolédano & Dmitriev (1996).

If there is no symbol (La) and/or (Li) below the symbol of the R -irep Γ_η (i.e. if both Landau and Lifshitz conditions are fulfilled), then the R -irep is called an *active representation*. In the opposite case, the R -irep is a *passive representation* (Lyubarskii, 1960; Kociński, 1983, 1990).

Standard variables: components of the order parameter in the carrier space of the irreducible representation Γ_η expressed in so-called *standard variables* (see the manual of the software *GI★KoBo-1*). Upper and lower indices and the typeface of standard variables allow one to identify to which irreducible representation Γ_η they belong. Standard variables of one-

dimensional representations are denoted by x (Sans Serif typeface), two- or three-dimensional R -ireps by x , y or x , y , z , respectively. Upper indices $+$ and $-$ correspond to the lower indices g (*gerade*) and u (*ungerade*) of spectroscopic notation, respectively. The lower index specifies to which irreducible representation the variable belongs.

For multidimensional representations, a general vector of the carrier space V_η is given in the last row; this vector is invariant under the kernel of Γ_η that appears as a low-symmetry group in column F_1 . The other rows contain special vectors defined by equal or zero values of some standard variables; these vectors are invariant under epikernels of Γ_n given in column F_1 .

F_1 : short international (Hermann–Mauguin) and Schoenflies symbol of the point group F_1 which describes the symmetry of the first single domain state of the ferroic (low-symmetry) phase. The subscripts define the orientation of symmetry elements (generators) of F_1 in the Cartesian crystallophysical coordinate system of the group G (see Figs. 3.4.2.3 and 3.4.2.4, and Tables 3.4.2.5 and 3.4.2.6). This specifies the orientation of the group F_1 , which is a prerequisite for domain structure analysis (see Chapter 3.4).

n_F : number of subgroups conjugate to F_1 under G . If $n_F = 1$, the group F_1 is a normal subgroup of G (see Section 3.2.3).

Principal tensor parameters: covariant tensor components, *i.e.* linear combinations of Cartesian tensor components that transform according to the same matrix R -irrep $D^{(\eta)}$ as the primary order parameter η . Principal tensor parameters are given in this form in the software *GIxKoBo-1* and in Kopský (2001).

This presentation is in certain situations not practical, since property tensors are usually described by numerical values of their Cartesian components. Then it is important to know morphic Cartesian tensor components and symmetry-breaking increments of nonzero Cartesian components that appear spontaneously in the ferroic phase. The bridge between these two presentations is

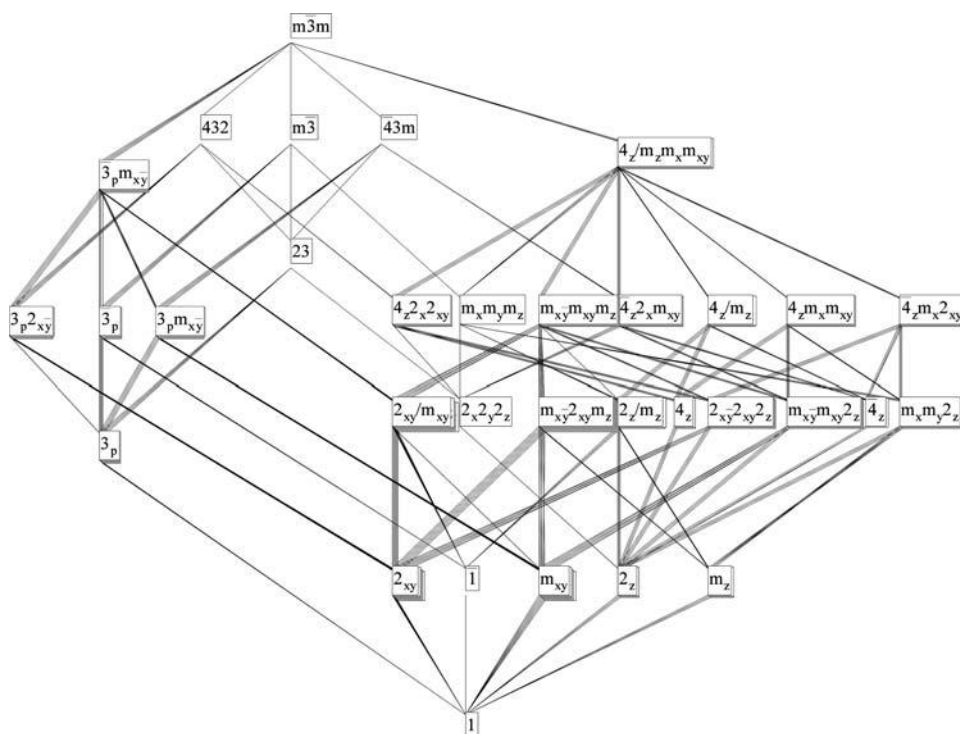


Fig. 3.1.3.1. Lattice of subgroups of the group $m\bar{3}m$. Conjugate subgroups are depicted as a pile of cards. In the software *GI★KoBo-1*, one can pull out individual conjugate subgroups by clicking on the pile. All conjugate subgroups are given explicitly in Table 3.4.2.7.

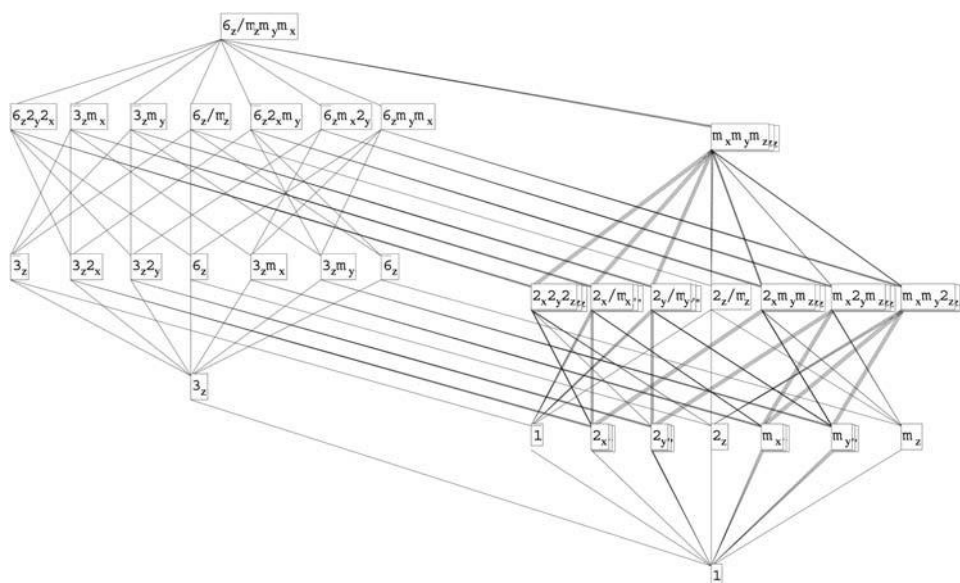


Fig. 3.1.3.2. Lattice of subgroups of the group $6/mmm$. Conjugate subgroups are depicted as a pile of cards. In the software *GI-KoBo-1*, one can pull out individual conjugate subgroups by clicking on the pile. All conjugate subgroups are given explicitly in Table 3.4.2.7.

3. PHASE TRANSITIONS, TWINNING AND DOMAIN STRUCTURES

provided by the *conversion equations* that express Cartesian tensor components as linear combinations of principal and secondary covariant components (for more details on tensorial covariants and conversion equations see Appendix E of the manual for *GI★KoBo-1* and Kopský, 2001).

We illustrate the situation on a transition with symmetry descent $4_z 2_x 2_{xy} \Downarrow 2_x 2_y 2_z$. In Table 3.1.3.1, we find that the principal tensor parameter transforms according to irreducible representation B_1 with standard variable x_3 . The corresponding covariant $u_3 = u_1 - u_2$ can be found in Appendix E of the manual of *GI★KoBo-1* (or in Kopský, 2001), where one also finds an invariant containing u_1 and u_2 : $u_{1,1} = u_1 + u_2$. The corresponding conversion equations are: $u_1 = \frac{1}{2}(u_{1,1} + u_3)$, $u_2 = \frac{1}{2}(u_{1,1} - u_3)$. In the parent phase $u_3 = u_1^{(p)} - u_2^{(p)} = 0$, hence $u_1^{(p)} = u_2^{(p)} = \frac{1}{2}u_{1,1}$, whereas in the ferroic phase $u_1^{(f)} = \frac{1}{2}(u_{1,1} + u_3) = u_1^{(p)} + \frac{1}{2}u_{1,1} = u_1^{(p)} + \delta u_1$, $u_2^{(f)} = u_2^{(p)} - \frac{1}{2}u_{1,1} = u_2^{(p)} + \delta u_2 = u_1^{(p)} - \delta u_1$. The symmetry-breaking increments $\delta u_1 = -\delta u_2$ describe thus the changes of the Cartesian components that correspond to the nonzero principal tensor component $u_1 - u_2$.

An analogous situation occurs frequently in trigonal and hexagonal parent groups, where $u_1 - u_2$ (or $g_1 - g_2$) transforms like the first or second component of the principal tensor parameter. In these cases, the corresponding symmetry-breaking increments of Cartesian components are again related: $\delta u_1 = -\delta u_2$ (or $\delta g_1 = -\delta g_2$).

We note that relations like $A_{11} = -A_{12} = -A_{26}$ do not imply that these components transform as the standard variable. Though these components are proportional to the principal tensor parameter in the first domain state, they cannot be transformed to corresponding components in other domain states as easily as covariant tensor components of the principal tensor parameter.

In general, it is useful to consider a tensor parameter as a vector in the carrier space of the respective representation. Then the Cartesian components are projections of this vector on the Cartesian basis of the tensor space.

The presentation of the principal tensor parameters in the column *Principal tensor parameters* of this table is a compromise: whenever conversion equations lead to simple relations between morphic Cartesian components and/or symmetry-breaking increments, we present these relations, in some cases together with corresponding covariants. In the more complicated cases, only the covariants are given. The corresponding conversion equations and labelling of covariants are given at the beginning of that part of the table which covers hexagonal and cubic parent groups G . In the main tables of the software *GI★KoBo-1*, the principal tensor parameters and the secondary tensor parameters up to rank 4 are given consistently in covariant form. Labelling of covariant components and conversion equations are given in Appendix E of the manual.

The principal tensor parameters presented in Table 3.1.3.1 represent a particular choice of property tensors for standard variables given in the second column. To save space, property tensors are selected in the following way: polarization \mathbf{P} and strain u are always listed; if none of their components transform according to $D^{(\eta)}$, then components of one axial and one polar tensor (if available) appearing in Table 3.1.3.3 are given. Principal parameters of two different property tensors are separated by a semicolon. If two different components of the same property tensor transform in the same way, they are separated by a comma.

As tensor indices we use integers 1, 2, 3 instead of vector components x, y, z and contracted indices 1, 2, 3, 4, 5, 6 in matrix notation for pairs $xx, yy, zz, yz \approx zy, zx \approx xz, xy \approx yx$, respectively

Important note: To make Table 3.1.3.1 compatible with the software *GI★KoBo-1* and with Kopský (2001), coefficients of property tensors in matrix notation with contracted indices 4, 5, 6 do not contain the numerical factors 2 and 4 which are usually

Table 3.1.3.3. *Important property tensors*

$i = 1, 2, 3; \mu, \nu = 1, 2, \dots, 6$.

| Tensor components | Property | Tensor components | Property |
|-------------------|------------------|--------------------|-------------------------|
| ε | enantiomorphism | P_i | chirality |
| P_i | polarization | ε_{ij} | pyroelectricity |
| u_μ | strain | $r_{i\mu}$ | dielectric permittivity |
| g_μ | optical activity | $Q_{\mu\nu}$ | electro-optics |
| $d_{i\mu}$ | piezoelectricity | | electrostriction |
| $A_{i\mu}$ | electrogyration | | |
| $\pi_{\mu\nu}$ | piezo-optics | | |

introduced to preserve a compact form (without these factors) of linear constitutive relations [see Chapter 1.1, Nye (1985) and especially Appendices E and F of Sirotn & Shaskolskaya (1982)]. This explains the differences in matrix coefficients appearing in Table 3.1.3.1 and those presented in Chapter 1.1 or in Nye (1985) and in Sirotn & Shaskolskaya (1982). Thus *e.g.* for the symmetry descent $6_z 2_x 2_y \Downarrow 3_z 2_x$, we find in Table 3.1.3.1 the principal tensor parameters $d_{11} = -d_{12} = -d_{26}$, whereas according to Chapter 1.1 or *e.g.* to Nye (1985) or Sirotn & Shaskolskaya (1982) these coefficients for $F_1 = 3_z 2_x$ are related by equations $d_{11} = -d_{12} = -2d_{26}$.

Property tensors and symbols of their components that can be found in Table 3.1.3.1 are given in the left-hand half of Table 3.1.3.3. The right-hand half presents other tensors that transform in the same way as those on the left and form, therefore, covariant tensor components of the same form as those given in the column *Principal tensor parameters*. Principal and secondary tensor parameters for all property tensors that appear in Table 3.1.3.3 are available in the software *GI★KoBo-1*.

n_f : number of ferroic single domain states that differ in the primary order parameter η and in the principal tensor parameters.

n_a : number of ferroelastic single domain states. If $n_a = n_f$, $n_a < n_f$ or $n_a = 1$, the ferroic phase is, respectively, a full, partial or non-ferroelastic one.

n_e : number of ferroelectric single domain states. If $n_e = n_f$, $n_e < n_f$ or $n_e = 0, 1$, the ferroic phase is, respectively, a full, partial or non-ferroelectric one ($n = 0$ or $n = 1$ correspond to a non-polar or to a polar parent phase, respectively) (see Section 3.4.2).

3.1.3.4. Examples

Example 3.1.3.4.1. Phase transition in triglycine sulfate (TGS). Assume that the space groups of both parent (high-symmetry) and ferroic (low-symmetry) phases are known: $\mathcal{G} = P2_1/c$ (C_{2h}^5), $\mathcal{F}_1 = P2_1$ (C_2^2). The same number of formula units in the primitive unit cell in both phases suggests that the transition is an equitranslational one. This conclusion can be checked in the lattice of equitranslational subgroups of the software *GI★KoBo-1*. There we find for the low-symmetry space group the symbol $P112_1(\mathbf{b}/4)$, where the vector in parentheses expresses the shift of the origin with respect to the conventional origin given in *IT A* (2002).

In Table 3.1.3.1, one finds that the corresponding point-group-symmetry descent $2_z/m_z \Downarrow 2_z$ is associated with irreducible representation $\Gamma_\eta = A_u$. The corresponding principal tensor parameters of lowest rank are the pseudoscalar ε (enantiomorphism or chirality) and the vector of spontaneous polarization with one nonzero morphic component P_3 – the transition is a proper ferroelectric one. The non-ferroelastic ($n_a = 1$) full ferroelectric phase has two ferroelectric domain states ($n_f = n_e = 2$). Other principal tensor parameters (morphic tensor components that transform according to Γ_η) are available in the software *GI★KoBo-1*: $g_1, g_2, g_3, g_6; d_{31}, d_{32}, d_{33}, d_{36}, d_{14}, d_{15}, d_{24}, d_{25}$. Property tensors with these components are listed in Table 3.1.3.3. As shown in Section 3.4.2, all these components

3.1. STRUCTURAL PHASE TRANSITIONS

change sign when one passes from one domain state to the other. Since there is no intermediate group between G and F , there are no secondary tensor parameters.

Example 3.1.3.4.2. Phase transitions in barium titanate (BaTiO_3). We shall illustrate the solution of the inverse Landau problem and the need to correlate the crystallographic system with the Cartesian crystallophysical coordinate system. The space-group type of the parent phase is $\mathcal{G} = Pm\bar{3}m$, and those of the three ferroic phases are $\mathcal{F}_1^{(1)} = P4mm$, $\mathcal{F}_1^{(2)} = Cm2m$, $\mathcal{F}_1^{(3)} = R3m$, all with one formula unit in the primitive unit cell.

This information is not complete. To perform mode analysis, we must specify these space groups by saying that the lattice symbol P in the first case and the lattice symbol R in the third case are given with reference to the cubic crystallographic basis $(\mathbf{a}, \mathbf{b}, \mathbf{c})$, while lattice symbol C in the second case is given with reference to crystallographic basis $[(\mathbf{a} - \mathbf{b}), (\mathbf{a} + \mathbf{b}), \mathbf{c}]$. If we now identify vectors of the cubic crystallographic basis with vectors of the Cartesian basis by $\mathbf{a} = a\mathbf{e}_x$, $\mathbf{b} = a\mathbf{e}_y$, $\mathbf{c} = a\mathbf{e}_z$, where $\mathbf{e}_x, \mathbf{e}_y, \mathbf{e}_z$ are three orthonormal vectors, we can see that the corresponding point groups are $F_1^{(1)} = 4_z m_x m_{xy}$, $F_1^{(2)} = m_{xy} 2_{xy} m_z$, $F_1^{(3)} = 3_p m_{xy}$.

Notice that without specification of crystallographic bases one could interpret the point group of the space group $Cm2m$ as $m_x 2_y m_z$. Bases are therefore always specified in lattices of equitranslational subgroups of the space groups that are available in the software *GI★KoBo-1*, where we can check that all three symmetry descents are equitranslational.

In Table 3.1.3.1, we find that these three ferroic subgroups are epikernels of the R -irep $\Gamma_\eta = T_{1u}$ with the following principal tensor components: P_3 , $P_1 = P_2$, $P_1 = P_2 = P_3$, respectively. Other principal tensor parameters can be found in the main tables of the software *GI★KoBo-1*. The knowledge of the representation Γ_η allows one to perform soft-mode analysis (see e.g. Rousseau *et al.*, 1981).

For the tetragonal ferroelectric phase with $F_1 = 4_z m_x m_y$, we find in Fig. 3.1.3.1 an intermediate group $L_1 = 4_z/m_z m_x m_{xy}$. In Table 3.1.3.1, we check that this is an epikernel of the R -irep E_g with secondary tensor parameter δu_3 . This phase is a full (proper) ferroelectric and partial ferroelastic one.

More details about symmetry aspects of structural phase transitions can be found in monographs by Izyumov & Szyrmaliuk (1990), Kociński (1983, 1990), Landau & Lifshitz (1969), Lyubarskii (1960), Tolédano & Dmitriev (1996) and Tolédano & Tolédano (1987). Group-subgroup relations of space groups are treated extensively in *IT A1* (2003).

3.1.4. Example of a table for non-equitranslational phase transitions

BY J.-C. TOLÉDANO

In the preceding Section 3.1.3, a systematic tabulation of possible symmetry changes was provided for the class of equitranslational phase transitions. This tabulation derives from the principles described in Section 3.1.2, and relates the enumeration of the symmetry changes at structural transitions to the characteristics of the irreducible representations of the space group \mathcal{G} of the ‘parent’ (highest-symmetry) phase adjacent to the transition. Systematic extension of this type of tabulation to the general case of transitions involving both a decrease of translational and of point-group symmetry has been achieved by several groups (Tolédano & Tolédano, 1976, 1977, 1980, 1982; Stokes & Hatch, 1988). The reader can refer, in particular, to the latter reference for an exhaustive enumeration of the characteristics of possible transitions. An illustration of the results obtained for a restricted class of parent phases (those associated with the point symmetry $4/m$ and to a simple Bravais lattice P) is presented here.

In order to clarify the content Table 3.1.4.1, let us recall (cf. Section 3.1.2) that Landau’s theory of continuous phase transitions shows that the order parameter of a transition transforms according to a physically irreducible representation of the space group \mathcal{G} of the high-symmetry phase of the crystal. A physically irreducible representation is either a real irreducible representation of \mathcal{G} or the direct sum of two complex-conjugate irreducible representations of \mathcal{G} . To classify the order-parameter symmetries of all possible transitions taking place between a given parent (high-symmetry) phase and another (low-symmetry) phase, it is therefore necessary, for each parent space group, to list the various relevant irreducible representations.

Each irreducible representation of a given space group can be denoted $\Gamma_n(k^*)$ and identified by two quantities. The star k^* , represented by a vector linking the origin of reciprocal space to a point of the first Brillouin zone, specifies the translational symmetry properties of the basis functions of $\Gamma_n(k^*)$. The dimension of $\Gamma_n(k^*)$ is equal to the number of components of the order parameter of the phase transition considered. A given space group has an infinite number of irreducible representations. However, physical considerations restrict a systematic enumeration to only a few irreducible representations. The restrictions arise from the fact that one focuses on continuous (or almost continuous) transitions between strictly periodic crystal structures (i.e. in particular, incommensurate phases are not considered), and have been thoroughly described previously (Tolédano & Tolédano, 1987, and references therein).

3.1.5. Microscopic aspects of structural phase transitions and soft modes

BY J. F. SCOTT

3.1.5.1. Introduction

Phase transitions in crystals are most sensitively detected *via* dynamic techniques. Two good examples are ultrasonic attenuation and internal friction. Unfortunately, while often exquisitely sensitive to subtle second-order phase transitions [e.g. the work of Spencer *et al.* (1970) on BaMnF_4], they provide no real structural information on the lattice distortions that occur at such phase transitions, or even convincing evidence that a real phase transition has occurred (e.g. transition from one long-range thermodynamically stable ordered state to another). It is not unusual for ultrasonic attenuation to reveal a dozen reproducible anomalies over a small temperature range, none of which might be a phase transition in the usual sense of the phrase. At the other extreme are detailed structural analyses *via* X-ray or neutron scattering, which give unambiguous lattice details but often totally miss small, nearly continuous rigid rotations of light ions, such as hydrogen bonds or oxygen or fluorine octahedra or tetrahedra. Intermediate between these techniques are phonon spectroscopies, notably infrared (absorption or reflection) and Raman techniques. The latter has developed remarkably over the past thirty years since the introduction of lasers and is now a standard analytical tool for helping to elucidate crystal structures and phase transitions investigated by chemists, solid-state physicists and materials scientists.

3.1.5.2. Displacive phase transitions

3.1.5.2.1. Landau–Devonshire theory

Landau (1937) developed a simple mean-field theory of phase transitions which implicitly assumes that each atom or ion in a system exerts a force on the other particles that is independent of the distance between them (see Section 3.1.2.2). Although this is a somewhat unphysical crude approximation to the actual forces, which are strongly dependent upon interparticle spacings, it allows the forces of all the other particles in the system to be replaced mathematically by an effective ‘field’, and for the

3. PHASE TRANSITIONS, TWINNING AND DOMAIN STRUCTURES

resulting equations to be solved exactly. This mathematical simplicity preserves the qualitative features of the real physical system and its phase transition without adding unnecessary cumbersome mathematics and had earlier been used to great advantage for fluids by Van der Waals (1873) and for magnetism by Weiss (1907). Landau's theory is a kind of generalization of those earlier theories. In it he defines an 'order parameter' x , in terms of which most physical quantities of interest may be expressed *via* free energies. In a ferromagnet, the order parameter corresponds to the net magnetization; it is zero above the Curie temperature T_c and increases monotonically with decreasing temperature below that temperature. In a liquid–gas phase transition the order parameter is the difference in density in the gas and liquid phases for the fluid.

Devonshire independently developed an equivalent theory for ferroelectric crystals around 1953 (Devonshire, 1954). For ferroelectrics, the order parameter is the spontaneous dielectric polarization P . In both his formalism and that of Landau, the ideas are most conveniently expressed through the free energy of the thermodynamic system:

$$F(P, T) = A(T - T_c)P^2 + BP^4 + CP^6, \quad (3.1.5.1a)$$

where A and C are positive quantities and B may have either sign. Scott (1999) shows that C changes sign at ferroelectric-to-

superionic conducting transition temperatures. As shown in Fig. 3.1.5.1, minimization of the free energy causes the expectation value of P to go from zero above the Curie temperature to a nonzero value below. If B is positive the transition is continuous ('second-order'), whereas if B is negative, the transition is discontinuous ('first-order'), as shown in Fig. 3.1.5.2. The coefficient B may also be a function of pressure p or applied electric field \mathbf{E} and may pass through zero at a critical threshold value of p or \mathbf{E} . Such a point is referred to as a 'tricritical point' and is marked by a change in the order of the transition from first-order to second-order. The term 'tri-critical' originates from the fact that in a three-dimensional graph with coordinates temperature T , pressure p and applied field \mathbf{E} , there are *three* lines marking the ferroelectric–paraelectric phase boundary that meet at a single point. Crossing any of these three lines produces a continuous phase transition (Fig. 3.1.5.3).

3.1.5.2.2. Soft modes

Minimization of the free energy above leads to the dependence of spontaneous polarization P upon temperature given by $P(T) = P(0)[(T_c - T)/T_c]$ for continuous transitions. In the more general case discussed by Landau, the polarization P is replaced by a generic 'order parameter' $\varphi(T)$ with the same dependence. Cochran's contribution (1960, 1961) was to show that for

Table 3.1.4.1. Possible symmetry changes across transitions from a parent phase with space group $P4/m$, $P4_2/m$, $P4/n$, $P4_2/n$, $I4/m$ or $I4_1/a$

Equitranslational symmetry changes are not included (*cf.* Section 3.1.3). The coordinates of the points in the second column are referred to the primitive unit cell of the reciprocal lattice. The terms used in the fifth column are introduced in Section 3.1.1. The last column is characteristic of non-equitranslational transitions.

| Parent space group | Irreducible representation | | Possible low-symmetry space groups | Macroscopic characteristics of the transition | Change in the number of atoms per primitive unit cell |
|--------------------|---|----------------------------------|------------------------------------|---|---|
| | Brillouin zone point | Dimension of the order parameter | | | |
| $P4/m$ | $\frac{1}{2}, \frac{1}{2}, 0$ | 2 | $P2/m; P2/b$ | Ferroelastic | 2 |
| | | 1 | $P4/m; P4/n$ | Non-ferroic | 2 |
| | $0, 0, \frac{1}{2}$ | 2 | $P2_1/m$ | Ferroelastic | 2 |
| | | 1 | $P4/m; P4_2/m$ | Non-ferroic | 2 |
| | $\frac{1}{2}, \frac{1}{2}, \frac{1}{2}$ | 2 | $B2/m$ | Ferroelastic | 2 |
| | | 1 | $I4/m$ | Non-ferroic | 2 |
| | $0, \frac{1}{2}, \frac{1}{2}$ | 2 | $B2/m$ | Ferroelastic | 2 |
| | | 1 | $I4/m$ | Non-ferroic | 4 |
| | $0, \frac{1}{2}, 0$ | 2 | $P2/m; P2/b$ | Ferroelastic | 2 |
| | | 1 | $P4/m; P4/n$ | Non-ferroic | 4 |
| $P4_2/m$ | $\frac{1}{2}, \frac{1}{2}, 0$ | 2 | $P2/m; P2/b$ | Ferroelastic | 2 |
| | | 1 | $P4_2/n; P4_2/m$ | Non-ferroic | 2 |
| | $0, 0, \frac{1}{2}$ | 2 | $P2_1/m$ | Ferroelastic | 2 |
| | | 2 | $P4_1; P4_3$ | Ferroelectric | 2 |
| | $\frac{1}{2}, \frac{1}{2}, \frac{1}{2}$ | 2 | $B2/m$ | Ferroelastic | 2 |
| | | 1 | $I4/m$ | Non-ferroic | 2 |
| | $0, \frac{1}{2}, \frac{1}{2}$ | 2 | $B2/m$ | Ferroelastic | 2 |
| | | 2 | $P4_1/a$ | Non-ferroic | 2 |
| | $0, \frac{1}{2}, 0$ | 2 | $P2/m; P2/b$ | Ferroelastic | 2 |
| | | 2 | $P4_2/m; P4_2/n$ | Non-ferroic | 2 |
| $P4/n$ | $\frac{1}{2}, \frac{1}{2}, 0$ | 2 | $P2/b$ | Ferroelastic | 2 |
| | | 2 | $P4$ | Ferroelectric | 2 |
| | $0, 0, \frac{1}{2}$ | 2 | $P2_1/b$ | Ferroelastic | 2 |
| | | 1 | $P4/n; P4_2/n$ | Non-ferroic | 2 |
| | $\frac{1}{2}, \frac{1}{2}, \frac{1}{2}$ | 2 | $B2/b$ | Ferroelastic | 2 |
| | | 2 | $I4$ | Ferroelectric | 2 |
| $P4_2/n$ | $\frac{1}{2}, \frac{1}{2}, 0$ | 2 | $P2/b$ | Ferroelastic | 2 |
| | $0, 0, \frac{1}{2}$ | 2 | $P2_1/b$ | Ferroelastic | 2 |
| | | 2 | $P4_1; P4_3$ | Ferroelectric | 2 |
| $I4/m$ | $\frac{1}{2}, -\frac{1}{2}, -\frac{1}{2}$ | 2 | $P2_1/m; P2_1/b$ | Ferroelastic | 2 |
| | | 1 | $P4/m; P4_2/m; P4/n; P4_2/n$ | Non-ferroic | 2 |
| | $\frac{1}{2}, \frac{1}{2}, 0$ | 2 | $B2/m; B2/b$ | Ferroelastic | 2 |
| | | 2 | $P4/m; P4_2/m; P4/n; P4_2/n$ | Non-ferroic | 4 |
| | $\frac{1}{2}, 0, 0$ | 4 | $B2/m$ | Ferroelastic | 2 |
| | | 4 | $P\bar{1}$ | Ferroelastic | 8 |
| $I4_1/a$ | | 4 | $I4/m; I4_1/a$ | Non-ferroic | 8 |
| | $\frac{3}{4}, \frac{1}{4}, -\frac{1}{4}$ | 2 | $I4/m; I4_1/a$ | Non-ferroic | 4 |
| | $\frac{1}{2}, -\frac{1}{2}, -\frac{1}{2}$ | 2 | $P2_1/b$ | Ferroelastic | 2 |
| | $\frac{1}{2}, 0, 0$ | 4 | $I4$ | Higher-order ferroic | 8 |
| | | 4 | $P\bar{1}$ | Ferroelastic | 2 |
| | | 4 | $P\bar{1}; B2/b$ | Ferroelastic | 4 |

3.1. STRUCTURAL PHASE TRANSITIONS

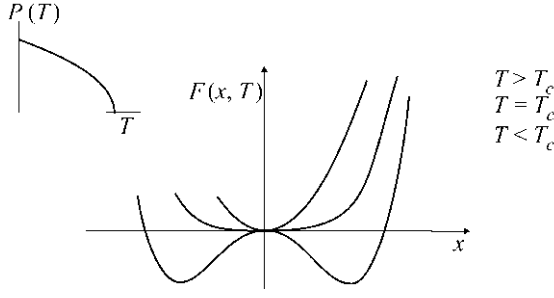


Fig. 3.1.5.1. Free energy $F(P, T)$ and order parameter $P(T)$ from the Landau–Devonshire theory [equation (3.1.5.1a)] for a continuous second-order ferroelectric phase transition [coefficient B positive in equation (3.1.5.1a)]. The insert shows the temperature dependence of the order parameter, i.e. the expectation value of the displacement $x(T)$.

continuous ‘displacive’ (as opposed to ‘order–disorder’) transitions, this order parameter is (or is proportional to) a normal mode of the lattice. One normal mode of the crystal must, in Cochran’s theory, literally soften: the generalized force constant for this mode weakens as a function of temperature, and its frequency consequently decreases. This soft-mode theory provided an important step from the macroscopic description of Landau and Devonshire to a microscopic theory, and in particular, to vibrational (phonon) spectroscopy.

Cochran illustrated this theory using a ‘shell’ model in which the electrons surrounding an ion were approximated by a rigid sphere; shell–shell force constants were treated as well as shell–core and core–core terms, in the general case. The initial application was to PbTe and other rock-salt cubic structures that undergo ferroelectric structural distortions.

For this simple case, the key equations relate the optical phonon frequencies of long wavelength to two terms: a short-range force constant R'_0 and a long-range Coulombic term. It is important that in general neither of these terms has a pathological temperature dependence; in particular, neither vanishes at the Curie temperature. Rather it is the subtle cancellation of the two terms at T_c that produces a ‘soft’ transverse optical phonon.

The longitudinal optical phonon frequency $\omega_{LO}(T)$ is positive definite and remains finite at all temperatures:

$$\mu\omega_{LO}^2 = R'_0 + \frac{8\pi Z^2 e^2}{9\epsilon V(T)}, \quad (3.1.5.1b)$$

where μ is a reduced mass for the normal mode; Ze is an effective charge for the mode, related to the valence state of the ions involved; ϵ is the high-frequency dielectric constant and $V(T)$ is the unit-cell volume, which is a function of temperature due to thermal expansion.

By comparison, the transverse optical phonon frequency

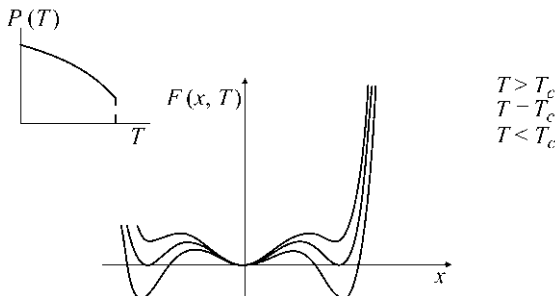


Fig. 3.1.5.2. Free energy $F(P, T)$ and order parameter $P(T)$ from the Landau–Devonshire theory [equation (3.1.5.1a)] for a discontinuous first-order ferroelectric phase transition [coefficient B negative in equation (3.1.5.1a)]. T_1 is the temperature (see Fig. 3.1.2.6) below which a secondary minimum appears in the free energy.

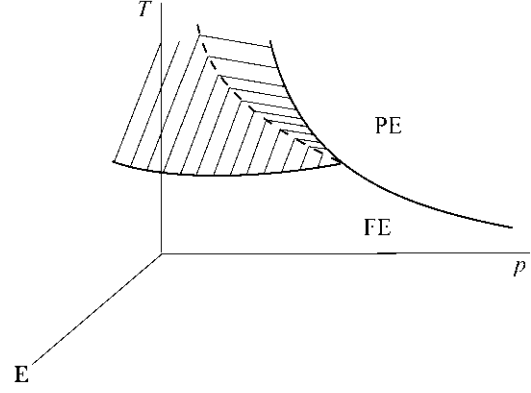


Fig. 3.1.5.3. Three-dimensional graph of phase boundaries as functions of temperature T , pressure p and applied electric field \mathbf{E} , showing a tricritical point where three continuous phase boundaries intersect.

$$\mu\omega_{TO}^2 = R'_0 - \frac{4\pi Z^2 e^2}{3\epsilon V(T)} \quad (3.1.5.1c)$$

can vanish accidentally when $V(T)$ reaches a value that permits cancellation of the two terms. Note that this does not require any unusual temperature dependence of the short-range interaction term R'_0 . This description appears to satisfy all well studied ferroelectrics except for the ‘ultra-weak’ ones epitomized by TSCC (tris-sarcosine calcium chloride), in which the Coulombic term in (3.1.5.1b) and (3.1.5.1c) is very small and the pathological dependence occurs in R'_0 . This leads to a situation in which the longitudinal optical phonon is nearly as soft as is the transverse branch.

Subsequent to Cochran’s shell-model developments, Cowley (1962, 1964, 1970) replaced this phenomenological modelling with a comprehensive many-body theory of phonon anharmonicity, in which the soft-mode temperature is dominated by Feynman diagrams emphasizing renormalization of phonon self-energies due to four-phonon interactions (two in and two out). This contrasts with the three-phonon interactions that dominate phonon linewidths under most conditions.

It is worth noting that the soft optical phonon branch is necessarily always observable in the low-symmetry phase *via* Raman spectroscopy in all 32 point-group symmetries. This was first proved by Worlock (1971), later developed in more detail by Pick (1969) and follows group-theoretically from the fact that the vibration may be regarded as a dynamic distortion of symmetry Γ_i which condenses at T_c to produce a static distortion of the same symmetry. Hence the vibration in the distorted phase has symmetry given by the product $\Gamma_i \times \Gamma_i$, which always contains the totally symmetric representation Γ_1 for any choice of Γ_i . If Γ_i is non-degenerate, its outer product with itself will contain only Γ_1 and there will be a single, totally symmetric soft mode; if Γ_i is degenerate, there will be two or three soft modes of different symmetries, at least one of which is totally symmetric.

Since the totally symmetric representation is Raman-active for all 32 point-group symmetries, this implies that the soft mode is always accessible to Raman spectroscopy at least in the distorted, low-symmetry phase of the crystal.

3.1.5.2.3. Strontium titanate, SrTiO_3

Among the perovskite oxides that are ferroelectric insulators, barium titanate has received by far the most attention from the scientific community since its independent characterization in several countries during World War II. The discovery of a ferroelectric that was robust, relatively inert (not water-soluble) and without hydrogen bonding was a scientific breakthrough, and its large values of dielectric constant and especially spontaneous polarization are highly attractive for devices. Although not ferroelectric in pure bulk form, strontium titanate has received

3. PHASE TRANSITIONS, TWINNING AND DOMAIN STRUCTURES

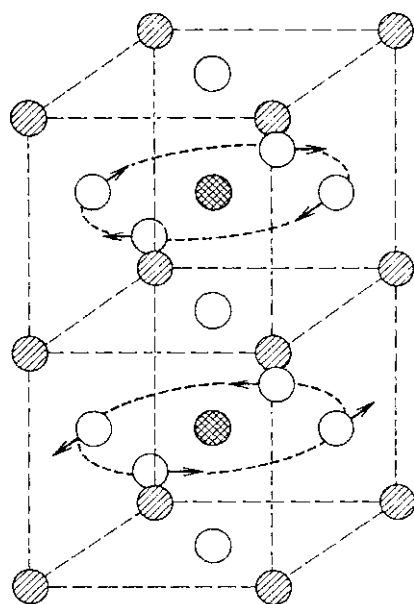


Fig. 3.1.5.4. Structure of strontium titanate above (undisplaced ions) and below (arrows) its anti-ferrodistortive phase transition at *ca.* 105 K. Below this temperature, the cubic primitive cell undergoes a tetragonal distortion and also doubles along the [001] cubic axis (domains will form along [100], [010] and [001] of the original cubic lattice). The ionic displacements approximate a rigid rotation of oxygen octahedra, out-of-phase in adjacent unit cells, except that the oxygens actually remain on the cube faces, so that a very small Ti—O bond elongation occurs.

the second greatest amount of attention of this family over the past thirty years. It also provides a textbook example of how optical spectroscopy can complement traditional X-ray crystallographic techniques for structural determination.

Fig. 3.1.5.4 shows the structure of strontium titanate above and below the temperature ($T_0 = 105$ K) of a non-ferroelectric phase transition. Note that there is an out-of-phase distortion of oxygen ions in adjacent primitive unit cells (referred to the single formula group ABO_3 in the high-temperature phase). This out-of-phase displacement approximates a rigid rotation of oxygen octahedra about a [100], [010] or [001] cube axis, except that the oxygens actually remain in the plane of the cube faces. We note three qualitative aspects of this distortion: Firstly, it doubles the primitive unit cell from one formula group to two; this will approximately double the number of optical phonons of very

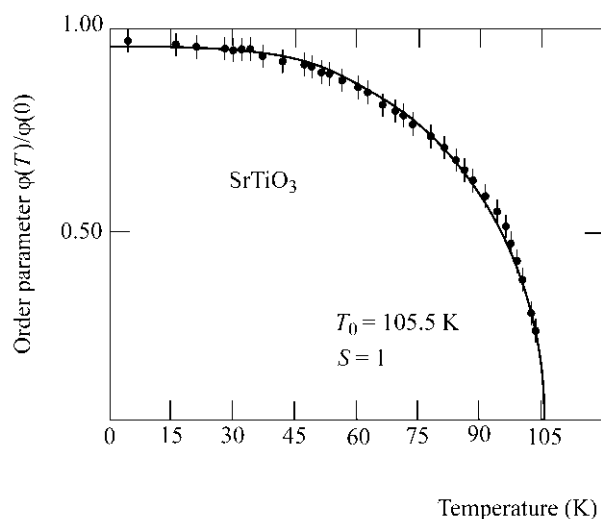


Fig. 3.1.5.5. Rotation angle *versus* temperature for the oxygen octahedron distortion below 105 K in strontium titanate described in Fig. 3.1.5.4. The solid curve is a mean-field least-squares fit to an $S = 1$ Brillouin function.

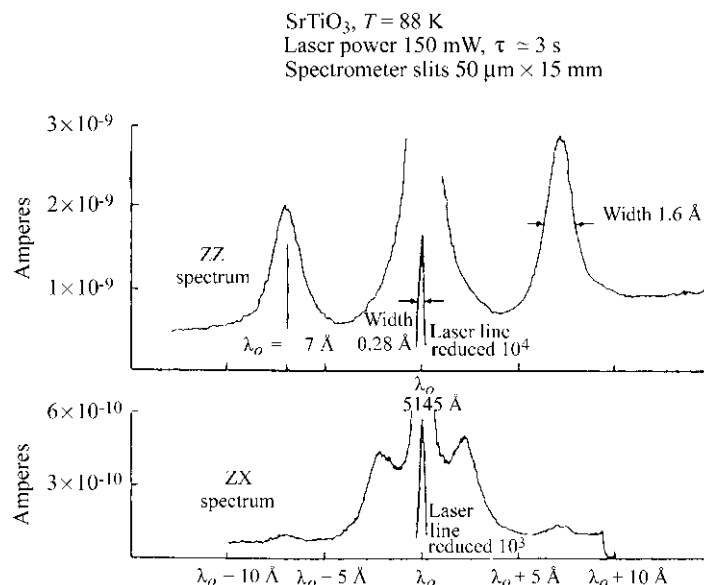


Fig. 3.1.5.6. Raman spectra of strontium titanate below its cubic-tetragonal phase transition temperature. These features disappear totally above the phase transition temperature, thereby providing a vivid indication of a rather subtle phase transition.

long wavelength ($q = 0$) permitted in infrared and/or Raman spectroscopy. Secondly, it makes the gross crystal class tetragonal, rather than cubic (although in specimens cooled through the transition temperature in the absence of external stress, we might expect a random collection of domains with tetragonal axes along the original [100], [010], [001] cube axes, which will give macroscopic cubic properties to the multidomain aggregate). Thirdly, the transition is perfectly continuous, as shown in Fig. 3.1.5.5, where the rotation angle of the oxygen octahedra about the cube axis is plotted *versus* temperature.

Fig. 3.1.5.4 does not correspond at all to the structure inferred earlier from X-ray crystallographic techniques (Lytle, 1964). The very small, nearly rigid rotation of light ions (oxygens) in multidomain specimens caused the X-ray study to overlook the primary characteristic of the phase transition and to register instead only the unmistakable change in the c/a ratio from unity. Thus, the X-ray study correctly inferred the cubic-tetragonal characteristic of the phase transition but it got both the space

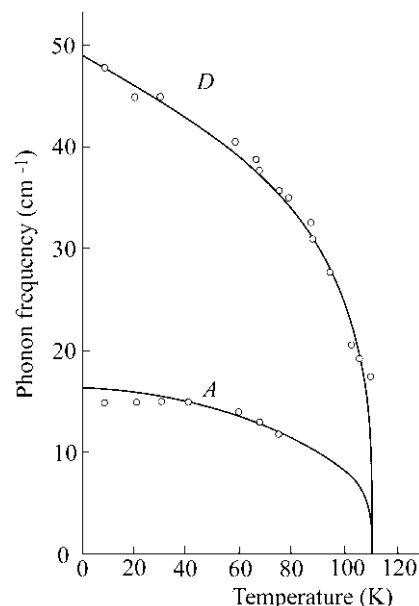


Fig. 3.1.5.7. Temperature dependence of phonon branches observed in the Raman spectra of tetragonal strontium titanate.

3.1. STRUCTURAL PHASE TRANSITIONS

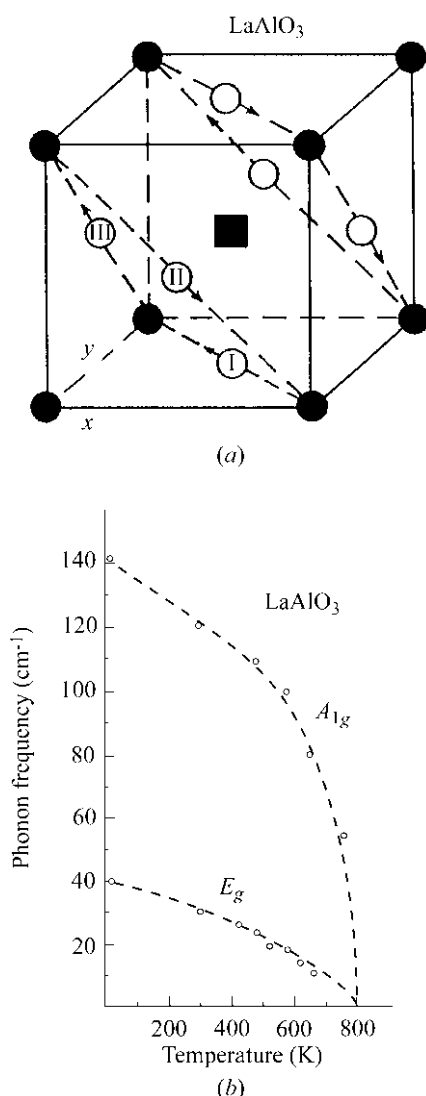


Fig. 3.1.5.8. (a) Structure of lanthanum aluminate above (undistorted) and below (arrows) its cubic-rhombohedral phase transition near 840 K. As in strontium titanate (Figs. 3.1.5.4–3.1.5.7), there is a nearly rigid rotation of oxygen octahedra (the oxygen ions actually remain on the cube faces); however, in the lanthanide aluminates ($\text{Ln} = \text{La}, \text{Pr}, \text{Nd}$) the rotation is about a cube [111] body diagonal, so that the resulting structure is rhombohedral, rather than tetragonal. The primitive unit cell doubles along the cubic [111] axis; domains will form with the unique axis along all originally equivalent body diagonals of the cubic lattice. (b) Optical phonon frequencies versus temperature in lanthanum aluminate.

group and the size of the primitive cell wrong. The latter error has many serious implications for solid-state physicists: For example, certain electronic transitions from valence to conduction bands are actually ‘direct’ (involving no change in wavevector) but would have erroneously been described as ‘indirect’ with the structure proposed by Lytle. More serious errors of interpretation arose with the microscopic mechanisms of ultrasonic loss proposed by Cowley based upon Lytle’s erroneous structure.

The determination of the correct structure of strontium titanate (Fig. 3.1.5.4) was actually made *via* EPR studies (Unoki & Sakudo, 1967) and confirmed *via* Raman spectroscopy (Fleury *et al.*, 1968). The presence of ‘extra’ $q = 0$ optical phonon peaks in the Raman spectra below T_0 (Fig. 3.1.5.6) is simple and unmistakable evidence of unit-cell multiplication. The fact that two optical phonon branches have frequencies that decrease continuously to zero (Fig. 3.1.5.7) as the transition temperature is approached from below shows further that the transition is ‘displacive’, that is, that the structures are perfectly ordered both above and below the transition temperature. This is a classic example of Cochran’s soft-mode theory discussed above.

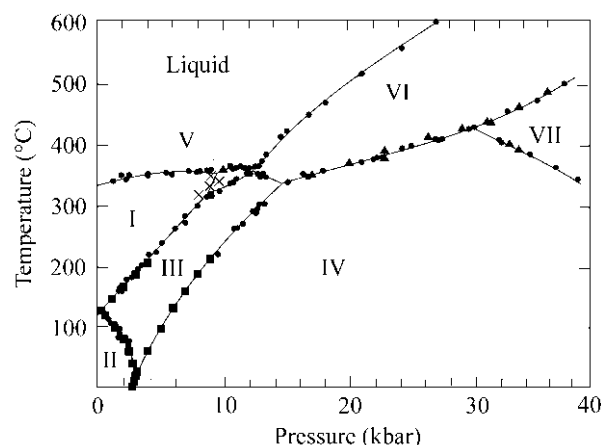


Fig. 3.1.5.9. Phase diagram of potassium nitrate, KNO_3 .

3.1.5.2.4. Lanthanum aluminate, LaAlO_3

A structural distortion related to that in strontium titanate is exhibited in lanthanum aluminate at approximately 840 K. As in strontium titanate, the distortion consists primarily of a nearly rigid rotation of oxygen octahedra. However, in the lanthanide aluminates (including NdAlO_3 and PrAlO_3) the rotation is about the [111] body diagonal(s) of the prototype cubic structure. The rotation, shown in Fig. 3.1.5.8, is out-of-phase in adjacent cubic unit cells, analogous to that in strontium titanate.

Historically, this phase transition and indeed the structure of lanthanum aluminate were incorrectly characterized by X-ray crystallography (Geller & Bala, 1956) and correctly assigned by Scott (1969) and Scott & Remeika (1970) *via* Raman spectroscopy. The causes were as in the case of strontium titanate, namely that it is difficult to assess small, nearly rigid rotations of light ions in twinned specimens. In the case of lanthanum aluminate, Geller and Bala incorrectly determined the space group to be $R\bar{3}m$ (D_{3d}^5), rather than the correct $R\bar{3}2/c$ (D_{3d}^6) shown in Fig. 3.1.5.8, and they had the size of the primitive unit cell as one formula group rather than two.

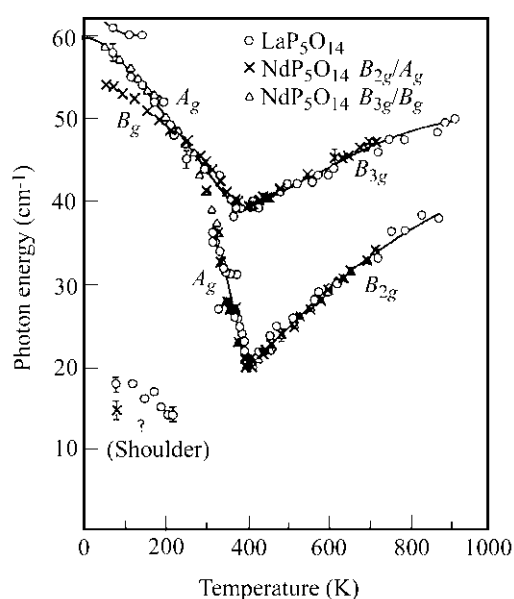
3.1.5.2.5. Potassium nitrate, KNO_3

Potassium nitrate has a rather simple phase diagram, reproduced in Fig. 3.1.5.9. Two different structures and space groups were proposed for the ambient temperature phase I: Shinnaka (1962) proposed D_{3d}^6 ($R\bar{3}2/c$) with two formula groups per primitive cell ($Z = 2$), whereas Tahvonen (1947) proposed D_{3d}^5 ($R\bar{3}m$) with one formula group per primitive cell. In fact, both are wrong. The correct space group is that of Nimmo & Lucas (1973): D_{3d}^6 ($R\bar{3}2/c$) with one formula group per primitive cell. Again, Raman spectroscopy of phonons shows that the Tahvonen structure predicts approximately twice as many spectral lines as can be observed. Balkanski *et al.* (1969) tried creatively but unsuccessfully to account for their spectra in terms of Tahvonen’s space-group symmetry assignment for this crystal; later Scott & Pouligny (1988) showed that all spectra were compatible with the symmetry assigned by Nimmo and Lucas. In this case, in contrast to the perovskites strontium titanate and lanthanum aluminate, the confusion regarding space-group symmetry arose from the large degree of structural disorder found in phase I of KNO_3 . The structures of phases II and III are unambiguous and are, respectively, aragonite D_{2h}^{16} ($Pnma$) with $Z = 4$ and C_{3v}^5 ($R3m$) with $Z = 1$.

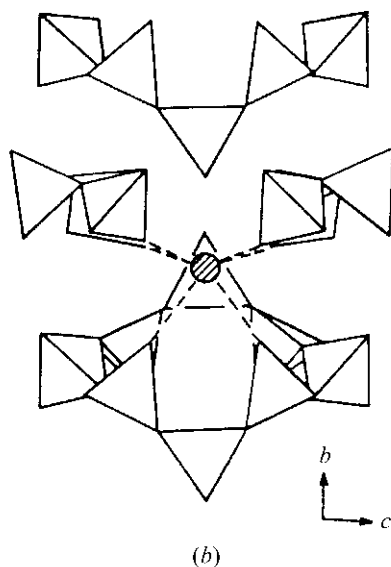
3.1.5.2.6. Lanthanum pentaphosphate

The lanthanide pentaphosphates ($\text{La}, \text{Pr}, \text{Nd}$ and $\text{TbP}_5\text{O}_{14}$) consist of linked ribbons of PO_4 tetrahedra. In each material a structural phase transition occurs from a high-temperature D_{2h}^7 ($Pncm$) point-group symmetry orthorhombic phase to a C_{2h}

3. PHASE TRANSITIONS, TWINNING AND DOMAIN STRUCTURES



(a)



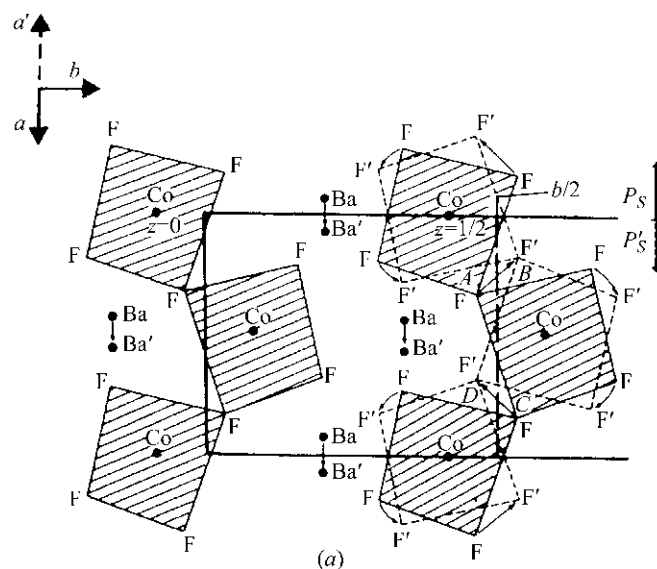
(b)

Fig. 3.1.5.10. (a) 'Soft' optical phonon frequency *versus* temperature in $\text{LaP}_5\text{O}_{14}$, showing displacive character of the phase transition. Large acousto-optic interaction prevents the optical phonon frequency from reaching zero at the transition temperature, despite the second-order character of the transition. (b) Lanthanum pentaphosphate structure, showing linked 'ribbons' of phosphate tetrahedra.

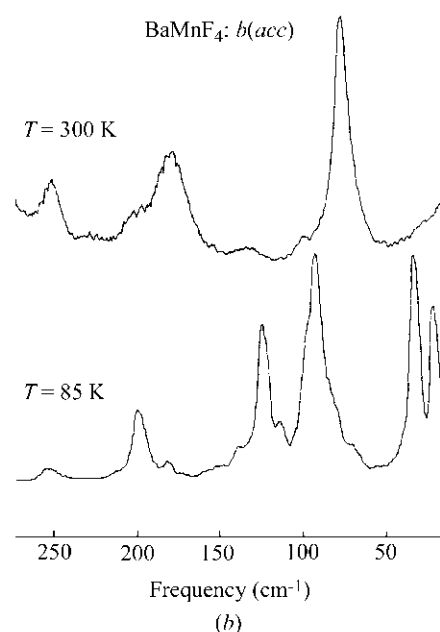
($P2_1/c$) monoclinic phase. The macroscopic order parameter for this transition is simply the monoclinic angle φ , or more precisely ($\varphi - 90^\circ$). In this family of materials, the X-ray crystallography was unambiguous in its determination of space-group symmetries and required no complementary optical information. However, the Raman studies (Fox *et al.*, 1976) provided two useful pieces of structural information. First, as shown in Fig. 3.1.5.10, they showed that the phase transition is entirely displacive, with no disorder in the high-symmetry phase; second, they showed that there is a microscopic order parameter that in mean field is proportional to the frequency of a 'soft' optical phonon of long wavelength ($q = 0$). This microscopic order parameter is in fact the eigenvector of that soft mode (normal coordinate), which approximates a rigid rotation of phosphate tetrahedra.

3.1.5.2.7. Barium manganese tetrafluoride

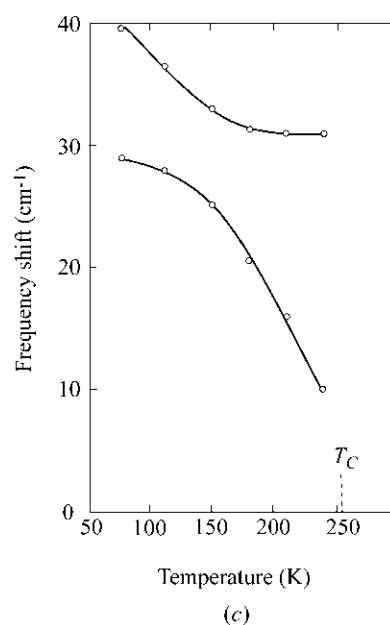
BaMnF_4 is an unusual material whose room-temperature structure is illustrated in Fig. 3.1.5.11(a). It consists of MnF_6 octahedra, linked by two shared corners along the polar a axis,



(a)



(b)



(c)

Fig. 3.1.5.11. (a) Structure of barium metal fluoride BaMF_4 ($M = \text{Co}, \text{Mn}, \text{Mg}, \text{Zn}, \text{Ni}$) at ambient temperature (300 K). (b) Raman spectroscopy of barium manganese fluoride above and below its structural phase transition temperature, ca. 251 K. (c) Temperature dependence of lower energy phonons in (b).

3.1. STRUCTURAL PHASE TRANSITIONS

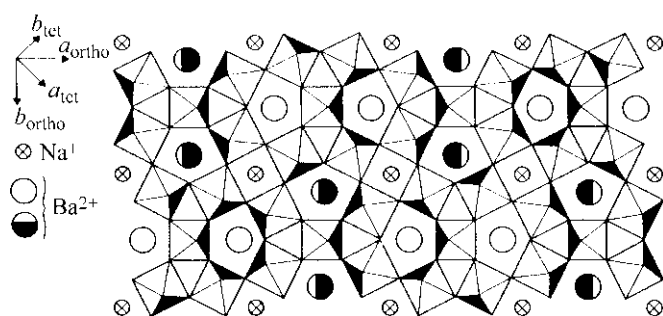


Fig. 3.1.5.12. Structure of the tungsten bronze barium sodium niobate $\text{Ba}_2\text{NaNb}_5\text{O}_{15}$ in its highest-temperature $P4/mbm$ phase above 853 K.

with ribbons of such octahedra rather widely separated by the large ionic radius barium ions in the b direction. The resulting structure is, both magnetically and mechanically, rather two-dimensional, with easy cleavage perpendicular to the b axis and highly anisotropic electrical (ionic) conduction.

Most members of the BaMF_4 family ($M = \text{Mg, Zn, Mn, Co, Ni, Fe}$) have the same structure, which is that of orthorhombic C_{2v} ($2mm$) point-group symmetry. These materials are all ferroelectric (or at least pyroelectric; high conductivity of some makes switching difficult to demonstrate) at all temperatures, with an 'incipient' ferroelectric Curie temperature extrapolated from various physical parameters (dielectric constant, spontaneous polarization *etc.*) to lie 100 K or more above the melting point (*ca.* 1050 K). The Mn compound is unique in having a low-temperature phase transition. The reason is that Mn^{+2} represents (Shannon & Prewitt, 1969) an end point in ionic size (largest) for the divalent transition metal ions Mn, Zn, Mg, Fe, Ni, Co; hence, the Mn ion and the space for it in the lattice are not a good match. This size mismatch can be accommodated by the r.m.s. thermal motion above room temperature, but at lower temperatures a structural distortion must occur.

This phase transition was first detected (Spencer *et al.*, 1970) *via* ultrasonic attenuation as an anomaly near 255 K. This experimental technique is without question one of the most sensitive in discovering phase transitions, but unfortunately it gives no direct information about structure and often it signals something that is not in fact a true phase transition (in BaMnF_4 Spencer *et al.* emphasized that they could find no other evidence that a phase transition occurred).

Raman spectroscopy was clearer (Fig. 3.1.5.11*b*), showing unambiguously additional vibrational spectra that arise from a doubling of the primitive unit cell. This was afterwards confirmed directly by X-ray crystallography at the Clarendon Laboratory, Oxford, by Wondre (1977), who observed superlattice lines indicative of cell doubling in the bc plane.

The real structural distortion near 250 K in this material is even more complicated, however. Inelastic neutron scattering at Brookhaven by Shapiro *et al.* (1976) demonstrated convincingly that the 'soft' optical phonon lies not at $(0, 1/2, 1/2)$ in the Brillouin zone, as would have been expected for the bc -plane cell doubling suggested on the basis of Raman studies, but at $(0.39, 1/2, 1/2)$. This implies that the actual structural distortion from the high-temperature C_{2v}^2 ($Cmc2_1$) symmetry does indeed double the primitive cell along the bc diagonal but in addition modulates the lattice along the a axis with a resulting repeat length that is incommensurate with the original (high-temperature) lattice constant a . The structural distortion microscopically approximates a rigid fluorine octahedra rotation, as might be expected. Hence, the chronological history of developments for this material is that X-ray crystallography gave the correct lattice structure at room temperature; ultrasonic attenuation revealed a possible phase transition near 250 K; Raman spectroscopy confirmed the transition and implied that it involved primitive

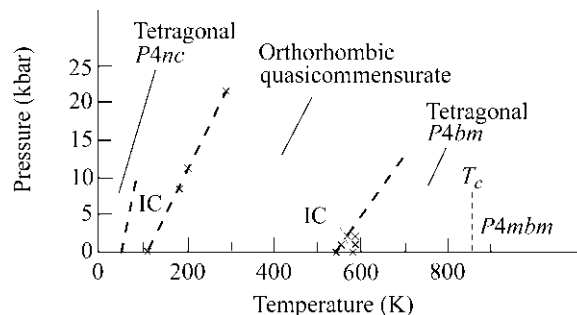


Fig. 3.1.5.13. Sequence of phases encountered with raising or lowering the temperature in barium sodium niobate.

cell doubling; X-ray crystallography confirmed directly the cell doubling; and finally neutron scattering revealed an unexpected incommensurate modulation as well. This interplay of experimental techniques provides a rather good model as exemplary for the field. For most materials, EPR would also play an important role in the likely scenarios; however, the short relaxation times for Mn ions made magnetic resonance of relatively little utility in this example.

3.1.5.2.8. Barium sodium niobate

The tungsten bronzes represented by $\text{Ba}_2\text{NaNb}_5\text{O}_{15}$ have complicated sequences of structural phase transitions. The structure is shown in Fig. 3.1.5.12 and, viewed along the polar axis, consists of triangular, square and pentagonal spaces that may or may not be filled with ions. In barium sodium niobate, the pentagonal channels are filled with Ba ions, the square channels are filled with sodium ions, and the triangular areas are empty.

The sequence of phases is shown in Fig. 3.1.5.13. At high temperatures (above $T_c = 853$ K) the crystal is tetragonal and paraelectric ($P4/mbm = D_{4h}^5$). When cooled below 853 K it becomes ferroelectric and of space group $P4bm = C_{4v}^2$ (still tetragonal). Between *ca.* 543 and 582 K it undergoes an incommensurate distortion. From 543 to *ca.* 560 K it is orthorhombic and has a '1*q*' modulation along a single orthorhombic axis. From 560 to 582 K it has a 'tweed' structure reminiscent of metallic lattices; it is still microscopically orthorhombic but has a short-range modulated order along a second orthorhombic direction and simultaneous short-range modulated order along an orthogonal axis, giving it an incompletely developed '2*q*' structure.

As the temperature is lowered still further, the lattice becomes orthorhombic but not incommensurate from 105–546 K; below 105 K it is incommensurate again, but with a microstructure quite different from that at 543–582 K. Finally, below *ca.* 40 K it becomes macroscopically tetragonal again, with probable space-group symmetry $P4nc$ (C_{4v}^6) and a primitive unit cell that is four times that of the high-temperature tetragonal phases above 582 K.

This sequence of phase transitions involves rather subtle distortions that are in most cases continuous or nearly continuous. Their elucidation has required a combination of experimental techniques, emphasizing optical birefringence (Schneck, 1982), Brillouin spectroscopy (Oliver, 1990; Schneck *et al.*, 1977; Tolédano *et al.*, 1986; Errandonea *et al.*, 1984), X-ray scattering, electron microscopy and Raman spectroscopy (Shawabkeh & Scott, 1991), among others. As with the other examples described in this chapter, it would have been difficult and perhaps impossible to establish the sequence of structures *via* X-ray techniques alone. In most cases, the distortions are very small and involve essentially only the oxygen ions.

3.1.5.2.9. Tris-sarcosine calcium chloride (TSCC)

Tris-sarcosine calcium chloride has the structure shown in Fig. 3.1.5.14. It consists of sarcosine molecules of formula

3. PHASE TRANSITIONS, TWINNING AND DOMAIN STRUCTURES

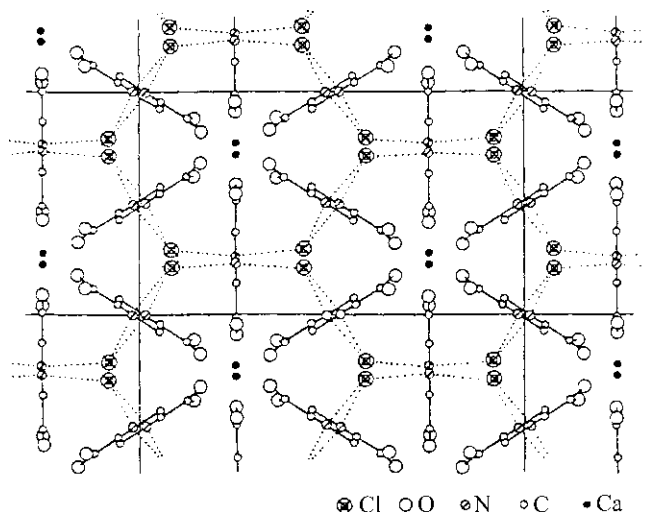


Fig. 3.1.5.14. Structure of tris-sarcosine calcium chloride, $(\text{CH}_3\text{NHCH}_2\text{COOH})_3\text{CaCl}_2$. The hydrogen ion (proton) on the COOH group is relocated in the crystal onto the N atom to form a zwitter ion, forming an $\text{H}-\text{N}-\text{H}$ group that hydrogen bonds to adjacent chlorine ions. Each nitrogen forms two such hydrogen bonds, whereas each chlorine has three, forming a very complex network of hydrogen bonding. The phase transition is actually displacive, involving a rather rigid rolling of whole sarcosine molecules, which stretches the $\text{N}-\text{H}$ bonds; it is not order-disorder of hydrogen ions in a $\text{Cl}\cdots\text{H}-\text{N}$ double well. (The $\text{Cl}\cdots\text{H}-\text{N}$ wells are apparently too asymmetric for that.)

$\text{CH}_3\text{NHCH}_2\text{COOH}$ in which the hydrogen ion comes off the COOH group and is used to hydrogen bond the nitrogen ion to a nearby chlorine, forming a zwitter ion. As is illustrated in this figure, this results in a relatively complex network of $\text{N}-\text{H}\cdots\text{Cl}$ bonds. The COO^- ion that results at the end group of each sarcosine is ionically bonded to adjacent calcium ions. The resulting structure is highly ionic in character and not at all that of a 'molecular crystal'. The structure at ambient temperatures is Pnma (D_{2h}^{16}) with $Z = 4$; below 127 K it distorts to $\text{Pna}2_1$ (C_{2v}^9) with Z still 4.

It had been supposed for some years on the basis of NMR studies of the Cl ions, as well as the conventional wisdom that 'hydrogen-bonded crystals exhibit order-disorder phase transitions', that the kinetics of ferroelectricity at the Curie temperature of 127 K in TSCC involved disorder in the proton positions along the $\text{N}-\text{H}\cdots\text{Cl}$ hydrogen bonds. In fact that is not correct; even the NMR data of Windsch & Volkel (1980), originally interpreted as order-disorder, actually show (Blinic *et al.*, 1970) a continuous, displacive evolution of the H-atom position along the $\text{H}\cdots\text{Cl}$ bond with temperature, rather than a statistical averaging

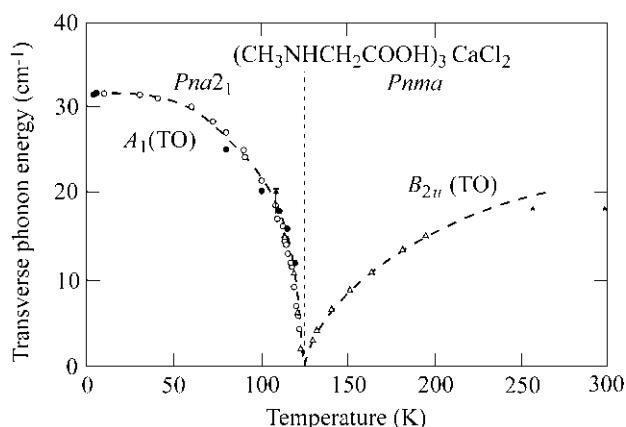


Fig. 3.1.5.15. 'Soft' optical phonon frequencies *versus* temperature in both ferroelectric and paraelectric phases of tris-sarcosine calcium chloride.

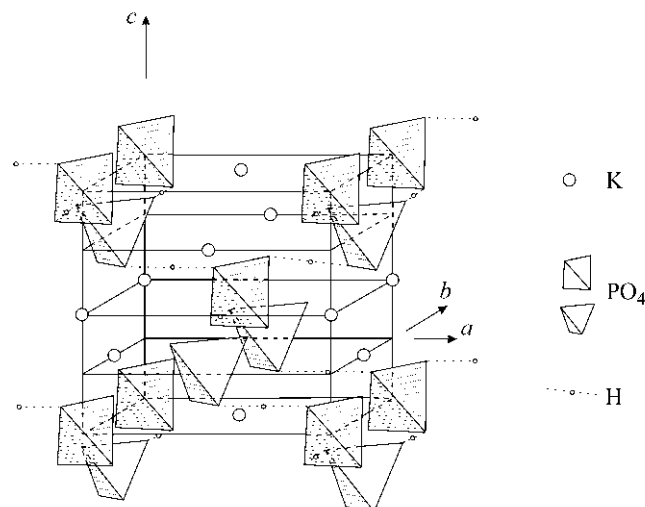


Fig. 3.1.5.16. The structure of potassium dihydrogen phosphate, KH_2PO_4 , showing the $\text{O}\cdots\text{H}\cdots\text{O}$ hydrogen bonds.

of two positions, which would characterize order-disorder dynamics. In addition, as shown in Fig. 3.1.5.15, there is (Kozlov *et al.*, 1983) a lightly damped 'soft' phonon branch in both the paraelectric and ferroelectric phases. TSCC is in fact a textbook example of a displacive ferroelectric phase transition. The hydrogen bonds do not exhibit disorder in the paraelectric phase. Rather, the transition approximates a rigid rotation of the sarcosine molecules, which stretches the $\text{N}-\text{H}\cdots\text{Cl}$ bond somewhat (Prokhorova *et al.*, 1980).

3.1.5.2.10. Potassium dihydrogen phosphate, KH_2PO_4

Potassium dihydrogen phosphate, colloquially termed 'KDP', has probably been the second most studied ferroelectric after barium titanate. It has been of some practical importance, and the relationship between its hydrogen bonds, shown in Fig. 3.1.5.16, the perpendicular displacement of heavier ions (K and P) and the Curie temperature has fascinated theoretical physicists, who generally employ a 'pseudo-spin model' in which the right and left displacements of the hydrogen ions along symmetric hydrogen bonds ($\text{O}\cdots\text{H}\cdots\text{O}$) can be described by a fictitious spin with up (+1/2) and down (-1/2) states.

Unlike TSCC, discussed above, KDP has perfectly symmetric hydrogen bonds. Therefore, one might expect that above a sufficiently high temperature the protons can quantum-mechanically tunnel between equivalent potential wells separated by a shallow (and temperature-dependent) barrier. Below T_C the protons order (all to the right or all to the left) in spatial regions that represent ferroelectric domains. This model, initially proposed by Blinc (1960), is correct and accounts for the large isotope shift in the Curie temperature noted for deuterated specimens. The complication is that the spontaneous polarization arises along a direction perpendicular to these proton displacements, so the dipoles do not arise from proton displacements directly. Instead, the proton coupling (largely Coulombic) to the potassium and phosphorus ions causes their displacements along the polar axis. This intricate coupling between protons along hydrogen bonds, which undergo an order-disorder transition, and K and P ions, which undergo purely displacive movements in their equilibrium positions, forms the basis of the theoretical interest in the lattice dynamics of KDP. Following Strukov & Levanyuk (1998), we would say that arguments over whether this transition is displacive or order-disorder are largely semantic; the correct description of KDP is that the thermal change in occupancy of the $\text{O}\cdots\text{H}\cdots\text{O}$ double wells modifies the free energy in such a way that the K and P ions undergo a displacive rearrangement.

3.1. STRUCTURAL PHASE TRANSITIONS

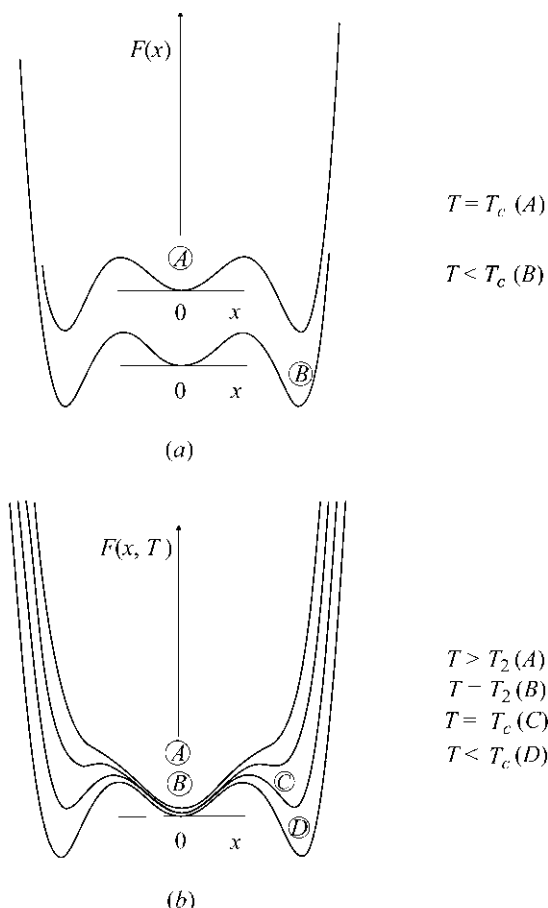


Fig. 3.1.5.17. Double-well models [circled letters show the time-averaged expectation values of the position $x(T)$ of the order parameter at each temperature]. (a) For purely order-disorder systems, the depth and separation of the wells is temperature-independent; only the thermal populations change, due to either true quantum-mechanical tunnelling (which only occurs for H or D ions) or thermally activated hopping (for heavier ions). (b) For purely displacive systems, all the temperature dependence is in the relative depths of the potential wells. [For mixed systems, such as KH_2PO_4 , both well depth(s) and thermal populations change with temperature.]

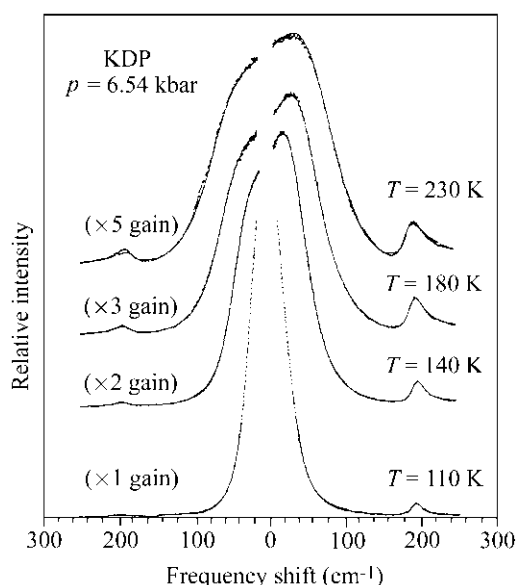


Fig. 3.1.5.18. Pressure dependence of the 'soft' optical phonon branch Raman spectra in potassium dihydrogen phosphate (after Peercy, 1975b), showing the displacive character of the phase transition [purely order-disorder phase transitions cannot exhibit propagating (underdamped) soft modes].

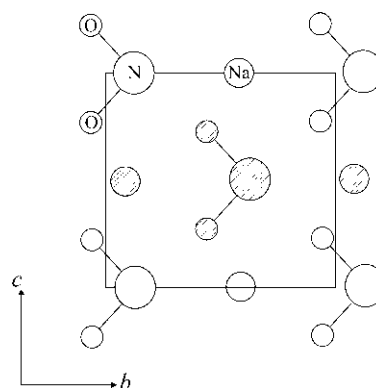


Fig. 3.1.5.19. Structure of sodium nitrite, NaNO_2 . The molecularly bonded NO_2 ions are shaped like little boomerangs. At high temperatures they are randomly oriented, pointing up or down along the polar b axis. At low temperatures they are (almost) all pointed in the same direction ($+b$ or $-b$ domains). Over a small range of intermediate temperatures their directions have a wave-like 'incommensurate' modulation with a repeat length L that is not an integral multiple of the lattice constant b .

The difficulty comes in recognizing that the normal-mode coordinate x corresponding to the soft mode in this case involves protons (H ions) and K and P ions. Therefore, the free-energy description (as in Fig. 3.1.5.17) will have partly displacive character and partly order-disorder. If the transition were purely displacive (as in TSCC, discussed above), all the important temperature changes would be in the shape of the free energy $F(x)$ with temperature T . Whereas if the transition were purely order-disorder (as in NaNO_2 , discussed below), the shape of the free-energy curves $F(x)$ would be quite independent of T ; only the relative populations of the two sides of the double well would be T -dependent. KDP is intermediate between these descriptions. Strictly, it is 'displacive' in the sense that its normal mode is a propagating mode, shown in Fig. 3.1.5.18 by Peercy's pressure-dependence Raman studies (Peercy, 1975a,b). If it were truly order-disorder, the mode would be a Debye relaxation with a spectral peak at zero frequency, independent of pressure or temperature. Only the width and intensity would depend upon these parameters.

As a final note on KDP, this material exhibits at ambient pressure and zero applied electric field a phase transition that is very slightly discontinuous. Application of modest pressure or field produces a truly continuous transition. That is, the tricritical point is easily accessible [at a critical field of 6 kV cm^{-1} , according to Western *et al.* (1978)].

3.1.5.2.11. Sodium nitrite, NaNO_2

Sodium nitrite exhibits a purely order-disorder transition and has been chosen for discussion to contrast with the systems in the sections above, which are largely displacive. The mechanism of its transition dynamics is remarkably simple and is illustrated in Fig. 3.1.5.19. There is a linear array of Na and N ions. At low temperatures, the arrow-shaped NO_2 ions (within each domain) point in the same direction; whereas above the Curie temperature they point in random directions with no long-range order. The flopping over of an NO_2 ion is a highly nonlinear response. Therefore the response function (spectrum) associated with this NO_2 flip-flop mode will consist of two parts: a high-frequency peak that looks like a conventional phonon response (lightly damped Lorentzian), plus a low-frequency Debye relaxation ('central mode' peaking at zero frequency). Most of the temperature dependence for this mode will be associated with the Debye spectrum. The spectrum of sodium nitrite is shown in Fig. 3.1.5.20.

Particularly interesting is its phase diagram, relating structure(s) to temperature and 'conjugate' field applied along the

3. PHASE TRANSITIONS, TWINNING AND DOMAIN STRUCTURES

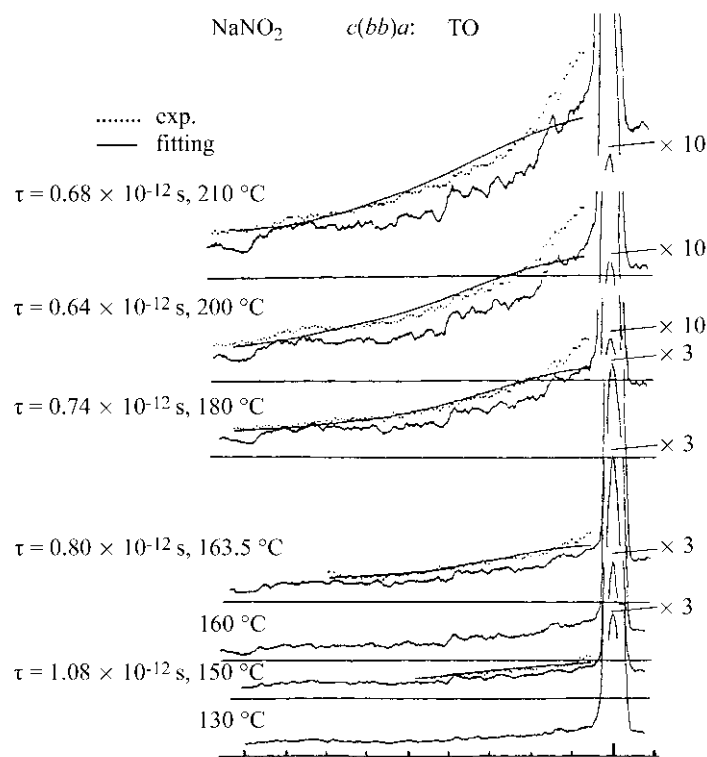
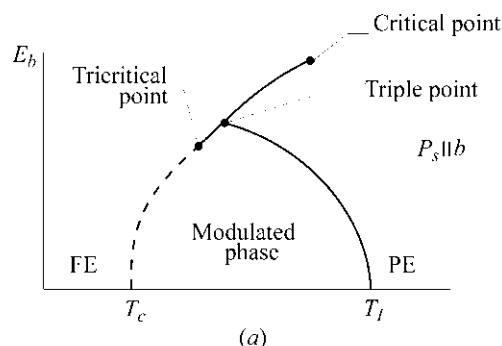
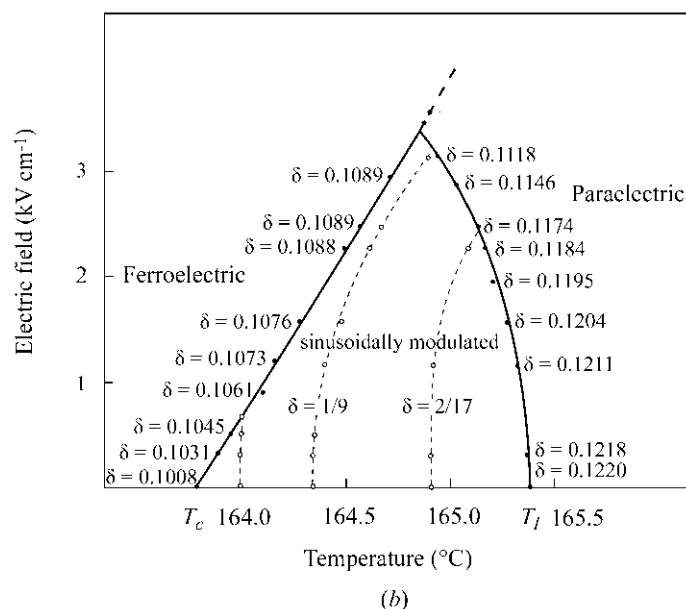


Fig. 3.1.5.20. Raman spectra of sodium nitrite, showing diffusive Debye-like response due to large-amplitude flopping over of nitrite ions [note that the high-frequency phonon-like response is due to the small-amplitude motion of this same normal mode; thus in this system N ions give rise not to $3N$ (non-degenerate) peaks in the spectral response function, but to $3N + 1$].



(a)



(b)

Fig. 3.1.5.21. Phase diagram for sodium nitrite for 'conjugate' electric fields applied along the polar b axis, showing triple point, tricritical point and critical end point. (a) Schematic; (b) real system.

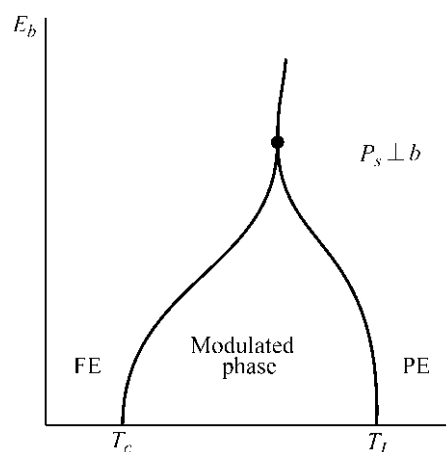


Fig. 3.1.5.22. Phase diagram for sodium nitrite for electric fields applied perpendicular to the polar b axis. In this situation, a Lifshitz point is possible where phase boundaries 'kiss' (touch tangentially).

polar axis. As Fig. 3.1.5.21 illustrates somewhat schematically, there are first-order phase boundaries, second-order phase boundaries, a tricritical point and a critical end point (as in a gas-liquid diagram). If the electric field is applied in a direction orthogonal to the polar axis, a Lifshitz point (Fig. 3.1.5.22) may be expected, in which the phase boundaries intersect tangentially. The ionic conductivity of sodium nitrite has made it difficult to make the figures in Figs. 3.1.5.21 and 3.1.5.22 precise.

3.1.5.2.12. Fast ion conductors

As exemplary of this class of materials, we discuss in this section the silver iodide compound $\text{Ag}_{13}\text{I}_9\text{W}_2\text{O}_8$. This material has the structure illustrated in Fig. 3.1.5.23. Conduction is *via* transport of silver ions through the channels produced by the W_4O_{16} ions (the coordination is not that of a simple tetrahedrally coordinated WO_4 tungstate lattice).

This crystal undergoes three structural phase transitions (Habbal *et al.*, 1978; Greer *et al.*, 1980; Habbal *et al.*, 1980), as illustrated in Fig. 3.1.5.24. The two at lower temperatures are first-order; that at the highest temperature appears to be perfectly continuous. Geller *et al.* (1980) tried to fit electrical data for this material ignoring the uppermost transition.

As in most of the materials discussed in this review, the phase transitions were most readily observed *via* optical techniques, Raman spectroscopy in particular. The subtle distortions involve oxygen positions primarily and are not particularly well suited to more conventional X-ray techniques. Silver-ion disorder sets in only above the uppermost phase transition, as indicated by the full spectral response (as in the discussion of sodium nitrite in the preceding section).

Infrared (Volkov *et al.*, 1985) and Raman (Shawabkeh & Scott, 1989) spectroscopy have similarly confirmed low-temperature phase transitions in RbAg_4I_5 at 44 and 30 K, in addition to the well studied $D_3^7-D_3^2$ ($R32-P321$) transition at 122 K. The two lower-temperature phases increase the size of the primitive cell, but their space groups cannot be determined from available optical data. The 44 K transition is signalled by the abrupt appearance of an intense phonon feature at 12 cm^{-1} in both infrared and Raman spectra.

3.1.5.2.13. High-temperature superconductors

It is useful to play Devil's Advocate and point out difficulties with the technique discussed, to indicate where caution might be exercised in its application. $\text{YBa}_2\text{Cu}_3\text{O}_{7-x}$ (YBaCuO) provides such a case. As in the case of BaMnF_4 discussed in Section 3.1.5.2.7, there was strong evidence for a structural phase transition near 235 K, first from ultrasonic attenuation (Wang, 1987;

3.1. STRUCTURAL PHASE TRANSITIONS

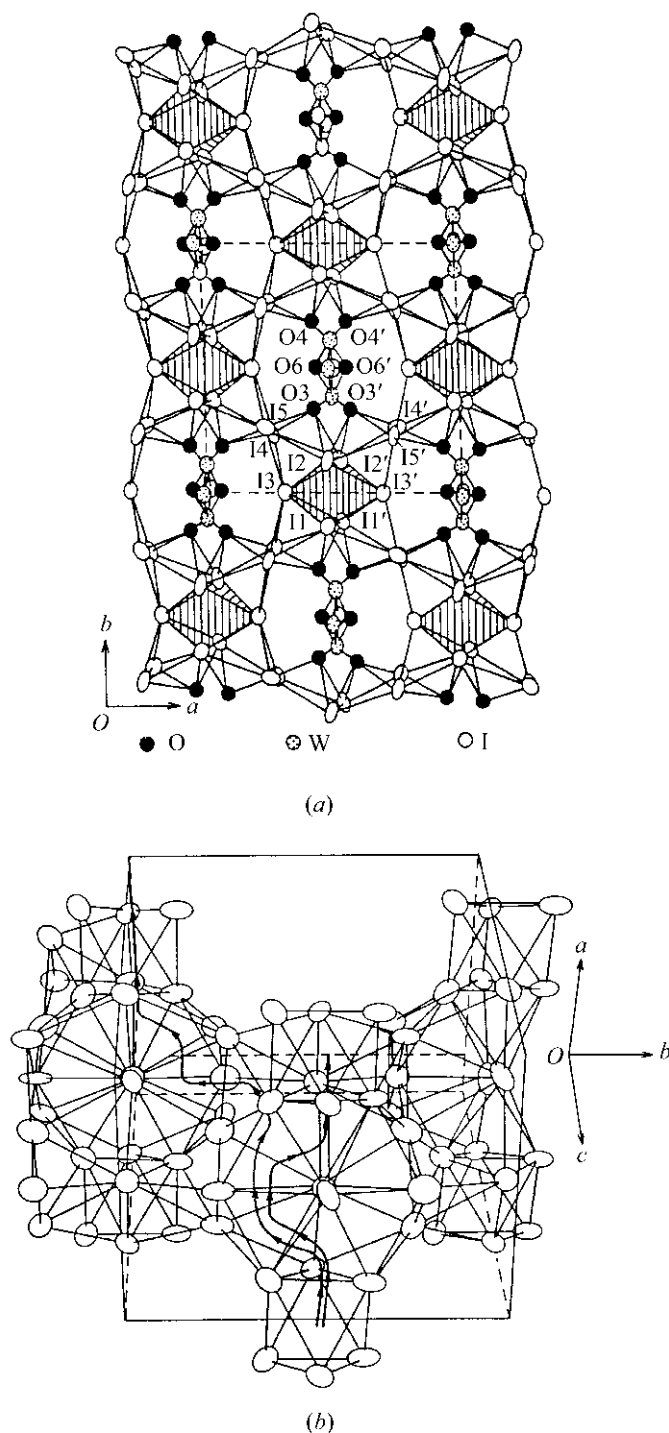


Fig. 3.1.5.23. (a) Crystal structure of silver iodide tungstate ($\text{Ag}_{13}\text{I}_9\text{W}_2\text{O}_8$); (b) showing conduction paths for Ag ions (after Chan & Geller, 1977).

Laegreid *et al.*, 1987) and then from Raman studies (Zhang *et al.*, 1988; Huang *et al.*, 1987; Rebane *et al.*, 1988). However, as years passed this was never verified *via* neutron or X-ray scattering. Researchers questioned (MacFarlane *et al.*, 1987) whether indeed a phase transition exists at such a temperature in this important material. At present it is a controversial and occasionally contentious issue. A difficulty is that light scattering in metals probes only the surface. No information is obtained on the bulk. Ultrasonic attenuation and internal friction probe the bulk, but give scanty information on mechanisms or structure.

In the specific case of YBaCuO , the 'extra' phonon line (Fig. 3.1.5.25) that emerges below 235 K is now known not to be from the superconducting $\text{YBa}_2\text{Cu}_3\text{O}_{7-x}$ material; its frequency of 644 cm^{-1} is higher than that of any bulk phonons in that material. However, this frequency closely matches that of the highest

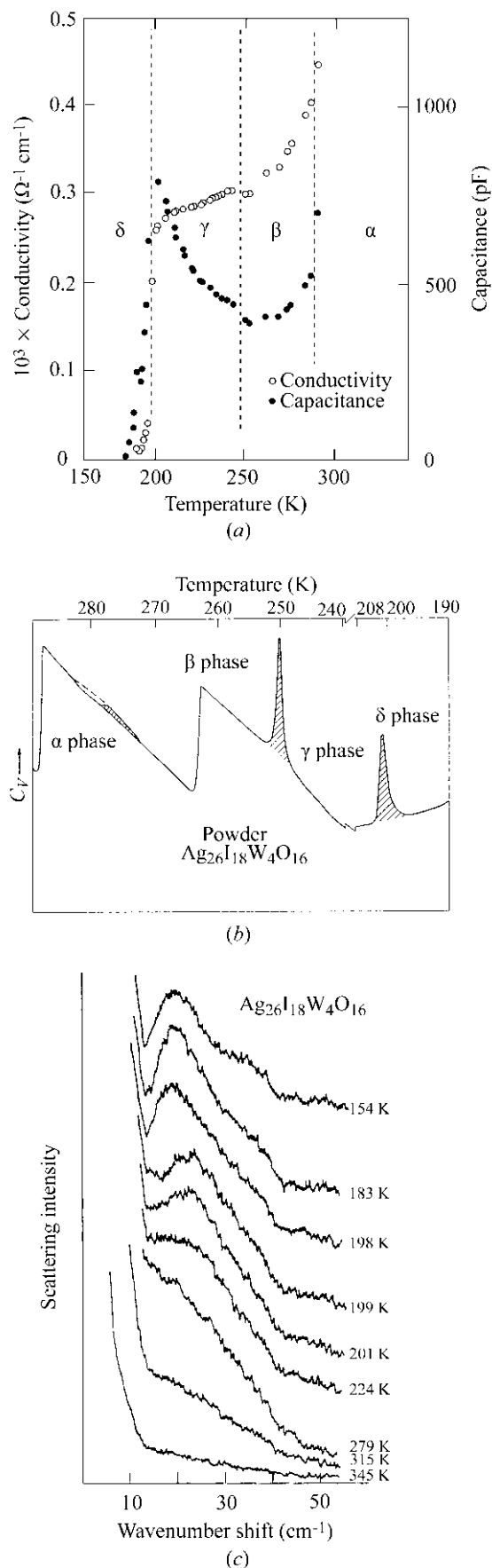


Fig. 3.1.5.24. Evidence for three phase transitions in silver iodide tungstate: (a) dielectric and conductivity data; (b) specific heat data; (c) Raman data. The lower transitions, at 199 and 250 K, are first order; the upper one, at 285 K, is second order.

3. PHASE TRANSITIONS, TWINNING AND DOMAIN STRUCTURES

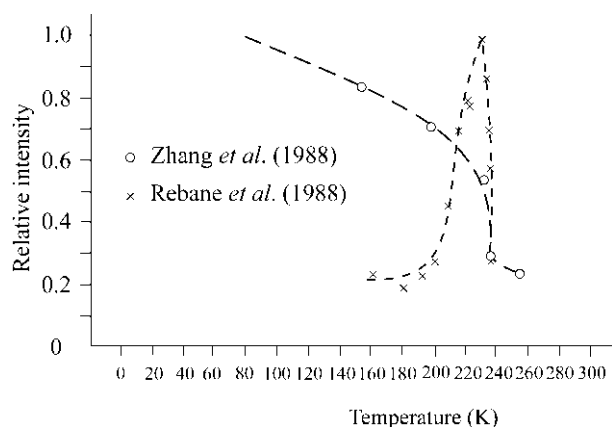


Fig. 3.1.5.25. Raman spectra of $\text{YBa}_2\text{Cu}_3\text{O}_{7-x}$ below an apparent phase transition at ca. 235 K (Zhang *et al.*, 1988).

LO (longitudinal optical) phonon in the semiconducting $\text{YBa}_2\text{Cu}_3\text{O}_{6+x}$ material, suggesting that the supposed phase transition at 235 K may be not a structural transition but instead a chemical transition in which oxygen is lost or gained at the surface with temperature cycling.

3.1.5.3. Low-temperature ferroelectric transitions

It has historically been difficult to establish the nature of ferroelectric phase transitions at cryogenic temperatures. This is simply because the coercive fields for most crystals rise as the temperature is lowered, often becoming greater than the breakdown fields below ca. 100 K. As a result, it is difficult to demonstrate *via* traditional macroscopic engineering techniques (switching) that a material is really ferroelectric. Some authors have proposed (*e.g.* Tokunaga, 1987) on theoretical grounds the remarkable (and erroneous) conjecture that no crystals have Curie temperatures much below 100 K. A rebuttal of this speculation is given in Table 3.1.5.1 in the form of a list of counter-examples. References may be found in the 1990 Landolt-Börnstein Encyclopedia of Physics (Vol. 28a). The original work on pure cadmium titanate and on lead pyrochlore (Hulm, 1950, 1953) did not demonstrate switching, but on the basis of more recent studies on mixed crystals $\text{Ca}_{2-2x}\text{Pb}_{2x}\text{Nb}_2\text{O}_7$ and $\text{Ca}_x\text{Cd}_{1-x}\text{TiO}_3$, it is clear that the pure crystals are ferroelectric at and below the stated temperatures.

Hence, in Table 3.1.5.1 we see examples where X-ray structural studies may establish the symmetries requisite for ferroelectricity without the macroscopic switching being demonstrated. This is the converse case to that primarily emphasized in this section (*i.e.* the use of techniques complementary to X-ray scattering to determine exact crystal symmetries); it is useful to see these reverse cases to demonstrate the full complementarity of X-ray crystallography and dynamic spectroscopic techniques.

3.1.6. Group informatics and tensor calculus

BY V. KOPSKÝ AND P. BOČEK

We shall briefly describe here the intentions and contents of the software package that constitutes part of the accompanying CD-ROM: *GI•KoBo-1* (*Group Informatics*, first two letters of authors names, release 1). A more detailed description is contained in the manual; the user may consult this file on the screen, but we recommend that it is printed out and that the printout is followed in order to become familiar with the theoretical background as well as with more detailed instructions for the use of the software.

The main purpose of this software is to describe the changes of tensor properties of crystalline materials during ferroic phase transitions, including basic information about domain states. The

Table 3.1.5.1. Low-temperature ferroelectrics

| Formula | Curie temperature T_c (K) | Curie constant C (K) | Entropy change ΔS (cal mol ⁻¹ K ⁻¹) |
|--|-----------------------------|------------------------|--|
| $\text{NH}_4\text{Al}(\text{SO}_4)_2 \cdot 12\text{H}_2\text{O}$ | 71 | ? | ? |
| $\text{NH}_4\text{Fe}(\text{SO}_4)_2 \cdot 12\text{H}_2\text{O}$ | 88 | 400 | 0.15 |
| $(\text{NH}_4)_2\text{Cd}(\text{SO}_4)_3$ | 95 | ? | ? |
| CdTiO_3 | 55 | 4.5×10^4 | ? |
| $\text{Pb}_2\text{Nb}_2\text{O}_7$ | 15.3 | ? | ? |
| $\text{LiTiC}_4\text{H}_4\text{O}_6 \cdot \text{H}_2\text{O}$ | 10.5 | ? | ? |
| $\text{K}_3\text{Li}_2\text{Nb}_5\text{O}_{15}$ | 7 | ? | ? |

software provides powerful information in a standardized manner and it is based on a few advanced methodical points that are not yet available in textbooks. These points are:

(i) The introduction of *typical variables*, which was inspired by the *symbolic method* of the old invariant theory (Weitzenböck, 1923).

(ii) The method of Clebsch–Gordan products (Kopský, 1976a,b). The name stems from Clebsch–Gordan coefficients, known in quantum mechanics as coefficients of momentum addition. In this case, the coefficients are connected with the orthogonal group $O(3)$; analogous coefficients were later introduced and calculated for crystal point groups (Koster *et al.*, 1963). They appear in Clebsch–Gordan products, which represent a better adaptation of results for our purposes.

(iii) Tables of *tensorial covariants* (Kopský, 1979a,b). The name covariant may sound rather unusual now, but it was originally used by Weyl (1946); it is equivalent to *symmetry-adapted bases* (*form-invariant bases* and other terms are also used). The term covariant is classical and its semantical use is easier.

(iv) Tables of *fine structures of domain states* (Kopský, 1982). These are contained in a booklet which is practically unknown though, together with tables of tensorial covariants, it contains all answers concerning changes of tensor properties at ferroic phase transitions.

Remark. The original term *fine domain structure* was amended because it is not quite accurate.

(v) *Extended integrity bases* (Patera *et al.*, 1978; Kopský, 1979c). These represent finite sets of polynomial invariants and covariants suitable for the calculation of all types of interactions in symmetric systems.

(vi) *Lattices of subgroups* (Ascher, 1968; Kopský, 1982). Subgroups of a group constitute a partially ordered set of special properties called a *lattice*. The unfortunate coincidence of the term (in English) with crystallographic lattices should be disregarded; it is always possible to see from the context what we mean by this term.

These methods provide good ammunition for all types of group-theoretical considerations where work with characters is insufficient and knowledge of the explicit bases of irreducible representations is necessary. This is exactly the case for the theory of structural phase transitions, and the consideration of domain states, pairs of domain states and domain walls or twin boundaries. The main results of the software are contained in tables of symmetry descents $G \Downarrow H$ and/or $G \Downarrow F_i$, where G is the parent point group, H its normal subgroup and F_i is the set of conjugate subgroups. These tables provide information about changes of tensors at ferroic phase transitions as well as basic information about interactions, and they are also supplemented by tables of equitranslational subgroups of space groups.

To make this exposition quite clear, we begin in the manual from the beginning with a brief review of elementary group-theoretical concepts used in the software. Relevant elementary tables (listed below in Section A) are followed by more advanced information proceeding towards the central goal of providing information for all symmetry descents (Section B). To achieve this goal, it was also necessary to introduce our own standard

3.1. STRUCTURAL PHASE TRANSITIONS

notation for specifically oriented groups, for their elements and for irreducible representations (ireps). The reasons for the introduction of these standards are twofold: (i) There is no unique and commonly accepted notation in the literature. The recent book by Altmann & Herzig (1994) contains slight inconsistencies (different symbols for elements in a group and in its subgroup) and is also not compatible with another prominent source (Bradley & Cracknell, 1972). (ii) We need a strict specification of groups and their subgroups with reference to a Cartesian coordinate system and a strict specification of matrix ireps; neither is available in the literature. This does not mean that we introduce brand-new symbols; we simply adapt those that are already in use and we take extreme care that every symbol has a unique meaning.

It is recommended that users follow the manual when first using the software. The tabular content is as follows:

A. General information

On opening the program, a panel *Crystallographic* appears on the screen. In the left-hand part are listed crystallographic geometric classes in a tree form wrapped to crystallographic systems (families). A click on a system brings to the screen a list of its crystallographic geometric classes as either Hermann–Mauguin, Schoenflies or Shubnikov symbols (the latter are used only on this level).

The default choice for the notation is set in a table *Options* under the pull-down menu *File*. Hermann–Mauguin or Schoenflies symbols are offered for groups, standard or spectroscopic notation for group elements, classes of ireps and classes of conjugate elements. The temporary notation, under the pull-down menu *Notation*, also includes the choice of Shubnikov symbols.

When the user clicks on a geometric class, all specifically oriented groups of this class used in the software appear in the right-hand part of the panel. At the top appear the groups in standard orientation that are further used as the standard parent groups, all remaining groups appearing below. For some groups two or three standard orientations are available, for reasons explained in the manual. The option of using Hermann–Mauguin or Schoenflies symbols for groups is available throughout; up to a certain point there are options for using either standard symbols of group elements and of ireps (as defined here) or spectroscopic symbols. A specific group is picked using the left mouse button, then a click with the right mouse button opens a pull-down menu. The following information is available under the titles:

(1) *Basic info*: This contains information relevant to each group of the geometric class, such as the number of elements, generators, isomorphism type, normalizer, number of conjugacy classes and the standard orientations.

(2) *Group elements*: Activates the group calculator, the keys of which list elements of the group. Performs calculation of products (strings) of up to ten elements by left or right multiplication.

(3) *Correlation std./spectro*: Symbols of groups, elements and classes of ireps for standard and spectroscopic notation are correlated.

(4) *Class structure*: Symbols of classes of conjugate elements are defined and elements of classes are listed.

(5) *Class multiplication table*: Displays class multiplication formulae.

(6) *Character table*: Standard and spectroscopic symbols of classes of ireps are specified and kernels of ireps are presented.

(7) *Kronecker products*: Tables of Kronecker products of classes of ireps are displayed. Up to this point, both standard and spectroscopic notation are used.

(8) *Ireps and standard variables*: Irreducible matrix representations (ireps) are explicitly defined. These also define the standard symbols of typical variables.

Brief: Brief tables specify matrices of ireps for generators of the group.

Full: Full tables provide these matrices for each group element. Kernels of ireps are presented. From this point onwards only the standard notation is used.

(9) *Clebsch–Gordan products*: Up to orthorhombic groups, one Clebsch–Gordan product table is given. For groups of higher systems, there are two options: *complex* Clebsch–Gordan tables, where variables $(\xi_\alpha, \eta_\alpha)$ are used, and *real* Clebsch–Gordan tables, with variables (x_α, y_α) for two-dimensional real ireps.

(10) *Tensorial covariants*: Decomposition of tensors up to fourth rank into their covariant components is displayed.

B. Ferroic phase transitions

(11) *Subgroups*: Choice of this item displays a panel with the lattice of subgroups of the originally chosen point group G either in Schoenflies or in Hermann–Mauguin symbols. The pull-down menu *Graph* in the upper bar enables handling of the lattice: each item can be picked and moved to another place, the rearranged lattice can be fixed as default or reset, and the lattice can be sent to a printer. Notice that sets of conjugate subgroups are stacked like a pile of sheets of paper and can be unstacked. Consecutive clicks activate individual subgroups of the set. In the upper part of the panel, ireps of the parent group G in spectroscopic symbols are listed; these are followed by boxes in which it is possible to scroll for special vectors of the respective carrier space in terms of typical variables. Clicking on a vector marks its stabilizer (epikernel of the irep) in the lattice and activates it at the same time. With each irep is associated a table of the extended integrity basis; the table is called either by the option *Integrity bases* under the pull-down menu *View* or directly by using the right mouse button in the box of this irep. If the Ctrl key is pressed after the choice of one vector, another vector may be chosen; as a result, an intersection of the respective epikernels is marked in the lattice.

Each subgroup of the lattice may also be activated independently. Lattices of subgroups serve themselves as menus for consideration of specific symmetry descents. Clicking on a subgroup H or on one of the stack of conjugate subgroups F_i activates the following information about symmetry descent $G \Downarrow H$ or $G \Downarrow F_i$:

(1) *Domain*: This option brings to the screen the main table that describes changes of tensor properties in chosen ferroic descent. The option is available under the pull-down menu *View* or directly at the subgroup in the case of normal subgroups. The change of tensor properties is given with reference to the first domain state and hence to the group F_1 from the set of conjugate subgroups. It is given for all tensors listed in Section 3.1.2.3 in a slightly different manner than in Table 3.1.3.1. Namely, principal and secondary tensor parameters of the transition are distinguished. In other words, the onsetting tensor components are distinguished according to the ireps to which they belong. From this information, one can deduce the *fine structure of domain states* with all possible crossovers when some tensor properties are identical in several domains. In tables for those symmetry descents where the subgroup is not an epikernel of a certain irep, expressions of the subgroup as possible intersection of epikernels are presented.

To each table is attached information about G -invariant forms of interactions. This consists of:

Integrity basis: of invariants in the primary order parameter.

Faint interactions: These are those interactions of the primary order parameter with secondary (faint) parameters that are responsible for the occurrence of faint parameters.

Electric switching interactions: The interactions of all order parameters with an external electric field.

Elastic switching interactions: The interactions of all order parameters with an external stress field.

(2) *Integrity bases*: Needs activation of the box of ireps as explained above. Displays the *extended integrity basis* of polynomials in variables of the chosen irep. This consists of the

3. PHASE TRANSITIONS, TWINNING AND DOMAIN STRUCTURES

integrity basis of polynomial invariants and of the linear bases of polynomial covariants.

(3) *Twinning group*: This option works for the first group of the set of conjugate subgroups only. It displays a table that contains consecutive normalizers of the set of conjugate subgroups, left, right and double coset resolutions of the parent group G with respect to the subgroup F_1 , and the twinning groups assigned to double cosets. This is the basic information concerning pairs of domain states.

Lattices of equitranslational subgroups of the space groups. The importance of these lattices was realized by Ascher (1968), who prepared the first tables. However, his tables do not contain full information about subgroups; neither the parent group nor the subgroups are completely specified. The current version gives the full information about subgroups including their settings and origins. The pull-down menu *Groups* contains two options: *Point* and *Space*. The choice of the second option brings to the screen another panel, in the right-hand part of which are listed space groups of the geometric class G through Hermann–Mauguin symbols corresponding to all settings and cell choices where applicable. The number of the space-group type, the Schoenflies symbol, the setting and the cell choice are shown in the left-hand part of the panel when you click on one of these Hermann–Mauguin symbols. At the same time, the symbols of the point groups in the lattice change to Schoenflies symbols of oriented space-group types. As you click on any of these subgroups, the Hermann–Mauguin symbol that specifies the subgroup completely appears in the lower bar of the panel, reserved for this information. Though the embellished lattice symbols used in this presentation are self-explanatory, consultation of the manual is recommended.

The option *Point* returns the lattice to its original form of the lattice of point groups.

The following is a list of tabular appendices contained in the manual:

Appendix A: correlation of various notations and Jones' faithful representation symbols;

Appendix B: Schoenflies and Hermann–Mauguin symbols of groups in standard orientations and of their subgroups;

Appendix C: isomorphisms used for defining irreducible representations;

Appendix D: standard polynomials;

Appendix E: labelling of covariants and conversion equations;

Appendix F: list of symmetry descents;

Appendix G: nonstandard lattice letters.

Our symbols for point-symmetry operations are compared with other sources in Appendix A. Symbols of all groups used in the software are given in Appendix B and isomorphisms in Appendix C. Standard polynomials in Appendix D are abbreviated symbols for more complicated polynomials that appear in the main tables. Appendix E is of primary importance for consideration of the relationship between tensor parameters and their contribution to Cartesian tensor components as already indicated in the text explaining Table 3.1.3.1. In Appendix F are listed and classified all symmetry descents considered in the main table. Consultation of Appendix G is strongly recommended to all users who want to use the lattices of equitranslational subgroups of the space groups.

3.1.7. Glossary

(a) Groups

| | |
|---------------|---|
| G | point-group symmetry of the parent (prototype, high-symmetry) phase |
| \mathcal{G} | space-group symmetry of the parent (prototype, high-symmetry) phase |

| | |
|---------------------------------------|---|
| F | point-group symmetry of the ferroic (low-symmetry) phase (domain state not specified) |
| \mathcal{F} | space-group symmetry of the ferroic (low-symmetry) phase (domain state not specified) |
| F_1 | point-group symmetry of the first ferroic single domain state |
| \mathcal{F}_1 | space-group symmetry of the first ferroic single domain state |
| $G \Downarrow F$ | point-group symmetry descent from G to F |
| $\mathcal{G} \Downarrow \mathcal{F}$ | space-group symmetry descent from \mathcal{G} to \mathcal{F} |
| $\mathcal{G} \Downarrow' \mathcal{F}$ | equitranslational symmetry descent from \mathcal{G} to \mathcal{F} |
| Γ_η | representation of \mathcal{G} (or of G) according to which η transforms |
| $D^{(\eta)}$ | irreducible matrix representation of the order parameter η |
| χ_η | character of the matrix representation $D^{(\eta)}$ |
| R -irep | physically irreducible representation |
| n_F | number of subgroups conjugate under G to subgroup F_1 |
| n_f | number of ferroic single domain states |
| n_a | number of ferroelastic single domain states |
| n_e | number of ferroelectric single domain states |

(b) Physical quantities

| | |
|--------------------|--|
| c | specific heat |
| $d_{i\mu}$ | piezoelectric tensor |
| F, G | free energy |
| g_μ | optical activity |
| P_i | dielectric polarization |
| S | entropy |
| s_{ij} | elastic compliance |
| T_c | Curie temperature |
| u_{ij}, u_μ | strain tensor |
| V | cell volume |
| χ | dielectric susceptibility |
| ε | enantiomorphism, chirality |
| ε_{ij} | high-frequency dielectric constant or permittivity |
| η | order parameter (primary) |
| λ | order parameter (secondary) |
| ω_{LO} | longitudinal optic mode frequency |
| ω_{TO} | transverse optic mode frequency |
| $\pi_{\mu\nu}$ | piezo-optic tensor |

References

- Aizu, K. (1969). *Possible species of ferroelastic crystals and of simultaneously ferroelectric and ferroelastic crystals*. *J. Phys. Soc. Jpn*, **27**, 387–396.
- Aizu, K. (1970). *Possible species of ferromagnetic, ferroelectric, and ferroelastic crystals*. *Phys. Rev. B*, **2**, 754–772.
- Aizu, K. (1973). *Second order ferroic states*. *J. Phys. Soc. Jpn*, **34**, 121–128.
- Altmann, S. L. & Herzig, P. (1994). *Point-group theory tables*. Oxford: Clarendon Press.
- Aroyo, M. I. & Perez-Mato, J. M. (1998). *Symmetry mode analysis of displacive phase transitions using International Tables for Crystallography*. *Acta Cryst.* **A54**, 19–30.
- Ascher, E. (1968). *Lattices of equi-translation subgroups of the space groups*. Geneva: Battelle.
- Ascher, E. & Kobayashi, J. (1977). *Symmetry and phase transitions: the inverse Landau problem*. *J. Phys. C: Solid State Phys.* **10**, 1349–1363.

3.1. STRUCTURAL PHASE TRANSITIONS

- Balkanski, M., Teng, M. K. & Nusimovici, M. (1969). *Lattice dynamics in KNO_3 , Phases I, II and III*. In *Light scattering spectra of solids*, edited by G. B. Wright, pp. 731–746. Paris: Flammarion.
- Blinic, R. (1960). *On the isotopic effects in the ferroelectric behaviour of crystals with short hydrogen bonds*. *J. Phys. Chem. Solids*, **13**, 204–211.
- Blinic, R., Jamsek-Vilfan, M., Lahajnar, G. & Hajdukovic, G. (1970). *Nuclear magnetic resonance study of the ferroelectric transition in diglycine nitrate and tris-sarcosine calcium chloride*. *J. Chem. Phys.* **52**, 6407–6411.
- Bradley, C. J. & Cracknell, A. P. (1972). *The mathematical theory of symmetry in solids. Representation theory for point groups and space groups*. Oxford: Clarendon Press.
- Chan, L. Y. Y. & Geller, S. (1977). *Crystal structure and conductivity of 26-silver 18-iodine tetrahydrate*. *J. Solid State Chem.* **21**, 331–347.
- Cochran, W. (1960). *Crystal stability and the theory of ferroelectricity; Part I*. *Adv. Phys.* **9**, 387–402.
- Cochran, W. (1961). *Crystal stability and the theory of ferroelectricity; Part II. Piezoelectric crystals*. *Adv. Phys.* **10**, 401–420.
- Cowley, R. A. (1962). *Temperature dependence of a transverse optic mode in strontium titanate*. *Phys. Rev. Lett.* **9**, 159–161.
- Cowley, R. A. (1964). *Lattice dynamics and phase transitions mode in strontium titanate*. *Phys. Rev. A*, **134**, 981–997.
- Cowley, R. A. (1970). *On the dielectric properties of an anharmonic crystal*. *J. Phys. Soc. Jpn*, **28**, Suppl., 205–209.
- Devonshire, A. F. (1954). *Theory of ferroelectrics*. *Adv. Phys.* **3**, 85.
- Dvořák, V. (1974). *Improper ferroelectrics*. *Ferroelectrics*, **7**, 1–9.
- Errandonea, G., Tolédano, J.-C., Litzler, A., Schneek, J., Savary, H. & Aubrée, J. (1984). *Kinetic characteristics of the thermal hysteresis in an incommensurate system*. *J. Phys. Lett.* **45**, L329–L334.
- Fleury, P. A., Scott, J. F. & Worlock, J. M. (1968). *Soft phonon modes and the 110 K phase transition in strontium titanate*. *Phys. Rev. Lett.* **21**, 16–19.
- Fox, D. L., Scott, J. F. & Bridenbaugh, P. M. (1976). *Soft modes in ferroelastic LaP_5O_{14} and NdP_5O_{14}* . *Solid State Commun.* **18**, 111–113.
- Geller, S. & Bala, V. B. (1956). *Crystallographic studies of perovskite-like compounds. II. Rare earth alluminates*. *Acta Cryst.* **9**, 1019–1024.
- Geller, S., Wilber, S. A., Ruse, G. F., Akridge, J. R. & Turkovic, A. (1980). *Anisotropic electrical conductivity and low-temperature phase transitions of the solid electrolyte $Ag_{26}I_{18}W_4O_{16}$* . *Phys. Rev. B*, **21**, 2506–2512.
- Greer, A. L., Habbal, F., Scott, J. F. & Takahashi, T. (1980). *Specific heat anomalies and phase transitions in the solid electrolyte $Ag_{26}I_{18}W_4O_{16}$* . *J. Chem. Phys.* **73**, 5833–5867.
- Habbal, F., Zvirgzds, J. A. & Scott, J. F. (1978). *Raman spectra of structural phase transitions in $Ag_{26}I_{18}W_4O_{16}$* . *J. Chem. Phys.* **69**, 4984–4989.
- Habbal, F., Zvirgzds, J. A. & Scott, J. F. (1980). *Ferroelectric phase transition in the superionic conductor $Ag_{26}I_{18}W_4O_{16}$* . *J. Chem. Phys.* **72**, 2760–2763.
- Huang, C. Y., Dries, L. T., Hor, P. H., Meng, R. I., Chu, C. W. & Frankel, R. B. (1987). *Observation of possible superconductivity at 230 K*. *Nature (London)*, **238**, 403–404.
- Hulm, J. K. (1950). *The dielectric properties of some alkaline earth titanates at low temperatures*. *Proc. Phys. Soc. London Ser. A*, **63**, 1184–1185.
- Hulm, J. K. (1953). *Low-temperature properties of cadmium and lead niobates*. *Phys. Rev.* **92**, 504.
- IEEE Standard on Piezoelectricity STD 176–1987. (1987). New York: The Institute of Electrical and Electronics Engineers, Inc. This IEEE Std 176–1987 is reproduced in *IEEE Transactions on Ultrasonics, Ferroelectrics, and Frequency Control*. (1996). **43**, No. 5.
- Indenbom, V. L. (1960). *Phase transitions without change in the number of atoms in the unit cell of the crystal*. *Sov. Phys. Crystallogr.* **5**, 105–115.
- International Tables for Crystallography (2002). Vol. A. *Space-group symmetry*, edited by Th. Hahn. Dordrecht: Kluwer Academic Publishers.
- International Tables for Crystallography (2003). Vol. A1. *Symmetry relations between space groups*, edited by H. Wondratschek & U. Müller. In preparation.
- Izyumov, Yu. A. & Syromiatnikov, V. N. (1990). *Phase transitions and crystal symmetry*. Dordrecht: Kluwer Academic Publishers.
- Janovec, V., Dvořák, V. & Petzelt, J. (1975). *Symmetry classification and properties of equi-translation structural phase transitions*. *Czech. J. Phys.* **B25**, 1362–1396.
- Jansen, L. & Boon, M. (1967). *Theory of finite groups. Applications in physics. Symmetry groups of quantum mechanical systems*. Amsterdam: North-Holland.
- Kociński, J. (1983). *Theory of symmetry changes at continuous phase transitions*. Warsaw: PWN – Polish Scientific Publishers; Amsterdam: Elsevier.
- Kociński, J. (1990). *Commensurate and incommensurate phase transitions*. Warsaw: PWN – Polish Scientific Publishers; Amsterdam: Elsevier.
- Kopský, V. (1976a). *The use of the Clebsch–Gordan reduction of the Kronecker square of the typical representation in symmetry problems of crystal physics. I. Theoretical foundations*. *J. Phys. C: Solid State Phys.* **9**, 3391–3405.
- Kopský, V. (1976b). *The use of the Clebsch–Gordan reduction of the Kronecker square of the typical representation in symmetry problems of crystal physics. II. Tabulation of Clebsch–Gordan products for classical and magnetic crystal point groups*. *J. Phys. C: Solid State Phys.* **9**, 3405–3420.
- Kopský, V. (1979a). *Tensorial covariants of the 32 crystal point groups*. *Acta Cryst.* **A35**, 83–95.
- Kopský, V. (1979b). *A simplified calculation and tabulation of tensorial covariants for magnetic point groups belonging to the same Laue class*. *Acta Cryst.* **A35**, 95–101.
- Kopský, V. (1979c). *Extended integrity bases of irreducible matrix groups. The crystal point groups*. *J. Phys. A: Math. Gen.* **12**, 943–957.
- Kopský, V. (1979d). *Representation generating theorem and interaction of improper quantities with order parameter*. *J. Phys. A: Math. Gen.* **12**, L291–L294.
- Kopský, V. (1982). *Group lattices, subduction of bases and fine domain structures for magnetic crystal point groups*. Prague: Academia.
- Kopský, V. (2000). *The change of tensor properties at ferroic phase transitions*. *Ferroelectrics*, **237**, 127–134.
- Kopský, V. (2001). *Tensor parameters of ferroic phase transitions. I. Theory and tables*. *Phase Transit.* **73**, No. 1–2, 1–422.
- Koster, G. F., Dimmock, J. O., Wheeler, R. E. & Statz, H. (1963). *Properties of the 32 groups*. Cambridge: MIT Press.
- Kozlov, G. V., Volkov, A. A., Scott, J. F. & Petzelt, J. (1983). *Millimeter wavelength spectroscopy of the ferroelectric phase transition in tris-sarcosine calcium chloride*. *Phys. Rev. B*, **28**, 255–261.
- Laegreid, T., Fossheim, K., Sandvold, E. & Juisrud, S. (1987). *Specific heat anomaly at 220 K connected with superconductivity at 90 K in ceramic $YBa_2Cu_3O_{7-x}$* . *Nature (London)*, **330**, 637–638.
- Landau, L. D. (1937). *Theory of phase transitions. I*. *Phys. Z. Sowjun.* **11**, 26–47; *II*. *Phys. Z. Sowjun.* **11**, 545–555.
- Landau, L. D. & Lifshitz, E. M. (1969). *Course in theoretical physics, Vol. 5, Statistical physics*, 2nd ed. Oxford: Pergamon Press.
- Levanyuk, A. P. & Sannikov, D. G. (1974). *Improper seignetolectrics*. *Uspekhi Fiz. Nauk.* **112**, 561–589. (In Russian.)
- Lines, M. E. & Glass, A. M. (1977). *Principles and applications of ferroelectrics and related materials*. Oxford University Press.
- Lytle, F. W. (1964). *X-ray diffractometry of low-temperature phase transformations in strontium titanate*. *J. Appl. Phys.* **35**, 2212–2214.
- Lyubarskii, G. Ya. (1960). *The application of group theory in physics*. Oxford: Pergamon Press.
- MacFarlane, R. M., Rosen, H. & Seki, H. (1987). *Temperature dependence of the Raman spectra of the high- T_c superconductor $YBa_2Cu_3O_{7-x}$* . *Solid State Commun.* **63**, 831–834.
- Nimmo, J. K. & Lucas, D. W. (1973). *The crystal structures of γ - and β - KNO_3 and the $\alpha \leftarrow \gamma \leftarrow \beta$ phase transformations*. *Acta Cryst.* **B32**, 1968–1971.
- Nowick, A. S. (1995). *Crystal properties via group theory*. Cambridge University Press.
- Nye, J. F. (1985). *Physical properties of crystals*. Oxford: Clarendon Press.
- Oliver, W. F. (1990). PhD thesis, University of Colorado.
- Patera, J., Sharp, R. T. & Winternitz, P. (1978). *Polynomial irreducible tensors for point groups*. *J. Math. Phys.* **19**, 2362–2376.
- Peercy, P. S. (1975a). *Soft mode and coupled modes in the ferroelectric phase of KH_2PO_4* . *Solid State Commun.* **16**, 439–442.
- Peercy, P. S. (1975b). *Measurement of the soft mode and coupled modes in the paraelectric and ferroelectric phases of KH_2PO_4* . *Phys. Rev. B*, **12**, 2741–2746.
- Pick, R. (1969). Private communication.
- Prokhorova, S. D., Smolensky, G. A., Siny, I. G., Kuzminov, E. G., Mikvabia, V. D. & Arndt, H. (1980). *Light scattering study of the phase transition in tris-sarcosine calcium chloride*. *Ferroelectrics*, **25**, 629–632.

3. PHASE TRANSITIONS, TWINNING AND DOMAIN STRUCTURES

- Rebane, L., Fimberg, T. A., Fefer, E. M., Blumberg, G. E. & Joon, E. R. (1988). *Raman scattering study of lattice instability in $YBa_2Cu_3O_{7-x}$ at 200–240 K*. *Solid State Commun.* **65**, 1535–1537.
- Rousseau, D. L., Bauman, R. P. & Porto, S. P. S. (1981). *Normal mode determination in crystals*. *J. Raman Spectrosc.* **10**, 253–290.
- Schneck, J. (1982). Thèse de Doctorat d'Etat ès Sciences Physiques, Université Pierre et Marie Curie (Paris).
- Schneck, J., Primot, J., Von der Muhl, R. & Ravez, J. (1977). *New phase transition with increasing symmetry on cooling in barium sodium niobate*. *Solid State Commun.* **21**, 57–60.
- Scott, J. F. (1969). *Raman study of trigonal–cubic phase transitions in rare-earth aluminates*. *Phys. Rev.* **183**, 823–825.
- Scott, J. F. (1999). *A comparison of Ag- and proton-conducting ferroelectrics*. *Solid State Ionics*, **125**, 141–146.
- Scott, J. F. & Pouligny, B. (1988). *Raman spectroscopic study of submicron KNO_3 films*. *J. Appl. Phys.* **64**, 1547–1551.
- Scott, J. F. & Remeika, J. P. (1970). *High-temperature Raman study of $SmAlO_3$* . *Phys. Rev. B*, **1**, 4182–4185.
- Shannon, R. D. & Prewitt, C. T. (1969). *Effective ionic radii in oxides and fluorides*. *Acta Cryst.* **B25**, 925–945.
- Shapiro, S. M., Cowley, R. A., Cox, D. E., Eibschutz, M. & Guggenheim, H. J. (1976). *Neutron scattering study of incommensurate $BaMnF_4$* . In *Proc. Natl Conf. Neutron Scat.* edited by R. M. Moon, pp. 399–406. Springfield, VA: Nat. Tech. Info. Serv.
- Shawabkeh, A. & Scott, J. F. (1989). *Raman spectra of low-temperature phase transitions in $RbAg_4I_5$* . *J. Raman Spectrosc.* **20**, 277–281.
- Shawabkeh, A. & Scott, J. F. (1991). *Raman spectroscopy of incommensurate $Ba_2NaNb_5O_{15}$* . *Phys. Rev. B*, **43**, 10999–11004.
- Shinnaka, Y. (1962). *X-ray study on the disordered structure above the ferroelectric Curie point in KNO_3* . *J. Phys. Soc. Jpn*, **17**, 820–828.
- Shuvalov, L. A. (1988). Editor. *Modern crystallography IV. Physical properties of crystals*. Berlin: Springer-Verlag.
- Sirotnin, Yu. I. & Shaskolskaya, M. P. (1982). *Fundamentals of crystal physics*. Moscow: Mir Publishers.
- Spencer, E. G., Guggenheim, H. J. & Kominiak, G. J. (1970). *$BaMnF_4$, a new crystal for microwave ultrasonics*. *Appl. Phys. Lett.* **17**, 300–301.
- Stokes, H. T. & Hatch, D. M. (1988). *Isotropy groups of the 230 crystallographic space groups*. Singapore: World Scientific.
- Strukov, B. A. & Levanyuk, A. P. (1998). *Ferroelectric phenomena in crystals*. Berlin: Springer.
- Tahvonen, P. E. (1947). *X-ray structure of potassium nitrate*. *Ann. Acad. Sci. Fenn. Ser. A*, 44–51.
- Tokunaga, M. (1987). *Two different mechanisms of the Curie–Weiss dielectric susceptibility in displacive-type ferroelectrics*. *J. Phys. Soc. Jpn*, **56**, 1653–1656.
- Tolédano, J.-C., Schneck, J. & Errandonea, G. (1986). *Incommensurate phase of barium sodium niobate*. In *Incommensurate phases in dielectric materials*, edited by R. Blinc & A. P. Levanyuk, pp. 233–252. Amsterdam: North-Holland.
- Tolédano, J.-C. & Tolédano, P. (1980). *Order parameter symmetries and free-energy expansions for purely ferroelastic transitions*. *Phys. Rev. B*, **21**, 1139–1172.
- Tolédano, J.-C. & Tolédano, P. (1987). *The Landau theory of phase transitions*. Singapore: World Scientific.
- Tolédano, P. & Dmitriev, V. (1996). *Reconstructive phase transitions*. Singapore: World Scientific.
- Tolédano, P. & Tolédano, J.-C. (1976). *Order parameter symmetries for ferroelectric nonferroelastic transitions*. *Phys. Rev. B*, **14**, 3097–3109.
- Tolédano, P. & Tolédano, J.-C. (1977). *Order parameter symmetries for the phase transitions of nonmagnetic secondary and higher order ferroics*. *Phys. Rev. B*, **16**, 386–407.
- Tolédano, P. & Tolédano, J.-C. (1982). *Non-ferroic phase transitions*. *Phys. Rev. B*, **25**, 1946–1964.
- Unoki, H. & Sakudo, T. (1967). *Electron spin resonance of Fe^{+3} in strontium titanate with specific reference to the 110 K phase transition*. *J. Phys. Soc. Jpn*, **23**, 546–552.
- Van der Waals, J. D. (1873). PhD thesis, University of Leiden.
- Volkov, A. A., Kozlov, G. V., Mirzoyants, G. I. & Petzelt, J. (1985). *Submicron dielectric spectroscopy of superionic conductors*. *Jpn. J. Appl. Phys.* **24**, Suppl. 24-2, 531–533.
- Wadhawan, V. K. (2000) *Introduction to ferroic materials*. Australia: Gordon and Breach Science Publishers.
- Wang, Y., Shen, H., Zhu, J., Xu, Z., Gu, M., Niu, Z. & Zhang, Z. (1987). *Ultrasonic anomaly in $YBa_2Cu_3O_{7-x}$ at 235 K*. *J. Phys. Condens. Mat.* **20**, L665.
- Weiss, P. (1907). *L'hypothèse du champ moléculaire et la propriété ferromagnétique*. *J. Phys. Radium*, **6**, 661–690.
- Weitzenböck, R. (1923). *Invariantentheorie*. Groningen: Noordhof.
- Western, A. B., Baker, A. G., Bacon, C. R. & Schmidt, V. H. (1978). *Pressure-induced critical point in the ferroelectric phase transition in KH_2PO_4* . *Phys. Rev. B*, **17**, 4461–4473.
- Weyl, H. (1946). *The classical groups*. Princeton: UP.
- Windsch, W. & Volkel, G. (1980). *EPR investigation of the dynamics of ferroelectric tris-sarcosine calcium chloride*. *Ferroelectrics*, **24**, 195–202.
- Wondre, F. R. (1977). Unpublished. Cited in Scott, J. F. (1978). *Spectroscopy of magnetoelectric $BaMnF_4$ and ferroelastic NdP_5O_{14}* . *Ferroelectrics*, **20**, 69–74.
- Worlock, J. M. (1971). *Light scattering studies of structural phase transitions*. In *Structural phase transitions and soft modes*, edited by E. Samuelsen, E. Andersen & Z. Feder, pp. 329–370. Oslo: Universitetsforlaget.
- Zhang, M.-S., Chen, Q., Sun, D., Ji, R.-F., Qin, Z.-K., Yu, Z. & Scott, J. F. (1988). *Raman studies of phonon anomalies at 235 K in $YBa_2Cu_3O_{7-x}$* . *Solid State Commun.* **65**, 487–490; see also Huang et al. (1987).

3.2. Twinning and domain structures

By V. JANOVEC, TH. HAHN AND H. KLAPPER

3.2.1. Introduction and history

Twins have been known for as long as mankind has collected minerals, admired their beauty and displayed them in museums and mineral collections. In particular, large specimens of contact and penetration twins with their characteristic re-entrant angles and simulated higher symmetries have caught the attention of mineral collectors, miners and scientists. *Twinning* as a special feature of crystal morphology, therefore, is a ‘child’ of mineralogy, and the terms and symbols in use for twinned crystals have developed during several centuries together with the development of mineralogy.

The first scientific description of *twinning*, based on the observation of re-entrant angles, goes back to Romé de l’Isle (1783). Haüy (1801) introduced symmetry considerations into twinning. He described *hemitropes* (twofold rotation twins) and *penetration twins*, and stated that the *twin face* is parallel to a possible crystal face. Much pioneering work was done by Weiss (1809, 1814, 1817/1818) and Mohs (1822/1824, 1823), who extended the symmetry laws of twinning and analysed the symmetry relations of many twins occurring in minerals. Naumann (1830) was the first to distinguish between twins with parallel axes (*Zwillinge mit parallelen Achsensystemen*) and twins with inclined (*crossed*) axes (*Zwillinge mit gekreuzten Achsensystemen*), and developed the mathematical theory of twins (Naumann, 1856). A comprehensive survey of the development of the concept and understanding of twinning up to 1869 is presented by Klein (1869).

At the beginning of the 20th century, several important mineralogical schools developed new and far-reaching ideas on twinning. The French school of Mallard (1879) and Friedel (1904) applied the lattice concept of Bravais to twinning. This culminated in the lattice classification of twins by Friedel (1904, 1926) and his introduction of the terms *macles par mériédrie* (twinning by merohedry), *macles par pseudo-mériédrie* (twinning by pseudo-merohedry), *macles par mériédrie réticulaire* [twinning by reticular (lattice) merohedry] and *macles par pseudo-mériédrie réticulaire* (twinning by reticular pseudo-merohedry). This concept of twinning was very soon taken up and further developed by Niggli in Zürich, especially in his textbooks (1919, 1920, 1924, 1941). The lattice theory of Mallard and Friedel was subsequently extensively applied and further extended by J. D. H. Donnay (1940), and in many later papers by Donnay & Donnay, especially Donnay & Donnay (1974). The Viennese school of Tschermak (1904, 1906), Tschermak & Becke (1915), and Tertsch (1936) thoroughly analysed the morphology of twins, introduced the *Kantennormalengesetz* and established the minimal conditions for twinning. The structural and energy aspects of twins and their boundaries were first accentuated and developed by Buerger (1945). Presently, twinning plays an important (but negative) role in crystal structure determination. Several sophisticated computer programs have been developed that correct for the presence of twinning in a small single crystal.

A comprehensive review of twinning is given by Cahn (1954); an extensive treatment of mechanical twinning is presented in the monograph by Klassen-Neklyudova (1964). A tensor classification of twinning was recently presented by Wadhawan (1997, 2000). Brief modern surveys are contained in the textbooks by Bloss (1971), Giacomazzo (1992) and Indenbom (see Vainshtein *et al.*, 1995), the latter mainly devoted to theoretical aspects. In previous volumes of *International Tables*, two articles on twinning

have appeared: formulae for the calculation of characteristic twin data, based on the work by Friedel (1926, pp. 245–252), are collected by Donnay & Donnay in Section 3 of Volume II of the previous series (Donnay & Donnay, 1972), and a more mathematical survey is presented by Koch in Chapter 1.3 of Volume C of the present series (Koch, 1999).

Independently from the development of the concept of twinning in mineralogy and crystallography, summarized above, the concept of *domain structures* was developed in physics at the beginning of the 20th century. This started with the study of *ferromagnetism* by Weiss (1907), who put forward the idea of a molecular field and formulated the hypothesis of differently magnetized regions, called *ferromagnetic domains*, that can be switched by an external magnetic field. Much later, von Hámos & Thiessen (1931) succeeded in visualizing magnetic domains by means of colloidal magnetic powder. For more details about magnetic domains see Section 1.6.4 of the present volume.

In 1921, Valasek (1921) observed unusual dielectric behaviour in Rochelle salt and pointed out its similarity with anomalous properties of ferromagnetic materials. This analogy led to a prediction of ‘electric’ domains, *i.e.* regions with different directions of spontaneous polarization that can be switched by an electric field. Materials with this property were called *Seignette electrics* (derived from the French, ‘*sel de Seignette*’, denoting Rochelle salt). The term *seignettelectrics* is still used in Russian, but in English has been replaced by the term *ferroelectrics* (Mueller, 1935). Although many experimental and theoretical results gave indirect evidence for *ferroelectric domain structure* [for an early history see Cady (1946)], it was not until 1944 that Zwicker & Scherrer (1944) reported the first direct optical observation of the domain structure in ferroelectric potassium dihydrogen phosphate (KDP). Four years later, Klassen-Neklyudova *et al.* (1948) observed the domain structure of Rochelle salt in a polarizing microscope (see Klassen-Neklyudova, 1964, p. 27). In the same year, Blattner *et al.* (1948), Kay (1948) and Matthias & von Hippel (1948) visualized domains and domain walls in barium titanate crystals using the same technique.

These early studies also gave direct evidence of the influence of mechanical stress and electric field on domain structure. Further, it was disclosed that a domain structure exists only below a certain temperature, called the *Curie point*, and that the crystal structures below and above the Curie point have different point-group symmetries. The Curie point thus marks a structural phase transition between a *paraelectric phase* without a domain structure and a *ferroelectric phase* with a ferroelectric domain structure. Later, the term ‘Curie point’ was replaced by the more suitable expression *Curie temperature* or *transition temperature*.

The fundamental achievement in understanding phase transitions in crystals is the *Landau theory* of continuous phase transitions (Landau, 1937). Besides a thermodynamic explanation of anomalies near phase transitions, it discloses that any continuous phase transition is accompanied by a discontinuous decrease of crystal symmetry. In consequence, a phase with lower symmetry can always form a domain structure.

The basic role of symmetry was demonstrated in the pioneering work of Zheludev & Shuvalov (1956), who derived by simple crystallographic considerations the point groups of paraelectric and ferroelectric phases of all possible ferroelectric phase transitions and gave a formula for the number of ferroelectric domain states.

3. PHASE TRANSITIONS, TWINNING AND DOMAIN STRUCTURES

A mechanical analogy to ferroelectric domains exists in the form of domains that differ in strain and can be switched by mechanical stress. This effect was studied under the name '*twinning with change of form*' in the monoclinic ferroelectric phase of Rochelle salt by Klassen-Neklyudova *et al.* (1948) and Chernysheva (1950). A detailed description of this work in English is presented by Klassen-Neklyudova (1964, pp. 27–30, 75–78) in her monograph on mechanical twinning of crystals. Indenbom (1960) has shown that such behaviour is not confined to ferroelectric crystals and has listed many symmetry changes of potential phase transitions accompanied by the appearance of a spontaneous strain that could give rise to domains with different strain. Aizu (1969) called such crystals *ferroelastic crystals* in analogy with ferroelectric crystals. *Ferroelastic domains* differ in spontaneous strain and can be switched by mechanical stress.

Generalization of the concepts of ferromagnetic, ferroelectric and ferroelastic crystals followed soon after (Aizu, 1970): A *ferroic crystal* has two or more *orientation states* (oriented bulk structures of domains) that can be switched by means of a magnetic field, an electric field, a mechanical stress or by a combination of these. *Ferroic domains* are distinct in some tensors describing the material properties of the crystal. Aizu has also shown that the type of domain structure is determined by the change of point-group symmetry at the structural phase transition from a *prototypic (parent, high-symmetry) phase* without domains to a *ferroic (distorted, low-symmetry, daughter) phase* in which domains appear.

A more detailed history of the research of ferromagnetic, ferroelectric, ferroelastic and ferroic materials in general can be found in the book by Wadhawan (2000).

The domain structure determines to a certain extent electric, elastic, electromechanical and other properties of ferroic crystals. The investigation of domain structures has thus become an inseparable part of the research of ferroelectrics, ferroelastics and ferroic crystalline materials in general.

Most of the work has been devoted to ferroelectrics, since their specific properties have found important applications, some of which (e.g. production of anisotropic ceramics, ferroelectric memories) are based on irreversible and hysteretic changes of the ferroelectric domain structure under an electric field. References to ferroelectric, ferroelastic and other domain structures are given at the end of Section 3.4.1.

Even though the basic concepts of *twinning* and *domain structures* are closely related and have many aspects in common, the study of both subjects has developed independently, using different terms and symbols to describe rather similar facts. There are many cases that can be treated equally well by both approaches, e.g. merohedral twins and non-ferroelastic domain structures. There are cases, however, which can only be understood with one of the two concepts, e.g. the (111) spinel twins cannot be interpreted as a domain structure, because a high-symmetry parent phase does not exist. Of the two topics, twinning is the older, whereas the younger topic domain structure has recently advanced to a more detailed physical understanding.

In the two following chapters, 3.3 and 3.4, the two topics are treated separately and in their own right. It will be apparent that the two approaches, despite the great similarity of their objects, are quite different: for *domain structures* the all-important theoretical basis is the existence of a – real or potential (hypothetical) – *parent (prototypic) phase* from which the *ferroic (distorted) phase* is derived. This lowering of symmetry, expressed by a group–subgroup relation between the symmetries of the parent and ferroic phases, is the source of an impressive theoretical edifice which allows the explanation, and even the prediction, of many crystallographic properties of a given domain structure.

The situation is different in *twinning*: whereas *transformation twins* are closely related to domain structures and hence can be treated with the same theoretical tools, many *growth twins* and

mechanical twins are characterized by the absence of an existing – and even a hypothetical – parent structure. From this it follows that growth and mechanical twins (which are the typical twin specimens of mineral collections) are to a much lesser extent amenable to group-theoretical analysis. Instead, each twinning case must be considered separately, and the orientation and contact relations of the twin partners must be individually ascertained. This requires discussion of many 'type cases'.

The present chapter continues with a short excursion into bicrystallography (Section 3.2.2), a topic not treated further in this article, followed by Section 3.2.3 with an exposition of basic concepts of set theory and group theory needed in Chapters 3.3 and 3.4.

3.2.2. A brief survey of bicrystallography

Both twinning and domain structures appear to be special cases of the relatively young research field of *bicrystallography* (Pond & Vlachavas, 1983), which has its origin in the study of *grain boundaries* in metals. Grains are coexisting crystals with identical composition and structure but with different orientations. Coexisting grains can be formally treated as generalized twins in which one of the conditions (*viz* a crystallographic relation between the twin components) is dropped.

A common feature of twins, domain structures and grain aggregates is the interface between coexisting crystals. The simplest edifice containing a crystalline interface is a bicrystal consisting of two semi-infinite perfect crystals (components) and a single planar interface along which the two crystals adjoin. For easier comprehension, one crystal of a bicrystal can be 'coloured' black and the other crystal white. Then the operations that leave both crystals unchanged are trivial colour-preserving symmetry operations, whereas the *symmetrizing operations*, which transform the black crystal into the white one and *vice versa*, are nontrivial colour-reversing operations. If one marks these colour-reversing operations by a prime or a star, then the symmetry group of a bicrystal has the structure of a *dichromatic (black-and-white) group* (see Section 3.2.3.2.7).

The dissymmetrization (symmetry reduction or lowering, symmetry descent) plays a basic role in bicrystallography. This is a process in which an object changes from a high-symmetry form into a low-symmetry form. As shown in Chapter 3.4, any dissymmetrization is accompanied by the formation of several symmetrically equivalent specimens of the low symmetry called *variants*. Variants are related by suppressed (lost) symmetry operations that are present in the low-symmetry form but are missing in the high-symmetry form. The set of all low-symmetry variants recovers the symmetry of the high-symmetry form. This general statement is referred to as the *law of symmetry compensation* and can be alternatively expressed by the following sentence (Shubnikov & Koptsik, 1974): If symmetry is reduced at one structural level, it arises and is recovered at another structural level. A paradigmatic example of dissymmetrization is a structural phase transition in which a high-symmetry parent (prototypic) phase changes into a low-symmetry distorted (ferroic) phase. The variants of the low-symmetry distorted phase are called single domain states or orientation states. The set of all single domain states recovers the high symmetry of the parent phase (see Chapter 3.4).

A systematic method for deriving the bicrystal symmetry, which is identical with the symmetry of the bicrystal interface, consists of four hierarchical stages (Pond & Vlachavas, 1983). At each stage, the bicrystal is represented by a construct (model) which is more detailed – and has, therefore, the same or lower symmetry – than the construct of the previous stage. These successive dissymmetrizations bring about at each stage equivalent variants of the bicrystal's construct. Different sets of variants

3.2. TWINNING AND DOMAIN STRUCTURES

at different stages have distinct physical significance and provide a basic generic classification of bicrystals and their interfaces.

The first stage deals with the so-called dichromatic pattern consisting of two interpenetrating black and white lattices of the two crystal components (Pond & Bollmann, 1979). The coinciding 'grey' points constitute the *coincidence site lattice* (CSL) (see Bollmann, 1970, 1982), which corresponds to the twin lattice in twinning (see Section 3.3.8). To find variants of the dichromatic pattern, bicrystallography replaces the symmetry group of a nonexistent previous 'zero stage' with a minimal group containing symmetries of the black crystal and the white crystal. This group is called the *embracing* or *fundamental group of dichromatic patterns* (Shubnikov & Koptsik, 1974; Pond & Vlachavas, 1983; Wadhawan, 2000). If the symmetry group of the dichromatic pattern is smaller than the embracing group, then this dissymmetrization produces orientational or translational variants of the dichromatic pattern.

In the second stage, black and white lattices are decorated by atoms and these crystal structures are represented by lattice complexes. [A lattice complex of a crystal is here defined as the set of points obtained by carrying out on each occupied atomic position all symmetry operations of the crystal's space group. Note that in crystallography the term 'lattice complex' has a different meaning; see *IT A* (2002), Parts 8 and 14.] Two interpenetrating black and white lattice complexes of crystal components form the dichromatic complex of a bicrystal. If the symmetry of the dichromatic complex is lower than that of the dichromatic pattern, the dissymmetrization gives rise to complex variants of the dichromatic complex. The concept of a dichromatic complex corresponds to the concept of a domain pair in domain structure analysis (see Section 3.4.3).

Mental constructions of the first two stages specify only the relation between the lattices and structures of crystal components of a bicrystal. In the third stage, an *ideal bicrystal* is formed by sectioning the black-and-white lattice (or structure) on the interface plane and discarding the black lattice (or structure) on one side of the section and the white lattice (structure) on the other side. If the interfacial plane is a crystallographic plane with two-dimensional periodicity, then the symmetry of this ideal bicrystal is described by a *dichromatic layer group* (see Sections 3.4.4.2 and 3.4.4.3). This group is smaller than the space-group symmetry of the dichromatic complex and this dissymmetrization gives rise to *morphological variants* of the ideal bicrystal. Operations suppressed at this dissymmetrization relate different morphological variants of the ideal bicrystal. An ideal bicrystal corresponds to a domain twin with zero-thickness domain wall (see Section 3.4.4).

All three preceding stages use geometrical models of an interface with fixed atomic positions. At the final fourth stage, these geometrical constraints are lifted and the ideal bicrystal relaxes to a *real* or *relaxed bicrystal* with a minimum free energy. During this relaxation process the interface plane may migrate into either crystal, one crystal may translate rigidly with respect to the other, and each atom may adjust its position to relax any resultant force acting on it. The relaxation may even include insertion or removal of additional material at the interface. If the symmetry of the relaxed bicrystal is lower than that of the ideal bicrystal, then relaxational variants of the relaxed bicrystal appear. The one-dimensional interface between two interfacial relaxational variants forms a line defect of the bicrystal interface. Relaxation variants of finite-thickness domain walls and line defects in these walls are discussed in Section 3.4.4.

Two main theoretical approaches have been used in examining the microscopic structure of a real bicrystal interface. In the older one, a real interface is treated as a *periodic array of dislocations*. This approach, still based on geometrical models, has explained successfully the microscopic structure of small-angle grain boundaries, but has failed in large-angle grain boundaries (misorientation angle larger than 15°).

More recent investigations utilizing computer simulations allow one to lift geometrical constraints and permit the calculation of equilibrium atomic positions directly from interatomic forces. These calculations have revealed that the lattice coincidence is almost always lost upon relaxation and that the microscopic structure of bicrystal interfaces can be described as an ordered sequence of coordination polyhedra. These conclusions have been confirmed by high-resolution electron microscopy. For more details see, for example, Fischmeister (1985), Sutton & Balluffi (1995) and Gottstein & Shvindlerman (1999).

The first three 'classical' stages of the bicrystallographical analysis already yield valuable conclusions. They disclose generic relations between different interfaces, specify crystallographically equivalent variants of an interface and classify line defects in interfaces. The symmetry of a bicrystal imposes constraints on tensor properties of the bicrystal interface, provides classification of the interfacial vibrational modes, discloses possible interfacial transitions *etc.* (see, for example, Kalonji, 1985).

The methodology of bicrystallography has many common features with the symmetry analysis of domain structures but, since both approaches have developed independently, they use a different terminology. Moreover, in comparison with bicrystals, domain structures and twins are more restricted by crystallographic constraints. This has resulted in more extensive application of group theory in domain structures than in bicrystallography. On the other hand, bicrystallography is more general and can even treat interfaces between two crystals belonging to different phases (heterophase interfaces).

A synoptic 'roadmap for the use of interfacial symmetry', compiled by Kalonji (1985), provides a quick guide to the possible applications of bicrystallography. A short introduction to bicrystallography can be found in Wadhawan (2000); a brief comparison of the concepts and terminologies of bicrystals, twins and domain structures is presented by Hahn *et al.* (1999). An extensive treatment of bicrystallography is available in the paper by Pond & Vlachavas (1983) and in the book by Sutton & Balluffi (1995), where other aspects of crystalline interfaces are also thoroughly covered.

3.2.3. Mathematical tools

Analysis of domain structures and twins does not deal primarily with single-crystal structures, as does classical crystallography, but studies collections of several crystal structures – which usually differ in orientation and position in space – and examines relations between these structures and their coexistence. The exact formulation of such an analysis uses mathematical concepts that are not yet quite common in crystallography. Thus, *e.g.*, a collection of crystallographic objects has to be decomposed into equivalence classes called orbits and strata, or the symmetry of an object (structure, domain wall, twin) has to be described with respect to a given group, which necessitates replacing the usual notion of a symmetry group by a 'stabilizer' (isotropy group). A prerequisite of introducing these terms is the concept of group action, which provides a basic and efficient tool for domain-structure analysis.

Another special feature of domain studies is that one can associate with a ferroic structure under study another structure, called the parent (prototypic) structure, from which the ferroic structure can be derived by small microscopic distortions. The fact that the symmetry of the ferroic phase is lower than that of the parent phase invokes the notion of a subgroup. Associated notions such as conjugate subgroups, normalizers and decomposition of a group into left and double cosets of a subgroup play an important role in the analysis.

Since some of these concepts are not available in standard texts, we present in this section the necessary mathematical

3. PHASE TRANSITIONS, TWINNING AND DOMAIN STRUCTURES

background and explanation of terms and relations that appear in Chapters 3.3 and 3.4.

Section 3.2.3.1 introduces the basic concepts of set theory and explains the notion of unordered and ordered pairs, mappings of sets and the partition of a set into equivalence classes. Section 3.2.3.2 deals with basic group theory and is devoted mainly to group–subgroup relations and relevant notions, of which the coset decompositions are of central importance. In Section 3.2.3.3, group theory is combined with set theory in the ‘action of a group on a set’ (for short, ‘group action’). Notions of stabilizer, orbit and stratum are explained and their significance is illustrated by several examples.

A simple exposition of the main group-theoretical concepts, including group action and orbits, can be found in the book by Hahn & Wondratschek (1994). A concise presentation of group actions and related notions with many examples has been given by Michel (1980). Other more detailed references are given at the end of each of the following sections.

3.2.3.1. Sets, pairs, mappings and equivalence classes

3.2.3.1.1. Sets

Definition 3.2.3.1. A *set* is a collection of distinguishable objects. The objects constituting a set are called *elements* (or *points*) of the set.

In Chapter 3.4 we encounter mainly two types of sets: sets the elements of which are crystalline objects (domain states, domain twins, domain walls *etc.*), and sets, like groups, with elements of mathematical nature, *e.g.* rotations, transformations, operations *etc.* The sets of crystalline objects will be denoted by capital sans-serif letters, *e.g.* $\mathbf{A}, \mathbf{B}, \dots$, and capital bold letters, *e.g.* $\mathbf{S}, \mathbf{M}, \mathbf{N}, \dots$ or $\mathbf{S}_1, \mathbf{S}_2, \mathbf{S}_3, \dots$, will be used to denote elements of such sets. Groups will be denoted by capital italic letters, *e.g.* G, F *etc.*, and their elements by lower-case italic letters, *e.g.* g, h, \dots . The exposition of this section is given for sets the elements of which are (crystalline) objects, but all notions and relations hold for any other sets.

If an element \mathbf{S} belongs to the set \mathbf{A} , one writes $\mathbf{S} \in \mathbf{A}$, in the opposite case $\mathbf{S} \notin \mathbf{A}$. Sets consisting of a small number of elements can be expressed explicitly by writing their elements between curly braces, $\mathbf{A} = \{\mathbf{S}, \mathbf{M}, \mathbf{N}, \mathbf{Q}\}$. The order of elements in the symbol of the set is irrelevant. From the definition of a set it follows that there are no equal elements in the set, or in other words, any two equal elements coalesce into one:

$$\{\mathbf{S}, \mathbf{S}\} = \{\mathbf{S}\}. \quad (3.2.3.1)$$

If a set contains many (or an infinite number of) elements, the elements are specified in another way, *e.g.* by stating that they have a certain property in common.

The number of elements in a set is the *order of the set*. A *finite set* \mathbf{A} consists of a finite number of elements and this number is denoted by $|\mathbf{A}|$. An *infinite set* contains infinite number of elements and an *empty set*, denoted by \emptyset , contains no element. In what follows, the term ‘set’ will mean a ‘finite nonempty set’ unless explicitly stated otherwise.

A set \mathbf{B} is a *subset* of \mathbf{A} , $\mathbf{B} \subseteq \mathbf{A}$ or $\mathbf{A} \supseteq \mathbf{B}$, if every element of \mathbf{B} is an element of \mathbf{A} . If each element of \mathbf{B} is an element of \mathbf{A} , and *vice versa*, then \mathbf{B} is *equal to* or *identical with* \mathbf{A} , $\mathbf{B} = \mathbf{A}$ or $\mathbf{A} = \mathbf{B}$. If there exists at least one element of \mathbf{A} which is not contained in \mathbf{B} , then \mathbf{B} is a *proper subset* of \mathbf{A} , $\mathbf{B} \subset \mathbf{A}$ or $\mathbf{A} \supset \mathbf{B}$. The subset \mathbf{B} is often defined by a restriction that specifies only some elements of \mathbf{A} as elements of \mathbf{B} . This is written in short as $\mathbf{B} = \{\mathbf{S} \in \mathbf{A} | \text{restriction on } \mathbf{S}\}$; the expression means that \mathbf{B} consists of *all* elements of \mathbf{A} that satisfy the restriction given behind the sign $|$.

The *intersection* of two sets \mathbf{A} and \mathbf{B} , $\mathbf{A} \cap \mathbf{B}$ or $\mathbf{B} \cap \mathbf{A}$, is a set comprising all elements that belong both to \mathbf{A} and to \mathbf{B} . If the sets

\mathbf{A} and \mathbf{B} have no element in common, $\mathbf{A} \cap \mathbf{B} = \emptyset$, then one says that the sets \mathbf{A} and \mathbf{B} are *disjoint*. The *union of sets* \mathbf{A} and \mathbf{B} , $\mathbf{A} \cup \mathbf{B}$ or $\mathbf{B} \cup \mathbf{A}$, is a set consisting of all elements that belong either to \mathbf{A} or to \mathbf{B} . Sometimes the symbol $+$ is used instead of the symbol \cup . The *difference of set* \mathbf{A} and \mathbf{B} , or the *complement of* \mathbf{B} *in* \mathbf{A} , $\mathbf{A} - \mathbf{B}$, comprises those elements of \mathbf{A} that do not belong to \mathbf{B} .

3.2.3.1.2. Pairs

A collection of two objects \mathbf{S}_i and \mathbf{S}_k constitutes an *unordered pair*. The objects of an unordered pair are called *elements* or *points*. A *trivial unordered pair* consists of two identical elements. A non-trivial unordered domain pair comprises two non-identical elements and is identical with a set of order two.

Note that we do not identify an unordered pair with a set of order two where, according to (3.2.3.1), two equal objects coalesce into one. In spite of this difference we shall use the same symbol for the unordered pair as for the set of order two, but reverse the symbol $\{\mathbf{S}, \mathbf{S}\}$ for the trivial unordered pair. With this reservation, the identity

$$\{\mathbf{S}_i, \mathbf{S}_k\} = \{\mathbf{S}_k, \mathbf{S}_i\} \quad (3.2.3.2)$$

holds for both unordered pairs and for sets of order two.

An *ordered pair*, denoted $(\mathbf{S}_i, \mathbf{S}_k)$, consists of the *first* and the *second member* of the pair. If $\mathbf{S}_i = \mathbf{S}_k$, the ordered pair is called a *trivial ordered pair*, $(\mathbf{S}_i, \mathbf{S}_i)$; if $\mathbf{S}_i \neq \mathbf{S}_k$ the pair $(\mathbf{S}_i, \mathbf{S}_k)$ is a *non-trivial ordered pair*. The ordered pair $(\mathbf{S}_k, \mathbf{S}_i)$ with a reversed order of elements is called a *transposed pair*. In contrast to unordered pairs, initial and transposed non-trivial ordered pairs are different objects,

$$(\mathbf{S}_i, \mathbf{S}_k) \neq (\mathbf{S}_k, \mathbf{S}_i) \text{ for } \mathbf{S}_i \neq \mathbf{S}_k. \quad (3.2.3.2a)$$

The members \mathbf{S}_i and \mathbf{S}_k of an ordered pair $(\mathbf{S}_i, \mathbf{S}_k)$ can either belong to one set, $\mathbf{S}_i \in \mathbf{A}, \mathbf{S}_k \in \mathbf{A}$, or each to a different set, $\mathbf{S}_i \in \mathbf{A}, \mathbf{S}_k \in \mathbf{B}$.

Two ordered pairs $(\mathbf{S}_i, \mathbf{S}_k)$ and $(\mathbf{S}_m, \mathbf{S}_p)$ are equal, $(\mathbf{S}_i, \mathbf{S}_k) = (\mathbf{S}_m, \mathbf{S}_p)$, if and only if $\mathbf{S}_i = \mathbf{S}_m$ and $\mathbf{S}_k = \mathbf{S}_p$.

We shall encounter ordered and unordered pairs in Sections 3.4.3 and 3.4.4, where the members of pairs are domain states or domain twins. However, pairs are also essential in introducing further concepts of set theory. The starting point is the following construction of a set of pairs that are formed from two sets:

A *Cartesian product* $\mathbf{A} \times \mathbf{B}$ of two sets \mathbf{A} and \mathbf{B} is a set of *all* ordered pairs (\mathbf{S}, \mathbf{M}) , where $\mathbf{S} \in \mathbf{A}, \mathbf{M} \in \mathbf{B}$. The sets \mathbf{A} and \mathbf{B} can be different or identical sets. If the sets \mathbf{A} and \mathbf{B} are finite, then the Cartesian product $\mathbf{A} \times \mathbf{B}$ consists of $|\mathbf{A}| \cdot |\mathbf{B}|$ ordered pairs.

3.2.3.1.3. Mappings

A *mapping* φ of a set \mathbf{A} into a set \mathbf{B} is a rule which assigns to each element $\mathbf{S} \in \mathbf{A}$ a unique element $\mathbf{M} \in \mathbf{B}$. This is written symbolically as $\varphi : \mathbf{S} \mapsto \mathbf{M}$ or $\mathbf{M} = \varphi(\mathbf{S})$, and one says that \mathbf{S} is mapped to \mathbf{M} under the mapping φ . The element \mathbf{M} is called the *image of the element* \mathbf{S} *under* φ . The assignment $\varphi : \mathbf{S} \mapsto \mathbf{M}$ can be expressed by an ordered pair (\mathbf{S}, \mathbf{M}) , if one ascribes \mathbf{S} to the first member of the pair and the element \mathbf{M} to the second member of the pair (\mathbf{S}, \mathbf{M}) . Then the mapping φ of a set \mathbf{A} into a set \mathbf{B} , symbolically written as $\varphi : \mathbf{A} \rightarrow \mathbf{B}$, can be identified with such a subset of ordered pairs of the Cartesian product $\mathbf{A} \times \mathbf{B}$ in which each element \mathbf{S} of \mathbf{A} occurs exactly once as the first member of the pair (\mathbf{S}, \mathbf{M}) . If \mathbf{A} is a finite set, then φ consists of $|\mathbf{A}|$ ordered pairs.

We note that in a mapping $\varphi : \mathbf{A} \rightarrow \mathbf{B}$ several elements of \mathbf{A} may be mapped to the same element of \mathbf{B} . In such a case, the mapping φ is called a *many-to-one mapping*. If the mapping $\varphi : \mathbf{A} \rightarrow \mathbf{B}$ is such that each element of \mathbf{B} is the image of some element of \mathbf{A} , then the mapping φ is called a *mapping of* \mathbf{A} *onto* \mathbf{B} . If φ is a mapping of \mathbf{A} onto \mathbf{B} and, moreover, each element of \mathbf{B} is

3.2. TWINNING AND DOMAIN STRUCTURES

the image of exactly one element of A , then the mapping φ becomes a *one-to-one correspondence between A and B* , $\varphi : A \leftrightarrow B$. In this case, A and B are of the same order.

One often encounters a situation in which one assigns to each ordered pair (S, M) an element N , where all three elements S, M, N are elements from the same set A , symbolically $\varphi : (S, M) \mapsto N$; $S, M, N \in A$ or $\varphi : A \times A \rightarrow A$. Such a mapping is called a *binary operation* or a *composition law* on the set A . A sum of two numbers $a + b = c$ or a product of two numbers $a \cdot b = c$, where a, b, c belong to the set of all real numbers, are elementary examples of binary operations.

3.2.3.1.4. Equivalence relation on a set, partition of a set

The notion of the ordered pair allows one to introduce another useful concept, namely the relation on a set. An example will illustrate this notion. Let \mathbb{Z} be a set of integers, $\mathbb{Z} = \{\dots, -2, -1, 0, 1, 2, \dots\}$. For each ordered pair (m, n) , $m, n \in \mathbb{Z}$, one can decide whether m is smaller than n , $m < n$, or not. All pairs (m, n) that fulfil the condition $m < n$ form a subset R of all possible ordered pairs $\mathbb{Z} \times \mathbb{Z}$. In other words, the relation $m < n$ defines a subset R of the set $\mathbb{Z} \times \mathbb{Z}$, $R \subset \mathbb{Z} \times \mathbb{Z}$. Similarly, the relation $|m| = |n|$ ($|n|$ denotes absolute value of n) defines another subset of $\mathbb{Z} \times \mathbb{Z}$.

To indicate that an element S is related to M by $\overset{R}{\sim}$, where $S, M \in A$, one writes $S \overset{R}{\sim} M$, where the relation R defines a subset R of all ordered pairs $A \times A$, $R \subset A \times A$ (the same letter R is used for the subset and for the relation on A). The opposite also holds: Each subset R of $A \times A$ defines a certain relation $\overset{R}{\sim}$ on A .

A relation $\overset{R}{\sim}$ is called an *equivalence relation on the set A* if it satisfies three conditions:

$$S \overset{R}{\sim} S \text{ for all } S \in A \text{ (reflexivity),} \quad (3.2.3.3)$$

$$\text{if } S, M \in A \text{ and } S \overset{R}{\sim} M, \text{ then } M \overset{R}{\sim} S \text{ (symmetry),} \quad (3.2.3.4)$$

$$\text{if } S, M, N \in A, S \overset{R}{\sim} M \text{ and } M \overset{R}{\sim} N, \text{ then } S \overset{R}{\sim} N \text{ (transitivity).} \quad (3.2.3.5)$$

Thus, for example, it is easy to corroborate that the relation $|m| = |n|$ on the set of integers \mathbb{Z} fulfils all three conditions (3.2.3.3) to (3.2.3.5) and is, therefore, an equivalence relation on the set \mathbb{Z} . On the other hand, the relation $m < n$ is not an equivalence relation on \mathbb{Z} since it fulfils neither the reflexivity (3.2.3.3) nor the symmetry condition (3.2.3.4).

Let $\overset{R}{\sim}$ be an equivalence relation on A and $S \in A$; all elements $M \in A$ such that $M \overset{R}{\sim} S$ constitute a subset of A denoted $[S]_R$ and called the *equivalence class of S with respect to $\overset{R}{\sim}$* (or the *R-equivalence class of S*). The element S is called the *representative* of the class $[S]_R$. Any other member of the class can be chosen as its representative. Any two elements of the equivalence class $[S]_R$ are *R-equivalent elements of A* .

From the definition of the equivalence class, it follows that any two elements $M, N \in A$ are either R-equivalent elements of A , $M \overset{R}{\sim} N$, and thus belong to the same class, $[M]_R = [N]_R$, or are not R-equivalent, and thus belong to two different classes that are disjoint, $[M]_R \cap [N]_R = \emptyset$. In this way, the equivalence relation $\overset{R}{\sim}$ divides the set A into disjoint subsets (equivalence classes), the union of which is equal to the set itself. Such a decomposition is called a *partition of the set A associated with the equivalence relation $\overset{R}{\sim}$* . For a finite set A this decomposition can be expressed as a union of equivalence classes,

$$A = [S]_R \cup [M]_R \cup \dots \cup [Q]_R, \quad (3.2.3.6)$$

where S, M, \dots, Q are representatives of the equivalence classes.

Generally, any decomposition of a set into a system of disjoint non-empty subsets such that every element of the set is a member of just one subset is called a *partition of the set*. To any partition of a set A there corresponds an equivalence relation $\overset{R}{\sim}$ such that the

R-equivalence classes of A form that partition. This equivalence relation defines two elements as equivalent if and only if they belong to the same subset.

The term ‘equivalent’ is often used when it is clear from the context what the relevant equivalence relation is. Similarly, the term ‘class’ is used instead of ‘equivalence class’. Sometimes equivalence classes have names that do not explicitly indicate that they are equivalence classes. For example, in group theory, conjugate subgroups, left, right and double cosets form equivalence classes (see Section 3.2.3.2). Often instead of the expression ‘partition of a set A ’ an equivalent expression ‘classification of the elements of a set A ’ is used. The most important equivalence classes in the symmetry analysis of domain structures are called orbits and will be discussed in Section 3.2.3.3.

More details on set theory can be found in Kuratowski & Mostowski (1968), Lipschutz (1981), and Opechowski (1986).

3.2.3.2. Groups and subgroups

3.2.3.2.1. Groups

Operations (isometries) that act on a body without changing its form and internal state combine in the same way as do elements of a group. Group theory is, therefore, the main mathematical tool for examining transformation properties – symmetry properties in particular – of crystalline objects. The basic concept of group theory is that of a group.

Definition 3.2.3.2. A group G is a set that satisfies four postulates:

(1) To each ordered pair (g_i, g_j) of two elements of G , there corresponds a unique element g_k of G , i.e. a binary operation (composition law) is defined on the set G . Usually, one writes the ordered pair simply as a ‘product’ $g_i g_j$ and the composition law as an equation,

$$g_i g_j = g_k, \quad g_i, g_j, g_k \in G. \quad (3.2.3.7)$$

This condition is referred to as *closure of G under multiplication*.

(2) The *multiplication is associative*, i.e. for any three elements g_i, g_j, g_k of G it holds that if $g_i g_j = g_l$ and $g_j g_k = g_m$ then $g_l g_k = g_i g_m$. This condition is usually written as one equation,

$$(g_i g_j) g_k = g_i (g_j g_k), \quad (3.2.3.8)$$

which expresses the requirement that the product of any three elements of G is the same, no matter which two of the three one multiplies first, as long as the order in which they stand is not changed. From postulate (2) it follows that the product of any finite sequence of group elements is determined uniquely if the order in which the elements are placed is preserved.

(3) The set G contains an *identity or unit element e* such that

$$eg = ge = g \text{ for any element } g \in G. \quad (3.2.3.9)$$

(4) For any element $g \in G$ there exists an *inverse element g^{-1}* such that

$$gg^{-1} = g^{-1}g = e. \quad (3.2.3.10)$$

The number of elements of a group G is called the *order of the group*. If the order of the group is finite, it is denoted by $|G|$.

The multiplication of group elements is, in general, not commutative, i.e. $g_i g_j \neq g_j g_i$ may hold for some $g_i, g_j \in G$. If the multiplication is commutative, i.e. if $g_i g_j = g_j g_i$ for all $g_i, g_j \in G$, then the group G is called a *commutative or Abelian group*. All groups of orders 1 to 5 are Abelian. In Abelian groups, an *additive notation* is sometimes used instead of the *multiplicative notation*, i.e. if g_i and g_k are elements of an Abelian group G then

3. PHASE TRANSITIONS, TWINNING AND DOMAIN STRUCTURES

one writes $g_i + g_k$ instead of $g_i g_k$. Additive notation is usually used in groups of translations.

The n th power g^n of an element $g \in G$, where n is a positive integer, is defined recursively in the following manner:

- (i) $g^0 = e$, $g^1 = g$, where e is a unit element of G ;
- (ii) $g^{n+1} = g^n g$;
- (iii) $g^{-n} = (g^n)^{-1}$.

If G is written additively, one writes ng instead of g^n and speaks of a *multiple of g* .

If m and n are integers and g is an element of G then the following *laws of exponents* hold:

$$g^m g^n = g^{m+n} = g^n g^m, \quad (3.2.3.11)$$

$$(g^m)^n = g^{mn} = (g^n)^m. \quad (3.2.3.12)$$

A set of elements $\{g_1, g_2, \dots\}$ of a group G is called a *set of generators of G* if any element of the group G can be written as a product of powers of these generators. In general, a group may have several sets of generators.

The *order of an element g* is the smallest positive integer m such that $g^m = e$. An element g and the inverse element g^{-1} have the same order. The order m of any element g of a finite group G is a factor of the order $|G|$.

Two groups G and G' with elements $g_1, g_2, \dots, g_i, \dots$ and $g'_1, g'_2, \dots, g'_i, \dots$, respectively, are *isomorphic* if there is an one-to-one correspondence φ between G and G' ,

$$\varphi : g_i \leftrightarrow g'_i \text{ for each } g_i \in G, \quad (3.2.3.13)$$

such that

$$\text{whenever } \varphi : g_i \leftrightarrow g'_i \text{ and } \varphi : g_j \leftrightarrow g'_j, \text{ then } \varphi : g_i g_j \leftrightarrow g'_i g'_j. \quad (3.2.3.14)$$

In other words, the *isomorphism of two groups G and G'* is a one-to-one mapping of G onto G' [(3.2.3.13)] which preserves the products of the elements of the two groups [(3.2.3.14)]. Two isomorphic groups G and G' are denoted as $G \cong G'$.

Isomorphism is an equivalence relation that divides the set of all groups into classes of isomorphic groups. Between two groups G and G' there may exist several isomorphisms.

Groups that appear in Chapters 3.3 and 3.4 are mostly *crystallographic groups* [for their definition and properties see Bradley & Cracknell (1972), Hahn & Wondratschek (1994), IT A (2002), IT A1 (2003), Janssen (1973), Opechowski (1986), and Vainshtein (1994)]. Elements of these groups are distance-preserving transformations (mappings) called *isometries*, *Euclidean transformations*, *motions* or *crystallographic operations*. Whenever we encounter crystallographic groups we shall use the term 'crystallographic operation' or just 'operation' or 'isometry' instead of 'element'.

In what follows, the group G may be a crystallographic point group or a crystallographic space group. Since we shall be mainly concerned with a continuum approach, we shall have in mind point groups. When we consider space groups, we shall mention this explicitly and, if possible, use calligraphic letters, e.g. \mathcal{G} , \mathcal{F} etc. for space groups.

Crystallographic operations of crystallographic point groups and products of these operations can be found by means of the multiplication calculator in the software *GI★KoBo-1* under the menu item *Group Elements* (see the manual for *GI★KoBo-1*).

3.2.3.2.2. Subgroups

Definition 3.2.3.3. Let G be a group. A subset F of G is a *subgroup of G* if it forms a group under the product rule of G , i.e. if it fulfils the group postulates (1) to (4).

For finite groups these requirements can be replaced by a single condition [see e.g. Opechowski (1986)]: The product of any two elements f_i, f_j of F belongs to F ,

$$f_i f_j = f_k, \quad f_k \in F \text{ for any } f_i, f_j \in F. \quad (3.2.3.15)$$

The groups G and F are denoted the *high-symmetry group* and the *low-symmetry group*, respectively. The pair 'group G – subgroup F ' is called the *symmetry descent $G \supset F$* , *dissymmetrization $G \supset F$* or *symmetry reduction $G \supset F$* . A symmetry descent is a basic specification of a phase transition and corresponding domain structure (see Chapters 3.1 and 3.4).

Each group G always has at least two subgroups: the group G itself (sometimes called the *improper subgroup*) and the *trivial subgroup* consisting of the unit element only. The symbol $F \subseteq G$ signifies that F is a subgroup of G including the improper subgroup G , whereas $F \subset G$ means that F is a *proper subgroup* of G which differs from G . By this definition, the trivial subgroup is a proper subgroup. This definition of a proper subgroup [used e.g. in Volume A of the present series (IT A, 2002) and by Opechowski (1986)] is convenient for our purposes, although often by the term 'proper subgroup' one understands a subgroup different from G and from the trivial subgroup.

A proper subgroup F of G is a *maximal subgroup of G* if it is not a proper subgroup of some other proper subgroup H , i.e. if there exists no group H such that $F \subset H \subset G$. A group can have more than one maximal subgroup.

A group P for which G is subgroup is called a *supergroup of G* , $G \subseteq P$. If G is a proper subgroup of Q , $G \subset Q$, then Q is a *proper supergroup of G* . If G is a maximal subgroup of P , then P is called a *minimal supergroup of G* .

Let a group L be a proper supergroup of a group F , $F \subset L$, and simultaneously a proper subgroup of a group G , $L \subset G$. Then the sequence of subgroups

$$F \subset L \subset G \quad (3.2.3.16)$$

will be called a *group–subgroup chain* and the group L an *intermediate group* of the chain (3.2.3.16).

Subgroups of crystallographic point groups are listed in Table 3.4.2.7 and are displayed in Figs. 3.1.3.1 and 3.1.3.2 (see also the software *GI★KoBo-1*, menu item *Subgroups*).

3.2.3.2.3. Left and right cosets

If F_1 is a proper subgroup of G and g_i is a fixed element of G , then the set of all products $g_i f$, where f runs over all elements of the subgroup F_1 , is denoted $g_i F_1$ and is called the *left coset of F_1 in G* ,

$$g_i F_1 = \{g_i f \mid \forall f \in F_1\}, \quad g_i \in G, \quad F_1 \subset G, \quad (3.2.3.17)$$

where the sign \forall means 'for all'. Similarly, one defines a *right coset of F_1 in G* :

$$F_1 g_i = \{f g_i \mid \forall f \in F_1\}, \quad g_i \in G, \quad F_1 \subset G. \quad (3.2.3.18)$$

[Some authors, e.g. Hall (1959), call the set $g_i F_1$ a right coset of F_1 in G and the set $F_1 g_i$ a left coset of F_1 in G .] Since in the application of cosets in the symmetry analysis of domain structures left cosets are used almost exclusively, all statements that follow are formulated for left cosets. Each statement about left cosets has a complementary statement about right cosets which can in most cases be obtained by replacing 'left' with 'right'.

The element g_i which appears explicitly in the symbol $g_i F_1$ of the left coset of F_1 is called a *representative of the left coset $g_i F_1$* . Any element of a left coset can be chosen as its representative.

Left coset criterion: Two elements g_i and g_j belong to the same left coset, $g_i F_1 = g_j F_1$, if and only if $g_i^{-1} g_j$ belongs to the subgroup F_1 , $g_i^{-1} g_j \in F_1$.

3.2. TWINNING AND DOMAIN STRUCTURES

The property of ‘belong to the same left coset’ is an equivalence relation, therefore two left cosets of the same subgroup are either identical or have no elements in common.

Proposition 3.2.3.4. The union of all distinct left cosets of F_1 in G constitutes a partition of G and is called the *decomposition of G into the left cosets of F_1* . If the set of left cosets of F_1 in G is finite, then the decomposition of G into the left cosets of F_1 can be expressed as

$$G = g_1 F_1 \cup g_2 F_1 \cup \dots \cup g_n F_1 = \bigcup_{i=1}^n g_i F_1, \quad (3.2.3.19)$$

where the symbol \cup is the set-theoretical union (see Section 3.2.3.1). For the representative g_1 of the first left coset the unit element e is usually chosen, $g_1 = e$. Then the first left coset is identical with the subgroup F_1 . The number of elements in each left coset of the decomposition is equal to the order of the group F_1 .

The set of left-coset representatives $\{g_1, g_2, \dots, g_n\}$ is sometimes called a *left transversal to F_1 in G* .

The number n of distinct left cosets is called the *index of the subgroup F_1 in the group G* and is denoted by the symbol $[G : F_1]$. If the groups G and F_1 are of finite order then

$$n = [G : F_1] = |G| : |F_1|, \quad (3.2.3.20)$$

where $|G|$ and $|F_1|$ are the orders of G and F_1 , respectively. From this equation follows:

Lagrange’s theorem: the order of a finite group is a multiple of the order of each of its subgroups. Alternatively, the index of a subgroup and the order of a finite subgroup are divisors of the group order.

We note that an infinite subgroup of an infinite group can have a finite index. Important examples are subgroups of translational groups of crystallographic space groups and subgroups of space groups (see Example [oC] 3.2.3.32 in Section 3.2.3.5).

The decompositions of crystallographic point groups into left and right cosets are available in the software *GI★KoBo-1*, under *Subgroups\View\Twinning Group*.

Proposition 3.2.3.5. Let L_1 be an intermediate group $F_1 \subset L_1 \subset G$. The group G can be decomposed into left cosets of L_1 ,

$$G = h_1 L_1 \cup h_2 L_1 \cup \dots \cup h_m L_1 = \bigcup_{j=1}^m h_j L_1, \quad (3.2.3.21)$$

where

$$m = [G : L_1] = |G| : |L_1|, \quad (3.2.3.22)$$

and the group L_1 into left cosets of F_1 ,

$$L_1 = p_1 F_1 \cup p_2 F_1 \cup \dots \cup p_d F_1 = \bigcup_{k=1}^d p_k F_1, \quad (3.2.3.23)$$

where

$$d = [L_1 : F_1] = |L_1| : |F_1|. \quad (3.2.3.24)$$

Then the decomposition of G into left cosets of F_1 can be written in the form

$$G = \bigcup_{j=1}^m \bigcup_{k=1}^d h_j p_k F_1 \quad (3.2.3.25)$$

and the index n of F_1 in G can be expressed as a product of indices m and d ,

$$n = [G : F_1] = [G : L_1][L_1 : F_1] = md. \quad (3.2.3.26)$$

Decompositions (3.2.3.19) and (3.2.3.21) of a group into left cosets enable one to divide a set of objects into classes of symmetrically equivalent objects (see Section 3.2.3.4). The concept of domain states is based on this result (see Section 3.4.2).

3.2.3.2.4. Conjugate subgroups

Two subgroups F_i and F_k are *conjugate subgroups* if there exists an element g of G such that

$$g F_i g^{-1} = F_k, \quad g \in G. \quad (3.2.3.27)$$

More explicitly, one says that the subgroup F_k is *conjugate by g* (or *conjugate under G*) *to the subgroup F_i* . Conjugate subgroups are isomorphic.

The property of ‘being conjugate’ is an equivalence relation. The set of all subgroups of a group G can therefore be partitioned into disjoint classes of conjugate subgroups. Conjugate subgroups of crystallographic point groups are given in Table 3.4.2.7 and in the software *GI★KoBo-1*, under *Subgroups\View\Twinning Group*.

3.2.3.2.5. Normalizers

The collection of all elements g that fulfil the relation

$$g F_i g^{-1} = F_i, \quad g \in G, \quad (3.2.3.28)$$

constitutes a group denoted by $N_G(F_i)$ and is called the *normalizer of F_i in G* . The normalizer $N_G(F_i)$ is a subgroup of G and a supergroup of F_i ,

$$F_i \subseteq N_G(F_i) \subseteq G. \quad (3.2.3.29)$$

The normalizer $N_G(F_i)$ determines the subgroups conjugate to F_i under G (see Example 3.2.3.10). The number m of subgroups conjugate to a subgroup F_i under G equals the index of $N_G(F_i)$ in G :

$$m = [G : N_G(F_i)] = |G| : |N_G(F_i)|, \quad (3.2.3.30)$$

where the last equation holds for finite G and F_i .

Normalizers of the subgroups of crystallographic point groups are available in Table 3.4.2.7 and in the software *GI★KoBo-1* under *Subgroups\View\Twinning Group*.

3.2.3.2.6. Normal subgroups

Among subgroups of a group, a special role is played by normal subgroups. A subgroup H of G is a *normal (invariant, self-conjugate) subgroup* of G if and only if it fulfils any of the following conditions:

(1) The subgroup H of G has no conjugate subgroups under G . (No subscript is therefore needed in the symbol of a normal subgroup H .)

(2) The normalizer $N_G(H)$ of H equals the group G ,

$$N_G(H) = G. \quad (3.2.3.31)$$

(3) Every element g of G commutes with H , or, equivalently, each left coset gH equals the right coset Hg :

$$gH = Hg \text{ for every } g \in G. \quad (3.2.3.32)$$

For a normal subgroup H of a group G a special symbol \triangleleft is often used instead of \subset , $H \triangleleft G$.

3. PHASE TRANSITIONS, TWINNING AND DOMAIN STRUCTURES

3.2.3.2.7. Halving subgroups and dichromatic (black-and-white) groups

Any subgroup H of a group G of index 2, called a *halving subgroup*, is a normal subgroup. The decomposition of G into left cosets of H consists of two left cosets,

$$G = H \cup gH. \quad (3.2.3.33)$$

Sometimes it is convenient to distinguish elements of the coset gH from elements of the halving subgroup H . This can be achieved by attaching a sign (usually written as a superscript) to all elements of the coset. We shall use for this purpose the sign \blacktriangle . To aid understanding, we shall also mark for a while the elements of the group H with another sign, \heartsuit . The multiplication law for these ‘decorated elements’ can be written in the following form:

$$g_1^{\heartsuit} g_2^{\heartsuit} = g_3^{\heartsuit}, \quad g_4^{\heartsuit} g_5^{\blacktriangle} = g_6^{\blacktriangle}, \quad g_7^{\blacktriangle} g_8^{\heartsuit} = g_9^{\heartsuit}, \quad g_{10}^{\blacktriangle} g_{11}^{\blacktriangle} = g_{12}^{\heartsuit}. \quad (3.2.3.34)$$

Now we replace the label \heartsuit by a dummy ‘no mark’ sign (*i.e.* we remove \heartsuit), but we still keep in mind the multiplication rules (3.2.3.34). Then the decomposition (3.2.3.33) becomes

$$G = H \cup g^{\blacktriangle} H, \quad (3.2.3.33a)$$

since the coset $g^{\blacktriangle} H$ assembles all marked elements and H consists of all bare elements of the group G .

The sign \blacktriangle can carry useful additional information, *e.g.* the application of labelled operations g^{\blacktriangle} is connected with some changes or new effects, whereas the application of a bare operation brings about no such changes or effects.

The label \blacktriangle can be replaced by various signs which can have different meanings. Thus in Chapter 3.3 a prime $'$ signifies a nontrivial twinning operation, in Chapter 1.5 it is associated with time inversion in magnetic structures, and in black-and-white patterns or structures a prime denotes an operation which exchanges black and white ‘colours’ (the qualifier ‘black-and-white’ concerns group operations, but not the black-and-white pattern itself). In Chapter 3.4, a star $*$ denotes a transposing operation which exchanges two domain states, while underlining signifies an operation exchanging two sides of an interface and underlined operations with a star signify twinning operations of a domain twin. Various interpretations of the label attached to the symbol of an operation have given rise to several designations of groups with partition (3.2.3.34): *black-and-white*, *dichromatic*, *magnetic*, *anti-symmetry*, *Shubnikov* or *Heech–Shubnikov* and other groups. For more details see Opechowski (1986).

3.2.3.2.8. Double cosets

Let F_1 and H_1 be two proper subgroups of the group G . The set of all distinct products $hg_j f$, where g_j is a fixed element of the group G and f and h run over all elements of the subgroups F_1 and H_1 , respectively, is called a *double coset of F_1 and H_1 in G* . The symbol of this double coset is $F_1 g_j F_1$,

$$F_1 g_j H_1 = \{fg_j h \mid \forall f \in F_1, \forall h \in H_1\}, \\ g_j \in G, F_1 \subset G, H_1 \subset G, \quad (3.2.3.35)$$

where the sign \forall means ‘for all’.

In the symmetry analysis of domain structures, only double cosets with $H_1 = F_1$ are used. We shall, therefore, formulate subsequent definitions and statements only for this special type of double coset.

The fixed element g_j is called the *representative of the double coset $F_1 g_j F_1$* . Any element of a double coset can be chosen as its representative.

Two double cosets are either identical or disjoint.

Proposition 3.2.3.6. The union of all distinct double cosets constitutes a partition of G and is called the *decomposition of the group G into double cosets of F_1* , since $F_1 F_1 = F_1$. If the set of double cosets of F_1 in G is finite, then the decomposition of G into the double cosets of F_1 can be written as

$$G = F_1 g_1 F_1 \cup F_1 g_2 F_1 \cup \dots \cup F_1 g_q F_1. \quad (3.2.3.36)$$

For the representative g_1 of the first double coset $F_1 g_1 F_1$ the unit element e is usually chosen, $g_1 = e$. Then the first double coset is identical with the subgroup F_1 .

A double coset $F_1 g_j F_1$ consists of left cosets of the form $f g_j F_1$, where $f \in F_1$. The number r of left cosets of F_1 in the double coset $F_1 g_j F_1$ is (Hall, 1959)

$$r = [F_1 : F_{1j}], \quad (3.2.3.37)$$

where

$$F_{1j} = F_1 \cap g_j F_1 g_j^{-1}. \quad (3.2.3.38)$$

The following definitions and statements are used in Chapter 3.4 for the double cosets $F_1 g_j F_1$ [for derivations and more details, see Janovec (1972)].

The inverse $(F_1 g_j F_1)^{-1}$ of a double coset $F_1 g_j F_1$ is a double coset $F_1 g_j^{-1} F_1$, which is either identical or disjoint with the double coset $F_1 g_j F_1$. The double coset that is its own inverse is called an *invertible (self-inverse, ambivalent) double coset*. The double coset that is disjoint with its inverse is called a *non-invertible (polar) double coset* and the double cosets $F_1 g_j F_1$ and $(F_1 g_j F_1)^{-1} = F_1 g_j^{-1} F_1$ are called *complementary polar double cosets*.

The inverse left coset $(g_j F_1)^{-1}$ contains representatives of all left cosets of the double coset $F_1 g_j^{-1} F_1$. If a left coset $g_j F_1$ belongs to an invertible double coset, then $(g_j F_1)^{-1}$ contains representatives of left cosets constituting the double coset $F_1 g_j F_1$. If a left coset $g_j F_1$ belongs to a non-invertible double coset, then $(g_j F_1)^{-1}$ contains representatives of left cosets constituting the complementary double coset $(F_1 g_j F_1)^{-1}$.

A double coset consisting of only one left coset,

$$F_1 g_j F_1 = g_j F_1, \quad (3.2.3.39)$$

is called a *simple double coset*. A double coset $F_1 g_j F_1$ is *simple* if and only if the inverse $(g_j F_1)^{-1}$ of the left coset $g_j F_1$ is again a left coset. For an invertible simple double coset $g_j F_1 = (g_j F_1)^{-1}$.

The union of all simple double cosets $F_1 g_j F_1 = g_j F_1$ in the double coset decomposition of G (3.2.3.36) constitutes the normalizer $N_G(F_1)$ (Speiser, 1927).

A double coset that comprises more than one left coset will be called a *multiple double coset*. Four types of double cosets FgF are displayed in Table 3.2.3.1. The double coset decompositions of all crystallographic point groups are available in the software *GI*KoBo-1* under *Subgroups\View\Twinning Group*.

Double cosets and the decomposition (3.2.3.36) of a group in double cosets are mathematical tools for partitioning a set of pairs of objects into equivalent classes (see Section 3.2.3.3.6). Such a division enables one to find possible twin laws and different types of domain walls that can appear in a domain structure resulting from a phase transition with a given symmetry descent (see Chapters 3.3 and 3.4).

More detailed introductions to group theory can be found in Budden (1972), Janssen (1973), Ledermann (1973), Rosen (1995), Shubnikov & Koptsik (1974), Vainshtein (1994) and Vainshtein *et*

Table 3.2.3.1. Four types of double cosets

| | $FgF = gF$ | $FgF \neq gF$ |
|-----------------------------------|-----------------------|-------------------------|
| $FgF = (FgF)^{-1}$ | Invertible simple | Invertible multiple |
| $FgF \cap (FgF)^{-1} = \emptyset$ | Non-invertible simple | Non-invertible multiple |

3.2. TWINNING AND DOMAIN STRUCTURES

al. (1995). More advanced books on group theory are, for example, Bradley & Cracknell (1972), Hall (1959), Lang (1965), Opechowski (1986), Robinson (1982) and Speiser (1927). Parts of group theory relevant to phase transitions and tensor properties are treated in the manual of the software *GI★KoBo-1*. Representations of the crystallographic groups are presented in Chapter 1.2 of this volume and in the software *GI★KoBo-1* (see the manual).

3.2.3.3. Action of a group on a set

3.2.3.3.1. Group action

A direct application of the set and group theory to our studies would hardly justify their presentation in the last two sections. However, an appropriate combination of these theories, called group action, forms a very useful tool for examining crystalline materials and domain structures in particular. In this section, the main concepts (action of a group on a set [a], orbits [o], stabilizers [s]) are explained and their application is illustrated with examples from crystallography, where the group G is either a crystallographic point group or space group (denoted \mathcal{G} , if necessary), and the set is the three-dimensional point space $E(3)$ [P], a crystal [C], a property tensor [T] and a subgroup of G [S]. Letters in square brackets in front of the sequential number of examples and definitions should aid navigation in the text.

Example [aP] 3.2.3.7. Crystals are objects in a three-dimensional space called point space. Points of this space form an infinite set which we denote $E(3)$. If one chooses a point O as the origin, then to each point $X \in E(3)$ one can assign the position vector $OX = \mathbf{r}$ of a vector space $V(3)$ [see, for example, *IT A* (2002), Part 8]. There is a one-to-one correspondence between points of the point space and corresponding position vectors of the vector space,

$$X \leftrightarrow OX = \mathbf{r}. \quad (3.2.3.40)$$

If one further selects three non-coplanar basic vectors $\mathbf{e}_1, \mathbf{e}_2, \mathbf{e}_3$, then the position vector \mathbf{r} can be written as

$$\mathbf{r} = x_1\mathbf{e}_1 + x_2\mathbf{e}_2 + x_3\mathbf{e}_3, \quad (3.2.3.41)$$

where x_1, x_2, x_3 are coordinates of the point X .

Let G be a point group. An operation (isometry) $g \in G$ transforms (moves) the point X to a point X' with the position vector

$$\mathbf{r}' = x'_1\mathbf{e}_1 + x'_2\mathbf{e}_2 + x'_3\mathbf{e}_3. \quad (3.2.3.42)$$

Coordinates of this image point are related to coordinates of the initial point by a linear relation,

$$x'_i = \sum_{j=1}^3 D(g)_{ij}x_j, \quad i = 1, 2, 3, \quad (3.2.3.43)$$

where $D(g)_{ij}$ are components of a 3×3 matrix representing the operation g .

The described motion of the point X under the operation g can be formally expressed as a simple relation

$$gX = X', \quad g \in G, \quad X, X' \in E(3), \quad (3.2.3.44)$$

the exact meaning of which can be formulated in terms introduced in Section 3.2.3.1 as a mapping φ that assigns to an ordered pair (g, X) a point X' of the set $E(3)$,

$$\varphi : (g, X) \mapsto X', \quad g \in G \text{ and } X, X' \in A. \quad (3.2.3.45)$$

The mapping φ – *i.e.* a prescription for how to determine from g and X the resulting point X' – is defined by (3.2.3.40) to (3.2.3.43). The relation (3.2.3.44) should be considered as only a shorthand version of the explicit relation (3.2.3.45).

The action of a group on a set generalizes the described procedure to any group and any set. In this section, we shall use the term ‘object’ for an element of a set and the term ‘operation’ for an element of a group.

Definition [a] 3.2.3.8. Let G be a group, A a set of objects S_i, S_j, S_k, \dots and $\varphi : G \times A \rightarrow A$ a mapping that assigns to an ordered pair (g, S_i) , where $g \in G, S_i$ and S_i are objects of the set A :

$$\varphi : (g, S_i) \mapsto S_k, \quad g \in G, \quad S_i, S_k \in A. \quad (3.2.3.46)$$

The ordered pair (g, S_i) can often be written simply as a product gS_i and the mapping as an equation. Then the relation (3.2.3.46) can be expressed in a simpler form:

$$gS_i = S_k, \quad g \in G, \quad S_i, S_k \in A. \quad (3.2.3.47)$$

If the mapping (3.2.3.46), expressed in this condensed way, fulfils two additional conditions,

$$eS_i = S_i \text{ for any } S_i \in A, \quad (3.2.3.48)$$

where e is the identity operation (unit element) of G , and

$$h(gS_i) = (hg)S_i \text{ for any } h, g \in G \text{ and any } S_i \in A, \quad (3.2.3.49)$$

then the mapping φ is called an *action* (or *operation*) of a group G on a set A , or just a *group action*.

We must note that the replacement of the explicit mapping (3.2.3.46) by a contracted version (3.2.3.47) is not always possible (see Example [aS] 3.2.3.11).

The condition (3.2.3.49) requires that the first action $gS_i = S_k$ followed by the second action $hS_k = S_m$ gives the same result as if one first calculates the product $hg = p$ and then applies it to S_i , $pS_i = S_m$.

When a group G , a set A , and a mapping φ fulfil the requirements (3.2.3.47) to (3.2.3.49), one says that G *acts* or *operates on* A and the set A is called a *G-set*.

Example [aC] 3.2.3.9. We shall examine the action of an isometry g on an ideal infinite crystal in the three-dimensional space. Let us choose four points (atoms) of the crystal that define three non-coplanar vectors $\mathbf{a}_1, \mathbf{a}_2, \mathbf{a}_3$ (*e.g.* basic lattice translations). These vectors will specify the *orientation of the crystal in space*. Let g be a point-group operation. This isometry g transforms (moves) points of the crystal to new positions and changes the orientation of the crystal to a new orientation specified by vectors $\mathbf{a}'_1, \mathbf{a}'_2, \mathbf{a}'_3$,

$$\mathbf{a}'_i = \sum_{j=1}^3 D(g)_{ji}\mathbf{a}_j, \quad i = 1, 2, 3, \quad (3.2.3.50)$$

where $D(g)_{ji}$ are coefficients of a 3×3 matrix representing the operation g . For non-trivial operations g , the resulting vectors $\mathbf{a}'_1, \mathbf{a}'_2, \mathbf{a}'_3$ always differ from the initial ones. If g is an improper rotation (rotoinversion), then these vectors have an opposite handedness to the vectors $\mathbf{a}_1, \mathbf{a}_2, \mathbf{a}_3$ of the initial orientation and, for enantiomorphous crystals, the transformed crystal is an enantiomorphous form of the crystal in the initial orientation.

We choose a *reference coordinate system* defined by the origin O and by three non-coplanar basis vectors $\mathbf{e}_1, \mathbf{e}_2, \mathbf{e}_3$. By the *state S of a crystal* we shall understand, in a continuum description, the set of all its properties expressed by components of physical property (matter) tensors in the reference coordinate system or, in a microscopic description, the positions of atoms in the elementary unit cell expressed in the reference coordinate system. States defined in this way may change with temperature and external fields, and also with the orientation of the crystal in

3. PHASE TRANSITIONS, TWINNING AND DOMAIN STRUCTURES

space. At constant temperature and external fields, the states are in one-to-one correspondence with the orientations of the crystal.

Application of an isometry on a state of a crystal can be treated as a group action: Let G be a point group and \mathbf{A} a set of all conceivable states of a crystal. We denote by \mathbf{S}_i the state of the crystal in an initial orientation. An operation g of G changes the orientation of the crystal and the resulting state \mathbf{S}_k of the crystal in a new orientation is determined by \mathbf{S}_i and g . This is, in mathematical terms, a mapping of a pair (g, \mathbf{S}_i) on a state \mathbf{S}_k from the set \mathbf{A} , $\varphi : (g, \mathbf{S}_i) \mapsto \mathbf{S}_k$, or in the shorthand notation,

$$g\mathbf{S}_i = \mathbf{S}_k, \quad g \in G, \quad \mathbf{S}_i, \mathbf{S}_k \in \mathbf{A}. \quad (3.2.3.51)$$

Since this mapping fulfils conditions (3.2.3.48) and (3.2.3.49), it is a group action. We note that for some g the resulting state \mathbf{S}_k can be identical with the initial state \mathbf{S}_i and that several operations can produce the same resulting state \mathbf{S}_k .

Group action of an isometry on a crystal applies in a natural way to domain structures, where the group G describes the symmetry of the parent (high-symmetry) phase and the states $\mathbf{S}_i, \mathbf{S}_k$ are crystallographically equivalent (G -equivalent) states of the distorted (low-symmetry) phase called *domain states*. This means that domain states are states that are crystallographically equivalent in G . In a continuum description, domain states differ in orientation and are called *ferroic domain states* or orientation states (see Section 3.4.3.2).

Example [aT] 3.2.3.10. Let us consider a property tensor τ (e.g. polarization, permittivity, piezoelectric coefficients) and let us denote by $\tau^{(i)}$ components of this tensor expressed in a fixed reference coordinate system. This set can be represented by a point in the corresponding tensor space. Let us denote by \mathbf{B} the set of all points of this tensor space and by G a point group. The mapping

$$g\tau^{(i)} = \tau^{(k)}, \quad g \in G, \quad \tau^{(i)}, \tau^{(k)} \in \mathbf{B}, \quad (3.2.3.52)$$

is defined by the transformation law of the tensor components (see Chapter 1.1). This mapping fulfils conditions (3.2.3.48) and (3.2.3.49), and can therefore be treated as a group action.

Example [aS] 3.2.3.11. Let G be a group, F a subgroup of G , $F \subset G$, and \mathbf{C} the set of all subgroups of G . The group G can act on the set \mathbf{C} by conjugation:

$$\varphi : (g, F) \mapsto gFg^{-1}, \quad g \in G, F \in \mathbf{C}. \quad (3.2.3.53)$$

In this case, one has to write the mapping explicitly since the abbreviated form gF would mean a left coset and not a conjugate subgroup gFg^{-1} . One also has to corroborate the validity of condition (3.2.3.49): $(h, (g, F)) \mapsto (h, (gFg^{-1})) \mapsto h(gFg^{-1})h^{-1} = hgF(hg)^{-1}$, which is the image of $((hg), F)$.

An action of a group G on a set \mathbf{A} introduces two basic notions, namely stabilizers and orbits.

3.2.3.3.2. Stabilizers (isotropy groups)

The concept of a stabilizer is closely connected with the notion of the symmetry group of an object. Under the *symmetry group* F of an object \mathbf{S} one understands the set of all operations (isometries) that map the object onto itself, i.e. leave this object \mathbf{S} invariant. In this approach, one usually ‘attaches’ the symmetry elements to the object. Then the symmetry group F of the object is its inherent property which does not depend on the orientation and position of the object in space. The term *eigensymmetry* is used in Chapter 3.3 for symmetry groups defined in this way.

The notion of a stabilizer describes the symmetry properties of an object from another standpoint, in which the object and the group of isometries are decoupled and introduced independently. One chooses a reference coordinate system and a group G of isometries, the operations of which have a defined orientation in this reference system. Usually, it is convenient to choose as the reference system the standard coordinate system (crystallographic or crystallophysical) of the group G . The object \mathbf{S}_i under consideration is specified not only *per se* but also by its orientation in the reference system. Those operations of G that map the object in this orientation onto itself form a group called the stabilizer of \mathbf{S}_i in the group G . An algebraic definition is formulated in the following way:

Definition [s] 3.2.3.12. The *stabilizer (isotropy group)* $I_G(\mathbf{S}_i)$ of an object \mathbf{S}_i of a G -set \mathbf{A} in group G is that subgroup of G comprised of all operations of G that do not change \mathbf{S}_i ,

$$I_G(\mathbf{S}_i) = \{g \in G | g\mathbf{S}_i = \mathbf{S}_i\}, \quad g \in G, \quad \mathbf{S}_i \in \mathbf{A}. \quad (3.2.3.54)$$

Unlike the ‘eigensymmetry’, the stabilizer $I_G(\mathbf{S}_i)$ depends on the group G , is generally a subgroup of G , $I_G(\mathbf{S}_i) \subseteq G$, and may change with the orientation of the object \mathbf{S}_i .

There is an important relation between stabilizers of two objects from a G -set (see e.g. Aizu, 1970; Kerber, 1991):

Proposition 3.2.3.13. Consider two objects $\mathbf{S}_i, \mathbf{S}_k$ from a G -set related by an operation g from the group G . The respective stabilizers $I_G(\mathbf{S}_i), I_G(\mathbf{S}_k)$ are conjugate by the same operation g ,

$$\text{if } \mathbf{S}_k = g\mathbf{S}_i, \text{ then } I_G(\mathbf{S}_k) = gI_G(\mathbf{S}_i)g^{-1}. \quad (3.2.3.55)$$

Let us illustrate the meaning of stabilizers with four examples of group action considered above.

Example [sP] 3.2.3.14. Let \mathcal{G} be a crystallographic space group and X a point of the three-dimensional point space $E(3)$ (see Example 3.2.3.7). The stabilizer $\mathcal{I}_{\mathcal{G}}(X)$, called the *site-symmetry group* of the point X in \mathcal{G} , consists of all symmetry operations of \mathcal{G} that leave the point X invariant. Consequently, the stabilizer $\mathcal{I}_{\mathcal{G}}(X)$ is a crystallographic point group. If the stabilizer $\mathcal{I}_{\mathcal{G}}(X)$ consists only of the identity operation, then the point X is called a *point of general position*. If $\mathcal{I}_{\mathcal{G}}(X)$ is a non-trivial point group, X is called a *point of special position* (IT A, 2002).

Example [sC] 3.2.3.15. The symmetry of domain states $\mathbf{S}_i, \mathbf{S}_k, \dots$, treated in Example [sP] 3.2.3.9, is adequately expressed by their stabilizers in the group G of the parent (high-symmetry) phase, $I_G(\mathbf{S}_i) = F_i, I_G(\mathbf{S}_k) = F_k, \dots$. These groups are called *symmetry groups of domain states*. If domain states $\mathbf{S}_i, \mathbf{S}_k$ are related by an operation $g \in G$, then their symmetry groups are, according to (3.2.3.55), conjugate by g ,

$$\text{if } \mathbf{S}_k = g\mathbf{S}_i \text{ then } F_k = gF_i g^{-1}. \quad (3.2.3.56)$$

Symmetry characterization of domain states by their stabilizers properly reflects a difference between ferroelastic single domain states and ferroelastic disoriented domain states (see Sections 3.4.3 and 3.4.4).

Example [sT] 3.2.3.16. The notion of the stabilizer enables one to formulate a basic relation between the symmetry group of the parent phase, the symmetry group of the first domain state \mathbf{S}_1 and order parameters of the transition. In a microscopic description, the symmetry of the parent phase is described by a space group \mathcal{G} and the symmetry of the first basic (microscopic) single domain

3.2. TWINNING AND DOMAIN STRUCTURES

state \mathbf{S}_1 by the stabilizer $\mathcal{I}_G(\mathbf{S}_1) = \mathcal{F}_1$. The stabilizer of the primary order parameter $\eta^{(1)}$ must fulfil the condition

$$I_G(\eta^{(1)}) = I_G(\mathbf{S}_1) = \mathcal{F}_1. \quad (3.2.3.57)$$

The appearance of nonzero $\eta^{(1)}$ in the ferroic phase thus fully accounts for the symmetry descent $\mathcal{G} \supset \mathcal{F}_1$ at the transition.

In a continuum description, a role analogous to $\eta^{(1)}$ is played by a *principal tensor parameter* $\mu^{(1)}$ (see Section 3.1.3). Its stabilizer $I_G(\mu^{(1)})$ in the parent point group G equals the point group F_1 of the first single domain state \mathbf{S}_1 ,

$$I_G(\mu^{(1)}) = I_G(\mathbf{S}_1) = F_1. \quad (3.2.3.58)$$

This contrasts with the *secondary order parameter* $\lambda^{(1)}$ (*secondary tensor parameter* in a continuum description). Its stabilizer

$$I_G(\lambda^{(1)}) = L_1 \quad (3.2.3.59)$$

is an intermediate group $F_1 \subset L_1 \subset G$, i.e. the appearance of $\lambda^{(1)}$ would lead only to a partial symmetry descent $G \supset L_1$ with $L_1 \supset F_1$.

Example [sS] 3.2.3.17. The stabilizer of a subgroup $F_i \subset G$ from Example [aS] 3.2.3.11 is the normalizer $N_G(F_i)$ defined in Section 3.2.3.2.5:

$$I_G(F_i) = \{g \in G | gF_i g^{-1} = F_i\} = N_G(F_i). \quad (3.2.3.60)$$

In general, a stabilizer, which is a subgroup of G , is an example of a structure which is induced by a group action on the group G . On the other hand, a group action exerts a partition of the set \mathbf{A} into equivalence classes called orbits.

3.2.3.3.3. Orbits

The group action allows one to specify the equivalence relation and the partition of a set into equivalence classes introduced in Section 3.2.3.1 [see (3.2.3.6)]. If G is a group and $\mathbf{S}_i, \mathbf{S}_k$ are two objects of a G -set \mathbf{A} , then one says that the *objects* $\mathbf{S}_i, \mathbf{S}_k$ are *G-equivalent*, $\mathbf{S}_i \sim^G \mathbf{S}_k$, if there exists an operation $g \in G$ that transforms \mathbf{S}_i into \mathbf{S}_k ,

$$\mathbf{S}_k = g\mathbf{S}_i, \quad \mathbf{S}_i, \mathbf{S}_k \in \mathbf{A}, \quad g \in G. \quad (3.2.3.61)$$

In our applications, the group G is most often a crystallographic group. In this situation we shall speak about *crystallographically equivalent objects*. Exceptionally, G will be the group of all isometries $O(3)$ (full orthogonal group in three dimensions); then we shall talk about *symmetrically equivalent objects*.

The relation \sim^G is an equivalence relation on a set \mathbf{A} and therefore divides a set \mathbf{A} into G -equivalence classes. These classes are called orbits and are defined in the following way:

Definition [o] 3.2.3.18. Let \mathbf{A} be a G -set and \mathbf{S}_i an object of the set \mathbf{A} . A *G-orbit* of \mathbf{S}_i , denoted GS_i , is a set of all objects of \mathbf{A} that are G -equivalent with \mathbf{S}_i ,

$$GS_i = \{g\mathbf{S}_i | \forall g \in G\}, \quad \mathbf{S}_i \in \mathbf{A}. \quad (3.2.3.62)$$

Important note: The object \mathbf{S}_i of the orbit GS_i is called the *representative of the orbit* GS_i . If the group G is known from the context, one simply speaks of an *orbit* of \mathbf{S}_i .

Any two objects of an orbit are G -equivalent and any object of the orbit can be chosen as a representative of this orbit. Two G -orbits GS_i, GS_j of a G -set \mathbf{A} are either identical or disjoint. The set \mathbf{A} can therefore be partitioned into disjoint orbits,

$$\mathbf{A} = GS_i \cup GS_k \cup \dots \cup GS_q. \quad (3.2.3.63)$$

Different groups G produce different partitions of the set \mathbf{A} .

Example [oP] 3.2.3.19. If X is a point in three-dimensional point space and G is a crystallographic point group (see Example [aP] 3.2.3.7), then the orbit $G(X)$ consisting of all crystallographically equivalent points is called a *point form* [see IT A (2002), Part 10]. If the group is a space group \mathcal{G} , then $\mathcal{G}(X)$ is called the *crystallographic orbit* of X with respect to \mathcal{G} . In this case, the crystallographic orbit is an infinite set of points due to the infinite number of translations in the space group \mathcal{G} [see IT A (2002), Part 8]. In this way, the infinite set of points of the point space is divided into an infinite number of disjoint orbits.

Example [oC] 3.2.3.20. Let \mathbf{S}_1 be a domain state from Example [aC] 3.2.3.9. The orbit GS_1 , where G is the parent phase symmetry, assembles all G -equivalent domain states,

$$GS_1 = \{\mathbf{S}_1, \mathbf{S}_2, \dots, \mathbf{S}_n\}. \quad (3.2.3.64)$$

The existence of several equivalent states is the main characteristic feature of domain states. Domain states of the orbit GS_1 represent all possible variants of the low-symmetry phase with the same energy and the same chance of appearance in the domain structure. Structurally, they represent the crystal structure \mathbf{S}_1 in all distinguishable orientations (and also positions in a microscopic description) related by isometries of the group G . If G contains rotoinversions and if \mathbf{S}_1 is an enantiomorphic structure, then the orbit GS_1 also comprises the enantiomorphic form of \mathbf{S}_1 .

Example [oT] 3.2.3.21. Let $\mu^{(1)}$ be a principal tensor parameter of the point-group-symmetry descent $G \supset F_1$ (see Example [sT] 3.2.3.16). The orbit $G\mu^{(1)}$ consists of all points in the tensor space of the principal tensor parameter that are crystallographically equivalent with respect to G ,

$$G\mu^{(1)} = \{\mu^{(1)}, \mu^{(2)}, \dots, \mu^{(n)}\}. \quad (3.2.3.65)$$

Example [oS] 3.2.3.22. The orbit GF_1 of a subgroup F_1 in Example [aS] 3.2.3.11 is the set of all subgroups conjugate under G to F_1 ,

$$GF_1 = \{F_1, g_2 F_1 g_2^{-1}, \dots, g_m F_1 g_m^{-1}\}. \quad (3.2.3.66)$$

From Proposition 3.2.3.13 and from Example [oS] 3.2.3.22, it follows that stabilizers of objects from one orbit GS_i constitute the orbit (3.2.3.66) of all subgroups conjugate under G . One can thus associate with each orbit GS_i an orbit GF_i of conjugate subgroups of G . The set of all objects with stabilizers from one orbit GF_i of conjugate subgroups is called a *stratum* of F_i in the set \mathbf{A} (Michel, 1980; Kerber, 1999). In crystallography, the term *Wyckoff position* is used for the stratum of points of the point space (IT A, 2002).

The notion of a stratum can be also applied to the classification of orbits of domain states treated in Example [oC] 3.2.3.22. Let G be the symmetry of the parent phase and \mathbf{A} the set of all states of the crystal. Orbits GS_i of domain states with stabilizers from one orbit GF_i of conjugate subgroups of G , $F_i = I_G(\mathbf{S}_i)$, are of the 'same type' and form a *stratum of domain states*. Domain states of different orbits belonging to the same stratum differ in the numerical values of parameters describing the states but have the same crystallographic and topological properties. All possible strata that can be formed from a given parent phase with

3. PHASE TRANSITIONS, TWINNING AND DOMAIN STRUCTURES

symmetry G can be identified with all different orbits of subgroups of G .

In a similar manner, points of the order-parameter space and tensor-parameter space from Examples [sC] 3.2.3.16 and [oT] 3.2.3.21 can be divided into strata which are characterized by the orbits of possible stabilizers.

Next, we formulate three propositions that are essential in the symmetry analysis of domain structures presented in Section 3.4.2.

3.2.3.3.4. Orbits and left cosets

Proposition 3.2.3.23. Let G be a finite group, \mathbf{A} a G -set and $I_G(\mathbf{S}_1) \equiv F_1$ the stabilizer of an object \mathbf{S}_1 of the set \mathbf{A} , $\mathbf{S}_1 \in \mathbf{A}$. The objects of the orbit

$$G\mathbf{S}_1 = \{\mathbf{S}_1, \mathbf{S}_2, \dots, \mathbf{S}_j, \dots, \mathbf{S}_n\} \quad (3.2.3.67)$$

and the left cosets $g_j F_1$ of the decomposition of G ,

$$G = g_1 F_1 \cup g_2 F_1 \cup \dots \cup g_j F_1 \cup \dots \cup g_n F_1 = \bigcup_{j=1}^n g_j F_1, \quad (3.2.3.68)$$

are in a one-to-one correspondence,

$$\mathbf{S}_j \leftrightarrow g_j F_1, \quad F_1 = I_G(\mathbf{S}_1), \quad j = 1, 2, \dots, n. \quad (3.2.3.69)$$

(See e.g. Kerber, 1991, 1999; Kopský, 1983; Lang, 1965.) The derivation of the bijection (3.2.3.69) consists of two parts:

(i) All operations of a left coset $g_j F_1$ transform \mathbf{S}_1 into the same $\mathbf{S}_j = g_j \mathbf{S}_1$, since $g_j \mathbf{S}_1 = g_j (F_1 \mathbf{S}_1) = (g_j F_1) \mathbf{S}_1$, where we use the relation

$$\begin{aligned} F_1 \mathbf{S}_1 &= \{f_1, f_2, \dots, f_q\} \mathbf{S}_1 \\ &= \{f_1 \mathbf{S}_1, f_2 \mathbf{S}_1, \dots, f_q \mathbf{S}_1\} \\ &= \{\mathbf{S}_1, \mathbf{S}_1, \dots, \mathbf{S}_1\} = \{\mathbf{S}_1\} = \mathbf{S}_1, \end{aligned} \quad (3.2.3.70)$$

which in the second line contains a generalization of the group action and in the third line reflects Definition 3.2.3.1 of a set as a collection of distinguishable objects, $\{\mathbf{S}_1, \mathbf{S}_1, \dots, \mathbf{S}_1\} = \mathbf{S}_1 \cup \mathbf{S}_1 \dots \cup \mathbf{S}_1 = \mathbf{S}_1$.

(ii) Any $g_r \in G$ that transforms \mathbf{S}_1 into $\mathbf{S}_j = g_j \mathbf{S}_1$ belongs to the left coset $g_j F_1$, since from $g_j \mathbf{S}_1 = g_r \mathbf{S}_1$ it follows that $g_r^{-1} g_j \mathbf{S}_1 = \mathbf{S}_1$, i.e. $g_r^{-1} g_j \in F_1$, which, according to the left coset criterion, holds if and only if g_r and g_j belong to the same left coset $g_j F_1$.

We note that the orbit $G\mathbf{S}_1$ depends on the stabilizer $I_G(\mathbf{S}_1) = F_1$ of the object \mathbf{S}_1 and not on the ‘eigensymmetry’ of \mathbf{S}_1 .

From Proposition 3.2.3.23 follow two corollaries:

Corollary 3.2.3.24. The order n of the orbit $G\mathbf{S}_1$ equals the index of the stabilizer $I_G(\mathbf{S}_1) = F_1$ in G ,

$$n = [G : I_G(\mathbf{S}_1)] = [G : F_1] = |G| : |F_1|, \quad (3.2.3.71)$$

where the last part of the equation applies to point groups only.

Corollary 3.2.3.25. All objects of the orbit $G\mathbf{S}_1$ can be generated by successive application of representatives of all left cosets $g_j F_1$ in the decomposition of G [see (3.2.3.68)] to the object \mathbf{S}_1 , $\mathbf{S}_j = g_j \mathbf{S}_1$, $j = 1, 2, \dots, n$. The orbit $G\mathbf{S}_1$ can therefore be expressed explicitly as

$$G\mathbf{S}_1 = \{\mathbf{S}_1, g_2 \mathbf{S}_1, \dots, g_j \mathbf{S}_1, \dots, g_n \mathbf{S}_1\}, \quad (3.2.3.72)$$

where the operations $g_1 = e, g_2, \dots, g_j, \dots, g_n$ (left transversal to F_1 in G) are the representatives of left cosets in the decomposition (3.2.3.68).

Example [oP] 3.2.3.26. The number of equivalent points of the point form $G\mathbf{X}$ (G orbit of the point \mathbf{X}) is called a *multiplicity* $m_G(\mathbf{X})$ of this point,

$$m_G(\mathbf{X}) = |G| : |I_G(\mathbf{X})|. \quad (3.2.3.73)$$

The multiplicity of a point of general position equals the order $|G|$ of the group G , since in this case $I_G(\mathbf{X}) = e$, a trivial group. Then points of the orbit $G\mathbf{X}$ and the operations of G are in a one-to-one correspondence. The multiplicity of a point of special position is smaller than the order $|G|$, $m_G(\mathbf{X}) < |G|$, and the operations of G and the points of the orbit $G\mathbf{X}$ are in a many-to-one correspondence. Points of a stratum have the same multiplicity; one can, therefore, talk about the multiplicity of the Wyckoff position [see IT A (2002)]. If G is a space group, the point orbit has to be confined to the volume of the primitive unit cell (Wondratschek, 1995).

Example [oC] 3.2.3.27. Corollaries 3.2.3.24 and 3.2.3.25 applied to domain states represent the basic relations of domain-structure analysis. According to (3.2.3.71), the index n of the stabilizer $I_G(\mathbf{S}_1)$ in the parent group G gives the number of domain states in the orbit $G\mathbf{S}_1$ and the relations (3.2.3.72) and (3.2.3.68) give a recipe for constructing domain states of this orbit.

Example [oT] 3.2.3.28. If $\mu^{(1)}$ is a principal tensor parameter associated with the symmetry descent $G \supset F_1$, then there is a one-to-one correspondence between the elements of the orbit of single domain states $G\mathbf{S}_1 = \{\mathbf{S}_1, \mathbf{S}_2, \dots, \mathbf{S}_j, \dots, \mathbf{S}_n\}$ and the elements of the orbit of the principal order parameter (points) $G\mu^{(1)} = \{\mu^{(1)}, \mu^{(2)}, \dots, \mu^{(j)}, \dots, \mu^{(n)}\}$ (see Example [oT] 3.2.3.21),

$$\mathbf{S}_j \leftrightarrow g_j F_1 \leftrightarrow \mu^{(j)}, \quad j = 1, 2, \dots, n. \quad (3.2.3.74)$$

Therefore, single domain states of the orbit $G\mathbf{S}_1$ can be represented by the principal tensor parameter of the orbit $G\mu^{(1)}$.

Example [oS] 3.2.3.29. Consider a subgroup F_1 of a group G . Since the stabilizer of F_1 in G is the normalizer $N_G(F_1)$ (see Example [sS] 3.2.3.17), the number m of conjugate subgroups is, according to (3.2.3.71),

$$m = [G : N_G(F_1)] = |G| : |N_G(F_1)|, \quad (3.2.3.75)$$

where the last part of the equation applies to point groups only. The orbit of conjugate subgroups is

$$\begin{aligned} GF_1 &= \{F_1, h_2 F_1 h_2^{-1}, \dots, h_j F_1 h_j^{-1}, \dots, h_m F_1 h_m^{-1}\}, \\ j &= 1, 2, \dots, m, \end{aligned} \quad (3.2.3.76)$$

where the operations $h_1 = e, h_2, \dots, h_j, \dots, h_m$ are the representatives of left cosets in the decomposition

$$G = N_G(F_1) \cup h_2 N_G(F_1) \cup \dots \cup h_j N_G(F_1) \cup \dots \cup h_m N_G(F_1). \quad (3.2.3.77)$$

3.2.3.3.5. Intermediate subgroups and partitions of an orbit into suborbits

Proposition 3.2.3.30. Let $G\mathbf{S}_1$ be a G orbit from Proposition 3.2.3.23 and L_1 an intermediate group,

$$F_1 \subset L_1 \subset G. \quad (3.2.3.78)$$

A successive decomposition of G into left cosets of L_1 and L_1 into left cosets of F_1 [see (3.2.3.25)] introduces a two-indices rela-

3.2. TWINNING AND DOMAIN STRUCTURES

bellings of the objects of a G orbit defined by the one-to-one correspondence

$$h_j p_k F_1 \leftrightarrow S_{jk}, \quad j = 1, 2, \dots, m, \quad k = 1, 2, \dots, d, \quad (3.2.3.79)$$

where $\{h_1, h_2, \dots, h_m\}$ are the representatives of the decompositions of G into left cosets of L_1 ,

$$G = h_1 L_1 \cup h_2 L_1 \cup \dots \cup h_j L_1 \cup \dots \cup h_m L_1, \quad m = [G : L_1], \quad (3.2.3.80)$$

and $\{p_1, p_2, \dots, p_d\}$ are the representatives of the decompositions of L_1 into left cosets of F_1 ,

$$L_1 = p_1 F_1 \cup p_2 F_1 \cup \dots \cup p_k F_1 \cup \dots \cup p_d F_1, \quad d = [L_1 : F_1]. \quad (3.2.3.81)$$

The index n of F_1 in G can be expressed as a product of indices m and d [see (3.2.3.26)],

$$n = [G : F_1] = [G : L_1][L_1 : F_1] = md. \quad (3.2.3.82)$$

If G is a finite group, then the index n can be expressed in terms of orders of groups G , F_1 and L_1 :

$$n = |G| : |F_1| = (|G| : |L_1|)(|L_1| : |F_1|) = md. \quad (3.2.3.83)$$

When one chooses $S_1 = S_{11}$, then the members of the orbit GS_{11} can be arranged into an $m \times d$ array,

$$\begin{array}{cccccc} S_{11} & S_{12} & \dots & S_{1k} & \dots & S_{1d} \\ S_{21} & S_{22} & \dots & S_{2k} & \dots & S_{2d} \\ \vdots & \vdots & \ddots & \vdots & \ddots & \vdots \\ S_{j1} & S_{j2} & \dots & S_{jk} & \dots & S_{jd} \\ \vdots & \vdots & \ddots & \vdots & \ddots & \vdots \\ S_{m1} & S_{m2} & \dots & S_{mk} & \dots & S_{md} \end{array} \quad (3.2.3.84)$$

The set of objects of the j th row of this array forms an L_j orbit with the representative S_{j1} ,

$$\begin{aligned} \{S_{j1}, S_{j2}, \dots, S_{jk}, \dots, S_{jd}\} \\ = \{h_j p_1 S_{11}, h_j p_2 S_{11}, \dots, h_j p_k S_{11}, \dots, h_j p_d S_{11}\} \\ = L_j S_{j1}, \end{aligned} \quad (3.2.3.85)$$

where

$$L_j = h_j L_1 h_j^{-1}, \quad S_{j1} = h_j S_{11}, \quad j = 1, 2, \dots, m. \quad (3.2.3.86)$$

The intermediate group L_1 thus induces a *splitting of the orbit* GS_{11} into m suborbits $L_j S_{j1}$, $j = 1, 2, \dots, m$:

$$GS_{11} = L_1 S_{11} \cup L_2 S_{21} \cup \dots \cup L_j S_{j1} \cup \dots \cup L_m S_{m1}, \quad m = [G : L_1]. \quad (3.2.3.87)$$

Aizu (1972) denotes this partitioning *factorization of species*.

The relation (3.2.3.79) is just the application of the correspondence (3.2.3.69) of Proposition 3.2.3.23 on the successive decomposition (3.2.3.25). Derivation of the second part of Proposition 3.2.3.30 can be sketched in the following way:

$$\begin{aligned} \{S_{j1}, S_{j2}, \dots, S_{jd}\} &= h_j \{p_1 S_{11}, p_2 S_{11}, \dots, p_d S_{11}\} \\ &= h_j \{p_1, p_2, \dots, p_d\} F_1 S_{11} \\ &= h_j L_1 S_{11} = h_j L_1 h_j^{-1} S_{j1} = L_j S_{j1}, \\ j &= 1, 2, \dots, m, \end{aligned} \quad (3.2.3.88)$$

where the relation (3.2.3.70) is used.

We note that the described partitioning of an orbit into suborbits depends on the choice of representative of the first suborbit S_{11} and that the number of conjugate subgroups L_j may be equal to or smaller than the number m of suborbits (see Example [oS] 3.2.3.34).

Each intermediate group L_1 in Proposition 3.2.3.30 can usually be associated with a certain attribute, *e.g.* a secondary order parameter, which specifies the suborbits.

Example [oP] 3.2.3.31. Let G be a point group and X_1 a point of general position ($I_G(X_1) = e$) in the point space. A symmetry descent to a subgroup $L_1 \subset G$ is accompanied by a splitting of the orbit GX_1 of $|G|$ equivalent points into $m = |G| : |L_1|$ suborbits each consisting of $|L_1|$ equivalent points. The first suborbit is $L_1 X_1$, the others are $L_j X_j$, $L_j = h_j L_1 h_j^{-1}$, $X_j = h_j X_1$, $j = 1, 2, \dots, m$, where h_j are representatives of left cosets of L_1 in the decomposition of G [see (3.2.3.80)].

Splitting of orbits of points of general position is a special case in which $I_L(X_1) = I_G(X_1)$. Splitting of orbits of points of special position is more complicated if $I_L(X_1) \subset I_G(X_1)$ (see Wondratschek, 1995).

Example [oC] 3.2.3.32. Let us consider a phase transition accompanied by a lowering of space-group symmetry from a parent space group \mathcal{G} with translation subgroup \mathbf{T} and point group G to a low-symmetry space group \mathcal{F} with translation subgroup \mathbf{U} and point group F . There exists a unique intermediate group \mathcal{M} , called the *group of Hermann*, which has translation subgroup \mathbf{T} and point group $M = F$ (see *e.g.* Hahn & Wondratschek, 1994; Wadhawan, 2000; Wondratschek & Aroyo, 2001).

The decomposition of \mathcal{G} into left cosets of \mathcal{M} , corresponding to (3.2.3.80), is in a one-to-one correspondence with the decomposition of G into left cosets of F , since \mathcal{G} and \mathcal{M} have the same translation subgroup \mathbf{T} and \mathcal{M} and \mathcal{F} have the same point group. Therefore, the index $n \equiv [\mathcal{G} : \mathcal{M}] = [G : F] = |G| : |F|$.

Since \mathcal{M} and \mathcal{F} have the same point group F , the decomposition of \mathcal{M} into left cosets of \mathcal{F} , corresponding to (3.2.3.81), is in a one-to-one correspondence with the decomposition of \mathbf{T} into left cosets of \mathbf{U} ,

$$\mathbf{T} = \mathbf{t}_1 \mathbf{U} + \mathbf{t}_2 \mathbf{U} + \dots + \mathbf{t}_d \mathbf{U}. \quad (3.2.3.89)$$

Representatives $\mathbf{t}_1, \mathbf{t}_2, \dots, \mathbf{t}_d$ are translations. The corresponding vectors lead from the origin of a 'superlattice' primitive unit cell of the low-symmetry phase to lattice points of \mathbf{T} located within or on the side faces of this 'superlattice' primitive unit cell (Van Tendeloo & Amelinckx, 1974). The number d_t of these vectors is equal to the ratio $v_{\mathcal{F}} : v_{\mathcal{G}} = Z_{\mathcal{F}} : Z_{\mathcal{G}}$, where $v_{\mathcal{F}}$ and $v_{\mathcal{G}}$ are the volumes of the *primitive* unit cell of the low-symmetry phase and the parent phase, respectively, and $Z_{\mathcal{F}}$ and $Z_{\mathcal{G}}$ are the number of chemical formula units in the *primitive* unit cell of the low-symmetry phase and the parent phase, respectively.

There is another useful formula for expressing $d_t = [\mathbf{T} : \mathbf{U}]$. The primitive basis vectors $\mathbf{b}_1, \mathbf{b}_2, \mathbf{b}_3$ of \mathbf{U} are related to the primitive basis vectors $\mathbf{a}_1, \mathbf{a}_2, \mathbf{a}_3$ of \mathbf{T} by a linear relation,

$$\mathbf{b}_i = \sum_{j=1}^3 \mathbf{a}_j m_{ij}, \quad i = 1, 2, 3, \quad (3.2.3.90)$$

where m_{ij} are integers. The volumes of primitive unit cells are $v_{\mathcal{G}} = \mathbf{a}_1(\mathbf{a}_2 \times \mathbf{a}_3)$ and $v_{\mathcal{F}} = \mathbf{b}_1(\mathbf{b}_2 \times \mathbf{b}_3)$. Using (3.2.3.90), one gets $v_{\mathcal{F}} = \det(m_{ij})v_{\mathcal{G}}$, where $\det(m_{ij})$ is the determinant of the (3×3) matrix of the coefficients m_{ij} . Hence the index $d_t = (v_{\mathcal{F}} : v_{\mathcal{G}}) = \det(m_{ij})$.

Thus we get for the index N of \mathcal{F} in \mathcal{G}

3. PHASE TRANSITIONS, TWINNING AND DOMAIN STRUCTURES

$$\begin{aligned} N &= [\mathcal{G} : \mathcal{F}] = [G : F][\mathbf{T} : \mathbf{U}] \\ &= (|G| : |F|)(v_{\mathcal{F}} : v_{\mathcal{G}}) = (|G| : |F|)(Z_{\mathcal{F}} : Z_{\mathcal{G}}) \\ &= (|G| : |F|)\det(m_{ij}) = nd_i. \end{aligned} \quad (3.2.3.91)$$

Each suborbit, represented by a row in the array (3.2.3.84), contains all basic (microscopic) domain states that are related by pure translations. These domain states exhibit the same tensor properties, *i.e.* they belong to the same ferroic domain state.

Example [sT] 3.2.3.33. Let us consider a phase transition with a symmetry descent $G \supset F_1$ with an orbit $G\mathbf{S}_{11}$ of domain states. Let L_1 be an intermediate group, $F_1 \subset L_1 \subset G$, and $\lambda^{(1)}$ the principal order parameter associated with the symmetry descent $G \supset L_1$ [cf. (3.2.3.58)], $I_G(\lambda^{(1)}) = L_1$. Since L_1 is an intermediate group, the quantity $\lambda^{(1)}$ represents a secondary order parameter of the symmetry descent $G \supset F_1$. The G orbit of $\lambda^{(1)}$ is

$$G\lambda^{(1)} = \{\lambda^{(1)}, \lambda^{(2)}, \dots, \lambda^{(m)}\}, \quad m = [G : L_1]. \quad (3.2.3.92)$$

As in Example [oT] 3.2.3.28, there is a bijection between left cosets of the decomposition of G into left cosets of L_1 [see (3.2.3.80)] and the G orbit of secondary order parameters (3.2.3.92). One can, therefore, associate with the suborbit $L_j\mathbf{S}_{j1}$ the value $\lambda^{(j)}$ of the secondary order parameter λ ,

$$L_j\mathbf{S}_{j1} \leftrightarrow \lambda^{(j)}, \quad j = 1, 2, \dots, m. \quad (3.2.3.93)$$

A suborbit $L_j\mathbf{S}_{j1}$ is thus comprised of objects of the orbit $G\mathbf{S}_{11}$ with the same value of the secondary order parameter $\lambda^{(j)}$.

Example [oS] 3.2.3.34. Let us choose for the intermediate group L_1 the normalizer $N_G(F_1)$. Then the suborbits equal

$$\begin{aligned} N_G(F_j)\mathbf{S}_{j1} &= \{h_j\mathbf{S}_{11}, h_jp_2\mathbf{S}_{11}, \dots, h_jp_d\mathbf{S}_{11}\}, \\ j &= 1, 2, \dots, m = [G : N_G(F_1)], \end{aligned} \quad (3.2.3.94)$$

where $p_1 = e, p_2, \dots, p_d$ are representatives of left cosets p_kF_1 in the decomposition of $N_G(F_1)$,

$$N_G(F_1) = p_1F_1 \cup p_2F_1 \cup \dots \cup p_dF_1, \quad d = [N_G(F_1) : F_1], \quad (3.2.3.95)$$

and h_j are representatives of the decomposition (3.2.3.77). The suborbit $F_j\mathbf{S}_{j1}$ consists of all objects with the same stabilizer F_j ,

$$\begin{aligned} I_G(\mathbf{S}_{j1}) &= I_G(\mathbf{S}_{j2}) = \dots = I_G(\mathbf{S}_{jd}) = F_j, \\ j &= 1, 2, \dots, m = [G : N_G(F_1)]. \end{aligned} \quad (3.2.3.96)$$

Propositions 3.2.3.23 and 3.2.3.30 are examples of structures that a group action induces from a group G on a G -set. Another important example is a permutation representation of the group G which associates operations of G with permutations of the objects of the orbit $G\mathbf{S}_i$ [see *e.g.* Kerber (1991, 1999); for application of the permutation representation in domain-structure analysis and domain engineering, see *e.g.* Fuksa & Janovec (1995, 2002)].

3.2.3.3.6. Orbits of ordered pairs and double cosets

An ordered pair $(\mathbf{S}_i, \mathbf{S}_k)$ is formed by two objects $\mathbf{S}_i, \mathbf{S}_k$ from the orbit $G\mathbf{S}_1$. Let \mathbf{P} denote the set of all ordered pairs that can be formed from the objects of the orbit $G\mathbf{S}_1$. The group action φ of group G on the set \mathbf{P} is defined by the following relation:

$$\begin{aligned} \varphi : g(\mathbf{S}_i, \mathbf{S}_k) &= (g\mathbf{S}_i, g\mathbf{S}_k) = (\mathbf{S}_r, \mathbf{S}_s), \\ g &\in G, \quad (\mathbf{S}_i, \mathbf{S}_k), (\mathbf{S}_r, \mathbf{S}_s) \in \mathbf{P}. \end{aligned} \quad (3.2.3.97)$$

The requirements (3.2.3.47) to (3.2.3.49) are fulfilled, mapping (3.2.3.97) defines an action of group G on the set \mathbf{P} .

The group action (3.2.3.97) introduces the G -equivalence of ordered pairs: Two ordered pairs $(\mathbf{S}_i, \mathbf{S}_k)$ and $(\mathbf{S}_r, \mathbf{S}_s)$ are crystallographically equivalent (with respect to the group G), $(\mathbf{S}_i, \mathbf{S}_k) \stackrel{G}{\sim} (\mathbf{S}_r, \mathbf{S}_s)$, if there exists an operation $g \in G$ that transforms $(\mathbf{S}_i, \mathbf{S}_k)$ into $(\mathbf{S}_r, \mathbf{S}_s)$,

$$g \in G \quad (g\mathbf{S}_i, g\mathbf{S}_k) = (\mathbf{S}_r, \mathbf{S}_s), \quad (\mathbf{S}_i, \mathbf{S}_k), (\mathbf{S}_r, \mathbf{S}_s) \in \mathbf{P}. \quad (3.2.3.98)$$

An orbit of ordered pairs $G(\mathbf{S}_i, \mathbf{S}_k)$ comprises all ordered pairs crystallographically equivalent with $(\mathbf{S}_i, \mathbf{S}_k)$. One can choose as a representative of the orbit $G(\mathbf{S}_i, \mathbf{S}_k)$ an ordered pair $(\mathbf{S}_1, \mathbf{S}_j)$ with the first member \mathbf{S}_1 since there is always an operation $g_{1i} \in G$ such that $g_{1i}\mathbf{S}_i = \mathbf{S}_1$. The orbit $F_1(\mathbf{S}_1, \mathbf{S}_j)$ assembles all ordered pairs with the first member \mathbf{S}_1 . This orbit can be expressed as

$$\begin{aligned} F_1(\mathbf{S}_1, \mathbf{S}_j) &= (F_1\mathbf{S}_1, F_1\mathbf{S}_j) = (\mathbf{S}_1, F_1(g_j\mathbf{S}_1)) \\ &= (\mathbf{S}_1, (F_1g_j)(F_1\mathbf{S}_1)) = (\mathbf{S}_1, (F_1g_jF_1)\mathbf{S}_1), \end{aligned} \quad (3.2.3.99)$$

where the identity $F_1\mathbf{S}_1 = \mathbf{S}_1$ [see relation (3.2.3.70)] has been used.

Thus the double coset $F_1g_jF_1$ contains all operations from G that produce all ordered pairs with the first member \mathbf{S}_1 that are G -equivalent with $(\mathbf{S}_1, \mathbf{S}_j = g_j\mathbf{S}_1)$. If one chooses $g_r \in G$ that is not contained in the double coset $F_1g_jF_1$, then the ordered pair $(\mathbf{S}_1, \mathbf{S}_r = g_r\mathbf{S}_1)$ must belong to another orbit $G(\mathbf{S}_1, \mathbf{S}_r) \neq G(\mathbf{S}_1, \mathbf{S}_j)$. Hence to distinct double cosets there correspond distinct classes of ordered pairs with the first member \mathbf{S}_1 , *i.e.* distinct orbits of ordered pairs. Since the group G can be decomposed into disjoint double cosets [see (3.2.3.36)], one gets

Proposition 3.2.3.35. Let G be a group and \mathbf{P} a set of all ordered pairs that can be formed from the objects of the orbit $G\mathbf{S}_1$. There is a one-to-one correspondence between the G orbits of ordered pairs of the set \mathbf{P} and the double cosets of the decomposition

$$G = F_1 \cup F_1g_2F_1 \cup \dots \cup F_1g_jF_1 \cup \dots \cup F_1g_qF_1, \quad j = 1, 2, \dots, q. \quad (3.2.3.100)$$

$$G(\mathbf{S}_1, \mathbf{S}_j) \leftrightarrow F_1g_jF_1 \text{ where } \mathbf{S}_j = g_j\mathbf{S}_1. \quad (3.2.3.101)$$

This bijection allows one to express the partition of the set \mathbf{P} of all ordered pairs into G orbits,

$$\mathbf{P} = G(\mathbf{S}_1, \mathbf{S}_1) \cup G(\mathbf{S}_1, g_2\mathbf{S}_1) \cup \dots \cup (\mathbf{S}_1, \mathbf{S}_j) \cup \dots \cup G(\mathbf{S}_1, g_q\mathbf{S}_1), \quad (3.2.3.102)$$

where $\{g_1 = e, g_2, \dots, g_j, \dots, g_q\}$ is the set of representatives of double cosets in the decomposition (3.2.3.100) (Janovec, 1972).

Proposition 3.2.3.35 applies directly to pairs of domain states (domain pairs) and allows one to find transposition laws that can appear in the low-symmetry phase (see Section 3.4.3).

For more details and other applications of group action see *e.g.* Kopský (1983), Lang (1965), Michel (1980), Opechowski (1986), Robinson (1982), and especially Kerber (1991, 1999).

References

- Aizu, K. (1969). Possible species of "ferroelastic" crystals and of simultaneously ferroelectric and ferroelastic crystals. *J. Phys. Soc. Jpn*, **27**, 387–396.

3.2. TWINNING AND DOMAIN STRUCTURES

- Aizu, K. (1970). *Possible species of ferromagnetic, ferroelectric and ferroelastic crystals*. *Phys. Rev. B*, **2**, 754–772.
- Aizu, K. (1972). *Electrical, mechanical and electromechanical orders of state shifts in nonmagnetic ferroic crystals*. *J. Phys. Soc. Jpn*, **32**, 1287–1301.
- Blattner, H., Känzig, W., Merz, W. & Sutter, H. (1948). *Die Domänenstruktur von BaTiO₃-Kristallen*. *Helv. Phys. Acta*, **21**, 207–209.
- Bloss, F. D. (1971). *Crystallography and crystal chemistry*, pp. 324–338. New York: Holt, Rinehart and Winston.
- Bollmann, W. (1970). *Crystal defects and crystalline interfaces*, ch. 12, pp. 143–148. Berlin: Springer.
- Bollmann, W. (1982). *Crystal lattices, interfaces, matrices*, pp. 111–249. Geneva: published by the author.
- Bradley, C. J. & Cracknell, A. P. (1972). *The mathematical theory of symmetry in solids*. Oxford: Clarendon Press.
- Budden, F. J. (1972). *Fascination of groups*. Cambridge University Press.
- Buerger, M. J. (1945). *The genesis of twin crystals*. *Am. Mineral.* **30**, 469–482.
- Cady, W. G. (1946). *Piezoelectricity*, ch. XXV. New York: McGraw-Hill.
- Cahn, R. W. (1954). *Twinned crystals*. *Adv. Phys.* **3**, 202–445.
- Chernysheva, M. A. (1950). *Mechanical twinning in crystals of Rochelle salt*. *Dokl. Akad. Nauk SSSR*, **74**, 247–249. (In Russian.)
- Donnay, G. & Donnay, J. D. H. (1974). *Classification of triperiodic twins*. *Can. Mineral.* **12**, 422–425.
- Donnay, J. D. H. (1940). *Width of albite-twinning lamellae*. *Am. Mineral.* **25**, 578–586.
- Donnay, J. D. H. & Donnay, G. (1972). *Crystal geometry*. In *International Tables for X-ray Crystallography*, Vol. II, 2nd edition, edited by J. C. Kasper & K. Lonsdale, Section 3. Birmingham: Kynoch Press.
- Fischmeister, H. F. (1985). *Structure and properties of high angle grain boundaries*. *J. Phys. (Paris)*, **46**, Suppl. C4-3–23.
- Friedel, G. (1904). *Etude sur les groupements cristallins*. *Extrait du Bulletin de la Société d'Industrie Minérale*, Quatrième Série, Tomes III et IV. Saint Etienne: Imprimerie Théolier J. et Cie.
- Friedel, G. (1926). *Leçons de cristallographie*. Nancy, Paris, Strasbourg: Berger-Levrault. [Reprinted (1964). Paris: Blanchard.]
- Fuksa, J. & Janovec, V. (1995). *Permutation classification of domain pairs*. *Ferroelectrics*, **172**, 343–350.
- Fuksa, J. & Janovec, V. (2002). *Macroscopic symmetries and domain configurations of engineered domain structures*. *J. Phys. Condens. Matter*, **14**, 3795–3812.
- Giacovazzo, C. (1992). Editor. *Fundamentals of crystallography*, pp. 80–87, 133–140. Oxford University Press.
- Gottstein, G. & Shvindlerman, L. S. (1999). *Grain boundary migration in metals*, ch. 2. London: CRC Press.
- Hahn, Th., Janovec, V. & Klapper, H. (1999). *Bicrystals, twins and domain structures – a comparison*. *Ferroelectrics*, **222**, 11–21.
- Hahn, Th. & Wondratschek, H. (1994). *Symmetry of crystals*. Sofia: Heron Press Ltd.
- Hall, M. Jr (1959). *The theory of groups*. New York: The Macmillan Company.
- Hámos, L. von & Thiessen, P. A. (1931). *Über die Sichtbarmachung von Bezirken verschiedenen ferromagnetischen Zustandes fester Körper*. *Z. Phys.* **71**, 442–444.
- Haüy, R.-J. (1801). *Traité de minéralogie I*, p. 273. Paris: Delance.
- Indenbom, V. L. (1960). *Phase transitions without change in the number of atoms in the unit cell of the crystal*. *Sov. Phys. Crystallogr.* **5**, 106–115.
- International Tables for Crystallography* (2002). Vol. A. *Space-group symmetry*, 5th edition, edited by Th. Hahn. Dordrecht: Kluwer Academic Publishers.
- International Tables for Crystallography* (2003). Vol. A1. *Symmetry relations between space groups*, edited by H. Wondratschek & U. Müller. In preparation.
- Janovec, V. (1972). *Group analysis of domains and domain pairs*. *Czech. J. Phys. B*, **22**, 974–994.
- Janssen, T. (1973). *Crystallographic groups*. Amsterdam: North-Holland.
- Kalonji, G. (1985). *A roadmap for the use of interfacial symmetry groups*. *J. Phys. (Paris) Colloq.* **46**, C4-249–255.
- Kay, H. F. (1948). *Preparation and properties of crystals of barium titanate, BaTiO₃*. *Acta Cryst.* **1**, 229–237.
- Kerber, A. (1991). *Algebraic combinatorics via finite group action*. Mannheim: B. I. Wissenschaftsverlag.
- Kerber, A. (1999). *Applied finite group actions*. Berlin: Springer.
- Klassen-Neklyudova, M. V. (1964). *Mechanical twinning of crystals*. New York: Consultants Bureau.
- Klassen-Neklyudova, M. V., Chernysheva, M. A. & Shternberg, A. A. (1948). *The real structure of crystals of Rochelle salt*. *Dokl. Akad. Nauk SSSR*, **63**, 527–530. (In Russian.)
- Klein, C. (1869). *Zwillingsverbindungen und Verzerrungen*. Heidelberg: G. Mohr.
- Koch, E. (1999). *Twinning*. In *International tables for crystallography*, Vol. C. *Mathematical, physical and chemical tables*, 2nd edition, edited by A. J. C. Wilson & E. Prince, Section 1.3. Dordrecht: Kluwer Academic Publishers.
- Kopský, V. (1983). *Algebraic investigations in Landau model of structural phase transitions, I, II, III*. *Czech. J. Phys. B*, **33**, 485–509, 720–744, 845–869.
- Kuratowski, K. & Mostowski, A. (1968). *Set theory*. Amsterdam: North-Holland.
- Landau, L. D. (1937). *On the theory of phase transitions. I and II*. *Zh. Eksp. Teor. Fiz.* **7**, pp. 19, 627 (in Russian); *Phys. Z. Sowjet.* **11**, pp. 26, 545 (in German). *Collected papers of L. D. Landau*, edited by D. Ter Haar (1967). New York: Gordon and Breach.
- Lang, S. (1965). *Algebra*. Reading, MA: Addison-Wesley.
- Ledermann, W. (1973). *Introduction to group theory*. London: Longman Group Ltd.
- Lipschutz, S. (1981). *Theory and problems of set theory and related topics*. Singapore: McGraw-Hill.
- Mallard, E. (1879). *Traité de cristallographie, géométrie et physique*. Vol. I. Paris: Dunod.
- Matthias, B. & von Hippel, A. (1948). *Domain structure and dielectric response of barium titanate single crystals*. *Phys. Rev.* **73**, 1378–1384.
- Michel, L. (1980). *Symmetry defects and broken symmetry. Configurations. Hidden symmetry*. *Rev. Mod. Phys.* **52**, 617–651.
- Mohs, F. (1822, 1824). *Grundriss der Mineralogie*, two volumes. Dresden: Arnold. [English translation by Haidinger, W. (1825): *Treatise on mineralogy*, three volumes. Edinburgh: Constable.]
- Mohs, F. (1823). *On the crystallographic discoveries and systems of Mohs and Weiss*. *Edinburgh Philos. J.* **8**, 275–290.
- Mueller, H. (1935). *Properties of Rochelle salt*. *Phys. Rev.* **47**, 175–191.
- Naumann, C. F. (1830). *Lehrbuch der reinen und angewandten Krystallographie*. Vol. II, p. 203. Leipzig: Brockhaus.
- Naumann, C. F. (1856). *Elemente der theoretischen Krystallographie*. p. 67. Leipzig: W. Engelmann.
- Niggli, P. (1919). *Geometrische Krystallographie des Diskontinuums*. Leipzig: Borntraeger. [Reprinted (1973). Wiesbaden: Sändig.]
- Niggli, P. (1920, 1924, 1941). *Lehrbuch der Mineralogie und Kristallchemie*, 1st ed. 1920, 2nd ed. 1924, 3rd ed., Part I, 1941, pp. 136–153, 401–414. Berlin-Zehlendorf: Gebrüder Borntraeger.
- Opechowski, W. (1986). *Crystallographic and metacrystallographic groups*. Amsterdam: North-Holland.
- Pond, R. C. & Bollmann, W. (1979). *The symmetry and interfacial structure of bicrystals*. *Philos. Trans. R. Soc. London Ser. A*, **292**, 449–472.
- Pond, R. C. & Vlachavas, D. S. (1983). *Bicrystallography*. *Proc. R. Soc. London Ser. A*, **386**, 95–143.
- Robinson, D. J. S. (1982). *A course in the theory of groups*. New York: Springer.
- Romé de l'Isle, J. B. L. (1783). *Cristallographie*. Vol. I, 2nd edition, p. 93. Paris: Imprimerie de Monsieur.
- Rosen, J. (1995). *Symmetry in science*. Berlin: Springer.
- Shubnikov, A. V. & Koptsik, V. A. (1974). *Symmetry in science and art*, pp. 348, 372. New York: Plenum.
- Speiser, A. (1927). *Theorie der Gruppen von endlicher Ordnung*. Berlin: Springer.
- Sutton, A. P. & Balluffi, R. W. (1995). *Interfaces in crystalline materials*, Section 1.5, pp. 25–41. Oxford: Clarendon Press.
- Tertsch, H. (1936). *Bemerkungen zur Frage der Verbreitung und zur Geometrie der Zwillingsbildungen*. *Z. Kristallogr.* **94**, 461–490.
- Tschermak, G. (1904). *Einheitliche Ableitung der Kristallisations- und Zwillingsgesetze*. *Z. Kristallogr.* **39**, 433–462.
- Tschermak, G. (1906). *Lehrbuch der Mineralogie*. Wien: Hölder.
- Tschermak, G. & Becke, F. (1915). *Lehrbuch der Mineralogie*. 7th edition, pp. 93–114. Wien: Hölder.
- Vainshtein, B. K. (1994). *Modern crystallography I. Symmetry of crystals*, 2nd edition. Berlin: Springer.

3. PHASE TRANSITIONS, TWINNING AND DOMAIN STRUCTURES

- Vainshtein, B. K., Fridkin, V. M. & Indenbom, V. L. (1995). *Modern crystallography II. Structure of crystals*, 2nd edition, Section 5.7. Berlin: Springer.
- Valasek, J. (1921). *Piezoelectricity and allied phenomena in Rochelle salt*. *Phys. Rev.* **17**, 475–481.
- Van Tendeloo, G. & Amelinckx, S. (1974). *Group-theoretical considerations concerning domain formation in ordered alloys*. *Acta Cryst.* **A30**, 431–440.
- Wadhawan, V. K. (1997). *A tensor classification of twinning in crystals*. *Acta Cryst.* **A53**, 546–555.
- Wadhawan, V. K. (2000). *Introduction to ferroic materials*. Amsterdam: Gordon and Breach.
- Weiss, Chr. S. (1809). *De Indagando Formarum Crystallinarum Characteres Geometrico Principali*. Dissertatio. Leipzig: Tauchnitz. [French translation by Brochant de Villiers, A. (1811): *Mémoire sur la détermination du caractère géométrique principal des formes cristallines*. *J. Mines*, **29**, 349–391, 401–444.]
- Weiss, Chr. S. (1814). *Schweigers Journal für Physik und Chemie*, Vol. X, p. 223.
- Weiss, Chr. S. (1817, 1818). *Magazin der Gesellschaft naturforschender Freunde zu Berlin*, Vol. VII, p. 183, Vol. VIII, p. 27.
- Weiss, P. (1907). *L'hypothèse du champ moléculaire et la propriété ferromagnétique*. *J. Phys. Radium*, **6**, 661–690.
- Wondratschek, H. (1995). *Splitting of Wyckoff positions (orbits)*. *Z. Kristallogr.* **210**, 567–573.
- Wondratschek, H. & Aroyo, M. (2001). *The application of Hermann's group \mathcal{M} in group-subgroup relations between space groups*. *Acta Cryst.* **A57**, 311–320.
- Zheludev, I. S. & Shuvalov, L. A. (1956). *Seignettelectric phase transitions and crystal symmetry*. *Kristallografiya*, **1**, 681–688. (In Russian.) [English translation: *Sov. Phys. Crystallogr.* **1**, 537–542].
- Zwicker, B. & Scherrer, P. (1944). *Elektrooptische Eigenschaften der seignette-elektrischen Kristalle KH_2PO_4 und KD_2PO_4* . *Helv. Phys. Acta*, **17**, 346–373.

3.3. Twinning of crystals

BY TH. HAHN AND H. KLAPPER

In this chapter, the basic concepts and definitions of twinning, as well as the morphological, genetic and lattice classifications of twins, are presented. Furthermore, twin boundaries are discussed extensively. The effect of twinning in reciprocal space, *i.e.* on diffraction and crystal-structure determinations, is outside the scope of the present edition. In the literature, the concept of twinning is very often used in a non-precise or ambiguous way. In order to clarify the terminology, this chapter begins with a section on the various kinds of crystal aggregates and intergrowths; in this context twinning appears as a special intergrowth with well defined crystallographic orientation relations.

3.3.1. Crystal aggregates and intergrowths

Minerals in nature and synthetic solid materials display different kinds of *aggregations*, in mineralogy often called *intergrowths*. In this chapter, we consider only aggregates of crystal grains of the same species, *i.e.* of the same (or nearly the same) chemical composition and crystal structure (homophase aggregates). Intergrowths of grains of different species (heterophase aggregates), *e.g.* heterophase bicrystals, epitaxy (two-dimensional oriented intergrowth on a surface), topotaxy (three-dimensional oriented precipitation or exsolution) or the paragenesis of different minerals in a rock or in a technical product are not treated in this chapter.

(i) *Arbitrary intergrowth*: Aggregation of two or more crystal grains with arbitrary orientation, *i.e.* without any systematic regularity. Examples are irregular aggregates of quartz crystals (*Bergkristall*) in a geode and intergrown single crystals precipitated from a solution. To this category also belong untextured polycrystalline materials and ceramics, as well as sandstone and quartzite.

(ii) *Parallel intergrowth*: Combination of two or more crystals with parallel (or nearly parallel) orientation of all edges and faces. Examples are dendritic intergrowths as well as parallel intergrowths of spinel octahedra (Fig. 3.3.1.1*a*) and of quartz prisms (Fig. 3.3.1.1*b*). Parallel intergrowths frequently exhibit re-entrant angles and are, therefore, easily misinterpreted as twins.

In this context the term *mosaic crystal* must be mentioned. It was introduced in the early years of X-ray diffraction in order to characterize the perfection of a crystal. A mosaic crystal consists of small blocks (size typically in the micron range) with orientations deviating only slightly from the average orientation of the

crystal; the term 'lineage structure' is also used for very small scale parallel intergrowths (Buerger, 1934, 1960*a*, pp. 69–73).

(iii) *Bicrystals*: This term is mainly used in metallurgy. It refers to the (usually synthetic) intergrowth of two single crystals with a well defined orientation relation. A bicrystal contains a *grain boundary*, which in general is also well defined. Usually, homophase bicrystals are synthesized in order to study the structure and properties of grain boundaries. An important tool for the theoretical treatment of bicrystals and their interfaces is the *coincidence-site lattice* (CSL). A brief survey of bicrystals is given in Section 3.2.2; a comparison with twins and domain structures is provided by Hahn *et al.* (1999).

(iv) *Growth sectors*: Crystals grown with planar faces (habit faces), *e.g.* from vapour, supercooled melt or solution, consist of regions crystallized on different growth faces (Fig. 3.3.1.2). These growth sectors usually have the shapes of pyramids with their apices pointing toward the nucleus or the seed crystal. They are separated by *growth-sector boundaries*, which represent inner surfaces swept by the crystal edges during growth. In many cases, these boundaries are imperfections of the crystal.

Frequently, the various growth sectors of one crystal exhibit slightly different chemical and physical properties. Of particular

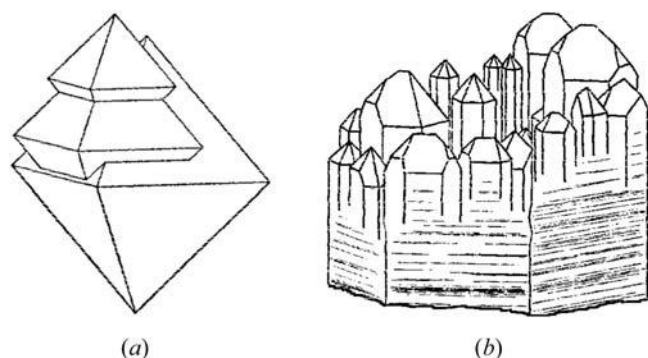


Fig. 3.3.1.1. Parallel intergrowth (a) of spinel octahedra and (b) of hexagonal quartz prisms. Part (a) after Phillips (1971, p. 172), part (b) after Tschermak & Becke (1915, p. 94).

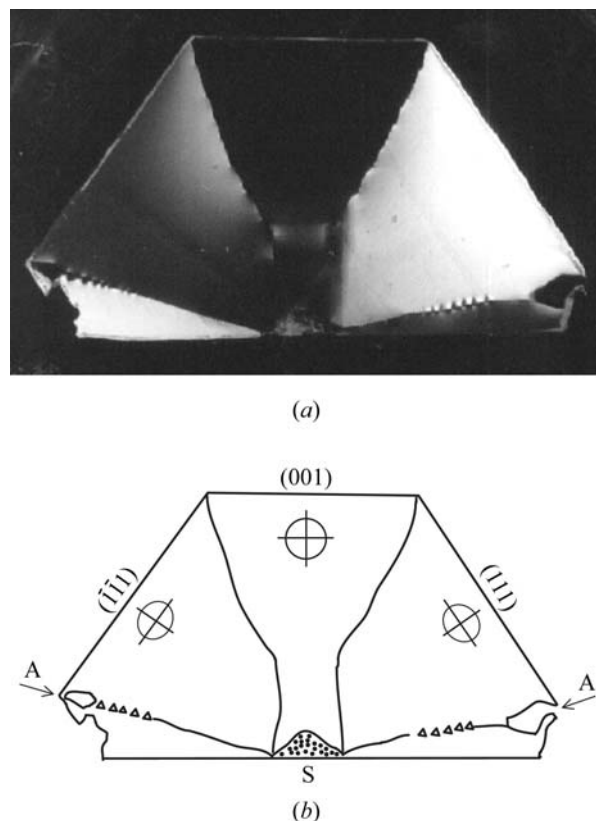


Fig. 3.3.1.2. (a) Optical anomaly of a cubic mixed (K,NH₄)-alum crystal grown from aqueous solution, as revealed by polarized light between crossed polarizers: (110) plate, 1 mm thick, horizontal dimension about 4 cm. (b) Sketch of growth sectors and their boundaries of the crystal plate shown in (a). The {111} growth sectors are optically negative and approximately uniaxial with their optical axes parallel to their growth directions {111} [birefringence Δn up to 5×10^{-5} ; Shtukenberg *et al.* (2001)]. The {001} growth sector is nearly isotropic ($\Delta n < 10^{-6}$). Along the boundaries A between {111} sectors a few small {110} growth sectors (resulting from small {110} facets) have formed during growth. S: seed crystal.

3. PHASE TRANSITIONS, TWINNING AND DOMAIN STRUCTURES

interest is a different optical birefringence in different growth sectors (optical anomaly) because this may simulate twinning. A typical example of this optical anomaly is shown in Fig. 3.3.1.2.

The phenomenon *optical anomaly* can be explained as follows: as a rule, impurities (or dopants) present in the solution are incorporated into the crystal during growth. Usually, the impurity concentrations differ in symmetrically *non-equivalent* growth sectors (which belong to different crystal forms), leading to slightly changed lattice parameters and physical properties of these sectors. Surprisingly, optical anomalies may occur also in symmetrically *equivalent* growth sectors (which belong to the same crystal form): as a consequence of growth fluctuations, layers of varying impurity concentrations parallel to the growth face of the sector ('growth striations') are formed. This causes a slight change of the interplanar spacing normal to the growth face. For example, a cubic NaCl crystal grown on {100} cube faces from an aqueous solution containing Mn ions consists of three pairs of (opposite) growth sectors exhibiting a slight tetragonal distortion with tetragonality 10^{-5} along their {100} growth directions, and, hence, are optically uniaxial (Ikeno *et al.*, 1968). Although this phenomenon closely resembles all features of twinning, it does not belong to the category 'twinning', because it is not an intrinsic property of the crystal species, but rather the result of different growth conditions (or growth mechanisms) on different faces of the same crystal (growth anisotropy).

An analogous effect may be observed in crystals grown from the melt on rounded and faceted interfaces (*e.g.* garnets). The regions crystallized on the rounded growth faces and on the different facets correspond to different growth sectors and may exhibit optical anomalies.

The relative lattice-parameter changes associated with these phenomena usually are smaller than 10^{-4} and cannot be detected in ordinary X-ray diffraction experiments. They are, however, accessible by high-resolution X-ray diffraction.

(v) *Translation domains*: Translation domains are homogeneous crystal regions that exhibit exact parallel orientations, but are displaced with respect to each other by a vector (frequently called a *fault vector*), which is a fraction of a lattice translation vector. The interface between adjoining translation domains is called the 'translation boundary'. Often the terms *antiphase domains* and *antiphase boundaries* are used. Special cases of translation boundaries are stacking faults. Translation domains are defined on an atomic scale, whereas the term parallel intergrowth [see item (ii) above] refers to macroscopic (morphological) phenomena; *cf.* Note (7) in Section 3.3.2.4.

(vi) *Twins*: A frequently occurring intergrowth of two or more crystals of the same species with well defined *crystallographic* orientation relations is called a *twin* (German: *Zwilling*; French: *macle*). Twins form the subject of the present chapter. The closely related topic of *domain structures* is treated in Chapter 3.4.

3.3.2. Basic concepts and definitions of twinning

Because twinning is a rather complex and widespread phenomenon, several definitions have been presented in the literature. Two of them are quoted here because of the particular engagement of their authors in this topic.

George Friedel (1904; 1926, p. 421): *A twin is a complex crystalline edifice built up of two or more homogeneous portions of the same crystal species in contact (juxtaposition) and oriented with respect to each other according to well-defined laws.*

These laws, as formulated by Friedel, are specified in his book (Friedel, 1926). His 'lattice theory of twinning' is discussed in Sections 3.3.8 and 3.3.9 of the present chapter.

Paul Niggli (1919, 1920/1924/1941): *If several crystal individuals of the same species are intergrown in such a way that all analogous faces and edges are parallel, then one speaks of parallel intergrowth. If for two crystal individuals not all but only some of the (morphological) elements (edges or faces), at least two independent ones, are parallel or antiparallel, and if such an intergrowth due to its frequent occurrence is not 'accidental', then one speaks of twins or twin formation. The individual partners of typical twins are either mirror images with respect to a common plane ('twin-plane law'), or they appear rotated by 180° around a (common) direction ('zone-axis law', 'hemitropic twins'), or both features occur together. These planes or axes, or both, for all frequently occurring twins turn out to be elements with relatively simple indices (referred to the growth morphology). (Niggli, 1924, p. 176; 1941, p. 137.)*

Both definitions are geometric. They agree in the essential fact that the 'well defined' laws, *i.e.* the orientation relations between two twin partners, refer to rational planes and directions. Morphologically, these relations find their expression in the parallelism of some crystal edges and crystal faces. In these and other classical definitions of twins, the structure and energy of twin boundaries were not included. This aspect was first introduced by Buerger in 1945.

3.3.2.1. Definition of a twin

In a more extended fashion we define twinning as follows:

An intergrowth of two or more macroscopic, congruent or enantiomorphic, individuals of the same crystal species is called a *twin*, if the orientation relations between the individuals occur frequently and are 'crystallographic'. The individuals are called twin components, twin partners or twin domains. A twin is characterized by the *twin law*, *i.e.* by the *orientation and chirality relation* of two twin partners, as well as by their *contact relation* (twin interface, composition plane, domain boundary).

3.3.2.2. Essential addenda to the definition

(a) The orientation relation between two partners is defined as *crystallographic* and, hence, the corresponding intergrowth is a *twin*, if the following two minimal conditions are *simultaneously* obeyed:

(i) at least *one* lattice row (crystal edge) $[uvw]$ is '*common*' to both partners I and II, either parallel or antiparallel, *i.e.* $[uvw]_I$ is parallel to $\pm[uvw]_{II}$;

(ii) at least *two* lattice planes (crystal faces) $(hkl)_I$ and $\pm(hkl)_{II}$, one from each partner, are '*parallel*', but not necessarily '*common*' (see below). This condition implies a *binary twin operation* (twofold rotation, reflection, inversion).

Both conditions taken together define the *minimal* geometric requirement for a twin (at least one common row and one pair of parallel planes), as originally pronounced by several classical authors (Tschermak, 1884, 1905; 1904; Tschermak & Becke, 1915; Mügge, 1911, p. 39; Niggli, 1920/1924/1941; Tertsch, 1936) and taken up later by Menzer (1955) and Hartman (1956). It is obvious that these crystallographic conditions apply even more to twins with two- and three-dimensional lattice coincidences, as described in Section 3.3.8. Other orientation relations, as they occur, for instance, in arbitrary intergrowths or bicrystals, are called '*noncrystallographic*'.

The terms '*common edge*' and '*common face*', as used in this section, are derived from the original morphological consideration of twins. Example: a re-entrant edge of a twin is common to both twin partners. In lattice considerations, the terms '*common lattice row*', '*common lattice plane*' and '*common lattice*' require a somewhat finer definition, in view of a possible *twin displacement vector* \mathbf{t} of the twin boundary, as introduced in Note (8) of

3.3. TWINNING OF CRYSTALS

Section 3.3.2.4 and in Section 3.3.10.3. For this distinction the terms 'parallel', 'common' and 'coincident' are used as follows:

Two lattice rows $[uvw]_I$ and $[uvw]_{II}$:

Common: rows parallel or antiparallel, with their lattice points possibly displaced with respect to each other parallel to the row by a vector $\mathbf{t} \neq \mathbf{0}$.

Coincident: common rows with pointwise coincidence of their lattice points, i.e. $\mathbf{t} = \mathbf{0}$.

Two lattice planes $(hkl)_I$ and $(hkl)_{II}$:

Parallel: 'only' the planes as such, but *not all* corresponding lattice rows in the planes, are mutually parallel or antiparallel.

Common: parallel planes with *all* corresponding lattice rows mutually parallel or antiparallel, but possibly displaced with respect to each other parallel to the plane by a vector $\mathbf{t} \neq \mathbf{0}$.

Coincident: common planes with pointwise coincidence of their lattice points, i.e. $\mathbf{t} = \mathbf{0}$.

Two point lattices I and II:

Parallel or *common*: all corresponding lattice rows are mutually parallel or antiparallel, but the lattices are possibly displaced with respect to each other by a vector $\mathbf{t} \neq \mathbf{0}$.

Coincident: parallel lattices with pointwise coincidence of their lattice points, i.e. $\mathbf{t} = \mathbf{0}$.

Note that for lattice rows and point lattices only two cases have to be distinguished, whereas lattice planes require three terms.

(b) A twinned crystal may consist of more than two individuals. All individuals that have the same orientation and handedness belong to the same *orientation state* (*component state*, *domain state*, *domain variant*). The term 'twin' for a crystal aggregate requires the presence of at least two orientation states.

(c) The orientation and chirality relation between two twin partners is expressed by the *twin law*. It comprises the set of *all twin operations* that transform the two orientation states into each other. A twin operation cannot be a symmetry operation of either one of the two twin components. The combination of a twin operation and the geometric element to which it is attached is called a *twin element* (e.g. twin mirror plane, twofold twin axis, twin inversion centre).

(d) An orientation relation between two individuals deserves the name '*twin law*' only if it occurs frequently, is reproducible and represents an inherent feature of the crystal species.

(e) One feature which facilitates the formation of twins is *pseudosymmetry*, apparent either in the crystal structure, or in special lattice-parameter ratios or lattice angles.

(f) In general, the twin interfaces are low-energy boundaries with good structural fit; very often they are low-index lattice planes.

3.3.2.3. Specifications and extensions of the orientation relations

In the following, the orientation and chirality relations of two or more twin components, only briefly mentioned in the definition, are explained in detail. Two categories of orientation relations have to be distinguished: those arising from *binary twin operations* (*binary twin elements*), i.e. operations of order 2, and those arising from *pseudo n-fold twin rotations* (*n-fold twin axes*), i.e. operations of order ≥ 3 .

3.3.2.3.1. Binary twin operations (twin elements)

The (crystallographic) orientation relation of two twin partners can be expressed either by a *twin operation* or by its corresponding *twin element*. Binary twin elements can be either *twin mirror planes* or *twofold twin axes* or *twin inversion centres*. The former two twin elements must be parallel or normal to (possible) crystal faces and edges (macroscopic description) or, equivalently, parallel or normal to lattice planes and lattice rows (microscopic lattice description). Twin elements may be either rational (integer indices) or irrational (irrational indices which, however, can always be approximated by sufficiently large integer indices). Twin reflection planes and twin axes *parallel* to lattice planes or lattice rows are always rational. Twin axes and twin mirror planes *normal* to lattice planes or lattice rows are either rational or irrational. In addition to planes and axes, points can also occur as twin elements: *twin inversion centres*.

There exist seven kinds of binary twin elements that define the seven general twin laws possible for noncentrosymmetric triclinic crystals (crystal class 1):

(i) *Rational twin mirror plane* (hkl) normal to an irrational line: *reflection twin* (Fig. 3.3.2.1a). The lattice plane hkl is common to both twin partners.

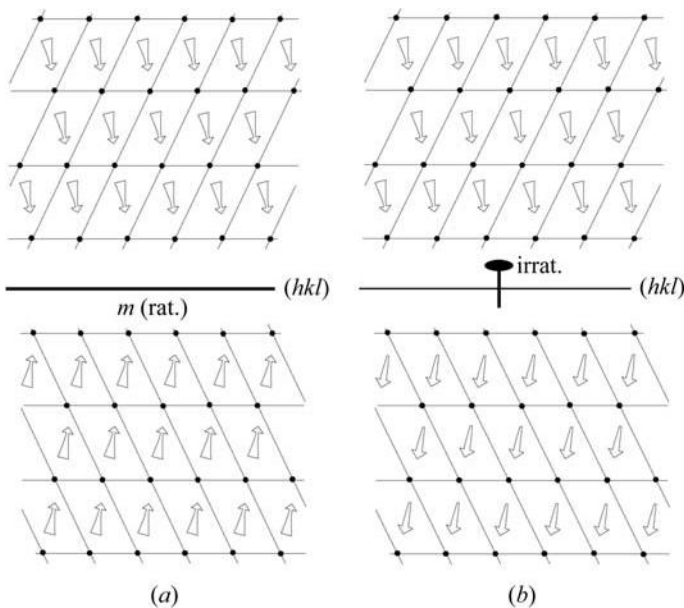


Fig. 3.3.2.1. Schematic illustration of the orientation relations of triclinic twin partners, see Section 3.3.2.3.1, (a) for twin element (i) 'rational twin mirror plane' and (b) for twin element (ii) 'irrational twofold twin axis' (see text); common lattice plane (hkl) for both cases. The noncentrosymmetry of the crystal is indicated by the tapering of the arrows. The sloping up and sloping down of the arrows is indicated by the tapering of their images. For centrosymmetry, both cases (a) and (b) represent the same orientation relation.

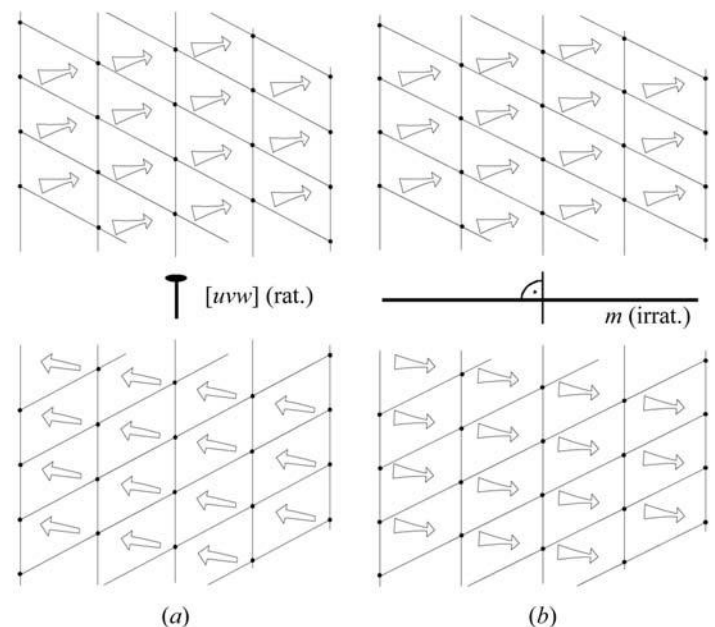


Fig. 3.3.2.2. As Fig. 3.3.2.1, (a) for twin element (iii) 'rational twofold twin axis' and (b) for twin element (iv) 'irrational twin mirror plane' (see text); common lattice row $[uvw]$ for both cases. For centrosymmetry, both cases represent the same orientation relation.

3. PHASE TRANSITIONS, TWINNING AND DOMAIN STRUCTURES

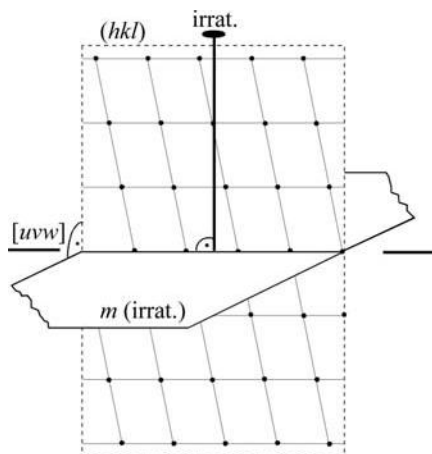


Fig. 3.3.2.3. Illustration of the *Kantennormalengesetz* (complex twin) for twin elements (v) and (vi) (see text); common lattice row $[uvw]$ for both cases. Note that both twin elements transform the net plane $(hkl)_I$ into its parallel but not pointwise coincident counterpart $(hkl)_{II}$. For centrosymmetry, both cases represent the same orientation relation.

(ii) *Irrational* twofold twin axis normal to a rational lattice plane hkl : *rotation twin* (Fig. 3.3.2.1b). The lattice plane hkl is common to both twin partners.

(iii) *Rational* twofold twin axis $[uvw]$ normal to an irrational plane: *rotation twin* (Fig. 3.3.2.2a). The lattice row $[uvw]$ is common to both twin partners.

(iv) *Irrational* twin mirror plane normal to a rational lattice row $[uvw]$: *reflection twin* (Fig. 3.3.2.2b). The lattice row $[uvw]$ is common to both twin partners.

(v) *Irrational* twofold twin axis normal to a rational lattice row $[uvw]$, both located in a rational lattice plane $(hkl)_I$; perpendicular to the irrational twin axis is an irrational plane: *complex twin*; German: *Kantennormalengesetz* (Fig. 3.3.2.3). The lattice row $[uvw]$ is 'common' to both twin partners; the planes $(hkl)_I$ and $(hkl)_{II}$ are 'parallel' but not 'common' (cf. Tschermak & Becke, 1915, p. 98; Niggli, 1941, p. 138; Bloss, 1971, pp. 228–230; Phillips, 1971, p. 178).

(vi) *Irrational* twin mirror plane containing a rational lattice row $[uvw]$; perpendicular to the twin plane is an irrational direction; the row $[uvw]$ and the perpendicular direction span a rational lattice plane (hkl) : *complex twin*; this 'inverted *Kantennormalengesetz*' is not described in the literature (Fig. 3.3.2.3). The row $[uvw]$ is 'common' to both twin partners; the planes $(hkl)_I$ and $(hkl)_{II}$ are 'parallel' but not 'common'.

(vii) *Twin inversion centre*: *inversion twin*. The three-dimensional lattice is common to both twin partners. Inversion twins are always merohedral (parallel-lattice) twins (cf. Section 3.3.8).

All these binary twin elements – no matter whether rational or irrational – lead to *crystallographic* orientation relations, as defined in Section 3.3.2.2, because the following lattice items belong to both twin partners:

(a) The rational lattice planes $(hkl)_I$ and $(hkl)_{II}$ are 'common' for cases (i) and (ii) (Fig. 3.3.2.1).

(b) The rational lattice rows $[uvw]_I$ and $[uvw]_{II}$ are 'common' and furthermore lattice planes $(hkl)_I/(hkl)_{II}$ in the zone $[uvw]$ are 'parallel', but not 'common' for cases (iii), (iv), (v) and (vi). Note that for cases (iii) and (iv) any two planes $(hkl)_I/(hkl)_{II}$ of the zone $[uvw]$ are parallel, whereas for cases (v) and (vi) only a single pair of parallel planes exists (cf. Figs. 3.3.2.2 and 3.3.2.3).

(c) The entire three-dimensional lattice is 'common' for case (vii).

In this context one realizes which wide range of twinning is covered by the requirement of a *crystallographic* orientation relation: the 'minimal' condition is provided by the *complex twins*

(v) and (vi): only a one-dimensional lattice row is 'common', two lattice planes are 'parallel' and all twin elements are irrational (Fig. 3.3.2.3). The 'maximal' condition, a 'common' three-dimensional lattice, occurs for *inversion twins* ('merohedral' or 'parallel-lattice twins'), case (vii).

In *noncentrosymmetric* triclinic crystals, the above twin elements define seven different twin laws, but for *centrosymmetric* crystals only three of them represent different orientation relations, because both in lattices and in centrosymmetric crystals a twin mirror plane defines the same orientation relation as the twofold twin axis normal to it, and *vice versa*. Consequently, the twin elements of the three pairs (i) + (ii), (iii) + (iv) and (v) + (vi) represent the same orientation relation. Case (vii) does not apply to centrosymmetric crystals, since here the inversion centre already belongs to the symmetry of the crystal.

For symmetries higher than triclinic, even more twin elements may define the same orientation relation, *i.e.* form the same twin law. Example: the dovetail twin of gypsum (point group $12/m1$) with twin mirror plane (100) can be described by the four alternative twin elements (i), (ii), (iii), (iv) (cf. Section 3.3.4, Fig. 3.3.4.1). Furthermore, with increasing symmetry, the twin elements (i) and (iii) may become even more special, and the nature of the twin type may change as follows:

(i) the line normal to a rational twin mirror plane (hkl) may become a *rational* line $[uvw]$;

(ii) the plane normal to a rational twofold twin axis $[uvw]$ may become a *rational* plane (hkl) .

In both cases, the three-dimensional lattice (or a sublattice of it) is now common to both twin partners, *i.e.* a 'merohedral' twin results.

There is one more binary twin type which seems to reduce even further the above-mentioned 'minimal' condition for a crystallographic orientation relation, the so-called '*median law*' (German: *Mediangesetz*) of Brögger (1890), described by Tschermak & Becke (1915, p. 99). So far, it has been found in one mineral only: hydrargillite (modern name gibbsite), $\text{Al}(\text{OH})_3$. The acceptability of this orientation relation as a twin law is questionable; see Section 3.3.6.10.

3.3.2.3.2. Pseudo n -fold twin rotations (twin axes) with $n \geq 3$

There is a long-lasting controversy in the literature, *e.g.* Hartman (1956, 1960), Buerger (1960b), Curien (1960), about the acceptance of three-, four- and sixfold rotation axes as twin elements, for the following reason:

Twin operations of order two (reflection, twofold rotation, inversion) are 'exact', *i.e.* in a component pair they transform the orientation state of one component exactly into that of the other. There occur, in addition, many cases of multiple twins, which can be described by three-, four- and sixfold twin axes. These axes, however, are *pseudo axes* because their rotation angles are close to but not exactly equal to 120, 90 or 60°, due to metrical deviations (no matter how small) from a higher-symmetry lattice. A well known example is the triple twin (German: *Drilling*) of orthorhombic aragonite, where the rotation angle $\gamma = 2 \arctan b/a = 116.2^\circ$ (which transforms the orientation state of one component exactly into that of the other) deviates significantly from the 120° angle of a proper threefold rotation (Fig. 3.3.2.4). Another case of $n = 3$ with a very small metrical deviation is provided by ammonium lithium sulfate ($\gamma = 119.6^\circ$).

All these (pseudo) n -fold rotation twins, however, can also be described by (exact) binary twin elements, *viz* by a cyclic sequence of twin mirror planes or twofold twin axes. This is also illustrated and explained in Fig. 3.3.2.4. This possibility of describing cyclic twins by 'exact' binary twin operations is the reason why Hartman (1956, 1960) and Curien (1960) do not consider 'non-exact' three-, four- and sixfold rotations as proper twin operations.

3.3. TWINNING OF CRYSTALS

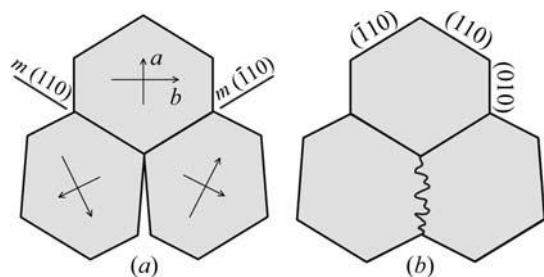


Fig. 3.3.2.4. (a) Triple growth twin of orthorhombic aragonite, CaCO_3 , with pseudo-threefold twin axis. The gap angle is 11.4° . The exact description of the twin aggregate by means of two symmetrically equivalent twin mirror planes (110) and $(\bar{1}\bar{1}0)$ is indicated. In actual crystals, the gap is usually closed as shown in (b).

The crystals forming twins with pseudo n -fold rotation axes always exhibit *metrical pseudosymmetries*. In the case of transformation twins and domain structures, the metrical pseudosymmetries of the low-symmetry (deformed) phase \mathcal{H} result from the *true structural symmetry* \mathcal{G} of the parent phase (cf. Section 3.3.7.2). This aspect caused several authors [e.g. Friedel, 1926, p. 435; Donnay (cf. Hurst *et al.*, 1956); Buerger, 1960b] to accept these pseudo axes for the treatment of twinning. The present authors also recommend including three-, four- and sixfold rotations as permissible twin operations. The consequences for the definition of the twin law will be discussed in Section 3.3.4 and in Section 3.4.3. For a further extension of this concept to fivefold and tenfold multiple growth twins, see Note (6) below and Example 3.3.6.8.

3.3.2.4. Notes on the definition of twinning

(1) The above definition of twinning covers twins with a *size range* from decimetres for large mineral specimens to fractions of microns of polydomain twins. The lower limit for a reasonable application of the twin concept lies in the nanometre range of 100–1000 Å. *Unit-cell twinning* is a limiting case closely related to superstructures or positional disorder and is not treated in this chapter. An extensive monograph on this topic under the name *Tropochemical cell-twinning* was recently published by Takeuchi (1997).

(2) *Rational twin elements* are designated by integer Miller indices (hkl) and integer direction indices $[uvw]$ for twin mirror planes and twin rotation axes, respectively; the values of these indices usually are small numbers, < 6 . Larger values should not be accepted without critical assessment. Irrational twin elements are described either by their rational ‘counterparts’ (perpendicular planes or lines) or are approximated by high integer values of the indices.

(3) For a twin, the *crystallographic orientation relation* is a property of the crystal structure, in contrast to bicrystals, where the given orientation relation is either accidental or enforced by the experiment. If such an orientation relation happens to be crystallographic, the bicrystal could formally be considered to be a twin. It is not recommended, however, to accept such a bicrystal as a twin because its orientation relation does not form ‘spontaneously’ as a property of the structure.

(4) There are some peculiarities about the *contact relations* between two twin components. Often quite different twin boundaries occur for one and the same orientation relation. The boundaries are either irregular (frequently in penetration twins) or planar interfaces. Even though crystallographic boundaries are the most frequent interfaces, the geometry of a contact relation is *not suitable as part of the twin definition*. Contact relations, however, play an important role for the morphological classification of twins (cf. Section 3.3.3.1). Frequently used alternative names for *twin boundaries* are *twin interfaces*, *contact planes*, *composition planes* or *domain boundaries*.

(5) Frequently, the term ‘twin plane (hkl) ’ is used for the characterization of a *reflection twin*. This term is justified only if the twin mirror plane and the composition plane coincide. It is, however, ambiguous if the twin mirror plane and the twin interface have different orientations. In twins of hexagonal KLiSO_4 , for example, the prominent composition plane (0001) is normal to the twin mirror plane $(10\bar{1}0)$ (cf. Klapper *et al.*, 1987). The short term ‘twin plane’ should be avoided in such cases and substituted by *twin mirror plane* or *twin reflection plane*. The frequently used term ‘twinning on (hkl) ’ [German: ‘Zwillingen nach (hkl) ’] refers to (hkl) as a twin mirror plane and not as a contact plane.

(6) There exist twins in which the twin operations can be regarded as *fivefold* or *tenfold* rotations (Ellner & Burkhardt, 1993; Ellner, 1995). These twins are due to pseudo-pentagonal or pseudo-decagonal metrical features of the lattice [$\gamma = \arctan(c/a) \approx 72^\circ$]. They can be treated in the same way as the three-, four- and sixfold rotation twins mentioned above. This includes the alternative (‘exact’) description of the twinning by a cyclic sequence of symmetrically equivalent twin reflection planes or twofold twin axes (cf. aragonite, Fig. 3.3.2.4). For this reason, we recommend that these intergrowths are accepted as (pseudo) n -fold rotation twins, even though the value of n is noncrystallographic.

(7) The classical treatment of twins considers only rotations, reflections and inversions as twin operations. In domain structures, relations between domain states exist that involve only *translations* (cf. Section 3.4.3), specifically those that are suppressed during a phase transition. Since every domain structure can be considered as a transformation twin, it seems legitimate to accept these translations as twin operations and speak of *translation twins* (T-twins according to Wadhawan, 1997, 2000). The translation vector of this twin operation is also known as the *fault vector* of the *translation boundary* (often called the *anti-phase boundary*) between two *translation domains* [cf. Section 3.3.1(v)]. It must be realized, however, that the acceptance of translation domains as twins would classify all stacking faults in metals, in diamond and in semiconductors as twin boundaries.

(8) The structural consideration of twin boundaries cannot be performed by employing only point-group twin elements as is sufficient for the description of the orientation relation. In structural discussions, in addition, a translational displacement of the two structures with respect to each other by a shift vector, which is called here the *twin displacement vector* \mathbf{t} , has to be taken into account. This displacement vector leads to a minimization of the twin-boundary energy. The components of this vector can have values between 0 and 1 of the basis vectors. In many cases, especially of transformation twins, glide planes or screw axes can occur as twin elements, whereby the glide or screw components may be relaxed, *i.e.* may deviate from their ideal values. The twin displacement vectors, as introduced here, include these glide or screw components and their relaxations. The role of the twin displacement vectors in the structure of the twin boundary is discussed in Section 3.3.10.4.

(9) In some cases the term ‘twin’ is used for systematic *oriented intergrowths* of crystals which are not twins as defined in this chapter. The following cases should be mentioned:

(i) *Allotwins* (Nespolo, Ferraris *et al.*, 1999): oriented crystal associations of different polytypes of the same compound. Different polytypes have the same chemistry and similar but nevertheless different structures. Well known examples are the micas, where twins and allotwins occur together (Nespolo *et al.*, 2000).

(ii) The oriented associations of two *polymorphs* (modifications) of the same compound across a phase boundary also do not deserve the name twin because of the different structures of their components. Note that this case is more general than the ‘allotwins’ of polytypes mentioned above. Interesting examples are the oriented intergrowths of the TiO_2 polymorphs rutile, anatase

3. PHASE TRANSITIONS, TWINNING AND DOMAIN STRUCTURES

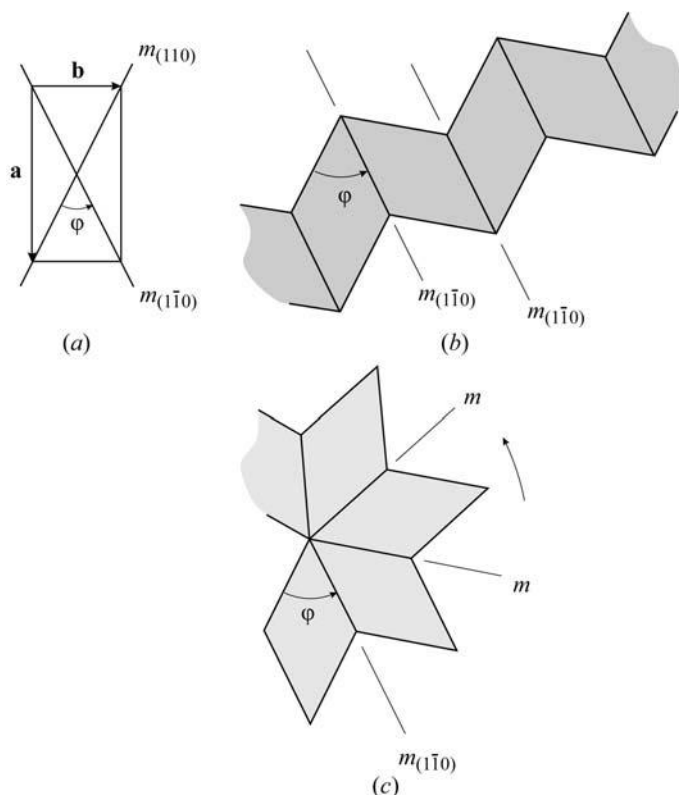


Fig. 3.3.3.1. Schematic illustration of simple (polysynthetic) and multiple (cyclic) twins. (a) Equivalent twin mirror planes (110) and $(1\bar{1}0)$ of an orthorhombic crystal. (b) Simple (polysynthetic) twin with two orientation states due to parallel repetition of the same twin mirror plane $(1\bar{1}0)$; the twin components are represented by {110} rhombs. (c) Multiple (cyclic) twin with several (more than two) orientation states due to cyclic repetition of equivalent twin mirror planes of type {110}.

and brookite. In this respect, the high-resolution transmission electron microscopy (HRTEM) studies of hydrothermally coarsened TiO_2 nanoparticles by Penn & Banfield (1998), showing the structures of anatase {121} reflection twin boundaries and of {112} anatase–(100) brookite interfaces on an atomic scale, are noteworthy.

(iii) *Plesiotwins* (Nespolo, Kogure & Ferraris, 1999): oriented crystal associations based on a large coincidence-site lattice (CSL). The composition plane has a low degree of restoration of lattice nodes and the relative rotations between individuals are noncrystallographic. In the phlogopite from Mutsure-jima, Japan, both ordinary twins and plesiotwins are reported (Sunagawa & Tomura, 1976).

3.3.3. Morphological classification, simple and multiple twinning

Before discussing the symmetry features of twinning in detail, it is useful to introduce the terms ‘simple’ and ‘multiple’ twins, which are sometimes grouped under the heading ‘repetitive or repeated twins’. This is followed by some morphological aspects of twinning.

Simple twins are aggregates that consist of domains of only two orientation states, irrespective of the number, size and shape of the individual domains, Fig. 3.3.3.1(b). Thus, only one orientation relation (one twin law) exists. Contact twins and polysynthetic twins (see below) are simple twins.

Multiple twins are aggregates that contain domains of three or more orientation states, i.e. at least two twin laws are involved. Two cases have to be distinguished:

(i) The twin elements are symmetrically *equivalent* with respect to the *eigensymmetry* group \mathcal{H} of the crystal (cf. Section 3.3.4.1). A typical example is provided by the equivalent (110) and $(1\bar{1}0)$

twin mirror planes of an orthorhombic crystal (e.g. aragonite), which frequently lead to *cyclic twins* (cf. Figs. 3.3.3.1a and c).

(ii) The twin elements are *not equivalent* with respect to the *eigensymmetry* of the crystal, i.e. several independent twin laws occur simultaneously in the twinned crystal. A typical example is provided by a Brazil twin of quartz, with each Brazil domain containing Dauphiné twins. This results in four domain states and three twin laws; cf. Example 3.3.6.3.

The distinction of simple and multiple twins is important for the following morphological classification. Further examples are given in Section 3.3.6.

3.3.3.1. Morphological classification

The morphology of twinned crystals, even for the same species and the same orientation relation, can be quite variable. For a given orientation relation the morphology depends on the geometry of the twin boundary as well as on the number of twin partners. A typical morphological feature of growth-twinned crystals is the occurrence of re-entrant angles. These angles are responsible for an increased growth velocity parallel to the twin boundary. This is the reason why twinned crystals often grow as platelets parallel to the composition plane (cf. Section 3.3.7.1). Detailed studies of the morphology of twins *versus* untwinned crystals were carried out as early as 1911 by Becke (1911). As a general observation, twinned crystals grow larger than untwinned crystals in the same batch.

The following classification of twins is in use:

(i) *Contact twins*. Two twin partners are in contact across a single composition plane $\pm(hkl)$, the Miller indices h, k, l of which have the same values for both partners (‘common’ plane). The contact plane usually has low indices. For reflection twins, the composition plane is frequently parallel to the twin mirror plane [see, however, Note (4) in Section 3.3.2.4]. Examples are shown in Fig. 3.3.6.1 for gypsum, in Fig. 3.3.6.5 for calcite and in Fig. 3.3.6.6(a) for a spinel (111) twin. In most cases, contact twins are growth twins.

(ii) *Polysynthetic (lamellar) twins* are formed by repetition of contact twins and consist of a linear sequence of domains with two alternating orientation states. The contact planes are parallel (lamellar twinning). This is typical for reflection twins if the twin mirror plane and the composition plane coincide. An illustrative example is the albite growth twin shown in Fig. 3.3.6.11. Polysynthetic twins may occur in growth, transformation and deformation twinning.

(iii) *Penetration twins*. The name ‘penetration twin’ results from the apparent penetration of two or more (idiomorphic) single crystals. The most prominent examples are twins of the spinel law in cubic crystals (e.g. spinels, fluorite, diamond). The spinel law is a reflection across (111) or a twofold rotation around [111]. Ideally these twins appear as two interpenetrating cubes with a common threefold axis, each cube representing one domain state (Fig. 3.3.6.6b). In reality, these twins usually consist of 12 pyramid-shaped domains, six of each domain state, all originating from a common point in the centre of the twinned crystal (as shown in Figs. 3.3.6.4 and 3.3.6.6). Another famous example is the Carlsbad twin of orthoclase feldspar with [001] as a twofold twin axis (Fig. 3.3.7.1). Penetration twins are always growth twins.

(iv) *Cyclic twins and sector twins*. In contrast to the linear sequence of domains in polysynthetic twins, *cyclic twins* form a circular arrangement of domains of suitable shape. They are always multiple twins (three or more orientations states) which are (formally) generated by successive application of equivalent twin laws. The twin aggregate may form a full circle or a fraction of a circle (see Figs. 3.3.3.1c, 3.3.6.7 and 3.3.6.10). Impressive examples are the ‘sixlings’ and ‘eightlings’ of rutile (Fig. 3.3.6.9, cf. Example 3.3.6.9).

3.3. TWINNING OF CRYSTALS

A special case of cyclic twins is provided by *sector twins*. Three or more domains of nearly triangular shape (angular sectors) extend from a common centre to form a twinned crystal with a more or less regular polygonal outline. The boundaries between two sector domains are usually planar and low-indexed. Such twins can be interpreted in two ways:

(a) they can be described by repeated action of (equivalent) reflection planes or twofold twin axes with suitable angular spacings;

(b) they can be described by approximate rotation axes of order three or more (including noncrystallographic axes such as fivefold); cf. Section 3.3.2.3.2 and Note (6) in Section 3.3.2.4.

Prominent examples are the growth twins of NH_4LiSO_4 (Fig. 3.3.7.2), aragonite (Fig. 3.3.2.4), K_2SO_4 (Fig. 3.3.6.7) and certain alloys with pseudo-fivefold twin axes (Fig. 3.3.6.8). Cyclic and sector twins are always growth twins.

(v) *Mimetic twins*. The term ‘mimetic’ is often applied to growth twins which, by their morphology, simulate a higher crystal symmetry. Regular penetration twins and sector twins are frequently also ‘mimetic’ twins. Particularly impressive examples are the harmotome and phillipsite twins, where monoclinic crystals, by multiple twinning, simulate higher symmetries up to a cubic rhomb-dodecahedron.

(vi) Common names of twins. In addition to the morphological description of twins mentioned above, some further shape-related names are in use:

(a) dovetail twins (prominent example: gypsum, cf. Fig. 3.3.4.1);

(b) elbow twins (rutile, cassiterite, cf. Fig. 3.3.6.9a);

(c) arrowhead twin (diamond);

(d) iron-cross twins (pyrite);

(e) butterfly twins (perovskite).

It is obvious from the morphological features of twins, described in this section, that crystals – by means of twinning – strive to simulate higher symmetries than they actually have. This will be even more apparent in the following section, which deals with the composite symmetry of twins and the twin law.

3.3.4. Composite symmetry and the twin law

In this section we turn our attention to the symmetry relations in twinning. The starting point of all symmetry considerations is the *eigensymmetry* \mathcal{H} of the untwinned crystal, i.e. the point group or space group of the single crystal, irrespective of its orientation and location in space. All domain states of a twinned crystal have the same (or the enantiomorphic) *eigensymmetry* but may exhibit different orientations. The orientation states of each two twin components are related by a twin operation k which cannot be part of the *eigensymmetry* \mathcal{H} . The term *eigensymmetry* is introduced here in order to provide a short and crisp distinction between the symmetry of the untwinned crystal (single-domain state) and the composite symmetry \mathcal{K} of a twinned crystal, as defined below. It should be noted that in morphology the term *eigensymmetry* is also used, but with another meaning, in connection with the symmetry of face forms of crystals (Hahn & Klapper, 2002).

3.3.4.1. Composite symmetry

For a comprehensive characterization of the symmetry of a twinned crystal, we introduce the important concept of *composite symmetry* \mathcal{K} . This symmetry is defined as the extension of the *eigensymmetry* group \mathcal{H} by a twin operation k . This extension involves, by means of left (or right) *coset composition* $k \times \mathcal{H}$, the generation of further twin operations until a supergroup is obtained. This supergroup is the composite symmetry group \mathcal{K} .

In the language of group theory, the relation between the composite symmetry group \mathcal{K} and the *eigensymmetry* group \mathcal{H}

can be expressed by a (left) coset decomposition of the supergroup \mathcal{K} with respect to the subgroup \mathcal{H} :

$$\mathcal{K} = k_1 \times \mathcal{H} \cup k_2 \times \mathcal{H} \cup k_3 \times \mathcal{H} \dots \cup k_i \times \mathcal{H},$$

where k_1 is the identity operation; $k_1 \times \mathcal{H} = \mathcal{H} \times k_1 = \mathcal{H}$.

The number i of cosets, including the subgroup \mathcal{H} , is the *index* $[i]$ of \mathcal{H} in \mathcal{K} ; this index corresponds to the number of different orientation states in the twinned crystal. If \mathcal{H} is a normal subgroup of \mathcal{K} , which is always the case if $i = 2$, then $k \times \mathcal{H} = \mathcal{H} \times k$, i.e. left and right coset decomposition leads to the same coset. The relation that the number of different orientation states n equals the index $[i]$ of \mathcal{H} in \mathcal{K} , i.e. $n = [i] = |\mathcal{K}| : |\mathcal{H}|$, was first expressed by Zheludev & Shuvalov (1956, p. 540) for ferroelectric phase transitions.

These group-theoretical considerations can be translated into the language of twinning as follows: although the *eigensymmetry* \mathcal{H} and the composite symmetry \mathcal{K} can be treated either as point groups (finite order) or space groups (infinite order), in this and the subsequent sections twinning is considered only in terms of point groups [see, however, Note (8) in Section 3.3.2.4, as well as Section 3.3.10.4]. With this restriction, the number of twin operations in each coset equals the order $|\mathcal{H}|$ of the *eigensymmetry* point group \mathcal{H} . All twin operations in a coset represent the same orientation relation, i.e. each one of them transforms orientation state 1 into orientation state 2. Thus, the complete coset characterizes the orientation relation comprehensively and is, therefore, defined here as the *twin law*. The different operations in a coset are called *alternative twin operations*. A further formulation of the twin law in terms of black–white symmetry will be presented in Section 3.3.5. Many examples are given in Section 3.3.6.

This extension of the ‘classical’ definition of a twin law from a single twin operation to a complete coset of alternative twin operations does not conflict with the traditional description of a twin by the one morphologically most prominent twin operation. In many cases, the morphology of the twin, e.g. re-entrant angles or the preferred orientation of a composition plane, suggests a particular choice for the ‘representative’ among the alternative

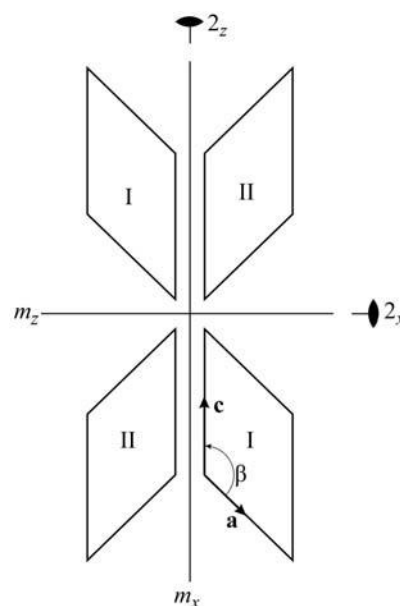


Fig. 3.3.4.1. Gypsum dovetail twin: schematic illustration of the coset of alternative twin operations. The two domain states I and II are represented by oriented parallelograms of *eigensymmetry* $2_y/m_y$. The subscripts x and z of the twin operations refer to the coordinate system of the orthorhombic composite symmetry \mathcal{K}_D of this twin; a and c are the monoclinic coordinate axes.

3. PHASE TRANSITIONS, TWINNING AND DOMAIN STRUCTURES

Table 3.3.4.1. Gypsum, dovetail twins: coset of alternative twin operations (twin law), given in orthorhombic axes of the composite symmetry \mathcal{K}_D

| \mathcal{H} | $k \times \mathcal{H}$ |
|---------------|----------------------------|
| 1 | $m_x \times 1 = m_x$ |
| 2_y | $m_x \times 2_y = m_z$ |
| m_y | $m_x \times m_y = 2_z$ |
| $\bar{1}$ | $m_x \times \bar{1} = 2_x$ |

twin operations. If possible, twin mirror planes are preferred over twin rotation axes or twin inversion centres.

The concept of the twin law as a coset of alternative twin operations, defined above, has been used in more or less complete form before. The following authors may be quoted: Mügge (1911, pp. 23–25); Tschermak & Becke (1915, p. 97); Hurst *et al.* (1956, p. 150); Raaz & Tertsch (1958, p. 119); Takano & Sakurai (1971); Takano (1972); Van Tendeloo & Amelinckx (1974); Donnay & Donnay (1983); Zikmund (1984); Wadhawan (1997, 2000); Nespolo *et al.* (2000). A systematic application of left and double coset decomposition to twinning and domain structures has been presented by Janovec (1972, 1976) in a key theoretical paper. An extensive group-theoretical treatment with practical examples is provided by Flack (1987).

Example: dovetail twin of gypsum. (Fig. 3.3.4.1.) Eigensymmetry:

$$\mathcal{H} = 1 \frac{2_y}{m_y} 1.$$

Twin reflection plane (100):

$$k_2 = k = m_x.$$

Composite symmetry group \mathcal{K}_D (orthorhombic):

$$\mathcal{K} = \mathcal{H} \cup k \times \mathcal{H},$$

given in orthorhombic axes, x, y, z . The coset $k \times \mathcal{H}$ contains all four alternative twin operations (Table 3.3.4.1) and, hence, represents the twin law. This is clearly visible in Fig. 3.3.6.1(a). In the symbol of the orthorhombic composite group,

$$\mathcal{K} = \frac{2'_x}{m'_x} \frac{2_y}{m_y} \frac{2'_z}{m'_z},$$

the primed operations indicate the coset of alternative twin operations. The above black-and-white symmetry symbol of the (orthorhombic) composite group \mathcal{K} is another expression of the twin law. Its notation is explained in Section 3.3.5. The twinning of gypsum is treated in more detail in Example 3.3.6.2.

It should be noted that among the four twin operations of the coset $k \times \mathcal{H}$ two are rational, m_x and 2_z , and two are irrational, m_z and 2_x (Fig. 3.3.4.1). All four are equally correct descriptions of the same orientation relation. From morphology, however, preference is given to the most conspicuous one, the twin mirror plane $m_x = (100)$, as the representative twin element.

The concept of composite symmetry \mathcal{K} is not only a theoretical tool for the extension of the twin law but has also practical aspects:

(i) *Morphology of growth twins.* In general, the volume fractions of the various twin domains are different and their distribution is irregular. Hence, most twins do not exhibit regular morphological symmetry. If, however, the twin aggregate consists of p components of equal volumes and shapes (p = ‘length’ of the coset of alternative twin operations) and if these components show a regular symmetrical distribution, the morphology of the twinned crystal displays the composite symmetry. In minerals, this is frequently very well approximated, as can be inferred from Fig. 3.3.6.1 for gypsum.

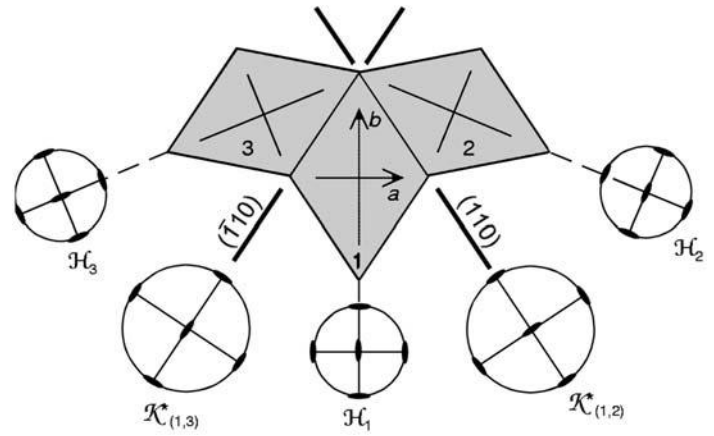


Fig. 3.3.4.2. Twinning of an orthorhombic crystal with equivalent twin mirror planes (110) and $\bar{1}\bar{1}0$. Three twin domains 1, 2 and 3, bound by {110} contact planes, are shown. The oriented eigensymmetries $\mathcal{H}_1, \mathcal{H}_2, \mathcal{H}_3$ and the reduced composite symmetries $\mathcal{K}^*(1, 2) = \mathcal{K}^*(110)$ and $\mathcal{K}^*(1, 3) = \mathcal{K}^*(\bar{1}\bar{1}0)$ of each domain pair are given in stereographic projection. The intersection symmetry of all domains is $\mathcal{H}^* = 112/m$.

(ii) *Diffraction pattern.* The ‘single-crystal diffraction pattern’ of a twinned crystal exhibits its composite symmetry \mathcal{K} if the volume fractions of all domain states are (approximately) equal.

(iii) *Permissible twin boundaries.* The composite symmetry \mathcal{K} in its black–white notation permits immediate recognition of the ‘permissible twin boundaries’ (W-type composition planes), as explained in Section 3.3.10.2.1.

3.3.4.2. Equivalent twin laws

In the example of the dovetail twin of gypsum above, the twin operation $k = m_x = m(100)$ is of a special nature in that it maps the entire eigensymmetry $\mathcal{H} = 12/m1$ onto itself and, hence, generates a *single* coset, a single twin law and a finite composite group \mathcal{K} of index [2] (simple twins). There are other twin operations, however, which do not leave the entire eigensymmetry invariant, but only a part (subgroup) of it, as shown for the hypothetical (111) twin reflection plane of gypsum in Example 3.3.6.2. In this case, extension of the complete group \mathcal{H} by such a twin operation k does not lead to a single twin law and a finite composite group, but rather generates in the same coset two or more twin operations k_2, k_3, \dots , which are *independent* (non-alternative) but symmetrically *equivalent* with respect to the eigensymmetry \mathcal{H} , each representing a different but equivalent twin law. If applied to the ‘starting’ orientation state 1, they generate two or more new orientation states 2, 3, 4, ... In the general case, continuation of this procedure would lead to an *infinite* set of domain states and to a composite group of infinite order (e.g. cylinder or sphere group). Specialized metrics of a crystal can, of course, lead to a ‘multiple twin’ of small finite order.

In order to overcome this problem of the ‘infinite sets’ and to ensure a finite composite group (of index [2]) for a pair of adjacent domains, we consider only that subgroup of the eigensymmetry \mathcal{H} which is left invariant by the twin operation k . This subgroup is the ‘intersection symmetry’ \mathcal{H}^* of the two ‘oriented eigensymmetries’ \mathcal{H}_1 and \mathcal{H}_2 of the domains 1 and 2 (shown in Fig. 3.3.4.2): $\mathcal{H}^* = \mathcal{H}_1 \cap \mathcal{H}_2$. This group \mathcal{H}^* is now extended by k and leads to the ‘reduced composite symmetry’ \mathcal{K}^* of the domain pair (1, 2): $\mathcal{K}^*(1, 2) = \mathcal{H}^* \cup k_2 \times \mathcal{H}^*$, which is a finite supergroup of \mathcal{H} of index [2]. In this way, the complete coset $k \times \mathcal{H}$ of the eigensymmetry \mathcal{H} is split into two (or more) smaller cosets $k_2 \times \mathcal{H}^*, k_3 \times \mathcal{H}^*$ etc., where k_2, k_3, \dots , are symmetrically equivalent twin operations in \mathcal{H} . Correspondingly, the differently oriented ‘reduced composite symmetries’ $\mathcal{K}^*(1, 2) = \mathcal{H}^* \cup k_2 \times \mathcal{H}^*, \mathcal{K}^*(1, 3) = \mathcal{H}^* \cup k_3 \times \mathcal{H}^*$ etc. of the domain pairs

3.3. TWINNING OF CRYSTALS

(1, 2), (1, 3) etc. are generated by the representative twin operations k_2, k_3 etc. These cosets $k_i \times \mathcal{H}^*$ are considered as the twin laws for the corresponding domain pairs.

As an example, an orthorhombic crystal of *eigensymmetry* $\mathcal{H} = 2/m2/m2/m$ with equivalent twin reflection planes $k_2 = m(110)$ and $k_3 = m(\bar{1}10)$ is shown in Fig. 3.3.4.2. From the ‘starting’ domain 1, the two domains 2 and 3 are generated by the two twin mirror planes (110) and ($\bar{1}10$), symmetrically equivalent with respect to the oriented *eigensymmetry* \mathcal{H}_1 of domain 1. The intersection symmetries of the two pairs of oriented *eigensymmetries* \mathcal{H}_1 & \mathcal{H}_2 and \mathcal{H}_1 & \mathcal{H}_3 are identical: $\mathcal{H}^* = 112/m$. The three oriented *eigensymmetries* $\mathcal{H}_1, \mathcal{H}_2, \mathcal{H}_3$, as well as the two differently oriented reduced composite symmetries $\mathcal{K}^*(1, 2) = \mathcal{K}^*(110)$ and $\mathcal{K}^*(1, 3) = \mathcal{K}^*(\bar{1}10)$ of the domain pairs (1, 2) and (1, 3), are all isomorphic of type $2/m2/m2/m$, but exhibit different orientations.

3.3.4.3. Classification of composite symmetries

The discussions and examples briefly presented in the previous section are now extended in a more general way. For the classification of composite symmetries \mathcal{K} we introduce the notion of *oriented eigensymmetry* \mathcal{H}_j of an orientation state j and attach to it its geometric representation, the *framework of oriented eigensymmetry elements*, for short *framework of oriented eigensymmetry*. Twin partners of different orientation states have the same *eigensymmetry* \mathcal{H} but exhibit different *oriented eigensymmetries* \mathcal{H}_j , which are geometrically represented by their frameworks of oriented *eigensymmetry*. The well known crystallographic term ‘framework of symmetry’ designates the spatial arrangement of the symmetry elements (planes, axes, points) of a point group or a space group, as represented by a stereographic projection or by a space-group diagram (cf. Hahn, 2002, Parts 6, 7 and 10).

Similarly, we also consider the *intersection group* $\mathcal{H}^* = \mathcal{H}_1 \cap \mathcal{H}_2$ of the oriented *eigensymmetries* \mathcal{H}_1 and \mathcal{H}_2 and its geometric representation, the *framework of intersection symmetry*. Two cases of intersection symmetries have to be distinguished:

Case (I): $\mathcal{H}^* = \mathcal{H}_1 \cap \mathcal{H}_2 = \mathcal{H}$. Here, all twin operations map the *complete* oriented frameworks of the two domain states 1 and 2 onto each other, i.e. the oriented *eigensymmetries* \mathcal{H}_1 and \mathcal{H}_2 and their intersection group \mathcal{H}^* coincide. Hence, for binary twin operations there is only one coset $k \times \mathcal{H} = k \times \mathcal{H}^*$ and one twin law. The composite symmetry $\mathcal{K} = \mathcal{H}^* \cup k \times \mathcal{H}^*$ is crystallographic. An example is provided by the dovetail twins of gypsum, described above (cf. Table 3.3.4.1).

Case (II): $\mathcal{H}^* = \mathcal{H}_1 \cap \mathcal{H}_2 < \mathcal{H}_1$ and $< \mathcal{H}_2$ (index $[i] \geq 2$). Here, the twin operations map only a *fraction* $1/i$ of the oriented symmetry elements of domain states 1 and 2 onto each other. Hence, the intersection group \mathcal{H}^* of the two oriented *eigensymmetries* \mathcal{H}_1 and \mathcal{H}_2 is a proper subgroup of index $[i] \geq 2$ of both \mathcal{H}_1 and \mathcal{H}_2 . The coset $k \times \mathcal{H}^*$ leads to the crystallographic *reduced composite symmetry*

$$\mathcal{K}^* = \mathcal{H}^* \cup k \times \mathcal{H}^*,$$

as for case (I) above. The number of twin laws, different but equivalent with respect to the ‘starting’ *eigensymmetry* \mathcal{H}_1 of the first domain state 1, equals the index $[i]$. This implies i differently oriented domain pairs (1, j) ($j = 1, 2, \dots, i$). The composite symmetry of such a domain pair is now defined by

Table 3.3.4.2. *Reduced composite symmetries* $\mathcal{K}^*(1, 2) = \mathcal{H}^* \cup k_2 \times \mathcal{H}^*$ and $\mathcal{K}^*(1, 3) = \mathcal{H}^* \cup k_3 \times \mathcal{H}^*$ for the orthorhombic example in Fig. 3.3.4.2

| \mathcal{H}^* | $k_2 \times \mathcal{H}^*$ | $k_3 \times \mathcal{H}^*$ |
|-----------------|----------------------------|----------------------------|
| 1 | $m(110)$ | $m(\bar{1}10)$ |
| 2_z | $m \perp [\bar{1}10]$ | $m \perp [110]$ |
| m_z | $2 \parallel [\bar{1}10]$ | $2 \parallel [110]$ |
| $\bar{1}$ | $2 \perp (110)$ | $2 \perp (\bar{1}10)$ |

$\mathcal{K}_{1,j}^* = \mathcal{H}^* \cup k_j \times \mathcal{H}^*$ and is called the *reduced composite symmetry* \mathcal{K}^* . All twin laws can be expressed by the black–white symbol of the reduced composite symmetry $\mathcal{K}_{1,j}^*$, as described in Section 3.3.5.

The orthorhombic example given in Section 3.3.4.1 (Fig. 3.3.4.2) is now extended as follows:

Eigensymmetry $\mathcal{H} = 2/m2/m2/m$, intersection symmetry $\mathcal{H}^* = 112/m$, $k_1 = \text{identity}$, $k_2 = m(110)$, $k_3 = m(\bar{1}10)$, $[i] = 2$. The two cosets $k_2 \times \mathcal{H}^*$ and $k_3 \times \mathcal{H}^*$ are listed in Table 3.3.4.2. From these cosets the two reduced composite symmetries $\mathcal{K}^*(1, 2)$ and $\mathcal{K}^*(1, 3)$ are derived as follows:

$$\mathcal{K}^*(1, 2) = \mathcal{H}^* \cup k_2 \times \mathcal{H}^* \quad \text{and} \quad \mathcal{K}^*(1, 3) = \mathcal{H}^* \cup k_3 \times \mathcal{H}^*.$$

These groups of reduced composite symmetry are always crystallographic and finite.

Note that the twin operations in these two reduced cosets would form *one* coset if one of the operations (k_2 or k_3) were applied to the *full eigensymmetry* \mathcal{H} (twice as long as \mathcal{H}^*): $k_2 \times \mathcal{H} = k_3 \times \mathcal{H} = k_2 \times \mathcal{H}^* \cup k_3 \times \mathcal{H}^*$. This process, however, would not result in a finite group, whereas the *two reduced* cosets lead to groups of finite order.

The two twin laws, based on $k_2(110)$ and $k_3(\bar{1}10)$, can be expressed by a black–white symmetry symbol of type $\mathcal{K}^* = 2'/m'2'/m'2/m$ with $\mathcal{H}^* = 112/m$. The frameworks of these two groups, however, are differently oriented (cf. Fig. 3.3.4.2).

In the limiting case, the intersection group \mathcal{H}^* consists of the identity alone (index $[i] = \text{order } |\mathcal{H}|$ of the *eigensymmetry* group), i.e. the two frameworks of oriented *eigensymmetry* have no symmetry element in common. The number of equivalent twin laws then equals the order $|\mathcal{H}|$ of the *eigensymmetry* group, and each coset consists of one twin operation only.

3.3.4.4. Categories of composite symmetries

After this preparatory introduction, the three categories of composite symmetry are treated.

(i) *Crystallographic composite symmetry*. According to case (I) above, only the following three types of twins have *crystallographic composite symmetry* \mathcal{K} with two orientation states, one coset and, hence, one twin law:

- (a) all merohedral twins (cf. Section 3.3.9);
- (b) twins of ‘monoaxial’ *eigensymmetry* \mathcal{H} that have either a twin reflection plane parallel or a twofold twin axis normal to the single *eigensymmetry* axis. Monoaxial *eigensymmetries* are $2, m = \bar{2}, 2/m, 3, \bar{3}, 4, \bar{4}, 4/m, 6, \bar{6} = 3/m, 6/m\bar{2}$;
- (c) the triclinic *eigensymmetry* groups 1 and $\bar{1}$; here any binary twin element leads to a crystallographic composite symmetry \mathcal{K} .

Examples, including some special cases of trigonal crystals, are given in Section 3.3.6.

(ii) *Noncrystallographic composite symmetry*. As shown below, a noncrystallographic composite symmetry \mathcal{K} results if the conditions of case (II) apply. Twins of this type are rather complicated because more than one twin law and more than two orientation states are involved. This case is illustrated in Figs. 3.3.3.1(c) and 3.3.4.2, where the twinning of an orthorhombic crystal with *eigensymmetry* $\mathcal{H} = 2/m2/m2/m$ and twin mirror plane (110) is considered. In case (II) above and in Fig. 3.3.4.2, domains 2 and 3 are generated from the starting domain 1 by the application of the equivalent twin elements $m_1(110)$ and $m_1(\bar{1}10)$. By applying the two twin elements $m_2(110)$ and $m_2(\bar{1}10)$ of domain 2, a new domain 4 is obtained and, at the same time, domain 1 is reproduced. Similarly, the twin elements $m_3(110)$ and $m_3(\bar{1}10)$ of domain 3 generate a further new domain 5, and domain 1 is reproduced again.

The continuation of this construction leads in the limit to a circular arrangement with an infinitely large number of domain

3. PHASE TRANSITIONS, TWINNING AND DOMAIN STRUCTURES

states. The group-theoretical treatment of this process, based on the *full eigensymmetry*, results in the infinite composite symmetry group $\mathcal{K} = \infty/mm$, with the rotation axis parallel to the twofold axis of the intersection symmetry $112/m$, common to all these infinitely many domains. In an even more general case, for example an orthorhombic crystal with twin reflection plane (111) , the infinite sphere group $\mathcal{K} = m\overline{\infty}$ would result as composite symmetry. Neither of these cases is physically meaningful and thus they are not considered further here. It is emphasized, however, that the *reduced* composite symmetry \mathcal{K}^* for any pair of domains in contact, as derived in case (II) above, is finite and crystallographic and, thus, of practical use.

(iii) *Pseudo-crystallographic composite symmetry*. Among twins with noncrystallographic composite symmetry, described above, those exhibiting structural or at least metrical pseudo-symmetries are of special significance. Again we consider an orthorhombic crystal with *eigensymmetry* $\mathcal{H} = 2/m\,2/m\,2/m$ and equivalent twin reflection planes (110) and $(\bar{1}\bar{1}0)$, but now with a special axial ratio $b/a \approx |\tan(360^\circ/n)|$ ($n = 3, 4$ or 6).

The procedure described above in (ii) leads to three different orientation states for $n = 3$ and 6 and to two different orientation states for $n = 4$, forming a cyclic arrangement of sector domains (for cyclic and sector twins see Section 3.3.3). The intersection group \mathcal{H}^* of all these domain states is $112/m$, with the twofold axis along the c axis. The reduced composite symmetry of any pair of domains in contact is orthorhombic of type $\mathcal{K}^* = 2'/m'\,2'/m'\,2/m$.

These multiple cyclic twins can be described in two ways (cf. Section 3.3.2.3.2):

(a) by repeated application of equivalent binary twin operations (reflections or twofold rotations) to a pseudosymmetrical crystal, as proposed by Hartman (1960) and Curien (1960). Note that each one of these binary twin operations is 'exact', whereas the closure of the cycle of sectors is only approximate; the deviation from $360^\circ/n$ depends on the (metrical) pseudosymmetry of the lattice;

(b) by successive application of pseudo n -fold twin rotations around the zone axis of the equivalent twin reflection planes. Note that the individual rotation angles are not exactly $360^\circ/n$, due to the pseudosymmetry of the lattice. This alternative description corresponds to the approach by Friedel (1926, p. 435) and Buerger (1960b).

It is now reasonable to define an *extended composite symmetry* $\mathcal{K}(n)$ by adding the n -fold rotation as a further generator to the reduced composite symmetry \mathcal{K}^* of a domain pair. This results in the composite symmetry $\mathcal{K}(n)$ of the complete twin aggregate, in the present case in a modification of the symmetry $\mathcal{K}^* = 2'/m'\,2'/m'\,2/m$ to:

$\mathcal{K}(6) = \mathcal{K}(3) = 6(2)/m\,2/m\,2/m$ (three orientation states, two twin laws) for $n = 3$ and $n = 6$;

$\mathcal{K}(4) = 4(2)/m\,2/m\,2/m$ (two orientation states, one twin law) for $n = 4$.

The *eigensymmetry* component of the main twin axis is given in parentheses.

This construction can also be applied to noncrystallographic twin rotations $n = 5, 7, 8$ etc. (cf. Section 3.3.6.8):

$\mathcal{K}(10) = \mathcal{K}(5) = 10(2)/m\,2/m\,2/m$ (five orientation states, four twin laws) for $n = 5$ and $n = 10$.

The above examples are based on a twofold *eigensymmetry* component along the n -fold twin axis. An example of a pseudo-hexagonal twin, monoclinic gibbsite, $\text{Al}(\text{OH})_3$, without a twofold *eigensymmetry* component along $[001]$, is treated as Example 3.3.6.10 and Fig. 3.3.6.10.

It is emphasized that the considerations of this section apply not only to the particularly complicated cases of multiple growth twins but also to transformation twins resulting from the loss of higher-order rotation axes that is accompanied by a small metrical deformation of the lattice. As a result, the extended

composite symmetries $\mathcal{K}(n)$ of the transformation twins resemble the symmetry \mathcal{G} of their parent phase. The occurrence of both multiple growth and multiple transformation twins of orthorhombic pseudo-hexagonal K_2SO_4 is described in Example 3.3.6.7.

Remark. It is possible to construct multiple twins that cannot be treated as a cyclic sequence of binary twin elements. This case occurs if a pair of domain states 1 and 2 are related only by an n -fold rotation or roto-inversion ($n \geq 3$). The resulting coset again contains the alternative twin operations, but in this case *only* for the orientation relation $1 \Rightarrow 2$, and not for $2 \Rightarrow 1$ ('non-transposable' domain pair). This coset procedure thus does not result in a composite group for a domain pair. In order to obtain the composite group, further cosets have to be constructed by means of the higher powers of the twin rotation under consideration. Each new power corresponds to a further domain state and twin law.

This construction leads to a composite symmetry $\mathcal{K}(n)$ of supergroup index $[i] \geq 3$ with respect to the *eigensymmetry* \mathcal{H} . This case can occur only for the following $\mathcal{H} \Rightarrow \mathcal{K}$ pairs: $1 \Rightarrow 3, \bar{1} \Rightarrow \bar{3}, 1 \Rightarrow 4, \bar{1} \Rightarrow \bar{4}, m \Rightarrow 4/m, 1 \Rightarrow 6, m \Rightarrow \bar{6} = 3/m, m \Rightarrow 6/m, 2/m \Rightarrow 6/m$ (monoaxial point groups), as well as for the two cubic pairs $222 \Rightarrow 23, mmm \Rightarrow 2/m\,3$. For the pairs $1 \Rightarrow 3, \bar{1} \Rightarrow \bar{3}, m \Rightarrow \bar{6} = 3/m, 2/m \Rightarrow 6/m$ and the two cubic pairs $222 \Rightarrow 23, mmm \Rightarrow 2/m\,3$, the \mathcal{K} relations are of index [3] and imply three non-transposable domain states. For the pairs $1 \Rightarrow 4, \bar{1} \Rightarrow \bar{4}, m \Rightarrow 4/m$, as well as $1 \Rightarrow 6$ and $m \Rightarrow 6/m$, four or six different domain states occur. Among them, however, domain pairs related by the second powers of 4 and 4 as well as by the third powers of 6 and 6 operations are transposable, because these twin operations correspond to twofold rotations.

No growth twins of this type are known so far. As transformation twin, langbeinite ($23 \Leftrightarrow 222$) is the only known example.

3.3.5. Description of the twin law by black-white symmetry

An alternative description of twinning employs the symbolism of colour symmetry. This method was introduced by Curien & Le Corre (1958) and by Curien & Donnay (1959). In this approach, a colour is attributed to each different domain state. Depending on the number of domain states, simple twins with two colours (*i.e.* 'black-white' or 'dichromatic' or 'anti-symmetry' groups) and multiple twins with more than two colours (*i.e.* 'polychromatic' symmetry groups) have to be considered. Two kinds of operations are distinguished:

(i) The symmetry operations of the *eigensymmetry* (point group) of the crystal. These operations are 'colour-preserving' and form the 'monochromatic' *eigensymmetry* group \mathcal{H} . The symbols of these operations are unprimed.

(ii) The twin operations, *i.e.* those operations which transform one orientation state into another, are 'colour-changing' operations. Their symbols are designated by a prime if of order 2: $2', m', \bar{1}'$.

For *simple twins*, all colour-changing (twin) operations are binary, hence the two domain states are transposable. The composite symmetry \mathcal{K} of these twins thus can be described by a 'black-and-white' symmetry group. The coset, which defines the twin law, contains only colour-changing (primed) operations. This notation has been used already in previous sections.

It should be noted that symbols such as $4'$ and $6'$, despite appearance to the contrary, represent *binary* black-and-white operations, because $4'$ contains 2, and $6'$ contains 3 and $2'$, with $2'$ being the twin operation. For this reason, these symbols are written here as $4'(2)$ and $6'(3)$, whereby the unprimed symbol in parentheses refers to the *eigensymmetry* part of the twin axis. In

3.3. TWINNING OF CRYSTALS

contrast, $6'(2)$ would designate a (polychromatic) twin axis which relates three domain states (three colours), each of *eigensymmetry* 2. Twin centres of symmetry $\bar{1}'$ are always added to the symbol in order to bring out an inversion twinning contained in the twin law. In the original version of Curien & Donnay (1959), the black–white symbols were only used for twinning by merohedry. In the present chapter, the symbols are also applied to non-merohedral twins, as is customary for (ferroelastic) domain structures. This has the consequence, however, that the *eigensymmetries* \mathcal{H} or \mathcal{H}^* and the composite symmetries \mathcal{K} or \mathcal{K}^* may belong to different crystal systems and, thus, are referred to different coordinate systems, as shown for the composite symmetry of gypsum in Section 3.3.4.1.

For the treatment of *multiple twins*, ‘polychromatic’ composite groups $\mathcal{K}(n)$ are required. These contain colour-changing operations of order higher than 2, *i.e.* they relate three or more colours (domain states). Consequently, not all pairs of domain states are transposable. This treatment of multiple twins is rather complicated and only sensible if the composite symmetry group is finite and contains twin axes of low order ($n \leq 8$). For this reason, the symbols for the composite symmetry \mathcal{K} of multiple twins are written without primes; see the examples in Section 3.3.4.4(iii).

3.3.6. Examples of twinned crystals

In order to illustrate the foregoing rather abstract deliberations, an extensive set of examples of twins occurring either in nature or in the laboratory is presented below. In each case, the twin law is described in two ways: by the coset of alternative twin operations and by the black–white symmetry symbol of the composite symmetry \mathcal{K} , as described in Sections 3.3.4 and 3.3.5.

For the description of a twin, the conventional crystallographic coordinate system of the crystal and its *eigensymmetry* group \mathcal{H} are used in general; exceptions are specifically stated. To indicate the orientation of the twin elements (both rational and irrational) and the composition planes, no specific convention has been adopted; rather a variety of intuitively understandable simple symbols are chosen for each particular case, with the additional remark ‘rational’ or ‘irrational’ where necessary. Thus, for twin reflection planes and (planar) twin boundaries symbols such as m_x , $m(100)$, $m \parallel (100)$ or $m \perp [100]$ are used, whereas twin rotation axes are designated by 2_z , $2_{[001]}$, $2 \parallel [001]$, $2 \perp (001)$, 3_z , $3_{[111]}$, $4_{[001]}$ *etc.*

3.3.6.1. Inversion twins in orthorhombic crystals

The (polar) 180° twin domains in a (potentially ferroelectric) crystal of *eigensymmetry* $\mathcal{H} = mm2$ ($m_x m_y 2_z$) and composite symmetry $\mathcal{K} = 2/m 2/m 2/m$ (*e.g.* in KTiOPO_4 , NH_4LiSO_4 , Li-formate monohydrate) result from a group–subgroup relation of index $[i] = 2$ with invariance of the symmetry framework (merohedral twins), but antiparallel orientation of the polar axes. The orientation relation between the two domain states is described by the coset $k \times \mathcal{H}$ of twin operations shown in Table 3.3.6.1, whereby the reflection in (001) , m_z , is considered as the ‘representative’ twin operation.

Table 3.3.6.1. Orthorhombic inversion twins: coset of alternative twin operations (twin law)

| \mathcal{H} | $k \times \mathcal{H} = m_z \times \mathcal{H}$ |
|---------------|---|
| 1 | m_z (normal to the polar axis $[001]$) |
| m_x | 2_x (normal to the polar axis) |
| m_y | 2_y (normal to the polar axis) |
| 2_z | $\bar{1}$ (inversion) |

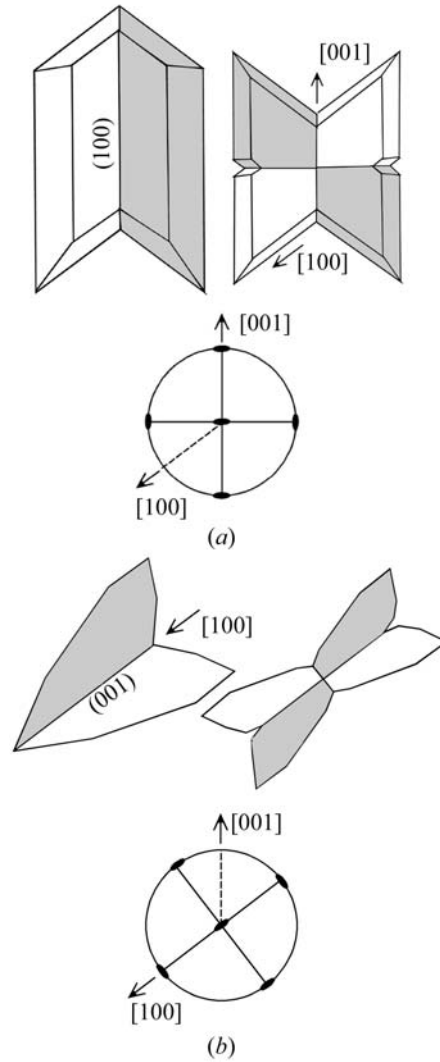


Fig. 3.3.6.1. Dovetail twin (a) and Montmartre twin (b) of gypsum. The two orientation states of each twin are distinguished by shading. For each twin type (a) and (b), the following aspects are given: (i) two idealized illustrations of each twin, on the left in the most frequent form with two twin components, on the right in the rare form with four twin components, the morphology of which displays the orthorhombic composite symmetry; (ii) the oriented composite symmetry in stereographic projection (dotted lines indicate monoclinic axes).

Hence, these twins can be regarded not only as reflection, but also as rotation or inversion twins. The composite symmetry, in black–white symmetry notation, is

$$\mathcal{K} = \frac{2'_x}{m_x} \frac{2'_y}{m_y} \frac{2_z}{m'_z} (\bar{1}'),$$

whereby the primed symbols designate the (alternative) twin operations (*cf.* Section 3.3.5).

3.3.6.2. Twinning of gypsum

The *dovetail twin* of gypsum [*eigensymmetry* $\mathcal{H} = 1 2/m 1$, with twin reflection plane $m \parallel (100)$], coset of twin operations $k \times \mathcal{H}$ and composite symmetry \mathcal{K} , was treated in Section 3.3.4. Gypsum exhibits an independent additional kind of growth twinning, the *Montmartre twin* with twin reflection plane $m \parallel (001)$. These two twin laws are depicted in Fig. 3.3.6.1. The two cosets of twin operations in Table 3.3.6.2 and the symbols of the composite symmetries \mathcal{K}_D and \mathcal{K}_M of both twins are referred, in addition to the monoclinic crystal axes, also to orthorhombic axes x_D, y, z_D for dovetail twins and x_M, y, z_M for Montmartre twins. This procedure brings out for each case the perpendicularity of the

3. PHASE TRANSITIONS, TWINNING AND DOMAIN STRUCTURES

Table 3.3.6.2. *Gypsum: cosets of alternative twin operations of the dovetail and the Montmartre twins, referred to their specific orthorhombic axes (subscripts D and M)*

| \mathcal{H} | Dovetail twins $m_{xD} \times \mathcal{H}$ | Montmartre twins $m_{zM} \times \mathcal{H}$ |
|--|--|--|
| 1 $2_y = 2 \parallel [010]$ $m_y = m \parallel (010)$ $\bar{1}$ | $m_{xD} = m \parallel (100)$ (rational) $m_{zD} = m \perp [001]$ (irrational) $2_{zD} = 2 \parallel [001]$ (rational) $2_{xD} = 2 \perp (100)$ (irrational) | $m_{zM} = m \parallel (001)$ (rational) $m_{xM} = m \perp [100]$ (irrational) $2_{xM} = 2 \parallel [100]$ (rational) $2_{zM} = 2 \perp [001]$ (irrational) |

rational and irrational twin elements, clearly visible in Fig. 3.3.6.1, as follows:

$$\mathcal{K}_D = \frac{2'_{xD} 2_y 2'_{zD}}{m'_{xD} m_y m'_{zD}} \quad \mathcal{K}_M = \frac{2'_{xM} 2_y 2'_{zM}}{m'_{xM} m_y m'_{zM}}$$

$$\begin{array}{ll} x_D \text{ (ortho)} \perp (100) \text{ (mono)} & x_M \text{ (ortho)} \parallel [100] \text{ (mono)} \\ z_D \text{ (ortho)} \parallel [001] \text{ (mono)} & z_M \text{ (ortho)} \perp (001) \text{ (mono)}. \end{array}$$

In both cases, the (*eigensymmetry*) framework $2_y/m_y$ is invariant under all twin operations; hence, the composite symmetries \mathcal{K}_D and \mathcal{K}_M are crystallographic of type $2/m2/m2/m$ (super-group index [2]) but differently oriented, as shown in Fig. 3.3.6.1. There is no physical reality behind the orthorhombic symmetry of the two \mathcal{K} groups: gypsum is neither structurally nor metrically pseudo-orthorhombic, the monoclinic angle being 128° . The two \mathcal{K} groups and their orthorhombic symbols, however, clearly reveal the two different twin symmetries and, for each case, the perpendicular orientations of the four twin elements, two rational and two irrational. The two twin types originate from independent nucleation in aqueous solutions.

It should be noted that for *all* (potential) twin reflection planes ($h0l$) in the zone $[010]$ (monoclinic axis), the oriented *eigensymmetry* $\mathcal{H} = 12/m1$ would be the same for all domain states, *i.e.* the intersection symmetry \mathcal{H}^* is identical with the oriented *eigensymmetry* \mathcal{H} and, thus, the composite symmetry would be always crystallographic.

For a more general twin reflection plane not belonging to the zone ($h0l$), such as (111), however, the oriented *eigensymmetry* \mathcal{H} would not be invariant under the twin operation. Consequently, an additional twin reflection plane ($\bar{1}\bar{1}1$), equivalent with respect to the *eigensymmetry* $12/m1$, exists. This (hypothetical) twin would belong to category (ii) in Section 3.3.4.4 and would formally lead to a noncrystallographic composite symmetry of infinite order. If, however, we restrict our considerations to the intersection symmetry $\mathcal{H}^* = \bar{1}$ of a domain pair, the reduced composite symmetry $\mathcal{K}^* = 2'/m'$ with $m' \parallel (111)$ and $2' \perp (111)$ (irrational) would result. Note that for these (hypothetical) twins the reduced composite symmetry \mathcal{K}^* and the *eigensymmetry* \mathcal{H} are isomorphic groups, but that their orientations are quite different.

Remark. In the domain-structure approach, presented in Chapter 3.4 of this volume, both gypsum twins, dovetail and Montmartre, can be derived together as a result of a single (hypothetical) ferroelastic phase transition from a (nonexistent) orthorhombic parent phase of symmetry $\mathcal{G} = 2/m2/m2/m$ to a monoclinic daughter phase of symmetry $\mathcal{H} = 12/m1$, with a very strong metrical distortion of 38° from $\beta = 90^\circ$ to $\beta = 128^\circ$ (Janovec, 2003). In this (hypothetical) transition the two mirror planes, (100) and (001), 90° apart in the orthorhombic form, become twin reflection planes of monoclinic gypsum, (100) for the dovetail, (001) for the Montmartre twin law, with an angle of 128° . It must be realized, however, that neither the orthorhombic parent phase nor the ferroelastic phase transition are real.

3.3.6.3. Twinning of low-temperature quartz (α -quartz)

Quartz is a mineral which is particularly rich in twinning. It has the noncentrosymmetric trigonal point group 32 with three polar

twofold axes and a non-polar trigonal axis. The crystals exhibit enantiomorphism (right- and left-handed quartz), piezoelectricity and optical activity. The lattice of quartz is hexagonal with holohedral (lattice) point group $6/m2/m2/m$. Many types of twin laws have been found (*cf.* Frondel, 1962), but only the four most important ones are discussed here:

- (a) Dauphiné twins;
- (b) Brazil twins;
- (c) Combined-law (Leydolt, Liebisch) twins;
- (d) Japanese twins.

The first three types are merohedral (parallel-lattice) twins and their composite symmetries belong to category (i) in Section 3.3.4.2, whereas the non-merohedral Japanese twins (twins with inclined lattices or inclined axes) belong to category (ii).

3.3.6.3.1. Dauphiné twins

This twinning is commonly described by a twofold twin rotation around the threefold symmetry axis $[001]$. The two orientation states are of equal handedness but their polar axes are reversed ('electrical twins'). Dauphiné twins can be transformation or growth or mechanical (ferrobieleastic) twins. The composite symmetry is $\mathcal{K} = 622$, the point group of high-temperature quartz (β -quartz). The coset decomposition of \mathcal{K} with respect to the *eigensymmetry* $\mathcal{H} = 32$ (index [2]) contains the operations listed in Table 3.3.6.3.

The left coset $2_z \times \mathcal{H}$ constitutes the twin law. Note that this coset contains four twofold rotations of which the first one, 2_z , is the standard description of Dauphiné twinning. In addition, the coset contains two sixfold rotations, 6^1 and $6^5 = 6^{-1}$. The black-white symmetry symbol of the composite symmetry is $\mathcal{K} = 6'(3)22'$ (super-group of index [2] of the *eigensymmetry* group $\mathcal{H} = 32$).

This coset decomposition $622 \Rightarrow 32$ was first listed and applied to quartz by Janovec (1972, p. 993).

3.3.6.3.2. Brazil twins

This twinning is commonly described by a twin reflection across a plane normal to a twofold symmetry axis. The two orientation states are of opposite handedness (*i.e.* the sense of the optical activity is reversed: optical twins) and the polar axes are reversed as well. The coset representing the twin law consists of the following six operations:

- (i) three reflections across planes $\{11\bar{2}0\}$, normal to the three twofold axes;
- (ii) three rotoinversions $\bar{3}$ around $[001]$: $\bar{3}^1, \bar{3}^3 = \bar{1}, \bar{3}^5 = \bar{3}^{-1}$.

The coset shows that Brazil twins can equally well be described as reflection or inversion twins. The composite symmetry

Table 3.3.6.3. *Dauphiné twins of α -quartz: coset of alternative twin operations (twin law)*

| \mathcal{H} | $2_z \times \mathcal{H}$ |
|-------------------|--|
| 1 | $2_z = 6^3$ |
| 3^1 | $6^5 (= 6^{-1})$ |
| 3^2 | 6^1 |
| $2_{[100]}$ | $2_z \times 2_{[100]} = 2_{[120]}$ |
| $2_{[010]}$ | $2_z \times 2_{[010]} = 2_{[210]}$ |
| $2_{[\bar{1}10]}$ | $2_z \times 2_{[\bar{1}10]} = 2_{[\bar{1}\bar{1}0]}$ |

3.3. TWINNING OF CRYSTALS

$$\mathcal{K} = \bar{3}'(3) \frac{2}{m'} 1(\bar{1}')$$

is a supergroup of index [2] of the *eigensymmetry* group 32.

3.3.6.3.3. Combined Dauphiné–Brazil (Leydolt, Liebis) twins

Twins of this type can be described by a twin reflection across the plane (0001), normal to the threefold axis [001]. The two orientation states of this twin are of opposite handedness (*i.e.* the optical activity is reversed, optical twin), but the polar axes are not reversed. The coset representing the twin law consists of the following six operations:

(i) three twin reflections across planes $\{10\bar{1}0\}$, parallel to the three twofold axes;

(ii) three rotoinversions $\bar{6}$ around [001]: $\bar{6}^1, \bar{6}^3 = m_z, \bar{6}^5 = \bar{6}^{-1}$.

The composite symmetry

$$\mathcal{K} = \bar{6}'(3)2m' = \frac{3}{m'} 2m'$$

is again a supergroup of index [2] of the *eigensymmetry* group 32. This twin law is usually described as a combination of the Dauphiné and Brazil twin laws, *i.e.* as the twofold Dauphiné twin rotation 2_z followed by the Brazil twin reflection $m(11\bar{2}0)$ or, alternatively, by the inversion $\bar{1}$. The product $2_z \times \bar{1} = m_z$ results in a particularly simple description of the combined law as a reflection twin on m_z .

Twin domains of the Leydolt type are very rarely intergrown in direct contact, *i.e.* with a common boundary. If, however, a quartz crystal contains inserts of Dauphiné and Brazil twins, the domains of these two types, even though not in contact, are related by the Leydolt law. In this sense, Leydolt twinning is rather common in low-temperature quartz. In contrast, GaPO_4 , a quartz homeotype with the berlinite structure, frequently contains Leydolt twin domains in direct contact, *i.e.* with a common boundary (Engel *et al.*, 1989).

In conclusion, the three merohedral twin laws of α -quartz described above imply four domain states with different orientations of important physical properties. These relations are shown in Fig. 3.3.6.2 for electrical polarity, optical activity and the orientation of etch pits on (0001). It is noteworthy that these three twin laws are the only possible merohedral twins of quartz, and that all three are realized in nature. Combined, they lead to the composite symmetry $\mathcal{K} = 6/m2/m2/m$ ('complete twin': Curien & Donnay, 1959).

In the three twin laws (cosets) above, only odd powers of 6, $\bar{3}$ and $\bar{6}$ (rotations and rotoinversions) occur as twin operations, whereas the even powers are part of the *eigensymmetry* 32. Consequently, repetition of any odd-power twin operation restores the original orientation state, *i.e.* each of these operations has the nature of a 'binary' twin operation and leads to a pair of *transposable* orientation states.

3.3.6.3.4. Japanese twins (or La Gardette twins)

Among the quartz twins with 'inclined axes' ('inclined lattices'), the Japanese twins are the most frequent and important

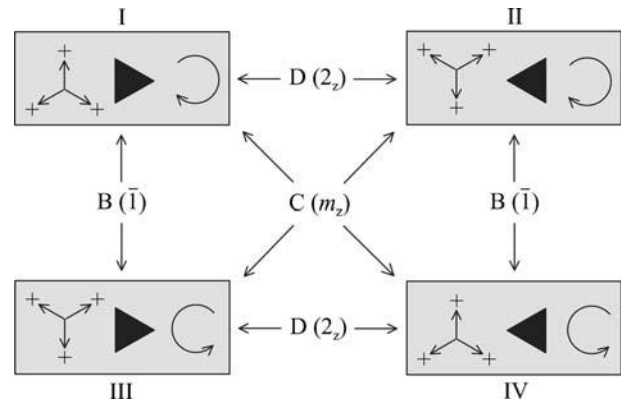


Fig. 3.3.6.2. Distinction of the four different domain states generated by the three merohedral twin laws of low-quartz and of quartz homeotypes such as GaPO_4 (Dauphiné, Brazil and Leydolt twins) by means of three properties: orientation of the three electrical axes (triangle of arrows), orientation of etch pits on (001) (solid triangle) and sense of the optical rotation (circular arrow). The twin laws relating two different domain states are indicated by arrows [D (2_z): Dauphiné law; B ($\bar{1}$): Brazil law; C (m_z): Leydolt law]. For GaPO_4 , see Engel *et al.* (1989).

ones. They are contact twins of two individuals with composition plane (11 $\bar{2}$ 2). This results in an angle of 84°33' between the two threefold axes. One pair of prism faces is parallel (coplanar) in both partners.

There exist four orientation relations, depending on

(i) the handedness of the two twin partners (equal or different);

(ii) the azimuthal difference (0 or 180°) around the threefold axis of the two partners.

These four variants are illustrated in Fig. 3.3.6.3 and listed in Table 3.3.6.4. The twin interface for all four twin laws is the same, (11 $\bar{2}$ 2), but only in type III do twin mirror plane and composition plane coincide.

In all four types of Japanese twins, the intersection symmetry (reduced *eigensymmetry*) \mathcal{H}^* of a pair of twin partners is 1. Consequently, the twin laws (cosets) consist of only one twin operation and the reduced composite symmetry \mathcal{K}^* is a group of order 2, represented by the twin element listed in Table 3.3.6.4. If one were to use the full *eigensymmetry* $\mathcal{H} = 32$, the infinite sphere group would result as composite symmetry \mathcal{K} .

Many further quartz twins with inclined axes are described by Frondel (1962). A detailed study of these inclined-axis twins in terms of coincidence-site lattices (CSLs) is provided by McLaren (1986).

3.3.6.4. Twinning of high-temperature quartz (β -quartz)

Upon heating quartz into the hexagonal high-temperature phase (point group 622) above 846 K, the Dauphiné twinning disappears, because the composite symmetry \mathcal{K} of the twinned low-temperature phase now becomes the *eigensymmetry* \mathcal{H} of the high-temperature phase. For Brazil twins, however, their nature as reflection or inversion twins is preserved during the transformation.

Table 3.3.6.4. The four different variants of Japanese twins according to Frondel (1962)

| Handedness of twin partners | Azimuthal difference (°) | Twin element = twin law | Label in Fig. 65 of Frondel (1962) |
|-----------------------------|--------------------------|---|------------------------------------|
| L–L or R–R | 0 | Irrational twofold twin axis normal to plane (11 $\bar{2}$ 2) | I(R), I(L) |
| | 180 | Rational twofold twin axis $[11\bar{1}] \equiv [11\bar{2}\bar{3}]^\dagger$ parallel to plane (11 $\bar{2}$ 2) | II(R), II(L) |
| L–R or R–L | 0 | Rational twin mirror plane (11 $\bar{2}$ 2) | III |
| | 180 | Irrational twin mirror plane normal to direction $[11\bar{1}] \equiv [11\bar{2}\bar{3}]^\dagger$ | IV |

† The line $[11\bar{1}] \equiv [11\bar{2}\bar{3}]$ is the edge between the faces $z(01\bar{1}1)$ and $r(10\bar{1}1)$ and is parallel to the composition plane (11 $\bar{2}$ 2). It is parallel or normal to the four twin elements. Transformation formulae between the three-index and the four-index direction symbols, UVW and uvw , are given by Barrett & Massalski (1966, p. 13).

3. PHASE TRANSITIONS, TWINNING AND DOMAIN STRUCTURES

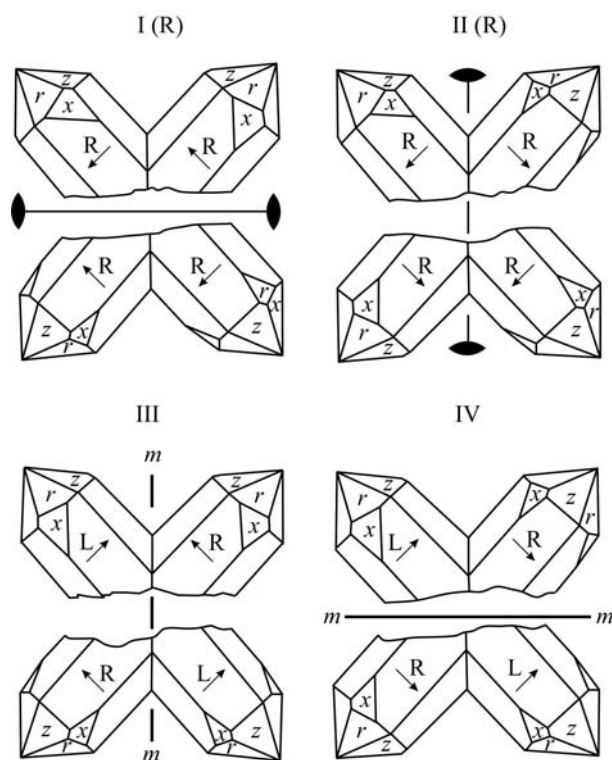


Fig. 3.3.6.3. The four variants of Japanese twins of quartz (after Frondel, 1962; cf. Heide, 1928). The twin elements 2 and m and their orientations are shown. In actual twins, only the upper part of each figure is realized. The lower part has been added for better understanding of the orientation relation. R, L: right-, left-handed quartz. The polarity of the twofold axis parallel to the plane of the drawing is indicated by an arrow. In addition to the cases I(R) and II(R), I(L) and II(L) also exist, but are not included in the figure. Note that a vertical line in the plane of the figure is the zone axis $[11\bar{1}]$ for the two rhombohedral faces r and z , and is parallel to the twin and composition plane ($11\bar{2}$) and the twin axis in variant II.

The *eigensymmetry* of high-temperature quartz is 622 (order 12). Hence, the coset of the Brazil twin law contains 12 twin operations, as follows:

- (i) the six twin operations of a Brazil twin in low-temperature quartz, as listed above in Example 3.3.6.3.2;
- (ii) three further reflections across planes $\{10\bar{1}0\}$, which bisect the three Brazil twin planes $\{11\bar{2}0\}$ of low-temperature quartz;
- (iii) three further rotoinversions around $[001]$: $\bar{6}^1$, $\bar{6}^3 = m_z$, $\bar{6}^5 = \bar{6}^{-1}$.

The composite symmetry is

$$\mathcal{K} = \frac{6}{m'} \frac{2}{m'} \frac{2}{m'} (\bar{1}'),$$

a supergroup of index [2] of the *eigensymmetry* 622 .

In high-temperature quartz, the combined Dauphiné–Brazil twins (Leydolt twins) are identical with Brazil twins, because the Dauphiné twin operation has become part of the *eigensymmetry* 622 . Accordingly, both kinds of twins of low-temperature quartz merge into one upon heating above 846 K. We recommend that these twins are called ‘Brazil twins’, independent of their type of twinning in the low-temperature phase. Upon cooling below 846 K, transformation Dauphiné twin domains may appear in both Brazil growth domains, leading to four orientation states as shown in Fig. 3.3.6.2. Among these four orientation states, two Leydolt pairs occur. Such Leydolt domains, however, are not necessarily in contact (cf. Example 3.3.6.3.3 above).

In addition to these twins with ‘parallel axes’ (merohedral twins), several kinds of growth twins with ‘inclined axes’ occur in high-temperature quartz. They are not treated here, but additional information is provided by Frondel (1962).

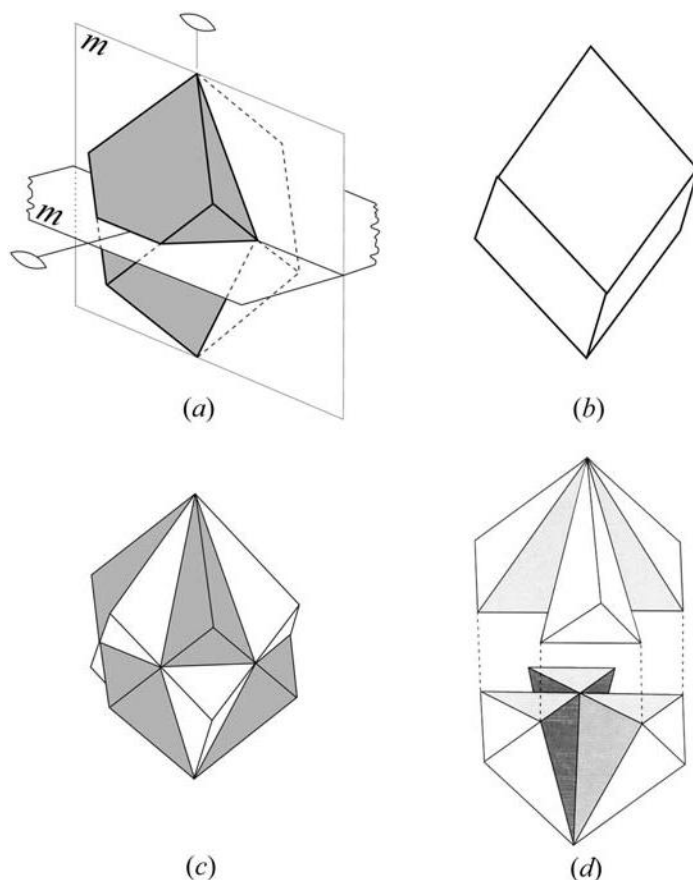


Fig. 3.3.6.4. Twin intergrowth of ‘obverse’ and ‘reverse’ rhombohedra of rhombohedral FeBO_3 . (a) ‘Obverse’ rhombohedron with four of the 12 alternative twin elements. (b) ‘Reverse’ rhombohedron (twin orientation). (c) Interpenetration of both rhombohedra, as observed in penetration twins of FeBO_3 . (d) Idealized skeleton of the six components (exploded along $[001]$ for better recognition) of the ‘obverse’ orientation state shown in (a). The components are connected at the edges along the threefold and the twofold eigensymmetry axes. The shaded faces are $\{10\bar{1}0\}$ and $\{0001\}$ coinciding twin reflection and contact planes with the twin components of the ‘reverse’ orientation state. Parts (a) to (c) courtesy of R. Diehl, Freiburg.

3.3.6.5. Twinning of rhombohedral crystals

In some rhombohedral crystals such as corundum Al_2O_3 (Wallace & White, 1967), calcite CaCO_3 or FeBO_3 (calcite structure) (Kotrbova *et al.*, 1985; Klapper, 1987), growth twinning with a ‘twofold twin rotation around the threefold symmetry axis $[001]$ ’ (similar to the Dauphiné twins in low-temperature quartz described above) is common. Owing to the *eigensymmetry* $\bar{3}2/m$ (order 12), the following 12 twin operations form the coset (twin law). They are described here in hexagonal axes:

- (i) three rotations around the threefold axis $[001]$: $\bar{6}^1$, $\bar{6}^3 = 2_z$, $\bar{6}^5 = \bar{6}^{-1}$;
- (ii) three twofold rotations around the axes $[120]$, $[210]$, $[1\bar{1}0]$;
- (iii) three reflections across the planes $(10\bar{1}0)$, $(1\bar{1}00)$, $(01\bar{1}0)$;
- (iv) three rotoinversions around the threefold axis $[001]$: $\bar{6}^1$, $\bar{6}^3 = m_z$ and $\bar{6}^5 = \bar{6}^{-1}$.

Some of these twin elements are shown in Fig. 3.3.6.4. They include the particularly conspicuous twin reflection plane m_z perpendicular to the threefold axis $[001]$. The composite symmetry is

$$\mathcal{K} = \frac{6'}{m'} (\bar{3}) \frac{2}{m} \frac{2'}{m'} \quad (\text{order } 24).$$

It is of interest that for FeBO_3 crystals this twin law always, without exception, forms penetration twins (Fig. 3.3.6.4), whereas for the isotypic calcite CaCO_3 only $\{0001\}$ contact twins are found (Fig. 3.3.6.5). This aspect is discussed further in Section 3.3.8.6.

3.3. TWINNING OF CRYSTALS

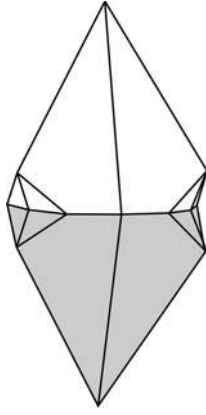


Fig. 3.3.6.5. Contact growth twin of calcite with the same twin law as FeBO_3 in Fig. 3.3.6.4. Conspicuous twin element: twin reflection plane (0001), coinciding with the composition plane (0001).

3.3.6.6. Spinel twins

The twinning of rhombohedral crystals described above also occurs for cubic crystals as the *spinel law* (spinel, CaF_2 , PbS, diamond, sphalerite-type structures such as ZnS, GaAs, CdTe, cubic face- and body-centred metals). In principle, all four threefold axes of the cube, which are equivalent with respect to the *eigensymmetry* \mathcal{H} , can be active in twinning. We restrict our considerations to the case where only one threefold axis, $[111]$, is involved. The most obvious twin operations are the twofold rotation around $[111]$ or the reflection across (111). For centrosymmetric crystals, they are alternative twin operations and belong to the same twin law. For noncentrosymmetric crystals, however, the two operations represent different twin laws. Both cases are covered by the term ‘spinel law’.

The orientation relation defined by the spinel law corresponds to the ‘obverse’ and ‘reverse’ positions of two rhombohedra (cubes), as shown in Fig. 3.3.6.6. For the two (differently) oriented *eigensymmetries* $4/m\bar{3}2/m$ of the domain states \mathcal{H}_1 and \mathcal{H}_2 , the intersection symmetry $\mathcal{H}^* = \bar{3}2/m$ (order 12) results.

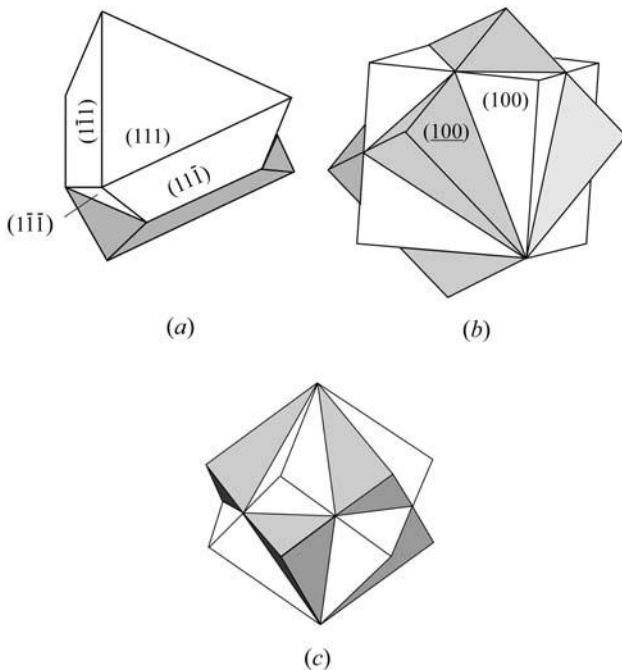


Fig. 3.3.6.6. Spinel (111) twins of cubic crystals (two orientation states). (a) Contact twin with (111) composition plane (two twin components). (b) and (c) Penetration twin (idealized) with one (111) and three $\{112\}$ composition planes (twelve twin components, six of each orientation state) in two different views, (b) with one $[001]$ axis vertical, (c) with the threefold twin axis $[111]$ vertical.

With this ‘reduced *eigensymmetry*’ \mathcal{H}^* , the coset of 12 alternative twin operations is the same as the one derived for twinning of rhombohedral crystals in Example 3.3.6.5.

In the following, we treat the spinel twins with the twin axis $[111]$ or the twin reflection plane (111) for the five cubic point groups (*eigensymmetries*) $\mathcal{H} = m\bar{3}m, \bar{4}3m, 432, m\bar{3}, 32$ in detail. The intersection groups are $\mathcal{H}^* = \bar{3}2/m, 3m, 32, \bar{3}$ and 3, respectively. For these ‘reduced *eigensymmetries*’, the cosets of the alternative twin operations are listed below with reference to cubic axes.

(a) *Eigensymmetry* $\mathcal{H} = 4/m\bar{3}2/m$ (order 48), reduced *eigensymmetry* $\mathcal{H}^* = \bar{3}2/m1$ (order 12).

Alternative twin operations:

- (1) three rotations $6^1, 6^3 = 2, 6^5 = 6^{-1}$ around the axis $[111]$;
- (2) three twofold rotations around the axes $[11\bar{2}], [\bar{2}11], [1\bar{2}1]$;
- (3) three reflections across the planes (112), $(\bar{2}11), (1\bar{2}1)$;
- (4) three rotoinversions around the axis $[111]$: $\bar{6}^1, \bar{6}^3 = m_z, \bar{6}^5 = \bar{6}^{-1}$.

Reduced composite symmetry $\mathcal{K}^* = 6'/m'(\bar{3})2/m'2'/m'$ (order 24).

(b) *Eigensymmetry* $\mathcal{H} = \bar{4}3m$ (order 24), reduced *eigensymmetry* $\mathcal{H}^* = 3m1$ (order 6).

Two different twin laws are possible:

- (1) Twin law representative: ‘twofold rotation around $[111]$ ’;
Alternative twin operations: lines (1) and (3) of case (a) above;
Reduced composite symmetry: $\mathcal{K}^* = 6'(3)mm'$ (order 12).
- (2) Twin law representative: ‘reflection across (111)’;
Alternative twin operations: lines (2) and (4) of case (a) above;
Reduced composite symmetry: $\mathcal{K}^* = 6'(3)m2' = 3/m'm'2'$ (order 12).

(c) *Eigensymmetry* $\mathcal{H} = 432$ (order 24), reduced *eigensymmetry* $\mathcal{H}^* = 321$ (order 6).

Again, two different twin laws are possible:

- (1) Twin law representative: ‘twofold rotation around $[111]$ ’;
Alternative twin operations: lines (1) and (2) of case (a) above;
Reduced composite symmetry: $\mathcal{K}^* = 6'(3)22'$ (order 12).
- (2) Twin law representative: ‘reflection across (111)’;
Alternative twin operations: lines (3) and (4) of case (a) above;
Reduced composite symmetry: $\mathcal{K}^* = 6'(3)2m' = 3/m'2m'$ (order 12).

(d) *Eigensymmetry* $\mathcal{H} = 2/m\bar{3}$ (order 24), reduced *eigensymmetry* $\mathcal{H}^* = \bar{3}$ (order 6).

Two different twin laws:

- (1) Twin law representative: ‘twofold rotation around $[111]$ ’ or ‘reflection across (111)’;
Alternative twin operations: lines (1) and (4) of case (a) above;
Reduced composite symmetry: $\mathcal{K}^* = 6'/m'(\bar{3})$ (order 12).
- (2) Twin law representative: ‘reflection across (112)’ or ‘twofold rotation around $[11\bar{2}]$ ’;
Alternative twin operations: lines (2) and (3) of case (a) above;
Reduced composite symmetry: $\mathcal{K}^* = \bar{3}12'/m'$ (order 12).

(e) *Eigensymmetry* $\mathcal{H} = 23$ (order 12), reduced *eigensymmetry* $\mathcal{H}^* = 3$ (order 3).

Four different twin laws are possible:

- (1) Twin law representative: ‘twofold rotation around $[111]$ ’;
Alternative twin operations: line (1) of case (a) above;
Reduced composite symmetry: $\mathcal{K}^* = 6'(3)$ (order 6).
- (2) Twin law representative: ‘reflection across (111)’.
Alternative twin operations: line (4) of case (a) above.
Reduced composite symmetry: $\mathcal{K}^* = \bar{6}'(3) = 3/m'$ (order 6).
- (3) Twin law representative: ‘twofold rotation around $[11\bar{2}]$ ’;
Alternative twin operations: line (2) of case (a) above;
Reduced composite symmetry $\mathcal{K}^* = 312'$ (order 6).

3. PHASE TRANSITIONS, TWINNING AND DOMAIN STRUCTURES

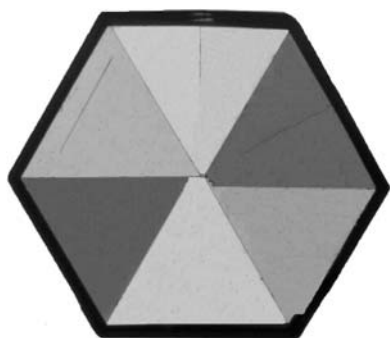


Fig. 3.3.6.7. Pseudo-hexagonal growth twin of K_2SO_4 showing six sector domains in three orientation states. (001) plate, about 1 mm thick and 5 mm in diameter, between polarizers deviating by 45° from crossed position for optimal contrast of all domains. The crystal was precipitated from aqueous K_2SO_4 solution containing 5% S_2O_3 ions. Courtesy of M. Moret, Milano.

- (4) Twin law representative: 'reflection across $(11\bar{2})$ ';
Alternative twin operations: line (3) of case (a) above;
Reduced composite symmetry: $\mathcal{K}^* = 31m'$ (order 6).

The restriction to only one of the four spinel twin axes $\langle 111 \rangle$ combined with the application of the coset expansion to the *reduced eigensymmetry* \mathcal{H}^* always leads to a crystallographic composite symmetry \mathcal{K}^* . The supergroup generated from the *full eigensymmetry*, however, would automatically include the other three spinel twin axes and thus would lead to the infinite sphere group $m\bar{3}c$, i.e. would imply infinitely many cosets and (equivalent) twin laws. Higher-order spinel twins are discussed in Section 3.3.8.3.

3.3.6.7. Growth and transformation twins of K_2SO_4

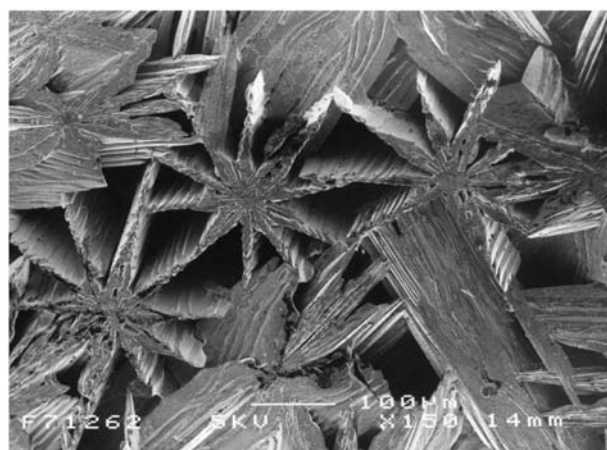
K_2SO_4 has an orthorhombic pseudo-hexagonal room-temperature phase with point group $\mathcal{H} = mmm$ and axial ratio $b/a = \tan 60.18^\circ$, and a hexagonal high-temperature phase (> 853 K) with supergroup $\mathcal{G} = 6/m2/m2/m$. It develops pseudo-hexagonal growth-sector twins with equivalent twin reflection planes (110) and $(1\bar{1}0)$ which are also composition planes, as shown in Fig. 3.3.6.7. As discussed in Sections 3.3.2.3.2 and 3.3.4.4 under (iii), this corresponds to a pseudo-threefold twin axis which, in combination with the twofold *eigensymmetry* axis, is also a pseudo-hexagonal twin axis. The extended composite symmetry is

$$\mathcal{K}(6) = \mathcal{K}(3) = 6(2)/m2/m2/m.$$

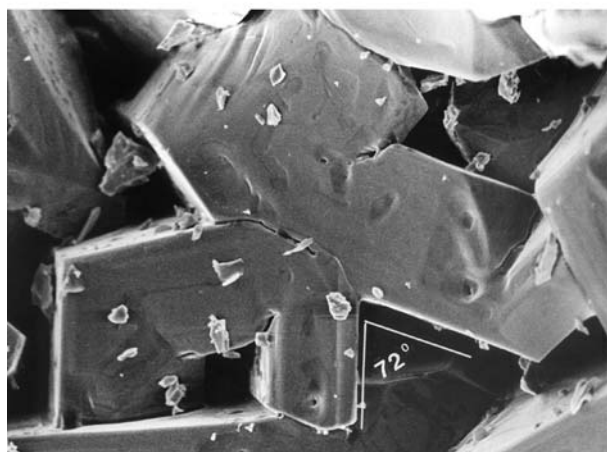
Upon heating above 853 K, the growth-sector twinning disappears. On cooling back into the low-temperature phase, transformation twinning ('domain structure') with three systems of lamellar domains appears. The three orientation states are identical for growth and transformation twins, but the morphology of the twins is not: sectors *versus* lamellae. The composite symmetry \mathcal{K} of the twins at room temperature is the true structural symmetry \mathcal{G} of the 'parent' phase at high temperatures.

3.3.6.8. Pentagonal–decagonal twins

As was pointed out in Note (8) of Section 3.3.2.4 and in part (iii) of Section 3.3.4.4, there exist twin axes with noncrystallographic multiplicities $n = 5, 7, 8$ etc. Twins with five- or tenfold rotations are frequent in intermetallic compounds. As an example, $FeAl_4$ is treated here (Ellner & Burkhardt, 1993; Ellner, 1995). This compound is orthorhombic, $2/m2/m2/m$, with an axial ratio close to $c/a = \tan 72^\circ$, corresponding to a pseudo-fivefold axis along $[010]$ and equivalent twin mirror planes (101) and $(\bar{1}01)$, which are about 36° apart. In an ideal intergrowth, this leads to a cyclic pseudo-pentagonal or pseudo-decagonal sector



(a)



(b)

Fig. 3.3.6.8. Pentagonal–decagonal twins. (a) Decagonal twins in the shape of tenfold stars on the surface of a bulk alloy, formed during the solidification of a melt of composition $Ru_8Ni_{15}Al_{77}$. Scanning electron microscopy picture. Typical diameter of stars *ca.* 200 μm . The arms of the stars show parallel intergrowth. (b) Pentagonal twin aggregate of Fe_4Al_{13} with morphology as grown in the orthorhombic high-temperature phase, showing several typical 72° angles between neighbouring twin partners (diameter of aggregate *ca.* 200 μm). Orthorhombic lattice parameters $a = 7.7510$, $b = 4.0336$, $c = 23.771$ Å, space group $Bmmm$. The parameters c and a approximate the relation $c/a = \tan 72^\circ$; the pseudo-pentagonal twin axis is $[010]$. On cooling, the monoclinic low-temperature phase is obtained. The twin reflection planes in the orthorhombic unit cell are (101) and $(10\bar{1})$, in the monoclinic unit cell (100) and (201) ; cf. Ellner & Burkhardt (1993, Fig. 10), Ellner (1995). Both parts courtesy of M. Ellner, Stuttgart.

twin (Fig. 3.3.6.8). All features of this twinning are analogous to those of pseudo-hexagonal aragonite, treated in Section 3.3.2.3.2, and of K_2SO_4 , described above as Example 3.3.6.7.

The intersection symmetry of all twin partners is $\mathcal{H}^* = 12/m1$; the reduced composite symmetry \mathcal{K}^* of a domain pair in contact is $2'/m2/m2'/m$. The extended composite symmetry of the ideal pentagonal sector twin is $\mathcal{K}(10) = \mathcal{K}(5) = 10(2)/m2/m2/m$.

3.3.6.9. Multiple twins of rutile

Rutile with *eigensymmetry* $4/m2/m2/m$ develops growth twins with coinciding twin reflection and composition plane $\{011\}$. Owing to its axial ratio $a/c = \tan 57.2^\circ$, the tetragonal c axes of the two twin partners form an angle of 114.4° . The intersection symmetry of the two domains is $\mathcal{H}^* = 2/m$ along the common direction $[100]$. The reduced composite symmetry of the domain pair is $\mathcal{K}^* = 2/m2'/m'2'/m'$, with the primed twin elements parallel and normal to the plane (011) . A twin of this type, consisting of two domains, is called an 'elbow twin' or a 'knee twin', and is shown in Fig. 3.3.6.9(a).

3.3. TWINNING OF CRYSTALS

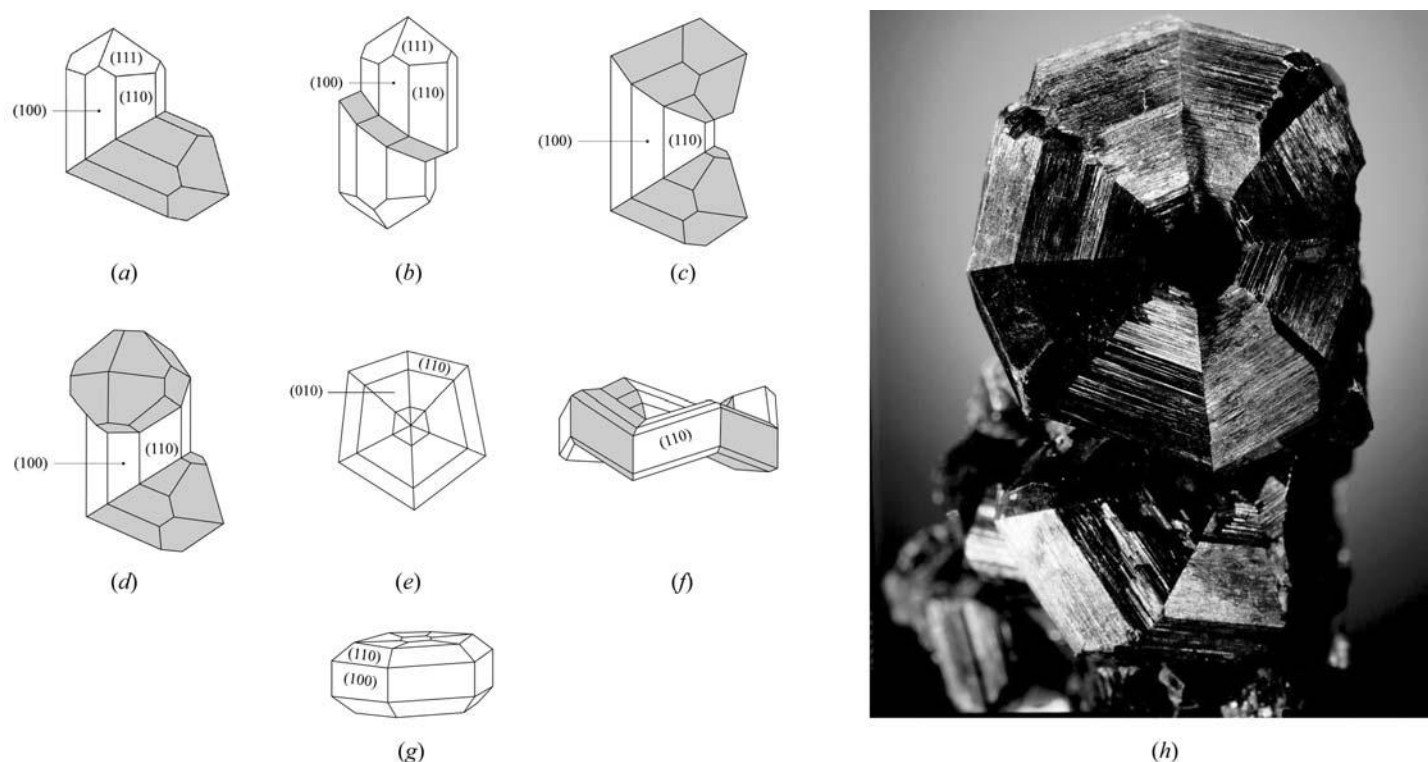


Fig. 3.3.6.9. Various forms of rutile (TiO_2) twins, with one or several equivalent twin reflection planes $\{011\}$. (a) Elbow twin (two orientation states). (b) Twin with two orientation states. One component has the form of an inserted lamella. (c) Triple twin (three orientation states) with twin reflection planes (011) and $(0\bar{1}1)$. (d) Triple twin with twin reflection planes (011) and (101) . (e) Cyclic sixfold twin with six orientation states. Two sectors appear strongly distorted due to the large angular excess of 35.6° . (f) Cyclic eightfold twin with eight orientation states. (g) Perspective view of the cyclic twin of (e). (h) Photograph of a rutile eightling (ca. 15 mm diameter) from Magnet Cove, Arkansas (Geologisk Museum, Kopenhagen). Parts (a) to (e) courtesy of H. Strunz, Unterwössen, cf. Ramdohr & Strunz, 1967, p. 512. Photograph (h) courtesy of M. Medenbach, Bochum.

In point group $4/m2/m2/m$, there exist four equivalent twin reflection planes $\{011\}$ (four different twin laws) with angles of 65.6° between (001) and $(0\bar{1}1)$ and 45° between (011) and (101) , leading to a variety of multiple twins. They may be linear polysynthetic or multiple elbow twins, or any combination thereof (Fig. 3.3.6.9). Very rare are complete cyclic sixfold twins with a large angular excess of $6 \times 5.6^\circ = 33.6^\circ$ (corresponding formally to a '5.5-fold' twin axis) and extended composite pseudosymmetry $\mathcal{K}(6) = 6(2)/m2/m2/m$, or cyclic eightfold twins with a nearly exact fit of the sectors and a morphological pseudo-8 twin axis. In the 'sixling', the tetragonal axes of the twin components are coplanar, whereas in the 'eightling' they alternate 'up and down', exhibiting in ideal development the morphological symmetry $82m$ of the twin aggregate. The extended composite symmetry is $\mathcal{K}(8) = 8(1)/m2/m2/m$ with eight twin components, each of different orientation state. These cyclic twins are depicted in Figs. 3.3.6.9(e), (f), (g) and (h).

The sketch of the 'eightling' in Fig. 3.3.6.9(f) suggests a hole in the centre of the ring, a fact which would pose great problems for the interpretation of the origin of the twin: how do the members of the ring 'know' when to turn and close the ring without an offset? Fig. 3.3.6.9(h) suggests that the ring is covered at the back, i.e. originates from a common point (nucleus). This was confirmed by a special investigation of another 'eightling' from Magnet Cove (Arkansas) by Lieber (2002): the 'eightling' started to grow from the nucleus and developed into the shape of a funnel with an opening of increasing diameter in the centre. This proves the nucleation growth of the ring (cf. Section 3.3.7.1.1).

3.3.6.10. Variety of twinning in gibbsite, $\text{Al}(\text{OH})_3$

Gibbsite (older name: hydrargillite) forms a pronounced layer structure with a perfect cleavage plane (001) . It is monoclinic with eigensymmetry $\mathcal{H} = 12/m1$, but strongly pseudo-hexagonal with

an axial ratio $b/a = \tan 30.4^\circ$. In contrast to most other pseudo-hexagonal crystals, the twofold eigensymmetry axis b is not parallel but normal to the pseudo-hexagonal c axis. The normal to the cleavage plane (001) is inclined by $\beta - 90^\circ = 4.5^\circ$ against $[001]$. Owing to the pseudo-hexagonal metrics of the plane (001) , the lattice planes (110) and $(\bar{1}10)$, equivalent with respect to the eigensymmetry $\mathcal{H} = 2/m$, form an angle of 60.8° .

The following four significant twin laws have been observed by Brögger (1890):

(i) *(001) reflection twin*: the cleavage plane (001) acts both as twin mirror and composition plane. The pseudo-hexagonal axes $[001]$ of both partners are inclined to each other by 9.0° . This twin law is quite common in natural and synthetic gibbsite.

(ii) *(100) reflection twin*: the twin mirror plane (100) is also the composition plane. The angle between the (001) planes of both partners is 9.0° , as in (i); the pseudo-hexagonal axes $[001]$ of both partners are parallel. This twin law is not common.

(iii) *(110) reflection twin*: again, twin mirror plane and composition plane coincide. The two (001) planes span an angle of 4.6° . This twin law is very rare in nature, but is often observed in synthetic materials. A sixfold sector twin of synthetic gibbsite, formed by cyclic repetition of $\{110\}$ twin reflection planes 60.8° apart, is shown in Fig. 3.3.6.10. The pseudo-hexagonal axis $[001]$ is common to all domains. Since the (001) plane is inclined towards this axis at 94.5° , the six (001) facets of the twinned crystal form a kind of 'umbrella' with $[001]$ as umbrella axis (Fig. 3.3.6.10a). This (001) umbrella faceting was recently observed in twinned synthetic gibbsite crystals by Sweegers *et al.* (1999).

In contrast to orthorhombic aragonite with only three pseudo-hexagonal orientation states, these gibbsite twins exhibit six different orientation states. This is due to the absence of any eigensymmetry element along the pseudo-hexagonal axis $[001]$. The intersection symmetry of all orientation states is $\bar{1}$. The reduced composite symmetry of a domain pair is $\mathcal{K}^* = 12'/m'1$, with m' the twin mirror plane (110) .

3. PHASE TRANSITIONS, TWINNING AND DOMAIN STRUCTURES

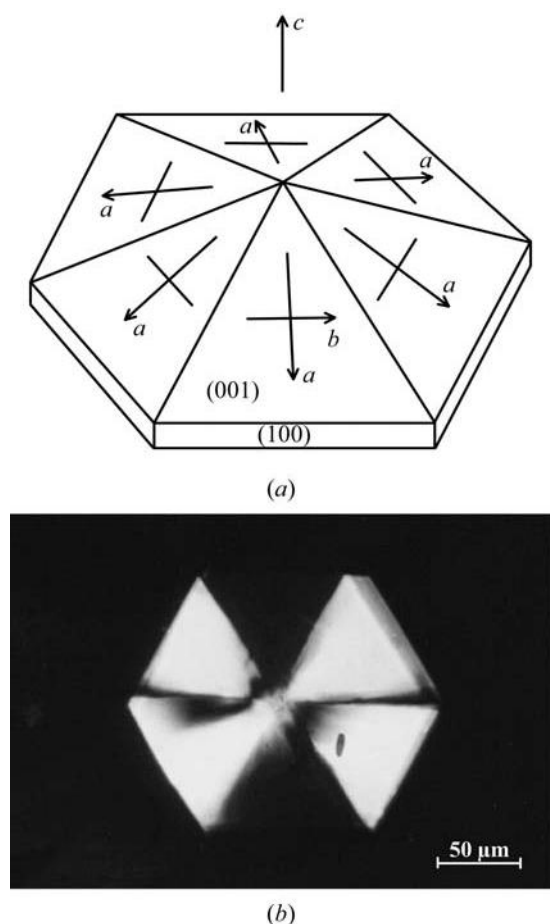


Fig. 3.3.6.10. Sixfold reflection twin of gibbsite, $\text{Al}(\text{OH})_3$, with equivalent (110) and $(\bar{1}\bar{1}0)$, both as twin mirror and composition planes. (a) Perspective view of a tabular sixfold sector twin with pseudo-hexagonal twin axis c . In each sector the monoclinic b axis is normal to the twin axis c , whereas the a axis slopes slightly down by about 4.5° ($\beta = 94.5^\circ$), leading to an umbrella-like shape of the twin. (b) Polarization micrograph of a sixfold twinned hexagon (six orientation states) of the shape shown in (a). Pairs of opposite twin components have the same optical extinction position. Courtesy of Ch. Sweepers, PhD thesis, University of Nijmegen, 2001.

(iv) ‘Median law’: According to Brögger (1890), this twin law implies exact parallelism of non-equivalent edges $[110]_{\text{I}}$ and $[010]_{\text{II}}$, and *vice versa*, of partners I and II. The twin element is an irrational twofold axis parallel to (001) , bisecting *exactly* the angle between $[110]$ and $[010]$, or alternatively, an irrational twin reflection plane normal to this axis. This interesting orientation relation, which has been observed so far only for gibbsite, does not obey the minimum condition for twinning as set out in Section 3.3.2.2. An alternative interpretation, treating these twins as *rational* $[130]$ rotation twins, is given by Johnsen (1907), *cf.* Tertsch (1936), pp. 483–484. Interestingly, this strange ‘twin law’ is the most abundant one among natural gibbsite twins.

3.3.6.11. Plagioclase twins

From the point of view of the relationship between pseudosymmetry and twinning, triclinic crystals are of particular interest. Classical mineralogical examples are the plagioclase feldspars with the ‘albite’ and ‘pericline’ twin laws of triclinic (crystal class $\bar{1}$) albite $\text{NaAlSi}_3\text{O}_8$ and anorthite $\text{CaAl}_2\text{Si}_2\text{O}_8$ (also microcline, triclinic KAlSi_3O_8), which all exhibit strong pseudosymmetries to the monoclinic feldspar structure of sanidine. Microcline undergoes a very sluggish monoclinic–triclinic phase transformation involving Si/Al ordering from sanidine to microcline, whereas albite experiences a quick, displacive transformation from monoclinic monalbite to triclinic albite.

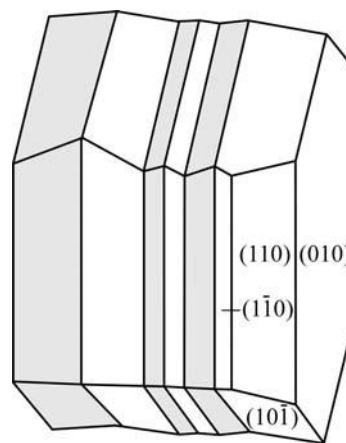


Fig. 3.3.6.11. Polysynthetic albite twin aggregate of triclinic feldspar, twin reflection and composition plane (010) .

The composite symmetries of these twins can be formulated as follows:

Albite law: reflection twin on (010) ; composition plane (010) rational (Fig. 3.3.6.11, Table 3.3.6.5). $\mathcal{K}_A = 2'/m'(\bar{1})$ with rational $m' \parallel (010)$.

Pericline law: twofold rotation twin along $[010]$; composition plane irrational $\parallel [010]$: ‘rhombic section’ (Fig. 3.3.6.12, Table 3.3.6.5). $\mathcal{K}_P = 2'/m'(\bar{1})$ with rational $2' \parallel [010]$.

Both twin laws resemble closely the monoclinic pseudosymmetry $2/m$ in two slightly different but distinct fashions: each twin law \mathcal{K} uses one rational twin element from $2/m$, the other one is irrational. The two frameworks of twin symmetry $2'/m'$ are inclined with respect to each other by about 4° , corresponding to the angle between b (direct lattice) and b^* (reciprocal lattice).

Both twins occur as growth and transformation twins: they appear together in the characteristic lamellar ‘transformation microclines’.

3.3.6.12. Staurolite

The mineral staurolite, approximate formula $\text{Fe}_2\text{Al}_9[\text{O}_6(\text{O},\text{OH})_2(\text{SiO}_4)_4]$, has ‘remained an enigma’ (Smith, 1968) to date with respect to the subtle details of symmetry, twinning, structure and chemical composition. A lively account of these problems is provided by Donnay & Donnay (1983). Staurolite is strongly pseudo-orthorhombic, C_{2mm} , and only detailed optical, morphological and X-ray experiments reveal monoclinic symmetry, $C_{12/m1}$, with $a = 7.87$, $b = 16.62$, $c = 5.65 \text{ \AA}$ and $\beta = 90^\circ$ within experimental errors (Hurst *et al.*, 1956; Smith, 1968).

Staurolite exhibits two quite different kinds of twins:

(i) *Twinning by high-order merohedry* (after Friedel, 1926, p. 56) was predicted by Hurst *et al.* (1956) in their detailed study of staurolite twinning. Staurolite crystals are supposed to consist of very fine scale monoclinic ($\mathcal{H} = 12/m1$) microtwins on $m(001)$, which yield a twin aggregate of orthorhombic composite symmetry $\mathcal{K} = 2'/m'2/m'2'/m'$. The coset consists of $m'(001)$, $m'(100)$, $2' \parallel [100]$ and $2' \parallel [001]$. Even though this twinning appears highly probable due to the pronounced structural pseudosymmetry (‘high-order merohedry’) of staurolite and has been mentioned by several authors (*e.g.* Smith, 1968), so far it has never been unambiguously proven. In particular, electron-microscopy investigations by Fitzpatrick (1976, quoted in

Table 3.3.6.5. Plagioclase: albite and pericline twins

| \mathcal{H} | $k \times \mathcal{H}$ (albite) | $k \times \mathcal{H}$ (pericline) |
|---------------|---------------------------------|------------------------------------|
| 1 | $m \parallel (010)$ rational | $2 \parallel [010]$ rational |
| $\bar{1}$ | $2 \perp (010)$ irrational | $m \perp [010]$ irrational |

3.3. TWINNING OF CRYSTALS

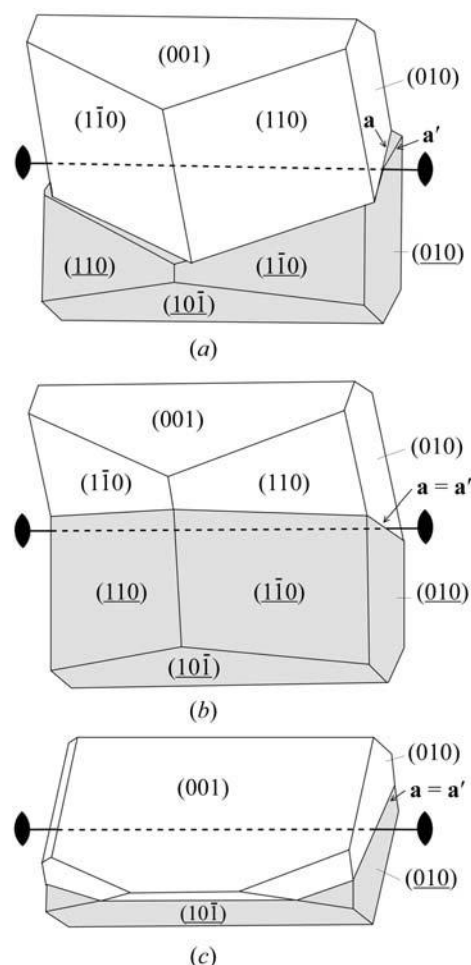


Fig. 3.3.6.12. Pericline twin of triclinic feldspar. Twofold twin axis [010]. (a) Twin with rational composition plane (001), exhibiting clearly the misfit (exaggerated) of the two adjacent (001) contact planes, as indicated by the crossing of lines **a** and **a'**. (b) The same (exaggerated) twin as in (a) but with irrational boundary along the 'rhombic section': fitting of contact planes from both sides (**a** and **a'** coincide and form a flat ridge). (c) Sketch of a real pericline twin with irrational interface ('rhombic section') containing the twin axis.

Bringhurst & Griffin, 1986, p. 1470) have failed to detect the submicroscopic twins.

(ii) Superimposed upon this first generation of microtwins very often occurs one or the other of two spectacular 'macroscopic' growth penetration twins in the shape of a cross, from which in 1792 the name 'stauros' of the mineral was given by Delam  theri  . The first detailed analysis of these twins was provided by Friedel (1926, p. 461).

(a) The 90  cross (Greek cross) with twin reflection and composition plane (031) is illustrated in Fig. 3.3.6.13(a) [cf. also the figures on p. 151 of Hurst *et al.* (1956) for less idealized drawings]. Plane (031) generates two twin components with an angle of $2 \arctan(b/3c) = 2 \arctan 0.9805 = 88.9^\circ$, very close to 90 , between their *c* axes. The equivalent twin reflection plane (  31) leads to the same angle, and both twin planes intersect along the lattice row [100].

With eigensymmetry $\mathcal{H} = 12/m1$, the intersection symmetry of the domain pair is $\mathcal{H}^* = 1$ and the reduced composite symmetry is $\mathcal{K}^* = 2'/m'$ [$m' = (031)$]. Owing to the special axial ratio $b/3c \approx 1$ mentioned above, the 90  cross is an excellent example of a pseudo-tetragonal twin. The extended composite symmetry of this twin is oriented along [100]:

$$\mathcal{K}(4) = 4(2)/m2/m2/m$$

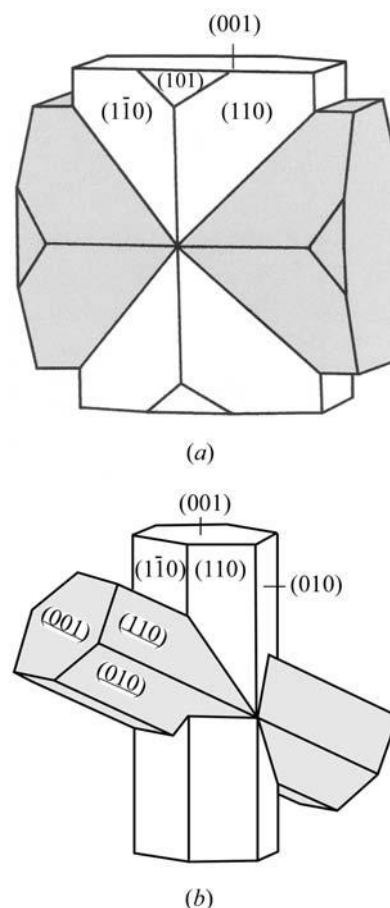


Fig. 3.3.6.13. Twinning of staurolite. (a) 90  cross ('Greek cross') with twin reflection and composition planes (031) and (  31). (b) 60  cross ('St Andrew's cross') with twin reflection and composition plane (231).

[cf. Section 3.3.4.2(iii)] with two domain states and all twin operations binary.

(b) The 60  cross (St Andrew's cross) with twin reflection plane (231) is illustrated in Fig. 3.3.6.13(b). It is the more abundant of the two crosses, with a ratio of 60  : 90  twins $\approx 9 : 1$ in one Georgia, USA, locality (cf. Hurst *et al.*, 1956, p. 152). Two equivalent twin mirror planes, (231) and (  31), intersecting in lattice row [102] exist. They include an angle of 60.4 . The action of one of these twin reflection planes leads to the 60  cross with an angle of 60  between the two *c* axes. The reduced composite symmetry of this twin pair is $\mathcal{K}^* = 2'/m'$ [$m' = (231)$].

In rare cases, penetration trillings occur by the action of both equivalent mirror planes, (231) and (  31), leading to three interpenetrating twin components with angles of about 60  between neighbouring arms.

Notes

(1) In many books, the twin reflection planes for the 90  cross and the 60  cross are given as (032) and (232) instead of (031) and (231). The former Miller indices refer to the morphological cell, which has a double *c* axis compared with the structural X-ray cell, used here.

(2) Friedel (1926) and Hurst *et al.* (1956) have derived both twin laws (031) and (231), mentioned above, from a multiple cubic pseudo-cell, the 'Mallard pseudo-cube'. This derivation will be presented in Section 3.3.9.2.4 as a characteristic example of 'twinning by reticular pseudo-merohedry'.

3.3.6.13. BaTiO  transformation twins

The perovskite family, represented by its well known member BaTiO , is one of the technically most important groups of dielectric materials, characterized by polar structures which

3. PHASE TRANSITIONS, TWINNING AND DOMAIN STRUCTURES

exhibit piezoelectricity, pyroelectricity and, most of all, ferroelectricity.

BaTiO₃ is cubic and centrosymmetric (paraelectric) above 393 K. Upon cooling below this temperature it transforms in one step (first-order transformation with small ΔH) into the ferroelectric tetragonal phase with polar space group $P4mm$. This transition is *translationengleich* of index $[i] = 6$. Hence there are domains of six possible orientation states at room temperature. The transformation can be theoretically divided into two steps:

(i) *Translationengleiche* symmetry reduction cubic $Pm\bar{3}m \rightarrow$ tetragonal $P4/mmm$ of index $[i_1] = 3$, leading to three sets of ferroelastic '90° domains', related by the (lost) cubic $\{110\}$ twin mirror planes or the (lost) cubic threefold axes. These three pseudo-merohedral orientation states point with their tetragonal c axes along the three former cube axes $[100]$, $[010]$ and $[001]$, thus including angles of nearly 90°.

(ii) Each of these centrosymmetric domains splits into two antiparallel polar ferroelectric '180° domains', whereby the space group $P4/mmm$ is *translationsgleich* reduced to $P4mm$ of index $[i_2] = 2$. The total index is: $[i] = [i_1] \cdot [i_2] = 6$.

The beautiful polysynthetic twin structure of BaTiO₃ is shown in the colour micrograph Fig. 3.4.1.1 in Chapter 3.4 of this volume.

3.3.6.14. Twins of twins

This term is due to Henke (2003) and refers to the simultaneous occurrence (superposition) of two or more different twin types (twin laws) in one and the same crystal. In *twins of twins*, one 'generation' of twin domains is superimposed upon the other, each with its own twin law. This may occur as a result of:

- (1) two successive phase transitions, each with its own twinning scheme, or
- (2) one phase transition with loss of two kinds of symmetry elements, or
- (3) a phase transition superimposed on an existing growth twin.

Typical examples are:

(i) the cubic–tetragonal ($m\bar{3}m \rightleftharpoons 4mm$) phase transition of BaTiO₃, described above. Here, 90° domains (due to the loss of the diagonal mirror planes) are superimposed by 180° domains (due to the loss of the inversion centres);

(ii) a similar case (tetragonal–monoclinic) is provided by the 'type case' of Henke (2003), (NO)₂VCl₆;

(iii) ammonium lithium sulfate exhibits pseudo-hexagonal growth-sector twins upon which lamellae of ferroelectric 180° domains are superimposed.

In this context, the term *complete twin* should be noted. It was coined by Curien & Donnay (1959) for the symmetry description of a crystal containing several merohedral twin laws. Their preferred example was quartz, but there are many relevant cases:

(i) The complete merohedral 'twins of twins' of quartz, *i.e.* the superposition of the Dauphiné, Brazil and Leydolt twins, can be formulated as follows:

Dauphine twin law: $321 \Rightarrow 6'(3)22'$

Brazil twin law: $321 \Rightarrow \bar{3}'(3)2/m'1(\bar{1}')$

Leydolt twin law: $321 \Rightarrow \bar{6}'(3)2m' = 3/m'2m'$.

Combination = 'complete twin': $6'(3)/m'2/m'2'/m'(\bar{1}')$; this symmetry corresponds to the hexagonal holohedral point group $6/m2/m2/m$, *cf.* Example 3.3.6.3.

(ii) Another example is provided by KLiSO₄ (crystal class 6), extensively investigated by Klapper *et al.* (1987):

Inversion twins: $6 \Rightarrow 6/m'(\bar{1}')$

Reflection twins: $6 \Rightarrow 6m'm'$

Rotation twins: $6 \Rightarrow 62'2'$.

Combination = 'complete twin': $6/m'2'/m'2'/m'(\bar{1}')$; this symmetry is isomorphic to the complete-twin symmetry of quartz, given above, and to the hexagonal holohedral point group $6/m2/m2/m$.

3.3.7. Genetic classification of twins

In Section 3.3.3, a classification of twins based on their morphological appearance was given. In the present section, twins are classified according to their origin. Genetic terms such as growth twins, transformation twins and mechanical twins were introduced by Buerger (1945) and are in widespread use. They refer to the *physical origin* of a given twin in contrast to its geometrical description in terms of a twin law. The latter can be the same for twins of different origin, but it will be seen that the generation of a twin has a strong influence on the shape and distribution of the twin domains. An extensive survey of the genesis of all possible twins is given by Cahn (1954).

3.3.7.1. Growth twinning

Growth twins can occur in nature (minerals), in technical processes or in the laboratory during growth from vapour, melt or solution. Two mechanisms of generation are possible for growth twins:

- (i) formation during nucleation of the crystal;
- (ii) formation during crystal growth.

3.3.7.1.1. Twinning by nucleation

In many cases, twins are formed during the first stages of spontaneous nucleation, possibly before the sub-critical nucleus reaches the critical size necessary for stable growth. This idea was originally proposed by Buerger (1945, p. 476) under the name *supersaturation twins*. There is strong evidence for twin formation during nucleation for penetration and sector twins, where all domains originate from one common well defined 'point' in the centre of the twinned crystal, which marks the location of the spontaneous nucleus.

Typical examples are the *penetration twins* of iron borate FeBO₃ (calcite structure), which are intergrowths of two rhombohedra, a reverse and an obverse one, and consist of 12 alternating twin domains belonging to two orientation states (see Example 3.3.6.5 and Fig. 3.3.6.4). Experimental details are presented by Klapper (1987) and Kotrbova *et al.* (1985). Further examples are the penetration twins of the spinel law (Example 3.3.6.6 and Fig. 3.3.6.6), the very interesting and complex [001] penetration twin of the monoclinic feldspar orthoclase (Fig. 3.3.7.1) and the *sector twins* of ammonium lithium sulfate with three orientation states (Fig. 3.3.7.2).

It should be emphasized that *all* iron borate crystals that are nucleated from flux or from vapour (chemical transport) exhibit penetration twinning. The occurrence of untwinned crystals has not been observed so far. Crystals of isostructural calcite and NaNO₃, on the other hand, do not exhibit penetration twins at all. In contrast, for ammonium lithium sulfate, NH₄LiSO₄, both sector-twinned and untwinned crystals occur in the same batch. In this case, the frequency of twin formation increases with higher supersaturation of the aqueous solution.

The formation of *contact twins* (such as the dovetail twins of gypsum) during nucleation also occurs frequently. This origin must always be assumed if both partners of the final twin have roughly the same size or if all spontaneously nucleated crystals in one batch are twinned. For example, all crystals of monoclinic

3.3. TWINNING OF CRYSTALS

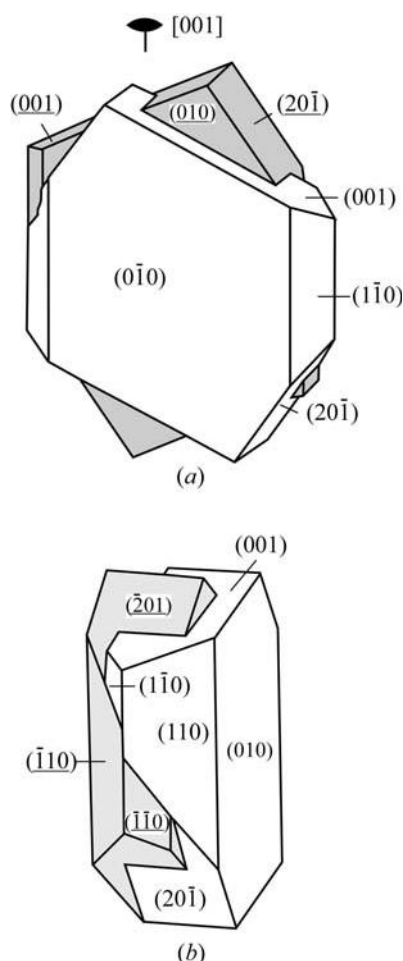


Fig. 3.3.7.1. Orthoclase (monoclinic K-feldspar). Two views, (a) and (b), of Carlsbad penetration twins (twofold twin axis $[001]$).

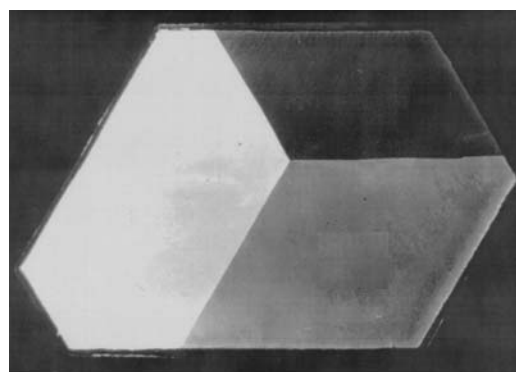
lithium hydrogen succinate precipitated from aqueous solution form dovetail twins without exception.

The process of twin formation during nucleation, as well as the occurrence of twins only for specific members of isostructural series (*cf.* Section 3.3.8.6), are not yet clearly understood. A hypothesis advanced by Senechal (1980) proposes that the nucleus first formed has a symmetry that is not compatible with the lattice of the (macroscopic) crystal. This symmetry may even be noncrystallographic. It is assumed that, after the nucleus has reached a critical size beyond which the translation symmetry becomes decisive, the nucleus collapses into a twinned crystal with domains of lower symmetry. This theory implies that for nucleation-twinned crystals, a metastable modification with a structure different from that of the stable macroscopic state may exist for very small dimensions. For this interesting theoretical model no experimental proof is yet available, but it appears rather reasonable; as a possible candidate of this kind of genesis, the rutile 'eightling' in Example 3.3.6.9 may be considered.

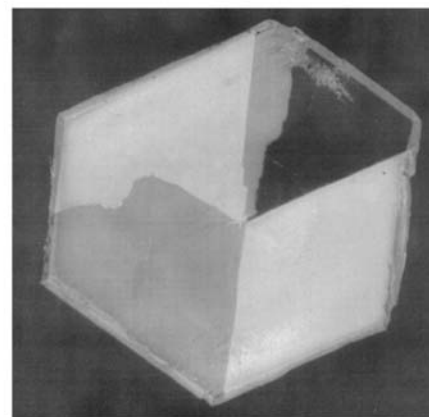
Recently, the ideas on twin nucleation have been experimentally substantiated by HRTEM investigations of multiple twins. The formation of these twins in nanocrystalline f.c.c. and diamond-type cubic materials, such as Ge, Ag and Ni, is explained by the postulation of various kinds of noncrystallographic nuclei, which subsequently 'collapse' into multiply twinned nanocrystals, *e.g.* fivefold twins of Ge; *cf.* Section 3.3.10.6. An extensive review is provided by Hofmeister (1998).

3.3.7.1.2. Twinning during crystal growth

(a) An alternative theory of twinning postulates the formation of a *two-dimensional nucleus* in twin position on a growth face of an existing macroscopic (previously untwinned) crystal. Such a



(a)



(b)

Fig. 3.3.7.2. Photographs of (001) plates (≈ 20 mm diameter, ≈ 1 mm thick) of NH_4LiSO_4 between crossed polarizers, showing sector growth twins due to metric hexagonal pseudosymmetry of the orthorhombic lattice. (a) Nearly regular threefold sector twin (three orientation states, three twin components). (b) Irregular sector twin (three orientation states, but five twin components).

mechanism was extensively described by Buerger (1945, pp. 472–475) and followed up by Menzer (1955) and Holser (1960). Obviously, this process is favoured by defects (inclusions, impurities) in the growth face. If the twin nucleus spreads out over the entire growth face, the twin boundary coincides with the growth face. This mechanism is generally assumed for the generation of large-area lamellar polysynthetic growth twins as observed for albite (Example 3.3.6.11 and Fig. 3.3.6.11). For a critical discussion of the origin of irrational twin interfaces in rotation twins such as the pericline twins see Cahn (1954, p. 408). It should be noted that this mechanism is possible only for twin boundaries of very low energy, since the boundary energy of the large interface has to be supplied in one step, *i.e.* during spreading out of one growth layer in twin position. It is obvious that this kind of twin formation can only occur if the twin boundary coincides with a prominent growth face (*F*-face, rarely *S*-face, according to Hartman, 1956).

(b) In the majority of growth twins, the twin boundary does *not* coincide with the growth face. This is the rule for merohedral twins, where the twin domains appear as 'inserts' in the shape of pyramids or lamellae extending from the initiating defects (mostly inclusions) into the direction of growth of the face on which the twin has started. Examples are the pyramid-shaped Brazil-twin inserts of quartz (Fronzel, 1962, Fig. 61 on p. 87) and the lamellar stripes of growth twins of KLiSO_4 (Klapper *et al.*, 1987, especially Fig. 5). Similar pyramidal twin inserts are observed for Dauphiné growth twins in natural and synthetic quartz. These twin morphologies in quartz, however, are often considerably modified after growth by (partial) ferroelastic switching of the domains, which is easily induced by stress at

3. PHASE TRANSITIONS, TWINNING AND DOMAIN STRUCTURES

elevated temperatures [cf. Section 3.3.7.3(iii)]. Illustrations of such Dauphiné twins are given by Frondel (1962, Fig. 49 on p. 78).

The growth-twin inserts as described above appear improbable for non-merohedral twins because unfavourable high-energy boundaries would be involved. As a consequence, it must be concluded that non-merohedral twins with boundaries *not* coinciding with a (prominent) growth face (e.g. dovetail twins of gypsum) must form during the nucleation stage of the crystal [Section 3.3.7.1.1 above].

(c) Another model of twin formation has been suggested by Schaskolsky & Schubnikow (1933). It is based on the idea that in the melt or solution the pre-existing small crystals make accidental contact with analogous faces $(hkl)_1$ and $(hkl)_2$ parallel, rotate and *agglutinate in twin position*, and continue to grow as a twin. This concept is also favoured by Buerger (1960*b*). The model of Schaskolsky & Schubnikow is based on their interesting experiments with many (≈ 1400) K-alum crystals (up to 0.5 mm in size), which sediment in solution on horizontal octahedron (111) and cube (100) faces of large alum crystals (20–30 mm in size). A statistical analysis of the orientation distribution of the sedimented crystals reveals a significantly increased frequency of (111)/(111) parallel intergrowths, of regular (001)/(111) intergrowths and of (111) spinel twins. The authors interpret this result as a rotation of the small crystals around the contact-face normal after deposition on the large crystal. This *initial contact plane* (ICP) model of twin formation was critically discussed by Senechal (1980) and considered as questionable, an opinion which is shared by the present authors.

(d) Finally, it is pointed out that twinning may drastically modify the regular *growth morphology* of (untwinned) crystals. A prominent example is the tabular shape of (111)-twinned cubic crystals with the large face parallel to the (111) contact plane. This is due to the increased lateral growth rate of the faces meeting in re-entrant edges (*re-entrant corner effect*; Hartman, 1956; Ming & Sunagawa, 1988). The (111) tabular shape of twinned cubic crystals plays an important role for photographic materials such as silver bromide, AgBr (Buerger, 1960*b*; Bögels *et al.*, 1997, 1998). A more extreme *habit modification* is exhibited by the $\langle 110 \rangle$ growth needles of cubic AgBr, which contain two $\{111\}$ twin planes intersecting along $\langle 110 \rangle$ (Bögels *et al.*, 1999).

The phenomenon of habit modification by twinning has been developed further by Senechal (1976, 1980), who presents an alternative model of the genesis of penetration twins (cf. Section 3.3.7.1.1 above): initial cubic (111) contact twins consisting of two octahedra change their habit during growth so as to form two interpenetrating cubes of the spinel law. As a further example, chabasite is cited.

(e) During *melt growth* of the important cubic semiconductors with the diamond structure (Si, Ge) and sphalerite (zinc sulfide) structure (e.g. indium phosphide, InP), twins of the spinel law [twin mirror plane (111) or twofold twin axis [111], cf. Section 3.3.10.3.3] are frequently formed. Whereas this twinning is relatively rare and can easily be avoided for Si and Ge, it is a persistent problem for the III–V and II–VI compound semiconductors, especially for InP and CdTe crystals, which have a particularly low $\{111\}$ stacking-fault energy (Gottschalk *et al.*, 1978). For Czochralsky growth, these twins are usually nucleated at ‘edge facets’ forming at the surface of the ‘shoulder’ (or ‘cone region’) where the growing crystal widens from the seed rod to its final diameter. Once nucleated, they proceed during further growth as bulk twins or, more frequently, as twin lamellae with sharp $\{111\}$ contact planes. For a [111] pulling direction, the three equivalent $\{111\}$ twin planes with inclination of 19.5° against the pull axis [111] are usually activated, whereas the perpendicular (111) twin plane does not or only rarely occurs (Bonner, 1981; Tohno & Katsui, 1986). These twins can be avoided by optimizing the growth conditions, in particular by the choice of a proper cone angle, which is the most crucial parameter. A mechanism of the $\{111\}$ twin formation of III–V compound semiconductors was

suggested by Hurle (1995) and experimentally confirmed for InP, using synchrotron-radiation topography combined with chemical etching and Normarski microscopy, by Chung *et al.* (1998) and Dudley *et al.* (1998). A comprehensive X-ray topographic study of (111) twinning in indium phosphide crystals, grown by the liquid-encapsulated Czochralski technique, and its interaction with dislocations is presented by Tohno & Katsui (1986).

(f) It should be noted lastly that ‘*annealing twins*’ (which are an important subject in metallurgy) are not treated in this section, because they are considered to be part of bicrystallography. These twins are formed during recrystallization and grain growth in annealed polycrystalline materials (cf. Cahn, 1954, pp. 399–401).

3.3.7.2. Transformation twinning

A solid-to-solid (polymorphic) phase transition is – as a rule – accompanied by a symmetry change. For displacive and order-disorder transitions, the symmetries of the ‘parent phase’ (prototype phase) \mathcal{G} and of the ‘daughter phase’ (deformed phase) \mathcal{H} exhibit frequently, but not always, a group-subgroup relation. During the transition to the low-symmetry phase the crystal usually splits into different domains. Three cases of transformation-twin domains are distinguished:

(i) The symmetry operations suppressed during the transition belong to the point group \mathcal{G} of the high-symmetry (prototype) phase, whereas the lattice, except for a small affine deformation, is unchanged (*translationengleiche subgroup*). In this case, the structures of the domains have different orientations and/or different handedness, both of which are related by the suppressed symmetry elements. Thus, the transition induces twins with the suppressed symmetry elements acting as twin elements (twin law). The number of *orientation states* is equal to the index $[i] = |\mathcal{G}|/|\mathcal{H}|$ of the group-subgroup relation, i.e. to the number of cosets of \mathcal{G} with respect to \mathcal{H} , including \mathcal{H} itself; cf. Section 3.3.4.1. If, for example, a threefold symmetry axis is suppressed, three domain states related by approximate 120° rotations will occur (for the problems of pseudo- n -fold twin axes, see Section 3.3.2.3.2). A further well known example is the α – β phase transformation of quartz at 846 K. On cooling from the hexagonal β phase (point group 622) to the trigonal α phase (point group 32), the twofold rotation $2_z = 6^\circ$, contained in the sixfold axis of β -quartz, is suppressed, and so are the other five rotations of the coset [cf. Example 3.3.6.3.1]. Consequently, two domain states appear (Dauphiné twins). These twins are usually described with the twofold axis along $[001]$ as twin element.

(ii) If a lattice translation is suppressed without change of the point-group symmetry (*klassengleiche subgroup*), i.e. due to loss of cell centring or to doubling (tripling *etc.*) of a lattice parameter, *translation domains* (antiphase domains) are formed (cf. Wondratschek & Jeitschko, 1976). The suppressed translation appears as the fault vector of the *translation boundary* (antiphase boundary) between the domains. Recently, translation domains were called ‘translation twins’ (T-twins, Wadhawan, 1997, 2000), cf. Section 3.3.2.4, Note (7).

(iii) The two cases can occur together, i.e. point-group symmetry and translation symmetry are both reduced in one phase transition (*general subgroup*). Here caution in the counting of the number of domain states is advisable since now orientation states and translation states occur together.

Well known examples of ferroelastic transformation twins are K_2SO_4 (Example 3.3.6.7) and various perovskites (Example 3.3.6.13). Characteristic for non-merohedral (ferroelastic) transformation twins are their planar twin boundaries and the many parallel (lamellar) twin domains of nearly equal size. In contrast, the twin boundaries of merohedral (non-ferroelastic) transformation twins, e.g. Dauphiné twins of quartz, often are curved, irregular and non-parallel.

3.3. TWINNING OF CRYSTALS

Transformation twins are closely related to the topic of *domain structures*, which is extensively treated in Chapter 3.4 of this volume.

A generalization of the concept of transformation twins includes twinning due to structural relationships in a family of related compounds ('structural twins'). Here the parent phase is formed by the high-symmetry 'basic structure' ('aristotype') from which the 'deformed structures' and their twin laws, occurring in other compounds, can be derived by subgroup considerations similar to those for actual transformation twins. Well known families are ABX_3 (perovskites) and A_2BX_4 (Na_2SO_4 - and K_2SO_4 -type compounds). In Example (3) of Section 3.3.9.2.4, growth twins among MeX_2 dichalcogenides are described in detail.

3.3.7.3. Mechanical twinning

Under mechanical load, some crystals can be 'switched' – partly or completely – from one orientation state into another. This change frequently proceeds in steps by the switching of domains. As a rule, the new orientation is related to the original one by an operation that obeys the definition of a twin operation (cf. Section 3.3.2.3). In many cases, the formation of *mechanical twins* (German: *Druckzwillinge*) is an essential feature of the plasticity of crystals. The deformation connected with the switching is described by a homogeneous shear. The domain arrangement induced by mechanical switching is preserved after the mechanical load is released. In order to re-switch the domains, a mechanical stress of opposite sign (coercive stress) has to be applied. This leads to a *hysteresis* of the stress–strain relation. In many cases, however, switching cannot be repeated because the crystal is shattered.

All aspects of mechanical twinning are reviewed by Cahn (1954, Section 3). A comprehensive treatment is presented in the monograph *Mechanical Twinning of Crystals* by Klassen-Neklyudova (1964). A brief survey of mechanical twinning in metals is given by Barrett & Massalski (1966).

With respect to symmetry, three categories of mechanical twins are distinguished in this chapter:

(i) *Mechanical twinning in the 'traditional' sense*. This kind of twinning has been studied by mineralogists and metallurgists under the name *deformation twins* for a long time. Well known examples are the deformation twins of calcite, galena, chalcopryrite and cubic metals. The characteristic feature is the non-existence of a real or virtual *parent phase* with a *crystallographic supergroup*. From a symmetry point of view, this means that the composite symmetry of the twin is noncrystallographic [cf. Section 3.3.4.4(ii)]. This case is illustrated by the famous deformation twins of calcite (Fig. 3.3.7.3): The *eigensymmetry* \mathcal{H} of calcite is $32/m$, and the most conspicuous twin element is the twin reflection plane $(01\bar{1}2)$ which is parallel to an edge of the cleavage rhombohedron $\{10\bar{1}1\}$. The extension of the *eigensymmetry* by this twin operation does not lead to a crystallographic composite symmetry, but the reduced composite symmetry is crystallographic, $\mathcal{K}^* = 2/m\ 2/m\ 2/m$.

Another famous case is that of the $\Sigma 3$ deformation twins of cubic metals that obey the spinel law of mineralogy [most conspicuous twin element: reflection plane parallel to (111)]. The extension of the *eigensymmetry* $4/m\bar{3}2/m$ by the twin operation leads to a noncrystallographic composite symmetry. The reduced composite symmetry \mathcal{K}^* , which is constructed from the intersection symmetry \mathcal{H}^* , however, is crystallographic (cf. Example 3.3.6.6).

A description of the (plastic) deformation by twinning in terms of strain ellipsoids is presented in Section 3.3.10.1.

(ii) *Ferroelastic twinning*. In 1970, a special category of mechanical twins was introduced and characterized by Aizu (1970a), who also coined the term *ferroelasticity*. This group of twins had already been treated, as part of the mechanical twins,

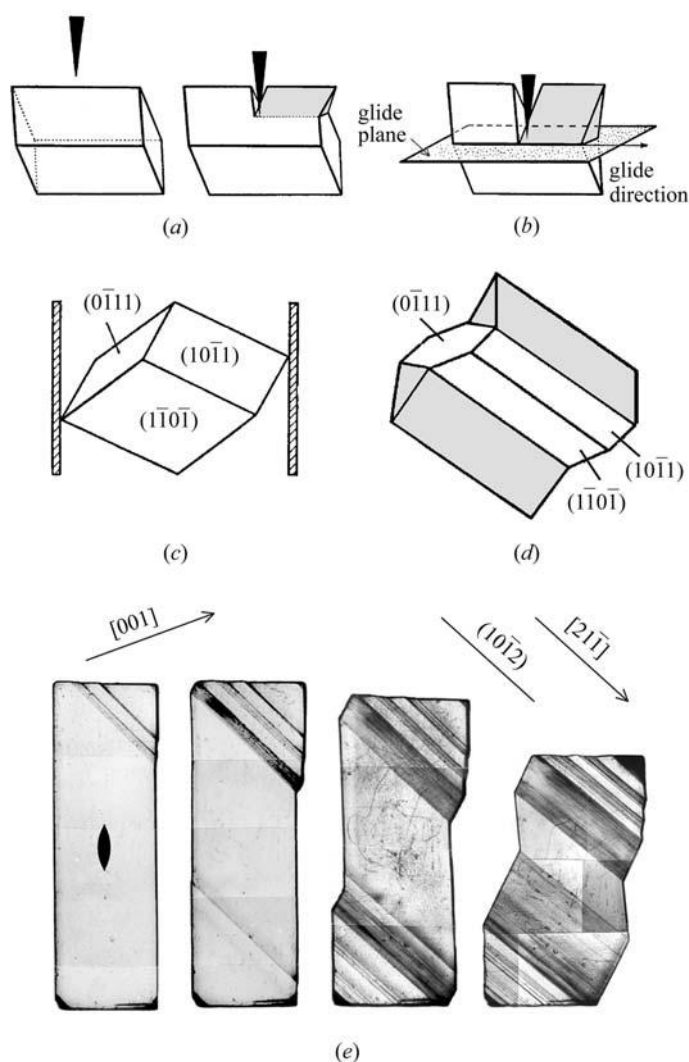


Fig. 3.3.7.3. Mechanical twins of calcite, CaCO_3 . All indices refer to the standard morphological cell [cf. Section 3.3.10.2.2, Example (5)]. (a) Generation of a deformation twin by a knife-edge impact (after Baumhauer, 1879). (b) Description as a glide process ('twin glide') on plane $(01\bar{1}2)$. (c), (d) Generation of deformation twins by compression of the cleavage rhombohedron $\{10\bar{1}1\}$ (Mügge, 1883). The shaded twin components have the same orientation. (e) Successive stages of deformation twinning of NaNO_3 (isotypic with calcite) by uniaxial compression. The compression axis (vertical) is chosen with an angle of 45° against the twin glide plane $(10\bar{1}2)$ and the glide direction $[21\bar{1}]$. The direction of the twofold axis is shown in the left-hand figure. Original size of the sample: ca. $3 \times 3 \times \sim 9.5$ mm. Part (e) courtesy of H. E. Hofer, PhD thesis, University of Cologne, 1989.

by Klassen-Neklyudova in her 1964 monograph mentioned above. The defining property of a ferroelastic crystal is the existence of a displacive (group–subgroup) transition, either real or virtual, from the parent phase into the ferroelastic phase with the essential requirement that parent and daughter phase belong to different crystal families (crystal systems). Only this symmetry feature allows for a *spontaneous shear strain* of the twin domains. The spontaneous deformations in a pair of domains have the same magnitude, but opposite signs. If the domain states can actually be switched into each other by a mechanical stress, the phase is called *ferroelastic*, otherwise it is called here *potentially ferroelastic*.

Ferroelastic twinning is not necessarily the result of a *real* phase transition. Switchable ferroelastic twins are frequently formed during growth. An example is orthorhombic ammonium sulfate, which can only be grown from aqueous solution and which frequently develops pseudo-hexagonal growth twins with three orientation states. Above about 353 K, the grown-in domains can easily be switched stepwise from one domain state into another by an appropriate shear stress, without the sample

3. PHASE TRANSITIONS, TWINNING AND DOMAIN STRUCTURES

ever undergoing a phase transition. Ammonium sulfate exhibits a virtual phase transition into a hexagonal prototype phase. It decomposes, however, at about 473 K, well before reaching the phase transition.

There are many examples (e.g. Rochelle salt) in which a ferroelastic domain structure can be generated by a real phase transition as well as by growth below the transition temperature. As a rule, the domain textures of growth and transformation twins are quite different. A detailed account of ferroelastic crystals is given by Salje (1993); a recent review is provided by Abrahams (1994).

(iii) *Ferrobielastic twinning*. Ferroelastic twinning implies a switchable spontaneous strain, i.e. a change of the unit-cell orientation in the different domains (*twinning with change of form*; Klassen-Neklyudova, 1964). In some species of crystals, however, mechanical twinning *without* change of the unit-cell orientation is possible (*twinning without change of form*). This can occur, for example, in trigonal crystals with a hexagonal *P* lattice. Here, the shape and orientation of the unit cell does not change from one domain to the other, and the twin is always merohedral (cf. Section 3.3.8). The atomic structure within the unit cell, however, is altered by the switching. The most famous example is the Dauphiné twinning of quartz, which can be induced by uniaxial stress along an appropriate direction. This effect was observed a long time ago by Judd (1888) and described in detail by Schubnikow & Zinserling (1932) and Zinserling & Schubnikow (1933). The ‘critical stress’ for the Dauphiné switching decreases with increasing temperature and becomes zero at the transition to the hexagonal phase at 846 K.

The property of a crystal to form ‘twins without change of form’ under mechanical stress was called *ferrobielasticity* by Newnham (1975). Aizu (1973) speaks of *second-order (ferro-elastic) state shifts*. It implies a change in the orientation of some tensorial properties. For Dauphiné twins of quartz, it is the elastic (fourth-rank) tensor that is responsible for the switching of the structure. Under uniaxial stress, a direction of high Young’s modulus¹ is transformed into a (compatible) direction of smaller Young’s modulus for which the material responds with a higher elastic yield. Note that this switching is induced by both compressive and tensile stress. A derivation of all crystal species capable of *second-order ferroic state shifts* by electric fields and mechanical stress, including a series of photographs showing the development of Dauphiné twins of quartz under stress, is presented by Aizu (1973).

For trigonal crystals with a *rhombohedral (R)* lattice, on the other hand, this switching implies the change of the obverse into the reverse rhombohedron and *vice versa*. In this case, the orientation of the primitive rhombohedral unit cell is changed, leading to ‘twinning with change of form’ (i.e. not to ferrobielasticity), even though the orientation of the triple hexagonal cell is not changed. This kind of twinning corresponds to the (0001) reflection twins of rhombohedral crystals and the (111) spinel twins of cubic crystals (cf. Examples 3.3.6.5 and 3.3.6.6). The switching from a cubic obverse rhombohedron into the reverse one actually takes place in the ‘ $\Sigma 3$ deformation twins’ of cubic metals [cf. part (i) above].

(iv) *Detwinning*. The generation of twins by mechanical stress allows, in reverse, the *detwinning* of crystals by the application of appropriate stress. This method has been extensively used for the elimination of Dauphiné twins in quartz (Thomas & Wooster, 1951; Klassen-Neklyudova, 1964, pp. 75–86). The presence of these ‘electrical’ twins impairs the function of piezoelectric devices, such as piezoelectric resonators, made from these crystals (Iliescu & Chirila, 1995; Iliescu *et al.*, 1997). Brazil twins of quartz, which also entail the reversal of the electric axes (cf. Fig. 3.3.6.2) cannot be detwinned. Mechanical detwinning by appropriate stress is also used to obtain single-domain crystals of the

ferroelastic $\text{YBa}_2\text{Cu}_3\text{O}_{7-\delta}$ high- T_c superconductor. In most cases, elevated temperatures reduce the critical stress required for domain switching.

It is characteristic of *ferroelectric* crystals that they can be switched into a single-domain state (i.e. ‘detwinned’ or ‘poled’) by a sufficiently strong (coercive) electric field of proper direction. It is, however, also possible to detwin *ferroelastic domains* by the application of electric fields. This occurs in *ferroelectric–ferroelastic* crystals, where ferroelectricity and ferroelasticity are coupled, i.e. where the reversal of the electric polarity is accompanied by (mechanical) switching of the ferroelastic domains into the other deformation state and *vice versa*. An outstanding and well known example is Rochelle salt, which undergoes an orthorhombic–monoclinic phase transition $222 \longleftrightarrow 2$ at about 297 K with coupled ferroelectricity and ferroelasticity in the monoclinic phase (cf. Zheludev, 1971, pp. 143, 226). An extensive crystal-optical study of the ferroelastic domain switching and detwinning in Rochelle salt by electric fields, including film records of the domain movements, was presented by Chernysheva [1951, 1955; quoted after Klassen-Neklyudova (1964), pp. 75–78 and Fig. 100].

(v) *Non-ferroelastic and co-elastic twins*. Phase transitions with symmetry changes within the same crystal family (crystal system) also exhibit a spontaneous deformation of the unit cell, but all orientation states have the same deformation, both in magnitude and orientation. Hence, a domain switching is not possible (except for ferrobielastic crystals treated above). Therefore, this kind of phase transition and its associated domain structure are called *non-ferroelastic*. Salje (1993) uses the term *co-elastic*. In crystallography, twins resulting from this kind of phase transition are grouped under *twins by merohedry* (cf. Section 3.3.8). Typical examples of non-ferroelastic and co-elastic materials are quartz (merohedral Dauphiné twins, phase transition $P3_121 \longleftrightarrow P622$ at 846 K) and calcite (transition $R\bar{3}c \longleftrightarrow R\bar{3}m$ at about 1523 K, cf. Salje, 1993, Chapter 2).

In conclusion, it is pointed out that twins with one and the same twin law can be generated in different ways. In addition to the twins of potassium sulfate mentioned above [growth twins, transformation twins and mechanical (ferroelastic) twins], the Dauphiné twinning of quartz is an example: it can be formed during crystal growth, by a phase transition and by mechanical stress [ferrobielasticity, cf. part (iii) above]. As a rule, the domain textures of a twinned crystal are quite different for growth twins, transformation twins and mechanical twins.

3.3.8. Lattice aspects of twinning

In the previous sections of this chapter, the symmetry relations and the morphological classification of twins have been presented on a macroscopic level, i.e. in terms of point groups. It would be ideal if this treatment could be extended to atomic dimensions, i.e. if twinning could be explained and even predicted in terms of space groups, crystal structures, interface structures and structural defects. This approach is presently only possible for a few specific crystals; for the majority of twins, however, only general rules are known and qualitative predictions can be made.

An early and very significant step towards this goal was the introduction of the lattice concept in the treatment of twinning (three-periodic twins). This was first done about a hundred years ago – based on the lattice analysis of Bravais – by Mallard (1879) and especially by Friedel (1904, 1926), in part before the advent of X-ray diffraction. The book by Friedel (1926), particularly Chapter 15, is the most frequently cited reference in this field. Later, Friedel (1933) sharpened his theories to include two further types of twins: ‘*macles monopériodiques*’ and ‘*macles dipériodiques*’, in addition to the previous ‘*macles tripériodiques*’,

¹ Defined in Section 1.3.3.1.

3.3. TWINNING OF CRYSTALS

see Section 3.3.8.2 below. These concepts were further developed by Niggli (1919, 1920/1924/1941).

The lattice aspects of twinning (*tri-periodic twins*) are discussed in this section and in Section 3.3.9. An important concept in this field is the *coincidence-site sublattice* of the twin in direct space and its counterpart in reciprocal space. Extensive use of the notion of coincidence-site lattices (CSLs) is made in *bicrystallography* for the study of grain boundaries, as briefly explained in Section 3.2.2.

The coincidence-site lattice and further related lattices (O- and DSC-lattices) were introduced into the study of bicrystals by Bollmann (1970, 1982) and were theoretically thoroughly developed by Grimmer (1989, 2003). Their applications to grain boundaries are contained in the works by Sutton & Balluffi (1995) and Gottstein & Shvindlerman (1999).

3.3.8.1. Basic concepts of Friedel's lattice theory

The basis of Friedel's (1904, 1926) lattice theory of twinning is the postulate that the coincidence-site sublattice common to the two twin partners (twin lattice) suffers no deviation (strict condition) or at most a slight deviation (approximate condition) in crossing the boundary between the two twin components (composition plane). This purely geometrical condition is often expressed as 'three-dimensional lattice control' (Santoro, 1974, p. 225), which is supposed to be favourable to the formation of twins.

In order to define the coincidence sublattice (twin lattice) of the two twin partners, it is assumed that their oriented point lattices are infinitely extended and interpenetrate each other. The lattice classification of twins is based on the degree of coincidence of these two lattices. The criterion applied is the dimension of the *coincidence-site subset* of the two interpenetrating lattices, which is defined as the set of all lattice points common to both lattices, provided that two initial points, one from each lattice, are brought to coincidence (common origin). This common origin has the immediate consequence that the concept of the twin displacement vector \mathbf{t} – as introduced in Note (8) of Section 3.3.2.4 – does not apply here. The existence of the coincidence subset of a twin results from the *crystallographic orientation relation* (Section 3.3.2.2), which is a prerequisite for twinning. This subset is one-, two- or three-dimensional (monoperiodic, diperiodic or triperiodic) twins.

If a coincidence relation exists between lattices in direct space, a complementary superposition relation occurs for their reciprocal lattices. This superposition can often, but not always, be detected in the diffraction patterns of twinned crystals.

3.3.8.2. Lattice coincidences, twin lattice, twin lattice index

Four types of (exact) *lattice coincidences* have to be distinguished in twinning:

(i) *No coincidence* of lattice points (except, of course, for the initial pair). This case corresponds to arbitrary intergrowth of two crystals or to a general bicrystal.

(ii) *One-dimensional coincidence*: Both lattices have only *one lattice row* in common. Of the seven binary twin operations listed in Section 3.3.2.3.1, the following three generate one-dimensional lattice coincidence:

(a) twofold rotation around a (rational) lattice row [twin operation (iii) in Section 3.3.2.3.1];

(b) reflection across an irrational plane normal to a (rational) lattice row (note that the coincidence would be three-dimensional if this plane were rational) [twin operation (iv)];

(c) twofold rotation around an irrational axis normal to a (rational) lattice row (complex twin, *Kantennormalengesetz*) [twin operations (v) and (vi)].

Lattices are always centrosymmetric; hence, for lattices, as well as for centrosymmetric crystals, the first two twin operations above belong to the same twin law. For noncentrosymmetric

crystals, however, the two twin operations define different twin laws.

(iii) *Two-dimensional coincidence*: Both lattices have only *one lattice plane* in common. The following two (of the seven) twin operations lead to two-dimensional lattice coincidence:

(a) reflection across a (rational) lattice plane [twin operation (i)];

(b) twofold rotation around an irrational axis normal to a (rational) lattice plane (note that the coincidence would be three-dimensional if this axis were rational) [twin operation (ii)].

Again, for lattices and centrosymmetric crystals both twin operations belong to the same twin law.

(iv) *Three-dimensional coincidence*: Here the coincidence subset is a three-dimensional lattice, the *coincidence-site lattice* or *twin lattice*. It is the three-dimensional sublattice common to the (equally or differently) oriented lattices of the two twin partners. The degree of three-dimensional lattice coincidence is defined by the *coincidence-site lattice index*, *twin lattice index* or *sublattice index* $[j]$, for short: *lattice index*. This index is often called Σ , especially in metallurgy. It is the volume ratio of the primitive cells of the twin lattice and of the (original) crystal lattice (*i.e.* $1/j$ is the 'degree of dilution' of the twin lattice with respect to the crystal lattice):

$$[j] = \Sigma = V_{\text{twin}}/V_{\text{crystal}}.$$

The lattice index is always an integer: $j = 1$ means *complete* coincidence (parallelism), $j > 1$ *partial* coincidence of the two lattices. The index $[j]$ can also be interpreted as elimination of the fraction $(j - 1)/j$ of the lattice points, or as index of the translation group of the twin lattice in the translation group of the crystal lattice. The coincidence lattice, thus, is the intersection of the oriented lattices of the two twin partners.

Twinning with $[j] = 1$ has been called by Friedel (1926, p. 427) *twinning by merohedry* ('*macles par mériédrie*') (for short: *merohedral twinning*), whereas twinning with $[j] > 1$ is called *twinning by lattice merohedry* or *twinning by reticular merohedry* ('*macles par mériédrie réticulaire*') (Friedel, 1926, p. 444). The terms for $[j] = 1$ are easily comprehensible and in common use. The terms for $[j] > 1$, however, are somewhat ambiguous. In the present section, therefore, the terms *sublattice*, *coincidence lattice* or *twin lattice* of index $[j]$ are preferred. Merohedral twinning is treated in detail in Section 3.3.9.

Complete and exact three-dimensional lattice coincidence ($[j] = 1$) always exists for inversion twins (of noncentrosymmetric crystals) [twin operation (vii)]. For reflection twins, complete or partial coincidence occurs if a (rational) lattice row $[uvw]$ is (exactly) perpendicular to the (rational) twin reflection plane (hkl); similarly for rotation twins if a (rational) lattice plane (hkl) is (exactly) perpendicular to the (rational) twofold twin axis $[uvw]$.

The systematic perpendicularity relations (*i.e.* relations valid independent of the axial ratios) for lattice planes (hkl) and lattice rows $[uvw]$ in the various crystal systems are collected in Table 3.3.8.1. No perpendicularity occurs for triclinic lattices (except for metrical accidents). The perpendicularity cases for monoclinic and orthorhombic lattices are trivial. For tetragonal (tet), hexagonal (hex) and rhombohedral (rhomb) lattices, systematic perpendicularity of planes and rows occurs only for the $[001]_{\text{tet}}$ and the $[001]_{\text{hex}}$ (or $[111]_{\text{rhomb}}$) zones, *i.e.* for planes parallel and rows perpendicular to these directions, in addition to the trivial cases $[001] \perp (001)$ or $[111] \perp (111)$. In cubic lattices, every lattice plane (hkl) is perpendicular to a lattice row $[uvw]$ (with $h = u$, $k = v$, $l = w$). More general coincidence relations were derived by Grimmer (1989, 2003).

The index $[j]$ of a coincidence or twin lattice can often be obtained by inspection; it can be calculated by using a formula for the auxiliary quantity j' as follows:

3. PHASE TRANSITIONS, TWINNING AND DOMAIN STRUCTURES

Table 3.3.8.1. Lattice planes (*hkl*) and lattice rows [*uvw*] that are mutually perpendicular (after Koch, 1999)

| Lattice | Lattice plane (<i>hkl</i>) | Lattice row [<i>uvw</i>] | Perpendicularity condition and quantity $j' = hu + kv + lw$ |
|---|------------------------------|----------------------------|---|
| Triclinic | — | — | — |
| Monoclinic (unique axis <i>b</i>) | (010) | [010] | — |
| Monoclinic (unique axis <i>c</i>) | (001) | [001] | — |
| Orthorhombic | (100) | [100] | — |
| | (010) | [010] | — |
| | (001) | [001] | — |
| Hexagonal and rhombohedral (hexagonal axes) | (<i>hki</i> 0) | [<i>uv</i> 0] | $u = 2h + k, v = h + 2k, j' = 2h^2 + 2k^2 + 2hk$ |
| | (0001) | [001] | — |
| Rhombohedral (rhombohedral axes) | (<i>h, k, -h - k</i>) | [<i>u, v, -u - v</i>] | $u = h, v = k, j' = 2h^2 + 2k^2 + 2hk$ |
| | (111) | [111] | — |
| Tetragonal | (<i>hk</i> 0) | [<i>uv</i> 0] | $u = h, v = k, j' = h^2 + k^2$ |
| | (001) | [001] | — |
| Cubic | (<i>hkl</i>) | [<i>uvw</i>] | $u = h, v = k, w = l; j' = h^2 + k^2 + l^2$ |

$$j' = hu + kv + lw \quad (\text{scalar product } \mathbf{r}_{hkl}^* \cdot \mathbf{t}_{uvw})$$

with sublattice index

$$\begin{aligned} [j] &= |j'| \text{ for } j' = 2n + 1 \\ &= |j'|/2 \text{ for } j' = 2n. \end{aligned}$$

Here, the indices of the plane (*hkl*) and of the perpendicular row [*uvw*] are referred to a primitive lattice basis (primitive cell). For centred lattices, described by conventional bases, modifications are required; these and further examples are given by Koch (1999). Formulae and tables are presented by Friedel (1926, pp. 245–252) and by Donnay & Donnay (1972). The various equations for the quantity j' are also listed in the last column of Table 3.3.8.1.

Note that in the tetragonal system for any (*hk*0) reflection twin and any [*uv*0] twofold rotation twin, the coincidence lattices are also tetragonal and have the same lattice parameter *c*. Further details are given by Grimmer (2003). An analogous relation applies to the hexagonal crystal family for (*hki*0) and [*uv*0] twins. In the cubic system, the following types of twin lattices occur:

- (111) and [111] twins: hexagonal *P* lattice (e.g. spinel twins);
- (*hk*0) and [*uv*0] twins: tetragonal lattice;
- (*hhl*) and [*uuw*] twins: orthorhombic lattice;
- (*hkl*) and [*uvw*] twins: monoclinic lattice.

Note that triclinic twin lattices are not possible for a cubic lattice.

After these general considerations of coincidence-site and twin lattices and their lattice index, specific cases of ‘triprimitive twins’ are treated in Section 3.3.8.3. In addition to the characterization of the twin lattice by its index [*j*], the Σ notation used in metallurgy is included.

3.3.8.3. Twins with three-dimensional twin lattices (‘triprimitive’ twins)

The following cases of exact superposition are distinguished:

(i) *Twins with* [*j*] = 1 ($\Sigma 1$ twins). Here, the crystal lattice and the twin lattice are identical, i.e. the coincidence (parallelism) of the two oriented crystal lattices is complete. Hence, any twin operation must be a symmetry operation of the point group of the lattice (holohedry), but not of the point group of the crystal. Consequently, this twinning can occur in ‘merohedral’ point groups only. This *twinning by merohedry (parallel-lattice twins, twins with parallel axes)* will be treated extensively in Section 3.3.9.

(ii) *Twins with* [*j*] = 2 ($\Sigma 2$ twins). This twinning does not occur systematically among the cases listed in Table 3.3.8.1, except for special metrical relations. Example: a primitive orthorhombic

lattice with $b/a = \sqrt{3}$ and twin reflection plane (110) or ($\bar{1}10$). The coincidence lattice is hexagonal with $a_{\text{hex}} = 2a$ and [*j*] = 2.

(iii) *Twins with* [*j*] = 3 ($\Sigma 3$ twins). Twins with [*j*] = 3 are very common among rhombohedral and cubic crystals (‘spinel law’) with the following two representative twin operations:

(a) twofold rotation around a threefold symmetry axis [111] (cubic or rhombohedral coordinate axes) or [001] (hexagonal axes);

(b) reflection across the plane (111) or (0001) normal to a threefold symmetry axis.

Both twin operations belong to the same twin law if the crystal is centrosymmetric. Well known examples are the (0001) contact twins of calcite, the penetration twins of iron borate, FeBO₃, with the calcite structure, and the spinel twins of cubic crystals (cf. Examples 3.3.6.5, 3.3.6.6 and Figs. 3.3.6.4–3.3.6.6). For crystals with a rhombohedral (*R*) lattice, the coincidence lattice is the primitive hexagonal (*P*) sublattice (whose unit cell is commonly used for the hexagonal description of rhombohedral crystals). Here, the two centring points inside the triple hexagonal *R* cell do not belong to the coincidence sublattice which is, hence, of index [*j*] = 3. The same holds for the spinel twins of cubic crystals, provided only one of the four threefold axes is involved in the twinning.

(iv) *Twins with* [*j*] > 3 ($\Sigma > 3$ twins). Whereas twins with [*j*] = 3 are very common and of high importance among minerals and metals, twins with higher lattice indices occur hardly at all. All these ‘high-index’ twins can occur systematically only in tetragonal, hexagonal, rhombohedral and cubic crystals, due to the geometric perpendicularity relations set out in Table 3.3.8.1. Note that for special lattice metrics (axial ratios and angles) they can occur, of course, in any crystal system. These special metrics, however, are not enforced by the crystal symmetry and hence the coincidences are not strict, but only ‘pseudo-coincidences’.

Examples

(1) Tetragonal twins with twin reflection planes {210} or {130}, or twofold twin axes $\langle 210 \rangle$ or $\langle 130 \rangle$ lead to [*j*] = 5, the largest value of [*j*] that has been found so far for tetragonal twins. The coincidence lattice is again tetragonal with $\mathbf{a}' = 2\mathbf{a} + \mathbf{b}$, $\mathbf{b}' = -\mathbf{a} + 2\mathbf{b}$, $\mathbf{c}' = \mathbf{c}$ and is shown in Fig. 3.3.8.1. An actual example, SmS_{1.9} (Tamazyan *et al.*, 2000b), is discussed in Section 3.3.9.2.4.

(2) There exist several old and still unsubstantiated indications for a [*j*] = 5 cubic garnet twin with twin reflection plane (210), cf. Arzruni (1887); Tschermak & Becke (1915, p. 594).

(3) *Klockmannite*, CuSe (Taylor & Underwood, 1960; Takeda & Donnay, 1965). This hexagonal mineral seems to be the only example for a hexagonal twin with [*j*] > 3. X-ray diffraction experiments indicate a reflection twin on (1340), corresponding

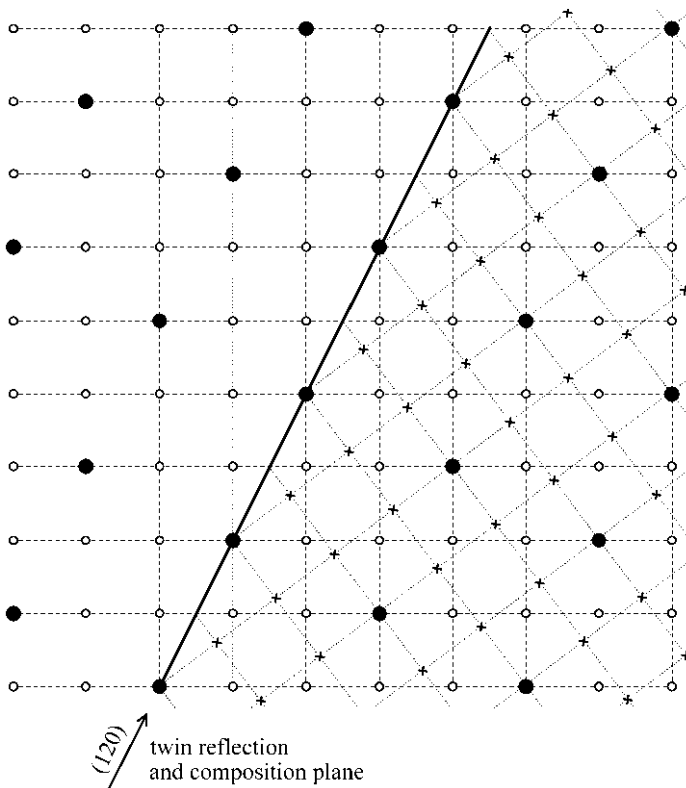


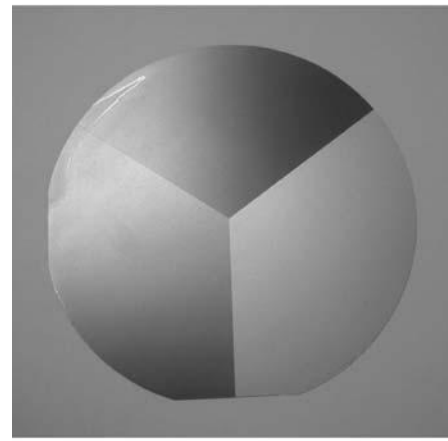
Fig. 3.3.8.1. Lattice relations of $\Sigma 5$ twins of tetragonal crystals with primitive lattice: twin mirror plane and composition plane (120) with twin displacement vector $\mathbf{t} = \mathbf{0}$. Small dots: lattice points of domain 1; small x: lattice points of domain 2; large black dots: $\Sigma 5$ coincidence lattice.

to $[j] = 13$. Later structural studies, however, suggest the possibility of disorder instead of twinning.

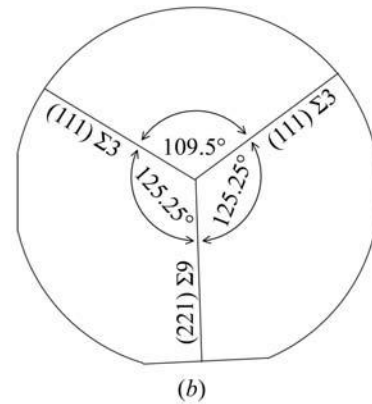
(4) *Galena, PbS* (NaCl structure). Galena crystals from various localities often exhibit lamellae parallel to the planes {441} which are interpreted as (441) reflection twins with $[j] = 33$ ($\Sigma 33$ twin) (cf. Niggli, 1926, Fig. 9k on p. 53). These natural twins are deformation and not growth twins. In laboratory deformation experiments, however, these twins could not be generated. A detailed analysis of twinning in PbS with respect to plastic deformation is given by Seifert (1928).

(5) For cubic metals and alloys *annealing twins* (*recrystallization twins*) with $[j] > 3$ are common. Among them *high-order twins* (*high-generation twins*) are particularly frequent. They are based on the $\Sigma 3$ (spinel) twins (first generation) which may coalesce and form 'new twins' with $\Sigma 9 = 3^2$ [second generation, with twin reflection plane (221)], $\Sigma 27 = 3^3$ [third generation, twin reflection plane (115)], $\Sigma 81 = 3^4$ [fourth generation, twin reflection plane (447)] etc. Every step to a higher generation increases Σ by a factor of three (Gottstein, 1984). An interesting and actual example is the artificial silicon *tricrystal* shown in Fig. 3.3.8.2, which contains three components related by two (111) reflection planes (first generation, two $\Sigma 3$ boundaries) and one (221) reflection plane (second generation, one $\Sigma 9$ boundary).

(6) The same type of tricrystal has been found in cubic magnetite (Fe_3O_4) nanocrystals grown from the biogenic action of magnetotactic bacteria in an aquatic environment (Devouard *et al.*, 1998). Here, HRTEM micrographs (Fig. 6 of the paper) show the same triple-twin arrangement as in the Si tricrystal above. The authors illustrate this triple twin by (111) spinel-type intergrowth of three octahedra exhibiting two $\Sigma 3$ and one $\Sigma 9$ domain pairs. The two $\Sigma 3$ interfaces are (111) twin reflection planes, whereas the $\Sigma 9$ boundary is very irregular and not a compatible planar (221) interface (i.e. not a twin reflection plane).



(a)



(b)

Fig. 3.3.8.2. (a) A (110) silicon slice (10 cm diameter, 0.3 mm thick), cut from a Czochralski-grown tricrystal for solar-cell applications. As seed crystal, a cylinder of three coalesced Si single-crystal sectors in (111) and (221) reflection-twin positions was used. Pulling direction [110] (Courtesy of M. Krühler, Siemens AG, München). (b) Sketch of the tricrystal wafer showing the twin relations [twin laws $m(111)$ and $m(221)$] and the Σ characters of the three domain pairs. The atomic structures of these (111) and (221) twin boundaries are discussed by Kohn (1956, 1958), Hornstra (1959, 1960) and Queisser (1963).

(7) A third instructive example is provided by the fivefold cyclic 'cozonal' twins (zone axis $[1\bar{1}0]$) of Ge nanocrystals (Neumann *et al.*, 1996; Hofmeister, 1998), which are treated in Section 3.3.10.6.5 and Fig. 3.3.10.11. All five boundaries between neighbouring domains (sector angles 70.5°) are of the $\Sigma 3(111)$ type. Second nearest ($2 \times 70.5^\circ$), third nearest ($3 \times 70.5^\circ$) and fourth nearest ($4 \times 70.5^\circ$) neighbours exhibit $\Sigma 9$, $\Sigma 27$ and $\Sigma 81$ coincidence relations (second, third and fourth Σ generation), respectively, as introduced above in (5). These relations can be described by the 'cozonal' twin reflection planes (111), (221), (115) and (447). Since $5 \times 70.5^\circ = 352.5^\circ$, an angular gap of 7.5° would result. In actual crystals this gap is compensated by stacking faults as shown in Fig. 3.3.10.11. A detailed treatment of all these cases, including structural models of the interfaces, is given by Neumann *et al.* (1996).

(8) Examples of (hypothetical) twins with $[j] > 1$ due to metrical specialization of the lattice are presented by Koch (1999).

3.3.8.4. Approximate (pseudo-)coincidences of two or more lattices

In part (iv) of Section 3.3.8.2, three-dimensional lattice coincidences and twin lattices (sublattices) were considered under two restrictions:

(a) the lattice coincidences (according to the twin lattice index $[j]$) are *exact* (not approximate);

3. PHASE TRANSITIONS, TWINNING AND DOMAIN STRUCTURES

(b) only *two* lattices are superimposed to form the twin lattice. In the present section these two conditions are relaxed as follows:

(1) In addition to exact lattice coincidences (as they occur for all merohedral twins) *approximate* lattice coincidences (pseudo-coincidences) are taken into account.

In this context, it is important to explain the meaning of the terms *approximate lattice coincidences* or *pseudo lattice coincidences* as used in this section. Superposition of two or more equal lattices (with a common origin) that are slightly misoriented with respect to each other leads to a three-dimensional moiré pattern of coincidences and anti-coincidences. The *beat period* of this pattern increases with decreasing misorientation. It appears sensible to use the term approximate or pseudo-coincidences only if the 'splitting' of lattice points is small within a sufficiently large region around the common origin of the two lattices. Special cases occur for reflection twins and rotation twins of pseudosymmetrical lattices. For the former, exact two-dimensional coincidences exist parallel to the (rational) twin reflection plane and the moiré pattern is only one-dimensional in the direction normal to this plane. Hence, the region of 'small splitting' is a two-dimensional (infinitely extended) thin layer of the twin lattice on both sides of the twin reflection plane [example: pseudo-monoclinic albite (010) reflection twins]. For rotation twins, the region of 'small splitting' is an (infinitely long) cylinder around the twin axis. On the axis the lattice points coincide exactly.

In general, a typical measure of this region, in terms of the reciprocal lattice, could be the size of a conventional X-ray diffraction photograph. Whereas the slightest deviations from exact coincidence lead to pseudo-coincidences, the 'upper limit of the splitting', up to which two lattices are considered as pseudo-coincident, is not definable on physical grounds and thus is a matter of convention and personal preference. As an angular measure of the splitting the *twin obliquity* has been introduced by Friedel (1926). This concept and its use in twinning will be discussed below in Section 3.3.8.5.

(2) The previous treatment of superposition of only two lattices is extended to multiple twins with several interpenetrating lattices which are related by a pseudo n -fold twin axis. Such a twin axis cannot be 'exact', no matter how close its rotation angle comes to the exact angular value. For this reason, twin axes of order $n > 2$ necessarily lead to *pseudo* lattice coincidences.

Here it is assumed that such pseudo-coincidences exist for any pair of neighbouring twin domains. As a consequence, pseudo-coincidences occur for all n domains. For this case, the following rules exist:

(i) Only n -fold twin axes with the crystallographic values $n = 3, 4$ and 6 lead to pseudo lattice coincidences of all domains. Example: cyclic triplets of aragonite.

(ii) The number of (interpenetrating) lattices equals the number of different domain states [cf. Section 3.3.4.4(iii)], viz.

6, 3 or 2 lattices for $n = 6$,

3 lattices for $n = 3$,

4 or 2 lattices for $n = 4$,

whereby the case '2 lattices' for $n = 6$ leads to exact lattice coincidence (merohedral twinning, e.g. Dauphiné twins of quartz).

(iii) There always exists *exact* (one-dimensional) coincidence of all lattice rows along the twin axis.

(iv) If there is a (rational) lattice plane normal to the twin axis, the splitting of the lattice points occurs only parallel to this plane. If, however, this lattice plane is pseudo-normal (i.e. slightly inclined) to the twin axis, the splitting of lattice points also has a small component along the twin axis.

3.3.8.5. Twin obliquity and lattice pseudosymmetry

The concept of *twin obliquity* has been introduced by Friedel (1926, p. 436) to characterize (metrical) pseudosymmetries of lattices and their relation to twinning. The obliquity ω is defined as the angle between the normal to a given lattice plane (hkl) and a lattice row $[uvw]$ that is not parallel to (hkl) and, *vice versa*, as the angle between a given lattice row $[uvw]$ and the normal to a lattice plane (hkl) that is not parallel to $[uvw]$. The twin obliquity is thus a quantitative (angular) measure of the pseudosymmetry of a lattice and, hence, of the deviation which the twin lattice suffers in crossing the composition plane (cf. Section 3.3.8.1).

The smallest mesh of the net plane (hkl) together with the shortest translation period along $[uvw]$ define a unit cell of a sublattice of lattice index $[j]$; j may be $= 1$ or > 1 [cf. Section 3.3.8.2(iv)]. The quantities ω and j can be calculated for any lattice and any (hkl)/ $[uvw]$ combination by elementary formulae, as given by Friedel (1926, pp. 249–252) and by Donnay & Donnay (1972). Recently, a computer program has been written by Le Page (1999, 2002) which calculates for a given lattice all (hkl)/ $[uvw]$ / ω / j combinations up to given limits of ω and j . In the theory of Friedel and the French School, a (metrical) pseudosymmetry of a lattice or sublattice is assumed to exist if the twin obliquity ω as well as the twin lattice index j are 'small'. This in turn means that the pair lattice plane (hkl)/lattice row $[uvw]$ is the better suited as twin elements (twin reflection plane/twofold twin axis) the smaller ω and j are.

The term 'small' obviously cannot be defined in physical terms. Its meaning rather depends on conventions and actual analyses of triperiodic twins. In his textbook, Friedel (1926, p. 437) quotes frequently observed twin obliquities of $3\text{--}4^\circ$ (albite $4^\circ 3'$, aragonite $3^\circ 44'$) with 'rare exceptions' of $5\text{--}6^\circ$. In a paper devoted to the quartz twins with 'inclined axes', Friedel (1923, pp. 84 and 86) accepts the La Gardette (Japanese) and the Esterel twins, both with large obliquities of $\omega = 5^\circ 27'$ and $\omega = 5^\circ 48'$, as pseudo-merohedral twins only because their lattice indices $[j] = 2$ and 3 are ('*en revanche*') remarkably small. He considers $\omega = 6^\circ$ as a limit of acceptance ['*limite prohibitive*'; Friedel (1923, p. 88)].

Lattice indices $[j] = 3$ are very common (in cubic and rhombohedral crystals), $[j] = 5$ twins are rare and $[j] = 6$ seems to be the maximal value encountered in twinning (Friedel, 1926, pp. 449, 457–464; Donnay & Donnay, 1974, Table 1). In his quartz paper, Friedel (1923, p. 92) rejects all pseudo-merohedral quartz twins with $[j] \geq 4$ despite small ω values, and he points out, as proof that high j values are particularly unfavourable for twinning, that strictly merohedral quartz twins with $[j] = 7$ do not occur, i.e. that $\omega = 0$ cannot 'compensate' for high j values.

In agreement with all these results and later experiences (e.g. Le Page, 1999, 2002), we consider in Table 3.3.8.2 only lattice pseudosymmetries with $\omega \leq 6^\circ$ and $[j] \leq 6$, preferably $[j] \leq 3$. (It should be noted that, on purely mathematical grounds, arbitrarily small ω values can always be obtained for sufficiently large values of h, k, l and u, v, w , which would be meaningless for twinning.) The program by Le Page (1999, 2002) enables for the first time systematic calculations of many ('all possible') (hkl)/ $[uvw]$ combinations for a given lattice and, hence, statistical and geometrical evaluations of existing and particularly of (geometrically) 'permissible' but not observed twin laws. In Table 3.3.8.2, some examples are presented that bring out both the merits and the problems of lattice geometry for the theory of twinning. The 'permissibility criteria' $\omega \leq 6^\circ$ and $[j] \leq 6$, mentioned above, are observed for most cases.

The following comments on these data should be made.

Gypsum: The calculations result in nearly 70 'permissible' (hkl)/ $[uvw]$ combinations. For the very common (100) dovetail twin, four (100)/ $[uvw]$ combinations are obtained. Only the two combinations with smallest ω and $[j]$ are listed in the table; similarly for the less common (001) Montmartre twin. In addition, two cases of low-index (hkl) planes with small obliquities and

3.3. TWINNING OF CRYSTALS

small lattice indices are listed, for which twinning has never been observed.

Rutile: Here nearly twenty ‘permissible’ $(hkl)/[uvw]$ combinations with $\omega \leq 6^\circ$, $[j] \leq 6$ occur. For the frequent (101) reflection twins, five permissible cases are calculated, of which two are given in the table. For the rare (301) reflection twins, only the one case listed, with high obliquity $\omega = 5.4^\circ$, is permissible. For the further two cases of low obliquity and lattice index [5], twins are not known. Among them is one case of (strict) ‘reticular merohedry’, (210) or (130), with $\omega = 0$ and $[j] = 5$ (cf. Fig. 3.3.8.1).

Quartz: The various quartz twins with inclined axes were studied extensively by Friedel (1923). The two most frequent cases, the Japanese (1122) twin (called La Gardette twin by Friedel) and the (1011) Esterel twin, are considered here. In both cases, several lattice pseudosymmetries occur. Following Friedel, those with the smallest lattice index, but relatively high obliquity close to 6° are listed in the table. Again, a twin of (strict) ‘reticular merohedry’ with $\omega = 0$ and $[j] = 7$ does not occur [cf. Section 3.3.9.2.3, Example (2)].

Staurolite: Both twin laws occurring in nature, (031) and (231), exhibit small obliquities but rather high lattice indices [6] and [12]. The frequent (231) 60° twin with $[j] = 12$ falls far outside the ‘permissible’ range. The further two planes listed in the table, (201) and (101), exhibit favourably small obliquities and lattice indices, but do not form twins. The existing (031) and (231) twins of staurolite are discussed again in Section 3.3.9.2 under the aspect of ‘reticular pseudo-merohedry’.

Calcite: For calcite, 19 lattice pseudosymmetries obeying Friedel’s ‘permissible criteria’ are calculated. Again, only a few are mentioned here (indices referred to the structural cell). For the primary deformation twin (0118), e-twin after Bueble & Schmahl (1999), cf. Section 3.3.10.2.2, Example (5), one permis-

sible lattice pseudosymmetry with small obliquity 0.59 but high lattice index [5] is found. For the less frequent secondary deformation twin (1014), r-twin, the situation is similar. The planes (0112) and (1011) permit small obliquities and lattice indices $\leq [5]$, but do not appear as twin planes.

The discussion of the examples in Table 3.3.8.2 shows that, with one exception [staurolite (231) twin], the obliquities and lattice indices of common twins fall within the $\omega/[j]$ limits accepted for lattice pseudosymmetry. Three aspects, however, have to be critically evaluated:

(i) For most of the lattice planes (hkl) , several pseudo-normal rows $[uvw]$ with different values of ω and $[j]$ within the $6^\circ/[6]$ limit occur, and *vice versa*. Friedel (1923) discussed this in his theory of quartz twinning. He considers the $(hkl)/[uvw]$ combination with the smallest lattice index as responsible for the observed twinning.

(ii) Among the examples given in the table, low-index $(hkl)/[uvw]$ combinations with more favourable $\omega/[j]$ values than for the existing twins can be found that never form twins. A prediction of twins on the basis of ‘lattice control’ alone, characterized by low ω and $[j]$ values, would fail in these cases.

(iii) All examples in the table were derived solely from lattice geometry, none from structural relations or other physical factors.

Note. As a mathematical alternative to the term ‘obliquity’, another more general measure of the deviation suffered by the twin lattice in crossing the twin boundary was presented by Santoro (1974, equation 36). This measure is the difference between the metric tensors of lattice 1 and of lattice 2, the latter after retransformation by the existing or assumed twin operation (or more general orientation operation).

Table 3.3.8.2. Examples of calculated obliquities ω and lattice indices $[j]$ for selected $(hkl)/[uvw]$ combinations and their relation to twinning

Calculations were performed with the program *OBLIQUE* written by Le Page (1999, 2002).

| Crystal | (hkl) | Pseudo-normal $[uvw]$ | Obliquity $[\omega]$ | Lattice index $[j]$ | Remark |
|---|------------------|-------------------------------|-------------------------|------------------------|------------------------------------|
| Gypsum $A2/a$ $a = 6.51, b = 15.15, c = 6.28 \text{ \AA}$ $\beta = 127.5^\circ$ | (100) | [302] [805] | 2.47 0.42 | 3 4 | Dovetail twin (very frequent) |
| | (001) | [203] [305] | 5.92 0.95 | 3 5 | Montmartre twin (less frequent) |
| | (101) | [101] | 2.60 | 2 | No twin |
| | (111) | [314] | 1.35 | 4 | No twin |
| Rutile $P4_2/mnm$ $a = 4.5933, c = 2.9592 \text{ \AA}$ | (101) | [102] [307] | 5.02 0.84 | 3 5 | Frequent twin |
| | (301) | [101] | 5.43 | 2 | Rare twin |
| | (201) | [304] | 2.85 | 5 | No twin |
| | (210) or (130) | [210] or [130] | 0 | 5 | No twin |
| Quartz $P3_121$ $a = 4.9031, c = 5.3967 \text{ \AA}$ | (1122) | [111] | 5.49 | 2 | Japanese twin (La Gardette) (rare) |
| | (1011) | [211] | 5.76 | 3 | Esterel twin (rare) |
| | (1012) | [212] | 5.76 | 3 | Sardinia twin (very rare) |
| | (2130) or (1450) | [540] or [230] | 0 | 7 | No twin |
| Staurolite $C2/m$ $a = 7.781, b = 16.620, c = 5.656 \text{ \AA}$ $\beta = 90.00^\circ$ | (031) | [013] | 1.19 | 6 | 90° twin (rare) |
| | (231) | [313] | 0.90 | 12 | 60° twin (frequent) |
| | (201) | [101] | 0.87 | 3 | No twin |
| | (101) | [102] | 0.87 | 3 | No twin |
| Calcite $R3c$ $a = 4.989, c = 17.062 \text{ \AA}$ [hexagonal axes, structural X-ray cell; cf. Section 3.3.10.2.2, Example (5)] | (0112) | [5,10,1] [7,14,2] [481] | 5.31 2.57 0.59 | 2 3 5 | No twin |
| | (1014) | [421] | 0.74 | 4 | Rare deformation twin (r-twin) |
| | (0118) | [121] | 0.59 | 5 | Frequent deformation twin (e-twin) |
| | (1011) | [14.7.1] | 1.54 | 5 | No twin |
| | | | | | |

3. PHASE TRANSITIONS, TWINNING AND DOMAIN STRUCTURES

3.3.8.6. Twinning of isostructural crystals

In the present section, the critical discussion of the lattice theory of twinning is extended from the individual crystal species, treated in Section 3.3.8.5, to the occurrence of *merohedral twinning in series of isotypic and homeotypic crystals*. The crystals in each series have the same (or closely related) structure, space group, lattice type and lattice coincidences. The following cases are of interest here:

(i) Quartz (SiO_2), quartz-homeotypic gallium phosphate (GaPO_4) and benzil [$(\text{C}_6\text{H}_5\text{CO})_2$, so-called ‘organic quartz’] crystallize under normal conditions in the enantiomorphic space groups $P3_121$ and $P3_221$. In quartz, merohedral Dauphiné and Brazil $\Sigma 1$ twins are very frequent, whereas twins of the Leydolt (or ‘combined’) law are very rare (cf. Example 3.3.6.3). In gallium phosphate, Leydolt twins occur as frequently as Dauphiné and Brazil twins (Engel *et al.*, 1989). In benzil crystals, however, these twins are never observed, although the same space-group symmetries and conditions for systematic lattice coincidences as in quartz and in gallium phosphate exist. The reason is the completely different structure and chemical bonding of benzil, which is not capable of forming low-energy boundaries for these three twin laws.

(ii) Iron borate FeBO_3 , calcite CaCO_3 and sodium nitrate NaNO_3 crystallize under normal conditions in the calcite structure with space group $R32/c$. The rhombohedral lattice allows twinning with a hexagonal $\Sigma 3$ coincidence lattice (cf. Example 3.3.6.5). Practically all spontaneously nucleated FeBO_3 crystals grown from vapour (chemical transport) or solution (flux) are $\Sigma 3$ -twinned and form intergrowths of reverse and obverse rhombohedra (penetration twins). This kind of twinning is comparatively rare in calcite, where the twins usually appear with another morphology [contact twins on (0001)]. Interestingly, this $\Sigma 3$ twinning does not occur (or is extremely rare) in sodium nitrate. This shows that even for isotypic crystals, the tendency to form $\Sigma 3$ twins is extremely different. This can also be observed for crystals with the sodium chloride structure. Crystals of the silver halogenides AgCl and AgBr , precipitated from aqueous solution, develop multiple $\Sigma 3$ twins with high frequency (Bögels *et al.*, 1999), and so does galena PbS , whereas the isotypic alkali halogenides (e.g. NaCl , LiF) practically never (or only extremely rarely) form $\Sigma 3$ twins.

(iii) Another instructive example is provided by the $\Sigma 3$ (111) spinel twins in the sphalerite (ZnS) structure of III–V and II–VI semiconductor crystals (cf. Example 3.3.6.6). In some of these compounds this kind of twinning is quite rare (e.g. in GaAs), but in others (e.g. InP , CdTe) it is very frequent. Gottschalk *et al.* (1978) have quantitatively shown that the ease and frequency of twin formation is governed by the (111) stacking-fault energy [which is the energy of the (111) twin boundary]. They have calculated the (111) stacking-fault energies of various III–V semiconductors, taking into account the different ionicities of the bonds. The results prove quantitatively that the frequency of the $\Sigma 3$ twin formation is correlated with the (111) boundary energy.

These examples corroborate the early observations of Cahn (1954, pp. 387–388). The present authors agree with his elegantly formulated conclusion, ‘that the fact that two substances are isostructural is but a slender guide to a possible similarity in their twinning behaviour’.

3.3.8.7. Conclusions

In conclusion, the *lattice theory of twinning*, presented in this section, can be summarized as follows:

(i) The lattice theory represents one of the first systematic theories of twinning; it is based on a clear and well defined concept and thus has found widespread acceptance, especially for the description, characterization and classification of ‘triperiodic’ (merohedral and pseudo-merohedral) twins.

(ii) The concept, however, is purely *geometrical* and has as its object a mathematical, not a physical, item, the *lattice*. It takes into account neither the crystal structure nor the orientation and energy of the twin interface. This deficit has been pointed out and critically discussed by Buerger (1945), Cahn (1954, Section 1.3), Hartman (1956) and Holser (1958, 1960); it is the major reason for the limitations of the theory and its low power of prediction for actual cases of twinning.

(iii) The relations between twinning and lattice (pseudo-) symmetries, however, become immediately obvious and are proven by many observations as soon as *structural pseudo-symmetries* exist. Twinning is always facilitated if a real or hypothetical ‘parent structure’ exists from which the twin law and the interface can be derived. Here, the *lattice pseudosymmetry* appears as a necessary consequence of the *structural pseudo-symmetry*, which usually involves only small deformations of the parent structure, resulting in small obliquities of twin planes and twin axes (which are symmetry elements of the parent structure) and, hence, in twin interfaces of low energy. These structural pseudosymmetries are the result either of actual or hypothetical phase transitions (domain structures, cf. Chapter 3.4) or of structural relationships to a high-symmetry ‘prototype’ structure, as explained in Section 3.3.9.2 below.

(iv) On the other hand, twinning quite often occurs without recognizable structural pseudosymmetry, e.g. the (100) dovetail twins and the (001) Montmartre twins of gypsum, as well as the (101) and (301) reflection twins of rutile and some further examples listed in Table 3.3.8.2. In all these cases, it can be concluded that the lattice theory of twinning is not the suitable tool for the characterization and prediction of the twins; in the terminology of Friedel: the twins are not ‘triperiodic’ but only ‘diperiodic’ or ‘monoperiodic’.

3.3.9. Twinning by merohedry and pseudo-merohedry

We now resume the discussion of Section 3.3.8 on three-dimensional coincidence lattices and pseudo-coincidence lattices and apply it to actual cases of twinning, i.e. we treat in the present section *twinning by merohedry* (*‘macles par méridrie’*) and *twinning by pseudo-merohedry* (*‘macles par pseudo-méridrie’*), both for lattice index $[j] = 1$ and $[j] > 1$, as introduced by Friedel (1926, p. 434). Often (strict) merohedral twins are called ‘parallel-lattice twins’ or ‘twins with parallel axes’. Donnay & Donnay (1974) have introduced the terms *twinning by twin-lattice symmetry* (TLS) for merohedral twinning and *twinning by twin-lattice quasi-symmetry* (TLQS) for pseudo-merohedral twinning, but we shall use here the original terms introduced by Friedel.

3.3.9.1. Definitions of merohedry

In the context of twinning, the term ‘merohedry’ is applied with two different meanings which should be clearly distinguished in order to avoid confusion. The two cases are:

Case (1): ‘Merohedry’ of point groups

A merohedral point group is a subgroup of the holohedral point group (lattice point group) of a given crystal system (crystal family), i.e. group and subgroup belong to the same crystal system. This is the original sense of the term *merohedry*, which has the morphological meaning of reduction of the number of faces of a given crystal form as compared with a *holohedral* crystal form. The degree of merohedry is given by the subgroup index $[i]$. For point groups within the same crystal family, possible indices $[i]$ are 2 (hemihedry), 4 (tetartohedry) and 8 (ogdohedry). The only example for $[i] = 8$ is the point group 3 in the hexagonal holohedry $6/m\ 2/m\ 2/m$.

If the point group of a crystal is reduced to such an extent that the subgroup belongs to a crystal family of lower symmetry, this subgroup is called a *pseudo-merohedral* point group, provided that the structural differences and, hence, also the metrical

3.3. TWINNING OF CRYSTALS

changes of the lattice (axial ratios) are small. Twinning by merohedry corresponds to non-ferroelastic phase transitions, twinning by pseudo-merohedry to ferroelastic phase transitions.

Both merohedral and pseudo-merohedral subgroups of point groups are listed in Section 10.1.3 and Fig. 10.1.3.2 of Volume A of this series (Hahn & Klapper, 2002); cf. also Koch (1999), Table 1.3.4.1.

Case (2): 'Merohedry' of translation groups (lattices)

The term 'reticular' or 'lattice merohedry' designates the relation between a lattice and its 'diluted' sublattice (without consideration of their lattice point groups). A sublattice² is a three-dimensional subset of lattice points of a given lattice and corresponds to a subgroup of index $[j] > 1$ of the original translation group. This kind of group-subgroup relation has been called 'reticular merohedry' ('*mériédrie réticulaire*') by Friedel (1926, p. 444). Note that the lattice and its sublattice may belong to different crystal systems, and that the lattice point groups (holohedries) of lattice and sublattice generally do not obey a group-subgroup relation. This is illustrated by a cubic P lattice (lattice point group $4/m\bar{3}2/m$) and one of its monoclinic sublattices (lattice point group $2/m$) defined by a general lattice plane (hkl) and the lattice row $[hkl]$ normal to it. The symmetry direction $[hkl]$ of the monoclinic sublattice does not coincide with any of the symmetry directions of the cubic lattice, i.e. there is no group-subgroup relation of the lattice point groups. The subgroup common to both (the intersection group) is only $\bar{1}$. A somewhat more complicated example is the $[j] = 5$ ($\Sigma 5$) sublattice obtained by a (210) twin reflection of a tetragonal crystal lattice; cf. Fig. 3.3.8.1. Both lattice and sublattice are tetragonal, $4/mmm$, with common c axes, but the intersection group of their holohedries is only $4/m$, the further symmetry elements are oriented differently.

Friedel (1926, p. 449) also introduced the term 'reticular pseudo-merohedry' ('*pseudo-mériédrie réticulaire*'). This notion, however, can not be applied to a single lattice and its sublattice (a single lattice can be *truly* diluted but not *pseudo*-diluted), but requires pseudo-coincidence of two or more superimposed lattices, which form a 'pseudo-sublattice' of index $[j] > 1$, as described in Section 3.3.8.4.

Because of this complicating and confusing situation we avoid here the term *merohedry* in connection with lattices and translation groups. Instead, the terms *coincidence(-site) lattice*, *twin lattice* or *sublattice* of index $[j]$ are preferred, as explained in Section 3.3.8.2(iv). Note that we also use two different symbols $[i]$ and $[j]$ to distinguish the subgroup indices of point groups and of lattices.

3.3.9.2. Types of twins by merohedry and pseudo-merohedry

Both kinds of merohedries and pseudo-merohedries were used by Mallard (1879) and especially by Friedel (1904, 1926) and the French School in their treatment of twinning. Based on the concepts of exact coincidence (merohedry), approximate coincidence (pseudo-merohedry) and partial coincidence (twin lattice index $[j] > 1$), four major categories of 'triprismatic' twins were distinguished by Friedel and are explained below.

3.3.9.2.1. Merohedral twins of lattice index $[j] = 1$

Here the lattices of all twin partners are parallel and *coincide exactly*. Consequently, all twin operations are symmetry operations of the lattice point symmetry (holohedral point group), but not of the point group of the structure. Here the term 'merohedry' refers to point groups only, i.e. to Case (1) above. Experimentally, in single-crystal X-ray diffraction diagrams all

reflections coincide exactly, and tensorial properties of second rank (e.g. birefringence, dielectricity, electrical conductivity) are not influenced by this kind of twinning.

Typical examples of merohedral twins are:

(1) *Quartz*: Dauphiné, Brazil and Leydolt twins (cf. Example 3.3.6.3).

(2) *Pyrite*, iron-cross twins: crystals of cubic *eigensymmetry* $2/m\bar{3}$ form penetration twins of peculiar morphology by reflection on (110), with $[i] = 2$.

(3) *KLiSO₄*: the room-temperature phase III of *eigensymmetry* 6 exhibits four domain states related by three merohedral twin laws. These growth twins of index $[i] = 4$ have been characterized in detail by optical activity, pyroelectricity and X-ray topography (Klapper *et al.*, 1987).

(4) *Potassium titanyl phosphate*, *KTiOPO₄*: point group $mm2$, forms inversion twins (ferroelectric domains) below its Curie temperature of 1209 K.

3.3.9.2.2. Pseudo-merohedral twins of lattice index $[j] = 1$

These twins are characterized by pseudo-merohedry of point groups, Case (1) in Section 3.3.9.1. The following examples are based on *structural pseudosymmetry* and consequently also on lattice pseudosymmetry, either as the result of phase transformations or of structural relationships:

(1) Transformation twins of *Rochelle salt*: this ferroelastic/ferroelectric transformation at about 295 K follows the group-subgroup relation orthorhombic $2'2'2' \longleftrightarrow$ monoclinic 121 (index $[i] = 2$) with $\beta \approx 90^\circ$. The primed operations form the coset of the group-subgroup relation and thus the twin law. Owing to the small deviation of the angle β from 90° , the lattices of both twin partners nearly coincide. Note that this group-subgroup relation involves both an orthorhombic merohedral and a monoclinic merohedral point group, viz 222 and 2.

(2) Transformation twins orthorhombic $2'/m'2/m2'/m' \longleftrightarrow$ monoclinic $12/m1$ with $\beta \approx 90^\circ$. This is a case analogous to that of Rochelle salt, except that the point groups involved are the holohedries of the orthorhombic and of the monoclinic crystal system, mmm and $2/m$ [example: $\text{KH}_3(\text{SeO}_3)_2$].

(3) Pseudo-hexagonal growth twins of an orthorhombic C -centred crystal with $b/a \approx \sqrt{3}$ and twin reflection planes $m'(110)$ and $m'(1\bar{1}0)$. The lattices of the three domain states nearly coincide and form a 'pseudo-coincidence lattice' of lattice index $[j] = 1$, but of point-group index $[i] = 3$, with subgroup $\mathcal{H} = 2/m2/m2/m$ and supergroup $\mathcal{K}(6) = 6(2)/m2/m2/m$ (cf. Example 3.3.6.7). Here, in contrast to exact merohedry, in single-crystal X-ray diffraction patterns most reflection spots will be split into three. Note that the term 'index' appears twice, first as the subgroup index $[i] = 3$ of the point groups and second as the lattice index $[j] = 1$ of the twin lattice.

3.3.9.2.3. Twinning with partial lattice coincidence (lattice index $[j] > 1$)

For these twins with partial but *exact* coincidence Friedel has coined the terms 'twinning by reticular merohedry' or 'by lattice merohedry'. Here the term merohedry refers only to the sublattice, i.e. to Case (2) above. Typical examples with $[j] = 3$ and $[j] > 3$ were described in Section 3.3.8.3. In addition to the sublattice relations, it is reasonable to include the point-group relations as well. Four examples are presented:

(1) Twinning of rhombohedral crystals (lattice index $[j] = 3$, example FeBO_3). The *eigensymmetry* point groups of the structure and of the R lattice (of the untwinned crystal) are both $\mathcal{H} = \bar{3}2/m$. The extension of the *eigensymmetry* by the (binary) twin operation 2_z , as described in Example 3.3.6.5, leads to the composite symmetry $\mathcal{K} = 6'/m'(3)2/m2'/m'$, i.e. the point-group index is $[i] = 2$. The sublattice index is $[j] = 3$, because of the elimination of the centring points of the original triple R lattice in forming the hexagonal P twin lattice.

² Some authors use the term *superlattice* instead of *sublattice* because of its larger unit cell, or the term *derivative lattice*; for the latter term see Chapter 13.2 of Volume A of this series (Billiet & Bertaut, 2002)

3. PHASE TRANSITIONS, TWINNING AND DOMAIN STRUCTURES

(2) Reflection twinning across $\{21\bar{3}0\}$ or $\{14\bar{5}0\}$, or twofold rotation twinning around $\langle 540 \rangle$ or $\langle 230 \rangle$ of a hexagonal crystal with a P lattice (lattice symmetry $6/m2/m2/m$). The twin generates a hexagonal coincidence lattice of index $[j] = 7$ ($\Sigma 7$) with $\mathbf{a}' = 3\mathbf{a} + 2\mathbf{b}$, $\mathbf{b}' = -2\mathbf{a} + \mathbf{b}$, $\mathbf{c}' = \mathbf{c}$. The hexagonal axes \mathbf{a}' and \mathbf{b}' are rotated around $[001]$ by an angle of 40.9° with respect to \mathbf{a} and \mathbf{b} . The intersection lattice point group of both twin partners is $6/m$. The extension of this group by the twin operation 'reflection across $\{21\bar{3}0\}$ ' leads to the point group of the coincidence lattice $6/m2'/m'2'/m'$ (referred to the coordinate axes \mathbf{a}' , \mathbf{b}' , \mathbf{c}'). The primed operations define the coset (twin law). For hexagonal lattices rotated around $[001]$, the $\Sigma 7$ coincidence lattice ($[j] = 7$) is the smallest sublattice with lattice index $[j] > 1$ (least-diluted hexagonal sublattice). No example of a hexagonal $\Sigma 7$ twin seems to be known.

(3) Tetragonal growth twins with $[j] = 5$ ($\Sigma 5$ twins) in $\text{SmS}_{1.9}$ (Tamazyan *et al.*, 2000b). This rare twin is illustrated in Fig. 3.3.8.1 and is described, together with the twins of the related phase PrS_2 , in Example (3) of Section 3.3.9.2.4 below.

(4) Reflection twins across a general net plane (hkl) of a cubic P lattice. This example has been treated already in Section 3.3.9.1, Case (2).

3.3.9.2.4. Twinning with partial lattice pseudo-coincidence (lattice index $[j] > 1$)

This type can be derived from the category in Section 3.3.9.2.3 above by relaxation of the condition of exact lattice coincidence, resulting in two nearly, but not exactly, coinciding lattices (pseudo-coincidence, *cf.* Section 3.3.8.4). In this sense, the two Sections 3.3.9.2.3 and 3.3.9.2.4 are analogous to the two Sections 3.3.9.2.1 and 3.3.9.2.2.

The following four examples are characteristic of this group:

(1) *(110) reflection twins of a pseudo-hexagonal orthorhombic crystal with a P lattice*: If the axial ratio $b/a = \sqrt{3}$ were exact, the lattices of both twin partners would coincide exactly on a sublattice of index $[j] = 2$ (due to the absence of the C centring); *cf.* Koch (1999), Fig. 1.3.2.2. If b/a deviates slightly from $\sqrt{3}$, the exact coincidence lattice changes to a pseudo-coincidence lattice of lattice index $[j] = 2$. Examples are ammonium lithium sulfate, NH_4LiSO_4 , many members of the K_2SO_4 -type series (*cf.* Docherty *et al.*, 1988) and aragonite, CaCO_3 .

(2) *Staurolite twinning*: This topic has been extensively treated as Example 3.3.6.12. The famous 90° - and 60° -twin 'crosses' are a complicated and widely discussed example for Friedel's notion of 'twinning by reticular merohedry' (Friedel, 1926, p. 461). It was followed up by an extensive analysis by Hurst *et al.* (1956). Both twin laws (90° and 60° crosses) can be geometrically derived from a multiple pseudo-cubic cell \mathbf{a}'_c , \mathbf{b}'_c , \mathbf{c}'_c (so-called 'Mallard's pseudo-cube') which is derived from the structural monoclinic C -centred cell \mathbf{a}_m , \mathbf{b}_m , \mathbf{c}_m as follows, involving a rotation of $\sim 45^\circ$ around $[100]$:

$$\mathbf{a}'_c = \mathbf{b}_m + 3\mathbf{c}_m, \quad \mathbf{b}'_c = -\mathbf{b}_m + 3\mathbf{c}_m, \quad \mathbf{c}'_c = 3\mathbf{a}_m.$$

Using Smith's (1968) lattice constants for the structural monoclinic cell with space group $C2/m$ and $a = 7.871$, $b = 16.620$, $c = 5.656$ Å, $\beta = 90^\circ$ (within the limits of error), $V_m = 740$ Å³, the pseudo-cube has the following lattice constants:

$$\begin{array}{lll} a'_c = 23.753 & b'_c = 23.753 & c'_c = 23.613 \text{ Å} \\ \alpha_c = 90 & \beta_c = 90 & \gamma_c = 88.81^\circ \quad V'_c = 13323 \text{ Å}^3. \end{array}$$

The volume ratio V'_c/V_m of the two cells is 18, *i.e.* the sublattice index is $[j] = 18$. If, however, the primitive monoclinic unit cell is used, the volume ratio doubles and the sublattice index used in the twin analysis increases to $[j] = 36$. The (metrical) *eigensym-*

metry of the pseudo-cube is orthorhombic (due to $\beta_c = 90^\circ$), $(2/m)_{[001]}(2/m)_{[110]}(2/m)_{[1\bar{1}0]}$, referred to \mathbf{a}'_c , \mathbf{b}'_c , \mathbf{c}'_c .

Note, however, that this pseudo-cube in reality is C -centred because the C -centring vector $1/2(\mathbf{a}'_c + \mathbf{b}'_c) = 3\mathbf{c}_m$ is a lattice vector of the monoclinic lattice. This C -centring has not been considered by Friedel, Hurst and Donnay, who have based their analysis on the primitive pseudo-cube.

According to Friedel, the 'symmetry elements' of the pseudo-cube are potential twin elements of staurolite, except for $(2/m)_{[110]}$, which is the monoclinic symmetry direction of the structure. In Table 3.3.9.1, the twin operations of the 90° and 60° twins are compared with the 'symmetry operations' of the pseudo-cube with respect to obliquities ω and lattice indices $[j]$, referred to both sets of axes, pseudo-cubic \mathbf{a}'_c , \mathbf{b}'_c , \mathbf{c}'_c and monoclinic (but metrically orthorhombic) \mathbf{a}_m , \mathbf{b}_m , \mathbf{c}_m . The calculations were again performed with the program *OBLIQUE* by Le Page (1999, 2002). In order to keep agreement with the interpretation of Friedel and Hurst *et al.*, the pseudo-cube is treated as primitive, with $[j] = 36$.

The following interpretations can be given (*cf.* Fig. 13 in Hurst *et al.*, 1956):

(a) 90° cross (Table 3.3.9.1a, Fig. 3.3.6.13a):

(i) The pseudo-tetragonal 90° cross can be explained and visualized very well with eight twin operations, a fourfold twin axis along $[100]_m = [001]_c$ with operations 4^1 , 4^3 , 4^1 , 4^3 and two pairs of 'diagonal' twin operations 2 and m . They form the coset of the (metrically) 'orthorhombic' ($\beta = 90^\circ$) *eigensymmetry* $\mathcal{H} = mmm$ which results in the composite symmetry $\mathcal{K} = 4'(2)/m2/m2'/m'$.

(ii) The obliquities for all twin operations are at most 1.2° , the lattice index is $[j]_m = 1$ for the twin axis, but for the 'diagonal' twin elements it is $[j]_m = 6$, which is at the limit of the permissible range. Because of these facts, Friedel prefers to consider the 90° cross as a 90° rotation twin around $[100]_m$ rather than as a (diagonal) reflection twin across $(031)_m$ or $(0\bar{3}1)_m$.

(iii) Note that for the interpretation of the 90° cross the complete pseudo-cube with lattice index $[j] = 36$ is not required. Because $\mathbf{c}'_c = 3\mathbf{a}_m$, a pseudo-tetragonal unit cell with axes \mathbf{a}'_c , \mathbf{b}'_c , $(1/3)\mathbf{c}'_c$ and $[j] = 12$ is sufficient.

(b) 60° cross (Table 3.3.9.1b, Fig. 3.3.6.13b):

(iv) The widespread 60° cross is much more difficult to interpret and visualize. The four threefold twin axes around $\langle 111 \rangle$ of the pseudo-cube split into two pairs, both with very small obliquities $< 1^\circ$. One pair, $[102]_m$ and $[\bar{1}02]_m$, has a favourable index $[j]_m = 3$; however, the other one, $[320]_m$ and $[\bar{3}20]_m$ is with $[j]_m = 9$ unacceptably high. According to Friedel's theory, this makes $[102]_m$ the best choice as threefold twin axis.

(v) There is a further $\pm 90^\circ$ twin rotation around $[100]_c$ or $[013]_m$ with small obliquity, $\omega = 1.2^\circ$, but very high lattice index, $[j]_m = 6$. Note that this is the same axis that has been used already for the 90° twin, but with a 180° rotation.

(vi) The greatest deviation from the 'permissibility' criterion is exhibited by the twin axes $2[101]_c = 2[313]_m$ and $2[011]_c = 2[3\bar{1}3]_m$ and the twin planes, pseudo-normal to them, $(231)_m$ and $(2\bar{3}1)_m$. The obliquity $\omega = 0.9^\circ$ is very good but the twin index is $[j] = 12$, a value far outside Friedel's '*limite prohibitive*'. These operations, however, are the 'standard' twin operations that are always quoted for the 60° twins. Following Friedel (1926, p. 462), the best definition of the 60° twin is the $\pm 120^\circ$ rotations around $[102]_m$ with $\omega = 0.87^\circ$ and $[j]_m = 3$.

(vii) If the (true) C -centring of the pseudo-cube is taken into account, however, no $\langle 111 \rangle$ pseudo-threefold axes remain; hence, the 60° cross cannot be explained by the lattice construction of the pseudo-cube.

(3) *Growth twins of monoclinic PrS_2 and of tetragonal $\text{SmS}_{1.9}$* : These two rather complicated examples belong to the structural family of MeX_2 dichalcogenides which is rich in structural rela-

3.3. TWINNING OF CRYSTALS

tionships and different kinds of twins. The ‘basic structure’ and ‘aristotype’ of this family is the tetragonal ZrSSi structure with axes $a_b = b_b \approx 3.8$, $c_b \approx 7.9$ Å, $V_b \approx 114$ Å³, space group $P4/nmm$ (b stands for basic). The crystal chemistry of this structural family is discussed by Böttcher *et al.* (2000).

(a) PrS_2 (Tamazyan *et al.*, 2000a)

PrS_2 is a monoclinic member of this series with space group $P2_1/b11$ (unique axis $a!$) and axes $a \approx 4.1$, $b \approx 8.1$, $c \approx 8.1$ Å, $\alpha \approx 90.08^\circ$, $V \approx 269$ Å³. The structure is strongly pseudo-tetragonal along $[001]$ (with cell a , $b/2$, c) and is a ‘derivative structure’ of ZrSSi. Hence pseudo-merohedral twinning that makes use of this structural tetragonal pseudosymmetry would be expected, with twin elements $4[001]$ or $m(210)$ or $2[120]$ *etc.* and $[j] = 2$ because $b \approx 2a$, but, surprisingly, this twinning has not been observed so far. It may occur in other PrS_2 samples or in other isostructural crystals of this series.

Instead, the monoclinic crystal uses another structural pseudosymmetry, the approximate *orthorhombic* symmetry along $[100]$ with $\alpha \approx 90^\circ$, to twin on 2_y , 2_z , m_y or m_z (coset of $2_x/m_x$) with composite symmetry $\mathcal{K} = 2/m'2'/m'2'/m'$, $[j] = 1$ and $[i] = 2$ (*cf.* Fig. 4 of the paper).

The monoclinic PrS_2 cell has a third kind of pseudosymmetry that is not structural, only metrical. The cell is pseudo-tetragonal along $[100]$ due to $b \approx c$ and $\alpha \approx 90^\circ$. This pure lattice pseudosymmetry, not surprisingly, is not used for twinning, *e.g.* via $4[100]$ or $m(011)$ or $m(0\bar{1}1)$ or $2[011]$ or $2[0\bar{1}1]$.

(b) $SmS_{1.9}$ (Tamazyan *et al.*, 2000b)

This structure is (strictly) tetragonal with axes $a = b \approx 8.8$, $c \approx 15.9$ Å, $V \approx 1238$ Å³ and space group $P4_2/n$. It is a tenfold superstructure of ZrSSi with the following basis-vector relations:

$$\mathbf{a} = 2\mathbf{a}_b + \mathbf{b}_b, \quad \mathbf{b} = -\mathbf{a}_b + 2\mathbf{b}_b, \quad \mathbf{c} = 2\mathbf{c}_b,$$

leading to lattice constants $a \approx \sqrt{5}a_b$, $b \approx \sqrt{5}b_b$, $c \approx 2c_b$. This well ordered tetragonal supercell now twins on $m(210)$ or $2[210]$ or $m(130)$ or $2[130]$ (which is equivalent to a rotation around $[001]$ of 36.87°) to form a $\Sigma 5$ twin by ‘reticular merohedry’ ($[j] = 5$) with lattice constants $a' = a\sqrt{5} = 19.72$, $b' = b\sqrt{5} = 19.72$, $c' = c = 15.93$ Å, $V = 6192$ Å³. This is illustrated in Fig. 3.3.8.1.

$SmS_{1.9}$ represents the first thoroughly investigated and documented tetragonal $[j] = 5$ ($\Sigma 5$) twin known to us. The sublattice of this twin is the tetragonal coincidence lattice with smallest

lattice index $[j] > 1$, *i.e.* the ‘least-diluted’ systematic tetragonal sublattice.

(4) *Growth twins of micas*: A rich selection of different twin types, both merohedral and pseudo-merohedral, with $[j] = 1$ and 3, is provided by the mineral family of micas, which includes several polytypes. A review of these complicated and interesting twinning phenomena is presented by Nespolo *et al.* (1997). Detailed theoretical derivations of mica twins and allotwins, both in direct and reciprocal space, are published by Nespolo *et al.* (2000).

In conclusion, it is pointed out that the above four categories of twins, described in Sections 3.3.9.2.1 to 3.3.9.2.4, refer only to cases with exact or approximate *three-dimensional* lattice coincidence (*triperiodic twins*). Twins with only two- or one-dimensional lattice coincidence (*diperiodic* or *monoperiodic* twins) [*e.g.* the (100) reflection twins of gypsum and the (101) rutile twins] belong to other categories, *cf.* Section 3.3.8.2. The examples above have shown that for triperiodic twins *structural* pseudosymmetries are an essential feature, whereas purely *metrical* (*lattice*) pseudosymmetries are not a sufficient tool in explaining and predicting twinning, as is evidenced by the case of staurolite, discussed above in detail.

3.3.9.3. Pseudo-merohedry and ferroelasticity

The large group of pseudo-merohedral twins (irrespective of their lattice index) contains a very important subset which is characterized by the physical property *ferroelasticity*. Ferroelastic twins result from a real or virtual phase transition involving a change of the crystal family (crystal system). These transitions are displacive, *i.e.* they are accompanied by only small structural distortions and small changes of lattice parameters. The structural symmetries lost in the phase transition are preserved as pseudosymmetries and are thus candidates for twin elements. This leads to a pseudo-coincidence of the lattices of the twin partners and thus to pseudo-merohedral twinning. Because of the small structural changes involved in the transformation, domains usually switch under mechanical stress, *i.e.* they are ferroelastic. A typical example for switchable ferroelastic domains is Rochelle salt, the first thoroughly investigated ferroelastic transformation twin, discussed in Section 3.3.9.2.2, Example (1).

Table 3.3.9.1. *Staurolite*, 60° and 90° twins

Comparison of the twin operations with the ‘symmetry operations’ of the primitive pseudo-cube with respect to obliquity ω and lattice index $[j]$, referred both to the pseudo-cubic axes, $\mathbf{a}'_c, \mathbf{b}'_c, \mathbf{c}'_c$, and the monoclinic (metrically orthorhombic) axes, $\mathbf{a}_m, \mathbf{b}_m, \mathbf{c}_m$. The calculations were performed with the program *OBLIQUE* by Le Page (1999, 2002).

(a) 90° cross (eight twin operations).

| Twin operations referred to | | Obliquity ω [°] | Lattice index $[j]$ referred to | | Remarks |
|---|--|---------------------------|---|--|--|
| $\mathbf{a}'_c, \mathbf{b}'_c, \mathbf{c}'_c$ | $\mathbf{a}_m, \mathbf{b}_m, \mathbf{c}_m$ | | $\mathbf{a}'_c, \mathbf{b}'_c, \mathbf{c}'_c$ | $\mathbf{a}_m, \mathbf{b}_m, \mathbf{c}_m$ | |
| $4[001]_c$ | $4[100]_m$ | 0 | 1 | 1 | Four collinear twin operations $4^1, 4^3, \bar{4}^1, \bar{4}^3$ |
| $2[100]_c$ | $2[013]_m$ | 1.19 | 1 | 6 | Four ‘diagonal’ (with respect to the monoclinic unit cell) twin operations intersecting in $[001]_c = [100]_m$ |
| $m(100)_c$ | $m(031)_m$ | 1.19 | 1 | 6 | |
| $2[010]_c$ | $2[0\bar{1}3]_m$ | 1.19 | 1 | 6 | |
| $m(010)_c$ | $m(0\bar{3}1)_m$ | 1.19 | 1 | 6 | |

(b) 60° cross.

| Twin operations referred to | | Obliquity ω [°] | Lattice index $[j]$ referred to | | Equivalent directions |
|---|--|---------------------------|---|--|---|
| $\mathbf{a}'_c, \mathbf{b}'_c, \mathbf{c}'_c$ | $\mathbf{a}_m, \mathbf{b}_m, \mathbf{c}_m$ | | $\mathbf{a}'_c, \mathbf{b}'_c, \mathbf{c}'_c$ | $\mathbf{a}_m, \mathbf{b}_m, \mathbf{c}_m$ | |
| $3[111]_c (\pm 120^\circ)$ | $3[102]_m$ | 0.87 | 3 | 3 | $[11\bar{1}]_c = [\bar{1}102]_m$ |
| $3[1\bar{1}1]_c (\pm 120^\circ)$ | $3[320]_m$ | 0.25 | 3 | 9 | $[111]_c = [3\bar{2}0]_m$ |
| $4[100]_c (\pm 90^\circ)$ | $4[013]_m$ | 1.19 | 1 | 6 | $[010]_c = [0\bar{1}3]_m$ |
| $m(100)_c$ | $m(031)_m$ | 1.19 | 1 | 6 | |
| $2[101]_c$ | $2[313]_m$ | 0.90 | 1 | 12 | $[011]_c = [3\bar{1}3]_m$ $[10\bar{1}]_c = [313]_m$ $[01\bar{1}]_c = [313]_m$ |
| $m(101)_c$ | $m(231)_m$ | 0.90 | 1 | 12 | |

3. PHASE TRANSITIONS, TWINNING AND DOMAIN STRUCTURES

3.3.10. Twin boundaries

3.3.10.1. Contact relations in twinning

So far, twinning has been discussed only in terms of symmetry and orientation relations of the (bulk) twin components. In this chapter, the very important aspect of *contact relations* is discussed. This topic concerns the orientation and the structure of the *twin boundary*, which is also called twin interface, composition plane, contact plane, domain boundary or domain wall. It is the twin boundary and its structure and energy which determine the occurrence or non-occurrence of twinning. In principle, for each crystal species an infinite number of orientation relations obey the requirements for twinning, as set out in Section 3.3.2, because any rational lattice plane (hkl), as well as any rational lattice row $[uvw]$, common to both partners would lead to a legitimate reflection or rotation twin. Nevertheless, only a relatively small number of crystal species exhibit twinning at all, and, if so, with only a few twin laws. This wide discrepancy between theory and reality shows that a permissible crystallographic orientation relation (twin law) is a necessary, but not at all a sufficient, condition for twinning. In other words, the *contact relations* play the decisive role: a permissible orientation relation can only lead to actual twinning if a twin interface of good structural fit and low energy is available.

In principle, a twin boundary is a special kind of grain boundary connecting two 'homophase' component crystals which exhibit a crystallographic orientation relation, as defined in Section 3.3.2. For a given orientation relation of the twin partners, crystallographic or general, the interface energy depends on the orientation of their boundary. It is intuitively clear that crystallographic orientation relations lead to energetically more favourable boundaries than noncrystallographic ones. As a rule, twin boundaries are planar (at least in segments), but for certain types of twins curved and irregular interfaces have been observed. This is discussed later in this section.

In order to determine theoretically for a given twin law the optimal interface, the interface energy has to be calculated or at least estimated for various boundary orientations. This problem has not been solved for the general case so far. The special situation of reflection twins with coinciding twin mirror and composition planes has recently been treated by Fleming *et al.* (1997). These authors calculated the interface energies for three possible reflection twin laws in each of aragonite, gibbsite, corundum, rutile and sodium oxalate, and they compared the results with the observed twinning. In all cases, the twin law with lowest boundary energy corresponds to the twin law actually observed. Another calculation of the twin interface energy has been performed by Lieberman *et al.* (1998) for the $(10\bar{2})$ reflection twins of monoclinic saccharin crystals. In this study, the $(10\bar{2})$ boundary energy was calculated for different shifts of the two twin components with respect to each other. It was shown that a minimum of the boundary energy is achieved for a particular 'twin displacement vector' (*cf.* Section 3.3.10.4.1).

Calculations of interface energies, as performed by Fleming *et al.* (1997) and Lieberman *et al.* (1998), however, require knowledge of the atomic potentials and their parameters for each pair of bonded atoms. They are, therefore, restricted to specific crystals for which these parameters are known. Similarly, high-resolution electron microscopy (HRTEM) images of twin boundaries have been obtained so far for only a small number of crystals.

It is possible, however, to predict for a given twin law low-energy twin boundaries on the basis of symmetry considerations, even without knowledge of the crystal structure, as discussed in the following section. This prediction has been carried out by Sapriel (1975) for *ferroelastic* crystals. His treatment assumes a phase transition from a real or hypothetical parent phase (supergroup \mathcal{G}) to a 'distorted' (daughter) phase of lower *eigensymmetry* (subgroup \mathcal{H}), leading to two (or more) domain

states of equal but opposite shear strain. The subgroup \mathcal{H} must belong to a lower-symmetry crystal system than the supergroup \mathcal{G} , as explained in Section 3.3.7.3(ii). Similar criteria, but restricted to ferroelectric materials, had previously been devised in 1969 by Fousek & Janovec (1969). A review of ferroelastic domains and *domain walls* is provided by Boulesteix (1984) and an extension of the Sapriel procedure to *phase boundaries* between a ferroelastic and its 'prototypic' (parent) phase is given by Boulesteix *et al.* (1986).

3.3.10.2. Strain compatibility of interfaces

For a simple derivation of stress-free contact planes, we go back to the classical description of mechanical twinning by a homogeneous shear, which is illustrated by a deformation ellipsoid as shown in Fig. 3.3.10.1(a) (*cf.* Liebsch, 1891; Niggli, 1941; Klassen-Neklyudova, 1964). In a modification of this approach, we consider two parts of a homogeneous, crystalline or noncrystalline, solid body, which are subjected to equal but opposite shear deformations $-\varepsilon$ and $+\varepsilon$. The undeformed state of the body and the deformed states of its two parts are represented by a sphere ($\varepsilon = 0$) and by two ellipsoids $-\varepsilon$ and $+\varepsilon$, as shown in Fig. 3.3.10.1(b). We now look for stress-free contact planes between the two deformed parts, *i.e.* planes for which line segments of any direction parallel to the planes experience the same length change in both parts during the shear. This criterion is obeyed by those planes that exhibit identical cross sections through both ellipsoids. Mathematically, this is expressed by the equation (Sapriel, 1975)

$$(\varepsilon_{ij}^I - \varepsilon_{ij}^{II})x_i x_j = 2\varepsilon x_1 x_2 = 0$$

($\varepsilon_{ij}^I = \varepsilon_{12}^I = +\varepsilon$, $\varepsilon_{ij}^{II} = \varepsilon_{12}^{II} = -\varepsilon$; x_1, x_2, x_3 are Cartesian coordinates) which has as solutions the two planes $x_1 = 0$ (plane *BB* in Fig. 3.3.10.1b) and $x_2 = 0$ (plane *AA*). These planes are called 'planes of strain compatibility' or 'permissible' planes. From the solutions of the above equation and Fig. 3.3.10.1(b) it is apparent that two such planes, *AA* and *BB*, normal to each other exist. The intersection line of the two compatible planes is called the shear axis of the shear deformation.

It is noted that during a shear deformation induced by the (horizontal) translations shown in Fig. 3.3.10.1(b), only the plane *AA*, parallel to the arrows, can be generated as a contact plane between the two domains. A contact plane *BB*, normal to the arrows, cannot be formed by this process, because this would lead to a gap on one side and a penetration of the material on the other side. Plane *BB*, however, could be formed during a (virtual) switching between $+\varepsilon$ and $-\varepsilon$ with 'vertical' translations, parallel to *BB*, which would formally result in the same mutual arrangement of the ellipsoids. The compatibility criterion, as expressed by the equation above (which applies to elastic continua), does not distinguish between these two cases. Note that the planes *AA* and *BB* are mirror planes relating the deformations $+\varepsilon$ and $-\varepsilon$. Both contact planes often occur simultaneously in *growth twins*, see for example the dovetail and the Montmartre twins of gypsum (Fig. 3.3.6.1). In general, each interface coinciding with a twin mirror plane or a plane normal to a twin axis is a (mechanically) compatible contact plane.

It should be emphasized that the criterion 'strain compatibility' is a purely mechanical one for which only stress and strain are considered. It leads to 'mechanical' low-energy boundaries. Other physical properties, such as electrical polarization, may reduce the number of mechanically permissible boundaries, *e.g.* due to energetically unfavourable head-to-head or tail-to-tail orientation of the axis of spontaneous polarization in polar crystals. The mechanical compatibility criterion is, however, always applicable to centrosymmetric materials.

3.3. TWINNING OF CRYSTALS

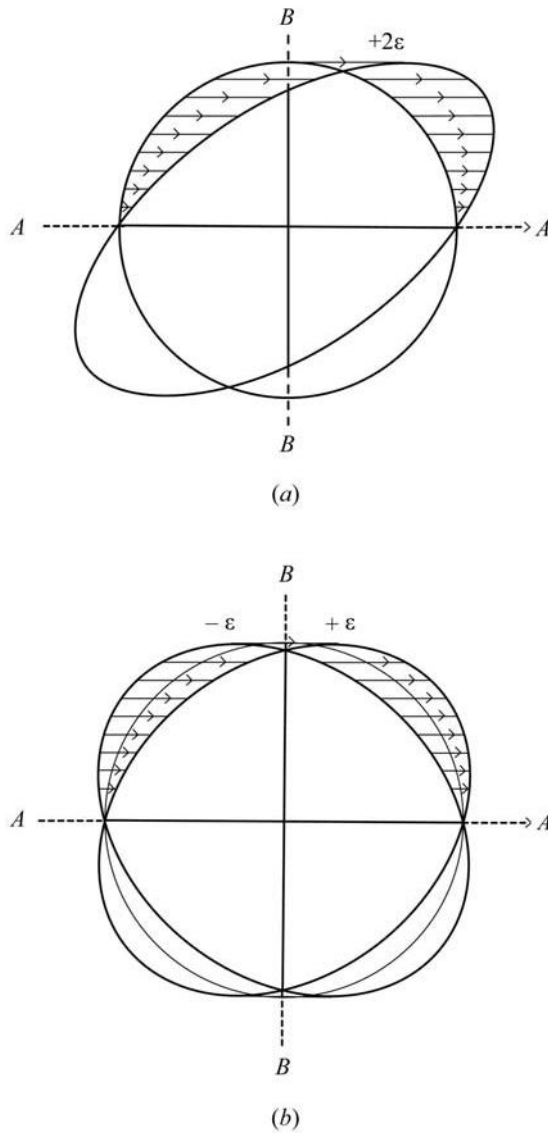


Fig. 3.3.10.1. (a) Classical description of mechanical twinning by homogeneous shear deformation (Liebisch, 1891, pp. 104–118; Niggli, 1941, pp. 145–149; Klassen-Neklyudova, 1964, pp. 4–10). The shear deforms a sphere into an ellipsoid of equal volume by translations (arrows) parallel to the twin (glide) plane AA . The translations are proportional to the distance from the plane AA . Shear angle 2ε . (Only the translations in the upper half of the diagram are shown, in the lower half they are oppositely directed.) (b) Ellipsoids representing the (spontaneous) shear deformations $-\varepsilon$ and $+\varepsilon$ of two orientation states, referred to the (real or hypothetical) intermediate (prototypic) state with $\varepsilon = 0$ (sphere). The switching of orientation state $-\varepsilon$ into state $+\varepsilon$ through the shear angle 2ε is, analogous to (a), indicated by arrows. The shear ellipsoids $-\varepsilon$ and $+\varepsilon$ have common cross sections along the perpendicular planes AA and BB which are both, therefore, mechanically compatible contact planes of the $+\varepsilon$ and $-\varepsilon$ twin domains.

3.3.10.2.1. Sapriel approach to permissible (compatible) boundaries in ferroelastic (non-merohedral) transformation twins

The general approach to strain compatibility, as given above, can be employed to derive the permissible composition planes for twins with inclined axes (non-merohedral twins; for merohedral twins see Section 3.3.10.2.3 below). This concept was applied by Sapriel (1975) to the 94 Aizu species of *ferroelastic transformation* twins. According to Aizu (1969, 1970a,b), each species is represented by a pair of symmetry groups, separated by the letter F (= ferroic) in the form KFH , e.g. $2/m2/m2/mF12/m1$ or $m\bar{3}mF\bar{3}m$. The parent phase with symmetry \mathcal{G} represents the undeformed (zero-strain) reference state (the sphere in Fig. 3.3.10.1b), whereas the spontaneous strain of the two orientation states of phase \mathcal{H} is represented by the two ellipsoids. Details of the calculation of the permissible domain boundaries for all

ferroelastic transformation twins are given in the paper by Sapriel (1975).

Two kinds of permissible boundaries are distinguished by Sapriel:

(a) *W boundaries*. These interfaces are parallel to symmetry planes of the parent phase (supergroup \mathcal{K}), which are lost in the transition and have become twin reflection planes (F operations) of the deformed phase (subgroup \mathcal{H}), i.e. they are ‘crystallographically prominent planes of fixed indices’ (Sapriel, 1975, p. 5129), which are fixed by the symmetry of the parent phase. A rational lattice plane perpendicular to a lost twofold symmetry axis of the parent phase is also a W boundary. W boundaries are crystallographically invariant with respect to temperature and pressure.

(b) *W' boundaries*. In contrast to W boundaries, W' interfaces are not fixed by the symmetry of the parent phase, i.e. they do not correspond to lost symmetry elements. Their orientation depends on the direction of the spontaneous shear strain and thus changes with temperature and pressure. In general, W' boundaries are irrational planes.

Example. The distinction between these two types of boundaries is illustrated by the example of the (triclinic) Aizu species $2/mF\bar{1}$. Here, the lost mirror plane of the monoclinic parent phase (F operation) yields the permissible prominent W twin boundary (010). The second permissible boundary, perpendicular to the first, is an irrational W' composition plane in the zone of the direction normal to triclinic (010), i.e. of the triclinic reciprocal \mathbf{b}^* axis. The azimuthal orientation of this boundary around the zone axis is not determined by symmetry but depends on the direction of the spontaneous shear strain of the deformed triclinic phase.

Sapriel (1975) has shown that for ferroelastic crystals the pair of perpendicular permissible domain boundaries can consist either of two W planes, or of one W and one W' plane, or of two W' planes. Examples are the Aizu species $2/m2/m2/mF12/m1$, $2/mF\bar{1}$ and $4F2$, respectively. There are even four Aizu cases without any permissible boundaries: $3F1$, $\bar{3}F\bar{1}$, $23F222$, $m\bar{3}Fmmm$. An example is langbeinite ($23F222$), which was discussed at the end of Section 3.3.4.4.

Note. The two members of a pair of permissible twin boundaries are always exactly perpendicular to each other. Frequently observed slight deviations from the strict 90° orientation have been interpreted as relaxation of the perpendicularity condition in the deformed phase, resulting from the ferroelastic phase transition (cf. Sapriel, 1975, p. 5138). This, however, is not the reason for the deviation from 90° , but rather a splitting of the two (exactly) perpendicular symmetry planes in the parent phase \mathcal{G} into two pairs of compatible twin boundaries (i.e. two independent twin laws) in the deformed phase \mathcal{H} , whereby the pairs are *nearly* perpendicular to each other. From each pair only one interface (usually the rational one) is realized in the twin, whereas the other compatible twin boundary (usually the irrational one) is suppressed because of its unfavourable energetic situation.

Examples

(1) Phase transition orthorhombic ($\mathcal{G} = 2/m2/m2/m$) \Rightarrow monoclinic ($\mathcal{H} = 12/m1$, $\beta \approx 90^\circ$), in Aizu notation $2/m2/m2/mF12/m1$. Whereas in \mathcal{G} the mirror planes m_x and m_z are exactly perpendicular, these planes deviate slightly (by $\beta - 90^\circ$) from perpendicularity in \mathcal{H} and split into two different twin laws (cosets), the first one containing twin plane m_x , the second one m_z . Each twin law contributes its rational twin boundary, m_x or m_z , to the observed twin aggregate, whereas in each pair the perpendicular irrational plane is suppressed.

(2) In a tetragonal–orthorhombic phase transition, the two *exactly* perpendicular mirror planes (110) and ($\bar{1}\bar{1}0$) of the tetragonal prototype phase \mathcal{G} split into two independent

3. PHASE TRANSITIONS, TWINNING AND DOMAIN STRUCTURES

(rational) twin boundaries in the deformed orthorhombic phase \mathcal{H} , which are now *nearly* perpendicular to each other.

The most famous example of this type of twinning is the 1023 K ferroelastic phase transition of the high- T_c superconductor $\text{YBa}_2\text{Cu}_3\text{O}_{7-\delta}$. The twinning on $\{110\}$ in this compound was first extensively studied by Roth *et al.* (1987), both in direct space (TEM) and in reciprocal space (electron and X-ray diffraction), and by Schmid *et al.* (1988); see also Shekhtman (1993).

3.3.10.2.2. Extension to non-merohedral growth and mechanical twins

The treatment by Sapriel (1975) was directed to (switchable) ferroelastics with a real structural phase transition from a parent phase \mathcal{G} to a deformed daughter phase \mathcal{H} . This procedure can be extended to those *non-merohedral* twins that lack a (real or hypothetical) parent phase, in particular to growth twins as well as to mechanical twins in the traditional sense [cf. Section 3.3.7.3(i)]. Here, the missing supergroup \mathcal{G} formally has to be replaced by the ‘full’ or ‘reduced’ composite symmetry \mathcal{K} or \mathcal{K}^* of the twin, as defined in Section 3.3.4. Furthermore, we replace the spontaneous shear strain by one half of the imaginary shear deformation which would be required to transform the first orientation state into the second *via* a hypothetical intermediate (zero-strain) reference state. Note that this is a formal procedure only and does not occur in reality, except in mechanical twinning (cf. Section 3.3.7.3). With respect to this intermediate reference state, the two twin orientations possess equal but opposite ‘spontaneous’ strain. With these definitions, the Sapriel treatment can be applied to non-merohedral twins in general. This extension even permits the generalization of the Aizu notation of ferroelastic species to $\mathcal{K}\mathcal{F}\mathcal{H}$ and $\mathcal{K}^*\mathcal{F}\mathcal{H}^*$ (e.g. $mmmF2/m$), whereby now \mathcal{H} and \mathcal{H}^* represent the *eigensymmetry* and the intersection symmetry, and \mathcal{K} and \mathcal{K}^* the (possibly reduced) composite symmetry of the domain pair. With these modifications, the tables of Sapriel (1975) can be used to derive the permissible boundaries W and W' for general non-merohedral twins.

It should be emphasized that this extension of the Sapriel treatment requires a modification of the definition of the W boundary as given above in Section 3.3.10.2.1: The (rational) symmetry operations of the parent phase, becoming F operations in the phase transformation, have to be replaced by the (growth) twin operations contained in the coset of the twin law. These twin operations now correspond to either rational or irrational twin elements. Consequently, the W boundaries defined by these twin elements can be either rational or irrational, whereas by Sapriel they are defined as rational. The Sapriel definition of the W' boundaries, on the other hand, is not modified: W' boundaries depend on the direction of the spontaneous shear strain and are always irrational. They cannot be derived from the twin operations in the coset and, hence, do not appear as primed twin elements in the black–white symmetry symbol of the composite symmetry \mathcal{K} or \mathcal{K}^* .

In many cases, the derivation of the permissible twin boundaries W can be simplified by application of the following rules:

- (i) any twin mirror plane, rational or irrational, is a permissible composition plane W ;
- (ii) the plane perpendicular to any twofold twin axis, rational or irrational, is a permissible composition plane W ;
- (iii) all these twin mirror planes and twofold twin axes can be identified in the coset of any twin law, for example by the primed twin elements in the black–white symmetry symbol of the composite symmetry \mathcal{K} (cf. Section 3.3.5).

In conclusion, the following differences in philosophy between the Sapriel approach in Section 3.3.10.2.1 and its extension in the present section are noted: Sapriel starts from the supergroup \mathcal{G} of

the parent phase and determines all permissible domain walls at once by means of the symmetry reduction $\mathcal{G} \rightarrow \mathcal{H}$ during the phase transition. This includes group–subgroup relations of index $[i] > 2$. The present extension to general twins takes the opposite direction: starting from the *eigensymmetry* \mathcal{H} of a twin component and the twin law $k \times \mathcal{H}$, a symmetry increase to the composite symmetry \mathcal{K} of a twin domain pair is obtained. From this composite symmetry, which is always a supergroup of \mathcal{H} of index $[i] = 2$, the two permissible boundaries between the two twin domains are derived. Repetition of this process, using further twin laws one by one, determines the permissible boundaries in multiple twins of index $[i] > 2$.

Examples

(1) *Gypsum dovetail twin*, *eigensymmetry* $\mathcal{H} = 2/m$, twin element: reflection plane (100) (cf. Example 3.3.6.2, Fig. 3.3.6.1).

Intersection symmetry of two twin domains: $\mathcal{H}^* = 12/m1$ (= *eigensymmetry* \mathcal{H}); composite symmetry: $\mathcal{K} = 2'/m'2/m2'/m'$ (referred to orthorhombic axes); corresponding Aizu notation: $2/m2/m2/mF12/m1$; alternative twin elements in the coset: rational twin reflection plane $m' \parallel (100)$ and irrational plane m' normal to $[001]$, as well as the twofold axes normal to these planes, all referred to monoclinic axes. The two alternative twin reflection planes are at the same time permissible W boundaries.

In most dovetail and Montmartre twins of gypsum only the rational (100) or (001) twin boundary is observed. In some cases, however, both permissible W boundaries occur, whereby the irrational interface is usually distinctly smaller and less perfect than the rational one, cf. Fig. 3.3.6.1.

(2) *Multiple twins* with orthorhombic *eigensymmetry* $\mathcal{H} = 2/m2/m2/m$ and equivalent twin mirror planes (110) and $(\bar{1}\bar{1}0)$.

Intersection symmetry of two or more domain states: $\mathcal{H}^* = 112/m$; reduced composite symmetry: $\mathcal{K}^* = 2'/m'2'/m'2/m$.

Reference is made to Fig. 3.3.4.2 in Section 3.3.4.2, where the complete cosets for *both* twin laws (110) and $(\bar{1}\bar{1}0)$ are shown. For each twin law, the two perpendicular twin mirror planes are at the same time the two permissible W twin boundaries. The (110) boundary is rational, the second permissible boundary, perpendicular to (110), is irrational; similarly for $(\bar{1}\bar{1}0)$. The rational boundary is always observed. This rule remains valid for multiple twins, in particular for the spectacular cyclic twins with pseudo n -fold twin axes: $\arctan b/a \approx 60^\circ$ (aragonite), 72° (AlMn alloy), 90° (staurolite 90° cross), \dots , $360^\circ/n$. A pentagonal twin is shown in Fig. 3.3.6.8.

(3) *Twins of triclinic feldspars*, *eigensymmetry* $\mathcal{H} = \bar{1}$ (cf. Example 3.3.6.11, Figs. 3.3.6.11 and 3.3.6.12).

(a) *Albite law*: twin reflection plane (010) (referred to triclinic, pseudo-monoclinic axes), Fig. 3.3.6.11.

Intersection symmetry: $\mathcal{H}^* = \mathcal{H} = \bar{1}$; composite symmetry: $\mathcal{K} = 2'/m'(\bar{1})$.

The two permissible twin boundaries are the W twin plane (010) (fixed and rational) and a W' plane perpendicular to the first in the zone of the reciprocal axis $\mathbf{b}^* = [010]^*$, but ‘floating’ with respect to its azimuth. The rational W plane (010) is always observed in the form of large-area, polysynthetic twin aggregates.

(b) *Pericline law*: twofold twin rotation axis $[010]$ (referred to triclinic, pseudo-monoclinic axes), Fig. 3.3.6.12.

Intersection symmetry: $\mathcal{H}^* = \mathcal{H} = \bar{1}$; composite symmetry: $\mathcal{K} = 2'/m'(\bar{1})$.

The two permissible contact planes are:

- (i) the irrational W plane normal to the twin axis $[010]$ [parallel to the reciprocal $(010)^*$ plane];
- (ii) the irrational W' plane, normal to the first W plane, in the zone of the $[010]$ twin axis, but ‘floating’ with respect to its azimuth.

The latter composition plane is the famous ‘rhombic section’ which is always observed. The azimuthal angle of the rhombic section around $[010]$ depends on the Na/Ca ratio of the plagioclase.

3.3. TWINNING OF CRYSTALS

clase crystal and is used for the determination of its chemical composition.

Remark. Both twin laws (albite and pericline) occur simultaneously in microcline, KAlSi_3O_8 ('transformation microcline') as the result of a slow Si/Al order-disorder phase transition from monoclinic sanidine to triclinic microcline, forming crosshatched lamellae of albite and pericline twins (Aizu species $2/m\bar{1}$).

(4) *Carlsbad twins* of monoclinic orthoclase KAlSi_3O_8 (cf. Fig. 3.3.7.1).

Eigensymmetry: $\mathcal{H} = 12/m\bar{1}$; twin element: twofold axis $\{001\}$ (referred to monoclinic axes); intersection symmetry: $\mathcal{H}^* = \mathcal{H} = 12/m\bar{1}$; composite symmetry: $\mathcal{K} = 2'/m'2/m2'/m'$ (referred to orthorhombic axes).

Permissible W twin boundaries (referred to monoclinic axes):

(i) $m \perp [001]$ (irrational),

(ii) $m \parallel (100)$ (rational).

Carlsbad twins are penetration twins. The twin boundaries are more or less irregular, as is indicated by the re-entrant edges on the surface of the crystals. From some of these edges, it can be concluded that boundary segments parallel to the permissible (100) planes as well as parallel to the non-permissible (010) planes (which are symmetry planes of the crystal) occur. This is possibly due to complications arising from the penetration morphology.

(5) *Calcite deformation twins (e-twins)* [cf. Section 3.3.7.3(i) and Fig. 3.3.7.3].

The deformation twinning in calcite has been extensively studied by Barber & Wenk (1979). Recently, these twins were discussed by Bueble & Schmahl (1999) from the viewpoint of Sapriel's strain compatibility theory of domain walls.

For calcite (space group $R\bar{3}c$) three unit cells are in use:

(i) *Structural* triple hexagonal R -centred cell ('X-ray cell'): $a_{\text{hex}} = 4.99$, $c_{\text{hex}} = 17.06$ Å. This cell is used by both Barber & Wenk and Bueble & Schmahl.

(ii) *Morphological* cell: $a_{\text{morph}} = a_{\text{hex}} = 4.99$, $c_{\text{morph}} = 1/4c_{\text{hex}} = 4.26$ Å. This cell is used in many mineralogical textbooks for the description of the calcite morphology and twinning.

(iii) *Rhombohedral (pseudo-cubic)* cell, F -centred, corresponding to the cleavage rhombohedron and the cell of the cubic NaCl structure: $a_{\text{pc}} = 3.21$ Å, $\alpha_{\text{pc}} = 101.90^\circ$.

Eigensymmetry: $\mathcal{H} = \bar{3}2/m\bar{1}$; twin reflection and interface plane: $(01\bar{1}8)_{\text{hex}} = (01\bar{1}2)_{\text{morph}} = (110)_{\text{pc}}$ (similar for the two other equivalent planes); intersection symmetry: $\mathcal{H}^* = 2/m$ along $[010]_{\text{hex}} = [10\bar{1}]_{\text{pc}}$; reduced composite symmetry: $\mathcal{K}^* = 2/m2'/m'_12'/m'_2$, with $m_1 = (0118)_{\text{hex}} = (0112)_{\text{morph}} = (110)_{\text{pc}}$ rational and m_2 an irrational plane normal to the edge of the cleavage rhombohedron (cf. Fig. 3.3.7.3). Planes m_1 and m_2 are compatible W twin boundaries, of which the rational plane m_1 is the only one observed.

Bueble & Schmahl (1999) treated the mechanical twinning of calcite by using the Sapriel formalism for ferroelastic crystals. The authors devised a virtual prototypic phase of cubic $m\bar{3}m$ symmetry with the NaCl unit cell (iii) mentioned above. From a virtual ferroelastic phase transition $m\bar{3}m \Rightarrow \bar{3}2/m$, they derived four orientation states (corresponding to compression axes along the four cube diagonals). The W boundaries are of type $\{110\}_{\text{pc}} = \{0118\}_{\text{hex}} = \{0112\}_{\text{morph}}$ and $\{001\}_{\text{pc}} = \{0114\}_{\text{hex}} = \{0111\}_{\text{morph}}$ (cleavage faces). These boundaries are observed. The *e*-twins (primary twins) with $\{110\}_{\text{pc}}$ W walls, however, dominate in calcite (primary deformation twin lamellae), whereas the secondary *r*-twins with $\{001\}_{\text{pc}}$ W boundaries are relatively rare.

A comparison with the compatible twin boundaries m_1 and m_2 derived from the reduced composite symmetry \mathcal{K}^* shows that the $m_1 = \{110\}_{\text{pc}} = \{0118\}_{\text{hex}}$ boundary is predicted by both approaches, whereas m_2 and $\{001\}_{\text{pc}} = \{0114\}_{\text{hex}}$ differ by an angle of 26.2° . The twin reflection planes $\{110\}_{\text{pc}}$ (*e*-twin) and $\{001\}_{\text{pc}}$ (*r*-twin) represent different twin laws and are not alter-

native twin elements of the same twin law, as are $m_1 = \{110\}_{\text{pc}}$ and m_2 . They would be alternative elements if the rhombohedron (pseudo-cube), keeping its structural $\bar{3}2/m$ symmetry, were re-distorted into an exact cube.

This situation explains the rather complicated deformation twin texture of calcite. Whereas two *e*-twin components can be stress-free attached to each other along a boundary consisting of compatible $m_1 = \{110\}_{\text{pc}}$ and m_2 segments, a boundary of $\{110\}_{\text{pc}}$ and (incompatible) $\{001\}_{\text{pc}}$ segments would generate stress, which is extraordinarily high due to the extreme shear angle of 26.2° . The irrational m_2 boundary, though mechanically compatible, is not observed in calcite and is obviously suppressed due to bad structural fit. As a consequence, the stress in the boundary regions between the mutually incompatible *e* $\{110\}_{\text{pc}}$ and *r* $\{001\}_{\text{pc}}$ twin systems is often buffered by the formation of needle twin lamellae (Salje & Ishibashi, 1996) or structural channels along crystallographic directions ('Rose channels'; Rose, 1868). Twinning dislocations and cracks (Barber & Wenk, 1979) also relax high stress. In 'real' ferroelastic crystals with their small shear (usually below 1°) these stress-relaxing phenomena usually do not occur.

3.3.10.2.3. Permissible boundaries in merohedral twins (lattice index $[j] = 1$)

In merohedral twins (lattice index $[j] = 1$), the twin elements map the entire lattice exactly upon itself. Hence there is no spontaneous strain, in which the twin domains would differ. The mechanical compatibility criterion means in this case that any orientation of a twin boundary is permissible, because interfaces of any orientation obey the mechanical compatibility criterion, no matter whether the planes are rational, irrational or even curved interfaces. This variety of interfaces is brought out by many actual cases, as shown by the following examples:

(1) Quartz.

The boundaries of Dauphiné *transformation* twins ($622 \Rightarrow 32$) are usually irregular, curved interfaces without macroscopically flat parts (segments) (Fron del, 1962). The boundaries of Dauphiné *growth* twins are usually curved too, but sometimes they exhibit large segments roughly parallel to the rhombohedron faces $r\{10\bar{1}1\}$ and $z\{10\bar{1}1\}$. Inserts of growth-twin domains often have the shape of rounded cones with apices located at the nucleating perturbation (usually an inclusion). X-ray topography has shown that Dauphiné boundaries are sometimes stepped on a fine scale just above the topographic resolution of a few μm (Lang, 1967*a,b*).

In contrast to Dauphiné boundaries, the contact faces of Brazil twins (which are always *growth* twins) strictly adopt low-index lattice planes, preferentially those of the major rhombohedron $r\{10\bar{1}1\}$, less frequently of the minor rhombohedron $z\{10\bar{1}1\}$. More rarely observed are boundary segments parallel to $\{10\bar{1}0\}$, $\{11\bar{2}1\}$ and $\{0001\}$ (Fron del, 1962). A special case are the differently dyed $r\{10\bar{1}1\}$ Brazil-twin lamellae of amethyst (Fron del, 1962).

(2) Triglycine sulfate (TGS).

This crystal exhibits a ferroelectric transition $2/m \Leftrightarrow 2$ with antipolar (merohedral) inversion twins (180° domains). The domains usually have the shape of irregular cylinders parallel to the polar axis. All boundaries parallel to the polar axis are observed, whereas boundaries inclined or normal to the polar axis are 'electrically forbidden' (they would be head-to-head and tail-to-tail boundaries, cf. Section 3.3.10.3), even though they are mechanically permissible.

(3) Lithium formate monohydrate (polar point group $mm2$).

The crystals grown from aqueous solutions exhibit inversion twins in the shape of sharply defined (010) lamellae (non-switchable 180° domains). Other boundaries of these growth twins have not been observed (Klapper, 1973).

3. PHASE TRANSITIONS, TWINNING AND DOMAIN STRUCTURES

(4) $KLiSO_4$ (polar point group 6).

Among the three different merohedral twin laws, one type, with twin reflection plane m parallel to the hexagonal axis $[001]$, stands out. The numerous grown-in twin lamellae are bounded by large planar (0001) interfaces (normal to the polar axis). It should be noted that these very prominent twin boundaries are perpendicular to the twin reflection plane. This is a rather rare case of boundary orientation. These planes are oriented normal to the polar axis but are not electrically forbidden, due to the twin law $m \parallel [001]$ which preserves the polar direction (Klapper *et al.*, 1987).

These examples demonstrate that in many merohedral twins only a small number of rational, well defined boundaries occur, even though *any* boundary is permitted by the mechanical compatibility criterion. This shows that the latter criterion is a necessary, but not a sufficient, condition and that further influences, in particular electrical or structural ones, are effective.

3.3.10.2.4. Permissible twin boundaries in twins with lattice index $[j] > 1$

In contrast to the mechanical compatibility of *any* composition plane in merohedral twins (lattice index $[j] = 1$), twins of higher lattice index $[j] > 1$ are more restricted with respect to the orientation of permissible twin boundaries. In fact, these special twins can be treated in the same way as the general non-merohedral twins described in Section 3.3.10.2.2 above. Again, we attribute equal but opposite spontaneous shear strain to the two twin domains 1 and 2. This 'spontaneous' shear strain (referred to an intermediate state of zero strain) is half the shear deformation necessary to transform the orientation of domain 1 into that of domain 2. This also means that the lattice of domain 1 is transformed into the lattice of domain 2. The essential difference to the case in Section 3.3.10.2.2 is the fact that by this deformation only a subset of lattice points is 'restored'. This subset forms the sublattice of index $[j] \geq 2$ common to both domains (coincidence-site sublattice, twin lattice). With this analogy, the Sapriel formalism can be applied to the derivation of the mechanically compatible (permissible) twin boundaries. Again, the easiest way to find the permissible planes is the construction of the black-white symmetry symbol of the twin law, in which planes parallel to primed mirror planes or normal to primed twofold axes constitute the permissible W interfaces.

It is emphasized that the concept of a deformation from domain state 1 to domain state 2 is not always a mere mental construction, as it is for growth twins. It is physical reality in some deformation twins, for example in the famous $\Sigma 3$ deformation twins (spinel law) of cubic metals which are essential elements of the plasticity of these metals. During the $\Sigma 3$ deformation, the $\{100\}$ cube (a 90° rhombohedron) is switched from its 'reverse'

into its 'obverse' orientation and *vice versa*, whereby the hexagonal P sublattice of index $[j] = 3$ is restored and, thus, is common to both twin domains.

Exact lattice coincidences of twin domains result from special symmetry relations of the lattice. Such relations are systematically provided by n -fold symmetry axes of order $n > 2$, *i.e.* by three-, four- and sixfold axes. In other words: twins of lattice index $[j] > 2$ occur systematically in trigonal, hexagonal, tetragonal and cubic crystals. This may lead to trigonal, tetragonal and hexagonal intersection symmetries \mathcal{H}^* (reduced *eigensymmetries*) of domain pairs. Consequently, if there exists one pair of permissible composition planes, all pairs of planes equivalent to the first one with respect to the intersection symmetry are permissible twin boundaries as well. This is illustrated by three examples in Table 3.3.10.1.

For the cubic and rhombohedral $\Sigma 3$ twins (spinel law), due to the threefold axis of the intersection symmetry, three pairs of permissible planes occur. The plane (111), normal to this threefold axis, is common to the three pairs of boundaries (threefold degeneracy), *i.e.* in total four different permissible W twin boundaries occur. These composition planes (111), $(1\bar{1}\bar{2})$, $(\bar{2}11)$, $(1\bar{2}1)$ are indeed observed in the $\Sigma 3$ spinel-type penetration twins, recognizable by their re-entrant edges (Fig. 3.3.6.6). They also occur as twin glide planes of cubic metals. For the tetragonal $\Sigma 5$ twin, two pairs of perpendicular permissible W composition planes result, (120) & (210) and (310) & ($\bar{1}30$), one pair bisecting the other pair under 45° . For the cubic $\Sigma 33$ twin [galena PbS, *cf.* Section 3.3.8.3, example (4)], due to the low intersection symmetry, only one pair of permissible W boundaries results.

3.3.10.3. Electrical constraints of twin interfaces

As mentioned before, the mechanical compatibility of twin boundaries is a necessary but not a sufficient criterion for the occurrence of stress-free low-energy twin interfaces. An additional restriction occurs in materials with a permanent (spontaneous) electrical polarization, *i.e.* in crystals belonging to one of the ten pyroelectric crystal classes which include all ferroelectric materials. In these crystals, domains with different directions of the spontaneous polarization may occur and lead to 'electrically charged boundaries'.

3.3.10.3.1. Merohedral twins

Of particular significance are *merohedral* twins with polar domains of antiparallel spontaneous polarization $\pm \mathbf{P}$ (180° domains). The charge density ρ at a boundary between two twin domains is given by

$$\rho = \pm 2P_n,$$

where P_n is the component of the polarization normal to the boundary. The interfaces with positive charge are called 'head-to-

Table 3.3.10.1. Examples of permissible twin boundaries for higher-order merohedral twins ($[j] > 1$)

| | $\Sigma 3$ growth and deformation twins of cubic crystals, twin mirror plane (111) (spinel law) | $\Sigma 5$ growth twins of tetragonal rare-earth sulfides ($\text{SmS}_{1.9}$), twin mirror plane (120) | $\Sigma 33$ deformation twins of cubic galena (PbS), twin mirror plane (441) [†] |
|--|--|---|---|
| Eigensymmetry \mathcal{H} | $4/m\bar{3}2/m$ | $4/m2/m2/m$ | $4/m\bar{3}2/m$ |
| Intersection symmetry \mathcal{H}^* ‡ | $\bar{3}2/m$ parallel to $[111]$ | $4/m$ parallel to $[001]$ | $2/m$ parallel to $[1\bar{1}0]$ |
| Reduced composite symmetry \mathcal{K}^* ‡ | $6'/m'_1(\bar{3})2/m'2'/m'_3$ | $4/m2'/m'_12'/m'_2$ | $2'/m'_12'/m'2'/m'_2$ |
| Permissible twin boundaries | Three pairs of perpendicular planes $m_1 = (111) \text{ \& } m_3 = (11\bar{2})$ $m_1 = (111) \text{ \& } m_3 = (\bar{2}11)$ $m_1 = (111) \text{ \& } m_3 = (1\bar{2}1)$ | Two pairs of perpendicular planes $m_1 = (120) \text{ \& } (210)$ $m_2 = (310) \text{ \& } (\bar{1}30)$ | One pair of permissible planes $m_1 = (441) \text{ \& } m_2 = (11\bar{8})$ |
| Reference system | Cubic axes | Tetragonal axes | Cubic axes |

[†] The existence of this deformation twin is still in doubt (*cf.* Seifert, 1928). [‡] The intersection symmetry \mathcal{H}^* and the permissible boundaries are referred to the coordinate system of the *eigensymmetry*; the reduced composite symmetries \mathcal{K}^* are based on their own conventional coordinate system derived from the intersection symmetry \mathcal{H}^* plus the twin law (*cf.* Section 3.3.4).

3.3. TWINNING OF CRYSTALS

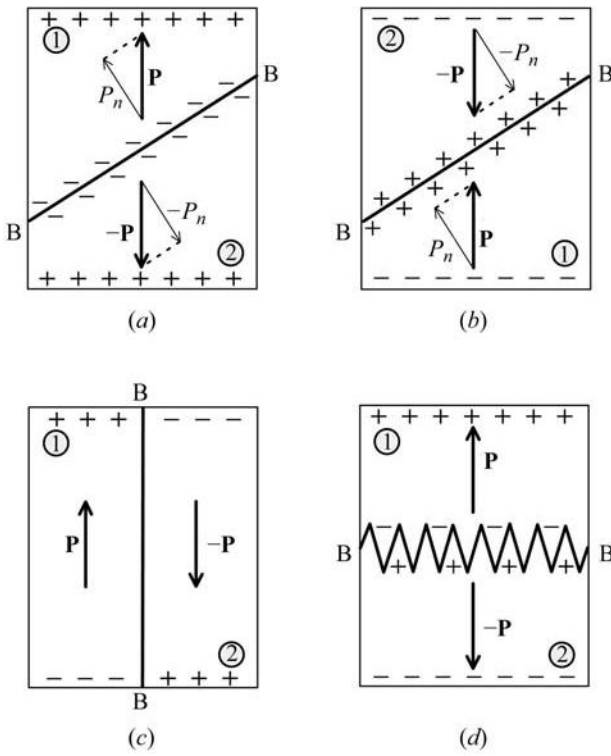


Fig. 3.3.10.2. Boundaries B-B between 180° domains (merohedral twins) of pyroelectric crystals. (a) Tail-to-tail boundary. (b) Head-to-head boundary. (c) Uncharged boundary ($P_n = 0$). (d) Charged zigzag boundary, with average orientation normal to the polar axis. The charge density is significantly reduced. Note that the charges at the boundaries are usually compensated by stray charges of opposite sign.

head' boundaries, those with negative charge 'tail-to-tail' boundaries. Interfaces parallel to the polarization direction are uncharged ($P_n = 0$) (Fig. 3.3.10.2).

The electrical charges on a twin boundary constitute an additional (now electrostatic) energy of the twin boundary and are 'electrically forbidden'. Only boundaries parallel to the polar axes are 'permitted'. This is in fact mostly observed: practically all 180° domains originating during a phase transition from a paraelectric parent phase to the polar (usually ferroelectric) daughter phase exhibit uncharged boundaries parallel to the spontaneous polarization. Uncharged boundaries have also been found in inversion growth twins obtained from aqueous solutions, such as lithium formate monohydrate and ammonium lithium sulfate. Both crystals possess the polar *eigensymmetry* $mm2$ and contain grown-in inversion twin lamellae (180° domains) parallel to their polar axis.

'Charged' boundaries, however, may occur in crystals that are electrical conductors. In such cases, the polarization charges accumulating along head-to-head or tail-to-tail boundaries are compensated by opposite charges obtained through the electrical conductivity. This compensation may lead to a considerable reduction of the interface energy. Note that the term 'charged' is often used for boundaries of head-to-head and tail-to-tail character, even if they are uncharged due to charge compensation.

Examples

(1) *Lithium niobate* LiNbO_3 exhibits a phase transition from $\bar{3}2/m$ to $3m$ between 1323 and 1473 K (depending on the Li/Nb stoichiometry). Crystals are grown from the melt ($T_m = 1538$ K) by Czochralski pulling along the trigonal axis $[001]$ in the paraelectric phase. They transform into the ferroelectric polar phase when cooled below the Curie temperature. The crystals are electrically conductive at high temperatures and can be poled by an electric field parallel to the polar axis. By applying an alternating rectangular voltage between seed crystal and melt, a

sequence of 180° domains is formed during the subsequent transition. The domain boundaries follow the curved growth front (crystal-melt interface) and have alternating head-to-head and tail-to-tail character (Räuber, 1978).

(2) Orthorhombic polar *potassium titanyl phosphate*, KTiOPO_4 (KTP), exhibits a para- to ferroelectric phase transition ($mmm \rightleftharpoons mm2$) and a considerable conductivity of potassium ions. In this material, head-to-head and tail-to-tail boundaries are common. Sometimes strongly folded, charged zigzag boundaries occur, which contain large segments of faces nearly parallel to the spontaneous polarization (Scherf *et al.*, 1999). The average orientation of these boundaries is roughly normal to the polar axis (Fig. 3.3.10.2d), but their charge density is considerably reduced by the zigzag geometry.

(3) Head-to-head and tail-to-tail twin boundaries are also found in crystals grown from aqueous solutions. In such cases, the polarization charges are compensated by the opposite charges present in the electrolytic solution. An interesting example is hexagonal *potassium lithium sulfate* KLiSO_4 (point group 6) which exhibits, among other types of twins, anti-polar domains of inversion twins. The twin boundaries often have head-to-head or tail-to-tail character and frequently coincide with the growth-sector boundaries (Klapper *et al.*, 1987).

3.3.10.3.2. Non-merohedral twins

Charged and uncharged boundaries may also occur in *non-merohedral* twins of pyroelectric crystals. In this case, the polar axes of the two twin domains 1 and 2 are not parallel. The charge density ρ of the boundary is given by

$$\rho = P_n(2) - P_n(1),$$

with $P_n(1)$ and $P_n(2)$ the components of the spontaneous polarization normal to the boundary. An example of both charged and uncharged boundaries is provided by the growth twins of *ammonium lithium sulfate* with *eigensymmetry* $m2m$. These crystals exhibit, besides the inversion twinning mentioned above, growth-sector twins with twin laws 'reflection plane (110)' and 'twofold twin axis normal to (110)'. (Both twin elements would constitute the same twin law if the crystal were centrosymmetric.) The observed and permissible composition plane for both laws is (110) itself. As is shown in Fig. 3.3.10.3, the (110) boundary is charged for the reflection twin and uncharged for the rotation twin. Both cases are realized for ammonium lithium sulfate. The charges of the reflection-twin boundary are compensated by the charges contained in the electrolytic aqueous solution from which the crystal is grown. On heating (cooling), however, positive (negative) charges appear along the twin boundary.

3.3.10.3.3. Non-pyroelectric acentric crystals

Finally, it is pointed out that electrical constraints of twin boundaries do not occur for *non-pyroelectric acentric* crystals. This is due to the absence of spontaneous polarization and, consequently, of electrical boundary charges. This fact is apparent for the Dauphiné and Brazil twins of quartz: they exhibit boundaries normal to the polar twofold axes which are reversed by the twin operations.

Nevertheless, it seems that among possible twin laws those leading to opposite directions of the polar axes are avoided. This can be explained for spinel twins of cubic crystals with the sphalerite structure and *eigensymmetry* $\bar{4}3m$. Two twin laws, different due to the lack of the symmetry centre, are possible:

- (i) twofold twin rotation around $[111]$,
- (ii) twin reflection across the plane (111).

In the first case, the sense of the polar axis $[111]$ is not reversed, in the second case it is reversed. All publications on this kind of twinning, common in III-V and II-VI compound semiconductors (GaAs, InP, ZnS, CdTe *etc.*), report the twofold axis along $[111]$ as

3. PHASE TRANSITIONS, TWINNING AND DOMAIN STRUCTURES

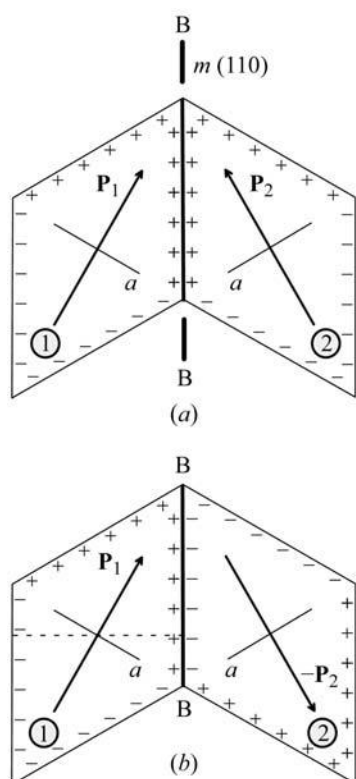


Fig. 3.3.10.3. Charged and uncharged boundaries B-B of non-merohedral twins of pseudo-hexagonal NH_4LiSO_4 . Point group $m2m$, spontaneous polarization \mathbf{P} along twofold axis $[010]$. (a) Twin element mirror plane (110): electrically charged boundary of head-to-head character. (b) Twin element twofold twin axis normal to plane (110): uncharged twin boundary ('head-to-tail' boundary).

the true twin element, not the mirror plane (111); this was discussed very early on in a significant paper by Aminoff & Broomé (1931).

3.3.10.4. Displacement and fault vectors of twin boundaries

The statements of the preceding sections on the permissibility of twin boundaries are very general and derived without any regard to the crystal structure. For example, *any arbitrary reflection plane* relating two partners of a crystal aggregate or even of an anisotropic continuous elastic medium represents a mechanically permissible boundary. For twin boundaries in crystals, however, additional aspects have to be taken into account, *viz* the atomic structure of the twin interface, *i.e.* the geometrical configuration of atoms, ions and molecules and their crystal-chemical interactions (bonding topology) in the transition region between the two twin partners. Only if the configurations and interactions of the atoms lead to boundaries of good structural fit and, consequently, of low energy, will the interfaces occur with the reproducibility and frequency that are prerequisites for a twin. In this respect, the mechanical and electrical permissibility conditions given in the preceding sections are necessary but not sufficient conditions for the occurrence of a twin boundary and – in the end – of the twin itself. In the following considerations, all twin boundaries are assumed to be permissible in the sense discussed above.

3.3.10.4.1. Twin displacement vector \mathbf{t}

As a first step of the structural elucidation of a reflection-twin boundary, the mutual relation of the two lattices of the twin partners 1 and 2 at the boundary is considered. It is assumed that the unit cells of both lattices have the same origin with respect to their crystal structure, *i.e.* that the lattice points are located in the same structural sites of both partners. Three cases of lattice

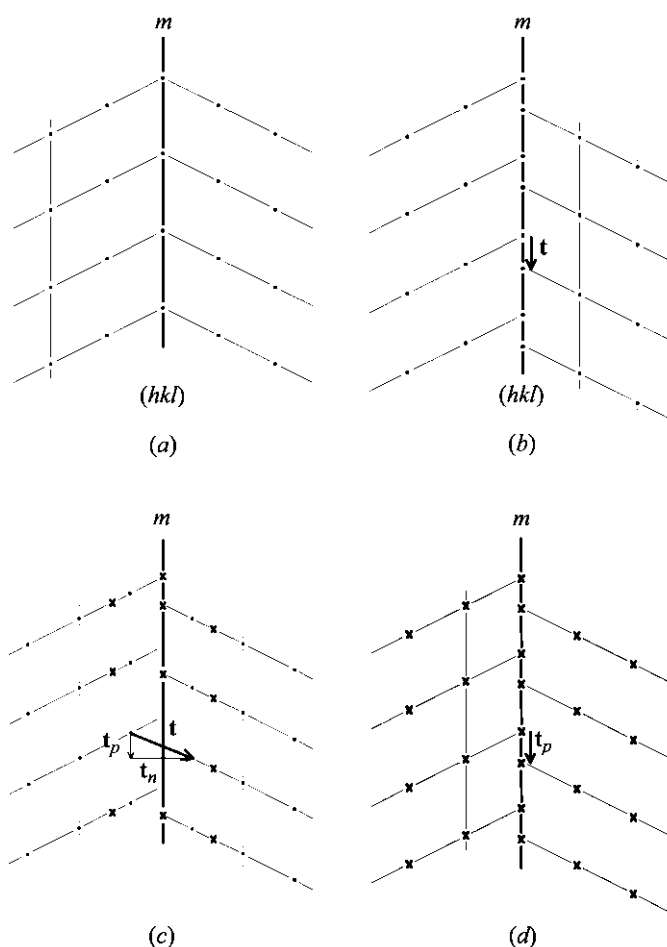


Fig. 3.3.10.4. Lattice representation of twin displacement vectors. (a) Lattice representation of a 'pure' twin reflection plane ($\mathbf{t} = 0$). (b) Twin reflection plane with parallel displacement vector \mathbf{t} (generalized twin glide plane). (c) Twin reflection plane with a general twin displacement vector with parallel and normal components: $\mathbf{t} = \mathbf{t}_n + \mathbf{t}_p$. By choosing a suitable new lattice point x (origin shift), the normal component \mathbf{t}_n disappears, preserving the parallel component \mathbf{t}_p as the true twin displacement vector and leading to case (b), as shown in (d).

relations across the rational composition plane (hkl) (assumed to be parallel to the twin reflection plane) are considered, as outlined in Fig. 3.3.10.4 [see also Section 3.3.2.4, Note (8)].

(a) The composition lattice planes (hkl)₁ and (hkl)₂ of domains 1 and 2 coincide *pointwise* (Fig. 3.3.10.4a), *i.e.* the lattices of the two twin partners coincide in the twin boundary.

(b) The composition lattice planes (hkl)₁ and (hkl)₂ are *common* but not *pointwise* coincident, *i.e.* the two lattices are displaced by a non-integer vector \mathbf{t} (*twin displacement vector*) *parallel* to the composition plane (Fig. 3.3.10.4b).

(c) The composition lattice planes (hkl)₁ and (hkl)₂ are displaced – in addition to the parallel component – by a component *normal* to the composition plane (Fig. 3.3.10.4c). By an appropriate choice of the lattice points with respect to the structure, this normal component vanishes and, hence, this general case reduces to case (b) (Fig. 3.3.10.4d).

This shows that for the characterization of a twin with coinciding twin reflection and contact plane only the component of a twin displacement vector *parallel* to the twin boundary is significant. Thus, on an atomic scale, not only twin reflection planes ($\mathbf{t} \approx 0$) but also 'twin glide planes' ($\mathbf{t} \approx 1/2\mathbf{v}_L$, where \mathbf{v}_L is a lattice translation vector), as well as all intermediate cases, have to be considered. In principle, these considerations also apply to irrational twin reflection and composition planes. Moreover, twin displacement vectors also have to be admitted for the other types of twins, *viz* rotation and inversion twins. Examples are given below.

3.3. TWINNING OF CRYSTALS

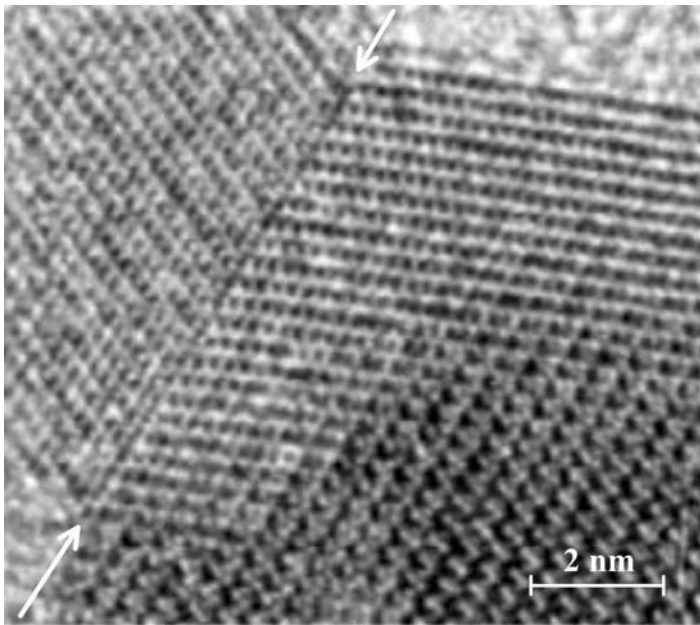


Fig. 3.3.10.5. HRTEM micrograph of anatase, TiO_2 , with a (112) reflection twin boundary (arrows), viewed edge-on along $[1\bar{3}1]$. The twin displacement vector $\mathbf{t} = 1/2$ of the boundary translation period is clearly visible. Courtesy of R. L. Penn, Madison, Wisconsin; cf. Penn & Banfield, 1998.

So far, the considerations about twin boundaries are based on the idealized concept that the bulk structure extends without any deformation up to the twin boundary. In reality, however, near the interface the structures are more or less deformed (relaxed), and so are their lattices. This transition region may even contain a central slab exhibiting a different structure, which is often close to a real or hypothetical polymorph or to the parent structure. [Examples: the Dauphiné twin boundary of α -quartz resembles the structure of β -quartz; the iron-cross (110) twin interface of pyrite, FeS_2 , resembles the structure of marcasite, another polymorph of FeS_2 .]

Whereas the twin displacement vector keeps its significance for small distortions of the boundary region, it loses its usefulness for large structural deformations. It should be noted that *rational* twin interfaces are usually observed as ‘good’, whereas *irrational* twin boundaries, despite mechanical compatibility, usually exhibit irregular features and macroscopically visible deformations.

Twin displacement vectors are a consequence of the minimization of the boundary energy. This has been proven by a theoretical study of the boundary energy of reflection twins of monoclinic saccharine crystals with (102) as twin reflection and composition plane (Lieberman *et al.*, 1998). The authors calculated the boundary energy as a function of the lattice displacement vector \mathbf{t} , which was varied within the mesh of the (102) composition plane, admitting also a component normal to the composition plane. The calculations were based on a combination of Lennard–Jones and Coulomb potentials and result in a flat energy minimum for a displacement vector $\mathbf{t} = [0.05/0.71/0.5]$ (referred to the monoclinic axes). The calculations were carried out for the undistorted bulk structure. The actual deformation of the structure near the twin boundary is not known and, hence, cannot be taken into account. Nevertheless, this model calculation shows that in general twin displacement vectors $\mathbf{t} \neq \mathbf{0}$ are required for the minimization of the boundary energy.

Twin displacement vectors have been considered as long as structural models of boundaries have been derived. One of the oldest examples is the model of the (110) growth-twin boundary of aragonite, suggested by Bragg (1924) (cf. Section 3.3.10.5 below). An even more instructive model is presented by Bragg (1937, pp. 246–248) and Bragg & Claringbull (1965, pp. 302–303) for the Baveno (021) twin reflection and interface plane of

feldspars. It shows that the tetrahedral framework can be continued without interruption across the twin boundary only if the twin reflection plane is a glide plane parallel to (021). A model of a twin boundary requiring a displacement vector $\mathbf{t} \neq \mathbf{0}$ was reported by Black (1955) for the (110) twin reflection boundary of the alloy $\text{Fe}_4\text{Al}_{13}$.

In their interesting theoretical study of the morphology and twinning of gypsum, Bartels & Follner (1989, especially Fig. 4) conclude that the (100) twin interface of Montmartre twins is a pure twin reflection plane without displacement vector, whereas the dovetail twins exhibit a ‘twin glide component’ $\mathbf{a}/2 + \mathbf{b}/2 + \mathbf{c}/2$ parallel to the twin reflection plane $(\bar{1}01)$. [Note that in the present chapter, due to a different choice of coordinate system, the Montmartre twins are given as (001) and the dovetail twins as (100), cf. Example 3.3.6.2.]

The occurrence of twin displacement vectors can be visualized by high-resolution transmission electron microscopy (HRTEM) studies of twin boundaries. Fig. 3.3.10.5 shows an HRTEM micrograph of a (112) twin reflection boundary of anatase TiO_2 , viewed edge on (arrows) along $[1\bar{3}1]$ (Penn & Banfield, 1998). The offset of the lattices along the twin boundary is clearly visible. This result is confirmed by the structural model presented by the authors, which indicates a parallel displacement vector $\mathbf{t} \approx 1/2\mathbf{v}_L$. Twin displacement vectors have also been observed on HRTEM micrographs of sputtered $\text{Fe}_4\text{Al}_{13}$ alloys by Tsuchimori *et al.* (1992).

3.3.10.4.2. Fault vectors of twin boundaries in merohedral twins

Twin displacement vectors can occur in twin boundaries of both non-merohedral (see above) and merohedral twins. For *merohedral* twins, the displacement vector is usually called the ‘fault vector’, because of the close similarity of these twin boundaries with antiphase boundaries and stacking faults (cf. Section 3.3.2.4, Note 7). In contrast to non-merohedral twins, for merohedral twins these displacement vectors can be determined by imaging the twin boundaries by means of electron or X-ray diffraction methods. The essential reason for this possibility is the exact parallelism of the lattices of the two twin partners 1 and 2, so that for any reflection hkl the electron and X-ray diffraction conditions are always simultaneously fulfilled for both partners. Thus, in transmission electron microscopy and X-ray topography, both domains 1 and 2 are simultaneously imaged under the same excitation conditions. By a proper choice of imaging reflections, both twin domains exhibit the same diffracted intensity (no ‘domain contrast’), and the twin boundary is imaged by fringe contrast analogously to the imaging of stacking faults and antiphase boundaries (‘stacking fault contrast’).

This contrast results from the ‘phase jump’ of the structure factor upon crossing the boundary. For stacking faults and antiphase boundaries this phase jump is $2\pi\mathbf{f} \cdot \mathbf{g}_{hkl}$, with \mathbf{f} the fault vector of the boundary and \mathbf{g}_{hkl} the diffraction vector of the reflection used for imaging. For (merohedral) twin boundaries the total phase jump Ψ_{hkl} is composed of two parts,

$$\Psi_{hkl} = \phi_{hkl} + 2\pi\mathbf{f} \cdot \mathbf{g}_{hkl},$$

with ϕ_{hkl} the phase change due to the twin operation and $2\pi\mathbf{f} \cdot \mathbf{g}_{hkl}$ the phase change resulting from the lattice displacement vector \mathbf{f} . The boundary contrast is strongest if the phase jump Ψ_{hkl} is an odd integer multiple of π , and it is zero if Ψ_{hkl} is an integer multiple of 2π . By imaging the boundary in various reflections hkl and analysing the boundary contrast, taking into account the known phase change ϕ_{hkl} (calculated from the structure-factor phases of the reflections hkl_1 and hkl_2 related by the twin operation), the fault vector \mathbf{f} can be determined (see the examples below). This procedure has been introduced into transmission electron microscopy by McLaren & Phakey (1966, 1969) and into X-ray topography by Lang (1967a,b) and McLaren & Phakey (1969).

3. PHASE TRANSITIONS, TWINNING AND DOMAIN STRUCTURES

In the equation given above, for each reflection hkl the total phase jump Ψ_{hkl} is independent of the origin of the unit cell. The individual quantities ϕ_{hkl} and $2\pi\mathbf{f} \cdot \mathbf{g}_{hkl}$, however, vary with the choice of the origin but are coupled in such a way that Ψ_{hkl} (which alone has a physical meaning) remains constant. This is illustrated by the following simple example of an inversion twin.

The twin operation relates reflections hkl_1 and $hkl_2 = \bar{h}\bar{k}\bar{l}_1$. Their structure factors are (assuming Friedel's rule to be valid)

$$F_1 = |F| \exp(-i\varphi) \quad \text{and} \quad F_2 = |F| \exp(+i\varphi).$$

The phase difference of the two structure factors is $\phi_{hkl} = 2\varphi$ and depends on the choice of the origin. If the origin is chosen at the twin inversion centre (superscript o), the phase jump Ψ_{hkl} at the boundary is given by

$$\Psi_{hkl} = \phi_{hkl}^o = 2\varphi^o.$$

This is the total phase jump occurring for reflection pairs $hkl_1/hkl_2 = hkl/\bar{h}\bar{k}\bar{l}$ at the twin boundary.

If the origin is not located at the twin inversion centre but is displaced from it by a vector $\frac{1}{2}\mathbf{f}$, the phases of the structure factors of reflections hkl_1 and hkl_2 are

$$\begin{aligned} \varphi_1 &= \varphi^o - 2\pi(\tfrac{1}{2}\mathbf{f}) \cdot \mathbf{g}_{hkl} \quad \text{and} \\ \varphi_2 &= -\varphi_1 = -[\varphi^o - 2\pi(\tfrac{1}{2}\mathbf{f}) \cdot \mathbf{g}_{hkl}]. \end{aligned}$$

From these equations the phase difference of the structure factors is calculated as

$$\phi_{hkl} = \varphi_1 - \varphi_2 = 2\varphi^o - 2\pi\mathbf{f} \cdot \mathbf{g}_{hkl},$$

and the total phase jump at the boundary is

$$\Psi_{hkl} = 2\varphi^o = \phi_{hkl} + 2\pi\mathbf{f} \cdot \mathbf{g}_{hkl}.$$

This shows that here the fault vector \mathbf{f} has no physical meaning. It merely compensates for the phase contributions that result from an 'improper' choice of the origin. If, by the procedures outlined above, a fault vector \mathbf{f} is determined, the true twin inversion centre is located at the endpoint of the vector $\frac{1}{2}\mathbf{f}$ attached to the chosen origin.

Similar considerations apply to reflection and twofold rotation twins. In these cases, the components of the fault vectors normal to the twin plane or to the twin axis can also be eliminated by a proper choice of the origin. The parallel components, however, cannot be modified by changes of the origin and have a real physical significance for the structure of the boundary.

Particularly characteristic fault vectors occur in (merohedral) 'antiphase domains' (APD). Often the fault vector is the lattice-translation vector lost in a phase transition.

3.3.10.4.3. Examples of fault-vector determinations

(1) Inversion boundaries (180° domain walls) of ferroelectric *lithium ammonium sulfate* (LAS), LiNH_4SO_4 (Klapper, 1987), cf. Example 3.3.6.1.

LAS is ferroelectric at room temperature (point group $m2m$) and transforms into the paraelectric state (point group mmm) at 459 K. Crystals grown from aqueous solution at about 313 K contain grown-in inversion twins with boundaries exactly parallel to (001), appearing on X-ray topographs by stacking-fault fringe contrast. It was found that the boundaries are invisible in reflections of type $h0l$ (zone of the polar axis [010]), but show contrast in reflections with $k \neq 0$ with some exceptions (e.g. no contrast for reflection 040). The 'zero-contrast' reflections are particularly helpful for the determination of the fault vector. Applying the procedure described above, a fault vector $\mathbf{f} = 1/2[010]$ (parallel to the polar axis) was derived for the chosen origin, which is located on the polar twofold symmetry axis. Thus, the true twin inversion centre is located at the

endpoint of the vector $\frac{1}{2}\mathbf{f} = 1/4[010]$. An inspection of the LAS structure shows that this point is the location of the inversion centre of the paraelectric parent phase above 459 K. Thus, during the transition from the para- to the ferroelectric phase the structural inversion centres vanish in the bulk of the domains, but are preserved in the domain boundaries as *twin inversion centres*.

For this (001) twin interface, a reasonable structural model without any breaking of the framework of SO_4 and LiO_4 tetrahedra could be derived easily. The tetrahedra adopt a staggered orientation across the boundary, compared with a nearly eclipsed orientation in the bulk structure.

(2) Brazil twin boundaries of quartz.

Brazil twins are commonly classified as $\{11\bar{2}0\}$ reflection twins but can alternatively be considered as inversion twins, as explained in Section 3.3.6.3.2. The twin boundaries are usually strictly planar and mainly parallel to one of the major rhombohedron faces $\{10\bar{1}1\}$ but, less frequently, to one of the minor rhombohedron faces $\{1011\}$ or prism faces $\{10\bar{1}0\}$. From electron microscopy studies of polysynthetic (lamellar) Brazil twins in amethyst (McLaren & Phakey, 1966), fault vectors of type $\mathbf{f} = 1/2\langle 010 \rangle$, i.e. one half of one of the three translations along the twofold axes, were obtained for twin boundaries parallel to $\{10\bar{1}1\}$, where \mathbf{f} is parallel to the boundary. The same but slightly shorter fault vector $\mathbf{f} = 0.4\langle 010 \rangle$ for $\{10\bar{1}1\}$ Brazil boundaries was determined in X-ray topographic studies by Lang (1967a,b) and Lang & Miuskov (1969). Another detailed X-ray topographic investigation was carried out by Phakey (1969). He confirmed the existence of the fault vector $\mathbf{f} = 1/2\langle 010 \rangle$ but proved also the occurrence of further fault vectors of type $\mathbf{f} = \langle 0, \frac{1}{2}, \frac{1}{3} \rangle$ for $\{10\bar{1}1\}$ twin boundaries. Based on these fault vectors, the structures of the Brazil twin boundaries could be derived: it was shown that no Si—O bonds are broken and that the left- and right-handed partner structures join each other with only small distortions of the tetrahedral framework. It is worth mentioning that the structural channels along the threefold axes do not continue smoothly across the boundary but are mutually displaced by the fault-vector component parallel to the basal plane (0001). McLaren, Phakey and Lang, however, did not consider the location of the twin elements (twin inversion centre or twin reflection plane) in the structure, which can be determined from the fault vectors.

These structural studies of the Brazil twin boundaries have shown that the fault vectors \mathbf{f} are different for different orientations of the interface. As a consequence, a 'stair-rod' dislocation must occur along the bend of the twin interface from one orientation to the other. Stair-rod dislocations have been observed and characterized in the X-ray topographic study of Brazil boundaries by Phakey (1969).

3.3.10.5. Examples of structural models of twin boundaries

Until the rather recent advent of high-resolution transmission electron microscopy (HRTEM), no experimental method for the direct elucidation of the atomic structures of twin interfaces existed. Thus, many authors have devised structural models of twin interfaces based upon the (undeformed) bulk structure of the crystals and the experimentally determined orientation and contact relations. The criterion of good structural fit and low energy of a boundary was usually applied in a rather intuitive manner to the specific case in question. The first and classic example is the model of the aragonite (110) boundary by Bragg (1924).

Some examples of twin-boundary models from the literature are given below. They are intended to show the wide variety of substances and kinds of models. Examples for the direct observation of twin-interface structures by HRTEM follow in Section 3.3.10.6.

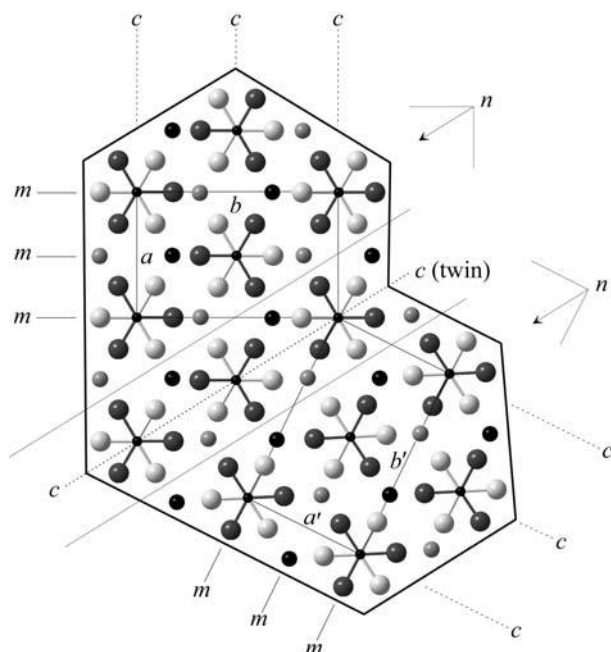


Fig. 3.3.10.6. Structural model of the (110) twin boundary of aragonite (after Bragg, 1924), projected along the pseudo-hexagonal c axis. The orthorhombic unit cells of the two domains with *eigensymmetry* $Pmcn$, as well as their glide/reflection planes m and c , are indicated. The slab centred on the (110) interface between the thin lines is common to both partners. The interface coincides with a twin glide plane c and is shown as a dotted line (twin displacement vector $\mathbf{t} = 1/2\mathbf{c}$). The model is based on a hexagonal cell with $\gamma = 120^\circ$, the true angle is $\gamma = 116.2^\circ$. The origin of the orthorhombic cell is chosen at the inversion centre halfway between two CO_3 groups along c .

3.3.10.5.1. Aragonite, CaCO_3

The earliest structural model of a twin boundary was derived for aragonite by Bragg (1924), reviewed in Bragg (1937, pp. 119–121) and Bragg & Claringbull (1965, pp. 131–133). Aragonite is orthorhombic with space group $Pmcn$. It exhibits a pronounced hexagonal pseudosymmetry, corresponding to a (hypothetical) parent phase of symmetry $P6_3/mmc$, in which the Ca ions form a hexagonal close-packed structure with the CO_3 groups filling the octahedral voids along the 6_3 axes. By eliminating the threefold axis and the C -centring translation of the orthohexagonal unit cell, the above orthorhombic space group results, where the lost centring translation now appears as the glide component n . Of the three mirror planes parallel to $\{11\bar{2}0\}_{\text{hex}}$ and the three c -glide planes parallel to $\{1010\}_{\text{hex}}$, one of each set is retained in the orthorhombic structure, whereas the other two appear as possible twin mirror planes $\{110\}_{\text{orth}}$ and $\{130\}_{\text{orth}}$. It is noted that predominantly planes of type $\{110\}_{\text{orth}}$ are observed as twin boundaries, but less frequently those of type $\{130\}_{\text{orth}}$.

From this structural pseudosymmetry the atomic structure of the twin interface was easily derived by Bragg. It is shown in Fig. 3.3.10.6. In reality, small relaxations at the twin boundary have to be assumed. It is clearly evident from the figure that the twin operation is a glide reflection with glide component $\frac{1}{2}\mathbf{c}$ (= twin displacement vector \mathbf{t}).

3.3.10.5.2. Dauphiné twins of α -quartz

For this merohedral twin (*eigensymmetry* 32) a real parent phase, hexagonal β -quartz (622), exists. The structural relation between the two Dauphiné twin partners of α -quartz is best seen in projection along $[001]$, as shown in Fig. 3.3.10.7 and in Figure 3 of McLaren & Phakey (1966), assuming a fault vector $\mathbf{f} = \mathbf{0}$ in both cases. These figures reveal that only small deformations occur upon passing from one twin domain to the other, irrespective of the orientation of the boundary. This is in agreement with the general observation that Dauphiné boundaries are

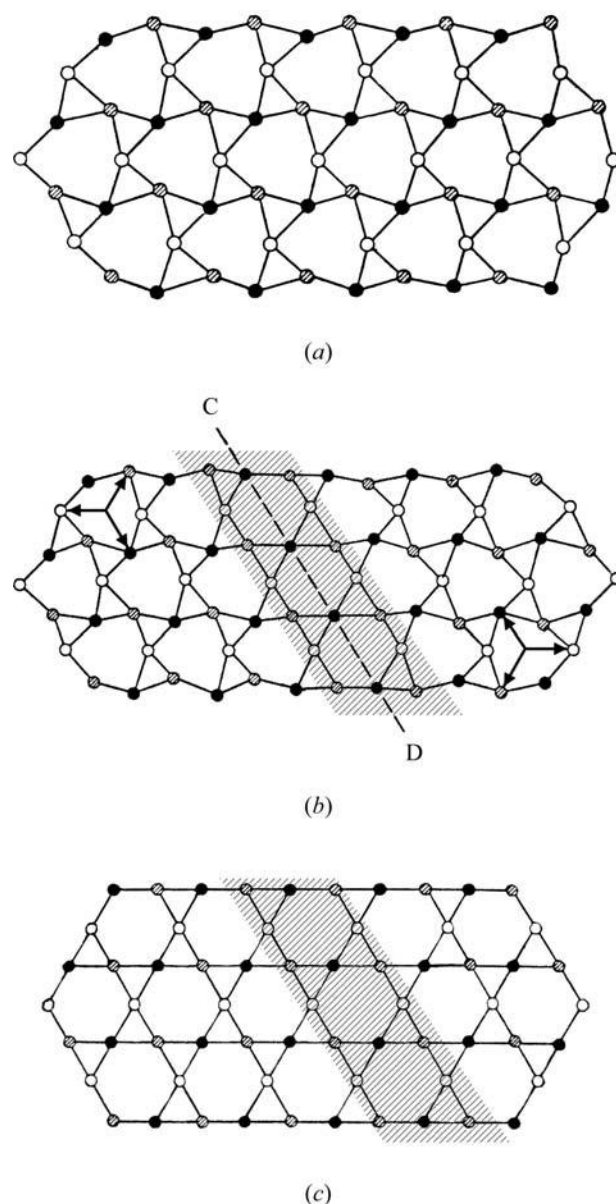


Fig. 3.3.10.7. Simplified structural model of a $\{10\bar{1}0\}$ Dauphiné twin boundary in quartz (after Klassen-Neklyudova, 1964). Only Si atoms are shown. (a) Arrangement of Si atoms in the low-temperature structure of quartz viewed along the trigonal axis $[001]$. (b) Model of the Dauphiné twin boundary C–D. Note the opposite orientation of the three electrical axes shown in the upper left and lower right corner of part (b). In this model, the structural slab centred along the twin boundary has the structure of the hexagonal high-temperature phase of quartz which is shown in (c).

usually irregular and curved and can adopt any orientation. The electron microscopy study of Dauphiné boundaries by McLaren & Phakey confirms the fault vector $\mathbf{f} = \mathbf{0}$. It is noteworthy that the two models of the boundary structure by Klassen-Neklyudova (1964) and McLaren & Phakey (1966) imply a slab with the β -quartz structure in the centre of the transition zone (Fig. 3.3.10.7b). This is in agreement with the assumption voiced by several authors, first by Aminoff & Broomé (1931), that the central zone of a twin interface often exhibits the structure of a different (real or hypothetical) polymorph of the crystal.

There are, however, X-ray topographic studies by Lang (1967a,b) and Lang & Miuskov (1969) which show that curved Dauphiné boundaries may be fine-stepped on a scale of a few tens of microns and exhibit a pronounced change of the X-ray topographic contrast of one and the same boundary from strong to zero (invisibility), depending on the boundary orientation. This observation indicates a change of the fault vector with the boundary orientation. It is in contradiction to the electron

3. PHASE TRANSITIONS, TWINNING AND DOMAIN STRUCTURES

microscopy results of McLaren & Phakey (1966) and requires further experimental elucidation.

3.3.10.5.3. Potassium lithium sulfate, KLiSO_4

The room-temperature phase of KLiSO_4 is hexagonal with space group $P6_3$. It forms a 'stuffed' tridymite structure, consisting of a framework of alternating SO_4 and LiO_4 tetrahedra with the K ions 'stuffed' into the framework cavities. Crystals grown from aqueous solutions exhibit merohedral growth twins with twin reflection planes $\{10\bar{1}0\}$ (alternatively $\{11\bar{2}0\}$) with extended and sharply defined (0001) twin boundaries. The twins consist of left- and right-handed partners with the same polarity. The left- and right-handed structures, projected along the polar hexagonal c axis, are shown in Figs. 3.3.10.8(a) and (b) (Klapper *et al.*, 1987). The tetrahedra of the two tetrahedral layers within one translation period c are in a staggered orientation. A model of the twin boundary is shown in Fig. 3.3.10.8(c): the tetrahedra on both sides of the twin interface (0001), parallel to the plane of the figure, now adopt an eclipsed position, leading to an uninterrupted framework and a conformation change in second coordination across the interface. It is immediately obvious that this (0001) interface permits an excellent low-energy fit of the two partner structures. Note that all six (alternative) twin reflection planes $\{10\bar{1}0\}$ and $\{11\bar{2}0\}$ are normal to the twin boundary. It is not possible to establish a similar low-energy structural model of a boundary which is parallel to one of these twin mirror planes (Klapper *et al.*, 1987).

Inspection of the boundary structure in Fig. 3.3.10.8(c) shows that the tetrahedra related by the twin reflection plane $\{10\bar{1}0\}$ (one representative plane is indicated by the dotted line) are

shifted with respect to each other by a twin displacement vector $\mathbf{t} = 1/2[001]$. Thus, on an atomic scale, these twin reflection planes are in reality twin c -glide planes, bringing the right- and left-hand partner structures into coincidence.

Interestingly, upon cooling below 233 K, KLiSO_4 undergoes a (very) sluggish phase transition from the $P6_3$ phase III into the trigonal phase IV with space group $P31c$ by suppression of the twofold axis parallel $[001]$ and by addition of a c -glide plane. Structure determinations show that the bulk structure of IV is exactly the atomic arrangement of the grown-in twin boundary of phase III, as presented in Fig. 3.3.10.8(c). Moreover, X-ray topography reveals transformation twins $\text{III} \rightarrow \text{IV}$, exhibiting extended and sharply defined polysynthetic (0001) twin lamellae in IV. From the X-ray topographic domain contrast, it is proven that the twin element is the twofold rotation axis parallel to $[001]$. The structural model of the (0001) twin interfaces is given in Figs. 3.3.10.8(a) and (b). They show that across the (0001) twin boundary the tetrahedra are staggered, in contrast to the bulk structure of IV where they are in an eclipsed orientation (Fig. 3.3.10.8c). It is immediately recognized that the two tetrahedral layers, one above and one below the (0001) twin boundary in Fig. 3.3.10.8(a) or (b), are related by 2_1 screw axes.

Thus, the (idealized) (0001) twin boundary of the transformation twins of phase IV is represented by the bulk structure of the hexagonal room-temperature phase III, whereas the twin boundary of the growth twins of the hexagonal phase III is represented by the bulk structure of the trigonal low-temperature phase IV. Upon cooling from $P6_3$ (phase III) to $P31c$ (phase IV), the 2_1 axes are suppressed as symmetry elements, but they now act as twin elements. In the model they are located as in space group $P6_3$, one type being contained in the 6_3 axes, the other type halfway in between. Upon heating, the re-transformation $\text{IV} \rightarrow \text{III}$ restores the $\{10\bar{1}0\}/\{11\bar{2}0\}$ reflection twins with the same large (0001) boundaries in the same geometry as existed before the transition cycle, but now as result of a phase transition, not of crystal growth (strong memory effect).

Thus, KLiSO_4 is another particularly striking example of the phenomenon, mentioned above for the Dauphiné twins of quartz, that the twin-interface structure of one polymorph may resemble the bulk structure of another polymorph.

The structural models of both kinds of twin boundaries do not exhibit a fault vector $\mathbf{f} \neq \mathbf{0}$. This may be explained by the compensation of the glide component $\frac{1}{2}c$ of the c -glide plane in phase IV by the screw component $\frac{1}{2}c$ of the 2_1 screw axis in phase III and *vice versa*.

3.3.10.5.4. Twin models of molecular crystals

An explanation for the occurrence of twinning based on the 'conflict' between the energetically most favourable (hence stable) crystal structure and the arrangement with the highest possible symmetry was proposed by Krafczyk *et al.* (1997 and references therein) for some molecular crystals. According to this theory, pseudosymmetrical structures exhibit 'structural instabilities', *i.e.* *symmetrically* favourable structures occur, whereas the *energetically* more stable structures are not realized, but

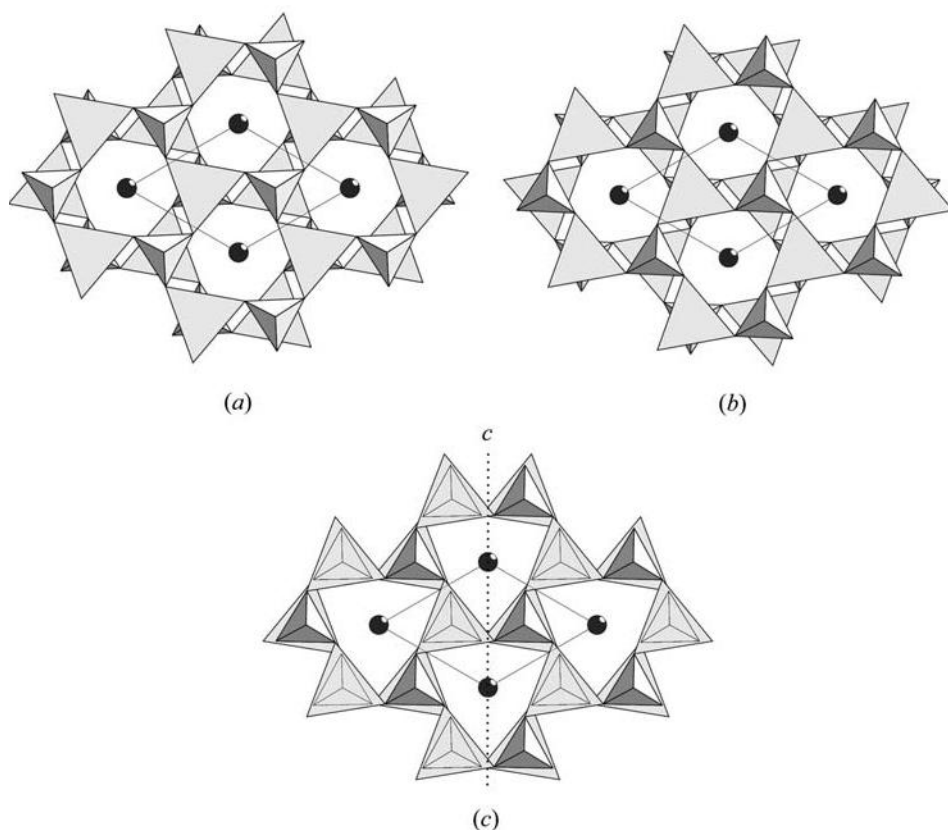


Fig. 3.3.10.8. KLiSO_4 : Bulk tetrahedral framework structures and models of (0001) twin boundary structures of phases III and IV. Small tetrahedra: SO_4 ; large tetrahedra: LiO_4 ; black spheres: K. All three figures play a double role, both as bulk structure and as (0001) twin-boundary structures. (a) and (b) Left- and right-handed bulk structures of phase III ($P6_3$), as well as possible structures of the (0001) twin boundary in phase IV. (c) Bulk structure of phase IV ($P31c$), as well as possible structure of the (0001) twin boundary in phase III. The SO_4 tetrahedra covered by the LiO_4 tetrahedra are shown by thin lines. Dotted line: $\{10\bar{1}0\}$ c -glide plane. In all cases, the (0001) twin boundary is located between the two tetrahedral layers parallel to the plane of the figure.

3.3. TWINNING OF CRYSTALS

were theoretically derived by lattice-energy calculations. The differences between the two structures provide the explanation for the occurrence of twins. The twin models contain characteristic 'shift vectors' (twin displacement vectors). The theory was successfully applied to pentaerythrite, 1,2,4,5-tetrabromobenzene, maleic acid and 3,5-dimethylbenzoic acid.

3.3.10.6. Observations of twin boundaries by transmission electron microscopy

In the previous sections of this chapter, twin boundaries have been discussed from two points of view: *theoretically* in terms of 'compatibility relations', *i.e.* of mechanically and electrically 'permissible' interfaces (Sections 3.3.10.2 and 3.3.10.3), followed by *structural* aspects, *viz* by displacement and fault vectors (Section 3.3.10.4), as well as atomistic models of twin boundaries (Section 3.3.10.5), in each case accompanied by actual examples.

In the present section, a recent and very powerful method of direct experimental elucidation of the atomistic structure of twin interfaces is summarized, *transmission electron microscopy* (TEM), in particular *high-resolution* transmission electron microscopy (HRTEM). This method enjoys wider and wider application because it can provide in principle – if applied with proper caution and criticism – direct evidence for the problems discussed in earlier sections: 'good structural fit', 'twin displacement vector', 'relaxation of the structure' across the boundary *etc.*

The present chapter is not a suitable place to introduce and explain the methods of TEM and HRTEM and the interpretation of the images obtained. Instead, the following books, containing treatments of the method in connection with materials science, are recommended: Wenk (1976), especially Sections 2.3 and 5; Amelinckx *et al.* (1978), especially pp. 107–151 and 217–314; McLaren (1991); Buseck *et al.* (1992), especially Chapter 11; and Putnis (1992), especially pp. 67–80.

The results of HRTEM investigations of twin interfaces are not yet numerous and representative enough to provide a complete and coherent account of this topic. Instead, a selection of typical examples is provided below, from which an impression of the method and its usefulness for twinning can be gained.

3.3.10.6.1. Anatase, TiO_2 (Penn & Banfield, 1998, 1999)

This investigation has been presented already in Section 3.3.10.4.1 and Fig. 3.3.10.5 as an example of the occurrence of a twin displacement vector, leading to $\mathbf{t} \approx 1/2\mathbf{v}_L$, where \mathbf{v}_L is a lattice translation vector parallel to the (112) twin reflection plane of anatase. Another interesting result of this HRTEM study by Penn & Banfield is the formation of anatase–brookite intergrowths during the hydrothermal coarsening of TiO_2 nanoparticles. The preferred contact plane is (112) of anatase and (100) of brookite, with [131] of anatase parallel to [011] of brookite in the intergrowth plane. Moreover, it is proposed that brookite may nucleate at (112) twin boundaries of anatase and develop into (100) brookite slabs sandwiched between the anatase twin components. Similarly, after hydrothermal treatment at 523 K, nuclei of rutile at the anatase (112) twin boundary were also observed by HRTEM (Penn & Banfield, 1999). A detailed structural model for this anatase-to-rutile phase transition is proposed by the authors, from which a sluggish nucleation of rutile followed by rapid growth of this phase was concluded.

3.3.10.6.2. SnO_2 (rutile structure)

Twin interfaces (011) of the closely related tetragonal SnO_2 (cassiterite) were investigated by Smith *et al.* (1983). A very close agreement between HRTEM images and corresponding computer simulations was obtained for $\mathbf{t} = 1/2[1\bar{1}1](011)$. This twin is termed 'glide twin' by the authors, because the twin operation is a reflection across (011) followed by a displacement vector $\mathbf{t} = 1/2[1\bar{1}1](011)$ parallel to the twin plane (011).

3.3.10.6.3. $\Sigma 3$ (111) twin interface in BaTiO_3 [cf. Section 3.3.8.3(iii)]

In cubic crystals, twins of the $\Sigma 3$ (111) spinel type are by far the most common. A technologically very important phase, BaTiO_3 perovskite, was investigated by Rečnik *et al.* (1994) employing HRTEM, computer simulations and EELS (spatially resolved electron-energy-loss spectroscopy). The samples were prepared by sintering at 1523 K, *i.e.* in the cubic phase, whereby $\Sigma 3$ (111) growth twins were formed. These twins are preserved during the transition into the tetragonal phase upon cooling below $T_c = 398$ K. Note that these (now tetragonal) (111) twins are not transformation twins, as are the (110) ferroelastic twins.

Fig. 3.3.10.9(a) shows an HRTEM micrograph and Fig. 3.3.10.9(b) the structural model of the (111) twin boundary, both projected along $[1\bar{1}0]$. The main results of this study can be summarized as follows.

(1) The twin boundary coincides exactly with the twin reflection plane (111). It is very sharp and consists of one atomic layer only, common to both twin components. It is fully 'coherent' (cf. Section 3.3.10.9).

(2) The twin boundary is formed by a close-packed BaO_3 layer, and the TiO_6 octahedra on both sides share faces to form Ti_2O_9 groups. These groups occur also in the hexagonal high-temperature modification of BaTiO_3 , *i.e.* this is a further example of a twin interface having the structure of another polymorph of the same compound.

(3) The EELS results suggest a reduction in the valence state of the Ti^{4+} ions in the interface towards Ti^{3+} which is compensated by some oxygen vacancies, leading to the composition of the interface layer $\text{BaO}_{3-x}(\text{V}_\text{O})_x$ instead of BaO_3 . This result indicates that the stoichiometry of a boundary, even of a coherent one, may differ from that of the bulk.

A very interesting structural feature of the BaTiO_3 (111) twin interface was discovered by Jia & Thust (1999), applying sophisticated HRTEM methods to thin films of nanometre thickness (grown by the pulsed-laser deposition technique). The distance of the nearest Ti plane on either side of the (111) twin reflection plane (which is formed by a BaO_3 layer, see above) from this twin plane is *increased* by 0.19 Å, *i.e.* the distance between the Ti atoms in the Ti_2O_9 groups, mentioned above under (2), is increased from the hypothetical value of 2.32 Å for Ti in the ideal octahedral centres to 2.70 Å in the actual interface structure. This expansion is due to the strong repulsion between the two neighbouring Ti ions in the Ti_2O_9 groups. A similar expansion of the Ti–Ti distance in the Ti_2O_9 groups (from 2.34 to 2.67 Å), again due to the strong repulsion between the Ti atoms, has been observed in the bulk crystal structure of the hexagonal modification of BaTiO_3 .

In addition, a *decrease* by 0.16 Å of the distance between the two nearest BaO planes across the twin interface was found, which corresponds to a *contraction* of this pair of BaO planes from 2.32 Å in the bulk to 2.16 Å at the twin interface (corresponding closely to the value of 2.14 Å in the hexagonal phase).

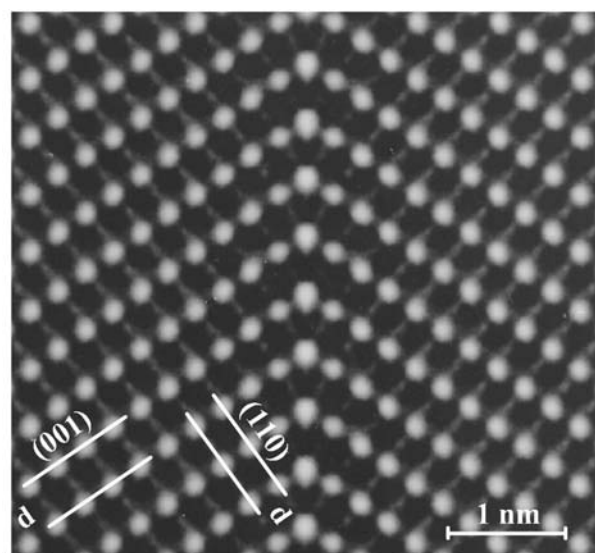
It is remarkable that no significant (*i.e.* > 0.05 Å) displacements were found for second and higher pairs of both Ti–Ti and BaO–BaO layers. Moreover, no significant lateral shifts, *i.e.* no twin displacements vectors $\mathbf{t} \neq 0$ parallel to the (111) twin interface, were observed.

Note that BaTiO_3 is treated again in Section 3.3.10.7.5 below, with respect to its twin texture in polycrystalline aggregates.

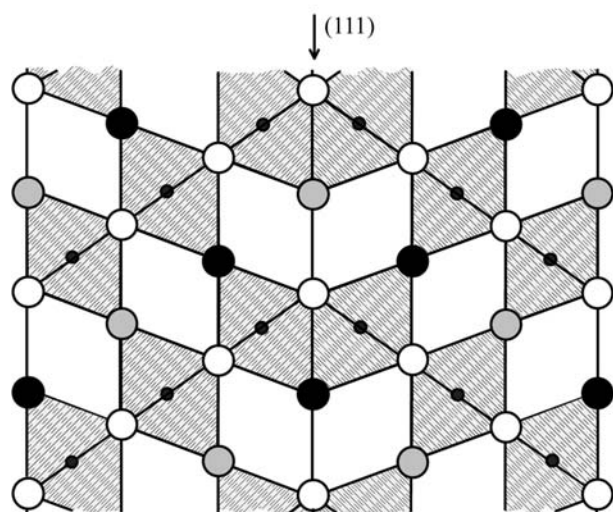
3.3.10.6.4. $\Sigma = 3$ bicrystal boundaries in Cu and Ag

Differently oriented interfaces in $\Sigma 3$ bicrystals of Cu and Ag were elucidated by Hoffmann & Ernst (1994) and Ernst *et al.* (1996). They prepared bicrystals of fixed $\Sigma 3$ orientation relationship [corresponding to the (111) spinel twin law] but with different contact planes. The inclinations of these contact planes

3. PHASE TRANSITIONS, TWINNING AND DOMAIN STRUCTURES



(a)



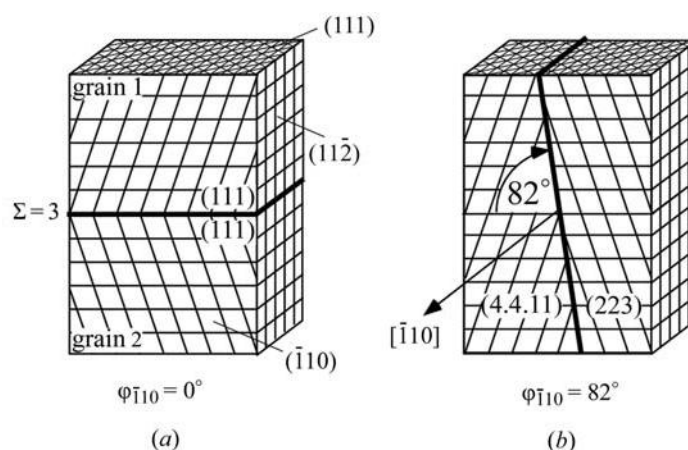
● Ba, O ● O, Ba ● Ti⁴⁺ ○ O

(b)

Fig. 3.3.10.9. (a) HRTEM micrograph of a coherent (111) twin boundary in BaTiO₃, projected along $[\bar{1}10]$. The intense white spots represent the $[\bar{1}10]$ Ba–O columns, the small weak spots in between represent the Ti columns. Thickness of specimen 4 nm. (b) Structural model of the (111) twin boundary (arrow), as derived from the micrograph (a) and confirmed by computer simulation. Note that the pure oxygen columns (open circles) are not visible in the micrograph (a), due to the low scattering power of oxygen. Some slight structural deformations along the twin boundary are discussed in the text. Courtesy of W. Mader, Bonn; cf. Rečnik *et al.* (1994).

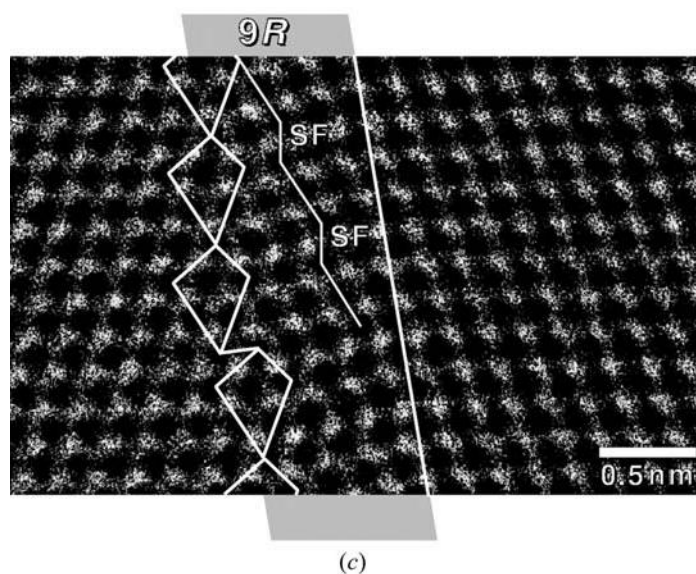
vary by rotations around the two directions $[\bar{1}10]$ and $[11\bar{2}]$ [both parallel to the (111) twin reflection plane] in the range $\Phi = 0^\circ$ – 90° , where $\Phi = 0^\circ$ corresponds to the (111) ‘coherent twin plane’, as illustrated in Figs. 3.3.10.10(a) and (b).

The boundary energies were determined from the surface tension derived from the characteristic angles of surface grooves formed along the boundaries by thermal etching. The theoretical energy values were obtained by molecular statics calculations. The measured and calculated energy curves show a deep and sharp minimum at $\Phi = 0^\circ$ for rotations around both $[\bar{1}10]$ and $[11\bar{2}]$. This corresponds to the coherent (111) $\Sigma 3$ twin boundary and is to be expected. It is surprising, however, that a second, very shallow energy minimum occurs in both cases at high Φ angles: $\Phi_{[\bar{1}10]} \approx 82^\circ$ and $\Phi_{[11\bar{2}]} \approx 84^\circ$, rather than at the



(a)

(b)



(c)

Fig. 3.3.10.10. (a) Schematic block diagram of a $\Sigma = 3$ bicrystal (spinel twin) for $\phi_{[\bar{1}10]} = 0^\circ$, i.e. for coinciding (111) twin reflection and composition plane. (b) Schematic block diagram of the $\Sigma = 3$ bicrystal for $\phi_{[\bar{1}10]} = 82^\circ$. (c) HRTEM micrograph of the $\Sigma = 3$ boundary of Cu for $\phi_{[\bar{1}10]} = 82^\circ$, projected along $[\bar{1}10]$. The black spots coincide with the $[\bar{1}10]$ Cu-atom columns. The micrograph reveals a thin (≈ 10 Å) interface slab of a rhombohedral 9R structure, which can be derived from the bulk cubic 3C structure by introducing a stacking fault SF on every third (111) plane. The (111) planes are horizontal, the interface is roughly parallel to (4.4.11) and (223), respectively. Courtesy of F. Ernst, Stuttgart; cf. Ernst *et al.* (1996).

compatible (112) contact plane for $\Phi_{[\bar{1}10]} = 90^\circ$ [the contact plane $(\bar{1}\bar{1}0)$ for $\Phi_{[11\bar{2}]} = 90^\circ$ is not compatible]. For these two angular inclinations, the boundaries, as determined by HRTEM and computer modelling, exhibit complex three-dimensional boundary structures with thin slabs of unusual Cu arrangements: the $\Phi_{[\bar{1}10]} \approx 82^\circ$ slab has a rhombohedral structure of nine close-packed layers (9R) with a thickness of about 10 Å (in contrast to the f.c.c. bulk structure, which is 3C). This is shown and explained in Fig. 3.3.10.10(c). Similarly, for the $\Phi_{[11\bar{2}]} \approx 84^\circ$ slab a b.c.c. structure (as for α -Fe) was found, again with a thickness of ≈ 10 Å.

3.3.10.6.5. Fivefold cyclic twins in nanocrystalline materials

Multiply twinned particles occur frequently in nanocrystalline (sphere-like or rod-shaped) particles and amorphous thin films (deposited on crystalline substrates) of cubic face-centred metals, diamond-type semiconductors (C, Si, Ge) and alloys. Hofmeister & Junghans (1993) and Hofmeister (1998) have carried out extensive HRTEM investigations of nanocrystalline Ge particles

3.3. TWINNING OF CRYSTALS

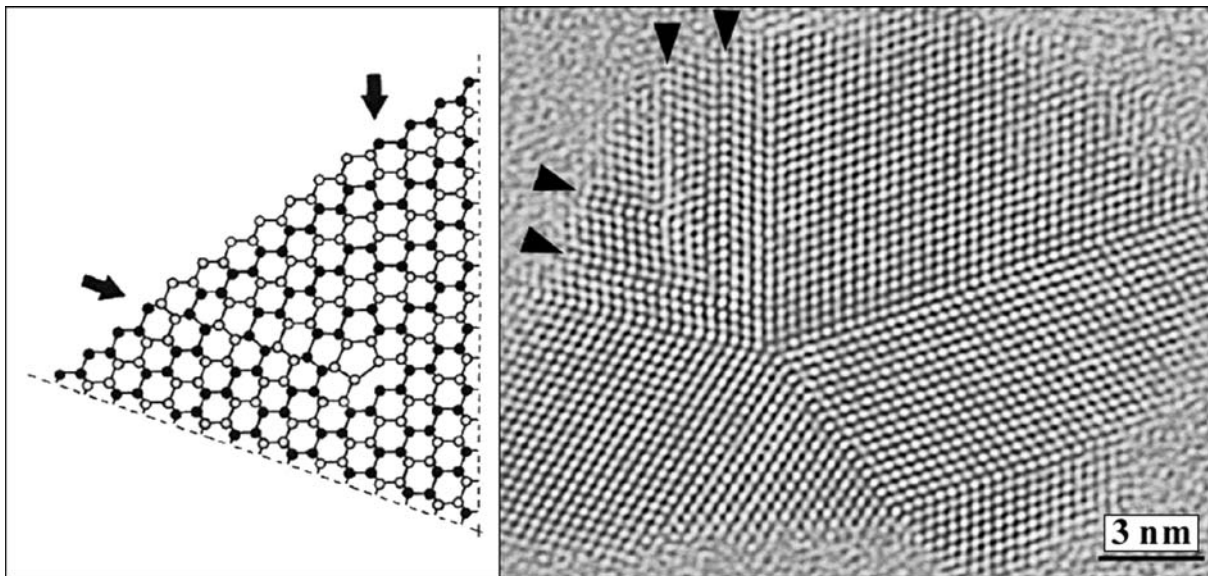


Fig. 3.3.10.11. HRTEM micrograph of a fivefold-twinned Ge nanocrystal (right) in an amorphous Ge film formed by vapour deposition on an NaCl cleavage plane. Projection along a $[1\bar{1}0]$ lattice row that is the junction of the five twin sectors; plane of the image: $(1\bar{1}0)$. The coinciding $\{111\}$ twin reflection and composition planes (spinel law) are clearly visible. In one twin sector, two pairs of stacking faults (indicated by arrows) occur. They reduce the stress introduced by the angular misfit of the twin sectors. The atomic model (left) shows the structural details of the bulk and of one pair of stacking faults. Courtesy of H. Hofmeister, Halle; cf. Hofmeister & Junghans (1993); Hofmeister (1998).

in amorphous Ge films. The particles reveal, among others, *five-fold cyclic twins* with coinciding (111) twin reflection planes and twin boundaries (spinel type). A typical example of a fivefold twin is presented in Fig. 3.3.10.11: The five different $\{111\}$ twin boundaries are perpendicular to the image plane $(1\bar{1}0)$ and should theoretically form dihedral angles of 70.5° (supplement to the tetrahedral angle 109.5°), which would lead to an angular gap of about 7.5° . In reality, the five twin sectors are more or less distorted with angles ranging up to 76° . The stress due to the angular mismatch is often relaxed by defects such as stacking faults (marked by arrows in Fig. 3.3.10.11). The $[110]$ junction line of the five sectors can be considered as a pseudo-fivefold twin axis (similar to the pseudo-trigonal twin axis of aragonite, cf. Fig. 3.3.2.4; see also the fivefold twins in the alloy FeAl_4 , described in Example 3.3.6.8 and Fig. 3.3.6.8).

For the formation of fivefold twins, different mechanisms have been suggested by Hofmeister (1998): *nucleation* of noncrystallographic clusters, which during subsequent growth collapse into cyclic twins; successive growth twinning on alternate cozoal (111) twin planes; and deformation twinning (cf. Section 3.3.7).

The fivefold multiple twins provide an instructive example of a *twin texture*, a subject which is treated in the following section.

3.3.10.7. Twin textures

So far in Section 3.3.10, ‘free’ twin interfaces have been considered with respect to their mechanical and electrical compatibility, their twin displacement vectors and their structural features, experimentally and by modelling. In the present section, the ‘textures’ of twin domains, both in a ‘single’ twin crystal and in a polycrystalline material or ceramic, are considered. With the term ‘twin texture’, often also called ‘twin pattern’, ‘domain pattern’ or ‘twin microstructure’, the size, shape and spatial distribution of the twin domains in a twinned crystal aggregate is expressed. In a (polycrystalline) ceramic, the interaction of the twin interfaces in each grain with the grain boundary is a further important aspect. Basic factors are the ‘form changes’ and the resulting space-filling problems of the twin domains compared to the untwinned crystal. These interactions can occur during crystal growth, phase transitions or mechanical deformations.

From the point of view of form changes, two categories of twins, described in Sections 3.3.10.7.1 and 3.3.10.7.2 below, have

to be distinguished. Discussions of the most important twin cases follow in Sections 3.3.10.7.3 to 3.3.10.7.5.

3.3.10.7.1. Merohedral (non-ferroelastic) twins (see Sections 3.3.9 and 3.3.10.2.3)

In these twins, the lattices of all domains are exactly parallel (‘parallel-lattice twins’). Hence, no lattice deformations (spontaneous strain) occur and the development of the domain pattern of the twins is not infringed by spatial constraints. As a result, the twin textures can develop freely, without external restraints [cf. Section 3.3.10.7.5 below].

It should be noted that these features apply to *all* merohedral twins, irrespective of origin, *i.e.* to growth and transformation twins and, among mechanical twins, to ferroelastic twins [for the latter see Section 3.3.7.3(iii)].

3.3.10.7.2. Non-merohedral (ferroelastic) twins

Here, the lattices of the twin domains are not completely parallel (‘twins with inclined axes’). As a result, severe space problems may arise during domain formation. Several different cases have to be considered:

(1) Only *one* twin law, *i.e.* only *two* domain states occur which can form two-component twins (*e.g.* dovetail twins of gypsum, Carlsbad twins of orthoclase) or multi-component twins (*e.g.* lamellar, polysynthetic twins of albite). For these twins, no spatial constraints are imposed and, hence, the twin crystal can develop freely, without external restraints. Again, this applies to both growth and transformation twins.

(2) *Two or more* twin laws, *i.e.* *three or more* domain states coexist. Here, the free development of a twin domain is impeded by the space requirements of its neighbours. For *growth twins*, typical cases are sector and cyclic twins (*e.g.* K_2SO_4 and aragonite). More complicated examples are the famous harmotome and phillipsite growth twins, where the combined action of several twin laws leads to a pseudo-cubic twin texture and twin morphology.

Transformation and deformation twins are extensively treated in the following Section 3.3.10.7.3.

3. PHASE TRANSITIONS, TWINNING AND DOMAIN STRUCTURES

3.3.10.7.3. Fitting problems of ferroelastic twins

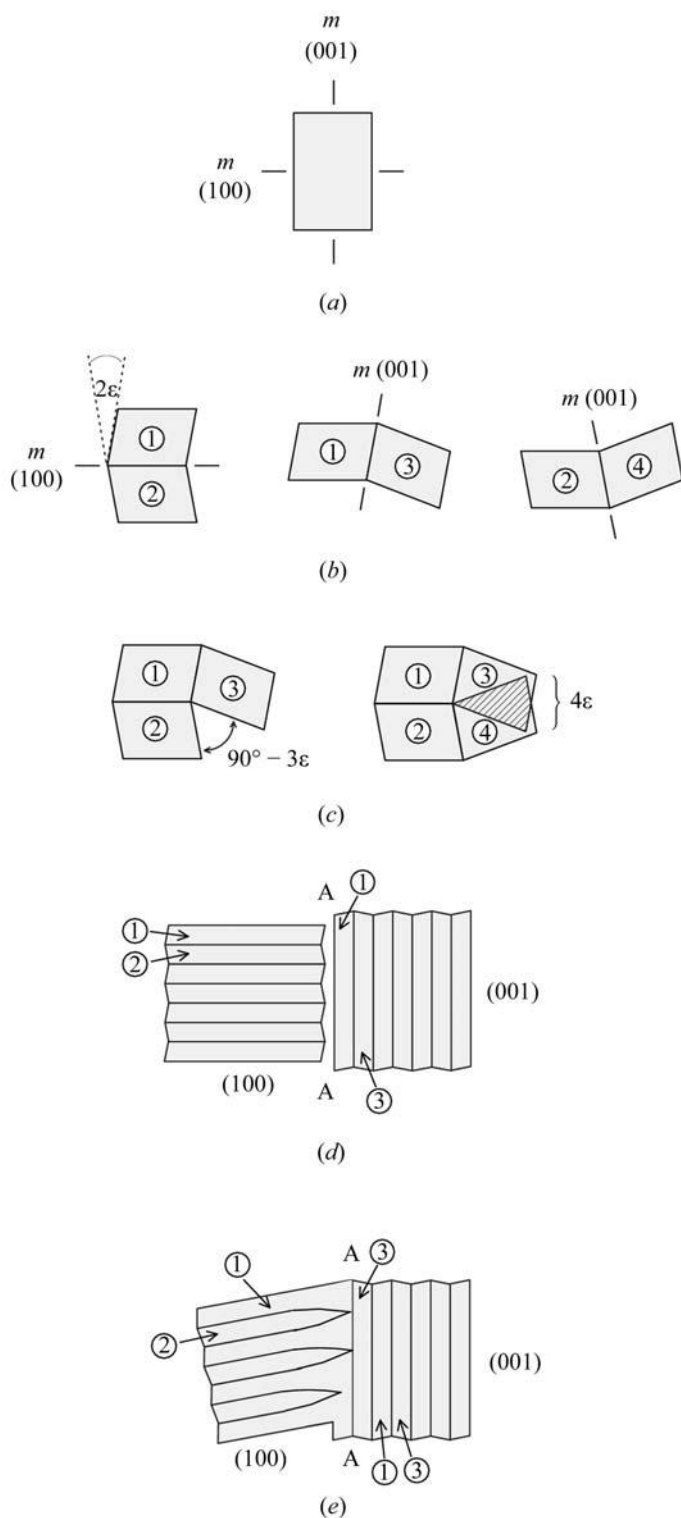


Fig. 3.3.10.12. Illustration of space-filling problems of domains for a (ferroelastic) orthorhombic \rightarrow monoclinic phase transition with an angle ε (exaggerated) of spontaneous shear. (a) Orthorhombic parent crystal with symmetry $2/m2/m2/m$. (b) Domain pairs 1 + 2, 1 + 3 and 2 + 4 of the monoclinic daughter phase ($\beta = 90^\circ + \varepsilon$) with independent twin reflection planes (100) and (001). (c) The combination of domain pairs 1 + 2 and 1 + 3 leads to a gap with angle $90^\circ - 3\varepsilon$, whereas the combination of the three domain pairs 1 + 2, 1 + 3 and 2 + 4 generates a wedge-shaped overlap (hatched) of domains 3 and 4 with angle 4ε . (d) Twin lamellae systems of domain pairs 1 + 2 (left) and 1 + 3 (or 2 + 4) (right) with low-energy contact planes (100) and (001). Depending on the value of ε , adaptation problems with more or less strong lattice distortions arise in the boundary region A–A between the two lamellae systems. (e) Stress relaxation and reduction of strain energy in the region A–A by the tapering of domains 2 ('needle domains') on approaching the (nearly perpendicular) boundary of domains 3 + 1. The tips of the needle lamellae may impinge on the boundary or may be somewhat withdrawn from it, as indicated in the figure. The angle between the two lamellae systems is $90^\circ - \varepsilon$.

The real problem of space-constrained twin textures, however, is provided by non-merohedral (ferroelastic) *transformation* and *deformation* twins (including the cubic deformation twins of the spinel law). This is schematically illustrated in Fig. 3.3.10.12 for the very common case of orthorhombic \rightarrow monoclinic transformation twins ($\beta = 90^\circ + \varepsilon$).

Figs. 3.3.10.12(a) and (b) show the 'splitting' of two mirror planes (100) and (001) of parent symmetry mmm , as a result of a phase transition $mmmF12/m1$, into the two independent and symmetrically *non-equivalent* twin reflection planes (100) and (001), each one representing a different (monoclinic) twin law. The two orientation states of each domain pair differ by the splitting angle 2ε . Note that in transformation twins the angle ε (spontaneous shear strain) is small, at most one or two degrees, due to the pseudosymmetry \mathcal{H} of the daughter phase with respect to the parent symmetry \mathcal{G} . It can be large, however, for deformation twins, e.g. calcite. The resulting fitting problems in ferroelastic textures are illustrated in Fig. 3.3.10.12(c). Owing to the splitting angle 2ε , twin domains would form gaps or overlaps, compared to a texture with $\varepsilon = 0$, where all domains fit precisely. In reality, the misfit due to $\varepsilon \neq 0$ leads to local stresses and associated elastic strains around the meeting points of three domains related by two twin laws [triple junctions, cf. Palmer *et al.* (1988), Figs. 3–6].

For the orthorhombic \rightarrow monoclinic transition considered here, the two different twin laws often lead to two and (for small ε) nearly perpendicular sets of polysynthetic twin lamellae. This is illustrated in Fig. 3.3.10.12(d). The boundaries in one set are formed by (100) planes, those in the other set by (001) planes, both of low energy. The misfit problems are located exclusively in the region AA where the two systems of lamellae meet. Here wedge-like domains (the so-called 'needle domains', see below) are formed, as shown in Fig. 3.3.10.12(e), i.e. the twin lamellae of one system taper on approaching the perpendicular twin system (right-angled twins), forming rounded or sharp needle tips. The tips of the needle lamellae may be in contact with the perpendicular lamella or may be somewhat withdrawn from it. These effects are the consequence of strain-energy minimization in the transition region of domain systems, as compared to the large-area contacts between parallel twin lamellae.

The formation of two lamellae systems with wedge-like domains was demonstrated very early on by the polarization-optical study of the orthorhombic \rightarrow monoclinic ($222 \rightarrow 2$) transformation of Rochelle salt at 297 K by Chernysheva (1950, 1955; quoted after Klassen-Neklyudova, 1964, pp. 27–30 and 76–77, Figs. 35, 38 and 100; see also Zheludev, 1971, pp. 180–185). The term 'needle domains' was coined by Salje *et al.* (1985) in their study of the monoclinic \rightarrow triclinic ($2/m \rightarrow 1$) transition of Na-feldspar. Another detailed description of needle domains is provided by Palmer *et al.* (1988) for the cubic \rightarrow tetragonal ($4/m\bar{3}2/m \rightarrow 4/m2/m2/m$) transformation of leucite at 878 K. The typical domain structure resulting from this transition is shown in Fig. 3.3.10.13.

A similar example is provided by the extensively investigated tetragonal \rightarrow orthorhombic transformation twinning of the high- T_c superconductor $\text{YBa}_2\text{Cu}_3\text{O}_{7-\delta}$ (YBaCu) below about 973 K (Roth *et al.*, 1987; Schmid *et al.*, 1988; Keester *et al.*, 1988, especially Fig. 6). Here two symmetrically equivalent systems of lamellae with twin laws $m(110)$ and $m(\bar{1}10)$ meet at nearly right angles ($\varepsilon \approx 1^\circ$). Interesting TEM observations of tapering, impinging and intersecting twin lamellae are presented by Müller *et al.* (1989). An extensive review on twinning of YBaCu, with emphasis on X-ray diffraction studies (including diffuse scattering), was published by Shekhtman (1993).

A particularly remarkable case occurs for hexagonal \rightarrow orthorhombic ferroelastic transformation twins. Well known examples are the pseudo-hexagonal K_2SO_4 -type crystals

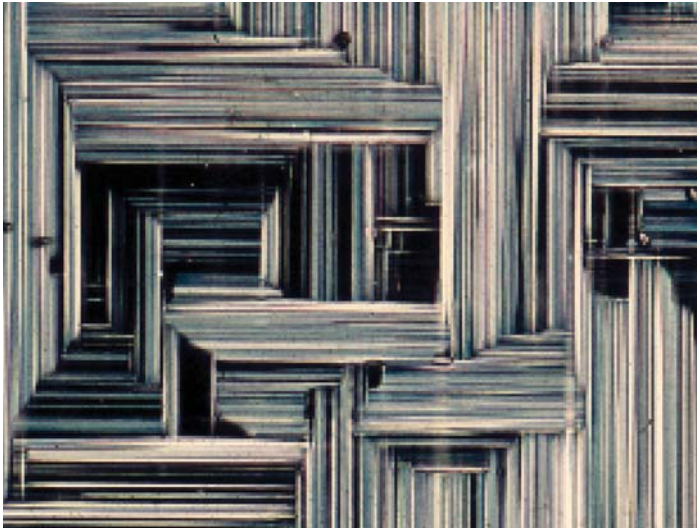


Fig. 3.3.10.13. Thin section of tetragonal leucite, $K(AlSi_2O_6)$, between crossed polarizers. The two nearly perpendicular systems of (101) twin lamellae result from the cubic-to-tetragonal phase transition at about 878 K. Width of twin lamellae 20–40 μm . Courtesy of M. Raith, Bonn.

(cf. Example 3.3.6.7). Three (cyclic) sets of orthorhombic twin lamellae with interfaces parallel to $\{10\bar{1}0\}_{hex}$ or $\{110\}_{orth}$ are generated by the transformation. More detailed observations on hexagonal–orthorhombic twins are available for the $III \rightarrow II$ (heating) and $I \rightarrow II$ (cooling) transformations of $KLiSO_4$ at about 712 and 938 K (Jennissen, 1990; Scherf *et al.*, 1997). The development of the three systems of twin lamellae of the orthorhombic phase II is shown by two polarization micrographs in Fig. 3.3.10.14. A further example, the cubic \rightarrow rhombohedral phase transition of the perovskite $LaAlO_3$, was studied by Bueble *et al.* (1998).

Another surprising feature is the penetration of two or more differently oriented nano-sized twin lamellae, which is often encountered in electron micrographs (cf. Müller *et al.*, 1989, Fig. 2b). In several cases, the penetration region is interpreted as a metastable area of the higher-symmetrical para-elastic parent phase.

In addition to the fitting problems discussed above, the resulting final twin texture is determined by several further effects, such as:

- (a) the nucleation of the (twinned) daughter phase in one or several places in the crystal;
- (b) the propagation of the phase boundary (transformation front, cf. Fig. 3.3.10.14);
- (c) the tendency of the twinned crystal to minimize the overall elastic strain energy induced by the fitting problems of different twin lamellae systems.

Systematic treatments of ferroelastic twin textures were first published by Boulesteix (1984, especially Section 3.3 and references cited therein) and by Shuvalov *et al.* (1985). This topic is extensively treated in Section 3.4.4 of the present volume. A detailed theoretical explanation and computational simulation of these twin textures, with numerous examples, was recently presented by Salje & Ishibashi (1996) and Salje *et al.* (1998). Textbook versions of these problems are available by Zheludev (1971) and Putnis (1992).

3.3.10.7.4. Tweed microstructures

The textures of ferroelastic twins and their fitting problems, discussed above, are ‘time-independent’ for both growth and deformation twins, *i.e.* after twin nucleation and growth or after the mechanical deformation there occurs in general no ‘ripening process’ with time before the final twin structure is produced.

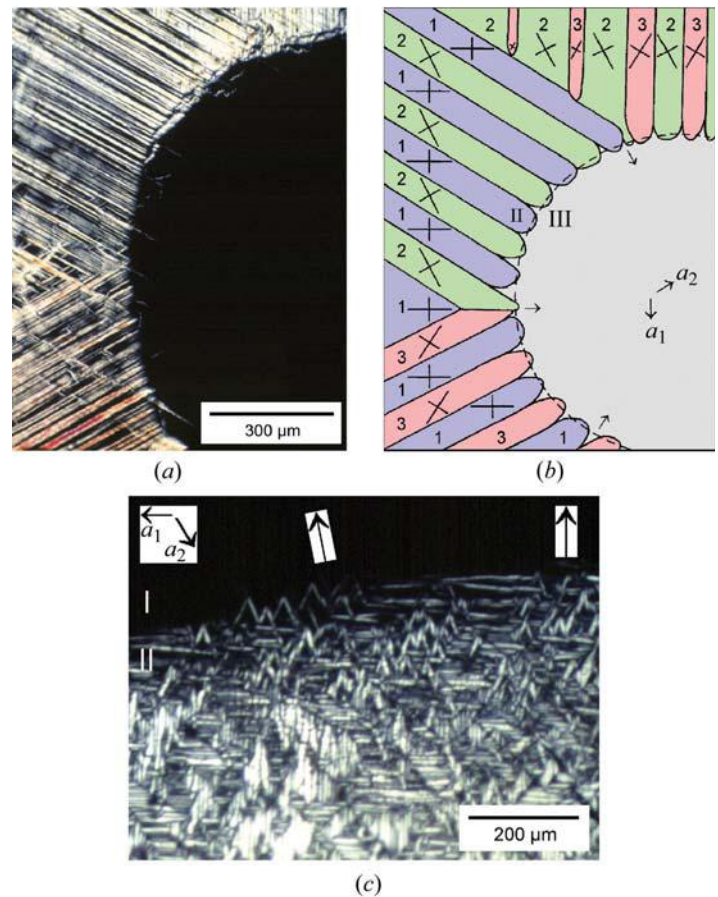


Fig. 3.3.10.14. Twin textures generated by the two different hexagonal-to-orthorhombic phase transitions of $KLiSO_4$. The figures show parts of $(0001)_{hex}$ plates (viewed along $[001]$) between crossed polarizers. (a) Phase boundary $III \rightarrow II$ with circular 712 K transition isotherm during heating. Transition from the inner (cooler) room-temperature phase III (hexagonal, dark) to the (warmer) high-temperature phase II (orthorhombic, birefringent). Owing to the loss of the threefold axis, lamellar $\{10\bar{1}0\}_{hex} = \{110\}_{orth}$ cyclic twin domains of three orientation states appear. (b) Sketch of the orientations states 1, 2, 3 and the optical extinction directions of the twin lamellae. Note the tendency of the lamellae to orient their interfaces normal to the circular phase boundary. Arrows indicate the direction of motion of the transition isotherm during heating. (c) Phase boundary $I \rightarrow II$ with 938 K transition isotherm during cooling. The dark upper region is still in the hexagonal phase I, the lower region has already transformed into the orthorhombic phase II (below 938 K). Note the much finer and more irregular domain structure compared with the $III \rightarrow II$ transition in (a). Courtesy of Ch. Scherf, PhD thesis, RWTH Aachen, 1999; cf. Scherf *et al.* (1997).

This is characteristically different for some transformation twins, both of the (slow) order–disorder and of the (fast) displacive type and for both metals and non-metals. Here, with time and/or with decreasing temperature, a characteristic microstructure is formed in between the high- and the low-temperature polymorph. This ‘precursor texture’ was first recognized and illustrated by Putnis in the investigation of cordierite transformation twinning and called ‘tweed microstructure’ (Putnis *et al.*, 1987; Putnis, 1992). In addition to the hexagonal–orthorhombic cordierite transformation, tweed structures have been investigated in particular in the K-feldspar orthoclase (monoclinic–triclinic transformation), in both cases involving (slow) Si–Al ordering processes. Examples of tweed structures occurring in (fast) displacive transformations are provided by tetragonal–orthorhombic Co-doped $YBaCu_3O_{7-d}$ (Schmahl *et al.*, 1989) and rhombohedral–monoclinic $(Pb,Sr)_3(PO_4)_2$ and $(Pb,Ba)_3(PO_4)_2$ (Bismayer *et al.*, 1995).

Tweed microstructures are precursor twin textures, intermediate between those of the high- and the low-temperature modifications, with the following characteristic features:

3. PHASE TRANSITIONS, TWINNING AND DOMAIN STRUCTURES

(a) With respect to *long-range order*, the tweed structure belongs to the (disordered) high-temperature form, as shown by synchrotron radiation powder diffraction; for instance, orthoclase has macroscopic monoclinic symmetry, and the tweed structure of cordierite is strictly hexagonal on a macroscopic scale.

(b) Experiments that reveal *short-range order*, especially TEM micrographs, infrared and Raman spectra and NMR spectra, show features of the ordered low-temperature modification; in orthoclase, very fine (nanometre-size) superposed triclinic albite and pericline microdomains occur, which may even fluctuate with time; similarly for cordierite.

With annealing or cooling time these tweed structures exhibit continuous 'coarsening' of their microdomains and 'sharpening' of their boundaries. The tweed microstructure of orthoclase develops into the well known crosshatched 'transformation microcline' texture discussed above in Section 3.3.10.2.2, example (3), and the cordierite tweed structure gives way to coarse twin lamellae in two orthogonal orientations of well ordered orthorhombic cordierite. Recently, interesting computer simulations of the time evolution of twin domains have been performed for alkali-metal feldspars by Tsatskis & Salje (1996) and for cordierite by Blackburn & Salje (1999). These papers also contain references to earlier work on tweed structures.

Textbook descriptions of tweed structures can be found in the following works: Putnis, 1992, Sections 7.3.5, 7.3.6 and 12.4.1; Salje, 1993, Sections 7.3 and pp. 116–201; Putnis & Salje, 1994.

3.3.10.7.5. Twin textures in polycrystalline aggregates

So far, twin textures have been treated independently of their occurrence in 'single crystals' or in polycrystalline aggregates. In the present section, the specific situation in polycrystalline materials such as ceramics, metals and rocks is discussed. This treatment is concerned with the extra effects that occur in addition to those discussed in Sections 3.3.10.7.1 to 3.3.10.7.4 above. These additional effects result from the fact that in a polycrystalline material a given crystal grain is surrounded by other grains and thus 'clamped' with respect to form and orientation changes arising from mechanical stress, electrical polarization or magnetization. Here, this effect is called 'neighbour clamping'.

Two cases of neighbour clamping occur, three-dimensional clamping of grains in the bulk of a sample and two-dimensional clamping at the surface of a sample. In addition, two-dimensional clamping can occur in thin films, either free or epitaxial. The result of this clamping is high elastic stress which is relaxed ('stress relief'; Arlt, 1990) by twinning, in particular by the formation of 'shape-preserving' twin textures.

Twinning in a ceramic is of great technical importance for the preparation and optimization of devices such as capacitors, piezoelectric elements and magnets. They often contain ferroelectric or ferromagnetic polycrystalline materials which undergo domain switching in an electric or magnetic field and, hence, can be poled.

In the following, we restrict our considerations to *non-metallic ceramics* where twinning is generated by a *ferroelastic* phase transition (e.g. perovskites). It is assumed that the ceramic is formed at temperatures far above the phase transition, which is accompanied on cooling by a considerable spontaneous lattice strain in the low-temperature phase, leading to the formation of *non-merohedral* twins. Without any formation of twins a considerable change of the grain shapes would occur and cause high inter-grain stress. The main mechanism of stress relaxation ('stress relief') is the formation of a ferroelastic twin texture which preserves the shape of the original (high-temperature phase) grain as far as possible. Note that the twin texture resulting from this 'neighbour clamping' is quite different from the twin texture of a free, unclamped grain. In the free grain, only

few twin lamellae with usually coherent boundaries are formed, whereas in the clamped grain several twin bands with narrow-spaced twin lamellae of different twin types occur.

In the clamped case, the significant effect of ferroelastic twin formation is the reduction of the elastic energy resulting from the clamping. On the other hand, the formation of new twin interfaces increases the twin-boundary energy. The competition of these effects leads to an energetic balance with a (relative) minimum of the overall energy of the sample. The process of twin formation does not occur sharply at the transition temperature T_c but continues over a considerable temperature range below T_c . The 'ideal' state of lowest energy is hardly ever reached due to the rigidity of the original grain structure (which remains rather unchanged) and to the existence of kinetic (coercive) barriers.

The group of materials for which these effects are most typical are the ferroelectric and ferroelastic perovskites, in particular BaTiO_3 . A detailed study is provided by Arlt (1990), who also presents extensive model calculations of relevant energy terms, as well as of average domain sizes and widths of twin bands.

Twinning phenomena in polycrystalline *metals* are treated by Christian (1965, Chapter 8).

Note. As mentioned above in Section 3.3.10.7.1, *non-ferroelastic* phase transitions cause no spontaneous lattice strain and, hence, the associated *merohedral* twins cannot act as 'stress relief' for a 'clamped' twin texture.

3.3.10.8. Twinning dislocations

In contrast to (low-angle) grain boundaries, twin boundaries do not require the existence of boundary dislocations as necessary constituents. Nevertheless, a special kind of dislocation, called '*twinning dislocation*', has been introduced in materials science for twin boundaries of deformation twins, i.e. for twins with a large shear angle 2ε and with a twin boundary parallel to a rational plane (hkl) which is simultaneously the twin reflection plane (Read, 1953, p. 109; Friedel, 1964, p. 173). Geometrically, a twinning dislocation is a step in the twin boundary (Fig. 3.3.10.15), i.e. a line along which the twin interface 'jumps' from one lattice plane to the next. As shown in Fig. 3.3.10.15, this 'dislocation line', which is located at the twin interface, is surrounded by lattice distortions, similar to the deformations around regular dislocations in an untwinned crystal.

Using the concept of a Burgers circuit for regular (perfect) dislocations, Burgers vectors \mathbf{b}_t of twinning dislocations can also be defined. Such a Burgers vector is parallel to the (rational) direction of shear (i.e. parallel to the intersection of the shear plane and the twin plane, as shown in Fig. 3.3.10.15). Its modulus is proportional to $\tan \varepsilon$ and has, in general, non-integer values. For small or zero values of the shear angle 2ε (pseudo-merohedral and merohedral twins) the Burgers vectors are small or zero, and the related 'twinning dislocations' are not physically meaningful. Note that in this approach steps in twin interfaces of (strictly) merohedral twins are not dislocations at all, because $\varepsilon = 0$ and $\mathbf{b}_t = 0$.

For classical deformation twins, the shear angles 2ε are large, and 'twinning dislocations' are well defined and have a significant influence on the deformation behaviour and on the shape of twin domains. Twin interfaces exactly parallel to the twin reflection plane are dislocation-free, whereas interfaces inclined to the reflection plane consist of segments parallel to the reflection plane separated by steps (i.e. twinning dislocations). For small inclinations, the twinning dislocations are widely spaced, whereas for curved interfaces their spacing varies. This feature plays an important role for lenticular domains (needle domains) of deformation twins. Twinning dislocations are also essential for the 'coherence' and 'incoherence' of twin boundaries as used in materials science. This aspect will be discussed in Section 3.3.10.9.

3.3. TWINNING OF CRYSTALS

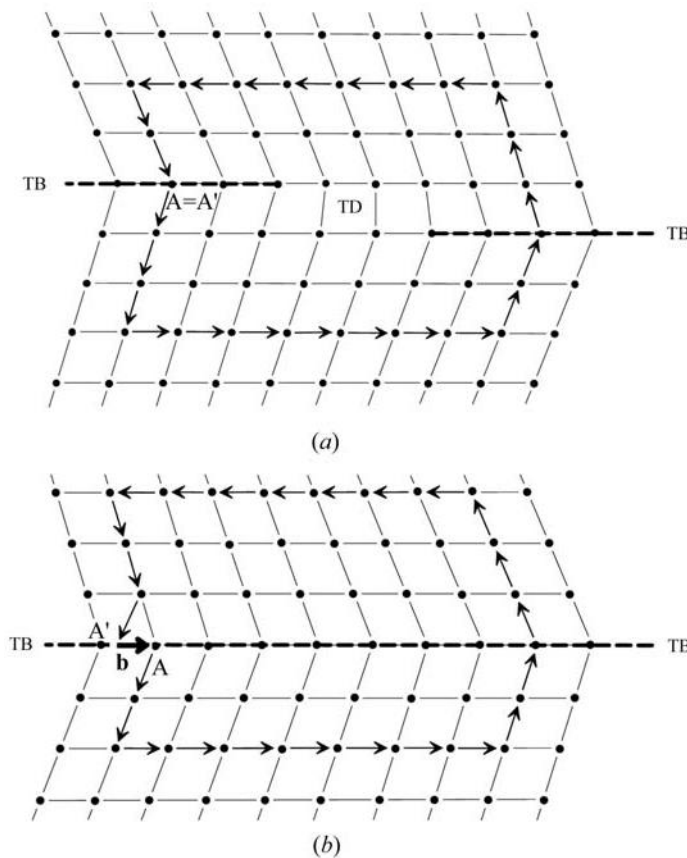


Fig. 3.3.10.15. Definition of the Burgers vector \mathbf{b} of a twinning dislocation TD (*i.e.* step of twin boundary TB). (a) Closed Burgers circuit ($A = A'$) encircling the twinning dislocation TD. (b) Analogous circuit in a reference crystal without dislocation (after Friedel, 1964, p. 140). The Burgers vector \mathbf{b} is defined as the closure error $A' \rightarrow A$ of the reference circuit.

An interesting study of twinning dislocations in deformation twins of calcite by means of X-ray topography has been carried out by Sauvage & Authier (1965), Authier & Sauvage (1966) and Sauvage (1968).

Twinning dislocations can interact with regular dislocations. Example: a twinning dislocation (*i.e.* the step between neighbouring interface planes) ending in an untwinned crystal. The end point must be a 'triple node' of three dislocations, *viz* of the twinning dislocation with Burgers vector \mathbf{b}_t , of a regular dislocation in twin partner 1 with Burgers vector \mathbf{b}_1 and of a regular dislocation in twin partner 2 with Burgers vector \mathbf{b}_2 . The three vectors obey Frank's conservation law of Burgers vectors at dislocation nodes:

$$\mathbf{b}_t + \mathbf{b}_1 + \mathbf{b}_2 = \mathbf{0}.$$

This reaction of dislocations is of great importance for the plastic deformation of crystals by twinning.

For more detailed information on twinning dislocations, reference is made to Read (1953, p. 109), Chalmers (1959, pp. 125 and 158), Friedel (1964, p. 173), Weertman & Weertman (1964, pp. 141–144), and the literature quoted therein.

In conclusion, it is pointed out that twinning dislocations may also occur in non-merohedral growth and transformation twins, but very little has been published on this topic so far. For transformation twins, however, twinning dislocations (in contrast to regular dislocations) as a rule are not physically meaningful because of the usually strong pseudosymmetry (*i.e.* small values of the shear angle 2ε) of these twins. Nevertheless, twinning dislocations allow the formation of the tapering twin walls of needle twins as described in Section 3.3.10.7.3.

3.3.10.9. Coherent and incoherent twin interfaces

At the start of Section 3.3.10, the terms *compatible* and *incompatible* twin boundaries were introduced and clearly defined. There exists another pair of terms, *coherent* and *incoherent* interfaces, which are predominantly used in bicrystallography and metallurgy for the characterization of grain boundaries, but less frequently in mineralogy and crystallography for twin boundaries. These terms, however, are defined in different and often rather diffuse ways, as the following examples show.

(1) Cahn (1954, p. 390), in his extensive review on twinning, defines *coherence* in metal twins as follows: 'An interface parallel to a twin (reflection) plane is called a coherent interface, while any other interface is termed *non-coherent*'. The same definition is given by Porter & Easterling (1992, p. 122), who consider twin boundaries as 'special high-angle boundaries'. This definition is widely used, especially in metallurgy, as evidenced by the following textbooks: Cottrell (1955, p. 212); Chalmers (1959, p. 125); Van Bueren (1961, pp. 251 and 450), Friedel (1964, p. 173); Klassen-Neklyudova (1964, p. 156); Kelly & Groves (1970, p. 308).

(2) Christian (1965, p. 332) distinguishes three levels of coherence of grain boundaries:

(a) *Incoherent* interfaces correspond to high-angle grain boundaries without any 'continuity conditions for lattice vectors or lattice planes across the interface'.

(b) *Semi-coherent* interfaces are low-angle boundaries formed by a regular network of dislocations. 'Such an interface consists of regions in which the two structures may be regarded as being in forced elastic coherence, separated by regions of misfit', *i.e.* there is *partial local register* across the boundary.

(c) *Fully coherent* interfaces correspond to the joining of two twin components along their rational or irrational composition plane in such a way that the lattices match exactly at the interface.

Very similar definitions are also used by Barrett & Massalski (1966, p. 493) and Sutton & Balluffi (1995, *Glossary*) for bicrystal boundaries. The third term, 'fully coherent', corresponds to the coherence definition of Cahn. It is noted that the terms 'fully coherent', 'semi-coherent' and 'incoherent' are also applied to the interfaces of grains of different phases ('interphase interfaces'), as well as to boundaries of second-phase precipitates, by Porter & Easterling (1992, Chapter 3.4).

(3) Putnis (1992, pp. 225 and 335) considers twin interfaces, as well as boundaries between matrix and precipitates, in minerals by their 'degree of lattice matching'. He uses the term *coherent* twin boundaries for 'perfect lattice plane matching across the interface, the strains being taken up by elastic distortions' (*i.e.* without the presence of dislocations). Dislocations along the twin boundary lead to a 'loss of coherence'. Interfaces containing dislocations are called *semi-coherent* (p. 336, Fig. 11.4), which is similar to the definition by Christian quoted above.

(4) Shekhtman (1993, p. 24) defines the term coherence only for ferroelastics (especially YBaCu) with different systems of lamellar twin domains: boundaries between (parallel) twin lamellae are defined as *coherent* interfaces, whereas boundaries between different lamellae systems are called *incoherent*.

The above definitions have one feature in common: coherent twin boundaries are planar interfaces, which are either rational or irrational, as stated explicitly by Christian (1965, p. 332). Beyond this, the various definitions are rather vague. In particular, they do not distinguish between ferroelastic and non-ferroelastic (strictly merohedral) twins and do not consider the twin displacement vector discussed in Section 3.3.10.4.

As an attempt to fill this gap, the following elucidations of the term '*coherence*' are suggested here. These proposals are based on the definitions summarized above, as well as on the concepts of compatibility of interfaces (Sections 3.3.10.1 and 3.3.10.3) and on the notion of twin displacement vector (Section 3.3.10.4).

3. PHASE TRANSITIONS, TWINNING AND DOMAIN STRUCTURES

(i) For *twin interfaces*, only the terms *coherent* and *incoherent* are used. In view of the fact that twin interfaces do not require regular (perfect) dislocations (but may contain twinning dislocations as described above in Section 3.3.10.8), the term ‘semi-coherent’ is reserved for grain boundaries and heterophase interfaces.

(ii) Twin boundaries are called *coherent* only if they are (mechanically) compatible. This holds for both rational and irrational twin boundaries, as suggested by Christian (1965, p. 332). Both cases may be distinguished by using qualifying adjectives such as ‘rationally coherent’ and ‘irrationally coherent’. Note that irrational (compatible) twin boundaries are usually less perfect and of higher energy than rational ones.

(iii) For strict merohedral (non-ferroelastic) twins (lattice index $[j] = 1$) any twin boundary, even a curved one, is compatible and, hence, is designated here as *coherent*, even if the contact plane does not coincide with the twin mirror plane.

(iv) For non-merohedral (ferroelastic) twins, a pair of (rational or irrational) perpendicular compatible interfaces occurs (Section 3.3.10.2.1). The same holds for merohedral twins of lattice index $[j] > 1$ (Section 3.3.10.2.4). All these compatible boundaries are considered here as *coherent*.

(v) In lattice and structural terms, a twin boundary is *coherent* if it exhibits a well defined matching of the two lattices along the entire boundary, *i.e.* continuity with respect to their lattice vectors and lattice planes. We want to stress that we consider the coherence of a twin boundary not as being destroyed by the presence of a nonzero twin displacement or fault vector as long as there is an optimal low-energy fit of the two partner structures. The twin displacement (fault) vector represents a ‘phase shift’ between the two structures with the same two-dimensional periodicity along their contact plane and thus defines the continuity relation across the boundary. This statement agrees with the general opinion that stacking faults, antiphase boundaries and many merohedral twin boundaries, all possessing nonzero fault vectors, are *coherent*. Well known examples are stacking faults in f.c.c and h.c.p metals and Brazil twin boundaries in quartz.

It is apparent from these discussions of *coherent* twin interfaces that several features have to be taken into account, some readily available by experiments and observations, whereas others require geometric models (lattice matching) or even physical models (structure matching), including determination of twin displacement vectors \mathbf{t} .

The definitions of *coherence*, as treated here, often do not satisfactorily agree with reality. Two examples are given:

(a) Japanese twins of quartz with twin mirror plane $(11\bar{2}2)$ or twofold twin axis normal to $(11\bar{2}2)$. According to the definitions given above, the observed $(11\bar{2}2)$ contact plane is *coherent*. Nevertheless, these $(11\bar{2}2)$ boundaries are always strongly disturbed and accompanied by extended lattice distortions. Thus, in reality they must be considered as *not coherent*.

(b) Sodium lithium sulfate, NaLiSO_4 , with polar point group $3m$ and a hexagonal lattice forms merohedral growth twins with twin mirror plane (0001) normal to the polar axis. The composition plane coincides with the twin plane and has head-to-head or tail-to-tail character. According to definition (iii) above, any twin boundary of this merohedral twin is *coherent*. The observed (0001) contact plane, however, despite coincidence with the twin mirror plane, is always strongly disturbed and cannot be considered as coherent. In this case, the observed *incoherence* is obviously due to the head-to-head orientation of the boundary, which is ‘electrically forbidden’.

These examples demonstrate that the above formal definitions of *coherence*, based on geometrical viewpoints alone, are not always satisfactory and require consideration of individual cases.

With these discussions of rather subtle features of twin interfaces, this chapter on twinning is concluded. It was our aim to

present this rather ancient topic in a way that progresses from classical concepts to modern considerations, from three dimensions to two and from macroscopic geometrical arguments to microscopic atomistic reasoning. Macroscopic derivations of orientation and contact relations of the twin partners (twin laws, as well as twin morphologies and twin genesis) were followed by lattice considerations and structural implications of twinning. Finally, the physical background of twinning was explored by means of the analysis of twin interfaces, their structural and energetic features. It is this latter aspect which in the future is most likely to bring the greatest progress toward the two main goals, an atomistic understanding of the phenomenon ‘twinning’ and the ability to predict correctly its occurrence and non-occurrence.

All considerations in this chapter refer to analysis of twinning in *direct space*. The complementary aspect, the effect of twinning in *reciprocal space*, lies beyond the scope of the present treatment and, hence, had to be omitted. This concerns in particular the recognition and characterization of twinning in diffraction experiments, especially by X-rays, as well as the consideration of the problems that twinning, especially merohedral twinning, may pose in single-crystal structure determination (*cf.* Buerger, 1960a). Several powerful computer programs for the solution of these problems exist. For a case study, see Herbst-Irmer & Sheldrick (1998).

3.3.11. Glossary

| | |
|--|---|
| (hkl) | crystal face, lattice plane, net plane (Miller indices) |
| $\{hkl\}$ | crystal form, set of symmetrically equivalent lattice (net) planes |
| $[uvw]$ | zone axis, crystal edge, lattice direction, lattice row (direction indices) |
| $\langle uvw \rangle$ | set of symmetrically equivalent lattice directions (rows) |
| \mathcal{G} | symmetry group of the (real or hypothetical) ‘parent structure’ or high-symmetry modification or ‘prototype phase’ of a crystal; group in general |
| \mathcal{H} | <i>eigensymmetry</i> group of an (untwinned) crystal; symmetry group of the deformed (‘daughter’) phase of a crystal; subgroup |
| $\mathcal{H}_1, \mathcal{H}_2, \dots, \mathcal{H}_j$ | oriented <i>eigensymmetries</i> of domain states 1, 2, \dots , j |
| $\mathcal{H}_{1,2}^*, \mathcal{H}^*$ | intersection symmetry group of the pair of oriented <i>eigensymmetries</i> \mathcal{H}_1 and \mathcal{H}_2 , reduced <i>eigensymmetry</i> of a domain |
| \mathcal{K} | composite symmetry group of a twinned crystal (domain pair); twin symmetry |
| $\mathcal{K}_{1,2}^*, \mathcal{K}^*$ | reduced composite symmetry of the domain pair (1, 2) |
| $\mathcal{K}(n)$ | extended composite symmetry of a twinned crystal with a pseudo n -fold twin axis |
| k, k_1, k_2, \dots, k_i | twin operations ($k_1 = \text{identity}$) |
| $2', m', \bar{1}', 4'(2), \bar{6}'(3), \bar{3}'(3), \bar{6}'(3)$ | twin operations of order two in colour-changing (black–white) symmetry notation |
| $ \mathcal{G} , \mathcal{H} , \mathcal{K} $ | order of group $\mathcal{G}, \mathcal{H}, \mathcal{K}$ |
| $[i]$ | index of \mathcal{H} in \mathcal{G} , or of \mathcal{H} in \mathcal{K} |
| $[j], \Sigma$ | index of coincidence-site lattice (twin lattice, sublattice) with respect to crystal lattice |
| ω | twin obliquity |
| \mathbf{b}_t | Burgers vector of twinning dislocations |
| \mathbf{f} | fault vector of a merohedral twin boundary |
| \mathbf{t} | twin displacement vector |

3.3. TWINNING OF CRYSTALS

| | |
|--------------------------|---|
| GFH | Aizu (1970a) symbol of a ferroic phase transition (ferroic species); F = ferroic |
| W, W' | designation of non-merohedral ferroelastic twin boundaries (according to Sapriel, 1975) |
| F_{hkl} | structure factor of reflection hkl |
| \mathbf{g}_{hkl} | diffraction vector (reciprocal-lattice vector) of reflection hkl |
| φ_{hkl} | phase angle of structure factor F_{hkl} |
| Ψ_{hkl}, Φ_{hkl} | difference of phase angles ('phase jump') across twin boundary |
| ρ | charge density of a ferroelectric twin boundary |
| \mathbf{P} | spontaneous polarization |

We are indebted to Elke Haque (Bonn), Zdenek Janovec (Prague) and Stefan Klumpp (Bonn) for preparing the figures. We are grateful to Vaclav Janovec (Prague) for fruitful discussions and to our editor André Authier for his patience and help in preparing the manuscript.

References

- Abrahams, S. C. (1994). *Structure relationship to dielectric, elastic and chiral properties*. *Acta Cryst.* **A50**, 658–685.
- Aizu, K. (1969). Possible species of 'ferroelastic' crystals and of simultaneously ferroelectric and ferroelastic crystals. *J. Phys. Soc. Jpn.*, **27**, 387–396.
- Aizu, K. (1970a). Possible species of ferromagnetic, ferroelectric and ferroelastic crystals. *Phys. Rev. B*, **2**, 754–772.
- Aizu, K. (1970b). Determination of the state parameters and formulation of spontaneous strain for ferroelastics. *J. Phys. Soc. Jpn.*, **28**, 706–716.
- Aizu, K. (1973). Second-order ferroic state shifts. *J. Phys. Soc. Jpn.*, **34**, 121–128.
- Amelinckx, S., Gevers, R. & Van Landuyt, J. (1978). Editors. *Diffraction and imaging techniques in materials science*, Vol. I. *Electron microscopy*, especially pp. 107–151. Amsterdam: North-Holland.
- Aminoff, G. & Broomé, B. (1931). *Strukturtheoretische Studien über Zwillinge I*. *Z. Kristallogr.* **80**, 355–376.
- Arlt, G. (1990). Twinning in ferroelectric and ferroelastic ceramics: stress relief. *J. Mater. Sci.* **25**, 2655–2666.
- Arzruni, A. (1887). Ein neues Zwillingsgesetz im regulären System. *Proc. Russ. Mineral. Soc. St. Petersburg*, **23**, 126–132. (In German.)
- Authier, A. & Sauvage, M. (1966). Dislocations de macle dans la calcite: interférences entre les champs d'onde créés à la traversée d'une lamelle de macle. *J. Phys. Rad. (France)*, **27**, 137–142.
- Barber, D. J. & Wenk, H.-R. (1979). Deformation twinning in calcite, dolomite, and other rhombohedral carbonates. *Phys. Chem. Miner.* **5**, 141–165.
- Barrett, C. S. & Massalski, T. B. (1966). *Structure of metals*, 3rd edition, especially pp. 406–414. New York: McGraw-Hill.
- Bartels, H. & Follner, H. (1989). Crystal growth and twin formation of gypsum. *Cryst. Res. Technol.* **24**, 1191–1196.
- Baumhauer, H. (1879). Über künstliche Kalkspath-Zwillinge nach -1/2R. *Z. Kristallogr.* **3**, 588–591.
- Becke, F. (1911). Über die Ausbildung der Zwillingskristalle. *Fortschr. Mineral. Kristallogr. Petrogr.* **1**, 48–65.
- Billiet, Y. & Bertaut, E. F. (2002). Isomorphic subgroups of space groups. Part 13 of *International tables for crystallography*, Vol. A. *Space-group symmetry*, edited by Th. Hahn, 5th ed. Dordrecht: Kluwer Academic Publishers.
- Bismayer, U., Röwer, R. W. & Wruck, B. (1995). Ferroelastic phase transition and renormalization effect in diluted lead phosphate, $(\text{Pb}_{1-x}\text{Sr}_x)_3(\text{PO}_4)_2$ and $(\text{Pb}_{1-x}\text{Ba}_x)_3(\text{PO}_4)_2$. *Phase Transit.* **55**, 169–179.
- Black, P. J. (1955). The structure of FeAl_3 . II. *Acta Cryst.* **8**, 175–182.
- Blackburn, J. & Salje, E. K. H. (1999). Time evolution of twin domains in cordierite: a computer simulation study. *Phys. Chem. Miner.* **26**, 275–296.
- Bloss, F. D. (1971). *Crystallography and crystal chemistry*, pp. 324–338. New York: Holt, Rinehart & Winston.
- Bögels, G., Buijnsters, J. G., Verhaegen, S. A. C., Meekes, H., Bennema, P. & Bollen, D. (1999). Morphology and growth mechanism of multiply twinned AgBr and AgCl needle crystals. *J. Cryst. Growth*, **203**, 554–563.
- Bögels, G., Meekes, H., Bennema, P. & Bollen, D. (1998). The role of {100} side faces for lateral growth of tabular silver bromide crystals. *J. Cryst. Growth*, **191**, 446–454.
- Bögels, G., Pot, T. M., Meekes, H., Bennema, P. & Bollen, D. (1997). Side-face structure and growth mechanism of tabular silver bromide crystals. *Acta Cryst.* **A53**, 84–94.
- Bollmann, W. (1970). *Crystal defects and crystalline interfaces*. ch. 12, pp. 143–148. Berlin: Springer.
- Bollmann, W. (1982). *Crystal lattices, interfaces, matrices*, pp. 111–249. Geneva: published by the author.
- Bonner, W. A. (1981). InP synthesis and LEC growth of twin-free crystals. *J. Cryst. Growth*, **54**, 21–31.
- Böttcher, P., Doert, Th., Arnold, H. & Tamazyan, R. (2000). Contributions to the crystal chemistry of rare-earth chalcogenides. I. The compounds with layer structures LnX_2 . *Z. Kristallogr.* **215**, 246–253.
- Boulesteix, C. (1984). A survey of domains and domain walls generated by crystallographic phase transitions causing a change of the lattice. *Phys. Status Solidi A*, **86**, 11–42.
- Boulesteix, C., Yangui, B., Ben Salem, M., Manolakis, C. & Amelinckx, S. (1986). The orientation relations of interfaces between a prototype phase and its ferroelastic derivatives: theoretical and experimental studies. *J. Phys.* **47**, 461–471.
- Bragg, W. L. (1924). The structure of aragonite. *Proc. R. Soc. London Ser. A*, **105**, 16–39.
- Bragg, W. L. (1937). *Atomic structure of minerals*. Ithaca, NY: Cornell University Press.
- Bragg, W. L. & Claringbull, G. F. (1965). *The crystalline state*, Vol. IV. *Crystal structures of minerals*, p. 302. London: Bell & Sons.
- Bringham, K. N. & Griffin, D. T. (1986). Staurolite-lukasite series. II. Crystal structure and optical properties of a cobaltoan staurolite. *Am. Mineral.* **71**, 1466–1472.
- Brögger, W. C. (1890). Hydrargillit. *Z. Kristallogr.* **16**, second part, pp. 16–43, especially pp. 24–43 and Plate 1.
- Bueble, S., Knorr, K., Brecht, E. & Schmahl, W. W. (1998). Influence of the ferroelastic twin domain structure on the 100 surface morphology of LaAlO_3 HTSC substrates. *Surface Sci.* **400**, 345–355.
- Bueble, S. & Schmahl, W. W. (1999). Mechanical twinning in calcite considered with the concept of ferroelasticity. *Phys. Chem. Miner.* **26**, 668–672.
- Buerger, M. J. (1934). The lineage structure of crystals. *Z. Kristallogr.* **89**, 195–220.
- Buerger, M. J. (1945). The genesis of twin crystals. *Am. Mineral.* **30**, 469–482.
- Buerger, M. J. (1960a). *Crystal-structure analyses*, especially ch. 3. New York: Wiley.
- Buerger, M. J. (1960b). Introductory remarks. Twinning with special regard to coherence. In *Symposium on twinning. Cursos y Conferencias*, Fasc. VII, pp. 3 and 5–7. Madrid: CSIC.
- Buseck, P. R., Cowley, J. M. & Eyring, L. (1992). Editors. *High-resolution transmission electron microscopy and associated techniques*, especially ch. 11. New York: Oxford University Press.
- Cahn, R. W. (1954). Twinned crystals. *Adv. Phys.* **3**, 202–445.
- Chalmers, B. (1959). *Physical metallurgy*, especially ch. 4.4. New York: Wiley.
- Chernysheva, M. A. (1950). Mechanical twinning in crystals of Rochelle salt. *Dokl. Akad. Nauk SSSR*, **74**, 247–249. (In Russian.)
- Chernysheva, M. A. (1951). Effects of an electric field on the twinned structure of Rochelle salt. *Dokl. Akad. Nauk SSSR*, **81**, 1965–1968. (In Russian.)
- Chernysheva, M. A. (1955). Twinning phenomena in crystals of Rochelle salt. PhD thesis, Moscow. (In Russian.)
- Christian, J. W. (1965). *The theory of transformations in metals and alloys*, especially chs. 8 and 20. Oxford: Pergamon.
- Chung, H., Dudley, M., Larson, D. J., Hurle, D. T. J., Bliss, D. F. & Prasad, V. (1998). The mechanism of growth-twin formation in zincblende crystals: insights from a study of magnetic-liquid encapsulated Czochralski grown InP single crystals. *J. Cryst. Growth*, **187**, 9–17.
- Cottrell, A. H. (1955). *Theoretical structural metallurgy*, 2nd edition, especially ch. 14.5. London: Edward Arnold.
- Curien, H. (1960). Sur les axes de macle d'ordre supérieur à deux. In *Symposium on twinning. Cursos y Conferencias*, Fasc. VII, pp. 9–11. Madrid: CSIC.

3. PHASE TRANSITIONS, TWINNING AND DOMAIN STRUCTURES

- Curien, H. & Donnay, J. D. H. (1959). *The symmetry of the complete twin*. *Am. Mineral.* **44**, 1067–1071.
- Curien, H. & Le Corre, Y. (1958). *Notation des macles à l'aide du symbolisme des groupes de couleurs de Choubnikov*. *Bull. Soc. Fr. Minéral. Cristallogr.* **81**, 126–132.
- Devouard, B., Pósai, M., Hua, X., Bazylnski, D. A., Frankel, R. B. & Buseck, P. R. (1998). *Magnetite from magnetotactic bacteria: size distributions and twinning*. *Am. Mineral.* **83**, 1387–1398.
- Docherty, R., El-Korashy, A., Jennissen, H.-D., Klapper, H., Roberts, K. J. & Scheffen-Lauenroth, T. (1988). *Synchrotron Laue topography studies of pseudo-hexagonal twinning*. *J. Appl. Cryst.* **21**, 406–415.
- Donnay, G. & Donnay, J. D. H. (1974). *Classification of triperiodic twins*. *Can. Mineral.* **12**, 422–425.
- Donnay, J. D. H. & Donnay, G. (1972). *Crystal geometry*, Section 3 (pp. 99–158). In *International tables for X-ray crystallography*, Vol. II, *Mathematical tables*, edited by J. C. Kasper & K. Lonsdale. Birmingham: Kynoch Press.
- Donnay, J. D. H. & Donnay, G. (1983). *The staurolite story*. *Tschermaks Mineral. Petrogr. Mitt.* **31**, 1–15.
- Dudley, M., Raghothamachar, B., Guo, Y., Huang, X. R., Chung, H., Hurl, D. T. J. & Bliss, D. F. (1998). *The influence of polarity on twinning in zincblende structure crystals: new insights from a study of magnetic liquid-encapsulated Czochralski-grown InP crystals*. *J. Cryst. Growth.* **192**, 1–10.
- Ellner, M. (1995). *Polymorphic phase transformation of Fe₄Al₁₃ causing multiple twinning with decagonal pseudo-symmetry*. *Acta Cryst.* **B51**, 31–36.
- Ellner, M. & Burkhardt, U. (1993). *Zur Bildung von Drehmehrlingen mit pentagonaler Pseudosymmetrie beim Erstarrungsvorgang des Fe₄Al₁₃*. *J. Alloy. Compd.* **198**, 91–100.
- Engel, G., Klapper, H., Krempel, P. & Mang, H. (1989). *Growth twinning in quartz-homeotypic gallium orthophosphate crystals*. *J. Cryst. Growth.* **94**, 597–606.
- Ernst, F., Finnis, M. W., Koch, A., Schmidt, C., Straumal, B. & Gust, W. (1996). *Structure and energy of twin boundaries in copper*. *Z. Metallkd.* **87**, 911–922.
- Flack, H. D. (1987). *The derivation of twin laws for (pseudo-)merohedry by coset decomposition*. *Acta Cryst.* **A43**, 564–568.
- Fleming, S. D., Parkinson, G. M. & Rohl, A. L. (1997). *Predicting the occurrence of reflection twins*. *J. Cryst. Growth.* **178**, 402–409.
- Fousek, J. & Janovec, V. (1969). *The orientation of domain walls in twinned ferroelectric crystals*. *J. Appl. Phys.* **40**, 135–142.
- Friedel, G. (1904). *Etude sur les groupements cristallins*. Extrait du *Bulletin de la Société d'Industrie Minérale*, Quatrième Série, Tomes III et IV. Saint Etienne: Imprimerie Théolier J. et Cie.
- Friedel, G. (1923). *Sur les macles du quartz*. *Bull. Soc. Fr. Minéral. Cristallogr.* **46**, 79–95.
- Friedel, G. (1926). *Leçons de cristallographie*, ch. 15. Nancy, Paris, Strasbourg: Berger-Levrault. [Reprinted (1964). Paris: Blanchard].
- Friedel, G. (1933). *Sur un nouveau type de macles*. *Bull. Soc. Fr. Minéral. Cristallogr.* **56**, 262–274.
- Friedel, J. (1964). *Dislocations*, especially ch. 6. Oxford: Pergamon.
- Fronzel, C. (1962). *The system of mineralogy*, 7th edition, Vol. III. *Silica minerals*, especially pp. 75–99. New York: Wiley.
- Gottschalk, H., Patzer, G. & Alexander, H. (1978). *Stacking fault energy and ionicity of cubic III–V compounds*. *Phys. Status Solidi A*, **45**, 207–217.
- Gottstein, G. (1984). *Annealing texture developments by multiple twinning in fcc crystals*. *Acta Metall.* **32**, 1117–1138.
- Gottstein, G. & Shvindlerman, L. S. (1999). *Grain boundary migration in metals*, ch. 2, pp. 105–123. Boca Raton, London, New York, Washington DC: CRC Press.
- Grimmer, H. (1989). *Systematic determination of coincidence orientations for all hexagonal lattices with axial ratio c/a in a given interval*. *Acta Cryst.* **A45**, 320–325.
- Grimmer, H. (2003). *Determination of all misorientations of tetragonal lattices with low multiplicity; connection with Mallard's rule of twinning*. *Acta Cryst.* **A59**, 287–296.
- Hahn, Th. (2002). Editor. *International tables for crystallography*, Vol. A. *Space-group symmetry*. 5th ed. Dordrecht: Kluwer Academic Publishers.
- Hahn, Th., Janovec, V. & Klapper, H. (1999). *Bicrystals, twins and domain structures – a comparison*. *Ferroelectrics*, **222**, 11–21.
- Hahn, Th. & Klapper, H. (2002). *Point groups and crystal classes*. Part 10 in *International tables for crystallography*, Vol. A. *Space-group symmetry*, edited by Th. Hahn, 5th edition. Dordrecht: Kluwer Academic Publishers.
- Hartman, P. (1956). *On the morphology of growth twins*. *Z. Kristallogr.* **107**, 225–237.
- Hartman, P. (1960). *Epitaxial aspects of the atacamite twin*. In *Symposium on twinning*. *Cursillos y Conferencias*, Fasc. VII, pp. 15–18. Madrid: CSIC.
- Heide, F. (1928). *Die Japaner-Zwillinge des Quarzes und ihr Auftreten im Quarzporphyr von Saubach i. V.* *Z. Kristallogr.* **66**, 239–281.
- Henke, H. (2003). *Crystal structures, order–disorder transition and twinning of the Jahn–Teller system (NO)₂VCl₆*. *Z. Kristallogr.* **218**, 617–625.
- Herbst-Irmer, R. & Sheldrick, G. M. (1998). *Refinement of twinned structures with SHELXL97*. *Acta Cryst.* **B54**, 443–449.
- Hoffmann, D. & Ernst, F. (1994). *Twin boundaries with 9R zone in Cu and Ag studied by quantitative HRTEM*. *Interface Sci.* **2**, 201–210.
- Hofmeister, H. (1998). *Forty years study of fivefold twinned structures in small particles and thin films*. *Cryst. Res. Technol.* **33**, 3–25, especially Section 4.
- Hofmeister, H. & Junghans, T. (1993). *Multiple twinning in the solid phase. Crystallisation of amorphous germanium*. *Mater. Sci. Forum*, **113–115**, 631–636.
- Holser, W. T. (1958). *Relation of structure to symmetry in twinning*. *Z. Kristallogr.* **110**, 250–265.
- Holser, W. T. (1960). *Relation of pseudosymmetry to structure in twinning*. In *Symposium on twinning*. *Cursillos y Conferencias*, Fasc. VII, pp. 19–30. Madrid: CSIC.
- Hornstra, J. (1959). *Models of grain boundaries in the diamond lattice I*. *Physica*, **25**, 409–422.
- Hornstra, J. (1960). *Models of grain boundaries in the diamond lattice II*. *Physica*, **26**, 198–208.
- Hurl, D. T. J. (1995). *A mechanism for twin formation during Czochralski and encapsulated vertical Bridgman growth of III–V compound semiconductors*. *J. Cryst. Growth*, **147**, 239–250.
- Hurst, V. J., Donnay, J. D. H. & Donnay, G. (1956). *Staurolite twinning*. *Mineral. Mag.* **31**, 145–163.
- Ikeno, S., Maruyama, H. & Kato, N. (1968). *X-ray topographic studies of NaCl crystals grown from aqueous solution with Mn ions*. *J. Cryst. Growth*, **3/4**, 683–693.
- Iliescu, B. & Chirila, R. (1995). *Electrical twinning of quartz by temperature gradient*. *Cryst. Res. Technol.* **30**, 231–235.
- Iliescu, B., Enculescu, I. & Chirila, R. (1997). *Dynamics of the Dauphiné twins in quartz crystals up to the transition point*. *Ferroelectrics*, **190**, 119–124.
- Janovec, V. (1972). *Group analysis of domains and domain pairs*. *Czech. J. Phys. B*, **22**, 974–994.
- Janovec, V. (1976). *A symmetry approach to domain structures*. *Ferroelectrics*, **12**, 43–53.
- Janovec, V. (2003). Personal communication.
- Jennissen, H.-D. (1990). *Phasenumwandlungen und Defektstrukturen in Kristallen mit tetraedrischen Baugruppen*. PhD thesis, Institut für Kristallographie, RWTH Aachen.
- Jia, C. L. & Thust, A. (1999). *Investigations of atomic displacements at a Σ₃ [111] twin boundary in BaTiO₃ by means of phase-retrieved electron microscopy*. *Phys. Rev. Lett.* **82**, 5052–5055.
- Johnsen, A. (1907). *Tschermak's Zwillingstheorie und das Gesetz der Glimmerzwillinge*. *Centralbl. Mineral. Geol. Palaeontol.* pp. 400–409, especially p. 407.
- Judd, J. W. (1888). *The development of a lamellar structure in quartz crystals by mechanical means*. *Mineral. Mag.* **8**, 1–9 and plate I.
- Keester, K. L., Housley, R. M. & Marshall, D. B. (1988). *Growth and characterization of large YBa₂Cu₃O_{7-x} single crystals*. *J. Cryst. Growth*, **91**, 295–301.
- Kelly, A. & Groves, G. W. (1970). *Crystallography and crystal defects*, especially chs. 10 and 12.5. London: Longman.
- Klapper, H. (1973). *Röntgentopographische Untersuchungen am Lithiumformiat-Monohydrat*. *Z. Naturforsch. A*, **28**, 614–622.
- Klapper, H. (1987). *X-ray topography of twinned crystals*. In *Progress in crystal growth and characterization*, Vol. 14, edited by P. Krishna. pp. 367–401. Oxford: Pergamon.
- Klapper, H., Hahn, Th. & Chung, S. J. (1987). *Optical, pyroelectric and X-ray topographic studies of twin domains and twin boundaries in KLiSO₄*. *Acta Cryst.* **B43**, 147–159.
- Klassen-Neklyudova, M. V. (1964). *Mechanical twinning of crystals*. New York: Consultants Bureau.

3.3. TWINNING OF CRYSTALS

- Koch, E. (1999). Twinning. Ch. 1.3 (pp. 10–14) in *International tables for crystallography*, Vol. C. Mathematical, physical and chemical tables, edited by A. J. C. Wilson & E. Prince, 2nd ed. Dordrecht: Kluwer Academic Publishers.
- Kohn, J. A. (1956). Twinning in diamond-type structures: high-order twinning in silicon. *Am. Mineral.* **41**, 778–784.
- Kohn, J. A. (1958). Twinning in diamond-type structures: a proposed boundary-structure model. *Am. Mineral.* **43**, 263–284.
- Kotrbova, M., Kadeckova, S., Novak, J., Bradler, J., Smirnov, G. V. & Shvydko, Yu. V. (1985). Growth and perfection of flux-grown FeBO_3 and $^{57}\text{FeBO}_3$ crystals. *J. Cryst. Growth*, **71**, 607–614.
- Krafczyk, S., Jacobi, H. & Föllner, H. (1997). Twinning of crystals as a result of differences between symmetrical and energetically most favourable structure arrangements. III. *Cryst. Res. Technol.* **32**, 163–173, and earlier references cited therein.
- Lang, A. R. (1967a). Some recent applications of X-ray topography. *Adv. X-ray Anal.* **10**, 91–107.
- Lang, A. R. (1967b). Fault surfaces in alpha quartz: their analysis by X-ray diffraction contrast and their bearing on growth history and impurity distribution. In *Crystal growth*, edited by H. S. Peiser, pp. 833–838. (Supplement to *Phys. Chem. Solids*.) Oxford: Pergamon Press.
- Lang, A. R. & Miuskov, V. F. (1969). Defects in natural and synthetic quartz. In *Growth of crystals*, edited by N. N. Sheftal, Vol. 7, 112–123. New York: Consultants Bureau.
- Le Page, Y. (1999). Low obliquity in pseudo-symmetry of lattices and structures, and in twinning by pseudo-merohedry. *Acta Cryst.* **A55**, Supplement. Abstract M12.CC001.
- Le Page, Y. (2002). Mallard's law recast as a Diophantine system: fast and complete enumeration of possible twin laws by [reticular] [pseudo] merohedry. *J. Appl. Cryst.* **35**, 175–181.
- Lieber, W. (2002). Personal communication.
- Lieberman, H. F., Williams, L., Davey, R. J. & Pritchard, R. G. (1998). Molecular configuration at the solid–solid interface: twinning in saccharine crystals. *J. Am. Chem. Soc.* **120**, 686–691.
- Liebisch, Th. (1891). *Physikalische Kristallographie*. Leipzig: Veit & Comp.
- McLaren, A. C. (1986). Some speculations on the nature of high-angle grain boundaries in quartz rocks. In *Mineral and rock deformation: laboratory studies*, edited by B. E. Hobbs & H. C. Heard. *Geophys. Monogr.* **36**, 233–245.
- McLaren, A. C. (1991). *Transmission electron microscopy of minerals and rocks*. Cambridge University Press.
- McLaren, A. C. & Phakey, P. P. (1966). Electron microscope study of Brazil twin boundaries in amethyst quartz. *Phys. Status Solidi*, **13**, 413–422.
- McLaren, A. C. & Phakey, P. P. (1969). Diffraction contrast from Dauphiné twin boundaries in quartz. *Phys. Status Solidi*, **31**, 723–737.
- Mallard, E. (1879). *Traité de cristallographie, géométrie et physique*. Vol. I. Paris: Dunod.
- Menzer, G. (1955). Über Kristallzwillingsgesetze. *Z. Kristallogr.* **106**, 193–198.
- Ming, N. B. & Sunagawa, I. (1988). Twin lamellae as possible self-perpetuating step sources. *J. Cryst. Growth*, **87**, 13–17.
- Mügge, O. (1883). Beiträge zur Kenntnis der Structurflächen des Kalkspathes. *Neues Jahrb. Mineral.* **81**, 32–54.
- Mügge, O. (1911). Über die Zwillingsbildung der Kristalle. *Fortschr. Mineral. Kristallogr. Petrogr.* **1**, 18–47.
- Müller, W. F., Wolf, Th. & Flükiger, R. (1989). Microstructure of superconducting ceramics of $\text{YBa}_2\text{Cu}_3\text{O}_{7-x}$. *Neues Jahrb. Mineral. Abh.* **161**, 41–67.
- Nespolo, M., Ferraris, G. & Takeda, H. (2000). Twins and allotwins of basic mica polytypes: theoretical derivation and identification in the reciprocal space. *Acta Cryst.* **A56**, 132–148.
- Nespolo, M., Ferraris, G., Takeda, H. & Takeuchi, Y. (1999). Plesiotwinning: oriented crystal associations based on a large coincidence-site lattice. *Z. Kristallogr.* **214**, 378–382.
- Nespolo, M., Kogure, T. & Ferraris, G. (1999). Allotwinning: oriented crystal association of polytypes – some warnings on consequences. *Z. Kristallogr.* **214**, 5–8.
- Nespolo, M., Takeda, H. & Ferraris, G. (1997). Crystallography of mica polytypes. In *EMU notes in mineralogy*, edited by St. Merlino, Vol. 1, ch. 2, pp. 81–118. Budapest: Eötvös University Press.
- Neumann, W., Hofmeister, H., Conrad, D., Scheerschmidt, K. & Ruvimov, S. (1996). Characterization of interface structures in nanocrystalline germanium by means of high-resolution electron microscopy and molecular dynamics simulation. *Z. Kristallogr.* **211**, 147–152.
- Newnham, R. E. (1975). *Structure–property relations*, pp. 106–107. Berlin: Springer.
- Niggli, P. (1919). *Geometrische Kristallographie des Diskontinuums*. Leipzig: Gebrüder Borntraeger. [Reprinted (1973). Wiesbaden: Sändig].
- Niggli, P. (1920/1924/1941). *Lehrbuch der Mineralogie und Kristallchemie*, 1st edition 1920, 2nd edition 1924, 3rd edition, Part I, 1941, especially pp. 136–153, 401–414. Berlin: Gebrüder Borntraeger.
- Niggli, P. (1926). *Lehrbuch der Mineralogie. Band II: Spezielle Mineralogie*, p. 53, Fig. 9. Berlin: Gebrüder Borntraeger.
- Palmer, D. C., Putnis, A. & Salje, E. K. H. (1988). Twinning in tetragonal leucite. *Phys. Chem. Mineral.* **16**, 298–303.
- Penn, R. L. & Banfield, J. F. (1998). Oriented attachment and growth, twinning, polytypism, and formation of metastable phases: insights from nano-crystalline TiO_2 . *Am. Mineral.* **83**, 1077–1082.
- Penn, R. L. & Banfield, J. F. (1999). Formation of rutile nuclei at anatase {112} twin interfaces and the phase transformation mechanism in nanocrystalline titania. *Am. Mineral.* **84**, 871–876.
- Phakey, P. P. (1969). X-ray topographic study of defects in quartz. I. Brazil twin boundaries. *Phys. Status Solidi*, **34**, 105–119.
- Phillips, F. C. (1971). *An introduction to crystallography*, 4th ed. London: Longman.
- Porter, D. A. & Easterling, K. E. (1992). *Phase transformations in metals and alloys*, 2nd edition, especially ch. 3. London: Chapman & Hall.
- Putnis, A. (1992). *Introduction to mineral sciences*, especially chs. 7.3 and 12.4. Cambridge University Press.
- Putnis, A. & Salje, E. K. H. (1994). Tweed microstructures: experimental observations and some theoretical models. *Phase Transit.* **48**, 85–105.
- Putnis, A., Salje, E. K. H., Redfern, S., Fyfe, C. & Strobl, H. (1987). Structural states of Mg-cordierite I: Order parameters from synchrotron X-ray and NMR data. *Phys. Chem. Miner.* **14**, 446–454.
- Queisser, H. J. (1963). Properties of twin boundaries in silicon. *J. Electrochem. Soc.* **110**, 52–56.
- Raaz, F. & Tertsch, H. (1958). *Einführung in die geometrische und physikalische Kristallographie*, 3rd edition. Wien: Springer.
- Ramdohr, P. & Strunz, H. (1967). *Klockmann's Lehrbuch der Mineralogie*, 15th edition, especially p. 512. Stuttgart: Enke.
- Räuber, A. (1978). Chemistry and physics of lithium niobate. In *Current topics in materials science*, Vol. 1, edited by E. Kaldis, pp. 548–550 and 585–587. Amsterdam: North Holland.
- Read, W. T. (1953). *Dislocations in crystals*, especially ch. 7. New York: McGraw-Hill.
- Rečnik, A., Brulay, J., Mader, W., Kolar, D. & Rühle, M. (1994). Structural and spectroscopic investigation of the (111) twins in barium titanite. *Philos. Mag. B*, **70**, 1021–1034.
- Rose, G. (1868). Über die im Kalkspath vorkommenden hohlen Canäle. *Abh. Königl. Akad. Wiss. Berlin*, **23**, 57–79.
- Roth, G., Ewert, D., Heger, G., Hervieu, M., Michel, C., Raveau, B., D'Yvoire, F. & Revcolevschi, A. (1987). Phase transformation and microtwinning in crystals of the high- T_c superconductor $\text{YBa}_2\text{Cu}_3\text{O}_{8-x}$, $x \approx 1.0$. *Z. Physik B*, **69**, 21–27.
- Salje, E. K. H. (1993). *Phase transformations in ferroelectric and co-elastic crystals*. Cambridge University Press.
- Salje, E. K. H., Buckley, A., Van Tendeloo, G., Ishibashi, Y. & Nord, G. L. (1998). Needle twins and right-angled twins in minerals: comparison between experiment and theory. *Am. Mineral.* **83**, 811–822.
- Salje, E. K. H. & Ishibashi, Y. (1996). Mesoscopic structures in ferroelastic crystals: needle twins and right-angled domains. *J. Phys. Condens. Matter*, **8**, 1–19.
- Salje, E. K. H., Kuscholke, B. & Wruck, B. (1985). Domain wall formation in minerals: I. Theory of twin boundary shapes in Na-feldspar. *Phys. Chem. Miner.* **12**, 132–140.
- Santoro, A. (1974). Characterization of twinning. *Acta Cryst.* **A30**, 224–231.
- Sapriel, J. (1975). Domain-wall orientations in ferroelastics. *Phys. Rev. B*, **12**, 5128–5140.
- Sauvage, M. (1968). Observations de sources et de réactions entre dislocations partielles de macles sur des topographies aux rayons X. *Phys. Status Solidi*, **29**, 725–736.
- Sauvage, M. & Authier, A. (1965). Etude des bandes de croissance et des dislocations de macles dans la calcite. *Bull. Soc. Fr. Minéral. Cristallogr.* **88**, 379–388.

3. PHASE TRANSITIONS, TWINNING AND DOMAIN STRUCTURES

- Schaskolsky, M. & Schubnikow, A. (1933). Über die künstliche Herstellung gesetzmässiger Kristallverwachsungen des Kalialauns. *Z. Kristallogr.* **85**, 1–16.
- Scherf, Ch., Hahn, Th., Heger, G., Becker, R. A., Wunderlich, W. & Klapper, H. (1997). Optical and synchrotron radiation white-beam topographic investigation during the high-temperature phase transition of KLiSO_4 . *Ferroelectrics*, **191**, 171–177.
- Scherf, Ch., Hahn, Th., Heger, G., Ivanov, N. R. & Klapper, H. (1999). Imaging of inversion twin boundaries in potassium titanyl phosphate (KTP) by liquid-crystal surface decoration and X-ray diffraction topography. *Philos. Trans. R. Soc. London Ser. A*, **357**, 2651–2658.
- Schmahl, W. W., Putnis, A., Salje, E. K. H., Freeman, P., Graeme-Barber, A., Jones, R., Singh, K. K., Blunt, J., Edwards, P. P., Loran, J. & Mirza, K. (1989). Twin formation and structural modulations in orthorhombic and tetragonal $\text{YBa}_2(\text{Cu}_{1-x}\text{Co}_x)_3\text{O}_{7-\delta}$. *Philos. Mag. Lett.* **60**, 241–251.
- Schmid, H., Burkhardt, E., Walker, E., Brixel, W., Clin, M., Rivera, J.-P., Jorda, J.-L., François, M. & Yvon, K. (1988). Polarized light and X-ray precession study of the ferroelastic domains of $\text{YBa}_2\text{Cu}_3\text{O}_{7-\delta}$. *Z. Phys. B*, **72**, 305–322.
- Schubnikow, A. & Zinserling, K. (1932). Über die Schlag- und Druckfiguren und über die mechanischen Quarzzwillinge. *Z. Kristallogr.* **83**, 243–264.
- Seifert, H. (1928). Über Schiebungen am Bleiglanz. *Neues Jahrb. Mineral. Geol. Palaeontol.* **57**, Beilage-Band, Abteilung A, Mineralogie und Petrographie, pp. 665–742.
- Senechal, M. (1976). The mechanism of formation of certain growth twins of the penetration type. *Neues Jahrb. Mineral. Monatsh.* pp. 518–525.
- Senechal, M. (1980). The genesis of growth twins. *Sov. Phys. Crystallogr.* **25**, 520–524.
- Shekhtman, V. Sh. (1993). Editor. *The real structure of high- T_c superconductors*, especially ch. 3, *Twins and structure of twin boundaries*, by I. M. Shmyt'ko & V. Sh. Shekhtman. Berlin: Springer.
- Shtukenberg, A. G., Punin, Yu. O., Haegeler, E. & Klapper, H. (2001). On the origin of inhomogeneity of anomalous birefringence in mixed crystals: an example of alums. *Phys. Chem. Miner.* **28**, 665–674.
- Shuvalov, L. A., Dudnik, E. F. & Wagin, S. V. (1985). Domain structure geometry of real ferroelastics. *Ferroelectrics*, **65**, 143–152.
- Smith, D. J., Bursill, L. A. & Wood, G. J. (1983). High resolution electron microscopy study of tin dioxide crystals. *J. Solid State Chem.* **50**, 51–69.
- Smith, J. V. (1968). The crystal structure of staurolite. *Am. Mineral.* **53**, 1139–1155.
- Sunagawa, I. & Tomura, S. (1976). Twinning in phlogopite. *Am. Mineral.* **61**, 939–943.
- Sutton, A. P. & Balluffi, R. W. (1995). *Interfaces in crystalline materials*, Section 1.5, pp. 25–41. Oxford: Clarendon Press.
- Sweegers, C., van Enkevort, W. J. P., Meekes, H., Bennema, P., Hiralal, I. D. K. & Rijkeboer, A. (1999). The impact of twinning on the morphology of $\gamma\text{-Al}(\text{OH})_3$ crystals. *J. Cryst. Growth*, **197**, 244–253.
- Takano, Y. (1972). Classification of twins IV. Ordinary twins. *J. Jpn. Assoc. Mineral. Petrogr. Econ. Geol.* **67**, 345–351.
- Takano, Y. & Sakurai, K. (1971). Classification of twins I. Bisecting twin axes and principal twin axes. *Mineral. J. (Jpn)*, **6**, 375–382.
- Takeda, H. & Donnay, J. D. H. (1965). Compound tessellations in crystal structures. *Acta Cryst.* **19**, 474–476.
- Takeuchi, Y. (1997). *Tropochemical cell-twinning*. Tokyo: Terra Scientific Publishing Company.
- Tamazyan, R., Arnold, H., Molchanov, V. N., Kuzmicheva, G. M. & Vasileva, I. G. (2000a). Contribution to the crystal chemistry of rare-earth chalcogenides. II. The crystal structure and twinning of rare-earth disulfide PrS_2 . *Z. Kristallogr.* **215**, 272–277.
- Tamazyan, R., Arnold, H., Molchanov, V. N., Kuzmicheva, G. M. & Vasileva, I. G. (2000b). Contribution to the crystal chemistry of rare-earth chalcogenides. III. The crystal structure and twinning of $\text{SmS}_{1.9}$. *Z. Kristallogr.* **215**, 346–351.
- Taylor, C. A. & Underwood, F. A. (1960). A twinning interpretation of 'superlattice' reflexions in X-ray photographs of synthetic klockmannite, CuSe . *Acta Cryst.* **13**, 361–362.
- Tertsch, H. (1936). Bemerkungen zur Frage der Verbreitung und zur Geometrie der Zwillingsbildungen. *Z. Kristallogr.* **94**, 461–490.
- Thomas, L. A. & Wooster, W. A. (1951). Piezocrescence - the growth of Dauphiné twinning in quartz under stress. *Proc. R. Soc. London Ser. A*, **208**, 43–62.
- Tohno, S. & Katsui, A. (1986). X-ray topographic study of twinning in InP crystals grown by the liquid-encapsulated Czochralski technique. *J. Cryst. Growth*, **74**, 362–374.
- Tsatskis, I. & Salje, E. K. H. (1996). Time evolution of pericline twin domains in alkali feldspars. A computer-simulation study. *Am. Mineral.* **81**, 800–810.
- Tschermak, G. (1884, 1905). *Lehrbuch der Mineralogie*, 1st ed. 1884, 6th ed. 1905. Wien: Alfred Hölder.
- Tschermak, G. (1904). Einheitliche Ableitung der Kristallisations- und Zwillingsgesetze. *Z. Kristallogr.* **39**, 433–462, especially 456–462.
- Tschermak, G. & Becke, F. (1915). *Lehrbuch der Mineralogie*, 7th edition, pp. 93–114. Wien: Alfred Hölder.
- Tsuchimori, M., Ishimasa, T. & Fukano, Y. (1992). Crystal structures of small Al-rich Fe alloy particles formed by a gas-evaporation technique. *Philos. Mag. B*, **66**, 89–108, especially Section 4.
- Van Bueren, H. G. (1961). *Imperfections in crystals*, especially chs. 13.4 and 19. Amsterdam: North-Holland.
- Van Tendeloo, G. & Amelinckx, S. (1974). Group-theoretical considerations concerning domain formation in ordered alloys. *Acta Cryst.* **A30**, 431–440.
- Wadhawan, V. K. (1997). A tensor classification of twinning in crystals. *Acta Cryst.* **A53**, 546–555.
- Wadhawan, V. K. (2000). *Introduction to ferroic materials*, ch. 7. Amsterdam: Gordon and Breach.
- Wallace, C. A. & White, E. A. D. (1967). The morphology and twinning of solution-grown corundum crystals. In *Crystal growth*, edited by H. S. Peiser (Supplement to *Phys. Chem. Solids*), pp. 431–435. Oxford: Pergamon.
- Weertman, J. & Weertman, J. R. (1964). *Elementary dislocation theory*, especially ch. 5. New York: MacMillan.
- Wenk, H.-R. (1976). Editor. *Electron microscopy in mineralogy*, especially ch. 2.3. Berlin: Springer.
- Wondratschek, H. & Jeitschko, W. (1976). Twin domains and antiphase domains. *Acta Cryst.* **A32**, 664–666.
- Zheludev, I. S. (1971). *Physics of crystalline dielectrics*, Vol. 1. *Crystallography and spontaneous polarization*. New York: Plenum Press.
- Zheludev, I. S. & Shuvalov, L. A. (1956). Seignettelectric phase transitions and crystal symmetry. *Kristallografiya*, **1**, 681–688. (In Russian.) (English translation: *Sov. Phys. Crystallogr.* **1**, 537–542.)
- Zikmund, Z. (1984). Symmetry of domain pairs and domain twins. *Czech. J. Phys. B*, **34**, 932–949.
- Zinserling, K. & Schubnikow, A. (1933). Über die Plastizität des Quarzes. *Z. Kristallogr.* **85**, 454–461.

3.4. Domain structures

BY V. JANOVEC AND J. PŘÍVRATSKÁ

3.4.1. Introduction

3.4.1.1. Basic concepts

It was demonstrated in Section 3.1.2 that a characteristic feature of structural phase transitions connected with a lowering of crystal symmetry is an anomalous behaviour near the transition, namely unusually large values of certain physical properties that vary strongly with temperature. In this chapter, we shall deal with another fundamental feature of structural phase transitions: the formation of a non-homogeneous, textured low-symmetry phase called a *domain structure*.

When a crystal homogeneous in the parent (prototypic) phase undergoes a phase transition into a ferroic phase with lower point-group symmetry, then this ferroic phase is almost always formed as a non-homogeneous structure consisting of homogeneous regions called *domains* and contact regions between domains called *domain walls*. All domains have the same or the enantiomorphous crystal structure of the ferroic phase, but this structure has in different domains a different orientation, and sometimes also a different position in space. When a domain structure is observed by a measuring instrument, different domains can exhibit different tensor properties, different diffraction patterns and can differ in other physical properties. The domain structure can be visualized optically (see Fig. 3.4.1.1) or by other experimental techniques. Powerful high-resolution electron microscopy (HREM) techniques have made it possible to visualize atomic arrangements in domain structures (see Fig. 3.4.1.2). The appearance of a domain structure, detected by any reliable technique, provides the simplest unambiguous experimental proof of a structural phase transition.

Under the influence of external fields (mechanical stress, electric or magnetic fields, or combinations thereof), the domain structure can change; usually some domains grow while others

decrease in size or eventually vanish. This process is called *domain switching*. After removing or decreasing the field a domain structure might not change considerably, *i.e.* the form of a domain pattern depends upon the field history: the domain structure exhibits *hysteresis* (see Fig. 3.4.1.3). In large enough fields, switching results in a reduction of the number of domains. Such a procedure is called *detwinning*. In rare cases, the crystal may consist of one domain only. Then we speak of a *single-domain crystal*.

There are two basic types of domain structures:

(i) Domain structures with one or several systems of parallel plane domain walls that can be observed in an optical or electron microscope. Two systems of perpendicular domain walls are often visible (see Fig. 3.4.1.4). In polarized light domains exhibit different colours (see Fig. 3.4.1.1) and in diffraction experiments splitting of reflections can be observed (see Fig. 3.4.3.9). Domains can be switched by external mechanical stress. These features are typical for a *ferroelastic domain structure* in which neighbouring domains differ in mechanical strain (deformation). Ferroelastic domain structures can appear only in ferroelastic phases, *i.e.* as a result of a phase transition characterized by a spontaneous shear distortion of the crystal.

(ii) Domain structures that are not visible using a polarized-light microscope and in whose diffraction patterns no splitting of reflections is observed. Special methods [*e.g.* etching, deposition of liquid crystals (see Fig. 3.4.1.5), electron or atomic force microscopy, or higher-rank optical effects (see Fig. 3.4.3.3)] are needed to visualize domains. Domains have the same strain and cannot usually be switched by an external mechanical stress. Such domain structures are called *non-ferroelastic domain structures*. They appear in all non-ferroelastic phases resulting from symmetry lowering that preserves the crystal family, and in partially ferroelastic phases.

Another important kind of domain structure is a *ferroelectric domain structure*, in which domains differ in the direction of the spontaneous polarization. Such a domain structure is formed at ferroelectric phase transitions that are characterized by the appearance of a new polar direction in the ferroic phase. Ferro-

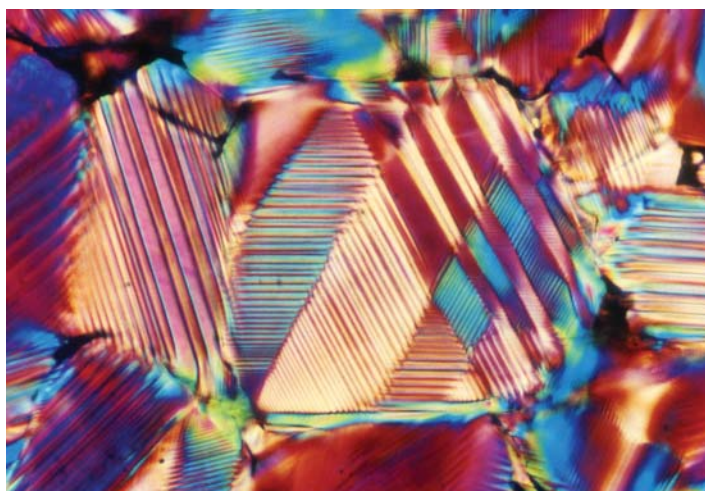


Fig. 3.4.1.1. Domain structure of tetragonal barium titanate (BaTiO_3). A thin section of barium titanate ceramic observed at room temperature in a polarized-light microscope (transmitted light, crossed polarizers). Courtesy of U. Töffner, Max-Planck-Institut für Metallforschung, Stuttgart. Different colours correspond to different ferroelastic domain states, connected areas of the same colour are ferroelastic domains and sharp boundaries between these areas are domain walls. Areas of continuously changing colour correspond to gradually changing thickness of wedge-shaped domains. An average distance between parallel ferroelastic domain walls is of the order of 1–10 μm .

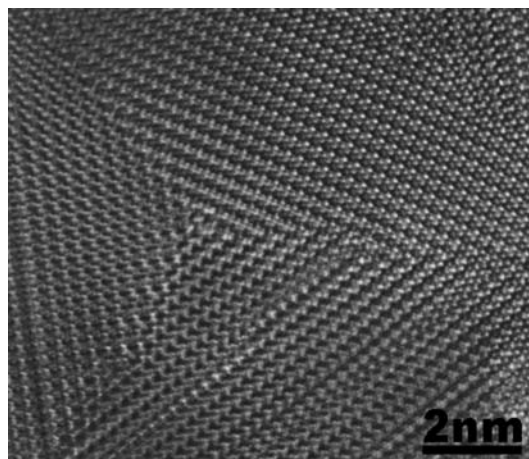


Fig. 3.4.1.2. Domain structure of a BaGa_2O_4 crystal seen by high-resolution transmission electron microscopy. Parallel rows are atomic layers. Different directions correspond to different ferroelastic domain states of domains, connected areas with parallel layers are different ferroelastic domains and boundaries between these areas are ferroelastic domain walls. Courtesy of H. Lemmens, EMAT, University of Antwerp.

3. PHASE TRANSITIONS, TWINNING AND DOMAIN STRUCTURES

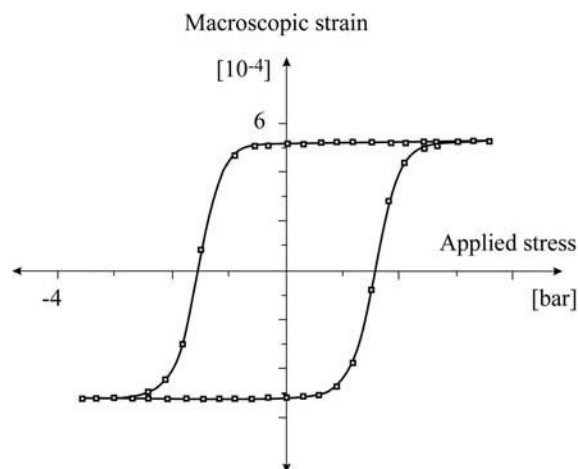


Fig. 3.4.1.3. Elastic hysteresis of ferroelastic lead phosphate $\text{Pb}_3(\text{PO}_4)_2$ (Salje, 1990). Courtesy of E. K. H. Salje, University of Cambridge. The dependence of strain on applied stress has the form of a loop. The states at the extreme left and right correspond to two ferroelastic domain states, steep parts of the loop represent switching of one state into the other by applied stress. The strain at zero stress corresponds to the last single-domain state formed in a field larger than the coercive stress defined by the stress at zero strain (the intersection of the loop with the axis of the applied stress). Similar dielectric hysteresis loops of polarization *versus* applied electric field are observed in ferroelectric phases (see *e.g.* Jona & Shirane, 1962).

electric domains can usually be switched by external electric fields. Two ferroelectric domains with different directions of spontaneous polarization can have different spontaneous strain [*e.g.* in dihydrogen phosphate (KDP) crystals, two ferroelectric domains with opposite directions of the spontaneous polarization have different spontaneous shear strain], or two ferroelectric domains with antiparallel spontaneous polarization can possess the same strain [*e.g.* in triglycine sulfate (TGS) crystals].

The physical properties of polydomain crystals are significantly influenced by their domain structure. The values of important material property tensor components, *e.g.* permittivity, piezoelectric and elastic constants, may be enhanced or diminished by the presence of a domain structure. Owing to switching and



Fig. 3.4.1.4. Transmission electron microscopy image of the ferroelastic domain structure in a $\text{YBa}_2\text{Cu}_3\text{O}_{7-y}$ crystal (Rosová, 1999). Courtesy of A. Rosová, Institute of Electrical Engineering, SAS, Bratislava. There are two systems ('complexes'), each of which is formed by almost parallel ferroelastic domain walls with needle-like tips. The domain walls in one complex are nearly perpendicular to the domain walls in the other complex.

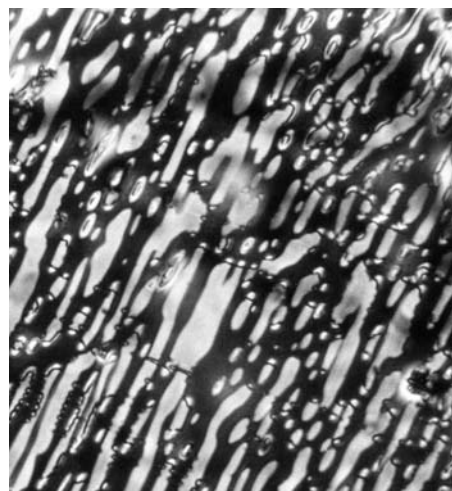


Fig. 3.4.1.5. Non-ferroelastic ferroelectric domains in triglycine sulfate (TGS) revealed by a liquid-crystal method. A thin layer of a nematic liquid crystal deposited on a crystal surface perpendicular to the spontaneous polarization is observed in a polarized-light microscope. Black and white areas correspond to ferroelectric domains with antiparallel spontaneous polarization. The typical size of the domains is of order of 1–10 μm . Courtesy of M. Połomska, Institute of Molecular Physics, PAN, Poznań. Although one preferential direction of domain walls prevails, the rounded shapes of the domains indicate that all orientations of non-ferroelastic walls are possible.

detwinning phenomena, polydomain materials exhibit hysteresis of material properties. These features have important practical implications, *e.g.* the production of anisotropic ceramic materials or ferroelectric memories.

The domain structure resulting from a structural phase transition belongs to a special type of twinning referred to as transformation twinning (see Section 3.3.7.2). Despite this, the current terminology used in domain-structure studies is different. The main terms were coined during the first investigations of ferroelectric materials, where striking similarities with the behaviour of ferromagnetic materials led researchers to introduce terms analogous to those used in studies of ferromagnetic domain structures that had been examined well at that time.

Bicrystallography (see Section 3.2.2) provides another possible frame for discussing domain structures. Bicrystallography and domain structure analysis have developed independently and almost simultaneously but different language has again precluded deeper confrontation. Nevertheless, there are common features in the methodology of both approaches, in particular, the principle of symmetry compensation (see Section 3.2.2), which plays a fundamental role in both theories.

In Chapter 3.1, it is shown that the anomalous behaviour near phase transitions can be explained in the framework of the Landau theory. In this theory, the formation of the domain structures follows from the existence of several equivalent solutions for the order parameter. This result is a direct consequence of a symmetry reduction at a ferroic phase transition. It is this dissymmetrization which is the genuine origin of the domain structure formation and which determines the basic static features of all domain structures.

3.4.1.2. Scope of this chapter

This chapter is devoted to the crystallographic aspects of static domain structures, especially to the symmetry analysis of these structures. The main aim is to explain basic concepts, derive relations that govern the formation of domain structures and provide tables with useful ready-to-use data on domain structures of ferroic phases. The exposition uses algebraic tools that are explained in Section 3.2.3, but the important points are illustrated with simple examples comprehensible even without mathematical details. The synoptic tables in Sections 3.4.2 and 3.4.3 present

3.4. DOMAIN STRUCTURES

the main results of the analysis for all possible ferroic domain structures. More detailed information on certain points can be found in the software *GI★KoBo-1*.

All these results are definite – their validity does not depend on any particular model or approximation – and form thus a firm basis for further more detailed quantitative treatments. ‘*For the most part, the only exact statements which can be made about a solid state system are those which arise as a direct consequence of symmetry alone.*’ (Knox & Gold, 1967.)

The exposition starts with domain states, continues with pairs of domain states and domain distinction, and terminates with domain twins and walls. This is also the sequence of steps in domain-structure analysis, which proceeds from the simplest to more complicated objects.

In Section 3.4.2, we explain the concept of *domain states* (also called variants or orientational states), define different types of domain states (principal, ferroelastic, ferroelectric, basic), find simple formulae for their number, and disclose their hierarchy and relation with symmetry lowering and with order parameters of the transition. Particular results for all possible ferroic phase transitions can be found in synoptic Table 3.4.2.7, which lists all possible crystallographically non-equivalent *point-group symmetry descents that may appear at a ferroic phase transition*. For each descent, all independent twinning groups (characterizing the relation between two domain states) are given together with the number of principal, ferroelastic and ferroelectric domain states and other data needed in further analysis.

Section 3.4.3 deals with *pairs of domain states* and with the relationship between two domain states in a pair. This relationship, in mineralogy called a ‘twin law’, determines the distinction between domain states, specifies switching processes between two domain states and forms a starting point for discussing domain walls and twins. We show different ways of expressing the relation between two domain states of a domain pair, derive a classification of domain pairs, find non-equivalent domain pairs and determine which tensor properties are different and which are the same in two domain states of a domain pair.

The presentation of non-equivalent domain pairs is divided into two parts. Synoptic Table 3.4.3.4 lists all representative *non-equivalent non-ferroelastic domain pairs*, and for each pair gives the twinning groups, and the number of tensor components that are different and that are the same in two domain states. These numbers are given for all important property tensors up to rank four. We also show how these data can be used to determine switching forces between two non-ferroelastic domain states.

Then we explain specific features of ferroelastic domain pairs: compatible (permissible) domain walls and disorientation of domain states in ferroelastic domain twins. A list of all non-equivalent ferroelastic domain pairs is presented in two tables. Synoptic Table 3.4.3.6 contains all *non-equivalent ferroelastic domain pairs with compatible (coherent) domain walls*. This table gives the orientation of compatible walls and their symmetry properties. Table 3.4.3.7 lists all *non-equivalent ferroelastic domain pairs with no compatible ferroelastic domain walls*.

Column K_{1j} in Table 3.4.2.7 specifies all representative non-equivalent domain pairs that can appear in each particular phase transition; in combination with Tables 3.4.3.4 and 3.4.3.6, it allows one to determine the main features of any ferroic domain structure.

Section 3.4.4 is devoted to domain twins and domain walls. We demonstrate that the symmetry of domain twins and domain walls is described by layer groups, give a classification of domain twins and walls based on their symmetry, and present possible layer groups of non-ferroelastic and ferroelastic domain twins and walls. Then we discuss the properties of finite-thickness domain walls. In an example, we illustrate the symmetry analysis of microscopic domain walls and present conclusions that can be drawn from this analysis about the microscopic structure of domain walls.

The exposition is given in the continuum description with crystallographic point groups and property tensors. In this approach, all possible cases are often treatable and where possible are covered in synoptic tables or – in a more detailed form – in the software *GI★KoBo-1*. Although the group-theoretical tools are almost readily transferable to the microscopic description (using the space groups and atomic positions), the treatment of an inexhaustible variety of microscopic situations can only be illustrated by particular examples.

Our attempt to work with well defined notions calls for introducing several new, and generalizing some accepted, concepts. Also an extended notation for the symmetry operations and groups has turned out to be indispensable. Since there is no generally accepted terminology on domain structures yet, we often have to choose a term from several existing more-or-less equivalent variants.

The specialized scope of this chapter does not cover several important aspects of domain structures. More information can be found in the following references. There are only two monographs on domain structures (both in Russian): Fesenko *et al.* (1990) and Sidorkin (2002). The main concepts of domain structures of ferroic materials are explained in the book by Wadhawan (2000) and in a review by Schranz (1995). Ferroelastic domain structures are reviewed in Boulesteix (1984) and Wadhawan (1991), and are treated in detail by Salje (1990, 1991, 2000a,b). Different aspects of ferroelectric domain structures are covered in books or reviews on ferroelectric crystals: Känzig (1957), Jona & Shirane (1962), Fatuzzo & Merz (1967), Mitsui *et al.* (1976), Lines & Glass (1977), Smolenskii *et al.* (1984), Zheludev (1988) and Strukov & Levanyuk (1998). Applications of ferroelectrics are described in the books by Xu (1991) and Uchino (2000). Principles and technical aspects of ferroelectric memories are reviewed by Scott (1998, 2000).

3.4.2. Domain states

3.4.2.1. Principal and basic domain states

As for all crystalline materials, domain structures can be approached in two ways: In the *microscopic description*, a crystal is treated as a regular arrangement of atoms. Domains differ in tiny differences of atomic positions which can be determined only indirectly, *e.g.* by diffraction techniques. In what follows, we shall pay main attention to the *continuum description*, in which a crystal is treated as an anisotropic continuum. Then the crystal properties are described by property tensors (see Section 1.1.1) and the crystal symmetry is expressed by crystallographic point groups. In this approach, domains exhibit different tensor properties that enable one to visualize domains by optical or other methods.

The domain structure observed in a microscope appears to be a patchwork of homogeneous regions – domains – that have various colours and shapes (see Fig. 3.4.1.1). Indeed, the usual description considers a domain structure as a collection of domains and contact regions of domains called domain walls. Strictly speaking, by a *domain* \mathbf{D}_i one understands a connected part of the crystal, called the *domain region*, which is filled with a homogeneous low-symmetry crystal structure. *Domain walls* can be associated with the boundaries of domain regions. The interior homogeneous bulk structure within a domain region will be called a *domain state*. Equivalent terms are *variant* or *structural variant* (Van Tendeloo & Amelinckx, 1974). We shall use different adjectives to specify domain states. In the microscopic description, domain states associated with the primary order parameter will be referred to as *primary (microscopic, basic) domain states*. In the macroscopic description, the primary domain states will be called *principal domain states*, which correspond to Aizu’s *orientation states*. (An exact definition of principal domain states is given below.)

3. PHASE TRANSITIONS, TWINNING AND DOMAIN STRUCTURES

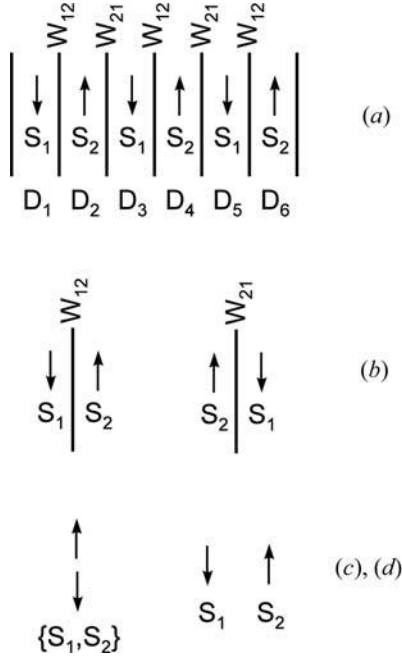


Fig. 3.4.2.1. Hierarchy in domain-structure analysis. (a) Domain structure consisting of domains D_1, D_2, \dots, D_6 and domain walls W_{12} and W_{21} ; (b) domain twin and reversed twin (with reversed order of domain states); (c) domain pair consisting of two domain states S_1 and S_2 ; (d) domain states S_1 and S_2 .

Further useful division of domain states is possible (though not generally accepted): Domain states that are specified by a constant value of the spontaneous strain are called *ferroelastic domain states*; similarly, *ferroelectric domain states* exhibit constant spontaneous polarization *etc.* Domain states that differ in some tensor properties are called *ferroic* or *tensorial domain states etc.* If no specification is given, the statements will apply to any of these domain states.

A domain D_i is specified by a domain state S_j and by domain region B_k : $D_i = D_i(S_j, B_k)$. Different domains may possess the same domain state but always differ in the domain region that specifies their shape and position in space.

The term ‘domain’ has also often been used for a domain state. Clear distinction of these two notions is essential in further considerations and is illustrated in Fig. 3.4.2.1. A ferroelectric domain structure (Fig. 3.4.2.1a) consists of six ferroelectric domains D_1, D_2, \dots, D_6 but contains only two domain states S_1, S_2 characterized by opposite directions of the spontaneous polarization depicted in Fig. 3.4.2.1(d). Neighbouring domains have different domain states but non-neighbouring domains may possess the same domain state. Thus domains with odd serial number have the domain state S_1 (spontaneous polarization ‘down’), whereas domains with even number have domain state S_2 (spontaneous polarization ‘up’).

A great diversity of observed domain structures are connected mainly with various dimensions and shapes of domain regions, whose shapes depend sensitively on many factors (kinetics of the phase transition, local stresses, defects *etc.*). It is, therefore, usually very difficult to interpret in detail a particular observed domain pattern. Domain states of domains are, on the other hand, governed by simple laws, as we shall now demonstrate.

We shall consider a ferroic phase transition with a symmetry lowering from a parent (prototypic, high-symmetry) phase with symmetry described by a point group G to a ferroic phase with the point-group symmetry F_1 , which is a subgroup of G . We shall denote this dissymmetrization by a group-subgroup symbol $G \supset F_1$ (or $G \Downarrow F_1$ in Section 3.1.3) and call it a *symmetry descent* or *dissymmetrization*. Aizu (1970a) calls these symmetry descents *species* and uses the letter F instead of the symbol \subset .

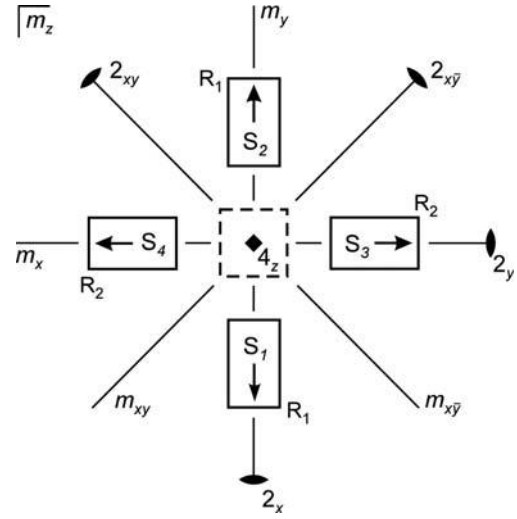


Fig. 3.4.2.2. Exploded view of single-domain states S_1, S_2, S_3 and S_4 (solid rectangles with arrows of spontaneous polarization) formed at a phase transition from a parent phase with symmetry $G = 4_z/m_z m_x m_{xy}$ to a ferroic phase with symmetry $F_1 = 2_x m_y m_z$. The parent phase is represented by a dashed square in the centre with the symmetry elements of the parent group $G = 4_z/m_z m_x m_{xy}$ shown.

As an illustrative example, we choose a phase transition with parent symmetry $G = 4_z/m_z m_x m_{xy}$ and ferroic symmetry $F_1 = 2_x m_y m_z$ (see Fig. 3.4.2.2). Strontium bismuth tantalate (SBT) crystals, for instance, exhibit a phase transition with this symmetry descent (Chen *et al.*, 2000). Symmetry elements in the symbols of G and F_1 are supplied with subscripts specifying the orientation of the symmetry elements with respect to the reference coordinate system. The necessity of this extended notation is exemplified by the fact that the group $G = 4_z/m_z m_x m_{xy}$ has six subgroups with the same ‘non-oriented’ symbol $mm2$: $m_x m_y 2_z$, $2_x m_y m_z$, $m_x 2_y m_z$, $m_{xy} m_{yz} 2_z$, $2_{xy} m_{xy} m_z$, $m_{yz} 2_{xy} m_z$. Lower indices thus specify these subgroups unequivocally and the example illustrates an important rule of domain-structure analysis: *All symmetry operations, groups and tensor components must be related to a common reference coordinate system and their orientation in space must be clearly specified.*

The physical properties of crystals in the continuum description are expressed by property tensors. As explained in Section 1.1.4, the crystal symmetry reduces the number of independent components of these tensors. Consequently, for each property tensor the number of independent components in the low-symmetry ferroic phase is the same or higher than in the high-symmetry parent phase. Those tensor components or their linear combinations that are zero in the high-symmetry phase and nonzero in the low-symmetry phase are called *morphic tensor components* or *tensor parameters* and the quantities that appear only in the low-symmetry phase are called *spontaneous quantities* (see Section 3.1.3.2). The morphic tensor components and spontaneous quantities thus reveal the difference between the high- and low-symmetry phases. In our example, the symmetry $F_1 = 2_x m_y m_z$ allows a nonzero spontaneous polarization $P_0^{(f)} = (P, 0, 0)$, which must be zero in the high-symmetry phase with $G = 4_z/m_z m_x m_{xy}$.

We shall now demonstrate in our example that the symmetry lowering at the phase transition leads to the existence of several equivalent variants (domain states) of the low-symmetry phase. In Fig. 3.4.2.2, the parent high-symmetry phase is represented in the middle by a dashed square that is a projection of a square prism with symmetry $4_z/m_z m_x m_{xy}$. A possible variant of the low-symmetry phase can be represented by an oblong prism with a vector representing the spontaneous polarization. In Fig. 3.4.2.2, the projection of this oblong prism is drawn as a rectangle which is shifted out of the centre for better recognition. We denote by S_1 a homogeneous low-symmetry phase with spontaneous polar-

3.4. DOMAIN STRUCTURES

ization $P_0^{(1)} = (P, 0, 0)$ and with symmetry $F_1 = 2_x m_y m_z$. Let us, mentally, increase the temperature to above the transition temperature and then apply to the high-symmetry phase an operation 2_z , which is a symmetry operation of this high-symmetry phase but not of the low-symmetry phase. Then decrease the temperature to below the transition temperature. The appearance of another variant of the low-symmetry phase S_2 with spontaneous polarization $P_0^{(2)} = (-P, 0, 0)$ obviously has the same probability of appearing as had the variant S_1 . Thus the two variants of the low-symmetry phase S_1 and S_2 can appear with the same probability if they are related by a symmetry operation suppressed (lost) at the transition, *i.e.* an operation that was a symmetry operation of the high-symmetry phase but is not a symmetry operation of the low-symmetry phase S_1 . In the same way, the lost symmetry operations 4_z and 4_z^3 generate from S_1 two other variants, S_3 and S_4 , with spontaneous polarizations $(0, P, 0)$ and $(0, -P, 0)$, respectively. Variants of the low-symmetry phase that are related by an operation of the high-symmetry group G are called *crystallographically equivalent (in G) variants*. Thus we conclude that *crystallographically equivalent (in G) variants of the low-symmetry phase have the same chance of appearing*.

We shall now make similar considerations for a general ferroic phase transition with a symmetry descent $G \supset F_1$. By the *state S of a crystal* we shall understand, in the continuum description, the set of all its properties expressed by property (matter) tensors in the reference Cartesian crystallophysical coordinate system of the parent phase (see Example 3.2.3.9 in Section 3.2.3.3.1). A state defined in this way may change not only with temperature and external fields but also with the orientation of the crystal in space.

We denote by S_1 a state of a homogeneous ferroic phase. If we apply to S_1 a symmetry operation g_i of the group G , then the ferroic phase in a new orientation will have the state S_j , which may be identical with S_1 or different. Using the concept of group action (explained in detail in Section 3.2.3.3.1) we express this operation by a simple relation:

$$g_j S_1 = S_j, \quad g_j \in G. \quad (3.4.2.1)$$

Let us first turn our attention to operations $f_j \in G$ that do not change the state S_1 :

$$f_j S_1 = S_1, \quad f_j \in G. \quad (3.4.2.2)$$

The set of all operations of G that leave S_1 invariant form a group called a *stabilizer* (or *isotropy group*) of a state S_1 in the group G . This stabilizer, denoted by $I_G(S_1)$, can be expressed explicitly in the following way:

$$I_G(S_1) \equiv \{g \in G | g S_1 = S_1\}, \quad (3.4.2.3)$$

where the right-hand part of the equation should be read as ‘a set of all operations of G that do not change the state S_1 ’ (see Section 3.2.3.3.2).

Here we have to explain the difference between the concept of a stabilizer of an object and the symmetry of that object. By the *symmetry group F of an object* one understands the set of all operations (isometries) that leave this object S invariant. The symmetry group F of an object is considered to be an inherent property that does not depend on the orientation and position of the object in space. (The term *eigensymmetry* is used in Chapter 3.3 for symmetry groups defined in this way.) In this case, the symmetry elements of F are ‘attached’ to the object.

A stabilizer describes the symmetry properties of an object in another way, in which the object and the group of isometries are decoupled. One is given a group G , the symmetry elements of which have a defined orientation in a fixed reference system. The object can have any orientation in this reference system. Those operations of G that map the object in a given orientation onto itself form the *stabilizer $I_G(S_1)$ of S_1 in the group G* . In this case,

the stabilizer depends on the orientation of the object in space and is expressed by an ‘oriented’ group symbol F_1 with subscripts defining the orientation of the symmetry elements of F_1 . Only for certain ‘prominent’ orientations will the stabilizer acquire a symmetry group of the same crystal class (crystallographic point group) as the *eigensymmetry* of the object.

We shall define a *single-domain orientation* as a prominent orientation of the crystal in which the stabilizer $I_G(S_1)$ of its state S_1 is equal to the symmetry group F_1 which is, after removing subscripts specifying the orientation, identical with the *eigensymmetry* of the ferroic phase:

$$I_G(S_1) = F_1. \quad (3.4.2.4)$$

This equation thus declares that the crystal in the state S_1 has a prominent single-domain orientation.

The concept of the stabilizer allows us to identify the ‘*eigensymmetry*’ of a domain state (or an object in general) S_i with the crystallographic class (non-oriented point group) of the stabilizer of this state in the group of all rotations $O(3)$, $I_{O(3)}(S_i)$.

Since we shall further deal mainly with states of the ferroic phase in single-domain orientations, we shall use the term ‘state’ for a ‘state of the crystal in a single-domain orientation’, unless mentioned otherwise. Then the stabilizer $I_G(S_1)$ will often be replaced by the group F_1 , although all statements have been derived and hold for stabilizers.

The difference between symmetry groups of a crystal and stabilizers will become more obvious in the treatment of secondary domain states in Section 3.4.2.2 and in discussing disoriented ferroelastic domain states (see Section 3.4.3.6.3).

As we have seen in our illustrative example, the suppressed operations generate from the first state S_1 other states. Let g_j be such a *suppressed operation*, *i.e.* $g_j \in G$ but $g_j \notin F_1$. Since all operations that retain S_1 are collected in F_1 , the operation g_j must transform S_1 into another state S_j ,

$$g_j S_1 = S_j \neq S_1, \quad g_j \in G, \quad g_j \notin F_1, \quad (3.4.2.5)$$

and we say that the state S_j is *crystallographically equivalent (in G) with the state S_1* , $S_j \stackrel{G}{\sim} S_1$.

We define *principal domain states* as crystallographically equivalent (in G) variants of the low-symmetry phase in single-domain orientations that can appear with the same probability in the ferroic phase. They represent possible macroscopic bulk structures of (1) ferroic single-domain crystals, (2) ferroic domains in non-ferroelastic domain structures (see Section 3.4.3.5), or (3) ferroic domains in any ferroic domain structure, if all spontaneous strains are suppressed [this is the so-called parent clamping approximation (PCA), see Section 3.4.2.5]. In what follows, *any statement formulated for principal domain states or for single-domain states applies to any of these three situations*. Principal domain states are identical with *orientation states* (Aizu, 1969) or *orientation variants* (Van Tendeloo & Amelinckx, 1974). The adjective ‘principal’ distinguishes these domain states from primary (microscopic, basic – see Section 3.4.2.5) domain states and secondary domain states, defined in Section 3.4.2.2, and implies that any two of these domain states differ in principal tensor parameters (these are linear combinations of morphic tensor components that transform as the primary order parameter of an equitranslational phase transition with a point-group symmetry descent $G \supset F_1$, see Sections 3.1.3.2 and 3.4.2.3). A simple criterion for a principal domain state S_1 is that its stabilizer in G is equal to the symmetry F_1 of the ferroic phase [see equation (3.4.2.4)].

When one applies to a principal domain state S_1 all operations of the group G , one gets all principal domain states that are crystallographically equivalent with S_1 . The set of all these states is denoted GS_1 and is called an *G -orbit of S_1* (see also Section 3.2.3.3.3),

3. PHASE TRANSITIONS, TWINNING AND DOMAIN STRUCTURES

$$GS_1 = \{S_1, S_2, \dots, S_n\}. \quad (3.4.2.6)$$

$$n = [G : F_1] = |G| : |F_1|, \quad (3.4.2.11)$$

In our example, the G -orbit is $4_z/m_z m_x m_{xy} S_1 = \{S_1, S_2, S_3, S_4\}$.

Note that any operation g from the parent group G leaves the orbit GS_1 invariant since its action results only in a permutation of all principal domain states. This change does not alter the orbit, since the orbit is a set in which the sequence (order) of objects is irrelevant. Therefore, the orbit GS_1 is invariant under the action of the parent group G , $GG S_1 = GS_1$.

A ferroic phase transition is thus a paradigmatic example of the law of symmetry compensation (see Section 3.2.2): The dissymmetrization of a high-symmetry parent phase into a low-symmetry ferroic phase produces variants of the low-symmetry ferroic phase (single-domain states). Any two single-domain states are related by some suppressed operations of the parent symmetry that are missing in the ferroic symmetry and the set of all single-domain states (G -orbit of domain states) recovers the symmetry of the parent phase. If the domain structure contains all domain states with equal partial volumes then the average symmetry of this polydomain structure is, in the first approximation, identical to the symmetry of the parent phase.

Now we find a simple formula for the number n of principal domain states in the orbit GS_1 and a recipe for an efficient generation of all principal domain states in this orbit.

The fact that all operations of the group $I_G(S_1) = F_1$ leave S_1 invariant can be expressed in an abbreviated form in the following way [see equation (3.2.3.70)]:

$$F_1 S_1 = S_1. \quad (3.4.2.7)$$

We shall use this relation to derive all operations that transform S_1 into $S_j = g_j S_1$:

$$g_j S_1 = g_j (F_1 S_1) = (g_j F_1) S_1 = S_j, \quad g_j \in G. \quad (3.4.2.8)$$

The second part of equation (3.4.2.8) shows that all lost operations that transform S_1 into S_j are contained in the left coset $g_j F_1$ (for left cosets see Section 3.2.3.2.3).

It is shown in group theory that two left cosets have no operation in common. Therefore, another left coset $g_k F_1$ generates another principal domain state S_k that is different from principal domain states S_1 and S_j . Equation (3.4.2.8) defines, therefore, a one-to-one relation between principal domain states of the orbit GS_1 and left cosets of F_1 [see equation (3.2.3.69)],

$$S_j \leftrightarrow g_j F_1, \quad F_1 = I_G(S_1), \quad j = 1, 2, \dots, n. \quad (3.4.2.9)$$

From this relation follow two conclusions:

(1) The number n of principal domain states equals the number of left cosets of F_1 . All different left cosets of F_1 constitute the decomposition of the group G into left cosets of F_1 [see equation (3.2.3.19)],

$$G = g_1 F_1 \cup g_2 F_1 \cup \dots \cup g_j F_1 \cup \dots \cup g_n F_1, \quad (3.4.2.10)$$

where the symbol \cup is a union of sets and the number n of left cosets is called the *index of G in F_1* and is denoted by the symbol $[G : F_1]$. Usually, one chooses for g_1 the identity operation e ; then the first left coset equals F_1 . Since each left coset contains $|F_1|$ operations, where $|F_1|$ is number of operations of F_1 (order of F_1), the number of left cosets in the decomposition (3.4.2.10) is

where $|G|, |F_1|$ are orders of the point groups G, F_1 , respectively. The index n is a quantitative measure of the degree of dissymmetrization $G \supset F_1$. Thus the number of principal domain states in orbit GS_1 is equal to the index of F_1 in G , i.e. to the number of operations of the high-symmetry group G divided by the number of operations of the low-symmetry phase F_1 . In our illustrative example we get $n = |4_z/m_z m_x m_{xy}| : |2_x m_y m_z| = 16 : 4 = 4$.

The basic formula (3.4.2.11) expresses a remarkable result: the number n of principal domain states is determined by how many times the number of symmetry operations increases at the transition from the low-symmetry group F_1 to the high-symmetry group G , or, the other way around, the fraction $\frac{1}{n}$ is a quantitative measure of the symmetry decrease from G to F_1 , $|F_1| = \frac{1}{n} |G|$. Thus it is not the concrete structural change, nor even the particular symmetries of both phases, but only the extent of dissymmetrization that determines the number of principal domain states. This conclusion illustrates the fundamental role of symmetry in domain structures.

(2) Relation (3.4.2.9) yields a recipe for calculating all principal domain states of the orbit GS_1 : One applies successively to the first principal domain states S_1 the representatives of all left cosets of F_1 :

$$GS_1 = \{S_1, g_2 S_1, \dots, g_j S_1, \dots, g_n S_1\}, \quad (3.4.2.12)$$

where the operations $g_1 = e, g_2, \dots, g_j, \dots, g_n$ are the representatives of left cosets in the decomposition (3.4.2.10) and e is an identity operation. We add that any operation of a left coset can be chosen as its representative, hence the operation g_j can be chosen arbitrarily from the left coset $g_j F_1, j = 1, 2, \dots, n$.

This result can be illustrated in our example. Table 3.4.2.1 presents in the first column the four left cosets $g_j \{2_x m_y m_z\}$ of the group $F_1 = 2_x m_y m_z$. The corresponding principal domain states $S_j, j = 1, 2, 3, 4$, and the values of spontaneous polarization in these principal domain states are given in the second and the third columns, respectively. It is easy to verify in Fig. 3.4.2.2 that all operations of each left coset transform the first principal domain state S_1 into one principal domain state $S_j, j = 2, 3, 4$.

The left coset decompositions of all crystallographic point groups and their subgroup symmetry are available in the software *GI★KoBo-1*, path: *Subgroups\View\Twinning Group*.

Let us turn briefly to the symmetries of the principal domain states. From Fig. 3.4.2.2 we deduce that two domain states S_1 and S_2 in our illustrative example have the same symmetry, $F_1 = F_2 = 2_x m_y m_z$, whereas two others S_3 and S_4 have another symmetry, $F_3 = F_4 = m_x 2_y m_z$. We see that symmetry does not specify the principal domain state in a unique way, although a principal domain state S_j has a unique symmetry $F_i = I_G(S_j)$.

It turns out that if g_j transforms S_1 into S_j , then the symmetry group F_j of S_j is conjugate by g_j to the symmetry group F_1 of S_1 [see Section 3.2.3.3, Proposition 3.2.3.13 and equation (3.2.3.55)]:

$$\text{if } S_j = g_j S_1, \text{ then } F_j = g_j F_1 g_j^{-1}. \quad (3.4.2.13)$$

One can easily check that in our example each operation of the second left coset of $F_1 = 2_x m_y m_z$ (second row in Table 3.4.2.1) transforms $F_1 = 2_x m_y m_z$ into itself, whereas operations from the

Table 3.4.2.1. Left and double cosets, principal and secondary domain states and their tensor parameters for the phase transition with $G = 4_z/m_z m_x m_{xy}$ and $F_1 = 2_x m_y m_z$

| Left cosets $g_j S_1$ | | | | Principal domain states | | | Secondary domain states | | |
|-----------------------|---------|---------------|----------|-------------------------|--------|-----------|-------------------------|-------------|-------------------|
| 1 | 2_x | m_y | m_z | S_1 | (P00) | (000g00) | R_1 | $u_1 - u_2$ | $Q_{11} - Q_{22}$ |
| $\bar{1}$ | m_x | 2_y | 2_z | S_2 | (-P00) | (000-g00) | | | |
| 2_{xy} | 4_z | $\bar{4}_z^3$ | m_{xy} | S_3 | (0P0) | (0000-g0) | R_2 | $u_2 - u_1$ | $Q_{22} - Q_{11}$ |
| $2_{\bar{xy}}$ | 4_z^3 | $\bar{4}_z$ | m_{xy} | S_4 | (0-P0) | (0000g0) | | | |

3.4. DOMAIN STRUCTURES

third and fourth left cosets yield $F_3 = F_4 = m_x 2_y m_z$. We shall return to this issue again at the end of Section 3.4.2.2.3.

3.4.2.2. Secondary domain states, partition of domain states

In this section we demonstrate that any morphic (spontaneous) property appears in the low-symmetry phase in several equivalent variants and find what determines their number and basic properties.

As we saw in Fig. 3.4.2.2, the spontaneous polarization – a principal tensor parameter of the $4_z/m_z m_x m_{xy} \supset 2_x m_y m_z$ phase transition – can appear in four different directions that define four principal domain states. Another morphic property is a spontaneous strain describing the change of unit-cell shape; it is depicted in Fig. 3.4.2.2 as a transformation of a square into a rectangle. This change can be expressed by a difference between two strain components $u_{11} - u_{22} = \lambda^{(1)}$, which is a morphic tensor parameter since it is zero in the parent phase and nonzero in the ferroic phase. The quantity $\lambda^{(1)} = u_{11} - u_{22}$ is a secondary order parameter of the transition $4_z/m_z m_x m_{xy} \supset 2_x m_y m_z$ (for secondary order parameters see Section 3.1.3.2).

From Fig. 3.4.2.2, we see that two domain states \mathbf{S}_1 and \mathbf{S}_2 have the same spontaneous strain, whereas \mathbf{S}_3 and \mathbf{S}_4 exhibit another spontaneous strain $\lambda^{(2)} = u_{22} - u_{11} = -\lambda^{(1)}$. Thus we can infer that a property ‘to have the same value of spontaneous strain’ divides the four principal domain states $\mathbf{S}_1, \mathbf{S}_2, \mathbf{S}_3$ and \mathbf{S}_4 into two classes: \mathbf{S}_1 and \mathbf{S}_2 with the same spontaneous strain $\lambda^{(1)}$ and \mathbf{S}_3 and \mathbf{S}_4 with the same spontaneous strain $\lambda^{(2)} = -\lambda^{(1)}$. Spontaneous strain appears in two ‘variants’: $\lambda^{(1)}$ and $\lambda^{(2)} = -\lambda^{(1)}$.

We can define a *ferroelastic domain state* as a state of the crystal with a certain value of spontaneous strain λ , irrespective of the value of the principal order parameter. Values $\lambda = \lambda^{(1)}$ and $\lambda^{(2)} = -\lambda^{(1)}$ thus specify two ferroelastic domain states \mathbf{R}_1 and \mathbf{R}_2 , respectively. The spontaneous strain in this example is a secondary order parameter and the ferroelastic domain states can therefore be called *secondary domain states*.

An algebraic version of the above consideration can be deduced from Table 3.4.2.1, where to each principal domain state (given in the second column) there corresponds a left coset of $F_1 = 2_x m_y m_z$ (presented in the first column). Thus to the partition of principal domain states into two subsets

$$\{\mathbf{S}_1, \mathbf{S}_2, \mathbf{S}_3, \mathbf{S}_4\} = \{\mathbf{S}_1, \mathbf{S}_2\}_{\lambda^{(1)}} \cup \{\mathbf{S}_3, \mathbf{S}_4\}_{\lambda^{(2)}}, \quad (3.4.2.14)$$

there corresponds, according to relation (3.4.2.9), a partition of left cosets

$$\begin{aligned} 4_z/m_z m_x m_{xy} \\ = \{ \{2_x m_y m_z\} \cup \bar{1}\{2_x m_y m_z\} \} \cup \{2_{xy}\{2_x m_y m_z\} \cup 2_{xy}\{2_x m_y m_z\} \} \\ = m_x m_y m_z \cup 2_{xy}\{m_x m_y m_z\}, \end{aligned} \quad (3.4.2.15)$$

where we use the fact that the union of the first two left cosets of $2_x m_y m_z$ is equal to the group $m_x m_y m_z$. This group is the stabilizer of the first ferroelastic domain state \mathbf{R}_1 , $I_G(\mathbf{R}_1) = m_x m_y m_z$. Two left cosets of $m_x m_y m_z$ correspond to two ferroelastic domain states, \mathbf{R}_1 and \mathbf{R}_2 , respectively. Therefore, the number n_a of ferroelastic domain states is equal to the number of left cosets of $m_x m_y m_z$ in $4_z/m_z m_x m_{xy}$, i.e. to the index of $m_x m_y m_z$ in $4_z/m_z m_x m_{xy}$, $n_a = [4_z/m_z m_x m_{xy} : m_x m_y m_z] = |4_z/m_z m_x m_{xy}| : |m_x m_y m_z| = 16 : 8 = 2$, and the number d_a of principal domain states in one ferroelastic domain state is equal to the index of $2_x m_y m_z$ in $m_x m_y m_z$, i.e. $d_a = [m_x m_y m_z : 2_x m_y m_z] = |m_x m_y m_z| : |2_x m_y m_z| = 8 : 4 = 2$.

A generalization of these considerations, performed in Section 3.2.3.3.5 (see especially Proposition 3.2.3.30 and Examples 3.2.3.10 and 3.2.3.33), yields the following main results.

Assume that $\lambda^{(1)}$ is a secondary order parameter of a transition with symmetry descent $G \supset F_1$. Then the stabilizer L_1 of this parameter $I_G(\lambda^{(1)}) \equiv L_1$ is an intermediate group,

$$F_1 \subseteq I_G(\lambda^{(1)}) \equiv L_1 \subseteq G. \quad (3.4.2.16)$$

Lattices of subgroups in Figs. 3.1.3.1 and 3.1.3.2 are helpful in checking this condition.

The set of n principal domain states (the orbit $G\mathbf{S}_1$) splits into n_λ subsets

$$n_\lambda = [G : L_1] = |G| : |L_1|. \quad (3.4.2.17)$$

Each of these subsets consists of d_λ principal domain states,

$$d_\lambda = [L_1 : F_1] = |L_1| : |F_1|. \quad (3.4.2.18)$$

The number d_λ is called a *degeneracy of secondary domain states*.

The product of numbers n_λ and d_λ is equal to the number n of principal domain states [see equation (3.2.3.26)]:

$$n_\lambda d_\lambda = n. \quad (3.4.2.19)$$

Principal domain states from each subset have the same value of the secondary order parameter $\lambda^{(j)}$, $j = 1, 2, \dots, n_\lambda$ and any two principal domain states from different subsets have different values of $\lambda^{(j)}$. A state of the crystal with a given value of the secondary order parameter $\lambda^{(j)}$ will be called a *secondary domain state* \mathbf{R}_j , $j = 1, 2, \dots, n_\lambda$. Equivalent terms are *degenerate* or *compound domain state*.

In a limiting case $L_1 = F_1$, the parameter $\lambda^{(1)}$ is identical with the principal tensor parameter and there is no degeneracy, $d_\lambda = 1$.

Secondary domain states $\mathbf{R}_1, \mathbf{R}_2, \dots, \mathbf{R}_j, \dots, \mathbf{R}_{n_\lambda}$ are in a one-to-one correspondence with left cosets of L_1 in the decomposition

$$G = h_1 L_1 \cup h_2 L_1 \cup \dots \cup h_j L_1 \cup \dots \cup h_{n_\lambda} L_1, \quad (3.4.2.20)$$

therefore

$$\mathbf{R}_j = h_j \mathbf{R}_1, \quad j = 1, 2, \dots, n_\lambda. \quad (3.4.2.21)$$

Principal domain states of the first secondary domain state \mathbf{R}_1 can be determined from the first principal domain state \mathbf{S}_1 :

$$\mathbf{S}_k = p_k \mathbf{S}_1, \quad k = 1, 2, \dots, d_\lambda, \quad (3.4.2.22)$$

where p_k is the representative of the k th left coset of F_1 of the decomposition

$$L_1 = p_1 F_1 \cup p_2 F_1 \cup \dots \cup p_k F_1 \cup \dots \cup p_{d_\lambda} F_1. \quad (3.4.2.23)$$

The partition of principal domain states according to a secondary order parameter offers a convenient labelling of principal domain states by two indices j, k , where the first index j denotes the sequential number of the secondary domain state and the second index k gives the sequential number of the principal domain state within the j th secondary domain state [see equation (3.2.3.79)]:

$$\mathbf{S}_{jk} = h_j p_k \mathbf{S}_{11}, \quad \mathbf{S}_{11} = \mathbf{S}_1, \quad j = 1, 2, \dots, n_\lambda, \quad k = 1, 2, \dots, d_\lambda, \quad (3.4.2.24)$$

where h_j and p_k are representatives of the decompositions (3.4.2.20) and (3.4.2.23), respectively.

The secondary order parameter λ can be identified with a principal order parameter of a phase transition with symmetry descent $G \subset L_1$ (see Section 3.4.2.3). The concept of secondary domain states enables one to define domain states that are characterized by a certain spontaneous property. We present the three most significant cases of such ferroic domain states.

3.4.2.2.1. Ferroelastic domain state

The distinction ferroelastic–non-ferroelastic is a basic division in domain structures. *Ferroelastic transitions* are ferroic transi-

3. PHASE TRANSITIONS, TWINNING AND DOMAIN STRUCTURES

tions involving a spontaneous distortion of the crystal lattice that entails a change of shape of the crystallographic or conventional unit cell (Wadhawan, 2000). Such a transformation is accompanied by a change in the number of independent nonzero components of a symmetric second-rank tensor u that describes spontaneous strain.

In discussing ferroelastic and non-ferroelastic domain structures, the concepts of crystal family and holohedry of a point group are useful (IT A, 2002). Crystallographic point groups (and space groups as well) can be divided into seven crystal systems and six *crystal families* (see Table 3.4.2.2). A symmetry descent within a crystal family does not entail a qualitative change of the spontaneous strain – the number of independent nonzero tensor components of the strain tensor u remains unchanged.

We shall denote the crystal family of a group M by the symbol $\text{Fam}M$. Then a simple criterion for a ferroic phase transition with symmetry descent $G \subset F$ to be a *non-ferroelastic phase transition* is

$$F \subset G, \quad \text{Fam}F = \text{Fam}G. \quad (3.4.2.25)$$

A necessary and sufficient condition for a *ferroelastic phase transition* is

$$F \subset G, \quad \text{Fam}F \neq \text{Fam}G. \quad (3.4.2.26)$$

A *ferroelastic domain state* \mathbf{R}_i is defined as a state with a homogeneous spontaneous strain $u^{(i)}$. [We drop the suffix ‘s’ or ‘(s)’ if the serial number of the domain state is given as the superscript (i). The definition of spontaneous strain is given in Section 3.4.3.6.1.] Different ferroelastic domain states differ in spontaneous strain. The symmetry of a ferroelastic domain state \mathbf{R}_i is specified by the stabilizer $I_G(u^{(i)})$ of the spontaneous strain $u^{(i)}$ of the principal domain state \mathbf{S}_i [see (3.4.2.16)]. This stabilizer, which we shall denote by A_i , can be expressed as an intersection of the parent group G and the holohedry of group F_i , which we shall denote $\text{Hol}F_i$ (see Table 3.4.2.2):

$$A_i \equiv I_G(u^{(i)}) = G \cap \text{Hol}F_i. \quad (3.4.2.27)$$

This equation indicates that the ferroelastic domain state \mathbf{R}_i has a prominent single-domain orientation. Further on, the term ‘ferroelastic domain state’ will mean a ‘ferroelastic domain state in single-domain orientation’.

In our illustrative example,

$$\begin{aligned} A_1 &= I_{4_z/m_z m_x m_y}(u_{11} - u_{22}) \\ &= \text{Hol}(2_x m_y m_z) \cap m 4_z / m_z m_x m_{xy} \\ &= m_x m_y m_z \cap 4_z / m_z m_x m_{xy} = m_x m_y m_z. \end{aligned}$$

The number n_a of ferroelastic domain states is given by

$$n_a = [G : A_1] = |G| : |A_1|. \quad (3.4.2.28)$$

In our example, $n_a = |4_z / m_z m_x m_{xy}| : |m_x m_y m_z| = 16 : 8 = 2$. In Table 3.4.2.7, last column, the number n_a of ferroelastic domain states is given for all possible ferroic phase transitions.

The number d_a of principal domain states compatible with one ferroelastic domain state (degeneracy of ferroelastic domain states) is given by

$$d_a = [A_1 : F_1] = |A_1| : |F_1|. \quad (3.4.2.29)$$

In our example, $d_a = |m_x m_y m_z| : |2_x m_y m_z| = 8 : 4 = 2$, i.e. two non-ferroelastic principal domain states are compatible with each of the two ferroelastic domain states (cf. Fig. 3.4.2.2).

The product of n_a and d_a is equal to the number n of all principal domain states [see equation (3.4.2.19)],

$$n_a d_a = [G : A_1][A_1 : F_1] = [G : F_1] = n. \quad (3.4.2.30)$$

The number d_a of principal domain states in one ferroelastic domain state can be calculated for all ferroic phase transitions from the ratio of numbers n and n_a that are given in Table 3.4.2.7.

According to Aizu (1969), we can recognize three possible cases:

(i) *Full ferroelastics*: All principal domain states differ in spontaneous strain. In this case, $n_a = n$, i.e. $A_1 = F_1$, ferroelastic domain states are identical with principal domain states.

(ii) *Partial ferroelastics*: Some but not all principal domain states differ in spontaneous strain. A necessary and sufficient condition is $1 < n_a < n$, or, equivalently, $F_1 \subset A_1 \subset G$. In this case, ferroelastic domain states are degenerate secondary domain states with degeneracy $n > d_a = |A_1| : |F_1| > 1$. In this case, the phase transition $G \supset F_1$ can also be classified as an *improper ferroelastic* one (see Section 3.1.3.2).

(iii) *Non-ferroelastics*: All principal domain states have the same spontaneous strain. The criterion is $n_a = 1$, i.e. $A_1 = G$.

A similar classification for ferroelectric domain states is given below. Both classifications are summarized in Table 3.4.2.3.

Example 3.4.2.1. Domain states in leucite. Leucite (KAlSi_2O_6) (see e.g. Hatch *et al.*, 1990) undergoes at about 938 K a ferroelastic phase transition from cubic symmetry $G = m\bar{3}m$ to tetragonal symmetry $L = 4/mmm$. This phase can appear in $|G = m\bar{3}m| : |4/mmm| = 3$ single-domain states, which we denote $\mathbf{R}_1, \mathbf{R}_2, \mathbf{R}_3$. The symmetry group of the first domain state \mathbf{R}_1 is $L_1 = 4_x / m_x m_y m_z$. This group equals the stabilizer $I_G(u^{(1)})$ of the spontaneous strain $u^{(1)}$ of \mathbf{R}_1 since $\text{Hol}(4_x / m_x m_y m_z) = 4_x / m_x m_y m_z$ (see Table 3.4.2.2), hence this phase is a full ferroelastic one.

At about 903 K, another phase transition reduces the symmetry $4/mmm$ to $F = 4/m$. Let us suppose that this transition has taken place in a domain state \mathbf{R}_1 with symmetry $L_1 = 4_x / m_x m_y m_z$; then the room-temperature ferroic phase has symmetry $F_1 = 4_x / m_x$. The $4_x / m_x m_y m_z \supset 4_x / m_x$ phase transition is a non-ferroelastic one [$\text{Hol}(4_x / m_x) = \text{Hol}(4_x / m_x m_y m_z) = 4_x / m_x m_y m_z$] with $|4_x / m_x m_y m_z| : |4_x / m_x| = 8 : 4 = 2$ non-ferroelastic domain states, which we denote \mathbf{S}_1 and \mathbf{S}_2 . Similar

Table 3.4.2.2. Crystal systems, holohedries, crystal families and number of spontaneous strain components

| Point group M | Crystal system | Holohedry $\text{Hol}M$ | Spontaneous strain components | | Crystal family $\text{Fam}M$ |
|---|----------------|-------------------------|-------------------------------|---------|------------------------------|
| | | | Independent | Nonzero | |
| 23, $m\bar{3}$, 432, $43m$, $m\bar{3}m$ | Cubic | $m\bar{3}m$ | 1 | 3 | Cubic |
| 6, $\bar{6}$, $6/m$, 622, $6mm$, $\bar{6}2m$, $6/mmm$ | Hexagonal | $6/mmm$ | 2 | 3 | Hexagonal |
| 3, $\bar{3}$, 32, $3m$, $\bar{3}m$ | Trigonal | $\bar{3}m$ | 2 | 3 | |
| 4, $\bar{4}$, $4/m$, 422, $4mm$, $\bar{4}2m$, $4/mmm$ | Tetragonal | $4/mmm$ | 2 | 3 | Tetragonal |
| 222, $mm2$, mmm | Orthorhombic | mmm | 3 | 3 | Orthorhombic |
| 2, m , $2/m$ | Monoclinic | $2/m$ | 4 | 4 | Monoclinic |
| 1, $\bar{1}$ | Triclinic | $\bar{1}$ | 6 | 6 | Triclinic |

3.4. DOMAIN STRUCTURES

Table 3.4.2.3. Aizu's classification of ferroic phases

n_a is the number of ferroelastic domain states, n_e is the number of ferroelectric domain states and n_f is the number of ferroic domain states.

| Ferroelastic | | | Ferroelectric | | |
|--------------|---------------|------------------|---------------|---------------|-------------------|
| Fully | Partially | Non-ferroelastic | Fully | Partially | Non-ferroelectric |
| $n_a = n$ | $1 < n_a < n$ | $n_a = 1$ | $n_e = n$ | $1 < n_e < n$ | $n_e = 0, 1$ |

considerations performed with initial domain states \mathbf{R}_2 and \mathbf{R}_3 generate another two couples of principal domain states \mathbf{S}_3 , \mathbf{S}_4 and \mathbf{S}_5 , \mathbf{S}_6 , respectively. Thus the room-temperature phase is a partially ferroelastic phase with three degenerate ferroelastic domain states, each of which can contain two principal domain states. Both ferroelastic domains and non-ferroelastic domains within each ferroelastic domain have been observed [see Fig. 3.3.10.13 in Chapter 3.3, Palmer *et al.* (1988) and Putnis (1992)].

3.4.2.2. Ferroelectric domain states

Ferroelectric domain states are defined as states with a homogeneous spontaneous polarization; different ferroelectric domain states differ in the direction of the spontaneous polarization. Ferroelectric domain states are specified by the stabilizer $I_G(\mathbf{P}_s^{(1)})$ of the spontaneous polarization $\mathbf{P}_s^{(1)}$ in the first principal domain state \mathbf{S}_1 [see equation (3.4.2.16)]:

$$F_1 \subseteq C_1 \equiv I_G(\mathbf{P}_s^{(1)}) \subseteq G. \quad (3.4.2.31)$$

The stabilizer C_1 is one of ten polar groups: 1, 2, 3, 4, 6, m , $mm2$, $3m$, $4mm$, $6mm$. Since F_1 must be a polar group too, it is simple to find the stabilizer C_1 fulfilling relation (3.4.2.31).

The number n_e of ferroelectric domain states is given by

$$n_e = [G : C_1] = |G| : |C_1|. \quad (3.4.2.32)$$

If the polar group C_1 does not exist, we put $n_e = 0$. The number n_e of ferroelectric domain states is given for all ferroic phase transitions in the eighth column of Table 3.4.2.7.

The number d_a of principal domain states compatible with one ferroelectric domain state (degeneracy of ferroelectric domain states) is given by

$$d_e = [C_1 : F_1] = |C_1| : |F_1|. \quad (3.4.2.33)$$

The product of n_e and d_e is equal to the number n of all principal domain states [see equation (3.4.2.19)],

$$n_e d_e = n. \quad (3.4.2.34)$$

The degeneracy d_e of ferroelectric domain states can be calculated for all ferroic phase transitions from the ratio of the numbers n and n_e that are given in Table 3.4.2.7.

According to Aizu (1969, 1970a), we can again recognize three possible cases (see also Table 3.4.2.3):

(i) *Full ferroelectrics*: All principal domain states differ in spontaneous polarization. In this case, $n_e = n$, i.e. $C_1 = F_1$, ferroelectric domain states are identical with principal domain states.

(ii) *Partial ferroelectrics*: Some but not all principal domain states differ in spontaneous polarization. A necessary and sufficient condition is $1 < n_e < n$, or equivalently, $F_1 \subset C_1 \subset G$. Ferroelectric domain states are degenerate secondary domain states with degeneracy $n > d_e > 1$. In this case, the phase transition $G \supset F_1$ can be classified as an *improper ferroelectric* one (see Section 3.1.3.2).

(iii) *Non-ferroelectrics*: No principal domain states differ in spontaneous polarization. There are two possible cases: (a) The parent phase is polar; then $C_1 = G$ and $n_e = 1$. (b) The parent phase is non-polar; in this case a polar stabilizer C_1 does not exist, then we put $n_e = 0$.

The classification of full-, partial- and non-ferroelectrics and ferroelastics is given for all Aizu's species in Aizu (1970a).

This classification for all symmetry descents is readily available from the numbers n , n_a , n_e in Table 3.4.2.7. One can conclude that partial ferroelectrics are rather rare.

Example 3.4.2.3. Domain structure in tetragonal perovskites. Some perovskites (e.g. barium titanate, BaTiO_3) undergo a phase transition from the cubic parent phase with $G = m\bar{3}m$ to a tetragonal ferroelectric phase with symmetry $F_1 = 4_x m_y m_z$. The stabilizer $A_1 = \text{Hol}(4_x m_y m_z) \cap m\bar{3}m = m_x m_y m_z$. There are $n_a = |m\bar{3}m| : |m_x m_y m_z| = 3$ ferroelastic domain states each compatible with $d_a = |m_x m_y m_z| : |4_x m_y m_z| = 2$ principal ferroelectric domain states that are related e.g. by inversion $\bar{1}$, i.e. spontaneous polarization is antiparallel in two principal domain states within one ferroelastic domain state.

A similar situation, i.e. two non-ferroelastic domain states with antiparallel spontaneous polarization compatible with one ferroelastic domain state, occurs in perovskites in the trigonal ferroic phase with symmetry $F = 3m$ and in the orthorhombic ferroic phase with symmetry $F_1 = m_{xy} 2_{xy} m_z$.

Many other examples are discussed by Newnham (1974, 1975), Newnham & Cross (1974a,b), and Newnham & Skinner (1976).

3.4.2.2.3. Domain states with the same stabilizer

In our illustrative example (see Fig. 3.4.2.2), we have seen that two domain states \mathbf{S}_1 and \mathbf{S}_2 have the same symmetry group (stabilizer) $2_x m_y m_z$. In general, the condition 'to have the same stabilizer (symmetry group)' divides the set of n principal domain states into equivalence classes. As shown in Section 3.2.3.3, the role of an intermediate group L_1 is played in this case by the normalizer $N_G(F_1)$ of the symmetry group F_1 of the first domain state \mathbf{S}_1 . The number d_F of domain states with the same symmetry group is given by [see Example 3.2.3.34 in Section 3.2.3.3.5 and equation (3.2.3.95)],

$$d_F = [N_G(F_1) : F_1] = |N_G(F_1)| : |F_1|. \quad (3.4.2.35)$$

The number n_F of subgroups that are conjugate under G to F_1 can be calculated from the formula [see equation (3.2.3.96)]

$$n_F = [G : N_G(F_1)] = |G| : |N_G(F_1)|. \quad (3.4.2.36)$$

The product of n_F and d_F is equal to the number n of ferroic domain states,

$$n = n_F d_F. \quad (3.4.2.37)$$

The normalizer $N_G(F_1)$ enables one not only to determine which domain states have the symmetry F_1 but also to calculate all subgroups that are conjugate under G to F_1 (see Examples 3.2.3.22, 3.2.3.29 and 3.2.3.34 in Section 3.2.3.3).

Normalizers $N_G(F_1)$ and the number d_F of principal domain states with the same symmetry are given in Table 3.4.2.7 for all symmetry descents $G \supset F_1$. The number n_F of subgroups conjugate to F_1 is given by $n_F = n : d_F$.

All these results obtained for point-group symmetry descents can be easily generalized to microscopic domain states and space-group symmetry descents (see Section 3.4.2.5).

3. PHASE TRANSITIONS, TWINNING AND DOMAIN STRUCTURES

3.4.2.3. Property tensors associated with ferroic domain states

In the preceding section we derived relations for domain states without considering their specific physical properties. Basic formulae for the number of principal and secondary domain states [see equations (3.4.2.11) and (3.4.2.17), respectively] and the transformation properties of these domain states [equations (3.4.2.12) and (3.4.2.21), respectively] follow immediately from the symmetry groups G , F_1 of the parent and ferroic phases, respectively. Now we shall examine which components of property tensors specify principal and secondary domain states and how these tensor components change in different domain states.

A property tensor τ is specified by its components. The number $m_i(\tau)$ of independent tensor components of a certain tensor τ depends on the point-group symmetry G of the crystal (see Chapter 1.1). The number $m_c(\tau)$ of nonzero Cartesian (rectangular) components depends on the orientation of the crystal in the reference Cartesian coordinate system and is equal to, or greater than, the number $m_i(\tau)$ of independent tensor components; this number $m_i(\tau)$ is independent of orientation. Then there are $m_c(\tau) - m_i(\tau)$ linear relations between Cartesian tensor components. The difference $m_c(\tau) - m_i(\tau)$ is minimal for a ‘standard’ orientation, in which symmetry axes of the crystal are, if possible, parallel to the axes of the reference coordinate system [for more on this choice, see Nye (1985) Appendix B, Sirotnin & Shaskolskaya (1982), Shuvalov (1988) and *IEEE Standards on Piezoelectricity* (1987)]. Even in this standard orientation, only for point groups of triclinic, monoclinic and orthorhombic crystal systems is the number $m_c(\tau)$ of nonzero Cartesian components of each property tensor equal to the number $m_i(\tau)$ of independent tensor components, *i.e.* all Cartesian tensor components are independent. For all other point groups $m_c(\tau) - m_i(\tau) > 0$, *i.e.* there are always relations between some Cartesian tensor components. One can verify this statement for the strain tensor in Table 3.4.2.2.

The relations between Cartesian tensor components can be removed when one uses *covariant tensor components*. [Kopský (1979); see also the manual of the software *GI★KoBo-1* and Kopský (2001). An analogous decomposition of Cartesian tensors into irreducible parts has been performed by Jerphagnon *et al.* (1978).] Covariant tensor components are linear combinations of Cartesian tensor components that transform according to irreducible matrix representations $D^{(\alpha)}(G)$ of the group G of the crystal (*i.e.* they form a basis of irreducible representations of G ; for irreducible representations see Chapter 1.2). The number of covariant tensor components equals the number of independent components of the tensor τ .

The advantage of expressing property tensors by covariant tensor components becomes obvious when one considers a change of a property tensor at a ferroic phase transition. A symmetry descent $G \supset F_1$ is accompanied by the preservation of, or an increase of, the number of independent Cartesian tensor components. The latter possibility can manifest itself either by the appearance of morphic Cartesian tensor components in the low-symmetry phase or by such changes of nonzero Cartesian components that break some relations between tensor components in the high-symmetry phase. This is seen in our illustrative example of the strain tensor u . In the high-symmetry phase with $G = 4_z/m_z m_x m_{xy}$, the strain tensor has two independent components and three nonzero components: $u_{11} \neq u_{22} = u_{33}$. In the low-symmetry phase with $F_1 = 2_x m_y m_z$, there are three independent and three nonzero components: $u_{11} \neq u_{22} \neq u_{33}$, *i.e.* the equation $u_{22} = u_{33}$ does not hold in the parent phase. This change cannot be expressed by a single Cartesian morphic component.

Since there are no relations between covariant tensor components, any change of tensor components at a symmetry descent can be expressed by morphic covariant tensor components, which are zero in the parent phase and nonzero in the

ferroic phase. In our example, the covariant tensor component of the spontaneous strain is $u_{11} - u_{22}$, which is a morphic component since $u_{11} - u_{22} = 0$ for the symmetry $4_z/m_z m_x m_{xy}$ but $u_{11} - u_{22} \neq 0$ for symmetry $2_x m_y m_z$.

Tensorial covariants are defined in an exact way in the manual of the software *GI★KoBo-1* and in Kopský (2001). Here we give only a brief account of this notion. Consider a crystal with symmetry G and a property tensor τ with n_τ independent tensor components. Let $D^{(\alpha)}(G)$ be a d_α -dimensional physically irreducible matrix representation of G . The $D^{(\alpha)}(G)$ *covariant of τ* consists of the following d_α *covariant tensor components*: $\tau_a^\alpha = (\tau_{a,1}^\alpha, \tau_{a,2}^\alpha, \dots, \tau_{a,d_\alpha}^\alpha)$, where $a = 1, 2, \dots$ and $m = n_\tau/d_\alpha$ numbers different d_α -tuples formed from n_τ components of τ . These covariant tensor components are linear combinations of Cartesian components of τ that transform as so-called typical variables of the matrix representation $D^{(\alpha)}(G)$, *i.e.* the transformation properties under operations $g \in G$ of covariant tensor components are expressed by matrices $D^\alpha(g)$.

The relation between two presentations of the tensor τ is provided by *conversion equations*, which express Cartesian tensor components as linear combinations of covariant tensor components and *vice versa* [for details see the manual and Appendix E of the software *GI★KoBo-1* and Kopský (2001)].

Tensorial covariants for all non-equivalent physically irreducible matrix representations of crystallographic point groups and all important property tensors up to rank four are listed in the software *GI★KoBo-1* and in Kopský (2001). Thus, for example, in Table D of the software *GI★KoBo-1*, or in Kopský (2001) p. 5, one finds for the two-dimensional irreducible representation E of group 422 the following tensorial covariants: (P_1, P_2) , (d_{11}, d_{22}) , (d_{12}, d_{21}) , (d_{13}, d_{23}) , (d_{26}, d_{16}) , (d_{35}, d_{34}) .

Let us denote by $\tau_a^{(\alpha)(1)}$ a tensorial covariant of τ in the first single-domain state \mathbf{S}_1 . A crucial role in the analysis is played by the stabilizer $I_G(\tau_a^{(\alpha)(1)})$ of these covariants, *i.e.* all operations of the parent group G that leave $\tau_a^{(\alpha)(1)}$ invariant. There are three possible cases:

(1) If

$$I_G(\tau_a^{(\alpha)(1)}) = G, \quad (3.4.2.38)$$

then all components of $\tau_a^{(\alpha)(1)}$ that are nonzero in the parent phase are also nonzero in the ferroic phase. All these components are the same in all principal domain states. For important property tensors and for all point groups G , these covariant tensor components are listed in the main tables of the software *GI★KoBo-1* and in Kopský (2001). The corresponding Cartesian tensor components are available in Section 1.1.4 and in standard textbooks (*e.g.* Nye, 1985; Sirotnin & Shaskolskaya, 1982).

(2) If

$$I_G(\tau_a^{(\alpha)(1)}) = F_1, \quad (3.4.2.39)$$

then any of $m = n_\tau/d_\alpha$ tensorial covariants $\tau_a^{(\alpha)}$, $a = 1, 2, \dots, m$, is a possible principal tensor parameter $\varphi^{(1)}$ of the transition $G \supset F_1$. Any two of $n_f = |G| : |F_1|$ principal domain states differ in some, or all, components of these covariants. The principal tensor parameter φ plays a similar symmetric (but generally not thermodynamic) role as the order parameter η does in the Landau theory. Only for equitranslational phase transitions is one of the principal tensor parameters (that with the temperature-dependent coefficient) identical with the primary order parameter of the Landau theory (see Section 3.1.3).

(3) If

$$I_G(\tau_a^{(\alpha)(1)}) = L_1, \quad F_1 \subset L_1 \subset G, \quad (3.4.2.40)$$

then $\tau_a^{(\alpha)(1)}$ represents the secondary tensor parameter λ (see Section 3.1.3.2). There exist $n_\lambda = |G| : |L_1|$ secondary domain states $\mathbf{R}_1, \mathbf{R}_2, \dots, \mathbf{R}_{n_\lambda}$ that differ in λ . Unlike in the two preceding cases (1) and (2), several intermediate groups

3.4. DOMAIN STRUCTURES

L_1, M_2, \dots (with secondary tensor parameters λ, μ, \dots) that fulfil condition (3.4.2.40) can exist.

Now we shall indicate how one can find particular property tensors that fulfil conditions (3.4.2.39) or (3.4.2.40). The solution of this group-theoretical task consists of three steps:

(i) For a given point-group symmetry descent $G \supset F_1$, or $G \supset L_1$, one finds the representation Γ_η that specifies the *transformation properties of the principal, or secondary, tensor parameter*, which plays the role of the order parameters in a continuum description. This task is called an inverse Landau problem (see Section 3.1.3 for more details). The solution of this problem is available in Tables 3.4.2.7 and 3.1.3.1, in the software *GI★KoBo-1* and in Kopský (2001), where the letters A, B signify one-dimensional irreducible representations, and letters E and T two- and three-dimensional ones. The dimensionality d_η or d_λ , of the representation Γ_η , or Γ_λ , specifies the maximal number of independent components of the principal, or secondary, tensor parameter φ , or λ , respectively. ‘Reducible’ indicates that Γ_η is a reducible representation.

(ii) In Table 3.1.3.1 one finds in the second column, for a given G and Γ_η , or Γ_λ (first column), the *standard variables* designating in a standardized way the covariant tensor components of the principal, or secondary, tensor parameters (for more details see Section 3.1.3.1 and the manual of the software *GI★KoBo-1*). For two- and three-dimensional irreducible representations, this column contains relations that restrict the values of the components and thus reduce the number of independent components.

(iii) *The association of covariant tensor components of property tensors with standard variables* is tabulated for all irreducible representations in an abridged version in Table 3.1.3.1, in the column headed *Principal tensor parameters*, and in full in the main table of the software *GI★KoBo-1* and of Kopský (2001).

Phase transitions associated with reducible representations are treated in detail only in the software *GI★KoBo-1* and in Kopský (2001). Fortunately, these phase transitions occur rarely in nature.

A rich variety of observed structural phase transitions can be found in Tomaszewski (1992). This database lists 3446 phase transitions in 2242 crystalline materials.

Example 3.4.2.4. Morphic tensor components associated with $4_z/m_z m_x m_{xy} \supset 2_x m_y m_z$ symmetry descent.

(1) *Principal tensor parameters $\varphi^{(1)}$.* The representation Γ_η that specifies the transformation properties of the principal tensor parameter $\varphi^{(1)}$ (and for equitranslational phase transitions also the primary order parameter $\eta^{(1)}$) can be found in the first column of Table 3.1.3.1 for $G = 4_z/m_z m_x m_{xy}$ and $F_1 = 2_x m_y m_z$; the R-irreducible representation (R-irep) $\Gamma_\eta = E_u$. Therefore, the principal tensor parameter $\varphi^{(1)}$ (or the primary order parameter $\eta^{(1)}$) has two components $(\varphi_1^{(1)}, \varphi_2^{(1)})$ [or $(\eta_1^{(1)}, \eta_2^{(1)})$]. The standard variables are in the second column: $(x_1^-, 0)$. This means that only the first component $\varphi_1^{(1)}$ (or $\eta_1^{(1)}$) is nonzero. In the column *Principal tensor parameters*, one finds that $\varphi_1^{(1)} = P_1$ (or

$\eta_1^{(1)} = P_1$), i.e. one principal tensor parameter is spontaneous polarization and the spontaneous polarization in the first domain state S_1 is $P_{(s)} = (P, 00)$. Other principal tensor parameters can be found in the software *GI★KoBo-1* or in Kopský (2001), p. 185: $(g_4, 0)$, $(d_{11}, 0)$, $(d_{12}, 0)$, $(d_{13}, 0)$, $(d_{26}, 0)$, $(d_{35}, 0)$ (the physical meaning of the components is explained in Table 3.4.3.5).

(2) *Secondary tensor parameters $\lambda^{(1)}, \mu^{(1)}, \dots$*

In the group lattice (group-subgroup chains) in Fig. 3.1.3.1, one finds that the only intermediate group between $4_z/m_z m_x m_{xy}$ and $2_x m_y m_z$ is $L_1 = m_x m_y m_z$. In the same table of the software *GI★KoBo-1* or in Kopský (2001), one finds $\Gamma_\lambda = B_{1g}$ and the following one-dimensional secondary tensor parameters: $u_1 - u_2$; $A_{14} + A_{25}$, A_{36} ; $s_{11} - s_{22}$, $s_{13} - s_{23}$, $s_{44} - s_{55}$; $Q_{11} - Q_{22}$, $Q_{12} - Q_{21}$, $Q_{13} - Q_{23}$, $Q_{31} - Q_{32}$, $Q_{44} - Q_{55}$.

The use of covariant tensor components has two practical advantages:

Firstly, the change of tensor components at a ferroic phase transition is completely described by the appearance of new nonzero covariant tensor components. If needed, Cartesian tensor components corresponding to covariant components can be calculated by means of *conversion equations*, which express Cartesian tensor components as linear combinations of covariant tensor components [for details on tensor covariants and conversion equations see the manual and Appendix E of the software *GI★KoBo-1* and Kopský (2001)].

Secondly, calculation of property tensors in various domain states is substantially simplified: transformations of Cartesian tensor components, which are rather involved for higher-rank tensors, are replaced by a simpler transformation of covariant tensor components by matrices $D^{(\eta)}$ of the matrix representation of Γ_η , or of Γ_λ [see again the software *GI★KoBo-1* and Kopský (2001)]. The determination of the tensor properties of all domain states is discussed in full in the book by Kopský (1982).

The relations between morphic properties, tensor parameters, order parameters and names of domain states are compared in Table 3.4.2.4, from which it is seen that what matters in distinguishing different domain states is the stabilizer of the spontaneous (morphic) property, where physically different parameters may possess a common stabilizer. The latter thermodynamic division, based on conditions of the stability, is finer than the former division, which is based on symmetry only. This difference manifests itself, for example, in the fact that two physically different tensor parameters, such as the principal order parameter φ and a ‘similar’ order parameter σ , transform according to different representations Γ_φ and Γ_σ but have the same stabilizer F_1 (such symmetry descents are listed in Table 3.1.3.2) and possess common domain states. This ‘degeneracy’ of domain states can be even more pronounced in the microscopic description, where the same stabilizer \mathcal{F}_1 and therefore a common basic domain state can be shared by three physically different order parameters: a primary order parameter η (the order parameter, components of which form a quadratic invar-

Table 3.4.2.4. *Morphic properties, tensor parameters, order parameters, stabilizers and domain states*

| Morphic property | Tensor or order parameter | Γ | Stabilizer of morphic property | Domain states |
|--------------------------------------|---------------------------|-----------------------------|--|-----------------------------|
| Principal tensor parameter | $\varphi^{(1)}$ | Γ_φ | F_1 | Principal |
| ‘Similar principal’ tensor parameter | $\sigma^{(1)}$ | Γ_σ | | |
| Secondary tensor parameter | $\lambda^{(1)}$ | Γ_λ | $L_1, F_1 \subset L_1 \subset G$ | Secondary ferroic |
| Spontaneous polarization | $\mathbf{P}_{(s)}$ | $\Gamma_{\mathbf{P}_{(s)}}$ | $C_1 = I_G(P_{(s)}^{(1)})$ | Ferroelectric |
| Spontaneous strain | $u_{(s)}$ | $\Gamma_{u_{(s)}}$ | $A_1 = \text{Hol} F_1 \cap G$ | Ferroelastic |
| Primary order parameter | $\eta^{(1)}$ | Γ_η | \mathcal{F}_1 | Primary, basic, microscopic |
| Pseudoproper order parameter | $\zeta^{(1)}$ | | | |
| ‘Similar’ order parameter | $\kappa^{(1)}$ | Γ_κ | | |
| Secondary order parameter | $\tau^{(1)}$ | Γ_τ | $\mathcal{M}_1, \mathcal{F}_1 \subset \mathcal{M}_1 \subset \mathcal{G}$ | Secondary microscopic |

3. PHASE TRANSITIONS, TWINNING AND DOMAIN STRUCTURES

iant with a temperature-dependent coefficient in the free energy), a pseudoproper order parameter ζ that transforms according to the same representation Γ_η as the primary order parameter but has a temperature coefficient that is not as strongly temperature-dependent as the primary order parameter, and a ‘similar’ order parameter κ with a representation Γ_κ different from Γ_η .

3.4.2.4. Synoptic table of ferroic transitions and domain states

The considerations of this and all following sections can be applied to any phase transition with point-group symmetry descent $G \supset F$. All such non-magnetic *crystallographically non-equivalent symmetry descents* are listed in Table 3.4.2.7 together with some other data associated with symmetry reduction at a ferroic phase transition. These symmetry descents can also be traced in lattices of point groups, which are displayed in Figs. 3.1.3.1 and 3.1.3.2.

The symmetry descents $G \supset F_1$ listed in Table 3.4.2.7 are analogous to Aizu’s ‘species’ (Aizu, 1970a), in which the symbol F stands for the symbol \supset in our symmetry descent, and the orientation of symmetry elements of the group F_1 with respect to G is specified by letters p, s, ps, pp etc.

As we have already stated, any systematic analysis of domain structures requires an unambiguous specification of the orientation and location of symmetry elements in space. Moreover, in a continuum approach, the description of crystal properties is performed in a rectangular (Cartesian) coordinate system, which differs in hexagonal and trigonal crystals from the crystallographic coordinate system common in crystallography. Last but not least, a ready-to-use and user-friendly presentation calls for symbols that are explicit and concise.

To meet these requirements, we use in this chapter, in Section 3.1.3 and in the software *GI★KoBo-1* a symbolism in which the orientations of crystallographic elements and operations are

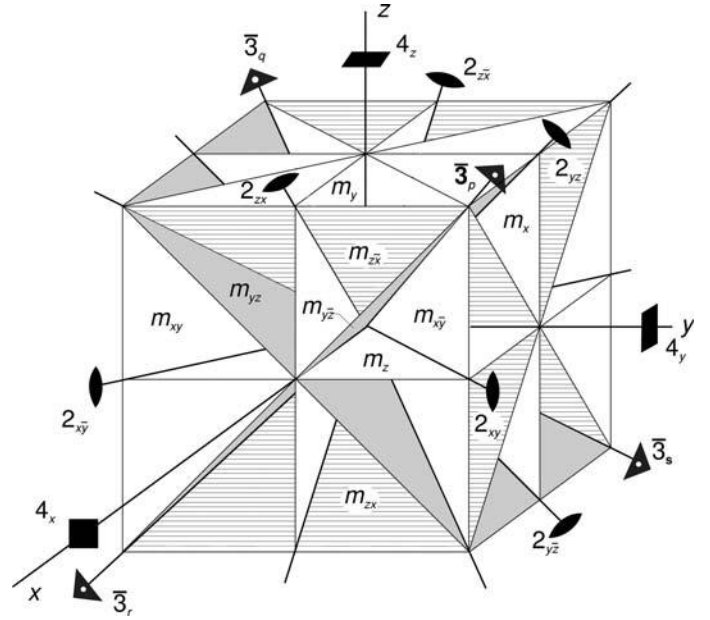


Fig. 3.4.2.3. Oriented symmetry operations of the cubic group $m\bar{3}m$ and of its subgroups. The Cartesian (rectangular) coordinate system x, y, z is identical with the crystallographic and crystallophysical coordinate systems. Correlation with other notations is given in Table 3.4.2.5.

expressed by means of suffixes related to a reference Cartesian coordinate system. The relation of this reference Cartesian coordinate system – called a *crystallophysical coordinate system* – to the usual crystallographic coordinate system is a matter of convention. We adhere to the generally accepted rules [see Nye (1985) Appendix B, Sirotin & Shaskolskaya (1982), Shuvalov (1988), and *IEEE Standards on Piezoelectricity*, 1987].

Table 3.4.2.5. Symbols of symmetry operations of the point group $m\bar{3}m$

Standard: symbols used in Section 3.1.3, in the present chapter and in the software; all symbols refer to the cubic crystallographic (Cartesian) basis, $p \equiv [111]$ (all positive), $q \equiv [\bar{1}\bar{1}\bar{1}]$, $r \equiv [11\bar{1}]$, $s \equiv [\bar{1}\bar{1}1]$. BC: Bradley & Cracknell (1972). AH: Altmann & Herzog (1994). IT A: IT A (2002). Jones: Jones’ faithful representation symbols express the action of a symmetry operation on a vector (xyz) (see e.g. Bradley & Cracknell, 1972).

| Standard | BC | AH | IT A | Jones | Standard | BC | AH | IT A | Jones |
|----------------------|------------|------------|--------------------------------------|-----------------------------|----------------------|---------------|---------------|-----------------------------------|-----------------------------|
| 1 or e | E | E | 1 | x, y, z | $\bar{1}$ or i | I | i | $\bar{1} \ 0, 0, 0$ | $\bar{x}, \bar{y}, \bar{z}$ |
| 2_z | C_{2z} | C_{2z} | 2 $0, 0, z$ | \bar{x}, \bar{y}, z | m_z | σ_z | σ_z | $m \ x, y, 0$ | x, y, \bar{z} |
| 2_x | C_{2x} | C_{2x} | 2 $x, 0, 0$ | x, \bar{y}, \bar{z} | m_x | σ_x | σ_x | $m \ 0, y, z$ | \bar{x}, y, z |
| 2_y | C_{2y} | C_{2y} | 2 $0, y, 0$ | \bar{x}, y, \bar{z} | m_y | σ_y | σ_y | $m \ x, 0, z$ | x, \bar{y}, z |
| 2_{xy} | C_{2a} | C'_{2a} | 2 $x, x, 0$ | y, x, \bar{z} | m_{xy} | σ_{da} | σ_{d1} | $m \ x, \bar{x}, z$ | \bar{y}, \bar{x}, z |
| $2_{\bar{x}\bar{y}}$ | C_{2b} | C'_{2b} | 2 $x, \bar{x}, 0$ | $\bar{y}, \bar{x}, \bar{z}$ | $m_{\bar{x}\bar{y}}$ | σ_{db} | σ_{d2} | $m \ x, x, z$ | y, x, z |
| 2_{zx} | C_{2c} | C'_{2c} | 2 $x, 0, x$ | z, \bar{y}, x | m_{zx} | σ_{dc} | σ_{d3} | $m \ \bar{x}, y, x$ | \bar{z}, y, \bar{x} |
| $2_{z\bar{x}}$ | C_{2e} | C'_{2e} | 2 $\bar{x}, 0, x$ | $\bar{z}, \bar{y}, \bar{x}$ | $m_{z\bar{x}}$ | σ_{de} | σ_{d5} | $m \ x, y, x$ | z, y, x |
| 2_{yz} | C_{2d} | C'_{2d} | 2 $0, y, y$ | \bar{x}, \bar{z}, y | m_{yz} | σ_{dd} | σ_{d4} | $m \ x, y, \bar{y}$ | x, \bar{z}, \bar{y} |
| $2_{y\bar{z}}$ | C_{2f} | C'_{2f} | 2 $0, y, \bar{y}$ | $\bar{x}, \bar{z}, \bar{y}$ | $m_{y\bar{z}}$ | σ_{df} | σ_{d6} | $m \ x, y, y$ | x, z, y |
| 3_p | C_{31}^+ | C_{31}^+ | 3 ⁺ x, x, x | z, x, y | $\bar{3}_p$ | S_{61}^- | S_{61}^- | $\bar{3}^+ \ x, x, x$ | $\bar{z}, \bar{x}, \bar{y}$ |
| 3_q | C_{32}^+ | C_{32}^+ | 3 ⁺ \bar{x}, \bar{x}, x | \bar{z}, x, \bar{y} | $\bar{3}_q$ | S_{62}^- | S_{62}^- | $\bar{3}^+ \ \bar{x}, \bar{x}, x$ | z, \bar{x}, y |
| 3_r | C_{33}^+ | C_{33}^+ | 3 ⁺ x, \bar{x}, \bar{x} | \bar{z}, \bar{x}, y | $\bar{3}_r$ | S_{63}^- | S_{63}^- | $\bar{3}^+ \ x, \bar{x}, \bar{x}$ | z, x, \bar{y} |
| 3_s | C_{34}^+ | C_{34}^+ | 3 ⁺ \bar{x}, x, \bar{x} | z, \bar{x}, \bar{y} | $\bar{3}_s$ | S_{64}^- | S_{64}^- | $\bar{3}^+ \ \bar{x}, x, \bar{x}$ | \bar{z}, x, y |
| 3_p^2 | C_{31}^- | C_{31}^- | 3 ⁻ x, x, x | y, z, x | $\bar{3}_p^5$ | S_{61}^+ | S_{61}^+ | $\bar{3}^- \ x, x, x$ | $\bar{y}, \bar{z}, \bar{x}$ |
| 3_q^2 | C_{32}^- | C_{32}^- | 3 ⁻ \bar{x}, \bar{x}, x | y, \bar{z}, \bar{x} | $\bar{3}_q^5$ | S_{62}^+ | S_{62}^+ | $\bar{3}^- \ \bar{x}, \bar{x}, x$ | \bar{y}, z, x |
| 3_r^2 | C_{33}^- | C_{33}^- | 3 ⁻ x, \bar{x}, \bar{x} | \bar{y}, z, \bar{x} | $\bar{3}_r^5$ | S_{63}^+ | S_{63}^+ | $\bar{3}^- \ x, \bar{x}, \bar{x}$ | y, \bar{z}, x |
| 3_s^2 | C_{34}^- | C_{34}^- | 3 ⁻ \bar{x}, x, \bar{x} | \bar{y}, \bar{z}, x | $\bar{3}_s^5$ | S_{64}^+ | S_{64}^+ | $\bar{3}^- \ \bar{x}, x, \bar{x}$ | y, z, \bar{x} |
| 4_z | C_{4z}^+ | C_{4z}^+ | 4 ⁺ $0, 0, z$ | \bar{y}, x, z | $\bar{4}_z$ | S_{4z}^- | S_{4z}^- | $\bar{4}^+ \ 0, 0, z$ | y, \bar{x}, \bar{z} |
| 4_x | C_{4x}^+ | C_{4x}^+ | 4 ⁺ $x, 0, 0$ | x, \bar{z}, y | $\bar{4}_x$ | S_{4x}^- | S_{4x}^- | $\bar{4}^+ \ x, 0, 0$ | \bar{x}, z, \bar{y} |
| 4_y | C_{4y}^+ | C_{4y}^+ | 4 ⁺ $0, y, 0$ | z, y, \bar{x} | $\bar{4}_y$ | S_{4y}^- | S_{4y}^- | $\bar{4}^+ \ 0, y, 0$ | \bar{z}, \bar{y}, x |
| 4_z^3 | C_{4z}^- | C_{4z}^- | 4 ⁻ $0, 0, z$ | y, \bar{x}, z | $\bar{4}_z^3$ | S_{4z}^+ | S_{4z}^+ | $\bar{4}^- \ 0, 0, z$ | \bar{y}, x, \bar{z} |
| 4_x^3 | C_{4x}^- | C_{4x}^- | 4 ⁻ $x, 0, 0$ | x, z, \bar{y} | $\bar{4}_x^3$ | S_{4x}^+ | S_{4x}^+ | $\bar{4}^- \ x, 0, 0$ | \bar{x}, \bar{z}, y |
| 4_y^3 | C_{4y}^- | C_{4y}^- | 4 ⁻ $0, y, 0$ | \bar{z}, y, x | $\bar{4}_y^3$ | S_{4y}^+ | S_{4y}^+ | $\bar{4}^- \ 0, y, 0$ | z, \bar{y}, \bar{x} |

3.4. DOMAIN STRUCTURES

We list all symbols of crystallographic symmetry operations and a comparison of these symbols with other notations in Tables 3.4.2.5 and 3.4.2.6 and in Figs. 3.4.2.3 and 3.4.2.4.

Now we can present the synoptic Table 3.4.2.7.

3.4.2.4.1. Explanation of Table 3.4.2.7

G : point group expressing the *symmetry of the parent (prototypic) phase*. Subscripts of generators in the group symbol specify their orientation in the Cartesian (rectangular) crystallophysical coordinate system of the group G (see Tables 3.4.2.5 and 3.4.2.6, and Figs. 3.4.2.3 and 3.4.2.4).

F_1 : this point group is a proper subgroup of G given in the first column and expresses the *symmetry of the ferroic phase in the first single-domain state S_1* . In accordance with *IT A* (2002), five groups are given in two orientations (bold and normal type). Subscripts of generators in the group symbol specify their orientation in the Cartesian (rectangular) crystallophysical coordinate system of the group G (see Tables 3.4.2.5 and 3.4.2.6, and Figs. 3.4.2.3 and 3.4.2.4). In the cubic groups, the direction of the body diagonal is denoted by abbreviated symbols: $p \equiv [111]$ (all positive), $q \equiv [\bar{1}\bar{1}1]$, $r \equiv [1\bar{1}\bar{1}]$, $s \equiv [\bar{1}1\bar{1}]$. In the hexagonal and trigonal groups, axes x' , y' and x'' , y'' of a Cartesian coordinate system are rotated about the z axis through 120 and 240°, respectively, from the crystallophysical Cartesian coordinate axes x and y .

Symmetry groups in parentheses are groups conjugate to F_1 under G (see Section 3.2.3.2). These are symmetry groups (stabilizers) of some domain states S_k different from S_1 (for more details see Section 3.4.2.2.3).

Γ_η : *physically irreducible representation of the group G* . This specifies the transformation properties of the principal tensor parameter of the phase transition in a continuum description and transformation properties of the primary order parameter η of the *equitranslational* phase transitions in the microscopic description. The letters A , B signify one-dimensional representations, and letters E and T two- and three-dimensional irreducible representations, respectively. Two letters T indicate that the symmetry descent $G \subset F_1$ can be accomplished by two non-equivalent three-dimensional irreducible representations (see Table 3.1.3.2). ‘Reducible’ denotes a reducible representation of G . In this case, there are always several non-equivalent reducible representations inducing the same descent $G \subset F_1$ [for more detailed information see the software *GI★KoBo-1* and Kopský (2001)].

Knowledge of Γ_η enables one to determine for all ferroic transitions property tensors and their components that are different in all principal domain states, and, for equitranslational

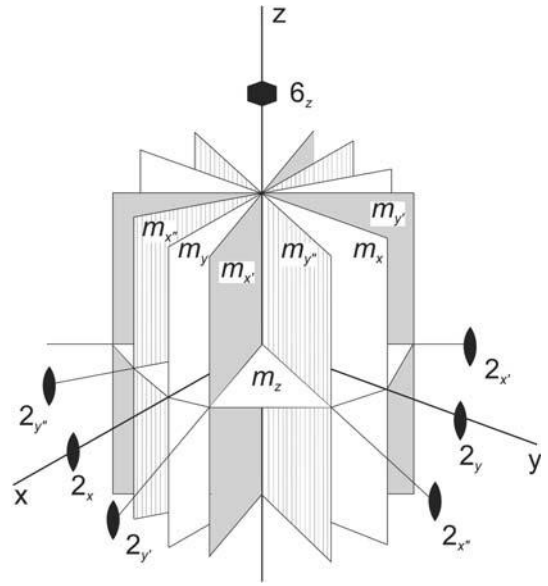


Fig. 3.4.2.4. Oriented symmetry operations of the hexagonal group 6/mmm and of its hexagonal and trigonal subgroups. The coordinate system x, y, z corresponds to the Cartesian crystallophysical coordinate system, the axes x, y, z of the crystallographic coordinate system are parallel to the twofold rotation axes $2_x, 2_y$ and to the sixfold rotation axis 6_z . Correlation with other notations is given in Table 3.4.2.6.

transitions only, microscopic displacements and/or ordering of atoms and molecules that are different in different basic (microscopic) domain states (for details see Section 3.1.3, especially Table 3.1.3.1, and Section 3.1.2).

$N_G(F_1)$: the *normalizer of F_1 in G* (defined in Section 3.2.3.2.4) determines subgroups conjugate to F_1 in G and specifies which domain states have the same symmetry (stabilizer in G). The number n_F of subgroups conjugate to F_1 in G is $n_F = [G : N_G(F_1)] = |G| : |N_G(F_1)|$ [see equation (3.4.2.36)] and the number d_F of principal domain states with the same symmetry is $d_F = [N_G(F_1) : F_1] = |N_G(F_1)| : |F_1|$ [see equation (3.4.2.35)]. There are three possible cases:

(i) $N_G(F_1) = G$. There are no subgroups conjugate to F_1 and the symmetry group F_i (stabilizer of S_i in G) of all principal domain states S_1, S_2, \dots, S_n is equal to G , $F_i = G$, for all $i = 1, 2, \dots, n$; hence domain states cannot be distinguished by their symmetry. The group F_1 is a normal subgroup of G , $F_1 \triangleleft G$ (see Section 3.2.3.2). This is always the case if there are just two single-domain states S_1, S_2 , i.e. if the index of F_1 in G equals two, $[G : F_1] = |G| : |F_1| = 2$.

Table 3.4.2.6. Symbols of symmetry operations of the point group 6/mmm

Standard: symbols used in Section 3.1.3, in the present chapter and in the software; suffixes (in *italic*) refer to the Cartesian crystallophysical coordinate system. BC: Bradley & Cracknell (1972). AH: Altmann & Herzog (1994). *IT A*: *IT A* (2002), coordinates (in Sans Serif) are expressed in a crystallographic hexagonal basis. Jones: Jones' faithful representation symbols express the action of a symmetry operation of a vector (xyz) in a crystallographic basis (see e.g. Bradley & Cracknell, 1972).

| Standard | BC | AH | <i>IT A</i> | Jones | Standard | BC | AH | <i>IT A</i> | Jones |
|-----------|------------|------------|-------------------|-----------------------------|------------------|---------------|---------------|-----------------------|-----------------------------|
| 1 or e | E | E | 1 | x, y, z | $\bar{1}$ or i | I | I | $\bar{1}$ 0, 0, 0 | $\bar{x}, \bar{y}, \bar{z}$ |
| 6_z | C_6^+ | C_6^+ | 6^+ 0, 0, z | $x - y, x, z$ | $\bar{6}_z$ | S_3^- | S_3^- | $\bar{6}^+$ 0, 0, z | $y - x, \bar{x}, \bar{z}$ |
| 3_z | C_3^+ | C_3^+ | 3^+ 0, 0, z | $\bar{y}, x - y, z$ | $\bar{3}_z$ | S_6^- | S_6^- | $\bar{3}^+$ 0, 0, z | $y, y - x, \bar{z}$ |
| 2_z | C_2 | C_2 | 2 0, 0, z | \bar{x}, \bar{y}, z | m_z | σ_h | σ_h | m $x, y, 0$ | x, y, \bar{z} |
| 3_z^2 | C_3^- | C_3^- | 3^- 0, 0, z | $y - x, \bar{x}, z$ | $\bar{3}_z^5$ | S_6^+ | S_6^+ | $\bar{3}^-$ 0, 0, z | $x - y, x, \bar{z}$ |
| 6_z^5 | C_6^- | C_6^- | 6^- 0, 0, z | $y, y - x, z$ | $\bar{6}_z^5$ | S_3^+ | S_3^+ | $\bar{6}^-$ 0, 0, z | $\bar{y}, x - y, \bar{z}$ |
| 2_x | C_{21}'' | C_{21}'' | 2 $x, 0, 0$ | $x - y, \bar{y}, \bar{z}$ | m_x | σ_{v1} | σ_{v1} | m $x, 2x, z$ | $y - x, y, z$ |
| $2_{x'}$ | C_{22}'' | C_{22}'' | 2 $0, y, 0$ | $\bar{x}, y - x, \bar{z}$ | $m_{x'}$ | σ_{v2} | σ_{v2} | m $2x, x, z$ | $x, x - y, z$ |
| $2_{x''}$ | C_{23}'' | C_{23}'' | 2 $x, x, 0$ | y, x, \bar{z} | $m_{x''}$ | σ_{v3} | σ_{v3} | m x, \bar{x}, z | $\bar{y}, \bar{x}, \bar{z}$ |
| 2_y | C_{21}' | C_{21}' | 2 $x, 2x, 0$ | $y - x, y, \bar{z}$ | m_y | σ_{d1} | σ_{d1} | m $x, 0, z$ | $x - y, \bar{y}, z$ |
| $2_{y'}$ | C_{22}' | C_{22}' | 2 $2x, x, 0$ | $x, x - y, \bar{z}$ | $m_{y'}$ | σ_{d2} | σ_{d2} | m $0, y, z$ | $\bar{x}, y - x, z$ |
| $2_{y''}$ | C_{23}' | C_{23}' | 2 $x, \bar{x}, 0$ | $\bar{y}, \bar{x}, \bar{z}$ | $m_{y''}$ | σ_{d3} | σ_{d3} | m x, x, z | y, x, z |

3. PHASE TRANSITIONS, TWINNING AND DOMAIN STRUCTURES

(ii) $N_G(F_1) = F_1$. Then any two domain states $\mathbf{S}_i, \mathbf{S}_k$ have different symmetry groups (stabilizers), $\mathbf{S}_i \neq \mathbf{S}_k \Leftrightarrow F_i \neq F_k$, i.e. there is a one-to-one correspondence between single-domain states and their symmetries, $\mathbf{S}_i \Leftrightarrow F_i$. In this case, principal domain states \mathbf{S}_i can be specified by their symmetries $F_i, i = 1, 2, \dots, n$. The number n_F of different groups conjugate to F_1 is equal to the index $[G : F_1] = |G| : |F_1| = n$.

(iii) $F_1 \subset N_G(F_1) \subset G$. Some, but not all, domain states $\mathbf{S}_i, \mathbf{S}_k$ have identical symmetry groups (stabilizers) $F_i = F_k$. The number d_F of domain states with the same symmetry group is $d_F = [N_G(F_1) : F_1] = |N_G(F_1)| : |F_1|$ [see equation (3.4.2.35)], $1 < d_F < n$. The number n_F of different groups conjugate to F_1 is equal to the index $n_F = [G : N_G(F_1)] = |G| : |N_G(F_1)|$ [see equation (3.4.2.36)] and in this case $1 < n_F < n$. It always holds that $n_F d_F = n$ [see equation (3.4.2.37)].

K_{ij} : *twinning group of a domain pair* ($\mathbf{S}_i, \mathbf{S}_j$). This group is defined in Section 3.4.3.2. It can be considered a colour (polychromatic) group involving c colours, where $c = [K_{ij} : F_1]$, and is, therefore, defined by two groups K_{ij} and F_1 , and its full symbol is $K_{ij}[F_1]$. In this column only K_{ij} is given, since F_1 appears in the second column of the table.

If the group symbol of K_{ij} contains generators with the star symbol, $*$, which signifies transposing operations of the domain pair ($\mathbf{S}_i, \mathbf{S}_j$), then the symbol $K_{ij}[F_1]$ denotes a dichromatic ('black-and-white') group signifying a completely transposable domain pair. In this special case, just the symbol K_{ij} containing stars $*$ specifies the group F_1 unequivocally.

The number in parentheses after the group symbol of K_{ij} is equal to the number of twinning groups K_{ik} equivalent with K_{ij} .

In the continuum description, a twinning group is significant in at least in two instances:

(1) A twinning group $K_{ij}[F_1]$ specifies the distinction of two domain states \mathbf{S}_i and $\mathbf{S}_j = g_{ij}\mathbf{S}_i$, where $g_{ij} \in G$ (see Sections 3.4.3.2 and 3.4.3.4).

(2) A twinning group $K_{ij}[F_1]$ may assist in signifying classes of equivalent domain pairs (orbits of domain pairs). In most cases, to a twinning group F_{ij} there corresponds just one class of equivalent domain pairs (an orbit) $G(\mathbf{S}_i, \mathbf{S}_j)$; then a twinning group can represent this class of equivalent domain pairs. Nevertheless, in some cases two or more classes of equivalent domain pairs have a common twinning group. Then one has to add a switching operation g_{ij} to the twinning group, $K_{ij}[F_1](g_{ij})$ (see the end of Section 3.4.3.2). In this way, classes of equivalent domain pairs $G(\mathbf{S}_i, \mathbf{S}_j)$ are denoted in synoptic Tables 3.4.2.7 and 3.4.3.6.

Twinning groups given in column K_{ij} thus specify *all G-orbits of domain pairs*. The number of G -orbits and representative domain pairs for each orbit are determined by double cosets of group F_1 (see Section 3.4.3.2). Representative domain pairs from each orbit of domain pairs are further analysed in synoptic Table 3.4.3.4 (non-ferroelastic domain pairs) and in synoptic Table 3.4.3.6 (ferroelastic domain pairs).

The set of the twinning groups K_{ij} given in this column is analogous to the concept of a *complete twin* defined as 'an edifice comprising in addition to an original crystal (domain state \mathbf{S}_i) as many twinned crystals (domain states \mathbf{S}_j) as there are possible twin laws' (see Curien & Le Corre, 1958). If a traditional definition of a twin law ['a geometrical relationship between two crystal components of a twin', see Section 3.3.2 and Koch (1999); Curien & Le Corre (1958)] is applied *sensu stricto* to domain twins then one gets the following correspondence:

(i) a twin law of a non-ferroelastic domain twin is specified by the twinning group K_{ij} (see Section 3.4.3.3 and Table 3.4.3.4);

(ii) two twin laws of two compatible ferroelastic domain twins, resulting from one ferroelastic single-domain pair $\{\mathbf{S}_i, \mathbf{S}_j\}$, are specified by two layer groups \bar{J}_{ij} associated with the twinning group K_{ij} of this ferroelastic single-domain pair $\{(\mathbf{S}_i, \mathbf{S}_j)\}$ (see Section 3.4.3.4 and Table 3.4.3.6).

n : *number of principal single-domain states*, the finest subdivision of domain states in a continuum description, $n = [G : F_1] = |G| : |F_1|$ [see equation (3.4.2.11)].

d_F : *number of principal domain states with the same symmetry group (stabilizer)*, $d_F = [N_G(F_1) : F_1] = |N_G(F_1)| : |F_1|$ [see equation (3.4.2.35)]. If $d_F > 1$, then the group F_1 does not specify the first single-domain state \mathbf{S}_1 . The number n_F of subgroups conjugate with F_1 is $n_F = n : d_F$.

n_e : *number of ferroelectric single-domain states*, $n_e = [G : C_1] = |G| : |C_1|$, where C_1 is the stabilizer (in G) of the spontaneous polarization in the first domain state \mathbf{S}_1 [see equation (3.4.2.32)]. The number d_e of principal domain states compatible with one ferroelectric domain state (degeneracy of ferroelectric domain states) equals $d_e = [C_1 : F_1] = |C_1| : |F_1|$ [see equation (3.4.2.33)].

Aizu's classification of ferroelectric phases (Aizu, 1969; see Table 3.4.2.3): $n_e = n$, fully ferroelectric; $1 < n_e < n$, partially ferroelectric; $n_e = 1$, non-ferroelectric, the parent phase is polar and the spontaneous polarization in the ferroic phase is the same as in the parent phase; $n_e = 0$, non-ferroelectric, parent phase is non-polar.

n_a : *number of ferroelastic single-domain states*, $n_a = [G : A_1] = |G| : |A_1|$, where A_1 is the stabilizer (in G) of the spontaneous strain in the first domain state \mathbf{S}_1 [see equation (3.4.2.28)]. The number d_a of principal domain states compatible with one ferroelastic domain state (degeneracy of ferroelastic domain states) is given by $d_a = [A_1 : F_1] = |A_1| : |F_1|$ [see equation (3.4.2.29)].

Aizu's classification of ferroelastic phases (Aizu, 1969; see Table 3.4.2.3): $n_a = n$, fully ferroelastic; $1 < n_a < n$, partially ferroelastic; $n_e = 1$, non-ferroelastic.

Example 3.4.2.5. Orthorhombic phase of perovskite crystals. The parent phase has symmetry $G = m\bar{3}m$ and the symmetry of the ferroic orthorhombic phase is $F_1 = m_{xy}2_{xy}m_z$. In Table 3.4.2.7, we find that $n = n_e$, i.e. the phase is fully ferroelectric. Then we can associate with each principal domain state a spontaneous polarization. In column K_{ij} there are four twinning groups. As explained in Section 3.4.3, these groups represent four 'twin laws' that can be characterized by the angle between the spontaneous polarization in single-domain state \mathbf{S}_i and $\mathbf{S}_j, j = 2, 3, 4, 5$. If we choose $\mathbf{P}_{(s)}^{(1)}$ along the direction $[110]$ (F_1 does not specify unambiguously this direction, since $d_F = 2!$), then the angles between $\mathbf{P}_{(s)}^{(1)}$ and $\mathbf{P}_{(s)}^{(j)}$, representing the 'twin law' for these four twinning groups $m\bar{3}m(m_{zx}), m\bar{3}m(2_{zx}), 4_z/m_zm_xm_{xy}, m_{xy}m_{xy}^*m_z$, are, respectively, 60, 120, 90 and 180°.

3.4.2.5. Basic (microscopic) domain states and their partition into translation subsets

The examination of principal domain states performed in the continuum approach can be easily generalized to a *microscopic description*. Let us denote the *space-group* symmetry of the parent (high-symmetry) phase by \mathcal{G} and the space group of the ferroic (low-symmetry) phase by \mathcal{F}_1 , which is a proper subgroup of $\mathcal{G}, \mathcal{F}_1 \subset \mathcal{G}$. Further we denote by \mathbf{S}_1 a *basic (microscopic)* low-symmetry structure described by positions of atoms in the unit cell. The stabilizer $\mathcal{I}_{\mathcal{G}}(\mathbf{S}_1)$ of the basic structure \mathbf{S}_1 in a single-domain orientation is equal to the space group \mathcal{F}_1 of the ferroic (low-symmetry) phase,

$$\mathcal{I}_{\mathcal{G}}(\mathbf{S}_1) = \mathcal{F}_1. \quad (3.4.2.41)$$

By applying a lost symmetry operation \mathbf{g}_j on \mathbf{S}_1 , one gets a crystallographically equivalent low-symmetry basic structure \mathbf{S}_j ,

$$\mathbf{g}_j\mathbf{S}_1 = \mathbf{S}_j \neq \mathbf{S}_1, \quad \mathbf{g}_j \in \mathcal{G}, \quad \mathbf{g}_j \notin \mathcal{F}_1. \quad (3.4.2.42)$$

We may recall that \mathbf{g}_j is a space-group symmetry operation consisting of a rotation (point-group operation) g_j and a non-

3.4. DOMAIN STRUCTURES

Table 3.4.2.7. Group-subgroup symmetry descents $G \supset F_1$

G : point-group symmetry of parent phase; F_1 : point-group symmetry of single-domain state \mathbf{S}_1 ; Γ_η : representation of G ; $N_G(F_1)$: normalizer of F_1 in G ; K_{ij} : twinning groups; n : number of principal single-domain states; d_F : number of principal domain states with the same symmetry; n_e : number of ferroelectric single-domain states; n_a : number of ferroelastic single-domain states.

| G | F_1 | Γ_η | $N_G(F_1)$ | K_{ij} | n | d_F | n_e | n_a |
|-------------------|---------------------------|--------------------------|---------------------------|---|-----|-------|-------|-------|
| $\bar{1}$ | 1 | A_u | $\bar{1}$ | $\bar{1}^*$ | 2 | 2 | 2 | 1 |
| 2_u^\dagger | 1 | B | 2_u | 2_u^* | 2 | 2 | 2 | 2 |
| m_u^\dagger | 1 | A'' | m_u | m_u^* | 2 | 2 | 2 | 2 |
| $2_u/m_u^\dagger$ | m_u | B_u | $2_u/m_u$ | $2_u^*/m_u$ | 2 | 2 | 2 | 1 |
| | 2_u | A_u | $2_u/m_u$ | $2_u/m_u^*$ | 2 | 2 | 2 | 1 |
| | $\bar{1}$ | B_g | $2_u/m_u$ | $2_u^*/m_u^*$ | 2 | 2 | 0 | 2 |
| | 1 | Reducible | $2_u/m_u$ | $m_u^*, 2_u^*, \bar{1}^*$ | 4 | 4 | 4 | 2 |
| $2_x 2_y 2_z$ | 2_z | B_{1g} | $2_x 2_y 2_z$ | $2_x^* 2_y^* 2_z$ | 2 | 2 | 2 | 2 |
| | 2_x | B_{3g} | $2_x 2_y 2_z$ | $2_x 2_y^* 2_z^*$ | 2 | 2 | 2 | 2 |
| | 2_y | B_{2g} | $2_x 2_y 2_z$ | $2_x^* 2_y 2_z^*$ | 2 | 2 | 2 | 2 |
| | 1 | Reducible | $2_x 2_y 2_z$ | $2_z^*, 2_x^*, 2_y^*$ | 4 | 4 | 4 | 4 |
| $m_x m_y 2_z$ | m_x | B_2 | $m_x m_y 2_z$ | $m_x m_y^* 2_z^*$ | 2 | 2 | 2 | 2 |
| | m_y | B_1 | $m_x m_y 2_z$ | $m_x^* m_y 2_z^*$ | 2 | 2 | 2 | 2 |
| | 2_z | A_2 | $m_x m_y 2_z$ | $m_x^* m_y^* 2_z^*$ | 2 | 2 | 1 | 2 |
| | 1 | Reducible | $m_x m_y 2_z$ | $m_x^*, m_y^*, 2_z^*$ | 4 | 2 | 4 | 4 |
| $m_x m_y m_z$ | $m_x m_y 2_z$ | B_{1u} | $m_x m_y m_z$ | $m_x m_y m_z^*$ | 2 | 2 | 2 | 1 |
| | $2_x m_y m_z$ | B_{3u} | $m_x m_y m_z$ | $m_x^* m_y m_z$ | 2 | 2 | 2 | 1 |
| | $m_x 2_y m_z$ | B_{2u} | $m_x m_y m_z$ | $m_x m_y^* m_z$ | 2 | 2 | 2 | 1 |
| | $2_x 2_y 2_z$ | A_{1u} | $m_x m_y m_z$ | $m_x^* m_y^* m_z^*$ | 2 | 2 | 0 | 1 |
| | $2_z/m_z$ | B_{1g} | $m_x m_y m_z$ | $m_x^* m_y^* m_z$ | 2 | 2 | 0 | 2 |
| | $2_x/m_x$ | B_{3g} | $m_x m_y m_z$ | $m_x m_y^* m_z^*$ | 2 | 2 | 0 | 2 |
| | $2_y/m_y$ | B_{2g} | $m_x m_y m_z$ | $m_x^* m_y m_z^*$ | 2 | 2 | 0 | 2 |
| | m_z | Reducible | $m_x m_y m_z$ | $2_x^* m_y^* m_z, m_x^* 2_y^* m_z, 2_z^*/m_z$ | 4 | 4 | 4 | 2 |
| | m_x | Reducible | $m_x m_y m_z$ | $m_x m_y^* 2_z^*, m_x^* 2_y^* m_z^*, 2_z^*/m_x$ | 4 | 4 | 4 | 2 |
| | m_y | Reducible | $m_x m_y m_z$ | $m_x^* m_y 2_z^*, 2_x^* m_y m_z^*, 2_y^*/m_y$ | 4 | 4 | 4 | 2 |
| | 2_z | Reducible | $m_x m_y m_z$ | $m_x^* m_y^* 2_z, 2_x^* 2_y^* 2_z, 2_z^*/m_z^*$ | 4 | 4 | 2 | 2 |
| | 2_x | Reducible | $m_x m_y m_z$ | $2_x m_y^* m_z^*, 2_x 2_y^* 2_z^*, 2_x^*/m_x^*$ | 4 | 4 | 2 | 2 |
| | 2_y | Reducible | $m_x m_y m_z$ | $m_x^* 2_y m_z^*, 2_x^* 2_y^* 2_z^*, 2_y^*/m_y^*$ | 4 | 4 | 2 | 2 |
| | $\bar{1}$ | Reducible | $m_x m_y m_z$ | $2_z^*/m_z^*, 2_x^*/m_x^*, 2_y^*/m_y^*$ | 4 | 4 | 0 | 4 |
| | 1 | Reducible | $m_x m_y m_z$ | $m_z^*, m_x^*, m_y^*, 2_z^*, 2_x^*, 2_y^*, \bar{1}^*$ | 8 | 8 | 8 | 4 |
| 4_z | 2_z | B | 4_z | 4_z^* | 2 | 2 | 1 | 2 |
| | 1 | ${}^1E \oplus {}^2E$ | 4_z | $4_z, 2_z^*$ | 4 | 4 | 4 | 4 |
| $\bar{4}_z$ | 2_z | B | $\bar{4}_z$ | $\bar{4}_z^*$ | 2 | 2 | 2 | 2 |
| | 1 | ${}^1E \oplus {}^2E$ | $\bar{4}_z$ | $\bar{4}_z, 2_z^*$ | 4 | 2 | 4 | 4 |
| $4_z/m_z$ | $\bar{4}_z$ | B_u | $4_z/m_z$ | $4_z^*/m_z^*$ | 2 | 2 | 0 | 1 |
| | 4_z | A_u | $4_z/m_z$ | $4_z/m_z^*$ | 2 | 2 | 2 | 1 |
| | $2_z/m_z$ | B_g | $4_z/m_z$ | $4_z^*/m_z$ | 2 | 2 | 0 | 2 |
| | m_z | ${}^1E_u \oplus {}^2E_u$ | $4_z/m_z$ | $4_z/m_z, 2_z^*/m_z$ | 4 | 4 | 4 | 2 |
| | 2_z | Reducible | $4_z/m_z$ | $\bar{4}_z^*, 4_z^*, 2_z^*/m_z^*$ | 4 | 4 | 2 | 2 |
| | $\bar{1}$ | ${}^1E_g \oplus {}^2E_g$ | $4_z/m_z$ | $4_z/m_z, 2_z^*/m_z^*$ | 4 | 4 | 0 | 4 |
| | 1 | Reducible | $4_z/m_z$ | $\bar{4}_z, 4_z, m_z^*, 2_z^*, \bar{1}^*$ | 8 | 8 | 8 | 4 |
| $4_z 2_x 2_{xy}$ | 4_z | A_2 | $4_z 2_x 2_{xy}$ | $4_z 2_x^* 2_{xy}$ | 2 | 2 | 2 | 1 |
| | $2_{xy} 2_{xy} 2_z$ | B_2 | $4_z 2_x 2_{xy}$ | $4_z^* 2_x^* 2_{xy}$ | 2 | 2 | 0 | 2 |
| | $2_x 2_y 2_z$ | B_1 | $4_z 2_x 2_{xy}$ | $4_z^* 2_x^* 2_{xy}$ | 2 | 2 | 0 | 2 |
| | $2_{xy} (2_{x\bar{y}})$ | E | $2_{xy} 2_{xy} 2_z$ | $4_z 2_x^* 2_{xy}, 2_{xy}^* 2_{xy} 2_z^*$ | 4 | 2 | 2 | 2 |
| | 2_z | Reducible | $4_z 2_x 2_{xy}$ | $4_z^*, 2_x^* 2_y^* 2_z, 2_{x\bar{y}}^* 2_{xy} 2_z$ | 4 | 4 | 2 | 2 |
| | $2_x (2_y)$ | E | $2_{xy} 2_{xy} 2_z$ | $4_z 2_x^* 2_{xy}, 2_x 2_y^* 2_z^*$ | 4 | 2 | 2 | 2 |
| | 1 | E | $4_z 2_x 2_{xy}$ | $4_z, 2_z^*, 2_x^*(2), 2_{xy}^*(2)$ | 8 | 8 | 8 | 8 |
| $4_z m_x m_{xy}$ | 4_z | A_2 | $4_z m_x m_{xy}$ | $4_z m_x^* m_{xy}$ | 2 | 2 | 1 | 1 |
| | $m_{x\bar{y}} m_{xy} 2_z$ | B_2 | $4_z m_x m_{xy}$ | $4_z^* m_x^* m_{xy}$ | 2 | 2 | 1 | 2 |
| | $m_x m_y 2_z$ | B_1 | $4_z m_x m_{xy}$ | $4_z^* m_x m_{xy}$ | 2 | 2 | 1 | 2 |
| | $m_{xy} (m_{x\bar{y}})$ | E | $m_{x\bar{y}} m_{xy} 2_z$ | $4_z m_x m_{xy}, m_{x\bar{y}}^* m_{xy} 2_z^*$ | 4 | 2 | 4 | 4 |
| | $m_x (m_y)$ | E | $m_x m_y 2_z$ | $4_z m_x m_{xy}, m_x m_y^* 2_z^*$ | 4 | 2 | 4 | 4 |
| | 2_z | Reducible | $4_z m_x m_{xy}$ | $4_z^*, m_x^* m_y^* 2_z, m_{x\bar{y}}^* m_{xy}^* 2_z$ | 4 | 4 | 2 | 2 |
| | 1 | E | $4_z m_x m_{xy}$ | $4_z, m_x^*(2), m_{xy}^*(2), 2_z^*$ | 8 | 8 | 8 | 8 |

$\dagger u = x, y, z, xy, yz, zx, x\bar{y}, y\bar{z}, z\bar{x}, x', x'', y', y''.$

3. PHASE TRANSITIONS, TWINNING AND DOMAIN STRUCTURES

Table 3.4.2.7 (cont.)

| G | F_1 | Γ_η | $N_G(F_1)$ | K_{Ij} | n | d_F | n_e | n_a |
|------------------------|---|---------------|------------------------|---|-----|-------|-------|-------|
| $\bar{4}_z 2_x m_{xy}$ | $\bar{4}_z$ | A_2 | $\bar{4}_z 2_x m_{xy}$ | $\bar{4}_z 2_x^* m_{xy}^*$ | 2 | 2 | 0 | 1 |
| | $m_{xy} m_{xy} 2_z$ | B_2 | $\bar{4}_z 2_x m_{xy}$ | $\bar{4}_z 2_x^* m_{xy}^*$ | 2 | 2 | 2 | 2 |
| | $2_x 2_y 2_z$ | B_1 | $\bar{4}_z 2_x m_{xy}$ | $\bar{4}_z 2_x^* m_{xy}^*$ | 2 | 2 | 0 | 2 |
| | $m_{xy} (m_{xy})$ | E | $m_{xy} m_{xy} 2_z$ | $\bar{4}_z 2_x m_{xy}, m_{xy}^* m_{xy} 2_z^*$ | 4 | 2 | 4 | 4 |
| | 2_z | Reducible | $\bar{4}_z 2_x m_{xy}$ | $\bar{4}_z^*, m_{xy}^* m_{xy} 2_z^*, 2_x^* 2_y^* 2_z^*$ | 4 | 4 | 2 | 2 |
| | $2_x (2_y)$ | E | $2_x 2_y 2_z$ | $\bar{4}_z 2_x m_{xy}, 2_x 2_y^* 2_z^*$ | 4 | 2 | 4 | 4 |
| | 1 | E | $\bar{4}_z 2_x m_{xy}$ | $\bar{4}_z, m_{xy}^*(2), 2_z^*, 2_x^*(2)$ | 8 | 8 | 8 | 8 |
| $\bar{4}_z m_x 2_{xy}$ | $\bar{4}_z$ | A_2 | $\bar{4}_z m_x 2_{xy}$ | $\bar{4}_z m_x^* 2_{xy}^*$ | 2 | 2 | 0 | 1 |
| | $m_x m_y 2_z$ | B_2 | $\bar{4}_z m_x 2_{xy}$ | $\bar{4}_z m_x^* 2_{xy}^*$ | 2 | 2 | 2 | 2 |
| | $2_{xy} 2_{xy} 2_z$ | B_1 | $\bar{4}_z m_x 2_{xy}$ | $\bar{4}_z m_x^* 2_{xy}^*$ | 2 | 2 | 0 | 2 |
| | $m_x (m_y)$ | E | $m_x m_y 2_z$ | $\bar{4}_z m_x 2_{xy}, m_x m_y^* 2_z^*$ | 4 | 2 | 4 | 4 |
| | $2_{xy} (2_{xy})$ | E | $2_{xy} 2_{xy} 2_z$ | $\bar{4}_z m_x 2_{xy}, 2_{xy}^* 2_{xy} 2_z^*$ | 4 | 2 | 4 | 4 |
| | 2_z | Reducible | $\bar{4}_z m_x 2_{xy}$ | $\bar{4}_z^*, m_x^* m_y^* 2_z^*, 2_{xy}^* 2_{xy} 2_z^*$ | 4 | 4 | 2 | 2 |
| | 1 | E | $\bar{4}_z m_x 2_{xy}$ | $\bar{4}_z, m_x^*(2), 2_{xy}^*(2), 2_z^*$ | 8 | 8 | 8 | 8 |
| $4_z/m_z m_x m_{xy}$ | $\bar{4}_z m_x 2_{xy}$ | B_{2u} | $4_z/m_z m_x m_{xy}$ | $4_z^*/m_z^* m_x^* m_{xy}^*$ | 2 | 2 | 0 | 1 |
| | $\bar{4}_z 2_x m_{xy}$ | B_{1u} | $4_z/m_z m_x m_{xy}$ | $4_z^*/m_z^* m_x^* m_{xy}^*$ | 2 | 2 | 0 | 1 |
| | $4_z m_x m_{xy}$ | A_{2u} | $4_z/m_z m_x m_{xy}$ | $4_z^*/m_z^* m_x^* m_{xy}^*$ | 2 | 2 | 2 | 1 |
| | $4_z 2_x 2_{xy}$ | A_{1u} | $4_z/m_z m_x m_{xy}$ | $4_z^*/m_z^* m_x^* m_{xy}^*$ | 2 | 2 | 0 | 1 |
| | $4_z/m_z$ | A_{2g} | $4_z/m_z m_x m_{xy}$ | $4_z^*/m_z^* m_x^* m_{xy}^*$ | 2 | 2 | 0 | 1 |
| | $\bar{4}_z$ | Reducible | $4_z/m_z m_x m_{xy}$ | $\bar{4}_z 2_x^* m_{xy}^*, \bar{4}_z m_x^* 2_{xy}^*, 4_z^*/m_z^*$ | 4 | 4 | 0 | 1 |
| | 4_z | Reducible | $4_z/m_z m_x m_{xy}$ | $4_z m_x^* m_{xy}^*, 4_z 2_x^* 2_{xy}^*, 4_z^*/m_z^*$ | 4 | 4 | 2 | 1 |
| | $m_{xy} m_{xy} m_z$ | B_{2g} | $4_z/m_z m_x m_{xy}$ | $4_z^*/m_z^* m_x^* m_{xy}^*$ | 2 | 2 | 0 | 2 |
| | $m_x m_y m_z$ | B_{1g} | $m_x m_y m_z$ | $4_z^*/m_z^* m_x^* m_{xy}^*$ | 2 | 2 | 0 | 2 |
| | $2_{xy} m_{xy} m_z (m_{xy} 2_{xy} m_z)$ | E_u | $m_{xy} m_{xy} m_z$ | $4_z/m_z m_x m_{xy}, m_{xy}^* m_{xy} m_z^*$ | 4 | 2 | 4 | 2 |
| | $2_x m_y m_z (m_x 2_y m_z)$ | E_u | $m_x m_y m_z$ | $4_z/m_z m_x m_{xy}, m_x^* m_y m_z^*$ | 4 | 2 | 4 | 2 |
| | $m_{xy} m_{xy} 2_z$ | Reducible | $4_z/m_z m_x m_{xy}$ | $\bar{4}_z 2_x^* m_{xy}^*, 4_z^* m_x^* m_{xy}^*, m_{xy} m_{xy} m_z^*$ | 4 | 4 | 2 | 2 |
| | $m_x m_y 2_z$ | Reducible | $4_z/m_z m_x m_{xy}$ | $\bar{4}_z^* m_x^* 2_{xy}^*, 4_z^* m_x^* m_{xy}^*, m_x m_y m_z^*$ | 4 | 4 | 2 | 2 |
| | $2_{xy} 2_{xy} 2_z$ | Reducible | $4_z/m_z m_x m_{xy}$ | $\bar{4}_z^* m_x^* 2_{xy}^*, 4_z^* 2_x^* 2_{xy}^*, m_{xy}^* m_{xy} m_z^*$ | 4 | 4 | 0 | 2 |
| | $2_x 2_y 2_z$ | Reducible | $4_z/m_z m_x m_{xy}$ | $\bar{4}_z^* 2_x^* m_{xy}^*, 4_z^* 2_x^* 2_{xy}^*, m_x^* m_y^* m_z^*$ | 4 | 4 | 0 | 2 |
| | $2_{xy}/m_{xy} (2_{xy}/m_{xy})$ | E_g | $m_{xy} m_{xy} m_z$ | $4_z/m_z m_x m_{xy}, m_{xy}^* m_{xy} m_z^*$ | 4 | 2 | 0 | 4 |
| | $2_z/m_z$ | Reducible | $4_z/m_z m_x m_{xy}$ | $4_z^*/m_z^*, m_{xy}^* m_{xy} m_z^*, m_x^* m_y^* m_z^*$ | 4 | 4 | 0 | 4 |
| | $2_x/m_x (2_y/m_y)$ | E_g | $m_x m_y m_z$ | $4_z/m_z m_x m_{xy}, m_x m_y m_z^*$ | 4 | 2 | 0 | 4 |
| | $m_{xy} (m_{xy})$ | Reducible | $m_{xy} m_{xy} m_z$ | $\bar{4}_z 2_x m_{xy}, 4_z m_x m_{xy}, 2_{xy}^* m_{xy} m_z^*, m_{xy}^* m_{xy} 2_z^*, 2_{xy}^*/m_{xy}$ | 8 | 4 | 8 | 4 |
| | m_z | Reducible | $4_z/m_z m_x m_{xy}$ | $4_z/m_z, 2_{xy}^* m_{xy} m_z^*(2), 2_x^* m_y^* m_z^*(2), 2_z^*/m_z$ | 8 | 8 | 8 | 4 |
| | $m_x (m_y)$ | Reducible | $m_x m_y m_z$ | $\bar{4}_z m_x 2_{xy}, 4_z m_x m_{xy}, m_x m_y^* 2_z^*, m_x^* m_y^* m_z^*, 2_x^*/m_x$ | 8 | 4 | 8 | 4 |
| | $2_{xy} (2_{xy})$ | Reducible | $m_{xy} m_{xy} m_z$ | $\bar{4}_z m_x 2_{xy}, 4_z 2_x 2_{xy}, m_{xy}^* 2_{xy} m_z^*, 2_{xy}^* 2_{xy} 2_z^*, 2_{xy}^*/m_{xy}$ | 8 | 4 | 8 | 4 |
| | 2_z | Reducible | $4_z/m_z m_x m_{xy}$ | $\bar{4}_z^*, 4_z^*, m_x^* m_y^* 2_z^*, m_{xy}^* m_{xy}^* 2_z^*, 2_x^* 2_y^* 2_z^*, 2_{xy}^* 2_{xy}^* 2_z^*, 2_z^*/m_z^*$ | 8 | 8 | 2 | 4 |
| | $2_x (2_y)$ | Reducible | $m_x m_y m_z$ | $\bar{4}_z 2_x m_{xy}, 4_z 2_x 2_{xy}, 2_x m_y^* m_z^*, 2_x^* 2_y^* 2_z^*, 2_x^*/m_x$ | 8 | 4 | 4 | 4 |
| | $\bar{1}$ | E_g | $4_z/m_z m_x m_{xy}$ | $4_z/m_z, 2_{xy}^*/m_{xy}^*(2), 2_z^*/m_z^*, 2_x^*/m_x^*(2)$ | 8 | 8 | 0 | 8 |
| | 1 | Reducible | $4_z/m_z m_x m_{xy}$ | $\bar{4}_z, 4_z^*, m_{xy}^*(2), m_z^*, m_x^*(2), 2_{xy}^*(2), 2_z^*, 2_x^*(2), 1^*$ | 16 | 16 | 16 | 8 |
| 3_z | 1 | E | 3_z | 3_z | 3 | 3 | 3 | 3 |
| $\bar{3}_z$ | 3_z | A_u | $\bar{3}_z$ | $\bar{3}_z$ | 2 | 2 | 2 | 1 |
| | $\bar{1}$ | E_g | $\bar{3}_z$ | $\bar{3}_z$ | 3 | 3 | 0 | 3 |
| | 1 | E_u | $\bar{3}_z$ | $\bar{3}_z, 3_z, \bar{1}^*$ | 6 | 6 | 6 | 3 |
| $3_z 2_x$ | 3_z | A_2 | $3_z 2_x$ | $3_z 2_x^*$ | 2 | 2 | 2 | 1 |
| | $2_x (2_{x'}, 2_{x''})$ | E | 2_x | $3_z 2_x$ | 3 | 1 | 3 | 3 |
| | 1 | E | $3_z 2_x$ | $3_z, 2_x^*(3)$ | 6 | 6 | 6 | 6 |
| $3_z 2_y$ | 3_z | A_2 | $3_z 2_y$ | $3_z 2_y^*$ | 2 | 2 | 2 | 1 |
| | $2_y (2_{y'}, 2_{y''})$ | E | 2_y | $3_z 2_y$ | 3 | 1 | 3 | 3 |
| | 1 | E | $3_z 2_y$ | $3_z, 2_y^*(3)$ | 6 | 6 | 6 | 6 |
| $3_z m_x$ | 3_z | A_2 | $3_z m_x$ | $3_z m_x^*$ | 2 | 2 | 1 | 1 |
| | $m_x (m_{x'}, m_{x''})$ | E | m_x | $3_z m_x$ | 3 | 1 | 3 | 3 |
| | 1 | E | $3_z m_x$ | $3_z, m_x^*(3)$ | 6 | 6 | 6 | 6 |
| $3_z m_y$ | 3_z | A_2 | $3_z m_y$ | $3_z m_y^*$ | 2 | 2 | 1 | 1 |
| | $m_y (m_{y'}, m_{y''})$ | E | m_y | $3_z m_y$ | 3 | 1 | 3 | 3 |
| | 1 | E | $3_z m_y$ | $3_z, m_y^*(3)$ | 6 | 6 | 6 | 6 |

3.4. DOMAIN STRUCTURES

Table 3.4.2.7 (cont.)

| G | F_1 | Γ_η | $N_G(F_1)$ | K_{1j} | n | d_F | n_e | n_a |
|---------------------|--|---------------|---------------------|---|-----|-------|-------|-------|
| $\bar{3}_z m_x$ | $3_z m_x$ | A_{2u} | $\bar{3}_z m_x$ | $\bar{3}_z^* m_x$ | 2 | 2 | 2 | 1 |
| | $3_z 2_x$ | A_{1u} | $\bar{3}_z m_x$ | $\bar{3}_z^* m_x^*$ | 2 | 2 | 0 | 2 |
| | $\bar{3}_z$ | A_{2g} | $\bar{3}_z m_x$ | $\bar{3}_z m_x^*$ | 2 | 2 | 0 | 1 |
| | 3_z | Reducible | $\bar{3}_z m_x$ | $3_z m_x^*, 3_z 2_x^*, \bar{3}_z^*$ | 4 | 4 | 2 | 1 |
| | $2_x/m_x (2_{x'}/m_{x'}, 2_{x''}/m_{x''})$ | E_g | $2_x/m_x$ | $\bar{3}_z m_x$ | 3 | 1 | 0 | 3 |
| | $m_x (m_{x'}, m_{x''})$ | E_u | $2_x/m_x$ | $\bar{3}_z m_x, 3_z m_x, 2_x^*/m_x(3)$ | 6 | 2 | 6 | 3 |
| | $2_x (2_{x'}, 2_{x''})$ | E_u | $2_x/m_x$ | $\bar{3}_z m_x, 3_z 2_x, 2_x/m_x^*(3)$ | 6 | 2 | 6 | 3 |
| | $\bar{1}$ | E_g | $\bar{3}_z m_x$ | $\bar{3}_z, 2_x^*/m_x^*(3)$ | 6 | 6 | 0 | 6 |
| | 1 | E_u | $\bar{3}_z m_x$ | $\bar{3}_z, 3_z, m_x^*(3), 2_x^*(3), \bar{1}^*$ | 12 | 12 | 12 | 6 |
| $\bar{3}_z m_y$ | $3_z m_y$ | A_{2u} | $\bar{3}_z m_y$ | $\bar{3}_z^* m_y$ | 2 | 2 | 2 | 1 |
| | $3_z 2_y$ | A_{1u} | $\bar{3}_z m_y$ | $\bar{3}_z^* m_y^*$ | 2 | 2 | 0 | 1 |
| | $\bar{3}_z$ | A_{2g} | $\bar{3}_z m_y$ | $\bar{3}_z m_y^*$ | 2 | 2 | 0 | 1 |
| | 3_z | Reducible | $\bar{3}_z m_y$ | $3_z m_y^*, 3_z 2_y^*, \bar{3}_z^*$ | 4 | 4 | 0 | 1 |
| | $2_y/m_y (2_{y'}/m_{y'}, 2_{y''}/m_{y''})$ | E_g | $2_y/m_y$ | $\bar{3}_z m_y$ | 3 | 1 | 2 | 1 |
| | $m_y (m_{y'}, m_{y''})$ | E_u | $2_y/m_y$ | $\bar{3}_z m_y, 3_z m_y, 2_y^*/m_y(3)$ | 6 | 2 | 0 | 3 |
| | $2_y (2_{y'}, 2_{y''})$ | E_u | $2_y/m_y$ | $\bar{3}_z m_y, 3_z 2_y, 2_y/m_y^*(3)$ | 6 | 2 | 6 | 3 |
| | $\bar{1}$ | E_g | $\bar{3}_z m_y$ | $\bar{3}_z, 2_y^*/m_y^*(3)$ | 6 | 6 | 0 | 3 |
| | 1 | E_u | $\bar{3}_z m_y$ | $\bar{3}_z, 3_z, m_y^*(3), 2_y^*(3), \bar{1}^*$ | 12 | 12 | 12 | 6 |
| 6_z | 3_z | B | 6_z | 6_z^* | 2 | 2 | 1 | 1 |
| | 2_z | E_2 | 6_z | 6_z | 3 | 3 | 1 | 3 |
| | 1 | E_1 | 6_z | $6_z, 3_z, 2_z^*$ | 6 | 6 | 6 | 6 |
| $\bar{6}_z$ | 3_z | A'' | $\bar{6}_z$ | $\bar{6}_z^*$ | 2 | 2 | 2 | 1 |
| | m_z | E' | $\bar{6}_z$ | $\bar{6}_z$ | 3 | 2 | 3 | 3 |
| | 1 | E'' | $\bar{6}_z$ | $\bar{6}_z, 3_z, m_z^*$ | 6 | 6 | 6 | 6 |
| $6_z/m_z$ | $\bar{6}_z$ | B_u | $6_z/m_z$ | $6_z^*/m_z$ | 2 | 2 | 0 | 1 |
| | 6_z | A_u | $6_z/m_z$ | $6_z/m_z^*$ | 2 | 2 | 2 | 1 |
| | $\bar{3}_z$ | B_g | $6_z/m_z$ | $6_z^*/m_z^*$ | 2 | 2 | 0 | 1 |
| | 3_z | Reducible | $6_z/m_z$ | $\bar{6}_z^*, 6_z^*, \bar{3}_z^*$ | 4 | 4 | 2 | 1 |
| | $2_z/m_z$ | E_{2g} | $6_z/m_z$ | $6_z/m_z$ | 3 | 3 | 0 | 3 |
| | m_z | E_{1u} | $6_z/m_z$ | $6_z/m_z, \bar{6}_z, 2_z^*/m_z$ | 6 | 6 | 6 | 3 |
| | 2_z | E_{2u} | $6_z/m_z$ | $6_z/m_z, 6_z, 2_z/m_z^*$ | 6 | 6 | 2 | 3 |
| | $\bar{1}$ | E_{1g} | $6_z/m_z$ | $6_z/m_z, \bar{3}_z, 2_z^*/m_z^*$ | 6 | 6 | 0 | 6 |
| | 1 | Reducible | $6_z/m_z$ | $\bar{6}_z, 6_z, \bar{3}_z, 3_z, m_z^*, 2_z^*, \bar{1}^*$ | 12 | 12 | 12 | 6 |
| $6_z 2_x 2_y$ | 6_z | A_2 | $6_z 2_x 2_y$ | $6_z 2_x^* 2_y^*$ | 2 | 2 | 2 | 1 |
| | $3_z 2_x$ | B_1 | $6_z 2_x 2_y$ | $6_z^* 2_x^* 2_y^*$ | 2 | 2 | 0 | 1 |
| | $3_z 2_y$ | B_2 | $6_z 2_x 2_y$ | $6_z^* 2_x^* 2_y$ | 2 | 2 | 0 | 1 |
| | 3_z | Reducible | $6_z 2_x 2_y$ | $6_z^*, 3_z 2_x^*, 3_z 2_y^*$ | 4 | 4 | 2 | 1 |
| | $2_x 2_y 2_z (2_{x'} 2_{y'} 2_z, 2_{x''} 2_{y''} 2_z)$ | E_2 | $2_x 2_y 2_z$ | $6_z 2_x 2_y$ | 3 | 1 | 0 | 3 |
| | 2_x | E_2 | $6_z 2_x 2_y$ | $6_z, 2_x^* 2_y^* 2_z(3)$ | 6 | 6 | 2 | 6 |
| | $2_x (2_{x'}, 2_{x''})$ | E_1 | $2_x 2_y 2_z$ | $6_z 2_x 2_y, 3_z 2_x, 2_x^* 2_y^* 2_z^*$ | 6 | 2 | 6 | 6 |
| | $2_y (2_{y'}, 2_{y''})$ | E_1 | $2_x 2_y 2_z$ | $6_z 2_x 2_y, 3_z 2_y, 2_x^* 2_y^* 2_z^*$ | 6 | 2 | 6 | 6 |
| | 1 | E_1 | $6_z 2_x 2_y$ | $6_z, 3_z, 2_z^*, 2_x^*(3), 2_y^*(3)$ | 12 | 12 | 12 | 12 |
| $6_z m_x m_y$ | 6_z | A_2 | $6_z m_x m_y$ | $6_z m_x^* m_y^*$ | 2 | 2 | 1 | 1 |
| | $3_z m_x$ | B_2 | $6_z m_x m_y$ | $6_z^* m_x^* m_y^*$ | 2 | 2 | 1 | 1 |
| | $3_z m_y$ | B_1 | $6_z m_x m_y$ | $6_z^* m_x^* m_y$ | 2 | 2 | 1 | 1 |
| | 3_z | Reducible | $6_z m_x m_y$ | $6_z^*, 3_z m_x^*, 3_z m_y^*$ | 4 | 4 | 1 | 1 |
| | $m_x m_y 2_z (m_{x'} m_{y'} 2_z, m_{x''} m_{y''} 2_z)$ | E_2 | $m_x m_y 2_z$ | $6_z m_x m_y$ | 3 | 1 | 1 | 3 |
| | $m_x (m_{x'}, m_{x''})$ | E_1 | $m_x m_y 2_z$ | $6_z m_x m_y, 3_z m_x, m_x m_y^* 2_z^*$ | 6 | 2 | 6 | 6 |
| | $m_y (m_{y'}, m_{y''})$ | E_1 | $m_x m_y 2_z$ | $6_z m_x m_y, 3_z m_y, m_x^* m_y^* 2_z^*$ | 6 | 2 | 6 | 6 |
| | 2_z | E_2 | $6_z m_x m_y$ | $6_z, m_x^* m_y^* 2_z(3)$ | 6 | 6 | 1 | 6 |
| | 1 | E_1 | $6_z m_x m_y$ | $6_z, 3_z, 2_z^*, m_x^*(3), m_y^*(3)$ | 12 | 12 | 12 | 12 |
| $\bar{6}_z m_x 2_y$ | $\bar{6}_z$ | A_2' | $\bar{6}_z m_x 2_y$ | $\bar{6}_z m_x^* 2_y^*$ | 2 | 2 | 0 | 1 |
| | $3_z m_x$ | A_2'' | $\bar{6}_z m_x 2_y$ | $\bar{6}_z^* m_x^* 2_y^*$ | 2 | 2 | 2 | 1 |
| | $3_z 2_y$ | A_1' | $\bar{6}_z m_x 2_y$ | $\bar{6}_z^* m_x^* 2_y$ | 2 | 2 | 0 | 1 |
| | 3_z | Reducible | $\bar{6}_z m_x 2_y$ | $\bar{6}_z^*, 3_z m_x^*, 3_z 2_y^*$ | 4 | 4 | 2 | 1 |
| | $m_x 2_y m_z (m_{x'} 2_{y'} m_z, m_{x''} 2_{y''} m_z)$ | E' | $m_x 2_y m_z$ | $\bar{6}_z m_x 2_y$ | 3 | 1 | 3 | 3 |
| | m_z | E' | $\bar{6}_z m_x 2_y$ | $\bar{6}_z, m_x^* 2_y^* m_z(3)$ | 6 | 6 | 6 | 6 |
| | $m_x (m_{x'}, m_{x''})$ | E'' | $m_y 2_y m_z$ | $\bar{6}_z m_x 2_y, 3_z m_x, m_x 2_y^* m_z^*$ | 6 | 2 | 6 | 6 |
| | $2_y (2_{y'}, 2_{y''})$ | E'' | $m_y 2_y m_z$ | $\bar{6}_z m_x 2_y, 3_z 2_y, m_x^* 2_y^* m_z^*$ | 6 | 2 | 3 | 6 |
| | 1 | E'' | $\bar{6}_z m_x 2_y$ | $\bar{6}_z, 3_z, m_z^*, m_x^*(3), 2_y^*(3)$ | 12 | 12 | 12 | 12 |

3. PHASE TRANSITIONS, TWINNING AND DOMAIN STRUCTURES

Table 3.4.2.7 (cont.)

| G | F_1 | Γ_η | $N_G(F_1)$ | K_{1j} | n | d_F | n_e | n_a |
|------------------------------|--|---------------|---------------------|---|-----|-------|-------|-------|
| $\bar{6}_z 2_x m_y$ | $\bar{6}_z$ | A_2' | $\bar{6}_z 2_x m_y$ | $\bar{6}_z 2_x^* m_y^*$ | 2 | 2 | 0 | 1 |
| | $3_z m_y$ | A_2' | $\bar{6}_z 2_x m_y$ | $\bar{6}_z 2_x^* m_y^*$ | 2 | 2 | 2 | 1 |
| | $3_z 2_x$ | A_1'' | $\bar{6}_z 2_x m_y$ | $\bar{6}_z 2_x^* m_y^*$ | 2 | 2 | 0 | 1 |
| | 3_z | Reducible | $\bar{6}_z 2_x m_y$ | $\bar{6}_z^*, 3_z m_y^*, 3_z 2_x^*$ | 4 | 4 | 2 | 1 |
| | $2_x m_y m_z (2_x m_y m_z, 2_{x'} m_{y'} m_z)$ | E' | $m_x 2_y m_z$ | $\bar{6}_z 2_x m_y$ | 3 | 1 | 3 | 3 |
| | m_z | E' | $\bar{6}_z 2_x m_y$ | $\bar{6}_z, 2_x^* m_y^* m_z(3)$ | 6 | 6 | 6 | 6 |
| | $m_y (m_{y'}, m_{y''})$ | E'' | $m_x 2_y m_z$ | $\bar{6}_z 2_x m_y, 3_z m_y, 2_x^* m_y m_z^*$ | 6 | 2 | 6 | 6 |
| | $2_x (2_{x'}, 2_{x''})$ | E'' | $m_x 2_y m_z$ | $\bar{6}_z 2_x m_y, 3_z 2_x, 2_x^* m_y m_z^*$ | 6 | 2 | 3 | 6 |
| | 1 | E'' | $\bar{6}_z 2_x m_y$ | $\bar{6}_z, 3_z, m_z^*, m_y^*(3), 2_x^*(3)$ | 12 | 12 | 12 | 12 |
| $6_z/m_z m_x m_y$ | $\bar{6}_z m_x 2_y$ | B_{2u} | $6_z/m_z m_x m_y$ | $6_z^*/m_z m_x m_y^*$ | 2 | 2 | 0 | 1 |
| | $\bar{6}_z 2_x m_y$ | B_{1u} | $6_z/m_z m_x m_y$ | $6_z^*/m_z m_x^* m_y$ | 2 | 2 | 0 | 1 |
| | $6_z m_x m_y$ | A_{2u} | $6_z/m_z m_x m_y$ | $6_z/m_z^* m_x m_y$ | 2 | 2 | 2 | 1 |
| | $6_z 2_x 2_y$ | A_{1u} | $6_z/m_z m_x m_y$ | $6_z/m_z^* m_x^* m_y^*$ | 2 | 2 | 0 | 1 |
| | $6_z/m_z$ | A_{2g} | $6_z/m_z m_x m_y$ | $6_z/m_z m_x^* m_y^*$ | 2 | 2 | 0 | 1 |
| | $\bar{6}_z$ | Reducible | $6_z/m_z m_x m_y$ | $\bar{6}_z m_x^* 2_y^*, \bar{6}_z 2_x^* m_y^*, 6_z^*/m_z$ | 4 | 4 | 0 | 1 |
| | 6_z | Reducible | $6_z/m_z m_x m_y$ | $6_z m_x^* m_y^*, 6_z 2_x^* 2_y^*, 6_z/m_z^*$ | 4 | 4 | 2 | 1 |
| | $\bar{3}_z m_x$ | B_{1g} | $6_z/m_z m_x m_y$ | $6_z^*/m_z^* m_x m_y^*$ | 2 | 2 | 0 | 1 |
| | $\bar{3}_z m_y$ | B_{2g} | $6_z/m_z m_x m_y$ | $6_z^*/m_z^* m_x^* m_y$ | 2 | 2 | 0 | 1 |
| | $3_z m_x$ | Reducible | $6_z/m_z m_x m_y$ | $\bar{6}_z^* m_x 2_y^*, 6_z^* m_x m_y^*, \bar{3}_z^* m_x$ | 4 | 4 | 2 | 1 |
| | $3_z m_y$ | Reducible | $6_z/m_z m_x m_y$ | $\bar{6}_z^* 2_x^* m_y, 6_z^* m_x^* m_y, \bar{3}_z^* m_y$ | 4 | 4 | 2 | 1 |
| | $3_z 2_x$ | Reducible | $6_z/m_z m_x m_y$ | $\bar{6}_z^* 2_x m_y^*, 6_z^* 2_x 2_y^*, \bar{3}_z^* m_x^*$ | 4 | 4 | 0 | 1 |
| | $3_z 2_y$ | Reducible | $6_z/m_z m_x m_y$ | $\bar{6}_z^* m_x^* 2_y, 6_z^* 2_x^* 2_y, \bar{3}_z^* m_y^*$ | 4 | 4 | 0 | 1 |
| | $\bar{3}_z$ | Reducible | $6_z/m_z m_x m_y$ | $6_z^*/m_z^*, \bar{3}_z m_x^*, \bar{3}_z m_y^*$ | 4 | 4 | 0 | 1 |
| | 3_z | Reducible | $6_z/m_z m_x m_y$ | $\bar{6}_z^*, 6_z^*, 3_z m_x^*, 3_z m_y^*, 3_z 2_x^*, 3_z 2_y^*, \bar{3}_z^*$ | 8 | 8 | 2 | 1 |
| | $m_x m_y m_z (m_{x'} m_{y'} m_z, m_{x''} m_{y''} m_z)$ | E_{2g} | $m_x m_y m_z$ | $6_z/m_z m_x m_y$ | 3 | 1 | 0 | 3 |
| | $m_x m_y 2_z (m_{x'} m_{y'} 2_z, m_{x''} m_{y''} 2_z)$ | E_{2u} | $m_x m_y m_z$ | $6_z/m_z m_x m_y, 6_z m_x m_y, m_x m_y m_z^*$ | 6 | 2 | 2 | 3 |
| | $2_x m_y m_z (2_{x'} m_{y'} m_z, 2_{x''} m_{y''} m_z)$ | E_{1u} | $m_x m_y m_z$ | $6_z/m_z m_x m_z, \bar{6}_z 2_x m_y, m_x^* m_y m_z$ | 6 | 2 | 6 | 3 |
| | $m_x 2_y m_z (m_{x'} 2_{y'} m_z, m_{x''} 2_{y''} m_z)$ | E_{1u} | $m_x m_y m_z$ | $6_z/m_z m_x m_z, \bar{6}_z m_x 2_y, m_x m_y^* m_z$ | 6 | 2 | 6 | 3 |
| | $2_x 2_y 2_z (2_{x'} 2_{y'} 2_z, 2_{x''} 2_{y''} 2_z)$ | E_{2u} | $m_x m_y m_z$ | $6_z/m_z m_x m_y, 6_z 2_x 2_y, m_x^* m_y^* m_z^*$ | 6 | 6 | 0 | 3 |
| | $2_z/m_z$ | E_{2g} | $6_z/m_z m_x m_y$ | $6_z/m_z, m_x^* m_y^* m_z(3)$ | 6 | 6 | 0 | 6 |
| | $2_x/m_x (2_{x'}/m_{x'}, 2_{x''}/m_{x''})$ | E_{1g} | $m_x m_y m_z$ | $6_z/m_z m_x m_y, \bar{3}_z m_x, m_x m_y m_z^*$ | 6 | 2 | 0 | 6 |
| | $2_y/m_y (2_{y'}/m_{y'}, 2_{y''}/m_{y''})$ | E_{1g} | $m_x m_y m_z$ | $6_z/m_z m_x m_y, \bar{3}_z m_y, m_x m_y m_z^*$ | 6 | 2 | 0 | 6 |
| | m_z | E_{1u} | $6_z/m_z m_x m_y$ | $6_z/m_z, \bar{6}_z, 2_x^* m_y^* m_z, m_x^* 2_y^* m_z, 2_z^*/m_z$ | 12 | 12 | 12 | 6 |
| | $m_x (m_{x'}, m_{x''})$ | Reducible | $m_x m_y m_z$ | $\bar{6}_z m_x 2_y, 6_z m_x m_y, \bar{3}_z m_x, 3_z m_x, m_x m_y^* 2_z^*, m_x 2_y^* m_z^*, 2_x^*/m_x$ | 12 | 4 | 12 | 6 |
| | $m_y (m_{y'}, m_{y''})$ | Reducible | $m_x m_y m_z$ | $\bar{6}_z 2_x m_y, 6_z m_x m_y, \bar{3}_z m_y, 3_z m_y, m_x m_y^* 2_z^*, 2_x^* m_y m_z^*, 2_y^*/m_y$ | 12 | 4 | 12 | 6 |
| | 2_z | E_{2u} | $6_z/m_z m_x m_y$ | $6_z/m_z, 6_z, m_x^* m_y^* 2_z(3), 2_x^* 2_y^* 2_z(3), 2_z/m_z^*$ | 12 | 12 | 2 | 6 |
| | $2_x (2_{x'}, 2_{x''})$ | Reducible | $m_x m_y m_z$ | $\bar{6}_z 2_x m_y, 6_z 2_x 2_y, \bar{3}_z m_x, 3_z 2_x, 2_x m_y^* m_z^*, 2_x 2_y^* 2_z^*, 2_x/m_x$ | 12 | 4 | 6 | 6 |
| | $2_y (2_{y'}, 2_{y''})$ | Reducible | $m_x m_y m_z$ | $\bar{6}_z m_x 2_y, 6_z 2_x 2_y, \bar{3}_z m_y, 3_z 2_y, m_x^* 2_y m_z^*, 2_x^* 2_y^* 2_z^*, 2_y/m_y$ | 12 | 4 | 6 | 6 |
| | $\bar{1}$ | E_{1g} | $6_z/m_z m_x m_y$ | $6_z/m_z, \bar{3}_z, 2_z^*/m_z^*, 2_x^*/m_x^*(3), 2_y^*/m_y^*(3)$ | 12 | 12 | 0 | 12 |
| | 1 | Reducible | $6_z/m_z m_x m_y$ | $\bar{6}_z, 6_z, \bar{3}_z, 3_z, m_z^*, m_x^*(3), m_y^*(3), 2_z^*, 2_x^*(3), 2_y^*(3), \bar{1}^*$ | 24 | 24 | 24 | 12 |
| 23 | $3_p (3_q, 3_r, 3_s)$ | T | 3_p | 23 | 4 | 1 | 4 | 4 |
| | $2_x 2_y 2_z$ | E | 23 | 23 | 3 | 3 | 0 | 3 |
| | $2_z (2_x, 2_y)$ | T | $2_x 2_y 2_z$ | $23, 2_x^* 2_y^* 2_z$ | 6 | 2 | 6 | 6 |
| | 1 | T | 23 | $3_p(4), 2_z^*(3)$ | 12 | 12 | 12 | 12 |
| $m\bar{3}$ | 23 | A_u | $m\bar{3}$ | $m^* \bar{3}^*$ | 2 | 2 | 0 | 1 |
| | $\bar{3}_p (\bar{3}_q, \bar{3}_r, \bar{3}_s)$ | T_g | $\bar{3}_p$ | $m\bar{3}$ | 4 | 1 | 0 | 4 |
| | $3_p (3_q, 3_r, 3_s)$ | T_u | $\bar{3}_p$ | $m\bar{3}, 23$ | 8 | 2 | 8 | 4 |
| | $m_x m_y m_z$ | E_g | $m\bar{3}$ | $m\bar{3}$ | 3 | 3 | 0 | 3 |
| | $m_x m_y 2_z (2_x m_y m_z, m_x 2_y m_z)$ | T_u | $m_x m_y m_z$ | $m\bar{3}, m_x m_y m_z^*$ | 6 | 2 | 6 | 3 |
| | $2_x 2_y 2_z$ | E_u | $m\bar{3}$ | $m\bar{3}, 23, m_x^* m_y^* m_z^*$ | 6 | 6 | 0 | 3 |
| | $2_z/m_z (2_x/m_x, 2_y/m_y)$ | T_g | $m_x m_y m_z$ | $m\bar{3}, m_x^* m_y^* m_z$ | 6 | 2 | 0 | 6 |
| | $m_z (m_x, m_y)$ | Reducible | $m_x m_y m_z$ | $m\bar{3}, 2_x^* m_y^* m_z, m_x^* 2_y^* m_z, 2_z^*/m_z$ | 12 | 4 | 12 | 6 |
| | $2_z (2_x, 2_y)$ | Reducible | $m_x m_y m_z$ | $m\bar{3}, 23, m_x^* m_y^* 2_z, 2_x^* 2_y^* 2_z, 2_z/m_z^*$ | 12 | 4 | 6 | 6 |
| | $\bar{1}$ | T_g | $m\bar{3}$ | $\bar{3}_p(4), 2_z^*/m_z^*(3)$ | 12 | 12 | 0 | 12 |
| | 1 | T_u | $m\bar{3}$ | $\bar{3}_p(4), 3_p(4), m_z^*(3), 2_z^*(3), \bar{1}^*$ | 24 | 24 | 24 | 12 |

3.4. DOMAIN STRUCTURES

Table 3.4.2.7 (cont.)

| G | F_1 | Γ_η | $N_G(F_1)$ | K_{Ij} | n | d_F | n_e | n_a |
|-------------------------------|---|------------------|---------------------------|---|-----|-------|-------|-------|
| 432 | 23 | A_2 | 432 | 4^*32^* | 2 | 2 | 0 | 1 |
| | $3_p 2_{x\bar{y}} (3_q 2_{x\bar{y}}, 3_r 2_{xy}, 3_s 2_{xy})$ | T_2 | $3_p 2_{x\bar{y}}$ | 432 | 4 | 1 | 0 | 4 |
| | $3_p (3_q, 3_r, 3_s)$ | T_1 | $3_p 2_{x\bar{y}}$ | $23, 3_p 2_{x\bar{y}}^*$ | 8 | 2 | 8 | 4 |
| | $4_z 2_x 2_{xy} (4_x 2_y 2_{yz}, 4_y 2_z 2_{xz})$ | E | $4_z 2_x 2_{xy}$ | 432 | 3 | 1 | 0 | 3 |
| | $4_z (4_x, 4_y)$ | T_1 | $4_z 2_x 2_{xy}$ | $432, 4_z 2_x 2_{xy}^*$ | 6 | 2 | 6 | 3 |
| | $2_x 2_y 2_z$ | E | 432 | $23, 4_z^* 2_x^* 2_{xy}^*$ | 6 | 6 | 0 | 6 |
| | $2_{xy} 2_{xy} 2_z (2_{yz} 2_{yz} 2_x, 2_{zx} 2_{zx} 2_y)$ | T_2 | $4_z 2_x 2_{xy}$ | $432, 4_z^* 2_x^* 2_{xy}^*$ | 6 | 2 | 0 | 6 |
| | $2_z (2_x, 2_y)$ | Reducible | $4_z 2_x 2_{xy}$ | $23, 4_y 2_z 2_{xy}, 4_z^*, 2_{xy}^* 2_{xy}^* 2_z, 2_x^* 2_y^* 2_z$ | 12 | 4 | 6 | 12 |
| | $2_{xy} (2_{yz}, 2_{zx}, 2_{x\bar{y}}, 2_{y\bar{z}}, 2_{z\bar{x}})$ | T_1, T_2 | $2_{xy} 2_{xy} 2_z$ | $432, 3_r 2_{xy}, 3_s 2_{xy}, 4_z 2_x 2_{xy}, 2_{xy} 2_{xy}^* 2_z^*$ | 12 | 2 | 12 | 12 |
| | 1 | T_1, T_2 | 432 | $3_p(4), 4_z(3), 2_z^*(3), 2_{xy}^*(6)$ | 24 | 24 | 24 | 24 |
| $\bar{4}3m$ | 23 | A_2 | $\bar{4}3m$ | $\bar{4}^*3m^*$ | 2 | 2 | 0 | 1 |
| | $3_p m_{x\bar{y}} (3_q m_{x\bar{y}}, 3_r m_{xy}, 3_s m_{xy})$ | T_2 | $3_p m_{x\bar{y}}$ | $\bar{4}3m$ | 4 | 1 | 4 | 4 |
| | $3_p (3_q, 3_r, 3_s)$ | T_1 | $3_p m_{x\bar{y}}$ | $\bar{4}3m, 23, 3_p m_{x\bar{y}}^*$ | 8 | 2 | 4 | 4 |
| | $\bar{4}_z 2_x m_{xy} (\bar{4}_x 2_y m_{yz}, \bar{4}_y 2_z m_{zx})$ | E | $\bar{4}_z 2_x m_{xy}$ | $\bar{4}3m$ | 3 | 1 | 0 | 3 |
| | $\bar{4}_z (\bar{4}_x, \bar{4}_y)$ | T_1 | $\bar{4}_z 2_x m_{xy}$ | $\bar{4}3m, \bar{4}_z 2_x^* m_{xy}^*$ | 6 | 2 | 0 | 3 |
| | $m_{x\bar{y}} m_{xy} 2_z (m_{yz} m_{yz} 2_x, m_{zx} m_{zx} 2_y)$ | T_2 | $\bar{4}_z 2_x m_{xy}$ | $\bar{4}3m, \bar{4}_z^* 2_x^* m_{xy}^*$ | 6 | 2 | 6 | 6 |
| | $2_x 2_y 2_z$ | E | $\bar{4}3m$ | $23, \bar{4}_z^* 2_x^* m_{xy}^*$ | 6 | 6 | 0 | 6 |
| | $m_{xy} (m_{yz}, m_{zx}, m_{x\bar{y}}, m_{y\bar{z}}, m_{z\bar{x}})$ | T_1, T_2 | $m_{x\bar{y}} m_{xy} 2_z$ | $\bar{4}3m, 3, m_{xy}, 3, m_{xy}, \bar{4}_z 2_x m_{xy}, m_{x\bar{y}}^* m_{xy} 2_z^*$ | 12 | 2 | 12 | 12 |
| | $2_z (2_x, 2_y)$ | Reducible | $\bar{4}_z 2_x m_{xy}$ | $23, \bar{4}_z^*, 4_z^*, m_{x\bar{y}}^* m_{xy}^* 2_z, 2_x^* 2_y^* 2_z$ | 12 | 4 | 6 | 12 |
| | 1 | T_1, T_2 | $\bar{4}3m$ | $3_p(4), \bar{4}_z(3), m_{xy}^*(6), 2_z^*(3)$ | 24 | 24 | 24 | 24 |
| $m\bar{3}m$ | $\bar{4}3m$ | A_{2u} | $m\bar{3}m$ | $m^* \bar{3}^* m$ | 2 | 2 | 0 | 1 |
| | 432 | A_{1u} | $m\bar{3}m$ | $m^* \bar{3}^* m^*$ | 2 | 2 | 0 | 1 |
| | $m\bar{3}$ | A_{2g} | $m\bar{3}m$ | $m\bar{3}m^*$ | 2 | 2 | 0 | 1 |
| | 23 | Reducible | $m\bar{3}m$ | $\bar{4}^*3m^*, 4^*32^*, m_z^* \bar{3}_p$ | 4 | 4 | 0 | 1 |
| | $\bar{3}_p m_{x\bar{y}} (\bar{3}_q m_{x\bar{y}}, \bar{3}_r m_{xy}, \bar{3}_s m_{xy})$ | T_{2g} | $\bar{3}_p m_{x\bar{y}}$ | $m\bar{3}m$ | 4 | 1 | 0 | 4 |
| | $3_p m_{x\bar{y}} (3_q m_{x\bar{y}}, 3_r m_{xy}, 3_s m_{xy})$ | T_{1u} | $\bar{3}_p m_{x\bar{y}}$ | $m\bar{3}m, \bar{4}3m, \bar{3}_p^* m_{x\bar{y}}$ | 8 | 2 | 8 | 4 |
| | $3_p 2_{x\bar{y}} (3_q 2_{x\bar{y}}, 3_r 2_{xy}, 3_s 2_{xy})$ | T_{2u} | $\bar{3}_p m_{x\bar{y}}$ | $m\bar{3}m, 432, \bar{3}_p^* m_{x\bar{y}}$ | 8 | 2 | 0 | 4 |
| | $\bar{3}_p (\bar{3}_q, \bar{3}_r, \bar{3}_s)$ | T_{1g} | $\bar{3}_p m_{x\bar{y}}$ | $m\bar{3}m, m\bar{3}, \bar{3}_p^* m_{x\bar{y}}$ | 8 | 2 | 0 | 4 |
| | $3_p (3_q, 3_r, 3_s)$ | Reducible | $\bar{3}_p m_{x\bar{y}}$ | $\bar{4}3m, 432, m\bar{3}, 23, 3_p m_{x\bar{y}}, 3_p 2_{x\bar{y}}, \bar{3}_p^*$ | 16 | 4 | 8 | 4 |
| | $4_z / m_z m_x m_{xy} (4_x / m_x m_y m_{yz}, 4_y / m_y m_z m_{zx})$ | E_g | $4_z / m_z m_x m_{xy}$ | $m\bar{3}m$ | 3 | 1 | 0 | 3 |
| | $\bar{4}_z 2_x m_{xy} (\bar{4}_x 2_y m_{yz}, \bar{4}_y 2_z m_{zx})$ | E_u | $4_z / m_z m_x m_{xy}$ | $m\bar{3}m, \bar{4}3m, 4_z^* / m_z^* m_x^* m_{xy}^*$ | 6 | 2 | 0 | 3 |
| | $\bar{4}_z m_z 2_{xy} (\bar{4}_x m_y 2_{yz}, \bar{4}_y m_z 2_{zx})$ | T_{2u} | $4_z / m_z m_x m_{xy}$ | $m\bar{3}m, 4_z^* / m_z^* m_x^* m_{xy}^*$ | 6 | 2 | 0 | 3 |
| | $4_z m_x m_{xy} (4_x m_y m_{yz}, 4_y m_z m_{zx})$ | T_{1u} | $4_z / m_z m_x m_{xy}$ | $m\bar{3}m, 4_z / m_z^* m_x^* m_{xy}^*$ | 6 | 2 | 6 | 3 |
| | $4_z 2_x 2_{xy} (4_x 2_y 2_{yz}, 4_y 2_z 2_{zx})$ | E_u | $4_z / m_z m_x m_{xy}$ | $m\bar{3}m, 432, 4_z / m_z^* m_x^* m_{xy}^*$ | 6 | 2 | 0 | 3 |
| | $4_z / m_z (4_x / m_x, 4_y / m_y)$ | T_{1g} | $4_z / m_z m_x m_{xy}$ | $m\bar{3}m, 4_z / m_z^* m_x^* m_{xy}^*$ | 6 | 2 | 0 | 3 |
| | $\bar{4}_z (\bar{4}_x, \bar{4}_y)$ | Reducible | $4_z / m_z m_x m_{xy}$ | $m\bar{3}m, \bar{4}3m, \bar{4}_z 2_x^* m_{xy}^*, \bar{4}_z m_z^* 2_{xy}^*, 4_z^* / m_z^*$ | 12 | 4 | 0 | 3 |
| | $4_z (4_x, 4_y)$ | Reducible | $4_z / m_z m_x m_{xy}$ | $m\bar{3}m, 432, 4_z m_z^* m_{xy}^*, 4_z 2_x^* 2_{xy}^*, 4_z / m_z^*$ | 12 | 4 | 6 | 3 |
| | $m_x m_y m_z$ | E_g | $m\bar{3}m$ | $m\bar{3}, 4_z^* / m_z^* m_x^* m_{xy}^*$ | 6 | 6 | 0 | 6 |
| | $m_{x\bar{y}} m_{xy} m_z (m_{yz} m_{yz} m_x, m_{zx} m_{zx} m_y)$ | T_{2g} | $4_z / m_z m_x m_{xy}$ | $m\bar{3}m, 4_z^* / m_z^* m_x^* m_{xy}^*$ | 6 | 2 | 0 | 6 |
| | $m_x m_y 2_z (2_x m_x m_z, m_x 2_y m_z)$ | Reducible | $4_z / m_z m_x m_{xy}$ | $m\bar{3}, 4_y / m_y m_z m_{zx}, \bar{4}_z^* m_x^* 2_{xy}^*, 4_z^* m_x^* m_{xy}^*, m_x m_y m_z^*$ | 12 | 4 | 6 | 6 |
| | $m_{x\bar{y}} m_{xy} 2_z (m_{yz} m_{yz} 2_x, m_{zx} m_{zx} 2_y)$ | Reducible | $4_z / m_z m_x m_{xy}$ | $m\bar{3}m, \bar{4}3m, \bar{4}_z^* 2_x^* m_{xy}^*, 4_z^* m_x^* m_{xy}^*, m_{x\bar{y}}^* m_{xy} m_z^*$ | 12 | 4 | 6 | 6 |
| | $m_{x\bar{y}} 2_{xy} m_z (m_{yz} 2_{yz} m_x, m_{zx} 2_{zx} m_y, 2_{x\bar{y}} m_{xy} m_z, 2_{y\bar{z}} m_{yz} m_x, 2_{z\bar{x}} m_{zx} m_y)$ | T_{1u}, T_{2u} | $m_{x\bar{y}} m_{xy} m_z$ | $m\bar{3}m(m_{zx}), m\bar{3}m(2_{zx}), 4_z / m_z m_x m_{xy}, m_{x\bar{y}} m_{xy} m_z$ | 12 | 2 | 12 | 6 |
| | $2_x 2_y 2_z$ | E_u | $m\bar{3}m$ | $m\bar{3}, 23, \bar{4}_z^* 2_x^* m_{xy}^*, 4_z^* 2_{xy}^* 2_{xy}^*, m_x^* m_y^* m_z^*$ | 12 | 12 | 0 | 6 |
| | $2_{xy} 2_{xy} 2_z (2_{yz} 2_{yz} 2_x, 2_{zx} 2_{zx} 2_y)$ | E_u | $4_z / m_z m_x m_{xy}$ | $m\bar{3}m, 432, \bar{4}_z m_x^* 2_{xy}, 4_z^* 2_x^* 2_{xy}, m_{x\bar{y}}^* m_{xy}^* m_z^*$ | 12 | 4 | 0 | 6 |
| | $2_z / m_z (2_x / m_x, 2_y / m_y)$ | Reducible | $4_z / m_z m_x m_{xy}$ | $m\bar{3}, 4_y / m_y m_z m_{zx}, 4_z^* / m_z, m_x^* m_y^* m_z^*, m_{x\bar{y}}^* m_{xy}^* m_z^*$ | 12 | 4 | 0 | 12 |
| | $2_{xy} / m_{xy} (2_{yz} / m_{yz}, 2_{zx} / m_{zx}, 2_{x\bar{y}} / m_{x\bar{y}}, 2_{y\bar{z}} / m_{y\bar{z}}, 2_{z\bar{x}} / m_{z\bar{x}})$ | T_{1g}, T_{2g} | $m_{x\bar{y}} m_{xy} m_z$ | $m\bar{3}m, \bar{3}_p m_{xy}(2), 4_z / m_z m_x m_{xy}, m_{x\bar{y}}^* m_{xy} m_z^*$ | 12 | 2 | 0 | 12 |
| | $m_z (m_x, m_y)$ | T_{1u}, T_{2u} | $4_z / m_z m_x m_{xy}$ | $m\bar{3}, \bar{4}_z m_z 2_{yz}, 4_y m_z m_{zx}, 4_z / m_z, 2_x^* m_y^* m_z(2), m_{x\bar{y}}^* 2_{xy}^* m_z(2), 2_z^* / m_z$ | 24 | 8 | 24 | 12 |
| | $m_{xy} (m_{yz}, m_{zx}, m_{x\bar{y}}, m_{y\bar{z}}, m_{z\bar{x}})$ | T_{1u} | $m_{x\bar{y}} m_{xy} m_z$ | $m\bar{3}m, \bar{4}3m, 4_z 2_x m_{xy}, 4_z m_x m_{xy}, \bar{3}_p m_{xy}, \bar{3}_s m_{xy}, 3, m_{xy}, m_{x\bar{y}}^* m_{xy}^* 2_z^*, 2_{xy}^* / m_{xy}$ | 24 | 4 | 24 | 12 |
| | $2_z (2_x, 2_y)$ | Reducible | $4_z / m_z m_x m_{xy}$ | $m\bar{3}, 23, 4_z 2_x m_{zx}, 4_y 2_z 2_{zx}, 4_z^*, 4_z^*, m_x^* m_y^* 2_z^*, m_{x\bar{y}}^* m_{xy}^* 2_z^*, 2_x^* 2_y^* 2_z^*, 2_{xy}^* 2_{xy}^* 2_z^*, 2_z / m_z^*$ | 24 | 8 | 6 | 12 |
| | $2_{xy} (2_{yz}, 2_{zx}, 2_{x\bar{y}}, 2_{y\bar{z}}, 2_{z\bar{x}})$ | T_{2u} | $m_{x\bar{y}} m_{xy} m_z$ | $m\bar{3}m, 432, 3, m_{xy}, 3, m_{xy}, 3, 2_{xy}, 3, 2_{xy}, 4_z m_x 2_{xy}, 4_z 2_x 2_{xy}, m_{x\bar{y}}^* 2_{xy}^* m_z^*, 2_{xy}^* 2_{xy}^* 2_z^*, 2_{xy} / m_{xy}$ | 24 | 4 | 12 | 12 |
| | $\bar{1}$ | T_{1g}, T_{2g} | $m\bar{3}m$ | $\bar{3}_p(4), 4_z / m_z(3), 2_z^* / m_z^*(3), 2_{xy}^* / m_{xy}^*(6)$ | 24 | 24 | 0 | 24 |
| | 1 | T_{1u}, T_{2u} | $m\bar{3}m$ | $\bar{3}_p(4), \bar{4}_z(3), 4_z(3), m_z^*(3), m_{xy}^*(6), 2_z^*(3), 2_{xy}^*(6), 1^*$ | 48 | 48 | 48 | 24 |

3. PHASE TRANSITIONS, TWINNING AND DOMAIN STRUCTURES

primitive translation $\mathbf{u}(g_j)$, $\mathbf{g}_j = \{g_j | \mathbf{u}(g_j)\}$ (see Section 1.2.3). The symbol $\{g_j | \mathbf{u}(g_j)\}$ is called a *Seitz space-group symbol* (Bradley & Cracknell, 1972). The product (composition law) of two Seitz symbols is

$$\{g_1 | \mathbf{u}(g_1)\} \{g_2 | \mathbf{u}(g_2)\} = \{g_1 g_2 | g_1 \mathbf{u}(g_2) + \mathbf{u}(g_1)\}. \quad (3.4.2.43)$$

All crystallographically equivalent low-symmetry basic structures form a \mathcal{G} -orbit and can be calculated from the first basic structure \mathbf{S}_1 in the following way:

$$\mathcal{G}\mathbf{S}_1 = \{\mathbf{S}_1, \mathbf{S}_2, \dots, \mathbf{S}_j, \dots, \mathbf{S}_N\} = \{\mathbf{e}\mathbf{S}_1, \mathbf{g}_2\mathbf{S}_1, \dots, \mathbf{g}_j\mathbf{S}_1, \dots, \mathbf{g}_N\mathbf{S}_1\}, \quad (3.4.2.44)$$

where $\mathbf{g}_1 = \mathbf{e}$, $\mathbf{g}_2, \dots, \mathbf{g}_j, \dots, \mathbf{g}_N$ are the representatives of the left cosets $\mathbf{g}_j\mathcal{F}_1$ of the decomposition of \mathcal{G} ,

$$\mathcal{G} = \mathcal{F}_1 \cup \mathbf{g}_2\mathcal{F}_1 \cup \dots \cup \mathbf{g}_j\mathcal{F}_1 \cup \dots \cup \mathbf{g}_N\mathcal{F}_1. \quad (3.4.2.45)$$

These crystallographically equivalent low-symmetry structures are called *basic (elementary) domain states*.

The number N of basic domain states is equal to the number of left cosets in the decomposition (3.4.2.45). As we shall see in next section, this number is finite [see equation (3.4.2.60)], though the groups \mathcal{G} and \mathcal{F}_1 consist of an infinite number of operations.

In a microscopic description, a *basic (elementary) domain state* is described by positions of atoms in the unit cell. Basic domain states that are related by translations suppressed at the phase transition are called *translational* or *antiphase domain states*. These domain states have the same macroscopic properties. The attribute 'to have the same macroscopic properties' divides all basic domain states into classes of translational domain states.

In a microscopic description, a ferroic phase transition is accompanied by a lowering of space-group symmetry from a parent space group \mathcal{G} , with translation subgroup \mathcal{T} and point group G , to a low-symmetry space group \mathcal{F}_1 , with translation subgroup \mathcal{U}_1 and point group F_1 . There exists a unique intermediate group \mathcal{M}_1 , called the *Hermann group*, which has translation subgroup \mathcal{T} and point group $M_1 = F_1$ (see e.g. Hahn & Wondratschek, 1994; Wadhawan, 2000; Wondratschek & Aroyo, 2001):

$$\mathcal{F}_1 \stackrel{c}{\subseteq} \mathcal{M}_1 \stackrel{t}{\subseteq} \mathcal{G}, \quad (3.4.2.46)$$

$$F_1 = M_1 \subseteq G, \quad (3.4.2.47)$$

$$\mathcal{U}_1 \subseteq \mathcal{T} = \mathcal{T}, \quad (3.4.2.48)$$

where $\stackrel{c}{\subseteq}$ denotes an equiclass subgroup (a descent at which only the translational subgroup is reduced but the point group is preserved) and $\stackrel{t}{\subseteq}$ signifies an equitranslational subgroup (only the point group descends but the translational subgroup does not change). Group \mathcal{M}_1 is a maximal subgroup of \mathcal{G} that preserves all macroscopic properties of the basic domain state \mathbf{S}_1 with symmetry \mathcal{F}_1 .

At this point we have to make an important note. Any space-group symmetry descent $\mathcal{G} \subset \mathcal{F}_1$ requires that the lengths of the basis vectors of the translation group \mathcal{U}_1 of the ferroic space group \mathcal{F}_1 are commensurate with basic vectors of the translational group \mathcal{T} of the parent space group \mathcal{G} . It is usually tacitly assumed that this condition is fulfilled, although in real phase transitions this is never the case. Lattice parameters depend on temperature and are, therefore, different in parent and ferroic phases. At ferroelastic phase transitions the spontaneous strain changes the lengths of the basis vectors in different ways and at first-order phase transitions the lattice parameters change abruptly.

To assure the validity of translational symmetry descents, we have to suppress all distortions of the crystal lattice. This condition, called the *high-symmetry approximation* (Zikmund, 1984) or *parent clamping approximation* (PCA) (Janovec *et al.*, 1989;

Wadhawan, 2000), requires that the lengths of the basis vectors $\mathbf{a}^f, \mathbf{b}^f, \mathbf{c}^f$ of the translation group \mathcal{U}_1 of the ferroic space group \mathcal{F}_1 are either exactly the same as, or are integer multiples of, the basic vectors $\mathbf{a}^p, \mathbf{b}^p, \mathbf{c}^p$ of the translational group \mathcal{T} of the parent space group \mathcal{G} . Then the relation between the primitive basis vectors $\mathbf{a}^f, \mathbf{b}^f, \mathbf{c}^f$ of \mathcal{U}_1 and the primitive basis vectors $\mathbf{a}^p, \mathbf{b}^p, \mathbf{c}^p$ of \mathcal{T} can be expressed as

$$(\mathbf{a}^f, \mathbf{b}^f, \mathbf{c}^f) = (\mathbf{a}^p, \mathbf{b}^p, \mathbf{c}^p) \begin{pmatrix} m_{11} & m_{12} & m_{13} \\ m_{21} & m_{22} & m_{23} \\ m_{31} & m_{32} & m_{33} \end{pmatrix}, \quad (3.4.2.49)$$

where m_{ij} , $i, j = 1, 2, 3$, are integers.

Throughout this part, the parent clamping approximation is assumed to be fulfilled.

Now we can return to the partition of the set of basic domain states into translational subsets. Let $\{\mathbf{S}_1, \mathbf{S}_2, \dots, \mathbf{S}_n\}$ be the set of all basic translational domain states that can be generated from \mathbf{S}_1 by lost translations. The stabilizer (in \mathcal{G}) of this set is the Hermann group,

$$\mathcal{I}_{\mathcal{G}}\{\mathbf{S}_1, \mathbf{S}_2, \dots, \mathbf{S}_n\} = \mathcal{M}_1, \quad (3.4.2.50)$$

which plays the role of the intermediate group. The number of translational subsets and the relation between these subsets is determined by the decomposition of \mathcal{G} into left cosets of \mathcal{M}_1 :

$$\mathcal{G} = \{g_1 | \mathbf{v}(g_1)\} \mathcal{M}_1 \cup \{g_2 | \mathbf{v}(g_2)\} \mathcal{M}_1 \cup \dots \cup \{g_j | \mathbf{v}(g_j)\} \mathcal{M}_1 \cup \dots \cup \{g_n | \mathbf{v}(g_n)\} \mathcal{M}_1. \quad (3.4.2.51)$$

Representatives $\mathbf{g}_j = \{g_j | \mathbf{u}(g_j)\}$ are space-group operations, where g_j is a point-group operation and $\mathbf{u}(g_j)$ is a non-primitive translation (see Section 1.2.3).

We note that the Hermann group \mathcal{M}_1 can be found in the software *GI★KoBo-1* as the equitranslational subgroup of \mathcal{G} with the point-group descent $G \subset F_1$ for any space group \mathcal{G} and any point group F_1 of the ferroic phase.

The decomposition of the point group G into left cosets of the point group F_1 is given by equation (3.4.2.10):

$$G = g_1 F_1 \cup g_2 F_1 \cup \dots \cup g_j F_1 \cup \dots \cup g_n F_1. \quad (3.4.2.52)$$

Since the space groups \mathcal{M}_1 and \mathcal{F}_1 have identical point groups, $M_1 = F_1$, the decomposition (3.4.2.51) is identical with a decomposition of G into left cosets of M_1 ; one can, therefore, choose for the representatives in (3.4.2.10) the point-group parts of the representatives $\{g_j | \mathbf{u}(g_j)\}$ in decomposition (3.4.2.51). Both decompositions comprise the same number of left cosets, *i.e.* corresponding indices are equal; therefore, the number of subsets, comprising only translational basic domain states, is equal to the number n of principal domain states:

$$n = [\mathcal{G} : \mathcal{M}_1] = [G : F_1] = |G| : |F_1|, \quad (3.4.2.53)$$

where $|G|$ and $|F_1|$ are the number of operations of G and F_1 , respectively.

The first 'representative' basic domain state \mathbf{S}_j of each subset can be obtained from the first basic domain state \mathbf{S}_1 :

$$\mathbf{S}_j = \{g_j | \mathbf{v}(g_j)\} \mathbf{S}_1, \quad j = 1, 2, \dots, n, \quad (3.4.2.54)$$

where $\{g_j | \mathbf{v}(g_j)\}$ are representatives of left cosets of \mathcal{M}_1 in the decomposition (3.4.2.51).

Now we determine basic domain states belonging to the first subset (first principal domain state). Equiclass groups \mathcal{M}_1 and \mathcal{F}_1 have the same point-group operations and differ only in translations. The decomposition of \mathcal{M}_1 into left cosets of \mathcal{F}_1 can therefore be written in the form

3.4. DOMAIN STRUCTURES

$$\mathcal{M}_1 = \{e|\mathbf{t}_1\}\mathcal{F}_1 \cup \{e|\mathbf{t}_2\}\mathcal{F}_1 \cup \dots \cup \{e|\mathbf{t}_k\}\mathcal{F}_1 \cup \dots \cup \{e|\mathbf{t}_{d_t}\}\mathcal{F}_1, \quad (3.4.2.55)$$

where e is the identity point-group operation and \mathcal{T}_k , $k = 1, 2, \dots, d_t$, are lost translations that can be identified with the representatives in the decomposition of \mathcal{T} into left cosets of \mathcal{U}_1 :

$$\mathcal{T} = \mathbf{t}_1\mathcal{U}_1 + \mathbf{t}_2\mathcal{U}_1 + \dots + \mathbf{t}_k\mathcal{U}_1 + \dots + \mathbf{t}_{d_t}\mathcal{U}_1. \quad (3.4.2.56)$$

The number d_t of basic domain states belonging to one principal domain state will be called a *translational degeneracy*. For the translations $\mathbf{t}_1, \mathbf{t}_2, \dots, \mathbf{t}_k, \dots, \mathbf{t}_{d_t}$, one can choose vectors that lead from the origin of a ‘superlattice’ primitive unit cell of \mathcal{U}_1 to lattice points of \mathcal{T} located within or on the side faces of this ‘superlattice’ primitive unit cell. The number d_t of such lattice points is equal to the ratio $v_{\mathcal{F}} : v_{\mathcal{G}}$, where $v_{\mathcal{F}}$ and $v_{\mathcal{G}}$ are the volumes of the *primitive* unit cells of the low-symmetry and parent phases, respectively.

The number d_t can be also expressed as the determinant $\det(m_{ij})$ of the (3×3) matrix of the coefficients m_{ij} that in equation (3.4.2.49) relate the primitive basis vectors $\mathbf{a}^f, \mathbf{b}^f, \mathbf{c}^f$ of \mathcal{U}_1 to the primitive basis vectors $\mathbf{a}^p, \mathbf{b}^p, \mathbf{c}^p$ of \mathcal{T} (Van Tendeloo & Amelinckx, 1974; see also Example 2.5 in Section 3.2.3.3). Finally, the number d_t equals the ratio $Z_{\mathcal{F}} : Z_{\mathcal{G}}$, where $Z_{\mathcal{F}}$ and $Z_{\mathcal{G}}$ are the numbers of chemical formula units in the *primitive* unit cell of the ferroic and parent phases, respectively. Thus we get for the translational degeneracy d_t three expressions:

$$d_t = [\mathcal{M}_1 : \mathcal{F}_1] = [\mathcal{T} : \mathcal{U}] = v_{\mathcal{F}} : v_{\mathcal{G}} = \det(m_{ij}) = Z_{\mathcal{F}} : Z_{\mathcal{G}}. \quad (3.4.2.57)$$

The basic domain states belonging to the first subset of translational domain states are

$$\mathbf{S}_j = \{e|\mathbf{t}_k\}\mathbf{S}_1, \quad k = 1, 2, \dots, d_t, \quad (3.4.2.58)$$

where $\{e|\mathbf{t}_k\}$ is a representative from the decomposition (3.4.2.55).

The partitioning we have just described provides a useful labelling of basic domain states: Any basic domain state can be given a label ab , where the first integer $a = 1, 2, \dots, n$ specifies the principal domain state (translational subset) and the integer $b = 1, 2, \dots, d_t$ designates the domain state within a subset. With this convention the k th basic domain state in the j th subset can be obtained from the first basic domain state $\mathbf{S}_1 = \mathbf{S}_{11}$ (see Proposition 3.2.3.30 in Section 3.2.3.3):

$$\mathbf{S}_{jk} = \{g_j|\mathbf{v}(g_j)\}\{e|\mathbf{t}_k\}\mathbf{S}_{11}, \quad j = 1, 2, \dots, n, \quad k = 1, 2, \dots, d_t. \quad (3.4.2.59)$$

In a shorthand version, the letter \mathbf{S} can be omitted and the symbol can be written in the form a_b , where the ‘large’ number a signifies the principal domain state and the subscript b (translational index) specifies a basic domain state compatible with the principal domain state a .

The number n of translational subsets (which can be associated with principal domain states) times the translational degeneracy d_t (number of translational domain states within one translational subset) is equal to the total number N of all basic domain states:

$$N = nd_t = (|G| : |F_1|)(v_{\mathcal{F}} : v_{\mathcal{G}}) = (|G| : |F_1|)\det(m_{ij}) = (|G| : |F_1|)(Z_{\mathcal{F}} : Z_{\mathcal{G}}). \quad (3.4.2.60)$$

Example 3.4.2.6. Basic domain states in gadolinium molybdate (GMO). Gadolinium molybdate $[\text{Gd}_2(\text{MoO}_4)_3]$ undergoes a non-equitranslational ferroic phase transition with parent space group $\mathcal{G} = P42_1m$ (D_{2d}^3) and with ferroic space group $\mathcal{F}_1 = Pba2$ (C_{2v}^8)

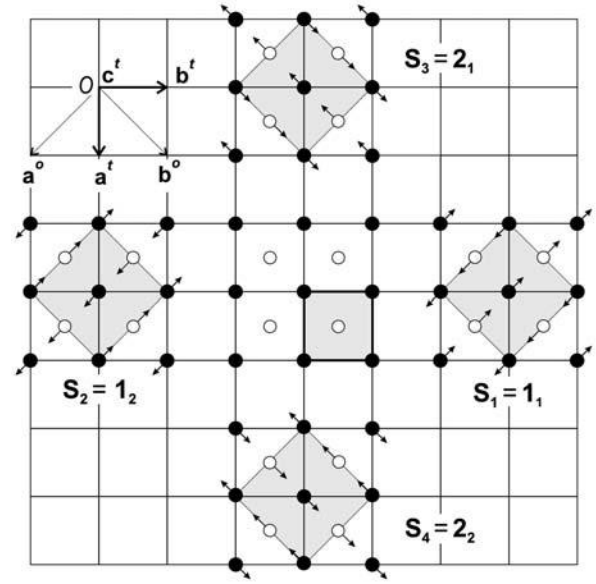


Fig. 3.4.2.5. Four basic single-domain states $\mathbf{S}_1 \equiv 1_1$, $\mathbf{S}_2 \equiv 1_2$, $\mathbf{S}_3 \equiv 2_1$, $\mathbf{S}_4 \equiv 2_2$ of the ferroic phase of a calomel (Hg_2Cl_2) crystal. Full \bullet and empty \circ circles represent centres of gravity of Hg_2Cl_2 molecules at the levels $z = 0$ and $z = c/2$, respectively, projected onto the $z = 0$ plane. The parent tetragonal phase is depicted in the centre of the figure with a full square representing the primitive unit cell. Arrows are exaggerated spontaneous shifts of molecules in the ferroic phase. Dotted squares depict conventional unit cells of the orthorhombic basic domain states in the parent clamping approximation. If the parent clamping approximation is lifted, these unit cells would be represented by rectangles elongated parallel to the arrows.

(see Section 3.1.2). From equation (3.4.2.53) we get $n = |42m| : |mm2| = 8 : 4 = 2$, i.e. there are two subsets of translational domain states corresponding to two principal domain states. In the software *GI★KoBo-1* one finds for the space group $P42_1m$ and the point group $mm2$ the corresponding equitranslational subgroup $\mathcal{M}_1 = Cmm2$ (C_{2v}^{11}) with vectors of the conventional orthorhombic unit cell (in the parent clamping approximation) $\mathbf{a}^o = \mathbf{a}^t - \mathbf{b}^t$, $\mathbf{b}^o = \mathbf{a}^t + \mathbf{b}^t$, $\mathbf{c}^o = \mathbf{c}^t$, where $\mathbf{a}^t, \mathbf{b}^t, \mathbf{c}^t$ is the basis of the tetragonal space group $P42_1m$. Hence, according to equation (3.4.2.49),

$$(\mathbf{a}^o, \mathbf{b}^o, \mathbf{c}^o) = (\mathbf{a}^t, \mathbf{b}^t, \mathbf{c}^t) \begin{pmatrix} 1 & 1 & 0 \\ -1 & 1 & 0 \\ 0 & 0 & 1 \end{pmatrix}. \quad (3.4.2.61)$$

The determinant of the transformation matrix equals two, therefore, according to equation (3.4.2.57), each principal domain state can contain $d_t = 2$ translational domain states that are related by lost translation \mathbf{a}^t or \mathbf{b}^t . In all, there are four basic domain states (for more details see Barkley & Jeitschko, 1973; Janovec, 1976; Wondratschek & Jeitschko, 1976).

Example 3.4.2.7. Basic domain states in calomel crystals. Crystals of calomel, Hg_2Cl_2 , consist of almost linear $\text{Cl}-\text{Hg}-\text{Hg}-\text{Cl}$ molecules aligned parallel to the c axis. The centres of gravity of these molecules form in the parent phase a tetragonal body-centred parent phase with the conventional tetragonal basis $\mathbf{a}^t, \mathbf{b}^t, \mathbf{c}^t$ and with space group $\mathcal{G} = I4/mmm$. The structure of this phase projected onto the $z = 0$ plane is depicted in the middle of Fig. 3.4.2.5 as a solid square with four full circles and one empty circle representing the centres of gravity of the Hg_2Cl_2 molecules at the levels $z = 0$ and $z = c/2$, respectively.

The ferroic phase has point-group symmetry $F_1 = m_{xy}m_{xz}2_z$, hence there are $n = |42m| : |m_{xy}m_{xz}2_z| = 2$ ferroelastic principal domain states. The conventional orthorhombic basis is $\mathbf{a}^o = \mathbf{a}^t - \mathbf{b}^t$, $\mathbf{b}^o = \mathbf{a}^t + \mathbf{b}^t$, $\mathbf{c}^o = \mathbf{c}^t$ (see upper left corner of Fig.

3. PHASE TRANSITIONS, TWINNING AND DOMAIN STRUCTURES

3.4.2.5). This is the same situation as in the previous example, therefore, according to equations (3.4.2.57) and (3.4.2.61), the translational degeneracy $d_t = 2$, i.e. each ferroelastic domain state can contain two basic domain states.

The structure S_1 of the ferroic phase in the parent clamping approximation is depicted in the left-hand part of Fig. 3.4.2.5 with a dotted orthorhombic conventional unit cell. The arrows represent exaggerated spontaneous shifts of the molecules. These shifts are frozen-in displacements of a transverse acoustic soft mode with the \mathbf{k} vector along the $[110]$ direction in the first domain state S_1 , hence all molecules in the (110) plane passing through the origin O are shifted along the $[1\bar{1}0]$ direction, whereas those in the neighbouring parallel planes are shifted along the antiparallel direction $[\bar{1}10]$ (the indices are related to the tetragonal coordinate system). The symmetry of S_1 is described by the space group $\mathcal{F}_1 = Amam (D_{2h}^{17})$; this symbol is related to the conventional orthorhombic basis and the origin of this group is shifted by $\mathbf{a}'/2$ or \mathbf{b} with respect to the origin 0 of the group $\mathcal{G} = I4/mmm$.

Three more basic domain states S_2 , S_3 and S_4 can be obtained, according to equation (3.4.2.44), from S_1 by applying representatives of the left cosets in the resolution of \mathcal{G} [see equation (3.4.2.42)], for which one can find the expression

$$\mathcal{G} = \{1|000\}\mathcal{F}_1 \cup \{1|100\}\mathcal{F}_1 \cup \{4_z|000\}\mathcal{F}_1 \cup \{4_z^3|000\}\mathcal{F}_1. \quad (3.4.2.62)$$

All basic domain states S_1 , S_2 , S_3 and S_4 are depicted in Fig. 3.4.2.5. Domain states S_1 and S_2 , and similarly S_3 and S_4 , are related by lost translation \mathbf{a}' or \mathbf{b}' . Thus the four basic domain states S_1 , S_2 , S_3 and S_4 can be partitioned into two translational subsets $\{S_1, S_2\}$ and $\{S_3, S_4\}$. Basic domain states forming one subset have the same value of the secondary macroscopic order parameter λ , which is in this case the difference $\varepsilon_{11} - \varepsilon_{22}$ of the components of a symmetric second-rank tensor ε , e.g. the permittivity or the spontaneous strain (which is zero in the parent clamping approximation).

This partition provides a useful labelling of basic domain states: $S_1 \equiv 1_1$, $S_2 \equiv 1_2$, $S_3 \equiv 2_1$, $S_4 \equiv 2_2$, where the first number signifies the ferroic (orientational) domain state and the subscript (translational index) specifies the basic domain state with the same ferroic domain state.

Symmetry groups (stabilizers in \mathcal{G}) of basic domain states can be calculated from a space-group version of equation (3.4.2.13):

$$\begin{aligned} \mathcal{F}_2 &= \{1|100\}\mathcal{F}_2\{1|100\}^{-1} = \mathcal{F}_1; \\ \mathcal{F}_3 &= \{4_z|000\}\mathcal{F}_2\{4_z|000\}^{-1} = Bbmm, \end{aligned}$$

with the same conventional basis, and $\mathcal{F}_4 = \{1|100\}\mathcal{F}_3\{1|100\}^{-1} = \mathcal{F}_3$, where the origin of these groups is shifted by $\mathbf{a}'/2$ or \mathbf{b} with respect to the origin 0 of the group $\mathcal{G} = I4/mmm$.

In general, a space-group-symmetry descent $\mathcal{G} \supset \mathcal{F}_1$ can be performed in two steps:

(1) An equitranslational symmetry descent $\mathcal{G} \stackrel{t}{\supset} \mathcal{M}_1$, where \mathcal{M}_1 is the equitranslational subgroup of \mathcal{G} (Hermann group), which is unequivocally specified by space group \mathcal{G} and by the point group F_1 of the space group \mathcal{F}_1 . The Hermann group \mathcal{M}_1 can be found in the software *GL*KoBo-1* or, in some cases, in *IT A* (2002) under the entry ‘Maximal non-isomorphic subgroups, type I’.

(2) An equiclass symmetry descent $\mathcal{M}_1 \stackrel{c}{\supset} \mathcal{F}_1$, which can be of three kinds [for more details see *IT A* (2002), Section 2.2.15]:

(i) Space groups \mathcal{M}_1 and \mathcal{F}_1 have the same conventional unit cell. These descents occur only in space groups \mathcal{M}_1 with centred conventional unit cells and the lost translations are some or all centring translations of the unit cell of \mathcal{M}_1 . In many cases, the descent $\mathcal{M}_1 \supseteq \mathcal{F}_1$ can be found in the main tables of *IT A* (2002),

under the entry ‘Maximal non-isomorphic subgroups, type IIa’. Gadolinium molybdate belongs to this category.

(ii) The conventional unit cell of \mathcal{M}_1 is larger than that of \mathcal{F}_1 . Some vectors of the conventional unit cell of \mathcal{U}_1 are multiples of that of \mathcal{T} . In many cases, the descent $\mathcal{M}_1 \supseteq \mathcal{F}_1$ can be found in the main tables of *IT A* (2002), under the entry ‘Maximal non-isomorphic subgroups, type IIb’.

(iii) Space group \mathcal{F}_1 is an isomorphic subgroup of \mathcal{M}_1 , i.e. both groups are of the same space-group type (with the same Hermann–Mauguin symbol) or of the enantiomorphic space-group type. Each space group has an infinite number of isomorphic subgroups. Maximal isomorphic subgroups of lowest index are tabulated in *IT A* (2002), under the entry ‘Maximal non-isomorphic subgroups, type IIc’.

3.4.3. Domain pairs: domain twin laws, distinction of domain states and switching

Different domains observed by a single apparatus can exhibit different properties even though their crystal structures are either the same or enantiomorphic and differ only in spatial orientation. Domains are usually distinguished by their bulk properties, i.e. according to their domain states. Then the problem of domain distinction is reduced to the distinction of domain states. To solve this task, we have to describe in a convenient way the distinction of any two of all possible domain states. For this purpose, we use the concept of domain pair.

Domain pairs allow one to express the geometrical relationship between two domain states (the ‘twin law’), determine the distinction of two domain states and define switching fields that may induce a change of one state into the other. Domain pairs also present the first step in examining domain twins and domain walls.

In this section, we define domain pairs, ascribe to them symmetry groups and so-called twinning groups, and give a classification of domain pairs. Then we divide domain pairs into equivalence classes (G -orbits of domain pairs) – which comprise domain pairs with the same inherent properties but with different orientations and/or locations in space – and examine the relation between G -orbits and twinning groups.

A qualitative difference between the coexistence of two domain states provides a basic division into non-ferroelastic and ferroelastic domain pairs. The synoptic Table 3.4.3.4 lists representatives of all G -orbits of *non-ferroelastic domain pairs*, contains information about the distinction of non-ferroelastic domain states by means of diffraction techniques and specifies whether or not important property tensors can distinguish between domain states of a non-ferroelastic domain pair. These data also determine the external fields needed to switch the first domain state into the second domain state of a domain pair. Synoptic Table 3.4.3.6 contains representative *ferroelastic domain pairs* of G -orbits of domain pairs for which there exist compatible (permissible) domain walls and gives for each representative pair the orientation of the *two compatible domain walls*, the expression for the disorientation angle (obliquity) and other data. Table 3.4.3.7 lists representatives of all classes of ferroelastic domain pairs for which *no compatible domain walls* exist. Since Table 3.4.2.7 contains for each symmetry descent $\mathcal{G} \supset \mathcal{F}$ all twinning groups that specify different G -orbits of domain pairs which can appear in the ferroic phase, one can get from this table and from Tables 3.4.3.4, 3.4.3.6 and 3.4.3.7 the significant features of the domain structure of any ferroic phase.

3.4.3.1. Domain pairs and their symmetry, twin law

A pair of two domain states, in short a *domain pair*, consists of two domain states, say S_i and S_k , that are considered irrespective of their possible coexistence (Janovec, 1972). Geometrically,

3.4. DOMAIN STRUCTURES

domain pairs can be visualized as two interpenetrating structures of \mathbf{S}_i and \mathbf{S}_k . Algebraically, two domain states \mathbf{S}_i and \mathbf{S}_k can be treated in two ways: as an ordered or an unordered pair (see Section 3.2.3.1.2).

An *ordered domain pair*, denoted $(\mathbf{S}_i, \mathbf{S}_k)$, consists of the first domain state \mathbf{S}_i and the second domain state. Occasionally, it is convenient to consider a *trivial ordered domain pair* $(\mathbf{S}_i, \mathbf{S}_i)$ composed of two identical domain states \mathbf{S}_i .

An ordered domain pair is a construct that in bicrystallography is called a *dichromatic complex* (see Section 3.3.3; Pond & Vlachavas, 1983; Sutton & Balluffi, 1995; Wadhwani, 2000).

An ordered domain pair $(\mathbf{S}_i, \mathbf{S}_k)$ is defined by specifying \mathbf{S}_i and \mathbf{S}_k or by giving \mathbf{S}_i and a *switching operation* g_{ik} that transforms \mathbf{S}_i into \mathbf{S}_k ,

$$\mathbf{S}_k = g_{ik}\mathbf{S}_i, \quad \mathbf{S}_i, \mathbf{S}_k \in GS_1, \quad g_{ik} \in G. \quad (3.4.3.1)$$

For a given \mathbf{S}_i and \mathbf{S}_k , the switching operation g_{ik} is not uniquely defined since each operation from the left coset $g_{ik}F_i$ [where F_i is the stabilizer (symmetry group) of \mathbf{S}_i] transforms \mathbf{S}_i into \mathbf{S}_k , $g_{ik}\mathbf{S}_i = (g_{ik}F_i)\mathbf{S}_i = \mathbf{S}_k$.

An ordered domain pair $(\mathbf{S}_k, \mathbf{S}_i)$ with a reversed order of domain states is called a *transposed domain pair* and is denoted $(\mathbf{S}_i, \mathbf{S}_k)^t \equiv (\mathbf{S}_k, \mathbf{S}_i)$. A non-trivial ordered domain pair $(\mathbf{S}_i, \mathbf{S}_k)$ is different from the transposed ordered domain pair,

$$(\mathbf{S}_k, \mathbf{S}_i) \neq (\mathbf{S}_i, \mathbf{S}_k) \text{ for } i \neq k. \quad (3.4.3.2)$$

If g_{ik} is a switching operation of an ordered domain pair $(\mathbf{S}_i, \mathbf{S}_k)$, then the inverse operation g_{ik}^{-1} of g_{ik} is a switching operation of the transposed domain pair $(\mathbf{S}_k, \mathbf{S}_i)$:

$$\text{if } (\mathbf{S}_i, \mathbf{S}_k) = (\mathbf{S}_i, g_{ik}\mathbf{S}_i) \text{ and } (\mathbf{S}_k, \mathbf{S}_i) = (\mathbf{S}_k, g_{ki}\mathbf{S}_k), \text{ then } g_{ki} = g_{ik}^{-1}. \quad (3.4.3.3)$$

An *unordered domain pair*, denoted by $\{\mathbf{S}_i, \mathbf{S}_k\}$, is defined as an *unordered* set consisting of two domain states \mathbf{S}_i and \mathbf{S}_k . In this case, the sequence of domains states in a domain pair is irrelevant, therefore

$$\{\mathbf{S}_i, \mathbf{S}_k\} = \{\mathbf{S}_k, \mathbf{S}_i\}. \quad (3.4.3.4)$$

In what follows, we shall omit the specification ‘ordered’ or ‘unordered’ if it is evident from the context, or if it is not significant.

A domain pair $(\mathbf{S}_i, \mathbf{S}_k)$ can be transformed by an operation $g \in G$ into another domain pair,

$$g(\mathbf{S}_i, \mathbf{S}_k) \equiv (g\mathbf{S}_i, g\mathbf{S}_k) = (\mathbf{S}_l, \mathbf{S}_m), \quad \mathbf{S}_i, \mathbf{S}_k, \mathbf{S}_l, \mathbf{S}_m \in GS_1, \quad g \in G. \quad (3.4.3.5)$$

These two domain pairs will be called *crystallographically equivalent (in G) domain pairs* and will be denoted $(\mathbf{S}_i, \mathbf{S}_k) \stackrel{G}{\sim} (\mathbf{S}_l, \mathbf{S}_m)$.

If the transformed domain pair is a transposed domain pair $(\mathbf{S}_k, \mathbf{S}_i)$, then the operation g will be called a *transposing operation*,

$$g^*(\mathbf{S}_i, \mathbf{S}_k) = (g^*\mathbf{S}_i, g^*\mathbf{S}_k) = (\mathbf{S}_k, \mathbf{S}_i), \quad \mathbf{S}_i, \mathbf{S}_k \in GS_1, \quad g^* \in G. \quad (3.4.3.6)$$

We see that a transposing operation $g^* \in G$ exchanges domain states \mathbf{S}_i and \mathbf{S}_k :

$$g^*\mathbf{S}_i = \mathbf{S}_k, \quad g^*\mathbf{S}_k = \mathbf{S}_i, \quad \mathbf{S}_i, \mathbf{S}_k \in GS_1, \quad g^* \in G. \quad (3.4.3.7)$$

Thus, comparing equations (3.4.3.1) and (3.4.3.7), we see that a transposing operation g^* is a switching operation that transforms \mathbf{S}_i into \mathbf{S}_k , and, in addition, switches \mathbf{S}_k into \mathbf{S}_i . Then a product of two transposing operations is an operation that changes neither \mathbf{S}_i nor \mathbf{S}_k .

What we call in this chapter a *transposing operation* is usually denoted as a *twin operation* (see Section 3.3.5 and e.g. Holser, 1958a; Curien & Donnay, 1959; Koch, 1999). We are reserving the term ‘twin operation’ for operations that exchange domain states of a simple domain twin in which two ferroelastic domain states *coexist* along a domain wall. Then, as we shall see, the transposing operations are identical with the twin operations in non-ferroelastic domains (see Section 3.4.3.5) but may differ in ferroelastic domain twins, where only some transposing operations of a single-domain pair survive as twin operations of the corresponding ferroelastic twin with a nonzero disorientation angle (see Section 3.4.3.6.3).

Transposing operations are marked in this chapter by a star, $*$ (with five points), which should be distinguished from an asterisk, $*$ (with six points), used to denote operations or symmetry elements in reciprocal space. The same designation is used in the software *GI★KoBo-1* and in the tables in Kopský (2001). A prime, $'$, is often used to designate transposing (twin) operations (see Section 3.3.5; Curien & Le Corre, 1958; Curien & Donnay, 1959). We have reserved the prime for operations involving time inversion, as is customary in magnetism (see Chapter 1.5). This choice allows one to analyse domain structures in magnetic and magnetoelectric materials (see e.g. Přívratská & Janovec, 1997).

In connection with this, we invoke the notion of a *twin law*. Since this term is not yet common in the context of domain structures, we briefly explain its meaning.

In crystallography, a twin is characterized by a twin law defined in the following way (see Section 3.3.2; Koch, 1999; Cahn, 1954):

(i) A *twin law* describes the geometrical relation between twin components of a twin. This relation is expressed by a *twin operation* that brings one of the twin components into parallel orientation with the other, and *vice versa*. A symmetry element corresponding to the twin operation is called the *twin element*. (Requirement ‘and *vice versa*’ is included in the definition of Cahn but not in that of Koch; for the most common twin operations of the second order the ‘*vice versa*’ condition is fulfilled automatically.)

(ii) The relation between twin components deserves the name ‘twin law’ only if it occurs frequently, is reproducible and represents an inherent feature of the crystal.

An analogous definition of a *domain twin law* can be formulated for domain twins by replacing the term ‘twin components’ by ‘domains’, say $\mathbf{D}_i(\mathbf{S}_i, B_k)$ and $\mathbf{D}_m(\mathbf{S}_m, B_p)$, where \mathbf{S}_i, B_k and \mathbf{S}_m, B_p are, respectively, the domain state and the domain region of the domains $\mathbf{D}_i(\mathbf{S}_i, B_k)$ and $\mathbf{D}_m(\mathbf{S}_m, B_p)$, respectively (see Section 3.4.2.1). The term ‘transposing operation’ corresponds to transposing operation g_{12}^* of domain pair $(\mathbf{S}_1, \mathbf{S}_2) = (\mathbf{S}_j, g_{jn}^*\mathbf{S}_n)$ as we have defined it above if two domains with domain states \mathbf{S}_1 and \mathbf{S}_2 *coexist* along a domain wall of the domain twin.

Domain twin laws can be conveniently expressed by crystallographic groups. This specification is simpler for non-ferroelastic twins, where a twin law can be expressed by a dichromatic space group (see Section 3.4.3.5), whereas for ferroelastic twins with a compatible domain wall dichromatic layer groups are adequate (see Section 3.4.3.6.3).

Restriction (ii), formulated by Georges Friedel (1926) and explained in detail by Cahn (1954), expresses a necessity to exclude from considerations crystal aggregates (intergrowths) with approximate or accidental ‘nearly exact’ crystal components resembling twins (Friedel’s *macles d’imagination*) and thus to restrict the definition to ‘true twins’ that fulfil condition (i) exactly and are characteristic for a given material. If we confine our considerations to domain structures that are formed from a *homogeneous* parent phase, this requirement is fulfilled for *all* aggregates consisting of two or more domains. Then the definition of a ‘domain twin law’ is expressed only by condition (i). Condition (ii) is important for growth twins.

We should note that the definition of a twin law given above involves only domain states and does not explicitly contain

3. PHASE TRANSITIONS, TWINNING AND DOMAIN STRUCTURES

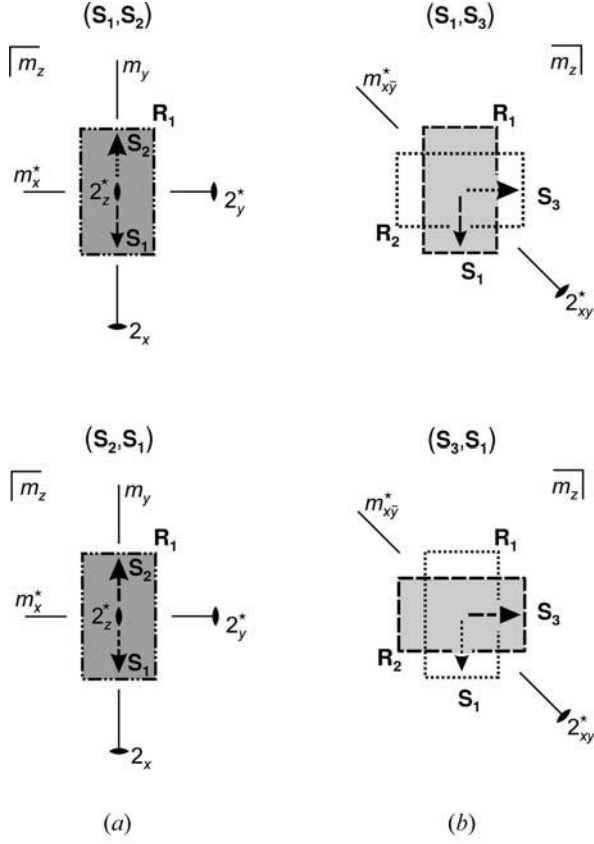


Fig. 3.4.3.1. Transposable domain pairs. Single-domain states are those from Fig. 3.4.2.2. (a) Completely transposable non-ferroelastic domain pair. (b) Partially transposable ferroelastic domain pair.

specification of the contact region between twin components or neighbouring domains. The concept of domain state is, therefore, relevant for discussing the twin laws. Moreover, there is no requirement on the coexistence of interpenetrating structures in a domain pair. One can even, therefore, consider cases where no real coexistence of both structures is possible. Nevertheless, we note that the characterization of twin laws used in mineralogy often includes specification of the contact region (e.g. twin plane or diffuse region in penetrating twins).

Ordered domain pairs (S_1, S_2) and (S_1, S_3) , formed from domain states of our illustrative example (see Fig. 3.4.2.2), are displayed in Fig. 3.4.3.1(a) and (b), respectively, as two superposed rectangles with arrows representing spontaneous polarization. In ordered domain pairs, the first and the second domain state are distinguished by shading [the first domain state is grey ('black') and the second clear ('white')] and/or by using dashed and dotted lines for the first and second domain state, respectively.

In Fig. 3.4.3.2, the ordered domain pair (S_1, S_2) and the transposed domain pair (S_2, S_1) are depicted in a similar way for another example with symmetry descent $G = 6_z/m_z \supset 2_z/m_z = F_1$.

Let us now examine the *symmetry of domain pairs*. The *symmetry group* F_{ik} of an ordered domain pair $(S_i, S_k) = (S_i, g_{ik}S_i)$ consists of all operations that leave invariant both S_i and S_k , i.e. F_{ik} comprises all operations that are common to stabilizers (symmetry groups) F_i and F_k of domain states S_i and S_k , respectively,

$$F_{ik} \equiv F_i \cap F_k = F_i \cap g_{ik}F_i g_{ik}^{-1}, \quad (3.4.3.8)$$

where the symbol \cap denotes the intersection of groups F_i and F_k . The group F_{ik} is in Section 3.3.4 denoted by \mathcal{H}^* and is called an intersection group.

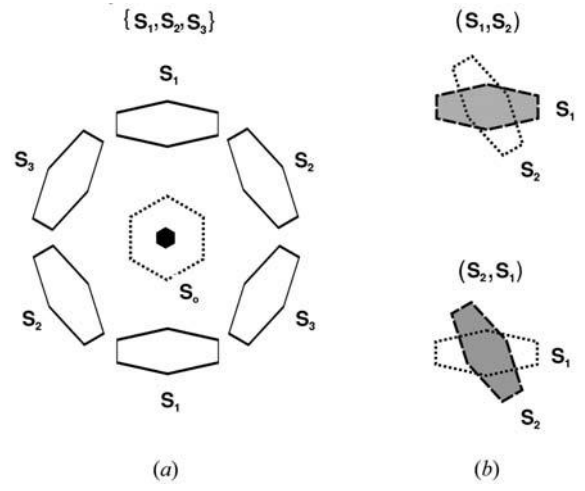


Fig. 3.4.3.2. Non-transposable domain pairs. (a) The parent phase with symmetry $G = 6_z/m_z$ is represented by a dotted hexagon and the three ferroelastic single-domain states with symmetry $F_1 = F_2 = F_3 = 2_z/m_z$ are depicted as drastically squeezed hexagons. (b) Domain pair (S_1, S_2) and transposed domain pair (S_2, S_1) . There exists no operation from the group $6_z/m_z$ that would exchange domain states S_1 and S_2 , i.e. that would transform one domain pair into a transposed domain pair.

From equation (3.4.3.8), it immediately follows that the symmetry F_{ki} of the transposed domain pair (S_k, S_i) is the same as the symmetry F_{ik} of the initial domain pair (S_i, S_k) :

$$F_{ki} = F_k \cap F_i = F_i \cap F_k = F_{ik}. \quad (3.4.3.9)$$

Symmetry operations of an unordered domain pair $\{S_i, S_k\}$ include, besides operations of F_{ik} that do not change either S_i or S_k , all transposing operations, since for an unordered domain pair a transposed domain pair is identical with the initial domain pair [see equation (3.4.3.4)]. If g_{ik}^* is a transposing operation of (S_i, S_k) , then all operations from the left coset $g_{ik}^*F_{ik}$ are transposing operations of that domain pair as well. Thus the *symmetry group* J_{ik} of an unordered domain pair $\{S_i, S_k\}$ can be, in a general case, expressed in the following way:

$$J_{ik} = F_{ik} \cup g_{ik}^*F_{ik}, \quad g_{ik}^* \in G. \quad (3.4.3.10)$$

Since, for an unordered domain, the order of domain states in a domain pair is not significant, the transposition of indices i, k in J_{ik} does not change this group,

$$J_{ik} = F_{ik} \cup g_{ik}^*F_{ik} = F_{ki} \cup g_{ki}^*F_{ki} = J_{ki}, \quad (3.4.3.11)$$

which also follows from equations (3.4.3.3) and (3.4.3.9).

A *basic classification of domain pairs* follows from their symmetry. Domain pairs for which at least one transposing operation exists are called *transposable* (or *ambivalent*) *domain pairs*. The symmetry group of a transposable unordered domain pair $\{S_i, S_k\}$ is given by equation (3.4.3.10).

The star in the symbol J_{ik}^* indicates that this group contains transposing operations, i.e. that the corresponding domain pair (S_i, S_k) is a transposable domain pair.

A transposable domain pair (S_i, S_k) and transposed domain pair (S_k, S_i) belong to the same G -orbit:

$$G(S_i, S_k) = G(S_k, S_i). \quad (3.4.3.12)$$

If $\{S_i, S_k\}$ is a transposable pair and, moreover, $F_i = F_k = F_{ik}$, then *all* operations of the left coset $g_{ik}^*F_i$ simultaneously switch S_i into S_k and S_k into S_i . We call such a pair a *completely transposable domain pair*. The symmetry group J_{ik} of a completely transposable pair $\{S_i, S_k\}$ is

$$J_{ik}^* = F_i \cup g_{ik}^*F_i, \quad g_{ik}^* \in G, \quad F_i = F_k. \quad (3.4.3.13)$$

3.4. DOMAIN STRUCTURES

We shall use for symmetry groups of completely transposable domain pairs the symbol J_{ik}^* .

If $F_i \neq F_k$, then $F_{ik} \subset F_i$ and the number of transposing operations is smaller than the number of operations switching \mathbf{S}_i into \mathbf{S}_k . We therefore call such pairs *partially transposable domain pairs*. The symmetry group J_{ik} of a partially transposable domain pair $\{\mathbf{S}_i, \mathbf{S}_k\}$ is given by equation (3.4.3.10).

The symmetry groups J_{ik} and J_{ik}^* , expressed by (3.4.3.10) or by (3.4.3.13), respectively, consists of two left cosets only. The first is equal to F_{ik} and the second one $g_{ik}^* F_{ik}$ comprises all the transposing operations marked by a star. An explicit symbol $J_{ik}[F_{ik}]$ of these groups contains both the group J_{ik} and F_{ik} , which is a subgroup of J_{ik} of index 2.

If one 'colours' one domain state, e.g. \mathbf{S}_i , 'black' and the other, e.g. \mathbf{S}_k , 'white', then the operations without a star can be interpreted as 'colour-preserving' operations and operations with a star as 'colour-exchanging' operations. Then the group $J_{ik}[F_{ik}]$ can be treated as a 'black-and-white' or dichromatic group (see Section 3.2.3.2.7). These groups are also called Shubnikov groups (Bradley & Cracknell, 1972), two-colour or Heesch-Shubnikov groups (Opechowski, 1986), or antisymmetry groups (Vainshtein, 1994).

The advantage of this notation is that instead of an explicit symbol $J_{ik}[F_{ik}]$, the symbol of a dichromatic group specifies both the group J_{ik} and the subgroup F_{ij} or F_1 , and thus also the transposing operations that define, according to equation (3.4.3.7), the second domain state \mathbf{S}_j of the pair.

We have agreed to use a special symbol J_{ik}^* only for completely transposable domain pairs. Then the star in this case indicates that the subgroup F_{ik} is equal to the symmetry group of the first domain state \mathbf{S}_i in the pair, $F_{ik} = F_i$. Since the group F_i is usually well known from the context (in our main tables it is given in the first column), we no longer need to add it to the symbol of J_{ik} .

Domain pairs for which an exchanging operation g_{ik}^* cannot be found are called *non-transposable* (or *polar*) *domain pairs*. The symmetry J_{ij} of a non-transposable domain pair is reduced to the usual 'monochromatic' symmetry group F_{ik} of the corresponding ordered domain pair $(\mathbf{S}_i, \mathbf{S}_k)$. The G -orbits of mutually transposed polar domain pairs are disjoint (Janovec, 1972):

$$G(\mathbf{S}_i, \mathbf{S}_k) \cap G(\mathbf{S}_k, \mathbf{S}_i) = \emptyset. \quad (3.4.3.14)$$

Transposed polar domain pairs, which are always non-equivalent, are called *complementary domain pairs*.

If, in particular, $F_{ik} = F_i = F_k$, then the symmetry group of the unordered domain pair is

$$J_{ik} = F_i = F_k. \quad (3.4.3.15)$$

In this case, the unordered domain pair $\{\mathbf{S}_i, \mathbf{S}_k\}$ is called a *non-transposable simple domain pair*.

If $F_i \neq F_k$, then the number of operations of F_{ik} is smaller than that of F_i and the symmetry group J_{ik} is equal to the symmetry group F_{ik} of the ordered domain pair $(\mathbf{S}_i, \mathbf{S}_k)$,

$$J_{ik} = F_{ik}, \quad F_{ik} \subset F_i. \quad (3.4.3.16)$$

Such an unordered domain pair $\{\mathbf{S}_i, \mathbf{S}_k\}$ is called a *non-transposable multiple domain pair*. The reason for this designation will be given later in this section.

We stress that domain states forming a domain pair are not restricted to single-domain states. Any two domain states with a defined orientation in the coordinate system of the parent phase can form a domain pair for which all definitions given above are applicable.

Example 3.4.3.1. Now we examine domain pairs in our illustrative example of a phase transition with symmetry descent $G = 4_z/m_z m_{xy} \supset 2_x m_y m_z = F_1$ and with four single-domain states $\mathbf{S}_1, \mathbf{S}_2, \mathbf{S}_3$ and \mathbf{S}_4 , which are displayed in Fig. 3.4.2.2. The domain

pair $\{\mathbf{S}_1, \mathbf{S}_2\}$ depicted in Fig. 3.4.3.1(a) is a completely transposable domain pair since transposing operations exist, e.g. $g_{12}^* = m_x^*$, and the symmetry group F_{12} of the ordered domain pair $(\mathbf{S}_1, \mathbf{S}_2)$ is

$$F_{12} = F_1 \cap F_2 = F_1 = F_2 = 2_x m_y m_z. \quad (3.4.3.17)$$

The symmetry group J_{12} of the unordered pair $\{\mathbf{S}_1, \mathbf{S}_2\}$ is a dichromatic group,

$$J_{12}^* = 2_x m_y m_z \cup m_x^* \{2_x m_y m_z\} = m_x^* m_y m_z. \quad (3.4.3.18)$$

The domain pair $\{\mathbf{S}_1, \mathbf{S}_3\}$ in Fig. 3.4.3.1(b) is a partially transposable domain pair, since there are operations exchanging domain states \mathbf{S}_1 and \mathbf{S}_3 , e.g. $g_{13}^* = m_{xy}^*$, but the symmetry group F_{13} of the ordered domain pair $(\mathbf{S}_1, \mathbf{S}_3)$ is smaller than F_1 :

$$F_{13} = F_1 \cap F_3 = 2_x m_y m_z \cap m_x 2_y m_z = \{1, m_z\} \equiv \{m_z\}, \quad (3.4.3.19)$$

where 1 is an identity operation and $\{1, m_z\}$ denotes the group m_z . The symmetry group of the unordered domain pair $\{\mathbf{S}_1, \mathbf{S}_3\}$ is equal to a dichromatic group,

$$J_{13} = \{m_z\} \cup 2_{xy}^* \{m_z\} = 2_{xy}^* m_{xy} m_z. \quad (3.4.3.20)$$

The domain pair $(\mathbf{S}_1, \mathbf{S}_2)$ in Fig. 3.4.3.2(b) is a non-transposable simple domain pair, since there is no transposing operation of $G = 6_z/m_z$ that would exchange domain states \mathbf{S}_1 and \mathbf{S}_2 , and $F_1 = F_2 = 2_z/m_z$. The symmetry group J_{12} of the unordered domain pair $\{\mathbf{S}_1, \mathbf{S}_2\}$ is a 'monochromatic' group,

$$J_{12} = F_{12} = F_1 = F_2 = 2_z/m_z. \quad (3.4.3.21)$$

The G -orbit $6_z/m_z(\mathbf{S}_1, \mathbf{S}_2)$ of the pair $(\mathbf{S}_1, \mathbf{S}_2)$ has no common domain pair with the G -orbit $6_z/m_z(\mathbf{S}_2, \mathbf{S}_1)$ of the transposed domain pair $(\mathbf{S}_2, \mathbf{S}_1)$. These two 'complementary' orbits contain mutually transposed domain pairs.

Symmetry groups of domain pairs provide a basic classification of domain pairs into the four types introduced above. This classification applies to microscopic domain pairs as well.

3.4.3.2. Twinning group, distinction of two domain states

We have seen that for transposable domain pairs the symmetry group J_{ij} of a domain pair $(\mathbf{S}_i, \mathbf{S}_j)$ specifies transposing operations $g_{ij}^* F_1$ that transform \mathbf{S}_i into \mathbf{S}_j . This does not apply to non-transposable domain pairs, where the symmetry group $J_{ij} = F_{ij}$ does not contain any switching operation. Another group exists, called the twinning group, which is associated with a domain pair and which does not have this drawback. The twinning group determines the distinction of two domain states, specifies the external fields needed to switch one domain state into another one and enables one to treat domain pairs independently of the transition $G \supset F_1$. This facilitates the tabulation of the properties of non-equivalent domain pairs that appear in all possible ferroic phases.

The *twinning group* K_{ij} of a *domain pair* $(\mathbf{S}_i, \mathbf{S}_j)$ is defined as the *minimal* subgroup of G that contains both F_1 and a switching operation g_{ij} of the domain pair $(\mathbf{S}_i, \mathbf{S}_j)$, $\mathbf{S}_j = g_{ij} \mathbf{S}_i$ (Fuksa & Janovec, 1995; Janovec *et al.*, 1995; Fuksa, 1997),

$$F_1 \subset K_{ij} \subseteq G, \quad g_{ij} \in K_{ij}, \quad (3.4.3.22)$$

where no group K'_{ij} exists such that

$$F_1 \subset K'_{ij} \subset K_{ij}, \quad g_{ij} \in K'_{ij}. \quad (3.4.3.23)$$

The twinning group K_{ij} is identical to the embracing (fundamental) group used in bicrystallography (see Section 3.2.2). In Section 3.3.4 it is called a composite symmetry of a twin.

3. PHASE TRANSITIONS, TWINNING AND DOMAIN STRUCTURES

Since K_{1j} is a group, it must contain all products of g_{1j} with operations of F_1 , i.e. the whole left coset $g_{1j}F_1$. For completely transposable domain pairs, the union of F_1 and $g_{1j}^*F_1$ forms a group that is identical with the symmetry group J_{1j}^* of the unordered domain pair $\{\mathbf{S}_1, \mathbf{S}_j\}$:

$$K_{1j}^* = J_{1j}^* = F_1 \cup g_{1j}^*F_1, \quad g_{1j}^* \in K_{1j}, \quad F_1 = F_j. \quad (3.4.3.24)$$

In a general case, the twinning group K_{1j} , being a supergroup of F_1 , can always be expressed as a decomposition of the left cosets of F_1 ,

$$K_{1j} = F_1 \cup g_{1j}F_1 \cup g_{1k}F_1 \cup \dots \cup g_{1c}F_1 \in G. \quad (3.4.3.25)$$

We can associate with the twinning group a set of c domain states, the K_{1j} -orbit of \mathbf{S}_1 , which can be generated by applying to \mathbf{S}_1 the representatives of the left cosets in decomposition (3.4.3.25),

$$K_{1j}\mathbf{S}_1 = \{\mathbf{S}_1, \mathbf{S}_j, \dots, \mathbf{S}_c\}. \quad (3.4.3.26)$$

This orbit is called the *generic orbit of domain pair* $(\mathbf{S}_1, \mathbf{S}_j)$.

Since the generic orbit (3.4.3.26) contains both domain states of the domain pair $(\mathbf{S}_1, \mathbf{S}_j)$, one can find different and equal nonzero *tensor components in two domain states* \mathbf{S}_1 and \mathbf{S}_j by a similar procedure to that used in Section 3.4.2.3 for ascribing principal and secondary tensor parameters to principal and secondary domain states. All we have to do is just replace the group G of the parent phase by the twinning group K_{1j} . There are, therefore, three kinds of nonzero tensor components in \mathbf{S}_1 and \mathbf{S}_j :

(1) Domain states \mathbf{S}_1 and \mathbf{S}_j differ in the principal tensor parameters κ_a of the ‘virtual’ phase transition with symmetry descent $K_{1j} \supset F_1$,

$$\kappa_a^{(1)} \neq \kappa_a^{(j)}, \quad a = 1, 2, \dots, \quad (3.4.3.27)$$

where $\kappa_a^{(1)}$ and $\kappa_a^{(j)}$ are the principal tensor parameters in domain states \mathbf{S}_1 and \mathbf{S}_j ; in the symbol of the principal tensor parameter κ_a we explicitly write only the lower index a , which numbers different principal tensor parameters, but omit the upper index labelling the representation of K_{1j} , according to which κ_a transforms, and the second lower index denoting the components of the principal tensor parameter (see Section 3.4.2.3 and the manual of the software *GI★KoBo-1*, path: *Subgroups\View\Domains* and Kopský (2001)).

The principal tensor parameters $\kappa_a^{(1)}$ of lower rank in domain state \mathbf{S}_1 can be found for $G = K_{1j}$ in Table 3.1.3.1 of Section 3.1.3.3, where we replace G by K_{1j} , and for all important property tensors in the software *GI★KoBo-1*, path: *Subgroups\View\Domains* and in Kopský (2001), where we again replace G by K_{1j} . Tensor parameters in domain state \mathbf{S}_j can be obtained by applying to the principal tensor parameters in \mathbf{S}_1 the operation g_{1j} .

(2) If there exists an intermediate group L_{1j} in between F_1 and K_{1j} that does not – contrary to K_{1j} – contain the switching operation g_{1j} of the domain pair $(\mathbf{S}_1, \mathbf{S}_j)$,

$$F_1 \subset L_{1j} \subseteq K_{1j}, \quad g_{1j} \in L_{1j}, \quad (3.4.3.28)$$

[cf. relation (3.4.3.23)] then domain states \mathbf{S}_1 and \mathbf{S}_j differ not only in the principal tensor parameters κ_a , but also in the secondary tensor parameters λ_b :

$$\lambda_b^{(1)} \neq \lambda_b^{(j)}, \quad I_{K_{1j}}(\lambda_b^{(1)}) = L_{1j}, \quad b = 1, \dots, \quad (3.4.3.29)$$

where $\lambda_b^{(1)}$ and $\lambda_b^{(j)}$ are the secondary tensor parameters in domain states \mathbf{S}_1 and \mathbf{S}_j ; the last equation, in which $I_{K_{1j}}(\lambda_b^{(1)})$ is the stabilizer of $\lambda_b^{(1)}$ in K_{1j} , expresses the condition that λ_b is the principal tensor parameter of the transition $K_{1j} \supset L_{1j}$ [see equation (3.4.2.40)].

The secondary tensor parameters $\lambda_b^{(1)}$ of lower rank in domain state \mathbf{S}_1 can be found for $G = K_{1j}$ in Table 3.1.3.1 of Section

3.1.3.3, and for all important property tensors in the software *GI★KoBo-1*, path: *Subgroups\View\Domains* and in Kopský (2001). Tensor parameters $\lambda_b^{(j)}$ in domain state \mathbf{S}_j can be obtained by applying to the secondary tensor parameters $\lambda_b^{(1)}$ in \mathbf{S}_1 the operation g_{1j} .

(3) All nonzero tensor components that are the same in domain states \mathbf{S}_1 and \mathbf{S}_j are identical with nonzero tensor components of the group K_{1j} . These components are readily available for all important material tensors in Section 1.1.4, in the software *GI★KoBo-1*, path: *Subgroups\View\Domains* and in Kopský (2001).

Cartesian tensor components corresponding to the tensor parameters can be calculated by means of conversion equations [for details see the manual of the software *GI★KoBo-1*, path: *Subgroups\View\Domains* and Kopský (2001)].

Let us now illustrate the above recipe for finding tensor distinctions by two simple examples.

Example 3.4.3.2. The domain pair $(\mathbf{S}_1, \mathbf{S}_2)$ in Fig. 3.4.3.1(a) is a completely transposable pair, therefore, according to equations (3.4.3.24) and (3.4.3.18),

$$K_{12}^* = J_{12}^* = 2_x m_y m_z \cup m_x^* \{2_x m_y m_z\} = m_x^* m_y m_z. \quad (3.4.3.30)$$

In Table 3.1.3.1, we find that the first principal tensor parameter $\kappa^{(1)}$ of the transition $G = K_{1j} = m_x m_y m_z \supset 2_x m_y m_z = F_1$ is the x -component P_1 of the spontaneous polarization, $\kappa_1^{(1)} = P_1$. Since the switching operation g_{12}^* is for example the inversion $\bar{1}$, the tensor parameter $\kappa_1^{(2)}$ in the second domain state \mathbf{S}_2 is $\kappa_1^{(2)} = -P_1$.

Other principal tensor parameters can be found in the software *GI★KoBo-1* or in Kopský (2001), p. 185. They are: $\kappa_2^{(1)} = d_{12}$, $\kappa_3^{(1)} = d_{13}$, $\kappa_4^{(1)} = d_{26}$, $\kappa_5^{(1)} = d_{35}$ (the physical meaning of the components is explained in Table 3.4.3.5). In the second domain state \mathbf{S}_2 , these components have the opposite sign. No other tensor components exist that would be different in \mathbf{S}_1 and \mathbf{S}_2 , since there is no intermediate group L_{1j} in between F_1 and K_{1j} .

Nonzero components that are the same in both domain states are nonzero components of property tensors in the group mmm and are listed in Section 1.1.4.7 or in the software *GI★KoBo-1* or in Kopský (2001).

The numbers of independent tensor components that are different and those that are the same in two domain states are readily available for all non-ferroelastic domain pairs and important property tensors in Table 3.4.3.4.

Example 3.4.3.3. The twinning group of the partially transposable domain pair $(\mathbf{S}_1, \mathbf{S}_3)$ in Fig. 3.4.3.1(b) with $\mathbf{S}_3 = 2_{xy}\mathbf{S}_1$ has the twinning group

$$K_{13} = 2_x m_y m_z \cup 2_{xy} \{2_x m_y m_z\} \cup 2_z \{2_x m_y m_z\} \cup 2_{x\bar{y}} \{2_x m_y m_z\} \\ = 4_z / m_z m_x m_{xy}. \quad (3.4.3.31)$$

Domain states \mathbf{S}_1 and \mathbf{S}_3 differ in the principal tensor parameter of the transition $4_z / m_z m_x m_{xy} \subset 2_x m_y m_z$, which is two-dimensional and which we found in Example 3.4.2.4: $\kappa_1^{(1)} = (P, 0)$. Then in the domain state \mathbf{S}_3 it is $\kappa_1^{(3)} = D(2_{xy})(P, 0) = (0, P)$. Other principal tensors are: $\kappa_2^{(1)} = (g_4, 0)$, $\kappa_3^{(1)} = (d_{11}, 0)$, $\kappa_4^{(1)} = (d_{12}, 0)$, $\kappa_5^{(1)} = (d_{13}, 0)$, $\kappa_6^{(1)} = (d_{26}, 0)$, $\kappa_7^{(1)} = (d_{35}, 0)$ (the physical meaning of the components is explained in Table 3.4.3.5). In the domain state \mathbf{S}_3 they keep their absolute value but appear as the second nonzero components, as with spontaneous polarization.

There is an intermediate group $L_{13} = m_x m_y m_z$ between $F_1 = 2_x m_y m_z$ and $K_{13} = 4_z / m_z m_x m_{xy}$, since $L_{13} = m_x m_y m_z$ does not contain $g_{13} = 2_{xy}$. The one-dimensional secondary tensor parameters for the symmetry descent $K_{13} = 4_z / m_z m_x m_{xy} \supset L_{13} = m_x m_y m_z$ was also found in Example 3.4.2.4: $\lambda_1^{(1)} = u_1 - u_2$;

3.4. DOMAIN STRUCTURES

$\lambda_2^{(1)} = A_{14} + A_{25}, A_{36}; \quad \lambda_3^{(1)} = s_{11} - s_{22}, \quad s_{13} - s_{23}, \quad s_{44} - s_{55};$
 $\lambda_4^{(1)} = Q_{11} - Q_{22}, Q_{12} - Q_{21}, Q_{13} - Q_{23}, Q_{31} - Q_{32}, Q_{44} - Q_{55}.$
 All these parameters have the opposite sign in S_3 .

The tensor distinction of two domain states S_1 and S_j in a domain pair (S_1, S_j) provides a useful *classification of domain pairs* given in the second and the third columns of Table 3.4.3.1. This classification can be extended to ferroic phases which are named according to domain pairs that exist in this phase. Thus, for example, if a ferroic phase contains ferroelectric (ferroelastic) domain pair(s), then this phase is a ferroelectric (ferroelastic) phase. Finer division into full and partial ferroelectric (ferroelastic) phases specifies whether all or only some of the possible domain pairs in this phase are ferroelectric (ferroelastic) ones. Another approach to this classification uses the notions of principal and secondary tensor parameters, and was explained in Section 3.4.2.2.

A discussion of and many examples of secondary ferroic phases are available in papers by Newnham & Cross (1974a,b) and Newnham & Skinner (1976), and tertiary ferroic phases are discussed by Amin & Newnham (1980).

We shall now show that the tensor distinction of domain states is closely related to the switching of domain states by external fields.

3.4.3.3. Switching of ferroic domain states

We saw in Section 3.4.2.1 that all domain states of the orbit GS_1 have the same chance of appearing. This implies that they have the same free energy, *i.e.* they are degenerate. The same conclusion follows from thermodynamic theory, where domain states appear as equivalent solutions of equilibrium values of the order parameter, *i.e.* all domain states exhibit the same free energy Ψ (see Section 3.1.2). These statements hold under a tacit assumption of absent external electric and mechanical fields. If these fields are nonzero, the degeneracy of domain states can be partially or completely lifted.

The free energy $\Psi^{(k)}$ per unit volume of a ferroic domain state S_k , $k = 1, 2, \dots, n$, with spontaneous polarization $\mathbf{P}_0^{(k)}$ with components $P_{0i}^{(k)}$, $i = 1, 2, 3$, and with spontaneous strain components $u_{0\mu}^{(k)}$, $\mu = 1, 2, \dots, 6$, is (Aizu, 1972)

$$\Psi^{(k)} = \Psi_0 - P_{0i}^{(k)} E_i - u_{0\mu}^{(k)} \sigma_\mu - d_{i\mu}^{(k)} E_i \sigma_\mu - \frac{1}{2} \varepsilon_0 \kappa_{ik}^{(k)} E_i E_k - \frac{1}{2} s_{\mu\nu}^{(k)} \sigma_\mu \sigma_\nu - \frac{1}{2} Q_{ik\mu} E_i E_k \sigma_\mu - \dots, \quad (3.4.3.32)$$

where the Einstein summation convention (summation with respect to suffixes that occur twice in the same term) is used with $i, j = 1, 2, 3$ and $\mu, \nu = 1, 2, \dots, 6$. The symbols in equation (3.4.3.32) have the following meaning: E_i and u_μ are components of the external electric field and of the mechanical stress, respectively, $d_{i\mu}^{(k)}$ are components of the piezoelectric tensor, $\varepsilon_0 \kappa_{ij}^{(k)}$ are components of the electric susceptibility, $s_{\mu\nu}^{(k)}$ are

compliance components, and $Q_{ij\mu}^{(k)}$ are components of electrostriction (components with Greek indices are expressed in matrix notation) [see Section 3.4.5 (Glossary), Chapter 1.1 or Nye (1985); Sirotnin & Shaskolskaya (1982)].

We shall examine two domain states S_1 and S_j , *i.e.* a domain pair (S_1, S_j) , in electric and mechanical fields. The difference of their free energies is given by

$$\begin{aligned} \Psi^{(j)} - \Psi^{(1)} = & -(P_{0i}^{(j)} - P_{0i}^{(1)}) E_i - (u_{0\mu}^{(j)} - u_{0\mu}^{(1)}) \sigma_\mu - (d_{i\mu}^{(j)} - d_{i\mu}^{(1)}) E_i \sigma_\mu \\ & - \frac{1}{2} \varepsilon_0 (\kappa_{ik}^{(j)} - \kappa_{ik}^{(1)}) E_i E_k - \frac{1}{2} (s_{\mu\nu}^{(j)} - s_{\mu\nu}^{(1)}) \sigma_\mu \sigma_\nu \\ & - \frac{1}{2} (Q_{ik\mu}^{(j)} - Q_{ik\mu}^{(1)}) E_i E_k \sigma_\mu - \dots \end{aligned} \quad (3.4.3.33)$$

For a domain pair (S_1, S_j) and given external fields, there are three possibilities:

(1) $\Psi^{(j)} = \Psi^{(1)}$. Domain states S_1 and S_j can coexist in equilibrium in given external fields.

(2) $\Psi^{(j)} < \Psi^{(1)}$. In given external fields, domain state S_j is more stable than S_1 ; for large enough fields (higher than the coercive ones), the state S_1 switches into the state S_j .

(3) $\Psi^{(j)} > \Psi^{(1)}$. In given external fields, domain state S_j is less stable than S_1 ; for large enough fields (higher than the coercive ones), the state S_j switches into the state S_1 .

A typical dependence of applied stress and corresponding strain in ferroelastic materials has a form of a elastic hysteresis loop (see Fig. 3.4.1.3). Similar dielectric hysteresis loops are observed in ferroelectric materials; examples can be found in books on ferroelectric crystals (*e.g.* Jona & Shirane, 1962).

A classification of switching (state shifts in Aizu's terminology) based on equation (3.4.3.33) was put forward by Aizu (1972, 1973) and is summarized in the second and fourth columns of Table 3.4.3.1. The order of the state shifts specifies the switching fields that are necessary for switching one domain state of a domain pair into the second state of the pair.

Another distinction related to switching distinguishes between *actual* and *potential* ferroelectric (ferroelastic) phases, depending on whether or not it is possible to switch the spontaneous polarization (spontaneous strain) by applying an electric field (mechanical stress) lower than the electrical (mechanical) breakdown limit under reasonable experimental conditions (Wadhawan, 2000). We consider in our classification always the potential ferroelectric (ferroelastic) phase.

A closer look at equation (3.4.3.33) reveals a correspondence between the difference coefficients in front of products of field components and the tensor distinction of domain states S_1 and S_j in the domain pair (S_1, S_j) : If a morphic Cartesian tensor component of a *polar* tensor is different in these two domain states, then the corresponding difference coefficient is nonzero and defines components of fields that can switch one of these domain states into the other. A similar statement holds for the symmetric tensors of rank two (*e.g.* the spontaneous strain tensor).

Table 3.4.3.1. *Classification of domain pairs, ferroic phases and of switching (state shifts)*

$P_{0i}^{(k)}$ and $u_{0\mu}^{(k)}$ are components of the spontaneous polarization and spontaneous strain in the domain state S_k , where $k = 1$ or $k = j$; similarly, $d_{i\mu}^{(k)}$ are components of the piezoelectric tensor, $\varepsilon_0 \kappa_{ij}^{(k)}$ are components of electric susceptibility, $s_{\mu\nu}^{(k)}$ are compliance components and $Q_{ij\mu}^{(k)}$ are components of electrostriction (components with Greek indices are expressed in matrix notation) [see Chapter 1.1 or *e.g.* Nye (1985) and Sirotnin & Shaskolskaya (1982)]. Text in *italics* concerns the classification of ferroic phases. \mathbf{E} is the electric field and σ is the mechanical stress.

| Ferroic class | Domain pair – at least in one pair | Domain pair – phase | Switching (state shift) | Switching field |
|---------------|---|---------------------|---------------------------------|------------------------|
| Primary | At least one $P_{0i}^{(j)} - P_{0i}^{(1)} \neq 0$ | Ferroelectric | Electrically first order | \mathbf{E} |
| | At least one $u_{0\mu}^{(j)} - u_{0\mu}^{(1)} \neq 0$ | Ferroelastic | Mechanically first order | σ |
| Secondary | At least one $P_{0i}^{(j)} - P_{0i}^{(1)} \neq 0$ and at least one $u_{0\mu}^{(j)} - u_{0\mu}^{(1)} \neq 0$ | Ferroelastoelectric | Electromechanically first order | $\mathbf{E}\sigma$ |
| | All $P_{0i}^{(j)} - P_{0i}^{(1)} = 0$ and at least one $\varepsilon_0 (\kappa_{ik}^{(j)} - \kappa_{ik}^{(1)}) \neq 0$ | Ferrobioelectric | Electrically second order | $\mathbf{E}\mathbf{E}$ |
| | All $u_{0\mu}^{(j)} - u_{0\mu}^{(1)} = 0$ and at least one $s_{\mu\nu}^{(j)} - s_{\mu\nu}^{(1)} \neq 0$ | Ferrobielastic | Mechanically second order | $\sigma\sigma$ |
| ... | ... | ... | ... | ... |

$i, j = 1, 2, 3; \mu, \nu = 1, 2, \dots, 6.$

3. PHASE TRANSITIONS, TWINNING AND DOMAIN STRUCTURES

Table 3.4.3.2. Four types of domain pairs

| F_{ij} | J_{ij} | K_{ij} | Double coset | Domain pair name symbol |
|----------------------|-------------------------------|---|--|--|
| $F_1 = F_j$ | $F_1 \cup g_{ij}^* F_1$ | $F_1 \cup g_{ij}^* F_1$ | $F_1 g_{ij} F_1 = g_{ij} F_1 = (g_{ij} F_1)^{-1}$ | <u>t</u> ransposable <u>c</u> ompletely tc |
| $F_{ij} \subset F_1$ | $F_{ij} \cup g_{ij}^* F_{ij}$ | $F_1 \cup g_{ij}^* F_1 \cup \dots$ | $F_1 g_{ij} F_1 = (F_1 g_{ij} F_1)^{-1}$ | <u>t</u> ransposable <u>p</u> artially tp |
| $F_1 = F_j$ | F_1 | $F_1 \cup g_{ij} F_1 \cup g_{ij}^{-1} F_1$ | $F_1 g_{ij} F_1 = g_{ij} F_1 \cap (g_{ij} F_1)^{-1} = \emptyset$ | <u>n</u> on-transposable <u>s</u> imple ns |
| $F_{ij} \subset F_1$ | F_{ij} | $F_1 \cup g_{ij} F_1 \cup (g_{ij} F_1)^{-1} \cup \dots$ | $F_1 g_{ij} F_1 \cap (F_1 g_{ij} F_1)^{-1} = \emptyset$ | <u>n</u> on-transposable <u>m</u> ultiple nm |

Tensor distinction for all representative non-ferroelastic domain pairs is available in the synoptic Table 3.4.3.4. These data also carry information about the switching fields.

3.4.3.4. Classes of equivalent domain pairs and their classifications

Two domain pairs that are crystallographically equivalent, $(\mathbf{S}_i, \mathbf{S}_k) \sim^G (\mathbf{S}_l, \mathbf{S}_m)$ [see equation (3.4.3.5)], have different orientations in space but their inherent properties are the same. It is, therefore, useful to divide all domain pairs of a ferroic phase into classes of equivalent domain pairs. All domain pairs that are equivalent (in G) with a given domain pair, say $(\mathbf{S}_i, \mathbf{S}_k)$, can be obtained by applying to $(\mathbf{S}_i, \mathbf{S}_k)$ all operations of G , i.e. by forming a G -orbit $G(\mathbf{S}_i, \mathbf{S}_k)$.

One can always find in this orbit a domain pair $(\mathbf{S}_1, \mathbf{S}_j)$ that has in the first place the first domain state \mathbf{S}_1 . We shall call such a pair a *representative domain pair of the orbit*. The initial orbit $G(\mathbf{S}_i, \mathbf{S}_k)$ and the orbit $G(\mathbf{S}_1, \mathbf{S}_j)$ are identical:

$$G(\mathbf{S}_i, \mathbf{S}_k) = G(\mathbf{S}_1, \mathbf{S}_j).$$

The set \mathbf{P} of n^2 ordered pairs (including trivial ones) that can be formed from n domain states can be divided into G -orbits (classes of equivalent domain pairs):

$$\mathbf{P} = G(\mathbf{S}_1, \mathbf{S}_1) \cup G(\mathbf{S}_1, g_2 \mathbf{S}_1) \cup \dots \cup (\mathbf{S}_1, g_j \mathbf{S}_1) \cup \dots \cup G(\mathbf{S}_1, g_q \mathbf{S}_1). \quad (3.4.3.34)$$

Similarly, as there is a one-to-one correspondence between domain states and left cosets of the stabilizer (symmetry group) F_1 of the first domain state [see equation (3.4.2.9)], there is an analogous relation between G -orbits of domain pairs and so-called double cosets of F_1 .

A *double coset* $F_1 g_j F_1$ of F_1 is a set of left cosets that can be expressed as $f g_j F_1$, where $f \in F_1$ runs over all operations of F_1 (see Section 3.2.3.2.8). A group G can be decomposed into disjoint double cosets of $F_1 \subset G$:

$$G = F_1 e F_1 \cup F_1 g_2 F_1 \cup \dots \cup F_1 g_j F_1 \cup \dots \cup F_1 g_q F_1, \quad j = 1, 2, \dots, q, \quad (3.4.3.35)$$

where $g_1 = e, g_2, \dots, g_j, \dots, g_q$ is the set of representatives of double cosets.

There is a one-to-one correspondence between double cosets of the decomposition (3.4.3.35) and G -orbits of domain pairs (3.4.3.34) (see Section 3.2.3.3.6, Proposition 3.2.3.35):

$$G(\mathbf{S}_1, \mathbf{S}_j) \leftrightarrow F_1 g_j F_1, \quad \text{where } \mathbf{S}_j = g_j \mathbf{S}_1, \quad j = 1, 2, \dots, q. \quad (3.4.3.36)$$

We see that the representatives g_j of the double cosets in decomposition (3.4.3.35) define domain pairs $(\mathbf{S}_1, g_j \mathbf{S}_1)$ which represent all different G -orbits of domain pairs. Just as different left cosets $g_i F_1$ specify all domain states, different double cosets determine all classes of equivalent domain pairs (G -orbits of domain pairs).

The properties of double cosets are reflected in the properties of corresponding domain pairs and provide a natural classification of domain pairs. A specific property of a double coset is that it is either identical or disjoint with its inverse. A double coset that is identical with its inverse,

$$(F_1 g_j F_1)^{-1} = F_1 g_j^{-1} F_1 = F_1 g_j F_1, \quad (3.4.3.37)$$

is called an *invertible (ambivalent) double coset*. The corresponding class of domain pairs consists of transposable (ambivalent) domain pairs.

A double coset that is disjoint with its inverse,

$$(F_1 g_j F_1)^{-1} = F_1 g_j^{-1} F_1 \cap F_1 g_j F_1 = \emptyset, \quad (3.4.3.38)$$

is a *non-invertible (polar) double coset* (\emptyset denotes an empty set) and the corresponding class of domain pairs comprises non-transposable (polar) domain pairs. A double coset $F_1 g_j F_1$ and its inverse $(F_1 g_j F_1)^{-1}$ are called *complementary double cosets*. Corresponding classes called *complementary classes of equivalent domain pairs* consist of transposed domain pairs that are non-equivalent.

Another attribute of a double coset is the number of left cosets which it comprises. If an invertible double coset consists of one left coset,

$$F_1 g_j F_1 = g_j F_1 = (g_j F_1)^{-1}, \quad (3.4.3.39)$$

then the domain pairs in the G -orbit $G(\mathbf{S}_1, g_j \mathbf{S}_1)$ are completely transposable. An invertible double coset comprising several left cosets is associated with a G -orbit consisting of partially transposable domain pairs. Non-invertible double cosets can be divided into simple non-transposable double cosets (complementary double cosets consist of one left coset each) and multiple non-transposable double cosets (complementary double cosets comprise more than one left coset each).

Thus there are four types of double cosets (see Table 3.2.3.1 in Section 3.2.3.2) to which there correspond the four basic types of domain pairs presented in Table 3.4.3.2.

These results can be illustrated using the example of a phase transition with $G = 4_z/m_z m_x m_{xy} \supset 2_x m_y m_z = F_1$ with four domain states (see Fig. 3.4.2.2). The corresponding four left cosets of $2_x m_y m_z$ are given in Table 3.4.2.1. Any operation from the first left coset (identical with F_1) transforms the second left coset into itself, i.e. this left coset is a double coset. Since it consists of an operation of order two, it is a simple invertible double coset. The corresponding representative domain pair is $(\mathbf{S}_1, \bar{\mathbf{S}}_1) = (\mathbf{S}_1, \mathbf{S}_2)$. By applying operations of $G = 4_z/m_z m_x m_{xy}$ on $(\mathbf{S}_1, \mathbf{S}_2)$, one gets the class of equivalent domain pairs (G -orbit): $(\mathbf{S}_1, \mathbf{S}_2) \sim^G (\mathbf{S}_2, \mathbf{S}_1) \sim^G (\mathbf{S}_3, \mathbf{S}_4) \sim^G (\mathbf{S}_4, \mathbf{S}_3)$. These domain pairs can be labelled as '180° pairs' according to the angle between the spontaneous polarization in the two domain states.

When one applies operations from the first left coset on the third left coset, one gets the fourth left coset, therefore a double coset consists of these two left cosets. An inverse of any operation of this double coset belongs to this double coset, hence it is a multiple invertible double coset. Corresponding domain pairs are partially transposable ones. A representative pair is, for example,

Table 3.4.3.3. Decomposition of $G = 6_z/m_z$ into left cosets of $F_1 = 2_z/m_z$

| Left coset | | | | Principal domain state |
|------------|---------|---------------|---------------|------------------------|
| 1 | 2_z | $\bar{1}$ | m_z | \mathbf{S}_1 |
| 3_z | 6_z^5 | $\bar{3}_z$ | $\bar{6}_z^5$ | \mathbf{S}_2 |
| 3_z^2 | 6_z | $\bar{3}_z^5$ | $\bar{6}_z$ | \mathbf{S}_3 |

3.4. DOMAIN STRUCTURES

$(\mathbf{S}_1, 2_{xy}\mathbf{S}_1) = (\mathbf{S}_1, \mathbf{S}_3)$ which is indeed a partially transposable domain pair [cf. (3.4.3.19) and (3.4.3.20)]. The class of equivalent ordered domain pairs is $(\mathbf{S}_1, \mathbf{S}_3) \stackrel{G}{\sim} (\mathbf{S}_3, \mathbf{S}_1) \stackrel{G}{\sim} (\mathbf{S}_1, \mathbf{S}_4) \stackrel{G}{\sim} (\mathbf{S}_4, \mathbf{S}_1) \stackrel{G}{\sim} (\mathbf{S}_3, \mathbf{S}_2) \stackrel{G}{\sim} (\mathbf{S}_2, \mathbf{S}_3) \stackrel{G}{\sim} (\mathbf{S}_2, \mathbf{S}_4) \stackrel{G}{\sim} (\mathbf{S}_4, \mathbf{S}_2)$. These are ‘90° domain pairs’.

An example of non-invertible double cosets is provided by the decomposition of the group $G = 6_z/m_z$ into left and double cosets of $F_1 = 2_z/m_z$ displayed in Table 3.4.3.3. The inverse of the second left coset (second line) is equal to the third left coset (third line) and *vice versa*. Each of these two left cosets thus corresponds to a double coset and these double cosets are complementary double cosets. Corresponding representative simple non-transposable domain pairs are $(\mathbf{S}_1, \mathbf{S}_2)$ and $(\mathbf{S}_2, \mathbf{S}_1)$, and are depicted in Fig. 3.4.3.2.

We conclude that *double cosets determine classes of equivalent domain pairs that can appear in the ferroic phase resulting from a phase transition with a symmetry descent $G \supset F_1$* . Left coset and double coset decompositions for all crystallographic point-group descents are available in the software *GI★KoBo-1*, path: *Subgroups\View\Twining groups*.

A double coset can be specified by any operation belonging to it. This representation is not very convenient, since it does not reflect the properties of corresponding domain pairs and there are many operations that can be chosen as representatives of a double coset. It turns out that in a continuum description the twinning group K_{ij} can represent classes of equivalent domain pairs $G(\mathbf{S}_1, \mathbf{S}_j)$ with two exceptions:

(i) Two complementary classes of non-transposable domain pairs have the same twinning group. This follows from the fact that if a twinning group contains the double coset, then it must comprise also the inverse double coset.

(ii) Different classes of transposable domain pairs have different twinning groups except in the following case (which corresponds to the orthorhombic ferroelectric phase in perovskites): the group $F_1 = m_{xy}2_{xy}m_z$ generates with switching operations $g = 2_{yz}$ and $g_3 = m_{yz}$ two different double cosets with the same twinning group $K_{12} = K_{13} = m\bar{3}m$ (one can verify this in the software *GI★KoBo-1*, path: *Subgroups\View\Twining groups*). Domain states are characterized in this ferroelectric phase by the direction of the spontaneous polarization. The angles between the spontaneous polarizations of the domain states in domain pairs $(\mathbf{S}_1, 2_{yz}\mathbf{S}_1)$ and $(\mathbf{S}_1, m_{yz}\mathbf{S}_1)$ are 120 and 60°, respectively; this shows that these representative domain pairs are not equivalent and belong to two different G -orbits of domain pairs. To distinguish these two cases, we add to the twinning group $m\bar{3}m[m_{xy}2_{xy}m_z]$ either the switching operation 2_{yz} or m_{yz} , i.e. the two distinct orbits are labelled by the symbols $m\bar{3}m(2_{yz})$ and $m\bar{3}m(m_{yz})$, respectively.

Bearing in mind these two exceptions, *one can, in the continuum description, represent G -orbits of domain pairs $G(\mathbf{S}_1, \mathbf{S}_j)$ by twinning groups $K_{ij}[F_1]$* .

We have used this correspondence in synoptic Table 3.4.2.7 of symmetry descents at ferroic phase transitions. For each symmetry descent $G \supset F_1$, the twinning groups given in column K_{ij} specify possible G -orbits of domain pairs that can appear in the domain structure of the ferroic phase (Litvin & Janovec, 1999). We divide all orbits of domain pairs (represented by corresponding twinning groups K_{ij}) that appear in Table 3.4.2.7 into classes of non-ferroelastic and ferroelastic domain pairs and present them with further details in the three synoptic Tables 3.4.3.4, 3.4.3.6 and 3.4.3.7 described in Sections 3.4.3.5 and 3.4.3.6.

As we have seen, a classification of domain pairs according to their internal symmetry (summarized in Table 3.4.3.2) introduces a partition of all domain pairs that can be formed from domain states of the G -orbit $G\mathbf{S}_1$ into equivalence classes of pairs with the same internal symmetry. Similarly, any inherent physical property of domain pairs induces a partition of all domain pairs into corresponding equivalence classes. Thus, for example, the

classification of domain pairs, based on tensor distinction or switching of domain states (see Table 3.4.3.1, columns two and three), introduces a division of domain pairs into corresponding equivalence classes.

3.4.3.5. Non-ferroelastic domain pairs: twin laws, domain distinction and switching fields, synoptic table

Two domain states \mathbf{S}_1 and \mathbf{S}_j form a *non-ferroelastic domain pair* $(\mathbf{S}_1, \mathbf{S}_j)$ if the spontaneous strain in both domain states is the same, $\mathbf{u}_0^{(1)} = \mathbf{u}_0^{(j)}$. This is so if the twinning group K_{ij} of the pair and the symmetry group F_1 of domain state \mathbf{S}_1 belong to the same crystal family (see Table 3.4.2.2):

$$\text{Fam}K_{ij} = \text{Fam}F_1. \quad (3.4.3.40)$$

It can be shown that *all non-ferroelastic domain pairs are completely transposable domain pairs* (Janovec et al., 1993), i.e.

$$F_{ij} = F_1 = F_j \quad (3.4.3.41)$$

and the twinning group K_{ij} is equal to the symmetry group J_{ij} of the unordered domain pair [see equation (3.4.3.24)]:

$$K_{ij}^* = J_{ij}^* = F_1 \cup g_{ij}^*F_1. \quad (3.4.3.42)$$

(Complete transposability is only a necessary, but not a sufficient, condition of a non-ferroelastic domain pair, since there are also ferroelastic domain pairs that are completely transposable – see Table 3.4.3.6.)

The relation between domain states in a non-ferroelastic domain twin, in which two domain states coexist, is the same as that of a corresponding non-ferroelastic domain pair consisting of *single-domain* states. Transposing operations g_{ij}^* are, therefore, also *twining operations*.

Synoptic Table 3.4.3.4 lists representative domain pairs of all orbits of non-ferroelastic domain pairs. Each pair is specified by the first domain state \mathbf{S}_1 with symmetry group F_1 and by transposing operations g_{ij}^* that transform \mathbf{S}_1 into \mathbf{S}_j , $\mathbf{S}_j = g_{ij}^*\mathbf{S}_1$. Twin laws in dichromatic notation are presented and basic data for tensor distinction and switching of non-ferroelastic domains are given.

3.4.3.5.1. Explanation of Table 3.4.3.4

The first three columns specify domain pairs.

F_1 : point-group symmetry (stabilizer in K_{ij}) of the first domain state \mathbf{S}_1 in a single-domain orientation. There are two domain states with the same F_1 ; one has to be chosen as \mathbf{S}_1 . Subscripts of generators in the group symbol specify their orientation in the Cartesian (rectangular) crystallophysical coordinate system of the group K_{ij} (see Tables 3.4.2.5, 3.4.2.6 and Figs. 3.4.2.3, 3.4.2.4).

g_{ij}^* : switching operations that specify domain pair $(\mathbf{S}_1, g_{ij}^*\mathbf{S}_1) = (\mathbf{S}_1, \mathbf{S}_j)$. Subscripts of symmetry operations specify the orientation of the corresponding symmetry element in the Cartesian (rectangular) crystallophysical coordinate system of the group K_{ij} . In hexagonal and trigonal systems, x' , y' and x'' , y'' denote the Cartesian coordinate system rotated about the z axis through 120 and 240°, respectively, from the Cartesian coordinate axes x and y ; diagonal directions are abbreviated: $p = [111]$, $q = [\bar{1}\bar{1}1]$, $r = [1\bar{1}1]$, $s = [\bar{1}11]$ (for further details see Tables 3.4.2.5 and 3.4.2.6, and Figs. 3.4.2.3 and 3.4.2.4).

All switching operations of the second order are given, switching operations of higher order are omitted. The star symbol signifies that the operation is both a transposing and a twinning operation.

$K_{ij}^* = J_{ij}^*$: twinning group of the domain pair $(\mathbf{S}_1, \mathbf{S}_j)$. This group is equal to the symmetry group J_{ij}^* of the completely transposable unordered domain pair $\{\mathbf{S}_1, \mathbf{S}_j\}$ [see equation (3.4.3.24)]. The dichromatic symbol of the group $K_{ij}^* = J_{ij}^*$ designates the *twin law of the non-ferroelastic domain pair* $\{\mathbf{S}_1, \mathbf{S}_j\}$ and the *twin law of all*

3. PHASE TRANSITIONS, TWINNING AND DOMAIN STRUCTURES

Table 3.4.3.4. *Non-ferroelastic domain pairs, domain twin laws and distinction of non-ferroelastic domains*

F_1 : symmetry of \mathbf{S}_1 ; g_{1j}^* : twinning operations of second order; K_{1j}^* : twinning group signifying the twin law of domain pair $(\mathbf{S}_1, g_{1j}^*\mathbf{S}_1)$; J_{1j}^* : symmetry group of the pair; Γ_α : irreducible representation of K_{1j}^* ; ϵ , \mathbf{P}_i , \dots , $\mathbf{Q}_{ij\mu}$: components of property tensors (see Table 3.4.3.5); $a|c$: number of distinct|equal nonzero tensor components of property tensors.

| F_1 | g_{1j}^* | $K_{1j}^* = J_{1j}^*$ | Γ_α | Diffraction intensities | ϵ | \mathbf{P}_i | g_μ | $\mathbf{d}_{i\mu}$ | $\mathbf{A}_{i\mu}$ | $\mathbf{s}_{\mu\nu}$ | $\mathbf{Q}_{ij\mu}$ |
|------------------------|--|----------------------------|-----------------|-------------------------|------------|----------------|---------|---------------------|---------------------|-----------------------|----------------------|
| 1 | $\bar{1}^*$ | $\bar{1}^*$ | A_u | = | 1 0 | 3 0 | 6 0 | 18 0 | 0 18 | 0 21 | 0 36 |
| 2_u^\dagger | $\bar{1}^*, m_u^*$ | $2_u/m_u^*$ | A_u | = | 1 0 | 1 0 | 4 0 | 8 0 | 0 8 | 0 13 | 0 20 |
| m_u^\dagger | $\bar{1}^*, 2_u^*$ | $2_u^*/m_u$ | B_u | = | 0 0 | 2 0 | 2 0 | 10 0 | 0 8 | 0 13 | 0 20 |
| $2_x 2_y 2_z$ | $\bar{1}^*, m_x^*, m_y^*, m_z^*$ | $m_x^* m_y^* m_z^*$ | A_u | = | 1 0 | 0 0 | 3 0 | 3 0 | 0 3 | 0 9 | 0 12 |
| $2_{xy} 2_{xy} 2_z$ | $\bar{1}^*, m_{xy}^*, m_{xy}^*, m_z^*$ | $m_{xy}^* m_{xy}^* m_z^*$ | A_u | = | 1 0 | 0 0 | 3 0 | 3 0 | 0 3 | 0 9 | 0 12 |
| $m_x m_y 2_z$ | $\bar{1}^*, m_z^*, 2_x^*, 2_y^*$ | $m_x m_y m_z^*$ | B_{1u} | = | 0 0 | 1 0 | 1 0 | 5 0 | 0 3 | 0 9 | 0 12 |
| $2_x m_y m_z$ | $\bar{1}^*, m_x^*, 2_y^*, 2_z^*$ | $m_x^* m_y m_z$ | B_{1u} | = | 0 0 | 1 0 | 1 0 | 5 0 | 0 3 | 0 9 | 0 12 |
| $m_x 2_y m_z$ | $\bar{1}^*, m_y^*, 2_x^*, 2_z^*$ | $m_x m_y^* m_z$ | B_{1u} | = | 0 0 | 1 0 | 1 0 | 5 0 | 0 3 | 0 9 | 0 12 |
| $m_{xy} m_{xy} 2_z$ | $\bar{1}^*, m_z^*, 2_{xy}^*, 2_{xy}^*$ | $m_{xy} m_{xy} m_z^*$ | B_{1u} | = | 0 0 | 1 0 | 1 0 | 5 0 | 0 3 | 0 9 | 0 12 |
| 4_z | $\bar{1}^*, m_z^*$ | $4_z/m_z^*$ | A_u | = | 1 0 | 1 0 | 2 0 | 4 0 | 0 4 | 0 7 | 0 10 |
| 4_z | $2_x^*, 2_y^*, 2_{xy}^*, 2_{xy}^*$ | $4_z 2_x^* 2_{xy}^*$ | A_2 | \neq | 0 1 | 1 0 | 0 2 | 3 1 | 3 1 | 1 6 | 3 7 |
| 4_z | $m_x^*, m_y^*, m_{xy}^*, m_{xy}^*$ | $4_z m_x^* m_{xy}^*$ | A_2 | \neq | 1 0 | 0 1 | 2 0 | 1 3 | 3 1 | 1 6 | 3 7 |
| $\bar{4}_z$ | $\bar{1}^*, m_z^*$ | $4_z^*/m_z^*$ | B_u | = | 0 0 | 0 0 | 2 0 | 4 0 | 0 4 | 0 7 | 0 10 |
| $\bar{4}_z$ | $m_{xy}^*, m_{xy}^*, 2_x^*, 2_y^*$ | $\bar{4}_z 2_x^* m_{xy}^*$ | A_2 | \neq | 0 0 | 0 0 | 1 1 | 2 2 | 3 1 | 1 6 | 3 7 |
| $\bar{4}_z$ | $m_x^*, m_y^*, 2_{xy}^*, 2_{xy}^*$ | $\bar{4}_z m_x^* 2_{xy}^*$ | A_2 | \neq | 0 0 | 0 0 | 1 1 | 2 2 | 3 1 | 1 6 | 3 7 |
| $4_z/m_z$ | $m_x^*, m_y^*, m_{xy}^*, m_{xy}^*, 2_x^*, 2_y^*, 2_{xy}^*, 2_{xy}^*$ | $4_z/m_z m_x^* m_{xy}^*$ | A_{2g} | \neq | 0 0 | 0 0 | 0 0 | 0 0 | 3 1 | 1 6 | 3 7 |
| $4_z 2_x 2_{xy}$ | $\bar{1}^*, m_z^*, m_x^*, m_y^*, m_{xy}^*, m_{xy}^*$ | $4_z/m_z^* m_x^* m_{xy}^*$ | A_{1u} | = | 1 0 | 0 0 | 2 0 | 1 0 | 0 1 | 0 6 | 0 7 |
| $4_z m_x m_{xy}$ | $\bar{1}^*, m_z^*, 2_x^*, 2_y^*, 2_{xy}^*, 2_{xy}^*$ | $4_z/m_z^* m_x m_{xy}$ | A_{2u} | = | 0 0 | 1 0 | 0 0 | 3 0 | 0 1 | 0 6 | 0 7 |
| $\bar{4}_z 2_x m_{xy}$ | $\bar{1}^*, m_z^*, m_x^*, m_y^*, 2_{xy}^*, 2_{xy}^*$ | $4_z^*/m_z^* m_x^* m_{xy}$ | B_{1u} | = | 0 0 | 0 0 | 1 0 | 2 0 | 0 1 | 0 6 | 0 7 |
| $\bar{4}_z m_x 2_{xy}$ | $\bar{1}^*, m_z^*, m_{xy}^*, m_{xy}^*, 2_x^*, 2_y^*$ | $4_z^*/m_z^* m_x m_{xy}$ | B_{1u} | = | 0 0 | 0 0 | 1 0 | 2 0 | 0 1 | 0 6 | 0 7 |
| 3_v^\ddagger | $\bar{1}^*$ | $\bar{3}_v^*$ | A_u | = | 1 0 | 1 0 | 2 0 | 6 0 | 0 6 | 0 7 | 0 12 |
| 3_z | $2_x^*, 2_{x'}^*, 2_{x''}^*$ | $3_z 2_x^*$ | A_2 | \neq | 0 1 | 1 0 | 0 2 | 4 2 | 4 2 | 1 6 | 4 8 |
| 3_z | $2_y^*, 2_{y'}^*, 2_{y''}^*$ | $3_z 2_y^*$ | A_2 | \neq | 0 1 | 1 0 | 0 2 | 4 2 | 4 2 | 1 6 | 4 8 |
| 3_p | $2_{xy}^*, 2_{y\bar{z}}^*, 2_{z\bar{x}}^*$ | $3_p 2_{xy}^*$ | A_2 | \neq | 0 1 | 1 0 | 0 2 | 4 2 | 4 2 | 1 6 | 4 8 |
| 3_z | $m_x^*, m_{x'}^*, m_{x''}^*$ | $3_z m_x^*$ | A_2 | \neq | 1 0 | 0 1 | 2 0 | 2 4 | 4 2 | 1 6 | 4 8 |
| 3_z | $m_y^*, m_{y'}^*, m_{y''}^*$ | $3_z m_y^*$ | A_2 | \neq | 1 0 | 0 1 | 2 0 | 2 4 | 4 2 | 1 6 | 4 8 |
| 3_p | $m_{xy}^*, m_{y\bar{z}}^*, m_{z\bar{x}}^*$ | $3_p m_x^*$ | A_2 | \neq | 1 0 | 0 1 | 2 0 | 2 4 | 4 2 | 1 6 | 4 8 |
| 3_z | 2_z^* | 6_z^* | B | \neq | 0 1 | 0 1 | 0 2 | 2 4 | 2 4 | 2 5 | 4 8 |
| 3_z | m_z^* | $\bar{6}_z^*$ | A'' | \neq | 1 0 | 1 0 | 2 0 | 4 2 | 2 4 | 2 5 | 4 8 |
| $\bar{3}_z$ | $m_x^*, m_{x'}^*, m_{x''}^*, 2_x^*, 2_{x'}^*, 2_{x''}^*$ | $\bar{3}_z m_x^*$ | A_{2g} | \neq | 0 0 | 0 0 | 0 0 | 0 0 | 4 2 | 1 6 | 4 8 |
| $\bar{3}_z$ | $m_y^*, m_{y'}^*, m_{y''}^*, 2_y^*, 2_{y'}^*, 2_{y''}^*$ | $\bar{3}_z m_y^*$ | A_{2g} | \neq | 0 0 | 0 0 | 0 0 | 0 0 | 4 2 | 1 6 | 4 8 |
| $\bar{3}_p$ | $m_{xy}^*, m_{y\bar{z}}^*, m_{z\bar{x}}^*, 2_{xy}^*, 2_{y\bar{z}}^*, 2_{z\bar{x}}^*$ | $\bar{3}_p m_x^*$ | A_{2g} | \neq | 0 0 | 0 0 | 0 0 | 0 0 | 4 2 | 1 6 | 4 8 |
| $\bar{3}_z$ | $m_z^*, 2_z^*$ | $6_z^*/m_z^*$ | B_g | \neq | 0 0 | 0 0 | 0 0 | 0 0 | 2 4 | 2 5 | 4 8 |
| $3_z 2_x$ | $\bar{1}^*, m_x^*, m_{x'}^*, m_{x''}^*$ | $\bar{3}_z^* m_x^*$ | A_{1u} | = | 1 0 | 0 0 | 2 0 | 2 0 | 0 2 | 0 6 | 0 8 |
| $3_z 2_y$ | $\bar{1}^*, m_y^*, m_{y'}^*, m_{y''}^*$ | $\bar{3}_z^* m_y^*$ | A_{1u} | = | 1 0 | 0 0 | 2 0 | 2 0 | 0 2 | 0 6 | 0 8 |
| $3_z 2_x$ | $2_z^*, 2_y^*, 2_{y'}^*, 2_{y''}^*$ | $6_z^* 2_y^*$ | B_1 | \neq | 0 1 | 0 0 | 0 2 | 1 1 | 1 1 | 1 5 | 2 6 |
| $3_z 2_y$ | $2_z^*, 2_x^*, 2_{x'}^*, 2_{x''}^*$ | $6_z^* 2_x^*$ | B_1 | \neq | 0 1 | 0 0 | 0 2 | 1 1 | 1 1 | 1 5 | 2 6 |
| $3_p 2_{xy}$ | $\bar{1}^*, m_{xy}^*, m_{y\bar{z}}^*, m_{z\bar{x}}^*$ | $\bar{3}_p^* m_x^*$ | A_{1u} | = | 1 0 | 0 0 | 2 0 | 2 0 | 0 2 | 0 6 | 0 8 |
| $3_z 2_x$ | $m_z^*, m_y^*, m_{y'}^*, m_{y''}^*$ | $\bar{6}_z^* 2_y m_y^*$ | A_1'' | \neq | 1 0 | 0 0 | 2 0 | 1 1 | 1 1 | 1 5 | 2 6 |
| $3_z 2_y$ | $m_z^*, m_x^*, m_{x'}^*, m_{x''}^*$ | $\bar{6}_z^* m_x 2_y^*$ | A_1'' | \neq | 1 0 | 0 0 | 2 0 | 1 1 | 1 1 | 1 5 | 2 6 |
| $3_p m_{xy}$ | $\bar{1}^*, 2_{xy}^*, 2_{y\bar{z}}^*, 2_{z\bar{x}}^*$ | $\bar{3}_p^* m_x$ | A_{2u} | = | 0 0 | 1 0 | 0 0 | 4 0 | 0 2 | 0 6 | 0 8 |
| $3_z m_x$ | $\bar{1}^*, 2_x^*, 2_{x'}^*, 2_{x''}^*$ | $\bar{3}_z^* m_x$ | A_{2u} | = | 0 0 | 1 0 | 0 0 | 4 0 | 0 2 | 0 6 | 0 8 |
| $3_z m_y$ | $\bar{1}^*, 2_y^*, 2_{y'}^*, 2_{y''}^*$ | $\bar{3}_z^* m_y$ | A_{2u} | = | 0 0 | 1 0 | 0 0 | 4 0 | 0 2 | 0 6 | 0 8 |
| $3_z m_x$ | $2_z^*, m_y^*, m_{y'}^*, m_{y''}^*$ | $6_z^* m_x m_y^*$ | B_2 | \neq | 0 0 | 0 1 | 0 0 | 1 3 | 1 1 | 1 5 | 2 6 |
| $3_z m_y$ | $m_x^*, m_{x'}^*, m_{x''}^*$ | $6_z^* m_x^* m_y$ | B_2 | \neq | 0 0 | 0 1 | 0 0 | 1 3 | 1 1 | 1 5 | 2 6 |
| $3_z m_x$ | $m_z^*, 2_y^*, 2_{y'}^*, 2_{y''}^*$ | $\bar{6}_z^* m_x 2_y^*$ | A_2'' | \neq | 0 0 | 1 0 | 0 0 | 3 1 | 1 1 | 1 5 | 2 6 |
| $3_z m_y$ | $m_z^*, 2_x^*, 2_{x'}^*, 2_{x''}^*$ | $\bar{6}_z^* 2_x m_y$ | A_2'' | \neq | 0 0 | 1 0 | 0 0 | 3 1 | 1 1 | 1 5 | 2 6 |
| $\bar{3}_z m_x$ | $m_z^*, m_y^*, m_{y'}^*, m_{y''}^*$ | $6_z^*/m_z^* m_x m_y^*$ | B_{1g} | \neq | 0 0 | 0 0 | 0 0 | 0 0 | 1 1 | 1 5 | 2 6 |
| $\bar{3}_z m_y$ | $m_z^*, m_x^*, m_{x'}^*, m_{x''}^*$ | $6_z^*/m_z^* m_x^* m_y$ | B_{1g} | \neq | 0 0 | 0 0 | 0 0 | 0 0 | 1 1 | 1 5 | 2 6 |
| 6_z | $\bar{1}^*, m_z^*$ | $6_z/m_z^*$ | A_u | = | 1 0 | 1 0 | 2 0 | 4 0 | 0 4 | 0 5 | 0 8 |
| 6_z | $2_x^*, 2_{x'}^*, 2_{x''}^*, 2_y^*, 2_{y'}^*, 2_{y''}^*$ | $6_z 2_x^* 2_y^*$ | A_2 | \neq | 0 1 | 1 0 | 0 2 | 3 1 | 3 1 | 0 5 | 2 6 |
| 6_z | $m_x^*, m_{x'}^*, m_{x''}^*, m_y^*, m_{y'}^*, m_{y''}^*$ | $6_z m_x^* m_y^*$ | A_2 | \neq | 1 0 | 0 1 | 2 0 | 1 3 | 3 1 | 0 5 | 2 6 |
| $\bar{6}_z$ | $\bar{1}^*, 2_z^*$ | $6_z^*/m_z^*$ | B_u | = | 0 0 | 0 0 | 0 0 | 2 0 | 0 4 | 0 5 | 0 8 |
| $\bar{6}_z$ | $m_x^*, m_{x'}^*, m_{x''}^*, 2_y^*, 2_{y'}^*, 2_{y''}^*$ | $\bar{6}_z m_x^* 2_y^*$ | A_2' | \neq | 0 0 | 0 0 | 0 0 | 1 1 | 3 1 | 0 5 | 2 6 |
| $\bar{6}_z$ | $m_y^*, m_{y'}^*, m_{y''}^*, 2_x^*, 2_{x'}^*, 2_{x''}^*$ | $\bar{6}_z 2_x^* m_y^*$ | A_2' | \neq | 0 0 | 0 0 | 0 0 | 1 1 | 3 1 | 0 5 | 2 6 |

$\dagger u = z, x(x', x''), y(y', y''), xy(xy\bar{y}, zx, z\bar{x}, yz, y\bar{z})$. $\ddagger v = z, p(q, r, s)$.

3.4. DOMAIN STRUCTURES

Table 3.4.3.4 (cont.)

| F_1 | g_{ij}^* | $K_{ij}^* = J_{ij}^*$ | Γ_α | Diffraction intensities | ϵ | P_i | g_μ | $d_{i\mu}$ | $A_{i\mu}$ | $s_{\mu\nu}$ | $Q_{ij\mu}$ |
|---------------------|--|-----------------------|-----------------|-------------------------|------------|-------|---------|------------|------------|--------------|-------------|
| $6_z/m_z$ | $m_x^*, m_x^*, m_{x'}^*, m_y^*, m_y^*, m_{y'}^*, 2_x^*, 2_x^*, 2_{x'}^*, 2_y^*, 2_y^*, 2_{y'}^*$ | $6_z/m_z m_x^* m_y^*$ | A_{2g} | \neq | 0 0 | 0 0 | 0 0 | 0 0 | 3 1 | 0 5 | 2 6 |
| $6_z 2_x 2_y$ | $\bar{1}^*, m_x^*, m_x^*, m_x^*, m_{x'}^*, m_y^*, m_y^*, m_{y'}^*$ | $6_z/m_z m_x^* m_y^*$ | A_{1u} | $=$ | 1 0 | 0 0 | 2 0 | 1 0 | 0 1 | 0 5 | 0 6 |
| $6_z m_x m_y$ | $\bar{1}^*, m_x^*, 2_x^*, 2_{x'}^*, 2_y^*, 2_{y'}^*, 2_{y'}^*$ | $6_z/m_z m_x m_y$ | A_{2u} | $=$ | 0 0 | 1 0 | 0 0 | 3 0 | 0 1 | 0 5 | 0 6 |
| $\bar{6}_z 2_x m_y$ | $\bar{1}^*, 2_x^*, m_x^*, m_x^*, m_{x'}^*, 2_y^*, 2_{y'}^*, 2_{y'}^*$ | $6_z/m_z m_x^* m_y^*$ | B_{2u} | $=$ | 0 0 | 0 0 | 0 0 | 1 0 | 0 1 | 0 5 | 0 6 |
| $\bar{6}_z m_x 2_y$ | $\bar{1}^*, 2_x^*, m_y^*, m_y^*, m_{y'}^*, 2_x^*, 2_{x'}^*, 2_{x'}^*$ | $6_z/m_z m_x m_y^*$ | B_{2u} | $=$ | 0 0 | 0 0 | 0 0 | 1 0 | 0 1 | 0 5 | 0 6 |
| 23 | $\bar{1}^*, m_x^*, m_y^*, m_z^*$ | $m^* \bar{3}$ | A_u | $=$ | 1 0 | 0 0 | 1 0 | 1 0 | 0 1 | 0 3 | 0 4 |
| 23 | $2_{xy}^*, 2_{yz}^*, 2_{zx}^*, 2_{x'y'}^*, 2_{y'z'}^*, 2_{z'x'}^*$ | $4^* 32^*$ | A_2 | \neq | 0 1 | 0 0 | 0 1 | 1 0 | 1 0 | 0 3 | 1 3 |
| 23 | $m_{xy}^*, m_{yz}^*, m_{zx}^*, m_{x'y'}^*, m_{y'z'}^*, m_{z'x'}^*$ | $\bar{4}^* 3m^*$ | A_2 | \neq | 1 0 | 0 0 | 1 0 | 0 1 | 1 0 | 0 3 | 1 3 |
| $m\bar{3}$ | $m_{xy}^*, m_{yz}^*, m_{zx}^*, m_{x'y'}^*, m_{y'z'}^*, m_{z'x'}^*, 2_{xy}^*, 2_{yz}^*, 2_{zx}^*, 2_{x'y'}^*, 2_{y'z'}^*, 2_{z'x'}^*$ | $m\bar{3}m^*$ | A_{2g} | \neq | 0 0 | 0 0 | 0 0 | 0 0 | 1 0 | 0 3 | 1 3 |
| 432 | $\bar{1}^*, m_x^*, m_x^*, m_x^*, m_{xy}^*, m_{yz}^*, m_{zx}^*, m_{x'y'}^*, m_{y'z'}^*, m_{z'x'}^*$ | $m^* \bar{3}m^*$ | A_{1u} | $=$ | 1 0 | 0 0 | 1 0 | 0 0 | 0 0 | 0 3 | 0 3 |
| $\bar{4}3m$ | $\bar{1}^*, m_x^*, m_y^*, m_z^*, 2_{xy}^*, 2_{yz}^*, 2_{zx}^*, 2_{x'y'}^*, 2_{y'z'}^*, 2_{z'x'}^*$ | $m^* \bar{3}m$ | A_{2u} | $=$ | 0 0 | 0 0 | 0 0 | 1 0 | 0 0 | 0 3 | 0 3 |

non-ferroelastic twins with domains containing \mathbf{S}_1 and \mathbf{S}_j (see Section 3.4.3.1).

The second part of the table concerns the *distinction and switching* of domain states of the non-ferroelastic domain pair $(\mathbf{S}_1, \mathbf{S}_j) = (\mathbf{S}_1, g_{ij}^* \mathbf{S}_1)$.

Γ_α : irreducible representation of K_{ij} that defines the transformation properties of the principal tensor parameters of the symmetry descent $K_{ij} \supset F_1$ and thus specifies the components of principal tensor parameters that are given explicitly in Table 3.1.3.1, in the software *GI★KoBo-1* and in Kopský (2001), where one replaces G by K_{ij} .

Diffraction intensities: the entries in this column characterize the differences of diffraction intensities from two domain states of the domain pair:

$=$ signifies that the twinning operations belong to the Laue class of F_1 . Then the reflection intensities per unit volume are the same for both domain states if anomalous scattering is zero, *i.e.* if Friedel's law is valid. For nonzero anomalous scattering, the intensities from the two domain states differ, but when the partial volumes of both states are equal the diffraction pattern is centrosymmetric;

\neq signifies that the twinning operations do not belong to the Laue class of F_1 . Then the reflection intensities per unit volume of the two domain states are different [for more details, see Chapter 3.3; Catti & Ferraris (1976); Koch (1999)].

$\epsilon, P_i, g_\mu, \dots, Q_{ij\mu}$: components (in matrix notation) of important *property tensors* that are specified in Table 3.4.3.5. The same symbol may represent several property tensors (given in the same row of Table 3.4.3.5) of the same rank and intrinsic symmetry. Bold-face symbols signify polar tensors. For each type of property tensor two numbers $a|c$ are given; number a in front of the vertical bar $|$ is the *number of independent covariant components* (in most cases identical with Cartesian components) that have the *same absolute value but different sign in domain states* \mathbf{S}_1 and \mathbf{S}_j . The number c after the vertical bar $|$ gives the *number of independent nonzero tensor parameters that have equal values in both domain states* of the domain pair $(\mathbf{S}_1, \mathbf{S}_j)$. These tensor components are already nonzero in the parent phase.

Table 3.4.3.5. *Property tensors and switching fields*

$i = 1, 2, 3; \mu, \nu = 1, 2, \dots, 6$.

| Symbol | Property tensor | Symbol | Property tensor | Switching fields |
|-----------------|---------------------|---------------|-----------------|------------------|
| ϵ | Enantiomorphism | | | |
| P_i | Polarization | p_i | Chirality | E |
| ϵ_{ij} | Permittivity | | Pyroelectricity | EE |
| g_μ | Optical activity | | | |
| $d_{i\mu}$ | Piezoelectricity | r_{ijk} | Electro-optics | Eu |
| $A_{i\mu}$ | Electrogyration | | | |
| $s_{\mu\nu}$ | Elastic compliances | | | uu |
| $Q_{ij\mu}$ | Electrostriction | $\pi_{ij\mu}$ | Piezo-optics | EEu |

The principal tensor parameters are one-dimensional and have the same absolute value but opposite sign in \mathbf{S}_1 and $\mathbf{S}_j = g_{ij}^* \mathbf{S}_1$. Principal tensor parameters for symmetry descents $K_{ij} \supset F_1$ and the associated Γ_α of all non-ferroelastic domain pairs can be found for property tensors of lower rank in Table 3.1.3.1 and for all tensors appearing in Table 3.4.3.4 in the software *GI★KoBo-1* and in Kopský (2001), where one replaces G by K_{ij} .

When $a \neq 0$ for a polar tensor (in bold-face components), then *switching fields* exist in the combination given in the last column of Table 3.4.3.5. Components of these fields can be determined from the explicit form of corresponding principal tensor parameters expressed in Cartesian components.

Table 3.4.3.5 lists important property tensors up to fourth rank. Property tensor components that appear in the column headings of Table 3.4.3.4 are given in the first column, where bold face is used for the polar tensors significant for specifying the switching fields appearing in schematic form in the last column. In the third and fourth columns, those property tensors appear for which hold all the results presented in Table 3.4.3.4 for the symbols given in the first column of Table 3.4.3.5.

We turn attention to Section 3.4.5 (Glossary), which describes the difference between the notation of tensor components in matrix notation given in Chapter 1.1 and those used in the software *GI★KoBo-1* and in Kopský (2001).

The numbers a in front of the vertical bar $|$ in Table 3.4.3.4 provide global information about the tensor distinction of two domain states and enables one to classify domain pairs. Thus, for example, the first number a in column P_i gives the number of nonzero components of the spontaneous polarization that differ in sign in both domain states; if $a \neq 0$, this domain pair can be classified as a *ferroelectric domain pair*.

Similarly, the first number a in column g_μ determines the number of independent components of the tensor of optical activity that have opposite sign in domain states \mathbf{S}_1 and \mathbf{S}_j ; if $a \neq 0$, the two domain states in the pair can be distinguished by optical activity. Such a domain pair can be called a *gyrotropic domain pair*. As in Table 3.4.3.1 for the ferroelectric (ferroelastic) domain pairs, we can define a *gyrotropic phase* as a ferroic phase with gyrotropic domain pairs. The corresponding phase transition to a gyrotropic phase is called a *gyrotropic phase transition* (Koňák *et al.*, 1978; Wadhawan, 2000). If it is possible to switch gyrotropic domain states by an external field, the phase is called a *ferrogyrotropic phase* (Wadhawan, 2000). Further division into full and partial subclasses is possible.

One can also define *piezoelectric (electro-optic) domain pairs*, *electrostrictive (elasto-optic) domain pairs* and corresponding phases and transitions.

As we have already stated, domain states in a domain pair $(\mathbf{S}_1, \mathbf{S}_j)$ differ in principal tensor parameters of the transition $K_{ij} \supset F_1$. These principal tensor parameters are Cartesian tensor

3. PHASE TRANSITIONS, TWINNING AND DOMAIN STRUCTURES

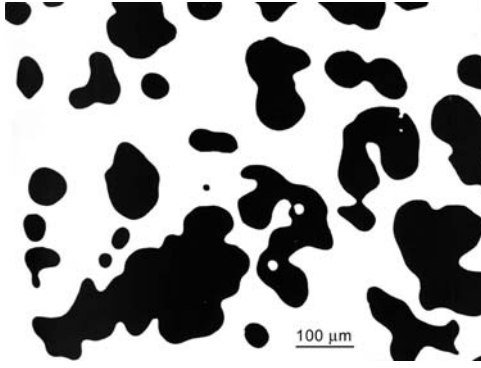


Fig. 3.4.3.3. Domain structure in lead germanate observed using a polarized-light microscope. Visualization based on the opposite sign of the optical activity coefficient in the two domain states. Courtesy of V.I. Shur, Ural State University, Ekaterinburg.

components or their linear combinations that transform according to an irreducible representation Γ_α specifying the primary order parameter of the transition $K_{ij} \supset F_1$ (see Section 3.1.3). Owing to a special form of K_{ij} expressed by equation (3.4.3.42), this representation is a real one-dimensional irreducible representation of K_{ij} . Such a representation associates +1 with operations of F_1 and -1 with operations from the left coset g_{ij}^* . This means that the principal tensor parameters are one-dimensional and have the same absolute value but opposite sign in \mathbf{S}_1 and $\mathbf{S}_j = g_{ij}^* \mathbf{S}_1$. Principal tensor parameters for symmetry descents $K_{ij} \supset F_1$ and associated Γ_α 's of all non-ferroelastic domain pairs can be found for property tensors of lower rank in Table 3.1.3.1 and for all tensors appearing in Table 3.4.3.5 in the software *GI★KoBo-1* and in Kopský (2001).

These specific properties of non-ferroelastic domain pairs allow one to formulate simple rules for tensor distinction that do not use principal tensor parameters and that are applicable for property tensors of lower rank.

(i) Symmetry descents $K_{ij} \supset F_1$ of non-ferroelastic domain pairs for lower-rank property tensors lead only to the appearance of independent Cartesian morphic tensor components and not to the breaking of relations between these components. These morphic Cartesian tensor components can be found by comparing matrices of property tensors in the twinning group K_{ij} and the low-symmetry group F_1 as those components that appear in F_1 but are zero in K_{ij} .

(ii) As follows from Table 3.4.3.4, one can always find a twinning operation that is either inversion, or a twofold axis or a mirror plane with a prominent crystallographic orientation. By applying the method of direct inspection (see Section 1.1.4.6.3), one can in most cases easily find morphic Cartesian components in the second domain state of the domain pair considered and prove that they differ only in sign.

Example 3.4.3.4. Tensor distinction of domains and switching in lead germanate. Lead germanate ($\text{Pb}_5\text{Ge}_3\text{O}_{11}$) undergoes a phase transition with symmetry descent $G = 6 \supset 3 = F_1$ for which we find in Table 3.4.2.7, column K_{ij} , just one twinning group $K_{ij} = \bar{6}^*$, i.e. $K_{ij}^* = G$. This means that there is only one G -orbit of domain pairs. Since $\text{Fam}3 = \text{Fam}\bar{6}$ [see Table 3.4.2.2 and equation (3.4.3.40)] this orbit comprises non-ferroelastic domain pairs. In Table 3.4.3.4, we find for $F_1 = 3$ and $F_{ij}^* = \bar{6}$ that the two domain states differ in some components of all property tensors listed in this table. The first polar tensor is the spontaneous polarization (the pair is ferroelectric) with one component ($a = 1$) that has opposite sign in the two domain states. In Table 3.1.3.1, we find for $G (= K_{ij}) = \bar{6}$ and $F_1 = 3$ that this component is $P_3 = P_z$. From Table 3.4.3.1, it follows that the state shift is electrically first order with switching field $\mathbf{E} = (0, 0, E_z)$.

The first optical tensor, which could enable the visualization of the domain states, is the optical activity g_μ with two independent components which have opposite sign in the two domain states. In the software *GI★KoBo-1*, path: *Subgroups\View\Domains* or in Kopský (2001) we find these components: $g_3, g_1 + g_2$. Shur *et al.* (1989) have visualized in this way the domain structure of lead germanate with excellent black and white contrast (see Fig. 3.4.3.3). Other examples are given in Shuvalov & Ivanov (1964) and especially in Koňák *et al.* (1978).

Table 3.4.3.4 can be used readily for twinning by merohedry [see Chapter 3.3 and e.g. Cahn (1954); Koch (1999)], where it enables an easy determination of the tensor distinction of twin components and the specification of external fields for possible switching and detwinning.

Example 3.4.3.5. Tensor distinction and switching of Dauphiné twins in quartz. Quartz undergoes a phase transition from $G = 6_z 2_x 2_y$ to $F_1 = 3_z 2_x$. Using the same procedure as in the previous example, we come to following conclusions: There are only two domain states $\mathbf{S}_1, \mathbf{S}_2$ and the twinning group, expressing the twin law, is equal to the high-symmetry group $K_{12}^* = 6_z 2_x 2_y$. In Table 3.4.3.4, we find that these two states differ in one independent component of the piezoelectric tensor and in one elastic compliance component. Comparison of the matrices for $6_z 2_x 2_y$ and $3_z 2_x$ (see Sections 1.1.4.10.3 and 1.1.4.10.4) yields the following morphic tensor components in the first domain state \mathbf{S}_1 : $d_{11}^{(1)} = -d_{12}^{(1)} = -2d_{26}^{(1)}$ and $s_{14}^{(1)} = -s_{24}^{(1)} = 2s_{56}^{(1)}$. According to the rule given above, the values of morphic components in the second domain state \mathbf{S}_2 are $d_{11}^{(2)} = -d_{11}^{(1)} = -d_{12}^{(2)} = d_{12}^{(1)} = -2d_{26}^{(2)} = 2d_{26}^{(1)}$ and $s_{14}^{(2)} = -s_{14}^{(1)} = -s_{24}^{(2)} = s_{24}^{(1)} = 2s_{56}^{(2)} = -2s_{56}^{(1)}$ [see Section 3.4.5 (Glossary)]. These results show that there is an elastic state shift of second order and an electromechanical state shift of second order. Nonzero components $d_{14} = -d_{25}$ in $6_z 2_x 2_y$ are the same in both domain states. Similarly, one can find five independent components of the tensor $s_{\mu\nu}$ that are nonzero in $6_z 2_x 2_y$ and equal in both domain states. For the piezo-optic tensor $\pi_{\mu\nu}$, one can proceed in a similar way. Aizu (1973) has used the ferroelastic character of the domain pairs for visualizing domains and realizing switching in quartz. Other methods for switching and visualizing domains in quartz are known (see e.g. Bertagnolli *et al.*, 1978, 1979).

3.4.3.6. Ferroelastic domain pairs

A *ferroelastic domain pair* consists of two domain states that have different spontaneous strain. A domain pair $(\mathbf{S}_1, \mathbf{S}_j)$ is a ferroelastic domain pair if the crystal family of its twinning group K_{ij} differs from the crystal family of the symmetry group F_1 of domain state \mathbf{S}_1 ,

$$\text{Fam}K_{ij} \neq \text{Fam}F_1. \quad (3.4.3.43)$$

Before treating compatible domain walls and disorientations, we explain the basic concept of spontaneous strain.

3.4.3.6.1. Spontaneous strain

A *strain* describes a *change* of crystal shape (in a macroscopic description) or a change of the unit cell (in a microscopic description) under the influence of mechanical stress, temperature or electric field. If the relative changes are small, they can be described by a second-rank symmetric tensor \mathbf{u} called the *Lagrangian strain*. The values of the strain components u_{ik} , $i, k = 1, 2, 3$ (or in matrix notation u_μ , $\mu = 1, \dots, 6$) can be calculated from the 'undeformed' unit-cell parameters before deformation and 'deformed' unit-cell parameters after deformation (see Schlenker *et al.*, 1978; Salje, 1990; Carpenter *et al.*, 1998).

3.4. DOMAIN STRUCTURES

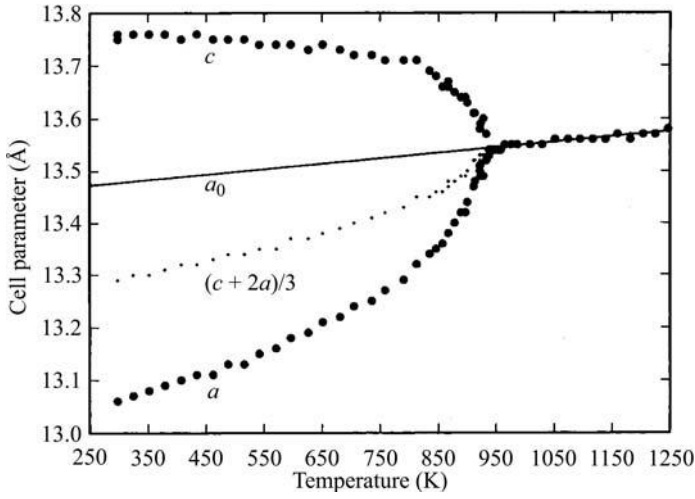


Fig. 3.4.3.4. Temperature dependence of lattice parameters in leucite. Courtesy of E. K. H Salje, University of Cambridge.

A *spontaneous strain* describes the change of an ‘undeformed’ unit cell of the high-symmetry phase into a ‘deformed’ unit cell of the low-symmetry phase. To exclude changes connected with thermal expansion, one demands that the parameters of the undeformed unit cell are those that the high-symmetry phase would have at the temperature at which parameters of the low-symmetry phase are measured. To determine these parameters directly is not possible, since the parameters of the high-symmetry phase can be measured only in the high-symmetry phase. One uses, therefore, different procedures in order to estimate values for the high-symmetry parameters under the external conditions to which the measured values of the low-symmetry phase refer (see *e.g.* Salje, 1990; Carpenter *et al.*, 1998). Three main strategies are illustrated using the example of leucite (see Fig. 3.4.3.4):

(i) The lattice parameters of the high-symmetry phase are extrapolated from values measured in the high-symmetry phase (a straight line a_0 in Fig. 3.4.3.4). This is a preferred approach.

(ii) For certain symmetry descents, it is possible to approximate the high-symmetry parameters in the low-symmetry phase by average values of the lattice parameters in the low-symmetry phase. Thus for example in cubic \rightarrow tetragonal transitions one can take for the cubic lattice parameter $a_0 = (2a + c)/3$ (the dotted curve in Fig. 3.4.3.4), for cubic \rightarrow orthorhombic transitions one may assume $a_0 = (abc)^{1/3}$, where a, b, c are the lattice parameters of the low-symmetry phase. Errors are introduced if there is a significant volume strain, as in leucite.

(iii) Thermal expansion is neglected and for the high-symmetry parameters in the low-symmetry phase one takes the lattice parameters measured in the high-symmetry phase as close as possible to the transition. This simplest method gives better results than average values in leucite, but in general may lead to significant errors.

Spontaneous strain has been examined in detail in many ferroic crystals by Carpenter *et al.* (1998).

Spontaneous strain can be divided into two parts: one that is different in all ferroelastic domain states and the other that is the same in all ferroelastic domain states. This division can be achieved by introducing a *modified strain tensor* (Aizu, 1970b), also called a *relative spontaneous strain* (Wadhawan, 2000):

$$\mathbf{u}_{(s)}^{(i)} = \mathbf{u}^{(i)} - \mathbf{u}_{(s)}^{(av)}, \quad (3.4.3.44)$$

where $\mathbf{u}_{(s)}^{(i)}$ is the matrix of relative (modified) spontaneous strain in the ferroelastic domain state \mathbf{R}_i , $\mathbf{u}^{(i)}$ is the matrix of an ‘absolute’ spontaneous strain in the same ferroelastic domain state \mathbf{R}_i and $\mathbf{u}_{(s)}^{(av)}$ is the matrix of an *average spontaneous strain*

that is equal to the sum of the matrices of absolute spontaneous strains over all n_a ferroelastic domain states,

$$\mathbf{u}^{(av)} = \frac{1}{n_a} \sum_{j=1}^{n_a} \mathbf{u}^{(j)}. \quad (3.4.3.45)$$

The relative spontaneous strain $\mathbf{b}_{(s)}^{(i)}$ is a *symmetry-breaking strain* that transforms according to a non-identity representation of the parent group G , whereas the average spontaneous strain is a *non-symmetry breaking strain* that transforms as the identity representation of G .

Example 3.4.3.6. We illustrate these concepts with the example of symmetry descent $4_z/m_z m_x m_{xy} \supset 2_x m_y m_z$ with two ferroelastic domain states \mathbf{R}_1 and \mathbf{R}_2 (see Fig. 3.4.2.2). The absolute spontaneous strain in the first ferroelastic domain state \mathbf{R}_1 is

$$\mathbf{u}^{(1)} = \begin{pmatrix} \frac{a-a_0}{a_0} & 0 & 0 \\ 0 & \frac{b-a_0}{a_0} & 0 \\ 0 & 0 & \frac{c-c_0}{c_0} \end{pmatrix} = \begin{pmatrix} u_{11} & 0 & 0 \\ 0 & u_{22} & 0 \\ 0 & 0 & u_{33} \end{pmatrix}, \quad (3.4.3.46)$$

where a, b, c and a_0, b_0, c_0 are the lattice parameters of the orthorhombic and tetragonal phases, respectively.

The spontaneous strain $\mathbf{u}^{(2)}$ in domain state \mathbf{R}_2 is obtained by applying to $\mathbf{u}^{(1)}$ any switching operation that transforms \mathbf{R}_1 into \mathbf{R}_2 (see Table 3.4.2.1),

$$\mathbf{u}^{(2)} = \begin{pmatrix} u_{22} & 0 & 0 \\ 0 & u_{11} & 0 \\ 0 & 0 & u_{33} \end{pmatrix}. \quad (3.4.3.47)$$

The average spontaneous strain is, according to equation (3.4.3.45),

$$\mathbf{u}^{(av)} = \frac{1}{2} \begin{pmatrix} u_{11} + u_{22} & 0 & 0 \\ 0 & u_{11} + u_{22} & 0 \\ 0 & 0 & u_{33} + u_{33} \end{pmatrix}. \quad (3.4.3.48)$$

This deformation is invariant under any operation of G .

The relative spontaneous strains in ferroelastic domain states \mathbf{R}_1 and \mathbf{R}_2 are, according to equation (3.4.3.44),

$$\mathbf{u}_{(s)}^{(1)} = \mathbf{u}^{(1)} - \mathbf{u}^{(av)} = \begin{pmatrix} \frac{1}{2}(u_{11} - u_{22}) & 0 & 0 \\ 0 & -\frac{1}{2}(u_{11} - u_{22}) & 0 \\ 0 & 0 & 0 \end{pmatrix}, \quad (3.4.3.49)$$

$$\mathbf{u}_{(s)}^{(2)} = \mathbf{u}^{(2)} - \mathbf{u}^{(av)} = \begin{pmatrix} -\frac{1}{2}(u_{11} - u_{22}) & 0 & 0 \\ 0 & \frac{1}{2}(u_{11} - u_{22}) & 0 \\ 0 & 0 & 0 \end{pmatrix}. \quad (3.4.3.50)$$

Symmetry-breaking nonzero components of the relative spontaneous strain are identical, up to the factor $\frac{1}{2}$, with the secondary tensor parameters $\lambda_b^{(1)}$ and $\lambda_b^{(2)}$ of the transition $4_z/m_z m_x m_{xy} \supset 2_x m_y m_z$ with the stabilizer $I_{4_z/m_z m_x m_{xy}}(\mathbf{R}_1) = I_{4_z/m_z m_x m_{xy}}(\mathbf{R}_2) = m_x m_y m_z$. The non-symmetry-breaking component u_{33} does not appear in the relative spontaneous strain.

The form of relative spontaneous strains for all ferroelastic domain states of all full ferroelastic phases are listed in Aizu (1970b).

3.4.3.6.2. Equally deformed planes of a ferroelastic domain pair

We start with the example of a phase transition with the symmetry descent $G = 4_z/m_z m_x m_{xy} \supset 2_x m_y m_z$, which generates two ferroelastic single-domain states \mathbf{R}_1 and \mathbf{R}_2 (see Fig. 3.4.2.2).

3. PHASE TRANSITIONS, TWINNING AND DOMAIN STRUCTURES

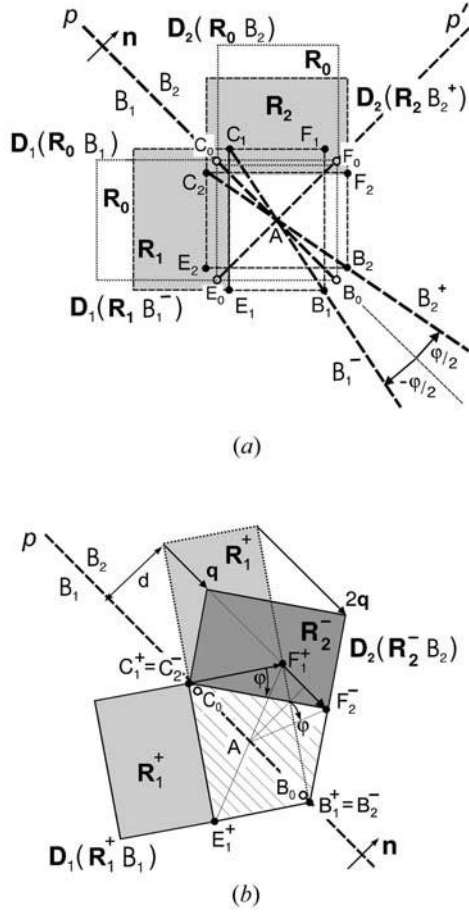


Fig. 3.4.3.5. Formation of a ferroelastic domain twin. (a) Formation of ferroelastic single-domain states R_1, R_2 from the parent phase R_0 ; p and p' are two perpendicular planes of equal deformation. (b) Formation of a ferroelastic twin: (i) by rotating the single-domain states S_1, S_2 in (a) through an angle $\pm \frac{1}{2}\varphi$ about the domain-pair axis A (R_1^+ and R_2^- are the resulting disoriented ferroelastic domain states); (ii) by a simple shear deformation with a shear angle (obliquity) φ .

An 'elementary cell' of the parent phase is represented in Fig. 3.4.3.5(a) by a square $B_0E_0C_0F_0$ and the corresponding domain state is denoted by R_0 .

In the ferroic phase, the square $B_0E_0C_0F_0$ can change either under spontaneous strain $u^{(1)}$ into a spontaneously deformed rectangular cell $B_1E_1C_1F_1$ representing a domain state R_1 , or under a spontaneous strain $u^{(2)}$ into rectangular $B_2E_2C_2F_2$ representing domain state R_2 . We shall use the letter R_0 as a symbol of the parent phase and R_1, R_2 as symbols of two ferroelastic single-domain states.

Let us now choose in the parent phase a vector $\overrightarrow{AB_0}$. This vector changes into $\overrightarrow{AB_1}$ in ferroelastic domain state R_1 and into $\overrightarrow{AB_2}$ in ferroelastic domain state R_2 . We see that the resulting vectors $\overrightarrow{AB_1}$ and $\overrightarrow{AB_2}$ have different direction but equal length: $|\overrightarrow{AB_1}| = |\overrightarrow{AB_2}|$. This consideration holds for any vector in the plane p , which can therefore be called an *equally deformed plane* (EDP). One can find that the perpendicular plane p' is also an equally deformed plane, but there is no other plane with this property.

The intersection of the two perpendicular equally deformed planes p and p' is a line called an *axis of the ferroelastic domain pair* (R_1, R_2) (in Fig. 3.4.3.5 it is a line at A perpendicular to the paper). This axis is the only line in which any vector chosen in the parent phase exhibits equal deformation and has its direction unchanged in both single-domain states R_1 and R_2 of a ferroelastic domain pair.

This consideration can be expressed analytically as follows (Fousek & Janovec, 1969; Sapriel, 1975). We choose in the parent phase a plane p and a unit vector $\mathbf{v}(x_1, x_2, x_3)$ in this plane. The

changes of lengths of this vector in the two ferroelastic domain states R_1 and R_2 are $u_{ik}^{(1)}x_ix_k$ and $u_{ik}^{(2)}x_ix_k$, respectively, where $u_{ik}^{(1)}$ and $u_{ik}^{(2)}$ are spontaneous strains in R_1 and R_2 , respectively (see e.g. Nye, 1985). (We are using the Einstein summation convention: when a letter suffix occurs twice in the same term, summation with respect to that suffix is to be understood.) If these changes are equal, i.e. if

$$u_{ik}^{(1)}x_ix_k = u_{ik}^{(2)}x_ix_k, \quad (3.4.3.51)$$

for any vector $\mathbf{v}(x_1, x_2, x_3)$ in the plane p this plane will be an equally deformed plane. If we introduce a *differential spontaneous strain*

$$\Delta u_{ik} \equiv u_{ik}^{(2)} - u_{ik}^{(1)}, \quad i, k = 1, 2, 3, \quad (3.4.3.52)$$

the condition (3.4.3.51) can be rewritten as

$$\Delta u_{ik}x_ix_j = 0. \quad (3.4.3.53)$$

This equation describes a cone with the apex at the origin. The cone degenerates into two planes if the determinant of the differential spontaneous strain tensor equals zero,

$$\det \Delta u_{ik} = 0. \quad (3.4.3.54)$$

If this condition is satisfied, two solutions of (3.4.3.53) exist:

$$Ax_1 + Bx_2 + Cx_3 = 0, \quad A'x_1 + B'x_2 + C'x_3 = 0. \quad (3.4.3.55)$$

These are equations of two planes p and p' passing through the origin. Their normal vectors are $\mathbf{n} = [ABC]$ and $\mathbf{n}' = [A'B'C']$. It can be shown that from the equation

$$\Delta u_{11} + \Delta u_{22} + \Delta u_{33} = 0, \quad (3.4.3.56)$$

which holds for the trace of the matrix $\det \Delta u_{ik}$, it follows that these two planes are perpendicular:

$$AA' + BB' + CC' = 0. \quad (3.4.3.57)$$

The intersection of these equally deformed planes (3.4.3.53) is the *axis of the ferroelastic domain pair* (R_1, R_2).

Let us illustrate the application of these results to the domain pair (R_1, R_2) depicted in Fig. 3.4.3.1(b) and discussed above. From equations (3.4.3.41) and (3.4.3.47), or (3.4.3.49) and (3.4.3.50) we find the only nonzero components of the difference strain tensor are

$$\Delta u_{11} = u_{22} - u_{11}, \quad \Delta u_{22} = u_{11} - u_{22}. \quad (3.4.3.58)$$

Condition (3.4.3.54) is fulfilled and equation (3.4.3.53) is

$$\Delta u_{11}x_1^2 + \Delta u_{22}x_2^2 = (u_{22} - u_{11})x_1^2 + (u_{11} - u_{22})x_2^2 = 0. \quad (3.4.3.59)$$

There are two solutions of this equation:

$$x_1 = x_2, \quad x_1 = -x_2. \quad (3.4.3.60)$$

These two equally deformed planes p and p' have the normal vectors $\mathbf{n} = [110]$ and $\mathbf{n}' = [1\bar{1}0]$. The axis of this domain pair is directed along $[001]$.

Equally deformed planes in our example have the same orientations as have the mirror planes m_{xy} and m_{xy} lost at the transition $4_z/m_z m_x m_{xy} \supset m_x m_y m_z$. From Fig. 3.4.3.5(a) it is clear why: reflection m_{xy} , which is a transposing operation of the domain pair (R_1, R_2), ensures that the vectors $\overrightarrow{AB_1}$ and $\overrightarrow{AB_2}$ arising from $\overrightarrow{AB_0}$ have equal length. A similar conclusion holds for a 180° rotation and a plane perpendicular to the corresponding twofold axis. Thus we come to two useful rules:

Any reflection through a plane that is a transposing operation of a ferroelastic domain pair ensures the existence of two planes of

3.4. DOMAIN STRUCTURES

equal deformation: one is parallel to the corresponding mirror plane and the other one is perpendicular to this mirror plane.

Any 180° rotation that is a transposing operation of a ferroelastic domain pair ensures the existence of two equally deformed planes: one is perpendicular to the corresponding twofold axis and the other one is parallel to this axis.

A reflection in a plane or a 180° rotation generates at least one equally deformed plane with a fixed prominent *crystallographic orientation* independent of the magnitude of the spontaneous strain; the other perpendicular equally deformed plane may have a *non-crystallographic orientation* which depends on the spontaneous strain and changes with temperature. If between switching operations there are two reflections with corresponding perpendicular mirror planes, or two 180° rotations with corresponding perpendicular twofold axes, or a reflection and a 180° rotation with a corresponding twofold axis parallel to the mirror, then both perpendicular equally deformed planes have fixed crystallographic orientations. If there are no switching operations of the second order, then both perpendicular equally deformed planes may have non-crystallographic orientations, or equally deformed planes may not exist at all.

Equally deformed planes in ferroelastic-ferroelectric phases have been tabulated by Fousek (1971). Sapriel (1975) lists equations (3.4.3.55) of equally deformed planes for all ferroelastic phases. Table 3.4.3.6 contains the orientation of equally deformed planes (with further information about the walls) for representative domain pairs of all orbits of ferroelastic domain pairs. Table 3.4.3.7 lists representative domain pairs of all ferroelastic orbits for which no compatible walls exist.

3.4.3.6.3. Disoriented domain states, ferroelastic domain twins and their twin laws

To examine another possible way of forming a ferroelastic domain twin, we return once again to Fig. 3.4.3.5(a) and split the space along the plane p into a half-space B_1 on the negative side of the plane p (defined by a negative end of normal \mathbf{n}) and another half-space B_2 on the positive side of p . In the parent phase, the whole space is filled with domain state \mathbf{R}_0 and we can, therefore, treat the crystal in region B_1 as a domain $\mathbf{D}_1(\mathbf{R}_0, B_1)$ and the crystal in region B_2 as a domain $\mathbf{D}_2(\mathbf{R}_0, B_2)$ (we remember that a domain is specified by its domain region, e.g. B_1 , and by a domain state, e.g. \mathbf{R}_1 , in this region; see Section 3.4.2.1).

Now we cool the crystal down and exert the spontaneous strain $\mathbf{u}^{(1)}$ on domain $\mathbf{D}_1(\mathbf{R}_0, B_1)$. The resulting domain $\mathbf{D}_1(\mathbf{R}_1, B_1^-)$ contains domain state \mathbf{R}_1 in the domain region B_1^- with the planar boundary along $(B_1^- C_1^-)$ (the overbar ‘ $-$ ’ signifies a rotation of the boundary in the positive sense). Similarly, domain $\mathbf{D}_2(\mathbf{R}_0, B_2)$ changes after performing spontaneous strain $\mathbf{u}^{(2)}$ into domain $\mathbf{D}_2(\mathbf{R}_2, B_2^+)$ with domain state \mathbf{R}_2 and the planar boundary along $(B_2^+ C_2^+)$. This results in a disruption in the sector $B_1 A B_2$ and in an overlap of \mathbf{R}_1 and \mathbf{R}_2 in the sector $C_1 A C_2$.

The overlap can be removed and the continuity recovered by rotating the domain $\mathbf{D}_1(\mathbf{R}_1, B_1^-)$ through angle $\varphi/2$ and the domain $\mathbf{D}_2(\mathbf{R}_2, B_2^+)$ through $-\varphi/2$ about the domain-pair axis A (see Fig. 3.4.3.5a and b). This rotation changes the domain $\mathbf{D}_1(\mathbf{R}_1, B_1^-)$ into domain $\mathbf{D}_1(\mathbf{R}_1^+, B_1)$ and domain $\mathbf{D}_2(\mathbf{R}_2, B_2^+)$ into domain $\mathbf{D}_2(\mathbf{R}_2^-, B_2)$, where \mathbf{R}_1^+ and \mathbf{R}_2^- are domain states rotated away from the single-domain state orientation through $\varphi/2$ and $-\varphi/2$, respectively. Domains $\mathbf{D}_1(\mathbf{R}_1, B_1)$ and $\mathbf{D}_2(\mathbf{R}_2, B_2)$ meet without additional strains or stresses along the plane p and form a *simple ferroelastic twin* with a *compatible domain wall* along p . This wall is stress-free and fulfils the conditions of mechanical compatibility.

Domain states \mathbf{R}_1^+ and \mathbf{R}_2^- with new orientations are called *disoriented (misoriented) domain states* or *suborientational states* (Shuvalov *et al.*, 1985; Dudnik & Shuvalov, 1989) and the angles

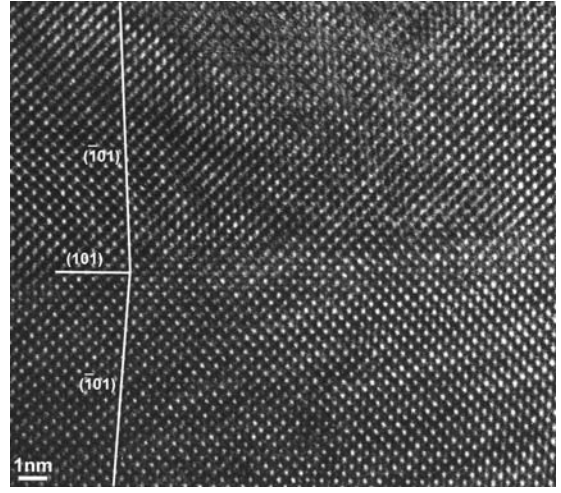


Fig. 3.4.3.6. High-resolution electron microscopy image of a ferroelastic twin in the orthorhombic phase of WO_3 . Courtesy of H. Lemmens, EMAT, University of Antwerp.

$\varphi/2$ and $-\varphi/2$ are the *disorientation angles* of \mathbf{R}_1^+ and \mathbf{R}_2^- , respectively.

We have described the formation of a ferroelastic domain twin by rotating single-domain states into new orientations in which a stress-free compatible contact of two ferroelastic domains is achieved. The advantage of this theoretical construct is that it provides a visual interpretation of disorientations and that it works with ferroelastic single-domain states which can be easily derived and transformed.

There is an alternative approach in which a domain state in one domain is produced from the domain state in the other domain by a shear deformation. The same procedure is used in mechanical twinning [for mechanical twinning, see Section 3.3.8.4 and e.g. Cahn (1954); Klassen-Neklyudova (1964); Christian (1975)].

We illustrate this approach again using our example. From Fig. 3.4.3.5(b) it follows that domain state \mathbf{R}_2^- in the second domain can be obtained by performing a simple shear on the domain state \mathbf{R}_1^+ of the first domain. In this simple shear, a point is displaced in a direction parallel to the equally deformed plane p (in mechanical twinning called a *twin plane*) and to a plane perpendicular to the axis of the domain pair (*plane of shear*). The displacement \mathbf{q} is proportional to the distance d of the point from the domain wall. The *amount of shear* is measured either by the absolute value of this displacement at a unit distance, $s = q/d$, or by an angle φ called a *shear angle* (sometimes 2φ is defined as the shear angle). There is no change of volume connected with a simple shear.

The angle φ is also called an *obliquity* of a twin (Cahn, 1954) and is used as a convenient measure of pseudosymmetry of the ferroelastic phase.

The high-resolution electron microscopy image in Fig. 3.4.3.6 reveals the relatively large shear angle (obliquity) φ of a ferroelastic twin in the monoclinic phase of tungsten trioxide (WO_3). The plane (101) corresponds to the plane p of a ferroelastic wall in Fig. 3.4.3.5(b). The planes $(\bar{1}01)$ are crystallographic planes in the lower and upper ferroelastic domains, which correspond in Fig. 3.4.3.5(b) to domain $\mathbf{D}_1(\mathbf{R}_1^+, B_1)$ and domain $\mathbf{D}_2(\mathbf{R}_2^-, B_2)$, respectively. The planes $(\bar{1}01)$ in these domains correspond to the diagonals of the elementary cells of \mathbf{R}_1^+ and \mathbf{R}_2^- in Fig. 3.4.3.5(b) and are nearly perpendicular to the wall. The angle between these planes equals 2φ , where φ is the shear angle (obliquity) of the ferroelastic twin.

Disorientations of domain states in a ferroelastic twin bring about a deviation of the optical indicatrix from a strictly perpendicular position. Owing to this effect, ferroelastic domains exhibit different colours in polarized light and can be easily visualized. This is illustrated for a domain structure of

3. PHASE TRANSITIONS, TWINNING AND DOMAIN STRUCTURES

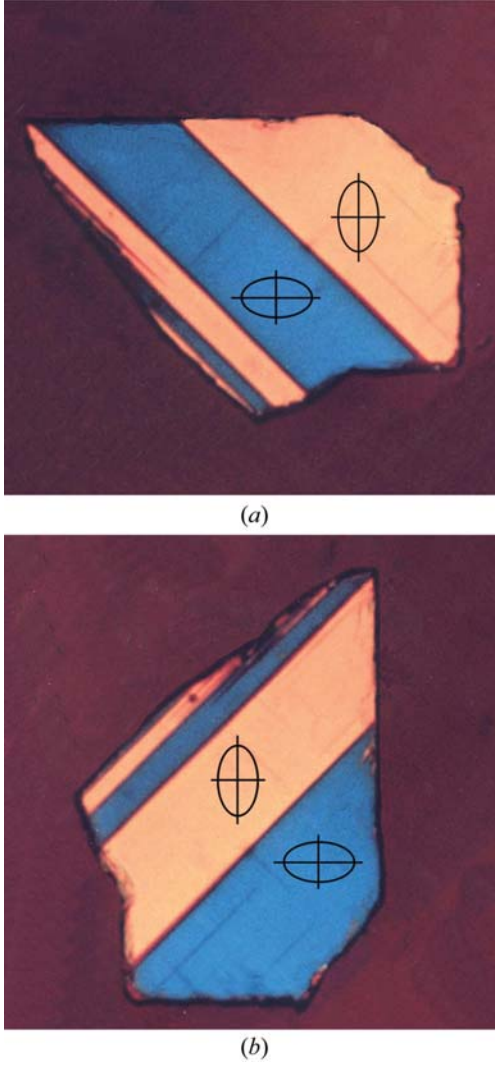


Fig. 3.4.3.7. Ferroelastic twins in a very thin $\text{YBa}_2\text{Cu}_3\text{O}_{7-\delta}$ crystal observed in a polarized-light microscope. Courtesy of H. Schmid, Université de Genève.

$\text{YBa}_2\text{Cu}_3\text{O}_{7-\delta}$ in Fig. 3.4.3.7. The symmetry descent $G = 4_z/m_z m_x m_{xy} \supset m_x m_y m_z = F_1 = F_2$ gives rise to two ferroelastic domain states \mathbf{R}_1 and \mathbf{R}_2 . The twinning group K_{12} of the non-trivial domain pair $(\mathbf{R}_1, \mathbf{R}_2)$ is

$$K_{12}[m_x m_y m_z] = J_{12}^* = m_x m_y m_z \cup 4_z^*[2_x m_y m_z] = 4_z^*/m_z m_x m_{xy}^*. \quad (3.4.3.61)$$

The colour of a domain state observed in a polarized-light microscope depends on the orientation of the index ellipsoid (indicatrix) with respect to a fixed polarizer and analyser. This index ellipsoid transforms in the same way as the tensor of spontaneous strain, *i.e.* it has different orientations in ferroelastic domain states. Therefore, different ferroelastic domain states exhibit different colours: in Fig. 3.4.3.7, the blue and pink areas (with different orientations of the ellipse representing the spontaneous strain in the plane of the figure) correspond to two different ferroelastic domain states. A rotation of the crystal that does not change the orientation of ellipses (*e.g.* a 180° rotation about an axis parallel to the fourfold rotation axis) does not change the colours (ferroelastic domain states). If one neglects disorientations of ferroelastic domain states (see Section 3.4.3.6) – which are too small to be detected by polarized-light microscopy – then none of the operations of the group $F_1 = F_2 = m_x m_y m_z$ change the single-domain ferroelastic domain states $\mathbf{R}_1, \mathbf{R}_2$, hence there is no change in the colours of domain regions of the crystal. On the other hand, all operations with a

star symbol (operations lost at the transition) exchange domain states \mathbf{R}_1 and \mathbf{R}_2 , *i.e.* also exchange the two colours in the domain regions. The corresponding permutation is a transposition of two colours and this attribute is represented by a star attached to the symbol of the operation. This exchange of colours is nicely demonstrated in Fig. 3.4.3.7 where a -90° rotation is accompanied by an exchange of the pink and blue colours in the domain regions (Schmid, 1991, 1993).

It can be shown (Shuvalov *et al.*, 1985; Dudnik & Shuvalov, 1989) that for small spontaneous strains the amount of shear s and the angle φ can be calculated from the second invariant Λ_2 of the differential tensor Δu_{ik} :

$$s = 2\sqrt{-\Lambda_2}, \quad (3.4.3.62)$$

$$\varphi = \sqrt{-\Lambda_2}, \quad (3.4.3.63)$$

where

$$\Lambda_2 = \begin{vmatrix} \Delta u_{11} & \Delta u_{12} \\ \Delta u_{21} & \Delta u_{22} \end{vmatrix} + \begin{vmatrix} \Delta u_{22} & \Delta u_{23} \\ \Delta u_{32} & \Delta u_{33} \end{vmatrix} + \begin{vmatrix} \Delta u_{11} & \Delta u_{13} \\ \Delta u_{31} & \Delta u_{33} \end{vmatrix}. \quad (3.4.3.64)$$

In our example, where there are only two nonzero components of the differential spontaneous strain tensor [see equation (3.4.3.58)], the second invariant $\Lambda_2 = -(\Delta u_{11} \Delta u_{22}) = -(u_{22} - u_{11})^2$ and the angle φ is

$$\varphi = \pm |u_{22} - u_{11}|. \quad (3.4.3.65)$$

In this case, the angle φ can also be expressed as $\varphi = \pi/2 - 2 \arctan a/b$, where a and b are lattice parameters of the orthorhombic phase (Schmid *et al.*, 1988).

The shear angle φ ranges in ferroelastic crystals from minutes to degrees (see *e.g.* Schmid *et al.*, 1988; Dudnik & Shuvalov, 1989).

Each equally deformed plane gives rise to two compatible domain walls of the same orientation but with opposite sequence of domain states on each side of the plane. We shall use for a *simple domain twin* with a planar wall a symbol $(\mathbf{R}_1^+ | \mathbf{n} | \mathbf{R}_2^-)$ in which \mathbf{n} denotes the normal to the wall. The bra-ket symbol $(|$ and $|)$ represents the half-space domain regions on the negative and positive sides of \mathbf{n} , respectively, for which we have used letters \mathcal{B}_1 and \mathcal{B}_2 , respectively. Then $(\mathbf{R}_1^+ |$ and $| \mathbf{R}_2^-)$ represent domains $\mathbf{D}_1(\mathbf{R}_1^+, \mathcal{B}_1)$ and $\mathbf{D}_2(\mathbf{R}_2^-, \mathcal{B}_2)$, respectively. The symbol $(\mathbf{R}_1^+ | \mathbf{R}_2^-)$ properly specifies a domain twin with a zero-thickness domain wall.

A domain wall can be considered as a domain twin with domain regions restricted to non-homogeneous parts near the plane p . For a domain wall in domain twin $(\mathbf{R}_1^+ | \mathbf{R}_2^-)$ we shall use the symbol $[\mathbf{R}_1^+ | \mathbf{R}_2^-]$, which expresses the fact that a domain wall of zero thickness needs the same specification as the domain twin.

If we exchange domain states in the twin $(\mathbf{R}_1^+ | \mathbf{n} | \mathbf{R}_2^-)$, we get a *reversed twin (wall)* with the symbol $(\mathbf{R}_2^- | \mathbf{n} | \mathbf{R}_1^+)$. These two ferroelastic twins are depicted in the lower right and upper left parts of Fig. 3.4.3.8, where – for ferroelastic–non-ferroelectric twins – we neglect spontaneous polarization of ferroelastic domain states. The reversed twin $\mathbf{R}_2^- | \mathbf{n} | \mathbf{R}_1^+$ has the opposite shear direction.

Twin and reversed twin can be, but may not be, crystallographically equivalent. Thus *e.g.* ferroelastic–non-ferroelectric twins $(\mathbf{R}_1^+ | \mathbf{n} | \mathbf{R}_2^-)$ and $(\mathbf{R}_2^- | \mathbf{n} | \mathbf{R}_1^+)$ in Fig. 3.4.3.8 are equivalent, *e.g.* via 2_z , whereas ferroelastic–ferroelectric twins $(\mathbf{S}_1^+ | \mathbf{n} | \mathbf{S}_3^-)$ and $(\mathbf{S}_3^- | \mathbf{n} | \mathbf{S}_1^+)$ are not equivalent, since there is no operation in the group K_{12} that would transform $(\mathbf{S}_1^+ | \mathbf{n} | \mathbf{S}_3^-)$ into $(\mathbf{S}_3^- | \mathbf{n} | \mathbf{S}_1^+)$.

As we shall show in the next section, the symmetry group $T_{12}(\mathbf{n})$ of a twin and the symmetry group $T_{21}(\mathbf{n})$ of a reverse twin are equal,

$$T_{12}(\mathbf{n}) = T_{21}(\mathbf{n}). \quad (3.4.3.66)$$

3.4. DOMAIN STRUCTURES

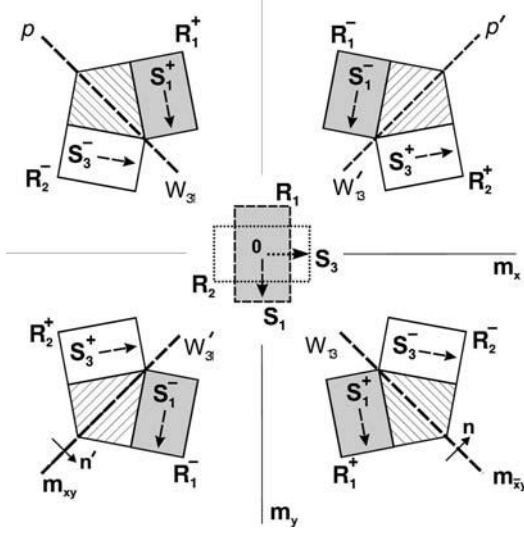


Fig. 3.4.3.8. Exploded view of four ferroelastic twins with disoriented ferroelastic domain states \mathbf{R}_1^+ , \mathbf{R}_2^- and \mathbf{R}_1^- , \mathbf{R}_2^+ formed from a single-domain pair (\mathbf{S}_1 , \mathbf{S}_2) (in the centre).

A sequence of repeating twins and reversed twins

$$\dots \mathbf{R}_1^+ | \mathbf{n} | \mathbf{R}_2^- | \mathbf{n} | \mathbf{R}_1^+ | \mathbf{n} | \mathbf{R}_2^- | \mathbf{n} | \mathbf{R}_1^+ | \mathbf{n} | \mathbf{R}_2^- | \mathbf{n} | \mathbf{R}_1^+ | \mathbf{n} | \mathbf{R}_2^- \dots \quad (3.4.3.67)$$

forms a *lamellar ferroelastic domain structure* that is very common in ferroelastic phases (see e.g. Figs. 3.4.1.1 and 3.4.1.4).

Similar considerations can be applied to the second equally deformed plane p' that is perpendicular to p . The two twins and corresponding compatible domain walls for the equally deformed plane p' have the symbols $(\mathbf{R}_1^- | \mathbf{n}' | \mathbf{R}_2^+)$ and $(\mathbf{R}_2^- | \mathbf{n}' | \mathbf{R}_1^+)$, and are also depicted in Fig. 3.4.3.8. The corresponding lamellar domain structure is

$$\dots \mathbf{R}_1^- | \mathbf{n}' | \mathbf{R}_2^+ | \mathbf{n}' | \mathbf{R}_1^- | \mathbf{n}' | \mathbf{R}_2^+ | \mathbf{n}' | \mathbf{R}_1^- | \mathbf{n}' | \mathbf{R}_2^+ | \mathbf{n}' | \mathbf{R}_1^- | \mathbf{n}' | \mathbf{R}_2^+ \dots \quad (3.4.3.68)$$

Thus from one ferroelastic single-domain pair $(\mathbf{R}_1, \mathbf{R}_2)$ depicted in the centre of Fig. 3.4.3.8 four different ferroelastic domain twins can be formed. It can be shown that these four twins have the same shear angle φ and the same amount of shear s . They differ only in the direction of the shear.

Four disoriented domain states $\mathbf{R}_1^-, \mathbf{R}_1^+$ and $\mathbf{R}_2^-, \mathbf{R}_2^+$ that appear in the four domain twins considered above are related by lost operations (e.g. diagonal, vertical and horizontal reflections), i.e. they are crystallographically equivalent. This result can readily be obtained if we consider the stabilizer of a disoriented domain state \mathbf{R}_1^+ , which is $I_{4/mmm}(\mathbf{R}_1^+) = 2_z/m_z$. Then the number n_a^{dis} of disoriented ferroelastic domain states is given by

$$n_a^{\text{dis}} = [G : I_g(\mathbf{R}_1^+)] = |4_z/m_z m_x m_{xy}| : |2_z/m_z| = 16 : 4 = 4. \quad (3.4.3.69)$$

All these domain states appear in ferroelastic polydomain structures that contain coexisting lamellar structures (3.4.3.67) and (3.4.3.68).

Disoriented domain states in ferroelastic domain structures can be recognized by diffraction techniques (e.g. using an X-ray precession camera). The presence of these four disoriented domain states results in splitting of the diffraction spots of the high-symmetry tetragonal phase into four or two spots in the orthorhombic ferroelastic phase. This splitting is schematically depicted in Fig. 3.4.3.9. For more details see e.g. Shmyt'ko *et al.* (1987), Rosová *et al.* (1993), and Rosová (1999).

Finally, we turn to *twin laws of ferroelastic domain twins with compatible domain walls*. In a ferroelastic twin, say $(\mathbf{R}_1^+ | \mathbf{n} | \mathbf{R}_2^-)$,

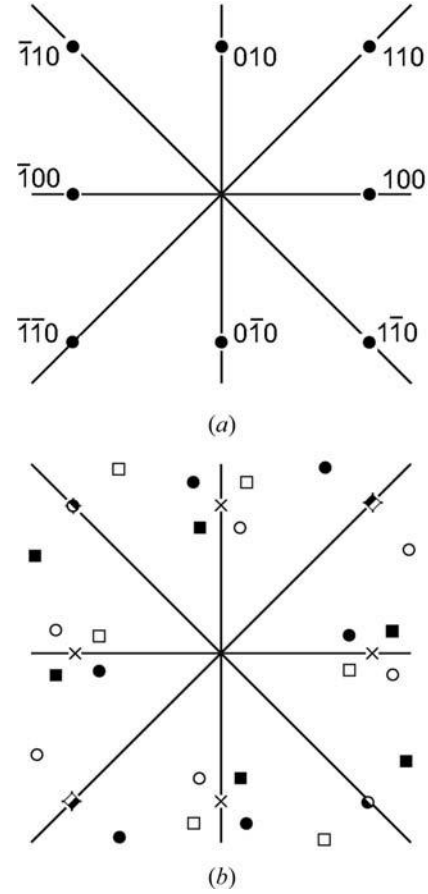


Fig. 3.4.3.9. Splitting of diffraction spots from the four domain twins in Fig. 3.4.3.8. (a) Diffraction spots of the tetragonal parent phase of the domain state \mathbf{R}_1 . (b) Diffraction pattern of the domain structure with four domain twins: white circles, \mathbf{R}_1^+ ; black circles, \mathbf{R}_1^- ; white squares, \mathbf{R}_2^+ ; black squares, \mathbf{R}_2^- .

there are just two possible *twinning operations* that interchange two ferroelastic domain states \mathbf{R}_1^+ and \mathbf{R}_2^- of the twin: reflection through the plane of the domain wall (m_{xy}^* in our example) and 180° rotation with a rotation axis in the intersection of the domain wall and the plane of shear (2_{xy}^*). These are the only transposing operations of the domain pair $(\mathbf{R}_1, \mathbf{R}_2)$ that are preserved by the shear; all other transposing operations of the domain pair $(\mathbf{R}_1, \mathbf{R}_2)$ are lost. (This is a difference from non-ferroelastic twins, where all transposing operations of the pair become twinning operations of a non-ferroelastic twin.)

Consider the twin $(\mathbf{S}_1^+ | \mathbf{n} | \mathbf{S}_3^-)$ in Fig. 3.4.3.8. By *non-trivial twinning operations* we understand transposing operations of the domain pair $(\mathbf{S}_1^+, \mathbf{S}_3^-)$, whereas *trivial twinning operations* leave invariant \mathbf{S}_1^+ and \mathbf{S}_3^- . As we shall see in the next section, the union of trivial and non-trivial twinning operations forms a group $T_{1+2}(\mathbf{n})$. This group, called the *symmetry group of the twin* $(\mathbf{S}_1^+ | \mathbf{n} | \mathbf{S}_3^-)$, comprises all symmetry operations of this twin and we shall use it for designating the *twin law of the ferroelastic twin*, just as the group J_{ij} of the domain pair $(\mathbf{S}_1, \mathbf{S}_j)$ specifies the twin law of a non-ferroelastic twin. This group $T_{1+2}(\mathbf{n})$ is a layer group (see Section 3.4.4.2) that keeps the plane p invariant, but for characterizing the twin law, which specifies the relation of domain states of two domains in the twin, one can treat $T_{1+2}(\mathbf{n})$ as an ordinary (dichromatic) point group $T_{1+2}(\mathbf{n})$. Thus the twin law of the domain twin $(\mathbf{S}_1^+ | \mathbf{n} | \mathbf{S}_3^-)$ is designated by the group

$$T_{1+3}(\mathbf{n}) = 2_{xy}^* m_{xy}^* m_z = T_{3-1}(\mathbf{n}), \quad (3.4.3.70)$$

where (3.4.3.70) expresses the fact that a twin and the reversed twin have the same symmetry, see equation (3.4.3.66). We see that

3. PHASE TRANSITIONS, TWINNING AND DOMAIN STRUCTURES

this group coincides with the symmetry group J_{1+2-} of the single-domain pair $(\mathbf{S}_1, \mathbf{S}_3)$ (see Fig. 3.4.3.1b).

The twin law of two twins $(\mathbf{S}_1^-|\mathbf{n}'|\mathbf{S}_3^+)$ and $(\mathbf{S}_3^+|\mathbf{n}'|\mathbf{S}_1^-)$ with the same equally deformed plane p' is expressed by the group

$$T_{1-3+}(\mathbf{n}') = m_z = T_{3-1+}(\mathbf{n}'), \quad (3.4.3.71)$$

which is different from the $T_{1+3-}(\mathbf{n})$ of the twin $(\mathbf{S}_1^+|\mathbf{n}|\mathbf{S}_3^-)$.

Representative domain pairs of all orbits of ferroelastic domain pairs (Litvin & Janovec, 1999) are listed in two tables. Table 3.4.3.6 contains representative domain pairs for which compatible domain walls exist and Table 3.4.3.7 lists ferroelastic domain pairs where compatible coexistence of domain states is not possible. Table 3.4.3.6 contains, beside other data, for each ferroelastic domain pair the orientation of two equally deformed planes and the corresponding symmetries of the corresponding four twins which express two twin laws.

3.4.3.6.4. Ferroelastic domain pairs with compatible domain walls, synoptic table

As we have seen, for each ferroelastic domain pair for which condition (3.4.3.54) for the existence of coherent domain walls is fulfilled, there exist two perpendicular equally deformed planes. On each of these planes two ferroelastic twins can be formed; these two twins are in a simple relation (one is a reversed twin of the other), have the same symmetry, and can therefore be represented by one of these twins. Then we can say that from one ferroelastic domain pair two different twins can be formed. Each of these twins represents a different ‘twin law’ that has arisen from the initial domain pair. All four ferroelastic twins can be described in terms of mechanical twinning with the same value of the shear angle φ .

3.4.3.6.4.1. Explanation of Table 3.4.3.6

Table 3.4.3.6 presents representative domain pairs of all classes of ferroelastic domain pairs for which compatible domain walls exist. The first five columns concern the domain pair. In subsequent columns, each row splits into two rows describing the orientation of two associated perpendicular equally deformed planes and the symmetry properties of the four domain twins that can be formed from the given domain pair. We explain the meaning of each column in detail.

The first three columns specify *domain pairs*.

F_1 : point-group symmetry (stabilizer in K_{1j}) of the first domain state \mathbf{S}_1 in a single-domain orientation.

g_{1j} : switching operations (if available) that specify the domain pair $(\mathbf{S}_1, \mathbf{S}_j = g_{1j}\mathbf{S}_1)$. Subscripts x, y, z specify the orientation of the symmetry operations in the Cartesian coordinate system of K_{1j} . Subscripts x', y' and x'', y'' denote a Cartesian coordinate system rotated about the z axis through 120 and 240°, respectively, from the Cartesian coordinate axes x and y . Diagonal directions are abbreviated: $p = [111]$, $q = [\bar{1}\bar{1}1]$, $r = [\bar{1}\bar{1}\bar{1}]$. Where possible, reflections and 180° rotations are chosen such that the two perpendicular permissible walls have crystallographic orientations.

K_{1j} : twinning group of the domain pair $(\mathbf{S}_1, \mathbf{S}_j)$. For the pair with $F_1 = m_{xy}2_{xy}m_z$ and $K = m\bar{3}m$, where the twinning group does not specify the domain pair unambiguously, we add after K_{1j} in parentheses a switching operation 2_{xz}^* or m_{xz}^* that defines the domain pair.

Axis: axis of ferroelastic domain pair around which single-domain states must be rotated to establish a contact along a compatible domain wall. This axis is parallel to the intersection of the two compatible domain walls given in the column *Wall*

Table 3.4.3.6. Ferroelastic domain pairs and twins with compatible walls

F_1 : symmetry of \mathbf{S}_1 ; g_{1j} : twinning operations; K_{1j} : twinning group; *Axis*: axis of domain pair; *Equation*:† direction of the axis; φ :† disorientation angle; \bar{J}_{1j} : symmetry of the twin pair; ℓ_{1j}^* : twinning operation; \bar{T}_{1j} : symmetry of the twin and wall, twin law of the twin; Classification: see Table 3.4.4.3.

| F_1 | g_{1j} | K_{1j} | Axis | Equation | Wall normals | φ | \bar{J}_{1j} | ℓ_{1j}^* | \bar{T}_{1j} | Classification |
|-----------|-------------------------------|----------------------|---------------------------|----------|--|-----------|------------------------------------|--------------------|--------------------|----------------|
| 1 | 2_z^* | 2_z^* | $[B\bar{1}0]$ | (a) | $[001]$ $[1B0]_e$ | (1) | 2_z^* 2_z^* | 2_z^* | 1 2_z^* | AR* SI |
| 1 | m_z^* | m_z^* | $[B\bar{1}0]$ | (a) | $[001]_e$ $[1B0]$ | (1) | m_z^* m_z^* | m_z^* | m_z^* 1 | SI AR* |
| $\bar{1}$ | $m_z^*, 2_z^*$ | $2_z^*/m_z^*$ | $[B\bar{1}0]$ | (a) | $[001]$ $[1B0]$ | (1) | $2_z^*/m_z^*$ $2_z^*/m_z^*$ | m_z^* 2_z^* | m_z^* 2_z^* | SR SR |
| 2_z | $2_x^*, 2_y^*$ | $2_x^*2_y^*2_z$ | $[001]$ | | $[100]$ $[010]$ | (2) | $2_x^*2_y^*2_z$ $2_x^*2_y^*2_z$ | 2_x^* 2_x^* | 2_y^* 2_y^* | SR SR |
| 2_z | m_x^*, m_y^* | $m_x^*m_y^*2_z$ | $[001]$ | | $[100]$ $[010]$ | (2) | $m_x^*m_y^*2_z$ $m_x^*m_y^*2_z$ | m_x^* m_y^* | m_y^* m_x^* | SR SR |
| 2_z | $4_z^*, 4_z^{*3}$ | 4_z^* | $[001]$ | (b) | $[1B0]$ $[B\bar{1}0]$ | (3) | 2_z 2_z | | 1 1 | AR AR |
| 2_z | $\bar{4}_z^*, \bar{4}_z^{*3}$ | $\bar{4}_z^*$ | $[001]$ | (b) | $[1B0]$ $[B\bar{1}0]$ | (3) | 2_z 2_z | | 1 1 | AR AR |
| 2_z | $3_z, 6_z^5$ | 6_z | $[001]$ | (c) | $[1B0]$ $[B\bar{1}0]$ | (4) | 2_z 2_z | | 1 1 | AR AR |
| | $3_z^2, 6_z$ | 6_z | $[001]$ | (c) | $[1B0]$ $[B\bar{1}0]$ | (4) | 2_z 2_z | | 1 1 | AR AR |
| 2_z | $\bar{3}_z^5, \bar{6}_z$ | $6_z/m_z$ | $[001]$ | (c) | $[1B0]$ $[B\bar{1}0]$ | (4) | 2_z 2_z | | 1 1 | AR AR |
| | $\bar{3}_z, \bar{6}_z^5$ | $6_z/m_z$ | $[001]$ | (c) | $[1B0]$ $[B\bar{1}0]$ | (4) | 2_z 2_z | | 1 1 | AR AR |
| 2_x | $2_{xy}^*, 4_z$ | $4_z2_x2_{xy}$ | $[\bar{C}C2]$ | (d) | $[110]$ $[\bar{1}\bar{1}C]_e$ | (5) | 2_{xy}^* 2_{xy}^* | 2_{xy}^* | 1 2_{xy}^* | AR* SI |
| 2_x | $m_{xy}^*, \bar{4}_z$ | $\bar{4}_z2_xm_{xy}$ | $[\bar{C}C2]$ | (d) | $[110]_e$ $[\bar{1}\bar{1}C]$ | (5) | m_{xy}^* m_{xy}^* | m_{xy}^* | m_{xy}^* 1 | SI AR* |
| 2_x | $2_x^*, 3_z^2$ | 3_z2_x | $[\sqrt{3}C, C, \bar{4}]$ | (e) | $[\bar{1}\sqrt{3}0]$ $[\sqrt{3}1C]_e$ | (6) | 2_x^* 2_x^* | 2_x^* | 1 2_x^* | AR* SI |

3.4. DOMAIN STRUCTURES

Table 3.4.3.6 (cont.)

| F_l | g_{lj} | K_{lj} | Axis | Equation | Wall normals | φ | \bar{J}_{lj} | \bar{t}_{lj} | \bar{T}_{lj} | Classification |
|---------------------|-------------------------|----------------------------|---------------------------------|----------|--|-----------|--|--|--|----------------|
| 2_x | $m_x^*, \bar{3}_z^5$ | $\bar{3}_z m_x$ | $[\sqrt{3}C, C, \bar{4}]$ | (e) | $[\bar{1}\sqrt{3}0]_e$ $[\sqrt{3}1C]$ | (6) | \underline{m}_x^* \underline{m}_x^* | \underline{m}_x^* 1 | \underline{m}_x^* 1 | SI AR* |
| 2_x | $2_{y'}^*, 6_z$ | $6_z 2_{xy}$ | $[\bar{C}, \sqrt{3}C, \bar{4}]$ | (f) | $[\sqrt{3}10]_e$ $[\bar{1}\sqrt{3}C]_e$ | (7) | $2_{y'}^*$ $2_{y'}^*$ | $2_{y'}^*$ $2_{y'}^*$ | 1 $2_{y'}^*$ | AR* SI |
| 2_x | $m_{y'}^*, \bar{6}_z$ | $\bar{6}_z 2_{xy}$ | $[\bar{C}, \sqrt{3}C, \bar{4}]$ | (f) | $[\sqrt{3}10]_e$ $[\bar{1}\sqrt{3}C]$ | (7) | $\underline{m}_{y'}^*$ $\underline{m}_{y'}^*$ | $\underline{m}_{y'}^*$ 1 | $\underline{m}_{y'}^*$ 1 | SI AR* |
| 2_{xy} | $m_x^*, \bar{4}_z^3$ | $\bar{4}_z m_x 2_{xy}$ | $[0C\bar{1}]$ | (g) | $[100]_e$ $[01C]$ | (8) | \underline{m}_x^* \underline{m}_x^* | \underline{m}_x^* 1 | \underline{m}_x^* 1 | SI AR* |
| m_z | $m_x^*, 2_y^*$ | $m_x^* 2_y^* m_z$ | $[001]$ | | $[100]_e$ $[010]$ | (2) | $\underline{m}_x^* 2_y^* m_z$ $\underline{m}_x^* 2_y^* m_z$ | \underline{m}_x^* \underline{m}_x^* | $\underline{m}_x^* 2_y^* m_z$ \underline{m}_z | SI AR* |
| m_z | $4_z, \bar{4}_z^3$ | $4_z/m_z$ | $[001]$ | (b) | $[1B0]_{e0}$ $[B10]_{0e}$ | (3) | m_z m_z | | m_z m_z | AI AI |
| | $4_z^3, \bar{4}_z$ | $4_z/m_z$ | $[001]$ | (b) | $[1B0]_{e0}$ $[B10]_{0e}$ | (3) | m_z m_z | | m_z m_z | AI AI |
| m_z | $3_z, \bar{6}_z^5$ | $\bar{6}_z$ | $[001]$ | (c) | $[1B0]_{e0}$ $[B10]_{0e}$ | (4) | m_z m_z | | m_z m_z | AI AI |
| | $3_z^2, \bar{6}_z$ | $\bar{6}_z$ | $[001]$ | (c) | $[1B0]_{e0}$ $[B10]_{0e}$ | (4) | m_z m_z | | m_z m_z | AI AI |
| m_z | $\bar{3}_z, 6_z^5$ | $6_z/m_z$ | $[001]$ | (c) | $[1B0]_{e0}$ $[B10]_{0e}$ | (4) | m_z m_z | | m_z m_z | AI AI |
| | $\bar{3}_z^5, 6_z$ | $6_z/m_z$ | $[001]$ | (c) | $[1B0]_{e0}$ $[B10]_{0e}$ | (4) | m_z m_z | | m_z m_z | AI AI |
| m_x | $m_{xy}^*, 4_z$ | $4_z m_x m_{xy}$ | $[\bar{C}C2]$ | (d) | $[110]_e$ $[11C]$ | (5) | \underline{m}_{xy}^* \underline{m}_{xy}^* | \underline{m}_{xy}^* 1 | \underline{m}_{xy}^* 1 | SI AR* |
| m_x | $2_{xy}^*, \bar{4}_z$ | $\bar{4}_z m_x 2_{xy}$ | $[\bar{C}C2]$ | (d) | $[110]_e$ $[11C]_e$ | (5) | 2_{xy}^* 2_{xy}^* | 2_{xy}^* 2_{xy}^* | 1 2_{xy}^* | AR* SI |
| m_x | $m_{x'}^*, 3_z^2$ | $3_z m_x$ | $[\sqrt{3}C, C, \bar{4}]$ | (e) | $[\bar{1}\sqrt{3}0]_e$ $[\sqrt{3}1C]$ | (6) | $\underline{m}_{x'}^*$ $\underline{m}_{x'}^*$ | $\underline{m}_{x'}^*$ 1 | $\underline{m}_{x'}^*$ 1 | SI AR* |
| m_x | $2_{x'}^*, \bar{3}_z^5$ | $\bar{3}_z m_x$ | $[\sqrt{3}C, C, \bar{4}]$ | (e) | $[\bar{1}\sqrt{3}0]_e$ $[\sqrt{3}1C]_e$ | (6) | $2_{x'}^*$ $2_{x'}^*$ | $2_{x'}^*$ $2_{x'}^*$ | 1 $2_{x'}^*$ | AR* SI |
| m_x | $m_{y'}^*, 6_z$ | $6_z m_x m_{y'}$ | $[\bar{C}, \sqrt{3}C, \bar{4}]$ | (f) | $[\sqrt{3}10]_e$ $[\bar{1}\sqrt{3}C]$ | (7) | $\underline{m}_{y'}^*$ $\underline{m}_{y'}^*$ | $\underline{m}_{y'}^*$ 1 | $\underline{m}_{y'}^*$ 1 | SI AR* |
| m_x | $2_{y'}^*, \bar{6}_z$ | $\bar{6}_z m_x 2_{y'}$ | $[\bar{C}, \sqrt{3}C, \bar{4}]$ | (f) | $[\sqrt{3}10]_e$ $[\bar{1}\sqrt{3}C]_e$ | (7) | $2_{y'}^*$ $2_{y'}^*$ | $2_{y'}^*$ $2_{y'}^*$ | 1 $2_{y'}^*$ | AR* SI |
| m_{xy} | $2_x^*, \bar{4}_z^3$ | $\bar{4}_z 2_x m_{xy}$ | $[0C\bar{1}]$ | (g) | $[100]_e$ $[01C]_e$ | (8) | 2_x^* 2_{xy}^* | 2_x^* 2_x^* | 1 2_x^* | AR* SI |
| $2_z/m_z$ | m_x^*, m_y^* | $m_x^* m_y^* m_z$ | $[001]$ | | $[100]_e$ $[010]$ | (2) | $\underline{m}_x^* m_y^* m_z$ $\underline{m}_x^* m_y^* m_z$ | \underline{m}_x^* \underline{m}_y^* | $\underline{m}_x^* 2_y^* m_z$ $\underline{2}_x^* m_y^* m_z$ | SR SR |
| $2_z/m_z$ | $4_z^*, 4_z^{3*}$ | $4_z^*/m_z$ | $[001]$ | (b) | $[1B0]_{e0}$ $[B10]_{0e}$ | (3) | $2_z/m_z$ $2_z/m_z$ | | m_z m_z | AR AR |
| $2_z/m_z$ | $3_z, 6_z^5$ | $6_z/m_z$ | $[001]$ | (c) | $[1B0]_{e0}$ $[B10]_{0e}$ | (4) | $2_z/m_z$ $2_z/m_z$ | | m_z m_z | AR AR |
| | $3_z^2, 6_z$ | $6_z/m_z$ | $[001]$ | (c) | $[1B0]_{e0}$ $[B10]_{0e}$ | (4) | $2_z/m_z$ $2_z/m_z$ | | m_z m_z | AR AR |
| $2_x/m_x$ | $m_{xy}^*, 4_z$ | $4_z/m_x m_x m_{xy}$ | $[\bar{C}C2]$ | (d) | $[110]_e$ $[11C]$ | (5) | $2_{xy}^*/m_{xy}^*$ $2_{xy}^*/m_{xy}^*$ | \underline{m}_{xy}^* $\underline{2}_{xy}^*$ | \underline{m}_{xy}^* $\underline{2}_{xy}^*$ | SR SR |
| $2_x/m_x$ | $m_{x'}^*, 3_z^2$ | $\bar{3}_z m_x$ | $[\sqrt{3}CC\bar{4}]$ | (e) | $[\bar{1}\sqrt{3}0]_e$ $[\sqrt{3}1C]$ | (6) | $2_{x'}^*/m_{x'}^*$ $2_{x'}^*/m_{x'}^*$ | $\underline{m}_{x'}^*$ $\underline{2}_{x'}^*$ | $\underline{m}_{x'}^*$ $\underline{2}_{x'}^*$ | SR SR |
| $2_x/m_x$ | $m_{y'}^*, 6_z$ | $6_z/m_x m_x m_{y'}$ | $[\bar{C}, \sqrt{3}C, \bar{4}]$ | (f) | $[\sqrt{3}10]_e$ $[\bar{1}\sqrt{3}C]$ | (7) | $2_{y'}^*/m_{y'}^*$ $2_{y'}^*/m_{y'}^*$ | $\underline{m}_{y'}^*$ $\underline{2}_{y'}^*$ | $\underline{m}_{y'}^*$ $\underline{2}_{y'}^*$ | SR SR |
| $2_x 2_y 2_z$ | $2_{xy}^*, 2_{xy}^*$ | $4_z^* 2_x 2_{xy}^*$ | $[001]$ | | $[110]_e$ $[110]_e$ | (10) | $2_{xy}^* 2_{xy}^* 2_z$ $2_{xy}^* 2_{xy}^* 2_z$ | 2_{xy}^* 2_{xy}^* | 2_{xy}^* 2_{xy}^* | SR SR |
| $2_x 2_y 2_z$ | m_{xy}^*, m_{xy}^* | $\bar{4}_z^* 2_x m_{xy}^*$ | $[001]$ | | $[110]_e$ $[110]_e$ | (10) | $\underline{m}_{xy}^* m_{xy}^* 2_z$ $\underline{m}_{xy}^* m_{xy}^* 2_z$ | \underline{m}_{xy}^* \underline{m}_{xy}^* | \underline{m}_{xy}^* \underline{m}_{xy}^* | SR SR |
| $2_x 2_y 2_z$ | $2_x^*, 2_y^*$ | $6_z 2_x 2_y$ | $[001]$ | | $[\bar{1}\sqrt{3}0]_e$ $[\sqrt{3}10]_e$ | (9) | $2_x^* 2_y^* 2_z$ $2_x^* 2_y^* 2_z$ | 2_x^* 2_x^* | 2_x^* 2_x^* | SR SR |
| $2_x 2_y 2_z$ | $m_{x'}^*, m_{y'}^*$ | $6_z/m_x m_x m_{y'}$ | $[001]$ | | $[\bar{1}\sqrt{3}0]_e$ $[\sqrt{3}10]_e$ | (9) | $\underline{m}_{x'}^* m_{y'}^* 2_z$ $\underline{m}_{x'}^* m_{y'}^* 2_z$ | $\underline{m}_{x'}^*$ $\underline{m}_{y'}^*$ | $\underline{m}_{x'}^*$ $\underline{m}_{y'}^*$ | SR SR |
| $2_{xy} 2_{xy} 2_z$ | m_x^*, m_y^* | $\bar{4}_z^* m_x^* 2_{xy}$ | $[001]$ | | $[100]_e$ $[010]_e$ | (12) | $\underline{m}_x^* m_y^* 2_z$ $\underline{m}_x^* m_y^* 2_z$ | \underline{m}_x^* \underline{m}_y^* | \underline{m}_x^* \underline{m}_y^* | SR SR |

3. PHASE TRANSITIONS, TWINNING AND DOMAIN STRUCTURES

Table 3.4.3.6 (cont.)

| F_1 | g_{ij} | K_{ij} | Axis | Equation | Wall normals | φ | \bar{J}_{ij} | \bar{t}_{ij} | \bar{T}_{ij} | Classification |
|------------------------|-----------------------|-----------------------------------|---------------|----------|--|-----------|--|--------------------------|--|----------------|
| $2_{xy}2_{xy}2_z$ | $2_{xz}^*, 4_y$ | $4_z 3_p 2_{xy}$ | $[B2\bar{B}]$ | (h) | $[101]$ $[\bar{1}B1]$ | (11) | 2_{xz}^* 2_{xz} | 2_{xz}^* 2_{xz} | 1 2_{xz} | AR* SI |
| $2_{xy}2_{xy}2_z$ | $m_{xz}^*, \bar{4}_y$ | $m_z \bar{3}_p m_{xy}$ | $[B2\bar{B}]$ | (h) | $[101]$ $[\bar{1}B1]$ | (11) | m_{xz}^* m_{xz} | m_{xz}^* m_{xz} | m_{xz} 1 | SI AR* |
| $m_x m_y 2_z$ | m_{xy}^*, m_{xy}^* | $4_z^* m_x m_{xy}^*$ | [001] | | $[110]$ $[\bar{1}\bar{1}0]$ | (10) | $m_{xy}^* m_{xy}^* 2_z$ $m_{xy}^* m_{xy}^* 2_z$ | m_{xy}^* m_{xy}^* | m_{xy}^* m_{xy}^* | SR SR |
| $m_x m_y 2_z$ | $2_{xy}^*, 2_{xy}^*$ | $4_z^* m_x 2_{xy}^*$ | [001] | | $[110]$ $[\bar{1}\bar{1}0]$ | (10) | $2_{xy}^* 2_{xy}^* 2_z$ $2_{xy}^* 2_{xy}^* 2_z$ | 2_{xy}^* 2_{xy}^* | 2_{xy}^* 2_{xy}^* | SR SR |
| $m_x m_y 2_z$ | $m_{x'}^*, m_{y'}^*$ | $6_z m_x m_y$ | [001] | | $[\bar{1}\sqrt{3}0]$ $[\sqrt{3}10]$ | (9) | $m_{x'}^* m_{y'}^* 2_z$ $m_{x'}^* m_{y'}^* 2_z$ | $m_{x'}^*$ $m_{y'}^*$ | $m_{x'}^*$ $m_{y'}^*$ | SR SR |
| $m_x m_y 2_z$ | $2_{x'}^*, 2_{y'}^*$ | $6_z / m_z m_x m_y$ | [001] | | $[\bar{1}\sqrt{3}0]$ $[\sqrt{3}10]$ | (9) | $2_{x'}^* 2_{y'}^* 2_z$ $2_{x'}^* 2_{y'}^* 2_z$ | $2_{y'}^*$ $2_{x'}^*$ | $2_{y'}^*$ $2_{x'}^*$ | SR SR |
| $m_x 2_y m_z$ | $m_{x'}^*, 2_{y'}^*$ | $\bar{6}_z m_x 2_y$ | [001] | | $[\bar{1}\sqrt{3}0]_e$ $[\sqrt{3}10]_e$ | (9) | $m_{x'}^* 2_{y'}^* m_z$ $m_{x'}^* 2_{y'}^* m_z$ | $m_{x'}^*$ $m_{x'}^*$ | $m_{x'}^* 2_{y'}^* m_z$ m_z | SI AR* |
| $2_x m_y m_z$ | $m_{xy}^*, 2_{xy}^*$ | $4_z / m_z m_x m_{xy}$ | [001] | | $[110]$ $[\bar{1}\bar{1}0]_e$ | (10) | $2_{xy}^* m_{xy}^* m_z$ $2_{xy}^* m_{xy}^* m_z$ | m_{xy}^* m_{xy}^* | m_z $2_{xy}^* m_{xy}^* m_z$ | AR* SI |
| $2_x m_y m_z$ | $m_{y'}^*, 2_{x'}^*$ | $\bar{6}_z 2_x m_y$ | [001] | | $[\bar{1}\sqrt{3}0]$ $[\sqrt{3}10]_e$ | (9) | $2_{x'}^* m_{y'}^* m_z$ $2_{x'}^* m_{y'}^* m_z$ | $m_{y'}^*$ $m_{y'}^*$ | m_z $2_{x'}^* m_{y'}^* m_z$ | AR* SI |
| $2_x m_y m_z$ | $m_{x'}^*, 2_{y'}^*$ | $6_z / m_z m_x m_y$ | [001] | | $[\bar{1}\sqrt{3}0]_e$ $[\sqrt{3}10]_e$ | (9) | $m_{x'}^* 2_{y'}^* m_z$ $m_{x'}^* 2_{y'}^* m_z$ | $m_{x'}^*$ $m_{x'}^*$ | $m_{x'}^* 2_{y'}^* m_z$ m_z | SI AR* |
| $m_{xy} m_{xy} 2_z$ | $2_x^*, 2_y^*$ | $4_z^* 2_x^* m_{xy}$ | [001] | | $[100]$ $[010]$ | (12) | $2_x^* 2_y^* 2_z$ $2_x^* 2_y^* 2_z$ | 2_y^* 2_x^* | 2_y^* 2_x^* | SR SR |
| $m_{xy} m_{xy} 2_z$ | $m_{xz}^*, \bar{4}_y$ | $\bar{4}_z 3_p m_{xy}$ | $[B2\bar{B}]$ | (h) | $[101]_e$ $[\bar{1}B1]$ | (11) | m_{xz}^* m_{xz} | m_{xz}^* m_{xz} | m_{xz} 1 | SI AR* |
| $m_{xy} m_{xy} 2_z$ | $2_{xz}^*, 4_y$ | $m_z \bar{3}_p m_{xy}$ | $[B2\bar{B}]$ | (h) | $[101]$ $[\bar{1}B1]_e$ | (11) | 2_{xz}^* 2_{xz} | 2_{xz}^* 2_{xz} | 1 2_{xz} | AR* SI |
| $m_{xy} 2_{xy} m_z$ | $m_{xz}^*, 4_y$ | $m_z \bar{3}_p m_{xy} (m_{xz}^*)$ | $[B2\bar{B}]$ | (h) | $[101]_e$ $[\bar{1}B1]$ | (11) | m_{xz}^* m_{xz} | m_{xz}^* m_{xz} | m_{xz} 1 | SI AR* |
| $m_{xy} 2_{xy} m_z$ | $2_{xz}^*, \bar{4}_y$ | $m_z \bar{3}_p m_{xy} (2_{xz}^*)$ | $[B2\bar{B}]$ | (h) | $[101]$ $[\bar{1}B1]_e$ | (11) | 2_{xz}^* 2_{xz} | 2_{xz}^* 2_{xz} | 1 2_{xz} | AR* SI |
| $m_x m_y m_z$ | m_{xy}^*, m_{xy}^* | $4_z^* / m_z m_x m_{xy}^*$ | [001] | | $[110]$ $[\bar{1}\bar{1}0]$ | (10) | $m_{xy}^* m_{xy}^* m_z$ $m_{xy}^* m_{xy}^* m_z$ | m_{xy}^* m_{xy}^* | $2_{xy}^* m_{xy}^* m_z$ $m_{xy}^* 2_{xy}^* m_z$ | SR SR |
| $m_x m_y m_z$ | $m_{x'}^*, m_{y'}^*$ | $6_z / m_z m_x m_y$ | [001] | | $[\bar{1}\sqrt{3}0]$ $[\sqrt{3}10]$ | (9) | $m_{x'}^* m_{y'}^* m_z$ $m_{x'}^* m_{y'}^* m_z$ | $m_{y'}^*$ $m_{y'}^*$ | $m_{x'}^* 2_{y'}^* m_z$ $2_{x'}^* m_{y'}^* m_z$ | SR SR |
| $m_{xy} m_{xy} m_z$ | $m_{xz}^*, 4_y$ | $m_z \bar{3}_p m_{xy}$ | $[B2\bar{B}]$ | (h) | $[101]$ $[\bar{1}B1]$ | (11) | $2_{xz}^* / m_{xz}$ $2_{xz}^* / m_{xz}$ | m_{xz}^* 2_{xz}^* | m_{xz} 2_{xz} | SR SR |
| 4_z | $2_{xz}^*, 4_y$ | $4_z 3_p 2_{xy}$ | [010] | | $[101]$ $[\bar{1}01]_e$ | (13) | 2_{xz}^* 2_{xz} | 2_{xz}^* 2_{xz} | 1 2_{xz} | AR* SI |
| 4_z | $m_{xz}^*, \bar{4}_y$ | $m_z \bar{3}_p m_{xy}$ | [010] | | $[101]_e$ $[\bar{1}01]$ | (13) | m_{xz}^* m_{xz} | m_{xz}^* m_{xz} | m_{xz} 1 | SI AR* |
| $\bar{4}_z$ | $m_{xz}^*, \bar{4}_y$ | $\bar{4}_z 3_p m_{xy}$ | [010] | | $[101]$ $[\bar{1}01]$ | (13) | m_{xz}^* m_{xz} | m_{xz}^* m_{xz} | m_{xz} 1 | SI AR* |
| $\bar{4}_z$ | $2_{xz}^*, 4_y$ | $m_z \bar{3}_p m_{xy}$ | [010] | | $[101]$ $[\bar{1}01]_e$ | (13) | 2_{xz}^* 2_{xz} | 2_{xz}^* 2_{xz} | 1 2_{xz} | AR* SI |
| $4_z / m_z$ | $m_{xz}^*, 4_y$ | $m_z \bar{3}_p m_{xy}$ | [010] | | $[101]$ $[\bar{1}01]$ | (13) | $2_{xz}^* / m_{xz}$ $2_{xz}^* / m_{xz}$ | m_{xz}^* 2_{xz}^* | m_{xz} 2_{xz} | SR SR |
| $4_z 2_x 2_{xy}$ | $2_{xz}^*, 2_{xz}^*$ | $4_z 3_p 2_{xy}$ | [010] | | $[101]$ $[\bar{1}01]$ | (13) | $2_{xz}^* 2_{xz}^* 2_y$ $2_{xz}^* 2_{xz}^* 2_y$ | 2_{xz}^* 2_{xz}^* | 2_{xz}^* 2_{xz}^* | SR SR |
| $4_z 2_x 2_{xy}$ | m_{xz}^*, m_{xz}^* | $m_z \bar{3}_p m_{xy}$ | [010] | | $[101]$ $[\bar{1}01]$ | (13) | $m_{xz}^* m_{xz}^* 2_y$ $m_{xz}^* m_{xz}^* 2_y$ | m_{xz}^* m_{xz}^* | m_{xz} m_{xz} | SR SR |
| $4_z m_x m_{xy}$ | $m_{xz}^*, 2_{xz}^*$ | $m_z \bar{3}_p m_{xy}$ | [010] | | $[101]$ $[\bar{1}01]_e$ | (13) | $2_{xz}^* m_{xz}^* m_y$ $2_{xz}^* m_{xz}^* m_y$ | 2_{xz}^* 2_{xz}^* | m_y $2_{xz}^* m_{xz}^* m_y$ | AR* SI |
| $\bar{4}_z 2_x m_{xy}$ | m_{xz}^*, m_{xz}^* | $\bar{4}_z 3_p m_{xy}$ | [010] | | $[101]$ $[\bar{1}01]$ | (13) | $m_{xz}^* m_{xz}^* 2_y$ $m_{xz}^* m_{xz}^* 2_y$ | m_{xz}^* m_{xz}^* | m_{xz} m_{xz} | SR SR |
| $\bar{4}_z m_x 2_{xy}$ | $m_{xz}^*, 2_{xz}^*$ | $m_z \bar{3}_p m_{xy}$ | [010] | | $[101]$ $[\bar{1}01]$ | (13) | $2_{xz}^* m_{xz}^* m_y$ $2_{xz}^* m_{xz}^* m_y$ | m_{xz}^* m_{xz}^* | m_y $2_{xz}^* m_{xz}^* m_y$ | AR* SR |
| $\bar{4}_z 2_x m_{xy}$ | $2_{xz}^*, 2_{xz}^*$ | $m_z \bar{3}_p m_{xy}$ | [010] | | $[101]$ $[\bar{1}01]$ | (13) | $2_{xz}^* 2_{xz}^* 2_y$ $2_{xz}^* 2_{xz}^* 2_y$ | 2_{xz}^* 2_{xz}^* | 2_{xz}^* 2_{xz}^* | SR SI |

3.4. DOMAIN STRUCTURES

Table 3.4.3.6 (cont.)

| F_1 | g_{1j} | K_{1j} | Axis | Equation | Wall normals | φ | \bar{J}_{1j} | \bar{t}_{1j} | \bar{T}_{1j} | Classification |
|----------------------|-----------------------|------------------------|-------|----------|--|-----------|---|-----------------------------|---|----------------|
| $4_z/m_z m_x m_{xy}$ | m_{xz}^*, m_{xz}^* | $m_z \bar{3}_p m_{xy}$ | [010] | | $\begin{bmatrix} [101] \\ [\bar{1}01] \end{bmatrix}$ | (13) | $\frac{m_{xz}^* m_{xz}^* m_y}{m_{xz}^* m_{xz}^* m_y}$ | $\frac{m_{xz}^*}{m_{xz}^*}$ | $\frac{m_{xz}^* 2_{xz}^* m_y}{2_{xz}^* m_{xz}^* m_y}$ | SR SR |
| 3_p | $2_x^*, 3_r$ | $2_z 3_p$ | [011] | | $\begin{bmatrix} [100] \\ [011]_e \end{bmatrix}$ | (14) | $\frac{2_x^*}{2_x^*}$ | $\frac{2_x^*}{2_x^*}$ | $\frac{1}{2_x^*}$ | AR* SI |
| 3_p | $m_x^*, \bar{3}_r$ | $m_z \bar{3}_p$ | [011] | | $\begin{bmatrix} [100]_e \\ [011] \end{bmatrix}$ | (14) | $\frac{m_x^*}{m_x^*}$ | $\frac{m_x^*}{m_x^*}$ | $\frac{m_x^*}{1}$ | SI AR* |
| 3_p | $2_{xy}^*, 4_y$ | $4_z 3_p 2_{xy}$ | [110] | | $\begin{bmatrix} [001]_e \\ [110] \end{bmatrix}$ | (14) | $\frac{2_{xy}^*}{2_{xy}^*}$ | $\frac{2_{xy}^*}{2_{xy}^*}$ | $\frac{2_{xy}^*}{1}$ | SI AR* |
| 3_p | $m_{xy}^*, \bar{4}_y$ | $\bar{4}_z 3_p m_{xy}$ | [110] | | $\begin{bmatrix} [001] \\ [110]_e \end{bmatrix}$ | (14) | $\frac{m_{xy}^*}{m_{xy}^*}$ | $\frac{m_{xy}^*}{m_{xy}^*}$ | $\frac{1}{m_{xy}^*}$ | AR* SI |
| $\bar{3}_p$ | $m_x^*, 3_r$ | $m_z \bar{3}_p$ | [011] | | $\begin{bmatrix} [100] \\ [011] \end{bmatrix}$ | (14) | $\frac{2_x^*/m_x^*}{2_x^*/m_x^*}$ | $\frac{m_x^*}{2_x^*}$ | $\frac{m_x^*}{2_x^*}$ | SR SR |
| $\bar{3}_p$ | $m_{xy}^*, 4_y$ | $m_z \bar{3}_p m_{xy}$ | [110] | | $\begin{bmatrix} [001] \\ [110] \end{bmatrix}$ | (14) | $\frac{2_{xy}^*/m_{xy}^*}{2_{xy}^*/m_{xy}^*}$ | $\frac{2_{xy}^*}{m_{xy}^*}$ | $\frac{2_{xy}^*}{m_{xy}^*}$ | SR SR |
| $3_p 2_{xy}$ | $2_x^*, 2_{yz}^*$ | $4_z 3_p 2_{xy}$ | [011] | | $\begin{bmatrix} [100] \\ [011] \end{bmatrix}$ | (14) | $\frac{2_x^* 2_{yz}^* 2_{yz}^*}{2_x^* 2_{yz}^* 2_{yz}^*}$ | $\frac{2_{yz}^*}{2_x^*}$ | $\frac{2_{yz}^*}{2_x^*}$ | SR SR |
| $3_p 2_{xy}$ | m_x^*, m_{yz}^* | $m_z \bar{3}_p m_{xy}$ | [011] | | $\begin{bmatrix} [100] \\ [011] \end{bmatrix}$ | (14) | $\frac{m_x^* m_{yz}^* 2_{yz}^*}{m_x^* m_{yz}^* 2_{yz}^*}$ | $\frac{m_x^*}{m_{yz}^*}$ | $\frac{m_x^*}{m_{yz}^*}$ | SR SR |
| $3_p m_{xy}$ | $2_x^*, m_{yz}^*$ | $\bar{4}_z 3_p m_{xy}$ | [011] | | $\begin{bmatrix} [100] \\ [011]_e \end{bmatrix}$ | (14) | $\frac{m_{yz}^* m_{yz}^* 2_x^*}{m_{yz}^* m_{yz}^* 2_x^*}$ | $\frac{m_{yz}^*}{m_{yz}^*}$ | $\frac{m_{yz}^*}{m_{yz}^* 2_x^*}$ | AR* SI |
| $3_p m_{xy}$ | $m_x^*, 2_{yz}^*$ | $m_z \bar{3}_p m_{xy}$ | [011] | | $\begin{bmatrix} [100]_e \\ [011] \end{bmatrix}$ | (14) | $\frac{m_x^* 2_{yz}^* m_{yz}^*}{m_x^* 2_{yz}^* m_{yz}^*}$ | $\frac{m_x^*}{m_{yz}^*}$ | $\frac{m_x^* 2_{yz}^* m_{yz}^*}{m_{yz}^*}$ | SI AR* |
| $\bar{3}_p m_{xy}$ | m_x^*, m_{yz}^* | $m_z \bar{3}_p m_{xy}$ | [011] | | $\begin{bmatrix} [100] \\ [011] \end{bmatrix}$ | (14) | $\frac{m_x^* m_{yz}^* m_{yz}^*}{m_x^* m_{yz}^* m_{yz}^*}$ | $\frac{m_x^*}{m_{yz}^*}$ | $\frac{m_x^* 2_{yz}^* m_{yz}^*}{2_x^* m_{yz}^* m_{yz}^*}$ | SR SR |

† Equations for directions of axes and shear angle φ :

$$\begin{aligned}
 & \begin{pmatrix} a & f & e \\ f & b & d \\ e & d & c \end{pmatrix} & \begin{pmatrix} a & d & 0 \\ d & b & 0 \\ 0 & 0 & c \end{pmatrix} & \begin{pmatrix} a & 0 & 0 \\ 0 & b & d \\ 0 & d & c \end{pmatrix} \\
 (a) & [001] \quad [1 \frac{d}{e} 0] & (b) & [\bar{1}\alpha 0] \quad [\alpha 10] & (d) & [110] \quad [1\bar{1} \frac{2d}{a-b}] \\
 & & \alpha = & \frac{2d + \sqrt{(a-b)^2 + 4d^2}}{a-b} & (e) & [\bar{1}\sqrt{3}0] \quad [\sqrt{3}1 \frac{4d}{b-a}] \\
 (c) & [\bar{1}\beta 0] \quad [\beta 10] & (f) & [\sqrt{3}10] \quad [\bar{1}\sqrt{3} \frac{4\sqrt{3}}{3(a-b)}] \\
 \beta = & \frac{(a-b) + 2\sqrt{3}d + 4\sqrt{(a-b)^2 + 4d^2}}{\sqrt{3}(a-b) - 2d} \\
 (1) & 2\sqrt{d^2 + e^2} & (2) & 2|d| & (5) & \sqrt{(a-b)^2 + 2d^2} \\
 (3) & \frac{1}{2}\sqrt{(a-b)^2 + 4d^2} & (6) & \frac{\sqrt{3}}{2}\sqrt{(a-b)^2 + 4d^2} & (7) & 2|d| \\
 (4) & \frac{\sqrt{3}}{2}\sqrt{(a-b)^2 + 4d^2} & & & & \\
 & & & & & \\
 & \begin{pmatrix} a & b & -d \\ b & a & d \\ -d & d & c \end{pmatrix} & \begin{pmatrix} a & 0 & 0 \\ 0 & b & 0 \\ 0 & 0 & c \end{pmatrix} & \begin{pmatrix} a & d & 0 \\ d & a & 0 \\ 0 & 0 & c \end{pmatrix} \\
 (g) & [100] \quad [0\bar{1} \frac{d}{b}] & (h) & [101] \quad [\bar{1} \frac{2d}{c-d} 1] \\
 (8) & 2\sqrt{a^2 + b^2} & (9) & \frac{\sqrt{3}}{2}|a-b| & (11) & \sqrt{(a-c)^2 + 2d^2} \\
 & & (10) & |a-b| & (12) & 2|d| \\
 & & & & & \\
 & \begin{pmatrix} a & 0 & 0 \\ 0 & a & 0 \\ 0 & 0 & c \end{pmatrix} & \begin{pmatrix} a & d & d \\ d & a & d \\ d & d & a \end{pmatrix} & & & \\
 (13) & |a-c| & (14) & 2\sqrt{2}|d| & & &
 \end{aligned}$$

normals and its direction \mathbf{h} is defined by a vector product $\mathbf{h} = \mathbf{n}_1 \times \mathbf{n}_2$ of normal vectors \mathbf{n}_1 and \mathbf{n}_2 of these walls. Letters B and C denote components of \mathbf{h} which depend on spontaneous strain.

Equation: a reference to an expression, given at the end of the table, for the direction \mathbf{h} of the axis, where parameters B and C in the column *Axis* are expressed as functions of spontaneous strain components. The matrices above these expressions give the form of the ‘absolute’ spontaneous strain.

Wall normals: orientation of equally deformed planes. As explained above, each plane represents two mutually reversed compatible domain walls. Numbers or parameters B , C given in parentheses can be interpreted either as components of normal

vectors to compatible walls or as intercepts analogous to Miller indices: Planes of compatible domain walls $Ax_1 + Bx_2 + Cx_3 = 0$ and $A'x_1 + B'x_2 + C'x_3 = 0$ [see equations (3.4.3.55)] pass through the origin of the Cartesian coordinate system of K_{1j} and have normal vectors $\mathbf{n}_1 = [ABC]$ and $\mathbf{n}_2 = [A'B'C']$. It is possible to find a plane with the same normal vector $[ABC]$ but not passing through the origin, e.g. $Ax_1 + Bx_2 + Cx_3 = 1$. Then parameters A , B and C can be interpreted as the reciprocal values of the oriented intercepts on the coordinate axes cut by this plane, $[x_1/(1/A)] + [x_2/(1/B)] + [x_3/(1/C)] = 1$. In analogy with Miller indices, the symbol (ABC) is used for expressing the orientation of a wall. However, parameters A , B and C are not Miller indices, since they are expressed in an orthonormal and

3. PHASE TRANSITIONS, TWINNING AND DOMAIN STRUCTURES

not a crystallographic coordinate system. A left square bracket [in front of two equally deformed planes signifies that the two domain walls (domain twins) associated with one equally deformed plane are crystallographically equivalent (in K_{ij}) with two domain walls (twins) associated with the perpendicular equally deformed plane, *i.e.* all four compatible domain walls (domain twins) that can be formed from domain pair (S_1, S_j) are crystallographically equivalent in K_{ij} .

The subscript e indicates that the wall carries a nonzero polarization charge, $\text{Div } \mathbf{P} \neq 0$. This can happen in ferroelectric domain pairs with spontaneous polarization not parallel to the axis of the pair. If one domain wall is charged then the perpendicular wall is not charged. In a few cases, polarization and/or orientation of the domain wall is not determined by symmetry; then it is not possible to specify which of the two walls is charged. In such cases, a subscript $e0$ or $0e$ indicates that one of the two walls is charged and the other is not.

φ : reference to an expression, given at the end of the table, in which the shear angle φ (in radians) is given as a function of the ‘absolute’ spontaneous strain components, which are defined in a matrix given above the equations.

\bar{J}_{ij} : symmetry of the ‘twin pair’. The meaning of this group and its symbol is explained in the next section. This group specifies the symmetry properties of a ferroelastic domain twin and the reversed twin with compatible walls of a given orientation and with domain states S_1^+ , S_j^- and S_1^- , S_j^+ . This group can be used for designating a twin law of the ferroelastic domain twin.

\bar{I}_{ij}^* : one non-trivial twinning operation of the twin $S_1[ABC]S_j$ and the wall. An underlined symbol with a star symbol signifies an operation that inverts the wall normal and exchanges the domain states (see the next section).

\bar{T}_{ij} : layer-group symmetry of the ferroelastic domain twin and the reversed twin with compatible walls of a given orientation. Contains all trivial and non-trivial symmetry operations of the domain twin (see the next section).

Classification: symbol that specifies the type of domain twin and the wall. Five types of twins and domain walls are given in Table 3.4.4.3. The letter S denotes a symmetric domain twin (wall) in which the structures in two half-spaces are related by a symmetry operation of the twin, A denotes an asymmetric twin where there is no such relation. The letters R (reversible) and I (irreversible) signify whether a twin and reversed twin are, or are not, crystallographically equivalent in K_{ij} .

Example 3.4.3.7. The rhombohedral phase of perovskite crystals. Examples include PZN-PT and PMN-PT solid solutions (see *e.g.* Erhart & Cao, 2001) and BaTiO_3 below 183 K. The phase transition has symmetry descent $m\bar{3}m \supset 3m$.

In Table 3.4.2.7 we find that there are eight domain states and eight ferroelectric domain states. In this fully ferroelectric phase, domain states can be specified by unit vectors representing the direction of spontaneous polarization. We choose $S_1 \equiv [111]$ with corresponding symmetry group $F_1 = 3_p m_{z\bar{y}}$.

From eight domain states one can form $7 \times 8 = 56$ domain pairs. These pairs can be divided into classes of equivalent pairs which are specified by different twinning groups. In column K_{ij} of Table 3.4.2.7 we find three twinning groups:

(i) The first twin law $\bar{3}_p m_{x\bar{y}}$ characterizes a non-ferroelastic pair ($\text{Fam} \bar{3}_p m_{x\bar{y}} = \text{Fam} \bar{3}_p^* m_{x\bar{y}}$) with inversion $\bar{1}$ as a twinning operation of this pair. A representative domain pair is $(S_1, g_{12} S_1 = S_2) = ([111], [\bar{1}\bar{1}\bar{1}])$, domain pairs consist of two domain states with antiparallel spontaneous polarization (‘180° pairs’). Domain walls of low energy are not charged, *i.e.* they are parallel with the spontaneous polarization.

(ii) The second twinning group $K_{13} = \bar{4}3m$ characterizes a ferroelastic domain pair ($\text{Fam} \bar{4}3m = m\bar{3}m \neq \text{Fam} F_1 = \bar{3}_p m_{z\bar{y}}$). In Table 3.4.3.6, we find $g_{13}^* = 2_x^*$, which defines the representative pair $([111], [\bar{1}\bar{1}\bar{1}])$ (‘109° pairs’). Orientations of compatible

Table 3.4.3.7. Ferroelastic domain pairs with no compatible domain walls

F_i is the symmetry of S_i , g_{ij} is the switching operation, K_{ij} is the twinning group. Pair is the domain pair type, where ns is non-transposable simple and nm is non-transposable multiple (see Table 3.4.3.2). $v = z$, $p = [111]$, $q = [\bar{1}\bar{1}\bar{1}]$, $r = [\bar{1}\bar{1}\bar{1}]$, $s = [\bar{1}\bar{1}\bar{1}]$ (see Table 3.4.2.5 and Fig. 3.4.2.3).

| F_i | g_{ij} | K_{ij} | Pair |
|-----------------|--------------------------|------------------------|------|
| 1 | 4_z | 4_z | ns |
| 1 | $\bar{4}_z$ | $\bar{4}_z$ | ns |
| 1 | 3_v | 3_v | ns |
| 1 | $\bar{3}_v$ | $\bar{3}_v$ | ns |
| 1 | 6_z | 6_z | ns |
| 1 | $\bar{6}_z$ | $\bar{6}_z$ | ns |
| $\bar{1}$ | $4_z, 4_z^3$ | $4_z/m_z$ | ns |
| $\bar{1}$ | $3_v, 3_v^2$ | $\bar{3}_v$ | ns |
| $\bar{1}$ | $6_z, 6_z^2$ | $6_z/m_z$ | ns |
| 2_z | $3_p, 3_p^2$ | $2_z 3_p$ | nm |
| 2_z | $\bar{3}_p, \bar{3}_p^2$ | $m_z \bar{3}_p$ | nm |
| 2_{xy} | $3_p, 3_p^2$ | $4_z 3_p 2_{xy}$ | nm |
| 2_{xy} | $\bar{3}_p, \bar{3}_p^2$ | $m_z \bar{3}_p m_{xy}$ | nm |
| m_z | $3_p, 3_p^2$ | $m_z 3_p^2$ | nm |
| m_{xy} | $3_p, 3_p^2$ | $\bar{4}_z 3_p m_{xy}$ | nm |
| m_{xy} | $4_x, 4_x^3$ | $m_z \bar{3}_p m_{xy}$ | nm |
| $2_z/m_z$ | $3_p, 3_p^2$ | $m_z \bar{3}_p$ | nm |
| $2_{xy}/m_{xy}$ | $3_p, 3_p^2$ | $m_z \bar{3}_p m_{xy}$ | nm |
| $2_x 2_y 2_z$ | $3_p, 3_p^2$ | $2_z 3_p$ | ns |
| $2_x 2_y 2_z$ | $\bar{3}_p, \bar{3}_p^2$ | $m_z \bar{3}_p$ | ns |
| $m_x m_y 2_z$ | $3_p, 3_p^2$ | $m_z \bar{3}_p$ | nm |
| $m_x m_y m_z$ | $3_p, 3_p^2$ | $m_z \bar{3}_p$ | ns |

domain walls of this domain pair are (100) and (011)_e (this wall is charged). All equivalent orientations of these compatible walls will appear if all crystallographically equivalent pairs are considered.

(iii) The third twinning group $K_{14} = m\bar{3}m$ also represents ferroelastic domain pairs with representative pair $([111], m_x^*[111]) = ([111], [\bar{1}\bar{1}\bar{1}])$ (‘71° pairs’) and compatible wall orientations (100)_e and (011). We see that for a given crystallographic orientation both charged and non-charged domain walls exist; for a given orientation the charge specifies to which class the domain wall belongs.

These conclusions are useful in deciphering the ‘domain-engineered structures’ of these crystals (Yin & Cao, 2000).

3.4.3.6.5. Ferroelastic domain pairs with no compatible domain walls, synoptic table

Ferroelastic domain pairs for which condition (3.4.3.54) for the existence of coherent domain walls is violated are listed in Table 3.4.3.7. All these pairs are non-transposable pairs. It is expected that domain walls between ferroelastic domain states would be stressed and would contain dislocations. Dudnik & Shuvalov (1989) have shown that in thin samples, where elastic stresses are reduced, ‘almost coherent’ ferroelastic domain walls may exist.

Example 3.4.3.8. Ferroelastic crystal of langbeinite. Langbeinite $\text{K}_2\text{Mg}_2(\text{SO}_4)_3$ undergoes a phase transition with symmetry descent $23 \supset 222$ that appears in Table 3.4.3.7. The ferroelastic phase has three ferroelastic domain states. Dudnik & Shuvalov (1989) found, in accord with their theoretical predictions, nearly linear ‘almost coherent’ domain walls accompanied by elastic stresses in crystals thinner than 0.5 mm. In thicker crystals, elastic stresses became so large that crystals were cracking and no domain walls were observed.

Similar effects were reported by the same authors for the partial ferroelastic phase of $\text{CH}_3\text{NH}_3\text{Al}(\text{SO}_4)_2 \cdot 12\text{H}_2\text{O}$ (MASD)

3.4. DOMAIN STRUCTURES

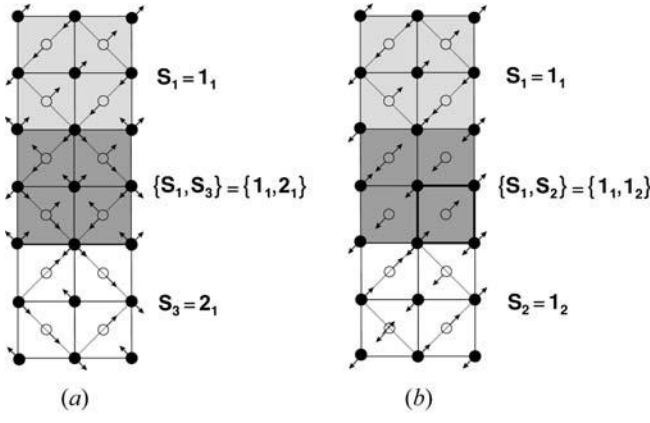


Fig. 3.4.3.10. Domain pairs in calomel. Single-domain states in the parent clamping approximation are those from Fig. 3.4.2.5. The first domain state of a domain pair is shown shaded in grey ('black'), the second domain state is colourless ('white'), and the domain pair of two interpenetrating domain states is shown shaded in dark grey. (a) Ferroelastic domain pair (S_1, S_3) in the parent clamping approximation. This is a partially transposable domain pair. (b) Translational domain pair (S_1, S_2) . This is a completely transposable domain pair.

with symmetry descent $\bar{3}m \supset mmm$, where ferroelastic domain walls were detected only in thin samples.

3.4.3.7. Domain pairs in the microscopic description

In the *microscopic description*, two microscopic domain states S_i and S_k with space-group symmetries \mathcal{F}_i and \mathcal{F}_k , respectively, can form an ordered domain pair (S_i, S_k) and an unordered domain pair $\{S_i, S_k\}$ in a similar way to in the continuum description, but one additional aspect has to be considered. The definition of the symmetry group \mathcal{F}_{ik} of an ordered domain pair (S_i, S_k) ,

$$\mathcal{F}_{ik} = \mathcal{F}_i \cap \mathcal{F}_k, \quad (3.4.3.72)$$

is meaningful only if the group \mathcal{F}_{ik} is a space group with a three-dimensional translational subgroup (three-dimensional *twin lattice* in the classical description of twinning, see Section 3.3.8)

$$\mathcal{T}_{ik} = \mathcal{T}_i \cap \mathcal{T}_k, \quad (3.4.3.73)$$

where \mathcal{T}_i and \mathcal{T}_k are translation subgroups of \mathcal{F}_i and \mathcal{F}_k , respectively. This condition is fulfilled if both domain states S_i and S_k have the same spontaneous strains, *i.e.* in non-ferroelastic domain pairs, but in ferroelastic domain pairs one has to suppress spontaneous deformations by applying the parent clamping approximation [see Section 3.4.2.2, equation (3.4.2.49)].

Example 3.4.3.9. Domain pairs in calomel. Calomel undergoes a non-equitranslational phase transition from a tetragonal parent phase to an orthorhombic ferroelastic phase (see Example 3.4.2.7 in Section 3.4.2.5). Four basic microscopic single-domain states are displayed in Fig. 3.4.2.5. From these states, one can form 12 non-trivial ordered single-domain pairs that can be partitioned (by means of double coset decomposition) into two orbits of domain pairs.

Representative domain pairs of these orbits are depicted in Fig. 3.4.3.10, where the first microscopic domain state S_i participating in a domain pair is displayed in the upper cell (light grey) and the second domain state S_j , $j = 2, 3$, in the lower white cell. The overlapping structure in the middle (dark grey) is a geometrical representation of the domain pair $\{S_i, S_j\}$.

The domain pair $\{S_1, S_3\}$, depicted in Fig. 3.4.3.10(a), is a ferroelastic domain pair in the parent clamping approximation. Then two overlapping structures of the domain pair have a common three-dimensional lattice with a common unit cell (the

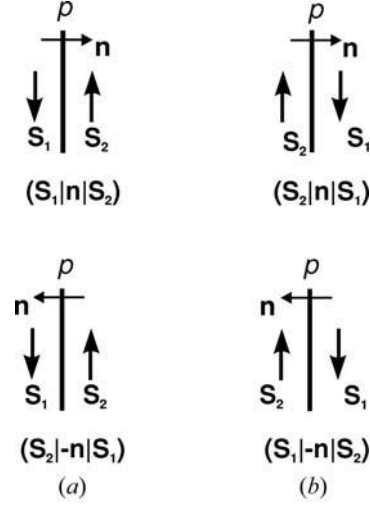


Fig. 3.4.4.1. Symbols of a simple twin. (a) Two different symbols with antiparallel normal \mathbf{n} . (b) Symbols of the reversed twin.

dotted square), which is the same as the unit cells of domain states S_1 and S_3 .

Domain pair $\{S_1, S_2\}$, shown in Fig. 3.4.3.10(b), is a translational (antiphase) domain pair in which domain states S_1 and S_2 differ only in location but not in orientation. The unit cell (heavily outlined small square) of the domain pair $\{S_1, S_2\}$ is identical with the unit cell of the tetragonal parent phase (*cf.* Fig. 3.4.2.5).

The two arrows attached to the circles in the domain pairs represent exaggerated displacements within the wall.

Domain pairs represent an intermediate step in analyzing microscopic structures of domain walls, as we shall see in Section 3.4.4.

3.4.4. Domain twins and domain walls

3.4.4.1. Formal description of simple domain twins and planar domain walls of zero thickness

In this section, we examine crystallographic properties of planar compatible domain walls and simple domain twins. The symmetry of these objects is described by layer groups. Since this concept is not yet common in crystallography, we briefly explain its meaning in Section 3.4.4.2. The exposition is performed in the continuum description, but most of the results apply with slight generalizations to the microscopic treatment that is illustrated with an example in Section 3.4.4.7.

We shall consider a *simple domain twin* \mathbf{T}_{12} that consists of two domains \mathbf{D}_1 and \mathbf{D}_2 which meet along a planar domain wall \mathbf{W}_{12} of zero thickness. Let us denote by p a *plane of the domain wall*, in brief *wall plane* of \mathbf{W}_{12} . This plane is specified by Miller indices (hkl) , or by a normal \mathbf{n} to the plane which also defines the sidedness (plus and minus side) of the plane p . By *orientation of the plane* p we shall understand a specification which can, but may not, include the sidedness of p . If both the orientation and the sidedness are given, then the plane p divides the space into two half-spaces. Using the bra-ket symbols, mentioned in Section 3.4.3.6, we shall denote by $(|$ the half-space on the negative side of p and by $|)$ the half-space on the positive side of p .

A *simple twin* consists of two (theoretically semi-infinite) domains \mathbf{D}_1 and \mathbf{D}_2 with domain states S_1 and S_2 , respectively, that join along a planar domain wall the orientation of which is specified by the wall plane p with normal \mathbf{n} . A symbol $(S_1|\mathbf{n}|S_2)$ specifies the domain twin unequivocally: domain $(S_1|$, with domain region $(|$ filled with domain state S_1 , is on the negative side of p and domain $|S_2)$ is on the positive side of p (see Fig. 3.4.4.1a).

3. PHASE TRANSITIONS, TWINNING AND DOMAIN STRUCTURES

If we were to choose the normal of opposite direction, *i.e.* $-\mathbf{n}$, the same twin would have the symbol $(\mathbf{S}_2 | -\mathbf{n} | \mathbf{S}_1)$ (see Fig. 3.4.4.1a). Since these two symbols signify the same twin, we have the identity

$$(\mathbf{S}_1 | \mathbf{n} | \mathbf{S}_2) \equiv (\mathbf{S}_2 | -\mathbf{n} | \mathbf{S}_1). \quad (3.4.4.1)$$

Thus, if we invert the normal \mathbf{n} and simultaneously exchange domain states \mathbf{S}_1 and \mathbf{S}_2 in the twin symbol, we obtain an identical twin (see Fig. 3.4.4.1a). This identity expresses the fact that the specification of the twin by the symbol introduced above does not depend on the chosen direction of the wall normal \mathbf{n} .

The full symbol of the twin can be replaced by a shorter symbol $\mathbf{T}_{12}(\mathbf{n})$ if we accept a simple convention that the first lower index signifies the domain state that occupies the half space (|) on the negative side of \mathbf{n} . Then the identity (3.4.4.1) in short symbols is

$$\mathbf{T}_{12}(\mathbf{n}) \equiv \mathbf{T}_{21}(-\mathbf{n}). \quad (3.4.4.2)$$

If the orientation and sidedness of the plane p of a wall is known from the context or if it is not relevant, the specification of \mathbf{n} in the symbol of the domain twin and domain wall can be omitted.

A twin $(\mathbf{S}_1 | \mathbf{n} | \mathbf{S}_2)$, or $\mathbf{T}_{12}(\mathbf{n})$, can be formed by sectioning the ordered domain pair $(\mathbf{S}_1, \mathbf{S}_2)$ by a plane p with normal \mathbf{n} and removing the domain state \mathbf{S}_2 on the negative side and domain state \mathbf{S}_1 on the positive side of the normal \mathbf{n} . This is the same procedure that is used in bicrystallography when an ideal bicrystal is derived from a dichromatic complex (see Section 3.2.2).

A twin with reversed order of domain states is called a *reversed twin*. The symbol of the twin reversed to the initial twin $(\mathbf{S}_1 | \mathbf{n} | \mathbf{S}_2)$ is

$$(\mathbf{S}_2 | \mathbf{n} | \mathbf{S}_1) \equiv (\mathbf{S}_1 | -\mathbf{n} | \mathbf{S}_2) \quad (3.4.4.3)$$

or

$$\mathbf{T}_{21}(\mathbf{n}) \equiv \mathbf{T}_{12}(-\mathbf{n}). \quad (3.4.4.4)$$

A reversed twin $(\mathbf{S}_2 | \mathbf{n} | \mathbf{S}_1) \equiv (\mathbf{S}_1 | -\mathbf{n} | \mathbf{S}_2)$ is depicted in Fig. 3.4.4.1(b).

A *planar domain wall* is the interface between the domains \mathbf{D}_1 and \mathbf{D}_2 of the associated simple twin. Even a domain wall of zero thickness is specified not only by its orientation in space but also by the domain states that adhere to the minus and plus sides of the wall plane p . The symbol for the wall is, therefore, analogous to that of the twin, only in the explicit symbol the brackets () are replaced by square brackets [] and \mathbf{T} in the short symbol is replaced by \mathbf{W} :

$$[\mathbf{S}_1 | \mathbf{n} | \mathbf{S}_2] \equiv [\mathbf{S}_2 | -\mathbf{n} | \mathbf{S}_1] \quad (3.4.4.5)$$

or by a shorter equivalent symbol

$$\mathbf{W}_{12}(\mathbf{n}) \equiv \mathbf{W}_{21}(-\mathbf{n}). \quad (3.4.4.6)$$

3.4.4.2. Layer groups

An adequate concept for characterizing symmetry properties of simple domain twins and planar domain walls is that of layer groups. A layer group describes the symmetry of objects that exist in a three-dimensional space and have two-dimensional translation symmetry. Typical examples are two-dimensional planes in three-dimensional space [two-sided planes and sectional layer groups (Holser, 1958a,b), domain walls and interfaces of zero thickness], layers of finite thickness (*e.g.* domain walls and interfaces of finite thickness) and two semi-infinite crystals joined along a planar and coherent (compatible) interface [*e.g.* simple domain twins with a compatible (coherent) domain wall, bicrystals].

Table 3.4.4.1. Crystallographic layer groups with continuous translations

| International | Non-coordinate |
|---------------|-------------------------------|
| 1 | 1 |
| $\bar{1}$ | $\bar{1}$ |
| 112 | 2 |
| 11m | \underline{m} |
| 112/m | $2/\underline{m}$ |
| 211 | $\underline{2}$ |
| m11 | \underline{m} |
| 2/m11 | $\underline{2}/\underline{m}$ |
| 222 | $\underline{222}$ |
| mm2 | $\underline{mm2}$ |
| m2m | $\underline{m2m}$ |
| mmm | \underline{mmm} |
| 4 | 4 |
| $\bar{4}$ | $\bar{4}$ |
| 4/m | $4/\underline{m}$ |
| 422 | $\underline{422}$ |
| 4mm | $\underline{4mm}$ |
| $\bar{4}2m$ | $\bar{4}\underline{2m}$ |
| 4/mmm | $4/\underline{mmm}$ |
| 3 | 3 |
| $\bar{3}$ | $\bar{3}$ |
| 32 | $\underline{32}$ |
| 3m | $\underline{3m}$ |
| $\bar{3}m$ | $\bar{3}\underline{m}$ |
| 6 | 6 |
| $\bar{6}$ | $\bar{6}$ |
| 6/m | $6/\underline{m}$ |
| 622 | $\underline{622}$ |
| 6mm | $\underline{6mm}$ |
| $\bar{6}m2$ | $\bar{6}\underline{m2}$ |
| 6/mmm | $6/\underline{mmm}$ |

A *crystallographic layer group* comprises symmetry operations (isometries) that leave invariant a chosen crystallographic plane p in a crystalline object. There are two types of such operations:

(i) *side-preserving operations* keep invariant the normal \mathbf{n} of the plane p , *i.e.* map each side of the plane p onto the same side. This type includes translations (discrete or continuous) in the plane p , rotations of $360^\circ/n$, $n = 2, 3, 4, 6$, around axes perpendicular to the plane p , reflections through planes perpendicular to p and glide reflections through planes perpendicular to p with glide vectors parallel to p . The corresponding symmetry elements are not related to the location of the plane p in space, *i.e.* they are the same for all planes parallel to p .

(ii) *side-reversing operations* invert the normal \mathbf{n} of the plane *i.e.* exchange sides of the plane. Operations of this type are: an inversion through a point in the plane p , rotations of $360^\circ/n$, $n = 3, 4, 6$ around axes perpendicular to the plane followed by inversion through this point, 180° rotation and 180° screw rotation around an axis in the plane p , reflection and glide reflections through the plane p , and combinations of these operations with translations in the plane p . All corresponding symmetry elements are located in the plane p .

A layer group \mathcal{L} consists of two parts:

$$\mathcal{L} = \hat{\mathcal{L}} \cup \underline{s}\hat{\mathcal{L}}, \quad (3.4.4.7)$$

where $\hat{\mathcal{L}}$ is a subgroup of \mathcal{L} that comprises all side-preserving operations of \mathcal{L} ; this group is isomorphic to a plane group and is called a *trivial layer group* or a *face group*. An underlined character \underline{s} denotes a side-reversing operation and the left coset $\underline{s}\hat{\mathcal{L}}$ contains all side-reversing operations of \mathcal{L} . Since $\hat{\mathcal{L}}$ is a halving subgroup, the layer group \mathcal{L} can be treated as a dichromatic (black-and-white) group in which side-preserving operations are

3.4. DOMAIN STRUCTURES

colour-preserving operations and side-reversing operations are colour-exchanging operations.

There are 80 layer groups with discrete two-dimensional translation subgroups [for a detailed treatment see *IT E* (2002), or *e.g.* Vainshtein (1994), Shubnikov & Kopcik (1974), Holser (1958a)]. Equivalent names for these layer groups are *net groups* (Opechowski, 1986), *plane groups in three dimensions* (Grell *et al.*, 1989), *groups in a two-sided plane* (Holser, 1958a,b) and others.

To these layer groups there correspond 31 point groups that describe the symmetries of crystallographic objects with two-dimensional continuous translations. Holser (1958b) calls these groups *point groups in a two-sided plane*, Kopský (1993) coins the term *point-like layer groups*. We shall use the term 'layer groups' both for layer groups with discrete translations, used in a microscopic description, and for crystallographic 'point-like layer groups' with continuous translations in the continuum approach. The geometrical meaning of these groups is similar and most of the statements and formulae hold for both types of layer groups.

Crystallographic layer groups with a continuous translation group [point groups of two-sided plane (Holser, 1958b)] are listed in Table 3.4.4.1. The *international notation* corresponds to international symbols of layer groups with discrete translations; this notation is based on the Hermann–Mauguin (international) symbols of three-dimensional space groups, where the *c* direction is the direction of missing translations and the character '1' represents a symmetry direction in the plane with no associated symmetry element (see *IT E*, 2002).

In the *non-coordinate notation* (Janovec, 1981), side-reversing operations are underlined. Thus *e.g.* $\underline{2}$ denotes a 180° rotation around a twofold axis in the plane *p* and \underline{m} a reflection through this plane, whereas 2 is a side-preserving 180° rotation around an axis perpendicular to the plane and *m* is a side-preserving reflection through a plane perpendicular to the plane *p*. With exception of $\underline{1}$ and $\underline{2}$, the symbol of an operation specifies the orientation of the plane *p*. This notation allows one to signify layer groups with different orientations in one reference coordinate system. Another non-coordinate notation has been introduced by Shubnikov & Kopcik (1974).

If a crystal with point-group symmetry *G* is bisected by a crystallographic plane *p*, then all operations of *G* that leave the plane *p* invariant form a *sectional layer group* = $\overline{G(p)}$ of the plane *p* in *G*. Operations of the group $\overline{G(p)}$ can be divided into two sets [see equation (3.4.4.7)]:

$$\overline{G(p)} = \widehat{G(p)} \cup \underline{\widehat{G(p)}}, \quad (3.4.4.8)$$

where the trivial layer group $\widehat{G(p)}$ expresses the symmetry of the crystal face with normal **n**. These face symmetries are listed in *IT A* (2002), Part 10, for all crystallographic point groups *G* and all orientations of the plane expressed by Miller indices (*hkl*). The underlined operation \underline{g} is a side-reversing operation that inverts the normal **n**. The left coset $\underline{\widehat{G(p)}}$ contains all side-reversing operations of $\overline{G(p)}$.

The number n_p of planes symmetrically equivalent (in *G*) with the plane *p* is equal to the index of $\overline{G(p)}$ in *G*:

$$n_p = [G : \overline{G(p)}] = |G| : |\overline{G(p)}|. \quad (3.4.4.9)$$

Example 3.4.4.1. As an example, we find the sectional layer group of the plane (010) in the group $G = 4_z/m_x m_y m_z$ (see Fig. 3.4.2.2).

$$\begin{aligned} 4_z/m_x m_y m_z(010) &= m_x 2_y m_z \cup \underline{m_y} \{m_x 2_y m_z\} \\ &= m_x 2_y m_z \cup \{\underline{m_y}, \underline{2_z}, \underline{1}, \underline{2_x}\} \\ &= m_x \underline{m_y} m_z. \end{aligned} \quad (3.4.4.10)$$

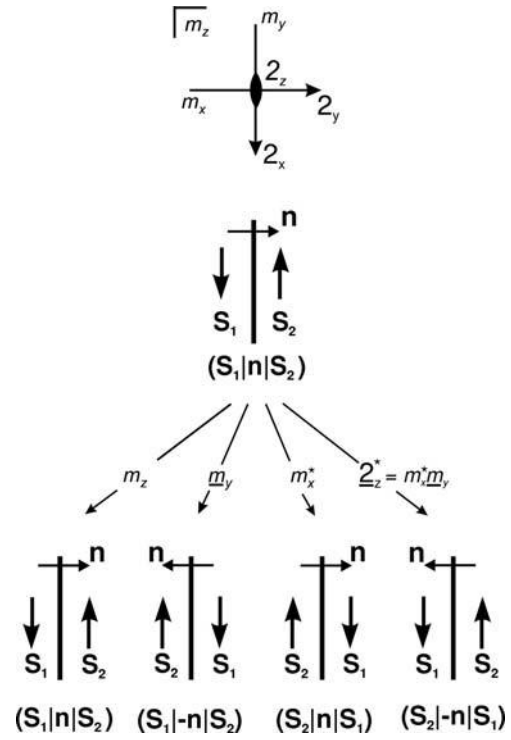


Fig. 3.4.4.2. A simple twin under the action of four types of operation that do not change the orientation of the wall plane *p*. Compare with Table 3.4.4.2.

In this example $n_p = |4_z/m_x m_y m_z| : |m_x \underline{m_y} m_z| = 16 : 8 = 2$ and the plane crystallographically equivalent with the plane (010) is the plane (100) with sectional symmetry $\underline{m_x} m_y m_z$.

3.4.4.3. Symmetry of simple twins and planar domain walls of zero thickness

We shall examine the symmetry of a twin $(S_1|n|S_2)$ with a planar zero-thickness domain wall with orientation and location defined by a plane *p* (Janovec, 1981; Zikmund, 1984; Zieliński, 1990). The symmetry properties of a planar domain wall W_{1j} are the same as those of the corresponding simple domain twin. Further, we shall consider twins but all statements also apply to the corresponding domain walls.

Operations that express symmetry properties of the twin must leave the orientation and location of the plane *p* invariant. We shall perform our considerations in the continuum description and shall assume that the plane *p* passes through the origin of the coordinate system. Then point-group symmetry operations leave the origin invariant and do not change the position of *p*.

If we apply an operation $g \in G$ to the twin $(S_1|n|S_2)$, we get a crystallographically equivalent twin $(S_1|n_m|S_k) \sim^G (S_1|n|S_2)$ with other domain states and another orientation of the domain wall,

$$g(S_1|n|S_2) = (gS_1|g n|gS_2) = (S_1|n_m|S_k), \quad g \in G. \quad (3.4.4.11)$$

It can be shown that the transformation of a domain pair by an operation $g \in G$ defined by this relation fulfils the conditions of an action of the group *G* on a set of all domain pairs formed from the orbit GS_1 (see Section 3.2.3.3). We can, therefore, use all concepts (stabilizer, orbit, class of equivalence *etc.*) introduced for domain states and also for domain pairs.

Operations *g* that describe symmetry properties of the twin $(S_1|n|S_2)$ must not change the orientation of the wall plane *p* but can reverse the sides of *p*, and must either leave invariant both domain states *S*₁ and *S*₂ or exchange these two states. There are four types of such operations and their action is summarized in Table 3.4.4.2. It is instructive to follow this action in Fig. 3.4.4.2

3. PHASE TRANSITIONS, TWINNING AND DOMAIN STRUCTURES

Table 3.4.4.2. Action of four types of operations g on a twin $(S_1|n|S_j)$

Operation g keeps the orientation of the plane p unchanged.

| g | gS_1 | gS_j | gn | $g(S_1 $ | $g S_j)$ | $g(S_1 n S_j) = (gS_1 gn gS_j)$ | Resulting twin |
|------------------------|--------|--------|------|----------|----------|-----------------------------------|----------------|
| f_{1j} | S_1 | S_j | n | $(S_1 $ | $ S_j)$ | $(S_1 n S_j)$ | Initial twin |
| \underline{s}_{1j} | S_1 | S_j | $-n$ | $(S_1 $ | $ S_j)$ | $(S_1 -n S_j) \equiv (S_j n S_1)$ | Reversed twin |
| r_{1j}^* | S_j | S_1 | n | $(S_j $ | $ S_1)$ | $(S_j n S_1)$ | Reversed twin |
| \underline{t}_{1j}^* | S_j | S_1 | $-n$ | $(S_j $ | $ S_1)$ | $(S_j -n S_1) \equiv (S_1 n S_j)$ | Initial twin |

using an example of the twin $(S_1[010]S_2)$ with domain states S_1 and S_2 from our illustrative example (see Fig. 3.4.2.2).

(1) An operation f_{1j} which leaves invariant the normal n and both domain states S_1, S_j in the twin $(S_1|n|S_j)$; such an operation does not change the twin and is called the *trivial symmetry operation of the twin*. An example of such an operation of the twin $(S_1[010]S_2)$ in Fig. 3.4.4.2 is the reflection m_z .

(2) An operation \underline{s}_{1j} which inverts the normal n but leaves invariant both domain states S_1 and S_j . This *side-reversing operation* transforms the initial twin $(S_1|n|S_j)$ into $(S_1|-n|S_j)$, which is, according to (3.4.4.1), identical with the inverse twin $(S_j|n|S_1)$. As in the non-coordinate notation of layer groups (see Table 3.4.4.1) we shall underline the side-reversing operations. The reflection \underline{m}_y in Fig. 3.4.4.2 is an example of a side-reversing operation.

(3) An operation r_{1j}^* which exchanges domain states S_1 and S_j but does not change the normal n . This *state-exchanging operation*, denoted by a star symbol, transforms the initial twin $(S_1|n|S_j)$ into a reversed twin $(S_j|n|S_1)$. A state-exchanging operation in our example is the reflection m_x^* .

(4) An operation \underline{t}_{1j}^* which inverts n and simultaneously exchanges S_1 and S_j . This operation, called the *non-trivial symmetry operation of a twin*, transforms the initial twin into $(S_j|-n|S_1)$, which is, according to (3.4.4.1), identical with the initial twin $(S_1|n|S_j)$. An operation of this type can be expressed as a product of a side-exchanging operation (underlined) and a state-exchanging operation (with a star), and will, therefore, be underlined and marked by a star. In Fig. 3.4.4.2, a non-trivial symmetry operation is for example the 180° rotation $\underline{2}_z^*$.

We note that the star and the underlining do not represent any operation; they are just suitable auxiliary labels that can be omitted without changing the result of the operation.

To find all trivial symmetry operations of the twin $(S_1|n|S_j)$, we recall that all symmetry operations that leave both S_1 and S_j invariant constitute the symmetry group F_{1j} of the ordered domain pair (S_1, S_j) , $F_{1j} = F_1 \cap F_j$, where F_1 and F_j are the symmetry groups of S_1 and S_j , respectively. The sectional layer group of the plane p in group F_{1j} is (if we omit p)

$$\bar{F}_{1j} = \hat{F}_{1j} \cup \underline{s}_{1j}\hat{F}_{1j}. \quad (3.4.4.12)$$

The trivial (side-preserving) subgroup \hat{F}_{1j} assembles all trivial symmetry operations of the twin $(S_1|n|S_j)$. The left coset $\underline{s}_{1j}\hat{F}_{1j}$, where \underline{s}_{1j} is a side-reversing operation, contains all side-reversing operations of this twin. In our example $\hat{F}_{12} = \{1, m_z\}$ and $\underline{s}_{1j}\hat{F}_{1j} = \underline{m}_y\{1, m_z\} = \{\underline{m}_y, \underline{2}_x\}$ (see Fig. 3.4.4.2).

Similarly, the left coset $r_{1j}^*\hat{F}_{1j}$ contains all state-exchanging operations, and $\underline{t}_{1j}^*\hat{F}_{1j}$ all non-trivial symmetry operations of the twin $(S_1|n|S_j)$. In the illustrative example, $r_{1j}^*\hat{F}_{1j} = m_x^*\{1, m_z\} = \{m_x^*, 2_y^*\}$ and $\underline{t}_{1j}^*\hat{F}_{1j} = \underline{2}_z^*\{1, m_z\} = \{\underline{2}_z^*, \underline{1}^*\}$.

The trivial group \hat{F}_{1j} and its three cosets constitute the sectional layer group \bar{J}_{1j} of the plane p in the symmetry group $J_{1j} = F_{1j} \cup g_{1j}^*F_{1j}$ of the unordered domain pair $\{S_1, S_j\}$,

$$\bar{J}_{1j} = \hat{J}_{1j} \cup \underline{s}_{1j}\hat{J}_{1j} = \hat{F}_{1j} \cup r_{1j}^*\hat{F}_{1j} \cup \underline{s}_{1j}\hat{F}_{1j} \cup \underline{t}_{1j}^*\hat{F}_{1j}, \quad (3.4.4.13)$$

where r_{1j}^* is an operation of the left coset $g_{1j}^*F_{1j}$ that leaves the normal n invariant and $\underline{t}_{1j}^* = \underline{s}_{1j}r_{1j}^*$.

Group \bar{J}_{1j} can be interpreted as a symmetry group of a *twin pair* $(S_1, S_j|n|S_j, S_1)$ consisting of a domain twin $(S_1|n|S_j)$ and a superposed reversed twin $(S_j|n|S_1)$ with a common wall plane p . This construct is analogous to a domain pair (dichromatic complex in bicrystallography) in which two homogeneous domain states S_1 and S_j are superposed (see Section 3.4.3.1). In the same way as the group J_{1j} of domain pair $\{S_1, S_j\}$ is divided into two cosets with different results of the action on this domain pair, the symmetry group \bar{J}_{1j} of the twin pair can be decomposed into four cosets (3.4.4.13), each of which acts on a domain twin $(S_j|n|S_1)$ in a different way, as specified in Table 3.4.4.2.

We can associate with operations from each coset in (3.4.4.13) a label. If we denote operations from \bar{F}_{1j} without a label by e , underlining by a and star by b , then the multiplication of labels is expressed by the relations

$$a^2 = b^2 = e, \quad ab = ba. \quad (3.4.4.14)$$

The four different labels e, a, b, ab can be formally viewed as four colours, the permutation of which is defined by relations (3.4.3.14); then the group \bar{J}_{1j} can be treated as a four-colour layer group.

Since the symbol of a point group consists of generators from which any operation of the group can be derived by multiplication, one can derive from the international symbol of a sectional layer group, in which generators are supplied with adequate labels, the coset decomposition (3.4.4.13).

Thus for the domain pair $\{S_1, S_2\}$ in Fig. 3.4.4.2 with $J_{12}^* = m_x^*m_y m_z$ [see equation (3.4.3.18)] and $p(010)$ we get the sectional layer group $\bar{J}_{12}(010) = m_x^*\underline{m}_y m_z$. Operations of this group (besides generators) are $m_x^*\underline{m}_y = \underline{2}_z^*$, $\underline{m}_y m_z = \underline{2}_x$, $m_x^* m_z = \underline{2}_y^*$, $m_x^*\underline{2}_x = \underline{1}^*$.

All operations $g \in G$ that transform a twin into itself constitute the *symmetry group* $T_{1j}(n)$ (or in short T_{1j}) of the twin $(S_1|n|S_j)$. This is a layer group consisting of two parts:

$$T_{1j} = \hat{F}_{1j} \cup \underline{t}_{1j}^*\hat{F}_{1j}, \quad (3.4.4.15)$$

where \hat{F}_{1j} is a face group comprising all trivial symmetry operations of the twin and the left coset $\underline{t}_{1j}^*\hat{F}_{1j}$ contains all non-trivial operations of the twin that reverse the sides of the wall plane p and simultaneously exchange the states $(S_1$ and $S_j)$.

One can easily verify that the symmetry $T_{1j}(n)$ of the twin $(S_1|n|S_j)$ is equal to the symmetry $T_{j1}(n)$ of the reversed twin $(S_j|n|S_1)$,

$$T_{1j}(n) = T_{j1}(n). \quad (3.4.4.16)$$

Similarly, for sectional layer groups,

$$\bar{F}_{1j}(n) = \bar{F}_{j1}(n) \quad \text{and} \quad \bar{J}_{1j}(n) = \bar{J}_{j1}(n). \quad (3.4.4.17)$$

Therefore, the symmetry of a twin $T_{1j}(p)$ and of sectional layer groups $\bar{F}_{1j}(p), \bar{J}_{1j}(p)$ is specified by the orientation of the plane p [expressed e.g. by Miller indices (hkl)] and not by the sidedness of p . However, the two layer groups $\bar{F}_{1j}(p)$ and $\bar{F}_{j1}(p)$, and $T_{1j}(p)$ and $T_{j1}(p)$ express the symmetry of *two different* objects, which can in special cases (non-transposable pairs and irreversible twins) be symmetrically non-equivalent.

The symmetry $T_{1j}(n)$ also expresses the symmetry of the wall $W_{1j}(n)$. This symmetry imposes constraints on the form of tensors

3.4. DOMAIN STRUCTURES

Table 3.4.4.3. Classification of domain walls and simple twins

| T_{ij} | \bar{J}_{ij} | Classification | Symbol |
|---|---|-----------------------------|--------|
| $\hat{F}_{ij} \cup \hat{L}_{ij}^* \hat{F}_{ij}$ | $\hat{F}_{ij} \cup \hat{L}_{ij}^* \hat{F}_{ij} \cup r_{ij}^* \hat{F}_{ij} \cup \hat{L}_{ij} \hat{F}_{ij}$ | Symmetric reversible | SR |
| $\hat{F}_{ij} \cup \hat{L}_{ij}^* \hat{F}_{ij}$ | $\hat{F}_{ij} \cup \hat{L}_{ij}^* \hat{F}_{ij}$ | Symmetric irreversible | SI |
| \hat{F}_{ij} | $\hat{F}_{ij} \cup \hat{L}_{ij} \hat{F}_{ij}$ | Asymmetric side-reversible | AR |
| \hat{F}_{ij} | $\hat{F}_{ij} \cup r_{ij}^* \hat{F}_{ij}$ | Asymmetric state-reversible | AR* |
| \hat{F}_{ij} | \hat{F}_{ij} | Asymmetric irreversible | AI |

describing the properties of walls. In this way, the appearance of spontaneous polarization in domain walls has been examined (Přivratská & Janovec, 1999; Přivratská *et al.*, 2000).

According to their symmetry, twins and walls can be divided into two types: For a *symmetric twin (domain wall)*, there exists a non-trivial symmetry operation \hat{L}_{ij}^* and its symmetry is expressed by equation (3.4.4.15). A symmetric twin can be formed only from transposable domain pairs.

For an *asymmetric twin (domain wall)*, there is no non-trivial symmetry operation and its symmetry group is, therefore, confined to trivial group \hat{F}_{ij} .

$$T_{ij} = \hat{F}_{ij}. \quad (3.4.4.18)$$

The difference between symmetric and asymmetric walls can be visualized in domain walls of finite thickness treated in Section 3.4.4.6.

The symmetry T_{ij} of a symmetric twin (wall), expressed by relation (3.4.4.15), is a layer group but not a sectional layer group of any point group. It can, however, be derived from the sectional layer group \bar{F}_{ij} of the corresponding ordered domain pair $\{S_1, S_j\}$ [see equation (3.4.4.12)] and the sectional layer group \bar{J}_{ij} of the unordered domain pair $\{S_1, S_j\}$ [see equation (3.4.4.13)],

$$T_{ij} = \bar{J}_{ij} - \{\bar{F}_{ij} - \hat{F}_{ij}\} - \{\hat{J}_{ij} - \hat{F}_{ij}\}. \quad (3.4.4.19)$$

This is particularly useful in the microscopic description, since sectional layer groups of crystallographic planes in three-dimensional space groups are tabulated in IT E (2002), where one also finds an example of the derivation of the twin symmetry in the microscopic description.

The treatment of twin (wall) symmetry based on the concept of domain pairs and sectional layer groups of these pairs (Janovec, 1981; Zikmund, 1984) is analogous to the procedure used in treating interfaces in bicrystals (see Section 3.2.2; Pond & Bollmann, 1979; Pond & Vlachavas, 1983; Kalonji, 1985; Sutton & Balluffi, 1995). There is the following correspondence between terms: domain pair \rightarrow dichromatic complex; domain wall \rightarrow interface; domain twin with zero-thickness domain wall \rightarrow ideal bicrystal; domain twin with finite-thickness domain wall \rightarrow real (relaxed) bicrystal. Terms used in bicrystallography cover more general situations than domain structures (e.g. grain boundaries of crystals with non-crystallographic relations, phase interfaces). On the other hand, the existence of a high-symmetry phase, which is missing in bicrystallography, enables a more detailed discussion of crystallographically equivalent variants (orbits) of various objects in domain structures.

The symmetry group T_{ij} is the stabilizer of a domain twin (wall) in a certain group, and as such determines a class (orbit) of domain twins (walls) that are crystallographically equivalent with this twin (wall). The number of crystallographically equivalent twins is equal to the number of left cosets (index) of T_{ij} in the corresponding group. Thus the number $n_{W(p)}$ of equivalent domain twins (walls) with the same orientation defined by a plane p of the wall is

$$n_{W(p)} = [\overline{G(p)} : T_{ij}] = |\overline{G(p)}| : |T_{ij}|, \quad (3.4.4.20)$$

where $\overline{G(p)}$ is a sectional layer group of the plane p in the parent group G , $[\overline{G(p)} : T_{ij}]$ is the index of T_{ij} in $\overline{G(p)}$ and absolute value denotes the number of operations in a group.

The set of all domain walls (twins) crystallographically equivalent in G with a given wall $[S_1 | n | S_j]$ forms a G -orbit of walls, $GW_{ij} \equiv G[S_1 | n | S_j]$. The number n_w of walls in this G -orbit is

$$\begin{aligned} n_w &= [G : T_{ij}] = |G| : |T_{ij}| = (|G| : |\overline{G(p)}|)(|\overline{G(p)}| : |T_{ij}|) \\ &= n_p n_{W(p)}, \end{aligned} \quad (3.4.4.21)$$

where n_p is the number of planes equivalent with plane p expressed by equation (3.4.4.9) and $n_{W(p)}$ is the number of equivalent domain walls with the plane p [see equation (3.4.4.20)]. Walls in one orbit have the same scalar properties (e.g. energy) and their structure and tensor properties are related by operations that relate walls from the same orbit.

Another aspect that characterizes twins and domain walls is the relation between a twin and the reversed twin. A twin (wall) which is crystallographically equivalent with the reversed twin (wall) will be called a *reversible twin (wall)*. If a twin and the reversed twin are not crystallographically equivalent, the twin will be called an *irreversible twin (wall)*. If a domain wall is reversible, then the properties of the reversed wall are fully specified by the properties of the initial wall, for example, these two walls have the same energy and their structures and properties are mutually related by a crystallographic operation. For irreversible walls, no relation exists between a wall and the reversed wall. Common examples of irreversible walls are electrically charged ferroelectric walls (walls carrying a nonzero polarization charge) and domain walls or discommensurations in phases with incommensurate structures.

A necessary and sufficient condition for reversibility is the existence of side-reversing and/or state-exchanging operations in the sectional layer group \bar{J}_{ij} of the unordered domain pair $\{S_1, S_j\}$ [see equation (3.4.4.13)]. This group also contains the symmetry group T_{ij} of the twin [see equation (3.4.4.15)] and thus provides a full symmetry characteristic of twins and walls,

$$\bar{J}_{ij} = T_{ij} \cup \hat{L}_{ij} \hat{F}_{ij} \cup \hat{L}_{ij}^* \hat{F}_{ij}. \quad (3.4.4.22)$$

Sequences of walls and reversed walls appear in simple lamellar domain structures which are formed by domains with two alternating domain states, say S_1 and S_2 , and parallel walls W_{12} and reversed walls W_{21} (see Fig. 3.4.2.1).

The distinction ‘symmetric–asymmetric’ and ‘reversible–irreversible’ provides a natural classification of domain walls and simple twins. *Five prototypes of domain twins and domain walls*, listed in Table 3.4.4.3, correspond to five subgroups of the sectional layer group \bar{J}_{ij} : the sectional layer group \bar{J}_{ij} itself, the layer group of the twin $T_{ij} = \hat{F}_{ij} \cup \hat{L}_{ij}^* \hat{F}_{ij}$, the sectional layer group $\bar{F}_{ij} = \hat{F}_{ij} \cup \hat{L}_{ij} \hat{F}_{ij}$, the trivial layer group $\hat{J}_{ij} = \hat{F}_{ij} \cup r_{ij}^* \hat{F}_{ij}$ and the trivial layer group \hat{F}_{ij} .

An example of a symmetric reversible (SR) twin (and wall) is the twin $(S_1[010]S_2)$ in Fig. 3.4.4.2 with a non-trivial twinning operation \hat{L}_{ij}^* and with reversing operations \hat{m}_{ij} and \hat{m}_{ij}^* . The twin $(S_1^+[110]S_3^-)$ and reversed twin $(S_3^-[110]S_1^+)$ in Fig. 3.4.3.8 are symmetric and irreversible (SI) twins with a twinning operation

3. PHASE TRANSITIONS, TWINNING AND DOMAIN STRUCTURES

Table 3.4.4.4. Symmetries of non-ferroelastic domain twins and walls

| T_{ij} | \bar{J}_{ij} | Classification |
|-----------------------------------|-----------------------------------|----------------|
| 1 | 1 | AI |
| 1 | $\bar{1}$ | AR |
| | $\underline{2}$ | AR |
| | 2^* | AR* |
| | m^* | AR* |
| $\bar{1}^*$ | $\bar{1}^*$ | SI |
| | $\underline{2}/m^*$ | SR |
| | $2^*/\underline{m}$ | SR |
| 2 | $2m^*m^*$ | AR* |
| $\underline{2}^*$ | $\underline{2}^*$ | SI |
| | $\underline{2}^*/m^*$ | SR |
| | $2^*\underline{2}^*\underline{2}$ | SR |
| | $\underline{2}^*\underline{m}m^*$ | SR |
| m | m | AI |
| | $\underline{2}/m$ | AR |
| | 2^*mm^* | AR* |
| \underline{m}^* | \underline{m}^* | SI |
| | $2^*/\underline{m}^*$ | SR |
| | $\underline{m}^*m^*\underline{2}$ | SR |
| $\underline{2}^*/m$ | $\underline{2}^*/m$ | SI |
| | $mm^*\underline{m}^*$ | SR |
| $2/\underline{m}^*$ | $2/\underline{m}^*$ | SI |
| | $m^*m^*\underline{m}^*$ | SR |
| | $4^*/\underline{m}^*$ | SR |
| $2\underline{2}^*\underline{2}^*$ | $2\underline{2}^*\underline{2}^*$ | SI |
| | $\underline{m}m^*m^*$ | SR |
| | $4^*2\underline{2}^*$ | SR |
| | $\bar{4}2^*m^*$ | SR |
| $\underline{m}^*m\underline{2}^*$ | $\underline{m}^*m\underline{2}^*$ | SI |
| | \underline{m}^*mm^* | SR |
| mmm^* | mmm^* | SI |
| | $4^*/\underline{m}^*m^*m$ | SR |
| 4 | $4m^*m^*$ | AR* |
| $\bar{4}^*$ | $\bar{4}^*2m^*$ | SR |
| $4/\underline{m}^*$ | $4/\underline{m}^*$ | SI |
| | $4/\underline{m}^*m^*m^*$ | SR |
| $4\underline{2}^*\underline{2}^*$ | $4\underline{2}^*\underline{2}^*$ | SI |
| | $4/\underline{m}m^*m^*$ | SR |
| $\bar{4}^*2^*m$ | $4^*/\underline{m}m^*m$ | SR |
| $4/\underline{m}^*mm$ | $4/\underline{m}^*mm$ | SI |
| 3 | $3m^*$ | AR* |
| | 6^* | AR* |
| $\bar{3}^*$ | $\bar{3}^*$ | SI |
| | $\bar{3}^*m^*$ | SR |
| | $6^*/\underline{m}$ | SR |
| $3m$ | 6^*mm^* | AR* |
| $3\underline{2}^*$ | $3\underline{2}^*$ | SI |
| | $\bar{3}m^*$ | SR |
| | $6^*2\underline{2}^*$ | SR |
| | $\bar{6}2^*m^*$ | SR |
| $\bar{3}^*m$ | $\bar{3}^*m$ | SI |
| | $6^*/\underline{m}m^*m^*$ | SR |
| 6 | $6m^*m^*$ | AR* |
| $\bar{6}^*$ | $\bar{6}^*$ | SI |
| | $6^*/\underline{m}^*$ | SR |
| | $\bar{6}^*2m^*$ | SR |
| $6/\underline{m}^*$ | $6/\underline{m}^*$ | SI |
| | $6/\underline{m}^*m^*m^*$ | SR |
| $6\underline{2}^*\underline{2}^*$ | $6\underline{2}^*\underline{2}^*$ | SI |
| | $6/\underline{m}m^*m^*$ | SR |
| $\bar{6}^*m\underline{2}^*$ | $\bar{6}^*m\underline{2}^*$ | SI |
| | $6^*/\underline{m}^*mm^*$ | SR |
| $6/\underline{m}^*mm$ | $6/\underline{m}^*mm$ | SI |

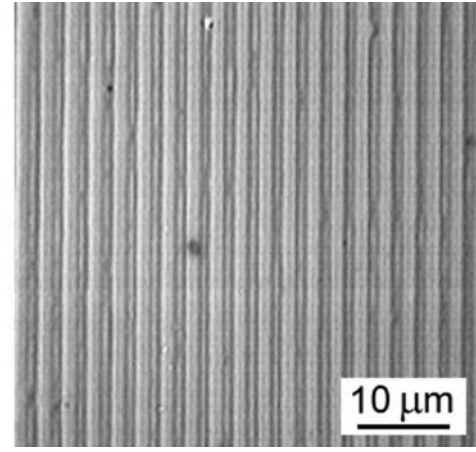


Fig. 3.4.4.3. Engineered periodic non-ferroelastic ferroelectric stripe domain structure within a lithium tantalate crystal with symmetry descent $\bar{6} \supset 3$. The domain structure is revealed by etching and observed in an optical microscope (Shur *et al.*, 2001). Courtesy of V.I. Shur, Ural State University, Ekaterinburg.

\underline{m}_{xy}^* ; no reversing operations exist (walls are charged and charged walls are always irreversible, since a charge is invariant with respect to any transformation of the space). The twin ($S_1^+[110]S_3^+$) and reversed twin ($S_3^+[110]S_1^-$) in the same figure are asymmetric state-reversible twins with state-reversing operation \underline{m}_{xy}^* and with no non-trivial twinning operation.

The same classification also applies to domain twins and walls in a microscopic description.

As in the preceding section, we shall now present separately the symmetries of non-ferroelastic simple domain twins [‘twinning without a change of crystal shape (or form)’] and of ferroelastic simple domain twins [‘twinning with a change of crystal shape (or form)’]; Klassen-Neklyudova (1964), Indenbom (1982)].

3.4.4.4. Non-ferroelastic domain twins and domain walls

Compatibility conditions impose no restriction on the orientation of non-ferroelastic domain walls. Any of the non-ferroelastic domain pairs listed in Table 3.4.3.4 can be sectioned on any crystallographic plane p and the sectional group \bar{J}_{ij} specifies the symmetry properties of the corresponding twin and domain wall. The analysis can be confined to one representative orientation of each class of equivalent planes, but a listing of all possible cases is too voluminous for the present article. We give, therefore, in Table 3.4.4.4 only possible symmetries T_{ij} and \bar{J}_{ij} of non-ferroelastic domain twins and walls, together with their classification, without specifying the orientation of the wall plane p .

Non-ferroelastic domain walls are usually curved with a slight preference for certain orientations (see Figs. 3.4.1.5 and 3.4.3.3). Such shapes indicate a weak anisotropy of the wall energy σ , *i.e.* small changes of σ with the orientation of the wall. The situation is different in ferroelectric domain structures, where charged domain walls have higher energies than uncharged ones.

A small energetic anisotropy of non-ferroelastic domain walls is utilized in producing *tailored domain structures* (Newnham *et al.*, 1975). A required domain pattern in a non-ferroelastic ferroelectric crystal can be obtained by evaporating electrodes of a desired shape (*e.g.* stripes) onto a single-domain plate cut perpendicular to the spontaneous polarization P_0 . Subsequent poling by an electric field switches only regions below the electrodes and thus produces the desired antiparallel domain structure.

Periodically poled ferroelectric domain structures fabricated by this technique are used for example in quasi-phase-matching optical multipliers (see *e.g.* Shur *et al.*, 1999, 2001; Rosenman *et*

3.4. DOMAIN STRUCTURES

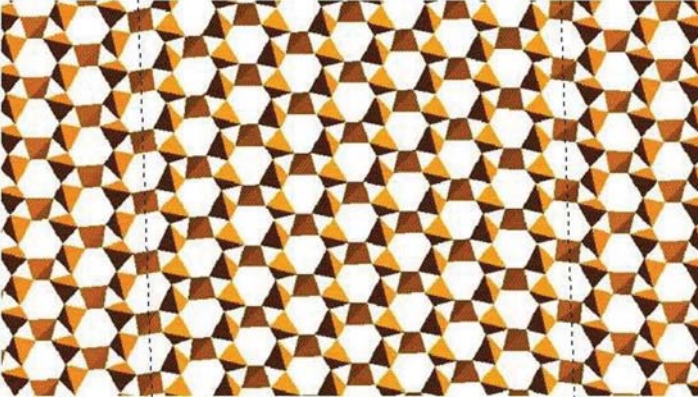


Fig. 3.4.4.4. Microscopic structure of two domain states and two parallel mutually reversed domain walls in the α phase of quartz. The left-hand vertical dotted line represents the domain wall W_{12} , the right-hand line is the reversed domain wall W_{21} . To the left of the left-hand line and to the right of the right-hand line are domains with domain state S_1 , the domain between the lines has domain state S_2 . For more details see text. Courtesy of M. Calleja, University of Cambridge.

al., 1998). An example of such an *engineered domain structure* is presented in Fig. 3.4.4.3.

Anisotropic domain walls can also appear if the Landau free energy contains a so-called Lifshitz invariant (see Section 3.1.3.3), which lowers the energy of walls with certain orientations and can be responsible for the appearance of an incommensurate phase (see e.g. Dolino, 1985; Tolédano & Tolédano, 1987; Tolédano & Dmitriev, 1996; Strukov & Levanyuk, 1998). The irreversible character of domain walls in a commensurate phase of crystals also containing (at least theoretically) an incommensurate phase has been confirmed in the frame of phenomenological theory by Ishibashi (1992). The incommensurate structure in quartz that demonstrates such an anisotropy is discussed at the end of the next example.

Example 3.4.4.2. Domain walls in α -phase of quartz. Quartz (SiO_2) undergoes a structural phase transition from the parent β phase (symmetry group $6_z 2_x 2_y$) to the ferroic α phase (symmetry $3_z 2_x$). The α phase can appear in two domain states S_1 and S_2 , which have the same symmetry $F_1 = F_2 = 3_z 2_x$. The symmetry J_{12} of the unordered domain pair $\{S_1, S_2\}$ is given by $J_{12}^* = 3_z 2_x \cup 2_y^* \{3_z 2_x\} = 6_z^* 2_x 2_y^*$.

Table 3.4.4.5 summarizes the results of the symmetry analysis of domain walls (twins). Each row of the table contains data for one representative domain wall $W_{12}(\mathbf{n}_{12})$ from one orbit $GW_{12}(\mathbf{n}_{12})$. The first column of the table specifies the normal \mathbf{n} of the wall plane p , further columns list the layer groups \widehat{F}_{12} , T_{12} and \bar{J}_{12} that describe the symmetry properties and classification of the wall (defined in Table 3.4.4.3), and n_w is the number of symmetrically equivalent domain walls [cf. equation (3.4.4.21)].

The last two columns give possible components of the spontaneous polarization \mathbf{P} of the wall $W_{12}(\mathbf{n})$ and the reversed wall $W_{21}(\mathbf{n})$. Except for walls with normals $[001]$ and $[100]$, all walls



Fig. 3.4.4.5. Transmission electron microscopy (TEM) image of the incommensurate triangular ($3 - q$ modulated) phase of quartz. The black and white triangles correspond to domains with domain states S_1 and S_2 , and the transition regions between black and white areas to domain walls (discommensurations). For a domain wall of a certain orientation there are no reversed domain walls with the same orientation but reversed order of black and white; the walls are, therefore, non-reversible. Domain walls in regions with regular triangular structures are related by 120 and 240° rotations about the z direction and carry parallel spontaneous polarizations (see text). Triangular structures in two regions (blocks) with different orientations of the triangles are related e.g. by 2_x and carry, therefore, antiparallel spontaneous polarizations and behave macroscopically as two ferroelectric domains with antiparallel spontaneous polarization. Courtesy of E. Snoeck, CEMES, Toulouse and P. Saint-Grégoire, Université de Toulon.

are polar, i.e. they can be spontaneously polarized. The reversal of the polarization in reversible domain walls requires the reversal of domain states. In irreversible domain walls, the reversal of W_{12} into W_{21} is accompanied by a change of the polarization \mathbf{P} into \mathbf{P}' , which may have a different absolute value and direction different to that of \mathbf{P} .

The structure of two domain states and two mutually reversed domain walls obtained by molecular dynamics calculations are depicted in Fig. 3.4.4.4 (Calleja *et al.*, 2001). This shows a projection on the ab plane of the structure represented by SiO_4 tetrahedra, in which each tetrahedron shares four corners. The threefold symmetry axes in the centres of distorted hexagonal channels and three twofold symmetry axes (one with vertical orientation) perpendicular to the threefold axes can be easily seen. The two vertical dotted lines are the wall planes p of two mutually reversed walls $[S_1[010]S_2] = W_{12}[010]$ and $[S_2[010]S_1] = W_{21}[010]$. In Table 3.4.4.5 we find that these walls have the symmetry $T_{12}[010] = T_{21}[010] = 2_x 2_y^* 2_z^*$, and in Fig. 3.4.4.4 we can verify that the operation 2_x is a ‘side-reversing’ operation \underline{s}_{12} of the wall (and the whole twin as wall), operation 2_y^* is a ‘state-exchanging operation’ r_{12}^* and the operation 2_z^* is a non-trivial ‘side-and-state reversing’ operation \underline{t}_{12}^* of the wall. The walls

Table 3.4.4.5. Symmetry properties of domain walls in quartz

| $ \mathbf{P} \neq \mathbf{P}' $, $P'_\alpha \neq -P_\alpha$, $\alpha = x, y, z$. | | | | | | | |
|---|--------------------|-------------------|-------------------|----------------|-------|----------------------|----------------------|
| \mathbf{n} | \widehat{F}_{12} | T_{12} | \bar{J}_{12} | Classification | n_w | $\mathbf{P}(W_{12})$ | $\mathbf{P}(W_{21})$ |
| [001] | 3_z | $3_z 2_y^*$ | $6_z^* 2_x 2_y^*$ | SR | 2 | | |
| [100] | 2_x | $2_x 2_y^* 2_z^*$ | $2_x 2_y^* 2_z^*$ | SI | 3 | | |
| [010] | 1 | 2_z^* | $2_x 2_y^* 2_z^*$ | SR | 6 | $0, 0, P_z$ | $0, 0, -P_z$ |
| [0vw] | 1 | 1 | 2_x | AR | 12 | P_x, P_y, P_z | $P_x, -P_y, -P_z$ |
| [u0w] | 1 | 2_y^* | 2_y^* | SI | 6 | $0, P_y, 0$ | $0, -P_y, 0$ |
| [uv0] | 1 | 2_z^* | 2_z^* | SI | 6 | $0, 0, P_z$ | $0, 0, P_z'$ |
| [uvw] | 1 | 1 | 1 | AI | 12 | P_x, P_y, P_z | P_x', P_y', P_z' |

3. PHASE TRANSITIONS, TWINNING AND DOMAIN STRUCTURES

Table 3.4.4.6. Symmetry properties of ferroelastic domain twins and compatible domain walls

| T_{ij} | \bar{J}_{ij} | Classification | | $K_{ij}[F_1]$ |
|-----------------------|-----------------------|----------------|-----|--|
| 1 | $\underline{2}$ | V | AR | $4^*[2], \bar{4}^*[2], 6[2], 6/m[2]$ |
| 1 | $\underline{2}$ | V | AR | |
| 1 | 2^* | W | AR* | { $2^*[1], 422[2], \bar{4}2m[m], 32[2], \bar{3}m[m], 622[2], \bar{6}m2[m],$ $432[222], m\bar{3}m[mm2], m\bar{3}m[2_{xy}][mm2]$ |
| 2^* | 2^* | V | SI | |
| 1 | 2^* | W | AR* | $23[3], 432[4], 432[3], m\bar{3}m[\bar{4}]$ |
| 2^* | 2^* | W | SI | |
| 1 | m^* | V | AR* | { $m^*[1], 4mm[m], \bar{4}2m[2], 3m[m], \bar{3}m[2], 6mm[m], \bar{6}m2[2],$ $43m[mm2], m\bar{3}m[222], m\bar{3}m[m^*_{xy}][m2m]$ |
| \underline{m}^* | \underline{m}^* | W | SI | |
| 1 | m^* | W | AR* | $m\bar{3}[3], \bar{4}3m[\bar{4}], \bar{4}3m[3], m\bar{3}m[4]$ |
| \underline{m}^* | 2^* | W | SI | |
| 2^* | 2^*2^*2 | W | SR | { $2^*2^*2[2], 4^*22^*[222], \bar{4}^*2^*m[mm2], 622[222], 6/mmm[mm2],$ $432[422], 432[32], m\bar{3}m[42m]$ |
| 2^* | 2^*2^*2 | W | SR | |
| 2^* | $2^*/m^*$ | V | SR | $2^*/m^*[\bar{1}], 4/mmm[2/m], \bar{3}m[2/m], 6/mmm[2/m],$ $m\bar{3}m[mmm]$ |
| \underline{m}^* | $2^*/\underline{m}^*$ | W | SR | |
| 2^* | $2^*/m^*$ | W | SR | $m\bar{3}[\bar{3}], m\bar{3}m[4/m], m\bar{3}m[\bar{3}]$ |
| \underline{m}^* | $2^*/\underline{m}^*$ | W | SR | |
| m | m | V | AI | $4/m[m], \bar{6}[m], 6/m[m]$ |
| m | m | V | AI | |
| m | $\underline{2}/m$ | V | AR | $4^*/m[2/m], 6/m[2/m]$ |
| m | $\underline{2}/m$ | V | AR | |
| \underline{m}^* | $m^*\underline{m}^*2$ | W | SR | { $m^*m^*2[2], 4^*mm^*[mm2], \bar{4}^*2m^*[222], 6mm[mm2],$ $6/mmm[222], 43m[42m], m\bar{3}m[422], m\bar{3}m[32]$ |
| \underline{m}^* | \underline{m}^*m^*2 | W | SR | |
| m | m^*2^*m | W | AR* | { $m^*2^*m[m], 4/mmm[2mm], \bar{6}m2[m2m], 6/mmm[m2m],$ $43m[3m], m\bar{3}m[4mm], m\bar{3}m[42m], m\bar{3}m[3m]$ |
| \underline{m}^*2^*m | \underline{m}^*2^*m | W | SI | |
| \underline{m}^*2^*m | \underline{m}^*m^*m | W | SR | { $m^*m^*m[2/m], 4^*/mmm^*[mmm], 6/mmm[mmm],$ $m\bar{3}m[4/mmm], m\bar{3}m[3m]$ |
| 2^*m^*m | m^*m^*m | W | SR | |

$\mathbf{W}_{12}[010]$ and $\mathbf{W}_{21}[010]$ are, therefore, symmetric and reversible walls.

During a small temperature interval above the appearance of the α phase at 846 K, there exists an incommensurate phase that can be treated as a regular domain structure, consisting of triangular columnar domains with domain walls (discommensurations) of negative wall energy σ (see *e.g.* Dolino, 1985). Both theoretical considerations and electron microscopy observations (see *e.g.* Van Landuyt *et al.*, 1985) show that the wall normal has the $[uv0]$ direction. From Table 3.4.4.5 it follows that there are six equivalent walls that are symmetric but irreversible, therefore any two equivalent walls differ in orientation.

This prediction is confirmed by electron microscopy in Fig. 3.4.4.5, where black and white triangles correspond to domains with domain states \mathbf{S}_1 and \mathbf{S}_2 , and the transition regions between black and white areas to domain walls (discommensurations). To a domain wall of a certain orientation no reversible wall appears with the same orientation but with a reversed order of black and white. Domain walls in homogeneous triangular parts of the structure are related by 120 and 240° rotations and carry, therefore, parallel spontaneous polarizations; wall orientations in two differently oriented blocks (the middle of the right-hand part and the rest on the left-hand side) are related by 180° rotations about the axis 2_x in the plane of the photograph and are, therefore, polarized in antiparallel directions (for more details see Saint-Grégoire & Janovec, 1989; Snoeck *et al.*, 1994). After cooling down to room temperature, the wall energy becomes positive and the regular domain texture changes into a coarse domain structure in which these six symmetry-related wall orientations still prevail (Van Landuyt *et al.*, 1985).

3.4.4.5. Ferroelastic domain twins and walls. Ferroelastic twin laws

As explained in Section 3.4.3.6, from a domain pair $(\mathbf{S}_1, \mathbf{S}_j)$ of ferroelastic single-domain states with two perpendicular equally deformed planes p and p' one can form four different ferroelastic

twins (see Fig. 3.4.3.8). Two mutually reversed twins $(\mathbf{S}_1|\mathbf{n}|\mathbf{S}_j)$ and $(\mathbf{S}_j|\mathbf{n}|\mathbf{S}_1)$ have the same twin symmetry $T_{ij}(p)$ and the same symmetry $\bar{J}_{ij}(p)$ of the twin pair $(\mathbf{S}_1, \mathbf{S}_j|\mathbf{n}|\mathbf{S}_j, \mathbf{S}_1)$. The *ferroelastic twin laws* can be expressed by the layer group $\bar{J}_{ij}(p)$ or, in a less complete way (without specification of reversibility), by the twin symmetry $T_{ij}(p)$. The same holds for two mutually reversed twins $(\mathbf{S}_1|\mathbf{n}'|\mathbf{S}_j)$ and $(\mathbf{S}_j|\mathbf{n}'|\mathbf{S}_1)$ with a twin plane p' perpendicular to p .

Table 3.4.4.6 summarizes possible symmetries T_{ij} of ferroelastic domain twins and corresponding ferroelastic twin laws \bar{J}_{ij} . Letters V and W signify strain-dependent and strain-independent (with a fixed orientation) domain walls, respectively. The classification of domain walls and twins is defined in Table 3.4.4.3. The last column contains twinning groups $K_{ij}[F_1]$ of ordered domain pairs $(\mathbf{S}_1, \mathbf{S}_j)$ from which these twins can be formed. The symbol of K_{ij} is followed by a symbol of the group F_1 given in square brackets. The twinning group $K_{ij}[F_1]$ specifies, up to two cases, a class of equivalent domain pairs [orbit $G(\mathbf{S}_1, \mathbf{S}_j)$] (see Section 3.4.3.4). More details on particular cases (orientation of domain walls, disorientation angle, twin axis) can be found in synoptic Table 3.4.3.6. From this table follow two general conclusions:

(1) All layer groups describing the symmetry of compatible ferroelastic domain walls are polar groups, therefore *all compatible ferroelastic domain walls in dielectric crystals can be spontaneously polarized*. The direction of the spontaneous polarization is parallel to the intersection of the wall plane p and the plane of shear (*i.e.* a plane perpendicular to the axis of the ferroelastic domain pair, see Fig. 3.4.3.5b and Section 3.4.3.6.2).

(2) *Domain twin $(\mathbf{S}_1|\mathbf{n}|\mathbf{S}_j)$ formed in the parent clamping approximation from a single-domain pair $(\mathbf{S}_1, \mathbf{S}_j)$ and the relaxed domain twin $(\mathbf{S}_1^+|\mathbf{n}|\mathbf{S}_j^-)$ with disoriented domain states have the same symmetry groups T_{ij} and \bar{J}_{ij} .*

This follows from simple reasoning: all twin symmetries T_{ij} in Table 3.4.4.6 have been derived in the parent clamping approximation and are expressed by the orthorhombic group $mm2$ or by some of its subgroups. As shown in Section 3.4.3.6.2, the maximal symmetry of a mechanically twinned crystal is also $mm2$. An

3.4. DOMAIN STRUCTURES

additional simple shear accompanying the lifting of the parent clamping approximation cannot, therefore, decrease the symmetry $\bar{T}_{ij}(p)$ derived in the parent clamping approximation. In a similar way, one can prove the statement for the group $\bar{J}_{ij}(p)$ of the twin pairs $(S_1, S_j | n | S_j, S_1)$ and $(S_1^+, S_j^- | n | S_j^-, S_1^+)$.

3.4.4.6. Domain walls of finite thickness – continuous description

A domain wall of zero thickness is a geometrical construct that enabled us to form a twin from a domain pair and to find a layer group that specifies the *maximal symmetry* of that twin. However, real domain walls have a finite, though small, thickness. Spatial changes of the structure within a wall may, or may not, lower the wall symmetry and can be conveniently described by a *phenomenological theory*.

We shall consider the simplest case of a one nonzero component η of the order parameter (see Section 3.1.2). Two nonzero equilibrium homogeneous values of $-\eta_0$ and $+\eta_0$ of this parameter correspond to two domain states S_1 and S_2 . Spatial changes of the order parameter in a domain twin $(S_1 | n | S_2)$ with a zero-thickness domain wall are described by a step-like function $\eta(\xi) = -\eta_0$ for $\xi < 0$ and $\eta(\xi) = +\eta_0$ for $\xi > 0$, where ξ is the distance from the wall of zero thickness placed at $\xi = 0$.

A domain wall of finite thickness is described by a function $\eta(\xi)$ with limiting values $-\eta_0$ and η_0 :

$$\lim_{\xi \rightarrow -\infty} \eta(\xi) = -\eta_0, \quad \lim_{\xi \rightarrow +\infty} \eta(\xi) = \eta_0. \quad (3.4.4.23)$$

If the wall is symmetric, then the profile $\eta(\xi)$ in one half-space, say $\xi < 0$, determines the profile in the other half-space $\xi > 0$. For continuous $\eta(\xi)$ fulfilling conditions (3.4.4.23) this leads to the condition

$$\eta(\xi) = -\eta(-\xi), \quad (3.4.4.24)$$

i.e. $\eta(\xi)$ must be an odd function. This requirement is fulfilled if there exists a non-trivial symmetry operation of a domain wall (twin): a side reversal ($\xi \rightarrow -\xi$) combined with an exchange of domain states [$\eta(\xi) \rightarrow -\eta(\xi)$] results in an identical wall profile.

A particular form of the wall profile $\eta(\xi)$ can be deduced from Landau theory. In the simplest case, the dependence $\eta(\xi)$ of the domain wall would minimize the free energy

$$\int_{-\infty}^{\infty} \left(\Phi_0 + \frac{1}{2} \alpha (T - T_c) \eta^2 + \frac{1}{4} \beta \eta^4 + \frac{1}{2} \delta \left(\frac{d^2 \eta}{d\xi^2} \right)^2 \right) d\xi, \quad (3.4.4.25)$$

where α , β , δ are phenomenological coefficients and T and T_c are the temperature and the temperature of the phase transition, respectively. The first three terms correspond to the homogeneous part of the Landau free energy (see Section 3.2.1) and the last term expresses the energy of the spatially changing order parameter. This variational task with boundary conditions (3.4.4.23) has the following solution (see e.g. Salje, 1990, 2000b; Ishibashi, 1990; Strukov & Levanyuk, 1998)

$$\eta(\xi) = \eta_0 \tanh(\xi/w), \quad (3.4.4.26)$$

where the value w specifies one half of the *effective thickness* $2w$ of the domain wall and is given by

$$w = \sqrt{2\delta/\alpha(T_c - T)}. \quad (3.4.4.27)$$

This dependence, expressed in relative dimensionless variables ξ/w and η/η_0 , is displayed in Fig. 3.4.4.6.

The wall profile $\eta(\xi)$ expressed by solution (3.4.4.26) is an odd function of ξ ,

$$\eta(-\xi) = \eta_0 \tanh(-\xi/w) = -\eta_0 \tanh(\xi/w) = -\eta(\xi), \quad (3.4.4.28)$$

and fulfils thus the condition (3.4.4.24) of a symmetric wall.

The wall thickness can be estimated from electron microscopy observations, or more precisely by a diffuse X-ray scattering

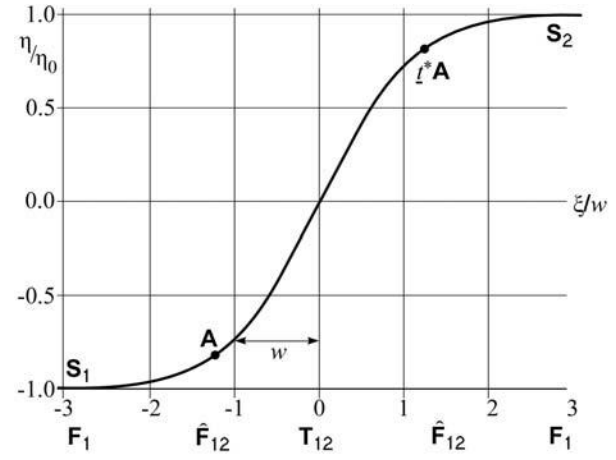


Fig. 3.4.4.6. Profile of the one-component order parameter $\eta(\xi)$ in a symmetric wall (S). The effective thickness of the wall is $2w$.

technique (Locherer *et al.*, 1998). The effective thickness $2w$ [see equation (3.4.4.26)] in units of crystallographic repetition length A normal to the wall ranges from $2w/A = 2$ to $2w/A = 12$, i.e. $2w$ is about 10–100 nm (Salje, 2000b). The temperature dependence of the domain wall thickness expressed by equation (3.4.4.27) has been experimentally verified, e.g. on LaAlO_3 (Chrosch & Salje, 1999).

The energy σ of the domain wall per unit area equals the difference between the energy of the twin and the energy of the single-domain crystal. For a one nonzero component order parameter with the profile (3.4.4.26), the wall energy σ is given by (Strukov & Levanyuk, 1998)

$$\sigma = \int_{-\infty}^{\infty} [\Phi(\eta(\xi)) - \Phi(\eta_0)] d\xi = \frac{2\sqrt{2}\delta}{3\beta} [\alpha(T_c - T)]^{3/2}, \quad (3.4.4.29)$$

where $2w$ is the effective thickness of the wall [see equation (3.4.4.27)] and the coefficients are defined in equation (3.4.4.25).

The order of magnitude of the wall energy σ of ferroelastic and non-ferroelastic domain walls is typically several millijoule per square metre (Salje, 2000b).

Example 3.4.4.3. In our example of a ferroelectric phase transition $4_z/m_z m_x m_{xy} \supset 2_x m_y m_z$, one can identify η with the P_1 component of spontaneous polarization and ξ with the axis y . One can verify in Fig. 3.4.4.6 that the symmetry $\bar{T}_{12}[010] = \bar{2}_z^*/m_z$ of the twin $(S_1[010]S_2)$ with a zero-thickness domain wall is retained in the domain wall with symmetric profile (3.4.4.26): both non-trivial symmetry operations $\bar{2}_z^*$ and $\bar{1}^*$ transform the profile $\eta(y)$ into an identical function.

This example illustrates another feature of a symmetric wall: All non-trivial symmetry operations of the wall are located at the central plane $\xi = 0$ of the finite-thickness wall. The sectional group \bar{T}_{12} of this plane thus expresses the *symmetry of the central layer* and also the *global symmetry* of a symmetric wall (twin). The *local symmetry* of the off-centre planes $\xi \neq 0$ is equal to the face group \bar{F}_{12} of the the layer group \bar{T}_{12} (in our example $\bar{F}_{12} = \{1, m_z\}$).

The relation between a wall profile $\eta(\xi)$ of a *symmetric reversible* (SR) wall and the profile $\eta^{\text{rev}}(\xi)$ of the reversed wall is illustrated in Fig. 3.4.4.7, where the dotted curve is the wall profile $\eta^{\text{rev}}(\xi)$ of the reversed wall. The profile $\eta^{\text{rev}}(\xi)$ of the reversed wall is completely determined by the the profile $\eta(\xi)$ of the initial wall, since both profiles are related by equations

$$\eta^{\text{rev}}(\xi) = -\eta(\xi) = \eta(-\xi). \quad (3.4.4.30)$$

3. PHASE TRANSITIONS, TWINNING AND DOMAIN STRUCTURES

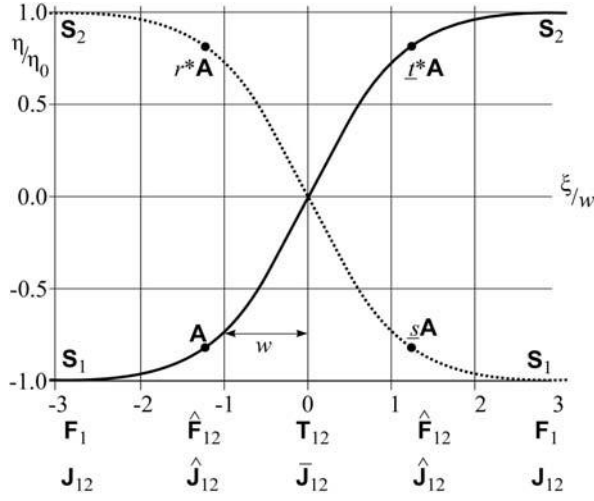


Fig. 3.4.4.7. Profiles of the one-component order parameter $\eta(\xi)$ in a symmetric wall (solid curve) and in the reversed wall (dotted curve). The wall is symmetric and reversible (SR).

The first part of the equation corresponds to a state-exchanging operation r_{12}^* (cf. point r^*A in Fig. 3.4.4.7) and the second one to a side-reversing operation s_{12} (point sA in the same figure). In a symmetric reversible wall, both types of reversing operations exist (see Table 3.4.4.3).

In a *symmetric irreversible* (SI) wall both initial and reversed wall profiles fulfil symmetry condition (3.4.4.24) but equations (3.4.4.30) relating both profiles do not exist. The profiles $\eta(\xi)$ and $\eta^{\text{rev}}(\xi)$ may differ in shape and surface wall energy. Charged domain walls are always irreversible.

A possible profile of an *asymmetric domain wall* is depicted in Fig. 3.4.4.8 (full curve). There is no relation between the negative part $\eta(\xi) < 0$ and positive part $\eta(\xi) > 0$ of the wall profile $\eta(\xi)$. Owing to the absence of non-trivial twin operations, there is no central plane with higher symmetry. The local symmetry (sectional layer group) at any location ξ within the wall is equal to the face group \hat{F}_{12} . This is also the global symmetry T_{12} of the entire wall, $T_{12} = \hat{F}_{12}$.

The dotted curve in Fig. 3.4.4.8 represents the reversed-wall profile of an *asymmetric state-reversible* (AR*) wall that is related to the initial wall by state-exchanging operations $r_{12}^* \hat{F}_{12}$ (see Table 3.4.4.5),

$$\eta^{\text{rev}}(\xi) = -\eta(\xi). \quad (3.4.4.31)$$

An example of an *asymmetric side-reversible* (AR) wall is shown in Fig. 3.4.4.9. In this case, an asymmetric wall (full curve) and reversed wall (dotted curve) are related by side-reversing operations $s_{12} \hat{F}_{12}$:

$$\eta^{\text{rev}}(\xi) = \eta(-\xi). \quad (3.4.4.32)$$

In an *asymmetric irreversible* (AI) wall, both profiles $\eta(\xi)$ and $\eta^{\text{rev}}(\xi)$ are asymmetric and there is no relation between these two profiles.

The *symmetry* $T_{12}(\eta)$ of a finite-thickness wall with a profile $\eta(\xi)$ is equal to or lower than the symmetry T_{12} of the corresponding zero-thickness domain wall, $T_{12} \supseteq T_{12}(\eta)$. A symmetry descent $T_{12} \supset T_{12}(\eta)$ can be treated as a phase transition in the domain wall (see e.g. Bul'bich & Gufan, 1989a,b; Sonin & Tagancev, 1989). There are $n_{W(\eta)}$ equivalent *structural variants of the finite-thickness domain wall* with the same orientation and the same energy but with different structures of the wall,

$$n_{W(\eta)} = [T_{12} : T_{12}(\eta)] = |T_{12}| : |T_{12}(\eta)|. \quad (3.4.4.33)$$

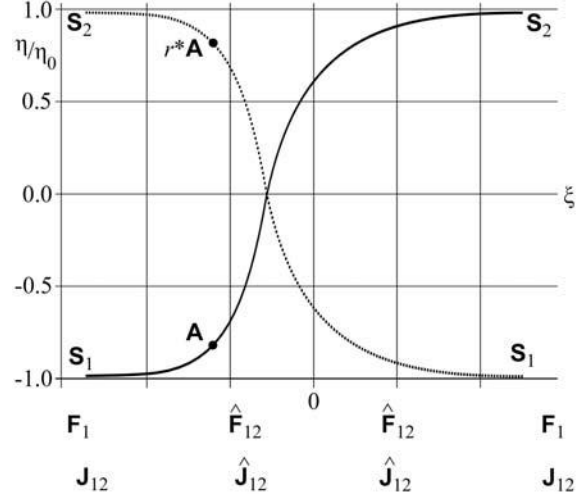


Fig. 3.4.4.8. Profiles of the one-component order parameter $\eta(\xi)$ in an asymmetric wall (solid curve) and in the reversed asymmetric wall (dotted curve). The wall is asymmetric and state-reversible (AR*).

Domain-wall variants – two-dimensional analogues of domain states – can coexist and meet along line defects – one-dimensional analogues of a domain wall (Tagancev & Sonin, 1989).

Symmetry descent in domain walls of finite thickness may occur if the order parameter η has more than one nonzero component. We can demonstrate this on ferroic phases with an order parameter with two components η_1 and η_2 . The profiles $\eta_1(\xi)$ and $\eta_2(\xi)$ can be found, as for a one-component order parameter, from the corresponding Landau free energy (see e.g. Cao & Barsch, 1990; Houchmandzadeh *et al.*, 1991; Ishibashi, 1992, 1993; Rychetský & Schranz, 1993, 1994; Schranz, 1995; Huang *et al.*, 1997; Strukov & Levanyuk, 1998; Hatt & Hatch, 1999; Hatch & Cao, 1999).

Let us denote by $T_{12}(\eta_1)$ the symmetry of the profile $\eta_1(\xi)$ and by $T_{12}(\eta_2)$ the symmetry of the profile $\eta_2(\xi)$. Then the symmetry of the entire wall $T_{12}(\eta)$ is a common part of the symmetries $T_{12}(\eta_1)$ and $T_{12}(\eta_2)$,

$$T_{12}(\eta) = T_{12}(\eta_1) \cap T_{12}(\eta_2). \quad (3.4.4.34)$$

Example 3.4.4.4. In our illustrative phase transition $4_z/m_z m_x m_{xy} \supset 2_x m_y m_z$, the order parameter has two components η_1, η_2 that can be associated with the x and y components P_1 and P_2 of the

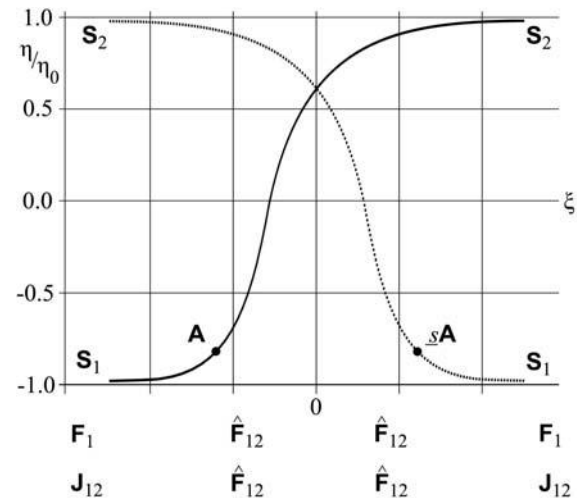


Fig. 3.4.4.9. Profiles of the one-component order parameter $\eta(\xi)$ in an asymmetric wall (solid curve) and in the reversed asymmetric wall (dotted curve). The wall is asymmetric and side-reversible (AR).

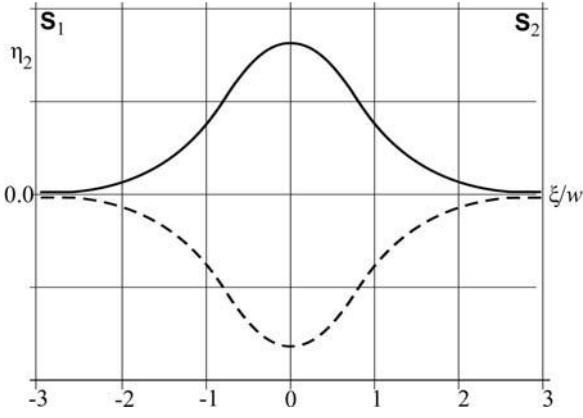


Fig. 3.4.4.10. A profile of the second order parameter component in a degenerate domain wall.

spontaneous polarization (see Table 3.1.3.1 and Fig. 3.4.2.2). We have seen that the domain wall $[S_1[010]S_2]$ of zero thickness has the symmetry $T_{12} = \underline{2}_z^*/m_z$. If one lets $\eta_1(y)$ relax and keeps $\eta_2(y) = 0$ (a so-called *linear structure*), then $T_{12}(\eta_1) = \underline{2}_z^*/m_z$ (see Fig. 3.4.4.2 with $\xi = y$). If the last condition is lifted, a possible profile of a relaxed $\eta_2(y)$ is depicted by the full curve in Fig. 3.4.4.10. If both components $\eta_1(y)$ and $\eta_2(y)$ are nonzero within the wall, one speaks about a *rotational structure* of domain wall. In this relaxed domain wall the spontaneous polarization rotates in the plane (001), resembling thus a Néel wall in magnetic materials. The even profile $\eta_2(-y) = \eta_2(y)$ has the symmetry $T_{12}(\eta_2) = m_x^* \underline{2}_y^* m_z$. Hence, according to (3.4.4.34), the symmetry of a relaxed wall with a rotational structure is $T_{12}(\eta) = \underline{2}_z^*/m_z \cap m_x^* \underline{2}_y^* m_z = \{1, m_z\}$. This is an asymmetric state-reversible (AR*) wall with two chiral variants [see equation (3.4.4.33)] that are related by $\underline{1}^*$ and $\underline{2}_z^*$; the profile $\eta_2(y)$ of the second variant is depicted in Fig. 3.4.4.10 by a dashed curve.

Similarly, one gets for a zero-thickness domain wall $[S_1[001]S_2]$ perpendicular to z the symmetry $T_{12} = \underline{2}_y^*/m_y$. For a relaxed domain wall with profiles $\eta_1(z)$ and $\eta_2(z)$, displayed in Figs. 3.4.4.6 and 3.4.4.10 with $\xi = z$, one gets $T_{12}(\eta_1) = \underline{2}_y^*/m_y$, $T_{12}(\eta_2) = m_x^* \underline{2}_y^* m_z$ and $T_{12}(\eta) = \{1, \underline{2}_y^*\}$. The relaxed domain wall with rotational structure has lower symmetry than the zero-thickness wall or the wall with linear structure, but remains a symmetric and reversible (SR) domain wall in which spontaneous polarization rotates in a plane (001), resembling thus a Bloch wall in magnetic materials. Two chiral right-handed and left-handed variants are related by operations m_z and $\underline{1}^*$. This example illustrates that the structure of domain walls may differ with the wall orientation.

We note that the stability of a domain wall with a rotational structure and with a linear structure depends on the values of the coefficients in the Landau free energy, on temperature and on external fields. In favourable cases, a phase transition from a symmetric linear structure to a less symmetric rotational structure can occur. Such phase transitions in domain walls have been studied theoretically by Bul'bich & Gufan (1989a,b) and by Sonin & Tagancev (1989).

3.4.4.7. Microscopic structure and symmetry of domain walls

The thermodynamic theory of domain walls outlined above is efficient in providing quantitative results (wall thickness, energy) in any specific material. However, since this is a continuum theory, it is not able to treat local structural changes on a microscopic level and, moreover, owing to the small thickness of domain walls (several lattice constants), the reliability of its conclusions is to some extent uncertain.

Discrete theories either use simplified models [e.g. pseudospin ANNNI (axial next nearest neighbour Ising) model] that yield

quantitative results on profiles, energies and interaction energies of walls but do not consider real crystal structures, or calculate numerically for a certain structure the atomic positions within a wall from interatomic potentials.

Symmetry analysis of domain walls provides useful qualitative conclusions about the microscopic structure of walls. Layer groups with discrete two-dimensional translations impose, *via* the site symmetries, restrictions on possible displacements and/or ordering of atoms or molecules. From these conclusions, combined with a reasonable assumption that these shifts or ordering vary continuously within a wall, one gets *topological constraints on the field of local displacements and/or ordering of atoms or molecules in the wall*. The advantage of this treatment is its simplicity and general validity, since no approximations or simplified models are needed. The analysis can also be applied to domain walls of zero thickness, where thermodynamic theory fails. However, this method does not yield any quantitative results, such as values of displacements, wall thickness, energy *etc*.

The procedure is similar to that in the continuum description. The main relations equations (3.4.4.12)–(3.4.4.17) and the classification given in Table 3.4.4.3 hold for a microscopic description as well; one has only to replace point groups by space groups.

A significant difference is that the sectional layer groups and the wall symmetry depend on the location of the plane p in the crystal lattice. This position can be expressed by a vector $s\mathbf{d}$, where \mathbf{d} is the *scanning vector* (see IT E, 2002 and the example below) and s is a non-negative number smaller than 1, $0 \leq s < 1$. An extended symbol of a twin in the microscopic description, corresponding to the symbol (3.4.4.1) in the continuum description, is

$$(S_1 | \mathbf{n}; s\mathbf{d} | S_2) \equiv (S_2 | -\mathbf{n}; s\mathbf{d} | S_1). \quad (3.4.4.35)$$

The main features of the analysis are demonstrated on the following example.

Example 3.4.4.5. Ferroelastic domain wall in calomel. We examine a ferroelastic compatible domain wall in a calomel crystal (Janovec & Zikmund, 1993; IT E, 2002, Chapter 5). In Section 3.4.2.5, Example 3.4.2.7, we found the microscopic domain states (see Fig. 3.4.2.5) and, in Section 3.4.3.7, the corresponding ordered domain pair (S_1, S_3) and unordered domain pair $\{S_1, S_3\}$ (depicted in Fig. 3.4.3.10). These pairs have symmetry groups $\mathcal{F}_{13} = Pn_{xy} \cdot n_{xy} m_z$ and $\mathcal{J}_{13} = P4_{2z}^*/m_z n_{xy} m_x^*$, respectively. Both groups have an orthorhombic basis $\mathbf{a}^o = \mathbf{a}' - \mathbf{b}'$, $\mathbf{b}^o = \mathbf{a}' + \mathbf{b}'$, $\mathbf{c}^o = \mathbf{c}'$, with a shift of origin $\mathbf{b}'/2$ for both groups.

Compatible domain walls in this ferroelastic domain pair have orientations (100) and (010) in the tetragonal coordinate system (see Table 3.4.3.6). We shall examine the former case – the latter is crystallographically equivalent. Sectional layer groups of this plane in groups \mathcal{F}_{13} and \mathcal{J}_{13} have a two-dimensional translation group (net) with basic vectors $\mathbf{a}^s = 2\mathbf{b}'$ and $\mathbf{b}^s = \mathbf{c}'$, and the scanning vector $\mathbf{d} = 2\mathbf{a}'$ expresses the repetition period of the layer structure (*cf.* Fig. 3.4.3.10a). From the diagram of symmetry elements of the group \mathcal{F}_{13} and \mathcal{J}_{13} , available in IT A (2002), one can deduce the sectional layer groups at any location $s\mathbf{d}$, $0 \leq s < 1$. These sectional layer groups are listed explicitly in IT E (2002) in the *scanning tables* of the respective space groups.

The resulting sectional layer groups $\overline{\mathcal{F}}_{13}$ and $\overline{\mathcal{J}}_{13}$ are given in Table 3.4.4.7 in two notations, in which the letter p signifies a two-dimensional net with the basic translations \mathbf{a}^s , \mathbf{b}^s introduced above. Standard symbols are related to the basis \mathbf{a}^s , \mathbf{b}^s , $\mathbf{c}^s = \mathbf{d}$. Subscripts in non-coordinate notation specify the orientation of symmetry elements in the reference Cartesian coordinate system of the tetragonal phase, the partial translation in the glide plane a and in the screw axis 2_1 is equal to $\frac{1}{2}\mathbf{a}^s = \mathbf{b}'$, *i.e.* the symbols a and 2_1 are also related to the basis \mathbf{a}^s , \mathbf{b}^s , \mathbf{c}^s . At special locations $s\mathbf{d} = 0\mathbf{d}$, $\frac{1}{2}\mathbf{d}$ and $s\mathbf{d} = \frac{1}{4}\mathbf{d}$, $\frac{3}{4}\mathbf{d}$, sectional groups contain both side-

3. PHASE TRANSITIONS, TWINNING AND DOMAIN STRUCTURES

Table 3.4.4.7. Sectional layer groups and twin (wall) symmetries of the twin ($S_1|[100]$; $sd|S_3$) in a calomel crystal

| Location sd | $\overline{\mathcal{F}}_{13}$ | | $\overline{\mathcal{J}}_{13}$ | | T_{13} | | Classification |
|------------------------------|-------------------------------|--------------------|-------------------------------|---------------------------|----------|-------------------------|----------------|
| | Standard | Non-coordinate | Standard | Non-coordinate | Standard | Non-coordinate | |
| $\frac{1}{4}d, \frac{3}{4}d$ | $p12/m1$ | $p2_z/m_z$ | $pmma$ | $pm_y^*m_z a_x^*$ | $p2_1ma$ | $p2_{\pm y}^*m_z a_x^*$ | SR |
| $0d, \frac{1}{4}d$ | $p12/m1^\dagger$ | $p2_z/m_z^\dagger$ | $pmmm^\dagger$ | $pm_y^*m_z m_x^*^\dagger$ | $p2nm$ | $p2_y^*m_z m_x^*$ | SR |
| sd | $p1m1$ | pm_z | $pm2$ | $p2_x^*m_y^*m_z$ | $p1m1$ | pm_z | AR* |

† Shift of origin $b_f/2$.

preserving and side-reversing operations, whereas for any other location sd these layer groups are trivial (face) layer groups consisting of side-preserving operations only and are, therefore, also called *floating groups* in the direction d (IT E, 2002).

The wall (twin) symmetry T_{13} can be easily deduced from sectional layer groups $\overline{\mathcal{F}}_{13}$ and $\overline{\mathcal{J}}_{13}$: the floating group $\widehat{\mathcal{F}}_{13}$ is just the sectional layer group $\overline{\mathcal{F}}_{13}$ at a general location, $\widehat{\mathcal{F}}_{13} = \overline{\mathcal{F}}_{13}(sd) = pm_z$. Two other generators in the group symbol of T_{13} are non-trivial twinning operations (underlined with a star) of $\overline{\mathcal{J}}_{13}$. The classification in the last column of Table 3.4.4.7 is defined in Table 3.4.4.3.

Local symmetry exerts constraints on possible displacements of the atoms within a wall. The site symmetry of atoms in a wall of zero thickness, or at the central plane of a finite-thickness domain wall, are defined by the layer group T_{13} . The site symmetry of the off-centre atoms at $0 < |\xi| < \infty$ are determined by floating group $\widehat{\mathcal{F}}_{13}$ and the limiting structures at $\xi \rightarrow -\infty$ and $\xi \rightarrow \infty$ by space groups \mathcal{F}_1 and \mathcal{F}_3 , respectively. A reasonable condition that the displacements of atoms change continuously if one passes through the wall from $\xi \rightarrow -\infty$ to $\xi \rightarrow \infty$ allows one to deduce a qualitative picture of the displacements within a wall.

Symmetry groups of domain pairs, sectional layer groups and the twin symmetry have been derived in the parent clamping approximation (PCA) (see Section 3.4.2.5). As can be seen from Fig. 3.4.3.5, a relaxation process, accompanying a lifting of this approximation, consists of a simple shear (shear vector parallel to q) and an elongation (or contraction) in the domain wall along the shear direction (change of the vector AB_0 into the vector AB_1^\dagger). These deformations influence neither the layer group T_{13} nor its floating group $\widehat{\mathcal{F}}_{13}$. Hence the wall (twin) symmetry T_{13} derived in the parent clamping approximation expresses also the symmetry of a ferroelastic domain wall (twin) with nonzero spontaneous shear unless the simple shear is accompanied by a reshuffling of atoms or molecules in both domains. This useful statement holds for any ferroelastic domain wall (twin).

A microscopic structure of the ferroelastic domain wall in two symmetrically prominent positions is depicted in Fig. 3.4.4.11. For better recognition, displacements of molecules are exaggerated

and the changes of the displacement lengths are neglected. Since the symmetry of all groups involved contains a reflection m_z , the atomic shifts are confined to planes (001). It can be seen in the figure that when one moves through the wall in the direction $[110]$ or $[1\bar{1}0]$, the vector of the molecular shift experiences rotations through $\frac{1}{2}\pi$ about the c' direction in opposite senses for the ‘black’ and ‘white’ molecules.

The ‘black’ molecules in the central layer at location $\frac{1}{4}d$ or $\frac{3}{4}d$ [wall (a) on the left-hand side of Fig. 3.4.4.11] exhibit nearly antiparallel displacements perpendicular to the wall. Strictly perpendicular shifts would represent ‘averaged’ displacements compatible with the layer symmetry $\overline{\mathcal{J}}_{13} = p2_{1y}^*m_z a_x^*$, which is, however, broken by a simple shear that decreases the symmetry to $T_{13} = p2_{1y}^*m_z a_x^*$, which does not require perpendicular displacements of ‘black’ molecules.

The wall with central plane location $0d$ or $\frac{1}{4}d$ (Fig. 3.4.4.11b) has symmetry $T_{13} = p2_y^*m_z m_x^*$, which restricts displacements of ‘white’ molecules of the central layer to the y direction only; the ‘averaged’ displacements compatible with $\overline{\mathcal{J}}_{13} = pm_y^*m_z m_x^*$ (origin shift $b_f/2$) would have equal lengths of shifts in the $+y$ and $-y$ directions, but the relaxed central layer with symmetry $T_{13} = p2_y^*m_z m_x^*$ allows unequal shifts in the $-y$ and $+y$ directions.

Walls (a) and (b) with two different prominent locations have different layer symmetries and different structures of the central layer. These two walls have extremal energy, but symmetry cannot decide which one has the minimum energy. The two walls have the same polar point-group symmetry $m_z 2_y^*m_z$, which permits a spontaneous polarization along y .

Similar analysis of the displacement and ordering fields in domain walls has been performed for KSCN crystals (Janovec *et al.*, 1989), sodium superoxide NaO_2 (Zieliński, 1990) and for the simple cubic phase of fullerene C_{60} (Saint-Grégoire *et al.*, 1997).

3.4.5. Glossary

Note: the correspondence between contracted Greek indices and the Cartesian vector components used in Sections 3.1.3, in the present chapter and in the software *GI★KoBo-1*, is defined in the following way:

| | | | | | | |
|----------------------|----|----|----|--------|--------|--------|
| Cartesian components | 11 | 22 | 33 | 23, 32 | 31, 13 | 12, 21 |
| Contracted notation | 1 | 2 | 3 | 4 | 5 | 6 |

In this designation, coefficients with contracted indices 4, 5, 6 appear two times, *e.g.* index 4 replaces yz in one coefficient and zy in the other coefficient. With this convention, the coefficients transform in tensor space as vector components, but some coefficients differ from the usual matrix notation (Voigt matrices) by numerical factors [see Section 1.1.4.10; Nye (1985); Sirotnin & Shaskolskaya, Appendix E (1982)].

(a) Objects

B_m

d

$D_i(S_k, B_m)$

GS_1

domain region

scanning vector (basis vector of a scanning group)

the i th domain, with domain state S_k in the m th domain region B_m

G -orbit of principal single-domain states

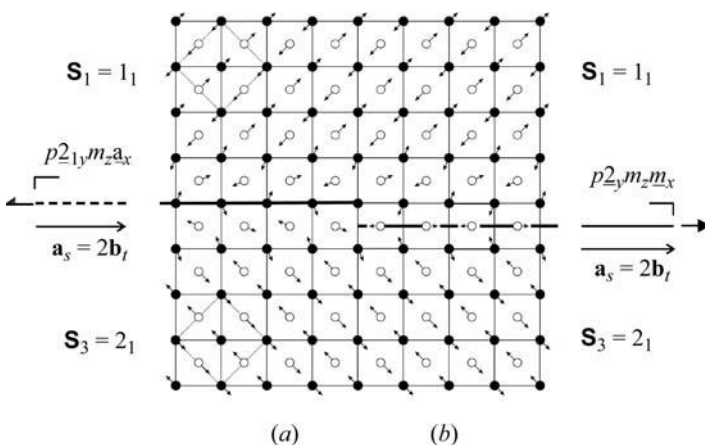


Fig. 3.4.4.11. Microscopic structure of a ferroelastic domain wall in calomel. (a) and (b) show a domain wall at two different locations with two different layer groups and two different structures of the central planes.

3.4. DOMAIN STRUCTURES

| | |
|--|---|
| $G(\mathbf{S}_1, \mathbf{S}_j)$ | G -orbit of domain pairs |
| $G(\mathbf{S}_1 \mathbf{n} \mathbf{S}_j)$ | G -orbit of simple domain twins |
| \mathbf{n} | normal to a plane p |
| p | plane of a domain wall, domain wall plane |
| $\mathbf{R}_1, \mathbf{R}_2, \dots, \mathbf{R}_i, \dots$ | secondary ferroic single-domain states |
| $\mathbf{R}_1^+, \mathbf{R}_1^-, \mathbf{R}_2^+, \dots, \mathbf{R}_2^-, \dots$ | disoriented secondary ferroic domain states |
| $\mathbf{s}\mathbf{d}$ ($0 \leq s < 1$) | location of a plane in crystal lattice |
| $\mathbf{S}_1, \mathbf{S}_2, \dots, \mathbf{S}_i, \dots$ | principal single-domain states (orientation states, variants) |
| $\mathbf{S}_1^+, \mathbf{S}_1^-, \mathbf{S}_2^+, \mathbf{S}_2^-, \dots$ | disoriented domain states |
| $\mathbf{S}_1, \mathbf{S}_2, \dots, \mathbf{S}_i, \dots$ | basic (microscopic) single-domain states (structural variants) |
| $(\mathbf{S}_i, \mathbf{S}_k)$ | ordered domain pair = ordered pair of domain states \mathbf{S}_i and \mathbf{S}_k |
| $\{\mathbf{S}_i, \mathbf{S}_k\}$ | unordered domain pair = unordered pair of domain states \mathbf{S}_i and \mathbf{S}_k |
| $(\mathbf{S}_i \mathbf{n} \mathbf{S}_k)$ | simple domain twin formed from single-domain states |
| $(\mathbf{S}_i^+ \mathbf{n} \mathbf{S}_k^-)$ | simple ferroelastic domain twin with a compatible domain wall |
| $[\mathbf{S}_i \mathbf{n} \mathbf{S}_k]$ | domain wall in the simple twin $(\mathbf{S}_i \mathbf{n} \mathbf{S}_k)$ |
| $\mathbf{T}_{ik}(\mathbf{n})$ or \mathbf{T}_{ik} | simple domain twin – short symbol |
| $\mathbf{W}_{ik}(\mathbf{n})$ or \mathbf{W}_{ik} | domain wall – short symbol |
| φ | shear angle, obliquity |
| $\pm \frac{1}{2}\varphi$ | disorientation angle of a domain state |

(b) Symmetry groups – point groups in a continuum description and space groups in a microscopic description

| | |
|---|---|
| F | point-group symmetry of the ferroic phase (domain state not specified) |
| \mathcal{F} | space-group symmetry of the ferroic phase (domain state not specified) |
| F_i | point-group symmetry of a principal domain state \mathbf{S}_i |
| \mathcal{F}_i | space-group symmetry of a basic (microscopic) domain state \mathbf{S}_i |
| F_{ik} | point-group symmetry (stabilizer in G) of the ordered domain pair $(\mathbf{S}_i, \mathbf{S}_k)$ |
| \mathcal{F}_{ik} | space-group symmetry (stabilizer in \mathcal{G}) of the ordered domain pair $(\mathbf{S}_i, \mathbf{S}_k)$ |
| \bar{F}_{ik} | sectional layer group of F_{ik} |
| \widehat{F}_{ik} | face group, trivial layer group, scanning group of F_{ik} |
| $\text{Fam } G$ | crystal family of the group G |
| G | point-group symmetry of the parent phase |
| \mathcal{G} | space-group symmetry of the parent phase |
| g | point-group symmetry operation of the group $G(\mathcal{G})$ |
| \mathbf{g} | space-group symmetry operation of the group \mathcal{G} |
| g_{ik} | switching operation in domain pair $(\mathbf{S}_i, \mathbf{S}_k)$, transforms \mathbf{S}_i into \mathbf{S}_k |
| g_{ik}^* | transposing operation in domain pair $(\mathbf{S}_i, \mathbf{S}_k)$, exchanges \mathbf{S}_i and \mathbf{S}_k , twinning operation of a non-ferroelastic domain pair $(\mathbf{S}_i, \mathbf{S}_k)$ |
| $I_G(\mathbf{S}_i)$ | stabilizer (isotropy group) of \mathbf{S}_i in G |
| $\mathcal{I}_{\mathcal{G}}(\mathbf{S}_i)$ | stabilizer (isotropy group) of \mathbf{S}_i in \mathcal{G} |
| J_{ik} | point-group symmetry (stabilizer in G) of the unordered domain pair $\{\mathbf{S}_i, \mathbf{S}_k\}$ |
| J_{ik}^* | point-group symmetry (stabilizer in G) of a completely transposable domain pair $\{\mathbf{S}_i, \mathbf{S}_k\}$ |
| \mathcal{J}_{ik} | space-group symmetry (stabilizer in \mathcal{G}) of the unordered domain pair $\{\mathbf{S}_i, \mathbf{S}_k\}$ |
| K_{ik} | twinning group of the domain pair $(\mathbf{S}_i, \mathbf{S}_k)$ |
| K_{ik}^* | twinning group of a completely transposable domain pair $(\mathbf{S}_i, \mathbf{S}_k)$ |
| L_i | intermediate group, $F_i \in L_i \in G$ |

| | |
|-------------------------------|---|
| \bar{J}_{ik} | sectional layer group of J_{ik} |
| \widehat{J}_{ik} | face group, trivial subgroup, floating subgroup of sectional group of J_{ik} |
| r_{ik}^* | symmetry operation of \bar{J}_{ik} that exchanges \mathbf{S}_i and \mathbf{S}_k |
| \underline{s}_{ik} | symmetry operation of \bar{J}_{ik} that inverts \mathbf{n} into $-\mathbf{n}$ |
| \underline{t}_{ik}^* | symmetry operation of \bar{J}_{ik} that exchanges \mathbf{S}_i and \mathbf{S}_k and inverts \mathbf{n} into $-\mathbf{n}$ |
| $\mathbf{T}_{ik}(\mathbf{n})$ | symmetry group of the twin $\mathbf{T}_{ik}(\mathbf{n})$ |
| $\mathbf{W}_{ik}(\mathbf{n})$ | symmetry group of the domain wall $\mathbf{W}_{ik}(\mathbf{n})$ |
| \mathcal{T}_i | translational subgroup of \mathcal{F}_i |
| \mathcal{T}_{ik} | translational subgroup of \mathcal{F}_{ik} |

(c) Components of property tensors

| | |
|---------------|-------------------|
| ε | enantiomorphism |
| P_i | polarization |
| u_μ | strain |
| g_μ | optical activity |
| $d_{i\mu}$ | piezoelectricity |
| A_{iv} | electrogyration |
| $s_{\mu\nu}$ | linear elasticity |
| $Q_{\mu\nu}$ | electrostriction |

$i = 1, 2, 3; \mu, \nu = 1, 2, \dots, 6.$

In the final period this work was supported by Ministry of Education of the Czech Republic under project MCM242200002.

References

- Aizu, K. (1969). Possible species of 'ferroelastic' crystals and of simultaneously ferroelectric and ferroelastic crystals. *J. Phys. Soc. Jpn*, **27**, 387–396.
- Aizu, K. (1970a). Possible species of ferromagnetic, ferroelectric and ferroelastic crystals. *Phys. Rev. B*, **2**, 754–772.
- Aizu, K. (1970b). Determination of the state parameters and formulation of spontaneous strain for ferroelastics. *J. Phys. Soc. Jpn*, **28**, 706–716.
- Aizu, K. (1972). Electrical, mechanical and electromechanical orders of state shifts in nonmagnetic ferroic crystals. *J. Phys. Soc. Jpn*, **32**, 1287–1301.
- Aizu, K. (1973). Second-order ferroic state shifts. *J. Phys. Soc. Jpn*, **34**, 121–128.
- Altmann, S. L. & Herzig, P. (1994). *Point-group theory tables*. Oxford: Clarendon Press.
- Amin, A. & Newnham, R. E. (1980). Tertiary ferroics. *Phys. Status Solidi A*, **61**, 215–219.
- Barkley, J. R. & Jeitschko, W. (1973). Antiphase boundaries and their interactions with domain walls in ferroelastic–ferroelectric $\text{Gd}_2(\text{MoO}_4)_3$. *J. Appl. Phys.* **44**, 938–944.
- Bertagnolli, E., Kittinger, E. & Tichý, J. (1978). Observation of reversible elastic Dauphiné twinning in alpha-quartz. *J. Phys. (Paris) Lett.* **39**, 295–297.
- Bertagnolli, E., Kittinger, E. & Tichý, J. (1979). Ferrobielastic hysteresis in alpha-quartz. *J. Appl. Phys.* **50**, 6267–6271.
- Boulesteix, C. (1984). A survey of domains and domain walls generated by crystallographic phase transitions causing a change of the lattice. *Phys. Status Solidi A*, **86**, 11–42.
- Bradley, C. J. & Cracknell, A. P. (1972). *The mathematical theory of symmetry in solids*. Oxford: Clarendon Press.
- Bul'bich, A. A. & Gufan, Yu. M. (1989a). Inevitable symmetry lowering in a domain wall near a reordering phase transition. *Sov. Phys. JETP*, **67**, 1153–1157.
- Bul'bich, A. A. & Gufan, Yu. M. (1989b). Phase transition in domain walls. *Ferroelectrics*, **172**, 351–359.
- Cahn, R. W. (1954). Twinned crystals. *Adv. Phys.* **3**, 363–445.
- Calleja, M., Dove, M. T. & Salje, E. K. H. (2001). Anisotropic ionic transport in quartz: the effect of twin boundaries. *J. Phys. Condens. Matter*, **13**, 9445–9454.

3. PHASE TRANSITIONS, TWINNING AND DOMAIN STRUCTURES

- Cao, W. & Barsch, G. R. (1990). Landau–Ginzburg model of interphase boundaries in improper ferroelastic perovskites of D_{4h}^{18} symmetry. *Phys. Rev. B*, **41**, 4334–4348.
- Carpenter, M. A., Salje, E. K. H. & Graeme-Barber, A. (1998). Spontaneous strain as a determinant of thermodynamic properties for phase transitions in minerals. *Eur. J. Mineral.* **10**, 621–691.
- Catti, M. & Ferraris, G. (1976). Twinning by merohedry and X-ray structure determination. *Acta Cryst.* **A32**, 163–165.
- Chen, X. J., Liu, J. S., Zhu, J. S. & Wang, Y. N. (2000). Group theoretical analysis of the domain structure of $\text{SrBi}_2\text{Ta}_2\text{O}_9$ ferroelectric ceramic. *J. Phys. Condens. Matter*, **12**, 3745–3749.
- Christian, J. W. (1975). *The theory of transformations in metals and alloys*. Oxford: Pergamon Press.
- Chrosch, J. & Salje, E. K. H. (1999). Temperature dependence of the domain wall width in LaAlO_3 . *J. Appl. Phys.* **85**, 722–727.
- Curien, H. & Donnay, J. D. H. (1959). The symmetry of the complete twin. *Am. Mineral.* **44**, 1067–1070.
- Curien, H. & Le Corre, Y. (1958). Notation des macles à l'aide du symbolisme des groupes de couleurs de Chubnikov. *Bull. Soc. Fr. Mineral. Cristallogr.* **81**, 126–132.
- Dolino, G. (1985). In *Modern problems in condensed matter sciences*. Vol. 2, *Incommensurate phases in dielectrics*, edited by R. Blinc & A. P. Levanyuk, pp. 207–231. Amsterdam: North-Holland.
- Dudnik, E. F. & Shuvalov, L. A. (1989). Domain structure and phase boundaries in ferroelastics. *Ferroelectrics*, **98**, 207–234.
- Erhart, J. & Cao, W. (2001). Effective symmetry and physical properties of twinned perovskite ferroelectric single crystals. *J. Mater. Res.* **16**, 570–578.
- Fatuzzo, E. & Merz, W. J. (1967). *Ferroelectricity*. Amsterdam: North-Holland.
- Fesenko, E. G., Gavrilachenko, B. G. & Semenchov, A. F. (1990). *Domain structure in multiaxial ferroelectric crystals*. Rostov on Don: Publishing House of the Rostov University (in Russian).
- Fousek, J. (1971). Permissible domain walls in ferroelectric species. *Czech. J. Phys. B*, **21**, 955–968.
- Fousek, J. & Janovec, V. (1969). The orientation of domain walls in twinned ferroelectric crystals. *J. Appl. Phys.* **40**, 135–142.
- Friedel, G. (1926). *Leçons de cristallographie*. Nancy, Paris, Strasbourg: Berger-Levrault. Reprint (1964). Paris: Blanchard.
- Fuksa, J. (1997). The role of the twinning group of a domain pair in tensor distinction of domain states. *Ferroelectrics*, **204**, 135–155.
- Fuksa, J. & Janovec, V. (1995). Permutation classification of domain pairs. *Ferroelectrics*, **172**, 343–350.
- Grell, H., Krause, C. & Grell, J. (1989). *Tables of the 80 plane space groups in three dimensions*. Berlin: Akademie der Wissenschaften der DDR.
- Hahn, Th. & Wondratschek, H. (1994). *Symmetry of crystals. Introduction to International Tables for Crystallography Vol. A*. Sofia: Heron Press.
- Hatch, D. M. & Cao, W. (1999). Determination of domain and domain wall formation at ferroic transitions. *Ferroelectrics*, **222**, 1–10.
- Hatch, D. M., Ghose, S. & Stokes, H. (1990). Phase transitions in leucite, KAl_2O_6 . I. Symmetry analysis with order parameter treatment and the resulting microscopic distortions. *Phys. Chem. Mineral.* **17**, 220–227.
- Hatt, R. A. & Hatch, D. M. (1999). Order parameter profiles in ferroic phase transitions. *Ferroelectrics*, **226**, 61–78.
- Holser, W. T. (1958a). Relation of symmetry to structure in twinning. *Z. Kristallogr.* **110**, 249–265.
- Holser, W. T. (1958b). Point groups and plane groups in a two-sided plane and their subgroups. *Z. Kristallogr.* **110**, 266–281.
- Houchmandzadeh, B., Lajzerowicz, J. & Salje, E. K. H. (1991). Order parameter coupling and chirality of domain walls. *J. Phys. Condens. Matter*, **3**, 5163–5169.
- Huang, X. R., Jiang, S. S., Hu, X. B. & Liu, W. J. (1997). Theory of twinning structures in the orthorhombic phase of ferroelectric perovskites. *J. Phys. Condens. Matter*, **9**, 4467–4482.
- IEEE Standards on Piezoelectricity (1987). IEEE Std 176-987. New York: The Institute of Electrical and Electronics Engineers, Inc.
- Indenbom, V. L. (1982). In *Modern crystallography II*, edited by B. K. Vainshtein, V. M. Fridkin & V. L. Indenbom, pp. 387–396. Berlin: Springer.
- International Tables for Crystallography (2002). Vol. A, *Space-group symmetry*, 5th edition, edited by Th. Hahn. Dordrecht: Kluwer Academic Publishers.
- International Tables for Crystallography (2002). Vol. E, *Subperiodic groups*, edited by V. Kopský & D. B. Litvin. Dordrecht: Kluwer Academic Publishers.
- Ishibashi, Y. (1990). Structure and physical properties of domain walls. *Ferroelectrics*, **104**, 299–310.
- Ishibashi, Y. (1992). Domain walls in crystals with incommensurate phases. II. *J. Phys. Soc. Jpn.* **61**, 357–362.
- Ishibashi, Y. (1993). The 90° -wall in the tetragonal phase of BaTiO_3 -type ferroelectrics. *J. Phys. Soc. Jpn.* **62**, 1044–1047.
- Janovec, V. (1972). Group analysis of domains and domain pairs. *Czech. J. Phys. B*, **22**, 974–994.
- Janovec, V. (1976). Symmetry approach to domain structures. *Ferroelectrics*, **12**, 43–53.
- Janovec, V. (1981). Symmetry and structure of domain walls. *Ferroelectrics*, **35**, 105–110.
- Janovec, V., Litvin, D. B. & Fuksa, J. (1995). Transposable domain pairs and domain distinction. *Ferroelectrics*, **172**, 351–359.
- Janovec, V., Richterová, L. & Litvin, D. B. (1993). Non-ferroelastic twin laws and distinction of domains in non-ferroelastic phases. *Ferroelectrics*, **140**, 95–100.
- Janovec, V., Schranz, W., Warhanek, H. & Zikmund, Z. (1989). Symmetry analysis of domain structure in KSCN crystals. *Ferroelectrics*, **98**, 171–189.
- Janovec, V. & Zikmund, Z. (1993). Microscopic structure of domain walls and antiphase boundaries in calomel crystals. *Ferroelectrics*, **140**, 89–93.
- Jerphagnon, J., Chemla, D. & Bonneville, R. (1978). The description of the physical properties of condensed matter using irreducible tensors. *Adv. Phys.* **27**, 609–650.
- Jona, F. & Shirane, G. (1962). *Ferroelectric crystals*. Oxford: Pergamon Press.
- Kalonji, G. (1985). A roadmap for the use of interfacial symmetry groups. *J. Phys. (Paris) Colloq.* **46**, 49–556.
- Känzig, W. (1957). *Ferroelectrics and antiferroelectrics*. In *Solid state physics IV*, edited by F. Seitz & D. Turnbull, pp. 1–197. New York: Academic Press.
- Klassen-Neklyudova, M. V. (1964). *Mechanical twinning of crystals*. New York: Consultants Bureau.
- Knox, R. S. & Gold, A. (1967). *Symmetry in the solid state. Introduction*. New York: W. A. Benjamin.
- Koch, E. (1999). Twinning. In *International tables for crystallography*, Vol. C, *Mathematical, physical and chemical tables*, 2nd edition, edited by A. J. C. Wilson & E. Prince, Section 1.3. Dordrecht: Kluwer Academic Publishers.
- Koňák, Č., Kopský, V. & Smutný, F. (1978). Gyrotropic phase transitions. *J. Phys. Solid State Phys.* **11**, 2493–2518.
- Kopský, V. (1979). Tensorial covariants for the 32 crystal point groups. *Acta Cryst.* **A35**, 83–95.
- Kopský, V. (1982). Group lattices, subduction of bases and fine domain structures for magnetic point groups. Prague: Academia.
- Kopský, V. (1993). Translation normalizers of Euclidean motion groups. *J. Math. Phys.* **34**, 1548–1576.
- Kopský, V. (2001). Tensor parameters of ferroic phase transitions I. Theory and tables. *Phase Transit.* **73**, 1–422.
- Lines, M. E. & Glass, A. M. (1977). *Principles and applications of ferroelectric and related materials*. Oxford: Clarendon Press.
- Litvin, D. B. & Janovec, V. (1999). Classification of domain pairs and tensor distinction. *Ferroelectrics*, **222**, 87–93.
- Locherer, K. R., Chrosch, J. & Salje, E. K. H. (1998). Diffuse X-ray scattering in WO_3 . *Phase Transit.* **67**, 51–63.
- Mitsui, T., Tatsuzaki, I. & Nakamura, E. (1976). *An introduction to the physics of ferroelectrics*. New York: Gordon & Breach.
- Newnham, R. E. (1974). Domains in minerals. *Am. Mineral.* **59**, 906–918.
- Newnham, R. E. (1975). Structure–property relations. Berlin: Springer.
- Newnham, R. E. & Cross, L. E. (1974a). Symmetry of secondary ferroics I. *Mater. Res. Bull.* **9**, 927–934.
- Newnham, R. E. & Cross, L. E. (1974b). Symmetry of secondary ferroics II. *Mater. Res. Bull.* **9**, 1021–1032.
- Newnham, R. E., Miller, C. S., Cross, L. E. & Cline, T. W. (1975). Tailored domain patterns in piezoelectric crystals. *Phys. Status Solidi A*, **32**, 69–78.
- Newnham, R. E. & Skinner, D. P. Jr (1976). Polycrystalline secondary ferroics. *Mater. Res. Bull.* **11**, 1273–1284.
- Nye, J. F. (1985). *Physical properties of crystals*. Oxford: Clarendon Press.
- Opechowski, W. (1986). *Crystallographic and metacystallographic groups*. Amsterdam: North-Holland.

3.4. DOMAIN STRUCTURES

- Palmer, D. C., Putnis, A. & Salje, E. K. H. (1988). Twinning in tetragonal leucite. *Phys. Chem. Mineral.* **16**, 298–303.
- Pond, R. C. & Bollmann, W. (1979). *The symmetry and interfacial structure of bicrystals*. *Philos. Trans. R. Soc. London Ser. A*, **292**, 449–472.
- Pond, R. C. & Vlachavas, D. S. (1983). *Bicrystallography*. *Proc. R. Soc. London Ser. A*, **386**, 95–143.
- Privratská, J. & Janovec, V. (1997). Pyromagnetic domain walls connecting antiferromagnetic non-ferroelastic domains. *Ferroelectrics*, **204**, 321–331.
- Privratská, J. & Janovec, V. (1999). Spontaneous polarization and/or magnetization in non-ferroelastic domain walls: symmetry predictions. *Ferroelectrics*, **222**, 23–32.
- Privratská, J., Janovec, V. & Machonský, L. (2000). Tensor properties discriminating domain walls from non-ferroelastic domains. *Ferroelectrics*, **240**, 83–92.
- Putnis, A. (1992). *Introduction to mineral sciences*. Cambridge University Press.
- Rosenman, G., Skliar, A., Eger, D., Oron, M. & Katz, M. (1998). Low temperature periodic electrical poling of flux-grown KTiOPO_4 and isomorphic crystals. *Appl. Phys. Lett.* **73**, 3650–3652.
- Rosová, A. (1999). Real domain structure origination in (110) mechanical twinning in $\text{YBa}_2\text{Cu}_3\text{O}_{7-y}$. In *Studies of high temperature superconductors*, Vol. 28, edited by A. Narlikar, pp. 125–148. New York: Nova Science Publishers.
- Rosová, A., Boulesteix, C. & Vávra, I. (1993). Role of microtwins in twin lamella intersections and interconnections in $\text{YBa}_2\text{Cu}_3\text{O}_{7-y}$. *Physica C*, **214**, 247–256.
- Rychetský, I. & Schranz, W. (1993). Antiphase boundaries in Hg_2Br_2 and KSCN . *J. Phys. Condens. Matter*, **5**, 1455–1472.
- Rychetský, I. & Schranz, W. (1994). Ferroelastic domain walls in Hg_2Br_2 and KSCN . *J. Phys. Condens. Matter*, **6**, 11159–11165.
- Saint-Grégoire, P. & Janovec, V. (1989). Modulated phases in crystals: Symmetry of walls and wall lattices. Example of quartz. In *Nonlinear coherent structures*, edited by M. Barts & J. Léon. Lecture notes in physics, Vol. 353, pp. 117–126. Berlin: Springer.
- Saint-Grégoire, P., Janovec, V. & Kopský, V. (1997). A sample analysis of domain walls in simple cubic phase of C_{60} . *Ferroelectrics*, **191**, 73–78.
- Salje, E. K. H. (1990). *Phase transitions in ferroelastic and co-elastic crystals*, 1st edition. Cambridge University Press.
- Salje, E. K. H. (1991). Strain-related transformation twinning in minerals. *Neues Jahrb. Mineral. Abh.* **163**, 43–86.
- Salje, E. K. H. (2000a). Mesoscopic twin patterns in ferroelastic and co-elastic minerals. *Rev. Mineral. Geochem.* **39**, 65–84.
- Salje, E. K. H. (2000b). Ferroelasticity. *Contemp. Phys.* **41**, 79–91.
- Sapriel, J. (1975). Domain-wall orientations in ferroelastics. *Phys. Rev. B*, **12**, 5128–5140.
- Schlenker, J. L., Gibbs, G. V. & Boisen, M. B. (1978). Strain-tensor components expressed in terms of lattice parameters. *Acta Cryst.* **A34**, 52–54.
- Schmid, H. (1991). Polarized light microscopy of the ferroelastic domains of $\text{YBa}_2\text{Cu}_3\text{O}_{7-x}$. *Phase Transit.* **30**, 205–214.
- Schmid, H. (1993). Polarized light microscopy (PLM) of ferroelectric and ferroelastic domains in transmitted and reflected light. In *Ferroelectric ceramics*, edited by N. Setter & E. L. Colla, pp. 107–126. Basel: Birkhäuser.
- Schmid, H., Burkhardt, E., Walker, E., Brixel, W., Clin, M., Rivera, J.-P., Jorda, J.-L., François, M. & Yvon, K. (1988). Polarized light and X-ray precession study of the ferroelastic domains of $\text{YBa}_2\text{Cu}_3\text{O}_{7-\delta}$. *Z. Phys. B Condens. Matter*, **72**, 305–322.
- Schranz, W. (1995). Domains and interfaces near ferroic phase transitions. *Key Eng. Mater.* **101–102**, 41–60.
- Scott, J. (1998). The physics of ferroelectric ceramic thin films for memory applications. *Ferroelectrics Rev.* **1**, 1–129.
- Scott, J. (2000). *Ferroelectric memories*. Heidelberg: Springer.
- Shmyt'ko, I. M., Shekhtman, V. Sh., Ossipyan, Yu. A. & Afonikova, N. S. (1987). Twin structure and structure of twin boundaries in 1-2-3- $\text{O}_{7-\delta}$ crystals. *Ferroelectrics*, **97**, 151–170.
- Shubnikov, A. V. & Kopcik, V. A. (1974). *Symmetry in science and art*. New York: Plenum Press.
- Shur, V. Ya., Batchko, R. G., Rumyantsev, E. L., Miller, G. D., Fejer, M. M. & Byer, R. L. (1999). Domain engineering: periodic domain patterning in lithium niobate. *Proc. 11th ISAF*, pp. 399–406. Piscataway, NJ: IEEE.
- Shur, V. Ya., Gruverman, A. L., Letuchev, V. V., Rumyantsev, E. L. & Subbotin, A. L. (1989). Domain structure of lead germanate. *Ferroelectrics*, **98**, 29–49.
- Shur, V. Ya., Rumyantsev, E. L., Nikolaeva, E. V., Shishkin, E. I., Batchko, R. G., Fejer, M. M. & Byer, R. L. (2001). Recent achievements in domain engineering in lithium niobate and lithium tantalate. *Ferroelectrics*, **257**, 191–202.
- Shuvalov, L. A. (1988). Editor. *Modern crystallography IV. Physical properties of crystals*. Berlin: Springer.
- Shuvalov, L. A., Dudnik, E. F. & Wagin, S. V. (1985). Domain structure geometry of real ferroelastics. *Ferroelectrics*, **65**, 143–152.
- Shuvalov, L. A. & Ivanov, N. R. (1964). Change in the optical activity of ferroelectric crystals on reversal of polarization. *Sov. Phys. Crystallogr.* **9**, 290–299. (*Kristallografiya*, **9**, 363–372.)
- Sidorkin, A. S. (2002). *Domain structure in ferroelectrics and related materials*. Moscow: Fizmatlit (in Russian).
- Sirotnin, Yu. I. & Shaskolskaya, M. P. (1982). *Fundamentals of crystal physics*. Moscow: Mir.
- Smolenskii, G. A., Bokov, V. A., Isupov, V. A., Krainik, N. N., Pasynkov, R. E. & Shur, M. S. (1984). *Physics of ferroelectric phenomena*. New York: Gordon & Breach.
- Snoeck, E., Saint-Grégoire, P., Janovec, V. & Roucau, C. (1994). TEM study of 3-q modulated phase of quartz-type under electric field. *Ferroelectrics*, **155**, 171–176.
- Sonin, E. B. & Tagancev, A. K. (1989). Structure and phase transitions in antiphase boundaries of improper ferroelectrics. *Ferroelectrics*, **98**, 291–295.
- Strukov, B. A. & Levanyuk, A. P. (1998). *Ferroelectric phenomena in crystals*. Berlin: Springer.
- Sutton, A. P. & Balluffi, R. W. (1995). *Interfaces in crystalline materials*. Oxford: Clarendon Press.
- Tagancev, A. R. & Sonin, E. B. (1989). Linear singularities and their motion in improper ferroelectrics. *Ferroelectrics*, **98**, 297–300.
- Tolédano, J.-C. & Tolédano, P. (1987). *The Landau theory of phase transitions*. Singapore: World Scientific.
- Tolédano, P. & Dmित्रiev, V. (1996). *Reconstructive phase transitions*. Singapore: World Scientific.
- Tomaszewski, P. E. (1992). Structural phase transitions in crystals. I. Database. II. Statistical analysis. *Phase Transit.* **38**, 127–220, 221–228.
- Uchino, K. (2000). *Ferroelectric devices*. New York: Marcel Dekker.
- Vainshtein, B. K. (1994). *Modern crystallography I. Symmetry of crystals*. Berlin: Springer.
- Van Landuyt, J., Van Tendeloo, G., Amelinckx, S. & Walker, M. B. (1985). Interpretation of Dauphiné-twin-domain configurations resulting from the α - β phase transition in quartz and aluminium phosphate. *Phys. Rev. B*, **31**, 2986–2992.
- Van Tendeloo, G. & Amelinckx, S. (1974). Group-theoretical considerations concerning domain formation in ordered alloys. *Acta Cryst.* **A30**, 431–440.
- Wadhawan, V. K. (1991). Ferroelasticity: introductory survey and present status. *Phase Transit.* **34**, 3–18.
- Wadhawan, V. K. (2000). *Introduction to ferroic materials*. The Netherlands: Gordon and Breach.
- Wondratschek, H. & Aroyo, M. I. (2001). The application of Hermann's group \mathcal{M} in group-subgroup relations between space groups. *Acta Cryst.* **A57**, 311–320.
- Wondratschek, H. & Jeitschko, W. (1976). Twin domains and antiphase domains. *Acta Cryst.* **A32**, 664–666.
- Xu, Y. (1991). *Ferroelectric materials and their applications*. Amsterdam: North-Holland.
- Yin, J. & Cao, W. (2000). Domain configurations in domain engineered $0.995\text{Pb}(\text{Zn}_{1/3}\text{Nb}_{2/3})\text{O}_3$ - 0.045PbTiO_3 single crystals. *J. Appl. Phys.* **87**, 7438–7441.
- Zheludev, I. S. (1988). Electrical properties of crystals. In *Modern crystallography IV. Physical properties of crystals*, edited by L. A. Shuvalov, pp. 178–266. Berlin: Springer-Verlag.
- Zieliński, P. (1990). Group-theoretical description of domains and phase boundaries in crystalline solids. *Surf. Sci. Rep.* **11**, 179–223.
- Zikmund, Z. (1984). Symmetry of domain pairs and domain walls. *Czech. J. Phys. B*, **34**, 932–949.

List of terms and symbols used in this volume

(1) Vector spaces and tensor analysis

| | |
|---|-------------------------------------|
| Basis vectors in direct space (covariant) | $\mathbf{e}_i, \mathbf{a}_i$ |
| Basis vectors in reciprocal space (contravariant) | $\mathbf{e}^i, \mathbf{a}_i^*$ |
| Contravariant components of vectors in direct space | x^i |
| Covariant components of vectors in reciprocal space | x_i |
| Direction indices (of a lattice row) | $[uvw]$ |
| Dual (or reciprocal) space (n dimensions) | E_n (Chapter 1.1) |
| Element of | \in |
| Euclidian space, direct space (n dimensions) | E^n |
| Hermitian conjugate of matrix M | M^+ |
| Integers (positive) | \mathbb{Z}^+ |
| Integers (ring of) | \mathbb{Z} |
| Kronecker symbol | δ_i^j |
| Metric tensor | g_{ij} |
| Miller indices (of a lattice plane) | (hkl) |
| Nabla operator | ∇ |
| Orthogonal transformation | R |
| Outer product | \wedge |
| Partial derivative with respect to x_i | ∂_i |
| Permutation tensor | $\varepsilon_{ijk}, \hat{e}_{ijk}$ |
| Position vector in reciprocal space | \mathbf{G}, \mathbf{k} |
| Reciprocal lattice vector | \mathbf{g}_{hkl} |
| Sum of spaces | \oplus |
| Tensor of rank n, p times covariant and q times contravariant ($n = p + q$) | $t_{i_1 \dots i_p}^{j_1 \dots j_q}$ |
| Tensor product | \otimes |
| Transpose of matrix M | M^T |
| Unit transformation, matrix or element | E |
| Vector in superspace | \mathbf{a}_{si} |
| Vector in reciprocal superspace | \mathbf{a}_{si}^* |
| Vector product | \wedge, \times |
| Volume element | $d\tau$ |
| Volume of unit cell in direct (reciprocal) space | $V (V^*)$ |

(2) Group theory

| | |
|--|--|
| Character | χ |
| Character (irreducible) | χ_α |
| Character (value at R) | $\chi(R)$ |
| Class multiplication constants | c_{ijk} |
| Conjugacy class | C_i |
| Cyclic group of order m | C_m |
| Dihedral group of order $2n$ | D_n |
| Dimension of irreducible representation α | d_α |
| Lattice translation subgroup | $T(n)$ |
| Matrix representation of point group K | $\Gamma(K)$ |
| Multiplicity | m_α |
| Octahedral group | O |
| Order of class C_i | n_i |
| Orthogonal group | $O(n)$ |
| Orthogonal group (special) | $SO(n)$ |
| Physically irreducible representation | $R\text{-irep}$ |
| Point group | K (Chapter 1.2), G_o (Chapter 2.1), G (Part 3) |
| Point group (order of) | $ K , N$ |

| | |
|-----------------------------------|---------------------------|
| Representation of point group K | $D(K)$ |
| Space group | G, \mathcal{G} (Part 3) |
| Tetrahedral group | T |

(3) Physical properties

(a) Elastic properties

| | |
|--|--|
| Bulk modulus (volume isothermal compressibility) | κ |
| Components of the displacement vector | u_i |
| Elastic compliances (second-order) | s_{ijkl} |
| Elastic compliances (second-order adiabatic) | $(s_{ijkl})^\sigma$ |
| Elastic compliances (second-order reduced) | $s_{\alpha\beta}$ |
| Elastic compliances (third-order) | s_{ijklmn} |
| Elastic stiffnesses (second-order) | c_{ijkl}, C_{ijkl} |
| Elastic stiffnesses (second-order adiabatic) | $(c_{ijkl})^\sigma$ |
| Elastic stiffnesses (second-order reduced) | $c_{\alpha\beta}$ |
| Elastic stiffnesses (third-order) | c_{ijklmn} |
| Lamé coefficients | λ |
| Normal stress | $\bar{\nu}$ |
| Poisson's ratio | ν |
| Pressure | p |
| Shear stress | $\bar{\tau}$ |
| Strain tensor | S_{ij}, u_{ij} (Chapters 1.4, 1.5 and 3.1), η_{ij} (Chapter 2.3) |
| Strain Voigt matrix | S_α |
| Stress tensor | T_{ij}, τ_{ij} (Chapter 1.4), σ_{ij} (Chapters 2.1, 2.3, 2.4) |
| Stress Voigt matrix | T_α |
| Velocity of sound | v |
| Volume | V |
| Volumic mass | ρ |
| Young's modulus | E |

(b) Electric properties

| | |
|--|---------------------------------|
| Charge density | $\rho(\mathbf{r})$ |
| Charge of the electron | e |
| Current density | $\mathbf{j}(\mathbf{r}), J$ |
| Dielectric impermeability | η_{ij} |
| Dielectric permittivity or constant | ε |
| Dielectric permittivity of vacuum | ε_0 |
| Dielectric permittivity tensor | ε_{ij} |
| Dielectric permittivity tensor (adiabatic) | $(\varepsilon_{ij})^\sigma$ |
| Dielectric susceptibility | $\chi_{ij}^e, \chi_{ijk} \dots$ |
| Dielectric susceptibility (n th-order) | $\chi^{(n)}$ |
| Effective mass of the electron | m^* |
| Electric dipole operator | \hat{p} |
| Electric displacement | \mathbf{D} |
| Electric field | \mathbf{E} |
| Electric polarization | \mathbf{P} |
| Electric polarization (n th-order) | \mathbf{P}_n |
| Electric polarization (nonlinear) | \mathbf{P}^{NL} |
| Electro-optic tensor | r_{ijk} |
| Electrostriction tensor | Q_{ijkl} |
| Electrostriction tensor (reduced) | $Q_{\alpha\beta}$ |
| Hall constant | $R_{H \text{ } ijk}$ |
| Piezoelectric tensor | d_{ijk} |
| Piezoelectric tensor at constant strain | e_{ijk} |

LIST OF TERMS AND SYMBOLS USED IN THIS VOLUME

| | | | |
|---|--------------------------------|--|---|
| Piezoelectric tensor (reduced) | d_{ia} | Refractive indices for biaxial indicatrix | $n_x, n_\alpha, \alpha; n_y, n_\beta, \beta;$ |
| Piezoelectric tensor (reduced adiabatic) | $(d_{ijk})^\sigma$ | Velocity of light in a vacuum | n_z, n_γ, γ |
| Piezoelectric tensor (reduced inverse) | d_{ai} | Velocity (group) | c |
| Pyroelectric tensor | p_i | Wavelength of light | ν_g |
| | | Wavevector of light propagating in crystal | λ |
| (c) <i>Magnetic properties</i> | | | $\mathbf{k} (k = 2\pi/\lambda)$ |
| Antiferromagnetic vector | \mathbf{L}_i | | |
| Bohr magneton | μ_B | (e) <i>Thermodynamic properties</i> | |
| Constant describing magnetostriction | λ | Anisotropy energy | U_a |
| Effective number of Bohr magnetons | p (Section 1.6.1) | Atomic Debye–Waller factor (static) | S_α |
| Landé g -factor | g | Atomic Debye–Waller factor (thermal) | T_α |
| Magnetic birefringence | Δn | Boltzmann constant | k_B |
| Magnetic field | \mathbf{H} | Debye frequency | ω_D |
| Magnetic induction | \mathbf{B} | Debye temperature | Θ_D |
| Magnetic moment | μ | Einstein frequency | ω_E |
| Magnetic moment density | $\mathbf{m}(\mathbf{r})$ | Einstein temperature | Θ_E |
| Magnetic permeability | μ_{ij} | Elastic energy | U_{el} |
| Magnetic permeability of vacuum | μ_o | Entropy | σ, S |
| Magnetic susceptibility | χ_{ij}, χ_{ij}^m | Free energy | $\mathcal{G}, \mathcal{F}, F, A$ |
| Magnetization (= magnetic moment per unit volume = ferromagnetic vector) | \mathbf{M} | Grüneisen parameter | $\bar{\gamma}, \gamma$ |
| Magnetoelastic energy | U_{me} | Grüneisen parameter (averaged mode) | $\gamma_{q,j}$ |
| Magnetoelectric tensor (linear) | α_{ij} | Grüneisen parameter (generalized mode) | $\gamma_{\mathbf{q},kl}$ |
| Magnetoelectric tensor (nonlinear) <i>EHH</i> | β_{ijk} | Hamiltonian | H |
| Magnetoelectric tensor (nonlinear) <i>HEE</i> | γ_{ijk} | Heat current | J_Q |
| Magneto-optic tensor | \mathbf{f} | Internal energy | U, \mathcal{U} |
| Néel temperature | T_N | Lattice energy | E_{ph} |
| Orbital angular momentum | \mathbf{L} (Section 1.6.1.1) | Partition function | Z |
| Piezomagnetic components | Λ_{ijk} | Phonon wavevector | q |
| Piezomagnetic components (reduced) | Λ_{ia} | Seebeck coefficient | S |
| Piezomagnetoelectric tensor | π_{ijkl} | Specific heat at constant strain (volume) | c^S, c_V |
| Spin angular momentum (of an atom or ion) | \mathbf{S} | Specific heat at constant stress (pressure) | c^T, c_p |
| Spin density | $\mathbf{S}(\mathbf{r})$ | Specific heat at constant volume (according to the Debye model) | c_V^{Debye} |
| Sum of the magnetic moments in a unit cell | \mathbf{m} | Specific heat at constant volume (according to the Einstein model) | c_V^{Einstein} |
| Sum of the magnetic moments in a unit cell, in which some of the moments are taken with opposite sign | \mathbf{l}_i | Temperature | Θ, T |
| Total angular momentum | \mathbf{J} | Temperature-stress components | λ_{ij} |
| Weiss constant | Δ | Thermal conductivity | K |
| | | Thermal expansion | α_{ij} |
| | | Thermal expansion (volume) | β |
| | | Thermodynamic potential | Φ |
| (d) <i>Optical properties</i> | | Zero-point energy | E_o |
| Angle between optic axes | $2V$ | | |
| Cyclic (or circular) frequency | ω | (4) <i>Phase transformations: for details see Sections 3.1.7, 3.3.11 and 3.4.5</i> | |
| Elasto-optic (strain-optic) tensor | p_{ijkl} | Aizu symbol of a ferroic phase transition | $GF\mathcal{H}$ (Chapter 3.3) |
| Elasto-optic (strain-optic) tensor, reduced | $p_{\alpha\beta}$ | Eigensymmetry of untwinned crystal or daughter phase | \mathcal{H} (Chapter 3.3) |
| Electro-optic tensor | r_{ijk} | Order parameter (primary) | η |
| Ellipticity of wave | κ | Order parameter (secondary) | λ |
| Gyration susceptibility | γ_{ijl} | Point group of ferroic (low-symmetry) phase | F (Chapters 3.1 and 3.4) |
| Gyration tensor | g_{ij}, G_{ij} | Point group of parent (high-symmetry) phase | G |
| Gyration vector | \mathbf{G} | Space group of ferroic (low-symmetry) phase | \mathcal{F} (Chapters 3.1 and 3.4) |
| Optical rotatory power | ρ | Space group of parent (high-symmetry) phase | \mathcal{G} |
| Phase difference of light | Δ | Symmetry descent from G to F (point groups) | $G \Downarrow F$ |
| Piezo-optic tensor | π_{ijkl} | Symmetry descent from \mathcal{G} to \mathcal{F} (space groups) | $\mathcal{G} \Downarrow \mathcal{F}$ |
| Piezo-optic tensor (reduced) | $\pi_{\alpha\beta}$ | Transition temperature, in particular: Curie temperature | T_C |
| Polarizability operator | $\hat{\alpha}$ | | |
| Poynting vector | \mathbf{S} | | |
| Poynting vector (unit) | $\mathbf{s}, \hat{\mathbf{s}}$ | | |
| Raman tensor | $R^j(\mathbf{q})$ | | |
| Rayleigh length | Z_r | | |
| Refractive index (extraordinary) | n_e | | |
| Refractive index of light | n | | |
| Refractive index (ordinary) | n_o | | |

Author index

Entries refer to chapter number.

- Abed, M., 1.7
 Abrahams, S. C., 1.9, 1.10, 3.3
 Absar, I., 1.9
 Achenbach, G. D., 1.5
 Afonikova, N. S., 3.4
 Agafonov, A. P., 1.5
 Agranovich, V. M., 1.6, 2.3
 Agranovskaia, A. I., 1.5
 Ahn, C. H., 1.8
 Aizu, K., 1.5, 3.1, 3.2, 3.3, 3.4
 Akai, H., 2.2
 Akai, M., 2.2
 Akhmanov, S. A., 1.7
 Akridge, J. R., 3.1
 Akulov, N., 1.5
 Alba, M., 2.1
 Albrecht, A. C., 1.7
 Alcantara Bonfim, O. F. de 1.5
 Alder, B. J., 2.2
 Alexander, H., 3.3
 Allen, P. B., 1.8
 Al'shin, B. I., 1.5
 Altmann, S. L., 1.2, 2.2, 3.1, 3.4
 Ambrosch-Draxl, C., 2.2
 Amelinckx, S., 3.2, 3.3, 3.4
 Amin, A., 3.4
 Aminoff, G., 3.3
 Anastassakis, E. M., 2.3
 Andersen, O. K., 2.2
 Anderson, J. C., 1.5
 Andratskii, V. P., 1.5
 Andreadza, P., 1.7
 Andreev, A. F., 1.5
 Anthony, T. R., 1.8
 Antonetti, A., 1.7
 Arbman, G. O., 2.2
 Arlt, G., 3.3
 Armstrong, J. A., 1.7
 Arndt, H., 3.1
 Arnold, H., 3.3
 Aroyo, M. I., 3.1, 3.2, 3.4
 Arzruni, A., 3.3
 Asaumi, K., 1.7
 Ascher, E., 1.5, 3.1
 Ashkin, A., 1.7
 Astrov, D. N., 1.5
 Aubrée, J., 3.1
 Authier, A., 1.1, 1.3, 3.3
- Bacon, C. R., 3.1
 Badan, J., 1.7
 Bak, P., 1.10
 Baker, A. G., 3.1
 Bala, V. B., 3.1
 Balkanski, M., 3.1
 Balluffi, R. W., 3.2, 3.3, 3.4
 Banerjee, P. P., 1.7
 Banfield, J. F., 3.3
 Banholzer, W. F., 1.8
 Barbara, B., 1.5
 Barber, D. J., 3.3
 Barkley, J. R., 3.4
 Baroni, S., 2.1
 Barrett, C. S., 3.3
 Barron, T. H. K., 1.4
 Barsch, G. R., 3.4
 Bartels, H., 3.3
 Barth, U. von 2.2
 Baruchel, J., 1.5
 Bass, J., 1.8
 Batchko, R. G., 3.4
 Bauer, P., 1.5
 Bauman, R. P., 2.3, 3.1
 Baumgartner, R. A., 1.7
 Baumhauer, H., 3.3
 Bazan, Ch., 1.5
 Bazhan, A. N., 1.5
 Bazylinski, D. A., 3.3
 Beasley, M. R., 1.8
- Beaulac, T. P., 1.8
 Becke, F., 3.2, 3.3
 Becker, R., 1.5
 Becker, R. A., 3.3
 Beest, B. W. van 1.10
 Beier, B., 1.7
 Belov, N. V., 1.5
 Belova, E. N 1.5
 Belyi, L. I., 1.5
 Ben Salem, M., 3.3
 Benedek, G., 2.4
 Bennema, P., 3.3
 Berger, H., 1.8
 Berman, R., 1.8
 Bernstein, J. L., 1.7
 Bertagnolli, E., 3.4
 Bertaut, E. F., 1.5, 3.3
 Bethea, C. G., 1.7
 Bhagavantam, S., 1.1
 Bichurin, M., 1.5
 Bickford, L. R. Jr 1.5
 Billiet, Y., 3.3
 Billings, A., 1.1
 Bilz, H., 2.1
 Birman, J. L., 1.10, 2.3
 Birss, R. R., 1.5
 Bismayer, U., 3.3
 Bisson, S. E., 1.7
 Blachman, R., 1.7
 Black, P. J., 3.3
 Blackburn, J., 3.3
 Blaha, P., 2.2
 Blattner, H., 3.2
 Blech, I., 1.10
 Blinc, R., 1.10, 3.1
 Bliss, D. F., 3.3
 Blit, S., 1.7
 Blöchl, P. E., 2.2
 Bloembergen, N., 1.5, 1.7
 Bloss, F. D., 1.6, 3.2, 3.3
 Blügel, S., 2.2
 Blumberg, G. E., 3.1
 Blunt, J., 3.3
 Boček, P., 3.1
 Bögels, G., 3.3
 Boisen, M. B., 1.4, 3.4
 Bokhenkov, E. L., 2.1
 Bokov, V. A., 3.4
 Bolle, K. J., 1.7
 Bollen, D., 3.3
 Bollmann, W., 3.2, 3.3, 3.4
 Bonner, W. A., 3.3
 Bonneville, R., 1.7, 3.4
 Bonnini, C., 1.7
 Boon, M., 3.1
 Bordui, P. F., 1.7
 Born, M., 1.6, 2.4
 Borovik-Romanov, A. S., 1.5
 Bosenberg, W. R., 1.7
 Bosshard, C., 1.7
 Böttcher, P., 3.3
 Bouckaert, L. P., 2.2
 Boulanger, B., 1.7
 Boulesteix, C., 3.3, 3.4
 Bourges, P., 2.1
 Boyd, G. D., 1.7
 Boyd, R. W., 1.7
 Boyer, L., 1.3, 2.4
 Bradler, J., 3.3
 Bradley, C. J., 2.1, 2.2, 3.1, 3.2, 3.4
 Bragg, W. L., 1.6, 3.3
 Brandmüller, J., 2.3
 Brasselet, S., 1.7
 Breazeale, M. A., 1.3
 Brecht, E., 3.3
 Breitenbach, G., 1.7
 Brenier, A., 1.7
 Bridenbaugh, P. M., 3.1
 Brillouin, L., 1.1, 1.3, 2.4
- Bringhurst, K. N., 3.3
 Brixel, W., 3.3, 3.4
 Brögger, W. C., 3.3
 Broomé, B., 3.3
 Brosnan, S. J., 1.7
 Brugger, K., 1.3
 Brulay, J., 3.3
 Bruls, G. J. C. L., 1.8
 Buckley, A., 3.3
 Buda, F., 1.4
 Budden, F. J., 3.2
 Bueble, S., 3.3
 Buerger, M. J., 3.2, 3.3
 Buijsters, J. G., 3.3
 Bul'bich, A. A., 3.4
 Burckhardt, J. J., 1.5
 Bürgi, H.-B., 1.9
 Burke, K., 2.2
 Burkhardt, E., 3.3, 3.4
 Burkhardt, U., 3.3
 Bursill, L. A., 3.3
 Burstein, E., 2.3
 Burzlaff, H., 1.9
 Burzo, E., 1.5
 Buseck, P. R., 3.3
 Butcher, P. N., 1.6, 1.7
 Butler, P. H., 1.2
 Butler, W. H., 1.8
 Byer, R. L., 1.7, 3.4
- Cabirol, X., 1.7
 Cady, W. G., 1.1, 3.2
 Cahn, J. W., 1.10
 Cahn, R. W., 3.2, 3.3, 3.4
 Calleja, M., 3.4
 Callen, H., 2.3
 Canali, C., 1.8
 Cao, W., 3.4
 Car, R., 1.4, 2.2
 Cardona, M., 2.3
 Cardwell, M. J., 1.5
 Carpenter, M. A., 3.4
 Catti, M., 3.4
 Cecchi, L., 2.4
 Ceperley, D. M., 2.2
 Chabbal, R., 2.4
 Chakraborty, B., 1.8
 Chalmers, B., 3.3
 Chan, L. Y. Y., 3.1
 Chantrel, H., 2.4
 Chappert, J., 1.5
 Chauvet, O., 1.8
 Chemla, D., 3.4
 Chemla, D. S., 1.7
 Chen, Q., 3.1
 Chen, X. J., 3.4
 Cheng, K., 1.7
 Chernysheva, M. A., 3.2, 3.3
 Chirila, R., 3.3
 Christian, J. W., 3.3, 3.4
 Chrosch, J., 3.4
 Chu, C. W., 3.1
 Chung, H., 3.3
 Chung, J., 1.7
 Chung, S. J., 3.3
 Claringbull, G. F., 3.3
 Clark, A. E., 1.5
 Claus, R., 2.3
 Clin, M., 3.3, 3.4
 Cline, T. W., 3.4
 Cochran, W., 3.1
 Colle, R., 2.2
 Collin, G., 2.1
 Condon, E. U., 2.2
 Connes, P., 2.4
 Conrad, D., 3.3
 Cooper, B. R., 1.5
 Coquillay, A., 1.7
 Cotter, D., 1.6, 1.7
- Cottrell, A. H., 3.3
 Courtens, E., 2.4
 Cowley, J. M., 3.3
 Cowley, R. A., 3.1
 Cox, D. E., 1.5, 3.1
 Cox, K. G., 1.6
 Cracknell, A. P., 1.5, 2.1, 2.2, 3.1, 3.2, 3.4
 Cross, L. E., 3.4
 Cummins, H. Z., 2.4
 Curie, J., 1.1
 Curie, P., 1.1, 1.5
 Curien, H., 3.3, 3.4
- Davey, R. J., 3.3
 De Launay, J., 1.3
 Debuisschert, T., 1.7
 Dederichs, P. H., 2.2
 Dénoyer, F., 1.10
 DeSavage, B. F., 1.5
 Devanarayanan, S., 1.4
 Devarajan, V., 1.6
 Devonshire, A. F., 3.1
 Devouard, B., 3.3
 Dimmock, J. O., 3.1
 Ding, D.-H., 1.10
 Dmitriev, V., 3.1, 3.4
 Dmitriev, V. G., 1.7
 Docherty, R., 3.3
 Dodge, J. S., 1.8
 Doert, Th., 3.3
 Dolinichuk, S. G., 1.7
 Dolino, G., 3.4
 Donaldson, W., 1.7
 Donnay, G., 3.2, 3.3
 Donnay, J. D. H., 3.2, 3.3, 3.4
 Donnelly, R. A., 2.2
 Döring, W., 1.5
 Dorner, B., 2.1
 Dou, S. X., 1.7
 Douady, J., 1.7
 Dougherty, J. P., 1.7
 Dove, M. T., 2.1, 3.4
 Drabold, D. A., 2.2
 Dreizler, R. M., 2.2
 Dries, L. T., 3.1
 Driscoll, T. A., 1.7
 Drittler, B., 2.2
 Drobyshchev, L. A., 1.5
 Ducuing, J., 1.7
 Dudley, M., 3.3
 Dudnik, E. F., 3.3, 3.4
 Dufek, P., 2.2
 Dunitz, J. D., 1.9
 Dunn, M. H., 1.7
 Dvořák, V., 3.1
 D'Yvoire, F., 3.3
 Dziedzic, J. M., 1.7
 Dzyaloshinskii, I. E., 1.5
- Easterling, K. E., 3.3
 Ebert, H., 2.2
 Ebrahimzadeh, M., 1.7
 Eckardt, R. C., 1.7
 Eckold, G., 2.1
 Edwards, P. P., 3.3
 Edwards, T. J., 1.7
 Egelstaff, P. A., 2.4
 Eger, D., 1.7, 3.4
 Eibschutz, M., 3.1
 Eimerl, D., 1.7
 El-Korashy, A., 3.3
 Ellis, D. E., 2.2
 Ellner, M., 3.3
 Elsässer, C., 2.2
 Enckevort, W. J. P. van, 3.3
 Enculescu, I., 3.3
 Engel, G., 3.3
 Ephraïm, M., 1.2

AUTHOR INDEX

- Eremenko, V. V., 1.5
Erhart, J., 3.4
Ernst, F., 3.3
Ernzerhof, M., 2.2
Errandonea, G., 3.1
Etchepare, J., 1.7
Evans, J. S. O., 1.4
Ewald, P. P., 1.6
Ewert, D., 3.3
Eyring, L., 3.3
- Faber, J., 1.5
Fabre, C., 1.7
Fahlen, T. S., 1.7
Fähnle, M., 2.2
Fatuzzo, E., 3.4
Fedosejevs, R., 1.7
Fefer, E. M., 3.1
Feigelson, R. S., 1.7
Fejer, M. M., 1.7, 3.4
Ferrari, J. M., 1.5
Ferraris, G., 3.3, 3.4
Ferré, J., 1.3, 1.5
Fesenko, E. G., 3.4
Fève, J. P., 1.7
Fimberg, T. A., 3.1
Finnis, M. W., 3.3
Fischer, M., 1.3
Fischmeister, H. F., 3.2
Fisher, M. E., 1.5
Fix, A., 1.7
Flack, H. D., 3.3
Fleischer, J. F., 1.8
Fleming, S. D., 3.3
Fleury, P. A., 3.1
Flükiger, R., 3.3
Folen, V. J., 1.5
Follner, H., 3.3
Foner, S., 1.5
Forro, L., 1.8
Fossheim, K., 3.1
Fousek, J., 3.3, 3.4
Fox, D. L., 3.1
François, M., 3.3, 3.4
Frankel, R. B., 3.1, 3.3
Franken, P., 1.7
Franz, R., 1.8
Freeman, A. J., 1.5
Freeman, P., 3.3
Frey, T., 1.9
Fridkin, V. M., 3.2
Friedel, G., 2.4, 3.2, 3.3, 3.4
Friedel, J., 3.3
Fritsch, K., 2.4
Fronde, C., 3.3
Frota-Pessoa, S., 2.2
Fukano, Y., 3.3
Fuksa, J., 3.2, 3.4
Fumi, F. G., 1.1, 1.3
Fyfe, C., 3.3
- Gaal, P. S., 1.4
Gagulin, V. V., 1.5
Garito, A. F., 1.7
Gavril'yachenko, B. G., 3.4
Geballe, T. H., 1.8
Gehring, G. A., 1.5
Gelatt, C. D. Jr 2.2
Geldart, D. J. W., 1.8
Gelder, A. P. van, 1.8
Geller, S., 3.1
Gerson, R., 1.5
Gesland, J. Y., 1.3
Geusic, J. E., 1.7
Gevers, R., 3.3
Ghose, S., 3.4
Giacobino, E., 1.7
Giacovazzo, C., 3.2
Giannozzi, P., 2.1
Gibbs, G. V., 1.4, 3.4
Gignoux, D., 1.5
Gijssman, H. M., 1.5
Gillert, M., 1.7
Ginzburg, V., 1.6, 2.3
- Gironcoli, S. de, 1.4, 2.1
Girvin, S. M., 1.8
Glass, A. M., 1.6, 3.1, 3.4
Glazer, A. M., 1.6
Gnatchenko, S. L., 1.5
Godby, R. W., 2.2
Gold, A., 3.4
Goldsmid, H. J., 1.8
Gorbatsevich, A. A., 1.5
Gordon, L. A., 1.7
Gornall, W. S., 2.4
Gottschalk, H., 3.3
Gottstein, G., 3.2, 3.3
Graeme-Barber, A., 3.3, 3.4
Gramaccioli, C. M., 1.9
Gratias, D., 1.10
Green, R. E., 1.3
Greer, A. L., 3.1
Gregora, I., 2.3
Grell, H., 3.4
Grell, J., 3.4
Griffin, D. T., 3.3
Grillon, G., 1.7
Grimmer, H., 1.5, 3.3
Grimvall, G., 1.8
Gross, E., 2.4
Gross, E. K. U., 2.2
Grossmann, G., 2.2
Groth, P., 1.6
Groves, G. W., 3.3
Grumbach, M. P., 2.2
Gruverman, A. L., 3.4
Gu, M., 3.1
Guccione, R., 1.5
Guenzburger, D., 2.2
Gufan, Yu. M., 3.4
Guggenheim, H. J., 3.1
Gunnarsson, O., 2.2
Güntherodt, G., 2.3
Guo, Y., 3.3
Gupta, P. K., 1.7
Gurzadian, G. G., 1.7
Gust, W., 3.3
Gustafson, E. K., 1.7
- Habbal, F., 3.1
Hadni, A., 1.7
Haegele, E., 3.3
Hahn, T. A., 1.4
Hahn, Th., 1.10, 2.1, 3.2, 3.3, 3.4
Hajdukovic, G., 3.1
Halbout, J. M., 1.7
Hall, M. Jr 3.2
Hámos, L. von 3.2
Hariharan, P., 2.4
Harmon, B. N., 2.2
Harris, S. E., 1.7
Hartman, P., 3.3
Hartshorne, N. H., 1.6
Hatanaka, T., 1.7
Hatch, D. M., 1.2, 3.1, 3.4
Hatt, R. A., 3.4
Haüy, R.-J., 3.2
Hayden, L. M., 1.7
Hayes, W., 2.3, 2.4
Hazell, R. G., 1.9
Hedin, L., 2.2
Heesch, H., 1.5
Heger, G., 3.3
Heide, F., 3.3
Heiming, A., 2.1
Hellström, J., 1.7
Henderson, A. J., 1.7
Henke, H., 3.3
Herbst-Irmer, R., 3.3
Hercher, M., 2.4
Herman, W. N., 1.7
Hervieu, M., 3.3
Herzig, C., 2.1
Herzig, P., 1.2, 2.2, 3.1, 3.4
Hierle, R., 1.7
Hill, A. E., 1.7
Hippel, A. von, 3.2
Hiralal, I. D. K., 3.3
- Hobden, M. V., 1.7
Hoffmann, D., 3.3
Hoffmann, R., 2.2
Hofmeister, H., 3.3
Hohenberg, P., 2.2
Holser, W. T., 3.3, 3.4
Hor, P. H., 3.1
Horiuchi, N., 1.7
Hornstra, J., 3.3
Hou, S. L., 1.5
Houchmandzadeh, B., 3.4
Housley, R. M., 3.3
Hu, C.-Z., 1.10
Hu, X. B., 3.4
Hua, X., 3.3
Huang, C. Y., 3.1
Huang, X. R., 3.3, 3.4
Hulin, D., 1.7
Hulm, J. K., 3.1
Hummel, W., 1.9
Hummeler, K., 2.2
Hurle, D. T. J., 3.3
Hurst, V. J., 3.3
Hybertsen, M. S., 2.2
- Ibanez, A., 1.7
Iida, S., 1.5
Ikeda, T., 1.1
Ikeno, S., 3.3
Iliescu, B., 3.3
Indenbom, V. L., 1.5, 3.1, 3.2, 3.4
Ipatova, I. P., 2.1
Ishibashi, Y., 3.3, 3.4
Ishimasa, T., 3.3
Isupov, V. A., 1.5, 3.4
Ito, H., 1.7
Ito, R., 1.7
Ivanov, A. S., 2.1
Ivanov, N. R., 3.3, 3.4
Izyumov, Yu. A., 1.5, 3.1
- Jaccard, D., 1.8
Jackson, J. D., 1.5
Jacobi, H., 3.3
Jacoboni, C., 1.8
Jahn, H. A., 1.9
James, W. J., 1.5
Jamsek-Vilfan, M., 3.1
Janak, J. F., 2.2
Janner, A., 1.2, 1.5, 1.10
Janovec, V., 3.1, 3.2, 3.3, 3.4
Jansen, H. B., 2.2
Jansen, L., 3.1
Janssen, T., 1.2, 1.10, 3.2
Jarlborg, T., 1.8
Jeitschko, W., 3.3, 3.4
Jennissen, H.-D., 3.3
Jerphagnon, J., 1.7, 3.4
Jessen, S. M., 1.4
Ji, R.-F., 3.1
Jia, C. L., 3.3
Jiang, S. S., 3.4
Johnsen, A., 3.3
Johnson, C. K., 1.9
Jona, F., 1.6, 3.4
Jones, R., 3.3
Jones, R. C., 1.6
Jonson, M., 1.8
Joon, E. R., 3.1
Jorda, J.-L., 3.3, 3.4
Joshua, S. J., 1.5
Josse, D., 1.7
Judd, J. W., 3.3
Juisrud, S., 3.1
Julliard, J., 1.3
Jundt, D. H., 1.7
Junghans, T., 3.3
Junod, A., 1.8
- Kadeckova, S., 3.3
Kadomtseva, A. M., 1.5
Kalonji, G., 3.2, 3.4
Kalus, J., 2.1
Kaminow, I. P., 1.6
- Kaminsky, W., 1.6
Kaned, Y., 1.7
Känzig, W., 3.2, 3.4
Kapitulnik, A., 1.8
Karlssohn, H., 1.7
Kato, K., 1.7
Kato, N., 3.3
Katsui, A., 3.3
Katz, M., 1.7, 3.4
Kaufmann, E. N., 2.2
Kawakami, S., 1.5
Kawase, K., 1.7
Kay, H. F., 3.2
Kaz, A., 1.7
Kazei, Z. A., 1.5
Kearley, G., 2.4
Keester, K. L., 3.3
Kelly, A., 3.3
Kempen, H. van, 1.8
Kennedy, G. T., 1.7
Kerber, A., 3.2
Kerr, P. F., 1.6
Khan, F. S., 1.8
Kharchenko, N. F., 1.5
Khodja, S., 1.7
Kiselev, S. V., 1.5
Kittinger, E., 3.4
Klapper, H., 3.2, 3.3
Klassen-Neklyudova, M. V., 3.2, 3.3, 3.4
Klein, C., 3.2
Klein, L., 1.8
Kleinman, D. A., 1.7
Klemens, P. G., 1.8
Knappe, R., 1.7
Knorr, K., 3.3
Knox, R. S., 3.4
Kobayashi, J., 3.1
Koch, A., 3.3
Koch, E., 3.2, 3.3, 3.4
Koch, K., 1.7
Kociński, J., 3.1
Koelling, D. D., 2.2
Kogure, T., 3.3
Kohn, J. A., 3.3
Kohn, W., 2.2
Kolar, D., 3.3
Kominiak, G. J., 3.1
Koňák, Č., 3.4
Kondo, T., 1.7
Kopaev, Yu. V., 1.5
Kopský, V., 1.5, 1.10, 3.1, 3.2, 3.4
Koptsik, J. N., 1.5
Koptsik, V. A., 1.5, 1.10, 3.2, 3.4
Kornienko, N. E., 1.7
Korringa, J., 2.2
Koshino, S., 1.8
Koster, G. F., 3.1
Kotler, Z., 1.7
Kotrbova, M., 3.3
Kouvel, J. S., 1.5
Kovalev, O. V., 1.2, 1.5, 2.1
Kovrygin, A. I., 1.7
Kozlov, G. V., 3.1
Krafczyk, S., 3.3
Krainik, N. N., 3.4
Krause, C., 3.4
Krempel, P., 3.3
Kress, W., 2.1
Krisch, M. H., 2.4
Krishnamurthy, N., 1.1
Krishnan, R. S., 1.4
Krynetskii, I. B., 1.5
Kübler, J., 2.2
Kuks, W. F., 1.9
Kulp, T. J., 1.7
Kumaraswamy, K., 1.1
Kuo, P. K., 1.8
Küppers, H., 1.4
Kuratsuowski, K., 3.2
Kurki-Suonio, K., 2.2
Kurtz, S. K., 1.7
Kuscholke, B., 3.3
Kuzhukeev, Zh.-N. M., 1.5

AUTHOR INDEX

- Kuzmicheva, G. M., 3.3
Kuzminov, E. G., 3.1
Kuznetsov, P. I., 1.9
- Laegreid, T., 3.1
Lahajnar, G., 3.1
Lajzerowicz, J., 3.4
Landau, L. D., 1.5, 3.1, 3.2
Lander, G. H., 1.5
Lang, A. R., 3.3
Lang, S., 3.2
Larson, D. J., 3.3
Laurell, F., 1.7
Lax, M., 2.4
Lax, M. J., 2.3
Lazay, P. D., 2.4
Lazzeri, M., 1.4
Le Corre, Y., 3.3, 3.4
Le Gall, H., 1.5
Le Page, Y., 3.3
Lecomte, M., 1.3
Ledermann, W., 3.2
Ledoux, I., 1.7
Lee, E. W., 1.5
Lee, G., 1.5
Lefaucheux, F., 1.7
LeGarrec, B., 1.7
Leibfried, G., 2.1
Lepers, C., 1.7
Letuchev, V. V., 3.4
Levanyuk, A. P., 3.1, 3.4
Levin, K. H., 1.7
Levine, B. F., 1.7
Levinstein, H. J., 1.7
Levitin, R. Z., 1.5
Levy, H. A., 1.9
Levy, M., 2.2
Lewis, J. G., 1.6
Leycuras, C., 1.5
Lichnerowicz, A., 1.1
Lieber, W., 3.3
Lieberman, H. F., 3.3
Liebisch, Th., 3.3
Lifshitz, E. M., 1.5, 3.1
Lindsay, I. D., 1.7
Lines, M. E., 1.6, 3.1, 3.4
Lipschutz, S., 3.2
Lipscomb, G. F., 1.7
Litvin, D. B., 3.4
Litvinenko, Yu. G., 1.5
Litzler, A., 3.1
Liu, J. S., 3.4
Liu, W. J., 3.4
Locherer, K. R., 3.4
Loran, J., 3.3
Loucks, T. L., 2.2
Loudon, R., 2.3, 2.4
Louie, G., 2.2
Louisell, W. H., 1.7
Love, W. F., 1.2
Lowry, T. M., 1.6
Lubensky, T. C., 1.10
Lucas, D. W., 3.1
Lukina, M. M., 1.5
Lundqvist, B. I., 2.2
Lynch, R. T., 1.7
Lytle, F. W., 3.1
Lyubarskii, G. Ya., 3.1
Lyubimov, V. N., 1.5
- MacDonald, A. H., 1.8
MacFarlane, R. M., 3.1
Mach, J. E., 2.4
Machonský, L., 3.4
Mackenzie, G. A., 2.1
Mader, W., 3.3
Magel, G. A., 1.7
Mahan, G. D., 1.8
Maisch, W. G., 1.5
Mallard, E., 3.2, 3.3
Mang, H., 3.3
Man'ko, V. I., 1.5
Manolakis, C., 3.3
Maradudin, A. A., 2.1
- Marchenko, V. I., 1.5
Marnier, G., 1.7
Marshall, D. B., 3.3
Marshall, L. R., 1.7
Martin, R. A., 2.2
Maruyama, H., 3.3
Mary, T. A., 1.4
Masciovecchio, C., 2.4
Mason, W. P., 1.1, 1.5
Massalski, T. B., 3.3
Masse, R., 1.7
Matarrese, L. M., 1.5
Mathieu, J. P., 2.3
Matthias, B., 3.2
Matthiessen, A., 1.8
McLaren, A. C., 3.3
McNutt, D. P., 2.4
McSkimmin, H. J., 1.3
Meekes, H., 3.3
Mehendale, S. C., 1.7
Melcher, R. L., 1.3
Ménaert, B., 1.7
Meng, R. I., 3.1
Menzer, G., 3.3
Mercier, M., 1.5
Mercier, R., 1.5
Merkulov, V. S., 1.5
Merten, L., 2.3
Merz, W., 3.2
Merz, W. J., 3.4
Methfessel, M., 2.2
Meyer, B., 2.2
Michard, F., 1.3
Michel, C., 3.3
Michel, Ch., 1.5
Michel, L., 3.2
Midwinter, J. E., 1.7
Miekeley, W., 2.1
Migus, A., 1.7
Mikvabia, V. D., 3.1
Miller, A., 1.7
Miller, C. S., 3.4
Miller, G. D., 3.4
Miller, S. C., 1.2
Milov, V. N., 1.5
Milton, J. T., 1.7
Minella, D., 1.5
Ming, N. B., 3.3
Mirza, K., 3.3
Mirzoyants, G. I., 3.1
Mitrofanov, N. L., 2.1
Mitsui, T., 3.4
Miuskov, V. F., 3.3
Mlynek, J., 1.7
Mohs, F., 3.2
Molchanov, V. N., 3.3
Monaco, G., 2.4
Montroll, E. W., 2.1
Mooij, J. H., 1.8
Moore, G. T., 1.7
Moreau, J.-M., 1.5
Morin, F. J., 1.5
Morita, R., 1.7
Moriya, T., 1.5
Morrell, J. A., 1.7
Moskvin, A. S., 1.5
Mostowski, A., 3.2
Moxon, J. R. L., 1.6
Mueller, H., 3.2
Mügge, O., 3.3
Mukhin, A. A., 1.5
Müller, W. F., 3.3
Münster, C., 1.6
Murnaghan, F. D., 1.3
Myers, L. E., 1.7
- Naish, V. E., 1.5
Nakamura, E., 3.4
Nakamura, K., 1.7
Narang, R. S., 1.7
Narasimhamurty, T. S., 1.6
Natkaniec, I., 2.1
Naumann, C. F., 3.2
Naumenko, V. M., 1.5
- Nebel, A., 1.7
Néel, L., 1.5
Nelmes, R. J., 1.9
Nelson, D. F., 2.4
Neronova, N. N., 1.5
Nespolo, M., 3.3
Neumann, F., 1.1
Neumann, W., 3.3
Newnham, R. E., 3.3, 3.4
Nicoud, J. F., 1.7
Niggli, P., 3.2, 3.3
Nikogosyan, D. N., 1.7
Nikolaeva, E. V., 3.4
Nimmo, J. K., 3.1
Niu, Z., 3.1
Nord, G. L., 3.3
Nouet, J., 1.3
Novak, J., 3.3
Nowick, A. S., 1.1, 3.1
Nusair, M., 2.2
Nusimovici, M., 3.1
Nussbaum, A., 1.6
Nye, J. F., 1.1, 1.4, 1.7, 2.3, 3.1, 3.4
- O'Dell, T. H., 1.5
Offenberger, A., 1.7
Ogasawara, N., 1.7
Oliver, W. F., 3.1
Onsager, L., 1.1
Opechowski, W., 1.5, 3.2, 3.4
Ordejon, P., 2.2
Orlova, M. P., 1.5
Oron, M., 1.7, 3.4
Ossipyan, Yu. A., 3.4
Ottaviani, G., 1.8
Oudar, J. L., 1.7
Ozerov, R. P., 1.5
Ozhogin, V. I., 1.5
- Pacaud, O., 1.7
Pach, K., 1.9
Palke, W. A., 2.2
Palm, J. H., 1.9
Palmer, D. C., 3.3, 3.4
Pappis, J., 1.5
Parkinson, G. M., 3.3
Parr, R., 2.2
Parrinello, M., 1.4, 2.2
Pasiskevicius, V., 1.7
Pasteur, L., 1.1
Pasynkov, R. E., 3.4
Patera, J., 3.1
Patzner, G., 3.3
Paufler, P., 1.1
Pauthenet, R., 1.5
Pavone, P., 2.1
Pawley, G. S., 2.1
Percy, P. S., 3.1
Penn, R. L., 3.3
Penzkofer, A., 1.7
Perdew, J. P., 2.2
Perez-Mato, J. M., 3.1
Perigaud, A., 1.7
Perkins, P. E., 1.7
Perry, J. W., 1.7
Perry, T. T., 1.7
Pershan, P., 1.7
Peterlin-Neumaier, T., 1.5
Peters, C. W., 1.7
Peterse, W. J. A. M., 1.9
Petrilli, H. M., 2.2
Petrov, S. B., 1.5
Petry, W., 2.1
Petzelt, J., 3.1
Phakey, P. P., 3.3
Phillips, F. C., 3.3
Phillips, R. A., 1.6
Pick, R., 3.1
Pierce, J. W., 1.7
Pinczuk, A., 2.3
Pine, A. S., 2.4
Pinski, F. J., 1.8
Pintschovius, L., 2.1
Pisani, C., 2.2
- Pisarev, R. V., 1.3
Pliszka, P., 1.7
Pohalski, C. C., 1.7
Pond, R. C., 3.2, 3.4
Popov, S. N., 1.5
Popov, Yu. F., 1.5
Porter, D. A., 3.3
Porto, S. P. S., 2.3, 3.1
Pósfai, M., 3.3
Pot, T. M., 3.3
Poulet, H., 2.3
Poulligny, B., 3.1
Poulis, N. J., 1.5
Powers, P. E., 1.7
Prasad, V., 3.3
Pratt, W. P., 1.8
Prewitt, C. T., 3.1
Price, P. F., 1.9
Primot, J., 3.1
Pritchard, R. G., 3.3
Přívratká, J., 3.4
Prokhorov, A. S., 1.5
Prokhorova, S. D., 3.1
Pryor, A. W., 1.9
Pryor, R. W., 1.8
Puccetti, G., 1.7
Punin, Yu. O., 3.3
Putnis, A., 3.3, 3.4
Pyka, N., 2.1
Pyykkö, P., 2.2
- Qin, Z.-K., 3.1
Qiu, P., 1.7
Quaranta, A. A., 1.8
Queisser, H. J., 3.3
- Raaz, F., 3.3
Rado, G. T., 1.5
Raghothamachar, B., 3.3
Raj, R., 1.7
Ramaswamy, S., 1.10
Ramdohr, P., 3.3
Raselli, A., 1.9
Räuber, A., 3.3
Raveau, B., 3.3
Ravez, J., 3.1
Raymakers, R. J., 1.7
Razé, G., 1.7
Read, W. T., 3.3
Rebane, L., 3.1
Rečnik, A., 3.3
Redfern, S., 3.3
Reichardt, W., 2.1
Reid, D. T., 1.7
Reintjes, J., 1.7
Reissland, J. A., 2.1
Remeika, J. P., 3.1
Renard, M., 1.7
Renshaw, A. R., 1.6
Revaz, B., 1.8
Revcolevschi, A., 3.3
Richterová, L., 3.4
Rieder, H., 1.5
Rijkeboer, A., 3.3
Ripamonti, C., 1.1
Rivera, J.-P., 1.5, 3.3, 3.4
Roberts, K. J., 3.3
Robinson, D. J. S., 3.2
Rode, D. L., 1.8
Roessler, F. L., 2.4
Rohl, A. L., 3.3
Romé de l'Isle, J. B. L., 3.2
Rose, G., 3.3
Rosen, H., 3.1
Rosen, J., 3.2
Rosenman, G., 1.7, 3.4
Rosker, M. J., 1.7
Rosová, A., 3.4
Rostocker, N., 2.2
Roth, G., 3.3
Roth, W. L., 1.8
Roucau, C., 3.4
Rousseau, D. L., 2.3, 3.1
Rousseau, I., 1.7

AUTHOR INDEX

- Rousseau, M., 1.3
Route, R. K., 1.7
Rowe, D. M., 1.8
Röwer, R. W., 3.3
Rudashevskii, E. G., 1.5
Ruffing, B., 1.7
Rühle, M., 3.3
Rumiantsev, A. Yu., 2.1
Rumyantsev, E. L., 3.4
Ruocco, G., 2.4
Ruse, G. F., 3.1
Ruvimov, S., 3.3
Rychetský, I., 3.4
Rytz, D., 1.7
- Saint-Grégoire, P., 3.4
Sakudo, T., 3.1
Sakurai, K., 3.3
Salamon, M. B., 1.8
Salje, E. K. H., 1.3, 3.3, 3.4
Salvetti, O., 2.2
Sandercock, J. R., 2.4
Sandratskii, L. M., 2.2
Sands, D. E., 1.1
Sandvold, E., 3.1
Sannikov, D. G., 3.1
Santi, G., 1.8
Santoro, A., 3.3
Sapriel, J., 1.6, 3.3, 3.4
Sauvage, M., 3.3
Savary, H., 3.1
Saxena, S. K., 1.4
Schaskolsky, M., 3.3
Scheerschmidt, K., 3.3
Scheffen-Lauenroth, T., 3.3
Scheidt, M., 1.7
Schell, A. J., 1.7
Scherf, Ch., 3.3
Scheringer, C., 1.9
Scherrer, P., 3.2
Schiller, S., 1.7
Schlenker, J. L., 1.4, 3.4
Schlenker, M., 1.5
Schlüter, M., 2.2
Schmahl, W. W., 3.3
Schmelzer, U., 2.1
Schmid, H., 1.5, 3.3, 3.4
Schmidt, C., 3.3
Schmidt, V. H., 3.1
Schneck, J., 3.1
Schober, H. R., 2.1
Schoen, P. E., 2.4
Schranz, W., 3.4
Schroeder, P. A., 1.8
Schubnikow, A., 3.3
Schulz, H., 1.9
Schwartz, L., 1.1, 1.7
Schwarz, K., 2.2
Schwarzenberger, R. L. E., 1.5
Scott, B. A., 1.3
Scott, J., 3.4
Scott, J. F., 3.1
Scott, R. A. M., 1.5
Seifert, H., 3.3
Seitz, F., 2.2
Seki, H., 3.1
Semenchev, A. F., 3.4
Semenov, V. A., 1.5
Sen, J., 2.4
Senechal, M., 1.10, 3.3
Sette, F., 2.4
Sham, L. J., 2.2
Shannon, R. D., 3.1
Shapiro, S. M., 3.1
Sharp, R. T., 3.1
Shaskol'skaya, M. P., 1.1, 1.5, 3.1, 3.4
Shawabkeh, A., 3.1
Shchurov, V. A., 1.5
Shechtman, D., 1.10
Sheka, E. F., 2.1
Shekhtman, V. Sh., 3.3, 3.4
Sheldrick, G. M., 3.3
Shen, G., 1.4
Shen, H., 3.1
- Shen, Y. R., 1.7
Sher, E. S., 1.5
Shinnaka, Y., 3.1
Shirane, G., 1.6, 3.4
Shishkin, E. I., 3.4
Shmueli, U., 1.9
Shmyt'ko, I. M., 3.4
Shortley, G. H., 2.2
Shternberg, A. A., 3.2
Shtukenberg, A. G., 3.3
Shubnikov, A. V., 1.5, 3.2, 3.4
Shur, M. S., 3.4
Shur, V. Ya., 3.4
Shuvalov, L. A., 1.1, 1.5, 1.7, 3.1, 3.2, 3.3, 3.4
Shvindlerman, L. S., 3.2, 3.3
Shvydko, Yu. V., 3.3
Sibbett, W., 1.7
Sidorkin, A. S., 3.4
Siegman, A. E., 1.7
Siegman, E., 1.7
Sierro, J., 1.8
Sievers, A. J., 1.8
Sigelle, M., 1.7
Singh, D. J., 2.2
Singh, K. K., 3.3
Singh, S., 1.7
Siny, I. G., 3.1
Sirotnin, Yu. I., 1.1, 1.5, 1.9, 3.1, 3.4
Sizmann, A., 1.7
Skinner, D. P. Jr 3.4
Skliar, A., 1.7, 3.4
Skriver, H. L., 2.2
Slack, G. A., 1.8
Slater, J. C., 2.2
Sleight, A. W., 1.4
Smirnov, G. V., 3.3
Smirnova, T. S., 1.5
Smith, D. J., 3.3
Smith, J. V., 3.3
Smith, R. G., 1.7
Smith, V. H. Jr 1.9
Smolenskii, G. A., 1.5, 3.1, 3.4
Smoluchowski, R., 2.2
Smutný, F., 3.4
Snoeck, E., 3.4
Snyder, G. J., 1.8
Socular, J. E. S., 1.10
Sonin, E. B., 3.4
Sorantin, P., 2.2
Sosnovska, I., 1.5
Speiser, A., 3.2
Spencer, E. G., 3.1
Spitzer, D. P., 1.8
Springborg, M., 2.2
Srinivasan, R., 1.4
Srivastava, G. P., 2.1
Stadnicka, K., 1.6
Stalder, E. W., 1.5
Statz, H., 3.1
Steichele, E., 1.5
Stein-Arsic, M., 2.1
Steinhardt, P. J., 1.10
Stoicheff, B. P., 2.4
Stokes, H., 1.2, 3.1, 3.4
Stolypin, Yu. E., 1.5
Stössel, H., 1.5
Stothard, D. J. M., 1.7
Stout, J. W., 1.5
Stratonovich, R. L., 1.9
Strauch, D., 2.1
Straumal, B., 3.3
Strobl, H., 3.3
Strukov, B. A., 3.1, 3.4
Strunz, H., 3.3
Stuart, A., 1.6
Stull, J. L. 1.5
Subbotin, A. L., 3.4
Suck, J.-B., 2.4
Sugihashi, A., 1.7
Sukhorukov, A. P. 1.7
Sun, D., 3.1
Sunagawa, I., 3.3
Sussner, H., 2.4
- Sutter, H., 3.2
Sutton, A. P., 3.2, 3.3, 3.4
Sweegers, C., 3.3
Swihart, J. C., 1.8
Syromiatnikov, V. N., 1.5, 3.1
Szivessy, G., 1.6
- Tagancev, A., 3.4
Tahvonen, P. E., 3.1
Takahashi, H., 1.7
Takahashi, T., 3.1
Takano, Y., 3.3
Takeda, H., 3.3
Takeuchi, Y., 3.3
Tamazyan, R., 3.3
Tang, C. L., 1.7
Taniuchi, T., 1.7
Tarkhova, T. N., 1.5
Tatsuzaki, I., 3.4
Tavger, B. A., 1.5
Taylor, C. A., 3.3
Taylor, P. L., 1.8
Taylor, R., 1.8
Tebbutt, I. J., 1.6
Teng, M. K., 3.1
Terakura, K., 2.2
Tertsch, H., 3.2, 3.3
Thiers, A., 1.2
Thiessen, P. A., 3.2
Thomas, L. A., 3.3
Thomas, R. L., 1.8
Thro, P. Y., 1.7
Thurmond, C. D., 1.7
Thurston, R. N., 1.3
Thust, A., 3.3
Tichý, J., 3.4
Tikhonov, V. I., 1.9
Tohno, S., 3.3
Tokunaga, M., 3.1
Tolédano, J.-C., 3.1, 3.4
Tolédano, P., 3.1, 3.4
Tomaszewski, P. E., 3.4
Tomov, I. V., 1.7
Tomura, S., 3.3
Toner, J., 1.10
Toupin, R., 1.3
Townsend Smith, T., 1.5
Trampenau, J., 2.1
Trickey, S. B., 2.2
Trueblood, K. N., 1.9
Truesdell, C., 1.3
Tsatskis, I., 3.3
Tschermak, G., 3.2, 3.3
Tsuchimori, M., 3.3
Tsuei, C. C., 1.8
Tsuya, N., 1.5
Turkovic, A., 3.1
Turnbull, G. A., 1.7
Turov, E. A., 1.5
Turrell, G., 2.3
- Uchino, K., 3.4
Umegaki, S., 1.7
Underwood, F. A., 3.3
Unoki, H., 3.1
Unschel, R., 1.7
- Vacher, R., 1.3, 2.4
Vainshtein, B. K., 3.2, 3.4
Valasek, J., 3.2
Van Bueren, H. G., 3.3
Van den Handel, J., 1.5
Van der Waals, J. D., 3.1
Van Landuyt, J., 3.3, 3.4
Van Tendeloo, G., 3.2, 3.3, 3.4
Van Uiter, L. G., 1.7
Vasileva, I. G., 3.3
Vávra, I., 3.4
Velsko, S. P., 1.7
Venetsev, Yu. N., 1.5
Verger-Gaugry, J. L., 1.10
Verhaegen, S. A. C., 3.3
Vettier, C., 1.5
Vianden, R. J., 2.2
- Villeval, P., 1.7
Vlachavas, D. S., 3.2, 3.4
Vogt, C., 1.8
Vogt, T., 1.4
Voigt, W., 1.1, 1.3, 1.5
Volk, G., 3.1
Volkov, A. A., 3.1
Von der Muhl, R., 3.1
Vosko, S. H., 2.1, 2.2
- Wadhawan, V. K., 3.1, 3.2, 3.3, 3.4
Waerden, B. L. van der 1.5
Wagin, S. V., 3.3, 3.4
Wahlstrom, E. E., 1.6
Walker, E., 3.3, 3.4
Walker, M. B., 3.4
Wallace, C. A., 3.3
Wallace, D. C., 1.3
Wallenstein, R., 1.7
Wang, R.-H., 1.10
Wang, Y., 3.1
Wang, Y. N., 3.4
Wang, Z., 1.8
Warhanek, H., 3.4
Warner, J., 1.7
Warren, J. L., 2.1
Weber, H. J., 2.1
Weertman, J., 3.3
Weertman, J. R., 3.3
Wei, L., 1.8
Weigel, D., 1.10
Weinert, M., 2.2
Weinreich, G., 1.7
Weiss, Chr. S., 3.2
Weiss, G. H., 2.1
Weiss, P., 3.1, 3.2
Weitzenböck, R., 3.1
Wenk, H.-R., 3.3
Western, A. B., 3.1
Weyl, H., 3.1
Wheeler, R. E., 3.1
White, E. A. D., 3.3
White, G. K., 1.4
White, R. L., 1.5
Wiedemann, G., 1.8
Wigner, E., 2.2
Wijn, H. P. J., 1.5
Wilber, S. A., 3.1
Wilk, L., 2.2
Williams, A. R., 2.2
Williams, L., 3.3
Willis, B. T. M., 1.9
Winchell, A. N., 1.6
Windsch, W., 3.1
Winkler, B., 2.2
Winternitz, P., 3.1
Wiser, N., 1.8
Wolf, E., 1.6, 2.4
Wolf, Th., 3.3
Wondratschek, H., 1.9, 3.2, 3.3, 3.4
Wondre, F. R., 3.1
Wood, G. J., 3.3
Wood, I. G., 1.6
Woods, G. L., 1.7
Wooster, W. A., 1.1, 3.3
Worlock, J. M., 3.1
Worlton, T. G., 2.1
Wruck, B., 3.3
Wu, J. W., 1.8
Wunderlich, W., 3.3
Wyder, P., 1.8
- Xu, Y., 3.4
Xu, Z., 3.1
- Yamamoto, A., 1.10
Yang, S. T., 1.7
Yang, W.-G., 1.10
Yangui, B., 3.3
Yao, J. Q., 1.7
Yao, T., 1.8
Yariv, A., 1.6, 1.7
Yavelov, B. E., 1.5
Ye, Z.-G., 1.5

AUTHOR INDEX

- | | | | |
|-------------------------|-----------------------|-------------------------------------|----------------------|
| Yeh, P., 1.6, 1.7 | Zaitsev, V. M., 1.5 | Zheludev, I. S., 1.1, 3.2, 3.3, 3.4 | Zorin, I. A., 1.5 |
| Yin, J., 3.4 | Zalessky, A. V., 1.5 | Zhitomirsky, I. D., 1.5 | Zorin, R. V., 1.5 |
| Youden, J. P. A., 2.4 | Zamorzaev, A. M., 1.5 | Zhu, J., 3.1 | Zucker, U. H., 1.9 |
| Yu, Z., 3.1 | Zarembowitch, A., 1.3 | Zhu, J. S., 3.4 | Zvezdin, A. K., 1.5 |
| Yudin, V. M., 1.5 | Zarembowitch, J., 1.3 | Zieliński, P., 3.4 | Zvirgzds, J. A., 3.1 |
| Yvon, K., 3.3, 3.4 | Zeller, R., 2.2 | Zikmund, Z., 3.3, 3.4 | Zwicker, B., 3.2 |
| | Zhang, M.-S., 3.1 | Ziman, J. M., 1.8 | Zyss, J., 1.7 |
| Zaccaro, J., 1.7 | Zhang, Z., 3.1 | Zinserling, K., 3.3 | Zysset, B., 1.7 |
| Zadorozhnii, V. I., 1.7 | Zhdanov, G. S., 1.5 | Zondy, J. J., 1.7 | |

Subject index

- Ab initio* calculations, 103, 271, 291, 299, 302
ABDP and Kleinmann symmetries, **181**, 188
Absorption colours, 166
 ABX_3 structure type, 415
 A_2BX_4 structure type, 415
Acceptance bandwidths, 197–199, 201, 204, 212
 angular, 198–200, 208, 212
 spectral, 200, 208, 212
 thermal, 200, 212
Acoustic activity, 14
Acoustic branches, **101**, 222, **269**, 272, 288, 315
Acoustic modes, 222, **268**, 272, 317, 470
Acoustic phonons, 91, **223–225**, 270, 282, 314, 326, 329–330
Acousto-optic effect, 3, **175**, *see also* elasto-optic effect
 linear, 152
Acousto-optic interaction, 366
Acousto-optic materials, 175–176
 figure of merit, 176
Actinide elements, 106
Active representation, 359
Acute bisectrix figure, **162**, 164–165
Adiabatic coefficients, 32
Aggregates, 364, 378, **393**, 395, 432, 437, 439, 442, 471
 twin, 397–398, 400, 402, **408–410**, 427–428
Aizu classification, 127, **456–457**, 462
Aizu notation, 427, **428**
Aizu species, **427**, 429, 452, 457, 460
Albite ($\text{NaAlSi}_3\text{O}_8$), 413, 420, 439, 442
 growth twin 398
 twin law, 410, 428–429
Alkali metals, 221, 224
Allotwins, 397, 425
AlMn alloys, 244, 428
Alternative twin operations, 399–400, 402–403, 407–408
Aluminium, 84, 89
Amethyst, 429, 434
Ammonium lithium sulfate (NH_4LiSO_4), 396, 403, 412, 424, 431, 434
Ammonium sulfate $[(\text{NH}_4)_2\text{SO}_4]$, 415–416
Analyser, **154**, 155–157, 159–161
Analyser plane, 156
Anatase (TiO_2), 397, 433, 437
 to rutile phase transition, 437
Angular phase, 131, 136
Anharmonic deformation density, 239
Anharmonic interactions, 224, **225**
Anharmonic potentials, 90–91, 103
Anharmonicity, 80, 100, 228, 266, 272, 363
Anisotropy, 307, 309–310
 energy, **118–120**, 125–127, 131–132, 143, 145–146
 factor, 83–84
Annealing twins, 414, 419
Antibonding states, 306, 309
Anticrossing, 286
Antiferromagnetic crystals, 105, 132
Antiferromagnetic domains, 126, 136–137
Antiferromagnetic ferroelectrics, 106, 130, 141–142
Antiferromagnetic helical structure, **108**, 109, 122
Antiferromagnetic order, 114, 122
Antiferromagnetic phase, 91, 118, 125
Antiferromagnetic structure, 105, **108**, 109, 118, 123, 127, 130, 132, 306
Antiferromagnetic vector, 105, **118–119**, 122–127, 129–132, 135–137, 139–140, 142–144
Antiferromagnetism, 115, 141
Antiferromagnets, **105–109**, 116, 119–120, 122, 126–132, 134, 136–137, 140–141
 nuclear, 108
 uniaxial, 123–124, 137
Antiphase
 boundaries, 394, 397, 433, 444
 domains, 394, 414, 434
Anti-Stokes process, 316–317, 327
Antisymmetric tensors, 10, **13**, 29, 38, 42, 51, 68, 168, *see also* axial tensors
 rank 3, 168
 rank 3 (unit), 168
Antisymmetry groups, 109
Approximate lattice coincidence, *see* pseudo-coincidence
Aragonite (CaCO_3), 153, 396–399, 408–409, 420, 424, 426, 428, 433–434, **435**, 439
Aristotype, 415, 425
Arrott–Belov–Kouvel plots, 123
Arrowhead twin, 399
Asymmetry parameter, 308
Atom transformation table, 276, 279
Atomic displacement
 contribution, 321, 325–326
 ellipsoid (*ORTEP* ellipsoid), 239
 parameters (ADPs), 228
 Raman tensor, 326
 tensors, 229, 232, 239
 vector, 228
Atomic level, 299
Atomic orbitals, 299, 301, 305
Atomic sphere approximation, 299, 302
Aufbau principle, 300
Augmented plane wave (APW), 302, *see also* linearized augmented plane wave (LAPW)
Axial force, 322
Axial plane, 154, 160, 163–166
Axial scalar, 14
Axial tensors, 5, 10, **13**, 24, 29–30, 132, 138, 168, 322, 360
 time-antisymmetric, 136
Axial vectors, 3, **10**, 12–13, 106, 112, 120, 138, 168, 318, 324
Babinet compensator, 160
Back focal plane, 161
Band index, 298–299
Band structure, 220, 291, 294, **305**, 310, 312
Barium boron oxide (BBO) (BaB_2O_4), 189, 210
Barium gallate (BaGa_2O_4), 449
Barium magnesium tetrafluoride (BaMgF_4), 366
Barium sodium niobate ($\text{Ba}_2\text{NaNb}_5\text{O}_{15}$), 206, 214, 367
Barium titanate (BaTiO_3), 339, 361, 377, 411–412, 437, 442, 449, 457, 490
Basic structure, *see* aristotype
Baveno twin, 433
Becke line, 156, 161
Benzil $[(\text{C}_6\text{H}_5\text{CO})_2]$, 422
Berek compensator, 160
Berlinite (AlPO_4), 405
Bertrand lens, **154**, 161
Biaxial classes, **160**, 165, 185–186, 194–196, 200
Biaxial crystals, **154**, 156, 160, 162, 165–166, 185–187, 189, 193–194, 196, 199–201, 212
 negative, **154**, 186, 191–192, 199
 positive, **154**, 186, 191–192, 199
Biaxial figure, **162**, 163–165
Biaxial indicatrix, **154**, 173, 176
Biaxial medium, 11
Bicrystallography, **378**, 414, 417, 443, 450, 471, 473, 492, 494–495
Bicrystals, **378–379**, 393–394, 397, 417, 437, 443, 492, 495
Bilinear forms, 7–8, 13
Biot–Fresnel construction, 162–163
Biotite, 156, 166
Birefringence, 3, **152–167**, 170, 172–175, 185–186, 188, 199, 210–211, 315, 330–331, 367, 394
 circular, 167, 170
 determination of, 157, 160
 linear, **153–154**, 167, 170, 172, 174
 magnetic, *see* Cotton–Mouton effect
 strain or stress, 3, 174
Black and white symmetry groups, 109, 141, 378, 384, 399–401, **402**, 403–404, 428, 430, 473, *see also* antisymmetry groups, colour symmetry
Bloch condition, 296–297
Bloch function, 295–297, **299**, 301, 303, 305–306
Bloch states, 296–299, **305**
Bloch theorem, **295**, 306
Bloch wall, 501
Bloch waves, 281
Block-diagonal form, 282, 284
Body forces, 76, 94
Bonding character, 306
Bonding states, 306, 309
Boracite, 130, 139, 142
Born–Oppenheimer approximation, 302
Born–von Karman boundary conditions, *see* periodic boundary conditions
Bose factor, 271, 273
Bose–Einstein factor, 100, 221, 316
Boundary contrast, 433
Boundary energy, **413**, 422, 426, 438, 442
 minimization, 397, 433
Bravais lattices, **294**, 298, 340, 347, 361
 magnetic, 105, **113–114**, 116, 121, 130, 140
Brazil twin, 398, **404–406**, 412–413, 416, 422–423, 429, 431, 434, 444
Brillouin scattering, 88, 317, 326, **329**
Brillouin zone, **47–50**, 62, 121, 221, 223–224, 226, 249, 268, 270, 274, 277, 282, 286, 288–290, **294**, 298, 303, 315, 317, 327
 symmetry of, 298
Brookite (TiO_2), 397, 437
Brugger constants, 93
Brugger stiffness coefficients, 93
Bulk modulus, 83
Burgers vector, 442–443
Burnside’s theorem, 39
Butterfly twin, 399
Cadmium sulfide (CdS), 223
Cadmium telluride (CdTe), 407
Calcite (CaCO_3), 84, 103, 153, 155–156, 160–161, 398, 406, 412, 415–416, 418, 421–422, 429, 440, 443
Calcium gadolinium borate $[\text{CaGd}_4(\text{BO}_3)_3\text{O}]$, 214
Calomel (Hg_2Cl_2), 469, 491, 501–502
Capacitance method, 102, **103**
Carlsbad twins, 398, 429, 439
Car–Parrinello method, 302
Cartesian coordinates, 92, 102, 118, 134, 138, 183, 200, 232, 249, 251, 266, 283, 304, 315, 351, 358, 361, 373, 453, 460–461
Cartesian product, 380
Cartesian tensors, **51**, 249, 322, 351, 359, 458, 459
Cassiterite (SnO_2), 399, 437
Cauchy relation, 77, 82
Ceramics, 393, 439, 442
Chalcopyrite, 415
Character tables, **40–41**, 44–45, **56–58**, 66–68, 251–252, 256, 283, 291, 373
 for quasicrystals, 256
Characters, **39–42**, 44, 46, 54, 57, 62, 66, 68, 249, 282, 288–291
Charge density, 302–305, 307–309
 nuclear, 308
Charged boundaries, 430–431
Chemical bonding, 299, 301, 305, 311
Chirality, 166–167, 352
Chirality relation, 394–395
Christoffel determinant, 86–88
Christoffel matrix, 86
Chromium oxide (Cr_2O_3), 117, 130, 139
Circular birefringence, 167, 170
Circularly polarized light, **160**, 166–167, 170, 172
 left, 166, 170
 right, 166, 169–170
Clamping, 442
Class multiplication constants, 40
Class multiplication table, 373
Class structure, 373
Clebsch–Gordan coefficients, **52**, 372
Clebsch–Gordan products, 372–373
Cobalt, 131, 143, 145
Co-elastic twins, 416
Coherence
 of grain boundaries, 443
 of twin boundaries, 442–444
Coherence length, **188**, 193, 198, 212, 214, 243
Coherent domain walls, **451**, 486, 492

SUBJECT INDEX

- Coherent interface, 443
- Coincidence
 - one-dimensional, 417
 - three-dimensional, 417
 - two-dimensional, 417
- Coincidence lattice, 417–418, 422
 - index, 417
- Coincidence-site lattice (CSL), **379**, 393, 398, 405, 417, 423
- Coincidence-site sublattice, 417
- Coincidence-site subset, 417
- Colour-changing operations, 402–403
- Colour-preserving operations, 402
- Colour symmetry, 109, 402, *see also* black and white symmetry groups, dichromatic groups
- Commutator group, 41
- Compatibility relations, 266, **289**, 298, 305, 310, 317, 321, 323
- Compatible planes, 426
- Compensating gauge transformations, 248
- Compensator
 - Babinet, 160
 - Berek, 160
 - Ehringhaus, 160
 - Sénarmont, 160
- Complete twin, 402, 405, **412**, 462
- Complex twin, 396, 417
- Component state, *see* orientation state
- Composite pseudosymmetry, 409
- Composite symmetry, **399–406**, 408, 410, 415, 423–425, 428
 - classification, 401
 - crystallographic, **401**, 404, 408
 - extended, **402**, 408–409, 411
 - noncrystallographic, **401**, 402, 404, 415
 - pseudo-crystallographic, 402
 - reduced, **400–402**, 404–405, 407–409, 411, 415, 428
- Composition plane, 394, **397–400**, 403, 405, 408–411, 417, 420, 426–428, 430–433, 443–444
- Compressibility, 272
 - isothermal, 273
 - linear, 83
 - volume, 82–83, 100, 103
- Condenser, **154**, 157, 160
- Conductivity
 - electrical, 5, **220**, 223–224, 226, 431
 - ionic, 370
 - metallic, 306
 - thermal, 5, 9, 13, 220, **224**
- Conjugate subgroups, 359, 372–374, 379, 381, **383**, 386–389
- Conoscopic configuration, 154–155, **160–162**
- Contact plane, **397–398**, 414, 426, 428, 432, 437–438, 444
 - initial, 414
- Contact relations, 378, 394, 397, **426**, 434
- Contact twins, 377, **398**, 405–406, 412, 414, 418, 422
- Contracted product, **8**, 9–10, 14, 24, 26, *see also* contraction
- Contraction, **8**, 182, *see also* contracted product
- Contragredient, 38
- Contravariant, 5, 6–9, 13, *see also* contragredient
- Conversion efficiency, **197**, 198, 200–208, 210–212, 214
- Conversion equations, 360, 374, 458–459, 474
- Copper, 298, 306, 310, 312, 437
- Cordierite ($\text{Mg}_2\text{Al}_4\text{Si}_5\text{O}_{18}$), 441–442
- Core electrons, 297, 302, 305–306
 - spectra, 312
- Co-representations, 55
- Corundum (Al_2O_3), 406, 426
- Coset composition, 399
- Coset decomposition, 380, 388
- Cosets, **382–384**, 388, 454–455, 468, 471–474, 476, 494–495, *see also* double cosets
- Cotton–Mouton effect, 137, 152
- Coulomb energy, 300
- Coulomb potential, 299–301, 309
- Coulomb repulsion, 306
- Coulombic term, 363, 368
- Covariance, 9–10, 239
- Covariant, **5–10**, 13, 228–229, 239, *see also* tensorial covariants
- Critical phenomena, 340
- Critical point, 327
- 60° Cross, 411, 424, *see also* St Andrew's cross
- 90° Cross, 411, 424, 428, *see also* Greek cross
- Cross wires, 155, 161
- Crossed polars (Nicols), 156–157, 160, 166, 174
- Crystal family, 415–416, 418, 422, 425
- Crystal-field effects, 311
- Crystal-field splitting, 141
- Crystal harmonics, 303–304, 308, 311
- Crystal optics, 152
 - classical, 150
- Crystal system, 416
- CuAu alloys, 244
- Cubic dilatation, 72, 75–76, 82
- Cumulants, 228, **229**
- Curie laws, 4, **11**
- Curie temperature, 123, 347, 362–363, 367–369, 372, 377
- Curie–Weiss law, 106–107, 141
- Current density, 220, 224
- Cyclic twins, 396, **398**, 399, 402, 428, 439
 - eightfold, 409
 - fivefold, 419, 438
 - sixfold, 409
- Cylindrical symmetry, 11
- Daughter phase, 378, 404, 414, 440
- Dauphiné twins, 398, **404–406**, 412–414, 416, 420, 422–423, 429, 431, 433, 435, 480
- Dauphiné–Brazil twin, **405**, 406
- Debye frequency, 272
- Debye model, 90, 101, 223, 272
- Debye temperature, 89–90, 221, 224–225, 272
- Debye–Waller factor, 228, 232, 239
 - static, 228
 - thermal, 228
- Debye–Waller temperature, 228
- Deformation twins, 398, **415**, 419, 421, 429–430, 440–443, *see also* mechanical twins
 - $\Sigma 3$, 415–416
- Degeneracy, 282–283, 286, 288–289
 - accidental, 286
 - of lattice vibrations, 286
 - time-reversal, 286, 289
- Degenerate eigenvalues, 274, 282
- Degenerate phonon branches, 268
- Demagnetizing field, 125
- Density functional theory (DFT), 294, **299–300**, 302–303, 305–306, 308
- Density of states (DOS), 306, 312, 327
- Detwinning, **416**, 449–450, 480, *see also* switching
- Dextrorotation, 166–168
- Dextrorotatory solution, 169
- Diamagnetic susceptibility, 106–107
- Diamagnets, **105–107**, 109, 115–116, 132, 138, 140
- Diamond, 82, 103, 224–225, 338, 397–399
- Dichalcogenides MeX_2 , 415, 424
- Dichroism, 166
 - circular, 167
 - linear, 167
- Dichromatic complex, **379**, **471**, 492, 494–495
- Dichromatic groups, 378–379, **384**, 402, 462, 471, 473, 477, 485, 492, *see also* black and white symmetry groups
- Dichromatic pattern, 379
- Dielectric constant, 3–5, 8–9, 13, 31, 151
- Dielectric displacement, 152, 168
- Dielectric impermeability, 8, 26, 172–174
 - relative, 154
- Dielectric impermeability tensor, 154, 172, 175
- Dielectric permittivity, 137, 140–141, 340, 450, *see also* dielectric constant
- Dielectric (or electric) polarization, **3**, 4, 8, 11–12, 24, 31, 54, 137–140, 151, 178, 340, 342, 349, 351, 358, 360, 362
 - spontaneous, *see* spontaneous polarization
 - third-order, 178
- Dielectric susceptibility, **3–4**, 151, 192, 314, 342–344, 347, 349, 351, *see also* susceptibility
 - linear, **180**, 314, 323, 325
 - magnetic field dependence, 140
 - nonlinear, **179–180**, 314, 316
 - n th order, 180–181
- Dielectric susceptibility
 - second-order, 180–181, 316
 - tensor, *see* dielectric tensor
- Dielectric tensor, 3, 38, 42, **152–154**, 167–168, 178, 182–183, 187, 193, 195–196, 321, 324, 329–330
 - effective, 167–168
 - effective, symmetry of, 168
 - second-order, 178
 - third-order, 178
- Difference-frequency generation (DFG), 178, 189, 197, **208**
- Differential cross section, 315–316, 327
- Diffraction pattern of a twinned crystal, 400, 417, 423
- Diperic twins, **417**, 422, 425
- Direct inspection method, 14, **16**, 18, 20
- Dirichlet construction, 294
- Dirichlet region, 46, 294
- Discommensurations, 495, 498
- Dislocation arrays, 379
- Dislocation node, 443
- Dislocation reactions, 443
- Dislocations
 - perfect, 442, 444
 - stair-rod, 434
 - twinning, 429
- Dispersion, 156, 166
 - birefringent, 167
 - directional, 321–322
 - optical rotatory, 167
 - phonon, 268, 281
 - spatial, 167, 322–323, 325
 - static, 228
 - volume, 82–83, 100, 103
 - X-ray anomalous, 167
- Dispersion curves, **270**, 321, 327
- Dispersion relation, 314
- Displacive modulation, 243–245
- Dissymmetrization, **378**, 379, 382, 450, 452, 454, *see also* symmetry descent
- Distorted phase, 426
- Domain boundary, 394, 397, 426–427, 434
- Domain pairs, 451, 462, **470**, 492–495, 497–499, 501–502
 - elasto-optic, 479
 - electro-optic, 479
 - electrostrictive, 479
 - ferroelastic, 451, **462**, 470, 475, 477, 480–481, 486, 490
 - ferroelectric, 479
 - gyrotropic, 479
 - microscopic description of, 491
 - non-ferroelastic, 451, 462, **470**, 474, 476–477, 480, 496
 - piezoelectric, 479
- Domain states, 120, 136, 351, 358–361, 372–374, 377–378, 386–388, 397–405, 420, 423, 426, 428, 430, 439, **451**, 471, 501, *see also* orientation state
 - ferroelastic, 351, 356, **451–453**, 455–457, 469, 471, 481
 - ferroelectric, 351, 356, 360, **452**, 457, 490
 - ferroic, **351**, 356, 358, 452, 455, 457–458, 460, 470, 475
 - non-ferroelastic, 451, **456–457**, 470
 - non-ferroelectric, 457
 - tensor distinction, 355
- Domain structures, 338, 340, 351, 359, 372, **377**, 393–394, 397, 400, 403, 408, 415, 422, **449**
 - ferroelastic, 416, **449**, 451, 456
 - ferroelectric, 377–378, **449**, 451–452, 496
 - ferroic, **450–451**, 453
 - non-ferroelastic, 378, 449, 453, 456
- Domain switching, *see* switching
- Domain texture, 416
- Domain twins, 379–380, 384, 451, 462, **470**, 471, 483, 486, 490–491
 - ferroelastic, 451, **462**, 471, 483, 485, 490, 498
 - non-ferroelastic, 451, 462, 477, 496
- Domain walls, 125–126, 377, 426, 429, 434, 449, 451, 470, 480, 484–486, **490–491**
 - coherent, **451**, 486, 492
 - ferroelastic, 451, **491**, 498
 - non-ferroelastic, 451, 496

SUBJECT INDEX

- Domains
 - 180°, 105, **125**, 127, 139
 - antiferromagnetic, 126, 136–137
 - antiphase, 394, 414, 434
 - anti-polar, 431
 - ferroelastic, **340**, 378, 386, 412, 416, 425–426
 - ferroelectric, 368, **377**, 412, 423, 449
 - ferroic, 127, **378**, 386, 390, 453
 - ferromagnetic, 377
 - needle, **440**, 442
 - S-, 126, 135, 139
 - T-, *see* twin domains
- Doppler shift, 308
- Double cosets, 379, 381, **384**, 390, 454, 462, 476–477, 491
- Double groups, **45**, 55, 61
- Double refraction, 10, 153, **155**, 157, 178, 184–185, 187, 193
- Double space groups, 50
- Dovetail twin, 396, 399, **400**, 401, 403–404, 412, 414, 420, 422, 426, 428, 433, 439
- Druckzwillinge*, *see* mechanical twins
- Dual basis, 6–7, 47
- Dual lattice, 62
- Dual space, 6, 9, 37–38
- Dual vectors, 38
- Dummy index, 4, 13, 31, 72, 81
- Dynamic elasticity, nonlinear, 94
- Dynamical matrix, 86, **266–267**, 270, 274, 284, 321
 - block-diagonalized, 284
 - eigenvalues, 268, 274
 - eigenvectors, 268, 274, 281
 - symmetry constraints, 276
 - transformation law, 275
- Dzyaloshinskii–Moriya interaction, 128

- Easy-axis magnetic, 119–120, 125–128, 131
- Easy-plane magnetic, 119–120, 125–126, 128, 131
- Edgeworth series, 229, 232
- Effective charge
 - matrix, 315
 - tensor, 318, 324
- Effective coefficient, 188, **193**, 197–198, 201, 209, 214
- Ehringhaus compensator, 160
- Eigensymmetry*, 386, **398–409**, 411, 415, 423–424, 427–428, 453
 - full, **401–402**, 405, 408
 - monochromatic, 402
 - oriented, 400–401
 - reduced, **405**, 407–408
- Einstein convention, 4–5, 8, 72
- Einstein model, 90, 271
- Einstein temperature, 272
- Elastic coefficients, 81, 331, *see also* elastic stiffnesses
 - in piezoelectric materials, 331
- Elastic compliances, 26–27, 31, **81–82**, 84, 143, 480
 - fourth-order, 81
 - second-order, 93
 - third-order, 81
- Elastic constants, 3–5, 13–14, 26, **81–82**, 88, 450
 - adiabatic, 90
 - dynamic, 88
 - fifth-order, 91
 - fourth-order, 91
 - frequency dependence of, 88
 - higher-order, 91, 94
 - higher-order, measure of, 97
 - in icosahedral quasicrystals, 255
 - in octagonal quasicrystals, 254
 - in quasiperiodic structures, 252
 - measure of, 86, 88
 - pressure dependence of, 89–91
 - second-order, 93
 - static, 88
 - temperature dependence of, 89–90
 - third-order, 81, 91, 93, 94
 - third-order, measure of, 97
- Elastic energy, 142–143, 145
- Elastic limit, 80
- Elastic moduli, 81, *see also* elastic compliances
- Elastic stiffnesses, 3, 26–27, 32, **80–82**, 84, 86–87, 89, 91, 143, 145–146, 174, 250, 270, 273, 288, 325
 - adiabatic, 88
 - dynamic, 86
- Elastic stiffnesses
 - fourth-order, 81
 - higher-order, 93
 - in piezoelectric media, 330
 - isentropic, 93
 - isothermal, 88, 93
 - pressure dependence of, 89, 91
 - relation with velocity of waves, 87
 - second-order, 93
 - temperature dependence of, 89
 - third-order, 81, 93
- Elastic strain energy, 82, 91, 93–95
- Elastic waves, 86, 94, 329–330
 - in piezoelectric media, 329
- Elasticity
 - dynamic, 86
 - linear, 80, 91, 93
 - nonlinear, 91
- Elasto-optic domain pairs, 479
- Elasto-optic effect, 26–27, **152**, 172, 174–175, *see also* photoelastic effect
- Elasto-optic material, 152
- Elasto-optic tensor, 174, 324–325
 - linear, 174
- Elbow twins, 399, 408
- Electric dipole operator, 167
- Electric effect
 - linear, 151
 - quadratic, 151
- Electric field, 3–4, 38, 220, 223–224
 - crystalline, 106–108
 - symmetry of, 11
- Electric field gradient (EFG), 294, 302, 305, **307**, 308–310
 - in quasiperiodic structures, 252–253
 - lattice, 309
- Electrical conductivity, 5, **220**, 224, 226, 431
 - intrinsic, 223
- Electrical constraints, 430
- Electrical resistivity, 220
 - intrinsic, 221
- Electrocaloric effect, 3–4, 31
- Electrogyration, 352, 503
- Electronic structure, 294–295, 298–303, 305–307, 309, 312
- Electro-optic contribution, 321–323, 325–326
- Electro-optic domain pairs, 479
- Electro-optic effect, 3, 31, 150, **172**, 173, 330
 - linear, 150–151, 172, 175, 323
 - nonlinear, 150
 - quadratic, 151–152, 323
- Electro-optic materials, 172
- Electro-optic tensor, 172
 - linear, 172–173
 - quadratic, 326
 - rank 3, 330
- Electrostriction, 3, 24, 26–27, 31, 475, 503
- Electrostrictive domain pairs, 479
- Ellipticity, 170, 172
- Elongations, 73, 75, 83, 86
 - principal, 74
 - quadratic of, 73, 75–76, 83
 - simple, 75–76
- Enantiomorphic groups, **31**, 422, 470
- Enantiomorphism, **352**, 360, 387, 404, 479
- Enantiomorphous crystals, 385, 394, 449
- Energy bands, 294, 298, 305, 308
- Energy density, 79, 94
- Energy gap, 301
- Entropy, 3–4, 31
- Epikernel, 350–351, 356, 359, 361, 373
- Equitranslational phase transitions, **350–361**, 453, 458–459, 461
- Equitranslational subgroups, 350, **358**, 360–361, 372, 374, 414, 468, 470
- Equivalence class, **39**, 42, 53, **379**, 380–381, 387, 493
- Equivalence relation, 381–383, 387
- Esterel twin, 420–421
- Euclidean group, 46, 51, 53
- Euclidean space, 46, 51
- Euclidean transformation, **50–51**, 53–54, 248, 382
- Eulerian description, 92
- Even parity, 319–320, 323, 325–326

- Exchange
 - energy, 108, 116, 118, 125–126
 - interaction, 107–108, 119, 122–123, 129
 - symmetry, 116, 122
- Exchange–correlation
 - energy, 300–301
 - potential, 300
 - treatment, 299, 303
- Excitations, 314–316, 320–323, 326–328
 - vibrational, 314
- Extended zone scheme, 288
- Extensive quantity (parameter), **3–5**, 31
- External forces, 322
- Extinction
 - straight, 165
 - symmetrical, 165
- Extinction position, 156–157, 159, 165–166
- Eye piece, 154–155, 160–161

- Fabry–Perot interferometer, 205, 329, 332
 - planar, 331
 - spherical, 332
- Faraday rotation, 152
- Fast ray, 155–156, 159–160, 166
- Fault vector, 394, 397, 414, **432–433**, 435–437, 444
 - determination, 434
- Fe₄Al₁₃, 408, 433
- Feldspars, 398, 410, 433, 442
 - K-, 441
 - monoclinic, 412
 - Na-, 440
 - triclinic, 428
- Fermi energy, 305, 307–309
- Fermi exclusion principle, 301
- Fermi golden rule, 220, 225, 312
- Fermi hole, 301
- Fermi surface, 220, 222, 224, 226
- Fermi velocity, 221
- Fermi–Dirac statistics, 107, 226
- Ferrimagnetism, 109, 141
- Ferrimagnets, **105–107**, 112, 122, 125, 139–141, 306
- Ferrobielastic switching, 413
- Ferrobielastic twinning, 416
- Ferrobielastic twins, 404, 439
- Ferrobielasticity, 416, 480
- Ferroelastic domain pairs, 451, **462**, 470, 475, 477, 480–481, 486, 490
- Ferroelastic domain states, 351, 356, **451–453**, 455–457, 469, 471, 481
- Ferroelastic domain structure, 416, **449**, 451, 456
- Ferroelastic domain twins, 451, **462**, 471, 483, 485, 490, 498
- Ferroelastic domain walls, 451, **491**, 498
- Ferroelastic domains, **340**, 378, 386, 412, 416, 425–426
- Ferroelastic–ferroelectric phases, **416**, 423, 483
- Ferroelastic materials, 72, **339**, 349, 378, 415–416, 428–429, 443, 475
 - fully, 127, 456, 475
 - improper, 456
 - partial, 456, 475
- Ferroelastic phase, 174, **415**, 426, 449, 475, 491
 - full, **351**, 358, 360–361
 - partial, **355**, 358, 360–361, 449
 - potentially, 415
- Ferroelastic single-domain states, 360, 386, **462**, 481, 498
- Ferroelastic transition, 174, 339, **351**, 362, 404, 423, 427–428, 442, 455–456, 468
 - improper, **351**, 358
 - proper, **351**, 358
- Ferroelastic twins, **414–415**, 425, 427, **439–442**, 444, 471, *see also* mechanical twins
- Ferroelasticity, **415–416**, 425
- Ferroelectric antiferromagnets, 106, 130, 141–142
- Ferroelectric domain pairs, 479
- Ferroelectric domain states, 351, 356, 360, **452**, 457, 490
- Ferroelectric domain structure, 377–378, **449**, 451–452, 496
- Ferroelectric domains, 368, **377**, 412, 423, 449

SUBJECT INDEX

- Ferroelectric materials, 10, 12, 72, 88, 130, 141, **151**, 174, 193, 349, **362–363**, 367–368, 377–378, 416, 426, 430–442, 450, 475
 low-temperature, 372
 potentially, 403
- Ferroelectric phase, **351**, 368, 377, 412, 431, 434, 449, 457, 475, 477
 full, **351**, 358, 360–361, 457, 462, 475, 490
 improper, 457
 partial, **355**, 358, 361, 457, 475
 proper, 361
- Ferroelectric single-domain states, 360, 462
- Ferroelectric transition, 339, **351**, 362–363, 368, 399, 429, 431, 434, 449, 499
 improper, **351**, 358
 low-temperature, 372
 proper, **351**, 358, 360
- Ferroelectricity, 412, 416
- Ferrogrotropic phase, 479
- Ferroic classes, **339–340**, 349
- Ferroic crystals, 378
- Ferroic domain states, **351**, 356, 358, 452, 455, 457–458, 460, 470, 475
- Ferroic domain structure, **450–451**, 453
- Ferroic domains, 127, **378**, 386, 390, 453
- Ferroic materials, **378**, 451, 481
- Ferroic phase, **339**, 350–351, 358–361, 378–379, 387, 449, 452–453, 455–458, 461–462, 468–470, 475–477, 482, 500
 low-symmetry, 359–360
- Ferroic single-domain states, **351**, 360
- Ferroic species, 127
- Ferroic symmetry, **350**, 356
- Ferroic transition, 338–340, **350**, 372–373, 450–454, 456–461, 468
- Ferromagnetic domains, 377
- Ferromagnetic ferroelectrics, 105, 141
- Ferromagnetic helical structure, 108, 122
- Ferromagnetic materials, 72, **105**, 306, 325, 377–378, 442, 450
- Ferromagnetic phase, 118
- Ferromagnetic structure, 118, 123
- Ferromagnetic vector, 105, **118–119**, 122, 129, 142
- Ferromagnetism, 109, **112**, 114, 116, 122, 127, 141, 151, 377
 weak, 109, 117–118, **127–132**, 135–137, 140–142
- Ferromagnetoelectrics, 141–142
- Ferromagnets, **105–107**, 112, 114, 116, 119, 122, 125, 127, 131–132, 137, 139–141, 144–146, 362
 nuclear, 108
 uniaxial, 123
 weak, 108, 128, 130–132
- Fick's law, 5
- Field tensors, **4**, 13, 178, 193–197, 214
- Figure of merit, **197**, 198, 206
 for acousto-optic materials, 176
- Fivefold rotation, 397
- Fizeau interferometer, 102
- Flash figure, 156, 162, 165–166
 uniaxial, 165
- Fluorite (CaF₂), 398, 407
- Focal plane (back), 161
- Force constants, 266–267, 272, 274, 286
 matrix of, 266–268, 270, 274–275
- Four-wave mixing, 151
- Fourier module, 243–246, 248–250, 253
- Fourier's law, 5
- Free-electron model, 297, 299
- Free energy, 31, 340–344, 346–349, 358, 362, 368–369
- Fresnel equation, 184
- Friedel's lattice theory, 417
- Fringe contrast, 433–434
- Fringe counting, 158
- Full-potential methods, 299, 302–304
 linearized augmented plane wave (LAPW), 303
- Fullerene (C₆₀), 502
- Gadolinium molybdate (GMO) [Gd₂(MoO₄)₃], 347, 349–351, 469–470
- Galena (PbS), 407, 415, 419, 422, 430
- Gallium arsenide (GaAs), 175–176, 223, 225, 272, 407
- Gallium phosphate (GaPO₄), 405, 422
- Garnet twin, 418
- Garnets, 141
- Gaussian beams, 197, 201, **202**, 205
- Gaussian system of units, 106, 139, 146
- Generalized gradient approximation, 301
- Germanium, 82, 223, 225, 419, 438
- Gibbs function, 31–32
- Gibbsite [Al(OH)₃], 396, 402, **409**, 426
- Glide twin, 437
- Grain boundaries, 378–379, 393
- Gram–Charlier series, 229, 232
- Graphite, 103, 338
- Greek cross, 411, *see also* 90° cross
- Ground state, 294, 301, 308, 312
- Group calculator, 373
- Growth face, 413
- Growth morphology, 414
- Growth-sector boundary, 393, 431
- Growth-sector twins, 408, 412
- Growth sectors, 393
- Growth twins, 378, **397–400**, 412–416, 423–426, 428–431, 436, 439, 444, 471
 pseudo-hexagonal, 423
- Grüneisen model, 90
- Grüneisen parameter, 101, 272
 averaged-mode, 273
 generalized-mode, 273
 mean, 273
- Grüneisen relation, 100, 103
- Gypsum (CaSO₄·2H₂O), 396, 398–401, **403**, 412, 414, 420, 422, 425–426, 428, 433, 439
- Gyration, 151, 166, 168
 tensor, 14, 30, 168, 170, 172
 vector, 168, 170
- Gyrotropic domain pair, 479
- Gyrotropic materials, 14, 30–31, 166, 168, *see also* optical activity
- Gyrotropic transition, 479
- Habit modification, 414
- Haematite (Fe₂O₃), 117, 127, 131, 135–137
- Hall constant, 14, **224**
- Hall effect, 14, 220, **223**, 224
- Hamiltonian, 266, 270
- Harmonic approximation, 266
- Harmonic generation (ultrasonic) 94, 96–97
- Harmonic oscillators, 270, 273
- Harmotome twin, 399, 439
- Hartree–Fock (HF) methods, 299, 301, 305–306
- Head-to-head boundaries, 431
- Heat capacity, 271–272, 274
- Heat current, 220
- Heat flow, 220, 224
- Helical structure, 108, 122, 130–131
 antiferromagnetic, **108**, 109, 122
- Helmholtz free energy, 273
- Hermann–Mauguin symbols, 111, 134, 358–359, 373–374
- Hexagonal crystals, 397, 405, 408, 418, 424, 430–431, 435–437
- Hg_{3–x}AsF₆, 244
- High-order twins, 419
- High-resolution transmission electron microscopy (HRTEM), 398, 413, 419, 426, 433–434, **437**, 438, 498
- High-symmetry phase, 340, 343, 350, 360–361, 366
- High-temperature superconductors, *see* superconductors
- Holmium, 244
- Holohedral groups, 49, 62, 404, 412, 422
- Homogeneous deformation, 72
- Homogeneous shear, 415
- Hooke's law, 3, **80**, 91–92, 270
 generalized, 81
- Huang conditions, 267
- Hydrargillite, *see* gibbsite [Al(OH)₃]
- Hyperfine interactions, 307
- Hypersthene [(Mg,Fe)₂Si₂O₆], 166
- Hysteresis, 415, 449–450, 475
- Icosahedral quasicrystals, 246, 252, 255
- Icosahedral tensors, 252
- Incoherence of twin boundaries, 442, 444
- Incoherent interfaces, 443
- Incommensurate composite structures, 244
- Incommensurate crystal (IC), 243–248, 251, 253
- Incommensurate magnetic system, 244
- Incommensurate structure, 108–109, 115–116, 121–**122**, 131, **243**, 495, 497–498
- Index of a group–subgroup relation, 399, 414
- Index of refraction, 9, *see also* refractive index
- Index surface, 183, 186–187, 189, 194, 197, 211
- Indicatrix, 9, 11, 17, **153**, 154–155, 160–162, 165–166, 172, 174, 176
 biaxial, **154**, 173, 176
 uniaxial, 154, 174, *see also* uniaxial ellipsoid
- Indium phosphide (InP), 414
- Inelastic scattering, **314**, 318, 326–327
- Infrared absorption, 290
- Infrared activity, 290, 318, 320–321, 324, 326
- Infrared spectroscopy, 290
- Inner symmetry, 232
- Integrity bases, 358, 373
 extended, 372–373
- Intensive quantity (parameter), **3**, 4–5, 24, 31
- Interface energy, 426
- Interference figures, **160**, 165–166
- Interferometers
 Fabry–Perot, *see* Fabry–Perot interferometer
 Fizeau, 102
 Michelson, 102
- Interferometry, 88, 102
- Intergrowths, 393
 arbitrary, 393
 oriented, 397
 parallel, 393
- Intermediate group, 351, 358, 361
- Internal energy, 271
- Intersection group, 401
- Intersection symmetry, 400–401
- Intrinsic electrical conductivity, 223
- Intrinsic electrical resistivity, 221
- Intrinsic mobility, **222**, 223–224
- Intrinsic symmetry, **13**, 26
- Invariance
 rotational, 267
 time-reversal, 286, 288
 translational, 267, 269
- Invariant tensors, 34, 52, 67–68
- Invariants, 52, 229, 239
- Inversion, 277, 281
- Inversion boundaries, 434
- Inversion operator, 297
- Inversion twins, **396**, 403–405, 417, 423, 429, 431–432, 434
- Ionization potential, 301
- Ireps, 373, *see also* irreducible representations
- Iron, 143–144
- Iron borate (FeBO₃), 127, 406, 412, 418, 422–423
- Iron-cross twin, 399, 423, 433
- Irreducible multiplier representation, 282–283, 288–289, 291
- Irreducible representations, **36–42**, 49, 67, 122, 276, 283–291, 296–298, 317–319, 328, 347–348, 355, 372–374, 458–459, 479–480
 in quasiperiodic structures, **251**, 255
 of lattice translation groups, 47
 of space groups, **47**, 105, 120–122, 248, 289–290, 327, 361
 of tensors, 51, 179, 251
 physically, **41–42**, 57, 350, 356, 358, 361, 458, 461
 tables, **57–61**, 63, 122, 255, 258, 289–290, 348, 352, 358
- Irreducible tensors, 51
- Irreducible vector space, 284
- Irreducible wedge, 298
- Isogyres, **161**, 162–166
- Isostructural crystals, 422
- Itinerant electrons, 306
- Jahn–Teller phase transition, 91
- Japanese twins, **404**, 405, 421, 444, *see also* La Gardette twins
- Jones matrix, 169
- Kantennormalengesetz*, 377, 396, 417
- Kernel, 350, 359, 373
- Kerr effect, 151, *see also* electro-optic effect (quadratic)
- Klassengleiche* subgroup, 414

SUBJECT INDEX

- Klockmannite (CuSe), 418
 Knee twin, 408
 Kohn–Sham equations, 301, 303
 Kohn–Sham orbitals, 302
 Koopman’s theorem, 301
 Korrínga–Kohn–Rostocker (KKR) method, **302**, 305, 307
 Kronecker products, 373
 Kronecker symbol, 5
 Kund tube, 88
- La Gardette twins, **405**, 420
 Laevorotation, 166, 168
 Lagrangian description, 92
 Lagrangian strain, 92–95
 Lamé constants
 second-order, 85, 94
 third-order, 93
 Lamellar twinning, 398
 Landau condition, 358–359
 Landau polynomial expansion, 345
 Landau problem
 direct, 358
 inverse, 356, 358, 361
 Landau theory, 105, 118, 120, 122–123, **340**, 347, 350, 361, 377, 450, 458, 499
 Landau–Devonshire theory, 361
 Landé *g*-factor, 106–107, 137
 Langbeinite [K₂Mg₂(SO₄)₃], 402, 427, 490
 Lanthanum aluminate (LaAlO₃), 365, 441
 Lanthanum pentaphosphate (LaP₃O₁₄), 365
 Latent heat, 342, 344
 Lattice coincidence, 394, 417, 419, 425, 430
 Lattice concept of twinning, 416
 Lattice dynamics, 228, 266
 Lattice index, 417
 Lattice pseudosymmetry, 420
 Lattice translation subgroup, 35, 46–48, 295–296, 298
 Lattice vibrations, *see* phonons
 Lattices of subgroups, 351, 356, 358, 360–361, 372–374
 Laue class, 15, 16, 82, 329, 331
 Layer groups, 451, 462, 485, **490–495**, 497–502
 dichromatic, 379, 471
 sectional, 492–495, 500–502
 Lead germanate (Pb₅Ge₃O₁₁), 480
 Lead phosphate [Pb₃(PO₄)₂], 449
 Leucite (KAlSi₂O₆), 440, 456, 481
 Leydolt twins, **404**, 406, 412, 422–423, *see also* Dauphiné–Brazil twin
 Liebsch twins, 404, *see also* Dauphiné–Brazil twin
 Lifshitz condition, 358–359
 Ligand-field theory, 305
 Linear birefringence, **153–154**, 167, 170, 172, 174
 Linear combination of atomic orbitals (LCAO), 299, **301**, 305, 310, 312
 Linear combination of muffin-tin orbitals (LMTO), 299, **302**, 305, 307
 Linear forms, 7–8
 Linearized augmented plane wave (LAPW), 302, **303**, 304–308, 310, 312
 Lineshape function, 316
 Lithium formate monohydrate [Li(CHO₂)·H₂O], 403, 429, 431
 Lithium niobate (LiNbO₃), 172, 193, 211, 214, 431
 Local coordinate system, 303, **304**, 305–307, 310–311
 Local density approximation, 300
 Local orbitals, 303, 310
 Localized electrons, 306
 Longitudinal optic mode (LO), 316, 321, 363, 372
 Low-energy boundaries, 395, 422, 426
 Low-symmetry phase, 338, 340, **343**, 347, 349–350, 360–361, 363
- Macles*, 394, 471, *see also* twins
 dipériodiques, 416, *see also* diperiodic twins
 monopériodiques, 416, *see also* monopерiodic twins
 par mériédrie, 377, 417, 422, *see also* twinning by merohedry
 par mériédrie réticulaire, 377, 417, *see also* twinning by reticular merohedry
 par pseudo-mériédrie, 377, 422, *see also* twinning by pseudo-merohedry
- Macles*
 par pseudo-mériédrie réticulaire, 377, *see also* twinning by reticular pseudo-merohedry
 tripériodiques, 416, *see also* triperiodic twins
 Magnetic anisotropy energy, 118
 Magnetic birefringence, 137, *see also* Cotton–Mouton effect
 Magnetic Bravais lattices, 105, **113–114**, 116, 121, 130, 140
 Magnetic cell, 113, 116
 Magnetic field, 3–4, 12, 54, 106, 220, 223–224
 Magnetic induction, 3–4, 106, 152
 symmetry of, 12
 Magnetic lattices, 112
 Magnetic moment density, 105
 Magnetic permeability, 106
 Magnetic point groups, **53**, 55, 62, 66, **109**
 grey, 109
 white, 109
 Magnetic space groups, 53, 115
 Magnetic spin–spin interaction, 119
 Magnetic sublattice, 107
 Magnetic susceptibility, 4, 13, 54, **106–107**, 124, 130, 140–141
 Magnetic symmetry, 105, **109**, 116, 131–132
 linear, 137
 Magnetite (Fe₃O₄), 107, 419
 Magnetization, 3
 Magnetocaloric effect, 4
 Magnetoelastic energy, 120, 132, 135, 142–143, 145
 Magnetolectric effect, 4, 117, 137
 linear, 126, 138
 nonlinear, 140
 Magnetolectric susceptibility, 141
 Magneto-optic effect, 3, 150
 linear, 150
 nonlinear, 150
 quadratic, 152
 Magneto-optic tensor, 324–325
 Magnetostatic energy, 125
 Magnetostriction, 3, 136, **142**, 144
 linear, 126, 132, 136–137
 spontaneous, 142–145
 Magnons, 314, 318
 Maker fringes, **212**, 214
 Mallard pseudo-cube, 411
 Manley–Rowe relations, **182**, 188, 204
 Many-body problem, 300
 Mappings, **380**, 382
 Martensitic transformation, 338
 Material tensors, **4**, 351, 378, 474, *see also* physical property tensors (or property tensors)
 Matrix of physical properties, **4**, 13, 31
 symmetry of, 4
 Matrix method, 14, 16, 18
 Matter tensors, *see* material tensors
 Matthiessen’s rule, 220, 224
 Maxwell’s equations, 152, 178, 183
 Mean-square displacements, 228, 239
 Mechanical twins, 377–378, 412, **415–416**, 428–429, *see also* deformation twins
 Median law, 396, 410
Mediangesetz, *see* median law
Mériédrie réticulaire, 423
 Merohedral twins, 378, 404–406, 412–414, 417–418, 420, **422**, 423, 425, 429–430, 433, 435–436, 439, 442–444
 of lattice index [*j*] = 1, 423
 Merohedry, 422
 of translation groups (lattices), 423
 Metric tensor, **5**, 6, 9, 13, 35, 67, 249–250
 for a quasicrystal, 253
 tensor nature of, 9
 Mica, 425
 Michelson interferometer, 102
 Microcline (KAlSi₃O₈), 429
 Microtwins, 410
 Mimetic twins, 399
 Mobility, **222**, 223–224
 intrinsic, **222**, 223–224
 Modulated structures, 243, 249
 Modulation
 composition, 244
 displacive, *see* displacive modulation
- Modulation wavevector, **243**, 244–246, 249
 Moiré pattern, 420
 Moments, 228–229
 Momentum of the electron, 297
 Monoperiodic twins, **417**, 422, 425
 Montmartre twin, 403–404, 422, 426, 428, 433
 Morphic effects, 143, **322**, 325, 327, 351, 359–360
 Morphic properties, 455, 459
 Morphic tensor components, 452–453, 455, 458–459, 475, 480
 Morphological classification, 398
 Mosaic crystal, 393
 Mössbauer spectroscopy, 307–308
 Muffin-tin approximation (MTA), 299, 302–304
 Muffin-tin orbitals, 299
 Multilinear forms, 7
 Multiple twins, 396, **398**, 399–400, 402–403, 408, 413, 420, 422, 428
 fivefold, 439
 Multiplicator group, 43–44
 Multiplicity, 282, 289
 Multiplier co-representation, 277
 Multiplier representation, 276
 Murnaghan constants, 93–94
 Mutual exclusion rule, 320
- Nanocrystalline materials, 413, 419, 438
 Needle domains, **440**, 442
 Néel temperature, 124, 126, 130, 140
 Neumann’s principle, **11**, 13–15
 Neutron inelastic scattering, 269, 271, 290
 Nickel, 120, 144
 Niobium dioxide (NbO₂), 339
 Nonbonding states, 306, 310
 Non-crossing rule, 310
 Noncrystallographic symmetry, 244, 250
 Non-equitranslational phase transitions, 358, 361, 469, 491
 Non-ferroelastic domain pairs, 451, 462, **470**, 474, 476–477, 480, 496
 Non-ferroelastic domain states, 451, **456–457**, 470
 Non-ferroelastic domain structure, 378, 449, 453, 456
 Non-ferroelastic domain twins, 451, 462, 477, 496
 Non-ferroelastic domain walls, 451, 496
 Non-ferroelastic materials, 340, 416, 456
 Non-ferroelastic phase, 355, 360, 449, 462
 Non-ferroelastic transitions, 423, 442, 456
 Non-ferroelastic twins, 414, **416**, **439**, 444, 471
 Non-ferroelectric domain states, 457
 Non-ferroelectric phase, 360, 364, 457
 Non-ferroic transition, 338–339
 Nonlinear crystals, 178, **187**, 188, 198–200, 202, 204–206, 208–212, 214
 Nonlinear elasticity, 31
 Nonlinear optics, 10, 15, 31, 150, 152, **178**, 314
 Nonlinear polarization, 178, 181, 187–188, 193, 212
 Nonlinear susceptibility, 192, 212
 Non-merohedral twins, 404, 414, **427**, 428, 431, 439–440, 442, 444
 Non-pyroelectric acentric crystals, 431
 Non-symmorphic space group, 48, 50, 277, 288, 295, 311
 Normal coordinates, 270, 314–318, 321, 324–327
 Normalizer, 379, **383**, 384, 387–388, 390, 457, 461
 Nuclear antiferromagnets, 108
 Nuclear charge density, 308
 Nuclear quadrupole moment, **307**, 308
 Nuclear spin quantum number, 307
 Numerical aperture, 154
- Objective lens, 154
 Obtuse bisectrix figure, 165
 Octagonal quasicrystals, 253–254
 Octagonal tiling, 244, 246, 254
 Odd parity, 319–320, 323
 Off-site contribution, 310, 312
 Ohm’s law, 5
 Olivine, 156
 Onsager relations, **5**, 220, 324
 Optic axes, 154, 156–157, 160–162, 164–166, 169–170, 172
 Optic axial plane, *see* axial plane
 Optic axis figure, 161, 164, 166
 uniaxial, 161–162, 165

SUBJECT INDEX

- Optic branches, 269, 315
- Optic modes, 323
 - longitudinal, LO, 316, 321, 363, 372
 - polar, 316
 - Raman-active, 326
 - transverse, TO, 316, 321, 363
- Optical activity, 11, 14, 151, **166–167**, 352, 423, 503, *see also* gyration
- Optical anisotropy, 153
- Optical anomaly, 394
- Optical indicatrix, *see* indicatrix
- Optical microscope, *see* polarizing microscope
- Optical parametric oscillation, 178, 197, **208**
- Optical path difference, 157
- Optical phonons, 223, 225, 314, 318, 321–324, 327
- Optical rectification, 151
- Optical rotation, 14, 151, **161**, 168, 170, *see also* gyration
- Optical rotatory dispersion, 167
- Optical rotatory power, 14, 30, **168–169**
- Optical spectroscopy, 269, 290
- Optics
 - linear, 150, 152
 - nonlinear, *see* nonlinear optics
- Orbit, 379–381, 385–386, **387**, 388, 390, 453–455, 462, 468, 470, 472–477, 480, 483, 486, 491, 493, 495, 497–498
- Orbital magnetic moment, 105
- Order parameter, 120–121, 139, 340, **341**, 342–351, 359, 361–363, 366, 373, 386
 - fluctuations, 123
 - primary, 350–351, 356, 358–360, 373, 387
 - principal, 388, 390
 - secondary, 351, 358, 387, 389–390
- Orientation relation, 394–395
 - crystallographic, 393–394, 396–397, 417, 426
 - noncrystallographic, 394
- Orientation state, 378, 386, **395**, 396, 398–402, 404–406, 408–409, 412, 414–416, 427–429, 440, 451, 453
- ORTEP*, 232, 239
- Orthochromites, 129, 131, 136
- Orthoclase (KAlSi_3O_8), 398, 412, 429, 439, 441–442
- Orthoferrites, 118, 129–131, 136, 141
- Orthogonality, 301, 303, 310
- Orthogonality relations, **38**, 39–41, 44, 52, 56
- Orthoscopic configuration, 154, **160**, 161–162, 164–165
- Outer product, 9, 41
- Outer symmetry, 232
- Overtone, 327
- Paraelectric phase, 377
- Parallel-lattice twins, 404
- Paramagnetic susceptibility, 106–107
- Paramagnetoelectric effect, 141
- Paramagnets, 105, **106**, 107, 109, 115–116, 138, 140–141
- Parametric amplification, 151, 178, 197, 208
- Parent clamping approximation, 453, **468**, 469–470, 491, 498, 502
- Parent phase, 339, **350–351**, 358, 361–362, **378–379**, 386–387, 414–415, 434–435, 449, 461–463, *see also* prototype (or high-symmetry) phase
- Parent symmetry, **352–358**, 440, 452, 454
- Partial charges, **306**, 307, 309–310
- Partition (of a set), 380–381, 383–384, 387–388, 390, 455
- Partition function, 273
- Passive representation, 359
- Penetration trillings, 411
- Penetration twins, 377, **397–399**, 406, 411–412, 414, 418, 422–423, 429–430
- Penrose tiling, 244
 - icosahedral, 247
- Pentagonal–decagonal twins, 408
- Pericline, 442
 - twin law, 410, 428–429
- Periodic boundary conditions, 267, 296, 298–299
- Permissible boundaries, 427, 429–430
- Permissible composition planes, 427
- Permissible domain boundaries, 427
- Permissible domain walls, 428
- Permissible planes, 426
- Permissible twin boundaries, 400, 428
- Permittivity of vacuum, 152, 183
- Permutation tensor, 10, 14, 70, 77, 168
- Perovskites, 141, 174, 363, 399, 411, 414–415, 437, 441–442, 457, 462, 477, 490
- Phase conjugation, 152
- Phase jump, 433–434
- Phase matching, 178, 184, **188**, 193–194, 196–212, 214
- Phase mismatch, **187**, 188, 197–199, 202–204, 206–207, 209, 214
- Phase transformation (polymorphic), 414
- Phase transitions
 - antiferromagnetic, 91
 - continuous, 120, **340**, 343, 346–347, 350–351, 361–362, 369
 - diffusion-assisted, 338
 - diffusionless, 338
 - discontinuous, 340, **344**, 347, 350, 356, 362
 - displacive, 273, 338, **361**, 363, 365–366, 368–369, 414–415
 - equitranslational, **350–361**, 453, 458–459, 461
 - first-order, 344, 350, 362
 - magnetic, 116
 - non-equitranslational, 358, 361, 469, 491
 - non-reconstructive, 338
 - order–disorder, **338**, 368–369, 414
 - reconstructive, 338
 - second-order, **340**, 350, 361–362
 - second-order magnetic, 116, 128
 - structural, 338–340, 361
- Phason, 250–251, 255
 - degrees of freedom, 250, 252
 - elasticity tensor, 252, 255
 - strain tensor, 254–255
- Phillipsite twin, 399, 439
- Phonon bands (or branches), 221
 - degenerate, 268
 - LA, **222**, 329, 331
 - LO, **222**, 316, 321–322, 326, 363, 372
 - TA, **222**, 329, 331
 - TO, **222**, 316, 321–322, 326
- Phonon contribution to elastic constants, 250, 254
- Phonon degrees of freedom, 250, 252
- Phonon density of states, 271
- Phonon dispersion, 268, 281
- Phonon drag, 222, 224
- Phonon scattering, 223–224
- Phonons, **266**, 314–316, 318, 321, 326–327
 - acoustic, 91, **223–225**, 270, 314, 326, 329–330
 - E, 322
 - electron scattering by, 221, 223
 - optical, 223, 225, 314, 318, 321–324, 327
 - Raman-active, 320
- Photoelastic effect, 3, 26, 150, *see also* piezo-optic effect
 - linear, 152, 173
- Photoelasticity, 78
- Physical irreducibility, 350
- Physical property tensors (or property tensors), 4, 13, **14**, 31, **350**, 351–352, 358–360, 450–452, 458, 461, 470, 474, 479–480, 503, *see also* material tensors
- Piezocaloric effect, 3–4, 31
- Piezoelectric constants, 24, 32, 450
- Piezoelectric crystals, 223, 321, 324, 326, 329–331
- Piezoelectric domain pairs, 479
- Piezoelectric effect, 4–5, 8, **24**, 31–32, 172, 323
- Piezoelectric resonators, 32
- Piezoelectric stress coefficients, 32
- Piezoelectric tensor, **24**, 26, 151, 172, 321, 323, 329, 352, 475, 480
 - in octagonal quasicrystals, 254
 - in quasicrystalline structures, 251
- Piezoelectric transducer, 86, 88–89
- Piezoelectricity, 3–4, **11–12**, 15, 78, 223, 412, 503
- Piezomagnetic effect, 4, 29, 126, **132**, 137
- Piezomagnetism, 3, 15
- Piezomagnetoelectric effect, 141
- Piezo-optic effect, 8, **31**, 152, **173**, 330, *see also* photoelastic effect
- Piezo-optic tensor, **26**, 27, **174**, 325, 330, 352
- Plagioclase, 156, 166, 429
- Plagioclase twins, 410
- Planes of strain compatibility, 426
- Plasmons, 314, 317, 326
- Pleochroism, 155–156, 166
- Plesiotwins, 398
- PMN-PT, 490
- Pockels effect, 331, *see also* electro-optic effect (linear)
- Pockels tensor, 331, *see also* piezo-optic tensor
- Point-charge model, 307, 309
- Point groups for quasicrystals, 251
- Poisson's ratio, 3, 83
- Polar force, 322
- Polar tensors, **24**, 25–26, 317–319, 321–323, 326
- Polar vectors, **10**, 12, 317–319, 321, 324, 326
- Polaritons, 314, 321
- Polarizability, 290
- Polarizability operator, 167
- Polarization
 - acoustic, 14
 - circular, 169–170
 - dielectric, *see* dielectric (or electric) polarization
 - elliptical, 170
 - of elastic waves, 86
 - nonlinear, 178, 181, 187–188, 193, 212
 - n*th order, 179
 - rotatory, 3
 - spontaneous, *see* spontaneous polarization
- Polarization colours, 156–160, 166
- Polarization selection rules, 317, 320, 322, 326
- Polarization vector, 267
- Polarizer, 154–156, 159–161
- Polarizing microscope, 154–155, 160, 166
- Polycrystalline aggregates, 437, 442
- Polycrystalline materials, 99–100, 393, 414, 439
- Polymorphs, 397, 433, 435–437, 441
- Polysynthetic twins, **398**, 409, 412–413, 428, 434, 436, 439–440
- Potassium dihydrogen phosphate (KDP) (KH_2PO_4), 202, 214, 368, 377, 450
- Potassium lithium sulfate (KLiSO_4), 397, 412–413, 423, 430–431, **436**, 441
- Potassium nickel fluoride (KNiF_3), 91
- Potassium niobate (KNbO_3), 209
- Potassium nitrate (KNO_3), 365
- Potassium selenate (K_2SeO_4), 243
- Potassium sulfate (K_2SO_4), 408, 415–416, 424, 439
- Potassium thiocyanate (KSCN), 502
- Potassium titanyl phosphate (KTP) (KTiOPO_4), 200–201, 205–206, 210–211, 214, 403, 423, 431
- Potassium trihydrogen selenite ($[\text{KH}_3(\text{SeO}_3)_2]$), 423
- Potassium zinc fluoride (KZnF_3), 89, 91
- Poynting vector, 184, 200–201
- Praeseodymium sulfide (PrS_2), 424
- Principle of superposition, 170
- Probability density function (p.d.f.), 229, 239
- Projection operator, 283–286
- Propagation tensor, 270
- Prototype (or high-symmetry) phase, 127, 144–145, **339**, 350, 365, 416, 422, 427, 429, *see also* parent phase
- Prototype structure, 339, 365
- Pseudo-coincidence, 418–419, 422–423, 425
- Pseudo-fivefold axis, 408
- Pseudo-mériédrie réticulaire*, 423
- Pseudo-merohedral twins, 420, **422**, 423, 425, 442
 - of lattice index $[j] = 1$, 423
- Pseudo-merohedry, 425
- Pseudomomentum, 297, 299
- Pseudo-potential, 299, **302**
- Pseudoscalar, 14, 30
- Pseudosymmetry, 395
 - composite, 409
- Pseudotensors, 54, 64, 67, *see also* axial tensors
- Pseudovectors, 10, 13–14, 51, 54, *see also* axial vectors
- Pulse-echo technique, 88
- Pulse-superposition method, 89
- Pure deformation, 73
- Pushrod dilatometry, **102**, 103
- Pyrite (FeS_2), 399, 423, 433
- Pyroelectric coefficients, 32
- Pyroelectric effect, 4, 12, 31–32
- Pyroelectric materials, 367
- Pyroelectricity, 3–4, **12**, 412, 423, 430–431
- Pyromagnetic effect, 4, 13
- PZN-PT, 490

SUBJECT INDEX

- q-dependent terms, 322, 326
- Quadrilinear forms, 8
- Quantum-mechanical treatment, 294–295, **299**, 312
- Quartz, 155, 160, 168, 170, 172, 178, 214, 269, 393, 398, 412–414, 416, 420–421, 423, 429, 431, 434, 444, 480, 497
 - alpha- (high-temperature), 404, 433, 435
 - beta- (low-temperature), 405, 414, 433
 - X-cut, 88
 - Y-cut, 88
- Quartz wedge, 154, 158–160
- Quasicrystals, 244–247, 251–255
 - icosahedral, 246, 252, 255
- Quasi-harmonic approximation, 90, 100, 273, 316
- Quasi-harmonic model, 266, 272
- Quasimoments, 229
- Quasiparticles, 270
- Quasiperiodic structures, 243
- Quasi phase matching, **192**, 198, 210–211
- Quasi-static limit, 317, 327
- R-irreducible representations (*R*-ireps), 351, 358–359, 459, *see also* irreducible representations (physically)
- Raman activity, 290–291, **317**, 318, 320, 323, 327, 358, 363
 - field-induced, 323
 - force-induced, 322–323
 - intrinsic, 324
- Raman scattering, 178, **314**
 - antisymmetric, 318, 320
 - electric-field-induced, 323
 - first-order, 315, 322, 327
 - forbidden, 326
 - force-induced, 322–323
 - higher-order, 326
 - in a magnetic field, 324
 - magnetic-field-induced, 324
 - second-order, 326–327
 - strain-induced, 325
 - stress-induced, 325
 - symmetric, 320, 323, 325
- Raman shift, 314–315
- Raman spectral line shape, 316
- Raman spectroscopy, **290**, 361, 363–365, 367, 370
- Raman tensor, 314, 316, **317**, 318, 321–323, 325–327
 - electric-field-induced, 324–326
 - field-induced, 323–325
 - first-order, 316
 - force-induced, 322–323
 - intrinsic, 322, 324–326
 - magnetic-field-induced, 324–325
 - q-induced, 325
 - strain-induced, 325
 - symmetry of, 317–318
 - zero-field, 325
- Rare-earth metals, 106, 108, 129, 143
- Rayleigh length, 200, 202
- Reciprocal basis, 6–7, 38, 62, 243, 245–247, 249
- Reciprocal cell, 7
- Reciprocal lattice, 10, 47, 49, 243–248, 294, 296–298, 303
- Reciprocal space, 6–7, 10, 38, 245, 249
- Recrystallization twins, *see* annealing twins
- Reducible representations, 36, 118, 350, 356
- Reduction of tensor components, 15–16
 - rank 2, 15–16
 - rank 2 axial tensors, 29
 - rank 3, 15, 17
 - rank 3 reduced polar tensors, 24
 - rank 4, 15, 20
 - rank 4 reduced polar tensors, 26
- Reflection twins, **395–398**, 404–405, 409–410, 416–422, 424–426, 431–434, 436
- Refractive index, 151–152
 - calculation of, 167
 - changes due to strain, 174
 - extraordinary, 153
 - measurement of, 156
 - ordinary, 153
 - real and imaginary components, 167
 - variation with wavelength, 166
- Relativistic effects, **300**, 302
- Relativistic interactions, 108, 119, 122–123
- Relief, 156, 161
- Reorientation transition (magnetic), **131**, 136
- Repetitive twins, 398
- Representation quadric, 99
- Representation surface, 8, 99, 232, 239
- Representations, **34**, 297
 - active, 359
 - contragredient, 38
 - gerade*, 41
 - irreducible, *see* irreducible representations
 - of double groups, 45, 61
 - of double space groups, 50
 - of point groups, 40, 49, 61
 - of space groups, 49
 - of the first kind, 287
 - of the second kind, 288
 - of the third kind, 288
 - projective, 43, 62
 - reducible, *see* reducible representations
 - regular, 36
 - small, 298
 - spin, 61
 - tensor, 42, 291, 305, 310
 - ungerade*, 41
 - vector, 290
- Resonance technique, 88
- Response function, 316, 327
- Retardation, 157, 160
 - effective, 160
 - relative, 157, 159–160
- Reticular merohedry, 425
- Reticular pseudo-merohedry, 423
- Rhombic section, 410, **428**
- Rhombohedral crystals, 406, 416, 418, 420, 423, 430
- Rigidity modulus, 82
- Ripening process, 441
- Rochelle salt, 377–378, 416, 423, 425, 440
- Rotating stage, 154
- Rotation matrix, 5
- Rotation twins, **396–397**, 410, 413, 417–418, 420, 424, 426, 431–432, 434
- Ru₅Ni₂₅Al₇₇, 408
- Rutile (TiO₂), 305, 310–311, 397–399, 408, 421–422, 425–426, 437
 - to anatase phase transition, 437
- Saccharine, 433
- Sanidine, 429
- Sapriel approach, 427
- Satellites, 243–244, 247
- Scattering angle, 314
- Scattering cross section, 330
- Scattering cross section (Raman), 314, 317–318, 320–322
 - first-order, 316–317
 - second-order, 327
 - symmetry properties, 316
- Scattering frequency, 314, 317
- Scattering geometry, 315, 317, 321–322, 326
- Scattering wavevector, 314–315, 317, 321–322
- Schoenflies symbols, 110–111, 358–359, 373–374
- Schrödinger equation, 295, 297, 299–300, 303
- Schrödinger group, 295
- Schur's lemma, **37**, 38, 41, 44, 53, 55
- S-domains, 126, 135, 139
- Second harmonic generation (SHG), 151, 178, 181–182, 191, **197**, 206–207
 - electric-field induced, 151
 - non-resonant, 197, 202–203
 - resonant, 205
 - ultrasonic, 96
- Sector twins, **398**, 399, 402, 408–409, 412, 439
- Seebeck coefficient, 220, **226**
- Seignettelectrics, 377
- Seitz operator, **295**, 297
- Sel de Seignette*, 377
- Selection rules, 312
 - for Brillouin scattering, 329
 - optical, 290
 - polarization, 317, 320, 322, 326
 - Raman scattering, 319, 322, 327
 - Raman tensor, 317
- Self-interaction, 299, 301
- Sellmeier equations, 184, 211, **212**
- Semiconductors, 14, 222, 224, 226, 299, 317, 326
- Semi-core states, 303, 305–306, 310
- Sénarmont compensator, 160
- Sensitive tint, 157, 159
- Sensitive tint plate, 154, 157, 159, 161, 164, 166
- Sets, 380
- Shear
 - homogeneous, 415
 - pure, 76
 - simple, 76
- Shear strain, 101, 349, 426
- Short-range force, 363
- Shubnikov group, 53
- Shubnikov symbols, 111, 373
- SI units, 146
- Sigma notation, 417–418
- Σ1 twins, 418, 422
- Σ2 twins, 418
- Σ3 bicrystal boundaries, 437
- Σ3 twin interface, 437
- Σ3 twins, 415–416, 418–419, 422, 430
- Σ > 3 twins, 418
- Σ5 twins, 424–425, 430
- Σ7 twins, 424
- Σ9 twins, 419
- Σ27 twins, 419
- Σ33 twins, 419, 430
- Σ81 twins, 419
- Silicon, 82, 103, 222–223, 225
- Silicon trichloride, 419
- Silver, 437
- Simple twins, 398, 400, 402
- Sing around method, 89
- Single particle approach, 295
- Sinusoidal structures, 109
- Site symmetry, 229, 232, 386
- Site-symmetry restrictions, 232
- Slater's transition state, 301
- Slow ray, 155, 159–160, 166
- Small representations, 298, 305, 310
- SmS_{1.9}, 418, 424
- Sodium chloride (NaCl), 84, 88
- Sodium nitrate (NaNO₃), 412, 422
- Sodium nitrite (NaNO₂), 244, 369
- Sodium sulfate (Na₂SO₄), 415
- Sodium superoxide (NaO₂), 502
- Soft modes, 338, 350, 358, **361**
- Sommerfeld model, 303, *see also* free-electron model
- Specific heat, 3–4, 31
- Spectral differential cross section, 314–316
- Sphalerite (ZnS), 407, 422
- Spherical harmonics, 302–309
- Spherical symmetry, 11
- Spin density waves, 109
- Spin flip, 124, 127
- Spin flop, 124, 132, 139
- Spinel, 393, 398, 407
- Spinel law, 398, 407, 412, 414, 430
- Spinel twins, 398, 407, 414, 416, 418, 422, 431
- Spin-orbit coupling, 119, 142, 300, 306
- Spin representations, 61
- Spontaneous magnetization, **107**, 109, 116, 119, 125, 127, 131, 140
- Spontaneous magnetostriction, 120, 127, **143**
- Spontaneous nucleation, 412
- Spontaneous parametric emission, 209
- Spontaneous polarization, 12, 140–142, **151**, 193, 351, 362, 393, 430, 449, 452, 472, 490, 495–499, 501
- Spontaneous properties, 452, 455, *see also* morphic properties
- Spontaneous shear, **415**, 427, 440, 449, 502
- Spontaneous strain, **72**, 127, 174, 340, 351, 378, 452, 455–456, 458, 470, 489–491
- St Andrew's cross, 411, *see also* 60° cross
- Stabilizers, 379, **386**, 453, 455–459, 470–472, 474, 476–477, 493, 495
- Stacking fault contrast, 433
- Stacking faults, 394, 397, 419, 433
- Standard variables, 359–360
- Star, **47**, 48–50, 121, 130, 297–298, 305–306
- Static disorder, 228
- Static displacements, 228
- Staurolite, **410**, 421, 424–425
- Stokes process, 316–317, 327

SUBJECT INDEX

- Strain (spontaneous), *see* spontaneous strain
- Strain birefringence, 3, 174
- Strain ellipsoid, 99
- Strain field, 72
- Strain tensor, 4, 13, 24, **72**, 78, 81–85, 90–93, 99, 101, 250–251, 272–273, 349, 351
- Strain-optic tensor, 174
- Stress quadric, 79
- Stress relaxation, *see* stress relief
- Stress relief, 442
- Stress tensor, 4, 13, 24, **76**, 81–82, 84, 90–92, 250, 273
 - local properties, 79
 - Piola–Kirchhoff, 95
 - special forms, 78
 - symmetry of, 77
 - Voigt notation, 78
- Strontium bismuth tantalate ($\text{Sr}_x\text{Bi}_{3-x}\text{Ta}_2\text{O}_9$), 452
- Strontium titanate (SrTiO_3), 351, 363
- Structural twins, 415
- Sublattice index, 418
- Sum-frequency generation (SFG), 178, 182, 189, 197, 206–208
- Superconductors, 268, 307, 309, 370, 416, 428, 440
- Superlattice reflections, 338, 348–349
- Supersaturation twins, 412
- Superspace, 244–246, 250–251
- Superspace groups, 247–249, 252–253
- Susceptibility, 151–152, 168, *see also* dielectric susceptibility
 - electro-optic, third-order, 151
 - higher-order, 150
 - nonlinear, 192, 212
 - optical, third-order, 151
 - paramagnetic, 106–107
- Susceptibility derivatives, 314, 317, 322, 324, 327
 - first-order, 326
 - higher-order, 322
 - second-order, 324
- Susceptibility tensor, 173
- Switching, 373, 450, **470**
- Switching of domains, 127, **415–416**, 442, 449
- Symmetric tensors, 5, 13, 24, 30, 34, 38, 42, 51
 - rank 2, 17, 26, 34, 42, 51–52
 - rank 4, 22
- Symmetry-adapted bases, 372
- Symmetry-breaking increments, 351, 359–360
- Symmetry descent, **350–351**, 378, 382, 384, 452, 470, 477, 500
 - equitranslational 350, 356
- Symmetry species, 318, 320–322, 324–325
- Symmorphic space groups, 48–49, 277, 282, 288, 295
- Systematic extinctions, 248

- Tail-to-tail boundaries, 431
- T-domains, *see* twin domains
- Temperature factor, *see* Debye–Waller factor
- Temperature-stress constants, 32
- Tenfold rotation, 397
- Tensor contraction, 229
- Tensor derivatives, 10
- Tensor expansion, 229
- Tensor parameter, 350, 358, 374, 452, 459
 - principal, 351, 356, 358–361, 373, 387–388, 453, 455, 458–459, 461, 474, 479–480
 - secondary, 351, 355, 358, 360–361, 373, 387, 458–459, 474, 481
- Tensor product, 7–10, 24, 37–38, 41–42, 51–52, 68, 178, 193, 251, 254
- Tensor product space, 42–43, 52–53, 253
- Tensor representation, 42, 291, 305, 310
- Tensorial covariants, 351, 359–360, 372–374, 458–459, 479
- Tensors
 - in higher-dimensional spaces, 249
 - in quasiperiodic structures, 243
 - in superspace, 250–251
 - mathematical definition, 7
 - transformation properties of, 38, 42, 51
 - transformation rules, 7
- Tetragonal crystals, 430
- Thermal conductivity, 5, 9, 13, 220, **224**
- Thermal diffusion, 5
- Thermal displacements, 228
- Thermal expansion, 3–4, 9, 12, 31, 72, 90, **99**, 221, 225, 272–273
 - negative, 103
 - volume, 99
- Thermal motion, 228–229, 232
 - ellipsoid, 239
- Thermal resistance, 224–226
- Thermal resistivity, 224–225
- Third harmonic generation (THG), 178, 181–182, 196–197, **206**, 207
- Threshold oscillation intensity, 209–210
- Tight binding, 301
- Tilings, 244
- Time inversion, 105, 109, 114, 138–139
- Time-reversal degeneracy, 286, 289
- Time-reversal group, 53
- Time-reversal operator, 53–54, 56
- Tin, 84
- TO–LO splitting, 321, 326
- Toroidal moment, 138
- Total cross section, 315
- Tourmaline, 12
- Transformation microcline, 410, 429, 442
- Transformation twins, 378, 397–398, 408, 410–411, **414**, 416, 427, 436, 439–440
- Transition-metal carbonates, 117, 127
- Transition-metal fluorides, 128, 132, 134–137
- Transition-metal oxides, 107, 117, 119, 127
- Transition metals, 106–107, 129
- Transition probability, 312
- Transition region, 433
- Transition susceptibility, 314–315, 317, 321, 325–327
 - first-order, 322
- Transition susceptibility tensor, 315
- Transition temperature, 342, 346, 349–350, 362, 364–365
- Translation boundary, 397, 414
- Translation domains, 394, 397, 414
- Translation group, 423
- Translation twins (T-twins), 397, 414
- Translational symmetry, 294–295, 298–299, 301, 305
- Translationengleiche* subgroups, *see* equitranslational subgroups
- Transverse optic mode (TO), 316, 321, 363
- Triaxial ellipsoid, 154
- Trichroic crystals, 166
- Tricritical point, 362, 369–370
- Triglycine sulfate (TGS), 339, 360, 429, 449–450
- Trilinear forms, 7–8, 14
- Triperiodic twins, 417, **418**, 420, 422–423, 425
- Triple scalar product, 6, 14, 73
- Tris-sarcosine calcium chloride (TSCC), 363, **367**, 369
- Tropochemical cell twinning, 397
- Tungsten, 84
- Tweed microstructure, 441
- Twin axes, 396
 - of order $n > 2$, 420
 - n -fold, 395, 420
 - pseudo-fivefold, 399
 - pseudo n -fold, 428
 - sixfold, 396
 - threefold, 424
 - twofold, 395–397, 399, 418, 428
 - with noncrystallographic multiplicities, 408
- Twin boundaries, 372, 393–394, 397–398, 403, 413–414, 421–422, **426**, 430, 432–433
 - coherent, 443
 - compatible, 429–430, 443, *see also* permissible boundaries
 - incompatible, 429, 443
 - irrational, 433
 - rational, 427
 - structural model, 434
 - three-dimensional structure, 438
- Twin component, 394
- Twin displacement vector, 394, 397, 426, 432, 437
- Twin domains, 126, 174, 394, 400, 403, 405, 412–415, 420, 428, 430–431, 433, 435, 439–440, 442
- Twin elements, 395
 - binary, **395**, 396
 - irrational, 397
 - rational, 397
- Twin formation
 - by nucleation, 412
 - during crystal growth, 413
- Twin inserts, 413
- Twin interface, 394–395, 397, 422, 426, 430, 436–437, 439
 - coherent, 443
 - incoherent, 443
 - irrational, 413
 - rational, 433
- Twin inversion centre, 395, 434
- Twin lamellae, 413–414, 419, 429–431, 434, 436, 440–443
- Twin lattice index, 417
- Twin law, 394, **395**, 399, 405, 409, 451, 462, 470–471, 477–478, 480, 483, 485–486, 490, 498
- Twin microstructure, 72
- Twin mirror plane, 395
- Twin obliquity, 420
- Twin operations, 395, 397
 - alternative, 399–400, 402–403, 407–408
 - binary, 395–396, 401–402
- Twin partner, 394, 398, 401, 405, 408, 417, 423, 425, 432–433
- Twin pattern, 439
- Twin planes, 162, 165
- Twin rotations
 - noncrystallographic, 402
 - pseudo n -fold, 396, 402
- Twin textures, 439
- Twin with lattice index $[j] > 1$, 430
- Twinkling, 156
- Twinning, 174, 338–339, 377, **393**
 - by high-order merohedry, 410
 - by lattice merohedry, 417
 - by merohedry, 377, 416–417, 422, 480
 - by pseudo-merohedry, 377, 422
 - by reticular merohedry, 377, 417, 423–424
 - by reticular pseudo-merohedry, 377, 411
 - by twin-lattice pseudo-symmetry, 422
 - by twin-lattice symmetry, 422
 - definition of, 394
 - lattice aspects of, 416
 - mirror plane, 397
 - with a change of form, 416
 - with partial lattice coincidence (lattice index $[j] > 1$), 423
 - with partial lattice pseudo-coincidence (lattice index $[j] > 1$), 424
 - without a change of form, 416
- Twinning dislocations, 429, 442, 444
- Twinning group, 374, 451, 462, 470, **473**, 477, 480, 484, 486, 490, 498
- Twinning pattern, 339
- Twins, 338, 377, **394**, 451
 - genetic classification of, 412
 - with inclined axes, 404–405
- Twins of twins, 412
- Two-dimensional nucleus, 413
- Two-wave mixing, 151

- Undepleted pump approximation, **196**, 197, 202, 205–207
- Uniaxial antiferromagnets, 123–124, 137
- Uniaxial classes, **160**, 165, 185, 194–195
- Uniaxial crystals, **11**, 118, 153, **155–156**, 165–166, 168, 170, 185–186, 189, 196, 199–201, 212, 318
- Uniaxial ellipsoid, 153
- Uniaxial figure, 161, 165
- Uniaxial negative, 161
- Uniaxial positive, 161
- Unit-cell twinning, 397
- Universal stage, 166

- Valence electrons, 297, 299, 302, 305–307, 312
- Valence states, 300, 303, 305, 312
- Variants, *see* domain states
- Variational principle, 300–301, 303
- Vector product, 9–10, 12–13
- Vector representation, 290

SUBJECT INDEX

- Vector spaces, 5, 7
- Velocity of elastic waves, 270
- Velocity of sound, 176
- Vibration direction, 154, **155**, 156
 - fast, 159
 - slow, 159
- Voigt effect, *see* Cotton–Mouton effect
- Voigt matrix, 24, 502
- Voigt notation, 24, 78–79, 81–82, 172–173
- Voigt strain matrix, 24–27, 75
- Voigt stress matrix, 24, 78
- Voronoi cell, 46–47, 294
- W boundary, 427–428
- W' boundary, 427–428
- Walk-off, 184–187, 194, 197, 200–203, 206–208, 211–212
- Wigner–Seitz cell, 46, 294
- Wurtzite, 223
- Wyckoff position, 49, 62, 232
- X-ray absorption spectra, 312
- X-ray anomalous dispersion, 167
- X-ray emission spectra, 312
- X-ray topography, 423, 429, 433, 436, 443
- Young’s modulus, 3, 80–81, **83**, 416
 - variation with orientation, 83
- Yttrium aluminium borate [$\text{YAl}(\text{BO}_3)_4$], 214
- Yttrium barium copper oxide (YBaCuO), 309–310, 370, 416, 428, 440–441, 443, 449, 484
- Yttrium manganese oxide (YMnO_3), 142
- Zero-point motion, 228
- Zinc, 84
- Zinc oxide, 223
- Zwilling*, *see* twins